Flares

SUVI data as an alternative source for EUV imaging data:
SUVI data guide for SDO/AIA users

GOES images and movies Sun now
https://lasp.colorado.edu/space-weather-portal/now/sun

GOES, access *via* https://www.ngdc.noaa.gov/stp/satellite/goes/index.html

Секундные данные GOES в двух каналах 1-8 А и 0.5-4 А брали с сайта **https://umbra.nascom.nasa.gov/goes/fits/** . Для вычисления приращения потока в канале 1-8 А использовались процедуры по работе с данными GOES пакета SolarSoft https://hesperia.gsfc.nasa.gov/rhessidatacenter/complementary_data/goes.html .

Данные GOES
ftp://satdat.ngdc.noaa.gov/sem/goes/data/avg/
https://satdat. ngdc.noaa.gov/sem/goes/data/new_full/
Old "satdat" base URL -> New base URL
https://satdat.ngdc.noaa.gov/sem/goes/ -> **https://www.ncei.noaa.gov/data/goes-space-environment-monitor/access/**
https://satdat.ngdc.noaa.gov/sxi/ -> **https://www.ncei.noaa.gov/data/goes-solar-xray-imager/access/**
https://satdat.ngdc.noaa.gov/dmsp/ -> **https://www.ncei.noaa.gov/data/dmsp-space-weather-sensors/access/**
https://satdat.ngdc.noaa.gov/sem/poes/ -> **https://www.ncei.noaa.gov/data/poes-metop-space-environment-monitor/access/**

The standard two-dimensional CSHKP model of flares:
Carmichael 1964, NASA Special Publication, 50, 451, https://articles.adsabs.harvard.edu/pdf/1964NASSP..50..451C ;
Sturrock 1966, Nature, 211, 695, https://sci-hub.ru/10.1038/211695a0 ;
Hirayama 1974, Solar Physics, 34, 323, https://sci-hub.ru/10.1007/BF00153671 ;
Kopp & Pneuman 1976, Solar Physics, 50, 85, doi: https://sci-hub.ru/10.1007/BF00206193

Space Weather Live
https://www.spaceweatherlive.com/en.html

Solar Demon **https://www.sidc.be/solardemon/**
Flares, Dimmings and EUV waves event detection

Preliminary Current Catalogue of Solar Flare Events, 2018,
www.wdcb.ru/stp/data/Solar_Flare_Events/Fl_XXIV.pdf

V.N.Ishkov Catalog of Solar Flare Events with X-ray Classes M1 - X>17.5 XXIV Cycle of Solar Activity (I.2009 – I2.2019 …)

The data center for the Spectrometer and Telescope for Imaging X-rays (STIX) on board Solar Orbiter https://datacenter.stix.i4ds.net/stix

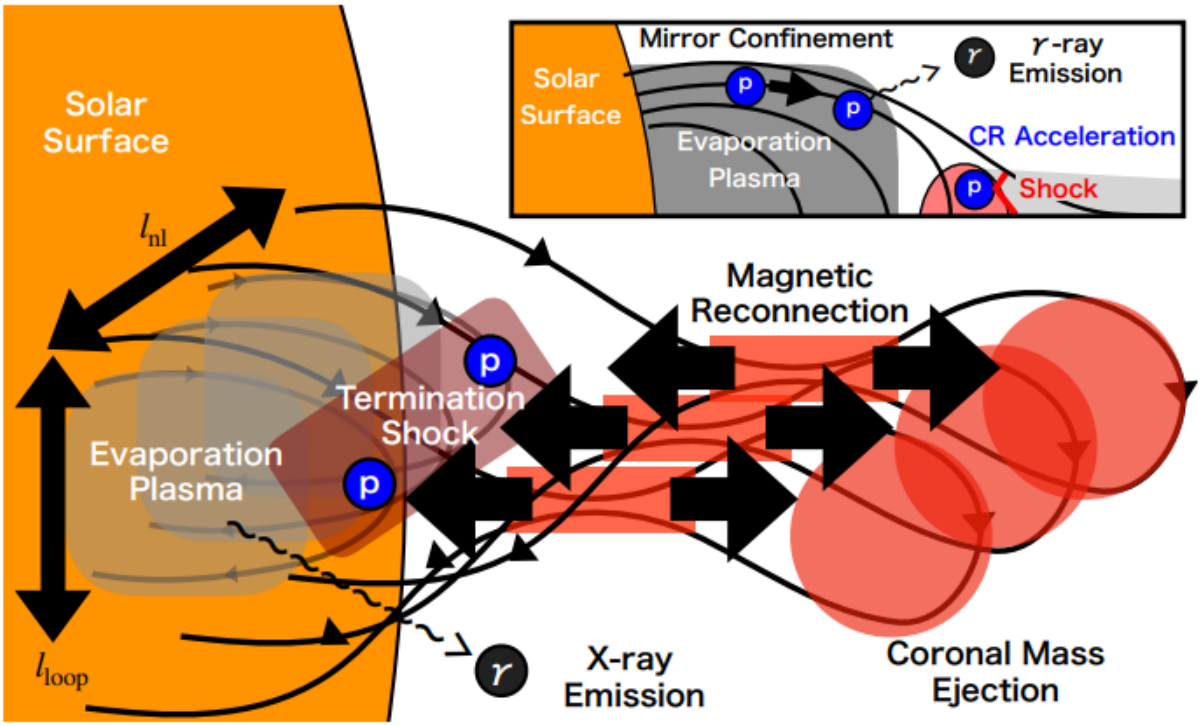

Figure 1. Schematic picture of our hadronic gamma-ray emission model from the impulsive phase of solar flares. The magnetic reconnection event produces bipolar outflows. One outflow is ejected to interplanetary space, which is known as CME. The other outflow collides with the magnetic field loops, which leads to the formation of a termination shock. Non-thermal electron beam and thermal conduction by the shocked gas heat up the chromospheric plasma. This leads to the hot plasma upflows (so-called chromospheric evaporation), and the flare loops are filled with the evaporation plasma. In our model, CR protons are accelerated at the shock and confined inside the flare loop owing to the magnetic mirror effect, as seen in the inset of the figure. These CR protons produce hadronic gamma rays via hadronuclear interactions with the evaporation plasma.

Kimura et al. 2022 Хорошее описание импульсной и постепенной фаз вспышек
https://arxiv.org/pdf/2211.13891.pdf

A Database of Magnetic and Thermodynamic Properties of Confined And Eruptive Solar Flares

Maria D. **Kazachenko**
ApJ **2023**
https://arxiv.org/pdf/2310.02878.pdf **File**
I.Introduction
RibbonDB dataset (Kazachenko et al. 2017) http://solarmuri.ssl.berkeley.edu/~kazachenko/RibbonDB/
SolarErupDB database **http://solarmuri.ssl.berkeley.edu/~kazachenko/SolarErupDB/**

Probability Distribution Functions of Solar and Stellar Flares

Takashi **Sakurai**
Physics, vol. 5, issue 1, pp. 11-23 **2022**
https://arxiv.org/ftp/arxiv/papers/2212/2212.02678.pdf
https://www.mdpi.com/2624-8174/5/1/2
We studied the soft X-ray data flare fluence

http://solarwww.mtk.nao.ac.jp/sakurai/tar/goesfluence_datalist.zip
for the flare fluence above 5×10–5 J m–2 (1997-2020) and peak flux above 1×10–7 W m–2 (1980-2020), respectively.
Data Availability Statement: **The GOES flare peak flux data are available at** https://www.ngdc.noaa.gov/stp/space-weather/solar-data/solar-features/solar-flares/x- rays/goes/xrs/ for the years 1975-2016, and at ftp://ftp.swpc.noaa.gov/pub/warehouse/ for 2017 and later. **The fluence data are included in these data after 1997.**
The X-ray background data for the years 1983-2011 are given in ftp://ftp.ngdc.noaa.gov/STP/SOLAR_DATA/SATELLITE_ENVIRONMENT/Daily_Fluences/Fluence. **The background data for 2011-2019** are available at https://satdat.ngdc.noaa.gov/sem/goes/data/science/xrs/ and at https://data.ngdc.noaa.gov/platforms/solar-space-observing-satellites/goes/ for 2020. The background values between 1983 March and 1987 were calculated from the 1-minute intensities given at https://satdat.ngdc.noaa.gov/sem/goes/data/avg.

Flare Index Catalog Data (1976-2021)
https://astronomi.boun.edu.tr/flare-index

A new catalogue of solar flare events from soft x-ray GOES signal in the period 1986-2020
Nicola **Plutino**, Francesco Berrilli, Dario Del Moro, Luca Giovannelli
Advances in Space Research **2022**
https://arxiv.org/pdf/2211.10189.pdf

List of GOES flares and CMEs
https://www.ngdc.noaa.gov/stp/space-weather/solar-data/solar-features/solar-flares/x-rays/goes/xrs/
https://cdaw.gsfc.nasa.gov/pub/yashiro/flare_cme/fclist_pub.txt
```
Yashiro et al. 2006, ApJ, 650, L143
# http://adsabs.harvard.edu/abs/2006ApJ...650L.143Y
```

List of high-cadence IRIS flare observations: 15 Dec 2021-… 2022
https://docs.google.com/document/d/1iPQPTYPULzrnjbnN38j6j0p2AccPTJc1xbqEXZmr0mU/edit

Space Sci. Rev. 2020-**2022** Topical Collection : Oscillatory Processes in Solar and Stellar Corona.
Seven comprehensive review papers
https://link.springer.com/journal/11214/topicalCollection/AC_b5bf4ca939ef807534e522d3c54d129f

We conduct **a post hoc analysis** of solar flare predictions

SDO/AIA

Table A1: AIA wavelength bands.

Channel name	Primary ion(s)	Region of atmosphere*	Char. log(T)
white light	continuum	photosphere	3.7
1700Å	continuum	temperature minimum, photosphere	3.7
304Å**	He II	chromosphere, transition region	4.7
1600Å**	C IV+cont.	transition region + upper photosphere	5.0
171Å**	Fe IX	quiet corona, upper transition region	5.8
193Å**	Fe XII, XXIV	corona and hot flare plasma	6.1, 7.3
211Å**	Fe XIV	active-region corona	6.3
335Å**	Fe XVI	active-region corona	6.4
94Å**	Fe XVIII	flaring regions (partial readout possible)	6.8
131Å**	Fe VIII, XX, XXIII	flaring regions (partial readout possible)	5.6, 7.0, 7.2

* Absorption allows imaging of chromospheric material within the corona; ** in baseline program

---

Magnetohydrodynamic (MHD) Waves and Oscillations in the Sun's Corona and MHD Coronal Seismology
Solar Phys. **2021** Topical collection (23 articles)
link.springer.com/journal/11207/topicalCollection/AC_dd43639faf4f387889037783ce77c71b/page/1

SDO JSOC Data-Product FITS File Changes
http://jsoc.stanford.edu/

Space Weather Database Of Notifications, Knowledge, Information (DONKI)
One-stop on-line **tool for space weather** researchers and forecasters.
https://ccmc.gsfc.nasa.gov/donki/

Data files of **soft X-rays** from NOAA (ftp://satdat.ngdc.noaa.- gov/sem/goes/data/avg/) with a 1-minute cadence
GOES solar flare catalogue (ftp://ftp.ngdc. noaa.gov/STP/space-weather/solar-data/solar-features/solar-flares/ x-rays/goes/)

The GOES, PAMELA and STEREO data are available at
https://www.ngdc.noaa.gov/stp/satellite/goes/
https://www.ssdc.asi.it/pamela/ and
http://www.srl.caltech.edu/STEREO/, respectively.

Top 50 solar flares by years and Cycles
https://www.spaceweatherlive.com/en/solar-activity/top-50-solar-flares.html

GOES, access via https: //www.ngdc.noaa.gov/stp/satellite/goes/index.html

The basic soft X-ray photometry of solar flares comes from NOAA's GOES satellites, which began systematic flare observations from space in the 1970s and continue to the present with

approximately the same instrumentation, detecting few-keV X-rays in two standard wavelength bands: 1-8 Â ("soft") and 0.5-4 Â ("hard").
As is well known, flares occur in a broad distribution of magnitudes, which NOAA simplifies by the "ABCMX" logarithmic flux scale; these magnitude levels range from 10-8 to 10-4 W/m2, respectively.

Table 1. Event catalogs currently implemented in the Interactive Multi-Instrument Database of Solar Flares (https://solarflare.njit.edu/).

Source Name	Dates presented	Source web link
Primary flare lists		
GOES flare list	Jan, 2002 — current time	ftp://ftp.swpc.noaa.gov/pub/warehouse/
RHESSI flare list	Feb, 2002 — current time	http://hesperia.gsfc.nasa.gov/hessidata/dbase/
HEK flare list	Feb, 2010 — current time	https://www.lmsal.com/isolsearch
Secondary event catalogs		
IRIS observing logs	Jul, 2013 — current time	http://iris.lmsal.com/search/
Hinode flare catalog	Nov, 2006 — July, 2016	http://st4a.stelab.nagoya-u.ac.jp/hinode_flare/
Fermi GBM flare catalog	Nov, 2008 — current time	https://hesperia.gsfc.nasa.gov/fermi/gbm/qlook/
Nobeyama coverage check	Jan, 2010 — current time	ftp://solar-pub.nao.ac.jp/pub/nsro/norp/xdr/
OVSA flare catalog	Jan, 2002 — Dec, 2003	http://www.ovsa.njit.edu/data/
CACTus CME catalog	Jan, 2002 — current time	http://sidc.oma.be/cactus/
Filament eruption catalog	Apr, 2010 — Oct, 2014	http://aia.cfa.harvard.edu/filament/
Konus-Wind flare catalog	Jan, 2002 — Jul, 2016	http://www.ioffe.ru/LEA/Solar/index.html

Guide to SDO Data Analysis
edited by Marc DeRosa & Greg Slater
September 14, **2020**
https://www.lmsal.com/sdodocs/doc/dcur/SDOD0060.zip/zip/entry/index.html

Multi-Instrument Database of Solar Flares (this https URL).
Interactive Multi-Instrument Database of Solar Flares
Viacheslav M **Sadykov**, Rishabh Gupta, Alexander G Kosovichev, Vincent Oria, Gelu M Nita
Astrophysical Journal Supplement Series, Volume 231, Issue 1, article id. 6 **2017**
https://arxiv.org/pdf/1702.02991.pdf
https://iopscience.iop.org/article/10.3847/1538-4365/aa79a9/pdf

KW-Sun: Konus-Wind Solar Flare Database
http://www.ioffe.ru/LEA/kwsun/

A Catalog of Solar Flare Events Observed by the SOHO/EIT
Sumanth A. **Rotti**, Petrus C.H. Martens, Berkay Aydin
ApJS **249** 20 **2020**
https://arxiv.org/pdf/2007.05586.pdf
https://doi.org/10.3847/1538-4365/ab9a42

Секундные данные GOES в двух каналах 1-8 А и 0.5-4 А брали с сайта https://umbra.nascom.nasa.gov/goes/fits/ . Для вычисления приращения потока в канале 1-8 А использовались процедуры по работе с данными GOES пакета SolarSoft https://hesperia.gsfc.nasa.gov/rhessidatacenter/complementary_data/goes.html .

GOES, access *via* https://www.ngdc.noaa.gov/stp/satellite/goes/index.html;
RHESSI via https://hesperia.gsfc.nasa.gov/ssw/hessi/doc/guides/hessi_data_access.htm, and

SDO/AIA via https://sdo.gsfc.nasa.gov/data/.

1Список событий GOES ftp://ftp.swpc.noaa.gov/pub/indices/events/

ftp://ftp.ngdc.noaa.gov/STP/space-weather/solar-data/solar-features/solar-flares/x-rays/goes/xrs

Solar Ultraviolet Imager (SUVI) on board the NOAA GOESR satellite
(Seaton & Darnel 2018), https://iopscience.iop.org/article/10.3847/2041-8213/aaa28e/pdf

Science-Quality GOES 13-15 XRS Data Set Released
https://www.ngdc.noaa.gov/stp/satellite/goes-r.html
https://solarnews.nso.edu/science-quality-goes-13-15-xrs-data-set-released/
https://satdat.ngdc.noaa.gov/sem/goes/data/**plots**/ Месячные профили

X-ray data from Solar X-Ray Sensor (XRS) event files of GOES-15 satellite observations on the **NOAA database** https://satdat.ngdc.noaa.gov/sem/goes/data/full/
See Ravishankar and Michałek A&A 638, A42 (**2020**) **File**

Данные GOES
ftp://satdat.ngdc.noaa.gov/sem/goes/data/avg/

Public release of co-aligned IRIS/SST data sets
Posted by Luc Rouppe van der Voort | June 12, 2020 | General news
Since the launch of IRIS in 2013, researchers from the University of Oslo and the Lockheed Martin Solar and Astrophysics Laboratory (LMSAL) have conducted coordinated observing campaigns with IRIS and the Swedish 1-m Solar Telescope (SST) on La Palma. Co-aligned IRIS/SST datasets are now available in the search engine at https://iris.lmsal.com/search/ (click on the More button, Coordinated Observations). Details of the released datasets are described in https://arxiv.org/abs/2005.14175 and IRIS Technical Note 47 (https://iris.lmsal.com/documents.html)

Flares, active regions and related activity

Списки вспышек 1955-2020

https://www.ngdc.noaa.gov/stp/space-weather/solar-data/solar-features/solar-flares/

```
The Catalog of Solar Flare Events with X-ray Class M1 - X>17.5

        XXIII cycle of Solar Activity (1996 - 2008)
```

http://www.wdcb.ru/stp/data/Solar_Flare_Events/FI_XXIII.txt

Вспышки цикла 24 (2009-2017)

http://www.wdcb.ru/stp/data/Solar_Flare_Events/FI_XXIV.txt

the GOES flare catalog
https://hesperia.gsfc.nasa.gov/goes/goes_event_listings/

Hinode Flare Catalog (https://hinode.isee.nagoya-u.ac.jp/flare_catalogue/),
which is maintained by ISAS/JAXA and Institute for SpaceEarth Environmental Research (ISEE), Nagoya University.

Ioffe Institute. Laboratory for Experimental Astrophysics
KW-Sun: Konus-Wind Solar Flare Database (1994-2017)
Solar Flare Database – All Data Are On-line Now
http://www.ioffe.ru/LEA/kwsun/

Interactive Multi-Instrument Database of Solar Flares
Viacheslav M **Sadykov**, Rishabh Gupta, Alexander G Kosovichev, Vincent Oria, Gelu M Nita
Solar Phys. **2017**
https://arxiv.org/pdf/1702.02991.pdf

The Coronas-F Space Mission **Book**
Key Results for Solar Terrestrial Physics
Vladimir **Kuznetsov**
in Astrophysics and Space Science Library (**2014**)
2014, XII, 483 p. 319 illus., 48 illus. in color.
http://link.springer.com/book/10.1007/978-3-642-39268-9

Recent results from Hinode:
PASJ special issue, Volume 66 Issue SP1 December **2014**
http://pasj.oxfordjournals.org/content/66/SP1.toc

Solar Phys., **257**, Number 1, May 2012.
Solar Flare Magnetic Fields and Plasmas / Guest Editors: Y. Fan and G. H. Fisher

---

Solar Phys.
Numbers 1-2 / Май 2009 г.
STEREO Science Results at Solar Minimum | Guest Editors: E. R. Christian, M. L. Kaiser, T. A. Kucera, O. C. St. Cyr

---

Hinode "a new solar observatory in space"
Saku **Tsuneta**1, Louise K. Harra2, and Satoshi Masuda3
Climate andWeather of the Sun-EarthSystem(CAWSES):SelectedPapers from the2007KyotoSymposium, Edited by T. Tsuda, R. Fujii, K. Shibata, and M. A. Geller, pp. 63–75.
c_TERRAPUB, Tokyo, **2009, File.**

Since its launch in September 2006, the Japan-US-UK solar physics satellite, Hinode, has continued its observation of the sun, sending back solar images of unprecedented clarity every day. Hinode is equipped with three telescopes, a visible light telescope, an X-ray telescope, and an extreme ultraviolet imaging spectrometer. The Hinode optical telescope has a large primary mirror measuring 50 centimeters in diameter and is the world's largest space telescope for observing the sun and its vector magnetic fields. The impact of Hinode as an optical telescope on solar physics is comparable to that of the Hubble Space Telescope on optical astronomy. While the optical telescope observes the sun's surface, the Hinode X-ray telescope captures images of the corona and the high-temperature flares that range between several million and several tens of millions of degrees. The telescope has captured coronal structures that are clearer than ever. The Hinode EUV imaging spectrometer possesses approximately ten times the sensitivity and four times the resolution of a similar instrument on the SOHO satellite. The source of energy for the sun is in the nuclear fusion reaction that takes place at its core. Here temperature drops closer to the surface, where the temperature measures about 6,000 degrees. Mysteriously, the temperature starts rising again above the surface, and the temperature of the corona is exceptionally high, several millions of degrees. It is as if water were boiling fiercely in a kettle placed on a stove with no fire, inconceivable as it may sound. The phenomenon is referred to as the coronal heating problem, and it is one of the major astronomical mysteries. The Hinode observatory was designed to solve this mystery. It is expected that Hinode would also provide clues to unraveling why strong magnetic fields are formed and how solar flares are triggered. An overview on the initial results from Hinode is presented. Dynamic video pictures captured by Hinode can be viewed on the website of the National Astronomical Observatory of Japan (NAOJ) at http://hinode.nao.ac.jp/index e.shtml.

The Hinode Mission

Sakurai, Takashi (Ed.)
Reprinted from Solar Physics Journal, Vol. 243/1, 2007 and Vol. 249/2, 2008
2009, IV, 208 p. 140 illus., 45 in color., Hardcover
ISBN: 978-0-387-88738-8

The Solar-B satellite was launched in 2006 by the Institute of Space and Astronautical Science, Japan Aerospace Exploration Agency (ISAS/JAXA), and was renamed Hinode ('sunrise' in Japanese). Hinode carries three instruments: the X-ray telescope (XRT), the EUV imaging spectrometer (EIS), and the Solar Optical Telescope (SOT). These instruments were developed by ISAS/JAXA in cooperation with the National Astronomical Observatory of Japan as domestic partner, and NASA and the Science and Technology Facilities Council (UK) as international partners. ESA and the Norwegian Space Center have been providing a downlink station.

The Hinode (Solar-B) Mission gives a comprehensive description of the Hinode mission and its instruments onboard. This book is most useful for researchers, professionals, and graduate students working in the field of solar physics, astronomy, and space instrumentation. This is the only book that carefully describes the details of the Hinode mission; it is richly illustrated with full-color images and figures.

This volume combines the first set of instrumental papers on the mission overview, EIS, XRT, and the database system along with the second set of papers on SOT and XRT.

A Topical Issue on the Hinode Mission

"Solar Physics", Volume **249**, Number 2, **2008**
http://springerlink.com/content/hg3825426kx8/?p=0dd9afd47ba747c59caa6b78641b2467&pi=0

- The Solar Optical Telescope for the Hinode Mission: An Overview
- The Solar Optical Telescope of Solar-B (Hinode): The Optical Telescope Assembly
- Image Stabilization System for Hinode (Solar-B) Solar Optical Telescope
- Polarization Calibration of the Solar Optical Telescope onboard Hinode
- The Hinode X-Ray Telescope (XRT): Camera Design, Performance and Operations

---

---------- Hinode description

The *Hinode* (Solar-B) Mission: An Overview

T. **Kosugi** · K. Matsuzaki · T. Sakao · T. Shimizu · Y. Sone · S. Tachikawa · T. Hashimoto · K. Minesugi · A. Ohnishi · T. Yamada · S. Tsuneta · H. Hara · K. Ichimoto · Y. Suematsu · M. Shimojo · T.Watanabe · S. Shimada · J.M. Davis · L.D. Hill · J.K. Owens · A.M. Title · J.L. Culhane · L.K. Harra · G.A. Doschek · L. Golub
Solar Phys (**2007**) **243**: 3–17, **File**

The EUV Imaging Spectrometer for Hinode

J.L. **Culhane** · L.K. Harra · A.M. James · K. Al-Janabi · L.J. Bradley · R.A. Chaudry · K. Rees · J.A. Tandy · P. Thomas · M.C.R. Whillock · B.Winter · G.A. Doschek · C.M. Korendyke · C.M. Brown · S. Myers · J. Mariska · J. Seely · J. Lang · B.J. Kent · B.M. Shaughnessy · P.R. Young · G.M. Simnett · C.M. Castelli · S. Mahmoud · H. Mapson-Menard · B.J. Probyn · R.J. Thomas · J. Davila · K. Dere · D. Windt · J. Shea · R. Hagood · R. Moye · H. Hara · T.Watanabe · K. Matsuzaki · T. Kosugi · V. Hansteen · Ø. Wikstol
Solar Phys (2007) 243: 19–61

The EUV Imaging Spectrometer (EIS) on Hinode will observe solar corona and upper transition region emission lines in the wavelength ranges 170 – 210 Å and 250 – 290 Å.
EIS can scan a field of 6 x 8.5 arc min with spatial and velocity scales of 1 arc sec and 25 km s^{-1} per pixel.

http://www.springerlink.com/content/x4455n22v12u0kqw/

The X-Ray Telescope (XRT) for the *Hinode* Mission

L. **Golub** · E. DeLuca · G. Austin · J. Bookbinder · D. Caldwell · P. Cheimets · J. Cirtain · M. Cosmo · P. Reid · A. Sette · M. Weber · T. Sakao · R. Kano · K. Shibasaki · H. Hara · S. Tsuneta · K. Kumagai · T. Tamura · M. Shimojo · J. McCracken · J. Carpenter · H. Haight · R. Siler · E. Wright · J. Tucker · H. Rutledge · M. Barbera · G. Peres · S. Varisco
Solar Phys (2007) 243: 63–86
http://www.springerlink.com/content/553m078nl22u6562/

Data Archive of the Hinode Mission

K. **Matsuzaki** · M. Shimojo · T.D. Tarbell · L.K. Harra · E.E. Deluca
Solar Phys (2007) 243: 87–92
http://www.springerlink.com/content/m54m42754357796m/

Special Issue: Initial Results from Hinode

PUBLICATIONS OF THE ASTRONOMICAL SOCIETY OF JAPAN
Vol. 59, No. SP3 (2007 November 30)

http://pasj.asj.or.jp/v59/v59sp3.html

Rapid Fluctuations in Solar Flares

Proceedings of a workshop held at the Ramada Hotel Lanham, Maryland September 30-October 4,1985, NASA Conference Publication 2449, **1987**
Edited by Brian R. Dennis, Larry E.Orwig, AlanL.Kiplinger,
Section 1 - X-rays, Section 2 - Radio and Microwaves
https://www.academia.edu/24803822/Rapid_spectral_and_flux-time_variations_in_a_solar_burst_observed_at_various_dm-mm_wavelengths_and_at_hard_x_rays?auto=download

---

A Deep Learning Approach to Operational Flare Forecasting

Yasser **Abduallah**, Jason T. L. Wang
2024
https://arxiv.org/pdf/2405.16080

Solar flares are explosions on the Sun. They happen when energy stored in magnetic fields around solar active regions (ARs) is suddenly released. In this paper, we present a transformer-based framework, named SolarFlareNet, for predicting whether an AR would produce a gamma-class flare within the next 24 to 72 hours. We consider three gamma classes, namely the >=M5.0 class, the >=M class and the >=C class, and build three transformers separately, each corresponding to a gamma class. Each transformer is used to make predictions of its corresponding gamma-class flares. The crux of our approach is to model data samples in an AR as time series and to use transformers to capture the temporal dynamics of the data samples. Each data sample consists of magnetic parameters taken from Space-weather HMI Active Region Patches (SHARP) and related data products. We survey flare events that occurred from May 2010 to December 2022 using the Geostationary Operational Environmental Satellite X-ray flare catalogs provided by the National Centers for Environmental Information (NCEI), and build a database of flares with identified ARs in the NCEI flare catalogs. This flare database is used to construct labels of the data samples suitable for machine learning. We further extend the deterministic approach to a calibration-based probabilistic forecasting method. The SolarFlareNet system is fully operational and is capable of making near real-time predictions of solar flares on the Web.

Search for Solar Flare Neutrinos with the KamLAND detector

S. **Abe**, S. Asami, A. Gando, Y. Gando, T. Gima, A. Goto, ….
ApJ **924** 103 **2022**
https://arxiv.org/pdf/2105.02458.pdf
https://iopscience.iop.org/article/10.3847/1538-4357/ac35d1/pdf
We report the result of a search for neutrinos in coincidence with solar flares from the GOES flare database. The search was performed on a 10.8 kton-year exposure of KamLAND collected from 2002 to 2019. We found no statistical excess of neutrinos and established 90\% confidence level upper limits of 8.4×107\,cm−2 (3.0×109\,cm−2) on electron anti-neutrino (electron neutrino) fluence at 20\,MeV normalized to the X12 flare, assuming that the neutrino fluence is proportional to the X-ray intensity. The 90\% C.L. upper limits from this work exclude the entire region of parameter space associated with the Homestake event excess for the large solar flare in 1991. **2004 Feb 26**

Signature of the turbulent component of solar dynamo on active region scales and its association with flaring activity

Valentina I. **Abramenko**
MNRAS Volume 507, Issue 3, Pages 3698–3706, **2021**
https://arxiv.org/pdf/2111.04425.pdf
https://watermark.silverchair.com/stab2404.pdf
https://doi.org/10.1093/mnras/stab2404
It is a challenging problem to obtain observational evidence of the turbulent component of solar dynamo operating in the convective zone because the dynamo action is hidden below the photosphere. Here we present results of a statistical study of flaring active regions (ARs) that produced strong solar flares of an X-ray class X1.0 and higher during a time period that covered solar cycles 23 and 24. We introduced a magneto-morphological classification of ARs, which allowed us to estimate the possible contribution of the turbulent component of the dynamo into the structure of an AR. We found that in 72 per cent of cases, flaring ARs do not comply with the empirical laws of the global dynamo (frequently they are not bipolar ARs or, if they are, they violate the Hale polarity law, the Joy law, or the leading sunspot prevalence rule). This can be attributed to the influence of the turbulent dynamo action inside the convective zone on spatial scales of typical ARs. Thus, it appears that the flaring is governed by the turbulent component of the solar dynamo. The contribution into the flaring from these AR 'violators' (irregular ARs) is enhanced during the second maximum and the descending phase of a solar cycle, when the toroidal field weakens and the influence of the turbulent component becomes more pronounced. These observational findings are in consensus with a concept of the essential role of non-linearities and turbulent intermittence in the magnetic fields generation inside the convective zone, which follows from dynamo simulations. **16 Oct 1999, 15 Feb 2011, 26 Sep 2011, 27 Oct 2013, 6 Sep 2017**
Table 2. ARs with X-class flares in the 23rd cycle (1996-2006)
Table 3. ARs with X-class flares in the 24th cycle (2011-2017)

Possibilities of predicting flare productivity based on magnetic field power spectra in active regions

Abramenko, V. I.
Geomagnetism and Aeronomy, Volume 55, Issue 7, pp.860-865, **2015**
Photospheric plasma is in a state of developed turbulence. Chaotic motions in the photosphere and below are among the main sources of eruptive processes in the solar atmosphere. The magnetic field power spectra, as measured in the active region (AR) photosphere, were used as a source of information on the photospheric plasma turbulent state and as a tool for predicting AR flare productivity. It was shown that, first, ARs with the Kolmogorov power spectrum evolve mainly without catastrophes—strong flares—and have rather regular and simple magnetic configurations. At the same time, ARs with a spectrum steeper than the Kolmogorov have increased flare productivity and complex magnetic configurations. Second, a steep non-Kolmogorov spectrum in the early stage of AR development indicates that the AR flare productivity is high over the followingdays. Third, the time fluctuations in the spectral index in flare-active regions reach 30% and are much higher than the fluctuations in low-flaring ARs. Periods with an increased absolute value of the spectral index, i.e., periods with a steeper spectrum, are observed approximately 1-2 days before a powerful flare. The data make it possible to assume that an energy relationship exists between the photosphere and the overlying atmosphere and to use the magnetic power spectrum as a tool for predicting AR flare activity.

INTERMITTENCY AND MULTIFRACTALITY SPECTRA OF THE MAGNETIC FIELD IN SOLAR ACTIVE REGIONS

Valentyna **Abramenko** and Vasyl Yurchyshyn
Astrophysical Journal, 722:122–130, **2010**
We present the results of a study of intermittency and multifractality of magnetic structures in solar active regions (ARs). Line-of-sight magnetograms for 214 ARs of different flare productivity observed at the center of the solar disk from 1997 January until 2006 December are utilized. Data from the Michelson Doppler Imager (MDI)

instrument on board the *Solar and Heliospheric Observatory* operating in the high resolution mode, the Big Bear Solar Observatory digital magnetograph, and the *Hinode* SOT/SP instrument were used. Intermittency spectra were derived from high-order structure functions and flatness functions. The flatness function exponent is a measure of the degree of intermittency. We found that the flatness function exponent at scales below approximately 10 Mm is correlated with flare productivity (the correlation coefficient is −0.63). The *Hinode* data show that the intermittency regime is extended toward small scales (below 2 Mm) as compared to the MDI data. The spectra of multifractality, derived from the structure functions and flatness functions, are found to be broader for ARs of higher flare productivity as compared to those of low flare productivity. The magnetic structure of high-flaring ARs consists of a voluminous set of monofractals, and this set is much richer than that for low-flaring ARs. The results indicate the relevance of the multifractal organization of the photospheric magnetic fields to the flaring activity. The strong intermittency observed in complex and high-flaringARs is a hint that we observe a photospheric imprint of enhanced sub-photospheric dynamics.

Features of Microwave Radiation and Magnetographic Characteristics of Solar Active Region NOAA 12242 Before the X1.8 Flare on December 20, 2014

V.E.**Abramov-Maximov** (1), V.N.Borovik (1), L.V.Opeikina (2), A.G.Tlatov (1), L.V.Yasnov (3) ((1) Central Astronomical Observatory at Pulkovo, Saint-Petersburg, Russia, (2) Special Astrophysical Observatory, Nizhnii Arkhyz, Russia, (3) St. Petersburg State University, Saint-Petersburg, Russia)
Geomagnetism and Aeronomy, **2017**, Vol. 57, No. 8, p.978
https://arxiv.org/pdf/1711.09134.pdf

This paper continues the cycle of authors' works on the detection of precursors of large flares (M5 and higher classes) in active regions (ARs) of the Sun by their microwave radiation and magnetographic characteristics. Generalization of the detected precursors of strong flares can be used to develop methods for their prediction. This paper presents an analysis of the development of NOAA AR 12242, in which an X1.8 flare occurred on **December 20, 2014**. The analysis is based on regular multiazimuth and multiwavelength observations with the RATAN-600 radio telescope in the range 1.65-10 cm with intensity and circular polarization analysis and data from the Solar Dynamics Observatory (SDO). It was found that a new component appeared in the AR microwave radiation two days before the X-flare. It became dominant in the AR the day before the flare and significantly decreased after the flare. The use of multiazimuth observations from RATAN-600 and observations at 1.76 cm from the Nobeyama Radioheliograph made it possible to identify the radio source that appeared before the X-flare with the site of the closest convergence of opposite polarity fields near the neutral line in the AR. It was established that the X-flare occurred 20 h after the total gradient of the magnetic field of the entire region calculated from SDO/HMI data reached its maximum value. Analysis of the evolution of the microwave source that appeared before the X-flare in AR 12242 and comparison of its parameters with the parameters of other components of the AR microwave radiation showed that the new source can be classified as neutral line associated source (NLS), which were repeatedly detected by the RATAN-600 and other radio telescopes 1-3 days before the large flares.

Dynamics of Microwave Sources Associated with the Neutral Line and the Magnetic-Field Parameters of Sunspots as a Factor in Predicting Large Flares

V. E. **Abramov-Maximov**, V. N. Borovik, L. V. Opeikina, A. G. Tlatov
Solar Phys., **2014**

We studied the evolution of five active regions (ARs) where strong X-class flares occurred in 2011 – 2012 (NOAA ARs **11158, 11166, 11263, 11283 and 11520**). Our study focuses on the pre-flare phase of these ARs (during a few days before the flare) to reveal features in the microwave radiation and magnetic-field characteristics of the ARs that indicate that a powerful flare is about to take place. One well-developed AR (NOAA AR 11654) that did not produce large flares was also studied. We used daily multiwavelength spectral-polarization solar observations in the range of 1.65 – 6.0 cm
made with the RATAN-600 radio telescope and data obtained by the Solar Dynamics Observatory/Helioseismic and Magnetic Imager (SDO/HMI). Whenever X-class flares occurred, we found that a new compact microwave source developed that was associated with the neutral line of the photospheric magnetic field (neutral line associated source – NLS) above the place with highest gradient of magnetic field. In some cases this became predominant in radio emission of the AR one to two days before a large flare. No such source was detected in AR without a powerful flare. An analysis of magnetic-field characteristics of sunspots (based on SDO/HMI data) showed that the large X-flares we investigated occurred in ARs with high magnetic flux (~ 1022 Mx) and with an increasing magnetic-field gradient. We first identified the positions of the developing microwave source (NLS) with the location of the large flare that was registered in the AR one to two days later. Radio characteristics and dynamics of NLS detected before large flares possibly reflect the place in the corona where the energy for flaring is stored. Thus, an early detection of a rapidly developing microwave source NLS and an increasing magnetic-field gradient can be used as a factor in predicting large flares.

Fermi-LAT Observations of High-energy Behind-the-limb Solar Flares

M. **Ackermann**1, A. Allafort2, L. Baldini3, G. Barbiellini4,5, D. Bastieri6,7, R. Bellazzini8, E. Bissaldi9, R. Bonino10,11, E. Bottacini2, J. Bregeon12Show full author list

2017 ApJ 835 219

http://sci-hub.cc/doi/10.3847/1538-4357/835/2/219

https://arxiv.org/pdf/1702.00641v1.pdf

We report on the Fermi-LAT detection of high-energy emission from the behind-the-limb (BTL) solar flares that occurred on **2013 October 11, and 2014 January 6 and September 1**. The Fermi-LAT observations are associated with flares from active regions originating behind both the eastern and western limbs, as determined by STEREO. All three flares are associated with very fast coronal mass ejections (CMEs) and strong solar energetic particle events. We present updated localizations of the >100 MeV photon emission, hard X-ray (HXR) and EUV images, and broadband spectra from 10 keV to 10 GeV, as well as microwave spectra. We also provide a comparison of the BTL flares detected by Fermi-LAT with three on-disk flares and present a study of some of the significant quantities of these flares as an attempt to better understand the acceleration mechanisms at work during these occulted flares. We interpret the HXR emission to be due to electron bremsstrahlung from a coronal thin-target loop top with the accelerated electron spectra steepening at semirelativistic energies. The >100 MeV gamma-rays are best described by a pion-decay model resulting from the interaction of protons (and other ions) in a thick-target photospheric source. ***The protons are believed to have been accelerated (to energies >10 GeV) in the CME environment and precipitate down to the photosphere from the downstream side of the CME shock and landed on the front side of the Sun, away from the original flare site and the HXR emission.***

HIGH-ENERGY GAMMA-RAY EMISSION FROM SOLAR FLARES: SUMMARY OF FERMI LAT DETECTIONS AND ANALYSIS OF TWO M-CLASS FLARES

M. **Ackermann**2, M. Ajello3, A. Albert4, A. Allafort5,1, L. Baldini6, G. Barbiellini7,8, D. Bastieri et al. **Fermi-LAT collaboration**

E-print, April **2013, File**; **2014** ApJ 787 15

We present the detections of 19 solar flares detected in high-energy gamma rays (above 100 MeV) with the Fermi Large Area Telescope (LAT) during its first four years of operation. Interestingly, all flares are associated with fairly fast Coronal Mass Ejections (CMEs) and are not all powerful X-ray flares. We then describe the detailed temporal, spatial and spectral characteristics of the first two long-lasting events: the **2011 March 7** flare, a moderate (M3.7) impulsive flare followed by slowly varying gamma-ray emission over 13 hours, and the **2011 June 7** M2.5 flare, which was followed by gamma-ray emission lasting for 2 hours. We compare the Fermi-LAT data with X-ray and proton data measurements from GOES and RHESSI. We argue that a hadronic origin of the gamma rays is more likely than a leptonic origin and find that the energy spectrum of the proton distribution softens after the 2011 March 7 flare, favoring a scenario with continuous acceleration at the flare site. This work suggests that proton acceleration in solar flares is more common than previously thought, occurring for even modest X-ray flares, and for longer durations.

FERMI DETECTION OF γ-RAY EMISSION FROM THE M2 SOFT X-RAY FLARE ON 2010 JUNE 12

M. **Ackermann** et al.

2012 ApJ 745 144

The Geostationary Operational Environmental Satellite (GOES) M2-class solar flare, **SOL2010-06-12T00:57**, was modest in many respects yet exhibited remarkable acceleration of energetic particles. The flare produced an ~50 s impulsive burst of hard X- and γ-ray emission up to at least 400 MeV observed by the Fermi Gamma-ray Burst Monitor and Large Area Telescope experiments. The remarkably similar hard X-ray and high-energy γ-ray time profiles suggest that most of the particles were accelerated to energies 300 MeV with a delay of ~10 s from mildly relativistic electrons, but some reached these energies in as little as ~3 s. The γ-ray line fluence from this flare was about 10 times higher than that typically observed from this modest GOES class of X-ray flare. *There is no evidence for time-extended >100 MeV emission as has been found for other flares with high-energy γ-rays.*

Large Scale Evaluation of Deep Learning-based Explainable Solar Flare Forecasting Models with Attribution-based Proximity Analysis

Temitope **Adeyeha**, Chetraj Pandey, Berkay Aydin

IEEE International Conference on Big Data **2024**

https://arxiv.org/pdf/2411.18070

Accurate and reliable predictions of solar flares are essential due to their potentially significant impact on Earth and space-based infrastructure. Although deep learning models have shown notable predictive capabilities in this domain, current evaluations often focus on accuracy while neglecting interpretability and reliability--factors that are especially

critical in operational settings. To address this gap, we propose a novel proximity-based framework for analyzing post hoc explanations to assess the interpretability of deep learning models for solar flare prediction. Our study compares two models trained on full-disk line-of-sight (LoS) magnetogram images to predict ≥M-class solar flares within a 24-hour window. We employ the Guided Gradient-weighted Class Activation Mapping (Guided Grad-CAM) method to generate attribution maps from these models, which we then analyze to gain insights into their decision-making processes. To support the evaluation of explanations in operational systems, we introduce a proximity-based metric that quantitatively assesses the accuracy and relevance of local explanations when regions of interest are known. Our findings indicate that the models' predictions align with active region characteristics to varying degrees, offering valuable insights into their behavior. This framework enhances the evaluation of model interpretability in solar flare forecasting and supports the development of more transparent and reliable operational systems. **2015-01-01**

Hybrid data-driven magnetofrictional and magnetohydrodynamic simulations of an eruptive solar active region

A. **Afanasyev**, Y. Fan, M. Kazachenko, M. Cheung
ApJ **952** 136 **2023**
https://arxiv.org/pdf/2306.05388.pdf
https://iopscience.iop.org/article/10.3847/1538-4357/acd7e9/pdf
We present first results of the hybrid data-driven magnetofrictional (MF) and data-constrained magnetohydrodynamic (MHD) simulations of solar active region NOAA 11158, which produced an X-class flare and coronal mass ejection on **2011 February 15**. First, we apply the MF approach to build the coronal magnetic configuration corresponding to the SDO/HMI photospheric magnetograms by using the JSOC PDFI SS electric field inversions at the bottom boundary of the simulation domain. We then use the pre-eruptive MF state at about 1.5 hour before the observed X-class flare as the initial state for the MHD simulation, assuming a stratified polytropic solar corona. The MHD run shows that the initial magnetic configuration containing twisted magnetic fluxes and a 3D magnetic null point is out of equilibrium. We find the eruption of a complex magnetic structure consisting of two magnetic flux ropes, as well as the development of flare ribbons, with their morphology being in good agreement with observations. We conclude that the combination of the data-driven MF and data-constrained MHD simulations is a useful practical tool for understanding the 3D magnetic structures of real solar ARs that are unobservable otherwise.

Validation of the PDFI_SS method for electric field inversions using a magnetic flux emergence simulation

Andrey N. **Afanasyev**, Maria D. Kazachenko, Yuhong Fan, George H. Fisher, Benoit Tremblay
ApJ Volume 919, Issue 1, id.7, **2021**
https://arxiv.org/pdf/2106.10579.pdf
https://iopscience.iop.org/article/10.3847/1538-4357/ac0d01/pdf
Knowledge of electric fields in the photosphere is required to calculate the electromagnetic energy flux through the photosphere and set up boundary conditions for data-driven magnetohydrodynamic (MHD) simulations of solar eruptions. Recently, the PDFI_SS method for inversions of electric fields from a sequence of vector magnetograms and Doppler velocity measurements was improved to incorporate spherical geometry and a staggered-grid description of variables. The method was previously validated using synthetic data from anelastic MHD (ANMHD) simulations. In this paper, we further validate the PDFI_SS method, using approximately one-hour long MHD simulation data of magnetic flux emergence from the upper convection zone into the solar atmosphere. We reconstruct photospheric electric fields and calculate the Poynting flux, and compare those to the actual values from the simulations. We find that the accuracy of the PDFI_SS reconstruction is quite good during the emergence phase of the simulated ephemeral active region evolution and decreases during the shearing phase. Analysing our results, we conclude that the more complex nature of the evolution (compared to the previously studied ANMHD case) that includes the shearing evolution phase is responsible for the obtained accuracy decrease.

Solar flare observations with the Radio Neutrino Observatory Greenland (RNO-G)

S. **Agarwal**, J. A. Aguilar, S. Ali, P. Allison, M. Betts, +++
A&A **2024**
https://arxiv.org/pdf/2404.14995.pdf
The science program of the Radio Neutrino Observatory-Greenland (RNO-G) extends beyond particle astrophysics to include radioglaciology and, as we show herein, solar physics, as well. Impulsive solar flare observations not only permit direct measurements of light curves, spectral content, and polarization on time scales significantly shorter than most extant dedicated solar observatories, but also offer an extremely useful above-surface calibration source, with pointing precision of order tens of arc-minutes. Using the early RNO-G data from 2022-2023, observed flare characteristics are compared to well-established solar observatories. Also, a number of individual flares are used to highlight angular reconstruction and calibration methods. RNO-G observes signal excesses during solar flares reported by the solar-observing Callisto network and in coincidence with about 60% of the brightest excesses recorded by the SWAVES satellite, when the Sun is above the horizon for RNO-G. In these observed flares, there is significant

impulsivity in the time-domain. In addition, the solar flares are used to calibrate the RNO-G absolute pointing on the radio signal arrival direction to sub-degree resolution. **2022-09-29**

Study of Reconnection Dynamics and Plasma Relaxation in MHD simulation of a Solar Flare

Satyam **Agarwal**, Ramit Bhattacharyya, Shangbin Yang

Solar Phys. **299**, 15 **2024**

https://arxiv.org/pdf/2401.11417.pdf

https://doi.org/10.1007/s11207-024-02255-5

Self-organization in continuous systems is associated with dissipative processes. In particular, for magnetized plasmas, it is known as magnetic relaxation, where the magnetic energy is converted into heat and kinetic energy of flow through the process of magnetic reconnection. An example of such a system is the solar corona, where reconnection manifests as solar transients like flares and jets. Consequently, toward investigation of plasma relaxation in solar transients, we utilize a novel approach of data-constrained MHD simulation for an observed solar flare. The selected active region NOAA 12253 hosts a GOES M1.3 class flare. The investigation of extrapolated coronal magnetic field in conjunction with the spatiotemporal evolution of the flare reveals a hyperbolic flux tube (HFT), overlying the observed brightenings. MHD simulation is carried out with the EULAG-MHD numerical model to explore the corresponding reconnection dynamics. The overall simulation shows signatures of relaxation. For a detailed analysis, we consider three distinct sub-volumes. We analyze the magnetic field line dynamics along with time evolution of physically relevant quantities like magnetic energy, current density, twist, and gradients in magnetic field. In the terminal state, none of the sub-volumes are seen to reach a force-free state, thus remaining in non-equilibrium, suggesting the possibility of further relaxation. We conclude that the extent of relaxation depends on the efficacy and duration of reconnection, and hence, on the energetics and time span of the flare. **04 January, 2015**

How to Train Your Flare Prediction Model: Revisiting Robust Sampling of Rare Events

Azim **Ahmadzadeh**, Berkay Aydin, Manolis K. Georgoulis, Dustin J. Kempton, Sushant S. Mahajan, Rafal A. Angryk

ApJS **254** 23 **2021**

https://arxiv.org/pdf/2103.07542.pdf

https://agupubs.onlinelibrary.wiley.com/doi/epdf/10.1029/2021SW002841

https://doi.org/10.3847/1538-4365/abec88

We present a case study of solar flare forecasting by means of metadata feature time series, by treating it as a prominent class-imbalance and temporally coherent problem. Taking full advantage of pre-flare time series in solar active regions is made possible via the Space Weather Analytics for Solar Flares (SWAN-SF) benchmark dataset; a partitioned collection of multivariate time series of active region properties comprising 4075 regions and spanning over 9 years of the Solar Dynamics Observatory (SDO) period of operations. We showcase the general concept of temporal coherence triggered by the demand of continuity in time series forecasting and show that lack of proper understanding of this effect may spuriously enhance models' performance. We further address another well-known challenge in rare event prediction, namely, the class-imbalance issue. The SWAN-SF is an appropriate dataset for this, with a 60:1 imbalance ratio for GOES M- and X-class flares and a 800:1 for X-class flares against flare-quiet instances. We revisit the main remedies for these challenges and present several experiments to illustrate the exact impact that each of these remedies may have on performance. Moreover, we acknowledge that some basic data manipulation tasks such as data normalization and cross validation may also impact the performance -- we discuss these problems as well. In this framework we also review the primary advantages and disadvantages of using true skill statistic and Heidke skill score, as two widely used performance verification metrics for the flare forecasting task. In conclusion, we show and advocate for the benefits of time series vs. point-in-time forecasting, provided that the above challenges are measurably and quantitatively addressed.

Challenges with Extreme Class-Imbalance and Temporal Coherence: A Study on Solar Flare Data

Azim **Ahmadzadeh**, Maxwell Hostetter, Berkay Aydin, Manolis K. Georgoulis, Dustin J. Kempton, Sushant S. Mahajan, Rafal A. Angryk

IEEE BigData **2019**

https://arxiv.org/pdf/1911.09061.pdf

In analyses of rare-events, regardless of the domain of application, class-imbalance issue is intrinsic. Although the challenges are known to data experts, their explicit impact on the analytic and the decisions made based on the findings are often overlooked. This is in particular prevalent in interdisciplinary research where the theoretical aspects are sometimes overshadowed by the challenges of the application. To show-case these undesirable impacts, we conduct a series of experiments on a recently created benchmark data, named Space Weather ANalytics for Solar Flares (SWAN-SF). This is a multivariate time series dataset of magnetic parameters of active regions. As a remedy for the imbalance issue, we study the impact of data manipulation (undersampling and oversampling) and model manipulation (using class weights). Furthermore, we bring to focus the auto-correlation of time series that is inherited from the use of sliding

window for monitoring flares' history. Temporal coherence, as we call this phenomenon, invalidates the randomness assumption, thus impacting all sampling practices including different cross-validation techniques. We illustrate how failing to notice this concept could give an artificial boost in the forecast performance and result in misleading findings. Throughout this study we utilized Support Vector Machine as a classifier, and True Skill Statistics as a verification metric for comparison of experiments. We conclude our work by specifying the correct practice in each case, and we hope that this study could benefit researchers in other domains where time series of rare events are of interest. **Feb. 24, 2014**

Solar Flare Prediction Using Advanced Feature Extraction, Machine Learning, and Feature Selection

Omar W. **Ahmed**, Rami Qahwaji, Tufan Colak, Paul A. Higgins, Peter T. Gallagher, D. Shaun Bloomfield
Solar Physics , March **2013**, Volume 283, Issue 1, pp 157-175
Novel machine-learning and feature-selection algorithms have been developed to study: i) the flare-prediction-capability of magnetic feature (MF) properties generated by the recently developed Solar Monitor Active Region Tracker (SMART); ii) SMART's MF properties that are most significantly related to flare occurrence. Spatiotemporal association algorithms are developed to associate MFs with flares from April 1996 to December 2010 in order to differentiate flaring and non-flaring MFs and enable the application of machine-learning and feature-selection algorithms. A machine-learning algorithm is applied to the associated datasets to determine the flare-prediction-capability of all 21 SMART MF properties. The prediction performance is assessed using standard forecast-verification measures and compared with the prediction measures of one of the standard technologies for flare-prediction that is also based on machine-learning: Automated Solar Activity Prediction (ASAP). The comparison shows that the combination of SMART MFs with machine-learning has the potential to achieve more accurate flare-prediction than ASAP. Feature-selection algorithms are then applied to determine the MF properties that are most related to flare occurrence. It is found that a reduced set of six MF properties can achieve a similar degree of prediction accuracy as the full set of 21 SMART MF properties.

Active Region Coronal Rain Event Observed by the Fast Imaging Solar Spectrograph on the NST

Kwangsu **Ahn**, Jongchul Chae, Kyung-Suk Cho, Donguk Song, Heesu Yang, Philip R. Goode, Wenda Cao, Hyungmin Park, Jakyung Nah, Bi-Ho Jang, Young-Deuk Park
Solar Physics, Volume 289, Issue 11, pp 4117-4136 **2014**
http://link.springer.com/article/10.1007%2Fs11207-014-0559-x
The Fast Imaging Solar Spectrograph (FISS) is being operated on the New Solar Telescope of the Big Bear Solar Observatory. It simultaneously records spectra of Hα and Ca ii 8542 Å lines, and this dual-spectra measurement provides an estimate of the temperature and nonthermal speed components. We observed a loop structure in **AR 11305** using the FISS, SDO/AIA, and STEREO/EUVI in 304 Å, and found plasma material falling along the loop from a coronal height into the umbra of a sunspot, which accelerated up to 80 km s−1. We also observed **C2 and C7 flare** events near the loop. The temperature of the downflows was in the range of 10 000 – 33 000 K, increasing toward the umbra. The temperature of the flow varied with time, and the temperature near the footpoint rose immediately after the C7 flare, but the temperature toward the umbra remained the same. There seemed to be a temporal correlation between the amount of downflow material and the observed C-class flares. The downflows decreased gradually soon after the flares and then increased after a few hours. These high-speed red-shift events occurred continuously during the observations. The flows observed on-disk in Hα and Ca ii 8542 Å appeared as fragmented, fuzzy condensed material falling from the coronal heights when seen off-limb with STEREO/EUVI at 304 Å. Based on these observations, we propose that these flows were an on-disk signature of coronal rain.

Impulsive and Long Duration High-energy Gamma-Ray Emission from the Very Bright 2012 March 7 Solar Flares

M. **Ajello**1, A. Albert2, A. Allafort2,
E-print, April **2013, File**; **2014** ApJ 789 20
The Fermi Large Area Telescope (LAT) detected gamma-rays up to 4 GeV from two bright X-class solar flares on 2012 March 7, showing both an impulsive and temporally extended emission phases. The gamma-rays appear to originate from the same active region as the X-rays associated with these flares. The >100 MeV gamma-ray flux decreases monotonically during the first hour (impulsive phase) followed by a slower decrease for the next 20 hr. A power law with a high-energy exponential cutoff can adequately describe the photon spectrum. Assuming that the gamma rays result from the decay of pions produced by accelerated protons and ions with a power-law spectrum, we find that the index of that spectrum is ~3, with minor variations during the impulsive phase. During the extended phase the photon spectrum softens monotonically, requiring the proton index varying from ~4 to >5. The >30 MeV proton flux observed

by the GOES satellites also shows a flux decrease and spectral softening, but with a harder spectrum (index ~2-3). Based on these observations, we explore the relative merits of prompt or continuous acceleration scenarios, hadronic or leptonic emission processes, and acceleration at the solar corona or by the fast coronal mass ejections. **We conclude that the most likely scenario is continuous acceleration of protons in the solar corona that penetrate the lower solar atmosphere and produce pions that decay into gamma rays. However, acceleration in the downstream of the shock cannot be definitely ruled out.**

Electric Current Approach Studying Both Auroral Substorms and Solar Flares Together

Syun-Ichi **Akasofu*** **Review**

Front. Astron. Space Sci., 06 March **2020** | https://doi.org/10.3389/fspas.2020.00004

https://www.frontiersin.org/articles/10.3389/fspas.2020.00004/pdf

Auroral substorms and solar flares are basically various manifestations of electromagnetic energy dissipation processes, so it is useful to consider both phenomena in terms of a chain of processes, consisting of power supply (dynamo), transmission (currents/circuits), and dissipation (auroral substorms, solar flares), the electric current approach. In this short review, we briefly describe both phenomena together on the basis of the chain process. It is shown that the introduction of a dynamo process in this consideration provides a step-by-step way of studying both phenomena. It is shown that (a) both the solar wind–magnetosphere dynamo and a photospheric dynamo proposed by Lee et al. (1995) have enough power to accumulate enough energy for the explosive features of both phenomena, respectively. (b) For substorms, the power is accumulated in the inner magnetosphere and inflates it, and for flares, the power is likely to be accumulated in a loop current along and above two-ribbon flares. (c) For substorms, the energy release (unloading) process deflates the inner magnetosphere, resulting in an earthward electric field, and for flares, the disruption of the loop current suggested by Alfven (1950) may be responsible for the energy release.

A new and quantitative prediction scheme for solar flares

Syun-Ichi **Akasofu**

Journal of Atmospheric and Solar-Terrestrial Physics Volume 174, September **2018**, Pages 66-70

https://reader.elsevier.com/reader/sd/C6242C7F5E9BDE0F090DD73FEC0C41BED507809788F6C553CE4B20F88CD9E37B34BED4E254836400DAF7A9F76DF18976

At the present time, there is no quantitative way to predict not only the onset time of solar flares, but also their intensity. In the past, most solar flare prediction studies have searched for various precursors of the onset of flares. In this paper, we consider a new and quantitative approach to predict the onset of the explosive process of solar flares and their intensity, based on the principle that solar flares are basically various manifestations of electromagnetic energy dissipation, so that a dynamo process in the photosphere as its power supply is essential. The power is a basic physical quantity (erg/s), so that it can, at least in principle, be universally applicable for all flares. The power of the photospheric dynamo is given by the Poynting flux $P= V(B2/8\pi)S$ erg/s, where V and B are the plasma speed and magnetic field intensity, and S is the dimension of the plasma flow; these quantities are in principle observable simultaneously all together, in addition to the dissipation rate δ (for example, the Hα emission rate). In fact, if one can follow the development of the power P(t) and $[\int P(t)dt - \int \delta(t)dt]$, it may be possible, together with various precursors, to predict in principle the onset time and the intensity of flares at least semi-quantitatively, although this task will require much experience on the basis of a large number of flares. Unfortunately, however, all the needed simultaneous data set (V, B, S, δ) is not available in the present literature, so that one incomplete case is examined. This concept has been examined for auroral substorms, which are also manifestations of electromagnetic energy dissipation and have the explosive feature. This was possible, because the simultaneous data sets (V, B, S, δ) are available.

Incorporating Polar Field Data for Improved Solar Flare Prediction

Mehmet **Aktukmak**, Zeyu Sun, Monica Bobra, Tamas Gombosi, Ward B. Manchester, Yang Chen, Alfred Hero

Frontiers **2022**

https://arxiv.org/pdf/2212.01730.pdf

In this paper, we consider incorporating data associated with the sun's north and south polar field strengths to improve solar flare prediction performance using machine learning models. When used to supplement local data from active regions on the photospheric magnetic field of the sun, the polar field data provides global information to the predictor. While such global features have been previously proposed for predicting the next solar cycle's intensity, in this paper we propose using them to help classify individual solar flares. We conduct experiments using HMI data employing four different machine learning algorithms that can exploit polar field information. Additionally, we propose a novel probabilistic mixture of experts model that can simply and effectively incorporate polar field data and provide on-par prediction performance with state-of-the-art solar flare prediction algorithms such as the Recurrent Neural Network (RNN). Our experimental results indicate the usefulness of the polar field data for solar flare prediction, which can improve Heidke Skill Score (HSS2) by as much as 10.1%.

Reduction of the downward energy flux of non-thermal electrons in the solar flare corona due to co-spatial return current losses

Meriem **Alaoui**, Gordon D. Holman, Marc Swisdak

ApJ **974** 177 **2024**

https://arxiv.org/abs/2407.17955

https://iopscience.iop.org/article/10.3847/1538-4357/ad71cb/pdf

High energy electrons carry much of a solar flare's energy. Therefore, understanding changes in electron beam distributions during their propagation is crucial. A key focus of this paper is how the co-spatial return current reduces the energy flux carried by these accelerated electrons. We systematically compute this reduction for various beam and plasma parameters relevant to solar flares. Our 1D model accounts for collisions between beam and plasma electrons, return current electric-field deceleration, thermalization in a warm target approximation, and runaway electron contributions. The results focus on the classical (Spitzer) regime, offering a valuable benchmark for energy flux reduction and its extent. Return current losses are only negligible for the lowest nonthermal fluxes. We calculate the conditions for return current losses to become significant and estimate the extent of the modification to the beam's energy flux density. We also calculate two additional conditions which occur for higher injected fluxes: (1) where runaway electrons become significant, and (2) where current-driven instabilities might become significant, requiring a model that self-consistently accounts for them. Condition (2) is relaxed and the energy flux losses are reduced in the presence of runaway electrons. All results are dependent on beam and co-spatial plasma parameters. We also examine the importance of the reflection of beam electrons by the return-current electric field. We show that the interpretation of a number of flares needs to be reviewed to account for the effects of return currents.

RHESSI Nuggets #477 **2024** https://heliowiki.smce.nasa.gov/wiki/index.php/How_much_of_the_energy_in_flare-accelerated_electrons_reaches_the_chromosphere%3F

How much of the energy in flare-accelerated electrons reaches the chromosphere? Keeping flare-accelerated electrons out of the chromosphere.

Role of Suprathermal Runaway Electrons Returning to the Acceleration Region in Solar Flares

Meriem **Alaoui**, Gordon D. Holman, Joel C. Allred, Rafael T. Eufrasio

ApJ **917** 74 **2021**

https://arxiv.org/pdf/2103.13999.pdf

https://iopscience.iop.org/article/10.3847/1538-4357/ac0820/pdf

https://doi.org/10.3847/1538-4357/ac0820

During solar flares, a large flux of energetic electrons propagate from the tops of reconnecting magnetic flux tubes toward the lower atmosphere. Over the course of the electrons' transport, a co-spatial counter-streaming return current is induced, thereby balancing the current density. In response to the return current electric field, a fraction of the ambient electrons will be accelerated into the runaway regime. However, models describing the accelerated electron beam/return-current system have generally failed to take these suprathermal runaway electrons into account self-consistently. We develop a model in which an accelerated electron beam drives a steady-state, sub-Dreicer co-spatial return-current electric field, which locally balances the direct beam current and freely accelerates a fraction of background (return-current) electrons. The model is self-consistent, i.e., the electric field induced by the co-evolution of the direct beam and the runaway current is considered. We find that (1) the return current electric field can return a significant number of suprathermal electrons to the acceleration region, where they can be further accelerated to higher energies, runaway electrons can be a few tens of percent of the return current flux returning to the nonthermal beam's acceleration region, (2) the energy gain of the suprathermal electrons can be up to 10−35\,keV, (3) the heating rate in the corona can be reduced by an order of magnitude in comparison to models which neglect the runaway component. The results depend on the injected beam flux density, the temperature and density of the background plasma.

Statistical Study of Hard X-Ray Spectral Breaks in Solar Flares

Meriem **Alaoui**, Säm Krucker, Pascal Saint-Hilaire

Solar Physics August **2019**, 294:105

sci-hub.se/10.1007/s11207-019-1495-6

The Reuven Ramaty High Energy Solar Spectroscopic Imager (RHESSI) provides hard X-ray spectral observations with ≈1 keV≈1 keV resolution to study flare-accelerated (>10 keV>10 keV) electrons through their bremsstrahlung emission. Here we report on a statistical study of RHESSI flares with emission above 150 keV, focusing on the spectral shape at the hard X-ray peak. Spectral parameters are derived by fitting the photon spectrum with a broken power law and by the standard thick-target fit. Consistent with previous studies, the most common spectral shape of the photon spectrum (52 out of 65 events) is a double power law with a downward break (“knee”), with ten events showing a single power law and three events having an upward break (“ankle”). The spectral breaks occur typically around 55 keV and the difference of the spectral index above and below the break, γ2 and γ1, is typically between 0.3 and 1. We show correlations between the downward break parameters. The most prominent correlation, with a rank order coefficient of ρ=0.92ρ=0.92, is between the power-law indices above and below the break: γ1=(0.74±0.04)γ2+(0.34±0.14).

Applying a thick target fit to the photon spectrum, a similar correlation is also found for the flare-accelerated electron spectra with $\delta 1=(0.85\pm0.08)\delta 2-(0.3\pm0.3)$ ($\rho=0.67$). Spectral breaks could be a property of the acceleration mechanism itself or they could be a secondary effect produced by particle transport or wave-particle interactions. Any theoretical models should be consistent with these correlations. In addition, we find that one upward and 23 (49%) downward breaks are consistent with nonuniform ionization within the thick target. **2004/07/16, 2002/04/10, 2004/07/15**
Table (2002-2006)

Understanding breaks in solar flares x-ray spectra: Evaluation of a co-spatial return-current model

Meriem **Alaoui**, Gordon Holman
2017 *ApJ* **851** 78
https://arxiv.org/pdf/1706.03897.pdf
We investigate the possibility of explaining hard x-ray spectral breaks in terms of a 1D model with a co-spatial return current. We choose 19 flares observed by the Ramaty High Energy Solar Spectroscopic Imager (RHESSI) with strong spectral breaks at lower energies, around a few deka-keV, that cannot be explained by Compton back-scattering or non-uniform ionization alone. We identify these strong breaks at the HXR peak time, but we obtain 8 s cadence spectra of the entire impulsive phase. We then fit these spectra using a model in which electrons with an initially power-law distribution lose energy through return-current losses until they reach the thick-target chromosphere, where they lose all of their remaining energy through Coulomb collisions. Our main results are: (1) The return-current collisional thick-target model provides an acceptable fit for spectra with a strong flattening at lower energies; (2) the resistivity is found to be typically 2 orders of magnitude higher than Spitzer values (3) in the upper limit of the low-energy cutoff Ec, any runaway population of return-current electrons is negligible, and the anomalous Dreicer field is at least an order of magnitude higher than the return-current electric field. This also suggests that instability of the return current might not be responsible for the "enhanced" resistivity; (4) in the lower limit of Ec, a non-negligible runaway population can contribute to carrying the return current, but the background thermal electrons carry the return current in most cases; (5) in the upper limit of the cutoff energy, the drift velocity of the beam electrons is low enough to keep the return current stable to the generation of standard current-driven instabilities; (6) it is possible that the return current is carried by the beam electrons, which would require relaxing the 1D assumption, thus invalidating the anomalous resistivity result.
Table 1: Event list and spectral fit parameters at the time of peak emission.
19- and 20-Jan-2005
RHESSI Science Nuggets # 330 **2018**
http://sprg.ssl.berkeley.edu/~tohban/wiki/index.php/Understanding_the_co-spatial_return_current_in_solar_flares

Return-current Model Spectra and Enhanced Plasma Resistivity

Meriem **Alaoui** and Gordon Holman
RHESSI Science Nuggets #259 August, **2015**
http://sprg.ssl.berkeley.edu/~tohban/wiki/index.php/Return-current_Model_Spectra_and_Enhanced_Plasma_Resistivity
Solar flares involve sudden brightening across the whole range of the electromagnetic spectrum, and in particular the hard X-ray emission has proved to be a crucial factor in deciphering flare physics. The most common hard X-ray emission is an "impulsive" source that seems to define the main energy release of a flare, although other more gradual energy releases may also take place. The hard X-rays come from bremsstrahlung, a very inefficient emission mechanism, and the mere existence of hard X-ray sources implies a large amount of energy in energetic electrons.
We have found (Ref. [2]) that spectra with strong breaks can be fitted with a return current model.

Inferring Fundamental Properties of the Flare Current Sheet Using Flare Ribbons: Oscillations in the Reconnection Flux Rates

Marcel F. Corchado **Albelo**, Maria D. Kazachenko, Benjamin J. Lynch
ApJ **965** 16 **2024**
https://arxiv.org/pdf/2402.03567.pdf
https://iopscience.iop.org/article/10.3847/1538-4357/ad25f4/pdf
Magnetic reconnection is understood to be the main physical process that facilitates the transformation of magnetic energy into heat, motion, and particle acceleration during solar eruptions. Yet, observational constraints on reconnection region properties and dynamics are limited due to lack of high-cadence and high-spatial-resolution observations. By studying the evolution and morphology of post-reconnected field-lines footpoints, or flare ribbons and vector photospheric magnetic field, we estimate the magnetic reconnection flux and its rate of change with time to study the flare reconnection process and dynamics of the current sheet above. We compare high-resolution imaging data to study the evolution of the fine structure in flare ribbons as ribbons spread away from the polarity inversion line. Using data from two illustrative events (one M- and X-class flare), we explore the relationship between the ribbon-front fine structure and the temporal development of bursts in the reconnection region. Additionally, we use the RibbonDB database to perform statistical analysis of 73 (C- to X-class) flares and identify QPP's properties using the Wavelet

Transform. Our main finding is the discovery of quasi-periodic pulsations (QPP) signatures in the derived magnetic reconnection rates in both example events and the large flare sample. We find that the oscillations' periods range from one to four minutes. Furthermore, we find nearly co-temporal bursts in Hard X-ray (HXR) emission profiles. We discuss how dynamical processes in the current sheet involving plasmoids can explain the nearly-co-temporal signatures of quasi periodicity in the reconnection rates and HXR emission. **2014-09-10, 2015-11-04**
Table 2. Magnetic reconnection rate oscillation period for each of the 73 flares included in our study. 2010-2015
IRIS Nugget Aug 2024 https://iris.lmsal.com/nugget

An automated classification approach to ranking photospheric proxies of magnetic energy build-up

Amani **Al-Ghraibah**, Laura. E. Boucheron, R.T.James McAteer
A&A 579, A64 (**2015**)
http://arxiv.org/pdf/1506.08717v1.pdf
We study the photospheric magnetic field of ~2000 active regions in solar cycle 23 to search for parameters indicative of energy build-up and subsequent release as a solar flare. We extract three sets of parameters: snapshots in space and time- total flux, magnetic gradients, and neutral lines; evolution in time- flux evolution; structures at multiple size scales- wavelet analysis. This combines pattern recognition and classification techniques via a relevance vector machine to determine whether a region will flare. We consider classification performance using all 38 extracted features and several feature subsets. Classification performance is quantified using both the true positive rate and the true negative rate. Additionally, we compute the true skill score which provides an equal weighting to true positive rate and true negative rate and the Heidke skill score to allow comparison to other flare forecasting work.
We obtain a true skill score of ~0.5 for any predictive time window in the range 2-24hr, with a TPR of ~0.8 and a TNR of ~0.7. These values do not appear to depend on the time window, although the Heidke skill score (<0.5) does. Features relating to snapshots of the distribution of magnetic gradients show the best predictive ability over all predictive time windows. Other gradient-related features and the instantaneous power at various wavelet scales also feature in the top five ranked features in predictive power. While the photospheric magnetic field governs the coronal non-potentiality (and likelihood of flaring), photospheric magnetic field alone is not sufficient to determine this uniquely. Furthermore we are only measuring proxies of the magnetic energy build up. We still lack observational details on why energy is released at any particular point in time. We may have discovered the natural limit of the accuracy of flare predictions from these large scale studies. **15 June 2002, 28-31October 2003**

Numerical MHD Simulation of the Coupled Evolution of Collisional Plasma and Magnetic Field in the Solar Chromosphere. I. Gradual and Impulsive Energisation

L.M. **Alekseeva**, S.P. Kshevetskii
Solar Phys. Volume 290, Issue 11, pp 3295-3318 **2015**
http://arxiv.org/pdf/1508.03626v1.pdf
The dynamical coupling between the solar chromospheric plasma and magnetic field is investigated by numerically solving a fully self-consistent, two-dimensional initial-value problem for the nonlinear collisional MHD equations including electric resistivity, thermal conduction, and, in some cases, gas-dynamic viscosity. The processes in the contact zone between two horizontal magnetic fields of opposite polarities are considered. The plasma is assumed to be initially motionless and having a temperature of 50,000 K uniform throughout the plasma volume; the characteristic magnetic field corresponds to a plasma $\beta \gtrsim 1$. In a physical-time interval of 17~seconds typically covered by a computational run, the plasma temperature gradually increases by a factor of two to three. Against this background, an impulsive (in 0.1 seconds or less) increase in the current-aligned plasma velocity occurs at the site of the current-layer thinning (sausage-type deformation, or m=0 pinch instability). Such a "velocity burst" can be interpreted physically as an event of suprathemal-proton generation. Further development of the sausage instability results in an increase in the kinetic temperature of the protons to high values, even to those observed in flares. The form of our system of MHD equations indicates that such increases are a property of the exact solution of the system at an appropriate choice of the parameters. Magnetic reconnection does not manifest itself in this solution: it would generate flows forbidden by the chosen geometry. Therefore, the pinch-sausage effect can act as an energiser of the upper chromosphere and be an alternative to the magnetic-reconnection process as the producer of flares.

ARTop: an open-source tool for measuring active region topology at the solar photosphere

K **Alielden**, D MacTaggart, Q Ming, C Prior, B Raphaldini
RAS Techniques and Instruments, Volume 2, Issue 1, January **2023**, Pages 398–407,
https://doi.org/10.1093/rasti/rzad029
https://watermark.silverchair.com/rzad029.pdf

The importance of measuring topological quantities, such as magnetic helicity, in solar observations has long been recognized. In particular, topological quantities play an important role in both understanding and predicting solar eruptions. In this paper, we present ARTop (Active Region Topology), an open-source and end-to-end software tool that allows researchers to calculate the fluxes of topological quantities based on solar magnetograms. In addition to this, ARTop also allows for the efficient analysis of these quantities in both 2D maps and time series. ARTop calculates the fluxes of magnetic helicity and magnetic winding, together with particular decompositions of these quantities. To perform these calculations, SHARP magnetograms are downloaded and velocity maps are created using the DAVE4VM method. Visualization tools, written in Python, are provided to aid in the selection of appropriate output variables and for the straightforward creation of maps and time series. Additionally, other analysis functions are included to facilitate and aid solar flare investigations. This software offers researchers a powerful tool for investigating the behaviour of active regions and the origins of space weather.

Automatic detection of small-scale EUV brightenings observed by the Solar Orbiter/EUI

N. **Alipour**, H. Safari, C. Verbeeck, D. Berghmans, F. Auchère, L. P. Chitta, P. Antolin, K. Barczynski, É. Buchlin, R. Aznar Cuadrado, L. Dolla, M. K. Georgoulis, S. Gissot, L. Harra, A. C. Katsiyannis, D. M. Long, S. Mandal, S. Parenti, O. Podladchikova, E. Petrova, É. Soubrié, U. Schühle, C. Schwanitz, L. Teriaca, M. J. West, A. N. Zhukov

A&A 663, A128 **2022**

https://arxiv.org/pdf/2204.04027.pdf

https://www.aanda.org/articles/aa/pdf/2022/07/aa43257-22.pdf

Context. Accurate detections of frequent small-scale extreme ultraviolet (EUV) brightenings are essential to the investigation of the physical processes heating the corona. Aims. We detected small-scale brightenings, termed campfires, using their morphological and intensity structures as observed in coronal EUV imaging observations for statistical analysis. Methods. We applied a method based on Zernike moments and a support vector machine classifier to automatically identify and track campfires observed by Solar Orbiter/Extreme Ultraviolet Imager (EUI) and SDO/AIA. Results. This method detected 8678 campfires (with length scales between 400 km and 4000 km) from a sequence of 50 High Resolution EUV telescope (HRIEUV) 174Å images. From 21 near co-temporal AIA images covering the same field of view as EUI, we found 1131 campfires, 58% of which were also detected in HRIEUV images. In contrast, about 16% of campfires recognized in HRIEUV were detected by AIA. We obtain a campfire birthrate of 2*10-16m-2s-1. About 40% of campfires show a duration longer than 5 s, having been observed in at least two HRIEUV images. We find that 27% of campfires were found in coronal bright points and the remaining 73% have occurred out of coronal bright points. We detected 23 EUI campfires with a duration greater than 245 s. We found that about 80% of campfires are formed at supergranular boundaries, and the features with the highest total intensities are generated at network junctions and intense H I Lyman-{\alpha} emission regions observed by EUI/HRILya. The probability distribution functions for the total intensity, peak intensity, and projected area of campfires follow a power law behavior with absolute indices between 2 and 3. This self-similar behavior is a possible signature of self-organization, or even self-organized criticality, in the campfire formation process. **30 May 2020**

Prediction of Flares within 10 Days before They Occur on the Sun

Nasibe **Alipour**, Faranak Mohammadi, and Hossein Safari

2019 ApJS 243 20

sci-hub.se/10.3847/1538-4365/ab289b

Prediction of solar flares due to the effects on Earth and satellites is an important topic for scientists. We develop a method and a tool for flare prediction by applying the support vector machine classifier to unique and independent Zernike moments extracted from active region (AR) images. In the analysis, we used the Helioseismic and Magnetic Imager (HMI) line-of-sight magnetograms, the Atmospheric Imaging Assembly (AIA) ultraviolet (UV at 1600 Å) and extreme ultraviolet (EUV at 304, 171, 193, 211, 335, 94, and 131 Å) images for a period of eight years of the solar cycle 24 (2010 June to 2018 September). The power-law behavior for the frequency distribution of the large flaring time window—the time interval between the occurrence of an AR and first large flare (X- and M-class) therein—indicated that most of the large flares appeared within 150 hr. The True Skill Score (TSS) metric for the performance of the win classifier that (uses the outputs of the HMI and AIA at 193, 211, 94, and 131 Å classifiers) was obtained as 0.86 ± 0.04. We also showed that the maximum value of the TSS for prediction of large flares for the win classifiers was about 0.95 ± 0.03 on the flaring day and decreased to 0.76 ± 0.1 within 4 to 10 days before flaring. **15 July 2010, 29 June 2014, 10 Sept 2014, 3 Sept 2017**

From 1D fields to Vlasov equilibria: Theory and application of Hermite Polynomials

O. **Allanson**, T. Neukirch, S. Troscheit and F. Wilson

Plasma Physics, 82, 905820306 (**2016**) [28 pages, Open Access])

We consider the theory and application of a solution method for the inverse problem in collisionless equilibria, namely that of calculating a Vlasov"Maxwell equilibrium for a given macroscopic (fluid) equilibrium. Using Jeans" theorem,

the equilibrium distribution functions are expressed as functions of the constants of motion, in the form of a Maxwellian multiplied by an unknown function of the canonical momenta. In this case it is possible to reduce the inverse problem to inverting Weierstrass transforms, which we achieve by using expansions over Hermite polynomials. A sufficient condition on the pressure tensor is found which guarantees the convergence and the boundedness of the candidate solution, when satisfied. This condition is obtained by elementary means, and it is clear how to put it into practice. We also argue that for a given pressure tensor for which our method applies, there always exists a positive distribution function solution for a sufficiently magnetised plasma. Illustrative examples of the use of this method with both force-free and non-force-free macroscopic equilibria are presented, including the full verification of a recently derived distribution function for the force-free Harris sheet (Allanson et al., Phys. Plasmas, vol. 22 (10), 2015, 102116). In the effort to model equilibria with lower values of the plasma \beta, solutions for the same macroscopic equilibrium in a new gauge are calculated, with numerical results presented for βpl=0.05.

A New Analysis Procedure for Detecting Periodicities within Complex Solar Coronal Arcades

Farhad **Allian**, Rekha Jain, B.W Hindman

ApJ **880** 3 **2019**

https://arxiv.org/pdf/1902.06644.pdf

We study intensity variations, as measured by the Atmospheric Imaging Assembly (AIA) on board the Solar Dynamics Observatory (SDO), in a solar coronal arcade using a newly developed analysis procedure that employs spatio-temporal auto-correlations. We test our new procedure by studying large-amplitude oscillations excited by nearby flaring activity within a complex arcade and detect a dominant periodicity of 12.5 minutes. We compute this period in two ways: from the traditional time-distance fitting method and using our new auto-correlation procedure. The two analyses yield consistent results. The auto-correlation procedure is then implemented on time series for which the traditional method would fail due to the complexity of overlapping loops and a poor contrast between the loops and the background. Using this new procedure, we discover the presence of small-amplitude oscillations within the same arcade with 8-minute and 10-minute periods prior and subsequent to the large-amplitude oscillations, respectively. Consequently, we identify these as "decayless" oscillations that have only been previously observed in non-flaring loop systems. **2014 January 27**

Solar Flare Heating with Turbulent Suppression of Thermal Conduction

Joel C. **Allred**, Graham S. Kerr, A. Gordon Emslie

ApJ **2022**

https://arxiv.org/pdf/2204.11684.pdf

During solar flares plasma is typically heated to very high temperatures, and the resulting redistribution of energy via thermal conduction is a primary mechanism transporting energy throughout the flaring solar atmosphere. The thermal flux is usually modeled using Spitzer's theory, which is based on local Coulomb collisions between the electrons carrying the thermal flux and those in the background. However, often during flares, temperature gradients become sufficiently steep that the collisional mean free path exceeds the temperature gradient scale size, so that thermal conduction becomes inherently non-local. Further, turbulent angular scattering, which is detectable in nonthermal widths of atomic emission lines, can also act to increase the collision frequency and so suppress the heat flux. Recent work by Emslie & Bian (2018) extended Spitzer's theory of thermal conduction to account for both non-locality and turbulent suppression. We have implemented their theoretical expression for the heat flux (which is a convolution of the Spitzer flux with a kernel function) into the RADYN flare-modeling code and performed a parameter study to understand how the resulting changes in thermal conduction affect flare dynamics and hence the radiation produced. We find that models with reduced heat fluxes predict slower bulk flows, less intense line emission, and longer cooling times. By comparing features of atomic emission lines predicted by the models with Doppler velocities and nonthermal line widths deduced from a particular flare observation, we find that models with suppression factors between 0.3 to 0.5 relative to the Spitzer value best reproduce observed Doppler velocities across emission lines forming over a wide range of temperatures. Interestingly, the model that best matches observed nonthermal line widths has a kappa-type velocity distribution function.

Modeling the Transport of Nonthermal Particles in Flares Using Fokker–Planck Kinetic Theory

Joel C. **Allred**1, Meriem Alaoui2, Adam F. Kowalski3,4,5, and Graham S. Kerr2

2020 ApJ 902 16

https://doi.org/10.3847/1538-4357/abb239

We describe a new approach for modeling the transport of high-energy particles accelerated during flares from the acceleration region in the solar corona until their eventual thermalization in the flare footpoint. Our technique numerically solves the Fokker–Planck equation and includes forces corresponding to Coulomb collisions in a flux loop with nonuniform ionization, synchrotron emission reaction, magnetic mirroring, and a return current electric field. Our solution to the Fokker–Planck equation includes second-order pitch angle and momentum diffusion. It is applicable to particles of arbitrary mass and charge. By tracking the collisions, we predict the bremsstrahlung produced as these particles interact with the ambient stellar atmosphere. This can be compared directly with observations and used to

constrain the accelerated particle energy distribution. We have named our numerical code FP and distributed it for general use. We demonstrate its effectiveness in several test cases.

A 3D Model of AR 11726 Heated by Nanoflares

Joel **Allred**, Adrian Daw, Jeffrey Brosius
2018
https://arxiv.org/pdf/1807.00763.pdf
The Extreme Ultraviolet Normal Incidence Spectrograph (EUNIS) and the Hinode/ EUV Imaging Spectrometer (EIS) observed AR 11726 on **2013 April 23**. We present intensity images in numerous atomic lines constructed from these observations. These lines are formed over a wide range of temperatures, and we use their relative intensities to constrain a parameterization of nanoflare heating. We construct a 3D model of the magnetic field in this active region by extrapolating the surface magnetic field into the corona and using SDO/AIA images of coronal loops to ensure that extrapolated magnetic field lines co-align with observed coronal loops. We trace 2848 magnetic field lines within the volume of this active region and model how they fill with hot plasma in response to nanoflare heating. We perform a parameter study to determine how the frequency and energy released in nanoflares scale with magnetic field strength and loop length. From our 3D model, we construct synthetic images of the lines observed by EUNIS and EIS and constrain the parameter study by minimizing the difference between the synthetic and observed images.

An exact collisionless equilibrium for the Force-Free Harris Sheet with low plasma beta

O. **Allanson**, T. Neukirch, F. Wilson and S. Troscheit
Physics of Plasmas, 22, 102116 (**2015**) [11 pages, Open Access])
http://scitation.aip.org/content/aip/journal/pop/22/10/10.1063/1.4934611
We present a first discussion and analysis of the physical properties of a new exact collisionless equilibrium for a one-dimensional nonlinear force-free magnetic field, namely, the force-free Harris sheet. The solution allows any value of the plasma beta, and crucially below unity, which previous nonlinear force-free collisionless equilibria could not. The distribution function involves infinite series of Hermite polynomials in the canonical momenta, of which the important mathematical properties of convergence and non-negativity have recently been proven. Plots of the distribution function are presented for the plasma beta modestly below unity, and we compare the shape of the distribution function in two of the velocity directions to a Maxwellian distribution.

Solar Flare Heating with Turbulent Suppression of Thermal Conduction

Joel C. **Allred**1, Graham S. Kerr1,2, and A. Gordon Emslie3
2022 ApJ 931 60
https://iopscience.iop.org/article/10.3847/1538-4357/ac69e8/pdf
During solar flares, plasma is typically heated to very high temperatures, and the resulting redistribution of energy via thermal conduction is a primary mechanism transporting energy throughout the flaring solar atmosphere. The thermal flux is usually modeled using Spitzer's theory, which is based on local Coulomb collisions between the electrons carrying the thermal flux and those in the background. However, often during flares, temperature gradients become sufficiently steep that the collisional mean free path exceeds the temperature-gradient scale size, so that thermal conduction becomes inherently nonlocal. Further, turbulent angular scattering, which is detectable in nonthermal widths of atomic emission lines, can also act to increase the collision frequency and thus suppress the heat flux. Recent work by Emslie & Bian extended Spitzer's theory of thermal conduction to account for both nonlocality and turbulent suppression. We have implemented their theoretical expression for the heat flux (which is a convolution of the Spitzer flux with a kernel function) into the RADYN flare-modeling code and performed a parameter study to understand how the resulting changes in thermal conduction affect the flare dynamics and hence the radiation produced. We find that models with reduced heat fluxes predict slower bulk flows, less intense line emission, and longer cooling times. By comparing the features of atomic emission lines predicted by the models with Doppler velocities and nonthermal line widths deduced from a particular flare observation, we find that models with suppression factors between 0.3 and 0.5 relative to the Spitzer value best reproduce the observed Doppler velocities across emission lines forming over a wide range of temperatures. Interestingly, the model that best matches the observed nonthermal line widths has a kappa-type velocity distribution function.

Modeling the Transport of Nonthermal Particles in Flares Using Fokker-Planck Kinetic Theory

Joel C. **Allred**, Meriem Alaoui, Adam F. Kowalski, Graham S. Kerr
ApJ **2020**
https://arxiv.org/pdf/2008.10671.pdf
We describe a new approach for modeling the transport of high energy particles accelerated during flares from the acceleration region in the solar corona until their eventual thermalization in the flare footpoint. Our technique numerically solves the Fokker-Planck equation and includes forces corresponding to Coulomb collisions in a flux loop

with nonuniform ionization, synchrotron emission reaction, magnetic mirroring and a return current electric field. Our solution to the Fokker-Planck equation includes second-order pitch angle and momentum diffusion. It is applicable to particles of arbitrary mass and charge. By tracking the collisions, we predict the bremsstrahlung produced as these particles interact with the ambient stellar atmosphere. This can be compared directly with observations and used to constrain the accelerated particle energy distribution. We have named our numerical code FP and have distributed it for general use. We demonstrate its effectiveness in several test cases.

A Unified Computational Model for Solar and Stellar Flares

Joel C. **Allred**, Adam F. Kowalski, Mats Carlsson
ApJ **809** 104 **2015**
http://arxiv.org/pdf/1507.04375v1.pdf
We present a unified computational framework which can be used to describe impulsive flares on the Sun and on dMe stars. The models assume that the flare impulsive phase is caused by a beam of charged particles that is accelerated in the corona and propagates downward depositing energy and momentum along the way. This rapidly heats the lower stellar atmosphere causing it to explosively expand and dramatically brighten. Our models consist of flux tubes that extend from the sub-photosphere into the corona. We simulate how flare-accelerated charged particles propagate down one-dimensional flux tubes and heat the stellar atmosphere using the Fokker-Planck kinetic theory. Detailed radiative transfer is included so that model predictions can be directly compared with observations. The flux of flare-accelerated particles drives return currents which additionally heat the stellar atmosphere. These effects are also included in our models. We examine the impact of the flare-accelerated particle beams on model solar and dMe stellar atmospheres and perform parameter studies varying the injected particle energy spectra. We find the atmospheric response is strongly dependent on the accelerated particle cutoff energy and spectral index.

Identifying Flare-indicative Photospheric Magnetic Field Parameters from Multivariate Time-series Data of Solar Active Regions

Khaznah **Alshammari**1, Shah Muhammad Hamdi2, and Soukaina Filali Boubrahimi2
2024 ApJS 271 39
https://iopscience.iop.org/article/10.3847/1538-4365/ad21e4/pdf
Photospheric magnetic field parameters are frequently used to analyze and predict solar events. Observation of these parameters over time, i.e., representing solar events by multivariate time-series (MVTS) data, can determine relationships between magnetic field states in active regions and extreme solar events, e.g., solar flares. We can improve our understanding of these events by selecting the most relevant parameters that give the highest predictive performance. In this study, we propose a two-step incremental feature selection method for MVTS data using a deep-learning model based on long short-term memory (LSTM) networks. First, each MVTS feature (magnetic field parameter) is evaluated individually by a univariate sequence classifier utilizing an LSTM network. Then, the top performing features are combined to produce input for an LSTM-based multivariate sequence classifier. Finally, we tested the discrimination ability of the selected features by training downstream classifiers, e.g., Minimally Random Convolutional Kernel Transform and support vector machine. We performed our experiments using a benchmark data set for flare prediction known as Space Weather Analytics for Solar Flares. We compared our proposed method with three other baseline feature selection methods and demonstrated that our method selects more discriminatory features compared to other methods. Due to the imbalanced nature of the data, primarily caused by the rarity of minority flare classes (e.g., the X and M classes), we used the true skill statistic as the evaluation metric. Finally, we reported the set of photospheric magnetic field parameters that give the highest discrimination performance in predicting flare classes.

New cases of super-flares on slowly rotating solar-type stars and large amplitude super-flares in G- and M-type main-sequence stars.

A.k. **Althukair**1,2 ID and D. Tsiklauri1
Research in Astron. Astrophys. **2023**
https://arxiv.org/pdf/2306.02292.pdf
In our previous work, we searched for super-flares on different types of stars while focusing on G-type dwarfs using entire Kepler data to study statistical properties of the occurrence rate of super-flares. Using these new data, as a by-product, we found fourteen cases of super-flare detection on thirteen slowly rotating Sun-like stars with rotation periods of 24.5 to 44 days. This result supports earlier conclusion by others that the Sun may possibly have a surprise super-flare. Moreover, we found twelve and seven new cases of detection of exceptionally large amplitude super-flares on six and four main-sequence stars of G- and M-type, respectively. No large-amplitude flares were detected in A, F, or K main-sequence stars. Here we present preliminary analysis of these cases. The super-flare detection, i.e. an estimation of flare energy, is based on a more accurate method compared to previous studies. We fit an exponential decay function to flare light curves and study the relation between e-folding decay time, τ , vs. flare amplitude and flare energy. We find that for slowly rotating Sun-like stars, large values of τ correspond to small flare energies and small values of τ correspond to high flare energies considered. Similarly, τ is large for small flare amplitudes and τ is small for large amplitudes considered. However, there is no clear relation between these parameters for large amplitude super-flares in

the main sequence G- and M-type stars, as we could not establish clear functional dependence between the parameters via standard fitting algorithms.

THERMAL TO NONTHERMAL ENERGY PARTITION AT THE EARLY RISE PHASE OF SOLAR FLARES

Alexander A. **Altyntsev**1, Gregory D. Fleishman2,3, Sergey V. Lesovoi1, and Nataliia S. Meshalkina
2012 ApJ 758 138

In some flares, the thermal component appears much earlier than the nonthermal component in the X-ray range. Using sensitive microwave observations, we revisit this finding made by Battaglia et al. based on a thorough analysis of RHESSI data. We have found that nonthermal microwave emission produced by accelerated electrons with energy of at least several hundred keV appears as early as the thermal soft X-ray emission, indicating that the electron acceleration takes place at the very early flare phase. The non-detection of the hard X-rays at that early stage of the flares is thus an artifact of a limited RHESSI sensitivity. In all of the considered events, the microwave emission intensity increases at the early flare phase. We found that either thermal or nonthermal gyrosynchrotron emission can dominate the low-frequency (optically thick) part of the microwave spectrum below the spectral peak occurring at 3-10 GHz. In contrast, the high-frequency optically thin part of the spectrum is always formed by the nonthermal, accelerated electron component, whose power-law energy spectrum can extend up to a few MeV at this early flare stage. This means that even though the total number of accelerated electrons is small at this stage, their nonthermal spectrum is fully developed. This implies that an acceleration process of available seed particles is fully operational. While creation of this seed population (the process commonly called "injection" of the particles from the thermal pool into the acceleration process) has a rather low efficiency at this stage, the plasma heating efficiency is high. This imbalance between the heating and acceleration (in favor of the heating) is difficult to reconcile within most of available flare energization models. Being reminiscent of the trade off between the Joule heating and runaway electron acceleration, it puts additional constraints on the electron injection into the acceleration process. As a byproduct of this study, we demonstrate that for those cases when the optically thick part of the radio spectrum is dominated by the thermal contribution, the microwave spectral data yield reliable estimates of the magnetic field and source area at the early flare phase.

Magneto-Acoustic Energetics Study of the Seismically Active Flare of 15 February 2011

J.D. **Alvarado-G?mez**, J.C. Buitrago-Casas, J.C. Mart?nez-Oliveros, C. Lindsey, H. Hudson, B. Calvo-Mozo
E-pront, March **2012**, Solar Phys. October **2012**, Volume 280, Issue 2, pp 335-345

Multi--wavelength studies of energetic solar flares with seismic emissions have revealed interesting common features between them. We studied the first GOES X--class flare of the 24th solar cycle, as detected by the Solar Dynamics Observatory (SDO). For context, seismic activity from this flare (SOL2011-02-15T01:55-X2.2, in NOAA AR 11158) has been reported in the literature (Kosovichev, 2011; Zharkov et al., 2011). Based on Dopplergram data from the Helioseismic and Magnetic Imager (HMI), we applied standard methods of local helioseismology in order to identify the seismic sources in this event. RHESSI hard X-ray data are used to check the correlation between the location of the seismic sources and the particle precipitation sites in during the flare. Using HMI magnetogram data, the temporal profile of fluctuations in the photospheric line-of-sight magnetic field is used to estimate the magnetic field change in the region where the seismic signal was observed. This leads to an estimate of the work done by the Lorentz-force transient on the photosphere of the source region. In this instance this is found to be a significant fraction of the acoustic energy in the attendant seismic emission, suggesting that Lorentz forces can contribute significantly to the generation of sunquakes. However, there are regions in which the signature of the Lorentz-force is much stronger, but from which no significant acoustic emission emanates.

Rapid Variability in the SOL2011-08-04 Flare: Implications for Electron Acceleration

Alexander T. **Altyntsev**, Nataliia S. Meshalkina, Alexandra L. Lysenko, Gregory D. Fleishman
ApJ **883** 38 **2019**
https://arxiv.org/pdf/1909.03593.pdf
sci-hub.se/10.3847/1538-4357/ab3808

Particle acceleration in solar flares remains an outstanding problem in solar physics. It is yet unclear which of the acceleration mechanisms dominates and how exactly is the excessive magnetic energy transferred to the nonthermal and other forms of energy. We emphasize, that the ultimate acceleration mechanism must be capable of efficiently working in the most extreme conditions, such as the shortest detected time scales and the highest acceleration efficiency. Here we focus on detailed multiwavelength analysis of a very initial phase of the SOL**2011-08-04** flare, which demonstrated prominent short subpeaks of nonthermal emission during filament eruption associated with the flare. We demonstrate that the three-dimensional configuration of the flare, combined with timing and spectral behavior of the rapidly varying component, put very stringent constraints on the acceleration regime. Specifically, the rapid subpeaks are generated by short injections of nonthermal electrons with a reasonably hard, single power-law spectrum and a relatively narrow spread of pitch-angles along the mean magnetic field. The acceleration site is a compact volume located near the top of extended coronal loop(s). The electrons are accelerated up to several hundreds of keV promptly, with the characteristic acceleration time shorter than 50 ms. We show, that these properties are difficult to reconcile with widely adopted stochastic acceleration models, while the data inescapably require acceleration by a super-Dreicer electric field, whether regular or random.

Sources of Quasi-Periodic Pulses in the 18 August 2012 Flare

A. **Altyntsev**, N. Meshalkina, H. Meszarosova, M. Karlicky, V. Palshin, S. Lesovoi
Solar Physics, **2016**
http://arxiv.org/pdf/1601.02332v1.pdf

We analyzed spatial and spectral characteristics of quasi-periodic pulses (QPP) for the **18 August 2012** limb are, using new data from a complex of spectral and imaging instruments developed by the Siberian Solar Radio Telescope team and the Wind/Konus gamma-ray spectrometer. A sequence of broadband pulses with periods of approximately ten seconds were observed in X-rays at energies between 25 keV and 300 keV, and in microwaves at frequencies from a few GHz up to 34 GHz during an interval of one minute. The QPP X-ray source was located slightly above the limb where the south legs of large and small EUV loop systems were close to each other. Before the QPPs the soft X-ray emission and the Ramaty High Energy Solar Spectroscopic Imager signal from the energy channels below 25 keV were gradually arising for several minutes at the same location. It was found that each X-ray pulse showed the soft-hard-soft behavior. The 17 and 34 GHz microwave source were at footpoints of the small loop system and the source emitting in the 4.2 {7.4 GHz band in the large one. The QPPs were probably generated by modulation of acceleration processes in the energy release site. Analyzing radio spectra we determined the plasma parameters in the radio sources. The microwave pulses could be explained by relatively weak variations of the spectrum hardness of emitting electrons.

Image Synthesis for Solar Flare Prediction

Elad **Amar**1 and Ohad Ben-Shahar2
ApJS 271 29 **2024**
https://iopscience.iop.org/article/10.3847/1538-4365/ad1dd4/pdf

Solar flare prediction is a topic of interest to many researchers owing to the potential of solar flares to affect various technological systems, both terrestrial and in orbit. In recent years, the forecasting task has become progressively more reliant on data-driven computations and machine-learning algorithms. Although these efforts have improved solar flare predictions, they still falter in doing so for large solar flares, in particular under operational conditions, since large-flare data are very scarce and labeled data are heavily imbalanced. In this work, we seek to address this fundamental issue and present a scheme for generating synthetic magnetograms to reduce the imbalance in the data. Our method consists of (1) synthetic oversampling of line-of-sight magnetograms using Gaussian mixture model representation, followed by (2) a global optimization technique to ensure consistency of both physical features and flare precursors, and (3) the mapping of the generated representations to realistic magnetogram images using deep generative models. We show that these synthetically generated data indeed improve the capacity of solar flare prediction models and that, when tested on such a state-of-the-art model, it significantly enhances its forecasting performance, achieving an F1-score as high as 0.43 ± 0.08 and a true skill statistic of 0.64 ± 0.10 for X-class flares in the 24 hr operational solar flare data split. **2011 February 15, 2014 November 6, 2014 October 26**

Magnetic cage and rope as the key for solar eruptions.

Amari T, Canou A, Aly JJ, Delyon F, Alauzet F.
2018 Nature 554, Issue 7691, 211–215. doi: 10.1038/nature24671
sci-hub.tw/10.1038/nature24671
https://www.nature.com/articles/nature24671

Solar flares are spectacular coronal events that release large amounts of energy. They are classified as either eruptive or confined, depending on whether they are associated with a coronal mass ejection. Two types of model have been developed to identify the mechanism that triggers **confined flares**, although it has hitherto not been possible to decide between them because the magnetic field at the origin of the flares could not be determined with the required accuracy. In the first type of model, the triggering is related to the topological complexity of the flaring structure, which implies the presence of magnetically singular surfaces. This picture is observationally supported by the fact that radiative emission occurs near these features in many flaring regions. The second type of model attributes a key role to the formation of a twisted flux rope, which becomes unstable. Its plausibility is supported by simulations, by interpretations of some observations and by laboratory experiments. Here we report modelling of a confined event that uses the measured photospheric magnetic field as input. We first use a static model to compute the slowly evolving magnetic state of the corona before the eruption, and then use a dynamical model to determine the evolution during the eruption itself. We find that a magnetic flux rope must be present throughout the entire event to match the field measurements. This rope evolves slowly before saturating and suddenly erupting. Its energy is insufficient to break through the overlying field, whose lines form a confining cage, but its twist is large enough to trigger a kink instability, leading to the confined flare, as previously suggested. Topology is not the main cause of the flare, but it traces out the locations of the X-ray emission. We show that a weaker magnetic cage would have produced a more energetic eruption with a coronal mass ejection, associated with a predicted energy upper bound for a given region.

Magnetic diffusion in Solar atmosphere produces measurable electric fields

Tetsu **Anan**, Roberto Casini, Han Uitenbroek, Thomas A. Schad, +++
Nature Communications **2024**
https://arxiv.org/pdf/2410.09221
The efficient release of magnetic energy in astrophysical plasmas, such as during solar flares, can in principle be achieved through magnetic diffusion, at a rate determined by the associated electric field. However, attempts at measuring electric fields in the solar atmosphere are scarce, and none exist for sites where the magnetic energy is presumably released. Here, we present observations of an energetic event using the National Science Foundation's Daniel K. Inouye Solar Telescope, where we detect the polarization signature of electric fields associated with magnetic diffusion. We measure the linear and circular polarization across the hydrogen H-epsilon Balmer line at 397 nm at the site of a brightening event in the solar chromosphere. Our spectro-polarimetric modeling demonstrates that the observed polarization signals can only be explained by the presence of electric fields, providing conclusive evidence of magnetic diffusion, and opening a new window for the quantitative study of this mechanism in space plasmas. **23 February 2022**

Measurement of Vector Magnetic Field in a Flare kernel with a Spectropolarimetric Observation in He I 10830 A

Tetsu **Anan**, Takurou Yoneya, Kiyoshi Ichimoto, Satoru Ueno, Daikou Shiota, Satoshi Nozawa, Shinsuke Takasao, Tomoko Kawate
PASJ (Hida topical issue) 70, Issue 6, 101 **2018**
https://arxiv.org/pdf/1808.06821.pdf
A flare kernel associated with a C4 class flare was observed in a spectral window including the He I triplet 10830 A and Si I 10827 A with a spectropolarimeter on the Domeless Solar Telescope at Hida Observatory on **August 9th, 2015**. Observed Stokes profiles of the He I triplet in the flare kernel in its post-maximum phase are well reproduced through inversions considering the Zeeman and the Paschen-Back effects with a three slab model of the flare kernel, in which two slabs having up and downward velocities produce emissions and one slab produces an absorption. The magnetic field strength inferred from the emission components of the He I line is 1400 G, which is significantly stronger than 690 G that is observed at the same location in the same line 6.5 hours before the flare. In addition, photospheric magnetic field vector derived from the Si I10827 A is similar to that of the flare kernel. To explain this results, we suggest that the emission in the He I triplet during the flare is produced in the deep layer, around which bombardment of non-thermal electrons leads to the formation of a coronal temperature plasma. Assuming a hydrogen column density at the location where the He I emissions are formed, and a power-law index of non-thermal electron energy distribution, we derived the low-energy cutoff of the non-thermal electron as 20 - 30 keV, which is consistent with that inferred from hard X-ray data obtained by RHESSI.

Predicting Flares and Solar Energetic Particle Events: The FORSPEF Tool

A. **Anastasiadis**, A. Papaioannou, I. Sandberg, M. Georgoulis, K. Tziotziou, A. Kouloumvakos, P. Jiggens
Solar Physics September **2017**, 292:134
A novel integrated prediction system for solar flares (SFs) and solar energetic particle (SEP) events is presented here. The tool called forecasting solar particle events and flares (FORSPEF) provides forecasts of solar eruptive events, such as SFs with a projection to occurrence and velocity of coronal mass ejections (CMEs), and the likelihood of occurrence of an SEP event. In addition, the tool provides nowcasting of SEP events based on actual SF and CME near real-time data, as well as the SEP characteristics (e.g. peak flux, fluence, rise time, and duration) per parent solar event. The prediction of SFs relies on the effective connected magnetic field strength (BeffBeff) metric, which is based on an assessment of potentially flaring active-region (AR) magnetic configurations, and it uses a sophisticated statistical

analysis of a large number of AR magnetograms. For the prediction of SEP events, new statistical methods have been developed for the likelihood of the SEP occurrence and the expected SEP characteristics. The prediction window in the forecasting scheme is 24 hours with a refresh rate of 3 hours, while the respective prediction time for the nowcasting scheme depends on the availability of the near real-time data and ranges between 15 – 20 minutes for solar flares and 6 hours for CMEs. We present the modules of the FORSPEF system, their interconnection, and the operational setup. Finally, we demonstrate the validation of the modules of the FORSPEF tool using categorical scores constructed on archived data, and we also discuss independent case studies. **26 Oct-$ Nov 2003, 20 Jan 2005, 7 March 2012, 2014-12-18**
http://tromos.space.noa.gr/forspef/ 26 Oct-$ Nov 2003, 20 Jan 2005, 7 March 2012, 2014-12-18
CESRA Highlight #1551, Oct 2017 http://www.astro.gla.ac.uk/users/eduard/cesra/?p=1551

REMOTE OSCILLATORY RESPONSES TO A SOLAR FLARE
A. **Andić** and R. T. J. McAteer
2013 ApJ 772 54
The processes governing energy storage and release in the Sun are both related to the solar magnetic field. We demonstrate the existence of a magnetic connection between the energy released by a flare and increased oscillatory power in the lower solar atmosphere. The oscillatory power in active regions tends to increase in response to explosive events at other locations, but not in the active region itself. We carry out timing studies and show that this effect is probably caused by a large-scale magnetic connection between the regions, instead of a globally-propagating wave. We show that oscillations tend to exist in longer-lived wave trains with short periods (P < 200 s) at the time of a flare. These wave trains may be mechanisms by which flare energy can be redistributed throughout the solar atmosphere.

UMBRAL DYNAMICS IN THE NEAR-INFRARED CONTINUUM
A. **Anđić**1, W. Cao1 and P. R. Goode
2011 ApJ 736 79
We detected peaks of oscillatory power at 3 and ~6.5 minutes in the umbra of the central sunspot of the active region NOAA AR 10707 in data obtained in the near-infrared (NIR) continuum at 1565.7 nm. The NIR data set captured umbral dynamics around 50 km below the $\tau 500 = 1$ level. The umbra does not oscillate as a whole, but rather in distinct parts that are distributed over the umbral surface. The most powerful oscillations, close to a period of ~6.5, do not propagate upward. We noted a plethora of large umbral dots (UDs) that persisted for ≥30 minutes and stayed in the same locations. The peaks of oscillatory power above the detected UDs are located at 3 and 5 minute oscillations, but are very weak in comparison with the oscillations of ~6.5 minutes.

Semiempirical photospheric models of a solar flare on May 28, 2012
E.S. **Andriets**, , N.N. Kondrashova
Advances in Space Research, Volume 55, Issue 3, 1 February **2015**, Pages 871–878
http://www.sciencedirect.com/science/article/pii/S0273117714004827
The variation of the photosphere physical state during the decay phase of SF/B6.8-class solar flare on May 28, 2012 in active region NOAA 11490 is studied.
We used the data of the spectropolarimetric observations with the French–Italian solar telescope THEMIS (Tenerife, Spain). Semi-empirical model atmospheres are derived from the inversion with SIR (Stokes Inversion based on Response functions) code. The inversion was based on Stokes profiles of six photospheric lines. Each model atmosphere has a two-component structure: a magnetic flux tube and non-magnetic surroundings. The Harvard Smithsonian Reference Atmosphere (HSRA) has been adopted for the surroundings. The macroturbulent velocity and the filling factor were assumed to be constant with the depth. The optical depth dependences of the temperature, magnetic field strength, and line-of-sight velocity are obtained from inversion.
According to the received model atmospheres, the parameters of the magnetic field and the thermodynamical parameters changed during the decay phase of the flare. The model atmospheres showed that the photosphere remained in a disturbed state during observations after the maximum of the flare. There are temporal changes in the temperature and the magnetic field strength optical depth dependences. The temperature enhancement in the upper photospheric layers is found in the flaring atmospheres relative to the quiet-Sun model. The downflows are found in the low and upper photosphere at the decay phase of the flare.

Novel data analysis techniques in coronal seismology **Review**
Sergey A. **Anfinogentov**, Patrick Antolin, Andrew R. Inglis, Dmitrii Kolotkov, Elena G. Kupriyanova, James A. McLaughlin, Giuseppe Nisticò, David J. Pascoe, S. Krishna Prasad, Ding Yuan
2022
https://arxiv.org/pdf/2112.13577.pdf

We review novel data analysis techniques developed or adapted for the field of coronal seismology. We focus on methods from the last ten years that were developed for extreme ultraviolet (EUV) imaging observations of the solar corona, as well as for light curves from radio and X-ray. The review covers methods for the analysis of transverse and longitudinal waves; spectral analysis of oscillatory signals in time series; automated detection and processing of large data sets; empirical mode decomposition; motion magnification; and reliable detection, including the most common pitfalls causing artefacts and false detections. We also consider techniques for the detailed investigation of MHD waves and seismological inference of physical parameters of the coronal plasma, including restoration of the three-dimensional geometry of oscillating coronal loops, forward modelling and Bayesian parameter inference. **May 9, 2007, June 27, 2007., 2013-01-21**

Multivariate time series dataset for space weather data analytics

Angryk, Rafal A. ; Martens, Petrus C. ; Aydin, Berkay et al. ;
Scientific Data, Volume 7, Issue 1, article id.227, **2020**
https://www.nature.com/articles/s41597-020-0548-x.pdf
DOI: 10.1038/s41597-020-0548-x
We introduce and make openly accessible a comprehensive, multivariate time series (MVTS) dataset extracted from solar photospheric vector magnetograms in Spaceweather HMI Active Region Patch (SHARP) series. Our dataset also includes a cross-checked NOAA solar flare catalog that immediately facilitates solar flare prediction efforts. We discuss methods used for data collection, cleaning and pre-processing of the solar active region and flare data, and we further describe a novel data integration and sampling methodology. Our dataset covers 4,098 MVTS data collections from active regions occurring between May 2010 and December 2018, includes 51 flare-predictive parameters, and integrates over 10,000 flare reports. Potential directions toward expansion of the time series, either "horizontally" - by adding more prediction-specific parameters, or "vertically" - by generalizing flare into integrated solar eruption prediction, are also explained. The immediate tasks enabled by the disseminated dataset include: optimization of solar flare prediction and detailed investigation for elusive flare predictors or precursors, with both operational (research-to-operations), and basic research (operations-to-research) benefits potentially following in the future.

Magnetic Helicity Signs and Flaring Propensity: Comparing Force-free Parameter with the Helicity signs of Hα Filaments and X-ray Sigmoids

V. **Aparna**, Manolis K. Georgoulis, Petrus C. Martens
ApJ **967** 134 **2024**
https://arxiv.org/ftp/arxiv/papers/2403/2403.17075.pdf
https://iopscience.iop.org/article/10.3847/1538-4357/ad38c1/pdf
Sigmoids produce strong eruptive events. Earlier studies have shown that the ICME axial magnetic field Bz can be predicted with some credibility by observing the corresponding filament or the polarity inversion line in the region of eruption and deriving the magnetic field direction from that. Sigmoids are coronal structures often associated with filaments in the sigmoidal region. In this study, firstly we compare filament chirality with sigmoid handedness to observe their correlation. Secondly, we perform non-linear force-free approximations of the coronal magnetic connectivity using photospheric vector magnetograms underneath sigmoids to obtain a weighted-average value of the force-free parameter and to correlate it with filament chirality and the observed coronal sigmoid handedness. Importantly, we find that the sigmoids and their filament counterparts do not always have the same helicity signs. Production of eruptive events by regions that do not have the same signs of helicities is ∼3.5 times higher than when they do. A case study of magnetic energy/ helicity evolution in NOAA AR 12473 is also presented. **2011-11-24, 2012-05-05, 2012-06-15, Dec 23, 2015 - Jan 01, 2016**.

Clusters of Small Eruptive Flares Produced by Magnetic Reconnection in the Sun

V. **Archontis**1 and V. Hansteen
2014 ApJ 788 L2
http://arxiv.org/pdf/1405.6420v1.pdf
We report on the formation of small solar flares produced by patchy magnetic reconnection between interacting magnetic loops. A three-dimensional (3D) magnetohydrodynamic (MHD) numerical experiment was performed, where a uniform magnetic flux sheet was injected into a fully developed convective layer. The gradual emergence of the field into the solar atmosphere results in a network of magnetic loops, which interact dynamically forming current layers at their interfaces. The formation and ejection of plasmoids out of the current layers leads to patchy reconnection and the spontaneous formation of several small (size 1-2 Mm) flares. We find that these flares are short-lived (30 s–3 minutes) bursts of energy in the range O(1025-1027) erg, which is basically the nanoflare-microflare range. Their persistent formation and co-operative action and evolution leads to recurrent emission of fast EUV/X-ray jets and considerable plasma heating in the active corona.

Recurrent solar jets in active regions

V. **Archontis**1, K. Tsinganos2, and C. Gontikakis3

A&A 512, L2 (**2010**)

Aims: We study the emergence of a toroidal flux tube into the solar atmosphere and its interaction with a pre-existing field of an active region. We investigate the emission of jets as a result of repeated reconnection events between colliding magnetic fields.

Methods: We perform 3D simulations by solving the time-dependent, resistive MHD equations in a highly stratified atmosphere.

Results: A small active region field is constructed by the emergence of a toroidal magnetic flux tube. A current structure is build up and reconnection sets in when new emerging flux comes into contact with the ambient field of the active region. The topology of the magnetic field around the current structure is drastically modified during reconnection. The modification results in a formation of new magnetic systems that eventually collide and reconnect. We find that reconnection jets are taking place in successive recurrent phases in directions perpendicular to each other, while in each phase they release magnetic energy and hot plasma into the solar atmosphere. After a series of recurrent appearance of jets, the system approaches an equilibrium where the efficiency of the reconnection is substantially reduced. We deduce that the emergence of new magnetic flux introduces a perturbation to the active region field, which in turn causes reconnection between neighboring magnetic fields and the release of the trapped energy in the form of jet-like emissions. This is the first time that self-consistent recurrency of jets in active regions is shown in a three-dimensional experiment of magnetic flux emergence.

On the structure and evolution of complexity in sigmoids: a flux emergence model

Archontis, V., Hood, A., Savcheva, A., Golub, L, Deluca, E.

E-print, Oct **2008**, ApJ

Sigmoids are structures with a forward or inverse S-shape, generally observed in the solar corona in soft X-ray emission. It is believed that the appearance of a sigmoid in an active region is an important factor in eruptive activity. The association of sigmoids with dynamic phenomena such as flares and coronal mass ejections (CMEs) make the study of sigmoids important. Recent observations of a coronal sigmoid, obtained with the X-Ray Telescope (XRT) on board Hinode, showed the formation and eruption phase with high spatial resolution. These observations revealed that the topological structure of the sigmoid is complex : it consists of many, differently oriented, loops that all together form two opposite {it J-like} bundles or an overal S-shaped structure. A series of theoretical and numerical models have been proposed, over the past years, to explain the nature of sigmoids but there is no explanation on how the afore-mentioned complexity in sigmods is build up. In this paper we present a flux emergence model that leads to the formation of a sigmoid, whose structure and evolution of complexity are in good qualitative agreement with the recent observations.

The emission in the region E>0.1MeV during disk and limb faint solar flares

Arkhangelskaja Irenea, Arkhangelskiy Andrewa, , Kotov Yurya, Glyanenko Alexandra, Kolchina Mariaa, Kirichenko Alexey

Advances in Space Research, Volume 51, Issue 11, 1 June **2013**, Pages 1996–2001

Hard X-ray and gamma-ray emission in energy band E>50E>50 keV was first observed by AVS-F apparatus onboard CORONAS-F satellite (detector SONG-D) during some solar flares with classes B and C by GOES classification. Such component registered in flares with duration less than 30 min. However γ-emission up to several tens of MeV was observed during some classes B and C events, which temporal profiles were not corresponded to Neupert effect. For example, during class B2.3 limb solar flare **January 7, 2005** maximum observed energy was Emax~36 MeV and during class B4.6 disk solar event **January 12, 2005** maximum observed energy was Emax~ 7 MeV. Properties of temporal profiles and energy spectra of faint solar flares, during which emission in the energy band of E>0.1E>0.1 MeV were registered are discussed in the presented work. There is not any strong correlation between presence or absence of hard X-ray and γ-ray emission and the intensity of soft X-ray emission during solar flares. The one of illustration of this fact is the absence of any observed statistically significant count rate exceed above background level during some class M flares in the energy band E>0.1E>0.1 MeV. The typical example of such flares is event **November 8, 2001** (class M4.2, lasts from 14:59 UT up to 16:00 UT, maximum of soft X-ray emission was at 15:35 UT on GOES data).

A Machine Learning Approach to Correcting Atmospheric Seeing in Solar Flare Observations

John A. **Armstrong**, Lyndsay Fletcher

MNRAS 501, Issue 2, February **2021**, Pages 2647–2658

https://arxiv.org/pdf/2011.12814.pdf

https://doi.org/10.1093/mnras/staa3742
Current post-processing techniques for the correction of atmospheric seeing in solar observations -- such as Speckle interferometry and Phase Diversity methods -- have limitations when it comes to their reconstructive capabilities of solar flare observations. This, combined with the sporadic nature of flares meaning observers cannot wait until seeing conditions are optimal before taking measurements, means that many ground-based solar flare observations are marred with bad seeing. To combat this, we propose a method for dedicated flare seeing correction based on training a deep neural network to learn to correct artificial seeing from flare observations taken during good seeing conditions. This model uses transfer learning, a novel technique in solar physics, to help learn these corrections. Transfer learning is when another network already trained on similar data is used to influence the learning of the new network. Once trained, the model has been applied to two flare datasets: one from AR12157 on **2014/09/06** and one from AR12673 on **2017/09/06**. The results show good corrections to images with bad seeing with a relative error assigned to the estimate based on the performance of the model. Further discussion takes place of improvements to the robustness of the error on these estimates.

Visco-Resistive Dissipation in Strongly Driven Transient Reconnection

C. K. **Armstrong**, I. J. D. Craig
Solar Physics, March **2014**, Volume 289, Issue 3, pp 869-877
Solar flare energy release mechanisms often neglect the role played by viscous effects. Here we perform incompressible planar reconnection simulations, driven by the Orszag–Tang vortex, for both classical and Braginskii forms of the viscosity. We show that strongly driven “saturated” flux pile-up current layers, which lead to weak reconnection rates at small resistivities, are accompanied by invariant global viscous losses. These results support the notion that viscous dissipation in flaring plasmas can account for a significant fraction of the flare energy release.

Slow Shock Formation Upstream of Reconnecting Current Sheets

H. **Arnold**1, J. F. Drake1, M. Swisdak1, F. Guo2, J. T. Dahlin3, and Q. Zhang2
2022 ApJ 926 24
https://iopscience.iop.org/article/10.3847/1538-4357/ac423b/pdf
The formation, development, and impact of slow shocks in the upstream regions of reconnecting current layers are explored. Slow shocks have been documented in the upstream regions of magnetohydrodynamic (MHD) simulations of magnetic reconnection as well as in similar simulations with the kglobal kinetic macroscale simulation model. They are therefore a candidate mechanism for preheating the plasma that is injected into the current layers that facilitate magnetic energy release in solar flares. Of particular interest is their potential role in producing the hot thermal component of electrons in flares. During multi-island reconnection, the formation and merging of flux ropes in the reconnecting current layer drives plasma flows and pressure disturbances in the upstream region. These pressure disturbances steepen into slow shocks that propagate along the reconnecting component of the magnetic field and satisfy the expected Rankine–Hugoniot jump conditions. Plasma heating arises from both compression across the shock and the parallel electric field that develops to maintain charge neutrality in a kinetic system. Shocks are weaker at lower plasma β, where shock steepening is slow. While these upstream slow shocks are intrinsic to the dynamics of multi-island reconnection, their contribution to electron heating remains relatively minor compared with that from Fermi reflection and the parallel electric fields that bound the reconnection outflow.

A Statistical Study of Low-frequency Solar Radio Type-III Bursts

Mahender **Aroori**, K. Sasikumar Raja, R. Ramesh, Vemareddy Panditi, Christian Monstein, Yellaiah Ganji
Solar Phys. **2020**
https://arxiv.org/pdf/2009.05755.pdf
We have studied low-frequency (45 - 410 MHz) type III solar radio bursts observed using the e-CALLISTO spectrometer located at Gauribidanur radio observatory, India during 2013 - 2017. After inspecting the 1531 type III bursts we found that 426 bursts were associated with flares, while the other bursts might have triggered by small scale features / weak energy events present in the solar corona. In this study, we have carried out a statistical analysis of various observational parameters like start time, lower and upper-frequency cut-offs of type III bursts and their association with flares, variation of such parameters with flare parameters such as location, class, onset and peak timings. From this study, we found that most of the high-frequency bursts (whose upper-frequency cut-off >350 MHz) are originated from the western longitudes. We interpret that it could be due to the fact that Parker spirals from these longitudes are directed towards the earth and high-frequency bursts are more directive. Further, we report that number of bursts that reach earth from western longitudes are higher than eastern longitudes.

Comparative study of electric currents and energetic particle fluxes in a solar flare and Earth magnetospheric substorm

Anton **Artemyev**, Ivan Zimovets, Ivan Sharykin, Yukitoshi Nishimura, Cooper Downs, James Weygand, Robyn Fiori, Xiao-Jia Zhang, Andrei Runov, Marco Velli, Vassilis Angelopoulos, Olga

Panasenco, Christopher Russell, Yoshizumi Miyoshi, Satoshi Kasahara, Ayako Matsuoka, Shoichiro Yokota, Kunihiro Keika, Tomoaki Hori, Yoichi Kazama, Shiang-Yu Wang, Iku Shinohara, Yasunobu Ogawa
https://arxiv.org/pdf/2105.03772.pdf
ApJ **923** 151 **2021**
https://arxiv.org/pdf/2105.03772.pdf
https://iopscience.iop.org/article/10.3847/1538-4357/ac2dfc/pdf
https://doi.org/10.3847/1538-4357/ac2dfc
Magnetic field-line reconnection is a universal plasma process responsible for the conversion of magnetic field energy to the plasma heating and charged particle acceleration. Solar flares and Earth's magnetospheric substorms are two most investigated dynamical systems where magnetic reconnection is believed to be responsible for global magnetic field reconfiguration and energization of plasma populations. Such a reconfiguration includes formation of a long-living current systems connecting the primary energy release region and cold dense conductive plasma of photosphere/ionosphere. In both flares and substorms the evolution of this current system correlates with formation and dynamics of energetic particle fluxes. Our study is focused on this similarity between flares and substorms. Using a wide range of datasets available for flare and substorm investigations, we compare qualitatively dynamics of currents and energetic particle fluxes for one flare and one substorm. We showed that there is a clear correlation between energetic particle bursts (associated with energy release due to magnetic reconnection) and magnetic field reconfiguration/formation of current system. We then discuss how datasets of in-situ measurements in the magnetospheric substorm can help in interpretation of datasets gathered for the solar flare. **2015 June 22**

Electron trapping and acceleration by kinetic Alfvén waves in solar flares

A. V. **Artemyev**1,2, I. V. Zimovets1 and R. Rankin3
A&A 589, A101 (**2016**) DOI 10.1051/0004-6361/201527617
Context. Theoretical models and spacecraft observations of solar flares highlight the role of wave-particle interaction for non-local electron acceleration. In one scenario, the acceleration of a large electron population up to high energies is due to the transport of electromagnetic energy from the loop-top region down to the footpoints, which is then followed by the energy being released in dense plasma in the lower atmosphere.
Aims. We consider one particular mechanism of non-linear electron acceleration by kinetic Alfvén waves. Here, waves are generated by plasma flows in the energy release region near the loop top. We estimate the efficiency of this mechanism and the energies of accelerated electrons.
Methods. We use analytical estimates and test-particle modelling to investigate the effects of electron trapping and acceleration by kinetic Alfvén waves in the inhomogeneous plasma of the solar corona.
Results. We demonstrate that, for realistic wave amplitudes, electrons can be accelerated up to 10−1000 keV during their propagation along magnetic field lines. Here the electric field that is parallel to the direction of the background magnetic field is about 10 to 103 times the amplitude of the Dreicer electric field. The acceleration mechanism strongly depends on electron scattering which is due to collisions that only take place near the loop footpoints.
Conclusions. The non-linear wave-particle interaction can play an important role in the generation of relativistic electrons within flare loops. Electron trapping and coherent acceleration by kinetic Alfvén waves represent the energy cascade from large-scale plasma flows that originate at the loop-top region down to the electron scale. The non-diffusive character of the non-linear electron acceleration may be responsible for the fast generation of high-energy particles.

Chaotic Charged Particle Motion and Acceleration in Reconnected Current Sheet

A. V. **Artemyev**, A. I. Neishtadt, I. V. Zimovets, L. M. Zelenyi
Solar Phys. Volume 290, Issue 3, pp 787-810 **2015**
We investigate charged particle dynamics and acceleration in the current sheet located in the reconnection outflow region. We consider parameter ranges corresponding to current sheets in the solar corona. We demonstrate a new effect of fast chaotization of charged particle motion due to effective geometrical destruction of adiabatic invariants in current sheets in the presence of a quite strong sheared magnetic field and a finite electric field. This fast chaotization results in particle acceleration and enhancement of effective collisionless conductivity. Additionally, chaotization of charged particle motion could lead to particle escape from the current sheet and corresponding formation of field-aligned beams. We also discuss different regimes of charged particle motion in the reconnected current sheet for wide parameter ranges.

Preferential acceleration of heavy ions in the reconnection outflow region Drift and surfatron ion acceleration

A. V. **Artemyev**1,2, G. Zimbardo3, A. Y. Ukhorskiy4 and M. Fujimoto
A&A 562, A58 (**2014**)
Context. Many observations show that heating in the solar corona should be more effective for heavy ions than for protons. Moreover, the efficiency of particle heating also seems to be larger for a larger particle electric charge. The transient magnetic reconnection is one of the most natural mechanisms of charged particle acceleration in the solar corona. However, the role of this process in preferential acceleration of heavy ions has still yet to be investigated.
Aims. In this paper, we consider charged particle acceleration in the reconnection outflow region. We investigate the dependence of efficiency of various mechanisms of particle acceleration on particle charge and mass.
Methods. We take into account recent in situ spacecraft observations of the nonlinear magnetic waves that have originated in the magnetic reconnection. We use analytical estimates and test-particle trajectories to study resonant and nonresonant particle acceleration by these nonlinear waves.
Results. We show that resonant acceleration of heavy ions by nonlinear magnetic waves in the reconnection outflow region is more effective for heavy ions and/or for ions with a larger electric charge. Nonresonant acceleration can be considered as a combination of particle reflections from the front of the nonlinear waves. Energy gain for a single reflection is proportional to the particle mass, while the maximum possible gain of energy corresponds to the classical betatron heating.
Conclusions. Small-scale transient magnetic reconnections produce nonlinear magnetic waves propagating away from the reconnection region. These waves can effectively accelerate heavy ions in the solar corona via resonant and nonresonnat regimes of interactions. This mechanism of acceleration is more effective for ions with a larger mass and/or with a larger electric charge.

Stability of Current Sheets in the Solar Corona

A. **Artemyev** and I. Zimovets
Solar Physics, Volume 277, Number 2, 283-298, **2012**
This work aims at investigating unstable modes of oscillation of quasi-vertical two-dimensional current sheets with sheared magnetic fields under physical conditions typical for the solar corona. We use linear magnetohydrodynamic equations to obtain sets of unstable modes related to the longitudinal inhomogeneity of the current sheet. It is shown that these modes of current sheet oscillations can modulate the current sheet thickness along the polarity inversion line. Based on the obtained results, we propose a scenario which can naturally explain both the quasi-periodic pulsations of hard X-ray emission and the parallel movement of their double footpoint-like sources along the polarity inversion line observed in some eruptive two-ribbon solar flares.

TEMPORAL AND SPATIAL ANALYSES OF SPECTRAL INDICES OF NONTHERMAL EMISSIONS DERIVED FROM HARD X-RAYS AND MICROWAVES

Ayumi **Asai**1, Junko Kiyohara2, Hiroyuki Takasaki2,3, Noriyuki Narukage4, Takaaki Yokoyama5, Satoshi Masuda6, Masumi Shimojo7, and Hiroshi Nakajima
2013 ApJ 763 87
We studied electron spectral indices of nonthermal emissions seen in hard X-rays (HXRs) and microwaves. We analyzed 12 flares observed by the Hard X-Ray Telescope aboard Yohkoh, Nobeyama Radio Polarimeters, and the Nobeyama Radioheliograph (NoRH), and compared the spectral indices derived from total fluxes of HXRs and microwaves. Except for four events, which have very soft HXR spectra suffering from the thermal component, these flares show a gap $\Delta\delta$ between the electron spectral indices derived from HXRs δ_X and those from microwaves δ_μ ($\Delta\delta = \delta_X - \delta_\mu$) of about 1.6. Furthermore, from the start to the peak times of the HXR bursts, the time profiles of the HXR spectral index δ_X evolve synchronously with those of the microwave spectral index δ_μ, keeping the constant gap. We also examined the spatially resolved distribution of the microwave spectral index by using NoRH data. The microwave spectral index δ_μ tends to be larger, which means a softer spectrum, at HXR footpoint sources with stronger magnetic field than that at the loop tops. These results suggest that the electron spectra are bent at around several hundreds of keV, and become harder at the higher energy range that contributes the microwave gyrosynchrotron emission.

Flare Onset Observed with Hinode in the 2006 December 13 Flare.

Asai A, Hara H, Watanabe T, Imada S
(**2012a**) In: Sekii T, Watanabe T, Sakurai T (eds) Hinode-3: The 3rd Hinode Science Meeting, Proceedings of the conference held 1-4 December 2009 at Hitotsubashi Memorial Hall, Tokyo, Japan. ASP Conference Series, vol 454, Astronomical Society of the Pacific, San Francisco, p 303

A Study on Red Asymmetry of H-alpha Flare Ribbons Using Narrowband Filtergram in the 2001 April 10 Solar Flare

Asai, A., Ichimoto, K., Kitai, R., Kurokawa, H., and Shibata, K.

E-print, Oct **2011**; PASJ, (publication in April 2012, V64 No2 issue)
We report a detailed examination of the ``red asymmetry'' of H-alpha emission line seen during the 2001 April 10 solar flare by using a narrowband filtergram. We investigated the temporal evolution and the spatial distribution of the red asymmetry by using the H-alpha data taken with the 60cm Domeless Solar Telescope at Hida Observatory, Kyoto University. We confirmed that the red asymmetry clearly appeared all over the flare ribbons, and the strong red asymmetry is located on the outer narrow edges of the flare ribbons, with the width of about 1.5" - 3.0" (1000 - 2000 km), where the strong energy releases occur. Moreover, we found that the red asymmetry, which also gives a measure of the Doppler shift of the H-alpha emission line concentrates on a certain value, not depending on the intensity of the H-alpha kernels. This implies not only that the temporal evolutions of the red asymmetry and those of the intensity are not in synchronous in each flare kernel, but also that the peak asymmetry (or velocity of the chromospheric condensation) of individual kernel is not a strong function of their peak intensity.

IMAGING SPECTROSCOPY ON PREFLARE CORONAL NONTHERMAL SOURCES ASSOCIATED WITH THE 2002 JULY 23 FLARE
Ayumi **Asai**1, Hiroshi Nakajima1, Masumi Shimojo1, Takaaki Yokoyama2, Satoshi Masuda3, and S¨am Krucker4
Astrophysical Journal, 695:1623–1630, **2009** April
http://www.iop.org/EJ/toc/-alert=43190/0004-637X/695/2
We present a detailed examination on the coronal nonthermal emissions **during the preflare phase** of the X4.8 flare that occurred on **2002 July 23**. The microwave (17 GHz and 34 GHz) data obtained with Nobeyama Radioheliograph, at Nobeyama Solar Radio Observatory and the hard X-ray (HXR) data taken with *RHESSI* obviously showed nonthermal sources that are located above the flare loops during the preflare phase. We performed imaging spectroscopic analyses on the nonthermal emission sources both in microwaves and in HXRs, and confirmed that electrons are accelerated from several tens of keV to more than 1 MeV even in this phase. If we assume the thin-target model for the HXR emission source, the derived electron spectral indices (~ 4.7) is the same value as that from microwaves (~ 4.7) within the observational uncertainties, which implies that the distribution of the accelerated electrons follows a single power law. The number density of the microwave-emitting electrons is, however, larger than that of the HXR-emitting electrons, unless we assume low-ambient plasma density of about 1.0 Ч 10^9 cm^{-3} for the HXR-emitting region. If we adopt the thick-target model for the HXR emission source, on the other hand, the electron spectral index (~ 6.7) is much different, while the gap of the number density of the accelerated electrons is somewhat reduced.

Evolution of the anemone AR NOAA 10798 and the related geo-effective flares and CMEs
Ayumi **Asai**, Kazunari Shibata,4 Takako T. Ishii,4 Mitsuo Oka,4,5 Ryuho Kataoka,6
Ken'ichi Fujiki,7 and Nat Gopalswamy
JOURNAL OF GEOPHYSICAL RESEARCH, VOL. 114, A00A21, doi:10.1029/2008JA013291, **2009**
We present a detailed examination of the features of the active region (AR) NOAA 10798. This AR generated coronal mass ejections (CMEs) that caused a large geomagnetic storm on 24 August 2005 with the minimum **Dst index of _216 nT**. We examined the evolution of the AR and the features on/near the solar surface and in the interplanetary space. The AR emerged in the middle of a small coronal hole, and formed a sea anemone like configuration. Ha filaments were formed in the AR, which have southward axial field. Three M class flares were generated, and the first two that occurred on 22 August 2005 were followed by Halo-type CMEs. The speeds of the CMEs were fast, and recorded about 1200 and 2400 km s_1, respectively. The second CME was especially fast, and
caught up and interacted with the first (slower) CME during their travelings toward Earth. These acted synergically to generate an interplanetary disturbance with strong southward magnetic field of about _50 nT, which was followed by the large geomagnetic storm.
22 Aug 2005

STRONGLY BLUESHIFTED PHENOMENA OBSERVED WITH HINODE EIS IN THE 2006 DECEMBER 13 SOLAR FLARE
Ayumi **Asai**,1, 2,3 Hirohisa Hara,2,3 Tetsuya Watanabe,2,3 Shinsuke Imada,2 Taro Sakao,4
Noriyuki Narukage,4 J. L. Culhane,5 and G. A. Doschek6
E-print, June **2008;** Astrophysical Journal, 685:622-628, **2008**
http://arxiv.org/pdf/astro-ph/0209106v1.pdf
We present a detailed examination of strongly blueshifted emission lines observed with the EUV Imaging Spectrometer on board the Hinode satellite. We found two kinds of blueshifted phenomenon associated with the X3.4 flare that occurred on 2006 December 13. One was related to a plasmoid ejection seen in soft X-rays. It was very bright in all the lines used for the observations. The other was associated with the faint arc-shaped ejection seen in soft X-rays. The soft

X-ray ejection is thought to be a magnetohydrodynamic (MHD) fast-mode shock wave. This is therefore the first spectroscopic observation of an MHD fast-mode shock wave associated with a flare.

Loop top nonthermal emission sources associated with an over-the-limb flare observed with NoRH and RHESSI
Adv. Space Res. 39(9),Pages 1398-1401, **2007**
Ayumi **Asai**, Hiroshi Nakajima, Mitsuo Oka, Keisuke Nishida and Yasuyuki T. Tanaka
We studied the M3.7 class flare which occurred on 2005 July 27, in the active region NOAA 10792. This flare is an over-the-limb flare, and the footpoints are entirely occulted by the solar disk. The microwave and the hard X-ray images obtained with the Nobeyama Radioheliograph and the RHESSI satellite, respectively, clearly showed emission sources above the post-flare loop system. We examined the emission sources in detail spatially, temporally, and spectroscopically. As a result, one of the hard X-ray emission sources and the microwave emission source are nonthermal.

Preflare Nonthermal Emission Observed in Microwaves and Hard X-Rays
A. **ASAI** et al. PASJ: **P**ubl. Astron. Soc. Japan 58, L1-L5, **2006**, File
We discuss the temporal and spatial features of the nonthermal emissions in the preflare phase, and their relation with the ejection

Flare Ribbon Expansion and Energy Release,
A. **Asai** et al., Journal of Astrophysics and Astronomy, 27, 167-173, **2006**, **File**
A detailed examination about the relationship between the evolution of the Halpha flare ribbons and the released magnetic energy during the April 10 2001 flare.

Difference between Spatial Distributions of the H-alpha Kernels and Hard X-Ray Sources in a Solar Flare
Ayumi **Asai**, Satoshi Masuda, Takaaki Yokoyama, Masumi Shimojo, Hiroaki Isobe, Hiroki Kurokawa, Kazunari Shibata
Astrophys.J. 578 (**2002**) L91
http://arxiv.org/pdf/astro-ph/0209106v1.pdf
We present the relation of the spatial distribution of H-alpha kernels with the distribution of hard X-ray (HXR) sources seen during the **2001 April 10** solar flare. This flare was observed in H-alpha with the (Sartorius) telescope at Kwasan Observatory, Kyoto University, and in hard X-rays (HXRs) with the Hard X-ray Telescope (HXT) onboard Yohkoh. We compared the spatial distribution of the HXR sources with that of the H-alpha kernels. While many H-alpha kernels are found to brighten successively during the evolution of the flare ribbons, only a few radiation sources are seen in the HXR images. We measured the photospheric magnetic field strengths at each radiation source in the H-alpha images, and found that the H-alpha kernels accompanied by HXR radiation have magnetic strengths about 3 times larger than those without HXR radiation. We also estimated the energy release rates based on the magnetic reconnection model. The release rates at the H-alpha kernels with accompanying HXR sources are 16-27 times larger than those without HXR sources. These values are sufficiently larger than the dynamic range of HXT, which is about 10, so that the difference between the spatial distributions of the Hα kernels and the HXR sources can be explained.

Interface Region Imaging Spectrograph (IRIS) Observations of the Fractal Dimension in the Solar Atmosphere
Markus **Aschwanden** and Vilangot Nived
Front. Astron. Space Sci. 9:999319. **2022**
https://arxiv.org/pdf/2207.12894.pdf
https://www.lmsal.com/~aschwand/eprints/2022_iris.pdf
https://doi.org/10.3389/fspas.2022.999319
https://www.frontiersin.org/articles/10.3389/fspas.2022.999319/pdf
We focus here on impulsive phenomena and Quiet-Sun features in the solar transition region, observed with the Interface Region Imaging Spectrograph (IRIS) at 1,400 Å (at formation temperatures of Te ≈ 104–106 K). Summarizing additional literature values we find the following fractal dimensions (in increasing order): DA = 1.23 ± 0.09 for photospheric granulation, DA =1.40 ± 0.09 for chromospheric (network) patterns, DA = 1.54 ± 0.04 for plages in the transition region, DA = 1.56 ± 0.08 for extreme ultra-violet (EUV) nanoflares, DA = 1.59 ± 0.20 for active regions in

photospheric magnetograms, and DA = 1.76 ± 0.14 for large solar flares. We interpret low values of the fractal dimension (1.0 ≲ DA ≲ 1.5) in terms of sparse curvi-linear flow patterns, while high values of the fractal dimension (1.5 ≲ DA ≲ 2.0) indicate quasi-space-filling transport processes, such as chromospheric evaporation in flares. Phenomena in the solar transition region appear to be consistent with self-organized criticality (SOC) models, based on their fractality and their size distributions of fractal areas A and (radiative) energies E, which show power law slopes of αobsA=2.51±0.21αAobs=2.51±0.21 (with αtheoA=2.33αAtheo=2.33 predicted), and αobsE=2.03±0.18αEobs=2.03±0.18 (with αtheoE=1.80αEtheo=1.80 predicted). This agreement suggests that brightenings detected with IRIS at 1,400 Å reveal the same nonlinear SOC statistics as their coronal counterparts in EUV.

Reconciling Power Law Slopes in Solar Flare and Nanoflare Size Distributions

Markus J. **Aschwanden**

ApJL 934 L3 **2022**

https://www.lmsal.com/~aschwand/eprints/2022_reconcile.pdf

https://iopscience.iop.org/article/10.3847/2041-8213/ac7b8d/pdf

We unify the power laws of size distributions of solar flare and nanoflare energies. We present three models that predict the power law slopes α _E of flare energies defined in terms of the 2-D and 3-D fractal dimensions (D_A, D_V): (i) The spatio-temporal standard SOC model, defined by the power law slope α E1=1+2/(D_V+2)=(13/9)≈ 1.44; (ii) the 2-D thermal energy model, α E2=1+2/D_A=(7/3)≈ 2.33, and (iii) the 3-D thermal energy model, α E3=1+2/D_V=(9/5)≈ 1.80. The theoretical predictions of energies are consistent with the observational values of these three groups, i.e., α E1=1.47 ± 0.07; α E2=2.38 ± 0.09, and α E3=1.80 ± 0.18. These results corroborate that the energy of nanoflares does not diverge at small energies, since (α E1<2) and (α E3<2), except for the unphyiscal 2-D model (α E2>2). *This conclusion adds an additional argument against the scenario of coronal heating by nanoflares.*

The Fractality and Size Distributions of Astrophysical Self-Organized Criticality Systems

Markus J. **Aschwanden**

2022 *ApJ* **934** 33

https://arxiv.org/pdf/2203.12484.pdf

https://iopscience.iop.org/article/10.3847/1538-4357/ac6bf2/pdf

The statistics of nonlinear processes in avalanching systems, based on the {\sl self-organized criticality (SOC)} concept of Bak et al.~(1987), predicts power law-like size (or occurrence frequency) distribution functions. Following up on previous work we define a {\sl standard SOC model} in terms of six assumptions: (i) multi-fractality; (ii) the length-area-volume relationship of Mandelbrot (1977); (iii) the flux-volume relationship, (iv) classical diffusion, (v) the Euclidean volume limit at the event peak time, and (vi) the spatio-temporal fluence or energy of an avalanche event. We gather data of the fractal dimension and power law slopes from 162 publications and assemble them in 28 groups (e.g., solar and stellar flare energies), from which we find that 75\% of the groups are consistent with the standard SOC model. Alternative SOC models (Levy-flight, flat-world, non-fractal) are slightly less correlated with the data. The remaining discrepancies are attributed to outliers caused by small-number statistics, background subtraction problems, inadequate fitting ranges, and deviations from ideal power laws.

Global energetics of solar flares. XIII. The Neupert effect and acceleration of coronal mass ejections

Markus J. **Aschwanden**

ApJ **2021**

https://arxiv.org/pdf/2112.07759.pdf **File**

Our major aim is a height-time model r(t) of the propagation of {\sl Coronal Mass Ejections (CMEs)}, where the lower corona is self-consistently connected to the heliospheric path. We accomplish this task by using the Neupert effect to derive the peak time, duration, and rate of the CME acceleration phase, as obtained from the time derivative of the {\sl soft X-ray (SXR)} light curve. This novel approach offers the advantage to obtain the kinematics of the CME height-time profile r(t), the CME velocity profile v(t)=dr(t)/dt, and the CME acceleration profile a(t)=dv(t)/dt from {\sl Geostationary Orbiting Earth Satellite (GOES)} and white-light data, without the need of {\sl hard X-ray (HXR)} data. We apply this technique to a data set of 576 (GOES X and M-class) flare events observed with GOES and the {\sl Large Angle Solar Coronagraph (LASCO)}. Our analysis yields acceleration rates in the range of aA=0.1−13 km s−2, acceleration durations of τA=1.2−45 min, and acceleration distances in the range of dA=3−1063 Mm, with a median of dA=39 Mm, which corresponds to the hydrostatic scale height of a corona with a temperature of Te≈0.8 MK. The results are consistent with standard flare/CME models that predict magnetic reconnection and synchronized (primary) acceleration of CMEs in the low corona (at a height of ~0.1 R_sun), while secondary (weaker) acceleration may occur further out at heliospheric distances. **2011-03-09, 2011-03-12, 2011-08-09, 2011-09-05, 2011-11-15, 2011-12-30, 2012-**

01-23, 2012-03-06, 2012-03-07, 2012-07-06, 2012-07-09, 2012-07-14, 2013-05-14, 2013-05-31, 2013-10-15, 2013-11-05, 2014-02-02, 2014-02-13, 2014-02-25, 2014-05-06, 2014-10-20
Table 1. Measurements of timing [tA, tB, t1, tn], distances from Sun center [rA, rB, r1, rn], velocity [vB], and acceleration rate [aA] of CMEs and solar flares based on predictions by the Neupert effect, for 24 selected flares (Table 1 and Figures 1-6).
Table 2. Measurements of timing [tA, tB, t1, tn], altitudes [rA, rB, r1, rn], velocity [vB], and acceleration rate [aA] of CME kinematics. The full table of 576 events is available as a machine-readable file.
RHESSI Science Nuggets #422 **2021 Bridging solar flares to coronal mass ejections**
https://sprg.ssl.berkeley.edu/~tohban/wiki/index.php/Bridging_solar_flares_to_coronal_mass_ejections
1996-12-23

The Solar Memory From Hours to Decades

Markus J. **Aschwanden**, Jay R. Johnson
ApJ **921** 82 **2021**
https://arxiv.org/pdf/2107.13621.pdf
https://iopscience.iop.org/article/10.3847/1538-4357/ac2a29/pdf
https://doi.org/10.3847/1538-4357/ac2a29
Waiting time distributions allow us to distinguish at least three different types of dynamical systems, such as (i) linear random processes (with no memory); (ii) nonlinear, avalanche-type, nonstationary Poisson processes (with memory during the exponential growth of the avalanche rise time); and (iii) chaotic systems in the state of a nonlinear limit cycle (with memory during the oscillatory phase). We describe the temporal evolution of the flare rate λ(t)∝tp with a polynomial function, which allows us to distinguish linear (p≈1) from nonlinear ($p \gapprox 2$) events. The power law slopes α of observed waiting times (with full solar cycle coverage) cover a range of α=2.1−2.4, which agrees well with our prediction of α=2.0+1/p=2.3−2.5. The memory time can also be defined with the time evolution of the logistic equation, for which we find a relationship between the nonlinear growth time τG=τrise/(4p) and the nonlinearity index p. We find a nonlinear evolution for most events, in particular for the clustering of solar flares (p=2.2±0.1), partially occulted flare events (p=1.8±0.2), and the solar dynamo (p=2.8±0.5). The Sun exhibits memory on time scales of $\lapprox$2 hours to 3 days (for solar flare clustering), 6 to 23 days (for partially occulted flare events), and 1.5 month to 1 year (for the rise time of the solar dynamo).

The Poissonian origin of power laws in solar flare waiting time distributions

Aschwanden,M.J., Johnson,J.R., and Nurhan,Y.
ApJ **921** 166 **2021**
https://www.lmsal.com/~aschwand/eprints/2021_wait.pdf
https://arxiv.org/pdf/2107.13065
https://iopscience.iop.org/article/10.3847/1538-4357/ac19a9/pdf
https://doi.org/10.3847/1538-4357/ac19a9
In this study we aim for a deeper understanding of the power law slope, α, of waiting time dis8 tributions. Statistically independent events with linear behavior can be characterized by binomial, 9 Gaussian, exponential, or Poissonian size distribution functions. In contrast, physical processes with 10 nonlinear behavior exhibit spatio-temporal coherence (or memory) and “fat tails” in their size distribu11 tions that fit power law-like functions, as a consequence of the time variability of the mean event rate, 12 as demonstrated by means of Bayesian block decomposition in the work of Wheatland et al. (1998). 13 In this study we conduct numerical simulations of waiting time distributions N(τ) in a large pa14 rameter space for various (polynomial, sinusoidal, Gaussian) event rate functions λ(t), parameterized with an exponent p that expresses the degree of the polynomial function λ(t) ∝ t p 15 . We derive an 16 analytical exact solution of the waiting time distribution function in terms of the incomplete gamma 17 function, which is similar to a Pareto type-II function and has a power law slope of α = 2 + 1/p, in 18 the asymptotic limit of large waiting times. Numerically simulated random distributions reproduce 19 this theoretical prediction accurately. Numerical simulations in the nonlinear regime (p ≥ 2) predict 20 power law slopes in the range of 2.0 ≤ α ≤ 2.5. The self-organized criticality model yields a prediction 21 of α = 2. Observations of solar flares and coronal mass ejections (over at least a half solar cycle) are 22 found in the range of αobs ≈ 2.1 − 2.4. Deviations from strict power law functions are expected due 23 to the variability of the flare event rate λ(t), and deviations from theoretically predicted slope values 24 α occur due to the Poissonian weighting bias of power law fits.

Self-organized Criticality in Stellar Flares

Markus J. **Aschwanden**1 and Manuel Güdel2
2021 ApJ 910 41
https://www.lmsal.com/~aschwand/eprints/2021_stellar.pdf
https://doi.org/10.3847/1538-4357/abdec7
https://iopscience.iop.org/article/10.3847/1538-4357/abdec7/pdf
https://arxiv.org/pdf/2106.06490.pdf

Power-law size distributions are the hallmarks of nonlinear energy dissipation processes governed by self-organized criticality (SOC). Here we analyze 75 data sets of stellar flare size distributions, mostly obtained from the Extreme-Ultraviolet Explorer and the Kepler mission. We aim to answer the following questions for size distributions of stellar flares. (i) What are the values and uncertainties of power-law slopes? (ii) Do power-law slopes vary with time? (iii) Do power-law slopes depend on the stellar spectral type? (iv) Are they compatible with solar flares? (v) Are they consistent with SOC models? We find that the observed size distributions of stellar flare fluences (or energies) exhibit power-law slopes of αE = 2.09 ± 0.24 for optical data sets observed with Kepler. The observed power-law slopes do not show much time variability and do not depend on the stellar spectral type (M, K, G, F, A, giants). In solar flares, we find that background subtraction lowers the uncorrected value of αE = 2.20 ± 0.22 to αE = 1.57 ± 0.19. Furthermore, most of the stellar flares are temporally not resolved in low-cadence (30 minutes) Kepler data, which causes an additional bias. Taking these two biases into account, the stellar flare data sets are consistent with the theoretical prediction $N(x) \propto x^{-\alpha_x}$ of SOC models, i.e., αE = 1.5. Thus, accurate power-law fits require automated detection of the inertial range and background subtraction, which can be modeled with the generalized Pareto distribution, finite-system size effects, and extreme event outliers.

Correlation of the sunspot number and the waiting time distribution of solar flares, coronal mass ejections, and solar wind switchback events observed with the Parker Solar Probe

Markus J. **Aschwanden**, Thierry Dudok de Wit

ApJ **912** 94 **2021**

https://arxiv.org/pdf/2102.02305.pdf
https://www.lmsal.com/~aschwand/eprints/2021_parker.pdf
https://doi.org/10.3847/1538-4357/abef69

Waiting time distributions of solar flares and {\sl coronal mass ejections (CMEs)} exhibit power law-like distribution functions with slopes in the range of ατ≈1.4−3.2, as observed in annual data sets during 4 solar cycles (1974-2012). We find a close correlation between the waiting time power law slope ατ and the {\sl sunspot number (SN)}, i.e., ατ = 1.38 + 0.01 × SN. The waiting time distribution can be fitted with a Pareto-type function of the form N(τ)=N0 (τ0+τ)−ατ, where the offset τ0 depends on the instrumental sensitivity, the detection threshold of events, and pulse pile-up effects. The time-dependent power law slope ατ(t) of waiting time distributions depends only on the global solar magnetic flux (quantified by the sunspot number) or flaring rate, independent of other physical parameters of {\sl self-organized criticality (SOC)} or {\sl magneto-hydrodynamic (MHD)} turbulence models. Power law slopes of ατ≈1.2−1.6 were also found in solar wind switchback events, as observed with the {\sl Parker Solar Probe (PSP)}. We conclude that the annual variability of switchback events in the heliospheric solar wind is modulated by flare and CME rates originating in the photosphere and lower corona.

Finite System-Size Effects in Self-Organized Criticality Systems

Markus J. **Aschwanden**

2021 *ApJ* **909** 69

https://arxiv.org/pdf/2101.03124.pdf
https://www.lmsal.com/~aschwand/eprints/2021_finite.pdf
https://iopscience.iop.org/article/10.3847/1538-4357/abef69/pdf
https://doi.org/10.3847/1538-4357/abda48

We explore upper limits for the largest avalanches or catastrophes in nonlinear energy dissipation systems governed by self-organized criticality (SOC). We generalize the idealized "straight" power low size distribution and Pareto distribution functions in order to accomodate for incomplete sampling, limited instrumental sensitivity, finite system-size effects, "Black-Swan" and "Dragon-King" extreme events. Our findings are: (i) Solar flares show no finite system-size limits up to L < 200 Mm, but solar flare durations reveal an upper flare duration limit of < 6 hrs; (ii) Stellar flares observed with KEPLER exhibit inertial ranges of E≈1034−1037 erg, finite system-size ranges at E≈1037−1038 erg, and extreme events at E=(1−5)×1038 erg; (iii) The maximum flare energy of different spectral-type stars (M, K, G, F, A, Giants) reveal a positive correlation with the stellar radius, which indicates a finite system-size limit imposed by the stellar surface area. Fitting our finite system-size models to terrestrial data sets (Earth quakes, wildfires, city sizes, blackouts, terrorism, words, surnames, web-links) yields evidence (in half of the cases) for finite system-size limits and extreme events, which can be modeled with dual power law size distributions.

Global Energetics of Solar Flares. XII. Physical Scaling Laws

Markus J. **Aschwanden**

ApJ **903** 23 **2020**

https://arxiv.org/pdf/2007.04419.pdf
https://www.lmsal.com/~aschwand/eprints/2020_scaling.pdf
https://doi.org/10.3847/1538-4357/abb946

In this study we test 30 variants of 5 physical scaling laws that describe different aspects of solar flares. We express scaling laws in terms of the magnetic potential field energy Ep, the mean potential field strength Bp, the free energy Efree, the dissipated magnetic flare energy Ediss, the mean loop length scale L, the mean helically twisted flux tube radius R, the sunspot radius r, the emission measure-weighted flare temperature Tw, the electron density ne, and the total emission measure EM, measured from a data set of $\lapprox 400$ GOES M- and X-class flare events. The 5 categories of physical scaling laws include (i) a scaling law of the potential-field energy, (ii) a scaling law for helical twisting, (iii) a scaling law for Petschek-type magnetic reconnection, (iv) the Rosner-Tucker-Vaiana scaling law, and (v) the Shibata-Yokoyama scaling law. We test the self-consistency of these theoretical scaling laws with observed parameters by requiring two conditions: a cross-corrleation coefficient of CCC>0.5 between the observed and theoretically predicted scaling laws, and a linear regression fit with a slope of α≈1. With these two criteria we find that 10 out of the 30 tested scaling law variants are consistent with the observed data, which strongly corroborates the existence and validity of the tested flare scaling laws.

Global Energetics of Solar Flares. XI. Flare Magnitude Predictions of the GOES Class

Markus J. **Aschwanden**

2020 ApJ 897 16

sci-hub.do/10.3847/1538-4357/ab9630 **File**

https://arxiv.org/pdf/2007.04413.pdf

https://iopscience.iop.org/article/10.3847/1538-4357/ab9630/pdf

In this study we determine scaling relationships of observed solar flares that can be used to predict upper limits of the Geostationary Orbiting Earth Satellite (GOES)–class magnitude of solar flares. The flare prediction scheme is based on the scaling of the slowly varying potential energy Ep(t), which is extrapolated in time over an interval of Δt 24 hr. The observed scaling of the dissipated energy Ediss scales with the potential field energy as Ediss µ Ep 1.32. In addition, the observed scaling relationship of the flare volume, V µ Ediss 1.17, the multi-thermal energy, Eth ∝ V0.76, the flare emission measure (EM) µ Eth 0.79, the EM-weighted temperature Tw, and the GOES flux, Ft Et 8() () µ p 0.92, allows us then to predict an upper limit of the GOES-class flare magnitude in the extrapolated time window. We find a good correlation (cross-correlation coefficient (CCC) ≈ 0.7) between the observed and predicted GOES-class flare magnitudes (in 172 X- and M-class events). This is the first algorithm that employs observed scaling laws of physical flare parameters to predict GOES flux upper limits, an important capability that complements previous flare prediction methods based on machine-learning algorithms used in space-weather forecasting.

Table 1 Observed and Predicted Upper Limits of the GOES 1–8 Å Flux during the Month of **2011 February 1–28**, Containing a Total of 14 X- and M-class Flares

Global Energetics of Solar Flares, X. Petschek Reconnection Rate and Alfvén Mach Number of Magnetic Reconnection Outflows

Markus J. **Aschwanden**

ApJ **895** 134 **2020**

https://www.lmsal.com/~aschwand/eprints/2020_petschek.pdf

https://doi.org/10.3847/1538-4357/ab8aec

https://arxiv.org/pdf/2007.04404.pdf

We investigate physical scaling laws for magnetic energy dissipation in solar flares, in the framework of the Sweet-Parker model and the Petschek model. We find that the total dissipated magnetic energy Ediss in a flare depends on the mean magnetic field component Bf associated with the free energy Ef, the length scale L of the magnetic area, the hydrostatic density scale height lambda of the solar corona, the Alfvén Mach number M_A=v_1/vA (the ratio of the inflow speed v1 to the Alfvénic outflow speed vA), and the flare duration au_f, i.e., Ediss = (1/4π) B_f^2 L lambda vA M_A au_f, where the Alfvén speed depends on the nonpotential field strength Bnp and the mean electron density ne in the reconnection outflow. Using MDI/SDO and AIA/SDO observations and 3-D magnetic field solutions obtained with the vertical-current approximation nonlinear force-free field code (VCA-NLFFF) we measure all physical parameters necessary to test scaling laws, which represents a new method to measure Alfvén Mach numbers MA, the reconnection rate, and the total free energy dissipated in solar flares.

Torsional Alfvénic Oscillations Discovered in the Magnetic Free Energy During Solar Flares

Markus J. **Aschwanden**, Tongjiang Wang

2020 *ApJ* **891** 99

https://arxiv.org/pdf/2001.10103.pdf

https://doi.org/10.3847/1538-4357/ab7120

We report the discovery of torsional Alfvénic oscillations in solar flares, which modulate the time evolution of the magnetic free energy Ef(t), while the magnetic potential energy Ep(t) is uncorrelated, and the nonpotential energy varies as Enp(t)=Ep+Ef(t). The mean observed time period of the torsional oscillations is Pobs=15.1±3.9 min, the mean field line length is L=135±35 Mm, and the mean phase speed is vphase=315±120 km s−1, which we interpret as torsional Alfvénic waves in flare loops with enhanced electron densities. Most of the torsional oscillations are found to be decay-

less, but exhibit a positive or negative trend in the evolution of the free energy, indicating new emerging flux (if positive), magnetic cancellation, or flare energy dissipation (if negative). The time evolution of the free energy has been calculated in this study with the {\sl Vertical-Current Approximation (Version 4) Nonlinear Force-Free Field (VCA4-NLFFF)} code, which incorporates automatically detected coronal loops in the solution and bypasses the non-forcefreeness of the photospheric boundary condition, in contrast to traditional NLFFF codes.
We analyze the same subset of 11 GOES X-class flares presented in previous papers (Aschwanden et al. 2014a; Aschwanden 2019c), which represents all X-class flares observed with the SDO during the first 3.5 years of the mission (2010 June 1 to 2014 January 31)

Non-Stationary Fast-Driven Self-Organized Criticality in Solar Flares

Markus J. **Aschwanden**
ApJ **887** 57 **2019**
http://www.lmsal.com/~aschwand/eprints/2019_wait.pdf
https://arxiv.org/pdf/1909.08673.pdf
sci-hub.se/10.3847/1538-4357/ab5371
The original concept of self-organized criticality (Bak et al. 1987), applied to solar flare statistics (Lu and Hamilton 1991), assumed a slow-driven and stationary flaring rate, which warrants time scale separation (between flare durations and inter-flare waiting times), it reproduces power-law distributions for flare peak fluxes and durations, but predicts an exponential waiting time distribution. In contrast to these classical assumptions we observe: (i) multiple energy dissipation episodes during most flares, (ii) violation of the principle of time scale separation, (iii) a fast-driven and non-stationary flaring rate, (iv) a power law distribution for waiting times Δ t, with a slope of α Δ t $\approx$ 2.0, as predicted from the universal reciprocality between mean flaring rates and mean waiting times; and (v) pulses with rise times and decay times of the dissipated magnetic free energy on time scales of 12±6 min, up to 13 times in long-duration (\lapprox 4 hrs) flares. These results are inconsistent with coronal long-term energy storage (Rosner and Vaiana 1978), but require photospheric-chromospheric current injections into the corona.

Global Energetics of Solar Flares. IX. Refined Magnetic Modeling

Markus J. **Aschwanden**
ApJ **885** 49 **2019**
http://www.lmsal.com/~aschwand/eprints/2019_global9.pdf
https://arxiv.org/pdf/1909.08672.pdf
https://doi.org/10.3847/1538-4357/ab46c1
A more accurate analytical solution of the vertical-current approximation nonlinear force-free field (VCA3-NLFFF) model is presented that includes besides the radial (B_r) and the azimuthal (B_ϕ) magnetic field components a poloidal component (B\theta \neq 0) also. This new analytical solution is of second-order accuracy in the divergence-freeness condition, and of third-order accuracy in the force-freeness condition. We re-analyze the sample of 173 GOES M- and X-class flares observed with the Atmospheric Imaging Assembly (AIA) and Helioseismic and Magnetic Imager (HMI) onboard the Solar Dynamics Observatory (SDO). The new code reproduces helically twisted loops with a low winding number below the kink instability consistently, avoiding unstable, highly-twisted structures of the Gold-Hoyle flux rope type. The magnetic energies agree within EVCA3/E_W=0.99±0.21 with the Wiegelmann (W-NLFFF) code. The time evolution of the magnetic field reveals multiple, intermittent energy build-up and releases in most flares, contradicting both the Rosner-Vaiana model (with gradual energy storage in the corona) and the principle of time scale separation (τflare $\ll$ τstorage) postulated in self-organized criticality models. The mean dissipated flare energy is found to amount to 7%±3% of the potential energy, or 60%±26% of the free energy, a result that can be used for predicting flare magnitudes based on the potential field of active regions. **2010-08-07, 2010-10-16, 2011/02/13-18**

Self-Organized Criticality in Solar and Stellar Flares: Are Extreme Events Scale-Free ?

Markus J. **Aschwanden**
2019 ApJ **880** 105
https://arxiv.org/pdf/1906.05840.pdf
http://www.lmsal.com/~aschwand/eprints/2019_extreme.pdf
sci-hub.se/10.3847/1538-4357/ab29f4
We search for outliers in extreme events of statistical size distributions of astrophysical data sets, motivated by the {\sl Dragon-King hypothesis} of Sornette (2009), which suggests that the most extreme events in a statistical distribution may belong to a different population, and thus may be generated by a different phyiscal mechanism, in contrast to the strict power law behavior of {\sl self-organized criticality (SOC)} models. Identifying such disparate outliers is important for space weather predictions. Possible physical mechanisms to produce such outliers could be generated by sympathetic flaring. However, we find that Dragon-King events are not common in solar and stellar flares, identified in 4 out of 25 solar and stellar flare data sets only. Consequently, small, large, and extreme flares are essentially scale-free and can be modeled with a single physical mechanism. In very large data sets ($N \gapprox 10^4$) we find significant

deviations from ideal power laws in almost all data sets. Neverthess, the fitted power law slopes constrain physcial scaling laws in terms of flare areas and volumes, which have the highest nonlinearity in their scaling laws.

Global Energetics of Solar Flares: VIII. The Low-Energy Cutoff

Markus **Aschwanden**, Eduard P. Kontar, Natasha L.S. Jeffrey
2019 ApJ 881 1
https://arxiv.org/pdf/1906.05835.pdf
http://www.lmsal.com/~aschwand/eprints/2019_global8.pdf
One of the key problems in solar flare physics is the determination of the low-energy cut-off; the value that determines the energy of nonthermal electrons and hence flare energetics. We discuss different approaches to determine the low-energy cut-off in the spectrum of accelerated electrons: (i) the total electron number model, (ii) the time-of-flight model (based on the equivalence of the time-of-flight and the collisional deflection time); (iii) the warm target model of Kontar et al.~(2015), and (iv) the model of the spectral cross-over between thermal and nonthermal components. We find that the first three models are consistent with a low-energy cutoff with a mean value of ≈10 keV, while the cross-over model provides an upper limit for the low-energy cutoff with a mean value of ≈21 keV. Combining the first three models we find that the ratio of the nonthermal energy to the dissipated magnetic energy in solar flares has a mean value of qE=0.57±0.08, which is consistent with an earlier study based on the simplified approximation of the warm target model alone (qE=0.51±0.17). This study corroborates the self-consistency between three different low-energy cutoff models in the calculation of nonthermal flare energies.

Global Energetics of Solar Flares. VII. Aerodynamic Drag in Coronal Mass Ejections

Markus J. **Aschwanden**1 and Nat Gopalswamy
2019 ApJ 877 149
sci-hub.se/10.3847/1538-4357/ab1b39
https://arxiv.org/pdf/1906.05804.pdf
The free energy that is dissipated in a magnetic reconnection process of a solar flare, generally accompanied by a coronal mass ejection (CME), has been considered as the ultimate energy source of the global energy budget of solar flares in previous statistical studies. Here we explore the effects of the aerodynamic drag force on CMEs, which supplies additional energy from the slow solar wind to a CME event, besides the magnetic energy supply. For this purpose, we fit the analytical aerodynamic drag model of Cargill and Vršnak et al. to the height–time profiles r(t) of LASCO/SOHO data in 14,316 CME events observed during the first 8 yr (2010–2017) of the Solar Dynamics Observatory era (ensuring EUV coverage with AIA). Our main findings are (1) a mean solar wind speed of w = 472 ± 414 km s−1, (2) a maximum drag-accelerated CME energy of $E_{drag} \lesssim 2 \times 1032$ erg, (3) a maximum flare-accelerated CME energy of $E_{flare} \lesssim 1.5 \times 1033$ erg, (4) the ratio of the summed kinetic energies of all flare-accelerated CMEs to the drag-accelerated CMEs amounts to a factor of 4, (5) the inclusion of the drag force slightly lowers the overall energy budget of CME kinetic energies in flares from ≈7% to ≈4%, and (6) the arrival times of CMEs at Earth can be predicted with an accuracy of ≈23%.
Table 1 Statistics of CME Parameters for 14,316 Eruptive CME Events Detected with LASCO/SOHO during 2010–2017

Helical Twisting Number and Braiding Linkage Number of Solar Coronal Loops

Markus J. **Aschwanden**
2019
https://arxiv.org/pdf/1902.10612.pdf
Coronal loops in active regions are often characterized by quasi-circular and helically twisted (sigmoidal) geometries, which are consistent with dipolar potential field models in the former case, and with nonlinear force-free field models with vertical currents in the latter case. Alternatively, Parker-type nanoflare models of the solar corona hypothesize that a braiding mechanism operates between unresolved loop strands, which is a more complex topological model. In this study we use the vertical-current approximation of a nonpotential magnetic field solution (that fulfills the divergence-free and force-free conditions) to characterize the number of helical turns Ntwist in twisted coronal loops. We measure the helical twist in 15 active regions observed with AIA and HMI/SDO and find a mean nonpotentiality angle (between the potential and nonpotential field directions) of μNP=15∘±3∘. The resulting mean rotational twist angle is φ=49∘±11∘, which corresponds to Ntwist=φ/360∘=0.14±0.03 turns with respect to the untwisted potential field, with an absolute upper limit of $N_{twist} \lapprox 0.5$, which is far below the kink instability limit of $|N_{twist}| \gapprox 1$. The number of twist turns Ntwist corresponds to the Gauss linkage number Nlink in braiding topologies. We conclude that any braided topology (with |Nlink|≥1) cannot explain the observed stability of loops in a force-free corona, nor the observed low twist number. Parker-type nanoflaring can thus occur in non-forcefree environments only, such as in the chromosphere and transition region. **2011 November 08**
Table 1: Data (2010-2011)

The Minimum Energy Principle Applied to Parker's Coronal Braiding and Nanoflaring Scenario

M.J. **Aschwanden**, A.A van Ballegooijen

2018

https://arxiv.org/pdf/1808.05269.pdf

http://www.lmsal.com/~aschwand/eprints/2018_parker.pdf

Parker's coronal braiding and nanoflaring scenario predicts the development of tangential discontinuities and highly misaligned magnetic field lines, as a consequence of random buffeting of their footpoints due to the action of sub-photospheric convection. The increased stressing of magnetic field lines is thought to become unstable above some critical misalignment angle and to result into local magnetic reconnection events, which is generally referred to as Parker's `nanoflaring scenario'. In this study we show that the {\sl minimum (magnetic) energy principle} leads to a bifurcation of force-free field solutions for helical twist angles at $|\varphi(t)|=\pi$, which prevents the build-up of arbitrary large free energies and misalignment angles. The minimum energy principle predicts that neighbored magnetic field lines are almost parallel (with misalignment angles of $\Delta\mu \approx 1.6^\circ - 1.8^\circ$), and do not reach a critical misalignment angle prone to nanoflaring. Consequently, no nanoflares are expected in the divergence-free and force-free parts of the solar corona, while they are more likely to occur in the chromosphere and transition region.

Global Energetics of Solar Flares: VI. Refined Energetics of Coronal Mass Ejections

Markus J. **Aschwanden**

ApJ 847, Issue 1, article id. 27 **2017**

https://arxiv.org/pdf/1704.01993.pdf

https://iopscience.iop.org/article/10.3847/1538-4357/aa8952/pdf

In this study we refine a CME model presented in an earlier study on the global energetics of solar flares and associated CMEs, and apply it to all (860) GOES M- and X-class flare events observed during the first 7 years (2010-2016) of the Solar Dynamics Observatory (SDO) mission, which doubles the statistics of the earlier study. The model refinements include: (1) the CME geometry in terms of a 3D sphere undergoing self-similar adiabatic expansion; (2) the inclusion of solar gravitational deceleration during the acceleration and propagation of the CME, which discriminates eruptive and confined CMEs; (4) a self-consistent relationship between the CME center-of-mass motion detected during EUV dimming and the leading-edge motion observed in white-light coronagraphs; (5) the equi-partition of the CME kinetic and thermal energy; and (6) the Rosner-Tucker-Vaiana (RTV) scaling law. The refined CME model is entirely based on EUV dimming observations (using AIA/SDO data) and complements the traditional white-light scattering model (using LASCO/SOHO data), and both models are independently capable to determine fundamental CME parameters such as the CME mass, speed, and energy. Comparing the two methods we find that: (1) LASCO is less sensitive than AIA in detecting CMEs (in 24% of the cases); (2) CME masses below mcme~1014 g are under-estimated by LASCO; (3) AIA and LASCO masses, speeds, and energy agree closely in the statistical mean after elimination of outliers; (4) the CMEs parameters of the speed v, emission measure-weighted flare peak temperature Te, and length scale L are consistent with the following scaling laws (derived from first principles): v∝T1/2e, v∝(mcme)1/4, and mcme∝L2.

Global Energetics of Solar Flares and CMEs: V. Energy Closure in Flares and Coronal Mass Ejections

Markus J. **Aschwanden**, Amir Campi, Christina M.S. Cohen, Gordon Holman, Ju Jing, Matthieu Kretzschmar, Eduard P. Kontar, James McTiernan, Richard A. Mewaldt, Aidan O'Flannagain, Ian G. Richardson, Daniel Ryan, Harry P. Warren, Yan Xu

ApJ 836, Issue 1, article id. 17 **2017**

https://arxiv.org/pdf/1701.01176v1.pdf

https://iopscience.iop.org/article/10.3847/1538-4357/836/1/17/pdf

In this study we synthesize the results of four previous studies on the global energetics of solar flares and associated coronal mass ejections (CMEs), which include magnetic, thermal, nonthermal, and CME energies in 399 solar M and X-class flare events observed during the first 3.5 years of the Solar Dynamics Observatory (SDO) mission. Our findings are: (1) The sum of the mean nonthermal energy of flare-accelerated particles (Ent), the energy of direct heating (Edir), and the energy in coronal mass ejections (ECME), which are the primary energy dissipation processes in a flare, is found to have a ratio of (Ent+Edir+ECME)/Emag=0.87±0.18, compared with the dissipated magnetic free energy Emag, which confirms energy closure within the measurement uncertainties and corroborates the magnetic origin of flares and CMEs; (2) The energy partition of the dissipated magnetic free energy is: 0.51±0.17 in nonthermal energy of ≥6 keV electrons, 0.17±0.17 in nonthermal ≥1 MeV ions, 0.07±0.14 in CMEs, and 0.07±0.17 in direct heating; (3) The thermal energy is almost always less than the nonthermal energy, which is consistent with the thick-target model; (4) The bolometric luminosity in white-light flares is comparable with the thermal energy in soft X-rays (SXR); (5) Solar Energetic Particle (SEP) events carry a fraction ≈0.03 of the CME energy, which is consistent with CME-driven shock acceleration; and (6) The warm-target model predicts a lower limit of the low-energy cutoff

at ec≈6 keV, based on the mean differential emission measure (DEM) peak temperature of Te=8.6 MK during flares. This work represents the first statistical study that establishes energy closure in solar flare/CME events.
2011-Feb-15, 2011-Aug-04, 2011-Sep-22, 2012-Jan-23, 2012-Jan-27, 2012-Mar-07, 2012-May-17, 2013-May-13, 2013-Jun-21
Table 1. SEP kinetic energies for selected 3-spacecraft events from 2011-2013. The higher value of the two lower limits of CME/LASCO (column 6) and CME/AIA energies (column 7) is used in the SEP/CME ratio (column 8).

Global Energetics of Solar Flares: III. Non thermal Energies

Markus J. **Aschwanden**, Gordon Holman, Aidan O'Flannagain, Amir Campi, James M. McTiernan, Eduard Konter
ApJ 832 27 **2016**
http://arxiv.org/pdf/1607.06488v1.pdf
http://iopscience.iop.org/article/10.3847/0004-637X/832/1/27/pdf
This study entails the third part of a global flare energetics project, in which RHESSI data of 193 M and X-class flare events from the first 3.5 yrs of the SDO) mission are analyzed. We fit a thermal and a nonthermal component to RHESSI spectra, yielding the temperature of the differential emission measure (DEM) tail, the nonthermal power law slope and flux, and the thermal/nonthermal cross-over energy. From these parameters we calculate the total non thermal energy in electrons with two different methods: (i) using the observed cross-over energy as low-energy cutoff, and (ii) using the low-energy cutoff predicted by the warm thick-target bremsstrahlung model of Kontar et al. We find commensurable ranges of the low-energy or 21+/-6 keV for the cross-over method, and 18+/-6 keV for the warm-target model. Comparing with the statistics of magnetically dissipated energies and thermal energies in the two previous studies, we find the following mean (logarithmic) energy ratios: E_nt=0.07 E_mag, and E_th=0.74 E_Na, with a logarithmic standard deviation corresponding to a factor of 8. A new finding is that the thermal energy exceeds the nonthermal energy in 40% of the flares, with the energy ratio E_th/E_nt being anti-correlated with the flare size or GOES class. This implies an insufficiency of the electron beam thick-target model in those events to explain the full amount of thermal flare plasma, as it has been noted earlier and interpreted as failure of the "theoretical Neupert effect". Additional heating of the thermal flare plasma is needed besides the chromospheric evaporation process, such as by thermal conduction fronts or direct heating processes. However, the total dissipated magnetic energy, most likely to be produced by a magnetic reconnection process, is still found to be sufficient to explain both the thermal and non thermal energies in flares. **2011-Feb-15 , 2012-Jul-10 , 2014-Jan-27**
Table 1. Nonthermal energy parameters measured in 193 flare events observed with RHESSI. June 2010 – January 2014

Global Energetics of Solar Flares: IV. Coronal Mass Ejection Energetics

Markus J. **Aschwanden**
ApJ 831..105A **2016**
http://arxiv.org/pdf/1605.04952v1.pdf **File**
http://www.lmsal.com/~aschwand/eprints/2016_global4.pdf
https://iopscience.iop.org/article/10.3847/0004-637X/831/1/105/pdf
This study entails the fourth part of a global flare energetics project, in which the mass mcme, kinetic energy Ekin, and the gravitational potential energy Egrav of coronal mass ejections (CMEs) is measured in 399 M and X-class flare events observed during the first 3.5 yrs of the Solar Dynamics Observatory (SDO) mission, using *a new method based on the EUV dimming effect*. The EUV dimming is modeled in terms of a radial adiabatic expansion process, which is fitted to the observed evolution of the total emission measure of the CME source region. The model derives the evolution of the mean electron density, the emission measure, the bulk plasma expansion velocity, the mass, and the energy in the CME source region. The EUV dimming method is truly complementary to the Thomson scattering method in white light, which probes the CME evolution in the heliosphere at r>2R⊙, while the EUV dimming method tracks the CME launch in the corona. We compare the CME parameters obtained in white light with the LASCO/C2 coronagraph with those obtained from EUV dimming with the Atmospheric Imaging Assembly (AIA) onboard SDO for all identical events in both data sets. We investigate correlations between CME parameters, the relative timing with flare parameters, frequency occurrence distributions, and the energy partition between magnetic, thermal, nonthermal, and CME energies. CME energies are found to be systematically lower than the dissipated magnetic energies, which is consistent with a magnetic origin of CMEs. **2010-10-16, 2010-06-12, 2011-05-29, 2011-08-02, 2011-09-24, 2011-09-28, 2011-11-09, 2012-01-27, 2012-03-10, 2012-03-13, 2012-06-06, 2012-07-05, 2012-07-19, 2012-08-11, 2012-09-09, 2012-11-13, 2013-05-22, 2013-08-17, 2013-10-24, 2013-11-01, 2013-11-03, 2013-11-06, 2013-11-19, 2014-01-07**
Table 3. Temporal and spatial parameters of the first 10 entries (out of the 399 events) listed in the complete machine-readable data file.
Table 4. CME parameters of the first 10 entries (out of the 399 events) listed in the complete machine-readable data file.

The Vertical Current Approximation Nonlinear Force-Free Field Code - Description, Performance Tests, and Measurements of Magnetic Energies Dissipated in Solar Flares

Markus J. **Aschwanden**

2016

http://arxiv.org/pdf/1602.00635v1.pdf

In this work we provide an updated description of the Vertical Current Approximation Nonlinear Force-Free Field (VCA-NLFFF) code, which is designed to measure the evolution of the potential, nonpotential, free energies, and the dissipated magnetic energies during solar flares. This code provides a complementary and alternative method to existing traditional NLFFF codes. The chief advantages of the VCA-NLFFF code over traditional NLFFF codes are the circumvention of the unrealistic assumption of a force-free photosphere in the magnetic field extrapolation method, the capability to minimize the misalignment angles between observed coronal loops (or chromospheric fibril structures) and theoretical model field lines, as well as computational speed. In performance tests of the VCA-NLFFF code, by comparing with the NLFFF code of Wiegelmann (2004), we find agreement in the potential, nonpotential, and free energy within a factor of about 1.3, but the Wiegelmann code yields in the average a factor of 2 lower flare energies. The VCA-NLFFF code is found to detect decreases in flare energies in most X, M, and C-class flares. The successful detection of energy decreases during a variety of flares with the VCA-NLFFF code indicates that current-driven twisting and untwisting of the magnetic field is an adequate model to quantify the storage of magnetic energies in active regions and their dissipation during flares. - The VCA-NLFFF code is also publicly available in the Solar SoftWare (SSW). **2011 Febr 12-17, 2014 Mar 29**,

Table 2. Data sets used in performance tests of the VCA-NLFFF code in this study: X-class flares

25 Years of Self-Organized Criticality: Solar and Astrophysics **Review**

Markus J. **Aschwanden** , Norma B. Crosby, Michaila Dimitropoulou, Manolis K. Georgoulis, Stefan Hergarten, James McAteer, Alexander V. Milovanov, Shin Mineshige, Laura Morales and 6 more

Space Science Reviews January **2016**, Volume 198, Issue 1, pp 47-166 **Open Access**

Shortly after the seminal paper “Self-Organized Criticality: An explanation of 1/f noise” by Bak et al. (1987), the idea has been applied to solar physics, in “Avalanches and the Distribution of Solar Flares” by Lu and Hamilton (1991). In the following years, an inspiring cross-fertilization from complexity theory to solar and astrophysics took place, where the SOC concept was initially applied to solar flares, stellar flares, and magnetospheric substorms, and later extended to the radiation belt, the heliosphere, lunar craters, the asteroid belt, the Saturn ring, pulsar glitches, soft X-ray repeaters, blazars, black-hole objects, cosmic rays, and boson clouds. The application of SOC concepts has been performed by numerical cellular automaton simulations, by analytical calculations of statistical (powerlaw-like) distributions based on physical scaling laws, and by observational tests of theoretically predicted size distributions and waiting time distributions. Attempts have been undertaken to import physical models into the numerical SOC toy models, such as the discretization of magneto-hydrodynamics (MHD) processes. The novel applications stimulated also vigorous debates about the discrimination between SOC models, SOC-like, and non-SOC processes, such as phase transitions, turbulence, random-walk diffusion, percolation, branching processes, network theory, chaos theory, fractality, multi-scale, and other complexity phenomena. We review SOC studies from the last 25 years and highlight new trends, open questions, and future challenges, as discussed during two recent ISSI workshops on this theme.

Global Energetics of Solar Flares: VI. Refined Energetics of Coronal Mass Ejections

Markus J. **Aschwanden**

ApJ 847 27 **2017**

https://arxiv.org/pdf/1704.01993.pdf

sci-hub.se/10.3847/1538-4357/aa8952

In this study we refine a CME model presented in an earlier study on the global energetics of solar flares and associated CMEs, and apply it to all (860) GOES M- and X-class flare events observed during the first 7 years (2010-2016) of the Solar Dynamics Observatory (SDO) mission, which doubles the statistics of the earlier study. The model refinements include: (1) the CME geometry in terms of a 3D sphere undergoing self-similar adiabatic expansion; (2) the inclusion of solar gravitational deceleration during the acceleration and propagation of the CME, which discriminates eruptive and confined CMEs; (4) a self-consistent relationship between the CME center-of-mass motion detected during EUV dimming and the leading-edge motion observed in white-light coronagraphs; (5) the equi-partition of the CME kinetic and thermal energy; and (6) the Rosner-Tucker-Vaiana (RTV) scaling law. The refined CME model is entirely based on EUV dimming observations (using AIA/SDO data) and complements the traditional white-light scattering model (using LASCO/SOHO data), and both models are independently capable to determine fundamental CME parameters such as the CME mass, speed, and energy. Comparing the two methods we find that: (1) LASCO is less sensitive than AIA in detecting CMEs (in 24% of the cases); (2) CME masses below mcme~1014 g are under-estimated by LASCO; (3) AIA

and LASCO masses, speeds, and energy agree closely in the statistical mean after elimination of outliers; (4) the CMEs parameters of the speed v, emission measure-weighted flare peak temperature Te, and length scale L are consistent with the following scaling laws (derived from first principles): v∝T1/2e, v∝(mcme)1/4, and mcme∝L2.

Global Energetics of Solar Flares: V. Energy Closure in Flares and Coronal Mass Ejections

Markus J. **Aschwanden**, Amir Campi, Christina M.S. Cohen, Gordon Holman, Ju Jing, Matthieu Kretzschmar, Eduard P. Kontar, James McTiernan, Richard A. Mewaldt, Aidan O'Flannagain, Ian G. Richardson, Daniel Ryan, Harry P. Warren, Yan Xu

ApJ 836 17 **2017**

https://arxiv.org/pdf/1701.01176v1.pdf

http://iopscience.iop.org/article/10.3847/1538-4357/836/1/17/pdf

In this study we synthesize the results of four previous studies on the global energetics of solar flares and associated coronal mass ejections (CMEs), which include magnetic, thermal, nonthermal, and CME energies in 399 solar M and X-class flare events observed during the first 3.5 years of the Solar Dynamics Observatory (SDO) mission. Our findings are: (1) The sum of the mean nonthermal energy of flare-accelerated particles (Ent), the energy of direct heating (Edir), and the energy in coronal mass ejections (ECME), which are the primary energy dissipation processes in a flare, is found to have a ratio of (Ent+Edir+ECME)/Emag=0.87±0.18, compared with the dissipated magnetic free energy Emag, which confirms energy closure within the measurement uncertainties and corroborates the magnetic origin of flares and CMEs; (2) The energy partition of the dissipated magnetic free energy is: 0.51±0.17 in nonthermal energy of ≥6 keV electrons, 0.17±0.17 in nonthermal ≥1 MeV ions, 0.07±0.14 in CMEs, and 0.07±0.17 in direct heating; (3) The thermal energy is almost always less than the nonthermal energy, which is consistent with the thick-target model; (4) The bolometric luminosity in white-light flares is comparable with the thermal energy in soft X-rays (SXR); (5) Solar Energetic Particle (SEP) events carry a fraction ≈0.03 of the CME energy, which is consistent with CME-driven shock acceleration; and (6) The warm-target model predicts a lower limit of the low-energy cutoff at ec≈6 keV, based on the mean differential emission measure (DEM) peak temperature of Te=8.6 MK during flares. This work represents the first statistical study that establishes energy closure in solar flare/CME events.
2011-Feb-15, 2011-Aug-04, 2011-Sep-22, 2012-Jan-23, 2012-Jan-27, 2012-Mar-07, 2012-May-17, 2013-May-13, 2013-Jun-21

Table 1. SEP kinetic energies for selected 3-spacecraft events from 2011-2013. The higher value of the two lower limits of CME/LASCO (column 6) and CME/AIA energies (column 7) is used in the SEP/CME ratio (column 8).

Global Energetics of Solar Flares: IV. Coronal Mass Ejection Energetics

Markus J. **Aschwanden**

ApJ 831 105 **2016**

http://arxiv.org/pdf/1605.04952v1.pdf **File**

http://www.lmsal.com/~aschwand/eprints/2016_global4.pdf

This study entails the fourth part of a global flare energetics project, in which the mass mcme, kinetic energy Ekin, and the gravitational potential energy Egrav of coronal mass ejections (CMEs) is measured in 399 M and X-class flare events observed during the first 3.5 yrs of the Solar Dynamics Observatory (SDO) mission, *using a new method based on the EUV dimming effect*. The EUV dimming is modeled in terms of a radial adiabatic expansion process, which is fitted to the observed evolution of the total emission measure of the CME source region. The model derives the evolution of the mean electron density, the emission measure, the bulk plasma expansion velocity, the mass, and the energy in the CME source region. The EUV dimming method is truly complementary to the Thomson scattering method in white light, which probes the CME evolution in the heliosphere at r>2R⊙, while the EUV dimming method tracks the CME launch in the corona. We compare the CME parameters obtained in white light with the LASCO/C2 coronagraph with those obtained from EUV dimming with the Atmospheric Imaging Assembly (AIA) onboard SDO for all identical events in both data sets. We investigate correlations between CME parameters, the relative timing with flare parameters, frequency occurrence distributions, and the energy partition between magnetic, thermal, nonthermal, and CME energies. CME energies are found to be systematically lower than the dissipated magnetic energies, which is consistent with a magnetic origin of CMEs. **2010-10-16, 2010-06-12, 2011-05-29, 2011-08-02, 2011-09-24, 2011-09-28, 2011-11-09, 2012-01-27, 2012-03-10, 2012-03-13, 2012-06-06, 2012-07-05, 2012-07-19, 2012-08-11, 2012-09-09, 2012-11-13, 2013-05-22, 2013-08-17, 2013-10-24, 2013-11-01, 2013-11-03, 2013-11-06, 2013-11-19, 2014-01-07**

Table 3. Temporal and spatial parameters of the first 10 entries (out of the 399 events) listed in the complete machine-readable data file.

Table 4. CME parameters of the first 10 entries (out of the 399 events) listed in the complete machine-readable data file.

Thresholded Power Law Size Distributions of Instabilities in Astrophysics

Aschwanden, M.J.,

ApJ **2015**

http://www.lmsal.com/~aschwand/eprints/2015_powerlaw.pdf
Power law-like size distributions are ubiquitous in astrophysical instabilities. There are at least four natural effects that cause deviations from ideal power law size distributions, which we model here in a generalized way: (1) a physical threshold of an instability; (2) incomplete sampling of the smallest events below a threshold x_0; (3) contamination by an event-unrelated background x_b; and (4) truncation effects at the largest events due to a finite system size. These effects can be modeled in simplest terms with a ``thresholded power law'' distribution function (also called generalized Pareto [type II] or Lomax distribution), N(x) dx \propto (x+x_0)-a dx, where x_0 > 0 is positive for a threshold effect, while x_0 < 0 is negative for background contamination. We analytically derive the functional shape of this thresholded power law distribution function from an exponential-growth evolution model, which produces avalanches only when a disturbance exceeds a critical threshold x_0. We apply the thresholded power law distribution function to terrestrial, solar (HXRBS, BATSE, RHESSI), and stellar flare (Kepler) data sets. We find that the thresholded power law model provides an adequate fit to most of the observed data. Major advantages of this model are the automated choice of the power law fitting range, diagnostics of background contamination, physical inastability thresholds, instrumental detection thresholds, and finite system size limits. When testing self-organized criticality models, which predict ideal power laws, we suggest to include these natural truncation effects. **4.2. Solar Data, Flares**

Benchmark Test of Differential Emission Measure Codes and Multi-Thermal Energies in Solar Active Regions

Aschwanden,M.J., Boerner,P., Caspi,A., McTiernan,J.M., Ryan,D., and Warren,H.P.
Solar Phys. Volume 290, Issue 10, pp 2733-2763 **2015**
http://www.lmsal.com/~aschwand/eprints/2015_dem.pdf
http://arxiv.org/pdf/1509.07546v1.pdf
We compare the ability of 11 Differential Emission Measure (DEM) forward-fitting and inversion methods to constrain the properties of active regions and solar flares by simulating synthetic data using the instrumental response functions of SDO/AIA, SDO/EVE, RHESSI, and GOES/XRS. The codes include the single-Gaussian DEM, a bi-Gaussian DEM, a fixed-Gaussian DEM, a linear spline DEM, the spatial synthesis DEM, the Monte-Carlo Markov chain DEM, the regularized DEM inversion, the Hinode/XRT method, a polynomial spline DEM, an EVE+GOES, and an EVE+RHESSI method. Averaging the results from all 11 DEM methods, we find the following accuracies in the inversion of physical parameters: the EM-weighted temperature T_wfit/T_wsim=0.9±0.1, the peak emission measure EM_pfit/EM_psim=0.6±0.2, the total emission measure EM_tfit/EM_tsim=0.8±0.3, and the multi-thermal energies Ethfit/EMthsim=1.2±0.4. We find that the AIA spatial synthesis, the EVE+GOES, and the EVE+RHESSI method yield the most accurate results.

Magnetic Energy Dissipation during the 2014 March 29 Solar Flare

M.J. **Aschwanden**
ApJL **804** L20 **2015**
http://www.lmsal.com/~aschwand/eprints/2015_iris.pdf
http://arxiv.org/pdf/1504.03301v1.pdf
We calculated the time evolution of the free magnetic energy during the 2014-Mar-29 flare (SOL2014-03-29T17:48), the first X-class flare detected by IRIS. The free energy was calculated from the difference between the nonpotential field, constrained by the geometry of observed loop structures, and the potential field. We use AIA/SDO and IRIS images to delineate the geometry of coronal loops in EUV wavelengths, as well as to trace magnetic field directions in UV wavelengths in the chromosphere and transition region. We find an identical evolution of the free energy for both the coronal and chromospheric tracers, as well as agreement between AIA and IRIS results, with a peak free energy of Efree(tpeak) ≈ (45 ± 2) x 1030 erg, which decreases by an amount of Δ Efree ≈ (29 ± 3) x 1030 erg during the flare decay phase. The consistency of free energies measured from different EUV and UV wavelengths for the first time here, demonstrates that vertical electric currents (manifested in form of helically twisted loops) can be detected and measured from both chromospheric and coronal tracers.

Global Energetics of Solar Flares: II. Thermal Energies

M.J. **Aschwanden**, P. Boerner, D. Ryan, A. Caspi, J.M. McTiernan, H.P. Warren
ApJ **802** 53 **2015**
http://arxiv.org/pdf/1502.05941v1.pdf
https://iopscience.iop.org/article/10.1088/0004-637X/802/1/53/pdf
We present the second part of a project on the global energetics of solar flares and CMEs that includes about 400 M- and X-class flares observed with AIA/SDO during the first 3.5 years of its mission. In this Paper II we compute the differential emission measure (DEM) distribution functions and associated multi-thermal energies, using a spatially-synthesized Gaussian DEM forward-fitting method. The multi-thermal DEM function yields a significantly higher (by

an average factor of ≈14), but more comprehensive (multi-)thermal energy than an isothermal energy estimate from the same AIA data. We find a statistical energy ratio of Eth/Ediss≈2%−40% between the multi-thermal energy Eth and the magnetically dissipated energy Ediss, which is an order of magnitude higher than the estimates of Emslie et al.~2012. For the analyzed set of M and X-class flares we find the following physical parameter ranges: L=108.2−109.7cm for the length scale of the flare areas, Tp=105.7−107.4 K for the DEM peak temperature, Tw=106.8−107.6 K for the emission measure-weighted temperature, np=1010.3−1011.8 cm−3for the average electron density, EMp=1047.3−1050.3 cm−3 for the DEM peak emission measure, and Eth=1026.8−1032.0 erg for the multi-thermal energies. The deduced multi-thermal energies are consistent with the RTV scaling law Eth,RTV=7.3×10−10 T3pL2p, which predicts extremal values of Eth,max≈1.5×1033 erg for the largest flare and Eth,min≈1×1024 erg for the smallest coronal nanoflare. The size distributions of the spatial parameters exhibit powerlaw tails that are consistent with the predictions of the fractal-diffusive self-organized criticality model combined with the RTV scaling law. **2011-02-15**

Table 1. **Thermal energy parameters of 28 X-class flare events.**

Table 2. **Thermal energy parameters of 391 M and X-class flare events. The full list is available from a machine-readable file, from which only the first 10 entries are listed here.**

Global Energetics of Solar Flares: I. Magnetic Energies

Markus J. **Aschwanden**, Yan Xu, and Ju Jing

ApJ, 797 50 **2014**

http://www.lmsal.com/~aschwand/eprints/2014_global1.pdf

http://arxiv.org/pdf/1410.8013v1.pdf

https://iopscience.iop.org/article/10.1088/0004-637X/797/1/50/pdf

We present the first part of a project on the global energetics of solar flares and coronal mass ejections (CMEs) that includes about 400 M- and X-class flares observed with AIA and HMI onboard SDO. We calculate the potential (E_p), the nonpotential (Enp) or free energies (Efree =Enp-E_p), and the flare-dissipated magnetic energies (Ediss). We calculate these magnetic parameters using two different NLFFF codes: The COR-NLFFF code uses the line-of-sight magnetic field component B_z from HMI to define the potential field, and the 2D coordinates of automatically detected coronal loops in 6 coronal wavelengths from AIA to measure the helical twist of coronal loops caused by vertical currents, while the PHOT-NLFFF code extrapolates the photospheric 3D vector fields. We find agreement between the two codes in the measurement of free energies and dissipated energies within a factor of \lapprox 3. The size distributions of magnetic parameters exhibit powerlaw slopes that are approximately consistent with the fractal-diffusive self-organized criticality model. The magnetic parameters exhibit scaling laws for the nonpotential energy, Enp \propto E_p1.02, for the free energy, Efree \propto E_p1.7 and $Efree \propto B\varphi1.0 L1.5$, for the dissipated energy, Ediss \propto E_p1.6 and Ediss \propto Efree0.9, and the energy dissipation volume, V \propto Ediss1.2. The potential energies vary in the range of E_p = 1 \times 1031 - 4 \times 1033 erg, while the free energy has a ratio of Efree/E_p \approx 1\%-25\%. The Poynting flux amounts to Fflare \approx 5 \times 108 - 1010 erg cm-2 s-1 during flares, which averages to FAR \approx 6 \times 10^6 erg cm-2 s-1 during the entire observation period and is comparable with the coronal heating rate requirement in active regions. **20110215, 20120306**

Table 3. Magnetic energy parameters calculated with the COR-NLFFF code for **172 M and X-class flares** with a longitude difference of < 45◦ to the central meridian.

25 Years of Self-Organized Criticality: Solar and Astrophysics **Review**

Aschwanden, M.J., Crosby, N., Dimitropoulou, M., Geogoulis, M.K., Hergarten, S., McAteer, J., Milovanov, A.V., Mineshige, S., Morales, L., Nishizuka, N., Pruessner, G., Sanchez, R., Sharma, S., Strugarek, A., and Uritsky, V.

Space Science Reviews, **2014**

http://www.lmsal.com/~aschwand/eprints/2014_soc25.pdf

http://arxiv.org/pdf/1403.6528v1.pdf

Shortly after the seminal paper ``Self-Organized Criticality: An explanation of 1/f noise" by Bak, Tang, and Wiesenfeld (1987), the idea has been applied to solar physics, in``Avalanches and the Distribution of Solar Flares" by Lu and Hamilton (1991). In the following years, an inspiring cross-fertilization from complexity theory to solar and astrophysics took place, where the SOC concept was initially applied to solar flares, stellar flares, and magnetospheric substorms, and later extended to the radiation belt, the heliosphere, lunar craters, the asteroid belt, the Saturn ring, pulsar glitches, soft X-ray repeaters, blazars, black-hole objects, cosmic rays, and boson clouds. The application of SOC concepts has been performed by numerical cellular automaton simulations, by analytical calculations of statistical (powerlaw-like) distributions based on physical scaling laws, and by observational tests of theoretically predicted size distributions and waiting time distributions. Attempts have been undertaken to import physical models into the numerical SOC toy models, such as the discretization of magneto-hydrodynamics (MHD) processes. The novel

applications stimulated also vigorous debates about the discrimination between SOC models, SOC-like, and non-SOC processes, such as phase transitions, turbulence, random-walk diffusion, percolation, branching processes, network theory, chaos theory, fractality, multi-scale, and other complexity phenomena. We review SOC studies from the last 25 years and highlight new trends, open questions, and future challenges, as discussed during two recent ISSI workshops on this theme.

The Magnetic Field of Active Region 11158 During the 2011 February 12-17 Flares : Differences between Photospheric Extrapolation and Coronal Forward-Fitting Methods

Aschwanden, M.J., Sun, X.D., and Liu, Y.

E-print, Feb **2014**; ApJ

We developed a {\sl coronal non-linear force-free field (COR-NLFFF)} forward-fitting code that fits an approximate {\sl non-linear force-free field (NLFFF)} solution to the observed geometry of automatically traced coronal loops. In contrast to photospheric NLFFF codes, which calculate a magnetic field solution from the constraints of the transverse photospheric field, this new code uses coronal constraints instead, and this way provides important information on systematic errors of each magnetic field calculation method, as well as on the non-forcefreeness in the lower chromosphere. In this study we applied the COR-NLFFF code to active region NOAA 11158, during the time interval of 2011 Feb 12 to 17, which includes an X2.2 GOES-class flare plus 35 M and C-class flares. We calcuated the free magnetic energy with a 6-minute cadence over 5 days. We find good agreement between the two types of codes for the total nonpotential E_N and potential energy E_P, but find up to a factor of 4 discrepancy in the free energy Efree=E_N-E_P, and up to a factor of 10 discrepancy in the decrease of the free energy \Delta Efree during flares. The coronal NLFFF code exhibits a larger time variability, and yields a decrease of free energy during the flare that is sufficient to satisfy the flare energy budget, while the photospheric NLFFF code shows much less time variability and an order of magnitude less free energy decrease during flares. The discrepancy may partly be due to the pre-processing of photospheric vector data, but more likely due to the non-forcefreeness in the lower chromosphere. We conclude that the coronal field cannot be correctly calculated based on photospheric data alone, but requires additional information on coronal loop geometries.

STEREO/ *Extreme Ultraviolet Imager* (EUVI) Event Catalog 2006-2012

Markus J. **Aschwanden**1, Jean-Pierre W.ulser1, Nariaki V. Nitta1, James R. Lemen1, Sam Freeland1, and William T. Thompson2

Solar Physics, March **2014**, Volume 289, Issue 3, pp 919-938; **File**

An event catalog is generated with an automated detection algorithm based on the entire EUVI image database observed with the two STEREO/A and B spacecraft over the first six years of the mission (2006-2012). The event catalog includes the heliographic positions of some 20,000 EUV events, transformed from spacecraft coordinates to Earth coordinates, and information on associated GOES flare events (down to the level of GOES A-class flares). The 304°A wavelength turns out to be most efficient channel for flare detection (79%), while the 171 °A (4%), 195 °A (10%), and the 284 °A channel (7%), retrieve substantially less flare events, partially due to the suppressing effect of EUV dimming, and partially due to the lower cadence they were operated in the later years of the mission. Due to the Sun-circling orbits of STEREO/A and B, a large number of flares have been detected on the back-side of the Sun, invisible from Earth, or seen as partially occulted events. The statistical size distributions of EUV peak fluxes (with a powerlaw slope of $\alpha_P = 2.5 \pm 0.2$) and event durations (with a powerlaw slope of $\alpha_T = 2.4 \pm 0.3$) are found to be consistent with the fractal-diffusive self-organized criticality model. The EUVI event catalog is available on-line at secchi.lmsal.com/EUVI/euvi_autodetection/euvi_events.txt and may serve as a comprehensive tool to identify stereoscopically observed flare events for 3D reconstruction and to study occulted flare events.

A Macroscopic Description of Self-Organized Criticality Systems and Astrophysical Applications

Markus J. **Aschwanden**

E-print, Oct **2013**; ApJ

We suggest a generalized definition of self-organized criticality (SOC) systems: SOC is a critical state of a nonlinear energy dissipation system that is slowly and continuously driven towards a critical value of a system-wide instability threshold, producing scale-free, fractal-diffusive, and intermittent avalanches with powerlaw-like size distributions. We develop here a macroscopic description of SOC systems that provides an equivalent description of the complex microscopic fine structure, in terms of fractal-diffusive transport (FD-SOC). Quantitative values for the size distributions of SOC parameters (length scales L, time scales T, fluxes F, and energies E) are derived from first principles, using the scale-free probability theorem, $N(L) dL propto L-d, for Euclidean space dimension d$. We apply this model to astrophysical SOC systems, such as lunar craters, the asteroid belt, Saturn ring particles, magnetospheric substorms, radiation belt electrons, solar flares, stellar flares, pulsar glitches, soft gamma-ray repeaters, black-hole

objects, blazars, and cosmic rays. The FD-SOC model predicts correctly the size distributions of 7 out of these 12 astrophysical phenomena, and indicates non-standard scaling laws and measurement biases for the others.

Multi-Wavelength Observations of the Spatio-Temporal Evolution of Solar Flares with AIA/SDO: II. Hydrodynamic Scaling Laws and Thermal Energies

Markus J. **Aschwanden** and Toshifumi Shimizu

E-print, Aug **2013**; **2013** ApJ 776 132

http://iopscience.iop.org/article/10.1088/0004-637X/776/2/132

In this study we measure physical parameters of the same set of 155 M and X-class solar flares observed with AIA/SDO as analyzed in Paper I, by performing a {sl differential emission measure (DEM)} analysis to determine the flare peak emission measure EM_p, peak temperature T_p, electron density n_p, and thermal energy Eth, in addition to the spatial scales L, areas A, and volumes V measured in Paper I. The parameter ranges for M and X-class flares are: log(EM_p)=47.0-50.5, T_p=5.0-17.8 MK, n_p=4 x 10^9-9 x 1011 cm-3, and thermal energies of Eth=1.6 x 1028-1.1 x 1032 erg. We find that these parameters obey the Rosner-Tucker-Vaiana (RTV) scaling law T_p^2 propto n_p L and H propto T7/2 L-2 during the peak time t_p of the flare density n_p, when energy balance between the heating rate H and the conductive and radiative loss rates is achieved for a short instant, and thus enables the applicability of the RTV scaling law. The application of the RTV scaling law predicts powerlaw distributions for all physical parameters, which we demonstrate with numerical Monte-Carlo simulations as well as with analytical calculations. A consequence of the RTV law is also that we can retrieve the size distribution of heating rates, for which we find N(H) propto H-1.8, which is consistent with the magnetic flux distribution N(Phi) propto Phi-1.85 observed by Parnell et al.~(2009) and the heating flux scaling law F_H propto H L propto B/L of Schrijver et al.~(2004). The fractal-diffusive self-organized criticality model in conjunction with the RTV scaling law reproduces the observed powerlaw distributions and their slopes for all geometrical and physical parameters and can be used to predict the size distributions for other flare datasets, instruments, and detection algorithms.

Multi-Wavelength Observations of the Spatio-Temporal Evolution of Solar Flares with AIA/SDO:I. Universal Scaling Laws of Space and Time Parameters

Aschwanden,J.M., Zhang, J., Liu,K.

E-print, Aug **2013**; **2013** ApJ 775 23

http://www.lmsal.com/~aschwand/eprints/2013_spatio1.pdf

http://iopscience.iop.org/article/10.1088/0004-637X/775/1/23/pdf

We extend a previous statistical solar flare study of 155 GOES M- and X-class flares observed with AIA/SDO (Aschwanden 2012) to all 7 coronal wavelengths (94, 131, 171, 193, 211, 304, 335 ang) to test the wavelength-dependence of scaling laws and statistical distributions. Except for the 171 and 193 ang wavelengths, which are affected by EUV dimming caused by coronal mass ejections (CMEs), we find near-identical size distributions of geometric (lengths L, flare areas A, volumes V, fractal dimension D_2), temporal (flare durations T), and spatio-temporal parameters (diffusion coefficient kappa, spreading exponent eta, and maximum expansion velocities vmax) in different wavelengths, which are consistent with the universal predictions of the fractal-diffusive avalanche model of a slowly-driven self-organized criticality (FD-SOC) system, i.e., N(L) propto L-3, N(A) propto A-2, N(V) propto V-5/3, N(T) propto T-2, D_2=3/2, for a Euclidean dimension d=3. Empirically we find also a new strong correlation $kappa propto L0.94pm0.01 and the 3-parameter scaling law L propto kappa T0.1$, which is more consistent with the logistic-growth model than with classical diffusion. The findings suggest long-range correlation lengths in the FD-SOC system that operate in the vicinity of a critical state, which could be used for predictions of individual extreme events. We find also that eruptive flares (with accompanying CMEs), have larger volumes V, longer flare durations T, higher EUV and soft X-ray fluxes, and somewhat larger diffusion coefficients kappa than confined flares (without CMEs).

STEREO/EUVI Event Catalog 2006-2012

Markus J. **Aschwanden**1, Jean-Pierre W.ulser1, Nariaki V. Nitta1, James R., Lemen1, Sam Freeland1, and William T. Thompson

Solar Phys., **2013, File**

An event catalog is generated with an automated detection algorithm based on the entire EUVI image database observed with the two STEREO/A and B spacecraft over the first six years of the mission (2006-2012). The event catalog includes the heliographic positions of some 20,000 EUV events, transformed from spacecraft coordinates to Earth coordinates, and information on associated GOES flare events (down to the level of GOES A-class flares). The 304°A wavelength turns out to be most efficient channel for flare detection (79%), while the 171 °A (4%), 195 °A (10%), and the

284 °A channel (7%), retrieve substantially less flare events, partially due to the suppressing effect of EUV
dimming, and partially due to the lower cadence they were operated in the later years of the mission. Due to the Sun-circling orbits of STEREO/A and B, a large number of flares have been detected on the back-side of the Sun, invisible from Earth, or seen as partially occulted events. The statistical size distributions of EUV peak fluxes (with a powerlaw slope of _P = 2.5 ± 0.2) and event durations (with a powerlaw slope of _T = 2.4 ± 0.3) are found to be consistent with the fractal-diffusive self-organized criticality model. The EUVI event catalog is available on-line and may serve as a comprehensive tool to identify stereoscopically observed flare events for 3D reconstruction and to study occulted flare events.

!! GeV Particle Acceleration in Solar Flares and Ground Level Enhancement (GLE) Events

Markus J. **Aschwanden** **Review**

Space Sci. Rev. Space Science Reviews, Volume 171, Numbers 1-4 (**2012**), 3-21, **File**

{sl Ground Level Enhancement (GLE)} events represent the most energetic class of {sl solar energetic particle (SEP)} events, requiring acceleration processes to boost gapprox 1 GeV ions in order to produce showers of secondary particles in the Earth's atmosphere with sufficient intensity to be detected by ground-level neutron monitors, above the background of cosmics rays. Although the association of GLE events with both solar flares and coronal mass ejections (CMEs) is undisputed, the question arises about the location of the responsible acceleration site: **coronal flare reconnection sites**, coronal CME shocks, or interplanetary shocks? To investigate the first possibility we explore the timing of GLE events with respect to hard X-ray production in solar flares, considering the height and magnetic topology of flares, the role of extended acceleration, and particle trapping. **We find that 50\% (6 out of 12) of recent (non-occulted) GLE events are accelerated during the impulsive flare phase, while the remaining half are accelerated significantly later. It appears that the prompt GLE component, which is observed in virtually all GLE events according to a recent study by Vashenyuk et al. (Astrophys. Space Sci. Trans. 7(4):459–463, 2011), is consistent with a flare origin in the lower corona, while the delayed gradual GLE component can be produced by both, either by extended acceleration and/or trapping in flare sites, or by particles accelerated in coronal and interplanetary shocks.**

See **2.5** Magnetic Topology of Acceleration Regions

(2) The magnetic field lines above the vertical current sheet of the main reconnection regions are likely ***to be open, which allows escape of accelerated particles*** into interplanetary space and along Earth-connected magnetic field lines;

2.6 Extended Particle Acceleration and Trapping **Extended γ -ray emission**

A statistical fractal-diffusive avalanche model of a slowly-driven self-organized criticality system

M. J. **Aschwanden**

A&A 539, A2 (**2012**)

Aims. We develop a statistical analytical model that predicts the occurrence frequency distributions and parameter correlations of avalanches in nonlinear dissipative systems in the state of a slowly-driven self-organized criticality (SOC) system.

Methods. This model, called the fractal-diffusive SOC model, is based on the following four assumptions: (i) the avalanche size L grows as a diffusive random walk with time T, following L ∝ T1/2; (ii) the energy dissipation rate f(t) occupies a fractal volume with dimension DS; (iii) the mean fractal dimension of avalanches in Euclidean space S = 1,2,3 is DS ≈ (1 + S)/2; and (iv) the occurrence frequency distributions N(x) ∝ x − αx based on spatially uniform probabilities in a SOC system are given by N(L) ∝ L − S, with S being the Eudlidean dimension. We perform cellular automaton simulations in three dimensions (S = 1,2,3) to test the theoretical model.

Results. The analytical model predicts the following statistical correlations: F ∝ LDS ∝ TDS/2 for the flux, P ∝ LS ∝ TS/2 for the peak energy dissipation rate, and E ∝ FT ∝ T1 + DS/2 for the total dissipated energy; the model predicts powerlaw distributions for all parameters, with the slopes αT = (1 + S)/2, αF = 1 + (S − 1)/DS, αP = 2 − 1/S, and αE = 1 + (S − 1)/(DS + 2). The cellular automaton simulations reproduce the predicted fractal dimensions, occurrence frequency distributions, and correlations within a satisfactory agreement within ≈ 10% in all three dimensions.

Conclusions. One profound prediction of this universal SOC model is that the energy distribution has a powerlaw slope in the range of αE = 1.40 − 1.67, and the peak energy distribution has a slope of αP = 1.67 (for any fractal dimension DS = 1,...,3 in Euclidean space S = 3), and thus predicts that the bulk energy is always contained in the largest events, which rules out significant nanoflare heating in the case of solar flares.

THE SPATIO-TEMPORAL EVOLUTION OF SOLAR FLARES OBSERVED WITH AIA/SDO: FRACTAL DIFFUSION, SUB-DIFFUSION, OR LOGISTIC GROWTH?

Markus J. **Aschwanden**

2012 ApJ 757 94

We explore the spatio-temporal evolution of solar flares by fitting a radial expansion model r(t) that consists of an exponentially growing acceleration phase, followed by a deceleration phase that is parameterized by the generalized diffusion function r(t)κ(t – t 1)β/2, which includes the logistic growth limit (β = 0), sub-diffusion (β = 0-1), classical diffusion (β = 1), super-diffusion (β = 1-2), and the linear expansion limit (β = 2). We analyze all M- and X-class flares observed with Geostationary Operational Environmental Satellite and Atmospheric Imaging Assembly/Solar Dynamics Observatory (SDO) during the first two years of the SDO mission, amounting to 155 events. We find that most flares operate in the sub-diffusive regime (β = 0.53 ± 0.27), which we interpret in terms of anisotropic chain reactions of intermittent magnetic reconnection episodes in a low plasma-β corona. We find a mean propagation speed of v = 15 ± 12 km s–1, with maximum speeds of v max = 80 ± 85 km s–1 per flare, which is substantially slower than the sonic speeds expected for thermal diffusion of flare plasmas. The diffusive characteristics established here (for the first time for solar flares) is consistent with the fractal-diffusive self-organized criticality model, which predicted diffusive transport merely based on cellular automaton simulations**.**

AUTOMATED SOLAR FLARE STATISTICS IN SOFT X-RAYS OVER 37 YEARS OF GOES OBSERVATIONS: THE INVARIANCE OF SELF-ORGANIZED CRITICALITY DURING THREE SOLAR CYCLES

Markus J. **Aschwanden** and Samuel L. Freeland

2012 ApJ 754 112

http://arxiv.org/pdf/1205.6712v1.pdf

https://iopscience.iop.org/article/10.1088/0004-637X/754/2/112/pdf

We analyzed the soft X-ray light curves from the Geostationary Operational Environmental Satellites over the last 37 years (1975-2011) and measured with an automated flare detection algorithm over 300,000 solar flare events (amounting to 5 times higher sensitivity than the NOAA flare catalog). We find a power-law slope of $\alpha_F = 1.98 \pm 0.11$ for the (background-subtracted) soft X-ray peak fluxes that is invariant through three solar cycles and agrees with the theoretical prediction $\alpha_F = 2.0$ of the fractal-diffusive self-organized criticality (FD-SOC) model. For the soft X-ray flare rise times, we find a power-law slope of $\alpha_T = 2.02 \pm 0.04$ during solar cycle minima years, which is also consistent with the prediction $\alpha_T = 2.0$ of the FD-SOC model. During solar cycle maxima years, the power-law slope is steeper in the range of α_T 2.0-5.0, which can be modeled by a solar-cycle-dependent flare pile-up bias effect. These results corroborate the FD-SOC model, which predicts a power-law slope of $\alpha_E = 1.5$ for flare energies and thus rules out significant nanoflare heating. While the FD-SOC model predicts the probability distribution functions of spatio-temporal scaling laws of nonlinear energy dissipation processes, additional physical models are needed to derive the scaling laws between the geometric SOC parameters and the observed emissivity in different wavelength regimes, as we derive here for soft X-ray emission. The FD-SOC model also yields statistical probabilities for solar flare forecasting.

The State of Self-organized Criticality of the Sun during the Last Three Solar Cycles. II. Theoretical Model

Markus J. **Aschwanden**

Solar Physics, Volume 274, Numbers 1-2, 119-129, **2011**

The observed power-law distributions of solar-flare parameters can be interpreted in terms of a nonlinear dissipative system in a state of self-organized criticality (SOC). We present a universal analytical model of an SOC process that is governed by three conditions: i) a multiplicative or exponential growth phase, ii) a randomly interrupted termination of the growth phase, and iii) a linear decay phase. This basic concept approximately reproduces the observed frequency distributions. We generalize it to a randomized exponential growth model, which also includes a (log-normal) distribution of threshold energies before the instability starts, as well as randomized decay times, which can reproduce both the observed occurrence-frequency distributions and the scatter of correlated parameters more realistically. With this analytical model we can efficiently perform Monte-Carlo simulations of frequency distributions and parameter correlations of SOC processes, which are simpler and faster than the iterative simulations of cellular automaton models. Solar-cycle modulations of the power-law slopes of flare-frequency distributions can be used to diagnose the thresholds and growth rates of magnetic instabilities responsible for solar flares.

The State of Self-organized Criticality of the Sun During the Last Three Solar Cycles. I. Observations

Markus **J. Aschwanden**

Solar Physics, Volume 274, Numbers 1-2, 99-117, **2011**

We analyze the occurrence-frequency distributions of peak fluxes [P], total fluxes [E], and durations [T] of solar flares over the last three solar cycles (during 1980−2010) from SMM/HXRBS, CGRO/BATSE, and RHESSI hard X-ray data. From the synthesized data we find powerlaw slopes with mean values of $\alpha_P = 1.73 \pm 0.07$ for the peak flux, $\alpha_E = 1.62 \pm 0.12$ for the total flux, and $\alpha_T = 1.99 \pm 0.35$ for flare durations. We find a tendency of an anti-correlation of the powerlaw slope of peak fluxes with the flare rate or sunspot number as a function of the solar cycle. The occurrence powerlaw slope is always steeper by $\Delta\alpha \approx 0.1$ during a solar-cycle minimum compared with the previous solar-cycle maximum, but the relative amplitude varies for each cycle or instrument. Since each solar cycle has been observed with a different instrument, part of the variation could be attributed to instrumental characteristics and different event selection criteria used in generating the event catalogs. The relatively flatter powerlaw slopes during solar maxima could indicate more energetic flares with harder electron-energy spectra, probably due to a higher magnetic complexity of the solar corona. This would imply a non-stationarity (or solar-cycle dependence) of the coronal state of self-organized criticality.

3-D reconstruction of active regions with STEREO

Markus J. **Aschwanden**, a, , and Jean-Pierre Wülsera

Journal of Atmospheric and Solar-Terrestrial Physics, Volume 73, Issue 10, **2011**, Pages 1082-1095

We **review** data analysis and physical modeling related to the 3-D reconstruction of active regions in the solar corona, using stereoscopic image pairs from the STEREO/EUVI instrument. This includes the 3-D geometry of coronal loops (with measurements of the loop inclination plane, coplanarity, circularity, and hydrostaticity), the 3-D electron density and temperature distribution (which enables diagnostics of hydrostatic, hydrodynamic, and heating processes), the 3-D magnetic field (independent of any theoretical model based on photospheric extrapolations), as well as the 3-D reconstruction of CME phenomena, such as EUV dimming, CME acceleration, CME bubble expansion, and associated Lorentz forces that excite MHD kink-mode oscillations in the surroundings of a CME launch site. The mass of CMEs, usually measured from white-light coronagraphs, can be determined independently from the EUV dimming in the CME source region. The detailed 3-D density and temperature structure of an active region can be modeled using the method of instant stereoscopic tomography with orders of magnitude higher spatial resolution than with standard solar-rotation tomography.

Research highlights

►First 3D reconstruction of coronal loops in a solar active region with STEREO spacecraft. ►Electron density and temperature diagnostics with DEM in temperature range of 10(5)-10(7) K. ►Diagnostic of hydrostatic equilibrium and super-hydrostatic non-equilibrium in coronal loops. ►3D magnetic modeling with forward-fitting to STEREO-triangulated coronal loops. ►3D reconstruction of EUV dimming, Coronal mass ejection (CME) mass, and kinematics.

The State of Self-Organized Criticality of the Sun During the Last Three Solar Cycles. II. Theoretical Model

Markus J. **Aschwanden**

E-print, 5 Oct **2010,** Solar Physics, WIH Topical Issue,

The observed powerlaw distributions of solar flare parameters can be interpreted in terms of a nonlinear dissipative system in the state of self-organized criticality (SOC). We present a universal analytical model of a SOC process that is governed by three conditions: (i) a multiplicative or exponential growth phase, (ii) a randomly interrupted termination of the growth phase, and (iii) a linear decay phase. This basic concept approximately reproduces the observed frequency distributions. We generalize it to a randomized exponential-growth model, which includes also a (log-normal) distribution of threshold energies before the instability starts, as well as randomized decay times, which can reproduce both the observed occurrence frequency distributions and the scatter of correlated parametyers more realistically. With this analytical model we can efficiently perform Monte-Carlo simulations of frequency distributions and parameter correlations of SOC processes, which are simpler and faster than the iterative simulations of cellular automaton models. Solar cycle modulations of the powerlaw slopes of flare frequency distributions can be used to diagnose the thresholds and growth rates of magnetic instabilities responsible for solar flares.

A Universal Scaling Law for the Fractal Energy Dissipation Domain in Self-Organized Criticality Systems

Markus J. **Aschwanden**

E-print, 4 Aug **2010,** ApJL

Nonlinear dissipative systems in the state of self-organized criticality release energy sporadically in avalanches of all sizes, such as in earthquakes, auroral substorms, solar and stellar flares, soft gamma-ray repeaters, and pulsar glitches. The statistical occurrence frequency distributions of event energies E generally exhibit a powerlaw-like function $N(E)propto E^{-alpha_E}$ with a powerlaw slope of $alpha_E approx 1.5$. The powerlaw slope $alpha_E$ of

energies can be related to the fractal dimension D of the spatial energy dissipation domain by $D=3/alpha_E$, which predicts a powerlaw slope $alpha_E=1.5$ for area-rupturing or area-spreading processes with $D=2$. For solar and stellar flares, 2-D area-spreading dissipation domains are naturally provided in current sheets or separatrix surfaces in a magnetic reconnection region. Thus, this universal scaling law provides a useful new diagnostic on the topology of the spatial energy dissipation domain in geophysical and astrophysical observations.

RECONCILIATION OF WAITING TIME STATISTICS OF SOLAR FLARES OBSERVED IN HARD X-RAYS

Markus J. **Aschwanden**1 and James M. McTiernan2

Astrophysical Journal, 717:683–692, **2010** July

We study the waiting time distributions of solar flares observed in hard X-rays with *ISEE-3/ICE*, HXRBS/*SMM*, WATCH/GRANAT, BATSE/*CGRO*, and *RHESSI*. Although discordant results and interpretations have been published earlier, based on relatively small ranges (<2 decades) of waiting times, we find that all observed distributions, spanning over 6 decades of waiting times ($\Delta t \approx 10^{-3}$–103 hr), can be reconciled with a single distribution function, $N(\Delta t) \propto \lambda 0(1 + \lambda 0 \Delta t)^{-2}$, which has a power-law slope of $p \approx 2.0$ at large waiting times ($\Delta t \approx 1$–1000 hr) and flattens out at short waiting times Δt _ $\Delta t0 = 1/\lambda 0$.We find a consistent breakpoint at $\Delta t0 = 1/\lambda 0 = 0.80 \pm 0.14$ hr from the WATCH, HXRBS, BATSE, and *RHESSI* data. The distribution of waiting times is invariant for sampling with different flux thresholds, while the mean waiting time scales reciprocically with the number of detected events, $\Delta t0 \propto 1/n$det. This waiting time distribution can be modeled with a nonstationary Poisson process with a flare rate $\lambda = 1/\Delta t$ that varies as $f(\lambda) \propto \lambda^{-1} \exp{-(\lambda/\lambda 0)}$. This flare rate distribution requires a highly intermittent flare productivity in short clusterswith high rates, separated by relatively long quiescent intervalswith very lowflare rates.

3D Reconstruction of Active Regions with STEREO (Invited Review)

Markus J. **Aschwanden** and Jean-Pierre Wuelser

E-print, Feb **2010**, J. Atmos. Solar-Terr. Physics,

We review data analysis and physical modeling related to the 3D reconstruction of active regions in the solar corona, using stereoscopic image pairs from the STEREO/EUVI instrument. This includes the 3D geometry of coronal loops (with measurements of the loop inclination plane, coplanarity, circularity, and hydrostaticity), the 3D electron density and temperature distribution (which enables diagnostics of hydrostatic, hydrodynamic, and heating processes), the 3D magnetic field (independent of any theoretical model based on photospheric extrapolations), as well as the 3D reconstruction of CME phenomena, such as EUV dimming, CME acceleration, CME bubble expansion, and associated Lorentz forces that excite MHD kink-mode oscillations in the surroundings of a CME launch site. The mass of CMEs, usually measured from white-light coronagraphs, can be determined independently from the EUV dimming in the CME source region. The full 3D density and temperature structure of an active region can be reconstructed in unprecedented detail with instant stereoscopic tomography.

2. 3D Geometry of Active Regions
3. 3D Density Reconstruction of Active Regions
4. 3D Temperature Diagnostics of Active Regions
5. 3D Magnetic Field Modeling of Active Regions
6. **3D Reconstruction of EUV Dimming and CME mass**
7. 3D Motion of Loop Oscillations and Waves

THE HYDRODYNAMIC EVOLUTION OF IMPULSIVELY HEATED CORONAL LOOPS: EXPLICIT ANALYTICAL APPROXIMATIONS

Markus J. Aschwanden1 and David Tsiklauri2

2009 ApJS 185 171-185

We derive simple analytical approximations (in explicit form) for the hydrodynamic evolution of the electron temperature $T(s, t)$ and electron density $n(s, t)$, for one-dimensional coronal loops that are subject to impulsive heating with subsequent cooling. Our analytical approximations are derived from first principles, using (1) the hydrodynamic energy balance equation, (2) the loop scaling laws of Rosner-Tucker-Vaiana and Serio, (3) the Neupert effect, and (4) the Jakimiec relationship. We compare our analytical approximations with 56 numerical cases of time-dependent hydrodynamic simulations from a parametric study of Tsiklauri et al., covering a large parameter space of heating rates, heating timescales, heating scale heights, loop lengths, for both footpoint and apex heating, mostly applicable to flare conditions. The average deviations from the average temperature and density values are typically $\approx$20% for our analytical expressions. The analytical approximations in explicit form provide an efficient tool to mimic time-dependent hydrodynamic simulations, to model observed soft X-rays and extreme-ultraviolet light curves of heated and cooling loops in the solar corona and in flares by forward fitting, to model microflares, to infer the coronal heating function

from light curves of multi-wavelength observations, and to provide physical models of differential emission measure distributions for solar and stellar flares, coronae, and irradiance.

Flare Acceleration for GeV Particles

Markus **Aschwanden**

Presentation at "Ground Level Enhancement (GLE)"

Comparative Data Analysis Workshop (CDAW), LMSAL, Jan 6-9, **2009**

Conclusion:

1) The maximum energy of accelerated particles in flares is observed up to 100 MeV for electron bremsstrahlung and up to 1 GeV for protons and pions.

2) The maximum energy of accelerated particles observed in solar flare gamma rays implies severe constraints for sub-Dreicer electric field acceleration mechanisms, but is achievable with super-Dreicer fields or stochastic acceleration.

3) The altitude of acceleration regions in flare sites is confined to hacc=5000-35,000 km (<0.05 solar radii) according to time-of-flight measurements and direct hard X-ray imaging. Acceleration sites at larger distances to the Sun (as inferred for GLE events) are likely to be associated with CME shocks.

4) The vertical symmetry of acceleration sites warrants simultaneous acceleration in upward and downward direction (e.g., electric DC fields, wave turbulence regions, fast shocks in Petschek-type) and **allows charged particles to escape into interplanetary space and produce GLEs.**

The escape of flare-accelerated particles into interplanetary is faciliated on one hand by temporarily opened fields during the magnetic reconnetion process. For instance, during the "magnetic break-out model" (Antiochos et al. 1999), a temporary opening of a secondary arcade occurs during the reconnection process.

On the other hand, there are also pre-existing open field lines that allow particles to escape. Schrijver & DeRosa (2003) found from potential field extrapolations that a fraction of the IMF connects directly to plages of active regions (<10% in solar min. 30-50% at cycle max.)

FIRST THREE-DIMENSIONAL RECONSTRUCTIONS OF CORONAL LOOPS WITH THE *STEREO A+B* SPACECRAFT. III. INSTANT STEREOSCOPIC TOMOGRAPHY OF ACTIVE REGIONS

Markus J. **Aschwanden**, Jean-Pierre Wuelser, Nariaki V. Nitta, James R. Lemen, and Anne Sandman

Astrophysical Journal, 695:12–29, **2009** April

http://www.iop.org/EJ/toc/-alert=43190/0004-637X/695/1

Here we develop a novel three-dimensional (3D) reconstruction method of the coronal plasma of an active region by combining stereoscopic triangulation of loops with density and temperature modeling of coronal loops with a filling factor equivalent to tomographic volume rendering. Because this method requires only a stereoscopic image pair in multiple temperature filters, which are sampled within ≈ 1 minute with the recent *STEREO*/EUVI instrument, this method is about four orders of magnitude faster than conventional solar rotation-based tomography.We reconstruct the 3D density and temperature distribution of active region NOAA 10955 by stereoscopic triangulation of 70 loops, which are used as a skeleton for a 3D field interpolation of some 7000 loop components, leading to a 3D model that reproduces the observed fluxes in each stereoscopic image pair with an accuracy of a few percents (of the average flux) in each pixel. With the stereoscopic tomography we infer also a differential emission measure distribution over the entire temperature range of $T \approx 10^4$–10^7, with predictions for the transition region and hotter corona in soft X-rays. The tomographic 3D model provides also large statistics of physical parameters. We find that the extreme-ultraviolet loops with apex temperatures of T_m _ 3.0 MK tend to be super-hydrostatic, while hotter loops with $T_m \approx 4$–7 MK are near-hydrostatic. The new 3D reconstruction model is fully independent of any magnetic field data and is promising for future tests of theoretical magnetic field models and coronal heating models.

Solar Flare and CME Observations with STEREO/EUVI

M.J. **Aschwanden**, · J.P. Wuelser, N.V. Nitta, · J.R. Lemen1

E-print, Dec 2008; Solar Phys. (2009) **256**: 3-40 DOI 10.1007/s11207-009-9347-4, **2009, File**

STEREO/EUVI observed 185 flare events (detected above the GOES class C1 level or at >25 keV with RHESSI) during the first two years of the mission (Dec 2006 - Nov 2008), while coronal mass ejections (CME) were reported in about a third of these events. We compile a **comprehensive catalog of these EUVI-observed events**, containing the peak fluxes in soft X-rays, hard X-rays, and EUV, as well as a classification and statistics of prominent EUV features: 79% show impulsive EUV emission (coincident with hard X-rays), 73% show delayed EUV emission from postflare loops and arcades, 24% represent occulted flares, 17% exhibit EUV dimming, 5% show loop oscillations or propagating waves, and at least 3% show erupting filaments. We analyze an example of each EUV feature by stereoscopic modeling of their 3D geometry. We find that impulsive EUV emission indicates compression of cold coronal plasma during the

flare energy release, in contrast to the delayed postflare EUV emission that results from cooling of the soft X-ray emitting flare loops. Occulted flares allow us to determine CME-related coronal dimming uncontaminated from flare-related EUV emission. From modeling the time evolution of EUV dimming we can accurately quantify the initial expansion of CMEs and determine their masses. Further we find evidence that coronal loop oscillations are excited by the rapid initial expansion of CMEs. These examples demonstrate that stereoscopic
EUV data provide powerful new methods to model the 3D aspects in the hydrodynamics of flares and kinematics of CMEs.

FIRST 3D RECONSTRUCTIONS OF CORONAL LOOPS WITH THE STEREO A+B SPACECRAFT. II. ELECTRON DENSITY AND TEMPERATURE MEASUREMENTS
Markus J. **Aschwanden**, Nariaki V. Nitta, Jean-Pierre Wuelser, and James R. Lemen
The Astrophysical Journal, 680:1477-1495, **2008**
http://www.journals.uchicago.edu/doi/pdf/10.1086/588014
Using the stereoscopically derived three-dimensional (3D) geometry of 30 loops observed with STEREO EUVI (described in Paper I) we determine here the electron density profiles $n_e(s)$ and electron temperature profiles $T_e(s)$ from a triple-filter analysis of the stereoscopic images taken in the wavelengths of 171, 195, and 284 A.
We find that the observations are not consistent with equilibrium solutions, but rather display the typical overpressures of loops that have been previously heated to higher temperatures and cool down in a nonequilibriumstate, similar to earlier EIT and TRACE measurements.

New Aspects on Particle Acceleration in Solar Flares from RHESSI Observations
Markus J. **Aschwanden**
E-print, May **2008**; Asian Journal of Physics, Special Issue on Flare Phenomena, (ed. Rajmal Jain), **File**
In this review we highlight a number of recent RHESSI observations that are directly relevant to the study of particle acceleration processes in solar flares. Many observations confirm our basic standard models of acceleration in various types of coronal magnetic reconnection regions, but reveal a number of unexpected features that either require more detailed magnetic, hydrodynamic, and kinetic modeling or rethinking in terms of alternative models.

THE LOCALIZATION OF PARTICLE ACCELERATION SITES IN SOLAR FLARES AND CMES
MARKUS J. **ASCHWANDEN**
Space Science Reviews (**2006**) 124: 361–372, **File**

Observations of Nonthermal Velocities and Comparisons with an Alfvén Wave Turbulence Model in Solar Active Regions
M. **Asgari-Targhi**1, D. H. Brooks6,2, M. Hahn3, S. Imada4, E. Tajfirouze5, and D. W. Savin3
2024 ApJ 968 7
https://iopscience.iop.org/article/10.3847/1538-4357/ad434a/pdf
We present a study of spectral line width measurements from the Extreme-ultraviolet Imaging Spectrometer on Hinode. We used spectral line profiles of Fe xvi 262.984 Å, Fe xiv 264.787 Å, Fe xiv 270.519 Å, Fe xiv 274.203 Å, and Fe xv 284.160 Å, and studied 11 active regions. Previous studies of spectral line widths have shown that in hot loops in the cores of active regions, the observed nonthermal velocities are smaller than predicted from models of reconnection jets in the corona or shock heating associated with Alfvén waves. The observed line widths are also inconsistent with models of chromospheric evaporation due to coronal nanoflares. We show that recent advances in higher resolution Alfvén wave turbulence modeling enables us to obtain nonthermal velocities similar to those measured in active regions. The observed nonthermal velocities for the 11 active regions in our study are in the range of 17–30 km s−1, consistent with the spectral line nonthermal widths predicted from our model of 16 interacting flux tubes, which are in the range of 15–37 km s−1.

Modeling of Hot Plasma in the Solar Active Region Core
M. **Asgari-Targhi**1, J. T. Schmelz2, S. Imada3, S. Pathak2, and G. M. Christian
2015 ApJ 807 146
Magnetically confined plasma with temperatures $\geqslant 5$ MK are a feature of hot coronal loops observed in the core of active regions. In this paper, using observations and MHD modeling of coronal loops, we investigate whether wave heating (Alternating Current) models can describe the high temperature loops observed in the active region of **2012 September 7**. We construct three-dimensional MHD models for the Alfvén wave turbulence within loops with high temperature. We find that for the Alfvén waves to create enough turbulence to heat the corona, the rms velocity at the

footpoints must be 5–6 $\mathrm{km\ s^{-1}}$. We conclude that the Alfvén wave turbulence model may be a candidate for explaining how the hot loops are heated, provided the loops have a high velocity at their photospheric footpoints.

Non-thermal Observations of a Flare Loop-top using IRIS Fe XXI: Implications for Turbulence and Electron Acceleration

William **Ashfield** IV, Vanessa Polito, Sijie Yu, Hannah Collier, Laura Hayes
ApJ **973** 96 **2024**
https://arxiv.org/pdf/2407.12174
https://iopscience.iop.org/article/10.3847/1538-4357/ad64ca/pdf
The excess broadening of high-temperature spectral lines, long observed near the tops of flare arcades, is widely considered to result from magnetohydrodynamic (MHD) turbulence. According to different theories, plasma turbulence is also believed to be a candidate mechanism for particle acceleration during solar flares. However, the degree to which this broadening is connected to the acceleration of non-thermal electrons remains largely unexplored outside of recent work, and many observations have been limited by limited spatial resolution and cadence. Using the Interface Region Imaging Spectrometer (IRIS), we present spatially resolved observations of loop-top broadenings using hot (11MK) Fe XXI 1354.1 Å line emission at ~9s cadence during the **2022 March 30** X1.3 flare. We find non-thermal velocities upwards of 65km/s that decay linearly with time, indicating the presence and subsequent dissipation of plasma turbulence. Moreover, the initial Fe XXI signal was found to be co-spatial and co-temporal with microwave emission measured by the Expanded Owens Valley Solar Array (EOVSA), placing a population of non-thermal electrons in the same region as the loop-top turbulence. Evidence of electron acceleration at this time is further supported by hard X-ray measurements from the Spectrometer/Telescope for Imaging X-rays (STIX) aboard Solar Orbiter. Using the decay of non-thermal broadenings as a proxy for turbulent dissipation, we found the rate of energy dissipation to be consistent with the power of non-thermal electrons deposited into the chromosphere, suggesting a possible connection between turbulence and electron acceleration.
IRIS Nugget 13 Sep **2024** https://iris.lmsal.com/nugget

A Model for Gradual Phase Heating Driven by MHD Turbulence in Solar Flares

William **Ashfield** IV, Dana Longcope
ApJ **944** 147 **2023**
https://arxiv.org/pdf/2301.04592.pdf
https://iopscience.iop.org/article/10.3847/1538-4357/acb1b2/pdf
Coronal flare emission is commonly observed to decay on timescales longer than those predicted by impulsively-driven, one-dimensional flare loop models. This discrepancy is most apparent during the gradual phase, where emission from these models decays over minutes, in contrast to the hour or more often observed. Magnetic reconnection is invoked as the energy source of a flare, but should deposit energy into a given loop within a matter of seconds. Models which supplement this impulsive energization with a long, persistent ad hoc heating have successfully reproduced long-duration emission, but without providing a clear physical justification. Here we propose a model for extended flare heating by the slow dissipation of turbulent Alfvén waves initiated during the retraction of newly-reconnected flux tubes through a current sheet. Using one-dimensional simulations, we track the production and evolution of MHD wave turbulence trapped by reflection from high-density gradients in the transition region. Turbulent energy dissipates through non-linear interaction between counter-propagating waves, modeled here using a phenomenological one-point closure model. AIA EUV light curves synthesized from the simulation were able to reproduce emission decay on the order of tens of minutes. We find this simple model offers a possible mechanism for generating the extended heating demanded by observed coronal flare emissions self-consistently from reconnection-powered flare energy release.

Connecting Chromospheric Condensation Signatures to Reconnection Driven Heating Rates in an Observed Flare

William H. **Ashfield** IV, Dana W. Longcope, Chunming Zhu, Jiong Qiu
ApJ **926** 164 **2022**
https://arxiv.org/pdf/2112.02150.pdf
https://iopscience.iop.org/article/10.3847/1538-4357/ac402d/pdf
Observations of solar flare reconnection at very high spatial and temporal resolution can be made indirectly at the footpoints of reconnected loops into which flare energy is deposited. The response of the lower atmosphere to this energy input includes a downward-propagating shock called chromospheric condensation, which can be observed in the UV and visible. In order to characterize reconnection using high-resolution observations of this response, one must develop a quantitative relationship between the two. Such a relation was recently developed and here we test it on observations of chromospheric condensation in a single footpoint from a flare ribbon of the X1.0 flare on **25 Oct. 2014** (SOL2014-10-25T16:56:36). Measurements taken of Si iv 1402.77 Å emission spectra using the Interface Region Imaging Spectrograph (IRIS) in a single pixel show red-shifted component undergoing characteristic condensation

evolution. We apply the technique called the Ultraviolet Footpoint Calorimeter (UFC) to infer energy deposition into the one footpoint. This energy profile, persisting much longer than the observed condensation, is input into a one-dimensional, hydrodynamic simulation to compute the chromospheric response, which contains a very brief condensation episode. From this simulation we synthesize Si iv spectra and compute the time-evolving Doppler velocity. The synthetic velocity evolution is found to compare reasonably well with the IRIS observation, thus corroborating our reconnection-condensation relationship. The exercise reveals that the chromospheric condensation characterizes a particular portion of the reconnection energy release rather than its entirety, and that the time scale of condensation does not necessarily reflect the time scale of energy input.

Relating the Properties of Chromospheric Condensation to Flare Energy Transported by Thermal Conduction

W. H. **Ashfield**1 and D. W. Longcope1
2021 ApJ 912 25
https://iopscience.iop.org/article/10.3847/1538-4357/abedb4/pdf
https://doi.org/10.3847/1538-4357/abedb4
Chromospheric condensation is a brief episode of downflow often accompanying energy release and evaporation in a solar flare. While this component of a flare reflects the energy release process only indirectly, it can be observed at high spatial and temporal resolution, even from the ground. It appears in spectroscopic observations of cooler lines, formed below ~105 K, as a redshift that peaks and decays after less than 1 minute. In order to use this signature to infer characteristics of solar flare energy release, it is important to establish quantitative relationships with properties of the condensation. The initial investigation reported here does so after restricting consideration to energy transport via thermal conduction into a simplified, stratified chromosphere. We develop an analytical expression for the decay of a condensation propagating into a stratified atmosphere. This model provides a relationship between shock velocity and preshock density structure. We also use one-dimensional gasdynamic simulations to explore the dynamics of these shocks as they penetrate into the stratified chromosphere. We find that the peak downflow speed primarily reflects the energy flux into the chromosphere, while the product of this velocity and the redshift duration is proportional to the preshock density scale height as H $\simeq$ 0.6u0τ.

FOXSI-2 Solar Microflares. I. Multi-instrument Differential Emission Measure Analysis and Thermal Energies

P. S. **Athiray**1,2, Juliana Vievering1, Lindsay Glesener1, Shin-nosuke Ishikawa3, Noriyuki Narukage4, Juan Camilo Buitrago-Casas5, Sophie Musset1, Andrew Inglis6, Steven Christe7, Säm Krucker5,8Show full author list
2020 ApJ 891 78
https://doi.org/10.3847/1538-4357/ab7200
In this paper we present the differential emission measures (DEMs) of two sub-A class microflares observed in hard X-rays (HXRs) by the FOXSI-2 sounding rocket experiment, on **2014 December 11**. The second Focusing Optics X-ray Solar Imager (FOXSI) flight was coordinated with instruments X-ray Telescope (Hinode/XRT) and Solar Dynamics Observatory/Atmospheric Imaging Assembly (AIA), which provided observations in soft X-rays and Extreme Ultraviolet. This unique data set offers an unprecedented temperature coverage, useful for characterizing the plasma temperature distribution of microflares. By combining data from FOXSI-2, XRT, and AIA, we determined a well-constrained DEM for the microflares. The resulting DEMs peak around 3 MK and extend beyond 10 MK. The emission measures determined from FOXSI-2 were lower than 1026 cm−5 for temperatures higher than 5 MK; faint emission in this range is best measured in HXRs. The coordinated FOXSI-2 observations produce one of the few definitive measurements of the distribution and the amount of plasma above 5 MK in microflares. We utilize the multi-thermal DEMs to calculate the amount of thermal energy released during both the microflares as ~5.0 × 1028 erg for Microflare 1 and ~1.6 × 1028 erg for Microflare 2. We also show the multi-thermal DEMs provide more comprehensive thermal energy estimates than isothermal approximation, which systematically underestimates the amount of thermal energy released.
RHESSI Nuggets #396 Dec **2020** https://sprg.ssl.berkeley.edu/~tohban/wiki/index.php/Investigation_of_Small-Scale_Energy_Releases_in_Hard_X-rays_with_%E2%80%8BFOXSI

Drifting of the line-tied footpoints of CME flux-ropes

Guillaume **Aulanier**, Jaroslav Dudik
A&A 621, A72 (**2019**)
https://arxiv.org/pdf/1811.04253.pdf
http://www.lesia.obspm.fr/perso/guillaume-aulanier/Aulanier_Dudik_2018_AeA.pdf
sci-hub.tw/10.1051/0004-6361/201834221
Context. Bridging the gap between heliospheric and solar observations of eruptions requires to map ICME footpoints down to the Sun's surface. But this not straightforward. Improving the understanding of the spatio-temporal evolutions

of eruptive flares requires a comprehensive standard model. But the current one is two-dimensional only and it cannot address the question of CME footpoints.
Aims. Existing 3D extensions to the standard model show that flux-rope footpoints are surrounded by curved-shaped QSL-footprints that can be related with hook-shaped flare-ribbons. We build upon this finding and further address the joint questions of their timeevolution, and of the formation of flare loops at the ends of flaring PILs of the erupting bipole, which are both relevant for flare understanding in general and for ICME studies in particular.
Methods. We calculate QSLs and relevant field lines in an MHD simulation of a torus-unstable flux-rope. The evolving QSL footprints are used to define the outer edge of the flux rope at different times, and to identify and characterize new 3D reconnection geometries and sequences that occur above the ends of the flaring PIL. We also analyse flare-ribbons as observed in EUV by SDO/AIA and IRIS during two X-class flares.
Results. The flux-rope footpoints are drifting during the eruption, which is unexpected due to line-tying. This drifting is due to a series of coronal reconnections that erode the flux rope on one side and enlarge it on the other side. Other changes in the flux-rope footpoint-area are due to multiple reconnections of individual field lines whose topology can evolve sequentially from arcade to flux rope and finally to flare loop. These are associated with deformations and displacements of QSL footprints, which resemble those of the studied flare ribbons.
Conclusions. Our model predicts continuous deformations and a drifting of ICME flux-rope footpoints whose areas are surrounded by equally-evolving hooked-shaped flare-ribbons, as well as the formation of flare loops at the ends of flaring PILs which originate from the flux-rope itself, both of which being due to purely three-dimensional reconnection geometries. The observed evolution of flare-ribbons in two events supports the model, but more observations are required to test all its predictions. **July 12, 2012, September 10, 2014**

The standard flare model in three dimensions, II. Upper limit on solar flare energy

G. **Aulanier**, P. D?moulin, C.J. Schrijver, M. Janvier, E. Pariat, B. Schmieder
E-print, Nov **2012**, http://solar.physics.montana.edu/cgi-bin/eprint/index.pl?entry=16890
A&A, 549, A66 (**2013**)
Solar flares strongly affect the Sun's atmosphere as well as the Earth's environment. Quantifying the maximum possible energy of solar flares of the present-day Sun, if any, is thus a key issue in heliophysics. The largest solar flares observed over the past few decades have reached energies of a few times 10^32 ergs, possibly up to 10^33 ergs. Flares in active Sun-like stars reach up to about 10^36 ergs. In the absence of direct observations of solar flares within this range, complementary methods of investigation are needed to assess the probability of solar flares beyond those in the observational record. Using historical reports for sunspot and solar active region properties in the photosphere we scale to observed solar values a realistic dimensionless 3D MHD simulation for eruptive flares, which originate from a highly sheared bipole. This enables us to calculate the magnetic fluxes and flare energies in the model in a wide paramater space. Firstly, commonly observed solar conditions lead to modeled magnetic fluxes and flare energies that are comparable to those estimated from observations. Secondly, we evaluate from observations that 30% of the area of sunspot groups are typically involved in flares. This is related to the strong fragmentation of such groups, which naturally results from sub-photospheric convection. When the model is scaled to 30\% of the area of the largest sunspot group ever reported, with its peak magnetic field being set to the strongest value ever measured in a sunspot, it produces a flare with a maximum energy of ~ 6x10^33 ergs. The results of the model suggest that the Sun is able to produce flares up to about six times as energetic in TSI fluence as the strongest directly-observed flare from Nov 4, 2003. Sunspot groups larger than historically reported would yield superflares for spot pairs that would exceed tens of degrees in extent. We thus conjecture that superflare-productive Sun-like stars should have a much stronger dynamo than in the Sun.

The standard flare model in three dimensions
I. Strong-to-weak shear transition in post-flare loops

G. **Aulanier**, M. Janvier, and B. Schmieder
E-print, 20 May, **2012, File**; A&A 543, A110 (**2012**)
The standard CSHKP model for eruptive flares is two-dimensional. Yet observational interpretations of photospheric currents in pre-eruptive sigmoids, shear in post-flare loops, and relative positioning and shapes flare ribbons,all together require three-dimensional extensions to the model. The paper focuses on the strong-to-weak shear transition in post-flare loop, and on the time-evolution of the geometry of photospheric electric currents, which occur during the development of eruptive flares. The objective is to understand the three-dimensional physical processes which cause them, and to know how much the post-flare and the pre-eruptive distributions of shear depend on each other. The strong-to-weak shear transition in post-flare loops is identified and quantified in a flare observed by STEREO, as well as in a magnetohydrodynamic simulation of CME initiation performed with the OHM code. In both approaches, the magnetic shear is evaluated with field line footpoints. In the simulation, the shear is also estimated from ratios between magnetic field components. The modeled strong-to-weak shear transition in post-flare loops comes from two effects. Firstly, a reconnection-driven transfer of the differential magnetic shear, from the pre- to the post-eruptive configuration. Secondly, a vertical straightening of the inner legs of the CME, which induces an outer shear weakening.

The model also predicts the occurrence of narrow electric current layers inside J-shaped flare ribbons, which are dominated by direct currents. Finally, the simulation naturally accounts for energetics and time-scales for weak and strong flares, when typical scalings for young and decaying solar active regions are applied. The results provide three-dimensional extensions to the standard flare model. These extensions involve MHD processes that should be tested with observations. **May 9, 2011**

The Late Gradual Phase of Large Flares: The Case of November 3, 2003

H. **Aurass**

Solar Phys., **2014**

http://www.aip.de/mitglieder/haurass/paper/the-late-gradual-phase-of-solar-flares/view

The hard X-ray time profiles of most solar eruptive events begin with an {\it impulsive phase} which may be followed by a {\it late gradual phase}. In a recent article (Aurass {\it et al.} 2013, {\it Astron. Astrophys.} {\bf 555}, A40) we analyzed the impulsive phase of the solar eruptive event on November 3, 2003 in radio and X-ray emission. We find evidence of magnetic breakout reconnection using the radio diagnostic of the common effect of the flare current sheet and, at heights of ±0.4\Rs, of a coronal breakout current sheet (a source site that we call X). In this article we investigate the radio emission during the late gradual phase of the previously analyzed event. The work is based on 40--400~MHz dynamic spectra ({\it Radio Spectrograph} Observatorium Tremsdorf, Leibniz Institut f\"ur Astrophysik Potsdam, AIP) combined with radio images obtained by the French {\it Nan\c{c}ay Multifrequency Radio Heliograph} (NRH) of the Observatoire de Paris, Meudon. Additionally we use {\it Ramaty High Energy Solar Spectroscopic Imager} (RHESSI) hard X-ray (HXR) flux records, and {\it Solar and Heliospheric Observatory} (SOHO) {\it Large Angle and Spectrometric Coronagraph} (LASCO) and {\it Extreme ultraviolet Imaging Telescope} (EIT) images. The analysis shows that the late gradual phase is subdivided into two distinct stages. Stage 1 (here lasting five minutes) is restricted to reoccurring radio emission at source site X. We observe plasma emission and an azimuthally moving source (from X toward the NE; speed \ab1200\kms) at levels radially ordered {\it against} the undisturbed coronal density gradient. These radio sources mark the lower boundary of an overdense region with a huge azimuthal extent. By the end of its motion, the source decays and reappears at point X. This is the onset of stage 2 traced here during its first 13~minutes. By this time, NRH sources observed at frequencies \le236.6~MHz radially lift off with a speed of \ab400\kms (one third of the front speed of the coronal mass ejection (CME)) as one slowly decaying broadband source. This speed is still observable in SOHO/LASCO~C3 difference frames in the wake of the CME four hours later. In stage 2, the radio sources at higher frequencies appear directly above the active region with growing intensity. We interpret the observations as the transit of the lower boundary of the CME body through the height range of the coronal breakout current sheet. The relaxing global coronal field reconnects with the magnetic surroundings of the current sheets still connecting the CME in its wake with the Sun. The accelerated particles locally excite plasma emission but can escape also toward the active region, the CME, and the large-scale solar magnetic field. The breakout relaxation process may be a source of reconnection- and acceleration rate modulations. In this view, the late gradual phase is a certain stage of the coronal breakout relaxation after the release of the CME. This article is, to our best knowledge, the first observational report of the coronal breakout recovery. Our interpretation of the radio observations agrees with some predictions of magnetic breakout simulations ({\it e.g.} Lynch {\it et al.} 2008, {\it Astrophys. Journ.} {\bf 683}, 1192). Again, combined spectral and imaging radio observations give a unique access to dynamic coronal processes which are invisible in other spectral ranges.

Radio evidence for breakout reconnection in solar eruptive events

H. **Aurass**, G. Holman, S. Braune, G. Mann, P. Zlobec

E-print, May **2013, File**; A&A, 555, A40

Magnetic reconnection is understood to be fundamental to energy release in solar eruptive events (SEEs). In these events reconnection produces a magnetic flux rope above an arcade of hot flare loops. Breakout reconnection, a secondary reconnection high in the corona between this flux rope and the overlying magnetic field, has been hypothesized. Direct observational evidence for breakout reconnection has been elusive, however. The aim of this study is to establish a plausible interpretation of the combined radio and hard X-ray (HXR) emissions observed during the impulsive phase of the near-limb X3.9-class SEE on **2003 November 03**. We study radio spectra (AIP), simultaneous radio images (Nanc{c}ay Multi-frequency Radio Heliograph, NRH), and single-frequency polarimeter data (OAT). The radio emission is nonthermal plasma radiation with a complex structure in frequency and time. Emphasis is on the time interval when the HXR flare loop height was observed by the Ramaty High Energy Solar Spectroscopic Imager (RHESSI) to be at its minimum and an X-ray source was observed above the top of the arcade loops. Two stationary, meter-wavelength sources are observed radially aligned at 0.18 and 0.41Rs above the active region and hard X-ray sources. The lower source is apparently associated with the upper reconnection jet of the flare current sheet (CS), and the upper source is apparently associated with breakout reconnection. Sources observed at lower radio frequencies surround the upper source at the expected locations of the breakout reconnection jets. We believe the upper radio source is the most compelling evidence to date for the onset of breakout reconnection during a SEE. The height stationarity of the breakout sources and their dynamic radio spectrum discriminate them from propagating disturbances. Timing and location arguments reveal for the first time that both the earlier described ``above the flare loop top'' HXR source and the lower radio source are emission from the upper reconnection jet above the vertical flare CS.

Coronal current sheet signatures during the 17 May 2002 CME-flare

H. **Aurass**1, F. Landini2, G. Poletto

E-print, Aug 2009; A&A, 506, 901–911 (**2009**), **File**

Context. The relation between current sheets (CSs) associated with flares, revealed by characteristic radio signatures, and current sheets associated with coronal mass ejections (CMEs), detected in coronal ultraviolet (UV) and white light data, has not been analyzed, yet.
Aims. We aim at establishing the relationship between CSs associated with a limb flare and CSs associated with the CME that apparently develops after the flare. We use a unique data set, acquired on May 17, 2002, which includes radio and extreme ultraviolet (XUV) observations.
Methods. Spectral radio diagnostics, UV spectroscopic techniques, white light coronograph imaging, and (partly) radio imaging are used to illustrate the relation between the CSs and to infer the physical parameters of the radially aligned features that develop in the aftermath of the CME.
Results. During the flare, several phenomena are interpreted in accordance with earlier work and with reference to the common eruptive flare scenario as evidence of flare CSs in the low corona. These are drifting pulsating structures in dynamic radio spectra, an erupting filament, expanding coronal loops morphologically recalling the later white light CME, and associated with earlier reported hard X-ray source sites. In the aftermath of the CME, UV spectra allowed us to estimate the CS temperature and density, over the 1.5 - 2.1 R☉ interval of heliocentric altitudes. The UV detected CS, however, appears to be only one of many current sheets that exist underneath the erupting flux rope. A type II burst following the CME radio continuum in time at lower frequencies is considered as the radio signature of a coronal shock excited at the flank of the CME.
Conclusions. *The results show that we can build an overall scenario where the CME is interpreted in terms of an erupting arcade crossing the limb of the Sun and connected to underlying structures via multiple CSs. Eventually, the observed limb flare seems to be a consequence of the ongoing CME.*

Electric Current Neutralization in Solar Active Regions and Its Relation to Eruptive Activity

Ellis A. **Avallone**, Xudong Sun

ApJ **893** 123 **2020**

https://arxiv.org/pdf/2003.02814.pdf

https://doi.org/10.3847/1538-4357/ab7afa

It is well established that magnetic free energy associated with electric currents powers solar flares and coronal mass ejections (CMEs) from solar active regions (ARs). However, the conditions that determine whether an AR will produce an eruption are not well understood. Previous work suggests that the degree to which the driving electric currents, or the sum of all currents within a single magnetic polarity, are neutralized may serve as a good proxy for assessing the ability of ARs to produce eruptions. Here, we investigate the relationship between current neutralization and flare/CME production using a sample of 15 flare-active and 15 flare-quiet ARs. All flare-quiet and 4 flare-active ARs are also CME-quiet. We additionally test the relation of current neutralization to the degree of shear along polarity inversion lines (PILs) in an AR. We find that flare-productive ARs are more likely to exhibit non-neutralized currents, specifically those that also produce a CME. We find that flare/CME-active ARs also exhibit higher degrees of PIL shear than flare/CME-quiet ARs. We additionally observe that currents become more neutralized during magnetic flux emergence in flare-quiet ARs. Our investigation suggests that current neutralization in ARs is indicative of their eruptive potential. **2011.02.15, 2013.06.19-20, 2017.09.4-7**

HMI Science Nuggets #138 March **2020** http://hmi.stanford.edu/hminuggets/?p=3224

RHESSI NUGGETS #391 Oct **2020** https://iopscience.iop.org/article/10.3847/1538-4357/ab7afa/pdf

Relative yield of thermal and nonthermal emission during weak flares observed by STIX during September 20-25, 2021

Arun Kumar **Awasthi** (1), Tomasz Mrozek (1), Sylwester Kołomański (2), Michalina Litwicka (3,1), Marek Stęślicki (1), Karol Kułaga (2)

ApJ **2024**

https://arxiv.org/pdf/2402.01936.pdf

The disparate nature of thermal-nonthermal energy partition during flares, particularly during weak flares, is still an open issue. Following the Neupert effect, quantifying the relative yield of X-ray emission in different energy bands can enable inferring the underlying energy release mechanism. During **September 20-25, 2021**, the Solar Orbiter mission - being closer to the Sun (∼0.6 AU) and having a moderate separation angle (<40∘) from the Sun-Earth line provided a unique opportunity to analyze multi-wavelength emission from ∼200 (mostly weak) flares, commonly observed by the Spectrometer Telescope for Imaging X-rays (STIX), STEREO-A, GOES, and SDO observatories. Associating the quotient (qf) of hard X-ray fluence (12-20 keV) and soft X-ray flux (4-10 keV) with the peak SXR flux enabled us to

identify strongly non-thermal flares. Multi-wavelength investigation of spectral and imaging mode observations of the 20 strongly non-thermal weak flares reveals an inverse relationship of qf with the emission measure (EM) (and density), and a positive relationship with the flare plasma temperature. This indicates that plasma in tenuous loops attains higher temperatures compared to that in the denser loops, in response to nonthermal energy deposition. This is in agreement with the plasma parameters of the coronal loops, as derived by applying the one-dimensional Palermo Harvard (PH) hydrodynamical code to the coronal loop plasma having different initial coronal loop base pressures when subjected to similar heating input. Our investigation, therefore, indicates that the plasma parameters of the flaring loop in the initial phase have a decisive role in thermal-nonthermal energy partitioning.

Effects of supra-arcade downflows interacting with the post-flare arcade

Arun Kumar **Awasthi**, Rui Liu, Tingyu Gou
ApJ **941** 158 **2022**
https://arxiv.org/pdf/2211.08592.pdf
https://iopscience.iop.org/article/10.3847/1538-4357/aca3a8/pdf
Supra-arcade downflows (SADs) are dark voids descending through plasma above the post-flare arcade. Although they are generally viewed as byproducts of flare reconnections in the corona, the nature of SADs is under debate. Here we investigated six distinct episodes of SADs observed in the post-maximum phase of an M-class flare of **April 11, 2013**. Differential emission measure analysis revealed that SAD cases occurring close to the flare maximum contain an enhanced hot plasma component at 5--7~MK whereas those occurring later exhibited a depression in hot plasma at 7--12~MK compared to the ambient supra-arcade plasma. On-disk location of the flare enabled us to examine in detail the interaction of SADs with the post-flare arcade, whose effects include 1) transverse oscillations of period ~160~s in the supra-arcade rays in the wake of voids, 2) footpoint brightening in 1700{~Å} whose peak is delayed by 22-46~s with respect to the SAD's arrival at the top of the arcade, and 3) EUV intensity perturbations expanding and propagating with a speed ~400 km~s−1. On the other hand, due to line-of-sight confusion in the optically thin corona, the ribbon enhancement following the interaction produces an illusion of plasma rebound at the top of the arcade, where the interaction fails to yield significant plasma heating. These effects indicate that the interaction mainly generates MHD waves propagating toward the surface, which may further produce quasi-periodic brightening at flare ribbons, therefore contributing to quasi-periodic flare gradual phase emission in EUV.

Chromospheric response during the precursor and the main phase of a B6.4 flare on August 20, 2005

Arun Kumar **Awasthi**, Pawel Rudawy, Robert Falewicz, Arkadiusz Berlicki, Rui Liu
ApJ **858** 98 **2018**
https://arxiv.org/pdf/1804.02632.pdf
Solar flare precursors depict constrained rate of energy release contrasting the imminent rapid energy release which calls for different regime of plasma processes to be at play. Due to subtle emission during the precursor phase, its diagnostics remain delusive, revealing either the non-thermal electrons (NTEs) or the thermal conduction to be the driver. In this regard, we investigate the chromospheric response during various phases of a B6.4 flare on **August 20, 2005**. Spatio-temporal investigation of flare ribbon enhancement during the precursor phase, carried out using spectra-images recorded in several wavelength positions on the H-alpha line profile, revealed its delayed response (180 seconds) compared to the X-ray emission, as well as sequential increment in the width of the line-profile which are indicative of a slow heating process. However, energy contained in the H-alpha emission during the precursor phase reach as high as 80% of that estimated during the main phase. Additionally, the plasma hydrodynamics during the precursor phase, as resulted from the application of a single-loop one-dimensional model, revealed the presence of power-law extension in the model generated X-ray spectra, with flux lower than the RHESSI background. Therefore, our multi-wavelength diagnostics and hydrodynamical modeling of the precursor emission indicates the role of a two-stage process. Firstly, reconnection triggered NTEs, although too small in flux to overcome the observational constraints, thermalize in the upper chromosphere. This leads to the generation of a slow conduction front which causes plasma heating during the precursor phase.

Thermal characteristics and the differential emission measure distribution during a B8.3 flare on July 04, 2009

Arun Kumar **Awasthi**, Barbara Sylwester, Janusz Sylwester, Rajmal Jain
ApJ 823 126 **2016**
http://arxiv.org/pdf/1604.01935v1.pdf
See http://arxiv.org/pdf/1604.01926v1.pdf
We investigate the evolution of differential emission measure distribution (DEM[T]) in various phases of a B8.3 flare, which occurred on **July 04, 2009**. We analyze the soft X-ray (SXR) emission in 1.6-8.0 keV range, recorded collectively by Solar Photometer in X-rays (SphinX; Polish) and Solar X-ray Spectrometer (SOXS; Indian) instruments. We make a comparative investigation of the best-fit DEM[T] distributions derived by employing various inversion schemes viz. single gaussian, power-law, functions and Withbroe-Sylwester (W-S) maximum likelihood algorithm. In

addition, SXR spectrum in three different energy bands viz. 1.6-5.0 keV (low), 5.0-8.0 keV (high) and 1.6-8.0 keV (combined) is analyzed to determine the dependence of the best-fit DEM[T] distribution on the selection of energy interval. The evolution of DEM[T] distribution, derived using W-S algorithm, reveals the plasma of multi-thermal nature during the rise to the maximum phase of the flare, while of isothermal nature in the post-maximum phase of the flare. Thermal energy content is estimated considering the flare plasma to be of 1) iso-thermal and 2) multi-thermal nature. We find that the energy content during the flare, estimated from the multi-thermal approach, is in good agreement with that derived using the iso-thermal assumption except during the maximum of the flare. Further, (multi-) thermal energy estimated employing low-energy band of the SXR spectrum result in higher values than that derived from the combined-energy band. On the contrary, the analysis of high-energy band of SXR spectrum lead to lower thermal energy than that estimated from the combined-energy band.

Multiwavelength diagnostics of the precursor and main phases of an M1.8 flare on 2011 April 22

Awasthi, A. K.; Jain, R.; Gadhiya, P. D.; Aschwanden, M. J.; Uddin, W.; Srivastava, A. K.; Chandra, R.; Gopalswamy, N.; Nitta, N. V.; Yashiro, S.; Manoharan, P. K.; Choudhary, D. P.; Joshi, N. C.; Dwivedi, V. C.; Mahalakshmi, K.

MNRAS, Volume 437, Issue 3, p.2249-2262, **2014**

http://arxiv.org/pdf/1310.6029v1.pdf

We study the temporal, spatial and spectral evolution of the M1.8 flare, which occurred in the active region 11195 (S17E31) on 2011 April 22, and explore the underlying physical processes during the precursor phase and their relation to the main phase. The study of the source morphology using the composite images in 131 Å wavelength observed by the Solar Dynamics Observatory/Atmospheric Imaging Assembly and 6-14 keV [from the Reuven Ramaty High Energy Solar Spectroscopic Imager (RHESSI)] revealed a multiloop system that destabilized systematically during the precursor and main phases. In contrast, hard X-ray emission (20-50 keV) was absent during the precursor phase, appearing only from the onset of the impulsive phase in the form of foot-points of emitting loops. This study also revealed the heated loop-top prior to the loop emission, although no accompanying foot-point sources were observed during the precursor phase. We estimate the flare plasma parameters, namely temperature (T), emission measure (EM), power-law index (γ) and photon turn-over energy ($\varepsilon$to), and found them to be varying in the ranges 12.4-23.4 MK, 0.0003-0.6 × 1049 cm-3, 5-9 and 14-18 keV, respectively, by forward fitting RHESSI spectral observations. The energy released in the precursor phase was thermal and constituted ≈1 per cent of the total energy released during the flare. The study of morphological evolution of the filament in conjunction with synthesized T and EM maps was carried out, which reveals (a) partial filament eruption prior to the onset of the precursor emission and (b) heated dense plasma over the polarity inversion line and in the vicinity of the slowly rising filament during the precursor phase. Based on the implications from multiwavelength observations, we propose a scheme to unify the energy release during the precursor and main phase emissions in which the precursor phase emission was originated via conduction front that resulted due to the partial filament eruption. Next, the heated leftover S-shaped filament underwent slow-rise and heating due to magnetic reconnection and finally erupted to produce emission during the impulsive and gradual phases.

Studies of the atmospheric structure of the solar white-light flare of August 9, 2011

A. N. **Babin**, E. A. Baranovskii, A. N. Koval'

Astronomy Reports August **2016**, Volume 60, Issue 8, pp 768-775

Semi-empirical models for three kernels emitting in the continuum during the pre-impulsive and impulsive phases of the white-light flare of **August 9, 2011** have been calculated, based on observations of the continuum brightness near 6579 Å, Hα profiles, and photospheric iron lines. These computations show that, in order to achieve agreement between the computed and observed profiles and the contrast of the continuum emission of the impulsive kernels of the white-light flare, the temperature must be increased in both the lower chromosphere and the upper photosphere. The most efficient heating is located deeper in the photosphere in the pre-impulsive than in the impulsive phase, and chromospheric heating is negligible in the pre-impulsive phase. Spectral data and the results of model computations indicate that it is difficult to explain the emission of the white-light flare kernels as the effect of heating by energy transported from the corona into lower-lying, deep layers of the atmosphere by canonical transport mechanisms.

Particle Trapping and Acceleration in Turbulent Post-flare Coronal Loops

Fabio **Bacchini**, Wenzhi Ruan, Rony Keppens

MNRAS Volume 529, Issue 3, April 2024, Pages 2399–2412, **2024**

https://arxiv.org/pdf/2403.07107.pdf

https://academic.oup.com/mnras/article-pdf/529/3/2399/57019812/stae723.pdf

We present a study of energetic-electron trapping and acceleration in the Kelvin-Helmholtz-induced magnetohydrodynamic (MHD) turbulence of post-flare loops in the solar corona. Using the particle-tracing capabilities of MPI-AMRVAC 3.0, we evolve ensembles of test electrons (i.e. without feedback to the underlying MHD) inside the turbulent looptop, using the guiding-center approximation. With the MHD looptop model of Ruan et al. 2018, we investigate the relation between turbulence and particle trapping inside the looptop structure, showing that better-developed turbulent cascades result in more efficient trapping primarily due to mirror effects. We then quantify the electron acceleration in the time-evolving MHD turbulence, and find that ideal-MHD processes inside the looptop can produce nonthermal particle spectra from an initial Maxwellian distribution. Electrons in this turbulence are preferentially accelerated by mirror effects in the direction perpendicular to the local magnetic field while remaining confined within small regions of space between magnetic islands. Assuming dominance of Bremsstrahlung radiation mechanisms, we employ the resulting information from accelerated electrons (combined with the MHD background) to construct HXR spectra of the post-flare loop that include nonthermal-particle contributions. Our results pave the way to constructing more realistic simulations of radiative coronal structure for comparison with current and future observations.

MULTI-WAVELENGTH OBSERVATIONS OF A SUBARCSECOND PENUMBRAL TRANSIENT BRIGHTENING EVENT

X. Y. **Bai**1,2, J. T. Su2, W. D. Cao3, S. Q. Liu1, Y. Y. Deng2, and T. G. Priya

2016 ApJ 823 60

We report a subarcsecond penumbral transient brightening event with the high-spatial resolution observations from the 1.6 m New Solar Telescope (NST), Interface Region Imaging Spectrograph(IRIS), and the Solar Dynamics Observatory. The transient brightening, whose thermal energy is in the range of nanoflares, has signatures in the chromosphere, the transient region, and the corona. NST's Hα channel reveals the fine structure of the event with a width as narrow as 101 km (0″.14), which is much smaller than the width from the previous observation. The transient brightening lasts for about 3 minutes. It is associated with a redshift of about 17 km s−1, found in the Si iv 1402.77 Å line and exhibits an inward motion to the umbra with a speed of 87 km s−1. The small-scale energy released from the event has a multi-temperature component. Spectral analysis of the brightening region from IRIS shows that not only the transition region lines such as Si iv 1402.77 Å and C ii 1334.53 Å, but also the chromospheric Mg ii k 2796.35 Å line are significantly enhanced and broadened. In addition, the event can be found in all the extreme-ultraviolet passbands of the Atmospheric Imaging Assembly and the derived differential emission measure profile increases between 4 and 15 MK (or $6.6 \leq \log T \leq 7.2$) in the transient brightening phase. It is possible that the penumbral transient brightening event is caused by magnetic reconnection.

Hard X-ray emission from a flare-related jet:

H.═M.═**Bain** and L.═Fletcher

A&A 508 (**2009**) 1443-1452

http://www.aanda.org/10.1051/0004-6361/200911876

Aims. We aim to understand the physical conditions in a jet event which occurred on the **22nd of August 2002**, paying particular attention to evidence for non-thermal electrons in the jet material.

Methods. We investigate the flare impulsive phase using multiwavelength observations from the Transition Region and Coronal Explorer (TRACE) and the Reuven Ramaty High Energy Spectroscopic Imager (RHESSI) satellite missions, and the ground-based Nobeyama Radioheliograph (NoRH) and Radio Polarimeters (NoRP).

Results. We report what we believe to be the first observation of hard X-ray emission formed in a coronal jet. We present radio observations which confirm the presence of non-thermal electrons present in the jet at this time. The evolution of the event is best compared with the magnetic reconnection jet model in which emerging magnetic field interacts with the pre-existing coronal field. We calculate an apparent jet velocity of ~500 km s-1 which is consistent with model predictions for jet material accelerated by the JxB force resulting in a jet velocity of the order of the Alfvén speed (~100–1000 km s-1).

First joint X-ray solar microflare observations with NuSTAR and Solar Orbiter/STIX

Natália **Bajnoková**, Iain G. Hannah, Kristopher Cooper, Säm Krucker, Brian W. Grefenstette, David M. Smith, Natasha L. S. Jeffrey, Jessie Duncan

MNRAS Volume 533, Issue 3 **2024** Pages 3742–3755

, https://doi.org/10.1093/mnras/stae2029

https://arxiv.org/pdf/2409.04722

We present the first joint spectral and imaging analysis of hard X-ray (HXR) emission from 3 microflares observed by the Nuclear Spectroscopic Telescope ARray (NuSTAR) and Solar Orbiter/Spectrometer/Telescope for Imaging X-rays (STIX). We studied 5 joint spectra from GOES A7, B1 and B6 class microflares from active region AR12765 on **2020 June 6 and 7**. As these events are very bright for NuSTAR, resulting in extremely low (<1%) livetime, we introduce a pile-up correction method. All five joint spectra were fitted with an isothermal model finding temperatures in the 9-11

MK range. Furthermore, three joint spectra required an additional non-thermal thick-target model finding non-thermal powers of 1025-1026 erg s−1. All the fit parameters were within the ranges expected for HXR microflares. The fit results give a relative scaling of STIX and NuSTAR mostly between 6-28% (one outlier at 52%) suggesting each instrument are well calibrated. In addition to spectral analysis, we performed joint HXR imaging of the June 6 and one of the June 7 microflares. In NuSTAR's field of view (FOV), we observed two separate non-thermal sources connected by an elongated thermal source during the June 6 microflares. In STIX's FOV (44 degrees W with respect to NuSTAR), we imaged thermal emission from the hot flare loops which when reprojected to an Earth viewpoint matches the thermal sources seen with NuSTAR and in the hotter EUV channels with the Solar Dynamic Observatory's Atmospheric Imaging Assembly.

Plasma Upflows Induced by Magnetic Reconnection Above an Eruptive Flux Rope

Deborah **Baker**, Teodora Mihailescu, Pascal Demoulin, Lucie M. Green, Lidia van Driel-Gesztelyi, Gherardo Valori, David H. Brooks, David M. Long, Miho Janvier

Solar Physics (**2021**) 296:103

https://arxiv.org/ftp/arxiv/papers/2106/2106.16137.pdf

https://link.springer.com/content/pdf/10.1007/s11207-021-01849-7.pdf

https://doi.org/10.1007/s11207-021-01849-7

One of the major discoveries of Hinode's Extreme-ultraviolet Imaging Spectrometer (EIS) is the presence of upflows at the edges of active regions. As active regions are magnetically connected to the large-scale field of the corona, these upflows are a likely contributor to the global mass cycle in the corona. Here we examine the driving mechanism(s) of the very strong upflows with velocities in excess of 70 km/s, known as blue-wing asymmetries, observed during the eruption of a flux rope in AR 10977 (eruptive flare SOL**2007-12-07**T04:50). We use Hinode/EIS spectroscopic observations combined with magnetic-field modeling to investigate the possible link between the magnetic topology of the active region and the strong upflows. A Potential Field Source Surface (PFSS) extrapolation of the large-scale field shows a quadrupolar configuration with a separator lying above the flux rope. Field lines formed by induced reconnection along the separator before and during the flux-rope eruption are spatially linked to the strongest blue-wing asymmetries in the upflow regions. The flows are driven by the pressure gradient created when the dense and hot arcade loops of the active region reconnect with the extended and tenuous loops overlying it. In view of the fact that separator reconnection is a specific form of the more general quasi-separatrix (QSL) reconnection, we conclude that the mechanism driving the strongest upflows is, in fact, the same as the one driving the persistent upflows of approx. 10 - 20 km/s observed in all active regions.

Can Subphotospheric Magnetic Reconnection Change the Elemental Composition in the Solar Corona?

Deborah **Baker**1, Lidia van Driel-Gesztelyi1,2,3, David H. Brooks4, Pascal Démoulin2, Gherardo Valori1, David M. Long1, J. Martin Laming5, Andy S. H. To1, and Alexander W. James

2020 ApJ 894 35

https://doi.org/10.3847/1538-4357/ab7dcb

Within the coronae of stars, abundances of those elements with low first ionization potential (FIP) often differ from their photospheric values. The coronae of the Sun and solar-type stars mostly show enhancements of low-FIP elements (the FIP effect) while more active stars such as M dwarfs have coronae generally characterized by the inverse-FIP effect (I-FIP). Here we observe patches of I-FIP effect solar plasma in AR 12673, a highly complex βγδ active region. We argue that the umbrae of coalescing sunspots, and more specifically strong light bridges within the umbrae, are preferential locations for observing I-FIP effect plasma. Furthermore, the magnetic complexity of the active region and major episodes of fast flux emergence also lead to repetitive and intense flares. The induced evaporation of the chromospheric plasma in flare ribbons crossing umbrae enables the observation of four localized patches of I-FIP effect plasma in the corona of AR 12673. These observations can be interpreted in the context of the ponderomotive force fractionation model which predicts that plasma with I-FIP effect composition is created by the refraction of waves coming from below the chromosphere. We propose that the waves generating the I-FIP effect plasma in solar active regions are generated by subphotospheric reconnection of coalescing flux systems. Although we only glimpse signatures of I-FIP effect fractionation produced by this interaction in patches on the Sun, on highly active M stars it may be the dominant process.

Transient Inverse-FIP Plasma Composition Evolution within a Confined Solar Flare

Deborah **Baker**, Lidia van Driel-Gesztelyi, David H. Brooks, Gherardo Valori, Alexander W. James, J. Martin Laming, David M. Long, Pascal Demoulin, Lucie M. Green, Sarah A. Matthews, Katalin Olah, Zsolt Kovari

2019 *ApJ* **875** 35

https://arxiv.org/pdf/1902.06948.pdf

https://iopscience.iop.org/article/10.3847/1538-4357/ab07c1/pdf

Understanding elemental abundance variations in the solar corona provides an insight into how matter and energy flow from the chromosphere into the heliosphere. Observed variations depend on the first ionization potential (FIP) of the main elements of the Sun's atmosphere. High-FIP elements (>10 eV) maintain photospheric abundances in the corona, whereas low-FIP elements have enhanced abundances. Conversely, inverse FIP (IFIP) refers to the enhancement of high-FIP or depletion of low-FIP elements. We use spatially resolved spectroscopic observations, specifically the Ar XIV/Ca XIV intensity ratio, from Hinode's Extreme-ultraviolet Imaging Spectrometer to investigate the distribution and evolution of plasma composition within two confined flares in a newly emerging, highly sheared active region. During the decay phase of the first flare, patches above the flare ribbons evolve from the FIP to the IFIP effect, while the flaring loop tops show a stronger FIP effect. The patch and loop compositions then evolve toward the pre-flare basal state. We propose an explanation of how flaring in strands of highly sheared emerging magnetic fields can lead to flare-modulated IFIP plasma composition over coalescing umbrae which are crossed by flare ribbons. Subsurface reconnection between the coalescing umbrae leads to the depletion of low-FIP elements as a result of an increased wave flux from below. This material is evaporated when the flare ribbons cross the umbrae. Our results are consistent with the ponderomotive fractionation model (Laming2015) for the creation of IFIP-biased plasma. **2012 March 3-6**
UKSP Nugget #105 Oct **2019** http://www.uksolphys.org/uksp-nugget/105-transient-inverse-fip-effect-observed-during-a-solar-flare/
Hinode/ EIS Nugget, Feb **2020** http://solarb.mssl.ucl.ac.uk/SolarB/nuggets/nugget_2020mar.jsp

FIP Bias Evolution in a Decaying Active Region

D. **Baker**, D. H. Brooks, P. Démoulin, S. L. Yardley, L. van Driel-Gesztelyi, D. M. Long, L. M. Green
ApJ **2015**
http://arxiv.org/pdf/1501.07397v1.pdf
Solar coronal plasma composition is typically characterized by first ionization potential (FIP) bias. Using spectra obtained by Hinode's EUV Imaging Spectrometer (EIS) instrument, we present a series of large-scale, spatially resolved composition maps of active region (AR) 11389. The composition maps show how FIP bias evolves within the decaying AR from **2012 January 4-6**. Globally, FIP bias decreases throughout the AR. We analyzed areas of significant plasma composition changes within the decaying AR and found that small-scale evolution in the photospheric magnetic field is closely linked to the FIP bias evolution observed in the corona. During the AR's decay phase, small bipoles emerging within supergranular cells reconnect with the pre-existing AR field, creating a pathway along which photospheric and coronal plasmas can mix. The mixing time scales are shorter than those of plasma enrichment processes. Eruptive activity also results in shifting the FIP bias closer to photospheric in the affected areas. Finally, the FIP bias still remains dominantly coronal only in a part of the AR's high-flux density core. We conclude that in the decay phase of an AR's lifetime, the FIP bias is becoming increasingly modulated by episodes of small-scale flux emergence, i.e. decreasing the AR's overall FIP bias. Our results show that magnetic field evolution plays an important role in compositional changes during AR development, revealing a more complex relationship than expected from previous well-known Skylab results showing that FIP bias increases almost linearly with age in young ARs (Widing & Feldman, 2001, ApJ, 555, 426).

Plasma composition of a sigmoidal anemone active region

D. **Baker**, D. H. Brooks, P. Demoulin, L. Gesztelyi, L. M. Green, J. Carlyle
E-print, Oct **2013**; **2013** ApJ 778 69
Using spectra obtained by the EIS instrument onboard Hinode, we present a detailed spatially resolved abundance map of an active region (AR) - coronal hole (CH) complex that covers an area of 359 arcsec x 485 arcsec. The abundance map provides fi rst ionization potential (FIP) bias levels in various coronal structures within the large EIS fi eld of view. Overall, FIP bias in the small, relatively young AR is 2-3. This modest FIP bias is a consequence of the AR age, its weak heating, and its partial reconnection with the surrounding CH. Plasma with a coronal composition is concentrated at AR loop footpoints, close to where fractionation is believed to take place in the chromosphere. In the AR, we found a moderate positive correlation of FIP bias with nonthermal velocity and magnetic flux density, both of which are also strongest at the AR loop footpoints. Pathways of slightly enhanced FIP bias are traced along some of the loops connecting opposite polarities within the AR. We interpret the traces of enhanced FIP bias along these loops to be the beginning of fractionated plasma mixing in the loops. Low FIP bias in a sigmoidal channel above the AR's main polarity inversion line where ongoing flux cancellation is taking place, provides new evidence of a bald patch magnetic topology of a sigmoid/flux rope configuration. **2007 October 17**.

MAGNETIC RECONNECTION ALONG QUASI-SEPARATRIX LAYERS AS A DRIVER OF UBIQUITOUS ACTIVE REGION OUTFLOWS

D. Baker1, L. van Driel-Gesztelyi1,2,3, C. H. Mandrini4, P. Démoulin2 and M. J. Murray1

ApJ 705 926-935, **2009** doi: 10.1088/0004-637X/705/1/926

H*inode's* EUV Imaging Spectrometer (EIS) has discovered ubiquitous outflows of a few to 50 km s^{-1} from active regions (ARs). These outflows are most prominent at the AR boundary and appear over monopolar magnetic areas. They are linked to strong non-thermal line broadening and are stronger in hotter EUV lines. The outflows persist for at least several days. Using *Hinode* EIS and X-Ray Telescope observations of AR 10942 coupled with magnetic modeling, we demonstrate that the outflows originate from specific locations of the magnetic topology where field lines display strong gradients of magnetic connectivity, namely quasi-separatrix layers (QSLs), or in the limit of infinitely thin QSLs, separatrices. We found the strongest AR outflows to be in the vicinity of QSL sections located over areas of strong magnetic field. We argue that magnetic reconnection at QSLs separating closed field lines of the AR and either large-scale externally connected or "open" field lines is a viable mechanism for driving AR outflows which are likely sources of the slow solar wind.

Energy Release During Slow Long-Duration Flares Observed by RHESSI

U. **Bak-Steslicka** · T. Mrozek · S. Kołoma´ nski

Solar Phys (**2011**) 271:75–89

Slow long-duration events (SLDEs) are flares characterized by the long duration of their rising phase. In many such cases the impulsive phase is weak without typical shortlasting pulses. Instead, smooth, long-lasting hard X-ray (HXR) emission is observed. We analyzed hard X-ray emission and morphology of six selected SLDEs. In our analysis we utilized data from the RHESSI and GOES satellites. The physical parameters of HXR sources were obtained from imaging spectroscopy and were used for the energy balance analysis. The characteristic decay time of the heating rate, after reaching its maximum value, is very long, which explains the long rising phase of these flares.

24 Oct. 2003, 18 Nov. 2003 (10:11), 13 Jul. 2005, 23 Aug. 2005, 06 Sep. 2005, 25 Jan. 2007

See RHESSI Scince Nuggets, No. 162, Slowly but surely towards the huge amount of energy I, by Urszula Bak-Steslicka, Tomasz Mrozek, and Sylwester Kolomanski: **The energetics of "slow LDEs"**.

http://sprg.ssl.berkeley.edu/~tohban/wiki/index.php/Slowly_but_surely_towards_the_huge_amount_of_energy_I

21 Apr 2002, 10 Nov 2004, SOL2005-09-06

Investigation of Slow Rising LDE Flares and Associated CMEs

Bak-Steslicka, U.; Kolomanski, S.; Jakimiec, J

Freiburg ESP Meeting **2008, Poster**

We investigated limb long duration flares with slow rising phases (slow LDE) accompanied with CMEs. It was shown by other authors that acceleration phase of CME lasts as long as the rising phase of associated flare. Thus, slow evolution of slow rising flares allows to study earliest stages of CME evolution in details. Using LASCO data we examined statistical properties of these CME while SXT, EIT and TRACE data were utilized to analyse structure and evolution of associated slow LDE flares. The SXT, EIT and TRACE data allow us to identify CME related structures visible in EUV and SXR

Impact of nanoflare heating in the lower solar atmosphere

H. **Bakke**

RHESSI Science Nuggets #458 **2023**

https://sprg.ssl.berkeley.edu/~tohban/wiki/index.php/Impact_of_nanoflare_heating_in_the_lower_solar_atmosphere

Chromospheric emission from nanoflare heating in RADYN simulations

H. **Bakke**1,2, M. Carlsson1,2, L. Rouppe van der Voort1,2, B. V. Gudiksen1,2, V. Polito3,4, P. Testa5 and B. De Pontieu4,1,2

A&A 659, A186 (**2022**)

https://www.aanda.org/articles/aa/pdf/2022/03/aa42842-21.pdf

https://doi.org/10.1051/0004-6361/202142842

Context. Heating signatures from small-scale magnetic reconnection events in the solar atmosphere have proven to be difficult to detect through observations. Numerical models that reproduce flaring conditions are essential in understanding how nanoflares may act as a heating mechanism of the corona.

Aims. We study the effects of non-thermal electrons in synthetic spectra from 1D hydrodynamic RADYN simulations of nanoflare heated loops to investigate the diagnostic potential of chromospheric emission from small-scale events.

Methods. The Mg II h and k, Ca II H and K, Ca II 854.2 nm, and Hα and Hβ chromospheric lines were synthesised from various RADYN models of coronal loops subject to electron beams of nanoflare energies. The contribution function to the line intensity was computed to better understand how the atmospheric response to the non-thermal electrons affects the formation of spectral lines and the detailed shape of their spectral profiles.
Results. The spectral line signatures arising from the electron beams highly depend on the density of the loop and the lower cutoff energy of the electrons. Low-energy (5 keV) electrons deposit their energy in the corona and transition region, producing strong plasma flows that cause both redshifts and blueshifts of the chromospheric spectra. Higher-energy (10 and 15 keV) electrons deposit their energy in the lower transition region and chromosphere, resulting in increased emission from local heating. Our results indicate that effects from small-scale events can be observed with ground-based telescopes, expanding the list of possible diagnostics for the presence and properties of nanoflares.

Non-thermal electrons from solar nanoflares
In a 3D radiative MHD simulation

H. **Bakke**1,2, L. Frogner1,2 and B. V. Gudiksen1,2
A&A 620, L5 (**2018**)
https://www.aanda.org/articles/aa/pdf/2018/12/aa34129-18.pdf
https://arxiv.org/pdf/1811.12404.pdf
Context. We introduce a model for including accelerated particles in pure magnetohydrodynamics (MHD) simulations of the solar atmosphere.
Aims. We show that the method is viable and produces results that enhance the realism of MHD simulations of the solar atmosphere.
Methods. The acceleration of high-energy electrons in solar flares is an accepted fact, but is not included in the most advanced 3D simulations of the solar atmosphere. The effect of the acceleration is not known, and here we introduce a simple method to account for the ability of the accelerated electrons to move energy from the reconnection sites and into the dense transition zone and chromosphere.
Results. The method was only run for a short time and with low reconnection energies, but this showed that the reconnection process itself changes, and that there is a clear effect on the observables at the impact sites of the accelerated electrons. Further work will investigate the effect on the reconnection sites and the impact sites in detail.

Characterising Solar Magnetic Reconnection in Confined and Eruptive Flares

Kanniah **Balamuralikrishna**, John Y. H. Soo, Norhaslinda Mohamed Tahrin, Abdul Halim Abdul Aziz
Astrophys. Space Sci. 368 (**2023**) 94
https://arxiv.org/ftp/arxiv/papers/2312/2312.12873.pdf
https://doi.org/10.1007/s10509-023-04251-w
Magnetic reconnection is a fundamental mechanism through which energy stored in magnetic fields is released explosively on a massive scale, they could be presented as eruptive or confined flares, depending on their association with coronal mass ejections (CMEs). Several previous works have concluded that there is no correlation between flare duration and flare class, however, their sample sizes are skewed towards B and C classes; they hardly represent the higher classes. Therefore, we studied a sample without extreme events in order to determine the correlation between flare duration and flare type (confined and eruptive). We examined 33 flares with classes between M5 to X5 within 45◦ of the disk centres, using data from the Atmospheric Imaging Assembly (AIA) and the Helioseismic and Magnetic Imager (HMI). We find that the linear correlation between flare class against flare duration by full width half maximum (FWHM) in general is weak (r=0.19); however, confined flares have a significant correlation (r=0.58) compared to eruptive types (r=0.08). Also, the confined M class flares' average duration is less than half of the eruptive flares. Similarly, confined flares have a higher correlation (r=0.89) than eruptive flares (r=0.60) between flare classes against magnetic reconnection flux. In this work, a balanced sample size between flare types is an important strategy for obtaining a reliable quantitative comparison. **7-3-2012, 4-2-2014, 10-9-2014**
Table 1: The list of solar flare events used in this work. Events 1-17 are confined (no CME), while events 18-33 are eruptive (with CME). 2011-2017

Universality in solar flare, magnetic storm and earthquake dynamics using Tsallis statistical mechanics

G. **Balasis**, I. A. Daglis, A. Anastasiadis, C. Papadimitriou, M. Mandea, K. Eftaxias
E-print, Sept 2010; Accepted for publication in : Physica A (**2010**)
The universal character of the dynamics of various extreme phenomena is an outstanding scientific challenge. We show that X-ray flux and Dst time series during powerful solar flares and intense magnetic storms, respectively, obey a nonextensive energy distribution function for earthquake dynamics with similar values for the Tsallis entropic index q. Thus, evidence for uni- versality in solar flares, magnetic storms and earthquakes arise naturally in the framework of Tsallis statistical mechanics. The observed similarity sug- gests a common approach to the interpretation of these diverse phenomena in terms of driving physical mechanisms that have the same character.

Statistical relationship between the succeeding solar flares detected by the RHESSI satellite

L. G. **Balázs**, N. Gyenge, M. B. Korsós, T. Baranyi, E. Forgács-Dajka, I. Ballai

2014

http://arxiv.org/pdf/1403.6964v1.pdf

The Reuven Ramaty High Energy Solar Spectroscopic Imager (RHESSI) has observed more than 80,000 solar energetic events since its launch on February 12 th, 2002. Using this large sample of observed flares, we studied the spatio-temporal relationship between succeeding flares. Our results show that the statistical relationship between the temporal and spatial differences of succeeding flares can be described as a power law of the form R(t)~tp with p=0.327±0.007. We discuss the possible interpretations of this result as a characteristic function of a supposed underlying physics. Different scenarios are considered to explain this relation, including the case where the connectivity between succeeding events is realised through a shock wave in the post Sedov-Taylor phase or where the spatial and temporal relationship between flares is supposed to be provided by an expanding flare area in the sub-diffusive regime. Furthermore, we cannot exclude the possibility that the physical process behind the statistical relationship is the reordering of the magnetic field by the flare or it is due to some unknown processes.

Intrusion of Magnetic Peninsula toward the Neighboring Opposite-polarity Region That Triggers the Largest Solar Flare in Solar Cycle 24

Yumi **Bamba**1,2, Satoshi Inoue2, and Shinsuke Imada2

2020 ApJ 894 29

https://doi.org/10.3847/1538-4357/ab85ca

https://arxiv.org/pdf/2005.00688.pdf

The largest X9.3 solar flare in solar cycle 24 and the preceding X2.2 flare occurred on **2017 September 6**, in the solar active region NOAA 12673. This study aims to understand the onset mechanism of these flares via analysis of multiple observational data sets from the Hinode and Solar Dynamics Observatory and results from a nonlinear force-free field extrapolation. The most noticeable feature is the intrusion of a major negative-polarity region, appearing similar to a peninsula, oriented northwest into a neighboring opposite-polarity region. We also observe proxies of magnetic reconnection related to the intrusion of the negative peninsula: rapid changes of the magnetic field around the intruding negative peninsula; precursor brightening at the tip of the negative peninsula, including a cusp-shaped brightening that shows a transient but significant downflow (~100 km s−1) at a leg of the cusp; a dark tube-like structure that appears to be a magnetic flux rope that erupted with the X9.3 flare; and coronal brightening along the dark tube-like structure that appears to represent the electric current generated under the flux rope. Based on these observational features, we propose that (1) the intrusion of the negative peninsula was critical in promoting the push-mode magnetic reconnection that forms and grows a twisted magnetic flux rope that erupted with the X2.2 flare, and (2) the continuing intrusion progressing even beyond the X2.2 flare is further promoted to disrupt the equilibrium that leads the reinforcement of the magnetic flux rope that erupted with the X9.3 flare.

Hinode/EIS Nugget July **2020** http://solarb.mssl.ucl.ac.uk/SolarB/nuggets/nugget_2020july.jsp

Evaluation of Applicability of a Flare Trigger Model based on Comparison of Geometric Structures

Yumi **Bamba**, Kanya Kusano

ApJ **856** 43 **2018**

https://arxiv.org/pdf/1802.00134.pdf

The triggering mechanism(s) and critical condition(s) of solar flares are still not completely clarified, although various studies have attempted to elucidate them. We have also proposed a theoretical flare-trigger model based on MHD simulations Kusano et al. 2012, in which two types of small-scale bipole field, the so-called Opposite Polarity (OP) and Reversed Shear (RS) types of field, can trigger flares. In this study, we evaluated the applicability of our flare-trigger model to observation of 32 flares that were observed by the Solar Dynamics Observatory (SDO), by focusing on geometrical structures. We classified the events into six types, including the OP and RS types, based on photospheric magnetic field configuration, presence of precursor brightenings, and shape of the initial flare ribbons. As a result, we found that approximately 30% of the flares were consistent with our flare-trigger model, and the number of RS type triggered flares is larger than that of the OP type. We found none of the sampled events contradicts our flare model, although we cannot clearly determine the trigger mechanism of 70% of the flares in this study. We carefully investigated the applicability of our flare-trigger model and the possibility that other models can explain the other 70% of the events. Consequently, we concluded that our flare-trigger model has certainly proposed important conditions for flare-triggering. **2011-08-07, 2012-03-06, 2012-03-07, 2012-07-02, 2013-04-11, 2013-10-24**

Table 1: Event list

CESRA #96 **2018** http://hmi.stanford.edu/hminuggets/?p=2436

Study on Precursor Activity of the X1.6 Flare in the Great AR 12192 with SDO, IRIS, and Hinode

Y. **Bamba**, K. S. Lee, S. Imada, K. Kusano
2017 ApJ 840 116
https://arxiv.org/pdf/1704.05158.pdf

The physical properties and its contribution to the onset of solar flare are still unclear although chromospheric brightening is considered a precursor phenomenon of flare. Many studies suggested that photospheric magnetic field changes cause destabilization of large-scale coronal structure. We aim to understand how a small photospheric change contributes to a flare and to reveal how the intermediary chromosphere behaves in the precursor phase. We analyzed the precursor brightening of the X1.6 flare on **2014 October 22** in the AR 12192 using the Interface Region Imaging Spectrograph (IRIS) and Hinode/EUV Imaging Spectrometer (EIS) data. We investigated a localized jet with the strong precursor brightening, and compared the intensity, Doppler velocity, and line width in C II, Mg II k, Si IV lines by IRIS and He II, Fe XII, Fe XV lines by Hinode/EIS. We also analyzed photospheric magnetic field and chromospheric/coronal structures using Solar Dynamics Observatory (SDO)/Helioseismic and Magnetic Imager (HMI) and Atmospheric Imaging Assembly (AIA). We found a significant blueshift (~ 100 km/s), which is related to the strong precursor brightening over a characteristic magnetic field structure, and the blueshift was observed at all the temperature. This might indicate that the flow is accelerated by Lorentz force. Moreover, the large-scale coronal loop that connects the foot-points of the flare ribbons was destabilized just after the precursor brightening with the blueshift. It suggests that magnetic reconnection locally occurred in the lower chromosphere and it triggered magnetic reconnection of the X1.6 flare in the corona.

Triggering Process of the X1.0 Three-ribbon Flare in the Great Active Region NOAA 12192

Yumi **Bamba**1,2, Satoshi Inoue2, Kanya Kusano2, and Daikou Shiota
2017 ApJ 838 134
http://sci-hub.cc/10.3847/1538-4357/aa6682
https://arxiv.org/pdf/1704.00877.pdf

The solar magnetic field in a flare-producing active region (AR) is much more complicated than theoretical models, which assume a very simple magnetic field structure. The X1.0 flare, which occurred in AR 12192 on **2014 October 25**, showed a complicated three-ribbon structure. To clarify the trigger process of the flare and to evaluate the applicability of a simple theoretical model, we analyzed the data from Hinode/Solar Optical Telescope and the Solar Dynamics Observatory/Helioseismic and Magnetic Imager, Atmospheric Imaging Assembly. We investigated the spatio-temporal correlation between the magnetic field structures, especially the non-potentiality of the horizontal field, and the bright structures in the solar atmosphere. As a result, we determined that the western side of the positive polarity, which is intruding on a negative polarity region, is the location where the flare was triggered. This is due to the fact that the sign of the magnetic shear in that region was opposite that of the major shear of the AR, and the significant brightenings were observed over the polarity inversion line (PIL) in that region before flare onset. These features are consistent with the recently proposed flare-trigger model that suggests that small reversed shear (RS) magnetic disturbances can trigger solar flares. Moreover, we found that the RS field was located slightly off the flaring PIL, contrary to the theoretical prediction. We discuss the possibility of an extension of the RS model based on an extra numerical simulation. Our result suggests that the RS field has a certain flexibility for displacement from a highly sheared PIL, and that the RS field triggers more flares than we expected.

Comparison between Hinode/SOT and SDO/HMI, AIA Data for the Study of the Solar Flare Trigger Process

Yumi **Bamba**, Kanya Kusano, Shinsuke Imada, Yusuke Iida
PASJ, Hinode special issue, 66 (SP1), S16 (1–9) **2014**
http://arxiv.org/pdf/1407.1887v1.pdf
http://pasj.oxfordjournals.org/content/66/SP1/S16.full.pdf+html

Understanding the mechanism that produces solar flares is important not only from the scientific point of view but also for improving space weather predictability. There are numerous observational and computational studies, which attempted to reveal the onset mechanism of solar flares. However, the underlying mechanism of flare onset remains elusive. To elucidate the flare trigger mechanism, we have analyzed several flare events which were observed by Hinode/Solar Optical Telescope (SOT), in our previous study. Because of the limitation of SOT field of view, however, only four events in the Hinode data sets have been utilizable. Therefore, increasing the number of events is required for evaluating the flare trigger models. We investigated the applicability of data obtained by the Solar Dynamics Observatory (SDO) to increase the data sample for a statistical analysis of the flare trigger process. SDO regularly observes the full disk of the sun and all flares although its spatial resolution is lower than that of Hinode. We investigated the M6.6 flare which occurred on **13 February 2011** and compared the analyzed data of SDO with the results of our previous study using Hinode/SOT data. Filter and vector magnetograms obtained by the Helioseismic and

Magnetic Imager (HMI) and filtergrams from the Atmospheric Imaging Assembly (AIA) 1600Å were employed. From the comparison of small-scale magnetic configurations and chromospheric emission prior to the flare onset, we confirmed that the trigger region is detectable with the SDO data. We also measured the magnetic shear angles of the active region and the azimuth and strength of the flare-trigger field. The results were consistent with our previous study. We concluded that statistical studies of the flare trigger process are feasible with SDO as well as Hinode data. We also investigated the temporal evolution of the magnetic field before the flare onset with SDO.

Study on Triggering Process of Solar Flares Based on Hinode/SOT Observations

Y. **Bamba**, K. Kusano, T. T. Yamamoto, and T. J. Okamoto
E-print, Sept **2013; 2013** ApJ 778 48
We investigated four major solar flare events that occurred in active regions NOAA 10930 (**December 13 and 14, 2006**) and NOAA 11158 (**February 13 and 15, 2011**) by using data observed by the Solar Optical Telescope (SOT) onboard the Hinode satellite. To reveal the trigger mechanism of solar flares, we analyzed the spatio-temporal correlation between the detailed magnetic field structure and the emission image of the Ca H line at the central part of flaring regions for several hours prior to the onset of flares. We observed in all the flare events that the magnetic shear angle in the flaring regions exceeded 70 degrees, as well as that characteristic magnetic disturbances developed at the centers of flaring regions in the pre-flare phase. These magnetic disturbances can be classified into two groups depending on the structure of their magnetic polarity inversion lines; the so-called "Opposite-Polarity" and "Reversed-Shear" magnetic field recently proposed by our group, although the magnetic disturbance in one event of the four samples is too subtle to clearly recognize the detailed structure. The result suggests that some major solar flares are triggered by rather small magnetic disturbances. We also show that the critical size of the flare-trigger field varies among flare events and briefly discuss how the flare-trigger process depends on the evolution of active regions.

Transverse Oscillation of Coronal Loops Induced by Eruptions of a Magnetic Flux Tube and a Plasmoid

K. Safna **Banu**, Ram Ajor Maurya & P. T. Jain Jacob
Solar Physics volume 297, Article number: 134 (**2022**)
https://doi.org/10.1007/s11207-022-02065-7
We studied transverse oscillations in hot coronal loops of active region NOAA 12673 located at the west limb. Loop oscillations were associated with a plasmoid ejection from the same location. During the rising phase of the plasmoid, a magnetic flux tube was seen to be rising and bending towards the loop system that erupted before the plasmoid ejection. In addition to the plasmoid ejection, a large coronal mass ejection (CME) and an X8.2 flare were observed in the same active region for several hours (≈7≈7 hours). After the plasmoid ejection, a follow-up shock wave from the flare site was triggered by a sudden momentum transfer towards the solar disk. It was found to be propagating across the entire solar disk with an average speed of ≈1290 kms−1≈1290 kms−1. By analyzing the time sequence of these events, we found that a plasmoid ejection perturbed the loops from their equilibrium and set them in oscillation. We found different oscillations of the fundamental mode in two loops, fast decaying (with a period of 7.93 minutes and an average damping time of ≈19≈19 minutes) and slow decaying (with a period of 6.31 minutes and an average damping time of ≈34≈34 minutes). The two different oscillations could be due to their lengths, magnetic fields, and plasma densities. Using the methods of coronal seismology, we estimated the average magnetic field in the coronal loops to be 29 G and 36 G, which is consistent with the order of the coronal magnetic fields found in other studies. **10 Sep 2017**

Scaling of electron heating by magnetization during reconnection and applications to dipolarization fronts and super-hot solar flares

M. Hasan **Barbhuiya**, Paul. A. Cassak, Michael. A. Shay, Vadim Roytershteyn, Marc Swisdak, Amir Caspi, Andrei Runov, Haoming Liang
JGR 127, e30610 **2023**
https://arxiv.org/pdf/2208.00559.pdf
DOI: 10.1029/2022JA030610
Electron ring velocity space distributions have previously been seen in numerical simulations of magnetic reconnection exhausts and have been suggested to be caused by the magnetization of the electron outflow jet by the compressed reconnected magnetic fields [Shuster et al., Geophys. Res. Lett.,41, 5389 (2014)]. We present a theory of the dependence of the major and minor radii of the ring distributions solely in terms of upstream (lobe) plasma conditions, thereby allowing a prediction of the associated temperature and temperature anisotropy of the rings in terms of upstream parameters. We test the validity of the prediction using 2.5-dimensional particle-in-cell (PIC) simulations with varying upstream plasma density and temperature, finding excellent agreement between the predicted and simulated values. We confirm the Shuster et al. suggestion for the cause of the ring distributions, and also find that the ring distributions are located in a region marked by a plateau, or shoulder, in the reconnected magnetic field profile. The predictions of the temperature are consistent with observed electron temperatures in dipolarization fronts, and may provide an explanation

for the generation of plasma with temperatures in the 10s of MK in super-hot solar flares. A possible extension of the model to dayside reconnection is discussed. Since ring distributions are known to excite whistler waves, the present results should be useful for quantifying the generation of whistler waves in reconnection exhausts.

Electric current evolution at the footpoints of solar eruptions

Krzysztof **Barczynski**, Guillaume Aulanier, Miho Janvier, Brigitte Schmieder, Sophie Masson
ApJ **895** 18 **2020**
https://arxiv.org/pdf/2004.07990.pdf
https://doi.org/10.3847/1538-4357/ab893d
Electric currents play a critical role in the triggering of solar flares and their evolution. The aim of the present paper is to test whether the surface electric current has a surface or subsurface fixed source as predicts the circuit approach of flare physics, or is the response of the surface magnetic field to the evolution of the coronal magnetic field as the MHD approach proposes. Out of all 19 X-class flares as observed by SDO from 2011 to 2016 near the disk center, we analyzed the only 9 eruptive flares for which clear ribbon-hooks were identifiable. Flare ribbons with hooks are considered to be the footprints of eruptive flux ropes in MHD flare models. For the first time, fine measurements of time-evolution of electric currents inside the hooks in the observations as well as in the OHM 3D MHD simulation are performed. Our analysis shows a decrease of the electric current in the area surrounded by the ribbon hooks during and after the eruption. We interpret the decrease of the electric currents as due to the expansion of the flux rope in the corona during the eruption. Our analysis brings a new contribution to the standard flare model in 3D. **15 February 2011, 7 September 2011, 29th March 2014, 10th September 2014, 7 November 2014, 11 March 2015**
Table 1. Properties of flares, ribbon and ribbon hooks visibility for 19 flares (2011-2015).

Flare reconnection-driven magnetic field and Lorentz force variations at the Sun's surface

Krzysztof **Barczynski**, Guillaume Aulanier, Sophie Masson, Michael S. Wheatland
ApJ **877** 67 **2019**
https://arxiv.org/pdf/1904.05447.pdf
sci-hub.se/10.3847/1538-4357/ab1b3d
During eruptive flares, vector magnetograms show increasing horizontal magnetic field and downward Lorentz force in the Sun's photosphere around the polarity-inversion line. Such behavior has often been associated with the implosion conjecture and interpreted as the result of either momentum conservation while the eruption moves upward, or of the contraction of flare loops. We characterize the physical origin of these observed behaviors by analyzing a generic 3D MHD simulation of an eruptive flare. Even though the simulation was undesigned to recover the magnetic field and Lorentz force properties, it is fully consistent with them, and it provides key additional informations to understand them. The area where the magnetic field increases gradually develops between current ribbons, which spread away from each other and are connected to the coronal region. This area is merely the footprint of the coronal post-flare loops, whose contraction increases their shear field component and the magnetic energy density in line with the ideal induction equation. For simulated data, we computed the Lorentz force density map by applying the method used in observations. We obtained increase of the downward component of the Lorentz force density around the PIL -consistent with observations. However, this significantly differs from the Lorentz force density maps obtained directly from the 3D magnetic field and current. These results altogether question previous interpretations based on the implosion conjecture and momentum conservation with the CME, and rather imply that the observed increases in photospheric horizontal magnetic fields result from the reconnection-driven contraction of sheared flare-loops.

The Flare-Energy Distributions Generated by Kink-Unstable Ensembles of Zero-Net-Current Coronal Loops

M. R. **Bareford**, P. K. Browning and R. A. M. Van der Linden
Solar Physics, Volume 273, Number 1, 93-115, **2011**
It has been proposed that the million-degree temperature of the corona is due to the combined effect of barely detectable energy releases, called nanoflares, that occur throughout the solar atmosphere. Unfortunately, the nanoflare density and brightness implied by this hypothesis means that conclusive verification is beyond present observational abilities. Nevertheless, we investigate the plausibility of the nanoflare hypothesis by constructing a magnetohydrodynamic (MHD) model that can derive the energy of a nanoflare from the nature of an ideal kink instability. The set of energy-releasing instabilities is captured by an instability threshold for linear kink modes. Each point on the threshold is associated with a unique energy release; thus we can predict a distribution of nanoflare energies. When the linear instability threshold is crossed, the instability enters a nonlinear phase as it is driven by current sheet reconnection. As the ensuing flare erupts and declines, the field transitions to a lower energy state, which is modelled by relaxation theory; i.e., helicity is conserved and the ratio of current to field becomes invariant within the loop. We apply the model so that all the loops within an ensemble achieve instability followed by energy-releasing relaxation. The result is a nanoflare energy distribution. Furthermore, we produce different distributions by varying the loop aspect ratio, the nature of the path to instability taken by each loop and also the level of radial expansion that may accompany loop

relaxation. The heating rate obtained is just sufficient for coronal heating. In addition, we also show that kink instability cannot be associated with a critical magnetic twist value for every point along the instability threshold.

A Comparison of Flare Forecasting Methods, I: Results from the "All-Clear" Workshop

G. **Barnes**, K.D. Leka, C.J. Schrijver, T. Colak, R. Qahwaji, O.W. Ashamari, Y.Yuan, J. Zhang, R.T.J. McAteer, D.S. Bloomfield, P.A. Higgins, P.T. Gallagher, D.A. Falconer, M.K. Georgoulis, M.S. Wheatland,C. Balch, T. Dunn, E.L. Wagner

ApJ **829** 89 **2016**

http://arxiv.org/pdf/1608.06319v1.pdf

Solar flares produce radiation which can have an almost immediate effect on the near-Earth environment, making it crucial to forecast flares in order to mitigate their negative effects. The number of published approaches to flare forecasting using photospheric magnetic field observations has proliferated, with varying claims about how well each works. Because of the different analysis techniques and data sets used, it is essentially impossible to compare the results from the literature. This problem is exacerbated by the low event rates of large solar flares. The challenges of forecasting rare events have long been recognized in the meteorology community, but have yet to be fully acknowledged by the space weather community. During the interagency workshop on "all clear" forecasts held in Boulder, CO in 2009, the performance of a number of existing algorithms was compared on common data sets, specifically line-of-sight magnetic field and continuum intensity images from MDI, with consistent definitions of what constitutes an event. We demonstrate the importance of making such systematic comparisons, and of using standard verification statistics to determine what constitutes a good prediction scheme. When a comparison was made in this fashion, no one method clearly outperformed all others, which may in part be due to the strong correlations among the parameters used by different methods to characterize an active region. For M-class flares and above, the set of methods tends towards a weakly positive skill score (as measured with several distinct metrics), with no participating method proving substantially better than climatological forecasts.

Inference of Heating Properties from "Hot" Non-flaring Plasmas in Active Region Cores. II. Nanoflare Trains

W. T. **Barnes**, P. J. Cargill, S. J. Bradshaw

ApJ 833 217 **2016**

https://arxiv.org/pdf/1610.06150v1.pdf

Despite its prediction over two decades ago, the detection of faint, high-temperature ("hot") emission due to nanoflare heating in non-flaring active region cores has proved challenging. Using an efficient two-fluid hydrodynamic model, this paper investigates the properties of the emission expected from repeating nanoflares (a nanoflare train) of varying frequency as well as the separate heating of electrons and ions. If the emission measure distribution (EM(T)) peaks at T=Tm, we find that EM(Tm) is independent of details of the nanoflare train, and EM(T) above and below Tm reflects different aspects of the heating. Below Tm the main influence is the relationship of the waiting time between successive nanoflares to the nanoflare energy. Above Tm power-law nanoflare distributions lead to an extensive plasma population not present in a monoenergetic train. Furthermore, in some cases characteristic features are present in EM(T). Such details may be detectable given adequate spectral resolution and a good knowledge of the relevant atomic physics. In the absence of such resolution we propose some metrics that can be used to infer the presence of "hot" plasma.

Inference of Heating Properties from "Hot" Non-flaring Plasmas in Active Region Cores I. Single Nanoflares

W. T. **Barnes**, P. J. Cargill, S. J. Bradshaw

ApJ 829 31 **2016**

http://arxiv.org/pdf/1608.04776v1.pdf

The properties expected of "hot" non-flaring plasmas due to nanoflare heating in active regions are investigated using hydrodynamic modeling tools, including a two-fluid development of the EBTEL code. Here we study a single nanoflare and show that while simple models predict an emission measure distribution extending well above 10 MK that is consistent with cooling by thermal conduction, many other effects are likely to limit the existence and detectability of such plasmas. These include: differential heating between electrons and ions, ionization non-equilibrium and, for short nanoflares, the time taken for the coronal density to increase. The most useful temperature range to look for this plasma, often called the "smoking gun" of nanoflare heating, lies between 106.6 and 107 K. Signatures of the actual heating may be detectable in some instances.

SPONTANEOUS CURRENT-LAYER FRAGMENTATION AND CASCADING RECONNECTION IN SOLAR FLARES. I. MODEL AND ANALYSIS

Miroslav **Bárta**1,2, Jörg Büchner1, Marian Karlický2 and Jan Skála

2011 ApJ 737 24

Magnetic reconnection is commonly considered to be a mechanism of solar (eruptive) flares. A deeper study of this scenario reveals, however, a number of open issues. Among them is the fundamental question of how the magnetic energy is transferred from large, accumulation scales to plasma scales where its actual dissipation takes place. In order to investigate this transfer over a broad range of scales, we address this question by means of a high-resolution MHD simulation. The simulation results indicate that the magnetic-energy transfer to small scales is realized via a cascade of consecutively smaller and smaller flux ropes (plasmoids), analogous to the vortex-tube cascade in (incompressible) fluid dynamics. Both tearing and (driven) "fragmenting coalescence" processes are equally important for the consecutive fragmentation of the magnetic field (and associated current density) into smaller elements. At the later stages, a dynamic balance between tearing and coalescence processes reveals a steady (power-law) scaling typical of cascading processes. It is shown that cascading reconnection also addresses other open issues in solar-flare research, such as the duality between the regular large-scale picture of (eruptive) flares and the observed signatures of fragmented (chaotic) energy release, as well as the huge number of accelerated particles. Indeed, spontaneous current-layer fragmentation and the formation of multiple channelized dissipative/acceleration regions embedded in the current layer appear to be intrinsic to the cascading process. The multiple small-scale current sheets may also facilitate the acceleration of a large number of particles. The structure, distribution, and dynamics of the embedded potential acceleration regions in a current layer fragmented by cascading reconnection are studied and discussed.

SPONTANEOUS CURRENT-LAYER FRAGMENTATION AND CASCADING RECONNECTION IN SOLAR FLARES. II. RELATION TO OBSERVATIONS
Miroslav **Bárta**1,2,3, Jörg Büchner1, Marian Karlický2 and Pavel Kotrč2
2011 ApJ 730 47
In a paper by Bárta et al., the authors addressed by means of high-resolution MHD simulations some open questions on the CSHKP scenario of solar flares. In particular, they focused on the problem of energy transfer from large to small scales in the decaying flare current sheet (CS). Their calculations suggest that magnetic flux ropes (plasmoids) are formed in a full range of scales by a cascade of tearing and coalescence processes. Consequently, the initially thick current layer becomes highly fragmented. Thus, the tearing and coalescence cascade can cause an effective energy transfer across the scales. In this paper, we investigate whether this mechanism actually applies in solar flares. We extend the MHD simulation by deriving model-specific features that can be searched for in observations. The results of the underlying MHD model show that the plasmoid cascade creates a specific hierarchical distribution of non-ideal/acceleration regions embedded in the CS. We therefore focus on the features associated with the fluxes of energetic particles, in particular on the structure and dynamics of emission regions in flare ribbons. We assume that the structure and dynamics of diffusion regions embedded in the CS imprint themselves into the structure and dynamics of flare-ribbon kernels by means of magnetic field mapping. Using the results of the underlying MHD simulation, we derive the expected structure of ribbon emission and extract selected statistical properties of the modeled bright kernels. Comparing the predicted emission and its properties with the observed ones, we obtain a good agreement between the two.

Plasmoid Dynamics in Flare Reconnection and the Frequency Drift of the Drifting Pulsating Structure
M. **Bárta** · M. Karlický · R. Žemli˘cka
Solar Phys (**2008**) 253: 173–189
In the paper by Kliem, Karlický, and Benz (*Astron. Astrophys.* **360**, 715, 2000) it was suggested, that plasmoids formed during the bursty regime of solar flare reconnection can be “visualised” in the radio spectra as drifting pulsating structures via accelerated particles trapped inside the plasmoid. In the present paper we investigate this idea in detail. First, simple statistical analysis supporting this hypothesis is presented. Then, by using the 2.5-D MHD (including gravity) model solar flare reconnection in the inhomogeneous, stratified atmosphere is simulated and the formation and subsequent ejection of the plasmoid is demonstrated. The ejected plasmoid, which is considered to be a trap for accelerated electrons, is traced and its plasma parameters are computed. To estimate the associated plasma radio emission we need to know locations of accelerated electrons and corresponding plasma frequencies. General considerations predict that these electrons should be distributed mainly along the magnetic separatrix surfaces and this was confirmed by using a particle-in-cell simulation. Finally, under some simplifying assumptions the model dynamic radio spectrum is constructed. The relation between the global frequency drift and the plasmoid motion in the inhomogeneous ambient atmosphere is studied. The results are discussed with respect to the observed drifting pulsation structures and their possible utilisation for flare magnetic field diagnostics.

Dynamics of plasmoids formed by the current sheet tearing:
M. **Barta**, B. Vrsnak and M. Karlicky
A&A 477 (**2008**) 649-655
http://www.aanda.org/10.1051/0004-6361:20078266

Moving blob-like features observed in the soft X-ray and EUV range above flare-loops are often interpreted as signatures of plasmoids formed by the current sheet tearing in the flare-associated reconnection process.
We investigate the evolution of the flare-associated current sheet numerically in order to analyse the kinematics and dynamics of plasmoids.
The presented results explain, qualitatively and quantitatively, the broad spectrum of kinematical properties of various observational features attributed to the current-sheet plasmoids.

RADIO SPECTRAL EVOLUTION OF AN X-RAYYPOOR IMPULSIVE SOLAR FLARE: IMPLICATIONS FOR PLASMA HEATING AND ELECTRON ACCELERATION

T. S. **Bastian**, G. D. Fleishman, and D. E. Gary
The Astrophysical Journal, 666:1256-1267, **2007**
https://iopscience.iop.org/article/10.1086/520106/pdf
We present radio and X-ray observations of an impulsive solar flare that was moderately intense in microwaves, yet showed very meager EUV and X-ray emission. The flare occurred on **2001 October 24** and was well observed at radio wavelengths by the Nobeyama Radioheliograph (NoRH), the Nobeyama Radio Polarimeters (NoRP), and the Owens Valley Solar Array (OVSA). It was also observed in EUV and X-ray wavelength bands by the TRACE, GOES, and Yohkoh satellites. We find that the impulsive onset of the radio emission is progressively delayed with increasing frequency relative to the onset of hard X-ray emission. In contrast, the time of flux density maximum is progressively delayed with decreasing frequency. The decay phase is independent of radio frequency. The simple source morphology and the excellent spectral coverage at radio wavelengths allowed us to employ a nonlinear χ2-minimization scheme to fit the time series of radio spectra to a source model that accounts for the observed radio emission in terms of gyrosynchrotron radiation from MeV-energy electrons in a relatively dense thermal plasma. We discuss plasma heating and electron acceleration in view of the parametric trends implied by the model fitting. We suggest that stochastic acceleration likely plays a role in accelerating the radio-emitting electrons.

On the proton precipitation sites in solar flares

Andrea Francesco **Battaglia**, Säm Krucker
A&A **2024**
https://arxiv.org/pdf/2412.11490
The Reuven Ramaty High Energy Solar Spectrocopy Imager (RHESSI) γ-ray observations of the extraordinary GOES X25 flare SOL2003-10-28T11:10 are revisited to investigate previously reported conclusions that flare-accelerated electrons and protons precipitate along spatially separated flare loops. In contrast to previous works which reconstructed 2.223 MeV images over extended time periods ($\sim$20 minutes), we selected shorter integration times of the order of 2 to 3 minutes. Using simulations of the 2.223 MeV profile by Murphy et al. (2003) in combination with observations of the prompt γ-ray lines from the INTEGRAL mission, we obtain two separated integration time ranges representing the peak of the flare and the start of the decay, respectively. The resulting γ-ray images are then compared to GONG white-light (WL) observations to identify where along the flaring ribbons electrons and protons precipitation occurs. We point out that previously reported results comparing RHESSI hard X-ray (HXR) and γ-ray images only hold if the relative time evolution in the two energy ranges is the same. As the decay times for the **28 October 2003** is different at the considered two energy ranges (200-300 keV and around 2.223 MeV), the previously published conclusion that electrons and protons precipitate at different locations is an overstatement. Using shorter integration times reveals that the γ-ray and HXR sources spatially coincide with the WL flare ribbons. Our key conclusion is that electron and proton precipitation sites coincide with the flare ribbons, suggesting that the electron and proton precipitation sites are the same, at least within RHESSI's imaging capabilities. This result solves the twenty-years-long mystery around the previously reported different electron and proton precipitation sites.

The observational evidence that all microflares that accelerate electrons to high-energies are rooted in sunspots

Andrea Francesco **Battaglia**, Säm Krucker, Astrid M. Veronig, Muriel Zoë Stiefel, Alexandar Warmuth, Arnold O. Benz, Daniel F. Ryan, Hannah Collier, Louise Harra
A&A **2024**
https://arxiv.org/pdf/2409.14466
In general, large solar flares are more efficient at accelerating high-energy electrons than microflares. Nonetheless, we sometimes observe microflares that accelerate electrons to high energies. We statistically characterize 39 microflares with strikingly hard spectra in the hard X-ray (HXR) range, which means that they are efficient in accelerating high-energy electrons. We refer to these events as "hard microflares." The statistical analysis is built upon spectral and imaging information from STIX, combined with EUV and magnetic field maps from SDO. The key observational result is that all hard microflares in this dataset have one of the footpoints rooted directly within a sunspot (either in the umbra or the penumbra). This clearly indicates that the underlying magnetic flux densities are large. For the events with the classic two-footpoints morphology, the absolute value of the mean line-of-sight magnetic flux density (and vector magnetic field strength) at the footpoint rooted within the sunspot ranges from 600 to 1800 G (1500 to 2500 G),

whereas the outer footpoint measures from 10 to 200 G (100 to 400 G), therefore about 10 times weaker. Approximately 78% of hard microflares, which exhibited two HXR footpoints, have similar or even stronger HXR flux from the footpoint rooted within the sunspot. This contradicts the magnetic mirroring scenario. In addition, about 74% of the events could be approximated by a single loop geometry, demonstrating that hard microflares typically have a relatively simple morphology. We conclude that all hard microflares are rooted in sunspots, which implies that the magnetic field strength plays a key role in efficiently accelerating high-energy electrons, with hard HXR spectra associated with strong fields. This key result will allow us to further constrain our understanding of the electron acceleration mechanisms in flares and space plasmas. **2021-06-30, 2021-Oct-04, 2021-10-08-09, 2022-02-03, 2022-03-30, 2022-Nov-12, 2022-Dec-22-23, 2023-02-12**

Table A.1. List of all the hard microflares analyzed in this paper 2021-2023

Solar Orbiter Science Nuggets #39 Sep **2024** https://www.cosmos.esa.int/web/solar-orbiter/-/science-nugget-all-microflares-that-accelerate-electrons-to-high-energies-are-rooted-in-sunspots

RHESSI Science Nuggets #471 **2024**

https://sprg.ssl.berkeley.edu/~tohban/wiki/index.php/All_microflares_that_accelerate_electrons_to_high_energies_are_rooted_in_sunspots

The existence of hot X-ray onsets in solar flares

Andrea Francesco **Battaglia**, Hugh Hudson, Alexander Warmuth, Hannah Collier, Natasha L. S. Jeffrey, Amir Caspi, Ewan C. M. Dickson, Jonas Saqri, Stefan Purkhart, Astrid M. Veronig, Louise Harra, Säm Krucker

A&A 679, A139 **2023**

https://arxiv.org/pdf/2310.04234.pdf

https://www.aanda.org/articles/aa/pdf/2023/11/aa47706-23.pdf

It is well known among the scientific community that solar flare activity often begins well before the main impulsive energy release. Our aim is to investigate the earliest phase of four distinct flares observed by Solar Orbiter/STIX and determine the relationships of the newly heated plasma to flare structure and dynamics. The analysis focuses on four events that were observed from both Earth and Solar Orbiter, which allows for a comparison of STIX observations with those of GOES/XRS and SDO/AIA. The early phases of the events were studied using STIX and GOES spectroscopic analysis to investigate the evolution of the physical parameters of the plasma, including the isothermal temperature and emission measure. Furthermore, to determine the location of the heated plasma, STIX observations were combined with AIA images. The events with clear emission prior to the impulsive phase show elevated temperatures (>10MK) from the very beginning, which indicates that energy release started before any detection by STIX. Although the temperature shows little variation during the initial phase, the emission measure increases by about two orders of magnitude, implying a series of incrementally greater energy releases. The spectral analysis of STIX and GOES from the very first time bins suggests that the emission has a multi-thermal nature, with a hot component of more than 10MK. This analysis confirms the existence of "hot onsets," with STIX detecting the hot onset pattern even earlier than GOES. These elevated temperatures imply that energy release actually begins well before any detection by STIX. Therefore, hot onsets may be significant in the initiation, early development, or even prediction of solar flares. **2021-05-07, 2021-09-23, 2021-10-09, 2022-03-11**

HOT X-RAY ONSET OBSERVATIONS IN SOLAR FLARES WITH SOLAR ORBITER/STIX

Andrea Francesco **Battaglia**1,2, Hugh Hudson3,4, Säm Krucker1,4, Hannah Collier1,2, and the Solar Orbiter/STIX team

Solar Orbiter nugget #5 **2023** https://www.cosmos.esa.int/web/solar-orbiter/science-nuggets/hot-x-ray-onset-observations-in-solar-flares-with-solar-orbiter-stix

9 Oct 2021

Identifying the energy release site in a Solar microflare with a jet

Andrea Francesco **Battaglia**, Wen Wang, Jonas Saqri, Tatiana Podladchikova, Astrid M. Veronig, Hannah Collier, Ewan C. M. Dickson, Olena Podladchikova, Christian Monstein, Alexander Warmuth, Frédéric Schuller, Louise Harra, Säm Krucker

A&A 670, A56 **2023**

https://arxiv.org/pdf/2212.11098.pdf

https://www.aanda.org/articles/aa/pdf/2023/02/aa44996-22.pdf

One of the main science questions of the Solar Orbiter and Parker Solar Probe missions deals with understanding how electrons in the lower solar corona are accelerated and how they subsequently access interplanetary space. We aim to investigate the electron acceleration and energy release sites as well as the manner in which accelerated electrons access the interplanetary space in the case of the **SOL2021-02-18**T18:05 event, a GOES A8 class microflare associated with a coronal jet. This study takes advantage of three different vantage points, Solar Orbiter, STEREO-A, and Earth, with

observations ranging from radio to X-ray. Multi-wavelength timing analysis combined with UV/EUV imagery and X-ray spectroscopy by Solar Orbiter/STIX (Spectrometer/Telescope for Imaging X-rays) is used to investigate the origin of the observed emission during different flare phases. The event under investigation satisfies the classical picture of the onset time of the acceleration of electrons coinciding with the jet and the radio type III bursts. This microflare features prominent hard X-ray nonthermal emission down to at least 10 keV and a spectrum that is much harder than usual for a microflare with a spectral index of 2.9. From Earth's vantage point, the microflare is seen near the limb, revealing the coronal energy release site above the flare loop in EUV, which, from STIX spectroscopic analysis, turns out to be hot (at roughly the same temperature of the flare). Moreover, this region is moving toward higher altitudes over time (about 30 km/s). During the flare, the same region spatially coincides with the origin of the coronal jet. We conclude that the energy release site observed above-the-loop corresponds to the electron acceleration site, corroborating that interchange reconnection is a viable candidate for particle acceleration in the low corona on field lines open to interplanetary space.

A demonstration of STIX hard X-ray imaging spectroscopy capabilities for an X-class flare (SOL2021-10-28)

Andrea **BATTAGLIA**, Hannah COLLIER, and Säm KRUCKER
RHESSI Science Nuggets #426 **2022**
https://sprg.ssl.berkeley.edu/~tohban/wiki/index.php/A_demonstration_of_STIX_hard_X-ray_imaging_spectroscopy_capabilities_for_an_X-class_flare_(SOL2021-10-28)
The Solar Orbiter observatory, launched just two years ago, carries a hard X-ray imager (STIX)] that now extends RHESSI's hard X-ray record. Although not as powerful as RHESSI in some regards, STIX has remarkable advantages - it approaches the Sun closely, and it can observe stereoscopically when combined with Earth-bound instruments. This Nugget reports on the first X-class event observed, the flare SOL**2021-10-28**.

Multiple electron acceleration instances during a series of solar microflares observed simultaneously at X-rays and microwaves

Marina **Battaglia**, Rohit Sharma, Yingjie Luo, Bin Chen, Sijie Yu, Säm Krucker
ApJ **922** 134 **2021**
https://arxiv.org/pdf/2109.12847.pdf
https://iopscience.iop.org/article/10.3847/1538-4357/ac2aa6/pdf
https://doi.org/10.3847/1538-4357/ac2aa6
Even small solar flares can display a surprising level of complexity regarding their morphology and temporal evolution. Many of their properties, such as energy release and electron acceleration can be studied using highly complementary observations at X-ray and radio wavelengths. We present X-ray observations from the Reuven Ramaty High Energy Solar Spectroscopic Imager (RHESSI) and radio observations from the Karl G. Jansky Very Large Array (VLA) of a series of GOES A3.4 to B1.6 class flares observed on **2013 April 23**. The flares, as seen in X-ray and extreme ultraviolet (EUV), originated from multiple locations within active region NOAA 11726. A veritable zoo of different radio emissions between 1 GHz and 2 GHz was observed co-temporally with the X-ray flares. In addition to broad-band continuum emission, broad-band short-lived bursts and narrow-band spikes, indicative of accelerated electrons, were observed. However, these sources were located up to 150 arcsec away from the flaring X-ray sources but only some of these emissions could be explained as signatures of electrons that were accelerated near the main flare site. For other sources, no obvious magnetic connection to the main flare site could be found. These emissions likely originate from secondary acceleration sites triggered by the flare, but may be due to reconnection and acceleration completely unrelated to the co-temporally observed flare. Thanks to the extremely high sensitivity of the VLA, not achieved with current X-ray instrumentation, it is shown that particle acceleration happens frequently and at multiple locations within a flaring active region.
RHESSI Nuggets #417 **2021** https://sprg.ssl.berkeley.edu/~tohban/wiki/index.php/Manifold_Nonthermality

STIX X-ray microflare observations during the Solar Orbiter commissioning phase

Andrea Francesco **Battaglia**, Jonas Saqri, Paolo Massa, Emma Perracchione, Ewan C. M. Dickson, Hualin Xiao, Astrid M. Veronig, Alexander Warmuth, ……
A&A Volume 656, id.A4, **2021**
https://arxiv.org/pdf/2106.10058.pdf
https://ui.adsabs.harvard.edu/link_gateway/2021A%26A...656A...4B/EPRINT_PDF
https://doi.org/10.1051/0004-6361/202140524
The Spectrometer/Telescope for Imaging X-rays (STIX) is the HXR instrument onboard Solar Orbiter designed to observe solar flares over a broad range of flare sizes, between 4-150 keV. We report the first STIX observations of microflares recorded during the instrument commissioning phase in order to investigate the STIX performance at its detection limit. This first result paper focuses on the temporal and spectral evolution of STIX microflares occuring in the AR12765 in June 2020, and compares the STIX measurements with GOES/XRS, SDO/AIA, and Hinode/XRT. For the observed microflares of the GOES A and B class, the STIX peak time at lowest energies is located in the impulsive phase of the flares, well before the GOES peak time. Such a behavior can either be explained by the higher sensitivity

of STIX to higher temperatures compared to GOES, or due to the existence of a nonthermal component reaching down to low energies. The interpretation is inconclusive due to limited counting statistics for all but the largest flare in our sample. For this largest flare, the low-energy peak time is clearly due to thermal emission, and the nonthermal component seen at higher energies occurs even earlier. This suggests that the classic thermal explanation might also be favored for the majority of the smaller flares. In combination with EUV and SXR observations, STIX corroborates earlier findings that an isothermal assumption is of limited validity. Future diagnostic efforts should focus on multi-wavelength studies to derive differential emission measure distributions over a wide range of temperatures to accurately describe the energetics of solar flares. Commissioning observations confirm that STIX is working as designed. As a rule of thumb, STIX detects flares as small as the GOES A class. For flares above the GOES B class, detailed spectral and imaging analyses can be performed. **Jun 2020: 7, 13**
RHESSI Nuggets #410 https://sprg.ssl.berkeley.edu/~tohban/wiki/index.php/STIX,_the_Hard_X-Ray_Telescope_on_board_Solar_Orbiter

Electron distribution and energy release in magnetic reconnection outflow regions during the pre-impulsive phase of a solar flare

Marina **Battaglia**, Eduard P. Kontar, Galina Motorina
ApJ **872** 204 **2019**
https://arxiv.org/pdf/1901.07767.pdf
We present observations of electron energization in magnetic reconnection outflows during the pre-impulsive phase of solar flare SOL**2012-07-19**T05:58. During a time-interval of about 20 minutes, starting 40 minutes before the onset of the impulsive phase, two X-ray sources were observed in the corona, one above the presumed reconnection region and one below. For both of these sources, the mean electron distribution function as a function of time is determined over an energy range from 0.1~keV up to several tens of keV, for the first time. This is done by simultaneous forward fitting of X-ray and EUV data. Imaging spectroscopy with RHESSI provides information on the high-energy tail of the electron distribution in these sources while EUV images from SDO/AIA are used to constrain the low specific electron energies. The measured electron distribution spectrum in the magnetic reconnection outflows is consistent with a time-evolving kappa-distribution with κ=3.5−5.5. The spectral evolution suggests that electrons are accelerated to progressively higher energies in the source above the reconnection region, while in the source below, the spectral shape does not change but an overall increase of the emission measure is observed, suggesting density increase due to evaporation. The main mechanisms by which energy is transported away from the source regions are conduction and free-streaming electrons. The latter dominates by more than one order of magnitude and is comparable to typical non-thermal energies during the hard X-ray peak of solar flares, suggesting efficient acceleration even during this early phase of the event.
RHESSI Nuggets #345 February **2019** http://sprg.ssl.berkeley.edu/~tohban/wiki/index.php/An_energetic_pre-flare:_electron_distributions_in_magnetic_reconnection_outflows

The Solar X-ray Limb

Marina **Battaglia**, Hugh S. Hudson, Gordon J. Hurford, Säm Krucker, Richard A. Schwartz
ApJ **2017**
https://arxiv.org/pdf/1705.11044.pdf
We describe a new technique to measure the height of the X-ray limb with observations from occulted X-ray flare sources as observed by the RHESSI (the Reuven Ramaty High-Energy Spectroscopic Imager) satellite. This method has model dependencies different from those present in traditional observations at optical wavelengths, which depend upon detailed modeling involving radiative transfer in a medium with complicated geometry and flows. It thus provides an independent and more rigorous measurement of the "true" solar radius, meaning that of the mass distribution. RHESSI's measurement makes use of the flare X-ray source's spatial Fourier components (the visibilities), which are sensitive to the presence of the sharp edge at the lower boundary of the occulted source. We have found a suitable flare event for analysis, SOL2011-10-20T03:25 (M1.7), and report a first result from this novel technique here. Using a 4-minute integration over the 3-25 keV photon energy range, we find RX−ray=964.05 ± 0.15±0.29 arcsec, where the uncertainties include statistical uncertainties from the method and a systematic error. The standard VAL-C model predicts a value of 963.48 arcsec, about 2σ below our value. **2011-10-20**

Multi-thermal representation of the kappa-distribution of solar flare electrons and application to simultaneous X-ray and EUV observations

Marina **Battaglia**, Galina Motorina, Eduard P. Kontar
ApJ 815 73 **2015**
http://arxiv.org/pdf/1511.01328v1.pdf
Acceleration of particles and plasma heating is one of the fundamental problems in solar flare physics. An accurate determination of the spectrum of flare energized electrons over a broad energy range is crucial for our understanding of aspects such as the acceleration mechanism and the total flare energy. Recent years have seen a growing interest in the kappa-distribution as representation of the total spectrum of flare accelerated electrons. In this work we present the kappa-distribution as a differential emission measure. This allows for inferring the electron distribution from X-ray

observations and EUV observations by simultaneously fitting the proposed function to RHESSI and SDO/AIA data. This yields the spatially integrated electron spectra of a coronal source between less than 0.1 keV up to several tens of keV. The method is applied to a single-loop GOES C4.1 flare. The results show that the total energy can only be determined accurately by combining RHESSI and AIA observations. Simultaneously fitting the proposed representation of the kappa-distribution reduces the electron number density in the analyzed flare by a factor of ~30 and the total flare energy by a factor of ~5 compared with the commonly used fitting of RHESSI spectra. The spatially integrated electron spectrum of the investigated flare between 0.043 keV and 24 keV is consistent with the combination of a low-temperature (~2 MK) component and a hot (~11 MK) kappa-like component with spectral index 4, reminiscent of solar wind distributions. **14 Aug 2010**

How important are electron beams in driving chromospheric evaporation in the 2014 March 29 flare?

Marina **Battaglia**, Lucia Kleint, Säm Krucker, David Graham
ApJ 813 113 **2015**
http://arxiv.org/pdf/1509.09186v1.pdf

We present high spatial resolution observations of chromospheric evaporation in the flare SOL2014-03-29T17:48. Interface Region Imaging Spectrograph (IRIS) observations of the FeXXI 1354.1 A line indicate evaporating plasma at a temperature of 10 MK along the flare ribbon during the flare peak and several minutes into the decay phase with upflow velocities between 30 km s−1 and 200 km s−1. Hard X-ray (HXR) footpoints were observed by RHESSI for two minutes during the peak of the flare. Their locations coincided with the locations of the upflows in parts of the southern flare ribbon but the HXR footpoint source preceded the observation of upflows in FeXXI by 30-75 seconds. However, in other parts of the southern ribbon and in the northern ribbon the observed upflows were not coincident with a HXR source in time nor space, most prominently during the decay phase. In this case evaporation is likely caused by energy input via a conductive flux that is established between the hot (25 MK) coronal source, which is present during the whole observed time-interval, and the chromosphere. The presented observations suggest that conduction may drive evaporation not only during the decay phase but also during the flare peak. Electron beam heating may only play a role in driving evaporation during the initial phases of the flare.

Where is the chromospheric response to conductive energy input from a hot pre-flare coronal loop?

Marina **Battaglia**, Lyndsay Fletcher, Paulo J. A. Simoes
E-print, May **2014**, ApJ, 789 47, **2014**
http://arxiv.org/pdf/1405.4621v1.pdf

Before the onset of a flare is observed in hard X-rays there is often a prolonged pre-flare or pre-heating phase with no detectable hard X-ray emission but pronounced soft X-ray emission suggesting that energy is being released and deposited into the corona and chromosphere already at this stage. This work analyses the temporal evolution of coronal source heating and the chromospheric response during this pre-heating phase to investigate the origin and nature of early energy release and transport during a solar flare. Simultaneous X-ray, EUV, and microwave observations of a well observed flare with a prolonged pre-heating phase are analysed to study the time evolution of the thermal emission and to determine the onset of particle acceleration. During the 20 minutes duration of the pre-heating phase we find no hint of accelerated electrons, neither in hard X-rays nor in microwave emission. However, the total energy budget during the pre-heating phase suggests that energy must be supplied to the flaring loop to sustain the observed temperature and emission measure. Under the assumption of this energy being transported toward the chromosphere via thermal conduction, significant energy deposition at the chromosphere is expected. However, no detectable increase of the emission in the AIA wavelength channels sensitive to chromospheric temperatures is observed. The observations suggest energy release and deposition in the flaring loop before the onset of particle acceleration, yet a model in which energy is conducted to the chromosphere and subsequent heating of the chromosphere is not supported by the observations. **August 9th 2011**

Electron Distribution Functions in Solar Flares from combined X-ray and EUV Observations

Marina **Battaglia** & Eduard P. Kontar
E-print, Oct **2013**, http://arxiv.org/pdf/1310.3930v1.pdf; 2013 ApJ 779 107

Simultaneous solar flare observations with SDO and RHESSI provide spatially resolved information about hot plasma and energetic particles in flares. RHESSI allows the properties of both hot (> 8 MK) thermal plasma and nonthermal electron distributions to be inferred, while SDO/AIA is more sensitive to lower temperatures. We present and implement a new method to reconstruct electron distribution functions from SDO/AIA data. The combined analysis of RHESSI and AIA data allows the electron distribution function to be inferred over the broad energy range from ~0.1 keV up to a few tens of keV. The analysis of two well observed flares suggests that the distributions in general agree to

within a factor of three when the RHESSI values are extrapolated into the intermediate range 1-3 keV, with AIA systematically predicting lower electron distributions. Possible instrumental and numerical effects, as well as potential physical origins for this discrepancy are discussed. The inferred electron distribution functions in general show one or two nearly Maxwellian components at energies below ~ 15 keV and a non-thermal tail above.
2010-08-14, 2012-07-19

RHESSI AND SDO/AIA OBSERVATIONS OF THE CHROMOSPHERIC AND CORONAL PLASMA PARAMETERS DURING A SOLAR FLARE

M. **Battaglia**1,2 and E. P. Konta
E-print, Oct **2012; 2012** ApJ 760 142 http://arxiv.org/pdf/1210.3367v1.pdf
X-ray and extreme ultraviolet (EUV) observations are an important diagnostic of various plasma parameters of the solar atmosphere during solar flares. Soft X-ray and EUV observations often show coronal sources near the top of flaring loops, while hard X-ray emission is mostly observed from chromospheric footpoints. Combining RHESSI with simultaneous Solar Dynamics Observatory/Atmospheric Imaging Assembly (AIA) observations, it is possible for the first time to determine the density, temperature, and emission profile of the solar atmosphere over a wide range of heights during a flare, using two independent methods. Here we analyze a near limb event during the first of three hard X-ray peaks. The emission measure, temperature, and density of the coronal source is found using soft X-ray RHESSI images while the chromospheric density is determined using RHESSI visibility analysis of the hard X-ray footpoints. A regularized inversion technique is applied to AIA images of the flare to find the differential emission measure (DEM). Using DEM maps, we determine the emission and temperature structure of the loop, as well as the density, and compare it with RHESSI results. The soft X-ray and hard X-ray sources are spatially coincident with the top and bottom of the EUV loop, but the bulk of the EUV emission originates from a region without cospatial RHESSI emission. The temperature analysis along the loop indicates that the hottest plasma is found near the coronal loop-top source. The EUV observations suggest that the density in the loop legs increases with increasing height while the temperature remains constant within uncertainties.
*We consider a well observed limb-flare that happened on **2011 February 24** with three HXR peaks between 07:29 and 07:33 UT.*

NUMERICAL SIMULATIONS OF CHROMOSPHERIC HARD X-RAY SOURCE SIZES IN SOLAR FLARES

M. **Battaglia**1,2, E. P. Kontar1, L. Fletcher1, and A. L. MacKinnon
2012 ApJ 752 4
X-ray observations are a powerful diagnostic tool for transport, acceleration, and heating of electrons in solar flares. Height and size measurements of X-ray footpoint sources can be used to determine the chromospheric density and constrain the parameters of magnetic field convergence and electron pitch-angle evolution. We investigate the influence of the chromospheric density, magnetic mirroring, and collisional pitch-angle scattering on the size of X-ray sources. The time-independent Fokker-Planck equation for electron transport is solved numerically and analytically to find the electron distribution as a function of height above the photosphere. From this distribution, the expected X-ray flux as a function of height, its peak height, and full width at half-maximum are calculated and compared with RHESSI observations. A purely instrumental explanation for the observed source size was ruled out by using simulated RHESSI images. We find that magnetic mirroring and collisional pitch-angle scattering tend to change the electron flux such that electrons are stopped higher in the atmosphere compared with the simple case with collisional energy loss only. However, the resulting X-ray flux is dominated by the density structure in the chromosphere and only marginal increases in source width are found. Very high loop densities (>1011 cm–3) could explain the observed sizes at higher energies, but are unrealistic and would result in no footpoint emission below about 40 keV, contrary to observations. We conclude that within a monolithic density model the vertical sizes are given mostly by the density scale height and are predicted smaller than the RHESSI results show.

X-ray, EUV & WL emission heights observed by RHESSI & SDO

Marina **Battaglia** and Eduard Kontar
RHESSI science Nugget, No. 156, **2011**
http://sprg.ssl.berkeley.edu/~tohban/wiki/index.php/X-ray,_EUV_%26_WL_emission_heights_observed_by_RHESSI_%26_SDO
High resolution allows us to determine source heights for the first time

Height structure of X-ray, EUV and white-light emission in a solar flare

Marina **Battaglia**, Eduard P. Kontar
E-print 21 July **2011**; A&A, 533, L2 (**2011**)
Context: The bulk of solar flare emission originates from very compact sources located in the lower solar atmosphere and seen in various wavelength ranges: near optical, UV, EUV, soft and hard X-rays, and gamma-ray emission, yet very

few spatially resolved imaging observations to determine the structure of these compact regions exist. Aims: We investigate the above-the-photosphere heights of hard X-ray (HXR), EUV and white-light (6173 A) continuum sources in the low atmosphere and the corresponding densities at these heights. Considering collisional transport of solar energetic electrons we also determine where and how much energy is deposited and compare these values with the emissions observed in HXR, EUV and continuum. Methods: Simultaneous EUV/continuum images from AIA/HMI on-board SDO and HXR RHESSI images are compared to study a well observed gamma-ray limb flare. Using RHESSI X-ray visibilities we determine the height of the HXR sources as a function of energy above the photosphere. Co-aligning AIA/SDO and HMI/SDO images with RHESSI we infer, for the first time, the heights and characteristic densities of HXR, EUV and continuum (white-light) sources in the flaring footpoint of the loop. Results: 35-100 keV HXR sources are found at heights between 1.7 and 0.8 Mm above the photosphere, below the 6173 A continuum emission which appears at heights 1.5-3 Mm, and the peak of EUV emission originating near 3 Mm. Conclusions: The EUV emission locations are consistent with energy deposition from low energy electrons of ~12 keV occurring in the top layers of the fully ionized chromosphere/low corona and not by > 20 keV electrons that produce HXR footpoints in the lower neutral chromosphere. The maximum of white-light continuum emission appears between the HXR and EUV emission, presumably in the transition between ionized and neutral atmospheres suggesting free-bound and free-free continuum emission. We note that the energy deposited by low energy electrons is sufficient to explain the energetics of optical and UV emissions.

HARD X-RAY FOOTPOINT SIZES AND POSITIONS AS DIAGNOSTICS OF FLARE ACCELERATED ENERGETIC ELECTRONS IN THE LOW SOLAR ATMOSPHERE

M. **Battaglia** and E. P. Kontar

2011 ApJ 735 42

The hard X-ray (HXR) emission in solar flares comes almost exclusively from a very small part of the flaring region, the footpoints of magnetic loops. Using RHESSI observations of solar flare footpoints, we determine the radial positions and sizes of footpoints as a function of energy in six near-limb events to investigate the transport of flare accelerated electrons and the properties of the chromosphere. HXR visibility forward fitting allows us to find the positions/heights and the sizes of HXR footpoints along and perpendicular to the magnetic field of the flaring loop at different energies in the HXR range. We show that in half of the analyzed events, a clear trend of decreasing height of the sources with energy is found. Assuming collisional thick-target transport, HXR sources are located between 600 and 1200 km above the photosphere for photon energies between 120 and 25 keV, respectively. In the other events, the position as a function of energy is constant within the uncertainties. The vertical sizes (along the path of electron propagation) range from 1.3 to 8 arcsec which is up to a factor four larger than predicted by the thick-target model even in events where the positions/heights of HXR sources are consistent with the collisional thick-target model. Magnetic mirroring, collisional pitch-angle scattering, and X-ray albedo are discussed as potential explanations of the findings.

The influence of albedo on the size of hard X-ray flare sources

M. **Battaglia**, E. P. Kontar and I. G. Hannah

A&A 526, A3 (**2011**)

Context. Hard X-rays from solar flares are an important diagnostic of particle acceleration and transport in the solar atmosphere. However, any observed X-ray flux from on-disc sources is composed of direct emission plus Compton backscattered photons (albedo). This affects both the observed spectra and images and the physical quantities derived from them, such as the spatial and spectral distributions of accelerated electrons or characteristics of the solar atmosphere (e.g. density).

Aims. We propose a new indirect method to measure albedo and to infer the directivity of X-rays in imaging using RHESSI data. We describe this method and demonstrate its application to a compact disc event observed with RHESSI.

Methods. Visibility forward fitting is used to determine the size (second moment) of a disc event observed by RHESSI as a function of energy. Using a Monte Carlo simulation code of photon transport in the chromosphere, maps for different degrees of downward directivity and true source sizes are computed. The resulting sizes from the simulated maps are compared with the sizes from the observations to find limits on the true source size and the directivity.

Results. The observed full width half maximum of the source varies in size between 7.4 arcsec and 9.1 arcsec with the maximum between 30 and 40 keV. Such behaviour is expected in the presence of albedo and is found in the simulations. The uncertainties in the data are not small enough to make unambiguous statements about the true source size and the directivity simultaneously. However, a source size smaller than 6 arcsec is improbable for modest directivities, and the true source size is likely to be around 7 arcsec for small directivities.

Conclusions. While it is difficult to image the albedo patch directly, the effect of backscattered photons on the observed source size can be estimated. This is demonstrated here on observations for the first time. The increase in source size caused by albedo has to be accounted for when computing physical quantities that include the size as a parameter, such as flare energetics. At the same time, studying the albedo signature provides vital information about the directivity of X-rays and related electrons.

Do solar decimetric spikes originate in coronal X-ray sources?

Marina **Battaglia** and Arnold O. Benz

E-print, April **2009**; A&A

Context: In the standard solar flare scenario, a large number of particles are accelerated in the corona. Nonthermal electrons emit both X-rays and radio waves. Thus, correlated signatures of the acceleration process are predicted at both wavelengths, coinciding either close to the footpoints of a magnetic loop or near the coronal X-ray source. Aims: We attempt to study the spatial connection between coronal X-ray emission and decimetric radio spikes to determine the site and geometry of the acceleration process.
Methods: The positions of radio-spike sources and coronal X-ray sources are determined and analyzed in a well-observed limb event. Radio spikes are identified in observations from the Phoenix-2 spectrometer. Data from the Nancay radioheliograph are used to determine the position of the radio spikes. RHESSI images in soft and hard X-ray wavelengths are used to determine the X-ray flare geometry. Those observations are complemented by images from GOES/SXI.
Results: We find that the radio emission originates at altitudes much higher than the coronal X-ray source, having an offset from the coronal X-ray source amounting to 90 arcsec and to 113 arcsec and 131 arcsec from the two footpoints, averaged over time and frequency. Conclusions: Decimetric spikes do not originate from coronal X-ray flare sources contrary to previous expectations. However, the observations suggest a causal link between the coronal X-ray source, related to the major energy release site, and simultaneous activity in the higher corona.

Observations of conduction driven evaporation in the early rise phase of solar flares

Battaglia, M., Fletcher, L., Benz, A. O.

E-print, March **2009**; A&A

The classical flare picture features a beam of electrons, which were accelerated in a site in the corona, hitting the chromosphere. The electrons are stopped in the dense chromospheric plasma, emitting bremsstrahlung in hard X-rays. The ambient material is heated by the deposited energy and expands into the magnetic flare loops, a process termed chromospheric evaporation. In this view hard X-ray emission from the chromosphere is succeeded by soft-X-ray emission from the hot plasma in the flare loop, the soft X-ray emission being a direct consequence of the impact of the non-thermal particle beam. However, observations of events exist in which a pronounced increase in soft X-ray emission is observed minutes before the onset of the hard X-ray emission. Such pre-flare emission clearly contradicts the classical flare picture. For the first time, the pre-flare phase of such solar flares is studied in detail. The aim is to understand the early rise phase of these events. We want to explain the time evolution of the observed emission by means of alternative energy transport mechanisms such as heat conduction. RHESSI events displaying pronounced pre-flare emission were analyzed in imaging and spectroscopy. The time evolution of images and full sun spectra was investigated and compared to the theoretical expectations from conduction driven chromospheric evaporation. The pre-flare phase is characterized by purely thermal emission from a coronal source with increasing emission measure and density. After this earliest phase, a small non-thermal tail to higher energies appears in the spectra, becoming more and more pronounced. However, images still only display one X-ray source, implying that this non-thermal emission is coronal. The increase of emission measure and density indicates that material is added to the coronal region. The most plausible origin is evaporated material from the chromosphere. Energy provided by a heat flux is capable of driving chromospheric evaporation. We show that the often used classical Spitzer treatment of the conductive flux is not applicable. The conductive flux is saturated. During the preflare-phase, the temperature of the coronal source remains constant or increases. Continuous heating in the corona is necessary to explain this observation. The observations of the pre-flare phase of four solar flares are consistent with chromospheric evaporation driven by a saturated heat flux. Additionally, continuous heating in the corona is necessary to sustain the observed temperature.

On the Sweet-Parker model for incompressible visco-resistive magnetic reconnection in two dimensions associated to ideal magnetohydrodynamic instabilities

Hubert **Baty**

ApJ **2022**

https://arxiv.org/pdf/2201.01135.pdf

We revisit the well known Sweet-Parker (SP) model for magnetic reconnection in the framework of two dimensional incompressible magnetohydrodynamics. The steady-state solution is re-derived by considering a non zero viscosity via the magnetic Prandtl number Pm. Moreover, contrary to the original SP model, a particular attention is paid to the possibility that the inflowing magnetic field Be and the length of the current layer L are not necessarily fixed and may depend on the dissipation parameters. Using two different ideally unstable setups to form the current sheet, namely the tilt and coalescence modes, we numerically explore the scaling relations with resistivity η and Prandtl number Pm during the magnetic reconnection phase, and compare to the generalized steady-state SP theoretical solution. The usual Sweet-Parker relations are recovered in the limit of small Pm and η values, with in particular the normalized reconnection rate being simply $S^{-1/2}(1+Pm)^{-1/4}$, where S represents the Lundquist number $S=LV_A/\eta$ (V_A being the characteristic Alfvén speed). In the opposite limit of higher Pm and/or η values, a significant deviation from the SP model is obtained with a complex dependence $B_e(\eta,Pm)$ that is explored depending on

the setup considered. We discuss the importance of these results in order to correctly interpret the numerous exponentially increasing numerical studies published in the literature, with the aim of explaining eruptive phenomena observed in the solar corona.

On the growth rate of plasmoid chains during nonlinear viscoresistive evolution of the tilt instability

Hubert **Baty**
2020
https://arxiv.org/pdf/2003.08660.pdf
We investigate by means of two-dimensional incompressible magnetohydrodynamic (MHD) numerical simulations, the onset phase of the fast collisional magnetic reconnection regime that is supported by the formation of plasmoid chains when the Lundquist number S exceeds a critical value. The present study extends previous results obtained at magnetic Prandtl number Pm = 1 (Baty 2020) to a range of different Pm values. We use FINMHD code where a set of reduced visco-resistive MHD equations is employed to form two quasi-singular current layers as a consequence of the tilt instability. The results reinforce the conclusion that, a phase of sudden super-Alfvenic growth (when Pm is not too high) of plasmoid chains is obtained, following a previous quiescent phase during current sheet formation on a slower Alfvenic time scale. We compare our results with predictions from the general theory of the plasmoid instability. We also discuss the importance of this onset phase to reach the ensuing stochastic time-dependent reconnection regime, where a fast time-averaged rate independent of S is obtained. Finally, we briefly discuss the relevance of our results to explain the flaring activity in solar corona and internal disruptions in tokamaks.
See https://arxiv.org/pdf/2001.07036.pdf

FINMHD: An Adaptive Finite-element Code for Magnetic Reconnection and Formation of Plasmoid Chains in Magnetohydrodynamics

Hubert **Baty**
2019 ApJS 243 23
sci-hub.se/10.3847/1538-4365/ab2cd2
Solving the problem of fast eruptive events in magnetically dominated astrophysical plasmas requires the use of particularly well adapted numerical tools. Indeed, the central mechanism based on magnetic reconnection is determined by a complex behavior with quasi-singular forming current layers enriched by their associated small-scale magnetic islands called plasmoids. A new code is thus presented for the solution of two-dimensional dissipative magnetohydrodynamics (MHD) equations in cartesian geometry specifically developed to this end. A current–vorticity formulation representative of an incompressible model is chosen in order to follow the formation of the current sheets and the ensuing magnetic reconnection process. A finite-element discretization using triangles with quadratic basis functions on an unstructured grid is employed, and implemented via a highly adaptive characteristic-Galerkin scheme. The adaptivity of the code is illustrated on simplified test equations and finally for magnetic reconnection associated with the nonlinear development of the tilt instability between two repelling current channels. Varying the Lundquist number S has allowed us to study the transition between the steady-state Sweet–Parker reconnection regime (for $S \lesssim 10^4$) and the plasmoid-dominated reconnection regime (for $S \gtrsim 10^5$). The implications for the understanding of the mechanism explaining the fast conversion of free magnetic energy in astrophysical environments such as the solar corona are briefly discussed.

KINETIC MODELING OF PARTICLE ACCELERATION IN A SOLAR NULL-POINT RECONNECTION REGION

G. **Baumann**1, T. Haugbølle1,2, and Å. Nordlund
2013 ApJ 771 93
The primary focus of this paper is on the particle acceleration mechanism in solar coronal three-dimensional reconnection null-point regions. Starting from a potential field extrapolation of a Solar and Heliospheric Observatory (SOHO) magnetogram taken on **2002 November 16**, we first performed magnetohydrodynamics (MHD) simulations with horizontal motions observed by SOHO applied to the photospheric boundary of the computational box. After a build-up of electric current in the fan plane of the null point, a sub-section of the evolved MHD data was used as initial and boundary conditions for a kinetic particle-in-cell model of the plasma. We find that sub-relativistic electron acceleration is mainly driven by a systematic electric field in the current sheet. A non-thermal population of electrons with a power-law distribution in energy forms in the simulated pre-flare phase, featuring a power-law index of about –1.78. This work provides a first step toward bridging the gap between macroscopic scales on the order of hundreds of Mm and kinetic scales on the order of centimeter in the solar corona, and explains how to achieve such a cross-scale coupling by utilizing either physical modifications or (equivalent) modifications of the constants of nature. With their exceptionally high resolution—up to 135 billion particles and 3.5 billion grid cells of size 17.5 km—these simulations offer a new opportunity to study particle acceleration in solar-like settings.

3D Solar Null Point Reconnection MHD Simulations

G. **Baumann**, K. Galsgaard, Å. Nordlund

Solar Physics, June **2013**, Volume 284, Issue 2, pp 467-487

Numerical MHD simulations of 3D reconnection events in the solar corona have improved enormously over the last few years, not only in resolution, but also in their complexity, enabling more and more realistic modeling. Various ways to obtain the initial magnetic field, different forms of solar atmospheric models as well as diverse driving speeds and patterns have been employed. This study considers differences between simulations with stratified and non-stratified solar atmospheres, addresses the influence of the driving speed on the plasma flow and energetics, and provides quantitative formulas for mapping electric fields and dissipation levels obtained in numerical simulations to the corresponding solar quantities. The simulations start out from a potential magnetic field containing a null-point, obtained from a Solar and Heliospheric Observatory (SOHO) Michelson Doppler Imager (MDI) magnetogram magnetogram extrapolation approximately 8 hours before a C-class flare was observed. The magnetic field is stressed with a boundary motion pattern similar to – although simpler than – horizontal motions observed by SOHO during the period preceding the flare. The general behavior is nearly independent of the driving speed, and is also very similar in stratified and non-stratified models, provided only that the boundary motions are slow enough. The boundary motions cause a build-up of current sheets, mainly in the fan-plane of the magnetic null-point, but do not result in a flare-like energy release. The additional free energy required for the flare could have been partly present in non-potential form at the initial state, with subsequent additions from magnetic flux emergence or from components of the boundary motion that were not represented by the idealized driving pattern.

PARTICLE-IN-CELL SIMULATION OF ELECTRON ACCELERATION IN SOLAR CORONAL JETS

G. **Baumann** and Å. Nordlund

2012 ApJ 759 L9

We investigate electron acceleration resulting from three-dimensional magnetic reconnection between an emerging, twisted magnetic flux rope and a pre-existing weak, open magnetic field. We first follow the rise of an unstable, twisted flux tube with a resistive MHD simulation where the numerical resolution is enhanced by using fixed mesh refinement. As in previous MHD investigations of similar situations, the rise of the flux tube into the pre-existing inclined coronal magnetic field results in the formation of a solar coronal jet. A snapshot of the MHD model is then used as an initial and boundary condition for a particle-in-cell simulation, using up to half a billion cells and over 20 billion charged particles. Particle acceleration occurs mainly in the reconnection current sheet, with accelerated electrons displaying a power law in the energy probability distribution with an index of around –1.5. The main acceleration mechanism is a systematic electric field, striving to maintaining the electric current in the current sheet against losses caused by electrons not being able to stay in the current sheet for more than a few seconds at a time.

On the factors determining the eruptive character of solar flares

Christian **Baumgartner**, Julia K. Thalmann, Astrid M. Veronig

ApJ **2017**

https://arxiv.org/pdf/1712.05106.pdf

We investigated how the magnetic field in solar active regions (ARs) controls flare activity, i.e., whether a confined or eruptive flare occurs. We analyzed 44 flares of GOES class M5.0 and larger that occurred during 2011–2015. We used 3D potential magnetic field models to study their location (using the flare distance from the flux-weighted AR center dFC) and the strength of the magnetic field in the corona above (via decay index n and flux ratio). We also present a first systematic study of the orientation of the coronal magnetic field, using the orientation ϕ of the flare-relevant polarity inversion line as a measure. We analyzed all quantities with respect to the size of the underlying dipole field, characterized by the distance between the opposite-polarity centers, dPC. Flares originating from underneath the AR dipole (dFC/dPC < 0.5) tend to be eruptive if launched from compact ARs (dPC $\leq$ 60 Mm) and confined if launched from extended ARs. Flares ejected from the periphery of ARs (dFC/dPC > 0.5) are predominantly eruptive. In confined events the flare-relevant field adjusts its orientation quickly to that of the underlying dipole with height ($\Delta\phi$ & 40◦ until the apex of the dipole field), in contrast to eruptive events where it changes more slowly with height. The critical height for torus instability, hcrit = h(n = 1.5), discriminates best between confined (hcrit & 40 Mm) and eruptive flares (hcrit . 40 Mm). It discriminates better than $\Delta\phi$, implying that the decay of the confining field plays a stronger role than its orientation at different heights. **2014-10-25**

Table 1. Event list (**Flares ≥M5.0** that occurred between January 2011 and December 2015.)

ESTIMATES OF DENSITIES AND FILLING FACTORS FROM A COOLING TIME ANALYSIS OF SOLAR MICROFLARES OBSERVED WITH RHESSI

R. N. **Baylor**1, P. A. Cassak1, S. Christe2, I. G. Hannah3, Säm Krucker4,5, D. J. Mullan6, M. A. Shay6, H. S. Hudson3,4 and R. P. Lin

2011 ApJ 736 75

High-resolution imaging-spectroscopy movies of solar active region NOAA 10998 obtained with the Crisp Imaging Spectropolarimeter at the Swedish 1-m Solar Telescope show very bright, rapidly flickering, flame-like features that appear intermittently in the wings of the Balmer Hα line in a region with moat flows and likely some flux emergence. They show up at regular Hα blue-wing bright points that outline the magnetic network, but flare upward with much larger brightness and distinct "jet" morphology seen from aside in the limbward view of these movies. We classify these features as Ellerman bombs and present a morphological study of their appearance at the unprecedented spatial, temporal, and spectral resolution of these observations. The bombs appear along the magnetic network with footpoint extents up to 900 km. They show apparent travel away from the spot along the pre-existing network at speeds of about 1 km s–1. The bombs flare repetitively with much rapid variation at timescales of seconds only, in the form of upward jet-shaped brightness features. These reach heights of 600-1200 km and tend to show blueshifts; some show bi-directional Doppler signature and some seem accompanied with an Hα surge. They are not seen in the core of Hα due to shielding by overlying chromospheric fibrils. The network where they originate has normal properties. The morphology of these jets strongly supports deep-seated photospheric reconnection of emergent or moat-driven magnetic flux with pre-existing strong vertical network fields as the mechanism underlying the Ellerman bomb phenomenon.

Detecting quasi-periodic pulsations in solar and stellar flares with a neural network

Sergey A. **Belov**, Dmitrii Y. Kolotkov, Valery M. Nakariakov, Anne-Marie Broomhal

ApJS **274** 31 **2024**

https://arxiv.org/pdf/2408.05038

https://iopscience.iop.org/article/10.3847/1538-4365/ad6f98/pdf

Quasi-periodic pulsations (QPP) are often detected in solar and stellar flare lightcurves. These events may contain valuable information about the underlying fundamental plasma dynamics as they are not described by the standard flare model. The detection of QPP signals in flare lightcurves is hindered by their intrinsically non-stationary nature, contamination by noise, and the continuously increasing amount of flare observations. Hence, the creation of automated techniques for QPP detection is imperative. We implemented the Fully Convolution Network (FCN) architecture to classify the flare lightcurves whether they have exponentially decaying harmonic QPP or not. To train the FCN, 90,000 synthetic flare lightcurves with and without QPP were generated. After training, it showed an accuracy of 87.2% on the synthetic test data and did not experience overfitting. To test the FCN performance on real data, we used the subset of stellar flare lightcurves observed by Kepler, with strong evidence of decaying QPP identified hitherto with other methods. Then, the FCN was applied to find QPPs in a larger-scale Kepler flare catalogue comprised of 2274 events, resulting in a 7% QPP detection rate with a probability above 95%. The FCN, implemented in Python, is accessible through a browser application with a user-friendly graphical interface and detailed installation and usage guide. The obtained results demonstrate that the developed FCN performs well and successfully detects exponentially decaying harmonic QPP in real flare data, and can be used as a tool for preliminary sifting of the QPP events of this type in future large-scale observational surveys.

Solar nanoflares in different spectral ranges

S. A. Belov1,2, S. A. Bogachev1,3, L. S. Ledentsov1,4 and D. I. Zavershinskii1,2

A&A, 684, A60 (**2024**)

https://www.aanda.org/articles/aa/pdf/2024/04/aa48199-23.pdf

Aims. The rates and other characteristics of solar nanoflares were measured for the same area of the Sun in different extreme-ultravioilet (EUV) channels to find how the main properties of nanoflares depend on the spectral range.
Methods. We used images of the quiet Sun obtained by the Atmospheric Imaging Assembly (AIA) on board the Solar Dynamics Observatory (SDO) in seven spectral channels, 94 Å, 131 Å, 171 Å, 193 Å, 211 Å, 304 Å, and 335 Å. We analyzed 300 images for each AIA/SDO channel covering one hour from 12:00 UT to 13:00 UT on 20 May 2019 with a 12 s cadence. We searched for nanoflares in two 360″×720″ fields of view above (N) and below (S) the Sun's equator to measure nanoflare latitudinal distributions and their N–S asymmetry. To detect nanoflares, we used a threshold-based algorithm with 5σ threshold.
Results. The integral nanoflare rate measured in seven spectral ranges is 3.53 × 10−21 cm−1 s−1; the corresponding frequency is 215 events s−1 for the entire surface of the Sun. A search for nanoflares in any single AIA-channel leads to significant underestimation of their frequency and rate: 171 Å −34% of the total value; 193 Å −33%; 211 Å −24%; other channels – less than 16%. Most EUV nanoflares are single-pixel (∼78%) and mono-channel (∼86%) events. In channel 304 Å, multipixel events dominate over single-pixel events (68% vs. 32%). The average duration of nanoflares is in the range of (89 − 141)±(40 − 61) s depending on the spectral region with the mean value being 129 ± 59 s. The latitudinal distribution of nanoflares is approximately uniform in the range from 0° to 45° for all channels. We find a

slight difference between the N and S hemispheres (up to 20% depending on channel), but we do not find it to be statistically significant.
Conclusions. We demonstrate that solar nanoflares can be found in all AIA EUV channels. The detection probability strongly depends on the spectral range and the channels can be approximately ranked as follows (from high to low probability): 171 Å, 193 Å, 211 Å, 131 Å, 304 Å, 335 Å, and 94 Å. The first three channels, 171, 193, and 211 Å, allow the detection of ~78% of all the nanoflares. The remaining four add only 22%. Other characteristics of nanoflares, including duration and spatial distribution, weakly depend on spectral range. **20 May 2019**
Table 1. Nanoflare observations.

On the Estimation of the SHARP Parameter MEANALP from AIA Images Using Deep Neural Networks

B. **Benson**, W. D. Pan, A. Prasad, G. A. Gary & Q. Hu
Solar Physics volume 296, Article number: 163 (**2021**)
https://link.springer.com/content/pdf/10.1007/s11207-021-01912-3.pdf
https://doi.org/10.1007/s11207-021-01912-3
Space-weather HMI Active Region Patches (SHARPs) data from the Helioseismic and Magnetic Imager (HMI) on board the Solar Dynamics Observatory (SDO) provides high cadence data from the full-disk photospheric magnetic field. The SHARP's MEANALP (αmαm) parameter, which characterizes the twist, can provide a measure of nonpotentiality of an active region, which can be a condition for the occurrence of solar flares. The SDO/Atmospheric Imaging Assembly (AIA) captures images at a higher cadence (12 or 24 seconds) than the SDO/HMI. Hence, if the αmαm can be inferred from the AIA data, we can estimate the magnetic field evolution of an active region at a higher temporal cadence. Shortly before a flare occurs, we observed a change in the αmαm in some active regions that produced stronger (M- or X-class) flares. Therefore, we study the ability of neural networks to estimate the αmαm parameter from SDO/AIA images. We propose a classification and regression scheme to train deep neural networks using AIA filtergrams of active regions with the objective to estimate the αmαm of active regions outside our training set. Our results show a classification accuracy greater than 85% within two classes to identify the range of the αmαm parameter. We also attempt to understand the nature of the solar images using variational autoencoders. Thus, this study opens a promising new application of neural networks which can be extended to other SHARP parameters in the future. **25 October 2010**

A hybrid supervised/unsupervised machine learning approach to solar flare prediction

Federico **Benvenuto**, Michele Piana, Cristina Campi, Anna Maria Massone
2017
https://arxiv.org/pdf/1706.07103.pdf
We introduce a hybrid approach to solar flare prediction, whereby a supervised regularization method is used to realize feature importance and an unsupervised clustering method is used to realize the binary flare/no-flare decision. The approach is validated against NOAA SWPC data.

Observations of a Radio-quiet Solar Preflare

A. O. **Benz**, M. Battaglia, M. Guedel
Solar Phys. **2017**
https://arxiv.org/pdf/1709.06417.pdf
The preflare phase of the flare SOL2011-08-09T03:52 is unique in its long duration, its coverage by the {\it Reuven Ramaty High Energy Solar Spectroscopic Imager (RHESSI) and the Nobeyama Radioheliograph}, and the presence of three well-developed soft X-ray (SXR) peaks. No hard X-rays (HXR) are observed in the preflare phase. Here we report that also no associated radio emission at 17 GHz was found despite the higher sensitivity of the radio instrument. The ratio between the SXR peaks and the upper limit of the radio peaks is larger by more than one order of magnitude compared to regular flares. The result suggests that the ratio between acceleration and heating in the preflare phase was different than in regular flares. Acceleration to relativistic energies, if any, occurred with lower efficiency.

Flare Observations **Review**

Arnold O. **Benz**
Living Reviews in Solar Physics December **2017?**, 14:2 **File**
This article is a revised version of http://dx.doi.org/10.12942/lrsp-2008-1.
https://link.springer.com/content/pdf/10.1007%2Fs41116-016-0004-3.pdf
Solar flares are observed at all wavelengths from decameter radio waves to gamma-rays beyond 1 GeV. This review focuses on recent observations in EUV, soft and hard X-rays, white light, and radio waves. Space missions such as RHESSI, Yohkoh, TRACE, SOHO, and more recently Hinode and SDO have enlarged widely the observational base. They have revealed a number of surprises: Coronal sources appear before the hard X-ray emission in chromospheric footpoints, major flare acceleration sites appear to be independent of coronal mass ejections, electrons, and ions may be

accelerated at different sites, there are at least 3 different magnetic topologies, and basic characteristics vary from small to large flares. Recent progress also includes improved insights into the flare energy partition, on the location(s) of energy release, tests of energy release scenarios and particle acceleration. The interplay of observations with theory is important to deduce the geometry and to disentangle the various processes involved. There is increasing evidence supporting magnetic reconnection as the basic cause. While this process has become generally accepted as the trigger, it is still controversial how it converts a considerable fraction of the energy into non-thermal particles. Flare-like processes may be responsible for large-scale restructuring of the magnetic field in the corona as well as for its heating. Large flares influence interplanetary space and substantially affect the Earth's ionosphere. Flare scenarios have slowly converged over the past decades, but every new observation still reveals major unexpected results, demonstrating that solar flares, after 150 years since their discovery, remain a complex problem of astrophysics including major unsolved questions. **March 19, 1980, 1980-03-27, 3 Feb 1986, 1992-08-18, 2002-04-15, 2002-04-21, 2002-04-30, Jul 23 2002, 2002-11-09, 2003-10-23, 20Jan 2005, 2006-07-13, 2006-12-05, 2006-12-09, April 30, 2007, 13 May 2013,**

Decimetric pulsations and coronal X-ray sources
A. **Benz**, M. Battaglia, and N. Vilmer
RHESSI Science Nugget, No 150, April **2011**
http://sprg.ssl.berkeley.edu/~tohban/wiki/index.php/Decimetric_pulsations_and_coronal_X-ray_sources
Pulsations are the strongest flare emissions at decimeter radio wavelengths, and they are common. Coherent stellar radio emissions are of a similar type. Sometimes they are regular oscillations with periods of the order of one second, at other times, and especially at high frequencies, they are irregular and faster. The question may come to the mind of the gentle Nugget reader, how such radio emissions may complement our picture of flare physics. Although decimetric pulsations are generally believed to originate from non-thermal electrons, they often do not correlate in time with non-thermal X-rays. We have decided to select cases where the two emissions do correlate within a few seconds and investigate the spatial relations more closely, using flares that occurred near the limb. This simplifies the geometry and the interpretation of the spatial relations. **5 December 2006**

Flare Observations A Review
Arnold O. **Benz**
Living **Reviews** in Solar Physics (**2008**); **File**
E-print, Feb 2008
http://solarphysics.livingreviews.org/Articles/lrsp-2008-1/
Solar flares are observed at all wavelengths from decameter radio waves to gamma-rays at 100 MeV. This review focuses on recent observations in EUV, soft and hard X-rays, white light and radio waves. Space missions such as RHESSI, Yohkoh, TRACE, and SOHO have enlarged widely the observational base. They have revealed a number of surprises: Coronal sources appear before the hard X-ray emission in chromospheric footpoints, major flare acceleration sites appear to be independent of coronal mass ejections (CMEs), electrons and ions may be accelerated at different sites, and basic characteristics vary from small to large flares. Recent progress also includes improved insights into the flare energy partition, on the location(s) of energy release, tests of energy release scenarios and particle acceleration. The interplay of observations with theory is important to deduce the geometry and to disentangle the various processes involved. There is increasing evidence supporting reconnection of magnetic field lines as the basic cause. While this process has become generally accepted as the trigger, it does not explain the huge energy involved, nor the impulsive acceleration of charged particles. Flare-like processes may be responsible for large-scale restructuring of the magnetic field in the corona as well as for its heating. Large flares influence interplanetary space and substantially affect the Earth's lower ionosphere. While flare scenarios have slowly converged over the past decades, every new observation still reveals major unexpected results, demonstrating that solar flares, after 150 years since their discovery, remain an unexplained problem of astrophysics.

Machine learning as a flaring storm warning machine: Was a warning machine for the September 2017 solar flaring storm possible?
Federico **Benvenuto**, Cristina Campi, Anna Maria Massone, Michele Piana
ApJL **904** L7 **2020**
https://arxiv.org/pdf/2007.02425.pdf
https://doi.org/10.3847/2041-8213/abc5b7
Machine learning is nowadays the methodology of choice for flare forecasting and supervised techniques, in both their traditional and deep versions, are becoming the most frequently used ones for prediction in this area of space weather. Yet, machine learning has not been able so far to realize an operating warning system for flaring storms and the scientific literature of the last decade suggests that its performances in the prediction of intense solar flares are not optimal.
The main difficulties related to forecasting solar flaring storms are probably two. First, most methods are conceived to provide probabilistic predictions and not to send binary yes/no indications on the consecutive occurrence of flares along an extended time range. Second, flaring storms are typically characterized by the explosion of high energy events,

which are seldom recorded in the databases of space missions; as a consequence, supervised methods are trained on very imbalanced historical sets, which makes them particularly ineffective for the forecasting of intense flares. Yet, in this study we show that supervised machine learning could be utilized in a way to send timely warnings about the most violent and most unexpected flaring event of the last decade, and even to predict with some accuracy the energy budget daily released by magnetic reconnection during the whole time course of the storm. Further, we show that the combination of sparsity-enhancing machine learning and feature ranking could allow the identification of the prominent role that energy played as an Active Region property in the forecasting process.

A Hybrid Supervised/Unsupervised Machine Learning Approach to Solar Flare Prediction

Federico **Benvenuto**1, Michele Piana2, Cristina Campi3, and Anna Maria Massone3
2018 ApJ 853 90
http://sci-hub.tw/10.3847/1538-4357/aaa23c
This paper introduces a novel method for flare forecasting, combining prediction accuracy with the ability to identify the most relevant predictive variables. This result is obtained by means of a two-step approach: first, a supervised regularization method for regression, namely, LASSO is applied, where a sparsity-enhancing penalty term allows the identification of the significance with which each data feature contributes to the prediction; then, an unsupervised fuzzy clustering technique for classification, namely, Fuzzy C-Means, is applied, where the regression outcome is partitioned through the minimization of a cost function and without focusing on the optimization of a specific skill score. This approach is therefore hybrid, since it combines supervised and unsupervised learning; realizes classification in an automatic, skill-score-independent way; and provides effective prediction performances even in the case of imbalanced data sets. Its prediction power is verified against NOAA Space Weather Prediction Center data, using as a test set, data in the range between 1996 August and 2010 December and as training set, data in the range between 1988 December and 1996 June. To validate the method, we computed several skill scores typically utilized in flare prediction and compared the values provided by the hybrid approach with the ones provided by several standard (non-hybrid) machine learning methods. The results showed that the hybrid approach performs classification better than all other supervised methods and with an effectiveness comparable to the one of clustering methods; but, in addition, it provides a reliable ranking of the weights with which the data properties contribute to the forecast.

RELATION BETWEEN THE CORONAL MASS EJECTION ACCELERATION AND THE NON-THERMAL FLARE CHARACTERISTICS

S. **Berkebile-Stoiser**, A. M. Veronig, B. M. Bein, and M. Temmer
2012 ApJ 753 88, **File**
We investigate the relationship between the main acceleration phase of coronal mass ejections (CMEs) and the particle acceleration in the associated flares as evidenced in Reuven Ramaty High Energy Solar Spectroscopic Imager non-thermal X-rays for a set of 37 impulsive flare-CME events. Both the CME peak velocity and peak acceleration yield distinct correlations with various parameters characterizing the flare-accelerated electron spectra. The highest correlation coefficient is obtained for the relation of the CME peak velocity and the total energy in accelerated electrons (c = 0.85), supporting the idea that the acceleration of the CME and the particle acceleration in the associated flare draw their energy from a common source, probably magnetic reconnection in the current sheet behind the erupting structure. In general, the CME peak velocity shows somewhat higher correlations with the non-thermal flare parameters than the CME peak acceleration, except for the spectral index of the accelerated electron spectrum, which yields a higher correlation with the CME peak acceleration (c –0.6), indicating that the hardness of the flare-accelerated electron spectrum is tightly coupled to the impulsive acceleration process of the rising CME structure. We also obtained high correlations between the CME initiation height h 0 and the non-thermal flare parameters, with the highest correlation of h 0 to the spectral index δ of flare-accelerated electrons (c 0.8). This means that CMEs erupting at low coronal heights, i.e., in regions of stronger magnetic fields, are accompanied by flares that are more efficient at accelerating electrons to high energies. In the majority of events (~80%), the non-thermal flare emission starts after the CME acceleration, on average delayed by 6 minutes, in line with the standard flare model where the rising flux rope stretches the field lines underneath until magnetic reconnection sets in. We find that the current sheet length at the onset of magnetic reconnection is 21 ± 7 Mm. The flare hard X-ray peaks are well synchronized with the peak of the CME acceleration profile, and in 75% of the cases they occur within ±5 minutes. Our findings provide strong evidence for the tight coupling between the CME dynamics and the particle acceleration in the associated flare in impulsive events, with the total energy in accelerated electrons being closely correlated with the peak velocity (and thus the kinetic energy) of the CME, whereas the number of electrons accelerated to high energies is decisively related to the CME peak acceleration and the height of the pre-eruptive structure.

Multi-wavelength fine structure and mass flows in solar microflares

Berkebile-Stoiser, S. ; G?m?ry, P.; Veronig, A.M.; Ryb?ak, J.; S?tterlin, P.
E-print, Aug **2009;** A&A 505 (**2009**) 811-823
http://www.aanda.org/10.1051/0004-6361/200912100

Aims. We study the multi-wavelength characteristics at high spatial resolution, as well as chromospheric evaporation signatures of solar microflares. To this end, we analyze the fine structure and mass flow dynamics in the chromosphere, transition region and corona of three homologous microflares (GOES class <A9/0.7 with/without background), which occurred on **July 4, 2006** in AR 10898.
Methods. A multi-wavelength analysis using temporally and spatially highly resolved imaging data from the Dutch open telescope (H alpha, Ca II H), the transition region and coronal explorer (17.1 nm), the extreme-ultraviolet imaging telescope (19.5 nm), and the Reuven Ramaty high energy solar spectroscopic imager (>3 keV) was carried out. EUV line spectra provided by the coronal diagnostic spectrometer are searched for Doppler shifts in order to study associated plasma flows at chromospheric (He I, T ~ 3.9 ? 10^4 K), transition region (e.g. O V, T ~ 2.6 ? 10^5 K), and coronal temperatures (Si XII, T ~ 2 ? 10^6 K). RHESSI X-ray spectra provide information about non-thermal electrons.
Results. The multi-wavelength appearance of the microflares is in basic agreement with the characteristics of large flares. For the first event, a complex flare sequence is observed in TRACE 17.1 nm images (T ~ 1 MK), which show several brightenings, narrow loops of enhanced emission, and an EUV jet. EIT 19.5 nm data (T ~ 1.5 MK) exhibit similar features for the third event. DOT measurements show finely structured chromospheric flare brightenings for all three events, loop-shaped fibrils of increased emission between H alpha brightenings, as well as a similar feature in Ca II. For all three events, a RHESSI X-ray source (3?8 keV, T ~ 10 MK) is located in between two chromospheric brightenings situated in magnetic flux of opposite polarity. We find the flow dynamics associated with the events to be very complex. In the chromosphere and transition region, CDS observed downflows for the first (v < 40 km s^−1), and upflows for the second event (v < 40 km s^−1). During the third microflare, we find upflows of <20 km s^−1 and also weak downflows of <20 km s^−1 in two separate brightenings. For all three microflares, multi-component fitting is needed for several profiles of He I, O V, and Ne VI lines observed at the flare peaks, which indicate spatially unresolved, oppositely directed flows of <180 km s^−1. We interpret these flows as twisting motions of the flare loops. Loop-shaped fibrils in between H alpha brightenings showing opposite flow directions (v ~ 5 km s^−1) are also observed in DOT H alpha Dopplergrams. RHESSI X-ray spectra show evidence of non-thermal bremsstrahlung for two of the three microflares. The electron beam flux density deposited in the chromosphere for these events is estimated to straddle the threshold heating flux between gentle and explosive evaporation.

White-light continuum emission from a solar flare and plage

Arkadiusz **Berlicki** (1,2), Arun Kumar Awasthi (1), Petr Heinzel (2), Michal Sobotka
International Astronomical Union#320 Proceedings **2016**
http://arxiv.org/pdf/1604.04186v1.pdf
Observations of flare emissions in the optical continuum are very rare. Therefore, the analysis of such observations is useful and may contribute to our understanding of the flaring chromosphere and photosphere. We study the white light continuum emission observed during the X6.9 flare which occurred on **August 09, 2011**. This emission comes not only from the flare ribbons but also from the nearby plage area. The main aim of this work is to disentangle the flare and plage (facula) emission. We analyzed the spatial, spectral and temporal evolution of the flare and plage properties by analyzing multi-wavelength observations. We study the morphological correlation of the whitelight continuum emission observed with different instruments. We found that some active region areas which produce the continuum emission correspond rather to plages than to the flare kernels. We showed that in some cases the continuum emission from the WL flare kernels is very similar to the continuum emission of faculae.

THREE-DIMENSIONAL SPONTANEOUS MAGNETIC RECONNECTION

Andrey **Beresnyak**
2017 ApJ 834 47
Magnetic reconnection is best known from observations of the Sun where it causes solar flares. Observations estimate the reconnection rate as a small, but non-negligible fraction of the Alfvén speed, so-called fast reconnection. Until recently, the prevailing pictures of reconnection were either of resistivity or plasma microscopic effects, which was contradictory to the observed rates. Alternative pictures were either of reconnection due to the stochasticity of magnetic field lines in turbulence or the tearing instability of the thin current sheet. In this paper we simulate long-term three-dimensional nonlinear evolution of a thin, planar current sheet subject to a fast oblique tearing instability using direct numerical simulations of resistive-viscous magnetohydrodynamics. The late-time evolution resembles generic turbulence with a −5/3 power spectrum and scale-dependent anisotropy, so we conclude that the tearing-driven reconnection becomes turbulent reconnection. The turbulence is local in scale, so microscopic diffusivity should not affect large-scale quantities. This is confirmed by convergence of the reconnection rate toward with increasing Lundquist number. In this spontaneous reconnection, with mean field and without driving, the dissipation rate per unit area also converges to …, and the dimensionless constants 0.015 and 0.006 are governed only by self-driven nonlinear dynamics of the sheared magnetic field. Remarkably, this also means that a thin current sheet has a universal fluid resistance depending only on its length to width ratio and to …

Current State of Seismic Emission Associated with Solar Flares **Review**

Diana **Besliu-Ionescu** 1 , Alina Donea 2, Paul Cally
Sun and Geosphere, **2017**; 12/1: 59 -67
http://newserver.stil.bas.bg/SUNGEO//00SGArhiv/SG_v12_No1_2017-pp-59-67.pdf
Certain solar flares are followed by photospheric seismic emission, also known as sunquakes. Sunquakes were predicted more than 40 years ago, but observed for the first time 20 years ago. A valid scenario that would fit all discoveries made so far is still missing. This paper summarises the current state of the literature concerning sunquakes. It describes all published reports of known seismic sources to date and presents possible triggering mechanisms. **2011-02-15**
Table 1: List of the events used in the regression model. In bold are shown the events used for validation

Generalized analytical models of Syrovatskii's current sheet

Bezrodnykh, Vlasov, Somov,
Astronomy Lett. 37, 113, **2011**.
Two-dimensional stationary magnetic reconnection models that include a thin Syrovatskii-type current sheet and four discontinuous magnetohydrodynamic flows of finite length attached to its endpoints are considered. The flow pattern is not specified but is determined from a self-consistent solution of the problem in the approximation of a strong magnetic field. Generalized analytical solutions that take into account the possibility of a current sheet discontinuity in the region of anomalous plasma resistivity have been found. The global structure of the magnetic field in the reconnection region and its local properties near the current sheet and attached discontinuities are studied. In the reconnection regime in which reverse currents are present in the current sheet, the attached discontinuities are trans-Alfvénic shock waves near the current sheet endpoints. Two types of transitions from nonevolutionary shocks to evolutionary ones along discontinuous flows are shown to be possible, depending on the geometrical model parameters. The relationship between the results obtained and numerical magnetic reconnection experiments is discussed.

Transient Phenomena in the Energetic Behind-the-Limb Solar Flare of September 29, 1989

Bhatnagar, A.; Jain, R. M.; Burkepile, J. T.; Chertok, I. M.; Magun, A.; Urbarz, H.; Zlobec, P.
ASTROPHYSICS AND SPACE SCIENCE I Vol. 243 No. 1 **1996**; edited by S. Ananthakrishnan; A. Pramesh Rao., p.209-213
https://ui.adsabs.harvard.edu/link_gateway/1996Ap%26SS.243..209B/ADS_PDF
The powerful cosmic ray flare of **Sept. 29, 1989** occurred behind the limb and was observed over a wide spectral range. The analysis of optical, radio, and other relevant data suggest two phases of energy release. After an impulsive phase a prolonged post eruption energy release occurred in an extended region of the corona following the eruption of a large coronal mass ejection (CME). This phase is responsible for numerous coronal and interplanetary phenomena including the ground-level increase of cosmic rays.

Solar flares associated coronal mass ejections in case of type II radio bursts

Beena **Bhatt** , Lalan Prasad, Harish Chandra, Suman Garia
Astrophysics and Space Science August **2016**, 361:265
We have statistically studied 220 events from 1996 to 2008 (i.e. solar cycle 23). Two set of flare-CME is examined one with Deca-hectometric (DH) type II and other without DH type II radio burst. Out of 220 events 135 (flare-halo CME) are accompanied with DH type II radio burst and 85 are without DH type II radio burst. Statistical analysis is performed to examine the distribution of solar flare-halo CME around the solar disk and to investigate the relationship between solar flare and halo CME parameters in case of with and without DH type II radio burst. In our analysis we have observed that: (i) 10–20° latitudinal belt is more effective than the other belts for DH type II and without DH type II radio burst. In this belt, the southern region is more effective in case of DH type II radio burst, whereas in case of without DH type II radio burst dominance exits in the northern region. (ii) 0–10° longitudinal belt is more effective than the other belts for DH type II radio burst and without DH type II radio burst. In this belt, the western region is more effective in case of DH type II radio burst, while in case of without DH type II radio burst dominance exits in the eastern region. (iii) Mean speed of halo CMEs (1382 km/s) with DH type II radio burst is more than the mean speed of halo CMEs (775 km/s) without DH type II radio burst. (iv) Maximum number of M-class flares is found in both the cases. (v) Average speed of halo CMEs in each class accompanied with DH type II radio burst is higher than the average speed of halo CMEs in each class without DH type II radio burst. (vi) Average speed of halo CMEs, associated with X-class flares, is greater than the other class of solar flares in both the cases.

Supervised convolutional neural networks for classification of flaring and nonflaring active regions using line-of-sight magnetograms

Shamik **Bhattacharjee**, Rasha Alshehhi, Dattaraj B. Dhuri, Shravan M. Hanasoge

ApJ **898** 98 **2020**
https://arxiv.org/pdf/2005.13333.pdf
https://doi.org/10.3847/1538-4357/ab9c29
Solar flares are explosions in the solar atmosphere that release intense bursts of short-wavelength radiation and are capable of producing severe space-weather consequences. Flares release free energy built up in coronal fields, which are rooted in active regions (ARs) on the photosphere, via magnetic reconnection. The exact processes that lead to reconnection are not fully known and therefore reliable forecasting of flares is challenging. Recently, photospheric magnetic-field data has been extensively analysed using machine learning (ML) and these studies suggest that flare-forecasting accuracy does not strongly depend on how long in advance flares are predicted (Bobra & Couvidat 2015; Raboonik et al. 2017; Huang et al. 2018). Here, we use ML to understand the evolution of AR magnetic fields before and after flares. We explicitly train convolutional neural networks (CNNs) to classify SDO/HMI line-of-sight magnetograms into ARs producing at least one M- or X-class flare or as nonflaring. We find that flaring ARs remain in flare-productive states -- marked by recall >60% with a peak of ~ 80% -- days before and after flares. We use occlusion maps and statistical analysis to show that the CNN pays attention to regions between the opposite polarities from ARs and the CNN output is dominantly decided by the total unsigned line-of-sight flux of ARs. Using synthetic bipole magnetograms, we find spurious dependencies of the CNN output on magnetogram dimensions for a given bipole size. Our results suggest that it is important to use CNN designs that eliminate such artifacts in CNN applications for processing magnetograms and, in general, solar image data. **2013.04.08, 2014.01.05, 2014.03.19, 2014.03.26, 2014.04.14, 2015.07.10**

Morphological evidence for nanoflares heating warm loops in the solar corona

Y. **Bi**, J. J. Yang, Y. Qin, Z. P. Qiang, J. C. Hong, B. Yang, Z. Xu, H. Liu, K. F. Ji
A&A **2023**
https://arxiv.org/pdf/2309.10049.pdf
Nanoflares are impulsive energy releases by magnetic reconnection in the braided coronal magnetic field, which is a potential mechanism for heating the corona. However, there are still sporadic observations of the interchange of braiding structure segments and footpoints inside coronal loops, which is predicted to be the morphological evolution of the reconnecting magnetic bundles in the nanoflare picture. This work aims to detect the evolutions of the pairs of braiding strands within the apparent single coronal loops observed in Atmospheric Imaging Assembly (AIA) images. The loop strands are detected on two kinds of upsampled AIA 193 Å images, which are obtained by upscaling the Point Spread Function matched AIA images via Bicubic interpolation and are generated using a super-resolution convolutional neural network, respectively. The architecture of the network is designed to map the AIA images to unprecedentedly high spatial resolution coronal images taken by High-resolution Coronal Imager (Hi-C) during its brief flight. At times, pairs of separate strands that appear braided together later evolved into pairs of almost parallel strands with completely exchanged parts. These evolutions offer morphological evidence that magnetic reconnections between the braiding strands have taken place, which is further supported by the appearance of transient hot emissions containing significant high-temperature components (T > 5MK) at the footpoints of the braiding structures. The brief appearances of the two rearranging strands support that magnetic reconnections have occurred within what appears to be a single AIA loop. **22 Jun 2010, 30 Aug 2011, 5 January 2012**

A Survey of Changes in Magnetic Helicity Flux on the Photosphere During Relatively Low Class Flares

Yi **Bi**, Ying D Liu, Yanxiao Liu, Jiayan Yang, Zhe Xu, Kaifan JI
ApJ **865** 139 **2018**
https://arxiv.org/pdf/1808.04591.pdf
Using the 135-second cadence of the photospheric vector data provided by the Helioseismic and Magnetic Imager telescope on board the Solar Dynamic Observatory, we examined the time-evolution of magnetic helicity fluxes across the photosphere during 16 flares with the energy class lower than M5.0. During the flare in 4 out of 16 events, we found impulsive changes in the helicity fluxes. This indicates that even the flare with less energy could be associated with anomalistic transportation of the magnetic helicity across the photosphere. Accompanying the impulsive helicity fluxes, the poynting fluxes across the photosphere evolved from positive to negative. As such, the transportations of magnetic energy across the photosphere were toward solar interior during these flares. In each of the 4 events, the impulsive change in the helicity flux was always mainly contributed by abrupt change in horizontal velocity field on a sunspot located near the flaring polarity inversion line. The velocity field on each sunspot shows either an obvious vortex patten or an shearing patten relative to the another magnetic polarity, which tended to relax the magnetic twist or shear in the corona. During these flares, abrupt change in the Lorentz force acting on these sunspots were found. The rotational motions and shearing motions of these sunspots always had the same directions with the resultant Lorentz forces. These results support the view that the impulsive helicity transportation during the flare could be driven by the change in the Lorentz force applied on the photosphere. **2011-11-15, 2013-12-28, 2014-08-25, 2015-11-09**
Table 1. A list of flares surveyed (2011-2015)

The Photospheric Vortex Flows during a Solar Flare

Yi **Bi**, Jiayan Yang, Yunchun Jiang, Junchao Hong, Zhe Xu, Zhining Qu, and Kaifang Ji
2017 ApJL 849 L35

The rotational motions of the photospheric magnetic flux play a role in magnetic twist transportation between the corona and the solar interior. Using observations from the Helioseismic and Magnetic Imager on board the Solar Dynamic Observatory (SDO), we found one counterclockwise and two clockwise vortex flows on the photosphere in the NOAA active region 12371 during the flare SOL**2015-06-22**T18:23 (M6.5). The counterclockwise vortex was located on the footpoint of the erupting hot channels observed by the Atmospheric Imaging Assembly (AIA) Telescope on board SDO. The two clockwise vortices resided on either side of the polarity inversion line. At these vortices, the impulsive and irreversible change in the photospheric vector magnetic field were detected. The resulting change in the photospheric Lorentz force provides a torque in each vortex, which has the same direction with each vortex. A magnetic field extrapolation model shows that the coronal field starting from the two clockwise vortices suffered significant shrinkage during the changeover period of the photospheric field. Moreover, some of the modeled field rooted in the counterclockwise vortex displays a pronounced expansion during the flare. These results suggest that the clockwise vortices could result from the contraction of the magnetic field lines during the flare, while the counterclockwise vortex may be attributed to the expansion of the eruptive flux rope as observed in the AIA images.

Heating and cooling of coronal loops with turbulent suppression of parallel heat conduction

Nicolas **Bian**, A. Gordon Emslie, Duncan Horne, Eduard P. Kontar
ApJ **852** 127 **2017**
https://arxiv.org/pdf/1711.11388.pdf

Using the "enthalpy-based thermal evolution of loops" (EBTEL) model, we investigate the hydrodynamics of the plasma in a flaring coronal loop in which heat conduction is limited by turbulent scattering of the electrons that transport the thermal heat flux. The EBTEL equations are solved analytically in each of the two (conduction-dominated and radiation-dominated) cooling phases. Comparison of the results with typical observed cooling times in solar flares shows that the turbulent mean free-path λ_T lies in a range corresponding to a regime in which classical (collision-dominated) conduction plays at most a limited role. We also consider the magnitude and duration of the heat input that is necessary to account for the enhanced values of temperature and density at the beginning of the cooling phase and for the observed cooling times. We find through numerical modeling that in order to produce a peak temperature $\simeq 1.5\times 10^7$ K and a 200 s cooling time consistent with observations, the flare heating profile must extend over a significant period of time; in particular, its lingering role must be taken into consideration in any description of the cooling phase. Comparison with observationally-inferred values of post-flare loop temperatures, densities, and cooling times thus leads to useful constraints on both the magnitude and duration of the magnetic energy release in the loop, as well as on the value of the turbulent mean free-path λ_T.

The Power of Turbulence

Nic **Bian**
RHESSI Nuggets #308 September **2017**
http://sprg.ssl.berkeley.edu/~tohban/wiki/index.php/The_Power_of_Turbulence

Turbulent energy content may underlie flare energy transfer, recconnection, and particle acceleration.
2013-05-13

The role of diffusion in the transport of energetic electrons during solar flares

Nicolas H. **Bian**, A. Gordon Emslie, Eduard P. Kontar
ApJ 835 262 **2017**
https://arxiv.org/pdf/1612.09456v1.pdf

The transport of the energy contained in suprathermal electrons in solar flares plays a key role in our understanding of many aspects of flare physics, from the spatial distributions of hard X-ray emission and energy deposition in the ambient atmosphere to global energetics. Historically the transport of these particles has been largely treated through a deterministic approach, in which first-order secular energy loss to electrons in the ambient target is treated as the dominant effect, with second-order diffusive terms (in both energy and angle) being generally either treated as a small correction or even neglected. We here critically analyze this approach, and we show that spatial diffusion through pitch-angle scattering necessarily plays a very significant role in the transport of electrons. We further show that a satisfactory treatment of the diffusion process requires consideration of non-local effects, so that the electron flux depends not just on the local gradient of the electron distribution function but on the value of this gradient within an extended region encompassing a significant fraction of a mean free path. Our analysis applies generally to pitch-angle scattering by a variety of mechanisms, from Coulomb collisions to turbulent scattering. We further show that the spatial transport of electrons along the magnetic field of a flaring loop can be modeled rather effectively as a Continuous Time Random Walk with velocity-dependent probability distribution functions of jump sizes and occurrences, both of which can be expressed in terms of the scattering mean free path.

Anomalous Cooling of Coronal Loops with Turbulent Suppression of Thermal Conduction

Nicolas H. **Bian**, Jonathan M. Watters, Eduard P. Kontar, A. Gordon Emslie

ApJ 833 76 **2016**

https://arxiv.org/pdf/1610.04732v1.pdf

We investigate the impact of turbulent suppression of parallel heat conduction on the cooling of post-flare coronal loops. Depending on the value of the mean free path λT associated with the turbulent scattering process, we identify four main cooling scenarios. The overall temperature evolution, from an initial temperature in excess of 107~K, is modeled in each case, highlighting the evolution of the dominant cooling mechanism throughout the cooling process. Comparison with observed cooling times allows the value of λT to be constrained, and interestingly this range corresponds to situations where collision-dominated conduction plays a very limited role, or even no role at all, in the cooling of post-flare coronal loops.

Suppression of parallel transport in turbulent magnetized plasmas and its impact on non-thermal and thermal aspects of solar flares

Bian, Nicolas H., Kontar, Eduard P., and Emslie, A. Gordon

ApJ 824 78 **2016**

http://arxiv.org/pdf/1603.08672v1.pdf

The transport of the energy contained in electrons, both thermal and suprathermal, in solar flares plays a key role in our understanding of many aspects of the flare phenomenon, from the spatial distribution of hard X-ray emission to global energetics. Motivated by recent *RHESSI* observations that point to the existence of a mechanism that confines electrons to the coronal parts of flare loops more effectively than Coulomb collisions, we here consider the impact of pitch-angle scattering off turbulent magnetic fluctuations on the parallel transport of electrons in flaring coronal loops. It is shown that the presence of such a scattering mechanism in addition to Coulomb collisional scattering can significantly reduce the parallel thermal and electrical conductivities relative to their collisional values. We provide illustrative expressions for the resulting thermoelectric coefficients that relate the thermal flux and electrical current density to the temperature gradient and the applied electric field. We then evaluate the effect of these modified transport coefficients on the flare coronal temperature that can be attained, on the post-impulsive-phase cooling of heated coronal plasma, and on the importance of the beam-neutralizing return current on both ambient heating and the energy loss rate of accelerated electrons. We also discuss the possible ways in which anomalous transport processes have an impact on the required overall energy associated with accelerated electrons in solar flares.

The Formation of Kappa Distributions in Solar Flares

Nicolas **Bian** and Duncan Stackpole

RHESSI Science Nugget, No. 238, Oct **2014**

It turns out that a kappa distribution can arise naturally from Coulomb collisions, as in a coronal thick target.

The Formation of Kappa-Distribution Accelerated Electron Populations in Solar Flares

Bian, Nicolas H., Emslie, A. Gordon, Stackhouse, Duncan J., Kontar, Eduard P.

ApJ, 796 142 **2014**

http://arxiv.org/pdf/1410.0819v2.pdf

Driven by recent RHESSI observations of confined loop-top hard X-ray sources in solar flares, we consider stochastic acceleration of electrons in the presence of Coulomb collisions. If electron escape from the acceleration region can be neglected, the electron distribution function is determined by a balance between diffusive acceleration and collisions. Such a scenario admits a stationary solution for the electron distribution function that takes the form of a kappa distribution. We show that the evolution toward this kappa distribution involves a "wave front" propagating forwards in velocity space, so that electrons of higher energy are accelerated later; the acceleration time scales with energy according to \tau\rm acc \sim E3/2. At sufficiently high energies escape from the finite-length acceleration region will eventually dominate. For such energies, the electron velocity distribution function is obtained by solving a time-dependent Fokker-Planck equation in the "leaky-box" approximation. Solutions are obtained in the limit of a small escape rate from an acceleration region that can effectively be considered a thick target.

Stochastic Acceleration by Multi-Island Contraction during Turbulent Magnetic Reconnection

Bian, Nicolas H.; Kontar, Eduard P.
Physical Review Letters, vol. 110, Issue 15, id. 151101, **2013**
https://arxiv.org/pdf/1302.6090.pdf
DOI: 10.1103/PhysRevLett.110.151101
The acceleration of charged particles in magnetized plasmas is considered during turbulent multi-island magnetic reconnection. The particle acceleration model is constructed for an ensemble of islands which produce adiabatic compression of the particles. The model takes into account the statistical fluctuations in the compression rate experienced by the particles during their transport in the acceleration region. The evolution of the particle distribution function is described as a simultaneous first- and second-order Fermi acceleration process. While the efficiency of the first-order process is controlled by the average rate of compression, the second-order process involves the variance in the compression rate. Moreover, the acceleration efficiency associated with the second-order process involves both the Eulerian properties of the compression field and the Lagrangian properties of the particles. The stochastic contribution to the acceleration is nonresonant and can dominate the systematic part in the case of a large variance in the compression rate. The model addresses the role of the second-order process, how the latter can be related to the large-scale turbulent transport of particles, and explains some features of the numerical simulations of particle acceleration by multi-island contraction during magnetic reconnection.

A CLASSIFICATION SCHEME FOR TURBULENT ACCELERATION PROCESSES IN SOLAR FLARES

Nicolas **Bian**1, A. Gordon Emslie2, and Eduard P. Kontar
2012 ApJ 754 103
We establish a classification scheme for stochastic acceleration models involving low-frequency plasma turbulence in a strongly magnetized plasma. This classification takes into account both the properties of the accelerating electromagnetic field, and the nature of the transport of charged particles in the acceleration region. We group the acceleration processes as either resonant, non-resonant, or resonant-broadened, depending on whether the particle motion is free-streaming along the magnetic field, diffusive, or a combination of the two. Stochastic acceleration by moving magnetic mirrors and adiabatic compressions are addressed as illustrative examples. We obtain expressions for the momentum-dependent diffusion coefficient D(p), both for general forms of the accelerating force and for the situation when the electromagnetic force is wave-like, with a specified dispersion relation $\omega = \omega(k)$. Finally, for models considered, we calculate the energy-dependent acceleration time, a quantity that can be directly compared with observations of the time profile of the radiation field produced by the accelerated particles, such as those occuring during solar flares.

Turbulent cross-field transport of non-thermal electrons in coronal loops: theory and observations

N. H. **Bian**, E. P. Kontar and A. L. MacKinnon
A&A 535, A18 (**2011**)
Context. A fundamental problem in astrophysics is the interaction between magnetic turbulence and charged particles. It is now possible to use Ramaty High Energy Solar Spectroscopic Imager (RHESSI) observations of hard X-rays (HXR) emitted by electrons to identify the presence of turbulence and to estimate the magnitude of the magnetic field line diffusion coefficient at least in dense coronal flaring loops.
Aims. We discuss the various possible regimes of cross-field transport of non-thermal electrons resulting from broadband magnetic turbulence in coronal loops. The importance of the Kubo number K as a governing parameter is emphasized and results applicable in both the large and small Kubo number limits are collected.
Methods. Generic models, based on concepts and insights developed in the statistical theory of transport, are applied to the coronal loops and to the interpretation of hard X-ray imaging data in solar flares. The role of trapping effects, which become important in the non-linear regime of transport, is taken into account in the interpretation of the data.
Results. For this flaring solar loop, we constrain the ranges of parallel and perpendicular correlation lengths of turbulent magnetic fields and possible Kubo numbers. We show that a substantial amount of magnetic fluctuations with energy ~1% (or more) of the background field can be inferred from the measurements of the magnetic diffusion coefficient inside thick-target coronal loops.

Analysis of the Stellar Occultations During the Unprecedented Long-Duration Flare

Kamil **Bicz**, Robert Falewicz, Petr Heinzel, Małgorzata Pietras, Paweł Preś
ApJL **2024**
https://arxiv.org/pdf/2408.02649

In strong stellar and solar flares flare loops typically appear during the decay phase, providing an additional contribution to the flare emission and, possibly, obscuring the flare emission. Super-flares, common in active, cool stars, persist mostly from minutes to several hours and alter the star's luminosity across the electromagnetic spectrum. Recent observations of a young main-sequence star reveal a distinctive cool loop arcade forming above the flaring region during a 27-hour superflare event, obscuring the region multiple times. Analysis of these occultations enables the estimation of the arcade's geometry and physical properties. The arcade's size expanded from 0.213 to 0.391 R∗ at a speed of approximately 3.5km/s. The covering structure exhibited a thickness below 12200km, with electron densities ranging from 1013 to 1014cm−3 and temperatures below 7600K, 6400K, and 5077K for successive occultations. Additionally, the flare's maximum emission temperature has to exceed 12000K for the occultations to appear. Comparing these parameters with known values from other stars and the Sun suggests the structure's nature as an arcade of cool flare loops. For the first time, we present the physical parameters and the reconstructed geometry of the cool flare loops that obscure the flaring region during the gradual phase of a long-duration flare on a star other than the Sun.

HELIOSEISMOLOGY OF PRE-EMERGING ACTIVE REGIONS. II. AVERAGE EMERGENCE PROPERTIES

A. C. **Birch**1,2, D. C. Braun1, K. D. Leka1, G. Barnes1, and B. Javornik
2013 ApJ 762 131
We report on average subsurface properties of pre-emerging active regions as compared to areas where no active region emergence was detected. Helioseismic holography is applied to samples of the two populations (pre-emergence and without emergence), each sample having over 100 members, which were selected to minimize systematic bias, as described in Leka et al. We find that there are statistically significant signatures (i.e., difference in the means of more than a few standard errors) in the average subsurface flows and the apparent wave speed that precede the formation of an active region. The measurements here rule out spatially extended flows of more than about 15 m s–1 in the top 20 Mm below the photosphere over the course of the day preceding the start of visible emergence. These measurements place strong constraints on models of active region formation.

Can Substorm Particle Acceleration Be Applied to Solar Flares?

J. **Birn**1,2, M. Battaglia3, L. Fletcher4, M. Hesse5, and T. Neukirch6
2017 ApJ 848 116
Using test particle studies in the electromagnetic fields of three-dimensional magnetohydrodynamic (MHD) simulations of magnetic reconnection, we study the energization of charged particles in the context of the standard two-ribbon flare picture in analogy to the standard magnetospheric substorm paradigm. In particular, we investigate the effects of the collapsing field ("collapsing magnetic trap") below a reconnection site, which has been demonstrated to be the major acceleration mechanism that causes energetic particle acceleration and injections observed in Earth's magnetotail associated with substorms and other impulsive events. We contrast an initially force-free, high-shear field (low beta) with low and moderate shear, finite-pressure (high-beta) arcade structures, where beta represents the ratio between gas (plasma) and magnetic pressure. We demonstrate that the energization affects large numbers of particles, but the acceleration is modest in the presence of a significant shear field. Without incorporating loss mechanisms, the effect on particles at different energies is similar, akin to adiabatic heating, and thus is not a likely mechanism to generate a power-law tail onto a (heated or not heated) Maxwellian velocity distribution.

ENERGY RELEASE AND TRANSFER IN SOLAR FLARES: SIMULATIONS OF THREE-DIMENSIONAL RECONNECTION

J. **Birn**1, L. Fletcher2, M. Hesse3, and T. Neukirch4
Astrophysical Journal, 695:1151–1162, **2009**
http://www.iop.org/EJ/toc/-alert=43190/0004-637X/695/2
Using three-dimensional magnetohydrodynamic simulations we investigate energy release and transfer in a threedimensional extension of the standard two-ribbon flare picture. In this scenario, reconnection is initiated in a thin current sheet (suggested to form below a departing coronal mass ejection) above a bipolar magnetic field. Two cases are contrasted: an initially force-free current sheet (low beta) and a finite-pressure current sheet (high beta), where beta represents the ratio between gas (plasma) and magnetic pressure. The energy conversion process from reconnection consists of incoming Poynting flux turned into up- and downgoing Poynting flux, enthalpy flux, and bulk kinetic energy flux. In the low-beta case, the outgoing Poynting flux is the dominant contribution, whereas the outgoing enthalpy flux dominates in the high-beta case. The bulk kinetic energy flux is only a minor contribution in the downward direction. The dominance of the downgoing Poynting flux in the low-beta case is consistent with an alternative to the thick target electron beam model for solar flare energy transport, suggested recently by Fletcher & Hudson, whereas the enthalpy flux may act as an alternative transport mechanism. For plausible characteristic parameters of the reconnecting field configuration, we obtain energy release timescales and energy output rates that compare favorably with those inferred from observations for the

impulsive phase of flares. Significant enthalpy flux and heating are found even in the initially force-free case with very small background beta, resulting mostly from adiabatic compression rather than Ohmic dissipation. The energy conversion mechanism is most easily understood as a two-step process (although the two steps may occur essentially simultaneously): the first step is the acceleration of the plasma by Lorentz forces in layers akin to the slow shocks in the Petschek reconnection model, involving the conversion of magnetic energy to bulk kinetic energy. However, due to pressure gradient forces that oppose the Lorentz forces in approximate, or partial force balance, the accelerated plasma becomes slowed down and compressed, whereby the bulk kinetic energy is converted to heat, either locally deposited or transported away by enthalpy flux and deposited later. This mechanism is most relevant in the downflow region, which is more strongly governed by force balance; it is less important in the outflow above the reconnection site, where more energy remains in the form of fast bulk flow.

Book: J. **Birn** and E. R. Priest, Editors,
"**Reconnection of Magnetic Fields, Magnetohydrodynamics and Collisionless Theory and Observations**," Cambridge University Press, **2007**, ISBN-13 978-0-521-85420-7 or ISBN-10 0-521-85420-2

Case studies on pre-eruptive X-class flares using R-value in the lower solar atmosphere

Shreeyesh **Biswal**, Marianna B. Korsós, Manolis K. Georgoulis, Alexander Nindos, Spiros Patsourakos, Robertus Erdélyi
ApJ **974** 259 **2024**
https://arxiv.org/pdf/2408.04018
https://iopscience.iop.org/article/10.3847/1538-4357/ad6c33/pdf
The R-value is a measure of the strength of photospheric magnetic Polarity Inversion Lines (PILs) in Active Regions (ARs). This work investigates the possibility of a relation between R-value variations and the occurrence of X-class flares in ARs, not in the solar photosphere, as usual, but above it in regions, closer to where flares occur. The modus operandi is to extrapolate the Solar Dynamic Observatory's (SDO) Helioseismic and Magnetic Imager (HMI) magnetogram data up to a height of 3.24 Mm above the photosphere and then compute the R-value based on the extrapolated magnetic field. Recent studies have shown that certain flare-predictive parameters such as the horizontal gradient of the vertical magnetic field and magnetic helicity may improve flare prediction lead times significantly if studied at a specific height range above the photosphere, called the Optimal Height Range (OHR). Here we define the OHR as a collection of heights where a sudden but sustained increase in R-value is found. For the eight case studies discussed in this paper, our results indicate that it is possible for OHRs to exist in the low solar atmosphere (between 0.36 - 3.24 Mm), where R-value spikes occur 48-68 hrs before the first X-class flare of an emerging AR. The temporal evolution of R-value before the first X-class flare for an emerging AR is also found to be distinct from that of non-flaring ARs. For X-class flares associated with non-emerging ARs, an OHR could not be found. **13-15 Feb 2011, 2011/03/06-09, 2014/03/28-29, 2017/09/03-06**

Performance of Major Flare Watches from the Max Millennium Program (2001-2010)

D. Shaun **Bloomfield**, Peter T. Gallagher, William H. Marquette, Ryan O. Milligan, Richard C. Canfield
Solar Phys. Vol. 291, Issue 2 **2016**
http://arxiv.org/pdf/1512.04518v1.pdf
The physical processes that trigger solar flares are not well understood and significant debate remains around processes governing particle acceleration, energy partition, and particle and energy transport. Observations at high resolution in energy, time, and space are required in multiple energy ranges over the whole course of many flares in order to build an understanding of these processes. Obtaining high-quality, co-temporal data from ground- and space- based instruments is crucial to achieving this goal and was the primary motivation for starting the Max Millennium program and Major Flare Watch (MFW) alerts, aimed at coordinating observations of all flares >X1 GOES X-ray classification (including those partially occulted by the limb). We present a review of the performance of MFWs from 1 February 2001 to 31 May 2010, inclusive, that finds: (1) 220 MFWs were issued in 3,407 days considered (6.5% duty cycle), with these occurring in 32 uninterrupted periods that typically last 2-8 days; (2) 56% of flares >X1 were caught, occurring in 19% of MFW days; (3) MFW periods ended at suitable times, but substantial gain could have been achieved in percentage of flares caught if periods had started 24 h earlier; (4) MFWs successfully forecast X-class flares with a true skill statistic (TSS) verification metric score of 0.500, that is comparable to a categorical flare/no-flare interpretation of the NOAA Space Weather Prediction Centre probabilistic forecasts (TSS = 0.488).
Table 2. Details of >X1 flares missed by MFWs and their source active regions.

Mysteries of Flare/CME Initiation **Interesting**

Shaun **Bloomfield** and HughHudson

RHESSI Science Nugget, No. 228, June **2014**
http://sprg.ssl.berkeley.edu/~tohban/wiki/index.php/RHESSI_Science_Nuggets
nearby major flares can occur in pairs - but how? **10 June 2014**

TOWARD RELIABLE BENCHMARKING OF SOLAR FLARE FORECASTING METHODS

D. Shaun **Bloomfield**1, Paul A. Higgins1, R. T. James McAteer2 and Peter T. Gallagher
2012 ApJ 747 L41
http://arxiv.org/pdf/1202.5995v1.pdf
Solar flares occur in complex sunspot groups, but it remains unclear how the probability of producing a flare of a given magnitude relates to the characteristics of the sunspot group. Here, we use Geostationary Operational Environmental Satellite X-ray flares and McIntosh group classifications from solar cycles 21 and 22 to calculate average flare rates for each McIntosh class and use these to determine Poisson probabilities for different flare magnitudes. Forecast verification measures are studied to find optimum thresholds to convert Poisson flare probabilities into yes/no predictions of cycle 23 flares. A case is presented to adopt the true skill statistic (TSS) as a standard for forecast comparison over the commonly used Heidke skill score (HSS). In predicting flares over 24 hr, the maximum values of TSS achieved are 0.44 (C-class), 0.53 (M-class), 0.74 (X-class), 0.54 (≥M1.0), and 0.46 (≥C1.0). The maximum values of HSS are 0.38 (C-class), 0.27 (M-class), 0.14 (X-class), 0.28 (≥M1.0), and 0.41 (≥C1.0). These show that Poisson probabilities perform comparably to some more complex prediction systems, but the overall inaccuracy highlights the problem with using average values to represent flaring rate distributions.

Predicting Coronal Mass Ejections Using Machine Learning Methods

Monica G. **Bobra**, Stathis Ilonidis
ApJ 821, Issue 2, article id. 127 **2016**
http://arxiv.org/pdf/1603.03775v1.pdf **File**
https://iopscience.iop.org/article/10.3847/0004-637X/821/2/127/pdf
Of all the activity observed on the Sun, two of the most energetic events are flares and Coronal Mass Ejections (CMEs). Usually, solar active regions that produce large flares will also produce a CME, but this is not always true (Yashiro et al., 2005). Despite advances in numerical modeling, it is still unclear which circumstances will produce a CME (Webb & Howard, 2012). Therefore, it is worthwhile to empirically determine which features distinguish flares associated with CMEs from flares that are not. At this time, no extensive study has used physically meaningful features of active regions to distinguish between these two populations. As such, we attempt to do so by using features derived from [1] photospheric vector magnetic field data taken by the Solar Dynamics Observatory's Helioseismic and Magnetic Imager instrument and [2] X-ray flux data from the Geostationary Operational Environmental Satellite's X-ray Flux instrument. We build a catalog of active regions that either produced both a flare and a CME (the positive class) or simply a flare (the negative class). We then use machine-learning algorithms to [1] determine which features distinguish these two populations, and [2] forecast whether an active region that produces an M- or X-class flare will also produce a CME. We compute the True Skill Statistic, a forecast verification metric, and find that it is a relatively high value of approximately 0.8 plus or minus 0.2. We conclude that a combination of six parameters, which are all intensive in nature, will capture most of the relevant information contained in the photospheric magnetic field.

Solar Flare Prediction Using SDO/HMI Vector Magnetic Field Data with a Machine-Learning Algorithm

Monica G. **Bobra**, Sebastien Couvidat
ApJ, 798, Issue 2, article id. 135 **2015**
http://arxiv.org/pdf/1411.1405v1.pdf
https://iopscience.iop.org/article/10.1088/0004-637X/798/2/135/pdf
We attempt to forecast M-and X-class solar flares using a machine-learning algorithm, called Support Vector Machine (SVM), and four years of data from the Solar Dynamics Observatory's Helioseismic and Magnetic Imager, the first instrument to continuously map the full-disk photospheric vector magnetic field from space. Most flare forecasting efforts described in the literature use either line-of-sight magnetograms or a relatively small number of ground-based vector magnetograms. This is the first time a large dataset of vector magnetograms has been used to forecast solar flares. We build a catalog of flaring and non-flaring active regions sampled from a database of 2,071 active regions, comprised of 1.5 million active region patches of vector magnetic field data, and characterize each active region by 25 parameters. We then train and test the machine-learning algorithm and we estimate its performances using forecast verification metrics with an emphasis on the True Skill Statistic (TSS). We obtain relatively high TSS scores and overall predictive abilities. We surmise that this is partly due to fine-tuning the SVM for this purpose and also to an advantageous set of features that can only be calculated from vector magnetic field data. We also apply a feature selection algorithm to determine which of our 25 features are useful for discriminating between flaring and non-flaring active regions and conclude that only a handful are needed for good predictive abilities. **March 7, 2012,**

Solar Flare Forecasting Using HMI Vector Magnetic Field Data with a Support Vector Machine Algorithm

Monica **Bobra** and Sebastien Couvidat
HMI Science Nuggets, #25, **2014**
http://hmi.stanford.edu/hminuggets/?p=911
We attempt to forecast M-and X-class flares using a machine-learning algorithm, called Support Vector Machine (SVM), and four years of HMI data.

The motions of the hard X-ray sources in solar flares: Images and statistics,

Bogachev, S.A., Somov, B.V., Kosugi, T., and Sakao, T.,
Astrophys. J., **2005**, vol. 630, p. 561.

SoFAST: Automated Flare Detection with the PROBA2/SWAP EUV Imager

K. **Bonte**, D. Berghmans, A. De Groof, K. Steed, S. Poedts
Solar Physics, August **2013**, Volume 286, Issue 1, pp 185-199
The Sun Watcher with Active Pixels and Image Processing (SWAP) EUV imager onboard PROBA2 provides a non-stop stream of coronal extreme-ultraviolet (EUV) images at a cadence of typically 130 seconds. These images show the solar drivers of space-weather, such as flares and erupting filaments. We have developed a software tool that automatically processes the images and localises and identifies flares. On one hand, the output of this software tool is intended as a service to the Space Weather Segment of ESA's Space Situational Awareness (SSA) program. On the other hand, we consider the PROBA2/SWAP images as a model for the data from the Extreme Ultraviolet Imager (EUI) instrument prepared for the future Solar Orbiter mission, where onboard intelligence is required for prioritising data within the challenging telemetry quota. In this article we present the concept of the software, the first statistics on its effectiveness and the online display in real time of its results. Our results indicate that it is not only possible to detect EUV flares automatically in an acquired dataset, but that quantifying a range of EUV dynamics is also possible. The method is based on thresholding of macropixelled image sequences. The robustness and simplicity of the algorithm is a clear advantage for future onboard use.

The Effects of Oscillations and Collisions of Emerging Bipolar Regions on the Triggering of Solar Flares

C. **Boocock**1, K. Kusano2, and D. Tsiklauri1
2020 ApJ 900 65
https://doi.org/10.3847/1538-4357/aba61a
https://arxiv.org/pdf/2009.05457.pdf
https://iopscience.iop.org/article/10.3847/1538-4357/aba61a/pdf
The ability to predict the occurrence of solar flares in advance is important to humankind due to the potential damage they can cause to Earth's environment and infrastructure. It has been shown in Kusano et al. that a small-scale bipolar region (BR), with its flux reversed relative to the potential component of the overlying field, appearing near the polarity inversion line (PIL) is sufficient to effectively trigger a solar flare. In this study we perform further 3D magnetohydrodynamic simulations to study the effect that the motion of these small-scale BRs has on the effectiveness of flare triggering. The effect of two small-scale BRs colliding is also simulated. The results indicate that the strength of the triggered flare is dependent on how much of the overlying field is disrupted by the BR. Simulations of linear oscillations of the BR showed that oscillations along the PIL increase the flare strength while oscillations across the PIL detract from the flare strength. The flare strength is affected more by larger amplitude oscillations but is relatively insensitive to the frequency of oscillations. In the most extreme case the peak kinetic energy of the flare increased more than threefold compared to a non-oscillating BR. Simulations of torsional oscillations of the BR showed a very small effect on the flare strength. Finally, simulations of colliding BRs showed the generation of much stronger flares as the flares triggered by each individual BR coalesce. These results show that significantly stronger flares can result from motion of the BR along the PIL of a sheared field or from the presence of multiple BRs in the same region.

Comparison of the Hall Magnetohydrodynamics and Magnetohydrodynamics evolution of a flaring solar active region

Kamlesh **Bora**, Ramit Bhattacharyya, Avijeet Prasad, Bhuwan Joshi, Qiang Hu
ApJ **925** 197 **2021**
https://arxiv.org/pdf/2112.01785.pdf
https://iopscience.iop.org/article/10.3847/1538-4357/ac3bce/pdf

This work analyzes the Hall magnetohydrodynamics (HMHD) and magnetohydrodynamics (MHD) numerical simulations of a flaring solar active region as a testbed while idealizing the coronal Alfvén speed to be of two orders of magnitude lesser. HMHD supports faster magnetic reconnection and shows richer complexity in magnetic field line evolution compared to the MHD. The magnetic reconnections triggering the flare are explored by numerical simulations augmented with relevant multi-wavelength observations. The initial coronal magnetic field is constructed by non-force-free extrapolation of photospheric vector magnetic field. Magnetic structure involved in the flare is identified to be a flux rope, with its overlying magnetic field lines constituting the quasi-separatrix layers (QSLs) along with a three-dimensional null point and a null line. Compared to the MHD simulation, the HMHD simulation shows a higher and faster ascend of the rope together with the overlying field lines, which further reconnect at the QSL located higher up in the corona. The foot points of the field lines match better with the observations for the HMHD case with the central part of the flare ribbon located at the chromosphere. Additionally, field lines are found to rotate in a circular pattern in the HMHD, whereas no such rotation is seen in the MHD results. Interestingly, plasma is also observed to be rotating in a co-spatial chromospheric region, which makes the HMHD simulation more credible. Based on the aforementioned agreements, HMHD simulation is found to agree better with observations and, thus, opens up a novel avenue to explore.

Particle acceleration with anomalous pitch angle scattering in 3D separator reconnection

Alexei **Borissov**, Thomas Neukirch, Eduard Kontar, James Threlfall, Clare Parnell
A&A **2020**
https://arxiv.org/pdf/2001.07548.pdf

Understanding how the release of stored magnetic energy contributes to the generation of non-thermal high energy particles during solar flares is an important open problem in solar physics. Magnetic reconnection plays a fundamental role in the energy release and conversion processes taking place during flares. A common approach for investigating particle acceleration is to use test particles in fields derived from magnetohydrodynamic (MHD) simulations of reconnection. These MHD simulations use anomalous resistivities that are much larger than the Spitzer resistivity based on Coulomb collisions. The processes leading to enhanced resistivity should also affect the test particles. We explore the link between resistivity and particle orbits building on a previous study using a 2D MHD simulation of magnetic reconnection. This paper extends the previous investigation to a 3D magnetic reconnection configuration and to study the effect on test particle orbits. We carried out orbit calculations using a 3D MHD simulation of separator reconnection. We use the relativistic guiding centre approximation including stochastic pitch angle scattering. The effects of varying the resistivity and the models for pitch angle scattering on particle orbit trajectories, final positions, energy spectra, final pitch angle distribution, and orbit duration are all studied in detail. Pitch angle scattering widens collimated beams of orbit trajectories, allowing orbits to access previously unaccessible field lines; this causes final positions to spread to topological structures that were previously inaccessible. Scattered orbit energy spectra are found to be predominantly affected by the level of anomalous resistivity, with the pitch angle scattering model only playing a role in isolated cases. Scattering is found to play a crucial role in determining the pitch angle and orbit duration distributions.

Particle acceleration with anomalous pitch angle scattering in 2D MHD reconnection simulations

Alexei **Borissov**, Eduard P. Kontar, James Threlfall, Thomas Neukirch
A&A 605, A73 **2017**
https://arxiv.org/pdf/1709.00305.pdf
https://www.aanda.org/articles/aa/pdf/2017/09/aa31183-17.pdf

The conversion of magnetic energy into other forms during solar flares is one of the outstanding open problems in solar physics. It is generally accepted that magnetic reconnection plays a crucial role in these conversion processes. To achieve the rapid energy release required in solar flares, an anomalous resistivity, orders of magnitude higher than the Spitzer resistivity, is often used in MHD simulations of reconnection. Spitzer resistivity is based on Coulomb scattering, which becomes negligible at the high energies achieved by accelerated particles. As a result, simulations of particle acceleration in reconnection events are often performed in the absence of any interaction between accelerated particles and any background plasma. This need not be the case for scattering associated with anomalous resistivity caused by turbulence within solar flares, as the higher resistivity implies an elevated scattering rate. We present results of test particle calculations, with and without pitch angle scattering, subject to fields derived from MHD simulations of two-dimensional (2D) X-point reconnection. Scattering rates proportional to the ratio of the anomalous resistivity to the local Spitzer resistivity, as well as at fixed values, are considered. Pitch angle scattering, which is independent of the anomalous resistivity, causes higher maximum energies in comparison to those obtained without scattering. Scattering rates which are dependent on the local anomalous resistivity tend to produce fewer highly energised particles due to weaker scattering in the separatrices, even though scattering in the current sheet may be stronger when compared to resistivity-independent scattering. Strong scattering also causes an increase in the number of particles exiting the computational box in the reconnection outflow region, as opposed to along the separatrices as is the case in the absence of scattering.

Particle Acceleration in Collapsing Magnetic Traps with a Braking Plasma Jet

Alexei **Borissov**, Thomas Neukirch, James Threlfall
Solar Phys. Volume 291, Issue 5, pp 1385-1404 **2016**
http://arxiv.org/pdf/1605.06343v1.pdf

Collapsing magnetic traps (CMTs) are one proposed mechanism for generating non-thermal particle populations in solar flares. CMTs occur if an initially stretched magnetic field structure relaxes rapidly into a lower-energy configuration, which is believed to happen as a by-product of magnetic reconnection. A similar mechanism for energising particles has also been found to operate in the Earth's magnetotail. One particular feature proposed to be of importance for particle acceleration in the magnetotail is that of a braking plasma jet, i.e. a localised region of strong flow encountering stronger magnetic field which causes the jet to slow down and stop. Such a feature has not been included in previously proposed analytical models of CMTs for solar flares. In this work we incorporate a braking plasma jet into a well studied CMT model for the first time. We present results of test particle calculations in this new CMT model. We observe and characterise new types of particle behaviour caused by the magnetic structure of the jet braking region, which allows electrons to be trapped both in the braking jet region and the loop legs. We compare and contrast the behaviour of particle orbits for various parameter regimes of the underlying trap by examining particle trajectories, energy gains and the frequency with which different types of particle orbit are found for each parameter regime.

ELECTRON ACCELERATION IN CONTRACTING MAGNETIC ISLANDS DURING SOLAR FLARES

D. **Borovikov**1, V. Tenishev1, T. I. Gombosi1, S. E. Guidoni2,3, C. R. DeVore3, J. T. Karpen3, and S. K. Antiochos3
2017 ApJ 835 48
http://sci-hub.cc/doi/10.3847/1538-4357/835/1/48

Electron acceleration in solar flares is well known to be efficient at generating energetic particles that produce the observed bremsstrahlung X-ray spectra. One mechanism proposed to explain the observations is electron acceleration within contracting magnetic islands formed by magnetic reconnection in the flare current sheet. In a previous study, a numerical magnetohydrodynamic simulation of an eruptive solar flare was analyzed to estimate the associated electron acceleration due to island contraction. That analysis used a simple analytical model for the island structure and assumed conservation of the adiabatic invariants of particle motion. In this paper, we perform the first-ever rigorous integration of the guiding-center orbits of electrons in a modeled flare. An initially isotropic distribution of particles is seeded in a contracting island from the simulated eruption, and the subsequent evolution of these particles is followed using guiding-center theory. We find that the distribution function becomes increasingly anisotropic over time as the electrons' energy increases by up to a factor of five, in general agreement with the previous study. In addition, we show that the energized particles are concentrated on the Sunward side of the island, adjacent to the reconnection X-point in the flare current sheet. Furthermore, our analysis demonstrates that the electron energy gain is dominated by betatron acceleration in the compressed, strengthened magnetic field of the contracting island. Fermi acceleration by the shortened field lines of the island also contributes to the energy gain, but it is less effective than the betatron process.

PREDICTION OF SOLAR FLARE SIZE AND TIME-TO-FLARE USING SUPPORT VECTOR MACHINE REGRESSION

Laura E. **Boucheron**1, Amani Al-Ghraibah1, and R. T. James McAteer
2015 ApJ 812 51
http://arxiv.org/pdf/1511.01941v1.pdf

We study the prediction of solar flare size and time-to-flare using 38 features describing magnetic complexity of the photospheric magnetic field. This work uses support vector regression to formulate a mapping from the 38-dimensional feature space to a continuous-valued label vector representing flare size or time-to-flare. When we consider flaring regions only, we find an average error in estimating flare size of approximately half a geostationary operational environmental satellite (GOES) class. When we additionally consider non-flaring regions, we find an increased average error of approximately three-fourths a GOES class. We also consider thresholding the regressed flare size for the experiment containing both flaring and non-flaring regions and find a true positive rate of 0.69 and a true negative rate of 0.86 for flare prediction. The results for both of these size regression experiments are consistent across a wide range of predictive time windows, indicating that the magnetic complexity features may be persistent in appearance long before flare activity. This is supported by our larger error rates of some 40 hr in the time-to-flare regression problem. The 38 magnetic complexity features considered here appear to have discriminative potential for flare size, but their persistence in time makes them less discriminative for the time-to-flare problem.

Radio Observations of the 20 January 2005 X-class Flare

C. **Bouratzis** · P. Preka-Papadema · A. Hillaris · P. Tsitsipis · A. Kontogeorgos · V.G. Kurt · X. Moussas
Solar Phys, 267: 343–359, **2010; File**
We present a multi-frequency and multi-instrument study of the **20 January 2005** event. We focus mainly on the complex radio signatures and their association with the active phenomena taking place: flares, CMEs, particle acceleration, and magnetic restructuring. As a variety of energetic-particle accelerators and sources of radio bursts are present, in the flare – ejecta combination, we investigate their relative importance in the progress of this event. The dynamic spectra of ARTEMIS-IV – Wind/Waves – HiRAS, with 2000 MHz – 20 kHz frequency coverage, were used to track the evolution of the event from the low corona to the interplanetary space; these were supplemented with SXR, HXR, and γ-ray recordings. The observations were compared with the expected radio signatures and energetic-particle populations envisaged by the Standard Flare – CME model and the reconnection outflow termination shock model. A proper combination of these mechanisms seems to provide an adequate model for the interpretation of the observational data.

Coronal energy input and dissipation in a solar active region 3D MHD model

Ph.-A. **Bourdin**1,2, S. Bingert3 and H. Peter2
A&A 580, A72 (**2015**)
http://www.aanda.org/articles/aa/pdf/2015/08/aa25839-15.pdf
Context. We have conducted a 3D MHD simulation of the solar corona above an active region (AR) in full scale and high resolution, which shows coronal loops, and plasma flows within them, similar to observations.
Aims. We want to find the connection between the photospheric energy input by field-line braiding with the coronal energy conversion by Ohmic dissipation of induced currents.
Methods. To this end we compare the coronal energy input and dissipation within our simulation domain above different fields of view, e.g. for a small loops system in the AR core. We also choose an ensemble of field lines to compare, e.g., the magnetic energy input to the heating per particle along these field lines.
Results. We find an enhanced Ohmic dissipation of currents in the corona above areas that also have enhanced upwards-directed Poynting flux. These regions coincide with the regions where hot coronal loops within the AR core are observed. The coronal density plays a role in estimating the coronal temperature due to the generated heat input. A minimum flux density of about 200 Gauss is needed in the photosphere to heat a field line to coronal temperatures of about 1 MK.
Conclusions. This suggests that the field-line braiding mechanism provides the coronal energy input and that the Ohmic dissipation of induced currents dominates the coronal heating mechanism.
14 Nov. 2007

Observationally driven 3D magnetohydrodynamics model of the solar corona above an active region⋆

Ph.-A. **Bourdin**1,2, S. Bingert1 and H. Peter
A&A 555, A123 **(2013)**
Aims. The goal is to employ a 3D magnetohydrodynamics (MHD) model including spectral synthesis to model the corona in an observed solar active region. This will allow us to judge the merits of the coronal heating mechanism built into the 3D model.
Methods. Photospheric observations of the magnetic field and horizontal velocities in an active region are used to drive our coronal simulation from the bottom. The currents induced by this heat the corona through Ohmic dissipation. Heat conduction redistributes the energy that is lost in the end through optically thin radiation. Based on the MHD model, we synthesized profiles of coronal emission lines which can be directly compared to actual coronal observations of the very same active region.
Results. In the synthesized model data we find hot coronal loops which host siphon flows or which expand and lose mass through draining. These synthesized loops are at the same location as and show similar dynamics in terms of Doppler shifts to the observed structures. This match is shown through a comparison with Hinode data as well as with 3D stereoscopic reconstructions of data from STEREO.
Conclusions. The considerable match to the actual observations shows that the field-line braiding mechanism leading to the energy input in our corona provides the proper distribution of heat input in space and time. From this we conclude that in an active region the field-line braiding is the dominant heating process, at least at the spatial scales available to current observations.

FLOWS AT THE EDGE OF AN ACTIVE REGION: OBSERVATION AND INTERPRETATION

C. **Boutry**1,2, E. Buchlin1,2, J.-C. Vial1,2, and S. Régnier
2012 ApJ 752 13

Upflows observed at the edges of active regions have been proposed as the source of the slow solar wind. In the particular case of Active Region (AR) 10942, where such an upflow has been already observed, we want to evaluate the part of this upflow that actually remains confined in the magnetic loops that connect AR 10942 to AR 10943. Both active regions were visible simultaneously on the solar disk and were observed by STEREO/SECCHI EUVI. Using Hinode/EIS spectra, we determine the Doppler shifts and densities in AR 10943 and AR 10942 in order to evaluate the mass flows. We also perform magnetic field extrapolations to assess the connectivity between AR 10942 and AR 10943. AR 10943 displays a persistent downflow in Fe XII. Magnetic extrapolations including both ARs show that this downflow can be connected to the upflow in AR 10942. We estimate that the mass flow received by AR 10943 areas connected to AR 10942 represents about 18% of the mass flow from AR 10942. We conclude that the upflows observed on the edge of active regions represent either large-scale loops with mass flowing along them (accounting for about one-fifth of the total mass flow in this example) or open magnetic field structures where the slow solar wind originates.

MULTI-WAVELENGTH OBSERVATIONS OF SOLAR FLARES WITH A CONSTRAINED PEAK X-RAY FLUX

Trevor A. **Bowen**1,2, Paola Testa1, and Katharine K. Reeves
2013 ApJ 770 126
We present an analysis of soft X-ray (SXR) and extreme-ultraviolet (EUV) observations of solar flares with an approximate C8 Geostationary Operational Environmental Satellite (GOES) class. Our constraint on peak GOES SXR flux allows for the investigation of correlations between various flare parameters. We show that the duration of the decay phase of a flare is proportional to the duration of its rise phase. Additionally, we show significant correlations between the radiation emitted in the flare rise and decay phases. These results suggest that the total radiated energy of a given flare is proportional to the energy radiated during the rise phase alone. This partitioning of radiated energy between the rise and decay phases is observed in both SXR and EUV wavelengths. Though observations from the EUV Variability Experiment show significant variation in the behavior of individual EUV spectral lines during different C8 events, this work suggests that broadband EUV emission is well constrained. Furthermore, GOES and Atmospheric Imaging Assembly data allow us to determine several thermal parameters (e.g., temperature, volume, density, and emission measure) for the flares within our sample. Analysis of these parameters demonstrate that, within this constrained GOES class, the longer duration solar flares are cooler events with larger volumes capable of emitting vast amounts of radiation. The shortest C8 flares are typically the hottest events, smaller in physical size, and have lower associated total energies. These relationships are directly comparable with several scaling laws and flare loop models.
November 4, 2015

Solar neutrinos as indicators of the Sun's activity

O.M.**Boyarkin**, I.O.Boyarkina
International Journal of Modern Physics A, Vol. 35 (**2019**) 1950448
https://arxiv.org/pdf/2004.10056.pdf
Opportunity of the solar flares (SF's) prediction observing the solar neutrino fluxes is investigated. In three neutrino generations the evolution of the neutrino flux traveling the coupled sunspots (CS's) which are the SF source is considered. It is assumed that the neutrinos possess both the dipole magnetic moment and the anapole moment while the magnetic field above the CS's may reach the values 105−106 Gs, displays the twisting nature and has the nonpotential character. The possible resonance conversions of the solar neutrino flux are examined. Since the νeL→νμL resonance takes place before the convective zone, its existence can in no way be connected with the SF. However, when the solar neutrino flux moves through the CS's in the preflare period, then it may undergo the additional resonance conversions and, as a result, depleting the electron neutrinos flux may be observed.

PATTERNS OF ACTIVITY IN A GLOBAL MODEL OF A SOLAR ACTIVE REGION

S. J. **Bradshaw**1 and N. M. Viall
2016 ApJ 821 63 DOI: 10.3847/0004-637X/821/1/62
In this work we investigate the global activity patterns predicted from a model active region heated by distributions of nanoflares that have a range of frequencies. What differs is the average frequency of the distributions. The activity patterns are manifested in time lag maps of narrow-band instrument channel pairs. We combine hydrodynamic and forward modeling codes with a magnetic field extrapolation to create a model active region and apply the time lag method to synthetic observations. Our aim is not to reproduce a particular set of observations in detail, but to recover some typical properties and patterns observed in active regions. Our key findings are the following. (1) Cooling dominates the time lag signature and the time lags between the channel pairs are generally consistent with observed values. (2) Shorter coronal loops in the core cool more quickly than longer loops at the periphery. (3) All channel pairs show zero time lag when the line of sight passes through coronal loop footpoints. (4) There is strong evidence that plasma must be re-energized on a timescale comparable to the cooling timescale to reproduce the observed coronal activity, but it is likely that a relatively broad spectrum of heating frequencies are operating across active regions. (5) Due to their highly dynamic nature, we find nanoflare trains produce zero time lags along entire flux tubes in our model active region that are seen between the same channel pairs in observed active regions.

Patterns of Activity in a Global Model of a Solar Active Region

Stephen J. **Bradshaw**, Nicholeen M. Viall

2016

http://arxiv.org/pdf/1603.06670v1.pdf

In this work we investigate the global activity patterns predicted from a model active region heated by distributions of nanoflares that have a range of frequencies. What differs is the average frequency of the distributions. The activity patterns are manifested in time lag maps of narrow-band instrument channel pairs. We combine hydrodynamic and forward modeling codes with a magnetic field extrapolation to create a model active region and apply the time lag method to synthetic observations. Our aim is not to reproduce a particular set of observations in detail, but to recover some typical properties and patterns observed in active regions. Our key findings are the following. 1. cooling dominates the time lag signature and the time lags between the channel pairs are generally consistent with observed values. 2. shorter coronal loops in the core cool more quickly than longer loops at the periphery. 3. all channel pairs show zero time lag when the line-of-sight passes through coronal loop foot-points. 4. there is strong evidence that plasma must be re-energized on a time scale comparable to the cooling timescale to reproduce the observed coronal activity, but it is likely that a relatively broad spectrum of heating frequencies are operating across active regions. 5. due to their highly dynamic nature, we find nanoflare trains produce zero time lags along entire flux tubes in our model active region that are seen between the same channel pairs in observed active regions. **2013-01-01**

CHROMOSPHERIC NANOFLARES AS A SOURCE OF CORONAL PLASMA. II. REPEATING NANOFLARES

S. J. **Bradshaw**1 and J. A. Klimchuk

2015 ApJ 811 129

http://arxiv.org/pdf/1603.06673v1.pdf

The million degree plasma of the solar corona must be supplied by the underlying layers of the atmosphere. The mechanism and location of energy release, and the precise source of coronal plasma, remain unresolved. In earlier work, we pursued the idea that warm plasma is supplied to the corona via direct heating of the chromosphere by nanoflares, contrary to the prevailing belief that the corona is heated in situ and the chromosphere is subsequently energized and ablated by thermal conduction. We found that single (low-frequency) chromospheric nanoflares could not explain the observed intensities, Doppler-shifts, and red/blue asymmetries in Fe xii and xiv emission lines. In the present work, we follow up on another suggestion that the corona could be powered by chromospheric nanoflares that repeat on a timescale substantially shorter than the cooling/draining timescale. That is, a single magnetic strand is re-supplied with coronal plasma before the existing plasma has time to cool and drain. We perform a series of hydrodynamic experiments and predict the Fe xii and xiv line intensities, Doppler-shifts, and red/blue asymmetries. We find that our predicted quantities disagree dramatically with observations and fully developed loop structures cannot be created by intermediate- or high-frequency chromospheric nanoflares. We conclude that the mechanism ultimately responsible for producing coronal plasma operates above the chromosphere, but this does not preclude the possibility of a similar mechanism powering the chromosphere, extreme examples of which may be responsible for heating chromospheric plasma to transition region temperatures (e.g., type II spicules).

Collisional and Radiative Processes in Optically Thin Plasmas

Stephen J. **Bradshaw**, John C. Raymond

E-print, March **2013**

Most of our knowledge of the physical processes in distant plasmas is obtained through measurement of the radiation they produce. Here we provide an overview of the main collisional and radiative processes and examples of diagnostics relevant to the microphysical processes in the plasma. Many analyses assume a time-steady plasma with ion populations in equilibrium with the local temperature and Maxwellian distributions of particle velocities, but these assumptions are easily violated in many cases. We consider these departures from equilibrium and possible diagnostics in detail.

DIAGNOSING THE TIME-DEPENDENCE OF ACTIVE REGION CORE HEATING FROM THE EMISSION MEASURE. I. LOW-FREQUENCY NANOFLARES

S. J. **Bradshaw**1, J. A. Klimchuk2, and J. W. Reep

2012 ApJ 758 53

Observational measurements of active region emission measures contain clues to the time dependence of the underlying heating mechanism. A strongly nonlinear scaling of the emission measure with temperature indicates a large amount of hot plasma relative to warm plasma. A weakly nonlinear (or linear) scaling of the emission measure indicates a relatively large amount of warm plasma, suggesting that the hot active region plasma is allowed to cool and so the

heating is impulsive with a long repeat time. This case is called low-frequency nanoflare heating, and we investigate its feasibility as an active region heating scenario here. We explore a parameter space of heating and coronal loop properties with a hydrodynamic model. For each model run, we calculate the slope α of the emission measure distribution EM(T)T α. Our conclusions are: (1) low-frequency nanoflare heating is consistent with about 36% of observed active region cores when uncertainties in the atomic data are not accounted for; (2) proper consideration of uncertainties yields a range in which as many as 77% of observed active regions are consistent with low-frequency nanoflare heating and as few as zero; (3) low-frequency nanoflare heating cannot explain observed slopes greater than 3; (4) the upper limit to the volumetric energy release is in the region of 50 erg cm–3 to avoid unphysical magnetic field strengths; (5) the heating timescale may be short for loops of total length less than 40 Mm to be consistent with the observed range of slopes; (6) predicted slopes are consistently steeper for longer loops.

Viewpoint: **A New Twist in Simulating Solar Flares**
Brandenburg, A.
Physics 9, 26 (**2016**)
http://arxiv.org/pdf/1603.01917v1.pdf
Simulations show for the first time how the magnetic fields that produce solar flares can extend out of the Sun by acquiring a twist.

OBSERVATION AND ANALYSIS OF BALLISTIC DOWNFLOWS IN AN M-CLASS FLARE WITH THE INTERFACE REGION IMAGING SPECTROGRAPH
Sean R. **Brannon**
2016 ApJ 833 101 DOI 10.3847/1538-4357/833/1/101
Despite significant advances in instrumentation, there remain no studies that analyze observations of on-disk flare loop plasma flows covering the entire evolution from chromospheric evaporation, through plasma cooling, to draining downflows. We present results from an imaging and spectroscopic observation from the Interface Region Imaging Spectrograph(IRIS) of the SOL**2015–03–12T11**:50:00 M-class flare, at high spatial resolution and time cadence. Our analysis of this event reveals initial plasma evaporation at flare temperatures indicated by 100–200 km s−1 blueshifts in the Fe xxi line. We subsequently observe plasma cooling into chromospheric lines (Si iv and O iv) with ~11 minute delay, followed by loop draining at ~40 km s−1 as indicated by a "C"-shaped redshift structure and significant (~60 km s−1) non-thermal broadening. We use density-sensitive lines to calculate a plasma density for the flare loops, and estimate a theoretical cooling time approximately equal to the observed delay. Finally, we use a simple elliptical free-fall draining model to construct synthetic spectra, and perform what we believe to be the first direct comparison of such synthetic spectra to observations of draining downflows in flare loops.

Spectroscopic observations of evolving flare ribbon substructure suggesting origin in current sheet waves
S. R. **Brannon**, D. W. Longcope, J. Qiu
ApJ **810** 4 **2015**
http://arxiv.org/pdf/1507.01554v1.pdf
We present imaging and spectroscopic observations from the Interface Region Imaging Spectrograph (IRIS) of the evolution of the flare ribbon in the SOL**2014-04-18**T13:03 M-class flare event, at high spatial resolution and time cadence. These observations reveal small-scale substructure within the ribbon, which manifests as coherent quasi-periodic oscillations in both position and Doppler velocities. We consider various alternative explanations for these oscillations, including modulation of chromospheric evaporation flows. Among these we find the best support for some form of wave localized to the coronal current sheet, such as a tearing mode or Kelvin-Helmholtz instability.

Modeling properties of chromospheric evaporation driven by thermal conduction fronts from reconnection shocks
Sean **Brannon**, Dana Longcope
2014, ApJ 792 50
http://arxiv.org/pdf/1408.1705v1.pdf
Magnetic reconnection in the corona results in contracting flare loops, releasing energy into plasma heating and shocks. The hydrodynamic shocks so produced drive thermal conduction fronts (TCFs) which transport energy into the chromosphere and drive upflows (evaporation) and downflows (condensation) in the cooler, denser footpoint plasma. Observations have revealed that certain properties of the transition point between evaporation and condensation (the "flow reversal point" or FRP), such as temperature and velocity-temperature derivative at the FRP, vary between different flares. These properties may provide a diagnostic tool to determine parameters of the coronal energy release mechanism and the loop atmosphere. In this study, we develop a 1-D hydrodynamical flare loop model with a simplified three-region atmosphere (chromosphere/transition region/corona), with TCFs initiated by shocks introduced in the corona. We investigate the effect of two different flare loop parameters (post-shock temperature and transition

region temperature ratio) on the FRP properties. We find that both of the evaporation characteristics have scaling-law relationships to the varied flare parameters, and we report the scaling exponents for our model. This provides a means of using spectroscopic observations of the chromosphere as quantitative diagnostics of flare energy release in the corona.

Short Duration Stellar Flares in GALEX Data

C. E. **Brasseur**, Rachel A. Osten, Scott W. Fleming
2019 *ApJ* **883** 88
https://arxiv.org/pdf/1908.08377.pdf
We report on a population of short duration near-ultraviolet (NUV) flares in stars observed by the Kepler and GALEX missions. We analyzed NUV light curves of 34,276 stars observed from 2009-2013 by both the GALEX (NUV) and Kepler (optical) space missions with the eventual goal of investigating multi-wavelength flares. From the GALEX data we constructed light curves with a 10 second cadence, and ultimately detected 1,904 short duration flares on 1,021 stars. The vast majority (94.5\%) of these flares have durations less than five minutes, with flare flux enhancements above the quiescent flux level ranging from 1.5 to 1700. The flaring stars are primarily solar-like, with Teff ranging from 3,000-11,000 K and radii between 0.5-15 R⊙. This set of flaring stars is almost entirely distinct from that of previous flare surveys of Kepler data and indicates a previously undetected collection of small flares contained within the Kepler sample. The range in flare energies spans 1.8×1032-8.9×1037 erg, with associated relative errors spanning 2-87\%. The flare frequency distribution by energy follows a power-law with index α=1.72±0.05, consistent with results of other solar and stellar flare studies at a range of wavelengths. This supports the idea that the NUV flares we observe are governed by the same physical processes present in solar and optical flares. The relationship between flare duration and associated flare energy extends results found for solar and stellar white-light flares, and suggests that these flares originate in regions with magnetic field strengths of several hundred Gauss, and length scales of order 1010 cm.

A Helioseismic Survey of Near-surface Flows Around Active Regions and their Association with Flares

D. C. **Braun**
ApJ 819 106 **2015**
http://arxiv.org/pdf/1602.00038v1.pdf
We use helioseismic holography to study the association of shallow flows with solar flare activity in about 250 large sunspot groups observed between 2010 and 2014 with the Helioseismic and Magnetic Imager on the Solar Dynamics Observatory. Four basic flow parameters: horizontal speed, horizontal component of divergence, vertical component of vorticity, and a vertical kinetic helicity proxy, are mapped for each active region during its passage across the solar disk. Flow indices are derived representing the mean and standard deviation of these parameters over magnetic masks and compared with contemporary measures of flare X-ray flux. A correlation exists for several of the flow indices, especially those based on the speed and the standard deviation of all flow parameters. However, their correlation with X-ray flux is similar to that observed with the mean unsigned magnetic flux density over the same masks. The temporal variation of the flow indices are studied, and a superposed epoch analysis with respect to the occurrence to 70 M and X-class flares is made. While flows evolve with the passage of the active regions across the disk, no discernible precursors or other temporal changes specifically associated with flares are detected. 2011 Sept 1-10, 1-10 Dec 2011

FarNet-II: An improved solar far-side active region detection method

E. G. **Broock**, A. Asensio Ramos, T. Felipe
A&A **2022**
https://arxiv.org/pdf/2209.14789.pdf
Context. Activity on the far side of the Sun is routinely studied through the analysis of the seismic oscillations detected on the near side using helioseismic techniques such as phase shift sensitive holography. Recently, the neural network FarNet was developed to improve these detections. Aims. We aim to create a new machine learning tool, FarNet II, which further increases the scope of FarNet, and to evaluate its performance in comparison to FarNet and the standard helioseismic method for detecting far side activity. Methods. We developed FarNet II, a neural network that retains some of the general characteristics of FarNet but improves the detections in general, as well as the temporal coherence among successive predictions. The main novelties are the implementation of attention and convolutional long short term memory (ConvLSTM) modules. A cross validation approach, training the network 37 times with a different validation set for each run, was employed to leverage the limited amount of data available. We evaluate the performance of FarNet II using three years of extreme ultraviolet observations of the far side of the Sun acquired with the Solar Terrestrial Relations Observatory (STEREO) as a proxy of activity. The results from FarNet II were compared with those obtained from FarNet and the standard helioseismic method using the Dice coefficient as a metric. Results. FarNet II achieves a Dice coefficient that improves that of FarNet by over 0.2 points for every output position on the sequences from the evaluation dates. Its improvement over FarNet is higher than that of FarNet over the standard method. Conclusions. The new network is a very promising tool for improving the detection of activity on the far side of the Sun given by pure

helioseismic techniques. Space weather forecasts can potentially benefit from the higher sensitivity provided by this novel method.

Spectroscopic Observations of Coronal Rain Formation and Evolution following an X2 Solar Flare

David H. **Brooks**, Jeffrey W. Reep, Ignacio Ugarte-Urra, John E. Unverferth, Harry P. Warren
ApJ **962** 105 **2024**
https://arxiv.org/pdf/2401.04537.pdf
https://iopscience.iop.org/article/10.3847/1538-4357/ad18be/pdf
A significant impediment to solving the coronal heating problem is that we currently only observe active region (AR) loops in their cooling phase. Previous studies showed that the evolution of cooling loop densities and apex temperatures are insensitive to the magnitude, duration, and location of energy deposition. Still, potential clues to how energy is released are encoded in the cooling phase properties. The appearance of coronal rain, one of the most spectacular phenomena of the cooling phase, occurs when plasma has cooled below 1MK, which sets constraints on the heating frequency, for example. Most observations of coronal rain have been made by imaging instruments. Here we report rare Hinode/EUV Imaging Spectrometer (EIS) observations of a loop arcade where coronal rain forms following an X2.1 limb flare. A bifurcation in plasma composition measurements between photospheric at 1.5MK and coronal at 3.5MK suggests that we are observing post-flare driven coronal rain. Increases in non-thermal velocities and densities with decreasing temperature (2.7MK to 0.6MK) suggest that we are observing the formation and subsequent evolution of the condensations. Doppler velocity measurements imply that a 10% correction of apparent flows in imaging data is reasonable. Emission measure analysis at 0.7MK shows narrow temperature distributions, indicating coherent behaviour reminiscent of that observed in coronal loops. The space-time resolution limitations of EIS suggest that we are observing the largest features or rain showers. These observations provide insights into the heating rate, source, turbulence, and collective behaviour of coronal rain from observations of the loop cooling phase. **2023, March 3**

On orbit performance of the solar flare trigger for the Hinode EUV Imaging Spectrometer

David H. **Brooks**, Jeffrey W. Reep, Ignacio Ugarte-Urra, Harry P. Warren
Frontiers in Astronomy and Space Sciences 10: 1149831. **2023**
https://arxiv.org/pdf/2303.13155.pdf
https://www.frontiersin.org/articles/10.3389/fspas.2023.1149831/pdf
We assess the on-orbit performance of the flare event trigger for the Hinode EUV Imaging Spectrometer. Our goal is to understand the time-delay between the occurrence of a flare, as defined by a prompt rise in soft X-ray emission, and the initiation of the response observing study. Wide (266″) slit patrol images in the He II 256.32A spectral line are used for flare hunting, and a reponse is triggered when a pre-defined intensity threshold is reached. We use a sample of 13 > M-class flares that succesfully triggered a response, and compare the timings with soft X-ray data from GOES, and hard X-ray data from RHESSI and Fermi. Excluding complex events that are difficult to interpret, the mean on orbit response time for our sample is 2 min 10 s, with an uncertainty of 84 s. These results may be useful for planning autonomous operations for future missions, and give some guidance as to how improvements could be made to capture the important impulsive phase of flares. **6 Nov 2011, 6 Mar 2012, 9 May 2012, 2 Nov 2013, 7 Nov 2013, 31 Dec 2013, 2014, January 1, 2 Feb 2014, 6 Feb 2014, 1 Oct 2015, 6 Sep 2017, 5 May 2022**
Table 1. GOES-15 start time

The Formation and Lifetime of Outflows in a Solar Active Region

David H. **Brooks**, Louise Harra, Stuart D. Bale, Krzysztof Barczynski, Cristina Mandrini, Vanessa Polito, Harry P. Warren
ApJ **2021**
https://arxiv.org/pdf/2106.03318.pdf
Active regions are thought to be one contributor to the slow solar wind. Upflows in EUV coronal spectral lines are routinely osberved at their boundaries, and provide the most direct way for upflowing material to escape into the heliosphere. The mechanisms that form and drive these upflows, however, remain to be fully characterised. It is unclear how quickly they form, or how long they exist during their lifetimes. They could be initiated low in the atmosphere during magnetic flux emergence, or as a response to processes occuring high in the corona when the active region is fully developed. On **2019, March 31**, a simple bipolar active region (AR 12737) emerged and upflows developed on each side. We used observations from Hinode, SDO, IRIS, and Parker Solar Probe (PSP) to investigate the formation and development of the upflows from the eastern side. We used the spectroscopic data to detect the upflow, and then used the imaging data to try to trace its signature back to earlier in the active region emergence phase. We find that the upflow forms quickly, low down in the atmosphere, and that its initiation appears associated with a small field-opening eruption and the onset of a radio noise storm detected by PSP. We also confirmed that the upflows existed for the vast majority of the time the active region was observed. These results suggest that the contribution to the solar wind occurs even when the region is small, and continues for most of its lifetime. **31 Mar- 1 Apr 2019**

A diagnostic of coronal elemental behavior during the inverse FIP effect in solar flares

David H. **Brooks**

ApJ **863** 140 **2018**

https://arxiv.org/pdf/1807.04408.pdf

The solar corona shows a distinctive pattern of elemental abundances that is different from that of the photosphere. Low first ionization potential (FIP) elements are enhanced by factors of several. A similar effect is seen in the atmospheres of some solar-like stars, while late type M stars show an inverse FIP effect. This inverse effect was recently detected on the Sun during solar flares, potentially allowing a very detailed look at the spatial and temporal behavior that is not possible from stellar observations. A key question for interpreting these measurements is whether both effects act solely on low FIP elements (a true inverse effect predicted by some models), or whether the inverse FIP effect arises because high FIP elements are enhanced. Here we develop a new diagnostic that can discriminate between the two scenarios, based on modeling of the radiated power loss, and applying the models to a numerical hydrodynamic simulation of coronal loop cooling. We show that when low/high FIP elements are depleted/enhanced, there is a significant difference in the cooling lifetime of loops that is greatest at lower temperatures. We apply this diagnostic to a post X1.8 flare loop arcade and inverse FIP region, and show that for this event, low FIP elements are depleted. We discuss the results in the context of stellar observations, and models of the FIP and inverse FIP effect. We also provide the radiated power loss functions for the two inverse FIP effect scenarios in machine readable form to facilitate further modeling. **2014, December 20**

Measurements of Non-Thermal Line Widths in Solar Active Regions

David H. **Brooks**, Harry P. Warren

ApJ 820 63 **2016**

http://arxiv.org/pdf/1511.02313v1.pdf

Spectral line widths are often observed to be larger than can be accounted for by thermal and instrumental broadening alone. This excess broadening is a key observational constraint for both nanoflare and wave dissipation models of coronal heating. Here we present a survey of non-thermal velocities measured in the high temperature loops (1--5MK) often found in the cores of solar active regions. This survey of Hinode Extreme Ultraviolet Imaging Spectrometer (EIS) observations covers 15 non-flaring active regions that span a wide range of solar conditions. We find relatively small non-thermal velocities, with a mean value of 17km s−1, and no significant trend with temperature or active region magnetic flux. These measurements appear to be inconsistent with those expected from reconnection jets in the corona, chromospheric evaporation induced by coronal nanoflares, and Alfv\'en wave turbulence models. Furthermore, because the observed non-thermal widths are generally small their measurements are difficult and susceptible to systematic effects. **2011, April 11, 2011, April 19**

ESTABLISHING A CONNECTION BETWEEN ACTIVE REGION OUTFLOWS AND THE SOLAR WIND: ABUNDANCE MEASUREMENTS WITH EIS/*HINODE*

David H. **Brooks**1,3 and Harry P. Warren2

Astrophysical Journal Letters, 727:L13 (5pp), **2011** January

One of the most interesting discoveries from *Hinode* is the presence of persistent high-temperature high-speed outflows from the edges of active regions (ARs). EUV imaging spectrometer (EIS) measurements indicate that the outflows reach velocities of 50 kms-1 with spectral line asymmetries approaching 200 km s-1. It has been suggested that these outflows may lie on open field lines that connect to the heliosphere, and that they could potentially be a significant source of the slow speed solar wind. A direct link has been difficult to establish, however. We use EIS measurements of spectral line intensities that are sensitive to changes in the relative abundance of Si and S as a result of the first ionization potential (FIP) effect, to measure the chemical composition in the outflow regions of AR 10978 over a 5 day period in 2007 December. We find that Si is always enhanced over S by a factor of 3–4. This is generally consistent with the enhancement factor of low FIP elements measured in situ in the slow solar wind by non-spectroscopic methods. Plasma with a slow wind-like composition was therefore flowing from the edge of the AR for at least 5 days. Furthermore, on December 10 and 11, when the outflow from the western side was favorably oriented in the Earth direction, the Si/S ratio was found to match the value measured a few days later by the *Advanced Composition Explorer*/Solar Wind Ion Composition Spectrometer. *These results provide strong observational evidence for a direct connection between the solar wind, and the coronal plasma in the outflow regions.*

MODELING OF THE EXTREME-ULTRAVIOLET AND SOFT X-RAY EMISSION IN A SOLAR CORONAL BRIGHT POINT

David H. **Brooks**1 and Harry P. Warren

Astrophysical Journal, 687:1363Y1372, **2008**

http://www.journals.uchicago.edu/doi/abs/10.1086/591834

Previous studies have been able to reproduce both the observed intensities and the morphology of high-temperature solar plasma using steady state heating models. These models, however, have been unable to reproduce the lower temperature emission observed in active regions. Here we present results from numerical simulations of a coronal bright point.

An H alpha Surge Provoked by Moving Magnetic Features near an Emerging Flux Region

D. H. **Brooks**, H. Kurokawa, and T. E. Berger
The Astrophysical Journal, Volume 656, Number 2, Page 1197, **2007**
[http://www.journals.uchicago.edu/cgi-bin/resolve?ApJ61682]
We present a detailed study of Hα surges from cotemporal high-resolution multiwavelength images of NOAA *AR 8227, May-June 1998*

A Blueprint of State-of-the-art Techniques for Detecting Quasi-periodic Pulsations in Solar and Stellar Flares

Anne-Marie **Broomhall**1,2, James R. A. Davenport3,4, Laura A. Hayes5,6, Andrew R. Inglis6, Dmitrii Y. Kolotkov1, James A. McLaughlin7, Tishtrya Mehta1, Valery M. Nakariakov1,8, Yuta Notsu9,10,11,13, David J. Pascoe1
2019 ApJS 244 44
sci-hub.se/10.3847/1538-4365/ab40b3
Quasi-periodic pulsations (QPPs) appear to be a common feature observed in the light curves of both solar and stellar flares. However, their quasi-periodic nature, along with the fact that they can be small in amplitude and short-lived, makes QPPs difficult to unequivocally detect. In this paper, we test the strengths and limitations of state-of-the-art methods for detecting QPPs using a series of hare-and-hounds exercises. The hare simulated a set of flares, both with and without QPPs of a variety of forms, while the hounds attempted to detect QPPs in blind tests. We use the results of these exercises to create a blueprint for anyone who wishes to detect QPPs in real solar and stellar data. We present eight clear recommendations to be kept in mind for future QPP detections, with the plethora of solar and stellar flare data from new and future satellites. These recommendations address the key pitfalls in QPP detection, including detrending, trimming data, accounting for colored noise, detecting stationary-period QPPs, detecting QPPs with nonstationary periods, and ensuring that detections are robust and false detections are minimized. We find that QPPs can be detected reliably and robustly by a variety of methods, which are clearly identified and described, if the appropriate care and due diligence are taken.

Temperature and differential emission measure evolution of a limb flare on 13 January 2015

M. **Bröse**1,2,3, A. Warmuth1, T. Sakao4,5 and Y. Su6,7
A&A 663, A18 (**2022**)
https://www.aanda.org/articles/aa/pdf/2022/07/aa41868-21.pdf
https://arxiv.org/pdf/2406.13339
Context. Spatially unresolved observations show that the cooling phase in solar flares can be much longer than theoretical models predict. It has not yet been determined whether this is also the case for different subregions within the flare structure.
Aims. We aim to investigate whether or not the cooling times, which are observed separately in coronal loops and the supra-arcade fan (SAF), are in accordance with the existing cooling models, and whether the temperature and emission measure of supra-arcade downflows (SADs) are different from their surroundings.
Methods. We analysed the M5.6 limb flare on **13 January 2015** using SDO/AIA observations. We applied a differential emission measure (DEM) reconstruction code to derive spatially resolved temperature and emission measure maps, and used the output to investigate the thermal evolution of coronal loops, the SAF, and the SADs.
Results. In the event of 13 January 2015, the observed cooling times of the loop arcade and the SAF are significantly longer than predicted by the Cargill model, even with suppressed plasma heat conduction. The observed SADs show different temperature characteristics, and in all cases a lower density than their surroundings.
Conclusions. In the limb flare event studied here, continuous heating likely occurs in both loops and SAF during the gradual flare phase and leads to an extended cooling phase.

Localized Quasi-periodic Fluctuations in C ii, Si iv, and Fe xxi Emission during Chromospheric Evaporation in a Flare Ribbon Observed by IRIS on 2017 September 9

Jeffrey W. **Brosius** and Andrew R. Inglis
2018 ApJ 867 85
sci-hub.tw/10.3847/1538-4357/aae5f5

We investigate the onset of a GOES M3.7 flare on **2017 September 9** with rapid-cadence (9.4 s) UV stare spectra obtained with IRIS in five 1" slit segments. Our analysis is based primarily on integrated intensities and Doppler velocities of C ii λ1334.5 (T ≈ 2.5 × 104 K), Si iv λ1402.7 (7.9 × 104 K), and Fe xxi λ1354.1 (1.1 × 107 K). The four segments within the ribbon show systematically earlier starting times for the low-T lines (C ii and Si iv) than Fe xxi; further, the velocities derived for Fe xxi are generally directed upward along the line of sight. This is consistent with the standard flare model, in which beams of nonthermal particles ionize and heat the chromosphere and drive chromospheric evaporation: as the temperature and ionization stages of the chromospheric plasma increase, intensities of emission lines also increase, first from lines in lower stages of ionization, and later from lines in higher stages of ionization. Where quasi-periodic fluctuations were observed in the ribbon in both low-T and Fe xxiemission, peaks in the low-T intensity preceded those in the Fe xxi intensity, and peaks in the Fe xxi upward velocity typically also preceded those in the Fe xxi intensity. Thus, the behavior of each individual fluctuation was similar to that of a standard flare, suggesting that each individual fluctuation was due to a separate injection of nonthermal particles into the chromosphere. Based on RHESSI hard X-ray observations, we estimate sufficient beam energy flux (≥1.5 × 1010 erg cm−2 s−1) to drive explosive chromospheric evaporation.

Explosive Chromospheric Evaporation and Warm Rain in a C3.1 Flare Observed by IRIS, Hinode/EIS, and RHESSI

Jeffrey W. **Brosius** and Andrew R. Inglis
2017 ApJ 848 39

IRIS and EIS observed a GOES C3.1 flare in stare mode on **2014 March 15**. The GOES flare started at 00:21:35 and peaked at 00:26:30 UT. The IRIS slit pointed near the center of the flare, while the EIS slit pointed $35''$ to its west. About 4 minutes before the GOES flare start, the IRIS C ii and Si iv intensities became (and remained) greater than their pre-flare averages, indicating that the flare had begun and that the chromosphere and transition region were involved. IRISfirst detected blueshifted Fe xxi emission at 00:22:42 UT, by which time the C ii and Si ivintensities had increased by factors around 100 and their profiles were redshifted. Simultaneous, cospatial blueshifted Fe xxi emission with redshifted C ii and Si iv emission indicates explosive chromospheric evaporation. EIS spectra reveal Fe xxiii emission that is too weak to measure velocities, and intensity enhancements by factors about 1.7 in the Fe xiv and Fe xvi emission. Lines from both of these coronal ions show redshifts ≈9 km s−1 around 00:24:00 UT, and the Fe xiv 264.7/274.2 intensity ratio reveals an increase of n e from $(1.03 \pm 0.20) \times 10^9$ before to $(3.58 \pm 0.68) \times 10^9$ cm−3 during the flare. The redshifted coronal line emission and increased n e are consistent with warm rain falling and accumulating in the remote area observed by EIS. A fit to the RHESSI hard X-ray spectrum yields a nonthermal energy injection rate of 4.9×10^{26} erg s−1, from which we estimate a HXR beam energy flux range consistent with explosive evaporation.

Hinode/ EIS Nugget Feb 2018 http://solarb.mssl.ucl.ac.uk/SolarB/nuggets/nugget_2018feb.jsp

QUASI-PERIODIC FLUCTUATIONS AND CHROMOSPHERIC EVAPORATION IN A SOLAR FLARE RIBBON OBSERVED BY HINODE/EIS, IRIS, AND RHESSI

Jeffrey W. **Brosius**1, Adrian N. Daw2, and Andrew R. Inglis1
2016 ApJ 830 101

The Hinode/Extreme-ultraviolet Imaging Spectrometer (EIS) obtained rapid cadence (11.2 s) EUV stare spectra of an M7.3 flare ribbon in AR 12036 on **2014 April 18**. Quasi-periodic (P ≈ 75.6 ± 9.2 s) intensity fluctuations occurred in emission lines of O iv, Mg vi, Mg vii, Si vii, Fe xiv, and Fe xvi during the flare's impulsive rise, and ended when the maximum intensity in Fe xxiii was reached. The profiles of the O iv–Fe xvi lines reveal that they were all redshifted during most of the interval of quasi-periodic intensity fluctuations, while the Fe xxiii profile revealed multiple components including one or two highly blueshifted ones. This indicates that the flare underwent explosive chromospheric evaporation during its impulsive rise. Fluctuations in the relative Doppler velocities were seen, but their amplitudes were too subtle to extract significant quasi-periodicities. RHESSI detected 25–100 keV hard-X-ray sources in the ribbon near the EIS slit's pointing position during the peaks in the EIS intensity fluctuations. The observations are consistent with a series of energy injections into the chromosphere by nonthermal particle beams. Electron densities derived with Fe xiv (4.6 × 1010 cm−3) and Mg vii (7.8 × 109 cm−3) average line intensity ratios during the interval of quasi-periodic intensity fluctuations, combined with the radiative loss function of an optically thin plasma, yield radiative cooling times of 32 s at 2.0 × 106 K, and 46 s at 6.3 × 105 K (about half the quasi-period); assuming Fe xiv's density for Fe xxiii yields a radiative cooling time of 103 s (13 times the quasi-period) at 1.4 × 107 K.

See Hinode/EIS Nugget, 24 Nov 2016 http://solarb.mssl.ucl.ac.uk/SolarB/nuggets/nugget_2016dec.jsp

QUASI-PERIODIC FLUCTUATIONS AND CHROMOSPHERIC EVAPORATION IN A SOLAR FLARE RIBBON OBSERVED BY IRIS

Jeffrey W. **Brosius**1 and Adrian N. Daw
ApJ 810(1) 45 **2015**
The Interface Region Imaging Spectrograph (IRIS) satellite obtained rapid cadence (9.4 s) stare spectra of an M7 flare ribbon in AR 12036 on **2014 April 18**. Chromospheric and transition region line emission exhibited quasi-periodic intensity and velocity fluctuations in the ribbon prior to the appearance of Fe xxi emission. Seven intensity peaks were observed in light curves from small ($0\farcs333 \times 0\farcs333$) tracked spatial locations in the ribbon, the first four of which show variable time separations around 3 minutes, and the last four of which show variable time separations about half that value, i.e., the frequency appears to have doubled. The Fe xxi intensity increased rapidly and impulsively after the quasi-periodic fluctuations in chromospheric and transition region lines. The entire Fe xxi line profile was blueshifted when the line first appeared, corresponding to an upward velocity around −100 km s−1. This upward velocity increased to a maximum of about −150 km s−1 before diminishing to zero around the time of maximum intensity. Simultaneous, cospatial velocities observed with Si iv line emission were directed downward, consistent with explosive chromospheric evaporation. During this flare the Fe xxiline's profile is well fit with only one Gaussian component that is either wholly blueshifted or wholly at rest; no significant secondary blueshifted or redshifted components are observed. This suggests that IRIS may have sufficient spatial resolution to resolve loop strands in these flare observations. Under the assumption that the Fe xxi line is at rest when its width is thermal, we derive a rest wavelength of 1354.0714 ± 0.0108 Å for this forbidden line.

EUNIS Sees Pervasive Faint Fe XIX Emission: Evidence for Nanoflare Heating

Jeff **Brosius**
RHESSI Science Nugget, No. 233, Aug **2014**
http://sprg.ssl.berkeley.edu/~tohban/wiki/index.php/RHESSI_Science_Nuggets
Observations with the Extreme Ultraviolet Normal Incidence Spectrograph (EUNIS) sounding rocket instrument during its 2013 flight now have provided strong evidence for "nanoflare heating" as the explanation. **23 April 2013**

Rapid Evolution of the Solar Atmosphere during the Impulsive Phase of a Microflare Observed with the Extreme-ultraviolet Imaging Spectrometer aboard Hinode: Hints of Chromospheric Magnetic Reconnection

Jeffrey W. **Brosius**
2013 ApJ 777 135
We obtained rapid cadence (11.2 s) EUV stare spectra of a solar microflare with the Extreme-ultraviolet Imaging Spectrometer aboard Hinode. The intensities of lines formed at temperatures too cool to be found in the corona brightened by factors around 16 early during this event, indicating that we observed a site of energy deposition in the chromosphere. We derive the density evolution of the flare plasma at temperature around 2 MK from the intensity ratio of Fe XIV lines at 264.789 Å and 274.204 Å. From both lines we removed the bright pre-flare quiescent emission, and from 274.204 we removed the blended emission of Si VII λ274.180 based on the Si VII λ274.180/275.361 intensity ratio, which varies only slightly with density. In this way the flare electron density is derived with emission from only the flare plasma. The density increased by an order of magnitude from its pre-flare quiescent average of (3.43 ± 0.19) × 109 cm–3 to its maximum impulsive phase value of (3.04 ± 0.57) × 1010 cm–3 in 2 minutes. The fact that this rapid increase in density is not accompanied by systematic, large upward velocities indicates that the density increase is not due to the filling of loops with evaporated chromospheric material, but rather due to material being directly heated in the chromosphere, likely by magnetic reconnection. The density increase may be due to a progression of reconnection sites to greater depths in the chromosphere, where it has access to larger densities, or it may be due to compression of 2 MK plasma by the 10 MK plasma as it attempts to expand against the high-density chromospheric plasma.

Rapid Evolution of the Solar Atmosphere During a Microflare Observed with EIS: Hints of Chromospheric Magnetic Reconnection

Jeffrey W. **Brosius**
EIS Nugget - November **2013**, http://solarb.mssl.ucl.ac.uk/SolarB/nuggets/nugget_2013nov.jsp
In the standard model of solar flares, energy stored in non-potential magnetic fields is released by reconnection in the corona. This energy heats the local plasma to temperatures around 10 MK and/or accelerates nonthermal particles, and is subsequently transported by thermal conduction and/or particle beams (and possibly also Alfven waves) through the relatively tenuous corona to the chromosphere, where it is stopped in the cooler, denser plasma. The possibility that flare reconnection occurs in the chromosphere itself has been mentioned by Brosius & Holman (2009).
2012 November 21

CHROMOSPHERIC EVAPORATION IN SOLAR FLARE LOOP STRANDS OBSERVED WITH THE EXTREME-ULTRAVIOLET IMAGING SPECTROMETER ON BOARD HINODE
Jeffrey W. **Brosius**
2013 ApJ 762 133
The entire profile of the Fe XXIII line at 263.8 Å, formed at temperature 14 MK, was blueshifted by an upward velocity –122 ± 33 km s–1 when it was first detected by the Extreme-ultraviolet Imaging Spectrometer operating in rapid cadence (11.18 s) stare mode during a C1 solar flare. The entire profile became even more blueshifted over the next two exposures, when the upward velocity reached its maximum of –208 ± 14 km s–1 before decreasing to zero over the next 12 exposures. After that, a weak, secondary blueshifted component appeared for five exposures, reached a maximum upward velocity of –206 ± 33 km s–1, and disappeared after the maximum line intensity (stationary plus blueshifted) was achieved. Velocities were measured relative to the intense stationary profile observed near the flare's peak and early during its decline. The initial episode during which the entire profile was blueshifted lasted about 156 s, while the following episode during which a secondary blueshifted component was detected lasted about 56 s. The first episode likely corresponds to chromospheric evaporation in a single loop strand, while the second corresponds to evaporation in an additional strand, as described in multi-strand flare loop models proposed by Hori et al. and Warren & Doschek. Line emission from progressively cooler ions (Fe XVII, XVI, and XIV) brightened at successively later times, consistent with cooling of flare-heated plasma.

Episodic Chromospheric Evaporation in Flare Loop Strands Observed with EIS
Jeff **Brosius**
EIS nugget, Dec **2012**
http://msslxr.mssl.ucl.ac.uk:8080/SolarB/nuggets/nugget_2012nov.jsp
2012 March 7

EXTREME-ULTRAVIOLET SPECTROSCOPIC OBSERVATION OF DIRECT CORONAL HEATING DURING A C-CLASS SOLAR FLARE
Jeffrey W. **Brosius**
2012 ApJ 754 54
With the Coronal Diagnostic Spectrometer operating in rapid cadence (9.8 s) stare mode during a C6.6 flare on the solar disk, we observed a sudden brightening of Fe XIX line emission (formed at temperature T 8 MK) above the pre-flare noise without a corresponding brightening of emission from ions formed at lower temperatures, including He I (0.01 MK), O V (0.25 MK), and Si XII (2 MK). The sudden brightening persisted as a plateau of Fe XIX intensity that endured more than 11 minutes. The Fe XIX emission at the rise and during the life of the plateau showed no evidence of significant bulk velocity flows, and hence cannot be attributed to chromospheric evaporation. However, the line width showed a significant broadening at the rise of the plateau, corresponding to nonthermal velocities of at least 89 km s–1 due to reconnection outflows or turbulence. During the plateau He I, O V, and Si XII brightened at successively later times starting about 3.5 minutes after Fe XIX, which suggests that these brightenings were produced by thermal conduction from the plasma that produced the Fe XIX line emission; however, we cannot rule out the possibility that they were produced by a weak beam of nonthermal particles. We interpret an observed shortening of the O V wavelength for about 1.5 minutes toward the middle of the plateau to indicate new upward motions driven by the flare, as occurs during gentle chromospheric evaporation; relative to a quiescent interval shortly before the flare, the O V upward velocity was around –10 km s–1.

Using SDO's AIA to investigate energy transport from a flare's energy release site to the chromosphere⋆
J. W. **Brosius**1 and G. D. Holman
A&A 540, A24 **(2012)**
Context. Coordinated observations of a GOES B4.8 microflare with SDO's Atmospheric Imaging Assembly (AIA) and the Ramaty High Energy Solar Spectroscopic Imager (RHESSI) on **2010 July 31** show that emission in all seven of AIA's EUV channels brightened simultaneously nearly 6 min before RHESSI or GOES detected emission from plasma at temperatures around 10 MK.
Aims. To help interpret these and AIA flare observations in general, we characterized the expected temporal responses of AIA's 94, 131, 171, 193, 211, and 335 Å channels to solar flare brightenings by combining (1) AIA's nominal temperature response functions available through SSWIDL with (2) EUV spectral line data observed in a flare loop footpoint on 2001 April 24 with the Coronal Diagnostic Spectrometer (CDS) on timescales comparable to AIA's image cadence.
Methods. The nine emission lines observed by CDS cover a wide range of formation temperature from about 0.05 to 8 MK. Line brightenings observed early during the CDS flare occurred at temperatures less than about 0.7 MK, with the largest values around 0.1 MK. These brightenings were consistent with the flare's energy transport being dominated by

nonthermal particle beams. Because all of AIA's EUV channels are sensitive to emission from plasma in the 0.1 to 0.7 MK temperature range, we show that all of AIA's EUV channels will brighten simultaneously during flares like this, in which energy transport is dominated by nonthermal particle beams.
Results. The 2010 July 31 flare observed by AIA and RHESSI displays this behavior, so we conclude that such beams likely dominated the flare's energy transport early during the event. When thermal conduction from a reconnection-heated, hot (~10 MK) plasma dominates the energy transport, the AIA channels that are sensitive to emission from such temperatures (particularly the 94 and 131 Å channels) will brighten earlier than the channels that are not sensitive to such temperatures (171 and 211 Å).
Conclusions. Thus, based on the differences expected between AIA's response to flares whose energy transport is dominated by nonthermal particle beams from those whose energy transport is dominated by thermal conduction, AIA can be used to determine the dominant energy transport mechanism for any given event.

CONVERSION FROM EXPLOSIVE TO GENTLE CHROMOSPHERIC EVAPORATION DURING A SOLAR FLARE

Jeffrey W. **Brosius** **2009** ApJ 701 1209-1218 doi: 10.1088/0004-637X/701/2/1209

A *GOES* M1.5 solar flare was observed in NOAA AR 10652 on **2004 July 27** around 20:00 UT with the Coronal Diagnostic Spectrometer (CDS) aboard the *Solar and Heliospheric Observatory* (*SOHO*) spacecraft. Images obtained with *SOHO*'s Extreme-ultraviolet Imaging Telescope and with the *Transition Region And Coronal Explorer* satellite show that the CDS slit was positioned within the flare, whose emission extended 1 arcmin along the slit. Rapid cadence (9.8 s) stare spectra obtained with CDS include emission from the upper chromosphere (He I at 584.3 Å), transition region (O V at 629.7 Å), corona (Si XII at 520.7 Å), and hot flare plasma (Fe XIX at 592.2 Å), and reveal that (1) the flare brightened in its southern parts before it did so in the north; (2) chromospheric evaporation was "explosive" during the first rapid intensity increase observed in Fe XIX, but converted to "gentle" during the second; (3) chromospheric evaporation did not occur in the northern portion of the flare observed by CDS: the brightening observed there was due to flare material moving into that location from elsewhere. We speculate that the initial slow, steady increase of Fe XIX intensity that was observed to start several minutes before its rapid increase was due to direct coronal heating. The change from explosive to gentle evaporation was likely due to either an increased absorption of beam energy during the gentle event because the beam passed through an atmosphere modified by the earlier explosive event, or to a weakening of the coronal magnetic field's ability to accelerate nonthermal particle beams (via reconnection) as the flare progressed, or both.

Modelling Of The Hydrogen Lyman Lines In Solar Flares

Stephen A **Brown**, Lyndsay Fletcher, Graham S Kerr, Nicolas Labrosse, Adam F Kowalski, Jaime De La Cruz Rodríguez

2018 *ApJ* **862** 59

https://arxiv.org/pdf/1807.03373.pdf
http://iopscience.iop.org/article/10.3847/1538-4357/aacc29/pdf

The hydrogen Lyman lines (91.2 nm < lambda < 121.6 nm) are significant contributors to the radiative losses of the solar chromosphere, and are enhanced during flares. We have shown previously that the Lyman lines observed by the Extreme Ultraviolet Variability instrument onboard the Solar Dynamics Observatory exhibit Doppler motions equivalent to speeds on the order of 30 km/s. But contrary to expectation, no dominant flow direction was observed, with both redshifts and blueshifts present. To understand the formation of the Lyman lines, particularly their Doppler motions, we have used the radiative hydrodynamic code, RADYN, and the radiative transfer code, RH, to simulate the evolution of the flaring chromosphere and the response of the Lyman lines during solar flares. We find that upflows in the simulated atmospheres lead to blueshifts in the line cores, which exhibit central reversals. We then model the effects of the instrument on the profiles using the EVE instrument's properties. What may be interpreted as downflows (redshifted emission) in the lines after they have been convolved with the instrumental line profile may not necessarily correspond to actual downflows. Dynamic features in the atmosphere can introduce complex features in the line profiles which will not be detected by instruments with the spectral resolution of EVE, but which leave more of a signature at the resolution of the Spectral Investigation of the Coronal Environment (SPICE) instrument on Solar Orbiter.

Doppler speeds of the hydrogen Lyman lines in solar flares from EVE

Stephen A **Brown**, Lyndsay Fletcher, Nicolas Labrosse

A&A 596, A51 **2016**

https://arxiv.org/pdf/1610.04007v1.pdf

The hydrogen Lyman lines provide important diagnostic information about the dynamics of the chromosphere, but there have been few systematic studies of their variability during flares. We investigate Doppler shifts in these lines in several flares, and use these to calculate plasma speeds. We use spectral data from the Multiple EUV Grating Spectrograph B (MEGS-B) detector of the Extreme-Ultraviolet Variability Experiment (EVE) instrument on the Solar Dynamics Observatory. MEGS-B obtains full-disk spectra of the Sun at a resolution of 0.1nm in the range 37-105 nm, which we

analyse using three independent methods. The first method performs Gaussian fits to the lines, and compares the quiet-Sun centroids with the flaring ones to obtain the Doppler shifts. The second method uses cross-correlation to detect wavelength shifts between the quiet-Sun and flaring line profiles. The final method calculates the "center-of-mass" of the line profile, and compares the quiet-Sun and flaring centroids to obtain the shift. In a study of 6 flares we find strong signatures of both upflow and downflow in the Lyman lines, with speeds measured in Sun-as-a-Star data of around 10 km/s, and speeds in the flare excess signal of around 30 km/s All events showing upflows in Lyman lines are associated with some kind of eruption or coronal flow in imaging data, which may be responsible for the net blueshifts. Events showing downflows in the Lyman lines may be associated with loop contraction or faint downflows, but it is likely that chromospheric condensation flows are also contributing. **2011-02-15, 2011-03-07, 2011-11-03, 7 March 2012, 2014-01-01, 2014-01-07**

Local re-acceleration and a modified thick target model of solar flare electrons:

J. C. **Brown**, R. Turkmani, E. P. Kontar, A. L. MacKinnon and L. Vlahos
A&A 508 (**2009**) 993-1000
http://www.aanda.org/10.1051/0004-6361/200913145

Context. The collisional thick target model (CTTM) of solar hard X-ray (HXR) bursts has become an almost “standard model” of flare impulsive phase energy transport and radiation. However, it faces various problems in the light of recent data, particularly the high electron beam density and anisotropy it involves.
Aims. We consider how photon yield per electron can be increased, and hence fast electron beam intensity requirements reduced, by local re-acceleration of fast electrons throughout the HXR source itself, after injection.
Methods. We show parametrically that, if net re-acceleration rates due to e.g. waves or local current sheet electric ($\mathcal{E}$) fields are a significant fraction of collisional loss rates, electron lifetimes, and hence the net radiative HXR output per electron can be substantially increased over the CTTM values. In this local re-acceleration thick target model (LRTTM) fast electron number requirements and anisotropy are thus reduced. One specific possible scenario involving such re-acceleration is discussed, viz, a current sheet cascade (CSC) in a randomly stressed magnetic loop.
Results. Combined MHD and test particle simulations show that local $\mathcal{E}$ fields in CSCs can efficiently accelerate electrons in the corona and and re-accelerate them after injection into the chromosphere. In this HXR source scenario, rapid synchronisation and variability of impulsive footpoint emissions can still occur since primary electron acceleration is in the high Alfvén speed corona with fast re-acceleration in chromospheric CSCs. It is also consistent with the energy-dependent time-of-flight delays in HXR features.
Conclusions. Including electron re-acceleration in the HXR source allows an LRTTM modification of the CTTM in which beam density and anisotropy are much reduced, and alleviates theoretical problems with the CTTM, while making it more compatible with radio and interplanetary electron numbers. The LRTTM is, however, different in some respects such as spatial distribution of atmospheric heating by fast electrons.

Non-thermal recombination - a neglected source of flare hard X-rays and fast electron diagnostic

J. C. **Brown** and P. C. V. Mallik
A&A 481, 507-518 (**2008**)
http://www.aanda.org/index.php?option=article&access=doi&doi=10.1051/0004-6361:20078103

Flare Hard X-rays (HXRs) from non-thermal electrons are commonly treated as solely bremsstrahlung (free-free = f-f), recombination (free-bound = f-b) being neglected. This assumption is shown to be substantially in error, especially in hot sources, mainly due to recombination onto Fe ions.

RHESSI Results – Time for a Rethink?

J.C. **Brown**, E.P. Kontar, A.M. Veronig
Lecture Notes in Physics (LNP), volume 725, **2007**
https://link.springer.com/chapter/10.1007/978-3-540-71570-2_4
https://arxiv.org/pdf/astro-ph/0607440.pdf

Hard X-rays and γ-rays are the most direct signatures of energetic electrons and ions in the sun’s atmosphere which is optically thin at these energies and their radiation involves no coherent processes. Being collisional they are complementary to gyro-radiation in probing atmospheric density as opposed to magnetic field and the electrons are primarily 10–100~keV in energy, complementing the (>100 keV) electrons likely responsible for microwave bursts. The pioneering results of the Ramaty High Energy Solar Spectroscopic Imager (RHESSI) are raising the first new major questions concerning solar energetic particles in many years. Some highlights of these results are discussed – primarily around RHESSI topics on which the authors have had direct research involvement – particularly when they are raising the need for re-thinking of entrenched ideas. Results and issues are broadly divided into discoveries in the spatial, temporal and spectral domains, with the main emphasis on flare hard X-rays/fast electrons but touching also on γ-

rays/ions, non-flare emissions, and the relationship to radio bursts. **4 Dec 1978, Feb 20, 2002; 14 March 2002, 2002 April 14/15, July 23, 2002**

Helicity-conserving relaxation in unstable and merging magnetic flux ropes

Philippa **Browning**, Mykola Gordovskyy, Alan Hood
2023
https://arxiv.org/pdf/2308.08277.pdf
Twisted magnetic flux ropes are reservoirs of free magnetic energy. In a highly-conducting plasma such as the solar corona, energy release through multiple magnetic reconnections can be modelled as a helicity-conserving relaxation to a minimum energy state. One possible trigger for this relaxation is the ideal kink instability in a twisted flux rope. We show that this provides a good description for confined solar flares, and develop from idealised cylindrical models to realistic models of coronal loops. Using 3D magnetohydrodynamic simulations combined with test-particle simulations of non-thermal electrons and ions, we predict multiple observational signatures of such flares. We then show how interactions and mergers of flux ropes can release free magnetic energy, using relaxation theory to complement simulations of merging-compression formation in spherical tokamaks and heating avalanches in the solar corona.

New classification parameter of solar flares based on the maximum flux in soft X-rays and on duration of flare.

Bruevich, E.A.:
2020, J. Astrophys. Astron. 41, 3. DOI. ADS.
https://arxiv.org/pdf/1805.07158.pdf
https://doi.org/10.1007/s12036-020-9623-0
https://sci-hub.ru/10.1007/s12036-020-9623-0
Solar flare activity is characterised by different classification systems, both in optical and X-ray ranges. The most generally accepted classifications of solar flares describe important parameters of flares such as the maximum of brightness of the flare in the in optical range - Hα flare class (change from F to B), area of the flare in Hα (change from S for areas less than 2 square degrees to 4 for areas more than 24.7 square degrees) and the maximum amplitude of the soft X-ray (SXR-flux) in the band 0.1 – 0.8 nm (F max 0.1−0.8) – X-ray flares of classes from C to X. A new classification parameter of solar flares is proposed here – the X-ray index of flare XI, based on GOES measurements of solar radiation in the SXR-range. The XI-index has a clear physical interpretation associated with the total flare energy in the SXRrange. XI is easily calculated for each flare with use of available GOES data. The XI-index can be used along with other geoeffective parameters of Solar activity to assess both flares and Coronal mass ejections (CMEs) that are connected with them.
Table 1. Parameters of 96 flares of 23rd and 24th cycles and subsequent solar proton events affecting the earth environment

Powerful solar flares in September 2017. Comparison with the largest flares in cycle 24

E. A. **Bruevich**, V. V. Bruevich
2018
https://arxiv.org/pdf/1807.01271.pdf
Solar flare activity in cycle 24 is studied. Satellite observations of x-ray fluxes from GOES-15 and UV emission lines from the SDO/EVE experiment are used. The most powerful flares of cycle 24 in classes X9.3 and X8.2 in September 2017 are compared with powerful flares in classes M5-X6.9. The times at which the fluxes in the 30.4 and 9.4 nm lines and in the 0.1-0.8 nm x-ray range begin to increase are compared for 21 of the large flares. The total energies arriving at the earth from flares in the 30.4 and 9.4 nm lines and in the 0.1-0.9 nm x-ray range, E30.4, E9.4, and E0.1−0.8, from 25 flares during 2011 and 2012 are calculated. It is shown that the calculated energies of the flares in the analyzed lines from SDO/EVE and in the x-ray range from GOES-15 are closely interrelated. **24.02.2011, 09.03.2011, 03.11.2011, 23.01.2012, 06.09.2017, 10.09.2017**

New classification of solar flares based on the maximum flux in Soft X-rays and on duration of flare

Elena **Bruevich**
2018
https://arxiv.org/pdf/1805.07158.pdf
Solar flare activity is characterized by classification systems, both in optical and Soft X-ray ranges. The most generally accepted classifications of solar flares describe important parameters of flare such as the maximum of brightness of the flare in optical range in Hα (flare class in Hα is changed from F to B), area of the flare in Hα which is changed from S (less than 2 square degrees) to 4 (more than 24.7 square degrees) and the maximum amplitude of the Soft X-ray flux in the band 0.1-0.8 nm (X-ray flare of classes from C to X). A new classification of solar flares which is proposed in this paper -- the X-ray index of flare XI, based on measurements of radiation in the range 0.1-0.8 nm on the GOES satellites.

The XI index has a clear physical interpretation associated with the total flare energy in the range 0.1-0.8 nm. XI is easily calculated for each flare with use of available GOES data. The XI index can be used to assess flares along with other important geoeffective parameters.
Section 4 XI – X-RAY SOLAR FLARE INDEX AND SOLAR PROTON EVENTS (SPE)
09.03.2011, 12.07.2012
Table 1: Parameters of 36 flares of 24-th cycle 92011-2017)
Table 2: Parameters of 84 flares of 23-rd and 24-th cycles and subsequent Solar Proton Events affecting the earth environment (1998-2017)

Flare activity of the Sun and variations in its UV emission during cyrcle 24

E.A. **Bruevich**, G.V. Yakunina
2017
https://arxiv.org/pdf/1711.06262.pdf
The flare activity and the ultraviolet emission of the sun during its 24-th cycle are analysed. As compared to cycles 21-23, where the most powerful flares were observed during the decay phase, in cycle 24 the greatest number of powerful flares (>X2.7) occurred in the rising phase and at the maximum with the exception of the two largest flares of cycle 24 X9.3 and X8.2 in September 2017. We showed that regression fits of solar UV indices to the overall radiation level from the sun are substantially different for cycle 24 compared to cycles 21-23. It is found that for the flare of August 9, 2011 (SDO and GOES-15 observations), the flare propagates in a direction from the upper corona to the transition region and to the chromosphere. A study of the N-S asymmetry in the distribution of the flares in cycle 24 reveals a strong predominance of flares in the N-hemisphere in 2011 and in the S-hemisphere in 2014. It is also found that during cycles 23 and 24, the delays in the onset of proton events relative to the onset of the flares that cause them have a distribution with a distinct maximum corresponding to a delay of 2 hours for protons with energies >10 MeV, as well as for those with energies >100 MeV. **August 9, 2011**
Table 2: Flares in Cycle 24 Accompanied by the Largest-scale Proton Events

Large flares (M1 - X7) in solar cycle 24

E.A. **Bruevich**, T.V. Kazachevskaya, G.V. Yakunina
2017
https://arxiv.org/pdf/1706.01421.pdf
The large (X-ray class > M1) and very large (X-ray class >X1) flares (according to the observations of GOES-15 and Preliminary data from Current Catalog of Flare Events) in solar activity cycle 24 were analyzed. The monthly average values of optical Flare Index for 2010 - 2016 were calculated. The values of the total energy of the flare E (J m-2) in the 0.1 -- 0.8 nm range at the level of the earth's atmosphere were estimated. The energy spectrum (the dependence of the number of flares with the full energy E from the value of this full energy) for 115 flares of M5 - X7 classes was built. The comparative study of monthly averaged values of several indices of solar activity in current cycle 24: the relative sunspot numbers (SSN), the 10.7 cm radio flux, the radiation flux in the Lyman-alpha line, the solar constant (TSI) and the Flare Index (FI) was made. **9.08.2011**

3He-Rich Solar Energetic Particles in Helical Jets on the Sun

Radoslav **Bucik**, Davina E. Innes, Glenn M. Mason, Mark E. Wiedenbeck, Raul Gomez-Herrero, Nariaki V. Nitta
ApJ **2017**
https://arxiv.org/pdf/1711.09394.pdf
Particle acceleration in stellar flares is ubiquitous in the Universe, however, our Sun is the only astrophysical object where energetic particles and their source flares can both be observed. The acceleration mechanism in solar flares, tremendously enhancing (up to a factor of ten thousand) rare elements like 3He and ultra-heavy nuclei, has been puzzling for almost 50 years. Here we present some of the most intense 3He- and Fe-rich solar energetic particle events ever reported. The events were accompanied by non-relativistic electron events and type III radio bursts. The corresponding high-resolution, extreme-ultraviolet imaging observations have revealed for the first time a helical structure in the source flare with a jet-like shape. The helical jets originated in relatively small, compact active regions, located at the coronal hole boundary. A mini-filament at the base of the jet appears to trigger these events. The events were observed with the two Solar Terrestrial Relations Observatories STEREO on the backside of the Sun, during the period of increased solar activity in 2014. The helical jets may be a distinct feature of these intense events that is related to the production of high 3He and Fe enrichments. **2014 Apr 30, 17July 2014, 2014 Jul 19, 2014 Jul 20**

On the faintest solar coronal hard X-rays observed with FOXSI

Juan Camilo **Buitrago-Casas**, Lindsay Glesener, Steven Christe, Säm Krucker, et al.
A&A 665, A103 **2022**
https://arxiv.org/pdf/2205.04291.pdf
https://www.aanda.org/articles/aa/pdf/2022/09/aa43272-22.pdf

Solar nanoflares are small eruptive events releasing magnetic energy in the quiet corona. If nanoflares follow the same physics as their larger counterparts, they should emit hard X-rays (HXRs) but with a rather faint intensity. A copious and continuous presence of nanoflares would deliver enormous amounts of energy into the solar corona, possibly accounting for its high temperatures. To date, there has not been any direct observation of such sustained and persistent HXRs from the quiescent Sun. However, Hannah et al. in 2010 constrained the quiet Sun HXR emission using almost 12 days of quiescent solar-off-pointing observations by RHESSI. These observations set upper limits at 3.4×10^{-2} photons^{-1} s^{-1} cm^{-2} keV^{-1} and 9.5×10^{-4} photons^{-1} s^{-1} cm^{-2} keV^{-1} for the 3-6 keV and 6-12 keV energy ranges, respectively. Observing feeble HXRs is challenging because it demands high sensitivity and dynamic range instruments in HXRs. The Focusing Optics X-ray Solar Imager (FOXSI) sounding rocket experiment excels in these two attributes. Particularly, FOXSI completed its third successful flight (FOXSI-3) on **September 7th, 2018**. During FOXSI-3's flight, the Sun exhibited a fairly quiet configuration, displaying only one aged non-flaring active region. Using the entire ∼6.5 minutes of FOXSI-3 data, we constrained the quiet Sun emission in HXRs. We found 2σ upper limits in the order of $\sim10^{-3}$ photons^{-1} s^{-1} cm^{-2} keV^{-1} for the 5-10 keV energy range. FOXSI-3's upper limit is consistent with what was reported by Hannah et al., 2010, but FOXSI-3 achieved this result using ∼1/2640 less time than RHESSI. A possible future spacecraft using FOXSI's concept would allow enough observation time to constrain the current HXR quiet Sun limits further or perhaps even make direct detections.

A statistical correlation of sunquakes based on their seismic, white light, and X-ray emission

J.C. **Buitrago-Casas**, J.C. Martinez Oliveros, C. Lindsey, B. Calvo-Mozo, S. Krucker, L. Glesener,S. Zharkov

Solar Phys. Volume 290, Issue 11, pp 3151-3162 **2015**

http://arxiv.org/pdf/1502.07798v1.pdf

Several mechanisms have been proposed to explain the transient seis- mic emission, i.e., sunquakes, from some solar flares. Some theories associate high-energy electrons and/or white-light emission with sunquakes. High-energy charged particles and their subsequent heating of the photosphere and/or chro- mosphere could induce acoustic waves in the solar interior. We carried out a correlative study of solar flares with emission in hard-X rays (HXRs), enhanced continuum emission at 6173{\AA}, and transient seismic emission. We selected those flares observed by RHESSI (Reuven Ramaty High Energy Solar Spectroscopic Imager) with a considerable flux above 50 keV between January 1, 2010 and June 26, 2014. We then used data from the Helioseismic and Magnetic Imager onboard the Solar Dynamic Observatory (SDO/HMI) to search for excess visible continuum emission and new sunquakes not previously reported. We found a total of 18 sunquakes out of 75 investigated. All of the sunquakes were associated with a enhancement of the visible continuum during the flare time. Finally, we calculated a coefficient of correlation for a set of dichotomic variables related to these observations. We found a strong correlation between two of the standard helioseismic detection techniques, and between sunquakes and visible continuum enhancements. We discuss the phenomenological connectivity between these physical quantities and the observational difficulties of detecting seismic signals and excess continuum radiation. **Table 1. Times and locations of the seismically active solar flares**
November 7, 2013

Effect of binary collisions on electron acceleration in magnetic reconnection

C. A. **Burge**1,3, A. L. MacKinnon1 and P. Petkak

A&A 561, A107 **(2014)**

Context. The presence of energetic X-ray sources in the solar corona indicates there are additional transport effects in the acceleration region. A prime method of investigation is to add collisions into models of particle behaviour at the reconnection region.

Aims. We investigate electron test particle acceleration in a simple model of an X-type reconnection region. In particular, we explore the possibility that collisions will cause electrons to re-enter the acceleration more frequently, in turn causing particles to be accelerated to high energies.

Methods. The deterministic (Lorentz) description of particle gyration and acceleration has been coupled to a model for the effects of collisions. The resulting equations are solved numerically using Honeycutt's extension of the RK4 method to stochastic differential equations. This approach ensures a correct description of collisional energy loss and pitch-angle scattering combined with a sufficiently precise description of gyro-motion and acceleration.

Results. Even with initially mono-energetic electrons, the competition between collisions and acceleration results in a distribution of electron energies. When realistic model parameters are used, electrons achieve X-ray energies. A possible model for coronal hard X-ray sources is indicated.

Conclusions. Even in competition with energy losses, pitch-angle scattering results in a small proportion of electrons reaching higher energies than they would in a collisionless situation.

Particle Acceleration in the Presence of Weak Turbulence at an X-Type Neutral Point

C. A. **Burge**, P. Petkaki, A. L. MacKinnon

Solar Physics, October **2012**, Volume 280, Issue 2, pp 575-590

We simulate the likely noisy situation near a reconnection region by superposing many 2D linear reconnection eigenmodes. The superposition of modes on the steady state X-type magnetic field creates multiple X- and O-type neutral points close to the original neutral point and so increases the size of the non-adiabatic region. We study test particle trajectories of initially thermal protons in these fields. Protons become trapped in this region and are accelerated by the turbulent electric field to energies up to 1 MeV in time scales relevant to solar flares. Higher energies are achieved due to the interaction of particles with increasingly turbulent electric and magnetic fields.

Search for a Signature of Twist-removal in the Magnetic Field of Sunspots in Relation with Major Flares

Olga **Burtseva**1, Sanjay Gosain1, and Alexei A. Pevtsov
2017 ApJ 849 103 DOI 10.3847/1538-4357/aa8dfc
https://arxiv.org/pdf/1711.02166.pdf
We investigate the restructuring of the magnetic field in sunspots associated with two flares: the X6.5 flare on **2006 December 6** and the X2.2 flare on **2011 February 15**. The observed changes were evaluated with respect to the so-called twist-removal model, in which helicity (twist) is removed from the corona as the result of an eruption. Since no vector magnetograms were available for the X6.5 flare, we applied the azimuthal symmetry approach to line-of-sight magnetograms to reconstruct the pseudo-vector magnetic field and investigate the changes in average twist and inclination of magnetic field in the sunspot around the time of the flare. For the X2.2 flare, results from the full vector magnetograms were compared with the pseudo-vector field data. For both flares, the data show changes consistent with the twist-removal scenario. We also evaluate the validity of the azimuthal symmetry approach on simple isolated round sunspots. In general, the derivations based on the azimuthal symmetry approach agree with true-vector field data though we find that even for symmetric sunspots the distribution of the magnetic field may deviate from an axially symmetric distribution.

Hard X-ray Emission During Flares and Photospheric Field Changes

O. **Burtseva**, J. C. Martínez-Oliveros, G. J. D. Petrie, A. A. Pevtsov
ApJ **806** 173 **2015**
http://arxiv.org/pdf/1505.00509v1.pdf
We study the correlation between abrupt permanent changes of magnetic field during X-class flares observed by the GONG and HMI instruments, and the hard X-ray (HXR) emission observed by RHESSI, to relate the photospheric field changes to the coronal restructuring and investigate the origin of the field changes. We find that spatially the early RHESSI emission corresponds well to locations of the strong field changes. The field changes occur predominantly in the regions of strong magnetic field near the polarity inversion line (PIL). The later RHESSI emission does not correspond to significant field changes as the flare footpoints are moving away from the PIL. Most of the field changes start before or around the start time of the detectable HXR signal, and they end at about the same time or later than the detectable HXR flare emission. Some of the field changes propagate with speed close to that of the HXR footpoint at a later phase of the flare. The propagation of the field changes often takes place after the strongest peak in the HXR signal when the footpoints start moving away from the PIL, i.e. the field changes follow the same trajectory as the HXR footpoint, but at an earlier time. Thus, the field changes and HXR emission are spatio-temporally related but not co-spatial nor simultaneous. We also find that in the strongest X-class flares the amplitudes of the field changes peak a few minutes earlier than the peak of the HXR signal. We briefly discuss this observed time delay in terms of the formation of current sheets during eruptions.

Magnetic Flux Changes and Cancellation Associated with X-Class and M-Class Flares

Olga **Burtseva**, Gordon Petrie
Solar Physics, April **2013**, Volume 283, Issue 2, pp 429-452
We perform a statistical study of permanent changes in longitudinal fields associated with solar flares by tracking magnetic features. The YAFTA feature tracking algorithm is applied to GONG++ 1-minute magnetograms for 77 X-class and M-class flares to analyze the evolution and interaction of the magnetic features and to estimate the amount of canceled magnetic flux. We find that significantly more magnetic flux decreases than increases occurred during the flares, consistent with a model of collapsing loop structure for flares. Correlations between both total (unsigned) and net (signed) flux changes and the GOES peak X-ray flux are dominated by X-class flares at limb locations. The flux changes were accompanied in most cases by significant cancellation, most of which occurred during the flares. We find that the field strength and complexity near the polarity inversion line are approximately equally important in the flux cancellation processes that accompany the flares. We do not find a correlation between the flux cancellation events and the stepwise changes in the magnetic flux in the region.
Table, 6 December 2006

Decay Timescales of Chromospheric Condensations in Solar Flare Footpoints

Elizabeth C. **Butler**1 and Adam F. Kowalski2,3

2024 ApJ 970 33
https://iopscience.iop.org/article/10.3847/1538-4357/ad3dfb/pdf
Chromospheric condensations (CCs) are a prominent feature of flare footpoint heating in the solar flare standard model, yet their timescales and velocities are not well understood. Fisher derived several important analytical relationships, which have rarely been examined with modern spectral observations. The Interface Region Imaging Spectrograph (IRIS) provides a wealth of flare data with a high enough cadence to sufficiently capture CC evolution. We analyzed Doppler shifts in Mg ii 2791 and Fe ii 2814 from a sample of flare footpoint pixels observed by IRIS to compare with Fisher's analytics and recent flare models. We found a detection lifetime of 1 minute occurs in 50% of the sample, with Mg ii showing several pixels with longer values and Fe ii almost categorically shorter, and both growing with the maximum velocity, vmax. The shifts' half-life is commonly <40 s and is inversely related to vmax, indicating that the first half of the CC evolution has more efficient kinetic energy loss. The lifetime's wide range and growth with vmax indicate that the footpoint atmospherics and heating scenarios can vary more widely than first postulated in Fisher. Around 90% of the sample had observable acceleration periods, lasting an average of 38 and 32 s for Mg ii and Fe ii, respectively. These acceleration periods, as well as serving as flare model diagnostics themselves, could potentially be used to calculate other model diagnostics such as the initially accelerated mass. **10 Sep 2014**
IRIS Nugget 14 Nov **2024** https://iris.lmsal.com/nugget

PARTICLE ACCELERATION BY STRONG TURBULENCE IN SOLAR FLARES: THEORY OF SPECTRUM EVOLUTION

A. M. **Bykov** and G. D. Fleishman
ApJ 692 L45-L49 **2009**
http://www.iop.org/EJ/abstract/1538-4357/692/1/L45
We propose a nonlinear self-consistent model of the turbulent nonresonant particle acceleration in solar flares. We simulate temporal evolution of the spectra of charged particles accelerated by strong long-wavelength MHD turbulence taking into account the back-reaction of the accelerated particles on the turbulence. The main finding is that the nonlinear coupling of accelerated particles with MHD turbulence results in prominent evolution of the spectra of accelerated particles, which can be either soft-hard-soft or soft-hard-harder depending on the particle injection efficiency. Such evolution patterns are widely observed in hard X-ray and gamma-ray emission from solar flares.

Automatic Tracking of Active Regions and Detection of Solar Flares in Solar EUV Images

C. **Caballero**, M. C. Aranda
Solar Physics, May **2014**, Volume 289, Issue 5, pp 1643-1661
Solar catalogs are frequently handmade by experts using a manual approach or semi-automated approach. The appearance of new tools is very useful because the work is automated. Nowadays it is impossible to produce solar catalogs using these methods, because of the emergence of new spacecraft that provide a huge amount of information. In this article an automated system for detecting and tracking active regions and solar flares throughout their evolution using the Extreme UV Imaging Telescope (EIT) on the Solar and Heliospheric Observatory (SOHO) spacecraft is presented. The system is quite complex and consists of different phases: i) acquisition and preprocessing; ii) segmentation of regions of interest; iii) clustering of these regions to form candidate active regions which can become active regions; iv) tracking of active regions; v) detection of solar flares. This article describes all phases, but focuses on the phases of tracking and detection of active regions and solar flares. The system relies on consecutive solar images using a rotation law to track the active regions. Also, graphs of the evolution of a region and solar evolution are presented to detect solar flares. The procedure developed has been tested on 3500 full-disk solar images (corresponding to 35 days) taken from the spacecraft. More than 75 % of the active regions are tracked and more than 85 % of the solar flares are detected.

Dynamic Processes of the Moreton Wave on 2014 March 29

Denis P. **Cabezas**, Ayumi Asai, Kiyoshi Ichimoto, Takahito Sakaue, Satoru UeNo, Jose K. Ishitsuka, Kazunari Shibata
ApJ **883** 32 **2019**
https://arxiv.org/pdf/1908.03534.pdf
https://doi.org/10.3847/1538-4357/ab3a35
On **2014 March 29**, an intense solar flare classified as X1.0 occurred in the active region 12017. Several associated phenomena accompanied this event, among them a fast-filament eruption, large-scale propagating disturbances in the corona and the chromosphere including a Moreton wave, and a coronal mass ejection. This flare was successfully detected in multiwavelength imaging in H-alpha line by the Flare Monitoring Telescope (FMT) at Ica University, Peru. We present a detailed study of the Moreton wave associated with the flare in question. Special attention is paid to the Doppler characteristics inferred from the FMT wing (H-alpha±0.8~Å) observations, which are used to examine the downward/upward motion of the plasma in the chromosphere. Our findings reveal that the downward motion of the chromospheric material at the front of the Moreton wave attains a maximum velocity of 4 km/s, whereas the

propagation speed ranges between 640 and 859 km/s. Furthermore, utilizing the weak shock approximation in conjunction with the velocity amplitude of the chromospheric motion induced by the Moreton wave, we derive the Mach number of the incident shock in the corona. We also performed the temperature-emission measure analysis of the coronal wave based on the Atmospheric Imaging Assembly (AIA) observations, which allowed us to derive the compression ratio, and to estimate the Alfvén and fast-mode Mach numbers of the order of 1.06-1.28 and 1.05-1.27. Considering these results and the MHD linear theory we discuss the characteristics of the shock front and the interaction with the chromospheric plasma.
RHESSI Science Nugget #357 **2019**
http://sprg.ssl.berkeley.edu/~tohban/wiki/index.php/Dynamic_Processes_of_the_Moreton_Wave_on_2014_March_29

Heating Mechanisms for Intermittent Loops in Active Region Cores from AIA/SDO EUV Observations

A.C. **Cadavid**, J.K. Lawrence, D.J. Christian, D.B. Jess, G. Nigro
2014
http://arxiv.org/pdf/1404.7824v1.pdf
We investigate intensity variations and energy deposition in five coronal loops in active region cores. These were selected for their strong variability in the AIA/SDO 94 {\AA} intensity channel. We isolate the hot Fe XVIII and Fe XXI components of the 94 {\AA} and 131 {\AA} by modeling and subtracting the "warm" contributions to the emission. HMI/SDO data allow us to concentrate on "inter-moss" regions in the loops. The detailed evolution of the inter-moss intensity time series reveals loops that are impulsively heated in a mode compatible with a nanoflare storm, with a spike in the hot 131 {\AA} signals leading and the other five EUV emission channels following in progressive cooling order. A sharp increase in electron temperature tends to follow closely after the hot 131 {\AA} signal confirming the impulsive nature of the process. A cooler process of growing emission measure follows more slowly. The Fourier power spectra of the hot 131 {\AA} signals, when averaged over the five loops, present three scaling regimes with break frequencies at (0.1/min) and (0.7/min). The low frequency regime corresponds to 1/f noise; the intermediate indicates a persistent scaling process and the high frequencies show white noise. Very similar results are found for the energy dissipation in a 2-D "hybrid" shell model of loop magneto-turbulence, based on reduced magnetohydrodynamics, which is compatible with nanoflare statistics. We suggest that such turbulent dissipation is the energy source for our loops. **2011 July 13, 14, 15.**

Statistics of Solar White-Light Flares I: Optimization of Identification Methods and Application

Yingjie **Cai**, Yijun Hou, Ting Li, Jifeng Liu
ApJ **975** 69 **2024**
https://arxiv.org/pdf/2408.05381
https://iopscience.iop.org/article/10.3847/1538-4357/ad793b/pdf
White-light flares (WLFs) are energetic activity in stellar atmosphere. However, the observed solar WLF is relatively rare compared to stellar WLFs or solar flares observed at other wavelengths, limiting our further understanding solar/stellar WLFs through statistical studies. By analyzing flare observations from the \emph{Solar Dynamics Observatory (SDO)}, here we improve WLF identification methods for obtaining more solar WLFs and their accurate light curves from two aspects: 1) imposing constraints defined by the typical temporal and spatial distribution characteristics of WLF-induced signals; 2) setting the intrinsic threshold for each pixel in the flare ribbon region according to its inherent background fluctuation rather than a fixed threshold for the whole region. Applying the optimized method to 90 flares (30 C-class ones, 30 M-class ones, and 30 X-class ones) for a statistical study, we identified a total of 9 C-class WLFs, 18 M-class WLFs, and 28 X-class WLFs. The WLF identification rate of C-class flares reported here reaches 30\%, which is the highest to date to our best knowledge. It is also revealed that in each GOES energy level, the proportion of WLFs is higher in confined flares than that in eruptive flares. Moreover, a power-law relation is found between the WLF energy (\emph{E}) and duration (τ): $\tau \propto E^{0.22}$, similar to those of solar hard/soft X-ray flares and other stellar WLFs. These results indicate that we could recognize more solar WLFs through optimizing the identification method, which will lay a base for future statistical and comparison study of solar and stellar WLFs. **2011-12-31, 2014-09-17, 2015-11-01, 2015-12-29, 2017-09-06**
Table 1. List of Flares (First 20 events)
HMI Nuggets #202 Sep **2024** http://hmi.stanford.edu/hminuggets/?p=4264

Variations of the Plasma Environment Revealed by the Evolution of the Supra-arcade Fan in the 2017 September 10 Flare

Qiangwei **Cai**1,2, Jing Ye3,4, Hengqiang Feng1,2, and Guoqing Zhao1,2
2022 ApJ 929 99
https://iopscience.iop.org/article/10.3847/1538-4357/ac5fa4/pdf

Based on observations from the Interface Region Imaging Spectrograph and Hinode, we analyze the thermodynamic evolution of the supra-arcade fan (SAF) in the **2017 September 10** flare. The SAF presents discontinuous characters during the rising process, indicating a nonuniform process of magnetic reconnection in the solar eruption. The intensity peaks of the high-temperature spectral lines (Fe xxi 1354.08 Å, Fe xxiii 263.76 Å, and Fe xxiv 255.10 Å) basically correspond to the valley of the Doppler velocity and Doppler width. The temperature and density increase spatially at the upper boundary of the SAF. These results indicate that a compressed interface may exist in the SAF, where the plasma environment shows remarkable changes in density, temperature, and turbulence. In view of the fact that the height of the SAF is close to the hard X-ray source, we conclude that the interface could be related to termination shocks (TSs), taking into account the synthetic spectral profiles obtained from numerical experiments. In turn, the variations of the spectral profiles might be useful tools for identifying TSs from EUV spectral observations.
IRIS Nugget 12 Jul **2022** https://iris.lmsal.com/nugget

Dynamical and Thermal Manifestations of the Region above the Top of the Post-flare Loops: MHD Simulations

Qiangwei **Cai**1,2, Hengqiang Feng1,2, Jing Ye3,4, and Chengcai Shen5
2021 ApJ 912 79
https://iopscience.iop.org/article/10.3847/1538-4357/abee27/pdf
https://doi.org/10.3847/1538-4357/abee27
Observations proved that a distributed structure named a supra-arcade fan (SAF) exists above post-flare loops in solar eruptions. The locations of the SAF are spatially consistent with various emission sources. Termination shocks (TSs) that are often regarded as an efficient driver for particle acceleration possibly exist in the SAF. We performed the numerical simulations of solar flares based on the standard flare model to study the dynamical and thermal manifestations of the SAF, as well as the possibility of detecting TSs in extreme-ultraviolet (EUV) images. In the simulations, the SAF and TSs can be clearly identified. The motion history and temperature evolution of plasmas inside the SAF indicate that the mass of the SAF comes from the corona and the plasmas are heated in the current sheet. The height of the SAF decreases with the speed of about 64.6 km s−1 when the rate of magnetic reconnection quickly increases, and then increases with a slightly lower velocity of about 50.5 km s−1 after the peak of the rate of magnetic reconnection. The descent–ascent path of the SAF is due to the unbalance of the Lorentz force and the pressure force inside the magnetic loops. In synthetic EUV images, emission intensity variations in the area surrounding TSs are significant, indicating that, depending on the viewing angle, TSs could be identifiable in EUV observations. The results of numerical simulations are generally consistent with observations, helping us to better understand the characteristics of the SAF and the physical natures behind it.

Energy Partition in Four Confined Circular-Ribbon Flares

Z. M. **Cai**, Q. M. Zhang, Z. J. Ning, Y. N. Su, H. S. Ji
Solar Phys. **296**, Article number: 61 **2021**
https://arxiv.org/pdf/2102.09819.pdf
https://link.springer.com/content/pdf/10.1007/s11207-021-01805-5.pdf
https://doi.org/10.1007/s11207-021-01805-5
In this study, we investigated the energy partition of four confined circular-ribbon flares (CRFs) near the solar disk center, which are observed simultaneously by SDO, GOES, and RHESSI. We calculated different energy components, including the radiative outputs in 1–8, 1–70, and 70–370 Å, total radiative loss, peak thermal energy derived from GOES and RHESSI, nonthermal energy in flare-accelerated electrons, and magnetic free energy before flares. It is found that the energy components increase systematically with the flare class, indicating that more energies are involved in larger flares. The magnetic free energies are larger than the nonthermal energies and radiative outputs of flares, which is consistent with the magnetic nature of flares. The ratio Enth/Emag of the four flares, being 0.70–0.76, is considerably higher than that of eruptive flares. Hence, this ratio may serve as an important factor that discriminates confined and eruptive flares. The nonthermal energies are sufficient to provide the heating requirements including the peak thermal energy and radiative loss. Our findings impose constraint on theoretical models of confined CRFs and have potential implication for the space weather forecast. **10–May–2012, 07–Nov–2013, 29–Dec–2013, 05–Mar–2014**

Investigations of a supra-arcade fan and termination shock above the top of the flare-loop system of the 2017 September 10 event

Qiangwei **Cai**, Chengcai Shen, John C Raymond, Zhixing Mei, Alexander Warmuth, Ilia I Roussev, Jun Lin
MNRAS Volume 489, Issue 3, November **2019**, Pages 3183–3199
https://doi.org/10.1093/mnras/stz2167
https://watermark.silverchair.com/stz2167.pdf
On **2017 September 10**, a major eruption on the west solar limb produced a class X-8.2 flare and a superfast coronal mass ejection (CME). During the eruptive process, the geometric topology of the erupting magnetic configuration presented a clear flare-current sheet (CS)–CME structure. Analysing the images and spectral data from the Solar

Dynamics Observatory/Atmospheric Imaging Assembly (SDO/AIA), the Interface Region Imaging Spectrograph (IRIS) and Hinode/EUV Imaging Spectrometer (EIS), we studied the supra-arcade fan (SAF) region between the bottom of the CS and the top of the flare loops in the south part of the erupting configuration. Our results indicated that the SAF contained hot plasma of temperature up to 107 K and mean electron density 3.5×109 cm−33.5×109 cm−3 and the fast variation component (FVC) of the SAF light curve shown by the IRIS slit-jaw images (SJI) displayed a quasi-periodic oscillating feature with a period of 76.8 s. We utilized the ATHENA code to simulate the detailed evolutionary features of the magnetic structure of a typical two-ribbon flare. The numerical experiments duplicate the observational features in many respects, including the spatial distribution and evolution in the structure of the plasma and magnetic field, the turbulence and the termination shock (TS) in the SAF. Our results suggest that the SAF is a high-temperature structure that possibly contains the TS.

Feature ranking of active region source properties in solar flare forecasting and the uncompromised stochasticity of flare occurrence

Cristina **Campi**, Federico Benvenuto, Anna Maria Massone, D Shaun Bloomfield, Manolis K Georgoulis, Michele Piana
2019 *ApJ* **883** 150
https://arxiv.org/pdf/1906.12094.pdf
https://doi.org/10.3847/1538-4357/ab3c26
Solar flares originate from magnetically active regions but not all solar active regions give rise to a flare. Therefore, the challenge of solar flare prediction benefits by an intelligent computational analysis of physics-based properties extracted from active region observables, most commonly line-of-sight or vector magnetograms of the active-region photosphere. For the purpose of flare forecasting, this study utilizes an unprecedented 171 flare-predictive active region properties, mainly inferred by the Helioseismic and Magnetic Imager onboard the Solar Dynamics Observatory (SDO/HMI) in the course of the European Union Horizon 2020 FLARECAST project. Using two different supervised machine learning methods that allow feature ranking as a function of predictive capability, we show that: i) an objective training and testing process is paramount for the performance of every supervised machine learning method; ii) most properties include overlapping information and are therefore highly redundant for flare prediction; iii) solar flare prediction is still - and will likely remain - a predominantly probabilistic challenge.

Major Flare Watch Evaluation

Dick **Canfield** & Shaun Bloomfield, **2010**
http://sprg.ssl.berkeley.edu/~tohban/wiki/index.php/Major_Flare_Watch_Evaluation
Major flares that produce gamma-ray emission are the highest priority target of the RHESSI Mission. As such, multi-wavelength imaging and spectroscopic observations from other spacecraft and ground-based observatories before, during and after such flares are crucial to the interpretation of RHESSI data from these events. If a region is likely to produce a major event, the MM_COs declare that a **Major Flare Watch campaign** is in effect. How effective have these campaigns been over the course of the RHESSI mission? That's the subject of this **Nugget**.

Yohkoh SXT Full-Resolution Observations of Sigmoids: Structure, Formation, and Eruption

Richard C. **Canfield**, Maria D. Kazachenko, Loren W. Acton, D. H. Mackay, Ji Son, Tanya L. Freeman
E-print, Aug. 2007

Magnetic Reconnection Rate in the M6.5 Solar Flare on 2015 June 22

Bryce **Cannon**1, Ju Jing1,2, Qin Li1,2, Nian Liu1,2, Jeongwoo Lee1,2, Wenda Cao1,2, and Haimin Wang1,2
2023 ApJ 950 144
https://iopscience.iop.org/article/10.3847/1538-4357/accf9f/pdf
Magnetic reconnection is regarded as the mechanism for the rapid release of magnetic energy stored in active regions during solar flares, and quantitative measurements of the magnetic reconnection rate are essential for understanding solar flares. In the context of the standard two-ribbon flare model, we derive the coronal magnetic reconnection rate of the M6.5 flare on **2015 June 22** in two terms, reconnection flux change rate and reconnection electric field, both of which can be obtained from observations of the flare morphology. Data used include a sequence of chromospheric Hα images with unprecedented resolution during the flare from the Visual Imaging Spectrometer of the Goode Solar Telescope (GST) at the Big Bear Solar Observatory and a preflare line-of-sight photospheric magnetogram from the GST Near-InfraRed Imaging Spectropolarimeter along with hard X-ray data from the Ramaty High Energy Solar Spectroscopic Imager. The temporal correlation between the magnetic reconnection rate and nonthermal emission is found, and the variation of the reconnection electric field is mainly determined by the ribbon speed, not by the local magnetic field encountered by the ribbon front. Spatially, the hard X-ray source overlaps with the location of the

strongest electric field obtained at the same time. The ribbon motion shows abundant fine structures, including a local acceleration at the location of a light bridge with a weaker magnetic field.
RHESSI_Science_Nuggets #452 2023
https://sprg.ssl.berkeley.edu/~tohban/wiki/index.php/Spatial_Distribution_of_Magnetic_Reconnection_Rate_in_an_M6.5_Solar_Flare

EVIDENCE FOR A PRE-ERUPTIVE TWISTED FLUX ROPE USING THE THEMIS VECTOR MAGNETOGRAPH
A. **Canou**, T. Amari, V. Bommier, B. Schmieder, G. Aulanier, and H. Li
ApJ 693 L27-L30, **2009**
http://www.iop.org/EJ/abstract/1538-4357/693/1/L27
Although there is evidence that twisted structures form during large-scale eruptive events, it is not yet clear whether these exist in the pre-eruptive phase as twisted flux ropes (TFRs) in equilibrium. This question has become a major issue since several theoretical mechanisms can lead to the formation of TFRs. These models consider either the evolution of a coronal configuration driven by photospheric changes or the emergence of TFR from the convection zone. We consider as a target for addressing this issue the active region NOAA AR 10808 known at the origin of several large-scale eruptive phenomena, and associated with the emergence of a δ-spot. Using the THEMIS vector magnetogram as photospheric boundary conditions for our nonlinear force-free reconstruction model of the low corona and without any other assumption, we show that the resulting pre-eruptive configuration exhibits a TFR above the neutral line of the emerging δ-spot. In addition, the free magnetic energy of this configuration could even be large enough to explain such resulting large-scale eruptive events. **2005 September 13**

Slow and sausage loop mode excitation due to local and global spontaneous perturbations
H. **Capettini**, M. Cécere, A. Costa, G. Krause, O. Reula
A&A 644, A106 **2020**
https://arxiv.org/pdf/2011.00140.pdf
We analyse the capability of different type of perturbations -associated with usual environment energy fluctuations of the solar corona- to excite slow and sausage modes in solar flaring loops. We perform numerical simulations of the MHD ideal equations considering straight plasma magnetic tubes subject to local and global energy depositions. We find that local loop energy depositions of typical microflares [~(1027-1030) erg] are prone to drive slow shock waves that induce slow mode patterns. The slow mode features are obtained for every tested local energy deposition inside the loop. Meanwhile, to obtain an observable sausage mode pattern a global perturbation, capable to modify instantaneously the internal loop temperature, is required, i.e. the characteristic conductive heating time must be much smaller than the radiative cooling one. Experiments carried out by varying parameter β show us that the excitation of sausage modes does not depend significantly on the value of this parameter but on the global or local character of the energy source.

Hα and Hβ emission in a C3.3 solar flare: comparison between observations and simulations
Vincenzo **Capparelli**, Francesca Zuccarello, Paolo Romano, Paulo J. A. Simoes, Lyndsay Fletcher, David Kuridze, Mihalis Mathioudakis, Peter H. Keys,Gianna Cauzzi, Mats Carlsson
2017 *ApJ* **850** 36
https://arxiv.org/pdf/1710.04067.pdf
http://iopscience.iop.org/article/10.3847/1538-4357/aa9187/pdf
The Hydrogen Balmer series is a basic radiative loss channel from the flaring solar chromosphere. We report here on the analysis of an extremely rare set of simultaneous observations of a solar flare in the Hα and Hβ lines at high spatial and temporal resolution, which were acquired at the Dunn Solar Telescope. Images of the C3.3 flare (SOL**2014-04-22**T15:22) made at various wavelengths along the Hα line profile by the Interferometric Bidimensional Spectrometer (IBIS) and in the Hβ with the Rapid Oscillations in the Solar Atmosphere (ROSA) broadband imager are analyzed to obtain the intensity evolution. The Hα and Hβ intensity excesses in three identified flare footpoints are well correlated in time. We examine the ratio of Hα to Hβ flare excess, which was proposed by previous authors as a possible diagnostic of the level of electron beam energy input. In the stronger footpoints, the typical value of the the Hα/Hβ intensity ratio observed is ~0.4−0.5, in broad agreement with values obtained from a RADYN non-LTE simulation driven by an electron beam with parameters constrained (as far as possible) by observation. The weaker footpoint has a larger Hα/Hβ ratio, again consistent with a RADYN simulation but with a smaller energy flux. The Hα line profiles observed have a less prominent central reversal than is predicted by the RADYN results, but can be brought into agreement if the Hα-emitting material has a filling factor of around 0.2--0.3.

Active Region Emission Measure Distributions and Implications for Nanoflare Heating
P. J. **Cargill**
2014 ApJ 784 49

The temperature dependence of the emission measure (EM) in the core of active regions coronal loops is an important diagnostic of heating processes. Observations indicate that EM(T) ~ Ta below approximately 4 MK, with 2 < a < 5. Zero-dimensional hydrodynamic simulations of nanoflare trains are used to demonstrate the dependence of a on the time between individual nanoflares (TN) and the distribution of nanoflare energies. If TN is greater than a few thousand seconds, a < 3. For smaller values, trains of equally spaced nanoflares cannot account for the observed range of a if the distribution of nanoflare energies is either constant, randomly distributed, or a power law. Power law distributions where there is a delay between consecutive nanoflares proportional to the energy of the second nanoflare do lead to the observed range of a. However, TN must then be of the order of hundreds to no more than a few thousand seconds. If a nanoflare leads to the relaxation of a stressed coronal field to a near-potential state, the time taken to build up the required magnetic energy is thus too long to account for the EM measurements. Instead, it is suggested that a nanoflare involves the relaxation from one stressed coronal state to another, dissipating only a small fraction of the available magnetic energy. A consequence is that nanoflare energies may be smaller than previously envisioned.

Current Fragmentation and Particle Acceleration in Solar Flares **Review**

P. J. **Cargill**, L. Vlahos, G. Baumann, J. F. Drake and Å. Nordlund
Space Science Reviews, **2012**, 173, Issue 1-4, pp 223-245, **File**

Particle acceleration in solar flares remains an outstanding problem in plasma physics and space science. While the observed particle energies and timescales can perhaps be understood in terms of acceleration at a simple current sheet or turbulence site, the vast number of accelerated particles, and the fraction of flare energy in them, defies any simple explanation. The nature of energy storage and dissipation in the global coronal magnetic field is essential for understanding flare acceleration. Scenarios where the coronal field is stressed by complex photospheric motions lead to the formation of **multiple current sheets**, rather than the single monolithic current sheet proposed by some. The currents sheets in turn can fragment into multiple, smaller dissipation sites. MHD, kinetic and cellular automata models are used to demonstrate this feature. Particle acceleration in this environment thus involves interaction with many distributed accelerators. A series of examples demonstrate how acceleration works in such an environment. As required, acceleration is fast, and relativistic energies are readily attained. It is also shown that accelerated particles do indeed interact with multiple acceleration sites. Test particle models also demonstrate that a large number of particles can be accelerated, with a significant fraction of the flare energy associated with them. However, in the absence of feedback, and with limited numerical resolution, these results need to be viewed with caution. Particle in cell models can incorporate feedback and in one scenario suggest that acceleration can be limited by the energetic particles reaching the condition for firehose marginal stability. Contemporary issues such as footpoint particle acceleration are also discussed. It is also noted that the idea of a "standard flare model" is ill-conceived when the entire distribution of flare energies is considered.

Radio Diagnostics of electron acceleration sites during the eruption of a flux rope in the solar corona
Eoin **Carley**∗1,2, Nicole Vilmer3 , and Peter Gallagher2
2016 ApJ 833 87
http://arxiv.org/pdf/1609.01463v1.pdf

Electron acceleration in the solar corona is often associated with flares and the eruption of twisted magnetic structures known as flux ropes. However, the locations and mechanisms of such particle acceleration during the flare and eruption are still subject to much investigation. Observing the exact sites of particle acceleration can help confirm how the flare and eruption are initiated are initiated and how they evolve. Here we use the Atmospheric Imaging Assembly to analyse a flare and erupting flux rope on **2014-April-18**, while observations from the Nancay Radio Astronomy Facility allows us to diagnose the sites of electron acceleration during the eruption. Our analysis shows evidence for a pre-formed flux rope which slowly rises and becomes destabilised at the time of a C-class flare, plasma jet and the escape of >75 keV electrons from rope center into the corona. As the eruption proceeds, continued acceleration of electrons with energies of ~5 keV occurs above the flux rope for a period over 5 minutes. At flare peak, one site of electron acceleration is located close to the flare site while another is driven by the erupting flux rope into the corona at speeds of up to 400 km/s. Energetic electrons then fill the erupting volume, eventually allowing the flux rope legs to be clearly imaged from radio sources at 150-445MHz. Following the analysis of Joshi et al. (2015), we conclude that the sites of energetic electrons are consistent with flux rope eruption via a tether-cutting or flux cancellation scenario inside a magnetic fan-spine structure. In total, our radio observations allow us to better understand the evolution of a flux rope eruption and its associated electron acceleration sites, from eruption initiation to propagation into the corona.
See CESRA **2016** p.39
http://cesra2016.sciencesconf.org/conference/cesra2016/pages/CESRA2016_prog_abs_book_v3.pdf
See **CESRA highlight** #1188, March **2017** http://www.astro.gla.ac.uk/users/eduard/cesra/?p=1188

Quasiperiodic acceleration of electrons by a plasmoid-driven shock in the solar atmosphere

Eoin P. **Carley**, David M. Long, Jason P. Byrne, Pietro Zucca, D. Shaun Bloomfield, Joseph McCauley, Peter T. Gallagher
(**2013**). Nature Physics, 9, 811-816
http://arxiv.org/pdf/1406.0743v1.pdf ; **File** (**2014**)

Cosmic rays and solar energetic particles may be accelerated to relativistic energies by shock waves in astrophysical plasmas. On the Sun, shocks and particle acceleration are often associated with the eruption of magnetized plasmoids, called coronal mass ejections (CMEs). However, the physical relationship between CMEs and shock particle acceleration is not well understood. Here, we use extreme ultraviolet, radio and white-light imaging of a solar eruptive event on **22 September 2011** to show that a CME-induced shock (Alfv\'en Mach number 2.4+0.7−0.8) was coincident with a coronal wave and an intense metric radio burst generated by intermittent acceleration of electrons to kinetic energies of 2-46 keV (0.1-0.4 c). Our observations show that plasmoid-driven quasi-perpendicular shocks are capable of producing quasi-periodic acceleration of electrons, an effect consistent with a turbulent or rippled plasma shock surface.

A statistical search for a uniform trigger threshold in solar flares from individual active regions

Julian B. **Carlin**, Andrew Melatos, Michael S. Wheatland
ApJ **948** 76 **2023**
https://arxiv.org/pdf/2303.07512.pdf
https://iopscience.iop.org/article/10.3847/1538-4357/acc387/pdf
Solar flares result from the sudden release of energy deposited by sub-photospheric motions into the magnetic field of the corona. The deposited energy accumulates secularly between events. One may interpret the observed event statistics as resulting from a state-dependent Poisson process, in which the instantaneous flare rate is a function of the stress in the system, and a flare becomes certain as the stress approaches a threshold set by the micro-physics of the flare trigger. If the system is driven fast, and if the threshold is static and uniform globally, a cross-correlation is predicted between the size of a flare and the forward waiting time to the next flare. This cross-correlation is broadly absent from the \emph{Geostationary Operational Environmental Satellite} (\emph{GOES}) soft X-ray flare database. One also predicts higher cross-correlations in active regions where the shapes of the waiting time and size distributions match. Again there is no evidence for such an association in the \emph{GOES} data. The data imply at least one of the following: i) the threshold at which a flare is triggered varies in time; ii) the rate at which energy is driven into active regions varies in time; iii) historical flare catalogs are incomplete; or iv) the description of solar flares as resulting from a build-up and release of energy, once a threshold is reached, is incomplete.
Erratum: **2023** ***ApJ*** 953 **120** **https://iopscience.iop.org/article/10.3847/1538-4357/ace82c/pdf**

Investigating the Dynamics and Density Evolution of Returning Plasma Blobs from the 2011 June 7 Eruption

Jack **Carlyle**, David R. Williams, Lidia van Driel-Gesztelyi, Davina Innes, Andrew Hillier, Sarah Matthews
E-print, Jan **2014**; ApJL 788 L31 **2014**
This work examines infalling matter following an enormous Coronal Mass Ejection (CME) on 2011 June 7. The material formed discrete concentrations, or blobs, in the corona and fell back to the surface, appearing as dark clouds against the bright corona. In this work we examined the density and dynamic evolution of these blobs in order to formally assess the intriguing morphology displayed throughout their descent. The blobs were studied in five wavelengths (94, 131, 171, 193 and 211 Angstrom) using the Solar Dynamics Observatory Atmospheric Imaging Assembly (SDO/AIA), comparing background emission to attenuated emission as a function of wavelength to calculate column densities across the descent of four separate blobs. We found the material to have a column density of hydrogen of approximately 2 ? 1019 cm−2, which is comparable with typical pre-eruption filament column densities. Repeated splitting of the returning material is seen in a manner consistent with the Rayleigh-Taylor instability. Furthermore, the observed distribution of density and its evolution are also a signature of this instability. By approximating the three-dimensional geometry (with data from STEREO-A), volumetric densities were found to be approximately 2 ? 10−14 g cm−3, and this, along with observed dominant length-scales of the instability, was used to infer a magnetic field of the order 1 G associated with the descending blobs.

Largest flare of past 9 years erupts from Sun,

Cartier, K. M. S.
(2017), Eos, 98,https://doi.org/10.1029/2017EO081863. Published on 08 September 2017.
https://eos.org/articles/largest-flare-of-past-9-years-erupts-from-sun
12:02 p.m. UTC on 6 September
Good movie
https://eos.org/wp-content/uploads/2017/09/Earth_to_Scale_short_500.gif?x35494

Measuring X-ray anisotropy in solar flares. Prospective stereoscopic capabilities of STIX and MiSolFA

Stereoscopic measurements of X-ray anisotropy in solar flares with STIX and MiSolFA
Diego **Casadei**, Natasha L. S. Jeffrey, Eduard P. Kontar
A&A 606, A2 **2017**

https://arxiv.org/pdf/1702.08795.pdf
https://www.aanda.org/articles/aa/pdf/2017/10/aa30629-17.pdf
Context. During a solar flare, a large fraction of the magnetic energy released goes into the kinetic energy of non-thermal particles, with X-ray observations providing a direct diagnostic tool of keV flare-accelerated electrons. However, the electron angular distribution, a prime diagnostic tool of the acceleration mechanism and transport, is poorly known.
Aims. During the next solar maximum, two upcoming space-borne X-ray missions, STIX onboard Solar Orbiter and MiSolFA, will perform stereoscopic X-ray observations of solar flares at two di_erent locations: STIX at 0.28 AU (at perihelion) and up to inclinations of _ 25_, and MiSolFA at low-Earth orbit. The combined observations from these cross-calibrated detectors, will allow us to confidently detect the electron anisotropy of individual flares for the first time.
Methods. Both instrumental and physical effects are simulated for STIX and MiSolFA including thermal shielding, background and X-ray Compton backscattering (albedo effect) in the solar photosphere. We predict the expected number of observable flares and stereoscopic measurements during the next solar maximum. The range of useful spacecraft observation angles is estimated, for the challenging case of close-to-isotropic flare anisotropy.
Results. The simulated results show that STIX and MiSolFA will be capable of detecting low levels of flare anisotropy, even with a relatively small (_20–30_) angular separation of the spacecrafts, and will directly measure the flare electron anisotropy of about 40 M- and X-class solar flares during the next solar maximum.
Conclusions. Near-future stereoscopic observations with Solar Orbiter/STIX and MiSolFA will help distinguish between competing flare-acceleration mechanisms, and provide information regarding collisional and non-collisional transport processes occurring in the flaring atmosphere for individual solar flares.

Hard X-ray Directivity Measurements with STIX and MiSolFA

Diego **Casadei,** Hugh Hudson
RHESSI Science Nugget No. 266, Dec **2015**
http://sprg.ssl.berkeley.edu/~tohban/wiki/index.php/Hard_X-ray_Directivity_Measurements_with_STIX_and_MiSolFA
Current studies show that energy-dependent signatures related to different viewing angles may be detectable with flares of GOES M and X class. The useful energy range goes from the end of the thermally-dominated region until the background-dominated region, where the counts due to high-energy photons are not much larger than the background counts. This spectral range depends on the flare observed. For example, an X-class flare is expected to have higher counts in the high-energy region, but at the same time its thermal component extends to higher energy than softer flares. On the other hand, the non-thermal spectrum is visible at lower energies for M-class flares, but it might produce not enough counts at high energy (one should not forget about the variability of the spectral index too). From the statistical point of view, one expects to get few tens of useful flares during solar maximum, which means that there is a good chance to observe several "good" flares with both instruments.
Solar X-ray emission has inherent directivity, but it has not yet been very well studied. We know of useful information embedded in this property, but indeed we are likely to be surprised by what we see. STIX will lead the way by going into deep space, and MiSolFA can provide its stereoscopic complement. **2005-01-20**

Solar Flare Measurements with STIX and MiSolFA

Diego **Casadei**
Astrophysics and Space Instrumentation session, 2014 Nuclear Science Symposium and Medical Imaging Conference, 11 Nov **2014**
http://arxiv.org/pdf/1411.0901v1.pdf
Solar flares are the most powerful events in the solar system and the brightest sources of X-rays, often associated with emission of particles reaching the Earth and causing geomagnetic storms, giving problems to communication, airplanes and even black-outs. X-rays emitted by accelerated electrons are the most direct probe of solar flare phenomena. The Micro Solar-Flare Apparatus (MiSolFA) is a proposed compact X-ray detector which will address the two biggest issues in solar flare modeling. Dynamic range limitations prevent simultaneous spectroscopy with a single instrument of all X-ray emitting regions of a flare. In addition, most X-ray observations so far are inconsistent with the high anisotropy predicted by the models usually adopted for solar flares. Operated at the same time as the STIX instrument of the ESA Solar Orbiter mission, at the next solar maximum (2020), they will have the unique opportunity to look at the same flare from two different directions: Solar Orbiter gets very close to the Sun with significant orbital inclination; MiSolFA is in a near-Earth orbit. To solve the cross-calibration problems affecting all previous attempts to combine data from different satellites, MiSolFA will adopt the same photon detectors as STIX, precisely quantifying the anisotropy of the X-ray emission for the first time. By selecting flares whose footpoints (the brightest X-ray sources, at the chromosphere) are occulted by the solar limb for one of the two detectors, the other will be able to study the much fainter coronal emission, obtaining for the first time simultaneous observations of all

interesting regions. MiSolFA shall operate on board of a very small satellite, with several launch opportunities, and will rely on moir\'e imaging techniques.

Magnetic Energy Powers the Corona: How We Can Understand its 3D Storage & Release

Amir **Caspi**, Daniel B. Seaton, Roberto Casini, Cooper Downs, Sarah E. Gibson, Holly Gilbert, Lindsay Glesener, Silvina E. Guidoni, J. Marcus Hughes, David McKenzie, Joseph Plowman, Katharine K. Reeves, Pascal Saint-Hilaire, Albert Y. Shih, Matthew J. West

White paper to the Decadal Survey for Solar and Space Physics (Heliophysics) 2024-2033 **2023**

https://arxiv.org/pdf/2305.17146.pdf

The coronal magnetic field is the prime driver behind many as-yet unsolved mysteries: solar eruptions, coronal heating, and the solar wind, to name a few. It is, however, still poorly observed and understood. We highlight key questions related to magnetic energy storage, release, and transport in the solar corona, and their relationship to these important problems. We advocate for new and multi-point co-optimized measurements, sensitive to magnetic field and other plasma parameters, spanning from optical to γ-ray wavelengths, to bring closure to these long-standing and fundamental questions. We discuss how our approach can fully describe the 3D magnetic field, embedded plasma, particle energization, and their joint evolution to achieve these objectives.

Hard X-Ray Imaging of Individual Spectral Components in Solar Flares

Amir **Caspi**, Albert Y. Shih, James M. McTiernan, Säm Krucker

2015 811 L1 ApJL

http://arxiv.org/ftp/arxiv/papers/1508/1508.06003.pdf

We present a new analytical technique, combining Reuven Ramaty High Energy Solar Spectroscopic Imager (RHESSI) high-resolution imaging and spectroscopic observations, to visualize solar flare emission as a function of spectral component (e.g., isothermal temperature) rather than energy. This computationally inexpensive technique is applicable to all spatially-invariant spectral forms and is useful for visualizing spectroscopically-determined individual sources and placing them in context, e.g., comparing multiple isothermal sources with nonthermal emission locations. For example, while extreme ultraviolet images can usually be closely identified with narrow temperature ranges, due to the emission being primarily from spectral lines of specific ion species, X-ray images are dominated by continuum emission and therefore have a broad temperature response, making it difficult to identify sources of specific temperatures regardless of the energy band of the image. We combine RHESSI calibrated X-ray visibilities with spatially-integrated spectral models including multiple isothermal components to effectively isolate the individual thermal sources from the combined emission and image them separately. We apply this technique to the **2002 July 23** X4.8 event studied in prior works, and image for the first time the super-hot and cooler thermal sources independently. The super-hot source is farther from the footpoints and more elongated throughout the impulsive phase, consistent with an in situ heating mechanism for the super-hot plasma.

Constraining solar flare differential emission measures with EVE and RHESSI

Amir **Caspi**, James M. McTiernan, Harry P. Warren

E-print, May **2014**; ApJL

http://www.ssl.berkeley.edu/~cepheid/eprints/Caspi_McTiernan_Warren_2014_ApJL.pdf

http://arxiv.org/pdf/1405.7068v1.pdf

Deriving a well-constrained differential emission measure (DEM) distribution for solar flares has historically been difficult, primarily because no single instrument is sensitive to the full range of coronal temperatures observed in flares, from <2 to >50 MK. We present a new technique, combining extreme ultraviolet (EUV) spectra from the EUV Variability Experiment (EVE) onboard the Solar Dynamics Observatory with X-ray spectra from the Reuven Ramaty High Energy Solar Spectroscopic Imager (RHESSI), to derive, for the first time, a self-consistent, well-constrained DEM for jointly-observed solar flares. EVE is sensitive to ~2-25 MK thermal plasma emission, and RHESSI to >10 MK; together, the two instruments cover the full range of flare coronal plasma temperatures. We have validated the new technique on artificial test data, and apply it to two X-class flares from solar cycle 24 to determine the flare DEM and its temporal evolution; the constraints on the thermal emission derived from the EVE data also constrain the low-energy cutoff of the non-thermal electrons, a crucial parameter for flare energetics. The DEM analysis can also be used to predict the soft X-ray flux in the poorly-observed ~0.4-5 nm range, with important applications for geospace science. **2011 Feb 15, 2011 Mar 09**

Statistical Properties of Super-hot Solar Flares

Amir **Caspi**, S?m Krucker, R. P. Lin

E-print, Dec **2013**; **2014** ApJ 781 43

We use RHESSI high-resolution imaging and spectroscopy observations from ~6 to 100 keV to determine the statistical relationships between measured parameters (temperature, emission measure, etc.) of hot, thermal plasma in 37 intense (GOES M- and X-class) solar flares. The RHESSI data, most sensitive to the hottest flare plasmas, reveal a strong correlation between the maximum achieved temperature and the flare GOES class, such that ?super-hot? temperatures

>30 MK are achieved almost exclusively by X-class events; the observed correlation differs significantly from that of GOES-derived temperatures, and from previous studies. A nearly-ubiquitous association with high emission measures, electron densities, and instantaneous thermal energies suggests that super-hot plasmas are physically distinct from cooler, ~10?20 MK GOES plasmas, and that they require substantially greater energy input during the flare. High thermal energy densities suggest that super-hot flares require strong coronal magnetic fields, exceeding ~100 G, and that both the plasma beta and volume filling factor f cannot be much less than unity in the super-hot region.
Table: 2002-2003

RHESSI LINE AND CONTINUUM OBSERVATIONS OF SUPER-HOT FLARE PLASMA

A. **Caspi**1 and R. P. Lin1,2
Astrophysical Journal Letters, 725:L161–L166, **2010**

We use *RHESSI* high-resolution imaging and spectroscopy observations from ~5 to 100 keV to characterize the hot thermal plasma during the **2002 July 23** X4.8 flare. These measurements of the steeply falling thermal X-ray continuum are well fit throughout the flare by two distinct isothermal components: a super-hot (T_e > 30 MK) component that peaks at ~44 MK and a lower-altitude hot (T_e _ 25 MK) component whose temperature and emission measure closely track those derived from *GOES* measurements. The two components appear to be spatially distinct, and their evolution suggests that the super-hot plasma originates in the corona, while the *GOES* plasma results from chromospheric evaporation. Throughout the flare, the measured fluxes and ratio of the Fe and Fe–Ni excitation line complexes at ~6.7 and ~8 keV show a close dependence on the super-hot continuum temperature. During the pre-impulsive phase, when the coronal thermal and non-thermal continua overlap both spectrally and spatially, we use this relationship to obtain limits on the thermal and non-thermal emission.

Super-hot (T > 30 MK) Thermal Plasma in Solar Flares

A. **Caspi**
E-print, Aug **2010**, Ph.D. Dissertation

The Sun offers a convenient nearby laboratory to study the physical processes of particle acceleration and impulsive energy release in magnetized plasmas that occur throughout the universe, from planetary magnetospheres to black hole accretion disks. Solar flares are the most powerful explosions in the solar system, releasing up to 10^32-10^33 ergs over only 100-1,000 seconds. These events can accelerate electrons up to hundreds of MeV and can heat plasma to tens of MK, exceeding ~40 MK in the most intense flares. The accelerated electrons and the hot plasma each contain tens of percent of the total flare energy, indicating an intimate link between particle acceleration, plasma heating, and flare energy release. X-ray emission is the most direct signature of these processes; accelerated electrons emit hard X-ray bremsstrahlung as they collide with the ambient atmosphere, while hot plasma emits soft X-rays from both bremsstrahlung and excitation lines of highly-ionized atoms. The Reuven Ramaty High Energy Solar Spectroscopic Imager (RHESSI) observes this emission from ~3 keV to ~17 MeV with unprecedented spectral, spatial, and temporal resolution, providing the most precise measurements of the X-ray flare spectrum and enabling the most accurate characterization of the X-ray-emitting hot and accelerated electron populations. RHESSI observations show that ?super-hot? temperatures exceeding ~30 MK are common in large flares but are achieved almost exclusively by X-class events and appear to be strictly associated with coronal magnetic field strengths exceeding ~170 Gauss; these results suggest a direct link between the magnetic field and heating of super-hot plasma, and that super-hot flares may require a minimum threshold of field strength and overall flare intensity. Imaging and spectroscopic observations of **the 2002 July 23 X4.8** event show that the super-hot plasma is both spectrally and spatially distinct from the usual ~10-20 MK plasma observed in nearly all flares, and is located above rather than at the top of the loop containing the cooler plasma. It exists with high density even during the pre-impulsive phase, which is dominated by coronal non-thermal emission with negligible footpoints, suggesting that particle acceleration and plasma heating are intrinsically related but that, rather than the traditional picture of chromospheric evaporation, the origins of super-hot plasma may be the compression and subsequent thermalization of ambient material accelerated in the reconnection region above the flare loop, a physically-plausible process not detectable with current instruments but potentially observable with future telescopes. Explaining the origins of super-hot plasma would thus ultimately help to understand the mechanisms of particle acceleration and impulsive energy release in solar flares.

On the Cause of Supra-Arcade Downflows in Solar Flares

P. A. **Cassak**, J. F. Drake, J. T. Gosling, T.-D. Phan, M. A. Shay, L. S. Shepherd
E-print, Sept **2013**; **2013** ApJ 775 L14

A model of supra-arcade downflows (SADs), dark low density regions also known as tadpoles that propagate sunward during solar flares, is presented. It is argued that the regions of low density are flow channels carved by sunward-directed outflow jets from reconnection. The solar corona is stratified, so the flare site is populated by a lower density plasma than that in the underlying arcade. As the jets penetrate the arcade, they carve out regions of depleted plasma density which appear as SADs. The present interpretation differs from previous models in that reconnection is localized

in space but not in time. Reconnection is continuous in time to explain why SADs are not filled in from behind as they would if they were caused by isolated descending flux tubes or the wakes behind them due to temporally bursty reconnection. Reconnection is localized in space because outflow jets in standard two-dimensional reconnection models expand in the normal (inflow) direction with distance from the reconnection site, which would not produce thin SADs as seen in observations. On the contrary, outflow jets in spatially localized three-dimensional reconnection with an out-of-plane (guide) magnetic field expand primarily in the out-of-plane direction and remain collimated in the normal direction, which is consistent with observed SADs being thin. Two-dimensional proof-of-principle simulations of reconnection with an out-of-plane (guide) magnetic field confirm the creation of SAD-like depletion regions and the necessity of density stratification. Three-dimensional simulations confirm that localized reconnection remains collimated.

THE IMPACT OF MICROSCOPIC MAGNETIC RECONNECTION ON PRE-FLARE ENERGY STORAGE

P. A. Cassak and J. F. Drake2
2009 ApJ 707 L158-L162
It is widely accepted that magnetic reconnection releases a large amount of energy during solar flares. Studies of reconnection usually assume that the length scale over which the global (macroscopic) magnetic field reverses is identical to the thickness of the reconnection site. However, in spatially extended high-Lundquist number plasmas such as the solar corona, this scenario is untenable; the reconnection site is microscopic and embedded inside the macroscopic current set up by global fields. We use numerical simulations and scaling arguments to show that embedded effects on reconnection could have a profound influence on energy storage before a flare. From large-scale high-Lundquist number resistive magnetohydrodynamics simulations of reconnection with a diffusion region on a much smaller scale than the macroscopic current sheet, we find that the generation of secondary islands is governed by the local magnetic field immediately upstream of the diffusion region rather than the (potentially much larger) global field. This diminishes the production of secondary islands and leads to a thicker diffusion region than those predicted using the global field strength. Such considerations are crucial for understanding the onset of solar eruptions and how energy accumulates before such eruptions. We argue that if reconnection with secondary islands is fast, the energy storage times before an eruption are too small to explain observations. If reconnection with secondary islands remains slow, embedded effects cause the diffusion region to begin far wider than kinetic scales, so energy storage before a flare can occur while collisional (Sweet-Parker) reconnection with secondary islands proceeds.

3D MHD Simulation of Flare Supra-Arcade Downflows in a Turbulent Current Sheet Medium

M. **Cécere**1,2, E. Zurbriggen1,2, A. Costa1,2,3, and M. Schneiter
2015 ApJ 807 6
Supra-arcade downflows (SADs) are sunward, generally dark, plasma density depletions originated above posteruption flare arcades. In this paper, using 3D MHD simulations we investigate whether the SAD cavities can be produced by a direct combination of the tearing mode and Kelvin–Helmholtz instabilities leading to a turbulent current sheet (CS) medium or if the current sheet is merely the background where SADs are produced, triggered by an impulsive deposition of energy. We find that to give an account of the observational dark lane structures an addition of local energy, provided by a reconnection event, is required. We suggest that there may be a closed relation between characteristic SAD sizes and CS widths that must be satisfied to obtain an observable SAD.

SIMULATION OF DESCENDING MULTIPLE SUPRA-ARCADE RECONNECTION OUTFLOWS IN SOLAR FLARES

M. **Cécere**1,2, M. Schneiter1,3,4, A. Costa1,3,4, S. Elaskar1,4, and S. Maglione
2012 ApJ 759 79
After recent Atmospheric Imaging Assembly observations by Savage, McKenzie, and Reeves, we revisit the scenario proposed by us in previous papers. We have shown that sunward, generally dark plasma features that originated above posteruption flare arcades are consistent with a scenario where plasma voids (which we identify as supra-arcade reconnection outflows, SAROs) generate the bouncing and interfering of shocks and expansion waves upstream of an initial localized deposition of energy that is collimated in the magnetic field direction. In this paper, we analyze the multiple production and interaction of SAROs and their individual structures that make them relatively stable features while moving. We compare our results with observations and with the scenarios proposed by other authors.

THE NAKED EMERGENCE OF SOLAR ACTIVE REGIONS OBSERVED WITH SDO/HMI

Rebecca **Centeno**
2012 ApJ 759 72

We take advantage of the HMI/SDO instrument to study the naked emergence of active regions (ARs) from the first imprints of the magnetic field on the solar surface. To this end, we followed the first 24 hr in the life of two rather isolated ARs that appeared on the surface when they were about to cross the central meridian. We analyze the correlations between Doppler velocities and the orientation of the vector magnetic field, consistent finding that the horizontal fields connecting the main polarities are dragged to the surface by relatively strong upflows and are associated with elongated granulation that is, on average, brighter than its surroundings. The main magnetic footpoints, on the other hand, are dominated by vertical fields and downflowing plasma. The appearance of moving dipolar features (MDFs, of opposite polarity to that of the AR) in between the main footpoints is a rather common occurrence once the AR reaches a certain size. The buoyancy of the fields is insufficient to lift up the magnetic arcade as a whole. Instead, weighted by the plasma that it carries, the field is pinned down to the photosphere at several places in between the main footpoints, giving life to the MDFs and enabling channels of downflowing plasma. MDF poles tend to drift toward each other, merge and disappear. This is likely to be the signature of a reconnection process in the dipped field lines, which relieves some of the weight allowing the magnetic arcade to finally rise beyond the detection layer of the Helioseismic and Magnetic Imager spectral line.

Superpenumbral Fibrils Powered by Sunspot Oscillations

Jongchul **Chae**1, Heesu Yang1, Hyungmin Park1, Ram Ajor Maurya1, Kyung-Suk Cho2, and Vasyl Yurchysyn

2014 ApJ 789 108

It is still a mystery how the solar chromosphere can stand high above the photosphere. The dominant portion of this layer must be dynamically supported, as is evident by the common occurrence of jets such as spicules and mottles in quiet regions, and fibrils and surges in active regions. Hence, revealing the driving mechanism of these chromospheric jets is crucial for our understanding of how the chromosphere itself exists. Here, we report our observational finding that fibrils in the superpenumbra of a sunspot are powered by sunspot oscillations. We find patterns of outward propagation that apparently originate from inside the sunspot, propagate like running penumbral waves, and develop into the fibrils. Redshift ridges seen in the time-distance plots of velocity often merge, forming a fork-like pattern. The predominant period of these shock waves increases, often jumping with distance, from 3 minutes to 10 minutes. This short-to-long period transition seems to result from the selective suppression of shocks by the falling material of their preceding shocks. Based on our results, we propose that the fibrils are driven by slow shock waves with long periods that are produced by the merging of shock waves with shorter periods propagating along the magnetic canopy.

A TEST OF THREE OPTICAL FLOW TECHNIQUES—LCT, DAVE, AND NAVE

Jongchul **Chae** and Takashi Sakurai

Astrophysical Journal, 689:593Y612, **2008**

Atime sequence of high-quality images currently produced by high-resolution observations either from the ground or in space may be utilized to determine the transverse flow field on the plane of the sky with the help of optical flow techniques. We have examined the performance of three different methods—a well-known technique called local correlation tracking (LCT), a recently developed technique called the differential affine velocity estimator (DAVE), and a new technique called the nonlinear affine velocity estimator (NAVE)—using three kinds of image data: mapping-based synthetic images, a set of MHD simulation data, and real images (magnetograms) taken by the Solar Optical Telescope on board **Hinode..**

Solar Ultraviolet Irradiance Observations of the Solar Flares During the Intense September 2017 Storm Period

P. C. **Chamberlin**, T. N. Woods, L. Didkovsky, F. G. Eparvier, A. R. Jones, J. L. Machol, J. P. Mason, M. Snow, E. M. B. Thiemann, R. A. Viereck, D. L. Woodraska

Space Weather Volume16, Issue10 Pages 1470-1487 **2018**

http://sci-hub.tw/https://agupubs.onlinelibrary.wiley.com/doi/abs/10.1029/2018SW001866

sci-hub.tw/10.1029/2018SW001866

A large outburst of flares occurred between 4–10 September 2017 when new magnetic flux emerged into and strengthened an existing active region, National Oceanic and Atmospheric Administration Region 12673. This intense solar storm period included X9.3 (6 September) and X8.2 (10 September) flares, the largest flares that have occurred during Solar Cycle 24, as well as 39 M-class flares and three additional X-class flares. Another X-class flare from this active region was observed on the farside of the Sun from Mars Atmosphere and Volatile EvolutioN prior to the September events, along with other large M-class flares, showing the potential for how farside irradiance monitoring can improve flare prediction at Earth for 1- to 13-day forecasts. This September 2017 flare period is similar to other famous storm periods such as the 18 October to 5 November 2003 Halloween storm that produced 14 X-class flares and 137 M-class flares and the 6–10 September 2005 period that had 11 X-class and 68 M-class flares. All of these storm

periods occurred in the declining phase of the solar cycle when solar activity had decreased significantly from solar maximum levels. This paper focuses on a number of solar irradiance observations at ultraviolet (0–190 nm) wavelengths during the September 2017 storm period and the advantages that an ensemble of measurements and models have for studying solar flares.

Thermal Evolution and Radiative Output of Solar Flares Observed by the EUV Variability Experiment (EVE)

Chamberlin, P. C., R. O. Milligan, and T. N. Woods
E-print, Apr **2012**, Solar Phys. Volume 279, Number 1 (**2012**), 23-42
This paper describes the methods used to obtain the thermal evolution and radiative output during solar flares as observed by the Extreme ultraviolet Variability Experiment (EVE) onboard the Solar Dynamics Observatory (SDO). How EVE measurements, due to the temporal cadence, spectral resolution and spectral range, can be used to determine how the thermal plasma radiates at various temperatures throughout the impulsive and gradual phase of flares is presented and discussed in detail. EVE can very accurately determine the radiative output of flares due to pre- and in-flight calibrations. Events are presented that show that the total radiated output of flares depends more on the flare duration than the typical GOES X-ray peak magnitude classification. With SDO observing every flare throughout its entire duration and over a large temperature range, new insights into flare heating and cooling as well as the radiative energy release in EUV wavelengths support existing research into understanding the evolution of solar flares.

"SDO EVE spectroscopy of solar flares,"

Phil **Chamberlin** and Tom Woods.
RHESSI Science Nugget, **2010**
See http://sprg.ssl.berkeley.edu/~tohban/wiki/index.php/SDO_EVE_Flare_Observation
The lack of routine observations of the solar spectrum, as it varies in many interesting ways, has always held back solar research. Now the new Solar Dynamics Observatory, launched in February 2010, is providing a 24/7 view of the the all-important UV/EUV part of the solar spectrum via its EVE instrument.
As seen in Figure 1, the EUV solar spectral irradiance is provided by the EVE instrument from 6-106 nm at 0.1 nm spectral resolution, providing many temperature, density, and energetic diagnostics of solar flares over a wide temperature range that covers chromospheric to hot coronal emission. The EVE observations of two GOES M-class flares, one compact and one two-ribbon, are the focus of this Nugget, demonstrating the observation capabilities of SDO EVE that are very complementary to RHESSI
M2.0 Compact flare on 2010 June 12, M1.0 Two-Ribbon flare on 2010 August 7

A Study of a long duration B9 flare-CME event and associated piston-driven shock

R. **Chandra**, P. F. Chen, A. Fulara, A. K. Srivastava, W. Uddin
Adv. Space Research Volume 61, Issue 2, 15 January **2018**, Pages 705-714
https://arxiv.org/pdf/1710.08734.pdf
We present and discuss here the observations of a small long duration GOES B- class flare associated with a quiescent filament eruption, a global EUV wave and a CME on **2011 May 11**. The event was well observed by the Solar Dynamics Observatory (SDO), GONG H{\alpha}, STEREO and HiRAS spectrograph. As the fil- ament erupted, ahead of the filament we observed the propagation of EIT wave fronts, as well as two flare ribbons on both sides of the polarity inversion line (PIL) on the solar surface. The observations show the co-existence of two types of EUV waves, i.e., a fast and a slow one. A type II radio burst with up to the third harmonic component was also associated with this event. The evolution of pho- tospheric magnetic field showed flux emergence and cancellation at the filament site before its eruption.

Homologous Flares and Magnetic Field Topology in Active Region NOAA 10501 on 20 November 2003

R. **Chandra**, B. Schmieder, C.H. Mandrini, P. Demoulin, E. Pariat, T. Torok, W. Uddin
E-print Nov **2010**, Solar Phys. (**2011**) 269: 83–104
We present and interpret observations of two morphologically homologous flares that occurred in active region (AR) NOAA 10501 on **20 November 2003**. Both flares displayed four homologous H-alpha ribbons and were both accompanied by coronal mass ejections (CMEs). The central flare ribbons were located at the site of an emerging bipole in the center of the active region. The negative polarity of this bipole fragmented in two main pieces, one rotating around the positive polarity by ~ 110 deg within 32 hours. We model the coronal magnetic field and compute its topology, using as boundary condition the magnetogram closest in time to each flare. In particular, we calculate the location of quasiseparatrix layers (QSLs) in order to understand the connectivity between the flare ribbons. Though several polarities were present in AR 10501, the global magnetic field topology corresponds to a quadrupolar magnetic field distribution without magnetic null points. For both flares, the photospheric traces of QSLs are similar and match well the locations of the four H-alpha ribbons. This globally unchanged topology and the continuous shearing by the

rotating bipole are two key factors responsible for the flare homology. However, our analyses also indicate that different magnetic connectivity domains of the quadrupolar configuration become unstable during each flare, so that magnetic reconnection proceeds differently in both events.

How can a Negative Magnetic Helicity Active Region Generate a Positive Helicity Magnetic Cloud ?

R. **Chandra** · E. Pariat · B. Schmieder · C.H. Mandrini · W. Uddin ·
E-print, Oct **2009, File**

The geoeffective magnetic cloud (MC) of **20 November 2003**, has been associated to the **18 November 2003**, solar active events in previous studies. In some of these, it was estimated that the magnetic helicity carried by the MC had a positive sign, as well as its solar source, active region (AR) NOAA 10501. In this paper we show that the large-scale magnetic field of AR 10501 had a negative helicity sign. Since coronal mass ejections (CMEs) are one of the means by which the Sun ejects magnetic helicity excess into the interplanetary space, the signs of magnetic helicity in the AR and MC should agree. Therefore, this finding contradicts what is expected from magnetic helicity conservation. However, using for the first time correct helicity density maps to determine the spatial distribution of magnetic helicity injection, we show the existence of a localized flux of positive helicity in the southern part of AR 10501. We conclude that positive helicity was ejected from this portion of the AR leading to the observed positive helicity MC.

Evidence of Magnetic Helicity in Emerging Flux and Associated Flare

R. **Chandra**, B. Schmieder, G. Aulanier, J.M. Malherbe
E-print, June **2009**; Solar Phys., 258: 53–67, **2009**

The aim of this paper is to look at the magnetic helicity structure of an emerging active region and show that both emergence and flaring signatures are consistent with a same sign for magnetic helicity. We present a multi-wavelength analysis of an M1.6 flare occurring in the active region NOAA 10365 on **27 May, 2003**, in which a large new bipole emerges in a decaying active region. The diverging flow pattern and the ``tongue'' shape of the magnetic field in the photosphere with elongated polarities are highly suggestive of the emergence of a twisted flux tube. The orientation of these tongues indicates the emergence of a flux tube with a right hand twist, i.e. positive magnetic helicity. The flare signatures in the chromosphere are ribbons observed in H-alpha by the MSDP spectrograph in the Meudon solar tower and in 1600 A by TRACE. These ribbons have a `J' shape and are shifted along the inversion line. The pattern of these ribbons suggests that the flare was triggered by magnetic reconnection at coronal heights below a twisted flux tube of positive helicity, corresponding to that of the observed emergence. It is the first time that such a consistency between the signatures of the emerging flux through the photosphere and flare ribbons is clearly identified in observations. Another type of ribbons observed during the flare at the periphery of the active region by the MSDP and SOHO/EIT are related to the existence of a null point, which is found high in the corona in a potential field extrapolation. We discuss the interpretation of these secondary brightenings in terms of the ``breakout'' model and in terms of plasma compression/heating within large-scale separatrices.

RESONANT INTERACTIONS BETWEEN PROTONS AND OBLIQUE ALFV´EN/ION-CYCLOTRON WAVES IN THE SOLAR CORONA AND SOLAR FLARES

Benjamin D. G. **Chandran**, Peera Pongkitiwanichakul, Philip A. Isenberg, Martin A. Lee, Sergei A. Markovskii, Joseph V. Hollweg, and Bernard J. Vasquez
Astrophysical Journal, 722:710–720, **2010**

We consider interactions between protons and Alfv´en/ion-cyclotron (A/IC) waves in collisionless low-β plasmas in which the proton distribution function f is strongly modified by wave pitch-angle scattering. If the angle θ between the wave vector and background magnetic field is zero for all the waves, then strong scattering causes f to become approximately constant on surfaces of constant η, where $\eta \_ v_{2\perp}$ + 1.5 $v_{2/3A}$ $|v\_|_{4/3}$. Here, $v_\perp$ and $v\_$ are thevelocity components perpendicular and parallel to the background magnetic field, and v_A is the Alfv´en speed. If $f = f(\eta)$, then A/IC waves with $\theta = 0$ are neither damped nor amplified by resonant interactions with protons. In this paper, we argue that if some mechanism generates high-frequency A/IC waves with a range of θ values, then
wave–particle interactions initially cause the proton distribution function to become so anisotropic that the plasma becomes unstable to the growth of waves with $\theta = 0$. The resulting amplification of $\theta = 0$ waves leads to an angular distribution of A/IC waves that is sharply peaked around $\theta = 0$ at the large wavenumbers at which A/IC waves resonate with protons. Scattering by this angular distribution of A/IC waves subsequently causes f to become approximately constant along surfaces of constant η, which in turn causes oblique A/IC waves to be damped by protons. We calculate the proton and electron contributions to the damping rate analytically, assuming Maxwellian electrons and $f = f(\eta)$. Because the plasma does not relax to a state inwhich proton damping of obliqueA/ICwaves ceases, oblique A/IC waves can be significantly more effective at heating protons than A/IC waves with $\theta = 0$.

Modelling repeatedly flaring delta-sunspots

Piyali **Chatterjee**, Viggo Hansteen, Mats Carlsson
Physical Review Letters **2016**
http://arxiv.org/pdf/1601.00749v1.pdf
Active regions (AR) appearing on the surface of the Sun are classified into α, β, γ, and δ by the rules of the Mount Wilson Observatory, California on the basis of their topological complexity. Amongst these, the δ-sunspots are known to be super-active and produce the most X-ray flares. Here, we present results from a simulation of the Sun by mimicking the upper layers and the corona, but starting at a more primitive stage than any earlier treatment. We find that this initial state consisting of only a thin sub-photospheric magnetic sheet breaks into multiple flux-tubes which evolve into a colliding-merging system of spots of opposite polarity upon surface emergence, similar to those often seen on the Sun. The simulation goes on to produce many exotic δ-sunspot associated phenomena: repeated flaring in the range of typical solar flare energy release and ejective helical flux ropes with embedded cool-dense plasma filaments resembling solar coronal mass ejections.
See Viewpoint: A New Twist in Simulating Solar Flares,
Axel **Brandenburg**
to be published in Physics. Edited by Jessica Thomas **2016**
http://arxiv.org/pdf/1603.01917v1.pdf**,**

The Flare Irradiance Spectral Model - Version 2 (FISM2)

P. C. **Chamberlin**, F. G. Eparvier, V. Knoer, H. Leise, A. Pankratz, M. Snow, B. Templeman, E. M. B. Thiemann, D. L. Woodraska, T. N. Woods
Space Weather e2020SW002588 **2020**
https://doi.org/10.1029/2020SW002588
https://agupubs.onlinelibrary.wiley.com/doi/epdf/10.1029/2020SW002588
The Flare Irradiance Spectral Model (FISM) is an important tool for estimating solar variability for a myriad of space weather research studies and applications, and FISM Version 2 (FISM2) recently was released. FISM2 is an empirical model of the solar ultraviolet irradiance created to fill spectral and temporal gaps in the satellite observations. FISM2 estimates solar ultraviolet irradiance variations due to the solar cycle, solar rotations, and solar flares. The major improvement provided by FISM2 is that it is based on multiple new, more accurate instruments that have now captured almost a full solar cycle and thousands of flares, drastically improving the accuracy of the modeled FISM2 solar irradiance spectra. Specifically, these new instruments are SDO EVE, SORCE XPS, and SORCE SOLSTICE. FISM2 is also improved to 0.1 nm spectral bins across the same 0-190 nm spectral range, and is already being used in research to estimate space weather changes due to solar irradiance variability in planetary thermospheres and ionospheres.

Solar Ultraviolet Irradiance Observations of the Solar Flares During the Intense September 2017 Storm Period

P. C. **Chamberlin**, T. N. Woods, L. Didkovsky, F. G. Eparvier, A. R. Jones, J. L. Machol, J. P. Mason, M. Snow, E. M. B. Thiemann, R. A. Viereck, D. L. Woodraska
Space Weather **2018**
http://sci-hub.tw/https://agupubs.onlinelibrary.wiley.com/doi/abs/10.1029/2018SW001866
A large outburst of flares occurred between 4-10 September 2017 when new magnetic flux emerged into and strengthened an existing active region, NOAA Region 12673. This intense solar storm period included X9.3 (**6 September**) and X8.2 (**10 September)** flares, the largest flares that have occurred during solar cycle 24, as well as 39 M-class flares and 3 additional X-class flares. Another X-class flare from this active region was observed on the far-side of the Sun from MAVEN prior to the September events, along with other large M-class flares, showing the potential for how far-side irradiance monitoring can improve flare prediction at Earth for 1 to 13 day forecasts. This September 2017 flare period is similar to other famous storm periods such as the *18 October to 5 November 2003* Halloween storm that produced 14 X-class flares and 137 M-class flares and the *6-10 September 2005* period that had 11 X-class and 68 M-class flares. All of these storm periods occurred in the declining phase of the solar cycle when solar activity had decreased significantly from solar maximum levels. This paper focuses on a number of solar irradiance observations at ultraviolet (0-190 nm) wavelengths during the September 2017 storm period and the advantages that an ensemble of measurements and models have for studying solar flares.

Solar flares associated coronal mass ejection accompanied with DH type II radio burst in relation with interplanetary magnetic field, geomagnetic storms and cosmic ray intensity

Harish **Chandra**, Beena Bhatt
New Astronomy Volume 60, April **2018**, Pages 22-32
sci-hub.tw/10.1016/j.newast.2017.10.001

In this paper, we have selected 114 flare-CME events accompanied with Deca-hectometric (DH) type II radio burst chosen from 1996 to 2008 (i.e., solar cycle 23). Statistical analyses are performed to examine the relationship of flare-CME events accompanied with DH type II radio burst with Interplanetary Magnetic field (IMF), Geomagnetic storms (GSs) and Cosmic Ray Intensity (CRI). The collected sample events are divided into two groups. In the first group, we considered 43 events which lie under the CME span and the second group consists of 71 events which are outside the CME span. Our analysis indicates that flare-CME accompanied with DH type II radio burst is inconsistent with CSHKP flare-CME model. We apply the Chree analysis by the superposed epoch method to both set of data to find the geo-effectiveness. We observed different fluctuations in IMF for arising and decay phase of solar cycle in both the cases. Maximum decrease in Dst during arising and decay phase of solar cycle is different for both the cases. It is noted that when flare lie outside the CME span CRI shows comparatively more variation than the flare lie under the CME span. Furthermore, we found that flare lying under the CME span is more geo effective than the flare outside of CME span. We noticed that the time leg between IMF Peak value and GSs, IMF and CRI is on average one day for both the cases. Also, the time leg between CRI and GSs is on average 0 to 1 day for both the cases. In case flare lie under the CME span we observed high correlation (0.64) between CRI and Dst whereas when flare lie outside the CME span a weak correlation (0.47) exists. Thus, flare position with respect to CME span play a key role for geo-effectiveness of CME.

Multi-wavelength view of an M2.2 Solar Flare on 26 November 2000

R. **Chandra**, V. K. Verma, S. Rani, R. A. Maurya
2016
http://arxiv.org/pdf/1608.05796v1.pdf
In this paper, we present a study of an M2.2 class solar flare of **26 November 2000** from NOAA AR 9236. The flare was well observed by various ground based observatories (ARIES, Learmonths Solar Observatory) and space borne instruments (SOHO, HXRS, GOES) in time interval between 02:30 UT to 04:00 UT. The flare started with long arc-shape outer flare ribbon. Afterwards the main flare starts with two main ribbons. Initially the outer ribbons start to expand with an average speed (∼ 20 km s−1) and later it shows contraction. The flare was associated with partial halo coronal mass ejection (CMEs) which has average speed of 495 km s−1. The SOHO/MDI observations show that the active region was in quadrupolar magnetic configuration. The flux cancellation was observed before the flare onset close to flare site. Our analysis indicate the flare was initiated by the magnetic breakout mechanism.

Ion Acceleration and the Development of a Power-law Energy Spectrum in Magnetic Reconnection

H. **Che**1,2, G. P. Zank1,2, and A. O. Benz3,4
2021 ApJ 921 135
https://doi.org/10.3847/1538-4357/ac1fe7
How charged particles are accelerated efficiently and form a power-law energy spectrum in magnetic reconnection is a problem that is not well understood. In a previous paper, it was shown that the electron Kelvin–Helmholtz instability (EKHI) in force-free magnetic reconnection generates fast-expanding vortices that can accelerate electrons in a few tens of ion gyroperiods (less than 1 ms in the solar corona) to form a power-law energy distribution. In this paper, we present a particle-in-cell (PIC) simulation study of ion acceleration in force-free magnetic reconnection in the presence of the EKHI-induced turbulence. We find that ions are not significantly accelerated by the EKHI-induced stochastic electric field until the magnetic vortices expand to sizes comparable to the ion gyroradius. The Alfvén waves generated by the EKHI couple with the magnetic vortices, leading to resonance between the ions inside the magnetic vortices and Alfvén waves and enhanced ion heating. The induced Alfvén wave resonance results in a broken power-law energy spectrum with a breakpoint at $\sim m_i v_A^2$, where vA is the Alfvén velocity. We show that the process that forms the nonthermal tail is a second-order Fermi mechanism and the mean spectral index is α = (1 + 4a2D/R)/2, where D is the spatial scale of the inductive electric field, R is that of vortices, and a = Bg/B0, with ratio of guide field Bg and asymptotic B0.

The Formation of Electron Outflow Jets with Power-law Energy Distribution in Guide-field Magnetic Reconnection

H. **Che**1,2, G. P. Zank1,2, A. O. Benz3,4, B. Tang1,2, and C. Crawford1,2
2021 ApJ 908 72
https://iopscience.iop.org/article/10.3847/1538-4357/abcf29/pdf
https://doi.org/10.3847/1538-4357/abcf29
Observationally, electron beams with power-law energy spectra are commonly associated with solar flares. Previous studies have found that during magnetic reconnection with a guide field B g larger than 0.1 times the asymptotic field B 0, electron beams are unable to develop due to the strong deflection caused by the guide field. Using particle-in-cell simulations we show that in force-free reconnection, the development of an electron Kelvin–Helmholz instability can suppress the Hall effect and produce a flute-like outflow exhaust, in which both electrons and ions are nearly frozen-in with the magnetic field. The coupling of a continuously growing electron velocity shear and E × B drift drive the electrons out of magnetic vortices and results in collimated jets with a power-law energy spectrum in the elongated

exhaust. The spatial density of electron jets is comparable to the background and is highly inhomogeneous, signifying on asymmetric density structure in guide field reconnection.

The Solar Wind Electron Halo as Produced by Electron Beams Originating in the Lower Corona: Beam Density Dependence

H. **Che**1,2, M. L. Goldstein3, C. S. Salem4, and A. F. Viñas2
2019 ApJ 883 151
https://doi.org/10.3847/1538-4357/ab3b5a
It has been suggested that the isotropic electron halo observed in the solar wind electron velocity distribution function may originate from nanoflare-accelerated electron beams below 1.1 R ⊙ from the solar surface through the nonlinear electron two-stream instability (ETSI). This model unifies the origins of kinetic waves, the electron halo, and the coronal weak Type III bursts, and establishes a link between the solar wind observables and the electron dynamics in nanoflares. One of the important predictions of this model is that the halo-core temperature ratio is anticorrelated with the density ratio, and the minimum ratio is ~4, a relic of the ETSI heating and has been found to be consistent with solar wind observations. However, how the density and relative drift of the electron beams determine the thermal properties of solar wind electrons is unclear. In this paper, using a set of particle-in-cell simulations and kinetic theory, we show that a necessary condition for an isotropic halo to develop is that the ratio of beam density n b and the background n 0 be lower than a critical value N c ~ 0.3. Heating of the core electrons becomes weaker with decreasing beam density, while the heating of halo electrons becomes stronger. As a result, the temperature ratio of the halo and core electrons increases with the decrease of the beam density, explaining the physical meaning of the predicted anticorrelated relation. We apply these results to the current observations and discuss the possible electron beam density produced in the nanoflares.

A Brief Review on Particle Acceleration in Multi-island Magnetic Reconnection **Review**

H. **Che**, G. P. Zank
2019
https://arxiv.org/pdf/1908.09155.pdf
The basic physics and recent progresses in theoretical and particle-in-cell (PIC) simulation studies of particle acceleration in multi-island magnetic reconnection are briefly reviewed. Particle acceleration in multi-island magnetic reconnection is considered a plausible mechanism for the acceleration of energetic particles in solar flares and the solar wind. Theoretical studies have demonstrated that such a mechanism can produce the observed power-law energy distribution of energetic particles if the particle motion is sufficiently randomized in the reconnection event. However, PIC simulations seem to suggest that the first-order Fermi acceleration mechanism is unable to produce a power-law particle energy distribution function in mildly relativistic multi-island magnetic reconnections. On the other hand, while simulations of highly relativistic reconnections appear to be able to produce a power-law energy spectrum, the spectral indices obtained are generally harder than the soft power-law spectra with indices ∼−5 commonly observed in the solar wind and solar flare events. In addition, the plasma heating due to kinetic instabilities in 3D magnetic reconnection may "thermalize" the power-law particles, making it even more difficult for multi-island reconnections to generate a power-law spectrum. We discuss the possible reasons that may lead to these problems.

How Nanoflares Produce Kinetic Waves, Nano-Type III Radio Bursts, and Non-Thermal Electrons in the Solar Wind

H. **Che**
Proceedings of 17th Annual International Astrophysics Conference, Santa Fe, 2018 **2018**
https://arxiv.org/pdf/1807.10942.pdf
Observations of the solar corona and the solar wind discover that the solar wind is unsteady and originates from the impulsive events near the surface of the Sun's atmosphere. How solar coronal activities affect the properties of the solar wind is a fundamental issue in heliophysics. We report a simulation and theoretical investigation of how nanoflare accelerated electron beams affect the kinetic-scale properties of the solar wind and generate coherent radio emission. We show that nanoflare-accelerated electron beams can trigger a nonlinear electron two stream instability, which generates kinetic Alfv\'en and whistler waves, as well as a non-Maxwellian electron velocity distribution function, consistent with observations of the solar wind. The plasma coherent emission produced in our model agrees well with the observations of Type III, J and V solar radio bursts. Open questions in the kinetic solar wind model are also discussed.

On the Rates of Steady, Quasi-steady and Impulsive Magnetic Reconnection

H. **Che**
ApJL **2018**
https://arxiv.org/pdf/1802.07748.pdf

Magnetic reconnection (MR) is considered as a major source of particle energization in astrophysical plasma. In the past, analysis of MR often assumes the magnetostatic condition, i.e. $\partial_t = 0$. We show that under the Sweet-Parker-Petschek framework, steady state is an over-constraint and is not achievable. On the other hand, the quasi-steady state defined as $\partial_t \mathbf{E} = 0$ but $\partial_t \mathbf{B} \neq 0$ or equivalently $\partial_t\mathbf{j}\neq 0$ better describes the asymptotic behaviour of MR without turbulence. The upper limit of MR rate for quasi-steady MR is found to be $\sim 1/3\sqrt{3} \sim 0.19$. The limit does not apply to impulsive or turbulent MR of which $\partial_t\mathbf{B} \neq 0$ and $\partial_t\mathbf{E} \neq 0$. In impulsive MR the rate can be higher or lower than 0.19 depending on the state of the turbulence. Our results may explain the apparent discrepancy in observations of solar flare MR rates. The analysis is independent of mass ratio and thus the results are applicable to pair plasma.

Common Origin of Kinetic Scale Turbulence and the Electron Halo in the Solar Wind -- Connection to Nanoflares

Haihong **Che**

Proceedings of the Fourteenth International Solar Wind Conference **2016**

http://arxiv.org/pdf/1603.00549v1.pdf

We summarize our recent studies on the origin of solar wind kinetic scale turbulence and electron halo in the electron velocity distribution function. Increasing observations of nanoflares and microscopic type III radio bursts strongly suggest that nanoflares and accelerated electron beams are common in the corona. Based on particle-in-cell simulations, we show that both the core-halo feature and kinetic scale turbulence observed in the solar wind can be produced by the nonlinear evolution of electron two-stream instability driven by nanoflare accelerated electron beams. The energy exchange between waves and particles reaches equilibrium in the inner corona and the key features of the turbulence and velocity distribution are preserved as the solar wind escapes into interplanetary space along open magnetic field lines. Observational tests of the model and future theoretical work are discussed.

The Origin of Non-Maxwellian Solar Wind Electron Velocity Distribution Function: Connection to Nanoflares in the Solar Corona

H. **Che** and M. L. Goldstein

2014 ApJ 795 L38

The formation of the observed core-halo feature in the solar wind electron velocity distribution function is a long-time puzzle. In this Letter, based on the current knowledge of nanoflares, we show that the nanoflare-accelerated electron beams are likely to trigger a strong electron two-stream instability that generates kinetic Alfvén wave and whistler wave turbulence, as we demonstrated in a previous paper. We further show that the core-halo feature produced during the origin of kinetic turbulence is likely to originate in the inner corona and can be preserved as the solar wind escapes to space along open field lines. We formulate a set of equations to describe the heating processes observed in the simulation and show that the core-halo temperature ratio of the solar wind is insensitive to the initial conditions in the corona and is related to the core-halo density ratio of the solar wind and to the quasi-saturation property of the two-stream instability at the time when the exponential decay ends. This relation can be extended to the more general core-halo-strahl feature in the solar wind. The temperature ratio between the core and hot components is nearly independent of the heliospheric distance to the Sun. We show that the core-halo relative drift previously reported is a relic of the fully saturated two-stream instability. Our theoretical results are consistent with the observations while new tests for this model are provided.

Using Flare-Induced Modulation of Three- and Five-Minute Oscillations for Studying Wave Propagation in the Solar Atmosphere

Andrei **Chelpanov**, Nikolai Kobanov

Solar Physics volume 296, Article number: 180 (**2021**)

https://arxiv.org/pdf/2110.12732.pdf

https://link.springer.com/content/pdf/10.1007/s11207-021-01910-5.pdf

https://doi.org/10.1007/s11207-021-01910-5

We propose a method for diagnosing the physical conditions in the solar atmosphere using a small increase in oscillation amplitudes resulting from minuscule solar flares. As an example, we consider a B2 flare, which caused a sharp short-lived increase in the amplitude of three- and five-minute oscillations in the lower layers of the solar atmosphere. Enhanced three- and five-minute oscillations propagated from the lower layers of the atmosphere into the corona. Such short oscillation trains made it possible to remove the uncertainties arising in the measurements of the phase and group lags between the layers. In addition, the amplification of the oscillations that reach the corona may add to the likelihood of a repeated flare. Studying oscillations in small flare events has the advantage of exploring the atmosphere in its quasi-quiet condition as opposed to powerful flares, which cause substantial and prolonged disturbance of the environment. In addition, small flares are much more common than powerful flares, which allows one to choose from a larger sample of observational material. **21 September 2012**

Oscillations accompanying a He I 10830 Å negative flare in a solar facula

Andrei **Chelpanov**, Nikolai Kobanov

Solar Physics **2018** November 2018, 293:157

https://arxiv.org/pdf/1810.10153.pdf

https://link.springer.com/content/pdf/10.1007%2Fs11207-018-1378-2.pdf

On **September 21, 2012**, we carried out spectral observations of a solar facula in the Si I 10827 {\AA}, He I 10830 {\AA}, and H{\alpha} spectral lines. Later, in the process of analyzing the data, we found a small-scale flare in the middle of the time series. Due to an anomalous increase in the absorption of the He I 10830 {\AA} line, we identified this flare as a negative flare.

The aim of this paper is to study the influence of the negative flare on the oscillation characteristics in the facular photosphere and chromosphere.

We measured line-of-sight (LOS) velocity and intensity of all the three lines as well as half-width of the chromospheric lines. We also used SDO/HMI magnetic field data. The flare caused modulation of all the studied parameters. In the location of the negative flare, the amplitude of the oscillations increased four times on average. In the adjacent magnetic field local maxima, the chromospheric LOS velocity oscillations appreciably decreased during the flare. The facula region oscillated as a whole with a 5-minute period before the flare, and this synchronicity was disrupted after the flare. The flare changed the spectral composition of the line-of-sight magnetic field oscillations, causing an increase in the low-frequency oscillation power.

Simultaneous Eruption and Shrinkage of Pre-existing Flare Loops during a Subsequent Solar Eruption

Huadong **Chen**, Lyndsay Fletcher, Guiping Zhou, Xin Cheng, Ya Wang, Sargam Mulay, Ruisheng Zheng, Suli Ma, Xiaofan Zhang

ApJ **2024**

https://arxiv.org/pdf/2410.12202

We investigated two consecutive solar eruption events in the solar active region (AR) 12994 at the solar eastern limb on **2022 April 15**. We found that the flare loops formed by the first eruption were involved in the second eruption. During the initial stage of the second flare, the middle part of these flare loops (E-loops) erupted outward along with the flux ropes below, while the parts of the flare loops (I-loops1 and I-loops2) on either side of the E-loops first rose and then contracted. Approximately 1 hour after the eruption, the heights of I-loops1 and I-loops2 decreased by 9 Mm and 45 Mm, respectively, compared to before the eruption. Their maximum descent velocities were 30 km/s and 130 km/s, respectively. The differential emission measure (DEM) results indicate that the plasma above I-loops1 and I-loops2 began to be heated about 23 minutes and 44 minutes after the start of the second flare, respectively. Within 20 minutes, the plasma temperature in these regions increased from ~3 MK to 6 MK. We proposed an adiabatic heating mechanism that magnetic energy would be converted into thermal and kinetic energy when the pre-stretched loops contract. Our calculations show that the magnetic energy required to heat the two high-temperature regions are 10^29-10^30 erg, which correspond to a loss of field strength of 2-3 G.

Energetic Electrons Accelerated and Trapped in a Magnetic Bottle above a Solar Flare Arcade

Bin **Chen** (1), Xiangliang Kong (2), Sijie Yu (1), Chengcai Shen (3), Xiaocan Li (4), Fan Guo (5), Yixian Zhang (6), Lindsay Glesener (6), Säm Krucker (7, 8) EOVSA

ApJ **971** 85 **2024**

https://arxiv.org/pdf/2406.00109 **File**

https://iopscience.iop.org/article/10.3847/1538-4357/ad531a/pdf

Where and how flares efficiently accelerate charged particles remains an unresolved question. Recent studies revealed that a "magnetic bottle" structure, which forms near the bottom of a large-scale reconnection current sheet above the flare arcade, is an excellent candidate for confining and accelerating charged particles. However, further understanding its role requires linking the various observational signatures to the underlying coupled plasma and particle processes. Here we present the first study combining multi-wavelength observations with data-informed macroscopic magnetohydrodynamics and particle modeling in a realistic eruptive flare geometry. The presence of an above-the-looptop magnetic bottle structure is strongly supported by the observations, which feature not only a local minimum of magnetic field strength but also abruptly slowing down plasma downflows. It also coincides with a compact hard X-ray source and an extended microwave source that bestrides above the flare arcade. Spatially resolved spectral analysis suggests that nonthermal electrons are highly concentrated in this region. Our model returns synthetic emission signatures that are well-matched to the observations. The results suggest that the energetic electrons are strongly trapped in the magnetic bottle region due to turbulence, with only a small fraction managing to escape. The electrons are primarily accelerated by plasma compression and facilitated by a fast-mode termination shock via the Fermi mechanism. Our results provide concrete support for the magnetic bottle as the primary electron acceleration site in eruptive solar flares. They also offer new insights into understanding the previously reported small population of flare-accelerated electrons entering interplanetary space. **2017 September 10**

Can the Parker Solar Probe Detect a CME-flare Current Sheet?

Yuhao **Chen**, Zhong Liu, Pengfei Chen, David F. Webb, Qi Hao, Jialiang Hu, Guanchong Cheng, Zhixing Mei, Jing Ye, Qian Wang, Jun Lin

ApJS **269** 22 **2023**

https://arxiv.org/pdf/2309.06432.pdf

https://iopscience.iop.org/article/10.3847/1538-4365/acf8c7/pdf

A current sheet (CS) is the central structure in the disrupting magnetic configuration during solar eruptions. More than 90\% of the free magnetic energy (the difference between the energy in the non-potential magnetic field and that in the potential one) stored in the coronal magnetic field beforehand is converted into heating and kinetic energy of the plasma, as well as accelerating charged particles, by magnetic reconnection occurring in the CS. However, the detailed physical properties and fine structures of the CS are still unknown since there is no relevant information obtained via in situ detections. The Parker Solar Probe (PSP) may provide us such information should it traverse a CS in the eruption. The perihelion of PSP's final orbit is located at about 10 solar radii from the center of the Sun, so it can observe the CS at a very close distance, or even traverses the CS, which provides us a unique opportunity to look into fine properties and structures of the CS, helping reveal the detailed physics of large-scale reconnection that was impossible before. We evaluate the probability that PSP can traverse a CS, and examine the orbit of a PSP-like spacecraft that has the highest probability to traverse a CS.

1. INTRODUCTION

An Atypical Plateau-like Extreme-ultraviolet Late-phase Solar Flare Driven by the Non-radial Eruption of a Magnetic Flux Rope

Yuehong **Chen**, Yu Dai, Mingde Ding

A&A 675, A147 **2023**

https://arxiv.org/pdf/2305.14980.pdf

https://www.aanda.org/articles/aa/pdf/2023/07/aa45914-23.pdf

Recent observations in extreme-ultraviolet (EUV) wavelengths reveal an EUV late phase in some solar flares, which is characterized by a second peak in the warm coronal emissions (about 3 MK) occurring several tens of minutes to a few hours after the corresponding main flare peak. We aim to clarify the physical origin of an atypical plateau-like EUV late phase in an X1.8-class solar flare occurring on **2011 September 7** from active region (AR) 11283. We first characterize the plateau-like late phase using EUV Variability Experiment (EVE) full-disk integrated irradiance observations and Atmospheric Imaging Assembly (AIA) spatially-resolved imaging observations on board the Solar Dynamics Observatory (SDO). Then we perform a nonlinear force-free-field (NLFFF) extrapolation, from which a filament-hosting magnetic flux rope (MFR) is revealed. The eruption of the MFR is tracked both in the plane of the sky (POS) and along the line of sight (LOS) through visual inspection and spectral fitting, respectively. Finally, we carry out differential emission measure (DEM) analysis to explore the thermodynamics of the late-phase loops. The MFR shows a non-radial eruption from a fan-spine magnetic structure. The eruption of the MFR and its interaction with overlying arcades invoke multiple magnetic reconnections, which are responsible for the production of different groups of late-phase loops. Afterwards, the late-phase loops enter a long-lasting cooling stage, appearing sequentially in AIA passbands of decreasing response temperatures. Due to their different lengths, the different groups of late-phase loops cool down at different cooling rates, which makes their warm coronal emission peaks temporally separated from each other. Combing the emissions from all late-phase loops together, an elongated plateau-like late phase is formed.

Editorial: Machine Learning and Statistical Methods for Solar Flare Predictions

Editorial on the Research Topic

Yang **Chen**, Shane Maloney, Enrico Camporeale, Xin Huang, and Zhenjun Zhou

Front. Astron. Space Sci. 10: 1121615. **2023**

doi: 10.3389/fspas.2023.1121615

https://www.frontiersin.org/articles/10.3389/fspas.2023.1121615/pdf

Eruption of a Magnetic Flux Rope in a Comprehensive Radiative Magnetohydrodynamic Simulation of flare-productive active regions

Feng **Chen**, Matthias Rempel, Yuhong Fan

ApJL **950** L3 **2023**

https://arxiv.org/pdf/2303.05405.pdf

https://iopscience.iop.org/article/10.3847/2041-8213/acda2e/pdf

Radiative magnetohydrodynamic simulation includes sufficiently realistic physics to allow for the synthesis of remote sensing observables that can be quantitatively compared with observations. We analyze the largest flare in a simulation

of the emergence of large flare-productive active regions described by Chen et al. The flare is accompanied by a spectacular coronal mass ejection and reaches M2 class, as measured from synthetic soft X-ray flux. The eruption reproduces many key features of observed solar eruptions. A pre-existing magnetic flux rope is formed along the highly sheared polarity inversion line between a sunspot pair and is covered by an overlying multi-pole magnetic field. During the eruption, the progenitor flux rope actively reconnects with the canopy field and evolves to the large-scale multi-thermal flux rope that is observed in the corona. Meanwhile, the magnetic energy released via reconnection is channeled down to the lower atmosphere and gives rise to bright soft X-ray post-flare loops and flare ribbons that reproduce the morphology and dynamic evolution of observed flares. The model helps to shed light on questions of where and when the a flux rope may form and how the magnetic structures in an eruption are related to observable emission properties.

Quantifying Energy Release in Solar Flares and Solar Eruptive Events: New Frontiers with a Next-Generation Solar Radio Facility

Bin **Chen** (1), Dale E. Gary (1), Sijie Yu (1), Surajit Mondal (1), Gregory D. Fleishman (1), Xiaocan Li (2), Chengcai Shen (3), Fan Guo (4), Stephen M. White (5), Timothy S. Bastian (6), Pascal Saint-Hilaire (7), James F. Drake (8), Joel Dahlin (9), Lindsay Glesener (10), Hantao Ji (11), Astrid Veronig (12), Mitsuo Oka (7), Katharine K. Reeves (3), Judith Karpen (9)

Science white paper to the 2024 Solar and Space Physics Decadal Survey **2023**

https://arxiv.org/pdf/2301.12192.pdf

Solar flares and the often associated solar eruptive events serve as an outstanding laboratory to study the magnetic reconnection and the associated energy release and conversion processes under plasma conditions difficult to reproduce in the laboratory, and with considerable spatiotemporal details not possible elsewhere in the universe. In the past decade, thanks to advances in multi-wavelength imaging spectroscopy, as well as developments in theories and numerical modeling, significant progress has been made in improving our understanding of solar flare/eruption energy release. In particular, broadband imaging spectroscopy at microwave wavelengths offered by the Expanded Owens Valley Solar Array (EOVSA) has enabled the revolutionary capability of measuring the time-evolving coronal magnetic fields at or near the flare reconnection region. However, owing to EOVSA's limited dynamic range, imaging fidelity, and angular resolution, such measurements can only be done in a region around the brightest source(s) where the signal-to-noise is sufficiently large. In this white paper, after a brief introduction to the outstanding questions and challenges pertinent to magnetic energy release in solar flares and eruptions, we will demonstrate how a next-generation radio facility with many (~100-200) antenna elements can bring the next revolution by enabling high dynamic range, high fidelity broadband imaging spectropolarimetry along with a sub-second time resolution and arcsecond-level angular resolution. We recommend to prioritize the implementation of such a ground-based instrument within this decade. We also call for facilitating multi-wavelength, multi-messenger observations and advanced numerical modeling in order to achieve a comprehensive understanding of the "system science" of solar flares and eruptions. **2017 Sept. 10**

Coronal loop kink oscillation periods derived from the information of density, magnetic field, and loop geometry

G. Y. **Chen**1, L. Y. Chen1, Y. Guo1, M. D. Ding1, P. F. Chen1 and R. Erdélyi2,3,4

A&A 664, A48 (**2022**)

https://www.aanda.org/articles/aa/pdf/2022/08/aa42711-21.pdf

Context. Coronal loop oscillations can be triggered by solar eruptions, for example, and are observed frequently by the Atmospheric Imaging Assembly (AIA) on board Solar Dynamics Observatory (SDO). The Helioseismic and Magnetic Imager (HMI) on board SDO offers us the opportunity to measure the photospheric vector magnetic field and carry out solar magneto-seismology (SMS).

Aims. By applying SMS, we aim to verify the consistency between the observed period and the one derived from the information of coronal density, magnetic field, and loop geometry, that is, the shape of the loop axis.

Methods. We analysed the data of three coronal loop oscillation events detected by SDO/AIA and SDO/HMI. First, we obtained oscillation parameters by fitting the observational data. Second, we used a differential emission measure (DEM) analysis to diagnose the temperature and density distribution along the coronal loop. Subsequently, we applied magnetic field extrapolation to reconstruct the three-dimensional magnetic field and then, finally, used the shooting method to compute the oscillation periods from the governing equation.

Results. The average magnetic field determined by magnetic field extrapolation is consistent with that derived by SMS. A new analytical solution is found under the assumption of exponential density profile and uniform magnetic field. The periods estimated by combining the coronal density and magnetic field distribution and the associated loop geometry are closest to the observed ones, and are more realistic than when the loop geometry is regarded as being semi-circular or having a linear shape.

Conclusions. The period of a coronal loop is sensitive to not only the density and magnetic field distribution but also the loop geometry. **2010 October 16, 6 Sep 2011, 7 Mar 2012**

Flare Index Prediction with Machine Learning Algorithms

Anqin **Chen**, Qian Ye & Jingxiu Wang

Solar Physics volume 296, Article number: 150 (**2021**)
https://link.springer.com/content/pdf/10.1007/s11207-021-01895-1.pdf
https://doi.org/10.1007/s11207-021-01895-1
Solar flares are one of the most important sources of disastrous space weather events, leading to negative effects on spacecrafts and living organisms. It is very important to predict solar flares to minimize the potential losses. In this paper, we use three different machine learning algorithms: K-Nearest Neighbors (KNN), Random Forest (RF), and XGBoost (XGB) to predict the total flare index TflareTflare and the maximum flare index MflareMflare of an active region (AR) within the subsequent of 24, 48, and 72 hrs. First, we selected 54514 vector magnetograms of 129 ARs on the visible solar hemisphere in solar cycle 24 whose maximum sunspot groups' area was larger than 400 μh. Then the following four magnetic parameters of each magnetogram were calculated: 1) the total magnetic flux |Φtot|, 2) the total photospheric free magnetic energy density Efree, 3) the gradient-weighted integral length of the neutral line with horizontal magnetic gradient of line-of-sight magnetic field larger than 0.1 G km−1 (WLSG), and 4) the area with magnetic shear angle larger than 40∘ (AΨ), as well as Tflare and Mflare corresponding to each magnetogram. Afterward, we split samples randomly into training (85% of the whole data) and testing (15%) data sets. After hyperparameter tuning and model construction we found that RF is an optimal algorithm for the prediction task and that the coefficients of determination (R2) of test data set via the majority of RF models are beyond 0.97. In addition, the feature importance of RF and XGB models indicates that |Φtot| and Efree are two optimal parameters to predict both Tflare and Mflare, and |Φtot| and Efree are the best parameters for Mflare and Tflare, respectively.

A Possible Selection Rule for Flares Causing Sunquakes

Ruizhu **Chen** and Junwei Zhao
2021 ApJ 908 182
https://arxiv.org/pdf/2103.08158.pdf
https://iopscience.iop.org/article/10.3847/1538-4357/abd240/pdf
https://doi.org/10.3847/1538-4357/abd240
Sunquakes are helioseismic power enhancements initiated by solar flares, but not all flares generate sunquakes. It is curious why some flares cause sunquakes while others do not. Here we propose a hypothesis to explain the disproportionate occurrence of sunquakes: during a flare's impulsive phase when the flare's impulse acts upon the photosphere, delivered by shock waves, energetic particles from higher atmosphere, or by downward Lorentz Force, a sunquake tends to occur if the background oscillation at the flare footpoint happens to oscillate downward in the same direction with the impulse from above. To verify this hypothesis, we select 60 strong flares in Solar Cycle 24, and examine the background oscillatory velocity at the sunquake sources during the flares' impulsive phases. Since the Doppler velocity observations at sunquake sources are usually corrupted during the flares, we reconstruct the oscillatory velocity in the flare sites using helioseismic holography method with an observation-based Green's function. A total of 24 flares are found to be sunquake active, giving a total of 41 sunquakes. It is also found that in 3–5 mHz frequency band, 25 out of 31 sunquakes show net downward oscillatory velocities during the flares' impulsive phases, and in the 5–7 mHz frequency band, 33 out of 38 sunquakes show net downward velocities. These results support the hypothesis that a sunquake more likely occurs when a flare impacts a photospheric area with a downward background oscillation.
2012 October 23
Table 1: Statistics of all the sunquakes found in this survey and the flares that triggered them. (2011-2017)
HMI Science Nuggets #154 March **2021** **http://hmi.stanford.edu/hminuggets/?p=3500**

Energetic Electron Distribution of the Coronal Acceleration Region: First results from Joint Microwave and Hard X-ray Imaging Spectroscopy

Bin **Chen** (1), Marina Battaglia (2), Säm Krucker (2), Katharine K. Reeves (3), Lindsay Glesener (4)
ApJL **908** L55 **2021**
https://arxiv.org/pdf/2102.05173.pdf
https://iopscience.iop.org/article/10.3847/2041-8213/abe471/pdf
https://doi.org/10.3847/2041-8213/abe471
Nonthermal sources located above bright flare arcades, referred to as the "above-the-loop-top" sources, have been often suggested as the primary electron acceleration site in major solar flares. The X8.2 limb flare on **2017 September 10** features such an above-the-loop-top source, which was observed in both microwaves and hard X-rays (HXRs) by the Expanded Owens Valley Solar Array (EOVSA) and the Reuven Ramaty High Energy Solar Spectroscopic Imager (RHESSI), respectively. By combining the microwave and HXR imaging spectroscopy observations with multi-filter extreme ultraviolet and soft X-ray imaging data, we derive the energetic electron distribution of this source over a broad energy range from <10 keV up to ~MeV during the early impulsive phase of the flare. The best-fit electron distribution consists of a thermal "core" from ~25 MK plasma. Meanwhile, a nonthermal power-law "tail" joins the thermal core at ~16 keV with a spectral index of ~3.6, which breaks down at above ~160 keV to >6.0. In addition, temporally resolved analysis suggests that the electron distribution above the break energy rapidly hardens with the spectral index decreasing from >20 to ~6.0 within 20 s, or less than ~10 Alfvén crossing times in the source. These results provide

strong support for the above-the-loop-top source as the primary site where an on-going bulk acceleration of energetic electrons is taking place very early in the flare energy release.

The Electron Acoustic Wave and Its Role in Solar Flaring Loops Heating

L. **Chen**1,2, D. J. Wu1, L. Xiang3,4, C. Shi1, B. Ma5,6, J. F. Tang7, and J. Huang2
2020 ApJ 904 193
https://doi.org/10.3847/1538-4357/abc00b
From soft X-ray emission, the solar flare temperatures are from several MK to dozens of times MK, which are higher than the preflare coronal temperatures. A combination of several heating mechanisms may contribute to the heating problem in solar flare loops. In this paper, we propose an important mechanism of solar flaring loops heating, in which the excited electron acoustic wave (EAW) by flare-accelerated fast electron beams can lead to electron heating via collisionless Landau damping effect produced by wave–particle resonant interaction. Taking account of the return-current effect of fast electron beams, by use of numerical and analytic solutions, the plasma wave instability driven by fast electron beams is investigated in typical solar flare loop plasma parameters. The results show that the EAW is the strongest unstable wave mode rather than other wave modes. The dissipation of EAW via collisionless Landau damping and its application to solar flaring loops heating are discussed in detail.

Measurement of magnetic field and relativistic electrons along a solar flare current sheet

Bin **Chen**, Chengcai Shen, Dale E. Gary, Katharine K. Reeves, Gregory D. Fleishman, Sijie Yu, Fan Guo, Säm Krucker, Jun Lin, Gelu Nita, Xiangliang Kong
Nature Astronomy, Advanced Online Publication **4**, pages1140–1147 **2020**
2020 Nature Astronomy **4**, pages1140–1147
https://arxiv.org/pdf/2005.12757.pdf **File**
https://www.nature.com/articles/s41550-020-1147-7
https://sci-hub.st/10.1038/s41550-020-1147-7
In the standard model of solar flares, a large-scale reconnection current sheet is postulated as the central engine for powering the flare energy release and accelerating particles. However, where and how the energy release and particle acceleration occur remain unclear due to the lack of measurements for the magnetic properties of the current sheet. Here we report the measurement of spatially-resolved magnetic field and flare-accelerated relativistic electrons along a current-sheet feature in a solar flare. The measured magnetic field profile shows a local maximum where the reconnecting field lines of opposite polarities closely approach each other, known as the reconnection X point. The measurements also reveal a local minimum near the bottom of the current sheet above the flare loop-top, referred to as a "magnetic bottle". This spatial structure agrees with theoretical predictions and numerical modeling results. A strong reconnection electric field of ~4000 V/m is inferred near the X point. This location, however, shows a local depletion of microwave-emitting relativistic electrons. These electrons concentrate instead at or near the magnetic bottle structure, where more than 99% of them reside at each instant. Our observations suggest that the loop-top magnetic bottle is likely the primary site for accelerating and/or confining the relativistic electrons. **2017 September 10**
Video http://harp.njit.edu/~binchen/download/publications/Chen+2020_RCS/Chen_Supplementary_Video_1.mp4

Rejuvenating Solar Flare Termination Shocks as Particle Accelerators

Bin **CHEN**
RHESSI Science Nuggets #378 **2020**
http://sprg.ssl.berkeley.edu/~tohban/wiki/index.php/Rejuvenating_Solar_Flare_Termination_Shocks_as_Particle_Accelerators
3 Mar 2012

Microwave Spectral Imaging of an Erupting Magnetic Flux Rope: Implications for the Standard Solar Flare Model in Three Dimensions

Bin **Chen** (1), Sijie Yu (1), Katharine K. Reeves (2), Dale E. Gary (1)
2020 *ApJL* **895** L50
https://arxiv.org/pdf/2005.01900.pdf
https://doi.org/10.3847/2041-8213/ab901a
https://iopscience.iop.org/article/10.3847/2041-8213/ab901a/pdf
We report microwave spectral imaging observations of an erupting magnetic flux rope during the early impulsive phase of the X8.2-class limb flare on **2017 September 10**, obtained by the Expanded Owens Valley Solar Array (EOVSA). A few days prior to the eruption, when viewed against the disk, the flux rope appeared as a reverse S-shaped dark filament along the magnetic polarity inversion line. During the eruption, the rope exhibited a "hot channel" structure in extreme ultraviolet and soft X-ray passbands sensitive to ~10 MK plasma. The central portion of the flux rope was nearly aligned with the line of sight, which quickly developed into a teardrop-shaped dark cavity during the early phase of the eruption. A long and thin plasma sheet formed below the cavity, interpreted as the reconnection current sheet viewed

edge-on. A nonthermal microwave source was present at the location of the central current sheet, which extended upward encompassing the dark cavity. A pair of nonthermal microwave sources were observed for several minutes at both sides of the main flaring region. They shared a similar temporal behavior and spectral property to the central microwave source below the cavity, interpreted as the conjugate footpoints of the erupting flux rope. These observations are broadly consistent with the magnetic topology and the associated energy release scenario suggested in the three-dimensional standard model for eruptive solar flares. In particular, our detection of nonthermal emission at conjugate flux rope footpoints provides solid evidence of particle transport along an erupting magnetic flux rope.

Solar Flare Observations with the Karl G. Jansky Very Large Array

Bin **Chen**
Presentation at the Fleishman's Webinar, April **2020**
http://www.ioffe.ru/LEA/SF_AR/files/Chen_solarwebinar_20200401.pdf

Tracing fast electron beams - Chen et al. 2018, ApJ, 866, 62 - Chen et al. 2013, ApJL, 763, 21 ⊙

Mapping solar flare termination shocks - Luo et al., in prep - Chen et al. 2019, ApJ, 884, 63 - Chen et al. 2015, Science, 350, 1238 ⊙

Imaging waves and oscillations - Yu & Chen, 2019, ApJ, 872, 71 - Wang, Chen & Gary 2017, ApJ, 848, 77 ⊙

Microflares - Battaglia et al., in prep - Sharma et al., in prep

Extreme Ultraviolet Late Phase of Solar Flares

Jun **Chen**, Rui Liu, Kai Liu, Arun Kumar Awasthi, Pejin Zhang, Yuming Wang, Bernhard Kliem
ApJ **890** 158 **2020**
https://arxiv.org/pdf/2001.06929.pdf
sci-hub.si/10.3847/1538-4357/ab6def
A second peak in extreme ultraviolet sometimes appears during the gradual phase of solar flares, which is known as EUV late phase (ELP). Stereotypically ELP is associated with two separated sets of flaring loops with distinct sizes, and it has been debated whether ELP is caused by additional heating or extended plasma cooling in the longer loop system. Here we carry out a survey of 55 M-and-above GOES-class flares with ELP during 2010--2014. Based on the flare-ribbon morphology, these flares are categorized as circular-ribbon (19 events), two-ribbon (23 events), and complex-ribbon (13 events) flares. Among them, 22 events (40%) are associated with coronal mass ejections, while the rest are confined. An extreme ELP, with the late-phase peak exceeding the main-phase peak, is found in 48% of two-ribbon flares, 37% of circular-ribbon flares, and 31% of complex-ribbon flares, suggesting that additional heating is more likely present during ELP in two-ribbon than in circular-ribbon flares. Overall, cooling may be the dominant factor causing the delay of the ELP peak relative to the main-phase peak, because the loop system responsible for the ELP emission is generally larger than, and well separated from, that responsible for the main-phase emission. All but one of the circular-ribbon flares can be well explained by a composite "dome-plate" quasi-separatrix layer (QSL). Only half of these show a magnetic null point, with its fan and spine embedded in the dome and plate, respectively. The dome-plate QSL, therefore, is a general and robust structure characterizing circular-ribbon flares. **2010 October 16, 2013 March 6**
Table 2. Flare list (2010-2014)
RHESSI Nuggets #381 June **2020**
http://sprg.ssl.berkeley.edu/~tohban/wiki/index.php/Extreme-Ultraviolet_Late_Phase_of_Solar_Flares

Identifying Solar Flare Precursors Using Time Series ofSDO/HMI Images and SHARP Parameters

Yang **Chen**1, Ward B. Manchester2, Alfred O. Hero3, Gabor Toth2, Benoit DuFumier3,Tian Zhou1, Xiantong Wang2, Haonan Zhu3,ZeyuSun3, and Tamas I. Gombosi2
Space Weather Volume17, Issue10 October **2019** Pages 1404-1426
https://agupubs.onlinelibrary.wiley.com/doi/epdf/10.1029/2019SW002214
In this paper we present several methods to identify precursors that show great promise for early predictions of solar flare events. A data preprocessing pipeline is built to extract useful data from multiple sources, Geostationary Operational Environmental Satellites and Solar Dynamics Observatory (SDO)/Helioseismic and Magnetic Imager (HMI), to prepare inputs for machine learning algorithms. Two classification models are presented: classification of flares from quiet times for active regions and classification of strong versus weak flare events. We adopt deep learning algorithms to capture both spatial and temporal information from HMI magnetogram data. Effective feature extraction and feature selection with raw magnetogram data using deep learning and statistical algorithms enable us to train classification models to achieve almost as good performance as using active region parameters provided in HMI/Space-Weather HMI-Active Region Patch (SHARP) data files. Case studies show a significant increase in the prediction score around 20 hr before strong solar flare events. **2011/04/22, 2014/02/03, 2015/05/19-20, 2017/09/07**

Energy origination and triggering mechanism of a series of homologous confined flares

Guorong **Chen**, Xiaoli Yan

ApJ **887** 99 **2019**

https://arxiv.org/pdf/1910.09147.pdf

https://doi.org/10.3847/1538-4357/ab4f76

Using the Hα data from the New Vacuum Solar Telescope (NVST) at the Fuxian Solar Observatory together with multi-wavelength images and magnetograms obtained by Solar Dynamics Observatory (SDO), we study the detailed process of three homologous confined flares in active-region (AR) NOAA 11861 on **2013 October 12**. All of the three flares occurred at same location, with similar morphologies and comparable class. Through analyzing the evolution of magnetic field and flow field, we found an emergence of magnetic flux and a strong shearing motion between two opposite polarities near the following sunspot. The magnetic flux and the average transverse field strength exhibited a decrease before each eruption and reached the lowest point at the onset of each eruption. By calculating the shearing and the emergence energy in the photosphere, we found that the integral of energy injected from the photosphere, for a few hours, could provide enough energy for the flares. The reconnection between different loops was observed in Hα images during the occurrence of each flare. These results suggest that the emerging magnetic flux and the shearing motion in the photosphere can inject the energy to the sheared magnetic loops and the energy finally was released via magnetic reconnection to power the solar flares.

Observing Current Sheet Formation Forced by Non-radial Rotating Motion of Mini-filaments

Hechao **Chen**1,2,3, Jiayan Yang1,3, Yadan Duan4, and Kaifan Ji1,3

2019 ApJ 879 74

sci-hub.se/10.3847/1538-4357/ab24ce

In this paper, we study two externally forced magnetic reconnection events near NOAA active region 12494 for their current sheet (CS) formation. In both events, small-scale reconnection happened between mini-filaments and other preexisting magnetic fields. Initially, mini-filaments underwent obvious non-radial rotating motion due to their loss of equilibrium. With their clockwise/anti-clockwise rotation, the axial fluxes of the mini-filaments slowly came to squeeze the anti-parallel ambient fields, leading to an X-shaped structure. As the squeezing effect strengthened, CS regions gradually formed and grew in length, with a temperature around 1.8 MK. Afterward, clear cusp regions, plasma heating (~5 MK), and newborn magnetic structures came to be in sequence. Finally, mini-filaments erupted in a complex fashion due to the involvement of external reconnection. Based on the multiwavelength imaging observations, the apparent thickness/length, temperature/emission of the CS regions and their related plasma flows are carefully analyzed. Their reconnection rates are roughly estimated as 0.01–0.06 and 0.01–0.02. In particular, a chain of high-speed plasmoid ejections was detected along with a set of the reconnected field lines in Event1, implying the onset of tearing-mode instability inside its CS region. These observations indicate that non-radial rotating motion of filaments can serve as external flows to drive reconnection, and also provide a basic scenario of CS formation within small-scale magnetic reconnetion processes. **2016 February 6**

Quasi-periodic Pulsations before and during a Solar Flare in AR 12242

Xingyao **Chen**, Yihua Yan, Baolin Tan, Jing Huang, Wei Wang, Linjie Chen, Yin Zhang, Chengming Tan, Donghao Liu, and Satoshi Masuda

2019 ApJ 878 78

https://iopscience.iop.org/article/10.3847/1538-4357/ab1d64/pdf

Quasi-periodic pulsations (QPPs) are frequently observed in solar flares, which may reveal some essential characteristics of both thermal and nonthermal energy releases. This work presents multi-wavelength imaging observations of an M8.7 flare in active region AR 12242 on **2014 December 17**. We found that there were three different QPPs: UV QPPs with a period of about 4 minutes at 1600 Å images near the center of the active region lasting from the preflare phase to the impulsive phase; EUV QPPs with a period of about 3 minutes along the circular ribbon during the preflare phase; and radio QPPs with a period of about 2 minutes at frequencies of 1.2–2.0 GHz around the flaring source region during the impulsive phase. The observations include the radio images observed by the Mingantu Spectral Radioheliograph in China at frequencies of 1.2–2.0 GHz for the first time, microwave images by the Nobeyama Radioheliograph, UV and EUV images by AIA/SDO, and a magnetogram by HMI/SDO. We suggest that the 4 minute UV QPPs should be modulated by the sunspot oscillations, and the 3 minute EUV QPPs are closely related to the 2 minute radio QPPs for their source regions connected by a group of coronal loops. We propose that the intermittent magnetic reconnecting downward and upward plasmoids may be the possible trigger of both the preflare 3 minute EUV QPPs and the impulsive 2 minute radio QPPs. The other possible mechanism is LRC oscillation, which is associated with the current-carrying coronal loops. The latter mechanism implies that the existence of preflare QPPs may be a possible precursor to solar flares.

Identifying Solar Flare Precursors Using Time Series of SDO/HMI Images and SHARP Parameters

Yang **Chen**, Ward B. Manchester, Alfred O. Hero, Gabor Toth, Benoit DuFumier, Tian Zhou, Xiantong Wang, Haonan Zhu, Zeyu Sun, Tamas I. Gombosi
Space Weather **2019**
https://arxiv.org/pdf/1904.00125.pdf
sci-hub.se/10.1029/2019SW002214
https://agupubs.onlinelibrary.wiley.com/doi/epdf/10.1029/2019SW002214
Space Weather Quarterly Volume 16, Issue 3 p. 20-42, **2019**
https://agupubs.onlinelibrary.wiley.com/doi/epdf/10.1002/swq.23
We present several methods towards construction of precursors, which show great promise towards early predictions, of solar flare events in this paper. A data pre-processing pipeline is built to extract useful data from multiple sources (Geostationary Operational Environmental Satellites (GOES) and Solar Dynamics Observatory (SDO)/Helioseismic and Magnetic Imager (HMI) to prepare inputs for machine learning algorithms. Two classification models are presented: classification of flares from quiet times for active regions and classification of strong versus weak flare events. We adopt deep learning algorithms to capture both the spatial and temporal information from HMI magnetogram data. Effective feature extraction and feature selection with raw magnetogram data using deep learning and statistical algorithms enable us to train classification models to achieve almost as good performance as using active region parameters provided in HMI/Space-Weather HMI-Active Region Patch (SHARP) data files. The results show great promise towards accurate, reliable, and timely predictions of solar flare events. The use of Atmospheric Imaging Assembly (AIA) data will be the topic of future studies.

Astro2020 Science White Paper: Probing Magnetic Reconnection in Solar Flares - New Perspectives from Radio Dynamic Imaging Spectroscopy **Review**

Bin **Chen** (1), Tim Bastian (2), Joel Dahlin (3), James F. Drake (4), Gregory D. Fleishman (1), Dale E. Gary (1), Lindsay Glesener (5), Fan Guo (6), Hantao Ji (7), Pascal Saint-Hilaire (8), Chengcai Shen (9), Stephen M. White
Astro2020 Decadal Survey call for science white papers **2019**
https://arxiv.org/pdf/1903.11192.pdf
Magnetic reconnection is a fundamental physical process in many laboratory, space, and astrophysical plasma contexts. Solar flares serve as an outstanding laboratory to study the magnetic reconnection and the associated energy release and conversion processes under plasma conditions difficult to reproduce in the laboratory, and with considerable spatiotemporal details not possible elsewhere in astrophysics. Here we emphasize the unique power of remote-sensing observations of solar flares at radio wavelengths. In particular, we discuss the transformative technique of broadband radio dynamic imaging spectroscopy in making significant contributions to addressing several outstanding challenges in magnetic reconnection, including the capability of pinpointing magnetic reconnection sites, measuring the time-evolving reconnecting magnetic fields, and deriving the spatially and temporally resolved distribution function of flare-accelerated electrons.

Magnetic Reconnection Null Points as the Origin of Semi-relativistic Electron Beams in a Solar Jet

Bin **Chen**, Sijie Yu, Marina Battaglia, Samaiyah Farid, Antonia Savcheva, Katharine K. Reeves, Säm Krucker, T. S. Bastian, Fan Guo, Svetlin Tassev
ApJ 866(1), 62 **2018**
https://arxiv.org/pdf/1808.05951.pdf
https://iopscience.iop.org/article/10.3847/1538-4357/aadb89/pdf
https://web.njit.edu/~binchen/download/publications/Chen+2018_TP3/Chen_et_al_2018_type3_apj.pdf
Magnetic reconnection, the central engine that powers explosive phenomena throughout the Universe, is also perceived as one of the principal mechanisms for accelerating particles to high energies. Although various signatures of magnetic reconnection have been frequently reported, observational evidence that links particle acceleration directly to the reconnection site has been rare, especially for space plasma environments currently inaccessible to in situ measurements. Here we utilize broadband radio dynamic imaging spectroscopy available from the Karl G. Jansky Very Large Array to observe decimetric type III radio bursts in a solar jet with high angular (~20″), spectral (~1 %), and temporal resolution (50 milliseconds). These observations allow us to derive detailed trajectories of semi-relativistic (tens of keV) electron beams in the low solar corona with unprecedentedly high angular precision (<0″.65). We found that each group of electron beams, which corresponds to a cluster of type III bursts with 1-2-second duration, diverges from an extremely compact region (~600 km2) in the low solar corona. The beam-diverging sites are located behind the erupting jet spire and above the closed arcades, coinciding with the presumed location of magnetic reconnection in the jet eruption picture supported by extreme ultraviolet/X-ray data and magnetic modeling. We interpret each beam-diverging site as a reconnection null point where multitudes of magnetic flux tubes join and reconnect. Our data suggest that the null points likely consist of a high level of density inhomogeneities possibly down to 10-km scales. These results, at least in the present case, strongly favor a reconnection-driven electron acceleration scenario. **2014 November 1**

Thermodynamics of supra-arcade downflows in solar flares

Xin **Chen**, Rui Liu, Na Deng, Haimin Wang

A&A 606, A84 **2017**

https://arxiv.org/pdf/1706.03452.pdf

Context. Supra-arcade downflows (SADs) have been frequently observed during the gradual phase of solar flares near the limb. In coronal emission lines sensitive to flaring plasmas, they appear as tadpole-like dark voids against the diffuse fan-shaped "haze" above, flowing toward the well-defined flare arcade.
Aims. We aim to investigate the evolution of SADs' thermal properties, and to shed light on the formation mechanism and physical processes of SADs.
Methods. We carefully studied several selected SADs from two flare events and calculated their differential emission measures (DEMs) as well as DEM-weighted temperatures using data obtained by the Atmospheric Imaging Assembly (AIA) onboard the Solar Dynamic Observatory.
Results. Our analysis shows that SADs are associated with a substantial decrease in DEM above 4 MK, which is 1-3 orders of magnitude smaller than the surrounding haze as well as the region before or after the passage of SADs, but comparable to the quiet corona. There is no evidence for the presence of the SAD-associated hot plasma (> 20 MK) in the AIA data, and this decrease in DEM does not cause any significant change in the DEM distribution as well as the DEM-weighted temperature, which supports this idea that SADs are density depletion. This depression in DEM rapidly recovers in the wake of the SADs studied, generally within a few minutes, suggesting that they are discrete features. In addition, we found that SADs in one event are spatio-temporally associated with the successive formation of post-flare loops along the flare arcade. **2013 October 2**

Double Coronal X-ray and Microwave Sources Associated With A Magnetic Breakout Solar Eruption

Yao **Chen**, Zhao Wu, Wei Liu, Richard A. Schwartz, Di Zhao, Bing Wang, Guohui Du

2017 *ApJ* **843** 8

https://arxiv.org/pdf/1705.06074.pdf

http://sci-hub.cc/10.3847/1538-4357/aa7462

Double coronal hard X-ray (HXR) sources are believed to be critical observational evidence of bi-directional energy release through magnetic reconnection in a large-scale current sheet in solar ares. Here we present a study on double coronal sources observed in both HXR and microwave regimes, revealing new characteristics distinct from earlier reports. This event is associated with a footpoint-occulted X1.3-class flare (**25 April 2014**, starting at 00:17 UT) and a coronal mass ejection that are likely triggered by the magnetic breakout process, with the lower source extending upward from the top of the partially-occulted flare loops and the upper source co-incident with rapidly squeezing-in side lobes (at a speed of ~250 km/s on both sides). The upper source can be identified at energies as high as 70-100 keV. The X-ray upper source is characterized by flux curves different from the lower source, a weak energy dependence of projected centroid altitude above 20 keV, a shorter duration and a HXR photon spectrum slightly-harder than those of the lower source. In addition, the microwave emission at 34 GHz also exhibits a similar double source structure and the microwave spectra at both sources are in line with gyro-synchrotron emission given by non- thermal energetic electrons. These observations, especially the co-incidence of the very-fast squeezing-in motion of side lobes and the upper source, indicate that the upper source is associated with (possibly caused by) this fast motion of arcades. This sheds new lights on the origin of the corona double-source structure observed in both HXRs and microwaves.

See RHESSI Science Nuggets #301 May **2017**

http://sprg.ssl.berkeley.edu/~tohban/wiki/index.php/Double_Coronal_X-ray_and_Microwave_Sources_Associated_With_A_Magnetic_Breakout_Solar_Eruption

Fast sausage modes in magnetic tubes with continuous transverse profiles: effects of a finite plasma beta

Shao-Xia **Chen**, Bo Li, Ming Xiong, Hui Yu, Ming-Zhe Guo

ApJ **2016**

https://arxiv.org/abs/1610.03254

While standing fast sausage modes in flare loops are often invoked to interpret quasi-periodic pulsations (QPPs) in solar flares, it is unclear as to how they are influenced by the combined effects of a continuous transverse structuring and a finite internal plasma beta (βi). We derive a generic dispersion relation (DR) governing linear sausage waves in straight magnetic tubes for which plasma pressure is not negligible and the density and temperature inhomogeneities of essentially arbitrary form take place in a layer of arbitrary width. Focusing on fast modes, we find that βi only weakly influences kc, the critical longitudinal wavenumber separating the leaky from trapped modes. Likewise, for both trapped and leaky modes, the periods P in units of the transverse fast time depend only weakly on βi, which is compatible with the fact that the effective wavevectors of fast sausage modes are largely perpendicular to the

background magnetic field. However, a weak βi dependence of the damping times τ is seen only when the length-to-radius ratio L/R is ∼50% larger than some critical value π/(kcR), which itself rather sensitively depends on the density contrast, profile steepness as well as on how the transverse structuring is described. In the context of QPPs, we conclude that the much simpler zero-beta theory can be employed for trapped modes, as long as one sees the deduced internal Alfv\'en speed as actually being the fast speed. In contrast, effects due to a finite beta in flare loops should be considered when leaky modes are exploited.

Particle Acceleration by a Solar Flare Termination Shock

Bin **Chen** (1), Timothy S. Bastian (2), Chengcai Shen (1), Dale E. Gary (3), Sam Krucker (4, 5), Lindsay Glesener

Science 4 December **2015**: Vol. 350 no. 6265 pp. 1238-1242

http://arxiv.org/ftp/arxiv/papers/1512/1512.02237.pdf

https://science.sciencemag.org/content/350/6265/1238.full

Solar flares—the most powerful explosions in the solar system—are also efficient particle accelerators, capable of energizing a large number of charged particles to relativistic speeds. A termination shock is often invoked in the standard model of solar flares as a possible driver for particle acceleration, yet its existence and role have remained controversial. We present observations of a solar flare termination shock and trace its morphology and dynamics using high-cadence radio imaging spectroscopy. We show that a disruption of the shock coincides with an abrupt reduction of the energetic electron population. The observed properties of the shock are well reproduced by simulations. These results strongly suggest that a termination shock is responsible, at least in part, for accelerating energetic electrons in solar flares. **2012 March 3**

Supplementary Movie S1 is available at this https URL

RHESSI Science Nuggets #378 **2020**

http://sprg.ssl.berkeley.edu/~tohban/wiki/index.php/Rejuvenating_Solar_Flare_Termination_Shocks_as_Particle_Accelerators

Standing Sausage Modes In Nonuniform Magnetic Tubes: An Inversion Scheme For Inferring Flare Loop Parameters

Shao-Xia **Chen**, Bo Li, Ming Xiong, Hui Yu, Ming-Zhe Guo

ApJ 812 22 **2015**

http://arxiv.org/pdf/1509.01442v1.pdf

Standing sausage modes in flare loops are important for interpreting quasi-periodic pulsations (QPPs) in solar flare lightcurves. We propose an inversion scheme that consistently uses their periods P and damping times τ to diagnose flare loop parameters. We derive a generic dispersion relation governing linear sausage waves in pressure-less straight tubes, for which the transverse density inhomogeneity takes place in a layer of arbitrary width l and is of arbitrary form. We find that P and τ depend on the combination of [R/vAi,L/R,l/R, ρi/ρe], where R is the loop radius, L is the looplength, vAi is the internal Alfv\'en speed, and ρi/ρe is the density contrast. For all the density profiles examined, P and τ experience saturation when $L/R \gg 1$, yielding an inversion curve in the [R/vAi,l/R, ρi/ρe] space with a specific density profile when L/R is sufficiently large. When applied to a spatially unresolved QPP event, the scheme yields that R/vAi is the best constrained, whereas l/R corresponds to the other extreme. For spatially resolved QPPs, while $L/R \gg 1$ cannot be assumed beforehand, an inversion curve remains possible due to additional geometrical constraints. When a spatially resolved QPP event involves another mode, as is the case for a recent event, the full set of [vAi,l, ρi/ρe] can be inferred. We conclude that the proposed scheme provides a useful tool for magneto-seismologically exploiting QPPs.

Periods and Damping Rates of Fast Sausage Oscillations in Multishelled Coronal Loops

Shao-Xia **Chen**, Bo Li, Li-Dong Xia, Hui Yu

Solar Phys. Volume 290, Issue 8, pp 2231-2243 **2015**

http://arxiv.org/pdf/1507.02169v1.pdf

Standing sausage modes are important in interpreting quasi-periodic pulsations in the light curves of solar flares. Their periods and damping times play an important role in seismologically diagnosing key parameters like the magnetic field strength in regions where flare energy is released. Usually, such applications are based on theoretical results neglecting unresolved fine structures in magnetized loops. However, the existence of fine structuring is suggested on both theoretical and observational grounds. Adopting the framework of cold magnetohydrodynamics (MHD), we model coronal loops as magnetized cylinders with a transverse equilibrium density profile comprising a monolithic part and a modulation due to fine structuring in the form of concentric shells. The equation governing the transverse velocity perturbation is solved with an initial-value-problem approach, and the effects of fine structuring on the periods P and damping times τ of global, leaky, standing sausage modes are examined. A parameter study shows that fine structuring, be it periodically or randomly distributed, brings changes of only a few percents to P and τ when there are more than about ten shells. The monolithic part, its steepness in particular, plays a far more important role in determining P and τ.

We conclude that when measured values of P and τ of sausage modes are used for seismological purposes, it is justified to use theoretical results where the effects due to fine structuring are neglected.

Confined Flares in Solar Active Region 12192 from 2014 October 18 to 29

Huadong **Chen**, Jun Zhang, Suli Ma, Shuhong Yang, Leping Li, Xin Huang, Junmin Xiao
ApJL **808** L24 **2015**
http://arxiv.org/pdf/1507.00651v1.pdf
Using the observations from the Atmospheric Imaging Assembly (AIA) and Helioseismic and Magnetic Imager (HMI) aboard the Solar Dynamics Observatory (SDO), we investigate six X-class and twenty- nine M-class flares occurring in solar active region (AR) 12192 from October 18 to 29. Among them, thirty (including six X- and twenty-four M-class) flares originated from the AR core and the other five M-flares appeared at the AR periphery. Four of the X-flares exhibited similar flaring structures, indicating they were homologous flares with analogous triggering mechanism. The possible scenario is: photospheric motions of emerged magnetic fluxes lead to shearing of the associated coronal magnetic field, which then yields a tether-cutting favorable configuration. Among the five periphery M-flares, four were associated with jet activities. The HMI vertical magnetic field data show that the photospheric fluxes of opposite magnetic polarities emerged, converged and canceled with each other at the footpoints of the jets before the flares. Only one M-flare from the AR periphery was followed by a coronal mass ejection (CME). From October 20 to 26, the mean decay index of the horizontal background field within the height range of 40?105 Mm is below the typical threshold for torus instability onset. This suggests that a strong confinement from the overlying magnetic field might be responsible for the poor CME production of AR 12192.
Table 1. X- and M-class flares in Solar AR 12192

Direct Observations of Tether-cutting Reconnection During a Major Solar Event From 2014 February 24 to 25

Huadong **Chen**, Jun Zhang, Xin Cheng, Suli Ma, Shuhong Yang, Ting Li
ApJL, **201**4
http://arxiv.org/pdf/1411.4454v1.pdf
Using the multi-wavelength data from Atmospheric Imaging Assembly on board the Solar Dynamic Observatory, we investigated two successive solar flares, a C5.1 confined flare and an X4.9 ejective flare with a halo coronal mass ejection,in NOAA AR 11990 from **2014 Feb 24 to 25**. Before the confined are onset, EUV brightening beneath the filament was detected. As the are began, a twisted helical flux rope (FR) wrapping around the filament moved upward and then stopped, and in the meantime an obvious X-ray source below it was observed. Prior to the ejective X4.9 flare, some pre-existing loop structures in the active region interacted with each other, which produced a brightening region beneath the filament. Meanwhile, a small flaring loop appeared below the interaction region and some new helical lines connecting the far ends of the loop structures was gradually formed and continually added into the former twisted FR. Then, due to the resulting imbalance between the magnetic pressure and tension, the new FR together with the filament erupted outward. Our observations coincide well with tether-cutting model, suggesting that the two flares probably have the same triggering mechanism, i.e., tether-cutting reconnection. To our knowledge, this is the first direct observation of tether-cutting reconnection occurring between the pre-existing loops in active region. In the ejective flare case, the erupting filament exhibited an omega-like kinked structure and underwent an exponential rise after a slow-rise phase, indicating the kink instability might be also responsible for the eruption initiation.

A model for the formation of the active region corona driven by magnetic flux emergence

F. **Chen**, H. Peter, S. Bingert, M. C. M. Cheung
E-print, Feb **2014**, A&A
We present the first model that couples the formation of the corona of a solar active region to a model of the emergence of a sunspot pair. This allows us to study when, where, and why active region loops form, and how they evolve. We use a 3D radiation MHD simulation of the emergence of an active region through the upper convection zone and the photosphere as a lower boundary for a 3D MHD coronal model. The latter accounts for the braiding of the magnetic fieldlines, which induces currents in the corona heating up the plasma. We synthesize the coronal emission for a direct comparison to observations. Starting with a basically field-free atmosphere we follow the filling of the corona with magnetic field and plasma. Numerous individually identifiable hot coronal loops form, and reach temperatures well above 1 MK with densities comparable to observations. The footpoints of these loops are found where small patches of magnetic flux concentrations move into the sunspots. The loop formation is triggered by an increase of upwards-directed Poynting flux at their footpoints in the photosphere. In the synthesized EUV emission these loops develop within a few minutes. The first EUV loop appears as a thin tube, then rises and expands significantly in the horizontal direction. Later, the spatially inhomogeneous heat input leads to a fragmented system of multiple loops or strands in a growing envelope.

Determination of Stochastic Acceleration Model Characteristics in Solar Flares

Qingrong **Chen** and Vahe' Petrosian
E-print, July **2013**, **2013** ApJ 777 33
https://iopscience.iop.org/article/10.1088/0004-637X/777/1/33/pdf
Following our recent paper (Petrosian & Chen 2010), we have developed an inversion method to determine the basic characteristics for the model of stochastic acceleration of particles by plasma waves or turbulence directly and non-parametrically from observations in the framework of the leaky box version of the Fokker-Planck kinetic equation. These characteristics are determined by wave-particle interactions as described by the momentum and pitch angle diffusion coefficients. Our method relates these coefficients directly to observations. In particular, we show that by inverting the Fokker-Planck equation to its integral form, one can derive the energy diffusion coefficient and direct acceleration rate by turbulence in terms of the accelerated and escaping particle spectra. We apply the analytic formulas to the suprathermal electrons in solar flares, which produce hard X-ray emission at the coronal loop top (LT) region and two thick target footpoint regions of the flare loop. We utilize the regularized electron flux spectral images recently developed for the Reuven Ramaty High Energy Solar Spectroscopic Imager ({it RHESSI}). From the spatially resolved electron flux spectra, we determine the electron escape time, which is related to the pitch angle scattering rate, and the energy diffusion coefficient at the LT acceleration region. Results obtained from two relatively intense {it RHESSI} events indicate that the escape time increases with energy and the energy diffusion (or direct acceleration) time and scattering time have dramatically different energy dependences. Such behaviors may be difficult to explain by existing wave-particle interaction models, and may indicate that a different acceleration mechanism is at work or imply a breakdown of the basic interpretation of the escape of electrons being a random walk process. The discrepant energy dependences can be alleviated somewhat by a turbulence spectrum that is much steeper than the Kolmogorov-type spectrum. On the other hand, a more likely explanation could be that the escape of electrons out of the LT acceleration region is governed by converging field lines in a magnetic mirror geometry, in which the escape time is proportional to scattering time. The results demonstrate the critical importance of combined modeling of electron acceleration by plasma wave turbulence and the large scale magnetic field variations in a reconnection environment.

Quantifying solar superactive regions with vector magnetic field observations

A. Q. **Chen**, and J. X. Wang
E-print, 29 May **2012**; A&A 543, A49 (**2012**)
The vector magnetic field characteristics of superactive regions (SARs) hold the key for understanding why SARs are extremely active and provide the guidance in space weather prediction. We aim to quantify the characteristics of SARs using the vector magnetograms taken by the Solar Magnetic Field Telescope at Huairou Solar Observatory Station. The vector magnetic field characteristics of 14 SARs in solar cycles 22 and 23 were analyzed using the following four parameters: 1) the magnetic flux imbalance between opposite polarities, 2) the total photospheric free magnetic energy, 3) the length of the magnetic neutral line with its steep horizontal magnetic gradient, and 4) the area with strong magnetic shear. Furthermore, we selected another eight large and inactive active regions (ARs), which are called fallow ARs (FARs), to compare them with the SARs. We found that most of the SARs have a net magnetic flux higher than 7.0*10^21 Mx, a total photospheric free magnetic energy higher than 1.0*10^24 erg/cm, a magnetic neutral line with a steep horizontal magnetic gradient (>= 300 G/Mm) longer than 30 Mm, and an area with strong magnetic shear (shear angle >= 80◦) greater than 100 Mm^2. In contrast, the values of these parameters for the FARs are mostly very low. The Pearson X^2 test was used to examine the significance of the difference between the SARs and FARs, and the results indicate that these two types of ARs can be fairly distinguished by each of these parameters. The significance levels are 99.55%, 99.98%, 99.98%, and 99.96%, respectively. However, no single parameter can distinguish them perfectly. Therefore we propose a composite index based on these parameters, and find that the distinction between the two types of ARs is also significant with a significance level of 99.96%. These results are useful for a better physical understanding of the SAR and FAR.

THE ROLE OF INVERSE COMPTON SCATTERING IN SOLAR CORONAL HARD X-RAY AND γ-RAY SOURCES

Bin **Chen**1 and T. S. Bastian
2012 ApJ 750 35
Coronal hard X-ray (HXR) and continuum γ-ray sources associated with the impulsive phase of solar flares have been the subject of renewed interest in recent years. They have been interpreted in terms of thin-target, non-thermal bremsstrahlung emission. This interpretation has led to rather extreme physical requirements in some cases. For example, in one case, essentially all of the electrons in the source must be accelerated to non-thermal energies to account for the coronal HXR source. In other cases, the extremely hard photon spectra of the coronal continuum γ-ray emission suggest that the low-energy cutoff of the electron energy distribution lies in the MeV energy range. Here, we consider the role of inverse Compton scattering (ICS) as an alternate emission mechanism in both the ultra- and mildly relativistic regimes. It is known that relativistic electrons are produced during powerful flares; these are capable of upscattering soft photospheric photons to HXR and γ-ray energies. Previously overlooked is the fact that mildly relativistic electrons, generally produced in much greater numbers in flares of all sizes, can upscatter extreme-ultraviolet/soft X-ray photons to HXR energies. We also explore ICS on anisotropic electron distributions and show that

the resulting emission can be significantly enhanced over an isotropic electron distribution for favorable viewing geometries. We briefly review results from bremsstrahlung emission and reconsider circumstances under which non-thermal bremsstrahlung or ICS would be favored. Finally, we consider a selection of coronal HXR and γ-ray events and find that in some cases the ICS is a viable alternative emission mechanism.

IMPULSIVE PHASE CORONAL HARD X-RAY SOURCES IN AN X3.9 CLASS SOLAR FLARE
Qingrong **Chen**1 and Vahé Petrosian
2012 ApJ 748 33, **File**
We present the analysis of a pair of unusually energetic coronal hard X-ray (HXR) sources detected by the Reuven Ramaty High Energy Solar Spectroscopic Imager during the impulsive phase of an X3.9 class solar flare on **2003 November 3**, which simultaneously shows two intense footpoint (FP) sources. A distinct loop top (LT) coronal source is detected up to ~150 keV and a second (upper) coronal source up to ~80 keV. These photon energies, which were not fully investigated in earlier analysis of this flare, are much higher than commonly observed in coronal sources and pose grave modeling challenges. The LT source in general appears higher in altitude with increasing energy and exhibits a more limited motion compared to the expansion of the thermal loop. The high-energy LT source shows an impulsive time profile and its nonthermal power-law spectrum exhibits soft-hard-soft evolution during the impulsive phase, similar to the FP sources. The upper coronal source exhibits an opposite spatial gradient and a similar spectral slope compared to the LT source. These properties are consistent with the model of stochastic acceleration of electrons by plasma waves or turbulence. However, the LT and FP spectral index difference (varying from ~0 to 1) is much smaller than commonly measured and than that expected from a simple stochastic acceleration model. Additional confinement or trapping mechanisms of high-energy electrons in the corona are required. Comprehensive modeling including both kinetic effects and the macroscopic flare structure may shed light on this behavior. These results highlight the importance of imaging spectroscopic observations of the LT and FP sources up to high energies in understanding electron acceleration in solar flares. Finally, we show that the electrons producing the upper coronal HXR source may very likely be responsible for the type III radio bursts at the decimetric/metric wavelength observed during the impulsive phase of this flare.

An Analysis of the Formation of Interconnecting Loops
Jie **Chen**, Henrik Lundstedt, Yuanyong Deng, Peter Wintoft and Yin Zhang
Solar Physics, Volume 273, Number 1, 51-68, **2011**
Fifty interconnecting loops (ILs) that are induced by new-born active regions are investigated. The formation period of four ILs including two same-hemisphere interconnecting loops (HILs) and two transequatorial loops (TLs) are analyzed. The magnetic flux related with these loops is studied. Considering the active region pairs related with the IL as a magnetic system, the total magnetic flux has a tendency of increasing for this system, the signs of net magnetic flux tend to be opposite for the active region pairs. There is no difference between HILs and TLs in this aspect.

Statistical properties of superactive regions during solar cycles 19–23⋆
A. Q. **Chen**1,2, J. X. Wang1, J. W. Li2, J. Feynman3 and J. Zhang
A&A 534, A47 (**2011**)
Context. Each solar activity cycle is characterized by a small number of superactive regions (SARs) that produce the most violent of space weather events with the greatest disastrous influence on our living environment.
Aims. We aim to re-parameterize the SARs and study the latitudinal and longitudinal distributions of SARs.
Methods. We select 45 SARs in solar cycles 21–23, according to the following four parameters: 1) the maximum area of sunspot group, 2) the soft X-ray flare index, 3) the 10.7 cm radio peak flux, and 4) the variation in the total solar irradiance. Another 120 SARs given by previous studies of solar cycles 19–23 are also included. The latitudinal and longitudinal distributions of the 165 SARs in both the Carrington frame and the dynamic reference frame during solar cycles 19–23 are studied statistically.
Results. Our results indicate that these 45 SARs produced 44% of all the X class X-ray flares during solar cycles 21–23, and that all the SARs are likely to produce a very fast CME. The latitudinal distributions of SARs display the Maunder butterfly diagrams and SARs occur preferentially in the maximum period of each solar cycle. Northern hemisphere SARs dominated in solar cycles 19 and 20 and southern hemisphere SARs dominated in solar cycles 21 and 22. In solar cycle 23, however, SARs occurred about equally in each hemisphere. There are two active longitudes in both the northern and southern hemispheres, about 160°–200° apart. Applying the improved dynamic reference frame to SARs, we find that SARs rotate faster than the Carrington rate and there is no significant difference between the two hemispheres. The synodic periods are 27.19 days and 27.25 days for the northern and southern hemispheres, respectively. The longitudinal distribution of SARs is significantly non-axisymmetric and about 75% SARs occurred near two active longitudes with half widths of 45°.

Scattered Light: Inverse Compton Scattering and Coronal Hard X-ray Sources

B. **Chen** and T. S. Bastian

RHESSI Nugget, No. 157, 17 July **2011**

http://sprg.ssl.berkeley.edu/~tohban/wiki/index.php/Scattered_Light:_Inverse_Compton_Scattering_and_Coronal_Hard_X-ray_Sources

We conclude that for certain coronal HXR/γ-ray sources, ICS emission may be a viable alternative to thin-target bremsstrahlung emission, particularly if the responsible energetic electron distribution is anisotropic. If ICS indeed plays a role in the production of coronal HXR/γ−ray sources, it represents a new opportunity to diagnose the properties of energetic electrons.

EVIDENCE OF EXPLOSIVE EVAPORATION IN A MICROFLARE OBSERVED BY *HINODE*/EIS

F. **Chen**[1,2] and M. D. Ding

Astrophysical Journal, 724:640–648, **2010**

We present a detailed study of explosive chromospheric evaporation during a microflare which occurred on **2007 December 7** as observed with the Extreme-ultraviolet Imaging Spectrometer on board *Hinode*. We find temperature-dependent upflows for lines formed from 1.0 to 2.5 MK and downflows for lines formed from 0.05 to 0.63 MK in the impulsive phase of the flare. Both the line intensity and the nonthermal line width appear enhanced in most of the lines and are temporally correlated with the evaporation velocity. Our results are consistent with the numerical simulations of flare models, which take into account a strong nonthermal electron beam in producing the explosive chromospheric evaporation. The explosive evaporation observed in this microflare implies that the same dynamic processes may exist in events with very different magnitudes.

Statistical study of twist values of transequatorial loops and the relationship with flares

Jie **Chen**, Henrik Lundstedt, Hongqi Zhang

Advances in Space Research, Volume 45, Issue 4, 15 February **2010**, Pages 537-540

In this paper, the twist values of 'S'-shape transequatorial loops (TLs) from 1991 to 2001 are calculated, GOES soft X-ray flares dataset of the active regions connected by these TLs are investigated. The result shows the twist value of the TLs has a weak relation with the flare flux. There is no clear correlation between the twist value and the distance between the footpoint of TLs and location of flare in the corresponding active regions.

Observations of H^{α} surges and ultraviolet jets above satellite sunspots

H. D. **Chen**, Y. C. Jiang[1], and S. L. Ma[1, 2]

A&A 478, 907-913 (**2008**)

http://www.aanda.org/index.php?option=article&access=doi&doi=10.1051/0004-6361:20078641

To know more about the physical origin of surges and jets, we investigated seven successive surge events, which occurred above the satellite sunspots of active region NOAA 10720 on **2005 January 15**.

The seven H-alpha surges we studied repeatedly occurred where the photospheric longitudinal fluxes of opposite magnetic polarities emerged, converged and were canceled by each other. Correspondingly, a small satellite spot emerged, decayed and disappeared during a period of about 2 hours in the white-light observations. In morphology, all surges displayed almost linear ejective structures. Their dynamic properties, such as the transverse velocity, projected maximum length and lifetime, varied in wide ranges. They are 30-200 km s^{-1}, 38 000-220 000 km and from several to tens of minutes, respectively. Correspondingly, the intensities of their correlated microflares were different too. The surges of major velocities or maximum lengths seemed to be accompanied by processes of more energy release. Prior to these surge events, a small H-alpha arch filament connecting the opposite flux elements was found at the base region. Instead of erupting completely, it gradually disappeared during the surges. Its role in the surge activities is very like a bipolar flux, which contained the cool plasma and reconnected with the ambient magnetic fields. In 1600 Å, three surge events exhibited the composite structures of bright jets and nearby small flaring loops, which provides direct evidence of magnetic reconnection origin of the surges. A careful comparison revealed that the ends of the arch filament, the UV jets and the small flaring loops just corresponded to the interacting longitudinal fluxes in the photosphere.

*Conclusions.*These observational results support the magnetic reconnection model of surges and jets.

Magnetic reconnection configurations and particle acceleration in solar flares

P. F. **Chen**, W. J. Liu, & C. Fang

E-print **2008**, File;

Adv. Space Res., 39, 1421, **2007**
Numerical simulations of two types of flares indicate that magnetic reconnection can provide environments favorable for various particle acceleration mechanisms to work. This paper reviews recent test particle simulations of DC electric field mechanism, and discusses how the **flare particles can escape into the interplanetary space** under different magnetic configurations.

Evidence for Plasmoid-mediated Magnetic Reconnection during a Small-scale Flare in the Partially Ionized Low Solar Atmosphere

Guanchong **Cheng**, Lei Ni, Zehao Tang, Yajie Chen, Yuhao Chen, Jialiang Hu, Jun Lin
ApJL **966** L29 **2024**
https://arxiv.org/pdf/2404.18983
https://iopscience.iop.org/article/10.3847/2041-8213/ad4027/pdf
Magnetic reconnection plays a crucial role in the energy release process for different kinds of solar eruptions and activities. The rapid solar eruption requires a fast reconnection model. Plasmoid instability in the reconnecting current sheets is one of the most acceptable fast reconnection mechanisms for explaining the explosive events in the magnetohydrodynamics (MHD) scale, which is also a potential bridge between the macroscopic MHD reconnection process and microscale dissipations. Plenty of high resolution observations indicate that the plasmoid-like structures exist in the high temperature solar corona, but such evidences are very rare in the lower solar atmosphere with partially ionized plasmas. Utilizing joint observations from the Goode Solar Telescope (GST) and the Solar Dynamics Observatory (SDO), we discovered a small-scale eruptive phenomenon in NOAA AR 13085, characterized by clear reconnection cusp structures, supported by Nonlinear Force-Free Field (NLFFF) extrapolation results. The plasmoid-like structures with a size about 150 km were observed to be ejected downward from the current sheet at a maximum velocity of 24 km·s−1 in the Hα line wing images, followed by enhanced emissions at around the post flare loop region in multiple wave lengths. Our 2.5D high-resolution MHD simulations further reproduced such a phenomenon and revealed reconnection fine structures. These results provide comprehensive evidences for the plasmoid mediated reconnection in partially ionized plasmas, and suggest an unified reconnection model for solar flares with different length scales from the lower chromosphere to corona.

Plasma Motion inside Flaring Regions Revealed by Doppler Shift Information from SDO/EVE Observations

Zhixun **Cheng**1,2, Yuming Wang1,2, Rui Liu1,2, Zhenjun Zhou2,3, and Kai Liu1,2
2019 ApJ 875 93
sci-hub.se/10.3847/1538-4357/ab0f2d
Plasma motions within flaring regions provide key information for us to understand the flare processes. Here, we study two X-class flares near the solar disk center, one on **2014 January 7** and the other on **2012 March 7**, by using 10 extreme ultraviolet (EUV) emission lines from the Solar Dynamics Observatory/EUV Variability Experiment (EVE). The EVE plasma dynamic spectrum chart, a 2D map of Doppler shift against temperature and time, is constructed based on a spectroscopic analysis of the EUV lines. Three kinds of plasma motion are identified in the plasma dynamic spectrum charts: chromospheric evaporation (100–200 km s−1) above 1 MK, cooling inside post-flare loops (approximately 150 km s−1) between 0.3 and 1 MK, and condensation at footpoints (<30 km s−1) below 0.3 MK. We find that the chromospheric evaporation and condensation at footpoints started in the impulsive phase almost simultaneously, while the cooling occurred later in the gradual phase, with a time delay of more than 10 minutes, probably implying the timescale of evaporation movement and heat loss. Atmospheric Imaging Assembly observations and differential emission measure (DEM) analyses suggest that the cooled plasma moves downward within the cold transition region (TR) loops, from top to feet, which are below the hot coronal loops. Besides, the reversal temperature between blue/redshifts is close to 1 MK, implying that the boundary of upflowing/downflowing plasma is located at the lower corona or the upper TR.

Observations of Turbulent Magnetic Reconnection Within a Solar Current Sheet

X. **Cheng**, Y. Li, L. F. Wan, M. D. Ding, P. F. Chen, J. Zhang, J. J. Liu
ApJ **866** 64 **2018**
https://arxiv.org/pdf/1808.06071.pdf
http://iopscience.iop.org/article/10.3847/1538-4357/aadd16/pdf
Magnetic reconnection is a fundamental physical process in various astrophysical, space, and laboratory environments. Many pieces of evidence for magnetic reconnection have been uncovered. However, its specific processes that could be fragmented and turbulent have been short of direct observational evidence. Here, we present observations of a super-hot current sheet during SOL**2017-09-10**T X8.2-class solar flare that display the fragmented and turbulent nature of magnetic reconnection. As bilateral plasmas converge toward the current sheet, significant plasma heating and non-thermal motions are detected therein. Two oppositely directed outflow jets are intermittently expelled out of the fragmenting current sheet, whose intensity shows a power-law distribution in spatial frequency domain. The intensity and velocity of the sunward outflow jets also display a power-law distribution in temporal frequency domain. The

length-to-width ratio of the current sheet is estimated to be larger than theoretical threshold of and thus ensures occurrence of tearing mode instability. The observations therefore suggest fragmented and turbulent magnetic reconnection occurring in the long stretching current sheet.
Erratum 2019 ApJ 874 108 https://iopscience.iop.org/article/10.3847/1538-4357/ab1079/pdf

A Two-ribbon White-light Flare Associated with a Failed Solar Eruption Observed by ONSET, SDO, and IRIS

X. **Cheng**, Q. Hao, M. D. Ding, K. Liu, P. F. Chen, C. Fang, Y. D. Liu
ApJ **809** 46 **2015**
http://arxiv.org/pdf/1507.02109v1.pdf
http://iopscience.iop.org/article/10.1088/0004-637X/809/1/46/pdf
Two-ribbon brightenings are one of the most remarkable characteristics of an eruptive solar flare and are often used for predicting the occurrence of coronal mass ejections (CMEs). Nevertheless, it was called in question recently whether all two-ribbon flares are eruptive. In this paper, we investigate a two ribbon-like white-light (WL) flare that is associated with a failed magnetic flux rope (MFR) eruption on **2015 January 13**, which has no accompanying CME in the WL coronagraph. Observations by \textit{Optical and Near-infrared Solar Eruption Tracer} and \textit{Solar Dynamics Observatory} reveal that, with the increase of the flare emission and the acceleration of the unsuccessfully erupting MFR, two isolated kernels appear at the WL 3600 {\AA} passband and quickly develop into two elongated ribbon-like structures. The evolution of the WL continuum enhancement is completely coincident in time with the variation of \textit{Fermi} hard X-ray 26--50 keV flux. Increase of continuum emission is also clearly visible at the whole FUV and NUV passbands observed by \textit{Interface Region Imaging Spectrograph}. Moreover, in one WL kernel, the \ion{Si}{4}, \ion{C}{2}, and \ion{Mg}{2} h/k lines display significant enhancement and non-thermal broadening. However, their Doppler velocity pattern is location-dependent. At the strongly bright pixels, these lines exhibit a blueshift; while at moderately bright ones, the lines are generally redshifted. These results show that the failed MFR eruption is also able to produce a two-ribbon flare and high-energy electrons that heat the lower atmosphere, causing the enhancement of the WL and FUV/NUV continuum emissions and chromospheric evaporation.
See RHESSI Science Nugget No 257, July **2015**
http://sprg.ssl.berkeley.edu/~tohban/wiki/index.php/A_Two-ribbon_White-light_Flare_Associated_with_a_Failed_Solar_Eruption

Solar flare hard X-ray spikes observed by RHESSI: a statistical study

J. X. **Cheng**1,2, J. Qiu3, M. D. Ding1,4 and H. Wang
A&A 547, A73 **(2012)**
Context. Hard X-ray (HXR) spikes refer to fine time structures on timescales of seconds to milliseconds in high-energy HXR emission profiles during solar flare eruptions.
Aims. We present a preliminary statistical investigation of temporal and spectral properties of HXR spikes.
Methods. Using a three-sigma spike selection rule, we detected 184 spikes in 94 out of 322 flares with significant counts at given photon energies, which were detected from demodulated HXR light curves obtained by the Reuven Ramaty High Energy Solar Spectroscopic Imager (RHESSI). About one fifth of these spikes are also detected at photon energies higher than 100 keV.
Results. The statistical properties of the spikes are as follows. (1) HXR spikes are produced in both impulsive flares and long-duration flares with nearly the same occurrence rates. Ninety percent of the spikes occur during the rise phase of the flares, and about 70% occur around the peak times of the flares. (2) The time durations of the spikes vary from 0.2 to 2 s, with the mean being 1.0 s, which is not dependent on photon energies. The spikes exhibit symmetric time profiles with no significant difference between rise and decay times. (3) Among the most energetic spikes, nearly all of them have harder count spectra than their underlying slow-varying components. There is also a weak indication that spikes exhibiting time lags in high-energy emissions tend to have harder spectra than spikes with time lags in low-energy emissions.

HARD X-RAY AND ULTRAVIOLET OBSERVATIONS OF THE 2005 JANUARY 15 TWO-RIBBON FLARE

J. X. **Cheng**1,2, G. Kerr3 and J. Qiu
2012 ApJ 744 48
It is well known that two-ribbon flares observed in Hα and ultraviolet (UV) wavelengths mostly exhibit compact and localized hard X-ray (HXR) sources. In this paper, we present comprehensive analysis of a two-ribbon flare observed in UV 1600 Å by Transition Region and Coronal Explorer and in HXRs by Reuven Ramaty High Energy Solar Spectroscopic Imager. HXR (25-100 keV) imaging observations show two kernels of size (FWHM) 15" moving along

the two UV ribbons. We find the following results. (1) UV brightening is substantially enhanced wherever and whenever the compact HXR kernel is passing, and during the HXR transit across a certain region, the UV count light curve in that region is temporally correlated with the HXR total flux light curve. After the passage of the HXR kernel, the UV light curve exhibits smooth monotonical decay. (2) We measure the apparent motion speed of the HXR sources and UV ribbon fronts, and decompose the motion into parallel and perpendicular motions with respect to the magnetic polarity inversion line (PIL). It is found that HXR kernels and UV fronts exhibit similar apparent motion patterns and speeds. The parallel motion dominates during the rise of the HXR emission, and the perpendicular motion starts and dominates at the HXR peak, the apparent motion speed being 10-40 km s–1. (3) We also find that UV emission is characterized by a rapid rise correlated with HXRs, followed by a long decay on timescales of 15-30 minutes. The above analysis provides evidence that UV brightening is primarily caused by beam heating, which also produces thick-target HXR emission. The thermal origin of UV emission cannot be excluded, but would produce weaker heating by one order of magnitude. The extended UV ribbons in this event are most likely a result of sequential reconnection along the PIL, which produces individual flux tubes (post-flare loops), subsequent non-thermal energy release and heating in these flux tubes, and then the very long cooling time of the transition region at the feet of these flux tubes.
25 Jan 2005

A COMPARATIVE STUDY OF CONFINED AND ERUPTIVE FLARES IN NOAA AR 10720
X. **Cheng**1,2,3, J. Zhang2, M. D. Ding1,3, Y. Guo1,3 and J. T. Su
E-print March **2011**, **2011** ApJ 732 87, **File**
We investigate the distinct properties of two types of flares: eruptive flares associated with coronal mass ejections (CMEs) and confined flares without CMEs. Our study sample includes nine M- and X-class flares, all from the same active region (AR), six of which are confined and three others which are eruptive. The confined flares tend to be more impulsive in the soft X-ray time profiles and show slenderer shapes in the Extreme-ultraviolet Imaging Telescope 195 Å images, while the eruptive ones are long-duration events and show much more extended brightening regions. The location of the confined flares is closer to the center of the AR, while the eruptive flares are at the outskirts. This difference is quantified by the displacement parameter, which is the distance between the AR center and the flare location; the average displacement of the six confined flares is 16 Mm, while that of the eruptive ones is as large as 39 Mm. Further, through nonlinear force-free field extrapolation, we find that the decay index of the transverse magnetic field in the low corona (~10 Mm) is larger for eruptive flares than for confined ones. In addition, the strength of the transverse magnetic field over the eruptive flare sites is weaker than it is over the confined ones. These results demonstrate that the strength and the decay index of the background magnetic field may determine whether or not a flare is eruptive or confined. The implication of these results on CME models is discussed in the context of torus instability of the flux rope.
14-17 Jan 2005

Re-flaring of a Post-Flare Loop System Driven by Flux Rope Emergence and Twisting
X. **Cheng**, M. D. Ding, Y. Guo, J. Zhang, J. Jing, T. Wiegelmann
E-print, 11 May **2010**, ApJL ApJL.,716,68, **2010**
In this letter, we study in detail the evolution of the post-flare loops on **2005 January 15** that occurred between two consecutive solar eruption events, both of which generated a fast halo CME and a major flare. The post-flare loop system, formed after the first CME/flare eruption, evolved rapidly, as manifested by the unusual accelerating rise motion of the loops. Through nonlinear force-free field (NLFFF) models, we obtain the magnetic structure over the active region. It clearly shows that the flux rope below the loops also kept rising accompanied with increasing twist and length. Finally, the post-flare magnetic configuration evolved to a state that resulted in the second CME/flare eruption. This is an event in which the post-flare loops can re-flare in a short period of _16 hr following the first CME/flare eruption. The observed re-flaring at the same location is likely driven by the rapid evolution of the flux rope caused by the magnetic flux emergence and the rotation of the sunspot. This observation provides valuable information on CME/flare models and their prediction.

RADIATIVE HYDRODYNAMIC SIMULATION OF THE CONTINUUM EMISSION IN SOLAR WHITE-LIGHT FLARES
J. X. Cheng1, M. D. Ding1,2 and Mats Carlsson3
2010 ApJ 711 185-191
http://iopscience.iop.org/0004-637X/711/1/185/pdf/0004-637X_711_1_185.pdf
It is believed that solar white-light flares (WLFs) originate in the lower chromosphere and upper photosphere. In particular, some recently observed WLFs show a large continuum enhancement at 1.56 μm where the opacity reaches its minimum. Therefore, it is important to clarify how the energy is transferred to the lower layers responsible for the

production of WLFs. Based on radiative hydrodynamic simulations, we study the role of non-thermal electron beams in increasing the continuum emission. We vary the parameters of the electron beam and disk positions and compare the results with observations. The electron beam heated model can explain most of the observational white-light enhancements. For the most energetic WLFs observed so far, however, a very large electron beam flux and a high low-energy cutoff, which are possibly beyond the parameter space in our simulations, are required in order to reproduce the observed white-light emission.

Long- and Mid-Term Variations of the Soft X-ray Flare Type in Solar Cycles

I.M. **Chertok** (1), A.V. Belov (1),
Solar Phys. 292:144 **2017**
http://www.izmiran.ru/~ichertok/FlareVariations/preprint.pdf
https://arxiv.org/abs/1710.06837
Using data from the GOES spacecraft in the 1-8 A wavelength range for Solar Cycles 23, 24, and part of Cycles 21 and 22, we compare mean temporal parameters (rising, decay times, duration) and the proportion of impulsive short-duration events (SDE) and gradual long-duration events (LDE) among C- and ≥M1.0-class flares. It is found that the fraction of the SDE ≥M1.0-class flares (including spikes) in Cycle 24 exceeds that in Cycle 23 in all three temporal parameters at the maximum phase and in the decay time during the ascending cycle phase. However, Cycles 23 and 24 barely differ in the fraction of the SDE C-class flares. The temporal parameters of SDEs, their fraction, and consequently the relationship between the SDE and LDE flares do not remain constant, but they reveal regular changes within individual cycles and during the transition from one cycle to another. In all phases of all four cycles, these changes have the character of pronounced, large-amplitude "quasi-biennial" oscillations (QBOs). In different cycles and at the separate phases of individual cycles, such QBOs are superimposed on various systematic trends displayed by the analyzed temporal flare parameters. In Cycle 24, the fraction of the SDE ≥M1.0-class flares from the N- and S-hemispheres displays the most pronounced synchronous QBOs. The QBO amplitude and general variability of the intense ≥M1.0-class flares almost always markedly exceeds those of the moderate C-class flares. The ordered quantitative and qualitative variations of the flare type revealed in the course of the solar cycles are discussed within the framework of the concept that the SDE flares are associated mainly with small sunspots (including those in developed active regions) and that small and large sunspots behave differently during cycles and form two distinct populations.
Correction Solar Phys (**2018**) 293:43 https://link.springer.com/content/pdf/10.1007%2Fs11207-018-1266-9.pdf

A Simple Way to Estimate the Soft X-ray Class of Far-Side Solar Flares Observed with STEREO/EUVI

I.M. **Chertok** (1), A.V. Belov (1), V.V. Grechnev (2)
Solar Phys. Volume 290, Issue 7, pp 1947-1961 **2015**
http://arxiv.org/pdf/1505.01649v1.pdf
Around the peaks of substantial flares, bright artifact nearly horizontal saturation streaks (B-streaks) corresponding to the brightest parts of the flare sources appear in the STEREO/EUVI 195 A images. We show that the length of such B-streaks can be used for the solution of an actual problem of evaluating the soft X-ray flux and class of far-side flares registered with double STEREO spacecraft but invisible from Earth. For this purpose from data on about 350 flares observed from January 2007 to July 2014 (mainly exceeding the GOES M1.0 level) both with GOES and STEREO, an empirical relation is established correlating the GOES 1-8 A peak flux and the B-streak length. This allowed us for the same years to estimate the soft X-ray classes for approximately 65 strong far-side flares observed by STEREO. The results of this simple and prompt method are consistent with the estimations of Nitta et al. (Solar Phys., 288, 241, 2013) based on the calculations of the EUVI full-disk digital number output. In addition, we studied some features of the B-streaks in impulsive and long-duration flares and demonstrated that B-streaks in several consecutive EUVI images can be used to reconstruct a probable time history of strong far-side flares.

Probing the Physics of the Solar Atmosphere with the Multi-slit Solar Explorer (MUSE): II. Flares and Eruptions

Mark C. M. **Cheung**, Juan Martínez-Sykora, Paola Testa, Bart De Pontieu, ……..
ApJ **926** 53 **2021**
https://arxiv.org/pdf/2106.15591.pdf
https://iopscience.iop.org/article/10.3847/1538-4357/ac4223/pdf
Current state-of-the-art spectrographs cannot resolve the fundamental spatial (sub-arcseconds) and temporal scales (less than a few tens of seconds) of the coronal dynamics of solar flares and eruptive phenomena. The highest resolution coronal data to date are based on imaging, which is blind to many of the processes that drive coronal energetics and dynamics. As shown by IRIS for the low solar atmosphere, we need high-resolution spectroscopic measurements with simultaneous imaging to understand the dominant processes. In this paper: (1) we introduce the Multi-slit Solar Explorer (MUSE), a spaceborne observatory to fill this observational gap by providing high-cadence (<20 s), sub-arcsecond resolution spectroscopic rasters over an active region size of the solar transition region and corona; (2) using advanced numerical models, we demonstrate the unique diagnostic capabilities of MUSE for exploring solar coronal

dynamics, and for constraining and discriminating models of solar flares and eruptions; (3) we discuss the key contributions MUSE would make in addressing the science objectives of the Next Generation Solar Physics Mission (NGSPM), and how MUSE, the high-throughput EUV Solar Telescope (EUVST) and the Daniel K Inouye Solar Telescope (and other ground-based observatories) can operate as a distributed implementation of the NGSPM. This is a companion paper to De Pontieu et al. (2021a), which focuses on investigating coronal heating with MUSE. **2014 05 01**

A comprehensive three-dimensional radiative magnetohydrodynamic simulation of a solar flare

Cheung, M. C. M.; Rempel, M.; Chintzoglou, G.; Chen, F.; Testa, P.; Martínez-Sykora, J.; Sainz Dalda, A.; DeRosa, M. L.; Malanushenko, A.; Hansteen, V.; De Pontieu, B.; Carlsson, M.; Gudiksen, B.; McIntosh, S. W.

Nature Astronomy, Volume 3, p. 160-166, **2019**

https://www.nature.com/articles/s41550-018-0629-3.epdf?author_access_token=gr3ZY26ebIzUR2WcqRelLtRgN0jAjWel9jnR3ZoTv0Ml0vLceeS715erqhTpFvw2HotukX4DnLjV72vef04rbrBNiKT8IpB-xuD7Br3cS_76LBoSAtE-Jvzb_BTU2AfQS-zu-EmkHfeGYupBmflp6w%3D%3D

Solar and stellar flares are the most intense emitters of X-rays and extreme ultraviolet radiation in planetary systems1,2. On the Sun, strong flares are usually found in newly emerging sunspot regions3. The emergence of these magnetic sunspot groups leads to the accumulation of magnetic energy in the corona. When the magnetic field undergoes abrupt relaxation, the energy released powers coronal mass ejections as well as heating plasma to temperatures beyond tens of millions of kelvins. While recent work has shed light on how magnetic energy and twist accumulate in the corona4 and on how three-dimensional magnetic reconnection allows for rapid energy release5,6, a self-consistent model capturing how such magnetic changes translate into observable diagnostics has remained elusive. Here, we present a comprehensive radiative magnetohydrodynamics simulation of a solar flare capturing the process from emergence to eruption. The simulation has sufficient realism for the synthesis of remote sensing measurements to compare with observations at visible, ultraviolet and X-ray wavelengths. This unifying model allows us to explain a number of well-known features of solar flares7, including the time profile of the X-ray flux during flares, origin and temporal evolution of chromospheric evaporation and condensation, and sweeping of flare ribbons in the lower atmosphere. Furthermore, the model reproduces the apparent non-thermal shape of coronal X-ray spectra, which is the result of the superposition of multi-component super-hot plasmas8 up to and beyond 100 million K. **April 2014**

Thermal Diagnostics with the Atmospheric Imaging Assembly onboard the Solar Dynamics Observatory: A Validated Method for Differential Emission Measure Inversions

Mark C. M. **Cheung**, P. Boerner, C. J. Schrijver, P. Testa, F. Chen, H. Peter, A. Malanushenko

ApJ **807** 143 **2015**

http://arxiv.org/pdf/1504.03258v1.pdf

We present a new method for performing differential emission measure (DEM) inversions on narrow-band EUV images from the Atmospheric Imaging Assembly (AIA) onboard the Solar Dynamics Observatory (SDO). The method yields positive definite DEM solutions by solving a linear program. This method has been validated against a diverse set of thermal models of varying complexity and realism. These include (1) idealized gaussian DEM distributions, (2) 3D models of NOAA Active Region 11158 comprising quasi-steady loop atmospheres in a non-linear force-free field, and (3) thermodynamic models from a fully-compressible, 3D MHD simulation of AR corona formation following magnetic flux emergence. We then present results from the application of the method to AIA observations of Active Region 11158, comparing the region's thermal structure on two successive solar rotations. Additionally, we show how the DEM inversion method can be adapted to simultaneously invert AIA and XRT data, and how supplementing AIA data with the latter improves the inversion result. The speed of the method allows for routine production of DEM maps, thus facilitating science studies that require tracking of the thermal structure of the solar corona in time and space.
2011-02-15, 2011-03-15

A METHOD FOR DATA-DRIVEN SIMULATIONS OF EVOLVING SOLAR ACTIVE REGIONS

Mark C. M. **Cheung** and Marc L. DeRosa

2012 ApJ 757 147

We present a method for performing data-driven simulations of solar active region formation and evolution. The approach is based on magnetofriction, which evolves the induction equation assuming that the plasma velocity is proportional to the Lorentz force. The simulations of active region (AR) coronal field are driven by temporal sequences of photospheric magnetograms from the Helioseismic Magnetic Imager instrument on board the Solar Dynamics Observatory (SDO). Under certain conditions, the data-driven simulations produce flux ropes that are ejected from the modeled AR due to loss of equilibrium. Following the ejection of flux ropes, we find an enhancement of the photospheric horizontal field near the polarity inversion line. We also present a method for the synthesis of mock coronal images based on a proxy emissivity calculated from the current density distribution in the model. This method

yields mock coronal images that are somewhat reminiscent of images of ARs taken by instruments such as SDO's Atmospheric Imaging Assembly at extreme ultraviolet wavelengths.

Signatures of Type III Solar Radio Bursts from Nanoflares: Modeling

Sherry **Chhabra**, James A. Klimchuk, Dale E. Gary
ApJ **2021**
https://arxiv.org/pdf/2109.03355.pdf
There is a wide consensus that the ubiquitous presence of magnetic reconnection events and the associated impulsive heating (nanoflares) is a strong candidate for solving the solar coronal heating problem. Whether nanoflares accelerate particles to high energies like full-sized flares is unknown. We investigate this question by studying the type III radio bursts that the nanoflares may produce on closed loops. The characteristic frequency-drifts that type III bursts exhibit can be detected using a novel application of the time-lag technique developed by Viall & Klimchuk (2012) even when there are multiple overlapping bursts. We present a simple numerical model that simulates the expected radio emission from nanoflares in an active region (AR), which we use to test and calibrate the technique. We find that in the case of closed loops the frequency spectrum of type III bursts is expected to be extremely steep such that significant emission is produced at a given frequency only for a rather narrow range of loop lengths. We also find that the signature of bursts in the time-lag signal diminishes as: (1)the variety of participating loops within that range increases; (2)the occurrence rate of bursts increases; (3) the duration of bursts increases; and (4) the brightness of the bursts decreases relative to noise. In addition, our model suggests a possible origin of type I bursts as a natural consequence of type III emission in a closed-loop geometry.

Direct measurement of non-thermal electron acceleration from magnetically driven reconnection in a laboratory plasma

Abraham **Chien**, Lan Gao, Shu Zhang, Hantao Ji, Eric G. Blackman, William Daughton, Adam Stanier, Ari Le, Fan Guo, Russ Follett, Hui Chen, Gennady Fiksel, Gabriel Bleotu, Robert C. Cauble, Sophia N. Chen, Alice Fazzini, Kirk Flippo, Omar French, Dustin H. Froula, Julien Fuchs, Shinsuke Fujioka, Kenneth Hill, Sallee Klein, Carolyn Kuranz, Philip Nilson, Alexander Rasmus, Ryunosuke Takizawa
2022
https://arxiv.org/pdf/2201.10052.pdf
Magnetic reconnection is a ubiquitous astrophysical process that rapidly converts magnetic energy into some combination of plasma flow energy, thermal energy, and non-thermal energetic particles, including energetic electrons. Various reconnection acceleration mechanisms in different low-β (plasma-to-magnetic pressure ratio) and collisionless environments have been proposed theoretically and studied numerically, including first- and second-order Fermi acceleration, betatron acceleration, parallel electric field acceleration along magnetic fields, and direct acceleration by the reconnection electric field. However, none of them have been heretofore confirmed experimentally, as the direct observation of non-thermal particle acceleration in laboratory experiments has been difficult due to short Debye lengths for \textit{in-situ} measurements and short mean free paths for \textit{ex-situ} measurements. Here we report the direct measurement of accelerated non-thermal electrons from low-β magnetically driven reconnection in experiments using a laser-powered capacitor coil platform. We use kiloJoule lasers to drive parallel currents to reconnect MegaGauss-level magnetic fields in a quasi-axisymmetric geometry. The angular dependence of the measured electron energy spectrum and the resulting accelerated energies, supported by particle-in-cell simulations, indicate that the mechanism of direct electric field acceleration by the out-of-plane reconnection electric field is at work. Scaled energies using this mechanism show direct relevance to astrophysical observations. Our results therefore validate one of the proposed acceleration mechanisms by reconnection, and establish a new approach to study reconnection particle acceleration with laboratory experiments in relevant regimes.

An active region jet observed with Hinode

C. **Chifor**[1], P. R. Young[2], H. Isobe[3], H. E. Mason[1], D. Tripathi[1], H. Hara[4], T. Yokoyama[3]
E-print, Jan 2008; A&A
http://www.damtp.cam.ac.uk/user/christina/papers/Chifor-Jet_AA_letter_jan08.pdf
Conclusions.The high-velocity up-flows, together with the density dependence on velocity support an evaporation scenario for the acceleration of this jet. The large density and small filling factor, coupled with the large Doppler velocities are strongly suggestive of multiple small-scale magnetic reconnection events being responsible for the production of both EUV and X-ray jets.

Magnetic flux cancellation associated with a recurring solar jet observed with *Hinode*, *RHESSI*, and *STEREO*/EUVI

C. **Chifor**[1], H. Isobe[2], H. E. Mason[1], I. G. Hannah[3], P. R. Young[4], G. Del Zanna[5], S. Krucker[6], K. Ichimoto[2], Y. Katsukawa[7], and T. Yokoyama[8]
A&A 491, 279-288 (2008), DOI: 10.1051/0004-6361:200810265
http://www.aanda.org/10.1051/0004-6361:200810265

Aims. We study the physical properties of a recurring solar active region jet observed in X-rays and extreme-ultraviolet (EUV).
Methods. Multi-wavelength data from all three instruments on board Hinode were analysed. X-ray imaging and spectroscopy of the microflaring emission associated with the jets was performed with the Reuven Ramaty High Energy Spectroscopic Imager (RHESSI). Associated EUV jets were observed with the Sun Earth Connection Coronal and Heliospheric Investigation (SECCHI)/Extreme Ultraviolet Imager (EUVI) on board STEREO.
Results. We found a correlation between recurring magnetic flux cancellation close to a pore, the X-ray jet emission, and associated Ca II H ribbon brightenings. We estimated the lower limit for the decrease in magnetic energy associated with the X-ray jet emission at 3x1029 erg. The recurring plasma ejection was observed simultaneously at EUV and X-ray temperatures, associated with type III radio bursts and microflaring activity at the jet footpoint.
Conclusions. The recurring jet (EUV and X-ray) emissions can be attributed to chromospheric evaporation flows due to recurring coronal magnetic reconnection. In this process, the estimated minimum loss in the magnetic energy is sufficient to account for the total energy required to launch the jet.

X-ray precursors to flares and filament eruptions

C. **Chifor**, D. Tripathi, H. E. Mason, B. R. Dennis
E-print, July 2007, A&A 472 (2007) 967-979
The preflare brightenings are precursors to the flare and filament eruption. These precursors represent distinct, localised instances of energy release, rather than a gradual energy release prior to the main flare. The X-ray precursors represent clearly observable signatures in the early stages of the eruption. Together with the timing of the filament fast-rise at or after the main flare onset, the X-ray precursors provide evidence for a tether-cutting mechanism initially manifested as localised magnetic reconnection being a common trigger for both flare emission and filament eruption.

The Origin of Major Solar Activity - Collisional Shearing Between Nonconjugated Polarities of Multiple Bipoles Emerging Within Active Regions

Georgios **Chintzoglou**, Jie Zhang, Mark C. M. Cheung, Maria Kazachenko
ApJ **871** 67 **2019**
https://arxiv.org/pdf/1811.02186.pdf
sci-hub.tw/10.3847/1538-4357/aaef30
Active Regions (ARs) that exhibit compact Polarity Inversion Lines (PILs) are known to be very flare-productive. However, the physical mechanisms behind this statistical inference have not been demonstrated conclusively. We show that such PILs can occur due to the collision between two emerging flux tubes nested within the same AR. In such multipolar ARs, the flux tubes may emerge simultaneously or sequentially, each initially producing a bipolar magnetic region (BMR) at the surface. During each flux tube's emergence phase, the magnetic polarities can migrate such that opposite polarities belonging to different BMRs collide, resulting in shearing and cancellation of magnetic flux. We name this process 'collisional shearing' to emphasize that the shearing and flux cancellation develops due to the collision. Collisional shearing is a process different from the known concept of flux cancellation occurring between polarities of a single bipole, a process that has been commonly used in many numerical models. High spatial and temporal resolution observations from the Solar Dynamics Observatory for two emerging ARs, **AR11158 and AR12017**, show the continuous cancellation of up to 40% of the unsigned magnetic flux of the smallest BMR, which occurs at the collisional PIL for as long as the collision persists. The flux cancellation is accompanied by a succession of solar flares and CMEs, products of magnetic reconnection along the collisional PIL. Our results suggest that the quantification of magnetic cancellation driven by collisional shearing needs to be taken into consideration in order to improve the prediction of solar energetic events and space weather. **11-16 Feb 2011, 23-28 Mar 2014**
HMI Science Nuggets #121 Feb 2019 http://hmi.stanford.edu/hminuggets/?p=2846

Formation of Magnetic Flux Ropes during Confined Flaring Well Before the Onset of a Pair of Major Coronal Mass Ejections

Georgios **Chintzoglou**, Spiros Patsourakos, Angelos Vourlidas
ApJ **2015**
http://arxiv.org/pdf/1507.01165v1.pdf
NOAA Active Region (AR) 11429 was the source of twin super-fast Coronal Mass Ejections (CMEs). The CMEs took place within a hour from each other, with the onset of the first taking place in the beginning of **March 7, 2012**. This AR fulfills all the requirements for a "super active region"; namely, Hale's law incompatibility and a δ-spot magnetic configuration. One of the biggest storms of Solar Cycle 24 to date (Dst=−143 nT) was associated with one of these events. Magnetic Flux Ropes (MFRs) are twisted magnetic structures in the corona, best seen in∼10 MK hot plasma emission and are often considered the core of erupting structures. However, their "dormant" existence in the solar atmosphere (i.e. prior to eruptions), is an open question. Aided by multi-wavelength observations (SDO/HMI/AIA and STEREO EUVI B) and a Non-Linear Force-Free (NLFFF) model for the coronal magnetic field, our work uncovers two

separate, weakly-twisted magnetic flux systems which suggest the existence of pre-eruption MFRs that eventually became the seeds of the two CMEs. The MFRs could have been formed during confined (i.e. not leading to major CMEs) flaring and sub-flaring events which took place the day before the two CMEs in the host AR 11429.

Hard X-rays from the deep solar atmosphere: An unusual UV burst with flare properties

L. P. **Chitta**, I. G. Hannah, L. Fletcher, H. S. Hudson, P. R. Young, S. Krucker, H. Peter
A&A Letters 688, L9 **2024**
https://arxiv.org/pdf/2407.06140
https://www.aanda.org/articles/aa/pdf/2024/08/aa50866-24.pdf
Explosive transient events occur throughout the solar atmosphere. The differing manifestations range from coronal mass ejections to Ellermann bombs. The former may have negligible signatures in the lower atmosphere, and the latter may have negligible nonthermal emissions such as hard X-radiation. A solar flare generally involves a broad range of emission signatures. Using a suite of four space-borne telescopes, we report a solar event that combines aspects of simple UV bursts and hard X-ray emitting flares at the same time. The event is a compact C-class flare in active region AR11861, SOL**2013-10-12**T00:30. By fitting a combined isothermal and nonthermal model to the hard X-ray spectrum, we inferred plasma temperatures in excess of 15\,MK and a nonthermal power of about 3×1027\,erg\,s−1 in this event. Despite these high temperatures and evidence for nonthermal particles, the flare was mostly confined to the chromosphere. However, the event lacked clear signatures of UV spectral lines, such as the Fe\,{\sc xii} 1349\,Å and Fe\,{\sc xxi} 1354\,Å emission lines, which are characteristic of emission from hotter plasma with a temperature over 1\,MK. Moreover, the event exhibited very limited signatures in the extreme-UV wavelengths. Our study indicates that a UV burst -- hard X-ray flare hybrid phenomenon exists in the low solar atmosphere. Plasma that heats to high temperatures coupled with particle acceleration by magnetic energy that is released directly in the lower atmosphere sheds light on the nature of active region core heating and on inferences of flare signatures.

From formation to disruption: observing multi-phase evolution of a solar flare current sheet

L. P. **Chitta**, E. R. Priest, X. Cheng
ApJ Volume 911, Issue 2, id.133 **2021**
https://arxiv.org/pdf/2103.02352.pdf
https://iopscience.iop.org/article/10.3847/1538-4357/abec4d/pdf
A current sheet, where magnetic energy is liberated through reconnection and is converted to other forms, is thought to play the central role in solar flares, the most intense explosions in the heliosphere. However, the evolution of a current sheet and its subsequent role in flare related phenomena such as particle acceleration is poorly understood. Here we report observations obtained with NASA's Solar Dynamics Observatory that reveal a multi-phase evolution of a current sheet in the early stages of a solar flare, from its formation to quasi-stable evolution and disruption. Our observations have implications for the understanding of onset and evolution of reconnection in early stages of eruptive solar flares. **2020 November 29**

Extreme ultraviolet bursts and nanoflares in the quiet solar transition region and corona

L. P. **Chitta**, H. Peter, P. R. Young
A&A **2021**
https://arxiv.org/pdf/2102.00730.pdf
The quiet solar corona consists of a myriad of loop-like features with magnetic fields originating from network and internetwork regions on the solar surface. Based on HRTS, Yohkoh, SOHO, and TRACE observations, there is a rich literature on a variety of such burst phenomena in the solar atmosphere. However, it remains unclear whether such transients, mostly observed in the extreme ultraviolet (EUV), play a significant role in atmospheric heating. We revisit the issue of these bursts as a prelude to the new high resolution EUV imagery expected from the recently launched Solar Orbiter. We use EUV images recorded by the SDO/AIA to investigate statistical properties of the bursts. We detect the bursts in the 171 Å filter images of AIA in an automated way through a pixel-wise analysis by imposing different intensity thresholds. By exploiting the high cadence (12 s) of the AIA observations, we find that the distribution of lifetime of these events peaks at about 120 s, nevertheless, there are a significant number of events also at timescales shorter than 60 s. The sizes of the detected bursts are limited by the spatial resolution, hinting at a larger number of hidden events in the AIA data. We estimate that there appear about 100 new bursts per second on the whole Sun. The detected bursts have nanoflare-like energies of 1024 erg per event. Based on this we estimate that at least 100 times more events of similar nature would be required to account for energy required to heat the corona. Thus, considering AIA observations alone, the EUV bursts discussed here have no significant role in the quiet-Sun coronal heating. If the quiet-Sun coronal heating is mainly bursty, then the high-resolution EUV observations from the Solar Orbiter may be able to reduce, at least partly, the deficit in the number of EUV bursts seen with SDO/AIA, by detecting more such events. **2011-01-25, 2017-03-21**

Onset of turbulent fast magnetic reconnection observed in the solar atmosphere

L. P. **Chitta**, A. Lazarian

ApJL **890** L2 **2020**
https://arxiv.org/pdf/2001.08595.pdf
sci-hub.si/10.3847/2041-8213/ab6f0a
Fast magnetic reconnection powers explosive events throughout the universe, from gamma-ray bursts to solar flares. Despite its importance, the onset of astrophysical fast reconnection is the subject of intensive debates and remains an open question in plasma physics. Here we report high cadence observations of two reconnection-driven solar microflares obtained by the Interface Region Imaging Spectrograph that show persistent turbulent flows preceding flaring. The speeds of these flows are comparable to the local sound speed initially, suggesting the onset of fast reconnection in a highly turbulent plasma environment. Our results are in close quantitative agreement with the theory of turbulence-driven reconnection as well as with numerical simulations in which fast magnetic reconnection is induced by turbulence. **2014 May 25, 2016 July 18**
CESRA #2539 Apr **2020** http://www.astro.gla.ac.uk/users/eduard/cesra/?p=2539

The nature of energy source powering solar coronal loops driven by nanoflares

L. P. **Chitta**, H. Peter, S. K. Solanki
A&A Letters **2018**
https://arxiv.org/pdf/1806.11045.pdf
Magnetic energy is required to heat the outer atmosphere of the Sun, the corona, to millions of degrees. We study the nature of the magnetic energy source that is probably responsible for the brightening of coronal loops driven by nanoflares in the cores of solar active regions. We consider observations of two active regions (AR) 11890 and 12234 in which nanoflares were stated to be detected. To this end, we use ultraviolet and extreme ultraviolet (EUV) images from the Atmospheric Imaging Assembly (AIA) onboard the Solar Dynamics Observatory (SDO) for coronal loop diagnostics. These images are combined with the co-temporal line-of-sight magnetic field maps from the Helioseismic and Magnetic Imager (HMI) onboard SDO to investigate the connection between coronal loops and their magnetic roots in the photosphere. The core of these ARs exhibited loop brightening in multiple EUV channels of AIA, particularly in its 9.4 nm filter. The HMI magnetic field maps show the presence of a complex mixed polarity magnetic field distribution at the base of these loops. We detect the cancellation of photospheric magnetic flux at these locations at a rate of about 1015 Mx s−1. The associated compact coronal brightenings directly above the cancelling magnetic features are indicative of plasma heating due to chromospheric magnetic reconnection. We suggest that the complex magnetic topology and the evolution of magnetic field such as flux cancellation in the photosphere and the resulting chromospheric reconnection can play an important role in energizing active region coronal loops driven by nanoflares. Our estimates of magnetic energy release during flux cancellation in the quiet Sun suggests that chromospheric reconnection can also power the quiet corona. **09 November 2013, 11 December 2014**
RHESSI Science Nuggets #326 **2018**
http://sprg.ssl.berkeley.edu/~tohban/wiki/index.php/Coronal_nanoflares_powered_by_footpoint_reconnection

A Statistical Study of the IRIS Observational Signatures of Nanoflares and Non-thermal Particles

Kyuhyoun **Cho**, Paola Testa, Bart De Pontieu, Vanessa Polito
ApJ **2022**
https://arxiv.org/pdf/2211.06832.pdf
Nanoflares are regarded as one of the major mechanisms of magnetic energy release and coronal heating in the solar outer atmosphere. We conduct a statistical study on the response of the chromosphere and transition region to nanoflares, as observed by the Interface Region Imaging Spectrograph (IRIS), by using an algorithm for the automatic detection of these events. The initial atmospheric response to these small heating events is observed, with IRIS, as transient brightening at the footpoints of coronal loops heated to high temperatures (>4 MK). For four active regions, observed over 143 hours, we detected 1082 footpoint brightenings under the IRIS slit, and for those we extracted physical parameters from the IRIS Mg II and Si IV spectra that are formed in the chromosphere and transition region, respectively. We investigate the distribution of the spectral parameters, and the relationship between the parameters, also comparing them with predictions from RADYN numerical simulations of nanoflare-heated loops. We find that these events, and the presence of non-thermal particles, tend to be more frequent in flare productive active regions, and where the hot AIA 94Å emission is higher. We find evidence for highly dynamic motions characterized by strong \siiv\ non-thermal velocity (not dependent on the heliocentric x coordinate, i.e., on the angle between the magnetic field and the line-of-sight) and asymmetric \mgii\ spectra. These findings provide tight new constraints on the properties of nanoflares, and non-thermal particles, in active regions, and their effects on the lower atmosphere. **18 Sep 2015, 28 Dec 2015, 21 Mar 2016, 13 Apr 2016,**
IRIS Nugget Feb **2023** https://iris.lmsal.com/nugget

Strong Blue Asymmetry in Hα Line as a Preflare Activity

Kyuhyoun **Cho**, Jeongwoo Lee, Jongchul Chae, Haimin Wang, Kwangsu Ahn,

Heesu Yang, Eun-kyung Lim, Ram Ajor Maurya
Solar Phys. Volume 291, Issue 8, pp 2391–2406 **2016**
https://arxiv.org/pdf/2005.06404.pdf
Chromospheric activities before solar flares provide important clues to the mechanisms that initiate solar flares, but are as yet poorly understood. We report a significant and rapid Hαα line broadening before the solar flare **SOL2011-09-29**T18:08 that was detected using the unprecedented high-resolution Hα imaging spectroscopy with the Fast Imaging Solar Spectrograph (FISS) installed on the 1.6 m New Solar Telescope (NST) at Big Bear Solar Observatory. The strong Hαα broadening extends as a blue excursion up to −4.5 Å and as a red excursion up to 2.0 Å, which implies a mixture of velocities in the range of −130 kms−1−130 kms−1 to 38 km s−1 derived by applying the cloud model, comparable to the highest chromospheric motions reported before. The Hαα blueshifted broadening lasts for about six minutes and is temporally and spatially correlated with the start of a rising filament, which is later associated with the main phase of the flare as detected by the Atmosphere Imaging Assembly (AIA) onboard the Solar Dynamics Observatory (SDO). The potential importance of this Hααblueshifted broadening as a preflare chromospheric activity is briefly discussed within the context of the two-step eruption model.

Comparison of damped oscillations in solar and stellar X-ray flares

Cho, I.-H., Cho, K.-S., Nakariakov, V.M., Kim, S., Kumar, P.
ApJ 830 110 **2016**
http://www2.warwick.ac.uk/fac/sci/physics/research/cfsa/people/valery/cho2016.pdf
We explore the similarity and difference of the quasi-periodic pulsations (QPPs) observed in the decay phase of solar and stellar flares at X-rays. We identified 42 solar flares with pronounced QPPs, observed with the Reuven Ramaty High-Energy Solar Spectroscopic Imager (RHESSI) and 36 stellar flares with QPPs, observed with X-ray Multi Mirror Newton observatory (XMM-Newton). The Empirical Mode Decomposition (EMD) method and least-square fit by a damped sine function were applied to obtain the periods (P) and damping times (\tau) of the QPPs. We found that (1) the periods and damping times of the stellar QPPs are $5.00^{+70.45}_{-4.57}$ min and $17.29^{+60.80}_{-17.02}$ min, which are comparable with those of the solar QPPs ($0.57^{+3.01}_{-0.30}$ and $1.20^{+2.77}_{-0.76}$ min). (2) The ratio of the damping times to the periods (\tau/P) observed in the stellar QPPs ($1.46^{+2.54}_{-0.48}$) are statistically identical to those of solar QPPs ($1.49^{+2.49}_{-0.66}$). (3) The scalings of the QPP damping time with the period are well described by the power law in both solar and stellar cases. The power indices of the solar and stellar QPPs are 0.96±{0.10} and 0.98±{0.05}, respectively. This scaling is consistent with the scalings found for standing slow magnetoacoustic and kink modes in solar coronal loops. Thus, we propose that the underlying mechanism responsible for the stellar QPPs is the natural magnetohydrodynamic oscillations in the flaring or adjacent coronal loops, as in the case of solar flares. **30 Oct 2014**
Table 1. RHESSI Flare list for the Solar QPPs

Study of temporal and spectral characteristics of the X-ray emission from solar flares

Veena **Choithani**, Rajmal Jain, Arun Kumar Awasthi, Geetanjali Singh, Sneha Chaudhari, Som Kumar Sharma
Research in Astronomy and Astrophysics (RAA) **2018**
https://arxiv.org/pdf/1804.08431.pdf
Temporal and spectral characteristics of X-ray emission from 60 flares of intensity ≥C class observed by Solar X-ray Spectrometer (SOXS) during 2003-2011 are presented. We analyse the X-ray emission observed in four and three energy bands by the Si and CZT detectors, respectively. The number of peaks in the intensity profile of the flares varies between 1 and 3. We find moderate correlation (R≃0.2) between the rise time and the peak flux of the first peak of the flare irrespective to energy band, which is indicative of its energy-independent nature. Moreover, magnetic field complexity of the flaring region is found to be anti-correlated (R=0.61) with the rise time of the flares while positively correlated (R=0.28) with the peak flux of the flare. The time delay between the peak of the X-ray emission in a given energy band and that in the 25-30 keV decreases with increasing energy suggesting conduction cooling to be dominant in the lower energies. Analysis of 340 spectra from 14 flares reveals that the peak of Differential Emission Measure (DEM) evolution delays by 60-360 s relative to that of the temperature, and this time delay is inversely proportional to the peak flux of the flare. We conclude that temporal and intensity characteristics of flares are energy dependent as well as magnetic field configuration of the active region. **14 Aug2004, 17 September 2005, 06 April 2006**
Table 1: Physical Properties of solar flares under current investigation (2003-2011)

Different Periodicities in the Sunspot Area and the Occurrence of Solar Flares and Coronal Mass Ejections in Solar Cycle 23 – 24

D. P. **Choudhary**, J. K. Lawrence, M. Norris, A. C. Cadavid
Solar Physics, February **2014**, Volume 289, Issue 2, pp 649-656
In order to investigate the relationship between magnetic-flux emergence, solar flares, and coronal mass ejections (CMEs), we study the periodicity in the time series of these quantities. It has been known that solar flares, sunspot area, and photospheric magnetic flux have a dominant periodicity of about 155 days, which is confined to a part of the phase

of the solar cycle. These periodicities occur at different phases of the solar cycle during successive phases. We present a time-series analysis of sunspot area, flare and CME occurrence during Cycle 23 and the rising phase of Cycle 24 from 1996 to 2011. We find that the flux emergence, represented by sunspot area, has multiple periodicities. Flares and CMEs, however, do not occur with the same period as the flux emergence. Using the results of this study, we discuss the possible activity sources producing emerging flux.

Flux emergence, flux imbalance, magnetic free energy and solar flares

Debi Prasad **Choudhary**, Sanjay Gosain, Nat Gopalswamy, P.K. Manoharan, R. Chandra, W. Uddin, A.K. Srivastava, S. Yashiro, N.C. Joshi, P. Kayshap, V.C. Dwivedi, K. Mahalakshmi, E. Elamathi, Max Norris, A.K. Awasthi, R. Jain

Advances in Space Research, Volume 52, Issue 8, 15 October **2013**, Pages 1561–1566

Emergence of complex magnetic flux in the solar active regions lead to several observational effects such as a change in sunspot area and flux embalance in photospheric magnetograms. The flux emergence also results in twisted magnetic field lines that add to free energy content. The magnetic field configuration of these active regions relax to near potential-field configuration after energy release through solar flares and coronal mass ejections. In this paper, we study the relation of flare productivity of active regions with their evolution of magnetic flux emergence, flux imbalance and free energy content. We use the sunspot area and number for flux emergence study as they contain most of the concentrated magnetic flux in the active region. The magnetic flux imbalance and the free energy are estimated using the HMI/SDO magnetograms and Virial theorem method. We find that the active regions that undergo large changes in sunspot area are most flare productive. The active regions become flary when the free energy content exceeds 50% of the total energy. Although, the flary active regions show magnetic flux imbalance, it is hard to predict flare activity based on this parameter alone.

Study of multi-periodic coronal pulsations during an X-class solar flare

Partha **Chowdhury**, A.K. Srivastava, B.N. Dwivedi, Robert Sych, Y.-J. Moon

Advances in Space Research, Volume 56, Issue 12, 15 December 2015, Pages 2769–2778 **2015**

http://arxiv.org/pdf/1507.02009v1.pdf

http://www.sciencedirect.com/science/article/pii/S0273117715005682

We investigate quasi-periodic coronal pulsations during the decay phase of an X 3.2 class flare on **14 May 2013**, using soft X-ray data from the RHESSI satellite. Periodogram analyses of soft X-ray light curves show that 53 s and 72 s periods co-exist in the 3-6, 6-12 and 12-25 KeV energy bands. Considering the typical length of the flaring loop system and observed periodicities, we find that they are associated with multiple (first two harmonics) of fast magnetoacoustic sausage waves. The phase relationship of soft X-ray emissions in different energy bands using cross-correlation technique show that these modes are standing in nature as we do not find the phase lag. Considering the period ratio, we diagnose the local plasma conditions of the flaring region by invoking MHD seismology. The period ratio P1/2P2 is found to be 0.65, which indicates that such oscillations are most likely excited in longitudinal density stratified loops.

Exploring impulsive solar magnetic energy release and particle acceleration with focused hard X-ray imaging spectroscopy

Steven **Christe**, Samuel Krucker, Lindsay Glesener, Albert Shih, Pascal Saint-Hilaire, Amir Caspi, Joel Allred, Marina Battaglia, Bin Chen, James Drake, Brian Dennis, Dale Gary, Szymon Gburek, Keith Goetz, Brian Grefenstette, Mikhail Gubarev, Iain Hannah, Gordon Holman, Hugh Hudson, Andrew Inglis, Jack Ireland, Shinosuke Ishikawa, James Klimchuk, Eduard Kontar, Adam Kowalski, Dana Longcope, Anna-Maria Massone, Sophie Musset, Michele Piana, Brian Ramsey, Daniel Ryan, Richard Schwartz, Marek Stęślicki, Paul Turin, Alexander Warmuth, Colleen Wilson-Hodge, Stephen White, Astrid Veronig, Nicole Vilmer, Tom Woods

Next Generation Solar Physics Mission white paper **2017**

https://arxiv.org/pdf/1701.00792v1.pdf

How impulsive magnetic energy release leads to solar eruptions and how those eruptions are energized and evolve are vital unsolved problems in Heliophysics. The standard model for solar eruptions summarizes our current understanding of these events. Magnetic energy in the corona is released through drastic restructuring of the magnetic field via reconnection. Electrons and ions are then accelerated by poorly understood processes. Theories include contracting loops, merging magnetic islands, stochastic acceleration, and turbulence at shocks, among others. Although this basic model is well established, the fundamental physics is poorly understood. HXR observations using grazing-incidence focusing optics can now probe all of the key regions of the standard model. These include two above-the-looptop (ALT) sources which bookend the reconnection region and are likely the sites of particle acceleration and direct heating. The science achievable by a direct HXR imaging instrument can be summarized by the following science questions and objectives which are some of the most outstanding issues in solar physics (1) How are particles accelerated at the Sun? (1a) Where are electrons accelerated and on what time scales? (1b) What fraction of electrons is accelerated out of the ambient medium? (2) How does magnetic energy release on the Sun lead to flares and eruptions? A Focusing Optics X-

ray Solar Imager (FOXSI) instrument, which can be built now using proven technology and at modest cost, would enable revolutionary advancements in our understanding of impulsive magnetic energy release and particle acceleration, a process which is known to occur at the Sun but also throughout the Universe.

Solving the Coronal Heating Problem using X-ray Microcalorimeters

Steven **Christe**, Simon Bandler, Edward DeLuca, Amir Caspi, Leon Golub, Randall Smith, Joel Allred, Jeffrey W. Brosius, Brian Dennis, James Klimchuk
Next Generation Solar Physics Mission **2017**
https://arxiv.org/pdf/1701.00795v1.pdf

Even in the absence of resolved flares, the corona is heated to several million degrees. However, despite its importance for the structure, dynamics, and evolution of the solar atmosphere, the origin of this heating remains poorly understood. Several observational and theoretical considerations suggest that the heating is driven by small, impulsive energy bursts which could be Parker-style "nanoflares" (Parker 1988) that arise via reconnection within the tangled and twisted coronal magnetic field. The classical "smoking gun" (Klimchuk 2009; Cargill et al. 2013) for impulsive heating is the direct detection of widespread hot plasma (T > 6 MK) with a low emission measure. In recent years there has been great progress in the development of Transition Edge Sensor (TES) X-ray microcalorimeters that make them more ideal for studying the Sun. When combined with grazing-incidence focusing optics, they provide direct spectroscopic imaging over a broad energy band (0.5 to 10 keV) combined with extremely impressive energy resolution in small pixels, as low as 0.7 eV (FWHM) at 1.5 keV (Lee 2015), and 1.56 eV (FWHM) at 6 keV (Smith 2012), two orders of magnitude better than the current best traditional solid state photon-counting spectrometers. Decisive observations of the hot plasma associated with nanoflare models of coronal heating can be provided by new solar microcalorimeters. These measurements will cover the most important part of the coronal spectrum for searching for the nanoflare-related hot plasma and will characterize how much nanoflares can heat the corona both in active regions and the quiet Sun. Finally, microcalorimeters will enable to study all of this as a function of time and space in each pixel simultaneously a capability never before available.

The RHESSI Microflare Height Distribution

S. **Christe**, S. Krucker and P. Saint-Hilaire
Solar Physics, Volume 270, Number 2, 493-502, **2011**

We present the first in-depth statistical survey of flare source heights observed by RHESSI. Flares were found using a flare-finding algorithm designed to search the 6 – 10 keV count-rate when RHESSI's full sensitivity was available in order to find the smallest events (Christe et al. in Astrophys. J. 677, 1385, 2008). Between March 2002 and March 2007, a total of 25 006 events were found. Source locations were determined in the 4 – 10 keV, 10 – 15 keV, and 15 – 30 keV energy ranges for each event. In order to extract the height distribution from the observed projected source positions, a forward-fit model was developed with an assumed source height distribution where height is measured from the photosphere. We find that the best flare height distribution is given by $g(h) \propto \exp(-h/\lambda)$ where $\lambda = 6.1 \pm 0.3$ Mm is the scale height. A power-law height distribution with a negative power-law index, $\gamma = 3.1 \pm 0.1$ is also consistent with the data. Interpreted as thermal loop-top sources, these heights are compared to loops generated by a potential-field model (PFSS). The measured flare heights distribution are found to be much steeper than the potential-field loop height distribution, which may be a signature of the flare energization process.

M is for Magnifique Part Deux

Steven **Christe**, Andy Inglis
RHESSI nugget, 21 Feb **2011**
http://sprg.ssl.berkeley.edu/~tohban/wiki/index.php/M_is_for_Magnifique_Part_Deux
we continue our analysis of the M class flare of **October 16th, 2010** (SOL2010-10-16T19:12)

RHESSI Microflare Statistics. I. Flare-Finding and Frequency Distributions

S. **Christe**, I. G. Hannah, S. Krucker, J. McTiernan, and R. P. Lin
The Astrophysical Journal, Vol. 677, No. 2: 1385-1394, **2008**.
http://www.journals.uchicago.edu/doi/pdf/10.1086/529011

Multi-wavelength observations of the 2014 June 11 M3.9 flare: temporal and spatial characteristics

Damian J. **Christian**, David Kuridze, David B. Jess, Menoa Yousefi, Mihalis Mathioudakis
Research in Astronomy and Astrophysics Vol 19, No 7, 101, **2019**
https://arxiv.org/pdf/1811.07077.pdf
We present multi-wavelength observations of an M-class flare (M3.9) that occurred on **2014 June 11**. Our observations were conducted with the Dunn Solar Telescope (DST), adaptive optics, the multi-camera system ROSA (Rapid Oscillations in Solar Atmosphere) and new HARDcam (Hydrogen-Alpha Rapid Dynamics) camera in various wavelengths, such as Ca II K, Mg I b2 (at 5172.7 Å), and Hα narrow-band, and G-band continuum filters. Images were re-constructed using the Kiepencheuer-Institut Speckle Interferometry Package (KISIP) code, to improve our image resolution. We observed intensity increases of ≈120-150\% in the Mg, Ca K and Hα narrow band filters during the flare. Intensity increases for the flare observed in the SDO EUV channels were several times larger, and the GOES X-rays increased over a factor of 30 for the harder band. Only a modest delay is found between the onset of flare ribbons of a nearby sympathetic flare and the main flare ribbons observed in these narrow-band filters. The peak flare emission occurs within a few seconds for the Ca K, Mg, and Hα bands. Time-distance techniques find propagation velocities of ≈60 km/s and as high as 300 km/s for regions of the main flare ribbon. This result and delays and velocities observed with SDO (≈100 km/s) for different coronal heights agree well with the simple model of energy propagation versus height, although a more detailed model for the flaring solar atmosphere is needed. Future high time resolution observations of solar flares (such as those available with DKIST) are important for disentangling the detailed flare-physics.

THE CURRENT SHEET ASSOCIATED WITH THE 2003 NOVEMBER 4 CORONAL MASS EJECTION: DENSITY, TEMPERATURE, THICKNESS, AND LINE WIDTH

A. **Ciaravella**1, 2 and J. C. Raymond2
Astrophysical Journal, 686:1372Y1382, 2008
http://www.journals.uchicago.edu/doi/pdf/10.1086/590655
In the wake of the 2003 November 4 coronal mass ejection associated with the largest solar flare of the last sunspot cycle, a current sheet (CS) was observed by the Ultraviolet Coronagraph Spectrometer (UVCS) as a narrow bright feature in the [Fe xviii] ($10^{6.8}$ K) line. This is the first UVobservation in which the CS evolution is followed from its onset. UV spectra provide diagnostics of electron temperature, emission measure, Doppler shift, line width, and size of the CS as function of time. Since the UVCS slit was inside the Mark IV K-coronameter (MK4) field of view, the combination of UV spectra and MK4 white light data provides estimates of the electron density and depth along the line of sight of the CS. The thickness of the CS in the [Fe xviii] line is far larger than classical or anomalous resistivity would predict, and it might indicate an effective resistivity much larger than anomalous resistivity, such as that due to hyperdiffusion. The broad [Fe xviii] line profiles in the CS cannot be explained as thermal widths. They result from a combination of bulk motions and turbulence. The Petschek reconnection mechanism and turbulent reconnection may be consistent with the observations.

Flare Forecasting Algorithms Based on High-Gradient Polarity Inversion Lines in Active Regions

Domenico **Cicogna**, Francesco Berrilli, Daniele Calchetti, Dario Del Moro, Luca Giovannelli, Federico Benvenuto, Cristina Campi, Sabrina Guastavino, Michele Piana
ApJ **915** 38 **2021**
https://arxiv.org/pdf/2105.00897.pdf
https://iopscience.iop.org/article/10.3847/1538-4357/abfafb/pdf
https://doi.org/10.3847/1538-4357/abfafb
Solar flares emanate from solar active regions hosting complex and strong bipolar magnetic fluxes. Estimating the probability of an active region to flare and defining reliable precursors of intense flares is an extremely challenging task in the space weather field. In this work, we focus on two metrics as flare precursors, the unsigned flux R, tested on MDI/SOHO data and one of the most used parameters for flare forecasting applications, and a novel topological parameter D representing the complexity of a solar active region. More in detail, we propose an algorithm for the computation of the R value which exploits the higher spatial resolution of HMI maps. This algorithm leads to a differently computed R value, whose functionality is tested on a set of cycle 24th solar flares. Furthermore, we introduce a topological parameter based on the automatic recognition of magnetic polarity-inversion lines in identified active regions, and able to evaluate its magnetic topological complexity. We use both a heuristic approach and a supervised machine learning method to validate the effectiveness of these two descriptors to predict the occurrence of X- or M- class flares in a given solar active region during the following 24 hours period. Our feature ranking analysis shows that both parameters play a significant role in prediction performances. Moreover, the analysis demonstrates that the new topological parameter D is the only one, among 173 overall predictors, which is always present for all test subsets and is systematically ranked within the top-ten positions in all tests concerning the computation of the weighs with which each predictor impacts the flare forecasting. **5 September 2017**

A Framework for Designing and Evaluating Solar Flare Forecasting Systems

T. **Cinto** (1 and 2), A. L. S. Gradvohl (1), G. P. Coelho (1), A. E. A. da Silva

Monthly Notices of the Royal Astronomical Society, Volume 495, Issue 3, July **2020**, Pages 3332–3349, https://doi.org/10.1093/mnras/staa1257

https://arxiv.org/pdf/2005.02493.pdf

Disturbances in space weather can negatively affect several fields, including aviation and aerospace, satellites, oil and gas industries, and electrical systems, leading to economic and commercial losses. Solar flares are the most significant events that can affect the Earth's atmosphere, thus leading researchers to drive efforts on their forecasting. The related literature is comprehensive and holds several systems proposed for flare forecasting. However, most techniques are tailor-made and designed for specific purposes, not allowing researchers to customize them in case of changes in data input or in the prediction algorithm. This paper proposes a framework to design, train, and evaluate flare prediction systems which present promising results. Our proposed framework involves model and feature selection, randomized hyper-parameters optimization, data resampling, and evaluation under operational settings. Compared to baseline predictions, our framework generated some proof-of-concept models with positive recalls between 0.70 and 0.75 for forecasting ≥M class flares up to 96 hours ahead while keeping the area under the ROC curve score at high levels.

Solar Flares Forecasting Using Time Series and Extreme Gradient Boosting Ensembles

T. **Cinto** (1 and 2), A. L. S. Gradvohl (1), G. P. Coelho (1), A. E. A. da Silva

2020 *Solar Physics* **volume 295**, Article number: 93

https://arxiv.org/pdf/2004.13299.pdf

https://link.springer.com/content/pdf/10.1007/s11207-020-01661-9.pdf

Space weather events may cause damage to several fields, including aviation, satellites, oil and gas industries, and electrical systems, leading to economic and commercial losses. Solar flares are one of the most significant events, and refer to sudden radiation releases that can affect the Earth's atmosphere within a few hours or minutes. Therefore, it is worth designing high-performance systems for forecasting such events. Although in the literature there are many approaches for flare forecasting, there is still a lack of consensus concerning the techniques used for designing these systems. Seeking to establish some standardization while designing flare predictors, in this study we propose a novel methodology for designing such predictors, further validated with extreme gradient boosting tree classifiers and time series. This methodology relies on the following well-defined machine learning based pipeline: (i) univariate feature selection; (ii) randomized hyper-parameter optimization; (iii) imbalanced data treatment; (iv) adjustment of cut-off point of classifiers; and (v) evaluation under operational settings. To verify our methodology effectiveness, we designed and evaluated three proof-of-concept models for forecasting ≥C class flares up to 72 hours ahead. Compared to baseline models, those models were able to significantly increase their scores of true skill statistics (TSS) under operational forecasting scenarios by 0.37 (predicting flares in the next 24 hours), 0.13 (predicting flares within 24-48 hours), and 0.36 (predicting flares within 48-72 hours). Besides increasing TSS, the methodology also led to significant increases in the area under the ROC curve, corroborating that we improved the positive and negative recalls of classifiers while decreasing the number of false alarms.

Quasi-Periodic Particle Acceleration in a Solar Flare

Brendan P. **Clarke**, Laura A. Hayes, Peter T. Gallagher, Shane A. Maloney, Eoin P. Carley

ApJ **910** 123 **2021**

https://arxiv.org/pdf/2102.04267.pdf

https://iopscience.iop.org/article/10.3847/1538-4357/abe463/pdf

https://doi.org/10.3847/1538-4357/abe463

A common feature of electromagnetic emission from solar flares is the presence of intensity pulsations that vary as a function of time.

Here, we analyse a GOES M3.7 class flare exhibiting pronounced QPPs across a broad band of wavelengths using imaging and time-series analysis. We identify QPPs in the timeseries of X-ray, low frequency radio and EUV wavelengths using wavelet analysis, and localise the region of the flare site from which the QPPs originate via X-ray and EUV imaging. It was found that the pulsations within the 171 Å, 1600 Å, soft X-ray (SXR), and hard X-ray (HXR) light curves yielded similar periods of ∼122 s, ∼131s, ∼123 s, and ∼137 s, respectively, indicating a common progenitor. The low frequency radio emission at 2.5 MHz contained a longer period of ∼231 s. Imaging analysis indicates that the location of the X-ray and EUV pulsations originates from a HXR footpoint linked to a system of nearby open magnetic field lines. Our results suggest that intermittent particle acceleration, likely due to 'bursty' magnetic reconnection, is responsible for the QPPs. The precipitating electrons accelerated towards the chromosphere produce the X-ray and EUV pulsations, while the escaping electrons result in low frequency radio pulses in the form of type III radio bursts. The modulation of the reconnection process, resulting in episodic particle acceleration, explains the presence of these QPPs across the entire spatial range of flaring emission. **2015 Nov 4**

RHESSI Nuggets #411 **2021**

https://sprg.ssl.berkeley.edu/~tohban/wiki/index.php/Flare_Pulsation_and_the_Heliosphere

CESRA #3019 **2021** http://www.astro.gla.ac.uk/users/eduard/cesra/?p=3019

Extreme solar events **Review**

Edward W. **Cliver**, Carolus J. Schrijver, Kazunari Shibata & Ilya G. Usoskin
Living Reviews in Solar Physics volume 19, Article number: 2 (**2022**)
https://arxiv.org/ftp/arxiv/papers/2205/2205.09265.pdf
https://link.springer.com/content/pdf/10.1007/s41116-022-00033-8.pdf

We trace the evolution of research on extreme solar and solar-terrestrial events from the 1859 Carrington event to the rapid development of the last twenty years. Our focus is on the largest observed/inferred/theoretical cases of sunspot groups, flares on the Sun and Sun-like stars, coronal mass ejections, solar proton events, and geomagnetic storms. The reviewed studies are based on modern observations, historical or long-term data including the auroral and cosmogenic radionuclide record, and Kepler observations of Sun-like stars. We compile a table of 100- and 1000-year events based on occurrence frequency distributions for the space weather phenomena listed above. Questions considered include the Sun-like nature of superflare stars and the existence of impactful but unpredictable solar "black swans" and extreme "dragon king" solar phenomena that can involve different physics from that operating in events which are merely large.
774 AD, 17 Sep 1770, 1 September 1859, 4 Feb 1872, 14-15 May 1921, 28 Feb 1942, 5 April 1947, 23 May 1967, 2–11 August 1972 , 29 Apr 1973, 21 Apr 2002, 28 October 2003; 6, 13, 14 Dec 2006, 9 Nov 2011, 28 Oct 2013, 4 Nov 2015
Table 5 Historical fast transit ICME events

On the Size of the Flare Associated with the Solar Proton Event in 774 AD

E. W. **Cliver**1,2, H. Hayakawa3,4,5,6, Jeffrey J. Love7, and D. F. Neidig8,9
2020 ApJ 903 41
https://doi.org/10.3847/1538-4357/abad93

The 774 AD solar proton event (SPE) detected in cosmogenic nuclides had an inferred >1 GV (>430 MeV) fluence estimated to have been ~30–70 times larger than that of the 1956 February 23 ground level event (GLE). The 1956 GLE was itself ~2.5 times larger at >430 MeV than the episode of strong GLE activity from 1989 August–October. We use an inferred soft X-ray (SXR) class of X20 ± 10 for the 1956 February 23 eruptive flare as a bridge to the source flare for the 774 SPE. A correlation of the >200 MeV proton fluences of hard-spectra post-1975 GLEs with the SXR peak fluxes of their associated flares yields an **SXR flare class of X285 ± 140** (bolometric energy of ~(1.9 ± 0.7) × 1033 erg) for the 774 flare. This estimate is within theoretical determinations of the largest flare the Sun could produce based on the largest spot group yet observed. Assuming a single eruptive flare source for the 774 SPE, the above estimate indicates that the Sun can produce a threshold-level 1033 erg superflare. If the 774 event originated in two closely timed, equal-fluence SPEs, the inferred flare size drops to X180 ± 90 (~(1.4 ± 0.5) × 1033 erg). We speculate on favorable solar conditions that can lead to enhanced shock acceleration of high-energy protons in eruptive flares.

ABRUPT CHANGES OF THE PHOTOSPHERIC MAGNETIC FIELD IN ACTIVE REGIONS AND THE IMPULSIVE PHASE OF SOLAR FLARES

E. W. **Cliver**1, G. J. D. Petrie2, and A. G. Ling
2012 ApJ 756 144
http://iopscience.iop.org/0004-637X/756/2/144/pdf/apj_756_2_144.pdf

We compared time profiles of changes of the unsigned photospheric magnetic flux in active regions with those of their associated soft X-ray (SXR) bursts for a sample of 75 ≥ M5 flares well observed by Global Oscillation Network Group longitudinal magnetographs. Sixty-six of these events had stepwise changes in the spatially integrated unsigned flux during the SXR flares. In superposed epoch plots for these 66 events, there is a sharp increase in the unsigned magnetic flux coincident with the onset of the flare impulsive phase while the end of the stepwise change corresponds to the time of peak SXR emission. We substantiated this result with a histogram-based comparison of the timing of flux steps (onset, midpoint of step, and end) for representative points in the flaring regions with their associated SXR event time markers (flare onset, onset of impulsive phase, time of peak logarithmic derivative, maximum). On an individual event basis, the principal part of the stepwise magnetic flux change occurred during the main rise phase of the SXR burst (impulsive phase onset to SXR peak) for ~60% of the 66 cases. We find a close timing agreement between magnetic flux steps and >100 keV emission for the three largest hard X-ray (>100 keV) bursts in our sample. These results identify the abrupt changes in photospheric magnetic fields as an impulsive phase phenomenon and indicate that the coronal magnetic field changes that drive flares are rapidly transmitted to the photosphere.

Solar Gradual Hard X-Ray Bursts and Associated Phenomena

Cliver, E. W.; Dennis, B. R.; Kiplinger, A. L.; Kane, S. R.; Neidig, D. F.; Sheeley, N. R., Jr.; Koomen, M. J.
1986 ApJ...305..920-935
http://articles.adsabs.harvard.edu/full/1986ApJ...305..920C
DOI: 10.1086/164306

White-light coronagraph, H-alpha and radio data are presented as well as hard X-ray data for a sample of 10 gradual hard X-ray bursts (GHBs) in an attempt to better understand the nature of these events. It is found that: (1) the hard X-

ray photon energy spectrum began to harden near the onset of the GHBs and continued in this fashion during the decay phase; (2) a coronal mass ejection (CME) occurred in association with at least nine of the GHBs; (3) the GHBs occurred in the late phase of major flares; (4) the centimeter wavelength bursts associated with the GHBs had relatively low frequency spectral maxima, and in relation to the observed hard X-ray emission, they were microwave-rich; (5) the associated decimetric bursts showed significant intensity variations on time scales ranging from 0.1 to approximately greater than 1 minute; and (6) the GHBs were most strongly associated with type IV events. It is concluded that the acceleration and trapping of radiating electrons occurs in the postflare loop systems following CMEs. **6 Apr 1980, 1 May 1980, 24 Apr 1981, 26 Apr 1981, 13 May 1981, 14 Nov 1981, 7 Mar 1982, 6 Jun 1982, 10 Jun 1982, 17 Dec 1982**
Table

Interplay of Boltzmann equation and continuity equation for accelerated electrons in solar flares

Anna **Codispoti** and Nicola Pinamonti
SIAM/ASA Journal on Uncertainty Quantification, **2015**
http://arxiv.org/pdf/1502.04534v1.pdf
During solar flares a large amount of electrons are accelerated within the plasma present in the solar atmosphere. Accurate measurements of the motion of these electrons start becoming available from the analysis of hard X-ray imaging-spectroscopy observations. In this paper, we discuss the linearized perturbations of the Boltzmann kinetic equation describing an ensemble of electrons accelerated by the energy release occurring during solar flares. Either in the limit of high energy or at vanishing background temperature such an equation reduces to a continuity equation equipped with an extra force of stochastic nature. This stochastic force is actually described by the well known energy loss rate due to Coulomb collision with ambient particles, but, in order to match the collision kernel in the linearized Boltzmann equation it needs to be treated in a very specific manner. In the second part of the paper the derived continuity equation is solved with some hyperbolic techniques, and the obtained solution is written in a form suitable to be compared with data gathered by hard X-ray imaging-spectroscopy telescopes. Finally, a first validation of the model with NASA Reuven Ramaty High Energy Solar Spectroscopic Imager spectrometer measurements is provided.

RETURN CURRENTS AND ENERGY TRANSPORT IN THE SOLAR FLARING ATMOSPHERE

Anna **Codispoti**1, Gabriele Torre1,2, Michele Piana1,2, and Nicola Pinamonti
2013 ApJ 773 121
According to the standard Ohmic perspective, the injection of accelerated electrons into the flaring region violates local charge equilibrium and therefore, in response, return currents are driven by an electric field to equilibrate such charge violation. In this framework, the energy loss rate associated with these local currents has an Ohmic nature and significantly shortens the accelerated electron path. In the present paper, we adopt a different viewpoint and, specifically, we study the impact of the background drift velocity on the energy loss rate of accelerated electrons in solar flares. We first utilize the Rutherford cross-section to derive the formula of the energy loss rate when the collisional target has a finite temperature and the background instantaneously and coherently moves up to equilibrate the electron injection. We then use the continuity equation for electrons and imaging spectroscopy data provided by RHESSI to validate this model. We show that this new formula for the energy loss rate provides a better fit of the experimental data with respect to the model based on the effects of standard Ohmic return currents.

RADIATIVE LOSSES OF SOLAR CORONAL PLASMAS

J. **Colgan**, J. Abdallah, Jr., M. E. Sherrill, and M. Foster, C. J. Fontes, and U. Feldman
Astrophysical Journal, 689:585-592, 2008
A comprehensive set of calculations of the radiative losses of solar coronal plasmas is presented. The Los Alamos suite of atomic structure and collision codes is used to generate collisional data for 15 coronal elements. These data are used in the Los Alamos plasma kinetics code ATOMIC to compute the radiative power loss as a function of electron temperature. We investigate the sensitivity of the loss curves to the quality of the atomic data and changes in the coronal elemental abundances, and we compare our results with previous work.

Solar flares in the Solar Orbiter Era: Short exposure EUI/FSI observations of STIX flares

Hannah **Collier**, Laura A. Hayes, Stefan Purkhart, Säm Krucker, Daniel F. Ryan, Vanessa Polito, Astrid M. Veronig, Louise K. Harra, David Berghmans, Emil Kraaikamp, Marie Dominique, Laurent R. Dolla, Cis Verbeeck
A&A 692, A176 **2024**
https://arxiv.org/pdf/2411.09319
https://www.aanda.org/articles/aa/pdf/2024/12/aa51838-24.pdf

Aims: This paper aims to demonstrate the importance of short-exposure extreme ultraviolet (EUV) observations of solar flares in the study of particle acceleration, heating and energy partition in flares. This work highlights the observations now available from the Extreme Ultraviolet Imager (EUI) instrument suite onboard Solar Orbiter while operating in short exposure mode.
Methods: A selection of noteworthy flares observed simultaneously by the Spectrometer Telescope for Imaging X-rays (STIX) and the Full Sun Imager of EUI (EUI/FSI) are detailed. New insights are highlighted and potential avenues of investigation are demonstrated, including forward modelling the atmospheric response to a non-thermal beam of electrons using the RADYN 1D hydrodynamic code, in order to compare the predicted and observed EUV emission.
Results: The examples given in this work demonstrate that short exposure EUI/FSI observations are providing important diagnostics during flares. A dataset of more than 9000 flares observed by STIX (from November 2022 until December 2023) with at least one short exposure EUI/FSI 174 Å image is currently available. The observations reveal that the brightest parts of short-exposure observations consist of substructure in flaring ribbons which spatially overlap with the hard X-ray emission observed by STIX in the majority of cases. We show that these observations provide an opportunity to further constrain the electron energy flux required for flare modelling, among other potential applications**. 2022-11-13, 2023-04-22, 2023-07-16,**

Localising pulsations in the hard X-ray and microwave emission of an X-class flare

Hannah **Collier**, Laura A. Hayes, Sijie Yu, Andrea F. Battaglia, William Ashfield, Vanessa Polito, Louise K. Harra, Säm Krucker
A&A 684, A215 **2024**
https://arxiv.org/pdf/2402.10546.pdf
https://www.aanda.org/articles/aa/pdf/2024/04/aa48652-23.pdf
Aims: This work aims to identify the mechanism driving pulsations in hard X-ray (HXR) and microwave emission during solar flares. Here, by using combined HXR and microwave observations from Solar Orbiter/STIX and EOVSA we investigate an X1.3 GOES class flare, **2022-03-30**T17:21:00, which displays pulsations on timescales evolving from ~ 7 s in the impulsive phase to ~ 35 s later in the flare.
Methods: The temporal, spatial and spectral evolution of the HXR and microwave pulsations during the impulsive phase of the flare are analysed. Images are reconstructed for individual peaks in the impulsive phase and spectral fitting is performed at high cadence throughout the first phase of pulsations.
Results: Imaging analysis demonstrates that the HXR and microwave emission originates from multiple sites along the flare ribbons. The brightest sources and the location of the emission changes in time. Through HXR spectral analysis, the electron spectral index is found to be anti-correlated with the HXR flux showing a "soft-hard-soft" spectral index evolution for each pulsation. The timing of the associated filament eruption coincides with the early impulsive phase.
Conclusions: Our results indicate that periodic acceleration and/or injection of electrons from multiple sites along the flare arcade is responsible for the pulsations observed in HXR and microwave. The evolution of pulsation timescales is likely a result of changes in the 3D magnetic field configuration in time related to the associated filament eruption.
SO Nugget #28 May **2024** https://www.cosmos.esa.int/web/solar-orbiter/-/science-nugget-hard-x-ray-and-microwave-pulsations-a-signature-of-the-flare-energy-release-process

Characterising fast-time variations in the hard X-ray time profiles of solar flares using Solar Orbiter's STIX

Hannah **Collier**, Laura A. Hayes, Andrea F. Battaglia, Louise K. Harra, Säm Krucker
A&A 671, A79 **2023**
https://arxiv.org/pdf/2301.08040.pdf
https://www.aanda.org/articles/aa/pdf/2023/03/aa45293-22.pdf
Aims: The aim of this work is to develop a method to systematically detect and characterise fast-time variations ($\gtrsim$1s) in the non-thermal hard X-ray (HXR) time profiles of solar flares using high-resolution data from Solar Orbiter's Spectrometer/Telescope for Imaging X-rays (STIX).
Methods: The HXR time profiles were smoothed using Gaussian Process (GP) regression. The time profiles were then fitted with a linear combination of Gaussians to decompose the time profile. From the Gaussian decomposition, key characteristics such as the periodicity, full width at half maximum (FWHM), time evolution, and amplitude can be derived.
Results: We present the outcome of applying this method to four M and X GOES-class flares from the first year of Solar Orbiter science operations. The HXR time profiles of these flares were decomposed into individual Gaussians and their periods were derived. The quality of fit is quantified by the standard deviation of the residuals (difference between observed and fitted curve, normalised by the error on the observed data), for which we obtain $\leq$1.8 for all flares presented. In this work, the first detection of fast-time variations with Solar Orbiter's STIX instrument has been made on timescales across the range of 4-128s.
Conclusions: A new method for identifying and characterising fast-time variations in the non-thermal HXR profiles of solar flares has been developed, in which the time profiles are fit with a linear combination of Gaussian bursts. The

opportunity to study time variations in flares has greatly improved with the new observations from STIX on Solar Orbiter. **2021-09-23, 2021-10-09, 2022-03-30, 2022-05-04**
RHESSI #443 **2023** https://sprg.ssl.berkeley.edu/~tohban/wiki/index.php/Hard_X-ray_Pulsations_via_Gaussian_Decomposition

Plasmoid Instability in Forming Current Sheets

L. **Comisso**1,2, M. Lingam3,4, Y.-M. Huang1,2, and A. Bhattacharjee1
2017 ApJ 850 142
The plasmoid instability has revolutionized our understanding of magnetic reconnection in astrophysical environments. By preventing the formation of highly elongated reconnection layers, it is crucial in enabling the rapid energy conversion rates that are characteristic of many astrophysical phenomena. Most previous studies have focused on Sweet–Parker current sheets, which are unattainable in typical astrophysical systems. Here we derive a general set of scaling laws for the plasmoid instability in resistive and visco-resistive current sheets that evolve over time. Our method relies on a principle of least time that enables us to determine the properties of the reconnecting current sheet (aspect ratio and elapsed time) and the plasmoid instability (growth rate, wavenumber, inner layer width) at the end of the linear phase. After this phase the reconnecting current sheet is disrupted and fast reconnection can occur. The scaling laws of the plasmoid instability are notsimple power laws, and they depend on the Lundquist number (S), the magnetic Prandtl number (Pm), the noise of the system (ψ_0), the characteristic rate of current sheet evolution ($1/\tau$), and the thinning process. We also demonstrate that previous scalings are inapplicable to the vast majority of astrophysical systems. We explore the implications of the new scaling relations in astrophysical systems such as the solar corona and the interstellar medium. In both of these systems, we show that our scaling laws yield values for the growth rate, wavenumber, and aspect ratio that are much smaller than the Sweet–Parker–based scalings.

Study of transverse oscillations in coronal loops excited by flares and eruptions

Sandra M. **Conde** C, Rekha Jain, Vera Jatenco-Pereira
ApJ **2022**
https://arxiv.org/pdf/2205.12063.pdf
We present measurements of periodicity for transverse loop oscillations during the periods of activity of two remote and separated (both temporally and spatially) flares. The oscillations are observed in the same location more than 100 Mm away from the visible footpoints of the loops. Evidence for several possible excitation sources is presented. After close examination, we find that the eruptions during the flaring activities play an important role in triggering the oscillations. We investigate periodicities using time-distance, Fast Fourier Transform, and Wavelet techniques. Despite different excitation sources in the vicinity of the loops and the changing nature of amplitudes, the periodicity of multiple oscillations is found to be 4 - 6 minutes. **27-28 Jan 2014**

Excitation Sources of Oscillations in Solar Coronal Loops: A Multi-wavelength Analysis

Sandra M. **Conde** C.1,2, Rekha Jain3, and Vera Jatenco-Pereira1
2020 ApJL 890 L21
https://doi.org/10.3847/2041-8213/ab7348
An investigation into the excitation sources of oscillations detected in a coronal loop structure is carried out using the images obtained with Interface Region Imaging Spectrometer (IRIS) and the Atmospheric Imaging Assembly (AIA) instrument on board the Solar Dynamics Observatory (SDO). A loop structure in the active region AR 11967 on **2014 January 28**, oscillating in the vicinity of a strong eruption and an M3.6 class flare site, is clearly noticeable in SDO/AIA 171 Å images. We study in detail, the oscillations with detected periods between 4 and 13 minutes and their connection in IRIS SJI 1330 Å and SDO/AIA 1700 Å images; both of these wavelengths sample the lower parts of the solar atmosphere. The simultaneous presence of many oscillations in the region of interest in all three wavelength passbands suggest that these oscillations were excited in the lower-chromosphere–photosphere plasma connected to the loop structure and then propagated at higher heights. We further investigate the Doppler velocity measurements from the spectrograph snapshots in IRIS C ii 1336 Å, Si iv 1403 Å and Mg ii k 2796 Å. These show signatures of upflows in the vicinity of the loop structure's endpoints estimated from 171 Å images. We suggest that some of the oscillations observed in AIA 171 Å have been triggered by plasma ejections and perturbations seen in the lower layers of the solar atmosphere. Based on the estimated phase speeds, the oscillations are likely to be slow magnetoacoustic in nature.

QUANTIFYING THE EVOLVING MAGNETIC STRUCTURE OF ACTIVE REGIONS

Paul A. **Conlon**1, R.T. James McAteer1,2, Peter T. Gallagher1, and Linda Fennell1
Astrophysical Journal, 722:577–585, **2010**
The topical and controversial issue of parameterizing the magnetic structure of solar active regions has vital implications in the understanding of how these structures form, evolve, produce solar flares, and decay. This interdisciplinary and ill-constrained problem of quantifying complexity is addressed by using a two-dimensional wavelet transform modulus maxima (WTMM) method to study the multifractal properties of active region photospheric magnetic fields.TheWTMMmethod provides an adaptive space-scale partition of a fractal distribution,

from which one can extract the multifractal spectra. The use of a novel segmentation procedure allows us to remove the quiet Sun component and reliably study the evolution of active region multifractal parameters. It is shown that prior to the onset of solar flares, the magnetic field undergoes restructuring as Dirac-like features (with a H¨older exponent, $h = -1$) coalesce to form step functions (where $h = 0$). The resulting configuration has a higher concentration of gradients along neutral line features. We propose that when sufficient flux is present in an active region for a period of time, it must be structured with a fractal dimension greater than 1.2, and a H¨older exponent greater than -0.7, in order to produce M- and X-class flares. This result has immediate applications in the study of the underlying physics of active region evolution and space weather forecasting.

RHESSI and TRACE observations of an M2.5 flare: a direct application of the *Kopp and Pneuman model:*

L. **Contarino**, P. Romano and F. Zuccarello
A&A 458 (2006) 297-300 (File)
an M2.5 flare that occurred in NOAA 9901 on 16 April 2002
The event shows a simple morphology in which the EUV and X-ray sources change from an *X* to a *Y* configuration; the formation of a thin, filamentary structure, compatible with what is expected from the collapse of an *X*-point in a current sheet

Detecting non-thermal emission in a solar microflare using nested sampling

Kristopher **Cooper**, Iain G. Hannah, Lindsay Glesener, Brian W. Grefenstette
MNRAS **2024**
https://arxiv.org/pdf/2402.05426.pdf
Microflares are energetically smaller versions of solar flares, demonstrating the same processes of plasma heating and particle acceleration. However, it remains unclear down to what energy scales this impulsive energy release continues, which has implications for how the solar atmosphere is heated. The heating and particle acceleration in microflares can be studied through their X-ray emission, finding predominantly thermal emission at lower energies; however, at higher energies it can be difficult to distinguish whether the emission is due to hotter plasma and/or accelerated elections. We present the first application of nested sampling to solar flare X-ray spectra, an approach which provides a quantitative degree of confidence for one model over another. We analyse NuSTAR X-ray observations of a small active region microflare (A0.02 GOES/XRS class equivalent) that occurred on **2021 November 17**, with a new Python package for spectral fitting, sunkit-spex, to compute the parameter posterior distributions and the evidence of different models representing the higher energy emission as due to thermal or non-thermal sources. Calculating the Bayes factor, we show there is significantly stronger evidence for the higher energy microflare emission to be produced by non-thermal emission from flare accelerated electrons than by an additional hot thermal source. Qualitative confirmation of this non-thermal source is provided by the lack of hotter (10 MK) emission in SDO/AIA's EUV data. The nested sampling approach used in this paper has provided clear support for non-thermal emission at the level of 3x1024 erg s−1 in this tiny microflare.

NuSTAR Observation of a Minuscule Microflare in a Solar Active Region

Kristopher **Cooper**1, Iain G. Hannah1, Brian W. Grefenstette2, Lindsay Glesener3, Säm Krucker4,5, Hugh S. Hudson1,5, Stephen M. White6, and David M. Smith7
2020 ApJL 893 L40
https://doi.org/10.3847/2041-8213/ab873e
https://arxiv.org/pdf/2004.11176.pdf
We present X-ray imaging spectroscopy of one of the weakest active region (AR) microflares ever studied. The microflare occurred at ~11:04 UT on **2018 September 9** and we studied it using the Nuclear Spectroscopic Telescope ARray (NuSTAR) and the Solar Dynamic Observatory's Atmospheric Imaging Assembly (SDO/AIA). The microflare is observed clearly in 2.5–7 keV with NuSTAR and in Fe xviii emission derived from the hotter component of the 94 Å SDO/AIA channel. We estimate the event to be three orders of magnitude lower than a GOES A class microflare with an energy of 1.1 × 1026 erg. It reaches temperatures of 6.7 MK with an emission measure of 8.0 × 1043 cm−3. Non-thermal emission is not detected but we instead determine upper limits to such emission. We present the lowest thermal energy estimate for an AR microflare in literature, which is at the lower limits of what is still considered an X-ray microflare.

COOL-PLASMA JETS THAT ESCAPE INTO THE OUTER CORONA

Gianni **Corti**,1 Giannina Poletto,1 Steve T. Suess,2 Ronald L. Moore,2 and Alphonse C. Sterling2
The Astrophysical Journal, 659:1702Y1712, **2007**
http://adsabs.harvard.edu/abs/2007ApJ...659.1702C

Numerical simulation of dark lanes in post–flare supra–arcade

Costa, Andrea, Elaskar, Sergio, Fern?ndez, Carlos, Mart?nez, Guadalupe
E-print, Oct **2009**

We integrate the MHD ideal equations to simulate dark void sunwardly moving structures in post–flare supra–arcades. We study the onset and evolution of the internal plasma instability to compare with observations and to gain insight into physical processes and characteristic parameters of these phenomena. The numerical approach uses a finite-volume Harten-Yee TVD scheme to integrate the 1D1 2 MHD equations specially designed to capture supersonic flow discontinuities. The integration is performed in both directions, the sunward radial one and the transverse to the magnetic field. For the first time, we numerically reproduce observational dark voids described in Verwichte et al. (2005). We show that the dark tracks are plasma vacuums generated by the bouncing and interfering of shocks and expansion waves, upstream an initial slow magnetoacoustic shock produced by a localized deposition of energy modeled with a pressure perturbation. The same pressure perturbation produces a transverse to the field or perpendicular magnetic shock giving rise to nonlinear waves that compose the kink–like plasma void structures, with the same functional sunward decreasing phase speed and constancy with height of the period, as those determined by the observations.

Coronal energy release by MHD avalanches
II. EUV line emission from a multi-threaded coronal loop

G. **Cozzo**, J. Reid, P. Pagano, F. Reale, P. Testa, A. W. Hood, C. Argiroffi, A. Petralia, E. Alaimo, F. D'Anca, L. Sciortino, M. Todaro, U. Lo Cicero, M. Barbera, B. De Pontieu, J. Martinez-Sykora
A&A **2024**
https://arxiv.org/pdf/2406.11701

MHD kink instability can trigger the fragmentation of a twisted magnetic flux tube into small-scale current sheets that dissipate as aperiodic impulsive heating events. This instability propagates as an avalanche to nearby flux tubes and leads to a nanoflare storm. Our previous work was devoted to related 3D MHD numerical modeling with a stratified and realistic atmosphere. This work addresses predictions for the EUV imaging spectroscopy of such structure and evolution of a loop, with an average temperature of 2.5 MK in the solar corona. We set a particular focus on the forthcoming MUSE mission. From the output of the numerical simulations, we synthesized the intensities, Doppler shifts, and non-thermal line broadening in 3 EUV spectral lines in the MUSE passbands: Fe IX 171A, Fe XV 284 A, and Fe XIX 108 A, at 1 MK, 2 MK, and 10 MK, respectively, according to the MUSE expected pixel size, temporal resolution, and temperature response functions. We provide maps showing different view angles and realistic spectra. Finally, we discuss the relevant evolutionary processes from the perspective of possible observations. We find that the MUSE observations might be able to detect the fine structure determined by tube fragmentation. In particular, the Fe IX line is mostly emitted at the loop footpoints, where we track the motions that drive the magnetic stressing and detect the upward motion of evaporating plasma from the chromosphere. In Fe XV, we see the bulk of the loop with increasing intensity. The Fe XIX line is very faint within the chosen simulation parameters; thus, any transient brightening around the loop apex may possibly be emphasized by the folding of sheet-like structure. In conclusion, we show that coronal loop observations with MUSE can pinpoint some crucial features of MHD-modeled ignition processes, such as the related dynamics, helping to identify the heating processes.

Coronal energy release by MHD avalanches
Effects on a structured, active region, multi-threaded coronal loop

G. **Cozzo**1, J. Reid2, P. Pagano1,3, F. Reale1,3 and A. W. Hood2
A&A 678, A40 (**2023**)
https://www.aanda.org/articles/aa/pdf/2023/10/aa46689-23.pdf

Context. A possible key element for large-scale energy release in the solar corona is a magnetohydrodynamic (MHD) kink instability in a single twisted magnetic flux tube. An initial helical current sheet progressively fragments in a turbulent way into smaller-scale sheets. Dissipation of these sheets is similar to a nanoflare storm. Since the loop expands in the radial direction during the relaxation process, an unstable loop can disrupt nearby stable loops and trigger an MHD avalanche.

Aims. Exploratory investigations have been conducted in previous works with relatively simplified loop configurations. In this work, we address a more realistic environment that comprehensively accounts for most of the physical effects involved in a stratified atmosphere typical of an active region. The questions we investigate are whether the avalanche process will be triggered, with what timescales, and how will it develop as compared with the original, simpler approach.

Methods. We used three-dimensional MHD simulations to describe the interaction of magnetic flux tubes, which have a stratified atmosphere with chromospheric layers, a thin transition region to the corona, and a related transition from high-β to dlow-β regions. The model also includes the effects of thermal conduction and of optically thin radiation.

Results. Our simulations address the case where one flux tube amongst a few is twisted at the footpoints faster than its neighbours. We show that this flux tube becomes kink unstable first in conditions in agreement with those predicted by analytical models. It then rapidly affects nearby stable tubes, instigating significant magnetic reconnection and dissipation of energy as heat. In turn, the heating brings about chromospheric evaporation as the temperature rises up to about 107 K, close to microflare observations.
Conclusions. This work confirms, in more realistic conditions, that avalanches are a viable mechanism for the storing and release of magnetic energy in plasma confined in closed coronal loops as a result of photospheric motions.

Current Singularities at Quasi-separatrix Layers and Three-dimensional Magnetic Nulls

I. J. D. **Craig** and Frederic Effenberger
2014 ApJ 795 129.
http://arxiv.org/pdf/1410.6545v1.pdf
The open problem of how singular current structures form in line-tied, three-dimensional magnetic fields is addressed. A Lagrangian magneto-frictional relaxation method is employed to model the field evolution toward the final near-singular state. Our starting point is an exact force-free solution of the governing magnetohydrodynamic equations that is sufficiently general to allow for topological features like magnetic nulls to be inside or outside the computational domain, depending on a simple set of parameters. Quasi-separatrix layers (QSLs) are present in these structures and, together with the magnetic nulls, they significantly influence the accumulation of current. It is shown that perturbations affecting the lateral boundaries of the configuration lead not only to collapse around the magnetic null but also to significant QSL currents. Our results show that once a magnetic null is present, the developing currents are always attracted to that specific location and show a much stronger scaling with resolution than the currents that form along the QSL. In particular, the null-point scalings can be consistent with models of "fast" reconnection. The QSL currents also appear to be unbounded but give rise to weaker singularities, independent of the perturbation amplitude.

Magnetic evolution of superactive regions: Complexity and potentially unstable magnetic discontinuities

S. **Criscuoli**1, P. Romano2, F. Giorgi1, and F. Zuccarello3
A&A 506, 1429-1436 (**2009**)
Context. It is widely accepted that solar flares are manifestations of magnetic reconnection events taking place in the solar atmosphere. Several aspects of these events remain unclear, although many efforts have been devoted to the investigation of magnetic field configurations at flare occurrence sites.
Aims. In this work, we have studied the temporal evolution of some properties of a sample of superactive regions with the aim to single out the most significant for flare activity forecasting.
Methods. We have investigated properties of 14 superactive regions, observed between January 1st 2000 and December 31st 2006 with MDI/SOHO instrument and characterized by a particularly intense flare activity during their passage on the solar disk. We have analyzed the temporal evolution of fractal and multifractal properties of photospheric magnetic fields, namely the generalized fractal dimension and the contribution and dimensional diversities, which describe geometrical properties of the magnetic field, as well as the potential unstable volumes of magnetic discontinuities above the studied ARs, which may provide information about the magnetic field configuration in upper layers of the atmosphere. Correlations of these quantities with the flare index, which provides information about the flare activity of a region, have also been estimated.
Results. We found that in 50% of our sample the generalized fractal dimension is correlated with the flare index computed over windows of 50 h, while the contribution diversity and the dimensional diversity are anticorrelated with the same index. A clear increase of the potential unstable volume of magnetic discontinuities in the corona is observed before the phases characterized by more frequent and intense flares. We also found that the free energy distribution functions of unstable volumes of the analyzed superactive regions can be fitted with straight lines whose slope is larger than the values found in previous works for less active magnetic regions.
Conclusions. The generalized fractal dimension and the potential unstable volume of magnetic discontinuities are the most suitable for statistical investigations of relations with flare activity over longer (50 h) and shorter (few hours) time intervals, respectively.

The Scaling of Vortical Electron Acceleration in Thin-current Magnetic Reconnection and Its Implications in Solar Flares

C. **Crawford**1,2, H. Che1,2, and A. O. Benz3,4
2024 ApJ 961 25
https://iopscience.iop.org/article/10.3847/1538-4357/ad09e6/pdf
To investigate how magnetic reconnection (MR) accelerates electrons to a power-law energy spectrum in solar flares, we explore the scaling of a kinetic model proposed by Che & Zank (CZ) and compare it to observations. Focusing on thin current sheet MR particle-in-cell (PIC) simulations, we analyze the impact of domain size on the evolution of the electron Kelvin–Helmholtz instability (EKHI). We find that the duration of the growth stage of the EKHI

(��~Ω�−1) is short and remains nearly unchanged because the electron gyrofrequency Ωe is independent of domain size. The quasi-steady stage of the EKHI (tMR) dominates the electron acceleration process and scales linearly with the size of the simulations as L/vA0, where vA0 is the Alfvén speed. We use the analytical results obtained by CZ to calculate the continuous temporal evolution of the electron energy spectra from PIC simulations and linearly scale them to solar flare observational scales. For the first time, an electron acceleration model predicts the sharp two-stage transition observed in typical soft–hard–harder electron energy spectra, implying that the electron acceleration model must be efficient with an acceleration timescale that is a small fraction of the duration of solar flares. Our results suggest that we can use PIC MR simulations to investigate the observational electron energy spectral evolution of solar flares if the ratio tMR/tG is sufficiently small, i.e., ≲10%.

Validation of the NOAA Space Weather Prediction Center's solar flare forecasting look-up table and forecaster-issued probabilities

Crown, Misty D.

Space Weather, VOL. 10, S06006, 4 PP., **2012**

This paper provides an assessment of the operational solar flare look-up table currently in use at the National Oceanic and Atmospheric Administration (NOAA) Space Weather Prediction Center (SWPC) during solar cycle 23 (May 1996 – December 2008). To assess the value of human interaction, a validation of subjective flare probability forecasts was conducted and compared to the results obtained from the climatological look-up table used at SWPC. Probabilistic flare forecasts are evaluated using the Brier Skill Score, then discretized and entered into contingency tables from which a variety of verification measures are calculated. The ultimate goal of this report is to provide an operational baseline, whereby the scores and statistics from this paper can be used as the basis for future evaluation of models presented to the operational community.

Oscillations in the Flaring Active Region NOAA 11272

S. M. Conde **Cuellar**, J. E. R. Costa, C. E. Cedeño Montaña

Solar Phys. Volume 291, Issue 11, pp 3289–3302 **2016**

https://arxiv.org/pdf/1611.08707v1.pdf

We studied waves seen during the class C1.9 flare that occurred in Active Region NOAA 11272 on SOL**2011-08-17**. We found standing waves with periods in the 9- and 19-minute band in six extreme ultraviolet (EUV) wavelengths of the SDO/AIA instrument. We succeeded in identifying the magnetic arc where the flare started and two neighbour loops that were disturbed in sequence. The analysed standing waves spatially coincide with these observed EUV loops. To study the wave characteristics along the loops, we extrapolated field lines from the line-of-sight magnetograms using the force-free approximation in the linear regime. We used atmosphere models to determine the mass density and temperature at each height of the loop. Then, we calculated the sound and Alfvén speeds using densities \(10^{8} \lesssim n_{i} \lesssim 10^{17}\mbox{ cm}^{-3}\) and temperatures \(10^{3} \lesssim T \lesssim 10^{7}~\mbox{K}\). The brightness asymmetry in the observed standing waves resembles the Alfvén speed distribution along the loops, but the atmospheric model we used needs higher densities to explain the observed periods.

Flare parameters inferred from a 3D loop model data base

Valente A **Cuambe** J E R Costa P J A Simões

Monthly Notices of the Royal Astronomical Society, Volume 477, Issue 2, 21 June **2018**, Pages 1508–1519

https://sci-hub.tw/10.1093/mnras/sty867

We developed a data base of pre-calculated flare images and spectra exploring a set of parameters which describe the physical characteristics of coronal loops and accelerated electron distribution. Due to the large number of parameters involved in describing the geometry and the flaring atmosphere in the model used, we built a large data base of models (∼250 000) to facilitate the flare analysis. The geometry and characteristics of non-thermal electrons are defined on a discrete grid with spatial resolution greater than 4 arcsec. The data base was constructed based on general properties of known solar flares and convolved with instrumental resolution to replicate the observations from the Nobeyama radio polarimeter spectra and Nobeyama radioheliograph (NoRH) brightness maps. Observed spectra and brightness distribution maps are easily compared with the modelled spectra and images in the data base, indicating a possible range of solutions. The parameter search efficiency in this finite data base is discussed. 8 out of 10 parameters analysed for 1000 simulated flare searches were recovered with a relative error of less than 20 per cent on average. In addition, from the analysis of the observed correlation between NoRH flare sizes and intensities at 17 GHz, some statistical properties were derived. From these statistics, the energy spectral index was found to be δ ∼ 3, with non-thermal electron densities showing a peak distribution ≲107 cm−3, and Bphotosphere ≳ 2000 G. Some bias for larger loops with heights as great as ∼2.6 × 109 cm, and looptop events were noted. An excellent match of the spectrum and the brightness distribution at 17 and 34 GHz of the **2002 May 31** flare is presented as well.

Statistical Study of Magnetic Topology for Eruptive and Confined Solar Flares

Yanmei **Cui**, Haimin Wang, Yan Xu, Siqing Liu

JGR **Volume123, Issue3** March **2018** Pages 1704-1714

http://sci-hub.tw/http://onlinelibrary.wiley.com/doi/10.1002/2017JA024710/abstract;jsessionid=1B28DD312655626B6C73EE27929AA447.f03t01

Large flares and halo CMEs can often cause strong space environment disturbances and sequently a series of space environment effects. The X-class flares associated with halo CMEs are particular prone to these effects. In this paper, 58 X-class flares were collected and studied with the source locations in 30 degrees from the disk center, which were observed from 1996 to 2015. Among these events, *48 flares were associated with CMEs and defined as "eruptive"* events. The other *10 flares without CMEs were defined as "confined" flares.* By comparing the properties of flares and associated magnetic fields for the two sets of samples, we found: (1) Magnetic free energy and overlying transverse fields play important roles in producing solar eruptions. Eruptive flares with high-speed CMEs tend to occur in active regions with more free energy and larger decay index. (2) CME speeds are affected by magnetic free energy, which are described by parameters of the unsigned magnetic flux, the area of polarity inversion region, and the strength of transverse fields in the low altitude. These parameters have moderate positive correlations with CME speeds.
Table 1: Selected X-Class Flares and the associated CMEs from 1996 to 2015

Explosive Events: Swirling Transition Region Jets

W. **Curdt**, H. Tian, S. Kamio

Solar Physics, October **2012**, Volume 280, Issue 2, pp 417-424

In this paper, we extend our earlier work to provide additional evidence for an alternative scenario to explain the nature of events called 'explosive events'. The bidirected, fast Doppler motion of explosive events observed spectroscopically in the transition region emission is classically interpreted as a pair of bidirectional jets moving upward and downward from a reconnection site. We discuss the problems of this model. In our previous work, we focused basically on the discrepancy of fast Doppler motion without detectable motion in the image plane. We now suggest an alternative scenario for the explosive events, based on our observations of spectral line tilts and bifurcated structure in some events. Both features are indicative of rotational motion in narrow structures. We explain the bifurcation as the result of rotation of hollow cylindrical structures and demonstrate that this kind of sheath model can also be applied to explain the nature of the puzzling 'explosive events'. We find that the spectral tilt, the lack of apparent motion, the bifurcation, and a rapidly growing number of direct observations support an alternative scenario of linear, spicular-sized jets with a strong spinning motion.

Confirming geomagnetic Sfe by means of a solar flare detector based on GNSS

Juan José **Curto**1*, José Miguel Juan2 and Cristhian Camilo Timoté2

J. Space Weather Space Clim. **2019**, 9, A42

https://www.swsc-journal.org/articles/swsc/pdf/2019/01/swsc190038.pdf

Solar Flares (SF) refer to sudden increases of electromagnetic radiation from the Sun lasting from minutes to hours. Irradiance in the Extremely Ultra-Violet (EUV) or X band is enhanced and it can produce a sudden over-ionization in the ionosphere, which can be tracked by several techniques. On the one hand, this over-ionization increases the ionospheric delays of GNSS signals in such a way as can be monitored using measurements collected by dual-frequency GNSS receivers. On the other hand, this over-ionization of the ionosphere is the origin of electrical currents which, in turn, induce magnetic fields which can be monitored with ground magnetometers. In this work we propose the use of a GNSS Solar Flare Monitor (GNSS-SF) for its utility to confirm the presence of ionospheric ionization which is able to produce Solar Flare Effects (Sfe) in geomagnetism. A period of 11 years (2008–2018) has been analyzed and contingency tables are shown. Although most of the GNSS-SF detections coincide with SF and most of the Sfe have a detected origin in the ionosphere, there are some paradoxes: sometimes small flares produce disturbances which are clearly detected by both methods while other disturbances, originated by powerful flares, go by virtually unnoticed. We analyzed some of these cases and proposed some explanations. We found that suddenness in the variation is a key factor for detection. Threshold values of the velocity of change to remove the background noise and the use of the acceleration of change instead of the velocity of change as the key performance detector are other topics we deal with in this paper. We conclude that the GNSS-SF detector could provide warnings of ionization disturbances from SF covering the time when the Sfe detectors are "blind", and can help to confirm Sfe events when Sfe detectors are not able to give a categorical answer.

Comments: https://www.swsc-journal.org/articles/swsc/pdf/2020/01/swsc190087.pdf
https://www.swsc-journal.org/articles/swsc/pdf/2020/01/swsc200005.pdf

SFE: waiting for the big one

Juan José **Curto***, Josep Castell and Ferran Del Moral

J. Space Weather Space Clim., 6, A23 (**2016**)
http://www.swsc-journal.org/articles/swsc/pdf/2016/01/swsc150071.pdf
Accurate measurements of the radiation delivered during the two largest solar flares ever observed are unavailable. In the case of the Carrington event (1858) the X-ray and UV radiation was not recorded, while in the case of the big flare which happened after the storm of **29–31 October 2003** we will call from now on as Halloween event (2003) the radiation saturated the X-ray radiometer. Despite many studies, a consensus regarding the real values of these events at the moment of maximum radiation has never been reached.
In this paper, we used an alternative approach to try and determine these values. We estimated the values from the perturbations they produced in the Earth's magnetism – these are known as **Solar Flare Effects (Sfe)**. Firstly, we established an empirical relationship between the variation in the radiation (cause) and its effect on the magnetism (consequence). Then, using the inverse function, we estimated the energy flux of both events. We found that both flares can actually be classified as being larger than X45.
Finally, we also calculated the return period for a Carrington-like flare. Assuming that this event had an intensity of about X45 – according to our calculations – we estimated the return period to be 90 ± 60 years.

Data-driven radiative hydrodynamic modeling of SOL2014-03-29

Fatima Rubio **da Costa**
RHESSI Science Nugget No. 274, May **2016**
http://sprg.ssl.berkeley.edu/~tohban/wiki/index.php/Data-driven_radiative_hydrodynamic_modeling_of_SOL2014-03-29

Data-driven Radiative Hydrodynamic Modeling of the 2014 March 29 X1.0 Solar Flare

Fatima Rubio **da Costa**, Lucia Kleint, Vahé Petrosian, Wei Liu and Joel C. Allred
ApJ **827** 38 **2016**
http://arxiv.org/pdf/1603.04951v1.pdf
Spectroscopic observations of solar flares provide critical diagnostics of the physical conditions in the flaring atmosphere. Some key features in observed spectra have not yet been accounted for in existing flare models. Here we report a data-driven simulation of the well-observed X1.0 flare on **2014 March 29** that can reconcile some well-known spectral discrepancies. We analyzed spectra of the flaring region from the Interface Region Imaging Spectrograph (IRIS) in MgII h&k, the Interferometric BIdimensional Spectropolarimeter at the Dunn Solar Telescope (DST/IBIS) in Hα 6563 Å and CaII 8542 Å, and the Reuven Ramaty High Energy Solar Spectroscope Imager (RHESSI) in hard X-rays. We constructed a multi-threaded flare loop model and used the electron flux inferred from RHESSI data as the input to the radiative hydrodynamic code RADYN to simulate the atmospheric response. We then synthesized various chromospheric emission lines and compared them with the IRIS and IBIS observations. In general, the synthetic intensities agree with the observed ones, especially near the northern footpoint of the flare. The simulated MgII line profile has narrower wings than the observed one. This discrepancy can be reduced by using a higher microturbulent velocity (27 km s-1) in a narrow chromospheric layer. In addition, we found that an increase of electron density in the upper chromosphere within a narrow height range of ~800 km below the transition region can turn the simulated MgII line core into emission and thus reproduce the single peaked profile, which is a common feature in all IRIS flares

Combined Modeling of Acceleration, Transport, and Hydrodynamic Response in Solar Flares. II. Inclusion of Radiative Transfer with RADYN

Fatima Rubio **da Costa**, Wei Liu, Vahe' Petrosian, Mats Carlsson
ApJ 813 133 **2015**
http://arxiv.org/pdf/1505.01549v1.pdf
Solar flares involve complex processes that are coupled together and span a wide range of temporal, spatial, and energy scales. Modeling such processes self-consistently has been a challenge in the past. Here we present such a model to simulate the coupling of high-energy particle kinetics with hydrodynamics of the atmospheric plasma. We combine the Stanford unified Fokker-Planck code that models particle acceleration, transport, and bremsstrahlung radiation with the RADYN hydrodynamic code that models the atmospheric response to collisional heating by non-thermal electrons through detailed radiative transfer calculations. We perform simulations using different injection electron spectra, including an {\it ad hoc} power law and more realistic spectra predicted by the stochastic acceleration model due to turbulence or plasma waves. Surprisingly, stochastically accelerated electrons, even with energy flux $\ll$1010 erg s$-$1 cm$-$2, cause "explosive" chromospheric evaporation and drive stronger up- and downflows (and hydrodynamic shocks). We synthesize emission line profiles covering different heights in the lower atmosphere, including Hα 6563 \AA, HeII 304 \AA, CaII K 3934 \AA\ and SiIV 1393 \AA. One interesting result is the unusual high temperature (up to a few 105 K) of the formation site of HeII 304 \AA, which is expected due to photonionization-recombination under flare conditions, compared to those in the quiet Sun dominated by collisional excitation. When compared with

observations, our results can constrain the properties of non-thermal electrons and thus the poorly understood particle acceleration mechanism.

Solar Flare Chromospheric Line Emission: Comparison Between IBIS High-resolution Observations and Radiative Hydrodynamic Simulations

Fatima Rubio **da Costa**, Lucia Kleint, Vah? Petrosian, Alberto Sainz Dalda, Wei Liu
2014
http://arxiv.org/pdf/1412.1815v1.pdf
Solar flares involve impulsive energy release, which results in enhanced radiation in a broad spectral and at a wide height range. In particular, line emission from the chromosphere (lower atmosphere) can provide critical diagnostics of plasma heating processes. Thus, a direct comparison between high-resolution spectroscopic observations and advanced numerical modeling results can be extremely valuable, but has not been attempted so far. We present in this paper such a self-consistent investigation of an M3.0 flare observed by the Dunn Solar Telescope's (DST) Interferometric Bi-dimensional Spectrometer (IBIS) on 2011 September 24 that we have modeled with the radiative hydrodynamic code RADYN (Carlsson & Stein 1992, 1997; Abbett & Hawley 1999; Allred et al. 2005). We obtained images and spectra of the flaring region with IBIS in Hα 6563 ? and Ca II 8542 ?, and with the Reuven Ramaty High Energy Solar Spectroscope Imager (RHESSI)in X-rays. The latter was used to infer the non-thermal electron population, which was passed to RADYN to simulate the atmospheric response to electron collisional heating. We then synthesized spectral lines and compared their shapes and intensities with those observed by IBIS and found that they exhibit an agreement in general. In particular, the synthetic Ca II 8542 ? profile fits well to the observed profile, while the synthetic Hα profile is fainter in the core than the observation. This indicates that Hα emission is more responsive to the non-thermal electron flux than the Ca II 8542 ? emission. We suggest that a refinement of the energy input and other processes is necessary to resolve this discrepancy. **2011 September 24**

Observations of a solar flare and filament eruption in Lyman α and X-rays

Rubio **da Costa**, F.; Fletcher, L.; Labrosse, N.; Zuccarello, F.
Astronomy and Astrophysics, Volume 507, Issue 2, **2009**, pp.1005-1014
Context: Lα is a strong chromospheric emission line, which has been relatively rarely observed in flares. The Transition Region and Coronal Explorer (TRACE) has a broad “Lyman α” channel centered at 1216 Å used primarily at the beginning of the mission. A small number of flares were observed in this channel.
Aims: We aim to characterise the appearance and behaviour of a flare and filament ejection which occurred on 8th September 1999 and was observed by TRACE in Lα, as well as by the Yohkoh Soft and Hard X-ray telescopes. We explore the flare energetics and its spatial and temporal evolution. We have in mind the fact that the Lα line is a target for the Extreme Ultraviolet Imaging telescope (EUI) which has been selected for the Solar Orbiter mission, as well as the LYOT telescope on the proposed SMESE mission.
Methods: We use imaging data from the TRACE 1216 Å, 1600 Å and 171 Å channels, and the Yohkoh hard and soft X-ray telescopes. A correction is applied to the TRACE data to obtain a better estimate of the pure Lα signature. The Lα power is obtained from a knowledge of the TRACE response function, and the flare electron energy budget is estimated by interpreting Yohkoh/HXT emission in the context of the collisional thick target model.
Results: We find that the Lα flare is characterised by strong, compact footpoints (smaller than the UV ribbons) which correlate well with HXR footpoints. The Lα power radiated by the flare footpoints can be estimated, and is found to be on the order of 1026 erg s-1 at the peak. This is less than 10% of the power inferred for the electrons which generate the co-spatial HXR emission, and can thus readily be provided by them. The early stages of the filament eruption that accompany the flare are also visible, and show a diffuse, roughly circular spreading sheet-like morphology, with embedded denser blobs.
Conclusions: On the basis of this observation, we conclude that flare and filament observations in the Lα line with the planned EUI and LYOT telescopes will provide valuable insight into solar flare evolution and energetics, especially when accompanied by HXR imaging and spectroscopy.

Complex Network for Solar Active Regions

Farhad **Daei**, Hossein Safari, and Neda Dadashi
2017 ApJ 845 36
http://sci-hub.cc/10.3847/1538-4357/aa7ddf
In this paper we developed a complex network of solar active regions (ARs) to study various local and global properties of the network. The values of the Hurst exponent (0.8–0.9) were evaluated by both the detrended fluctuation analysis and the rescaled range analysis applied on the time series of the AR numbers. The findings suggest that ARs can be considered as a system of self-organized criticality (SOC). We constructed a growing network based on locations, occurrence times, and the lifetimes of 4227 ARs recorded from 1999 January 1 to 2017 April 14. The behavior of the clustering coefficient shows that the AR network is not a random network. The logarithmic behavior of

the length scale has the characteristics of a so-called small-world network. It is found that the probability distribution of the node degrees for undirected networks follows the power law with exponents of about 3.7–4.2. This indicates the scale-free nature of the AR network. The scale-free and small-world properties of the AR network confirm that the system of ARs forms a system of SOC. Our results show that the occurrence probability of flares (classified by GOES class $C > 5$, M, and X flares) in the position of the AR network hubs takes values greater than that obtained for other nodes.

Variability of the Reconnection Guide Field in Solar Flares

Joel T. **Dahlin**, Spiro K. Antiochos, Jiong Qiu, C. Richard DeVore
ApJ **932** 94 **2021**
https://arxiv.org/pdf/2110.04132.pdf
https://iopscience.iop.org/article/10.3847/1538-4357/ac6e3d/pdf
Solar flares may be the best-known examples of the explosive conversion of magnetic energy into bulk motion, plasma heating, and particle acceleration via magnetic reconnection. The energy source for all flares is the highly sheared magnetic field of a filament channel above a polarity inversion line (PIL). During the flare, this shear field becomes the so-called reconnection guide field (i.e., the non-reconnecting component), which has been shown to play a major role in determining key properties of the reconnection including the efficiency of particle acceleration. We present new high-resolution, three-dimensional, magnetohydrodynamics simulations that reveal the detailed evolution of the magnetic shear/guide field throughout an eruptive flare. The magnetic shear evolves in three distinct phases: shear first builds up in a narrow region about the PIL, then expands outward to form a thin vertical current sheet, and finally is transferred by flare reconnection into an arcade of sheared flare loops and an erupting flux rope. We demonstrate how the guide field may be inferred from observations of the sheared flare loops. Our results indicate that initially the guide field is larger by about a factor of 5 than the reconnecting component, but it weakens by more than an order of magnitude over the course of the flare. Instantaneously, the guide field also varies spatially over a similar range along the three-dimensional current sheet. We discuss the implications of our results for understanding observations of flare particle acceleration.

High-Resolution Three-Dimensional MHD Simulations of Plasmoid Formation in Solar Flares

Joel **Dahlin**, Spiro Antiochos, and C. Richard DeVore
EGU2020-10039 May **2020**
https://meetingorganizer.copernicus.org/EGU2020/displays/36057
In highly conducting plasmas, reconnecting current sheets are often unstable to the generation of plasmoids, small-scale magnetic structures that play an important role in facilitating the rapid release of magnetic energy and channeling that energy into accelerated particles. There is ample evidence for plasmoids throughout the heliosphere, from in situ observations of flux ropes in the solar wind and planetary magnetospheres to remote-sensing imaging of plasma ‘blobs’ associated with explosive solar activity such as eruptive flares and coronal jets. Accurate models for plasmoid formation and dynamics must capture the large-scale self-organization responsible for forming the reconnecting current sheet. However, due to the computational difficulty inherent in the vast separation between the global and current sheet scales, previous numerical studies have typically explored configurations with either reduced dimensionality or pre-formed current sheets. We present new three-dimensional MHD studies of an eruptive flare in which the formation of the current sheet and subsequent reconnection and plasmoid formation are captured within a single simulation. We employ Adaptive Mesh Refinement (AMR) to selectively resolve fine-scale current sheet dynamics. Reconnection in the flare current sheet generates many plasmoids that exhibit highly complex, three-dimensional structure. We show how plasmoid formation and dynamics evolve through the course of the flare, especially in response to the weakening of the reconnection “guide field” linked to the global reduction of magnetic shear. We discuss implications of our results for particle acceleration and transport in eruptive flares as well as for observations by Parker Solar Probe and the forthcoming Solar Orbiter.
Presentation # 10039 https://presentations.copernicus.org/EGU2020/presentations-ST1.7.zip

The role of three-dimensional transport in driving enhanced electron acceleration during magnetic reconnection

J. T. **Dahlin**, J. F. Drake, M. Swisdak
2017
https://arxiv.org/pdf/1706.00481.pdf
Magnetic reconnection is an important driver of energetic particles in many astrophysical phenomena. Using kinetic particle-in-cell (PIC) simulations, we explore the impact of three-dimensional reconnection dynamics on the efficiency of particle acceleration. In two-dimensional systems, Alfv\'enic outflows expel energetic electrons into flux ropes where they become trapped and disconnected from acceleration regions. However, in three-dimensional systems these flux ropes develop axial structure that enables particles to leak out and return to acceleration regions. This requires a finite

guide field so that particles may move quickly along the flux rope axis. We show that greatest energetic electron production occurs when the guide field is of the same order as the reconnecting component: large enough to facilitate strong transport, but not so large as to throttle the dominant Fermi mechanism responsible for efficient electron acceleration. This suggests a natural explanation for the envelope of electron acceleration during the impulsive phase of eruptive flares.

Generalized Coronal Loop Scaling Laws and Their Implication for Turbulence in Solar Active Region Loops

Y. **Dai**, J. J. Xiang, M. D. Ding
ApJ **2024**
https://arxiv.org/pdf/2403.02110.pdf
Recent coronal loop modeling has emphasized the importance of combining both Coulomb collisions and turbulent scattering to characterize field-aligned thermal conduction, which invokes a hybrid loop model. In this work we generalize the hybrid model by incorporating nonuniform heating and cross section that are both formulated by a power-law function of temperature. Based on the hybrid model solutions, we construct scaling laws that relate loop-top temperature (Ta) and heating rate (Ha) to other loop parameters. It is found that the loop-top properties for turbulent loops are additionally power-law functions of turbulent mean free path (λT), with the functional forms varying from situation to situation that depends on the specification of the heating and/or areal parameters. More importantly, both a sufficiently footpoint-concentrated heating and a cross-sectional expansion with height can effectively weaken (strengthen) the negative (positive) power-law dependence of Ta (Ha) on λT. The reason lies in a notable reduction of heat flux by footpoint heating and/or cross-sectional expansion in the turbulence-dominated coronal part, where turbulent scattering introduces a much weaker dependence of the conduction coefficient on temperature. In this region, therefore, the reduction of the heat flux predominately relies on a backward flattening of the temperature gradient. Through numerical modeling that incorporates more realistic conditions, this scenario is further consolidated. Our results have important implication for solar active region (AR) loops. With the factors of nonuniform heating and cross section taken into account, AR loops can bear relatively stronger turbulence while still keeping a physically reasonable temperature for nonflaring loops.

Transverse oscillation of a coronal loop induced by a flare-related jet

J. **Dai**, Q. M. Zhang, Y. N. Su, H. S. Ji
A&A **2020**
https://arxiv.org/pdf/2012.07074.pdf
In this work, we report our multi-wavelength observations of the transverse oscillation of a large scale coronal loop with a length of 350 Mm. The oscillation was induced by a blowout coronal jet, which was related to a circular ribbon flare (CRF) in AR 12434 on **2015 October 16**. We aim to determine the physical parameters in the coronal loop, including the Alfven speed and magnetic field strength. The jet induced kink oscillation was observed in extreme-ultraviolet (EUV) wavelengths by the Atmospheric Imaging Assembly (AIA) on board the Solar Dynamics Observatory (SDO). Line of sight magnetograms were observed by the Helioseismic and Magnetic Imager (HMI) on board SDO. We took several slices along the loop to assemble time-distance diagrams, and used an exponentially decaying sine function to fit the decaying oscillation. The initial amplitude, period, and damping time of kink oscillation were obtained. Coronal seismology of the kink mode was applied to estimate the Alfven speed and magnetic field strength in the oscillating loop. In addition, we measured the magnetic field of the loop through non-linear force free field (NLFFF) modeling using the flux rope insertion method. The oscillation is most pronounced in AIA 171 and 131. The oscillation is almost in phase along the loop with a peak initial amplitude of 13.6 Mm, meaning that the oscillation belong to the fast standing kink mode. The oscillation lasts for 3.5 cycles with an average period of 462 s and average damping time of 976 s. The values of t/P lie in the range of 1.5-2.5. Based on coronal seismology, the Alfven speed in the oscillating loop is estimated to be 1210 km. Two independent methods are applied to calculate the magnetic field strength of the loop, resulting in 30043 G using the coronal seismology and 21123 G using the NLFFF modeling, respectively.

Extremely Large Extreme-ultraviolet Late Phase Powered by Intense Early Heating in a Non-eruptive Solar Flare

Yu **Dai**, Mingde Ding, Weiguo Zong, Kai E. Yang
ApJ **863** 124 **2018**
https://arxiv.org/pdf/1807.01315.pdf
http://sci-hub.tw/10.3847/1538-4357/aad32e
We analyze and model an M1.2 non-eruptive solar flare on **2011 September 9**. The flare exhibits a strong late-phase peak of the warm coronal emissions (~3~MK) in extreme-ultraviolet (EUV), with peak emission over 1.3 times that of the main flare peak. Multiple flare ribbons are observed, whose evolution indicates a two-stage energy release process. A non-linear force-free field (NLFFF) extrapolation reveals the existence of a magnetic null point, a fan-spine structure, and two flux ropes embedded in the fan dome. Magnetic reconnections involved in the flare are driven by the destabilization and rise of one of the flux ropes. In the first stage, the fast ascending flux rope drives reconnections at

the null point and the surrounding quasi-separatrix layer (QSL), while in the second stage, reconnection mainly occurs between the two legs of the field lines stretched by the eventually stopped flux rope. The late-phase loops are mainly produced by the first-stage QSL reconnection, while the second-stage reconnection is responsible for the heating of main flaring loops. The first-stage reconnection is believed to be more powerful, leading to an extremely strong EUV late phase. We find that the delayed occurrence of the late-phase peak is mainly due to the long cooling process of the long late-phase loops. Using the model enthalpy-based thermal evolution of loops (EBTEL), we model the EUV emissions from a late-phase loop. The modeling reveals a peak heating rate of 1.1~erg~cm−3~s−1 for the late-phase loop, which is obviously higher than previous values.

Probing the Production of Extreme-ultraviolet Late Phase Solar Flares by Using the Enthalpy-Based Thermal Evolution of Loops Model

Yu **Dai**, Mingde Ding
ApJ **857** 99 **2018**
https://arxiv.org/pdf/1803.07210.pdf
http://sci-hub.tw/http://iopscience.iop.org/0004-637X/857/2/99/
Recent observations in extreme-ultraviolet (EUV) wavelengths reveal an EUV late phase in some solar flares, which is characterized by a second peak in warm coronal emissions (~3 MK) several tens of minutes to a few hours after the soft X-ray (SXR) peak. By using the enthalpy-based thermal evolution of loops (EBTEL) model, in this paper we numerically probe the production of EUV late phase solar flares. Starting from two main mechanisms of producing the EUV late phase, long-lasting cooling and secondary heating, we carry out two groups of numerical experiments to study the effects of these two processes on the emission characteristics in late phase loops. In either of the two processes an EUV late phase solar flare that conforms to the observational criteria can be numerically synthesized. However, the underlying hydrodynamic and thermodynamic evolutions in late phase loops are different between the two synthetic flare cases. The late phase peak due to a long-lasting cooling process always occurs during the radiative cooling phase, while that powered by a secondary heating is more likely to take place in the conductive cooling phase. We then propose a new method to diagnose the two mechanisms based on the shape of EUV late phase light curves. Moreover, from the partition of energy input, we discuss why most solar flares are not EUV late flares. Finally, by addressing some other factors that may potentially affect the loop emissions, we also discuss why the EUV late phase is mainly observed in warm coronal emissions.

Production of the Extreme-Ultraviolet Late Phase of an X Class Flare in a Three-Stage Magnetic Reconnection Process

Y. **Dai**, M. D. DIng, Y. Guo
E-print, July **2013, File**; 2013 ApJ 773 L21
We report observations of an X class flare on **2011 September 6** by the instruments onboard the Solar Dynamics Observatory (SDO). The flare occurs in a complex active region with multiple polarities. The Extreme-Ultraviolet (EUV) Variability Experiment (EVE) observations in the warm coronal emission reveal three enhancements, of which the third one corresponds to an EUV late phase. The three enhancements have a one-to-one correspondence to the three stages in flare evolution identified by the spatially-resolved Atmospheric Imaging Assembly (AIA) observations, which are characterized by a flux rope eruption, a moderate filament ejection, and the appearance of EUV late phase loops, respectively. The EUV late phase loops are spatially and morphologically distinct from the main flare loops. Multi-channel analysis suggests the presence of a continuous but fragmented energy injection during the EUV late phase resulting in the warm corona nature of the late phase loops. Based on these observational facts, We propose a three-stage magnetic reconnection scenario to explain the flare evolution. Reconnections in different stages involve different magnetic fields but show a casual relationship between them. The EUV late phase loops are mainly produced by the least energetic magnetic reconnection in the last stage.

Impact of 3D Structure on Magnetic Reconnection

Lars K. S. **Daldorff**, James E.Leake, James A. Klimchuk
ApJ **927** 196 **2022**
https://arxiv.org/pdf/2202.04761.pdf
https://iopscience.iop.org/article/10.3847/1538-4357/ac532d/pdf
Results from 2.5D and 3D studies of the onset and development of the tearing instability are presented, using high fidelity resistive MHD simulations. A limited parameter study of the strength of the reconnecting field (or shear angle) was performed. An initially simple 1D equilibrium was used, consisting of a modified force-free current sheet, with periodic boundary conditions in all directions. In all cases, the linear and non-linear evolution led to a primary current sheet between two large flux ropes. The global reconnection rate during this later stage was analyzed in all simulations. It was found that in 2.5D the primary current sheet fragmented due to plasmoids, and as expected, the global reconnection rate, calculated using multiple methods, increases with the strength of the reconnecting field due to a stronger Alfvén speed. In 3D, the presence of interacting oblique modes of the tearing instability complicates the simple 2.5D picture, entangling the magnetic field of the inflow and introducing a negative effect on the reconnection rate. The

two competing effects of stronger Alfvén speed and entangling, which both increase with the strength of the reconnecting field, resulted in a decrease in the reconnection rate with increasing reconnecting field. For all simulations, the 3D rates were less than in 2.5D, but suggest that as one goes to weak reconnecting field (or strong guide field), the system becomes more 2.5D like and the 2.5D and 3D rates converge. These results have relevance to situations like nano-flare heating and flare current sheets in the corona.

Flare productivity of newly-emerged paired and isolated solar active regions:

S.**Dalla**, L.Fletcher and N. A.Walton
A&A 468 (**2007**) 1103-1108

Studying the transfer of magnetic helicity in solar active regions with the connectivity-based helicity flux density method

K. **Dalmasse**, E. Pariat, G. Valori, J. Jing, P. Démoulin
ApJ **2017**
https://arxiv.org/pdf/1712.04691.pdf
In the solar corona, magnetic helicity slowly and continuously accumulates in response to plasma flows tangential to the photosphere and magnetic flux emergence through it. Analyzing this transfer of magnetic helicity is key for identifying its role in the dynamics of active regions (ARs). The connectivity-based helicity flux density method was recently developed for studying the 2D and 3D transfer of magnetic helicity in ARs. The method takes into account the 3D nature of magnetic helicity by explicitly using knowledge of the magnetic field connectivity, which allows it to faithfully track the photospheric flux of magnetic helicity. Because the magnetic field is not measured in the solar corona, modeled 3D solutions obtained from force-free magnetic field extrapolations must be used to derive the magnetic connectivity. Different extrapolation methods can lead to markedly different 3D magnetic field connectivities, thus questioning the reliability of the connectivity-based approach in observational applications. We address these concerns by applying this method to the isolated and internally complex AR 11158 with different magnetic field extrapolation models. We show that the connectivity-based calculations are robust to different extrapolation methods, in particular with regards to identifying regions of opposite magnetic helicity flux. We conclude that the connectivity-based approach can be reliably used in observational analyses and is a promising tool for studying the transfer of magnetic helicity in ARs and relate it to their flaring activity. **2011 February 14**

The origin of net electric currents in solar active regions

K. **Dalmasse**, G. Aulanier, P. Démoulin, B. Kliem, T. Török, E. Pariat
ApJ **810** 17 **2015**
http://arxiv.org/pdf/1507.05060v1.pdf
There is a recurring question in solar physics about whether or not electric currents are neutralized in active regions (ARs). This question was recently revisited using three-dimensional (3D) magnetohydrodynamic (MHD) numerical simulations of magnetic flux emergence into the solar atmosphere. Such simulations showed that flux emergence can generate a substantial net current in ARs. Another source of AR currents are photospheric horizontal flows. Our aim is to determine the conditions for the occurrence of net vs. neutralized currents with this second mechanism. Using 3D MHD simulations, we systematically impose line-tied, quasi-static, photospheric twisting and shearing motions to a bipolar potential magnetic field. We find that such flows: (1) produce both {\it direct} and {\it return} currents, (2) induce very weak compression currents - not observed in 2.5D - in the ambient field present in the close vicinity of the current-carrying field, and (3) can generate force-free magnetic fields with a net current. We demonstrate that neutralized currents are in general produced only in the absence of magnetic shear at the photospheric polarity inversion line - a special condition rarely observed. We conclude that, as magnetic flux emergence, photospheric flows can build up net currents in the solar atmosphere, in agreement with recent observations. These results thus provide support for eruption models based on pre-eruption magnetic fields possessing a net coronal current.

Can we explain atypical solar flares?⋆

K. **Dalmasse**1, R. Chandra2, B. Schmieder1 and G. Aulanier
A&A 574, A37 (**2015**)
http://www.aanda.org/articles/aa/pdf/2015/02/aa23206-13.pdf
http://arxiv.org/pdf/1410.8194v1.pdf
Context. We used multiwavelength high-resolution data from ARIES, THEMIS, and SDO instruments to analyze a non-standard, C3.3 class flare produced within the active region NOAA 11589 on **2012 October 16**. Magnetic flux emergence and cancellation were continuously detected within the active region, the latter leading to the formation of two filaments.
Aims. Our aim is to identify the origins of the flare taking the complex dynamics of its close surroundings into account.

Methods. We analyzed the magnetic topology of the active region using a linear force-free field extrapolation to derive its 3D magnetic configuration and the location of quasi-separatrix layers (QSLs), which are preferred sites for flaring activity. Because the active region's magnetic field was nonlinear force-free, we completed a parametric study using different linear force-free field extrapolations to demonstrate the robustness of the derived QSLs.
Results. The topological analysis shows that the active region presented a complex magnetic configuration comprising several QSLs. The considered data set suggests that an emerging flux episode played a key role in triggering the flare. The emerging flux probably activated the complex system of QSLs, leading to **multiple coronal magnetic reconnections within the QSLs.** This scenario accounts for the observed signatures: the two extended flare ribbons developed at locations matched by the photospheric footprints of the QSLs and were accompanied with flare loops that formed above the two filaments, which played no important role in the flare dynamics.
Conclusions. This is a typical example of a complex flare that can a priori show standard flare signatures that are nevertheless impossible to interpret with any standard model of eruptive or confined flare. We find that a topological analysis, however, permitted us to unveil the development of such complex sets of flare signatures.
Хорошее введение по confined and eruptive flares.

A confined flare above filaments

K. **Dalmasse**, R. Chandra, B. Schmieder and G. Aulanier
E-print, Oct **2013**; Proceedings of the IAU S300
http://arxiv.org/abs/1310.0667
We present the dynamics of two filaments and a C-class flare observed in NOAA 11589 on **2012 October 16**. We used the multi-wavelength high-resolution data from SDO, as well as THEMIS and ARIES ground-based observations. The observations show that the filaments are progressively converging towards each other without merging. We find that the filaments have opposite chirality which may have prevented them from merging. On October 16, a C3.3 class flare occurred without the eruption of the filaments. According to the standard solar flare model, after the reconnection, post-flare loops form {it below} the erupting filaments whether the eruption fails or not. However, the observations show the formation of post-flare loops {it above} the filaments, which is not consistent with the standard flare model. We analyze the topology of the active region's magnetic field by computing the quasi-separatrix layers (QSLs) using a linear force-free field extrapolation. We find a good agreement between the photospheric footprints of the QSLs and the flare ribbons. We discuss how slipping or slip-running reconnection at the QSLs may explain the observed dynamics.

HARD X-RAY ASYMMETRY LIMITS IN SOLAR FLARE CONJUGATE FOOTPOINTS

Antoun G. **Daou** and David Alexander
2016 ApJ 832 63
The transport of energetic electrons in a solar flare is modeled using a time-dependent one-dimensional Fokker–Planck code that incorporates asymmetric magnetic convergence. We derive the temporal and spectral evolution of the resulting hard X-ray (HXR) emission in the conjugate chromospheric footpoints, assuming thick target photon production, and characterize the time evolution of the numerically simulated footpoint asymmetry and its relationship to the photospheric magnetic configuration. The thick target HXR asymmetry in the conjugate footpoints is found to increase with magnetic field ratio as expected. However, we find that the footpoint HXR asymmetry saturates for conjugate footpoint magnetic field ratios ≥4. This result is borne out in a direct comparison with observations of 44 double-footpoint flares. The presence of such a limit has not been reported before, and may serve as both a theoretical and observational benchmark for testing a range of particle transport and flare morphology constraints, particularly as a means to differentiate between isotropic and anisotropic particle injection.

The GOES-R Solar UltraViolet Imager

Jonathan M. **Darnel**,Daniel B. Seaton,Christian Bethge,Laurel Rachmeler,Alison Jarvis,Steven M. Hill,Courtney L. Peck,J. Marcus Hughes,Jason Shapiro … See all authors
Space Weather **2022**
https://doi.org/10.1029/2022SW003044
https://agupubs.onlinelibrary.wiley.com/doi/epdf/10.1029/2022SW003044
The four Solar UltraViolet Imagers on board the GOES-16 and GOES-17 and the upcoming GOES-T and GOES-U weather satellites serve as NOAA's operational solar coronal imagers. These four identically designed solar EUV instruments are similar in design and capability to the SDO-AIA suite of solar telescopes, and are planned to operationally span two solar cycles or more, from 2017 through 2040. We present the concept of operations for the SUVI instruments, operational requirements, and constraints. The reader is also introduced to the instrument design, testing, and performance characteristics. Finally, the various data products are described along with their potential utility to the operational user or researcher. **21 Aug 2017, 10 Sep 2017, 29 Nov 2020, 29 Apr 2021**

Reconnection Process in the Sun and Heliosphere

A.C. **Das**

2010, In: Gopalswamy, N., Hasan, S.S., Ambastha, A. (eds.)
Heliophysical Processes, Astrophysics and Space Science Proceedings, Springer, Berlin, p. 99-118, **File**

Solar flare, coronal mass ejection and many other interesting plasma and magnetic field structures in the heliosphere are believed to be generated by a powerful plasma process widely known as reconnection of magnetic field lines. The basic understanding of this reconnection process is described by considering a simple model suggested by Dungey that contains a kind of consistent flow of plasma around an x-type neutral point. There are, however, several comprehensive MHD models, some of which are also discussed in this article. Spontaneous reconnection based on tearing mode instability is described very briefly for completeness. The crucial role played by magnetic reconnection in violent energy conversion occurring in solar flare, coronal mass ejection and other related phenomena like hard x-ray and soft x-ray emissions is highlighted. Several convincing observational evidences that support reconnectionmodel are presented. Numerical simulation is seen to be an essential part of this study that enhances our understanding of the evolution of plasmoid and multiple shocks due to reconnection of field lines. Some challenges are mentioned towards the end of the presentation.

The Evolution of Flare Activity with Stellar Age

Davenport, James R. A.; Covey, Kevin R.; Clarke, Riley W.; Boeck, Austin C.; Cornet, Jonathan; Hawley, Suzanne L.

Astrophysical Journal, Volume 871, Issue 2, article id. 241, 13 pp. (**2019**)
sci-hub.se/10.3847/1538-4357/aafb76

Using a recent census of flare stars from the Kepler survey, we have explored how flare activity evolves across stellar main-sequence lifetimes. We utilize a sample of 347 stars with robust flare activity detections and which have rotation periods measured via starspot modulations in their Kepler light curves. We consider three separate methods for quantifying flare activity from optical light curves and compare their utility for comparing flare activity between stars of differing ages and luminosities. These metrics include the fractional luminosity emitted in flares, the specific rate of flares emitted at a given energy, and a model for the entire flare frequency distribution (FFD). With all three approaches, we find that flare activity decreases for all low-mass stars as they spin down, and thus with age. Most striking is the evolution of the flare occurrence frequency distributions, which show no significant change in the power-law slope with age. Since our sample is preferentially constructed of younger, more active stars, our model overpredicts the superflare rate previously estimated for the Sun. Finally, we parameterize our best-fit model of the FFD for ease in predicting the rates of flares and their associated impacts on planet habitability and detection.

Correlation between decimetric radio emission and hard X-rays in=solar=flares:

B. P. **Dbrowski** and A. O. Benz
A&A 504 (**2009**) 565-573; **File**

Aims. The emission of decimetric flare radiation, in particular narrowband spikes and pulsations, is generally considered to originate in accelerated, non-thermal particles. On the other hand, non-thermal hard X-rays are also understood to be products of this acceleration. Do radio emission and hard X-ray signatures originate from the same acceleration process? A strong correlation between the light curves in the radio and HXR ranges may help answer this question.
Methods. The delay between the radio and hard X-ray emission was determined by cross-correlation. The time profiles of X-ray and radio emission include a wide range of energies and frequencies. Thus, correlation is not simply a yes/no question, but must be systematically searched for in various ranges. The high spectral resolution of RHESSI ensured that it was possible to carefully choose the energy range, excluding thermal emission. The broad bandwidth of *Phoenix-2* allowed the selection of any emission in the full decimetre range. The energy range and duration in hard X-rays, and the frequency range in radio spectrograms were chosen to optimize the correlation. The cross-correlation coefficient was then analyzed by a Gaussian fitting method.
Results. The measured delays have a distribution of *FWHM* 4.9 s and 4.7 s for pulsations and spikes, respectively, evaluated from such a Gaussian fitting method. The mean delay for pulsations was found to be -1.4 ± 0.9 s (minus indicates that hard X-ray emission comes first), and for narrowband spikes to -2.5 ± 2.5 s. There are broad wings in the distribution, which we interpret as chance coincidences. The delays do not depend on centre frequency, cross-correlation coefficient, duration of the correlating sequence, and position on the disk. However, we find an increase in the delay for the spikes with GOES magnitude (peak soft X-ray emission) of the flare and with peak hard X-ray flux. This was not the case for pulsations.
Conclusions. In contrast to previous reports, the average delays for all pulsations and all spike groups are consistent with zero. Thus, correlated decimetric pulsations and spikes are, on average, concomitant with non-thermal X-rays.

A parameter study for modeling MgII h and k emission during solar flares

Fatima Rubio **da Costa**, Lucia Kleint

ApJ **842** 82 **2017**

https://arxiv.org/pdf/1704.05874.pdf

Solar flares show highly unusual spectra, in which the thermodynamic conditions of the solar atmosphere are encoded. Current models are unable to fully reproduce the spectroscopic flare observations, especially the single-peaked spectral profiles of the MgII h and k lines. We aim at understanding the formation of the chromospheric and optically thick MgII h and k lines in flares through radiative transfer calculations. We take a flare atmosphere obtained from a simulation with the radiative hydrodynamic code RADYN as input for a radiative transfer modeling with the RH code. By iteratively changing this model atmosphere and varying thermodynamic parameters, such as temperature, electron density, and velocities, we study their effects on the emergent intensity spectra. We can reproduce the typical single-peaked MgII h and k flare spectral shape and their approximate intensity ratios to the subordinate MgII lines by either increasing densities, temperatures or velocities at the line core formation height range. Additionally, by combining unresolved up- and downflows up to ~250 km/s within one resolution element, we also reproduce the widely broadened line wings. While we cannot unambiguously determine which mechanism dominates in flares, future modeling efforts should investigate unresolved components, additional heat dissipation, larger velocities, and higher densities, and combine the analysis of multiple spectral lines. **2014 March 29**

COMBINED MODELING OF ACCELERATION, TRANSPORT, AND HYDRODYNAMIC RESPONSE IN SOLAR FLARES. II. Inclusion of Radiative Transfer with RADYN

Fatima Rubio **da Costa**, Wei Liu, Vah? Petrosian, Mats Carlsson

2015

http://arxiv.org/pdf/1505.01549v1.pdf

Solar flares involve complex processes that are coupled together and span a wide range of temporal, spatial, and energy scales. Modeling such processes self-consistently has been a challenge in the past. Here we present such a model to simulate the coupling of high-energy particle kinetics with hydrodynamics of the atmospheric plasma. We combine the Stanford unified Fokker-Planck code that models particle acceleration, transport, and bremsstrahlung radiation with the RADYN hydrodynamic code that models the atmospheric response to collisional heating by non-thermal electrons through detailed radiative transfer calculations. We perform simulations using different injection electron spectra, including an ad hoc power law and more realistic spectra predicted by the stochastic acceleration model due to turbulence or plasma waves. Surprisingly, stochastically accelerated electrons, even with energy flux 1010 (erg/s/cm^2), cause "explosive" chromospheric evaporation and drive stronger up- and downflows (and hydrodynamic shocks). We synthesize emission line profiles covering different heights in the lower atmosphere, including H α 6563 A, He II 304 Å, Ca II K 3934 A and Si IV 1393 A. One interesting result is the unusual high temperature (up to a few 105K) of the formation site of He II 304 Å, which is expected due to photonionization-recombination under flare conditions, compared to those in the quiet Sun dominated by collisional excitation. When compared with observations, our results can constrain the properties of non-thermal electrons and thus the poorly understood particle acceleration mechanism.

Solar Flare Chromospheric Line Emission: Comparison Between IBIS High-resolution Observations and Radiative Hydrodynamic Simulations

Fatima Rubio **da Costa**, Lucia Kleint, Vah? Petrosian, Alberto Sainz Dalda, Wei Liu

2015 *ApJ* 804 56

http://arxiv.org/pdf/1412.1815v1.pdf

Solar flares involve impulsive energy release, which results in enhanced radiation in a broad spectral and at a wide height range. In particular, line emission from the chromosphere (lower atmosphere) can provide critical diagnostics of plasma heating processes. Thus, a direct comparison between high-resolution spectroscopic observations and advanced numerical modeling results can be extremely valuable, but has not been attempted so far. We present in this paper such a self-consistent investigation of an M3.0 flare observed by the Dunn Solar Telescope's (DST) Interferometric Bi-dimensional Spectrometer (IBIS) on **2011 September 24** that we have modeled with the radiative hydrodynamic code RADYN (Carlsson & Stein 1992, 1997; Abbett & Hawley 1999; Allred et al. 2005). We obtained images and spectra of the flaring region with IBIS in Hα 6563 ? and Ca II 8542 ?, and with the Reuven Ramaty High Energy Solar Spectroscope Imager (RHESSI)in X-rays. The latter was used to infer the non-thermal electron population, which was passed to RADYN to simulate the atmospheric response to electron collisional heating. We then synthesized spectral lines and compared their shapes and intensities with those observed by IBIS and found that they exhibit an agreement in general. In particular, the synthetic Ca II 8542 ? profile fits well to the observed profile, while the synthetic Hα profile is fainter in the core than the observation. This indicates that Hα emission is more responsive to the non-thermal

electron flux than the Ca II 8542 ? emission. We suggest that a refinement of the energy input and other processes is necessary to resolve this discrepancy.

Observations of a solar flare and filament eruption in Lyman α and X-rays

F. Rubio **da Costa**1,2, L. Fletcher1, N. Labrosse1, and F. Zuccarello2
A&A 507, 1005–1014 (**2009**)

Context. Lα is a strong chromospheric emission line, which has been relatively rarely observed in flares. The Transition Region and Coronal Explorer (TRACE) has a broad "Lyman α" channel centered at 1216 Å used primarily at the beginning of the mission. A small number of flares were observed in this channel.

Aims.We aim to characterise the appearance and behaviour of a flare and filament ejection which occurred on **8th September 1999** and was observed by TRACE in Lα, as well as by the *Yohkoh* Soft and Hard X-ray telescopes. We explore the flare energetics and its spatial and temporal evolution. We have in mind the fact that the Lα line is a target for the Extreme Ultraviolet Imaging telescope (EUI) which has been selected for the Solar Orbiter mission, as well as the LYOT telescope on the proposed SMESE mission.

Methods.We use imaging data from the TRACE 1216 Å, 1600 Å and 171 Å channels, and the *Yohkoh* hard and soft X-ray telescopes. A correction is applied to the TRACE data to obtain a better estimate of the pure Lα signature. The Lα power is obtained from a knowledge of the TRACE response function, and the flare electron energy budget is estimated by interpreting *Yohkoh*/HXT emission in the context of the collisional thick target model.

Results.We find that the Lα flare is characterised by strong, compact footpoints (smaller than the UV ribbons) which correlate well with HXR footpoints. The Lα power radiated by the flare footpoints can be estimated, and is found to be on the order of 1026 erg s−1 at the peak. This is less than 10% of the power inferred for the electrons which generate the co-spatial HXR emission, and can thus readily be provided by them. The early stages of the filament eruption that accompany the flare are also visible, and show a diffuse, roughly circular spreading sheet-like morphology, with embedded denser blobs.

Conclusions.On the basis of this observation, we conclude that flare and filament observations in the Lα line with the planned EUI and LYOT telescopes will provide valuable insight into solar flare evolution and energetics, especially when accompanied by HXR imaging and spectroscopy.

Variability of the Reconnection Guide Field in Solar Flares

Joel T. **Dahlin**1,2, Spiro K. Antiochos1,3, Jiong Qiu4, and C. Richard DeVore1
2022 ApJ 932 94
https://iopscience.iop.org/article/10.3847/1538-4357/ac6e3d/pdf

Solar flares may be the best-known examples of the explosive conversion of magnetic energy into bulk motion, plasma heating, and particle acceleration via magnetic reconnection. The energy source for all flares is the highly sheared magnetic field of a filament channel above a polarity inversion line (PIL). During the flare, this shear field becomes the so-called reconnection guide field (i.e., the nonreconnecting component), which has been shown to play a major role in determining key properties of the reconnection, including the efficiency of particle acceleration. We present new high-resolution, three-dimensional, magnetohydrodynamics simulations that reveal the detailed evolution of the magnetic shear/guide field throughout an eruptive flare. The magnetic shear evolves in three distinct phases: shear first builds up in a narrow region about the PIL, then expands outward to form a thin vertical current sheet, and finally is transferred by flare reconnection into an arcade of sheared flare loops and an erupting flux rope. We demonstrate how the guide field may be inferred from observations of the sheared flare loops. Our results indicate that initially the guide field is larger by about a factor of 5 than the reconnecting component, but it weakens by more than an order of magnitude over the course of the flare. Instantaneously, the guide field also varies spatially over a similar range along the three-dimensional current sheet. We discuss the implications of the remarkable variability of the guide field for the timing and localization of efficient particle acceleration in flares.

Simultaneous Horizontal and Vertical Oscillation of a Quiescent Filament observed by CHASE and SDO

Jun **Dai**, Qingmin Zhang, Ye Qiu, Chuan Li, Zhentong Li, Shuting Li, Yingna Su, Haisheng Ji
ApJ **2023**
https://arxiv.org/pdf/2310.19228.pdf

In this paper, we present the imaging and spectroscopic observations of the simultaneous horizontal and vertical large-amplitude oscillation of a quiescent filament triggered by an EUV wave on **2022 October 02**. Particularly, the filament oscillation involved winking phenomenon in Ha images and horizontal motions in EUV images. Originally, a filament and its overlying loops across AR 13110 and 13113 erupted with a highly inclined direction, resulting in an X1.0 flare and a non-radial CME. The fast lateral expansion of loops excited an EUV wave and the corresponding Moreton wave propagating northward. Once the EUV wavefront arrived at the quiescent filament, the filament began to oscillate coherently along the horizontal direction and the winking filament appeared concurrently in Ha images. The horizontal oscillation involved an initial amplitude of 10.2 Mm and a velocity amplitude of 46.5 km/s, lasting for 3 cycles with a period of 18.2 minutes and a damping time of 31.1 minutes. The maximum Doppler velocities of the oscillating

filament are 18 km/s (redshift) and 24 km/s (blueshift), which was derived from the spectroscopic data provided by CHASE/HIS. The three-dimensional velocity of the oscillation is determined to be 50 km/s at an angle of 50 to the local photosphere plane. Based on the wave-filament interaction, the minimum energy of the EUV wave is estimated to be 2.7 10 20 J. Furthermore, this event provides evidence that Moreton wavesshould be excited by the highly inclined eruptions.

The Evolution of Flare Activity with Stellar Age

James R. A. **Davenport**, Kevin R. Covey, Riley W. Clarke, Austin C. Boeck, Jonathan Cornet, Suzanne L. Hawley

ApJ **2019**

https://arxiv.org/pdf/1901.00890.pdf

Using a recent census of flare stars from the Kepler survey, we have explored how flare activity evolves across stellar main sequence lifetimes. We utilize a sample of 347 stars with robust flare activity detections, and which have rotation periods measured via starspot modulations in their Kepler light curves. We consider three separate methods for quantifying flare activity from optical light curves, and compare their utility for comparing flare activity between stars of differing ages and luminosities. These metrics include: the fractional luminosity emitted in flares, the specific rate of flares emitted at a given energy, and a model for the entire flare frequency distribution. With all three approaches we find that flare activity decreases for all low-mass stars as they spin-down, and thus with age. Most striking is the evolution of the flare occurrence frequency distributions, which show no significant change in the power law slope with age. Since our sample is preferentially constructed of younger, more active stars, our model over-predicts the super-flare rate previously estimated for the Sun. Finally, we parameterize our best-fit model of the flare frequency distribution for ease in predicting the rates of flares and their associated impacts on planet habitability and detection.

Analysis of intermittency in submillimeter radio and Hard X-Rays during the impulsive phase of a solar flare

C. Guillermo Giménez **de Castro**, Paulo J. A. Simões, Jean-Pierre Raulin, Odilon M. Guimarães Jr

Solar Phys. **2016**

http://arxiv.org/pdf/1605.07677v1.pdf

We present an analysis of intermittent processes occurred during the impulsive phase of the flare SOL**2012-03-13**, using hard X-rays and submillimeter radio data. Intermittency is a key characteristic in turbulent plasmas and have been a analyzed recently for Hard X-rays data only. Since in a typical flare the same accelerated electron population is believed to produce both Hard X-rays and gyrosynchrotron, we compare both time profiles searching for intermittency signatures. For that we define a cross-wavelet power spectrum, that is used to obtain the Local Intermittency Measure or LIM. When greater than 3, the square LIM coefficients indicate a local intermittent process. The LIM 2 coefficient distribution in time and scale helps to identify avalanche or cascade energy release processes. We find two different and well separated intermittent behaviors in the submillimeter data: for scales greater than 20 s, a broad distribution during the rising and maximum phases of the emission seems to favor a cascade process; for scales below 1 s, short pulses centered on the peak time, are representative of avalanches. When applying the same analysis to Hard X-rays, we find only the scales above 10 s producing a distribution related to a cascade energy fragmentation. Our results suggest that different acceleration mechanisms are responsible for tens of keV and MeV energy ranges of electrons.

Submillimeter and X-ray observations of an X Class flare

Gimenez **de Castro**, C.G., Trottet, G., Silva-Valio, A., Krucker, S., Costa, J.E.R., Kaufmann, P., Correia, E., Levato, H

E-print, Aug **2009**; A&A

The GOES X1.5 class flare that occurred on **August 30,2002** at 1327:30 UT is one of the few events detected so far at submillimeter wavelengths. We present a detailed analysis of this flare combining radio observations from 1.5 to 212 GHz (an upper limit of the flux is also provided at 405 GHz) and X-ray. Although the observations of radio emission up to 212 GHz indicates that relativistic electrons with energies of a few MeV were accelerated, no significant hard X-ray emission was detected by RHESSI above ~250 keV. Images at 12-20 and 50-100 keV reveal a very compact, but resolved, source of about ~10"x10". EUV TRACE images show a multi-kernel structure suggesting a complex (multipolar) magnetic topology. During the peak time the radio spectrum shows an extended flatness from ~7 to 35 GHz. Modeling the optically thin part of the radio spectrum as gyrosynchrotron emission we obtained the electron spectrum (spectral index delta, instantaneous number of emitting electrons). It is shown that in order to keep the expected X-ray emission from the same emitting electrons below the RHESSI background at 250 keV, a magnetic field above 500 G is necessary. On the other hand, the electron spectrum deduced from radio observations >=50 GHz is harder than that deduced from ~70-250 keV X-ray data, meaning that there must exist a breaking energy around a few hundred keV. During the decay of the impulsive phase, a hardening of the X-ray spectrum is observed which is interpreted as a hardening of the electron distribution spectrum produced by the diffusion due to Coulomb collisions of the trapped electrons in a medium with an electron density of n_e ~ 3E10 - 5E10 cm-3.

Estimating the Maximum Intensities of Soft X-Ray Flares Using Extreme Value Theory

V. **De la Luz**, E. P. Balanzario, T. Tsiftsi

Solar Physics August **2018**, 293:119

http://sci-hub.tw/https://link.springer.com/article/10.1007/s11207-018-1342-1

Solar flares are one of the most energetic events in the solar system, their impact on Earth at ground level and its atmosphere remains under study. The repercussions of this phenomenon in our technological infrastructure includes radio blackouts and errors in geopositional and navigation systems that are considered natural hazards in ever more countries. Occurrence frequency and intensity of the most energetic solar flares are being taken into account in national programs for civil protection in order to reduce the risk and increase the resilience from space weather events. In this work we use the statistical theory of extreme values as well as other statistical methods in order to assess the magnitudes of the most extreme solar-flare events expected to occur in a given period of time. We found that the data set under study presents a dual tail behavior. Our results show that on average we can expect one solar flare greater than X23 each 25 years, that is to say, one such event each two solar cycles.

Cancellation analysis of current density in solar active region NOAA10019

Gaetano **De Vita**1,2, Antonio Vecchio3, Luca Sorriso-Valvo1*, Carine Briand4, Leonardo Primavera2, Sergio Servidio2, Fabio Lepreti2 and Vincenzo Carbone

J. Space Weather Space Clim., 5, A28 (**2015**)

http://www.swsc-journal.org/articles/swsc/pdf/2015/01/swsc140054.pdf

Solar flares are often associated with changes in the fine magnetic structure of the emitting active region. Such topological modification results in variations of both the scaling properties of the fields' fluctuations, and the fractal dimension of the associated gradients. The use of cancellation analysis of the current density has been attempted for the identification and quantitative estimation of such changes. The characteristics of the magnetic vector as measured by THEMIS telescope for the active region NOAA10019 have been studied in this paper, suggesting the presence of disrupted current filaments. The variation of the fractal dimension of the current structures, and in particular their smoothing, is discussed in relationship with occurrence of one flare in the active region. **3-6 July, 2002**

First search for GeV neutrinos from bright gamma-ray solar flares using the IceCube Neutrino Observatory

Gwenhaël **de Wasseige** (for the IceCube Collaboration)

the 36th International Cosmic Ray Conference (ICRC 2019). PoS-ICRC2019-1075 **2019**

https://arxiv.org/pdf/1908.08300.pdf

In response to a reported increase in the total neutrino flux in the Homestake experiment in coincidence with solar flares at the end of the eighties, solar neutrino detectors have searched for solar flare signals. Solar flares convert magnetic energy into thermal energy of plasma and kinetic energy of charged particles such as protons. As a consequence of magnetic reconnection, protons are injected downwards from the coronal acceleration region and can interact with dense plasma in the lower solar atmosphere, producing mesons that will subsequently decay into gamma rays and neutrinos at O(MeV-GeV) energies. The main motivation to search for solar flare neutrinos comes from their hadronic origin. As inherent products of high-energy proton collisions with the chromosphere, they are a direct probe of the proton accelerated towards the chromosphere. Using a multi-messenger approach, it is therefore possible to constrain the proton acceleration taking place in the solar flares, including the spectral index of the accelerated flux and its shape. We present the results of the first search for GeV neutrinos emitted during solar flares carried out with the IceCube Neutrino Observatory. We present a new approach which allows us to strongly lower the energy threshold of IceCube, originally designed to detect 10 GeV - PeV neutrinos. We compare the results with theoretical estimates of the corresponding flux. **Mar 7th, 2012, Feb 25th, 2014, Sep 1st, 2014, Sep 6th, 2017, Sep 10th, 2017**

See arXiv:1907.11699 for all IceCube contributions

On the Study of Solar Flares with Neutrino Observatories

G. **de Wasseige** (for the IceCube Collaboration)

2016

http://arxiv.org/pdf/1606.00681v1.pdf

Since the end of the eighties, in response to a reported increase of the total neutrino flux in the Homestake experiment in coincidence with solar flares, neutrino detectors have searched for signals of neutrinos associated with solar flare activity. Protons which are accelerated by the magnetic structures of such flares may collide with the solar atmosphere, producing mesons which subsequently decay, resulting in neutrinos at O(MeV-GeV) energies. The study of such neutrinos would provide a new window on the underlying physics of the acceleration process. The sensitivity to solar flares of the IceCube Neutrino Observatory, located at the geographical South Pole, is currently under study. We introduce a new approach for a time profile analysis. This is based on a stacking method of selected solar flares which are likely to be connected with pion production. An initial approach towards a neutrino search using the current IceCube experiment as well as first efforts to improve the detection efficiency in the future are presented.

Multiwavelength Observations by XSM, Hinode, and SDO of an Active Region. Chemical Abundances and Temperatures

G**. Del Zanna**1, B. Mondal2,3, Y. K. Rao1, N. P. S. Mithun2, S. V. Vadawale2, K. K. Reeves4, H. E. Mason1, A. Sarkar2, P. Janardhan2, and A. Bhardwaj2
2022 ApJ 934 159
https://iopscience.iop.org/article/10.3847/1538-4357/ac7a9a/pdf
We have reviewed the first year of observations of the Solar X-ray Monitor (XSM) on board Chandrayaan-2 and the available multiwavelength observations to complement the XSM data, focusing on the Solar Dynamics Observatory AIA and Hinode XRT and EIS observations. XSM has provided disk-integrated solar spectra in the 1–15 keV energy range, observing a large number of microflares. We present an analysis of multiwavelength observations of AR 12759 during its disk crossing. We use a new radiometric calibration of EIS to find that the quiescent active region (AR) core emission during its disk crossing has a distribution of temperatures and chemical abundances that does not change significantly over time. An analysis of the XSM spectra confirms the EIS results and shows that the low first ionization potential (FIP) elements are enhanced compared to their photospheric values. The frequent microflares produced by the AR did not affect the abundances of the quiescent AR core. We also present an analysis of one of the flares it produced, SOL2020-04-09T09:32. The XSM analysis indicates isothermal temperatures reaching 6 MK. The lack of very high-T emission is confirmed by AIA. We find excellent agreement between the observed XSM spectrum and the one predicted using an AIA DEM analysis. In contrast, the XRT Al-poly/Be-thin filter ratio gives lower temperatures for the quiescent and flaring phases. We show that this is due to the sensitivity of this ratio to low temperatures, as the XRT filter ratios predicted with a DEM analysis based on EIS and AIA give values in good agreement with the observed ones. **29 Mar-12 Apr 2020, 8-9 Apr 2020**

The Evolution of the EM Distribution in the Core of an Active Region

Giulio **Del Zanna**, Durgesh Tripathi, Helen Mason, Srividya Subramanian, Brendan O'Dwyer
A&A, 573, A104 **2015**
http://arxiv.org/pdf/1411.0128v1.pdf
We study the spatial distribution and evolution of the slope of the Emission Measure between 1 and 3~MK in the core active region NOAA~11193, first when it appeared near the central meridian and then again when it re-appeared after a solar rotation. We use observations recorded by the Extreme-ultraviolet Imaging Spectrometer (EIS) aboard Hinode, with a new radiometric calibration. We also use observations from the Atmospheric Imaging Assembly (AIA) aboard Solar Dynamics Observatory (SDO). We present the first spatially resolved maps of the EM slope in the 1--3~MK range within the core of the AR using several methods, both approximate and from the Differential Emission Measure (DEM). A significant variation of the slope is found at different spatial locations within the active region. We selected two regions that were not affected too much by any line-of-sight lower temperature emission. We found that the EM had a power law of the form EM~$\propto$Tb, with b = 4.4±0.4, and 4.6±0.4, during the first and second appearance of the active region, respectively. During the second rotation, line-of-sight effects become more important, although difficult to estimate. We found that the use of the ground calibration for Hinode/EIS and the approximate method to derive the Emission Measure, used in previous publications, produce an underestimation of the slopes. The EM distribution in active region cores is generally found to be consistent with high frequency heating, and stays more or less the same during the evolution of the active region. **Apr 19, 2011, 16 May 2011**

Elemental abundances and temperatures of quiescent solar active region cores from X-ray observations⋆

G. **Del Zanna** and H. E. Mason
A&A 565, A14 (**2014**)
E-print, May 2014
http://www.damtp.cam.ac.uk/user/astro/gd232/research/papers/delzanna_mason_2014.pdf
A brief review of studies of elemental abundances and emission measures in quiescent solar active region cores is presented. Hinode EUV Imaging Spectrometer (EIS) observations of strong iron spectral lines have shown sharply peaked distributions around 3 MK. EIS observations of lines emitted by a range of elements have allowed good estimates of abundances relative to iron. However, X-ray observations are required to measure the plasma emission above 3 MK and the abundances of oxygen and neon. We revisit, using up-to-date atomic data, older X-ray observations obtained by a sounding rocket and by the Solar Maximum Mission (SMM) Flat Crystal Spectrometer (FCS). We find that the Fe/O and Fe/Ne ratios are normally increased by a factor of 3.2, compared to the photospheric values. Similar results are obtained from FCS observations of six quiescent active region cores. The FCS observations also indicate that the emission measure above 3 MK has a very steep negative slope, with very little plasma observed at 5 MK or above.

The multi-thermal emission in solar active regions

G. **Del Zanna**

A&A 558, A73 (**2013)**

We present simultaneous SDO AIA and Hinode EIS observations of the hot cores of active regions (ARs) and assess the dominant contributions to the AIA EUV bands. This is an extension of our previous work. We find good agreement between SDO AIA, EVE and EIS observations, using our new EIS calibration and the latest EVE v.3 data. We find that all the AIA bands are multi-thermal, with the exception of the 171 and 335 Å, and provide ways to roughly estimate the main contributions directly from the AIA data. We present and discuss new atomic data for the AIA bands, showing that they are now sufficiently complete to obtain temperature information in the cores of ARs, with the exception of the 211 Å band. We found that the newly identified Fe xiv 93.61 Å line is the dominant contribution to the 94 Å band, whenever Fe xviii is not present. Three methods to estimate the Fe xviii emission in this band are presented, two using EIS and one directly from the AIA data. Fe xviii emission is often present in the cores of ARs, but we found cases where it is formed at 3 MK and not 7 MK, the temperature of peak ion abundance in equilibrium. The best EIS lines for elemental abundance determination and differential emission measure (DEM) analysis are discussed. A new set of abundances for many elements are obtained from EIS observations of hot 3 MK loops. The abundances of the elements with low first ionisation potential (FIP), relative to those of the high-FIP elements, are found to be enhanced by about a factor of three, compared to the photospheric values. A measurement of the path length implies that the absolute abundances of the low-FIP elements are higher than the photospheric values by at least a factor of three. We present a new DEM method customised for the AIA bands, to study the thermal structure of ARs at 1″ resolution. This was tested on a few ARs, including one observed during the Hi-C rocket flight. We found excellent agreement between predicted and observed AIA count rates and EIS radiances. Overall we found few differences between the AIA and Hi-C 193 Å images of coronal structures, despite the higher Hi-C resolution (0.25″). The Hi-C images and the AIA DEM modelling suggest that some of the cooler loops (below 1 MK) are already resolved by AIA, while the hotter (1.5–2.5 MK) “background” emission is in most places still unresolved even at the Hi-C resolution. This unresolved emission is significantly lower than previously observed with TRACE, the SOHO CDS, and Hinode EIS spectrometers. Its enhancement appears to be mostly due to increased iron abundance. We find an ubiquitous presence of emission at different temperatures that is not co-spatial, and suggest that future high-resolution imaging is carried out with isothermal bands.

Spectral diagnostics with the SDO EVE flare lines

G. **Del Zanna**, T.N. Woods

E-print, May **2013**, A&A

The diagnostic use of the soft X-ray and EUV lines observed with the Solar Dynamics Observatory (SDO) Extreme ultraviolet Variability Experiment (EVE) is discussed. We focus on all the flare lines observed in the 80-640 A range (mainly due to Fe XVIII - Fe XXIV), showing their use to measure temperatures, emission measures, densities, and chemical abundances. We discuss their identification at the EVE resolution, by using the latest atomic data, and by assessing possible sources of blending, taking into account higher-resolution solar spectra. We present observations of four flares, and study in more detail the gradual phase peak of the **7 March 2012** X5.6 flare. Good agreement between observations and theory is found in most cases, and the best lines for diagnostics are recommended. We found reasonable densities (10^11.2 cm^-3 from Fe XXI lines), but isothermal temperatures (12 MK) lower than those estimated with GOES. We show that EVE can be used to measure relative elemental abundance, and find photospheric argon/iron and calcium/iron abundances. We also show that lines normally formed in the quiet Sun in the low transition region such as O III are the best to study the impulsive phase.

A revised radiometric calibration for the Hinode/EIS instrument

G. **Del Zanna**

E-print, May **2013**, A&A

An assessment of the in-flight radiometric calibration of the Hinode EUV Imaging Spectrometer (EIS) is presented. This is done with the line ratio technique applied to a wide range of observations of the quiet Sun, active regions and flares from 2006 until 2012. The best diagnostic lines and the relevant atomic data are discussed in detail. Radiances over the quiet Sun are also considered, with comparisons with previous measurements. Some departures in the shapes of the ground calibration responsivities are found at the start of the mission. These shapes do not change significantly over time, with the exception of the shorter wavelengths of the EIS short-wavelength (SW) channel, which shows some degradation. The sensitivity of the SW channel at longer wavelengths does not show significant degradation, while that of the long-wavelength (LW) channel shows a significant degradation with time. By the beginning of 2010 the responsivity of the LW channel was already a factor of two or more lower than the values measured on the ground. A first-order correction is proposed. With this correction, the main ratios of lines in the two channels become constant to within a relative 20%, and the He II 256 A radiances over the quiet Sun also become constant over time. This correction removes long-standing discrepancies for a number of lines and ions, in particular those involving the strongest Fe X, Fe

XIII, Fe XIV, Fe XVI and Fe XXIV lines, where discrepancies of factors of more than two were found. These results have important implications for various EIS science analyses, in particular for measurements of temperatures, emission measures and elemental abundances.

The 22 May 2007 B-class flare: new insights from Hinode observations

G. **Del Zanna**1, U. Mitra-Kraev1, S. J. Bradshaw2,3,4, H. E. Mason1 and A. Asai
A&A 526, A1 (**2011**)

We present multi-wavelength observations of a small B-class flare which occurred on the Sun on **2007 May 22**. The observations include data from Hinode, GOES, TRACE and the Nobeyama Radioheliograph. We obtained spatially and spectrally-resolved information from the Hinode EUV Imaging Spectrometer (EIS) during this event. The temporal and temperature coverage of the EIS observations provides new insights into our understanding of chromospheric evaporation and cooling. The flare showed many "typical" features, such as brightenings in the ribbons, hot (10 MK) loop emission and subsequent cooling. We also observed a new feature, strong (up to 170 km s-1) blue-shifted emission in lines formed around 2–3 MK, located at the footpoints of the 10 MK coronal emission and within the ribbons. Electron densities at 2 MK in the kernels are high, of the order of 1011 cm-3, suggesting a very narrow layer where the chromospheric evaporation occurs. We have run a non-equilibrium hydrodynamic numerical simulation using the HYDRAD code to study the cooling of the 10 MK plasma, finding good agreement between the predicted and observed temperatures, densities and ion populations. Line blending for some potentially useful diagnostic lines for flares, which are observed with Hinode/EIS, is also discussed.

A single picture for solar coronal outflows and radio noise storms

G. **Del Zanna**1, G. Aulanier2, K.-L. Klein2, and T. T¨or¨ok2
E-print, Sept **2010, File**; A&A 526, A137 (**2011**)

We propose a unified interpretation for persistent coronal outflows and metric radio noise storms, two phenomena typically observed in association with quiescent solar active regions. Our interpretation is based on multi-wavelength observations of two such regions as they crossed the meridian in **May and July 2007**. For both regions, we observe a persistent pattern of blue-shifted coronal emission in high-temperature lines with Hinode/EIS, and a radio noise storm with the Nanc?ay Radioheliograph. The observations are supplemented by potential and linear force-free extrapolations of the photospheric magnetic field over large computational boxes, and by a detailed analysis of the coronal magnetic field topology. We find true separatrices in the coronal field and null points high in the corona, which are preferential locations for magnetic reconnection and electron acceleration. We suggest that the continuous growth of active regions maintains a steady reconnection across the separatrices at the null point. This interchange reconnection occurs between closed, high-density loops in the core of the active region and neighbouring open, low-density flux tubes. Thus, the reconnection creates strong pressure imbalances which are the main drivers of plasma upflows. Furthermore, the acceleration of low-energy electrons in the interchange reconnection region sustains the radio noise storm in the closed loop areas, as well as weak type III emission along the open field lines. For both active regions studied, we find a remarkable agreement between the observed places of persistent coronal outflows and radio noise storms with their locations as predicted by our interpretation.

A multi-wavelength study of the compact M1 flare on October 22, 2002

G. **Del Zanna**, A. Berlicki, B. Schmieder, H.E. Mason
2005-2006
http://www.damtp.cam.ac.uk/user/astro/gd232/research/papers/cflare/paper_sp.pdf

In this paper we present a further study of the M1 class flare observed on **October 22, 2002**. We focus on the SOHO Coronal Diagnostic Spectrometer (CDS) spectral observations performed during a multi-wavelength campaign with TRACE and ground-based instruments (VTT, THEMIS). Strong blue-shifts are observed in the CDS coronal lines in flare kernels during the impulsive phase of this flare. From a careful wavelength calibration we deduce upflows of 140 km/s for the Fe XIX flare emission, with a pattern of progressively smaller flows at lower temperatures. Large line-widths were observed, especially for the Fe XIX line, which indicate the existence of turbulent velocities. The strong upflows correspond to full shifts of the line profiles. These flows are observed at the initial phase of the flare, and correspond to the "explosive evaporation". The regions of the blueshifted kernels, a few arc seconds away from the flare onset location, could be explained by the chain reaction of successive magnetic reconnections of growing emerging field line with higher and higher overlying field. This interpretation is evidenced by the analysis of the magnetic topology of the a active region using a linear force-free-field extrapolation of THEMIS magnetograms.

What can we deduce from the 3D geometry of active region upflows?

P. **D_emoulin,** D. Baker, L. van Driel-Gesztelyi, and C.H. Mandrini
EIS Nugget, February **2013**
http://msslxr.mssl.ucl.ac.uk:8080/SolarB/nuggets/nugget_2013feb.jsp

One of the most intriguing Hinode/EIS results is the detection of high-speed upflows in coronal plasma at the edges of ARs (Doschek et al., 2007; Doschek et al., 2008; Del Zanna, 2008; Harra et al., 2008; Hara et al., 2008). These persistent upflows are located in regions of low electron density and low radiance over strong magnetic flux concentrations of a single polarity. Though the general characteristics of AR upflows are now well-known, key questions remain open - How are these flows oriented? How broad is the angular extent of the flows? Are upflows observed in different spectral lines related? How are they linked? In Démoulin et al., 2013, we attempt to address these questions by analyzing the limb-to-limb evolution of AR 10978 in order to constrain the geometry, nature, and physics of large-scale upflows present on both sides of ARs. **9-13 Dec 2007**

The 3D geometry of active region upflows deduced from their limb-to-limb evolution

P. **D_emoulin**1 _ D. Baker2 _C.H. Mandrini3;4 _ L. van Driel-Gesztelyi
E-print, Dec **2013**, Solar Phys. April **2013**, Volume 283, Issue 2, pp 341-367
We analyse the evolution of coronal plasma upflows from the edges of AR 10978, which has the best limb-to-limb data coverage with Hinode's EUV Imaging Spectrometer (EIS). We find that the observed evolution is largely due to the solar rotation progressively changing the viewpoint of nearly stationary flows. From the systematic changes in the upflow regions as a function of distance from disc centre, we deduce their 3D geometrical properties as inclination and angular spread in three coronal lines (SiVII, FeXII, FeXV). In agreement with magnetic extrapolations, we find that the flows are thin, fan-like structures rooted in quasi separatrix layers (QSLs). The fans are tilted away from the AR centre. The highest plasma velocities in these three spectral lines have similar magnitudes and their heights increase with temperature. The spatial location and extent of the upflow regions in the SiVII , FeXII and FeXV lines are different owing to (i) temperature stratification and (ii) line of sight integration of the spectral profiles with significantly different backgrounds. We conclude that we sample the same flows at different temperatures. Further, we find that the evolution of line widths during the disc passage is compatible with a broad range of velocities in the flows. Everything considered, our results are compatible with the AR upflows originating from reconnections along QSLs between over-pressure AR loops and neighboring under-pressure loops. The flows are driven along magnetic field lines by a pressure gradient in a stratified atmosphere. We propose that, at any given time, we observe the superposition of flows created by successive reconnections, leading to a broad velocity distribution. Movies are at:
http://www.lesia.obspm.fr/perso/pascal-demoulin/13/Movies_Vevol.zip

Initiation and Development of the white-light and radio CME on 15 April 2001

P. **Demoulin**, A. Vourlidas, M. Pick, A. Bouteille
E-print, 9 March **2012, File**; **2012** ApJ 750 147
The 2001 April 15 event was one of the largest of the last solar cycle. A former study (Maia et al., 2007) established that this event was associated with a coronal mass ejection (CME) observed both at white light and radio frequencies. This radio CME is illuminated by synchrotron emission from relativistic electrons. In this paper, we investigate the relation of the radio CME to its extreme ultraviolet (EUV) and white light counterpart and reach four main conclusions. i) The radio CME corresponds to the white light flux rope cavity. ii) The presence of a reconnecting current sheet behind the erupting flux rope is framed, both from below and above, by bursty radio sources. This reconnection is the source of relativistic radiating electrons which are injected down along the reconnected coronal arches and up along the flux rope border forming the radio CME. iii) Radio imaging reveals an important lateral over expansion in the low corona; this over expansion is at the origin of compression regions where type II and III bursts are imaged. iv) Already in the initiation phase, radio images reveal large scale interactions of the source active region with its surroundings, including another active region and open magnetic fields. Thus, these complementary radio, EUV, white light data validate the flux rope eruption model of CMEs.
ERRATUM: 2012 ApJ 754 156

Modelling and observations of photospheric magnetic helicity

P. **Démoulin** and E. Pariat
Advances in Space Research, Volume 43, Issue 7, 1 April **2009**, Pages 1013-1031
Mounting observational evidence of the emergence of twisted magnetic flux tubes through the photosphere have now been published. Such flux tubes, formed by the solar dynamo and transported through the convection zone, eventually reach the solar atmosphere. Their accumulation in the solar corona leads to flares and coronal mass ejections. Since reconnections occur during the evolution of the flux tubes, the concepts of twist and magnetic stress become inappropriate. Magnetic helicity, as a well preserved quantity, in particular in plasma with high magnetic Reynolds number, is a more suitable physical quantity to use, even if reconnection is involved.
Only recently, it has been realized that the flux of magnetic helicity can be derived from magnetogram time series. This paper reviews the advances made in measuring the helicity injection rate at the photospheric level, mostly in active regions. It relates the observations to our present theoretical understanding of the emergence process. Most of the helicity injection is found during magnetic flux emergence, whereas the effect of differential rotation is small, and the

long-term evolution of active regions is still puzzling. The photospheric maps of the injection of magnetic helicity provide new spatial information about the basic properties of the link between the solar activity and its sub-photospheric roots. Finally, the newest techniques to measure photospheric flows are reviewed.

Where will efficient energy release occur in 3-D magnetic configurations?

Adv. Space Res., 39(9) *Pages 1367-1377*
P. **Démoulin**

Recent theoretical and observational developments in magnetic helicity studies

Adv. Space Res. 39(11), *Pages 1674-1693, **2007*** **Обзор**
P. **Démoulin**

Magnetic helicity quantifies how the magnetic field is sheared and twisted compared to its lowest energy state (potential field). Such stressed magnetic fields are usually observed in association with flares, eruptive filaments, and coronal mass ejections (CMEs). Magnetic helicity plays a key role in magnetohydrodynamics because it is almost preserved on a timescale less than the global diffusion time scale. Its conservation defines a constraint to the magnetic field evolution.

Only relatively recently, scientists have realized that magnetic helicity can be computed from observations, and methods have been derived to bridge the gap between theory and observations. At the photospheric level, the rate (or flux) of magnetic helicity can be computed from the evolution of longitudinal magnetograms. The coronal helicity is estimated from magnetic extrapolation, while the helicity ejected in magnetic clouds (interplanetary counter-part of CMEs) is derived through modelling of in situ magnetic field measurements. Using its conserved property, a quantitative link between phenomena observed in the corona and then in the interplanetary medium has been achieved.

Some features of possible sources of the energy release in solar flares<<<

O. G. **Den** & I. V. Zimovets
Astronomy Reports, Volume 56, Number 6 (2012), 463-468
Astronomicheskii Zhurnal, **2012**, Vol. 89, No. 6, pp. 515–521**.**

Magnetic field singularities detected earlier as the self-intersection points of the F = 0 curves/surfaces are studied (where F is a certain differential factor calculated in the reference frame of the magnetic field at the given point); these singularities can be considered to be sources of the energy release in solar flares. Two types of such singularities, called transition points (TPs), have been found: the first type (TP1) corresponds to an intersection of the same type of components (terms) of the divergence of the magnetic field, and the second type (TP2) to the intersection of dissimilar components. There are some discontinuous spatial processes at these singularities, which produce jumps in the components of the divergence of the magnetic field (and their signs). TP2 singularities should result in much stronger effects than those resulting from TP1 singularities, which should give rise to the most powerful solar flares. The singularities studied are also compared with the null point of the magnetic field, when it exists. In particular, a model magnetic field containing a null point is considered. It is shown that the TP singularities do not coincide with the null point, but can be located in its vicinity; in the case considered, the TP1 singularity is located fairly close to the null point.

Two-stage Hierarchical Framework for Solar Flare Prediction

Hao **Deng**1,2, Yuting Zhong1, Hong Chen8,1,3,4, Jun Chen1, Jingjing Wang5, Yanhong Chen5,6, and Bingxian Luo5,6,7
2023 ApJS 268 43
https://iopscience.iop.org/article/10.3847/1538-4365/acebbe/pdf

Solar flares, often accompanied by coronal mass ejections and other solar phenomena, are one of the most important sources affecting space weather. It is important to investigate the forecast approach of solar flares to mitigate their destructive effect on the Earth. Statistical analysis, associated with data from 2010 to 2017 in Space-weather HMI Active Region Patches (SHARPs) collected by the Solar Dynamics Observatory's Helioseismic and Magnetic Imager, reveals that there is a distribution divergence between the two types of active regions (ARs) of solar flares. A two-stage hierarchical prediction framework is formulated to better utilize this intrinsic distribution information. Specially, we pick up the ARs where at least one solar flare event occurs within the next 48 hr as flaring ARs through balanced random forest and naive Bayesian methods and then predict the events from flaring ARs by a cascade module of learning models. The empirical evaluation of SHARPs data from 2016 to 2019 verifies the promising performance of our framework, e.g., 0.727 for the true skill statistic.

Fine-grained Solar Flare Forecasting Based on the Hybrid Convolutional Neural Networks

Zheng **Deng**, Feng Wang, Hui Deng, Lei Tan, Linhua Deng, Song Feng

ApJ **922** 232 **2021**
https://arxiv.org/pdf/2109.13428.pdf
https://iopscience.iop.org/article/10.3847/1538-4357/ac2b2b/pdf
https://doi.org/10.3847/1538-4357/ac2b2b
Improving the performance of solar flare forecasting is a hot topic in solar physics research field. Deep learning has been considered a promising approach to perform solar flare forecasting in recent years. We first used the Generative Adversarial Networks (GAN) technique augmenting sample data to balance samples with different flare classes. We then proposed a hybrid convolutional neural network (CNN) model M for forecasting flare eruption in a solar cycle. Based on this model, we further investigated the effects of the rising and declining phases for flare forecasting. Two CNN models, i.e., Mrp and Mdp, were presented to forecast solar flare eruptions in the rising phase and declining phase of solar cycle 24, respectively. A series of testing results proved: 1) Sample balance is critical for the stability of the CNN model. The augmented data generated by GAN effectively improved the stability of the forecast model. 2) For C-class, M-class, and X-class flare forecasting using Solar Dynamics Observatory (SDO) line-of-sight (LOS) magnetograms, the means of true skill statistics (TSS) score of M are 0.646, 0.653 and 0.762, which improved by 20.1%, 22.3%, 38.0% compared with previous studies. 3) It is valuable to separately model the flare forecasts in the rising and declining phases of a solar cycle. Compared with model M, the means of TSS score for No-flare, C-class, M-class, X-class flare forecasting of the Mrp improved by 5.9%, 9.4%, 17.9% and 13.1%, and the Mdp improved by 1.5%, 2.6%, 11.5% and 12.2%.

Periodic variation and phase analysis of grouped solar flare with sunspot activity
Hui **Deng**, Ying Mei, Feng Wang
Research in Astronomy and Astrophysics **2019**
https://arxiv.org/pdf/1910.02671.pdf
Studies on the periodic variation and the phase relationship between different solar activity indicators are useful for understanding the long-term evolution of solar activity cycle. Here we report the statistical analysis of grouped solar flare (GSF) and sunspot number (SN) during the time interval from January 1965 to March 2009. We find that, 1) the significant periodicities of both GSF and SN are related to the differential rotation periodicity, the quasi-biennial oscillation (QBO), and the eleven-year Schwabe cycle (ESC), but the specific values are not absolutely identical; 2) the ESC signal of GSF lags behind that of SN with an average of 7.8 months during the considered time interval, implying that the systematic phase delays between GSF and SN originate from the inter-solar-cycle signal. Our results may provide evidence about the storage of magnetic energy in the corona.

Phase and amplitude asymmetry in the quasi-biennial oscillation of solar Halpha flare activity
L. H. **Deng**, X. J. Zhang, G. Y. Li, H. Deng, F. Wang
MNRAS **2019**
https://arxiv.org/pdf/1910.02891.pdf
Quasi-biennial oscillation (QBO) of solar magnetic activities is intrinsic to dynamo mechanism, but still far from fully understood. In this work, the phase and amplitude asymmetry of solar QBO of Halpha flare activity in the northern and southern hemispheres is studied by the ensemble empirical mode decomposition, the cross-correlation analysis, and the wavelet transform technique. The following results are found: (1) solar QBO of Halpha flare index in the two hemispheres has a complicated phase relationship, but does not show any systematic regularity; (2) the solar cycle mode of solar Halpha flare index in the northern hemisphere generally leads that in the southern one by 9 months for the time interval from 1966 to 2014. The possible origin of these results is discussed.

Statistical properties of solar Hα flare activity
Linhua **Deng**, Xiaojuan Zhang, Jianmei An and Yunfang Cai
J. Space Weather Space Clim. **2017**, 7, A34
https://www.swsc-journal.org/articles/swsc/pdf/2017/01/swsc170008.pdf
Magnetic field structures on the solar atmosphere are not symmetric distribution in the northern and southern hemispheres, which is an important aspect of quasi-cyclical evolution of magnetic activity indicators that are related to solar dynamo theories. Three standard analysis techniques are applied to analyze the hemispheric coupling (north-south asymmetry and phase asynchrony) of monthly averaged values of solar Hα flare activity over the past 49 years (from 1966 January to 2014 December). The prominent results are as follows: (1) from a global point of view, solar Hα flare activity on both hemispheres are strongly correlated with each other, but the northern hemisphere precedes the southern one with a phase shift of 7 months; (2) the long-range persistence indeed exists in solar Hα flare activity, but the dynamical complexities in the two hemispheres are not identical; (3) the prominent periodicities of Hα flare activity are 17 years full-disk activity cycle and 11 years Schwabe solar cycle, but the short- and mid-term periodicities cannot determined by monthly time series; (4) by comparing the non-parametric rescaling behavior on a point-by-point basis, the hemispheric asynchrony of solar Hα flare activity are estimated to be ranging from several months to tens of months with an average value of 8.7 months. The analysis results could promote our knowledge on the long-range persistence,

the quasi-periodic variation, and the hemispheric asynchrony of solar Hα flare activity on both hemispheres, and possibly provide valuable information for the hemispheric interrelation of solar magnetic activity.

High-Cadence and High-Resolution Halpha Imaging Spectroscopy of a Circular Flare's Remote Ribbon with IBIS

Na **Deng**, Alexandra Tritschler, Ju Jing, Xin Chen, Chang Liu, Kevin Reardon, Carsten Denker, Yan Xu, and Haimin Wang

E-print, April **2013**; ApJ 769 112, **2013**;

We present an unprecedented high-resolution ha imaging spectroscopic observation of a C4.1 flare taken with the Interferometric Bidimensional Spectrometer (IBIS) in conjunction with the adaptive optics system at the 76~cm Dunn Solar Telescope on **2011 October 22** in active region NOAA 11324. Such a two-dimensional spectroscopic observation covering the entire evolution of a flare ribbon with high spatial (0.1arcpix image scale), cadence (4.8~s) and spectral (0.1~AA stepsize) resolution is rarely reported. The flare consists of a main circular ribbon that occurred in a parasitic magnetic configuration and a remote ribbon that was observed by the IBIS. Such a circular-ribbon flare with a remote brightening is predicted in 3D fan-spine reconnection but so far has been rarely observed. During the flare impulsive phase, we define ``core'' and ``halo'' structures in the observed ribbon based on IBIS narrowband images in the ha line wing and line center. Examining the ha emission spectra averaged in the flare core and halo areas, we find that only those from the flare cores show typical nonthermal electron beam heating characteristics that have been revealed by previous theoretical simulations and observations of flaring ha line profiles. These characteristics include: broad and centrally reversed emission spectra, excess emission in the red wing with regard to the blue wing (i.e., red asymmetry), and redshifted bisectors of the emission spectra. We also observe rather quick timescales for the heating (~30~s) and cooling (~14--33~s) in the flare core locations. Therefore, we suggest that the flare cores revealed by IBIS track the sites of electron beam precipitation with exceptional spatial and temporal resolution. The flare cores show two-stage motion (a parallel motion along the ribbon followed by an expansion motion perpendicular to the ribbon) during the two impulsive phases of the flare. Some cores jump quickly (30 kms) between discrete magnetic elements implying reconnection involving different flux tubes. We observe a very high temporal correlation (gtrsim0.9) between the integrated ha and HXR emission during the flare impulsive phase. A short time delay (4.6~s) is also found in the ha emission spikes relative to HXR bursts. The ionization timescale of the cool chromosphere and the extra time taken for the electrons to travel to the remote ribbon site may contribute to this delay.

RAPID ENHANCEMENT OF SHEARED EVERSHED FLOW ALONG THE NEUTRAL LINE ASSOCIATED WITH AN X6.5 FLARE OBSERVED BY HINODE

Na **Deng**1,2, Chang Liu2, Debi Prasad Choudhary1 and Haimin Wang

2011 ApJ 733 L14

We present G-band and Ca II H observations of NOAA AR 10930 obtained by Hinode/SOT on **2006 December 6** covering an X6.5 flare. The Local Correlation Tracking technique was applied to the foreshortening-corrected G-band image series to acquire horizontal proper motions in this complex βγδ active region. With the continuous high-quality, spatial and temporal resolution G-band data, we not only confirm the rapid decay of outer penumbrae and darkening of the central structure near the flaring neutral line, but also unambiguously detect for the first time the enhancement of the sheared Evershed flow (average horizontal flow speed increased from 330 ± 3.1 to 403 ± 4.6 m s–1) along the neutral line right after the eruptive white-light flare. Post-flare Ca II H images indicate that the originally fanning out field lines at the two sides of the neutral line get connected. Since penumbral structure and Evershed flow are closely related to photospheric magnetic inclination or horizontal field strength, we interpret the rapid changes of sunspot structure and surface flow as the result of flare-induced magnetic restructuring down to the photosphere. The magnetic fields turn from fanning out to inward connection causing outer penumbrae decay, meanwhile those near the flaring neutral line become more horizontal leading to stronger Evershed flow there. The inferred enhancement of horizontal magnetic field near the neutral line is consistent with recent magnetic observations and theoretical predictions of flare-invoked photospheric magnetic field change.

A Very Narrow RHESSI X-ray Flare on 25 September 2011

Brian R. **Dennis**, Anne K. Tolbert

ApJ **2019**

https://arxiv.org/pdf/1910.13308.pdf

The unusually narrow X-ray source imaged with RHESSI during an impulsive spike lasting for ~10~s during the GOES C7.9 flare on **25 September 2011** (SOL2011-09-25T03:32) was only ~2~ arcsec wide and ~10~arcsec long. Comparison with HMI magnetograms and AIA images at 1700~Å~shows that the X-ray emission was primarily from a long ribbon in the region of positive polarity with little if any emission from the negative polarity ribbon. However, a thermal plasma source density of ~1012 cm−3 estimated from the RHESSI-derived emission measure and source area showed that this could best be interpreted as a coronal hard X-ray source in which the accelerated electrons with energies lass than ~50~keV were stopped by Coulomb collisions in the corona, thus explaining the lack of the more usual bright X-ray footpoints. Analysis of RHESSI spectra shows greater consistency with a multi-temperature

distribution and a low energy cutoff to the accelerated electron spectrum of 22 keV compared to 12 keV if a single temperature distribution is assumed. This leads to a change in the lower limit on the total energy in electrons by an order of magnitude given the steepness of the best-fit electron spectrum with a power-law index of ~6.

Coronal hard X-ray sources revisited

Brian R. **Dennis**, Miguel A. Duval-Poo, Michele Piana, Andrew R. Inglis, A. Gordon Emslie, Jingnan Guo, Yan Xu
ApJ **867** 82 **2018**
https://arxiv.org/pdf/1809.04631.pdf
http://iopscience.iop.org/article/10.3847/1538-4357/aae0f5/pdf
This paper reports on the re-analysis of solar flares in which the hard X-rays (HXRs) come predominantly from the corona rather than from the more usual chromospheric footpoints. All of the 26 previously analyzed event time intervals, over 13 flares, are re-examined for consistency with a flare model in which electrons are accelerated near the top of a magnetic loop that has a sufficiently high density to stop most of the electrons by Coulomb collisions before they can reach the footpoints. Of particular importance in the previous analysis was the finding that the length of the coronal HXR source increased with energy in the 20 - 30 keV range. However, after allowing for the possibility that footpoint emission at the higher energies affects the inferred length of the coronal HXR source, and using analysis techniques that suppress the possible influence of such footpoint emission, we conclude that there is no longer evidence that the length of the HXR coronal sources increase with increasing energy. In fact, for the 6 flares and 12 time intervals that satisfied our selection criteria, the loop lengths decreased on average by 1.0 +/- 0.2 arcsec between 20 and 30 keV, with a standard deviation of 3.5 arcsec. We find strong evidence that the peak of the coronal HXR source increases in altitude with increasing energy. For the thermal component of the emission, this is consistent with the standard CHSKP flare model in which magnetic reconnection in a coronal current sheet results in new hot loops being formed at progressively higher altitudes. The explanation for the nonthermal emission is not so clear. **12 April 2002, 14/15 April 2002, 17 April 2002, 17 June 2003, 10 July 2003, 02 December 2003, 21 May 2004, 31 August 2004, 01 June 2005, 23 August 2005, 13 February 2011, 03 August 2011, 25 September 2011, 15 May 2013**
Table 1. Dates, times, and locations for all 14 analyzed flares. (Apr 2002-May 2013)
RHESSI Science Nuggets #333 October **2018**
http://sprg.ssl.berkeley.edu/~tohban/wiki/index.php/Coronal_Hard_X-ray_Sources_Revisited

Always a Farm Boy

Brian R. **Dennis**
Solar Phys. 294:2 **2019**
https://arxiv.org/pdf/1805.03248.pdf
This is the **memoir** of Brian Dennis - his life story to date, and his involvement with high energy solar physics.

RHESSI's 15th Anniversary

Brian **Dennis**, Säm Krucker and Albert Shih
RHESSI Science Nugget No. 292 Feb 2017
http://sprg.ssl.berkeley.edu/~tohban/wiki/index.php/RHESSI%27s_15th_Anniversary
2017-01-25 (B8.5), 21:26

Detection and Interpretation of Long-lived X-Ray Quasi-periodic Pulsations in the X-class Solar Flare on 2013 May 14

Brian R. **Dennis**1, Anne K. Tolbert1,2, Andrew Inglis1,2, Jack Ireland1,3, Tongjiang Wang1,2, Gordon D. Holman1, Laura A. Hayes3,4, and Peter T. Gallagher
2017 ApJ 836 84
http://iopscience.iop.org/article/10.3847/1538-4357/836/1/84/pdf
Quasi-periodic pulsations (QPP) seen in the time derivative of the GOES soft X-ray light curves are analyzed for the X3.2 event on **2013 May 14**. The pulsations are apparent for a total of at least two hours from the impulsive phase to well into the decay phase, with a total of 163 distinct pulses evident to the naked eye. A wavelet analysis shows that the characteristic timescale of these pulsations increases systematically from ~25 s at 01:10 UT, the time of the GOES peak, to ~100 s at 02:00 UT. A second "ridge" in the wavelet power spectrum, most likely associated with flaring emission from a different active region, shows an increase from ~40 s at 01:40 UT to ~100 s at 03:10 UT. We assume that the QPP that produced the first ridge result from vertical kink-mode oscillations of the newly formed loops following magnetic reconnection in the coronal current sheet. This allows us to estimate the magnetic field strength as a function of altitude given the density, loop length, and QPP timescale as functions of time determined from the GOES light curves and Ramaty High Energy Solar Spectroscopic Imager (RHESSI) images. The calculated magnetic field strength of the newly formed loops ranges from ~500 G at an altitude of 24 Mm to a low value of ~10 G at 60 Mm, in

general agreement with the expected values at these altitudes. Fast sausage-mode oscillations are also discussed and cannot be ruled out as an alternate mechanism for producing the QPP.

Fine Structure in Flare Soft X-ray Light Curves

Brian **Dennis** and Kim Tolbert:
RHESSI Science Nuggets, No. 262, Sept **2015**
http://sprg.ssl.berkeley.edu/~tohban/wiki/index.php/Fine_Structure_in_Flare_Soft_X-ray_Light_Curves
Thus, detailed comparisons between the soft X-ray structures with hard X-ray and microwave light curves have the potential for separating temporally the directly heated plasma from plasma heated by accelerated electrons..

Solar Flare Element Abundances from the Solar Assembly for X-rays (SAX) on MESSENGER

B. R. **Dennis**, K. J. H. Phillips, R. A. Schwartz, A. K. Tolbert, R. D. Starr, L. R. Nittler
ApJ **803** 67 **2015**
http://arxiv.org/pdf/1503.01602v1.pdf
X-ray spectra in the range 1.5−8.5~keV have been analyzed for 526 large flares detected with the Solar Assembly for X-rays (SAX) on the Mercury {\em MESSENGER} spacecraft between 2007 and 2013. For each flare, the temperature and emission measure of the emitting plasma were determined from the spectrum of the continuum. In addition, with the SAX energy resolution of 0.6 keV (FWHM) at 6~keV, the intensities of the clearly resolved Fe-line complex at 6.7~keV and the Ca-line complex at 3.9~keV were determined, along with those of unresolved line complexes from S, Si, and Ar at lower energies. Comparisons of these line intensities with theoretical spectra allow the abundances of these elements relative to hydrogen to be derived, with uncertainties due to instrument calibration and the unknown temperature distribution of the emitting plasma. While significant deviations are found for the abundances of Fe and Ca from flare to flare, the abundances averaged over all flares are found to be enhanced over photospheric values by factors of 1.66±0.34 (Fe), 3.89 ± 0.76 (Ca), 1.23 ± 0.45(S), 1.64 ± 0.66 (Si), and 2.48 ± 0.90 (Ar). These factors differ from previous reported values for Fe and Si at least. They suggest a more complex relation of abundance enhancement with the first ionization potential (FIP) of the element than previously considered, with the possibility that fractionation occurs in flares for elements with a FIP of less than ∼7~eV rather than ∼10~eV. **2007 June 1**

Which detectors can I use to analyze this flare?

Brian **Dennis** and Kim Tolbert
RHESSI Science Nuggets, #235, **2014**
http://sprg.ssl.berkeley.edu/~tohban/wiki/index.php/Which_detectors_can_I_use_to_analyze_this_flare%3F
A new Browser feature helps to answer this question.

RHESSI's Tenth Anniversary **A Review**

Brian **Dennis** and Bob Lin:
RHESSI Nugget No. 169, Feb **2012**
http://sprg.ssl.berkeley.edu/~tohban/wiki/index.php/RHESSI%27s_Tenth_Anniversary
A top-ten list of major RHESSI accomplishments in flare physics:
- Discovery of Gamma-Ray Footpoint Structures
- Energy Content & Spectrum of Flare Energetic Electrons
- Ubiquitous Nonthermal Emissions from the Corona, & Bulk Energization
- Double Coronal X-ray Sources
- Microflares and the Quiet Sun
- Initial Downward Motion of X-ray Sources
- HXR Flare Ribbons
- Location of Superhot X-ray Source
- Photosphere as a Compton or "Dentist's" Mirror
- Broadened 511-keV Positron Annihilation Line
Three serendipitous Non-flare-related Items:
- Solar Oblateness
- Magnetar Timing and Spectroscopy

- Magnetar Timing and Spectroscopy

Overview of the Volume **A Review**

B. R. **Dennis**1, A. G. Emslie2, and H. S. Hudson
Space Sci. Rev., 159:3–17, **2011, File**
In this introductory chapter, we provide a brief summary of the successes and remaining challenges in understanding the solar flare phenomenon and its attendant implications for particle acceleration mechanisms in astrophysical plasmas. We also provide a brief overview of the contents of the other chapters in this volume, with particular reference to the well-observed flare of **2002 July 23**.

- Observational Overview (Fletcher et al., 100 pp)
- Electron Acceleration and Propagation (Holman et al., 68 pp)
- Gamma Rays (Vilmer et al., 70 pp)
- Radio Astronomy (White et al., 36 pp)
- Microflares and Flare Statistics (Hannah et al., 40 pp)
- Deducing Electron Properties (Kontar et al., 64 pp)
- Particle Accleration (Zharkova et al., 62 pp)

Hard X-ray Flare Source Sizes Measured with *RHESSI*

Brian R. **Dennis**1 & Rick L. Pernak
E-print, Apr **2009**; ApJ
RHESSI observations of 18 double hard X-ray sources seen at energies above 25 keV are analyzed to determine the spatial extent of the most compact structures evident in each case. The following four image reconstruction algorithms were used: Clean, Pixon, and two routines using visibilities - Maximum Entropy and Forward Fit (VFF). All have been adapted for this study to optimize their ability to provide reliable estimates of the sizes of the more compact sources. The source fluxes, sizes, and morphologies obtained with each method are cross-correlated and the similarities and disagreements are discussed. The FWHM of the major axes of the sources with assumed elliptical Gaussian shapes are generally well correlated between the four image reconstruction routines and vary between the RHESSI resolution limit of ~2" up to ~20" with most below 10". The FWHM of the minor axes are generally at or just above the RHESSI limit and hence should be considered as unresolved in most cases. The orientation angles of the elliptical sources are also well correlated. These results suggest that the elongated sources are generally aligned along a flare ribbon with the minor axis perpendicular to the ribbon. This is verified for the one flare in our list with coincident TRACE images. There is evidence for significant extra flux in many of the flares in addition to the two identified compact sources, thus rendering the VFF assumption of just two Gaussians inadequate. A more realistic approximation in many cases would be of two line sources with unresolved widths. Recommendations are given for optimizing the RHESSI imaging reconstruction process to ensure that the finest possible details of the source morphology become evident and that reliable estimates can be made of the source dimensions.

Review of Selected RHESSI Solar Results

Brian R. **Dennis**, Hugh S. Hudson, Säm Krucker
Lecture Notes in Physics (LNP), volume 725, **2007** Pages 33-64
We review selected science results from RHESSI solar observations made since launch on 5 February 2002. A brief summary of the instrumentation is given followed by a sampling of the major science results obtained from the soft X-ray, hard X-ray, and gamma-ray energy domains. The thermal continuum measurements and detection of Fe-line features are discussed as they relate to parameters of the thermal flare plasma for several events, including microflares. Observations of X-ray looptop, and rising above-the-loop sources are discussed as they relate to standard models of eruptive events and the existence of a current sheet between the two. Hard X-ray spectra and images of footpoints and coronal sources are presented, showing how they can be used to separate thermal and nonthermal sources and determine the magnetic reconnection rate. Gamma-ray line images and spectra are presented as they relate to determining the location, spectra, and angular distribution of the accelerated ions and the temperature of the chromospheric target material. Finally, we discuss the overall energy budget for two of the larger events seen with RHESSI.

The Neupert effect - What can it tell us about the impulsive and gradual phases of solar flares?

Dennis, B..R., Zarro, D..M.:
1993, Solar Phys. 146, 177 – 190.

The plasma filling factor of coronal bright points - Coronal bright points:

K. P. **Dere**

A&A 491 (2008) 561-566
http://www.aanda.org/10.1051/0004-6361:200810000
Aims.We determine the volumetric plasma filling factor of coronal bright points.
Methods. Rastered spectra of the regions of the quiet Sun were recorded by the Extreme ultraviolet Imaging Spectrometer (EIS) during operations with the Hinode satellite. Calibrated intensities of Fe xii lines were obtained and images of the quiet corona were constructed. From the imaged spectra, the emission measures and geometrical widths of coronal bright points were obtained. Electron densities were determined from density-sensitive line ratios. A comparison of the emission measure and bright point widths with the electron densities yielded the plasma-filling factor.
Results.The median electron density of coronal bright points is 4 Ч 10^9 cm^{-3} at a temperature of 1.6Ч10^6 K. The volumetric plasma-filling factor of coronal bright points was found to vary from 4 Ч 10^{-5} to 0.2 with a median value of 0.015.
Conclusions. The current set of EIS coronal bright point observations indicates that the median value of their plasma filling-factor is 0.015. This can be interpreted as evidence of a considerable subresolution structure in coronal bright points or as the result of a single completely-filled plasma loop with a width on the order of 1–2 arcsec that has not been spatially resolved in these measurements.

Comparing feature sets and machine-learning models for prediction of solar flares Topology, physics, and model complexity

V. **Deshmukh**1, S. Baskar1, T. E. Berger2, E. Bradley1,3 and J. D. Meiss4
A&A 674, A159 (**2023**)
https://www.aanda.org/articles/aa/pdf/2023/06/aa45742-22.pdf
Context. Machine-learning methods for predicting solar flares typically employ physics-based features that have been carefully chosen by experts in order to capture the salient features of the photospheric magnetic fields of the Sun.
Aims. Though the sophistication and complexity of these models have grown over time, there has been little evolution in the choice of feature sets, or any systematic study of whether the additional model complexity leads to higher predictive skill.
Methods. This study compares the relative prediction performance of four different machine-learning based flare prediction models with increasing degrees of complexity. It evaluates three different feature sets as input to each model: a “traditional” physics-based feature set, a novel “shape-based” feature set derived from topological data analysis (TDA) of the solar magnetic field, and a combination of these two sets. A systematic hyperparameter tuning framework is employed in order to assure fair comparisons of the models across different feature sets. Finally, principal component analysis is used to study the effects of dimensionality reduction on these feature sets.
Results. It is shown that simpler models with fewer free parameters perform better than the more complicated models on the canonical 24-h flare forecasting problem. In other words, more complex machine-learning architectures do not necessarily guarantee better prediction performance. In addition, it is found that shape-based feature sets contain just as much useful information as physics-based feature sets for the purpose of flare prediction, and that the dimension of these feature sets – particularly the shape-based one – can be greatly reduced without impacting predictive accuracy.

Decreasing False Alarm Rates in ML-based Solar Flare Prediction using SDO/HMI Data

Varad **Deshmukh**, Natasha Flyer, Kiera Van Der Sande, Thomas Berger
ApJ **2021**
https://arxiv.org/pdf/2111.10704.pdf
A hybrid two-stage machine learning architecture that addresses the problem of excessive false positives (false alarms) in solar flare prediction systems is investigated. The first stage is a convolutional neural network (CNN) model based on the VGG-16 architecture that extracts features from a temporal stack of consecutive Solar Dynamics Observatory (SDO) Helioseismic and Magnetic Imager (HMI) magnetogram images to produce a flaring probability. The probability of flaring is added to a feature vector derived from the magnetograms to train an extremely randomized trees (ERT) model in the second stage to produce a binary deterministic prediction (flare/no flare) in a 12-hour forecast window. To tune the hyperparameters of the architecture a new evaluation metric is introduced, the "scaled True Skill Statistic". It specifically addresses the large discrepancy between the true positive rate and the false positive rate in the highly unbalanced solar flare event training datasets. Through hyperparameter tuning to maximize this new metric, our two-stage architecture drastically reduces false positives by ≈ 48% without significantly affecting the true positives (reduction by ≈ 12%), when compared with predictions from the first stage CNN alone. This, in turn, improves various traditional binary classification metrics sensitive to false positives such as the precision, F1 and the Heidke Skill Score. The end result is a more robust 12-hour flare prediction system that could be combined with current operational flare forecasting methods. Additionally, using the ERT-based feature ranking mechanism, we show that the CNN output probability is highly ranked in terms of flare prediction relevance. **1-7 Sep 2017**

RECONNECTION IN THREE DIMENSIONS: THE ROLE OF SPINES IN THREE ERUPTIVE FLARES

Angela **Des Jardins**1, Richard Canfield1, Dana Longcope1, Crystal Fordyce2, and Scott Waitukaitis3
Astrophysical Journal, 693:1628–1636, **2009** March
In order to better understand magnetic reconnection and particle acceleration in solar flares, we compare the

***RHESSI* hard X-ray (HXR) footpoint motions** of three flares with a detailed study of the corresponding topology given by a Magnetic Charge Topology model. We analyze the relationship between the footpoint motions and topological spine lines and find that the examined footpoint sources move along spine lines. We present a three dimensional topological model in which this movement can be understood. As reconnection proceeds, flux is transferred between the reconnecting domains, causing the separator to move. The movement of the separator's chromospheric ends, identified with the HXR footpoints, is along those spine lines on which the separator ends.

Does Nearby Open Flux Affect the Eruptivity of Solar Active Regions?

Marc L. **DeRosa**, Graham Barnes
ApJ **2018**
https://arxiv.org/pdf/1802.01199.pdf
The most energetic solar flares are typically associated with the ejection of a cloud of coronal material into the heliosphere in the form of a coronal mass ejection (CME). However, there exist large flares which are not accompanied by a CME. The existence of these non-eruptive flares raises the question of whether such flares suffer from a lack of access to nearby open fields in the vicinity above the flare (reconnection) site. In this study, we use a sample of 56 flares from Sunspot Cycles 23 and 24 to test whether active regions that produce eruptive X-class flares are preferentially located near coronal magnetic field domains that are open to the heliosphere, as inferred from a potential field source surface model. The study shows that X-class flares having access to open fields are eruptive at a higher rate than those for which access is lacking. The significance of this result should be moderated due to the small number of non-eruptive X-class flares in the sample, based on the associated Bayes factor. **2001-04-15, 2002-08-21 , 2013-11-10, 2014-12-20, 2017-09-06**
Table 1. Sample of flaring active regions

Decreasing False-alarm Rates in CNN-based Solar Flare Prediction Using SDO/HMI Data

Varad **Deshmukh**1, Natasha Flyer2, Kiera van der Sande3, and Thomas Berger4
2022 ApJS 260 9
https://iopscience.iop.org/article/10.3847/1538-4365/ac5b0c/pdf
A hybrid two-stage machine-learning architecture that addresses the problem of excessive false positives (false alarms) in solar flare prediction systems is investigated. The first stage is a convolutional neural network (CNN) model based on the VGG-16 architecture that extracts features from a temporal stack of consecutive Solar Dynamics Observatory Helioseismic and Magnetic Imager magnetogram images to produce a flaring probability. The probability of flaring is added to a feature vector derived from the magnetograms to train an extremely randomized trees (ERT) model in the second stage to produce a binary deterministic prediction (flare/no-flare) in a 12 hr forecast window. To tune the hyperparameters of the architecture, a new evaluation metric is introduced: the "scaled True Skill Statistic." It specifically addresses the large discrepancy between the true positive rate and the false positive rate in the highly unbalanced solar flare event training data sets. Through hyperparameter tuning to maximize this new metric, our two-stage architecture drastically reduces false positives by ≈48% without significantly affecting the true positives (reduction by ≈12%), when compared with predictions from the first-stage CNN alone. This, in turn, improves various traditional binary classification metrics sensitive to false positives, such as the precision, F1, and the Heidke Skill Score. The end result is a more robust 12 hr flare prediction system that could be combined with current operational flare-forecasting methods. Additionally, using the ERT-based feature-ranking mechanism, we show that the CNN output probability is highly ranked in terms of flare prediction relevance.

Machine Learning Approaches to Solar-Flare Forecasting: Is Complex Better? **Review**

Varad **Deshmukh**, Srinivas Baskar, Elizabeth Bradley, Thomas Berger, James D. Meiss
ApJ **2022**
https://arxiv.org/pdf/2202.08776.pdf
Recently, there has been growing interest in the use of machine-learning methods for predicting solar flares. Initial efforts along these lines employed comparatively simple models, correlating features extracted from observations of sunspot active regions with known instances of flaring. Typically, these models have used physics-inspired features that have been carefully chosen by experts in order to capture the salient features of such magnetic field structures. Over time, the sophistication and complexity of the models involved has grown. However, there has been little evolution in the choice of feature sets, nor any systematic study of whether the additional model complexity is truly useful. Our goal is to address these issues. To that end, we compare the relative prediction performance of machine-learning-based, flare-forecasting models with varying degrees of complexity. We also revisit the feature set design, using topological data analysis to extract shape-based features from magnetic field images of the active regions. Using hyperparameter training for fair comparison of different machine-learning models across different feature sets, we show that simpler models with fewer free parameters \textit{generally perform better than more-complicated models}, ie., powerful machinery does not necessarily guarantee better prediction performance. Secondly, we find that \textit{abstract, shape-based features contain just as much useful information}, for the purposes of flare prediction, as the set of hand-crafted features developed by the solar-physics community over the years. Finally, we study the effects of dimensionality

reduction, using principal component analysis, to show that streamlined feature sets, overall, perform just as well as the corresponding full-dimensional versions. **1-7 Sep 2017**

Shape-based Feature Engineering for Solar Flare Prediction **Review**

Varad **Deshmukh**, Thomas Berger, James Meiss, Elizabeth Bradley
Proceedings for Innovative Applications of Artificial Intelligence Conference 2021 **2021**
https://arxiv.org/pdf/2012.14405.pdf
Solar flares are caused by magnetic eruptions in active regions (ARs) on the surface of the sun. These events can have significant impacts on human activity, many of which can be mitigated with enough advance warning from good forecasts. To date, machine learning-based flare-prediction methods have employed physics-based attributes of the AR images as features; more recently, there has been some work that uses features deduced automatically by deep learning methods (such as convolutional neural networks). We describe a suite of novel shape-based features extracted from magnetogram images of the Sun using the tools of computational topology and computational geometry. We evaluate these features in the context of a multi-layer perceptron (MLP) neural network and compare their performance against the traditional physics-based attributes. We show that these abstract shape-based features outperform the features chosen by the human experts, and that a combination of the two feature sets improves the forecasting capability even further. **4-7 Sep 2017**

Leveraging the Mathematics of Shape for Solar Magnetic Eruption Prediction

V. **Deshmukh**, T. E. Berger, E. Bradley, J. D. Meiss
Journal of Space Weather and Space Climate Volume 10, id.13, **2020**
https://arxiv.org/pdf/2003.05827.pdf
https://www.swsc-journal.org/articles/swsc/pdf/2020/01/swsc190060.pdf
Current operational forecasts of solar eruptions are made by human experts using a combination of qualitative shape-based classification systems and historical data about flaring frequencies. In the past decade, there has been a great deal of interest in crafting machine-learning (ML) flare-prediction methods to extract underlying patterns from a training set---e.g., a set of solar magnetogram images, each characterized by features derived from the magnetic field and labeled as to whether it was an eruption precursor. These patterns, captured by various methods (neural nets, support vector machines, etc.), can then be used to classify new images. A major challenge with any ML method is the \textit{featurization} of the data: pre-processing the raw images to extract higher-level properties, such as characteristics of the magnetic field, that can streamline the training and use of these methods. It is key to choose features that are informative, from the standpoint of the task at hand. To date, the majority of ML-based solar eruption methods have used physics-based magnetic and electric field features such as the total unsigned magnetic flux, the gradients of the fields, the vertical current density, etc. In this paper, we extend the relevant feature set to include characteristics of the magnetic field that are based purely on the geometry and topology of 2D magnetogram images and show that this improves the prediction accuracy of a neural-net based flare-prediction method. **2017 Sept 1-7**

Extreme-Ultraviolet Wave and Accompanying Loop Oscillations

Pooja **Devi**, Ramesh Chandra, Arun Kumar Awasthi, Brigitte Schmieder, Reetika Joshi
Solar Phys. **297**, Article number: 153 **2022**
https://arxiv.org/pdf/2211.07438.pdf
https://doi.org/10.1007/s11207-022-02082-6
We present the observations of an extreme-ultraviolet (EUV) wave, which originated from the active region (AR) NOAA 12887 on **28 October 2021** and its impact on neighbouring loops. The event was observed by the Atmospheric Imaging Assembly (AIA) on board the Solar Dynamics Observatory (SDO) satellite at various wavebands and by the Solar TErrestrial RElations Observatory-Ahead (STEREO-A) with its Extreme-Ultraviolet Imager (EUVI) and COR1 instruments with a different view angle than SDO. We show that the EUV wave event consists of several waves as well as non-wave phenomena. The wave components include: the fast-mode part of the EUV wave event, creation of oscillations in nearby loops, and the appearance of wave trains. The non-wave component consists of stationary fronts. We analyze selected oscillating loops and find that the periods of these oscillations range from 230 - 549 s. Further, we compute the density ratio inside and outside the loops and the magnetic field strength. The computed density ratio and magnetic field are found in the range of 1.08 - 2.92 and 5.75 - 8.79 G, respectively. Finally, by combining SDO and STEREO-A observations, we find that the observed EUV wave component propagates ahead of the CME leading edge.

Development of a Confined Circular-cum-parallel Ribbon Flare and Associated Pre-flare Activity

Pooja **Devi**, Bhuwan Joshi, Ramesh Chandra, Prabir K. Mitra, Astrid M. Veronig3, Reetika Joshi
Solar Phys. **295**, Article number: 75 **2020**
https://arxiv.org/pdf/2005.09586.pdf
https://link.springer.com/content/pdf/10.1007/s11207-020-01642-y.pdf

We study a complex GOES M1.1 circular ribbon flare and related pre-flare activity on **26 January 2015** [SOL26-01-2015] in solar active region NOAA 12268. This flare activity was observed by the AIA on board SDO and the RHESSI. The examination of photospheric magnetograms during the extended period, prior to the event, suggests the successive development of a so-called 'anemone' type magnetic configuration. NLFFF extrapolation reveals a fan-spine magnetic configuration with the presence of a coronal null-point. We found that the pre-flare activity in the active region starts ~15 min prior to the main flare in the form of localized bright patches at two locations. A comparison of locations and spatial structures of the pre-flare activity with magnetic configuration of the corresponding region suggests onset of magnetic reconnection at the null-point along with the low-atmosphere magnetic reconnection caused by the emergence and the cancellation of the magnetic flux. The main flare of M1.1 class is characterized by the formation of a well-developed circular ribbon along with a region of remote brightening. Remarkably, a set of relatively compact parallel ribbons formed inside the periphery of the circular ribbon which developed lateral to the brightest part of the circular ribbon. During the peak phase of the flare, a coronal jet is observed at the north-east edge of the circular ribbon which suggests interchange reconnection between large-scale field lines and low-lying closed field lines. Our investigation suggests a combination of two distinct processes in which ongoing pre-flare null-point reconnection gets further intensified as the confined eruption along with jet activity proceeded from within the circular ribbon region which results to the formation of inner parallel ribbons and corresponding post-reconnection arcade.

What Are the Causes of Super Activity of Solar Active Regions?

Suman K. **Dhakal**1 and Jie Zhang1
2024 ApJ 960 36
https://iopscience.iop.org/article/10.3847/1538-4357/ad07d2/pdf
https://arxiv.org/pdf/2312.15083.pdf
Flare productivity varies among solar active regions (ARs). This study analyzed 20 ARs of contrasting sunspot areas and flare productivities to understand the super flare productivity of certain ARs. We used the flare index (FI) as an indicator of flare activity. We examined the pattern of morphological evolution of magnetic features. Further, we derived a set of magnetic feature parameters to quantitatively characterize ARs. Our study found that the correlation coefficient is the highest (r = 0.78) between FI and the length of the strong gradient polarity inversion line (SgPIL), while the coefficient is the lowest (r = 0.14) between FI and the total unsigned magnetic flux. For the selected ARs, this study also found that the super flare productive ARs have SgPILs (R value) longer (greater) than 50 Mm (4.5). These results suggest that flare productivity is mainly controlled by the size of the subregion that comprises close interaction of opposite magnetic polarities and is weakly correlated with the size of the whole ARs. Further, even though magnetic flux emergence is important, this study shows that it alone is insufficient to increase flare productivity. New emergence can drive either the interaction of like or opposite magnetic polarities of nonconjugate pairs (i.e., polarities not from the same bipole). In the former case, the magnetic configuration remains simple, and flare productivity would be low. In the latter case, the convergence of opposite magnetic fluxes of nonconjugate pairs results in a magnetic configuration with long SgPIL and an increase in flare productivity. **2012.03.05-10, 2012.06.29–07.07, 2013.12.17-22, 2014.07.04-0.9**
Table 1 Average Value of Magnetic Field Parameters of Selected ARs

Deep-learning Reconstruction of Sunspot Vector Magnetic Fields for Forecasting Solar Storms

Dattaraj B. **Dhuri**1,2, Shamik Bhattacharjee1, Shravan M. Hanasoge1,2, and Sashi Kiran Mahapatra1
2022 ApJ 939 64
https://iopscience.iop.org/article/10.3847/1538-4357/ac9413/pdf
Solar magnetic activity produces extreme solar flares and coronal mass ejections, which pose grave threats to electronic infrastructure and can significantly disrupt economic activity. It is therefore important to appreciate the triggers of explosive solar activity and develop reliable space weather forecasting. Photospheric vector magnetic field data capture sunspot magnetic field complexity and can therefore improve the quality of space weather prediction. However, state-of-the-art vector field observations are consistently only available from Solar Dynamics Observatory/Helioseismic and Magnetic Imager (HMI) since 2010, with most other current and past missions and observational facilities, such as Global Oscillations Network Group (GONG), only recording line-of-sight (LOS) fields. Here, using an inception-based convolutional neural network (CNN), we reconstruct HMI sunspot vector field features from LOS magnetograms of HMI and GONG with high fidelity (∼90% correlation) and sustained flare forecasting accuracy. We rebuild vector field features during the 2003 Halloween storms, for which only LOS field observations are available, and the CNN-estimated electric current helicity accurately captures the observed rotation of the associated sunspot prior to the extreme flares, showing a striking increase. Our study thus paves the way for reconstructing three solar cycles worth of vector field data from past LOS measurements, which are of great utility in improving space weather forecasting models and gaining new insights about solar activity. **26-31 Oct 2003, 2-15 Feb 2011, 7-12 Mar 2011, 29 Jul-4 Aug 2011, 2-9 Sep 2011, 20-26 Oct 2013, 27 Oct-1 Nov, 2013, 6-10 Nov 2013, 16-20 Dec 2013, 6-11 Jan 2014, 3-7 Feb 2014, 2-6 Sep 2017**

Machine learning reveals systematic accumulation of electric current in lead-up to solar flares

Dattaraj B. **Dhuri**, Shravan M. Hanasoge, Mark C. M. Cheung

Proceedings of the National Academy of Sciences of the United States of America (PNAS)
2019
https://arxiv.org/pdf/1905.10167.pdf
Solar flares - bursts of high-energy radiation responsible for severe space-weather effects - are a consequence of the occasional destabilization of magnetic fields rooted in active regions (ARs). The complexity of AR evolution is a barrier to a comprehensive understanding of flaring processes and accurate prediction. Though machine learning (ML) has been used to improve flare predictions, the potential for revealing precursors and associated physics has been underexploited. Here, we train ML algorithms to classify between vector-magnetic-field observations from flaring ARs, producing at least one M-/X-class flare, and non-flaring ARs. Analysis of magnetic-field observations accurately classified by the machine presents statistical evidence for (1) ARs persisting in flare-productive states --- characterized by AR area --- for days, before and after M- and X-class flare events, (2) systematic pre-flare build-up of free energy in the form of electric currents, suggesting that associated subsurface magnetic field is twisted, (3) intensification of Maxwell stresses in the corona above newly emerging ARs, days before first flares. These results provide new insights into flare physics and improving flare forecasting.

The Effect of Limited Sample Sizes on the Accuracy of the Estimated Scaling Parameter for Power-Law-Distributed Solar Data

Elke **D'Huys**, David Berghmans, Daniel B. Seaton, Stefaan Poedts
Solar Phys. **2016**
http://arxiv.org/pdf/1605.06972v1.pdf
Many natural processes exhibit power-law behavior. The power-law exponent is linked to the underlying physical process and therefore its precise value is of interest. With respect to the energy content of nanoflares, for example, a power-law exponent steeper than 2 is believed to be a necessary condition to solve the enigmatic coronal heating problem. Studying power-law distributions over several orders of magnitudes requires sufficient data and appropriate methodology. In this paper we demonstrate the shortcomings of some popular methods in solar physics that are applied to data of typical sample sizes. We use synthetic data to study the effect of the sample size on the performance of different estimation methods and show that vast amounts of data are needed to obtain a reliable result with graphical methods (where the power-law exponent is estimated by a linear fit on a log-transformed histogram of the data). We **revisit published results on power laws for the angular width of solar coronal mass ejections and the radiative losses of nanoflares.** We demonstrate the benefits of the maximum likelihood estimator and advocate its use.

Measurements of Electron Anisotropy in Solar Flares Using Albedo with RHESSI X-Ray Data

E. C. M. **Dickson**, E. P. Kontar
Solar Physics, June **2013**, Volume 284, Issue 2, pp 405-425
The angular distribution of electrons accelerated in solar flares is a key parameter in the understanding of the acceleration and propagation mechanisms that occur there. However, the anisotropy of energetic electrons is still a poorly known quantity, with observational studies producing evidence for an isotropic distribution and theoretical models mainly considering the strongly beamed case. We use the effect of photospheric albedo to infer the pitch-angle distribution of X-ray emitting electrons using Hard X-ray data from RHESSI. A bi-directional approximation is applied and a regularised inversion is performed for eight large flare events to deduce the electron spectra in both downward (towards the photosphere) and upward (away from the photosphere) directions. The electron spectra and the electron anisotropy ratios are calculated for a broad energy range, from about ten up to ∼ 300 keV, near the peak of the flares. The variation of electron anisotropy over short periods of time lasting 4, 8 and 16 seconds near the impulsive peak has been examined. The results show little evidence for strong anisotropy and the mean electron flux spectra are consistent with the isotropic electron distribution. The 3σ level uncertainties, although energy and event dependent, are found to suggest that anisotropic distribution with anisotropy larger than ∼ three are not consistent with the hard X-ray data. At energies above 150 – 200 keV, the uncertainties are larger and thus the possible electron anisotropies could be larger.

Dynamic data-driven integrated flare model based on self-organized criticality

M. **Dimitropoulou**1, H. Isliker2, L. Vlahos2 and M. K. Georgoulis
A&A 553, A65 (**2013)**
Context. We interpret solar flares as events originating in active regions that have reached the self-organized critical state. We describe them with a dynamic integrated flare model whose initial conditions and driving mechanism are derived from observations.
Aims. We investigate whether well-known scaling laws observed in the distribution functions of characteristic flare parameters are reproduced after the self-organized critical state has been reached.
Methods. To investigate whether the distribution functions of total energy, peak energy, and event duration follow the expected scaling laws, we first applied the previously reported static cellular automaton model to a time series of seven

solar vector magnetograms of the NOAA active region 8210 recorded by the Imaging Vector Magnetograph on May 1 1998 between 18:59 UT and 23:16 UT until the self-organized critical state was reached. We then evolved the magnetic field between these processed snapshots through spline interpolation, mimicking a natural driver in our dynamic model. We identified magnetic discontinuities that exceeded a threshold in the Laplacian of the magnetic field after each interpolation step. These discontinuities were relaxed in local diffusion events, implemented in the form of cellular automaton evolution rules. Subsequent interpolation and relaxation steps covered all transitions until the end of the processed magnetograms' sequence. We additionally advanced each magnetic configuration that has reached the self-organized critical state (SOC configuration) by the static model until 50 more flares were triggered, applied the dynamic model again to the new sequence, and repeated the same process sufficiently often to generate adequate statistics. Physical requirements, such as the divergence-free condition for the magnetic field, were approximately imposed.
Results. We obtain robust power laws in the distribution functions of the modeled flaring events with scaling indices that agree well with observations. Peak and total flare energy obey single power laws with indices -1.65 ± 0.11 and -1.47 ± 0.13, while the flare duration is best fitted with a double power law (-2.15 ± 0.15 and -3.60 ± 0.09 for the flatter and steeper parts, respectively).
Conclusions. We conclude that well-known statistical properties of flares are reproduced after active regions reach the state of self-organized criticality. A significant enhancement of our refined cellular automaton model is that it initiates and further drives the simulation from observed evolving vector magnetograms, thus facilitating energy calculation in physical units, while a separation between MHD and kinetic timescales is possible by assigning distinct MHD timestamps to each interpolation step.

Simulating flaring events in complex active regions driven by observed magnetograms

M. **Dimitropoulou**1, H. Isliker2, L. Vlahos2 and M. K. Georgoulis
A&A 529, A101 (**2011**)
Context. We interpret solar flares as events originating in active regions that have reached the self organized critical state, by using a refined cellular automaton model with initial conditions derived from observations.
Aims. We investigate whether the system, with its imposed physical elements, reaches a self organized critical state and whether well-known statistical properties of flares, such as scaling laws observed in the distribution functions of characteristic parameters, are reproduced after this state has been reached.
Methods. To investigate whether the distribution functions of total energy, peak energy and event duration follow the expected scaling laws, we first applied a nonlinear force-free extrapolation that reconstructs the three-dimensional magnetic fields from two-dimensional vector magnetograms. We then locate magnetic discontinuities exceeding a threshold in the Laplacian of the magnetic field. These discontinuities are relaxed in local diffusion events, implemented in the form of cellular automaton evolution rules. Subsequent loading and relaxation steps lead the system to self organized criticality, after which the statistical properties of the simulated events are examined. Physical requirements, such as the divergence-free condition for the magnetic field vector, are approximately imposed on all elements of the model.
Results. Our results show that self organized criticality is indeed reached when applying specific loading and relaxation rules. Power-law indices obtained from the distribution functions of the modeled flaring events are in good agreement with observations. Single power laws (peak and total flare energy) are obtained, as are power laws with exponential cutoff and double power laws (flare duration). The results are also compared with observational X-ray data from the GOES satellite for our active-region sample.
Conclusions. We conclude that well-known statistical properties of flares are reproduced after the system has reached self organized criticality. A significant enhancement of our refined cellular automaton model is that it commences the simulation from observed vector magnetograms, thus facilitating energy calculation in physical units. The model described in this study remains consistent with fundamental physical requirements, and imposes physically meaningful driving and redistribution rules.

Comparison of the On-disk Apparent Current Sheets with the Limb Ones

Tao **Ding**1 and Jun Zhang1
2024 ApJ 974 104
https://iopscience.iop.org/article/10.3847/1538-4357/ad6df5/pdf
Based on observations from the Solar Dynamics Observatory (SDO) and the Solar and Heliospheric Observatory (SOHO), we investigate 30 apparent current sheets during 1999–2021, including 10 on-disk and 8 limb ones from the SDO, as well as 12 limb ones from the SOHO. Each on-disk current sheet is formed among an X-type configuration consisting of two sets of atmospheric structures, and each limb one is involved in a flare–coronal mass ejection event. During magnetic reconnection period, the on-disk apparent current sheet evolves from a bright point to an elongated line-like structure, and the structure becomes thin in the late stage of the reconnection. Subsequently, the plasma distribution within the current sheet manifests as a plasmoid chain. For the limb apparent current sheet, the length elongation is faster than that of the on-disk one, and the thinning process is also detected. Although the aspect ratios of the limb cases are comparable to the value for the occurrence of tearing mode instability from simulation research, no

obvious plasmoid chain is detected within these limb current sheets, and the density distribution is locally uniform. We suggest that due to the rapid extension of limb cases, the tearing mode instability is very fast, resulting in the formation of tiny plasmoids that are smaller than the instrument resolution. Moreover, there is another possible scenario. The observed limb apparent current sheet is just a bright ray, and the actual current sheet is only a small segment of the ray. **2001 September 21, 2012 January 1, 2017 September 10, 2019 November 1**
Table 1-3 Lists of Apparent Current Sheets

Preliminary Discussion on the Current Sheet

Tao **Ding**1, Jun Zhang1, Yuan Fang1, and Zhiying Ma1
2024 ApJ 964 58
https://iopscience.iop.org/article/10.3847/1538-4357/ad2683/pdf
The current sheet is a characteristic structure of magnetic energy dissipation during the magnetic reconnection process. So far, the width and depth of the current sheet are still indefinite. Here we investigate 64 current sheets observed by four telescopes from 1999 to 2022, and all of them have been well identified in the previous literature. In each current sheet, three width values are obtained at the quartering points. Based on these investigated cases, we obtain 192 values, which are in a wide range from hundreds to tens of thousands of kilometers. By calculating the pixel width (PW: the ratio of the current sheet width to the pixel resolution of corresponding observed data) of these current sheets, we find that more than 80% of the PW values concentrate on 2–4 pixels, indicating that the widths of the current sheets are dependent strongly on the instrument resolutions and all the sheets have no observable three-dimensional information. To interpret this result, we suggest that there are two probabilities. One is that the width of the current sheet is smaller than the instrument resolution, and the other is that the detected current sheet is only a small segment of the real one. Furthermore, there is another possible scenario. The so-called current sheet is just an emission-enhanced region. **5 Nov 2003, I Jan 2012, 3 Oct 2014, 8 Aug 2016**
Table 1 List of 64 Current Sheets and the Obtained Widths

The Evolution of Photospheric Magnetic Fields at the Footpoints of Reconnected Structures in the Solar Atmosphere

Tao **Ding**1, Jun Zhang1, Yue Fang1, Junchao Hong2, Yi Bi2, and Yongyuan Xiang2
2024 ApJ 964 16
https://iopscience.iop.org/article/10.3847/1538-4357/ad245f/pdf
Magnetic reconnection is believed to play an important role in the release and conversion of energy among magnetized plasma systems. So far, we have been unable to understand under what conditions magnetic reconnection can take place. Based on observations from the New Vacuum Solar Telescope and the Solar Dynamics Observatory (SDO), we study 16 magnetic reconnection events, and each event has a clear X-type configuration consisting of two sets of atmospheric structures. We focus on 38 footpoints that are relevant to these structures and can be clearly determined. By using SDO/Helioseismic and Magnetic Imager line-of-sight magnetograms, we track the field evolution of these footpoints. Prior to the occurrence of magnetic reconnection, the associated fields at the footpoints underwent convergence and shear motions, and thus became enhanced and complex. During the converging period, the rates of increase of the mean magnetic flux densities (MFDs) at these footpoints are 0.03–0.25 hr−1. While the unsigned mean MFDs are 70–300 G, magnetic reconnection in the solar atmosphere takes place. Subsequently, the photospheric fields of these footpoints diffuse and weaken, with rates of decrease of the MFDs from 0.03 to 0.18 hr−1. These results suggest that, due to the photospheric dynamical evolution at the footpoints, the footpoint MFDs increase from a small value to a large one, and the corresponding atmospheric magnetic fields become complicated and nonpotential; then reconnection happens and it releases the accumulated magnetic field energy. Our study supports the conjecture that magnetic reconnection releases free magnetic energy stored in the nonpotential fields. **3 Feb 2014, 9 Jan 2015, 6 Feb 2016,1 Nov 2019**
Table 1 Lists of 16 X-type Magnetic Reconnection Events and Associated Measured Parameters 2013-2016

Magnetic reconnection resulting from flux emergence: implications for jet formation in the lower solar atmosphere?

J. Y. **Ding**1,2, M. S. Madjarska1, J. G. Doyle1, Q. M. Lu2, K. Vanninathan1 and Z. Huang1
A&A 535, A95 **(2011)**
Aims. We aim at investigating the formation of jet-like features in the lower solar atmosphere, e.g. chromosphere and transition region, as a result of magnetic reconnection.
Methods. Magnetic reconnection as occurring at chromospheric and transition regions densities and triggered by magnetic flux emergence is studied using a 2.5D MHD code. The initial atmosphere is static and isothermal, with a temperature of 2 × 104 K. The initial magnetic field is uniform and vertical. Two physical environments with different magnetic field strength (25 G and 50 G) are presented. In each case, two sub-cases are discussed, where the environments have different initial mass density.
Results. In the case where we have a weaker magnetic field (25 G) and higher plasma density (Ne = 2 × 1011 cm-3), valid for the typical quiet Sun chromosphere, a plasma jet would be observed with a temperature of 2–3 × 104 K and a velocity as high as 40 kms-1. The opposite case of a medium with a lower electron density (Ne = 2 × 1010 cm-3), i.e. more typical for the transition region, and a stronger magnetic field of 50 G, up-flows with line-of-sight velocities as high as ~90 kms-1 and temperatures of 6 × 105 K, i.e. upper transition region – low coronal temperatures, are produced. Only in the latter case, the low corona Fe ix 171 Å shows a response in the jet which is comparable to the O v increase.
Conclusions. The results show that magnetic reconnection can be an efficient mechanism to drive plasma outflows in the chromosphere and transition region. The model can reproduce characteristics, such as temperature and velocity for a range of jet features like a fibril, a spicule, a hot X-ray jet or a transition region jet by changing either the magnetic field strength or the electron density, i.e. where in the atmosphere the reconnection occurs.

Chromospheric magnetic reconnection caused by photospheric flux emergence: implications for jet-like events formation

J. Y. **Ding**, M. S. Madjarska, J. G. Doyle and Q. M. Lu
A&A 510, A111 (**2010**)
Magnetic reconnection in the low atmosphere, e.g. chromosphere, is investigated in various physical environments. Its implications for the origination of explosive events (small-scale jets) are discussed. A 2.5-dimensional resistive magnetohydrodynamic (MHD) model in Cartesian coordinates is used. It is found that the temperature and velocity of the outflow jets as a result of magnetic reconnection are strongly dependent on the physical environments, e.g. the magnitude of the magnetic field strength and the plasma density. If the magnetic field strength is weak and the density is high, the temperature of the jets is very low (~10^4 K) as well as its velocity (~*40* km s^{-1}). However, if environments with stronger magnetic field strength (40 G) and smaller density (electron density $N_e = 2 \times 10^{10}$ cm^{-3}) are

considered, the outflow jets reach higher temperatures of up to 6×10^5 K and a line-of-sight velocity of up to *130* km s^{-1} which is comparable with the observational values of jet-like events.

Wavelets, Intermittency and Solar Flare Hard X-rays
2. LIM Analysis of High Time Resolution BATSE Data

A. N. **Dinkelaker**, A. L. MacKinnon
Solar Physics, February **2013**, Volume 282, Issue 2, pp 483-501
We apply local intermittency measure (LIM) analysis to 64 ms time resolved BATSE measurements of hard X-rays from several solar flares. LIM analysis yields information on the character of the processes giving rise to fluctuations in light curves, e.g. avalanche vs. cascade pictures. We present LIM scaleograms for several flares and summarise scaleogram morphological features. More detailed descriptions are given of the behaviour in the flare of 13 January 1992 (the well-known 'Masuda flare') and an interesting event on **22 November 1998**. All flares display episodes of intermittency across a range of scales. LIM scaleogram features may be consistent with both 'top-down' and 'bottom-up' scenarios for the development of small-scale structure, sometimes within the same flare. Thus neither class of model captures the totality of the events in a flare.

Wavelets, Intermittency and Solar Flare Hard X-rays
1. Local Intermittency Measure in Cascade and Avalanche Scenarios

A. N. **Dinkelaker**, A. L. MacKinnon
Solar Physics, February **2013**, Volume 282, Issue 2, pp 471-481
We introduce the local intermittency measure (LIM) as a tool for the investigation of solar flare hard X-ray light curves. Constructed from wavelet amplitudes, the LIM allows us to investigate the extent to which rapid fluctuations reveal an underlying, scale-invariant process, and to identify those episodes during a flare which definitely represent 'intermittent' behaviour (e.g. involvement of new spatial structures). We carry out two sets of simple simulations intended to provide generic examples of 'top-down' and 'bottom-up' scenarios for the development of flares, and show how LIM may discriminate between them.

Properties of Flare-Imminent versus Flare-Quiet Active Regions from the Chromosphere through the Corona I: Introduction of the AIA Active Region Patches (AARPs)

Karin **Dissauer**, KD Leka, Eric L. Wagner
ApJ **942** 83 **2023**
https://arxiv.org/pdf/2212.11251.pdf
https://iopscience.iop.org/article/10.3847/1538-4357/ac9c06/pdf
We begin here a series of papers examining the chromospheric and coronal properties of solar active regions. This first paper describes an extensive dataset of images from the Atmospheric Imaging Assembly on the Solar Dynamics Observatory curated for large-sample analysis of this topic. Based on (and constructed to coordinate with) the ``Active Region Patches" as identified by the pipeline data analysis system for the Helioseismic and Magnetic Imager (HMI) on the same mission, the ``HARPs"), the ``AIA Active Region Patches" (AARPs), described herein, comprise an unbiased multi-wavelength set of FITS files downsampled spatially only by way of HARP-centered patch extractions (full spatial sampling is retained), and downsampled in the temporal domain but still able to describe both short-lived kinematics and longer-term trends. The AARPs database enables physics-informed parametrization and analysis using Nonparametric Discriminant Analysis in Paper II of this series, and is validated for analysis using Differential Emission Measure techniques. The AARP dataset presently covers mid-2010 through December 2018, is approx 9TB in size, and available through the Solar Data Analysis Center. **2011.08.03 , March 07, 2012, 2012.03.12, March 29, 2014**

Uncovering Heterogeneity of Solar Flare Mechanism With Mixture Models

Bach Viet **Do**, Yang Chen, XuanLong Nguyen, Ward Manchester
2024
https://arxiv.org/pdf/2401.14345.pdf
The physics of solar flares occurring on the Sun is highly complex and far from fully understood. However, observations show that solar eruptions are associated with the intense kilogauss fields of active regions, where free energies are stored with field-aligned electric currents. With the advent of high-quality data sources such as the Geostationary Operational Environmental Satellites (GOES) and Solar Dynamics Observatory (SDO)/Helioseismic and Magnetic Imager (HMI), recent works on solar flare forecasting have been focusing on data-driven methods. In particular, black box machine learning and deep learning models are increasingly adopted in which underlying data structures are not modeled explicitly. If the active regions indeed follow the same laws of physics, there should be similar patterns shared among them, reflected by the observations. Yet, these black box models currently used in the literature do not explicitly characterize the heterogeneous nature of the solar flare data, within and between active regions. In this paper, we propose two finite mixture models designed to capture the heterogeneous patterns of active regions and their associated solar flare events. With extensive numerical studies, we demonstrate the usefulness of our

proposed method for both resolving the sample imbalance issue and modeling the heterogeneity for rare energetic solar flare events.

Updated analytical solutions of continuity equation for electron beams precipitation. I. Pure collisional and pure ohmic energy losses

R. R. **Dobranskis** and V. V. Zharkova
MNRAS, **2015**,453 (1): 229-241
http://mnras.oxfordjournals.org/content/453/1/229.short?rss=1;%20http://computing.unn.ac.uk/staff/slmv5/kinetics/DZ_Ohmic_Losses_Part1_v1.pdf
We present updated analytical solutions of continuity equations for power-law beam electrons precipitating in (a) purely collisional losses and (b) purely ohmic losses. The solutions of continuity equation (CE) normalized on electron density presented in Dobranskis & Zharkova are found by method of characteristics eliminating a mistake in the density characteristic pointed out by Emslie et al. The corrected electron beam differential densities (DD) for collisions are shown to have energy spectra with the index of -(γ + 1)/2, coinciding with the one derived from the inverse problem solution by Brown, while being lower by 1/2 than the index of -γ/2 obtained from CE for electron flux. This leads to a decrease of the index of mean electron spectra from -(γ - 2.5) (CE for flux) to -(γ - 2.0) (CE for electron density). The similar method is applied to CE for electrons precipitating in electric field induced by the beam itself. For the first time, the electron energy spectra are calculated for both constant and variable electric fields by using CE for electron density. We derive electron DD for precipitating electrons (moving towards the photosphere, μ = +1) and 'returning' electrons (moving towards the corona, μ = -1). The indices of DD energy spectra are reduced from -γ - 1 (CE for flux) to -γ (CE for electron density). While the index of mean electron spectra is increased by 0.5, from -γ + 0.5 (CE for flux) to -γ + 1(CE for electron density). Hard X-ray intensities are also calculated for relativistic cross-section for the updated differential spectra revealing closer resemblance to numerical Fokker-Planck (FP) solutions.

Exact Analytical Solutions of Continuity Equation for Electron Beams Precipitating in Coulomb Collisions

R. R. **Dobranskis** and V. V. Zharkova
2014 ApJ 788 42
The original continuity equation (CE) used for the interpretation of the power law energy spectra of beam electrons in flares was written and solved for an electron beam flux while ignoring an additional free term with an electron density. In order to remedy this omission, the original CE for electron flux, considering beam's energy losses in Coulomb collisions, was first differentiated by the two independent variables: depth and energy leading to partial differential equation for an electron beam density instead of flux with the additional free term. The analytical solution of this partial differential continuity equation (PDCE) is obtained by using the method of characteristics. This solution is further used to derive analytical expressions for mean electron spectra for Coulomb collisions and to carry out numeric calculations of hard X-ray (HXR) photon spectra for beams with different parameters. The solutions revealed a significant departure of electron densities at lower energies from the original results derived from the CE for the flux obtained for Coulomb collisions. This departure is caused by the additional exponential term that appeared in the updated solutions for electron differential density leading to its faster decrease at lower energies (below 100 keV) with every precipitation depth similar to the results obtained with numerical Fokker-Planck solutions. The effects of these updated solutions for electron densities on mean electron spectra and HXR photon spectra are also discussed.
ERRATUM: E-print, Aug **2014**
In this erratum letter we correct a mistake in the characteristics for differential density N obtained in \citet{2014ApJ...788...42D} from the updated continuity equation for electron density and compare the solutions for electron density N obtained from continuity equations (CEs) for electron flux Nv and for electron density. We show that the corrected solution for N obtained from CE for electron density still has an additional exponential term of (E2+2a\xi)-1/4 comparing to the solution found from continuity equation for electron flux. This updated solution produces power law differential spectra of beam electrons as function of E2+2a\xi having a spectral index equal to -\frac{\gamma+1}{2} and not to -\frac{\gamma+0.5}{2} as it appears from the continuity equation for electron flux Nv. This updated solution is exactly the one reported by \citet{Syrovatsky72} indicating that their solution has been derived from CE for electron density and not for electron flux as stated in their paper. The difference in the spectral indices in energy spectra is also reflected in the spectral indices for mean electron spectra with a spectral index to be equal to \gamma-2, similar to \citet{Syrovatsky72}, for the solutions from CE for electron density and equal to \gamma-2.5 if continuity equation for electron flux is used.

Measurements with STEREO/COR1 data of drag forces acting on small-scale blobs falling in the intermediate corona

S. **Dolei**1, A. Bemporad2 and D. Spadaro
A&A 562, A74 (**2014)**
In this work we study the kinematics of three small-scale (0.01 R⊙) blobs of chromospheric plasma falling back to the Sun after the huge eruptive event of **June 7, 2011**. From a study of 3D trajectories of blobs made with the Solar TErrestrial RElations Observatory (STEREO) data, we demonstrate the existence of a significant drag force acting on the blobs and calculate two drag coefficients, in the radial and tangential directions. The resulting drag coefficients CD are between 0 and 5, comparable in the two directions, making the drag force only a factor of 0.45–0.75 smaller than the gravitational force. To obtain a correct determination of electron densities in the blobs, we also demonstrate how, by combining measurements of total and polarized brightness, the Hα contribution to the white-light emission observed by the COR1 telescopes can be estimated. This component is significant for chromospheric plasma, being between 95 and 98% of the total white-light emission. Moreover, we demonstrate that the COR1 data can be employed even to estimate the Hα polarized component, which turns out to be in the order of a few percent of Hα total emission from the blobs. If the drag forces acting on small-scale blobs reported here are similar to those that play a role during the CME propagation, our results suggest that the magnetic drag should be considered even in the CME initiation modelling.

Solar flare forecasting from magnetic feature properties generated by Solar Monitor Active Region Tracker

Katarina **Domijan**, D. Shaun Bloomfield, Francois Pitie
Solar Phys. 294:6 **2019**
https://arxiv.org/pdf/1812.02652.pdf
https://link.springer.com/content/pdf/10.1007%2Fs11207-018-1392-4.pdf
We study the predictive capabilities of magnetic feature properties (MF) generated by Solar Monitor Active Region Tracker (SMART) for solar flare forecasting from two datasets: the full dataset of SMART detections from 1996 to 2010 that has been previously studied by Ahmed et al. (2011) and a subset of that dataset which only includes detections that are NOAA active regions (ARs). Main contributions: we use marginal relevance as a filter feature selection method to identify most useful SMART MF properties for separating flaring from non-flaring detections and logistic regression to derive classification rules to predict future observations. For comparison, we employ a Random Forest, Support Vector Machine and a set of Deep Neural Network models, as well as Lasso for feature selection. Using the linear model with three features we obtain significantly better results (TSS=0.84) to those reported by Ahmed et al.(2011) for the full dataset of SMART detections. The same model produced competitive results (TSS=0.67) for the dataset of SMART detections that are NOAA ARs which can be compared to a broader section of flare forecasting literature. We show that more complex models are not required for this data.

First Detection of Solar Flare Emission in Middle-Ultraviolet Balmer Continuum

Marie **Dominique**, Andrei N. Zhukov, Petr Heinzel, Ingolf E. Dammasch, Laurence Wauters, Laurent Dolla, Sergei Shestov, Matthieu Kretzschmar, Janet Machol, Giovanni Lapenta, Werner Schmutz
2018 *ApJL* **867** L24
https://arxiv.org/pdf/1810.09835.pdf
sci-hub.tw/10.3847/2041-8213/aaeace
We present the first detection of solar flare emission at middle-ultraviolet wavelengths around 2000 A by the channel 2 of the Large-Yield RAdiometer (LYRA) onboard the PROBA2 mission. The flare (SOL20170906) was also observed in the channel 1 of LYRA centered at the H I Lyman-{\alpha} line at 1216 A, showing a clear non-thermal profile in both channels. The flare radiation in channel 2 is consistent with the hydrogen Balmer continuum emission produced by an optically thin chromospheric slab heated up to 10000 K. Simultaneous observations in channels 1 and 2 allow the separation of the line emission (primarily from the Lyman-{\alpha} line) from the Balmer continuum emission. Together with the recent detection of the Balmer continuum emission in the near-ultraviolet by IRIS, the LYRA observations strengthen the interpretation of broadband flare emission as the hydrogen recombination continua originating in the chromosphere. **2017 September 6**

Detection of Quasi-Periodic Pulsations in Solar EUV Time Series

M. **Dominique**, A. N. Zhukov, L. Dolla, A. Inglis, G. Lapenta
Solar Physics April **2018**, 293:61
https://link.springer.com/content/pdf/10.1007%2Fs11207-018-1281-x.pdf
Quasi-periodic pulsations (QPPs) are intrinsically connected to the mechanism of solar flares. They are regularly observed in the impulsive phase of flares since the 1970s. In the past years, the studies of QPPs regained interest with the advent of a new generation of soft X-ray/extreme ultraviolet radiometers that pave the way for statistical surveys. Since the amplitude of QPPs in these wavelengths is rather small, detecting them implies that the overall trend of the time series needs to be removed before applying any Fourier or wavelet transform. This detrending process is known to

produce artificial detection of periods that must then be distinguished from real ones. In this paper, we propose a set of criteria to help identify real periods and discard artifacts. We apply these criteria to data taken by the Extreme Ultraviolet Variability Experiment (EVE)/ESP onboard the Solar Dynamics Observatory (SDO) and the Large Yield Radiometer (LYRA) onboard the PRoject for On-Board Autonomy 2 (PROBA2) to search for QPPs in flares stronger than **M5.0** that occurred during Solar Cycle 24. **2011-02-15, 2012-07-06**
Table

Forecasting solar flares with a transformer network.

Pelkum **Donahue** K and Inceoglu F
Front. Astron. Space Sci. 10:1298609. (**2024**)
doi: 10.3389/fspas.2023.1298609
https://www.frontiersin.org/articles/10.3389/fspas.2023.1298609/pdf
Space weather phenomena, including solar flares and coronal mass ejections, have significant influence on Earth. These events can cause satellite orbital decay due to heat-induced atmospheric expansion, disruption of GPS navigation and telecommunications systems, damage to satellites, and widespread power blackouts. The potential of flares and associated events to damage technology and disrupt human activities motivates prediction development. We use Transformer networks to predict whether an active region (AR) will release a flare of a specific class within the next 24 h. Two cases are considered: ≥C-class and ≥M-class. For each prediction case, separate models are developed. We train the Transformer to use time-series data to classify 24- or 48-h sequences of data. The sequences consist of 18 physical parameters that characterize an AR from the Space-weather HMI Active Region Patches data product. Flare event information is obtained from the Geostationary Operational Environmental Satellite flare catalog. Our model outperforms a prior study that similarly used only 24 h of data for the ≥C-class case and performs slightly worse for the ≥M-class case. When compared to studies that used a larger time window or additional data such as flare history, results are comparable. Using less data is conducive to platforms with limited storage, on which we plan to eventually deploy this algorithm.

Seismic Transients from Flares in Solar Cycle 23

Alina **Donea**
Space Science Reviews, Volume 158, Numbers 2-4, 451-469, **2011**
Some solar flares are known to drive seismic waves into the sub-photospheres of the magnetic regions that host them. Sunquakes, which are identified as a wave-packet of ripples are observed on the solar surface emanating from a focal region, known as seismic source or sometimes as a transient. Not all seismic transients from flares generate sunquakes. How these are produced is still a puzzle. In this paper, I will give an overview of the observed properties of sunquakes and efforts to understanding physics underlying them, including numerical modelling of flare-driven oscillations.

SEISMIC EMISSION FROM A M9.5-CLASS SOLAR FLARE

A.-C. **DONEA**, D. BESLIU-IONESCU, P.S. CALLY, C. LINDSEY, and V.V. ZHARKOVA
Solar Physics (**2006**) 239: 113–135.

Seismic Emission from the Solar Flares of 2003 October 28 and 29

Donea, A.-C.; Lindsey, C.
Astrophysical Journal, Volume 630, Issue 2, pp. 1168-1183, **2005**
We report the detection of seismic waves emitted from powerful solar flares that occurred in NOAA Active Region 10486 on 2003 October 28 and 29. We used helioseismic holography to image the seismic sources of the waves. This technique was previously used to image the source of seismic emission from the large solar flare of 1996 July 9. Egression power maps at 6 mHz with a 2 mHz bandwidth reveal multiple compact acoustic sources strongly associated with the footpoints of a coronal loop that hosted the flares. The total acoustic energy in the flare signatures is a very small fraction of the total energy radiated by the flares. The acoustic signatures are co-aligned with hard X-ray signatures, suggesting a direct link between energetic particles accelerated during the flare and the acoustic waves as a hydrodynamic response of the chromosphere, or possibly the underlying photosphere, to these particles at the footpoints of the loop. There is also evidence of high-energy protons impinging onto the chromosphere in the neighborhoods of the acoustic sources. Observations of emission in the D1 line of neutral sodium at the onset of the October 29 flare show evidence of a downward-propagating shock/condensation at the onset of the flare. Concurrent Global Oscillation Network Group (GONG) intensity observations show significant radiative emission with a sudden onset in the compact region encompassing the acoustic signature. Most flares appear to be acoustically inactive. Photospheric heating by high-energy protons is likely to be a major factor in seismic emission from acoustically active flares.

The Calibrations for the Chang'E-2 Solar X-Ray Monitor

Wu-Dong **Dong**, Xiaoping Zhang, Yong Li, Chi-Long Tang, Aoao Xu, Fan Zhang
Solar Physics September **2019**, 294:120

https://doi.org/10.1007/s11207-019-1508-5
The calibrations of the Solar X-ray Monitor (SXM) on the Chinese lunar mission Chang'E-2 are presented. The SXM payload uses a solid-state silicon PIN photodiode (Si-PIN) whose detection energy ranges from 0.5 keV to 10 keV. The energy resolution of SXM is 0.3 keV (FWHM) at 5.9 keV. The solar soft X-rays are collected in 976 channels every 10 seconds. The purpose of the calibrations is to specify the performance of SXM, which enables a reliable spectral analysis of the observed solar X-ray data. The characteristic lines of Fe at ≈6.7 keV≈6.7 keV and of the Fe/Ni complex at ≈8.0 keV≈8.0 keV are clearly determined during a solar flare. We compare the flux measured by SXM and the Geostationary Operational Environmental Satellite (GOES) series and find consistent results. The preliminary results of the analysis of observed spectra are also presented. The spectra are measured with high energy and time resolutions, which provide additional information such as element abundances in the solar flare region. This information could be very valuable for studying the dynamic evolution of solar flares.

Photospheric and Coronal Abundances in an X8.3 Class Limb Flare

G. A. **Doschek**1, H. P. Warren1, L. K. Harra2, J. L. Culhane2, T. Watanabe3, and H. Hara
2018 ApJ 853 178
http://sci-hub.tw/http://iopscience.iop.org/0004-637X/853/2/178/
We analyze solar elemental abundances in coronal post-flare loops of an X8.3 flare (SOL2017-09-10T16:06) observed on the west limb on **2017 September 10** near 18 UT using spectra recorded by the Extreme-ultraviolet Imaging Spectrometer (EIS) on the Hinode spacecraft. The abundances in the corona can differ from photospheric abundances due to the first ionization potential (FIP) effect. In some loops of this flare, we find that the abundances appear to be coronal at the loop apices or cusps, but steadily transform from coronal to photospheric as the loop footpoint is approached. This result is found from the intensity ratio of a low-FIP ion spectral line (Ca xiv) to a high-FIP ion spectral line (Ar xiv) formed at about the same temperature (4–5 MK). Both lines are observed close in wavelength. Temperature, which could alter the interpretation, does not appear to be a factor based on intensity ratios of Ca xv lines to a Ca xiv line. We discuss the abundance result in terms of the Laming model of the FIP effect, which is explained by the action of the ponderomotive force in magnetohydrodynamic (MHD) waves in coronal loops and in the underlying chromosphere.

THE MYSTERIOUS CASE OF THE SOLAR ARGON ABUNDANCE NEAR SUNSPOTS IN FLARES

G. A. **Doschek** and H. P. Warren
2016 ApJ 825 36
Recently we discussed an enhancement of the abundance of Ar xiv relative to Ca xiv near a sunspot during a flare, observed in spectra recorded by the Extreme-ultraviolet Imaging Spectrometer (EIS) on the Hinode spacecraft. The observed Ar xiv/Ca xiv ratio yields an argon/calcium abundance ratio seven times greater than expected from the photospheric abundance. Such a large abundance anomaly is unprecedented in the solar atmosphere. We interpreted this result as being due to an inverse first ionization potential (FIP) effect. In the published work, two lines of Ar xiv were observed, and one line was tentatively identified as an Ar xi line. In this paper, we report observing a similar enhancement in a full-CCD EIS flare spectrum in 13 argon lines that lie within the EIS wavelength ranges. The observed lines include two Ar xi lines, four Ar xiii lines, six Ar xiv lines, and one Ar xv line. The enhancement is far less than reported in Doschek et al. but exhibits similar morphology. The argon abundance is close to a photospheric abundance in the enhanced area, and the abundance could be photospheric. This enhancement occurs in association with a sunspot in a small area only a few arcseconds (1" = about 700 km) in size. There is no enhancement effect observed in the normally high-FIP sulfur and oxygen line ratios relative to lines of low-FIP elements available to EIS. Calculations of path lengths in the strongest enhanced area in Doschek et al. indicate a depletion of low-FIP elements.

Flare Footpoint Regions and a Surge Observed by the Hinode/EUV Imaging Spectrometer (EIS), RHESSI, and SDO/AIA

George A. **Doschek**, Harry P. Warren, Brian R. Dennis, Jeffrey W. Reep, Amir Caspi
2015 ApJ 813 32
http://arxiv.org/pdf/1510.07088v1.pdf
The Extreme-ultraviolet Imaging Spectrometer (EIS) on the Hinode spacecraft observed flare footpoint regions coincident with a surge for a M3.7 flare observed on **25 September 2011** at N12 E33 in active region 11302. The flare was observed in spectral lines of O VI, Fe X, Fe XII, Fe XIV, Fe XV, Fe XVI, Fe XVII, Fe XXIII and Fe XXIV. The EIS observations were made coincident with hard X-ray bursts observed by the Reuven Ramaty High Energy Solar Spectroscopic Imager (RHESSI). Overlays of the RHESSI images on the EIS raster images at different wavelengths show a spatial coincidence of features in the RHESSI images with the EIS upflow and downflow regions, as well as loop-top or near-loop-top regions. A complex array of phenomena was observed including multiple evaporation regions and the surge, which was also observed by the Solar Dynamics Observatory (SDO)/Atmospheric Imaging Assembly (AIA) telescopes. The slit of the EIS spectrometer covered several flare footpoint regions from which evaporative

upflows in Fe XXIII and Fe XXIV lines were observed with Doppler speeds greater than 500 km s−1. For ions such as Fe XV both evaporative outflows (~200 km s−1) and downflows (~30-50 km s−1) were observed. Non-thermal motions from 120 to 300 km s−1 were measured in flare lines. In the surge, Doppler speeds are found from about 0 to over 250 km s−1 in lines from ions such as Fe XIV. The non-thermal motions could be due to multiple sources slightly Doppler-shifted from each other or turbulence in the evaporating plasma. We estimate the energetics of the hard X-ray burst and obtain a total flare energy in accelerated electrons of ≥7×1028 ergs. This is a lower limit because only an upper limit can be determined for the low energy cutoff to the electron spectrum. We find that detailed modeling of this event would require a multi-threaded model due to its complexity.

Plasma Dynamics Above Solar Flare Soft X-Ray Loop Tops
G. A. **Doschek**1, D. E. McKenzie2, and H. P. Warren
ApJ 788 26, **2014**
We measure non-thermal motions in flare loop tops and above the loop tops using profiles of highly ionized spectral lines of Fe XXIV and Fe XXIII formed at multimillion-degree temperatures. Non-thermal motions that may be due to turbulence or multiple flow regions along the line of sight are extracted from the line profiles. The non-thermal motions are measured for four flares seen at or close to the solar limb. The profile data are obtained using the Extreme-ultraviolet Imaging Spectrometer on the Hinode spacecraft. The multimillion-degree non-thermal motions are between 20 and 60 km s–1 and appear to increase with height above the loop tops. Motions determined from coronal lines (i.e., lines formed at about 1.5 MK) tend to be smaller. The multimillion-degree temperatures in the loop tops and above range from about 11 MK to 15 MK and also tend to increase with height above the bright X-ray-emitting loop tops. The non-thermal motions measured along the line of sight, as well as their apparent increase with height, are supported by Solar Dynamics Observatory Atmospheric Imaging Assembly measurements of turbulent velocities in the plane of the sky.

Flows and Nonthermal Velocities in Solar Active Regions Observed with the EUV Imaging Spectrometer on Hinode: A Tracer of Active Region Sources of Heliospheric Magnetic Fields?
G. A. **Doschek**, H. P. Warren, J. T. Mariska, K. Muglach, J. L. Culhane,
H. Hara, and T. Watanabe
The Astrophysical Journal, Vol. 686, No. 2
http://www.journals.uchicago.edu/doi/abs/10.1086/591724

CHROMOSPHERIC EVAPORATION IN AN M1.8 FLARE OBSERVED BY THE EXTREME-ULTRAVIOLET IMAGING SPECTROMETER ON HINODE
G. A. **Doschek**1, H. P. Warren1, and P. R. Young
2013 ApJ 767 55
We discuss observations of chromospheric evaporation for a complex flare that occurred on **2012 March 9** near 03:30 UT obtained from the Extreme-ultraviolet Imaging Spectrometer (EIS) on board the Hinode spacecraft. This was a multiple event with a strong energy input that reached the M1.8 class when observed by EIS. EIS was in raster mode and fortunately the slit was almost at the exact location of a significant energy input. Also, EIS obtained a full-CCD spectrum of the flare, i.e., the entire CCD was readout so that data were obtained for about the 500 lines identified in the EIS wavelength ranges. Chromospheric evaporation characterized by 150-200 km s–1 upflows was observed in multiple locations in multi-million degree spectral lines of flare ions such as Fe XXII, Fe XXIII, and Fe XXIV, with simultaneous 20-60 km s–1 upflows in million degree coronal lines from ions such as Fe XII-Fe XVI. The behavior of cooler, transition region ions such as O VI, Fe VIII, He II, and Fe X is more complex, but upflows were also observed in Fe VIII and Fe X lines. At a point close to strong energy input in space and time, the flare ions Fe XXII, Fe XXIII, and Fe XXIV reveal an isothermal source with a temperature close to 14 MK and no strong blueshifted components. At this location there is a strong downflow in cooler active region lines from ions such as Fe XIII and Fe XIV, on the order of 200 km s–1. We speculate that this downflow may be evidence of the downward shock produced by reconnection in the current sheet seen in MHD simulations. A sunquake also occurred near this location. Electron densities were obtained from density sensitive lines ratios from Fe XIII and Fe XIV. Atmospheric Imaging Assembly (AIA) observations from the Solar Dynamics Observatory are used with JHelioviewer to obtain a qualitative overview of the flare. However, AIA data are not presented in this paper. In summary, spectroscopic data from EIS are presented that can be used for predictive tests of models of chromospheric evaporation as envisaged in the Standard Flare Model.

Superflares and Variability in Solar-Type Stars with TESS in the Southern Hemisphere
Lauren **Doyle**, Gavin Ramsay, J. Gerard Doyle

MNRAS **2020**
https://arxiv.org/pdf/2003.14410.pdf
Superflares on solar-type stars has been a rapidly developing field ever since the launch of Kepler. Over the years, there have been several studies investigating the statistics of these explosive events. In this study, we present a statistical analysis of stellar flares on solar-type stars made using photometric data in 2-min cadence from TESS of the whole southern hemisphere (sectors 1 - 13). We derive rotational periods for all stars in our sample from rotational modulations present in the lightcurve as a result of large starspot(s) on the surface. We identify 1980 stellar flares from 209 solar-type stars with energies in the range of 1031−1036erg (using the solar flare classification, this corresponds to X1 - X100,000) and conduct an analysis into their properties. We investigate the rotational phase of the flares and find no preference for any phase suggesting the flares are randomly distributed. As a benchmark, we use GOES data of solar flares to detail the close relationship between solar flares and sunspots. In addition, we also calculate approximate spot areas for each of our stars and compare this to flare number, rotational phase, and flare energy. Additionally, two of our stars were observed in the continuous viewing zone with lightcurves spanning one year, as a result, we examine the stellar variability of these stars in more detail.

Stellar Flares and Starspots
Lauren **Doyle**
RHESSI Nugget #339 Dec **2018**
http://sprg.ssl.berkeley.edu/~tohban/wiki/index.php/Stellar_Flares_and_Starspots
we find no correlation between the rotational phase and the number of flares in our sample of M dwarfs observed in short cadence by K2. Interestingly, our result indicates flares do not originate from the active region hosted by the large starspot. We outline three scenarios to explain this: polar spots, stellar binarity systems and the presence of orbiting. To test the three scenarios further we would need to investigate the inclination and potential star-planet or binary stars in greater detail.

The Diagnostic Potential of Transition Region Lines under-going Transient Ionization in Dynamic Events
J.G. **Doyle**, A. Giunta, A. Singh, M.S. Madjarska, H. Summers, B.J. Kellett & M. O'Mullane
E-print, May **2012**; Solar Phys. Volume 280, Number 1 (**2012**), 111-124
We discuss the diagnostic potential of high cadence ultraviolet spectral data when transient ionization is considered. For this we use high cadence UV spectra taken during the impulsive phase of a solar flares (observed with instruments on-board the Solar Maximum Mission) which showed excellent correspondence with hard X-ray pulses. The ionization fraction of the transition region ion O V and in particular the contribution function for the O V 1371A line are computed within the Atomic Data and Analysis Structure, which is a collection of fundamental and derived atomic data and codes which manipulate them. Due to transient ionization, the O V 1371A line is enhanced in the first fraction of a second with the peak in the line contribution function occurring initially at a higher electron temperature than in ionization equilibrium. The rise time and enhancement factor depend mostly on the electron density. The fractional increase in the O V 1371A emissivity due to transient ionization can reach a factor of 2--4 and can explain the fast response in the line flux of transition regions ions during the impulsive phase of flares solely as a result of transient ionization. This technique can be used to diagnostic the electron temperature and density of solar flares observed with the forth-coming Interface Region Imaging Spectrograph**.**

Electron acceleration during magnetic reconnection in macroscale systems
J. F. **Drake**
Fleishman's webinar 20-Nov-**2020**
https://www.youtube.com/watch?v=YXGDkw0tMJ0&feature=youtu.be
23 Jul 2002, 19 Jan 2005, 31 Dec 2007, 10 Sep 2017

A computational model for exploring particle acceleration during reconnection in macro-scale systems
J. F. **Drake**, H. Arnold, M. Swisdak, J. T. Dahlin
2018
https://arxiv.org/pdf/1809.04568.pdf
A new computational model is presented suitable for exploring the self- consistent production of energetic electrons during magnetic reconnection in macroscale systems. The equations are based on the recent discovery that parallel electric fields are ineffective drivers of energetic particles during reconnection so that the kinetic scales which control the development of such fields can be ordered out of the equations. The resulting equations consist of a magnetohydrodynamic (MHD) backbone with the energetic component represented by macro-particles described by the guiding center equations. Crucially, the energetic component feeds back on the MHD equations so that the total energy of the MHD fluid and the energetic particles is conserved. The equations correctly describe the firehose instability,

whose dynamics plays a key role in throttling reconnection and in controlling the spectra of energetic particles. The results of early tests of the model, including the propagation of Alfven waves in a system with pressure anisotropy and the growth of firehose modes, establish that the basic algorithm is stable and produces reliable physics results in preparation for further benchmarking with particle-in-cell models of reconnection.

A MAGNETIC RECONNECTION MECHANISM FOR ION ACCELERATION AND ABUNDANCE ENHANCEMENTS IN IMPULSIVE FLARES

J. F. **Drake**1, P. A. Cassak2, M. A. Shay3, M. Swisdak1, and E. Quataert4
The Astrophysical Journal, 700:L16–L20, **2009** July
The acceleration of ions during magnetic reconnection in solar flares is explored with simulations and analytic analysis. Ions crossing into Alfv´enic reconnection outflows can behave like pickup particles and gain an effective thermal velocity equal to the Alfv´en speed. However, with a sufficiently strong ambient out-of-plane magnetic field, which is the relevant configuration for flares, the ions can become adiabatic and their heating is then dramatically reduced. The threshold for nonadiabatic behavior, where ions are strongly heated, becomes a condition on the ion mass-to-charge ratio, $m_i/m_pZ_i > 10\sqrt{\beta_{0x}/2/\pi}$, where m_i and Z_i are the ion mass and charge state, m_p is the proton mass, and $\beta_{0x} = 8\pi nT/B_{20x}$ is the ratio of the plasma pressure to that of the reconnecting magnetic field B_{0x}. Thus, during flares high mass-to-charge particles gain energy more easily than protons and a simple model reveals that their abundances are enhanced, which is consistent with observations.

Connecting solar flare hard X-ray spectra to in situ electron spectra. A comparison of RHESSI and STEREO/SEPT observations

Nina **Dresing**, A. Warmuth, F. Effenberger, K.-L. Klein, S. Musset, L. Glesener, M. Brüdern
A&A 654, A92 **2021**
https://arxiv.org/pdf/2108.09045.pdf
https://www.aanda.org/articles/aa/pdf/2021/10/aa41365-21.pdf
https://doi.org/10.1051/0004-6361/202141365
We compare the characteristics of flare-accelerated energetic electrons at the Sun with those injected into interplanetary space. We have identified 17 energetic electron events well-observed with the SEPT instrument aboard STEREO which show a clear association with a hard X-ray (HXR) flare observed with the RHESSI spacecraft. We compare the spectral indices of the RHESSI HXR spectra with those of the interplanetary electrons. Because of the frequent double-power-law shape of the in situ electron spectra, we paid special attention to the choice of the spectral index used for comparison. The time difference between the electron onsets and the associated type III and microwave bursts suggests that the electron events are detected at 1 AU with apparent delays ranging from 9 to 41 minutes. While the parent solar activity is clearly impulsive, also showing a high correlation with extreme ultraviolet jets, most of the studied events occur in temporal coincidence with coronal mass ejections (CMEs). In spite of the observed onset delays and presence of CMEs in the low corona, we find a significant correlation of about 0.8 between the spectral indices of the HXR flare and the in situ electrons. The correlations increase if only events with significant anisotropy are considered. This suggests that transport effects can alter the injected spectra leading to a strongly reduced imprint of the flare acceleration. We conclude that interplanetary transport effects must be taken into account when inferring the initial acceleration of solar energetic electron events. Although our results suggest a clear imprint of flare acceleration for the analyzed event sample, a secondary acceleration might be present which could account for the observed delays. However, the limited and variable pitch-angle coverage of SEPT could also be the reason for the observed delays. **2011 Mar 24**
Table 1. Event list including the basic parameters of the correlated flare and SEE events (2007-2014)

Statistical results for solar energetic electron spectra observed over 12 years with STEREO/SEPT

Nina **Dresing**, Frederic Effenberger, Raul Gomez-Herrero, Bernd Heber, Andreas Klassen, Alexander Kollhoff, Ian Richardson, Solveig Theesen
ApJ **2020**
https://arxiv.org/pdf/1912.10279.pdf
We present a statistical analysis of near-relativistic (NR) solar energetic electron event spectra near 1au. We use measurements of the STEREO Solar Electron and Proton Telescope (SEPT) in the energyrange of 45-425 keV and utilize the SEPT electron event list containing all electron events observed bySTEREO A and STEREO B from 2007 through 2018. We select 781 events with significant signal tonoise ratios for our analysis and fit the spectra with single or broken power law functions of energy.We find 437 (344) events showing broken (single) power laws in the energy range of SEPT. The eventswith broken power laws show a mean break energy of about 120 keV. We analyze the dependence ofthe spectral index on the rise times and peak intensities of the events as well as on the presence ofrelativistic electrons. The results show a relation between the power law spectral index and the risetimes of the events with softer spectra belonging to rather impulsive events. Long rise-time events areassociated with hard spectra as well

as with the presence of higher energy (>0.7 MeV) electrons. Thisgroup of events cannot be explained by a pure flare scenario but suggests an additional accelerationmechanism, involving a prolonged acceleration and/or injection of the particles. A dependence of thespectral index on the longitudinal separation from the parent solar source region was not found. Astatistical analysis of the spectral indices during impulsively rising events (rise times<20 minutes) isalso shown.

Exploring self-consistent 2.5D flare simulations with MPI-AMRVAC⋆

Malcolm **Druett**, Wenzhi Ruan and Rony Keppens
A&A, 684, A171 (**2024**)
https://www.aanda.org/articles/aa/pdf/2024/04/aa47600-23.pdf

Context. Multidimensional solar flare simulations have not yet included a detailed analysis of the lower atmospheric responses, such as downflowing chromospheric compressions and chromospheric evaporation processes.
Aims. We present an analysis of multidimensional flare simulations, including an analysis of chromospheric upflows and downflows that provides important groundwork for comparing 1D and multidimensional models.
Methods. We followed the evolution of a magnetohydrodynamic standard solar flare model that includes electron beams and in which localized anomalous resistivity initiates magnetic reconnection. We varied the background magnetic field strength to produce simulations that cover a large span of observationally reported solar flare strengths. Chromospheric energy fluxes and energy density maps were used to analyze the transport of energy from the corona to the lower atmosphere, and the resultant evolution of the flare. Quantities traced along 1D field lines allowed for detailed comparisons with 1D evaporation models.
Results. The flares produced by varying the background coronal field strength between 20 G and 65 G have GOES classifications between B1.5 and M2.3. All produce a lobster claw reconnection outflow and a fast shock in the tail of this flow with a similar maximum Alfvén Mach number of ∼10. The impact of the reconnection outflow on the lower atmosphere and the heat conduction are the key agents driving the chromospheric evaporation and “downflowing chromospheric compressions”. The peak electron beam heating flux in the lower atmospheres varies between 1.4 × 109 and 4.7 × 1010 erg cm−2 s−1 across the simulations. The downflowing chromospheric compressions have kinetic energy signatures that reach the photosphere, but at subsonic speeds they would not generate sunquakes. The weakest flare generates a relatively dense flare loop system, despite having a negative net mass flux, through the top of the chromosphere, that is to say, more mass is supplied downward than is evaporated upward. The stronger flares all produce positive mass fluxes. Plasmoids form in the current sheets of the stronger flares due to tearing, and in all experiments the loop tops contain turbulent eddies that ring via a magnetic tuning fork process.
Conclusions. The presented flares have chromospheric evaporation driven by thermal conduction and the impact and rebound of the reconnection outflow, in contrast to most 1D models where this process is driven by the beam electrons. Several multidimensional phenomena are critical in determining plasma behavior but are not generally considered in 1D flare simulations. They include loop-top turbulence, reconnection outflow jets, heat diffusion, compressive heating from the multidimensional expansion of the flux tubes due to changing pressures, and the interactions of upward and downward flows from the evaporation meeting the material squeezed downward from the loop tops.

Chromospheric evaporation by particle beams in multi-dimensional flare models

Malcolm Keith **Druett**, Wenzhi Ruan, Rony Keppens
Solar Phys. 298, Article number: 134 **2023**
https://arxiv.org/pdf/2310.11226.pdf
https://doi.org/10.1007/s11207-023-02224-4

Evaporation of chromospheric plasma by particle beams has been a standard feature of models of solar flares for many decades, supported both by observations of strong hard X-ray bremsstrahlung signals, and detailed 1D hydrodynamic radiative transfer models with near-relativistic electron beams included. However in multi-dimensional models, evaporation, if included, has only been driven by heat conduction and by the impact and reflection of fast plasma outflows on the lower atmosphere. Here we present the first multi-dimensional flare simulation featuring evaporation driven by energetic electrons. We use a recent magnetohydrodynamic model that includes beam physics, but decrease the initial anomalous resistivity to create a gentler precursor phase, and improve on the dynamic resistivity treatment that determines where beams are injected. Beam-driven evaporation is achieved. The relevant factors are thermal conduction and electron beams, with the beam electrons more than doubling the kinetic energy flux, and adding 50% to the upward mass from the chromosphere. These findings finally pave the way for integrating detailed 1D flare modelling within a self-consistent 2D and 3D context. The beam fluxes from these self-consistent models can be used to directly compare multi-dimensional results with those from the externally injected beam fluxes of 1D models, as well as understand further evaporation-driven phenomena relating to beams of particles.

RHESSI Nuggets #464 Dec **2023**
https://sprg.ssl.berkeley.edu/~tohban/wiki/index.php/Solar_flares:_evaporation_and_simulation

Exploring self-consistent 2.5 D flare simulations with MPI-AMRVAC

Malcolm **Druett**, Wenzhi Ruan, Rony Keppens

A&A **2023**
https://arxiv.org/pdf/2310.09939.pdf
Context. The advent of multi-dimensional solar flare simulations has led to numerous investigations of coronal flows and new physical insights. These studies have not yet included detailed analysis of the lower atmospheric responses such as down-flowing chromospheric compressions and chromospheric evaporation processes.
Aims. In this work, we present an analysis of multi-dimensional flare simulations, including analysis of chromospheric up-flows and down-flows that help to elucidate multi-dimensional effects. We also provide important groundwork for comparing 1D and multi-dimensional models, with the aim that future multi-dimensional simulations can include detailed field-aligned physical processes.
Methods. A localized anomalous resistivity initiates magnetic reconnection, which drives the evolution of a standard solar flare model. We vary the background magnetic field strength, to produce four flare simulations that cover a large span of observationally reported solar flare strengths. Chromospheric energy fluxes, and energy density maps are used to analyse the transport of energy from the corona to the lower atmosphere, and the resultant evolution of the flare. Quantities traced along 1D field-lines allow for detailed comparison with 1D evaporation models. We highlight the similarities, stressing deficiencies from simplified physics along these 1D flux tubes, and crucial effects that enter by multi-dimensional effects. **Sept 10th 2017**

Non-thermal hydrogen Lyman line and continuum emission in solar flares generated by electron beams

Druett M. and Zharkova V.V.
A&A 623, A20 **2019**
http://computing.unn.ac.uk/staff/slmv5/kinetics/Druett_Zharkova_aa2019.pdf
Aims. Hydrogen Lyman continuum emission is greatly enhanced in the impulsive kernels of solar flares, with observations of Lyman lines showing impulsive brightening and both red and blue wing asymmetries, based on the images with low spatial resolution. A spate of proposed instruments will study Lyman emission in more detail from bright, impulsive flare kernels. In support of new instrumentation we aim to apply an improved interpretation of Lyman emission with the hydrodynamic radiative code, HYDRO2GEN, which has already successfully explained Hα emission with large redshifts and sources of white light emission in solar flares. The simulations can interpret the existing observations and propose observations in the forthcoming missions.
Methods. A flaring atmosphere is considered to be produced by a 1D hydrodynamic response to injection of an electron beam, defining depth variations of electron and ion kinetic temperatures, densities, and macro-velocities. Radiative responses in this flaring atmosphere affected by the beams with different parameters are simulated using a fully non-local thermodynamic equilibrium (NLTE) approach for a five-level plus continuum model hydrogen atom with excitation and ionisation by spontaneous, external, and internal diffusive radiation, and by inelastic collisions with thermal and beam electrons. Integral radiative transfer equations for all optically thick transitions are solved using the L2 approximation simultaneously with steady state equations.
Results. During a beam injection in the impulsive phase there is a large increase of collisional ionisation and excitation by nonthermal electrons that strongly (by orders of magnitude) increases excitation and the ionisation degree of hydrogen atoms from all atomic levels. These non-thermal collisions combined with plasma heating caused by beam electrons lead to an increase in Lyman line and continuum radiation, which is highly optically thick. During a beam injection phase the Lyman continuum emission is greatly enhanced in a large range of wavelengths resulting in a flattened distribution of Lyman continuum over wavelengths. After the beam is switched off, Lyman continuum emission, because of its large opacity, sustains, for a very long time, the high ionisation degree of the flaring plasma gained during the beam injection. This leads to a long enhancement of hydrogen ionisation, occurrence of white light flares, and an increase of Lyman line emission in cores and wings, whose shapes are moved closer to those from complete redistribution (CRD) in frequencies, and away from the partial ones (PRD) derived in the non-flaring atmospheres. In addition, Lyman line profiles can reflect macro-motions of a flaring atmosphere caused by downward hydrodynamic shocks produced in response to the beam injection reflected in the enhancements of Ly-line red wing emission. These red-shifted Ly-line profiles are often followed by the enhancement of Ly-line blue wing emission caused by the chromospheric evaporation. The ratio of the integrated intensities in the Lyα and Lyβ lines is lower for more powerful flares and agrees with reported values from observations, except in the impulsive phase in flaring kernels which were not resolved in previous observations, in which the ratio is even lower. These results can help observers to design the future observations in Lyman lines and continuum emission in flaring atmospheres.

HYDRO2GEN: Non-thermal hydrogen Balmer and Paschen emission in solar flares generated by electron beams

Druett M. and Zharkova V.V.
A&A 610, A68 **2018**
http://computing.unn.ac.uk/staff/slmv5/kinetics/druett_zharkova%20aa17.pdf
Aim. Sharp rises of hard X-ray (HXR) emission accompanied by Hα line profiles with strong red-shifts up to 4 Å from the central wavelength, often observed at the onset of flares with the Specola Solare Ticinese Telescope (STT) and the

Swedish Solar Telescope (SST), are not fully explained by existing radiative models. Moreover, observations of white light (WL) and Balmer continuum emission with the Interface Region Imaging Spectrograph (IRISH) reveal strong co-temporal enhancements and are often nearly co-spatial with HXR emission. These effects indicate a fast effective source of excitation and ionisation of hydrogen atoms in flaring atmospheres associated with HXR emission. In this paper, we investigate electron beams as the agents accounting for the observed hydrogen line and continuum emission. Methods. Flaring atmospheres are considered to be produced by a 1D hydrodynamic response to the injection of an electron beam defining their kinetic temperatures, densities, and macro velocities. We simulated a radiative response in these atmospheres using a fully non-local thermodynamic equilibrium (NLTE) approach for a 5-level plus continuum hydrogen atom model, considering its excitation and ionisation by spontaneous, external, and internal diffusive radiation and by inelastic collisions with thermal and beam electrons. Simultaneous steady-state and integral radiative transfer equations in all optically thick transitions (Lyman and Balmer series) were solved iteratively for all the transitions to define their source functions with the relative accuracy of 10−5. The solutions of the radiative transfer equations were found using the L2 approximation. Resulting intensities of hydrogen line and continuum emission were also calculated for Balmer and Paschen series.
Results. We find that inelastic collisions with beam electrons strongly increase excitation and ionisation of hydrogen atoms from the chromosphere to photosphere. This leads to an increase in Lyman continuum radiation, which has high optical thickness, and after the beam is off it governs hydrogen ionisation and leads to the long lasting orders of magnitude enhancement of emission in Balmer and Paschen continua. The ratio of Balmer-to-other-continuum head intensities are found to be correlated with the initial flux of the beam. The height distribution of contribution functions for Paschen continuum emission indicate a close correlation with the observations of heights of WL and HXR emission reported for limb flares. This process also leads to a strong increase of wing emission (Stark's wings) in Balmer and Paschen lines, which is superimposed on large red-shifted enhancements of Hα-Hγ line emission resulting from a downward motion by hydrodynamic shocks. The simulated line profiles are shown to fit closely the observations for various flaring events.

BEAM ELECTRONS AS A SOURCE OF H-alpha FLARE RIBBONS,
Druett M., Scullion E., Zharkova V., Matthews S., Zharkov S. and Van der Voort, L.P.
Nature Communications, Article number: 15905 **2017,**
https://www.nature.com/articles/ncomms15905
http://www.nature.com.sci-hub.cc/articles/ncomms15905
The observations of solar flare onsets show rapid increase of hard and soft X-rays, ultra-violet emission with large Doppler blue shifts associated with plasma upflows, and Hα hydrogen emission with red shifts up to 1–4 Å. Modern radiative hydrodynamic models account well for blue-shifted emission, but struggle to reproduce closely the red-shifted Hα lines. Here we present a joint hydrodynamic and radiative model showing that during the first seconds of beam injection the effects caused by beam electrons can reproduce Hα line profiles with large red-shifts closely matching those observed in a C1.5 flare by the Swedish Solar Telescope. The model also accounts closely for timing and magnitude of upward motion to the corona observed 29 s after the event onset in 171 Å by the Atmospheric Imaging Assembly/Solar Dynamics Observatory. **30th June 2013**

Bivariate Number Distribution of Solar Soft X-Ray Flares
Z. L. **Du**
2020 ApJ 896 5
https://doi.org/10.3847/1538-4357/ab8cca
https://sci-hub.tw/https://iopscience.iop.org/article/10.3847/1538-4357/ab8cca
Conventionally, researchers investigated the number distribution of solar flares by univariate analysis using all available data. For the first time, we investigate the bivariate number distribution of peak flux (f) and duration (T) of soft X-ray flares observed by the Geostationary Operational Environmental Satellite during the past 10 years. First, the univariate number distribution of f is found to obey a power law either for each class of flares or for the B or ≥C flares in a certain range of T. But the power-law index of B-class flares is much smaller than those of other higher-class ones. For the ≥C flares, the longer the duration, the smaller the power-law index. The univariate number distribution of T deviates from the power law at shorter durations and is better fitted by a skewed Gaussian function in logarithmic coordinates for almost any given range of f, reflecting the random phenomena in solar flares. Then, based on the univariate analysis, a linear Gaussian function is proposed to describe the bivariate logarithmic number distribution of f and T, from which the local power-law index with respect to either f or T can also be analyzed. The real number distribution of B flares should be in between the observed one and the power-law distribution of stronger flares (≥C). We suggest that nanoflare activity may not be the dominant source of coronal heating.

Towards understanding the frequency distribution of solar flares—part 1: a Stochastic-Diffusive model of solar flares
Z. L. **Du**
Astrophysics and Space Science September **2015**, 359:4

Systematic relationships of the subclass-averaged rise, decay times and durations of flare events as a function of the logarithmic peak flux (lnf) are investigated, employing the soft X-ray flares observed by GOES during the period from September 1975 to October 2014. Different behaviors are found before and after 1997. Since 1997 they all vary linearly with lnf, obeying the RV model. However, prior to 1997 they vary quadratically with lnf, implying a different energy storage/release process of flaring. The discrepancy may be related to the variation in the turbulence in the corona caused by the weakening magnetic field strength in the recent two decades. This motivates us to propose a Stochastic-Diffusive model for explaining the above result, by assuming that the temporal rate of flare energy resulted by external forces is proportional to the total energy already stored in the flare system and inversely proportional to the size scale of diffusion.

Are Solar Active Regions Born with Neutralized Currents?

Aiying **Duan**, Yaoyu Xing and Chaowei Jiang
2024 Res. Astron. Astrophys. Volume 24, Number 7 075005
DOI 10.1088/1674-4527/ad50b6
https://iopscience.iop.org/article/10.1088/1674-4527/ad50b6/pdf
Solar active regions (ARs) are formed by the emergence of current-carrying magnetic flux tubes from below the photosphere. Although for an isolated flux tube the direct and return currents flowing along the tube should balance with each other, it remains controversial whether such a neutralization of currents is also maintained during the emergence process. Here we present a systematic survey of the degrees of the current neutralization in a large sample of flux-emerging ARs which appeared on the solar disk around the central meridian from 2010 to 2022. The vector magnetograms taken by Helioseismic and Magnetic Imager onboard Solar Dynamic Observatory are employed to calculate the distributions of the vertical current density at the photosphere. Focusing on the main phase of flux emergence, i.e., the phase in which the total unsigned magnetic flux is continuously increased, we statistically examined the ratios of direct to return currents in all the ARs. Such a large-sample statistical study suggests that most of the ARs were born with currents close to neutralization. The degree of current neutralization seems to be not affected by the active-region size, the active-region growing rate, and the total unsigned current. The only correlation of significance as found is that the stronger the magnetic field nonpotentiality is, the further the AR deviates from current neutrality, which supports previous event studies that eruption-productive ARs often have non-neutralized currents.

The Initiation Mechanism of the First On-disk X-Class Flare of Solar Cycle 25

Aiying **Duan**, Chaowei Jiang, ZhenJun Zhou, Xueshang Feng
A&A 674, A192 **2023**
https://arxiv.org/pdf/2304.13241.pdf
https://www.aanda.org/articles/aa/pdf/2023/06/aa45583-22.pdf
In this paper we study the initiation mechanism of the first on-disk X-class eruptive flare in solar cycle 25. Coronal magnetic field reconstructions reveal a magnetic flux rope (MFR) with configuration highly consistent with a filament existing for a long period before the flare, and the eruption of the whole filament indicates that the MFR erupted during the flare. However, quantitative analysis shows that the pre-flare MFR resides in a height too low to trigger a torus instability (TI). The filament experienced a slow rise before the flare onset, for which we estimate evolution of the filament height using a triangulation method by combining the SDO and STEREO observations, and find it is also much lower than the critical height for triggering TI. On the other hand, the pre-flare evolution of the current density shows progressive thinning of a vertical current layer on top of the flare PIL, which suggests that a vertical current sheet forms before the eruption. Meanwhile, there is continuously shearing motion along the PIL under the main branch of the filament, which can drive the coronal field to form such a current sheet. As such, we suggest that the event follows a reconnection-based initiation mechanism as recently established using a high-accuracy MHD simulation, in which an eruption is initiated by reconnection in a current sheet that forms gradually within continuously-sheared magnetic arcade. The eruption should be further driven by TI as the filament quickly rises into the TI domain during the eruption.
28 Oct 2021

A Study of Pre-flare Solar Coronal Magnetic Fields: Magnetic Energy and Helicity

Aiying **Duan**, Chaowei Jiang, Xueshang Feng
ApJ **945** 102 **2023**
https://arxiv.org/pdf/2302.12478.pdf
https://iopscience.iop.org/article/10.3847/1538-4357/acbc1a/pdf
Solar flares fall into two types with eruptive ones associated with coronal mass ejection (CME) and confined ones without CME. To explore whether there are pre-flare conditions in terms of magnetic energy and helicity that can effectively determine the types of flares, here we analyzed a suite of related parameters of the reconstructed pre-flare coronal magnetic field of major solar flares, either eruptive or confined, from 2011 to 2017 near the solar disk center. The investigated parameters include the extensive-type quantities such as the total magnetic energy ET, the potential energy EP, the free energy EF, the relative helicity HR, and the non-potential helicity HJ, as well as the intensive-type indices EF/EP, |HJ/HR|, |HR/ϕ'^2| and |HJ/ϕ'^2|, where ϕ' is half of the total unsigned magnetic flux. We have the

following key findings: (1) None of the extensive parameters can effectively distinguish the eruptive and confined potential of the pre-flare coronal fields, though the confined events have averagely larger values; (2) All the intensive parameters have significantly larger average and median values for eruptive flares than the confined events, which indicates that the field for eruptive flares have overall higher degree of non-potentiality and complexity than that of the confined flares; (3) The energy ratio EF/EP and the normalized non-potential helicity |HJ/ϕ′2|, which are strongly correlated with each other, have among the highest capability of distinguishing the fields that possibly produce a major eruptive or confined flare, as over 75\% of all the events are successfully discriminated between eruptive and confined flares by using critical values of EF/EP≥0.27 and |HJ/ϕ′2|≥0.009.
Table 1. List of events and their pre-flare parameters. 2011-2017

Dynamic Property and Magnetic Nonpotentiality of Two Types of Confined Solar Flares

Xuchun **Duan**, Ting Li, Qihang Jing
ApJ,933(2),191,**2022**
https://arxiv.org/ftp/arxiv/papers/2207/2207.07004.pdf
https://iopscience.iop.org/article/10.3847/1538-4357/ac75c1/pdf
We analyze 152 large confined flares (GOES class ≥M1.0 and ≤45∘ from disk center) during 2010−2019, and classify them into two types according to the criterion taken from the work of Li et al. (2019). "Type I" flares are characterized by slipping motions of flare loops and ribbons and a stable filament underlying the flare loops. "Type II" flares are associated with the failed eruptions of the filaments, which can be explained by the classical 2D flare model. A total of 59 flares are "Type I" flares (about 40\%) and 93 events are "Type II" flares (about 60\%). There are significant differences in distributions of the total unsigned magnetic flux (ΦAR) of active regions (ARs) producing the two types of confined flares, with "Type I" confined flares from ARs with a larger ΦAR than "Type II". We calculate the mean shear angle ΨHFED within the core of an AR prior to the flare onset, and find that it is slightly smaller for "Type I" flares than that for "Type II" events. The relative non-potentiality parameter ΨHFED/ΦAR has the best performance in distinguishing the two types of flares. About 73\% of "Type I" confined flares have ΨHFED/ΦAR<1.0×10−21 degree Mx−1, and about 66\% of "Type II" confined events have ΨHFED/ΦAR≥1.0×10−21 degree Mx−1. We suggest that "Type I" confined flares cannot be explained by the standard flare model in 2D/3D, and the occurrence of multiple slipping magnetic reconnections within the complex magnetic systems probably leads to the observed flare. **2011 August 3, 2014 October 22, 2014 December 1, 2015 September 28**

Variation of Magnetic Flux Ropes Through Major Solar Flares

Aiying **Duan**, Chaowei Jiang, Zhenjun Zhou, Xueshang Feng, Jun Cui
ApJL **907** L23 **2021**
https://iopscience.iop.org/article/10.3847/2041-8213/abd638/pdf
https://arxiv.org/pdf/2012.14588.pdf
It remains unclear how solar flares are triggered and in what conditions they can be eruptive with coronal mass ejections. Magnetic flux ropes (MFRs) has been suggested as the central magnetic structure of solar eruptions, and their ideal instabilities including mainly the kink instability (KI) and torus instability (TI) provide important candidates for triggering mechanisms. Here using magnetic field extrapolations from observed photospheric magnetograms, we systematically studied the variation of coronal magnetic fields, focusing on MFRs, through major flares including 29 eruptive and 16 confined events. We found that nearly 90\% events possess MFR before flare and 70\% have MFR even after flare. We calculated the controlling parameters of KI and TI, including the MFR's maximum twist number and the decay index of its strapping field. Using the KI and TI thresholds empirically derived from solely the pre-flare MFRs, two distinct different regimes are shown in the variation of the MFR controlling parameters through flares. For the events with both parameters below their thresholds before flare, we found no systematic change of the parameters after the flares, in either the eruptive or confined events. In contrast, for the events with any of the two parameters exceeding their threshold before flare (most of them are eruptive), there is systematic decrease in the parameters to below their thresholds after flares. These results provide a strong constraint for the values of the instability thresholds and also stress the necessity of exploring other eruption mechanisms in addition to the ideal instabilities. **2014 February 4, 2017 September 6**
Table 1. List of events and parameters of their pre- and post-flare MFRs. (2011-2017)

A Study of Pre-Flare Solar Coronal Magnetic Fields: Magnetic Flux Ropes

Aiying **Duan**, Chaowei Jiang, Wen He, Xueshang Feng, Peng Zou, Jun Cui
ApJ **884** 73 **2019**
https://arxiv.org/pdf/1908.08643.pdf
https://doi.org/10.3847/1538-4357/ab3e33
Magnetic flux ropes (MFRs) are thought to be the central structure of solar eruptions, and their ideal MHD instabilities can trigger the eruption. Here we performed a study of all the MFR configurations that lead to major solar flares, either eruptive or confined, from 2011 to 2017 near the solar disk center. The coronal magnetic field is reconstructed from observed magnetograms, and based on magnetic twist distribution, we identified the MFR, which is defined as a

coherent group of magnetic field lines winding an axis with more than one turn. It is found that 90% of the events possess pre-flare MFRs, and their three-dimensional structures are much more complex in details than theoretical MFR models. We further constructed a diagram based on two parameters, the magnetic twist number which controls the kink instability (KI), and the decay index which controls the torus instability (TI). It clearly shows lower limits for TI and KI thresholds, which are ncrit=1.3 and |Tw|crit=2, respectively, as all the events above ncrit and nearly 90% of the events above |Tw|crit erupted. Furthermore, by such criterion, over 70% of the events can be discriminated between eruptive and confined flares, and KI seems to play a nearly equally important role as TI in discriminating between the two types of flare. There are more than half of events with both parameters below the lower limits, and 29% are eruptive. These events might be triggered by magnetic reconnection rather than MHD instabilities. **2011-02-15, 2011-03-09, 2011-08-03,2012-01-23, 2012-03-06, 2012-05-10, 2012-07-02, 2012-07-05, 2012-07-12, 2013-04-11, 2013-10-24, 2013-11-01, 2013-11-03, 2013-11-05, 2013-11-08, 2013-12-31, 2014-01-07, 2014-02-02, 2014-02-04, 2014-03-29, 2014-04-18, 2014-09-28, 2014-10-22, 2014-10-24, 2014-11-07, 2014-12-04, 2014-12-18, 2014-12-20, 2015-03-11/12, 2013-06-22, 2015-06-25, 2015-08-24, 2015-09-04,06, 2015-09-28, 2017-09-06**
Table 1. List of events and properties of their MFRs (2011-2017)

Expanding and Contracting Coronal Loops as Evidence of Vortex Flows Induced by Solar Eruptions

J. **Dudík**, F. P. Zuccarello, G. Aulanier, B. Schmieder, P. Démoulin
ApJ **2017**
https://arxiv.org/pdf/1706.04783.pdf
Eruptive solar flares were predicted to generate large-scale vortex flows at both sides of the erupting magnetic flux rope. This process is analogous to a well-known hydrodynamic process creating vortex rings. The vortices lead to advection of closed coronal loops located at peripheries of the flaring active region. Outward flows are expected in the upper part and returning flows in the lower part of the vortex. Here, we examine two eruptive solar flares, an X1.1-class flare SOL**2012-03-05**T03:20 and a C3.5-class SOL**2013-06-19**T07:29. In both flares, we find that the coronal loops observed by the Atmospheric Imaging Assembly in its 171\,\AA, 193\,\AA, or 211\,\AA~passbands show coexistence of expanding and contracting motions, in accordance with the model prediction. In the X-class flare, multiple expanding/contracting loops coexist for more than 35 minutes, while in the C-class flare, an expanding loop in 193\,\AA~appears to be close-by and co-temporal with an apparently imploding loop arcade seen in 171\,\AA. Later, the 193\,\AA~loop also switches to contraction. These observations are naturally explained by vortex flows present in a model of eruptive solar flares.

Non-Equilibrium Processes in the Solar Corona, Transition Region, Flares, and Solar Wind \textit{(Invited Review)}

Jaroslav **Dudík**, Elena Dzifčáková, Nicole Meyer-Vernet, Giulio Del Zanna, Peter R. Young, Alessandra Giunta, Barbara Sylwester, Janusz Sylwester, Mitsuo Oka, Helen E. Mason, Christian Vocks, Lorenzo Matteini, Säm Krucker, David R. Williams, Šimon Mackovjak
Solar Phys. **2017**
https://arxiv.org/pdf/1706.03396.pdf
We review the presence and signatures of the non-equilibrium processes, both non-Maxwellian distributions and non-equilibrium ionization, in the solar transition region, corona, solar wind, and flares. Basic properties of the non-Maxwellian distributions are described together with their influence on the heat flux as well as on the rates of individual collisional processes and the resulting optically thin synthetic spectra. Constraints on the presence of high-energy electrons from observations are reviewed, including positive detection of non-Maxwellian distributions in the solar corona, transition region, flares, and wind. Occurrence of non-equilibrium ionization is reviewed as well, especially in connection to hydrodynamic and generalized collisional-radiative modelling. Predicted spectroscopic signatures of non-equilibrium ionization depending on the assumed plasma conditions are summarized. Finally, we discuss the future remote-sensing instrumentation that can be used for detection of these non-equilibrium phenomena in various spectral ranges. **2012-07-19**

Slipping Magnetic Reconnection, Chromospheric Evaporation, Implosion, and Precursors in the 2014 September 10 X1.6-Class Solar Flare

Jaroslav **Dudik**, Vanessa Polito, Miho Janvier, Sargam M. Mulay, Marian Karlicky, Guillaume Aulanier, Giulio Del Zanna, Elena Dzifcakova, Helen E. Mason, Brigitte Schmieder
ApJ **823** 41 **2016**
http://arxiv.org/pdf/1603.06092v1.pdf **File**
We investigate the occurrence of slipping magnetic reconnection, chromospheric evaporation, and coronal loop dynamics in the **2014 September 10** X-class flare. The slipping reconnection is found to be present throughout the flare from its early phase. Flare loops are seen to slip in opposite directions towards both ends of the ribbons. Velocities of 20--40 km\,s−1 are found within time windows where the slipping is well resolved. The warm coronal loops exhibit expanding and contracting motions that are interpreted as displacements due to the growing flux rope that subsequently erupts. This flux rope existed and erupted before the onset of apparent coronal implosion. This indicates

that the energy release proceeds by slipping reconnection and not via coronal implosion. The slipping reconnection leads to changes in the geometry of the observed structures at the \textit{IRIS} slit position, from flare loop top to the footpoints in the ribbons. This results in variations of the observed velocities of chromospheric evaporation in the early flare phase. Finally, it is found that the precursor signatures including localized EUV brightenings as well as non-thermal X-ray emission are signatures of the flare itself, progressing from the early phase towards the impulsive phase, with the tether-cutting being provided by the slipping reconnection. The dynamics of both the flare and outlying coronal loops is found to be consistent with the predictions of the standard solar flare model in 3D.

Imaging and Spectroscopic Observations of a Transient Coronal Loop: Evidence for the Non-Maxwellian κ-Distributions

Jaroslav **Dudik**, Simon Mackovjak, Elena Dzifcakova, Giulio Del Zanna, David R. Williams, Marian Karlicky, Helen E. Mason, Juraj Lorincik, Pavel Kotrc, Frantisek Farnik, Alena Zemanova

ApJ **807** 123 **2015**

http://arxiv.org/pdf/1505.04333v1.pdf

We report on the SDO/AIA and Hinode/EIS observations of a transient coronal loop. The loop brightens up in the same location after the disappearance of an arcade formed during a B8.9-class microflare three hours earlier. EIS captures this loop during its brightening phase as observed in most of the AIA filters. We use the AIA data to study the evolution of the loop, as well as to perform the DEM diagnostics as a function of κ. Fe XI--XIII lines observed by EIS are used to perform the diagnostics of electron density and subsequently the diagnostics of κ. Using ratios involving the Fe XI 257.772\AA selfblend, we diagnose $\kappa \lesssim 2$, i.e., an extremely non-Maxwellian distribution. Using the predicted Fe line intensities derived from the DEMs as a function of κ, we show that, with decreasing κ, all combinations of ratios of line intensities converge to the observed values, confirming the diagnosed $\kappa \lesssim 2$. These results represent the first positive diagnostics of κ-distributions in the solar corona despite the limitations imposed by calibration uncertainties. **2013 March 30**

On the Area Expansion of Magnetic Flux-Tubes in Solar Active Regions

Dudik, J., Dzifcakova, E., Cirtain, J. W.

ApJ, 796 20 **2014**

http://arxiv.org/pdf/1409.6947v1.pdf

We calculated the 3D distribution of the area expansion factors in a potential magnetic field extrapolated from the high-resolution \textit{Hinode}/SOT magnetogram of a quiescent active region **NOAA 11482**. Retaining only closed loops within the computational box, we show that the distribution of area expansion factors show significant structure. Loop-like structures characterized by locally lower values of the expansion factor are embedded in a smooth background. These loop-like flux-tubes have squashed cross-sections and expand with height. The distribution of the expansion factors show overall increase with height, allowing an active region core characterized by low values of the expansion factor to be distinguished. The area expansion factors obtained from extrapolation of the SOT magnetogram are compared to those obtained from an approximation of the observed magnetogram by a series of 134 submerged charges. This approximation retains the general flux distribution in the observed magnetogram, but removes the small-scale structure in both the approximated magnetogram and the 3D distribution of the area expansion factors. We argue that the structuring of the expansion factor can be a significant ingredient in producing the observed structuring of the solar corona. However, due to the potential approximation used, these results may not be applicable to loops exhibiting twist neither to active regions producing significant flares. **18 May 2012**

Signatures of the non-Maxwellian kappa-distributions in optically thin line spectra I. Theory and synthetic Fe IX--XIII spectra

Dudik, J, Del Zanna, G., Mason, H.E., Dzifcakova, E.

A&A, 570, A124 **2014**

http://arxiv.org/pdf/1408.0950v1.pdf

We investigate the possibility of diagnosing the degree of departure from the Maxwellian distribution using single-ion spectra originating in astrophysical plasmas in collisional ionization equilibrium. New atomic data for excitation of Fe IX-XIII are integrated under the assumption of a kappa-distribution of electron energies. Diagnostic methods using lines of a single ion formed at any wavelength are explored. Such methods minimize uncertainties from the ionization and recombination rates, as well as the possible presence of non-equilibrium ionization. Approximations to the collision strengths are also investigated. The calculated intensities of most of the Fe IX-XIII EUV lines show consistent behaviour with kappa at constant temperature. Intensities of these lines decrease with kappa, with the vast majority of ratios of strong lines showing little or no sensitivity to kappa. Several of the line ratios, especially involving temperature-sensitive lines, show a sensitivity to kappa that is of the order of several tens of per cent, or, in the case of Fe IX, up to a factor of two. Forbidden lines in the near-ultraviolet, visible, or infrared parts of the spectrum are an exception, with smaller intensity changes or even a reverse behaviour with kappa. The most conspicuous example is the Fe X 6378A red line, whose intensity incerases with kappa. This line is a potentially strong indicator of departures from

the Maxwellian distribution. We find it possible to perform density diagnostics independently of kappa, with many Fe XI-XIII line ratios showing strong density-sensitivity and negligible sensitivity to kappa and temperature. We also tested different averaging of the collision strengths. It is found that averaging over 0.01 interval in log(E/Ryd) is sufficient to produce accurate distribution-averaged collision strengths at temperatures of the ion formation in ionization equilibrium.

Slipping reconnection during a solar flare

Jaroslav **Dudík**
UKSP Nugget: 44, Feb **2014**.

Slipping magnetic reconnection during an X-class solar flare observed by SDO/AIA

J. **Dudik**, M. Janvier, G. Aulanier, G. Del Zanna, M. Karlicky, H. Mason, B. Schmieder
E-print, Jan **2014, File**; **2014** ApJ 784 144
http://arxiv.org/pdf/1401.7529v1.pdf
We present SDO/AIA observations of an eruptive X-class flare of **July 12, 2012**, and compare its evolution with the predictions of a 3D numerical simulation. We focus on the dynamics of flare loops that are seen to undergo slipping reconnection during the flare. In the AIA 131A observations, lower parts of 10 MK flare loops exhibit an apparent motion with velocities of several tens of km/s along the developing flare ribbons. In the early stages of the flare, flare ribbons consist of compact, localized bright transition-region emission from the footpoints of the flare loops. A DEM analysis shows that the flare loops have temperatures up to the formation of Fe XXIV. A series of very long, S-shaped loops erupt, leading to a CME observed by STEREO. The observed dynamics are compared with the evolution of magnetic structures in the ``standard solar flare model in 3D". This model matches the observations well, reproducing both the apparently slipping flare loops, S-shaped erupting loops, and the evolution of flare ribbons. All of these processes are explained via 3D reconnection mechanisms resulting from the expansion of a torus-unstable flux rope. The AIA observations and the numerical model are complemented by radio observations showing a noise storm in the metric range. Dm-drifting pulsation structures occurring during the eruption indicate plasmoid ejection and enhancement of reconnection rate. The bursty nature of radio emission shows that the slipping reconnection is still intermittent, although it is observed to persist for more than an hour.
Хорошее Введение.

Is it possible to model observed active region coronal emission simultaneously in EUV and X-ray filters?

J. **Dudík**1,2, E. Dzifčáková2, M. Karlický2 and A. Kulinová
A&A 531, A115 **(2011)**
Aims. We investigate the possibility of modeling the active region coronal emission in the EUV and X-ray filters using one, universal, steady heating function, tied to the properties of the magnetic field.
Methods. We employ a simple, static model to compute the temperature and density distributions in the active region corona. The model allows us to explore a wide range of parameters of the heating function. The predicted EUV and X-ray emission in the filters of EIT/SOHO and XRT/Hinode are calculated and compared with observations. Using the combined improved filter-ratio (CIFR) method, a temperature diagnostic is employed to compare the modeled temperature structure of the active region with the temperature structure derived from the observations.
Results. The global properties of the observations are most closely matched for heating functions scaling as that depend on the spatially variable heating scale-length. The modeled X-ray emission originates from locations where large heating scale-lengths are found. However, the majority of the loops observed in the 171 and 195 filters can be modeled only by loops with very short heating scale-lengths. These loops are known to be thermally unstable. We are unable to find a model that both matches the observations in all EUV and X-ray filters, and contains only stable loops. As a result, although our model with a steady heating function can explain some of the emission properties of the 171 and 195 loops, it cannot explain their observed lifetimes. Thus, the model does not lead to a self-consistent solution. The performance of the CIFR method is evaluated and we find that the diagnosed temperature can be approximated with a geometric mean of the emission-measure weighted and maximum temperature along the line of sight.
Conclusions. We conclude that if one universal heating function exists, it should be at least partially time-dependent.

Wide-band fluctuations of solar active regions probed with SHARP magnetograms

G. **Dumbadze**1,2,3, B. M. Shergelashvili2,3,4, M. L. Khodachenko5 and S. Poedts1,6
A&A 683, A86 (**2024**)
https://www.aanda.org/articles/aa/pdf/2024/03/aa47225-23.pdf
Context. The power spectra of the fluctuation noise of the solar active region (AR) areas and magnetic fluxes sequentially observed in time contain information about their geometrical features and the related fundamental physical processes. These spectra are analysed for five different ARs with various magnetic field structures.

Aims. The goal of this work is to detect the characteristic properties of the Fourier and wavelet spectra evaluated for the time series of the fluctuating areas and radial magnetic fluxes of the active regions. Accordingly, this work gathers information on the properties of noise in the different cases considered.
Methods. The AR area and radial magnetic flux time series were built using SHARP magnetogram datasets that cover nearly the entire time of the ARs' transits over the solar disk. Then we applied Fourier and wavelet analyses to these time series using apodization and detrendization methods for the cross-comparison of the results. These methods allow for the detection and removal of the artefact data edge effects. Finally, we used a linear least-squares fitting method for the obtained spectra on a logarithmic scale to evaluate the power-law slopes of the fluctuation spectral power versus frequency (if any).
Results. According to our results, the fluctuation spectra of the areas and radial magnetic fluxes of the considered ARs differ from each other to a certain extent, both in terms of the values of the spectral power-law exponents and their frequency bands.
Conclusions. The characteristic properties of the fluctuation spectra for the compact, dispersed, and mixed-type ARs exhibit noticeable discrepancies amongst each other. It is plausible to conclude that this difference might be related to distinct physical mechanisms responsible for the vibrations of the AR areas and/or radial magnetic fluxes.
Table 1. Selected ARs

The catalog of Hvar Observatory solar observations

Mateja **Dumbovic**, Luci Karbonini, Jasa Calogovic, Filip Matkovic, Karmen Martinic, Akshay Kumar Remeshan, Roman Brajsa, Bojan Vrsnak
Solar Phys. **299**, 66 **2024**
https://arxiv.org/pdf/2404.18576
https://doi.org/10.1007/s11207-024-02304-z
We compile the catalog of Hvar Observatory solar observations in the time period corresponding to regular digitally stored chromospheric and photospheric observations 2010-2019. We make basic characterisation of observed phenomena and compare them to catalogs which are based on full disc solar images. We compile a catalog of observed ARs consisting of 1100 entries, where each AR is classified according to McIntosh and Mt Wilson classifications. We find that HVAR observations are biased towards more frequently observing more complex ARs and observing them in longer time periods, likely related to the small FOV not encompassing the whole solar disc. In Hα observations we catalog conspicuous filaments/prominences and flares. We characterise filaments according to their location, chirality (if possible) and eruptive signatures. Analysis of the eruptive filaments reveals a slight bias in HVAR catalog towards observation of partial eruptions, possibly related to the observers tendency to observe filament which already showed some activity. In the flare catalog we focus on their observed eruptive signatures (loops or ribbons) and their shape. In addition, we associate them to GOES soft X-ray flares to determine their corresponding class. We find that HVAR observations seem biased towards more frequently observing stronger flares and observing them in longer time periods. We demonstrate the feasibility of the catalog on a case study of the flare detected on **2 August 2011** in HVAR Hα observations and related Sun-to-Earth phenomena. Through flare-CME-ICME association we demonstrate the agreement of remote and in situ properties. The data used for this study, as well as the catalog, are made publicly available.

The 2019 International Women's Day event: A two-step solar flare with multiple eruptive signatures and low Earth impact

Dumbovic, M., Veronig, A. M., Podladchikova, T., Thalmann, J. K., Chikunova, G., Dissauer, K., Magdalenic, J., Temmer, M., Guo, J., Samara, E
A&A 652, A159 **2021**
https://arxiv.org/pdf/2106.15417.pdf
https://www.aanda.org/articles/aa/pdf/2021/08/aa40752-21.pdf
https://doi.org/10.1051/0004-6361/202140752
We present a detailed analysis of an eruptive event that occurred on early **2019 March 8** in active region AR 12734, to which we refer as the International Women's day event. The event under study is intriguing in several aspects: 1) low-coronal eruptive signatures come in "pairs" (a double-peak flare, two coronal dimmings, and two EUV waves); 2) although the event is characterized by a complete chain of eruptive signatures, the corresponding coronagraphic signatures are weak; 3) although the source region of the eruption is located close to the center of the solar disc and the eruption is thus presumably Earth-directed, heliospheric signatures are very weak with little Earth-impact. We analyze a number of multi-spacecraft and multi-instrument (both remote-sensing and in situ) observations, including Soft X-ray, (extreme-) ultraviolet (E)UV), radio and white-light emission, as well as plasma, magnetic field and particle measurements. We employ 3D NLFF modeling to investigate the coronal magnetic field configuration in and around the active region, the GCS model to make a 3D reconstruction of the CME geometry and the 3D MHD numerical model EUHFORIA to model the background state of the heliosphere. Our results indicate two subsequent eruptions of two systems of sheared and twisted magnetic fields, which merge already in the upper corona and start to evolve further out as a single entity. The large-scale magnetic field significantly influences both, the early and the interplanetary evolution

of the structure. During the first eruption the stability of the overlying field was disrupted which enabled the second eruption. We find that during the propagation in the interplanetary space the large-scale magnetic field, i.e. , the location of heliospheric current sheet between the AR and the Earth likely influences propagation and the evolution of the erupted structure(s).

The unipolar solar flares as a manifestation of the 'topological' magnetic reconnection

Yurii V. **Dumin**, Boris V. Somov
MNRAS, *Letters*, Volume 528, Issue 1, February **2024**, Pages L15–L19
https://arxiv.org/pdf/2309.16417.pdf
https://doi.org/10.1093/mnrasl/slad162
https://watermark.silverchair.com/slad162.pdf
The solar flares - which are the most prominent manifestation of the solar activity - typically manifest themselves as a single or a set of luminous arcs (magnetic flux tubes) rooted in the regions of opposite polarity in the photosphere. However, a careful analysis of the archival data by Hinode satellite sometimes reveals the surprising cases of the flaring arcs whose footpoints belong to the regions of the same polarity or to the areas without any appreciable magnetic field. Despite a counterintuitive nature of this phenomenon, it can be reasonably interpreted in the framework of the so-called 'topological model' of magnetic reconnection, where the magnetic null point is formed due to specific superposition of influences from the remote sources rather than by the local current systems. As a result, the energy release propagates along the separator of the flipping two-dome structure rather than along a fixed magnetic field line. Therefore, the luminous arc needs not to be associated anymore immediately with the magnetic sources. Here, we report both the observational cases of the above-mentioned type as well as provide their theoretical model and the numerical simulations. **2014 October 1**

New types of the chromospheric anemone microflares: Case study

Yu. V. **Dumin**, B. V. Somov
A&A **295**, Article number: 92 (**2020**)
https://arxiv.org/pdf/1904.09439.pdf
https://link.springer.com/article/10.1007/s11207-020-01662-8
Context: The chromospheric anemone microflares (AMF) are an interesting kind of the transient solar phenomena where the emission regions have a multi-ribbon configuration, as distinct from the ordinary flares usually possessing only two ribbons. The previously reported AMFs had typically three or, less frequently, four ribbons; and it was shown in our recent Letter [Yu.V. Dumin & B.V. Somov, A&A, 623, L4 (2019)] that they can be reasonably described by the so-called GKSS model of magnetic field, involving four magnetic sources with various polarity and arrangement.
Aims: An interesting question is if one can see more complex types of AMF (containing the grater number of the emission ribbons), which might be produced by more elaborated magnetic configurations?
Methods: To answer this question, we performed a visual inspection of the large set of the emission patterns in the chromospheric line CaII H recorded by Hinode/SOT and confronted them with the respective magnetograms obtained by SDO/HMI.
Results: As follows from our analysis, it is really possible to identify the AMFs with much more complex spatial configurations as compared to the previously-known ones, e.g., involving five luminous ribbons with a nontrivial arrangement. They are produced by the effective magnetic sources (sunspots) of different polarity with intermittent arrangement in the cross-like configuration, but their number is greater than in the standard GKSS model. **16 February 2014**

Ю.В. Думин (ГАИШ МГУ) "Анемонные" и "нетипичные многоленточные" вспышки: обзор литературы и новые результаты
В первой части доклада будет дан обзор исследований по солнечным вспышкам со сложной геометрической структурой, проводившихся в последние 10-15 лет. В частности, это - так называемые "нетипичные многоленточные" вспышки, состоящие из более чем двух светящихся лент, приблизительно параллельных друг другу [1], а также "анемонные" (звездообразные) микровспышки, в которых эмиссионные лепестки исходят, грубо говоря, из одного центра [2]. В то время как механизм формирования "нетипичных многоленточных" вспышек более или менее стандартен и связан с формированием нескольких систем магнитных аркад, процессы возникновения "анемонных" микровспышек остаются не до конца понятыми и, по-видимому, включают в себя несколько различных механизмов.
Первоначально анемонные вспышки были наблюдены в трехлепестковой конфигурации, ориентированной вертикально в виде перевернутой буквы "Y", и они были интерпретированы как "мини-эрупции", возникающие в процессе магнитного пересоединения. Однако последующие наблюдения со спутника Hinode выявили также случаи горизонтальной ориентации и, более того, возможность формирования не только трех, но и четырех эмиссионных лепестков, что делает их чисто "эруптивную" интерпретацию достаточно проблематичной. Для объяснения таких случаев была предложена картина расщепляющихся магнитных потоков, вдоль которых исходная область энерговыделения проектируется на нижележащие слои солнечной атмосферы [2]. Одной из конкретных и наиболее эффективных реализаций такого механизма является "топологическая неустойчивость"

определенных конфигураций магнитного поля, приводящая к весьма разнообразным структурам эмиссионных лепестков, качественно согласующимся с наблюдаемыми [3].
Во второй части доклада будут представлены некоторые наблюдательные результаты, полученные в последнее время в Отделе физики Солнца ГАИШ. Это, в частности - анемонные микровспышки с более чем четырьмя лепестками, которые являются сильным аргументом в пользу моделей с расщепляющимися потоками, а также анемонные микровспышки стандартной конфигурации, возникающие в областях с существенно несбалансированными магнитными источниками [4].
Библиография:
1. H. Wang, et al. Astrophys. J. Lett., v.781, p.L23 (2014)
2. K. Shibata, et al. Science, v.318, p.1591 (2007)
3. Yu.V. Dumin, B.V. Somov. Astron. & Astrophys., v.623, p.L4 (2019)
4. Yu.V. Dumin, B.V. Somov. Preprint arXiv:1904.09439 (2019)

Topological model of the anemone microflares in the solar chromosphere

Yu.V. **Dumin**, B.V. Somov
A&A 623, L4 **2019**
https://arxiv.org/pdf/1811.06214.pdf
https://www.aanda.org/articles/aa/pdf/2019/03/aa34645-18.pdf
The chromospheric anemone microflares, which were discovered by Hinode satellite about a decade ago, are the specific transient phenomena starting from a few luminous ribbons on the chromospheric surface and followed by the eruption upwards. While the eruptive stage was studied in sufficient detail, a quantitative theory of formation of the initial multi-ribbon structure remains undeveloped till now. Here, we construct a sufficiently simple but general model of the magnetic field sources that is able to reproduce all the observed types of the luminous ribbons by varying only a single parameter. As a working tool, we employ the Gorbachev-Kel'ner-Somov-Shvarts (GKSS) model of the magnetic field, which was originally suggested about three decades ago to explain fast ignition of the magnetic reconnection over considerable spatial scales by tiny displacements of the magnetic sources. Quite unexpectedly, this model turns out to be efficient also for the description of generic multi-ribbon structure in the anemone flares. As follows from our numerical simulation, displacement of a single magnetic source (sunspot) with respect to three other sources results in a complex transformation from three to four ribbons and, then, again to three ribbons but with an absolutely different arrangement. Such structures closely remind the observed patterns of emission in the anemone microflares.

Observation of "Topological" Microflares in the Solar Atmosphere

Yurii V. **Dumin**, Boris V. Somov
Research Notes of the American Astronomical Society **1** 15 **2017**
https://arxiv.org/pdf/1711.03140.pdf
http://iopscience.iop.org/article/10.3847/2515-5172/aa9928
We report on observation of the unusual kind of solar microflares, presumably associated with the so-called "topological trigger" of magnetic reconnection, which was theoretically suggested long time ago by Gorbachev et al. (Sov. Ast. 1988, v.32, p.308) but has not been clearly identified so far by observations. As can be seen in pictures by Hinode SOT in CaII line, there may be a bright loop connecting two sunspots, which looks at the first sight just as a magnetic field line connecting the opposite poles. However, a closer inspection of SDO HMI magnetograms shows that the respective arc is anchored in the regions of the same polarity near the sunspot boundaries. Yet another peculiar feature is that the arc flashes almost instantly as a thin strip and then begins to expand and decay, while the typical chromospheric flares in CaII line are much wider and propagate progressively in space. A qualitative explanation of the unusual flare can be given by the above-mentioned model of topological trigger. Namely, there are such configurations of the magnetic sources on the surface of photosphere that their tiny displacements result in the formation and fast motion of a 3D null point along the arc located well above the plane of the sources. So, such a null point can quickly ignite a magnetic reconnection along the entire its trajectory. Pictorially, this can be presented as flipping the so-called two-dome magnetic-field structure (which is just the reason why such mechanism was called topological). The most important prerequisite for the development of topological instability in the two-dome structure is a cruciform arrangement of the magnetic sources in its base, and this condition is really satisfied in the case under consideration.
1 October 2014

What is Generic Structure of the Three-dimensional Magnetic Reconnection?

Yurii V. **Dumin**, Boris V. Somov
2014
http://arxiv.org/pdf/1407.6039v1.pdf
The probability of occurrence of various topological configurations of the three-dimensional reconnection in a random magnetic field is studied. It is found that a specific six-tail spatial configuration should play the dominant role, while all other types of reconnection (in particular, the axially-symmetric fan-like structures) are realized with a much less probability. A characteristic feature of the six-tail configuration is that at the sufficiently large scales it is approximately

reduced to the well-known two-dimensional X-type structure; and this explains why the two-dimensional models of reconnection usually work quite well.

Evolution of Magnetic Nonpotentiality in NOAA AR 10486
J. **Dun,** H. Kurokawa, T. T. Ishii, Y. Liu, and H. Zhang
Astrophysical Journal, Volume 657, Number 1, Page 577, **2007.**
http://www.journals.uchicago.edu/cgi-bin/resolve?ApJ63861

Thermal Evolution of an Active Region through Quiet and Flaring Phases as Observed by NuSTAR XRT, and AIA

Jessie **Duncan**, Reed B. Masek, Albert Y. Shih, Lindsay Glesener, Will Barnes, Katharine K. Reeves, Yixian Zhang, Iain G. Hannah, Brian W. Grefenstette
2024 *ApJ* **966** 197
https://arxiv.org/pdf/2312.05109.pdf
https://iopscience.iop.org/article/10.3847/1538-4357/ad37f7/pdf
Solar active regions contain a broad range of temperatures, with the thermal plasma distribution often observed to peak in the few millions of kelvin. Differential emission measure (DEM) analysis can allow instruments with diverse temperature responses to be used in concert to estimate this distribution. NuSTAR HXR observations are uniquely sensitive to the highest-temperature components of the corona, and thus extremely powerful for examining signatures of reconnection-driven heating. Here, we use NuSTAR diagnostics in combination with EUV and SXR observations (from SDO/AIA and Hinode/XRT) to construct DEMs over 170 distinct time intervals during a five-hour observation of an alternately flaring and quiet active region (NOAA designation AR 12712). This represents the first HXR study to examine the time evolution of the distribution of thermal plasma in an active region. During microflares, we find that the initial microflare-associated plasma heating is dominantly heating of material that is already relatively hot, followed later on by broader heating of initially-cooler material. During quiescent times, we show that the amount of extremely hot (>10 MK) material in this region is significantly (~3 orders of magnitude) less than that found in the quiescent active region observed in HXRs by FOXSI-2 (Ishikawa et al. 2017). This result implies there can be radically different high-temperature thermal distributions in different active regions, and strongly motivates future HXR DEM studies covering a large number of these regions. **2018 May 29**

NuSTAR Observation of Energy Release in Eleven Solar Microflares

Jessie **Duncan**, Lindsay Glesener, Brian W. Grefenstette, Juliana Vievering, Iain G. Hannah, David M. Smith, Säm Krucker, Stephen M. White, Hugh Hudson
2021 *ApJ* **908** 29
https://arxiv.org/pdf/2011.06651.pdf
https://iopscience.iop.org/article/10.3847/1538-4357/abca3d/pdf
https://doi.org/10.3847/1538-4357/abca3d
Solar flares are explosive releases of magnetic energy. Hard X-ray (HXR) flare emission originates from both hot (millions of Kelvin) plasma and nonthermal accelerated particles, giving insight into flare energy release. The Nuclear Spectroscopic Telescope ARray (NuSTAR) utilizes direct focusing optics to attain much higher sensitivity in the HXR range than that of previous indirect imagers. This paper presents eleven NuSTAR microflares from two active regions (AR 12671 on 2017 August 21, and AR 12712 on 2018 May 29). The temporal, spatial, and energetic properties of each are discussed in context with previously published HXR brightenings. They are seen to display several 'large-flare' properties, such as impulsive time profiles and earlier peaktimes in higher energy HXRs. For two events where active region background could be removed, microflare emission did not display spatial complexity: differing NuSTAR energy ranges had equivalent emission centroids. Finally, spectral fitting showed a high energy excess over a single thermal model in all events. This excess was consistent with additional higher-temperature plasma volumes in 10/11 microflares, and consistent only with an accelerated particle distribution in the last. Previous NuSTAR studies focused on one or a few microflares at a time, making this the first to collectively examine a sizable number of events. Additionally, this paper introduces an observed variation in the NuSTAR gain unique to the extremely low-livetime (<1%) regime, and establishes a correction method to be used in future NuSTAR solar spectral analysis. **2017 August 21, 2018 May 29**
RHESSI Nuggets #401 February **2021**
https://sprg.ssl.berkeley.edu/~tohban/wiki/index.php/A_Collective_Study_of_11_NuSTAR_Microflares

The Statistical Relationship between White-light Emission and Photospheric Magnetic Field Changes in Flares

J. S. Castellanos **Durán**, L. Kleint
ApJ **904** 96 **2020**
https://arxiv.org/pdf/2007.02954.pdf

https://doi.org/10.3847/1538-4357/ab9c1e
Continuum emission, also called white-light emission (WLE), and permanent changes of the magnetic field (ΔBLOS) are often observed during solar flares. But their relation and their precise mechanisms are still unknown. We study statistically the relationship between ΔBLOS and WLE during 75 solar flares of different strengths and locations on the solar disk. We analyze SDO/HMI data and determine for each pixel in each flare if it exhibited WLE and/or ΔBLOS. We then investigate the occurrence, strength, and spatial size of the WLE, its dependence on flare energy, and its correlation to the occurrence of ΔBLOS. We detected WLE in 44/75 flares and ΔBLOS in 59/75 flares. We find that WLE and ΔBLOS are related, and their locations often overlap between 0-60\%. Not all locations coincide, thus potentially indicating differences in their origin. We find that the WL area is related to the flare class by a power law and extend the findings of previous studies, that the WLE is related to the flare class by a power law, to also be valid for C-class flares. To compare unresolved (Sun-as-a-star) WL measurements to our data, we derive a method to calculate temperatures and areas of such data under the black-body assumption. The calculated unresolved WLE areas improve, but still differ to the resolved flaring area by about a factor of 5-10 (previously 10-20), which could be explained by various physical or instrumental causes. This method could also be applied to stellar flares to determine their temperatures and areas independently. **2011-08-09, 2012-07-05, 23−Oct−12, 25 Feb 2014**
RHESSI Science Nuggets #385 Sep **2020** https://sprg.ssl.berkeley.edu/~tohban/wiki/index.php/White-light_emission_and_photospheric_magnetic_field_changes_in_flares

A Statistical Study of Photospheric Magnetic Field Changes During 75 Solar Flares

J. S. Castellanos **Durán**1,2, L. Kleint3,4, and B. Calvo-Mozo1
2018 ApJ 852 25
http://iopscience.iop.org.sci-hub.tw/0004-637X/852/1/25/
Abrupt and permanent changes of photospheric magnetic fields have been observed during solar flares. The changes seem to be linked to the reconfiguration of magnetic fields, but their origin is still unclear. We carried out a statistical analysis of permanent line-of-sight magnetic field ($B_{\rm LOS}$) changes during 18 X-, 37 M-, 19 C-, and 1 B-class flares using data from the Solar Dynamics Observatory/Helioseismic and Magnetic Imager. We investigated the properties of permanent changes, such as frequency, areas, and locations. We detected changes of $B_{\rm LOS}$ in 59/75 flares. We find that strong flares are more likely to show changes, with all flares ≥M1.6 exhibiting them. For weaker flares, permanent changes are observed in 6/17 C-flares. 34.3% of the permanent changes occurred in the penumbra and 18.9% in the umbra. Parts of the penumbra appeared or disappeared in 23/75 flares. The area where permanent changes occur is larger for stronger flares. Strong flares also show a larger change of flux, but there is no dependence of the magnetic flux change on the heliocentric angle. The mean rate of change of flare-related magnetic field changes is 20.7 Mx cm−2 min−1. The number of permanent changes decays exponentially with distance from the polarity inversion line. The frequency of the strength of permanent changes decreases exponentially, and permanent changes up to 750 Mx cm−2 were observed. We conclude that permanent magnetic field changes are a common phenomenon during flares, and future studies will clarify their relation to accelerated electrons, white-light emission, and sunquakes to further investigate their origin. **2011-02-15, 2011-07-30, 29 March 2014**
Table 1 List of Flares (2011)
HMI Science Nuggets #84 **2018** http://hmi.stanford.edu/hminuggets/?p=2172

Solar hard X-ray imaging by means of compressed sensing and finite isotropic wavelet transform

M. A. **Duval-Poo1**, M. Piana1,2 and A. M. Massone2
A&A 615, A59 (**2018**)
https://www.aanda.org/articles/aa/pdf/2018/07/aa31765-17.pdf
Aims. Compressed sensing realized by means of regularized deconvolution and the finite isotropic wavelet transform is effective and reliable in hard X-ray solar imaging.
Methods. The method uses the finite isotropic wavelet transform with the Meyer function as the mother wavelet. Furthermore, compressed sensing is realized by optimizing a sparsity-promoting regularized objective function by means of the fast iterative shrinkage-thresholding algorithm. Eventually, the regularization parameter is selected by means of the Miller criterion.
Results. The method is applied against both synthetic data mimicking measurements made with the Spectrometer/Telescope Imaging X-rays (STIX) and experimental observations provided by the Reuven Ramaty High Energy Solar Spectroscopic Imager (RHESSI). The performances of the method are qualitatively validated by comparing some morphological properties of the reconstructed sources with those of the corresponding synthetic configurations. Furthermore, the results concerning experimental data are compared with those obtained by applying other visibility-based reconstruction methods.
Conclusions. The results show that when the new method is applied to synthetic STIX visibility sets, it provides reconstructions with a spatial accuracy comparable to the accuracy provided by the most popular method in hard X-ray solar imaging and with a higher spatial resolution. Furthermore, when it is applied to experimental RHESSI data, the

reconstructions are characterized by reliable photometry and by a notable reduction of the ringing effects caused by the instrument point spread function**. 20 February 2002, 15 April 2002; July 23 2002, 2 December 2003, 31 August 2004,13 May 2013.**

A multiwavelength study of an M-class flare and the origin of an associated eruption from NOAA AR 11045

Dwivedi, B. N.; Srivastava, Abhishek K.; Kumar, Mukul; Kumar, Pankaj
E-print, March **2012**, New Astr. http://www.sciencedirect.com/science/article/pii/S1384107611001485
In this paper, we study multiwavelength observations of an M6.4 flare in Active Region NOAA 11045 on **7 February 2010**. The space- and ground-based observations from STEREO, SoHO/MDI, EIT, and Nobeyama Radioheliograph were used for the study. This active region rapidly appeared at the north-eastern limb with an unusual emergence of a magnetic field. We find a unique observational signature of the magnetic field configuration at the flare site. Our observations show a change from dipolar to quadrapolar topology. This change in the magnetic field configuration results in its complexity and a build-up of the flare energy. We did not find any signature of magnetic flux cancellation during this process. We interpret the change in the magnetic field configuration as a consequence of the flux emergence and photospheric flows that have opposite vortices around the pair of opposite polarity spots. The negative-polarity spot rotating counterclockwise breaks the positive-polarity spot into two parts. The STEREO-A 195 ? and STEREO-B 171 ? coronal images during the flare reveal that a twisted flux tube expands and erupts resulting in a coronal mass ejection (CME). The formation of co-spatial bipolar radio contours at the same location also reveals the ongoing reconnection process above the flare site and thus the acceleration of non-thermal particles. The reconnection may also be responsible for the detachment of a ring-shaped twisted flux tube that further causes a CME eruption with a maximum speed of 446 km/s in the outer corona.

Effects of electron distribution anisotropy in spectroscopic diagnostics of solar flares

E. **Dzifčáková** and M. Karlický
A&A 618, A176 (**2018**)
sci-hub.tw/10.1051/0004-6361/201833208
Aims. We analyzed effects of the bi-Maxwellian electron distribution representing electron temperature anisotropy along and across the magnetic field on the ionization and excitation equilibrium with consequences on the temperature diagnostics of the flare plasma.
Methods. The bi-Maxwellian energy distributions were calculated numerically. Synthetic X-ray line spectra of the bi-Maxwellian distributions were calculated using non-Maxwellian ionization, recombination, excitation and de-excitation rates.
Results. We found that the anisotropic bi-Maxwellian velocity distributions transform to the nonthermal energy distributions with a high-energy tail. Their maximum is shifted to lower energies and contains a higher number of the low-energy particles in comparison with the Maxwellian one. Increasing the deviation of the parameter $p = T_\parallel/T_\perp$ from 1, changes the shape of bi-Maxwellian distributions and ionization equilibrium, and relative line intensities also increase. The effects are more significant for the bi-Maxwellian distribution with $T_\parallel > T_\perp$. Moreover, considering different acceleration mechanisms and collisional isotropization it is possible that the bi-Maxwellian distributions with high deviations from the Maxwellian distribution are more probable for those with $p > 1$ than for those with $p < 1$. Therefore, distributions with $p > 1$ can be much more easily diagnosed than those with $p < 1$. Furthermore, we compared the effects of the bi-Maxwellian distributions on the ionization equilibrium and temperature diagnostics with those for the κ-distributions obtained previously. We found that they are similar and at the present state it is difficult to distinguish between the bi-Maxwellian and κ-distributions from the line ratios.

Spectroscopic diagnostics of the non-Maxwellian $κ$-distributions using SDO/EVE observations of the 2012 March 7 X-class flare

Elena **Dzifcakova**, Alena Zemanova, Jaroslav Dudik, Simon Mackovjak
ApJ **853** 158 **2018**
https://arxiv.org/pdf/1801.02936.pdf
Spectroscopic observations made by the Extreme Ultraviolet Variability Experiment (EVE) on board the Solar Dynamics Observatory (SDO) during the **2012 March 7** X5.4-class flare (SOL2012-03-07T00:07) are analyzed for signatures of the non-Maxwellian kappa-distributions. Observed spectra were averaged over 1 minute to increase photon statistics in weaker lines and the pre-flare spectrum was subtracted. Synthetic line intensities for the kappa-distributions are calculated using the KAPPA database. We find strong departures (kappa < 2) during the early and impulsive phases of the flare, with subsequent thermalization of the flare plasma during the gradual phase. If the temperatures are diagnosed from a single line ratio, the results are strongly dependent on the value of kappa. For kappa=2, we find temperatures about a factor of two higher than the commonly used Maxwellian ones. The non-Maxwellian effects could also cause the temperatures diagnosed from line ratios and from the ratio of GOES X-ray channels to be different. Multithermal analysis reveals the plasma to be strongly multithermal at all times with flat

DEMs. For lower kappa, the DEM_kappa are shifted towards higher temperatures. The only parameter that is nearly independent of kappa is electron density, where we find log(N_e) $\approx$ 11.5 almost independently of time. We conclude that the non-Maxwellian effects are important and should be taken into account when analyzing solar flare observations, including spectroscopic and imaging ones.
See RHESSI Science Nuggets # 317 Feb **2018**
http://sprg.ssl.berkeley.edu/~tohban/wiki/index.php/Non-Maxwellian_Diagnostics_from_SDO/EVE_Spectra_of_an_X-class_Flare

Shock-reflected electrons and X-ray line spectra

Elena **Dzifcakova**, Marek Vandas, Marian Karlicky
A&A 603, A17 **2017**
https://arxiv.org/pdf/1705.11007.pdf
The aim of this paper is to try to explain the physical origin of the non-thermal electron distribution that is able to form the enhanced intensities of satellite lines in the X-ray line spectra observed during the impulsive phases of some solar flares. Synthetic X-ray line spectra of the distributions composed of the distribution of shock reflected electrons and the background Maxwellian distribution are calculated in the approximation of non-Maxwellian ionization, recombination, excitation and de-excitation rates. The distribution of shock reflected electrons is determined analytically. We found that the distribution of electrons reflected at the nearly-perpendicular shock resembles, at its high-energy part, the so called n-distribution. Therefore it could be able to explain the enhanced intensities of Si XIId satellite lines. However, in the region immediately in front of the shock its effect is small because electrons in background Maxwellian plasma are much more numerous there. Therefore, we propose a model in which the shock reflected electrons propagate to regions with smaller densities and different temperatures. Combining the distribution of the shock-reflected electrons with the Maxwellian distribution having different densities and temperatures we found that spectra with enhanced intensities of the satellite lines are formed at low densities and temperatures of the background plasma when the combined distribution is very similar to the n-distribution also in its low-energy part. In these cases, the distribution of the shock-reflected electrons controls the intensity ratio of the allowed Si XIII and Si XIV lines to the Si XIId satellite lines. The high electron densities of the background plasma reduce the effect of shock-reflected electrons on the composed electron distribution function, which leads to the Maxwellian spectra.

Non-equilibrium ionization by a periodic electron beam
I. Synthetic coronal spectra and implications for interpretation of observations⋆

E. **Dzifčáková**1, J. Dudík1⋆⋆ and Š. Mackovjak
A&A 589, A68 (**2016**)
Context. Coronal heating is currently thought to proceed via the mechanism of nanoflares, small-scale and possibly recurring heating events that release magnetic energy.
Aims. We investigate the effects of a periodic high-energy electron beam on the synthetic spectra of coronal Fe ions.
Methods. Initially, the coronal plasma is assumed to be Maxwellian with a temperature of 1 MK. The high-energy beam, described by a κ-distribution, is then switched on every period P for the duration of P/ 2. The periods are on the order of several tens of seconds, similar to exposure times or cadences of space-borne spectrometers. Ionization, recombination, and excitation rates for the respective distributions are used to calculate the resulting non-equilibrium ionization state of Fe and the instantaneous and period-averaged synthetic spectra.
Results. Under the presence of the periodic electron beam, the plasma is out of ionization equilibrium at all times. The resulting spectra averaged over one period are almost always multithermal if interpreted in terms of ionization equilibrium for either a Maxwellian or a κ-distribution. Exceptions occur, however; the EM-loci curves appear to have a nearly isothermal crossing-point for some values of κs. The instantaneous spectra show fast changes in intensities of some lines, especially those formed outside of the peak of the respective EM(T) distributions if the ionization equilibrium is assumed.

Ionisation Equilibrium for the Non-Maxwellian Electron n -Distributions in Solar Flares: Updated Calculations

Elena **Dzifčáková**, Jaroslav Dudík
Solar Phys. Volume 290, Issue 12, pp 3545-3558 **2015**
We use the latest available atomic data to calculate the ionisation and recombination rates for the non-Maxwellian n-distributions, which were shown previously to provide a good fit to the enhanced intensities of dielectronic satellite lines during solar flares. The ionisation and recombination coefficients are subsequently used to derive the ionisation

equilibrium. To do so, we consider odd values of n ranging from 1 to 19, i.e., from Maxwellian to strongly non-Maxwellian cases. These calculations involve all elements with proton number up to 30, i.e., H to Zn. The n-distributions modify both the ionisation and the recombination rates. The ionisation rates decrease more steeply at lower pseudo-temperatures, while the radiative recombination rate is reduced due to a lower number of low-energy electrons. The peaks of the dielectronic recombination rates become narrower. These changes are reflected in the ionisation equilibrium. Ion abundance peaks become narrower and can also be shifted, mostly towards higher temperatures. The He-like ions are an important exception, as they are formed in a larger temperature range than that for the Maxwellian distribution. The ions Si xiii – xiv used previously for the diagnostics of the n-distributions are affected only weakly, confirming the determination of n. The ionisation equilibria are available as the electronic supplementary material in a format compatible with the CHIANTI database.
Erratum Solar Phys. 291(2) 2016

KAPPA: A Package for Synthesis of optically thin spectra for the non-Maxwellian kappa-distributions based on the CHIANTI database

Dzifcakova, E., Dudik, J., Kotrc, P., Farnik, F., Zemanova, A.
ApJSuppl **2015**
http://arxiv.org/pdf/1502.00853v1.pdf
The non-Maxwellian κ-distributions have been detected in the solar transition region and flares. These distributions are characterized by a high-energy tail and a near-Maxwellian core and are known to have significant impact on the resulting optically thin spectra arising from collisionally dominated astrophysical plasmas. We developed the KAPPA package (this http URL) for synthesis of such line and continuum spectra. The package is based on the freely available CHIANTI database and software, and can be used in a similar manner. Ionization and recombination rates together with the ionization equilibria are provided for a range of κ values. Distribution-averaged collision strengths for excitation are obtained by an approximate method for all transitions in all ions available within CHIANTI. The validity of this approximate method is tested by comparison with direct calculations. Typical precisions of better than 5% are found, with all cases being within 10%. Tools for calculation of synthetic line and continuum intensities are provided and described. Examples of the synthetic spectra and SDO/AIA responses to emission for the κ-distributions are given.

Dielectronic satellite lines and double layers in solar flares

E. **Dzifčáková**1, M. Karlický1 and J. Dudík
A&A 550, A60 (**2013**)
Context. Particle acceleration during solar flares results in departures of the distribution of particle energies from the Maxwellian distribution. Apart from the high-energy tail, the bulk of the distribution was recently also found to be significantly affected, due, e.g., to the presence of double layers.
Aims. We investigate the influence of several proposed non-Maxwellian distribution functions on the X-ray flare line spectra. The distribution functions considered are sharply peaked and include the n-distribution, the moving Maxwellian distribution, and the distribution formed in strong double layers in the flaring plasma.
Methods. Synthetic Si xiid–Si xiv spectra involving allowed and dielectronic transitions at 5 − 6 Å are calculated numerically. The parameters chosen for the calculations correspond to the impulsive phase of solar flares, as inferred by previous authors.
Results. The Si xiid λ5.56/Si xiii λ5.68 and Si xiid λ5.82/Si xiii λ5.68 ratios depend on the relative number of electrons at energies corresponding to the formation of the Si xiid lines. Therefore, these ratios increase with the increasing narrowness of the peak of the electron distribution function. The highest ratios are achieved for the distribution formed in double layers, while the moving Maxwellian distribution is less likely to reproduce the observed enhancement of Si xiid intensities. However, the ratio of the allowed Si xiv λ5.22/Si xiii λ5.68 transitions depends on the ionization equilibrium. This ratio is very small for the double-layer distribution. Combination of the double-layer distribution with a Maxwellian distribution with the same mean energy significantly enhances this ratio, while keeping the Si xiid intensities sufficiently increased to explain the characteristics of the observed spectra.
Conclusions. These results support the presence of double layers in the plasma during impulsive phase of solar flares.

Observation of kink waves and their reconnection-like origin in solar spicules

H. **Ebadi**, M. Ghiassi
Astrophysics and Space Science, **2014**
http://arxiv.org/pdf/1406.4661v1.pdf
We analyze the time series of Ca II H-line obtained from Hinode/SOT on the solar limb. We follow three cases of upwardly propagating kink waves along a spicule and inverted Y-shaped structures at the cusp of it. The time-distance analysis shows that the axis of spicule undergoes quasi-periodic transverse displacement at different heights from the photosphere. The mean period of transverse displacement is ~ 175 s and the mean amplitude is 1 arc\,sec. The oscillation periods are increasing linearly with height which may be counted as the signature that the spicule is working as a low pass filter and allows only the low frequencies to propagate towards higher heights. The oscillations amplitude

is increasing with height due to decrease in density. The phase speeds are increasing until some heights and then decreasing which may be related to the small scale reconnection at the spicule basis. We conclude that transversal displacement of spicules axis can be related to the propagation of kink waves along them. Moreover, we observe signatures of small-scale magnetic reconnection at the cusp of spicules which may excite kink waves.

Properties of magnetic null points associated with X-class flares during solar cycle 24

R. L. **Edgar**, S. Regnier
MNRAS **2024**
https://arxiv.org/pdf/2410.16778
Since the launch of the Solar Dynamics Observatory (SDO) in 2010 and throughout the solar cycle 24, the Sun has produced few tens of xclass flares, which are the most energetic solar events. Those flares are produced in regions where the magnetic flux/energy is large and the magnetic configurations are complex. To provide more insights into the flaring process, we investigate the properties of magnetic null points (MNPs) and their correlation with the energy release sites. During solar cycle 24, we identify 17 xclass flares satisfying selection criteria. From SDO/HMI magnetograms, we perform potential extrapolations around the peak time of the flare to access the 3D coronal magnetic field and thus investigate the existence of coronal MNPs. We then correlate the flaring sites with the existing MNPs using SDO/AIA 171A EUV observations, and deduce their properties (sign, spine, fan). Six active regions out of 10 possess at least one MNP, which is stable and with large magnetic field gradients: this implies that 35% of xclass flares are associated with a MNP; of which 87.5% of MNPs are of positive type. The MNPs associated with the flare sites are predominantly located ata height between 05 and 2 Mm, and with a vertical/radial spine field line. We also find a slight correlation between the MNPs not associated with a flare and negative-type MNPs (55%) within the active region. Regarding the physics of flares, the association between the enhanced intensity at the flaring site and a MNP represents about a third of the possible scenarios for triggering xclass flares. , **7 March 2012, 22 October 2014**
Table 1. Properties of the 17 X-class flares selected 2011-2014
Table 2. Characterisation of X-class flares associated with a magnetic null point

Properties of magnetic null points associated with X-class flares during solar cycle 24

R L **Edgar**, S Régnier
MNRAS, Volume 532, Issue 1, July **2024**, Pages 755–762,
https://doi.org/10.1093/mnras/stae1470
https://watermark.silverchair.com/stae1470.pdf
Since the launch of the Solar Dynamics Observatory (SDO) in 2010 and throughout the solar cycle 24, the Sun has produced few tens of X-class flares, which are the most energetic solar events. Those flares are produced in regions where the magnetic flux/energy is large and the magnetic configurations are complex. To provide more insights into the flaring process, we investigate the properties of magnetic null points (MNPs) and their correlation with the energy release sites. During solar cycle 24, we identify 17 X-class flares satisfying selection criteria. From SDO/HMI magnetograms, we perform potential extrapolations around the peak time of the flare to access the 3D coronal magnetic field and thus investigate the existence of coronal MNPs. We then correlate the flaring sites with the existing MNPs using SDO/AIA 171 Å; EUV observations, and deduce their properties (sign, spine, and fan). Six active regions out of 10 possess at least one MNP which is stable and with large magnetic field gradients: this implies that 35 per cent of X-class flares are associated with an MNP; of which 87.5 per cent of MNPs are of positive type. The MNPs associated with the flare sites are predominantly located at a height between 0.5 and 2 Mm, and with a vertical/radial spine field line. We also find a slight correlation between the MNPs not associated with a flare and negative-type MNPs (55 per cent) within the active region. Regarding the physics of flares, the association between the enhanced intensity at the flaring site and an MNP represents about a third of the possible scenarios for triggering X-class flares. **2012-03-07, 2014-10-22**
Table 1. Properties of the 17 X-class flares selected 2011-2014
Table 2. Characterization of X-class flares associated with an MNP

Assessment of a planetary model to predict Rieger periodicity in sunspots and flares

Ian R. **Edmonds**
2018
https://arxiv.org/ftp/arxiv/papers/1811/1811.10703.pdf
This paper develops a planetary model to predict the occurrence of intermediate range periodicity in solar activity, in particular the ~155 day Rieger periodicity in flare activity. It is shown that periodicity at half integer multiples of the period of Mercury occurs consistently in indices of solar activity. For this reason the planetary model is based on the triggering of sunspot emergence when planetary tides peak at times of conjunction of Mercury with Venus, Earth and/or Jupiter. The periodicity of components in the planetary model match reasonably well the observed intermediate periodicity in sunspot and flare activity with the strongest model component occurring at 155 day period. A comparison of filtered versions of the model and

the N.O.A.A. flare index at 155 day periodicity demonstrates the potential for both short term, (within a solar cycle), and longer term, (over several solar cycles), predictive capability of the model. However, this assessment finds that prediction of 155 day periodicity in flare activity is effective only when the north and south hemispheric components of flare activity are in-phase.

Revisiting 154-day periodicity in the occurrence of hard flares. A planetary influence?
Ian **Edmonds**
2016
https://arxiv.org/pdf/1611.04240v1.pdf
Rieger et al (1984) reported observations of a 154 day periodicity in flares during solar cycle 21. This paper discusses the observations in the light of a simple empirical planetary model of sunspot emergence. The planetary model predicts sunspot emergence when Mercury and Earth approach conjunction and Mercury approaches the Sun. We show that the reported times of flare activity are coherent with the planetary model. While the base period of the model is 170 days, the average model period, over the interval of flare recordings, is 157 days due to a 180 degree phase change in the planetary forcing near the middle of the record interval. We conclude that the periodicity at 154 days arises when the phase change in planetary forcing and the resulting progressive phase change in total sunspot area emergence and flare occurrence shifts the major peak in the flare spectrum from the planetary forcing period, 170 days, to 154 days.

Formation and Reconnection of Three-dimensional Current Sheets with a Guide Field in the Solar Corona

Justin K. **Edmondson**, Benjamin J. Lynch
ApJ **849** 28 **2017**
https://arxiv.org/pdf/1708.03690.pdf
We analyze a series of three-dimensional magnetohydrodynamic numerical simulations of magnetic reconnection in a model solar corona to study the effect of the guide field component on quasi-steady state interchange reconnection in a pseudostreamer arcade configuration. This work extends the analysis of \citet{Edmondson2010b} by quantifying the mass density enhancement coherency scale in the current sheet associated with magnetic island formation during the nonlinear phase of plasmoid-unstable reconnection. We compare the results of four simulations of a zero, weak, moderate, and a strong guide field, BGF/B0={0.0,0.1,0.5,1.0}, to quantify the plasmoid density enhancement's longitudinal and transverse coherency scales as a function of the guide field strength. We derive these coherency scales from autocorrelation and wavelet analyses, and demonstrate how these scales may be used to interpret the density enhancement fluctuation's Fourier power spectra in terms of a structure formation range, an energy continuation range, and an inertial range---each population with a distinct spectral slope. We discuss the simulation results in the context of solar and heliospheric observations of pseudostreamer solar wind outflow and possible signatures of reconnection-generated structure.
Erratum: ApJ 850:210, **2017** http://iopscience.iop.org/article/10.3847/1538-4357/aa9927/pdf

FORMATION AND RECONNECTION OF THREE-DIMENSIONAL CURRENT SHEETS IN THE SOLAR CORONA

J. K. **Edmondson**1, S. K. Antiochos2, C. R. DeVore3, and T. H. Zurbuchen4
Astrophysical Journal, 718:72–85, **2010** July
Current-sheet formation and magnetic reconnection are believed to be the basic physical processes responsible for much of the activity observed in astrophysical plasmas, such as the Sun’s corona. We investigate these processes for a magnetic configuration consisting of a uniform background field and an embedded line dipole, a topology that is expected to be ubiquitous in the corona. This magnetic system is driven by a uniform horizontal flow applied at the line-tied photosphere. Although both the initial field and the driver are translationally symmetric, the resulting evolution is calculated using a fully three-dimensional (3D) magnetohydrodynamic simulation with adaptive mesh refinement that resolves the current sheet and reconnection dynamics in detail. The advantage of our approach is that it allows us to directly apply the vast body of knowledge gained from the many studies of two-dimensional (2D) reconnection to the fully 3D case. We find that a current sheet forms in close analogy to the classic Syrovatskii 2D mechanism, but the resulting evolution is different than expected. The current sheet is globally stable, showing no evidence for a disruption or a secondary instability even for aspect ratios as high as 80:1. The global evolution generally follows the standard Sweet–Parker 2D reconnection model except for an accelerated reconnection rate at a very thin current sheet, due to the tearing instability and the formation ofmagnetic islands. An interesting conclusion is that despite the formation of fully 3D structures at small scales, the system remains close to 2D at global scales.We discuss the implications of our results for observations of the solar corona.

The Relation between Escape and Scattering Times of Energetic Particles in a Turbulent Magnetized Plasma: Application to Solar Flares

Frederic **Effenberger**1,2 and Vahé Petrosian3
2018 ApJL 868 L28
sci-hub.tw/10.3847/2041-8213/aaedb3

A knowledge of the particle escape time from the acceleration regions of many space and astrophysical sources is of critical importance in the analysis of emission signatures produced by these particles and in the determination of the acceleration and transport mechanisms at work. This Letter addresses this general problem, in particular in solar flares, where in addition to scattering by turbulence, the magnetic field convergence from the acceleration region toward its boundaries also influences the particle escape. We test an (approximate) analytic relation between escape and scattering times, and the field convergence rate, based on the work of Malyshkin & Kulsrud, valid for both strong and weak diffusion limits and isotropic pitch-angle distributions of the injected particles, with a numerical model of particle transport. To this end, a kinetic Fokker–Planck transport model of particles is solved with a stochastic differential equation scheme, assuming different initial pitch-angle distributions. This approach enables further insights into the phase-space dynamics of the transport process, which would otherwise not be accessible. We find that in general the numerical results agree well with the analytic equation for the isotropic case; however, there are significant differences in the weak diffusion regime for non-isotopic cases, especially for distributions beamed along the magnetic field lines. The results are important in the interpretation of observations of energetic particles in solar flares and other similar space and astrophysical acceleration sites, and for the determination of acceleration-transport coefficients, commonly used in Fokker–Planck–type kinetic equations.

Hard X-Ray Emission from Partially Occulted Solar Flares: RHESSI Observations in Two Solar Cycles

Frederic **Effenberger**, Fatima Rubio da Costa, Mitsuo Oka, Pascal Saint Hilaire, Wei Liu, Vahé Petrosian, Lindsay Glesener, Säm Krucker
ApJ 835 124 **2016** **File**
https://arxiv.org/pdf/1612.02856v1.pdf

Flares close to the solar limb, where the footpoints are occulted, can reveal the spectrum and structure of the coronal loop-top source in X-rays. We aim at studying the properties of the corresponding energetic electrons near their acceleration site, without footpoint contamination. To this end, a statistical study of partially occulted flares observed with RHESSI is presented here, covering a large part of solar cycles 23 and 24. We perform a detailed spectra, imaging and light curve analysis for 116 flares and include contextual observations from SDO and STEREO when available, providing further insights into flare emission that was previously not accessible. We find that most spectra are fitted well with a thermal component plus a broken power-law, non-thermal component. A thin-target kappa distribution model gives satisfactory fits after the addition of a thermal component. X-rays imaging reveals small spatial separation between the thermal and non-thermal components, except for a few flares with a richer coronal source structure. A comprehensive light curve analysis shows a very good correlation between the derivative of the soft X-ray flux (from GOES) and the hard X-rays for a substantial number of flares, indicative of the Neupert effect. The results confirm that non-thermal particles are accelerated in the corona and estimated timescales support the validity of a thin-target scenario with similar magnitudes of thermal and non-thermal energy fluxes. **11 Sept 2014, 22 Oct 2014, 31 Oct 2014, 3 March 2015**

Table 1. Partially occulted ares from solar cycle 24. See Table 2 in the Appendix for the are list from the previous cycle.
Table 2. Analysis results for partially occulted ares from KL2008
See RHESSI Science Nuggets #291, Jan **2017**
http://sprg.ssl.berkeley.edu/~tohban/wiki/index.php/Hard_X-ray_Emission_from_Partially_Occulted_Solar_Flares

Hard X-ray morphology of the X1.3 April 25, 2014 partially occulted limb solar flare

Frederic **Effenberger**, Fatima Rubio da Costa, Vahe Petrosian
proceedings for the 15th Annual International Astrophysics Conference **2016**
http://arxiv.org/pdf/1605.04858v1.pdf

At hard X-ray energies, the bright footpoint emission from solar flare loops often prevents a detailed analysis of the weaker loop-top source morphology due to the limited dynamic range available for X-ray imaging. Here, we study the X1.3 April 25, 2014 flare with the Reuven Ramaty High-Energy Solar Spectroscopic Imager (RHESSI). This partially occulted limb flare allows the analysis of the loop-top emission in isolation. We present results on the flare light curve at different energies, the source morphology from X-ray imaging and a detailed spectral analysis of the different source components by imaging spectroscopy. The loop-top source, a likely site of particle acceleration, shows a clear composition of different emission components. The results indicate the opportunities that detailed imaging of hard X-rays can provide to learn about particle acceleration, transport and heating processes in solar flares.

The Multifaceted M1.7 GOES-class Flare Event of 21 April 2023 in AR13283.

Elmhamdi, A., Marassi, A., Romano, P. et al.

Sol Phys 299, 109 (**2024**).
https://doi.org/10.1007/s11207-024-02355-2
On **21 April 2023**, a significant M1.7 solar flare erupted from Active Region 13283, accompanied by a filament eruption and a full-halo Coronal Mass Ejection, which reached Earth on **23 April**, triggering a severe geomagnetic storm, with Kp reaching 8 (G4) and Dst plummeting to −212 nT together with a sharply distinguished long-lasting negative double-dip behavior of the *z*-component of the interplanetary magnetic field. This event led to remarkable auroral displays, even at mid-latitudes in Europe. The flare-induced filament eruption caused distinct intensity dimming in the solar corona, observed in specific EUV wavelengths. We observed the dimming region growing at its fastest rate before the flare reached its peak of intensity. Notably, the proximity of the flare to a large southern coronal hole influenced the expansion and propagation of the coronal mass ejection toward Earth, probably impacting the solar wind speed and density. Additionally, we observed a sudden expansion of the coronal hole during the flare, leading us to speculating that the adjacent flare may have further stimulated the flow of solar-wind particles along the open magnetic-field lines. In accordance with the severe Dst-index disturbance, we also report changes in the potential of the pipeline of an Italian energy infrastructure company with respect to the surrounding soil as well as double-dip variation in the H-component of the terrestial magnetic field observed locally (reminiscent to what reported in Dst-index and IMF Bz) temporal profiles, confirming the effects of the geomagnetic storm at Italy mid-latitudes. Several solar radio events have been observed too. Therefore this study provides insights into the dynamic solar phenomena and their potential geomagnetic implications.

Twist and Writhe of the Magnetic Flux in the Super Active Region NOAA 11429

A. **Elmhamdi**, P. Romano, A. S. Kordi, H. A. Al-trabulsy
Solar Physics, Volume 289, Issue 8, pp 2957-2970 **2014**
We used full-disk line-of-sight magnetograms taken by the Helioseismic and Magnetic Imager (HMI) onboard the Solar Dynamics Observatory (SDO) to study the variation of coronal magnetic helicity in the Active Region (AR) NOAA 11429, where several GOES M- and X-class flares and coronal mass ejections (CMEs) occurred. The magnetic flux, total magnetic-helicity flux, and helicity accumulation over the period of interest, i.e. **6 to 11 March 2012**, were measured and are discussed. We also evaluated the tilt-angle evolution within the standard polarity flux-weighted centroids approach. The AR displays a shearing motion of the magnetic structures along the polarity inversion line, reaching values of about 1.0 km s−1. The variations of magnetic helicity flux and the tilt-angle seem to be time-correlated, and both display three-phase evolutionary patterns. We also found that the flare/CME activity is higher during the first observation phase when the tilt-angle decreases and the negative magnetic helicity is accumulated. The main changes in the accumulated helicity curve are observed only after the onset of the two strongest flare/CME events. After the major event (GOES X5.4 class/CME of 7 March) there was a decrease in the occurrence of flares and CMEs. This phase is marked by a decrease of the flux of magnetic helicity from the convection zone to the corona and a change in the orientation of the tilt of the AR. This behavior suggests that the combination of these two quantities might be important in the description of the magnetic complexity accumulated by an AR during its lifetime.

Using Extreme Value Theory for Determining the Probability of Carrington-Like Solar Flares

Sean **Elvidge**, Matthew J. Angling
Space Weather Volume16, Issue4 April **2018** Pages 417-421
http://sci-hub.tw/10.1002/2017SW001727
By their very nature, extreme space weather events occur rarely, and therefore, statistical methods are required to determine the probability of their occurrence. Space weather events can be characterized by a number of natural phenomena such as X-ray (solar) flares, solar energetic particle fluxes, coronal mass ejections, and various geophysical indices (such as Dst, Kp, and F10.7). In this paper extreme value theory (EVT) is used to investigate the probability of extreme solar flares. Previous work has assumed that the distribution of solar flares follows a power law. However, such an approach can lead to a poor estimation of the return times of flares due to uncertainties in the tails of the probability distribution function. Using EVT and Geostationary Operational Environmental Satellites X-ray flux data, it is shown that the expected 150 year return level is approximately an X60 flare while a Carrington-like flare is a one in a 100 year event. In the worst case the 150 year return level is an X90 flare while a Carrington flare is a one in 30 year event. It is also shown that the EVT results are consistent with flare data from the Kepler space telescope mission.
Nature **2016**
http://arxiv.org/pdf/1604.03325v1.pdf
Space weather events can negatively affect satellites, the electricity grid, satellite navigation systems and human health. As a consequence, extreme space weather has been added to the UK and other national risk registers. However, by their very nature, extreme events occur rarely and statistical methods are required to determine the probability of occurrence solar storms. Space weather events can be characterised by a number of natural phenomena such as X-ray (solar) flares, solar energetic particle (SEP) fluxes, coronal mass ejections and various geophysical indices (Dst, Kp, F10.7). Here we use extreme value theory (EVT) to investigate the probability of extreme solar flares. Previous work has suggested that the distribution of solar flares follows a power law. However such an approach can lead to overly "fat-tails" in the

probability distribution function and thus to an under estimation of the return time of such events. Using EVT and GOES X-ray flux data we find that the expected 150 year return level is an X60 flare (6x10^(-3) Wm-2, 1-8 {\AA} X-ray flux). We also show that the EVT results are consistent with flare data from the Kepler space telescope mission.

The Effects of Turbulent Electrical Resistivity on the Response of the Solar Atmosphere to Flare Energy Input. I. Results of Radiative Hydrodynamic Simulations

A. Gordon **Emslie**, Joel C. Allred, and Meriem Alaoui
2024 ApJ 977 246
https://iopscience.iop.org/article/10.3847/1538-4357/ad919c/pdf
A number of works have considered the role of turbulence in energy release and transport in solar flares, and in particular, on the transport of energy by thermal conduction. Here, we point out that for physical consistency, the effects of turbulence on the electrical conductivity, and hence on the ohmic heating by the return current that neutralizes the current in injected electron beams, must also be considered. Using radiative hydrodynamic simulations, in conjunction with thermal and electrical conductivities modified from their collisional values by turbulent processes, we model the heating rate along a flare loop. We derive the resulting temperature, pressure, velocity, and density profiles, and use them to calculate quantities such as the differential emission measure (DEM) and the emitted X-ray spectrum. For high levels of turbulence, the combination of high electrical resistivity and low thermal conductivity acts to create and sustain a region of very large temperature near the loop apex, creating a large overpressure that acts to suppress the upward evaporation of chromospheric material. Further, the associated large temperature gradients result in a reduction of the DEM at temperatures from 105 K to 107 K. The hard X-ray spectrum at high energies is reduced due to a lower electron flux reaching the chromosphere, but at low energies, it is enhanced due to thermal emission from the very hot coronal plasma. We assess the extent to which these results can be used to constrain the nature and role of turbulent motions in the flare volume.

Energy Deposition by Energetic Electrons in a Diffusive Collisional Transport Model

A. G. **Emslie**, N. H. Bian, E. P. Kontar
2018
https://arxiv.org/pdf/1806.08158.pdf
A considerable fraction of the energy in a solar flare is released as suprathermal electrons; such electrons play a major role in energy deposition in the ambient atmosphere and hence the atmospheric response to flare heating. Historically the transport of these particles has been approximated through a deterministic approach in which first-order secular energy loss to electrons in the ambient target is treated as the dominant effect, with second-order diffusive terms (in both energy and angle) being generally either treated as a small correction or neglected. However, it has recently been pointed out that while neglect of diffusion in energy may indeed be negligible, diffusion in angle is of the same order as deterministic scattering and hence must be included. Here we therefore investigate the effect of angular scattering on the energy deposition profile in the flaring atmosphere. A relatively simple compact expression for the spatial distribution of energy deposition into the ambient plasma is presented and compared with the corresponding deterministic result. For unidirectional injection there is a significant shift in heating from the lower corona to the upper corona; this shift is much smaller for isotropic injection. We also compare the heating profiles due to return current Ohmic heating in the diffusional and deterministic models.

Energy Partition in Large Solar Eruptive Events,

Gordon **Emslie** and Brian Dennis
RHESSI Science Nugget, No. 185, Oct **2012**
Where flare energy comes from, and where it goes to.
The paper also concludes that the energy radiated by the SXR-emitting plasma exceeds, by about half an order of magnitude, the peak energy content of the thermal plasma that produces this radiation, a situation that requires continuous re-energization of the hot plasma throughout the flare. Also, the energy contents in flare-accelerated electrons and ions are comparable, and together they are sufficient to supply the bolometric energy radiated across all wavelengths throughout the event. Finally, the paper finds that, in general, the available magnetic energy is sufficient to power the CME, the flare-accelerated particles, and the hot thermal plasma. This reaffirms the generally-held belief that the fundamental power source for SEEs lies in stressed active-region magnetic fields.

Global Energetics of Thirty-eight Large Solar Eruptive Events

Emslie, A. G.; Dennis, B. R.; Shih, A. Y.; Chamberlin, P. C.; Mewaldt, R. A.; Moore, C. S.; Share, G. H.; Vourlidas, A.; Welsch, B. T.
Astrophysical Journal, Volume 759, Issue 1, article id. 71, 18 pp. (**2012**); **File**
http://arxiv.org/abs/1209.2654
We have evaluated the energetics of 38 solar eruptive events observed by a variety of spacecraft instruments between 2002 February and 2006 December, as accurately as the observations allow. The measured energetic components

include: (1) the radiated energy in the Geostationary Operational Environmental Satellite 1-8 Å band, (2) the total energy radiated from the soft X-ray (SXR) emitting plasma, (3) the peak energy in the SXR-emitting plasma, (4) the bolometric radiated energy over the full duration of the event, (5) the energy in flare-accelerated electrons above 20 keV and in flare-accelerated ions above 1 MeV, (6) the kinetic and potential energies of the coronal mass ejection (CME), (7) the energy in solar energetic particles (SEPs) observed in interplanetary space, and (8) the amount of free (non-potential) magnetic energy estimated to be available in the pertinent active region. Major conclusions include: (1) the energy radiated by the SXR-emitting plasma exceeds, by about half an order of magnitude, the peak energy content of the thermal plasma that produces this radiation; (2) the energy content in flare-accelerated electrons and ions is sufficient to supply the bolometric energy radiated across all wavelengths throughout the event; (3) the energy contents of flare-accelerated electrons and ions are comparable; (4) the energy in SEPs is typically a few percent of the CME kinetic energy (measured in the rest frame of the solar wind); and (5) the available magnetic energy is sufficient to power the CME, the flare-accelerated particles, and the hot thermal plasma. **2002 February 20, 2002 May 22, 2002 November 9, 2003 May 27, 2003 October 28, 2004 July 15, 2004 July 25, 2005 January 20,**
Table 1. Event List with Component Energies (× 1030 ergs)

A Catalog of Suzaku/WAM Hard X-Ray Solar Flares

A. **Endo**, T. Minoshima, K. Morigami, M. Suzuki, A. Shimamori, Y. Sato, Y. Terada, M. S. Tashiro, Y. Urata, E. Sonoda, K. Yamaoka, S. Sugita, and K. Watanabe
Publ. Astron. Soc. Japan 62, pp.1341-1349 **(2010)**
We developed a catalog of solar flares in the hard X-ray band observed with the Wide-band All-sky Monitor (WAM) onboard the Suzaku satellite between 2005 July and 2009 November. During this period, 105 solar flares (GOES class X: 13, M: 29, C: 47, B: 16) were detected with WAM, including 10% of GOES-class C events reported during the same period. The observed photon flux ranged between 9 10 and 9 10photons scmkeV at 100 keV. The averaged hard X-ray spectrum for each solar flare was evaluated for 70 of the 105 events, and 43 of them were well fitted with a single power-law model with a photon index ranging between 7 and 3. We observed a weak trend where events with longer durations exhibited harder spectral slopes.

FLARES AND THEIR UNDERLYING MAGNETIC COMPLEXITY

Alexander J. **Engell**1, Marek Siarkowski2, Magda Gryciuk2, Janusz Sylwester2, Barbara Sylwester2, Leon Golub1,
Kelly Korreck1, and Jonathan Cirtain3
Astrophysical Journal, 726:12 (8pp), **2011**
SphinX (Solar PHotometer IN X-rays), a full-disk-integrated spectrometer, observed 137 flare-like/transient events with active region (AR) 11024 being the only AR on disk. The *Hinode* X-Ray Telescope (XRT) and Solar Optical Telescope observe 67 of these events and identified their location from 12:00 UT on **July 3 through 24:00 UT 2009 July 7**. We find that the predominant mechanisms for flares observed by XRT are (1) flux cancellation and (2) the shearing of underlying magnetic elements. Point- and cusp-like flare morphologies seen by XRT all occur in a magnetic environment where one polarity is impeded by the opposite polarity and vice versa, forcing the flux cancellation process. The shearing is either caused by flux emergence at the center of the AR and separation of polarities along a neutral line or by individual magnetic elements having a rotational motion. Both mechanisms are observed to contribute to single- and multiple-loop flares. We observe that most loop flares occur along a large portion of a polarity inversion line. Point- and cusp-like flares become more infrequent as the AR becomes organized with separation of the positive and negative polarities. SphinX, which allows us to identify when these flares occur, provides us with a statistically significant temperature and emission scaling law for A and B class flares: EM = 6.1 ↳ 1033 *T*1.9±0.1.

Energy Deposition by Energetic Electrons in a Diffusive Collisional Transport Model

A. Gordon **Emslie**1, Nicolas H. Bian1,2, and Eduard P. Kontar2
2018 ApJ 862 158
http://sci-hub.tw/10.3847/1538-4357/aaceaa
A considerable fraction of the energy in a solar flare is released as suprathermal electrons; such electrons play a major role in energy deposition in the ambient atmosphere, and hence the atmospheric response to flare heating. Historically, the transport of these particles has been approximated through a deterministic approach in which first-order secular energy loss to electrons in the ambient target is treated as the dominant effect, with second-order diffusive terms (in both energy and angle) being generally either treated as a small correction or neglected. However, it has recently been pointed out that while neglect of diffusion in energy may indeed be negligible, diffusion in angle is of the same order as deterministic scattering and hence must be included. Here we therefore investigate the effect of angular scattering on the energy deposition profile in the flaring atmosphere. A relatively simple compact expression for the spatial

distribution of energy deposition into the ambient plasma is presented and compared with the corresponding deterministic result. For unidirectional injection there is a significant shift in heating from the lower corona to the upper corona; this shift is much smaller for isotropic injection. We also compare the heating profiles due to return current ohmic heating in the diffusional and deterministic models.

On the Solution of the Continuity Equation for Precipitating Electrons in Solar Flares

A. Gordon **Emslie**1, Gordon D. Holman2, and Yuri E. Litvinenko
2014 ApJ 792 5
Electrons accelerated in solar flares are injected into the surrounding plasma, where they are subjected to the influence of collisional (Coulomb) energy losses. Their evolution is modeled by a partial differential equation describing continuity of electron number. In a recent paper, Dobranskis & Zharkova claim to have found an "updated exact analytical solution" to this continuity equation. Their solution contains an additional term that drives an exponential decrease in electron density with depth, leading them to assert that the well-known solution derived by Brown, Syrovatskii & Shmeleva, and many others is invalid. We show that the solution of Dobranskis & Zharkova results from a fundamental error in the application of the method of characteristics and is hence incorrect. Further, their comparison of the "new" analytical solution with numerical solutions of the Fokker-Planck equation fails to lend support to their result. We conclude that Dobranskis & Zharkova's solution of the universally accepted and well-established continuity equation is incorrect, and that their criticism of the correct solution is unfounded. We also demonstrate the formal equivalence of the approaches of Syrovatskii & Shmeleva and Brown, with particular reference to the evolution of the electron flux and number density (both differential in energy) in a collisional thick target. We strongly urge use of these long-established, correct solutions in future works.

Refinements to flare energy estimates: A followup to “Energy partition in two solar flare/CME events”

Emslie, A.G., Dennis, B.R., Holman, G.D., Hudson, H.S.,
2005. Journal of Geophysical Research (Space Physics) 110, A11103.

Energy partition in two solar flare/CME events

Emslie, A. G., Kucharek, H.; Dennis, B. R.; Gopalswamy, N.; Holman, G. D.; Share, G. H.; Vourlidas, A.; Forbes, T. G.; Gallagher, P. T.; Mason, G. M.; and 5 coauthors
Journal of Geophysical Research, Volume 109, Issue A10, CiteID A10104, **2004**
Using coordinated observations from instruments on the Advanced Composition Explorer (ACE), the Solar and Heliospheric Observatory (SOHO), and the Ramaty High Energy Solar Spectroscopic Imager (RHESSI), we have evaluated the energetics of two well-observed flare/CME events on 21 April 2002 and **23 July 2002**. For each event, we have estimated the energy contents (and the likely uncertainties) of (1) the coronal mass ejection, (2) the thermal plasma at the Sun, (3) the hard X-ray producing accelerated electrons, (4) the gamma-ray producing ions, and (5) the solar energetic particles. The results are assimilated and discussed relative to the probable amount of nonpotential magnetic energy available in a large active region.

Investigation of the Relationship between Solar Flares and Sunspot Groups

S. **Eren** 1 , A. Kilcik
Sun and Geosphere, **2017**; 12/1: 7 -10
http://newserver.stil.bas.bg/SUNGEO//00SGArhiv/SG_v12_No1_2017-pp-07-10.pdf
We studied the relationship between X-Ray flare numbers (C, M, and, X class flares) and sunspot counts in four categories (Simple (A + B), Medium (C), Large (D + E + F), and End (H)). All data sets cover the whole Solar Cycle 23 and the ascending and maximum phases of Cycle 24 (1996-2014). Pearson correlation analysis method was used to investigate the degree of relationship between monthly solar flare numbers and sunspot counts observed in different sunspot categories. We found that the C, M, and X class flares have highest correlation with the large group sunspot counts, while the small category does not any meaningful correlation. Obtained correlation coefficients between large groups and C, M, and X class flare numbers are 0.79, 0.74, and 0.4, respectively. Thus, we conclude that the main sources of X-Ray solar flares are the complex/large sunspot groups.

Flare-production potential associated with different sunspot groups

Eren, S.; Kilcik, A.; Atay, T.; Miteva, R.; Yurchyshyn, V.; Rozelot, J. P.; Özgüç, A

MNRAS. **2016**, 465, issue 1, pp. 68-75
http://sci-hub.cc/10.1093/mnras/stw2742
We analysed different types (C, M, and X classes) of X-ray solar flares occurring in sunspot groups. The data cover 1996?2014 time interval, and a total of 4262 active regions (ARs) were included in the data set. We defined the solar-flare-production potential as the ratio of the total number of flares observed in a sunspot group to the total number of the same-class sunspot groups. Our main findings are as follows: (1) large and complex sunspot groups (D+E+F) have the flare-production potential about eight times higher than the small and simple (A+B+C+H) ARs; (2) 79 per cent of all flares were produced by the large and complex sunspot groups, while only 21 per cent of flares were produced by the small groups; (3) the largest and the most complex F-class (very large and very complex) sunspot groups exhibit the highest flare-production potential (2.16 flare per sunspot group), while the smallest and the least complex A class sunspot groups show the lowest (0.05 flare per group) flare-production potential; (4) temporal variation of sunspot counts, sunspot group areas, and the total number of flares (including C flares) showed similar time profiles during both cycles with multiple peaks; (5) the mean area of ARs very well describes the flare-production potential of each group with the regression coefficient of R2 = 0.99. Most of these sunspot groups (>70 per cent) are, according to the Zurich Classification, complex ARs.

Fractal and Multifractal Properties of Active Regions as Flare Precursors: A Case Study Based on SOHO/MDI and SDO/HMI Observations

I. **Ermolli**, F. Giorgi, P. Romano, F. Zuccarello, S. Criscuoli, M. Stangalini
Solar Phys., **2014**, Volume 289, Issue 7, pp 2525-2545
Several studies indicate that fractal and multifractal parameters inferred from solar photospheric magnetic field measurements may help assessing the eruptive potential of Active Regions (ARs) and also predicting their flare activity. We further investigate this topic, by exploring the sensitivity of some parameters already used in the literature on data and methods employed for their estimation. In particular, we measured the generalized fractal dimensions D 0 and D 8, and the multifractal parameters C div and D div, on the time series of photospheric magnetograms of the flaring AR NOAA 11158 obtained with the SOHO/MDI and SDO/HMI. The observations by the latter instrument are characterized by a higher spatial and temporal resolution, as well as higher flux sensitivity, than the ones obtained from SOHO/MDI, which were widely employed in earlier studies. We found that the average and peak values of complexity parameters measured on the two data sets agree within measurement uncertainties. The temporal evolution of the parameters measured on the two data sets show rather similar trends, but the ones derived from the SOHO/MDI observations show larger and spurious variations over time than those deduced from analysis of the corresponding SDO/HMI data. We also found a larger sensitivity of these measurements to characteristics of the data analyzed than reported by earlier studies. In particular, analysis of the higher resolution and higher cadence SDO/HMI data allows us also to detect slight variations of the complexity indicators that cannot be derived from the analysis of the SOHO/MDI data. These variations occur right after the major events in the analyzed AR. They may be the signature of photospheric effects of coronal magnetic field re-arrangement. **12-15 February 2011**

Impacts of Data Preprocessing and Sampling Techniques on Solar Flare Prediction from Multivariate Time Series Data of Photospheric Magnetic Field Parameters

MohammadReza **EskandariNasab**1,2, Shah Muhammad Hamdi1, and Soukaina Filali Boubrahimi1
2024 ApJS 275 6
https://iopscience.iop.org/article/10.3847/1538-4365/ad7c4a/pdf
The accurate prediction of solar flares is crucial due to their risks to astronauts, space equipment, and satellite communication systems. Our research enhances solar flare prediction by employing sophisticated data preprocessing and sampling techniques for the Space Weather Analytics for Solar Flares (SWAN-SF) data set, a rich source of multivariate time series data of solar active regions. Our study adopts a multifaceted approach encompassing four key methodologies. Initially, we address over 10 million missing values in the SWAN-SF data set through our innovative imputation technique called fast Pearson correlation-based k-nearest neighbors imputation. Subsequently, we propose a precise normalization technique, called LSBZM normalization, tailored for time series data, merging various strategies (log, square root, Box–Cox, Z-score, and min–max) to uniformly scale the data set's 24 attributes (photospheric magnetic field parameters), addressing issues such as skewness. We also explore the "near decision boundary sample removal" technique to enhance the classification performance of the data set by effectively resolving the challenge of class overlap. Finally, a pivotal aspect of our research is a thorough evaluation of diverse oversampling and undersampling methods, including SMOTE, ADASYN, Gaussian noise injection, TimeGAN, Tomek links, and random undersampling, to counter the severe imbalance in the SWAN-SF data set, notably a 60:1 ratio of major (X and M) to minor (C, B, and FQ) flaring events in binary classification. To demonstrate the effectiveness of our methods, we use eight classification algorithms, including advanced deep-learning-based architectures. Our analysis shows significant true skill statistic scores, underscoring the importance of data preprocessing and sampling in time-series-based solar flare prediction.

Enhancing Multivariate Time Series-based Solar Flare Prediction with Multifaceted Preprocessing and Contrastive Learning

MohammadReza **EskandariNasab**, Shah Muhammad Hamdi, Soukaina Filali Boubrahimi
ICMLA **2024**
https://arxiv.org/pdf/2409.14016
Accurate solar flare prediction is crucial due to the significant risks that intense solar flares pose to astronauts, space equipment, and satellite communication systems. Our research enhances solar flare prediction by utilizing advanced data preprocessing and classification methods on a multivariate time series-based dataset of photospheric magnetic field parameters. First, our study employs a novel preprocessing pipeline that includes missing value imputation, normalization, balanced sampling, near decision boundary sample removal, and feature selection to significantly boost prediction accuracy. Second, we integrate contrastive learning with a GRU regression model to develop a novel classifier, termed ContReg, which employs dual learning methodologies, thereby further enhancing prediction performance. To validate the effectiveness of our preprocessing pipeline, we compare and demonstrate the performance gain of each step, and to demonstrate the efficacy of the ContReg classifier, we compare its performance to that of sequence-based deep learning architectures, machine learning models, and findings from previous studies. Our results illustrate exceptional True Skill Statistic (TSS) scores, surpassing previous methods and highlighting the critical role of precise data preprocessing and classifier development in time series-based solar flare prediction.

High-resolution observational analysis of flare ribbon fine structures

Jonas Thoen **Faber**, Reetika Joshi, Luc Rouppe van der Voort, Sven Wedemeyer, Lyndsay Fletcher, Guillaume Aulanier, Daniel Nóbrega-Siverio
A&A **2024**
https://arxiv.org/pdf/2411.18233
Context. Since the mechanism of energy release from solar flares is still not fully understood, the study of fine-scale features developing during flares becomes important for progressing towards a consistent picture of the essential physical mechanisms. Aims. We aim to probe the fine structures in flare ribbons at the chromospheric level using high-resolution observations with imaging and spectral techniques. Methods. We present a GOES C2.4 class solar flare observed with the Swedish 1-m Solar Telescope (SST), the Interface Region Imaging Spectrograph (IRIS), and the Atmospheric Imaging Assembly (AIA). The high-resolution SST observations offer spectroscopic data in the H-alpha, Ca II 8542 Å, and H-beta lines, which we use to analyse the flare ribbon. Results. Within the eastern flare ribbon, chromospheric bright blobs were detected and analysed in Ca II 8542 Å, H-alpha, and H-beta wavelengths. A comparison of blobs in H-beta observations and Si IV 1400 Å has also been performed. These blobs are observed as almost circular structures having widths from 140 km-200 km. The intensity profiles of the blobs show a red wing asymmetry. Conclusions. From the high spatial and temporal resolution H-beta observations, we conclude that the periodicity of the blobs in the flare ribbon, which are near-equally spaced in the range 330-550 km, is likely due to fragmented reconnection processes within a flare current sheet. This supports the theory of a direct link between fine-structure flare ribbons and current sheet tearing. We believe our observations represent the highest resolution evidence of fine-structure flare ribbons to date. **June 26, 2022**
RHESSI Science Nugget, No. **482**, Dec **2024** https://heliowiki.smce.nasa.gov/wiki/index.php/High-resolution_observational_analysis_of_flare_ribbon_fine_structures

The CUbesat Solar Polarimeter (CUSP) mission overview

Sergio **Fabiani**, Ettore Del Monte, Ilaria Baffo, Sergio Bonomo, +++
Proceeding of SPIE Conference "Astronomical Telescopes+ Instrumentation", Yokohama (Japan), 16-21 June **2024**
https://arxiv.org/pdf/2407.04748
The CUbesat Solar Polarimeter (CUSP) project is a future CubeSat mission orbiting the Earth aimed to measure the linear polarization of solar flares in the hard X-ray band, by means of a Compton scattering polarimeter. CUSP will allow us to study the magnetic reconnection and particle acceleration in the flaring magnetic structures of our star. The project is in the framework of the Italian Space Agency Alcor Program, which aims to develop new CubeSat missions. CUSP is approved for a Phase B study that will last for 12 months, starting in mid-2024. We report on the current status of the CUSP mission project as the outcome of the Phase A.

Towards imaging-spectro-polarimetry of solar flares in the X-rays

Sergio **Fabiani**, John Rankin, Stefano Basso, Enrico Costa, +++
Proceeding of SPIE Conference "Astronomical Telescopes+ Instrumentation", Yokohama (Japan), 16-21 June **2024**
https://arxiv.org/pdf/2407.04749

X-ray polarimetry of solar flares is still a not well established field of observation of our star. Past polarimeters were not able to measure with a high significance the polarization in X-rays from solar flares. Moreover, they had no imaging capabilities and measured only the polarization by integrating on all the image of the source. We propose a mission concept based on a gas photoelectric polarimeter, coupled with multilayer lobster-eye optics, to perform imaging-spectro-polarimetry of solar flares while monitoring the entire solar disc.

On the variations in the photospheric magnetic field in the vicinity of a solar flare as deduced from SDO/HMI measurements of the magnetic field vector

V.G. **Fainshtein**, Ya.I. Egorov, G.V. Rudenko, S.A. Anfinogentov
Solar Phys. **2016**
http://arxiv.org/pdf/1601.02310v1.pdf
We have considered temporal variations in the absolute value, radial and traverse components of magnetic induction, as well as those in the inclination angles between field lines and the radial direction from the solar center in the vicinity of the solar flare on **June 7, 2011** in the active region NOAA 11238. Our study has revealed that there appeared a relatively homogeneous region with a decreased absolute value of magnetic induction which extended along the future solar-flare ribbons, and with a neutral line, in the middle immediately before the solar flare onset in its future center. After the flare onset during approximately 40 minutes, this region revealed an increase in the absolute value of magnetic induction and traverse component of the magnetic field, and, at the same time, a 25-30 degree rise in the inclination angles between field lines and the radial direction from the solar center, as well as in the azimuth angle. Henceforward, the increased values of these magnetic field characteristics were observed during several hours. This result is qualitatively consistent with (Petrie and Sudol, 2010) where the increase in the traverse component and inclination angles has been predicted and has been indirectly confirmed by observations. After the flare onset, uncovered variations in the magnetic field characteristics were demonstrated to be very small or vanish in the regions with high values of the magnetic field on either side of the neutral line of the magnetic field.

IMPULSIVITY PARAMETER FOR SOLAR FLARES

W. G. **Fajardo-Mendieta**1,2, J. C. Mart?nez-Oliveros3, J. D. Alvarado-G?mez1,4,5, and B. Calvo-Mozo
2016 ApJ 818 56
http://arxiv.org/pdf/1602.03958v1.pdf
Three phases are typically observed during solar flares: the preflare, impulsive, and decay phases. During the impulsive phase, it is believed that the electrons and other particles are accelerated after the stored energy in the magnetic field is released by reconnection. The impulsivity of a solar flare is a quantifiable property that shows how quickly this initial energy release occurs. It is measured via the impulsivity parameter, which we define as the inverse of the overall duration of the impulsive phase. We take the latter as the raw width of the most prominent nonthermal emission of the flare. We computed this observable over a work sample of 48 M-class events that occurred during the current Solar Cycle 24 by using three different methods. The first method takes into account all of the nonthermal flare emission and gives very accurate results, while the other two just cover fixed energy intervals (30?40 keV and 25?50 keV) and are useful for fast calculations. We propose an alternative way to classify solar flares according to their impulsivity parameter values, defining three different types of impulsivity, namely, high, medium, and low. This system of classification is independent of the manner used to calculated the impulsivity parameter. Lastly, we show the relevance of this tool as a discriminator of different HXR generation processes. **2012-06-03**

Solar flare forecasting using morphological properties of sunspot groups

Mariachiara **Falco***, Pierfrancesco Costa and Paolo Romano
J. Space Weather Space Clim. **2019**, 9, A22
https://arxiv.org/pdf/1905.05759.pdf
sci-hub.se/10.1051/swsc/2019019
https://www.swsc-journal.org/articles/swsc/pdf/2019/01/swsc190005.pdf
We describe a new tool developed for solar flare forecasting on the base of some sunspot group properties. Assuming that the flare frequency follows the Poisson statistics, this tool uses a database containing the morphological characteristics of the sunspot groups daily observed by the Equatorial Spar of INAF – Catania Astrophysical Observatory since January 2002 up today. By means of a linear combination of the flare rates computed on the base of some properties of the sunspot groups, like area, number of pores and sunspots, Zurich class, relative importance between leading spot and density of the sunspot population, and type of penumbra of the main sunspot, we determine the probability percentages that a flare of a particular energy range may occur. Comparing our forecasts with the flares registered by GOES satellites in the 1–8 Å X-ray band during the subsequent 24 h we measured the performance of our method. We found that this method, which combines some morphological parameters and a statistical technique, has the best performances for the strongest events, which are more interesting for their implications in the Earth environment.
September 6, 2017
3.1 An example of flare forecasting: AR NOAA 12673

MAG4 versus alternative techniques for forecasting active region flare productivity

David A. **Falconer**, Ronald L. Moore, Abdulnasser F. Barghouty and Igor Khazanov
Space Weather, Volume 12, Issue 5, pages 306–317, **2014 File**
http://sci-hub.tw/10.1002/2013SW001024
MAG4 is a technique of forecasting an active region's rate of production of major flares in the coming few days from a free magnetic energy proxy. We present a statistical method of measuring the difference in performance between MAG4 and comparable alternative techniques that forecast an active region's major-flare productivity from alternative observed aspects of the active region. We demonstrate the method by measuring the difference in performance between the "Present MAG4" technique and each of three alternative techniques, called "McIntosh Active-Region Class," "Total Magnetic Flux," and "Next MAG4." We do this by using (1) the MAG4 database of magnetograms and major flare histories of sunspot active regions, (2) the NOAA table of the major-flare productivity of each of 60 McIntosh active-region classes of sunspot active regions, and (3) five technique performance metrics (Heidke Skill Score, True Skill Score, Percent Correct, Probability of Detection, and False Alarm Rate) evaluated from 2000 random two-by-two contingency tables obtained from the databases. We find that (1) Present MAG4 far outperforms both McIntosh Active-Region Class and Total Magnetic Flux, (2) Next MAG4 significantly outperforms Present MAG4, (3) the performance of Next MAG4 is insensitive to the forward and backward temporal windows used, in the range of one to a few days, and (4) forecasting from the free-energy proxy in combination with either any broad category of McIntosh active-region classes or any Mount Wilson active-region class gives no significant performance improvement over forecasting from the free-energy proxy alone (Present MAG4).
See Falconer_presentation, **2014**

PRIOR FLARING AS A COMPLEMENT TO FREE MAGNETIC ENERGY FOR FORECASTING SOLAR ERUPTIONS

David A. **Falconer**1,2, Ronald L. Moore1, Abdulnasser F. Barghouty1, and Igor Khazanov
2012 ApJ 757 32
From a large database of (1) 40,000 SOHO/MDI line-of-sight magnetograms covering the passage of 1300 sunspot active regions across the 30° radius central disk of the Sun, (2) a proxy of each active region's free magnetic energy measured from each of the active region's central-disk-passage magnetograms, and (3) each active region's full-disk-passage history of production of major flares and fast coronal mass ejections (CMEs), we find new statistical evidence that (1) there are aspects of an active region's magnetic field other than the free energy that are strong determinants of the active region's productivity of major flares and fast CMEs in the coming few days; (2) an active region's recent productivity of major flares, in addition to reflecting the amount of free energy in the active region, also reflects these other determinants of coming productivity of major eruptions; and (3) consequently, the knowledge of whether an active region has recently had a major flare, used in combination with the active region's free-energy proxy measured from a magnetogram, can greatly alter the forecast chance that the active region will have a major eruption in the next few days after the time of the magnetogram. The active-region magnetic conditions that, in addition to the free energy, are reflected by recent major flaring are presumably the complexity and evolution of the field.

A tool for empirical forecasting of major flares, coronal mass ejections, and solar particle events from a proxy of active-region free magnetic energy

Falconer, David; Barghouty, Abdulnasser F.; Khazanov, Igor; Moore, Ron
Space Weather, Vol. 9, No. 4, S04003, **2011, File**
This paper describes a new forecasting tool developed for and currently being tested by NASA's Space Radiation Analysis Group (SRAG) at Johnson Space Center, which is responsible for the monitoring and forecasting of radiation exposure levels of astronauts. The new software tool is designed for the empirical forecasting of M- and X-class flares, coronal mass ejections, and solar energetic particle events. For each type of event, the algorithm is based on the empirical relationship between the event rate and a proxy of the active region's free magnetic energy. Each empirical relationship is determined from a data set of ~40,000 active-region magnetograms from ~1300 active regions observed by SOHO/Michelson Doppler Imager (MDI) that have known histories of flare, coronal mass ejection, and solar energetic particle event production. The new tool automatically extracts each strong-field magnetic area from an MDI full-disk magnetogram, identifies each as a NOAA active region, and measures the proxy of the active region's free magnetic energy from the extracted magnetogram. For each active region, the empirical relationship is then used to convert the free-magnetic-energy proxy into an expected event rate. The expected event rate in turn can be readily converted into the probability that the active region will produce such an event in a given forward time window. Descriptions of the data sets, algorithm, and software in addition to sample applications and a validation test are presented. Further development and transition of the new tool in anticipation of SDO/HMI are briefly discussed.

THE "MAIN SEQUENCE" OF EXPLOSIVE SOLAR ACTIVE REGIONS: DISCOVERY AND INTERPRETATION

David A. Falconer1,2,3, Ronald L. Moore1, G. Allen Gary3 and Mitzi Adams1
ApJ 700 L166-L169, **2009**
We examine the location and distribution of the production of coronal mass ejections (CMEs) and major flares by sunspot active regions in the phase space of two whole-active-region magnetic quantities measured from 1897 SOHO/MDI magnetograms. These magnetograms track the evolution of 44 active regions across the central disk of radius 0.5 R Sun. The two quantities are LWLSG, a gauge of the total free energy in an active region's magnetic field, and LΦ, a measure of the active region's total magnetic flux. From these data and each active region's history of production of CMEs, X flares, and M flares, we find (1) that CME/flare-productive active regions are concentrated in a straight-line "main sequence" in (log LWLSG, log LΦ) space, (2) that main-sequence active regions have nearly their maximum attainable free magnetic energy, and (3) evidence that this arrangement plausibly results from equilibrium between input of free energy to an explosive active region's magnetic field in the chromosphere and corona by contortion of the field via convection in and below the photosphere and loss of free energy via CMEs, flares, and coronal heating, an equilibrium between energy gain and loss that is analogous to that of the main sequence of hydrogen-burning stars in (mass, luminosity) space.

MAGNETOGRAM MEASURES OF TOTAL NONPOTENTIALITY FOR PREDICTION OF SOLAR CORONAL MASS EJECTIONS FROM ACTIVE REGIONS OF ANY DEGREE OF MAGNETIC COMPLEXITY

D. A. **Falconer**,1 R. L. Moore, and G. A. Gary
Astrophysical Journal, 689:1433–1442, **2008**
For investigating the magnetic causes of coronal mass ejections (CMEs) and for forecasting the CME productivity of active regions, in previous work we have gauged the total nonpotentiality of a whole active region by either of two measures, L_{SSM} and L_{SGM}, two measures of the magnetic field along the main neutral line in a vector magnetogram of the active region. This previous work was therefore restricted to nominally bipolar active regions, active regions that have a clearly identifiable main neutral line. In the present paper, we show that our work can be extended to include multipolar active regions of any degree of magnetic complexity by replacing L_{SSM} and L_{SGM} with their generalized counterparts, WL_{SS} and WL_{SG}, which are corresponding integral measures covering all neutral lines in an active region instead of only the main neutral line. In addition, we show that for active regions within 30 heliocentric degrees of disk center, WL_{SG} can be adequately measured from line-of-sight magnetograms instead of vector magnetograms. This approximate measure of active-region total nonpotentiality, $_{L}WL_{SG}$, with the extensive set of 96 minute cadence full-disk line-of-sight magnetograms from SOHO MDI, can be used to study the evolution of active-region total nonpotentiality leading to the production of CMEs.

Time variations of observed Hα line profiles and precipitation depths of non-thermal electrons in a solar flare

R. **Falewicz**, K. Radziszewski, P. Rudawy, A. Berlicki
ApJ **847** 84 **2017**
https://arxiv.org/pdf/1708.09797.pdf
https://iopscience.iop.org/article/10.3847/1538-4357/aa89e9/pdf
We compare time variations of the Hα and X-ray emissions observed during the pre-impulsive and impulsive phases of the C1.1-class solar flare on **21 June 2013** with those of plasma parameters and synthesized X-ray emission from a one-dimensional hydro-dynamic numerical model of the flare. The numerical model was calculated assuming that the external energy is delivered to the flaring loop by non-thermal electrons. The Hαspectra and images were obtained using the Multi-channel Subtractive Double Pass spectrograph with a time resolution of 50~ms. The X-ray fluxes and spectra were recorded by the {\it Reuven Ramaty High-Energy Solar Spectroscopic Imager} ({\it RHESSI}). Pre-flare geometric and thermodynamic parameters of the model and the delivered energy were estimated using {\it RHESSI} data.
The time variations of the X-ray light curves in various energy bands and the those of the Hα intensities and line profiles were well correlated. The time scales of the observed variations agree with the calculated variations of the plasma parameters in the flaring loop footpoints, reflecting the time variations of the vertical extent of the energy deposition layer. Our result shows that the fast time variations of the Hα emission of the flaring kernels can be explained by momentary changes of the deposited energy flux and the variations of the penetration depths of the non-thermal electrons.

2D MHD and 1D HD models of a solar flare -- a comprehensive comparison of the results

R. **Falewicz**, P. Rudawy, K. Murawski, A. K. Srivastava
ApJ 813 70 **2015**
http://arxiv.org/pdf/1510.00254v1.pdf
Without any doubt solar flaring loops possess a multi-thread internal structure that is poorly resolved and there are no means to observe heating episodes and thermodynamic evolution of the individual threads. These limitations cause

fundamental problems in numerical modelling of flaring loops, such as selection of a structure and a number of threads, and an implementation of a proper model of the energy deposition process. A set of 1D hydrodynamic and 2D magnetohydrodynamic models of a flaring loop are developed to compare energy redistribution and plasma dynamics in the course of a prototypical solar flare. Basic parameters of the modeled loop are set according to the progenitor M1.8 flare recorded in the AR10126 on **September 20, 2002** between 09:21 UT and 09:50 UT. The non-ideal 1D models include thermal conduction and radiative losses of the optically thin plasma as energy loss mechanisms, while the non-ideal 2D models take into account viscosity and thermal conduction as energy loss mechanisms only. The 2D models have a continuous distribution of the parameters of the plasma across the loop, and are powered by varying in time and space along and across the loop heating flux. We show that such 2D models are a borderline case of a multi-thread internal structure of the flaring loop, with a filling factor equal to one. Despite the assumptions used in applied 2D models, their overall success in replicating the observations suggests that they can be adopted as a correct approximation of the observed flaring structures.

Plasma heating in solar flares and their soft and hard X-ray emissions

R. **Falewicz**

E-print, May **2014**; **2014** ApJ 789 71

http://arxiv.org/pdf/1405.6038v1.pdf

In this paper, the energy budgets of two single-loop like flares observed in X-ray are analysed under the assumption that non-thermal electrons (NTEs) are the only source of plasma heating during all phases of both events. The flares were observed by RHESSI and GOES on **February 20th, 2002** and **June 2nd, 2002**, respectively. Using a 1D hydrodynamic code for both flares the energy deposited in the chromosphere was derived applying RHESSI observational data. The use of the Fokker-Planck formalism permits the calculation of distributions of the non-thermal electrons in flaring loops, thus spatial distributions of the X-ray non-thermal emissions and integral fluxes for the selected energy ranges which were compared with the observed ones. Additionally, a comparative analysis of the spatial distributions of the signals in the RHESSI images was conducted for the footpoints and for the entire flare loops in selected energy ranges with these quantities fluxes obtained from the models. The best compatibility of the model and observations was obtained for the June 2nd, 2002 event in the 0.5-4 A GOES range and total fluxes in the 6-12 keV, 12-25 keV, 20-25 keV and 50-100 keV energy bands. Results of photometry of the individual flaring structures in a high energy range shows that the best compliance occurred for the June 2nd, 2002 flare, where the synthesized emissions were 30% or more higher than the observed emissions. For the February 20th, 2002 flare, synthesized emission is about 4 times lower than the observed one. However, in the low energy range the best conformity was obtained for the February 20th, 2002 flare, where emission from the model is about 11% lower than the observed one. The larger inconsistency occurs for the June 2nd, 2002 solar flare, where synthesized emission is about 12 times greater or even more than the observed emission. Some part of these differences may be caused by inevitable flaws of the applied methodology, like by an assumption that the model of the flare is symmetric and there are no differences in the emissions originating from the feet of the flare's loop and by relative simplicity of the applied numerical 1D code and procedures. No doubt a significant refinement of the applied numerical models and more sophisticated implementation of the various physical mechanisms involved are required to achieve a better agreement. Despite these problems, a collation of modelled results with observations shows that soft and hard X-ray emissions observed for analysed single-loop like events may be fully explained by electron beam-driven evaporation only.

PLASMA HEATING IN THE VERY EARLY AND DECAY PHASES OF SOLAR FLARES

R. **Falewicz**1, M. Siarkowski2 and P. Rudawy

2011 ApJ 733 37

In this paper, we analyze the energy budgets of two single-loop solar flares under the assumption that non-thermal electrons (NTEs) are the only source of plasma heating during all phases of both events. The flares were observed by RHESSI and GOES on **2002 September 20 and 2002 March 17**, respectively. For both investigated flares we derived the energy fluxes contained in NTE beams from the RHESSI observational data constrained by observed GOES light curves. We showed that energy delivered by NTEs was fully sufficient to fulfill the energy budgets of the plasma during the pre-heating and impulsive phases of both flares as well as during the decay phase of one of them. We concluded that in the case of the investigated flares there was no need to use any additional ad hoc heating mechanisms other than heating by NTEs.

Relationship between non-thermal electron energy spectra and GOES classes

R. **Falewicz**1, P. Rudawy1, and M. Siarkowski2

E-print, Apr **2009, File**; A&A, 500, 901-908 (**2009**)

Aims.We investigate the influence of the variations of energy spectrum of non-thermal electrons on the resulting *GOES* classes of solar flares.

Methods.Twelve observed flares with various soft to hard X-ray emission ratios were modeled using different non-thermal electron energy distributions. Initial values of the flare physical parameters including geometrical properties were estimated using observations.

Results.We found that, for a fixed total energy of non-thermal electrons in a flare, the resulting *GOES* class of the flare can be changed significantly by varying the spectral index and low energy cut-o_ of the non-thermal electron distribution. Thus, the *GOES* class of a flare depends not only on the total non-thermal electrons energy but also on the electron beam parameters. For example, we were able to convert a M2.7 class solar flare into a merely C1.4 class one and a B8.1 class event into a C2.6 class flare. The results of our work also suggest that the level of correlation between the cumulative time integral of HXR and SXR fluxes can depend on the considered HXR energy range.

STUDY OF THE POYNTING FLUX IN ACTIVE REGION 10930 USING DATA-DRIVEN MAGNETOHYDRODYNAMIC SIMULATION

Y. L. **Fan**1,2, H. N. Wang1, H. He1 and X. S. Zhu

2011 ApJ 737 39

Powerful solar flares are closely related to the evolution of magnetic field configuration on the photosphere. We choose the Poynting flux as a parameter in the study of magnetic field changes. We use time-dependent multidimensional MHD simulations around a flare occurrence to generate the results, with the temporal variation of the bottom boundary conditions being deduced from the projected normal characteristic method. By this method, the photospheric magnetogram could be incorporated self-consistently as the bottom condition of data-driven simulations. The model is first applied to a simulation datum produced by an emerging magnetic flux rope as a test case. Then, the model is used to study NOAA AR 10930, which has an X3.4 flare, the data of which has been obtained by the Hinode/Solar Optical Telescope on 2006 December 13. We compute the magnitude of Poynting flux (S total), radial Poynting flux (Sz), a proxy for ideal radial Poynting flux (S proxy), Poynting flux due to plasma surface motion (S sur), and Poynting flux due to plasma emergence (S emg) and analyze their extensive properties in four selected areas: the whole sunspot, the positive sunspot, the negative sunspot, and the strong-field polarity inversion line (SPIL) area. It is found that (1) the S total, Sz , and S proxy parameters show similar behaviors in the whole sunspot area and in the negative sunspot area. The evolutions of these three parameters in the positive area and the SPIL area are more volatile because of the effect of sunspot rotation and flux emergence. (2) The evolution of S sur is largely influenced by the process of sunspot rotation, especially in the positive sunspot. The evolution of S emg is greatly affected by flux emergence, especially in the SPIL area.

ON THE ORIGIN OF THE ASYMMETRIC HELICITY INJECTION IN EMERGING ACTIVE REGIONS

Y. Fan1, D. Alexander2 and L. Tian2

ApJ 707 604-611, **2009**

To explore the possible causes of the observed asymmetric helicity flux in emerging active regions between the leading and following polarities reported in a recent study by Tian & Alexander, we examine the subsurface evolution of buoyantly rising Ω-shaped flux tubes using three-dimensional, spherical-shell anelastic MHD simulations. We find that due to the asymmetric stretching of the Ω-shaped tube by the Coriolis force, the leading side of the emerging tube has a greater field strength, is more buoyant, and remains more cohesive compared to the following side. As a result, the magnetic field lines in the leading leg show more coherent values of local twist $\alpha \equiv (\nabla \times \mathbf{B}) \cdot \mathbf{B}/B^2$, whereas the values in the following leg show large fluctuations and are of mixed sign. On average, however, the field lines in the leading leg do not show a systematically greater mean twist compared to the following leg. Due to the higher rise velocity of the leading leg, the upward helicity flux through a horizontal cross section at each depth in the upper half of the convection zone is significantly greater in the leading polarity region than that in the following leg. This may contribute to the observed asymmetric helicity flux in emerging active regions. Furthermore, based on a simplified model of active region flux emergence into the corona by Longcope & Welsch, we show that a stronger field strength in the leading tube can result in a faster rotation of the leading polarity sunspot driven by torsional Alfvén waves during flux emergence into the corona, contributing to a greater helicity injection rate in the leading polarity of an emerging active region.

A MAGNETOHYDRODYNAMIC MODEL OF THE 2006 DECEMBER 13 ERUPTIVE FLARE

Y. **Fan**

2011 ApJ 740 68

We present a three-dimensional magnetohydrodynamic simulation that qualitatively models the coronal magnetic field evolution associated with the eruptive flare that occurred on 2006 **December 13** in the emerging δ-sunspot region NOAA 10930 observed by the Hinode satellite. The simulation is set up to drive the emergence of an east-west-oriented magnetic flux rope at the lower boundary into a preexisting coronal field constructed from the Solar and Heliospheric Observatory/Michelson Doppler Imager full-disk magnetogram at 20:51:01 UT on 2006 December 12. The resulting

coronal flux rope embedded in the ambient coronal magnetic field first settles into a stage of quasi-static rise and then undergoes a dynamic eruption, with the leading edge of the flux rope cavity accelerating to a steady speed of about 830 km s–1. The pre-eruption coronal magnetic field shows morphology that is in qualitative agreement with that seen in the Hinode soft X-ray observation in both the magnetic connectivity as well as the development of an inverse-S-shaped X-ray sigmoid. We examine the properties of the erupting flux rope and the morphology of the post-reconnection loops, and compare them with the observations.

THE EMERGENCE OF A TWISTED FLUX TUBE INTO THE SOLAR ATMOSPHERE: SUNSPOT ROTATIONS AND THE FORMATION OF A CORONAL FLUX ROPE

Y. **Fan**

2009 ApJ 697 1529-1542

We present a three-dimensional simulation of the dynamic emergence of a twisted magnetic flux tube from the top layer of the solar convection zone into the solar atmosphere and corona. It is found that after a brief initial stage of flux emergence during which the two polarities of the bipolar region become separated and the tubes intersecting the photosphere become vertical, significant rotational motion sets in within each polarity. The rotational motions of the two polarities are found to twist up the inner field lines of the emerged fields such that they change their orientation into an inverse configuration (i.e., pointing from the negative polarity to the positive polarity over the neutral line). As a result, a flux rope with sigmoid-shaped, dipped core fields forms in the corona, and the center of the flux rope rises in the corona with increasing velocity as the twisting of the flux rope footpoints continues. The rotational motion in the two polarities is a result of propagation of nonlinear torsional Alfvén waves along the flux tube, which transports significant twist from the tube's interior portion toward its expanded coronal portion. This is a basic process whereby twisted flux ropes are developed in the corona with increasing twist and magnetic energy, leading up to solar eruptions.

Modelling of Reflective Propagating Slow-mode Wave in a Flaring Loop

X. **Fang**, D. Yuan, T. Van Doorsselaere, R. Keppens, C. Xia

2015 ApJ 813 33

http://arxiv.org/pdf/1509.04536v1.pdf

Quasi-periodic propagating intensity disturbances have been observed in large coronal loops in EUV images over a decade, and are widely accepted to be slow magnetosonic waves. However, spectroscopic observations from Hinode/EIS revealed their association with persistent coronal upflows, making this interpretation debatable. We perform a 2.5D magnetohydrodynamic simulation to imitate the chromospheric evaporation and the following reflected patterns in a flare loop. Our model encompasses the corona, transition region, and chromosphere. We demonstrate that the quasi periodic propagating intensity variations captured by the synthesized \textit{Solar Dynamics Observatory}/Atmospheric Imaging Assembly (AIA) 131, 94~\AA~emission images match the previous observations well. With particle tracers in the simulation, we confirm that these quasi periodic propagating intensity variations consist of reflected slow mode waves and mass flows with an average speed of 310 km/s in an 80 Mm length loop with an average temperature of 9 MK. With the synthesized Doppler shift velocity and intensity maps of the \textit{Solar and Heliospheric Observatory}/Solar Ultraviolet Measurement of Emitted Radiation (SUMER) Fe XIX line emission, we confirm that these reflected slow mode waves are propagating waves.

Coronal Rain in Magnetic Arcades: Rebound Shocks, Limit Cycles, and Shear Flows

X. **Fang**, C. Xia, R. Keppens, and T. Van Doorsselaere

2015 ApJ 807 142

We extend our earlier multidimensional, magnetohydrodynamic simulations of coronal rain occurring in magnetic arcades with higher resolution, grid-adaptive computations covering a much longer (>6 hr) time span. We quantify how blob-like condensations forming in situ grow along and across field lines and show that rain showers can occur in limit cycles, here demonstrated for the first time in 2.5D setups. We discuss dynamical, multi-dimensional aspects of the rebound shocks generated by the siphon inflows and quantify the thermodynamics of a prominence–corona transition-region-like structure surrounding the blobs. We point out the correlation between condensation rates and the cross-sectional size of loop systems where catastrophic cooling takes place. We also study the variations of the typical number density, kinetic energy, and temperature while blobs descend, impact, and sink into the transition region. In addition, we explain the mechanisms leading to concurrent upflows while the blobs descend. As a result, there are plenty of shear flows generated with relative velocity difference around 80 km s−1 in our simulations. These shear flows are siphon flows set up by multiple blob dynamics and they in turn affect the deformation of the falling blobs. In particular, we show how shear flows can break apart blobs into smaller fragments, within minutes.

δ-Sunspot Formation in Simulation of Active-region-scale Flux Emergence

Fang **Fang** and Yuhong Fan

2015 ApJ 806 79

δ-sunspots, with highly complex magnetic structures, are very productive in energetic eruptive events, such as X-class flares and homologous eruptions. We here study the formation of such complex magnetic structures by numerical simulations of magnetic flux emergence from the convection zone into the corona in an active-region-scale domain. In our simulation, two pairs of bipolar sunspots form on the surface, originating from two buoyant segments of a single subsurface twisted flux rope, following the approach of Toriumi et al. Expansion and rotation of the emerging fields in the two bipoles drive the two opposite polarities into each other with apparent rotating motion, producing a compact δ-sunspot with a sharp polarity inversion line. The formation of theδ-sunspot in such a realistic-scale domain produces emerging patterns similar to those formed in observations, e.g., the inverted polarity against Hale's law, the curvilinear motion of the spot, and strong transverse field with highly sheared magnetic and velocity fields at the polarity inversion line (PIL). Strong current builds up at the PIL, giving rise to reconnection, which produces a complex coronal magnetic connectivity with non-potential fields in the δ-spot overlaid by more relaxed fields connecting the two polarities at the two ends.

BUILDUP OF MAGNETIC SHEAR AND FREE ENERGY DURING FLUX EMERGENCE AND CANCELLATION

Fang **Fang**1, Ward Manchester IV1, William P. Abbett2, and Bart van der Holst
2012 ApJ 754 15
We examine a simulation of flux emergence and cancellation, which shows a complex sequence of processes that accumulate free magnetic energy in the solar corona essential for the eruptive events such as coronal mass ejections, filament eruptions, and flares. The flow velocity at the surface and in the corona shows a consistent shearing pattern along the polarity inversion line (PIL), which together with the rotation of the magnetic polarities, builds up the magnetic shear. Tether-cutting reconnection above the PIL then produces longer sheared magnetic field lines that extend higher into the corona, where a sigmoidal structure forms. Most significantly, reconnection and upward-energy-flux transfer are found to occur even as magnetic flux is submerging and appears to cancel at the photosphere. A comparison of the simulated coronal field with the corresponding coronal potential field graphically shows the development of non-potential fields during the emergence of the magnetic flux and formation of sunspots.

Faraday's Law in Solar Flares: A Cautionary Message

Michael **FARADAY**
This Nugget was ghost-written by Declan Diver, Lyndsay Fletcher, Hugh Hudson, Adam Kowalski, and Rami Vainio.
RHESSI Nuggets #480 **2024**
https://heliowiki.smce.nasa.gov/wiki/index.php/Faraday%27s_Law_in_Solar_Flares:_A_Cautionary_Message
"Collapsing traps" (Ref. [5]) and many other examples of test particles exploring MHD structures abound, with descriptions of Fermi and betatron acceleration (and other mechanisms), but these theories are usually not self-consistent electrodynamically with the global configuration (e.g., they may use periodic boundary conditions). They describe steady-state fluids and do not include electrostatic potentials nor particle distribution functions. This Nugget just reminds us that there is likely to be rich physics to explore in the application of Faraday's Law in solar-flare plasma theory, and we speculate that the lack of much literature on this subject probably means that it involves difficult theoretical and modeling work.

A comparative study of resistivity models for simulations of magnetic reconnection in the solar atmosphere. II. Plasmoid formation

Øystein Håvard **Færder**, Daniel Nóbrega-Siverio, Mats Carlsson
A&A **2024**
https://arxiv.org/pdf/2401.01177.pdf
Plasmoid-mediated reconnection plays a fundamental role in different solar atmospheric phenomena. Numerical reproduction of this process is therefore essential for developing robust solar models. Our goal is to assess plasmoid-mediated reconnection across various numerical resistivity models in order to investigate how plasmoid numbers and reconnection rates depend on the Lundquist number. We used the Bifrost code to drive magnetic reconnection in a 2D coronal fan-spine topology, carrying out a parametric study of several experiments with different numerical resolution and resistivity models. We employed three anomalous resistivity models: (1) the original hyper-diffusion from Bifrost, (2) a resistivity proportional to current density, and (3) a resistivity quadratically proportional to electron drift velocity. For comparisons, experiments with uniform resistivity were also run. Plasmoid-mediated reconnection is obtained in most of the experiments. With uniform resistivity, increasing the resolution reveals higher plasmoid frequency with weaker scaling to the Lundquist number, obtaining 7.9-12 plasmoids per minute for SL∈[1.8×104,2.6×105] with a scaling of S0.210L in the highest-resolution resistivity cases, transcending into Petschek reconnection in the high-SL limit and Sweet-Parker reconnection in the low-SL limit. Anomalous resistivity leads to similar results even with lower resolution. The drift-velocity-dependent resistivity excellently reproduces Petschek reconnection for any Lundquist number, and similar results are seen with resistivity proportional to current-density. Among the different

resistivity models applied on the given numerical resolution, the hyper-diffusion model reproduced plasmoid characteristics in closest resemblance to those obtained with uniform resistivity at a significantly higher resolution.

A comparative study of resistivity models for simulations of magnetic reconnection in the solar atmosphere

Øystein Håvard **Færder**, Daniel Nóbrega-Siverio, Mats Carlsson
A&A 675, A97 **2023**
https://arxiv.org/pdf/2305.18895.pdf
https://www.aanda.org/articles/aa/pdf/2023/07/aa46447-23.pdf
Magnetic reconnection is a fundamental mechanism in astrophysics. A common challenge in mimicking this process numerically in particular for the Sun is that the solar electrical resistivity is small compared to the diffusive effects caused by the discrete nature of codes. We aim to study different anomalous resistivity models and their respective effects on simulations related to magnetic reconnection in the Sun. We used the Bifrost code to perform a 2D numerical reconnection experiment in the corona that is driven by converging opposite polarities at the solar surface. This experiment was run with three different commonly used resistivity models: 1) the hyper-diffusion model originally implemented in Bifrost, 2) a resistivity proportional to the current density, and 3) a resistivity proportional to the square of the electron drift velocity. The study was complemented with a 1D experiment of a Harris current sheet with the same resistivity models. The 2D experiment shows that the three resistivity models are capable of producing results in satisfactory agreement with each other in terms of the current sheet length, inflow velocity, and Poynting influx. Even though Petschek-like reconnection occurred with the current density-proportional resistivity while the other two cases mainly followed plasmoid-mediated reconnection, the large-scale evolution of thermodynamical quantities such as temperature and density are quite similar between the three cases. For the 1D experiment, some recalibration of the diffusion parameters is needed to obtain comparable results. Specifically the hyper-diffusion and the drift velocity-dependent resistivity model needed only minor adjustments, while the current density-proportional model needed a rescaling of several orders of magnitude.

Do Cellular Automaton Avalanche Models Simulate the Quasi-Periodic Pulsations of Solar Flares?

Nastaran **Farhang**, Farhad Shahbazi, Hossein Safari
ApJ **936** 87 **2022**
https://arxiv.org/pdf/2208.02493.pdf
https://iopscience.iop.org/article/10.3847/1538-4357/ac85ba/pdf
Quasi-periodic pulsations (QPPs) with various periods that originate in the underlying magnetohydrodynamic processes of the flaring structures are detected repeatedly in the solar flare emissions. We apply a 2D cellular automaton (CA) avalanche model to simulate QPPs as a result of a repetitive load/unload mechanism. We show that the frequent occurrence of magnetic reconnections in a flaring loop could induce quasi-periodic patterns in the detected emissions. We obtain that among 21070 simulated flares, 813 events endure over 50 seconds, scaled with the temporal resolution of the Yohkoh Hard X-ray Telescope, and about 70 percent of these rather long-lasting events exhibit QPPs. We also illustrate that the applied CA model provides a wide range of periodicities for QPPs. Furthermore, we observe the presence of multiple periods in nearly 50 percent of the cases applying the Lomb-Scargle periodogram. A lognormal distribution is fitted to the unimodal distribution of the periods as a manifestation of an underlying multiplicative mechanism that typifies the effect of the system's independent varying parameters. The global maximum of the periods' lognormal distribution is located at 29.29 seconds. We compare statistics of the simulated QPPs with parameters of the host flares and discuss the impacts of flare properties on QPPs' periods. Considering the intrinsic characteristic of CA models, namely the repetitive load/unload mechanism, and the obtained pieces of evidence, we suggest that CA models may generate QPPs. We also examine the applicability of the autoregressive integrated moving average models to describe the simulated and observational QPPs.

Energy Balance in Avalanche Models for Solar Flares

Nastaran **Farhang**, Michael S. Wheatland, Hossein Safari
ApJL **883** L20 **2019**
https://arxiv.org/pdf/1909.00195.pdf
https://doi.org/10.3847/2041-8213/ab40c3
The distributions of solar flare energies and waiting times have not been described simultaneously by a single physical model, yet. In this research, we investigate whether recent avalanche models can describe the distributions for both the released energies and waiting times of flares in an active region. Flaring events are simulated using the modified Lu and Hamilton model (Lu and Hamilton (1991), ApJ, 380, 89) and also the optimized model (Farhang et al. (2018), ApJ, 859, 41). Applying a probability balance equation approach, we study the statistics of the simulated flaring events and investigate the origin of the observed power law in the flare frequency-size distribution. The results indicate that the power law originates in the distribution of transition rates (the distribution of the probabilities of transitions between different energies) rather than the distribution of the energy of the active region. It is also observed that the waiting-time

distribution of simulated flaring events follows a q-exponential function which approximates a simple Poisson distribution.

Principle of Minimum Energy in Magnetic Reconnection in a Self-Organized Critical Model for Solar Flares

Nastaran **Farhang**, Hossein Safari, Michael S. Wheatland
2018 *ApJ* **859** 41
https://arxiv.org/pdf/1804.10356.pdf
Solar flares are an abrupt release of magnetic energy in the Sun's atmosphere due to reconnection of the coronal magnetic field. This occurs in response to turbulent flows at the photosphere which twist the coronal field. Similar to earthquakes, solar flares represent the behavior of a complex system, and expectedly their energy distribution follows a power law. We present a statistical model based on the principle of minimum energy in a coronal loop undergoing magnetic reconnection, which is described as an avalanche process. We show the distribution of peaks for the flaring events in this self-organized critical system is scale-free. The obtained power law index 1.84 $ \pm $ 0.02 for the peaks is in good agreement with satellite observations of soft X-ray flares. The principle of minimum energy can be applied for general avalanche models to describe many other phenomena.

Spatial and Temporal Analysis of 3 minute Oscillations in the Chromosphere Associated with the X2.2 Solar Flare on 2011 February 15

Laurel **Farris** and R. T. James McAteer
2020 ApJ 903 19
https://doi.org/10.3847/1538-4357/abb701
https://arxiv.org/pdf/2011.10074.pdf
Three minute oscillations in the chromosphere are attributed to both slow magnetoacoustic waves propagating from the photosphere and to oscillations generated within the chromosphere itself at its natural frequency as a response to a disturbance. Here we present an investigation of the spatial and temporal behavior of the chromospheric 3 minute oscillations before, during, and after the SOL2011-02-15T01:56 X2.2 flare. Observations in ultraviolet emission centered on 1600 and 1700 Å obtained at 24 s cadence from the Atmospheric Imaging Assembly on board the Solar Dynamics Observatory are used to create power maps as functions of both space and time. We observe higher 3 minute power during the flare, spatially concentrated in small areas ~10 pixels (~4") across. This implies that the chromospheric plasma is not oscillating globally as a single body. The locations of increased 3 minute power are consistent with observations of HXR flare emission from previous studies, suggesting that these small areas are manifestations of the chromosphere responding to injection of energy by nonthermal particles. This supports the theory that the chromosphere oscillates at the acoustic cutoff frequency in response to a disturbance.

The study of magnetic reconnection in solar spicules

Z. **Fazel**, H. Ebadi
Astrophysics and Space Science, **2014**
http://arxiv.org/pdf/1406.7265v1.pdf
This work is devoted to study the magnetic reconnection instability under solar spicule conditions. Numerical study of the resistive tearing instability in a current sheet is presented by considering the magnetohydrodynamic (MHD) framework. To investigate the effect of this instability in a stratified atmosphere of solar spicules, we solve linear and non-ideal MHD equations in the x-z plane. In the linear analysis it is assumed that resistivity is only important within the current sheet, and the exponential growth of energies takes place faster as plasma resistivity increases. We are interested to see the occurrence of magnetic reconnection during the lifetime of a typical solar spicule.

CAN THE COMPOSITION OF THE SOLAR CORONA BE DERIVED FROM HINODE/EXTREME-ULTRAVIOLET IMAGING SPECTROMETER SPECTRA?

U. **Feldman** et al
ApJ 695, 36-45, **2009** doi: 10.1088/0004-637X/695/1/36
Elemental abundances appear to be the same everywhere in the photosphere, but in the solar corona they vary in different regions. Abundances in quiet Sun (closed) flux tubes are different from those in coronal hole (CH, open) magnetic field regions, and therefore abundance variations might possibly be used to determine locations of slow and fast solar wind in the corona. In active regions, abundances can change from region to region and can vary with the age of the region. In the present paper, we evaluate the feasibility of determining relative elemental abundances in the corona using spectra acquired by the Extreme-ultraviolet Imaging Spectrometer (EIS) on Hinode. As test cases, we attempt to evaluate the coronal composition above the limb in an equatorial quiet region and in a polar CH. We also determine the elemental composition of coronal regions with moderate activity on the disk and at the limb. To estimate the accuracy of the instrumental calibration and the atomic physics used in the calculations, we compare the derived

composition with earlier derivations from spectra recorded by the Solar Ultraviolet Measurements of Emitted Radiation spectrometer in similar regions. We find that EIS can be used to determine relative abundance variations in the inner solar corona. The determination of absolute abundances can also be attempted after additional calibrations in space are accomplished.

A Compressed Sensing-based Image Reconstruction Algorithm for Solar Flare X-Ray Observations

Simon **Felix**, Roman Bolzern, Marina Battaglia
2017 *ApJ* **849** 10
https://arxiv.org/pdf/1709.08116.pdf
One way of imaging X-ray emission from solar flares is to measure Fourier components of the spatial X-ray source distribution. We present a new Compressed Sensing-based algorithm named VIS_CS, which reconstructs the spatial distribution from such Fourier components. We demonstrate the application of the algorithm on synthetic and observed solar flare X-ray data from the Reuven Ramaty High Energy Solar Spectroscopic Imager (RHESSI) satellite and compare its performance with existing algorithms. VIS_CS produces competitive results with accurate photometry and morphology, without requiring any algorithm- and X-ray source-specific parameter tuning. Its robustness and performance make this algorithm ideally suited for generation of quicklook images or large image cubes without user intervention, such as for imaging spectroscopy analysis. **19 July 2012**

Toward Model Compression for a Deep Learning–Based Solar Flare Forecast on Satellites

Kai **Feng**1,2, Long Xu1,3, Dong Zhao1, Sixuan Liu1,2, and Xin Huang1
2023 ApJS 268 59
https://iopscience.iop.org/article/10.3847/1538-4365/ace96a/pdf
Timely solar flare forecasting is challenged by the delay of transmitting vast amounts of data from the satellite to the ground. To avoid this delay, it is expected that forecasting models will be deployed on satellites. Thus, transmitting forecasting results instead of huge volumes of observation data would greatly save network bandwidth and reduce forecasting delay. However, deep-learning models have a huge number of parameters so they need large memory and strong computing power, which hinders their deployment on satellites with limited memory and computing resources. Therefore, there is a great need to compress forecasting models for efficient deployment on satellites. First, three typical compression methods, namely knowledge distillation, pruning, and quantization, are examined individually for compressing of solar flare forecasting models. And then, an assembled compression model is proposed for better compressing solar flare forecasting models. The experimental results demonstrate that the assembled compression model can compress a pretrained solar flare forecasting model to only 1.67% of its original size while maintaining forecasting accuracy.

MAGNETIC ENERGY PARTITION BETWEEN THE CORONAL MASS EJECTION AND FLARE FROM AR 11283

L. **Feng**1,2, T. Wiegelmann2, Y. Su3, B. Inhester2, Y. P. Li1, X. D. Sun4, and W. Q. Gan
2013 ApJ 765 37
On **2011 September 6**, an X-class flare and a halo coronal mass ejection (CME) were observed from Earth erupting from the same active region AR 11283. The magnetic energy partition between them has been investigated. SDO/HMI vector magnetograms were used to obtain the coronal magnetic field using the nonlinear force-free field (NLFFF) extrapolation method. The free magnetic energies before and after the flare were calculated to estimate the released energy available to power the flare and the CME. For the flare energetics, thermal and nonthermal energies were derived using the RHESSI and GOES data. To obtain the radiative output, SDO/EVE data in the 0.1-37 nm waveband were utilized. We have reconstructed the three-dimensional (3D) periphery of the CME from the coronagraph images observed by STEREO-A, B, and SOHO. The mass calculations were then based on a more precise Thomson-scattering geometry. The subsequent estimate of the kinetic and potential energies of the CME took advantage of the more accurate mass, and the height and speed in a 3D frame. The released free magnetic energy resulting from the NLFFF model is about 6.4 × 1031 erg, which has a possible upper limit of 1.8 × 1032 erg. The thermal and nonthermal energies are lower than the radiative output of 2.2 × 1031 erg from SDO/EVE for this event. The total radiation covering the whole solar spectrum is probably a few times larger. The sum of the kinetic and potential energy of the CME could go up to 6.5 × 1031 erg. Therefore, the free energy is able to power the flare and the CME in AR 11283. Within the uncertainty, the flare and the CME may consume a similar amount of free energy.

Particle kinetic analysis of a polar jet from SECCHI COR data

L. **Feng**1,2, B. Inhester2, J. de Patoul2, T. Wiegelmann2 and W. Q. Gan
A&A 538, A34 **(2012)**
Aims. We analyze coronagraph observations of a polar jet observed by the Sun Earth Connection Coronal and Heliospheric Investigation (SECCHI) instrument suite onboard the Solar TErrestrial RElations Observatory (STEREO) spacecraft.

Methods. In our analysis we compare the brightness distribution of the jet in white-light coronagraph images with a dedicated kinetic particle model. We obtain a consistent estimate of the time that the jet was launched from the solar surface and an approximate initial velocity distribution in the jet source. The method also allows us to check the consistency of the kinetic model. In this first application, we consider only gravity as the dominant force on the jet particles along the magnetic field.
Results. We find that the kinetic model explains the observed brightness evolution well. The derived initiation time is consistent with the jet observations by the EUVI telescope at various wavelengths. The initial particle velocity distribution is fitted by Maxwellian distributions and we find deviations of the high-energy tail from the Maxwellian distributions. We estimated the jet's total electron content to have a mass between 3.2 × 1014 and 1.8 × 1015 g. Mapping the integrated particle number along the jet trajectory to its source region and assuming a typical source region size, we obtain an initial electron density between 8 × 109 and 5 × 1010 cm-3 that is characteristic for the lower corona or the upper chromosphere. The total kinetic energy of all particles in the jet source region amounts from 2.1 × 1028 to 2.4 × 1029 erg.

First stereoscopic coronal loop reconstructions from STEREO/SECCHI images

L. **Feng**1,2, B. Inhester1, S. Solanki1, T. Wiegelmann1, B. Podlipnik1, R.A. Howard3, and J.-P. Wuelser
E-print, Nov. **2007**; ApJL
We present the first reconstruction of the three-dimensional shape of magnetic loops in an active region from two different vantage points based on simultaneously recorded images.

We demostrate that these data allow to obtain a reliable three-dimensional reconstruction of sufficiently bright loops. The result is compared with field lines derived from a coronal magnetic field model extrapolated from a photospheric magnetogram recorded nearly simultaneously by SOHO/MDI. We attribute discrepancies between reconstructed loops and extrapolated field lines to the inadequacy of the linear force-free field model used for the extrapolation.

Understanding the thermal and magnetic properties of a X-class flare in the low solar atmosphere

F. **Ferrente**, C. Quintero Noda, F. Zuccarello, S. L. Guglielmino
A&A 686, A244 **2024**
https://arxiv.org/pdf/2404.06231.pdf
https://www.aanda.org/articles/aa/pdf/2024/06/aa49512-24.pdf
We analyse the spatial distribution and vertical stratification of the physical parameters of the solar atmosphere when an X-class flare occurs. We made use of observations acquired by the Interferometric Bidimensional Spectropolarimeter instrument when observing the full Stokes parameters for the Fe I 6173 A and Ca II 8542 A transitions. We analysed the observed spectra using the newly developed DeSIRe code to infer the atmospheric parameters at photospheric and chromospheric layers over the entire observed field of view. Our findings reveal that the chromosphere is characterised by temperature enhancements and strong upflows in the flare ribbon area, which indicates that the flaring event is producing hot material that is moving outwards from the Sun. We did not detect any trace of temperature enhancements or strong velocities (of any sign) at photospheric layers, signalling that the impact of the flaring event mainly happens at the middle and upper layers. The information about the magnetic field vector revealed relatively smooth stratifications with height for both magnetic field strength and inclination. Still, when examining the spatial distribution of the magnetic field inclination, we observed the presence of large-scale mixed polarities in the regions where the flare ribbon is located. These results suggest that the interaction between those mixed polarities could be the flare's triggering mechanism. **2014 October 22**

Photospheric and Chromospheric Magnetic Field Evolution during the X1.6 Flare in Active Region NOAA 12192

F. **Ferrente**1, F. Zuccarello1,2, S. L. Guglielmino2, S. Criscuoli3, and P. Romano2
2023 ApJ 954 185
https://iopscience.iop.org/article/10.3847/1538-4357/ace9d1/pdf
We report on observations acquired by the Interferometric Bidimensional Spectropolarimeter (IBIS) during SOL**2014-10-22**T14:02, an X1.6 flare that occurred in active region NOAA 12192, taken in the Fe i 617.30 nm and Ca ii 854.2 nm line profiles. We analyze polarization signatures in the Stokes profiles of the two lines across one of the flare ribbons. Focusing our attention on the chromospheric signals and using the weak-field approximation (WFA), we study the temporal variation of the line-of-sight (LOS) magnetic field. We find variations of the magnetic field or the opacity along the flare ribbon, in most cases within the first 3 minutes of the observation just after the flare peak, during the tail of the flare impulsive phase. This result was validated by the STiC inversion of the pixels used for the WFA analysis. The analysis of the photospheric magnetic field shows that in this layer, the LOS magnetic field does not show the same changes observed in the chromosphere in the selected pixels, nor clear evidence of changes along the polarity inversion line around a magnetic polarity intrusion. In this respect, we also find that the temporal observing window is not

suitable for assessing the presence of stepwise changes. The nonlinear force-free field extrapolations, together with the analysis of the ribbons' isophotes obtained from Interface Region Imaging Spectrograph data, suggest that the region corresponding to the magnetic intrusion observed by IBIS is characterized by a complex magnetic connectivity and is almost cospatial with the area affected by the initial energy release.

Acceleration of Nonthermal Electrons in Coordinated Interaction with Whistler Turbulence in a Flare Loop.

Filatov, L.V., Melnikov, V.F.
Geomagn. Aeron. 63, 1079–1085 (**2023**).
https://doi.org/10.1134/S0016793223070071
This work is devoted to the study of the self-consistent interaction of nonthermal electrons injected into a flare loop and whistler turbulence in it. Both processes of redistribution of injected electrons by energy and pitch angles and processes of internal generation and damping of turbulence itself are considered. It is shown that both in the growth phase and in the decay phase of the injection, whistler generation occurs at relatively high frequencies. The interaction of nonthermal electrons with these waves leads to an increase in their concentration in the energy range of 50–150 keV due to efficient pitch-angle scattering and an additional stochastic acceleration process.

On the time evolution of brightness, volume and height of a coronal source in an M-class flare

Kazi A. **Firoz**, W. Q. Gan, Y. P. Li, J. Rodríguez-Pacheco & Y. Su
Astrophys Space Sci (**2017**) 362: 113.
http://sci-hub.cc/10.1007/s10509-017-3092-1
We study brightness, volume and heights of the X-ray thermal emission components for an M-class solar flare on **17 May 2012.** Based on the RHESSI data availability, we present the results for 01:42–01:58 UT over the late-flare phase. It is observed that the spatial evolution of the thermal emission components 6–12 and 12–18 keV are well associated with the hottest plasma in the corona. Results show that the ascending height (∼1.35×104 km∼1.35×104 km) and speed (∼14.0 kms−1∼14.0 kms−1) of coronal source component 6–12 keV is slightly smaller than the ascending height (∼1.45×104 km∼1.45×104 km) and speed (∼15.1 kms−1∼15.1 kms−1) of the coronal source component 12–18 keV. Mean flux intensity (ImeanImean) of the 6–12 keV maintained a good fit (χ2=0.41χ2=0.41) with the corresponding volume (VV) following strongly the power law [Imean=(15.8±0.21)V−1.28±0.03Imean=(15.8±0.21)V−1.28±0.03]. In contrast, the 12–18 keV maintained a weak fit (χ2=2.37χ2=2.37) following still the power law [Imean=(0.19±0.01)V−1.88±0.16Imean=(0.19±0.01)V−1.88±0.16]. The power law indices (−1.28±0.03;−1.88±0.16−1.28±0.03;−1.88±0.16) obtained by the observational analysis slightly differ from the power law index (−1.67) obtained by a theoretical model. The observations are consistent with adiabatic expansion of the coronal source component.

An explanation for the difference between physical conditions in two ribbons in the July 23, 2002 flare

N. M. **Firstova**
Astronomy Letters, **2015**
This study offers an explanation of the impact linear polarization observed during an impulsive phase of the 2??/4.8?? flare on **July 23, 2002**, with the Large Solar Vacuum Telescope (LSVT). A high degree of polarization and a deep central reversal of the ???? line were detected only in a small region of the flare's southern ribbon. An accurate comparison of LSVT high-resolution spectro-polarimetric data with the hard X-rays observed by the Reuven Ramaty High Energy Solar Spectroscopic (RHESSI) revealed that these effects on the ???? line profile were seen in the region (~10") which was located between two hard X-ray footpoints over the southern ribbon. At the same region, according to RHESSI data were locations of the gamma-ray sources (in the 0.3?C0.5 and 0.7?C1.4 MeV bands) which are caused by electron bremsstrahlung. We assume that two hard X-ray footpoints make a common footpoint of the southern branch of the loop, which is divided into two due to the high-energy electron flux. Injection of the high-energy and relativistic electron flux into the dense chromospheric layers might have caused the impact polarization and central reversal of the ???? line in the southern ribbon contrary to the northern one with no polarization and with a typical footpoint of ~20-120 keV hard X-rays.

Observation of H*α* line impact polarization in solar flares<<<

N. M. **Firstova**, V. I. Polyakov & A. V. Firstova
Astronomy Letters, July **2014**, Volume 40, Issue 7, pp 449-458
We present the results of studying the impact linear polarization of 32 solar flares of X-ray classes C, M, and X (two flares) observed with the Large Solar Vacuum Telescope. It has turned out that there is evidence for impact polarization only in 13 of them. The newly obtained data have confirmed that the linear Stokes parameters are predominantly 2–7%, while the spatial sizes of flaring points with nonzero Stokes parameters are small (1″-2″). Two features of the manifestation of impact polarization in flares revealed by these studies are of greatest interest: (1) at the two foot points

of a single flare loop or an arcade of loops, both the Hα intensity profiles and the Stokes profiles differ in behavior; (2) based on the Hα line, we have found for the first time that the sign of the Stokes parameters changes not only across the flare ribbon but also with depth of the chromosphere.

H alpha line impact linear polarization observed in the 23 July 2002 flare with the Large Solar Vacuum Telescope (LSVT)

Firstova N.M., Polyakov V.I., Firstova A.V.
E-print, 29 May **2012**; Solar Phys.
We represent results of research of proton flare 2B/X4.8, observed on the Large Solar Vacuum Telescope (LSVT) at the Baikal Astrophysical Observatory in a spectropolarimetric mode with high spatial and spectral resolution. We have found evidence for Hα line impact linear polarization in several cases, predominantly, during the initial moments of flare. Of the ?α line 606 cuts made along dispersion in 53 spectrograms, a polarizing signal was found more or less confidently found in 60 cuts (13 spectrograms). Mainly, polarization was observed in one kernel of flare. A typical feature of this kernel was that line was observed with a reversal in the central part of this kernel that created a dip in the kernel center in a photometric cut. The size of these dips and the size of sites with the linear polarization coincide and are equal 3 ? 6 arc sec. The maximum polarization degree in this kernel reached 15 %. The polarization direction in the kernel is radial except for first two frames with the polarization direction was both radial and tangential. Thus, there is an analogy of the effects observed at the chromospheric level in this kernel (polarization and depression in line cernel) with the temporal variation of the HXR sources

The PDFI_SS Electric Field Inversion Software

George H. **Fisher**, Maria D. Kazachenko, Brian T. Welsch, Xudong Sun, Erkka Lumme, David J. Bercik, Marc L. DeRosa, Mark C. M. Cheung
ApJS 248:2 (52pp) **2020**
https://arxiv.org/pdf/1912.08301.pdf
We describe the PDFI_SS software library, which is designed to find the electric field at the Sun's photosphere from a sequence of vector magnetogram and Doppler velocity measurements, and estimates of horizontal velocities obtained from local correlation tracking using the recently upgraded FLCT code. The library, a collection of Fortran subroutines, uses the "PDFI" technique described by Kazachenko et al. (2014), but modified for use in spherical, Plate-Carrée geometry on a staggered grid. The domain over which solutions are found is a subset of the global spherical surface, defined by user-specified limits of colatitude and longitude. Our staggered-grid approach, based on that of Yee (1966), is more conservative and self-consistent compared to the centered, Cartesian grid used by Kazachenko et al. (2014). The library can be used to compute an end-to-end solution for electric fields from data taken by the HMI instrument aboard NASA's SDO Mission. This capability has been incorporated into the HMI pipeline processing system operating at SDO's JSOC. The library is written in a general and modular way so that the calculations can be customized to modify or delete electric field contributions, or used with other data sets. Other applications include "nudging" numerical models of the solar atmosphere to facilitate assimilative simulations. The library includes an ability to compute "global" (whole-Sun) electric field solutions. The library also includes an ability to compute Potential Magnetic Field solutions in spherical coordinates. This distribution includes a number of test programs which allow the user to test the software.
February 14-15, 2011

The Coronal Global Evolutionary Model: Using HMI Vector Magnetogram and Doppler Data to Model the Buildup of Free Magnetic Energy in the Solar Corona

G. H. **Fisher**, W. P. Abbett, D. J. Bercik, M. D. Kazachenko, B. J. Lynch, B. T. Welsch, J. T. Hoeksema, K. Hayashi, Y. Liu, A. A. Norton, A. Sainz Dalda, X. Sun, M. L. DeRosa and M. C. M. Cheung
Space Weather Volume 13, Issue 6 June **2015** Pages 369–373
http://arxiv.org/ftp/arxiv/papers/1505/1505.06018.pdf
The most violent space weather events (eruptive solar flares and coronal mass ejections) are driven by the release of free magnetic energy stored in the solar corona. Energy can build up on timescales of hours to days, and then may be suddenly released in the form of a magnetic eruption, which then propagates through interplanetary space, possibly impacting the Earth's space environment. Can we use the observed evolution of the magnetic and velocity fields in the solar photosphere to model the evolution of the overlying solar coronal field, including the storage and release of magnetic energy in such eruptions? The objective of CGEM, the Coronal Global Evolutionary Model, funded by the NASA/NSF Space Weather Modeling program, is to develop and evaluate such a model for the evolution of the coronal magnetic field. The evolving coronal magnetic field can then be used as a starting point for magnetohydrodynamic (MHD) models of the corona, which can then be used to drive models of heliospheric evolution and predictions of magnetic field and plasma density conditions at 1AU.

Unusual Stokes V profiles during flaring activity of a delta sunspot

C. E. **Fischer**1, C. U. Keller2, F. Snik2, L. Fletcher3 and H. Socas-Navarro
A&A 547, A34 (**2012**)

Aims. We analyze a set of full Stokes profile observations of the flaring active region NOAA 10808. The region was recorded with the Vector-Spectromagnetograph of the Synoptic Optical Long-term Investigations of the Sun facility. The active region produced several successive X-class flares between 19:00 UT and 24:00 UT on **September 13, 2005** and we aim to quantify transient and permanent changes in the magnetic field and velocity field during one of the flares, which has been fully captured.

Methods. The Stokes profiles were inverted using the height-dependent inversion code LILIA to analyze magnetic field vector changes at the flaring site. We report multilobed asymmetric Stokes V profiles found in the δ-sunspot umbra. We fit the asymmetric Stokes V profiles assuming an atmosphere consisting of two components (SIR inversions) to interpret the profile shape. The results are put in context with Michelson Doppler Imager (MDI) magnetograms and reconstructed X-ray images from the Reuven Ramaty High Energy Solar Spectroscopic Imager.

Results. We obtain the magnetic field vector and find signs of restructuring of the photospheric magnetic field during the flare close to the polarity inversion line at the flaring site. At two locations in the umbra we encounter strong fields (~3 kG), as inferred from the Stokes I profiles, which, however, exhibit a low polarization signal. During the flare we observe in addition asymmetric Stokes V profiles at one of these sites. The asymmetric Stokes V profiles appear co-spatial and co-temporal with a strong apparent polarity reversal observed in MDI-magnetograms and a chromospheric hard X-ray source. The two-component atmosphere fits of the asymmetric Stokes profiles result in line-of-sight velocity differences in the range of ~12 km s-1 to 14 km s-1 between the two components in the photosphere. Another possibility is that local atmospheric heating is causing the observed asymmetric Stokes V profile shape. In either case our analysis shows that a very localized patch of ~5″ in the photospheric umbra, co-spatial with a flare footpoint, exhibits a subresolution fine structure.

Global Forces in Eruptive Solar Flares: The Lorentz Force Acting on the Solar Atmosphere and the Solar Interior

G. H. **Fisher**, D. J. Bercik, B. T. Welsch and H. S. Hudson
Solar Physics, Volume 277, Number 1, 59-76, **2012**

We compute the change in the Lorentz force integrated over the outer solar atmosphere implied by observed changes in vector magnetograms that occur during large, eruptive solar flares. This force perturbation should be balanced by an equal and opposite force perturbation acting on the solar photosphere and solar interior. The resulting expression for the estimated force change in the solar interior generalizes the earlier expression presented by Hudson, Fisher, and Welsch (Astron. Soc. Pac. CS-383, 221, 2008), providing horizontal as well as vertical force components, and provides a more accurate result for the vertical component of the perturbed force. We show that magnetic eruptions should result in the magnetic field at the photosphere becoming more horizontal, and hence should result in a downward (toward the solar interior) force change acting on the photosphere and solar interior, as recently argued from an analysis of magnetogram data by Wang and Liu (Astrophys. J. Lett. 716, L195, 2010). We suggest the existence of an observational relationship between the force change computed from changes in the vector magnetograms, the outward momentum carried by the ejecta from the flare, and the properties of the helioseismic disturbance driven by the downward force change. We use the impulse driven by the Lorentz-force change in the outer solar atmosphere to derive an upper limit to the mass of erupting plasma that can escape from the Sun. Finally, we compare the expected Lorentz-force change at the photosphere with simple estimates from flare-driven gasdynamic disturbances and from an estimate of the perturbed pressure from radiative backwarming of the photosphere in flaring conditions.

Wave Generation by Flare-accelerated Ions and Implications for 3He Acceleration

A. **Fitzmaurice**1,2, J. F. Drake2,3, and M. Swisdak1,2
2024 ApJ 964 97
https://arxiv.org/pdf/2311.12149.pdf
https://iopscience.iop.org/article/10.3847/1538-4357/ad217f/pdf

The waves generated by high-energy proton and alpha particles streaming from solar flares into regions of colder plasma are explored using particle-in-cell simulations. Initial distribution functions for the protons and alphas consist of two populations: an energetic, streaming population represented by an anisotropic ($T_\parallel > T_\perp$), one-sided kappa function and a cold, Maxwellian background population. The anisotropies and nonzero heat fluxes of these distributions destabilize oblique waves with a range of frequencies below the proton cyclotron frequency. These waves scatter particles out of the tails of the initial distributions along constant-energy surfaces in the wave frame. Overlap of the nonlinear resonance widths allows particles to scatter into near-isotropic distributions by the end of the simulations. The dynamics of 3He are explored using test particles. Their temperatures can increase by a factor of nearly 20. Propagation of such waves into regions above and below the flare site can lead to heating and transport of 3He into the flare acceleration region. The amount of heated 3He that will be driven into the flare site is proportional to the wave energy. Using values from our simulations, we show that the abundance of 3He driven into the acceleration region should

approach that of 4He in the corona. Therefore, waves driven by energetic ions produced in flares are a strong candidate to drive the enhancements of 3He observed in impulsive flares.

Data-constrained 3D modeling of a solar flare evolution: acceleration, transport, heating, and energy budget

Gregory D. **Fleishman**, Gelu M. Nita, Galina G. Motorina
ApJ **953** 174 **2023**
https://arxiv.org/pdf/2308.00149.pdf
https://iopscience.iop.org/article/10.3847/1538-4357/ace1f4/pdf
Solar flares are driven by release of the free magnetic energy and its conversion to other forms of energy -- kinetic, thermal, and nonthermal. Quantification of partitions between these energy components and their evolution is needed to understand the solar flare phenomenon including nonthermal particle acceleration, transport, and escape and the thermal plasma heating and cooling. The challenge of remote sensing diagnostics is that the data are taken with finite spatial resolution and suffer from line-of-sight (LOS) ambiguity including cases when different flaring loops overlap and project one over the other. Here we address this challenge by devising a data-constrained evolving 3D model of a multi-loop SOL**2014-02-16**T064620 solar flare of GOES class C1.5. Specifically, we employed a 3D magnetic model validated earlier for a single time frame and extended it to cover the entire flare evolution. For each time frame we adjusted the distributions of the thermal plasma and nonthermal electrons in the model, such as the observables synthesized from the model matched the observations. Once the evolving model has been validated this way, we computed and investigated the evolving energy components and other relevant parameters by integrating over the model volume. This approach removes the LOS ambiguity and permits to disentangle contributions from the overlapping loops. It reveals new facets of electron acceleration and transport, as well as heating and cooling the flare plasma in 3D. We find signatures of substantial direct heating of the flare plasma not associated with the energy loss of nonthermal electrons.

Energy budget of plasma motions, heating, and electron acceleration in a three-loop solar flare

Gregory D. **Fleishman**, Lucia Kleint, Galina G. Motorina, Gelu M. Nita, Eduard P. Kontar
ApJ **913** 97 **2021**
https://arxiv.org/pdf/2104.00811.pdf
https://iopscience.iop.org/article/10.3847/1538-4357/abf495/pdf
https://doi.org/10.3847/1538-4357/abf495
Non-potential magnetic energy promptly released in solar flares is converted to other forms of energy. This may include nonthermal energy of flare-accelerated particles, thermal energy of heated flaring plasma, and kinetic energy of eruptions, jets, up/down flows, and stochastic (turbulent) plasma motions. The processes or parameters governing partitioning of the released energy between these components is an open question. How these components are distributed between distinct flaring loops and what controls these spatial distributions is also unclear. Here, based on multi-wavelength data and 3D modeling, we quantify the energy partitioning and spatial distribution in the well observed SOL**2014-02-16**T064620 solar flare of class C1.5. Nonthermal emissions of this flare displayed a simple impulsive single-spike light curves lasting about 20\,s. In contrast, the thermal emission demonstrated at least three distinct heating episodes, only one of which was associated with the nonthermal component. The flare was accompanied by up and down flows and substantial turbulent velocities. The results of our analysis suggest that (i) the flare occurs in a multi-loop system that included at least three distinct flux tubes; (ii) the released magnetic energy is divided unevenly between the thermal and nonthermal components in these loops; (iii) only one of these three flaring loops contains an energetically important amount of nonthermal electrons, while two other loops remain thermal; (iv) the amounts of direct plasma heating and that due to nonthermal electron loss are comparable; (v) the kinetic energy in the flare footpoints constitute only a minor fraction compared with the thermal and nonthermal energies.
CESRA # 2967 Jul **2021** http://www.astro.gla.ac.uk/users/eduard/cesra/?p=2967

Mapping magnetic field and relativistic electrons along a solar flare current sheet

Gregory **Fleishman**, Bin Chen, Gary Dale, and Gelu Nita et al.
EGU2020-19937 May **2020**
https://meetingorganizer.copernicus.org/EGU2020/displays/36057
In the standard model of solar flares, a large-scale reconnection current sheet (RCS) is postulated as the central engine for powering the flare energy release and accelerating particles. However, where and how the energy release and particle acceleration occur remain unclear due to the lack of measurements for the magnetic properties of the RCS. Here we report the first measurement of spatially-resolved magnetic field and flare-accelerated relativistic electrons along a large-scale RCS in a solar flare. The measured magnetic field profile shows a local maximum where the reconnecting field lines of opposite polarities closely approach each other, known as the reconnection X point. The measurements also reveal a local minimum near the bottom of the RCS above the flare loop-top, referred to as a "magnetic bottle". This spatial structure agrees with theoretical predictions and numerical modeling results. A strong reconnection electric

field of over 4000 V/m is inferred near the X point. This location, however, shows a local depletion of microwave-emitting relativistic electrons. In contrast, the relativistic electrons concentrate at or near the magnetic bottle structure, where more than 99% of them reside at each instant. Our observations suggest crucial new input to the current picture of high energy electron acceleration.

Decay of the coronal magnetic field can release sufficient energy to power a solar flare

Gregory D. **Fleishman**[1,*], Dale E. Gary[1], Bin Chen[1], Natsuha Kuroda[2,3], Sijie Yu[1], Gelu M. Nita[1]
Science 17 Jan **2020**: Vol. 367, Issue 6475, pp. 278-280 **File**
sci-hub.si/10.1126/science.aax6874
https://science.sciencemag.org/content/367/6475/278/tab-pdf

Solar flares are powered by a rapid release of energy in the solar corona, thought to be produced by the decay of the coronal magnetic field strength. Direct quantitative measurements of the evolving magnetic field strength are required to test this. We report microwave observations of a solar flare, showing spatial and temporal changes in the coronal magnetic field. The field decays at a rate of ~5 Gauss per second for 2 minutes, as measured within a flare subvolume of ~1028 cubic centimeters. This fast rate of decay implies a sufficiently strong electric field to account for the particle acceleration that produces the microwave emission. The decrease in stored magnetic energy is enough to power the solar flare, including the associated eruption, particle acceleration, and plasma heating. **10 Sept 2017**

Revealing evolution of nonthermal electrons in solar flares using 3D modeling

Gregory D. **Fleishman**, Gelu M. Nita, Natsuha Kuroda, Sabina Jia, Kevin Tong, Richard R. Wen, Zhou Zhizhuo
ApJ **859** 17 **2018**
https://arxiv.org/pdf/1803.09847.pdf
http://sci-hub.tw/http://iopscience.iop.org/0004-637X/859/1/17/

Understanding nonthermal particle generation, transport, and escape in solar flares requires detailed quantification of the particle evolution in the realistic 3D domain where the flare takes place. Rather surprisingly, apart of standard flare scenario and integral characteristics of the nonthermal electrons, not much is known about actual evolution of nonthermal electrons in the 3D spatial domain. This paper attempts to begin to remedy this situation by creating sets of evolving 3D models, the synthesized emission from which matches the evolving observed emission. Here we investigate two contrasting flares: a dense, "coronal-thick-target" flare SOL**2002-04-12**T17:42, that contained a single flare loop observed in both microwave and X-ray, and a more complex flare, SOL**2015-06-22**T17:50, that contained at least four distinct flaring loops needed to consistently reproduce the microwave and X-ray emission. Our analysis reveals differing evolution pattern of the nonthermal electrons in the dense and tenuous loops; however, both of which imply the central role of resonant wave-particle interaction with turbulence. These results offer new constraints for theory and models of the particle acceleration and transport in solar flares.

A Large-scale Plume in an X-Class Solar Flare

Gregory D. **Fleishman**, Gelu M. Nita, Dale E. Gary
ApJ **845** 135 **2017**
https://arxiv.org/pdf/1707.06636.pdf

Ever-increasing multi-frequency imaging of solar observations suggests that solar flares often involve more than one magnetic fluxtube. Some of the fluxtubes are closed, while others can contain open field. The relative proportion of nonthermal electrons among those distinct loops is highly important for understanding the energy release, particle acceleration, and transport. The access of nonthermal electrons to the open field is further important as the open field facilitates the solar energetic particle (SEP) escape from the flaring site, and thus controls the SEP fluxes in the solar system, both directly and as seed particles for further acceleration. The large-scale fluxtubes are often filled with a tenuous plasma, which is difficult to detect in either EUV or X-ray wavelengths; however, they can dominate at low radio frequencies, where a modest component of nonthermal electrons can render the source optically thick and, thus, bright enough to be observed. Here we report detection of a large-scale `plume' at the impulsive phase of an X-class solar flare, **SOL2001-08-25T16**:23, using multi-frequency radio data from Owens Valley Solar Array. To quantify the flare spatial structure, we employ 3D modeling utilizing force-free-field extrapolations from the line-of-sight SOHO/MDI magnetograms with our modeling tool GX Simulator. We found that a significant fraction of the nonthermal electrons accelerated at the flare site low in the corona escapes to the plume, which contains both closed and open field. We propose that the proportion between the closed and open field at the plume is what determines the SEP population escaping into interplanetary space.

Particle acceleration and transport

Gregory **Fleishman**
CESRA **2016**
http://cesra2016.sciencesconf.org/conference/cesra2016/pages/CESRA2016_prog_abs_book_v1.pdf

Abstract The Sun is arguably the best astrophysical laboratory to study particle acceleration because of the relative proximity of the star and high efficiency of particle acceleration. A key difficulty of probing the particle acceleration at the sun is that we often observe the accelerated particles not in the very acceleration region, but from a remote location; thus, properties of the accelerated particles are modified by transport effects. The few reported detections of the flare acceleration sites raise new fundamental questions of exactly how flare energization works. What are the main driving physical parameters that control the initial partition between the nonthermal and thermal energies? Do waves or turbulence play a role? What is the role of the nonthermal particles in the flare energy release and plasma heating? What is the favorable magnetic morphology? In this talk I give a brief review of most likely acceleration mechanisms and most relevant transport effects and their observational signatures in radio and X-ray domains

A Cold Flare With Delayed Heating

Gregory D. **Fleishman**, Valentin D. Pal'shin, Natalia Meshalkina, Alexandra L. Lysenko, Larisa K. Kashapova, Alexander T. Altyntsev

ApJ **822** 71 **2016**

http://arxiv.org/pdf/1603.07273v1.pdf

https://iopscience.iop.org/article/10.3847/0004-637X/822/2/71/pdf **File**

Recently, a number of peculiar flares have been reported, which demonstrate significant non-thermal particle signatures with a low, if any, thermal emission, that implies close association of the observed emission with the primary energy release/electron acceleration region. This paper presents a flare that appears a "cold" one at the impulsive phase, while displaying a delayed heating later on. Using HXR data from \kw, microwave observations by SSRT, RSTN, NoRH and NoRP, context observations, and 3D modeling, we study the energy release, particle acceleration and transport, and the relationships between the nonthermal and thermal signatures. The flaring process is found to involve interaction between a small and a big loop and the accelerated particles divided in roughly equal numbers between them. Precipitation of the electrons from the small loop produced only weak thermal response because the loop volume was small, while the electrons trapped in the big loop lost most of their energy in the coronal part of the loop, which resulted in the coronal plasma heating but no or only weak chromospheric evaporation, and thus unusually weak soft X-ray emission. Energy losses of fast electrons in the big tenuous loop were slow resulting in the observed delay of the plasma heating. We determined that the impulsively accelerated electron population had a beamed angular distribution in the direction of electric force along the magnetic field of the small loop. The accelerated particle transport in big loop was primarily mediated by turbulent waves like in the other reported cold flares. **March 10, 2002**

Validation Of The Coronal Thick Target Source Model

Gregory D. **Fleishman**, Yan Xu, Gelu N. Nita, Dale E. Gary

ApJ **816** 62 **2016**

http://arxiv.org/pdf/1511.06947v1.pdf

We present detailed 3D modeling of a dense, coronal thick target X-ray flare using the GX Simulator tool, photospheric magnetic measurements, and microwave imaging and spectroscopy data. The developed model offers a remarkable agreement between the synthesized and observed spectra and images in both X-ray and microwave domains, which validates the entire model. The flaring loop parameters are chosen to reproduce the emission measure, temperature, and the nonthermal electron distribution at low energies derived from the X-ray spectral fit, while the remaining parameters, unconstrained by the X-ray data, are selected such as to match the microwave images and total power spectra. The modeling suggests that the accelerated electrons are trapped in the coronal part of the flaring loop, but away from where the magnetic field is minimal, and, thus, demonstrates that the data are clearly inconsistent with electron magnetic trapping in the weak diffusion regime mediated by the Coulomb collisions. Thus, the modeling supports the interpretation of the coronal thick-target sources as sites of electron acceleration in flares and supplies us with a realistic 3D model with physical parameters of the acceleration region and flaring loop. April 12, 2002

Energy Partitions and Evolution in a Purely Thermal Solar Flare

Gregory D. **Fleishman**, Gelu M. Nita, Dale E. Gary

ApJ **2015**

This paper presents a solely thermal flare, which we detected in the microwave range from the thermal gyro- and free-free emission it produced. An advantage of analyzing thermal gyro emission is its unique ability to precisely yield the magnetic field in the radiating volume. When combined with observationally-deduced plasma density and temperature, these magnetic field measurements offer a straightforward way of tracking evolution of the magnetic and thermal energies in the flare. For the event described here, the magnetic energy density in the radio-emitting volume declines over the flare rise phase, then stays roughly constant during the extended peak phase, but recovers to the original level over the decay phase. At the stage where the magnetic energy density decreases, the thermal energy density increases; however, this increase is insufficient, by roughly an order of magnitude, to compensate for the magnetic energy

decrease. When the magnetic energy release is over, the source parameters come back to nearly their original values. We discuss possible scenarios to explain this behavior. **2001 Apr 15**

PROBING DYNAMICS OF ELECTRON ACCELERATION WITH RADIO AND X-RAY SPECTROSCOPY, IMAGING, AND TIMING IN THE 2002 APRIL 11 SOLAR FLARE
Gregory D. **Fleishman**1,2, Eduard P. Kontar3, Gelu M. Nita1, and Dale E. Gary
2013 ApJ 768 190
Based on detailed analysis of radio and X-ray observations of a flare on **2002 April 11** augmented by realistic three-dimensional modeling, we have identified a radio emission component produced directly at the flare acceleration region. This acceleration region radio component has distinctly different (1) spectrum, (2) light curves, (3) spatial location, and, thus, (4) physical parameters from those of the separately identified trapped or precipitating electron components. To derive evolution of physical parameters of the radio sources we apply forward fitting of the radio spectrum time sequence with the gyrosynchrotron source function with five to six free parameters. At the stage when the contribution from the acceleration region dominates the radio spectrum, the X-ray- and radio-derived electron energy spectral indices agree well with each other. During this time the maximum energy of the accelerated electron spectrum displays a monotonic increase with time from ~300 keV to ~2 MeV over roughly one minute duration indicative of an acceleration process in the form of growth of the power-law tail; the fast electron residence time in the acceleration region is about 2-4 s, which is much longer than the time of flight and so requires a strong diffusion mode there to inhibit free-streaming propagation. The acceleration region has a relatively strong magnetic field, B ~ 120 G, and a low thermal density, ne 2 × 109 cm–3. These acceleration region properties are consistent with a stochastic acceleration mechanism.

Stochastic Particle Acceleration by Helical Turbulence in Solar Flares
Gregory D. **Fleishman** and Igor N. Toptygin
MNRAS (March 1, **2013**) 429 (3): 2515-2526
https://academic.oup.com/mnras/article/429/3/2515/1008708
Flaring release of magnetic energy in solar corona is only possible if the magnetic field deviates from a potential one. We show that the linear MHD modes excited on top of the non-potential magnetic field possess a nonzero kinetic helicity. Accordingly, this necessarily results in a noticeable kinetic helicity of the turbulence, composed of these linear modes with various scales and random phases, generated at the flare site by the primary energy release, which may be important for many applications. In particular, a nonzero turbulence helicity has a potentially strong effect on the particle acceleration because the helical component of the turbulence induces a mean regular large-scale (DC) electric field capable of directly accelerating the charged particles in addition to the commonly considered stochastic turbulent electric field. In this paper, we derive the kinetic helicity density of the linear MHD modes excited on top of a twisted large-scale magnetic field, estimate the corresponding turbulence helicity and take its effect on stochastic particle acceleration by the turbulence into consideration; in particular, we compare this induced mean electric field with the electron and estimated effective ion Dreicer fields. We have discovered that this, so far missing but highly important, ingredient of the turbulence at the flare site can be responsible for the thermal-to-nonthermal energy partition in flares by controlling the process of particle extraction from the thermal pool and formation of the seed particle population to be then stochastically accelerated to higher energies. In addition, it is naturally consistent with such puzzling flare manifestations as spatial separation of electron and proton emission sites, electron beam formation, and enrichment of the accelerated particle population by ^3He and other rare ions.

Cosmic Electrodynamics. **Book**
Gregory D. **Fleishman** and Igor N. Toptygin
Astrophysics and Space Science Library; Springer NY, Vol. 388, 712 p. **2013**
https://link.springer.com/content/pdf/10.1007%2F978-1-4614-5782-4.pdf
https://link.springer.com/book/10.1007%2F978-1-4614-5782-4#toc

New Interactive Solar Flare Modeling and Advanced Radio Diagnostics Tools
Gregory D. **Fleishman**1,2, Gelu M. Nita1 and Dale E. Gary1
BBSO Preprint # 1478, **2011**
http://solar.njit.edu/preprints/fleishman1478.pdf
Advances in Plasma Astrophysics, Proceedings IAU Symposium No. 274, 2010
A. Bonanno, E. de Gouveia Dal Pino & A. Kosovichev, eds.
The coming years will see routine use of solar data of unprecedented spatial and spectral resolution, time cadence, and completeness in the wavelength domain. To capitalize on the soon to be available radio facilities such as the expanded

OVSA, SSRT and FASR, and the challenges they present in the visualization and synthesis of the multi-frequency datasets, we propose that realistic, sophisticated 3D active region and flare modeling is timely now and will be a forefront of coronal studies over the coming years. Here we summarize our 3D modeling efforts, aimed at forward fitting of imaging spectroscopy data, and describe currently available 3D modeling tools. We also discuss plans for future generalization of our modeling tools.

Acceleration without Heating
G. **Fleishman** and E. Kontar
RHESSI science Nugget, 13 June, **2011**
http://sprg.ssl.berkeley.edu/~tohban/wiki/index.php/Acceleration_without_Heating
In this Nugget we describe an extreme solar flare, in the sense that its physical properties deviate strikingly from the normal behavior: it appeared mainly as a hard X-ray and radio source, without the usual GOES-type soft X-ray source. The event was well-observed by RHESSI and radio observatories, specifically the Owens Valley Solar Array (OVSA) and Phoenix-2. The flare could have the IAU designator **SOL2002-07-30T17:37:30**; normally the time field would be the GOES peak time, but in this case there was only a tiny GOES X-ray peak (Ref. [0]). It is quite rare not to see soft X-ray counterparts for strong solar hard X-ray bursts such as this one

A COLD, TENUOUS SOLAR FLARE: ACCELERATION WITHOUT HEATING
Gregory D. **Fleishman**1,2, Eduard P. Kontar3, Gelu M. Nita1 and Dale E. Gary
2011 ApJ 731 L19**; File**
https://iopscience.iop.org/article/10.1088/2041-8205/731/1/L19/pdf
We report the observation of an unusual cold, tenuous solar flare, which reveals itself via numerous and prominent non-thermal manifestations, while lacking any noticeable thermal emission signature. RHESSI hard X-rays and 0.1-18 GHz radio data from OVSA and Phoenix-2 show copious electron acceleration (1035 electrons s-1 above 10 keV) typical for GOES M-class flares with electrons energies up to 100 keV, but GOES temperatures not exceeding 6.1 MK. The imaging, temporal, and spectral characteristics of the flare have led us to a firm conclusion that the bulk of the microwave continuum emission from this flare was produced directly in the acceleration region. The implications of this finding for the flaring energy release and particle acceleration are discussed. **30-Jul-2002**

Dynamic Magnetography of Solar Flaring Loops
Gregory D. **Fleishman**, Gelu M. Nita and Dale E. Gary
BBSO preprint #1396, June **2009;** Astrophysical Journal, 698:L183–L187, **2009**
We develop a practical forward fitting method based on the *SIMPLEX algorithm with shaking*, which allows the derivation of the magnetic field and other parameters along a solar flaring loop using microwave imaging spectroscopy of gyrosynchrotron emission. We illustrate the method using a model loop with spatially varying magnetic field, filled with uniform ambient density and an evenly distributed fast electron population with an isotropic, power-law energy distribution.

Broadband Quasi-periodic Radio and X-Ray Pulsations in a Solar Flare
Gregory D. **Fleishman**1,2, T. S. Bastian3, and Dale E. Gary1
2008 ApJ 684 1433
https://iopscience.iop.org/article/10.1086/589821/pdf
We describe microwave and hard X-ray observations of strong quasi-periodic pulsations from the GOES X1.3 solar flare on 2003 June 15. The radio observations were made jointly by the Owens Valley Solar Array (OVSA), the Nobeyama Polarimeter (NoRP), and the Nobeyama Radioheliograph (NoRH). Hard X-ray observations were made by RHESSI. Using Fourier analysis, we study the frequency- and energy-dependent oscillation periods, differential phase, and modulation amplitudes of the radio and X-ray pulsations. Focusing on the more complete radio observations, we also examine the modulation of the degree of circular polarization and of the radio spectral index. The observed properties of the oscillations are compared with those derived from two simple models for the radio emission. In particular, we explicitly fit the observed modulation amplitude data to the two competing models. The first model considers the effects of MHD oscillations on the radio emission. The second model considers the quasi-periodic injection of fast electrons. We demonstrate that quasi-periodic acceleration and injection of fast electrons is the more likely cause of the quasi-periodic oscillations observed in the radio and hard X-ray emission, which has important implications for particle acceleration and transport in the flaring sources.

Preface (to Solar and Stellar Flares)
L. **Fletcher** , P. Heinzel, L. van Driel-Gesztelyi, C. H. Mandrini, F. Fárník
Solar Phys. 290:3379–3381 **2015**

FLARE RIBBON ENERGETICS IN THE EARLY PHASE OF AN SDO FLARE

L. **Fletcher**1, I. G. Hannah1, H. S. Hudson1,3, and D. E. Innes

2013 ApJ 771 104

The sites of chromospheric excitation during solar flares are marked by extended extreme ultraviolet ribbons and hard X-ray (HXR) footpoints. The standard interpretation is that these are the result of heating and bremsstrahlung emission from non-thermal electrons precipitating from the corona. We examine this picture using multi-wavelength observations of the early phase of an M-class flare **SOL2010-08-07**T18:24. We aim to determine the properties of the heated plasma in the flare ribbons, and to understand the partition of the power input into radiative and conductive losses. Using GOES, SDO/EVE, SDO/AIA, and RHESSI, we measure the temperature, emission measure (EM), and differential emission measure of the flare ribbons, and deduce approximate density values. The non-thermal EM, and the collisional thick target energy input to the ribbons are obtained from RHESSI using standard methods. We deduce the existence of a substantial amount of plasma at 10 MK in the flare ribbons, during the pre-impulsive and early-impulsive phase of the flare. The average column EM of this hot component is a few times 1028 cm–5, and we can calculate that its predicted conductive losses dominate its measured radiative losses. If the power input to the hot ribbon plasma is due to collisional energy deposition by an electron beam from the corona then a low-energy cutoff of ~5 keV is necessary to balance the conductive losses, implying a very large electron energy content. Independent of the standard collisional thick-target electron beam interpretation, the observed non-thermal X-rays can be provided if one electron in 103-104 in the 10 MK (1 keV) ribbon plasma has an energy above 10 keV. We speculate that this could arise if a non-thermal tail is generated in the ribbon plasma which is being heated by other means, for example, by waves or turbulence.

An Observational Overview of Solar Flares **A Review**

L. **Fletcher**1, B. R. Dennis2, H. S. Hudson3, S. Krucker3, K. Phillips4, A. Veronig5, M. Battaglia1, L. Bone4, A. Caspi3, Q. Chen7 , P. Gallagher8, P. T. Grigis9, · H. Ji10,11, W. Liu2,12, R. O. Milligan2, and M. Temmer5,13,14

Space Sci. Rev., 159:19–106, **2011, File**

https://link.springer.com/content/pdf/10.1007/s11214-010-9701-8.pdf

We present an overview of solar flares and associated phenomena, drawing upon a wide range of observational data primarily from the *RHESSI* era. Following an introductory discussion and overview of the status of observational capabilities, the article is split into topical sections which deal with different areas of flare phenomena (footpoints and ribbons, coronal sources, relationship to coronal mass ejections) and their interconnections. We also discuss flare soft X-ray spectroscopy and the energetics of the process. The emphasis is to describe the observations from multiple points of view, while bearing in mind the modelsthat link them to each other and to theory. The present theoretical and observational understanding of solar flares is far from complete, so we conclude with a brief discussion of models, and a list of missing but important observations.

Impulsive Phase Flare Energy Transport by Large-Scale Alfven Waves and the Electron Acceleration Problem

L. **Fletcher** and H. S. Hudson

The Astrophysical Journal, Vol. 675, No. 2: 1645-1655.

http://www.journals.uchicago.edu/doi/pdf/10.1086/527044

The impulsive phase of a solar flare marks the epoch of rapid conversion of energy stored in the preflare coronal magnetic field. Hard X-ray observations imply that a substantial fraction of flare energy released during the impulsive phase is converted to the kinetic energy of mildly relativistic electrons (10–100 keV). The liberation of the magnetic free energy can occur as the coronal magnetic field reconfigures and relaxes following reconnection. We investigate a scenario in which products of the reconfiguration—large-scale Alfve´n wave pulses—transport the energy and the magnetic field changes rapidly through the corona to the lower atmosphere. This offers two possibilities for electron acceleration. First, in a coronal plasma with_ < m_e/m_p, the waves propagate as inertial Alfve´n waves. In the presence of strong spatial gradients, these generate field-aligned electric fields that can accelerate electrons to energies on the order of 10 keVand above, including by repeated interactions between electrons and wave fronts. Second, when they reflect and mode-convert in the chromosphere, a cascade to high wavenumbers may develop. This will also accelerate electrons by turbulence, in a medium with a locally high electron number density. This concept, which bridges MHDbased and particle-based views of a flare, provides an interpretation of the recently observed rapid variations of the line-of-sight component of the photospheric magnetic field across the flare impulsive phase, and offers solutions to some perplexing flare problems, such as the flare ‘‘number problem’’ of finding and resupplying sufficient electrons to explain the impulsive-phase hard X-ray emission.

A TRACE White Light and RHESSI Hard X-Ray Study of Flare Energetics
L. **Fletcher**, I. G. Hannah, H. S. Hudson, and T. R. Metcalf
The Astrophysical Journal,Volume 656, Number 2,Page 1187, **2007**
http://www.journals.uchicago.edu/cgi-bin/resolve?ApJ70092

Forecasting Solar Flares Using Magnetogram-based Predictors and Machine Learning

Kostas **Florios**, Ioannis Kontogiannis, Sung-Hong Park, Jordan A. Guerra, Federico Benvenuto, D. Shaun Bloomfield, Manolis K. Georgoulis
Solar Phys. 293:28 **2018**
https://arxiv.org/pdf/1801.05744.pdf
https://link.springer.com/content/pdf/10.1007%2Fs11207-018-1250-4.pdf
We propose a forecasting approach for solar flares based on data from Solar Cycle 24, taken by the Helioseismic and Magnetic Imager (HMI) on board the Solar Dynamics Observatory (SDO) mission. In particular, we use the Space-weather HMI Active Region Patches (SHARP) product that facilitates cut-out magnetograms of solar active regions (AR) in the Sun in near-real-time (NRT), taken over a five-year interval (2012 - 2016). Our approach utilizes a set of thirteen predictors, which are not included in the SHARP metadata, extracted from line-of-sight and vector photospheric magnetograms. We exploit several Machine Learning (ML) and Conventional Statistics techniques to predict flares of peak magnitude >M1 and >C1, within a 24 h forecast window. The ML methods used are multi-layer perceptrons (MLP), support vector machines (SVM) and random forests (RF). We conclude that random forests could be the prediction technique of choice for our sample, with the second best method being multi-layer perceptrons, subject to an entropy objective function. A Monte Carlo simulation showed that the best performing method gives accuracy ACC=0.93(0.00), true skill statistic TSS=0.74(0.02) and Heidke skill score HSS=0.49(0.01) for >M1 flare prediction with probability threshold 15% and ACC=0.84(0.00), TSS=0.60(0.01) and HSS=0.59(0.01) for >C1 flare prediction with probability threshold 35%.
CESRA #95 **2018** http://hmi.stanford.edu/hminuggets/?p=2423

Statistical study of extreme-ultraviolet nanoflares in the quiet-Sun transition region

A. **Fludra**
A&A 674, A131 (**2023**)
https://www.aanda.org/articles/aa/pdf/2023/06/aa45306-22.pdf
Aims. We carried out a large statistical study of ubiquitous small-scale extreme-ultraviolet (EUV) brightenings in the nanoflare energy range in the quiet-Sun transition region to derive their properties, estimate their contribution to the heating of the solar atmosphere, and compare their numbers to the coronal events published in the literature. This is the first study of this magnitude at temperatures of about 2 × 105 K.
Methods. We applied a numerical method for detecting small-scale transient events in long 1D image time series. We used data recorded by the SOHO Coronal Diagnostic Spectrometer (CDS) in the transition region line O V 62.97 nm (220 000 K) and analysed 702 h of sit-and-stare time series obtained with a cadence of 15.6 s and 50 h with a cadence of 20.5 s in different quiet-Sun areas at a fixed slit position. These data span from 1996 to 2011. This analysis used a different method and a vastly larger number of data than the previous high-cadence CDS study of small events.
Results. We derive histograms of event durations, of the rise and decay time, of the peak intensity and thermal energy, and we obtain a continuous spectrum of their distributions for 117 000 events, spanning the nanoflare energy range with a linear spatial extent of 2−10 arcsec and with durations between 45 s and 40 min. The event peak intensity varied by a factor of 60. We demonstrated that all categories of small-scale events in the transition region are part of a continuum of activity. We obtain a total event rate of 460 s−1 on the entire surface of the Sun. This is more than four times greater than the coronal rate. The maximum value of the duration distribution occurs at 235 s, which is twice the duration of the coronal events. The decay time and rise time difference seen from the shortest to the longest events is symmetrical. We find two event populations: the power law of the smallest events that are confined to one pixel is far steeper for the peak count rates (index of −4.1) and thermal energy (index of −7) than the power law for combined larger events that extend over two or more pixels along the slit (thermal energy power-law index from −2.1 to −3.4).
Conclusions. The power law of the thermal energy of the smallest events, extrapolated to lower energies (picoflares), may provide a huge amount of energy for heating the entire transition region plasma at temperatures of about 220 000 K. An extrapolation of only the flatter power law of the larger events can also account for the entire observed emission.

Reconnection in the Post-Impulsive Phase of Solar Flares

Terry G. **Forbes**, Daniel B. Seaton, Katharine K. Reeves
ApJ **858** 70 **2018**
https://arxiv.org/pdf/1804.00324.pdf
https://iopscience.iop.org/article/10.3847/1538-4357/aabad4/pdf

Using a recently developed analytical procedure, we determine the rate of magnetic reconnection in the "standard" model of eruptive solar flares. During the late phase, the neutral line is located near the lower tip of the reconnection current sheet, and the upper region of the current sheet is bifurcated into a pair of Petschek-type shocks. Despite the presence of these shocks, the reconnection rate remains slow if the resistivity is uniform and the flow is laminar. Fast reconnection is achieved only if there is some additional mechanism that can shorten the length of the diffusion region at the neutral line. Observations of plasma flows by the X-Ray Telescope (XRT) on Hinode imply that the diffusion region is in fact quite short. Two possible mechanisms for reducing the length of the diffusion region are localized resistivity and MHD turbulence.

Solar Flare Models

Forbes, T.G.

"Encyclopedia of Astronomy and Astrophysics, Edited by Paul Murdin, article id. 2295. Bristol: Institute of Physics Publishing, **2001**. http://eaa.iop.org/abstract/0333750888/2295"

Even though FLARES have been observed on the Sun for nearly 150 years, their origin remains a mystery. At the present time there is no generally accepted model which explains why they occur, but there do exist models which successfully explain certain limited aspects such as the formation of flare loops and ribbons. Before discussing particular models, we review the constraints imposed on models ...

Reconnection and Field Line Shrinkage in Solar Flares

Forbes, T.G., Acton, L.W.:

1996, Astrophys. J. 459, 330

https://ui.adsabs.harvard.edu/link_gateway/1996ApJ...459..330F/ADS_PDF

We use images of flare loops taken by the Soft X-ray Telescope (SXT) on Yohkoh to estimate the decrease in height that open field lines undergo after they have reconnected to form closed loops. Following previous practice, we refer to this decrease as field line shrinkage and assume that intensity structures trace out the field lines. For this study, we examine two long-duration events near the limb which have flare loops that continually grow with time. The shrinkage is determined by comparing the height of a field line when it lies at the outermost edge of the flare loop system with the height it has later on when it lies at the innermost edge. We find that the field lines shrink by about 20% of their initial height in one flare and by about 32% in the other. These values are within 5% of the shrinkage predicted by a simple model of the reconnecting field which assumes that the field is potential everywhere except for a current sheet extending upward from the top of the loops. Numerical integration of the model density along the line of sight implies that most of the discrepancy between the observations and the theory is due to projection effects which occur when an arcade of loops is viewed at an arbitrary angle. Both flares have bright regions at the top of the loops, but in one flare the lower part of the region is cooler and denser than the rest of the loop, while in the other flare it is not. Consideration of the mapping of the bright regions to the footpoint of the loops implies that the cool region is formed by a thermal instability downstream of a reconnection outflow in the uppermost part of the loop. The absence of a cool, dense region in the other flare may be caused by the fact that it is a very weak event with temperatures and densities too low to trigger a thermal instability. **21 Feb 1992, 22-23 Apr 1993**

FROM LARGE-SCALE LOOPS TO THE SITES OF DENSE FLARING LOOPS: PREFERENTIAL CONDITIONS FOR LONG-PERIOD PULSATIONS IN SOLAR FLARES

C. **Foullon** 1, L. Fletcher 2, I. G. Hannah 2, E. Verwichte 1, B. Cecconi 3, V. M. Nakariakov 1, K. J. H. Phillips 4 and B. L. Tan

2010 ApJ 719 151

Long-period quasi-periodic pulsations (QPPs) of solar flares are a class apart from shorter period events. By involving an external resonator, the mechanism they call upon differs from traditional QPP models, but has wider applications. We present a multi-wavelength analysis of spatially resolved QPPs, with periods around 10 minutes, observed in the X-ray spectrum primarily at energies between 3 and 25 keV. Complementary observations obtained in Hα and radio emission in the kHz to GHz frequency range, together with an analysis of the X-ray plasma properties provide a comprehensive picture that is consistent with a dense flaring loop subject to periodic energization and thermalization. The QPPs obtained in Hα and type III radio bursts, with similar periods as the QPPs in soft X-rays, have the longest periods ever reported for those types of data sets. We also report 1-2 GHz radio emission, concurrent with but unrestricted to the QPP time intervals, which is multi-structured at regularly separated narrowband frequencies and modulated with ~18 minute periods. This radio emission can be attributed to the presence of multiple "quiet" large-scale loops in the background corona. Large scale but shorter inner loops below may act as preferential resonators for the QPPs. The observations support interpretations consistent with both inner and outer loops subject to fast kink magnetohydrodynamic waves. Finally, X-ray imaging indicates the presence of double coronal sources in the flaring sites, which could be the particular signatures of the magnetically linked inner loops. We discuss the preferential conditions and the driving mechanisms causing the repeated flaring.

Moreton and EUV Waves Associated with an X1.0 Flare and CME Ejection

Carlos **Francile**, Fernando M. López, Hebe Cremades, Cristina H. Mandrini, María Luisa Luoni, David M. Long
Solar Phys. Volume 291, Issue 11, pp 3217–3249 **2016 File**
A Moreton wave was detected in active region (AR) 12017 on **29 March 2014** with very high cadence with the H-Alpha Solar Telescope for Argentina (HASTA) in association with an X1.0 flare (SOL2014-03-29T17:48). Several other phenomena took place in connection with this event, such as low-coronal waves and a coronal mass ejection (CME). We analyze the association between the Moreton wave and the EUV signatures observed with the Atmospheric Imaging Assembly onboard the Solar Dynamics Observatory. These include their low-coronal surface-imprint, and the signatures of the full wave and shock dome propagating outward in the corona. We also study their relation to the white-light CME. We perform a kinematic analysis by tracking the wavefronts in several directions. This analysis reveals a high-directional dependence of accelerations and speeds determined from data at various wavelengths. We speculate that a region of open magnetic field lines northward of our defined radiant point sets favorable conditions for the propagation of a coronal magnetohydrodynamic shock in this direction. The hypothesis that the Moreton wavefront is produced by a coronal shock-wave that pushes the chromosphere downward is supported by the high compression ratio in that region. Furthermore, we propose a 3D geometrical model to explain the observed wavefronts as the chromospheric and low-coronal traces of an expanding and outward-traveling bubble intersecting the Sun. The results of the model are in agreement with the coronal shock-wave being generated by a 3D piston that expands at the speed of the associated rising filament. The piston is attributed to the fast ejection of the filament–CME ensemble, which is also consistent with the good match between the speed profiles of the low-coronal and white-light shock waves.

Multimodal Flare Forecasting with Deep Learning

Grégoire **Francisco**, Sabrina Guastavino, Teresa Barata, João Fernandes, Dario Del Moro
2024
https://arxiv.org/pdf/2410.16116
Solar flare forecasting mainly relies on photospheric magnetograms and associated physical features to predict forthcoming flares. However, it is believed that flare initiation mechanisms often originate in the chromosphere and the lower corona. In this study, we employ deep learning as a purely data-driven approach to compare the predictive capabilities of chromospheric and coronal UV and EUV emissions across different wavelengths with those of photospheric line-of-sight magnetograms. Our findings indicate that individual EUV wavelengths can provide discriminatory power comparable or better to that of line-of-sight magnetograms. Moreover, we identify simple multimodal neural network architectures that consistently outperform single-input models, showing complementarity between the flare precursors that can be extracted from the distinct layers of the solar atmosphere. To mitigate potential biases from known misattributions in Active Region flare catalogs, our models are trained and evaluated using full-disk images and a comprehensive flare event catalog at the full-disk level. We introduce a deep-learning architecture suited for extracting temporal features from full-disk videos.

Quantifying Turbulent Dynamics Found within the Plasma Sheets of Multiple Solar Flares

Michael S. **Freed**1,2 and David E. McKenzie1,3
2018 ApJ 866 29
http://sci-hub.tw/http://iopscience.iop.org/article/10.3847/1538-4357/aadee4/meta
It is vital to our understanding of solar flares that we discern how turbulent motion can affect the magnetic reconnection process. The objective of this study is to quantify the velocity and vorticity structures inherent in the observed motions found in a plasma sheet above arcades during a solar flare. The most noticeable features in these plasma sheets are the supra-arcade downflows (SADs) that sporadically enter the field of view. This work is also attempting to ascertain what effect these SADs have on the flow of plasma at different length scales. Contrast-enhanced images from five flares observed with the Solar Dynamics Observatory/Atmospheric Imaging Assembly (SDO/AIA) and Transition Region and Coronal Explorer (TRACE) were used to construct velocity maps—in the plane of the sky—via a Fourier local correlation tracking program. Power-law indices (α) were calculated from the power spectral densities (PSDs) associated with the intensity, kinetic energy, and enstrophy structures of these plasma sheets. Velocity oscillations are observed to be approximately three times stronger for velocities that are perpendicular (V_ϕ) instead of parallel (V_ρ) to the magnetic field's direction. Four of the flares observed were used for producing the following plasma sheet properties: kinetic energy PSD indices with only V_ρ were $-0.15 \leq \alpha_\rho \leq 0.08$, kinetic energy PSD indices with only V_ϕ were $-1.59 \leq \alpha_\phi \leq -1.46$, kinetic energy PSD indices with both velocities were $-0.89 \leq \alpha \leq -0.83$, enstrophy PSD indices were $0.87 \leq \alpha \leq 0.97$, kinetic energy density was 16.6 km2s−2 ≤ ϵ ≤ 60.0 km2 s−2, and enstrophy density was 1.2×10^{-6} s−2 ≤ ω ≤ 2.8×10^{-6} s−2. **2002-04-21, 2011 October 22, 2012-01-27, 2012-05-17, 2013-05-22**

A Record-Setting CMEless Flare

Sam **Freeland** and Greg Slater.
RHESSI_Science_Nuggets, No. 239, Oct **2014**
http://sprg.ssl.berkeley.edu/~tohban/wiki/index.php/RHESSI_Science_Nuggets

Active region 2192 has produced many major flares, but none with CMEs yet.

The Slowest Flare

Sam **Freeland** and Hugh Hudson:
RHESSI_Science_Nuggets, No. 180, July **2012**
http://sprg.ssl.berkeley.edu/~tohban/wiki/index.php/RHESSI_Science_Nuggets
SOL2012-07-17 had the slowest GOES rise time for any major flare (M or X) since 1995.
A flare with an exceptionally slow rise phase, more than 5 hours in GOES 1-8 A soft X-rays.

An overview of HMI off-disk flare observations

Dennis **Fremstad**, Juan Camilo Guevara Gómez, Hugh Hudson, Juan Carlos Martínez Oliveros
A&A 672, A32 **2023**
https://arxiv.org/pdf/2302.13632.pdf
https://www.aanda.org/articles/aa/pdf/2023/04/aa45788-22.pdf
Context: White-light continuum observations of solar flares often have coronal counterparts, including the classical "white-light prominence" (WLP) phenomenon. **Aims:** Coronal emissions by flares, seen in white-light continuum, have only rarely been reported previously. We seek to use modern data to understand the morphology of WLP events. **Methods**: We have identified a set of 14 examples of WLP detected by the HMI (Heliospheric and Magnetic Imager) experiment on board SDO (the Solar Dynamics Observatory satellite), using a new on-line catalogue covering 2011-2017. These invariably accompanied white-light flares (WLF) emission from the lower atmosphere by flares near the limb, as identified by hard X-ray images from RHESSI (the Reuven Ramaty High Energy Spectroscopic Imager). HMI provides full Stokes information, and we have used the linear polarisations (Q and U) to distinguish Thomson scattering from cool material, following the analysis pioneered by Saint-Hilaire et al. (2014). **Results**: The event morphologies fit roughly into three categories: Ejection, Loop, and Spike, but many events show multiple phenomena. **Conclusions**: The coronal white-light continuum, observed by HMI analogously to the observations made by a coronagraph, detects many examples of coronal emission and dynamics. Using the Stokes linear polarisation, we estimate the masses of hot coronal plasma in 11 of the 14 events and find them to be similar to typical CME masses, but not exceeding 1015 g. We note that the HMI observations do not occult the bright solar disk and were not designed for coronal observations, resulting in relatively low signal-to-noise ratios. We therefore believe that future such observations with better optimisation will be even more fruitful. **2012-11-20, 2013-05-13, 2015-10-02, 2017-09-10**
Table 1. On-disk flare kernel parameters

X-ray and Spectral UV Observations of Periodic Pulsations in a Solar Flare Fan/Looptop

Ryan J. **French**, Laura A. Hayes, Maria D. Kazachenko, Katharine K. Reeves, Chengcai Shen, Juraj Lörinčík
ApJ **2024**
https://arxiv.org/pdf/2411.02634
We present simultaneous X-ray and spectral ultraviolet (UV) observations of strikingly-coherent oscillations in emission from a coronal looptop and fan structure, during the impulsive phase of a long-duration M-class solar flare. The 50 s oscillations are observed near in-phase by Solar Orbiter/STIX, GOES, and IRIS Fe XXI intensity, Doppler and non-thermal velocity. For over 5 minutes of their approximate 35 minute duration, the oscillations are so periodic (2-sigma above the power law background), that they are better described as 'periodic pulsations' than the more-widely documented 'quasi-periodic pulsations' often observed during solar flares. By combining time-series analysis of the the multi-instrument datasets with comparison to MHD simulations, we attribute the oscillations to the magnetic tuning fork in the flare looptop-fan region, and betatron acceleration within the lower-altitude flare loops. These interpretations are possible due to the introduced 'Sliding Raster Method' (SliRM) for analysis of slit spectrometer (e.g. IRIS) raster data, to increase the temporal cadence of the observations at the expense of spatial information. **August 29 2022**

Doppler Signature of a Possible Termination Shock in an Off-Limb Solar Flare

Ryan J. **French**, Sijie Yu, Bin Chen, Chengcai Shen, Sarah A. Matthews
MNRAS **2024**
https://arxiv.org/pdf/2402.04445.pdf
We report striking Doppler velocity gradients observed during the well-observed **September 10th 2017** solar flare, and argue that they are consistent with the presence of an above-the-looptop termination shock beneath the flare current sheet. Observations from the Hinode Extreme-ultraviolet Imaging Spectrometer (EIS) measure plasma sheet Doppler shifts up to 35 km/s during the late-phase of the event. By comparing these line-of-sight flows with plane-of-sky measurements, we calculate total velocity downflows of 200+ km/s, orientated 6-10° out of the plane of sky. The observed velocities drop rapidly at the base of the hot plasma sheet seen in extreme ultraviolet, consistent with simulated velocity profiles predicted by our 2.5D magnetohydrodynamics model that features a termination shock at the same location. Finally, the striking velocity deceleration aligns spatially with the suppression of Fe XXIV non-thermal velocities, and a 35--50 keV hard X-ray looptop source observed by the Reuven Ramaty High Energy Solar

Spectroscopic Imager (RHESSI). Together, these observations are consistent with the presence of a possible termination shock within the X8.2-class solar flare.

Probing Current Sheet Instabilities from Flare Ribbon Dynamics

Ryan J. **French**, Sarah A. Matthews, I. Jonathan Rae, Andrew W. Smith
ApJ **922** 117 **2021**
https://arxiv.org/pdf/2109.03753.pdf
https://iopscience.iop.org/article/10.3847/1538-4357/ac256f/pdf
https://doi.org/10.3847/1538-4357/ac256f
The presence of current sheet instabilities, such as the tearing mode instability, are needed to account for the observed rate of energy release in solar flares. Insights into these current sheet dynamics can be revealed by the behaviour of flare ribbon substructure, as magnetic reconnection accelerates particles down newly reconnected field lines into the chromosphere to mark the flare footpoints. Behaviour in the ribbons can therefore be used to probe processes occurring in the current sheet.
In this study, we use high-cadence (1.7 s) IRIS Slit Jaw Imager observations to probe for the growth and evolution of key spatial scales along the flare ribbons - resulting from dynamics across the current sheet of a small solar flare on **December 6th 2016**. Combining analysis of spatial scale growth with Si IV non-thermal velocities, we piece together a timeline of flare onset for this confined event, and provide evidence of the tearing-mode instability triggering a cascade and inverse cascade towards a power spectrum consistent with plasma turbulence.
IRIS nugget Mar **2022** https://iris.lmsal.com/nugget

Dynamics of Late-Stage Reconnection in the 2017 September 10 Solar Flare

Ryan J. **French**, Sarah A. Matthews, Lidia van Driel-Gesztelyi, David M. Long, Philip G. Judge
ApJ **900** 192 **2020**
https://arxiv.org/pdf/2007.13377.pdf **File**
https://doi.org/10.3847/1538-4357/aba94b
In this multi-instrument paper, we search for evidence of sustained magnetic reconnection far beyond the impulsive phase of the X8.2-class solar flare on 2017 September 10. Using Hinode/EIS, CoMP, SDO/AIA, K-Cor, Hinode/XRT, RHESSI, and IRIS, we study the late-stage evolution of the flare dynamics and topology, comparing signatures of reconnection with those expected from the standard solar flare model. Examining previously unpublished EIS data, we present the evolution of non-thermal velocity and temperature within the famous plasma sheet structure, for the first four hours of the flare's duration. On even longer time scales, we use Differential Emission Measures and polarization data to study the longevity of the flare's plasma sheet and cusp structure, discovering that the plasma sheet is still visible in CoMP linear polarization observations on 2017 September 11, long after its last appearance in EUV. We deduce that magnetic reconnection of some form is still ongoing at this time - 27 hours after flare onset.
Hinode/EIS Nuggets Sep **2020** http://solarb.mssl.ucl.ac.uk/SolarB/nuggets/nugget_2020sep.jsp

Spectropolarimetric Insight into Plasma-Sheet Dynamics of a Solar Flare

Ryan J. **French**, Philip G. Judge, Sarah A. Matthews, Lidia van Driel-Gesztelyi
ApJL **887** L34 **2019**
https://arxiv.org/pdf/1911.12666.pdf
https://doi.org/10.3847/2041-8213/ab5d34
https://iopscience.iop.org/article/10.3847/2041-8213/ab5d34/pdf
We examine spectropolarimetric data from the CoMP instrument, acquired during the evolution of the **September 10th 2017** X8.2 solar flare on the western solar limb. CoMP captured linearly polarized light from two emission lines of Fe XIII at 1074.7 and 1079.8 nm, from 1.03 to 1.5 solar radii. We focus here on the hot plasma-sheet lying above the bright flare loops and beneath the ejected CME. The polarization has a striking and coherent spatial structure, with unexpectedly small polarization aligned with the plasma-sheet. By elimination, we find that small-scale magnetic field structure is needed to cause such significant depolarization, and suggest that plasmoid formation during reconnection (associated with the tearing mode instability) creates magnetic structure on scales below instrument resolution of 6 Mm. We conclude that polarization measurements with new coronagraphs, such as the upcoming DKIST, will further enhance our understanding of magnetic reconnection and development of turbulence in the solar corona. **2017-09-10**
RHESSI Science Nuggets #365 Dec **2019**
http://sprg.ssl.berkeley.edu/~tohban/wiki/index.php/Spectropolarimetric_Insight_into_Plasma-Sheet_Dynamics_of_a_Solar_Flare

Evidence from Hard X-Rays for Two-Stage Particle Acceleration in a Solar Flare

Frost, K. J. ; Dennis, B. R.
Astrophysical Journal, vol. 165, p.655, May **1971**
https://articles.adsabs.harvard.edu/pdf/1971ApJ...165..655F

A solar X-ray burst which evolves in time through two nonthermal phases is presented. The burst is considered to be bremostrablung from electrons accelerated in two stages in the solar atmosphere In the first stage, acceleration effectively to 100 keV occurs, perhaps by an induced electric field; in the second stage, the acceleration to higher energies could occur by a mechanism operating in a shock front. **1969 March 30**

Data-constrained MHD Simulation of a Multi-ribbon Flare Corresponding to a Successful and a Confined Eruption

Wentai **Fu**1,2, Yang Guo1,2, Mingde Ding1,2, Ze Zhong3, and Ye Qiu1,2
2023 ApJ 944 179
https://iopscience.iop.org/article/10.3847/1538-4357/acb6fb/pdf
The formation and eruption mechanisms of multi-ribbon flares are extremely complicated, especially when the flare is associated with homologous eruptions in the same region. In this paper, we investigate such an event, corresponding to a successful eruption and a confined eruption. This is an M7.1 flare, starting at 12:33 UT on **2011 September 24** in active region NOAA 11302. We obtain the coronal magnetic configuration for this region, using a nonlinear force-free field extrapolation based on the photospheric magnetogram at 12:00 UT. Taking this as the initial condition, we perform a data-constrained MHD simulation to study the evolution of the magnetic topology for this region. We analyze the magnetic null points and the 3D squashing degree for this region, indicating the existence of three flux ropes and two spine–fan structures. The model reproduces the rising processes of the two flux ropes, which form two homologous eruptions consistent with the observations as shown in 94 Å: a large-scale successful eruption that is followed by a small-scale confined eruption. By analyzing the magnetic configuration, the Lorentz force, and the decay index, we find that the torus instability plays an important role in driving the successful eruption of the large flux rope. The magnetic reconnection above the medium flux rope changes the direction of the overlying magnetic field, which provides a downward component of the Lorentz force to confine the eruption of the medium flux rope.

Active Region Emergence and Remote Flares

Yixing **Fu**, Brian T. Welsch
Solar Phys. Vol. 291, Issue 2 **2016**
http://arxiv.org/pdf/1504.06633v1.pdf
We study the effect of new emerging solar active regions on the large-scale magnetic environment of existing regions. We first present a theoretical approach to quantify the "interaction energy" between new and pre-existing regions as the difference between (i) the summed magnetic energies of their individual potential fields and (ii) the energy of their superposed potential fields. We expect that this interaction energy can, depending upon the relative arrangements of newly emerged and pre-existing magnetic flux, indicate the existence of "topological" free magnetic energy in the global coronal field that is independent of any "internal" free magnetic energy due to coronal electric currents flowing within the newly emerged and pre-existing flux systems. We then examine the interaction energy in two well-studied cases of flux emergence, but find that the predicted energetic perturbation is relatively small compared to energies released in large solar flares. Next, we present an observational study on the influence of the emergence of new active regions on flare statistics in pre-existing active regions, using NOAA's Solar Region Summary and GOES flare databases. As part of an effort to precisely determine the emergence time of active regions in a large event sample, we find that emergence in about half of these regions exhibits a two-stage behavior, with an initial gradual phase followed by a more rapid phase. Regarding flaring, we find that newly emerging regions produce a significant increase in the occurrence rate of X- and M-class flares in pre-existing regions. Given the relative weakness of the interaction energy, this effect suggests that perturbations in the large-scale magnetic field, such as topology changes invoked the "breakout" model of coronal mass ejections, might play a significant role in the occurrence of some flares.
25-30 Oct 2003, 11-15 Feb 2011

Magnetic Evolution of an Active Region Producing Successive Flares and Confined Eruptions

Marcelo López **Fuentes**, Mariano Poisson, Cristina H. Mandrini
Solar Phys. **299**, 52 **2024**
https://arxiv.org/pdf/2404.10517.pdf
https://doi.org/10.1007/s11207-024-02298-8
We analyze the magnetic evolution of solar active region (AR) NOAA 11476 that, between **9 and 10 May 2012**, produced a series of surge-type eruptions accompanied by GOES X-ray class M flares. Using force-free models of the AR coronal structure and observations in several wavelengths, in previous works we studied the detailed evolution of those eruptions, relating them to the characteristic magnetic topology of the AR and reconstructing the involved reconnection scheme. We found that the eruptions were due to the ejection of minifilaments, which were recurrently ejected and reformed at the polarity inversion line of a bipole that emerged in the middle of the positive main AR magnetic polarity. The bipole was observed to rotate for several tens of hours before the events. In this article we analyze, for the full AR and the rotating bipole, the evolution of a series of magnetic parameters computed using the Helioseismic and Magnetic Imager (HMI) vector magnetograms. We combine this analysis with estimations of the injection of magnetic energy and helicity obtained using the Differential Affine Velocity Estimator for Vector

Magnetograms (DAVE4VM) method that determines, from vector magnetograms, the affine velocity field constrained by the induction equation. From our results, we conclude that the bipole rotation was the main driver that provided the magnetic energy and helicity involved in the minifilament destabilizations and ejections. The results also suggest that the observed rotation is probably due to the emergence of a kinked magnetic flux rope with negative writhe helicity.

The effect of nanoflare flows on EUV spectral lines

Marcelo López **Fuentes**, James A. Klimchuk
ApJ **2022**
https://arxiv.org/pdf/2210.01896.pdf
The nanoflare model of coronal heating is one of the most successful scenarios to explain, within a single framework, the diverse set of coronal observations available with the present instrument resolutions. The model is based on the idea that the coronal structure is formed by elementary magnetic strands which are tangled and twisted by the displacement of their photospheric footpoints by convective motions. These displacements inject magnetic stress between neighbor strands that promotes current sheet formation, reconnection, plasma heating, and possibly also particle acceleration. Among other features, the model predicts the ubiquitous presence of plasma flows at different temperatures. These flows should, in principle, produce measurable effects on observed spectral lines in the form of Doppler-shifts, line asymmetries and non-thermal broadenings. In this work we use a Two-Dimensional Cellular Automaton Model (2DCAM) developed in previous works, in combination with the Enthalpy Based Thermal Evolution of Loops (EBTEL) model, to analyze the effect of nanoflare heating on a set of known EUV spectral lines. We find that the complex combination of the emission from plasmas at different temperatures, densities and velocities, in simultaneously evolving unresolved strands, produces characteristic properties in the constructed synthetic lines, such as Doppler-shifts and non-thermal velocities up to tens of km s−1 for the higher analyzed temperatures. Our results might prove useful to guide future modeling and observations, in particular, regarding the new generation of proposed instruments designed to diagnose plasmas in the 5 to 10 MK temperature range.

A nanoflare based cellular automaton model and the observed properties of the coronal plasma

Marcelo López **Fuentes**, James A. Klimchuk
ApJ 828 86 **2016**
http://arxiv.org/pdf/1607.03917v1.pdf
We use the cellular automaton model described in L\'opez Fuentes \& Klimchuk (2015, ApJ, 799, 128) to study the evolution of coronal loop plasmas. The model, based on the idea of a critical misalignment angle in tangled magnetic fields, produces nanoflares of varying frequency with respect to the plasma cooling time. We compare the results of the model with active region (AR) observations obtained with the Hinode/XRT and SDO/AIA instruments. The comparison is based on the statistical properties of synthetic and observed loop lightcurves. Our results show that the model reproduces the main observational characteristics of the evolution of the plasma in AR coronal loops. The typical intensity fluctuations have an amplitude of 10 to 15\% both for the model and the observations. The sign of the skewness of the intensity distributions indicates the presence of cooling plasma in the loops. We also study the emission measure (EM) distribution predicted by the model and obtain slopes in log(EM) versus log(T) between 2.7 and 4.3, in agreement with published observational values. **2011 January 18**

Two-dimensional Cellular Automaton Model for the Evolution of Active Region Coronal Plasmas

Marcelo López **Fuentes**1,3 and James A. Klimchuk
2015 ApJ 799 128
http://arxiv.org/pdf/1607.03883v1.pdf
We study a two-dimensional cellular automaton (CA) model for the evolution of coronal loop plasmas. The model is based on the idea that coronal loops are made of elementary magnetic strands that are tangled and stressed by the displacement of their footpoints by photospheric motions. The magnetic stress accumulated between neighbor strands is released in sudden reconnection events or nanoflares that heat the plasma. We combine the CA model with the Enthalpy Based Thermal Evolution of Loops model to compute the response of the plasma to the heating events. Using the known response of the X-Ray Telescope on board Hinode, we also obtain synthetic data. The model obeys easy-to-understand scaling laws relating the output (nanoflare energy, temperature, density, intensity) to the input parameters (field strength, strand length, critical misalignment angle). The nanoflares have a power-law distribution with a universal slope of –2.5, independent of the input parameters. The repetition frequency of nanoflares, expressed in terms of the plasma cooling time, increases with strand length. We discuss the implications of our results for the problem of heating and evolution of active region coronal plasmas.

Magnetic Twist and Writhe of Active Regions: On the Origin of Deformed Flux Tubes

M. López **Fuentes**, P. Démoulin, C.H. Mandrini, A.A. Pevtsov, L. van Driel-Gesztelyi
A&A, **201**4
http://arxiv.org/pdf/1411.5626v1.pdf
We study the long term evolution of a set of 22 bipolar active regions (ARs) in which the main photospheric polarities are seen to rotate one around the other during several solar rotations. We first show that differential rotation is not at the origin of this large change in the tilt angle. A possible origin of this distortion is the nonlinear development of a kink-instability at the base of the convective zone; this would imply the formation of a non-planar flux tube which, while emerging across the photosphere, would show a rotation of its photospheric polarities as observed. A characteristic of the flux tubes deformed by this mechanism is that their magnetic twist and writhe should have the same sign. From the observed evolution of the tilt of the bipoles, we derive the sign of the writhe of the flux tube forming each AR; while we compute the sign of the twist from transverse field measurements. Comparing the handedness of the magnetic twist and writhe, we find that the presence of kink-unstable flux tubes is coherent with no more than 35\% of the 20 cases for which the sign of the twist can be unambiguously determined. Since at most only a fraction of the tilt evolution can be explained by this process, we discuss the role that other mechanisms may play in the inferred deformation. We find that 36\% of the 22 cases may result from the action of the Coriolis force as the flux tube travels through the convection zone. Furthermore, because several bipoles overpass in their rotation the mean toroidal (East-West) direction or rotate away from it, we propose that a possible explanation for the deformation of all these flux tubes may lie in the interaction with large-scale vortical motions of the plasma in the convection zone, including also photospheric or shallow sub-photospheric large scale flows. **Tables**

Electromagnetic Turbulence in the Electron Current Layer to Drive Magnetic Reconnection

Keizo **Fujimoto**1,2 and Richard D. Sydora3
2021 ApJL 909 L15
https://iopscience.iop.org/article/10.3847/2041-8213/abe877/pdf
https://doi.org/10.3847/2041-8213/abe877
Magnetic reconnection is a natural energy converter that can have a significant impact on global processes in space, astrophysics, and fusion plasmas. Macroscopic modeling of reconnection is crucial in understanding the global responses to local kinetic processes. The key issue in developing the reconnection model is the description of the magnetic dissipation around the x-line to drive reconnection. In collisionless plasma, the dissipation can be generated by plasma turbulence through wave–particle interactions. However, the mechanisms to yield turbulence and dissipation in the reconnection current layer are currently poorly understood. In this study, we show, using three-dimensional particle-in-cell simulations, that the electron Kelvin–Helmholtz instability plays a primary role in driving intense electromagnetic turbulence leading to the dissipation and electron heating. We find that the ions hardly react to the turbulence, which indicates that the turbulence does not cause significant momentum exchange between electrons and ions resulting in electrical resistivity. It is demonstrated that the dissipation is mainly caused by viscosity associated with electron momentum transport across the current layer. The present results suggest a fundamental modification of the current magnetohydrodynamics models using the resistivity to generate the dissipation.

Distributed Electric Currents in Solar Active Regions

Yuriy A. **Fursyak,** Alexander S. Kutsenko, Valentina I. Abramenko
Solar Phys. **295**, Article number: 19 **2020**
https://arxiv.org/pdf/1912.07032.pdf
https://link.springer.com/content/pdf/10.1007/s11207-020-1584-6.pdf
Using magnetographic data provided by the Helioseismic and Magnetic Imager on board the Solar Dynamics Observatory, we analyzed the structure of magnetic fields and vertical electric currents in six active regions (ARs) with different level of flare activity. We found that electric currents are well balanced over the entire AR: for all of them the current imbalance is below 0.1%, which means that any current system is closed within an AR. Decomposition of the transverse magnetic field vector into two components allowed us to reveal the existence of large-scale vortex structures of the azimuthal magnetic field component around main sunspots of ARs. In each AR, we found a large-scale electric current system occupying a vast area of an AR, which we call distributed electric current. For ARs obeying the Hale polarity law and the hemispheric helicity sign rule, the distributed current is directed upward in the leading part of an AR and it appears to be closing back to the photosphere in the following part of an AR through the corona and chromosphere. Our analysis of the time variations of the magnitude of the distributed electric currents showed that low-flaring ARs exhibit small variations of the distributed currents in the range of ±20×1012 A, whereas the highly flaring ARs exhibited significant slow variations of the distributed currents in the range of 30−95×1012 A. Intervals of the enhanced flaring appear to be co-temporal with smooth enhancements of the distributed electric current. **2014 Sep 09–12, 2014 Oct 22–25, 2015 Jun 20–23, 2015 Jul 07–10, 2016 Feb 05–07, 2017 Sep 03–06**

Forward modelling of heating within a coronal arcade

Lianne **Fyfe**, Thomas Howson, Ineke De Moortel
A&A **2021**

https://arxiv.org/pdf/2110.14257

Aims. We investigate the synthetic observational signatures from numerical models of coronal heating in an arcade to determine what features are associated with such heating, and what tools can be used to identify them.
Methods. We consider two simulations of coronal arcades driven by footpoint motions with different characteristic timescales. Forward modelling is then used, and the synthetic emission data is analysed.
Results. The total intensity and Doppler velocities clearly show the magnetic structure of the coronal arcade. Contrasts in the local Doppler shift also highlight the locations of separatrix surfaces. The distinguishing feature of the AC and DC models is that of the frequencies. Through FFT analysis of the Doppler velocities, when short timescale footpoint motions are present, higher frequencies are observed. For longer timescale motions, the dominant signal is that of lower frequencies; however, higher frequencies were also detected, which matched the natural Alfvén frequency of the background magnetic field. Alfvénic wave signatures were identified in both models with fast wave signatures observable in the AC model. Finally, the estimates of the kinetic energy using the Doppler shifts were found to significantly underestimate within these models.
Conclusions. Observables identified within this article were from features such as Alfvén waves, fast waves, the arcade structure and separatrix surfaces. The two models were differentiated by examining the frequencies present. The Doppler velocities cannot provide accurate estimates of the total kinetic energy or the component parallel to the LOS. This is due to some plasma outside the formation temperature range of the ion, the multi-directional driver, and cancellation of the velocity along the LOS. The impact each factor has on the estimation is dependent on the set up of the model and the chosen emission line.

RHESSI AND TRACE OBSERVATIONS OF THE 21 APRIL 2002 X1.5 FLARE
PETER T. **GALLAGHER**1,2, BRIAN R. DENNIS1, SÄM KRUCKER3,
RICHARD A. SCHWARTZ1,4 and A. KIMBERLEY TOLBERT1,4
Solar Physics **210:** 341–356, **2002**, **File**.
Observations of the X1.5 flare on 21 April 2002 are reviewed using the Reuven Ramaty High-Energy Solar Spectroscopic Imager (RHESSI) and the Transition Region and Coronal Explorer (TRACE). The major findings are as follows: (1) The 3–25 keV X-rays started <4 min before the EUV (195 Å) emission suggesting that the initial energy release heated plasma directly to _20 MK, well above the 1.6 MK needed to produce the Fe XII (195 Å) line. (2) Using coaligned 12–25 keV RHESSI and TRACE images, further evidence is found for the existence of hot (15–20 MK) plasma in the 195 Å passband. This hot, diffuse emission is attributed to the presence of the Fe XXIV (192 Å) line within the TRACE 195 Å passband. (3) The 12–25 keV source centroid moves away from the limb with an apparent velocity of ~9.9 km s−1, slowing to ~1.7 km s−1 after 3 hours, its final altitude being ~140 Mm after ~12 hours. This suggests that the energy release site moves to higher altitudes in agreement with classical flare models. (4) The 50–100 keV emission correlates well with EUV flare ribbons, suggesting thick-target interactions at the footpoints of the magnetic arcade. The 50–100 keV time profile matches the time derivative of the GOES light curve (Neupert effect), which suggests that the same electrons that produced the thick-target hard X-ray emission also heat the plasma seen in soft X-rays. (5) X-ray footpoint emission has an E−3 spectrum down to ~10 keV suggesting a lower electron cutoff energy than previously thought. (6) The hard X-ray (25–200 keV) peaks have FWHM durations of ~1 min suggesting a more gradual energy release process than expected. (7) The TRACE images reveal a bright symmetric front propagating away from the main flare site at speeds of ≥120 km s−1. This may be associated with the fast CME observed several minutes later by LASCO. (8) Dark sinuous lanes are observed in the TRACE images that extend almost radially from the post-flare loop system. This ‘fan of spines’ becomes visible well into the decay phase of the flare and shows evidence for both lateral and downward motions.
See Electronic supplementary material
http://springerlink.metapress.com/content/j135842878532105/11207_2004_Article_5108116_ESM.html
See also
Rapid acceleration of a coronal mass ejection in the low corona and implications for propagation
Gallagher, P. T., G. R. Lawrence, and B. R. Dennis,
ApJL, *588*(1), L53–L56. (**2003**), **File**

Thermalisation and hard X-ray bremsstrahlung efficiency of self-interacting solar flare fast electrons

R. K. **Galloway**1*, P. Helander2, A. L. MacKinnon1 and J. C. Brown1
A&A 520, A72 (**2010**)
Context. Most theoretical descriptions of the production of solar flare bremsstrahlung radiation assume the collision of dilute accelerated particles with a cold, dense target plasma, neglecting interactions of the fast particles with each other.

This is inadequate for situations where collisions with this background plasma are not completely dominant, as may be the case in, for example, low-density coronal sources.
Aims. We aim to formulate a model of a self-interacting, entirely fast electron population in the absence of a dense background plasma, to investigate its implications for observed bremsstrahlung spectra and the flare energy budget.
Methods. We derive approximate expressions for the time-dependent distribution function of the fast electrons using a Fokker-Planck approach. We use these expressions to generate synthetic bremsstrahlung X-ray spectra as would be seen from a corresponding coronal source.
Results. We find that our model qualitatively reproduces the observed behaviour of some flares. As the flare progresses, the model's initial power-law spectrum is joined by a lower energy, thermal component. The power-law component diminishes, and the growing thermal component proceeds to dominate the total emission over timescales consistent with flare observations. The power-law exhibits progressive spectral hardening, as is seen in some flare coronal sources. We also find that our model requires a factor of 7–10 fewer accelerated electrons than the cold, thick target model to generate an equivalent hard X-ray flux.
Conclusions. This model forms the basis of a treatment of self-interactions among flare fast electrons, a process which affords a more efficient means to produce bremsstrahlung photons and so may reduce the efficiency requirements placed on the particle acceleration mechanism. It also provides a useful description of the thermalisation of fast electrons in coronal sources.

Active region upflows: 2. Data driven MHD modeling

K. **Galsgaard**, M. S. Madjarska, K. Vanninathan, Z. Huang, M. Presmann
ApJ (A&A) **2015**
http://arxiv.org/pdf/1509.05639v1.pdf
Context. Observations of many active regions show a slow systematic outflow/upflow from their edges lasting from hours to days. At present no physical explanation has been proven, while several suggestions have been put forward. Aims. This paper investigates one possible method for maintaining these upflows assuming that convective motions drive the magnetic field to initiate them through magnetic reconnection. Methods. We use Helioseismic and Magnetic Imager (HMI) data to provide an initial potential three dimensional magnetic field of the active region NOAA 11123 on **2010 November 13** where the characteristic upflow velocities are observed. A simple one-dimensional hydrostatic atmospheric model covering the region from the photosphere to the corona is derived. Local Correlation Tracking of the magnetic features in the HMI data is used to derive a proxy for the time dependent velocity field. The time dependent evolution of the system is solved using a resistive three-dimensional MagnetoHydro-Dynamic code. Results. The magnetic field contains several null points located well above the photosphere, with their fan planes dividing the magnetic field into independent open and closed flux domains. The stressing of the interfaces between the different flux domains is expected to provide locations where magnetic reconnection can take place and drive systematic flows. In this case, the region between the closed and open flux is identified as the region where observations find the systematic upflows. Conclusions. In the present experiment, the driving only initiates magneto-acoustic waves, without driving any systematic upflows at any of the flux interfaces.

On the motions of RHESSI flare footpoints

W.Q. **Gan**, Y.P. Li and L.I. Miroshnichenko
E-print, Oct 2006, File
Advances in Space Research, Volume 41, Issue 6, *Pages 908-913,* **2008**
The footpoint motions of flare hard X-ray (HXR) sources are directly related to the reconnection scenario of a solar flare. In this work, we tried to extract the information of footpoint motions for a number of flares observed with RHESSI. We found that the RHESSI flare results of the footpoint motions strongly support the classification proposed from the observations of YOHKOH/HXT. Furthermore, it is found that a flare can consist of two types of footpoint motions. We discussed the connections of the footpoint motions with the two-dimensional reconnection models.

Detection of decayless oscillations in solar transition region loops L4

Yuhang **Gao**, Zhenyong Hou, Tom Van Doorsselaere and Mingzhe Guo
A&A Letter Volume 681, L4, January **2024**
https://doi.org/10.1051/0004-6361/202348702
https://www.aanda.org/articles/aa/pdf/2024/01/aa48702-23.pdf
Context. Decayless kink oscillations have been frequently observed in coronal loops, serving as a valuable diagnostic tool for the coronal magnetic field. Such oscillations have never before been reported in low-lying loops of the transition region (TR).
Aims. The aim of this study is to detect decayless kink oscillations in TR loops for the first time.
Methods. We used the SI IV 1400 Å imaging data obtained from the Interface Region Imaging Spectrograph. We applied the Multiscale Gaussian Normalization method to highlight the TR loops, and generated time–distance maps to analyse the oscillation signals.

Results. Seven oscillation events detected here exhibit a small but sustained displacement amplitude (0.04–0.10 Mm) for more than three cycles. Their periods range from 3 to 5 min. The phase speed is found to increase with loop length, which is consistent with the decrease in Alfvén speed with height. With these newly detected oscillations, we obtain a rough estimate of the magnetic field in the transition region, which is about 5–10 G.
Conclusions. Our results further reveal the ubiquity of decayless kink oscillations in the solar atmosphere. These oscillations in TR loops have the potential to be a diagnostic tool for the TR magnetic field. **2013/09/24, 2013/09/25&26, 2013/10/25, 2013/11/07, 2013/12/27**

Association of X-class flares with sunspot groups of various classes in Cycles 22 and 23

P X **Gao**
MNRAS, Volume 484, Issue 4, 21 April **2019**, Pages 5692–5701,
sci-hub.tw/10.1093/mnras/stz362
We investigate the association between X-class flares and sunspot groups (SGs) of various classes in Solar Cycles (SCs) 22 and 23 and find the following results. (1) During SCs 22 and 23, 96.2 per cent and 94.3 per cent of X-class flares are associated with large SGs (Zurich classes D, E, and F), respectively; the percentages of large SGs associated with X-class flares are significantly higher than those of the other Zurich class SGs; however, the total number of large SGs in SC 22 is about 80 per cent of that in SC 23, while, the total number of X-class flares in SC 22 is 1.22 times that of SC 23. (2) During SCs 22 and 23, 83.1 per cent and 79.4 per cent of X-class flares are associated with penumbral class k SGs, respectively; the percentages of penumbral class k SGs associated with X-class flares are significantly higher than those of the other penumbral class SGs; however, the ratio of the maximum number of penumbral class k SGs during SC 22 to SC 23 is 1.10, while, the ratio of the maximum number of X-class flares during SC 22 to SC 23 is 2.73. (3) 49.3 per cent and 55.2 per cent of X-class flares occur in βδ or βγδ or γδ SGs in SCs 22 and 23, respectively; the total (maximum) numbers of βγδ and γδ SGs in SC 22 are about 63 per cent (53 per cent) and 33 per cent of those in SC 23, respectively; the total (maximum) number of βδ SGs in SC 22 is 3.03 (5.13) times that of SC 23.

The Broken Lane of a Type II Radio Burst Caused by Collision of a Coronal Shock with a Flare Current Sheet

Guannan **Gao**, Min Wang, Ning Wu, Jun Lin, E. Ebenezer, Baolin Tan
Solar Phys. Volume 291, Issue 11, pp 3369–3384 **2016**
http://link.springer.com/article/10.1007/s11207-016-1007-x
We investigated a peculiar metric type II solar radio burst with a broken lane structure that was observed on **November 13, 2012**. In addition to the radio data, we also studied the data in other wavelengths. The bursts were associated with two coronal mass ejections (CMEs) and two flares that originated from Active Region AR 11613. A long current sheet developed in the first CME, and the second CME collided with the current sheet first and then merged with the first CME. Combined information revealed by the multi-wavelength data indicated that a coronal shock was accountable for the type II radio burst and that the collision of this shock with the current sheet resulted in the broken lane of the type II radio burst. The type II burst lane re-formed after the shock passed through the current sheet. Furthermore, we estimated the thickness of the current sheet from a gap in the lane of the type II burst, and found that the result is consistent with previous ones obtained for various events observed in different wavelengths by different instruments. In addition, the regular type II burst associated with the first CME/flare was also studied, and the magnetic field in each source region of the two type II bursts was deduced in different ways.

A Study of Connections Between Solar Flares and Subsurface Flow Fields of Active Regions

Yu **Gao**, Junwei Zhao, Hongqi Zhang
Solar Physics, February **2014**, Volume 289, Issue 2, pp 493-502
We investigate the connections between the occurrence of major solar flares and subsurface dynamic properties of active regions. For this analysis, we select five active regions that produced a total of 11 flares with peak X-ray flux intensity higher than M5.0. The subsurface velocity fields are obtained from time–distance helioseismology analysis using SDO/HMI (Solar Dynamics Observatory/Helioseismic and Magnetic Imager) Doppler observations, and the X-ray flux intensity is taken from GOES (Geostationary Operational Environmental Satellites). It is found that among the eight amplitude bumps in the evolutionary curves of subsurface kinetic helicity, five (62.5%) of them had a flare stronger than M5.0 occurring within 8 hours, either before or after the bumps. Another subsurface parameter is the Normalized Helicity Gradient Variance (NHGV), reflecting kinetic helicity spread in different depth layers; it also shows bumps near the occurrence of these solar flares. Although there is no one-to-one correspondence between the flare and the subsurface properties, these observational phenomena are worth further studies to better understand the flares' subsurface roots, and to investigate whether the subsurface properties can be used for major flare forecasts**.**

ANALYSIS ON CORRELATIONS BETWEEN SUBSURFACE KINETIC HELICITY AND PHOTOSPHERIC CURRENT HELICITY IN ACTIVE REGIONS

Yu **Gao**1, Junwei Zhao2, and Hongqi Zhang

2012 ApJ 761 L9
An investigation on correlations between photospheric current helicity and subsurface kinetic helicity is carried out by analyzing vector magnetograms and subsurface velocities for two rapidly developing active regions. The vector magnetograms are from the Solar Dynamics Observatory/Helioseismic and Magnetic Imager (SDO/HMI) observed Stokes parameters, and the subsurface velocity is from time-distance data-analysis pipeline using HMI Dopplergrams. Over a span of several days, the evolution of the weighted current helicity shows a tendency similar to that of the weighted subsurface kinetic helicity, attaining a correlation coefficient above 0.60 for both active regions. Additionally, there seems to be a phase lag between the evolutions of the unweighted current and subsurface kinetic helicities for one of the active regions. The good correlation between these two helicities indicates that there is some intrinsic connection between the interior dynamics and photospheric magnetic twistedness inside active regions, which may help to interpret the well-known hemispheric preponderance of current-helicity distribution.

Flare heating of the chromosphere: Observations of flare continuum from GREGOR and IRIS

M. **García-Rivas**1,2,⋆, J. Kašparová1, A. Berlicki1,3, M. Švanda1,2, J. Dudík1, D. Čtvrtečka4, M. Zapiór1, W. Liu1, M. Sobotka1, M. Pavelková1 and G. G. Motorina1,⋆⋆
A&A, 690, A254 (**2024**)
https://www.aanda.org/articles/aa/pdf/2024/10/aa51219-24.pdf
Context. On **2022 May 4**, an M5.7 flare erupted in the active region NOAA 13004, which was the target of a coordinated campaign between GREGOR, IRIS, Hinode, and ground-based instruments at the Ondřejov observatory. A flare kernel located at the edge of a pore was co-observed by the IRIS slit and GREGOR HiFI+ imagers.
Aims. We investigated the flare continuum enhancement at different wavelength ranges in order to derive the temperature of the chromospheric layer heated during the flare.
Methods. All datasets were aligned to IRIS slit-jaw images. We selected a pixel along the IRIS slit where the flare kernel was captured and evaluated multi-wavelength light curves within it. We defined a narrow IRIS near-UV band that comprises only continuum emission. The method, which assumes that the flare continuum enhancement is due to optically thin emission from hydrogen recombination processes, was applied to obtain a lower limit on the temperature in the layer where the continuum enhancement was formed.
Results. We determined a lower limit for the temperature and its time evolution in the chromospheric layer heated during the flare in the range of (3–15) ×103 K. The mean electron density in that layer was estimated to be ∼1 × 1013 cm−3.
Conlcusions. Multi-wavelength flare co-observations are a rich source of diagnostics. Due to the rapidly evolving nature of flares, the sit-and-stare mode is key to achieving a high temporal cadence that allows one to thoroughly analyse the same flare structure.

Temperature and emission measure from GOES soft X-ray measurements.

Garcia HA.
1994b. Sol Phys 154: 275–308.
DOI: 10.1007/ BF00681100
https://articles.adsabs.harvard.edu/pdf/1994SoPh..154..275G
GOES (Geostationary Operational Environmental Satellite) X-ray sensors observe the Sun continuously in two broadband soft X-ray channels. These data are collected in real time and are used operationally to detect the onset and the intensity of solar flares. For these purposes it is usually sufficient to monitor only the soft channel (1–8 Å). The second, harder channel (0.5–4 Å) provides additional information on the state of the coronal plasma. The dual X-ray measurement data are archived and made available to external users for basic research.
The GOES X-ray sensors operate on the ion-chamber principle: measured ion-chamber electric current is proportional to the net ionization rate caused by incident X-ray flux on encapsulated noble gases. The ratio of the outputs of the two channels in electric current, therefore, is uniquely a function of the color temperature of the emitting plasma, and the magnitude of each of the currents is proportional to a quantity, known as the emission measure, that convolves the volume and the density of the emitting plasma.
This paper provides a detailed description of the procedure used for computing color temperature and emission measure from GOES X-ray data, including a table of constants for SMS and GOES X-ray sensors that are necessary for reducing the archived data from these satellites. Temperature and theoretical current tables were constructed, for individual GOES sensors, from laboratory calibrations of instrument responses and from synthetic solar X-ray spectra generated by two models of solar thermal X-ray emission: Raymond-Smith and Mewe-Alkemade. Example tables are shown and others are available on request.
Errors that may be incurred from the use of GOES X-ray data in the computation of flare temperatures and emission measures may be classified under four major groups: instrumentinduced errors, including errors of calibration and random measurement errors; environmentally induced errors, due primarily to the ambient energetic electron background; solar influences, including the consequences of the isothermal assumption and the single-source assumption; and uncertainties in the modelled solar synthetic spectrum. These error sources are discussed separately,

and a rough estimation of the collective error is made where this is quantitatively feasible. Finally, temperatures and emission measures are computed from GOES data and are compared with those derived from SMM andHinotori soft X-ray spectrometer data and from broadband photometric data from the PROGNOZ satellite.

Temperature and Emission Measure from GOES Soft X-Ray Measurements

Garcia, Howard A.

Solar Physics, Volume 154, Issue 2, pp.275-308,**1994**

https://link.springer.com/content/pdf/10.1007%2FBF00681100.pdf

GOES (Geostationary Operational Environmental Satellite) X-ray sensors observe the Sun continuously in two broadband soft X-ray channels. These data are collected in real time and are used operationally to detect the onset and the intensity of solar flares. For these purposes it is usually sufficient to monitor only the soft channel (1 8 Å). The second, harder channel (0.5 4 Å) provides additional information on the state of the coronal plasma. The dual X-ray measurement data are archived and made available to external users for basic research. The GOES X-ray sensors operate on the ion-chamber principle: measured ion-chamber electric current is proportional to the net ionization rate caused by incident X-ray flux on encapsulated noble gases. The ratio of the outputs of the two channels in electric current, therefore, is uniquely a function of the color temperature of the emitting plasma, and the magnitude of each of the currents is proportional to a quantity, known as the emission measure, that convolves the volume and the density of the emitting plasma. This paper provides a detailed description of the procedure used for computing color temperature and emission measure from GOES X-ray data, including a table of constants for SMS and GOES X-ray sensors that are necessary for reducing the archived data from these satellites. Temperature and theoretical current tables were constructed, for individual GOES sensors, from laboratory calibrations of instrument responses and from synthetic solar X-ray spectra generated by two models of solar thermal X-ray emission: Raymond-Smith and Mewe-Alkemade. Example tables are shown and others are available on request. Errors that may be incurred from the use of GOES X-ray data in the computation of flare temperatures and emission measures may be classified under four major groups: instrumentinduced errors, including errors of calibration and random measurement errors; environmentally induced errors, due primarily to the ambient energetic electron background; solar influences, including the consequences of the isothermal assumption and the single-source assumption; and uncertainties in the modelled solar synthetic spectrum. These error sources are discussed separately, and a rough estimation of the collective error is made where this is quantitatively feasible. Finally, temperatures and emission measures are computed from GOES data and are compared with those derived from SMM andHinotori soft X-ray spectrometer data and from broadband photometric data from the PROGNOZ satellite.

Prediction and warning system of SEP events and solar flares for risk estimation in space launch operations

Alberto **García-Rigo**1*, Marlon Núñez2, Rami Qahwaji3, Omar Ashamari3, Piers Jiggens4, Gustau Pérez1, Manuel Hernández-Pajares1 and Alain Hilgers

J. Space Weather Space Clim., 6, A28 (**2016**)

http://www.swsc-journal.org/articles/swsc/pdf/2016/01/swsc150014.pdf

A web-based prototype system for predicting solar energetic particle (SEP) events and solar flares for use by space launch operators is presented. The system has been developed as a result of the European Space Agency (ESA) project SEPsFLAREs (Solar Events Prediction system For space LAunch Risk Estimation). The system consists of several modules covering the prediction of solar flares and early SEP Warnings (labeled Warning tool), the prediction of SEP event occurrence and onset, and the prediction of SEP event peak and duration. In addition, the system acquires data for solar flare nowcasting from Global Navigation Satellite Systems (GNSS)-based techniques (GNSS Solar Flare Detector, GSFLAD and the Sunlit Ionosphere Sudden Total Electron Content Enhancement Detector, SISTED) as additional independent products that may also prove useful for space launch operators. **5-8 Dec 2006, 18th April, 2014**

Flare heating of the chromosphere: Observations of flare continuum from GREGOR and IRIS

M. **García-Rivas**, J. Kašparová, A. Berlicki, M. Švanda, J. Dudík, D. Čtvrtečka, M. Zapiór, W. Liu, M M. Sobotka, M. Pavelková, G. G. Motorina

A&A 690, A254 **2024**

https://arxiv.org/pdf/2408.10813

https://ui.adsabs.harvard.edu/link_gateway/2024A%26A...690A.254G/EPRINT_PDF

Context: On **2022 May 4**, an M5.7 flare erupted in the active region NOAA 13004, which was the target of a coordinated campaign between GREGOR, IRIS, Hinode, and ground-based instruments at the Ondřejov observatory. A flare kernel located at the edge of a pore was co-observed by the IRIS slit and GREGOR HiFI+ imagers. Aims: We investigated the flare continuum enhancement at different wavelength ranges in order to derive the temperature of the chromospheric layer heated during the flare. Methods: All datasets were aligned to IRIS slit-jaw images. We selected a pixel along the IRIS slit where the flare kernel was captured and evaluated multi-wavelength light curves within it. We

defined a narrow IRIS near-UV band that comprises only continuum emission. The method, which assumes that the flare continuum enhancement is due to optically thin emission from hydrogen recombination processes, was applied to obtain a lower limit on the temperature in the layer where the continuum enhancement was formed. Results: We determined a lower limit for the temperature and its time evolution in the chromospheric layer heated during the flare in the range of (3-15).10^3 K. The mean electron density in that layer was estimated to be about 1.10^(13) cm^(-3). Conclusions: Multi-wavelength flare co-observations are a rich source of diagnostics. Due to the rapidly evolving nature of flares, the sit-and-stare mode is key to achieving a high temporal cadence that allows one to thoroughly analyse the same flare structure.
IRIS Nugget Dec **2024** https://iris.lmsal.com/nugget

Evolution of Coronal Magnetic Field Parameters during X5.4 Solar Flare

Seth **Garland**, Vasyl Yurchyshyn, Robert Loper, Benjamin Akers, and Daniel Emmons
Astron. Space Sci. 10: 1148293. **2023** doi: 10.3389/fspas.2023.1148293
https://www.frontiersin.org/articles/10.3389/fspas.2023.1148293/pdf
https://www.frontiersin.org/articles/10.3389/fspas.2023.1148293/full
The coronal magnetic field over NOAA Active Region 11,429 during a X5.4 solar flare on **7 March 2012** is modeled using optimization based Non-Linear Force-Free Field extrapolation. Specifically, 3D magnetic fields were modeled for 11 timesteps using the 12-min cadence Solar Dynamics Observatory (SDO) Helioseismic and Magnetic Imager photospheric vector magnetic field data, spanning a time period of 1 hour before through 1 hour after the start of the flare. Using the modeled coronal magnetic field data, seven different magnetic field parameters were calculated for 3 separate regions: areas with surface |Bz|≥ 300 G, areas of flare brightening seen in SDO Atmospheric Imaging Assembly imagery, and areas with surface |B| ≥ 1000 G and high twist. Time series of the magnetic field parameters were analyzed to investigate the evolution of the coronal field during the solar flare event and discern pre-eruptive signatures. The data shows that areas with |B| ≥ 1000 G and |Tw|≥ 1.5 align well with areas of initial flare brightening during the pre-flare phase and at the beginning of the eruptive phase of the flare, suggesting that measurements of the photospheric magnetic field strength and twist can be used to predict the flare location within an active region if triggered. Additionally, the evolution of seven investigated magnetic field parameters indicated a destabilizing magnetic field structure that could likely erupt.

Quantifying the Empirical Relationship Between Loop Length and Duration of Solar Flares

Garcia, H. ; Farnik, F.
High Energy Solar Physics Workshop - Anticipating HESSI, ASP Conference Series, Vol. 206. Edited by R. Ramaty and N. Mandzhavidze. ISBN: 1-58381-033-1 (**2000**), p.252
https://articles.adsabs.harvard.edu/pdf/2000ASPC..206..252G

Abstract. A robust empirical relationship is found to exist between the length of a bright flare loop and the combined elements of the soft x-ray light curve, viz., rise time, decay time, and peak temperature. It is common knowledge that long duration (flare) events, LDEs, that have been observed by soft x-ray imaging telescopes, e.g., the Yohkoh SXT, exhibit unusually long loops. May it be inferred, therefore, that short duration flares have correspondingly short loops? The question of flare loop length vs. duration and temperature was addressed in a theory-based study by Hawley and coworkers and later by Metcalf and Fisher. A recent study was conducted by Garcia utilizing the 1992-1993 SXT measurements of the latter authors establishing an empirical validation of the concept. The present work extends that data set with SXT measurements obtained during the present solar cycle. The present work also considers several special characteristics of soft x-ray loops: single loop topology; quasi-stationary status; diffuseness; anti-correlations with maximum temperature and with maximum x-ray intensity.

Thermal-Spatial Analysis of Medium and Large Solar Flares, 1976 to 1996

Garcia, Howard A.
ApJ Supplement Series, Volume 127, Issue 1, pp. 189-210, **2000**

https://iopscience.iop.org/article/10.1086/313312/pdf

.Approximately 1100 moderate to large solar flares observed in soft X-rays by the GOES spacecraft, operating between 1976 and 1996, are analyzed individually for thermal and spatial structure by a model that utilizes discrete X-ray measurements, the ensemble X-ray light curve, and scaling laws relating certain thermal properties to spatial dimension. This method endeavors to reproduce a flare's thermal structure in terms of its loop geometry from spatially unresolved measurements, invoking a theoretically conceived and empirically confirmed relationship between the loop scale and temporal behavior of flares. Used in conjunction with a well-known, quasi-static equilibrium scaling law relating loop scale to key thermal parameters, a comprehensive solution of global thermal structure can be closed in the context of this model. The essential characteristics of this model were described by Garcia in an earlier paper showing the step by step procedure for computing the length, cross section, volume, density, mass, and thermal energy of an individual flare loop. The primary purpose of the present work is to utilize the model and method presented by Garcia, based on a small group of flares, to study a much larger sample of flares in order to determine their average characteristics of the above parameters over an extended range of X-ray intensity and size. The ability to utilize spatially unresolved X-ray data to analyze the structure of individual flares at small cost opens the possibility of investigating the average behavior of large populations of X-ray flares, exploiting the largely untapped reservoir of data accumulated since the advent of operational geosynchronous weather satellites.

Low-Temperature Soft X-ray Flares, Spectrally Hardening Hard X-ray Flares, and Energetic Interplanetary Protons

Garcia, H. A. ; Kiplinger, A. L.

Solar drivers of the interplanetary and terrestrial disturbances. Astronomical Society of the Pacific Conference Series, Proceedings of the 16th (sixteenth) international workshop National Solar Observatory/Sacramento Peak, Sunspot, New Mexico, USA, 16-20 October 1995, San Francisco: Astronomical Society of the Pacific (ASP), **1996**, edited by K. S. Balasubramaniam, Stephen L. Keil, and Raymond N. Smartt, p.91

https://articles.adsabs.harvard.edu/pdf/1996ASPC...95...91G

Abstract. Recent studies of soft x-ray emission (Garcia 1994) and hard x-ray spectroscopy (Kiplinger 1995) from samples of flares covering large portions of solar cycles 21 and 22 indicate that most solar energetic proton (SEP) events observed in the vicinity of Earth are highly associated with occurrences of particular types of solar flare characteristics. There are two apparent signatures of flares that are associated with SEP events that distinguish them from the common impulsive solar flare. Garcia's study showed that these flares have anomalously low temperatures in soft x-rays. Kiplinger's study revealed signatures of hard x-ray spectra that progressively harden during periods of decaying fluxes. Progressive hardening in hard x-rays may be the observable consequence of electron acceleration in large, low-density loops that are in close proximity to open field topologies. Low temperatures in soft x-rays are a newly discovered trait that may be interpreted as a thermal energy deficit in comparison with normal impulsive flares of the same soft x-ray intensity. Kiplinger (1995) noted that when an event exhibited a period of impulsive behavior and a period of progressive spectral hardening, the impulsive periods always occur first. Moreover, the relative flux contributions from the two periods varied widely from event to event. Some progressively hardening events showed no evidence of an impulsive component. This study compares soft x-ray flare peak temperatures with hard x-ray flares having differing relative intensities in the impulsive versus progressive hardening phases. This comparison revealed that the lowest temperature flares corresponded to hard x-ray events that had no, or weak, impulsive phases in relation to the hardening phase, and that the more intense soft x-ray flares corresponded to hard x-ray flares with a dominant impulsive phase.

Analysis of modeled 3D solar magnetic field during 30 X/M-class solar flares

Seth H. **Garland**1* Vasyl B. Yurchyshyn2 Robert D. Loper3 Benjamin F. Akers4 Daniel J. Emmons1

Front. Astron. Space Sci. 11: 1369749. **2024**

https://www.frontiersin.org/articles/10.3389/fspas.2024.1369749/pdf
https://doi.org/10.3389/fspas.2024.1369749
Using non-linear force free field (NLFFF) extrapolation, 3D magnetic fields were modeled from the 12-min cadence Solar Dynamics Observatory Helioseismic and Magnetic Imager (HMI) photospheric vector magnetograms, spanning a time period of 1 hour before through 1 hour after the start of 18 X-class and 12 M-class solar flares. Several magnetic field parameters were calculated from the modeled fields directly, as well as from the power spectrum of surface maps generated by summing the fields along the vertical axis, for two different regions: areas with photospheric |Bz|≥ 300 G (active region—AR) and areas above the photosphere with the magnitude of the non-potential field (BNP) greater than three standard deviations above |BNP|of the AR field and either the unsigned twist number |Tw| ≥ 1 turn or the shear angle Ψ ≥ 80° (non-potential region—NPR). Superposed epoch (SPE) plots of the magnetic field parameters were analyzed to investigate the evolution of the 3D solar field during the solar flare events and discern consistent trends across all solar flare events in the dataset, as well as across subsets of flare events categorized by their magnetic and sunspot classifications. The relationship between different flare properties and the magnetic field parameters was quantitatively described by the Spearman ranking correlation coefficient, rs. The parameters that showed the most consistent and discernable trends among the flare events, particularly for the hour leading up to the eruption, were the total unsigned flux ϕ), free magnetic energy (EFree), total unsigned magnetic twist (τTot), and total unsigned free magnetic twist (ρTot). Strong (|rs| ∈ [0.6, 0.8)) to very strong (|rs| ∈ [0.8, 1.0]) correlations were found between the magnetic field parameters and the following flare properties: peak X-ray flux, duration, rise time, decay time, impulsiveness, and integrated flux; the strongest correlation coefficient calculated for each flare property was 0.62, 0.85, 0.73, 0.82, −0.81, and 0.82, respectively. **2012-03-07, 2013-11-08**

Microwave and Hard X-Ray Observations of the 2017 September 10 Solar Limb Flare

Dale E. **Gary**, Bin Chen, Brian R. Dennis, Gregory D. Fleishman, Gordon J. Hurford, Sa"m Krucker, James M. McTiernan, Gelu M. Nita, Albert Y. Shih,Stephen M. White, Sijie Yu
ApJ **863** 83 **2018**
https://arxiv.org/pdf/1807.02498.pdf
http://sci-hub.tw/http://iopscience.iop.org/article/10.3847/1538-4357/aad0ef/meta
We report the first science results from the newly completed Expanded Owens Valley Solar Array (EOVSA), which obtained excellent microwave imaging spectroscopy observations of SOL2017-09-10, a classic partially-occulted solar limb flare associated with an erupting flux rope. This event is also well-covered by the Reuven Ramaty High Energy Solar Spectroscopic Imager (RHESSI) in hard X-rays (HXRs). We present an overview of this event focusing on microwave and HXR data, both associated with high-energy nonthermal electrons, and discuss them within the context of the flare geometry and evolution revealed by extreme ultraviolet (EUV) observations from the Atmospheric Imaging Assembly aboard the Solar Dynamics Observatory (SDO/AIA). The EOVSA and RHESSI data reveal the evolving spatial and energy distribution of high-energy electrons throughout the entire flaring region. The results suggest that the microwave and HXR sources largely arise from a common nonthermal electron population, although the microwave imaging spectroscopy provides information over a much larger volume of the corona.

PLASMA BETA ABOVE A SOLAR ACTIVE REGION: RETHINKING THE PARADIGM

G. ALLEN **GARY**
Solar Physics **203:** 71–86, **2001**.
In this paper, we present a model of the plasma beta above an active region and discuss its consequences in terms of coronal magnetic field modeling. The β-plasma model is representative and derived from a collection of sources. The resulting β variation with height in the solar atmosphere is used to emphasize that the assumption that the magnetic pressure dominates over the plasma pressure must be carefully employed when extrapolating the magnetic field. This paper points out (1) that the paradigm that the coronal magnetic field can be constructed from a force-free magnetic field must be used in the correct context, since the force-free region is sandwiched between two regions which have $\beta > 1$, (2) that the chromospheric Mg II–C IV magnetic measurements occur near the β-minimum, and (3) that, moving from the photosphere upwards, β can return to ~ 1 at relatively low coronal heights, e.g., $R \sim 1.2\ Rs$.

THREE-DIMENSIONAL RECONNECTION INVOLVING MAGNETIC FLUX ROPES

W. **Gekelman**1, E. Lawrence2, and B. Van Compernolle
2012 ApJ 753 131
Two and three magnetic flux ropes are created and studied in a well-diagnosed laboratory experiment. The twisted helical bundles of field lines rotate and collide with each other over time. In the two rope case, reverse current layers indicative of reconnection are observed. Using a high spatial and temporal resolution three-dimensional volume data set in both cases, quasi-separatrix layers (QSLs) are identified in the magnetic field. Originally developed in the context of solar magnetic reconnection, QSLs are thought to be preferred sites for reconnection. This is verified in these studies. In the case of three flux ropes there are multiple QSLs, which come and go in time. The divergence of the field lines

within the QSLs and the field line motion is presented. In all cases, it is observed that the reconnection is patchy in space and bursty in time. Although it occurs at localized positions it is the result of the nonlocal behavior of the flux ropes.

The Flare Likelihood and Region Eruption Forecasting (FLARECAST) Project: Flare forecasting in the big data & machine learning era **Review**

M. K. **Georgoulis**, D. S. Bloomfield, M. Piana, A. M. Massone, M. Soldati, P. T. Gallagher, E. Pariat, N. Vilmer, E. Buchlin, F. Baudin, A. Csillaghy, H. Sathiapal, D. R. Jackson, P. Alingery, F. Benvenuto, C. Campi, K. Florios, C. Gontikakis, C. Guennou, J. A. Guerra, I. Kontogiannis, V. Latorre, S. A. Murray, S.-H. Park, S. von Stachelski, A. Torbica, D. Vischi, M. Worsfold

Journal of Space Weather and Space Climate, **11**, 39 **2021**

https://arxiv.org/pdf/2105.05993.pdf

https://www.swsc-journal.org/articles/swsc/pdf/2021/01/swsc200032.pdf

https://doi.org/10.1051/swsc/2021023

The EU funded the FLARECAST project, that ran from Jan 2015 until Feb 2018. FLARECAST had a R2O focus, and introduced several innovations into the discipline of solar flare forecasting. FLARECAST innovations were: first, the treatment of hundreds of physical properties viewed as promising flare predictors on equal footing, extending multiple previous works; second, the use of fourteen (14) different ML techniques, also on equal footing, to optimize the immense Big Data parameter space created by these many predictors; third, the establishment of a robust, three-pronged communication effort oriented toward policy makers, space-weather stakeholders and the wider public. FLARECAST pledged to make all its data, codes and infrastructure openly available worldwide. The combined use of 170+ properties (a total of 209 predictors are now available) in multiple ML algorithms, some of which were designed exclusively for the project, gave rise to changing sets of best-performing predictors for the forecasting of different flaring levels. At the same time, FLARECAST reaffirmed the importance of rigorous training and testing practices to avoid overly optimistic pre-operational prediction performance. In addition, the project has (a) tested new and revisited physically intuitive flare predictors and (b) provided meaningful clues toward the transition from flares to eruptive flares, namely, events associated with coronal mass ejections (CMEs). These leads, along with the FLARECAST data, algorithms and infrastructure, could help facilitate integrated space-weather forecasting efforts that take steps to avoid effort duplication. In spite of being one of the most intensive and systematic flare forecasting efforts to-date, FLARECAST has not managed to convincingly lift the barrier of stochasticity in solar flare occurrence and forecasting: solar flare prediction thus remains inherently probabilistic. **12 Nov 2012, 2 January 2015, 5 Sep 2017**

Toward an Efficient Prediction of Solar Flares: Which Parameters, and How?

Georgoulis, M. K.

E-print, Nov **2013**; Entropy, 15(11), 5022-5052, **2013**

Solar flare prediction has become a forefront topic in contemporary solar physics, with numerous published methods relying on numerous predictive parameters, that can even be divided into parameter classes. Attempting further insight, we focus on two popular classes of flare-predictive parameters, namely multiscale (i.e., fractal and multifractal) and proxy (i.e., morphological) parameters, and we complement our analysis with a study of the predictive capability of fundamental physical parameters (i.e., magnetic free energy and relative magnetic helicity). Rather than applying the studied parameters to a comprehensive statistical sample of flaring and non-flaring active regions, that was the subject of our previous studies, the novelty of this work is their application to an exceptionally long and high-cadence time series of the intensely eruptive National Oceanic and Atmospheric Administration (NOAA) active region (AR) 11158, observed by the Helioseismic and Magnetic Imager on board the Solar Dynamics Observatory. Aiming for a detailed study of the temporal evolution of each parameter, we seek distinctive patterns that could be associated with the four largest flares in the AR in the course of its five-day observing interval. We find that proxy parameters only tend to show preflare impulses that are practical enough to warrant subsequent investigation with sufficient statistics. Combining these findings with previous results, we conclude that: (i) carefully constructed, physically intuitive proxy parameters may be our best asset toward an efficient future flare-forecasting; and (ii) the time series of promising parameters may be as important as their instantaneous values. Value-based prediction is the only approach followed so far. Our results call for novel signal and/or image processing techniques to efficiently utilize combined amplitude and temporal-profile information to optimize the inferred solar-flare probabilities. **13-16 Feb 2011**

NON-NEUTRALIZED ELECTRIC CURRENT PATTERNS IN SOLAR ACTIVE REGIONS: ORIGIN OF THE SHEAR-GENERATING LORENTZ FORCE

Manolis K. **Georgoulis**1,3, Viacheslav S. Titov2, and Zoran Mikić

2012 ApJ 761 61

Using solar vector magnetograms of the highest available spatial resolution and signal-to-noise ratio, we perform a detailed study of electric current patterns in two solar active regions (ARs): a flaring/eruptive and a flare-quiet one. We aim to determine whether ARs inject non-neutralized (net) electric currents in the solar atmosphere, responding to a debate initiated nearly two decades ago that remains inconclusive. We find that well-formed, intense magnetic polarity inversion lines (PILs) within ARs are the only photospheric magnetic structures that support significant net current. More intense PILs seem to imply stronger non-neutralized current patterns per polarity. This finding revises previous works that claim frequent injections of intense non-neutralized currents by most ARs appearing in the solar disk but also works that altogether rule out injection of non-neutralized currents. In agreement with previous studies, we also find that magnetically isolated ARs remain globally current-balanced. In addition, we confirm and quantify the preference of a given magnetic polarity to follow a given sense of electric currents, indicating a dominant sense of twist in ARs. This coherence effect is more pronounced in more compact ARs with stronger PILs and must be of sub-photospheric origin. Our results yield a natural explanation of the Lorentz force, invariably generating velocity and magnetic shear along strong PILs, thus setting a physical context for the observed pre-eruption evolution in solar ARs.

Are Solar Active Regions with Major Flares More Fractal, Multifractal, or Turbulent Than Others?

Manolis K. **Georgoulis**

Solar Physics, Volume 276, Numbers 1-2, 161-181, **2012**

Multiple recent investigations of solar magnetic-field measurements have raised claims that the scale-free (fractal) or multiscale (multifractal) parameters inferred from the studied magnetograms may help assess the eruptive potential of solar active regions, or may even help predict major flaring activity stemming from these regions. We investigate these claims here, by testing three widely used scale-free and multiscale parameters, namely, the fractal dimension, the multifractal structure function and its inertial-range exponent, and the turbulent power spectrum and its power-law index, on a comprehensive data set of 370 timeseries of active-region magnetograms (17733 magnetograms in total) observed by SOHO's Michelson Doppler Imager (MDI) over the entire Solar Cycle 23. We find that both flaring and non-flaring active regions exhibit significant fractality, multifractality, and non-Kolmogorov turbulence but none of the three tested parameters manages to distinguish active regions with major flares from flare-quiet ones. We also find that the multiscale parameters, but not the scale-free fractal dimension, depend sensitively on the spatial resolution and perhaps the observational characteristics of the studied magnetograms. Extending previous works, we attribute the flare-forecasting inability of fractal and multifractal parameters to i) a widespread multiscale complexity caused by a possible underlying self-organization in turbulent solar magnetic structures, flaring and non-flaring alike, and ii) a lack of correlation between the fractal properties of the photosphere and overlying layers, where solar eruptions occur. However useful for understanding solar magnetism, therefore, scale-free and multiscale measures may not be optimal tools for active-region characterization in terms of eruptive ability or, ultimately, for major solar-flare prediction.

SOLAR MAGNETIC HELICITY INJECTED INTO THE HELIOSPHERE: MAGNITUDE, BALANCE, AND PERIODICITIES OVER SOLAR CYCLE 23

M. K. **Georgoulis**[1,2], D. M. Rust[1], A. A. Pevtsov[3], P. N. Bernasconi[1], and K. M. Kuzanyan[4,5]

Astrophysical Journal, 705:L48–L52, **2009**

Relying purely on solar photospheric magnetic field measurements that cover most of solar cycle 23 (1996–2005), we calculate the total relative magnetic helicity injected into the solar atmosphere, and eventually shed into the heliosphere, over the latest cycle. Large active regions dominate the helicity injection process with ~5.7 × 10^{45} Mx^2 of total injected helicity. The net helicity injected is _1% of the above output. Peculiar active-region plasma flows account for ~80% of this helicity; the remaining ~20% is due to solar differential rotation. The typical helicity per active-region CME ranges between (1.8–7) × 10^{42} Mx^2 depending on the CME velocity. Accounting for various minor underestimation factors, we estimate a maximum helicity injection of ~6.6 × 10^{45} Mx^2 for solar cycle 23. Although no significant net helicity exists over both solar hemispheres, we recover the well-known hemispheric helicity preference, which is significantly enhanced by the solar differential rotation. We also find that helicity injection in the solar atmosphere is an inherently disorganized, impulsive, and aperiodic process.

Magnetic Complexity in Eruptive Solar Active Regions and Associated Eruption Parameters

Manolis K. **Georgoulis**

E-print Dec **2007**, GRL, File

Using an efficient magnetic complexity index in the active-region solar photosphere, we quantify the preflare strength of the photospheric magnetic polarity inversion lines in 23 eruptive active regions with flare/CME/ICME events tracked

all the way from the Sun to the Earth. We find that active regions with more intense polarity inversion lines host statistically stronger flares and faster, more impulsively accelerated, CMEs. No significant correlation is found between the strength of the inversion lines and the flare soft X-ray rise times, the ICME transit times, and the peak *Dst* indices of the induced geomagnetic storms. Corroborating these and previous results, we speculate on a possible interpretation for the connection between source active regions, flares, and CMEs. Further work is needed to validate this concept and uncover its physical details.

Quantitative Forecasting of Major Solar Flares,

Georgoulis, M. K., and Rust D. M. (**2007**),
Astrophys. J., 661, L109–L112.

Peculiarities of the Dynamics of Solar NOAA Active Region 12673

A. V. **Getling**
2019 *ApJ* **878** 127
https://arxiv.org/pdf/1904.08367.pdf
sci-hub.se/10.3847/1538-4357/ab21bd
The dynamics of active region (AR) 12673 is qualitatively studied using observational data obtained with the Helioseismic and Magnetic Imager of the Solar Dynamics Observatory on **August 31--September 8, 2017**. This AR was remarkable for its complex structure and extraodinary flare productivity. The sunspot group in this AR consisted of (1) an old, well-developed and highly stable, coherent sunspot, which had also been observed two solar rotations earlier, and (2) a rapidly developing cluster of umbral and penumbral fragments. Cluster (2) formed two elongated, arc-shaped chains of spot elements, skirting around the major sunspot (1), with two chains of magnetic elements spatially coinciding with the arcs. AR components (1) and (2) were in relative motion, cluster (2) overtaking spot (1), and their relative velocity agrees in order of magnitude with the velocity jump over the near-surface shear layer, or leptocline. The pattern of motion of the features about the main spot bears amazing resemblance to the pattern of a fluid flow about a roundish body. This suggests that spot (1) was dynamically coupled with the surface layers, while cluster (2) developed in deeper layers of the convection zone. The magnetic-flux emergence in cluster (2) appeared to be associated with fluid motions similar to roll convection. The mutual approach of components (1) and (2) gave rise to lights bridges in the umbrae of sunspots with the magnetic field having the same sign on both sides of the bridge.

X-ray Super-Flares From Pre-Main Sequence Stars: Flare Modeling

Konstantin V. **Getman** (1), Eric D. Feigelson (1), Gordon P. Garmire (2)
ApJ **2021**
https://arxiv.org/pdf/2106.08262.pdf
Getman et al. (2021) reports the discovery, energetics, frequencies, and effects on environs of >1000 X-ray super-flares with X-ray energies EX∼1034−1038∼erg from pre-main sequence (PMS) stars identified in the Chandra MYStIX and SFiNCs surveys. Here we perform detailed plasma evolution modeling of 55 bright MYStIX/SFiNCs super-flares from these events. This is the largest sample of highly energetic flares analyzed in a uniform fashion. They are compared with published X-ray super-flares from young stars in the Orion Nebula Cluster, older active stars, and the Sun. Several results emerge. First, the properties of PMS super-flares are independent of the presence or absence of protoplanetary disks, supporting the solar-type model of PMS flaring magnetic loops with both footpoints anchored in the stellar surface. Second, most PMS super-flares resemble solar long-duration events associated with coronal mass ejections. Slow rise PMS super-flares are an interesting exception. Third, strong correlations of super-flare peak emission measure and plasma temperature with the stellar mass are similar to established correlations for the PMS X-ray emission likely composed of numerous smaller flares. Fourth, a new correlation of loop geometry is linked to stellar mass; more massive stars have thicker flaring loops. Finally, the slope of a long-standing relationship between the X-ray luminosity and magnetic flux of various solar-stellar magnetic elements appears steeper in PMS super-flares than for solar events.

Solar Flares Complex Networks

Akbar **Gheibi**, Hossein Safari, Mohsen Javaherian
2017 *ApJ* **847** 115
https://arxiv.org/pdf/1709.01677.pdf
We investigate the characteristics of the solar flares complex network. The limited predictability, non-linearity, and self-organized criticality of the flares allow us to study systems of flares in the field of the complex systems. Both the occurrence time and the location of flares detected from January 1, 2006 to July 21, 2016 are used to design the growing flares network. The solar surface is divided into cells with equal areas. The cells, which include flare(s), are considered as nodes of the network. The related links are equivalent to sympathetic flaring. The extracted features present that the network of flares follows quantitative measures of complexity. The power-law nature of the connectivity distribution with a degree exponent greater than three reveals that flares form a scale-free and small-world network. The great value of the clustering coefficient, small characteristic path length, and slowly change of the diameter are all characteristics of the flares network. We show that the degree correlation of the flares network has the characteristics of a disassortative

network. About 11% of the large energetic flares (M and X types in GOES classification) that occurred in the network hubs cover 3% of the solar surface.

Fan Loops Observed by IRIS, EIS, and AIA

Avyarthana **Ghosh**1,2, Durgesh Tripathi1, G. R. Gupta1, Vanessa Polito3, Helen E. Mason3, and Sami K. Solanki4,

2017 ApJ 835 244

A comprehensive study of the physical parameters of active region fan loops is presented using the observations recorded with the Interface Region Imaging Spectrometer (IRIS), the EUV Imaging Spectrometer (EIS) on board Hinode, and the Atmospheric Imaging Assembly (AIA) and the Helioseismic and Magnetic Imager (HMI) on board the Solar Dynamics Observatory (SDO). The fan loops emerging from non-flaring AR 11899 (near the disk center) on **2013 November 19** are clearly discernible in AIA 171 Å images and in those obtained in Fe viii and Si vii images using EIS. Our measurements of electron densities reveal that the footpoints of these loops are at an approximately constant pressure with electron densities of cm−3 at (O iv), and cm−3 at (Si x). The electron temperature diagnosed across the fan loops by means of EM-Loci suggest that two temperature components exist at and 5.95 at the footpoints. These components are picked up by IRIS lines and EIS lines, respectively. At higher heights, the loops are nearly isothermal at , which remained constant along the loop. The measurement of the Doppler shift using IRIS lines suggests that the plasma at the footpoints of these loops is predominantly redshifted by 2–3 km s−1 in C ii, 10–15 km s−1 in Si iv, and 15–20 km s−1 in O iv, reflecting the increase in the speed of downflows with increasing temperature from to 5.15. These observations can be explained by low-frequency nanoflares or impulsive heating, and provide further important constraints on the modeling of the dynamics of fan loops.

The Free Energy of NOAA Solar Active Region AR 11029

S. A. **Gilchrist**, M. S. Wheatland and K. D. Leka

Solar Physics, Volume 276, Numbers 1-2, 133-160, **2012**

The NOAA active region (AR) 11029 was a small but highly active sunspot region which produced 73 GOES soft X-ray flares during its transit of the disk in late **October 2009**. The flares appear to show a departure from the well-known power law frequency-size distribution. Specifically, too few GOES C-class and no M-class flares were observed by comparison with a power law distribution (Wheatland, Astrophys. J. 710, 1324, 2010). This was conjectured to be due to the region having insufficient magnetic energy to power the missing large events. We construct nonlinear force-free extrapolations of the coronal magnetic field of AR 11029 using data taken on **24 October** by the SOLIS Vector SpectroMagnetograph (SOLIS/VSM) and data taken on **27 October** by the Hinode Solar Optical Telescope SpectroPolarimeter (Hinode/SP). Force-free modeling with photospheric magnetogram data encounters problems, because the magnetogram data are inconsistent with a force-free model. We employ a recently developed “self-consistency” procedure which addresses this problem and accommodates uncertainties in the boundary data (Wheatland and Régnier, Astrophys. J. 700, L88, 2009). We calculate the total energy and free energy of the self-consistent solution, which provides a model for the coronal magnetic field of the active region. The free energy of the region was found to be ≈4×1029 erg on 24 October and ≈7×1031 erg on 27 October. An order of magnitude scaling between RHESSI non-thermal energy and GOES peak X-ray flux is established from a sample of flares from the literature and is used to estimate flare energies from the observed GOES peak X-ray flux. Based on the scaling, we conclude that the estimated free energy of AR 11029 on 27 October when the flaring rate peaked was sufficient to power M-class or X-class flares; hence, the modeling does not appear to support the hypothesis that the absence of large flares is due to the region having limited energy.

Using Active Contours for Semi-Automated Tracking of UV and EUV Solar Flare Ribbons

C. D. Gill, L. Fletcher and S. Marshall

Solar Phys. 262(2), 355-371, **2010**

Solar-flare UV and EUV images show elongated bright “ribbons” that move over time. If these ribbons are assumed to locate the footpoints of magnetic-field lines reconnecting in the corona, then it is clear that studying their evolution can provide important insight into the reconnection process. An image-processing method based on active contours (commonly referred to as “snakes”) is proposed as a method for tracking UV and EUV flare ribbons and is tested on images from the *Transition Region and Coronal Explorer* (TRACE). This paper introduces the basic concepts of such an approach with a brief overview of the history and theory behind active contours. It then details the specifics of the snake algorithm developed for this work and shows the results of running the algorithm on test images. The results from the application of the developed algorithm are reported for six different TRACE flares (five in UV and one in EUV). The discussion of these results uses the output from an expert tracking the same ribbons by eye as a benchmark, and against these the snake algorithm is shown to compare favourably in certain conditions, but less so in others. The applicability of the automated snake algorithm to the general problem of ribbon tracking is discussed and suggestions for ways to improve the snake algorithm are proposed.

The Signature of Flare Activity in Multifractal Measurements of Active Regions Observed by SDO/HMI

F. **Giorgi**, I. Ermolli, P. Romano, M. Stangalini, F. Zuccarello, S. Criscuoli
Solar Phys. February **2015**, Volume 290, Issue 2, pp 507-525
https://arxiv.org/pdf/1705.06708.pdf

Recent studies indicate that measurements of fractal and multifractal parameters of active regions (ARs) are inefficient tools for distinguishing ARs on the basis of the flare activity or to predict flare events. In an attempt to validate this result on a large observation data set of higher spatial and temporal resolution and higher flux sensitivity than employed in previous studies, we analyzed high-cadence time series of line-of-sight magnetograms of 43 ARs characterized by different flare activity, which were observed with SDO/HMI from May 2010 to December 2013. On these data, we estimated four parameters, the generalized fractal dimensions D 0 and D 8, and the multifractal parameters C div and D div. We found distinct average values of the parameters measured on ARs that have hosted flares of different class. However, the dispersion of values measured on ARs that have produced the same class of events is such that the parameters deduced from distinct classes of flaring regions can also largely overlap. Based on the results of our measurements, C- and M-class flaring ARs are practically indistinguishable, and the same is true for M- and X-class flaring ARs. We only found consistent changes on the time series of the measured parameters on ≈ 50 % of the ARs and ≈ 50 % of the M- and X-class events. We show that these results hold for fractal and multifractal parameter estimates based on total unsigned and signed flux data of the ARs.

Table 1. ARs analyzed in this study accordingly to the NOAA catalog,

Sun CubE OnE: A multi-wavelength synoptic solar micro satellite

L. **Giovannelli** a, F. Berrilli a, M. Casolino b, F. Curti c, +++
Advances in Space Research Volume 71, Issue 4, 15 February **2023**, Pages 1995-2005
https://doi.org/10.1016/j.asr.2022.09.044

The Sun cubE onE (SEE) is a 12U CubeSat mission proposed for a phase A/B study to the Italian Space Agency that will investigate Gamma and X-ray fluxes and ultraviolet (UV) solar emission to support studies in Sun-Earth interaction and Space Weather from LEO. More in detail, SEE's primary goals are to measure the flares emission from soft-X to Gamma ray energy range and to monitor the solar activity in the Fraunhofer Mg II doublet at 280 nm, taking advantage of a full disk imager payload. The Gamma and X-ray fluxes will be studied with unprecedented temporal resolution and with a multi-wavelength approach thanks to the combined use of silicon photodiode and silicon photomultiplier (SiPM) -based detectors. The flare spectrum will be explored from the keV to the MeV range of energies by the same payload, and with a cadence up to 10 kHz and with single-photon detection capabilities to unveil the sources of the solar flares. The energy range covers the same bands used by GOES satellites, which are the standard bands for flare magnitude definition. At the same time SiPM detectors combined with scintillators allow to cover the non-thermal bremsstrahlung emission in the gamma energy range. Given its UV imaging capabilities, SEE will be a key space asset to support detailed studies on solar activity, especially in relation to ultraviolet radiation which strongly interacts with the upper layers of the Earth's atmosphere, and in relation to space safety, included in the field of human space exploration. The main goal for the UV payload is to study the evolution of the solar UV emission in the Mg II band at two different time scales: yearly variations along the solar cycle and transient variations during flare events. The Mg II index is commonly used as a proxy of the solar activity in the Sun-as-a-star paradigm, in which solar irradiance variations in the UV correlate with the variations in stratospheric ozone concentrations and other physical parameters of the Earth high atmosphere. SEE data will be used together with space and ground-based observatories that provide Solar data (e.g. Solar Orbiter, IRIS, GONG, TSST), high energy particle fluxes (e.g. GOES, MAXI, CSES) and geomagnetic data in a multi-instrument/multi-wavelength/multi-messenger approach.

N-body model of magnetic flux tubes reconnecting in the solar atmosphere

Luca **Giovannelli** (1), Francesco Berrilli (1), Dario Del Moro (1), Stefano Scardigli (1), Giuseppe Consolini (2), Marco Stangalini (3), Fabio Giannattasio (2), Adalia Caroli (1), Fulvia Pucci (1), Valentina Penza (
Journal of Physics: Conference Series **2016**
http://arxiv.org/pdf/1601.07105v1.pdf

The investigation of dynamics of the small scale magnetic field on the Sun photosphere is necessary to understand the physical processes occurring in the higher layers of solar atmosphere due to the magnetic coupling between the photosphere and the corona. We present a simulation able to address these phenomena investigating the statistics of magnetic loops reconnections. The simulation is based on N-body model approach and is divided in two computational layers. We simplify the convection problem, interpreting the larger convective scale, mesogranulation, as the result of the collective interaction of convective downflow of granular scale. The N-body advection model is the base to generate a synthetic time series of nanoflares produced by interacting magnetic loops. The reconnection of magnetic field lines is the result of the advection of the magnetic footpoints following the velocity field generated by the interacting downflows. The model gives a quantitative idea of how much energy is expected to be released by the reconfiguration of magnetic loops in the quiet Sun.

Diagnosing transient plasma status: from solar atmosphere to tokamak divertor

A. S. **Giuntaa**, S. Henderson , M. O'Mullane, J. Harrison, J. G. Doyle and H. P. Summers
2016
http://www.arm.ac.uk/~jgd/outgoing/PAPERS/ADAS/JINST_077P_0616_final_draft.pdf
This work strongly exploits the interdisciplinary links between astrophysical (such as the solar upper atmosphere) and laboratory plasmas (such as tokamak devices) by sharing the development of a common modelling for time-dependent ionisation. This is applied to the interpretation of solar flare data observed by the UVSP (Ultraviolet Spectrometer and Polarimeter), on-board the Solar Maximum Mission and the IRIS (Interface Region Imaging Spectrograph), and also to data from B2-SOLPS (Scrape Off Layer Plasma Simulations) for MAST (Mega Ampère Spherical Tokamak) Super-X divertor upgrade. The derived atomic data, calculated in the framework of the ADAS (Atomic Data and Analysis Structure) project, allow equivalent prediction in non-stationary transport regimes and transients of both the solar atmosphere and tokamak divertors, except that the tokamak evolution is about one thousand times faster. **2 Nov 1980**

The need for focused, hard X-ray investigations of the Sun

Lindsay **Glesener**, Albert Y. Shih, Amir Caspi, Ryan Milligan, Hugh Hudson, Mitsuo Oka, Juan Camilo Buitrago-Casas, Fan Guo, Dan Ryan, Eduard Kontar, Astrid Veronig, +++
White paper submitted to the Decadal Survey for Solar and Space Physics (Heliophysics) 2024-2033
2023
https://arxiv.org/ftp/arxiv/papers/2306/2306.05447.pdf
Understanding the nature of energetic particles in the solar atmosphere is one of the most important outstanding problems in heliophysics. Flare-accelerated particles compose a huge fraction of the flare energy budget; they have large influences on how events develop; they are an important source of high-energy particles found in the heliosphere; and they are the single most important corollary to other areas of high-energy astrophysics. Despite the importance of this area of study, this topic has in the past decade received only a small fraction of the resources necessary for a full investigation. For example, NASA has selected no new Explorer-class instrument in the past two decades that is capable of examining this topic. The advances that are currently being made in understanding flare-accelerated electrons are largely undertaken with data from EOVSA (NSF), STIX (ESA), and NuSTAR (NASA Astrophysics). This is despite the inclusion in the previous Heliophysics decadal survey of the FOXSI concept as part of the SEE2020 mission, and also despite NASA's having invested heavily in readying the technology for such an instrument via four flights of the FOXSI sounding rocket experiment. Due to that investment, the instrumentation stands ready to implement a hard X-ray mission to investigate flare-accelerated electrons. This white paper describes the scientific motivation for why this venture should be undertaken soon.

Accelerated Electrons Observed Down to <7 keV in a NuSTAR Solar Microflare

Lindsay **Glesener**1, Säm Krucker2,3, Jessie Duncan1, Iain G. Hannah4, Brian W. Grefenstette5, Bin Chen6, David M. Smith7, Stephen M. White8, and Hugh Hudson2,4
2020 ApJL 891 L34
sci-hub.si/10.3847/2041-8213/ab7341
https://arxiv.org/pdf/2003.12864.pdf
We report the detection of emission from a nonthermal electron distribution in a small solar microflare (GOES class A5.7) observed by the Nuclear Spectroscopic Telescope Array, with supporting observation by the Reuven Ramaty High Energy Solar Spectroscopic Imager (RHESSI). The flaring plasma is well accounted for by a thick-target model of accelerated electrons collisionally thermalizing within the loop, akin to the "coronal thick-target" behavior occasionally observed in larger flares. This is the first positive detection of nonthermal hard X-rays from the Sun using a direct imager (as opposed to indirectly imaging instruments). The accelerated electron distribution has a spectral index of 6.3 ± 0.7, extends down to at least 6.5 keV, and deposits energy at a rate of ~2 × 1027 erg s−1, heating the flare loop to at least 10 MK. The existence of dominant nonthermal emission in X-rays down to <5 keV means
that RHESSI emission is almost entirely nonthermal, contrary to what is usually assumed in RHESSI spectroscopy. The ratio of nonthermal to thermal energies is similar to that of large flares, in contrast to what has been found in previous studies of small RHESSI flares. We suggest that a coronal thick target may be a common property of many small microflares based on the average electron energy and collisional mean free path. Future observations of this kind will enable understanding of how flare particle acceleration changes across energy scales, and will aid the push toward the observational regime of nanoflares, which are a possible source of significant coronal heating. **2017 August 21**

Flare Energy Release at Small Scales

Lindsay **Glesener**
Fleishman's webinar 15 May **2020**
https://youtu.be/SlLbxgCTeSw

Electron Acceleration and Jet-Facilitated Escape in an M Class Solar Flare on 2002 August 19

Lindsay **Glesener**, Gregory D. Fleishman
ApJ **867** 84 **2018**
https://arxiv.org/pdf/1806.00858.pdf
sci-hub.tw/10.3847/1538-4357/aacefe
Sudden jets of collimated plasma arise from many locations on the Sun, including active regions. The magnetic field along which a jet emerges is often open to interplanetary space, offering a clear "escape route" for any flare-accelerated electrons and making jets lucrative targets for studying particle acceleration and the solar sources of transient heliospheric events. Bremsstrahlung hard X-rays (HXRs) could, in principle, trace the accelerated electrons that escape along the paths of the jets, but measurements of the escaping electron beams are customarily difficult due to the low densities of the corona. In this work, we augment HXR observations with gyrosynchrotron emission observed in microwaves, as well as extreme ultraviolet (EUV) emission and modeling to investigate flare-accelerated electrons in a coronal jet. HXR and microwave data from RHESSI and OVSA, respectively, give complementary insight into electron spectra and locations, including the presence of accelerated electrons in the jet itself. High-time-resolution HXR data from the Konus-Wind instrument suggest electron acceleration timescales on the order of 1 second or shorter. We model the energetic electron distributions in the GX Simulator framework using SoHO/MDI, RHESSI, TRACE, and OVSA data as constraints. The result is a modeled distribution, informed and constrained by measurements, of accelerated electrons as they escape the Sun. Combining the detection of microwave gyrosynchrotron emission from an open, rather than closed, magnetic configuration, with realistic 3D modeling constrained by magnetograms, EUV, and X-ray emission, we obtain the most stringent constraints to date on the accelerated electrons within a solar jet.

NuSTAR hard X-ray observation of a sub-A class solar flare

Lindsay **Glesener**, Sa"m Krucker, Iain G. Hannah, Hugh Hudson, Brian W. Grefenstette, Stephen M. White, David M. Smith, Andrew J. Marsh
ApJ **845** 122 **2017**
https://arxiv.org/pdf/1707.04770.pdf
We report a NuSTAR observation of a solar microflare, **SOL2015-09-01T04**. Although it was too faint to be observed by the GOES X-ray Sensor, we estimate the event to be an A0.1 class flare in brightness. This microflare, with only 5 counts per second per detector observed by RHESSI, is fainter than any hard X-ray (HXR) flare in the existing literature. The microflare occurred during a solar pointing by the highly sensitive NuSTAR astrophysical observatory, which used its direct focusing optics to produce detailed HXR microflare spectra and images. The microflare exhibits HXR properties commonly observed in larger flares, including a fast rise and more gradual decay, earlier peak time with higher energy, spatial dimensions similar to the RHESSI microflares, and a high-energy excess beyond an isothermal spectral component during the impulsive phase. The microflare is small in emission measure, temperature, and energy, though not in physical size; observations are consistent with an origin via the interaction of at least two magnetic loops. We estimate the increase in thermal energy at the time of the microflare to be 2.4x10^27 ergs. The observation suggests that flares do indeed scale down to extremely small energies and retain what we customarily think of as "flarelike" properties.

FOXSI Success

Lindsey **Glesener** and Sa"m Krucker
RHESSI Science Nuggets, No. 189, Dec **2012**
the FOXSI rocket soared, and right on schedule a B-class flare was detected. **November 2, 2012**

HARD X-RAY OBSERVATIONS OF A JET AND ACCELERATED ELECTRONS IN THE CORONA

Lindsay **Glesener**1, Säm Krucker2, and R. P. Lin
2012 ApJ 754 9
We report the first hard X-ray observation of a solar jet on the limb with flare footpoints occulted, so that faint emission from accelerated electrons in the corona can be studied in detail. In this event on **2003 August 21**, RHESSI observed a double coronal hard X-ray source in the pre-impulsive phase at both thermal and nonthermal energies. In the impulsive phase, the first of two hard X-ray bursts consists of a single thermal/nonthermal source coinciding with the lower of the two earlier sources, and the second burst shows an additional nonthermal, elongated source, spatially and temporally coincident with the coronal jet. Analysis of the jet hard X-ray source shows that collisional losses by accelerated electrons can deposit enough energy to generate the jet. The hard X-ray time profile above 20 keV matches that of the accompanying Type III and broadband gyrosynchrotron radio emission, indicating both accelerated electrons escaping outward along the jet path and electrons trapped in the flare loop. The double coronal hard X-ray source, the open field lines indicated by Type III bursts, and the presence of a small post-flare loop are consistent with significant electron acceleration in an interchange reconnection geometry.

Features of the Structure and Dynamics of the Active Region 12 673 Associated with Flares.

Golovko, A.A., Salakhutdinova, I.I.
Geomagn. Aeron. 63, 975–983 (**2023**).
https://doi.org/10.1134/S0016793223070083
The features of the structure and dynamics of the NOAA 12 673 active region, which is associated with flares, include a number of processes that are closely correlated in space and time: the formation of two main centers of activity, where the intermittency of the magnetic field and the velocity field is increased compared to the surrounding areas and a rapid stepwise decrease in the unsigned magnetic flux during flares, at velocities up to 4 × 1018 Mx/s in the X9.3 flare on **September 6, 2017**, against the background of a general downward trend at a rate of 1017 Mx/s. The magnitude of the stepwise fall correlates with the flare index; 1-minute bursts of the maximum magnetic field strength, the exit of thin magnetic ropes before the flares and the development of quasi-periodic 4-min pulsations after the X9.3 eruptive flare were detected.

Detecting the solar new magnetic flux regions on the base of vector magnetograms

A. A. **Golovko** & I. I. Salakhutdinova
Journal of Atmospheric and Solar-Terrestrial Physics Volume 179, November **2018**, Pages 120-127
http://sci-hub.tw/http://www.sciencedirect.com/science/article/pii/S1364682617307083
To understand better the origin of CME and other non-stationary processes, the detailed information about emerging flux regions must be known. The advanced method of mapping emerging magnetic flux regions through the multifractal segmentation of vector photospheric magnetograms, is created. It is free from influence of effects of projection. Maps of the vertical component of the field Hz and of the two transversal components Hx, Hy are processed separately and the computed segmented images are summarized. As a result, the detailed picture of distribution of new magnetic fluxes at the current time, is obtained. The SOT Hinode magnetograms for 2006-2015 were used. Observations of the flare-productive active regions NOAA 11158 and 11520 were processed. Hills of a new field in case of their birth have the considerable elongation which is possibly related to their rope-like geometry. In the centers of flare activity, in the vicinity of polarity inversion lines, exits of new magnetic flux alternate with processes of "magnetic cancellation".
February 15, 2011, 2012, July 13

Fractal properties of active regions

A. A. **Golovko** & I. I. Salakhutdinova
Astronomy Reports, 2012, Volume 56, Number 6, Pages 410-416
Astronomicheskii Zhurnal, **2012**, Vol. 89, No. 6, pp. 458–464.
The dynamics of active regions have been investigated using multi-fractal analysis methods, based on magnetograms of the full solar disk in the 630.2 nm line obtained with the SOLIS vector spectromagnetograph of Kitt Peak Observatory (USA) during 2006–2007 and January 1, 2009–April 12, 2010. The applied method of multi-fractal segmentation reveals the appearance of new magnetic fluxes on the Sun disk. A comparison of these fluxes with flare activity shows that the flares are generated in areas of interaction of emerging fluxes with existing structures.

Flare-induced changes of the photospheric magnetic field in a δ-spot deduced from ground-based observations

Peter **Gömöry**, Horst Balthasar, Christoph Kuckein, Július Koza, Astrid M. Veronig, Sergio J. González Manrique, Aleš Kučera, Pavol Schwartz, Arnold Hanslmeier
A&A 602, A60 **2017**
https://arxiv.org/pdf/1704.06089.pdf
Aims: Changes of the magnetic field and the line-of-sight velocities in the photosphere are being reported for an M-class flare that originated at a δ-spot belonging to active region NOAA 11865.
Methods: High-resolution ground-based near-infrared spectropolarimetric observations were acquired simultaneously in two photospheric spectral lines, Fe I 10783 \AA\ and Si I 10786 \AA, with the Tenerife Infrared Polarimeter at the Vacuum Tower Telescope (VTT) in Tenerife on **2013 October 15**. The observations covered several stages of the M-class flare. Inversions of the full-Stokes vector of both lines were carried out and the results were put into context using (extreme)-ultraviolet filtergrams from the Solar Dynamics Observatory (SDO).
Results: The active region showed high flaring activity during the whole observing period. After the M-class flare, the longitudinal magnetic field did not show significant changes along the polarity inversion line (PIL). However, an enhancement of the transverse magnetic field of approximately 550 G was found that bridges the PIL and connects umbrae of opposite polarities in the δ-spot. At the same time, a newly formed system of loops appeared co-spatially in the corona as seen in 171 \AA\ filtergrams of the Atmospheric Imaging Assembly (AIA) on board SDO. However, we cannot exclude that the magnetic connection between the umbrae already existed in the upper atmosphere before the M-class flare and became visible only later when it was filled with hot plasma. The photospheric Doppler velocities show a persistent upflow pattern along the PIL without significant changes due to the flare.
Conclusions: The increase of the transverse component of the magnetic field after the flare together with the newly formed loop system in the corona support recent predictions of flare models and flare observations.

Chromospheric evaporation flows and density changes deduced from Hinode/EIS during an M1.6 flare

P. **Gömöry**, A. M. Veronig, Y. Su, M. Temmer, J. K. Thalmann
A&A 588, A6 **2016**
http://arxiv.org/pdf/1602.02145v1.pdf
We analyzed high-cadence sit-and-stare observations acquired with the Hinode/EIS spectrometer and HXR measurements acquired with RHESSI during an M-class flare. During the flare impulsive phase, we observe no significant flows in the cooler Fe XIII line but strong upflows, up to 80-150 km/s, in the hotter Fe XVI line. The largest Doppler shifts observed in the Fe XVI line were co-temporal with the sharp intensity peak. The electron density obtained from a Fe XIII line pair ratio exhibited fast increase (within two minutes) from the pre-flare level of 5.01x10^(9) cm^(-3) to 3.16x10^(10) cm^(-3) during the flare peak. The nonthermal energy flux density deposited from the coronal acceleration site to the lower atmospheric layers during the flare peak was found to be 1.34x10^(10) erg/s/cm^(2) for a low-energy cut-off that was estimated to be 16 keV. During the decline flare phase, we found a secondary intensity and density peak of lower amplitude that was preceded by upflows of 15 km/s that were detected in both lines. The flare was also accompanied by a filament eruption that was partly captured by the EIS observations. We derived Doppler velocities of 250-300 km/s for the upflowing filament material.The spectroscopic results for the flare peak are consistent with the scenario of explosive chromospheric evaporation, although a comparatively low value of the nonthermal energy flux density was determined for this phase of the flare. This outcome is discussed in the context of recent hydrodynamic simulations. It provides observational evidence that the response of the atmospheric plasma strongly depends on the properties of the electron beams responsible for the heating, in particular the steepness of the energy distribution. **16 February 2011**

Rearrangement of sunspot magnetic field caused by an X1.5 solar flare

Liufan **Gong**, Xiaoli Yan, Hongfei Liang, Zhike Xue, Jincheng Wang, Liheng Yang, Yang Peng, Liping Yang, Xinsheng Zhang
MNRAS, Volume 530, Issue 4, June **2024**, Pages 3897–3905,
https://doi.org/10.1093/mnras/stae1020
https://watermark.silverchair.com/stae1020.pdf
Solar flares will cause the change of the photospheric magnetic field and sunspot structure. However, the exact physical processes involved remain unclear. Here, we study the changes of photospheric magnetic field before and after an X1.5 flare caused by a circular filament eruption in the active region NOAA 13006. The magnetic field structure of this active region is a fan-spine structure with a circular polarity inversion line (PIL). We found that the sunspot structure contracted towards the PIL as a whole after the flare. The penumbra away from the PIL gradually disappears, and the umbra and penumbra near the PIL gradually enhances. By analysing the local magnetic field, the Lorentz force (LF), and the photospheric velocity field in these three regions, we find that the magnetic flux in the region of the disappearing penumbra converges and contracts towards the PIL, leading to an enhancement of the umbra, while the enhancement of the penumbra potentially indicates that this region may be the footpoint of a reconnected magnetic field system. We suggest that this contracting motion is driven by the horizontal LF. **2022 May 10**

The Transition Region of Solar Flare Loops

C. **Gontikakis**, S. K. Antiochos, P. R. Young
ApJ **943** 120 **2023**
https://arxiv.org/pdf/2301.11020.pdf
https://iopscience.iop.org/article/10.3847/1538-4357/aca8a9/pdf
The transition region between the Sun's corona and chromosphere is important to the mass and energy transfer from the lower atmosphere to the corona; consequently, this region has been studied intensely with ultraviolet (UV) and extreme ultraviolet observations. A major result of these studies is that the amount of plasma at temperatures smaller than 100 000 K, is far too large to be compatible with the standard theory of thermal conductivity. However, it is not clear whether the disagreement lies with a problem in the observations or in the theory. We address this issue by analysing high-spatial and temporal resolution EUV observations from an X1.6-class flare taken with the Interface Region Imaging Spectrograph (IRIS) and the Solar Dynamic Observatory/Atmospheric Imaging Assembly (SDO/AIA). These data allow us to isolate the emission of flare loops from that of surrounding structures. We compare the Emission Measures (EMs) derived from the C II 1334.525Ang., Si IV 1402.770Ang transition region spectral lines, the Fe XXI 1354.066Ang flare line and the AIA 171Ang coronal images. We find that the EM ratios are incompatible with a standard conduction-dominated transition region model. Furthermore, the large increases in the EM magnitudes due to flare heating make it highly unlikely that the disagreement between data and theory is due to observational uncertainties in the source of the emission. We conclude that the standard Spitzer Harm thermal conductivity must be invalid for, at least, flare loops. We discuss the possibility that turbulent suppression of thermal conduction can account for our results. **10 Sep 2014**

Differential Emission Measure Evolution as a Precursor of Solar Flares

C. **Gontikakis** (1), I. Kontogiannis (2), M.K. Georgoulis (1,3), C. Guennou (4), P. Syntelis (5), S.H. Park (6), E. Buchlin

2020

https://arxiv.org/pdf/2011.06433.pdf

We analyse the temporal evolution of the Differential Emission Measure (DEM) of solar active regions and explore its usage in solar flare prediction. The DEM maps are provided by the Gaussian Atmospheric Imaging Assembly (GAIA-DEM) archive, calculated assuming a Gaussian dependence of the DEM on the logarithmic temperature. We analyse time-series of sixteen solar active regions and a statistically significant sample of 9454 point-in-time observations corresponding to hundreds of regions observed during solar cycle 24. The time-series analysis shows that the temporal derivatives of the Emission Measure dEM/dt and the maximum DEM temperature dTmax/dt frequently exhibit high positive values a few hours before M- and X-class flares, indicating that flaring regions become brighter and hotter as the flare onset approaches. From the point-in-time observations we compute the conditional probabilities of flare occurrences using the distributions of positive values of the dEM/dt, and dTmax/dt and compare them with corresponding flaring probabilities of the total unsigned magnetic flux, a conventionally used, standard flare predictor. For C-class flares, conditional probabilities have lower or similar values with the ones derived for the unsigned magnetic flux, for 24 and 12 hours forecast windows. For M- and X-class flares, these probabilities are higher than those of the unsigned flux for higher parameter values. Shorter forecast windows improve the conditional probabilities of dEM/dt, and dTmax/dt in comparison to those of the unsigned magnetic flux. We conclude that flare forerunner events such as preflare heating or small flare activity prior to major flares reflect on the temporal evolution of EM and Tmax. Of these two, the temporal derivative of the EM could conceivably be used as a credible precursor, or short-term predictor, of an imminent flare**. 2012-03-06, 6 June 2012, 2012 July 01-05, 2013-10-22, 2014-06-11**

Table 1: Active regions and flares of the first data set (2010-2013).

COMBINING PARTICLE ACCELERATION AND CORONAL HEATING VIA DATA-CONSTRAINED CALCULATIONS OF NANOFLARES IN CORONAL LOOPS

C. **Gontikakis**1, S. Patsourakos2, C. Efthymiopoulos1, A. Anastasiadis3, and M. K. Georgoulis

2013 ApJ 771 126

We model nanoflare heating of extrapolated active-region coronal loops via the acceleration of electrons and protons in Harris-type current sheets. The kinetic energy of the accelerated particles is estimated using semi-analytical and test-particle-tracing approaches. Vector magnetograms and photospheric Doppler velocity maps of NOAA active region 09114, recorded by the Imaging Vector Magnetograph, were used for this analysis. A current-free field extrapolation of the active-region corona was first constructed. The corresponding Poynting fluxes at the footpoints of 5000 extrapolated coronal loops were then calculated. Assuming that reconnecting current sheets develop along these loops, we utilized previous results to estimate the kinetic energy gain of the accelerated particles. We related this energy to nanoflare heating and macroscopic loop characteristics. Kinetic energies of 0.1-8 keV (for electrons) and 0.3-470 keV (for protons) were found to cause heating rates ranging from 10–6 to 1 erg s–1 cm–3. Hydrodynamic simulations show that such heating rates can sustain plasma in coronal conditions inside the loops and generate plasma thermal distributions that are consistent with active-region observations. We concluded the analysis by computing the form of X-ray spectra generated by the accelerated electrons using the thick-target approach. These spectra were found to be in agreement with observed X-ray spectra, thus supporting the plausibility of our nanoflare-heating scenario.

Improving the Spectral Resolution and Wavelength Scale of SDO/EVE MEGS-A Flare Observations.

Gonzalez, G., Chamberlin, P. & Herde, V.

Sol Phys 299, 151 (**2024**).

https://link.springer.com/content/pdf/10.1007/s11207-024-02394-9.pdf

https://doi.org/10.1007/s11207-024-02394-9

The Extreme ultraviolet Variability Experiment (EVE) is one of three instruments onboard the Solar Dynamics Observatory (SDO). This paper focuses on using the “A” channel on the Multiple EUV Grating Spectrographs (MEGS-A) on EVE, which measures wavelengths of 5 – 37 nm, to improve the wavelength scale accuracy and spectral resolution during solar flares. EVE’s least processed (Level 0B) data product is used to create updated wavelength scales that are shown, through this analysis, to make more precise spectral measurements compared to EVE Level 2 data. An X2.2 class flare that occurred on **15 February 2011**, SOL2011-02-15T0156, was used to derive the pixel-to-wavelength scales. An improvement range of 5.21% to 11.35% was found in the emission line widths. In the future, these measurements can be used for improved Doppler velocity calculations of the accelerated plasma of various temperatures during solar flares.

Numerical MHD simulations of solar flares and their associated small-scale structures

Mauricio **González-Servín**, J. J. González-Avilés

MNRAS Volume 528, Issue 3, March **2024**, Pages 5098–5113,
https://arxiv.org/pdf/2402.02161.pdf
https://academic.oup.com/mnras/article-pdf/528/3/5098/56672192/stae375.pdf
Using numerical simulations, we study the formation and dynamics of post-flare loops in a local region of the solar atmosphere. The MHD equations rule the post-flare structures' dynamic evolution, including space-dependent magnetic resistivity and highly anisotropic thermal conduction on a 2.5 D slice. We use an initial magnetic configuration consisting of a vertical current sheet, which helps trigger the magnetic reconnection process. Specifically, we study two scenarios, one with only resistivity and the second with resistivity plus thermal conduction. Numerical simulations show differences in the global morphology of the post-flare substructures in both cases. In particular, localized resistivity produces more substructure on the loops related to a Ritchmyer-Meshkov Instability (RMI). On the other hand, in the scenario with resistivity plus thermal conduction, the post-flare loops are smooth, and no apparent substructures develop. Besides, in the z−component of the current density for the Res+TC scenario, we observe the development of multiple small magnetic islands along the current sheet.

Flare Activity and Magnetic Feature Analysis of the Flare Stars

Hadis **Goodarzi**1, Ahmad Mehrabi1,2, Habib G. Khosroshahi1, and Han He3
2019 ApJS 244 37
https://doi.org/10.3847/1538-4365/ab44cd
We analyze the light curve of 1740 flare stars to study the relationship between the magnetic feature characteristics and the identified flare activity. Coverage and stability of magnetic features are inspired by rotational modulation of light-curve variations and flare activity of stars are obtained using our automated flare detection algorithm. The results show that: (i) the flare time occupation ratio (or flare frequency) and the total power of flares increase by increasing relative magnetic feature coverage and contrast in F–M-type stars; (ii) magnetic feature stability is highly correlated with the coverage and the contrast of the magnetic structures, as this is the case for the Sun; and (iii) stability, coverage, and contrast of the magnetic features, time occupation ratio, and total power of flares increases for G-, K-, and M-type stars by decreasing the Rossby number due to the excess of the produced magnetic field from dynamo procedure until reaching to the saturation level.

Investigating Performance Trends of Simulated Real-time Solar Flare Predictions: The Impacts of Training Windows, Data Volumes, and the Solar Cycle

Griffin T. **Goodwin**, Viacheslav M. Sadykov, Petrus C. Martens
ApJ **964** 163 **2024**
https://arxiv.org/pdf/2402.05288.pdf
https://iopscience.iop.org/article/10.3847/1538-4357/ad276c/pdf
This study explores the behavior of machine learning-based flare forecasting models deployed in a simulated operational environment. Using Georgia State University's Space Weather Analytics for Solar Flares benchmark dataset (Angryk et al. 2020a,b), we examine the impacts of training methodology and the solar cycle on decision tree, support vector machine, and multilayer perceptron performance. We implement our classifiers using three temporal training windows: stationary, rolling, and expanding. The stationary window trains models using a single set of data available before the first forecasting instance, which remains constant throughout the solar cycle. The rolling window trains models using data from a constant time interval before the forecasting instance, which moves with the solar cycle. Finally, the expanding window trains models using all available data before the forecasting instance. For each window, a number of input features (1, 5, 10, 25, 50, 120) and temporal sizes (5, 8, 11, 14, 17, 20 months) were tested. To our surprise, we found that for a 20-month window, skill scores were comparable regardless of the window type, feature count, and classifier selected. Furthermore, reducing the size of this window only marginally decreased stationary and rolling window performance. This implies that, given enough data, a stationary window can be chosen over other window types, eliminating the need for model retraining. Lastly, a moderately strong positive correlation was found to exist between a model's false positive rate and the solar X-ray background flux. This suggests that the solar cycle phase has a considerable influence on forecasting.

Extreme Solar Eruptions and their Space Weather Consequences **Review**

Nat **Gopalswamy**
2017, be published by Elsevier as a chapter in the book, "Extreme Events in the Geospace: Origins, Predictability and Consequences", Ed. Natalia Buzulukova
https://arxiv.org/ftp/arxiv/papers/1709/1709.03165.pdf **File**
Solar eruptions generally refer to coronal mass ejections (CMEs) and flares. Both are important sources of space weather. Solar flares cause sudden change in the ionization level in the ionosphere. CMEs cause solar energetic particle (SEP) events and geomagnetic storms. A flare with unusually high intensity and/or a CME with extremely high energy can be thought of examples of extreme events on the Sun. These events can also lead to extreme SEP events and/or geomagnetic storms. Ultimately, the energy that powers CMEs and flares are stored in magnetic regions on the Sun, known as active regions. Active regions with extraordinary size and magnetic field have the potential to produce

extreme events. Based on current data sets, we estimate the sizes of one-in-hundred and one-in-thousand year events as an indicator of the extremeness of the events. We consider both the extremeness in the source of eruptions and in the consequences. We then compare the estimated 100-year and 1000-year sizes with the sizes of historical extreme events measured or inferred.
Carrington flare , 2003 October 28, 2004 November 10, October 2014
Table 1. Integral fluence values for different models in units of 1010 p cm-2
Table 2. Expected 100-year and 1000-year event sizes estimated from the tail of observed distributions fitted to various functions.

Major Solar Flares without Coronal Mass Ejections

N. **Gopalswamy**1, S. Akiyama1,2 and S. Yashiro1,2,3
Proceedings IAU Symposium No. 257, **2008**, N. Gopalswamy, & D. Webb, eds.; **File**
We examine the source properties of X-class soft X-ray flares that were not associated with coronal mass ejections (CMEs). All the flares were associated with intense microwave bursts implying the production of high energy electrons. However, most (85%) of the flares were not associated with metric type III bursts, even though open field lines existed in all but two of the active regions. The X-class flares seem to be truly confined because there was no material ejection (thermal or nonthermal) away from the flaring region.

Energetic Phenomena on the Sun

Nat **Gopalswamy**
E-print, Nov. **2007**
AIP Conf. Proc. , Kodai School on Solar Physics, edited by S. S. Hasan and D. Banerjee, V. 919, pp. 275-313, 2007; **File**
Solar flares, coronal mass ejections (CMEs), solar energetic particles (SEPs), and fast solar wind represent the energetic phenomena on the Sun.
This paper provides an **over view** of the energetic phenomena on the Sun including their origin interplanetary propagation and space weather consequences.

Magnetic Reconnection Flux during Two Flares on September 6, 2017.

Gopasyuk, O.S., Volvach, A.E. & Yakubovskaya, I.V.
Geomagn. Aeron. 63, 1000–1006 (**2023**).
https://doi.org/10.1134/S0016793223070095
We analyzed the dynamics of the reconnection and energy release processes of the X2.2 and X9.3 flares that occurred on **September 6, 2017** in the active region NOAA 12673. We used SDO/AIA 1600 Å images together with SDO/HMI magnetograms. As a proxy for the flare energy release rate, we used the KRIM and RSTN microwave time profiles, GOES soft X-rays and its time derivative. Assuming that the chromospheric flare ribbons are located at the footpoints of magnetic field lines reconnecting in the corona and that the magnetic flux is conserved from the photosphere to the corona, we obtained magnetic reconnection fluxes and rates of its change. The cumulative positive and negative magnetic fluxes involved in the reconnection process were balanced. Temporal correlations are found between the calculated reconnection rate and the observed microwave emissions from for both events. An analysis of the total cumulative magnetic flux and SXR fluence of events showed that the magnitude of the magnetic flux involved in the reconnection process was greater in more energetic events and less in weaker ones.

Particle acceleration and their escape into the heliosphere in solar flares with open magnetic field

Mykola **Gordovskyy**, Philippa K. Browning, Kanya Kusano, Satoshi Inoue, Gregory E. Vekstein
ApJ **2023**
https://arxiv.org/pdf/2305.19449.pdf
Energetic particle populations in the solar corona and in the heliosphere appear to have different characteristics even when produced in the same solar flare. It is not clear what causes this difference: properties of the acceleration region, the large-scale magnetic field configuration in the flare, or particle transport effects, such as scattering. In this study we use a combination of magnetohydrodynamic and test-particle approaches to investigate magnetic reconnection, particle acceleration and transport in two solar flares: an M-class flare on **June 19th, 2013**, and an X-class flare on **September 6th, 2011**. We show that in both events , the same regions are responsible for the acceleration of particles remaining in the coronal and being ejected towards the heliosphere. However, the magnetic field structure around the acceleration region acts as a filter, resulting in different characteristics (such as energy spectra) acquired by these two populations. We argue that this effect is an intrinsic property of particle acceleration in the current layers created by the interchange reconnection and, therefore, may be ubiquitous, particularly, in non-eruptive solar flares with substantial particle emission into the heliosphere.

Forward Modeling of Particle Acceleration and Transport in an Individual Solar Flare

Mykola **Gordovskyy**1, Philippa K. Browning1, Satoshi Inoue2, Eduard P. Kontar3, Kanya Kusano2, and Grigory E. Vekstein1
2020 ApJ 902 147
https://arxiv.org/pdf/2009.10130.pdf
https://doi.org/10.3847/1538-4357/abb60e
https://iopscience.iop.org/article/10.3847/1538-4357/abb60e/pdf
The aim of this study is to generate maps of the hard X-ray emission produced by energetic electrons in a solar flare and compare them with observations. The ultimate goal is to test the viability of the combined MHD/test-particle approach for data-driven modeling of active events in the solar corona and their impact on the heliosphere. Based on an MHD model of X-class solar flare observed on **2017 September 6**, we calculate trajectories of a large number of electrons and protons using the relativistic guiding-center approach. Using the obtained particle trajectories, we deduce the spatial and energy distributions of energetic electrons and protons, and calculate bremsstrahlung hard X-ray emission using the "thin-target" approximation. Our approach predicts some key characteristics of energetic particles in the considered flare, including the size and location of the acceleration region, energetic particle trajectories and energy spectra. Most importantly, the hard X-ray bremsstrahlung intensity maps predicted by the model are in good agreement with those observed by RHESSI. Furthermore, the locations of proton and electron precipitation appear to be close to the sources of helioseismic response detected in this flare. Therefore, the adopted approach can be used for observationally driven modeling of individual solar flares, including manifestations of energetic particles in the corona, as well as the inner heliosphere. **2017 September 6**

Combining MHD and kinetic modelling of solar flares **Review**

M. **Gordovskyy**, P.K. Browning, R.F. Pinto
Advances in Space Research **2018**
https://arxiv.org/pdf/1809.05751.pdf
Solar flares are explosive events in the solar corona, representing fast conversion of magnetic energy into thermal and kinetic energy, and hence radiation, due to magnetic reconnection. Modelling is essential for understanding and predicting these events. However, self-consistent modelling is extremely difficult due to the vast spatial and temporal scale separation between processes involving thermal plasma (normally considered using magnetohydrodynamic (MHD) approach) and non-thermal plasma (requiring a kinetic approach). In this mini-review we consider different approaches aimed at bridging the gap between fluid and kinetic modelling of solar flares. Two types of approaches are discussed: combined MHD/test-particle (MHDTP) models, which can be used for modelling the flaring corona with relatively small numbers of energetic particles, and hybrid fluid-kinetic methods, which can be used for modelling stronger events with higher numbers of energetic particles. Two specific examples are discussed in more detail: MHDTP models of magnetic reconnection and particle acceleration in kink-unstable twisted coronal loops, and a novel reduced-kinetic model of particle transport.

Forward modelling of particle acceleration and transport in an individual solar flare

Mykola **Gordovskyy**, Philippa K. Browning, Satoshi Inoue, Eduard P. Kontar, Kanya Kusano, Grigory E. Vekstein
ApJ **2020**
https://arxiv.org/pdf/2009.10130.pdf
The aim of this study is to generate maps of the hard X-ray emission produced by energetic electrons in a solar flare and compare them with observations. The ultimate goal is to test the viability of the combined MHD/test-particle approach for data-driven modelling of active events in the solar corona and their impact on the heliosphere. Based on an MHD model of X-class solar flare observed on the **6th of September 2017**, we calculate trajectories of a large number of electrons and protons using the relativistic guiding-centre approach. Using the obtained particle trajectories, we deduce the spatial and energy distributions of energetic electrons and protons, and calculate bremsstrahlung hard X-ray emission using the 'thin target' approximation. Our approach predicts some key characteristics of energetic particles in the considered flare, including the size and location of the acceleration region, energetic particle trajectories and energy spectra. Most importantly, the hard X-ray bremsstrahlung intensity maps predicted by the model are in a good agreement with those observed by RHESSI. Furthermore, the locations of proton and electron precipitation appear to be close to the sources of helioseismic response detected in this flare. Therefore, the adopted approach can be used for observationally-driven modelling of individual solar flares, including manifestations of energetic particles in the corona, as well as inner heliosphere.

Combining MHD and kinetic modelling of solar flares

Mykola **Gordovskyy** a,⇑ , Philippa Browning a , Rui F. Pinto
Advances in Space Research 63 (**2019**) 1453–1465
Solar flares are explosive events in the solar corona, representing fast conversion of magnetic energy into thermal and kinetic energy, and hence radiation, due to magnetic reconnection. Modelling is essential for understanding and

predicting these events. However, selfconsistent modelling is extremely difficult due to the vast spatial and temporal scale separation between processes involving thermal plasma (normally considered using magnetohydrodynamic (MHD) approach) and non-thermal plasma (requiring a kinetic approach). In this mini-review we consider different approaches aimed at bridging the gap between fluid and kinetic modelling of solar flares. Two types of approaches are discussed: combined MHD/test-particle (MHDTP) models, which can be used for modelling the flaring corona with relatively small numbers of energetic particles, and hybrid fluid-kinetic methods, which can be used for modelling stronger events with higher numbers of energetic particles. Two specific examples are discussed in more detail: MHDTP models of magnetic reconnection and particle acceleration in kink-unstable twisted coronal loops, and a novel reduced-kinetic model of particle transport in converging magnetic fields.

Non-thermal line broadening in flaring coronal loops

Mykola **Gordovskyy**, Philippa Browning (University of Manchester) and Eduard Kontar
UKSP Nugget #76 **2017**
http://www.uksolphys.org/uksp-nugget/76-non-thermal-line-broadening-in-flaring-coronal-loops/
It is generally accepted that NTB represents spatially unresolved line-of-sight (LOS) motions (or LOS velocity dispersion), although there is no quantitative understanding of the physics of this effect in flares. In our study we exploit a numerical model of a solar flare [3] to investigate the velocity field in the flaring atmosphere. More specifically, we calculate the LOS velocities and LOS velocity dispersions for plasmas with different temperatures and compare them with observations (see [4] for more information).

Microwave polarisation as a detection tool for magnetic twist in solar flares

Mykola **Gordovskyy**∗1 , Philippa Browning1 , Eduard Kontar2 , Rui Pinto3 , and Nicole Vilmer4
CESRA **2016** p.59
http://cesra2016.sciencesconf.org/conference/cesra2016/pages/CESRA2016_prog_abs_book_v3.pdf
Reconnecting twisted coronal loops are a good alternative to the standard model for explaining some types of solar flares. Particularly, they can be a good candidate for interpreting smaller flares observed in isolated coronal loops. Furthermore, twisted flux ropes often form an essential element of the standard model for larger, eruptive flares. Therefore, it is important to be able to identify twisted magnetic fields in the flaring corona. We explore various observational features obtained using coupled MHD and test-particle models of thermal and non-thermal plasmas in reconnecting twisted coronal loops, developed using the Lare3D and GCA codes, and GX simulator. It is shown, that both thermal (EUV and SXR) and non-thermal (HXR and microwave) emission can be used for observational detection of twisted loops. In particular, I will discuss the microwave emission from twisted loops, and use of the cross-loop circular polarisation gradient of gyrosynchrotron emission (Sharykin & Kuznetsov 2016; Gordovskyy et al. 2016) as a potential detection tool, and its limitations for different field configurations and loop orientations.

Plasma motions and non-thermal line broadening in flaring twisted coronal loops

Mykola **Gordovskyy**, Eduard Kontar, Philippa Browning
A&A 589, A104 **2015**
http://arxiv.org/pdf/1508.06412v1.pdf
Observation of coronal EUV spectral lines offers an opportunity to evaluate the thermal structure and flows in flaring atmospheres. This, in turn, can be used to estimate the partitioning between the thermal and kinetic energies released in flares. Our aim is to forward-model large-scale (50-10000 km) velocity distributions in order to interpret non-thermal broadening of different spectral EUV lines observed in flares. The developed models allow us to understand the origin of the observed spectral line shifts and broadening, and link these features to particular physical phenomena in flaring atmospheres. We use ideal MHD to derive unstable twisted magnetic fluxtube configurations in a gravitationally-stratified atmosphere. The evolution of these twisted fluxtubes is followed using resistive MHD, with anomalous resistivity depending on the local density and temperature. The model also takes into account the thermal conduction and radiative losses. The model allows us to evaluate average velocities and velocity dispersions, which would be detected as 'non-thermal' velocities in observations, at different temperatures. Our models show qualitative and quantitative agreement with observations. Thus, the line-of-sight (LOS) velocity dispersions demonstrate substantial correlation with the temperature, increasing from about 20-30 km/s around 1 MK to about 200-400 km/s near 10-20 MK. The average velocities also correlate with velocity dispersions, although they demonstrate a very strong scattering, compared to observations. We also note that near foot-points the velocity dispersions across the magnetic field are systematically lower than that along the field. We conclude, that the correlation between the flow velocities, velocity dispersions and temperatures are likely to indicate that the same heating mechanism is responsible for heating the plasma, its turbulisation and expansion/evaporation.

Observational signatures of magnetic reconnection in kink-unstable coronal loops

Mykola **Gordovskyy**
UKSP Nugget #51, Oct **2014**
http://www.uksolphys.org/uksp-nugget/51-observational-signatures-of-magnetic-reconnection-in-twisted-coronal-loops/
What would the flare X-ray emission from a twisted loop look like?
Our numerical models provide two remarkable observational features, which should be observable in reconnecting twisted coronal loops (see [10,11] for more details). Firstly, we predict a 'twisted' pattern in thermal emission (EUV or SXR). However, the twist should be around 2π, i.e. much lower than the critical twist required for kink instability. This is consistent with observations: the twist angle visible in EUV is normally about few π. Secondly, the flaring loop should have expanding cross-section, which should be visible as a gradual increase in the horizontal size of HXR footpoints.

Observations of Unresolved Photospheric Magnetic Fields in Solar Flares Using Fe I and Cr I Lines

Mykola **Gordovskyy**, Vsevolod G. Lozitsky
Solar Phys., Volume 289, Issue 10, pp 3681-3701, **2014**
http://arxiv.org/pdf/1404.3938v1.pdf
The structure of the photospheric magnetic field during solar flares is examined using echelle spectropolarimetric observations. The study is based on several Fe I and Cr I lines observed at locations corresponding to brightest Hα emission during thermal phase of flares. The analysis is performed by comparing magnetic field values deduced from lines with different magnetic sensitivities, as well as by examining the fine structure of I±V Stokes profiles splitting. It is shown that the field has at least two components, with stronger unresolved flux tubes embedded in weaker ambient field. Based on a two-component magnetic field model, we compare observed and synthetic line profiles and show that the field strength in small-scale flux tubes is about 2−3 kG. Furthermore, we find that the small-scale flux tubes are associated with flare emission, which may have implications for flare phenomenology.

Particle acceleration and transport in reconnecting twisted loops in a stratified atmosphere

M. **Gordovskyy**1, P. K. Browning1, E. P. Kontar2 and N. H. Bian
A&A 561, A72 (**2014**)
http://arxiv.org/pdf/1501.06418v1.pdf
Context. Twisted coronal loops should be ubiquitous in the solar corona. Twisted magnetic fields contain excess magnetic energy, which can be released during magnetic reconnection, causing solar flares.
Aims. The aim of this work is to investigate magnetic reconnection, and particle acceleration and transport in kink-unstable twisted coronal loops, with a focus on the effects of resistivity, loop geometry and atmospheric stratification. Another aim is to perform forward-modelling of bremsstrahlung emission and determine the structure of hard X-ray sources.
Methods. We use a combination of magnetohydrodynamic (MHD) and test-particle methods. First, the evolution of the kinking coronal loop is considered using resistive MHD model, incorporating atmospheric stratification and loop curvature. Then, the obtained electric and magnetic fields and density distributions are used to calculate electron and proton trajectories using a guiding-centre approximation, taking into account Coulomb collisions.
Results. It is shown that electric fields in twisted coronal loops can effectively accelerate protons and electrons to energies up to 10 MeV. High-energy particles have hard, nearly power-law energy spectra. The volume occupied by high-energy particles demonstrates radial expansion, which results in the expansion of the visible hard X-ray loop and a gradual increase in hard X-ray footpoint area. Synthesised hard X-ray emission reveals strong footpoint sources and the extended coronal source, whose intensity strongly depends on the coronal loop density.

Effect of Collisions and Magnetic Convergence on Electron Acceleration and Transport in Reconnecting Twisted Solar Flare Loops

M. **Gordovskyy**, P. K. Browning, E. P. Kontar, N. H. Bian
Solar Physics, June **2013**, Volume 284, Issue 2, pp 489-498
http://arxiv.org/pdf/1501.06436v1.pdf
We study a model of particle acceleration coupled with an MHD model of magnetic reconnection in unstable twisted coronal loops. The kink instability leads to the formation of helical currents with strong parallel electric fields resulting in electron acceleration. The motion of electrons in the electric and magnetic fields of the reconnecting loop is investigated using a test-particle approach taking into account collisional scattering. We discuss the effects of Coulomb collisions and magnetic convergence near loop footpoints on the spatial distribution and energy spectra of high-energy electron populations and possible implications on the hard X-ray emission in solar flares.

Magnetic Relaxation and Particle Acceleration in a Flaring Twisted Coronal Loop

M. **Gordovskyy** and P. K. Browning

Solar Physics, Volume 277, Number 2, 299-316, **2012**

In the present work we aim to study particle acceleration in twisted coronal loops. For this purpose, an MHD model of magnetic reconnection in a linearly unstable twisted magnetic fluxtube is considered. Further, the electric and magnetic fields obtained in the MHD simulations are used to calculate proton and electron trajectories in the guiding-centre approximation. It is shown that particle acceleration in such a model is distributed rather uniformly along the coronal loop and the high-energy population remains generally neutral. It also follows from the model that the horizontal cross-section of the volume occupied by high-energy particles near the loop footpoints increases with time, which can be used as an observational proxy.

PARTICLE ACCELERATION BY MAGNETIC RECONNECTION IN A TWISTED CORONAL LOOP

Mykola **Gordovskyy** and Philippa K. Browning

Astrophysical Journal, 729:101 (6pp), **2011**

Photospheric motions may lead to twisted coronal magnetic fields which contain free energy that can be released by reconnection. Browning & Van der Linden suggested that such a relaxation event may be triggered by the onset of ideal kink instability. In the present work, we study the evolution of a twisted magnetic flux tube with zero net axial current following Hood et al. Based on the obtained magnetic and electric fields, proton and electron trajectories are calculated using the test-particle approach. We discuss resulting particle distributions and possible observational implications, for example, for small solar flares.

Solar Flare Occurrence Rate and Waiting Time Statistics

A. **Gorobets**, M. Messerotti

Solar Physics, December **2012**, Volume 281, Issue 2, pp 651-667

We use Renewal Theory for the estimation and interpretation of the flare rate from the Geostationary Operational Environmental Satellite (GOES) soft X-ray flare catalogue. It is found that, in addition to the flare rate variability with the solar cycles, a much faster variation occurs. The fast variation on time scales of days and hours down to minute scale appears to be comparable with time intervals between two successive flares (waiting times). The detected fast non-stationarity of the flaring rate is discussed in the framework of the previously published stochastic models of the waiting time dynamics.

EVIDENCE FOR COLLAPSING FIELDS IN THE CORONA AND PHOTOSPHERE DURING THE 2011 FEBRUARY 15 X2.2 FLARE: SDO/AIA AND HMI OBSERVATIONS

S. **Gosain**

2012 ApJ 749 85

We use high-resolution Solar Dynamics Observatory (SDO)/Atmospheric Imaging Assembly observations to study the evolution of the coronal loops in a flaring solar active region, NOAA 11158. We identify three distinct phases of the coronal loop dynamics during this event: (1) slow-rise phase: slow rising motion of the loop-tops prior to the flare in response to the slow rise of the underlying flux rope; (2) collapse phase: sudden contraction of the loop-tops, with the lower loops collapsing earlier than the higher loops; and (3) oscillation phase: the loops exhibit global kink oscillations after the collapse phase at different periods, with the period decreasing with the decreasing height of the loops. The period of these loop oscillations is used to estimate the field strength in the coronal loops. Furthermore, we also use SDO/Helioseismic and Magnetic Imager (HMI) observations to study the photospheric changes close to the polarity inversion line (PIL). The longitudinal magnetograms show a stepwise permanent decrease in the magnetic flux after the flare over a coherent patch along the PIL. Furthermore, we examine the HMI Stokes I, Q, U, V profiles over this patch and find that the Stokes-V signal systematically decreases while the Stokes-Q and U signals increase after the flare. These observations suggest that close to the PIL the field configuration became more horizontal after the flare. We also use HMI vector magnetic field observations to quantify the changes in the field inclination angle and find an inward collapse of the field lines toward the PIL by ~10°. These observations are consistent with the "coronal implosion" scenario and its predictions about flare-related photospheric field changes.

THE EVOLUTION OF THE TWIST SHEAR AND DIP SHEAR DURING X-CLASS FLARE OF 2006 DECEMBER 13: *HINODE* OBSERVATIONS

Sanjay **Gosain** and P. Venkatakrishnan

Astrophysical Journal Letters, 720:L137–L143, **2010**

The non-potentiality of solar magnetic fields is traditionally measured in terms of a magnetic shear angle, i.e., the angle between the observed and potential field azimuths. Here, we introduce another measure of the shear that has not been previously studied in solar active regions, i.e., the one that is associated with the inclination angle of the magnetic field. This form of the shear, which we call "dip shear," can be calculated by taking the difference between the observed and the potential field inclination. In this Letter, we study the evolution of the dip shear as well as the conventional twist shear in a δ-sunspot using high-resolution vector magnetograms from the *Hinode* space mission. We monitor these shears in a penumbral region located close to a flaring site during 2006 December 12 and 13. It is found that (1) the penumbral area close to the flaring site shows a high value of the twist shear and dip shear as compared with other parts of the penumbra, (2) after the flare, the value of the dip shear drops in this region while the twist shear tends to increase, (3) the dip shear and twist shear are correlated such that pixels with a large twist shear also tend to exhibit a large dip shear, and (4) the correlation between the twist shear and dip shear is tighter after the flare. The present study suggests that monitoring the twist shear alone during the flare is not sufficient, but we need to monitor it together with the dip shear.

HINODE OBSERVATIONS OF COHERENT LATERAL MOTION OF PENUMBRAL FILAMENTS DURING AN X-CLASS FLARE

S. **Gosain**, P. Venkatakrishnan, and Sanjiv Kumar Tiwari
Astrophysical Journal, 706:L240–L245, **2009** December

The X-3.4 class flare of **2006 December 13** was observed with a high cadence of 2 minutes at 0.2 arcsec resolution by *HINODE*/SOT FG instrument. The flare ribbons could be seen in G-band images also. A careful analysis of these observations after proper registration of images shows flare-related changes in penumbral filaments of the associated sunspot for the first time. The observations of sunspot deformation, decay of penumbral area, and changes in magnetic flux during large flares have been reported earlier in the literature. In this Letter, we report lateral motion of the penumbral filaments in a sheared region of the δ-sunspot during the X-class flare. Such shifts have not been seen earlier. The lateral motion occurs in two phases: (1) motion before the flare ribbons move across the penumbral filaments and (2) motion afterward. The former motion is directed away from expanding flare ribbons and lasts for about 4 minutes. The latter motion is directed in the opposite direction and lasts for more than 40 minutes. Further, we locate a patch in adjacent opposite polarity spot moving in opposite direction to the penumbral filaments. Together these patches represent conjugate footpoints on either side of the polarity inversion line, moving toward each other. This converging motion could be interpreted as shrinkage of field lines.

The solar flare myth.

Gosling, J.T.,
1993. J. Geophys. Res. 98, 18937–18950.

Evolution of solar surface inflows around emerging active regions

N. **Gottschling**, H. Schunker, A. C. Birch, B. Löptien, L. Gizon
A&A **2021**
https://arxiv.org/pdf/2105.10501.pdf

Solar active regions are associated with Evershed outflows in sunspot penumbrae, moat outflows surrounding sunspots, and extended inflows surrounding active regions. The latter have been identified on established active regions by various methods. The evolution of these inflows and their dependence on active region properties as well as their impact on the global magnetic field are not yet understood. We aim to understand the evolution of the average inflows around emerging active regions and to derive an empirical model for these inflows. We analyze horizontal flows at the surface of the Sun using local correlation tracking of solar granules observed in continuum images of SDO/HMI. We measure average flows of a sample of 182 isolated active regions up to seven days before and after their emergence onto the solar surface with a cadence of 12 hours. We investigate the average inflow properties with respect to active region characteristics of total flux and latitude. We fit a model to these observed inflows for a quantitative analysis. We find that converging flows of around 20 to 30 m/s are first visible one day prior to emergence, in agreement with recent results. These converging flows are present independently of active region properties of latitude or flux. We confirm a recently found prograde flow of about 40 m/s at the leading polarity during emergence. We find that the time after emergence when the latitudinal inflows increase in amplitude depends on the flux of the active region, ranging from one to four days after emergence and increasing with flux. The largest extent of the inflows is up to about 7±1∘ away from the center of the active region within the first six days after emergence. The inflow velocities have amplitudes of about 50 m/s.

Thermal Properties of Current Sheet Plasmas in Solar Flares

Tingyu **Gou**, Katharine K. Reeves
ApJ **972** 164 **2024**

https://arxiv.org/pdf/2407.01833
https://iopscience.iop.org/article/10.3847/1538-4357/ad5d61/pdf
The current sheet is an essential feature in solar flares and is the primary site for magnetic reconnetion and energy release. Imaging observations feature a long linear structure above the candle-flame-shaped flare loops, which resembles the standard flare model with the current sheet viewed edge-on. We investigate the thermal properties of plasmas surrounding the linear sheet during flares, using EUV observations from the Atmospheric Imaging Assembly (AIA) onboard the Solar Dynamics Observatory (SDO). The differential emission measure (DEM) analyses show evidence of high temperatures in the plasma sheets (PSs), containing hot emissions from only a narrow temperature range, suggestive of an isothermal feature. The sheet's temperature remains constant at different heights above the flare arcade, peaking at around logT=7.0-7.1; while the well-studied 2017 September 10 X8.2 flare exhibits as an exception in that the temperature decreases with an increasing height and peaks higher (logT=7.25) during the gradual phase. Most PS cases also hold similar emission measures and thicknesses; while the PS's emissions drop exponentially above the flare arcade, the sheet thicknesses show no significant height association as for all the measurements. The characteristics of isothermal and steady temperature suggests balanced heating and cooling processes along the current sheet, particularly additional heating may exist to compensate for the conductive and radiative cooling away from the reconenction site. Our results suggest a steady and uniform sheet structure in the macroscopic scale that results from flare reconnection. **2013 May 13, 2013 May 14, 2014 Feb 25, 2017 Sep 10, 2023 Feb 17,**

Solar Flare-CME Coupling Throughout Two Acceleration Phases of a Fast CME

Tingyu **Gou**, Astrid M. Veronig, Rui Liu, Bin Zhuang, Mateja Dumbovic, Tatiana Podladchikova, Hamish A. S. Reid, Manuela Temmer, Karin Dissauer, Bojan Vrsnak, Yuming Wang
ApJL **2020**
https://arxiv.org/pdf/2006.11707.pdf
Solar flares and coronal mass ejections (CMEs) are closely coupled through magnetic reconnection. CMEs are usually accelerated impulsively within the low solar corona, synchronized with the impulsive flare energy release. We investigate the dynamic evolution of a fast CME and its associated X2.8 flare occurring on **2013 May 13**. The CME experiences two distinct phases of enhanced acceleration, an impulsive one with a peak value of ~5 km s−2 followed by an extended phase with accelerations up to 0.7 km s−2. The two-phase CME dynamics is associated with a two-episode flare energy release. While the first episode is consistent with the "standard" eruption of a magnetic flux rope, the second episode of flare energy release is initiated by the reconnection of a large-scale loop in the aftermath of the eruption and produces stronger nonthermal emission up to γ-rays. In addition, this long-duration flare reveals clear signs of ongoing magnetic reconnection during the decay phase, evidenced by extended HXR bursts with energies up to 100--300 keV and intermittent downflows of reconnected loops for >4 hours. The observations reveal that the two-step flare reconnection substantially contributes to the two-phase CME acceleration, and the impulsive CME acceleration precedes the most intense flare energy release. The implications of this non-standard flare/CME observation are discussed.

Direct Observation of Two-step Magnetic Reconnection in a Solar Flare

Tingyu **Gou**, Astrid M. Veronig, Ewan C. Dickson, Aaron Hernandez-Perez, Rui Liu
ApJL, 845: L1 (**2017**)
http://sci-hub.cc/10.3847/2041-8213/aa813d
https://arxiv.org/pdf/1707.06198.pdf
We report observations of an eruptive X2.8 flare on **2013 May 13**, which shows two distinct episodes of energy release in the impulsive phase. The first episode is characterized by the eruption of a magnetic flux rope, similar to the energy-release process in most standard eruptive flares. The second episode, which is stronger than the first normal one and shows enhanced high-energy X-ray and even γ-ray emissions, is closely associated with magnetic reconnection of a large-scale loop in the aftermath of the eruption. The reconnection inflow of the loop leg is observed in the Solar Dynamics Observatory (SDO)/Atmospheric Imaging Assembly (AIA) 304 ? passband and accelerates toward the reconnection region to speeds as high as ~130 km s-1. Simultaneously, the corresponding outflow jets are observed in the AIA hot passbands with speeds of ~740 km s-1 and a mean temperature of ~14 MK. RHESSI observations show a strong burst of hard X-ray (HXR) and γ-ray emissions with hard electron spectra of $\delta \approx 3$, exhibiting a soft"hard"harder behavior. A distinct altitude decrease of the HXR loop-top source coincides with the inward swing of the loop leg observed in the AIA 304 ? passband, which is suggested to be related to the coronal implosion. This fast inflow of magnetic flux contained in the loop leg greatly enhances the reconnection rate and results in very efficient particle acceleration in the second-step reconnection, which also helps to achieve a second higher temperature peak up to $T \approx 30$ MK.

Stereoscopic Observation of Slipping Reconnection in A Double Candle-Flame-Shaped Solar Flare

Tingyu **Gou**, Rui Liu, Yuming Wang, Kai Liu, Bin Zhuang, Jun Chen, Quanhao Zhang, Jiajia Liu

ApJLetters **821** L28 **2016**
http://arxiv.org/pdf/1604.01457v1.pdf
The **2011 January 28** M1.4 flare exhibits two side-by-side candle-flame-shaped flare loop systems underneath a larger cusp-shaped structure during the decay phase, as observed at the northwestern solar limb by the Solar Dynamics Observatory (SDO). The northern loop system brightens following the initiation of the flare within the southern loop system, but all three cusp-shaped structures are characterized by ~ 10 MK temperatures, hotter than the arch-shaped loops underneath. The "Ahead" satellite of the Solar Terrestrial Relations Observatory (STEREO) provides a top view, in which the post-flare loops brighten sequentially, with one end fixed while the other apparently slipping eastward. By performing stereoscopic reconstruction of the post-flare loops in EUV and mapping out magnetic connectivities, we found that the footpoints of the post-flare loops are slipping along the footprint of a hyperbolic flux tube (HFT) separating the two loop systems, and that the reconstructed loops share similarity with the magnetic field lines that are traced starting from the same HFT footprint, where the field lines are relatively flexible. These results argue strongly in favor of slipping magnetic reconnection at the HFT. The slipping reconnection was likely triggered by the flare and manifested as propagative dimmings before the loop slippage is observed. It may contribute to the late-phase peak in Fe XVI 33.5 nm, which is even higher than its main-phase counterpart, and may also play a role in the density and temperature asymmetry observed in the northern loop system through heat conduction.

Do All Candle-Flame-Shaped Flares Have the Same Temperature Distribution?

Tingyu **Gou**, Rui Liu, Yuming Wang
Solar Phys. Volume 290, Issue 8, pp 2211-2230 **2015**
We performed a differential emission measure (DEM) analysis of candle-flame-shaped flares observed with the Atmospheric Imaging Assembly onboard the Solar Dynamic Observatory. The DEM profile of flaring plasmas generally exhibits a double peak distribution in temperature, with a cold component around logT≈6.2 and a hot component around logT≈7.0. Attributing the cold component mainly to the coronal background, we propose a mean temperature weighted by the hot DEM component as a better representation of flaring plasma than the conventionally defined mean temperature, which is weighted by the whole DEM profile. Based on this corrected mean temperature, the majority of the flares studied, including a confined flare with a double candle-flame shape sharing the same cusp-shaped structure, resemble the famous Tsuneta flare in temperature distribution, i.e., the cusp-shaped structure has systematically higher temperatures than the rounded flare arcade underneath. However, the M7.7 flare on **19 July 2012** poses a very intriguing violation of this paradigm: the temperature decreases with altitude from the tip of the cusp toward the top of the arcade; the hottest region is slightly above the X-ray loop-top source that is co-spatial with the emission-measure-enhanced region at the top of the arcade. This signifies that a different heating mechanism from the slow-mode shocks attached to the reconnection site operates in the cusp region during the flare decay phase.

A systematic examination of particle motion in a collapsing magnetic trap model for solar flares

K. J. **Grady**, T. Neukirch and P. Giuliani
A&A 546, A85 (**2012**)
Context. It has been suggested that collapsing magnetic traps may contribute to accelerating particles to high energies during solar flares.
Aims. We present a detailed investigation of the energization processes of particles in collapsing magnetic traps, using a specific model. We also compare for the first time the energization processes in a symmetric and an asymmetric trap model.
Methods. Particle orbits are calculated using guiding centre theory. We systematically investigate the dependence of the energization process on initial position, initial energy and initial pitch angle.
Results. We find that in our symmetric trap model particles can gain up to about 50 times their initial energy, but that for most initial conditions the energy gain is more moderate. Particles with an initial position in the weak field region of the collapsing trap and with pitch angles around 90° achieve the highest energy gain, with betatron acceleration of the perpendicular energy the dominant energization mechanism. For particles with smaller initial pitch angle, but still outside the loss cone, we find the possibility of a significant increase in parallel energy. This increase in parallel energy can be attributed to the curvature term in the parallel equation of motion and the associated energy gain happens in the centre of the trap, where the field line curvature has its maximum. We find qualitatively similar results for the asymmetric trap model, but with smaller energy gains and a larger number of particles escaping from the trap.

An extension of the theory of kinematic MHD models of collapsing magnetic traps to 2.5D with shear flow and to 3D:

K. J. **Grady** and T. Neukirch

A&A 508 (**2009**) 1461-1468
http://www.aanda.org/10.1051/0004-6361/200913230
Context. During solar flares a large number of charged particles are accelerated to high energies, but the exact mechanism responsible for this is, so far, still unclear. Acceleration in collapsing magnetic traps is one of the mechanisms proposed.
Aims. In the present paper we want to extend previous 2D models for collapsing magnetic traps to 3D models and to 2D models with shear flow.
Methods. We use analytic solutions of the kinematic magnetohydrodynamic (MHD) equations to construct the models. Particle orbits are calculated using the guiding centre approximation.
Results. We present a general theoretical framework for constructing kinematic MHD models of collapsing magnetic traps in 3D and in 2D with shear flow. A few illustrative examples of collapsing trap models are presented, together with some preliminary studies of particle orbits. For these example orbits, the energy increases roughly by a factor of 5 or 6, which is consistent with the energy increase found in previous 2D models.

Octupolar out-of-plane magnetic field structure generation during collisionless magnetic reconnection in a stressed X-point collapse

J. **Graf von der Pahlen**, D. Tsiklauri
Physics of Plasma, **2014**
http://arxiv.org/pdf/1406.3890v1.pdf
The out-of-plane magnetic field, generated by fast magnetic reconnection, during collisionless, stressed X-point collapse, was studied with a kinetic, 2.5D, fully electromagnetic, relativistic particle-in-cell numerical code, using both closed (flux conserving) and open boundary conditions on a square grid. It was discovered that the well known quadrupolar structure in the out-of-plane magnetic field gains four additional regions of opposite magnetic polarity, emerging near the corners of the simulation box, moving towards the X-point. The emerging, outer, magnetic field structure has opposite polarity to the inner quadrupolar structure, leading to an overall octupolar structure. Using Ampere's law and integrating electron and ion currents, defined at grid cells, over the simulation domain, contributions to the out-of-plane magnetic field from electron and ion currents were determined. The emerging regions of opposite magnetic polarity were shown to be the result of ion currents. Magnetic octupolar structure is found to be a signature of X-point collapse, rather than tearing mode, and factors relating to potential discoveries in experimental scenarios or space-craft observations are discussed.

Spectral signatures of chromospheric condensation in a major solar flare

David R. **Graham**, Gianna Cauzzi, Luca Zangrilli, Adam Kowalski, Paulo Simões, Joel Allred
ApJ **895** 6 **2020**
https://arxiv.org/pdf/2004.05075.pdf
https://doi.org/10.3847/1538-4357/ab88ad
We study the evolution of chromospheric line and continuum emission during the impulsive phase of the X-class SOL**2014-09-10**T17:45 solar flare. We extend previous analyses of this flare to multiple chromospheric lines of Fe I, Fe II, Mg II, C I, and Si II, observed with IRIS, combined with radiative-hydrodynamical (RHD) modeling. For multiple flaring kernels, the lines all show a rapidly evolving double-component structure: an enhanced, emission component at rest, and a broad, highly red-shifted component of comparable intensity. The red-shifted components migrate from 25-50 km s−1 towards the rest wavelength within ∼30 seconds.
Using Fermi hard X-ray observations, we derive the parameters of an accelerated electron beam impacting the dense chromosphere, using them to drive a RHD simulation with the RADYN code. As in Kowalski et al. 2017a, our simulations show that the most energetic electrons penetrate into the deep chromosphere, heating it to T∼10,000 K, while the bulk of the electrons dissipate their energy higher, driving an explosive evaporation, and its counterpart condensation -- a very dense (ne∼2×1014 cm−3), thin layer (30--40 km thickness), heated to 8--12,000 K, moving towards the stationary chromosphere at up to 50 km s−1.
The synthetic Fe II 2814.45A profiles closely resemble the observational data, including a continuum enhancement, and both a stationary and a highly red-shifted component, rapidly moving towards the rest wavelength. Importantly, the absolute continuum intensity, ratio of component intensities, relative time of appearance, and red-shift amplitude, are sensitive to the model input parameters, showing great potential as diagnostics.

Temporal evolution of multiple evaporating ribbon sources in a solar flare

D. R. **Graham**, G. Cauzzi
ApJL **807** L22 **2015**
http://arxiv.org/pdf/1506.03465v1.pdf
We present new results from the Interface Region Imaging Spectrograph showing the dynamic evolution of chromospheric evaporation and condensation in a flare ribbon, with the highest temporal and spatial resolution to date. IRIS observed the entire impulsive phase of the X-class flare **SOL2014-09-10**T17:45 using a 9.4 second cadence `sit-and-stare' mode. As the ribbon brightened successively at new positions along the slit, a unique impulsive phase

evolution was observed for many tens of individual pixels in both coronal and chromospheric lines. Each activation of a new footpoint displays the same initial coronal up-flows of up to ~300 km/s, and chromospheric downflows up to 40 km/s. Although the coronal flows can be delayed by over 1 minute with respect to those in the chromosphere, the temporal evolution of flows is strikingly similar between all pixels, and consistent with predictions from hydrodynamic flare models. Given the large sample of independent footpoints, we conclude that each flaring pixel can be considered a prototypical, `elementary' flare kernel.

Determining Energy Balance in the Flaring Chromosphere from Oxygen V Line Ratios

David R. **Graham**, Lyndsay Fletcher, Nicolas Labrosse
A&A, 584, A6 **2014**
http://arxiv.org/pdf/1411.4603v1.pdf
The impulsive phase of solar flares is a time of rapid energy deposition and heating in the lower solar atmosphere, leading to changes in the temperature and density structure of the region. We use an O V density diagnostic formed of the 192 to 248 line ratio, provided by Hinode EIS, to determine the density of flare footpoint plasma, at O V formation temperatures of 250,000 K, giving a constraint on the properties of the heated transition region. Hinode EIS rasters from 2 small flare events in December 2007 were used. Raster images were co-aligned to identify and establish the footpoint pixels, multiple-component Gaussian line fitting of the spectra was carried out to isolate the diagnostic pair, and the density was calculated for several footpoint areas. The assumptions of equilibrium ionization and optically thin radiation for the O V lines were found to be acceptable. Properties of the electron distribution, for one event, were deduced from earlier RHESSI hard X-ray observations and used to calculate the plasma heating rate, delivered by an electron beam adopting collisional thick-target assumptions, for 2 model atmospheres. Electron number densities of at least log n = 12.3 cm-3 were measured during the flare impulsive phase, far higher than previously expected. For one footpoint, the radiative loss rate for this plasma was found to exceed that which can be delivered by an electron beam implied by the RHESSI data. However, when assuming a completely ionised target atmosphere the heating rate exceeded the losses. A chromospheric thickness of 70-700 km was found to be required to balance a conductive input to the O V-emitting region with radiative losses. The analysis shows that for heating by collisional electrons, it is difficult, or impossible to raise the temperature of the chromosphere to explain the observed densities without assuming a completely ionised atmosphere. **2007-12-14**

THE EMISSION MEASURE DISTRIBUTION OF IMPULSIVE PHASE FLARE FOOTPOINTS

D. R. **Graham**1, I. G. Hannah1, L. Fletcher1, and R. O. Milligan
2013 ApJ 767 83
http://arxiv.org/pdf/1302.2514v1.pdf
The temperature distribution of the emitting plasma is a crucial constraint when studying the heating of solar flare footpoints. However, determining this for impulsive phase footpoints has been difficult in the past due to insufficient spatial resolution to resolve the footpoints from the loop structures, and a lack of spectral and temporal coverage. We use the capabilities of Hinode/Extreme Ultraviolet Imaging Spectrometer to obtain the first emission measure distributions (EMDs) from impulsive phase footpoints in six flares. Observations with good spectral coverage were analyzed using a regularized inversion method to recover the EMDs. We find that the EMDs all share a peak temperature of around 8 MK, with lines formed around this temperature having emission measures (EMs) peaking between 1028 and 1029 cm–5, indicating a substantial presence of plasma at very high temperatures within the footpoints. An EMD gradient of EM(T) ~ T is found in all events. Previous theoretical work on EM gradients shows this to be consistent with a scenario in which the deposited flare energy directly heats only the top layer of the flare chromosphere, while deeper layers are heated by conduction.

The density of EUV flare footpoints

David **Graham**, Lyndsay Fletcher & Iain Hannah
UKSP Nuggets 27 July **2011**
Density diagnostics of flare footpoints show a little bit of corona in the chromosphere.
http://www.uksolphys.org/?p=2987
SOL2007-06-05 (C6.6)

Hinode/EIS plasma diagnostics in the flaring solar chromosphere

D. R. **Graham**, L. Fletcher and I. G. Hannah
A&A 532, A27 (**2011**)

Context. The impulsive phase of solar flares is a time of rapid energy deposition and heating in the lower solar atmosphere, leading to changes in the temperature, density, ionisation and velocity structure of this region.
Aims. We aim to study the lower atmosphere during the impulsive phase of a flare using imaging and spectroscopic data from Hinode/EIS, RHESSI and TRACE. We place these observations in context by using a wide range of temperature observations from each instrument.
Methods. We analyse sparse raster data from the Hinode/EIS spectrometer to derive the density and line-of-sight velocity in flare footpoints, in a GOES C6.6 flare observed **on 05-June-2007**. The raster duration was 150s across the centre of a small active region, allowing multiple exposures of the flare ribbons and footpoints. Using RHESSI and Hinode/XRT we test both non-thermal and thermal models for the HXR emission.
Results. During the flare impulsive phase, we find evidence from XRT for flare footpoints at temperatures exceeding 7 MK. We measure the electron number density increasing up to a few ×1010 cm-3 in the footpoints, at temperatures of ~1.5−2 MK, accompanied by small downflows at temperatures below Fe XIII and upflows of up to ~140 km s-1 at temperatures above. This is reasonable in the context of HXR diagnostics of the flare electron beam. The electrons inferred have sufficient energy to affect the chromospheric ionisation structure.
Conclusions. EIS sparse raster data coupled with RHESSI imaging and spectroscopy prove useful here in studying the lower atmosphere of solar flares, and in this event suggest heat deposition relatively high in the chromosphere drives chromospheric evaporation while increasing the observed electron densities at footpoints. However, from RHESSI spectral fitting it is not possible to say whether the data are more consistent with a model including a non-thermal beam, or purely thermal model.

Strong Photospheric Heating Indicated by Fe I 6173 Å Line Emission During White-Light Solar Flares

Samuel **Granovsky**, Alexander G. Kosovichev, Viacheslav M. Sadykov, Graham S. Kerr, Joel C. Allred
ApJ **2024**
https://arxiv.org/pdf/2410.07440
Between 2017 and 2024, the Helioseismic and Magnetic Imager (HMI) onboard the Solar Dynamics Observatory has observed several white-light solar flares. Notably, for the X9.3 flare of **September 6, 2017**, HMI spectro-polarimetric observations reveal one or more locations within the umbra of the associated active region where the Fe I 6173 Å line goes into full emission, indicating significant heating of the photosphere and lower chromosphere. For these flares, we performed a spectro-polarimetric analysis at the aforementioned locations using HMI 90s cadence Stokes data. At the Fe I emission locations, line-core emission is observed to last for a single 90 s frame and is either concurrent with or followed by increases in the line continuum intensity lasting 90 to 180 seconds. This is followed by a smooth decay to pre-flare conditions over the next three to twenty minutes. For most locations, permanent changes to the Stokes Q, U, and/or V profiles were observed, indicating long-lasting non-transient changes to the photospheric magnetic field. These emissions coincided with local maxima in hard X-ray emission observed by the Konus instrument onboard the Wind spacecraft, as well as local maxima in the time derivative of soft X-ray emission observed by GOES satellites. Comparison of the Fe I 6173 Å line profile synthesis for the ad-hoc heating of the initial empirical VAL-S umbra model and quiescent Sun (VAL-C-like) model indicates that the Fe I 6173 Å line emission in the white-light flare kernels could be explained by the strong heating of initially cool photospheric regions.

A STATISTICAL STUDY OF SPECTRAL HARDENING IN SOLAR FLARES AND RELATED SOLAR ENERGETIC PARTICLE EVENTS

James A. **Grayson**, S¨am Krucker, and R. P. Lin1
Astrophysical Journal, 707:1588–1594, **2009** December; **File**
Using hard X-ray observations from the *Reuven Ramaty High Energy Solar Spectroscopic Imager* (*RHESSI*), we investigate the reliability of spectral hardening during solar flares as an indicator of related solar energetic particle (SEP) events at Earth. All *RHESSI* data are analyzed, from 2002 February through the end of Solar Cycle 23, thereby expanding upon recent work on a smaller sample of flares. Previous investigations have found very high success when associating soft–hard–harder (SHH) spectral behavior with energetic proton events, and confirmation of this link would suggest a correlation between electron acceleration in solar flares and SEPs seen in interplanetary space. In agreement with these past findings, we find that of 37 magnetically wellconnected flares (W30−W90), 12 of 18 flares with SHH behavior produced SEP events and none of 19 flares without SHH behavior produced SEPs. ***This demonstrates a statistically significant dependence of SHH and SEP observations, a link that is unexplained in the standard scenario of SEP acceleration at the shock front of coronal mass ejections and encourages further investigation of the mechanisms which could be responsible.***

On the Instrumental Discrepancies in Lyman-alpha Observations of Solar Flares

Harry J. **Greatorex**, Ryan O. Milligan, Ingolf E. Dammasch
Solar Phys. **299**, 162 **2024**

https://arxiv.org/pdf/2411.00736
https://link.springer.com/content/pdf/10.1007/s11207-024-02407-7.pdf
Despite the energetic significance of Lyman-alpha (Ly{\alpha}; 1216Å) emission from solar flares, regular observations of flare related Ly{\alpha} have been relatively scarce until recently. Advances in instrumental capabilities and a shift in focus over previous Solar Cycles mean it is now routinely possible to take regular co-observations of Ly{\alpha} emission in solar flares. Thus, it is valuable to examine how the instruments selected for flare observations may influence the conclusions drawn from the analysis of their unique measurements. Here, we examine three M-class flares each observed in Ly{\alpha} by GOES-14/EUVS-E, GOES-15/EUVS-E, or GOES-16/EXIS-EUVS-B, and at least one other instrument from PROBA2/LYRA, MAVEN/EUVM, ASO-S/LST-SDI, and SDO/EVE-MEGS-P. For each flare, the relative and excess flux, contrast, total energy, and timings of the Ly{\alpha} emission were compared between instruments. It was found that while the discrepancies in measurements of the relative flux between instruments may be considered minimal, the calculated contrasts, excess fluxes, and energetics may differ significantly - in some cases up to a factor of five. This may have a notable impact on multi instrument investigations of the variable Ly{\alpha} emission in solar flares and estimates of the contribution of Ly{\alpha} to the radiated energy budget of the chromosphere. The findings presented in this study will act as a guide for the interpretation of observations of flare-related Ly{\alpha} from upcoming instruments during future Solar Cycles and inform conclusions drawn from multi-instrument studies. **2010–02–08, 2016–04–18, 2023–05–09**

Observational Analysis of Lyman-alpha Emission in Equivalent Magnitude Solar Flares

Harry J. **Greatorex**, Ryan O. Milligan, Phillip C. Chamberlin
ApJ **954** 120 **2023**
https://arxiv.org/pdf/2306.16234.pdf
https://iopscience.iop.org/article/10.3847/1538-4357/acea7f/pdf
The chromospheric Lyman-alpha line of neutral hydrogen (Lyα; 1216 Å) is the most intense emission line in the solar spectrum, yet until recently observations of flare-related Lyα emission have been scarce. Here, we examine the relationship between nonthermal electrons accelerated during the impulsive phase of three M3 flares that were co-observed by RHESSI, GOES, and SDO, and the corresponding response of the chromosphere in Lyα. Despite having identical X-ray magnitudes, these flares show significantly different Lyα responses. The peak Lyα enhancements above quiescent background for these flares were 1.5%, 3.3%, and 6.4%. However, the predicted Lyα enhancements from FISM2 were consistently <2.5%. By comparing the properties of the nonthermal electrons derived from spectral analysis of hard X-ray observations, flares with a harder spectral index were found to produce a greater Lyα enhancement. The percentage of nonthermal energy radiated by the Lyα line during the impulsive phase was found to range from 2.0-7.9%. Comparatively, the radiative losses in He II (304 Å) were found to range from 0.6-1.4% of the nonthermal energy while displaying enhancements above the background of 7.3-10.8%. FISM2 was also found to underestimate the level of He II emission in two out of the three flares. These results may have implications for space weather studies and modelling the response of the terrestrial atmosphere to changes in the solar irradiance, and will guide the interpretation of flare-related Lyα observations that will become available during Solar Cycle 25. **16 Oct 2010, 24 Sep 2011, 1 Feb 2014**

Eruptive Flare, CME, and Shock Wave in the 25 August 2001 High-Energy Solar Event

V. V. **Grechnev**, A. A. Kochanov & A. M. Uralov
Solar Physics volume 298, Article number: 49 (**2023**)
https://doi.org/10.1007/s11207-023-02144-3
https://link.springer.com/content/pdf/10.1007/s11207-023-02144-3.pdf **File**
The major SOL**2001-08-25** event produced a fast coronal mass ejection (CME: 1430 km s−1), strong flare emissions in hard X-rays and γ-rays extending to high energies, and neutrons detected both on spacecraft and by a low-latitude neutron monitor. To supplement the probable picture of this outstanding event, we reconstruct kinematic plots of the eruption and the shock-wave history. The hard X-ray and γ-ray emissions exhibited soft-hard-soft evolution. The emissions were strongest and hardest during a two-minute interval soon after the highest change rate of the magnetic flux within the flare ribbons of 2.6×10^{19} Mx s−1, which was simultaneous with the reconstructed acceleration of the erupting flux rope. We reveal an indication of accelerated electrons injected into the erupting flux rope that then precipitated far from the main flare site, producing a hard X-ray source that moved along the footprint of a stretching flux-rope leg. These results suggest that the particle acceleration was governed by magnetic reconnection during the eruption. As in a typical situation, a piston shock was excited early in the impulsive phase and gradually transformed into a bow shock later. The frequency drift of a Type-II burst is shown to be proportional to a power of frequency f, $df/dt \propto -f^{\epsilon}$, with a typical range of ϵ being between 5/3 and 2. Overall, the SOL**2011-08-25** event was a typical eruptive two-ribbon flare. Its strength was determined mainly by the intensity of the reconnection processes.

Reconciliation of Observational Challenges to the Impulsive-Piston Shock-Excitation Scenario.
II. Shock Waves Produced in CME-less Events with a Null-Point Topology.

Grechnev, V.V., Kiselev, V.I., Uralov, A.M., Myshyakov, I.I.:
Solar Phys., **2022, File See movies of 16 Apr 2014**
Continuing Article I, we revisit challenging events previously identified by different authors, whose analysis led to conclusions about various mechanisms of the shock-wave excitation. Here we reconsider four events that involved fan–spine coronal configurations with a null-point topology (NPT). The presence of Type-II radio bursts in all events as well as extreme-ultraviolet disturbances (EUV waves) observed in three events evidence the presence of shock waves, whereas no coronal mass ejections (CMEs) were detected in most events. One idea proposed to explain observations was the shock-wave excitation by the straightening of a post-reconnection kinked loop. The Type-II burst in another event appeared in association with a compact flare with a high thermal pressure that looked in favor of a flare-generated blast wave. One event was associated with a possible pseudo-CME. All of these challenging events have been reconciled in terms of an impulsively excited piston shock. CME-less filament eruptions in NPT configurations appear to represent a distinct category of events responsible for some of the observed shock waves. **14 November 2005 , 28 February 2011 , 6 March 2014 , 16 April 2014**

Reconciliation of Observational Challenges to the Impulsive-Piston Shock-Excitation Scenario.
I. Kinematic Challenges

V.V. **Grechnev** · V.I. Kiselev · A.M. Uralov
Solar Phys. **297**, Article number: 106 **2022 File See movies of 8 December 2007**
Until now, there is no consensus on the origin of coronal shock waves. Questions also remain about the patterns that govern the propagation of the presumably related disturbances observed in the extreme ultraviolet (EUV waves). We present arguments in favor of the initial excitation of the waves by the impulsive acceleration of erupting structures. We consider two puzzling events that have been known thanks to the efforts of different research teams. Using recent findings and our methods, we aim to figure out what might actually have happened in these challenging events. In the first event, the expansion of the coronal mass ejection (CME) was determined by gravity starting from the low corona. The previous analysis led the authors to a conclusion about the flare-related origin of the associated shock wave. We also consider another event, in which an EUV wave had a strange kinematics. This was one of the weakest flares accompanied by EUV waves. Both of these challenging events have been reconciled in terms of an impulsively-excited piston shock. **24 December 1996, 8 December 2007**

Twin Null-Point-Associated Major Eruptive Three-Ribbon Flares with Unusual Microwave Spectra

V.V. **Grechnev**, N.S. Meshalkina, A.M. Uralov, A.A. Kochanov, S.V. Lesovoi, I.I. Myshyakov, V.I. Kiselev, D.A. Zhdanov, A.T. Altyntsev, M.V. Globa
Solar Phys. **295**, Article number: 128 **2020**
https://arxiv.org/pdf/2009.10350.pdf
https://link.springer.com/content/pdf/10.1007/s11207-020-01702-3.pdf
On **23 July 2016** after 05:00\,UTC, the first 48-antenna stage of the Siberian Radioheliograph detected two flares of M7.6 and M5.5 GOES importance that occurred within half an hour in the same active region. Their multi-instrument analysis reveals the following. The microwave spectra were flattened at low frequencies and the spectrum of the stronger burst had a lower turnover frequency. Each flare was eruptive, emitted hard X-rays and gamma-rays exceeding 800\,keV, and had a rare three-ribbon configuration. An extended hard X-ray source associated with a longest middle ribbon was observed in the second flare. The unusual properties of the microwave spectra are accounted for by a distributed multi-loop system in an asymmetric magnetic configuration that our modeling confirms. Microwave images did not to resolve compact configurations in these flares that may also be revealed incompletely in hard X-ray images because of their limited dynamic range. Being apparently simple and compact, non-thermal sources corresponded to the structures observed in the extreme ultraviolet. In the scenario proposed for two successive three-ribbon eruptive flares in a configuration with a coronal-null region, the first eruption causes a flare and facilitates the second eruption that also results in a flare.

Radio, Hard X-Ray, and Gamma-Ray Emissions Associated with a Far-Side Solar Event

V. **Grechnev**1 ¢ V. Kiselev1 ¢K. Kashapova1;2 ¢ A. Kochanov1;2 ¢I. Zimovets3;4;5 ¢ A. Uralov1 ¢ B. Nizamov6;7 ¢ I. Grigorieva8 ¢ D. Golovin3 ¢ M. Litvak3 ¢I. Mitrofanov3 ¢ A. Sanin3
Solar Phys. 293(10):133 **2018 File**
https://arxiv.org/abs/1808.10103
https://link.springer.com/content/pdf/10.1007%2Fs11207-018-1368-4.pdf
The **SOL2014-09-01** far-side solar eruptive event produced hard electromagnetic and radio emissions observed with detectors at near-Earth vantage points. Especially challenging was a long-duration > 100MeV gamma-ray burst probably produced by accelerated protons exceeding 300 MeV. This fact rose a question how high-energy protons could reach the Earth-facing solar surface. Some preceding studies discussed a scenario in which protons accelerated by a CME-driven shock high in the corona return to the solar surface. We continue with the analysis of this challenging event, involving radio images from the Nan»cay Radioheliograph and hard X-ray data from the High Energy Neutron Detector (HEND) of the Gamma-Ray Spectrometer onboard the Mars Odysseyspace observatory located near Mars. HEND recorded unocculted flare emission. The results indicate that the emissions observed from the Earth's direction were generated by flare-accelerated electrons and protons trapped in static long coronal loops. Their reacceleration is possible in these loops by a shock wave, which was excited by the eruption, being initially not CME-driven. The results highlight the ways to address remaining questions.

The 26 December 2001 Solar Eruptive Event Responsible for GLE63. III. CME, Shock Waves, and Energetic Particles

V.V. **Grechnev** (1), V.I. Kiselev (1), A.M. Uralov (1), K.-L. Klein (2), A.A. Kochanov (1)
Solar Phys. **2017**
https://arxiv.org/pdf/1612.04092v1.pdf **File**
The 26 December 2001 moderate solar eruptive event (GOES importance M7.1, microwaves up to 4000 sfu at 9.4 GHz, CME speed 1446 km/s) produced strong fluxes of solar energetic particles (SEPs) and ground-level enhancement of cosmic-ray intensity (GLE63). To find a possible reason for the atypically high proton outcome of this event, we study its multi-wavelength images and dynamic radio spectra, and quantitatively reconcile the findings with each other. An additional eruption probably occurred in the same active region about half an hour before the main eruption, which produced two blast-wave-like shocks during the impulsive phase. Later on, the two shock waves merged around the frontal direction into a single shock, which is traced up to 25R⊙ as a halo ahead of the expanding CME body, in agreement with an interplanetary type II event recorded by Wind/WAVES. The shape and kinematics of the halo indicate that the shock wave was in an intermediate regime between the blast wave and bow shock at these distances. The results show that i) the shock wave appeared during the flare rise and could accelerate particles earlier than usually assumed; ii) the particle event could be amplified by the preceding eruption, which stretched closed structures above the developing CME, facilitating its lift-off and escape of flare-accelerated particles, enabling a higher CME speed and a stronger shock ahead; iii) escape of flare-accelerated particles could be additionally facilitated by reconnection of the flux rope, where they were trapped, with a large coronal hole; iv) a rich seed population was provided by the first eruption for the acceleration by a trailing shock wave.

The 26 December 2001 Solar Eruptive Event Responsible for GLE63. II. Multi-Loop Structure of Microwave Sources in a Major Long-Duration Flare

V.V. **Grechnev** . A. M. Uralov, V. I. Kiselev, A.A. Kochanov
Solar Phys. January **2017**, 292:3 **File**
https://arxiv.org/pdf/1611.08349v1.pdf
Our analysis of the observations of the SOL2001-12-26 event, which was related to ground-level enhancement of cosmic-ray intensity GLE63, including microwave spectra and images from the Nobeyama Radioheliograph at 17 and 34 GHz, from the Siberian Solar Radio Telescope at 5.7 GHz, and from the Transition Region and Coronal Explorer in 1600 A, has led to the following results: A flare ribbon overlapped with the sunspot umbra, which is typical of large particle events. Atypical were i) the long duration of the flare, which lasted more than one hour; ii) the moderate intensity of the microwave burst, which was about 104 sfu; iii) the low peak frequency of the gyrosynchrotron spectrum, which was about 6 GHz; and its insensitivity to the flux increase by more than one order of magnitude. This was accompanied by a nearly constant ratio of the flux emitted by the volume in the high-frequency part of the spectrum to its elevated low-frequency part determined by the area of the source. With the self-similarity of the spectrum, a similarity was observed between the moving microwave sources and the brightest parts of the flare ribbons in 1600 A images. We compared the 17 GHz and 1600 A images and confirm that the microwave sources were associated with multiple flare loops, whose footpoints appeared in the ultraviolet as intermittent bright kernels. To understand the properties of the event, we simulated its microwave emission using a system of several homogeneous gyrosynchrotron sources above the ribbons. The scatter between the spectra and the sizes of the individual sources is determined by the inhomogeneity of the magnetic field within the ribbons. The microwave flux is mainly governed by the magnetic flux passing through the ribbons and the sources. The apparent simplicity of the microwave structures is caused by a poorer spatial resolution and dynamic range of the microwave imaging. The results indicate that microwave

manifestations of accelerated electrons correspond to the structures observed in thermal emissions, as well-known models predict.
See CESRA Highlight # 1375, May 2017 http://www.astro.gla.ac.uk/users/eduard/cesra/?p=1375

The 26 December 2001 Solar Event Responsible for GLE63. I. Observations of a Major Long-Duration Flare with the Siberian Solar Radio Telescope

V.V. **Grechnev** . A.A. Kochanov
Solar Phys. **2016 File**
http://arxiv.org/pdf/1609.02256v1.pdf
Ground Level Enhancements (GLEs) of cosmic-ray intensity occur, on average, once a year. Due to their rareness, studying the solar sources of GLEs is especially important to approach understanding their origin. The SOL2001-12-26 eruptive-flare event responsible for GLE63 seems to be challenging in some aspects. Deficient observations limited its perception. Analysis of extra observations found for this event provided new results presented in three companion papers. This paper, Paper I, addresses the observations of this flare with the Siberian Solar Radio Telescope (SSRT). Taking advantage of its instrumental particularities, we analyze the detailed SSRT observations of a major long-duration flare at 5.7 GHz without cleaning the images. The analysis confirms that the source of GLE63 was associated with an event in active region 9742 that was manifested in the first flare and the main flare. The first flare (04:30-05:03 UT) reached a GOES level of about M1.6. Two microwave sources have been revealed, whose brightness temperatures at 5.7 GHz exceeded 10 MK. The main flare, up to the M7.1 level, started at 05:04 UT, and occurred in strong magnetic .elds. The observed microwave sources reached about 250 MK. They appeared on the weaker-fi.eld periphery of the active region, approached each other nearly along the magnetic neutral line, coming closer to a stronger-field core of the active region, and then moved away from the neutral line like expanding ribbons. These motions rule out an association of the non-thermal microwave sources with a single flaring loop. These issues and the possible causes of the high proton productivity of this event are addressed in Paper II and Paper III.

Responsibility of a Filament Eruption for the Initiation of a Flare, CME, and Blast Wave, and its Possible Transformation into a Bow Shock

V. V. **Grechnev** (1), A. M. Uralov (1), I. V. Kuzmenko (2), A. A. Kochanov (1), I. M. Chertok (3), S. S. Kalashnikov
Solar Phys., **2014**
http://arxiv.org/pdf/1410.8696v1.pdf
Multi-instrument observations of two filament eruptions on **24 February and 11 May 2011** suggest the following updated scenario for eruptive flare, CME and shock wave evolution. An initial destabilization of a filament results in stretching out of magnetic threads belonging to its body and rooted in the photosphere along the inversion line. Their reconnection leads to i) heating of parts of the filament or its environment, ii) initial development of the flare arcade cusp and ribbons, and iii) increasing similarity of the filament to a curved flux rope and its acceleration. Then the pre-eruption arcade enveloping the filament gets involved in reconnection according to the standard model and continues to form the flare arcade and ribbons. The poloidal magnetic flux in the curved rope developing from the filament progressively increases and forces its toroidal expansion. This flux rope impulsively expands and produces an MHD disturbance, which rapidly steepens into a shock. The shock passes through the arcade expanding above the filament and then freely propagates ahead of the CME like a decelerating blast wave for some time. If the CME is slow, then the shock eventually decays. Otherwise, the frontal part of the shock changes into the bow-shock regime. This was observed for the first time in the 24 February 2011 event. When reconnection ceases, the flux rope relaxes and constitutes the CME core-cavity system. The expanding arcade develops into the CME frontal structure. We also found that reconnection in the current sheet of a remote streamer forced by the shock's passage results in a running flare-like process within the streamer responsible for a type II burst. The development of dimming and various associated phenomena are discussed.

The 17 February 2013 sunquake in the context of the active region's magnetic field configuration

Lucie M. **Green**, Gherardo Valori, Francesco P. Zuccarello, Sergei Zharkov, Sarah Matthews, Salvo L. Guglielmino
2017 ApJ 849 40
https://arxiv.org/pdf/1709.04874.pdf
Sunquakes are created by the hydrodynamic response of the lower atmosphere to a sudden deposition of energy and momentum. In this study we investigate a sunquake that occurred in NOAA active region 11675 on **17 February 2013**. Observations of the corona, chromosphere and photosphere are brought together for the first time with a non-linear force-free model of the active region's magnetic field in order to probe the magnetic environment in which the sunquake was initiated. We find that the sunquake was associated with the destabilization of a flux rope and an associated M-class

GOES flare. Active region 11675 was in its emergence phase at the time of the sunquake and photospheric motions caused by the emergence heavily modified the flux rope and its associated quasi-separatrix layers, eventually triggering the flux rope's instability. The flux rope was surrounded by an extended envelope of field lines rooted in a small area at the approximate position of the sunquake. We argue that the configuration of the envelope, by interacting with the expanding flux rope, created a "magnetic lens" that may have focussed energy in one particular location the photosphere, creating the necessary conditions for the initiation of the sunquake.

The First Focused Hard X-ray Images of the Sun with NuSTAR

Brian W. **Grefenstette**, Lindsay Glesener, S□äm Krucker, Hugh Hudson, Iain G. Hannah, David M. Smith, Julia K. Vogel, Stephen M. White, Kristin K. Madsen, Andrew J. Marsh, Amir Caspi, Bin Chen, Albert Shih, Matej Kuhar, Steven E. Boggs, Finn E. Christensen, William W. Craig, Karl Forster, Charles J. Hailey, Fiona A. Harrison, Hiromasa Miyasaka, Daniel Stern, William W. Zhang

ApJ **826** 20 **2016**

http://arxiv.org/pdf/1605.09738v1.pdf

We present results from the the first campaign of dedicated solar observations undertaken by the \textit{**Nuclear Spectroscopic Telescope ARray**} ({\em NuSTAR}) hard X-ray telescope. Designed as an astrophysics mission, {\em NuSTAR} nonetheless has the capability of directly imaging the Sun at hard X-ray energies (>3~keV) with an increase in sensitivity of at least two magnitude compared to current non-focusing telescopes. In this paper we describe the scientific areas where \textit{NuSTAR} will make major improvements on existing solar measurements. We report on the techniques used to observe the Sun with \textit{NuSTAR}, their limitations and complications, and the procedures developed to optimize solar data quality derived from our experience with the initial solar observations. These first observations are briefly described, including the measurement of the Fe K-shell lines in a decaying X-class flare, hard X-ray emission from high in the solar corona, and full-disk hard X-ray images of the Sun.

Bayesian Inference for Solar Flare Extremes

B. **Griffiths**,L. Fawcett,A.C. Green

Space Weather **Volume20, Issue3** e2021SW002886 **2022**

https://agupubs.onlinelibrary.wiley.com/doi/epdf/10.1029/2021SW002886

https://doi.org/10.1029/2021SW002886

While solar flares are a frequent occurrence, extreme flares are much rarer events and have the potential to cause disruption to life on Earth. In this paper we use Extreme Value Theory to model extreme solar flares, with inference performed in the Bayesian paradigm. The data used have been provided by the National Oceanic and Atmospheric Organisation and consist of recordings of peak flux measurements. After proposing several methods for analysis and selecting our preferred technique - which substantially increases the precision of estimates of key quantities of interest - we improve upon this technique still further by considering the use of informative prior distributions. Doing so, we estimate that a Halloween-type solar event, and a Carrington-type event, might occur once (on average) every 49 (29, 85) and 92 (50, 176) years respectively (95% credible intervals shown in parentheses). These findings are similar to those obtained by Tsiftsi and De la Luz (2018) and Elvidge and Angling (2018); however, the confidence intervals obtained in both are substantially wider than those found in our study, lending increased certainty to the estimated time between events of such magnitude in our work. We argue that taking the extremal index into account, even when this measure indicates weak temporal dependence, is beneficial to the analysis.

Spectral Hardening of Large Solar Flares

Paolo C. **Grigis** & Arnold O. Benz

E-print, August 2007, `Astrophysical Journal`, 683:1180–1191, **2008**

`http://www.journals.uchicago.edu/toc/apj/2008/683/2`

The evidence we find points toward a single acceleration mechanism acting in the two phases, rather than two different separated mechanisms, because the impulsive and gradual phases are closely interconnected in time and space.

Electron acceleration in solar flares: theory of spectral evolution:

P. C. **Grigis** and A. O. Benz

A&A 458 (**2006**) 641-651 (Section 'The Sun')

http://publish.edpsciences.org/abstract/aa/v458/p641

The coalescence of two rotating sunspots during the emergence of an active region

V. M. **Grigor'ev**, L. V. Ermakova, A. I. Khlystova

Astronomy Reports, December **2013**, Volume 57, Issue 12, pp 984-990

Astronomicheskii Zhurnal, **2013**, Vol. 90, No. 12, pp. 1066–1072.

The rare phenomenon of the coalescence of two rotating sunspots of the same magnetic polarity during the emergence of the active region NOAA 11117 is investigated using data from the SDO space observatory. The coalescing spots rotated in opposite directions. The leading spot which formed from this process rotated counterclockwise with an angular velocity of 4°/h. A possible explanation is presented, based on a model of the emerging, twisted magnetic Ω flux tube that interacts with convective flows as it crosses the convective zone.

Magnetic-field variations and solar flare activity

I.Yu. **Grigor'eva**, A. N. Shakhovskaya, M. A. Livshits, I. S. Knyazeva
Astronomy Reports, November **2012**, Volume 56, Issue 11, pp 887-894
Solar filtergrams obtained at the Crimean Astrophysical Observatory at the center and wings of the Hα line are used to study variations in filaments, in particular, in arch filament systems (AFSs). These are considered as an indicator of emerging new magnetic flux, providing information about the spatial locations of magnetic-field elements. Magnetic-field maps for the active region NOAA 10030 are analyzed as an example. A method developed earlier for detecting elements of emerging flux using SOHO/MDI magnetograms indicates a close link between the increase in flare activity in theNOAA 10030 group during **July 14–18, 2002** and variations in the topological disconnectedness of the magnetograms. Moreover, variations in the flare activity one day before a flare event are correlated with variations in the topological complexity of the field (the Euler characteristic) in regions with high field strengths (more than 700 G). Analysis of multi-wavelength polarization observations on the RATAN-600 radio telescope during July 13–17, 2002 indicate dominance of the radio emission above the central spot associated with the increase in flare activity. In addition to the flare site near the large spot in the group, numerous weak flares developed along an extended local neutral line, far from the central line of the large-scale field. The statistical characteristics of the magnetic-field maps analyzed were determined, and show flare activity of both types, i.e., localized in spot penumbras and above the neutral line of the field.

The Post-Eruptive Arcade Formation in The Limb Event on July 31, 2004 From Microwave Solar Observations with the RATAN-600 Radio Telescope.

Irina Yu. **Grigoryeva**1, Larisa K. Kashapova2, Valery N. Borovik1, Moisey A. Livshits3
Sun and Geosphere, **2010**; 5(2): 58-60
http://www.shao.az/SG/v5n2/SG_v5_No2_2010-pp-58-60.pdf
A CME/flare event occurred at the western limb on 31 July 2004. Five successive multi-wavelength scans in centimeter range were obtained with the RATAN-600 radio telescope starting at the early stage of post-eruptive arcade formation (24 min after a C8.3 flare peak) and lasting for 4 hours. Microwave radio emission of the arcade was rather intense at initial stage indicating a predominant contribution of thermal emission and then considerably decreased during the decay phase. Its maximum was co-spatial with the 195 E Fe XII loop tops. At the end of microwave observations the contribution of the emission from accelerated particles became significant. The similarity of microwave characteristics of two eruptive events (on **31 July 2004** at the western limb and on **25 January 2007** at the eastern limb) is shown.

Solar Flare Forecasting Based on Magnetogram Sequences Learning with Multiscale Vision Transformers and Data Augmentation Techniques.

Grim, L.F.L., Gradvohl, A.L.S.
Sol Phys 299, 33 (2024).
https://doi.org/10.1007/s11207-024-02276-0
Solar flares are releases of electromagnetic energy generally occurring in active solar regions with magnetic fields, known as sunspots. The burst of radiation released by a solar flare can reach Earth's atmosphere in a few minutes. High-intensity solar flares, M- or X-class flares, can significantly impact some of Earth's activities and technologies, such as satellites, telecommunications, and electrical power systems. Therefore driving efforts in high-intensity solar flare forecasting systems is crucial. A forecasting model that observes the evolution of active regions may analyze a set of attributes that indicate which active regions can be precursors to solar flares. Recent work has focused on deep-learning models that consider the evolution of active regions in the Sun. However, M- and X-class flares are spurious in the solar-cycle period. That situation leads to an imbalanced dataset, increasing the effort to develop machine-learning models for forecasting. Therefore we propose transformers-based models to forecast ≥M-class flares, taking sequences of line-of-sight magnetogram images as input. In addition, we apply data augmentation techniques and other methods to deal with training on imbalanced datasets. Our fine-tuned models outperformed state-of-the-art work using image processing to forecast ≥M-class flares in the next 48 h with an approximate True Skill Statistic (TSS) of 0.8. Moreover, the data augmentation techniques applied to the training set kept the TSS stable and improved most of the secondary performance metrics analyzed.

Sunspot Rotation in High- and Low-Flaring Active Regions

Richard **Grimes** & Balázs Pintér

Solar Physics volume 297, Article number: 109 (**2022**)
https://link.springer.com/content/pdf/10.1007/s11207-022-02040-2.pdf
Sunspot rotations are closely linked with flaring activity. They are thought to contribute to the accumulation of helicity in magnetic flux tubes and to triggering magnetic reconnection in large solar flares. This link to solar flares has led to sunspot rotations being used as a parameter in solar flare prediction methods, but analysis for long-period observations of rotations in the literature is scarce. In this study, the rotation profiles of sunspots in a selection of six active regions are studied over time periods of 5 – 10 days to measure how sunspot rotation varies as active regions develop. The active regions are divided into two categories: high-flaring groups, which produced at least one X-class flare, and low-flaring regions that had little flaring activity. Comparison of the rotation profiles in these regions showed that young complex sunspot groups exhibit faster angular velocities and more frequent changes in rotation than older single-spot groups and, although the most rotating groups were also the most flare-productive, sudden changes in rotation were found to not definitively indicate an imminent eruption. **2011-02-13-16, 2011-03-05-10, 2012-06-13-18, 2013-11-15-19, 2014-01-03-10**

Observation of Differential Rotation Within a Sunspot Umbra During an X-Class Flare

Richard **Grimes**, Balázs Pintér & Huw Morgan
Solar Physics volume 295, Article number: 87 (**2020**)
https://link.springer.com/content/pdf/10.1007/s11207-020-01657-5.pdf
Sunspots and their dynamics dominate the magnetic topology and evolution of both the photosphere and the overlying coronal active regions. Thus a comprehensive understanding of their behaviour is essential to understanding the solar magnetic field. A new technique is presented for applying multiple ellipse fits as a method for rotation tracking of sunspot umbrae. The method is applied to a sunspot in NOAA active region AR 12158 during an X-class flare event and the resulting rotation rate correlates well with other measurements from literature. The method also reveals an apparent difference in rotation rate between the edge and the innermost region of the sunspot umbra of up to 2 degrees per hour. Such differential rotation must lead to the large-scale twisting of sunspot magnetic flux tubes with implications for models of coronal loops and the build-up of instabilities that may lead to eruptions. **10th September 2014**
RHESSI Science Nuggets #384 Sep **2020**
https://sprg.ssl.berkeley.edu/~tohban/wiki/index.php/Sunspot_Differential_Rotation_in_an_X-class_Flare

A Decade of Questions About Magnetic Reconnection **Review**

Nicholas A. **Gross** and W. Jeffrey Hughes
Space Weather Volume 13, Issue 10 (pages 606–610) **2015**
Space Weather Quarterly Volume 13, Issue 2, **2016**
http://onlinelibrary.wiley.com/doi/10.1002/SWQv13i002/epdf
Students questions about reconnection are summarized

Quasi-Periodic Pulsations: Fermi/GBM Results

D. **Gruber** and Pawel Lachowicz
RHESSI Science Nuggets, No. 161, Oct **2011**
http://sprg.ssl.berkeley.edu/~tohban/wiki/index.php/Quasi-Periodic_Pulsations:_Fermi/GBM_Results
Here, we present time series and periodogram analyses of four solar flares which were observed by the Fermi Gamma-Ray Burst Monitor (GBM) and display compelling quasi-periodic behavior in their light curves. A more comprehensive analysis on this subject can be found here, and a general review of coronal waves and oscillations here.

Quasi-periodic pulsations in solar flares: new clues from the Fermi Gamma-Ray Burst Monitor

D. **Gruber**1, P. Lachowicz2, E. Bissaldi3, M. S. Briggs4, V. Connaughton4, J. Greiner1, A. J. van der Horst4, G. Kanbach1, A. Rau1, P. N. Bhat4, R. Diehl1, A. von Kienlin1, R. M. Kippen5, C. A. Meegan6, W. S. Paciesas4, R. D. Preece4 and C. Wilson-Hodge
A&A 533, A61 (**2011**)
http://sci-hub.tw/https://www.aanda.org/articles/aa/abs/2011/09/aa17077-11/aa17077-11.html
Aims. In the past four decades, it has been observed that solar flares display quasi-periodic pulsations (QPPs) from the lowest, i.e. radio, to the highest, i.e. gamma-ray, frequencies in the electromagnetic spectrum. It remains unclear which mechanism creates these QPPs. In this paper, we analyze four bright solar flares that display compelling signatures of quasi-periodic behavior and were observed with the Gamma-Ray Burst Monitor (GBM) onboard the Fermi satellite. Because GBM covers over three decades in energy (8 keV to 40 MeV), it is regarded as a key instrument in our attempt to understand the physical processes that drive solar flares.

Methods. We tested for periodicity in the time series of the solar flares observed by GBM by applying a classical periodogram analysis. However, in contrast to previous authors, we did not detrend the raw light curve before creating the power spectral density (PSD) spectrum. To assess the significance of the frequencies, we used a method that is commonly applied to X-ray binaries and Seyfert galaxies. This technique takes into account the underlying continuum of the PSD, which for all of these sources has a $P(f) \sim f^{-\alpha}$ dependence and is typically labeled red-noise.
Results. We checked the reliability of this technique by applying it to observations of a solar flare that had been observed by the Reuven Ramaty High-Energy Solar Spectroscopic Imager (RHESSI). These data contain, besides any potential periodicity from the Sun, a 4 s rotational period caused by the rotation of the spacecraft about its axis. We were unable to identify any intrinsic solar quasi-periodic pulsation but we did manage to reproduce the instrumental periodicity. Moreover, with the method adopted here, we do not detect significant QPPs in the four bright solar flares observed by GBM. We stress that for this kind of analyses it is of utmost importance to account appropriately for the red-noise component in the PSD of these astrophysical sources.

Flare Characteristics from X-ray Light Curves

M. **Gryciuk**, M. Siarkowski, J. Sylwester, S. Gburek, P. Podgorski, A. Kepa, B. Sylwester, T. Mrozek
Solar Physics June **2017**, 292:77 DOI: 10.1007/s11207-017-1101-8
https://link.springer.com/content/pdf/10.1007/s11207-017-1101-8.pdf
A new methodology is given to determine basic parameters of flares from their X-ray light curves. Algorithms are developed from the analysis of small X-ray flares occurring during the deep solar minimum of 2009, between Solar Cycles 23 and 24, observed by the Polish Solar Photometer in X-rays (SphinX) on the Complex Orbital Observations Near-Earth of Activity of the Sun-Photon (CORONAS-Photon) spacecraft. One is a semi-automatic flare detection procedure that gives start, peak, and end times for single ("elementary") flare events under the assumption that the light curve is a simple convolution of a Gaussian and exponential decay functions. More complex flares with multiple peaks can generally be described by a sum of such elementary flares. Flare time profiles in the two energy ranges of SphinX (1.16 – 1.51 keV, 1.51 – 15 keV) are used to derive temperature and emission measure as a function of time during each flare. The result is a comprehensive catalogue – the SphinX Flare Catalogue – which contains 1600 flares or flare-like events and is made available for general use. The methods described here can be applied to observations made by Geosynchronous Operational Environmental Satellites (GOES), the Reuven Ramaty High Energy Solar Spectroscopic Imager (RHESSI) and other broad-band spectrometers.

Operational solar flare forecasting via video-based deep learning

Sabrina **Guastavino**, Francesco Marchetti, Federico Benvenuto, Cristina Campi, and Michele Piana
Front. Astron. Space Sci. 9:1039805. **2023** doi: 10.3389/fspas.2022.1039805
https://www.frontiersin.org/articles/10.3389/fspas.2022.1039805/pdf
https://www.frontiersin.org/articles/10.3389/fspas.2022.1039805/full
Operational flare forecasting aims at providing predictions that can be used to make decisions, typically on a daily scale, about the space weather impacts of flare occurrence. This study shows that video-based deep learning can be used for operational purposes when the training and validation sets used for network optimization are generated while accounting for the periodicity of the solar cycle. Specifically, this article describes an algorithm that can be applied to build up sets of active regions that are balanced according to the flare class rates associated to a specific cycle phase. These sets are used to train and validate a long-term recurrent convolutional network made of a combination of a convolutional neural network and a long short-term memory network. The reliability of this approach is assessed in the case of two prediction windows containing the solar storms of March 2015, June 2015, and September 2017. **9-19 Mar 2015, 18-27 Jun 2015; 4-10 Sep 2017**

Implementation paradigm for supervised flare forecasting studies: A deep learning application with video data

Sabrina **Guastavino**1, Francesco Marchetti2, Federico Benvenuto1, Cristina Campi1 and Michele Piana1,3
A&A 662, A105 (**2022**)
https://doi.org/10.1051/0004-6361/202243617
https://www.aanda.org/articles/aa/pdf/2022/06/aa43617-22.pdf
Aims. In this study, we introduce a general paradigm for generating independent and well-balanced training, validation, and test sets for use in supervised machine and deep learning flare forecasting, to determine the extent to which video-based deep learning can predict solar flares.
Methods. We use this implementation paradigm in the case of a deep neural network, which takes videos of magnetograms recorded by the Helioseismic and Magnetic Imager onboard the Solar Dynamics Observatory (SDO/HMI) as input.
Results. The way the training and validation sets are prepared for network optimization has a significant impact on the prediction performances. Furthermore, deep learning is able to realize flare video classification with prediction performances that are in line with those obtained by machine learning approaches that require an a priori extraction of features from the HMI magnetograms.

Conclusions. To our knowledge, this is the first time that the solar flare forecasting problem is addressed by means of a deep neural network for video classification, which does not require any a priori extraction of features from the HMI magnetograms.

Desaturating EUV observations of solar flaring storms

Sabrina **Guastavino**, Michele Piana, Anna Maria Massone, Richard Schwartz, Federico Benvenuto
2019
https://arxiv.org/pdf/1904.04211.pdf
Image saturation has been an issue for several instruments in solar astronomy, mainly at EUV wavelengths. However, with the launch of the Atmospheric Imaging Assembly (AIA) as part of the payload of the Solar Dynamic Observatory (SDO) image saturation has become a big data issue, involving around 10^$ frames of the impressive dataset this beautiful telescope has been providing every year since February 2010. This paper introduces a novel desaturation method, which is able to recover the signal in the saturated region of any AIA image by exploiting no other information but the one contained in the image itself. This peculiar methodological property, jointly with the unprecedented statistical reliability of the desaturated images, could make this algorithm the perfect tool for the realization of a reconstruction pipeline for AIA data, able to work properly even in the case of long-lasting, very energetic flaring events. **September 10 2017**

Testing predictors of eruptivity using parametric flux emergence simulations

Chloé **Guennou**, Etienne Pariat, Nicole Vilmer, James E. Leake
2017
https://arxiv.org/pdf/1706.04915.pdf
Solar flares and coronal mass ejections (CMEs) are among the most energetic events in the solar system, impacting the near-Earth environment. Flare productivity is empirically known to be correlated with the size and complexity of active regions. Several indicators, based on magnetic-field data from active regions, have been tested for flare forecasting in recent years. None of these indicators, or combinations thereof, have yet demonstrated an unambiguous eruption or flare criterion. Furthermore, numerical simulations have been only barely used to test the predictability of these parameters. In this context, we used the 3D parametric MHD numerical simulations of the self-consistent formation of the flux emergence of a twisted flux tube, inducing the formation of stable and unstable magnetic flux ropes of Leake (2013, 2014). We use these numerical simulations to investigate the eruptive signatures observable in various magnetic scalar parameters and provide highlights on data analysis processing. Time series of 2D photospheric-like magnetograms are used from parametric simulations of stable and unstable flux emergence, to compute a list of about 100 different indicators. This list includes parameters previously used for operational forecasting, physical parameters used for the first time, as well as new quantities specifically developed for this purpose. Our results indicate that only parameters measuring the total non-potentiality of active regions associated with magnetic inversion line properties, such as the Falconer parameters , , and , as well as the new current integral and length parameters, present a significant ability to distinguish the eruptive cases of the model from the non-eruptive cases, possibly indicating that they are promising flare and eruption predictors.

Ensemble Forecasting of Major Solar Flares: Methods for Combining Models

Jordan A. **Guerra**, Sophie A. Murray, D. Shaun Bloomfield, Peter T. Gallagher
Journal of Space Weather and Space Climate 10, 38 **2020**
https://arxiv.org/pdf/2008.00382.pdf
https://www.swsc-journal.org/articles/swsc/pdf/2020/01/swsc200004.pdf
One essential component of operational space weather forecasting is the prediction of solar flares. With a multitude of flare forecasting methods now available online it is still unclear which of these methods performs best, and none are substantially better than climatological forecasts. Space weather researchers are increasingly looking towards methods used by the terrestrial weather community to improve current forecasting techniques. Ensemble forecasting has been used in numerical weather prediction for many years as a way to combine different predictions in order to obtain a more accurate result. Here we construct ensemble forecasts for major solar flares by linearly combining the full-disk probabilistic forecasts from a group of operational forecasting methods (ASAP, ASSA, MAG4, MOSWOC, NOAA, and MCSTAT). Forecasts from each method are weighted by a factor that accounts for the method's ability to predict previous events, and several performance metrics (both probabilistic and categorical) are considered. It is found that most ensembles achieve a better skill metric (between 5\% and 15\%) than any of the members alone. Moreover, over 90\% of ensembles perform better (as measured by forecast attributes) than a simple equal-weights average. Finally, ensemble uncertainties are highly dependent on the internal metric being optimized and they are estimated to be less than 20\% for probabilities greater than 0.2. This simple multi-model, linear ensemble technique can provide operational space weather centres with the basis for constructing a versatile ensemble forecasting system -- an improved starting point to their forecasts that can be tailored to different end-user needs.

Active Region Photospheric Magnetic Properties Derived from Line-of-sight and Radial Fields

Jordan A. **Guerra**, Sung-H. Park, Ioannis Kontogiannis, Peter T. Gallagher, Manolis Georgoulis, D. Shaun Bloomfield

Solar Physics January **2018**, 293:9

https://arxiv.org/pdf/1712.06902.pdf

The effect of using two representations of the normal-to-surface magnetic field to calculate photospheric measures that are related to active region (AR) potential for flaring is presented. Several AR properties were computed using line-of-sight (Blos) and spherical-radial (Br) magnetograms from the Spaceweather HMI Active Region Patch (SHARP) products of the Solar Dynamics Observatory, characterizing the presence and features of magnetic polarity inversion lines, fractality, and magnetic connectivity of the AR photospheric field. The data analyzed corresponds to ≈ 4,000 AR observations, achieved by randomly selecting 25% of days between September 2012 and May 2016 for analysis at 6-hr cadence. Results from this statistical study include: i) the Br component results in a slight upwards shift of property values in a manner consistent with a field-strength underestimation by the Blos component; ii) using the Br component results in significantly lower inter-property correlation in one-third of the cases, implying more independent information about the state of the AR photospheric magnetic field; iii) flaring rates for each property vary between the field components in a manner consistent with the differences in property-value ranges resulting from the components; iv) flaring rates generally increase for higher values of properties, except Fourier spectral power index that has flare rates peaking around a value of 5/3. These findings indicate that there may be advantages in using Br rather than Blos in calculating flare-related AR magnetic properties, especially for regions located far from central meridian.

HMI Science Nuggets, # 92 March **2018** http://hmi.stanford.edu/hminuggets/?p=2371

Ensemble Forecasting of Major Solar Flares

J. A. **Guerra**, A. Pulkkinen, V. M. Uritsky

Space Weather Volume 13, Issue 10 (pages 626–642) **2015**

http://arxiv.org/pdf/1504.04571v1.pdf

We present the results from the first ensemble prediction model for major solar flares (M and X classes). Using the probabilistic forecasts from three models hosted at the Community Coordinated Modeling Center (NASA-GSFC) and the NOAA forecasts, we developed an ensemble forecast by linearly combining the flaring probabilities from all four methods. Performance-based combination weights were calculated using a Monte Carlo-type algorithm by applying a decision threshold Pth to the combined probabilities and maximizing the Heidke Skill Score (HSS). Using the probabilities and events time series from 13 recent solar active regions (2012 - 2014), we found that a linear combination of probabilities can improve both probabilistic and categorical forecasts. Combination weights vary with the applied threshold and none of the tested individual forecasting models seem to provide more accurate predictions than the others for all values of Pth. According to the maximum values of HSS, a performance-based weights calculated by averaging over the sample, performed similarly to a equally weighted model. The values Pth for which the ensemble forecast performs the best are 25 \% for M-class flares and 15 \% for X-class flares. When the human-adjusted probabilities from NOAA are excluded from the ensemble, the ensemble performance in terms of the Heidke score, is reduced.

Round-the-world echo of earthquake and solar flare

Anatol **Guglielmi**, Vladimir Parkhomov

2019

https://arxiv.org/ftp/arxiv/papers/1905/1905.10644.pdf

We drew attention to the analogy between the round-the-world seismic echo on the Earth and on the Sun. The phenomenon of echo on the Earth is observed during earthquakes. It was found that the main shock of earthquake excites a circular surface wave, which having rounded the Earth returns to the epicenter and stimulates a repeated earthquake (aftershock) 3 hours after the main shock. Apparently, something similar happens on the Sun during a chromospheric flare. We found signs of a small increase in flare brightness approximately one hour after reaching maximum brightness. The phenomenon is explained by the fact that the converging surface wave, which has returned to the epicenter after the round-the-world trip, has a definite impact on the flare area. **September 10, 2005**

IRIS observations of magnetic interactions in the solar atmosphere between pre-existing and emerging magnetic fields. I. Overall evolution

Salvo L. **Guglielmino**, Francesca Zuccarello, Peter R. Young, Mariariata Murabito, Paolo Romano

ApJ **856** 127 **2018**

https://arxiv.org/pdf/1802.05657.pdf

http://sci-hub.tw/http://iopscience.iop.org/0004-637X/856/2/127/

We report multi-wavelength ultraviolet observations taken with the IRIS satellite, concerning the emergence phase in the upper chromosphere and transition region of an emerging flux region (EFR) embedded in the pre-existing field of

active region NOAA 12529. IRIS data are complemented by full-disk observations of the Solar Dynamics Observatory satellite, relevant to the photosphere and the corona. The photospheric configuration of the EFR is also analyzed by measurements taken with the spectropolarimeter aboard the Hinode satellite, when the EFR was fully developed. Recurrent intense brightenings that resemble UV bursts, with counterparts in all coronal passbands, are identified at the edges of the EFR. Jet activity is also observed at chromospheric and coronal levels, near the observed brightenings. The analysis of the IRIS line profiles reveals the heating of dense plasma in the low solar atmosphere and the driving of bi-directional high-velocity flows with speed up to 100 km/s at the same locations. Compared with previous observations and numerical models, these signatures suggest evidence of several long-lasting, small-scale magnetic reconnection episodes between the emerging bipole and the ambient field. This process leads to the cancellation of a pre-existing photospheric flux concentration and appears to occur higher in the atmosphere than usually found in UV bursts, explaining the observed coronal counterparts. **April 13 and 14 2016**

A MULTI-INSTRUMENT ANALYSIS OF A C4.1 FLARE OCCURRING IN A δ SUNSPOT

S. L. **Guglielmino**1, F. Zuccarello1, P. Romano2, A. Cristaldi3,4, I. Ermolli4, S. Criscuoli5, M. Falco1, andF. P. Zuccarello

2016 ApJ 819 157

We present an analysis of multi-instrument space- and ground-based observations relevant to a C4.1 solar flare that occurred in the active region (AR) NOAA 11267 on **2011 August 6**. Solar Dynamics Observatory observations indicate that at the flare's beginning, it was localized in the preceding sunspot of the AR, which exhibits a δ configuration. Along the polarity inversion line between its opposite polarities we find a large shear angle of about 80°. The helicity accumulation shows that the AR does not obey the general hemispheric helicity rule. At the flare peak, unique observations taken with the X-Ray Telescope aboard Hinode reveal that the bulk of the X-ray emission takes place in the δ-spot region, where the plasma heats up to $\approx 1.9 \cdot 10^7$ K. During the gradual phase, we observe the development of a Y-shaped structure in the corona and in the high chromosphere. An extruding structure forms, being directed from the emitting region above the δ spot toward the following sunspot. This structure cools down in a few tens of minutes while moving eastward along a direction opposite to the flare ribbon expansion. Finally, remote brightenings are found at the easternmost footpoint of this structure, appearing as a third flare ribbon in the chromosphere. After some minutes, RHESSImeasurements show that the X-ray emission is localized in the region close to the crossing point of the coronal Y-shaped structure. Simultaneously, high-resolution ($0''.15$) observations performed at the Swedish 1 m Solar Telescope indicate a decreasing trend of the Ca ii H intensity in the flare ribbons with some transient enhancements. All these findings suggest that this event is a manifestation of magnetic reconnection, likely induced by an asymmetric magnetic configuration in a highly sheared region.

MULTIWAVELENGTH OBSERVATIONS OF SMALL-SCALE RECONNECTION EVENTS TRIGGERED BY MAGNETIC FLUX EMERGENCE IN THE SOLAR ATMOSPHERE

S. L. **Guglielmino**1, L. R. Bellot Rubio2, F. Zuccarello1, G. Aulanier3, S. Vargas Dom´ınguez4, and S. Kamio5

Astrophysical Journal, 724:1083–1098, **2010**

The interaction between emerging magnetic flux and the pre-existing ambient field has become a “hot” topic for both numerical simulations and high-resolution observations of the solar atmosphere. The appearance of brightenings and surges during episodes of flux emergence is believed to be a signature of magnetic reconnection processes. We present an analysis of a small-scale flux emergence event in NOAA 10971, observed simultaneously with the Swedish 1 m Solar Telescope on La Palma and the *Hinode* satellite during a joint campaign in 2007 September. Extremely high-resolution *G*-band, Hα, and Ca ii H filtergrams, Fe i and Na i magnetograms, EUV raster scans, and X-ray images show that the emerging region was associated with chromospheric, transition region and coronal brightenings, as well as with chromospheric surges. We suggest that these features were caused by magnetic reconnection at low altitude in the atmosphere. To support this idea, we perform potential and linear force-free field extrapolations using the FROMAGE service. The extrapolations show that the emergence site is cospatial with a three-dimensional null point, from which a spine originates. This magnetic configuration and the overall orientation of the field lines above the emerging flux region are compatible with the structures observed in the different atmospheric layers and remain stable against variations of the force-free field parameter. Our analysis supports the predictions of recent three-dimensional numerical simulations that energetic phenomena may result from the interaction between emerging flux and the pre-existing chromospheric and coronal field.

Hinode Observations of Chromospheric Brightenings in the Ca ii H Line during Small-Scale Flux Emergence Events

S. L. **Guglielmino**, F. Zuccarello, P. Romano, and L. R. Bellot Rubio

The Astrophysical Journal Letters, Vol. 688, No. 2: L111-L114.
http://www.journals.uchicago.edu/doi/abs/10.1086/595657
Ca II H emission is a well-known indicator of magnetic activity in the Sun and other stars. It is also viewed as an important signature of chromospheric heating. However, the Ca II H line has not been used as a diagnostic of magnetic flux emergence from the solar interior. Here we report on *Hinode* observations of chromospheric Ca II H brightenings associated with a repeated, small-scale flux emergence event. We describe this process and investigate the evolution of the magnetic flux, G-band brightness, and Ca II H intensity in the emerging region. Our results suggest that energy is released in the chromosphere as a consequence of interactions between the emerging flux and the preexisting magnetic field, in agreement with recent 3D numerical simulations.

Double Power-law Formation by Sequential Particle Acceleration

S. E. **Guidoni**1,2, C. R. DeVore2, J. T. Karpen2, and M. Alaoui2,3
2024 ApJ 965 6
https://iopscience.iop.org/article/10.3847/1538-4357/ad2e8b/pdf
Spectral double power laws are common in solar high-energy phenomena such as flares and interplanetary energetic-electron events. However, the physical mechanism that produces the changes in power-law index within a single spectrum is unclear. We developed a fully analytical method of forming single power-law spectra from sequential acceleration of particles orbiting inside and hopping between simulated large-scale magnetic islands formed by flare reconnection. Here, we extend the analytical method to the formation of double power-law spectra by assuming sequential acceleration in two successive regions with different acceleration and particle-transport rates. The resulting spectral distribution is continuous and smooth, with a flattening at low energies, two power-law regions at mid-energies, and a steep rollover at high energies. The model provides analytical expressions for the spectral indices, all energy breaks, and normalization constants as functions of just three physical parameters of each acceleration region: (1) the energy gain in each accelerator, (2) the percentage of particles transferred between accelerators, and (3) the number of accelerators visited. One of the most salient predictions of our work is that the spectral index at high (low) energies is determined by the parameters of the first "seed" (second) acceleration region. By constructing the spectral distribution through an iterative analytical process, the evolution toward a double power law is easily characterized and explained. Our analytical model provides tools to interpret space- and ground-based observations from RHESSI, FOXSI, NuSTAR, Solar Orbiter/STIX, EOVSA, and future high-energy missions.

Spectral Power-law Formation by Sequential Particle Acceleration in Multiple Flare Magnetic Islands

Silvina E. **Guidoni**, Judith T. Karpen, C. Richard DeVore
ApJ **925** 191 **2022**
https://arxiv.org/pdf/2201.05564.pdf
https://iopscience.iop.org/article/10.3847/1538-4357/ac39a5/pdf
We present a first-principles model of pitch-angle and energy distribution function evolution as particles are sequentially accelerated by multiple flare magnetic islands. Data from magnetohydrodynamic (MHD) simulations of an eruptive flare/coronal mass ejection provide ambient conditions for the evolving particle distributions. Magnetic islands, which are created by sporadic reconnection at the self-consistently formed flare current sheet, contract and accelerate the particles. The particle distributions are evolved using rules derived in our previous work. In this investigation, we assume that a prescribed fraction of particles sequentially "hops" to another accelerator and receives an additional boost in energy and anisotropy. This sequential process generates particle number spectra that obey an approximate power law at mid-range energies and presents low- and high-energy breaks. We analyze these spectral regions as functions of the model parameters. We also present a fully analytic method for forming and interpreting such spectra, independent of the sequential acceleration model. The method requires only a few constrained physical parameters, such as the percentage of particles transferred between accelerators, the energy gain in each accelerator, and the number of accelerators visited. Our investigation seeks to bridge the gap between MHD and kinetic regimes by combining global simulations and analytic kinetic theory. The model reproduces and explains key characteristics of observed flare hard X-ray spectra as well as the underlying properties of the accelerated particles. Our analytic model provides tools to interpret high-energy observations for missions and telescopes, such as RHESSI, FOXSI, NuSTAR, Solar Orbiter, EOVSA, and future high-energy missions.

Magnetic-Island Contraction and Particle Acceleration in Simulated Eruptive Solar Flares

S. E. **Guidoni**, C. R. DeVore, J. T. Karpen, B. J. Lynch
ApJ 820 60 **2016**
http://arxiv.org/pdf/1603.01309v1.pdf
The mechanism that accelerates particles to the energies required to produce the observed high-energy impulsive emission in solar flares is not well understood. Drake et al. (2006) proposed a mechanism for accelerating electrons in contracting magnetic islands formed by kinetic reconnection in multi-layered current sheets. We apply these ideas to

sunward-moving flux ropes (2.5D magnetic islands) formed during fast reconnection in a simulated eruptive flare. A simple analytic model is used to calculate the energy gain of particles orbiting the field lines of the contracting magnetic islands in our ultrahigh-resolution 2.5D numerical simulation. We find that the estimated energy gains in a single island range up to a factor of five. This is higher than that found by Drake et al. for islands in the terrestrial magnetosphere and at the heliopause, due to strong plasma compression that occurs at the flare current sheet. In order to increase their energy by two orders of magnitude and plausibly account for the observed high-energy flare emission, the electrons must visit multiple contracting islands. This mechanism should produce sporadic emission because island formation is intermittent. Moreover, a large number of particles could be accelerated in each magnetohydrodynamic-scale island, which may explain the inferred rates of energetic-electron production in flares. We conclude that island contraction in the flare current sheet is a promising candidate for electron acceleration in solar eruptions.

Temperature and Electron Density Diagnostics of a Candle-flame-shaped Flare

S. E. **Guidoni**, D. E. McKenzie, D. W. Longcope, J. E. Plowman, and K. Yoshimura
ApJ 800 54 **2015**
Candle-flame-shaped flares are archetypical structures that provide indirect evidence of magnetic reconnection. A flare resembling Tsuneta's famous 1992 candle-flame flare occurred on **2011 January 28**; we present its temperature and electron density diagnostics. This flare was observed with Solar Dynamics Observatory/Atmospheric Imaging Assembly (SDO/AIA), Hinode/X-Ray Telescope (XRT), and Solar Terrestrial Relations Observatory Ahead (STEREO-A)/Extreme Ultraviolet Imager, resulting in high-resolution, broad temperature coverage, and stereoscopic views of this iconic structure. The high-temperature images reveal a brightening that grows in size to form a tower-like structure at the top of the posteruption flare arcade, a feature that has been observed in other long-duration events. Despite the extensive work on the standard reconnection scenario, there is no complete agreement among models regarding the nature of this high-intensity elongated structure. Electron density maps reveal that reconnected loops that are successively connected at their tops to the tower develop a density asymmetry of about a factor of two between the two legs, giving the appearance of "half-loops." We calculate average temperatures with a new fast differential emission measure (DEM) method that uses SDO/AIA data and analyze the heating and cooling of salient features of the flare. Using STEREO observations, we show that the tower and the half-loop brightenings are not a line-of-sight projection effect of the type studied by Forbes & Acton. This conclusion opens the door for physics-based explanations of these puzzling, recurrent solar flare features, previously attributed to projection effects. We corroborate the results of our DEM analysis by comparing them with temperature analyses from Hinode/XRT.

Flaring together: A preferred angular separation between sympathetic flares on the Sun

Louis-Simon **Guité**, Antoine Strugarek, Paul Charbonneau
A&A **2024**
https://arxiv.org/pdf/2412.10143
Sympathetic solar flares are eruptions that occur nearby in space and time, driven by an apparent interaction between the active regions in which they are triggered. Their statistical existence on the Sun has yet to be firmly established. The main goal of this paper is to identify a statistical signature of sympathetic flares, characterize their properties and determine a potential mechanism driving their interaction. We perform a statistical analysis of a large number of flares observed by the Atmospheric Imaging Assembly (AIA) onboard the Solar Dynamics Observatory (SDO), the Reuven Ramaty High Energy Solar Spectroscopic Imager (RHESSI) and the Spectrometer Telescope for Imaging X-rays (STIX) on Solar Orbiter during solar cycle 24 and 25. We examine the spatiotemporal distribution of consecutive flare pairs across solar cycle phases and hemispheres, along with the propagation velocity of potential causal interactions and the relationship between flare magnitudes. We observe an excess of hemispheric flares separated by about 30 degrees of longitude and triggered in less than 1.5 hours from each other. This peak in angular separation varies with the solar cycle phase and hemisphere. Moreover, we identify a deficit of transequatorial events separated by 25-30 degrees in latitude and less than 5 degrees in longitude, a phenomenon we term unsympathetic flares. We provide strong statistical evidence for the existence of sympathetic flares on the Sun, demonstrating that their occurrence rate reaches approximately 5% across the three instruments used in this study. Additionally, we propose an interpretation of the observed angular scale of the sympathetic phenomenon, based on the separation between magnetic field line footpoints derived from potential field source surface extrapolations. **October 23-24, 2013**
Table 2 Sample of SDO/AIA candidate sympathetic flares 2011-2016

The Role of Magnetic Skeleton in Solar Flare Filaments Activity

Juan **Guo**1,2, Huaning Wang3,4, Jingxiu Wang2,3,4, Xiaoshuai Zhu1,2, Jing Huang2,3, Shanqiang Chen1,2, Bingxian Luo1,2,4, Siqing Liu1,2,4, Yuanyong Deng2,3,4, and Jiaben Lin2,3
2024 ApJ 975 221
https://iopscience.iop.org/article/10.3847/1538-4357/ad7a67/pdf
We report an M9.3 flare and filaments activities from NOAA Active Region 11261 that are strongly modulated by the 3D magnetic skeleton. Magnetic field extrapolation from the vector magnetic field suggests complex magnetic

connectivity and the existence of a high coronal null point southeast of the active region. A small filament over the inversed V-shaped polarity inversion line erupted and resulted in the M9.3 flare associated with a weak ejection in the EUV hot channel and the formation of a relatively large filament. Both the weak ejection and the eruption of the large filament were toward the southeast. Comparative analyses have disclosed the following new facts. First, the trajectory of looptop hard X-ray emission provides solid evidence that the magnetic reconnection site propagated up toward the coronal null point as the flare and filaments erupted. Second, the EVU observations show coronal mass ejection-like eruption features in the ejection region of the magnetic skeleton. Third, the closed fan confined the west end of the large filament and the corresponding flare ribbons. We demonstrate a spatiotemporal relationship between the magnetic skeleton and the flare filament activity. We conclude that the magnetic skeleton can modulate and determine almost all the characteristics of the studied activity in the corresponding scale. **2011-07-30**

Fast Sausage Oscillations in Coronal Loops with Fine Structures

Mingzhe **Guo**, Bo Li, Mijie Shi
ApJ Letters **921** L17 **2021**
https://arxiv.org/pdf/2110.10021.pdf
https://iopscience.iop.org/article/10.3847/2041-8213/ac30e3/pdf
https://doi.org/10.3847/2041-8213/ac30e3
Fast sausage modes (FSMs) in flare loops have long been invoked to account for rapid quasi-periodic pulsations (QPPs) with periods of order seconds in flare lightcurves. However, most theories of FSMs in solar coronal cylinders assume a perfectly axisymmetric equilibrium, an idealized configuration apparently far from reality. In particular, it remains to examine whether FSMs exist in coronal cylinders with fine structures. Working in the framework of ideal magnetohydrodynamics (MHD), we numerically follow the response to an axisymmetric perturbation of a coronal cylinder for which a considerable number of randomly distributed fine structures are superposed on an axisymmetric background. The parameters for the background component are largely motivated by the recent IRIS identification of a candidate FSM in Fe XXI 1354 Å~observations. We find that the composite cylinder rapidly settles to an oscillatory behavior largely compatible with a canonical trapped FSM. This happens despite that kink-like motions develop in the fine structures. We further synthesize the Fe XXI 1354 Å~emissions, finding that the transverse Alfvén time characterizes the periodicities in the intensity, Doppler shift, and Doppler width signals. Distinct from the case without fine structuring, a non-vanishing Doppler shift is seen even at the apex. We conclude that density-enhanced equilibria need not be strictly axisymmetric to host FSM-like motions in general, and FSMs remain a candidate interpretation for rapid QPPs in solar flares.

Observations and modeling of the onset of fast reconnection in the solar transition region

L.-J. **Guo**, B. De Pontieu, Y.-M. Huang, H. Peter, A. Bhattacharjee
ApJ **901** 148 **2020**
https://arxiv.org/pdf/2009.11475.pdf
https://doi.org/10.3847/1538-4357/abb2a7
Magnetic reconnection is a fundamental plasma process that plays a critical role not only in energy release in the solar atmosphere, but also in fusion, astrophysical, and other space plasma environments. One of the challenges in explaining solar observations in which reconnection is thought to play a critical role is to account for the transition of the dynamics from a slow quasi-continuous phase to a fast and impulsive energetic burst of much shorter duration. Despite the theoretical progress in identifying mechanisms that might lead to rapid onset, a lack of observations of this transition has left models poorly constrained. High-resolution spectroscopic observations from NASA's Interface Region Imaging Spectrograph (IRIS) now reveal tell-tale signatures of the abrupt transition of reconnection from a slow phase to a fast, impulsive phase during UV bursts or explosive events in the Sun's atmosphere. Our observations are consistent with numerical simulations of the plasmoid instability, and provide evidence for the onset of fast reconnection mediated by plasmoids and new opportunities for remote-sensing diagnostics of reconnection mechanisms on the Sun. **13-Aug-2013, 4-Feb-2014, 15-Apr-2014, 2014 May 04-05**

The Role of a Magnetic Topology Skeleton in a Solar Active Region

Juan **Guo**1,2, Huaning Wang1,3, Jingxiu Wang3, Xiaoshuai Zhu1,4, Xinghua Dai1, Xin Huang1, Han He1, Yan Yan1, and Hui Zhao
2019 ApJ 874 181
sci-hub.se/10.3847/1538-4357/ab0aed
We investigate the 3D magnetic topology in the active region NOAA 11719 nine hours before and after a flare–coronal mass ejection (CME) event on **2013 April 11**. The extrapolated 3D coronal magnetic field is computed employing a boundary integrated model, and a complex magnetic topology skeleton comprising five fairly robust null points and their relevant structures are revealed with a mathematical method based on a Poincaré index of isolated 3D null points. Comparative analyses show that the magnetic topology skeleton in this active region determines geometries of post-flare loops and flare ribbons, and characterizes the initial stage of the CME. The present work demonstrates that the magnetic topology skeleton plays an important role in the process of the flare–CME eruption.

Solar Flare Termination Shock and Synthetic Emission Line Profiles of the Fe xxi 1354.08 Å Line

Lijia **Guo**1,2, Gang Li3,4, Kathy Reeves5, and John Raymond
2017 ApJL 846 L12
http://sci-hub.cc/10.3847/2041-8213/aa866a
Solar flares are among the most energetic phenomena that occur in the solar system. In the standard solar flare model, a fast mode shock, often referred to as the flare termination shock (TS), can exist above the loop-top source of hard X-ray emissions. The existence of the TS has been recently related to spectral hardening of a flare's hard X-ray spectra at energies >300 keV. Observations of the Fe xxi 1354.08 Å line during solar flares by the Interface Region Imaging Spectrograph (IRIS) spacecraft have found significant redshifts with >100 km s−1, which is consistent with a reconnection downflow. The ability to detect such a redshift with IRIS suggests that one may be able to use IRIS observations to identify flare TSs. Using a magnetohydrodynamic simulation to model magnetic reconnection of a solar flare and assuming the existence of a TS in the downflow of the reconnection plasma, we model the synthetic emission of the Fe xxi 1354.08 line in this work. We show that the existence of the TS in the solar flare may manifest itself in the Fe xxi 1354.08 Å line.

Direct Observation of Two-Step Magnetic Reconnection in a Solar Flare

Tingyu **Gou**, Astrid M. Veronig, Ewan Dickson, Aaron Hernandez-Perez, Rui Liu
ApJ **845** L1 **2017**
https://arxiv.org/pdf/1707.06198.pdf
http://iopscience.iop.org.sci-hub.cc/2041-8205/845/1/L1/
We report observations of an eruptive X2.8 flare on **2013 May 13**, which shows two distinct episodes of energy release in the impulsive phase. The first episode is characterized by the eruption of a magnetic flux rope, similar to the energy-release process in most standard eruptive flares. While the second episode, which is stronger than the first normal one and shows enhanced high-energy X-ray and even γ-ray emissions, is closely associated with magnetic reconnection of a large-scale loop in the aftermath of the eruption. The reconnection inflow of the loop leg is observed in the Solar Dynamics Observatory (SDO)/Atmospheric Imaging Assembly (AIA) 304 \r{A} passband and accelerates towards the reconnection region to a speed as high as ∼130 km/s. Simultaneously the corresponding outflow jets are observed in the AIA hot passbands with a speed of ∼740 km/s and mean temperature of ∼14 MK. RHESSI observations show a strong burst of hard X-ray (HXR) and γ-ray emissions with hard electron spectra of δ≈3, exhibiting a soft-hard-harder behavior. A distinct altitude decrease of the HXR loop-top source coincides with the inward swing of the loop leg observed in the AIA 304 \r{A} passband, which is suggested to be related to the coronal implosion. This fast inflow of magnetic flux contained in the loop leg greatly enhances the reconnection rate and results in very efficient particle acceleration in the second-step reconnection, which also helps to achieve a second higher temperature peak up to T ≈ 30 MK.

Operational solar flare forecasting via video-based deep learning

Sabrina **Guastavino**, Francesco Marchetti, Federico Benvenuto, Cristina Campi, Michele Piana
Frontiers **2022**
https://arxiv.org/pdf/2209.05128.pdf
Operational flare forecasting aims at providing predictions that can be used to make decisions, typically at a daily scale, about the space weather impacts of flare occurrence. This study shows that video-based deep learning can be used for operational purposes when the training and validation sets used for the network optimization are generated while accounting for the periodicity of the solar cycle. Specifically, the paper describes an algorithm that can be applied to build up sets of active regions that are balanced according to the flare class rates associated to a specific cycle phase. These sets are used to train and validate a Long-term Recurrent Convolutional Network made of a combination of a convolutional neural network and a Long-Short Memory network. The reliability of this approach is assessed in the case of two prediction windows containing the solar storm of **March 2015 and September 2017**, respectively.

Implementation paradigm for supervised flare forecasting studies: a deep learning application with video data

Sabrina **Guastavino**, Francesco Marchetti, Federico Benvenuto, Cristina Campi, Michele Piana
ApJ **2021**
https://arxiv.org/pdf/2110.12554.pdf
Solar flare forecasting can be realized by means of the analysis of magnetic data through artificial intelligence techniques. The aim is to predict whether a magnetic active region (AR) will originate solar flares above a certain class within a certain amount of time. A crucial issue is concerned with the way the adopted machine learning method is implemented, since forecasting results strongly depend on the criterion with which training, validation, and test sets are populated. In this paper we propose a general paradigm to generate these sets in such a way that they are independent

from each other and internally well-balanced in terms of AR flaring effectiveness. This set generation process provides a ground for comparison for the performance assessment of machine learning algorithms. Finally, we use this implementation paradigm in the case of a deep neural network, which takes as input videos of magnetograms recorded by the Helioseismic and Magnetic Imager on-board the Solar Dynamics Observatory (SDO/HMI). To our knowledge, this is the first time that the solar flare forecasting problem is addressed by means of a deep neural network for video classification, which does not require any a priori extraction of features from the HMI magnetograms.
Table 1. Description of twelve flare forecasting studies based on machine learning

Data-constrained Magnetohydrodynamic Simulation of an Intermediate Solar Filament Eruption

Yang **Guo**, Jinhan Guo, Yiwei Ni, M. D. Ding, P. F. Chen, Chun Xia, Rony Keppens, Kai E. Yang
ApJ **2023**
https://arxiv.org/pdf/2309.01325.pdf
Solar eruptive activities could occur in weak magnetic field environments and over large spatial scales, especially relevant to eruptions involving intermediate or quiescent solar filaments. To handle the large scales, we implement and apply a flux rope embedding method using regularized Biot-Savart laws in the spherical coordinate system. Combined with a potential field source surface model and a magneto-frictional method, a nonlinear force-free field comprising a flux rope embedded in a potential field is constructed. Using the combined nonlinear force-free field as the initial condition, we then perform a zero-β data-constrained magnetohydrodynamic (MHD) simulation for an M8.7 flare at 03:38 UT on **2012 January 23**. The MHD model reproduces the eruption process, flare ribbon evolution (represented by the quasi-separatrix layer evolution) and kinematics of the flux rope. This approach could potentially model global-scale eruptions from weak field regions.

Thermodynamic and Magnetic Topology Evolution of the X1.0 Flare on 2021 October 28 Simulated by a Data-driven Radiative Magnetohydrodynamic Model

Jin-han **Guo**, Yi-wei Ni, Ze Zhong, Yang Guo, Chun Xia, Hai-tang Li, Stefaan Poedts, Brigitte Schmieder, Peng-fei Chen
Astrophysical Journal Supplement **266** 3 **2023**
https://arxiv.org/pdf/2303.13980.pdf
https://iopscience.iop.org/article/10.3847/1538-4365/acc797/pdf
Solar filament eruptions, flares and coronal mass ejections (CMEs) are manifestations of drastic release of energy in the magnetic field, which are related to many eruptive phenomena from the Earth magnetosphere to black hole accretion disks. With the availability of high-resolution magnetograms on the solar surface, observational data-based modelling is a promising way to quantitatively study the underlying physical mechanisms behind observations. By incorporating thermal conduction and radiation losses in the energy equation, we develop a new data-driven radiative magnetohydrodynamic (MHD) model, which has the capability to capture the thermodynamic evolution compared to our previous zero-\b{eta} model. Our numerical results reproduce major observational characteristics of the X1.0 flare on **2021 October 28** in NOAA active region (AR) 12887, including the morphology of the eruption, kinematic of flare ribbons, extreme-ultraviolet (EUV) radiations, and two components of the EUV waves predicted by the magnetic stretching model, i.e., a fast-mode shock wave and a slower apparent wave due to successive stretching of magnetic field lines. Moreover, some intriguing phenomena are revealed in the simulation. We find that flare ribbons separate initially and ultimately stop at the outer stationary quasi-separatrix layers (QSLs). Such outer QSLs correspond to the border of the filament channel and determine the final positions of flare ribbons, which can be used to predict the size and the lifetime of a flare before it occurs. In addition, the side view of the synthesized EUV and white-light images exhibit typical three-part structures of CMEs, where the bright leading front is roughly cospatial with the non-wave component of the EUV wave, reinforcing the magnetic stretching model for the slow component of EUV waves.

Inferring flare loop parameters with measurements of standing sausage modes

Ming-Zhe **Guo**, Shao-Xia Chen, Bo Li, Li-Dong Xia, Hui Yu
Solar Phys. Volume 291, Issue 3, pp 877-896 **2016**
http://arxiv.org/pdf/1512.03692v1.pdf
Standing fast sausage modes in flare loops were suggested to account for a considerable number of quasi-periodic pulsations (QPPs) in the light curves of solar flares. This study continues our investigation into the possibility to invert the measured periods P and damping times τ of sausage modes to deduce the transverse Alfv\'en time R/vAi, density contrast ρi/ρe, and the steepness of the density distribution transverse to flare loops. A generic dispersion relation (DR) governing linear sausage modes is derived for pressureless cylinders where density inhomogeneity of arbitrary form takes place within the cylinder. We show that in general the inversion problem is under-determined for QPP events where only a single sausage mode exists, be the measurements spatially resolved or unresolved. While R/vAi can be inferred to some extent, the range of possible steepness parameters may be too broad to be useful. However, for spatially resolved measurements where an additional mode is present, it is possible to deduce self-consistently ρi/ρe, the profile steepness, and the internal Alfv\'en speed vAi. We show that at least for a recent QPP event that involves a

fundamental kink mode in addition to a sausage one, flare loop parameters are well constrained, even if the specific form of the transverse density distribution remains unknown. We conclude that spatially resolved, multi-mode QPP measurements need to be pursued for inferring flare loop parameters.

Non-thermal Electron Acceleration in Low Mach Number Collisionless Shocks. II. Firehose-mediated Fermi Acceleration and its Dependence on Pre-shock Conditions

Xinyi **Guo**, Lorenzo Sironi1, and Ramesh Narayan
2014 ApJ 797 47
Electron acceleration to non-thermal energies is known to occur in low Mach number (Ms 5) shocks in galaxy clusters and solar flares, but the electron acceleration mechanism remains poorly understood. Using two-dimensional (2D) particle-in-cell (PIC) plasma simulations, we showed in Paper?I that electrons are efficiently accelerated in low Mach number (Ms = 3) quasi-perpendicular shocks via a Fermi-like process. The electrons bounce between the upstream region and the shock front, with each reflection at the shock resulting in energy gain via shock drift acceleration. The upstream scattering is provided by oblique magnetic waves that are self-generated by the electrons escaping ahead of the shock. In the present work, we employ additional 2D PIC simulations to address the nature of the upstream oblique waves. We find that the waves are generated by the shock-reflected electrons via the firehose instability, which is driven by an anisotropy in the electron velocity distribution. We systematically explore how the efficiency of wave generation and of electron acceleration depend on the magnetic field obliquity, the flow magnetization (or equivalently, the plasma beta), and the upstream electron temperature. We find that the mechanism works for shocks with high plasma beta (20) at nearly all magnetic field obliquities, and for electron temperatures in the range relevant for galaxy clusters. Our findings offer a natural solution to the conflict between the bright radio synchrotron emission observed from the outskirts of galaxy clusters and the low electron acceleration efficiency usually expected in low Mach number shocks.

THE SPECIFIC ACCELERATION RATE IN LOOP-STRUCTURED SOLAR FLARES—IMPLICATIONS FOR ELECTRON ACCELERATION MODELS

Jingnan **Guo**1,2, A. Gordon Emslie3, and Michele Piana
2013 ApJ 766 28
We analyze electron flux maps based on RHESSI hard X-ray imaging spectroscopy data for a number of extended coronal-loop flare events. For each event, we determine the variation of the characteristic loop length L with electron energy E, and we fit this observed behavior with models that incorporate an extended acceleration region and an exterior "propagation" region, and which may include collisional modification of the accelerated electron spectrum inside the acceleration region. The models are characterized by two parameters: the plasma density n in, and the longitudinal extent L 0 of, the acceleration region. Determination of the best-fit values of these parameters permits inference of the volume that encompasses the acceleration region and of the total number of particles within it. It is then straightforward to compute values for the emission filling factor and for the specific acceleration rate (electrons s–1 per ambient electron above a chosen reference energy). For the 24 events studied, the range of inferred filling factors is consistent with a value of unity. The inferred mean value of the specific acceleration rate above E 0 = 20 keV is ~10–2 s–1, with a 1σ spread of about a half-order-of-magnitude above and below this value. We compare these values with the predictions of several models, including acceleration by large-scale, weak (sub-Dreicer) fields, by strong (super-Dreicer) electric fields in a reconnecting current sheet, and by stochastic acceleration processes.

Dense Loop Flares

Jingnan **Guo** and Gordon Emslie.
RHESSI Science Nugget, No. 181, Aug **2012**
http://sprg.ssl.berkeley.edu/~tohban/wiki/index.php/Dense_Loop_Flares
Direct electron mapping teaches us about the structure of electron acceleration in flares.

PROPERTIES OF THE ACCELERATION REGIONS IN SEVERAL LOOP-STRUCTURED SOLAR FLARES

Jingnan **Guo**1, A. Gordon Emslie2, Anna Maria Massone3, and Michele Piana
2012 ApJ 755 32
Using RHESSI hard X-ray imaging spectroscopy observations, we analyze electron flux maps for a number of extended coronal loop flares. For each event, we fit a collisional model with an extended acceleration region to the observed variation of loop length with electron energy E, resulting in estimates of the plasma density in, and longitudinal extent of, the acceleration region. These quantities in turn allow inference of the number of particles within the acceleration region and hence the filling factor f—the ratio of the emitting volume to the volume that encompasses the emitting

region(s). We obtain values of f that lie mostly between 0.1 and 1.0; the (geometric) mean value is f = 0.20 ×/÷ 3.9, somewhat less than, but nevertheless consistent with, unity. Further, coupling information on the number of particles in the acceleration region with information on the total rate of acceleration of particles above a certain reference energy (obtained from spatially integrated hard X-ray data) also allows inference of the specific acceleration rate (electron s–1 per ambient electron above the chosen reference energy). We obtain a (geometric) mean value of the specific acceleration rate η(20 keV) =(6.0 ×/÷ 3.4) × 10–3 electrons s–1 per ambient electron; this value has implications both for the global electrodynamics associated with replenishment of the acceleration region and for the nature of the particle acceleration process.

Determination of the acceleration region size in a loop-structured solar flare

J. **Guo**1, A. G. Emslie2, E. P. Kontar3, F. Benvenuto1, A. M. Massone4 and M. Piana
A&A 543, A53 (**2012**)

Aims. To study the acceleration and propagation of bremsstrahlung-producing electrons in solar flares, we analyze the evolution of the flare loop size with respect to energy at a variety of times. A GOES M3.7 loop-structured flare starting around 23:55 on **2002 April 14** is studied in detail using Ramaty High Energy Solar Spectroscopic Imager (RHESSI) observations.

Methods. We construct photon and mean-electron-flux maps in 2-keV energy bins by processing observationally-deduced photon and electron visibilities, respectively, through several image-processing methods: a visibility-based forward-fit (FWD) algorithm, a maximum entropy (MEM) procedure and the uv-smooth (UVS) approach. We estimate the sizes of elongated flares (i.e., the length and width of flaring loops) by calculating the second normalized moments of the intensity in any given map. Employing a collisional model with an extended acceleration region, we fit the loop lengths as a function of energy in both the photon and electron domains.

Results. The resulting fitting parameters allow us to estimate the extent of the acceleration region which is between ~ 13 arcsec and ~19 arcsec. Both forward-fit and uv-smooth algorithms provide substantially similar results with a systematically better fit in the electron domain.

Conclusions. The consistency of the estimates from these methods provides strong support that the model can reliably determine geometric parameters of the acceleration region. The acceleration region is estimated to be a substantial fraction (~1/2) of the loop extent, indicating that this dense flaring loop incorporates both acceleration and transport of electrons, with concurrent thick-target bremsstrahlung emission.

PARTICLE ACCELERATION AT A FLARE TERMINATION SHOCK: EFFECT OF LARGE-SCALE MAGNETIC TURBULENCE

Fan **Guo** and Joe Giacalone
2012 ApJ 753 28

We investigate the acceleration of charged particles (both electrons and protons) at collisionless shocks predicted to exist in the vicinity of solar flares. The existence of standing termination shocks has been examined by flare models and numerical simulations. We study electron energization by numerically integrating the equations of motion of a large number of test-particle electrons in the time-dependent two-dimensional electric and magnetic fields generated from hybrid simulations (kinetic ions and fluid electron) using parameters typical of the solar flare plasma environment. The shock is produced by injecting plasma flow toward a rigid piston. Large-scale magnetic fluctuations—known to exist in plasmas and known to have important effects on the nonthermal electron acceleration at shocks—are also included in our simulations. For the parameters characteristic of the flaring region, our calculations suggest that the termination shock formed in the reconnection outflow region (above post-flare loops) could accelerate electrons to a kinetic energy of a few MeV within 100 ion cyclotron periods, which is of the order of a millisecond. Given a sufficient turbulence amplitude level (δB 2/B 2 0 ~ 0.3), about 10% of thermal test-particle electrons are accelerated to more than 15 keV. We find that protons are also accelerated, but not to as high energy in the available time and the energy spectra are considerably steeper than that of the electrons for the parameters used in our simulations. Our results are qualitatively consistent with the observed hard X-ray emissions in solar flares.

EVOLUTION OF HARD X-RAY SOURCES AND ULTRAVIOLET SOLAR FLARE RIBBONS FOR A CONFINED ERUPTION OF A MAGNETIC FLUX ROPE

Y. **Guo**, M. D. Ding, B. Schmieder, P. Démoulin and H. Li
2012 ApJ 746 17, **File**

We study the magnetic field structures of hard X-ray (HXR) sources and flare ribbons of the M1.1 flare in active region NOAA 10767 on **2005 May 27**. We have found in a nonlinear force-free field extrapolation over the same polarity inversion line, a small pre-eruptive magnetic flux rope located next to sheared magnetic arcades. RHESSI and the Transition Region and Coronal Explorer (TRACE) observed this confined flare in the X-ray bands and ultraviolet (UV) 1600 Å bands, respectively. In this event magnetic reconnection occurred at several locations. It first started at the location of the pre-eruptive flux rope. Then, the observations indicate that magnetic reconnection occurred between the

pre-eruptive magnetic flux rope and the sheared magnetic arcades more than 10 minutes before the flare peak. This implies the formation of the larger flux rope, as observed with TRACE. Next, HXR sources appeared at the footpoints of this larger flux rope at the peak of the flare. The associated high-energy particles may have been accelerated below the flux rope in or around a reconnection region. Still, the close spatial association between the HXR sources and the flux rope footpoints favors an acceleration within the flux rope. Finally, a topological analysis of a large solar region, including active regions NOAA 10766 and 10767, shows the existence of large-scale Quasi-Separatrix Layers (QSLs) before the eruption of the flux rope. No enhanced emission was found at these QSLs during the flare, but the UV flare ribbons stopped at the border of the closest large-scale QSL.

RELATIONSHIP BETWEEN HARD AND SOFT X-RAY EMISSION COMPONENTS OF A SOLAR FLARE

Jingnan **Guo**1,2,3, Siming Liu1,3, Lyndsay Fletcher1, and Eduard P. Kontar1
Astrophysical Journal, 728:4 (12pp), **2011** February

X-ray observations of solar flares routinely reveal an impulsive high-energy and a gradual low-energy emission component, whose relationship is one of the key issues of solar flare study. The gradual and impulsive emission components are believed to be associated with, respectively, the thermal and nonthermal components identified in spectral fitting. In this paper, a prominent ~50 s hard X-ray (HXR) pulse of a simple *GOES* class C7.5 flare on **2002 February 20** is used to study the association between high-energy, non-thermal, and impulsive evolution, and low-energy, thermal, and gradual evolution. We use regularized methods to obtain time derivatives of photon fluxes to quantify the time evolution as a function of photon energy, obtaining a break energy between impulsive and gradual behavior. These break energies are consistent with a constant value of ~11 keV in agreement with those found spectroscopically between thermal and non-thermal components, but the relative errors of the former are greater than 15% and much greater than the few percent errors found from the spectral fitting. These errors only weakly depend on assuming an underlying spectral model for the photons, pointing to the current data being inadequate to reduce the uncertainties rather than there being a problem associated with an assumed model. The time derivative method is used to test for the presence of a "pivot energy" in this flare. Although these pivot energies are marginally consistent with a constant value of ~9 keV, its values in the HXR rise phase appear to be lower than those in the decay phase. Assuming that electrons producing the high-energy component have a power-law distribution and are accelerated from relatively hot regions of a background plasma responsible for the observed thermal component, a low limit is obtained for the low-energy cutoff. This limit is always lower than the break and pivot energies and is located in the tail of the Maxwellian distribution of the thermal component.

Is the 3-D magnetic null point with a convective electric field an efficient particle accelerator?

J.-N. **Guo**1,2,3, J. Büchner1, A. Otto4, J. Santos1, E. Marsch1 and W.-Q. Gan2
A&A 513, A73 (**2010**)

Aims. We study the particle acceleration at a magnetic null point in the solar corona, considering self-consistent magnetic fields, plasma flows and the corresponding convective electric fields.
Methods. We calculate the electromagnetic fields by 3-D magnetohydrodynamic (MHD) simulations and expose charged particles to these fields within a full-orbit relativistic test-particle approach. In the 3-D MHD simulation part, the initial magnetic field configuration is set to be a potential field obtained by extrapolation from an analytic quadrupolar photospheric magnetic field with a typically observed magnitude. The configuration is chosen so that the resulting coronal magnetic field contains a null. Driven by photospheric plasma motion, the MHD simulation reveals the coronal plasma motion and the self-consistent electric and magnetic fields. In a subsequent test particle experiment the particle energies and orbits (determined by the forces exerted by the convective electric field and the magnetic field around the null) are calculated in time.
Results. Test particle calculations show that protons can be accelerated up to 30 keV near the null if the local plasma flow velocity is of the order of 1000 km s-1 (in solar active regions). The final parallel velocity is much higher than the perpendicular velocity so that accelerated particles escape from the null along the magnetic field lines. Stronger convection electric field during big flare explosions can accelerate protons up to 2 MeV and electrons to 3 keV. Higher initial velocities can help most protons to be strongly accelerated, but a few protons also run the risk to be decelerated.
Conclusions. Through its convective electric field and due to magnetic nonuniform drifts and de-magnetization process, the 3-D null can act as an effective accelerator for protons but not for electrons. Protons are more easily de-magnetized and accelerated than electrons because of their larger Larmor radii. Notice that macroscopic MHD simulations are blind to microscopic magnetic structures where more non-adiabatic processes might be taking place. In the real solar corona, we expect that particles could have a higher probability to experience a de-magnetization process and get accelerated. To trigger a significant acceleration of electrons and even higher energetic protons, however, the existence of a resistive electric field mainly parallel to the magnetic field is required. A physically reasonable resistivity model included in

resistive MHD simulations is direly needed for the further investigations of electron acceleration by parallel electric fields.

A FLUX ROPE ERUPTION TRIGGERED BY JETS

Juan **Guo**1, Yu Liu2, Hongqi Zhang1, Yuanyong Deng1, Jiaben Lin1, and Jiangtao Su1
Astrophysical Journal, 711:1057–1061, **2010** March; **File**

We present an observation of a filament eruption caused by recurrent chromospheric plasma injections (surges/jets) on **2006 July 6**. The filament eruption was associated with an M2.5 two-ribbon flare and a coronal mass ejection (CME). There was a light bridge in the umbra of the main sunspot of NOAA 10898; one end of the filament was terminated at the region close to the light bridge, and recurrent surges were observed to be ejected from the light bridge. The surges occurred intermittently for about 8 hr before the filament eruption, and finally a clear jet was found at the light bridge to trigger the filament eruption. We analyzed the evolutions of the relative darkness of the filament and the loaded mass by the continuous surges quantitatively. It was found that as the occurrence of the surges, the relative darkness of the filament body continued growing for about 3–4 hr, reached its maximum, and kept stable for more than 2 hr until it erupted. If suppose 50% of the ejected mass by the surges could be trapped by the filament channel, then the total loaded mass into the filament channelwill be about 0.57×10^{16} g with a momentum of 0.57×10^{22} g cm s^{-1} by 08:08 UT, which is a non-negligible effect on the stability of the filament. Based on the observations, we present amodel showing the important role that recurrent chromospheric mass injection play in the evolution and eruption of a flux rope. Our study confirms that the surge activities can efficiently supply the necessary material for some filament formation. Furthermore, our study indicates that the continuous mass with momentum loaded by the surge activities to the filament channel could make the filament unstable and cause it to erupt.

Stability of the coronal magnetic field around large confined and eruptive solar flares

Manu **Gupta**, J. K. Thalmann, A. M. Veronig
A&A 686, A115 **2024**
https://arxiv.org/pdf/2402.12254.pdf
https://www.aanda.org/articles/aa/pdf/2024/06/aa46212-23.pdf

Context. The coronal magnetic field, which overlies the current-carrying field of solar active regions, straps the magnetic configuration below. The characteristics of this overlying field are crucial in determining if a flare will be eruptive and accompanied by a coronal mass ejection (CME), or if it will remain confined without a CME.
Aims. In order to improve our understanding on the pre-requisites of eruptive solar flares, we study and compare different measures that characterize the eruptive potential of solar active regions — the critical height for torus instability as a local measure and the helicity ratio as a global measure — with the structural properties of the underlying magnetic field, namely the altitude of the center of the current-carrying magnetic structure.
Methods. Using time series of 3D optimization-based nonlinear force-free magnetic field models for 10 different active regions (ARs) around the time of large solar flares, we determine the altitudes of the current-weighted centers of the non-potential model structures. Based on the potential magnetic field, we inspect the decay index, n, in multiple vertical planes oriented along of or perpendicular to the flare-relevant polarity inversion line, and estimate the critical height (hcrit) for torus instability (TI) using different thresholds of n. The critical heights are interpreted with respect to the altitudes of the current-weighted centers of the associated non-potential structures, as well as the eruptive character of the associated flares, and the eruptive potential of the host AR, as characterized by the helicity ratio.
Results. Our most important findings are that (i) hcrit is more segregated in terms of flare type than the helicity ratio, and that (ii) coronal field configurations with a higher eruptive potential (in terms of the helicity ratio) also appear to be more prone to TI. Furthermore, we find no pronounced differences in the altitudes of the non-potential structures prior to confined and eruptive flares. An aspect which requires further investigation is that, quite generally, the modeled non-potential structures hardly reside in a torusinstable regime, requiring further assessment regarding the applicability of the chosen NLFF modeling approach when targeted at the structural properties of the coronal magnetic field. **2011-02-15, 2011-03-09, 2011-09-26, 2011-11-05, 2012-03-07, 2014-10-24, 2015-01-30, 2015-03- 11, 2017-09-06**

Magnetic helicity and energy budget around large confined and eruptive solar flares

Manu **Gupta**, J. K. Thalmann, A. M. Veronig
A&A 653, A69 **2021**
https://arxiv.org/pdf/2106.08781.pdf
https://www.aanda.org/articles/aa/pdf/2021/09/aa40591-21.pdf
https://doi.org/10.1051/0004-6361/202140591

Context: In order to better understand the underlying process and prerequisites for solar activity, it is essential to study the time evolution of the coronal magnetic field of solar active regions (ARs) associated to flare activity.
Aims: We investigate the coronal magnetic energy and helicity budgets of ten solar ARs, around the times of large flares. In particular, we are interested in a possible relation of the derived quantities to the particular type of the flares that the AR produces, i.e., whether they are associated with a CME or they are confined.

Methods: Using an optimization approach, we employ time series of 3D nonlinear force-free magnetic field models of ten ARs, covering a time span of several hours around the time of occurrence of large solar flares (GOES class M1.0 and larger). We subsequently compute the 3D magnetic vector potentials associated to the model 3D coronal magnetic field using a finite-volume method. This allows us to correspondingly compute the coronal magnetic energy and helicity budgets, as well as related (intensive) quantities such as the relative contribution of free magnetic energy, EF/E (energy ratio), the fraction of non-potential (current-carrying) helicity, |HJ |/|HV | (helicity ratio), and the normalized current-carrying helicity, |HJ |/φ02 .
Results: The total energy and helicity budgets of flare-productive ARs (extensive parameters) cover a broad range of magnitudes, with no obvious relation to the eruptive potential of the individual ARs, i.e., whether or not a CME is produced in association with the flare. The intensive eruptivity proxies, EF/E and |HJ |/|HV |, and |HJ |/φ02 , however, seem to be distinctly different for ARs that produced CME-associated large flares compared to those which produced confined flares. For the majority of ARs in our sample, we are able to identify characteristic pre-flare magnitudes of the intensive quantities, clearly associated to subsequent CME-productivity.
Conclusions: If the corona of an AR exhibits characteristic values of h|HJ |/|HV |i > 0.1, hEF/Ei > 0.2, and h|HJ |/φ02 i > 0.005, then the AR is likely to produce large CME-associated flares. Conversely, confined large flares tend to originate from ARs that exhibit coronal values of h|HJ |/|HV |i . 0.1, hEF/Ei . 0.1, and h|HJ |/φ02 i . 0.002.

We investigate the coronal magnetic energy and helicity budgets of ten solar ARs, around the times of large flares. In particular, we are interested in a possible relation of the derived quantities to the particular type of the flares that the AR produces, i.e., whether they are associated with a CME or they are confined. Using an optimization approach, we employ time series of 3D nonlinear force-free magnetic field models of ten ARs, covering a time span of several hours around the time of occurrence of large solar flares (GOES class M1.0 and larger). We subsequently compute the 3D magnetic vector potentials associated to the model 3D coronal magnetic field using a finite-volume method. This allows us to correspondingly compute the coronal magnetic energy and helicity budgets, as well as related (intensive) quantities such as the relative contribution of free magnetic energy, EF/E (energy ratio), the fraction of non-potential (current-carrying) helicity, |HJ|/|HV| (helicity ratio), and the normalized current-carrying helicity, |HJ|/ϕ′2. The total energy and helicity budgets of flare-productive ARs (extensive parameters) cover a broad range of magnitudes, with no obvious relation to the eruptive potential of the individual ARs, i.e., whether or not a CME is produced in association with the flare. The intensive eruptivity proxies, EF/E and |HJ|/|HV|, and |HJ|/ϕ′2, however, seem to be distinctly different for ARs that produced CME-associated large flares compared to those which produced confined flares. For the majority of ARs in our sample, we are able to identify characteristic pre-flare magnitudes of the intensive quantities, clearly associated to subsequent CME-productivity. **2011-02-15, 2011-03-09, 2011-09-26, 2011-11-05, 2012-03-07, 2013-11-08, 2014-10-24, 2015-01-30, 2015-03-11, 2017-09-06**
Table. 1 List of flares under study

Observation and Modeling of Chromospheric Evaporation in a Coronal Loop Related to Active Region Transient Brightening

G. R. **Gupta**, Aveek Sarkar, Durgesh Tripathi
ApJ **857** 137 **2018**
https://arxiv.org/pdf/1803.11172.pdf
http://sci-hub.tw/http://iopscience.iop.org/0004-637X/857/2/137/
Using the observations recorded by Atmospheric Imaging Assembly (AIA) on-board the Solar Dynamics Observatory (SDO), the Interface Region Imaging Spectrograph (IRIS) and the Extreme-ultraviolet Imaging Spectrometer (EIS) and X-Ray Telescope (XRT) both on-board Hinode, we present the evidence of chromospheric evaporation in a coronal loop after the occurrence of two active region transient brightenings (ARTBs) at the two footpoints. The chromospheric evaporation started nearly simultaneously in all the three hot channels of AIA such as 131~{\AA}, 94~{\AA} and 335~{\AA}, which was observed to be temperature dependent, being fastest in the highest temperature channel. The whole loop became fully brightened following the ARTBs after ≈25~s in 131~{\AA}, ≈40~s in 94~{\AA}, and ≈6.5~min in 335~{\AA}. The DEM measurements at the two footpoints (i.e., of two ARTBs) and the loop-top suggest that the plasma attained a maximum temperature of ∼10~MK at all these locations. The spectroscopic observations from IRIS revealed the presence of redshifted emission of ∼20~km~s−1in cooler lines like \ion{C}{2} and \ion{Si}{4} during the ARTBs that was co-temporal with the evaporation flow at the footpoint of the loop. During the ARTBs, the line width of \ion{C}{2} and \ion{Si}{4} increased nearly by a factor of two during the peak emission. Moreover, enhancement in the line width preceded that in the Doppler shift which again preceded enhancement in the intensity. The observed results were qualitatively reproduced by 1-D hydrodynamic simulations where energy was deposited at both the footpoints of a monolithic coronal loop that mimicked the ARTBs identified in the observations.
2014 March 4

IRIS and SDO observation of recurrent explosive events

G. R. **Gupta**, Durgesh Tripathi
ApJ **809** 82 **2015**
http://arxiv.org/pdf/1506.05327v1.pdf

Observations of recurrent explosive events (EEs) with time scale of 3-5 minutes are reported. These EEs have been observed with the Interface Region Imaging Spectrograph (IRIS) and have a spatial dimension of ~1.5" along the slit. The spectral line profiles of \ion{C}{2}~1335/1336 \AA\ and \ion{Si}{4}~1394/1403\AA\ become highly broadened both in red as well as blue wings. Several absorption lines on top of the broadened profiles were identified. In addition, emission lines corresponding to neutral lines such as \ion{Cl}{1}~1351.66~{\AA}, \ion{C}{1}~1354.29~{\AA}, and \ion{C}{1}~1355.84~{\AA} were identified. The \ion{C}{1}~1354.29~{\AA}, and \ion{C}{1}~1355.84 {\AA} lines were found only during the EEs whereas \ion{Cl}{1}~1351.66~{\AA} broadens during the EEs. The estimated lower limit on electron number density obtained using the line ratios of \ion{Si}{4} and \ion{O}{4} is about 1013.5 cm−3, suggesting that the observed events are most likely occurring at heights corresponding to lower chromosphere. To the best of our knowledge, for the first time we have detected short-period variability (30 s and 60--90 s) within the EE bursts. Observations of photospheric magnetic field underneath EEs indicate that negative polarity field emerges in the neighbourhood of oppositely directed positive fields which undergo repetitive reconnection (magnetic flux cancellation) events. The dynamic changes observed in AIA 1700 \AA, 1600 \AA, \ion{C}{2} 1330 \AA\ and \ion{Si}{4} 1400 \AA\ intensity images corresponded very well with the emergence and cancellation of photospheric magnetic field (negative polarity) on the time scale of 3--5 min. The observations reported here suggests that these EEs are formed due to magnetic reconnection and are occurring in the lower chromosphere. **2014 March 4**

Periodic Recurrence Patterns In X-Ray Solar Flare Appearances

N. **Gyenge**, R. Erdélyi
2018 *ApJ* **859** 169
https://arxiv.org/pdf/1804.11229.pdf
http://sci-hub.tw/http://iopscience.iop.org/0004-637X/859/2/169/
The temporal recurrence of micro-flare events is studied for a time interval before and after of major solar flares. Our sample is based on the X-ray flare observations by the *Geostationary Operational Environmental Satellite* (*GOES*) and *Reuven Ramaty High Energy Solar Spectroscopic Imager*(*RHESSI*). The analyzed data contain 1330/301 M-class and X-class *GOES*/*RHESSI* energetic solar flares and 4062/4119 *GOES*/*RHESSI* micro-flares covering the period elapse since 2002. The temporal analysis of recurrence, by Fast Fourier Transform, of the micro-flares, shows multiple significant periods. Based on the *GOES* and *RHESSI* data, the temporal analysis also demonstrates that multiple periods manifest simultaneously in both statistical samples without any significant shift over time. In the *GOES* sample, the detected significant periods are: 11.33, 5.61, 3.75, 2.80, and 2.24 minutes. The *RHESSI* data show similar significant periods at 8.54, 5.28, 3.66, 2.88, and 2.19 minutes. The periods are interpreted as signatures of standing oscillations, with the longest period (P_1) being the fundamental and others being higher harmonic modes. The period ratio of the fundamental and higher harmonics ($P_1/P\,N$) is also analyzed. The standing modes may be signatures of global oscillations of the entire solar atmosphere encompassing magnetized plasma from the photosphere to the corona in active regions.

Statistical study of spatio-temporal distribution of precursor solar flares associated with major flares

N. **Gyenge**, I. Ballai, T. Baranyi
MNRAS **2016**
http://arxiv.org/pdf/1604.03384v1.pdf
The aim of the present investigation is to study the spatio-temporal distribution of precursor flares during the 24-hour interval preceding M- and X-class major flares and the evolution of follower flares. Information on associated (precursor and follower) flares is provided by Reuven Ramaty High Energy Solar Spectroscopic Imager (RHESSI). Flare List, while the major flares are observed by the Geostationary Operational Environmental Satellite (GOES) system satellites between 2002 and 2014. There are distinct evolutionary differences between the spatio-temporal distributions of associated flares in about one day period depending on the type of the main flare. The spatial distribution was characterised by the normalised frequency distribution of the quantity δ (the distance between the major flare and its precursor flare normalised by the sunspot group diameter) in four 6-hour time intervals before the major event. The precursors of X-class flares have a double-peaked spatial distribution for more than half a day prior to the major flare, but it changes to a lognormal-like distribution roughly 6 hours prior to the event. The precursors of M-class flares show lognormal-like distribution in each 6-hour subinterval. The most frequent sites of the precursors in the active region are within a distance of about 0.1 diameter of sunspot group from the site of the major flare in each case. Our investigation shows that the build-up of energy is more effective than the release of energy because of precursors.
2011−03−09

Active Longitude and Solar Flare Occurrences

N. **Gyenge**, A. Ludmány, T. Baranyi
2016 *ApJ* **818** 127

http://arxiv.org/pdf/1512.08124v1.pdf
The aim of the present work is to specify the spatio-temporal characteristics of flare activity observed by the Reuven Ramaty High Energy Solar Spectroscopic Imager (RHESSI) and Geostationary Operational Environmental Satellite (GOES) satellites in connection with the behaviour of the longitudinal domain of enhanced sunspot activity known as active longitude (AL). By using our method developed for this purpose, we identified the AL in every Carrington Rotation provided by the Debrecen Photoheliographic Data (DPD). The spatial probability of flare occurrence has been estimated depending on the longitudinal distance from AL in the northern and southern hemispheres separately. We have found that more than the 60\% of the RHESSI and GOES flares is located within ±36◦ from the active longitude. Hence, the most flare-productive active regions tend to be located in or close to the active longitudinal belt. This observed feature may allow predicting the geo-effective position of the domain of enhanced flaring probability. Furthermore, we studied the temporal properties of flare occurrence near the active longitude and several significant fluctuations were found. More precisely, the results of the method are the following fluctuations: 0.8 years, 1.3 years and 1.8 years. These temporal and spatial properties of the solar flare occurrence within the active longitudinal belts could provide us enhanced solar flare forecasting opportunity.

Automation of Tracking Various Sunspot Group Entities and Demonstrating Its Usage on the Flaring NOAA AR 11429

L. **Győri**

Solar Physics Volume 290, Issue 6, pp 1627-1645 **2015**

A method based on set and graph operations was developed to find and track related entities of sunspot groups on a series of consecutive solar images. Of course, if we can track entities of a sunspot group, we can also track various properties (e.g., position, area, magnetic field, and intensity) associated with them. A new higher-level sunspot-group entity belonging to the whole image series, a family, was introduced to cope with the mergings and separations of various sunspot group entities.

To demonstrate the usefulness of the method, it was applied to NOAA AR 11429 using Solar Dynamics Observatory/Helioseismic and Magnetic Imager (SDO/HMI) images. This large sunspot group produced several X, M, and C class flares, among others, an X5.4 class flare on **2012 March 7**. Abrupt transient and permanent variations in the mean line-of-sight (LOS) magnetic field of the large umbra families were found during the X5.4 flare. Two small umbra families immediately next to the polarity inversion line (PIL) and facing each other at opposite sides of the PIL exhibited abrupt stepwise changes in their mean LOS magnetic field during the X5.4 flare. The family with positive polarity decreased and the family with negative polarity increased. Some of the large umbra families also showed abrupt decrease in their darkness during the flare. We conjecture that an umbra family being a part of a long, narrow magnetic field strip pushing in an opposite magnetic polarity penumbral domain might be one of the triggering causes of several flares. Flare-related changes were observed at every spatial scale of the studied sunspot group. Two of the large opposite-polarity umbra families underwent shearing and converging motions. The break and the turning points of the motion curves of these families were related to flares. Some of the flares coincided with abrupt changes in the motion curves.

Toward Realistic Solar Flare Models: An explicit Particle-In-Cell solver in the DISPATCH framework

Michael **Haahr**, Boris V. Gudiksen, Åke Nordlund

A&A **2024**

https://arxiv.org/pdf/2409.02493

Context. Simulating solar flares, which involve large-scale dynamics and small-scale magnetic reconnection, poses significant computational challenges. Aims. This study aims to develop an explicit Particle-In-Cell (PIC) solver within the DISPATCH framework to model the small-scale kinetic processes in solar corona setting. This study in the first in a series with the ultimate goal to develop a hybrid PIC-MHD solver, to simulate solar flares. Methods. The PIC solver, inspired by the PhotonPlasma code, solves the Vlasov-Maxwell equations in a collisionless regime using explicit time-staggering and spatial-staggering techniques. Validation included unit tests, plasma frequency recovery, two-stream instability, and current sheet dynamics. Results. Validation tests confirmed the solver's accuracy and robustness in modeling plasma dynamics and electromagnetic fields. Conclusions. The integration of the explicit PIC solver into the DISPATCH framework is the first step towards bridging the gap between large and small scale dynamics, providing a robust platform for future solar physics research.

A Deep-Learning Approach for Operation of an Automated Realtime Flare Forecast

Yuko **Hada-Muranushi**, Takayuki Muranushi, Ayumi Asai, Daisuke Okanohara, Rudy Raymond, Gentaro Watanabe, Shigeru Nemoto, Kazunari Shibata

Space Weather **2016**

http://arxiv.org/pdf/1606.01587v1.pdf

Automated forecasts serve important role in space weather science, by providing statistical insights to flare-trigger mechanisms, and by enabling tailor-made forecasts and high-frequency forecasts. Only by realtime forecast we can experimentally measure the performance of flare-forecasting methods while confidently avoiding overlearning.
We have been operating unmanned flare forecast service since **August, 2015** that provides 24-hour-ahead forecast of solar flares, every 12 minutes. We report the method and prediction results of the system.

Reconnection Mediated by Magnetic Fractures and the Solar Flare

Gerhard **Haerendel**
2018 ApJ 855 95
http://sci-hub.tw/http://iopscience.iop.org/0004-637X/855/2/95/
Reconnection of sheared magnetic fields is commonly treated by regarding the component perpendicular to the antiparallel components as a largely inert guide field. In this paper an alternative is proposed in which the free energy residing in the shear field is being converted prior to reconnection. This happens in high-density, dissipative current sheets bordering the reconnection site. A global scenario is presented in which low-intensity currents out of the photosphere are converging into the narrow, high-intensity currents at high altitude. This is enabled by the obliqueness of the latter. The very short timescale of the energy conversion causes a lateral propagation of the current sheets. In a quasi-stationary situation, it balances the reconnection rate, which turns out to be much lower than in guide-field approaches. Another important consequence of the obliqueness is the field-parallel emission of runaway electrons. Accelerated up to tens of keV, they are possibly important contributors to the production of hard X-rays during the impulsive phase of a flare, but only in areas of upward-directed currents. Quantitative evaluation of the model predicts various potentially observable properties, such as width and propagation speed of the generated flare ribbons, spatial dependences of the electron spectrum, size of the area of energy deposition, and successive decrease of the shear angle between conjugate footpoints. The presented theoretical model can account for the observed brightness asymmetry of flare ribbons with respect to the direction of the vertical currents.

Field-parallel Acceleration: Comment on the Paper "Electric Currents on the Flare Ribbons: Observations and Standard Model" by Janvier et al. (2014, ApJ, 788, 60)

G. **Haerendel**
2017 ApJ 847 143
http://iopscience.iop.org/article/10.3847/1538-4357/aa81d3/pdf
It is proposed that the coincidence of higher brightness and upward electric current observed by Janvier et al. during a flare indicates electron acceleration by field-parallel potential drops sustained by extremely strong field-aligned currents of order 104 A m−2. A few consequences are discussed here.

Evidence for Field-parallel Electron Acceleration in Solar Flares

G. **Haerendel**
2017 ApJ 847 113
http://iopscience.iop.org/article/10.3847/1538-4357/aa8995/pdf
It is proposed that the coincidence of higher brightness and upward electric current observed by Janvier et al. during a flare indicates electron acceleration by field-parallel potential drops sustained by extremely strong field-aligned currents of the order of 104 A m−2. A consequence of this is the concentration of the currents in sheets with widths of the order of 1 m. The high current density suggests that the field-parallel potential drops are maintained by current-driven anomalous resistivity. The origin of these currents remains a strong challenge for theorists. **2011 February 15**

CHROMOSPHERIC EVAPORATION VIA ALFVÉN WAVES

Gerhard **Haerendel**
2009 ApJ 707 903-915
This paper presents a scenario for the chromospheric evaporation during solar flares, which is inspired by the chain of events leading to the formation of auroral arcs and ionospheric evacuation during magnetospheric substorms. The plasma, ejected from high coronal altitudes during a flare reconnection event, accumulates at the tops of coronal loops by braking of the reconnection flow, possibly by fast shock formation. A high-beta layer forms and distorts the magnetic field. Energy contained in magnetic shear stresses is transported as Alfvén waves from the loop-top toward the chromosphere. It is shown that under these conditions the Alfvén waves carry enough energy to feed the chromospheric evaporation process. The second subject of this investigation is identification of the most effective energy dumping or wave dissipation process. Several processes are being analyzed: ion-neutral collisions, classical and anomalous field-aligned current dissipation, and critical velocity ionization. All of them are being discarded, either because they turn out to be insufficient or imply very unlikely physical properties of the wave modes. It is finally concluded that turbulent fragmentation of the Alfvén waves entering the chromosphere can generate the required damping. The basic process would be phase mixing caused by a strongly inhomogeneous distribution of Alfvénic phase

speed and laminar flow breakup by Kelvin-Helmholtz (K-H) instability. The filamentary (fibril) structure of the chromosphere thus appears to be essential for the energy conversion, in which the K-H instability is the first step in a chain of processes leading to ion thermalization, electron heating, and neutral particle ionization. Quantitative estimates suggest that a transverse structure with scales not far below 100 km suffices to produce strong wave damping within a few seconds. Nonthermal broadening of some metallic ion lines observed during the pre-impulsive rise phase of a flare might be a residue of the turbulent breakup process.

Characteristics of Nanoflare Heating in a Coronal Bright Point

Michael **Hahn**1, Brandon Ho2, and Daniel Wolf Savin1
2022 ApJ 936 113
https://iopscience.iop.org/article/10.3847/1538-4357/ac897f/pdf
We have obtained constraints on the nanoflare energy distribution and timing for the heating of a coronal bright point. Observations of the bright point were made using the Extreme Ultraviolet Imaging Spectrometer on Hinode in slot mode, which collects a time series of monochromatic images of the region leading to unambiguous temperature diagnostics. The Enthalpy-Based Thermal Evolution of Loops model was used to simulate nanoflare heating of the bright point and generate a time series of synthetic intensities. The nanoflare heating in the model was parameterized in terms of the power-law index α of the nanoflare energy distribution, which is ∝ E−α; average nanoflare frequency f; and the number N of magnetic strands making up the observed loop. By comparing the synthetic and observed light curves, we inferred the region of the model parameter space (α, f, N) that was consistent with the observations. Broadly, we found that N and f are inversely correlated with one another, while α is directly correlated with either N or f. These correlations are likely a consequence of the region requiring a certain fixed energy input, which can be achieved in various ways by trading off among the different parameters. We also find hat a value of α > 2 generally gives the best match between the model and observations, which indicates that the heating is dominated by low-energy events. Our method of using monochromatic images, focusing on a relatively simple structure, and constraining nanoflare parameters on the basis of statistical properties of the intensity provides a versatile approach to better understand the nature of nanoflares and coronal heating. **2008 December 9**

Hard X-ray Polarimetry from Tian Gong 2

Wojtek **Hajdas**
RHESSI Science Nuggets #283 Oct **2016**
http://sprg.ssl.berkeley.edu/~tohban/wiki/index.php/Hard_X-ray_Polarimetry_from_Tian_Gong_2
The second Chinese space laboratory Tian Gong 2. Among the ten or more instruments onboard, and transported into space, resides [http://isdc.unige.ch/polar/ POLAR - the hard X-ray polarimeter, and the only non-Chinese experiment. POLAR is equipped with an array of 1600 plastic scintillators allowing for precise and efficient measurement of linear polarization in the hard X-ray energy range from 50 keV to 500 keV. It is also capable of the precise measurement of polarization in solar flares. **2016-10-12**

Probability of Solar Flares Turn Out to Form a Coronal Mass Ejections Events Due to the Characterization of Solar Radio Burst Type II and III **Book**

Zety Sharizat **Hamidi**
International Letters of Chemistry, Physics and Astronomy 16 (**2014**) 1-85
https://ui.adsabs.harvard.edu/search/filter_database_fq_database=OR&filter_database_fq_database=database%3A"astronomy"&filter_database_fq_database=database%3A"physics"&fq=%7B!type%3Daqp%20v%3D%24fq_database%7D&fq_database=(database%3A"astronomy"%20OR%20database%3A"physics")&q=author%3A("Hamidi")%20AND%20pubdate%3A%5B2014-01%20TO%202014-12%5D&sort=date%20desc%2C%20bibcode%20desc&p_=0
https://www.academia.edu/10330915/Probability_of_Solar_Flares_Turn_Out_to_Form_a_Coronal_Mass_Ejections_Events_Due_to_the_Characterization_of_Solar_Radio_Burst_Type_II_and_III?email_work_card=view-paper
The solar flare and Coronal Mass Ejections (CMEs) are well known as one of the most massiveeruptions which potentially create major disturbances in the interplanetary medium and initiate severe magnetic storms when they collide with the Earth‟s magnetosphere. However, how far the solar flarecan contribute to the formation of the CMEs is still not easy to be understood. These phenomena areassociated with II and III burst it also divided by sub-type of burst depending on the physicalcharacteristics and different mechanisms. In this work, we used a Compound Astronomical Low-costLow-frequency Instrument for Spectroscopy in Transportable Observatories (CALLISTO) system.The aim of the present study is to reveal dynamical properties of solar burst type II and III due toseveral mechanisms. Most of the cases of both solar radio bursts can be found in the range less that400 MHz. Based on solar flare monitoring within 24 hours, the CMEs that has the potential to explodewill dominantly be a class of M1 solar flare. Overall, the tendencies of SRBT III burst form the solarradio burst type III at 187 MHz to 449 MHz. Based on solar observations, it is evident that theexplosive, short time-scale energy release during flares and the long term, gradual energy releaseexpressed by CMEs can be reasonably understood only if both processes are taken as common
and probably not independent signatures of a destabilization of pre-existing coronal magnetic fieldstructures. The configurations of several active regions can be sourced regions of CMEs formation.The study of the formation,

acceleration and propagation of CMEs requires advanced and powerful observational tools in different spectral ranges as many „stages" as possible between the photosphere of the Sun and magnetosphere of the Sun and magnetosphere of the Earth. In conclusion, this range isa current regime of solar radio bursts during CMEs events. **9th March 2012, 13th November 2012, 23rd October 2012, 30th March 2013,**

Solar Flares with an Exponential Growth of the Emission Measure in the Impulsive Phase Derived from X-ray Observations

HAN Fei-ran LIU Si-ming

E-print, Aug **2013**; Published in Chinese Astronomy and Astrophysics

The light curves of solar flares in the impulsive phase are complex in general, indicating that multiple physical processes are involved in. With the GOES (Geostationary Operational Environmental Satellite) observations, we find that there are a subset of flares, whose impulsive phases are dominated by a period of exponential growth of the emission measure. The flares occurred from January 1999 to December 2002 are analyzed, and the results from the observations made with both GOES 8 and GEOS 10 satellites are compared to estimate the instrumental uncertainties. Their mean temperatures during this exponential growth phase have a normal distribution. Most flares within the 1σ range of this temperature distribution belong to the GOES class B or C, with the peak fluxes at the GOES low-energy channel following a log-normal distribution. The growth rate and duration of the exponential growth phase also follow a lognormal distribution, in which the duration is distributed in the range from half a minute to about half an hour. As expected, the growth time is correlated with the decay time of the soft X-ray flux. We also find that the growth rate of the emission measure is strongly anti-correlated with the duration of the exponential growth phase, and the mean temperature increases slightly with the increase of the growth rate. The implications of these results on the study of energy release in solar flares are discussed in the end.

Double-Loop Configuration of Solar Flares

Hanaoka, Yoichiro

1997 Sol. Ph..173..319-346

https://link.springer.com/content/pdf/10.1023/A:1004953003558.pdf

https://sci-hub.ru/10.1023/A:1004953003558

We analyzed several flares, which are presumed to be caused by interactions between an emerging loop and an overlying loop. We call such a basic combination of loops a 'double-loop configuration', and we reveal its topology on the basis of the microwave and soft X-ray observations of the flares and the magnetograms. In many cases, the magnetic field of the flare loops shows a 'bipolar + remote unipolar' structure, rather than a quadrapole structure. The footpoints of two loops are distributed in three magnetic patches, and two of the footpoints of the loops, one from the emerging loop and the other from the overlying loop, are included in a single magnetic polarity patch. Therefore, the two loops form a 'three-legged' structure, and the two loops are not anti-parallel as assumed in the traditional reconnection models. Typically, the emergence of a parasitic polarity near the major preceding-polarity region or the following one in an active region creates this configuration, but, in one of the analyzed flares, two active regions are involved in the configuration. Not only the flares, but various other active phenomena – microflares, thermal plasma flows like jets, and surges – occur in the same magnetic configuration. Hence, the interaction between two loops, which forms the three-legged structure, is an important source of the various types of activity. **1992 AUGUST 21 , 1992 OCTOBER 23 , 1992 December 15 , 1993 FEBRUARY 6 , 1993 April 10, 1993 April 11 , 1993 June 7, 1993 SEPTEMBER 30, 1994 December 14**

Flares and Plasma Flow Caused by Interacting Coronal Loops

Hanaoka, Yoichiro

1996 Sol. Ph..165..275-301

http://articles.adsabs.harvard.edu/pdf/1996SoPh..165..275H

Active region NOAA 7360 was observed in 1992 December with various instruments including the Yohkoh satellite. In this region, a small loop emerged near one of the footpoints of a pre-existing large coronal loop. These loops show evidence that interactions between coronal loops cause flares, microflares, and plasma flow. All of the four flares observed in this region show that brightenings in the small loop occurred first, and then the large loop flared up. The brightenings in the large loop can not occur by themselves, but must be triggered by the brightenings in the small loop. There must be interactions between the loops to cause these flares. As well as the flares, many microflares occurred in the small loop. More than half of them are accompanied by plasma ejection phenomena from the small loop into the large loop. The large loop is filled with ejected plasma with velocities of about 1000 km s-1. These ejection phenomena are considered as X-ray jets. The associated occurrences of the microflares and the jets suggest that they are also caused by interactions between the loops. The recurrent occurrences of the homologous flares and microflares mean that the magnetic field structure in this region inevitably causes the activity due to loop-loop interactions; the flares and jets occur under a common magnetic field structure. **14-17 Dec 1992**

Joint X-Ray, EUV, and UV Observations of a Small Microflare

Iain G. **Hannah**1, Lucia Kleint2,3, Säm Krucker2,4, Brian W. Grefenstette5, Lindsay Glesener6, Hugh S. Hudson1,4, Stephen M. White7, and David M. Smith8

2019 ApJ 881 109

https://iopscience.iop.org/article/10.3847/1538-4357/ab2dfa/pdf

We present the first joint observation of a small microflare in X-rays with the Nuclear Spectroscopic Telescope ARray (NuSTAR), in UV with the Interface Region Imaging Spectrograph (IRIS), and in EUV with the Solar Dynamics Observatory/Atmospheric Imaging Assembly (SDO/AIA). These combined observations allow us to study the hot coronal and cooler chromospheric/transition region emission from the microflare. This small microflare peaks from **2016 July 26** 23:35 to 23:36 UT, in both NuSTAR, SDO/AIA, and IRIS. Spatially, this corresponds to a small loop visible in the SDO/AIA Fe xviii emission, which matches a similar structure lower in the solar atmosphere seen by IRIS in SJI1330 and 1400 Å. The NuSTAR emission in both 2.5–4 and 4–6 keV is located in a source at this loop location. The IRIS slit was over the microflaring loop, and fits show little change in Mg ii but do show intensity increases, slight width enhancements, and redshifts in Si iv and O iv, indicating that this microflare had most significance in and above the upper chromosphere. The NuSTAR microflare spectrum is well fitted by a thermal component of 5.1 MK and 6.2 × 1044cm−3, which corresponds to a thermal energy of 1.5 × 1026 erg, making it considerably smaller than previously studied active region microflares. No non-thermal emission was detected but this could be due to the limited effective exposure time of the observation. This observation shows that even ordinary features seen in UV can remarkably have a higher-energy component that is clear in X-rays.

The first X-ray imaging spectroscopy of quiescent solar active regions with NuSTAR

I. G. **Hannah**, B. W. Grefenstette, D. M. Smith, L. Glesener, S. Krucker, H. S. Hudson, K. K. Madsen, A. Marsh, S. M. White, A. Caspi, A. Y. Shih, F. A. Harrison, D. Stern, S. E. Boggs, F. E. Christensen, W. W. Craig, C. J. Hailey, W. W. Zhang

ApJL 820 L14 **2016**

http://arxiv.org/pdf/1603.01069v1.pdf

We present the first observations of quiescent active regions (ARs) using NuSTAR, a focusing hard X-ray telescope capable of studying faint solar emission from high temperature and non-thermal sources. We analyze the first directly imaged and spectrally resolved X-rays above 2~keV from non-flaring ARs, observed near the west limb on **2014 November 1**. The NuSTAR X-ray images match bright features seen in extreme ultraviolet and soft X-rays. The NuSTAR imaging spectroscopy is consistent with isothermal emission of temperatures 3.1−4.4~MK and emission measures
1−8×1046~cm−3. We do not observe emission above 5~MK but our short effective exposure times restrict the spectral dynamic range. With few counts above 6~keV, we can place constraints on the presence of an additional hotter component between 5 and 12~MK of ∼1046cm−3 and ∼1043cm−3, respectively, at least an order of magnitude stricter than previous limits. With longer duration observations and a weakening solar cycle (resulting in an increased livetime), future NuSTAR observations will have sensitivity to a wider range of temperatures as well as possible non-thermal emission.

Minoflares

Iain **Hannah** and Hugh Hudson

RHESSI Science Nugget, No. 203, June **2013**

http://sprg.ssl.berkeley.edu/~tohban/wiki/index.php/Minoflares

We propose a new term ("minoflare") to aid researchers in making the distinction between flares and something else. At present we have no definitive way of distinguishing these possibilities, but we certainly look forward to FOXSI and NuSTAR observations, which will probe into entirely new domains in solar X-ray parameter space. These explorations may well resolve this issue.

The effect of turbulent density fluctuations on wave-particle interactions and solar flare X-ray spectrum

I. G. **Hannah**, E. P. Kontar, H. A. S. Reid

E-print, Nov **2012**, A&A, 550, A51 (**2013**)

http://arxiv.org/pdf/1211.6015v2.pdf

To demonstrate the effect of turbulent background density fluctuations on flare accelerated electron transport in the solar corona. Using the quasi-linear approximation, we numerically simulate the propagation of a beam of accelerated electrons from the solar corona to chromosphere, including the self-consistent response of the inhomogeneous background plasma in the form of Langmuir waves. We calculate the X-ray spectrum from these simulations using the bremsstrahlung cross-section and fit the footpoint spectrum using the collisional "thick-target" model, a standard approach adopted in observational studies. We find that the interaction of the Langmuir waves with the background electron density gradient shifts the waves to higher phase velocity where they then resonate with higher velocity

electrons. The consequence is that some of the electrons are shifted to higher energies, producing more high energy X-rays than expected in the cases where the density inhomogeneity is not considered. We find that the level of energy gain is strongly dependent on the initial electron beam density at higher energy and the magnitude of the density gradient in the background plasma. The most significant gains are for steep (soft) spectra which had few electrons initially at higher energies. If the X-ray spectrum of the simulated footpoint emission are fitted using the standard "thick-target" model some simulation scenarios produce more than an order-of-magnitude over estimate of the number of electrons >50keV in the source coronal distribution.

Microflares and the Statistics of X-ray Flares **A Review**

I. G. **Hannah**, H. S. Hudson, M. Battaglia, S. Christe, J. Kašparová, S. Krucker, M. R. Kundu and A. Veronig

Space Sci Rev (**2011**) 159:263–300, **File**

http://arxiv.org/pdf/1108.6203v1.pdf

https://link.springer.com/content/pdf/10.1007/s11214-010-9705-4.pdf

This review surveys the statistics of solar X-ray flares, emphasising the new views that RHESSI has given us of the weaker events (the microflares). The new data reveal that these microflares strongly resemble more energetic events in most respects; they occur solely within active regions and exhibit high-temperature/nonthermal emissions in approximately the same proportion as major events. We discuss the distributions of flare parameters (e.g., peak flux) and how these parameters correlate, for instance via the Neupert effect. We also highlight the systematic biases involved in intercomparing data representing many decades of event magnitude. The intermittency of the flare/microflare occurrence, both in space and in time, argues that these discrete events do not explain general coronal heating, either in active regions or in the quiet Sun.

The spectral difference between solar flare HXR coronal and footpoint sources due to wave-particle interactions

I. G. **Hannah** and E. P. Kontar

A&A 529, A109 (**2011**)

http://arxiv.org/pdf/1103.2257v1.pdf

Aims. We investigate the spatial and spectral evolution of hard X-ray (HXR) emission from flare accelerated electron beams subject to collisional transport and wave-particle interactions in the solar atmosphere.
Methods. We numerically follow the propagation of a power-law of accelerated electrons in 1D space and time with the response of the background plasma in the form of Langmuir waves using the quasilinear approximation.
Results. We find that the addition of wave-particle interactions to collisional transport for a transient initially injected electron beam flattens the spectrum of the footpoint source. The coronal source is unchanged and so the difference in the spectral indices between the coronal and footpoint sources is $\Delta\gamma > 2$, which is larger than expected from purely collisional transport. A steady-state beam shows little difference between the two cases, as has been previously found, as a transiently injected electron beam is required to produce significant wave growth, especially at higher velocities. With this transiently injected beam the wave-particle interactions dominate in the corona whereas the collisional losses dominate in the chromosphere. The shape of the spectrum is different with increasing electron beam density in the wave-particle interaction case whereas with purely collisional transport only the normalisation is changed. We also find that the starting height of the source electron beam above the photosphere affects the spectral index of the footpoint when Langmuir wave growth is included. This may account for the differing spectral indices found between double footpoints if asymmetrical injection has occurred in the flaring loop.

CONSTRAINING THE HARD X-RAY PROPERTIES OF THE QUIET SUN WITH NEW *RHESSI* OBSERVATIONS

I. G. **Hannah**1, H. S. Hudson2, G. J. Hurford2, and R. P. Lin3,4

Astrophysical Journal, 724:487–492, **2010**

We present new *RHESSI* upper limits in the 3–200 keV energy range for solar hard X-ray emission in the absence of flares and active regions, i.e., the quiet Sun, using data obtained between 2005 July and 2009 April. These newlimits, substantially deeper than any previous ones, constrain several physical processes that could produce hardX-ray emission. These include cosmic-ray effects and the generation of axions within the solar core. The data also limit the properties of “nanoflares,” a leading candidate to explain coronal heating.We find it unlikely for nanoflares involving nonthermal effects to heat the corona because such events would require a steep electron spectrum $E^{-\delta}$ with index$\delta > 5$ extending to very low energies (<1 keV), into the thermal energy range. We also use the limits to constrain the parameter space of an isothermal model and coronal thin-target emission models (power-law and kappa distributions).

THE EFFECT OF WAVE–PARTICLE INTERACTIONS ON LOW-ENERGY CUTOFFS IN SOLAR FLARE ELECTRON SPECTRA

I. G. **Hannah**1, E. P. Kontar1, and O. K. Sirenko2

Astrophysical Journal, 707:L45–L50, **2009** December

Solar flare hard X-ray (HXR) spectra from *Reuven Ramaty High Energy Solar Spectrometer* (*RHESSI*) are normally interpreted in terms of purely collisional electron beam propagation, ignoring spatial evolution and collective effects. In this Letter, we present self-consistent numerical simulations of the spatial and temporal evolution of an electron beam subject to collisional transport and beam-driven Langmuir wave turbulence. These wave–particle interactions represent the background plasma's response to the electron beam propagating from the corona to chromosphere and occur on a far faster timescale than Coulomb collisions. From these simulations, we derive the mean electron flux spectrum, comparable to such spectra recovered from high-resolution HXRs observations of solar flares with *RHESSI*. We find that a negative spectral index (i.e., a spectrum that increases with energy), or local minima when including the expected thermal spectral component at low energies, occurs in the standard thick-target model, when Coulomb collisions are only considered. The inclusion of wave–particle interactions does not produce a local minimum, maintaining a positive spectral index. These simulations are a step toward a more complete treatment of electron transport in solar flares and suggest that a flat spectrum (spectral index of 0–1) down to thermal energies maybe a better approximation instead of a sharp cutoff in the injected electron spectrum.

RHESSI MICROFLARE STATISTICS. II. X-RAY IMAGING, SPECTROSCOPY, AND ENERGY DISTRIBUTIONS

G. **Hannah**, S. Christe,1 S. Krucker, G. J. Hurford, H. S. Hudson, and R. P. Lin1

The Astrophysical Journal, 677:704Y718, **2008**

http://www.journals.uchicago.edu/doi/pdf/10.1086/529012

We present the first statistical analysis of the thermal and nonthermal X-ray emission of all 25,705 microflares (RHESSI) observed between 2002 March and 2007 March. These eventswere found by searching the 6Y12 keVenergy range (see Paper I) and are small active region flares, from low (GOES) C class to below A class. Each microflare is automatically analyzed at the peak time of the 6-12 keVemission: the thermal source size is found by forward-fitting the complex visibilities for 4-8 keV, and the spectral parameters (temperature, emission measure, power-law index) are found by forward-fitting a thermal plus nonthermal model. The resulting wealth of information we determine about the events allows a range of the thermal and nonthermal properties to be investigated. In particular, we find that there is no correlation between the thermal loop size and the flare magnitude, indicating that microflares are not necessarily spatially small.We present the first thermal energy distribution of RHESSI flares and compare it to previous thermal energy distributions of transient events.We also present the first nonthermal power distribution of RHESSI flares and find that a few microflares have unexpectedly large nonthermal powers up to 10_{28} erg s_{-1}. The total microflare nonthermal energy, however, is still small compared to that of large flares as it occurs for shorter durations. These large energies and difficulties in analyzing the steep nonthermal spectra suggest that a sharp broken power law and thicktarget bremsstrahlung model may not be appropriate for microflares.

Thermal Structure of Current Sheets and Supra-arcade Downflows in the Solar Corona

Will J. **Hanneman**1,2 and Katharine K. Reeves

2014 ApJ 786 95

After the peak intensity of many large solar flares, magnetic and thermodynamic processes give rise to a phenomenon known as supra-arcade downflows (SADs). SADs are sunward flowing density depletions, often observed in post-flare plasma sheets. Some models have suggested that the plasma in the dark lanes is heated to temperatures of 20-80 MK, which is much hotter than temperatures of the surrounding plasma. In this work, we use data from the Atmospheric Imaging Assembly on the Solar Dynamics Observatory and the X-Ray Telescope on the Hinode satellite to determine the thermal structure of SADs in the solar corona. We examine four flares that took place on **2011 October 22, 2012 January 14, 2012 January 16, and 2012 January 2**7. Differential emission measures are calculated for each flare and we compare the temperatures in the SADs to those of the surrounding plasma. We find that the SADs are hotter than the background, but cooler than the surrounding plasma in most cases, with only 1 out of the 11 SADs examined here having a slightly higher temperature than its surroundings.

On Mode Conversion, Reflection and Transmission of Magneto-Acoustic Waves from Above in an Isothermal Stratified Atmosphere

Shelley **Hansen**, Paul Cally, Alina Donea

MNRAS **201**5

http://arxiv.org/pdf/1511.07364v1.pdf

We use the exact solutions for magnetoacoustic waves in a two dimensional isothermal atmosphere with uniform inclined magnetic field to calculate the wave reflection, transmission, and conversion of slow and fast waves incident

from above (z=∞). This is relevant to the question of whether waves excited by flares in the solar atmosphere can penetrate the Alfv\'en/acoustic equipartition layer (which we identify as the canopy) to reach the photosphere with sufficient energy to create sunquakes. It is found that slow waves above the acoustic cutoff frequency efficiently penetrate (transmit) as acoustic (fast) waves if directed at a small attack angle to the magnetic field, with the rest converting to magnetic (slow) waves, in accord with Generalized Ray Theory. This may help explain the compact nature of seismic sources of sunquakes identified using seismic holography. The incident slow waves can also efficiently transmit at low frequency in inclined field due to the reduction in acoustic cutoff frequency (ramp effect). Incident fast (magnetic) "waves" from infinity with specified nonzero horizontal wavenumber are necessarily evanescent, but can carry energy to the equipartition level by tunnelling. It is found that this can then efficiently convert to acoustic (fast) energy that can again reach the photosphere as a travelling wave. Overall, there appear to be ample avenues for substantial compressive wave energy to penetrate the canopy and impact the photosphere.

Bombs and flares at the surface and lower atmosphere of the Sun

Viggo H. **Hansteen**, Vasilis Archontis, Tiago M.D. Pereira, Mats Carlsson, Luc Rouppe van der Voort, Jorrit Leenaarts

ApJ 839:22 (12pp), **2017**

https://arxiv.org/pdf/1704.02872.pdf

A spectacular manifestation of solar activity is the appearance of transient brightenings in the far wings of the Hα line, known as Ellerman bombs (EBs). Recent observations obtained by the Interface Region Imaging Spectrograph (IRIS) have revealed another type of plasma "bombs" (UV bursts) with high temperatures of perhaps up to 8×104 K within the cooler lower solar atmosphere. Realistic numerical modeling showing such events is needed to explain their nature. Here, we report on 3D radiative magneto-hydrodynamic simulations of magnetic flux emergence in the solar atmosphere. We find that ubiquitous reconnection between emerging bipolar magnetic fields can trigger EBs in the photosphere, UV bursts in the mid/low chromosphere and small (nano-/micro-) flares (106 K) in the upper chromosphere. These results provide new insights on the emergence and build up of the coronal magnetic field and the dynamics and heating of the solar surface and lower atmosphere.

Detecting and Classifying Flares in High-Resolution Solar Spectra with Supervised Machine Learning

Nicole **Hao**, Laura Flagg, Ray Jayawardhana

ApJ **973** 109 **2024**

https://arxiv.org/pdf/2406.15594

https://iopscience.iop.org/article/10.3847/1538-4357/ad5be3/pdf

Flares are a well-studied aspect of the Sun's magnetic activity. Detecting and classifying solar flares can inform the analysis of contamination caused by stellar flares in exoplanet transmission spectra. In this paper, we present a standardized procedure to classify solar flares with the aid of supervised machine learning. Using flare data from the RHESSI mission and solar spectra from the HARPS-N instrument, we trained several supervised machine learning models, and found that the best performing algorithm is a C-Support Vector Machine (SVC) with non-linear kernels, specifically Radial Basis Functions (RBF). The best-trained model, SVC with RBF kernels, achieves an average aggregate accuracy score of 0.65, and categorical accuracy scores of over 0.70 for the no-flare and weak-flare classes, respectively. In comparison, a blind classification algorithm would have an accuracy score of 0.33. Testing showed that the model is able to detect and classify solar flares in entirely new data with different characteristics and distributions from those of the training set. Future efforts could focus on enhancing classification accuracy, investigating the efficacy of alternative models, particularly deep learning models, and incorporating more datasets to extend the application of this framework to stars that host exoplanets.

A Circular White-Light Flare with Impulsive and Gradual White-Light Kernels

Q. **Hao**, K. Yang, X. Cheng, Y. Guo, C. Fang, M. D. Ding, P. F. Chen, Z. Li

Nature Communications Volume 8, id. 2202 **2017**

https://arxiv.org/pdf/1712.07279.pdf

sci-hub.tw/10.1038/s41467-017-02343-0

White-light flares are the flares with emissions visible in the optical continuum. They are thought to be rare and pose the most stringent requirements in energy transport and heating in the lower atmosphere. Here we present a nearly circular white-light flare on **2015 March 10** that was well observed by the Optical and Near-infrared Solar Eruption Tracer and Solar Dynamics Observatory. In this flare, there appear simultaneously both impulsive and gradual white-light kernels. The generally accepted thick-target model would be responsible for the impulsive kernels but not sufficient to interpret the gradual kernels. Some other mechanisms including soft X-ray backwarming or downward-propagating Alfven waves, acting jointly with electron beam bombardment, provide a possible interpretation. However, the origin of this kind of white-light kernels is still an open question that induces more observations and researches in the future to decipher it.

DIFFERENTIAL ROTATION RATE OF X-RAY BRIGHT POINTS AND SOURCE REGION OF THEIR MAGNETIC FIELDS

Hirohisa **Hara** **2009** ApJ 697 980-984

The differential rotation rate of the solar corona has statistically been estimated from the motion of X-ray bright points (XBPs) that were observed with the Yohkoh soft X-ray telescope and the source region of magnetic fields is discussed from the evaluated rotation rate. The rotation rate of a pair of XBPs in a given latitude band is calculated from the position of an XBP in an X-ray image and that of an arbitrary-chosen XBP in a different X-ray image obtained with a time lag Δt. We have made the histogram of rotation rate from such samples in each latitude band for many X-ray images, and it shows a symmetric distribution that is well fitted by a Voigt function, not a Gaussian function, with a background. The modal rates at various longitudes in a given latitude band become the same value when a height is adopted as a characteristic height of XBPs, and we define the modal value against latitude as the differential rotation rate of XBPs in the present study. The differential rotation rate shows a similar trend as that of photospheric magnetic fields evaluated from the local correlation technique. We find that the differential rotation rate changes with a parameter Δt that is associated with the lifetime of XBPs, and that it becomes smaller in height for shorter Δt with the lower end that approaches to the rotation rate determined from the photospheric Doppler measurements. This trend suggests that magnetic fields associated with XBPs with a short lifetime are rooted just below the surface of the Sun at the top of the convection zone, and that they have a different origin from active regions.

CHROMOSPHERIC MASS MOTIONS AND INTRINSIC SUNSPOT ROTATIONS FOR NOAA ACTIVE REGIONS 10484, 10486, AND 10488 USING ISOON DATA

Paul S. **Hardersen**1, K. S. Balasubramaniam2, and Svetlana Shkolyar

2013 ApJ 773 60

This work utilizes Improved Solar Observing Optical Network continuum (630.2 nm) and Hα (656.2 nm) data to: (1) detect and measure intrinsic sunspot rotations occurring in the photosphere and chromosphere, (2) identify and measure chromospheric filament mass motions, and (3) assess any large-scale photospheric and chromospheric mass couplings. Significant results from **2003 October 27-29**, using the techniques of Brown et al., indicate significant counter-rotation between the two large sunspots in NOAA AR 10486 on October 29, as well as discrete filament mass motions in NOAA AR 10484 on October 27 that appear to be associated with at least one C-class solar flare.

Fickle Fields: Are Transient Magnetic Reversals Real?

Brian J. **Harker** and Alexei A. Pevtsov

HMI Science Nuggets, **2014**

http://hmi.stanford.edu/hminuggets/?p=496

We present observations from SDO/HMI of a magnetic transient observed in NOAA 11429 during the M7.9 flare on 13 March 2012. The observed transient showed an impulsive rotation of the field vector in response to the white-light flare.

Case Study of a Magnetic Transient in NOAA 11429 Observed by SDO/HMI during the M7.9 Flare on 2012 March 13

Brian J. **Harker** and Alexei A. Pevtsov

2013 ApJ 778 175

NOAA 11429 was the source of an M7.9 X-ray flare at the western solar limb (N18° W63°) on 2012 March 13 at 17:12 UT. Observations of the line-of-sight magnetic flux and the Stokes I and V profiles from which it is derived were carried out by the Solar Dynamics Observatory Helioseismic and Magnetic Imager (SDO/HMI) with a 45 s cadence over the full disk, at a spatial sampling of 0."5. During flare onset, a transient patch of negative flux can be observed in SDO/HMI magnetograms to rapidly appear within the positive polarity penumbra of NOAA 11429. We present here a detailed study of this magnetic transient and offer interpretations as to whether this highly debated phenomenon represents a "real" change in the structure of the magnetic field at the site of the flare, or is instead a product of instrumental/algorithmic artifacts related to particular SDO/HMI data reduction techniques.

Coronal spectroscopy: Probing sources of slow solar wind in active regions, and the early phases of solar flares **Review**

Louise K. **Harra**

Advances in Space Research Volume 71, Issue 4, 15 February **2023**, Pages 1893-1899

https://doi.org/10.1016/j.asr.2022.05.061

Coronal spectroscopy has pushed forward the understanding of physical processes in all phenomena on the Sun. In this review we concentrate specifically on plasma parameters measured in sources of the slow solar wind in active regions

and the early phases of solar flares. These topics are a key part of the science goals of the Solar Orbiter mission (Müller et al., 2020) which has been designed to probe what drives the solar wind and solar transients that fill the heliosphere. Active regions, outside of flaring, have general characteristics that include closed loops showing red-shifted (down-flowing plasma), and the edges of the active regions showing blue-shifted (upflowing plasma). Constraining and understanding the evolution, behaviour and cause of the flows has been developed in the past years and are summarised. Of particular importance is the upflowing plasma which, in some cases, can contribute to the slow solar wind, and this review concentrates on recent results on this topic.
The early phases of solar flares and their energy sources are not yet fully understood. For decades, there has been a huge interest in pin-pointing the trigger of a solar flare. Coronal spectroscopy has revealed small-scale dynamics that occurs tens of minutes before the flare begins. The understanding of the trigger is key to improving flare predictions in the future, as well as understanding the physical processes.
Finally we look to the future of coronal spectroscopy, with new instruments and methodologies being developed that build on the current knowledge, and will improve significantly our physical understanding of processes at all scales on the Sun.

How Hot Can Small Solar Flares Get?

Louise **Harra**, Andrea F. Battaglia, Krzysztof Barczynski, Hannah Collier, Säm Krucker, Katharine K. Reeves & George Doschek
Solar Physics volume 298, Article number: 13 (**2023**)
https://link.springer.com/content/pdf/10.1007/s11207-022-02106-1.pdf
The temperature reached by solar flares is a key parameter to understanding the physical process that causes the energy release. In this work, we analysed data from a Hinode Observing Programme that focused on high cadence measurement of the flaring plasma. This was carried out when the X-ray imager and spectrometer (STIX) on Solar Orbiter was observing. We analysed 3 small microflares, and determined their evolution and temperature. The temperature of the B2.8 microflare reached 16 MK. There was evidence in the smaller B1.4 flare of Fe XXIV emission, indicating that hot plasma of 15 MK can be reached. **8 Oct 2021**,

Locating Hot Plasma in Small Flares using Spectroscopic Overlappogram Data from the Hinode EUV Imaging Spectrometer

Louise **Harra**, Sarah Matthews, David Long, Takahiro Hasegawa…
Solar Physics volume 295, Article number: 34 (**2020**)
sci-hub.si/10.1007/s11207-020-01602-6
https://arxiv.org/pdf/2003.02908.pdf
One of the key processes associated with the "standard" flare model is chromospheric evaporation, a process during which plasma heated to high temperatures by energy deposition at the flare footpoints is driven upwards into the corona. Despite several decades of study, a number of open questions remain, including the relationship between plasma produced during this process and observations of earlier "superhot" plasma. The Extreme ultraviolet Imaging Spectrometer (EIS) onboard Hinode has a wide slot, which is often used as a flare trigger in the He II emission-line band. Once the intensity passes a threshold level, the study will switch to one focussed on the flaring region. However, when the intensity is not high enough to reach the flare trigger threshold, these datasets are then available during the entire flare period and provide high-cadence spectroscopic observations over a large field of view. We make use of data from two such studies of a C4.7 flare and a C1.6 flare to probe the relationship between hot Fe XXIV plasma and plasmas observed by the Reuven Ramaty High Energy Solar Spectroscopic Imager (RHESSI) and the X-ray Telescope (XRT) to track where the emission comes from and when it begins. The flare trigger slot data used in our analysis has one-minute cadence. Although the spatial and spectral information are merged in the wide-slot data, it is still possible to extract when the hot plasma appears, through the appearance of the Fe Xxiv spectral image. It is also possible to derive spectrally pure Fe XXIV light curves from the EIS data, and compare them with those derived from hard X-rays, enabling a full exploration of the evolution of hot emission. The Fe XXIV emission peaks just after the peak in the hard X-ray lightcurve; consistent with an origin in the evaporation of heated plasma following the transfer of energy to the lower atmosphere. A peak was also found for the C4.7 flare in the RHESSI peak temperature, which occurred before the hard X-rays peaked. This suggests that the first peak in hot-plasma emission is likely to be directly related to the energy-release process. **10 and 13 March 2015**
RHESSI Nuggets #374 March **2020**
http://sprg.ssl.berkeley.edu/~tohban/wiki/index.php/Using_overlappogram_data_to_find_hot_flare_plasma

The Characteristics of Solar X-Class Flares and CMEs: A Paradigm for Stellar Superflares and Eruptions?

Louise K. **Harra**, Carolus J. Schrijver, Miho Janvier, Shin Toriumi, Hugh Hudson, Sarah Matthews, Magnus M. Woods, Hirohisa Hara, Manuel Guedel, Adam Kowalski, Rachel Osten, Kanya Kusano, Theresa Lueftinger

Solar Phys. Volume 291, Issue 6, pp 1761–1782 **2016** **Open Access File**
This paper explores the characteristics of **42 solar X-class flares** that were observed between February 2011 and November 2014, with data from the Solar Dynamics Observatory (SDO) and other sources. This flare list includes nine X-class flares that had no associated CMEs. In particular our aim was to determine whether a clear signature could be identified to differentiate powerful flares that have coronal mass ejections (CMEs) from those that do not. Part of the motivation for this study is the characterization of the solar paradigm for flare/CME occurrence as a possible guide to the stellar observations; hence we emphasize spectroscopic signatures. To do this we ask the following questions: Do all eruptive flares have long durations? Do CME-related flares stand out in terms of active-region size vs. flare duration? Do flare magnitudes correlate with sunspot areas, and, if so, are eruptive events distinguished? Is the occurrence of CMEs related to the fraction of the active-region area involved? Do X-class flares with no eruptions have weaker non-thermal signatures? Is the temperature dependence of evaporation different in eruptive and non-eruptive flares? Is EUV dimming only seen in eruptive flares? We find only one feature consistently associated with CME-related flares specifically: coronal dimming in lines characteristic of the quiet-Sun corona, i.e. 1 – 2 MK. We do not find a correlation between flare magnitude and sunspot areas. Although challenging, it will be of importance to model dimming for stellar cases and make suitable future plans for observations in the appropriate wavelength range in order to identify stellar CMEs consistently. **19-03-2011, 24-Sept-2011, 03-11-2011, 07-03-2012, 12-07-2012, 23-10-2012, 08-11-2013, 24-02-2014, 22-10-2014**
Table 1 The X-class flare sample.

Location of non-thermal velocity in the early phases of a large flare - revealing the pre-eruption flux rope?

Louise **Harra**, Sarah Matthews, J. L. Culhane, Mark Cheung, E. Kontar, Hiro Hara
EIS Nugget, Aug **2013**
http://solarb.mssl.ucl.ac.uk/SolarB/eisnuggets.jsp
24 Sept 2011

THE LOCATION OF NON-THERMAL VELOCITY IN THE EARLY PHASES OF LARGE FLARES—REVEALING PRE-ERUPTION FLUX ROPES

Louise K. **Harra**1, Sarah Matthews1, J. L. Culhane1, Mark C. M. Cheung2, Eduard P. Kontar3, and Hirohisa Hara
2013 ApJ 774 122
Non-thermal velocity measurements of the solar atmosphere, particularly from UV and X-ray emission lines have demonstrated over the decades that this parameter is important in understanding the triggering of solar flares. Enhancements have often been observed before intensity enhancements are seen. However, until the launch of Hinode, it has been difficult to determine the spatial location of the enhancements to better understand the source region. The Hinode EUV Imaging Spectrometer has the spectral and spatial resolution to allow us to probe the early stages of flares in detail. We analyze four events, all of which are GOES M- or X-classification flares, and all are located toward the limb for ease of flare geometry interpretation. Three of the flares were eruptive and one was confined. In all events, pre-flare enhancement in non-thermal velocity at the base of the active region and its surroundings has been found. These enhancements seem to be consistent with the footpoints of the dimming regions, and hence may be highlighting the activation of a coronal flux rope for the three eruptive events. In addition, pre-flare enhancements in non-thermal velocity were found above the looptops for the three eruptive events.

CORONAL NONTHERMAL VELOCITY FOLLOWING HELICITY INJECTION BEFORE AN X-CLASS FLARE

L. K. **Harra**, D. R. Williams, A. J. Wallace, T. Magara, H. Hara, S. Tsuneta, A. C. Sterling, and G. A. Doschek
ApJL 691 L99-L102 **2009**
http://www.iop.org/EJ/abstract/1538-4357/691/2/L99
We explore the "pre-flare" behavior of the corona in a three-day period building up to an X-class flare on **2006 December 13** by analyzing EUV spectral profiles from the Hinode EUV Imaging Spectrometer (EIS) instrument. We found an increase in the coronal spectral line widths, beginning after the time of saturation of the injected helicity as measured by Magara & Tsuneta. In addition, this increase in line widths (indicating nonthermal motions) starts before any eruptive activity occurs. The Hinode EIS has the sensitivity to measure changes in the buildup to a flare many hours before the flare begins.

Outflows at the Edges of Active Regions: Contribution to Solar Wind Formation?

L. K. **Harra**, T. Sakao, C. H. Mandrini, H. Hara, S. Imada, P. R. Young, L. van Driel–Gesztelyi, D. Baker
The Astrophysical Journal Letters
2008 April 1, Vol. 676, No. 2: pp. L147-L150б (doi: 10.1086/587485)

The formation of the slow solar wind has been debated for many years. In this Letter we show evidence of persistent outflow at the edges of an active region as measured by the EUV Imaging Spectrometer on board ***Hinode***. The Doppler velocity ranged between 20 and 50 km s^{-1} and was consistent with a steady flow seen in the X-Ray Telescope. The latter showed steady, pulsing outflowing material and some transverse motions of the loops. We analyze the magnetic field around the active region and produce a coronal magnetic field model. We determine from the latter that the outflow speeds adjusted for line-of-sight effects can reach over 100 km s^{-1}. We can interpret this outflow as expansion of loops that lie over the active region, which may either reconnect with neighboring large-scale loops or are likely to open to the interplanetary space. This material constitutes at least part of the slow solar wind.

Solar flares: the observations

Louise K. **Harra**
Mem. S.A.It. Vol. 78, 236, 2007, File
There is now strong observational evidence that magnetic reconnection is occurring. I will discuss the observational indicators of reconnection - and also the areas where the observations contradict the theory. The actual trigger for flares is not well understood and I will discuss how observations from the recently launched Hinode space mission will be able to address this problem.

How Does Large Flaring Activity from the Same Active Region Produce Oppositely Directed Magnetic Clouds?

Louise K. **Harra** · Nancy U. Crooker · Cristina H. Mandrini · Lidia van Driel-Gesztelyi · Sergio Dasso · Jingxiu Wang · Heather Elliott · Gemma Attrill · Bernard V. Jackson · Mario M. Bisi
Solar Phys, 244: 95–114, **2007**, DOI 10.1007/s11207-007-9002-x; **File**
We describe the interplanetary coronal mass ejections (ICMEs) that occurred as a result of a series of solar flares and eruptions from 4 to 8 November 2004. Two ICMEs/magnetic clouds occurring from these events had opposite magnetic orientations. This was despite the fact that the major flares related to these events occurred within the same active region that maintained the same magnetic configuration. The solar events include a wide array of activities: flares, trans-equatorial coronal loop disappearance and reformation, trans-equatorial filament eruption, and coronal hole interaction. The first major ICME/magnetic cloud was predominantly related to the active region 10696 eruption. The second major ICME/magnetic cloud was found to be consistent with the magnetic orientation of an erupting trans-equatorial filament or else a rotation of 160° of a flux rope in the active region.We discuss these possibilities and emphasize the importance of understanding the magnetic evolution of the solar source region before we can begin to predict geoeffective events with any accuracy.

Temporal Behaviors of Magnetic Helicity Injections by Self and Mutual Sunspot Rotations

Takahiro **Hasegawa**1,2 and Toshifumi Shimizu1,2
2023 ApJ 943 96
https://iopscience.iop.org/article/10.3847/1538-4357/aca800/pdf
Magnetic helicity is a physical parameter used to quantify the complexity of magnetic fields, providing an indication of the energy state in the coronal magnetic structure. We investigate the temporal evolution of magnetic helicity and its relationship to the occurrence of a variety of flares in the solar active region NOAA 12297, which was well observed using the Solar Dynamics Observatory/Helioseismic and Magnetic Imager in 2015 March. The active region produced many M-class flares and an X-class flare in two distinctive areas, both of which had a similar magnetic evolution, i.e., the opposite polarity of an emerging flux developed beside a preexisting sunspot, but exhibited flares with different magnitudes and frequencies. We derived the spatiotemporal evolution of the magnetic helicity injections and evaluated how spinning and braiding helicity injections evolved with time in the two areas. In one area, we observed a remarkable evolution, in which a negative spinning helicity injection in the preexisting sunspot increased in a positive helicity system, followed by the occurrence of the X-class flare. The negative helicity injection was clearly caused by the flux emergence that developed along the outer edge of the preexisting sunspot. The other area showed positive braiding helicity injections, with spinning helicity injections fluctuating concurrently with flux emergence, changing their signs several times, i.e., variable energy, and helicity input. The observed temporal behaviors of the helicity injections may explain different types of flare occurrences in the regions. **10-12 March 2015**

Magnetohydrodynamic Simulations for Solar Active Regions using Time-series Data of Surface Plasma Flow and Electric Field Inferred from Helioseismic Magnetic Imager Vector Magnetic Field Measurements

Keiji **Hayashi**1,2,3, Xueshang Feng2,4, Ming Xiong2,4, and Chaowei Jiang4
2019 ApJL 871 L28

Temporal evolution of magnetic structures of the solar active region (AR) NOAA AR 11158, is simulated with our magnetohydrodynamic (MHD) simulation models using time-dependent solar-surface electric field or plasma flow data. Using the Solar Dynamics Observatory/Helioseismic Magnetic Imager vector magnetogram data, the solar-surface boundary electric field maps are derived with our recently developed algorithm to reproduce the temporal evolution of solar-surface vector magnetic field as observed. The plasma motion velocity maps are calculated through the Differential Affine Velocity Estimator for Vector Magnetograms. In both data-driven models, the simulated evolutionary magnetic field structures at strong-field low-beta regions appear near force-free state, as the current helicity density ($\boldsymbol{J} \cdot \boldsymbol{B}/B^2$) are roughly constant along each field line. Although the magnetic energy simulated with the newly developed plasma-velocity-driven model is about 10% of that by the electric-field driven model, the plasma-velocity-driven model can maintain the frozen-in condition, and evolution of current and free energy generated by the solar-surface plasma motions can be spatially and temporally traced. The present MHD simulation models for AR system can be a step toward better, more realistic data-driven evolutionary modeling, in particular, establishing boundary treatments for introducing the time-dependent observation data in a physically and mathematically consistent manner. 11 February 2011

An MHD Simulation of Solar Active Region 11158 Driven with a Time-dependent Electric Field Determined from HMI Vector Magnetic Field Measurement Data

Keiji **Hayashi**1,2, Xueshang Feng1,3, Ming Xiong1,3, and Chaowei Jiang3
2018 ApJ 855 11

For realistic magnetohydrodynamics (MHD) simulation of the solar active region (AR), two types of capabilities are required. The first is the capability to calculate the bottom-boundary electric field vector, with which the observed magnetic field can be reconstructed through the induction equation. The second is a proper boundary treatment to limit the size of the sub-Alfvénic simulation region. We developed (1) a practical inversion method to yield the solar-surface electric field vector from the temporal evolution of the three components of magnetic field data maps, and (2) a characteristic-based free boundary treatment for the top and side sub-Alfvénic boundary surfaces. We simulate the temporal evolution of AR 11158 over 16 hr for testing, using Solar Dynamics Observatory/Helioseismic Magnetic Imager vector magnetic field observation data and our time-dependent three-dimensional MHD simulation with these two features. Despite several assumptions in calculating the electric field and compromises for mitigating computational difficulties at the very low beta regime, several features of the AR were reasonably retrieved, such as twisting field structures, energy accumulation comparable to an X-class flare, and sudden changes at the time of the X-flare. The present MHD model can be a first step toward more realistic modeling of AR in the future.
Erratum: ApJ 856:181, **2018** http://iopscience.iop.org/article/10.3847/1538-4357/aab787/pdf
HMI Science Nuggets #124 Apr **2019** http://hmi.stanford.edu/hminuggets/?p=2881

MHD simulations of the global solar corona around the Halloween event in 2003 using the synchronic frame format of the solar photospheric magnetic field

Keiji **Hayashi**, Xue Pu Zhao, Yang Liu
JOURNAL OF GEOPHYSICAL RESEARCH, VOL. 113, A07104, doi:10.1029/2007JA012814, **2008**
http://dx.doi.org/10.1029/2007JA012814

We performed two time-relaxation magnetohydrodynamics (MHD) simulations of the solar corona: one uses the boundary map representing the solar surface magnetic field distribution before the **Halloween event in 2003**, and the other uses map representing the postevent distribution. The aims of this study are to test a new concept of a solar surface magnetic field map capable of representing a particular time of interest and to examine the coronal responses to the solar photospheric magnetic field changes occurring over a few days. We used a new mapping scheme named "synchronic frame" that can include the longitudinal shift caused by the solar differential rotation and the solar surface variations occurring at the time of interest. These two time-relaxation MHD simulations using the two maps are separately performed to numerically obtain the quasi steady states of the solar corona before and after the Halloween event. Comparisons of the simulated coronal magnetic field structures to the SOHO/EIT measurements show that the combinations of our mapping method and simulation model reproduce the changes of the coronal structures well. We also find that the consequences of solar surface variations can be seen in the plasma quantities in the solar corona. These

results show the capability and importance of the solar surface magnetic field mapping scheme for better reconstruction of global coronal structures, parts of which are sensitive to the solar surface magnetic field variations.

The Spectrometer Telescope for Imaging X-rays (STIX) on Solar Orbiter

Laura A. **Hayes**, Sophie Musset, Daniel M üller, S äm Krucker
Book Chapter for Handbook of X-ray and Gamma-ray Astrophysics **2022**
https://arxiv.org/pdf/2207.02079.pdf
The Spectrometer/Telescope for Imaging X-rays (STIX) is one of the 10 instruments on-board the scientific payload of ESA's Solar Orbiter mission. STIX provides hard X-ray imaging spectroscopy in the 4-150~keV energy range, observing hard X-ray bremsstrahlung emission from the Sun. These observations provide diagnostics of the hottest thermal plasmas (>10~MK) and information on the non-thermal energetic electrons accelerated above 10~keV during solar flares. STIX has a spectral resolution of 1~keV, and employs the use of in-direct bi-grid Fourier imaging to spatially locate hard X-ray emission. Given that STIX provides critical information about accelerated electrons at the Sun through hard X-ray diagnostics, it is a powerful contribution to the Solar Orbiter suite and has a significant role to explore the dynamics of solar inputs to the heliosphere. This chapter describes the STIX instrument, its design, objectives, first observations and outlines the new perspectives STIX provides over the mission lifetime of Solar Orbiter. **27 May 2020, 7-9 May 2021, 28 Oct 2021**

Statistical Study of GOES X-ray Quasi-Periodic Pulsations in Solar Flares

Laura A. **Hayes**, Andrew R. Inglis, Steven Christe, Brian Dennis, Peter T. Gallagher
ApJ **895** 50 **2020**
https://arxiv.org/pdf/2004.11775.pdf
https://doi.org/10.3847/1538-4357/ab8d40
Small amplitude quasi-periodic pulsations (QPPs) detected in soft X-ray emission are commonplace in many flares. To date, the underpinning processes resulting in the QPPs are unknown. In this paper, we attempt to constrain the prevalence of \textit{stationary} QPPs in the largest statistical study to date, including a study of the relationship of QPP periods to the properties of the flaring active region, flare ribbons, and CME affiliation. We build upon the work of \cite{inglis2016} and use a model comparison test to search for significant power in the Fourier spectra of lightcurves of the GOES 1--8~Å\ channel. We analyze all X-, M- and C- class flares of the past solar cycle, a total of 5519 flares, and search for periodicity in the 6-300~s timescale range. Approximately 46\% of X-class, 29\% of M-class and 7\% of C-class flares show evidence of stationary QPPs, with periods that follow a log-normal distribution peaked at 20~s. The QPP periods were found to be independent of flare magnitude, however a positive correlation was found between QPP period and flare duration. No dependence of the QPP periods to the global active region properties was identified. A positive correlation was found between QPPs and ribbon properties including unsigned magnetic flux, ribbon area and ribbon separation distance. We found that both flares with and without an associated CME can host QPPs. Furthermore, we demonstrate that for X- and M- class flares, decay phase QPPs have statistically longer periods than impulsive phase QPPs. **2014-08-21, 2014-11-03, 2016-02-12**

Persistent Quasi-Periodic Pulsations During a Large X-Class Solar Flare

Laura A. **Hayes**, Peter T. Gallagher, Brian R. Dennis, Jack Ireland, Andrew Inglis, Diana E. Morosan
ApJ **875** 33 **2019**
https://arxiv.org/pdf/1903.01328.pdf
sci-hub.se/10.3847/1538-4357/ab0ca3
https://iopscience.iop.org/article/10.3847/1538-4357/ab0ca3/pdf
Solar flares often display pulsating and oscillatory signatures in the emission, known as quasi-periodic pulsations (QPP). QPP are typically identified during the impulsive phase of flares, yet in some cases, their presence is detected late into the decay phase. Here, we report extensive fine structure QPP that are detected throughout the large X8.2 flare from **2017 September 10**. Following the analysis of the thermal pulsations observed in the GOES/XRS and the 131 A channel of SDO/AIA, we find a pulsation period of ~65 s during the impulsive phase followed by lower amplitude QPP with a period of ~150 s in the decay phase, up to three hours after the peak of the flare. We find that during the time of the impulsive QPP, the soft X-ray source observed with RHESSI rapidly rises at a velocity of approximately 17 km/s following the plasmoid/coronal mass ejection (CME) eruption. We interpret these QPP in terms of a manifestation of the reconnection dynamics in the eruptive event. During the long-duration decay phase lasting several hours, extended downward contractions of collapsing loops/plasmoids that reach the top of the flare arcade are observed in EUV. We note that the existence of persistent QPP into the decay phase of this flare are most likely related to these features. The QPP during this phase are discussed in terms of MHD wave modes triggered in the post-flaring loops.
See movie https://www.dropbox.com/s/jyv71j0wredc1wz/animation1.mp4?dl=0
RHESSI Nuggets #347 March **2019** http://sprg.ssl.berkeley.edu/~tohban/wiki/index.php/Persistent_Quasi-Periodic_Pulsations_Detected_During_the_Large_X8.2_Solar_Flare

Pulsations in the Earth's Lower Ionosphere Synchronized with Solar Flare Emission

Laura A. **Hayes**, Peter T. Gallagher, Joseph McCauley, Brian R. Dennis, Jack Ireland, Andrew Inglis
JGR **2017**
https://arxiv.org/pdf/1710.01725.pdf
Solar flare emission at X-ray and extreme ultraviolet (EUV) energies can cause substantial enhancements in the electron density in the Earth's lower ionosphere. It has now become clear that flares exhibit quasi-periodic pulsations with timescales of minutes at X-ray energies, but to date, it has not been known if the ionosphere is sensitive to this variability. Here, using a combination of Very Low Frequency (24 kHz) measurement together with space-based X-ray and EUV observations, we report pulsations of the ionospheric D-region, which are synchronized with a set of pulsating flare loops. Modeling of the ionosphere show that the D-region electron density varies by up to an order of magnitude over the timescale of the pulsations (~ 20 mins). Our results reveal that the Earth's ionosphere is more sensitive to small-scale changes in solar soft X-ray flux than previously thought, and implies that planetary ionospheres are closely coupled to small-scale changes in solar/stellar activity. **24 July 2016**

Quasi-Periodic Pulsations during the Impulsive and Decay phases of an X-class Flare

Laura A. **Hayes**, Peter T. Gallagher, Brian R. Dennis, Jack Ireland, Andrew R. Inglis, Daniel F. Ryan
ApJL **827** L30 **2016**
http://arxiv.org/pdf/1607.06957v1.pdf
Quasi-periodic pulsations (QPP) are often observed in X-ray emission from solar flares. To date, it is unclear what their physical origins are. Here, we present a multi-instrument investigation of the nature of QPP during the impulsive and decay phases of the X1.0 flare of **28 October 2013**. We focus on the character of the fine structure pulsations evident in the soft X-ray time derivatives and compare this variability with structure across multiple wavelengths including hard X-ray and microwave emission. We find that during the impulsive phase of the flare, high correlations between pulsations in the thermal and non-thermal emissions are seen. A characteristic timescale of ~20 s is observed in all channels and a second timescale of ~55 s is observed in the non-thermal emissions. Soft X-ray pulsations are seen to persist into the decay phase of this flare, up to 20 minutes after the non-thermal emission has ceased. We find that these decay phase thermal pulsations have very small amplitude and show an increase in characteristic timescale from ~40 s up to ~70 s. We interpret the bursty nature of the co-existing multi-wavelength QPP during the impulsive phase in terms of episodic particle acceleration and plasma heating. The persistent thermal decay phase QPP are most likely connected with compressive MHD processes in the post-flare loops such as the fast sausage mode or the vertical kink mode.

Distinguishing between Flaring and Non-Flaring Active Regions: A Machine Learning Perspective

Soumitra **Hazra**, Gopal Sardar, Partha Choudhuri
A&A 639, A44 **2020**
https://arxiv.org/pdf/2003.03878.pdf
https://www.aanda.org/articles/aa/pdf/2020/07/aa37426-19.pdf
Context. Large-scale solar eruptions significantly affect space weather and damage space-based human infrastructures. It is necessary to predict large-scale solar eruptions; it will enable us to protect the vulnerable infrastructures of our modern society. Aims. We investigate the difference between flaring and nonflaring active regions. We also investigate whether it is possible to forecast a solar flare.
Methods. We used photospheric vector magnetogram data from the Solar Dynamic Observatory's Helioseismic Magnetic Imager to study the time evolution of photospheric magnetic parameters on the solar surface. We built a database of flaring and nonflaring active regions observed on the solar surface from 2010 to 2017. We trained a machine-learning algorithm with the time evolution of these active region parameters. Finally, we estimated the performance obtained from the machine-learning algorithm.
Results. The strength of some magnetic parameters such as the total unsigned magnetic flux, the total unsigned magnetic helicity, the total unsigned vertical current, and the total photospheric magnetic energy density in flaring active regions are much higher than those of the non-flaring regions. These magnetic parameters in a flaring active region evolve fast and are complex. We are able to obtain a good forecasting capability with a relatively high value of true skill statistic. We also find that time evolution of the total unsigned magnetic helicity and the total unsigned magnetic flux provides a very high ability of distinguishing flaring and nonflaring active regions.
Conclusions. We can distinguish a flaring active region from a nonflaring region with good accuracy. We confirm that there is no single common parameter that can distinguish all flaring active regions from the nonflaring regions. However, the time evolution of the top two magnetic parameters, the total unsigned magnetic flux and the total unsigned magnetic helicity, have a very high distinguishing capability. **2011-01-06, 2011-03-02, 2011-08-29**

The Relationship Between Solar Coronal X-Ray Brightness and Active Region Magnetic Fields: A Study Using High-Resolution Hinode Observations

Soumitra **Hazra**, Dibyendu Nandy, B. Ravindra
Solar Physics March **2015**, Volume 290, Issue 3, pp 771-785

By using high-resolution observations of nearly co-temporal and co-spatial Solar Optical Telescopespectropolarimeter and X-Ray Telescope coronal X-ray data onboard Hinode, we revisit the problematic relationship between global magnetic quantities and coronal X-ray brightness. Co-aligned vector magnetogram and X-ray data were used for this study. The total X-ray brightness over active regions is well correlated with integrated magnetic quantities such as the total unsigned magnetic flux, the total unsigned vertical current, and the area-integrated square of the vertical and horizontal magnetic fields. On accounting for the inter-dependence of the magnetic quantities, we inferred that the total magnetic flux is the primary determinant of the observed integrated X-ray brightness. Our observations indicate that a stronger coronal X-ray flux is not related to a higher non-potentiality of active-region magnetic fields. The data even suggest a slightly negative correlation between X-ray brightness and a proxy of active-region non-potentiality. Although there are small numerical differences in the established correlations, the main conclusions are qualitatively consistent over two different X-ray filters, the Al-poly and Ti-poly filters, which confirms the strength of our conclusions and validate and extend earlier studies that used low-resolution data. We discuss the implications of our results and the constraints they set on theories of solar coronal heating.

Coronal Magnetic Field Extrapolation and Topological Analysis of Fine-Scale Structures during Solar Flare Precursors

Wen **He**, Qiang Hu, Ju Jing, Haimin Wang, Chaowei Jiang, Sushree S. Nayak, Avijeet Prasad

ApJ **958** 90 **2023**

https://arxiv.org/pdf/2306.03226.pdf

https://iopscience.iop.org/article/10.3847/1538-4357/ad0236/pdf

Magnetic field plays an important role in various solar eruptions like flares, coronal mass ejections, etc. The formation and evolution of characteristic magnetic field topology in solar eruptions are critical problems that will ultimately help us understand the origination of these eruptions in the solar source regions. With the development of advanced techniques and instruments, observations with higher resolutions in different wavelengths and fields of view have provided more quantitative information for finer structures. So it is essential to improve our method to study the magnetic field topology in the solar source regions by taking advantage of high-resolution observations. In this study, we employ a nonlinear force-free field (NLFFF) extrapolation method based on a nonuniform grid setting for an M-class flare eruption event (SOL**2015-06-22**T17:39) with embedded magnetograms from the Solar Dynamics Observatory (SDO) and the Goode Solar Telescope (GST). The extrapolation results employing the embedded magnetogram for the bottom boundary are obtained by maintaining the native resolutions of the corresponding GST and SDO magnetograms. We compare the field line connectivity with the simultaneous GST/Hα and SDO/AIA observations for fine-scale structures associated with precursor brightenings. Then we perform a topological analysis of the field line connectivity corresponding to fine-scale magnetic field structures based on the extrapolation results. The results indicate that by combining the high-resolution GST magnetogram with a larger HMI magnetogram, the derived magnetic field topology is consistent with a scenario of magnetic reconnection among sheared field lines across the main polarity inversion line during solar flare precursors.

Electric Currents through J-shaped and Non-J-shaped Flare Ribbons

Yuwei **He**, Rui Liu, Lijuan Liu, Jun Chen, Wensi Wang, Yuming Wang

ApJ **900** 38 **2020**

https://arxiv.org/pdf/2007.05693.pdf

https://doi.org/10.3847/1538-4357/aba52a

Recently solar flares exhibiting a double J-shaped ribbons in the lower solar atmosphere have been paid increasing attention in the context of extending the two-dimensional standard flare model to three dimensions, as motivated by the spatial correlation between photospheric current channels and flare ribbons. Here we study the electric currents through the photospheric area swept by flare ribbons (termed synthesized ribbon area or SRA), with a sample of 71 two-ribbon flares, of which 36 are J-shaped. Electric currents flowing through one ribbon are highly correlated with those through the other, therefore belonging to the same current system. The non-neutrality factor of this current system is independent of the flare magnitude, implying that both direct and return currents participate in flares. J-shaped flares are distinct from non-J-shaped flares in the following aspects: 1) Electric current densities within J-shaped SRA are significantly smaller than those within non-J-shaped SRA, but J-shaped SRA and its associated magnetic flux are also significantly larger. 2) Electric currents through SRA are positively correlated with the flare magnitude, but J-shaped flares show stronger correlation than non-J-shaped flares. 3) The majority (75\%) of J-shaped flares are eruptive, while the majority (86\%) of non-J-shaped flares are confined; accordingly, hosting active regions of J-shaped flares are more likely to be sigmoidal than non-J-shaped flares. Thus, J-shaped flares constitute a distinct subset of two-ribbon flares, probably the representative of eruptive ones. Further, we found that combining SRA and its associated magnetic flux has the potential to differentiate eruptive from confined flares. **2013 April 12, 2013 August 12**

Data-driven MHD Simulation of the Formation and Initiation of a Large-scale Pre-flare Magnetic Flux Rope in Solar Active Region 12371

Wen **He**, Chaowei Jiang, Peng Zou, Aiying Duan, Xueshang Feng, Pingbing Zuo, Yi Wang

ApJ **2020**
https://arxiv.org/pdf/2002.04837.pdf
Solar eruptions are the most powerful drivers of space weather. To understand their cause and nature, it is crucial to know how the coronal magnetic field evolves before eruption. Here we study the formation process of a relatively large-scale magnetic flux rope (MFR) in active region NOAA~12371 that erupts with a major flare and coronal mass ejection on **2015 June 21**. A data-driven numerical magnetohydrodynamic model is employed to simulate three-dimensional coronal magnetic field evolution of one-day duration before the eruption. Comparison between the observed features and our modeled magnetic field discloses how the pre-eruption MFR forms. Initially, the magnetic field lines were weakly twisted as being simple sheared arcades. Then a long MFR was formed along the polarity inversion line due to the complex photospheric motion, which is mainly shearing rather than twisting. The presence of the MFR is evidenced by a coherent set of magnetic field lines with twist number above unity. Below the MFR a current sheet is shown in the model, suggesting that tether-cutting reconnection plays a key role in the MFR formation. The MFR's flux grows as more and more field lines are twisted due to continuous injection of magnetic helicity by the photospheric motions. Meanwhile, the height of the MFR's axis increases monotonely from its formation. By an analysis of the decay index of its overlying field, we suggest that it is because the MFR runs into the torus instability regime and becomes unstable that finally triggers the eruption.

Magnetic Configuration Associated with Two-Ribbon Solar Flares

Han **He**, Huaning Wang, Yihua Yan, Bo Li, P. F. Chen
2018
https://arxiv.org/pdf/1810.13124.pdf
Magnetic configuration of flare-bearing active regions (ARs) is one key aspect for understanding the initiation mechanism of solar flares. In this paper, we perform a comparative analysis between the magnetic configurations of two X-class two-ribbon flares happened in AR 10930 (on **2006 December 13**) and AR 11158 (on **2011 February 15**), whose photospheric magnetic fields were observed by Hinode and SDO satellites, respectively, and coronal magnetic fields were calculated based on nonlinear force-free field model. The analysis shows that both the flares initiated in local areas with extremely strong current density intensity, and the magnetic field chirality (indicated by sign of force-free factor α) along the main polarity inversion line (PIL) is opposite for the two ARs, that is, left-hand ($\alpha<0$) for AR 10930 and right-hand ($\alpha>0$) for AR 11158. Our previous study (He et al. 2014) showed that, for the flare of AR 10930, a prominent magnetic connectivity was formed above the main PIL before the flare and was totally broken after the flare eruption, and the two branches of broken magnetic connectivity combined with the isolated electric current at the magnetic connectivity breaking site compose a Z-shaped configuration. In this work, we find similar result for the flare of AR 11158 except that its magnetic configuration is inverse Z-shaped, which corresponds to the right-hand chirality of AR 11158 in contrast to the left-hand chirality of AR 10930. We speculate that two-ribbon flares can be generally classified to these two magnetic configurations by chirality (α signs) of ARs.

Variations of the 3-D coronal magnetic field associated with the X3.4-class solar flare event of AR 10930

Han **He**, Huaning Wang, Yihua Yan, P. F. Chen, Cheng Fang
JGR **2016**
http://arxiv.org/pdf/1605.00367v1.pdf
The variations of the 3-D coronal magnetic fields associated with the X3.4-class flare of active region 10930 are studied in this paper. The coronal magnetic field data are reconstructed from the photospheric vector magnetograms obtained by the Hinode satellite and using the nonlinear force-free field extrapolation method developed in our previous work (He et al., 2011). The 3-D force-free factor α, 3-D current density, and 3-D magnetic energy density are employed to analyze the coronal data. The distributions of α and current density reveal a prominent magnetic connectivity with strong negative α values and strong current density before the flare. This magnetic connectivity extends along the main polarity inversion line and is found to be totally broken after the flare. The distribution variation of magnetic energy density reveals the redistribution of magnetic energy before and after the flare. In the lower space of the modeling volume the increase of magnetic energy dominates, and in the higher space the decrease of energy dominates. The comparison with the flare onset imaging observation exhibits that the breaking site of the magnetic connectivity and site with the highest values of energy density increase coincide with the location of flare initial eruption. We conclude that a cramped positive α region appearing in the photosphere causes the breaking of the magnetic connectivity. A scenario for flare initial eruption is proposed in which the Lorentz force acting on the isolated electric current at the magnetic connectivity breaking site lifts the associated plasmas and causes the initial ejection. **13 December 2006**

Variations of the 3-D coronal magnetic field associated with the X3.4-class solar flare event of AR 10930

Han **He**1,2, Huaning Wang1, Yihua Yan1, P. F. Chen2,3 andCheng Fang

JGR, Volume 119, Issue 5, pages 3286–3315, May **2014**
The variations of the 3-D coronal magnetic fields associated with the X3.4-class flare of active region 10930 are studied in this paper. The coronal magnetic field data are reconstructed from the photospheric vector magnetograms obtained by the Hinode satellite and using the nonlinear force-free field extrapolation method developed in our previous work (He et al., 2011). The 3-D force-free factor α, 3-D current density, and 3-D magnetic energy density are employed to analyze the coronal data. The distributions of α and current density reveal a prominent magnetic connectivity with strong negative α values and strong current density before the flare. This magnetic connectivity extends along the main polarity inversion line and is found to be totally broken after the flare. The distribution variation of magnetic energy density reveals the redistribution of magnetic energy before and after the flare. In the lower space of the modeling volume the increase of magnetic energy dominates, and in the higher space the decrease of energy dominates. The comparison with the flare onset imaging observation exhibits that the breaking site of the magnetic connectivity and site with the highest values of energy density increase coincide with the location of flare initial eruption. We conclude that a cramped positive α region appearing in the photosphere causes the breaking of the magnetic connectivity. A scenario for flare initial eruption is proposed in which the Lorentz force acting on the isolated electric current at the magnetic connectivity breaking site lifts the associated plasmas and causes the initial ejection. **Dec 2006**

Reconfiguration of the coronal magnetic field by means of reconnection driven by photospheric magnetic flux convergence

J.-S. **He**1, E. Marsch1, C.-Y. Tu2, H. Tian1,2 and L.-J. Guo
A&A 510, A40 (**2010**)
Context. Magnetic reconnection is commonly believed to be responsible for flare-like events and plasma ejections in the solar atmosphere, but the field-line reconfiguration observed in association with magnetic reconnection has rarely been observed before.
Aims. We attempt to reconstruct the configuration of the magnetic field during a magnetic reconnection event, estimate the reconnection rate, and analyze the resulting X-ray burst and plasma ejection.
Methods. We use the local-correlation-tracking (LCT) method to track the convergence of magnetic fields with opposite polarities using photospheric observations from SOT/Hinode. The magnetic field lines are then extrapolated from the tracked footpoint positions into the corona, and the changes in field-line connections are marked. We estimate the reconnection rate by calculating the convective electric field in the photosphere, which is normalized to the product of the plasma jet speed and the coronal magnetic field strength inside the inflow region. The observed X-ray burst and plasma ejection are analysed with data from XRT/Hinode and TRACE, respectively.
Results. We find that in this reconnection event the two sets of approaching closed loops were reconfigured to a set of superimposed large-scale closed loops and another set of small-scale closed loops. Enhanced soft X-ray emission was seen to rapidly fill the reconnected loop after the micro-flare occurred at the reconnection site. Plasma was ejected from that site with a speed between 27 and 40 km s^{-1}. The reconnection rate is estimated to range between 0.03 and 0.09.
Conclusions. Our work presents a study of the magnetic field reconfiguration owing to magnetic reconnection driven by flux convergence in the photosphere. This observation of the magnetic structure change is helpful for future diagnosis of magnetic reconnection. The results obtained for the reconnection rate, the X-ray emission burst, and the plasma ejection provides new observational evidence, and places constraints on future theoretical study of magnetic reconnection in the Sun.

OBSERVATIONAL SIGNATURES OF SIMULATED RECONNECTION EVENTS IN THE SOLAR CHROMOSPHERE AND TRANSITION REGION

L. Heggland1, B. De Pontieu2 and V. H. Hansteen1,3
ApJ 702 1-18, **2009** doi: 10.1088/0004-637X/702/1/1\
We present the results of numerical simulations of wave-induced magnetic reconnection in a model of the solar atmosphere. In the magnetic field geometry we study in this paper, the waves, driven by a monochromatic piston and a driver taken from *Hinode* observations, induce periodic reconnection of the magnetic field, and this reconnection appears to help drive long-period chromospheric jets. By synthesizing spectra for a variety of wavelengths that are sensitive to a wide range of temperatures, we shed light on the often confusing relationship between the plethora of jet-like phenomena in the solar atmosphere, e.g., explosive events, spicules, and other phenomena thought to be caused by reconnection. Our simulations produce spicule-like jets with lengths and lifetimes that match observations, and the spectral signatures of several reconnection events are similar to observations of explosive events. We also find that in some cases, absorption from overlying neutral hydrogen can hide emission from matter at coronal temperatures.

Signatures of Helium continuum in cool flare loops observed by SDO/AIA

Petr **Heinzel** (1), Pavol Schwartz (2), Juraj Lörinčík (1, 3), Július Koza (2), Sonja Jejčič (4, 5, 1), David Kuridze (6)
ApJ **896** L35 **2020**
https://arxiv.org/pdf/2006.00574.pdf
https://sci-hub.tw/https://iopscience.iop.org/article/10.3847/2041-8213/ab9839
We present an analysis of off-limb cool flare loops observed by SDO/AIA during the gradual phase of SOL**2017-09-10**T16:06 X8.2-class flare. In the EUV channels starting from the 335 Å one, cool loops appear as dark structures against the bright loop arcade. These dark structures were precisely coaligned (spatially and temporally) with loops observed by SST in emission lines of hydrogen and ionized calcium. Recently published semi-empirical model of cool loops based on SST observations serves us to predict the level of hydrogen and helium recombination continua. The continua were synthesized using an approximate non-LTE approach and theoretical spectra were then transformed to AIA signals. Comparison with signals detected inside the dark loops shows that only in AIA 211 Å channel the computed level of recombination continua is consistent with observations for some models, while in all other channels which are more distant from the continua edges the synthetic continuum is far too low. In analogy with on-disk observations of flares we interpret the surplus emission as due to numerous EUV lines emitted from hot but faint loops in front of the cool ones. Finally we briefly comment on failure of the standard absorption model when used for analysis of the dark-loop brightness.

Can flare loops contribute to the white-light emission of stellar superflares ?

Petr **Heinzel**, Kazunari Shibata
ApJ **859** 143 **2018**
https://arxiv.org/pdf/1804.09656.pdf
Since the discovery of stellar superflares by Kepler satellite, these extremely energetic events have been studied in analogy to solar flares. Their white-light (WL) continuum emission has been interpreted as being produced by heated ribbons. In this paper we compute the WL emission from overlying flare loops depending on their density and temperature and show that, under conditions expected during superflares, the continuum brightening due to extended loop arcades can significantly contribute to stellar flux detected by Kepler. This requires electron densities in the loops 1012−1013 cm−3 or higher. We show that such densities, exceeding those typically present in solar flare loops, can be reached on M-dwarf and solar-type superflare stars with large starspots and much stronger magnetic fields. Quite importantly, the WL radiation of loops is not very sensitive to their temperature and thus both cool as well as hot loops may contribute. We show that the WL intensity emergent from optically-thin loops is lower than the blackbody radiation from flare ribbons, but the contribution of loops to total stellar flux can be quite important due to their significant emitting areas. This new scenario for interpreting superflare emission suggests that the observed WL flux is due to a mixture of the ribbon and loop radiation and can be even loop-dominated during the gradual phase of superflares.

On the nature of off-limb flare continuum sources detected by SDO/HMI

P.**Heinzel**, L. Kleint, J. Kasparova, S. Krucker
ApJ **847** 48 **2017**
https://arxiv.org/pdf/1709.06377.pdf
The Helioseismic and Magnetic Imager onboard the Solar Dynamics Observatory has provided unique observations of off-limb flare emission. White-light (WL) continuum enhancements were detected in the "continuum" channel of the Fe 6173 A line during the impulsive phase of the observed flares. In this paper we aim to determine which radiation mechanism is responsible for such an enhancement being seen above the limb, at chromospheric heights around or below 1000 km. Using a simple analytical approach, we compare two candidate mechanisms, the hydrogen recombination continuum (Paschen) and the Thomson continuum due to scattering of disk radiation on flare electrons. Both mechanisms depend on the electron density, which is typically enhanced during the impulsive phase of a flare as the result of collisional ionization (both thermal and also non-thermal due to electron beams). We conclude that for electron densities higher than 1012cm−3, the Paschen recombination continuum significantly dominates the Thomson scattering continuum and there is some contribution from the hydrogen free-free emission. This is further supported by detailed radiation-hydrodynamical (RHD) simulations of the flare chromosphere heated by the electron beams. We use the RHD code FLARIX to compute the temporal evolution of the flare heating in a semi-circular loop. The synthesized continuum structure above the limb resembles the off-limb flare structures detected by HMI, namely their height above the limb, as well as the radiation intensity. These results are consistent with recent findings related to hydrogen Balmer continuum enhancements, which were clearly detected in disk flares by the IRIS near-ultraviolet spectrometer.
20120719, 20121120
Helioseismic and Magnetic Imager (HMI) – **Science Nugget** #74 **2017** (hmi.stanford.edu/hminuggets/?p=2022)

Numerical RHD simulations of flaring chromosphere with Flarix

P. **Heinzel**, J. Kasparova, M. Varady, M. Karlicky, Z. Moravec
Proceedings IAU Symposium No. 320, **2016**

http://arxiv.org/pdf/1602.00016v1.pdf
Flarix is a radiation-hydrodynamical (RHD) code for modeling of the response of the chromosphere to a beam bombardment during solar flares. It solves the set of hydrodynamic conservation equations coupled with non-LTE equations of radiative transfer. The simulations are driven by high energy electron beams. We present results of the Flarix simulations of a flaring loop relevant to the problem of continuum radiation during flares. In particular we focus on properties of the hydrogen Balmer continuum which was recently detected by IRIS.

Hydrogen Balmer Continuum in Solar Flares Detected by the Interface Region Imaging Spectrograph (IRIS)

Petr **Heinzel**, Lucia Kleint
ApJL, 794 L23 **2014**
http://arxiv.org/pdf/1409.5680v1.pdf
We present a novel observation of the white-light flare (WLF) continuum, which was significantly enhanced during the X1 flare on **March 29, 2014** (SOL2014-03-29T17:48). Data from the Interface Region Imaging Spectrograph (IRIS) in its NUV channel show that at the peak of the continuum enhancement, the contrast at the quasi-continuum window above 2813 \AA\ reached 100 - 200 % and can be even larger closer to the Mg II lines. This is fully consistent with the hydrogen recombination Balmer continuum emission, which follows an impulsive thermal and non-thermal ionization caused by the precipitation of electron beams through the chromosphere. However, a less probable photospheric continuum enhancement cannot be excluded. The light curves of the Balmer continuum have an impulsive character with a gradual fading, similar to those detected recently in the optical region on Hinode/SOT. This observation represents a first Balmer-continuum detection from space far beyond the Balmer limit (3646 \AA), eliminating seeing effects known to complicate the WLF detection. Moreover, we use a spectral window so far unexplored for flare studies, which provides the potential to study the Balmer continuum, as well as many metallic lines appearing in emission during flares. Combined with future ground-based observations of the continuum near the Balmer limit, we will be able to disentangle between various scenarios of the WLF origin. IRIS observations also provide a critical quantitative measure of the energy radiated in the Balmer continuum, which constrains various models of the energy transport and deposition during flares.
See RHESSI Science Nuggets, #237, Sept **2014**
http://sprg.ssl.berkeley.edu/~tohban/wiki/index.php/The_Balmer_continuum_observed_from_IRIS!

Optical-to-Radio Continua in Solar Flares

P. **Heinzel** and E. H. Avrett
Solar Physics, Volume 277, Number 1, 31-44, **2012**
Spectral continua observed during solar flares may contain information about both thermal and non-thermal heating mechanisms. Using two semi-empirical flare models F2 and FLA, we synthesize the thermal continua from optical to mm–radio domains and compare their intensities with quiet-Sun values computed from a recent model C7. In this way, the far-infrared and sub-mm/mm continua are studied for the first time, and we present our results as a benchmark for further modeling and for planning new observations, especially with the ALMA instrument. Finally, we demonstrate how these continua are formed and show a close correspondence between their brightness temperature and the kinetic-temperature structure of the flaring atmosphere.

Flare line impact polarization

Na D2 589 nm line polarization in the 2001 June 15 flare⋆

J. C. **Hénoux**1 and M. Karlicky
E-print, Oct **2013**; A&A 556, A95 (**2013**)
Context. The impact polarization of optical chromospheric lines in solar flares is still being debated. For this reason, additional observations and improved flare atmosphere models are needed still.
Aims. The polarization-free telescope THEMIS used in multiline 2 MulTiRaies (MTR) mode allows accurate simultaneous linear polarization measurements in various spectral lines.
Methods. In the 2001 June 15 flare, Hα, Hβ, and Mg D2 lines linear impact polarization was reported as present in THEMIS 2 MTR observations. In this paper, THEMIS data analysis was extended to the Na D2 line. Sets of I ± U and I ± Q flare Stokes S 2D-spectra were corrected from dark-current, spectral-line curvature and from transmission differences. Then, we derived the linear polarization degree P and polarization orientation angle α 2D-spectra. No change in relative positioning could be found that would reduce the Stokes parameters U and Q values. No V and I crosstalks could explain our results either.
Results. The Na D2 line is linearly polarized with a polarization degree exceeding 5% at some locations. The polarization was found to be radial at outer ribbons edges, and tangential at their inner edges. This orientation change may be due to differences in electron distribution functions on the opposite borders of flare chromospheric ribbons. Electron beams propagating along magnetic field lines, together with return currents, could explain both radial and

tangential polarization. At the inner ribbon edges, intensity profile-width enlargements and blueshifts in polarization profiles are observed. This suggests chromospheric evaporation.

From solar to stellar flare characteristics
On a new peak size distribution for G-, K-, and M-dwarf star flares

Konstantin **Herbst**1, Athanasios Papaioannou2, Saša Banjac1 and Bernd Heber1
A&A 621, A67 (**2019**)
sci-hub.tw/10.1051/0004-6361/201832789

Context. The connection between solar energetic proton events and X-ray flares has been the focus of many studies over the past 13 yr. In the course of these investigations several peak size distribution functions based on Geostationary Operational Environmental Satellite (GOES) measurements of both quantities have been developed. In more recent studies one of these functions has been used to estimate the stellar proton fluence around the M-dwarf star AD Leonis. However, a comparison of the existing peak size distribution functions reveals strong discrepancies with respect to each other.
Aims. The aim of this paper is to derive a new peak size distribution function that can be utilized to give a more realistic estimate of the stellar proton flux of G-, K-, and M-dwarf stars.
Methods. By updating and extending the GOES-based peak size distribution down to B-class X-ray flare intensities with the help of SphinX data from the solar minimum conditions of 2009 and newly derived GOES data between 1975 and 2005, we developed a new power-law peak size distribution function for solar proton fluxes (E > 10 MeV). However, its resulting slope differs from values reported in the literature. Therefore, we also developed a double-power-law peak size distribution function. An extension to much higher X-ray flare intensities (10−1) W m−2 and above, for the first time, results in an approximation of best- and worst-case scenarios of the stellar proton flux around G-, K-, and M-dwarf stars.
Results. Investigating the impact of the newly developed peak size distribution function for G-, K-, and M-dwarf star flare intensities we show that in the worst-case scenario previous studies may underestimate the stellar proton flux by roughly one to five orders of magnitude.

Analysis of magnetic polarities in active regions for the prediction of solar flares

N. Granados **Hernández**, S. Vargas Domínguez
Rev. Acad. Colomb. Cienc. Ex. Fis. Nat. **2020**. 44(173):984-995
https://arxiv.org/ftp/arxiv/papers/2012/2012.04050.pdf

Solar active regions and the processes that occur in them have been extensively studied and analyzed and many types of models and characterizations have been proposed for the occurrence of different eruptive events that take place in the solar atmosphere. The most characteristic of these regions are those that have opposite magnetic polarity, which, in their majority, generate explosive events such as the so-called solar flares. The flares are intense explosions occurring in the solar atmosphere with adverse effects on the Earth and the technology developed by humans, and they are also determining factors in the so-called space weather. For this reason, attempts have been made to predict the occurrence of these events. In the present study, we developed a predictive model of solar flares higher than M5 based on the articles proposed by Korsos, et al. (2014, 2015) using the relationship between the flares and the bipolar active regions. The analysis took into account the areas of the umbrae of opposite polarity, their average magnetic field, and the magnetic barycenter from each sunspot in the region for a sample of three active regions to find the temporal variation due to the evolution of the sunspots, thus confirming previous results reported in the literature. We made a statistical analysis to determine whether after a flare occurs, another can arise in the subsequent hours. **2001-03-26**

A Hot Cusp-Shaped Confined Solar Flare

Aaron **Hernandez-Perez**, Yang Su, Julia K. Thalmann, Astrid M. Veronig, Ewan C. Dickson, Karin Dissauer, Bhuwan Joshi, Ramesh Chandra
ApJL **887** L28 **2019**
https://arxiv.org/pdf/1911.10859.pdf
https://doi.org/10.3847/2041-8213/ab5ba1

We analyze a confined flare that developed a hot cusp-like structure high in the corona (H ~ 66 Mm). A growing cusp-shaped flare arcade is a typical feature in the standard model of eruptive flares, caused by magnetic reconnection at progressively larger coronal heights. In contrast, we observe a static hot cusp during a confined flare. Despite an initial vertical temperature distribution similar to that in eruptive flares, we observe a distinctly different evolution during the late (decay) phase, in the form of prolonged hot emission. The distinct cusp shape, rooted at locations of non-thermal precursor activity, was likely caused by a magnetic field arcade that kinked near the top. Our observations indicate that the prolonged heating was a result of slow local reconnection and an increased thermal pressure near the kinked apexes due to continuous plasma upflows. **2014-01-13**
CESRA #371 Feb **2020** http://sprg.ssl.berkeley.edu/~tohban/wiki/index.php/A_Hot_Cusp-Shaped_Confined_Solar_Flare

Pre-eruption processes: heating, particle acceleration and the formation of a hot channel before the 2012 October 20 M9.0 limb flare

Aaron **Hernandez-Perez**, Yang Su, Astrid M. Veronig, Julia K. Thalmann, Peter Gömöry, Bhuwan Joshi
ApJ **874** 122 **2019**
https://arxiv.org/pdf/1902.08436.pdf
sci-hub.se/10.3847/1538-4357/ab09ed

We report a detailed study of the pre-eruption activities that led to the occurrence of an M9.0 flare/CME event on **2012 October 20** in NOAA AR 11598. This includes the study of the preceding confined C2.4 flare that occurred on the same AR ~25 minutes earlier. We observed that the M9.0 flare occurred as a consequence of two distinct triggering events well separated in time. The first triggering episode occurred as early as ~20 minutes before the onset of the M9.0 flare, evidenced by the destabilization and rise of a pre-existing filament to a new position of equilibrium at a higher coronal altitude during the decay phase of the C2.4 flare. This brought the system to a magnetic configuration where the establishment of the second triggering event was favorable. The second triggering episode occurred ~17 minutes later, during the early phase of the M9.0 flare, evidenced by the further rise of the filament and successful ejection. The second trigger is followed by a flare precursor phase, characterized by non-thermal emission and the sequential formation of a hot channel as shown by the SDO/AIA DEM (differential emission measure) maps, the RHESSI X-ray images and spectra. These observations are suggestive of magnetic reconnection and particle acceleration that can explain the precursor phase and can be directly related to the formation of the hot channel. We discuss on the triggering mechanisms, their implications during the early and precursor phases and highlight the importance of early activities and preceding small confined flares to understand the initiation of large eruptive flares.

Generation mechanisms of quasi-parallel and quasi-circular flare ribbons in a confined flare

Aaron **Hernandez-Perez**, Julia K. Thalmann, Astrid M. Veronig, Yang Su, Peter Gömöry, Ewan C. Dickson
ApJ 847 124 **2017**
https://arxiv.org/pdf/1708.08612.pdf
http://sci-hub.cc/http://iopscience.iop.org/0004-637X/847/2/124/

We analyze a confined multiple-ribbon M2.1 flare (SOL**2015-01-29**T11:42) that originated from a fan-spine coronal magnetic field configuration, within active region NOAA 12268. The observed ribbons form in two steps. First, two primary ribbons form at the main flare site, followed by the formation of secondary ribbons at remote locations. We observe a number of plasma flows at extreme-ultraviolet temperatures during the early phase of the flare (as early as 15 min before the onset) propagating towards the formation site of the secondary ribbons. The secondary ribbon formation is co-temporal with the arrival of the pre-flare generated plasma flows. The primary ribbons are co-spatial with RHESSI hard X-ray sources, whereas no enhanced X-ray emission is detected at the secondary ribbons sites. The (E)UV emission, associated with the secondary ribbons, peaks ~1 min after the last RHESSI hard X-ray enhancement. A nonlinear force-free model of the coronal magnetic field reveals that the secondary flare ribbons are not directly connected to the primary ribbons, but to regions nearby. Detailed analysis suggests that the secondary brightenings are produced due to dissipation of kinetic energy of the plasma flows (heating due to compression), and not due to non-thermal particles accelerated by magnetic reconnection, as is the case for the primary ribbons.

On the success rate of the farside seismic imaging of active regions

GonzAlez **HernAndez**, I.; Hill, F.; Scherrer, P. H.; Lindsey, C.; Braun, D. C.
Space Weather, Vol. 8, No. 6, S06002, **2010**

Seismic maps of the nonvisible side of the Sun (farside) have been used for almost a decade to follow large active regions before they rotate to face the Earth. Preliminary efforts to quantify the success rate of the technique (seismic holography) have been published with Michelson Doppler Imager (MDI) data. In this paper we present a thorough statistical analysis of 3 complete years of farside seismic maps (2003–2005) calculated using both Global Oscillation Network Group (GONG) data and a combined set of GONG and MDI data. A comparison with NOAA data of the frontside of the Sun during the same period shows that seismic maps detect about 40% of the total active regions that appear at the east limb of the Sun with a confidence level higher than 60%. The relationship found during this work between the seismic signature and the confidence level allows us to automatically highlight candidates in the farside seismic maps and to assign them the corresponding probability of appearance on the frontside.

Magnetic Reconnection in the Space Sciences: Past, Present, and Future **Review**

M. **Hesse**, P. A. Cassak
JGR Volume125, Issue2 February **2020** e2018JA025935
https://doi.org/10.1029/2018JA025935
https://agupubs.onlinelibrary.wiley.com/doi/epdf/10.1029/2018JA025935

Magnetic reconnection converts, often explosively, stored magnetic energy to particle energy in space and in the laboratory. Through processes operating on length scales that are tiny, it facilitates energy conversion over dimensions of, in some cases, hundreds of Earth radii. In addition, it is the mechanism behind large current disruptions in fusion machines, and it can explain eruptive behavior in astrophysics. We have known about the importance of magnetic reconnection for quite some time based on space observations. Theory and modeling employed magnetized fluids, a very simplistic description. While successful at modeling the large-scale consequences of reconnection, it is ill suited to describe the engine itself. This is because, at its heart, magnetic reconnection in space is kinetic, that is, governed by the intricate interaction of charged particles with the electromagnetic fields they create. This complex interaction occurs in very localized regions and involves very short temporal variations. Researching reconnection requires the ability to measure these processes as well as to express them in models vastly more complex than fluid approaches. Until very recently, neither of these capabilities existed. With the advent of NASA's Magnetospheric Multiscale mission and modern modeling advances, this has now changed, and we have now determined its small-scale structure in exquisite detail. In this paper, we review recent research results to predict what will be achieved in the future. We discuss how reconnection contributes to the evolution of larger-scale systems, and its societal impacts in the context of threatening space hazards, customarily referred to as “space weather.”

Solar Magnetic Feature Detection and Tracking for Space Weather Monitoring

Paul A. **Higgins**, Peter T. Gallagher, R.T. James McAteer, D. Shaun Bloomfield
E-print, July **2010**, Advances in Space Research, Volume 47, Issue 12, p. 2105-2117, **2011**.
We present an automated system for detecting, tracking, and cataloging emerging active regions throughout their evolution and decay using SOHO Michelson Doppler Interferometer (MDI) magnetograms. The SolarMonitor Active Region Tracking (SMART) algorithm relies on consecutive image differencing to remove both quiet-Sun and transient magnetic features, and region-growing techniques to group flux concentrations into classifiable features. We determine magnetic properties such as region size, total flux, flux imbalance, flux emergence rate, Schrijver's R-value, R* (a modified version of R), and Falconer's measurement of non-potentiality. A persistence algorithm is used to associate developed active regions with emerging flux regions in previous measurements, and to track regions beyond the limb through multiple solar rotations. We find that the total number and area of magnetic regions on disk vary with the sunspot cycle. While sunspot numbers are a proxy to the solar magnetic field, SMART offers a direct diagnostic of the surface magnetic field and its variation over timescale of hours to years. SMART will form the basis of the active region extraction and tracking algorithm for the Heliophysics Integrated Observatory (HELIO).

Connecting theory of plasmoid-modulated reconnection to observations of solar flares

Andrew **Hillier**, Shinsuke Takasao
Experimental Results (**2022**), 3, e26, 1–10
https://arxiv.org/ftp/arxiv/papers/2301/2301.03239.pdf
The short timescale of the solar flare reconnection process has long proved to be a puzzle. Recent studies suggest the importance of the formation of plasmoids in the reconnecting current sheet, with quantifying the aspect ratio of the width to length of the current sheet in terms of a negative power α of the Lundquist number, i.e. S−α, being key to understanding the onset of plasmoids formation. In this paper we make the first application of theoretical scalings for this aspect ratio to observed flares to evaluate how plasmoid formation may connect with observations. We find that for three different flares showing plasmoids a range of α values of α=0.27 to 0.31. The values in this small range implies that plasmoids may be forming before the theoretically predicted critical aspect ratio (α=1/3) has been reached, potentially presenting a challenge for the theoretical models. **August 18, 2010**

Statistical Properties of Ribbon Evolution and Reconnection Electric Fields in Eruptive and Confined Flares

Jürgen **Hinterreiter**, Astrid M. Veronig, Julia K. Thalmann, Johannes Tschernitz, Werner Pötzi
Solar Phys. 293:38 **2018**
https://arxiv.org/pdf/1801.03370.pdf
https://link.springer.com/content/pdf/10.1007%2Fs11207-018-1253-1.pdf
A statistical study of the chromospheric ribbon evolution in Hα two-ribbon flares is performed. The data set consists of 50 confined (62%) and eruptive (38%) flares that occurred from June 2000 to June 2015. The flares are selected homogeneously over the Hα and GOES (Geostationary Operational Environmental Satellite) classes, with an emphasis on including powerful confined flares and weak eruptive flares. Hα filtergrams from Kanzelh\"ohe Observatory in combination with MDI (Michelson Doppler Imager) and HMI (Helioseismic and Magnetic Imager) magnetograms are used to derive the ribbon separation, the ribbon-separation velocity, the magnetic-field strength, and the reconnection electric field. We find that eruptive flares reveal statistically larger ribbon separation and higher ribbon-separation velocities than confined flares. In addition, the ribbon separation of eruptive flares correlates with the GOES SXR flux, whereas no clear dependence was found for confined flares. The maximum ribbon-separation velocity is not correlated with the GOES flux, but eruptive flares reveal on average a higher ribbon-separation velocity (by ≈10 km s−1). The local reconnection electric field of confined (cc=0.50 ± 0.02) and eruptive (cc=0.77 ± 0.03) flares correlates with the

GOES flux, indicating that more powerful flares involve stronger reconnection electric fields. In addition, eruptive flares with higher electric-field strengths tend to be accompanied by faster coronal mass ejections. **9 November 2011, 22 October 2014**
Table 1. Results of ribbon tracking for all flares under study

Using SDO EVE data as a proxy for GOES XRS B 1–8 angstrom

Rachel A. **Hock**,1 Don Woodraska,2 and Thomas N. Woods2
SPACE WEATHER, VOL. 11, 262–271, doi:10.1002/swe.20042, **2013**
http://onlinelibrary.wiley.com/doi/10.1002/swe.20042/pdf
Solar soft X-ray irradiance measured by the GOES X-Ray Sensor (XRS) is a critical measurement for space weather operations. At present, there is a primary GOES XRS operating with a second XRS in storage on orbit. This configuration results in gaps in critical observational coverage when the primary XRS is nonoperational such as during satellite maneuvers and during the spring and fall eclipse seasons. EUV Variability Experiment (EVE) on NASA's Solar Dynamics Observatory provides near–real-time measurements of the solar soft X-ray irradiances at wavelengths similar to XRS. This study examines the accuracy in using EVE data as a proxy for GOES XRS. Using EVE data, we develop three different solar irradiance index models, which are then tested to determine how well they predict the XRS irradiances and magnitude (GOES class) of solar flares. The best performing index model has been implemented in Version 3 of EVE data and is publicly available within minimal latency through the EVE Science Processing and Operations Center.

The Origin of the EUV Late Phase: A Case Study of the C8.8 Flare on 2010 May 5

R. A. **Hock**, T. N. Woods, J. A. Klimchuk, F. G. Eparvier, A. R. Jones
ApJ **2012**
http://arxiv.org/pdf/1202.4819v1.pdf
One interesting feature observed by EVE is that a subset of flares exhibit an additional enhancement of the 2-3 million K emission several hours after the flare's soft X-ray emission. From the Atmospheric Imaging Assembly (AIA) images, we observe that this secondary emission, dubbed the EUV late phase, occurs in the same active region as the flare but not in the same coronal loops. Here, we examine the C8.8 flare that occurred on 2010 May 5 as a case study of EUV late phase flares. In addition to presenting detailed observations from both AIA and EVE, we develop a physical model of this flare and test it using the Enthalpy Based Thermal Evolution of Loops (EBTEL) model.

Scientific considerations for future spectroscopic measurements from space of activity on the Sun **Review**

Gordon D. **Holman**
JGR **2016**
http://sci-hub.cc/10.1002/2016JA022651
High-resolution UV and X-ray spectroscopy are important to understanding the origin and evolution of magnetic energy release in the solar atmosphere, as well as the subsequent evolution of heated plasma and accelerated particles. Electromagnetic radiation is observed from plasma heated to temperatures ranging from about 10 kK to above 10 MK, from accelerated electrons emitting photons primarily at X-ray energies, and from ions emitting in γ rays. These observations require space-based instruments sensitive to emissions at wavelengths shorter than the near UV. This article reviews some recent observations with emphasis on solar eruptive events, the models that describe them, and the measurements they indicate are needed for substantial progress in the future. Specific examples are discussed demonstrating that imaging spectroscopy with a cadence of seconds or better is needed to follow, understand, and predict the evolution of solar activity. Critical to substantial progress is the combination of a judicious choice of UV, EUV, and soft X-ray imaging spectroscopy sensitive to the evolution of this thermal plasma combined with hard X-ray imaging spectroscopy sensitive to suprathermal electrons. The major challenge will be to conceive instruments that, within the bounds of possible technologies and funding, have the flexibility and field of view to obtain spectroscopic observations where and when events occur while providing an optimum balance of dynamic range, spectral resolution and range, and spatial resolution.

Direct Spatial Association of an X-Ray Flare with the Eruption of a Solar Quiescent Filament

Gordon D. **Holman** & Adi Foord
ApJ **804** 108 **2015**
http://hesperia.gsfc.nasa.gov/~kim/Holman_Foord_2015_quiescent_filament_flare.pdf
are often associated with the eruption of active region filaments and coronal mass ejections (CMEs). CMEs can also be associated with the eruption of quiescent filaments, not located in active regions. Here we report the first identification of a solar X-ray flare outside an active region observed by the Ramaty High Energy Solar Spectroscopic Imager (RHESSI). The X-ray emission was directly associated with the eruption of a long, quiescent filament and fast CME.

Images from RHESSI show this flare emission to be located along a section of the western ribbon of the expanding, post-eruption arcade. EUV images from the Solar Dynamics Observatory (SDO) Atmospheric Imaging Assembly (AIA) show no connection between this location and nearby active regions. Therefore the flare emission is found to not be located in or associated with an active region. However, a nearby, small, magnetically strong dipolar region provides a likely explanation for the existence and location of the flare X-ray emission. This emerging dipolar region may have also triggered the filament eruption. **September 29, 2013**

RHESSI Detection of X-ray Emission from a Quiet-Sun Filament Eruption

Gordon **Holman** and Adi Foord
RHESSI Science Nugget No. 250, April **2015**
http://sprg.ssl.berkeley.edu/~tohban/wiki/index.php/RHESSI_Science_Nuggets
The event described in this Nugget reveals the presence of intense energy release even in the quiet Sun, in the form of an otherwise innocuous-looking quiescent filament. The power of the the CME that resulted, and its interplanetary development, do not have the same kind of associations with a solar flare as in an active-region event. Nevertheless high temperatures and non-thermal effects result, and hard X-ray observations such as those of RHESSI (or more sensitive ones) can diagnose them. **September 29, 2013**

Understanding the Impact of Return-Current Losses on the X-Ray Emission from Solar Flares

G.D. **Holman**
ApJ 745, Issue 1, article id. 52, 17 pp. (**2012**)
E-pint, 5 Nov **2011**
http://iopscience.iop.org/0004-637X/745/1/52/pdf/0004-637X_745_1_52.pdf
I obtain and examine the implications of one-dimensional analytic solutions for return-current losses on an initially power-law distribution of energetic electrons with a sharp low-energy cutoff in flare plasma with classical (collisional) resistivity. These solutions show, for example, that return-current losses are not sensitive to plasma density, but are sensitive to plasma temperature and the low-energy cutoff of the injected nonthermal electron distribution. A characteristic distance from the electron injection site, xrc, is derived. At distances less than xrc the electron flux density is not reduced by return-current losses, but plasma heating can be substantial in this region, in the upper, coronal part of the flare loop. Before the electrons reach the collisional thick-target region of the flare loop, an injected power-law electron distribution with a low-energy cutoff maintains that structure, but with a flat energy distribution below the cutoff energy, which is now determined by the total potential drop experienced by the electrons. Modifications due to the presence of collisional losses are discussed. I compare these results with earlier analytical results and with more recent numerical simulations. Emslie's 1980 conjecture that there is a maximum integrated X-ray source brightness on the order of 10-15 photons cm-2 s-1 cm-2 is examined. I find that this is not actually a maximum brightness and its value is parameter dependent, but it is nevertheless a valuable benchmark for identifying return-current losses in hard X-ray spectra. I discuss an observational approach to identifying return-current losses in flare data, including identification of a return-current "bump" in X-ray light curves at low photon energies.

Implications of X-ray Observations for Electron Acceleration and Propagation in Solar Flares

G.D. **Holman**1, M. J. Aschwanden2, H. Aurass3, M. Battaglia4, P. C. Grigis5, E. P. Kontar6, W. Liu1, P. Saint-Hilaire7, and V. V. Zharkova8
Space Sci. Rev., 159:107–166, **2011, File** **Review**
High-energy X-rays and g-rays from solar flares were discovered just over fifty years ago. Since that time, the standard for the interpretation of spatially integrated flare X-ray spectra at energies above several tens of keV has been the collisional thick-target model. After the launch of the *Reuven Ramaty High Energy Solar Spectroscopic Imager* (*RHESSI*) in early 2002, X-ray spectra and images have been of sufficient quality to allow a greater focus on the energetic electrons responsible for the X-ray emission, including their origin and their interactions with the flare plasma and magnetic field. The result has been new insights into the flaring process, as well as more quantitative models for both electron acceleration and propagation, and for the flare environment with which the electrons interact. In this article we review our current understanding of electron acceleration, energy loss, and propagation in flares. Implications of these new results for the collisional thick-target model, for general flare models, and for future flare studies are discussed.

An approximate recipe of chromospheric radiative losses for solar flares

Jie **Hong**, Mats Carlsson, M. D. Ding
A&A 661, A77 **2022**
https://arxiv.org/pdf/2203.07630.pdf

https://www.aanda.org/articles/aa/pdf/2022/05/aa42839-21.pdf
Radiative losses in the chromosphere are very important in the energy balance. There have been efforts to make simple lookup tables for chromospheric radiative losses in the quiet Sun. During solar flares, the atmospheric conditions are quite different, and the currently available recipe of Gan & Fang (1990) is constructed from semi-empirical models. It remains to be evaluated how these recipes work in flare conditions. We aim to construct an approximate recipe of chromospheric radiative losses for solar flares. We follow the method of Carlsson & Leenaarts (2012) to tabulate the optically thin radiative loss, escape probability, and ionization fraction, while using a grid of flare models from radiative hydrodynamic simulations as our dataset. We provide new lookup tables to calculate chromospheric radiative losses for flares. Compared with previous recipes, our recipe provides a better approximation to the detailed radiative losses for flares.

Multi-Wavelength Observations of Quasi-Periodic Pulsations in a Solar Flare

Zhenxiang **Hong**, Dong Li, Minghui Zhang, Chengming Tan, Suli Ma & Haisheng Ji
Solar Physics volume 296, Article number: 171 (**2021**)
https://link.springer.com/content/pdf/10.1007/s11207-021-01922-1.pdf
https://doi.org/10.1007/s11207-021-01922-1
We report our analysis of multi-wavelength observations of quasi-periodic pulsations (QPPs) during the impulsive phase of the C6.7 flare on **9 May 2019**. The flare was simultaneously observed by Fermi, the New Vacuum Solar Telescope, the Mingantu Spectral Radioheliograph, the Nobeyama Radio Polarimeters, and the Atmospheric Imaging Assembly (AIA) of the Solar Dynamics Observatory. Three well-pronounced pulsations are detected in full-disk hard X-ray and microwave fluxes, as well as the local light curves at wavelengths of the Hαα line core, AIA 304 Å, 171 Å, 211 Å, and 335 Å between ≈05:43:30 UT and ≈05:48:15 UT. The quasi-periods of about 90 – 110 seconds are determined from their Morlet wavelet power spectra. Meanwhile, a sequence of three groups of Type-III radio bursts is seen in the radio dynamic spectrum during the same time interval. Our observations suggest that the flare QPPs are possibly related to nonthermal electrons accelerated by the intermittent magnetic reconnection during the flare's impulsive phase.

Modeling the IRIS Lines During a Flare. I. The Blue-wing Enhancement in the Mg II k Line

Jie **Hong**1,2, Ying Li3, M. D. Ding1,2, and Yu-Hao Zhou4,1
2020 ApJ 890 115
https://doi.org/10.3847/1538-4357/ab6d05
The Interface Region Imaging Spectrograph (IRIS) Mg ii k line serves as a very good tool to diagnose the heating processes in solar flares. Recent studies have shown that apart from the usual red asymmetries that are interpreted as the result of condensation downflows, this line could also show a blue-wing enhancement. To investigate how such a blue asymmetry is formed, we perform a grid of radiative hydrodynamic simulations and calculate the corresponding line profiles. We find that such a spectral feature is likely to originate from the upward plasma motion in the upper chromosphere. However, the formation region that is responsible for the blue-wing enhancement could be located in an evaporation region, in an upward-moving blob, and even an upward-moving condensation region. We discuss how the electron beam parameters affect these different dynamics of the atmosphere.

The Response of the Lyman-Alpha Line in Different Flare Heating Models

Jie **Hong**, Ying Li, M. D. Ding, Mats Carlsson
ApJ **2019**
https://arxiv.org/pdf/1905.13356.pdf
The solar Lyα line is the strongest line in the ultraviolet waveband, and is greatly enhanced during solar flares. Here we present radiative hydrodynamic simulations of solar flares under different heating models, and calculate the response of this line taking into account non-equilibrium ionization of hydrogen and partial frequency redistribution. We find that in non-thermal heating models, the Lyα line can show a red or blue asymmetry corresponding to the chromospheric evaporation or condensation, respectively. The asymmetry may change from red to blue if the electron beam flux is large enough to produce a significant chromospheric condensation region. In the Lyα intensity lightcurve, there appears a dip when the change of asymmetry occurs. In thermal models, the Lyα line intensity peaks quickly and then falls, and the profile has an overall red asymmetry, which is similar to the profiles from heating by a soft electron beam. The Lyα profile shows a single red peak at the end of thermal heating, and the whole line is formed in a very small height range.

Bidirectional outflows as evidence of magnetic reconnection leading to a solar microflare

Jie **Hong**, M. D. Ding, Ying Li, Kai Yang, Xin Cheng, Feng Chen, Cheng Fang, Wenda Cao
ApJL 820 L17 **2016**
http://arxiv.org/pdf/1603.00941v1.pdf

Magnetic reconnection is a rapid energy release process that is believed to be responsible for flares on the Sun and stars. Nevertheless, such flare-related reconnection is mostly detected to occur in the corona, while there have been few studies concerning the reconnection in the chromosphere or photosphere. Here we present both spectroscopic and imaging observations of magnetic reconnection in the chromosphere leading to a microflare. During the flare peak time, chromospheric line profiles show significant blueshifted/redshifted components on the two sides of the flaring site, corresponding to upflows and downflows with velocities of ±(70--80) km s−1, comparable with the local Alfv\'{e}n speed as expected by the reconnection in the chromosphere. The three-dimensional nonlinear force-free field configuration further discloses twisted field lines (a flux rope) at a low altitude, cospatial with the dark threads in He I 10830 \r{A} images. The instability of the flux rope may initiate the flare-related reconnection. These observations provide clear evidence of magnetic reconnection in the chromosphere and show the similar mechanisms of a microflare to those of major flares.

Efficiency of Nonthermal Particle Acceleration in Magnetic Reconnection

Masahiro **Hoshino**

2022

https://arxiv.org/pdf/2203.15169.pdf

The nonthermal particle acceleration during magnetic reconnection remains a fundamental topic in several astrophysical phenomena, such as solar flares, pulsar wind, magnetars, etc, for more than half a century, and one of the unresolved questions is its efficiency. Recently, nonthermal particle acceleration mechanisms during reconnection have been extensively studied by particle-in-cell simulations, yet it is an intriguing enigma as to how the magnetic field energy is divided into thermally heated plasmas and nonthermal particles. Here we study both non-relativistic and relativistic magnetic reconnections using large-scale particle-in-cell simulation for a pair plasma, and indicate that the production of the nonthermal particle becomes efficient with increasing the plasma temperature. In the relativistic hot plasma case, we determine that the heated plasmas by reconnection can be approximated by a kappa distribution function with the kappa index of approximately 3 or less (equivalent to 2 or less for the power-law index), and the nonthermal energy density of reconnection is approximately over 95% of the total internal energy in the downstream exhaust.

A secondary fan-spine magnetic structure in active region 11897

Yijun **Hou**, Ting Li, Shuhong Yang, Jun Zhang

ApJ **871** 4 **2019**

https://arxiv.org/pdf/1811.11936.pdf

http://iopscience.iop.org/article/10.3847/1538-4357/aaf4f4/pdf

Fan-spine is a special topology in solar atmosphere and is closely related to magnetic null point as well as circular-ribbon flares, which can provide important information for understanding the intrinsic three-dimensional (3D) nature of solar flares. However, the fine structure within the fan has rarely been investigated. In present paper, we investigate a secondary fan-spine (SFS) structure within the fan of a larger fan-spine topology. On **2013 November 18**, this large fan-spine structure was traced out due to the partial eruption of a filament, which caused a circular-ribbon flare in active region 11897. The extrapolated 3D magnetic fields and squashing factor Q maps depict distinctly this fan-spine topology, its surrounding quasi-separatrix layer (QSL) halo, and a smaller quasi-circular ribbon with high Q located in the center, which implies the existence of fine structure within the fan. The imaging observations, extrapolated 3D fields, and Q maps on **November 17** show that there indeed exists an SFS surrounded by a QSL, which is enveloped by another QSL-halo corresponding to the overlying larger domeshaped fan. Moreover, the material flows caused by the null-point reconnection are also detected along this SFS. After checking the evolution of the underneath magnetic fields, we suggest that the continuous emergence of magnetic flux within the central parasitic region encompassed by the opposite-polarity fields results in the formation of the SFS under the large fan.

Eruption of a multi-flux-rope system in solar active region 12673 leading to the two largest flares in Solar Cycle 24

Y. J. **Hou**, J. Zhang, T. Li, S. H. Yang, X. H. Li

A&A 619, A100 **2018**

https://arxiv.org/pdf/1808.06795.pdf

Solar active region (AR) 12673 in 2017 September produced two largest flares in Solar Cycle 24: the X9.3 flare on **September 06** and the X8.2 flare on **September 10**. We attempt to investigate the evolutions of the two great flares and their associated complex magnetic system in detail. Aided by the NLFFF modeling, we identify a double-decker flux rope configuration above the polarity inversion line (PIL) in the AR core region. The north ends of these two flux ropes were rooted in a negative- polarity magnetic patch, which began to move along the PIL and rotate anticlockwise before the X9.3 flare on September 06. The strong shearing motion and rotation contributed to the destabilization of the two magnetic flux ropes, of which the upper one subsequently erupted upward due to the kink-instability. Then another two sets of twisted loop bundles beside these ropes were disturbed and successively erupted within 5 minutes like a chain reaction. Similarly, multiple ejecta components were detected to consecutively erupt during the X8.2 flare occurring in the same AR on September 10. We examine the evolution of the AR magnetic fields from **September 03 to 06** and find

that five dipoles emerged successively at the east of the main sunspot. The interactions between these dipoles took place continuously, accompanied by magnetic flux cancellations and strong shearing motions. In AR 12673, significant flux emergence and successive interactions between the different emerging dipoles resulted in a complex magnetic system, accompanied by the formations of multiple flux ropes and twisted loop bundles. We propose that the eruptions of a multi-flux-rope system resulted in the two largest flares in Solar Cycle 24.

A solar flare disturbing a light wall above a sunspot light bridge

Yijun **Hou**, Jun Zhang, Ting Li, Shuhong Yang, Leping Li, Xiaohong Li
2016 ApJ 829 L29
http://arxiv.org/pdf/1609.05412v1.pdf
With the high-resolution data from the Interface Region Imaging Spectrograph, we detect a light wall above a sunspot light bridge in the NOAA active region (AR) 12403. In the 1330 A slit-jaw images, the light wall is brighter than the ambient areas while the wall top and base are much brighter than the wall body, and it keeps oscillating above the light bridge. A C8.0 flare caused by a filament activation occurred in this AR with the peak at 02:52 UT on **2015 August 28**, and the flare's one ribbon overlapped the light bridge which was the observational base of the light wall. Consequently, the oscillation of the light wall was evidently disturbed. The mean projective oscillation amplitude of the light wall increased from 0.5 Mm to 1.6 Mm before the flare, and decreased to 0.6 Mm after the flare. We suggest that the light wall shares a group of magnetic field lines with the flare loops, which undergo a magnetic reconnection process, and they constitute a coupled system. When the magnetic field lines are pushed upwards at the pre-flare stage, the light wall turns to the vertical direction, resulting in the increase of the light wall's projective oscillation amplitude. After the magnetic reconnection takes place, a group of new field lines with smaller scales are formed underneath the reconnection site and the light wall inclines. Thus, the projective amplitude decreases remarkably at the post-flare stage.

CHALLENGING SOME CONTEMPORARY VIEWS OF CORONAL MASS EJECTIONS. I. THE CASE FOR BLAST WAVES

T. A. **Howard**1 and V. J. Pizzo
2016 ApJ 824 92 DOI: 10.3847/0004-637X/824/2/92
Since the closure of the "solar flare myth" debate in the mid-1990s, a specific narrative of the nature of coronal mass ejections (CMEs) has been widely accepted by the solar physics community. This narrative describes structured magnetic flux ropes at the CME core that drive the surrounding field plasma away from the Sun. This narrative replaced the "traditional" view that CMEs were blast waves driven by solar flares. While the flux rope CME narrative is supported by a vast quantity of measurements made over five decades, it does not adequately describe every observation of what have been termed CME-related phenomena. In this paper we present evidence that some large-scale coronal eruptions, particularly those associated with EIT waves, exhibit characteristics that are more consistent with a blast wave originating from a localized region (such as a flare site) rather than a large-scale structure driven by an intrinsic flux rope. We present detailed examples of CMEs that are suspected blast waves and flux ropes, and show that of our small sample of 22 EIT-wave-related CMEs, 91% involve a blast wave as at least part of the eruption, and 50% are probably blast waves exclusively. We conclude with a description of possible signatures to look for in determining the difference between the two types of CMEs and with a discussion on modeling efforts to explore this possibility.

Persistent Near-Surface Flow Structures from Local Helioseismology

Rachel **Howe**, R. W. Komm, D. Baker, L. Harra, L. van Driel-Gesztelyi, R. S. Bogart
Solar Phys. **2015**
Standing sausage modes are important in interpreting quasi-periodic pulsations in the light curves of solar flares. Their periods and damping times play an important role in seismologically diagnosing key parameters like the magnetic field strength in regions where flare energy is released. Usually, such applications are based on theoretical results neglecting unresolved fine structures in magnetized loops. However, the existence of fine structuring is suggested on both theoretical and observational grounds. Adopting the framework of cold magnetohydrodynamics (MHD), we model coronal loops as magnetized cylinders with a transverse equilibrium density profile comprising a monolithic part and a modulation due to fine structuring in the form of concentric shells. The equation governing the transverse velocity perturbation is solved with an initial-value-problem approach, and the effects of fine structuring on the periods P and damping times τ of global, leaky, standing sausage modes are examined. A parameter study shows that fine structuring, be it periodically or randomly distributed, brings changes of only a few percents to P and τ when there are more than about ten shells. The monolithic part, its steepness in particular, plays a far more important role in determining P and τ. We conclude that when measured values of P and τ of sausage modes are used for seismological purposes, it is justified to use theoretical results where the effects due to fine structuring are neglected.

The Slipping Magnetic Reconnection and Damped Quasiperiodic Pulsations in a Circular Ribbon Flare

Jing **Huang**1,2,3, Baolin Tan1,2,3, Yin Zhang1,2, Xiaoshuai Zhu2, Shangbin Yang1,2,3, and Yuanyong Deng1,2,
2024 ApJ 965 137
https://iopscience.iop.org/article/10.3847/1538-4357/ad3353/pdf
The study of circular ribbon (CR) flares is important to understand the three-dimensional magnetic reconnection in the solar atmosphere. We investigate the slipping brightenings and damped quasiperiodic pulsations in a CR flare by multiwavelength observations. During the flaring process, two extreme ultraviolet brightenings (SP1 and SP2) slip synchronously along the ribbon in a counterclockwise direction. The ribbon and fans between them show synchronous enhancement with the microwave and hard X-ray (HXR) CR source. In the magnetohydrostatic extrapolation results and observations, the dome and outer spine display an evident counterclockwise twisting feature. We propose the slipping reconnection occurs between the fan and outer spine in the null point, which covers the region from SP1 to SP2. The fan of SP1 shows the strongest twist and produces the most efficient reconnection. The ribbon after SP1 becomes weak due to the destruction of the fan configuration. The fan of SP2 is in the front of the slipping motion, which initiates new reconnection and brightens the local ribbon. The twisting of the dome continuously promotes new reconnection in the null point, which brightens the ribbon in sequence to display a counterclockwise slipping feature. Thus, the twist of the dome may trigger and dominate the slipping reconnection, and the rotation of the central positive pole could be one possible cause of the twist. After the peak, the microwave and HXR emission shows damped oscillations at a period of 15 s. The collapse of the fan–spine structure may lead to the standing kink oscillations of the fan to modulate the reconnection and particle acceleration process. **2014 June 11**.

Imaging and spectroscopic observations of extreme-ultraviolet brightenings using EUI and SPICE on board Solar Orbiter

Z. **Huang**, L. Teriaca, R. Aznar Cuadrado, et al.
A&A, 673, A82 **2023**
https://arxiv.org/pdf/2303.15979.pdf
https://doi.org/10.1051/0004-6361/202345988
https://www.aanda.org/articles/aa/pdf/forth/aa45988-23.pdf
https://www.aanda.org/articles/aa/pdf/2023/05/aa45988-23.pdf
The smallest extreme-ultraviolet (EUV) brightening events that were detected so far, called campfires, have recently been uncovered by the High Resolution EUV telescope (HRIEUV), which is part of the Extreme Ultraviolet Imager (EUI) on board Solar Orbiter. HRIEUV has a broad bandpass centered at 17.4 nm that is dominated by Fe ix and Fe x emission at about 1 MK. We study the thermal properties of EUI brightening events by simultaneously observing their responses at different wavelengths using spectral data from the Spectral Imaging of the Coronal Environment (SPICE) also on board Solar Orbiter and imaging data from EUI. We studied three EUI brightenings that were identified in HRIEUV data that lie within the small areas covered by the slit of the SPICE EUV spectrometer. We obtained the line intensities of the spectral profiles by Gaussian fitting. These diagnostics were used to study the evolution of the EUI brightenings over time at the different line-formation temperatures. We find that (i) the detection of these EUI brightenings is at the limit of the SPICE capabilities. They could not have been independently identified in the data without the aid of HRIEUV observations. (ii) Two of these EUI brightenings with longer lifetimes are observed up to Ne viii temperatures (0.6 MK). (iii) All of the events are detectable in O vi (0.3 MK), and the two longer-lived events are also detected in other transition region (TR) lines. (iv) In one case, we observe two peaks in the intensity light curve of the TR lines that are separated by 2.7 min for C iii and 1.2 min for O vi. The Ne viii intensity shows a single peak between the two peak times of the TR line intensity. Spectral data from SPICE allow us to follow the thermal properties of EUI brightenings. Our results indicate that at least some EUI brightenings barely reach coronal temperatures. **23 February 2021, 12-13 September 2021**
Solar Orbiter nugget #6 **2023** https://www.cosmos.esa.int/web/solar-orbiter/science-nuggets/euv-brightenings-using-eui-and-spice-on-board-solar-orbiter
23-Feb-2021, 12/13-Sep-2021

The Kinematic Evolution of Erupting Structures in Confined Solar Flares

Z. W. **Huang**1,2, X. Cheng1,2,3, and M. D. Ding1,2
2020 ApJL 904 L2
https://doi.org/10.3847/2041-8213/abc5b0
https://arxiv.org/pdf/2011.11929.pdf
In this Letter, we study the kinematic properties of ascending hot blobs associated with confined flares. Taking advantage of high-cadence extreme-ultraviolet images provided by the Atmospheric Imaging Assembly on board the Solar Dynamics Observatory, we find that for the 26 events selected here, the hot blobs are first impulsively accelerated outward, but then quickly slow down to motionlessness. Their velocity evolution is basically synchronous with the temporal variation of the Geostationary Operational Environmental Satellite soft X-ray flux of the associated flares, except that the velocity peak precedes the soft X-ray peak by minutes. Moreover, the duration of the acceleration phase of the erupting blobs is moderately correlated with that of the flare rise phase. For nine of the 26 cases, the erupting blobs even appear minutes prior to the onset of the associated flares. Our results show that a fraction of confined flares

also involve the eruption of a magnetic flux rope, which sometimes is formed and heated prior to the flare onset. We suggest that the initiation and development of these confined flares are similar to that of eruptive ones, and the main difference may lie in the background field constraint, which is stronger for the former than for the latter.

Comparison of Enhanced Absorption in He I 10830 Å in Observations and Modeling During the Early Phase of a Solar Flare

Nengyi **Huang**, Viacheslav M. Sadykov, Yan Xu, Ju Jing, Haimin Wang
ApJL **897** L6 **2020**
https://arxiv.org/pdf/2006.10218.pdf
https://sci-hub.tw/10.3847/2041-8213/ab9b7a
The \ion{He}{1} 10830~Å triplet is a very informative indicator of chromospheric activities as the helium is the second most abundant element in the solar atmosphere. Taking advantage of the high resolution of the 1.6 m Goode Solar Telescope (GST) at Big Bear Solar Observatory (BBSO), previous observations have shown clear evidence of the enhanced absorption, instead of typically-observed emission, for two M-class flares. In this study, we analyze the evolution of the \ion{He}{1} 10830~Å emission in numerical models and compare it with observations. The models represent the RADYN simulation results obtained from the F-CHROMA database. We consider the models with the injected electron spectra parameters close to observational estimates for the **2013-August-17** flare event (δ=8, Ec={15,20}keV, F={1×1011,3×1011}erg·cm−2) in detail, as well as other available models. The modeling results agree well with observations, in the sense of both the maximum intensity decrease (-17.1\%, compared to the observed value of -13.7\%) and the trend of temporal variation (initial absorption phase followed by the emission). All models demonstrate the increased number densities and decreased ratio of the upper and lower level populations of \ion{He}{1} 10830~Å transition in the initial phase, which enhances the opacity and forms an absorption feature. Models suggest that the temperatures and free electron densities at heights of 1.3-1.5\,Mm should be larger than ∼104\,K and 6×1011\,cm−3 thresholds for the line to start being in emission.

Spectral Diagnosis of Mg ii and Hα Lines during the Initial Stage of an M6.5 Solar Flare

Nengyi **Huang**, Yan Xu, Viacheslav M Sadykov, Ju Jing, and Haimin Wang
2019 ApJL 878 L15
https://iopscience.iop.org/article/10.3847/2041-8213/ab2330/pdf
Recent studies have shown special spectral properties during the initial stage of flare emissions, such as the enhanced absorption in He i 10830 Å line and a strong redshift in Hα. Using the high-resolution imaging spectroscopic data obtained by the Interface Region Imaging Spectrograph(IRIS), we investigate the Mg ii emission lines during an M6.5 flare (**SOL2015-06-22T18**:23), which was well covered by the joint observation of IRIS and the Goode Solar Telescope at Big Bear Solar Observatory. On the leading edge of the propagating ribbon, Mg ii lines are characterized by blue-wing enhancement and strong broadening. On the other hand, redshifts in Mg ii and Hα are found in the trailing areas of the flare ribbons. Numerical modeling, produced by combining RADYN and RH, suggests that the Mg ii line broadening is possibly caused by unresolved turbulence with velocities about 10 to 30 km s−1. The enhanced blue wing is likely due to a decrease of temperature and an increase of electron density, as consequences of electron precipitation. Based on the observations and simulation results, we discuss the possible response of the lower atmosphere to the electron precipitation, in terms of the evolution of temperature, electron density, and turbulence velocities.

Deep Learning Based Solar Flare Forecasting Model.
I. Results for Line-of-sight Magnetograms

Xin **Huang**1, Huaning Wang1,2, Long Xu1, Jinfu Liu3, Rong Li4, and Xinghua Dai1
2018 ApJ 856 7
http://iopscience.iop.org/article/10.3847/1538-4357/aaae00/pdf
Solar flares originate from the release of the energy stored in the magnetic field of solar active regions, the triggering mechanism for these flares, however, remains unknown. For this reason, the conventional solar flare forecast is essentially based on the statistic relationship between solar flares and measures extracted from observational data. In the current work, the deep learning method is applied to set up the solar flare forecasting model, in which forecasting patterns can be learned from line-of-sight magnetograms of solar active regions. In order to obtain a large amount of observational data to train the forecasting model and test its performance, a data set is created from line-of-sight magnetogarms of active regions observed by SOHO/MDI and SDO/HMI from 1996 April to 2015 October and corresponding soft X-ray solar flares observed by GOES. The testing results of the forecasting model indicate that (1) the forecasting patterns can be automatically reached with the MDI data and they can also be applied to the HMI data; furthermore, these forecasting patterns are robust to the noise in the observational data; (2) the performance of the deep learning forecasting model is not sensitive to the given forecasting periods (6, 12, 24, or 48 hr); (3) the performance of the proposed forecasting model is comparable to that of the state-of-the-art flare forecasting models, even if the duration of the total magnetograms continuously spans 19.5 years. Case analyses demonstrate that the deep learning based solar flare forecasting model pays attention to areas with the magnetic polarity-inversion line or the strong magnetic field in magnetograms of active regions. **2005 January 15, 2011 February 13,**

Solar Flare Loops: Observations and Interpretations **Book**

Guangli **Huang** • Victor F. Melnikov Haisheng Ji • Zongjun Ning
Science Press, Beijing and Springer Nature Singapore Pte Ltd. **2018**
https://link.springer.com/content/pdf/bfm%3A978-981-10-2869-4%2F1.pdf

Relationship between Intensity of White-light Flares and Proton Flux of Solar Energetic Particles

Nengyi **Huang**1,2, Yan Xu1,2, and Haimin Wang
2018 Res. Notes AAS 2 7
http://iopscience.iop.org/article/10.3847/2515-5172/aaa602
https://arxiv.org/pdf/1801.04316.pdf

In summary, our preliminary results show that most ($>83\%$) of WLFs and SEP events have no correspondence. Solar energetic particles (SEPs), including protons and heavy ions, are believed to be accelerated either by CME shock or by magnetic reconnection. The latter also produces solar flares, in which the white light flares (WLFs) are among the most energetic ones. Magnetic reconnections occur in the corona and the accelerated particles propagate both downward and upward along the magnetic loops. The former is the source of flare emission and the latter is thought to be SEPs. Therefore, a comparison between flare emission and SEP events provides valuable constraint in determining the acceleration site of SEPs. We collect 43 SEP events, observed from 2010 to 2017, and investigate their correlation with WL emission and SXR flus, observed by SDO/HMI and GOES, respectively. Our preliminary results show: 1) Among 47 SEP events, 39 of which do not have detectable flare emissions in white light and SXR. 2) Most strong WLFs are not associated with SEPs. 3) No clear correlation is found between the proton flux and the equivalent area, a quantity that measures the magnitude of WLF emission. A straightforward speculation is that the acceleration process could be different for SEPs and the energetic electrons powering WLFs in the events analyzed.
4.8. 2011, 9.8.2011, 23.01.2012, 13.03.2012, 2012 March 7 , 6.7.2012, 25-Jun 2015, 4.9.2017, 2017 September 6

Development of Turbulent Magnetic Reconnection in a Magnetic Island

Can **Huang**1,2, Quanming Lu1,2, Rongsheng Wang1,2, Fan Guo3, Mingyu Wu1,2, San Lu1,2, and Shui Wang1,2
2017 ApJ 835 245

In this paper, with two-dimensional particle-in-cell simulations, we report that the electron Kelvin–Helmholtz instability is unstable in the current layer associated with a large-scale magnetic island, which is formed in multiple X-line guide field reconnections. The current sheet is fragmented into many small current sheets with widths down to the order of the electron inertial length. Secondary magnetic reconnection then occurs in these fragmented current sheets, which leads to a turbulent state. The electrons are highly energized in such a process.

QUASI-PERIODIC ACCELERATION OF ELECTRONS IN THE FLARE ON 2012 JULY 19

Jing **Huang**1,2, Eduard P. Kontar3, Valery M. Nakariakov4, and Guannan Gao
2016 ApJ 831 119

Quasi-periodic pulsations (QPPs) of nonthermal emission in an M7.7 class flare on **2012 July 19** are investigated with spatially resolved observations at microwave and HXR bands and with spectral observations at decimetric, metric waves. Microwave emission at 17 GHz of two footpoints, HXR emission at 20–50 keV of the north footpoint and loop top, and type III bursts at 0.7–3 GHz show prominent in-phase oscillations at 270 s. The microwave emission of the loop leg has less pulsation but stronger emission. Through the estimation of plasma density around the loop top from EUV observations, we find that the local plasma frequency would be 1.5 GHz or even higher. Thus, type III bursts at 700 MHz originate above the loop top. Quasi-periodic acceleration or injection of energetic electrons is proposed to dominate these in-phase QPPs of nonthermal emission from footpoints, loop top, and above. In the overlying region, drifting pulsations (DPS) at 200–600 MHz oscillate at a distinct period (200 s). Its global structure drifts toward lower frequency, which is closely related to upward plasmoids observed simultaneously from EUV emission. Hence, nonthermal emission from overlying plasmoids and underlying flaring loops show different oscillating periods. Two individual systems of quasi-periodic acceleration of electrons are proposed to coincide in the bi-direction outflows from the reconnection region.

Explosive events in active region observed by IRIS and SST/CRISP

Z. **Huang**, M. S. Madjarska, E. M. Scullion, L.-D. Xia, J. G. Doyle, T. Ray

MNRAS **2016**
https://arxiv.org/pdf/1609.07698v1.pdf
Transition-region explosive events (EEs) are characterized by non-Gaussian line profiles with enhanced wings at Doppler velocities of 50-150 km s-1. They are believed to be the signature of solar phenomena that are one of the main contributors to coronal heating. The aim of this study is to investigate the link of EEs to dynamic phenomena in the transition region and chromosphere in an active region. We analyze observations simultaneously taken by the Interface Region Imaging Spectrograph (IRIS) in the Si IV 1394Å line and the slit-jaw (SJ) 1400Å images, and the Swedish 1-m Solar Telescope (SST) in the H α line. In total 24 events were found. They are associated with small-scale loop brightenings in SJ 1400Å images. Only four events show a counterpart in the H α -35 km s-1 and H α +35 km s-1 images. Two of them represent brightenings in the conjunction region of several loops that are also related to a bright region (granular lane) in the H α -35km s-1 and H α +35 km s-1 images. Sixteen are general loop brightenings that do not show any discernible response in the H α images. Six EEs appear as propagating loop brightenings, from which two are associated with dark jet-like features clearly seen in the H α -35 km s-1 images. We found that chromospheric events with jet-like appearance seen in the wings of the H α line can trigger EEs in the transition region and in this case the IRIS Si IV 1394Å line profiles are seeded with absorption components resulting from Fe II and Ni II. Our study indicates that EEs occurring in active regions have mostly upper-chromosphere/transition-region origin. We suggest that magnetic reconnection resulting from the braidings of small-scale transition region loops is one of the possible mechanisms of energy release that are responsible for the EEs reported in this paper. **2014 June 10**

The Energetics of White-light Flares Observed by SDO/HMI and RHESSI

Nengyi **Huang**, Yan Xu, Haimin Wang
Research in Astronomy and Astrophysics **16** 177 **2016**
http://arxiv.org/pdf/1608.06015v1.pdf
White-light (WL) flares have been observed and studied more than a century since the first discovery. However, some fundamental physics behind the brilliant emission remains highly controversial. One of the important facts in addressing the flare energetics is the spatialtemporal correlation between the white-light emission and the hard X-ray radiation, presumably suggesting that the energetic electrons are the energy sources. In this study, we present a statistical analysis of **25 strong flares** (?greater than or equal to M5) observed simultaneously by the Helioseismic and Magnetic Imager (HMI) on board the Solar Dynamics Observatory (SDO) and the Reuven Ramaty High Energy Solar Spectroscopic Imager (RHESSI). Among these events, WL emission was detected by SDO/HMI in 13 flares, associated with HXR emission. To quantitatively describe the strength of WL emission, equivalent area (EA) is defined as the integrated contrast enhancement over the entire flaring area. Our results show that the equivalent area is inversely proportional to the HXR power index, indicating that stronger WL emission tends to be associated with larger population of high energy electrons. However, no obvious correlation is found between WL emission and flux of non-thermal electrons at 50 keV. For the other group of 13 flares without detectable WL emission, the HXR spectra are softer (larger power index) than those flares with WL emission, especially for the X-class flares in this group. **2011.02.13 , 2011.02.15, 2011.03.09 , 2011.07.30, 2011.09.06, 2011.09.08, 2011.09.25 , 2012.03.09 , 2012.05.10 , 2012.07.04, 2012.07.05, 2012.07.12 , 2013.11.10, 2014.01.01 , 2014.01.07, 2014.03.29, 2014.04.18 , 2014.10.22, 2014.10.24, 2014.10.25, 2014.12.04, 2014.12.18, 2015.03.10, 2015.03.11**
Table 1 Properties White-Light Flares
Table 2 Properties of Flares without White-Light emission

Explosive events on subarcsecond scale in IRIS observations: a case study

Zhenghua **Huang**, Maria S. Madjarska, Lidong Xia, J. G. Doyle, Klaus Galsgaard, Hui Fu
ApJ **797** 88 **2014**
http://star.arm.ac.uk/preprints/2014/659.pdf
We present study of a typical explosive event (EE) at subarcsecond scale witnessed by strong non-Gaussian profiles with blue- and red-shifted emission of up to 150 km/s seen in the transition-region Si iv 1402.8 Å, and the chromospheric Mg ii k 2796.4 Å and C ii 1334.5 Å observed by the Interface Region Imaging Spectrograph (IRIS) at unprecedented spatial and spectral resolution. For the first time an EE is found to be associated with very small-scale (∼120 km wide) plasma ejection followed by retraction in the chromosphere. These small-scale jets originate from a compact bright-point-like structure of ∼1.5" size as seen in the IRIS 1330 Å images. SDO/AIA and SDO/HMI co-observations show that the EE lies in the footpoint of a complex loop-like brightening system. The EE is detected in the higher temperature channels of AIA 171 Å, 193 Å, and 131 Å suggesting that it reaches a higher temperature of log T = 5.36 ? 0.06 (K). Brightenings observed in the AIA channels with durations 90?120 s are probably caused by the plasma ejections seen in the chromosphere. The wings of the C ii line behave in a similar manner to the Si iv's, indicating close formation temperatures, while the Mg ii k wings show additional Doppler-shifted emission. Magnetic convergence or emergence followed by cancellation at a rate of 5 ?10^14 Mx/s is associated with the EE region. The combined changes of the locations and the flux of different magnetic patches suggest that magnetic reconnection must have taken place. Our results challenge several theories put forward in the past to explain non-Gaussian line profiles, i.e., EEs. Our case

study on its own, however, cannot reject these theories, thus further in-depth studies on the phenomena producing EEs are required. **2013 October 4**

Quasi-Periodic Pulsations with Varying Period in Multi-Wavelength Observations of an X-class Flare

Jing **Huang**1, Baolin Tan1, Yin Zhang1, Marian Karlický2, and Hana Mészárosová
2014 ApJ 791 44

This work presents an interesting phenomenon of the period variation in quasi-periodic pulsations (QPPs) observed during the impulsive phase of a coronal mass ejection-related X1.1 class flare on **2012 July 6**. The period of QPPs was changed from 21 s at soft X-rays (SXR) to 22-23 s at microwaves, to ~24 s at extreme ultraviolet emissions (EUV), and to 27-32 s at metric-decimetric waves. The microwave, EUV, and SXR QPPs, emitted from flare loops of different heights, were oscillating in phase. Fast kink mode oscillations were proposed to be the modulation mechanism, which may exist in a wide region in the solar atmosphere from the chromosphere to the upper corona or even to the interplanetary space. Changed parameters of flare loops through the solar atmosphere could result in the varying period of QPPs at different wavelengths. The first appearing microwave QPPs and quasi-periodic metric-decimetric type III bursts were generated by energetic electrons. This may imply that particle acceleration or magnetic reconnection were located between these two non-thermal emission sources. Thermal QPPs (in SXR and EUV emissions) occurred later than the nonthermal ones, which would suggest a some time for plasma heating or energy dissipation in flare loops during burst processes. At the beginning of flare, a sudden collapse and expansion of two separated flare loop structures occurred simultaneously with the multi-wavelength QPPs. An implosion in the corona, including both collapse and expansion of flare loops, could be a trigger of loop oscillations in a very large region in the solar atmosphere.

Energetic Electron Propagation in the Decay Phase of Non-thermal Flare Emission

Jing **Huang**1, Yihua Yan1, and Yuri T. Tsap
E-print, June **2014; 2014** ApJ 787 123

On the basis of the trap-plus-precipitation model, the peculiarities of non-thermal emission in the decay phase of solar flares have been considered. The calculation formulas for the escape rate of trapped electrons into the loss cone in terms of time profiles of hard X-ray (HXR) and microwave (MW) emission have been obtained. It has been found that the evolution of the spectral indices of non-thermal emission depend on the regimes of the pitch angle diffusion of trapped particles into the loss cone. The properties of non-thermal electrons related to the HXR and MW emission of the solar flare on **2004 November 3** are studied with Nobeyama Radioheliograph, Nobeyama Radio Polarimeters, RHESSI, and Geostationary Operational Environmental Satellite observations. The spectral indices of non-thermal electrons related to MW and HXR emission remained constant or decreased, while the MW escape rate as distinguished from that of the HXRs increased. This may be associated with different diffusion regimes of trapped electrons into the loss cone. New arguments in favor of an important role of the superstrong diffusion for high-energy electrons in flare coronal loops have been obtained.

H α spectroscopy and multi-wavelength imaging of a solar flare caused by filament eruption

Z. **Huang**, M. S. Madjarska, K. Koleva, J. G. Doyle, P. Duchlev, M. Dechev, and K. Reardon
E-print, May **2014**; A&A 566, A148, **2014**
http://star.arm.ac.uk/preprints/2014/652.pdf

We study a sequence of eruptive events including filament eruption, a GOES C4.3 flare and a coronal mass ejection. We aim to identify the possible trigger(s) and precursor(s) of the filament destabilisation; investigate flare kernel characteristics; flare ribbons/kernels formation and evolution; study the interrelation of the filament-eruption/flare/coronal-mass-ejection phenomena as part of the integral active-region magnetic field configuration; determine H α line profile evolution during the eruptive phenomena. Multi-instrument observations are analysed including H α line profiles, speckle images at H α -0.8 \AA\ and H$ α +0.8 \AA\ from IBIS at DST/NSO, EUV images and magnetograms from the SDO, coronagraph images from STEREO and the X-ray flux observations from FERMI and GOES. We establish that the filament destabilisation and eruption are the main trigger for the flaring activity. A surge-like event with a circular ribbon in one of the filament footpoints is determined as the possible trigger of the

filament destabilisation. Plasma draining in this footpoint is identified as the precursor for the filament eruption. A magnetic flux emergence prior to the filament destabilisation followed by a high rate of flux cancelation of 1.34\times1016 Mx s-1 is found during the flare activity. The flare X-ray lightcurves reveal three phases that are found to be associated with three different ribbons occurring consecutively. A kernel from each ribbon is selected and analysed. The kernel lightcurves and H α line profiles reveal that the emission increase in the line centre is stronger than that in the line wings. A delay of around 5-6 mins is found between the increase in the line centre and the occurrence of red asymmetry. Only red asymmetry is observed in the ribbons during the impulsive phases. Blue asymmetry is only associated with the dynamic filament. **11 Nov 2010**

Improving the performance of solar flare prediction using active longitudes information

X. **Huang**1, L. Zhang1,2, H. Wang1 and L. Li

A&A 549, A127 (**2013**)

Context. Solar flare prediction models normally depend on properties of active regions, such as sunspot area, McIntosh classifications, Mount Wilson classifications, and various measures of the magnetic field. Nevertheless, the positional information of active regions has not been used.

Aims. We define a metric, DARAL (distance between active regions and predicted active longitudes), to depict the positional relationship between active regions and predicted active longitudes and add DARAL to our solar flare prediction model to improve its performance.

Methods. Combining DARAL with other solar magnetic field parameters, we build a solar flare prediction model with the instance-based learning method, which is a simple and effective algorithm in machine learning. We extracted 70 078 active region instances from the Solar and Heliospheric Observatory (SOHO)/Michelson Doppler Imager (MDI) magnetograms containing 1055 National Oceanic and Atmospheric Administration (NOAA) active regions within 30° of the solar disk center from 1996 to 2007 and used them to train and test the solar flare prediction model.

Results. Using four performance measures (true positive rate, true negative rate, true skill statistic, and Heidke skill score), we compare performances of the solar flare prediction model with and without DARAL. True positive rate, true negative rate, true skill statistic, and Heidke skill score increase by 6.7% ± 1.3%, 4.2% ± 0.5%, 10.8% ± 1.4% and 8.7% ± 1.0%, respectively.

Conclusions. The comparison indicates that the metric DARAL is beneficial to performances of the solar flare prediction model.

CO-ANALYSIS OF SOLAR MICROWAVE AND HARD X-RAY SPECTRAL EVOLUTIONS. II. IN THREE SOURCES OF A FLARING LOOP

Guangli **Huang** and Jianping Li

2011 ApJ 740 46

Based on the spatially resolvable data of the Reuven Ramaty High Energy Solar Spectroscopic Imager (RHESSI) and Nobeyama Radio Heliograph (NoRH), co-analysis of solar hard X-ray and microwave spectral evolution is performed in three separate sources located in one looptop (LT) and two footpoints (FPs) of a huge flaring loop in the **2003 October 24** flare. The RHESSI image spectral evolution in 10-100 keV is always fitted by the well-known soft-hard-soft (SHS) pattern in the three sources. When the total energy is divided into four intervals similar to the Yohkoh/Hard X-ray Telescope, i.e., 12.5-32.5 keV, 32.5-52.5 keV, 52.5-72.5 keV, and 72.5-97.5 keV, the SHS pattern in lower energies is converted gradually to the hard-soft-hard (HSH) pattern in higher energies in all three sources. However, the break energy in the LT and the northeast FP (~32.5 keV) is evidently smaller than that in the southwest FP (~72.5 keV). Regarding microwave spectral evolution of the NoRH data, the well-known soft-hard-harder pattern appeared in the southwest FP, while the HSH pattern coexisted in the LT and the northeast FP. The different features of the hard X-ray and microwave spectral evolutions in the three sources may be explained by the loop-loop interaction with another huge loop in the LT and with a compact loop in the northeast FP, where the trapping effect is much stronger than that in the southwest FP. The comparison between the LT and FP spectral indices suggests that the radiation mechanism of X-rays may be quite different in different energy intervals and sources. The calculated electron spectral indices from the predicted mechanisms of X-rays gradually become closer to those from the microwave data with increasing X-ray energies.

Short-Term Solar Flare Prediction Using Predictor Teams

Xin **Huang** · Daren Yu · Qinghua Hu · Huaning Wang · Yanmei Cui

Solar Phys (**2010**) 263: 175–184

A short-term solar flare prediction model is built using predictor teams rather than an individual set of predictors. The information provided by the set of predictors could be redundant. So it is necessary to generate subsets of predictors which can keep the information constant. These subsets are called predictor teams. In the framework of rough set theory, predictor

teams are constructed from sequences of the maximum horizontal gradient, the length of neutral line and the number of singular points extracted from SOHO/MDI longitudinal magnetograms. Because of the instability of the decision tree algorithm, prediction models generated by the C4.5 decision tree for different predictor teams are diverse. The flaring sample, which is incorrectly predicted by one model, can be correctly forecasted by another one. So these base prediction models are used to construct an ensemble prediction model of solar flares by the majority voting rule. The experimental results show that the predictor team can keep the distinguishability of the original set, and the ensemble prediction model can obtain better performance than the model based on the individual set of predictors.

Simultaneous observations of second and sub-second time structures in H α , radio and hard X-ray data due to the periodical particle acceleration and MHD waves in the November 1, 2004 flare

Huang Guangli and Ji Haisheng
Astrophysics and Space Science, Volume 312, Numbers 1-2, 127-138, **2007**.
http://www.springerlink.com/content/u512lw1tp0160813/fulltext.pdf

Pitfalls of Periodograms: The Nonstationarity Bias in the Analysis of Quasiperiodic Oscillations

Moritz **Hübner**1,2, Daniela Huppenkothen3, Paul D. Lasky1,2, and Andrew R. Inglis4,5
2022 ApJS 259 32
https://iopscience.iop.org/article/10.3847/1538-4365/ac49ec/pdf
Quasiperiodic oscillations (QPOs) are an important key to understand the dynamic behavior of astrophysical objects during transient events like gamma-ray bursts, solar flares, and magnetar flares. Searches for QPOs often use the periodogram of the time series and perform spectral density estimation using a Whittle likelihood function. However, the Whittle likelihood is only valid if the time series is stationary since the frequency bins are otherwise not statistically independent. We show that if time series are nonstationary, the significance of QPOs can be highly overestimated and estimates of the central frequencies and QPO widths can be overconstrained. The effect occurs if the QPO is only present for a fraction of the time series and the noise level is varying throughout the time series. This can occur, for example, if background noise from before or after the transient is included in the time series or if the low-frequency noise profile varies strongly over the time series. Thus, we highlight the importance of careful segment selection prior to the analysis. We confirm the presence of this bias in previously reported results from solar flare data and show that significance can be highly overstated. Finally, we provide some suggestions that help identify whether an analysis is affected by this bias. **2013 May 12**

HOPE (hot onset precursor event) during high activity

Hugh **HUDSON**, Alphonse STERLING
RHESSI Nuggets #475 **2024**
https://heliowiki.smce.nasa.gov/wiki/index.php/HOPE_during_high_activity
The HOPE signature appears clearly even in extreme conditions; each impulsive event has a precursor hot phase. **2024-05-10**

An impulsive geomagnetic effect from an early-impulsive flare

Hugh S. **Hudson**, Edward. W. Cliver, Lyndsay Fletcher, Declan A. Diver, Peter T. Gallagher, Ying Li, Christopher M.J. Osborne, Craig Stark, Yang Su
MNRAS Volume 532, Issue 3, August **2024**, Pages 3120–3125, **2024**
https://arxiv.org/abs/2407.09233
https://doi.org/10.1093/mnras/stae1720
https://watermark.silverchair.com/stae1720.pdf
The geomagnetic "solar flare effect" (SFE) results from excess ionization in the Earth's ionosphere, famously first detected at the time of the Carrington flare in 1859. This indirect detection of a flare constituted one of the first cases of "multimessenger astronomy," whereby solar ionizing radiation stimulates ionospheric currents. Well-observed SFEs have few-minute time scales and perturbations of >10 nT, with the greatest events reaching above 100 nT. In previously reported cases the SFE time profiles tend to resemble those of solar soft X-ray emission, which ionizes the D-region; there is also a less-well-studied contribution from Lyman-alpha. We report here a specific case, from flare SOL**2024-03-10** (M7.4), in which an impulsive SFE deviated from this pattern. This flare contained an "early impulsive" component of exceptionally hard radiation, extending up to gamma-ray energies above 1 MeV, distinctly before the bulk of the flare soft X-ray emission. We can characterize the spectral distribution of this early-impulsive component in

detail, thanks to the modern extensive wavelength coverage. A more typical gradual SFE occurred during the flare's main phase. We suggest that events of this type warrant exploration of the solar physics in the "impulse response" limit of very short time scales. **2024-03-10**

Anticipating Solar Flares

Hugh S. **Hudson**
Solar Phys. **2024**
https://arxiv.org/pdf/2407.04567
Solar flares commonly have a hot onset precursor event" (HOPE), detectable from soft X-ray observations. Detecting this requires subtraction of pre-flare fluxes from the non-flaring Sun prior to the event, fitting an isothermal emission model to the flare excess fluxes by comparing the GOES passbands at 1-8 A and 0.5-4 A, and plotting the timewise evolution of the flare emission in a diagram of temperature \textit{vs} emission measure. The HOPE then appears as an initial "horizontal branch" in this diagram. It precedes the non-thermal impulsive phase of the flare and thus the flare peak in soft X-rays as well. We use this property to define a "flare anticipation index" (FAI), which can serve as an alert for observational programs aimed at solar flares based on near-real-time soft X-ray observations. This FAI gives lead times of a few minutes and produces very few false positive alerts even for flare brightenings too weak to merit NOAA classification. **2022-04-20, 2024-01-02-05**

Is there HOPE for Hyder flares?

Hugh **HUDSON**.
RHESSI Science Nuggets #468 **2024**
https://sprg.ssl.berkeley.edu/~tohban/wiki/index.php/Is_there_HOPE_for_Hyder_flares...
Filament eruptions/Hyder flares/disparitions brusques may all show Hot Onset Precursor Events
2014-11-01, *2022-05-10*

The greatest GOES soft X-ray flares: Saturation and recalibration over two Hale cycles

Hugh **Hudson**, Ed Cliver, Stephen White, Janet Machol, Courtney Peck, Kim Tolbert, Rodney Viereck, Dominic Zarro
Solar Phys. **299**, 39 (**2024**)
https://arxiv.org/pdf/2310.11457.pdf
https://doi.org/10.1007/s11207-024-02287-x
The solar soft X-ray observations from the GOES satellites provide one of the best quantitative records of solar activity, with nearly continuous flare records since 1975. We present a uniform analysis of the entire time series for 1975 to 2022 at NOAA class C1 level or above, to characterize the occurrence distribution function (ODF) of the flares observed in the 1-8 A spectral band. The analysis includes estimations of the peak fluxes of the 12 flares that saturated the 1-8 A time series. Our new estimates include NOAA's recently established correction factor (1.43) to adjust the GOES-1 through GOES-15 data covering 1975-2016. For each of the 12 saturated events we have made new estimates of peak fluxes based on fits to the rise and fall of the flare time profile, and have validated our extrapolation schemes by comparing with artificially truncated but unsaturated X10-class events. SOL**2003-11-04** now has a peak flux of 4.32e-3 W/m^2. This corresponds to X43 on the new scale, or X30 on the old scale. We provide a list in the Appendix for peak fluxes of all 38 events above 10^-3 W/m^2, the GOES X10 level, including the 12 saturated events. The full list now gives us a first complete sample from which we obtain an occurrence distribution function (ODF) for peak energy flux , often represented as a power law dF/dE ~ E^-alpha, for which we find alpha = 1.973 +- 0.014 in the range M1 to X3. The power-law description fails at the high end, requiring a downward break in the ODF above the X10 level. We give a tapered powerlaw description of the resulting CCDF (complementary cumulative distribution function) and extrapolate it into the domain of "superflares," i.e. flares with bolometric energies > 10^33 erg. Extrapolation of this fit provides estimates of 100-yr and 1000-yr GOES peak fluxes that agree reasonably well with other such estimates using different data sets and methodology. **1991-01-25, 2005-09-07**
Table 1. Test Events: Ten >X10 events
Table 2. Saturated Events
Table 7. The greatest GOES events (original)
Table 8. The greatest GOES events (augmentation)
RHESSI Science Nuggets #456 **2023**
https://sprg.ssl.berkeley.edu/~tohban/wiki/index.php/The_Greatest_GOES_Flares

A Glasgow geomagnetic observation of a solar flare

Hugh **HUDSON**, John MALONE-LEIGH, Graham WOAN, and Chris OSBORNE
RHESSI nugget #446 **2023**
https://sprg.ssl.berkeley.edu/~tohban/wiki/index.php/A_Glasgow_geomagnetic_observation_of_a_solar_flare
1859-09-01, 2022-05-10

A slow HOPE with microwave context

H. **Hudson**
RHESSI Science Nuggets #441 Feb **2023**
https://sprg.ssl.berkeley.edu/~tohban/wiki/index.php/A_slow_HOPE_with_microwave_context
A new microwave facility at Chashan Observatory, and a prototypical Hot Onset Precursor Event.
2022-04-20

Search for a Flare Anticipation Index (FAI)

Hugh **HUDSON**, Jim McTIERNAN
RHESSI Science Nuggets #460 **2023**
https://sprg.ssl.berkeley.edu/~tohban/wiki/index.php/Search_for_a_Flare_Anticipation_Index_(FAI)
To quantify the microwave and soft X-ray signatures of flare precursor activity, we have devised "flare anticipation indices" for soft X-ray and microwave data with some success. This clearly establishes the possibility of a joint FAI development, using both of these but also others of the signatures listed above, to establish a robust (and infallible?) few-minute FAI capability. Now some hard work is necessary to refine and improve on these findings. Also, it should go without saying, we need to figure out how these various precursors relate physically to their flares... it is certainly not simply "preheating," as we perhaps used to think. **4 Sep 2017**

The largest GOES solar soft X-ray bursts: saturated events, size distribution, and recalibration over two Hale cycles.

Hudson H, Cliver EW, Tolbert K, Machol J, Peck C, White S
(2022) Sol Phys (to be submitted)

Carrington Events **Review**

Hudson H.
Annual Review of Astronomy and Astrophysics, Volume 59, pp. 445-477, **2021**
https://www.annualreviews.org/doi/pdf/10.1146/annurev-astro-112420-023324
The Carrington event in 1859, a solar flare with an associated geomagnetic storm, has served as a prototype of possible superflare occurrence on the Sun. Recent geophysical (14C signatures in tree rings) and precise time-series photometry [the bolometric total solar irradiance (TSI) for the Sun, and the broadband photometry from Kepler and Transiting Exoplanet Survey Satellite, for the stars] have broadened our perspective on extreme events and the threats that they pose for Earth and for Earth-like exoplanets. This review assesses the mutual solar and/or stellar lessons learned and the status of our theoretical understanding of the new data, both stellar and solar, as they relate to the physics of the Carrington event. The discussion includes the event's implied coronal mass ejection, its potential "solar cosmic ray" production, and the observed geomagnetic disturbances based on the multimessenger information already available in that era. Taking the Carrington event as an exemplar of the most extreme solar event, and in the context of our rich modern knowledge of solar flare and/or coronal mass ejection events, we discuss the aspects of these processes that might be relevant to activity on solar-type stars, and in particular their superflares. The Carrington flare of 1859, though powerful, did not significantly exceed the magnitudes of the greatest events observed in the modern era. Stellar "superflare" events on solar-type stars may share common paradigms, and also suggest the possibility of a more extreme solar event at some time in the future. We benefit from comparing the better-known microphysics of solar flares and coronal mass ejections with the diversity of related stellar phenomena.

The Jakimiec Diagnostic Diagram

Hudson H.
RHESSI Nuggets #421 **2021**
https://sprg.ssl.berkeley.edu/~tohban/wiki/index.php/The_Jakimiec_Diagnostic_Diagram
The soft X-ray brightness of a solar flare has come to define flare occurrence in many cases. We have estimates of this brightness from 1975 via the GOES/XRS measurements, and in limited for earlier than that from SOLRAD. These basic data give us isothermal fits for the temperature and emission measure of the hot loops that appear in the corona when a flare happens. Thus we have two simple observable global parameters as functions of time from the basic measurements. One can represent these quite nicely as simple time series, but a diagnostic diagram that follows their joint evolution can give hints about the physics involved. This idea was elaborated first by Jerzy Jakimiec in Ref. [1], and here we describe how useful it is even today, some three decades later.

The great complexity shown by images of solar flares reveal all kinds of dynamic developments, but the energy the flare pumps into the hot coronal loops seems to have relatively simple patterns. These include a steady temperature at the very onset, a sharp increase during the hard X-ray emission (as described in many previous Nuggets, such as No. 403 recently, and then the complex clockwise pattern during the main phase of the flare before its systematic cooling patterns begin.) **2017-09-06**

Do Hot Onsets Predict Flare Magnitudes?

Hudson H. +
RHESSI Nuggets #415 **2021**
https://sprg.ssl.berkeley.edu/~tohban/wiki/index.php/Do_Hot_Onsets_Predict_Flare_Magnitudes%3F

Hot X-ray onsets of solar flares

Hugh S **Hudson**, Paulo J A Simões, Lyndsay Fletcher, Laura A Hayes, Iain G Hannah
Monthly Notices of the Royal Astronomical Society, Volume 501, Issue 1, February **2021**, Pages 1273–1281,
https://doi.org/10.1093/mnras/staa3664
https://arxiv.org/pdf/2007.05310.pdf
https://watermark.silverchair.com/staa3664.pdf
The study of the localized plasma conditions before the impulsive phase of a solar flare can help us understand the physical processes that occur leading up to the main flare energy release. Here, we present evidence of a hot X-ray 'onset' interval of enhanced isothermal plasma temperatures in the range of 10–15 MK over a period of time prior to the flare's impulsive phase. This 'hot onset' interval occurs during the initial soft X-ray increase and definitely before any detectable hard X-ray emission. The isothermal temperatures, estimated by the Geostationary Operational Environmental Satellite X-ray sensor, and confirmed with data from the Reuven Ramaty High Energy Solar Spectroscopic Imager, show no signs of gradual increase, and the 'hot onset' phenomenon occurs regardless of flare classification or configuration. In a small sample of four representative flare events, we tentatively identify this early hot onset soft X-ray emission to occur within footpoint and low-lying loop regions, rather than in coronal structures, based on images from the Atmospheric Imaging Assembly. We confirm this via limb occultation of a flaring region. These hot X-ray onsets appear before there is evidence of collisional heating by non-thermal electrons, and hence challenge the standard modelling techniques. **5 Nov 2010, 14 Feb 2011, 14 May 2012, 7 Jan 2014**
RHESSI Nuggets #392 Oct **2020** https://sprg.ssl.berkeley.edu/~tohban/wiki/index.php/Hot_Flare_Onsets
RHESSI Nuggets #415 **2021** **Do Hot Onsets Predict Flare Magnitudes?**
https://sprg.ssl.berkeley.edu/~tohban/wiki/index.php/Do_Hot_Onsets_Predict_Flare_Magnitudes%3F
2005-01-20

Grand Archive of Flare and CME Cartoons

Hugh S. **Hudson**
RHESSI Science Nuggets #389 Oct **2020** http://www.astro.gla.ac.uk/cartoons/thumbs.html

Solar Flare Build-Up and Release

Hugh S. **Hudson**
Solar Physics volume 295, Article number: 132 (**2020**)
https://doi.org/10.1007/s11207-020-01698-w
https://link.springer.com/content/pdf/10.1007/s11207-020-01698-w.pdf
Flares and coronal mass ejections should follow a pattern of build-up and release, with the build-up phase understood as the gradual addition of stress to the coronal magnetic field. Recently Hudson (Mon. Not. Roy. Astron. Soc. 491, 4435, 2020) presented observational evidence for this pattern in two isolated active regions from 1997 and 2006, finding a correlation between the waiting time after the event, and the event magnitude. In this article we systematically search for related evidence in the largest 14 active regions of Solar Cycle 24, chosen as those with peak sunspot area exceeding 1000 millionths of the solar hemisphere (MSH). The smallest of these regions, NOAA 12673, produced the exceptional flares SOL2017-09-06 and SOL2017-09-10. None of these regions showed significant correlations of waiting times and flare magnitudes, although two hinted at such an interval-size relationship. Correlations thus appear to be non-existent or intermittent, depending on presently unknown conditions. **2017-09-06, 2017-09-10**
Table 1 Active regions: Time spans (indicated as year-month-day-time) and flare occurrences

The "Last Best" Flares

Hugh **Hudson**, Ed Cliver, and Brian Dennis
RHESSI Science Nuggets #358 Oct **2019**
http://sprg.ssl.berkeley.edu/~tohban/wiki/index.php/The_"Last_Best"_Flares

This Nugget describes one of the peculiar properties of flare occurrence: often very powerful solar flares occur at the ends of solar cycles. We call these "last best" flares and list four of them, one per well-observed solar cycle, in the table

A correlation in the waiting-time distributions of solar flares

Hugh S. **Hudson**

MNRAS Volume 491, Issue 3, January **2020**, Pages 4435–4441

https://arxiv.org/pdf/1908.08749.pdf

sci-hub.se/10.1093/mnras/stz3121

In a limited sample of isolated solar active regions, we find that the waiting times between flares may correlate well with flare magnitudes as determined by the Geostationary Operational Environmental Satellites (GOES) soft X-ray fluxes. A 'build-up and release' (BUR) scenario for magnetic energy storage in the solar corona suggests the existence of such a relationship, relating the slowly varying subphotospheric energy sources to the sudden coronal energy releases of flares and coronal mass ejections (CMEs). Substantial amounts of research effort had not previously found any obvious observational evidence for such a BUR process. This has posed a puzzle since coronal magnetic energy storage represents the consensus view of the basic flare mechanism. We have revisited the GOES soft X-ray flare statistics for any evidence of correlations, using two isolated active regions, and have found significant evidence for a 'saturation' correlation. Rather than a 'reset' form of this relaxation, in which the time before a flare correlates with its magnitude, the 'saturation' relationship results in the time after the flare showing the correlation. The observed correlation competes with the 'obscuration' effect of reduced GOES sensitivity following a strong event, by which weaker events can be under-reported systematically. This complicates the observed correlation, and we discuss several approaches to remedy this. **2006 Dec 6-16**

RHESSI Science Nuggets #363 Nov **2019**

http://sprg.ssl.berkeley.edu/~tohban/wiki/index.php/Flare_waiting_times_depend_on_their_magnitudes

Chapter 9 - High-Energy Solar Physics **Review**

H.S. **Hudson** and A.L. MacKinnon

In: ***The Sun as a Guide to Stellar Physics*** ***Book***

Eds. Oddbjørn Engvold, Jean-Claude Vial, and Andrew Skumanich

Elsevier , November **2018**

https://www.sciencedirect.com/book/9780128143346/the-sun-as-a-guide-to-stellar-physics

This chapter deals generally with the high-energy astrophysics of the Sun, specifically with solar flares and coronal mass ejections (CMEs), but it also touches on the whole range of nonthermality or departures from Maxwellian distributions in solar plasmas. Radio, x-ray, and γ-ray observations provide primary remote-sensing observations of these departures, but such signatures can be hidden by brighter thermal emissions that may not be as fundamental in physics events. The solar paradigm for flare/CME development appears to match many of the new stellar observations of similar phenomena, but the limitations of observational sensitivity mean that we have few direct observations of the expected hard x-rays and none at all of the γ-rays that could confirm this.

The Relationship between Long-Duration Gamma-Ray Flares and Solar Cosmic Rays

Hugh S. **Hudson**

Space Weather of the Heliosphere: Processes and Forecasts (eds. Claire Foullon and Olga Malandraki), IAU Symposium 335, **2017**

https://arxiv.org/pdf/1711.05583.pdf

A characteristic pattern of solar hard X-ray emission, first identified in SOL1969-03-30 by Frost & Dennis (1971), turns out to have a close association with the prolonged high-energy gamma-ray emission originally observed by Forrest et al. (1985). This identification has become clear via the observations of long-duration gamma-ray flares by the Fermi/LAT experiment, for example in the event SOL2014-09-01. The distinctive features of these events include flat hard X-ray spectra extending well above 100 keV, a characteristic pattern of time development, low-frequency gyrosynchrotron peaks, CME association, and gamma-rays identifiable with pion decay originating in GeV ions. The identification of these events with otherwise known solar structures nevertheless remains elusive, in spite of the wealth of EUV imagery available from SDO/AIA. The quandary is that these events have a clear association with SEPs in the high corona, and yet the gamma-ray production implicates the photosphere itself, despite the strong mirror force that should focus the particles \textit{away} from the Sun We discuss the morphology of these phenomena and propose a solution to this problem. **1969-03-30, 1982-06-03, 2014-09-01**

Valderrama in the 21st Century,

Hugh **Hudson**

RHESSI Nugget No. 310, Oct **2017**

A newly-describd white-light flare from the 19th century, chronologically the third-ever observed flare. **1872-11-13, 1986-09-10, 1891-06-17, 1892-07-15, 2017-09-06, 17-09-09, 2017-09-10**

“Bastille Day 2017”
Hugh **Hudson** and Sa”m Krucker.
RHESSI Nugget No. 303 July **2017**
http://sprg.ssl.berkeley.edu/~tohban/wiki/index.php/Bastille_Day_2017
Interesting flares really do happen on Bastille Day…

GOES Hard X-rays?
Hugh **Hudson**, Janet Machol
RHESSI Science Nuggets, #290 Jan **2017**
http://sprg.ssl.berkeley.edu/~tohban/wiki/index.php/GOES_Hard_X-rays%3F
Solar minimum conditions reveal interesting properties of the GOES X-ray observations.

Syrovatskii's "constant density" approximation
Hugh **Hudson** and Paulo Simões
RHESSI Science Nuggets, #288 Dec **2016**
http://sprg.ssl.berkeley.edu/~tohban/wiki/index.php/Syrovatskii%27s_"constant_density"_approximation
In this Nugget we discuss one of the more minor contributions of the great astronomical theorist S. I. Syrovatskii (1925-1979). He could be considered as one of the main pioneers of plasma astrophysics, and he had a special interest in solar physics and, particularly, in solar flares. **11 July 1992, 9 Nov 2013**

Chasing White-Light Flares **Review**
H. S. **Hudson**
Solar Phys. Volume 291, Issue 5, pp 1273-1322 **2016** **Draft file**
In this memoir I describe my life in research, mostly in the area of solar physics. The recurring theme is “white-light flares,” and several sections of this paper deal with this and related phenomena; I wind up describing how I see the state of the art in this still-interesting and crucially important (as it has been since 1859) area of flare research. I also describe my participation in two long-lived satellite programs dedicated to solar observations (Yohkoh and RHESSI) and elaborate on their discoveries. These have both helped with white-light flares both directly and also with closely related X-ray and γ-ray emissions), with the result that this article leans heavily in that direction.

Extreme events, stellar evolution, and magnetic reconnection
Hugh **Hudson**
RHESSI Science Nuggets, #272, Apr **2016**
http://sprg.ssl.berkeley.edu/~tohban/wiki/index.php/Extreme_events,_stellar_evolution,_and_magnetic_reconnection

Soft and Hard X-rays, Flares, and the Corona
Hugh **Hudson**
RHESSI Science Nuggets, #263, Nov **2015**
http://sprg.ssl.berkeley.edu/~tohban/wiki/index.php/Soft_and_Hard_X-rays,_Flares,_and_the_Corona
Behavior of the X-ray Sun at low activity levels.
This Nugget has described how the quiet Sun appears in currently available X-ray data. The time-series view strongly suggests steady heating, rather than the episodic flare-like heating one sees at higher levels of activity, where hot flaring active regions dominate. This is not the end of the story, though; the heating could still be episodic, but just with more frequent episodes of weaker events.

The Fastest Flare
Hugh **Hudson** and Paulo Simões
RHESSI Science Nuggets, #256, June **2015**
Within the last week an extraordinarily fast GOES event happened (a burst within **SOL2015-06-20**T02:36, C2.3; for reference see also our earlier Nugget The Slowest Flare). We have checked, as described below, finding this to in fact have been the very fastest GOES burst for the entire month, 25-May through 24-June. What did this striking event look

like? In particular, could there have been a true impulsive-phase signature (non-thermal bremsstrahlung) from the fast electrons, detected by the GOES photometers? If so, that would be a remarkable first.
This "fastest" GOES event behaves for all the world like a major flare, with hard X-rays, white light, and gyroresonance microwave emission. It has interesting features that warrant further study. In this era of abundant data, an unusual event of this type ("striking similarities, and yet intriguing discrepancies") may enable us to learn interesting new things even from a single solar flare. There's definitely a problem to tackle here: how can the plasma cool so fast in this case? Presumably this means very strong conductive losses, but we need to confirm the feasibility of such an explanation.

Svestka's Research: Then and Now **Review**

Hugh S. **Hudson**
Solar Phys. Volume 290, Issue 12, pp 3383-3397 **2015**
http://arxiv.org/pdf/1503.04452v1.pdf
https://link.springer.com/content/pdf/10.1007/s11207-015-0669-0.pdf
Zdenek Svestka's research work influenced many fields of solar physics, especially in the area of flare research. In this article I take five of the areas that particularly interested him and assess them in a "then and now" style. His insights in each case were quite sound, although of course in the modern era we have learned things that he could not readily have envisioned. His own views about his research life have been published recently in this journal, to which he contributed so much, and his memoir contains much additional scientific and personal information (Svestka, 2010).
1980-05-21, 1992-08-28

The IAU Solar Target Identifier

Hugh **Hudson** and John Leibacher.
RHESSI Science Nuggets, #243, December **2014**
http://sprg.ssl.berkeley.edu/~tohban/wiki/index.php/The_IAU_Solar_Target_Identifier_-_A_Good_Thing
Standardized names for flares help a lot.

Back from the Far Side

Hugh **Hudson** and Greg Slater
RHESSI Science Nugget, No. 240, Nov **2014**
http://sprg.ssl.berkeley.edu/~tohban/wiki/index.php/Back_from_the_Far_Side
The return of AR 2192, well tracked by seismic imaging, has produced interesting flares but still no CMEs.
It is an extraordinary coincidence that exactly 11 years, or 4013.0 days (to be precise) after a major sunspot group in 2003, that we should have this cycle's largest one popping up. But that is not what is interesting. The flares themselves are remarkable and will be the subject of many studies, which we can try to follow as discoveries are made. It is most important for space weather applications to understand why this region could produce such powerful flares without CMEs. The added interest here is the tendency for homology, as described

Homing in on Flare Energy

Hugh **Hudson** and Ryan Milligan
RHESSI Science Nuggets, No. 223, **2014**
http://sprg.ssl.berkeley.edu/~tohban/wiki/index.php/Homing_in_on_Flare_Energy
representing the spectral energy distribution of a flare
This Nugget has no real conclusions, but does remind the solar community of the simple $\lambda f\lambda$ (or $\nu f\nu$) representation of the energy distribution. The gaps in our knowledge are now much smaller than they were a few years ago, but they are important ones and need to be understood before we can be sure that we have properly understood the radiant energy of a solar flare. Right now it seems likely that solar flares have a lot of energy in the UV, perhaps more than in the white-light continuum, but we don't really know yet for sure.

Instantaneous Flare Properties

Hugh **Hudson**
RHESSI Nuggets, No. 2018, **2014**
http://sprg.ssl.berkeley.edu/~tohban/wiki/index.php/Instantaneous_Flare_Properties
In this Nugget we descrbe a related method, that of the analysis of the instantaneous increment of the GOES signals. This essentially is a study of the time derivative of the data. **2013-01-05**

Remote sensing of low-energy SEPs via charge exchange

Hudson, H. S.; MacKinnon, A. L.; Badnell, N. R.

E-print, Feb **2014**; SOLAR WIND 13: Proceedings of the Thirteenth International Solar Wind Conference. AIP Conference Proceedings, Volume 1539, pp. 19-21 (**2013**)
Charge-exchange reactions at high energies provide new channels for the remote sensing of solar high-energy particles, as demonstrated by the recent detection of 1.8-5 MeV hydrogen atoms from a solar flare. Orrall and Zirker had earlier proposed the detection of low-energy protons via charge-exchange atomic reactions in the solar atmosphere, leading in the simplest case to extended red-wing emission in the Lymanα line. We discuss the analogous process for the He II 304 A line (forα particles) and also assess the feasibility of the analogous process in the solar wind, whereby ambient He and (C, N, O) ions allow low-energyα particles to undergo resonant charge exchange in the ambient corona and thereby produce 304 A wing emission close to the acceleration region.

Charge-exchange Limits on Low-energy α-particle Fluxes in Solar Flares
Hudson, H. S.; Fletcher, L.; MacKinnon, A. L.; Woods, T. N.
E-print, Feb **2014**; ApJ 752, 84 (**2012**)
http://arxiv.org/pdf/1401.6477v1.pdf
This paper reports on a search for flare emission via charge-exchange radiation in the wings of the Lyα line of He II at 304 ?, as originally suggested for hydrogen by Orrall & Zirker. Via this mechanism a primary α particle that penetrates into the neutral chromosphere can pick up an atomic electron and emit in the He II bound-bound spectrum before it stops. The Extreme-ultraviolet Variability Experiment on board the Solar Dynamics Observatory gives us our first chance to search for this effect systematically. The Orrall-Zirker mechanism has great importance for flare physics because of the essential roles that particle acceleration plays; this mechanism is one of the few proposed that would allow remote sensing of primary accelerated particles below a few MeV/nucleon. We study 10 events in total, including the γ-ray events SOL**2010-06-12** (M2.0) and SOL**2011-02-24** (M3.5) (the latter a limb flare), seven X-class flares, and one prominent M-class event that produced solar energetic particles. The absence of charge-exchange line wings may point to a need for more complete theoretical work. Some of the events do have broadband signatures, which could correspond to continua from other origins, but these do not have the spectral signatures expected from the Orrall-Zirker mechanism.

Cycle 23 Variation in Solar Flare Productivity
Hugh **Hudson**, Lyndsay Fletcher, Jim McTiernan
Solar Physics, April **2014**, Volume 289, Issue 4, pp 1341-1347
The NOAA listings of solar flares in cycles 21 – 24, including the GOES soft X-ray magnitudes, enable a simple determination of the number of flares each flaring active region produces over its lifetime. We have studied this measure of flare productivity over the interval 1975 – 2012. The annual averages of flare productivity remained approximately constant during cycles 21 and 22, at about two reported M- or X-flares per region, but then increased significantly in the declining phase of cycle 23 (the years 2004 – 2005). We have confirmed this by using the independent RHESSI flare catalog to check the NOAA events listings where possible. We note that this measure of solar activity does not correlate with the solar cycle. The anomalous peak in flare productivity immediately preceded the long solar minimum between cycles 23 and 24.

Flare Coronal Rain
Hugh **Hudson** and Sa"m Krucker
RHESSI Science Nuggets, No. 216, Dec **2013**
http://sprg.ssl.berkeley.edu/~tohban/wiki/index.php/Flare_Coronal_Rain
thermal collapse seen in flare loops in a wonderful new way.

Flare Productivity
Hugh **Hudson** and Lyndsay Fletcher
RHESSI Nugget, No. 90, Dec **2012**
the number of flares per active region fluctuated oddly in 2004-2005, and the RHESSI flare observations help to track such statistical features.

"Impulse Response Flares" and Gamma Rays
Hugh **Hudson** and Stephen White
RHESSI Nugget, No. 188, Nov **2012**
A simplifying paradigm may describe acceleration to the highest energies in flares

We've speculated in this Nugget that we can identify two distinct radiation signatures with the same process: the prompt acceleration of primary protons to energies above 100 MeV in regions of intense magnetic fields. The impulse-response time profile of this process may reveal a somewhat different paradigm for flare energetics, one that has a characteristic temporal signature on a time scale of about 20 s. If this is so, we may expect to see more such events with Fermi and at even shorter radio wavelengths with the new ALMA facility. RHESSI may also have signatures of this process that have not yet been disentangled from other features it detects at its highest energies.
mm-wave radio observations recorded at 86 GHz at the Hat Creek Observatory SOL2010-06-12

Dimmings and Sustained Gamma-Ray Events

Hugh **Hudson** and Nicola Omodei.
RHESSI Nugget, No. 179, July **2012**
http://sprg.ssl.berkeley.edu/~tohban/wiki/index.php/Dimmings_and_Sustained_Gamma-Ray_Events
Coronal disruptions reveal themselves as depletions and gamma-ray emissions
SOL2012-03-07

Momentum Distribution in Solar Flare Processes

H. S. **Hudson**, L. Fletcher, G. H. Fisher, W. P. Abbett and A. Russell
Solar Physics, Volume 277, Number 1, 77-88, **2012**
We discuss the consequences of momentum conservation in processes related to solar flares and coronal mass ejections (CMEs), in particular describing the relative importance of vertical impulses that could contribute to the excitation of seismic waves ("sunquakes"). The initial impulse associated with the primary flare energy transport in the impulsive phase contains sufficient momentum, as do the impulses associated with the acceleration of the evaporation flow (the chromospheric shock) or the CME itself. We note that the deceleration of the evaporative flow, as coronal closed fields arrest it, will tend to produce an opposite impulse, reducing the energy coupling into the interior. The actual mechanism of the coupling remains unclear at present.

The EVE Doppler Sensitivity and Flare Observations

H. S. **Hudson**, T. N. Woods, P. C. Chamberlin, L. Fletcher, G. Del Zanna, L. Didkovsky, N. Labrosse and D. Graham
Solar Physics, Volume 273, Number 1, 69-80, **2011**
The Extreme-ultraviolet Variability Experiment (EVE; see Woods et al., 2009) obtains continuous EUV spectra of the Sun viewed as a star. Its primary objective is the characterization of solar spectral irradiance, but its sensitivity and stability make it extremely interesting for observations of variability on time scales down to the limit imposed by its basic 10 s sample interval. In this paper we characterize the Doppler sensitivity of the EVE data. We find that the 30.4 nm line of He ii has a random Doppler error below 0.001 nm (1 pm, better than 10 km s−1 as a redshift), with ample stability to detect the orbital motion of its satellite, the Solar Dynamics Observatory (SDO). Solar flares also displace the spectrum, both because of Doppler shifts and because of EVE's optical layout, which (as with a slitless spectrograph) confuses position and wavelength. As a flare develops, the centroid of the line displays variations that reflect Doppler shifts and therefore flare dynamics. For the impulsive phase of the flare SOL2010-06-12, we find the line centroid to have a redshift of 16.8 ± 5.9 km s−1 relative to that of the flare gradual phase (statistical errors only). We find also that high-temperature lines, such as Fe xxiv 19.2 nm, have well-determined Doppler components for major flares, with decreasing apparent blueshifts as expected from chromospheric evaporation flows.

An Fe Cascade

Hugh **Hudson**
RHESSI Science Nugget, No. 171, Oct, **2012**
http://sprg.ssl.berkeley.edu/~tohban/wiki/index.php/An_Fe_Cascade
It seems sometimes as though the solar corona might be made entirely of iron, since its ions yield so many EUV and X-ray emission lines - a remark possibly first made by Werner Neupert. In reality, of course, the corona mostly consists of hydrogen, which therefore dominates the dynamics, and the iron is perhaps just there to be helpful diagnostically. In any case the high Z of iron gives us an opportunity to observe many states of ionization; in the corona (if we include the prominences) we could probably identify all 26 of the ions at one point or another. In particular we can watch the thermodynamic state of the corona evolve with space or time, ie see where and when it is hot or cold. Flares offer wonderful opportunities for temperature changes because of the heating resulting from the energy that they extract from the magnetic field.

The Fe cascade plots nicely characterize the expected time evolution of a post-flare loop system. The EVE data have enough signal-to-noise ratio for an X-class flare, such as this one, to learn much more about the time evolution of these systems, and so detailed analyses will be interesting. One virtue of the spectra is that they produce such a wealth of spectra for a single element, thus avoiding confusion due to possible abundance variations. These may also be able to "weigh" or find the mass of a coronal mass ejection, in a substantially different manner from the way a coronagraph does it. **SOL2011-02-15**

A Flare in 3D

Hugh **Hudson** and Juan Carlos Martinez Oliveros
RHESSI Science Nugget, No. 160, Oct, **2011**
http://sprg.ssl.berkeley.edu/~tohban/wiki/index.php/A_Flare_in_3D
24 February 2011

Hard X-rays and Sympathy

Hugh **Hudson**
RHESSI Science Nugget, 13 July **2011**
http://sprg.ssl.berkeley.edu/~tohban/wiki/index.php/Hard_X-rays_and_Sympathy
A hard X-ray spike elicits a sympathetic response.
SOL2011-07-11T10:56

EVE/ESP and the Neupert Effect

H. **Hudson**
RHESSI Science Nugget, 9 May **2011**
http://sprg.ssl.berkeley.edu/~tohban/wiki/index.php/EVE/ESP_and_the_Neupert_Effect
This Nugget follows a previous Nugget introducing EVE spectroscopy and its applications. Here we will look at the ESP component of EVE. The EVE data include a broad-band photometric observation of solar soft X-rays (nominally 0.1-5.9 nm), similar to the standard GOES photometry at 1-8A, but better in some ways. In illustrating these data we refer to the flare **SOL2011-02-24**, a limb event with white-light continuum emission (as in SOL2010-06-12, the subject of our previous Nugget). Because EVE (and its component ESP) observe in the extreme ultraviolet, where opacities are large, a limb event will systematically differ from a disk event in its morphology - not only because of [limb darkening], but also because of absorption by structures intervening on the line of sight.
The Neupert Effect works, sort of, in a limb gamma-ray flare.

The Alfven Speed above a Sunspot, and Gamma-rays

H. **Hudson**, L. Fletcher
RHESSI Science Nugget, 12 Apr **2011**
http://sprg.ssl.berkeley.edu/~tohban/wiki/index.php/The_Alfven_Speed_above_a_Sunspot,_and_Gamma-rays
It is common for powerful flares to occur actually within sunspots, with their H-alpha ribbons blithely crossing over these regions of very strong magnetic field. What does this association mean for flare theory, and what does it mean for the interesting differences RHESSI has discovered between flares with and without gamma-rays? We discuss these issues in the context of the X-class flare of **February 15, 2011**. This was only the second X-class flare of this solar maximum; it was not a gamma-ray event but it was the source of a clear sunquake.

Global Properties of Solar Flares **(A review)**

Hugh S. **Hudson**
Space Sci Rev., 158: 5–41, **2011**, **File**, DOI 10.1007/s11214-010-9721-4
https://link.springer.com/content/pdf/10.1007/s11214-010-9721-4.pdf
This article broadly reviews our knowledge of solar flares. There is a particular focus on their global properties, as opposed to the microphysics such as that needed for magnetic reconnection or particle acceleration as such. Indeed solar flares will always remain in the domain of remote sensing, so we cannot observe the microscales directly and must understand the basic physics entirely via the global properties plus theoretical inference. The global observables include the general energetics—radiation in flares and mass loss in coronal mass ejections (CMEs)—and the formation of different kinds of ejection and global wave disturbance: the type II radio-burst exciter, the Moreton wave, the EIT “wave”, and the “sunquake” acoustic waves in the solar interior. Flare radiation and CME kinetic energy can have comparable magnitudes, of order 1032 erg each for an X-class event, with the bulk of the radiant energy in the visible-UV continuum. We argue that the impulsive phase of the flare dominates the energetics of all of these manifestations, and also point out that energy and momentum in this phase largely reside in the electromagnetic field, not in the observable plasma.

Coronal Radiation Belts

Hudson, H. S.; MacKinnon, A. L.; De Rosa, M. L.; Frewen, S. F. N.
Astrophysical Journal Letters, Volume 698, Issue 2, pp. L86-L89 (**2009**)
https://arxiv.org/pdf/0905.3824.pdf
The magnetic field of the solar corona has a large-scale dipole character, which maps into the bipolar field in the solar wind. Using standard representations of the coronal field, we show that high-energy ions can be trapped stably in these large-scale closed fields. The drift shells that describe the conservation of the third adiabatic invariant may have complicated geometries. Particles trapped in these zones would resemble the Van Allen belts and could have detectable consequences. We discuss potential sources of trapped particles.

Flare Energy and Magnetic Field Variations

H.S. **Hudson**, G.H. Fisher, and B.T. Welsch
E-print, July **2007**

The unpredictability of the most energetic solar events

H.S. **Hudson**
E-print, July **2007**
These factors suggest that processes in the solar interior involved with the supply of magnetic flux up to the surface of the Sun have strong correlations in space and time, leading to a complex occurrence pattern that is presently unpredictable on timescales longer than active region lifetimes (weeks) and not correlated well with the solar cycle itself.

"Overview of solar flares," **Review**

Hudson, H. S., Fletcher, L., Khan, J. I., and Kosugi, T.,
in *Solar and Space Weather Radiophysics* (D. E. Gary and C. U. Keller, eds.), Kluwer, pp. 153-178, **2004, file**.
https://link.springer.com/content/pdf/10.1007%2F1-4020-2814-8.pdf
This chapter reviews the physics of solar flares, with special emphasis on the past decade. During this decade first Yohkoh and then TRACE have drastically improved our observational capabilities for flares, with contributions also from the essentially non-flare instrumentation on SOHO and of course the ground-based observatories. In this review we assess how these new observations have changed our understanding of the basic physics of flares and consider the implications of these results for future observations with FASR. The discussion emphasizes flaring loops, flare ejecta, particle acceleration, and microflares.

Second-stage acceleration in a limb-occulted flare

Hudson, H. S.; Lin, R. P.; Stewart, R. T.
Solar Physics, vol. 75, Jan. **1982**, p. 245-261.
From radio observations it is known that two distinct groups of phenomena occur in large solar flares. The phenomena are related to an impulsive phase of approximately 100 s duration in the early stage of a flare and a following second phase lasting for tens of minutes. A study is presented of the limb-occulted flare event of July 22, 1972, giving particular attention to the second stage particle acceleration. The study takes into account hard X-ray, energetic particle, and radio observations. The conducted analysis shows that second stage acceleration is physically distinct from the impulsive phase, and is characterized by continuous and widespread electron acceleration to high energies, most likely by the type II burst shock wave.

A purely coronal hard X-ray event

Hudson, H. S.
Astrophysical Journal, Part 1, vol. 224, Aug. 15, **1978**, p. 235-240.
OSO 7 observations of a hard X-ray event of coronal origin are described. This event had a duration of more than 42 min as well as an abnormally large hard/soft ratio and apparently occurred after the disappearance of a bright coronal streamer. This gradual hard X-ray event is tentatively associated with open field lines extending well above the closed loop structures that participated in the originating flare. It is noted that a gradual hardening of the hard X-ray spectral distribution occurred during the event. Physical conditions in the source are considered, and the results are compared with observations of other hard X-ray events associated with flares.

Using Multiple Instance Learning for Explainable Solar Flare Prediction

Cédric **Huwyler**, Martin Melchior

2022

https://arxiv.org/pdf/2203.13896.pdf

In this work we leverage a weakly-labeled dataset of spectral data from NASAs IRIS satellite for the prediction of solar flares using the Multiple Instance Learning (MIL) paradigm. While standard supervised learning models expect a label for every instance, MIL relaxes this and only considers bags of instances to be labeled. This is ideally suited for flare prediction with IRIS data that consists of time series of bags of UV spectra measured along the instrument slit. In particular, we consider the readout window around the Mg II h&k lines that encodes information on the dynamics of the solar chromosphere. Our MIL models are not only able to predict whether flares occur within the next ∼25 minutes with accuracies of around 90%, but are also able to explain which spectral profiles were particularly important for their bag-level prediction. This information can be used to highlight regions of interest in ongoing IRIS observations in real-time and to identify candidates for typical flare precursor spectral profiles. We use k-means clustering to extract groups of spectral profiles that appear relevant for flare prediction. The recovered groups show high intensity, triplet red wing emission and single-peaked h and k lines, as found by previous works. They seem to be related to small-scale explosive events that have been reported to occur tens of minutes before a flare.

Magnetic Structure and Nonthermal Electrons in the X6.9 Flare on 2011 August 9

Jung-Eun **Hwangbo**, Jeongwoo Lee, Sung-Hong Park, Sujin Kim, Dae-Young Lee, Su-Chan Bong, Yeon-Han Kim, Kyung-Suk Cho, and Young-Deuk Park

ApJ, 796 80, **2014**

The **2011 August 9** flare is one of the largest X-ray flares of sunspot cycle 24, but spatial information is rather limited due to its position close to the western limb. This paper presents information about the location of high-energy electrons derived from hard X-ray and microwave spectra obtained with the Reuven Ramaty High-Energy Solar Spectroscopic Imager (RHESSI) and the Korean Solar Radio Burst Locator (KSRBL), respectively. The KSRBL microwave spectrum shows significant fluxes at low frequencies, implying that the high-energy electrons reside in a coronal volume highly concentrated at strong magnetic fields, and rapidly expanding with decreasing magnetic fields. After a simple modeling of the microwave spectrum, we found that the microwave source should be located above the inner pair of magnetic poles in a large quadrupolar configuration. The time-dependent evolution of the magnetic field distribution and total nonthermal energy derived from the microwave spectra is also consistent with the standard picture of multiple magnetic reconnections recurring at a magnetic null point that forms above the magnetic quadrupoles and moves up with time.

Properties and relationship between solar eruptive flares and Coronal Mass Ejections during rising phase of Solar Cycles 23 and 24

M.Syed **Ibrahim**, A.Shanmugaraju, Y.-J.Moon, B.Vrsnak, S.Umapathy

Advances in Space Research Volume 61, Issue 1, 1 January **2018**, Pages 540-551

https://ac.els-cdn.com/S027311771730666X/1-s2.0-S027311771730666X-main.pdf?_tid=4faa2d64-de43-11e7-8054-00000aab0f01&acdnat=1512976814_f6b3fddde3a016b209ccb968996e7adf

Statistical relationship between major flares and the associated CMEs during rising phases of Solar Cycles 23 and 24 are studied. Totally more than 6000 and 10,000 CMEs were observed by SOHO/LASCO (Solar and Heliospheric Observatory/Large Angle Spectrometric Coronagraph) during 23rd [May 1996–June 2002] and 24th [December 2008–December 2014] solar cycles, respectively. In particular, we studied the relationship between properties of flares and CMEs using the limb events (longitude 70–85°) to avoid projection effects of CMEs and partial occultation of flares that occurred near 90°. After selecting a sample of limb flares, we used certain spatial and temporal constraints to find the flare-CME pairs. Using these constraints, we compiled 129 events in Solar Cycle 23 and 92 events in Solar Cycle 24. We compared the flare-CME relationship in the two solar cycles and no significant differences are found between the two cycles. We only found out that the CME mean width was slightly larger and the CME mean acceleration was slightly higher in cycle 24, and that there was somewhat a better relation between flare flux and CME deceleration in cycle 24 than in cycle 23.

Flare Ribbons Observed with G-band and FeI 6302Å, Filters of the Solar Optical Telescope on Board Hinode Vector Magnetic Fields and Doppler Velocity Structures Around a Cancellation Site in the Quiet Sun

Y. **Iida**, T. Yokoyama, and K. Ichimoto

ApJ **713** 325, **2010**

A cancellation is thought to be a basic process of the photospheric magnetic field and plays an important role in magnetic flux budget and in various solar activities. There are two major theoretical scenarios for this phenomena, the "U-loop emergence" and the "Ω-loop submergence" models. It is important to clarify which is the dominant process during the cancellation for the estimation of the solar magnetic flux transport through the surface. We study the vector magnetic field and velocity structures around a quiet-Sun cancellation by using the Solar Optical Telescope on board

the *Hinode* satellite. Transverse magnetic field connecting the canceling magnetic features and strong long-lasting Doppler redshift signal are found. The transverse field is observed in the first spectropolarimetric observation after the occurrence of the cancellation while the redshift is clearly delayed to the cancellation by 20 minutes. These results indicate that the observed cancellation is an "Ω-loop submergence."

The Properties of the Tilts of Bipolar Solar Regions

E. **Illarionov**, A. Tlatov, D. Sokoloff
Solar Phys., February **2015**, Volume 290, Issue 2, pp 351-361
http://arxiv.org/pdf/1410.4933v1.pdf
We investigate various properties associated with the tilt of isolated magnetic bipoles in magnetograms taken at the solar surface. We show that bipoles can be divided into two groups which have tilts of opposite signs, and reveal similar properties with respect to bipole area, flux and bipolar moment. Detailed comparison of these physical quantities shows that the dividing point between the two types of bipoles corresponds to a bipole area of about 300 millionths of the solar hemisphere (MHS). The time-latitude distribution of small bipoles differs substantially from that for large bipoles. Such behaviour in terms of dynamo theory may indicate that small and large bipoles trace different components of the solar magnetic field. The other possible viewpoint is that the difference in tilt data for small and large bipoles is connected with spectral helicity separation, which results in opposite tilts for small and large bipoles. We note that the data available do not provide convincing reasons to prefer either interpretation.

Giant white-light flares on fully convective stars occur at high latitudes

Ekaterina **Ilin**, Katja Poppenhaeger, Sarah J Schmidt, Silva P Järvinen, Elisabeth R Newton, Julián D Alvarado-Gómez, J Sebastian Pineda, James R A Davenport, Mahmoudreza Oshagh, Ilya Ilyin
Monthly Notices of the Royal Astronomical Society, Volume 507, Issue 2, October **2021**, Pages 1723–1745,
https://doi.org/10.1093/mnras/stab2159
White-light flares are magnetically driven localized brightenings on the surfaces of stars. Their temporal, spectral, and statistical properties present a treasury of physical information about stellar magnetic fields. The spatial distributions of magnetic spots and associated flaring regions help constrain dynamo theories. Moreover, flares are thought to crucially affect the habitability of exoplanets that orbit these stars. Measuring the location of flares on stars other than the Sun is challenging due to the lack of spatial resolution. Here we present four fully convective stars observed with the Transiting Exoplanet Survey Satellite that displayed large, long-duration flares in white-light which were modulated in brightness by the stars' fast rotation. This allowed us to determine the loci of these flares directly from the light curves. All four flares occurred at latitudes between 55° and 81°, far higher than typical solar flare latitudes. Our findings are evidence that strong magnetic fields tend to emerge close to the stellar rotational poles for fully convective stars, and suggest that the impact of flares on the habitability of exoplanets around small stars could be weaker than previously thought.

Detection of Emerging Sunspot Regions in the Solar Interior

Stathis **Ilonidis***, Junwei Zhao, Alexander Kosovichev
Science, 19 August **2011**: 333 (6045): 993-996
See http://science.nasa.gov/science-news/science-at-nasa/2011/25aug_sunspotbreakthrough/
Sunspots are regions where strong magnetic fields emerge from the solar interior and where major eruptive events occur. These energetic events can cause power outages, interrupt telecommunication and navigation services, and pose hazards to astronauts. We detected subsurface signatures of emerging sunspot regions before they appeared on the solar disc. Strong acoustic travel-time anomalies of an order of 12 to 16 seconds were detected as deep as 65,000 kilometers. These anomalies were associated with magnetic structures that emerged with an average speed of 0.3 to 0.6 kilometer per second and caused high peaks in the photospheric magnetic flux rate 1 to 2 days after the detection of the anomalies. Thus, synoptic imaging of subsurface magnetic activity may allow anticipation of large sunspot regions before they become visible, improving space weather forecast.

Non-Equilibrium Ionization Plasma During Large Solar Limb Flare Observed by Hinode/EIS

S. **Imada**
ApJL **914** L28 **2021**
https://arxiv.org/pdf/2105.14660.pdf
https://iopscience.iop.org/article/10.3847/2041-8213/ac063c/pdf
https://doi.org/10.3847/2041-8213/ac063c
This study on plasma heating considers the time-dependent ionization process during a large solar flare on **September 10, 2017**, observed by Hinode/EIS. The observed FeXXIV / FeXXIII ratios increase downstream of the reconnection outflow, and they are consistent with the time-dependent ionization effect at a constant electron temperature Te = 25 MK. Moreover, this study also shows that the non-thermal velocity, which can be related to the turbulent velocity,

reduces significantly along the downstream of the reconnection outflow, even when considering the time-dependent ionization process.
RHESSI Nuggets #409 **2021**
https://sprg.ssl.berkeley.edu/~tohban/wiki/index.php/Nonequilibrium_Ionization_of_Flare_Plasma_Observed_by_Hinode/EIS

Observation and numerical modeling of chromospheric evaporation during the impulsive phase of a solar flare

Shinsuke **Imada**, Izumi Murakami, Tetsuya Watanabe
Physics of Plasma **2015**
http://arxiv.org/pdf/1506.04674v1.pdf
We have studied the chromospheric evaporation flow during the impulsive phase of the flare by using the Hinode/EIS observation and 1D hydrodynamic numerical simulation coupled to the time-dependent ionization. The observation clearly shows that the strong redshift can be observed at the base of the flaring loop only during the impulsive phase. We performed two different numerical simulations to reproduce the strong downflows in FeXII and FeXV during the impulsive phase. By changing the thermal conduction coefficient, we carried out the numerical calculation of chromospheric evaporation in the thermal conduction dominant regime (conductivity coefficient kappa0 = classical value) and the enthalpy flux dominant regime (kappa0 = 0.1 x classical value). The chromospheric evaporation calculation in the enthalpy flux dominant regime could reproduce the strong redshift at the base of the flare during the impulsive phase. This result might indicate that the thermal conduction can be strongly suppressed in some cases of flare. We also find that time-dependent ionization effect is importance to reproduce the strong downflows in Fe XII and Fe XV. **6 November 2010**

Coronal Behavior Before the Large Flare Onset

Shinsuke **Imada**, Yumi Bamba, Kanya Kusano
PASJ, 66 (SP1), S17 (1–11) **2014**
http://arxiv.org/pdf/1408.2585v1.pdf
http://pasj.oxfordjournals.org/content/66/SP1/S17.full.pdf+html
Flares are a major explosive event in our solar system. They are often followed by coronal mass ejection that has a potential to trigger the geomagnetic storms. There are various studies aiming to predict when and where the flares are likely to occur. Most of these studies mainly discuss the photospheric and chromospheric activity before the flare onset. In this paper we study the coronal features before the famous large flare occurrence on **December 13th, 2006**. Using the data from Hinode/EUV Imaging Spectrometer (EIS), X-Ray Telescope (XRT), and Solar and Heliospheric Observatory (SOHO) /Extreme ultraviolet Imaging Telescope (EIT), we discuss the coronal features in the large scale (~ a few 100 arcsec) before the flare onset. Our findings are as follows: 1) The upflows in and around active region start growing from ~10 to 30 km /s a day before the flare. 2) The expanding coronal loops are clearly observed a few hours before the flare. 3) Soft X-ray and EUV intensity are gradually reduced. 4) The upflows are further enhanced after the flare. From these observed signatures, we conclude that the outer part of active region loops with low density were expanding a day before the flare onset, and the inner part with high density were expanding a few hours before the onset.

Evidence for Hot Fast Flow above a Solar Flare Arcade

S. **Imada**1,2, K. Aoki2,3, H. Hara2,3, T. Watanabe2, L. K. Harra4, and T. Shimizu
2013 ApJ 776 L11
EIS Nugget, Oct **2013**, http://solarb.mssl.ucl.ac.uk/SolarB/eisnuggets.jsp
Solar flares are one of the main forces behind space weather events. However, the mechanism that drives such energetic phenomena is not fully understood. The standard eruptive flare model predicts that magnetic reconnection occurs high in the corona where hot fast flows are created. Some imaging or spectroscopic observations have indicated the presence of these hot fast flows, but there have been no spectroscopic scanning observations to date to measure the two-dimensional structure quantitatively. We analyzed a flare that occurred on the west solar limb on **2012 January 27** observed by the Hinode EUV Imaging Spectrometer (EIS) and found that the hot (~30MK) fast (>500 km s–1) component was located above the flare loop. This is consistent with magnetic reconnection taking place above the flare loop.

Searching for rapid pulsations in solar flare X-ray data

Andrew R. **Inglis**, Laura A. Hayes
ApJ **971** 29 **2024**
https://arxiv.org/pdf/2406.07372

https://iopscience.iop.org/article/10.3847/1538-4357/ad54bb/pdf
Most studies of quasi-periodic pulsations in solar flares have identified characteristic periods in the 5 - 300s range. Due to observational limitations there have been few attempts to probe the < 5s period regime and understand the prevalence of such short-period quasi-periodic pulsations. However, the Fermi Gamma-ray Burst Monitor (GBM) has observed approximately 1500 solar flares to date in high cadence 16 Hz burst mode, providing us with an opportunity to study short-period quasi-periodic pulsations at X-ray energies. We systematically analyse every solar flare observed by Fermi/GBM in burst mode, estimating the prevalence of quasi-periodic pulsations in multiple X-ray energy bands. To better understand these results, we complement this with analysis of synthetic solar flare lightcurves, both with and without oscillatory signals present. Using these synthetic lightcurves, we can understand the likely false alarm and true positive rates in the real solar GBM data. We do not find strong evidence for widespread short-period quasi-periodic pulsations, indicating either a low base occurrence rate of such signatures or that their typical signal-to-noise ratios must be low - less than 1 - in Fermi/GBM data. Finally, we present a selection of the most interesting potential quasi-periodic pulsation events that were identified in the GBM solar X-ray data. **2011-06-16, 2012-05-10, 2013 October 28, 2014-10-20, 2015-09-29, 2022-05-20**

Quasi-periodic pulsations in solar flares: a key diagnostic of energy release on the Sun

Andrew **Inglis**, Laura Hayes, Silvina Guidoni, James McLaughlin, Valery M. Nakariakov, et al.
White paper submitted to the Decadal Survey for Solar and Space Physics (Heliophysics) 2024-2033
2023
https://arxiv.org/abs/2302.11549
Solar flares are among the most powerful and disruptive events in our solar system, however the physical mechanisms driving and transporting this energetic release are not fully understood. An important signature associated with flare energy release is highly variable emission on timescales of sub-seconds to minutes which often exhibit oscillatory behaviour, features collectively known as quasi-periodic pulsations (QPPs). To fully identify the driving mechanism of QPPs, exploit their potential as a diagnostic tool, and incorporate them into our understanding of solar and stellar flares, new observational capabilities and initiatives are required. There is a clear community need for flare-focused, rapid cadence, high resolution, multi-wavelength imaging of the Sun, with high enough sensitivity and dynamic range to observe small fluctuations in intensity in the presence of a large overall intensity. Furthermore, multidisciplinary funding and initiatives are required to narrow the gap between numerical models and observations. QPPs are direct signatures of the physics occurring in flare magnetic reconnection and energy release sites and hence are critical to include in a unified flare model. Despite significant modelling and theoretical work, no single mechanism or model can fully explain the presence of QPPs in flares. Moreover, it is also likely that QPPs fall into different categories that are produced by different mechanisms. At present we have insufficient information to observationally distinguish between mechanisms. The motivation to understand QPPs is strengthened by the geo-effectiveness of flares on the Earth's ionosphere, and by the fact that stellar flares exhibit similar QPP signatures. QPPs present a golden opportunity to better understand flare physics and exploit the solar-stellary analogy, benefiting both astrophysics, heliophysics, and the solar-terrestrial connection. **4 November 2015**

Evaluating Pointing Strategies for Future Solar Flare Missions

Andrew R. **Inglis**, Jack Ireland, Albert Y. Shih, Steven D. Christe
Solar Phys. **296**, Article number: 153 **2021**
https://arxiv.org/pdf/2110.13208.pdf
https://link.springer.com/content/pdf/10.1007/s11207-021-01896-0.pdf
https://doi.org/10.1007/s11207-021-01896-0
Solar flares are events of intense scientific interest. Although certain solar conditions are known to be associated with flare activity, the exact location and timing of an individual flare on the Sun cannot as yet be predicted with certainty. Missions whose science objectives depend on observing solar flares must often make difficult decisions on where to target their observations if they do not observe the full solar disk. Yet, little analysis exists in the literature which might guide these missions' operations to maximize their opportunities to observe flares. In this study we analyze and simulate the performance of different observation strategies using historical flare and active region data from 2011 to 2014. We test a number of different target selection strategies based on active region complexity and recent flare activity, each of which is examined under a range of operational assumptions. In each case we investigate various metrics such as the number of flares observed, the size of flares observed, and operational considerations such as the number of instrument re-points that are required. Overall, target selection methods based on recent flare activity showed the best overall performance, but required more repointings than other methods. The mission responsiveness to new information is identified as a strong factor determining flare observation performance. It is also shown that target selection methods based on active region complexities show a significant pointing bias towards the western solar hemisphere. The number of flares observed grows quickly with field-of-view size until the approximate size of an active region is reached, but further improvements beyond the active region size are much more incremental. These results provide valuable performance estimates for a future mission focused on solar flares, and inform the requirements that would ensure mission success.

Energy release from a stream of infalling prominence debris on 2011 September 7-8

Andrew R. **Inglis**, Holly R. Gilbert, Leon Ofman

ApJ **847** L17 **2017**

https://arxiv.org/pdf/1708.01555.pdf

http://sci-hub.cc/http://iopscience.iop.org/2041-8205/847/2/L17/

In recent years high-resolution and high-cadence EUV imaging has revealed a new phenomenon, impacting prominence debris, where prominence material from failed or partial eruptions can impact the lower atmosphere and release energy. We report a clear example of energy release and EUV brightening due to infalling prominence debris that occurred on **2011 September 7-8**. The initial eruption of prominence material was associated with an X1.8-class flare from AR11283, occurring at 22:30 UT on 2011 September 7. Subsequently, a semi-continuous stream of this material was observed to return to the solar surface with a velocity v > 150 km/s, impacting a region remote from the original active region between 00:20 - 00:40 UT on 2011 September 8. Using SDO/AIA, the differential emission measure of the plasma was estimated throughout this brightening event. We found that the radiated energy of the impacted plasma was L ~ 10^27 ergs, while the thermal energy peaked at ~ 10^28 ergs. From this we were able to determine the mass content of the debris to be in the range 2x10^14 < m < 2x10^15 g. Given typical prominence masses, the likely debris mass is towards the lower end of this range. This clear example of a prominence debris event shows that significant energy release takes place during these events, and that such impacts may be used as a novel diagnostic tool for investigating prominence material properties.

A large-scale search for evidence of quasi-periodic pulsations in solar flares

A. R. **Inglis**, J. Ireland, B. R. Dennis, L. A. Hayes, P. T. Gallagher

ApJ **2016**

https://arxiv.org/pdf/1610.07454v1.pdf

The nature of quasi-periodic pulsations in solar flares is poorly constrained, and critically the general prevalence of such signals in solar flares is unknown. Therefore, we perform a large-scale search for evidence of signals consistent with quasi-periodic pulsations in solar flares, focusing on the 1 - 300s timescale. We analyse 675 M- and X-class flares observed by GOES in 1-8\AA\ soft X-rays between 2011 February 1 and 2015 December 31. Additionally, over the same era we analyse Fermi/GBM 15-25 keV X-ray data for each of these flares that was associated with a Fermi/GBM solar flare trigger, a total of 261 events. Using a model comparison method, we determine whether there is evidence for a substantial enhancement in the Fourier power spectrum that may be consistent with a QPP signature, based on three tested models; a power-law plus a constant, a broken power-law plus constant, and a power-law-plus-constant with an additional QPP signature component. From this, we determine that ~30% of GOES events and ~8% of Fermi/GBM events show strong signatures consistent with classical interpretations of QPP. For the remaining events either two or more tested models cannot be strongly distinguished from each other, or the events are well-described by single power-law or broken power-law Fourier power spectra. For both instruments, a preferred characteristic timescale of ~5-30 s was found in the QPP-like events, with no dependence on flare magnitude in either GOES or GBM data. We also show that individual events in the sample show similar characteristic timescales in both GBM and GOES datasets. We discuss the implications of these results for our understanding of solar flares and possible QPP mechanisms. **2011-08-03, 2011-09-23, 2012-07-04, 2012-07-10, 2012-10-22, 2014-03-11**

Table 3 Abbreviated list of studied GOES events and analysis result parameters. The full table is available electronically.

Table 4 Abbreviated list of studied Fermi/GBM events and analysis result parameters. The full table is available electronically.

Quasi-periodic pulsations in solar and stellar flares: re-evaluating their nature in the context of power-law flare Fourier spectra

A. R. **Inglis**, J. Ireland, M. Dominique

ApJ, **798** 108 **2015**

http://arxiv.org/pdf/1410.8162v1.pdf

The nature of quasi-periodic pulsations in solar and stellar flares remains debated. Recent work has shown that power-law-like Fourier power spectra, also referred to as 'red' noise processes, are an intrinsic property of solar and stellar flare signals, a property that many previous studies of this phenomenon have not accounted for. Hence a re-evaluation of the existing interpretations and assumptions regarding QPP is needed. Here we adopt a Bayesian method for investigating this phenomenon, fully considering the Fourier power law properties of flare signals. Using data from the PROBA2/LYRA, Fermi/GBM, Nobeyama Radioheliograph and Yohkoh/HXT instruments, we study a selection of flares from the literature identified as QPP events. Additionally we examine optical data from a recent stellar flare that appears to exhibit oscillatory properties. We find that, for all but one event tested, an explicit oscillation is not required in order to explain the observations. Instead, the flare signals are adequately described as a manifestation of a power law in the Fourier power spectrum, rather than a direct signature of oscillating components or structures. However, for the flare of **1998 May 8**, strong evidence for the existence of an explicit oscillation with P ~ 14-16 s is found in the 17 GHz

radio data and the 13-23 keV Yohkoh HXT data. We conclude that, most likely, many previously analysed events in the literature may be similarly described in terms of power laws in the flare Fourier power spectrum, without the need to invoke a narrowband, oscillatory component. As a result the prevalence of oscillatory signatures in solar and stellar flares may be less than previously believed. The physical mechanism behind the appearance of the observed power laws is discussed.

Investigating the differential emission measure and energetics of microflares with combined SDO/AIA and RHESSI observations

A. R. **Inglis**, S. Christe
2014, ApJ 789 116
http://arxiv.org/pdf/1405.5262v1.pdf
An important question in solar physics is whether solar microflares, the smallest currently observable flare events in X-rays, possess the same energetic properties as large flares. Recent surveys have suggested that microflares may be less efficient particle accelerators than large flares, and hence contribute less nonthermal energy, which may have implications for coronal heating mechanisms. We therefore explore the energetic properties of microflares by combining Extreme Ultraviolet (EUV) and X-ray measurements.
We present forward-fitting differential emission measure (DEM) analysis of 10 microflares. The fitting is constrained by combining, for the first time, high temperature RHESSI observations and flux data from SDO/AIA. Two fitting models are tested for the DEM; a Gaussian distribution and a uniform DEM profile. A Gaussian fit proved unable to explain the observations for any of the studied microflares. However, 8 of 10 events studied were reasonably fit by a uniform DEM profile. Hence microflare plasma can be considered to be significantly multi-thermal, and may not be significantly peaked or contain resolvable fine structure, within the uncertainties of the observational instruments.
The thermal and non-thermal energy is estimated for each microflare, comparing the energy budget with an isothermal plasma assumption. From the multithermal fits the minimum non-thermal energy content was found to average approximately 30% of the estimated thermal energy. By comparison, under an isothermal model the non-thermal and thermal energy estimates were generally comparable. Hence, multi-thermal plasma is an important consideration for solar microflares that substantially alters their thermal and non-thermal energy content.

Hard X-ray and ultraviolet emission during the 2011 June 7 solar flare

A. R. **Inglis**, H. R. Gilbert
E-print, Sept **2013**, **2013** ApJ 777 30
The relationship between X-ray and UV emission during flares, particularly in the context of quasi-periodic pulsations, remains unclear. To address this, we study the impulsive X-ray and UV emission during the eruptive flare of **2011 June 7** utilising X-ray imaging from RHESSI and UV 1700A imaging from SDO/AIA. This event is associated with quasi-periodic pulsations in X-ray and possibly UV emission, as well as substantial parallel and perpendicular motion of the hard X-ray footpoints. The motion of the footpoints parallel to the flare ribbons is unusual; it is shown to reverse direction on at least two occasions. However, there is no associated short-timescale motion of the UV bright regions. Additionally, we find that the locations of the brightest X-ray and UV regions are different, particularly during the early portion of the flare impulsive phase, despite their integrated emission being strongly correlated in time. Correlation analysis of measured flare properties, such as the footpoint separation, flare shear, photospheric magnetic field and coronal reconnection rate, reveals that - in the impulsive phase - the 25 - 50 keV hard X-ray flux is only weakly correlated with these properties, in contrast to previous studies. We characterise this event in terms of long-term behaviour, where the X-ray nonthermal, thermal, and UV emission sources appear temporally and spatially consistent, and short-term behaviour, where the emission sources are inconsistent and quasi-periodic pulsations are a dominant feature requiring explanation. We suggest that the short timescale behaviour of hard X-ray footpoints, and the nature of the observed quasi-periodic pulsations, is determined by fundamental, as-yet unobserved properties of the reconnection region and particle acceleration sites. This presents a challenge for current three-dimensional flare reconnection models.
ERRATUM: **2014** ApJ 797 72

THE RELATIONSHIP BETWEEN HARD X-RAY PULSE TIMINGS AND THE LOCATIONS OF FOOTPOINT SOURCES DURING SOLAR FLARES

A. R. **Inglis** and B. R. Dennis
2012 ApJ 748 139
The cause of quasi-periodic pulsations in solar flares remains the subject of debate. Recently, Nakariakov & Zimovets proposed a new model suggesting that, in two-ribbon flares, such pulsations could be explained by propagating slow waves. These waves may travel obliquely to the magnetic field, reflect in the chromosphere, and constructively interfere at a spatially separate site in the corona, leading to quasi-periodic reconnection events progressing along the flaring arcade. Such a slow wave regime would have certain observational characteristics. We search for evidence of this phenomenon during a selection of two-ribbon flares observed by the Reuven Ramaty High Energy Solar Spectroscopic Imager, Solar and Heliospheric Observatory, and Transition Region and Coronal Explorer; the flares of **2002**

November 9, 2005 January 19, and 2005 August 22. We were not able to observe a clear correlation between hard X-ray footpoint separations and pulse timings during these events. Also, the motion of hard X-ray footpoints is shown to be continuous within the observational error, whereas a discontinuous motion might be anticipated in the slow wave model. Finally, we find that for a preferential slow wave propagation angle of 25°-28° that is expected for the fastest waves, the velocities of the hard X-ray footpoints lead to estimated pulse periods and ribbon lengths significantly larger than the measured values. Hence, for the three events studied, we conclude that the observational characteristics cannot be easily explained via the Nakariakov & Zimovets propagating slow wave model when only angles of 25°-28° are considered. We provide suggested flare parameters to optimize future studies of this kind.

Do Slow Waves Trigger Pulsations in Two-Ribbon Flares? An Observational Study,

Andrew **Inglis** and Brian Dennis
RHESSI Science Nugget No. 170, **2012**
http://sprg.ssl.berkeley.edu/~tohban/wiki/index.php/Do_slow_waves_trigger_pulsations_in_two-ribbon_flares%3F_An_observational_search
A recent Nugget by Nakariakov & Zimovets ([5]), suggested that quasi-periodic pulsations (QPP) might be explained in two-ribbon flares via slow MHD waves. A magnetized fluid can support a more complicated array of wave motions than a simple fluid, and in the MHD theory these are generically termed Alfvén waves. The QPP would be temporary standing waves corresponding to this theory; they can therefore be used to explain periodic-appearing variations in the emission from solar flares. QPP can be seen in flaring lightcurves at a variety of wavelengths, from radio waves to soft and hard X-rays. The characteristic timescale of these variations can vary from just a few seconds up to several minutes, but their root causes remain the subject of some debate.
Footpoint separation and pulse timings: **2002 November 9** (left), **2005 January 19** (centre) and **2005 August 22** (right).
Footpoint velocities at lightcurve peaks and valleys

Instrumental oscillations in RHESSI count rates during solar flares

A. R. **Inglis**1,5, I. V. Zimovets2, B. R. Dennis1, E. P. Kontar3, V. M. Nakariakov4,6, A. B. Struminsky2 and A. K. Tolbert
A&A 530, A47 **(2011**)
Aims. We seek to illustrate the analysis problems posed by RHESSI spacecraft motion by studying persistent instrumental oscillations found in the lightcurves measured by RHESSI's X-ray detectors in the 6–12 keV and 12–25 keV energy range during the decay phase of the flares of **2004 November 4 and 6.**
Methods. The various motions of the RHESSI spacecraft which may contribute to the manifestation of oscillations are studied. The response of each detector in turn is also investigated.
Results. We find that on 2004 November 6 the observed oscillations correspond to the nutation period of the RHESSI instrument. These oscillations are of greatest amplitude for detector 5, while in the lightcurves of many other detectors the oscillations are small or undetectable. We also find that the variation in detector pointing is much larger during this flare than the counterexample of 2004 November 4.
Conclusions. Sufficiently large nutation motions of the RHESSI spacecraft lead to clearly observable oscillations in count rates, posing a significant hazard for data analysis. This issue is particularly problematic for detector 5 due to its design characteristics. Dynamic correction of the RHESSI counts, accounting for the livetime, data gaps, and the transmission of the bi-grid collimator of each detector, is required to overcome this issue. These corrections should be applied to all future oscillation studies.

Iris si iv line profiles: An indication for the plasmoid instability during small-scale magnetic reconnection on the sun

Davina **Innes**, LiJia Guo, YiMin Huang, Amitava Bhattacharjee
ApJ 813 86 **2015**
http://arxiv.org/pdf/1509.08837v1.pdf
Our understanding of the process of fast reconnection has undergone a dramatic change in the last 10 years driven, in part, by the availability of high-resolution numerical simulations that have consistently demonstrated the break-up of current sheets into magnetic islands, with reconnection rates that become independent of Lundquist number, challenging the belief that fast magnetic reconnection in flares proceeds via the Petschek mechanism that invokes pairs of slow-mode shocks connected to a compact diffusion region. The reconnection sites are too small to be resolved with images but these reconnection mechanisms, Petschek and the plasmoid instability, have reconnection sites with very different density and velocity structures and so can be distinguished by high-resolution line-profiles observations. Using IRIS spectroscopic observations we obtain a survey of typical line profiles produced by small-scale events thought to be reconnection sites on the Sun. Slit-jaw images are used to investigate the plasma heating and re-configuration at the

sites. A sample of 15 events from two active regions is presented. The line profiles are complex with bright cores and broad wings extending to over 300 km/s. The profiles can be reproduced with the multiple magnetic islands and acceleration sites that characterise the plasmoid instability but not by bi-directional jets that characterise the Petschek mechanism. This result suggests that if these small-scale events are reconnection sites, then fast reconnection proceeds via the plasmoid instability, rather than the Petschek mechanism during small-scale reconnection on the Sun.
2014 April 15, 2014 May 03

Break up of returning plasma after the 7 June 2011 filament eruption by Rayleigh-Taylor instabilities⋆

D. E. **Innes**1, R. H. Cameron1, L. Fletcher2, B. Inhester1 and S. K. Solanki1
A&A 540, L10 (**2012**)
Context. A prominence eruption on **7 June 2011** produced spectacular curtains of plasma falling through the lower corona. At the solar surface they created an incredible display of extreme ultraviolet brightenings.
Aims. To identify and analyze some of the local instabilities which produce structure in the falling plasma.
Methods. The structures were investigated using SDO/AIA 171 Å and 193 Å images in which the falling plasma appeared dark against the bright coronal emission.
Results. Several instances of the Rayleigh-Taylor instability were investigated. In two cases the Alfvén velocity associated with the dense plasma could be estimated from the separation of the Rayleigh-Taylor fingers. A second type of feature, which has the appearance of self-similar branching horns was discussed.

EUV jets, type III radio bursts and sunspot waves investigated using SDO/AIA observations

D. E. **Innes**, R. H. Cameron and S. K. Solanki
E-print, June **2011**; A&A 531, L13 (**2011**) **, File**
Context. Quasi-periodic plasma jets are often ejected from the Sun into interplanetary space. The commonly observed signatures are day-long sequences of type III radio bursts.
Aims. The aim is to identify the source of quasi-periodic jets observed on **3 Aug. 2010** in the Sun's corona and in interplanetary space.
Methods. Images from the Solar Dynamics Observatory (SDO) at 211 Å are used to identify the solar source of the type III radio bursts seen in WIND/WAVES dynamic spectra. We analyse a 2.5 h period during which six strong bursts are seen. The radio signals are cross-correlated with emission from extreme ultraviolet (EUV) jets coming from the western side of a sunspot in AR 11092. The jets are further cross-correlated with brightening at a small site on the edge of the sunspot umbra, and the brightening with 3-min sunspot intensity oscillations.
Results. The radio bursts correlate very well with the EUV jets. The EUV jet emission also correlates well with brightening at what looks like their footpoint at the edge of the umbra. The jet emission lags the radio signals and the footpoint brightening by about 30 s because the EUV jets take time to develop. For 10–15 min after strong EUV jets are ejected, the footpoint brightens at roughly 3 min intervals. In both the EUV images and the extracted light curves, it looks as though the brightening is related to the 3-min sunspot oscillations, although the correlation coefficient is rather low. The only open field near the jets is rooted in the sunspot.
Conclusions. Active region EUV/X-ray jets and interplanetary electron streams originate on the edge of the sunspot umbra. They form along a current sheet between the sunspot open field and closed field connecting to underlying satellite flux. Sunspot running penumbral waves cause roughly 3-min jet footpoint brightening. The relationship between the waves and jets is less clear.

A Comparative Study of Solar Active Region 12371 with Data-constrained and Data-driven MHD Simulations

Satoshi **Inoue**, Keiji Hayashi, Takahiro Miyoshi, Ju Jing, Haimin Wang
ApJL **944** L44 **2023**
https://arxiv.org/pdf/2301.12336.pdf
https://iopscience.iop.org/article/10.3847/2041-8213/acb7f4/pdf
We performed two data-based magnetohydrodynamic (MHD) simulations for solar active region 12371 which produced an M6.5 flare. The first simulation is a full data-driven simulation where the initial condition is given by a nonlinear force-free field (NLFFF). This NLFFF was extrapolated from photospheric magnetograms approximately 1 hour prior to the flare, and then a time-varying photospheric magnetic field is imposed at the bottom surface. The second simulation is also a data-driven simulation, but it stops driving at the bottom before the time of flare onset and then switches to the data-constrained simulation, where the horizontal component of the magnetic field varies according to an induction equation while the normal component is fixed with time. Both simulations lead to an eruption, with both simulations producing highly twisted field lines before the eruption which were not found in the NLFFF alone. After the eruption, the first simulation based on the time-varying photospheric magneitic field, continues to produce sheared field lines after the flare without reproducing phenomena such as post-flare loops. The second simulation reproduces the phenomena associated with flares well. However in this case the evolution of the bottom magnetic field is inconsistent

with the evolution of the observed magnetic field. In this letter, we report potential advantages and disadvantages in data-constrained and data-driven MHD simulations that need to be taken into consideration by future studies. **June 15 2015**

An MHD Modeling of Successive X2.2 and X9.3 Solar Flares of 2017 September 6

Satoshi **Inoue**, Yumi Bamba
ApJ **914** 71 **2021**
https://arxiv.org/pdf/2104.06639.pdf
https://iopscience.iop.org/article/10.3847/1538-4357/abf835/pdf
https://doi.org/10.3847/1538-4357/abf835
Solar active region 12673 produced two successive X-class flares (X2.2 and X9.3) approximately 3 hours apart in September 2017. The X9.3 was the recorded largest solar flare in Solar Cycle 24. In this study we perform a data-constrained magnetohydrodynamic simulation taking into account the observed photospheric magnetic field to reveal the initiation and dynamics of the X2.2 and X9.3 flares. According to our simulation, the X2.2 flare is first triggered by magnetic reconnection at a local site where at the photosphere the negative polarity intrudes into the opposite-polarity region. This magnetic reconnection expels the innermost field lines upward beneath which the magnetic flux rope is formed through continuous reconnection with external twisted field lines. Continuous magnetic reconnection after the X2.2 flare enhances the magnetic flux rope, which is lifted up and eventually erupts via the torus instability. This gives rise to the X9.3 flare. **6 Sep 2017**

Magnetohydrodynamic Modeling of a Solar Eruption Associated with X9.3 Flare Observed in Active Region 12673

Satoshi **Inoue**, Daikou Shiota, Yumi Bamba, Sung-Hong Park
ApJ 867 83 **2018**
https://arxiv.org/pdf/1809.02309.pdf
sci-hub.tw/10.3847/1538-4357/aae079
On **2017 September 6**, the solar active region 12673 produced an X9.3 flare, regarded to be the largest to have occurred in solar cycle 24. In this work we have performed a magnetohydrodynamic (MHD) simulation in order to reveal the three-dimensional (3D) dynamics of the magnetic fields associated with the X9.3 solar flare. We first performed an extrapolation of the 3D magnetic field based on the observed photospheric magnetic field prior to the flare and then used this as the initial condition for the MHD simulation, which revealed a dramatic eruption. In particular, we found that a large coherent flux rope composed of highly twisted magnetic field lines formed during the eruption. A series of small flux ropes were found to lie along a magnetic polarity inversion line prior to the flare. Reconnection occurring between each flux rope during the early stages of the eruption formed the large, highly twisted flux rope. Furthermore, we observed a writhing motion of the erupting flux rope. Understanding these dynamics is important in the drive to increase the accuracy of space weather forecasting. We report on the detailed dynamics of the 3D eruptive flux rope and discuss the possible mechanisms of the writhing motion.
PSTEP Science Nuggets #20 **2019** http://www.pstep.jp/news_en/nuggets20en.html

Magnetohydrodynamics modeling of coronal magnetic field and solar eruptions based on the photospheric magnetic field **Review**

Satoshi **Inoue**
Progress in Earth and Planetary Science **2016** 3:19
http://progearthplanetsci.springeropen.com/articles/10.1186/s40645-016-0084-7
E-print, 4 July **2016**
In this paper, we summarize current progress on using the observed magnetic fields for magnetohydrodynamics (MHD) modeling of the coronal magnetic field and of solar eruptions, including solar flares and coronal mass ejections (CMEs). Unfortunately, even with the existing state-of-the-art solar physics satellites, only the photospheric magnetic field can be measured. We first review the 3D extrapolation of the coronal magnetic fields from measurements of the photospheric field. Specifically, we focus on the nonlinear force-free field (NLFFF) approximation extrapolated from the three components of the photospheric magnetic field. On the other hand, because in the force-free approximation the NLFFF is reconstructed for equilibrium states, the onset and dynamics of solar flares and CMEs cannot be obtained from these calculations. Recently, MHD simulations using the NLFFF as an initial condition have been proposed for understanding these dynamics in a more realistic scenario. These results have begun to reveal complex dynamics, some of which have not been inferred from previous simulations of hypothetical situations, and they have also successfully reproduced some observed phenomena. Although MHD simulations play a vital role in explaining a number of observed phenomena, there still remains much to be

understood. Herein, we review the results obtained by state-of-the-art MHD modeling combined with the NLFFF. **13 February 2011, 15 February 2011, 11 September 2011, 29 March 2014**

Structure and Stability of Magnetic Fields in Solar Active Region12192 Based on Nonlinear Force-Free Field Modeling

S. **Inoue**, K. Hayashi, K. Kusano
ApJ **2016**
http://arxiv.org/pdf/1601.00791v1.pdf
We analyze a three-dimensional (3D) magnetic structure and its stability in large solar active region(AR) 12192, using the 3D coronal magnetic field constructed under a nonlinear force-free field (NLFFF) approximation. In particular, we focus on the magnetic structure that produced an X3.1-class flare which is one of the X-class flares observed in AR 12192. According to our analysis, the AR contains multiple-flux-tube system, {\it e.g.}, a large flux tube, both of whose footpoints are anchored to the large bipole field, under which other tubes exist close to a polarity inversion line (PIL). These various flux tubes of different sizes and shapes coexist there. In particular, the later are embedded along the PIL, which produces a favorable shape for the tether-cutting reconnection and is related to the X-class solar flare. We further found that most of magnetic twists are not released even after the flare, which is consistent with the fact that no observational evidence for major eruptions was found. On the other hand, the upper part of the flux tube is beyond a critical decay index, essential for the excitation of torus instability before the flare, even though no coronal mass ejections (CMEs) were observed. We discuss the stability of the complicated flux tube system and suggest the reason for the existence of the stable flux tube. In addition, we further point out a possibility for tracing the shape of flare ribbons, on the basis of a detailed structural analysis of the NLFFF before a flare. **October 24, 2014**

Magnetohydrodynamic Simulation of the X2.2 Solar Flare on 2011 February 15: II. Dynamics Connecting the Solar Flare and the Coronal Mass Ejection

S. **Inoue**, K. Hayashi, T. Magara, G. S. Choe, Y. D. Park
ApJ **803** 73 **2015**
http://arxiv.org/pdf/1501.07663v2.pdf
We clarify a relationship of the dynamics of a solar flare and a growing Coronal Mass Ejection (CME) by investigating the dynamics of magnetic fields during the X2.2-class flare taking place in the solar active region 11158 on **2011 February 15**, based on simulation results obtained from Inoue et al. 2014. We found that the strongly twisted lines formed through the tether-cutting reconnection in the twisted lines of a nonlinear force-free field (NLFFF) can break the force balance within the magnetic field, resulting in their launch from the solar surface. We further discover that a large-scale flux tube is formed during the eruption as a result of the tether-cutting reconnection between the eruptive strongly twisted lines and these ambient weakly twisted lines. Then the newly formed large flux tube exceeds the critical height of the torus instability. The tether-cutting reconnection thus plays an important role in the triggering a CME. Furthermore, we found that the tangential fields at the solar surface illustrate different phases in the formation of the flux tube and its ascending phase over the threshold of the torus instability. We will discuss about these dynamics in detail.

Magnetohydrodynamic Simulation of the X2.2 Solar Flare on 2011 February 15: I. Comparison with the Observations

S. **Inoue**, K. Hayashi, T. Magara, G. S. Choe, Y. D. Park
E-print, June 2014; ApJ 788 182 **2014**
http://arxiv.org/pdf/1404.3257v1.pdf
We performed a magnetohydrodynamic (MHD) simulation using a nonlinear force-free field (NLFFF) in solar active region 11158 to clarify the dynamics of an X2.2-class solar flare. We found that the NLFFF never shows the drastic dynamics seen in observations, i.e., it is in stable state against the perturbations. On the other hand, the MHD simulation shows that when the strongly twisted lines are formed at close to the neutral line, which are produced via tether-cutting reconnection in the twisted lines of the NLFFF, consequently they erupt away from the solar surface via the complicated reconnection. This result supports the argument that the strongly twisted lines formed in NLFFF via tether-cutting reconnection are responsible for breaking the force balance condition of the magnetic fields in the lower solar corona. In addition to this the dynamical evolution of these field lines reveals that at the initial stage the spatial pattern of the footpoints caused by the reconnection of the twisted lines appropriately maps the distribution of the observed two-ribbon flares. Interestingly, after the flare the reconnected field lines convert into the structure like the post flare loops, which is analogous to EUV image taken by SDO. Eventually, we found that the twisted lines exceed a critical height at which the flux tube becomes unstable to the torus instability. These results illustrate the reliability of our simulation and also provide an important relationship between flare-CME dynamics.

MAGNETIC STRUCTURE PRODUCING X- AND M-CLASS SOLAR FLARES IN SOLAR ACTIVE REGION 11158

S. **Inoue**1, K. Hayashi2, D. Shiota3,4, T. Magara1, and G. S. Choe

2013 ApJ 770 79

We study the three-dimensional magnetic structure of the solar active region 11158, which produced one X-class and several M-class flares on **2011 February 13-16**. We focus on the magnetic twist in four flare events, **M6.6, X2.2, M1.0, and M1.1**. The magnetic twist is estimated from the nonlinear force-free field extrapolated from the vector fields obtained from the Helioseismic and Magnetic Imager on board the Solar Dynamic Observatory using the magnetohydrodynamic relaxation method developed by Inoue et al. We found that strongly twisted lines ranging from half-turn to one-turn twists were built up just before the M6.6 and X2.2 flares and disappeared after that. Because most of the twists remaining after these flares were less than a half-turn twist, this result suggests that the buildup of magnetic twist over the half-turn twist is a key process in the production of large flares. On the other hand, even though these strong twists were also built up just before the M1.0 and M1.1 flares, most of them remained afterward. Careful topological analysis before the M1.0 and M1.1 flares shows that the strongly twisted lines were surrounded mostly by the weakly twisted lines formed in accordance with the clockwise motion of the positive sunspot, whose footpoints are rooted in strong magnetic flux regions. These results imply that these weakly twisted lines might suppress the activity of the strongly twisted lines in the last two M-class flares.

BUILDUP AND RELEASE OF MAGNETIC TWIST DURING THE X3.4 SOLAR FLARE OF 2006 DECEMBER 13

S. **Inoue**1, D. Shiota2, T. T. Yamamoto3, V. S. Pandey1, T. Magara1, and G. S. Choe

2012 ApJ 760 17

We analyze the temporal evolution of the three-dimensional magnetic structure of the flaring active region (AR) NOAA 10930 by using the nonlinear force-free fields extrapolated from the photospheric vector magnetic fields observed by the Solar Optical Telescope on board Hinode. This AR consisted mainly of two types of twisted magnetic field lines: one has a strong negative (left-handed) twist due to the counterclockwise motion of the positive sunspot and is rooted in the regions of both polarities in the sunspot at a considerable distance from the polarity inversion line (PIL). In the flare phase, dramatic magnetic reconnection occurs in those negatively twisted lines in which the absolute value of the twist is greater than a half-turn. The other type consists of both positively and negatively twisted field lines formed relatively close to the PIL between two sunspots. A strong Ca II image began to brighten in this region of mixed polarity, in which the positively twisted field lines were found to be injected within one day across the pre-existing negatively twisted region, along which strong currents were embedded. Consequently, the central region near the PIL contains a mix of differently twisted field lines and the strong currents may play a prominent role in flare onset.

NONLINEAR FORCE-FREE MODELING OF A THREE-DIMENSIONAL SIGMOID OBSERVED ON THE SUN

S. **Inoue**1,2, T. Magara2, S. Watari1 and G. S. Choe

2012 ApJ 747 65, **File**

In this work, we analyze the characteristics of the three-dimensional magnetic structure of a sigmoid observed over an active region (AR 10930) and followed by X-class flares. This is accomplished by combining a nonlinear force-free field (NLFFF) model of a coronal magnetic field and the high-resolution vector-field measurement of a photospheric magnetic field by Hinode. The key findings of our analysis reveal that the value of the X-ray intensity associated with the sigmoid is more sensitive to the strength of the electric current rather than the twist of the field lines. The strong electric current flows along the magnetic field lines and composes the central part of the sigmoid, even though the twist of the field lines is weak in that region. On the other hand, the outer region (i.e., the elbow part) of the sigmoid is basically occupied by field lines of strong twist and weak current density. Consequently, weak X-ray emission is observed. As the initial Ca II illumination basically occurs from the central part of the sigmoid, this region plays an important role in determining the onset mechanism of the flare despite its weak twisted field-line configuration. We also compare our results with the magnetohydrodynamic simulation for the formation of a sigmoid. Although the estimated values of the twist from the simulation are found to be a little higher than the values obtained from the NLFFF, we find that the field-line configurations generated by the simulation and NLFFF are remarkably analogous as long as we deal with the lower coronal region. **2006 December 13**

TWIST AND CONNECTIVITY OF MAGNETIC FIELD LINES IN THE SOLAR ACTIVE REGION NOAA 10930

S. **Inoue**1, K. Kusano2,5, T. Magara3, D. Shiota4 and T. T. Yamamoto

2011 ApJ 738 161

Twist and connectivity of magnetic field lines in the flare-productive active region NOAA 10930 are investigated in terms of the vector magnetograms observed by the Solar Optical Telescope on board the Hinode satellite and the

nonlinear force-free field (NLFFF) extrapolation. First, we show that the footpoints of magnetic field lines reconstructed by the NLFFF correspond well to the conjugate pair of highly sheared flare ribbons on the Ca II images, which were observed by Hinode as an X3.4 class flare on **2006 December 13**. This demonstrates that the NLFFF extrapolation may be used to analyze the magnetic field connectivity. Second, we find that the twist of magnetic field lines anchored on the flare ribbons increased as the ribbons moved away from the magnetic polarity inversion line in the early phase of the flare. This suggests that magnetic reconnection might commence from a region located below the most strongly twisted field. Third, we reveal that the magnetic flux twisted more than a half turn and gradually increased during the last one day prior to the onset of the flare, and that it quickly decreased for two hours after the flare. This is consistent with the store-and-release scenario of magnetic helicity. However, within this active region, only a small fraction of the flux was twisted by more than one full turn and the field lines that reconnected first were twisted less than one turn. These results imply that the kink mode instability could hardly occur, at least before the onset of flare. Based on our results, we discuss the trigger process of solar flares.

ESTIMATING THE PROPERTIES OF HARD X-RAY SOLAR FLARES BY CONSTRAINING MODEL PARAMETERS

J. **Ireland**1, A. K. Tolbert2, R. A. Schwartz2, G. D. Holman3, and B. R. Dennis
2013 ApJ 769 89

We wish to better constrain the properties of solar flares by exploring how parameterized models of solar flares interact with uncertainty estimation methods. We compare four different methods of calculating uncertainty estimates in fitting parameterized models to Ramaty High Energy Solar Spectroscopic Imager X-ray spectra, considering only statistical sources of error. Three of the four methods are based on estimating the scale-size of the minimum in a hypersurface formed by the weighted sum of the squares of the differences between the model fit and the data as a function of the fit parameters, and are implemented as commonly practiced. The fourth method is also based on the difference between the data and the model, but instead uses Bayesian data analysis and Markov chain Monte Carlo (MCMC) techniques to calculate an uncertainty estimate. Two flare spectra are modeled: one from the Geostationary Operational Environmental Satellite X1.3 class flare of **2005 January 19**, and the other from the X4.8 flare of **2002 July 23**. We find that the four methods give approximately the same uncertainty estimates for the 2005 January 19 spectral fit parameters, but lead to very different uncertainty estimates for the 2002 July 23 spectral fit. This is because each method implements different analyses of the hypersurface, yielding method-dependent results that can differ greatly depending on the shape of the hypersurface. The hypersurface arising from the 2005 January 19 analysis is consistent with a normal distribution; therefore, the assumptions behind the three non-Bayesian uncertainty estimation methods are satisfied and similar estimates are found. The 2002 July 23 analysis shows that the hypersurface is not consistent with a normal distribution, indicating that the assumptions behind the three non-Bayesian uncertainty estimation methods are not satisfied, leading to differing estimates of the uncertainty. We find that the shape of the hypersurface is crucial in understanding the output from each uncertainty estimation technique, and that a crucial factor determining the shape of hypersurface is the location of the low-energy cutoff relative to energies where the thermal emission dominates. The Bayesian/MCMC approach also allows us to provide detailed information on probable values of the low-energy cutoff, Ec , a crucial parameter in defining the energy content of the flare-accelerated electrons. We show that for the 2002 July 23 flare data, there is a 95% probability that Ec lies below approximately 40 keV, and a 68% probability that it lies in the range 7-36 keV. Further, the low-energy cutoff is more likely to be in the range 25-35 keV than in any other 10 keV wide energy range. The low-energy cutoff for the 2005 January 19 flare is more tightly constrained to 107 ± 4 keV with 68% probability. Using the Bayesian/MCMC approach, we also estimate for the first time probability density functions for the total number of flare-accelerated electrons and the energy they carry for each flare studied. For the 2002 July 23 event, these probability density functions are asymmetric with long tails orders of magnitude higher than the most probable value, caused by the poorly constrained value of the low-energy cutoff. The most probable electron power is estimated at 1028.1 erg s–1, with a 68% credible interval estimated at 1028.1-1029.0 erg s–1, and a 95% credible interval estimated at 1028.0-1030.2 erg s–1. For the 2005 January 19 flare spectrum, the probability density functions for the total number of flare-accelerated electrons and their energy are much more symmetric and narrow: the most probable electron power is estimated at 1027.66 ± 0.01 erg s–1 (68% credible intervals). However, in this case the uncertainty due to systematic sources of error is estimated to dominate the uncertainty due to statistical sources of error.

X-Ray Flares and Activity Complexes on the Sun in Solar Cycle 24

Isaeva, E. S.; Tomozov, V. M.; Yazev, S. A.
Astronomy Reports, Volume 64, Issue 1, p.58-65, **2020**
https://link.springer.com/content/pdf/10.1134/S1063772920010035.pdf

The statistical relationship between activity complex (ACs) on the Sun and solar flares with GOES X-ray classes higher than M1.0 (744 events) is analyzed for the 24th solar-activity cycle (before January 2019). All groups of sunspots are divided into three classes, corresponding to those in cores and branches of ACs and those outside of ACs. It is shown that 78% of the flares considered occur predominantly in groups of sunspots in AC cores and branches. The specific number of flares in AC cores exceeds the corresponding number in AC branches and outside of ACs by a factor of 2.5. 87% of LDE flares of the indicated classes, 82% of all strong proton flares generating fluxes of energetic protons at the Earth's orbit, and 74% of all gamma-ray flares in Cycle 24 were associated with ACs.

Automatic Detection of Occulted Hard X-ray Flares Using Deep-Learning Methods

Shin-nosuke **Ishikawa**, Hideaki Matsumura, Yasunobu Uchiyama, Lindsay Glesener

Solar Phys. **296**, Article number: 39 **2021**
https://arxiv.org/pdf/2101.11550.pdf
https://link.springer.com/content/pdf/10.1007/s11207-021-01780-x.pdf

We present a concept for a machine-learning classification of hard X-ray (HXR) emissions from solar flares observed by the Reuven Ramaty High Energy Solar Spectroscopic Imager (RHESSI), identifying flares that are either occulted by the solar limb or located on the solar disk. Although HXR observations of occulted flares are important for particle-acceleration studies, HXR data analyses for past observations were time consuming and required specialized expertise. Machine-learning techniques are promising for this situation, and we constructed a sample model to demonstrate the concept using a deep-learning technique. Input data to the model are HXR spectrograms that are easily produced from RHESSI data. The model can detect occulted flares without the need for image reconstruction nor for visual inspection by experts. A technique of convolutional neural networks was used in this model by regarding the input data as images. Our model achieved a classification accuracy better than 90 %, and the ability for the application of the method to either event screening or for an event alert for occulted flares was successfully demonstrated.

Hot Plasma in a Quiescent Solar Active Region as Measured by RHESSI, XRT, and AIA

Shin-nosuke **Ishikawa**1 and Säm Krucker

2019 ApJ 876 111
http://sci-hub.se/10.3847/1538-4357/ab13a1

This paper investigates a quiescent (nonflaring) active region observed on 2010 July 13 in extreme ultraviolet (EUV), soft X-ray (SXR), and hard X-rays to search for a hot component that is speculated to be a key signature of coronal heating. We use a combination of Reuven Ramaty High Energy Solar Spectroscopic Imager (RHESSI) imaging and long-duration time integration (up to 40 minutes) to detect the active regions in the 3–8 keV range during apparently nonflaring times. The RHESSI imaging reveals a hot component that originates from the entire active region, as speculated for a nanoflare scenario where the entire active region is filled with a large number of unresolved small energy releases. An isothermal fit to the RHESSI data gives temperatures around ~7 MK with an emission measure of several times 1046 cm−3. Adding EUV and SXR observations taken by AIA and the X-ray Telescope, respectively, we derive a differential emission measure (DEM) that shows a peak between 2 and 3 MK with a steeply decreasing high-temperature tail, similar to what has been previously reported. The derived DEM reveals that a wide range of temperatures contributes to the RHESSI flux (e.g., 40% of the 4 keV emission being produced by plasma below 5 MK, while emission at 7 keV is almost exclusively from plasmas above 5 MK) indicating that the RHESSI spectrum should not be fitted with an isothermal. The hot component has a rather small emission measure (~0.1% of the total EM is above 5 MK), and the derived thermal energy content is of the order of 10% for a filling factor of unity, or potentially below 1% for smaller filling factors.

Detection of nanoflare-heated plasma in the solar corona by the FOXSI-2 sounding rocket

Ishikawa, Shin-nosuke; Glesener, Lindsay; Krucker, Säm; Christe, Steven; Buitrago-Casas, Juan Camilo; Narukage, Noriyuki; Vievering, Juliana

Nature Astronomy, Volume 1, p. 771-774, **2017**

The processes that heat the solar and stellar coronae to several million kelvins, compared with the much cooler photosphere (5,800 K for the Sun), are still not well known1. One proposed mechanism is heating via a large number of small, unresolved, impulsive heating events called nanoflares2. Each event would heat and cool quickly, and the average effect would be a broad range of temperatures including a small amount of extremely hot plasma. However, detecting these faint, hot traces in the presence of brighter, cooler emission is observationally challenging. Here we present hard X-ray data from the second flight of the Focusing Optics X-ray Solar Imager (FOXSI-2), which detected emission above 7 keV from an active region of the Sun with no obvious individual X-ray flare emission. Through differential emission measure computations, we ascribe this emission to plasma heated above 10 MK, providing evidence for the existence of solar nanoflares. The quantitative evaluation of the hot plasma strongly constrains the coronal heating models.

Hunting for Hidden Tiny Flares

Shin-nosuke **ISHIKAWA**

RHESSI Nuggets#312 November **2017**
http://sprg.ssl.berkeley.edu/~tohban/wiki/index.php/Hunting_for_Hidden_Tiny_Flares

One idea is to search for an extra hot component in the coronal plasma during in the absence of a time-series signature such as a flare (Ref. [2]). Since these weaker flares energy releases would need to cool from a maximum temperature, very hot (say, >10 MK) plasma could be present at all times if the tiny flares occur continuously. Therefore we coud

interpret any >10 MK "superhot" component as a signature of ensamble of such tiny flares. If we find them such high temperatures even in the absence of localized brightenings, it would suggest the presence of these tiny flares.
11 Dec 2014

Constraining hot plasma in a non-flaring solar active region with FOXSI hard X-ray observations

Shin-nosuke **ISHIKAWA**,1,∗ Lindsay GLESENER,2,∗ Steven CHRISTE,3,∗Kazunori ISHIBASHI,4,∗ David H. BROOKS,5,∗ David R. WILLIAMS,6,∗Masumi SHIMOJO,1,∗ Nobuharu SAKO,1,∗ and Sa.m KRUCKER2,7,∗

Publ. Astron. Soc. Japan (**2014**) 66 (SP1), S15 (1–7)

http://arxiv.org/pdf/1509.05288v1.pdf

We present new constraints on the high-temperature emission measure of a non-flaring solar active region using observations from the recently flown Focusing Optics X-ray Solar Imager (FOXSI) sounding rocket payload. FOXSI has performed the first focused hard X-ray (HXR) observation of the Sun in its first successful flight on **2012 November 2**. Focusing optics, combined with small strip detectors, enable high-sensitivity observations with respect to previous indirect imagers. This capability, along with the sensitivity of the HXR regime to high-temperature emission, offers the potential to better characterize high-temperature plasma in the corona as predicted by nanoflare heating models. We present a joint analysis of the differential emission measure (DEM) of active region 11602 using coordinated observations by FOXSI, Hinode/XRT, and Hinode/EIS. The Hinode-derived DEM predicts significant emission measure between 1MK and 3MK, with a peak in the DEM predicted at 2.0–2.5MK. The combined XRT and EIS DEM also shows emission from a smaller population of plasma above 8MK. This is contradicted by FOXSI observations that significantly constrain emission above 8 MK. This suggests that the Hinode DEM analysis has larger uncertainties at higher temperatures and that >8MK plasma above an emission measure of 3×1044 cm−3 is excluded in this active region.

SUZAKU/WAM AND RHESSI OBSERVATIONS OF NON-THERMAL ELECTRONS IN SOLAR MICROFLARES

Shin-nosuke **Ishikawa**1,2, Säm Krucker2,3, Masanori Ohno4, and Robert P. Lin

2013 ApJ 765 143

We report on hard X-ray spectroscopy of solar microflares observed by the Wide-band All-sky Monitor (WAM), on board the Suzaku satellite, and by RHESSI. WAM transient data provide wide energy band (50 keV-5 MeV) spectra over a large field of view (~2π sr) with a time resolution of 1 s. WAM is attractive as a hard X-ray solar flare monitor due to its large effective area (~800 cm2 at 100 keV, ~13 times larger than that of RHESSI). In particular, this makes it possible to search for high energy emission in microflares that is well below the RHESSI background. The WAM solar flare list contains six GOES B-class microflares that were simultaneously observed by RHESSI between the launch of Suzaku in 2005 July and 2010 March. At **100 keV**, the detected WAM fluxes are more than ~20 times below the typical RHESSI instrumental background count rates. The RHESSI and WAM non-thermal spectra are in good agreement with a single power law with photon spectral indices between 3.3 and 4.5. In a second step, we also searched the RHESSI microflare list for events that should be detectable by WAM, assuming that the non-thermal power-law emission seen by RHESSI extends to >50 keV. From the **12 detectable events** between 2005 July and 2007 February, 11 were indeed seen by WAM. This shows that microflares, similar to regular flares, can accelerate electrons to energies up to at least 100 keV.

ON THE RELATION OF ABOVE-THE-LOOP AND FOOTPOINT HARD X-RAY SOURCES IN SOLAR FLARES

S. **Ishikawa**1,2,3, Säm Krucker1,4, T. Takahashi2,3 and R. P. Lin

2011 ApJ 737 48

We report on the most prominent example of an above-the-loop hard X-ray source in the extensive solar flare database of RHESSI. The limb flare of **2003 October 22** around 20 UT resembles the famous Masuda flare, except that only one of the footpoint sources is visible with the other one occulted. However, even for this very prominent event, the above-the-loop source is only visible during one of the four hard X-ray peaks, highlighting the rare occurrence of above-the-loop sources that are equally bright as footpoint sources. The relative timing between the above-the-loop and footpoint sources shows that the coronal source peaks about 10 s before the footpoint source and decays during the time the footpoint source is most prominent. Furthermore, the derived number of non-thermal electrons within the above-the-loop source is large enough to provide the needed number of precipitating electrons to account for the footpoint emission over the duration of the hard X-ray peak. Hence, these observations support the simple scenario where bulk energization is accelerating all electrons within the above-the-loop source and precipitating electrons are emptying out of the above-the-loop source to produce the footpoint emissions

Suzaku Microflares

S. **Ishikawa**

RHESSI Science Nugget No. 154, **2011**

http://sprg.ssl.berkeley.edu/~tohban/wiki/index.php/Suzaku_Microflares

This Nugget introduces hard X-ray observations with the large effective area of the Wide-band All-sky Monitor (WAM) onboard the Suzaku satellite. The large effective area of the Suzaku/WAM instrument makes it attractive for solar flare observation. WAM has detected small flares down to the GOES B-class, i.e. microflares, and WAM data provide complementary information to RHESSI data. WAM time profiles are similar to RHESSI non-thermal observations and the joint spectra are well fitted by single power laws. Thus so far we can say that we have not detected any physical distinctions between flares and microflares. Microflares also strongly accelerate non-thermal electrons to comparably high energies. **Microflares too involve powerful particle acceleration.**

RHESSI IMAGING SURVEY OF γ -RAY BREMSSTRAHLUNG EMISSION IN SOLAR FLARES

S. **Ishikawa**[1,2], S¨am Krucker[3,4], T. Takahashi[1,2], and R. P. Lin

Astrophysical Journal, 728:22 (7pp), **2011** February

We present a high-energy (>150 keV) imaging survey of all solar γ -ray flares observed by the *Reuven Ramaty High Energy Solar Spectroscopic Imager* (*RHESSI*) to study bremsstrahlung emission from relativistic electrons. Using *RHESSI* rear segment data, images in the energy range from 150 to 450 keV integrated over the total duration of the impulsive phase of the flare are derived. Out of the 29 γ -ray peaks in 26 *RHESSI* flares, we successfully obtained images for 21 γ -ray peaks in 20 flares. The remaining eight peaks have >150 keV fluences of less than a few hundred photons per cm2 and counting statistics are too poor for detailed imaging. The flux ratio of the footpoint sources is found to be similar at 50 keV and above 150 keV, indicating that relativistic electrons are present in both footpoints of the flare loop. No correlation between the footpoint separation and the fluence ratio of the 2.2 MeV line and the >300 keV photons is found. This indicates that the relative efficiency of proton to electron acceleration does not depend on loop length, as could have been expected from stochastic acceleration models. As previously reported, the three flares with the best counting statistics show not only footpoint emission, but also a coronal γ -ray bremsstrahlung source. For events with lower counting statistics, no coronal source could be identified. However, instrumental limitation could easily hide a coronal source for events with lower statistics, suggesting that coronal γ -ray bremsstrahlung sources are nevertheless a general feature of γ -ray flares.

Table

Particle Acceleration and Heating in Regions of Magnetic Flux Emergence

Heinz **Isliker**, Vasilis Archontis, Loukas Vlahos

ApJ **2019**

https://arxiv.org/pdf/1907.04296.pdf

https://doi.org/10.3847/1538-4357/ab30c6

The interaction between emerging and pre-existing magnetic fields in the solar atmosphere can trigger several dynamic phenomena, such as eruptions and jets. A key element during this interaction is the formation of large scale current sheets and, eventually, their fragmentation that leads to the creation of a strongly turbulent environment. In this paper, we study the kinetic aspects of the interaction (reconnection) between emerging and ambient magnetic fields. We show that the statistical properties of the spontaneously fragmented and fractal electric fields are responsible for the efficient heating and acceleration of charged particles, which form a power law tail at high energies on sub-second time scales. A fraction of the energized particles escapes from the acceleration volume, with a super-hot component with temperature close to 150MK, and with a power law high energy tail with index between -2 and -3. We estimate the transport coefficients in energy space from the dynamics of the charged particles inside the fragmented and fractal electric fields, and the solution of a fractional transport equation, as appropriate for a strongly turbulent plasma, agrees with the test particle simulations. We also show that the acceleration mechanism is not related to Fermi acceleration, and the Fokker Planck equation is inconsistent and not adequate as a transport model. Finally, we address the problem of correlations between spatial transport and transport in energy space. Our results confirm the observations reported for high energy particles (hard X-rays, type III bursts and solar energetic particles) during the emission of solar jets.

H. **Isobe**, M. Kubo, T. Minoshima, K. Ichimoto, Y. Katsukawa, T. D. Tarbell, S. Tsuneta, T. E. Berger, B. Lites, S. Nagata, T. Shimizu, R. A. Shine, Y. Suematsu, and A. M. Title

*Publ. Astron. Soc. Japan 59, pp.S807-S813 (**2007**)*

[Abstract], [HTML], [PDF(3719kb)], [PS.gz(22286kb)] (Movie1, Movie2)

The Solar Optical Telescope (SOT) on board the Hinode satellite observed an X3.4 class flare on 2006 December 13. A typical two-ribbon structure was observed, not only in the chromospheric Ca II H line, but also in the G-band and Fe I 6302 °A line. The high-resolution, seeing-free images achieved by SOT revealed, for the first time, sub-arcsec fine structures of the “white light” flare. The G-band flare ribbons on sunspot umbrae showed a sharp leading edge, followed by a diffuse inside, as well as a previously known core–halo structure. The underlying structures, such as umbral dots, penumbral filaments, and granules, were visible in the flare ribbons. Assuming that the sharp leading edge was directly heated by a particle beam and the diffuse parts were heated by radiative back-warming, we estimated the depth of the diffuse flare emission using an intensity profile of the flare ribbon. We found that the depth of the diffuse emission was about 100km or less from the height of the source of radiative back-warming. The flare ribbons were also visible in the Stokes-V images of Fe I 6302 °A, as a transient polarity reversal. This is probably related to a “magnetic transient” reported in the literature. The intensity increase in Stokes-I images indicates that the Fe I 6302 °A line was significantly deformed by the flare, which may cause such a magnetic transient.

Numerical MHD Simulations of Reconnection in Solar Flares: Effects of the Magnetic-Field Strength in the Current Sheet

I. **Izquierdo-Guzmán**, J. J. González-Avilés & F. S. Guzmán
Solar Physics volume 298, Article number: 109 (**2023**)
https://doi.org/10.1007/s11207-023-02202-w
We simulate the evolution of reconnection in solar flares to study the influence of magnetic-field strength and thermal conduction on the dynamics of the magnetic-reconnection and energy-conversion processes. For this, we solve the 2.5D resistive magnetohydrodynamics (MHD) equations with thermal conduction on a domain that contains the chromosphere–corona interface. The flare is triggered at a null point where a Gaussian resistivity distribution is maximum, and further evolution is tracked. The parameter space considers magnetic-field strength [B0] between 22 G and 50 G, and thermal conductivity [κ] in the range from zero to 10−1110−11 W m−1K−7/2−7/2. In this parameter space, we find that the magnetic field determines the reconnection rate, which can change by a 100% in the range of B0, whereas thermal conduction can induce a rate change of at most 10%. We also measure the evolution of magnetic, internal, and kinetic energies in a region just above the reconnection point and measure their interplay. For all simulations, magnetic energy dominates initially and relaxes on a time scale of about 20 seconds. In this interval, the magnetic energy drops by ≈50%≈50%, whereas the internal energy grows by ≈100%≈100%. During the process, part of the energy becomes kinetic, which pushes the reconnection jet upwards and is bigger for the bigger B0 and smaller κ.

The Persistence of Apparent Non-Magnetostatic Equilibrium in NOAA 11035

Sarah A. **Jaeggli**
Proceedings of IAU Symposium 305: Polarimetry: From the Sun to Stars and Stellar Environments, **2015**
http://arxiv.org/pdf/1504.01325v1.pdf
NOAA 11035 was a highly sheared active region that appeared in December 2009 early in the new activity cycle. The leading polarity sunspot developed a highly unusual feature in its penumbra, an opposite polarity pore with a strong magnetic field in excess of 3500 G along one edge, which persisted for several days during the evolution of the region. This region was well observed by both space- and ground-based observatories, including Hinode, FIRS, TRACE, and SOHO. These observations, which span wavelength and atmospheric regimes, provide a complete picture of this unusual feature which may constitute a force-free magnetic field in the photosphere which is produced by the reconnection of magnetic loops low in the solar atmosphere. **2009-12-17**

Nanoflare Theory and Stochastic Reconnection

Amir **Jafari**1, Ethan T. Vishniac2, and Siyao Xu
2020 Res. Notes AAS 4 89
https://iopscience.iop.org/article/10.3847/2515-5172/ab9e02

Nanoflare Theory Revisited

Amir **Jafari**, Ethan Vishniac, Siyao Xu
ApJ **2020**
https://arxiv.org/pdf/2004.06186.pdf
Local magnetic reversals are an inseparable part of magnetohydrodynamic (MHD) turbulence whose collective outcome on an arbitrary scale in the inertial range may lead to a global stochastic reconnection event with a rate independent of small scale physics. We show that this picture is intimately related to the nanoflare theory of the solar corona. First, we argue that due to stochastic flux freezing, a generalized version of flux freezing in turbulence, the magnetic field follows the turbulent flow in a statistical sense. Bending and stretching an initially smooth field, therefore, the turbulence generally increases the magnetic spatial complexity. Strong magnetic shears associated with such a highly tangled field can trigger local reversals and field annihilations that convert magnetic energy into kinetic and thermal

energy respectively. The former maintains the turbulence, which incidentally continues to entangle the field completing the cycle, while the latter enhances the heat generation in the dissipative range. We support this theoretical picture invoking recent analytical and numerical studies which suggest a correlation between magnetic complexity and magnetic energy dissipation. The amplification of multiple local, in-phase reversals by super-linear Richardson diffusion may initiate a global reconnection at larger scales, however, even in the absence of such a global stochastic reconnection, the small scale reversals will continue to interact with the turbulence. We employ conventional scaling laws of MHD turbulence to illustrate that these local events are indeed efficient in both enhancing the turbulence and generating heat. Finally, using an MHD numerical simulation, we show that the time evolution of the magnetic complexity is statistically correlated with the kinetic energy injection rate and/or magnetic-to-thermal energy conversion rate.

Probing solar flare accelerated electron distributions with prospective X-ray polarimetry missions

Natasha L. S. **Jeffrey**, Pascal Saint-Hilaire, Eduard P. Kontar
A&A **2020**
https://arxiv.org/pdf/2008.07849.pdf
Solar flare electron acceleration is an extremely efficient process, but the method of acceleration is not well constrained. Two of the essential diagnostics: electron anisotropy (velocity angle to the guiding magnetic field) and the high energy cutoff (highest energy electrons produced by the acceleration conditions: mechanism, spatial extent, time), are important quantities that can help to constrain electron acceleration at the Sun but both are poorly determined. Here, using electron and X-ray transport simulations that account for both collisional and non-collisional transport processes such as turbulent scattering, and X-ray albedo, we show that X-ray polarization can be used to constrain the anisotropy of the accelerated electron distribution and the most energetic accelerated electrons together. Moreover, we show that prospective missions, e.g. CubeSat missions without imaging information, can be used alongside such simulations to determine these parameters. We conclude that a fuller understanding of flare acceleration processes will come from missions capable of both X-ray flux and polarization spectral measurements together. Although imaging polarimetry is highly desired, we demonstrate that spectro-polarimeters without imaging can also provide strong constraints on electron anisotropy and the high energy cutoff.

Probing Subsurface Flows in Active Region NOAA 12192 - Comparison with NOAA 10486

Kiran **Jain**, S.C. Tripathy, F. Hill
ApJ **849** 94 **2017**
https://arxiv.org/pdf/1710.02137.pdf
Active Region (AR) 12192 is the biggest AR observed in solar cycle 24 so far. This was a long-lived AR which survived for four Carrington rotations (CR) and exhibited several unusual phenomena. We measure the horizontal subsurface flows in this active region in multiple rotation using the ring-diagram technique of local helioseismology and the Global Oscillation Network Group (GONG+) Dopplergrams, and investigate how different was the plasma flow in AR 12192 from that in AR 10486. Both regions produced several high M- and X-class flares but had different CME productivity. Our analysis suggests that these ARs had unusually large horizontal flow amplitude with distinctly different directions. While meridional flow in AR 12192 was poleward that supports the flux transport to poles, it was equatorward in AR 10486. Furthermore, there was a sudden increase in the magnitude of estimated zonal flow in shallow layers in AR 12192 during the X3.1 flare, however, it reversed direction in AR 10486 with X17.2 flare. These flow patterns produced strong twists in horizontal velocity with depth in AR 10486 that persisted throughout the disk passage as opposed to AR 12192, which produced a twist only after the eruption of the X3.1 flare that disappeared soon after. Our study indicates that the sunspot rotation combined with the re-organization of magnetic field in AR 10486 was not sufficient to decrease the flow energy even after several large flares that might have triggered CMEs. Furthermore, in the absence of sunspot rotation in AR 12192, this re-organization of magnetic field contributed significantly to the substantial release of flow energy after the X3.1 flare. **2014/10/18-26, 2003/10/26-11/02**

Divergent Horizontal Sub-surface Flows within Active Region 11158

Kiran **Jain**, S.C. Tripathy, F. Hill
2015
http://arxiv.org/pdf/1508.00519v1.pdf
We measure the horizontal subsurface flow in a fast emerging active region (NOAA 11158) using the ring-diagram technique and the HMI high-spatial resolution Dopplergrams. This active region had a complex magnetic structure and displayed significant changes in the morphology during its disk passage. Over the period of six days from **2011 February 11 to 16**, the temporal variation in the magnitude of total velocity is found to follow the trend of magnetic field strength. We further analyze regions of individual magnetic polarity within AR 11158 and find that the horizontal velocity components in these sub-regions have significant variation with time and depth. The leading and trailing

polarity regions move faster than the mixed-polarity region. Further, both zonal and meridional components have opposite signs for trailing and leading polarity regions at all depths showing divergent flows within the active region. We also find a sharp decrease in the magnitude of total horizontal velocity in deeper layer around major flares. It is suggested that the re-organization of magnetic fields during flares combined with the sunspot rotation decreases the magnitude of horizontal flows or that the flow kinetic energy has been converted into the energy released by flares. After the decline in flare activity and the sunspot rotation, the flows tend to follow the pattern of the magnetic activity.We also observe less variation in the velocity components near the surface but these tend to increase with depth, further demonstrating that the deeper layers are more affected by the topology of active regions.

Probing the Role of Magnetic-Field Variations in NOAA AR 8038 in Producing a Solar Flare and CME on 12 May 1997

Rajmal **Jain**, Arun K. Awasthi, Babita Chandel, Lokesh Bharti, Y. Hanaoka & A. L. Kiplinger
Solar Physics, Volume 271, Numbers 1-2, 57-74, **2011**

We carried out a multi-wavelength study of a Coronal Mass Ejection (CME) and an associated flare, occurring on **12 May 1997**. We present a detailed investigation of magnetic-field variations in NOAA Active Region 8038 which was observed on the Sun during 7−16 May 1997. This region was quiet and decaying and produced only a very small flare activity during its disk passage. However, on 12 May 1997 it produced a CME and associated medium-size 1B/C1.3 flare. Detailed analyses of Hα filtergrams and SOHO/MDI magnetograms revealed continual but discrete surge activity, and emergence and cancellation of flux in this active region. The movie of these magnetograms revealed the two important results that the major opposite polarities of pre-existing region as well as in the emerging-flux region were approaching towards each other and moving magnetic features (MMF) were ejected from the major north polarity at a quasi-periodicity of about ten hours during 10−13 May 1997. These activities were probably caused by magnetic reconnection in the lower atmosphere driven by photospheric convergence motions, which were evident in magnetograms. The quantitative measurements of magnetic-field variations such as magnetic flux, gradient, and sunspot rotation revealed that in this active region, free energy was slowly being stored in the corona. Slow low-layer magnetic reconnection may be responsible for the storage of magnetic free energy in the corona and the formation of a sigmoidal core field or a flux rope leading to the eventual eruption. The occurrence of EUV brightenings in the sigmoidal core field prior to the rise of a flux rope suggests that the eruption was triggered by the inner tether-cutting reconnection, but not the external breakout reconnection. An impulsive acceleration, revealed from fast separation of the Hα ribbons of the first 150 seconds, suggests that the CME accelerated in the inner corona, which is also consistent with the temporal profile of the reconnection electric field. Based on observations and analysis we propose a qualitative model, and we conclude that the mass ejections, filament eruption, CME, and subsequent flare were connected with one another and should be regarded within the framework of a solar eruption.

Energy-Dependent Timing of Thermal Emission in Solar Flares

Rajmal **Jain**, Arun Kumar Awasthi, Arvind Singh Rajpurohit and Markus J. Aschwanden
Solar Physics, Volume 270, Number 1, 137-149, **2011**

We report solar flare plasma to be multi-thermal in nature based on the theoretical model and study of the energy-dependent timing of thermal emission in ten M-class flares. We employ high-resolution X-ray spectra observed by the Si detector of the “Solar X-ray Spectrometer” (SOXS). The SOXS onboard the Indian GSAT-2 spacecraft was launched by the GSLV-D2 rocket on 8 May 2003. Firstly we model the spectral evolution of the X-ray line and continuum emission flux F(ε) from the flare by integrating a series of isothermal plasma flux. We find that the multi-temperature integrated flux F(ε) is a power-law function of ε with a spectral index (γ)≈−4.65. Next, based on spectral-temporal evolution of the flares we find that the emission in the energy range E=4−15 keV is dominated by temperatures of T=12−50 MK, while the multi-thermal power-law DEM index (δ) varies in the range of −4.4 and −5.7. The temporal evolution of the X-ray flux F(ε,t) assuming a multi-temperature plasma governed by thermal conduction cooling reveals that the temperature-dependent cooling time varies between 296 and 4640 s and the electron density (n e) varies in the range of n e=(1.77−29.3)×1010 cm−3. Employing temporal evolution technique in the current study as an alternative method for separating thermal from nonthermal components in the energy spectra, we measure the break-energy point, ranging between 14 and 21±1.0 keV.

Investigation of the X-Ray Emission of the Large Arcade Flare of 2 March 1993

J. **Jakimiec**, M. Tomczak
Solar Physics, June **2014**, Volume 289, Issue 6, pp 2073-2089,

A large arcade flare, occurring on **2 March 1993**, has been investigated using X-ray observations recorded by the Yohkoh and GOES satellites and the Compton Gamma Ray Observatory. We analyzed the quasi-periodicity of the hard-X-ray (HXR) pulses in the impulsive phase of the flare and found a close similarity between the quasi-periodic sequence of the pulses to that observed in another large arcade flare, that of **2 November 1991**. This similarity helped to explain the strong HXR pulses which were recorded at the end of the impulsive phase as due to the inflow of dense plasma (coming from the chromospheric evaporation) into the acceleration volume inside the cusp. In HXR images a high flaring loop was seen with a triangular cusp structure at the top, where the electrons were efficiently accelerated. The sequence of HXR images allowed us to investigate complicated changes in the precipitation of the accelerated electrons toward the flare footpoints. We have shown that all these impulsive-phase observations can be easily explained in terms of the model of electron acceleration in oscillating magnetic traps located within the cusp structure. Some soft-X-ray (SXR) images were available for the late decay phase. They show a long arcade of SXR loops. Important information about the evolution of the flare during the slow decay phase is contained in the time variation of the temperature, T(t), and emission measure, EM(t). This information is the following: i) weak heating occurs during the slow decay phase and it slowly decreases; ii) the decrease in the heating determines a slow and smooth decrease in EM; iii) the coupling between the heating and the amount of the hot plasma makes the flare evolve along a sequence of quasi-steady states during the slow decay phase (QSS evolution).

Quasi-periodic Variations in the Hard X-ray Emission of a Large Arcade Flare

J. **Jakimiec**, M. Tomczak

Solar Physics, September **2013**, Volume 286, Issue 2, pp 427-440,

We investigated the quasi-periodic oscillations of the hard X-ray (HXR) emission of the large flare of **2 November 1991** using HXR light curves and soft X-ray and HXR images recorded with the Yohkoh X-ray telescopes. We analysed these observations and report five main results: i) The observations confirm that electrons are accelerated in oscillating magnetic traps that are contained within the cusp magnetic structure. ii) The chromospheric upflow increases the density within the magnetic traps, which in turn together with the higher amplitude of the trap oscillations increases the amplitude of the HXR pulses. iii) This increase stops when the density inside the traps increases progressively and inhibits the acceleration of electrons. iv) The model of oscillating magnetic traps is able to explain the time variation of the electron precipitation, the strong asymmetry in the precipitation of the accelerated electrons, and the systematic differences in the precipitation of 15 and 25 keV electrons. v) We have obtained direct observational evidence that strong HXR pulses are the result of the inflow into the accelerated volume of dense plasma from chromospheric evaporation.

Investigation of Quasi-periodic Variations in Hard X-Rays of Solar Flares. II. Further Investigation of Oscillating Magnetic Traps

J. **Jakimiec** and M. Tomczak

Solar Physics, Volume 278, Number 2 (**2012**), 393-410

In our recent paper (Jakimiec and Tomczak, Solar Physics 261, 233, 2010) we investigated quasi-periodic oscillations of hard X-rays during the impulsive phase of solar flares. We have come to the conclusion that they are caused by magnetosonic oscillations of magnetic traps within the volume of hard-X-ray (HXR) loop-top sources. In the present paper we investigate four flares that show clear quasi-periodic sequences of the HXR pulses. We also describe our phenomenological model of oscillating magnetic traps to show that it can explain the observed properties of the HXR oscillations. The main results are the following: i) Low-amplitude quasi-periodic oscillations occur before the impulsive phase of some flares. ii) The quasi-periodicity of the oscillations can change in some flares. We interpret this as being due to changes of the length of oscillating magnetic traps. iii) During the impulsive phase a significant part of the energy of accelerated (non-thermal) electrons is deposited within a HXR loop-top source. iv) The quick development of the impulsive phase is due to feedback between the pressure pulses by accelerated electrons and the amplitude of the magnetic-trap oscillation. v) The electron number density and magnetic field strength values obtained for the HXR loop-top sources in several flares fall within the limits of $N \approx (2-15)\times 1010$ cm−3, $B \approx (45-130)$ gauss. These results show that the HXR quasi-periodic oscillations contain important information about the energy release in solar flares.
18 Aug 1998

Investigation of Quasi-periodic Variations in Hard X-rays of Solar Flares

J. **Jakimiec** & M. Tomczak

Solar Phys., 261(2), 233–251, **2010**

The aim of the present paper is to use quasi-periodic oscillations in hard X-rays (HXRs) of solar flares as a diagnostic tool for the investigation of impulsive electron acceleration. We have selected a number of flares which showed quasi-periodic oscillations in hard X-rays and their loop-top sources could be easily recognized in HXR images. We have

considered MHD standing waves to explain the observed HXR oscillations. We interpret these HXR oscillations as being due to oscillations of magnetic traps within cusp-like magnetic structures. This is confirmed by the good correlation between periods of the oscillations and the sizes of the loop-top sources. We argue that a model of oscillating magnetic traps is adequate to explain the observations. During the compressions of a trap, particles are accelerated, but during its expansions plasma, coming from chromospheric evaporation, fills the trap, which explains the large number of electrons being accelerated during a sequence of strong pulses. The advantage of our model of oscillating magnetic traps is that it can explain both the pulses of electron acceleration and quasi-periodicity of their distribution in time.

Small electron acceleration episodes in the solar corona

Tomin **James**, Prasad Subramanian, Eduard P Kontar
MNRAS **2017**
https://arxiv.org/pdf/1706.04031.pdf
We study the energetics of nonthermal electrons produced in small acceleration episodes in the solar corona. We carried out an extensive survey spanning 2004--2015 and shortlisted 6 impulsive electron events detected at 1 AU that was not associated with large solar flares(GOES soft X-ray class > C1) or with coronal mass ejections. Each of these events had weak, but detectable hard Xray (HXR) emission near the west limb, and were associated with interplanetary type III bursts. In some respects, these events seem like weak counterparts of "cold/tenuous" flares. The energy carried by the HXR producing electron population was ≈1023 -- 1025 erg, while that in the corresponding population detected at 1 AU was ≈1024--1025 erg. The number of electrons that escape the coronal acceleration site and reach 1 AU constitute 6 % to 148 % of those that precipitate downwards to produce thick target HXR emission. **28-02-2004, 16-03-2004, 26-06-2004, 27-06-2004, 25-12-24**
Table 1. Impulsive electron events detected in-situ at 1 AU: first shortlist
Table 2. Final shortlist and spectral parameters

Two Distinct Types of CME-flare Relationships Based on SOHO and STEREO Observations

Soojoeng **Jang**1, Yong-Jae Moon1, Rok-Soon Kim2,3, Sujin Kim2,3, and Jae-Ok Lee2
2017 ApJ 845 169
https://iopscience.iop.org/article/10.3847/1538-4357/aa82b4/pdf
In this paper, we present two distinct types of coronal mass ejection (CME)-flare relationships according to their observing time differences using 107 events from 2010 to 2013. The observing time difference, ΔT, is defined as flare peak time minus CME first appearance time at Solar Terrestrial Relations Observatory (STEREO) COR1 field of view. There are 41 events for group A (ΔT < 0) and 66 events for group B (ΔT ≥ 0). We compare CME 3D parameters (speed and kinetic energy) based on multi-spacecraft data (SOlar and Heliospheric Observatory (SOHO) and STEREO A and B) and their associated flare properties (peak flux, fluence, and duration). Our main results are as follows. First, there are better relationships between CME and flare parameters for group B than that of group A. In particular, CME 3D kinetic energy for group B is well correlated with flare fluence with the correlation coefficient of 0.67, which is much stronger than that (cc = 0.31) of group A. Second, the events belonging to group A have short flare durations of less than 1 hr (mean = 21 minutes), while the events for group B have longer durations up to 4 hr (mean = 81 minutes). Third, the mean value of height at peak speed for group B is 4.05 Rs, which is noticeably higher than that of group A (1.89 Rs). This is well correlated with the CME acceleration duration (cc = 0.75). A higher height at peak speed and a longer acceleration duration of CME for group B could be explained by the fact that magnetic reconnections for group B continuously occur for a longer time than those for group A. **2011 September 7**

A multiple spacecraft detection of the 2 April 2022 M-class flare and filament eruption during the first close Solar Orbiter perihelion

M. **Janvier**, S. Mzerguat, P. R. Young, É. Buchlin, +++
A&A 677, A130 **2023**
https://arxiv.org/pdf/2307.02396.pdf
https://www.aanda.org/articles/aa/pdf/2023/09/aa46321-23.pdf
Context. The Solar Orbiter mission completed its first remote-sensing observation windows in the spring of 2022. On 2 April 2022, an M-class flare followed by a filament eruption was seen both by the instruments on board the mission and from several observatories in Earth's orbit, providing an unprecedented view of a flaring region with a large range of observations.
Aims. We aim to understand the nature of the flaring and filament eruption events via the analysis of the available dataset. The complexity of the observed features is compared with the predictions given by the standard flare model in 3D.
Methods. In this paper, we use the observations from a multi-view dataset, which includes extreme ultraviolet (EUV) imaging to spectroscopy and magnetic field measurements. These data come from the Interface Region Imaging Spectrograph, the Solar Dynamics Observatory, Hinode, as well as several instruments on Solar Orbiter.

Results. The large temporal coverage of the region allows us to analyse the whole sequence of the filament eruption starting with its pre-eruptive state. Information given by spectropolarimetry from SDO/HMI and Solar Orbiter PHI/HRT shows that a parasitic polarity emerging underneath the filament is responsible for bringing the flux rope to an unstable state. As the flux rope erupts, Hinode EIS captures blue-shifted emission in the transition region and coronal lines in the northern leg of the flux rope prior to the flare peak. This may be revealing the unwinding of one of the flux rope legs. At the same time, Solar Orbiter SPICE captures the whole region, complementing the Doppler diagnostics of the filament eruption. Analyses of the formation and evolution of a complex set of flare ribbons and loops, of the hard and soft X-ray emissions with STIX, show that the parasitic emerging bipole plays an important role in the evolution of the flaring region.
Conclusions. The extensive dataset covering this M-class flare event demonstrates how important multiple viewpoints and varied observations are in order to understand the complexity of flaring regions. While the analysed data are overall consistent with the standard flare model, the present particular magnetic configuration shows that surrounding magnetic activity such as nearby emergence needs to be taken into account to fully understand the processes at work. This filament eruption is the first to be covered from different angles by spectroscopic instruments, and provides an unprecedented diagnostic of the multi-thermal structures present before and during the flare. This complete dataset of an eruptive event showcases the capabilities of coordinated observations with the Solar Orbiter mission.

3D magnetic reconnection and its application to solar flares **Review**

Miho **Janvier**

Journal of Plasma Physics Special Collection on New Perspectives in Plasma Astrophysics **2017**

2017, J. Plasma Phys., 83, 535830101

https://arxiv.org/pdf/1612.06513v1.pdf

http://sci-hub.tw/10.1017/S0022377817000034

Solar flares are powerful radiations occuring in the Sun's atmosphere. They are powered by magnetic reconnection, a phemonenon that can convert magnetic energy into other forms of energy such as heat and kinetic energy, and it is believed to be ubiquitous in the universe. With the ever increasing spatial and temporal resolutions of solar observations, as well as numerical simulations benefiting from increasing computer power, we can now probe into the nature and the characteristics of magnetic reconnection in 3D to better understand its consequences during eruptive flares in our star's atmosphere. We review in the following the efforts made on different fronts to approach the problem of magnetic reconnection. In particular, we will see how understanding the magnetic topology in 3D helps locating the most probable regions for reconnection to occur, how the current layer evolves in 3D and how reconnection leads to the formation of flux ropes, plasmoids and flaring loops. **6 September 2011**

Evolution of Flare Ribbons, Electric Currents and Quasi-separatrix Layers During an X-class Flare

M. **Janvier**, A. Savcheva, E. Pariat, S. Tassev, S. Millholland, V. Bommier, P. McCauley, S. McKillop, F. Dougan

A&A 591, A141 **2016**

http://arxiv.org/pdf/1604.07241v1.pdf **File**

The standard model for eruptive flares has in the past few years been extended to 3D. It predicts typical J-shaped photospheric footprints of the coronal current layer, forming at similar locations as the Quasi-Separatrix Layers (QSLs). Such a morphology is also found for flare ribbons observed in the EUV band, as well as in non-linear force-free field (NLFFF) magnetic field extrapolations and models. We study the evolution of the photospheric traces of the current density and flare ribbons, both obtained with the SDO instruments. We investigate the photospheric current evolution during the **6 September 2011** X-class flare (SOL2011-09-06T22:20) from observational data of the magnetic field obtained with HMI. This evolution is compared with that of the flare ribbons observed in the EUV filters of the AIA. We also compare the observed electric current density and the flare ribbon morphology with that of the QSLs computed from the flux rope insertion method/NLFFF model.
The NLFFF model shows the presence of a fan-spine configuration of overlying field lines, due to the presence of a parasitic polarity, embedding an elongated flux rope that appears in the observations as two parts of a filament. The QSLs, evolved via a magnetofrictional method, also show similar morphology and evolution as both the current ribbons and the EUV flare ribbons obtained at several times during the flare. For the first time, we propose a combined analysis of the photospheric traces of an eruptive flare, in a complex topology, with direct measurements of electric currents and QSLs from observational data and a magnetic field model. The results, obtained by two diff?erent and independent approaches, 1) confirm previous results of current increase during the impulsive phase of the flare, 2) show how NLFFF models can capture the essential physical signatures of flares even in a complex magnetic field topology.

From coronal observations to MHD simulations, the building blocks for 3D models of solar flares **Review**

Miho **Janvier**, Guillaume Aulanier, Pascal Demoulin
Solar Phys. Volume 290, Issue 12, pp 3425-3456 **2015 File**
http://arxiv.org/pdf/1505.05299v1.pdf
https://link.springer.com/content/pdf/10.1007/s11207-015-0710-3.pdf
doi:10.1007/s11207-015-0710-3
Solar flares are energetic events taking place in the Sun's atmosphere, and their effects can greatly impact the environment of the surrounding planets. In particular, eruptive flares, as opposed to confined flares, launch coronal mass ejections into the interplanetary medium, and as such, are one of the main drivers of space weather. After briefly reviewing the main characteristics of solar flares, we summarize the processes that can account for the build up and release of energy during their evolution. In particular, we focus on the development of recent 3D numerical simulations that explain many of the observed flare features. These simulations can also provide predictions of the dynamical evolution of coronal and photospheric magnetic field. Here we present a few observational examples that, together with numerical modelling, point to the underlying physical mechanisms of the eruptions. **18 March 1999 , 27 Feb 2000, 2 March 2000, 19 October 2001, 16/11/2002 ,17=07=2004, 20 January 2005 , 12 February 2007 , 18 August 2010 , 15 February 2011, 09/05/2011, e 22 October 2011, 15/01/2012, 14 October 2012, 11/03/2014**

Electric current in flares ribbons: observations and 3D standard model

M. **Janvier**, G. Aulanier, V. Bommier, B. Schmieder, P. D?moulin, E. Pariat
ApJ, 788 60. **2014**
http://arxiv.org/pdf/1402.2010v3.pdf
We present for the first time the evolution of the photospheric electric currents during an eruptive X-class flare, accurately predicted by the standard 3D flare model. We analyze this evolution for the **February 15, 2011** flare using HMI/SDO magnetic observations and find that localized currents in \J-shaped ribbons increase to double their pre-flare intensity. Our 3D flare model, developed with the OHM code, suggests that these current ribbons, which develop at the location of EUV brightenings seen with AIA imagery, are driven by the collapse of the flare's coronal current layer. These findings of increased currents restricted in localized ribbons are consistent with the overall free energy decrease during a flare, and the shape of these ribbons also give an indication on how much twisted the erupting flux rope is. Finally, this study further enhances the close correspondence obtained between the theoretical predictions of the standard 3D model and flare observations indicating that the main key physical elements are incorporated in the model.
See: Field-parallel Acceleration: Comment on the Paper "Electric Currents on the Flare Ribbons: Observations and Standard Model" by Janvier et al. (2014, ApJ, 788, 60)
G. **Haerendel**
2017 ApJ 847 143 http://iopscience.iop.org/article/10.3847/1538-4357/aa81d3/pdf

The 3D standard model for eruptive flares

Miho **Janvier**
RHESSI Science Nuggets, No. 226, May, **2014**
http://sprg.ssl.berkeley.edu/~tohban/wiki/index.php/The_3D_standard_model_for_eruptive_flares
Eruptive solar flares, associated with coronal mass ejections (CMEs), are important energetic events taking place in the solar corona. The intense magnetic energy release originates from magnetic reconnection, which is also responsible for newly formed magnetic structures that are ejected as CMEs. Solar coronal observations reveal typical 3D magnetic structures during eruptive flares: flux ropes (twisted magnetic field lines structures), ultimately ejected in the interplanetary medium, and hot and dense flare loops. Magnetic reconnection takes place in regions of drastic changes in the magnetic connectivity: these are separatrices, defining different domains of connectivity, or quasi-separatrix layers (QSLs), which generalize in 3D the regions of strong connectivity gradients.
With an MHD numerical simulation recreating the evolution of a flux rope expansion during an eruptive flare [Ref. 1], we propose a 3D-extended, more complete version of the standard model for eruptive flares. We present below new understandings offered by this model.
Our 3D standard model, built from a 3D MHD simulation, extends our understanding of the observational characteristics, as well as the underlying physical mechanisms of eruptive flares. Its main characteristics are outlined in the cartoon of Figure 1. This model shows that both flare loops and flux rope are constructed by 3D reconnection, in the thin coronal current layer that maps as J-shaped current/flare ribbons onto the photosphere. Field lines entering this region reconnect successively, leading to a slipping motion, as recently seen in coronal observations. This change of connectivity allows shear transfer from dynamically evolving pre- to post- reconnected field lines, and is often observed as a strong-to-weak shear transfer in flare loops observations. The flux rope, on the other hand, is constantly growing as reconnected twisted field lines construct its outer shell. From its ejection in the interplanetary medium, a flux rope can be detected as a magnetic cloud by in situ instruments away from the Sun. **2011-05-09, 2011-02-15, 2012-12-07, See Aulanier, G.**

The standard flare model in three dimensions III. Slip-running reconnection properties

Janvier M., Aulanier G., Pariat E., Demoulin P.
E-print, May **2013**, A&A, 555, A77 (**2013**)
http://arxiv.org/pdf/1305.4053v1.pdf
A standard model for eruptive flares aims at describing observational 3D features of the reconnecting coronal magnetic field. Extensions to the 2D model require the physical understanding of 3D reconnection processes at the origin of the magnetic configuration evolution. However, the properties of 3D reconnection without null point and separatrices still need to be analyzed. We focus on magnetic reconnection associated with the growth and evolution of a flux rope and associated flare loops during an eruptive flare. We aim at understanding the intrinsic characteristics of 3D reconnection in the presence of quasi-separatrix layers (QSLs), how QSL properties are related to the slip-running reconnection mode in general, and how this applies to eruptive flares in particular. We studied the slip-running reconnection of field lines in a magnetohydrodynamic simulation of an eruptive flare associated with a torus-unstable flux rope. The squashing degree and the mapping norm are two parameters related to the QSLs. We computed them to investigate their relation with the slip-running reconnection speed of selected field lines. Field lines associated with the flux rope and the flare loops undergo a continuous series of magnetic reconnection, which results in their super-Alfvénic slipping motion. The time profile of their slippage speed and the space distribution of the mapping norm are shown to be strongly correlated. We find that the motion speed is proportional to the mapping norm. Moreover, this slip-running motion becomes faster as the flux rope expands, since the 3D current layer evolves toward a current sheet, and QSLs to separatrices. The present analysis extends our understanding of the 3D slip-running reconnection regime. We identified a controlling parameter of the apparent velocity of field lines while they slip-reconnect, enabling the interpretation of the evolution of post flare loops. This work completes the standard model for flares and eruptions by giving its 3D properties.

Magnetic Field Evolution of the Solar Active Region 13664

Robert **Jarolim**, Astrid Veronig, Stefan Purkhart, Peijin Zhang, Matthias Rempel
ApJ **976** L12 **2024**
https://arxiv.org/pdf/2409.08124
https://iopscience.iop.org/article/10.3847/2041-8213/ad8914/pdf
On **2024 May 10/11**, the strongest geomagnetic storm since November 2003 has occurred, with a peak Dst index of -412 nT. The storm was caused by NOAA Active Region (AR) 13664, which was the source of a large number of coronal mass ejections and flares, including 12 X-class flares. Starting from about May 7, AR 13664 showed a steep increase in its size and (free) magnetic energy, along with increased flare activity. In this study, we perform 3D magnetic field extrapolations with the NF2 nonlinear-force free code based on physics informed neural networks (Jarolim et al. 2023). In addition, we introduce the computation of the vector potential to achieve divergence-free solutions. We extrapolate vector magnetograms from SDO/HMI at the full 12 minute cadence from 2024 May 5-00:00 to 11-04:36 UT, in order to understand the active regions magnetic evolution and the large eruptions it produced. The computed change in magnetic energy and free magnetic energy shows a clear correspondence to the flaring activity. Regions of free magnetic energy and depleted magnetic energy indicate the flare origin and are in good correspondence with observations in Extreme Ultraviolet. Our results suggest that the modeled solar flares are related to significant topological reconfigurations. We provide a detailed analysis of the X4.0-class flare on May 10, where we show that the interaction between separated magnetic domains is directly linked to major flaring events. With this study, we provide a comprehensive data set of the magnetic evolution of AR 13664 and make it publicly available for further analysis. **May 2024: 5-11, 8, 10, 11**

Deconstructing Solar Super Active Region 13664 in the Context of the Historic Geomagnetic Storm of 2024 May 10-11

Priyansh **Jaswal**, Suvadip Sinha, Dibyendu Nandy
ApJ **2024**
https://arxiv.org/pdf/2409.14752
The impact of solar-stellar activity on planetary environments is a topic of great interest within the Sun-Earth system as well as exoplanetary systems. In particular, extreme events such as flares and coronal mass ejections have a profound effect on planetary atmospheres. In May this year, a magnetic active region on the Sun (AR 13664) -- with a size exceeding hundred times that of Earth -- unleashed a large number of high energy X-class flares and associated mass ejections. The resulting Earth impact (geomagnetic storm) on May 10-11 was the strongest in the last two decades. We perform the first comprehensive analysis of the magnetic properties of the active region that spawned these flares and identify this to be a super active region with very rare physical characteristics. We also demonstrate how the rate of energization of the system is related to the flaring process. Our work illuminates how flare productive super active regions on the Sun and stars can be identified and what are their salient physical properties. Specifically, we put AR 13664 in historical context over the cumulative period of 1874 May-2024 June. We find that AR 13664 stands at 99.95 percentile in the distribution of area over 1874 May-2024 June, and at 99.10 percentile in terms of flux content among all ARs over the period 1996 April-2024 June. Our analysis indicates that five of its magnetic properties rank highest among all ARs recorded in SHARP data series during 2010 May-2024 June by the Solar Dynamic Observatory. Furthermore, we demonstrate that AR 13664 reached its most dynamic flare productive state following a rapid rate of

rise of its flare-relevant parameters and that the X-class flares it spawned were more frequent near their peak values. Our analyses establish AR 13644 to be solar super active region and provide a paradigm for investigating their flare-relevant physical characteristics.

Multiple injections of energetic electrons associated with the flare/CME event on 9 October 2021

Immanuel Christopher **Jebaraj**, Athanasios Kouloumvakos, Nina Dresing, Alexander Warmuth, Nicolas Wijsen, Christian Palmroos, Jan Gieseler, Rami Vainio, Vratislav Krupar, Jasmina Magdalenic, Thomas Wiegelmann, Frederic Schuller, Andrea Battaglia, Annamaria Fedeli

A&A **2023**

https://arxiv.org/pdf/2301.03650.pdf File

We study the solar energetic particle (SEP) event observed on **9 October 2021**, by multiple spacecraft including Solar Orbiter (SolO). The event was associated with an M1.6 flare, a coronal mass ejection (CME) and a shock wave. During the event, high-energy protons and electrons were recorded by multiple instruments located within a narrow longitudinal cone. An interesting aspect of the event was the multi-stage particle energization during the flare impulsive phase and also what appears to be a separate phase of electron acceleration detected at SolO after the flare maximum. We aim to investigate and identify the multiple sources of energetic electron acceleration. We utilize SEP electron observations from the Energetic Particle Detector (EPD) and hard X-ray (HXR) observations from the Spectrometer/Telescope for Imaging X-rays (STIX) on-board SolO, in combination with radio observations at a broad frequency range. We focus on establishing an association between the energetic electrons and the different HXR and radio emissions associated with the multiple acceleration episodes. We have found that the flare was able to accelerate electrons for at least 20 minutes during the nonthermal phase observed in the form of five discrete HXR pulses. We also show evidence that the shock wave has contributed to the electron acceleration during and after the impulsive flare phase. The detailed analysis of EPD electron data shows that there was a time difference in the release of low- and high-energy electrons, with the high-energy release delayed. Also, the observed electron anisotropy characteristics suggest different connectivity during the two phases of acceleration.

See Introduction

A Modelling Investigation for Solar Flare X-ray Stereoscopy with Solar Orbiter/STIX and Earth Orbiting Missions

Natasha L. S. **Jeffrey**, Säm Krucker, Morgan Stores, Eduard P. Kontar, Pascal Saint-Hilaire, Andrea F. Battaglia, +++

ApJ **964** 145 **2024**

https://arxiv.org/pdf/2401.16032.pdf

https://iopscience.iop.org/article/10.3847/1538-4357/ad236f/pdf

The Spectrometer/Telescope for Imaging X-rays (STIX) on board Solar Orbiter (SolO) provides a unique opportunity to systematically perform stereoscopic X-ray observations of solar flares with current and upcoming X-ray missions at Earth. These observations will produce the first reliable measurements of hard X-ray (HXR) directivity in decades, providing a new diagnostic of the flare-accelerated electron angular distribution and helping to constrain the processes that accelerate electrons in flares. However, such observations must be compared to modelling, taking into account electron and X-ray transport effects and realistic plasma conditions, all of which can change the properties of the measured HXR directivity. Here, we show how HXR directivity, defined as the ratio of X-ray spectra at different spacecraft viewing angles, varies with different electron and flare properties (e.g., electron angular distribution, highest energy electrons, and magnetic configuration), and how modelling can be used to extract these typically unknown properties from the data. Lastly, we present a preliminary HXR directivity analysis of two flares, observed by the Fermi Gamma-ray Burst Monitor (GBM) and SolO/STIX, demonstrating the feasibility and challenges associated with such observations, and how HXR directivity can be extracted by comparison with the modelling presented here. **2021-08-28, 2021-11-01**

The role of turbulence in solar flares; Review

Natasha **Jeffrey**

Presentation at 16th ESPM September **2021**

https://indico.ict.inaf.it/event/794/contributions/9515/attachments/4978/10205/NJEFFREY_ESPM_SEPT_2021.pdf

Probing solar flare accelerated electron distributions with prospective X-ray polarimetry missions

Natasha L. S. **Jeffrey**, Pascal Saint-Hilaire, Eduard P. Kontar

A&A 642, A79 **2020**

https://arxiv.org/pdf/2008.07849.pdf

https://doi.org/10.1051/0004-6361/202038626

Solar flare electron acceleration is an extremely efficient process, but the method of acceleration is not well constrained. Two of the essential diagnostics: electron anisotropy (velocity angle to the guiding magnetic field) and the high energy cutoff (highest energy electrons produced by the acceleration conditions: mechanism, spatial extent, time), are important quantities that can help to constrain electron acceleration at the Sun but both are poorly determined. Here, using electron and X-ray transport simulations that account for both collisional and non-collisional transport processes such as turbulent scattering, and X-ray albedo, we show that X-ray polarization can be used to constrain the anisotropy of the accelerated electron distribution and the most energetic accelerated electrons together. Moreover, we show that prospective missions, e.g. CubeSat missions without imaging information, can be used alongside such simulations to determine these parameters. We conclude thata fuller understanding of flare acceleration processes will come from missions capable of both X-ray flux and polarization spectral measurements together. Although imaging polarimetry is highly desired, we demonstrate that spectro-polarimeters without imaging can also provide strong constraints on electron anisotropy and the high energy cutoff.
RHESSI Nuggets #398 January **2021** https://sprg.ssl.berkeley.edu/~tohban/wiki/index.php/Observing_Solar_Flare_X-ray_Polarization_with_Prospective_CubeSat_Missions

The Role of Energy Diffusion in the Deposition of Energetic Electron Energy in Solar and Stellar Flares

Natasha L. S. **Jeffrey**, Eduard P. Kontar, Lyndsay Fletcher
ApJ **880** 136 **2019** 10.3847/1538-4357/ab2764
https://arxiv.org/pdf/1906.01887.pdf
During solar flares, a large fraction of the released magnetic energy is carried by energetic electrons that transfer and deposit energy in the Sun's atmosphere. Electron transport is often approximated by a cold thick-target model (CTTM), assuming that electron energy is much larger than the temperature of the ambient plasma, and electron energy evolution is modeled as a systematic loss. Using kinetic modeling of electrons, we re-evaluate the transport and deposition of flare energy. Using a full collisional warm-target model (WTM), we account for electron thermalization and for the properties of the ambient coronal plasma such as its number density, temperature and spatial extent. We show that the deposition of non-thermal electron energy in the lower atmosphere is highly dependent on the properties of the flaring coronal plasma. In general, thermalization and a reduced WTM energy loss rate leads to an increase of non-thermal energy transferred to the chromosphere, and the deposition of non-thermal energy at greater depths. The simulations show that energy is deposited in the lower atmosphere initially by high energy non-thermal electrons, and later by lower energy non-thermal electrons that partially or fully thermalize in the corona, over timescales of seconds, unaccounted for in previous studies. This delayed heating may act as a diagnostic of both the injected non-thermal electron distribution and the coronal plasma, vital for constraining flare energetics. **2013-05-13**

The development of lower-atmosphere turbulence early in a solar flare

N. L. S. **Jeffrey**, L. Fletcher, N. Labrosse, P. J. A. Simões
Science Advances Vol. 4, no. 12, eaav2794
http://advances.sciencemag.org/content/4/12/eaav2794/tab-pdf
https://arxiv.org/ftp/arxiv/papers/1812/1812.09906.pdf
We present the first observational study of the onset and evolution of solar flare turbulence in the lower solar atmosphere on an unprecedented time scale of 1.7 s using the Interface Region Imaging Spectrograph observing plasma at a temperature of 80,000 K. At this time resolution, nonthermal spectral line broadening, indicating turbulent velocity fluctuations, precedes the flare onset at this temperature and is coincident with net blue-shifts. The broadening decreases as the flare brightens and then oscillates with a period of ~10 s. These observations are consistent with turbulence in the lower solar atmosphere at the flare onset, heating that region as it dissipates. This challenges the current view of energy release and transport in the standard solar flare model, suggesting that turbulence partly heats the lower atmosphere. **2016-12-06**
UKSP Nugget: #99 June **2019**
http://www.uksolphys.org/uksp-nugget/99-preflare-and-flare-turbulence-in-the-transition-region/

Non-Gaussian Velocity Distributions in Solar Flares from Extreme Ultraviolet Lines: A **Possible** Diagnostic of Ion Acceleration

Natasha L. S. **Jeffrey**, Lyndsay Fletcher, Nicolas Labrosse
ApJ 836 35 **2017**
https://arxiv.org/pdf/1701.02196v1.pdf
In a solar flare, a large fraction of the magnetic energy released is converted rapidly to the kinetic energy of non-thermal particles and bulk plasma motion. This will likely result in non-equilibrium particle distributions and turbulent plasma conditions. We investigate this by analysing the profiles of high-temperature extreme ultraviolet emission lines

from a major flare (SOL**2014-03-29**T17:44) observed by the EUV Imaging Spectrometer (EIS) on Hinode. We find that in many locations the line profiles are non-Gaussian, consistent with a kappa-distribution of emitting ions with properties that vary in space and time. At the flare footpoints, close to sites of hard X-ray emission from non-thermal electrons, the kappa-index for the Fe XVI 262.976 angstrom line at 3 MK takes values of 3-5. In the corona, close to a low-energy HXR source, the Fe XXIII 263.760 angstrom line at 15 MK shows kappa values of typically 4-7. The observed trends in the kappa parameter show that we are most likely detecting the properties of the ion population rather than any instrumental effects. We calculate that a non-thermal ion population could exist if locally accelerated on timescales < 0.1 s. However, observations of net redshifts in the lines also imply the presence of plasma downflows which could lead to bulk turbulence, with increased non-Gaussianity in cooler regions. Both interpretations have important implications for theories of solar flare particle acceleration.
See EIS nugget 17 Jan **2017 Measuring Solar Flare Non-Gaussian Velocities using EIS Spectroscopy**
http://solarb.mssl.ucl.ac.uk/SolarB/nuggets/nugget_2017jan.jsp

First evidence of non-Gaussian solar flare EUV spectral line profiles and accelerated non-thermal ion motion

Natasha **Jeffrey**, Lyndsay Fletcher, Nicolas Labrosse
A&A 590, A99 **2016**
http://arxiv.org/pdf/1601.07308v1.pdf
The properties of solar flare plasma can be determined from observations of optically thin EUV lines. The spectral line profiles emitted in a flaring MK plasma are expected to be dominated by Doppler broadening, producing Gaussian line profiles, if the underlying ion velocity distribution is Maxwellian. We look for non-Gaussian line profiles during a flare, that may indicate the presence of accelerated ion and/or plasma non-thermal velocity distributions. We study EUV spectral lines during a flare SOL**2013-05-15**T01:45 using the Hinode EUV Imaging Spectrometer (EIS). The flare is located close to the eastern solar limb. It has an extended loop structure, allowing different flare features: ribbons, hard X-ray (HXR) footpoints and the loop-top source to be clearly observed in EUV and X-rays. EUV line spectroscopy is performed in seven regions covering the flare features. We study the line profiles of isolated and unblended Fe XVI lines (262.9760 A) formed at temperatures of 2-4 MK. Suitable Fe XVI line profiles close to the time of peak soft X-ray emission and free of directed mass motions are examined using: 1. a higher moments analysis, 2. Gaussian fitting and 3. by fitting a kappa line profile convolved with a Gaussian to account for the EIS instrumental profile. The physical Fe XVI line profiles in the flaring loop-top, HXR footpoint and ribbon regions can be better fitted by a kappa line profile with low, non-thermal kappa values between 2-3.3. A higher moments analysis finds that many of the spectral line kurtosis values are higher than the Gaussian value of 3, even with the presence of a broad Gaussian instrumental profile. We discuss how an accelerated non-thermal ion population can account for the observed non-Gaussian line profiles, and for the Fe XVI excess broadening found from Gaussian fitting, if the emitting ions are interacting with a thermalised 4 MK electron population.

High-temperature differential emission measure and altitude variations in the temperature and density of solar flare coronal X-ray sources

Natasha **Jeffrey**, Eduard Kontar, Brian Dennis
A&A 584, A89 **2015**
http://arxiv.org/pdf/1510.04095v1.pdf
The detailed knowledge of plasma heating and acceleration region properties presents a major observational challenge in solar flare physics. Using the Ramaty High Energy Solar Spectroscopic Imager (RHESSI), the high temperature differential emission measure, DEM(T), and the energy-dependent spatial structure of solar flare coronal sources are studied quantitatively. The altitude of the coronal X-ray source is observed to increase with energy by ~+0.2 arcsec/keV between 10 and 25 keV. Although an isothermal model can fit the thermal X-ray spectrum observed by RHESSI, such a model cannot account for the changes in altitude, and multi-thermal coronal sources are required where the temperature increases with altitude. For the first time, we show how RHESSI imaging information can be used to constrain the DEM(T) of a flaring plasma. We develop a thermal bremsstrahlung X-ray emission model with inhomogeneous temperature and density distributions to simultaneously reproduce: i) DEM(T), ii) altitude as a function of energy, and iii) vertical extent of the flaring coronal source versus energy. We find that the temperature-altitude gradient in the region is ~+0.08 keV/arcsec (~1.3 MK/Mm). Similar altitude-energy trends in other flares suggest that the majority of coronal X-ray sources are multi-thermal and have strong vertical temperature and density gradients with a broad DEM(T). **2013-05-13**

The collisional relaxation of electrons in hot flaring plasma and inferring the properties of solar flare accelerated electrons from X-ray observations

Natasha **Jeffrey**, Eduard Kontar, Gordon Emslie, Nicolas Bian
14th Annual International Astrophysics Conference Tampa proceedings, **2015**
http://arxiv.org/pdf/1507.06785v1.pdf
X-ray observations are a direct diagnostic of fast electrons produced in solar flares, energized during the energy release process and directed towards the Sun. Since the properties of accelerated electrons can be substantially changed during their transport and interaction with the background plasma, a model must ultimately be applied to X-ray observations in order to understand the mechanism responsible for their acceleration. A cold thick target model is ubiquitously used for this task, since it provides a simple analytic relationship between the accelerated electron spectrum and the emitting electron spectrum in the X-ray source, with the latter quantity readily obtained from X-ray observations. However, such a model is inappropriate for the majority of solar flares in which the electrons propagate in a hot megaKelvin plasma, because it does not take into account the physics of thermalization of fast electrons. The use of a more realistic model, properly accounting for the properties of the background plasma, and the collisional diffusion and thermalization of electrons, can alleviate or even remove many of the traditional problems associated with the cold thick target model and the deduction of the accelerated electron spectrum from X-ray spectroscopy, such as the number problem and the need to impose an ad hoc low energy cut-off. **2005-08-23, 2013-05-13**

The spatial, spectral and polarization properties of solar flare X-ray sources

Natasha L. S. **Jeffrey**
Ph.D. **Thesis**, **2014**
http://arxiv.org/pdf/1412.8163v1.pdf
X-rays are a valuable diagnostic tool for the study of high energy accelerated electrons. Bremsstrahlung X-rays produced by, and directly related to, high energy electrons accelerated during a flare, provide a powerful diagnostic tool for determining both the properties of the accelerated electron distribution, and of the flaring coronal and chromospheric plasmas. This thesis is specifically concerned with the study of spatial, spectral and polarization properties of solar flare X-ray sources via both modelling and X-ray observations using the Ramaty High Energy Solar Spectroscopic Imager (RHESSI). Firstly, a new model is presented, accounting for finite temperature, pitch angle scattering and initial pitch angle injection. This is developed to accurately infer the properties of the acceleration region from the observations of dense coronal X-ray sources. Moreover, examining how the spatial properties of dense coronal X-ray sources change in time, interesting trends in length, width, position, number density and thermal pressure are found and the possible causes for such changes are discussed. Further analysis of data in combination with the modelling of X-ray transport in the photosphere, allows changes in X-ray source positions and sizes due to the X-ray albedo effect to be deduced. Finally, it is shown, for the first time, how the presence of a photospheric X-ray albedo component produces a spatially resolvable polarization pattern across a hard X-ray (HXR) source. It is demonstrated how changes in the degree and direction of polarization across a single HXR source can be used to determine the anisotropy of the radiating electron distribution. **13 January 1992, 14-15 Apr 2002, 23 July 2002, 20 September 2002, 21 May 2004, 10 Nov 2004, 23 Aug 2005**

On the variation of solar flare coronal x-ray source sizes with energy

Natasha L. S. **Jeffrey**, Eduard P. Kontar, Nicolas H. Bian, A. Gordon Emslie
ApJ, 787 86 **2014**
http://arxiv.org/pdf/1404.1962v1.pdf
Observations with {\em RHESSI} have enabled the detailed study of the structure of dense hard X-ray coronal sources in solar flares. The variation of source extent with electron energy has been discussed in the context of streaming of non-thermal particles in a one-dimensional cold-target model, and the results used to constrain both the physical extent of, and density within, the electron acceleration region. Here we extend this investigation to a more physically realistic model of electron transport that takes into account the finite temperature of the ambient plasma, the initial pitch-angle distribution of the accelerated electrons, and the effects of collisional pitch-angle scattering. The finite temperature results in the thermal diffusion of electrons, that leads to the observationally-inferred value of the acceleration region volume being an overestimate of its true value. The different directions of the electron trajectories, a consequence of both the non-zero injection pitch-angle and scattering within the target, cause the projected propagation distance parallel to the guiding magnetic field to be reduced, so that a one-dimensional interpretation can overestimate the actual density by a factor of up to ~6. The implications of these results for the determination of acceleration region properties (specific acceleration rate, filling factor, etc.) are discussed.

Three-phase life leads to corpulent X-ray loops

N. **Jeffrey** and E. Kontar
RHESSI Nugget No. 198, April **2013**
RHESSI reveals some of the secrets of the time development of coronal X-ray loops.
Using the VIS FWDFIT method, we decided to extend the investigation of loop spatial properties with a very simple study; observe for the first time how these X-ray loops changed with time during the X-ray rise, peak and decay phases

of the flare. For this we managed to find three suitable events with a simple loop shape: **23rd August 2005 from 14:22, 14/15th April 2002 from 23:58 and 21st May 2004 from 23:42.**

TEMPORAL VARIATIONS OF X-RAY SOLAR FLARE LOOPS: LENGTH, CORPULENCE, POSITION, TEMPERATURE, PLASMA PRESSURE, AND SPECTRA

Natasha L. S. **Jeffrey** and Eduard P. Kontar
2013 ApJ 766 75

The spatial and spectral properties of three solar flare coronal X-ray loops are studied before, during, and after the peak X-ray emission. Using observations from the Ramaty High Energy Solar Spectroscopic Imager (RHESSI), we deduce the temporal changes in emitting X-ray length, corpulence, volume, position, number density, and thermal pressure. We observe a decrease in the loop length, width, and volume before the X-ray peak, and an increasing number density and thermal pressure. After the X-ray peak, volume increases and loop corpulence grows due to increasing width. The volume variations are more pronounced than the position variations, often known as magnetic field line contraction. We believe this is the first dedicated study examining the temporal evolution of X-ray loop lengths and widths. Collectively, the observations also show for the first time three temporal phases given by peaks in temperature, X-ray emission, and thermal pressure, with the minimum volume coinciding with the X-ray peak. Although the volume of the flaring plasma decreases before the peak in X-ray emission, the relationship between temperature and volume does not support simple compressive heating in a collapsing magnetic trap model. Within a low β plasma, shrinking loop widths perpendicular to the guiding field can be explained by squeezing the magnetic field threading the region. Plasma heating leads to chromospheric evaporation and growing number density. This produces increasing thermal pressure and decreasing loop lengths as electrons interact at shorter distances and we believe after the X-ray peak, the increasing loop corpulence.

Modelling spatially resolved X-ray polarization

Natasha **Jeffrey**, Eduard Kontar
RHESSI Science Nugget, No. 165, Dec **2011**.

In conclusion, spatially resolved polarization could provide us with an effective method of determining the directivity of the radiating electron distribution, if and when in the future we have the instrumentation available to make reliable and sensitive polarization measurements. Our full results are shown in Jeffrey & Kontar (2011).

Spatially resolved hard X-ray polarization in solar flares: effects of Compton scattering and bremsstrahlung

Natasha **Jeffrey**, Eduard Kontar
Astronomy & Astrophysics, Volume 536, id.A93, **2011**

Aims: We study the polarization of hard X-ray (HXR) sources in the solar atmosphere, including Compton backscattering of photons in the photosphere (the albedo effect) and the spatial distribution of polarization across the source.

Methods: HXR photon polarization and spectra produced via electron-ion bremsstrahlung emission are calculated from various electron distributions typical for solar flares. Compton scattering and photoelectric absorption are then modelled using Monte Carlo simulations of photon transport in the photosphere to study the observed (primary and albedo) sources. Polarization maps across HXR sources (primary and albedo components) for each of the modelled electron distributions are calculated at various source locations from the solar centre to the limb.

Results: We show that Compton scattering produces a distinct polarization variation across the albedo patch at peak albedo energies of 20-50 keV for all anisotropies modelled. The results show that there are distinct spatial polarization changes in both the radial and perpendicular to radial directions across the extent of the HXR source at a given disk location. In the radial direction, the polarization magnitude and direction at specific positions along the HXR source will either increase or decrease with increased photon distribution directivity towards the photosphere. We also show how high electron cutoff energies influence the direction of polarization at above ~100 keV.

Conclusions: Spatially resolved HXR polarization measurements can provide important information about the directivity and energetics of the electron distribution. Our results indicate the preferred angular resolution of polarization measurements required to distinguish between the scattered and primary components. We also show how spatially resolved polarization measurements could be used to probe the emission pattern of an HXR source, using both the magnitude and the direction of the polarization.

High-Density Off-Limb Flare Loops Observed by SDO

S. **Jejčič**, L. Kleint, P. Heinzel
2018 ApJ 867 134

https://arxiv.org/pdf/1810.02431.pdf
sci-hub.tw/10.3847/1538-4357/aae650
The density distribution of flare loops and the mechanisms of their emission in the continuum are still open questions. On **September 10, 2017** a prominent loop system appeared during the gradual phase of an X8.2 flare (SOL2017-09-10), visible in all passbands of SDO/AIA and in the white-light continuum of SDO/HMI. We investigate its electron density by taking into account all radiation processes in the flare loops, i.e. the Thomson continuum, hydrogen Paschen and Brackett recombination continua, as well as free-free continuum emission. We derive a quadratic function of the electron density for a given temperature and effective loop thickness. By absolutely calibrating SDO/HMI intensities, we convert the measured intensities into electron density at each pixel in the loops. For a grid of plausible temperatures between cool (6000 K) and hot (10^6 K) structures, the electron density is computed for representative effective thicknesses between 200 and 20 000 km. We obtain a relatively high maximum electron density, about 10^13 cm^-3. At such high electron densities, the Thomson continuum is negligible and therefore one would not expect a significant polarization degree in dense loops. We conclude that the Paschen and Brackett recombination continua are dominant in cool flare loops, while the free-free continuum emission is dominant for warmer and hot loops.
HMI Science Nuggets #116 Nov **2018** http://hmi.stanford.edu/hminuggets/?p=2736

Turbulent plasma flow, its energies, and structures: Velocity vortices, magnetic field cocoons, and plasmoids

P. **Jelínek**1⋆ and M. Karlický2
A&A, 692, A116 (**2024**)
https://doi.org/10.1051/0004-6361/202449558
https://www.aanda.org/articles/aa/pdf/2024/12/aa49558-24.pdf
Context. Turbulent flows are believed to be present in the solar corona, especially in connection with solar flares and coronal mass ejections. They are supposed to be very effective processes in energy transportation and can contribute to the heating of the solar corona.
Aims. We study turbulence in reconnection outflows associated with flares and coronal mass ejections. We simulated the generation and evolution of the turbulent plasma flow and investigated its energies and formed plasma velocity and magnetic field structures.
Methods. For the numerical simulations, we adopted a three-dimensional (3D) magnetohydrodynamic (MHD) model, in which we solved a full set of the 3D time-dependent resistive and compressible MHD equations using the LARE3D numerical code.
Results. We numerically studied turbulence in the plasma flow in the model with the plasma parameters that could simulate processes in the magnetic reconnection outflows in solar flares. Starting from a non-turbulent plasma flow in the energetically closed system, we studied the evolution of the kinetic, internal, and magnetic energies during the turbulence generation. We found that most of the kinetic energy is transformed into the plasma heating (about 95%) and only a small part to the magnetic energy (about 5%). The turbulence in the system evolves to the saturation stage with the power-law index of the kinetic density spectrum, −5/3. Magnetic energy is also saturated due to its dissipation and reconnection in small and complex magnetic field structures. We show examples of the structures formed in studied turbulent flow: velocity vortices, magnetic field cocoons, and plasmoids.

Pulse-beam heating of deep atmospheric layers triggering their oscillations and upwards moving shocks that can modulate the reconnection in solar flares

P. **Jelínek**, M. Karlický
A&A 625, A3 **2019**
https://arxiv.org/pdf/1902.00292.pdf
https://sci-hub.se/10.0000/www.aanda.org/articles/aa/abs/2019/05/aa35188-19/aa35188-19.html
We study processes occurring after a sudden heating of the chromosphere at the flare arcade footpoints which is assumed to be caused by particle beams. For the numerical simulations we adopt a 2-D magnetohydrodynamic (MHD) model, in which we solve a full set of the time-dependent MHD equations by means of the FLASH code, using the Adaptive Mesh Refinement (AMR) method. In the initial state we consider a model of the solar atmosphere with densities according to the VAL-C model and the magnetic field arcade having the X-point structure above, where the magnetic reconnection is assumed. We found that the sudden pulse-beam heating of the chromosphere at the flare arcade footpoints generates magnetohydrodynamic shocks, one propagating upwards and the second one propagating downwards in the solar atmosphere. The downward moving shock is reflected at deep and dense atmospheric layers and triggers oscillations of these layers. These oscillations generate the upwards moving magnetohydrodynamic waves that can influence the above located magnetic reconnection in a quasi-periodic way. Because these processes require a sudden heating in very localized regions in the chromosphere therefore they can be also associated with seismic waves.

Oscillations excited by plasmoids formed during magnetic reconnection in vertical gravitationally stratified current-sheet

P. **Jelínek**, M. Karlický, T. Van Doorsselaere, M. Bárta

2017 ApJ 847 98
https://arxiv.org/pdf/1703.06674.pdf
Using the FLASH code, which solves the full set of the two-dimensional (2-D) non-ideal (resistive) time-dependent magnetohydrodynamic (MHD) equations, we study processes during the magnetic reconnection in a vertical gravitationally stratified current sheet. We show that during these processes, which correspond to processes in solar flares, plasmoids are formed due to the tearing mode instability of the current sheet. These plasmoids move upwards or downwards along the vertical current sheet, and some of them merge into larger plasmoids. We study the density and temperature structure of these plasmoids and their time evolution in details. We found that during the merging of two plasmoids the resulting larger plasmoid starts to oscillate; in our model with a ∼25 s period. On the other hand, the plasmoid moving downwards merges with the underlying flare arcade which also starts to oscillate during this process; in our model with a ∼35 s period. It is shown that the merging process of plasmoid with the flare arcade is a complex process as presented by complex density and temperature structures of the oscillating arcade. Moreover, all these processes are associated with magnetoacoustic waves produced by the motion and merging of plasmoids.

Electric current filamentation at a non-potential magnetic null-point due to pressure perturbation

P. **Jelinek**, M. Karlicky, K. Murawski
ApJ 812, 105, **2015**
An increase of electric current densities due to filamentation is an important process in any flare. We show that the pressure perturbation, followed by an entropy wave, triggers such a filamentation in the non-potential magnetic null-point. In the two-dimensional (2D), non-potential magnetic null-point, we generate the entropy wave by a negative or positive pressure pulse that is launched initially. Then, we study its evolution under the influence of the gravity field. We solve the full set of 2D time dependent, ideal magnetohydrodynamic equations numerically, making use of the FLASH code. The negative pulse leads to an entropy wave with a plasma density greater than in the ambient atmosphere and thus this wave falls down in the solar atmosphere, attracted by the gravity force. In the case of the positive pressure pulse, the plasma becomes evacuated and the entropy wave propagates upward. However, in both cases, owing to the Rayleigh?Taylor instability, the electric current in a non-potential magnetic null-point is rapidly filamented and at some locations the electric current density is strongly enhanced in comparison to its initial value. Using numerical simulations, we find that entropy waves initiated either by positive or negative pulses result in an increase of electric current densities close to the magnetic null-point and thus the energy accumulated here can be released as nanoflares or even flares.

Nanoflare Activity in the Solar Chromosphere

D. B. **Jess**, M. Mathioudakis, P. H. Keys
ApJ, 795 172 **2014**
http://arxiv.org/pdf/1409.6726v1.pdf
We use ground-based images of high spatial and temporal resolution to search for evidence of nanoflare activity in the solar chromosphere. Through close examination of more than 10^9 pixels in the immediate vicinity of an active region, we show that the distributions of observed intensity fluctuations have subtle asymmetries. A negative excess in the intensity fluctuations indicates that more pixels have fainter-than-average intensities compared with those that appear brighter than average. By employing Monte Carlo simulations, we reveal how the negative excess can be explained by a series of impulsive events, coupled with exponential decays, that are fractionally below the current resolving limits of low-noise equipment on high-resolution ground-based observatories. Importantly, our Monte Carlo simulations provide clear evidence that the intensity asymmetries cannot be explained by photon-counting statistics alone. A comparison to the coronal work of Terzo et al. (2011) suggests that nanoflare activity in the chromosphere is more readily occurring, with an impulsive event occurring every ~360s in a 10,000 km^2 area of the chromosphere, some 50 times more events than a comparably sized region of the corona. As a result, nanoflare activity in the chromosphere is likely to play an important role in providing heat energy to this layer of the solar atmosphere. **2011 December 10**

Microflare Activity Driven by Forced Magnetic Reconnection

D. B. **Jess**, M. Mathioudakis, P. K. Browning, P. J. Crockett, and F. P. Keenan
ApJ **712** L111-L115, **2010**
High cadence, multiwavelength, optical observations of a solar active region, obtained with the Swedish Solar Telescope, are presented. Two magnetic bright points are seen to separate in opposite directions at a constant velocity of 2.8 km s^{-1}. After a separation distance of ≈4400 km is reached, multiple Ellerman bombs are observed in both Hα and Ca-K images. As a result of the Ellerman bombs, periodic velocity perturbations in the vicinity of the magnetic neutral line, derived from simultaneous Michelson Doppler Imager data, are generated with amplitude ±6 km s^{-1} and wavelength ≈1000 km. The velocity oscillations are followed by an impulsive brightening visible in Hα and Ca-K, with a peak intensity enhancement of 63%. We interpret these velocity perturbations as the magnetic field deformation necessary to trigger forced reconnection. A time delay of ≈3 minutes between the Hα-wing and Ca-K observations indicates that the observed magnetic reconnection occurs at a height of ~200 km above the solar surface. These

observations are consistent with theoretical predictions and provide the first observational evidence of microflare activity driven by forced magnetic reconnection.

Do All Flares Have White-Light Emission?

D. B. **Jess**, M. Mathioudakis, P. J. Crockett, and F. P. Keenan
The Astrophysical Journal Letters, Vol. 688, No. 2: L119-L122.
http://www.journals.uchicago.edu/doi/abs/10.1086/595588

High-cadence, multiwavelength optical observations of a solar active region (NOAA AR 10969), obtained with the Swedish Solar Telescope, are presented. Difference imaging of white light continuum data reveals a white-light brightening, 2 minutes in duration, linked to a cotemporal and cospatial C2.0 flare event. The flare kernel observed in the white-light images has a diameter of 300 km, thus rendering it below the resolution limit of most space-based telescopes. Continuum emission is present only during the impulsive stage of the flare, with the effects of chromospheric emission subsequently delayed by ≈2 minutes. The localized flare emission peaks at 300% above the quiescent flux. This large, yet tightly confined, increase in emission is only resolvable due to the high spatial resolution of the Swedish Solar Telescope. An investigation of the line-of-sight magnetic field derived from simultaneous MDI data shows that the continuum brightening is located very close to a magnetic polarity inversion line. In addition, an Hα flare ribbon is directed along a region of rapid magnetic energy change, with the footpoints of the ribbon remaining cospatial with the observed white-light brightening throughout the duration of the flare. The observed flare parameters are compared with current observations and theoretical models for M- and X-class events and we determine the observed white-light emission is caused by radiative backwarming. We suggest that the creation of white-light emission is a common feature of all solar flares.

Active Region-based Flare Forecasting with Sliding Window Multivariate Time Series Forest Classifiers

Anli **Ji**, Berkay Aydin
2024
https://arxiv.org/pdf/2402.03474.pdf

Over the past few decades, many applications of physics-based simulations and data-driven techniques (including machine learning and deep learning) have emerged to analyze and predict solar flares. These approaches are pivotal in understanding the dynamics of solar flares, primarily aiming to forecast these events and minimize potential risks they may pose to Earth. Although current methods have made significant progress, there are still limitations to these data-driven approaches. One prominent drawback is the lack of consideration for the temporal evolution characteristics in the active regions from which these flares originate. This oversight hinders the ability of these methods to grasp the relationships between high-dimensional active region features, thereby limiting their usability in operations. This study centers on the development of interpretable classifiers for multivariate time series and the demonstration of a novel feature ranking method with sliding window-based sub-interval ranking. The primary contribution of our work is to bridge the gap between complex, less understandable black-box models used for high-dimensional data and the exploration of relevant sub-intervals from multivariate time series, specifically in the context of solar flare forecasting. Our findings demonstrate that our sliding-window time series forest classifier performs effectively in solar flare prediction (with a True Skill Statistic of over 85\%) while also pinpointing the most crucial features and sub-intervals for a given learning task.

Laboratory Study of Collisionless Magnetic Reconnection **Review**

H. **Ji**, J. Yoo, W. Fox, +++
Space Sci Rev **219**, 76 (**2023**).
https://doi.org/10.1007/s11214-023-01024-3
https://link.springer.com/content/pdf/10.1007/s11214-023-01024-3.pdf

A concise review is given on the past two decades' results from laboratory experiments on collisionless magnetic reconnection in direct relation with space measurements, especially by the Magnetospheric Multiscale (MMS) mission. Highlights include spatial structures of electromagnetic fields in ion and electron diffusion regions as a function of upstream symmetry and guide field strength, energy conversion and partitioning from magnetic field to ions and electrons including particle acceleration, electrostatic and electromagnetic kinetic plasma waves with various wavelengths, and plasmoid-mediated multiscale reconnection. Combined with the progress in theoretical, numerical, and observational studies, the physics foundation of fast reconnection in collisionless plasmas has been largely established, at least within the parameter ranges and spatial scales that were studied. Immediate and long-term future opportunities based on multiscale experiments and space missions supported by exascale computation are discussed, including dissipation by kinetic plasma waves, particle heating and acceleration, and multiscale physics across fluid and kinetic scales.

A Systematic Magnetic Polarity Inversion Line Data Set from SDO/HMI Magnetograms

Anli **Ji**1, Xumin Cai1, Nigar Khasayeva1, Manolis K. Georgoulis2, Petrus C. Martens3, Rafal A. Angryk1, and Berkay Aydin1
2023 ApJS 265 28
https://iopscience.iop.org/article/10.3847/1538-4365/acb43a/pdf
Magnetic polarity inversion lines (PILs) detected in solar active regions have long been recognized as arguably the most essential feature for triggering instabilities such as flares and eruptive events (i.e., eruptive flares and coronal mass ejections). In recent years, efforts have been focused on using features engineered from PILs for solar eruption prediction. However, PIL rasters and metadata are often generated as by-products and are not accessible for public use, which limits their utilization in data-intensive space weather analytics applications. We introduce a large-scale publicly available PIL data set covering practically the entire solar cycle 24 for applying to various space weather forecasting and analytics tasks. The data set is created using both radial magnetic field (B_r) and line-of-sight (B_LoS) magnetograms from the Solar Dynamics Observatory's Helioseismic and Magnetic Imager Active Region Patches (HARP) that involve 4090 HARP series ranging from 2010 May to 2019 March. This data set includes three PIL-related binary masks of rasters: the actual PILs as per the spatial analysis of the magnetograms, the region of polarity inversion, and the convex hull of PILs, along with time-series-structured metadata extracted from these masks. We also provide a preliminary exploratory analysis of selected features aiming to correlate time series of feature metadata and eruptive activity originating from active regions. We envision that this comprehensive PIL data set will complement existing data sets used for space weather forecasting and benefit research in related areas, specifically in better understanding the PIL structure, evolution, and role in eruptions. **2011 February 14**

Magnetic reconnection in the era of exascalecomputing and multiscale experiments,

Ji, H., Daughton, W., Jara-Almonte, J., et al.
2022, Nature **Reviews** Physics, 4, 263,
10.1038/s42254-021-00419-x
https://www.nature.com/articles/s42254-021-00419-x.pdf
Astrophysical plasmas have the remarkable ability to preserve magnetic topology, which inevitably gives rise to the accumulation of magnetic energy within stressed regions including current sheets. This stored energy is often released explosively through the process of magnetic reconnection, which produces a reconfiguration of the magnetic field, along with high-speed flows, thermal heating and nonthermal particle acceleration. Either collisional or kinetic dissipation mechanisms are required to overcome the topological constraints, both of which have been predicted by theory and validated with in situ spacecraft observations or laboratory experiments. However, major challenges remain in understanding magnetic reconnection in large systems, such as the solar corona, where the collisionality is weak and the kinetic scales are vanishingly small in comparison with macroscopic scales. The plasmoid instability or formation of multiple plasmoids in long, reconnecting current sheets is one possible multiscale solution for bridging this vast range of scales, and new laboratory experiments are poised to study these regimes. In conjunction with these efforts, we anticipate that the coming era of exascale computing, together with the next generation of observational capabilities, will enable new progress on a range of challenging problems, including the energy build-up and onset of reconnection, partially ionized regimes, the influence of magnetic turbulence and particle acceleration.

Major Scientific Challenges and Opportunities in Understanding Magnetic Reconnection and Related Explosive Phenomena in Solar and Heliospheric Plasmas **miniReview**

H. **Ji**, J. Karpen, A. Alt, S. Antiochos, S. Baalrud, S. Bale, et al.
White Paper for Heliophysics 2050 **2020**
https://arxiv.org/ftp/arxiv/papers/2009/2009.08779.pdf
Magnetic reconnection underlies many explosive phenomena in the heliosphere and in laboratory plasmas. The new research capabilities in theory/simulations, observations, and laboratory experiments provide the opportunity to solve the grand scientific challenges summarized in this whitepaper. Success will require enhanced and sustained investments from relevant funding agencies, increased interagency/international partnerships, and close collaborations of the solar, heliospheric, and laboratory plasma communities. These investments will deliver transformative progress in understanding magnetic reconnection and related explosive phenomena including space weather events.

A Hard X-Ray Sigmoidal Structure During the Initial Phase of the 2003 October 29 X10 Flare

Haisheng **Ji**, Haimin Wang, Chang Liu and Brian R. Dennis
BBSO, #1356, 2008
http://solar.njit.edu/preprints/Ji1356.pdf
We find a hard X-ray (HXR) sigmoidal (S-shaped) structure observed by *RHESSI* between 6 and 150 keV during the initial phase of the X10 flare of 2003 October 29.

The Relaxation of Sheared Magnetic Fields – A Contracting Process

Haisheng **Ji**, Guangli Huang and Haimin Wang
BBSO # 1331, Astrophysical Journal, Volume 660, Issue 1, pp. 893-900, **2007**
the contracting motion of flaring loops may be the result of the relaxation of the sheared magnetic field. In the framework of sheared linear force-free arcades, we establish a quantitative model to show that the release of magnetic energy will reduce magnetic shear of the arcades and less sheared arcades will have smaller height and span.

Reconstruction of a Highly Twisted Magnetic Flux Rope for an Inter-active-region X-Class Solar Flare

Chaowei **Jiang**1*, Aiying Duan2, Xueshang Feng3, Peng Zou1, Pingbing Zuo1 and Yi Wang1
Flare. Front. Astron. Space Sci. 6:63 **2019**
sci-hub.se/10.3389/fspas.2019.00063
Solar eruptions are manifestation of explosive release of magnetic energy in the Sun's corona. Large solar eruptions originate mostly within active regions, where strong magnetic fields concentrate on the solar surface. Here we studied the magnetic field structure for an exception, which is a peculiar GOES X1.2 flare accompanied with a very fast coronal mass ejection taking place between two active regions, where the magnetic field is relatively weak. The pre-flare magnetic field is reconstructed from the SDO/HMI vector magnetogram, using a non-linear force-free field extrapolation method. It is found that prior to the flare, there is a highly twisted magnetic flux rope with magnetic field lines winding over 6 turns, which connects the border of a leading sunspot of one active region and the following polarity of the neighboring active region. The basic configuration of the flux rope is consistent with the observed sigmoidal coronal loops and filament channels by SDO/AIA. It resides rather low-lying between the active regions such that the torus instability is not able to be triggered. Thus, it is likely that, due to the strong magnetic twist, the kink instability of the flux rope triggers the eruption. **2014 January 7**

Different contributions to space weather and space climate from different big solar active regions

Jie **Jiang**, Qiao Song, Jing-Xiu Wang, Tunde Baranyi
ApJ **2019**
https://arxiv.org/pdf/1901.00116.pdf
The purpose of this paper is to show that large active regions (ARs) with different magnetic configurations have different contributions to short-term and long-term variations of the Sun. As a case study, the complex δ-type AR 12673 and the simple β-type AR 12674 are investigated in detail. Since the axial dipole moment at cycle minimum determines the amplitude of the subsequent cycle and space climate, we have assimilated the individual observed magnetic configurations of these two ARs into a surface flux transport model to compare their contributions to the axial dipole moment D. We find that AR 12673 has a significant effect on D at the end of the cycle, making it weaker because of the abnormal and complicated magnetic polarities. An initial strongly positive D ends up with a strongly negative value. The flare-poor AR 12674 has a greater contribution to the long-term axial dipole moment than the flare-rich AR 12673. We then carry out a statistical analysis of ARs larger than 800 μHem from 1976 to 2017. We use the flare index FI and define an axial dipole moment index DI to quantify the effects of each AR on space weather and space climate, respectively. Whereas the FI has a strong dependence on the magnetic configuration, the DI shows no such dependence. The DI is mainly determined by the latitudinal location and the latitudinal separation of the positive and negative magnetic fluxes of the ARs. Simple ARs have the same possibility as complex ARs to produce big DI values affecting space climate. **2017 August 28 – September 10**

Magnetohydrodynamic Simulation of the X9.3 Flare on 2017 September 6: Evolving Magnetic Topology

Chaowei **Jiang**, Peng Zou, Xueshang Feng, Qiang Hu, Rui Liu, P. Vemareddy, Aiying Duan, Pingbing Zuo, Yi Wang, Fengsi Wei
ApJ **2018**
https://arxiv.org/pdf/1810.13095.pdf
Three-dimensional magnetic topology is crucial to understanding the explosive release of magnetic energy in the corona during solar flares. Much attention has been given to the pre-flare magnetic topology to identify candidate sites of magnetic reconnection, yet it is unclear how the magnetic reconnection and its attendant topological changes shape the eruptive structure and how the topology evolves during the eruption. Here we employed a realistic, data-constrained magnetohydrodynamic simulation to study the evolving magnetic topology for an X9.3 eruptive flare that occurred on **2017 September 6**. The simulation successfully reproduces the eruptive features and processes in unprecedented detail. The numerical results reveal that the pre-flare corona contains multiple twisted flux systems with different connections, and during the eruption, these twisted fluxes form a coherent flux rope through tether-cutting-like magnetic reconnection below the rope. Topological analysis shows that the rising flux rope is wrapped by a quasi-separatrix

layer, which intersects itself below the rope, forming a topological structure known as hyperbolic flux tube, where a current sheet develops, triggering the reconnection. By mapping footpoints of the newly-reconnected field lines, we are able to reproduce both the spatial location and, for the first time, the temporal separation of the observed flare ribbons, as well as the dynamic boundary of the flux rope's feet. Futhermore, the temporal profile of the total reconnection flux is comparable to the soft X-ray light curve. Such a sophisticated characterization of the evolving magnetic topology provides important insight into the eventual understanding and forecast of solar eruptions.

Decipher the Three-Dimensional Magnetic Topology of a Great Solar Flare

Chaowei **Jiang**, Peng Zou, Xueshang Feng, Qiang Hu, Aiying Duan, Pingbing Zuo, Yi Wang, Fengsi Wei
2018
https://arxiv.org/pdf/1802.02759.pdf
Three-dimensional magnetic topology of solar flare plays a crucial role in understanding its explosive release of magnetic energy in the corona. However, such three-dimensional coronal magnetic field is still elusive in direct observation. Here we realistically simulate the magnetic evolution during the eruptive process of a great flare, using a numerical magnetohydrodynamic model constrained by observed solar vector magnetogram. The numerical results reveal that the pre-flare corona contains multi-set twisted magnetic flux, which forms a coherent rope during the eruption. The rising flux rope is wrapped by a quasi-separatrix layer, which intersects itself below the rope, forming a hyperbolic flux tube and magnetic reconnection is triggered there. By tracing the footprint of the newly-reconnected field lines, we reproduce both the spatial location and its temporal evolution of flare ribbons with an expected accuracy in comparison of observed images. This scenario strongly confirms the three-dimensional version of standard flare model. **September 6 and 10, 2017**

Reconstruction of a Large-scale Pre-flare Coronal Current Sheet Associated with an Homologous X-shaped Flare

Chaowei **Jiang**, Xiaoli Yan, Xueshang Feng, Aiying Duan, Qiang Hu, Pingbing Zuo, Yi Wang
ApJ **850** 8 **2017**
https://arxiv.org/pdf/1710.02775.pdf
http://sci-hub.cc/10.3847/1538-4357/aa917a
As a fundamental magnetic structure in the solar corona, electric current sheets (CSs) can form either prior to or during solar flare, and they are essential for magnetic energy dissipation in the solar corona by enabling magnetic reconnection. However static reconstruction of CS is rare, possibly due to limitation inherent in available coronal field extrapolation codes. Here we present the reconstruction of a large-scale pre-flare CS in solar active region 11967 using an MHD-relaxation model constrained by SDO/HMI vector magnetogram. The CS is found to be associated with a set of peculiar homologous flares that exhibit unique X-shaped ribbons and loops occurring in a quadrupolar magnetic configuration. This is evidenced by that the field lines traced from the CS to the photosphere form an X shape which nearly precisely reproduces the shape of the observed flare ribbons, suggesting that the flare is a product of the dissipation of the CS through reconnection. The CS forms in a hyperbolic flux tube, which is an intersection of two quasi-separatrix layers. The recurrence of the X-shaped flares might be attributed to the repetitive formation and dissipation of the CS, as driven by the photospheric footpoint motions. These results demonstrate the power of data-constrained MHD model in reproducing CS in the corona as well as providing insight into the magnetic mechanism of solar flares.
2014 February 2

A Magnetic Bald-Patch Flare in Solar Active Region 11117

Chaowei **Jiang**, Xueshang Feng, S. T. Wu, Qiang Hu
RAA **2017**
https://arxiv.org/pdf/1705.10493.pdf
With SDO observations and a data-constrained MHD model, we identify a confined multi-ribbon flare occurred on **2010 October 25** in solar active region 11117 as a magnetic bald patch (BP) flare with strong evidences. From the photospheric magnetic field observed by SDO/HMI, we find there is indeed magnetic BPs on the PILs which match parts of the flare ribbons. From the 3D coronal magnetic field derived from a MHD relaxation model constrained by the vector magnetograms, we find strikingly good agreement of the BP separatrix surface (BPSS) footpoints with the flare ribbons, and the BPSS itself with the hot flaring loop system. Moreover, the triggering of the BP flare can be attributed to a small flux emergence under the lobe of the BPSS, and the relevant change of the coronal magnetic field through the flare is well reproduced by the pre-flare and post-flare MHD solutions, which match the corresponding pre and post-flare AIA observations, respectively. Our work contributes to the study of non-typical flares that constitute the majority of solar flares but cannot be explained by the standard flare model.

Analyses of the Photospheric Magnetic Dynamics in Solar Active Region 11117 Using an Advanced CESE-MHD Model

Chaowei **Jiang**1,2*, Shi T. Wu2,3* and Xueshang Feng1

http://journal.frontiersin.org.sci-hub.cc/article/10.3389/fspas.2016.00016/full
In this study, the photospheric vector magnetograms obtained by Helioseismic and Magnetic Imager on-board the Solar Dynamics Observatory are used as boundary conditions for a CESE-MHD model to investigate some photosphere characteristics around the time of a confined flare in solar active region NOAA AR 11117. We report our attempt of characterizing a more realistic solar atmosphere by including a plasma with temperature stratified from the photosphere to the corona in the CESE-MHD model. The resulted photospheric transverse flow is comparable to the apparent movements of the magnetic flux features that demonstrates shearing and rotations. We calculated the relevant parameters such as the magnetic energy flux and helicity flux, and with analysis of these parameters, we find that magnetic non-potentiality is transported across the photosphere into the corona in the simulated time interval, which might provide a favorable condition for producing the flare. **2010-10-25**

How did a Major Confined Flare Occur in Super Solar Active Region 12192?

Chaowei **Jiang**, Shi Tsan Wu, Vasyl B Yurchyshyn, Haimin Wang, Xueshang Feng, Qiang Hu
ApJ **828** 62 **2016 File**
http://arxiv.org/pdf/1606.09334v1.pdf
We study the physical mechanism of a major X-class solar flare that occurred in the super NOAA active region (AR) 12192 using a data-driven numerical magnetohydrodynamic (MHD) modeling complemented with observations. With the evolving magnetic fields observed at the solar surface as bottom boundary input, we drive an MHD system to evolve self-consistently in correspondence with the realistic coronal evolution. During a two-day time interval, the modeled coronal field has been slowly stressed by the photospheric field evolution,which gradually created a large-scale coronal current sheet, i.e., a narrow layer with intense current, in the core of the AR. The current layer was successively enhanced until it became so thin that a tether-cutting reconnection between the sheared magnetic arcades was set in, which led to a flare. The modeled reconnecting field lines and their footpoints match well the observed hot flaring loops and the flare ribbons, respectively, suggesting that the model has successfully "reproduced" the macroscopic magnetic process of the flare. In particular, with simulation, we explained why this event is a confined eruption-the consequent of the reconnection is the shared arcade instead of a newly formed flux rope. We also found much weaker magnetic implosion effect comparing to many other X-class flares. **2014 October 24,**

Interaction between an emerging flux region and a pre-existing fan-spine dome observed by \emph{IRIS} and \emph{SDO}

Fayu **Jiang**, Jun Zhang, Shuhong Yang
Publications of the Astronomical Society of Japan, **2015**
We present multi-wavelength observations of a fan-spine dome in the active region NOAA 11996 with the \textit{Interface Region Imaging Spectrograph} (\emph{IRIS}) and the Atmospheric Imaging Assembly on board the \textit{Solar Dynamics Observatory} (\emph{SDO}) on **March 9, 2014**. The destruction of the fan-spine topology owing to the interaction between its magnetic fields and an nearby emerging flux region (EFR) is firstly observed. The line-of-sight magnetograms from the Helioseismic and Magnetic Imager on board the \emph{SDO} reveal that the dome is located on the mixed magnetic fields, with its rim rooted in the redundant positive polarity surrounding the minority parasitic negative fields. The fan surface of the dome consists of a filament system and recurring jets are observed along its spine. The jet occurring around 13:54 UT is accompanied with a quasi-circular ribbon that brightens in the clockwise direction along the bottom rim of the dome, which may indicate an occurrence of slipping reconnection in the fan-spine topology. The EFR emerges continuously and meets with the magnetic fields of the dome. Magnetic cancellations take place between the emerging negative polarity and the outer positive polarity of the dome's fields, which lead to the rise of the loop connecting the EFR and brightenings related to the dome. A single Gaussian fit to the profiles of the \emph{IRIS} SI IV 1394 \AA\ line is used in the analysis. It appears that there are two rising components along the slit, except for the rise in the line-of-sight direction. The cancellation process repeats again and again. Eventually the fan-spine dome is destroyed and a new connectivity is formed. We suggest that magnetic reconnection between the EFR and the magnetic fields of the fan-spine dome in the process is responsible for the destruction of the dome.

Relationship between EUV microflares and small-scale magnetic fields in the quiet Sun

Fayu **Jiang**, Jun Zhang, Shuhong Yang
Publications of the Astronomical Society of Japan, **2015**
http://arxiv.org/pdf/1502.03568v1.pdf
Microflares are small dynamic signatures observed in X-ray and extreme-ultraviolet channels. Because of their impulsive emission enhancements and wide distribution, they are thought to be closely related to coronal heating. By using the high resolution 171 {\AA} images from the Atmospheric Imaging Assembly and the lines-of-sight

magnetograms obtained by the Helioseismic and Magnetic Imager on board the Solar Dynamics Observatory, we trace 10794 microflares in a quiet region near the disk center with a field of view of 960 arcsec × 1068 arcsec during 24 hr. The microflares have an occurrence rate of 4.4× 103 hr−1 extrapolated over the whole Sun. Their average brightness, size, and lifetime are 1.7 I0(of the quiet Sun), 9.6 Mm2, and 3.6 min, respectively. There exists a mutual positive correlation between the microflares' brightness, area and lifetime. In general, the microflares distribute uniformly across the solar disk, but form network patterns locally, which are similar to and matched with the magnetic network structures. Typical cases show that the microflares prefer to occur in magnetic cancellation regions of network boundaries. We roughly calculate the upper limit of energy flux supplied by the microflares and find that the result is still a factor of ~15 below the coronal heating requirement.

STUDY OF THE THREE-DIMENSIONAL CORONAL MAGNETIC FIELD OF ACTIVE REGION 11117 AROUND THE TIME OF A CONFINED FLARE USING A DATA-DRIVEN CESE-MHD MODEL

Chaowei **Jiang** (江朝伟)1, Xueshang Feng (冯学尚)1, S. T. Wu (吴式灿)2, and Qiang Hu

2012 ApJ 759 85

We apply a data-driven magnetohydrodynamics (MHD) model to investigate the three-dimensional (3D) magnetic field of NOAA active region (AR) 11117 around the time of a C-class confined flare that occurred on **2010 October 25**. The MHD model, based on the spacetime conservation-element and solution-element scheme, is designed to focus on the magnetic field evolution and to consider a simplified solar atomsphere with finite plasma β. Magnetic vector-field data derived from the observations at the photosphere is inputted directly to constrain the model. Assuming that the dynamic evolution of the coronal magnetic field can be approximated by successive equilibria, we solve a time sequence of MHD equilibria based on a set of vector magnetograms for AR 11117 taken by the Helioseismic and Magnetic Imager on board the Solar Dynamic Observatory around the time of the flare. The model qualitatively reproduces the basic structures of the 3D magnetic field, as supported by the visual similarity between the field lines and the coronal loops observed by the Atmospheric Imaging Assembly, which shows that the coronal field can indeed be well characterized by the MHD equilibrium in most cases. The magnetic configuration changes very little during the studied time interval of 2 hr. A topological analysis reveals that the small flare is correlated with a bald patch (BP, where the magnetic field is tangent to the photosphere), suggesting that the energy release of the flare can be understood by magnetic reconnection associated with the BP separatrices. The total magnetic flux and energy keep increasing slightly in spite of the flare, while the computed magnetic free energy drops during the flare by ~1030 erg, which seems to be adequate in providing the energy budget of a minor C-class confined flare.

NUMERICAL SIMULATION OF SOLAR MICROFLARES IN A CANOPY-TYPE MAGNETIC CONFIGURATION

R.-L. **Jiang**1,2, C. Fang1,2, and P.-F. Chen

2012 ApJ 751 152

Microflares are small activities in the solar low atmosphere; some are in the low corona while others are in the chromosphere. Observations show that some of the microflares are triggered by magnetic reconnection between the emerging flux and a pre-existing background magnetic field. We perform 2.5-dimensional, compressible, resistive magnetohydrodynamic simulations of the magnetic reconnection with gravity considered. The background magnetic field is a canopy-type configuration that is rooted at the boundary of the solar supergranule. By changing the bottom boundary conditions in the simulation, a new magnetic flux emerges at the center of the supergranule and reconnects with the canopy-type magnetic field. We successfully simulate the coronal and chromospheric microflares whose current sheets are located at the corona and the chromosphere, respectively. The microflare with a coronal origin has a larger size and a higher temperature enhancement than the microflare with a chromospheric origin. In the microflares with coronal origins, we also found a hot jet (~1.8 × 106 K), which is probably related to the observational extreme ultraviolet or soft X-ray jets, and a cold jet (~104 K), which is similar to the observational Hα/Ca surges. However, there is only a Hα/Ca bright point in the microflares that have chromospheric origins. The study of parameter dependence shows that the size and strength of the emerging magnetic flux are the key parameters that determine the height of the reconnection location, and they further determine the different observational features of the microflares.

RAPID SUNSPOT ROTATION ASSOCIATED WITH THE X2.2 FLARE ON 2011 FEBRUARY 15

Yunchun **Jiang**1, Ruisheng Zheng1,2, Jiayan Yang1,3, Junchao Hong1,2, Bi Yi1,2 and Dan Yang

2012 ApJ 744 50

We present observations of sunspot evolution associated with the first X-class flare of the present solar cycle 24, which occurred in AR 11158 on 2011 February 15. The active region consisted of four emerging bipoles that showed complicated sunspot motion. The preceding spot of a bipole underwent the fastest movement. It not only passed through the following end of another bipole, thus causing a shearing motion, but also merged with the same-polarity spots and formed a single, larger umbra. This led to the formation of a δ configuration with an S-shaped neutral line, above which

an extreme ultraviolet filament channel and a sigmoid formed and erupted to produce the flare. Along with the development of a clockwise (CW) spiral penumbra-filament pattern, the merged spot started rapid CW rotation around its umbral center 20 hr before the flare. The rotation persisted throughout the flare but stopped sharply about 1 hr after the flare ended, maintaining the twisted penumbra-filament pattern. The moving spot also caused continuous flux cancellation; in particular, its outer penumbra directly collided with small opposite-polarity spots only 100 minutes before the flare. When the shearing and rotational motions are main contributors to the energy buildup and helicity injection for the flare, the cancellation and collision might act as a trigger. Our observations support the idea that the rotation can be attributed to the emergence of twisted magnetic fields, as proposed in recent theories. Finally, the cause of its sudden halt is discussed.
15 Feb 2011

Detailed Analysis of Fan-Shaped jets in Three Dimensional Numerical Simulation

R. L. **Jiang**, K. Shibata, H. Isobe and C. Fang
E-print, Jan **2011**; Research in Astronomy and Astrophysics (RAA).
We performed three dimensional resistive magnetohydrodynamic simulations to study the magnetic reconnection using an initially shearing magnetic field configuration (force free field with a current sheet in the middle of the computational box). It is shown that there are two types of reconnection jets: the ordinary reconnection jets and fan-shaped jets, which are formed along the guide magnetic field. The fan-shaped jets are much different from the ordinary reconnection jets which are ejected by magnetic tension force. There are two driving forces for accelerating the fan-shaped jets. The one is the Lorentz force which dominates the motion of fluid elements at first and then the gas pressure gradient force accelerates the fluid elements in the later stage. The dependence on magnetic reconnection angle and resistivity value has also been studied. The formation and evolution of these jets provide a new understanding of dynamic magnetohydrodynamic jets.

The H-alpha surges and EUV jets from magnetic flux emergences and cancellations:

Y. C. **Jiang**, H. D. Chen, K. J. Li, Y. D. Shen and L. H. Yang
A&A 469 (**2007**) 331-337
http://www.aanda.org/10.1051/0004-6361:20053954

Solar Flare Intensity Prediction with Machine Learning Models

Zhenbang **Jiao**, Hu Su, Xiantong Wang, Ward Manchester, Tamas Gombosi, Alfred Hero, Yang Chen
Space Weather **Volume18, Issue7** e2020SW002440 **2020**
https://sci-hub.tw/https://agupubs.onlinelibrary.wiley.com/doi/abs/10.1029/2020SW002440
https://agupubs.onlinelibrary.wiley.com/doi/epdf/10.1029/2020SW002440
https://arxiv.org/pdf/1912.06120.pdf
https://doi.org/10.1029/2020SW002440
We develop a mixed Long Short Term Memory (LSTM) regression model to predict the maximum solar flare intensity within a 24-hour time window 0~24, 6~30, 12~36, 24~48 hours ahead of time using 6, 12, 24, 48 hours of data (predictors) for each HMI Active Region Patch (HARP). The model makes use of (1) the Space-weather HMI Active Region Patch (SHARP) parameters as predictors and (2) the exact flare intensities instead of class labels recorded in the Geostationary Operational Environmental Satellites (GOES) data set, which serves as the source of the response variables. Compared to solar flare classification, the model offers us more detailed information about the exact maximum flux level, i.e. intensity, for each occurrence of a flare. We also consider classification models built on top of the regression model and obtain encouraging results in solar flare classifications. Our results suggest that the most efficient time period for predicting the solar activity is within 24 hours before the prediction time under LSTM architecture using the SHARP parameters. **2011.02.11-20, 2011.07.25-29, 2011.09.23-29, 2017.03.27-04.04**

Homologous Microflares with Mass Ejection and Plasma Heating on the Quiet Sun

C. L. **Jin**1, G. P. Zhou1, and J. X. Wang1,2
2021 ApJL 914 L35
https://doi.org/10.3847/2041-8213/ac097c
Study of microflares on the quiet Sun is extremely important in learning the physics of both solar flare and atmospheric heating. Here, for the first time, we report the detailed observations of two homologous microflares from Atmospheric Imager Assembly (AIA) images and Heliospheric Magnetic Imager magnetograms in a very quiet region. The two microflares are observed clearly in the extreme ultraviolet and faintly in the ultraviolet in AIA images. They have an area of ~59 Mm2 and ~46 Mm2, and a duration of 25 minutes and 22 minutes. The magnetic cancellation continuously takes place during the microflares, and the magnetic flux decrease is apparent, with a value of ~4 × 1018 Mx. The obvious mass ejections are observed during the microflares, and dimming occurs during and after the microflares. The velocity of mass ejection is up to 160 km s−1. For the two microflares, the time of peak intensity in λ 30.4 nm precedes that of the coronal peak emission, up to 2.4–3.3 minutes. Their thermal energy is estimated to be 1.3 × 1027 erg and

2.5 × 1026 erg, respectively, which heats the corona up to 5.8 MK and 2.8 MK. There are many similarities of microflares on the quiet Sun to major flares in the active regions.

Data-driven Simulations of Magnetic Connectivity in Behind-the-Limb γ-ray Flares and Associated Coronal Mass Ejections

Meng **Jin**, Vahe Petrosian, Wei Liu, Nariaki V. Nitta, Nicola Omodei, Fatima Rubio da Costa, Frederic Effenberger, Gang Li, Melissa Pesce-Rollins, Alice Allafort, Ward Manchester IV

ApJ **2018**

https://arxiv.org/pdf/1807.01427.pdf

Recent detections of high-energy γ-rays by \emph{Fermi} from behind-the-limb (BTL) solar flares pose a puzzle on the particle acceleration/transport mechanisms in such events. Due to the large separation between the flare site and the location of γ-ray emission, it is suggested that the associated coronal mass ejections (CMEs) play an important role in accelerating and subsequently transporting particles back to the Sun to produce the observed γ-rays. We explore this scenario by simulating the CME associated with a BTL flare that occurred on **2014 September 1** about 40$\arcdeg$ behind the east solar limb. The flare was well observed by {\it Fermi}, {\it RHESSI}, {\it SDO}, and {\it STEREO}. \emph{Fermi}/LAT detected a substantial flux of >100 MeV γ-rays for more than an hour with an emission centroid located near the east limb but about 300$\arcsec$ north of the centroid of the \emph{RHESSI} HXR source. We utilize a data-driven global magnetohydrodynamics model (AWSoM: Alfv\'{e}n-wave Solar Model) and initiate the CME by the Gibson-Low flux rope to track the dynamic evolution of the global magnetic field during the event and investigate the magnetic connectivity between the CME/CME-driven shock and the \emph{Fermi}/LAT emission region. Moreover, we derive the time-varying shock parameters over the area that becomes magnetically connected to \emph{Fermi} γ-ray emission region on the visible solar disk. Our simulations show that the CME/CME-driven shock develops connections both to the flare region and the visible solar disk during the eruption, indicating that the CME's interaction with the global solar corona is critical for \emph{Fermi} BTL events and the associated long duration γ-ray emission.

Magnetic Eruption from a Three-ribbon Flare

Ju **Jing**1, Jeongwoo Lee1, Mia Mancuso1, Qin Li1, Nian Liu1, Satoshi Inoue1, Yan Xu1, and Haimin Wang1

2024 ApJ 972 110

https://iopscience.iop.org/article/10.3847/1538-4357/ad5ce3/pdf

A Statistical Study of Solar White-Light Flares Observed by the White-light Solar Telescope of the Lyman-alpha Solar Telescope on the Advanced Space-based Solar Observatory (ASO-S/LST/WST) at 360 nm

Zhichen **Jing**, Ying Li, Li Feng, Hui Li, Yu Huang, Youping Li, +++

Solar Phys. Volume 299, article number 1 **2024**

https://arxiv.org/pdf/2401.07275.pdf

https://link.springer.com/content/pdf/10.1007/s11207-024-02251-9.pdf

Solar white-light flares (WLFs) are those accompanied by brightenings in the optical continuum or integrated light. The White-light Solar Telescope (WST), as an instrument of the Lyman-alpha Solar Telescope (LST) on the Advanced Space-based Solar Observatory (ASO-S), provides continuous solar full-disk images at 360 nm, which can be used to study WLFs. We analyze 205 major flares above M1.0 from October 2022 to May 2023 and identify 49 WLFs at 360 nm from WST observations, i.e. with an occurrence rate of 23.9%. The percentages of WLFs for M1 - M4 (31 out of 180), M5 - M9 (11 out of 18), and above X1 (7 for all) flares are 17.2%, 61.1%, and 100%, respectively, namely the larger the flares, the more likely they are WLFs at 360 nm. We further analyze 39 WLFs among the identified WLFs and investigate their properties such as white-light enhancement, duration, and brightening area. It is found that the relative enhancement of the white-light emission at 360 nm is mostly (>90%) less than 30% and the mean enhancement is 19.4%. The WLFs' duration at 360 nm is mostly (>80%) less than 20 minutes and its mean is 10.3 minutes. The brightening area at 360 nm is mostly (>75%) less than 500 arcsecond2 and the median value is 225. We find that there exist good correlations between the white-light enhancement/duration/area and the peak soft X-ray (SXR) flux of the flare, with correlation coefficients of 0.68, 0.58, and 0.80, respectively. In addition, the white-light emission in most WLFs peaks around the same time as the temporal derivative of SXR flux as well as the hard X-ray emission at 20 - 50 keV, indicative of Neupert effect. It is also found that the limb WLFs are more likely to have a greater enhancement, which is consistent with numerical simulations. **11 February 2023**

Table 2. The 39 WLFs analyzed in detail. Nov 2022-May 2023

Understanding the Initiation of the M2.4 Flare on 2017 July 14

Ju **Jing**1, Satoshi Inoue1, Jeongwoo Lee1, Qin Li1, Gelu M. Nita1, Yan Xu1, Chang Liu1, Dale E. Gary1, and Haimin Wang1
2021 ApJ 922 108
https://iopscience.iop.org/article/10.3847/1538-4357/ac26c7/pdf
https://doi.org/10.3847/1538-4357/ac26c7
We present both the observation and the magnetohydrodynamics (MHD) simulation of the M2.4 flare (SOL2017-07-14T02:09) of NOAA active region (AR) 12665 with a goal to identify its initiation mechanism. The observation by the Atmospheric Image Assembly (AIA) on board the Solar Dynamics Observatory (SDO) shows that the major topology of the AR is a sigmoidal configuration associated with a filament/flux rope. A persistent emerging magnetic flux and the rotation of the sunspot in the core region were observed with Magnetic Imager (HMI) on board the SDO on the timescale of hours before and during the flare, which may provide free magnetic energy needed for the flare/coronal mass ejection (CME). A high-lying coronal loop is seen moving outward in AIA EUV passbands, which is immediately followed by the impulsive phase of the flare. We perform an MHD simulation using the potential magnetic field extrapolated from the measured pre-flare photospheric magnetic field as initial conditions and adopting the observed sunspot rotation and flux emergence as the driving boundary conditions. In our simulation, a sigmoidal magnetic structure and an overlying magnetic flux rope (MFR) form as a response to the imposed sunspot rotation, and the MFR rises to erupt like a CME. These simulation results in good agreement with the observation suggest that the formation of the MFR due to the sunspot rotation and the resulting torus and kink instabilities were essential to the initiation of this flare and the associated coronal mass ejection.

The Lyman-alpha Emission in Solar Flares. I. a Statistical Study on Its Relationship with the 1--8 Å Soft X-ray Emission

Zhichen **Jing**, Wuqi Pan, Yukun Yang, Dechao Song, Jun Tian, Y. Li, X. Cheng, Jie Hong, M. D. Ding
ApJ **904** 41 **2020**
https://arxiv.org/pdf/2009.10358.pdf
https://iopscience.iop.org/article/10.3847/1538-4357/abbacc/pdf
We statistically study the relationship between the Lyman-alpha (\lya) and 1--8 Å soft X-ray (SXR) emissions from 658 M- and X-class solar flares observed by the {\em Geostationary Operational Environmental Satellite} during 2006--2016. Based on the peak times of the two waveband emissions, we divide the flares into three types. Type I (III) has an earlier (a later) peak time in the \lya\ emission than that in the SXR emission, while type II has nearly a same peak time (within the time resolution of 10 s) between the \lya\ and SXR emissions. In these 658 flares, we find that there are 505 (76.8\%) type I flares, 10 (1.5\%) type II flares, and 143 (21.7\%) type III flares, and that the three types appear to have no dependence on the flare duration, flare location, or solar cycle. Besides the main peak, the \lya\ emission of the three type flares also shows sub-peaks which can appear in the impulsive or gradual phase of the flare. It is found that the main-peak (for type I) and sub-peak (for type III) emissions of \lya\ that appear in the impulsive phase follow the Neupert effect in general. This indicates that such \lya\ emissions are related to the nonthermal electron beam heating. While the main-peak (for type III) and sub-peak (for type I) emissions of \lya\ that appear in the gradual phase are supposed to be primarily contributed by the thermal plasma that cools down. **8 Sep 2011, 5 Mar 2012, 16 Apr 2012, 30 Jun 2012, 5 Jul 2012, 23 Oct 2012, 29 Oct 2013, 2 Oct 2014, 24 Oct 2014, 3 Nov 2014, 20 Sep 2015**

Witnessing a Large-scale Slipping Magnetic Reconnection along a Dimming Channel during a Solar Flare

Ju **Jing**, Rui Liu, Mark C. M. Cheung, Jeongwoo Lee, Yan Xu, Chang Liu, Chunming Zhu, Haimin Wang
2017 ApJL 842 L18
https://arxiv.org/pdf/1706.01355.pdf
We report the intriguing large-scale dynamic phenomena associated with the M6.5 flare~(SOL**2015-06-22**T18:23) in NOAA active region 12371, observed by RHESSI, Fermi, and the Atmospheric Image Assembly (AIA) and Magnetic Imager (HMI) on the Solar Dynamic Observatory (SDO). The most interesting feature of this event is a third ribbon (R3) arising in the decay phase, propagating along a dimming channel (seen in EUV passbands) towards a neighboring sunspot. The propagation of R3 occurs in the presence of hard X-ray footpoint emission, and is broadly visible at temperatures from 0.6~MK to over 10~MK through the Differential Emission Measure (DEM) analysis. The coronal loops then undergo an apparent slipping motion following the same path of R3, after a ~ 80~min delay. To understand the underlying physics, we investigate the magnetic configuration and the thermal structure of the flaring region. Our results are in favor of a slipping-type reconnection followed by the thermodynamic evolution of coronal loops. In comparison with those previously reported slipping reconnection events, this one proceeds across a particularly long distance (~60 Mm) over a long period of time (~50 min), and shows two clearly distinguished phases: the propagation of the footpoint brightening driven by nonthermal particle injection and the apparent slippage of loops governed by plasma heating and subsequent cooling.

Unprecedented Fine Structure of a Solar Flare Revealed by the 1.6 m New Solar Telescope

Ju **Jing**, Yan Xu, Wenda Cao, Chang Liu, Dale Gary & Haimin Wang
Scientific Reports 6, Article number: 24319 **2016**
http://www.nature.com/articles/srep24319#s2
http://arxiv.org/pdf/1604.08562v1.pdf
Solar flares signify the sudden release of magnetic energy and are sources of so called space weather. The fine structures (below 500 km) of flares are rarely observed and are accessible to only a few instruments world-wide. Here we present observation of a solar flare using exceptionally high resolution images from the 1.6 m New Solar Telescope (NST) equipped with high order adaptive optics at Big Bear Solar Observatory (BBSO). The observation reveals the process of the flare in unprecedented detail, including the flare ribbon propagating across the sunspots, coronal rain (made of condensing plasma) streaming down along the post-flare loops, and the chromosphere's response to the impact of coronal rain, showing fine-scale brightenings at the footpoints of the falling plasma. Taking advantage of the resolving power of the NST, we measure the cross sectional widths of flare ribbons, post-flare loops and footpoint brighenings, which generally lie in the range of 80-200 km, well below the resolution of most current instruments used for flare studies. Confining the scale of such fine structure provides an essential piece of information in modeling the energy transport mechanism of flares, which is an important issue in solar and plasma physics. **2015 June 22**

Comparison between the eruptive X2.2 flare on 2011 February 15 and confined X3.1 flare on 2014 October 24

Ju **Jing**, Yan Xu, Jeongwoo Lee, Nariaki V. Nitta, Chang Liu, Sung-Hong Park, Thomas Wiegelmann, Haimin Wang
Research in Astronomy and Astrophysics (RAA) Vol 15, No 9 1537-1546 **2015**
http://www.raa-journal.org/raa/index.php/raa/article/view/2313
We compare two contrasting X-class flares in terms of magnetic free energy, relative magnetic helicity and decay index of the active regions (ARs) in which they occurred. The events in question are the eruptive X2.2 flare from AR 11158 accompanied by a halo coronal mass ejection (CME) and the confined X3.1 flare from AR 12192 with no associated CME. These two flares exhibit similar behavior of free magnetic energy and helicity buildup for a few days preceding them. A major difference between the two flares is found to lie in the time-dependent change of magnetic helicity of the ARs that hosted them. AR 11158 shows a significant decrease in magnetic helicity starting ~4 hours prior to the flare, but no apparent decrease in helicity is observed in AR 12192. By examining the magnetic helicity injection rates in terms of sign, we confirmed that the drastic decrease in magnetic helicity before the eruptive X2.2 flare was not caused by the injection of reversed helicity through the photosphere but rather the CME-related change in the coronal magnetic field. Another major difference we find is that AR 11158 had a significantly larger decay index and therefore weaker overlying field than AR 12192. These results suggest that the coronal magnetic helicity and the decay index of the overlying field can provide a clue about the occurrence of CMEs.

EVOLUTION OF RELATIVE MAGNETIC HELICITY AND CURRENT HELICITY IN NOAA ACTIVE REGION 11158

Ju **Jing**1, Sung-Hong Park2, Chang Liu1, Jeongwoo Lee1,3, Thomas Wiegelmann4, Yan Xu1, Na Deng1, and Haimin Wang
2012 ApJ 752 L9
Both magnetic and current helicities are crucial ingredients for describing the complexity of active-region magnetic structure. In this Letter, we present the temporal evolution of these helicities contained in NOAA active region 11158 during five days from **2011 February 12 to 16**. The photospheric vector magnetograms of the Helioseismic and Magnetic Imager on board the Solar Dynamic Observatory were used as the boundary conditions for the coronal field extrapolation under the assumption of nonlinear force-free field, from which we calculated both relative magnetic helicity and current helicity. We construct a time-altitude diagram in which altitude distribution of the magnitude of current helicity density is displayed as a function of time. This diagram clearly shows a pattern of upwardly propagating current helicity density over two days prior to the X2.2 flare on February 15 with an average propagation speed of ~36 m s–1. The propagation is synchronous with the emergence of magnetic flux into the photosphere, and indicative of a gradual energy buildup for the X2.2 flare. The time profile of the relative magnetic helicity shows a monotonically increasing trend most of the time, but a pattern of increasing and decreasing magnetic helicity above the monotonic variation appears prior to each of two major flares, M6.6 and X2.2, respectively. The physics underlying this bump pattern is not fully understood. However, the fact that this pattern is apparent in the magnetic helicity evolution but not in the magnetic flux evolution makes it a useful indicator in forecasting major flares.

NONPOTENTIALITY OF CHROMOSPHERIC FIBRILS IN NOAA ACTIVE REGIONS 11092 AND 9661

Ju **Jing**1, Yuan Yuan1, Kevin Reardon2,3, Thomas Wiegelmann4, Yan Xu1 and Haimin Wang
2011 ApJ 739 67, **File**

In this paper, we present a method to automatically segment chromospheric fibrils from Hα observations and further identify their orientation. We assume that chromospheric fibrils are aligned with the magnetic field. By comparing the orientation of the fibrils with the azimuth of the embedding chromospheric magnetic field extrapolated from a potential field model, the shear angle, a measure of nonpotentiality, along the fibrils is readily deduced. Following this approach, we make a quantitative assessment of the nonpotentiality of fibrils in two NOAA active regions (ARs): (1) the relatively simple AR 11092, observed with very high resolution by Interferometric Bidimensional Spectrometer, and (2) a β-γ-δ AR 9661, observed with median resolution by Big Bear Solar Observatory before and after an X1.6 flare.

Free Magnetic Energy and Flare Productivity of Active Regions

Ju **Jing**, Changyi Tan, Yuan Yuan, Benjamin Wang, Thomas Wiegelmann, Yan Xu, and Haimin Wang
ApJ **713** 440, **2010**

In this study, the photospheric vector magnetograms, obtained with the Spectro-Polarimeter of the Solar Optical Telescope on board *Hinode*, are used as the boundary conditions to extrapolate the three-dimensional nonlinear force-free (NLFF) coronal magnetic fields. The observed non-force-free photospheric magnetic fields are preprocessed toward the nearly force-free chromospheric magnetic fields. The performance of the preprocessing procedure is evaluated by comparing with chromospheric magnetic fields obtained by the Vector SpectroMagnetograph instrument located on the Synoptic Optical Long-term Investigations of the Sun Tower. Then, the weighted optimization method is applied to the preprocessed boundary data to extrapolate the NLFF fields with which we are able to estimate the free magnetic energy stored in the active regions. The magnitude scaling correlation between the free magnetic energy and the soft X-ray flare index (FI) of active regions is then studied. The latter quantifies the impending flare production of active regions over the subsequent 1, 2, and 3 day time windows. Based on 75 samples, we find a positive correlation between the free energy and the FI. We also study the temporal variation of free magnetic energy for three active regions, of which two are flare-active and one is flare-quiet during the observation over a period of several days. While the magnitude of free magnetic energy unambiguously differentiates between the flare-active and the flare-quiet regions, the temporal variation of free magnetic energy does not exhibit a clear and consistent pre-flare pattern. This may indicate that the trigger mechanism of flares is as important as the energy storage in active regions

Temporal Evolution of Free Magnetic Energy Associated with Four X-class Flares

Ju **Jing**, P. F. Chen, Thomas Wiegelmann, Yan Xu, Sung-Hong Park, Haimin Wang
E-print, Feb **2009**; ApJ, **696** 84-90 doi: 10.1088/0004-637X/696/1/84, **2009**
BBSO, #1387, **2009,** **http://solar.njit.edu/preprints/jing1387.pdf**

We study the temporal variation of free magnetic energy E_{free} around the time of four X-class flares. The high-cadence photospheric vector magnetograms obtained by the digital vector magnegograph (DVMG) system at the Big Bear Solar Observatory (BBSO) are used as the boundary conditions to reconstruct the three-dimensional (3D) non-linear force-free (NLFF) coronal field. In order to remove the effect of the net Lorentz force and torque acting in the photosphere, the vector magnetograms are preprocessed using the method devised by Wiegelmann et al. (2006). Then a well-tested multigrid-like optimization code by Wiegelmann (2004) is applied to the preprocessed boundary data to extrapolate the NLFF coronal field with which we are able to estimate the free energy E_{free}. In all the four events, we find a significant drop of E_{free} starting sim15 min before the peak time of the associated non-thermal flare emission, although long term trend varies from event to event. We discuss the physical implication of the result, i.e., the magnetic relaxation is already going on in the corona well before the flare reconnection.

Spatial Distribution of Magnetic Reconnection in the 2006 December 13 Solar Flare As Observed by Hinode

Ju **Jing**1;2, Jongchul Chae3, and Haimin Wang1;2
Preprint BBSO #1352, **2007**, File; Ap.J.

A massive two-ribbon are and its source magnetic field region were well captured by Solar Optical Telescope (SOT) on board Hinode in Ca II H spectral line and by Spectro-Polarimeter (SP) of SOT, respectively. Using the high resolution Hinode data sets, we compare the spatial distribution of local magnetic reconnection rate and energy release rate along the ribbons with that of G-band kernels which serve as a proxy for the primary energy release. The G-band kernels spatially coincide with the maximum of both modelled quantities, which gives strong support for the reconnection model.

Changes of Magnetic Structure in 3-D Associated with the X3.4 Flare of 2006 December 13

Ju **Jing**1;2, Thomas Wiegelmann3, Yoshinori Suematsu4, Masahito Kubo5, and Haimin Wang
Preprint BBSO#1354, **2007**, The Astrophysical Journal, 676: L81–L84, 2008 March 20

http://www.journals.uchicago.edu/doi/pdf/10.1086/587058
Recent observations demonstrated that sunspot structure can change rapidly and irreversibly after ares. One of the most puzzling results is the increase in magnetic shear around aring magnetic polarity inversion line (PIL) after ares. However, all these observations were made at 2-dimensional (2-D) photosphere. In this letter, we study the altitude variation of the non-potentiality of the magnetic fields associated with the 4B/X3.4 are of 2006 December 13. The vector magnetograms with unprecedented quality from Hinode before and after the are are used as the boundary conditions to extrapolate the 3-dimensional (3-D) non-linear force-free (NLFF) magnetic fields and the potential fields. The former are computed with the optimization algorithm and the later with Green's function method. At the photosphere boundary, magnetic shear increases after the are in a local area close to the aring magnetic PIL. Two measures of the magnetic non-potentiality, the weighted mean shear _w and the total magnetic shear _wB, are calculated in this area at progressively higher altitude. By comparing their altitude variation pro_les before and after the are, we find that the non-potentiality of the local area increases after the are below 8,000 km and decreases from that height to _70,000 km. Beyond 70,000 km, the magnetic fields approach potential for both times.

Particle Acceleration in Magnetic Reconnection with Ad Hoc Pitch-angle Scattering

Grant **Johnson**1, Patrick Kilian2, Fan Guo3,4, and Xiaocan Li5
2022 ApJ 933 73
https://iopscience.iop.org/article/10.3847/1538-4357/ac7143/pdf
Particle acceleration during magnetic reconnection is a long-standing topic in space, solar, and astrophysical plasmas. Recent 3D particle-in-cell simulations of magnetic reconnection show that particles can leave flux ropes due to 3D field-line chaos, allowing particles to access additional acceleration sites, gain more energy through Fermi acceleration, and develop a power-law energy distribution. This 3D effect does not exist in traditional 2D simulations, where particles are artificially confined to magnetic islands due to their restricted motions across field lines. Full 3D simulations, however, are prohibitively expensive for most studies. Here, we attempt to reproduce 3D results in 2D simulations by introducing ad hoc pitch-angle scattering to a small fraction of the particles. We show that scattered particles are able to transport out of 2D islands and achieve more efficient Fermi acceleration, leading to a significant increase of energetic particle flux. We also study how the scattering frequency influences the nonthermal particle spectra. This study helps achieve a complete picture of particle acceleration in magnetic reconnection.

TRANSITION REGION EMISSION FROM SOLAR FLARES DURING THE IMPULSIVE PHASE

H. **Johnson**1,2, J. C. Raymond1, N. A. Murphy1, S. Giordano3, Y.-K. Ko4, A. Ciaravella5 and R. Suleiman
2011 ApJ 735 70
There are relatively few observations of UV emission during the impulsive phases of solar flares, so the nature of that emission is poorly known. Photons produced by solar flares can resonantly scatter off atoms and ions in the corona. Based on off-limb measurements by the Solar and Heliospheric Observatory/Ultraviolet Coronagraph Spectrometer, we derive the O VI λ1032 luminosities for 29 flares during the impulsive phase and the Lyα luminosities of 5 flares, and we compare them with X-ray luminosities from GOES measurements. The upper transition region and lower transition region luminosities of the events observed are comparable. They are also comparable to the luminosity of the X-ray emitting gas at the beginning of the flare, but after 10-15 minutes the X-ray luminosity usually dominates. In some cases, we can use Doppler dimming to estimate flow speeds of the O VI emitting gas, and five events show speeds in the 40-80 km s–1 range. The O VI emission could originate in gas evaporating to fill the X-ray flare loops, in heated chromospheric gas at the footpoints, or in heated prominence material in the coronal mass ejection. All three sources may contribute in different events or even in a single event, and the relative timing of UV and X-ray brightness peaks, the flow speeds, and the total O VI luminosity favor each source in one or more events.

A new approach for modelling chromospheric evaporation in response to enhanced coronal heating II. Non-uniform heating

C. D. **Johnston**1, A. W. Hood1, P. J. Cargill1, 2 and I. De Moortel1
A&A 605, A8 (**2017**)
http://www.aanda.org.sci-hub.cc/articles/aa/abs/2017/09/aa30486-17/aa30486-17.html
We proposed that the use of an approximate “jump condition” at the solar transition region permits fast and accurate numerical solutions of the one dimensional hydrodynamic equations when the corona undergoes impulsive heating. In particular, it eliminates the need for the very short timesteps imposed by a highly resolved numerical grid. This paper presents further examples of the applicability of the method for cases of non-uniform heating, in particular, nanoflare trains (uniform in space but non-uniform in time) and spatially localised impulsive heating, including at the loop apex and base of the transition region. In all cases the overall behaviour of the coronal density and temperature shows good agreement with a fully resolved one dimensional model and is significantly better than the equivalent results from a 1D code run without using the jump condition but with the same coarse grid. A detailed assessment of the errors introduced by the jump condition is presented showing that the causes of discrepancy with the fully resolved code are (i) the neglect of the terms corresponding to the rate of change of total energy in the unresolved atmosphere; (ii) mass motions

at the base of the transition region and (iii) for some cases with footpoint heating, an over-estimation of the radiative losses in the transition region.

A new approach for modelling chromospheric evaporation in response to enhanced coronal heating: 1 the method

C. D. **Johnston**, A. W. Hood, P. J. Cargill, I. De Moortel
2016
http://arxiv.org/pdf/1609.05075v1.pdf

We present a new computational approach that addresses the difficulty of obtaining the correct interaction between the solar corona and the transition region in response to rapid heating events. In the coupled corona, transition region and chromosphere system, an enhanced downward conductive flux results in an upflow (chromospheric evaporation). However, obtaining the correct upflow generally requires high spatial resolution in order to resolve the transition region. With an unresolved transition region, artificially low coronal densities are obtained because the downward heat flux jumps across the unresolved region to the chromosphere, underestimating the upflows. Here, we treat the lower transition region as a discontinuity that responds to changing coronal conditions through the imposition of a jump condition that is derived from an integrated form of energy conservation. To illustrate and benchmark this approach against a fully resolved one-dimensional model, we present field-aligned simulations of coronal loops in response to a range of impulsive (spatially uniform) heating events. We show that our approach leads to a significant improvement in the coronal density evolution than just when using coarse spatial resolutions insufficient to resolve the lower transition region. Our approach compensates for the jumping of the heat flux by imposing a velocity correction that ensures that the energy from the heat flux goes into driving the transition region dynamics, rather than being lost through radiation. Hence, it is possible to obtain improved coronal densities. The advantages of using this approach in both one-dimensional hydrodynamic and three-dimensional magnetohydrodynamic simulations are discussed.

ABRUPT LONGITUDINAL MAGNETIC FIELD CHANGES AND ULTRAVIOLET EMISSIONS ACCOMPANYING SOLAR FLARES

B. M. **Johnstone**1,2, G. J. D. Petrie1,2, and J. J. Sudol
2012 ApJ 760 29

We have used Transition Region and Coronal Explorer 1600 Å images and Global Oscillation Network Group (GONG) magnetograms to compare ultraviolet (UV) emissions from the chromosphere to longitudinal magnetic field changes in the photosphere during four X-class solar flares. An abrupt, significant, and persistent change in the magnetic field occurred across more than 10 pixels in the GONG magnetograms for each flare. These magnetic changes lagged the GOES flare start times in all cases, showing that they were consequences and not causes of the flares. Ultraviolet emissions were spatially coincident with the field changes. The UV emissions tended to lag the GOES start times for the flares and led the changes in the magnetic field in all pixels except one. The UV emissions led the photospheric field changes by 4 minutes on average with the longest lead being 9 minutes; however, the UV emissions continued for tens of minutes, and more than an hour in some cases, after the field changes were complete. The observations are consistent with the picture in which an Alfvén wave from the field reconnection site in the corona propagates field changes outward in all directions near the onset of the impulsive phase, including downward through the chromosphere and into the photosphere, causing the photospheric field changes, whereas the chromosphere emits in the UV in the form of flare kernels, ribbons, and sequential chromospheric brightenings during all phases of the flare.

Flare Prediction Using Photospheric and Coronal Image Data

Eric **Jonas**, Monica G. Bobra, Vaishaal Shankar, J. Todd Hoeksema, Benjamin Recht
Solar Physics March **2018**, 293:48
https://arxiv.org/pdf/1708.01323.pdf
https://link.springer.com/content/pdf/10.1007%2Fs11207-018-1258-9.pdf

The precise physical process that triggers solar flares is not currently understood. Here we attempt to capture the signature of this mechanism in solar-image data of various wavelengths and use these signatures to predict flaring activity. We do this by developing an algorithm that i) automatically generates features in 5.5 TB of image data taken by the Solar Dynamics Observatory of the solar photosphere, chromosphere, transition region, and corona during the time period between May 2010 and May 2014, ii) combines these features with other features based on flaring history and a physical understanding of putative flaring processes, and iii) classifies these features to predict whether a solar active region will flare within a time period of TT hours, where T=2 and 24T=2 and 24. Such an approach may be useful since, at the present time, there are no physical models of flares available for real-time prediction. We find that when optimizing for the True Skill Score (TSS), photospheric vector-magnetic-field data combined with flaring history yields the best performance, and when optimizing for the area under the precision–recall curve, all of the data are helpful. Our model performance yields a TSS of 0.84±0.030.84±0.03 and 0.81±0.030.81±0.03 in the T=2T=2- and 24-hour cases, respectively, and a value of 0.13±0.070.13±0.07 and 0.43±0.080.43±0.08 for the area under the precision–

recall curve in the T=2T=2- and 24-hour cases, respectively. These relatively high scores are competitive with previous attempts at solar prediction, but our different methodology and extreme care in task design and experimental setup provide an independent confirmation of these results. Given the similar values of algorithm performance across various types of models reported in the literature, we conclude that we can expect a certain baseline predictive capacity using these data. We believe that this is the first attempt to predict solar flares using photospheric vector-magnetic field data as well as multiple wavelengths of image data from the chromosphere, transition region, and corona, and it points the way towards greater data integration across diverse sources in future work.

The coupled tearing-thermal instability in coronal current sheets from the linear to the non-linear stage

Jordi De **Jonghe**, Samrat Sen
MNRAS **2024**
https://arxiv.org/pdf/2412.07427

In the solar corona, magnetically sheared structures are unstable to both tearing and thermal instabilities in a coupled fashion. However, how the choice of linear perturbation modes influences the time-scale to achieve the thermal runaway in a coupled tearing-thermal coronal current sheet is not well understood to date. Here, we model a force-free Harris current sheet under solar coronal conditions to investigate this coupling in the linear and non-linear regimes. In the linear regime, we adopt the magnetohydrodynamic spectroscopy code Legolas to compare the current sheet under thermal and thermoresistive conditions, after which we initialise non-linear simulations (with MPI-AMRVAC) with the unstable, linear tearing and thermal perturbations obtained with Legolas. It is shown that part of the unstable thermal quasi-continuum adopts tearing properties in the linear stage, but that it is not until the non-linear stage is reached that a true thermal 'runaway' effect leads to condensations inside tearing-induced flux ropes. Hence, the linear stage is governed by the dominant tearing instability whilst condensations form due to tearing-thermal coupling in the non-linear stage. Our results imply that perturbing an equilibrium current sheet with the fastest growing linear mode skips the mode mixing phase in which the dominant instability traditionally emerges, and significantly reduces the time-scale to enter into the non-linear stage and thermal runaway process from its equilibrium configuration.

Onset and evolution of solar flares: Application of 2D and 3D models of magnetic reconnection

Bhuwan **Joshi**, Prabir K. Mitra , Astrid M. Veronig , R. Bhattacharyya
the 3rd BINA workshop, to be published in the Bulletin of the Liège Royal Society of Sciences **2023**
https://arxiv.org/pdf/2310.00366.pdf

The contemporary multi-wavelength observations have revealed various important features during solar flares which, on one hand, support the two-dimensional (2D) "standard flare model" while, on other hand, also urge for the exploration of three-dimensional (3D) magnetic field topologies involved in flares. Traditionally, the formation of parallel ribbons on both side of the polarity inversion line (PIL) and associated overlying loop arcades have been recognized as the most prominent features of eruptive flares which has formed the basis for the development of the standard model providing a 2D description of the flare-associated phenomena. The actual flare, however, occurs in a more complicated 3D magnetic structure. Thus, despite the general applicability, the standard model has limited or no scope in explaining some of the features which exclusively requires a 3D description. In this context, the observations of "circular ribbon flares" stand out where one of the ribbons presents an almost fully closed quasi-circular or quasi-ellipsoidal shape, evidencing the involvement of a typical fan-spine magnetic configuration. In this article, we discuss observational features vis à vis theoretical understanding of solar flares in view of 2D and 3D models of magnetic reconnection. We highlight a few complex cases of circular ribbon flares exhibiting parallel ribbons, a coronal jet, and/or an erupting magnetic flux rope. Exploring various 3D topologies also enables us to probe similarities between the circumstances that govern the onset of jets, confined flares and CME-producing eruptive flares. **2004-08-17, 2013-04-11, 2014 February 11, 2014-12-17, 2015-03-12**

Origin of extreme solar eruptive activity from the active region NOAA 12673 and the largest flare of solar cycle 24

Bhuwan **Joshi**, Prabir K. Mitra (USO/PRL, India)
IAU S372 Proceedings Series **2022**
https://arxiv.org/pdf/2212.10795.pdf

During 2017, when the Sun was moving toward the minimum phase of solar cycle 24, an exceptionally eruptive active region (AR) NOAA 12673 emerged on the Sun during **August 28-September 10**. The AR 12673 produced four X-class and 27 M-class flares, along with numerous C-class flares, making it one of the most powerful ARs of solar cycle 24. Notably, it produced the largest flare of solar cycle 24, namely, the X9.3 event on 2017 September 6. In this work, we highlight the results of our comprehensive analysis involving multi-wavelength imaging and coronal magnetic field modeling to understand the evolution and eruptivity from AR 12673. We especially focus on the morphological,

spectral and kinematical evolution of the two X-class flares on **6 September 2017**. We explore various large- and small-scale magnetic field structures of the active region which are associated with the triggering and subsequent outbursts during the powerful solar transients.

Analysis of the Evolution of a Multi-Ribbon Flare and Failed Filament Eruption

Reetika **Joshi**, Cristina H. Mandrini, Ramesh Chandra, Brigitte Schmieder, Germán D. Cristiani, Cecilia Mac Cormack, Pascal Démoulin, Hebe Cremades

Solar Phys. **297**, Article number: 81 **2022**

https://arxiv.org/pdf/2206.00531.pdf

https://link.springer.com/content/pdf/10.1007/s11207-022-02021-5.pdf

How filaments form and erupt are topics about which solar researchers have wondered since more than a century and that are still open to debate. We present observations of a filament formation, its failed eruption, and the associated flare (SOL**2019-05-09**T05:51) that occurred in active region (AR) 12740 using data from SDO, STEREO-A, IRIS, and NSO/GONG. AR 12740 was a decaying region formed by a very disperse following polarity and a strong leading spot, surrounded by a highly dynamic zone where moving magnetic features (MMFs) were seen constantly diverging from the spot. Our analysis indicates that the filament was formed by the convergence of fibrils at a location where magnetic flux cancellation was observed. Furthermore, we conclude that its destabilization was also related to flux cancellation associated to the constant shuffling of the MMFs. A two-ribbon flare occurred associated to the filament eruption; however, because the large-scale magnetic configuration of the AR was quadrupolar, two additional flare ribbons developed far from the two main ones. We model the magnetic configuration of the AR using a force-free field approach at the AR scale size. This local model is complemented by a global potential-field source-surface one. Based on the local model, we propose a scenario in which the filament failed eruption and flare are due to two reconnection processes, one occurring below the erupting filament, leading to the two-ribbon flare, and another one above it between the filament flux-rope configuration and the large-scale closed loops. Our computation of the reconnected magnetic flux added to the erupting flux rope, compared to that of the large-scale field overlying it, lets us conclude that the latter was large enough to prevent the filament eruption. A similar conjecture can be drawn from the computation of the magnetic tension derived from the global field model.

Balmer continuum enhancement detected in a mini flare observed with IRIS

Reetika **Joshi**, Brigitte Schmieder, Petr Heinzel, James Tomin, Ramesh Chandra, Nicole Vilmer

A&A 654, A31 **2021**

https://arxiv.org/pdf/2107.11651.pdf

https://www.aanda.org/articles/aa/pdf/2021/10/aa41172-21.pdf

https://doi.org/10.1051/0004-6361/202141172

Optical and near-UV continuum emissions in flares contribute substantially to flare energy budget. Two mechanisms play an important role for continuum emission in flares: hydrogen recombination after sudden ionization at chromospheric layers and transportation of the energy radiatively from the chromosphere to lower layers in the atmosphere, the so called back-warming. The aim of the paper is to disentangle between these two mechanisms for the excess of Balmer continuum observed in a flare. Methods. We combine the observations of Balmer continuum obtained with IRIS (spectra and SJIs 2832 A) and hard X-ray (HXR) emission detected by FERMI Gamma Burst Monitor (GBM) during a mini flare. Calibrated Balmer continuum is compared to non-LTE radiative transfer flare models and radiated energy is estimated. Assuming thick target HXR emission, we calculate the energy of non-thermal electrons detected by FERMI GBM and compare it to the radiated energy. The favorable argument of a relationship between the Balmer continuum excess and the HXR emission is that there is a good time coincidence between both of them. In addition, the shape of the maximum brightness in the 2832 SJIs, which is mainly due to this Balmer continuum excess, is similar to the FERMI/GBM light curve. The electron-beam flux estimated from FERMI/GBM is consistent with the beam flux required in non-LTE radiative transfer models to get the excess of Balmer continuum emission observed in the IRIS spectra. The low energy input by non thermal electrons above 20 keV is sufficient to produce the enhancement of Balmer continuum emission. This could be explained by the topology of the reconnection site. The reconnection starts in a tiny bald patch region which is transformed dynamically in a X-point current sheet. The size of the interacting region would be under the spatial resolution of the instrument. **March 22, 2019**

Two-stage evolution of an extended C-class eruptive flaring activity from sigmoid active region NOAA 12734: SDO and Udaipur-CALLISTO observations

Bhuwan **Joshi** , Prabir K. Mitra , R. Bhattacharyya , Kushagra Upadhyay , Divya Oberoi , K. Sasikumar Raja , Christian Monstein

Solar Phys. **296**, Article number: 85 **2021**

https://arxiv.org/pdf/2104.10947.pdf

https://link.springer.com/content/pdf/10.1007/s11207-021-01820-6.pdf

https://doi.org/10.1007/s11207-021-01820-6

We present a multi-wavelength investigation of a C-class flaring activity that occurred in the active region NOAA 12734 on **8 March 2019**. The investigation utilises data from AIA and HMI on board the SDO and the Udaipur-CALLISTO solar radio spectrograph of the Physical Research Laboratory. This low intensity C1.3 event is characterised by typical features of a long duration event (LDE), viz. extended flare arcade, large-scale two-ribbon structures and twin coronal dimmings. The eruptive event occurred in a coronal sigmoid and displayed two distinct stages of energy release, manifested in terms of temporal and spatial evolution. The formation of twin dimming regions are consistent with the eruption of a large flux rope with footpoints lying in the western and eastern edges of the coronal sigmoid. The metric radio observations obtained from Udaipur-CALLISTO reveals a broad-band (≈50-180 MHz), stationary plasma emission for ≈7 min during the second stage of the flaring activity that resemble a type IV radio burst. A type III decametre-hectometre radio bursts with starting frequency of ≈2.5 MHz precedes the stationary type IV burst observed by Udaipur-CALLISTO by ≈5 min. The synthesis of multi-wavelength observations and Non-Linear Force Free Field (NLFFF) coronal modelling together with magnetic decay index analysis suggests that the sigmoid flux rope underwent a zipping-like uprooting from its western to eastern footpoints in response to the overlying asymmetric magnetic field confinement. The asymmetrical eruption of the flux rope also accounts for the observed large-scale structures viz. apparent eastward shift of flare ribbons and post flare loops along the polarity inversion line (PIL), and provides an evidence for lateral progression of magnetic reconnection site as the eruption proceeds.

Evolutionary stages and triggering process of a complex eruptive flare with circular and parallel ribbons

Navin Chandra **Joshi** (USO/PRL, Dept. of Phys./SRM Univ.), Bhuwan Joshi (USO/PRL), Prabir K. Mitra (USO/PRL, Dept. of Phys./Gujarat Univ.)

MNRAS Volume 501, Issue 4, March **2021**, Pages 4703–4721,

https://doi.org/10.1093/mnras/staa3480

https://arxiv.org/pdf/2101.09923.pdf

We report multi-wavelength study of a complex M-class solar eruptive flare that consists of three different sets of flare ribbons, viz. circular, parallel, and remote ribbons. Magnetic field modeling of source active region NOAA 12242 exhibits the presence of 3D null-point magnetic topology which encompasses an inner bipolar region. The event initiates with the faint signatures of the circular ribbon along with remote brightening right from the pre-flare phase which points toward the ongoing slow yet persistent null-point reconnection. We first detected flux cancellation and an associated brightening, which are likely signatures of tether-cutting reconnection that builds the flux rope near the polarity inversion line (PIL) of the inner bipolar region. In the next stage, with the onset of M8.7 flare, there is a substantial enhancement in the brightening of circular ribbon which essentially suggests an increase in the rate of ongoing null-point reconnection. Finally, the eruption of underlying flux rope triggers ``standard flare reconnection'' beneath it producing an abrupt rise in the intensity of the parallel ribbons as well as enhancing the rate of null-point reconnection by external forcing. We show that within the the fan dome, the region with magnetic decay index n>1.5 borders the null-point QSL. Our analysis suggests that both the torus instability and the breakout model have played role toward the triggering mechanism for the eruptive flare. This event is a nice example of the dynamical evolution of a flux rope initially confined in a null-point topology, that subsequently activates and erupts with the progression of the circular -- cum -- parallel ribbon flare. **2014 December 17**

Multi thermal atmosphere of a mini solar flare during magnetic reconnection observed with IRIS

Reetika **Joshi**, Brigitte Schmieder, Akiko Tei, Guillaume Aulanier, Juraj Lörinčík, Ramesh Chandra, Petr Heinzel

A&A 645, A80 **2021**

https://arxiv.org/pdf/2010.15401.pdf

https://www.aanda.org/articles/aa/pdf/2021/01/aa39229-20.pdf

https://doi.org/10.1051/0004-6361/202039229

The Interface Region Imaging Spectrograph(IRIS) with its high spatial and temporal resolution brings exceptional plasma diagnostics of solar chromospheric and coronal activity during magnetic reconnection. The aim of this work is to study the fine structure and dynamics of the plasma at a jet base forming a mini flare between two emerging magnetic fluxes (EMFs) observed with IRIS and the Solar Dynamics Observatory (SDO) instruments. We proceed to a spatio-temporal analysis of IRIS spectra observed in the spectral ranges of Mg II, C II, and Si IV ions. Doppler velocities from Mg II lines are computed by using a cloud model technique. Strong asymmetric Mg II and C II line profiles with extended blue wings observed at the reconnection site (jet base) are interpreted by the presence of two chromospheric temperature clouds, one explosive cloud with blueshifts at 290 km/s and one cloud with smaller Dopplershift (around 36 km/s). Simultaneously at the same location (jet base), strong emission of several transition region lines (e.g. O IV and Si IV), emission of the Mg II triplet lines of the Balmer-continuum and absorption of identified chromospheric lines in Si IV broad profiles have been observed and analysed. Such observations of IRIS line and continuum emissions allow us to propose a stratification model for the white-light mini flare atmosphere with multiple layers of different temperatures along the line of sight, in a reconnection current sheet. It is the first time that we could quantify the fast

speed (possibly Alfvénic flows) of cool clouds ejected perpendicularly to the jet direction by using the cloud model technique. We conjecture that the ejected clouds come from plasma which was trapped between the two EMFs before reconnection or be caused by chromospheric-temperature (cool) upflow material like in a surge, during reconnection.
March 22, 2019 Movies are available at https://www.aanda.org
IRIS Nugget June 2021 https://iris.lmsal.com/nugget

Generalisation of the Magnetic Field Configuration of typical and atypical Confined Flares

Navin Chandra **Joshi**, Xiaoshuai Zhu, Brigitte Schmieder, Guillaume Aulanier, Miho Janvier, Bhuwan Joshi, Tetsuya Magara, Ramesh Chandra, Satoshi Inoue
ApJ **871** 165 **2019**
https://arxiv.org/pdf/1811.01228.pdf
Atypical flares cannot be naturally explained with standard models. To predict such flares, we need to define their physical characteristics, in particular, their magnetic environment, and identify pairs of reconnected loops. Here, we present in detail a case-study of a confined flare preceded by flux cancellation that leads to the formation of a filament. The slow rise of the non-eruptive filament favours the growth and reconnection of overlying loops. The flare is only of C5.0 class but it is a long duration event. The reason is that it is comprised of three successive stages of reconnection. A non-linear force-free field extrapolation and a magnetic topology analysis allow us to identify the loops involved in the reconnection process and build a reliable scenario for this atypical confined flare. The main result is that a curved magnetic polarity inversion line in active regions is a key ingredient for producing such atypical flares. A comparison with previous extrapolations for typical and atypical confined flares leads us to propose a cartoon for generalizing the concept. **2014 May 15**

North-South Distribution and Asymmetry of GOES SXR Flares during Solar Cycle 24

Anita **Joshi**, Ramesh Chandra
Open Astron. 28, 228-235 (**2019**)
https://arxiv.org/ftp/arxiv/papers/2007/2007.06998.pdf
Here we present the results of the study of the north-south (N-S) distribution and asymmetry of GOES soft X-ray (SXR) flares during solar cycle 24. The period of study includes ascending, maximum and descending phases of the cycle. During the cycle double-peaked (2011, 2014) solar maximum has occurred. The cycle peak in the year 2011 is due to B-class flares excess activity in the northern hemisphere (NH) whereas C and M class flares excess activity in the southern hemisphere (SH) supported the second peak of the cycle in 2014. The data analysis shows that the SXR flares are more pronounced in 11 to 20 degree latitudes for each hemisphere. Cumulative values of SXR flare count show northern excess during the ascending phase of the cycle. However, in the descending phase of the cycle, southern excess occurred. In the cycle a significant SH dominated asymmetry exists. Near the maximum of the cycle, the asymmetry enhances pronouncedly and reverses in sign.

Observational and model analysis of a two-ribbon flare possibly induced by a neighbouring blowout jet

Bhuwan **Joshi** (USO/PRL, India), Julia K. Thalmann (Univ. of Graz, Austria), Prabir K. Mitra (USO/PRL, India), Ramesh Chandra (Kumaun Univ., India), Astrid M. Veronig (Univ. of Graz, Austria)
ApJ **851** 29 **2017**
https://arxiv.org/pdf/1710.08099.pdf
In this paper, we present unique observations of a blowout coronal jet that possibly triggered a two-ribbon confined C1.2 flare in a bipolar solar active region NOAA 12615 on **2016 December 5**. The jet activity initiates at chromospheric/transition-region heights with a small brightening that eventually grows in a larger volume with well developed standard morphological jet features, viz., base and spire. The spire widens up with a collimated eruption of cool and hot plasma components, observed in the 304 and 94 A channels of AIA, respectively. The speed of the plasma ejection, which forms the jet's spire, was higher for the hot component (~200 km/s) than the cooler one (~130 km/s). The NLFF model of coronal fields at pre- and post-jet phases successfully reveal opening of previously closed magnetic field lines with a rather inclined/low-lying jet structure. The peak phase of the jet emission is followed by the development of a two-ribbon flare that shows coronal loop emission in HXRs up to ~25 keV energy. The coronal magnetic fields rooted at the location of EUV flare ribbons, derived from the NLFF model, demonstrate the pre-flare phase to exhibit an "X-type" configuration while the magnetic fields at the post-flare phase are more or less parallel oriented. The comparisons of multi-wavelength measurements with the magnetic field extrapolations suggest that the jet activity likely triggered the two-ribbon flare by perturbing the field in the interior of the active region.

FORMATION AND ERUPTION OF A FLUX ROPE FROM THE SIGMOID ACTIVE REGION NOAA 11719 AND ASSOCIATED M6.5 FLARE: A MULTI-WAVELENGTH STUDY

Bhuwan **Joshi**1, Upendra Kushwaha1, Astrid M. Veronig2, Sajal Kumar Dhara1, A. Shanmugaraju3, and Yong-Jae Moon4

2017 ApJ 834 42
http://sci-hub.cc/doi/10.3847/1538-4357/834/1/42
We investigate the formation, activation, and eruption of a flux rope (FR) from the sigmoid active region NOAA 11719 by analyzing E(UV), X-ray, and radio measurements. During the pre-eruption period of ~7 hr, the AIA 94 Å images reveal the emergence of a coronal sigmoid through the interaction between two J-shaped bundles of loops, which proceeds with multiple episodes of coronal loop brightenings and significant variations in the magnetic flux through the photosphere. These observations imply that repetitive magnetic reconnections likely play a key role in the formation of the sigmoidal FR in the corona and also contribute toward sustaining the temperature of the FR higher than that of the ambient coronal structures. Notably, the formation of the sigmoid is associated with the fast morphological evolution of an S-shaped filament channel in the chromosphere. The sigmoid activates toward eruption with the ascent of a large FR in the corona, which is preceded by the decrease in photospheric magnetic flux through the core flaring region, suggesting tether-cutting reconnection as a possible triggering mechanism. The FR eruption results in a two-ribbon M6.5 flare with a prolonged rise phase of ~21 minutes. The flare exhibits significant deviation from the standard flare model in the early rise phase, during which a pair of J-shaped flare ribbons form and apparently exhibit converging motions parallel to the polarity inversion line, which is further confirmed by the motions of hard X-ray footpoint sources. In the later stages, the flare follows the standard flare model and the source region undergoes a complete sigmoid-to-arcade transformation. **2013-04-11**

The Role of Erupting Sigmoid in Triggering a Flare with Parallel and Large-Scale Quasi-Circular Ribbons

Navin Chandra **Joshi**, Chang Liu, Xudong Sun, Haimin Wang, Tetsuya Magara, Y.-J. Moon
ApJ 812 50 **2015**
http://arxiv.org/pdf/1509.01792v1.pdf
In this paper, we present observations and analysis of an interesting sigmoid formation, eruption and the associated flare that occurred on **2014 April 18** using multi-wavelength data sets. We discuss the possible role of the sigmoid eruption in triggering the flare, which consists of two different set of ribbons: parallel ribbons as well as a large-scale quasi-circular ribbon. Several observational evidence and nonlinear force-free field extrapolation results show the existence of a large-scale fan-spine type magnetic configuration with a sigmoid lying under a section of the fan dome. The event can be explained with the following two phases. During the pre-flare phase, we observed the formation and appearance of sigmoid via tether-cutting reconnection between the two sets of sheared fields under the fan dome. The second, main flare phase, features the eruption of the sigmoid, the subsequent flare with parallel ribbons, and a quasi-circular ribbon. We propose the following multi-stage successive reconnections scenario for the main flare. First, tether-cutting reconnection is responsible for the formation and the eruption of the sigmoid structure. Second, the reconnection occurred in the wake of the erupting sigmoid produces the parallel flare ribbons on the both sides of the circular polarity inversion line. Third, the null-type reconnection higher in the corona, possibly triggered by the erupting sigmoid, leads to the formation of a large quasi-circular ribbon. For the first time we suggest a mechanism for this type of flare consisting of a double set of ribbons triggered by an erupting sigmoid in a large scale fan-spine type magnetic configuration.

A Trio of Confined Flares in AR 11087

Anand D. **Joshi**1, Terry G. Forbes2, Sung-Hong Park1,3, and Kyung-Suk Cho
2015 ApJ 798 97
We investigate three flares that occurred in active region, AR 11087, observed by the Dutch Open Telescope (DOT) on **2010 July 13**, in a span of three hours. The first two flares have soft X-ray class B3, whereas the third flare has class C3. The third flare not only was the largest in terms of area and brightness but also showed a very faint coronal mass ejection (CME) associated with it, while the earlier two flares had no associated CME. The active region, located at 27° N, 26° E, has a small U-shaped active region filament to the south of the sunspot, and a quiescent filament is located to its west. Hα observations from DOT, as well as extreme-ultraviolet images and magnetograms from the STEREO spacecraft and Solar Dynamics Observatory, are used to study the dynamics of the active region during the three flares. Our observations imply that the first two flares are confined and that some filament material drains to the surface during these flares. At the onset of the third flare downflows are again observed within the active region, but a strong upflow is also observed at the northern end of the adjacent quiescent filament to the west. It is at the latter location that the CME originates. The temporal evolution of the flare ribbons and the dynamics of the filaments are both consistent with the idea that reconnection in a pre-existing current sheet leads to a loss of equilibrium.

RHESSI AND TRACE OBSERVATIONS OF MULTIPLE FLARE ACTIVITY IN AR 10656 AND ASSOCIATED FILAMENT ERUPTION

Bhuwan **Joshi**1, Upendra Kushwaha1, K.-S. Cho2, and Astrid M. Veronig
2013 ApJ 771 1

We present Reuven Ramaty High Energy Solar Spectroscopic Imager (RHESSI) and Transition Region and Coronal Explorer (TRACE) observations of multiple flare activity that occurred in the NOAA active region 10656 over a period of 2 hr on **2004 August 18**. Out of four successive flares, three were class C events, and the final event was a major X1.8 solar eruptive flare. The activities during the pre-eruption phase, i.e., before the X1.8 flare, are characterized by three localized episodes of energy release occurring in the vicinity of a filament that produces intense heating along with non-thermal emission. A few minutes before the eruption, the filament undergoes an activation phase during which it slowly rises with a speed of ~12 km s–1. The filament eruption is accompanied by an X1.8 flare, during which multiple hard X-ray (HXR) bursts are observed up to 100-300 keV energies. We observe a bright and elongated coronal structure simultaneously in E(UV) and 50-100 keV HXR images underneath the expanding filament during the period of HXR bursts, which provides strong evidence for ongoing magnetic reconnection. This phase is accompanied by very high plasma temperatures of ~31 MK, followed by the detachment of the prominence from the solar source region. From the location, timing, strength, and spectrum of HXR emission, we conclude that the prominence eruption is driven by the distinct events of magnetic reconnection occurring in the current sheet below the erupting prominence. These multi-wavelength observations also suggest that the localized magnetic reconnections associated with different evolutionary stages of the filament in the pre-eruption phase play an important role in destabilizing the active-region filament through the tether-cutting process, leading to large-scale eruption and X-class flare.

PRE-FLARE ACTIVITY AND MAGNETIC RECONNECTION DURING THE EVOLUTIONARY STAGES OF ENERGY RELEASE IN A SOLAR ERUPTIVE FLARE

Bhuwan **Joshi**1, Astrid M. Veronig2, Jeongwoo Lee3, Su-Chan Bong4, Sanjiv Kumar Tiwari5 and Kyung-Suk Cho

2011 ApJ 743 195

In this paper, we present a multi-wavelength analysis of an eruptive white-light M3.2 flare that occurred in active region NOAA 10486 on **2003 November 1**. The excellent set of high-resolution observations made by RHESSI and the TRACE provides clear evidence of significant pre-flare activities for ~9 minutes in the form of an initiation phase observed at EUV/UV wavelengths followed by an X-ray precursor phase. During the initiation phase, we observed localized brightenings in the highly sheared core region close to the filament and interactions among short EUV loops overlying the filament, which led to the opening of magnetic field lines. The X-ray precursor phase is manifested in RHESSI measurements below ~30 keV and coincided with the beginning of flux emergence at the flaring location along with early signatures of the eruption. The RHESSI observations reveal that both plasma heating and electron acceleration occurred during the precursor phase. The main flare is consistent with the standard flare model. However, after the impulsive phase, an intense hard X-ray (HXR) looptop source was observed without significant footpoint emission. More intriguingly, for a brief period, the looptop source exhibited strong HXR emission with energies up to ~50-100 keV and significant non-thermal characteristics. The present study indicates a causal relation between the activities in the pre-flare and the main flare. We also conclude that pre-flare activities, occurring in the form of subtle magnetic reorganization along with localized magnetic reconnection, played a crucial role in destabilizing the active region filament, leading to a solar eruptive flare and associated large-scale phenomena.

MAGNETIC RECONNECTION DURING THE TWO-PHASE EVOLUTION OF A SOLAR ERUPTIVE FLARE

Bhuwan **Joshi**1,2, Astrid Veronig3, K.-S. Cho1, S.-C. Bong1, B. V. Somov4, Y.-J. Moon5, Jeongwoo Lee6, P. K. Manoharan7, and Y.-H. Kim1

Astrophysical Journal, 706:1438–1450, **2009, File**

We present a detailed multi-wavelength analysis and interpretation of the evolution of an M7.6 flare that occurred near the southeast limb on **2003 October 24**. Pre-flare images at TRACE 195 Å show that the bright and complex system of coronal loops already existed at the flaring site. The X-ray observations of the flare taken from the *Reuven Ramaty High Energy Solar Spectroscopic Imager* (*RHESSI*) spacecraft reveal two phases of the flare evolution.

The first phase is characterized by the altitude decrease of the X-ray looptop (LT) source for ~11 minutes. Such a long duration of the descending LT source motion is reported for the first time. The EUV loops, located below the X-ray LT source, also undergo contraction with similar speed (~15 km s^{-1}) in this interval. During the second phase the two distinct hard X-ray footpoint (FP) sources are observed which correlate well with UV and Hα flare ribbons. The X-ray LT source now exhibits upward motion as anticipated from the standard flare model.

The *RHESSI* spectra during the first phase are soft and indicative of hot thermal emission from flaring loops with temperatures $T > 25$ MK at the early stage. On the other hand, the spectra at high energies (ε _ 25 keV) follow hard power laws during the second phase (γ = 2.6–2.8). We show that the observed motion of the LT and FP sources can be understood as a consequence of three-dimensional magnetic reconnection at a separator in the corona. During the first phase of the flare, the reconnection releases an excess of magnetic energy related to the magnetic tensions generated

before a flare by the shear flows in the photosphere. The relaxation of the associated magnetic shear in the corona by the reconnection process explains the descending motion of the LT source. During the second phase, the ordinary reconnection process dominates describing the energy release in terms of the standard model of large eruptive flares with increasing FP separation and upward motion of the LT source.

Multi-Wavelength Signatures of Magnetic Reconnection of a Flare-Associated Coronal Mass Ejection

Bhuwan **Joshi**, P. K. Manoharan, Astrid M. Veronig, P. Pant, Kavita Pandey
Solar Phys., 242(1-2), Page: 143 – 158, **2007**.
The study supports the standard CSHKP model of flares, which is consistent with nearly all eruptive flare models. More importantly, the results also contain evidence for breakout reconnection before the flare phase.

Multi-wavelength Analysis of an X2.7 Flare on 3 November 2003 from Active Region NOAA 10488

Bhuwan **Joshi**, P. K. Manoharan, A. M. Veronig, P. Pant, Kavita Pandey
Sun and Geosphere, **2006**; 1(2): 17-20 ISSN 1819-083917
http://newserver.stil.bas.bg/SUNGEO/00SGArhiv/SG_v1_No2_2006-pp-17-20.pdf
The evolution of an X2.7 solar flare, that occurred in a complex βγδ-type active region on 2003 November 3, isdiscussed utilizing multi-wavelength data set. The Hα images taken from solar tower telescope at ARIES,Nainital, India, reveal well-defined footpoint (FP) and looptop (LT) sources. As the flare evolves, LT sourcemoves upward and the separation between the two FP sources increases which is consistent with thereconnection models of solar flares. The coalignment of Hα with hard X-ray (HXR) images obtained from RHESSIshows spatial correlation between Hα and HXR footpoints, while the upward moving HXR LT source is alwayslocated above Hα LT source. The EUV images of flaring region at 195 Å taken from SOHO/EIT reveal intenseemission from low-lying loops near the active region during the impulsive phase. On the other hand, two brightloops are seen well outside the active region which undergo large scale reorganization during the flare. In radiowavelengths, type III radio bursts are observed few minutes prior to start of HXR LT emission indicating thepre-flare coronal activity. A type II radio burst followed the main phase of the event. The observations supportthe “break-out” model of solar eruptions proposed by S.Antiochos and coworkers.

Measuring the magnetic origins of solar flares, CMEs and Space Weather

Philip **Judge**, Matthias Rempel, Rana Ezzedine, Lucia Kleint, Ricky Egeland, Svetlana Berdyugina, Thomas Berger, Joan Burkepile, Rebecca Centeno, Giuliana de Toma, Mausumi Dikpati, Yuhong Fan, Holly Gilbert, Daniela Lacatus
ApJ **917** 27 **2021**
https://arxiv.org/pdf/2106.07786.pdf
https://iopscience.iop.org/article/10.3847/1538-4357/ac081f/pdf
https://doi.org/10.3847/1538-4357/ac081f
We take a broad look at the problem of identifying the magnetic solar causes of space weather. With the lackluster performance of extrapolations based upon magnetic field measurements in the photosphere, we identify a region in the near UV part of the spectrum as optimal for studying the development of magnetic free energy over active regions. Using data from SORCE, Hubble Space Telescope, and SKYLAB, along with 1D computations of the near-UV (NUV) spectrum and numerical experiments based on the MURaM radiation-MHD and HanleRT radiative transfer codes, we address multiple challenges. These challenges are best met through a combination of near UV lines of bright \ion{Mg}{2}, and lines of \ion{Fe}{2} and \ion{Fe}{1} (mostly within the 4s−4p transition array) which form in the chromosphere up to 2×104 K. Both Hanle and Zeeman effects can in principle be used to derive vector magnetic fields. However, for any given spectral line the τ=1 surfaces are generally geometrically corrugated owing to fine structure such as fibrils and spicules. By using multiple spectral lines spanning different optical depths, magnetic fields across nearly-horizontal surfaces can be inferred in regions of low plasma β, from which free energies, magnetic topology and other quantities can be derived. Based upon the recently-reported successful suborbital space measurements of magnetic fields with the CLASP2 instrument, we argue that a modest space-borne telescope will be able to make significant advances in the attempts to predict solar eruptions. Difficulties associated with blended lines are shown to be minor in an Appendix.

Are All Flare Ribbons Simply Connected to the Corona?

Philip G. **Judge**1, Alin Paraschiv2,3, Daniela Lacatus2,3, Alina Donea2, and Charlie Lindsey4
2017 ApJ 838 138
http://sci-hub.cc/10.3847/1538-4357/aa656c

https://arxiv.org/pdf/1707.07072.pdf
We consider the observational basis for the belief that flare ribbons in the chromosphere result from energy transport from the overlying corona. We study ribbons of small flares using magnetic and intensity data from the Hinode, Solar Dynamics Observatory, and IRIS missions. While most ribbons appear connected to the corona and overlie regions of significant vertical magnetic field, we examine one ribbon with no clear evidence for such connections. Evolving horizontal magnetic fields seen with Hinode suggest that reconnection with preexisting fields below the corona can explain the data. The identification of just one, albeit small, ribbon, with no apparent connection to the corona, leads us to conclude that at least two mechanisms are responsible for the heating that leads to flare ribbon emission. **2013 November 9.**

On helium line polarization during the impulsive phase of an X1 flare

Philip G. **Judge**, Lucia Kleint, Alberto Sainz-Dalda
ApJ **814** 100 **2015**
http://arxiv.org/pdf/1510.09218v1.pdf
We analyze spectropolarimetric data of the He I 1083~nm multiplet (1s2s3S1−1s2p3Po2,1,0) during the X1 flare SOL**2014-03-29**T17:48, obtained with the Facility Infrared Spectrometer (FIRS) at the Dunn Solar Telescope. While scanning active region NOAA 12017, the FIRS slit crossed a flare ribbon during the impulsive phase, when the helium line intensities turned into emission at < twice the continuum intensity. Their linear polarization profiles are of the same sign across the multiplet including 1082.9 nm, intensity-like, at <5\% of the continuum intensity. Weaker Zeeman-induced linear polarization is also observed. Only the strongest linear polarization coincides with hard X-ray (HXR) emission at 30-70 keV observed by the Reuven Ramaty High Energy Solar Spectroscope Imager. The polarization is generally more extended and lasts longer than the HXR emission. The upper J=0 level of the 1082.9~nm component is unpolarizable, thus lower level polarization is the culprit. We make non-LTE radiative transfer calculations in thermal slabs optimized to fit only intensities. The linear polarizations are naturally reproduced, through a systematic change of sign with wavelength of the radiation anisotropy when slab optical depths of the 1082.9 component are <1. Collisions with beams of particles are neither needed nor can they produce the same sign of polarization of the 1082.9 and 1083.0 nm components. The He I line polarization merely requires heating sufficient to produce slabs of the required thickness. Widely different polarizations of Hα, reported previously, are explained by different radiative anisotropies arising from slabs of different optical depths.

On the Origin of a Sunquake during the 29 March 2014 X1 Flare

Philip G. **Judge**, Lucia Kleint, Alina Donea, Alberto Sainz Dalda, Lyndsay Fletcher
ApJ 796 85 **2014**
http://arxiv.org/pdf/1409.6268v1.pdf
Helioseismic data from the HMI instrument have revealed a sunquake associated with the X1 flare SOL2014-03-29T17:48 in active region NOAA 12017. We try to discover if acoustic-like impulses or actions of the Lorentz force caused the sunquake. We analyze spectro-polarimetric data obtained with the Facility Infrared Spectrometer (FIRS) at the Dunn Solar Telescope (DST). Fortuitously the FIRS slit crossed the flare kernel close to the acoustic source, during the impulsive phase. The infrared FIRS data remain unsaturated throughout the flare. Stokes profiles of lines of Si I 1082.7 nm and He I 1083.0 nm are analyzed. At the flare footpoint, the Si I 1082.7 nm core intensity increases by a factor of several, the IR continuum increases by 4 +/- 1%. Remarkably, the Si I core resembles the classical Ca II K line's self-reversed profile. With nLTE radiative models of H, C, Si and Fe these properties set the penetration depth of flare heating to 100 +/- 100 km, i.e. photospheric layers. Estimates of the non-magnetic energy flux are at least a factor of two less than the sunquake energy flux. Milne-Eddington inversions of the Si I line show that the local magnetic energy changes are also too small to drive the acoustic pulse. Our work raises several questions: Have we "missed" the signature of downward energy propagation? Is it intermittent in time and/or non-local? Does the 1-2 s photospheric radiative damping time discount compressive modes?

Heating of the solar photosphere during a white-light flare

Jan **Jurcak**, Jana Kasparova, Michal Svanda, Lucia Kleint
A&A 620, A183 **2018** https://doi.org/10.1051/0004-6361/201833946
https://arxiv.org/pdf/1811.07794.pdf
The \ion{Fe}{i} lines observed by the Hinode/SOT spectropolarimeter were always seen in absorption, apart from the extreme solar limb. Here we analyse a unique dataset capturing these lines in emission during a solar white-light flare. We analyse the temperature stratification in the solar photosphere during a white-light flare and compare it with the post-white-light flare state. We used two scans of the Hinode/SOT spectropolarimeter to infer, by means of the LTE inversion code Stokes Inversion based on Response function (SIR), the physical properties in the solar photosphere during and after a white-light flare. The resulting model atmospheres are compared and the changes are related to the white-light flare. We show that the analysed white-light flare continuum brightening is probably not caused by the temperature increase at the formation height of the photospheric continuum. However, the photosphere is heated by the

flare approximately down to logτ=−0.5 and this results in emission profiles of the observed \ion{Fe}{i} lines. From the comparison with the post-white-light flare state of the atmosphere, we estimate that the major contribution to the increase in the continuum intensity originates in the heated chromosphere. **2017-Sept-06**
RHESSI Nuggets #372 March **2020**
http://sprg.ssl.berkeley.edu/~tohban/wiki/index.php/Heating_of_the_solar_photosphere_during_a_white-light_flare

The Role of Peak Temperatures in Solar X-Ray Flare Associations with CME Speeds and Widths and in Flare Size Distributions

S. W. **Kahler**1 and A. G. Ling2
2020 ApJ 901 63
https://doi.org/10.3847/1538-4357/abae5e
Recently, we reported that solar X-ray flares with relatively low peak (0.05–0.3 nm)/(0.1–0.8 nm) ratios R, a proxy for peak flare temperature T, were preferentially associated not only with solar energetic (E > 10 MeV) particle (SEP) events, but also with fast (Vcme ≥ 1000 km s−1) coronal mass ejections (CMEs) that produce the SEP events. Flares associated with a characteristic CME speed Vcme range from small and cool to large and hot, and cooler X-ray flares were preferentially associated with broader CME widths. Here we increase the list of analyzed Geostationary Operational Environmental Satellite flares from the previous 450 to 588 and validate the earlier results with flare peak X-ray temperatures T from the TEBBS (Temperature and Emission measure-based Background Subtraction) method catalog. Power-law size distributions of flare peak fluxes Fp are increasingly steeper for X-ray flares with (1) fast (Vcme ≥ 1000 km s−1); (2) slow (Vcme < 1000 km s−1); and (3) no CMEs; in each case flares of larger Fp are characteristically hotter. The power-law size distribution of SEP event peak intensities Ip is flatter than any of the X-ray Fp distributions or a distribution formed from the product of the steep SEP Ip dependence on Vcme and the Vcme number distributions.

Temperatures of Large Solar X-ray Events and Associated CME Speeds

S. **Kahler**,* A. Ling
36th International Cosmic Ray Conference -ICRC2019- July 24th - August 1st, **2019** Madison, WI, U.S.A.
https://pos.sissa.it/358/1089/pdf
Recently we [1] repeated an earlier analysis by [2,3] showing that large (> M3) solar X-ray flares associated with solar energetic particle (SEP) events have significantly lower peak X-ray flux ratios R of 0.04-0.5/0.1-0.8 nm, proxies for flare peak temperatures, than those without SEP events. Since we expect SEP events to be produced by shocks ahead of fast coronal mass ejections (CMEs), this would imply that an X-ray flare of a given peak flux is more likely to have a fast CME and associated SEP event when it has a relatively smaller R. We examine the role played by the ratios R in correlations between X-ray peak flare fluxes and CME speeds Vcme, and then compare CMEs widths W, speeds Vcme, X-ray flare durations ΔT, and R with each other. We resolve the apparent conflict between a global scaling model of eruptive events showing Vcme scaling with higher R and our confirmation that the [2,3] analysis implies faster CMEs are associated with flares of lower R.

SOLAR ENERGETIC PARTICLE EVENTS AND THE KIPLINGER EFFECT

S. W. **Kahler**
2012 ApJ 747 66, **File**
The Kiplinger effect is an observed association of solar energetic (E > 10 MeV) particle (SEP) events with a "soft-hard-harder" (SHH) spectral evolution during the extended phases of the associated solar hard (E > 30 keV) X-ray (HXR) flares. Besides its possible use as a space weather predictor of SEP events, the Kiplinger effect has been interpreted as evidence of SEP production in the flare site itself, contradicting the widely accepted view that particles of large SEP events are predominately or entirely accelerated in shocks driven by coronal mass ejections (CMEs). We review earlier work to develop flare soft X-ray (SXR) and HXR spectra as SEP event forecast tools and then examine recent Reuven Ramaty High-Energy Solar Spectroscopic Imager (RHESSI) evidence supporting the association of SHH HXR flares with large SEP events. We point out that ad hoc prediction criteria using the CME widths and SXR flare durations of associated RHESSI hard X-ray bursts (HXBs) can yield results comparable to those of the SHH prediction criteria. An examination of the RHESSI dynamic plots reveals several ambiguities in the determination of whether and when the SHH criteria are fulfilled, which must be quantified and applied consistently before an SHH-based predictive tool can be made. A comparative HXR spectral study beginning with the large population of relatively smaller SEP events has yet to be done, and we argue that those events will not be so well predicted by the SHH criteria. SHH HXR flares and CMEs are both components of large eruptive flare events, which accounts for the good connection of the SHH HXR flares with SEP events.

Solar flares and coronal mass ejections. (Review)

Kahler, S.W.,
1992. Ann Rev. Astron. Astrophys. 30, 113–141.

http://sci-hub.ru/10.1146/annurev.aa.30.090192.000553
This review addresses two basic questions. First, how did we form such a fundamentally incorrect view of the effects of flares after so much observational and theoretical work? Second, what is the observational and theoretical evidence to support a primary role for CMEs, and what can we say about the relationship between flares and CMEs? In Section 2 we present flare and CME observations in a historical context to show the changing perspective between the two phenomena. In Section 3 we discuss the coronal phenomena that bear on the relationship between flares and CMEs. Interplanetary effects are discussed in Section 4.

Continuous upflows and sporadic downflows observed in active regions

S. **Kamio**1, H. Peter1, W. Curdt1 and S. K. Solanki
A&A 532, A96 (**2011**)
Aims. We present a study of the temporal evolution of coronal loops in active regions and its implications for the dynamics in coronal loops.
Methods. We analyzed images of the Atmospheric Imaging Assembly (AIA) on the Solar Dynamics Observatory (SDO) at multiple temperatures to detect apparent motions in the coronal loops.
Results. Quasi-periodic brightness fluctuations propagate upwards from the loop footpoint in hot emission at 1 MK, while sporadic downflows are seen in cool emission below 1 MK. The upward motion in hot emission increases just after the cool downflows.
Conclusions. The apparent propagating pattern suggests a hot upflow from the loop footpoints, and is considered to supply hot plasma into the coronal loop, but a wavelike phenomenon cannot be ruled out. Coronal condensation occasionally happens in the coronal loop, and the cool material flows down to the footpoint. Emission from cool plasma could have a significant contribution to hot AIA channels in the event of coronal condensation.

Temporal evolution of microflares in bright points

Suguru **Kamio**
EIS Science Nugget for 1st July **2011**
http://msslxr.mssl.ucl.ac.uk:8080/SolarB/nuggets/nugget_2011jul.jsp
Recent observations by Hinode during the solar activity minimum revealed that quiet regions and coronal holes are not really quiet. X-ray bright points are found all over the Sun, and they occasionally undergo impulsive brightenings or microflares. Improved resolution of Hinode EIS and XRT allows us to follow a temporal evolution of the microflares. It is interesting to note that microflares in bright points and large flares in active regions share some common characteristics.

Onset Mechanism of M6.5 Solar Flare Observed in Active Region 12371

Jihye **Kang**, Satoshi Inoue, Kanya Kusano, Sung-Hong Park, Yong-Jae Moon
ApJ **887** 263 **2019**
https://arxiv.org/pdf/1911.05337.pdf
https://doi.org/10.3847/1538-4357/ab5582
sci-hub.tw/10.3847/1538-4357/ab5582
We studied a flare onset process in terms of stability of a three-dimensional (3D) magnetic field in active region 12371 producing an eruptive M6.5 flare in **2015 June 22**. In order to reveal the 3D magnetic structure, we first extrapolated the 3D coronal magnetic fields based on time series of the photospheric vector magnetic fields under a nonlinear force-free field (NLFFF) approximation. The NLFFFs nicely reproduced the observed sigmoidal structure which is widely considered as pre-eruptive magnetic configuration. We, in particular, found that the sigmoid is composed of two branches of sheared arcade loops. On the basis of the NLFFFs, we investigated the sheared arcade loops to explore the onset process of the eruptive flare using three representative MHD instabilities: the kink, torus and double arc instabilities. The double arc instability, recently proposed by Ishiguro & Kusano, is a double arc loop can be more easily destabilized than a torus loop. Consequently, the NLFFFs are found to be quite stable against the kink and torus instabilities. However, the sheared arcade loops formed prior to the flare possibly becomes unstable against the double arc instability. As a possible scenario on the onset process of the M6.5 flare, we suggest three-step process: (1) double arc loop are formed by the sheared arcade loops through the tether-cutting reconnection during an early phase of the flare, (2) the double arc instability contributes to the expansion of destabilized double arc loops and (3) finally, the torus instability makes the full eruption.

Sloshing Oscillations in Hot Coronal Loops Associated with M-Class Flares.

Karakotov, R., Kuznetsov, A., Anfinogentov, S. et al.
Sol Phys 299, 163 (**2024**).
https://doi.org/10.1007/s11207-024-02404-w

Analysis of more than 300 M-class solar flares observed with the Atmospheric Imaging Assembly onboard the Solar Dynamics Observatory in the 131 Å channel, revealed 16 events of sloshing oscillations in hot solar coronal loops. Time–distance maps made along the loops demonstrated EUV emission intensity blobs bouncing between the footpoints, i.e., showing characteristic zigzagging patterns, of the size shorter than 25% of the loop length. The oscillation periods are found to range from about 150 s to 1325 s. The average phase speed, estimated as the ratio of the oscillation period and the loop length, is about 500 km s−1. Parameters of the oscillations are consistent with the interpretation in terms of multi-harmonic slow magnetoacoustic oscillations.

Oscillatory Reconnection of a 2D X-point in a hot coronal plasma

Konstantinos **Karampelas**, James A. McLaughlin, Gert J. J. Botha, Stéphane Régnier
ApJ **925** 195 **2021**
https://arxiv.org/pdf/2112.05712.pdf
https://iopscience.iop.org/article/10.3847/1538-4357/ac3b53/pdf
Oscillatory reconnection (a relaxation mechanism with periodic changes in connectivity) has been proposed as a potential physical mechanism underpinning several periodic phenomena in the solar atmosphere including, but not limited to, quasi-periodic pulsations (QPPs). Despite its importance, however, the mechanism has never been studied within a hot, coronal plasma. We investigate oscillatory reconnection in a one million Kelvin plasma by solving the fully-compressive, resistive MHD equations for a 2D magnetic X-point under coronal conditions using the PLUTO code. We report on the resulting oscillatory reconnection including its periodicity and decay rate. We observe a more complicated oscillating profile for the current density compared to that found for a cold plasma, due to mode-conversion at the equipartition layer. We also consider, for the first time, the effect of adding anisotropic thermal conduction to the oscillatory reconnection mechanism, and we find this simplifies the spectrum of the oscillation profile and increases the decay rate. Crucially, the addition of thermal conduction does not prevent the oscillatory reconnection mechanism from manifesting. Finally, we reveal a relationship between the equilibrium magnetic field strength, decay rate, and period of oscillatory reconnection, which opens the tantalising possibility of utilizing oscillatory reconnection as a seismological tool.

3D Magnetic Free Energy and Flaring Activity Using 83 Major Solar Flares

Khojiakbar **Karimov**1, Harim Lee2, Hyun-Jin Jeong2, Yong-Jae Moon1,2, Jihye Kang2, Jihyeon Son1, Mingyu Jeon1, and Kanya Kusano3
2024 ApJL 965 L5
https://iopscience.iop.org/article/10.3847/2041-8213/ad3548/pdf
In this Letter, we examine the relationship between 3D magnetic free energy (MFE) and flaring activity using 83 major solar flares (M-class and X-class) in nine solar active regions (ARs). For this, we use 998 nonlinear force-free field extrapolations compiled by the "Institute for Space-Earth Environmental Research Database" at Nagoya University. These ARs produced at least three major flares with distinct rising and peak phases of 3D MFE. For each phase, the solar flare occurrence rate (FOR) is calculated as a ratio of the number of flares to the duration. The major results from this study are summarized as follows. First, there is no clear linear correlation (CC = 0.15) between 3D MFE and flare peak flux. Second, the FOR (3.4 day−1) of the rising phase is a little higher than that (3.1 day−1) of the peak phase, depending on AR. Third, for several flares, there are noticeable decreases in 3D MFE, which correspond to the typical energy of a major flare (about 1032 erg). Fourth, it is interesting to note that there are noticeable enhancements in FORs at several local maxima of 3D MFE, which may be associated with flux emergence and/or shearing motions. Fifth, the flare index rates, which are defined as the summation of flaring activity divided by the duration, of rising and peak phases are 151 day−1 and 314 day−1, respectively. Our results imply that the traditional and simple "storage and release" model does not apply to flare activities, and the random perturbation may be important for triggering flares.
2011/02/13-15, 2012/03/05-09, 2012/07/03-07, 2014/10/22-26, 2017/09/04-08, 2022/03/27-04/01

Intensity oscillations and heating of the coronal X-ray bright points from Hinode/XRT

R. **Kariyappa** and B. A. Varghese
A&A 485, 289–292 (**2008**)
DOI: 10.1051/0004-6361:20079127
We analysed a 7 h long time sequence of the soft X-ray images obtained on April 14, 2007 with a 2 min cadence using the X-Ray Telescope (XRT) on-board the Hinode mission.

Radio bursts observed during solar eruptive flares and their schematic summary **Review**

Marian **Karlický**
2023
https://arxiv.org/pdf/2307.07144.pdf

In this review we summarize results of our analysis of the observations of solar eruptive flares made by the Ondřejov radiospectrograph for more than twenty years. We also present some Potsdam-Tremsdorf radio spectra from our common studies. Considering a 3-dimensional model of eruptive flares together with the results of our magnetohydrodynamic and particle-in-cell simulations we show an importance of decimetric radio bursts for understanding of plasma processes in eruptive flares. We present drifting pulsation structures as signatures of plasmoids, an unusual zebra pattern in the very early flare stage, narrowband dm-spikes as the bursts generated in the reconnection plasma outflows, radio bursts indicating a merging of plasmoids, pair of decimetric type III bursts indicating the electron beams propagating upwards and downwards in the solar atmosphere from the acceleration site, and a special decimetric type III burst formed probably around the plasmoid. We present unusual radio bursts connected with the rising magnetic rope at the very beginning of eruptive flares. Furthermore, based on the analysis of decimetric continua we estimated the level of the plasma turbulence in a vicinity of the flare termination shock. Interpretations of all these bursts are based on models and time coincidences with observations in X-ray, UV and optical ranges; in most cases an information about positions of these radio sources is missing. To show an importance of positional information, we present a rare example of observations, where the drifting pulsation structure was observed simultaneously with the observations made by the EOVSA radiointerferometer. All the presented bursts are then summarized in a new scheme of bursts and compared with the schema commonly used. **18 August 1998, 28 March 2001, 12 April 2001, 24 September 2001, 28 September 2001, 26 September 2011, 25 June 2015, 6 September 2017, 10 September 2017, 2 April 2022**

The 2017 September 6 Flare: Radio Bursts and Pulsations in the 22-5000 MHz Range and Associated Phenomena

M. **Karlicky**, J. Rybak

ApJS **250** 31 **2020**

https://arxiv.org/pdf/2009.05756.pdf **File**

https://doi.org/10.3847/1538-4365/abb19f

For the **2017 September 6** flare (SOL2017-Sep-06T11:53) we present not only unusual radio bursts, but also their interesting time association with the other flare phenomena observed in EUV, white-light, X-ray, and γ-ray emissions. Using our new method based on wavelets we found quasi-periodic pulsations (QPPs) in several locations of the whole time-frequency domain of the analyzed radio spectrum (11:55-12:07 UT and 22-5000 MHz). Among them the drifting QPPs are new and the most interesting, especially a bi-directional QPP at the time of the hard X-ray and γ-ray peaks, and a sunquake start. In the pre-impulsive phase we show an unusual drifting pulsation structure (DPS) in association with the EUV brightenings caused by the interaction of magnetic ropes. In the flare impulsive phase we found an exceptional radio burst drifting from 5000 MHz to 800 MHz. In connection with this drifting burst, we show a U-burst at about the onset time of an EUV writhed structure and a drifting radio burst as a signature of a shock wave at high frequencies (1050-1350 MHz). In the peak flare phase we found an indication of an additional energy-release process located at higher altitudes in the solar atmosphere. These phenomena are interpreted considering a rising magnetic rope, magnetosonic waves and particle beams. Using a density model we estimated the density, wave velocities and source heights for the bi-directionally drifting QPPs, the density for the pre-impulsive DPS and U-burst, and the density and magnetic field strength for the drifting radio burst.

CESRA #2725 Nov **2020** http://www.astro.gla.ac.uk/users/eduard/cesra/?p=2725

Drifting Pulsation Structure at the Very Beginning of the 2017 September 10 Limb Flare

M. **Karlicky**, B. Chen, D. E. Gary, J. Kasparova, J. Rybak

ApJ **2020**

https://arxiv.org/pdf/1912.12518.pdf

Drifting pulsation structures (DPSs) are important radio fine structures usually observed at the beginning of eruptive solar flares. It has been suggested that DPSs carry important information on the energy release processes in solar flares. We study DPS observed in an X8.2-class flare on 2017 September 10 in the context of spatial and spectral diagnostics provided by microwave, EUV, and X-ray observations. We describe DPS and its sub-structures that were observed for the first time. We use a new wavelet technique to reveal characteristic periods in DPS and their frequency bands. Comparing the periods of pulsations found in this DPS with those in previous DPSs we found new very short periods in the 0.09-0.15 s range. We present EOVSA images and spectra of microwave sources observed during the DPS. This DPS at its very beginning has pulsations in two frequency bands (1000-1300 MHz and 1600--1800 MHz) which are interconnected by fast drifting bursts. We show that these double-band pulsations started just at the moment when the ejected filament splits apart in a tearing motion at the location where a signature of the flare current sheetlater appeared. Using the standard flare model and previous observations of DPSs, we interpret these double-band pulsations as a radio signature of superthermal electrons trapped in the rising magnetic rope and flare arcade at the moment when the flare magnetic reconnection starts. The results are discussed in a scenario with the plasmoid in the rising magnetic rope.

Radio, EUV, and X-Ray Observations during a Filament Rise in the 2011 June 7 Solar Flare

Marian **Karlický**1, Jana Kašparová1, and Robert Sych2

2020 ApJ 888 18
https://doi.org/10.3847/1538-4357/ab5801
The most energetic flares start with a filament rise followed by magnetic reconnection below this filament. The start of the reconnection corresponds to the beginning of the flare impulsive phase. In this paper we study processes before this phase. During the filament rise we recognize an unusual radio continuum with a starting boundary drifting toward lower frequencies. The estimated velocity of the agent generating this continuum boundary is about 400 km s−1, similar to that of the rising filament. In association with this filament rise, transient X-ray sources and extreme ultraviolet (EUV) brightenings are found near the filament footpoint and outside the locations where later two parallel flare ribbons appear. Moreover, oscillations with a ~30 s period are found simultaneously in radio, EUV, and X-ray observations. Around the end of these oscillations the flare impulsive phase starts as seen in observations of the drifting pulsation structure and X-ray source located at the upper part of the rising filament. We interpret the unusual radio continuum and transient X-ray sources, which are located outside the two parallel flare ribbons, as those generated during an interaction of the rising filament with the above-lying magnetic loops. The EUV brightening at the filament footpoint could be a signature of the magnetic reconnection inside the magnetic rope carrying the filament. Possible scenarios of the ~30 s period oscillations in radio, X-ray, and EUV are discussed.
RHESSI Nuggets #376 April **2020**
http://sprg.ssl.berkeley.edu/~tohban/wiki/index.php/Phenomena_in_the_unusually_long_pre-impulsive_phase_of_SOL2011-06-07

Oscillations in the 45-5000 MHz Radio Spectrum of the 18 April 2014 Flare

M. **Karlicky**, J. Rybak, C. Monstein
Solar Phys. **2017**
https://arxiv.org/pdf/1706.02836.pdf
study the 18 April 2014 M7.3 flare (SOL**2014-04-18**T13:03:00L245C017). We find a quasi-periodic character of this flare with periods in the range 65-115 seconds. At the very beginning of this flare, in connection with the drifting pulsation structure (plasmoid ejection) we find the 65-115 s oscillation phase drifting slowly towards lower frequencies, which indicates an upward propagating wave initiated at the start of the magnetic reconnection. In the drifting pulsation structure many periods (1-200 seconds) are found documenting multi-scale and multi-periodic processes. On this drifting structure fiber bursts with a characteristic period of about one second are superimposed, whose frequency drift is similar to that of the drifting 65-115 s oscillation phase. We also check periods found in this flare by EUV Imaging Spectrometer (EIS)/Hinode and Interface Region Imaging Spectrograph (IRIS) observations. We recognize the type III bursts (electron beams) as proposed, but their time coincidence with the EIS and IRIS peaks is not very good. This is probably due to the radio spectrum beeing a whole-disk record consisting of all bursts from any location while the EIS and IRIS peaks are emitted only from locations of slits in the EIS and IRIS observations.

Quasi-periodic processes in the flare loop generated by sudden temperature enhancements at loop footpoints

M. **Karlický**1 and P. Jelínek
A&A 590, A4 (**2016**)
Aims. During the impulsive flare phase, the plasma at the flare loop footpoints is rapidly heated by particle beams. In the present paper, we study processes that occur after this sudden heating in a two-dimensional magnetic loop.
Methods. We adopt a 2D magnetohydrodynamic (MHD) model, in which we solve a full set of the ideal time-dependent MHD equations by means of the FLASH code, using the adaptive mesh refinement (AMR) method. Periods in the processes are estimated by the wavelet analysis technique.
Results. We consider a model of the solar atmosphere with a symmetric magnetic loop. The length of this loop in the corona is approximately 21.5 Mm. At both loop footpoints, at the transition region, we initiate the Gaussian temperature (pressure) perturbation with the maximum temperature 14, 7, or 3.5 times higher than the unperturbed temperature. In the corona, the perturbations produce supersonic blast shocks with the Mach number of about 1.1, but well below Alfvén velocities. We consider cases with the same perturbations at both footpoints (symmetric case) and one with different perturbations (asymmetric case). In the symmetric case, the shocks move along both loop legs upwards to the top of the loop, where they interact and form a transient compressed region. Then they continue in their motion to the transition region at the opposite side of the loop, where they are reflected upwards, and so on. At the top of the loop, the shock appears periodically with the period of about 170 s. In the loop legs during this period, a double peak of the plasma parameters, which is connected with two arrivals of shocks, is detected: firstly, when the shock moves up and then when the shock, propagating from the opposite loop leg, moves down. Increasing the distance of the detection point in the loop leg from the top of the loop, the time interval between these shock arrivals increases. Thus, at these detection points, the processes with shorter periods can be detected. After ~500 s the process with the periodically interacting shocks slowly changes to slow mode magnetosonic free oscillation. Furthermore, we detected quasi-periodic processes, even in the chromosphere under the location of the pressure perturbation. These processes can be observed in

intensities and Doppler shifts of optical chromospheric lines. In the case with the asymmetric perturbations, we found that the processes are even more complex.

Thermal fronts in solar flares

M. **Karlicky**

ApJ 814, id. 153, 7 pp. (**2015**)

We studied the formation of a thermal front during the expansion of hot plasma into colder plasma. We used a three-dimensional electromagnetic particle-in-cell model that includes inductive effects. In early phases, in the area of the expanding hot plasma, we found several thermal fronts, which are defined as a sudden decrease of the local electron kinetic energy. The fronts formed a cascade. Thermal fronts with higher temperature contrast were located near plasma density depressions, generated during the hot plasma expansion. The formation of the main thermal front was associated with the return-current process induced by hot electron expansion and electrons backscattered at the front. A part of the hot plasma was trapped by the thermal front while another part, mainly with the most energetic electrons, escaped and generated Langmuir and electromagnetic waves in front of the thermal front, as shown by the dispersion diagrams. Considering all of these processes and those described in the literature, we show that anomalous electric resistivity is produced at the location of the thermal front. Thus, the thermal front can contribute to energy dissipation in the current-carrying loops of solar flares. We estimated the values of such anomalous resistivity in the solar atmosphere together with collisional resistivity and electric fields. We propose that the slowly drifting reverse drift bursts, observed at the beginning of some solar flares, could be signatures of the thermal front.

Solar flares: radio and X-ray signatures of magnetic reconnection processes **Review**

Marian **Karlický**

Research in Astronomy and Astrophysics, Volume 14, Number 7, 753-772, **2014**

DOI: 10.1088/1674-4527/14/7/002 ?

This review summarizes new trends in studies of magnetic reconnection in solar flares. It is shown that plasmoids play a very important role in this primary flare process. Using the results of magnetohydrodynamic and particle-in-cell simulations, we describe how the plasmoids are formed, how they move and interact, and how a flare current sheet is fragmented into a cascade of plasmoids. Furthermore, it is shown that during the interactions of these plasmoids electrons are not only very efficiently accelerated and heated, but electromagnetic (radio) emission is also produced. We also describe possible mechanisms for the triggering of magnetic reconnection. The relevant X-ray and radio signatures of these processes (such as radio drifting pulsation structures, narrowband dm-spikes, and the loop-top and above-the-loop-top X-ray sources) are then described. It is shown that plasmoids can also be formed in kinked magnetic ropes. A mapping of X-points of the magnetic reconnection on the chromosphere (as e.g. a splitting of flare ribbons) is mentioned. Supporting EUV and white-light observations of plasmoids are added. The significance of all these processes for the fast magnetic reconnection and electron acceleration is outlined. Their role in fusion experiments is briefly mentioned

Electron acceleration during three-dimensional relaxation of an electron beam-return current plasma system in a magnetic field

M. **Karlicky** and E.P. Kontar

E-print, July **2012**, A&A, 544, A148 (**2012**)

We investigate the effects of acceleration during non-linear electron-beam relaxation in magnetized plasma in the case of electron transport in solar flares. The evolution of electron distribution functions is computed using a three-dimensional particle-in-cell electromagnetic code. Analytical estimations under simplified assumptions are made to provide comparisons. We show that, during the non-linear evolution of the beam-plasma system, the accelerated electron population appears. We found that, although the electron beam loses its energy efficiently to the thermal plasma, a noticeable part of the electron population is accelerated. For model cases with initially monoenergetic beams in uniform plasma, we found that the amount of energy in the accelerated electrons above the injected beam-electron energy varies depending the plasma conditions and could be around 10-30% of the initial beam energy. This type of acceleration could be important for the interpretation of non-thermal electron populations in solar flares. Its neglect could lead to the over-estimation of accelerated electron numbers. The results emphasize that collective plasma effects should not be treated simply as an additional energy-loss mechanism, when hard X-ray emission in solar flares is interpreted, notably in the case of RHESSI data.

Fragmentation during merging of plasmoids in the magnetic field reconnection

M. **Karlický**, M. Bárta and D. Nickeler

A&A 541, A86 **(2012)**

Context. Application of the magnetic-reconnection theory onto large-scale events, such as solar flares, requires formation of very thin (kinetic-scale) current sheets within the rather thick flare current layer. Hence, some fragmentation/filamentation mechanisms has to be in action.
Aims. We aim at identifying fragmentation mechanisms for magnetic field and current density structures. Namely, we focus at detailed study of the processes during the merging of plasmoids that had been formed in the current layer.
Methods. A 2.5-D electromagnetic particle-in-cell model is used and its results analysed.
Results. It is shown that the merging process of plasmoids is not a simple process as presented in some previous studies. On the contrary, this process leads to a complex fragmentation. We found two types of fragmentation processes: a) fragmentation in the current sheet generated between the merging plasmoids and b) fragmentation at the boundary of plasma outflow from the reconnection between these plasmoids. While the first type of fragmentation is generated by the tearing-mode (plasmoid) instability of the secondary current sheet, the second one looks to be connected with an increase of the plasma β parameter during these processes. Thus, sheared high-β plasma flows produce this additional fragmentation.
Conclusions. The fragmentation and energy transport from large to small scales in a large-scale magnetic reconnection seem to be the result of interplay and positive feedback between instabilities driven by high gradients in both magnetic (intense current density) and velocity (high vorticity) fields.

THE n-DISTRIBUTION OF ELECTRONS AND DOUBLE LAYERS IN THE ELECTRON-BEAM-RETURN-CURRENT SYSTEM OF SOLAR FLARES
Marian **Karlický**
2012 ApJ 750 49
We investigate processes in the electron-beam-return-current system in the impulsive phase of solar flares to answer a question about the formation of the n-electron distribution detected in this phase of solar flares. An evolution of the electron-beam-return-current system with an initial local density depression is studied using a three-dimensional electromagnetic particle-in-cell model. In the system the strong double layer is formed. Its electric field potential increases with the electron beam flux. In this electric field potential, the electrons of background plasma are strongly accelerated and propagate in the return-current direction. The high-energy part of their distribution at the high-potential side of the strong double layer resembles that of the n-distribution. Thus, the detection of the n-distributions, where a form of the high-energy part of the distribution is the most important, can indicate the presence of strong double layers in solar flares. The similarity between processes in solar flare loops and those in the downward current region of the terrestrial aurora, where the double layers were observed by FAST satellite, supports this idea.

On the physical meaning of n-distributions in solar flares A36
M. **Karlický**, E. Dzifčáková and J. Dudík
A&A 537, A36 (**2012**)
Aims. We investigate the physical meaning of the n-distributions detected in solar flares.
Methods. We consider a Maxwellian velocity distribution with a velocity drift. This distribution is analytically integrated to obtain the energy distribution, and its stability is investigated numerically using a fully electromagnetic particle-in-cell code.
Results. It is shown that the derived moving Maxwellian energy distribution is very similar to the n-distribution, especially in their high-energy parts. Both these distributions are mutually fitted and a relation between their parameters found. Contrary to the n-distribution, the moving Maxwellian distribution has a simple physical meaning, e.g., the electron component of the return current in the beam-plasma system. However, for high drift velocities of such a component, the moving Maxwellian distribution is unstable. Therefore to keep the form of this distribution similar to the n-distribution, some stabilization processes are necessary. If so, then the high intensities of the Si xiid 5.56 Å and 5.82 Å satellite lines and their evolution in solar flares can be explained by moving Maxwellian distributions instead of the n-distributions. Thus, our previous results connected with the n-distributions can be understood in a new, physically profound way.

SUCCESSIVE MERGING OF PLASMOIDS AND FRAGMENTATION IN A FLARE CURRENT SHEET AND THEIR X-RAY AND RADIO SIGNATURES
Marian **Karlický**1 and Miroslav Bárta
2011 ApJ 733 107
http://www.pergamentum.com/eprint/ApJ2011suc_merg.pdf
Based on our recent MHD simulations, a conception of the successive merging of plasmoids and fragmentation in the current sheet in the standard flare model is presented. Then, using a 2.5-dimensional electromagnetic particle-in-cell model with free boundary conditions, these processes are modeled on the kinetic level of plasma description. We recognize the plasmoids that mutually interacted and finally merged into one large plasmoid. Between interacting plasmoids, additional plasmoids and current sheets on smaller spatial scales were formed, congruent with the

fragmentation found in MHD simulations. During interactions (merging-coalescences) between the plasmoids, the electrons were very efficiently accelerated and heated. We find that after a series of such merging processes, the electrons in some regions reached the energies necessary for emission in the hard X-ray range. Considering these energetic electrons and assuming a plasma density of 109-1010 cm–3 and a source volume equal to the **2007 December 31** flare, we compute the X-ray spectra as produced by the bremsstrahlung emission process. Comparing these spectra with observations, we think that these processes can explain the observed above-the-loop-top hard X-ray sources. Furthermore, we show that the process of fragmentation between two merging plasmoids can generate narrow-band dm-spikes. Formulae for schematic fractal reconnection structures are derived.

Tearing, coalescence and fragmentation processes in solar flare current sheet and drifting pulsating structures

M**. Karlický**

Advances in Space Research

Volume 46, Issue 4, 16 August **2010**, Pages 377-381

The paper presents a summary of results from two different simulations which study the tearing, coalescence and fragmentation of current sheets, the associated production of energetic electrons and of plasma waves from these electrons which could explain drifting pulsation structures observed at radio wavelengths. Using a 2.5-D particle-in-cell (PIC) model of the current sheet it is shown that due to the tearing mode instability the current sheet tears into plasmoids and these plasmoids later on coalesce into larger ones. During these processes electrons are accelerated and they produce observable electromagnetic waves. Furthermore, the 3-D PIC model with two current sheets extended in the electric current direction shows their fast fragmentation associated with the exponential dissipation of the free magnetic field energy. An example of the drifting pulsating structure which is considered to be a radio signature of the above mentioned processes in solar flares is shown.

Electron beam – plasma system with the return current and directivity of its X-ray emission

Karlicky, M., Kasparova, J.

E-print, Sept 2009; A&A, 506, 1437-1443 (**2009**)

Aims. An evolution of the electron distribution function in the beam-plasma system with the return current is computed numerically for different parameters. The X-ray bremsstrahlung corresponding to such an electron distribution is calculated and the directivity of the X-ray emission is studied.

Methods. For computations of the electron distribution functions we used a 3-D particle-in-cell electromagnetic code. The directivity of the X-ray emission was calculated using the angle-dependent electron-ion bremsstrahlung cross-section.

Results. It was found that the resulting electron distribution function depends on the magnetic field assumed along the electron beam propagation direction. For small magnetic fields the electron distribution function becomes broad in the direction perpendicular to the beam propagation due to the Weibel instability and the return current is formed by the electrons in a broad and shifted bulk of the distribution. On the other hand, for stronger magnetic fields the distribution is more extended in the beam-propagation direction and the return current is formed by the electrons in the extended distribution tail. In all cases, the anisotropy of the electron distribution decreases rapidly due to fast collisionless processes. However, the magnetic field reduces this anisotropy decrease. The X-ray directivity shows the same trend and it is always closer to the isotropic case than that in a simple beaming model.

Particle-in-cell simulations of return current in solar flares

M. **Karlický**, D. H. Nickeler, and M. Bárta

A&A 486, 325-329 (**2008**)

Results. In conditions of solar flares with the electron beam fluxes of $E_F = 9.1 \times 10^9$-4.55×10^{10} erg s^{-1} cm^{-2}, the beam-plasma interaction with the return current is studied. We found that the electron beam relaxes to the plateau distribution function as known from electrostatic simulations. Simultaneously, due to electromagnetic effects and the Buneman instability of the prescribed Maxwell-shifted return current, the electron distribution function evolves to a new stationary state with a new form of the return current. In this final state the return current is formed not only by electrons in the bulk of the electron distribution function, but also by electrons in the extended tail. We use the results of simulations to estimate the critical beam fluxes for the processes under study in the low corona, the transition region and the upper chromosphere.

Fragmentation of the Current Sheet, Anomalous Resistivity, and Acceleration of Particles

M. **Karlický**, M. Bárta
Solar Physics, Volume 247 Number 2, Page: 335 – 342, **2008**
http://springer.r.delivery.net/r/r?2.1.Ee.2Tp.1gRU2L.BwGL56..T.El%2aE.2xc6.DUBcEXf0

The morphology of average solar flare time profiles from observations of the Sun's lower atmosphere

Larisa K. **Kashapova**, Anne-Marie Broomhall, Alena I. Larionova, Elena G. Kupriyanova, Ilya D. Motyk
MNRAS Volume 502, Issue 3, April **2021**, Pages 3922–3931,
https://doi.org/10.1093/mnras/stab276
https://arxiv.org/pdf/2102.02596.pdf
https://watermark.silverchair.com/stab276.pdf

We study the decay phase of solar flares in several spectral bands using a method based on that successfully applied to white light flares observed on an M4 dwarf. We selected and processed 102 events detected in the Sun-as-a-star flux obtained with SDO/AIA images in the 1600~Å and 304~Å channels and 54 events detected in the 1700~Å channel. The main criterion for the selection of time profiles was a slow, continuous flux decay without significant new bursts. The obtained averaged time profiles were fitted with analytical templates, using different time intervals, that consisted of a combination of two independent exponents or a broken power law. The average flare profile observed in the 1700~Å channel decayed more slowly than the average flare profile observed on the M4 dwarf. As the 1700~Å emission is associated with a similar temperature to that usually ascribed to M dwarf flares, this implies that the M dwarf flare emission comes from a more dense layer than solar flare emission in the 1700~Å band. The cooling processes in solar flares were best described by the two exponents model, fitted over the intervals t1=[0, 0.5]t1/2 and t2=[3, 10]t1/2 where t1/2 is time taken for the profile to decay to half the maximum value. The broken power law model provided a good fit to the first decay phase, as it was able to account for the impact of chromospheric plasma evaporation, but it did not successfully fit the second decay phase.
In Appendix: **Table** A1 contains details of the flares in our sample. (2011-2017)
RHESSI Nuggets #412 **2021**
https://sprg.ssl.berkeley.edu/~tohban/wiki/index.php/The_Morphology_of_Flare_Time_Profiles

The origin of quasi-periodicities during circular ribbon flares

L. K. **Kashapova**, E. G. Kupriyanova, Z. Xu, H. A. S. Reid, D. Y. Kolotkov
A&A 642, A195 **2020**
https://warwick.ac.uk/fac/sci/physics/research/cfsa/people/kolotkov/eprints/kashapova_et_al_arxiv.pdf
https://arxiv.org/pdf/2008.02010.pdf

Context. Solar flares with a fan-spine magnetic topology can form circular ribbons. The previous study based on Hα line observations of the solar flares during **March 05, 2014** by Xu et al. (2017) revealed uniform and continuous rotation of the magnetic fan-spine. Preliminary analysis of the flare time profiles revealed quasi-periodic pulsations (QPPs) with similar properties in hard X-rays, Hα, and microwaves.
Aims. In this work, we address which process the observed periodicities are related to: periodic acceleration of electrons or plasma heating?
Methods. QPPs are analysed in the Hα emission from the centre of the fan (inner ribbon R1), a circular ribbon (R2), a remote source (R3), and an elongated ribbon (R4) located between R2 and R3. The methods of correlation, Fourier, wavelet, and empirical mode decomposition are used. QPPs in Hα emission are compared with those in microwave and X-ray emission.
Results. We found multi-wavelength QPPs with periods around 150 s, 125 s, and 190 s. The 150-s period is seen to co-exist in Hα, hard X-rays, and microwave emissions, that allowed us to connect it with flare kernels R1 and R2. These kernels spatially coincide with the site of the primary flare energy release. The 125-s period is found in the Hα emission of the elongated ribbon R4 and the microwave emission at 5.7 GHz during the decay phase. The 190-s period is present in the emission during all flare phases in the Hα emission of both the remote source R3 and the elongated ribbon R4, in soft X-rays, and microwaves at 4–8 GHz.
Conclusions. We connected the dominant 150-s QPPs with the slipping reconnection mechanism occurring in the fan. We suggested that the period of 125 s in the elongated ribbon can be caused by a kink oscillation of the outer spine connecting the primary reconnection site with the remote footpoint. The period of 190 s is associated with the 3-min sunspot oscillations.

Detection of Acceleration Processes During the Initial Phase of the 12 June 2010 Flare

L. K. **Kashapova**, N. S. Meshalkina, M. S. Kisil
Solar Physics, October **2012**, Volume 280, Issue 2, pp 525-535

We present an analysis of the plasma parameters during the initial phase of the 12 June 2010 flare (**SOL2010-06-12T00:57**). A peculiarity of the flare was the detection of γ-ray emission that is unusual for such weak and short event. The analysis revealed the presence of a flare precursor detected about five minutes before the flare onset in 94 Å images which spatially coincided with the non-polarized microwave (MW) source at 17 GHz (the Nobeyama Radio Heliograph) that is the Neutral Line associated Source (NLS). A comparison of the results obtained from MW data by the Nobeyama Radio Polarimeters and the multi-frequency Siberian Radioheliograph (the new 10-antenna radio heliograph prototype at 4.6 and 6.4 GHz) and hard X-ray (HXR) observations by the Fermi Gamma-ray Space Telescope reveal the presence of accelerated electrons during the flare's initial phase. The analysis of MW and HXR spectra also confirms the presence of accelerated particles. Moreover, a good temporal correlation between several light curves in different HXR energy bands and at MW frequencies indicates the generation of both HXR and MW emission by a common population of accelerated electrons. Detection of accelerated particles during the initial phase of the flare and soft-hard-harder (SHH) behavior of the spectra indicate several episodes of particle acceleration and confirm the non-impulsive type of the flare evolution.

Eruptive processes at the beginning of development of powerful flare-active regions on the sun

Astronomy Reports (2008) 52:1015-1026, December 01, **2008**
By **Kashapova, L. K.**; Livshits, M. A.
The evolution of large solar activity centers is studied, and the conditions resulting in powerful nonstationary processes are clarified. In addition to the factors that are usually considered (changes in sunspot area, the structure of magnetic fields, the character of motions), we examine to what extent observations of nonstationary processes (flares and associated coronal mass ejections) can be used to predict the development of such processes in the subsequent evolution of the activity center. We considered the example of a powerful group in October 2003, which could be observed before its appearance at the eastern limb using a spacecraft in near-Mars orbit. We plotted for events occurring in 2003 images of flares in various spectral ranges and analyzed high-energy processes in group 486, which was isolated at the beginning of its development, and then in the interrelated groups 486 and 484. The analysis of the peculiar early development of group 486 suggested that an intensification of the activity could be expected due to the emergence of new magnetic flux (and satellite groups), as well as the interaction and synchronization of two and then three large groups of the end of October 2003. In other words, in this case, extremely powerful nonstationary processes are associated with a relatively higher contribution of large-scale magnetic fields. We compare our results to analyses of motions and magnetic fields in this activity center throughout its transit across the disk from October 23 to November 5, 2003.
Download PDF

Solar and stellar flares: frequency, active regions and stellar dynamo

M.M. **Katsova**, V.N. Obridko, D.D. Sokoloff, I.M. Livshits
ApJ **936** 49 **2022**
https://arxiv.org/pdf/2208.03994.pdf
https://iopscience.iop.org/article/10.3847/1538-4357/ac85e3/pdf
We demonstrate that for weak flares the dependence on spottedness can be rather weak. The fact is that such flares can occur both in small and large active regions. At the same time, powerful large flares of classes M and X occur much more often in large active regions. In energy estimates, the mean magnetic field in starspots can also be assumed equal to the mean field in the sunspot umbra. So the effective mean magnetic field is 900 Mx/cm2 in sunspots and 2000 Mx/cm2 in starspots. Moreover, the height of the energy storage cannot be strictly proportional to A1/2. For stars, the fitting factor is an order of magnitude smaller. The analysis of the occurrence rate of powerful solar X-ray flares of class M and X and superflares on stars shows that, with allowance for the difference in the spottedness and compactness of active regions, both sets can be described by a single model. Thus, the problem of superflares on stars and their absence on the Sun is reduced to the problem of difference in the effectiveness of the dynamo mechanisms.

Superflares on Giant Stars

M.M.**Katsova**, L.L.Kitchatinov, D.Moss, K.Olah, D.D.Sokoloff
Astronomy Reports, **2018**, Vol.62, No.8 pp 513–519
https://arxiv.org/pdf/1804.06315.pdf
https://link.springer.com/content/pdf/10.1134%2FS1063772918080036.pdf
The Kepler mission identified huge flares on various stars including some of solar type. These events are substantially more energetic than solar flares, and so they are referred to as superflares. Even a small probability of such a superflare on the Sun would be a menace to modern society. A flare comparable in energy with that of superflares was observed on 24th and 25th September on the binary HK Lac. Unlike the Kepler stars, there are observations of differential rotation for HK Lac. This differential rotation appears to be anti-solar. For anti-solar differential rotation, dynamo

models can give magnetic activity waves of dipole symmetry as well as quasi-stationary magnetic configurations with quadrupole symmetry. The magnetic energy of such stationary configurations is usually about two orders of magnitude higher than that associated with activity waves. We believe that this mechanism could provide sufficient energy to produce superflares on late type stars, and present some simple models in support of this idea.

Can superflares occur on the Sun? A view from dynamo theory

M.M.**Katsova**, L.L.Kitchatinov, M.A.Livshits, D.L.Moss, D.D.Sokoloff, I.G.Usoskin
Astronomy Reports **2017**
https://arxiv.org/pdf/1710.00015.pdf
Recent data from the Kepler mission has revealed the occurrence of superflares in sun-like stars which exceed by far any observed solar flares in release of energy. A natural idea is that the dynamo mechanism in superflaring stars differs in some respect from that in the Sun. We search for a difference in the dynamo-related parameters between superflaring stars and the Sun to suggest a dynamo-mechanism as close as possible to the conventional solar/stellar dynamo but capable of providing much higher magnetic energy. Dynamo based on joint action of differential rotation and mirror asymmetric motions can in principle result in excitation of two types of magnetic fields. First of all, it is well-known in solar physics dynamo waves. The point is that another magnetic configuration with initial growth and further stabilisation is also possible for excitation. For comparable conditions, magnetic field strength of second configuration is much larger rather of the first one just because dynamo do not spend its efforts for periodic magnetic field inversions but use its for magnetic field growth. We analysed available data from the Kepler mission concerning the superflaring stars in order to find tracers of anomalous magnetic activity. Starting from the recent paper, we find that anti-solar differential rotation or anti-solar sign of the mirror-asymmetry of stellar convection can provide the desired strong magnetic field in dynamo models. We confirm this concept by numerical models of stellar dynamos with corresponding governing parameters. We conclude that the proposed mechanism can plausibly explain the superflaring events at least for some cool stars, including binaries, subgiants and, possibly, low-mass stars and young rapid rotators.

The Origin of Superflares on G-Type Dwarf Stars of Various Ages

M. M. **Katsova**, M. A. Livshits
Solar Phys. Volume 290, Issue 12, pp 3663-3682 **2015**
We analyze new observations of superflares on G-stars discovered in the optical and near-IR ranges with the Kepler mission. An evolution of solar-type activity is discussed. We give an estimate of the maximal total energy, Etot=1034 erg, of a flare that could have occurred on the young Sun at its age of 1 Gyr when the cycle was formed. We believe that the main source of the flare optical continuum is a low-temperature condensation forming in the course of the response of the chromosphere to an impulsive heating. For a superflare on the young Sun, we adopt an accelerated electron flux, Fe (E>20 keV)=3×1011 ergcm−2s−1, that is limited by the return current and obtain that the area of the optical continuum source on a G-star is S≈1019 cm2. This value is close to the area of the Hα ribbons in the largest solar flares, while the area of bright patches of a white-light flare on the contemporary Sun is lower by about two orders of magnitude. At the same electron flux and hard electron spectrum, a stellar flare of similar energy should be accompanied by a microwave source of about 2 mJy at frequencies 10 – 100 GHz at a distance of 100 pc. We discuss the possible detection of the flare-produced lithium in the course of spallation reactions. The detection of the flare microwave source and the emission in the Li resonant line could demonstrate how effective particle acceleration can be on stars in the lower part of the main sequence.

Inverse FIP Effects in Giant Solar Flares Found from Earth X-Ray Albedo with Suzaku/XIS

Satoru **Katsuda**, Masanori Ohno, Koji Mori, Tatsuhiko Beppu, Yoshiaki Kanemaru, Makoto S. Tashiro, Yukikatsu Terada, Kosuke Sato, Kae Morita, Hikari Sagara, Futa Ogawa, Haruya Takahashi, Hiroshi Murakami, Masayoshi Nobukawa, Hiroshi Tsunemi, Kiyoshi Hayashida, Hironori Matsumoto, Hirofumi Noda, Hiroshi Nakajima, Yuichiro Ezoe, Yohko Tsuboi, Yoshitomo Maeda, Takaaki Yokoyama, Noriyuki Narukage
ApJ **2020**
https://arxiv.org/pdf/2001.10643.pdf
We report X-ray spectroscopic results for four giant solar flares occurred on **2005 September 7** (X17.0), **2005 September 8** (X5.4), **2005 September 9** (X6.2), and 2006 December 5 (X9.0), obtained from Earth albedo data with the X-ray imaging spectrometer (XIS) onboard Suzaku. The good energy resolution of the XIS (FWHM~100 eV) enables us to separate a number of line-like features and detect the underlying continuum emission. These features include Si Heα, Si Lyα, S Heα, S Lyα, Ar Heα, and Ca Heα originating from solar flares as well as fluorescent Ar Kα and Ar Kβ from the Earth atmosphere. Absolute elemental abundances (X/H) averaged over the four flares are obtained to be ~2.0 (Ca), ~0.7 (Si), ~0.3 (S), and ~0.9 (Ar) at around flare peaks. This abundance pattern is similar to those of active stars' coronae showing inverse first ionization potential (i-FIP) effects, i.e., elemental abundances decrease with decreasing FIP with a turnover at the low end of FIP. The abundances are almost constant during the flares, with an exception of Si which increases by a factor of ~2 in the decay phase. The evolution of the Si abundance is consistent with a picture that the i-FIP plasma originates from the chromosphere evaporation and then mixes with the

surrounding low-FIP biased materials. Flare-to-flare abundance varied by a factor of 2, agreeing with past observations of solar flares. Finally, we emphasize that Earth albedo data acquired by X-ray astronomy satellites like Suzaku and XRISM can significantly contribute to studies of solar physics.

Unusual Emissions at Various Energies Prior to the Impulsive Phase of the Large Solar Flare and Coronal Mass Ejection of 4 November 2003

Pierre **Kaufmann**, Gordon D. Holman, Yang Su, C. Guillermo Gimenez de Castro, Emilia Correia, Luis O. T. Fernandes, Rodney V. de Souza, Adolfo Marun and Pablo Pereyra
Solar Physics, Volume 279, Number 2 (**2012**), 465-475
The GOES X28 flare of **4 November 2003** was the largest ever recorded in its class. It produced the first evidence for two spectrally separated emission components, one at microwaves and the other in the THz range of frequencies. We analyzed the pre-flare phase of this large flare, twenty minutes before the onset of the major impulsive burst. This period is characterized by unusual activity in X-rays, sub-THz frequencies, Hα, and microwaves. The CME onset occurred before the onset of the large burst by about 6 min. It was preceded by pulsations of 3 – 5 s periods at sub-THz frequencies together with X-ray and microwave enhancements. The sub-THz pulsations faded out as impulsive bursts were detected at 100 – 300 keV and 7 GHz, close to the time of the first Hα brightening and the CME onset. The activities detected prior to and at the CME onset were located nearly 2 arcmin south of the following large flare, suggesting they were separate events. This unusual activity brings new clues to understanding the complex energy buildup mechanisms prior to the CME onset, occurring at a distinct location and well before the major flare that exploded afterwards.

Sub-terahertz, Microwaves and High Energy Emissions During the 6 December 2006 Flare, at 18:40 UT

Pierre **Kaufmann** · Gérard Trottet · C. Guillermo Giménez de Castro · Jean-Pierre Raulin · Säm Krucker · Albert Y. Shih · Hugo Levato
Solar Phys (**2009**) 255: 131–142, DOI 10.1007/s11207-008-9312-7
The presence of a solar burst spectral component with flux density increasing with frequency in the sub-terahertz range, spectrally separated from the well-known microwave spectral component, bring new possibilities to explore the flaring physical processes, both observational and theoretical. The solar event of 6 December 2006, starting at about 18:30 UT, exhibited a particularly well-defined double spectral structure, with the sub-THz spectral component detected at 212 and 405 GHz by the Solar Submilimeter Telescope (SST) and microwaves (1 – 18 GHz) observed by the Owens Valley Solar Array (OVSA). Emissions obtained by instruments onboard satellites are discussed with emphasis to ultraviolet (UV) obtained by the Transition Region And Coronal Explorer (TRACE), soft X-rays from the Geostationary Operational Environmental Satellites (GOES) and X- and γ –rays from the Ramaty High Energy Solar Spectroscopic Imager (RHESSI). The sub-THz impulsive component had its closer temporal counterparts only in the higher energy X- and γ –rays ranges. The spatial positions of the centers of emission at 212 GHz for the first flux enhancement were clearly displaced by more than one arc-minute from positions at the following phases. The observed sub-THz fluxes and burst source plasma parameters were difficult to be reconciled with a purely thermal emission component. We discuss possible mechanisms to explain the double spectral components at microwaves and in the THz ranges.

Extrapolation of Three-dimensional Magnetic Field Structure in Flare-productive Active Regions with Different Initial Conditions

Y. **Kawabata**1, S. Inoue2, and T. Shimizu3,4
2020 ApJ 895 105
https://sci-hub.tw/https://iopscience.iop.org/article/10.3847/1538-4357/ab8ea9
Nonlinear force-free field (NLFFF) modeling has been extensively used as a tool to infer three-dimensional (3D) magnetic field structure. In this study, the dependency of the NLFFF calculation with respect to the initial guess of the 3D magnetic field is investigated. While major parts of the previous studies used the potential field as the initial guess in NLFFF modeling, we adopt linear force-free fields with different constant force-free alpha as the initial guesses. This method enables us to investigate the uniqueness of the magnetic field obtained by the NLFFF extrapolation with respect to the initial guess. The dependence of the initial conditions on NLFFF extrapolation is smaller in the strong magnetic field region. Therefore, the magnetic field at lower heights (<10 Mm) tends to be less affected by the initial conditions (correlation coefficient C > 0.9 with different initial conditions); although, the Lorentz force is concentrated at lower heights. **2013 March 15. 2014 February 3**

Statistical Relation between Solar Flares and Coronal Mass Ejections with Respect to Sigmoidal Structures in Active Regions

Y. **Kawabata**, Y. Iida, T. Doi, S. Akiyama, S. Yashiro, T. Shimizu
ApJ **869** 99 **2018** https://doi.org/10.3847/1538-4357/aaebfc
https://arxiv.org/pdf/1810.10808.pdf

Statistical dependencies among features of coronal mass ejections (CMEs), solar flares, and sigmoidal structures in soft-X-ray images were investigated. We applied analysis methods to all the features in the same way in order to investigate the reproducibility of the correlations among them, which may be found from the combination of previous statistical studies. The samples of 211 M-class and X-class flares, which were observed between 2006 and 2015 by Hinode/X-ray telescope, Solar and Heliospheric Observatory/Large Angle and Spectrometric Coronagraph, and GOES, were examined statistically. Five kinds of analysis were performed: Occurrence rate analysis, linear-correlation analysis, association analysis, the Kolmogorov--Smirnov test, and Anderson-Darling test. The analyses show three main results. First, the sigmoidal structure and long duration events (LDEs) has stronger dependency on the CME occurrence than large X-ray class events in on-disk events. Second, for the limb events, the significant dependency exists between LDEs and CME occurrence, and between X-ray class and CME occurrence. Third, there existed 32.4% of on-disk flare events, which had sigmoidal structure and were not accompanied by CMEs. However, the occurrence probability of CMEs without sigmoidal structures is very small, 8.8 %, in on-disk events. While the first and second results are consistent with previous studies, we newly provided the difference between the on-disk events and limb events. The third result that non-sigmoidal regions produce less eruptive events is also different from previous results. We suggest that sigmoidal structures in soft X-ray images will be a helpful feature for CME prediction regarding on-disk flare events.
13 December 2006
PSTEP Science Nuggets #18 **2019** http://www.pstep.jp/news_en/nuggets18en.html

Non-potential field formation in the X-shaped quadrupole magnetic field configuration

Yusuke **Kawabata**, Satoshi Inoue, Toshifumi Shimizu
ApJ **842** 106 **2017**
https://arxiv.org/pdf/1705.02560.pdf
http://iopscience.iop.org.sci-hub.cc/0004-637X/842/2/106/
Some types of solar flares are observed in X-shaped quadrupolar field configuration. To understand the magnetic energy storage in such a region, we studied non-potential field formation in an X-shaped quadrupolar field region formed in the active region NOAA 11967, which produced three X-shaped M-class flares on **February 2, 2014**. Nonlinear force-free field modeling was applied to a time series of vector magnetic field maps from the Solar Optical Telescope on board Hinode and Helioseismic and Magnetic Imager on board Solar Dynamics Observatory. Our analysis of the temporal three-dimensional magnetic field evolution shows that the sufficient free energy had already been stored more than 10 hours before the occurrence of the first M-class flare and that the storage was observed in a localized region. In this localized region, quasi-separatrix layers (QSLs) started to develop gradually from 9 hours before the first M-class flare. One of the flare ribbons that appeared in the first M-class flare was co-spatial with the location of the QSLs, suggesting that the formation of the QSLs is important in the process of energy release. These QSLs do not appear in the potential field calculation, indicating that they were created by the non-potential field. The formation of the QSLs was associated with the transverse photospheric motion of the pre-emerged flux and the emergence of a new flux. This observation indicates that the occurrence of the flares requires the formation of QSLs in the non-potential field in which free magnetic energy is stored in advance.

Factors That Determine the Power-law Index of an Energy Distribution of Solar Flares

Toshiki **Kawai**1 and Shinsuke Imada1,2
2022 ApJ 931 113
https://iopscience.iop.org/article/10.3847/1538-4357/ac6aca/pdf
The power-law index of an occurrence frequency distribution of flares as a function of energy is one of the most important indicators to evaluate the contribution of small-scale flares to coronal heating. For a few decades, many studies tried to derive the power-law index using various instruments and methods. However, these results are various and the cause of this uncertainty is unknown due to the variety of observation conditions. Therefore, we investigated the dependence of the index on the solar activity, coronal features, released energy range, and active region properties such as magnetic flux, twist, and size. Our findings are (1) annual power-law index derived from time series of total solar irradiance (Sun-as-a-star observation analysis) has a negative correlation with sunspot number; (2) power-law index in active region is smaller than that of the quiet Sun and coronal holes; (3) power-law index is almost constant in the energy range of $1025 \lesssim E \lesssim 1030$ erg; and (4) active regions that have more magnetic free energy density, unsigned magnetic flux, and shear angle tend to have smaller power-law indices. Based on the results and energy-scaling law of Petschek-type reconnection, we suggest that the power-law index of sunspot-scale events is smaller than that of granule-scale events. Moreover, we indicated that sunspot-scale events follow CSHKP flare model whereas granule-scale events follow Parker's nanoflare model.

Energy distribution of small-scale flares derived using genetic algorithm

Toshiki **Kawai**, Shinsuke Imada
2021 ApJ 906 2
https://iopscience.iop.org/article/10.3847/1538-4357/abc9ae/pdf
https://doi.org/10.3847/1538-4357/abc9ae

https://arxiv.org/pdf/2011.06390.pdf
To understand the mechanism of coronal heating, it is crucial to derive the contribution of small-scale flares, the so-called nanoflares, to the heating up of the solar corona. To date, several studies have tried to derive the occurrence frequency distribution of flares as a function of energy to reveal the contribution of small-scale flares. However, there are no studies that derive the distribution with considering the following conditions: (1) evolution of the coronal loop plasma heated by small-scale flares, (2) loops smaller than the spatial resolution of the observed image, and (3) multiwavelength observation. To take into account these conditions, we introduce a new method to analyze small-scale flares statistically based on a one-dimensional loop simulation and a machine learning technique, that is, genetic algorithm. First, we obtain six channels of SDO/AIA light curves of the active-region coronal loops. Second, we carry out many coronal loop simulations and obtain the SDO/AIA light curves for each simulation in a pseudo-manner. Third, using the genetic algorithm, we estimate the best combination of simulated light curves that reproduce the observation. Consequently, the observed coronal loops are heated by small-scale flares with energy flux larger than that typically required to heat up an active region intermittently. Moreover, we derive the occurrence frequency distribution which have various power-law indices in the range from 1 to 3, which partially supports the nanoflare heating model. In contrast, we find that 90% of the coronal heating is done by flares that have energy larger than 1025 erg. **30 May 2018**

Nowcast of an EUV dynamic spectrum during solar flares

Toshiki **Kawai**, Shinsuke Imada, Shohei Nishimoto, Kyoko Watanabe, Tomoko Kawate
2020
https://arxiv.org/pdf/2005.06099.pdf
In addition to X-rays, extreme ultraviolet (EUV) rays radiated from solar flares can cause serious problems, such as communication failures and satellite drag. Therefore, methods for forecasting EUV dynamic spectra during flares are urgently required. Recently, however, owing to the lack of instruments, EUV dynamic spectra have rarely been observed. Hence, we develop a new method that converts the soft X-ray light curve observed during large flare events into an EUV dynamic spectrum by using the Solar Dynamics Observatory / Atmospheric Imaging Assembly images, a numerical simulation, and atomic database. The simulation provides the solution for a coronal loop that is heated by a strong flare, and the atomic database calculates its dynamic spectrum, including X-ray and EUV irradiances. The coefficients needed for the conversion can be calculated by comparing the observed soft X-ray light curve with that of the simulation. We apply our new method to three flares that occurred in the active region 12673 on **September 06, 2017**. The results show similarities to those of the Flare Irradiance Spectral Model, and reconstruct some of the EUV peaks observed by the EUV Variability Experiment onboard the Solar Dynamics Observatory.

Infrequent Occurrence of Significant Linear Polarization in Hα Solar Flares

Tomoko **Kawate**, Yoichiro Hanaoka
ApJ **872** 74 **2019**
https://arxiv.org/pdf/1901.03441.pdf
We performed statistical and event studies of linear polarization in the Hα line during solar flares. The statistical study revealed that, among 71 Hα flares analyzed, including 64 GOES flares, only one event shows significant linear polarization signals. Such an infrequent occurrence of significant linear polarization in solar flares is consistent with the result by Bianda et al. (2005), who studied 30 flares and found no polarization signals. In the event showing the significant polarization, the maximum degree of linear polarization was 1.16±0.06\%, and the average direction of the polarization deviated by -142.5±6.0 degrees from the solar north. The observed polarization degrees and the directions are consistent with the preceding reports (e.g. Henoux et al. 1990; Emslie et al. 2000; Hanaoka 2003). These strong linear polarization signals did not appear at major flare ribbons, nor did they correlate with either hard or soft X-ray emissions temporally or spatially. Instead they appeared at a minor flare kernel, which corresponds to one of the footpoints of a coronal loop. The active region caused coronal dimming after the soft X-ray peak. The observed flare show no direct evidence that the linear polarization is produced by high energy particles, which are often considered to generate the polarization. On the other hand, our study suggests the possibility that coronal mass ejections, which have been often observed in flares showing linear polarization signals, play an important role for exciting linear polarization at Hα flare kernels. **2 Dec 2005**
Table 1. Eventlist (2004-2005)
RHESSI Science Nuggets #344 Feb **2019**
http://sprg.ssl.berkeley.edu/~tohban/wiki/index.php/Linear_Polarization_in_H-alpha_Flares

Temporal evolution and spatial distribution of white-light flare kernels in a solar flare

Tomoko **Kawate**, Takako T. Ishii, Yoshikazu Nakatani, Kiyoshi Ichimoto, Ayumi Asai, Satoshi Morita, Satoshi Masuda
ApJ 833 50 **2016**
https://arxiv.org/pdf/1610.04328v1.pdf
On **2011 September 6**, we observed an X2.1-class flare in continuum and Hα with a frame rate of about 30~Hz. After processing images of the event by using a speckle-masking image reconstruction, we identified white-light (WL) flare

ribbons on opposite sides of the magnetic neutral line. We derive the lightcurve decay times of the WL flare kernels at each resolution element by assuming that the kernels consist of one or two components that decay exponentially, starting from the peak time. As a result, 42% of the pixels have two decay-time components with average decay times of 15.6 and 587 s, whereas the average decay time is 254 s for WL kernels with only one decay-time component. The peak intensities of the shorter decay-time component exhibit good spatial correlation with the WL intensity, whereas the peak intensities of the long decay-time components tend to be larger in the early phase of the flare at the inner part of the flare ribbons, close to the magnetic neutral line. The average intensity of the longer decay-time components is 1.78 times higher than that of the shorter decay-time components. If the shorter decay time is determined by either the chromospheric cooling time or the nonthermal ionization timescale and the longer decay time is attributed to the coronal cooling time, this result suggests that WL sources from both regions appear in 42% of the WL kernels and that WL emission of the coronal origin is sometimes stronger than that of chromospheric origin.

Departure of high temperature iron lines from the equilibrium state in flaring solar plasmas

Tomoko **Kawate**, Francis P. Keenan, David B. Jess

ApJ 826 3 **2016**

http://arxiv.org/pdf/1606.02049v1.pdf

The aim of this study is to clarify if the assumption of ionization equilibrium and a Maxwellian electron energy distribution is valid in flaring solar plasmas. We analyze the **2014 December 20** X1.8 flare, in which the \ion{Fe}{xxi} 187~\AA, \ion{Fe}{xxii} 253~\AA, \ion{Fe}{xxiii} 263~\AA\ and \ion{Fe}{xxiv} 255~\AA\ emission lines were simultaneously observed by the EUV Imaging Spectrometer onboard the Hinode satellite. Intensity ratios among these high temperature Fe lines are compared and departures from isothermal conditions and ionization equilibrium examined. Temperatures derived from intensity ratios involving these four lines show significant discrepancies at the flare footpoints in the impulsive phase, and at the looptop in the gradual phase. Among these, the temperature derived from the \ion{Fe}{xxii}/\ion{Fe}{xxiv} intensity ratio is the lowest, which cannot be explained if we assume a Maxwellian electron distribution and ionization equilibrium, even in the case of a multi-thermal structure. This result suggests that the assumption of ionization equilibrium and/or a Maxwellian electron energy distribution can be violated in evaporating solar plasma around 10~MK.

THE RELATIONSHIP BETWEEN EXTREME ULTRAVIOLET NON-THERMAL LINE BROADENING AND HIGH-ENERGY PARTICLES DURING SOLAR FLARES

T. **Kawate**1,2 and S. Imada

2013 ApJ 775 122

http://arxiv.org/pdf/1308.3415v1.pdf

We have studied the relationship between the location of EUV non-thermal broadening and high-energy particles during large flares using the EUV Imaging Spectrometer on board Hinode, the Nobeyama Radio Polarimeter, the Nobeyama Radioheliograph, and the Atmospheric Imaging Assembly on board the Solar Dynamic Observatory. We have analyzed five large flare events that contain thermal-rich, intermediate, and thermal-poor flares classified by the definition discussed in the paper. We found that, in the case of thermal-rich flares, the non-thermal broadening of Fe XXIV occurred at the top of the flaring loop at the beginning of the flares. The source of 17 GHz microwaves is located at the footpoint of the flare loop. On the other hand, in the case of intermediate/thermal-poor flares, the non-thermal broadening of Fe XXIV occurred at the footpoint of the flare loop at the beginning of the flares. The source of 17 GHz microwaves is located at the top of the flaring loop. We discussed the difference between thermal-rich and intermediate/thermal-poor flares based on the spatial information of non-thermal broadening, which may provide clues that the presence of turbulence plays an important role in the pitch angle scattering of high-energy electrons.

HARD X-RAY AND MICROWAVE EMISSIONS FROM SOLAR FLARES WITH HARD SPECTRAL INDICES

T. **Kawate**1, N. Nishizuka2, A. Oi3, M. Ohyama4 and H. Nakajima

2012 ApJ 747 131

We analyze 10 flare events that radiate intense hard X-ray (HXR) emission with significant photons over 300 keV to verify that the electrons that have a common origin of acceleration mechanism and energy power-law distribution with solar flares emit HXRs and microwaves. Most of these events have the following characteristics. HXRs emanate from the footpoints of flare loops, while microwaves emanate from the tops of flare loops. The time profiles of the microwave emission show delays of peak with respect to those of the corresponding HXR emission. The spectral indices of microwave emissions show gradual hardening in all events, while the spectral indices of the corresponding HXR emissions are roughly constant in most of the events, though rather rapid hardening is simultaneously observed in some for both indices during the onset time and the peak time. These characteristics suggest that the microwave emission emanates from the trapped electrons. Then, taking into account the role of the trapping of electrons for the microwave emission, we compare the observed microwave spectra with the model spectra calculated by a

gyrosynchrotron code. As a result, we successfully reproduce the eight microwave spectra. From this result, we conclude that the electrons that have a common acceleration and a common energy distribution with solar flares emit both HXR and microwave emissions in the eight events, though microwave emission is contributed to by electrons with much higher energy than HXR emission.

A Database of Magnetic and Thermodynamic Properties of Confined And Eruptive Solar Flares

Maria D. **Kazachenko**
ApJ **958** 104 **2023**
https://arxiv.org/pdf/2310.02878.pdf **File**
https://iopscience.iop.org/article/10.3847/1538-4357/ad004e/pdf
Solar flares sometimes lead to coronal mass ejections that directly affect the Earth's environment. However, a large fraction of flares, including on solar-type stars, are confined flares. What are the differences in physical properties between confined and eruptive flares? For the first time, we quantify thermodynamic and magnetic properties of hundreds of confined and eruptive flares of GOES class C5.0 and above, 480 flares total. We first analyze large flares of GOES class M1.0 and above observed by the Solar Dynamics Observatory (SDO): 216 flares total, including 103 eruptive and 113 confined flares, from 2010 until 2016 April, we then look at the entire dataset above C5.0 of 480 flares. We compare GOES X-ray thermodynamic flare properties, including peak temperature and emission measure, and active-region and flare-ribbon magnetic field properties, including reconnected magnetic flux and peak reconnection rate. We find that for fixed peak X-ray flux, confined and eruptive flares have similar reconnection fluxes; however, for fixed peak X-ray flux confined flares have on average larger peak magnetic reconnection rates, are more compact, and occur in larger active regions than eruptive flares. These findings suggest that confined flares are caused by reconnection between more compact, stronger, lower lying magnetic-fields in larger active regions that reorganizes smaller fraction of these regions' fields. This reconnection proceeds at faster rates and ends earlier, potentially leading to more efficient flare particle acceleration in confined flares.
1. INTRODUCTION
RibbonDB dataset (Kazachenko et al. 2017) http://solarmuri.ssl.berkeley.edu/~kazachenko/RibbonDB/
SolarErupDB database **http://solarmuri.ssl.berkeley.edu/~kazachenko/SolarErupDB/**

Invited Review: Short-term Variability with the Observations from the Helioseismic and Magnetic Imager (HMI) Onboard the Solar Dynamics Observatory (SDO): Insights into Flare Magnetism

Maria D. **Kazachenko**, Marcel F. Albelo-Corchado, Cole A. Tamburri & Brian T. Welsch
Solar Physics volume 297, Article number: 59 (**2022**)
https://link.springer.com/content/pdf/10.1007/s11207-022-01987-6.pdf **File**
Continuous vector magnetic-field measurements by the Helioseismic and Magnetic Imager (HMI) onboard the Solar Dynamics Observatory (SDO) allow us to study magnetic-field properties of many flares. Here, we review new observational aspects of flare magnetism described using SDO data, including statistical properties of magnetic-reconnection fluxes and their rates, magnetic fluxes of flare dimmings, and magnetic-field changes during flares. We summarize how these results, along with statistical studies of coronal mass ejections (CMEs), have improved our understanding of flares and the flare/CME feedback relationship. Finally, we highlight future directions to improve the current state of understanding of solar-flare magnetism using observations. **14 Sep 2011, 7 March 2012, Sep 2014**
2. Flare Ribbons: Footpoints of Reconnected Fields
3. Coronal Dimmings: Footpoints of Expanding Coronal Structures
4. Flare-Associated Magnetic-Field Changes (FAMCs)
5. Relating CMEs and ICMEs to Their Source Regions

Toward Improved Understanding of Magnetic Fields Participating in Solar Flares: Statistical Analysis of Magnetic Field within Flare Ribbons

Maria D. **Kazachenko**, Benjamin J. Lynch, Antonia Savcheva, Xudong Sun, Brian T. Welsch
ApJ **926** 56 **2022**
https://arxiv.org/pdf/2111.06048.pdf
https://iopscience.iop.org/article/10.3847/1538-4357/ac3af3/pdf
Violent solar flares and coronal mass ejections (CMEs) are magnetic phenomena. However, how magnetic fields reconnecting in the flare differ from non-flaring magnetic fields remains unclear owing to the lack of studies of the flare magnetic properties. Here we present a first statistical study of flaring (highlighted by flare-ribbons) vector magnetic fields in the photosphere. Our systematic approach allows us to describe key physical properties of solar flare magnetism, including distributions of magnetic flux, magnetic shear, vertical current and net current over flaring versus

non-flaring parts of the active region, and compare these with flare/CME properties. Our analysis suggests that while flares are guided by the physical properties that scale with AR size, like the total amount of magnetic flux that participates in the reconnection process and the total current (extensive properties), CMEs are guided by mean properties, like the fraction of the AR magnetic flux that participates (intensive property), with little dependence on the amount of shear at polarity inversion line (PIL) or the net current. We find that the non-neutralized current is proportional to the amount of shear at PIL, providing direct evidence that net vertical currents are formed as a result of any mechanism that could generate magnetic shear along PIL. We also find that eruptive events tend to have smaller PIL fluxes and larger magnetic shears than confined events. Our analysis provides a reference for more realistic solar and stellar flare models. The database is available online and can be used for future quantitative studies of flare magnetism.

HMI Science Nuggets #174 Feb **2022** http://hmi.stanford.edu/hminuggets/?p=3839

A Database of Flare Ribbon Properties From Solar Dynamics Observatory I: Reconnection Flux

Maria D. **Kazachenko**, Benjamin J. Lynch, Brian T. Welsch, Xudong Sun

ApJ **845** 49 **2017**

https://arxiv.org/pdf/1704.05097.pdf

http://sci-hub.cc/10.3847/1538-4357/aa7ed6 **File**

We present a database of 3137 solar flare ribbon events corresponding to every flare of GOES class C1.0 and greater within 45 degrees from the disk center, from April 2010 until April 2016, observed by the Solar Dynamics Observatory. For every event in the database, we compare the GOES peak X-ray flux with corresponding active-region and flare-ribbon properties. We find that while the peak X-ray flux is not correlated with the active region unsigned magnetic flux, it is strongly correlated with the flare ribbon reconnection flux, flare ribbon area, and the fraction of active region flux that undergoes reconnection. We find the relationship between the peak X-ray flux and the flare ribbon reconnection flux to be IX, peak$\propto\Phi$1.3 ribbon for flares $\geq$M1 and IX,peak$\propto\Phi$1.5 ribbon over the entire flare set ($\geq$C1). This scaling law is consistent with earlier hydrodynamic simulations of impulsively heated flare loops. Using the flare reconnection flux as a proxy for the total released flare energy E, we find that the occurrence frequency of flare energies follows a power-law dependence: dN/dE$\propto$E$-$1.6 for 1031<E<1033 erg, consistent with earlier studies of solar and stellar flares. This database is available online and can be used for future quantitative studies of flares. **2011 February 15, 2011-03-31, 2012-03-07, 2012-06-17, 2013-04-11**.

1. INTRODUCTION

http://solarmuri.ssl.berkeley.edu/~kazachenko/RibbonDB/

HMI Science Nuggets #174 **2022** http://hmi.stanford.edu/hminuggets/?p=3839

Photospheric Electric Fields and Energy Fluxes in the Eruptive Active Region NOAA 11158

Kazachenko, Maria D.; Fisher, George H.; Welsch, Brian T.; Liu, Yang; Sun, Xudong

ApJ **811** 16 **2015**

http://arxiv.org/pdf/1505.05974v2.pdf

How much electromagnetic energy crosses the photosphere in evolving solar active regions? With the advent of high-cadence vector magnetic field observations, addressing this fundamental question has become tractable. In this paper, we apply the "PTD-Doppler-FLCT-Ideal" (PDFI) electric field inversion technique of Kazachenko et al. (2014) to a 6-day HMI/SDO vector magnetogram and Doppler velocity sequence, to find the electric field and Poynting flux evolution in active region NOAA 11158, which produced an X2.2 flare early on **2011 February 15**. We find photospheric electric fields ranging up to 2 V/cm. The Poynting fluxes range from $[-0.6$ to $2.3]\times10^{10}$ ergs$\cdot$cm^{-2}s^{-1}, mostly positive, with the largest contribution to the energy budget in the range of $[10^9$-$10^{10}]$ ergs$\cdot$cm^{-2}s^{-1}. Integrating the instantaneous energy flux over space and time, we find that the total magnetic energy accumulated above the photosphere from the initial emergence to the moment before the X2.2 flare to be $E=10.6\times10^{32}$ ergs, which is partitioned as 2.0 and 8.6×10^{32} ergs, respectively, between free and potential energies. Those estimates are consistent with estimates from preflare non-linear force-free field (NLFFF) extrapolations and the Minimum Current Corona estimates (MCC), in spite of our very different approach. This study of photospheric electric fields demonstrates the potential of the PDFI approach for estimating Poynting fluxes and opens the door to more quantitative studies of the solar photosphere and more realistic data-driven simulations of coronal magnetic field evolution.

See RHESSI Science Nuggets, #261, **2015**

http://sprg.ssl.berkeley.edu/~tohban/wiki/index.php/Photospheric_Electric_Fields_and_Energy_Fluxes_in_the_Eruptive_Active_Region_NOAA_11158

Predictions of Energy and Helicity in Four Major Eruptive Solar Flares

Maria D. **Kazachenko**, Richard C. Canfield, Dana W. Longcope and Jiong Qiu

Solar Physics, Volume 277, Number 1, 165-183, **2012, File**

In order to better understand the solar genesis of interplanetary magnetic clouds (MCs), we model the magnetic and topological properties of four large eruptive solar flares and relate them to observations. We use the three-dimensional Minimum Current Corona model (Longcope, 1996, Solar Phys. 169, 91) and observations of pre-flare photospheric magnetic field and flare ribbons to derive values of reconnected magnetic flux, flare energy, flux rope helicity, and orientation of the flux-rope poloidal field. We compare model predictions of those quantities to flare and MC observations, and within the estimated uncertainties of the methods used find the following: The predicted model reconnection fluxes are equal to or lower than the reconnection fluxes inferred from the observed ribbon motions. Both observed and model reconnection fluxes match the MC poloidal fluxes. The predicted flux-rope helicities match the MC helicities. The predicted free energies lie between the observed energies and the estimated total flare luminosities. The direction of the leading edge of the MC's poloidal field is aligned with the poloidal field of the flux rope in the AR rather than the global dipole field. These findings compel us to believe that magnetic clouds associated with these four solar flares are formed by low-corona magnetic reconnection during the eruption, rather than eruption of pre-existing structures in the corona or formation in the upper corona with participation of the global magnetic field. We also note that since all four flares occurred in active regions without significant pre-flare flux emergence and cancelation, the energy and helicity that we find are stored by shearing and rotating motions, which are sufficient to account for the observed radiative flare energy and MC helicity.

Sunspot Rotation, Flare Energetics and Flux Rope Helicity: The Halloween Flare on 2003 October 28

Maria D. **Kazachenko**1, Richard C. Canfield1, DanaW. Longcope1, Jiong Qiu1

ApJ, 722:1539–1546, **2010, File**

We study the X17 eruptive flare on **2003 October 28** using Michelson Doppler Imager observations of photospheric magnetic and velocity fields and *TRACE* 1600Å images of the flare in a three-dimensional model of energy buildup and release in NOAA 10486. The most dramatic feature of this active region is the 123◦ rotation of a large positive sunspot over 46 hr prior to the event. We apply a method for including such rotation in the framework of the minimum current corona model of the buildup of energy and helicity due to the observed motions. We distinguish between helicity and energy stored in the whole active region and that released in the flare itself. We find that while the rotation of a sunspot contributes significantly to the energy and helicity budgets of the whole active region, it makes only a minor contribution to that part of the region that flares. We conclude that in spite of the fast rotation, shearing motions alone store sufficient energy and helicity to account for the flare energetics and interplanetary coronal mass ejection helicity content within their observational uncertainties. Our analysis demonstrates that the relative importance of shearing and rotation in this flare depends critically on their location within the parent active region topology.

SUNSPOT ROTATION, FLARE ENERGETICS, AND FLUX ROPE HELICITY: THE ERUPTIVE FLARE ON 2005 MAY 13

Maria D. **Kazachenko**1, Richard C. Canfield1, Dana W. Longcope1, Jiong Qiu1, Angela DesJardins1, and Richard W. Nightingale2

Astrophysical Journal, 704:1146–1158, **2009** October

We use the Michelson Doppler Imager and *TRACE* observations of photospheric magnetic and velocity fields in NOAA 10759 to build a three-dimensional coronal magnetic field model. The most dramatic feature of this active region is the 34◦ rotation of its leading polarity sunspot over 40 hr. We describe a method for including such rotation in the framework of the Minimum Current Corona model. We apply this method to the buildup of energy and helicity associated with the eruptive flare of 2005 May 13. We find that including the sunspot rotation almost triples the modeled flare energy (1.0 Ч 1031 erg) and flux rope self-helicity (−7.1 Ч 1042 Mx2). This makes the results consistent with observations: the energy derived from *GOES* is 1.0 Ч 1031 erg, the magnetic cloud helicity from *WIND* is −5Ч1042 Mx2. Our combined analysis yields the first quantitative picture of the helicity and energy content processed through a flare in an active region with an obviously rotating sunspot and shows that rotation dominates the energy and helicity budget of this event.

X-ray line coincidence photopumping in a solar flare

F. P. **Keenan**, K. Poppenhaeger, M. Mathioudakis, S. J. Rose, J. Flowerdew, D. Hynes, D. J. Christian, J. Nilsen, W. R. Johnson

MNRAS **2017**

https://arxiv.org/pdf/1711.07761.pdf
Line coincidence photopumping is a process where the electrons of an atomic or molecular species are radiatively excited through the absorption of line emission from another species at a coincident wavelength. There are many instances of line coincidence photopumping in astrophysical sources at optical and ultraviolet wavelengths, with the most famous example being Bowen fluorescence (pumping of O III 303.80 A by He II), but none to our knowledge in X-rays. However, here we report on a scheme where a He-like line of Ne IX at 11.000 A is photopumped by He-like Na X at 11.003 A, which predicts significant intensity enhancement in the Ne IX 82.76 A transition under physical conditions found in solar flare plasmas. A comparison of our theoretical models with published X-ray observations of a solar flare obtained during a rocket flight provides evidence for line enhancement, with the measured degree of enhancement being consistent with that expected from theory, a truly surprising result. Observations of this enhancement during flares on stars other than the Sun would provide a powerful new diagnostic tool for determining the sizes of flare loops in these distant, spatially-unresolved, astronomical sources.

An assessment of Fe XX - Fe XXII emission lines in SDO/EVE data as diagnostics for high density solar flare plasmas using EUVE stellar observations

F. P. **Keenan**, R. O. Milligan, M. Mathioudakis, D. J. Christian
MNRAS **2017**
https://arxiv.org/pdf/1702.08714.pdf
The Extreme Ultraviolet Variability Experiment (EVE) on the Solar Dynamics Observatory obtains extreme-ultraviolet (EUV) spectra of the full-disk Sun at a spectral resolution of ~1 A and cadence of 10 s. Such a spectral resolution would normally be considered to be too low for the reliable determination of electron density (N_e) sensitive emission line intensity ratios, due to blending. However, previous work has shown that a limited number of Fe XXI features in the 90-60 A wavelength region of EVE do provide useful N_e-diagnostics at relatively low flare densities (N_e ~ 10^11-10^12 cm^-3). Here we investigate if additional highly ionised Fe line ratios in the EVE 90-160 A range may be reliably employed as N_e-diagnostics. In particular, the potential for such diagnostics to provide density estimates for high N_e (~10^13 cm^-3) flare plasmas is assessed. Our study employs EVE spectra for X-class flares, combined with observations of highly active late-type stars from the Extreme Ultraviolet Explorer (EUVE) satellite plus experimental data for well-diagnosed tokamak plasmas, both of which are similar in wavelength coverage and spectral resolution to those from EVE. Several ratios are identified in EVE data which yield consistent values of electron density, including Fe XX 113.35/121.85 and Fe XXII 114.41/135.79, with confidence in their reliability as N_e-diagnostics provided by the EUVE and tokamak results. These ratios also allow the determination of density in solar flare plasmas up to values of ~10^13 cm^-3. **2011 February 15**

Soft X-ray emission lines of Fe XV in solar flare observations and the Chandra spectrum of Capella

F. P. **Keenan**, J. J. Drake, S. Chung, N. S. Brickhouse, K. M. Aggarwal, A. Z. Msezane, R. S. I. Ryans, D. S. Bloomfield
ApJ **2006**
http://arxiv.org/pdf/astro-ph/0601591v1.pdf
Recent calculations of atomic data for Fe XV have been used to generate theoretical line ratios involving n = 3-4 transitions in the soft X-ray spectral region (52-83 A), for a wide range of electron temperatures and densities applicable to solar and stellar coronal plasmas. A comparison of these with solar flare observations from a rocket-borne spectrograph (XSST) reveals generally good agreement between theory and experiment. In particular, the 82.76 A emission line in the XSST spectrum is identified, for the first time to our knowledge in an astrophysical source. Most of the Fe XV transitions which are blended have had the species responsible clearly identified, although there remain a few instances where this has not been possible. The line ratio calculations are also compared with a co-added spectrum of Capella obtained with the Chandra satellite, which is probably the highest signal-to-noise observation achieved for a stellar source in the 25-175 A soft X-ray region. Good agreement is found between theory and experiment, indicating that the Fe XV lines are reliably detected in Chandra spectra, and hence may be employed as diagnostics to determine the temperature and/or density of the emitting plasma. However the line blending in the Chandra data is such that individual emission lines are difficult to measure accurately, and fluxes may only be reliably determined via detailed profile fitting of the observations. The co-added Capella spectrum is made available to hopefully encourage further exploration of the soft X-ray region in astronomical sources.

An investigation of Fe XV emission lines in solar flare spectra

F P **Keenan**, K M Aggarwal, D S Bloomfield, A Z Msezane, K G Widing
A&A **2005**
http://arxiv.org/pdf/astro-ph/0512571v1.pdf

Previously, large discrepancies have been found between theory and observation for Fe XV emission line ratios in solar flare spectra covering the 224-327 A wavelength range, obtained by the Naval Research Laboratory's S082A instrument on board Skylab. These discrepancies have been attributed to either errors in the adopted atomic data or the presence of additional atomic processes not included in the modelling, such as fluorescence. However our analysis of these plus other S082A flare observations (the latter containing Fe XV transitions between 321-482 A), performed using the most recent Fe XV atomic physics calculations in conjunction with a CHIANTI synthetic flare spectrum, indicate that blending of the lines is primarily responsible for the discrepancies. As a result, most Fe XV lines cannot be employed as electron density diagnostics for solar flares, at least at the spectral resolution of S082A and similar instruments (i.e. ~ 0.1 A). An exception is the intensity ratio I(321.8 A)/I(327.0 A), which appears to provide good estimates of the electron density at this spectral resolution.

Radiative hydrodynamic modelling and observations of the X-class solar flare on 2011 March 9

Michael B. **Kennedy**, Ryan O. Milligan, Joel C. Allred, Mihalis Mathioudakis, Francis P. Keenan
A&A 578, A72 **2015**
http://arxiv.org/pdf/1504.07541v1.pdf
We investigated the response of the solar atmosphere to non-thermal electron beam heating using the radiative transfer and hydrodynamics modelling code RADYN. The temporal evolution of the parameters that describe the non-thermal electron energy distribution were derived from hard X-ray observations of a particular flare, and we compared the modelled and observed parameters. The evolution of the non-thermal electron beam parameters during the X1.5 solar flare on **2011 March 9** were obtained from analysis of RHESSI X-ray spectra. The RADYN flare model was allowed to evolve for 110 seconds, after which the electron beam heating was ended, and was then allowed to continue evolving for a further 300s. The modelled flare parameters were compared to the observed parameters determined from extreme-ultraviolet spectroscopy. The model produced a hotter and denser flare loop than that observed and also cooled more rapidly, suggesting that additional energy input in the decay phase of the flare is required. In the explosive evaporation phase a region of high-density cool material propagated upward through the corona. This material underwent a rapid increase in temperature as it was unable to radiate away all of the energy deposited across it by the non-thermal electron beam and via thermal conduction. A narrow and high-density ($n_e \leq 10^{15}$ cm^{-3}) region at the base of the flare transition region was the source of optical line emission in the model atmosphere. The collision-stopping depth of electrons was calculated throughout the evolution of the flare, and it was found that the compression of the lower atmosphere may permit electrons to penetrate farther into a flaring atmosphere compared to a quiet Sun atmosphere.

Solar Flare Impulsive Phase Emission Observed with SDO/EVE

Michael B. **Kennedy**1, Ryan O. Milligan1,2,3, Mihalis Mathioudakis1, and Francis P. Keenan
2013 ApJ 779 84
http://arxiv.org/abs/1310.4649
Differential emission measures (DEMs) during the impulsive phase of solar flares were constructed using observations from the EUV Variability Experiment (EVE) and the Markov-Chain Monte Carlo method. Emission lines from ions formed over the temperature range log Te = 5.8-7.2 allow the evolution of the DEM to be studied over a wide temperature range at 10 s cadence. The technique was applied to several M- and X-class flares, where impulsive phase EUV emission is observable in the disk-integrated EVE spectra from emission lines formed up to 3-4 MK and we use spatially unresolved EVE observations to infer the thermal structure of the emitting region. For the nine events studied, the DEMs exhibited a two-component distribution during the impulsive phase, a low-temperature component with peak temperature of 1-2 MK, and a broad high-temperature component from 7 to 30 MK. A bimodal high-temperature component is also found for several events, with peaks at 8 and 25 MK during the impulsive phase. The origin of the emission was verified using Atmospheric Imaging Assembly images to be the flare ribbons and footpoints, indicating that the constructed DEMs represent the spatially average thermal structure of the chromospheric flare emission during the impulsive phase. **03-Aug-11, 16-Feb-11, 09-Mar-11, 25-Mar-11, 30-Jul-11, 04-Aug-11, 06-Sep-11, 07-Sep-11, 24-Sep-11, 28-Sep-11, 03-Nov-11, 06-Jul-12, 23-Oct-12**

Investigations of Flaring Plasma Parameters during an M-class Flare Using the Differential Evolution Method and XSM/Chandrayaan-2 Observations

Anna **Kępa**1, Marek Siarkowski1, Arun Kumar Awasthi1, Janusz Sylwester1, and Barbara Sylwester1
2023 ApJL 959 L29

https://iopscience.iop.org/article/10.3847/2041-8213/ad0f23/pdf
We employ the differential evolution (DE) method to analyze observations from the Solar X-Ray Monitor on board the Chandrayaan-2 spacecraft. DE belongs to the family of evolutionary algorithms that find solutions using mechanisms inspired by biological processes. This approach enables us to simultaneously calculate the distribution of the differential emission measure and elemental abundances through an iterative process. We establish a model for the emission sources of flaring plasma, incorporating temperature, emission measure, and abundances of eight elements: Mg, Al, Si, S, Ar, Ca, Fe, and Ni, for an M3.9 GOES-class solar flare that occurred on **2021 May 7** (SOL2021-05-07T19:04). Our analysis covers various phases of the flare, determining the evolution of temperature, emission measure, and elemental abundances. Additionally, utilizing data from the Spectrometer Telescope for Imaging X-rays on board the Solar Orbiter, we investigate the evolution of hard X-ray source morphology, source volume, electron density, and thermal behavior of the flaring plasma throughout the event. The results reveal notable variations in elemental abundances between photospheric and coronal values during different flare phases. This emphasizes the significance of elemental abundance information in comprehending X-ray emissions during solar flares.

On the Application of Differential Evolution to the Analysis of X-Ray Spectra

Anna **Kepa**, Barbara Sylwester, Marek Siarkowski, Janusz Sylwester
ApJ **2022**
https://arxiv.org/pdf/2202.09302.pdf
Using methods of differential evolution (DE,) we determined the coronal elemental abundances and the differential emission measure (DEM) distributions for the plasma flaring on **2003 January 21**. The analyses have been based on RESIK X-ray spectra. DE belongs to the family of evolutionary algorithms. DE is conceptually simple and easy to be implemented, so it has been applied to solve many problems in science and engineering. In this study we apply this method in a new context: simultaneous determination of plasma composition and DEM . In order to increase the confidence in the results obtained using DE, we tested the use of its algorithms by comparing the DE synthesized spectra with respective spectra observed by RESIK. Extensive discussion of the DE method used and the obtained physical characteristics of flaring plasma is presented.

RESIK and RHESSI observations of the 20 September 2002 flare

A. **Kepa**, R. Falewicz, M. Siarkowski, M. Pietras
A&A 642, A112 **2020**
https://arxiv.org/pdf/2008.05755.pdf
https://doi.org/10.1051/0004-6361/202038434
Soft X-ray spectra 3.33 A - 6.15 A from the RESIK instrument on CORONAS-F constitute a unique database for the study of the physical conditions of solar flare plasmas, enabling the calculation of differential emission measures. The two RESIK channels for the shortest wavelengths overlap with the lower end of RHESSI spectral energy range, which is located around 3 keV, making it possible to compare both data sets. We aim to compare observations from RESIK and RHESSI spectrometers and cross-correlate these instruments. Observations are compared with synthetic spectra calculated based on the results of one-dimensional hydrodynamical (1D-HD) modelling. The analysis was performed for the flare on **20 September 2002**. We estimated the geometry of the flaring loop, necessary for 1D-HD modelling, based on images from RHESSI and SOHO/EIT. The distribution of non-thermal electrons (NTEs) was determined from RHESSI spectra. The 1D-HD model assumes that non-thermal electrons with a power-law spectrum were injected at the apex of the flaring loop. The NTEs then heat and evaporate the chromosphere, filling the loop with hot and dense plasma radiating in soft X-rays. The total energy of electrons was constrained by comparing observed and calculated fluxes from GOES 1 - 8 A data. We determined the temperature and density at every point of the flaring loop throughout the evolution of the flare, calculating the resulting X-ray spectra. The synthetic spectra calculated based on the results of hydrodynamic modelling for the 20 September 2002 flare are consistent within a factor of two with the observed RESIK spectra during most of the duration of the flare. This discrepancy factor is probably related to the uncertainty on the cross-calibration between RESIK and RHESSI instruments.

A Multiwavelength Analysis of the Long-duration Flare Observed on 15 April 2002

A. **Kepa**, B. Sylwester, J. Sylwester, T. Mrozek, M. Siarkowski
Solar Phys. 295:22 **2020**
https://arxiv.org/pdf/1912.07984.pdf
https://doi.org/10.1007/s11207-020-1581-9
We present a multiwavelength analysis of the long duration flare observed on 15 April 2002 (soft X-ray peak time at 03:55 UT, **SOL2002-04-15T03**:55). This flare occurred on the disk (S15W01) in NOAA 9906 and was observed by a number of space instruments including the Extreme-Ultraviolet Imaging Telescope on the Solar and Heliospheric Observatory (SOHO/EIT), the RESIK spectrometer onboard the Coronas-F spacecraft, and the Ramaty High Energy Solar Spectroscopic Imager (RHESSI). We have performed a complex analysis of these measurements and studied the morphology and physical parameters characterizing the conditions in flaring plasmas. The 195 A SOHO/EIT images have been used to study evolution of flaring loops. Analysis of RHESSI data provided the opportunity for a detailed analysis of hard X-ray emission with 1 keV energy resolution. We have used Geostationary Operational Environmental

Satellite (GOES) observations for isothermal interpretation of the X-ray measurements. Temperature diagnostics of the flaring plasma have been carried out by means of a differential emission measure (DEM) analysis based on RESIK X-ray spectra.

Solar Flare Ribbon Fronts. II. Evolution of heating rates in individual flare footpoints

Graham S. **Kerr**, Vanessa Polito, Yan Xu, Joel C. Allred

ApJ **2024**

https://arxiv.org/pdf/2405.02799

Solar flare ribbon fronts appear ahead of the bright structures that normally characterise solar flares, and can persist for an extended period of time in spatially localised patches before transitioning to `regular' bright ribbons. They likely represent the initial onset of flare energy deposition into the chromosphere. Chromospheric spectra (e.g. He I 10830A and the Mg II near-UV lines) from ribbon fronts exhibit properties rather different to typical flare behaviour. In prior numerical modelling efforts we were unable to reproduce the long lifetime of ribbon fronts. Here we present a series of numerical experiments that are rather simple but which have important implications. We inject a very low flux of nonthermal electrons (F=5×108 erg s−1 cm−2) into the chromosphere for 100 s before ramping up to standard flare energy fluxes (F=1010−11 erg s−1 cm−2). Synthetic spectra not only sustained their ribbon front-like properties for significantly longer, in the case of harder nonthermal electron spectra the ribbon front behaviour persisted for the entirety of this weak-heating phase. Lengthening or shortening the duration of the weak-heating phase commensurately lengthened or shortened the ribbon front lifetimes. Ribbon fronts transitioned to regular bright ribbons when the upper chromosphere became sufficiently hot and dense, which happened faster for softer nonthermal electron spectra. Thus, the lifetime of flare ribbon fronts are a direct measure of the duration over which a relatively low flux of high energy electrons precipitates to the chromosphere prior to the bombardment of a much larger energy flux.

An Optically Thin View of the Flaring Chromosphere: Nonthermal widths in a chromospheric condensation during an X-class solar flare

Graham S. **Kerr**, Adam F. Kowalski, Joel C. Allred, Adrian N. Daw, Melissa R. Kane

MNRAS Volume 527, Issue 2, January **2024**, Pages 2523–2548

https://arxiv.org/pdf/2310.07111.pdf

https://doi.org/10.1093/mnras/stad3135

https://academic.oup.com/mnras/article-pdf/527/2/2523/53735634/stad3135.pdf

The bulk of solar flare energy is deposited in the chromosphere. Flare ribbons and footpoints in the chromosphere therefore offer great diagnostic potential of flare energy release and transport processes. High quality observations from the IRIS spacecraft have transformed our view of the Sun's atmospheric response to flares. Since most of the chromospheric lines observed by IRIS are optically thick, forward modelling is required to fully appreciate and extract the information they carry. Reproducing certain aspects of the Mg II lines remain frustratingly out of reach in state-of-the-art flare models, which are unable to satisfactorily reproduce the very broad line profiles. A commonly proposed resolution to this is to assert that very large values of `microturbulence' is present. We asses the validity of that approach by analysing optically thin lines in the flare chromosphere from the X-class flare SOL**2014-10-25**T17:08:00, using the derived value of nonthermal width as a constraint to our numerical models. A nonthermal width of the order 10~km~s−1 was found within the short-lived red wing components of three spectral lines, with relatively narrow stationary components. Simulations of this flare were produced, and in the post-processing spectral synthesis we include within the downflows a microturbulence of 10~km~s−1. While we can reproduce the O I 1355.598~Å line rather well, and we can capture the general shape and properties of the Mg II line widths, the synthetic lines are still too narrow.

IRIS Nugget Nov 2023 https://iris.lmsal.com/nugget

Prospects of Detecting Non-thermal Protons in Solar Flares via Lyman Line Spectroscopy: Revisiting the Orrall-Zirker Effect

Graham S. **Kerr**, Joel C. Allred, Adam F. Kowalski, Ryan O. Milligan, Hugh S. Hudson, Natalia Zambrana Prado, Therese A. Kucera, Jeffrey W. Brosius

ApJ **2023**

https://arxiv.org/pdf/2302.02017.pdf

Solar flares are efficient particle accelerators, with a substantial fraction of the energy released manifesting as non-thermal particles. While the role that non-thermal electrons play in transporting flare energy is well studied, the properties and importance of non-thermal protons is rather less well understood. This is in large part due to the paucity of diagnostics, particularly at the lower-energy (deka-keV) range of non-thermal proton distributions in flares. One means to identify the presence of deka-keV protons is by an effect originally described by \cite{1976ApJ...208..618O}. In the Orrall-Zirker effect, non-thermal protons interact with ambient neutral hydrogen, and via charge exchange produce a population of energetic neutral atoms (ENAs) in the chromosphere. These ENAs subsequently produce an extremely redshifted photon in the red wings of hydrogen spectral lines. We revisit predictions of the strength of this

effect using modern interaction cross-sections, and numerical models capable of self-consistently simulating the flaring non-equilibrium ionization stratification, and the non-thermal proton distribution (and, crucially, their feedback on each other). We synthesize both the thermal and non-thermal emission from \lya\ and \lyb, the most promising lines that may exhibit a detectable signal. These new predictions are are weaker and more transient than prior estimates, but the effects should be detectable in fortuitous circumstances. We degrade the \lyb\ emission to the resolution of the Spectral Imaging of the Coronal Environment (SPICE) instrument on board Solar Orbiter, demonstrating that though likely difficult, it should be possible to detect the presence of non-thermal protons in flares observed by SPICE.

Interrogating Solar Flare Loop Models with IRIS Observations 2: Plasma Properties, Energy Transport, and Future Directions **Review**

Graham S. **Kerr**

Frontiers in Astronomy and Space Sciences **2022**

https://arxiv.org/pdf/2212.06261.pdf

During solar flares a tremendous amount of magnetic energy is released and transported through the Sun's atmosphere and out into the heliosphere. Despite over a century of study, many unresolved questions surrounding solar flares are still present. Among those are how does the solar plasma respond to flare energy deposition, and what are the important physical processes that transport that energy from the release site in the corona through the transition region and chromosphere? Attacking these questions requires the concert of advanced numerical simulations and high spatial-, temporal-, and spectral- resolution observations. While flares are 3D phenomenon, simulating the NLTE flaring chromosphere in 3D and performing parameter studies of 3D models is largely outwith our current computational capabilities. We instead rely on state-of-the-art 1D field-aligned simulations to study the physical processes that govern flares. Over the last decade, data from the Interface Region Imaging Spectrograph (IRIS) have provided the crucial observations with which we can critically interrogate the predictions of those flare loop models. Here in Paper 2 of a two-part review of IRIS and flare loop models, I discuss how forward modelling flares can help us understand the observations from IRIS, and how IRIS can reveal where our models do well and where we are likely missing important processes, focussing in particular on the plasma properties, energy transport mechanisms, and future directions of flare modelling. **2014-Oct-25**

Interrogating Solar Flare Loop Models with IRIS Observations 1: Overview of the Models, and Mass flows **Review**

Graham S. **Kerr**

Frontiers in Astronomy and Space Sciences **2022**

https://arxiv.org/pdf/2212.06647.pdf

Solar flares are transient yet dramatic events in the atmosphere of the Sun, during which a vast amount of magnetic energy is liberated. This energy is subsequently transported through the solar atmosphere or into the heliosphere, and together with coronal mass ejections flares comprise a fundamental component of space weather. Thus, understanding the physical processes at play in flares is vital. That understanding often requires the use of forward modelling in order to predict the hydrodynamic and radiative response of the solar atmosphere. Those predictions must then be critiqued by observations to show us where our models are missing ingredients. While flares are of course 3D phenomenon, simulating the flaring atmosphere including an accurate chromosphere with the required spatial scales in 3D is largely beyond current computational capabilities, and certainly performing parameter studies of energy transport mechanisms is not yet tractable in 3D. Therefore, field-aligned 1D loop models that can resolve the relevant scales have a crucial role to play in advancing our knowledge of flares. In recent years, driven in part by the spectacular observations from the Interface Region Imaging Spectrograph (IRIS), flare loop models have revealed many interesting features of flares. For this review I highlight some important results that illustrate the utility of attacking the problem of solar flares with a combination of high quality observations, and state-of-the-art flare loop models, demonstrating: (1) how models help to interpret flare observations from IRIS, (2) how those observations show us where we are missing physics from our models, and (3) how the ever increasing quality of solar observations drives model improvements. Here in Paper 1 of this two part review I provide an overview of modern flare loop models, and of electron-beam driven mass flows during solar flares. **2014-September-10 , 2015-March-12**

He I 10830Å Dimming During Solar Flares, I: The Crucial Role of Non-Thermal Collisional Ionisations

Graham S. **Kerr**, Yan Xu, Joel C. Allred, Vanessa Polito, Viacheslav M. Sadykov, Nengyi Huang, Haimin Wang

ApJ **2021**

https://arxiv.org/pdf/2103.16686.pdf

While solar flares are predominantly characterised by an intense broadband enhancement to the solar radiative output, certain spectral lines and continua will, in theory, exhibit flare-induced dimmings. Observations of transitions of orthohelium He I λλ10830Å and the He I D3 lines have shown evidence of such dimming, usually followed by enhanced emission. It has been suggested that non-thermal collisional ionisation of helium by an electron beam,

followed by recombinations to orthohelium, is responsible for overpopulating the those levels, leading to stronger absorption. However it has not been possible observationally to preclude the possibility of overpopulating orthohelium via enhanced photoionisation of He I by EUV irradiance from the flaring corona followed by recombinations. Here we present radiation hydrodynamics simulations of non-thermal electron beam-driven flares where (1) both non-thermal collisional ionisation of Helium and coronal irradiance are included, and (2) only coronal irradiance is included. A grid of simulations covering a range of total energies deposited by the electron beam, and a range of non-thermal electron beam low-energy cutoff values, were simulated. In order to obtain flare-induced dimming of the He I 10830Å line it was necessary for non-thermal collisional ionisations to be present. The effect was more prominent in flares with larger low-energy cutoff values and longer lived in weaker flares and flares with a more gradual energy deposition timescale. These results demonstrate the usefulness of orthohelium line emission as a diagnostic of flare energy transport. **2013 Aug. 17**
RHESSI Nuggets #406 April **2021**
https://sprg.ssl.berkeley.edu/~tohban/wiki/index.php/Negative_He_10830_Flare_Ribbons_and_Non-thermal_Electrons

Solar Flare Energy Partitioning and Transport -- the Gradual Phase (a Heliophysics 2050 White Paper) miniReview

Graham S. **Kerr**, Meriem Alaoui, Joel C. Allred, Nicholas H. Bian, Brian R. Dennis, A. Gordon Emslie, Lyndsay Fletcher, Silvina Guidoni, Laura A. Hayes, Gordon D. Holman, Hugh S. Hudson, Judith T. Karpen, Adam F. Kowalski, Ryan O. Milligan, Vanessa Polito, Jiong Qiu, Daniel F. Ryan
Heliophysics 2050 Workshop **2020**
https://arxiv.org/pdf/2009.08407.pdf
Solar flares are a fundamental component of solar eruptive events (SEEs; along with solar energetic particles, SEPs, and coronal mass ejections, CMEs). Flares are the first component of the SEE to impact our atmosphere, which can set the stage for the arrival of the associated SEPs and CME. Magnetic reconnection drives SEEs by restructuring the solar coronal magnetic field, liberating a tremendous amount of energy which is partitioned into various physical manifestations: particle acceleration, mass and magnetic-field eruption, atmospheric heating, and the subsequent emission of radiation as solar flares. To explain and ultimately predict these geoeffective events, the heliophysics community requires a comprehensive understanding of the processes that transform and distribute stored magnetic energy into other forms, including the broadband radiative enhancement that characterises flares. This white paper, submitted to the Heliophysics 2050 Workshop, discusses the flare gradual phase part of SEEs, setting out the questions that need addressing via a combination of theoretical, modelling, and observational research. In short, the flare gradual phase persists much longer than predicted so, by 2050, we must identify the characteristics of the significant energy deposition sustaining the gradual phase, and address the fundamental processes of turbulence and non-local heat flux.

Solar Flare Energy Partitioning and Transport -- the Impulsive Phase (a Heliophysics 2050 White Paper) miniReview

Graham S. **Kerr**, Meriem Alaoui, Joel C. Allred, Nicholas H. Bian, Brian R. Dennis, A. Gordon Emslie, Lyndsay Fletcher, Silvina Guidoni, Laura A. Hayes, Gordon D. Holman, Hugh S. Hudson, Judith T. Karpen, Adam F. Kowalski, Ryan O. Milligan, Vanessa Polito, Jiong Qiu, Daniel F. Ryan
Heliophysics 2050 Workshop **2020**
https://arxiv.org/pdf/2009.08400.pdf
Solar flares are a fundamental component of solar eruptive events (SEEs; along with solar energetic particles, SEPs, and coronal mass ejections, CMEs). Flares are the first component of the SEE to impact our atmosphere, which can set the stage for the arrival of the associated SEPs and CME. Magnetic reconnection drives SEEs by restructuring the solar coronal magnetic field, liberating a tremendous amount of energy which is partitioned into various physical manifestations: particle acceleration, mass and magnetic-field eruption, atmospheric heating, and the subsequent emission of radiation as solar flares. To explain and ultimately predict these geoeffective events, the heliophysics community requires a comprehensive understanding of the processes that transform and distribute stored magnetic energy into other forms, including the broadband radiative enhancement that characterises flares. This white paper, submitted to the Heliophysics 2050 Workshop, discusses the flare impulsive phase part of SEEs, setting out the questions that need addressing via a combination of theoretical, modelling, and observational research. In short, by 2050 we must determine the mechanisms of particle acceleration and propagation, and must push beyond the paradigm of energy transport via nonthermal electron beams, to also account for accelerated protons & ions and downward directed Alfven waves.

Solar Flare Arcade Modelling: Bridging the gap from 1D to 3D Simulations of Optically Thin Radiation

Graham S. **Kerr**, Joel C. Allred, Vanessa Polito
ApJ **900** 18 **2020**
https://arxiv.org/pdf/2007.13856.pdf

https://doi.org/10.3847/1538-4357/abaa46
Solar flares are 3D phenomenon but modelling a flare in 3D, including many of the important processes in the chromosphere, is a computational challenge. Accurately modelling the chromosphere is important, even if the transition region and corona are the areas of interest, due to the flow of energy, mass, and radiation through the interconnected layers. We present a solar flare arcade model, that aims to bridge the gap between 1D and 3D modelling. Our approach is limited to the synthesis of optically thin emission. Using observed active region loop structures in a 3D domain we graft simulated 1D flare atmospheres onto each loop, synthesise the emission and then project that emission onto to the 2D observational plane. Emission from SDO/AIA, GOES/XRS, and IRIS/SG Fe XXI 1354.1A was forward modelled. We analyse the temperatures, durations, mass flows, and line widths associated with the flare, finding qualitative agreement but certain quantitative differences. Compared to observations, the Doppler shifts are of similar magnitude but decay too quickly. They are not as ordered, containing a larger amount of scatter compared to observations. The duration of gradual phase emission from GOES and AIA emission is also too short. Fe XXI lines are broadened, but not sufficiently. These findings suggest that additional physics is required in our model. The arcade model that we show here as a proof-of-concept can be extended to investigate other lines and global aspects of solar flares, providing a means to better test the coronal response to models of flare energy injection. **23rd April 2013, 2014-September-10**

Modelling Mg II During Solar Flares. II. Non-equilibrium Effects

Graham S. **Kerr**, Mats Carlsson, Joel C.Allred
ApJ **885** 119 **2019**
https://arxiv.org/pdf/1909.13300.pdf
sci-hub.se/10.3847/1538-4357/ab48ea
To extract the information that the Mg II NUV spectra (observed by the Interface Region Imaging Spectrograph; IRIS), carries about the chromosphere during solar flares, and to validate models of energy transport via model-data comparison, forward modelling is required. The assumption of statistical equilibrium is typically used to obtain the atomic level populations from snapshots of flare atmospheres, due to computational necessity. However it is possible that relying on statistical equilibrium could lead to spurious results. We compare solving the atomic level populations via statistical equilibrium versus a non-equilibrium time-dependent approach. This was achieved using flare simulations from RADYN alongside the minority species version, MS_RADYN, from which the time-dependent Mg II atomic level populations and radiation transfer were computed in complete frequency redistribution. The impacts on the emergent profiles, lightcurves, line ratios, and formation heights are discussed. In summary we note that non-equilibrium effects during flares are typically important only in the initial stages and for a short period following the cessation of the energy injection. An analysis of the timescales of ionisation equilibrium reveals that for most of the duration of the flare, when the temperatures and densities are sufficiently enhanced, the relaxation timescales are short ($\tau_{relax}<0.1$ s), so that the equilibrium solution is an adequate approximation. These effects vary with the size of the flare, however. In weaker flares effects can be more pronounced. We recommend that non-equilibrium effects be considered when possible, but that statistical equilibrium is sufficient at most stages of the flare.

Modelling Mg II During Solar Flares. I: Partial Frequency Redistribution, Opacity, and Coronal Irradiation

G. S. **Kerr**, Joel C. Allred, Mats Carlsson
ApJ **883** 57 **2019**
https://arxiv.org/pdf/1908.05329.pdf
sci-hub.se/10.3847/1538-4357/ab3c24
The Interface Region Imaging Spectrograph (IRIS) has routinely observed the flaring Mg II NUV spectrum, offering excellent diagnostic potential and a window into the location of energy deposition. A number of studies have forward modelled both the general properties of these lines and specific flare observations. Generally these have forward modelled radiation via post-processing of snapshots from hydrodynamic flare simulations through radiation transfer codes. There has, however, not been a study of how the physics included in these radiation transport codes affects the solution. A baseline setup for forward modelling MgII in flares is presented and contrasted with approaches that add or remove complexity. It is shown for Mg II: (1) PRD is still required during flare simulations despite the increased densities, (2) using full angle-dependent PRD affects the solution but takes significantly longer to process a snapshot, (3) including Mg I in NLTE results in negligible differences to the Mg II lines but does affect the NUV quasi-continuum, (4) only hydrogen and Mg II need to be included in NLTE, (5) ideally the non-equilibrium hydrogen populations, with non-thermal collisional rates, should be used rather than the statistical equilibrium populations, (6) an atom consisting of only the ground state, h & k upper levels, and continuum level is insufficient to model the resonance lines, and (7) irradiation from a hot, dense flaring transition region can affect the formation of Mg II. We discuss modifications to the RH code allowing straightforward inclusion of transition region and coronal irradiation in flares.

Si IV Resonance Line Emission During Solar Flares: Non-LTE, Non-equilibrium, Radiation Transfer Simulations

Graham S. **Kerr**, Mats Carlsson, Joel C. Allred, Peter R. Young, Adrian N. Daw

ApJ 871 23 **2018**
https://arxiv.org/pdf/1811.11075.pdf
sci-hub.tw/10.3847/1538-4357/aaf46e
The Interface Region Imaging Spectrograph (IRIS) routinely observes the Si IV resonance lines. When analyzing observations of these lines it has typically been assumed they form under optically thin conditions. This is likely valid for the quiescent Sun, but this assumption has also been applied to the more extreme flaring scenario. We used 36 electron beam driven radiation hydrodynamic solar flare simulations, computed using the RADYN code, to probe the validity of this assumption. Using these simulated atmospheres we solved the radiation transfer equations to obtain the non-LTE, non-equilibrium populations, line profiles, and opacities for a model Silicon atom, including charge exchange processes. This was achieved using the `minority species' version of RADYN. The inclusion of charge exchange resulted in a substantial fraction of Si IV at cooler temperatures than those predicted by ionisation equilibrium. All simulations with an injected energy flux F>5×1010 erg cm−2 s−1 resulted in optical depth effects on the Si IV emission, with differences in both intensity and line shape compared to the optically thin calculation. Weaker flares (down to F≈5×109 erg cm−2 s−1) also resulted in Si IV emission forming under optically thick conditions, depending on the other beam parameters. When opacity was significant, the atmospheres generally had column masses in excess of 5×10−6 g cm−2 over the temperature range 40 to 100 kK, and the Si IV formation temperatures were between 30 and 60 kK. We urge caution when analyzing Si IV flare observations, or when computing synthetic emission without performing a full radiation transfer calculation.

Simulations of the Mg II k and Ca II 8542 lines from an Alfvén Wave-heated flare chromosphere

Graham S. **Kerr**, Lyndsay Fletcher, Alexander J.B. Russell, Joel C. Allred
2016 *ApJ* **827** 101
We use radiation hydrodynamic simulations to examine two models of solar flare chromospheric heating: Alfv\'en wave dissipation and electron beam collisional losses. Both mechanisms are capable of strong chromospheric heating, and we show that the distinctive atmospheric evolution in the mid-to-upper chromosphere results in Mg II k-line emission that should be observably different between wave-heated and beam-heated simulations. We also present Ca II 8542A profiles which are formed slightly deeper in the chromosphere. The Mg II k-line profiles from our wave-heated simulation are quite different from those from a beam-heated model and are more consistent with IRIS observations. The predicted differences between the Ca II 8542A in the two models are small. We conclude that careful observational and theoretical study of lines formed in the mid-to-upper chromosphere holds genuine promise for distinguishing between competing models for chromospheric heating in flares.

IRIS Observations of the Mg II h & k Lines During a Solar Flare

Graham S. **Kerr**, Paulo J.A. Simões, Jiong Qiu, Lyndsay Fletcher
A&A 582, A50 **2015**
http://arxiv.org/pdf/1508.03813v1.pdf
The bulk of the radiative output of a solar flare is emitted from the chromosphere, which produces enhancements in the optical and UV continuum, and in many lines, both optically thick and thin. We have, until very recently, lacked observations of two of the strongest of these lines: the Mg II h & k resonance lines. We present a detailed study of the response of these lines to a solar flare. The spatial and temporal behaviour of the integrated intensities, k/h line ratios, line of sight velocities, line widths and line asymmetries were investigated during an M class flare (SOL**2014-02-13**T01:40). Very intense, spatially localised energy input at the outer edge of the ribbon is observed, resulting in redshifts equivalent to velocities of ~15-26km/s, line broadenings, and a blue asymmetry in the most intense sources. The characteristic central reversal feature that is ubiquitous in quiet Sun observations is absent in flaring profiles, indicating that the source function increases with height during the flare. Despite the absence of the central reversal feature, the k/h line ratio indicates that the lines remain optically thick during the flare. Subordinate lines in the Mg II passband are observed to be in emission in flaring sources, brightening and cooling with similar timescales to the resonance lines. This work represents a first analysis of potential diagnostic information of the flaring atmosphere using these lines, and provides observations to which synthetic spectra from advanced radiative transfer codes can be compared.

Physical Properties of White-Light Sources in the 2011 Feb 15 Solar Flare

Kerr, G.S & Fletcher, L.
E-print, Jan **2014**; **2014** ApJ 783 98
White light flares (WLFs) are observational rarities, making them understudied events. However, optical emission is a significant contribution to flare energy budgets and the emission mechanisms responsible could have important implications for flare models. Using Hinode SOT optical continuum data taken in broadband red, green and blue filters,

we investigate white-light emission from the X2.2 flare SOL2011-02-15T01:56:00. We develop a technique to robustly identify enhanced flare pixels and, using a knowledge of the RGB filter transmissions, determined the source color temperature and effective temperature. We investigated two idealized models of WL emission - an optically thick photospheric source, and an optically thin chromospheric slab. Under the optically thick assumption, the color temperature and effective temperature of flare sources in sunspot umbra and penumbra were determined as a function of time and position. Values in the range of 5000-6000K were found, corresponding to a blackbody temperature increase of a few hundred kelvin. The power emitted in the optical was estimated at ~10^26 ergs/s. In some of the white-light sources the color and blackbody temperatures are the same within uncertainties, consistent with a blackbody emitter. In other regions this is not the case, suggesting that some other continuum emission process is contributing. An optically thin slab model producing hydrogen recombination radiation is also discussed as a potential source of WL emission; it requires temperatures in the range 5,500 - 25,000K, and total energies of ~10^27 ergs/s.

Chromospheric velocities of a C-class flare⋆

P. H. **Keys**, D. B. Jess, M. Mathioudakis and F. P. Keenan
A&A 529, A127 (**2011**)
Aims. We use high spatial and temporal resolution observations from the Swedish Solar Telescope to study the chromospheric velocities of a C-class flare originating from active region NOAA 10969.
Methods. A time-distance analysis is employed to estimate directional velocity components in Hα and Ca ii K image sequences. Also, imaging spectroscopy has allowed us to determine flare-induced line-of-sight velocities. A wavelet analysis is used to analyse the periodic nature of associated flare bursts.
Results. Time-distance analysis reveals velocities as high as 64 km s-1 along the flare ribbon and 15 km s-1 perpendicular to it. The velocities are very similar in both the Hα and Ca ii K time series. Line-of-sight Hα velocities are red-shifted with values up to 17 km s-1. The high spatial and temporal resolution of the observations have allowed us to detect velocities significantly higher than those found in earlier studies. Flare bursts with a periodicity of ≈60 s are also detected. These bursts are similar to the quasi-periodic oscillations observed at hard X-ray and radio wavelength data.
Conclusions. Some of the highest velocities detected in the solar atmosphere are presented. Line-of-sight velocity maps show considerable mixing of both the magnitude and direction of velocities along the flare path. A change in direction of the velocities at the flare kernel has also been detected which may be a signature of chromospheric evaporation.
2007 August 24,

The relative timing of supra-arcade downflows in solar flares

J. I. **Khan**, H. M. Bain, and L. Fletcher
A&A 475, 333-340 (2007)
http://www.aanda.org/index.php?option=com_article&access=linkmanager&edpsname=aa&lang=en&volume=475&page=333
Supra-arcade downflows are generally dark, sunward-propagating features located above the bright arcade of loops in some solar flares.
Conclusions. Since the majority of supra-arcade downflows occur during the rise phase of the soft X-ray flare and the time of hard X-ray bursts, and have prior eruptive signatures this suggests that they are related to the main flare energy release process. Furthermore, the suggested association of supra-arcade downflows with recently reconnected magnetic field lines means they may indeed be considered as evidence for a magnetic reconnection process. The single supra-arcade downflow event which unambiguously started during the decay phase of the flare occurred during hard X-ray bursts and thus appears to be related to late energy release.

A Transient Coronal Sigmoid in Active Region NOAA 11909: Build-up Phase, M-class Eruptive Flare, and Associated Fast Coronal Mass Ejection

Hema **Kharayat**, Bhuwan Joshi, Prabir K. Mitra, P. K. Manoharan & Christian Monstein
Solar Physics volume 296, Article number: 99 (**2021**)
https://link.springer.com/content/pdf/10.1007/s11207-021-01830-4.pdf
https://doi.org/10.1007/s11207-021-01830-4
In this article, we investigate the formation and disruption of a coronal sigmoid from the active region (AR) NOAA 11909 on **07 December 2013**, by analyzing multi-wavelength and multi-instrument observations. Our analysis suggests that the formation of the sigmoid initiated ≈ 1 hour before its eruption through a coupling between two twisted coronal loop systems. This sigmoid can be well regarded as of 'transient' class due to its short lifetime as the eruptive activities started just after ≈ 20 min of its formation. A comparison between coronal and photospheric images suggests that the coronal sigmoid was formed over a simple ββ-type AR which also possessed dispersed magnetic field structure in the photosphere. The line-of-sight photospheric magnetograms also reveal small-scale flux cancellation events near the polarity inversion line, and overall flux cancellation during the extended pre-eruption phase which suggest the role of

tether-cutting reconnection toward the build-up of the flux rope. The disruption of the sigmoid proceeded with a two-ribbon eruptive M1.2 flare (SOL2013-12-07T07:29). In radio frequencies, we observe type III and type II bursts in meter wavelengths during the impulsive phase of the flare. The successful eruption of the flux rope leads to a fast coronal mass ejection (with a linear speed of ≈ 1085 km s−1) in SOHO/LASCO field-of-view. During the evolution of the flare, we clearly observe typical “sigmoid-to-arcade” transformation. Prior to the onset of the impulsive phase of the flare, flux rope undergoes a slow rise (≈ 15 km s−1) which subsequently transitions into a fast eruption (≈ 110 km s−1). The two-phase evolution of the flux rope shows temporal associations with the soft X-ray precursor and impulsive phase emissions of the M-class flare, respectively, thus pointing toward a feedback relationship between magnetic reconnection and early CME dynamics.

Temporal and Periodic Variation of the MCMESI for the Last Two Solar Cycles; Comparison with the Number of Different Class X-Ray Solar Flares

A. **Kilcik**, P. Chowdhury, V. Sarp, V. Yurchyshyn, B. Donmez, J.P. Rozelot, A. Ozguc
Solar Phys. **2020**
https://arxiv.org/ftp/arxiv/papers/2008/2008.11506.pdf
In this study we compared the temporal and periodic variations of the Maximum CME Speed Index (MCMESI) and the number of different class (C, M, and X) solar X-Ray flares for the last two solar cycles (Cycle 23 and 24). To obtain the correlation between the MCMESI and solar flare numbers the cross correlation analysis was applied to monthly data sets. Also to investigate the periodic behavior of all data sets the Multi Taper Method (MTM) and the Morlet wavelet analysis method were performed with daily data from 2009 to 2018. To evaluate our wavelet analysis Cross Wavelet Transform (XWT) and Wavelet Transform Coherence (WTC) methods were performed. Causal relationships between datasets were further examined by Convergence Cross Mapping (CCM) method. In results of our analysis we found followings; 1) The C class X-Ray flare numbers increased about 16 % during the solar cycle 24 compared to cycle 23, while all other data sets decreased; the MCMESI decreased about 16 % and the number of M and X class flares decreased about 32 %. 2) All the X-Ray solar flare classes show remarkable positive correlation with the MCMESI. While the correlation between the MCMESI and C class flares comes from the general solar cycle trend, it mainly results from the fluctuations in the data in case of the X class flares. 3) In general, all class flare numbers and the MCMESI show similar periodic behavior. 4) The 546 days periodicity detected in the MCMESI may not be of solar origin or at least the solar flares are not the source of this periodicity. 5) C and M Class solar flares have a stronger causative effect on the MCMESI compared to X class solar flares. However the only bidirectional causal relationship is obtained between the MCMESI and C class flare numbers.

The evolution of flaring and non-flaring active regions

A **Kilcik** V Yurchyshyn S Sahin V Sarp V Obridko A Ozguc J P Rozelot
Monthly Notices of the Royal Astronomical Society, Volume 477, Issue 1, 11 June **2018**, Pages 293–297,
http://sci-hub.tw/10.1093/mnras/sty388
According to the modified Zurich classification, sunspot groups are classified into seven different classes (A, B, C, D, E, F and H) based on their morphology and evolution. In this classification, classes A and B, which are small groups, describe the beginning of sunspot evolution, while classes D, E and F describe the large and evolved groups. Class C describes the middle phase of sunspot evolution and the class H describes the end of sunspot evolution. Here, we compare the lifetime and temporal evolution of flaring and non-flaring active regions (ARs), and the flaring effect on ARs in these groups in detail for the last two solar cycles (1996 through 2016). Our main findings are as follows: (i) Flaring sunspot groups have longer lifetimes than non-flaring ones. (ii) Most of the class A, B and C flaring ARs rapidly evolve to higher classes, while this is not applicable for non-flaring ARs. More than 50 per cent of the flaring A, B and C groups changed morphologically, while the remaining D, E, F and H groups did not change remarkably after the flare activity. (iii) 75 per cent of all flaring sunspot groups are large and complex. (iv) There is a significant increase in the sunspot group area in classes A, B, C, D and H after flaring activity. In contrast, the sunspot group area of classes E and F decreased. The sunspot counts of classes D, E and F decreased as well, while classes A, B, C and H showed an increase.

Temporal and Periodic Variations of Sunspot Counts in Flaring and Non-flaring Active Regions

A. **Kilcik**, V. Yurchyshyn, B. Donmez, V.N. Obridko, A. Ozguc, J.P. Rozelot
Solar Phys. 293:63 **2018**
https://arxiv.org/pdf/1705.09065.pdf
https://link.springer.com/content/pdf/10.1007%2Fs11207-018-1285-6.pdf
We analyzed temporal and periodic behavior of sunspot counts (SSCs) in flaring (C, M, or X class flares), and non-flaring active regions (ARs) for the almost two solar cycles (1996 through 2016). Our main findings are as follows: i) The temporal variation of monthly means of daily total SSCs in flaring and non-flaring ARs are different and these differences are also varying from cycle to cycle; temporal profile of non-flaring ARs are wider than the flaring ones during the solar cycle 23, while they are almost the same during the current cycle 24. The second peak (second

maximum) of flaring ARs are strongly dominate during current cycle 24, while this difference is not such a remarkable during cycle 23. The amplitude of SSCs in the non-flaring ARs are comparable during the first and second peaks (maxima) of the current solar cycle, while the first peak is almost not existent in case of the flaring ARs. ii) Periodic variations observed in SSCs of flaring and non-flaring ARs are quite different in both MTM spectrum and wavelet scalograms and these variations are also different from one cycle to another; the largest detected period in the flaring ARs is 113 days, while there are much higher periodicities (327, 312, and 256 days) in non-flaring ARs. There are no meaningful periodicities in MTM spectrum of flaring ARs exceeding 45 days during solar cycle 24, while a 113 days periodicity detected from flaring ARs of solar cycle 23. For the non-flaring ARs the largest period is 72 days during solar cycle 24, while the largest period is 327 days during current cycle.

Plasma Upflows and Microwave Emission in Hot Supra-arcade Structure Associated with an M1.6 Limb Flare

S. **Kim**, K. Shibasaki, H.-M. Bain, and K.-S. Cho
2014 ApJ 785 106
We have investigated a supra-arcade structure associated with an M1.6 flare, which occurred on the south-east limb on **2010 November 4**. It is observed in EUV with the Atmospheric Imaging Assembly (AIA) on board the Solar Dynamics Observatory, microwaves at 17 and 34 GHz with the Nobeyama Radioheliograph (NoRH), and soft X-rays of 8-20 keV with RHESSI. Interestingly, we found exceptional properties of the supra-arcade thermal plasma from the AIA 131 Å and the NoRH: (1) plasma upflows along large coronal loops and (2) enhancing microwave emission. RHESSI detected two soft X-ray sources, a broad one in the middle of the supra-arcade structure and a bright one just above the flare-arcade. We estimated the number density and thermal energy for these two source regions during the decay phase of the flare. In the supra-arcade source, we found that there were increases of the thermal energy and the density at the early and last stages, respectively. On the contrary, the density and thermal energy of the source on the top of the flare-arcade decreases throughout. The observed upflows imply that there is continuous energy supply into the supra-arcade structure from below during the decay phase of the flare. It is hard to explain by the standard flare model in which the energy release site is located high in the corona. Thus, we suggest that a potential candidate of the energy source for the hot supra-arcade structure is the flare-arcade, which has exhibited a predominant emission throughout.

Systematic Microwave Source Motions along a Flare-Arcade Observed by Nobeyama Radioheliograph and AIA/SDO

S. **Kim**, S. Masuda, K. Shibasaki, and S.-C. Bong
Publ. Astron. Soc. Japan 65, 2 [7 pages] (**2013**)
http://pasj.asj.or.jp/v65/sp1/65S002/65S002.pdf
We found systematic microwave source motions along a flare-arcade using Nobeyama Radioheliograph (NoRH) 17 GHz images. The motions were associated with an X-class disk flare that occurred on **2011 February 15**. For this study, we also used EUV images from Atmospheric Imaging Assembly (AIA) and magnetograms from Helioseismic and Magnetic Imager (HMI) onboard Solar Dynamics Observatory, and multi-channel microwave data from Nobeyama Radio Polarimeters (NoRP) and Korean Solar Radio Burst Locator (KSRBL). We traced centroids of the microwave source observed by NoRH 17 GHz during the flare, and found two episodes of the motion based on several facts: (1) The microwave source moved systematically along the flare-arcade, which was observed by the AIA 94 ˚A channel, in a direction parallel to the neutral line. (2) The period of each episode was 5 min and 14 min, respectively. (3) Estimated parallel speed was 34 kms$_{-1}$ for the first episode and 22 km s$_{-1}$ for the second episode. The spectral slope of the microwave flux above 10 GHz obtained by NoRP and KSRBL was negative for both episodes, and for the last phase of the second episodes it was flat with a flux of 150 sfu. The negative spectrum and the flat with high flux indicate that the gyrosynchrotron emission from accelerated electrons was dominant during the source motions. The sequential images from the AIA 304 ˚A and 94 ˚A channels revealed that there were successive plasma eruptions, and each eruption was initiated just before the start time of the microwave sources motion. Based on the results, we suggest that the microwave source motion manifests the displacement of the particle acceleration site caused by plasma eruptions.

PREFLARE ERUPTION TRIGGERED BY A TETHER-CUTTING PROCESS

Sujin **Kim**,1, 2 Y.-J. Moon,2 Y.-H. Kim,1 Y.-D. Park,1 K.-S. Kim,2 G. S. Choe,2, 3 and K.-H. Kim1
Astrophysical Journal, 683:510Y515, **2008**
http://www.journals.uchicago.edu/toc/apj/2008/683/1
We have examined the preflare activity of an M1.2 flare that occurred in NOAA active region 8440 on **1999 January 16,**

The series of TRACE images provides the following pieces of evidence for small-scale magnetic reconnections associated with the preflare activity.
In the aspects of the overall configuration and morphological change of UV loops, the preflare activity is quite consistent with the tether-cutting model with a single-bipole magnetic explosion. We suggest that the preflare activity and the main flare in this event not only have similar physical mechanisms, but also have a causal relation.

Two-Step Reconnections in a C3.3 Flare and Its Preflare Activity Observed by Hinode XRT

S. **Kim**, Y.-J. Moon, K.-H. Kim, Y.-H. Kim, T. Sakurai, J. Chae, K.-S. Kim, and G. Choe
*Publ. Astron. Soc. Japan 59, pp.S831-S836 (***2007***)*
[Abstract], [HTML], [PDF(526kb)], [PS.gz(4321kb)]
We investigated the evolution of a C3.3 impulsive flare and its preflare activity, which occurred in NOAA Active Region 10923 on **2006 November 12**, using Hinode X-Ray Telescope (XRT) data. For an extensive investigation, we also used GOES X-ray flux, TRACE 171 ° A, and SOHO MDI data. Examining the time-series of the XRT and TRACE images, we can identify the following evolutionary sequences: (1) There were three bundles of loops along the sheared polarity inversion line forming a sigmoidal structure during the preflare phase. (2) Preflare brightening occurred between two upper-loop bundles, and they consequently formed one larger bundle. (3) The main flare occurred near the location where this new loop bundle and the third bundle met together. (4) As a result, a single stacked loop structure was formed. This morphological evolution of the X-ray loops is quite consistent with a tether-cutting model involving a single-bipole explosion. Our result shows that the preflare and the main flare in this event are a two-step reconnection process, which strongly suggests that the preflare activity plays an important role in triggering the main flare.

Modeling Hadronic Gamma-ray Emissions from Solar Flares and Prospects for Detecting Non-thermal Signatures from Protostars

Shigeo S. **Kimura**, Shinsuke Takasao, Kengo Tomida
ApJ Volume 944, Issue 2, id.192 **2023**
https://arxiv.org/pdf/2211.13891.pdf
https://iopscience.iop.org/article/10.3847/1538-4357/acb649/pdf
We investigate gamma-ray emission in the impulsive phase of solar flares and the detectability of non-thermal signatures from protostellar flares. Energetic solar flares emit high-energy gamma rays of GeV energies, but their production mechanism and emission site are still unknown. Young stellar objects, including protostars, also exhibit luminous X-ray flares, but the triggering mechanism of the flaring activity is still unclear due to the strong obscuration. Non-thermal signatures in mm/sub-mm and gamma-ray bands are useful to probe protostellar flares owing to their strong penetration power. We develop a non-thermal emission model of the impulsive phase of solar flares, where cosmic-ray protons accelerated at the termination shock produce high-energy gamma rays via hadronuclear interaction with the evaporation plasma. This model can reproduce gamma-ray data in the impulsive phase of a solar flare. We apply our model to protostellar flares and show that Cherenkov Telescope Array will be able to detect gamma rays of TeV energies if particle acceleration in protostellar flares is efficient. Non-thermal electrons accelerated together with protons can emit strong mm and sub-mm signals via synchrotron radiation, whose power is consistent with the energetic mm/sub-mm transients observed from young stars. Future gamma-ray and mm/sub-mm observations from protostars, coordinated with a hard X-ray observation, will unravel the triggering mechanism of non-thermal particle production in protostellar flares.
Хорошее описание импульсной и постепенной (ПЭ) фаз вспышки

Comparative Studies of Hard X-Ray Spectral Evolution in Solar Flares with High-Energy Proton Events Observed at Earth

Kiplinger, Alan L.
Astrophysical Journal v.453, p.973, **1995**
https://articles.adsabs.harvard.edu/pdf/1995ApJ...453..973K
This paper presents the results of two extensive studies of hard X-ray spectral evolution in solar flares and their associations with energetic interplanetary proton events. The focus of this work is to establish the degree to which events that display progressively hardening hard X-ray spectra, at any time and over all observable timescales, are associated with high-energy interplanetary proton events. The first study examined a sample of 152 hard X-ray flares well observed with the HXRBS instrument on the Solar Maximum Mission (SMM). The study showed that 22 events revealed a progressive spectral hardening either over flux peaks (i.e., a soft-hard- harder spectral evolution) or during flux decays and that 18 of these 22 events (82%) had associated 10 MeV proton events or enhancements. Conversely, the absence of spectral hardening is associated with the absence of interplanetary protons with 124 of the 130 remaining flares (95.4%). Since the hard X-ray counting rate threshold of the first study was sufficiently high (5000 counts s-1) to

exclude many flares (more than 36%) associated with the largest interplanetary proton events, a second study was conducted using 193 less intense HXRBS events (a one out of three sample) and their associations with only large proton events. This study also identifies events with progressive spectral hardening. It also employs selection criteria suggested by the results of the first study to "predict" which flares would or would not have associated large proton events. This prescription for "predicting" proton events did so correctly for four large (SESC qualified) proton events, missed none, and produced only one "false alarm" in which the criteria were met but only a small proton event was seen at earth. Thus, a correct "prediction" was made for all but one of the 193 events. The results of the first study are then combined with the weighted results of the one out of three study, using the same selection criteria, to project correctly predicted associations of 22 out of 23 SESC events, for a 96% success rate, while 700 out of 708 flares were projected to be correct rejections with no associated proton events. The data suggest that progressive hardening is a diagnostic of high-energy particle acceleration of electrons and of protons and that it is not a manifestation of the "big flare syndrome" which asserts that the largest flares are associated with many or most known phenomena. There also appears to be an approximate relationship between the timescales (FWHM) of progressively hardening X-ray peaks and the cube of the interplanetary peak proton fluxes. The strong associations of particular hard X-ray characteristics and interplanetary proton events are of interest both on physical grounds and because the techniques employed can be directly adapted into a practical means of predicting which events are most likely to be associated with large interplanetary proton events that pose threats to humans in space and to spacecraft. **7 Dec 1982, 13 May 1983, 16 Dec 1988**
Tables 1980-1989

The Relation between Magnetic Fields and X-ray Emission for Solar Microflares and Active Regions

A.S. **Kirichenko**, S.A. Bogachev
Solar Phys. 292:120 **2017**
https://arxiv.org/pdf/1707.09144.pdf
We present the result of comparison between magnetic field parameters and the intensity of X-ray emission for solar microflares with Geosynchronous Operational Environmental Satellites (GOES) classes from A0.02 to B5.1. For our study, we used the monochromatic MgXII Imaging Spectroheliometer (MISH), Full-disk EUV Telescope (FET) and Solar PHotometer in X-rays (SphinX) instruments onboard the Complex Orbital Observations Near-Earth of Activity of the Sun-Photon (CORONAS-Photon) spacecraft because of their high sensitivity in soft X-rays. The peak flare flux (PFF) for solar microflares was found to depend on the strength of the magnetic field and total unsigned magnetic flux as a power-law function. In the spectral range 2.8-36.6 \AA\ which shows very little increase related to microflares the power-law index of the relation between the X-ray flux and magnetic flux for active regions is 1.48 ± 0.86, which is close to the value obtained previously by Pevtsov et al. (Astrophys. J. 598, 1387, 2003) for different types of solar and stellar objects. In the spectral range 1-8 \AA\ the power-law indices for PFF(B) and PFF(Φ) for microflares are 3.87 ± 2.16 and 3 ± 1.6 respectively. We also make suggestions on the heating mechanisms in active regions and microflares under the assumption of loops with constant pressure and heating using the Rosner-Tucker-Vaiana (RTV) scaling laws. **21 June 2009**

Plasma Heating in Solar Microflares: Statistics and Analysis

A. S. **Kirichenko** and S. A. Bogachev
2017 ApJ 840 45
http://sci-hub.cc/10.3847/1538-4357/aa6c2b
https://arxiv.org/pdf/1706.05852.pdf
In this paper we present the results of an analysis of 481 weak solar flares, from A0.01 class flares to the B GOES class, that were observed during the period of extremely low solar activity from 2009 April to July. For all flares we measured the temperature of the plasma in the isothermal and two-temperature approximations and tried to fit its relationship with the X-ray class using exponential and power-law functions. We found that the whole temperature distribution in the range from A0.01 to X-class cannot be fit by one exponential function. The fitting for weak flares below A1.0 is significantly steeper than that for medium and large flares. The power-law approximation seems to be more reliable: the corresponding functions were found to be in good agreement with experimental data both for microflares and for normal flares. Our study predicts that evidence of plasma heating can be found in flares starting from the A0.0002 X-ray class. Weaker events presumably cannot heat the surrounding plasma. We also estimated emission measures for all flares studied and the thermal energy for 113 events.

Qualities of Sequential Chromospheric Brightenings Observed in Hα and UV Images

Michael S. **Kirk**1,2, K. S. Balasubramaniam2,3, Jason Jackiewicz2, and R. T. James McAteer
2014 ApJ 796 78
http://arxiv.org/pdf/1411.4069v1.pdf

Chromospheric flare ribbons observed in Hα appear well-organized when first examined: ribbons impulsively brighten, morphologically evolve, and exponentially decay back to pre-flare levels. Upon closer inspection of the Hα flares, there is often a significant number of compact areas brightening in concert with the flare eruption but are spatially separated from the evolving flare ribbon. One class of these brightenings is known as sequential chromospheric brightenings (SCBs). SCBs are often observed in the immediate vicinity of erupting flares and are associated with coronal mass ejections. In the past decade there have been several previous investigations of SCBs. These studies have exclusively relied upon Hα images to discover and analyze these ephemeral brightenings. This work employs the automated detection algorithm of Kirk et al. to extract the physical qualities of SCBs in observations of ground-based Hα images and complementary Atmospheric Imaging Assembly images in He II, C IV, and 1700 Å. The metadata produced in this tracking process are then culled using complementary Doppler velocities to isolate three distinguishable types of SCBs. From a statistical analysis, we find that the SCBs at the chromospheric Hα layer appear earlier and last longer than their corresponding signatures measured in AIA. From this multi-layer analysis, we infer that SCBs are spatially constrained to the mid-chromosphere. We also derive an energy budget to explain SCBs which have a postulated energy of not more than 0.01% of the total flare energy. **2010 November 6**

An Automated Algorithm to Distinguish and Characterize Solar Flares and Associated Sequential Chromospheric Brightenings

M. S. **Kirk**, K. S. Balasubramaniam, J. Jackiewicz, B. J. McNamara, R. T. J. McAteer
Solar Phys. March **2013**, Volume 283, Issue 1, pp 97-111

We present a new automated algorithm to identify, track, and characterize small-scale brightening associated with solar eruptive phenomena observed in Hα. The temporal, spatially localized changes in chromospheric intensities can be separated into two categories: flare ribbons and sequential chromospheric brightenings (SCBs). Within each category of brightening we determine the smallest resolvable locus of pixels, a kernel, and track the temporal evolution of the position and intensity of each kernel. This tracking is accomplished by isolating the eruptive features, identifying kernels, and linking detections between frames into trajectories of kernels. We fully characterize the evolving intensity and morphology of the flare ribbons by observing the tracked flare kernels in aggregate. With the location of SCB and flare kernels identified, they can easily be overlaid on complementary data sets to extract Doppler velocities and magnetic-field intensities underlying the kernels. This algorithm is adaptable to any dataset to identify and track solar features.

Electron density of active region outflows measured by the EUV Imaging Spectrometer onboard Hinode

Naomasa **Kitagawa**, Takaaki Yokoyama
2015 *ApJ* **805** 97
http://arxiv.org/pdf/1502.07068v1.pdf

In order to better understand the nature of active region outflows, the electron density was measured by using a density-sensitive line pair Fe xiv 264.78A/274.20A.Since coronal line profiles of the outflow region are composed of a major component with a Doppler shift of < 10 km s^-1 and a minor component (enhanced blue wing: EBW) blueshifted by up to 100 km s^-1, we extracted EBW from the line profiles through double-Gaussian fitting. We tried applying the simultaneous fitting to those two Fe xiv lines with several physical restrictions. Electron density for both components (n_Major and n_EBW, respectively) was calculated by referring to the theoretical intensity ratio as a function of electron density as per the CHIANTI database. We studied six locations in the outflow regions around NOAA AR10978. The average electron density was n_Major = 10^(9.16 +- 0.16) cm^-3 and n_EBW = 10^(8.74 +- 0.29) cm^-3. The magnitude relationship between n_Major and n_EBW was opposite in the eastern and western outflow regions. The column depth was also calculated for each component, which leads to the result that the outflows possess only a small fraction (~ 0.1) in the eastern region, while they dominate over the major component in the line profiles by a factor of five in the western region. When taking into account the extending coronal structures, the western region can be thought to represent the mass leakage. In contrast, we suggest a possibility that the eastern region actually contributes to the mass supply to coronal loops.

Coronal upflows from edges of an active region observed with EUV Imaging Spectrometer onboard Hinode

Naomasa **Kitagawa**
PhD thesis, **2014**
http://arxiv.org/pdf/1411.4742v1.pdf

In order to better understand the plasma supply and leakage at active regions, we investigated physical properties of the upflows from edges of active region NOAA AR10978 observed with the EUV Imaging Spectrometer (EIS) onboard Hinode. Our observational aim is to measure two quantities of the outflows: Doppler velocity and electron density.

SOLAR MOSS PATTERNS: HEATING OF CORONAL LOOPS BY TURBULENCE AND MAGNETIC CONNECTION TO THE FOOTPOINTS
R. **Kittinaradorn**1, D. Ruffolo1,2, and W. H. Matthaeus3
Astrophysical Journal, 702:L138–L142, **2009** September
We address the origin of the patchy dark and bright emission structure, known as “moss,” observed by TRACE extreme ultraviolet observations of the solar disk. Here we propose an explanation based on turbulent, patchy heat conduction from the corona into the transition region. Computer simulations demonstrate that magnetic turbulence in coronal loops develops a flux rope structure with current sheets near the flux rope boundaries. Localized heating due to current sheet activity such as magnetic reconnection is followed by heat conduction along turbulent magnetic field lines. The field line trajectories tend to remain near the flux rope boundaries, resulting in selective heating of the plasma in the transition region. This can explain the network of bright regions in the observed moss morphology.

Eruptive Activity Related to Solar Energetic Particle Events **Review**
Karl-Ludwig **Klein**
In: O.E. Malandraki, N.B. Crosby (eds.), Solar Particle Radiation Storms Forecasting and Analysis Chapter 2, **2018**
https://link.springer.com/content/pdf/10.1007%2F978-3-319-60051-2.pdf
File Malandraki_Crosby_SEPs_Forecasting and Analysis_Book.pdf
Solar energetic particle events are associated with solar activity, especially flares and coronal mass ejections (CMEs). In this chapter a basic introduction is presented to the nature of flares and CMEs. Since both are manifestations of evolving magnetic fields in the solar corona, the chapter starts with a qualitative description of the magnetic structuring and electrodynamic coupling of the solar atmosphere. Flares and the radiative manifestations of energetic particles, i.e. bremsstrahlung, gyrosynchrotron and collective plasma emission of electrons, and nuclear gamma-ray emission are briefly presented. Observational evidence on the particle acceleration region in flares is given, as well as a very elementary qualitative overview of acceleration processes. Then CMEs, their origin and their association with shock waves are discussed, and related particle acceleration processes are briefly described.

Solar Flares and Space Weather,
Lucia **Kleint**
Presentation at ISWI Webinar 12, 28 June **2023**
https://youtu.be/gVhVI9FwSJw
The current, as well as all previous ISWI webinar sessions can be accessed through the website of the Office at:
https://www.unoosa.org/oosa/en/ourwork/psa/bssi/iswi_webinars.html

Nonlinear force-free modeling of flare-related magnetic field changes at the photosphere and chromosphere
Lucia **Kleint**, Michael S. Wheatland, Alpha Mastrano, Patrick I. McCauley
ApJ **865** 146 **2018**
https://arxiv.org/pdf/1808.07079.pdf
sci-hub.tw/10.3847/1538-4357/aadc5c
Rapid and stepwise changes of the magnetic field are often observed during flares but cannot be explained by models yet. Using a 45 min sequence of SDO/HMI 135 s fast-cadence vector magnetograms of the X1 flare on **2014-03-29** we construct, at each timestep, nonlinear force-free models for the coronal magnetic field. Observed flare-related changes in the line-of-sight magnetic field BLOS at the photosphere and chromosphere are compared with changes in the magnetic fields in the models. We find a moderate agreement at the photospheric layer (the basis for the models), but no agreement at chromospheric layers. The observed changes at the photosphere and chromosphere are surprisingly different, and are unlikely to be reproduced by a force-free model. The observed changes are likely to require a change in the magnitude of the field, not just in its direction.

The High Energy Solar Corona: Waves, Eruptions, Particles **Book**
Karl-Ludwig **Klein**, Alexander L. MacKinnon (Eds.)
Lecture Notes in Physics (LNP), volume 725, **2007**
https://link.springer.com/book/10.1007%2F978-3-540-71570-2

On the origin of the flare emission in IRIS' SJI 2832 filter: Balmer continuum or spectral lines?
Lucia **Kleint**, Petr Heinzel, Säm Krucker
ApJ **2017**
https://arxiv.org/pdf/1702.07167.pdf

Continuum ("White-light", WL) emission dominates the energetics of flares. Filter-based observations, such as the IRIS SJI 2832 filter, show WL-like brightenings during flares, but it is unclear whether the emission arises from real continuum emission or enhanced spectral lines, possibly turning into emission. The difficulty in filter-based observations, contrary to spectral observations, is to determine which processes contribute to the observed brightening during flares. Here we determine the contribution of the Balmer continuum and the spectral line emission to IRIS' SJI 2832 emission by analyzing the appropriate passband in simultaneous IRIS NUV spectra. We find that spectral line emission can contribute up to 100% to the observed SJI emission, that the relative contributions usually temporally vary, and that the highest SJI enhancements that are observed are most likely because of the Balmer continuum. We conclude that care should be taken when calling SJI 2832 a continuum filter during flares, because the influence of the lines on the emission can be significant. **2014-10-25**

First Detection of Chromospheric Magnetic Field Changes During an X1-Flare

Lucia **Kleint**
ApJ 834 26 **2016**
http://arxiv.org/pdf/1608.02552v1.pdf
Stepwise changes of the photospheric magnetic field, which often becomes more horizontal, have been observed during many flares. Previous interpretations include coronal loops that contract and it has been speculated that such jerks could be responsible for sunquakes. Here we report the detection of stepwise chromospheric line-of-sight magnetic field (BLOS) changes obtained through spectropolarimetry of Ca II 8542 \AA\ with DST/IBIS during the X1-flare SOL20140329T17:48. They are stronger (<640 Mx cm−2) and appear in larger areas than their photospheric counterparts (<320 Mx cm−2). The absolute value of BLOS more often decreases than increases. Photospheric changes are predominantly located near a polarity inversion line, chromospheric changes near footpoints of loops. The locations of changes are near, but not exactly co-spatial to hard X-ray (HXR) emission and neither to enhanced continuum emission, nor a small sunquake. Enhanced chromospheric and coronal emission is observed in nearly all locations that exhibit changes of BLOS, but the emission also occurs in many locations without any BLOS changes. Photospheric and chromospheric changes of BLOS show differences in timing, sign, and size and seem independent of each other. A simple model of contracting loops yields changes of opposite sign to those observed. An explanation for this discrepancy could be increasing loop sizes or loops that untwist in a certain direction during the flare. It is yet unclear which processes are responsible for the observed changes, their timing, size and locations, especially considering the incoherence between photosphere and chromosphere. **2014-03-29**
See HMI Science Nuggets #68 April **2017** http://hmi.stanford.edu/hminuggets/?p=1840

Continuum Enhancements in the Ultraviolet, the Visible and the Infrared during the X1 flare on 2014 March 29

Lucia **Kleint**, Petr Heinzel, Phil Judge, Säm Krucker
ApJ 816 88 **2016**
http://arxiv.org/pdf/1511.04161v1.pdf
Enhanced continuum brightness is observed in many flares ("white light flares"), yet it is still unclear which processes contribute to the emission. To understand the transport of energy needed to account for this emission, we must first identify both the emission processes and the emission source regions. Possibilities include heating in the chromosphere causing optically thin or thick emission from free-bound transitions of Hydrogen, and heating of the photosphere causing enhanced H− continuum brightness. To investigate these possibilities, we combine observations from IRIS, SDO/HMI, and the ground-based FIRS instrument, covering wavelengths in the far-UV, near-UV, visible, and infrared during the X1 flare SOL20140329T17:48. Fits of blackbody spectra to infrared and visible wavelengths are reasonable, yielding radiation temperatures ∼6000-6300 K. The NUV emission, formed in the upper photosphere under undisturbed conditions, exceeds these simple fits during the flare, requiring extra emission from the Balmer continuum in the chromosphere. Thus, the continuum originates from enhanced radiation from photosphere (visible-IR) and chromosphere (NUV). From the standard thick-target flare model, we calculate the energy of the nonthermal electrons observed by RHESSI and compare it to the energy radiated by the continuum emission. We find that the energy contained in most electrons >40 keV, or alternatively, of ∼10-20% of electrons >20 keV is sufficient to explain the extra continuum emission of 4−8×1010 erg s−1 cm−2. Also, from the timing of the RHESSI HXR and the IRIS observations, we conclude that the NUV continuum is emitted nearly instantaneously when HXR emission is observed with a time difference of no more than 15 s.

Flare Observed by a Dozen Instruments

Lucia **Kleint** and Kevin Reardon
RHESSI Science Nugget, No. 231, **2014**

http://sprg.ssl.berkeley.edu/~tohban/wiki/index.php/Flare_Observed_by_a_Dozen_Instruments
A wonderful flare observed by a grand set of instruments, including IRIS and IBIS.
2014-03-29 (X1.0)

SPECTROPOLARIMETRY OF C-CLASS FLARE FOOTPOINTS

L. **Kleint**
2012 ApJ 748 138
We investigate the decay phase of a C-class flare in full-Stokes imaging spectropolarimetry with quasi-simultaneous measurements in the photosphere (6302.5 Å line) and in the chromosphere (8542 Å line) with the IBIS instrument. We analyze data from two fields of view, each spanning about 40" × 80" and targeting the two footpoints of the flare. A region of interest is identified from V/I images: a patch of opposite polarity in the smaller sunspot's penumbra. We find unusual flows in this patch at photospheric levels: a Doppler shift of –4 km s–1, but also a possible radial inflow into the sunspot of 4 km s–1. Such patches seem to be common during flares, but only high-resolution observations allowed us to see the inflow, which may be related to future flares observed in this region. Chromospheric images show variable overlying emission and flows and unusual Stokes profiles. We also investigate the irregular penumbra, whose formation may be blocked by the opposite polarity patch and flux emergence. The 40 minute temporal evolution depicts the larger of the flare ribbons becoming fainter and changing its shape. Measurable photospheric magnetic fields remain constant and we do not detect flare energy transport down from the chromosphere. We find no clear indications of impact polarization in the 8542 Å line. We cannot exclude the possibility of impact polarization, because weaker signals may be buried in the prominent Zeeman signatures or it may have been present earlier during the flare.

Simulations of the CME-Flare Relationship

Kliem, B.1; Tötök, T.2
Freiburg ESP Meeting **2008, Presentation**
Observations of coronal mass ejections (CMEs) and solar flares have revealed a high correlation between the acceleration of the ejecta and the plasma heating and particle acceleration signified by the soft and hard X-ray emissions of the associated flare. The latter are generally thought to result from magnetic reconnection. This finding has stimulated the discussion of the CME-flare relationship, but at the same time it has made it difficult to find a conclusive answer as to whether magnetic reconnection or an ideal MHD instability is the prime cause of the eruptions. Numerical simulations of unstable flux ropes will be presented that are in very satisfactory quantitative agreement with erupting filaments, both, confined to the corona and ejective (i.e., developing into a CME). Some of these simulations indeed show a high degree of synchronization between the initial exponential acceleration of the flux rope, due to the ideal MHD instability, and the development of reconnection flows. However, others show a very delayed onset of reconnection, even after the flux rope's acceleration peak. In addition, the reconnection flows generally lag behind the motions driven by the ideal instability as the flux rope rise velocity nears the saturation phase. Both findings indicate that the ideal MHD process is the primary driver of the coupled CME-flare phenomenon.
The strong differences in the degree of synchronization, which the simulated systems show in the main rise phase of the eruption, are related to the magnetic topology prior to the eruption. Given the observational result of a high correlation between CME and flare development (Zhang & Dere 2006), these simulations yield constraints on the topology and lead us to conclude that a seed for a reconnecting current sheet must typically be present already at the onset of the eruption.

Nanoflare Heating: Observations and Theory **Review**

James A. **Klimchuk**
"Achievements of Hinode in the First Ten Years," PASJ, **2017**
https://arxiv.org/ftp/arxiv/papers/1709/1709.07320.pdf
This is a review of the observational and theoretical evidence for nanoflare heating of the magnetically-closed corona.

Chromospheric Nanoflares as the Source of Coronal Plasma

J. A. **Klimchuk**, S. J. Bradshaw
ApJ, 791 60, **2014**
http://arxiv.org/pdf/1405.1708v1.pdf
It has been suggested that the hot plasma of the solar corona comes primarily from impulsive heating events, or nanoflares, that occur in the lower atmosphere, either in the upper part of the ordinary chromosphere or at the tips of type II spicules. We test this idea with a series of hydrodynamic simulations. We find that synthetic Fe XII (195) and Fe XIV (274) line profiles generated from the simulations disagree dramatically with actual observations. The integrated line intensities are much too faint; the blue shifts are much too fast; the blue-red asymmetries are much too large; and the emission is confined to low altitudes. We conclude that chromospheric nanoflares are not a primary source of hot

coronal plasma. Such events may play an important role in producing the chromosphere and powering its intense radiation, but they do not, in general, raise the temperature of the plasma to coronal values. Those cases where coronal temperatures are reached must be relatively uncommon. The observed profiles of Fe XII and Fe XIV come primarily from plasma that is heated in the corona itself, either by coronal nanoflares or a quasi-steady coronal heating process. Chromospheric nanoflares might play a role in generating waves that provide this coronal heating.

131 and 304 Å Emission Variability Increases Hours Prior to Solar Flare Onset

Kara L. **Kniezewski**, Emily I. Mason, Vadim M. Uritsky, Seth H. Garland
ApJL **977** L29 **2024**
https://arxiv.org/pdf/2411.12704
https://iopscience.iop.org/article/10.3847/2041-8213/ad94dd/pdf
Thermal changes in coronal loops are well-studied, both in quiescent active regions and in flaring scenarios. However, relatively little attention has been paid to loop emission in the hours before the onset of a solar flare; here, we present the findings of a study of over 50 off-limb flares of GOES class C5.0 and above. We investigated the integrated emission variability for Solar Dynamics Observatory Atmospheric Imaging Assembly channels 131, 171, 193, and 304 Ångstroms for 6 hours before each flare, and compared these quantities to the same time range and channels above active regions without proximal flaring. We find significantly increased emission variability in the 2-3 hours before flare onset, particularly for the 131 and 304 channels. This finding suggests a potential new flare prediction methodology. The emission trends between the channels are not consistently well-correlated, suggesting a somewhat chaotic thermal environment within the coronal portion of the loops that disturbs the commonly-observed heating and cooling cycles of quiescent active region loops. We present our approach, the resulting statistics, and discuss the implications for heating sources in these pre-flaring active regions.

The Location and Angle Distribution of Magnetic Reconnection in the Solar Corona

Kalman J. **Knizhnik**1 and Logan C. Cabral-Pelletier2
2022 ApJ 937 93
https://iopscience.iop.org/article/10.3847/1538-4357/ac8d91/pdf
A major unresolved issue in solar physics is the nature of the reconnection events that may give rise to the extreme temperatures measured in the solar corona. In the nanoflare heating paradigm of coronal heating, localized reconnection converts magnetic energy into thermal energy, producing multithermal plasma in the corona. The properties of the corona produced by magnetic reconnection, however, depend on the details of the reconnection process. A significant challenge in understanding the details of reconnection in magnetohydrodynamic (MHD) models is that these models are frequently only able to tell us that reconnection has occurred, but there is significant difficulty in identifying precisely where and when it occurred. In order to properly understand the consequences of reconnection in MHD models, it is crucial to identify reconnecting field lines and where along the field lines reconnection occurs. In this work, we analyze a fully 3D MHD simulation of a realistic sunspot topology, driven by photospheric motions, and we present a model for identifying reconnecting field lines. We also present a proof-of-concept model for identifying the location of reconnection along the reconnecting field lines, and use that to measure the angle at which reconnection occurs in the simulation. We find evidence that magnetic reconnection occurs preferentially near field line footpoints, and discuss the implications of this for coronal heating models.

Nanoflare Diagnostics from Magnetohydrodynamic Heating Profiles

K. J. **Knizhnik**1, W. T. Barnes2, J. W. Reep1, and V. M. Uritsky3,4
2020 ApJ 899 156
https://doi.org/10.3847/1538-4357/aba959
https://arxiv.org/pdf/2009.00132.pdf
The nanoflare paradigm of coronal heating has proven extremely promising for explaining the presence of hot, multi-million degree loops in the solar corona. In this paradigm, localized heating events supply enough energy to heat the solar atmosphere to its observed temperatures. Rigorously modeling this process, however, has proven difficult because it requires an accurate treatment of both the magnetic field dynamics and reconnection as well as the plasma response to magnetic perturbations. In this paper, we combine fully 3D magnetohydrodynamic (MHD) simulations of coronal active region plasma driven by photospheric motions with spatially averaged, time-dependent hydrodynamic (HD) modeling of coronal loops to obtain physically motivated observables that can be quantitatively compared with observational measurements of active region cores. We take the behavior of reconnected field lines from the MHD simulation and use them to populate the HD model to obtain the thermodynamic evolution of the plasma and subsequently the emission measure distribution. We find that the photospheric driving of the MHD model produces only very low-frequency nanoflare heating that cannot account for the full range of active region core observations as measured by the low-temperature emission measure slope. Additionally, we calculate the spatial and temporal distributions of field lines exhibiting collective behavior, and argue that loops occur due to random energization occurring on clusters of adjacent field lines.

The Distribution of Time Delays Between Nanoflares in Magnetohydrodynamic Simulations

Kalman J. **Knizhnik** & Jeffrey W. Reep

Solar Physics volume 295, Article number: 21 (**2020**)

https://link.springer.com/content/pdf/10.1007/s11207-020-1588-2.pdf

Nanoflares are thought to be an important energy source for heating the solar corona. The exact amount of heating contributed by nanoflares depends, in part, on the frequency of the heating and the time interval between nanoflares. Several numerical models have attempted to constrain the frequency of the heating by fitting to observed emission measures. To date, however, no physically motivated value for the time interval between nanoflares has been obtained. In this paper, we calculate a physically motivated distribution of time intervals between successive “nanoflare” reconnection events in driven magnetohydrodynamic simulations. We show that this distribution follows a power law with a slope near −1, much shallower than previously inferred from observations and determined from loop model comparisons with observations. We show that the energy flux injected into the corona in our model is of order 107 ergcm−2s−1107 ergcm−2s−1, and that the heating rate due to these reconnection events reaches values of order 1--10 ergcm−3s−11--10 ergcm−3s−1. Additionally, we show that this power law slope is dependent only weakly on the amount of magnetic helicity injected into the solar magnetic field by the photospheric motions, but the rate of reconnection is about 45%45% higher if no magnetic helicity is injected.

The Role of Twist in Kinked Flux Rope Emergence and Delta-spot Formation

K. J. **Knizhnik**1, M. G. Linton2, and C. R. DeVore

2018 ApJ 864 89

https://arxiv.org/pdf/1808.05562.pdf

https://doi.org/10.3847/1538-4357/aad68c

It has been observationally well established that the magnetic configurations most favorable for producing energetic flaring events reside in δ-spots, a class of sunspots defined as having opposite-polarity umbrae sharing a common penumbra. They are frequently characterized by extreme compactness, strong rotation, and anti-Hale orientation. Numerous studies have shown that nearly all of the largest solar flares originate in δ-spots, making the understanding of these structures a fundamental step in predicting space weather. Despite their important influence on the space environment, surprisingly little is understood about the origin and behavior of δ-spots. In this paper, we perform a systematic study of the behavior of emerging flux ropes to test a theoretical model for the formation of δ-spots: the kink instability of emerging flux ropes. We simulated the emergence of highly twisted, kink-unstable flux ropes from the convection zone into the corona, and we compared their photospheric properties to those of emerged weakly twisted, kink-stable flux ropes. We show that the photospheric manifestations of the emergence of highly twisted flux ropes closely match the observed properties of δ-spots, and we discuss the resulting implications for observations. Our results strongly support and extend previous theoretical work that suggested that the kink instability of emerging flux ropes is a promising candidate to explain δ-spot formation, as it reproduces their key characteristics very well.

THE ACCELERATION OF IONS IN SOLAR FLARES DURING MAGNETIC RECONNECTION

K. **Knizhnik**1, M. Swisdak2 and J. F. Drake

2011 ApJ 743 L35

The acceleration of solar flare ions during magnetic reconnection is explored via particle-in-cell simulations that self-consistently and simultaneously follow the motions of both protons and α particles. We show that the dominant heating of thermal ions during guide field reconnection, the usual type in the solar corona, results from pickup behavior during the entry into reconnection exhausts. In contrast to anti-parallel reconnection, the temperature increment is dominantly transverse, rather than parallel, to the local magnetic field. A comparison of protons and α reveals a mass-to-charge (M/Q) threshold in pickup behavior that favors the heating of high-M/Q ions, which is consistent with impulsive flare observations.

Subsecond Spikes in Fermi GBM X-ray Flux as a Probe for Solar Flare Particle Acceleration

Trevor **Knuth**, Lindsay Glesener

ApJ **903** 63 **2020**

https://arxiv.org/pdf/2003.05007.pdf

https://doi.org/10.3847/1538-4357/abb779

Solar flares are known to release a large amount of energy into accelerating electrons. Studying small timescale (≤ 2s) fluctuations in nonthermal X-ray flux offers the opportunity to probe the nature of those acceleration mechanisms. By comparing the durations, differences in timing between energy bands, and the periodicity of these spikes against the relevant timescales called for by various acceleration mechanisms, a test for each mechanism's validity can be made. This work details the analysis of fast fluctuations in Fermi Gamma-ray Burst Monitor (Fermi GBM) data from 2 M9.3 class solar flares that occurred on **SOL2011-07-30 and SOL2011-08-04**. This study shows the usefulness of Fermi GBM data as a means of examining these small timescale spikes and presents a rigorous method of identifying, counting, and measuring the temporal properties of these subsecond X-ray spikes. In the 2 flares examined we found spikes to primarily occur in spans of 60-100 seconds in the impulsive phase. The relative spike intensity ranged from

5% to 46% of the total counts, depending on the energy band the spike was measured in. The average spike durations were 0.96 and 0.66 seconds and the median durations were 0.79 and 0.32 seconds for the 2 flares. The spike duration distribution for the SOL2011-08-04 flare was found to follow a power law with a -1.8 ± 0.5 index. Of the 3 spiking intervals identified, only 1 was found to have a periodicity, showing significant power at the 1.7 ± 0.1 Hz frequency.
RHESSI Nuggets #407 April **2021**
https://sprg.ssl.berkeley.edu/~tohban/wiki/index.php/Subsecond_Spikes_in_Solar_Flare_X-ray_Flux_as_Seen_by_Fermi_GBM

Oscillations Accompanying a He I 10830 Å Negative Flare in a Solar Facula II. Response of the Transition Region and Corona

Nikolai **Kobanov**, Andrei Chelpanov
2019 *Solar Physics* **volume 294**, Article number: 58
https://arxiv.org/pdf/1904.11142.pdf
https://link.springer.com/content/pdf/10.1007/s11207-019-1449-z.pdf
We studied oscillations related to flare SOL**2012-09-21**T02:19 in the transition region and chromosphere based on Reuven Ramaty High Energy Solar Spectroscopic Imager (RHESSI) and Solar Dynamics Observatory (SDO) data, as well as data from a ground-based observatory. We found that 2-minute oscillations triggered by the flare first appeared in the RHESSI channels then subsequently showed up in the SDO 171 {\AA} and 304 {\AA} channels and after that in the chromospheric He I 10830 {\AA} line. The delay of the chromospheric signal compared to the RHESSI signal is 7 minutes, which indicates that the wave perturbation propagated from the corona to the chromosphere. We used the sharp increase in 3- and 5-minute oscillations during the flare in the lower atmosphere to trace the propagation of the oscillation trains to the transition region and corona. The results show that the 171 {\AA} channel signals lagged behind the photospheric and chromospheric signals by 200 s on average. We suggest that we observed slow magnetoacoustic waves both in the case of 2-minute oscillations propagating downwards from the corona and in the case of 3- and 5-minute oscillations leaking to the corona from beneath.

Negative flare in the He I 10830 Å line in facula

Nikolai **Kobanov**, Andrei Chelpanov, Vasiliy Pulyaev
JASTP Volume 173, August **2018**, Pages 50-56
https://arxiv.org/pdf/1712.10117.pdf
A small-scale flare **SOL2012-09-21**T02:19 (B2) occurred in a spotless active region that we observed at a ground-based telescope equipped with a spectrograph. During the flare, we registered an increase in absorption in the He I 10830 \AA\ line by 25%, while other chromospheric and coronal spectral lines demonstrated increase in brightness at the same location. This phenomenon called negative flare had rarely been observed at the Sun before. In this paper, we describe the morphology of this flare and investigate its dynamics based on our spectral observations and space imaging data. The Hα and He I 10830 \AA\ lines reach their extreme intensities 5 and 6 minutes after the 171 \AA\ line. The brightening first occurred in the 171 \AA\ and 193 \AA\ Solar Dynamics Observatory (SDO) channels followed by the 94 \AA, 304 \AA, and 1600 \AA\ signals ∼2 minutes after (for the maximum phases). However, the abrupt changes in line-of-sight (LOS) velocities in the chromospheric lines occur simultaneously with the intensity changes in the 304 \AA\ and 1600 \AA\ lines: we observed a downward motion that was followed by two upward motions. The measured horizontal speed of the perturbation propagation was close to 70 km s−1 both in the chromospheric and coronal lines. We assume that we observed the photoionization-recombination process caused by UV radiation from the transition region during the coronal flare. With this, we point out the difficulties in interpreting the time lag between the emission maximum in the SDO UV channels and the second absorption maximum in the He I 10830 \AA\ line.

Oscillations in Solar Faculae. III. The Phase Relations Between Chromospheric and Photospheric Line-of-Sight Velocities

N. I. **Kobanov**, A. S. Kustov, S. A. Chupin and V. A. Pulyaev
Solar Physics, Volume 273, Number 1, 39-49, **2011**
An analysis of line-of-sight velocity oscillation in nine solar faculae was undertaken with the aim of studying phase relations between chromospheric (He i 10830 Å line) and photospheric (Si i 10827 Å line) five-minute oscillations. We found that the time lag of the chromospheric signal relative to photospheric one varies from −12 to 100 seconds and is about 50 seconds on average. We assume that the small observed lag can have three possible explanations: i) convergence of formation levels of He i 10830 Å and Si i 10827 Å in faculae; ii) significant increase of five-minute oscillation propagation velocity above faculae; iii) simultaneous presence of standing and travelling waves.

Forward Modeling Transient Brightenings and Microflares around an Active Region Observed with Hi-C

Adam R. **Kobelski**, David E. McKenzie

ApJ, 794 119 **2014**
http://arxiv.org/pdf/1408.5440v1.pdf
Small scale flare-like brightenings around active regions are among the smallest and most fundamental of energetic transient events in the corona, providing a testbed for models of heating and active region dynamics. In a previous study, we modeled a large collection of these microflares observed with Hinode/XRT using EBTEL and found that they required multiple heating events, but could not distinguish between multiple heating events on a single strand, or multiple strands each experiencing a single heating event. We present here a similar study, but with EUV data of Active Region 11520 from the High Resolution Coronal Imager (Hi-C) sounding rocket. Hi- C provides an order of magnitude improvement to the spatial resolution of XRT, and a cooler temperature sensitivity, which combine to provide significant improvements to our ability to detect and model microflare activity around active regions. We have found that at the spatial resolution of Hi-C (approximately 0.3 arcseconds), the events occur much more frequently than expected (57 events detected, only 1 or 2 expected), and are most likely made from strands of order 100 km wide, each of which is impulsively heated with multiple heating events. These findings tend to support bursty reconnection as the cause of the energy release responsible for the brightenings. **2012 July 11**,

Modeling Active Region Transient Brightenings Observed with XRT as Multi-Stranded Loops

Adam R **Kobelski**, David E McKenzie, Martin Donachie
ApJ 786 82, **2014**
http://arxiv.org/pdf/1403.7834v1.pdf
Strong evidence exists that coronal loops as observed in EUV and soft X-rays may not be monolithic isotropic structures, but can often be more accurately modeled as bundles of independent strands. Modeling the observed active region transient brightenings (ARTBs) within this framework allows exploration of the energetic ramifications and characteristics of these stratified structures. Here we present a simple method of detecting and modeling ARTBs observed with the Hinode/X-Ray Telescope (XRT) as groups of 0-dimensional strands, which allows us to probe parameter space to understand better the spatial and temporal dependence of strand heating in impulsively heated loops. This partially automated method can be used to analyze a large number of observations to gain a statistical insight into the parameters of coronal structures including the number of heating events required in a given model to fit the observations. In this article we present the methodology, and demonstrate its use in detecting and modeling ARTBs in a sample data set from Hinode/XRT. These initial results show that in general, multiple heating events are necessary to reproduce observed ARTBs, but the spatial dependence of these heating events could not yet be established**.**

Interplanetary Protons versus Interacting Protons in the 2017 September 10 Solar Eruptive Event

Leon **Kocharov**1, Melissa Pesce-Rollins2, Timo Laitinen3, Alexander Mishev1,4, Patrick Kühl5, Andreas Klassen5, Meng Jin6,7, Nicola Omodei8, Francesco Longo9,10, David F. Webb11
2020 ApJ 890 13
sci-hub.si/10.3847/1538-4357/ab684e
We analyze the relativistic proton emission from the Sun during the eruptive event on **2017 September 10**, which caused a ground-level enhancement (GLE 72) registered by the worldwide network of neutron monitors. Using the neutron monitor data and interplanetary transport modeling both along and across interplanetary magnetic field (IMF) lines, we deduce parameters of the proton injection into the interplanetary medium. The inferred injection profile of the interplanetary protons is compared with the profile of the >100 MeV γ-ray emission observed by the Fermi Large Area Telescope, attributed to pion production from the interaction of >300 MeV protons at the Sun. GLE 72 started with a prompt component that arrived along the IMF lines. This was followed by a more prolonged enhancement caused by protons arriving at the Earth across the IMF lines from the southwest. The interplanetary proton event is modeled using two sources—one source at the root of the Earth-connected IMF line and another source situated near the solar western limb. The maximum phase of the second injection of interplanetary protons coincides with the maximum phase of the prolonged >100 MeV γ-ray emission that originated from a small area at the solar western limb, below the current sheet trailing the associated coronal mass ejection (CME). A possible common source of interacting protons and interplanetary protons is discussed in terms of proton acceleration at the CME bow shock versus coronal (re-)acceleration in the wake of the CME.

Solar Interacting Protons Versus Interplanetary Protons in the Core Plus Halo Model of Diffusive Shock Acceleration and Stochastic Re-acceleration

L. **Kocharov**1, T. Laitinen2, R. Vainio3, A. Afanasiev3, K. Mursula4, and J. M. Ryan
2015 ApJ 806 80
https://iopscience.iop.org/article/10.1088/0004-637X/806/1/80/pdf
With the first observations of solar γ-rays from the decay of pions, the relationship of protons producing ground level enhancements (GLEs) on the Earth to those of similar energies producing the γ-rays on the Sun has been debated. These

two populations may be either independent and simply coincident in large flares, or they may be, in fact, the same population stemming from a single accelerating agent and jointly distributed at the Sun and also in space. Assuming the latter, we model a scenario in which particles are accelerated near the Sun in a shock wave with a fraction transported back to the solar surface to radiate, while the remainder is detected at Earth in the form of a GLE. Interplanetary ions versus ions interacting at the Sun are studied for a spherical shock wave propagating in a radial magnetic field through a highly turbulent radial ray (the acceleration core) and surrounding weakly turbulent sector in which the accelerated particles can propagate toward or away from the Sun. The model presented here accounts for both the first-order Fermi acceleration at the shock front and the second-order, stochastic re-acceleration by the turbulence enhanced behind the shock. We find that the re-acceleration is important in generating the γ-radiation and we also find that up to 10% of the particle population can find its way to the Sun as compared to particles escaping to the interplanetary space.

The Search for >35 MeV Neutrons from the June 3, 2012 Impulsive Flare

K. **Koga**, S. Masuda, H. Matsumoto, Y. Muraki, T. Obara O. Okudaira, S. Shibata, T. Yamamoto, T. Goka

Proceeding of the 34th International Cosmic Ray Conference in Hague in August, 2015, **2015**

http://arxiv.org/ftp/arxiv/papers/1508/1508.04930.pdf

We analyzed a highly impulsive solar flare observed **on June 3, 2012**. In association with this flare, emissions of hard X-rays, high-energy gamma rays, and neutrons were detected by the detectors onboard the FERMI, RHESSI satellites and the International Space Station. We compared those results with the pictures taken by the UV telescope onboard the Solar Dynamics Observatory satellite and found the crossing structure of two magnetic ropes at two positions on the solar surface almost at the same time. High-energy gamma rays were detected by the Fermi Large Area Telescope satellite, implying that the impulsive flare was one of a major source of proton acceleration processes on the solar surface. At the beginning of research, impulsive solar flares were considered to be the main source of particle acceleration processes; our current observations have confirmed this hypothesis.

Results of a Measurement of Solar Neutrons Emitted on March 5, 2012 using a Fiber-type neutron monitor onboard the SEDA-AP attached to the ISS

K. **Koga**, H. Matsumoto, O. Okudaira, T. Goka, T. Obara, S. Masuda, Y. Muraki, S. Shibata, T. Yamamoto

Proceeding of the 34th International Cosmic Ray Conference in Hague in August, 2015, **2015**

http://arxiv.org/ftp/arxiv/papers/1508/1508.04927.pdf

The solar neutron detector SEDA-FIB onboard the International Space Station (ISS) has detected several events from the solar direction associated with three large solar flares observed on **March 5th (X1.1), 7th (X5.4), and 9th (M6.3) of 2012**. In this study, we present the time profiles of those neutrons and discuss the physics that may be related to a possible acceleration scenario for ions over the solar surface. We compare our data with the dynamical pictures of the flares obtained by the ultra-violet telescope of the space-based Solar Dynamics Observatory.

Fine structure and long duration of a flare coronal X-ray source with RHESSI and SDO/AIA data

Sylwester **Kolomanski** (1), Tomasz Mrozek (1 and 2), Ewa Chmielewska (1)

A&A **2017**

https://arxiv.org/pdf/1701.09127v1.pdf

Coronal X-ray sources (CXSs) are phenomenon very often occurring in solar flares regardless of a flare size, duration or power. The nature of the sources was difficult to uncover for many years. It seems that at last, combining data from RHESSI and SDO/AIA, there is a unprecedented possibility to 'look inside' CXSs and to answer the questions about their formation, evolution and structure. We present a study of a CXS of the SOL**2011-10-22**T11:10 long-duration flare observed simultaneously with RHESSI and SDO/AIA. We focus our attention on the following questions: What was responsible for the CXS presence and long duration? Was there any fine structure in the CXS? Available data enables us to study a relation between the CXS and structures observed in EUV during the decay phase of the flare. X-ray emission recorded by RHESSI during the decay phase of the flare came from about 10 MK hot CXS. The source was observable for 5 hours. This long presence of the source could be supported by magnetic reconnection ongoing during the decay phase. Supra-arcade downflows, which are considered to be a manifestation of magnetic reconnection, were observed at the same time as the CXS. The source was co-spatial with the part of the hot supra-arcade region that had the highest emission measure and simultaneously the temperature within the range of RHESSI thermal-response. However, while the supra-arcade region was a dynamic region consisting of small-scale structures, the CXS seemed to be smooth, structureless. We run simulations using real and synthetic RHESSI data, but we did not find any strong evidence that the CXS had any small-scale structure.

Slowly and surely toward the huge amount of energy II
S. **Kolomanski** and T. Mrozek:
RHESSI Science Nugget, No. 164, **2011**
http://sprg.ssl.berkeley.edu/~tohban/wiki/index.php/Slowly_but_surely_towards_the_huge_amount_of_energy_II
How much energy does a solar flare need, to exist? How much energy must be accumulated in the magnetic field before a flare starts? And how fast must the accumulated energy be released? Should it be discharged in a short time during the flare initial (impulsive) stage? Or should it leak continuously out throughout the entire flare duration? These are several of the basic questions in flare physics, and the answers will help us to understand solar and stellar flares.
Analysis of the huge energies involved in loop-top sources in flares.
30 July 2005, 25 January 2007

RHESSI observations of long-duration flares with long-lasting X-ray loop-top sources

S. **Kołomański**, T. Mrozek and U. Bąk-Stęślicka
A&A 531, A57 (**2011**), **File**
Context. The Yohkoh /HXT observations of long duration events (LDEs) have shown that the HXR emission (14−23 keV) is present for tens of minutes after flare maximum. As a result, some heating process is expected to exist during that time. The higher energy resolution of RHESSI compared to HXT allow us to analyse LDEs in a more comprehensive way.
Aims. We selected three LDEs observed by RHESSI to answer the questions of how long HXR emission can be present, where it is emitted, what its nature is and how much energy should be released to sustain the emission.
Methods. We used RHESSI data to reconstruct images of the selected flares with an energy resolution as high as 1 keV. Next we estimated physical parameters of HXR sources through imaging spectroscopy. The physical parameters obtained were then used to calculate the energy balance of the observed sources.
Results. We found that HXR thermal emission can be present for many hours after LDE flare maximum. The emission comes from large and hot loop-top sources. The total energy that must be released to sustain the emission of the sources is as high as 1031 erg.
30 July 2005, 22 August 2005, 25 January 2007

The interaction of a plasmoid with a loop-top kernel

S. **Kolomanski**1, 2 and M. Karlický1
A&A 475, 685-693 (**2007**)
We study the interaction between a downward moving plasmoid and a loop-top kernel recognized in the 30 November 2000 flare. Such an interaction is predicted by some numerical models of solar flares.
Many details of this interaction are found, e.g., an increase of the X-ray and decimetric radio fluxes and an increase of the plasma temperature at the interaction site. Just after the coalescence of the plasmoid with the loop-top kernel, the 1-2 GHz pulsating radio structure and hard X-ray source above the coalescence site were observed.

Multi-wavelength quasi-periodic pulsations in a stellar superflare

Dmitrii Y. **Kolotkov**, Valery M. Nakariakov, Robin Holt, Alexey A. Kuznetsov
ApJ Letters **923** L33 **2021**
https://arxiv.org/pdf/2112.07734.pdf
https://iopscience.iop.org/article/10.3847/2041-8213/ac432e/pdf
https://doi.org/10.3847/2041-8213/ac432e
We present the first multi-wavelength simultaneous detection of QPP in a superflare (more than a thousand times stronger than known solar flares) on a cool star, in soft X-rays (SXR, with XMM-Newton) and white light (WL, with Kepler). It allowed for the first-ever analysis of oscillatory processes in a stellar flare simultaneously in thermal and non-thermal emissions, conventionally considered to come from the corona and chromosphere of the star, respectively. The observed QPP have periods 1.5 ± 0.15 hours (SXR) and 3 ± 0.6 hours (WL), and correlate well with each other. The unique relationship between the observed parameters of QPP in SXR and WL allowed us to link them with oscillations of the electric current in the flare loop, which directly affect the dynamics of non-thermal electrons and indirectly (via Ohmic heating) the thermal plasma. These findings could be considered in favour of the equivalent LCR-contour model of a flare loop, at least in the extreme conditions of a stellar superflare.

Quasi-periodic pulsations in the most powerful solar flare of Cycle 24

Dmitrii Y. **Kolotkov**, Chloe E. Pugh, Anne-Marie Broomhall, Valery M. Nakariakov
ApJL 858 L3 **2018**
https://arxiv.org/pdf/1804.04955.pdf

https://warwick.ac.uk/fac/sci/physics/research/cfsa/people/kolotkov/eprints/qpp_apjl_r2.pdf
http://sci-hub.tw/http://iopscience.iop.org/2041-8205/858/1/L3/
Quasi-periodic pulsations (QPP) are common in solar flares and are now regularly observed in stellar flares. We present the detection of two different types of QPP signals in the thermal emission light curves of the X9.3 class solar flare SOL**2017-09-06**T12:02, which is the most powerful flare of Cycle 24. The period of the shorter-period QPP drifts from about 12 to 25 seconds during the flare. The observed properties of this QPP are consistent with a sausage oscillation of a plasma loop in the flaring active region. The period of the longer-period QPP is about 4 to 5 minutes. Its properties are compatible with standing slow magnetoacoustic oscillations, which are often detected in coronal loops. For both QPP signals, other mechanisms such as repetitive reconnection cannot be ruled out, however. The studied solar flare has an energy in the realm of observed stellar flares, and the fact that there is evidence of a short-period QPP signal typical of solar flares along with a long-period QPP signal more typical of stellar flares suggests that the different ranges of QPP periods typically observed in solar and stellar flares is likely due to observational constraints, and that similar physical processes may be occurring in solar and stellar flares.

Kinetic model of force-free current sheets with non-uniform temperature

D. Y. **Kolotkov**, I. Y. Vasko, and V. M. Nakariakov
Physics of Plasmas **2015**
http://www2.warwick.ac.uk/fac/sci/physics/research/cfsa/people/kolotkov/eprints/kolotkov_vasko_281015.pdf
The kinetic model of a one-dimensional force-free current sheet (CS) developed recently by M. Harrison and T. Neukirch (Phys. Rev. Lett., vol. 6, 2009) predicts uniform distributions of the plasma temperature and density across the CS. However, in realistic physical systems inhomogeneities of these plasma parameters may arise quite naturally due to the boundary conditions or local plasma heating. Moreover, as the CS spatial scale becomes larger than the characteristic kinetic scales (the regime often referred to as the MHD limit) it should be possible to set arbitrary density and temperature profiles. Thus, an advanced model has to allow for inhomogeneities of the macroscopic plasma parameters across the CS, to be consistent with the MHD limit. In this paper we generalise the kinetic model of a force-free current sheet, taking into account the inhomogeneity of the density and temperature across the CS. In the developed model the density may either be enhanced or depleted in the CS central region. The temperature profile is prescribed by the density profile, keeping the plasma pressure uniform across the CS. All macroscopic parameters, as well as the distribution functions for the protons and electrons, are determined analytically. Applications of the developed model to current sheets observed in space plasmas are discussed.

Multi-mode quasi-periodic pulsations in a solar flare

D. Y. **Kolotkov**1, V. M. Nakariakov1,2,3, E. G. Kupriyanova3, H. Ratcliffe1 and K. Shibasaki
A&A 574, A53 (**2015**)
Context. Quasi-periodic pulsations (QPP) of the electromagnetic radiation emitted in solar and stellar flares are often detected in microwave, white light, X-ray, and gamma-ray bands. Mechanisms for QPP are intensively debated in the literature. Previous studies revealed that QPP may manifest non-linear, non-stationary and, perhaps, multi-modal processes operating in flares.
Aims. We study QPP of the microwave emission generated in an X3.2-class solar flare on **14 May, 2013**, observed with the Nobeyama Radioheliograph (NoRH), aiming to reveal signatures of the non-linear, non-stationary, and multi-modal processes in the signal.
Methods. The NoRH correlation signal obtained at the 17 GHz intensity has a clear QPP pattern. The signal was analysed with the Hilbert-Huang transform (HHT) that allows one to determine its instant amplitude and frequency, and their time variation.
Results. It was established that the QPP consists of at least three well-defined intrinsic modes, with the mean periods of 15, 45, and 100 s. All the modes have quasi-harmonic behaviour with different modulation patterns. The 100 s intrinsic mode is a decaying oscillation, with the decay time of 250 s. The 15 s intrinsic mode shows a similar behaviour, with the decay time of 90 s. The 45 s mode has a wave-train behaviour.
Conclusions. Dynamical properties of detected intrinsic modes indicate that the 100 s and 15 s modes are likely to be associated with fundamental kink and sausage modes of the flaring loop, respectively. The 100 s oscillation could also be caused by the fundamental longitudinal mode, while this interpretation requires the plasma temperature of about 30 million K and hence is not likely. The 45 s mode could be the second standing harmonics of the kink mode.

Multi-mode quasi-periodic pulsations in a solar flare

Kolotkov, D. Y., Nakariakov, V. M., Kupriyanova, E. G., Ratcliffe, H., Shibasaki, K.
A&A, **2015**
E-print, Dec **2014**
Context. Quasi-periodic pulsations (QPP) of the electromagnetic radiation emitted in solar and stellar flares are often detected in microwave, white light, X-ray and gamma-ray bands. Mechanisms for QPP are intensively debated in the literature. Previous studies revealed that QPP may manifest nonlinear, non-stationary and, perhaps, multi-modal processes operating in flares.

Aims. We study QPP of the microwave emission generated in an X3.2-class solar flare on **14 May, 2013**, observed with the Nobeyama Radioheliograph (NoRH), aiming to reveal signatures of the nonlinear, non-stationary, and multi-modal processes in the signal. Methods. The NoRH correlation signal obtained at the 17 GHz intensity has a clear QPP pattern. The signal was analysed with the Hilbert?Huang transform (HHT) that allows one to determine its instant amplitude and frequency, and their time variation. Results. It was established that the QPP consists of at least three well-defined intrinsic modes, with the mean periods of 15, 45 and 100 seconds. All the modes have quasi-harmonic behaviour with different modulation patterns. The 100-second intrinsic mode is a decaying oscillation, with the decay time of 250 seconds. The 15-second intrinsic mode shows a similar behaviour, with the decay time of 90 seconds. The 45-s mode has a wave-train behaviour. Conclusions. Dynamical properties of detected intrinsic modes indicate that the 100-s and 15-s modes are likely to be associated with fundamental kink and sausage modes of the flaring loop, respectively. The 100-s oscillation could also be caused by the fundamental longitudinal mode,while this interpretation requires the plasma temperature of about 30 million K and hence is not likely. The 45-s mode could be the second standing harmonics of the kink mode.

Active Regions with Superpenumbral Whirls or Sunspots Like Pinwheels

Rudi **Komm**
HMI Science Nuggets #23, **2014**
http://hmi.stanford.edu/hminuggets/?p=884

Solar flares and solar subphotospheric vorticity

Komm, R.; Hill, F.
J. Geophys. Res., Vol. 114, No. A6, A06105, **2009**
We explore the relation between surface magnetic flux of the sun and subsurface flow vorticity for flaring and nonflaring solar active regions. For this purpose, we use a data set consisting of 1009 active regions, including the vorticity measurements of their subsurface flows derived from high-resolution global oscillation network group (GONG) helioseismology data and the corresponding X-ray flare data from the geostationary operation environmental satellite (GOES). Using quantities averaged over the disk passage of active regions, we find that, while there is a considerable spread of the flux and vorticity values, they are more or less linearly related. We distinguish the level of flare activity by X-ray flare class and find that large flux or large vorticity values are sufficient for an active region to produce low-intensity C-class flares. Active regions that produce high-intensity X-class flares are characterized by large values of both flux and vorticity. Active regions that produce M-class flares of intermediate intensity are characterized by large vorticity values. The inclusion of solar subsurface vorticity thus helps to distinguish between flaring and nonflaring active regions.

Numerical Modeling of Energetic Electron Acceleration, Transport, and Emission in Solar Flares: Connecting Loop-top and Footpoint Hard X-Ray Sources

Xiangliang **Kong**, Bin Chen, Fan Guo, Chengcai Shen, Xiaocan Li, Jing Ye, Lulu Zhao, Zelong Jiang, Sijie Yu, Yao Chen, Joe Giacalone
ApJL **941** L22 **2022**
https://arxiv.org/pdf/2211.15333.pdf
https://iopscience.iop.org/article/10.3847/2041-8213/aca65c/pdf
The acceleration and transport of energetic electrons during solar flares is one of the outstanding topics in solar physics. Recent X-ray and radio imaging and spectroscopy observations have provided diagnostics of the distribution of nonthermal electrons and suggested that, in certain flare events, electrons are primarily accelerated in the loop-top and likely experience trapping and/or scattering effects. By combining the focused particle transport equation with magnetohydrodynamic (MHD) simulations of solar flares, we present a macroscopic particle model that naturally incorporates electron acceleration and transport. Our simulation results indicate that the physical processes such as turbulent pitch-angle scattering can have important impacts on both electron acceleration in the loop-top and transport in the flare loop, and their influences are highly energy dependent. A spatial-dependent turbulent scattering with enhancement in the loop-top can enable both efficient electron acceleration to high energies and transport of abundant electrons to the footpoints. We further generate spatially resolved synthetic hard X-ray (HXR) emission images and spectra, revealing both the loop-top and footpoint HXR sources. Similar to the observations, we show that the footpoint HXR sources are brighter and harder than the loop-top HXR source. We suggest that the macroscopic particle model provides new insights into understanding the connection between the observed loop-top and footpoint nonthermal emission sources by combining the particle model with dynamically evolving MHD simulations of solar flares.

A model of double coronal hard X-ray sources in solar flares

Xiangliang **Kong**, Jing Ye, Bin Chen, Fan Guo, Chengcai Shen, Xiaocan Li, Sijie Yu, Yao Chen, Joe Giacalone
ApJ **933** 93 **2022**
https://arxiv.org/pdf/2201.02293.pdf

https://iopscience.iop.org/article/10.3847/1538-4357/ac731b/pdf
A number of double coronal X-ray sources have been observed during solar flares by RHESSI, where the two sources reside at different sides of the inferred reconnection site. However, where and how are these X-ray-emitting electrons accelerated remains unclear. Here we present the first model of the double coronal hard X-ray (HXR) sources, where electrons are accelerated by a pair of termination shocks driven by bi-directional fast reconnection outflows. We model the acceleration and transport of electrons in the flare region by numerically solving the Parker transport equation using velocity and magnetic fields from the macroscopic magnetohydrodynamic simulation of a flux rope eruption. We show that electrons can be efficiently accelerated by the termination shocks and high-energy electrons mainly concentrate around the two shocks. The synthetic HXR emission images display two distinct sources extending to >100 keV below and above the reconnection region, with the upper source much fainter than the lower one. The HXR energy spectra of the two coronal sources show similar spectral slopes, consistent with the observations. Our simulation results suggest that the flare termination shock can be a promising particle acceleration mechanism in explaining the double-source nonthermal emissions in solar flares.

Dynamical modulation of solar flare electron acceleration due to plasmoid-shock interactions in the looptop region

Kong Xiangliang, Guo Fan, Shen Chengcai, Chen Bin, Chen Yao, Giacalone Joe
ApJL **905** L16 **2020**
https://arxiv.org/pdf/2011.09585.pdf
https://iopscience.iop.org/article/10.3847/2041-8213/abcbf5/pdf
A fast-mode shock can form in the front of reconnection outflows and has been suggested as a promising site for particle acceleration in solar flares. Recent development of magnetic reconnection has shown that numerous plasmoids can be produced in a large-scale current layer. Here we investigate the dynamical modulation of electron acceleration in the looptop region when plasmoids intermittently arrive at the shock by combining magnetohydrodynamics simulations with a particle kinetic model. As plasmoids interact with the shock, the looptop region exhibits various compressible structures that modulate the production of energetic electrons. The energetic electron population varies rapidly in both time and space. The number of 5−10 keV electrons correlates well with the area with compression, while that of >50 keV electrons shows good correlation with strong compression area but only moderate correlation with shock parameters. We further examine the impacts of the first plasmoid, which marks the transition from a quasi-steady shock front to a distorted and dynamical shock. The number of energetic electrons is reduced by ∼20% at 15−25 keV and nearly 40\% for 25−50 keV, while the number of 5−10 keV electrons increases. In addition, the electron energy spectrum above 10 keV evolves softer with time. We also find double or even multiple distinct sources can develop in the looptop region when the plasmoids move across the shock. Our simulations have strong implications to the interpretation of nonthermal looptop sources, as well as the commonly observed fast temporal variations in flare emissions, including the quasi-periodic pulsations.

The Acceleration and Confinement of Energetic Electrons by a Termination Shock in a Magnetic Trap: An Explanation for Nonthermal Loop-top Sources during Solar Flares

Xiangliang **Kong**, Fan Guo, Chengcai Shen, Bin Chen, Yao Chen, Sophie Musset, Lindsay Glesener, Peera Pongkitiwanichakul, Joe Giacalone
ApJL **887** L37 **2019**
https://arxiv.org/pdf/1911.08064.pdf
https://iopscience.iop.org/article/10.3847/2041-8213/ab5f67/pdf
Nonthermal loop-top sources in solar flares are the most prominent observational signature that suggests energy release and particle acceleration in the solar corona. Although several scenarios for particle acceleration have been proposed, the origin of the loop-top sources remains unclear. Here we present a model that combines a large-scale magnetohydrodynamic simulation of a two-ribbon flare with a particle acceleration and transport model for investigating electron acceleration by a fast-mode termination shock at the looptop. Our model provides spatially resolved electron distribution that evolves in response to the dynamic flare geometry. We find a concave-downward magnetic structure located below the flare termination shock, induced by the fast reconnection downflows. It acts as a magnetic trap to confine the electrons at the looptop for an extended period of time. The electrons are energized significantly as they cross the shock front, and eventually build up a power-law energy spectrum extending to hundreds of keV. We suggest that this particle acceleration and transport scenario driven by a flare termination shock is a viable interpretation for the observed nonthermal loop-top sources.

Electron Acceleration at a Coronal Shock Propagating Through a Large-scale Streamer-like Magnetic Field

Xiangliang **Kong**, Yao Chen, Fan Guo, Shiwei Feng, Guohui Du, Gang Li
ApJ **821** 32 **2016**
http://arxiv.org/pdf/1602.08170v1.pdf

With a test-particle simulation, we investigate the effect of large-scale coronal magnetic fields on electron acceleration at an outward-propagating coronal shock with a circular front. The coronal field is approximated by an analytical solution with a streamer-like magnetic field featured by partially open magnetic field and a current sheet at the equator atop the closed region. We show that the large-scale shock-field configuration, especially the relative curvature of the shock and the magnetic field line across which the shock is sweeping, plays an important role in the efficiency of electron acceleration. At low shock altitudes, when the shock curvature is larger than that of magnetic field lines, the electrons are mainly accelerated at the shock flanks; at higher altitudes, when the shock curvature is smaller, the electrons are mainly accelerated at the shock nose around the top of closed field lines. The above process reveals the shift of efficient electron acceleration region along the shock front during its propagation. It is also found that in general the electron acceleration at the shock flank is not so efficient as that at the top of closed field since at the top a collapsing magnetic trap can be formed. In addition, we find that the energy spectra of electrons is power-law like, first hardening then softening with the spectral index varying in a range of -3 to -6. Physical interpretations of the results and implications on the study of solar radio bursts are discussed**.**

A STATISTICAL STUDY OF THE SPECTRAL HARDENING OF CONTINUUM EMISSION IN SOLAR FLARES

X. **Kong**1,2, G. Li2, and Y. Chen
2013 ApJ 774 140
The observed hard X-ray and γ-ray continuum in solar flares is interpreted as Bremsstrahlung emission of accelerated non-thermal electrons. It has been noted for a long time that in many flares the energy spectra show hardening at energies around or above 300 keV. In this paper, we first conduct a survey of spectral hardening events that were previously studied in the literature. We then perform a systematic examination of 185 flares from the Solar Maximum Mission. We identify 23 electron-dominated events whose energy spectra show clear double power laws. A statistical study of these events shows that the spectral index below the break (γ1) anti-correlates with the break energy (ε b). Furthermore, γ1 also anti-correlates with Fr, the fraction of photons above the break compared to the total photons. A hardening spectrum, as well as the correlations between (γ1, ε b) and (γ1, Fr), provide stringent constraints on the underlying electron acceleration mechanism. Our results support a recent proposal that electrons are being accelerated diffusively at a flare termination shock with a width of the order of an ion inertial length scale.

The efficiency of electron acceleration during the impulsive phase of a solar flare

Eduard P. **Kontar**, A. Gordon Emslie, Galina G. Motorina, Brian R. Dennis
ApJ **947** L13 **2023**
https://arxiv.org/pdf/2304.01088.pdf
https://iopscience.iop.org/article/10.3847/2041-8213/acc9b7/pdf
Solar flares are known to be prolific electron accelerators, yet identifying the mechanism(s) for such efficient electron acceleration in solar flare (and similar astrophysical settings) presents a major challenge. This is due in part to a lack of observational constraints related to conditions in the primary acceleration region itself. Accelerated electrons with energies above ~20~keV are revealed by hard X-ray (HXR) bremsstrahlung emission, while accelerated electrons with even higher energies manifest themselves through radio gyrosynchrotron emission. Here we show, for a well-observed flare on **2017~September~10**, that a combination of \emph{RHESSI} hard X-ray and and SDO/AIA EUV observations provides a robust estimate of the fraction of the ambient electron population that is accelerated at a given time, with an upper limit of $\lapprox 10^{-2}$ on the number density of nonthermal (≥20~keV) electrons, expressed as a fraction of the number density of ambient protons in the same volume. This upper limit is about two orders of magnitude lower than previously inferred from microwave observations of the same event. Our results strongly indicate that the fraction of accelerated electrons in the coronal region at any given time is relatively small, but also that the overall duration of the HXR emission requires a steady resupply of electrons to the acceleration site. Simultaneous measurements of the instantaneous accelerated electron number density and the associated specific electron acceleration rate provide key constraints for a quantitative study of the mechanisms leading to electron acceleration in magnetic reconnection events.
RHESSI Nugget #449 2023
https://sprg.ssl.berkeley.edu/~tohban/wiki/index.php/Did_a_Solar_Flare_Accelerate_all_the_Ambient_Electrons_in_the_Coronal_Acceleration_Region%3F...
CESRA #3538 **2023** https://www.astro.gla.ac.uk/users/eduard/cesra/?p=3538

Determination of the total accelerated electron rate and power using solar flare hard X-ray spectra

Eduard P. **Kontar**, Natasha L. S. Jeffrey, A. Gordon Emslie
ApJ **871** 225 **2019**
https://arxiv.org/pdf/1812.09474.pdf
Solar flare hard X-ray spectroscopy serves as a key diagnostic of the accelerated electron spectrum. However, the standard approach using the collisional cold thick-target model poorly constrains the lower-energy part of the accelerated electron spectrum, and hence the overall energetics of the accelerated electrons are typically constrained

only to within one or two orders of magnitude. Here we develop and apply a physically self-consistent warm-target approach which involves the use of both hard X-ray spectroscopy and imaging data. The approach allows an accurate determination of the electron distribution low-energy cutoff, and hence the electron acceleration rate and the contribution of accelerated electrons to the total energy released, by constraining the coronal plasma parameters. Using a solar flare observed in X-rays by the {\em RHESSI} spacecraft, we demonstrate that using the standard cold-target methodology, the low-energy cutoff (and hence the energy content in electrons) is essentially undetermined. However, the warm-target methodology can determine the low-energy electron cutoff with ~7\% uncertainty at the 3σ level and hence permits an accurate quantitative study of the importance of accelerated electrons in solar flare energetics. **2013-05-13**

Turbulent kinetic energy in the energy balance of a solar flare

E. P. **Kontar**, J. E. Perez, L. K. Harra, A. A. Kuznetsov, A. G. Emslie, N. L. S. Jeffrey, N. H. Bian, B. R. Dennis

Physical Review Letters **2017**

https://arxiv.org/pdf/1703.02392.pdf

The energy released in solar flares derives from a reconfiguration of magnetic fields to a lower energy state, and is manifested in several forms, including bulk kinetic energy of the coronal mass ejection, acceleration of electrons and ions, and enhanced thermal energy that is ultimately radiated away across the electromagnetic spectrum from optical to X-rays. Using an unprecedented set of coordinated observations, from a suite of instruments, we here report on a hitherto largely overlooked energy component -- the kinetic energy associated with small-scale turbulent mass motions. We show that the spatial location of, and timing of the peak in, turbulent kinetic energy together provide persuasive evidence that turbulent energy may play a key role in the transfer of energy in solar flares. Although the kinetic energy of turbulent motions accounts, at any given time, for only ~(0.5−1)\% of the energy released, its relatively rapid (~1−10~s) energization and dissipation causes the associated throughput of energy (i.e., power) to rival that of major components of the released energy in solar flares, and thus presumably in other astrophysical acceleration sites.
2013 May 15
[CESRA] highlight #1409 June **2017** http://www.astro.gla.ac.uk/users/eduard/cesra/?p=1409

Non-thermal electrons in solar flares: Hot-Corona Cold Chromosphere Model

Eduard **Kontar**∗1 , Natasha Jeffrey , A. Gordon Emslie , and Nic Bian

CESRA **2016** p.61

http://cesra2016.sciencesconf.org/conference/cesra2016/pages/CESRA2016_prog_abs_book_v3.pdf

Extending previous studies of nonthermal electron transport in solar flares, which include the effects of collisional energy diffusion and thermalization of fast electrons, we present an analytic method to infer more accurate estimates of the accelerated electron spectrum in solar flares from observations of the hard X-ray spectrum. Unlike for the standard coldtarget model, the spatial characteristics of the flaring region, especially the necessity to consider a finite volume of hot plasma in the source, need to be taken into account in order to correctly obtain the injected electron spectrum from the source-integrated electron flux spectrum (a quantity straightforwardly obtained from hard X-ray observations). We present the new model and show that the effect of electron thermalization can be significant enough to nullify the need to introduce an ad hoc low-energy cutoff to the injected electron spectrum in order to keep the injected power in non-thermal electrons at a reasonable value. Hot-Corona Cold Chromosphere Model provides much needed the upper limit on the power and acceleration rate of electrons in solar flares.

How to better determine the power in non-thermal electrons from observed X-ray spectra

Eduard **Kontar**, Gordon Emslie, Natasha Jeffrey, Nic Bian

RHESSI Science Nuggets, #264, Nov **2015**

http://sprg.ssl.berkeley.edu/~tohban/wiki/index.php/How_to_better_determine_the_power_in_non-thermal_electrons_from_observed_X-ray_spectra

Incorporation of energy diffusion for electron transport helps to understand flare energetics.
Instead of using a cold thick-target model, we advocate the use of the more physically complete warm target model, including the effect of electron thermalization. We have developed a formula that allows explicit determination of this relationship, given the temperature T and extent L of the hot coronal region. A model fit routine f_warm_thick.pro has been developed for the standard RHESSI spectral-fitting softwre OSPEX. This routine allows the determination of the minimum cut-off value and hence the maximum (upper bound) power in non-thermal electrons. For some flares, the low energy cut-off is constrained with an uncertainty of only a couple of keV, providing an accurate estimate of the accelerated electron number/power.

Collisional relaxation of electrons in a warm plasma and accelerated nonthermal electron spectra in solar flares

E. P. **Kontar**, N. L. S. Jeffrey, A. G. Emslie, N. H. Bian

ApJ **809** 35 **2015**

http://arxiv.org/pdf/1505.03733v1.pdf

Extending previous studies of nonthermal electron transport in solar flares which include the effects of collisional energy diffusion and thermalization of fast electrons, we present an analytic method to infer more accurate estimates of the accelerated electron spectrum in solar flares from observations of the hard X-ray spectrum. Unlike for the standard cold-target model, the spatial characteristics of the flaring region, especially the necessity to consider a finite volume of hot plasma in the source, need to be taken into account in order to correctly obtain the injected electron spectrum from the source-integrated electron flux spectrum (a quantity straightforwardly obtained from hard X-ray observations). We show that, for a given source-integrated electron flux spectrum, the overall power in the injected electrons could be reduced by an order of magnitude or more relative to its cold-target value. Indeed, the extent of electron thermalization can be significant enough to nullify the need to introduce an {\it ad hoc} low-energy cutoff to the injected electron spectrum.

Turbulent pitch-angle scattering and diffusive transport of hard-X-ray producing electrons in flaring coronal loops

Kontar, E. P.; Bian, N. H.; Emslie, A. G.; Vilmer, N.

E-print, Dec **2013**; 2014 ApJ 780 176

Recent observations from {em RHESSI} have revealed that the number of non-thermal electrons in the coronal part of a flaring loop can exceed the number of electrons required to explain the hard X-ray-emitting footpoints of the same flaring loop. Such sources cannot, therefore, be interpreted on the basis of the standard collisional transport model, in which electrons stream along the loop while losing their energy through collisions with the ambient plasma; additional physical processes, to either trap or scatter the energetic electrons, are required. Motivated by this and other observations that suggest that high energy electrons are confined to the coronal region of the source, we consider turbulent pitch angle scattering of fast electrons off low frequency magnetic fluctuations as a confinement mechanism, modeled as a spatial diffusion parallel to the mean magnetic field. In general, turbulent scattering leads to a reduction of the collisional stopping distance of non-thermal electrons along the loop and hence to an enhancement of the coronal HXR source relative to the footpoints. The variation of source size L with electron energy E becomes weaker than the quadratic behavior pertinent to collisional transport, with the slope of L(E) depending directly on the mean free path lambda again pitch angle scattering. Comparing the predictions of the model with observations, we find that lambda sim(10^8-10^9) cm for sim30 keV, less than the length of a typical flaring loop and smaller than, or comparable to, the size of the electron acceleration region.

Wave-particle interactions in non-uniform plasma and the interpretation of hard X-ray spectra in solar flares

E. P. **Kontar**, H. Ratcliffe and N. H. Bian

A&A 539, A43 (**2012**)

Context. High-energy electrons accelerated during solar flares are abundant in the solar corona and in interplanetary space. Commonly, the number and energy of non-thermal electrons at the Sun is estimated through hard X-ray (HXR) spectral observations (e.g. RHESSI) and a single-particle collisional approximation.

Aims. We aim to investigate the role of the spectrally evolving Langmuir turbulence on the population of energetic electrons in the solar corona.

Methods. We numerically simulated the relaxation of a power-law non-thermal electron population in a collisional inhomogeneous plasma, including wave-particle and wave-wave interactions.

Results. The numerical simulations show that the long-time evolution of electron population above 20 keV deviates substantially from the collisional approximation when wave-particle interactions in non-uniform plasma are taken into account. The evolution of the Langmuir wave spectrum towards smaller wavenumbers, caused by large-scale density fluctuations and wave-wave interactions, leads to an effective acceleration of electrons. Furthermore, the time-integrated spectrum of non-thermal electrons, which is normally observed with HXR above 20 keV, is noticeably increased because of acceleration of non-thermal electrons through Langmuir waves.

Conclusions. The results show that the observed HXR spectrum, when interpreted in terms of collisional relaxation, can lead to an overestimated number and energy of energetic electrons accelerated in the corona.

Deducing Electron Properties from Hard X-ray Observations **A Review**

E. P. **Kontar**, J. C. Brown, A. G. Emslie, W. Hajdas, G. D. Holman, G. J. Hurford, J. Kašparová, P. C. V. Mallik, A. M. Massone and M. L. McConnell, et al.

Space Sci Rev (**2011**) 159:301–355, **File**
X-radiation from energetic electrons is the prime diagnostic of flare-accelerated electrons. The observed X-ray flux (and polarization state) is fundamentally a convolution of the cross-section for the hard X-ray emission process(es) in question with the electron distribution function, which is in turn a function of energy, direction, spatial location and time. To address the problems of particle propagation and acceleration one needs to infer as much information as possible on this electron distribution function, through a deconvolution of this fundamental relationship. This review presents recent progress toward this goal using spectroscopic, imaging and polarization measurements, primarily from the Reuven Ramaty High Energy Solar Spectroscopic Imager (RHESSI). Previous conclusions regarding the energy, angular (pitch angle) and spatial distributions of energetic electrons in solar flares are critically reviewed. We discuss the role and the observational evidence of several radiation processes: free-free electron-ion, free-free electron-electron, free-bound electron-ion, photoelectric absorption and Compton backscatter (albedo), using both spectroscopic and imaging techniques. This unprecedented quality of data allows for the first time inference of the angular distributions of the X-ray-emitting electrons and improved model-independent inference of electron energy spectra and emission measures of thermal plasma. Moreover, imaging spectroscopy has revealed hitherto unknown details of solar flare morphology and detailed spectroscopy of coronal, footpoint and extended sources in flaring regions. Additional attempts to measure hard X-ray polarization were not sufficient to put constraints on the degree of anisotropy of electrons, but point to the importance of obtaining good quality polarization data in the future.

ACCELERATION, MAGNETIC FLUCTUATIONS, AND CROSS-FIELD TRANSPORT OF ENERGETIC ELECTRONS IN A SOLAR FLARE LOOP

E. P. **Kontar**, I. G. Hannah, and N. H. Bian
Astrophysical Journal Letters, 730:L22 (6pp), **2011** April 1
sci-hub.tw/10.1088/2041-8205/730/2/L22
Plasma turbulence is thought to be associated with various physical processes involved in solar flares, including magnetic reconnection, particle acceleration, and transport. Using *RHESSI* observations and the X-ray visibility analysis, we determine the spatial and spectral distributions of energetic electrons for a flare (GOES M3.7 class, **2002 April 14**, 23:55 UT), which was previously found to be consistent with a reconnection scenario. It is demonstrated that because of the high density plasma in the loop, electrons have to be continuously accelerated about the loop apex of length ~2 Ч 10^9 cm and width ~7 Ч 10^8 cm. Energy-dependent transport of tens of keV electrons is observed to occur both along and across the guiding magnetic field of the loop.We show that the cross-field transport is consistent with the presence of **magnetic turbulence in the loop**, where electrons are accelerated, and estimate the magnitude of the field line diffusion coefficient for different phases of the flare. The energy density of magnetic fluctuations is calculated for given magnetic field correlation lengths and is larger than the energy density of the non-thermal electrons. The level of magnetic fluctuations peaks when the largest number of electrons is accelerated and is below detectability or absent at the decay phase. These hard X-ray observations provide the first observational evidence that magnetic turbulence governs the evolution of energetic electrons in a dense flaring loop and is suggestive of their turbulent acceleration.

THE SUB-ARCSECOND HARD X-RAY STRUCTURE OF LOOP FOOTPOINTS IN A SOLAR FLARE

E. P. **Kontar**, I. G. Hannah, N. L. S. Jeffrey, and M. Battaglia
Astrophysical Journal, 717:250–256, **2010** July
The newly developed X-ray visibility forward fitting technique is applied to the *RHESSI* data of a limb flare to investigate the energy and height dependence on sizes, shapes, and position of hard X-ray (HXR) chromospheric footpoint sources. This provides information about the electron transport and chromospheric density structure. The spatial distribution of two footpoint X-ray sources is analyzed using PIXON, Maximum Entropy Method, CLEAN, and visibility forward fit algorithms at nonthermal energies from ~20 to ~200 keV.We report, for the first time, the vertical extents and widths of HXR chromospheric sources measured as a function of energy for a limb event. Our observations suggest that both the vertical and horizontal sizes of footpoints are decreasing with energy. Higher energy emission originates progressively deeper in the chromosphere, consistent with downward flare accelerated streaming electrons. The ellipticity of the footpoints grows with energy from ~0.5 at ~20 keV to ~0.9 at ~150 keV. The positions of X-ray emission are in agreement with an exponential density profile of scale height ~150 km. The characteristic size of the HXR footpoint source along the limb decreases with energy, suggesting a converging magnetic field in the footpoint. The vertical sizes of X-ray sources are inconsistent with simple collisional transport in a single density scale height but can be explained using a multi-threaded density structure in the chromosphere.

PARTICLE ACCELERATION AND ENERGY RELEASE IN RHESSI ERA
Eduard **Kontar**
12th European Solar Physics Meeting, **2008**, Freiburg, Germany, **Presentation**
Since high energy emission (X-rays and gamma-rays) represents optically-thin radiation from energetic particles, it is a relatively straightforward, and hence extremely valuable, tool in the diagnostic study of flare-accelerated electrons and ions at the Sun. The observed X-ray/gamma-ray flux is fundamentally a convolution of the cross-section for the emission process(es) in question with the distribution function(s) of accelerated particles, which are in turn functions of energy, direction, spatial location and time. To address the key problems of particle acceleration, propagation as well as energy release one needs to infer as much information as possible on the particle distribution function, through a de-convolution of this fundamental relationship.
This **review** presents recent observational progress toward the understanding of energy release and particle acceleration using spectroscopic, imaging and polarization measurements, primarily from the Ramaty High Energy Solar Spectroscopic Imager (RHESSI). Previous conclusions regarding the energy, angular (pitch angle) and spatial distributions of energetic electrons and ions in solar flares are critically reviewed. The diagnostics of radiation processes, particle transport, and acceleration, using both spectroscopic and imaging techniques will be discussed. The unprecedented quality of the RHESSI data in combination with novel data analysis techniques have revealed previously unknown details of energetic particle distributions and imposed new challenging constraints on the particle acceleration.

The extremely strong non-neutralized electric currents of the unique solar active region NOAA 13664

Ioannis **Kontogiannis** (Leibniz-Institut für Astrophysik Potsdam (AIP) Germany)
A&A 690, L10 **2024**
https://www.aanda.org/articles/aa/pdf/2024/10/aa51627-24.pdf
In **May 2024**, the extremely complex active region National Oceanic and Atmospheric Administration (NOAA) 13664 produced the strongest geomagnetic storm since 2003. The aim of this study is to explore the development of the extreme magnetic complexity of NOAA 13664 in terms of its photospheric electric current. The non-neutralized electric current is derived from photospheric vector magnetograms, provided by the Helioseismic and Magnetic Imaged onboard the Solar Dynamics Observatory. The calculation method is based on image processing, thresholding and error analysis. The spatial and temporal evolution of the non-neutralized electric current of the region as well as its constituent sub-regions is examined. For context, a comparison with other complex, flare-prolific active regions is provided. Active region NOAA 13664 was formed by the emergence and interaction of three sub-regions, two of which were of notable individual complexity. It consisted of numerous persistent, current-carrying magnetic partitions that exhibited periods of conspicuous motions and strongly increasing electric current at many locations within the region. These periods were followed by intense and repeated flaring. The total unsigned non-neutralized electric currents and average injection rates reached 5.95·1013 A and 1.5·1013 A/day, and were the strongest observed so far, significantly surpassing other super-active regions of Solar Cycle 24 and 25. Active region NOAA 13664 presents a unique case of complexity. Further scrutiny of the spatial and temporal variation of the net electric currents during the emergence and development of super-active regions is paramount to understand the origin of complex regions and adverse space weather.
RHESSI Science Nuggets #473 **2024**
https://sprg.ssl.berkeley.edu/~tohban/wiki/index.php/An_extremely_complex_active_region_with_very_strong_non-neutralized_electric_currents

Solar active region evolution and imminent flaring activity through a color-coded visualization of photospheric vector magnetograms

I. **Kontogiannis** (1), A.G.M. Pietrow (1 and 2), M.K. Druett (2), E. Dineva (2), M. Verma (1), C. Denker (1)
A&A 691, A119 (**2024**)
https://arxiv.org/pdf/2408.07047
https://www.aanda.org/articles/aa/pdf/2024/11/aa51393-24.pdf
Context. The emergence of magnetic flux, its transition to complex configurations, and the pre-eruptive state of active regions are probed using photospheric magnetograms.
Aims. Our aim is to pinpoint different evolutionary stages in emerging active regions, explore their differences, and produce parameters that could advance flare prediction using color-coded maps of the photospheric magnetic field.
Methods. The three components of the photospheric magnetic field vector are combined to create color-combined magnetograms (COCOMAGs). From these, the areas occupied by different color hues are extracted, creating appropriate time series (color curves). These COCOMAGs and color curves are used as proxies of the active region evolution and its complexity.
Results. The morphology of COCOMAGs showcases typical features of active regions, such as sunspots, plages, and sheared polarity inversion lines. The color curves represent the area occupied by photospheric magnetic field of different orientation and contain information pertaining to the evolutionary stages of active regions. During emergence,

most of the region area is dominated by horizontal or highly inclined magnetic field, which is gradually replaced by more vertical magnetic field. In complex regions, large parts are covered by highly inclined magnetic fields, appearing as abrupt color changes in COCOMAGs. The decay of a region is signified by a domination of vertical magnetic field, indicating a gradual relaxation of the magnetic field configuration. The color curves exhibit a varying degree of correlation with active region complexity. Particularly the red and magenta color curves, which represent strong, purely horizontal magnetic field, are good indicators of future flaring activity.
Conclusions. Color-combined magnetograms facilitate a comprehensive view of the evolution of active regions and their complexity. They offer a framework for the treatment of complex observations and can be used in pattern recognition, feature extraction, and flare-prediction schemes. **20-24 May 2010, 23 Oct 2014, 7 Sep 2017**
Table 1. The sample of 33 active regions used for the statistics 2010-2017

The characteristics of flare- and CME-productive solar active regions **Review**

Ioannis **Kontogiannis**
Advances in Space Research Volume 71, Issue 4, 15 February **2023**, Pages 2017-2037
https://arxiv.org/pdf/2210.05453.pdf
https://doi.org/10.1016/j.asr.2022.10.008
Solar flares and coronal mass ejections (CMEs) cause immediate and adverse effects on the interplanetary space and geospace. The deeper understanding of the mechanisms that produce them and the construction of efficient prediction schemes are of paramount importance. The source regions of flares and CMEs exhibit some common morphological characteristics associated with strongly sheared magnetic polarity inversion lines, indicative of the complex magnetic configurations that store huge amounts of free magnetic energy and helicity. This knowledge is transformed into parameters that can help us distinguish efficiently between quiet, flare-, and CME-productive active regions. Nonetheless, flare and CME prediction still faces a number of challenges. The magnetic field information is constrained at the photosphere and accessed only from one vantage point of observation; the dynamic behavior of active regions is still not fully incorporated into predictions; the stochasticity of flares and CMEs renders their prediction probabilistic. To meet these challenges, new properties have been put forward to describe different aspects of magnetic energy storage mechanisms in active regions and offer the opportunity of parametric studies for over an entire solar cycle. This inventory of predictors now includes information from flow fields, transition region/coronal spectroscopy, data-driven modeling of the coronal magnetic field, as well as parameterizations of dynamic effects from time series. Further work towards these directions may help alleviate the current limitations in observing the magnetic field of higher atmospheric layers. This paper reviews these efforts as well as the importance of transforming new knowledge into more efficient predictors and including new types of data. **20-24 May 2010, 12-15 Feb 2011, 6 March 2012**

Testing and Improving a Set of Morphological Predictors of Flaring Activity

Ioannis **Kontogiannis**, Manolis K. Georgoulis, Sung-Hong Park, Jordan A. Guerra
Solar Phys. June **2018**, 293:96
https://link.springer.com/content/pdf/10.1007%2Fs11207-018-1317-2.pdf
https://arxiv.org/pdf/1807.06371.pdf
Efficient prediction of solar flares relies on parameters that quantify the eruptive capability of solar active regions. Several such quantitative predictors have been proposed in the literature, inferred mostly from photospheric magnetograms and/or white-light observations. Two of them are the Ising energy and the sum of the total horizontal magnetic field gradient. The former has been developed from line-of-sight magnetograms, while the latter uses sunspot detections and characteristics, based on continuum images. Aiming to include these parameters in an automated prediction scheme, we test their applicability on regular photospheric magnetic field observations provided by the Helioseismic and Magnetic Imager (HMI) instrument onboard the Solar Dynamics Observatory (SDO). We test their efficiency as predictors of flaring activity on a representative sample of active regions and investigate possible modifications of these quantities. The Ising energy appears to be an efficient predictor, and the efficiency is even improved if it is modified to describe interacting magnetic partitions or sunspot umbrae. The sum of the horizontal magnetic field gradient appears to be slightly more promising than the three variations of the Ising energy we implement in this article. The new predictors are also compared with two very promising predictors: the effective connected magnetic field strength and the total unsigned non-neutralized current. Our analysis shows that the efficiency of morphological predictors depends on projection effects in a nontrivial way. All four new predictors are found useful for inclusion in an automated flare forecasting facility, such as the Flare Likelihood and Region Eruption Forecasting (FLARECAST), but their utility, among others, will ultimately be determined by the validation effort underway in the framework of the FLARECAST project. **12 November 2012, 12 - 15 December 2013**

Non-neutralized electric currents in solar active regions and flare productivity

Ioannis **Kontogiannis**, Manolis K. Georgoulis, Sung-Hong Park, Jordan A. Guerra
Solar Phys. 292:159 **2017**
https://arxiv.org/pdf/1708.07087.pdf

We explore the association of non-neutralized currents with solar flare occurrence in a sizable sample of observations, aiming to show the potential of such currents in solar flare prediction. We use the regularly produced high quality vector magnetograms by the Helioseismic Magnetic Imager and more specifically the Space weather HMI Active Region Patches (SHARP). Through a newly established method, that incorporates detailed error analysis, we calculate the non-neutralized currents contained in active regions (AR). Two predictors are produced, namely the total and the maximum unsigned non-neutralized current. Both are tested in AR time-series and a representative sample of point-in-time observations during the interval 2012-2016. The average values of non-neutralized currents in flaring active regions are by more than an order of magnitude higher than in non-flaring regions and correlate very well with the corresponding flare index. The temporal evolution of these parameters appears to be connected to physical processes, such as flux emergence and/or magnetic polarity inversion line formation that are associated with increased solar flare activity. Using Bayesian inference of flaring probabilities, it is shown that the total unsigned non-neutralized current outperforms significantly the total unsigned magnetic flux and other well established current-related predictors. Thus, it shows good prospects for inclusion in an operational flare forecasting service. We plan to use the new predictor in the framework of the FLARECAST project along with other highly performing predictors.
Table 1. NOAA AR sample. tstart,tend are the starting and ending dates of each time-series. 2010-2013

On the Connection between Rieger-type and Magneto-Rossby Waves Driving the Frequency of the Large Solar Eruptions during Solar Cycles 19–25

Marianna B. **Korsós**1,2,3,4, Mausumi Dikpati5, Robertus Erdélyi2,4,6, Jiajia Liu7, and Francesca Zuccarello1,8
2023 ApJ 944 180
https://iopscience.iop.org/article/10.3847/1538-4357/acb64f/pdf
Global solar activity variation mainly occurs over about an 11 yr cycle. However, both longer and shorter periodicities than the solar cycle are also present in many different solar activity indices. The longer timescales may be up to hundreds of years, while the shorter timescales for global solar variability could be within 0.5–2 yr, which include, e.g., from the Rieger-type periods (150–160 days) to quasi-biennial oscillations of 2 yr. The most likely origin of this short-timescale quasi-periodicity is attributed to magnetic Rossby waves, which have periods of 0.8–2.4 yr. In this work, we present findings of a unique evolution of identified shorter periodicities, like the Rieger-type, arising from magnetic Rossby waves, throughout Solar Cycles 19–25. We report further observational evidence of the strong relationship between the Rieger-type periodicity, magneto-Rossby waves, and major solar flare activity. Moreover, this study also reveals that the global solar magnetic field has a continuous periodic longitudinal conveyor belt motion along the solar equator, together with an up-and-down movement in the latitudinal directions. We found that when these longitudinal and latitudinal movements have Rieger-type periodicity and magneto-Rossby waves during the same period of a solar cycle, major flare activity is present.

Magnetic Helicity Flux Oscillations in the Atmospheres of Flaring and Nonflaring Active Regions

M. B. **Korsós**1,2,3, R. Erdélyi2,3,4, X. Huang5, and H. Morgan1
2022 ApJ 933 66
https://iopscience.iop.org/article/10.3847/1538-4357/ac7469/pdf
Analyzing the evolution of magnetic helicity flux at different atmospheric heights is key for identifying its role in the dynamics of active regions (ARs). The three-dimensional (3D) magnetic field of both flaring and nonflaring ARs is constructed using potential field extrapolations, enabling the derivation of emergence, shearing, and total magnetic helicity components at a range of atmospheric heights. An analysis of temporal oscillations of the derived components shows that the largest significant period of the three helicity fluxes are common (within ±2 hr) from the photosphere up to at least 1 Mm for flaring ARs—being consistent with the presence of a coupled oscillatory behavior that is absent in the nonflaring ARs. We suggest that large, energetic solar eruptions may have been produced in ARs when the vertical and horizontal helicity flux components became a coupled oscillatory system in the low solar atmosphere. **2011.02.15, 2013.06.21**
Table 1 Summary Table of the Properties of the Studied 14 Flaring ARs: NOAA Number of AR
Table 2 Summary Table of the Properties of the Studied 10 Nonflaring ARs
Table 3 Summary Table of the Significance Ratio Interval of the Studied Largest Periods of the 14 Flaring and 10 Nonflaring ARs

Differences in periodic magnetic helicity injection behaviour between flaring and non-flaring Active Regions: Case Study

M. B. **Korsos**, P. Romano, H. Morgan, Y. Ye, R. Erdelyi, F. Zuccarello
2020 *ApJL* **897** L23
https://arxiv.org/pdf/2006.07659.pdf
https://doi.org/10.3847/2041-8213/ab9d7a

The evolution of magnetic helicity has a close relationship with solar eruptions and is of interest as a predictive diagnostic. In this case study, we analyse the evolution of the normalised emergence, shearing and total magnetic helicity components in the case of three flaring and three non-flaring active regions (ARs) using SHARPs (Spaceweather Helioseismic Magnetic Imager Active Region Patches) vector magnetic field data. The evolution of the three magnetic helicity components is analysed with wavelet transforms, revealing significant common periodicities of the normalised emergence, shearing and total helicity fluxes before flares in the flaring ARs. The three non-flaring ARs do not show such common periodic behaviour. This case study suggests that the presence of significant periodicities in the power spectrum of magnetic helicity components could serve as a valuable precursor for flares. **09/03/2011, 2013.07.04-07.12, 05-10/11/2013, 19-26/10/2014, 2015.12.15-12.22, 2017.03.29-04.07**

Testing and Validating Two Morphological Flare Predictors by Logistic Regression Machine Learning

M. B. **Korsos**, R. Erdelyi, J. Liu, H. Morgan
Front. Astron. Space Sci., 7:571186. **2021** |
https://www.frontiersin.org/articles/10.3389/fspas.2020.571186/full
https://doi.org/10.3389/fspas.2020.571186
2020 https://arxiv.org/pdf/2012.08164.pdf
Whilst the most dynamic solar active regions (ARs) are known to flare frequently, predicting the occurrence of individual flares and their magnitude, is very much a developing field with strong potentials for machine learning applications.
The present work is based on a method which is developed to define numerical measures of the mixed states of ARs with opposite polarities. The method yields compelling evidence for the assumed connection between the level of mixed states of a given AR and the level of the solar eruptive probability of this AR by employing two morphological parameters: (i) the separation parameter Sl−f and (ii) the sum of the horizontal magnetic gradient GS.
In this work, we study the efficiency of Sl−f and GS as flare predictors on a representative sample of ARs, based on the SOHO/MDI-Debrecen Data (SDD) and the SDO/HMI - Debrecen Data (HMIDD) sunspot catalogues. In particular, we investigate about 1000 ARs in order to test and validate the joint prediction capabilities of the two morphological parameters by applying the logistic regression machine learning method. Here, we confirm that the two parameters with their threshold values are, when applied together, good complementary predictors. Furthermore, the prediction probability of these predictor parameters is given at least 70\% a day before. **20 June 2013**

Solar Flare Prediction Using Magnetic Field Diagnostics Above the Photosphere

M. B. **Korsos**, M. K. Georgoulis, N. Gyenge, S. K. Bisoi, S. Yu, S. Poedts, C. J. Nelson, J. Liu, Y. Yan, R. Erdelyi
2020 *ApJ* **896** 119
https://arxiv.org/pdf/2005.12180.pdf
https://sci-hub.tw/10.3847/1538-4357/ab8fa2
In this article, we present the application of the weighted horizontal gradient of magnetic field (WGM) flare prediction method to 3-dimensional (3D) extrapolated magnetic configurations of 13 flaring solar active regions (ARs). The main aim is to identify an optimal height range, if any, in the interface region between the photosphere and lower corona, where the flare onset time prediction capability of WGM is best exploited. The optimal height is where flare prediction, by means of the WGM method, is achieved earlier than at the photospheric level. 3D magnetic structures, based on potential and non-linear force-free field extrapolations, are constructed to study a vertical range from the photosphere up to the low corona with a 45 km step size. The WGM method is applied as a function of height to all 13 flaring AR cases that are subject to certain selection criteria. We found that applying the WGM method between 1000 and 1800 km above the solar surface would improve the prediction of the flare onset time by around 2-8 hours.Certain caveats and an outlook for future work along these lines are also discussed. **15/02/2011, 09/03/2011, 06-07/09/2011, 22/10/2014, 11/03/2015,**

Investigation of pre-flare dynamics using the weighted horizontal magnetic gradient method: From small to major flare classes

Marianna B. **Korsos**, Shuhong Yang, Robert Erdelyi
Journal of Space Weather and Space Climate **9**, A6 **2019**
https://arxiv.org/pdf/1901.05984.pdf
https://www.swsc-journal.org/articles/swsc/pdf/2019/01/swsc170048.pdf
There is a wide range of eruptions in the solar atmosphere which contribute to space weather, including the major explosions of radiation known as flares. To examine pre-event behavior in delta-spot regions, we use here a method based on the weighted horizontal gradient of magnetic field (WG_M), defined between opposite polarity umbrae at the polarity inversion line of active regions (ARs) as measured using from the Debrecen Heliophysical Observatory catalogues. In this work, we extend the previous analysis of high-energy flares to include both medium (M) and low-

energy (C and B) flares. First, we found a logarithmic relationship between the log value of highest flare class intensity (from B- to X-class) in a δ-spot AR and the maximum value of WG_M of the 127 ARs investigated. We confirm a trend in the convergence-divergence phase of the barycenters of opposite polarities in the vicinity of the polarity inversion line. The extended sample (i) affirms the linear connection between the durations of the convergence-divergence phases of barycenters of opposite polarities in delta-spot regions up to flare occurrence and (ii) provides a geometric constraint for the location of flare emission around the polarity inversion line. The method provides a tool to possibly estimate the likelihood of a subsequent flare of the same or larger energy. **September 2, 2011 , June 13-14, 2012**

Applying the Weighted Horizontal Magnetic Gradient Method to a Simulated Flaring Active Region

M. B. **Korsós**1,2,3, P. Chatterjee4, and R. Erdélyi1,3
2018 ApJ 857 103
http://sci-hub.tw/http://iopscience.iop.org/0004-637X/857/2/103/
https://arxiv.org/pdf/1804.10351.pdf
Here, we test the weighted horizontal magnetic gradient (WG M) as a flare precursor, introduced by Korsós et al., by applying it to a magnetohydrodynamic (MHD) simulation of solar-like flares. The preflare evolution of the WG M and the behavior of the distance parameter between **the area-weighted barycenters** of opposite-polarity sunspots at various heights is investigated in the simulated δ-type sunspot. Four flares emanated from this sunspot. We found the optimum heights above the photosphere where the flare precursors of the WG M method are identifiable prior to each flare. These optimum heights agree reasonably well with the heights of the occurrence of flares identified from the analysis of their thermal and ohmic heating signatures in the simulation. We also estimated the expected time of the flare onsets from the duration of the approaching–receding motion of the barycenters of opposite polarities before each single flare. The estimated onset time and the actual time of occurrence of each flare are in good agreement at the corresponding optimum heights. This numerical experiment further supports the use of flare precursors based on the WG M method.

On the evolution of pre-flare patterns of a 3-dimensional model of AR 11429

M. B. **Korsos**, S. Poedts, N. Gyenge, M. K. Georgoulis, S. Yu, S. K. Bisoi, Y. Yan, M. S. Ruderman, R. Erdelyi
2018
https://arxiv.org/pdf/1801.00433.pdf
We apply a novel pre-flare tracking of sunspot groups towards improving the estimation of flare onset time by focusing on the evolution of the 3D magnetic field construction of AR 11429. The 3D magnetic structure is based on potential field extrapolation encompassing a vertical range from the photosphere through the chromosphere and transition region into the low corona. The basis of our proxy measure of activity prediction is the so-called weighted horizontal gradient of magnetic field (WG_M) defined between spots of opposite polarities close to the polarity inversion line of an active region. The temporal variation of the distance of the **barycenter** of the opposite polarities is also found to possess potentially important diagnostic information about the flare onset time estimation as function of height similar to its counterpart introduced initially in an application at the photosphere only in Korsos et al. (2015). We apply the photospheric pre-flare behavioural patterns of sunspot groups to the evolution of their associated 3D-constructed AR 11429 as function of height. We found that at a certain height in the lower solar atmosphere the onset time may be estimated much earlier than at the photosphere or at any other heights. Therefore, we present a tool and recipe that may potentially identify the optimum height for flare prognostic in the solar atmosphere allowing to improve our flare prediction capability and capacity. **2012.03.07-10**

An application of the weighted horizontal magnetic gradient to solar compact and eruptive events

M. B. **Korsos**, Michael S. Ruderman, R. Erdelyi
Advances in Space Research **2018** Volume 61, Issue 2, Pages 595-602
https://arxiv.org/pdf/1801.00281.pdf
We propose to apply the weighted horizontal magnetic gradient (WGM), introduced in Korsos et al (2015), for analysing the pre-flare and pre-CME behaviour and evolution of Active Regions (ARs) using the SDO/HMI-Debrecen Data catalogue. To demonstrate the power of investigative capabilities of the WGM method, in terms of flare and CME eruptions, we studied two typical ARs, namely, AR 12158 and AR 12192. The choice of ARs represent canonical cases. AR 12158 produced an X1.6 flare with fast "halo" CME (vlinear=1267 kms−1) while in AR 12192 there occurred a range of powerful X-class eruptions, i.e. X1.1, X1.6, X3.1, X1.0, X2.0 and X2.0-class energetic flares, interestingly, none with an accompanying CME. The value itself and temporal variation of WGM is found to possess potentially important diagnostic information about the intensity of the expected flare class. Furthermore, we have also estimated the flare onset time from the relationship of duration of converging and diverging motions of the area-weighted barycenters of two subgroups of opposite magnetic polarities. This test turns out not only to provide information about the intensity of the expected flare-class and the flare onset time but may also indicate whether a flare will occur

with/without fast CME.
We have also found that, in the case when the negative polarity **barycenter** has moved around and the positive one "remained" at the same coordinates preceding eruption, the flare occurred with fast "halo" CME.
Otherwise, when both the negative and the positive polarity barycenters have moved around, the AR produced flares without CME. If these properties found for the movement of the barycenters are generic pre-cursors of CME eruption (or lack of it), identifying them may serve as an excellent pre-condition for refining the forecast of the lift-off of CMEs.
9 September 2014, 22 October 2014

On Flare and CME Predictability Based on Sunspot Group Evolution

M. B. **Korsos**,1,2 and M. S. Ruderman2
Ground-based Solar Observations in the Space Instrumentation Era
ASP Conference Series, Vol. 504 p. 43, **2016**
http://aspbooks.org/publications/504/043.pdf
We propose to apply the weighted horizontal magnetic gradient (WGM), introduced in Korsós et al. (2015), for analysing the pre-flare and pre-CME behaviour and evolution of Active Regions (ARs) using the SDO/HMI-Debrecen Data catalogue. To demonstrate the power of investigative capabilities of the WGM method in terms of flare/CME eruptions, we show the results of studying three typical active regions, namely, AR11818, AR12017 and AR11495. The choice of ARs represent typical cases of flaring with a fast CME, flare eruption without a CME and non-flaring cases, respectively. AR11818 produced an M1.4 energetic flare with a fast "halo" CME (vlinear=1202 km/s) while in AR12017 occurred an X1.0 flare without a CME. The AR11495 is a good example for non-flaring ARs. The value and temporal variation of WGM is found to possess potentially important diagnostic information about the intensity of expected flares. However, this test turns out not only to provide information about the intensity of expected flares but may also show whether a flare will occur with/without a fast CME.**31 May-1 June 2012, 16-18 Aug 2013, 29 March 2014,**

ON THE STATE OF A SOLAR ACTIVE REGION BEFORE FLARES AND CMEs

M. B. **Korsós**1,2 and R. Erdélyi
2016 ApJ 823 153
Several attempts have been made to find reliable diagnostic tools to determine the state prior to flares and related coronal mass ejections (CMEs) in solar active regions (ARs). Characterization of the level of mixed states is carried out using the Debrecen sunspot Data for 116 flaring ARs. Conditional flare probabilities (CFPs) are calculated for different flaring classes. The association with slow/fast CMEs is examined. Two precursor parameters are introduced: (i) the sum of the (daily averaged) horizontal magnetic gradient G S (G DS) and (ii) the separation parameter . We found that if for a flaring AR then the CFP of the expected highest-intensity flare being X-class is more than 70%. If the CFP is more than 45% for the highest-intensity flare(s) to be M-class, and if there is larger than 60% CFP that C-class flare(s) may have the strongest intensity within 48 hr. Next, from analyzing G S for determining CFP we found: if 6.5, then it is very likely that C-class flare(s) may be the most intense; if then there is ~45% CFP that M-class could have the highest intensity; finally, if then there is at least 70% chance that the strongest energy release will be X-class in the next 48 hr. ARs are unlikely to produce X-class flare(s) if and log(G S) 5.5. Finally, in terms of providing an estimate of an associated slow/fast CME, we found that, if 0.4 or 6.5, there is no accompanying fast CME in the following 24 hr.

On flare predictability based on sunspot group evolution

Marianna **Korsos**, Andras Ludmany, Robert Erdelyi, Tunde Baranyi
2015 *ApJ* **802** L21
http://arxiv.org/pdf/1503.04634v1.pdf
The forecast method introduced by Kors\'os et al.(2014) is generalised from the horizontal magnetic gradient (GM), defined between two opposite polarity spots, to all spots within an appropriately defined region close to the magnetic neutral line of an active region. This novel approach is not limited to searching for the largest GM of two single spots as in previous methods. Instead, the pre-flare conditions of the evolution of spot groups is captured by the introduction of the weighted horizontal magnetic gradient, or W_GM. This new proxy enables the potential of forecasting flares stronger than M5. The improved capability includes (i) the prediction of flare onset time and (ii) an assessment whether a flare is followed by another event within about 18 hours. The prediction of onset time is found to be more accurate here. A linear relationship is established between the duration of converging motion and the time elapsed from the moment of closest position to that of the flare onset of opposite polarity spot groups. The other promising relationship is between the maximum of the W_GM prior to flaring and the value of W_GM at the moment of the initial flare onset in the case of multiple flaring. We found that when the W_GM decreases by about 54%, then there is no second flare. If, however, when the W_GM decreases less than 42%, then there will be likely a follow-up flare stronger than M5. This new capability may be useful for an automated flare prediction tool. **Nov. 23-26, 1999. Mar 26 - 03 Apr 2001.**
See http://aspbooks.org/publications/504/043.pdf

Dynamic Precursors of Flares in Active Region NOAA 10486

M. B. **Korsos**, N. Gyenge, T. Baranyi, A. Ludmany

2015

http://arxiv.org/pdf/1501.07257v1.pdf

Four different methods are applied here to study the precursors of flare activity in the Active Region NOAA 10486. Two approaches track the temporal behaviour of suitably chosen features (one, the weighted horizontal gradient WGM, is generalised form the horizontal gradient of the magnetic field, GM; another is the sum of the horizontal gradient of the magnetic field, GS, for all sunspot pairs). WGM is a photospheric indicator that is a proxy measure of magnetic non-potentiality of a specific area of the active region, i.e. it captures the temporal variation of the weighted horizontal gradient of magnetic flux summed up for the region where opposite magnetic polarities are highly mixed. The third one, referred to as the separateness parameter, S(lf), considers the overall morphology. Further, GS and S(lf) are photospheric newly defined quick-look indicators of the polarity mix of the entire active region. The fourth method is tracking the temporal variation of small x-ray flares, their times of succession and their energies observed by the Reuven Ramaty High Energy Solar Spectroscopic Imager instrument. All approaches yield specific pre-cursory signatures for the imminence of flares. **25 October- 3 November, 2003.**

Pre-Flare Dynamics of Sunspot Groups

M. B. **Korsos**, T. Baranyi, A. Ludmany

2014, ApJ 789 107

http://arxiv.org/pdf/1405.7485v1.pdf

Several papers provide evidences that the most probable sites of flare onset are the regions of high horizontal magnetic field gradients in solar active regions. Besides the localization of flare producing areas the present work intends to reveal the characteristic temporal variations in these regions prior to flares. This study uses sunspot data instead of magnetograms, it follows the behaviour of a suitable defined proxy measure representing the horizontal magnetic field gradient. The source of the data is the SDD (SOHO/MDI-Debrecen Data) sunspot catalogue. The most promising pre-flare signatures are the following properties of the gradient variation: i) steep increase, ii) high maximum, iii) significant fluctuation and iv) a gradual decrease between the maximum and the flare onset which can be related to the "pull mode" of the current layer. **These properties may yield a tool** for the assessment of flare probability and intensity within the next 8-10 hours. **28 March 2001, 17 Oct. 2001, 16-21 December, 2002**

Time Series of Magnetic Field Parameters of Merged MDI and HMI Space-Weather Active Region Patches as Potential Tool for Solar Flare Forecasting

Paul A. **Kosovich**, Viacheslav M. Sadykov, Alexander G. Kosovichev, Spiridon Kasapis, Irina N. Kitiashvili, Patrick M. O'Keefe, Aatiya Ali, Vincent Oria, Samuel Granovsky, Chun Jie Chong, Gelu M. Nita

2024

https://arxiv.org/pdf/2401.05591.pdf

Solar flare prediction studies have been recently conducted with the use of Space-Weather MDI (Michelson Doppler Imager onboard Solar and Heliospheric Observatory) Active Region Patches (SMARP) and Space-Weather HMI (Helioseismic and Magnetic Imager onboard Solar Dynamics Observatory) Active Region Patches (SHARP), which are two currently available data products containing magnetic field characteristics of solar active regions. The present work is an effort to combine them into one data product, and perform some initial statistical analyses in order to further expand their application in space weather forecasting. The combined data are derived by filtering, rescaling, and merging the SMARP with SHARP parameters, which can then be spatially reduced to create uniform multivariate time series. The resulting combined MDI-HMI dataset currently spans the period between April 4, 1996, and December 13, 2022, and may be extended to a more recent date. This provides an opportunity to correlate and compare it with other space weather time series, such as the daily solar flare index or the statistical properties of the soft X-ray flux measured by the Geostationary Operational Environmental Satellites (GOES). Time-lagged cross-correlation indicates that a relationship may exist, where some magnetic field properties of active regions lead the flare index in time. Applying the rolling window technique makes it possible to see how this leader-follower dynamic varies with time. Preliminary results indicate that areas of high correlation generally correspond to increased flare activity during the peak solar cycle.

Subsurface Flows Associated with Formation and Flaring Activity of Solar Active Regions

Alexander G. **Kosovichev**, Viacheslav M. Sadykov

Proc. IAU Symp. 365, **2024**
https://arxiv.org/pdf/2401.17598.pdf
We investigate the evolution of subsurface flows during the emergence and the active phase of sunspot regions using the time-distance helioseismology analysis of the full-disk Dopplergrams from the Helioseismic and Magnetic Imager (HMI) onboard the Solar Dynamics Observatory (SDO). We present an analysis of emerging active regions of various types, including delta-type active regions and regions with the reverse polarity order (`anti-Hale active regions'). The results reveal strong vortical and shearing flows during the emergence of magnetic flux, as well as the process of formation of large-scale converging flow patterns around developing active regions, predominantly in the top 6 Mm deep layers of the convection zone. Our analysis revealed a significant correlation between the flow divergence and helicity in the active regions with their flaring activity, indicating that measuring characteristics of subsurface flows can contribute to flare forecasting. **2011.02.12-14, 2017-09-03-06, 2021.10.07-10, 2022-05-05-09, 2022-12-29-31**

Spectro-Polarimetric Properties of Sunquake Sources in X1.5 Flare and Evidence for Electron and Proton Beam Impacts

Alexander G. **Kosovichev**, Viacheslav M. Sadykov, John T. Stefan
ApJ **958** 160 **2023**
https://arxiv.org/pdf/2309.07346.pdf
https://iopscience.iop.org/article/10.3847/1538-4357/acf9eb/pdf
The first significant sunquake event of Solar Cycle 25 was observed during the X1.5 flare of **May 10, 2022**, by the Helioseismic and Magnetic Imager (HMI) onboard the Solar Dynamics Observatory. We perform a detailed spectro-polarimetric analysis of the sunquake photospheric sources, using the Stokes profiles of the FeI 6173A line, reconstructed from the HMI linear and circular polarized filtergrams. The results show fast variations of the continuum emission with rapid growth and slower decay lasting 3-4 min, coinciding in time with the hard X-ray impulses observed by the Konus instrument onboard the Wind spacecraft. The variations in the line core appeared slightly ahead of the variations in the line wings, showing that the heating started in the higher atmospheric layers and propagated downward. The most significant feature of the line profile variations is the transient emission in the line core in three of the four sources, indicating intense, impulsive heating in the lower chromosphere and photosphere. In addition, the observed variations of the Stokes profiles reflect transient and permanent changes in the magnetic field strength and geometry in the sunquake sources. Comparison with the radiative hydrodynamics models shows that the physical processes in the impulsive flare phase are substantially more complex than those predicted by proton and electron beam flare models currently presented in the literature.
HMI Science Nuggets #495 **2024** http://hmi.stanford.edu/hminuggets/?p=4195

The Curious First Sunquake of Solar Cycle 25

Alexander **KOSOVICHEV**
RHESSI Science Nuggets #444 Mar **2023**
https://sprg.ssl.berkeley.edu/~tohban/wiki/index.php/The_Curious_First_Sunquake_of_Solar_Cycle_25
We have described sunquake sources associated with impulsive acceleration of high-energy particles in compact low-lying loops formed across the polarity inversion line. It is a challenge of flare physics to explain the acceleration of these high-energy particles in the first place, and it is another important challenge to explain the mechanism of their and their (sub)photospheric impact.**2022-05-10**

Initial Observations of Sunspot Oscillations Excited by Solar Flare

A. G. **Kosovichev**, T. Sekii
E-print, Oct 2007; Ap. J. http://arxiv.org/PS_cache/arxiv/pdf/0710/0710.1808v1.pdf
Observations of a large solar flare of December 13, 2006, using Solar Optical Telescope (SOT) on Hinode spacecraft revealed high-frequency oscillations excited by the flare in the sunspot chromosphere. These oscillations are observed in the region of strong magnetic field of the sunspot umbra, and may provide a new diagnostic tool for probing the structure of sunspots and understanding physical processes in solar flares.

The Cause of Photospheric and Helioseismic Responses to Solar Flares: High-Energy Electrons or Protons?

A. G. **Kosovichev**
E-print, Oct **2007**; Ap. J.
Analysis of the hydrodynamic and helioseismic effects in the photosphere during the solar flare **of July 23, 2002,** observed by Michelson Doppler Imager (MDI) on SOHO, and high-energy images from RHESSI shows that these effects are closely associated with sources of the hard X-ray emission, and that there are no such effects in the centroid

region of the flare gamma-ray emission. These results demonstrate that contrary to expectations the hydrodynamic and helioseismic responses ("sunquakes") are more likely to be caused by accelerated electrons than by high-energy protons. A series of multiple impulses of high-energy electrons forms a hydrodynamic source moving in the photosphere with a supersonic speed. The moving source plays a critical role in the formation of the anisotropic wave front of sunquakes.

Investigation of a Sunspot Complex by Helioseismology

A.G. **Kosovichev** and T.L. Duvall, Jr

E-print Feb. **2011**; to appear in Proc. IAU Symposium 273, Physics of Sun and Star Spots, Ventura, California 22-26 August 2010

Sunspot regions often form complexes of activity that may live for several solar rotations, and represent a major component of the Sun's magnetic activity. It had been suggested that the close appearance of active regions in space and time might be related to common subsurface roots, or "nests" of activity. EUV images show that the active regions are magnetically connected in the corona, but subsurface connections have not been established. We investigate the subsurface structure and dynamics of a large complex of activity, NOAA 10987-10989, observed during the SOHO/MDI Dynamics run in **March-April 2008**, which was a part of the Whole Heliospheric Interval (WHI) campaign. The active regions in this complex appeared in a narrow latitudinal range, probably representing a subsurface toroidal flux tube. We use the MDI full-disk Dopplergrams to measure perturbations of travel times of acoustic waves traveling to various depths by using time-distance helioseismology, and obtain sound-speed and flow maps by inversion of the travel times. The subsurface flow maps show an interesting dynamics of decaying active regions with persistent shearing flows, which may be important for driving the flaring and CME activity, observed during the WHI campaign. Our analysis, including the seismic sound-speed inversion results and the distribution of deep-focus travel-time anomalies, gave indications of diverging roots of the magnetic structures, as could be expected from Ω-loop structures. However, no clear connection in the depth range of 0-48 Mm among the three active regions in this complex of activity was detected.

Active Region Dynamics

A. G. **Kosovichev**, T. L. Duvall

Space Science Reviews, Volume 124, Number 1-4, 1-12

New methods of local helioseismology and uninterrupted time series of solar oscillation data from the Solar and Heliospheric Observatory (SOHO) have led to a major advance in our understanding of the structure and dynamics of active regions in the subsurface layers.

The Fine Structure of the Quasi-Biennial Oscillations of Sunspot Areas and the Double Magnetic Cycle of the Sun

Irina **Kostyuchenko** & Elena Bruevich

Solar Physics volume 296, Article number: 8 (**2021**)

https://link.springer.com/content/pdf/10.1007/s11207-020-01745-6.pdf

One of the basic features of solar activity is the quasi-biennial oscillations (QBOs)—variations with a period of about two years. The nature of the QBO remains unclear and the most puzzling is the high instability of the QBO period. We investigated a fine structure of the QBO period variability as manifested in sunspot area variations in Solar Cycles 19 – 23 using the wavelet transform with a real mother wavelet, Daubechies 10, that provided a high temporal resolution. We found that within every 11-yr solar cycle the QBO period varies not randomly, as it is widely accepted now, but it gradually decreases from the beginning of the solar cycle till the end, in phase with the shift of the average sunspots latitude to the equator. We have analyzed in a similar way the time series which were simulated using a combination of sine waves with different periods (constant and variable one) and red noise with a standard deviation as large as 40% of the sine amplitude. The analysis has shown that noise does not distort significantly the initial signal and noise itself does not form the structures with the properties which were observed in the case of the natural time series. We suppose that the revealed modification of the QBO period with the development of the solar cycle may be related to the latitudinal differential rotation in the solar convection zone and the possible influence of the rotational velocity in the region of the QBO generation on the QBO period value. Under this assumption, the process responsible for the QBO generation should operate in a layer with a substantial latitudinal shear which according to the helioseismology analysis is observed in the bulk of the convection zone and is getting smaller in the vicinity of the tachocline.

Thermodynamic properties of small flares in the quiet Sun observed by Hα and EUV: plasma motion of the chromosphere and time evolution of temperature/emission measure

Yuji **Kotani**, Takako T. Ishii, Daiki Yamasaki, Kenichi Otsuji, Kiyoshi Ichimoto, Ayumi Asai, Kazunari Shibata

MNRAS Volume 522, Issue 3, **2023**, Pages 4148–4160,

https://doi.org/10.1093/mnras/stad1232

https://arxiv.org/pdf/2304.12037.pdf

Small flares frequently occur in the quiet Sun. Previous studies have noted that they share many common characteristics with typical solar flares in active regions. However, their similarities and differences are not fully understood, especially their thermal properties. In this study, we performed imaging spectroscopic observations in the Hα line taken with the Solar Dynamics Doppler Imager on the Solar Magnetic Activity Research Telescope (SMART/SDDI) at the Hida Observatory and imaging observations with the Atmospheric Imaging Assembly onboard Solar Dynamics Observatory (SDO/AIA). We analysed 25 cases of small flares in the quiet Sun over the thermal energy range of 1024−1027erg, paying particular attention to their thermal properties. Our main results are as follows: (1) We observe a redshift together with line centre brightening in the Hα line associated with more than half of the small flares. (2) We employ differential emission measure analysis using AIA multi-temperature (channel) observations to obtain the emission measure and temperature of the small flares. The results are consistent with the Shibata & Yokoyama (1999, 2002) scaling law. From the scaling law, we estimated the coronal magnetic field strength of small flares to be 5 --15 G. (3) The temporal evolution of the temperature and the density shows that the temperature peaks precede the density peaks in more than half of the events. These results suggest that chromospheric evaporations/condensations play an essential role in the thermal properties of some of the small flares in the quiet Sun, as does for large flares. **2019-09-07**

Unified Relationship between Cold Plasma Ejections and Flare Energies Ranging from Solar Microflares to Giant Stellar Flares

Yuji **Kotani**, Kazunari Shibata, Takako T. Ishii, Daiki Yamasaki, Kenichi Otsuji, Kiyoshi Ichimoto, Ayumi Asai

ApJ **943** 143 **2023**

https://arxiv.org/pdf/2212.08850.pdf

https://iopscience.iop.org/article/10.3847/1538-4357/acac76/pdf

We often find spectral signatures of chromospheric cold plasma ejections accompanied by flares in a wide range of spatial scales in the solar and stellar atmospheres. However, the relationship between physical quantities (such as mass, kinetic energy, and velocity) of cold ejecta and flare energy has not been investigated in a unified manner for the entire range of flare energies to date. This study analyzed the spectra of cold plasma ejections associated with small-scale flares and solar flares (energy 1025−1029erg) to supply smaller energy samples. We performed Hα imaging spectroscopy observation by the Solar Dynamics Doppler Imager on the Solar Magnetic Activity Research Telescope (SMART/SDDI). We determined the physical quantities of the ejecta by cloud model fitting to the Hα spectrum. We determined flare energy by differential emission measure analysis using Atmospheric Imaging Assembly onboard Solar Dynamics Observatory (SDO/AIA) for small-scale flares and by estimating the bolometric energy for large-scale flares. As a result, we found that the ejection mass M and the total flare energy Etot follow a relation of M∝E2/3tot. We show that the scaling law derived from a simple physical model explains the solar and stellar observations with a coronal magnetic field strength as a free parameter. We also found that the kinetic energy and velocity of the ejecta correlate with the flare energy. These results suggest a common mechanism driven by magnetic fields to cause cold plasma ejections with flares on the Sun and stars. **2019-09-07**

New Observations of Balmer Continuum Flux in Solar Flares, Instrument Description and First Results

P. **Kotrč**, O. Procházka, P. Heinzel

Solar Physics Volume 291, Issue 3, pp 779-789 **2016**

http://arxiv.org/pdf/1601.04610v1.pdf

Increase in the Balmer continuum radiation during solar flares was predicted by various authors but never firmly confirmed observationally using ground-based slit spectrographs. Here we describe a new post-focal instrument - Image Selector - enabling to measure the Balmer continuum flux from the whole flare area, in analogy of successful detections of flaring dMe stars. The system was developed and put into operation at the horizontal solar telescope HSFA-2 of the Ond\v{r}ejov Observatory. We measure the total flux by a fast spectrometer from a limited but well defined region on the solar disk. Using a system of diaphragms, the disturbing contribution of a bright solar disk can be eliminated as much as possible. Light curves of the measured flux in the spectral range 350 - 440 nm are processed, together with the H{\alpha} images of the flaring area delimited by the appropriate diaphragm. The spectral flux data are flat-fielded, calibrated and processed to be compared with model predictions. Our analysis of the data proves that the described device is sufficiently sensitive to detect variations in the Balmer continuum during solar flares. Assuming that the Balmer-continuum kernels have at least a similar size as those visible in H\alpha, we find the flux increase in the Balmer continuum to reach 230 % - 550 % of the quiet continuum during the observed X-class flare. We also found temporal changes in the Balmer continuum flux starting well before the onset of the flare in H{\alpha}. **2014-06-11**

Microwave Imaging of Quasi-periodic Pulsations at Flare Current Sheet

Yuankun **Kou**, Xin Cheng, Yulei Wang, Sijie Yu, Bin Chen, Eduard P. Kontar, Mingde Ding

Nature Communications (**2022**) 13:7680

https://arxiv.org/pdf/2212.08318.pdf

https://www.nature.com/articles/s41467-022-35377-0.pdf
Quasi-periodic pulsations (QPPs) are frequently detected in solar and stellar flares, but the underlying physical mechanisms are still to be ascertained. Here, we show microwave QPPs during a solar flare originating from quasi-periodic magnetic reconnection at the flare current sheet. They appear as two vertically detached but closely related sources with the brighter ones located at flare loops and the weaker ones along the stretched current sheet. Although the brightness temperatures of the two microwave sources differ greatly, they vary in phase with periods of about 10--20 s and 30--60 s. The gyrosynchrotron-dominated microwave spectra also present a quasi-periodic soft-hard-soft evolution. These results suggest that relevant high-energy electrons are accelerated by quasi-periodic reconnection, likely arising from the modulation of magnetic islands within the current sheet as validated by a 2.5-dimensional magnetohydrodynamic simulation. **2017 July 13**

Stellar flares **Review**

Adam F. **Kowalski**
Living Reviews in Solar Physics 21: 1 **2024**
https://arxiv.org/pdf/2402.07885.pdf
https://link.springer.com/content/pdf/10.1007/s41116-024-00039-4
Magnetic storms on stars manifest as remarkable, randomly occurring changes of the luminosity over durations that are tiny in comparison to the normal evolution of stars. These stellar flares are bursts of electromagnetic radiation from X-ray to radio wavelengths, and they occur on most stars with outer convection zones. They are analogous to the events on the Sun known as solar flares, which impact our everyday life and modern technological society. Stellar flares, however, can attain much greater energies than those on the Sun. Despite this, we think that these phenomena are rather similar in origin to solar flares, which result from a catastrophic conversion of latent magnetic field energy into atmospheric heating within a region that is relatively small in comparison to normal stellar sizes. We review the last several decades of stellar flare research. We summarize multi-wavelength observational results and the associated thermal and nonthermal processes in flaring stellar atmospheres. Static and hydrodynamic models are reviewed with an emphasis on recent progress in radiation-hydrodynamics and the physical diagnostics in flare spectra. Thanks to their effects on the space weather of exoplanetary systems (and thus in our search for life elsewhere in the universe) and their preponderance in \emph{Kepler} mission data, white-light stellar flares have re-emerged in the last decade as a widely-impactful area of study within astrophysics. Yet, there is still much we do not understand, both empirically and theoretically, about the spectrum of flare radiation, its origin, and its time evolution. We conclude with several big-picture questions that are fundamental in our pursuit toward a greater understanding of these enigmatic stellar phonemena and, by extension, those on the Sun.

The Atmospheric Response to High Nonthermal Electron Beam Fluxes in Solar Flares. II. Hydrogen Broadening Predictions for Solar Flare Observations with the Daniel K. Inouye Solar Telescope

Adam F. **Kowalski** (1,2,3), Joel C. Allred (4), Mats Carlsson (5,6), Graham S. Kerr (7), Pier-Emmanuel Tremblay (8), Kosuke Namekata (9,10), David Kuridze (11,12,13), Han Uitenbroek (1)
ApJ **928** 190 **2022**
https://arxiv.org/pdf/2201.13349.pdf
https://iopscience.iop.org/article/10.3847/1538-4357/ac5174/pdf
Red-shifted components of chromospheric emission lines in the hard X-ray impulsive phase of solar flares have recently been studied through their 30 s evolution with the high resolution of IRIS. Radiative-hydrodynamic flare models show that these redshifts are generally reproduced by electron-beam generated chromospheric condensations. The models produce large ambient electron densities, and the pressure broadening of hydrogen Balmer series should be readily detected in observations. To accurately interpret upcoming spectral data of flares with the DKIST, we incorporate non-ideal, non-adiabatic line broadening profiles of hydrogen into the RADYN code. These improvements allow time-dependent predictions for the extreme Balmer line wing enhancements in solar flares. We study two chromospheric condensation models, which cover a range of electron beam fluxes ($1-5\times10^{11}$ erg s^{-1} cm^{-2}) and ambient electron densities ($1-60\times10^{13}$ cm^{-3}) in the flare chromosphere. Both models produce broadening and redshift variations within 10 s of the onset of beam heating. In the chromospheric condensations, there is enhanced spectral broadening due to large optical depths at Hα, Hβ, and Hγ, while the much lower optical depth of the Balmer series H12−H16 provides a translucent window into the smaller electron densities in the beam-heated layers below the condensation. The wavelength ranges of typical DKIST/ViSP spectra of solar flares will be sufficient to test the predictions of extreme hydrogen wing broadening and accurately constrain large densities in chromospheric condensations.

Spectral Evidence for Heating at Large Column Mass in Umbral Solar Flare Kernels I: IRIS NUV Spectra of the X1 Solar Flare of 2014 Oct 25

Adam F. **Kowalski** (1, 2, 3), Elizabeth Butler (1), Adrian N. Daw (4), Lyndsay Fletcher (5, 6), Joel C. Allred (4, 6), Bart De Pontieu (6, 7, 8), Graham S. Kerr (4), Gianna Cauzzi
ApJ **878** 135 **2019**
https://arxiv.org/pdf/1905.02111.pdf
sci-hub.se/10.3847/1538-4357/ab1f8b
The GOES X1 flare SOL**2014-10-25**T17:08:00 was a three-ribbon solar flare observed with IRIS in the near and far ultraviolet. One of the flare ribbons crossed a sunspot umbra, producing a dramatic, ~1000% increase in the near-ultraviolet (NUV) continuum radiation. We comprehensively analyze the ultraviolet spectral data of the umbral flare brightenings, which provide new challenges for radiative-hydrodynamic modeling of the chromospheric velocity field and the white-light continuum radiation. The emission line profiles in the umbral flare brightenings exhibit redshifts and profile asymmetries, but these are significantly smaller than in another, well-studied X-class solar flare. We present a ratio of the NUV continuum intensity to the \feii\ intensity. This continuum-to-line ratio is a new spectral diagnostic of significant heating at high column mass (log m/[g cm−2]>−2) during solar flares because the continuum and emission line radiation originate from relatively similar temperatures but moderately different optical depths. The full spectral readout of these IRIS data also allow for a comprehensive survey of the flaring NUV landscape: in addition to many lines of Fe II and Cr II, we identify a new solar flare emission line, He I λ2829.91 (as previously identified in laboratory and early-type stellar spectra). The Fermi/GBM hard X-ray data provide inputs to radiative-hydrodynamic models (which will be presented in Paper II) in order to better understand the large continuum-to-line ratios, the origin of the white-light continuum radiation, and the role of electron beam heating in the low atmosphere.

Parameterizations of Chromospheric Condensations in dG and dMe Model Flare Atmospheres

Adam F. **Kowalski** (1,2,3), Joel C. Allred (4) ((1) University of Colorado, (2) National Solar Observatory, (3) Laboratory for Atmospheric and Space Physics, (4) NASA Goddard Space Flight Center)
ApJ **2017**
https://arxiv.org/pdf/1711.09488.pdf
The origin of the near-ultraviolet and optical continuum radiation in flares is critical for understanding particle acceleration and impulsive heating in stellar atmospheres. Radiative-hydrodynamic simulations in 1D have shown that high energy deposition rates from electron beams produce two flaring layers at T~10^4 K that develop in the chromosphere: a cooling condensation (downflowing compression) and heated non-moving (stationary) flare layers just below the condensation. These atmospheres reproduce several observed phenomena in flare spectra, such as the red wing asymmetry of the emission lines in solar flares and a small Balmer jump ratio in M dwarf flares. The high beam flux simulations are computationally expensive in 1D, and the (human) timescales for completing NLTE models with adaptive grids in 3D will likely be unwieldy for a time to come. We have developed a prescription for predicting the approximate evolved states, continuum optical depth, and the emergent continuum flux spectra of radiative-hydrodynamic model flare atmospheres. These approximate prescriptions are based on an important atmospheric parameter: the column mass (m_ref) at which hydrogen becomes nearly completely ionized at the depths that are approximately in steady state with the electron beam heating. Using this new modeling approach, we find that high energy flux density (>F11) electron beams are needed to reproduce the brightest observed continuum intensity in IRIS data of the **2014-Mar-29** X1 solar flare and that variation in m_ref from 0.001 to 0.02 g/cm2 reproduces most of the observed range of the optical continuum flux ratios at the peaks of M dwarf flares.
See RHESSI Science Nuggets # 315 Jan **2018**
http://sprg.ssl.berkeley.edu/~tohban/wiki/index.php/Parameterized_Flare_Models_with_Chromospheric_Compressions

The Atmospheric Response to High Nonthermal Electron Beam Fluxes in Solar Flares I: Modeling the Brightest NUV Footpoints in the X1 Solar Flare of 2014 March 29

Adam F. **Kowalski** (University of Maryland College Park/NASA-GSFC, and University of Colorado Boulder/National Solar Observatory), Joel C. Allred (NASA Goddard Space Flight Center), Adrian N. Daw (NASA Goddard Space Flight Center), Gianna Cauzzi (INAF-Osservatorio Astrofisico di Arcetri), Mats Carlsson (University of Oslo)
ApJ 836 12 **2016**
http://arxiv.org/pdf/1609.07390v1.pdf
The **2014 March 29** X1 solar flare (SOL20140329T17:48) produced bright continuum emission in the far- and near-ultraviolet (NUV) and highly asymmetric chromospheric emission lines, providing long-sought constraints on the heating mechanisms of the lower atmosphere in solar flares. We analyze the continuum and emission line data from the Interface Region Imaging Spectrograph (IRIS) of the brightest flaring magnetic footpoints in this flare. We compare the NUV spectra of the brightest pixels to new radiative-hydrodynamic predictions calculated with the RADYN code using constraints on a nonthermal electron beam inferred from the collisional thick-target modeling of hard X-ray data from RHESSI. We show that the atmospheric response to a high beam flux density satisfactorily achieves the observed continuum brightness in the NUV. The NUV continuum emission in this flare is consistent with hydrogen (Balmer) recombination radiation that originates from low optical depth in a dense chromospheric condensation and from the

stationary beam-heated layers just below the condensation. A model producing two flaring regions (a condensation and stationary layers) in the lower atmosphere is also consistent with the asymmetric Fe II chromospheric emission line profiles observed in the impulsive phase.

New Insights into White-Light Flare Emission from Radiative-Hydrodynamic Modeling of a Chromospheric Condensation

Adam F. **Kowalski**, Suzanne L. Hawley, Mats Carlsson, Joel C. Allred, Han Uitenbroek, Rachel A. Osten, Gordon Holman

Solar Physics Volume 290, Issue 12, pp 3487-3523 **2015**

http://arxiv.org/pdf/1503.07057v1.pdf

(abridged) The heating mechanism at high densities during M dwarf flares is poorly understood. Spectra of M dwarf flares in the optical and near-ultraviolet wavelength regimes have revealed three continuum components during the impulsive phase: 1) an energetically dominant blackbody component with a color temperature of T ~ 10,000 K in the blue-optical, 2) a smaller amount of Balmer continuum emission in the near-ultraviolet at lambda < 3646 Angstroms and 3) an apparent pseudo-continuum of blended high-order Balmer lines. These properties are not reproduced by models that employ a typical "solar-type" flare heating level in nonthermal electrons, and therefore our understanding of these spectra is limited to a phenomenological interpretation. We present a new 1D radiative-hydrodynamic model of an M dwarf flare from precipitating nonthermal electrons with a large energy flux of 1013 erg cm−2 s−1. The simulation produces bright continuum emission from a dense, hot chromospheric condensation. For the first time, the observed color temperature and Balmer jump ratio are produced self-consistently in a radiative-hydrodynamic flare model. We find that a T ~ 10,000 K blackbody-like continuum component and a small Balmer jump ratio result from optically thick Balmer and Paschen recombination radiation, and thus the properties of the flux spectrum are caused by blue light escaping over a larger physical depth range compared to red and near-ultraviolet light. To model the near-ultraviolet pseudo-continuum previously attributed to overlapping Balmer lines, we include the extra Balmer continuum opacity from Landau-Zener transitions that result from merged, high order energy levels of hydrogen in a dense, partially ionized atmosphere. This reveals a new diagnostic of ambient charge density in the densest regions of the atmosphere that are heated during dMe and solar flares.

Optical Spectral Observations of a Flickering White-light Kernel in a C1 Solar Flare

Adam F. **Kowalski**1,4, Gianna Cauzzi2, and Lyndsay Fletcher

2015 ApJ 798 107

We analyze optical spectra of a two-ribbon, long-duration C1.1 flare that occurred on **2011 August 18** within AR 11271 (SOL2011-08-18T15:15). The impulsive phase of the flare was observed with a comprehensive set of space-borne and ground-based instruments, which provide a range of unique diagnostics of the lower flaring atmosphere. Here we report the detection of enhanced continuum emission, observed in low-resolution spectra from 3600 Å to 4550 Å acquired with the Horizontal Spectrograph at the Dunn Solar Telescope. A small, ≤0."5 (1015 cm2) penumbral/umbral kernel brightens repeatedly in the optical continuum and chromospheric emission lines, similar to the temporal characteristics of the hard X-ray variation as detected by the Gamma-ray Burst Monitor on the Fermi spacecraft. Radiative-hydrodynamic flare models that employ a nonthermal electron beam energy flux high enough to produce the optical contrast in our flare spectra would predict a large Balmer jump in emission, indicative of hydrogen recombination radiation from the upper flare chromosphere. However, we find no evidence of such a Balmer jump in the bluemost spectral region of the continuum excess. Just redward of the expected Balmer jump, we find evidence of a "blue continuum bump" in the excess emission which may be indicative of the merging of the higher order Balmer lines. The large number of observational constraints provides a springboard for modeling the blue/optical emission for this particular flare with radiative-hydrodynamic codes, which are necessary to understand the opacity effects for the continuum and emission line radiation at these wavelengths.

Spectral diagnostics of cool flare loops observed by SST: I. Inversion of the Ca II 8542 Å and Hβ lines

Július **Koza**, David Kuridze, Petr Heinzel, Sonja Jejčič, Huw Morgan, Maciej Zapiór

ApJ **885** 154 **2019**

https://arxiv.org/pdf/1909.07356.pdf

https://doi.org/10.3847/1538-4357/ab4426

Flare loops form an integral part of eruptive events, being detected in the range of temperatures from X-rays down to cool chromospheric-like plasmas. While the hot loops are routinely observed by the Solar Dynamics Observatory's Atmospheric Imaging Assembly (SDO/AIA), cool loops seen off-limb are rare. In this paper we employ unique observations of the SOL**2017-09-10**T16:06 X8.2-class flare which produced an extended arcade of loops. The Swedish 1-m Solar Telescope (SST) made a series of spectral images of the cool off-limb loops in the Ca II 8542 Å and the hydrogen Hβ lines. Our focus is on the loop apices. Non-LTE spectral inversion is achieved through the construction of

extended grids of models covering a realistic range of plasma parameters. The Multilevel Accelerated Lambda Iterations (MALI) code solves the non-LTE radiative-transfer problem in a 1D externally-illuminated slab, approximating the studied loop segment. Inversion of the Ca II 8542 Å and Hβ lines yields two similar solutions, both indicating high electron densities around 2×1012 cm−3 and relatively large microturbulence around 25 kms−1. These are in reasonable agreement with other independent studies of the same or similar events. In particular, the high electron densities in the range 1012−1013 cm−3 are consistent with those derived from the SDO's Helioseismic and Magnetic Imager white-light observations. The presence of such high densities in solar eruptive flares supports the loop interpretation of the optical continuum emission of stars which manifest superflares.

Solar Demon – an approach to detecting flares, dimmings, and EUV waves on SDO/AIA images

Emil **Kraaikamp*** and Cis Verbeeck
J. Space Weather Space Clim., 5, A18 (**2015**) **File**
http://www.swsc-journal.org/articles/swsc/pdf/2015/01/swsc140062.pdf
Flares, dimmings, and extreme ultraviolet (EUV) waves are three types of eruptive phenomena on the Sun, which are main drivers of space weather. Fast and reliable detection of these phenomena helps augment space weather predictions. In the current paper, we introduce Solar Demon, the first software that detects all three phenomena, using a modular design to exploit synergies. While Solar Demon runs in near real-time on SDO/AIA synoptic quick-look images to provide fast detections of flares, dimmings, and EUV waves for space weather purposes, it also processes new Atmospheric Imaging Assembly (AIA) synoptic science images on a regular basis to build dedicated science quality catalogs. An overview of Solar Demon is given, with a focus on the algorithms for EUV wave detection and characterization. Several first results, such as flare and dimming butterfly diagrams for the rising part of Solar Cycle 24, are presented. The main advantages, challenges, and future prospects for Solar Demon are outlined in the Section 5.
February 15, 2011, October 23, 2012, July 8, 2014, Oct 27, 2014, 2014-11-03, December 12, 2014,

Temperature Dependence of the Flare Fluence Scaling Exponent
On the variation of the scaling exponent of the flare fluence with temperature

M. **Kretzschmar**
Solar Phys. Volume 290, Issue 12, pp 3593-3609 **2015**
http://arxiv.org/pdf/1510.01975v1.pdf
Solar flares result in an increase of the solar irradiance at all wavelengths. While the distribution of the flare fluence observed in coronal emission has been widely studied and found to scale as f(E) ~ E^{-\alpha}, with \alpha slightly below 2, the distribution of the flare fluence in chromospheric lines is poorly known. We used the solar irradiance measurements observed by the SDO/EVE instrument at a 10s-cadence to investigate if there is a dependency of the scaling exponent on the formation region of the lines (or temperature). We analyzed all flares above the C1 level since the start of the EVE observation (May 2010) to determine the flare fluence distribution in 16 lines covering a large range of temperature, several of which were not studied before. Our results show a small downward trend with the temperature of the scaling exponent of the PDF, going from above 2 at lower temperature (a few 10^4 K) to about1.8 for hot coronal emission (several 10^6 K). However, because colder lines also have smaller contrast, we could not exclude that this behavior is caused by including more noise for smaller flare for these lines. We discuss the method and its limits and tentatively associate this possible trend to the different mechanisms responsible for the heating of the chromosphere and corona during flares.
See CESRA **2016**, p.96
http://cesra2016.sciencesconf.org/conference/cesra2016/pages/CESRA2016_prog_abs_book_v3.pdf

Thermal and kinetic coronal rain diagnostics with Mg II h & k lines⋆

M. **Kriginsky**1,2 and R. Oliver1,2
A&A 683, A127 (**2024**)
https://www.aanda.org/articles/aa/pdf/2024/03/aa48443-23.pdf
Aims. The aim of this work is to assess the temperature and velocity diagnostics of coronal rain clumps, as observed in the lines formed in the upper chromosphere.
Methods. We performed the temperature diagnostics using inversions of data from nine spectroscopic observations obtained with the IRIS spectrograph in the Mg II h & k lines. The sensitivity to the temperature of the emission peaks of these lines was exploited to determine the temperature of the coronal rain plasma using inversions of the spectroscopic profiles. Additional relationships between different spectral features of these lines, derived from the use of 3D radiative transfer line synthesis applied to simulations, were employed in order to derive the line-of-sight (LoS) velocities in different parts of the coronal rain plasma.

Results. For the first time, spectroscopic inversions of coronal rain were successfully performed. Temperatures derived from the inversions yield coronal rain clump temperatures at the formation height of the emission peaks of the Mg II h & k lines in the range between 5000 and 7000 K. This narrow range of values remains consistent among all the different observations used in this work. We obtained LoS velocities of up to 40 km s−1, which are consistent with the motion of the plasma being mostly constrained to the plane of the sky, as the coronal rain was mostly detected shortly after its formation and the observations took place in the disc. Furthermore, velocity diagnostics led to the detection of larger velocities at higher layers of the coronal rain plasma in some cases. This increased velocity seems to indicate that at some point (at least) during the fall of coronal rain clumps towards the chromosphere, the material in the upper part of the coronal rain plasma is falling with greater velocity than the material below it. The conditions of the temperature and density of the coronal rain plasma where the Mg II h line forms appear to be slightly different that those of the Mg II k line, with the former found at slightly colder and denser parts of the plasma.

A DEFT Way to Forecast Solar Flares

Larisza D. **Krista**1,2,3 and Matthew Chih4
2021 ApJ 922 218
https://iopscience.iop.org/article/10.3847/1538-4357/ac2840/pdf
https://doi.org/10.3847/1538-4357/ac2840
Solar flares have been linked to some of the most significant space weather hazards at Earth. These hazards, including radio blackouts and energetic particle events, can start just minutes after the flare onset. Therefore, it is of great importance to identify and predict flare events. In this paper we introduce the ***Detection and EUV Flare Tracking (DEFT) tool***, which allows us to identify flare signatures and their precursors using high spatial and temporal resolution extreme-ultraviolet (EUV) solar observations. The unique advantage of DEFT is its ability to identify small but significant EUV intensity changes that may lead to solar eruptions. Furthermore, the tool can identify the location of the disturbances and distinguish events occurring at the same time in multiple locations. The algorithm analyzes high temporal cadence observations obtained from the Solar Ultraviolet Imager instrument aboard the GOES-R satellite. In a study of 61 flares of various magnitudes observed in 2017, the "main" EUV flare signatures (those closest in time to the X-ray start time) were identified on average 6 minutes early. The "precursor" EUV signatures (second-closest EUV signatures to the X-ray start time) appeared on average 14 minutes early. Our next goal is to develop an operational version of DEFT and to simulate and test its real-time use. A fully operational DEFT has the potential to significantly improve space weather forecast times.

The Sun as a star: observations of white-light flares

M. **Kretzschmar**
A&A 530, A84 (**2011**)
Context. Solar flares radiate energy at all wavelengths, but the spectral distribution of this energy is still poorly known. White-light continuum emission is sometimes observed, and these flares are then called “white-light flares” (WLFs).
Aims. We investigate if all flares are WLFs and how the radiated energy is distributed spectrally.
Methods. We perform a superposed epoch analysis of spectral and total irradiance measurements obtained since 1996 by the SOHO and GOES spacecraft at various wavelengths, from soft X-rays to the visible domain.
Results. The long-term record of solar irradiance and the excellent duty cycle of the measurements allow us to detect a signal in visible irradiance even for moderate (C-class) flares mainly during the impulsive phase. We identify this signal as continuum emission emitted by WLFs and find that it is consistent with a blackbody emission at ~9000 K. We estimate the contribution of the WL continuum for several sets of flares and find it to be about 70% of the total radiated energy. We re-analyse the X17 flare that occurred on 28 October 2003 and find similar results.
Conclusions. We show that most of the flares – if not all – are WLFs and that the white-light continuum is the main contributor to the total radiated energy; this continuum is consistent with a blackbody spectrum at ~9000 K. These observational results are important for understanding the physical mechanisms during flares and possibly suggest a contribution of flares to the variations of the total solar irradiance (TSI).

Thermal and kinetic coronal rain diagnostics with MgII h & k lines

M. **Kriginsky**, R. Oliver
A&A **2024**
https://arxiv.org/pdf/2401.14859.pdf
We performed the temperature diagnostics using inversions of data from nine spectroscopic observations obtained with the IRIS spectrograph in the MgII h & k lines. The sensitivity to the temperature of the emission peaks of these lines was exploited to determine the temperature of the coronal rain plasma using inversions of the spectroscopic profiles. Additional relationships between different spectral features of these lines, derived from the use of 3D radiative transfer line synthesis applied to simulations, were employed in order to derive the line-of-sight (LoS) velocities in different parts of the coronal rain plasma. For the first time, spectroscopic inversions of coronal rain were successfully performed. Temperatures derived from the inversions yield coronal rain clump temperatures at the formation height of the emission peaks of the MgII h & k lines in the range between 5000 and 7000 K. This narrow range of values remains

consistent among all the different observations used in this work. We obtained LoS velocities of up to 40 km/s, which are consistent with the motion of the plasma being mostly constrained to the plane of the sky, as the coronal rain was mostly detected shortly after its formation and the observations took place in the disc. Furthermore, velocity diagnostics led to the detection of larger velocities at higher layers of the coronal rain plasma in some cases. This increased velocity seems to indicate that at some point (at least) during the fall of coronal rain clumps towards the chromosphere, the material in the upper part of the coronal rain plasma is falling with greater velocity than the material below it. The conditions of the temperature and density of the coronal rain plasma where the Mg II h line forms appear to be slightly different that those of the Mg II k line, with the former found at slightly colder and denser parts of the plasma.
Table 1. Description of the datasets used in this work. 2014-2015

Desaturated EUV Flare Ribbons in an X-class Flare

Säm **Krucker**1,2, Gabriele Torre1,3, and Richard A. Schwartz4,5
2021 ApJ 909 43
https://iopscience.iop.org/article/10.3847/1538-4357/ac2840/pdf
https://doi.org/10.3847/1538-4357/abcf30
This paper studies the energy dissipation of nonthermal electrons in the chromospheric flare ribbons during the peak time of a Geostationary Operational Environmental Satellite X-class flare (SOL**2011-09-06**) using desaturated Solar Dynamics Observatory/Atmospheric Imaging Assembly extreme-ultraviolet (EUV) narrow-band images. The temperature distribution in emission measure, called the differential emission measure (DEM), derived from the EUV fluxes from the flare ribbons shows an increase in the emission measure up to a temperature around 9 × 106 K, followed by a steep decline at higher temperatures. In contrast, the flare loop reaches temperatures up to 27 × 106 K. This result is in agreement with previously reported single-temperature measurements using soft X-ray filter images, as well as DEM distributions reported for smaller flares obtained from EUV line observations. The main difference between small and large flares appears to be an increased emission measure in the flare ribbons, while the ribbon peak temperature is similar for all flares. This is different from the flare loop temperatures, where the hottest temperatures occur in the largest flares. However, the physically relevant quantity for energy dissipation, the energy content of the heated plasma as a function of temperature, does not need to peak at the same temperature as the DEM. The poorly constrained source thickness in radial extent of the flare ribbons has a significant impact on the shape of the differential thermal energy distribution. In particular, if the highest temperatures occur over a wide radial extent as "evaporating" plasma starts expending, the largest amount of energy could potentially be hidden above the peak temperature of the DEM.

The Last Best Flare of Cycle 24?

Säm **Krucker**, Hugh Hudson
RHESSI Nuggets #306 September **2017**
http://sprg.ssl.berkeley.edu/~tohban/wiki/index.php/The_Last_Best_Flare_of_Cycle_24%3F
Cycle 24 has produced a great flare (and a GLE).
SOL**2017-09-06** (X9.3) and SOL**2017-09-10** (X8.2), both of which produced long-duration gamma-ray events observed by Fermi

RHESSI Heliophysics Senior Review 2015
High Energy Solar Spectroscopic Imager

Samuel **Krucker**, Brian Dennis, Albert Shih, Manfred Bester
http://hesperia.gsfc.nasa.gov/senior_review/2015/senior_review_proposal_2015.pdf
- Evolution of Solar Eruptive Events
- Flare-accelerated Electrons
- Flare-accelerated Ions
– Flare-heated Plasma
– Global Structure of the Photosphere
3 Nov 2010, 2011-03-07, 6 Sept 2011, 3 March 2012, 2012 July 19. 13 May 2013, 2014-01-28, March 29, 2014, 2014-04-19, 24 Sept 2014, 24 Oct 2014, 14 Dec 2014

First Images from the Focusing Optics X-Ray Solar Imager

Säm **Krucker**1,2, Steven Christe3, Lindsay Glesener1, Shin-nosuke Ishikawa4, Brian Ramsey5, Tadayuki Takahashi6,7, Shin Watanabe6,7, Shinya Saito6,7, Mikhail Gubarev5, Kiranmayee Kilaru5, Hiroyasu Tajima8, Takaaki Tanaka9, Paul Turin1, Stephen McBride1, David Glaser1, Jose Fermin1, Stephen White10, and Robert Lin
2014 ApJ 793 L32
The Focusing Optics X-ray Solar Imager (FOXSI) sounding rocket payload flew for the first time on **2012 November 2**, producing the first focused images of the Sun above 5 keV. To enable hard X-ray (HXR) imaging spectroscopy via

direct focusing, FOXSI makes use of grazing-incidence replicated optics combined with fine-pitch solid-state detectors. On its first flight, FOXSI observed several targets that included active regions, the quiet Sun, and a GOES-class B2.7 microflare. This Letter provides an introduction to the FOXSI instrument and presents its first solar image. These data demonstrate the superiority in sensitivity and dynamic range that is achievable with a direct HXR imager with respect to previous, indirect imaging methods, and illustrate the technological readiness for a spaceborne mission to observe HXRs from solar flares via direct focusing optics.

A Wonderful Cycle 24 Flare

Sa"m **Krucker** and Hugh Hudson
RHESSI Science Nugget, No. 2020, **2014**
http://sprg.ssl.berkeley.edu/~tohban/wiki/index.php/A_Wonderful_Cycle_24_Flare
Somewhat surprisingly, even this ostensibly weak Cycle 24 has produced 29 X-class flares thus far. Of these the third most powerful, GOES X4.9, just happened a week ago (**25 February 2014**). Reflecting the weakness of the solar cycle, the active region responsible (NOAA Region11990) had a relatively small sunspot area, only 250 millionths of the solar hemisphere - the biggest groups can be an order of magnitude larger.. But the flare itself was magnificent, and this Nugget just points to early views from RHESSI and other observatories.

Acceleration-region Densities

Sa"m **Krucker** and Marina Battaglia.
RHESSI Science Nugget, No. 205, Aug **2013**
http://sprg.ssl.berkeley.edu/~tohban/wiki/index.php/Acceleration-region_Densities
Clean examples of "above-the-loop-top" emission, as in the singular case of the Masuda flare, have been rare. The event discussed here (SOL**2012-07-19**T05:58, M7.7) is one of the best in the RHESSI database, and it had copious supporting observation - specifically, from SDO/AIA with its wonderful images of flare structures as seen in thermal emissions.
At last we have found a very clear example of the Masuda phenomenon, some 20 years after its original discovery (Ref. [1]), and one for which we have a great deal of modern data. This includes RHESSI and AIA, and the combination of these datasets has allowed us to understand the energetics of this new flare much better. We have come to the conclusion that the above-the-loop-top-source, well-observed here, contains a plasma that has a tail-dominated electron distribution function, ie that the acceleration process basically has worked on all of the electrons within its accessible volume: bulk acceleration.

RHESSI Heliophysics Senior Review 2013

Samuel **Krucker**, Brian Dennis, Manfred Bester, Laura Peticolas
http://hesperia.gsfc.nasa.gov/senior_review/2013/senior_review_proposal_2013.pdf**, 2013, File**
RHESSI was given an excellent rating by the Heliophysics Senior Review panel for both “overall scientific merit of the proposed extended mission” and for “Value to the Heliophysics System Observatory.” The Panel recommends “the continued operation of the RHESSI extended mission,” and states in its report that “RHESSI plays a unique role within the HSO, enabling system-wide studies of energy release and particle acceleration in flares/CMEs and their effects on the interplanetary medium, magnetosphere, and ITM.”

Solar flares at submillimeter wavelengths A review

Sam **Krucker** · C.G. Gimenez de Castro · H.S. Hudson · G. Trottet · T.S. Bastian · A.S. Hales · J. Kašparova · K.-L. Klein · M. Kretzschmar · T. Luthi · A. Mackinnon · S. Pohjolainen · S.M. White
Astronomy and Astrophysics Review, Volume 21, Issue 1, (**2013**) 21:58; **File**
We discuss the implications of the first systematic observations of solar flares at submillimeter wavelengths, defined here as observing wavelengths shorter than 3~mm (frequencies higher than 0.1 THz). The events observed thus far show that this wave band requires a new understanding of high-energy processes in solar flares. Several events, including observations from two different observatories, show during the impulsive phase of the flare a spectral component with a positive (increasing) slope at the highest observable frequencies (up to 405~GHz). To emphasize the increasing spectra and the possibility that these events could be even more prominent in the THz range, we term this spectral feature a ``THz component". Here we review the data and methods, and critically assess the observational evidence for such distinct component(s). This evidence is convincing. We also review the several proposed explanations for these feature(s), which have been reported in three distinct flare phases. These data contain important clues to flare development and particle acceleration as a whole, but many of the theoretical issues remain open. We generally have lacked systematic observations in the millimeter-wave to far-infrared range that are needed to complete our picture of these events, and encourage observations with new facilities. **2000-03-22T18:44; 2001-04-06T19:19, 2001-04-12T10:28, 2001-08-25T16:32; 2001-11-28T16:34; 2002-08-30T13:28; 2002-09-10T14:53; 2002-12-**

20T13:18; 2003-10-27T12:31; 2003-10-28T11:10; 2003-11-02T17:17; 2003-11-04T19:44; 2004-10-30T11:44; 2006-12-06T18:44

ELECTRON ACCELERATION ASSOCIATED WITH SOLAR JETS

Säm **Krucker**1,2, E. P. Kontar3, S. Christe4, L. Glesener1,5 and R. P. Lin
2011 ApJ 742 82

This paper investigates the solar source region of supra-thermal (few keV up to the MeV range) electron beams observed near Earth by combining in situ measurements of the three-dimensional Plasma and Energetic Particles experiment on the WIND spacecraft with remote-sensing hard X-ray observations by the Reuven Ramaty High Energy Solar Spectroscopic Imager. The in situ observations are used to identify events, and the hard X-ray observations are then searched for signatures of supra-thermal electrons radiating bremsstrahlung emission in the solar atmosphere. Only prompt events detected above 50 keV with a close temporal correlation between the flare hard X-ray emission and the electrons seen near Earth are selected, limiting the number of events to 16. We show that for 7 of these 16 events, hard X-ray imaging shows three chromospheric sources: two at the footpoints of the post-flare loop and one related to an apparently open field line. The remaining events show two footpoints (seven events, four of which show elongated sources possibly hiding a third source) or are spatially unresolved (two events). Out of the 16 events, 6 have a solar source region within the field of view of the Transition Region and Corona Explorer (TRACE). All events with TRACE data show EUV jets that have the same onset as the hard X-ray emission (within the cadence of tens of seconds). After the hard X-ray burst ends, the jets decay. These results suggest that escaping prompt supra-thermal electron events observed near Earth are accelerated in flares associated with reconnection between open and closed magnetic field lines, the so-called interchange reconnection scenario.

HIGH-RESOLUTION IMAGING OF SOLAR FLARE RIBBONS AND ITS IMPLICATION ON THE THICK-TARGET BEAM MODEL

Säm **Krucker**1,2, H. S. Hudson1,3, N. L. S. Jeffrey3, M. Battaglia3, E. P. Kontar3, A. O. Benz2, A. Csillaghy2 and R. P. Lin
2011 ApJ 739 96

We report on high-resolution optical and hard X-ray observations of solar flare ribbons seen during the GOES X6.5 class white-light flare of **2006 December 6**. The data consist of imaging observations at 430 nm (the Fraunhofer G band) taken by the Hinode Solar Optical Telescope with the hard X-rays observed by the Reuven Ramaty High Energy Solar Spectroscopic Imager. The two sets of data show closely similar ribbon structures, strongly suggesting that the flare emissions in white light and in hard X-rays have physically linked emission mechanisms. While the source structure along the ribbons is resolved at both wavelengths (length ~ 30"), only the G-band observations resolve the width of the ribbon, with values between ~05 and ~18. The unresolved hard X-ray observations reveal an even narrower ribbon in hard X-rays (the main footpoint has a width perpendicular to the ribbon of <11 compared to the G-band width of ~18) suggesting that the hard X-ray emission comes from the sharp leading edge of the G-band ribbon. Applying the thick-target beam model, the derived energy deposition rate is >5 × 1012 erg s–1 cm–2 provided by an electron flux of 1 × 1020 electrons s–1 cm–2 above 18 keV. This requires that the beam density of electrons above 18 keV be at least 1 × 1010 cm–3. Even if field lines converge toward the chromospheric footpoints, the required beam in the corona has too high a density to be described as a dilute tail population on top of a Maxwellian core. We discuss this issue and others associated with this extreme event, which poses serious questions to the standard thick target beam interpretation of solar flares.

TEMPERATURE AND DENSITY ESTIMATES OF EXTREME-ULTRAVIOLET FLARE RIBBONS DERIVED FROM TRACE DIFFRACTION PATTERNS

Säm **Krucker**1,2, Claire L. Raftery1 and Hugh S. Hudson
2011 ApJ 734 34

We report on Transition Region And Coronal Explorer 171 Å observations of the GOES X20 class flare on **2001 April 2** that shows EUV flare ribbons with intense diffraction patterns. Between the 11th to 14th order, the diffraction patterns of the compact flare ribbon are dispersed into two sources. The two sources are identified as emission from the Fe IX line at 171.1 Å and the combined emission from Fe X lines at 174.5, 175.3, and 177.2 Å. The prominent emission of the Fe IX line indicates that the EUV-emitting ribbon has a strong temperature component near the lower end of the 171 Å temperature response (~0.6–1.5 MK). Fitting the observation with an isothermal model, the derived temperature is around 0.65 MK. However, the low sensitivity of the 171 Å filter to high-temperature plasma does not provide estimates of the emission measure for temperatures above ~1.5 MK. Using the derived temperature of 0.65 MK, the observed 171 Å flux gives a density of the EUV ribbon of 3 × 1011 cm–3. This density is much lower than the density of the hard X-ray producing region (~1013 to 1014 cm–3) suggesting that the EUV sources, though closely related spatially, lie at higher altitudes.

Brilliant Timing

Säm **Krucker** & Hugh Hudson
RHESSI Science Nuggets, Dec **2010**
http://sprg.ssl.berkeley.edu/~tohban/wiki/index.php/Brilliant_Timing
We have described the hard X-ray and white light (actually the photospheric G-band) observations of a particular instant in a powerful solar flare. The excellent agreement between these two very different wave bands implies closely linked emission mechanisms. To the extent that this is borne out, our present model for the impulsive phase of a flare - its most powerful energy release - is seriously challenged by these observations.

MEASUREMENTS OF THE CORONAL ACCELERATION REGION OF A SOLAR FLARE

S¨am **Krucker**1, H. S. Hudson1, L. Glesener1,2, S. M. White3,4, S. Masuda5, J.-P. Wuelser6, and R. P. Lin1,2,7
Astrophysical Journal, 714:1108–1119, **2010** May; **File**
The *Reuven Ramaty High Energy Solar Spectroscopic Imager* (*RHESSI*) and the Nobeyama Radioheliograph (NoRH) are used to investigate coronal hard X-ray and microwave emissions in the partially disk-occulted solar flare of **2007 December 31**. The *STEREO* mission provides EUV images of the flare site at different viewing angles, establishing a two-ribbon flare geometry and occultation heights of the *RHESSI* and NoRH observations of ~16 Mm and ~25 Mm, respectively. Despite the occultation, intense hard X-ray emission up to ~80 keV occurs during the impulsive phase from a coronal source that is also seen in microwaves. The hard X-ray and microwave source during the impulsive phase is located ~6 Mm above thermal flare loops seen later at the soft X-ray peak time, similar in location to the above-the-loop-top source in the Masuda flare. A single nonthermal electron population with a power-law distribution (with spectral index of ~3.7 from ~16 keV up to the MeV range) radiating in both bremsstrahlung and gyrosynchrotron emission can explain the observed hard X-ray and microwave spectrum, respectively. This clearly establishes the non-thermal nature of the above-the-loop-top source. The large hard X-ray intensity requires a very large number ($>5 \times 10^{35}$ above 16 keV for the derived upper limit of the ambient density of $\sim 8 \times 10^{9}$ cm^{-3}) of suprathermal electrons to be present in this above-theloop-top source. This is of the same order of magnitude as the number of ambient thermal electrons. We show that collisional losses of these accelerated electrons would heat all ambient electrons to superhot temperatures (tens of keV) within seconds. Hence, the standard scenario, with hard X-rays produced by a beam comprising the tail of a dominant thermal core plasma, does not work. Instead, all electrons in the above-the-loop-top source seem to be accelerated, suggesting that the above-the-loop-top source is itself the electron acceleration region.

Co-Spatial White Light and Hard X-Ray Flare Footpoints Seen Above the Solar Limb

Säm **Krucker**1,2, Pascal Saint- Hilaire2, Hugh S. Hudson2,3, Margit Haberreiter4, Juan Carlos Martinez-Oliveros2, Martin D. Fivian2, Gordon Hurford1,2, Lucia Kleint1, Marina Battaglia1, Matej Kuhar1, and Nicolas G. Arnold
2015 ApJ 802 19
We report analysis of three solar flares that occur within 1° of limb passage, with the goal to investigate the source height of chromospheric footpoints in white light (WL) and hard X-rays (HXR). We find the WL and HXR (≥30 keV) centroids to be largely co-spatial and from similar heights for all events, with altitudes around 800 km above the photosphere or 300–450 km above the limb height. Because of the extreme limb location of the events we study, emissions from such low altitudes are influenced by the opacity of the atmosphere and projection effects. STEREO images reveal that for **SOL2012-11-20T12:36** the projection effects are smallest, giving upper limits of the absolute source height above the nominal photosphere for both wavelengths of ~1000 km. To be compatible with the standard thick target model, these rather low altitudes require very low ambient densities within the flare footpoints, in particular if the HXR-producing electrons are only weakly beamed. That the WL and HXR emissions are co-spatial suggests that the observed WL emission mechanism is directly linked to the energy deposition by flare accelerated electrons. If the WL emission is from low-temperature ($\leqslant 10^4$ K) plasma as currently thought, the energy deposition by HXR-producing electrons above ~30 keV seems only to heat chromospheric plasma to such low temperatures. This implies that the energy in flare-accelerated electrons above ~30 keV is not responsible for chromospheric evaporation of hot ($>10^6$ K) plasma, but that their energy is lost through radiation in the optical range.

Hard X–ray emission from the solar corona

S. **Krucker** · M. Battaglia · P. J. Cargill · L. Fletcher · H. S. Hudson · A. L. MacKinnon · S. Masuda · L. Sui · M. Tomczak · A. M. Veronig · L. Vlahos · S. M. White

E-print, July-Aug **2008**, **File**; Astronomy and Astrophysics Review

This **review** surveys hard X-ray emissions of non-thermal electrons in the solar corona. These electrons originate in flares and flare-related processes. Hard X-ray emission is the most direct diagnostic of electron presence in the corona, and such observations provide quantitative determinations of the total energy in the non-thermal electrons. The most intense flare emissions are generally observed from the chromosphere at footpoints of magnetic loops. Over the years, however, many observations of hard X-ray and even γ-ray emission directly from the corona have also been reported. These coronal sources are of particular interest as they occur closest to where the electron acceleration is thought to occur. Prior to the actual direct imaging observations, disk occultation was usually required to study coronal sources, resulting in limited physical information. Now RHESSI1 has given us a systematic view of coronal sources that combines high spatial and spectral resolution with broad energy coverage and high sensitivity. Despite the low density and hence low bremsstrahlung efficiency of the corona, we now detect coronal hard X-ray emissions from sources in all phases of solar flares. Because the physical conditions in such sources may differ substantially from those of the usual "footpoint" emission regions, we take the opportunity to revisit the physics of hard X-radiation and relevant theories of particle acceleration.

STEREO and RHESSI Observations of Electron Acceleration in a Partially Disk-Occulted Solar Flare

Krucker, S.1; Wuelser, J.-P.2; Vourlidas, A.3; Davila, J.4; Thompson, W.T.4; White, S.5; Lin, R.P.1

12th European Solar Physics Meeting, **2008**, Freiburg, Germany, **Presentation**

RHESSI hard X-ray observations of partially-disk occulted solar flares provide crucial information on faint coronal hard X-ray sources in the absence of generally much brighter emissions from footpoints of flare loops. Coronal hard X-ray sources can differ fundamentally from the classical footpoint sources of the flare impulsive phase and provide unique information about the supra-thermal electrons closest to the site in the corona where their acceleration is believed to occur. The different view-angles provided by the STEREO spacecraft allow us to put the partially occulted hard X-ray sources observed by RHESSI in context with the EUV flare ribbons and the EUV emission from CME observed by STEREO/EUVI.

In this presentation we report on the GOES C8 flare observed on **December 31, 2007** peaking around 01:11UT. From Earth-view (RHESSI), the flare occurs about 12 degrees behind the eastern limb giving an occultation height of 16 Mm. From STEREO B, the flare ribbons are seen on the disk (about 10 degrees from the limb), while the flare is highly occulted (130 Mm) for STEREO A observations so that emissions related to the associated CME are seen. Despite the occultation, RHESSI observes strong non-thermal emissions up to 100 keV that entirely originate from the corona. Initially, the coronal hard X-ray emission is seen from above the EUV flare ribbons similar to what is reported in the Masuda flare. Later on, emissions from a radially extended (approximately 20 Mm) source is seen. The radial extension is in the same direction as the current sheet of the outward moving CME suggesting that the HXR emission might be a direct signature of electrons accelerated in the reconnection process.

RHESSI AND *HINODE* X-RAY OBSERVATIONS OF A PARTIALLY OCCULTED SOLAR FLARE

Sa¨m **Krucker**,1 I. G. Hannah,1 and R. P. Lin1,2

The Astrophysical Journal, 671: L193–L196, **2007**

http://www.journals.uchicago.edu/doi/pdf/10.1086/525019

This Letter presents X-ray observations of a partially limb-occulted solar flare taken by the *Reuven Ramaty High-Energy Solar Spectroscopic Imager* and the X-ray telescope on board *Hinode*. Thermal emission originates from a simple loop at the western limb that rises slowly (~7 km s_{-1}) until the flare peak time. Above 18 keV, faint nonthermal emission with a hard/flat spectrum ( ) and fast time variations (of the order of tens of g ~ 4 seconds) is seen that comes from a loop slightly above (~2000 km) the thermal loop, if compared at the same time. However, the nonthermal loop agrees well in altitude with the thermal flare loop seen later, at the soft Xray peak time. This is consistent with simple flare models where nonthermal electrons in a flare loop produce thin-target hard X-ray emission in the corona as they travel to the loop footpoints. There they lose all their energy and heat chromospheric plasma that fills the loop earlier seen in nonthermal hard X-rays. This suggests that electron acceleration in solar flares occurs in the corona.

Hard X–ray emission from the solar corona Review

S. **Krucker** · M. Battaglia · P. J. Cargill · L. Fletcher · H. S. Hudson · A. L. MacKinnon · S. Masuda · L. Sui · M. Tomczak · A. M. Veronig · L. Vlahos · S. M. White

E-print, July-Aug **2008**; Astron Astrophys Rev (**2008**) 16:155–208, **File**

This **review** surveys hard X-ray emissions of non-thermal electrons in the solar corona. These electrons originate in flares and flare-related processes. Hard X-ray emission is the most direct diagnostic of electron presence in the corona, and such observations provide quantitative determinations of the total energy in the non-thermal electrons. The most intense flare emissions are generally observed from the chromosphere at footpoints of magnetic loops. Over the years, however, many observations of hard X-ray and even γ-ray emission directly from the corona have also been reported. These coronal sources are of particular interest as they occur closest to where the electron acceleration is thought to occur. Prior to the actual direct imaging observations, disk occultation was usually required to study coronal sources, resulting in limited physical information. Now RHESSI1 has given us a systematic view of coronal sources that combines high spatial and spectral resolution with broad energy coverage and high sensitivity. Despite the low density and hence low bremsstrahlung efficiency of the corona, we now detect coronal hard X-ray emissions from sources in all phases of solar flares. Because the physical conditions in such sources may differ substantially from those of the usual "footpoint" emission regions, we take the opportunity to revisit the physics of hard X-radiation and relevant theories of particle acceleration.

Are heating events in the quiet solar corona small flares? Multiwavelength observations of individual events.

Krucker, S., Benz, A.O.:

2000, Solar Phys. 191, 341 – 358.

Generation of Low-Frequency Kinetic Waves at the Footpoints of Pre-Flare Coronal Loops

Alexandr **Kryshtal**, Anna Voitsekhovska, Oleg Cheremnykh, Istvan Ballai, Gary Verth & Viktor Fedun

Solar Physics volume 295, Article number: 162 (**2020**)

https://link.springer.com/content/pdf/10.1007/s11207-020-01725-w.pdf

In this study we discuss the excitation of low-frequency plasma waves in the lower-middle chromosphere region of loop footpoints for the case when the plasma can be considered to be in a pre-flare state. It is shown that among the well-known semi-empirical models of the solar atmosphere, only the VAL (F) model together with a particular set of basic plasma parameters and amplitudes of the electric and magnetic fields supports generation of low-frequency wave instability. Our results show that it is possible to predict the onset of the flare process in the active region by using the interaction of kinetic Alfvén and kinetic ion-acoustic waves, which are solutions of the derived dispersion equation. The VAL (F) model allows situations when the main source of the aforementioned instability can be a sub-Dreicer electric field and drift plasma movements due to presence of spatial inhomogeneities. We also show that the generation of kinetic Alfvén and kinetic ion-acoustic waves can occur both, in plasma with a purely Coulomb conductivity and in the presence of small-scale Bernstein turbulence. The excitation of the small amplitude kinetic waves due to the development of low threshold instability in plasma with relatively low values of the magnetic field strength is also discussed.

The ion-acoustic instability in the pre-flare plasma near the loop footpoints at solar active regions

Kryshtal1, S. Gerasimenko1, A. Voitsekhovska1, and V. Fedun

Ann. Geophys., 31, 2193-2200, **2013**

www.ann-geophys.net/31/2193/2013/

The necessary physical conditions for development of the ion-acoustic instability in the chromospheric part of a flaring loop current circuit are investigated. Two possible scenarios have been studied. First, we consider that pre-flare loop plasma with the large-scale sub-Dreicer electric field has a classical Coulomb conductivity and, second, when anomalous resistance appears due to saturation of Bernstein turbulence. The Fontenla-Avrett-Loeser (FAL) model of the solar atmosphere was used to describe the pre-flare plasma. We have shown that investigated instability can grow and develop either in the presence of the Coulomb conductivity or saturated Bernstein turbulence. We demonstrate that in the case of small-scale instability, the threshold value for the degree of nonisothermality is high and, therefore, cannot be reached by inclusion of the ordinary Joule heating. The ion-acoustic instability can develop at the pre-flare loop footpoints provided the electrons are more than 10 times hotter than the ions there.

Why do some probabilistic forecasts lack reliability?

Yûki **Kubo**

J. Space Weather Space Clim. **2019**, 9, A17

https://www.swsc-journal.org/articles/swsc/pdf/2019/01/swsc180050.pdf

In this work, we investigate the reliability of the probabilistic binary forecast. We mathematically prove that a necessary, but not sufficient, condition for achieving a reliable probabilistic forecast is maximizing the Peirce Skill Score (PSS) at the threshold probability of the climatological base rate. The condition is confirmed by using artificially synthesized forecast–outcome pair data and previously published probabilistic solar flare forecast models. The condition gives a partial answer as to why some probabilistic forecast system lack reliability, because the system, which does not satisfy the proved condition, can never be reliable. Therefore, the proved condition is very important for the developers of a probabilistic forecast system. The result implies that those who want to develop a reliable probabilistic forecast system must adjust or train the system so as to maximize PSS near the threshold probability of the climatological base rate.

Verification of operational solar flare forecast: Case of Regional Warning Center Japan

Yûki **Kubo**, Mitsue Den, Mamoru Ishii
Journal of Space Weather and Space Climate **2017**
https://arxiv.org/pdf/1707.07903.pdf
In this article, we discuss a verification study of an operational solar flare forecast in the Regional Warning Center (RWC) Japan. The RWC Japan has been issuing four-categorical deterministic solar flare forecasts for a long time. In this forecast verification study, we used solar flare forecast data accumulated over 16 years (from 2000 to 2015). We compiled the forecast data together with solar flare data obtained with the Geostationary Operational Environmental Satellites (GOES). Using the compiled data sets, we estimated some conventional scalar verification measures with 95% confidence intervals. We also estimated a multi-categorical scalar verification measure. These scalar verification measures were compared with those obtained by the persistence method and recurrence method. As solar activity varied during the 16 years, we also applied verification analyses to four subsets of forecast-observation pair data with different solar activity levels. We cannot conclude definitely that there are significant performance difference between the forecasts of RWC Japan and the persistence method, although a slightly significant difference is found for some event definitions. We propose to use a scalar verification measure to assess the judgment skill of the operational solar flare forecast. Finally, we propose a verification strategy for deterministic operational solar flare forecasting.

Statistical Models for the Solar Flare Interval Distribution in Individual Active Regions

Y¯uki **Kubo**
Solar Phys (**2008**) 248: 85–98
http://www.springerlink.com/content/f712471x522k4914/fulltext.pdf
The results suggest that solar flares do not occur randomly in time; rather, solar flare intervals appear to be regulated by solar flare mechanisms. Determining a solar flare interval distribution is an essential step in probabilistic solar flare forecasting methods in space weather research. We briefly mention a probabilistic solar flare forecasting method as an application of a solar flare interval distribution analysis. The application of our distribution analysis to a probabilistic solar flare forecasting method is one of the main objectives of this study.

Modeling of Condensations in Coronal Loops Produced by Impulsive Heating

Therese A. **Kucera**, James A. Klimchuk, Manuel Luna
ApJ **965** 53 **2024**
https://arxiv.org/pdf/2402.06799.pdf
https://iopscience.iop.org/article/10.3847/1538-4357/ad25fc/pdf
We present the results of models of impulsively heated coronal loops using the 1-D hydrodynamic Adaptively Refined Godunov Solver (ARGOS) code. The impulsive heating events (which we refer to as "nanoflares") are modeled by discrete pulses of energy along the loop. We explore the occurrence of cold condensations due to the effective equivalent of thermal non-equilibrium (TNE) in loops with steady heating, and examine its dependence on nanoflare timing and intensity and also nanoflare location along the loop, including randomized distributions of nanoflares. We find that randomizing nanoflare distributions, both in time/intensity and location, diminishes the likelihood of condensations as compared to distributions with regularly occurring nanoflares with the same average properties. The usual criteria that condensations are favored for heating near loop footpoints and with high cadences are more strict for randomized (as opposed to regular) nanoflare distributions, and for randomized distributions the condensations stay in the loop for a shorter amount of time. That said, condensations can sometimes occur in cases where the average values of parameters (frequency or location) are beyond the critical limits above which condensations do not occur for corresponding steady, non-randomized values of those parameters. These properties of condensations occurring due to randomized heating can be used in the future to investigate diagnostics of coronal heating mechanisms.

Ca II 8542 Å brightenings induced by a solar microflare

C. **Kuckein** (1), A. Diercke (1 and 2), S. J. González Manrique (3 and 1 and 2), M. Verma (1), J. Löhner-Böttcher (4), H. Socas-Navarro (5), H. Balthasar (1), M. Sobotka (6), C. Denker (1)
A&A 608, A117 **2017**
https://arxiv.org/pdf/1709.06861.pdf

We study small-scale brightenings in Ca II 8542 \AA\ line-core images to determine their nature and effect on localized heating and mass transfer in active regions. High-resolution 2D spectroscopic observations of an active region in the Ca II 8542 \AA\ line were acquired with the GFPI attached to the 1.5-meter GREGOR telescope. Inversions of the spectra were carried out using NICOLE. We identified three brightenings of sizes up to 2"x2". We found evidence that the brightenings belonged to the footpoints of a microflare (MF). The properties of the observed brightenings disqualified the scenarios of Ellerman bombs or IRIS bombs. However, this MF shared some common properties with flaring active-region fibrils or flaring arch filaments (FAFs): (1) FAFs and MFs are both apparent in chromospheric and coronal layers according to the AIA channels, and (2) both show flaring arches with lifetimes of about 3.0-3.5 min and lengths of about 20". The inversions revealed heating by 600 K at the footpoint location in the ambient chromosphere during the impulsive phase. Connecting the footpoints, a dark filamentary structure appeared in the Ca II line-core images. Before the start of the MF, the spectra of this structure already indicated average blueshifts, meaning upward motions of the plasma along the LOS. During the impulsive phase, these velocities increased up to -2.2 km/s. Downflows dominated at the footpoints. However, in the upper photosphere, slight upflows occurred during the impulsive phase. Hence, bidirectional flows are present in the footpoints of the MF. Conclusions: We detected Ca II brightenings that coincided with the footpoint location of an MF. The MF event led to a rise of plasma in the upper photosphere, both before and during the impulsive phase. Excess mass, previously raised to at most chromospheric layers, slowly drained downward along arches toward the footpoints of the MF.

Full Stokes observations in the He I 1083 nm spectral region covering an M3.2 flare

C. **Kuckein** (1), M. Collados (2,3), R. Manso Sainz (2,3), A. Asensio Ramos
the conference proceedings of the IAUS 305: "Polarimetry: From the Sun to Stars and Stellar Environments"
2015
http://arxiv.org/pdf/1502.05505v1.pdf
We present an exceptional data set acquired with the Vacuum Tower Telescope (Tenerife, Spain) covering the pre-flare, flare, and post-flare stages of an M3.2 flare. The full Stokes spectropolarimetric observations were recorded with the Tenerife Infrared Polarimeter in the He I 1083.0 nm spectral region. The object under study was active region NOAA 11748 on **2013 May 17**. During the flare the chomospheric He I 1083.0 nm intensity goes strongly into emission. However, the nearby photospheric Si I 1082.7 nm spectral line profile only gets shallower and stays in absorption. Linear polarization (Stokes Q and U) is detected in all lines of the He I triplet during the flare. Moreover, the circular polarization (Stokes V) is dominant during the flare, being the blue component of the He I triplet much stronger than the red component, and both are stronger than the Si I Stokes V profile. The Si I inversions reveal enormous changes of the photospheric magnetic field during the flare. Before the flare magnetic field concentrations of up to 1500 G are inferred. During the flare the magnetic field strength globally decreases and in some cases it is even absent. After the flare the magnetic field recovers its strength and initial configuration.

Magnetic and Dynamical Photospheric Disturbances Observed During an M3.2 Solar Flare

C. **Kuckein**1, M. Collados2,3, and R. Manso Sainz
2015 ApJ 799 L25
http://arxiv.org/pdf/1501.04207v1.pdf
This Letter reports on a set of full-Stokes spectropolarimetric observations in the near-infrared He i 10830 Å spectral region covering the pre-flare, flare, and post-flare phases of an M3.2 class solar flare. The flare originated on **2013 May 17** and belonged to active region NOAA 11748. We detected strong He i 10830 Å emission in the flare. The red component of the He i triplet peaks at an intensity ratio to the continuum of about 1.86. During the flare,
He i Stokes V is substantially larger and appears reversed compared to the usually larger Si i Stokes V profile. The photospheric Si i inversions of the four Stokes profiles reveal the following: (1) the magnetic field strength in the photosphere decreases or is even absent during the flare phase, as compared to the pre-flare phase. However, this decrease is not permanent. After the flare, the magnetic field recovers its pre-flare configuration in a short time (i.e., 30 minutes after the flare). (2) In the photosphere, the line of sight velocities show a regular granular up- and downflow pattern before the flare erupts. During the flare, upflows (blueshifts) dominate the area where the flare is produced. Evaporation rates of $\sim 10^{-3}$ and $\sim 10^{-4}$ g cm−2 s−1 have been derived in the deep and high photosphere, respectively, capable of increasing the chromospheric density by a factor of two in about 400 s.

NuSTAR Detection of X-Ray Heating Events in the Quiet Sun

Matej **Kuhar**, Säm Krucker, Lindsay Glesener, Iain G. Hannah, Brian W. Grefenstette, David M. Smith, Hugh S. Hudson, Stephen M. White
ApJL 856 L32 **2018**
https://arxiv.org/pdf/1803.08365.pdf
The explanation of the coronal heating problem potentially lies in the existence of nanoflares, numerous small-scale heating events occuring across the whole solar disk. In this paper, we present the first imaging spectroscopy X-ray

observations of three quiet Sun flares during the NuSTAR solar campaigns on **2016 July 26** and **2017 March 21**, concurrent with SDO/AIA observations. Two of the three events showed time lags of a few minutes between peak X-ray and extreme ultraviolet (EUV) emissions. Isothermal fits with rather low temperatures in the range 3.2−4.1 MK and emission measures of (0.6−15)×1044 cm−3 describe their spectra well, resulting in thermal energies in the range (2−6)×1026 ergs. NuSTAR spectra did not show any signs of a nonthermal or higher temperature component. However, since the estimated upper limits of (hidden) nonthermal energy are comparable to the thermal energy estimates, the lack of a nonthermal component in the observed spectra is not a constraining result. The estimated GOES classes from the fitted values of temperature and emission measure fall between 1/1000 and 1/100 A class level, making them 8 orders of magnitude fainter in soft X-ray flux than the largest solar flares.
RHESSI Science Nuggets №319 March **2018**
http://sprg.ssl.berkeley.edu/~tohban/wiki/index.php/NuSTAR_detects_X-ray_flares_in_the_quiet_Sun

EVIDENCE OF SIGNIFICANT ENERGY INPUT IN THE LATE PHASE OF A SOLAR FLARE FROM NuSTAR X-RAY OBSERVATIONS

Matej **Kuhar**1,2, Säm Krucker1,3, Iain G. Hannah4, Lindsay Glesener5, Pascal Saint-Hilaire3,Brian W. Grefenstette6, Hugh S. Hudson3,7, Stephen M. White8, David M. Smith9, Andrew J. Marsh9
2017 ApJ 835 6
http://iopscience.iop.org.sci-hub.cc/0004-637X/835/1/6/
https://arxiv.org/pdf/1701.07759v1.pdf
https://iopscience.iop.org/article/10.3847/1538-4357/835/1/6/pdf
We present observations of the occulted active region AR 12222 during the third Nuclear Spectroscopic Telescope ARray (NuSTAR) solar campaign on 2014 December 11, with concurrent Solar Dynamics Observatory (SDO)/AIA and FOXSI-2 sounding rocket observations. The active region produced a medium-size solar flare 1 day before the observations, at ~18 UT on **2014 December 10**, with the post-flare loops still visible at the time of NuSTAR observations. The time evolution of the source emission in the SDO/AIA 335 Å channel reveals the characteristics of an extreme-ultraviolet late-phase event, caused by the continuous formation of new post-flare loops that arch higher and higher in the solar corona. The spectral fitting of NuSTAR observations yields an isothermal source, with temperature 3.8–4.6 MK, emission measure (0.3–1.8) × 1046 cm−3, and density estimated at (2.5–6.0) × 108 cm−3. The observed AIA fluxes are consistent with the derived NuSTARtemperature range, favoring temperature values in the range of 4.0–4.3 MK. By examining the post-flare loops' cooling times and energy content, we estimate that at least 12 sets of post-flare loops were formed and subsequently cooled between the onset of the flare andNuSTAR observations, with their total thermal energy content an order of magnitude larger than the energy content at flare peak time. This indicates that the standard approach of using only the flare peak time to derive the total thermal energy content of a flare can lead to a large underestimation of its value.

Correlation of hard X-ray and white light emission in solar flares

Matej **Kuhar**, Säm Krucker, Juan Carlos Martínez Oliveros, Marina Battaglia, Lucia Kleint, Diego Casadei, Hugh S. Hudson
ApJ 816 6 **2016**
http://arxiv.org/pdf/1511.07757v1.pdf
A statistical study of the correlation between hard X-ray and white light emission in solar flares is performed in order to search for a link between flare-accelerated electrons and white light formation. We analyze 43 flares spanning GOES classes M and X using observations from RHESSI (Reuven Ramaty High Energy Solar Spectroscopic Imager) and HMI (Helioseismic and Magnetic Imager). We calculate X-ray fluxes at 30 keV and white light fluxes at 6173 \r{A} summed over the hard X-ray flare ribbons with an integration time of 45 seconds around the peak hard-X ray time. We find a good correlation between hard X-ray fluxes and excess white light fluxes, with a highest correlation coefficient of 0.68 for photons with energy of 30 keV. Assuming the thick target model, a similar correlation is found between the deposited power by flare-accelerated electrons and the white light fluxes. The correlation coefficient is found to be largest for energy deposition by electrons above ~50 keV. At higher electron energies the correlation decreases gradually while a rapid decrease is seen if the energy provided by low-energy electrons is added. This suggests that flare-accelerated electrons of energy ~50 keV are the main source for white light production. **6 Sept 2011, 31 Dec 2011**
RHESSI Science Nugget No. 265, Nov 2015
http://sprg.ssl.berkeley.edu/~tohban/wiki/index.php/On_the_Correlation_of_HXR_and_WL_Emission_in_Solar_Flares

X-ray/Radio Quasi-periodic Pulsations Associated with Plasmoids in Solar Flare Current Sheets

Pankaj **Kumar**, Judith T. Karpen, Joel T. Dahlin
ApJ **2024**
https://arxiv.org/pdf/2412.05193

Plasmoids (or magnetic islands) are believed to play an important role in the onset of fast magnetic reconnection and particle acceleration during solar flares and eruptions. Direct imaging of flare current sheets and formation/ejection of multiple plasmoids in extreme ultraviolet (EUV) images, along with simultaneous X-ray and radio observations, offers significant insights into the mechanisms driving particle acceleration in solar flares. Here we present direct imaging of the formation and ejection of multiple plasmoids in flare plasma/current sheets and associated quasi-periodic pulsations (QPPs) observed in X-ray and radio wavelengths, using observations from SDO/AIA, RHESSI, and Fermi GBM. These plasmoids propagate bidirectionally upward and downward along the flare current sheet beneath the erupting flux rope during two successive flares associated with confined/failed eruptions. The flux rope exhibits evidence of helical kink instability with formation and ejection of multiple plasmoids in the flare current sheet, as predicted in an MHD simulation of a kink-unstable flux rope. RHESSI X-ray images show double coronal sources (``loop-top" and higher coronal sources) located at both ends of the flare current/plasma sheet. Moreover, we detected an additional transient faint X-ray source (6-12 keV) located between the double coronal sources, which was co-spatial with multiple plasmoids in the flare current sheet. X-ray (soft and hard) and radio (decimetric) observations unveil QPPs (periods≈10-s and 100-s) associated with the ejection and coalescence of plasmoids. These observations suggest that energetic electrons are accelerated during the ejection and coalescence of multiple plasmoids in the flare current sheet. **22 April 2015**

Direct Imaging of a Prolonged Plasma/Current Sheet and Quasiperiodic Magnetic Reconnection on the Sun

Pankaj **Kumar**, Judith T. Karpen, Vasyl Yurchyshyn, C. Richard DeVore, Spiro K. Antiochos
ApJ **2024**
https://arxiv.org/pdf/2407.07687
Magnetic reconnection is widely believed to be the fundamental process in the solar atmosphere that underlies magnetic energy release and particle acceleration. This process is responsible for the onset of solar flares, coronal mass ejections, and other explosive events (e.g., jets). Here, we report direct imaging of a prolonged plasma/current sheet along with quasiperiodic magnetic reconnection in the solar corona using ultra-high-resolution observations from the 1.6-meter Goode Solar Telescope (GST) at BBSO and Solar Dynamics Observatory/Atmospheric Imaging Assembly (SDO/AIA). The current sheet appeared near a null point in the fan-spine topology and persisted over an extended period (~20 hours). The length and apparent width of the current sheet were about 6 arcsec and 2 arcsec respectively, and the plasma temperature was ~10-20 MK. We observed quasiperiodic plasma inflows and outflows (bidirectional jets with plasmoids) at the reconnection site/current sheet. Furthermore, quasiperiodic reconnection at the long-lasting current sheet produced recurrent eruptions (small flares and jets) and contributed significantly to the recurrent impulsive heating of the active region. Direct imaging of a plasma/current sheet and recurrent null-point reconnection for such an extended period has not been reported previously. These unprecedented observations provide compelling evidence that supports the universal model for solar eruptions (i.e., the breakout model) and have implications for impulsive heating of active regions by recurrent reconnection near null points. The prolonged and sustained reconnection for about 20 hours at the breakout current sheet provides new insights into the dynamics and energy release processes in the solar corona. **August 22, 2022**

Direct Imaging of MHD Wave Mode Conversion Near a 3D Null Point on the Sun

Pankaj **Kumar**, Valery M. Nakariakov, Judith T. Karpen, Kyung-Suk Cho
ApJ **2024**
https://arxiv.org/pdf/2403.02250.pdf
Mutual conversion of various kinds of magnetohydrodynamic (MHD) waves can have profound impacts on wave propagation, energy transfer, and heating of the solar chromosphere and corona. Mode conversion occurs when an MHD wave travels through a region where the Alfvén and sound speeds are equal (e.g., a 3D magnetic null point). Here we report the first EUV imaging of mode conversion from a fast-mode to a slow-mode MHD wave near a 3D null point using Solar Dynamics Observatory/Atmospheric Imaging Assembly (SDO/AIA) observations. An incident fast EUV wavefront associated with an adjacent eruptive flare propagates laterally through a neighboring pseudostreamer. Shortly after the passage of the fast EUV wave through the null point, a slow-mode wave appears near the null that propagates upward along the open structures and simultaneously downward along the separatrix encompassing the fan loops of the pseudostreamer base. These observations suggest the existence of mode conversion near 3D nulls in the solar corona, as predicted by theory and MHD simulations. Moreover, we observe decaying transverse oscillations in both the open and closed structures of the pseudostreamer, along with quasiperiodic type III radio bursts indicative of repetitive episodes of electron acceleration. **May 9, 2014**

Velocity and Dissipation Characteristics of Turbulence in Solar-Flare Plasma: An Application of Stochastic Lagrangian Models

Pramod **Kumar**, R. K. Choudhary
Solar Physics volume 298, Article number: 128 (**2023**)

https://doi.org/10.1007/s11207-023-02221-7
Turbulence is one of the products of the magnetic-reconnection process in the solar-flare plasma. It intensely shifts the dynamics of the magnetic-reconnection process and rapidly transfers energy that facilitates plasma heating by over 10 MK and particle energization. In this study, using the results of a Monte Carlo experiment through the Euler–Maruyama approximation of stochastic Lagrangian models for inhomogeneous hydrodynamic turbulence, we present the velocity and dissipation (relaxation rate) characteristics of stochastic motions of particles (particles obeying a Gaussian distribution) in the turbulence of the solar-flare plasma. A Monte Carlo experiment was performed for a turbulent kinetic energy of 1030 erg, on a time scale of ten seconds and a length scale of the order of the full loop half-length [1010 cm] of the solar flare. The results of the velocity and dissipation (relaxation rate) are presented and analyzed in both one and two dimensions. We observed that the positive value of relaxation rate of (1--8)×10−4 s−1 for ≈ five seconds of dispersion time could lead to energy transfer and dissipation of the energy in the turbulence of the solar flare. The Monte Carlo mean relaxation rate of 4.5×10−4 s−1 shows that it dissipates ≈4.5×1027 erg energy into thermal energy in ten seconds, which is equal to ≈ 0.5% of the total injected kinetic energy. Velocities of the stochastic particles in the turbulence show the random fluctuations, which are unsteadily dispersive in nature. The range and mean values of particle velocities are ≈(0.5--3)×106 cms−1 and 1.5×106 cms−1, respectively, which indicates low-atmospheric turbulence (chromosphere) in the solar flare. The results obtained are in agreement with observations. Our analysis thus demonstrates that the turbulence in the solar flare dissipates ≈ 0.5% of the injected energy into thermal energy and low-atmospheric turbulence (chromosphere) in the solar flare. We surmise that the rest of the turbulent kinetic energy goes to the non-thermal particle energization (particle acceleration), generation of the termination shock, and other dynamical processes in the solar flare.

Magnetohydrodynamics evolution of three-dimensional magnetic null in NOAA active region 11515 initiated using non-force-free field extrapolation

Sanjay **Kumar**, Avijeet Prasad, Ranadeep Sarkar, and Ramit Bhattacharyya
Front. Astron. Space Sci. 9:1039061. **2022**
https://arxiv.org/pdf/2210.03957.pdf
doi: 10.3389/fspas.2022.1039061
https://www.frontiersin.org/articles/10.3389/fspas.2022.1039061/pdf
Magnetohydrodynamics simulation of active region NOAA 11515 is performed to examine the initiation of the M5.6 flaring event that starts around 10:43 UT on **2012 July 2**. The simulation is conducted using an extrapolated non-force-free magnetic field generated from the photospheric vector magnetogram of the active region as the initial magnetic field. The magnetic field shows the presence of a three-dimensional (3D) magnetic null with the corresponding dome overlying a filament and a low-lying magnetic flux rope, observed in 304~Å~ and 131~Å~ respectively.
The simulated dynamics, triggered by the initial Lorentz force, lead to the bifurcations of the flux rope, which is similar to the observed bifurcation in the 131 Å~ brightenings. Additionally, the rope exhibits a rise and reconnects at the 3D null. These reconnections convert field lines of the rope into the anchored outer spine of the 3D null -- explaining the occurrence of a nearby confined C-class flare. Further, the results show that the field lines of the flux rope reach the vicinity of the filament and become non-parallel to the field lines of the filament. This initiates the reconnections between the rope and the field lines of the filament -- activating the filament for the eruption. This interesting interaction of the flux rope and filament seems to contribute to the onset of the M-class flare.

A Study on the Various Modes of Parallel Heat Conduction in the Coronal Loops of Small and Large Solar Flares Using Scaling Laws

Pramod **Kumar** & R. K. Choudhary
Solar Physics volume 296, Article number: 147 (**2021**)
https://link.springer.com/content/pdf/10.1007/s11207-021-01884-4.pdf
https://doi.org/10.1007/s11207-021-01884-4
Recent studies show that the parallel heat conduction in the plasma of coronal loops associated with solar flares is controlled by the turbulence-dominated mode, in addition to the free streaming and collision-dominated modes. Using scaling laws, we have studied the relative importance of various modes of parallel heat conduction in the coronal loops of the small (B-class) and large (X-class) solar flares. The scaling laws relate the maximum loop temperature and heating rate to the loop pressure and loop half-length for collision, turbulence, and free streaming dominated modes of the parallel heat conduction. For a set of values of loop half-length ≈(2.0−3.0)×109 cm, loop pressure ≈(6.0−20.0) erg cm−3 for the small coronal loops, and loop half-length ≈(3.0−11.0)×109 cm, loop pressure ≈(1.0−103.0) erg cm−3 for the large coronal loops at a constant value of mean free path =107.5 cm, our results show that the estimated heating time is ≈ 40–125 s, which represents a fast heating rate. The estimated maximum loop temperature is found to be lower compared to the observed values for the coronal loops of the solar flares. The nature of positive and negative correlation between the scaling parameters show that the collision-dominated heat conduction is a dominant process in the loops of small flares while turbulence-dominated processes suppress the collision-dominated parallel heat conduction in the loops of large solar flares. The instabilities caused by the fast flow of evaporation from the footpoints are discussed as the source of the turbulence.

Magnetic reconnections in the presence of three-dimensional magnetic nulls and quasi-separatrix layers

Sanjay **Kumar**, Sushree S. Nayak, Avijeet Prasad, Ramit Bhattacharyya
Solar Phys. **296**, Article number: 26 **2021**
https://arxiv.org/pdf/2101.02065.pdf
https://link.springer.com/content/pdf/10.1007/s11207-021-01768-7.pdf
Three-dimensional (3D) magnetohydrodynamic simulations are carried out to explore magnetic reconnections in the presence of 3D magnetic nulls and quasi-separatrix layers (QSLs). The initial magnetic fields are created by superposing uniform vertical magnetic fields of two different magnitudes on a linear force-free field. The interior of the numerical box contains two 3D nulls with separatrix domes separated by a quasi-separator (or hyperbolic flux tube) with QSLs. In the first simulation, the uniform vertical field is so large that the nulls are located at low heights and the domes are separate. Initially unbalanced Lorentz forces drive rotational flows that form strong electric currents and strong torsional fan reconnection at the 3D nulls and weak QSL reconnection at the hyperbolic flux tube. Flipping or slipping of field lines is observed in both cases. In the second simulation, with a weaker vertical field and larger domes, the separatrix surfaces meet at the central quasi-separator and their rotation drives stronger QSL reconnection than before.

On the seismic emission in sunspots associated with Lorentz force changes accompanying major solar flares

Hirdesh **Kumar**, Brajesh Kumar
MNRAS **2020**
https://arxiv.org/pdf/2007.05231.pdf
Solar flares are known to generate seismic waves in the Sun. We present a detailed analysis of seismic emission in sunspots accompanying M- and X-class solar flares. For this purpose, we have used high-resolution Dopplergrams and line-of-sight magnetograms at a cadence of 45 s, along with vector magnetograms at a cadence of 135 s obtained from Helioseismic and Magnetic Imager (HMI) instrument aboard the Solar Dynamic Observatory (SDO) space mission. In order to identify the location of flare ribbons and hard X-ray foot-points, we have also used H-alpha chromospheric intensity observations obtained from Global Oscillation Network Group (GONG) instruments and hard X-ray images in 12-25 KeV band from the Reuvan Ramaty High Energy Solar Spectroscopic Imager (RHESSI) spacecraft. The Fast Fourier Transform (FFT) technique is applied to construct the acoustic velocity power map in 2.5-4 mHz band for pre-flare, spanning flare, and post flare epochs for the identification of seismic emission locations in the sunspots. In the power maps, we have selected only those locations which are away from the flare ribbons and hard X-rays foot-points. These regions are believed to be free from any flare related artefacts in the observational data. We have identified concentrated locations of acoustic power enhancements in sunspots accompanying major flares. Our investigation provides evidence that abrupt changes in the magnetic fields and associated impulsive changes in the Lorentz force could be the driving source for these seismic emissions in the sunspots during solar flares. **2011 February 15, 2011 August 03, 2013 October 28, 2014 December 04, 2014 December 18, 2014 December 20, 2015 March 11, 2015 June 22**
Table 1. Details of the active regions used in our analysis and information related to the flare evolution as seen in GOES soft X-ray (1–8 ˚A band).

On the signatures of flare-induced global waves in the Sun: GOLF and VIRGO observations

Brajesh **Kumar**, Savita Mathur, Rafael A. Garcia, Antonio Jimenez
MNRAS, Vol. 471, Issue 4, November **2017**
https://arxiv.org/pdf/1710.06245.pdf
Recently, several efforts have been made to identify the seismic signatures of flares and magnetic activity in the Sun and Sun-like stars. In this work, we have analyzed the disk-integrated velocity and intensity observations of the Sun obtained from the GOLF and VIRGO/SPM instruments, respectively, on board the SOHO space mission covering several successive flare events, for the period from **11 February 2011 to 17 February 2011**, of which 11 February 2011 remained a relatively quiet day and served as a "null test" for the investigation. Application of the spectral analysis to these disk-integrated Sun-as-a-star velocity and intensity signals indicates that there is enhanced power of the global modes of oscillations in the Sun during the flares, as compared to the quiet day. The GOLF instrument obtains velocity observations using the Na I D lines which are formed in the upper solar photosphere, while the intensity data used in our analysis are obtained by VIRGO/SPM instrument at 862~nm, which is formed within the solar photosphere. Despite the fact that the two instruments sample different layers of the solar atmosphere using two different parameters (velocity v/s intensity), we have found that both these observations show the signatures of flare-induced global waves in the Sun. These results could suffice in identifying the asteroseismic signatures of stellar flares and magnetic activity in the Sun-like stars.

Quasi-Periodic Radio Bursts Associated with Fast-mode Waves near a Magnetic Null Point

Pankaj **Kumar**, Valery M. Nakariakov, Kyung-Suk Cho

ApJ **2017**

https://arxiv.org/pdf/1706.09988.pdf

This paper presents an observation of quasi-periodic rapidly-propagating waves observed in the AIA 171/193 \AA~ channels during the impulsive phase of an M1.9 flare occurred on **7 May 2012**. The instant period was found to decrease from 240~s to 120~s, the speed of the wave fronts was in the range of ~664-1416 km/s. Almost simultaneously, quasi-periodic bursts with similar instant periods, ~70~s and ~140~s, occur in the microwave emission and in decimetric type IV, and type III radio bursts, and in the soft X-ray emission. The magnetic field configuration of the flare site was consistent with a breakout topology, i.e., a quadrupolar field along with a magnetic null point. The quasi-periodic rapidly-propagating wavefronts of the EUV emission are interpreted as a fast magnetoacoustic wave train. The observations suggest that the fast-mode waves are generated during the quasi-periodic magnetic reconnection in the cusp-region above the flare arcade loops. For the first time, we provide the evidence of a tadpole wavelet signature at about 70--140~s in decimetric (245/610~MHz) radio bursts, along with the direct observation of a coronal fast-mode wave train in EUV. In addition, at AIA 131/193 \AA\ we observed quasi-periodic EUV disturbances with the periods of 95~s and 240~s propagating downward at the apparent speed of 172-273 km/s. The nature of these downward propagating disturbances is not revealed, but they could be connected with magnetoacoustic waves or periodically shrinking loops.

Multiwavelength Observations of a Flux Rope Formation by Series of Magnetic Reconnection in the Chromosphere

Pankaj **Kumar**, Vasyl Yurchyshyn, Kyung-Suk Cho, Haimin Wang

A&A **2017**

https://arxiv.org/pdf/1703.09871.pdf

Using high-resolution observations from the 1.6 m New Solar Telescope (NST) operating at the Big Bear Solar Observatory (BBSO), we report direct evidence of merging/reconnection of cool Hα loops in the chromosphere during two homologous flares (B- and C-class) caused by a shear motion at the footpoint of two loops. The reconnection between these loops caused the formation of an unstable flux rope which showed counterclockwise rotation. The flux rope could not reach the height of torus instability and failed to form a coronal mass ejection. The HMI magnetograms revealed rotation of the negative/positive (N1/P2) polarity sunspots in the opposite directions, which increased the right and left-handed twist in the magnetic structures rooted at N1/P2. Rapid photospheric flux cancellation (duration∼20-30 min, rate≈3.44×1020 Mx h−1) was observed during and even after the first B6.0 flare and continued until the end of the second C2.3 flare. The RHESSI X-ray sources were located at the site of the loop's coalescence. To the best of our knowledge, such a clear interaction of chromospheric loops along with rapid flux cancellation has not been reported before. These high-resolution observations suggest the formation of a small flux rope by a series of magnetic reconnection within chromospheric loops associated with very rapid flux cancellation. **23 May 2015**

Preferential Heating and Acceleration of Heavy Ions in Impulsive Solar Flares

Rahul **Kumar**1,2, David Eichler2, Massimo Gaspari1,3, and Anatoly Spitkovsky1

2017 ApJ 835 295 Doi 10.3847/1538-4357/835/2/295

http://sci-hub.cc/doi/10.3847/1538-4357/835/2/295

We simulate decaying turbulence in a homogeneous pair plasma using a three-dimensional electromagnetic particle-in-cell method. A uniform background magnetic field permeates the plasma such that the magnetic pressure is three times larger than the thermal pressure and the turbulence is generated by counter-propagating shear Alfvén waves. The energy predominately cascades transverse to the background magnetic field, rendering the turbulence anisotropic at smaller scales. We simultaneously move several ion species of varying charge to mass ratios in our simulation and show that the particles of smaller charge to mass ratios are heated and accelerated to non-thermal energies at a faster rate. This is in accordance with the enhancement of heavy ions and a non-thermal tail in their energy spectrum observed in the impulsive solar flares. We further show that the heavy ions are energized mostly in the direction perpendicular to the background magnetic field, with a rate consistent with our analytical estimate of the rate of heating due to cyclotron resonance with the Alfvén waves, of which a large fraction is due to obliquely propagating waves.

Observation of a Short Period Quasi-Periodic Pulsation in Solar X-ray, Microwave and EUV Emissions

Pankaj **Kumar**, Valery M. Nakariakov, Kyung-Suk Cho

ApJ **836** 121 **2017**

https://arxiv.org/pdf/1701.02159v1.pdf

This paper presents the multi-wavelength analysis of a 13 s quasi-periodic pulsation (QPP) observed in hard X-ray (12-300 keV) and microwave (4.9-34 GHz) emissions during a C-class flare occurred on **21 September 2015**. AIA 304 and 171 \AA~ images show an emerging loop/flux tube (L1) moving radially outward, which interacts with preexisting structures within the active region. The QPP was observed during the expansion and rising motion of L1. The Nobeyama Radioheliograph (NoRH) microwave images in 17/34 GHz channels reveal a single radio source, which was co-spatial with a neighboring loop (L2). In addition, using AIA 304 \AA~ images, we detected intensity oscillations in the legs of loop L2 with a period of about 26 s. A similar oscillation period was observed in the GOES soft X-ray flux derivative. This oscillation period seems to increase with time. We suggest that the observed QPP is most likely generated by the interaction between loops L2 and L3 observed in the AIA hot channels (131 and 94 \AA). The merging speed of loops L2 and L3 was ~35 km/s. Loop L1 destroyed possibly by its interaction with preexisting structures in the active region and produced a cool jet with the speed ~106-118 km/s associated with a narrow CME (~770 km/s). Another mechanism of the QPP in terms of a sausage oscillation of the loop (L2) is also possible.

Analysis of sudden variations in photospheric magnetic fields during a large flare and their influences in the solar atmosphere

Brajesh **Kumar**, A. Raja Bayanna, P. Venkatakrishnan, Shibu K. Mathew
A&A **2016**
https://arxiv.org/pdf/1610.08294v1.pdf
The solar active region NOAA 11719 produced a large two-ribbon flare on **11 April 2013**. We have investigated the sudden variations in the photospheric magnetic fields in this active region during the flare employing the magnetograms obtained in the spectral line Fe I 6173 Angstrom by the Helioseismic and Magnetic Imager (HMI) onboard Solar Dynamics Observatory (SDO). The analysis of the line-of-sight magnetograms from HMI show sudden and persistent magnetic field changes at different locations of the active region before the onset of the flare and during the flare. The vector magnetic field observations available from HMI also show coincident variations in the total magnetic field strength and its inclination angle at these locations. Using the simultaneous Dopplergrams obtained from HMI, we observe perturbations in the photospheric Doppler signals following the sudden changes in the magnetic fields in the aforementioned locations. The power spectrum analysis of these velocity signals show enhanced acoustic power in these affected locations during the flare as compared to the pre-flare condition. Accompanying these observations, we have also used the near-simultaneous chromospheric observations obtained in the spectral line H-alpha 6562.8 Angstrom by the Global Oscillation Network Group (GONG) to study the evolution of flare ribbons and intensity oscillations in the active region. The H-alpha intensity oscillations also show enhanced oscillatory power during the flare in the aforementioned locations. These results indicate that the transient Lorentz force associated with the sudden changes in the magnetic fields could drive the localized photospheric and chromospheric oscillations, like the flare-induced oscillations in the solar atmosphere.

Effect of a Radiation Cooling and Heating Function on Standing Longitudinal Oscillations in Coronal Loops

Sanjay **Kumar**, V. M. Nakariakov, Y.-J. Moon
ApJ **2016**
http://arxiv.org/pdf/1603.08335v1.pdf
Standing long-period (with the periods longer than several minutes) oscillations in large hot (with the temperature higher than 3 MK) coronal loops have been observed as the quasi-periodic modulation of the EUV and microwave intensity emission and the Doppler shift of coronal emission lines, and have been interpreted as standing slow magnetoacoustic (longitudinal) oscillations. Quasi-periodic pulsations of shorter periods, detected in thermal and non-thermal emissions in solar flares could be produced by a similar mechanism. We present theoretical modelling of the standing slow magnetoacoustic mode, showing that this mode of oscillation is highly sensitive to peculiarities of the radiative cooling and heating function. We generalised the theoretical model of standing slow magnetoacoustic oscillations in a hot plasma, including the effects of the radiative losses, and accounting for plasma heating. The heating mechanism is not specified and taken empirically to compensate the cooling by radiation and thermal-conduction. It is shown that the evolution of the oscillations is described by a generalised Burgers equation. Numerical solution of an initial value problem for the evolutionary equation demonstrates that different dependences of the radiative cooling and plasma heating on the temperature lead to different regimes of the oscillations, including growing, quasi-stationary and rapidly decaying. Our findings provide a theoretical foundation for probing the coronal heating function, and may explain the observations of decayless long-period quasi-periodic pulsations in flares. The hydrodynamic approach employed in this study should be considered with caution in the modelling of non-thermal emission associated with flares, as it misses potentially important non-hydrodynamic effects.

Observation of a Quasi-periodic Pulsation in Hard X-ray, Radio and Extreme-ultraviolet Wavelengths

Pankaj **Kumar**, Valery M. Nakariakov, Kyung-Suk Cho

ApJ **822** 7 **2016**

http://arxiv.org/pdf/1603.03121v1.pdf

We present multi-wavelength analysis of a quasi-periodic pulsation (QPP) observed in the hard X-ray, radio, and extreme-ultraviolet (EUV) channels during an M1.9 flare occurred on **23-24 September 2011**. The non-thermal hard X-ray emission in 25-50 keV observed by RHESSI shows five distinct impulsive peaks of decaying amplitude with a period of about three minutes. Similar QPP was observed in the microwave emission recorded by the Nobeyama Radioheliograph and Polarimeter in the 8.8, 15, 17 GHz channels. Interestingly, the 3-min QPP was also observed in the metric and decimetric radio frequencies (25-180, 245, 610 MHz) as repetitive type III bursts. Multi-wavelength observations from the SDO/AIA, Hinode/SOT, and STEREO/SECCHI suggest a fan-spine topology at the eruption site, associated with the formation of a quasi-circular ribbon during the flare. A small filament was observed below the fan-loops before the flare onset. The filament rose slowly and interacted with the ambient field. This behaviour was followed by an untwisting motion of the filament. Two different structures of the filament showed ∼3-min periodic alternate rotation in the clockwise and counterclockwise directions. The 3-min QPP was found to highly correlate with 3-min oscillations in a nearby sunspot. We suggest that the periodic reconnection (modulated either by sunspot slow-mode wave or by untwisting filament) at a magnetic null-point most likely causes the repetitive particle acceleration, generating the QPP observed in hard X-ray, microwave and type III radio bursts.

See http://www.astro.gla.ac.uk/users/eduard/cesra/?p=646

X-ray and EUV Observations of Simultaneous Short and Long Period Oscillations in Hot Coronal Arcade Loops

Pankaj **Kumar**, Valery M. Nakariakov, Kyung-Suk Cho

ApJ **804** 4 **2015**

http://arxiv.org/pdf/1502.07117v1.pdf

We report decaying quasi-periodic intensity oscillations in the X-ray (6-12 keV) and extreme ultraviolet (EUV) channels (131, 94, 1600, 304 \AA) observed by the Fermi GBM (Gamma-ray Burst Monitor) and SDO/AIA, respectively, during a C-class flare. The estimated period of oscillation and decay time in the X-ray channel (6-12 keV) was about 202 s and 154 s, respectively. A similar oscillation period was detected at the footpoint of the arcade loops in the AIA 1600 and 304 \AA channels. Simultaneously, AIA hot channels (94 and 131 \AA) reveal propagating EUV disturbances bouncing back and forth between the footpoints of the arcade loops. The period of the oscillation and decay time were about 409 s and 1121 s, respectively. The characteristic phase speed of the wave is about 560 km/s for about 115 Mm loop length, which is roughly consistent with the sound speed at the temperature about 10-16 MK (480-608 km/s). These EUV oscillations are consistent with the SOHO/SUMER Doppler-shift oscillations interpreted as the global standing slow magnetoacoustic wave excited by a flare. The flare occurred at one of the footpoints of the arcade loops, where the magnetic topology was a 3D fan-spine with a null-point. Repetitive reconnection at this footpoint could cause the periodic acceleration of non-thermal electrons that propagated to the opposite footpoint along the arcade and precipitating there, causing the observed 202-s periodicity. Other possible interpretations, e.g. the second harmonics of the slow mode are also discussed. **20 July 2013**,

Multiwavelength observation of a large-scale flux rope eruption above kinked mini-filament

Pankaj **Kumar**, Kyung-Suk Cho

A&A, **2014**

http://arxiv.org/pdf/1409.7213v1.pdf

We analyse multiwavelength observations of a western limb flare (C3.9) occurred in AR NOAA 111465 on **30 April 2012**. The high resolution images recorded by SDO/AIA 304, 1600 \AA\ and Hinode/SOT Hα show the activation of a mini-filament (rising speed∼40 km s−1) associated with kink instability and the onset of a C-class flare near the southern leg of the filament. The first magnetic reconnection occurred at one of the footpoints of the filament causing the breaking of its southern leg. The filament shows unwinding motion of the northern leg and apex in the counterclockwise direction and failed to erupt. A flux-rope (visible only in hot channels, i.e., AIA 131 and 94 \AA\ channels and Hinode/SXT) structure was appeared along the neutral line during the second magnetic reconnection taking place above the kinked filament. Formation of the RHESSI hard X-ray source (12-25 keV) above the kinked filament and simultaneous appearance of the hot 131 \AA\ loops associated with photospheric brightenings (AIA 1700 \AA) suggest the particle acceleration along these loops from the top of the filament. In addition, EUV disturbances/waves observed above the filament in 171 \AA\ also show a close association with magnetic reconnection.

The flux rope rises slowly (∼100 km s−1) producing a rather big twisted structure possibly by reconnection with the surrounding sheared magnetic fields within ∼15-20 minutes, and showed an impulsive acceleration reaching a height of about 80--100 Mm. AIA 171 and SWAP 174 \AA\ images reveal a cool compression front (or CME frontal loop) surrounding the hot flux rope structure.

Simultaneous EUV and radio observations of bidirectional plasmoids ejection during magnetic reconnection⋆

Pankaj **Kumar** and Kyung-Suk Cho
A&A 557, A115 (**2013**)
We present a multiwavelength study of the X-class flare, which occurred in active region (AR) NOAA 11339 on **3 November 2011**. The extreme ultraviolet (EUV) images recorded by SDO/AIA show the activation of a remote filament (located north of the AR) with footpoint brightenings about 50 min prior to the flare's occurrence. The kinked filament rises up slowly, and after reaching a projected height of ~49 Mm, it bends and falls freely near the AR, where the X-class flare was triggered. Dynamic radio spectrum from the Green Bank Solar Radio Burst Spectrometer (GBSRBS) shows simultaneous detection of both positive and negative drifting pulsating structures (DPSs) in the decimetric radio frequencies (500–1200 MHz) during the impulsive phase of the flare. The global negative DPSs in solar flares are generally interpreted as a signature of electron acceleration related to the upward-moving plasmoids in the solar corona. The EUV images from AIA 94 Å reveal the ejection of multiple plasmoids, which move simultaneously upward and downward in the corona during the magnetic reconnection. The estimated speeds of the upward- and downward-moving plasmoids are ~152−362 and ~83–254 km s-1, respectively. These observations strongly support the recent numerical simulations of the formation and interaction of multiple plasmoids due to tearing of the current-sheet structure. On the basis of our analysis, we suggest that the simultaneous detection of both the negative and positive DPSs is most likely generated by the interaction or coalescence of the multiple plasmoids moving upward and downward along the current-sheet structure during the magnetic reconnection process. Moreover, the differential emission measure (DEM) analysis of the active region reveals a hot flux-rope structure (visible in AIA 131 and 94 Å) prior to the flare initiation and ejection of the multitemperature plasmoids during the flare impulsive phase.

Multiwavelength Observations of an Eruptive Flare: Evidence for Blast Waves and Break-Out

Pankaj **Kumar**, D. E. Innes
E-print, April **2013; File,** Solar Physics, November 2013, Volume 288, Issue 1, pp 255-268
Images of an east-limb flare on **3 November 2010** taken in the 131 Å channel of the Atmospheric Imaging Assembly onboard the Solar Dynamics Observatory provide a convincing example of a long current sheet below an erupting plasmoid, as predicted by the standard magnetic reconnection model of eruptive flares. However, the 171 Å and 193 Å channel images hint at an alternative scenario. These images reveal that large-scale waves with velocity greater than 1000 km s−1 propagated alongside and ahead of the erupting plasmoid. Just south of the plasmoid, the waves coincided with type-II radio emission, and to the north, where the waves propagated along plume-like structures, there was increased decimetric emission. Initially, the cavity around the hot plasmoid expanded. Later, when the erupting plasmoid reached the height of an overlying arcade system, the plasmoid structure changed, and the lower parts of the cavity collapsed inwards. Hot loops appeared alongside and below the erupting plasmoid. We consider a scenario in which the fast waves and the type-II emission were a consequence of a flare blast wave, and the cavity collapse and the hot loops resulted from the break-out of the flux rope through an overlying coronal arcade.

Eruption of a plasma blob, associated M-class flare, and large-scale extreme-ultraviolet wave observed by SDO⋆

P. **Kumar**1 and P. K. Manoharan
A&A 553, A109 (**2013**); **File**
We present a multiwavelength study of the formation and ejection of a plasma blob and associated extreme ultraviolet (EUV) waves in active region (AR) NOAA 11176, observed by SDO/AIA and STEREO on **25 March 2011**. The EUV images observed with the AIA instrument clearly show the formation and ejection of a plasma blob from the lower atmosphere of the Sun at ∼9 min prior to the onset of the M1.0 flare. This onset of the M-class flare happened at the site of the blob formation, while the blob was rising in a parabolic path with an average speed of ∼300 km s. The blob also showed twisting and de-twisting motion in the lower corona, and the blob speed varied from ∼10−540 km s. The faster and slower EUV wavefronts were observed in front of the plasma blob during its impulsive acceleration phase. The faster EUV wave propagated with a speed of ∼785 to 1020 km s, whereas the slower wavefront speed varied in

between ~245 and 465 km s. The timing and speed of the faster wave match the shock speed estimated from the drift rate of the associated type II radio burst. The faster wave experiences a reflection by the nearby AR NOAA 11177. In addition, secondary waves were observed (only in the 171 Å channel), when the primary fast wave and plasma blob impacted the funnel-shaped coronal loops. The Helioseismic Magnetic Imager (HMI) magnetograms revealed the continuous emergence of new magnetic flux along with shear flows at the site of the blob formation. It is inferred that the emergence of twisted magnetic fields in the form of arch-filaments/"anemone-type" loops is the likely cause for the plasma blob formation and associated eruption along with the triggering of M-class flare. Furthermore, the faster EUV wave formed ahead of the blob shows the signature of fast-mode MHD wave, whereas the slower wave seems to be generated by the field line compression by the plasma blob. The secondary wave trains originated from the funnel-shaped loops are probably the fast magnetoacoustic waves.
Three movies are available in electronic form at http://www.aanda.org

Multiwavelength Study of a Solar Eruption from AR NOAA 11112 I. Flux Emergence, Sunspot Rotation and Triggering of a Solar Flare

Pankaj **Kumar**, Sung-Hong Park, K.-S. Cho, S.-C. Bong
Solar Physics, February **2013**, Volume 282, Issue 2, pp 503-521
We analyze the multiwavelength observations of an M2.9/1N flare that occurred in the active region (AR) NOAA 11112 in the vicinity of a huge filament system on **16 October 2010**. SDO/HMI magnetograms reveal the emergence of a bipole (within the existing AR) 50 hours prior to the flare event. During the emergence, both the positive and negative sunspots in the bipole show translational as well as rotational motion. The positive-polarity sunspot shows significant motion/rotation in the south-westward/clockwise direction, and we see continuously pushing/sliding of the surrounding opposite-polarity field region. On the other hand, the negative-polarity sunspot moves/rotates in the westward/anticlockwise direction. The positive-polarity sunspot rotates ≈ 70∘ within 30 hours, whereas the one with negative polarity rotates ≈ 20∘ within 10 hours. SDO/AIA 94 Å EUV images show the emergence of a flux tube in the corona, consistent with the emergence of the bipole in HMI. The footpoints of the flux tube were anchored in the emerging bipole. The initial brightening starts at one of the footpoints (western) of the emerging loop system, where the positive-polarity sunspot pushes/slides towards a nearby negative-polarity field region. A high speed plasmoid ejection (speed ≈ 1197 km s−1) was observed during the impulsive phase of the flare, which suggests magnetic reconnection of the emerging positive-polarity sunspot with the surrounding opposite-polarity field region. The entire AR shows positive-helicity injection before the flare event. Moreover, the newly emerging bipole reveals the signature of a negative (left-handed) helicity. These observations provide unique evidence of the emergence of twisted flux tubes from below the photosphere to coronal heights, triggering a flare mainly due to the interaction between the emerging positive-polarity sunspot and a nearby negative-polarity sunspot by the shearing motion of the emerging positive sunspot towards the negative one. Our observations also strongly support the idea that the rotation can most likely be attributed to the emergence of twisted magnetic fields, as proposed by recent models.

ON THE FLARE-INDUCED SEISMICITY IN THE ACTIVE REGION NOAA 10930 AND RELATED ENHANCEMENT OF GLOBAL WAVES IN THE SUN

Brajesh **Kumar**1, P. Venkatakrishnan1, Savita Mathur2, Sanjiv Kumar Tiwari3 and R. A. García
2011 ApJ 743 29
A major flare (of class X3.4) occurred on **2006 December 13** in the active region NOAA 10930. This flare event has remained interesting to solar researchers for studies related to particle acceleration during the flare process and the reconfiguration of magnetic fields as well as fine-scale features in the active region. The energy released during flares is also known to induce acoustic oscillations in the Sun. Here, we analyze the line-of-sight velocity patterns in this active region during the X3.4 flare using the Dopplergrams obtained by the Global Oscillation Network Group (GONG) instrument. We have also analyzed the disk-integrated velocity observations of the Sun obtained by the Global Oscillation at Low Frequency (GOLF) instrument on board the Solar and Heliospheric Observatory spacecraft as well as full-disk collapsed velocity signals from GONG observations during this flare to study any possible connection between the flare-related changes seen in the local and global velocity oscillations in the Sun. We apply wavelet transform to the time series of the localized velocity oscillations as well as the global velocity oscillations in the Sun spanning the flare event. The line-of-sight velocity shows significant enhancement in some localized regions of the penumbra of this active region during the flare. The affected region is seen to be away from the locations of the flare ribbons and the hard X-ray footpoints. The sudden enhancement of this velocity seems to be caused by the Lorentz force driven by the "magnetic jerk" in the localized penumbral region. Application of wavelet analysis to these flare-induced localized seismic signals shows significant enhancement in the high-frequency domain ($5 < \nu < 8$ mHz) and a feeble enhancement in the p-mode oscillations ($2 < \nu < 5$ mHz) during the flare. On the other hand, the wavelet analysis of GOLF velocity data and the full-disk collapsed GONG velocity data spanning the flare event indicates significant post-flare enhancements in the high-frequency global velocity oscillations in the Sun, as evident from the wavelet

power spectrum and the corresponding scale-average variance. The present observations of the flare-induced seismic signals in the active region in context of the driving force are different as compared to previous reports on such cases. We also find indications of a connection between flare-induced localized seismic signals and the excitation of global high-frequency oscillations in the Sun.

Multi-Wavelength Observations of a Flux Rope Failed in the Eruption and Associated M-Class Flare from NOAA AR 11045

Pankaj **Kumar**1;2 _ A.K. Srivastava1;4 _B. Filippov3 _ R. Erdelyi4 _ Wahab Uddin1
E-print, July 2011**,** Volume 272, Number 2, 301-317, **2011, File**
We present the multiwavelength observations of a flux rope that was trying to erupt from NOAA AR 11045 and the associated M-class solar flare on **12 February 2010** using space-based and ground-based observations from TRACE, STEREO, SOHO/MDI, Hinode/XRT, and BBSO. While the flux rope was rising from the active region, an M1.1/2F class flare was triggered near one of its footpoints. We suggest that the flare triggering was due to the reconnection of a rising flux rope with the surrounding low-lying magnetic loops. The flux rope reached a projected height of ≈0.15R ⊙ with a speed of ≈90 km s−1 while the soft X-ray flux enhanced gradually during its rise. The flux rope was suppressed by an overlying field, and the filled plasma moved towards the negative polarity field to the west of its activation site. We found the first observational evidence of the initial suppression of a flux rope due to a remnant filament visible both at chromospheric and coronal temperatures that evolved a couple of days earlier at the same location in the active region. SOHO/MDI magnetograms show the emergence of a bipole ≈12 h prior to the flare initiation. The emerged negative polarity moved towards the flux rope activation site, and flare triggering near the photospheric polarity inversion line (PIL) took place. The motion of the negative polarity region towards the PIL helped in the build-up of magnetic energy at the flare and flux rope activation site. This study provides unique observational evidence of a rising flux rope that failed to erupt due to a remnant filament and overlying magnetic field, as well as associated triggering of an M-class flare.

Evidence of Solar Flare Triggering due to Loop-Loop Interaction Caused by Footpoint Shear-Motion

Kumar, Pankaj; Srivastava, A. K.; Somov, B. V.; Manoharan, P. K.; Erdelyi, R.; Uddin, Wahab
E-print, Sept **2010**, ApJ, ApJ 723 1651-1664, **2010**
We analyze multi-wavelength data of a M7.9/1N class solar flare which occurred on **27 April, 2006** from AR NOAA 10875. GOES soft X-ray images provide the most likely signature of two interacting loops and their reconnection, which triggers the solar flare. TRACE 195 A images also reveal the loop-loop interaction and the formation of `X' points with converging motion (~30 km/s) at the reconnection site in-between this interacting loop system. This provides the evidence of progressive reconnection and flare maximization at the interaction site in the active region. The absence of type III radio burst during this time period indicates no opening of magnetic field lines during the flare energy release, which implies only the change of field lines connectivity/orientation during the loop-loop interaction and reconnection process. The Ondrejov dynamic radio spectrum shows an intense decimetric (DCIM) radio burst (2.5--4.5 GHz, duration ~3 min) during flare initiation, which reveals the signature of particle acceleration from the reconnection site during loop-loop interaction. The double peak structures at 4.9 and 8.8 GHz provide the most likely confirmatory signature of the loop-loop interaction at the flare site in the active region. RHESSI hard X-ray images also show the loop-top and footpoint sources of the corresponding two loop system and their coalescence during the flare maximum, which act like the current carrying flux-tubes with resultant opposite magnetic fields and the net force of attraction. We also suggest that the shear motion/rotation of the footpoint of the smaller loop, which is anchored in the opposite polarity spot, may be responsible for the flare energy buildup and then its release due to the loop-loop interaction.

Multiwavelength Study of the M8.9/3B Solar Flare from AR NOAA 10960

Pankaj **Kumar** · A.K. Srivastava · B. Filippov · Wahab Uddin
Solar Phys (**2010**) 266: 39–58, DOI 10.1007/s11207-010-9586-4
We present a multiwavelength analysis of a long-duration, white-light solar flare (M8.9/3B) event that occurred on **04 June 2007** from AR NOAA 10960. The flare was observed by several spaceborne instruments, namely SOHO/MDI, *Hinode*/SOT, TRACE, and STEREO/SECCHI. The flare was initiated near a small, positive-polarity, satellite sunspot at the center of the active region, surrounded by opposite-polarity field regions. MDI images of the active region show a considerable amount of changes in the small positivepolarity sunspot of δ configuration during the flare event. SOT/G-band (4305 Å) images of the sunspot also suggest the rapid evolution of this positive-polarity sunspot with highly

twisted penumbral filaments before the flare event, which were oriented in a counterclockwise direction. It shows the change in orientation, and also the remarkable disappearance of twisted penumbral filaments (≈35 – 40%) and enhancement in umbral area (≈45 – 50%) during the decay phase of the flare. TRACE and SECCHI observations reveal the successive activation of two helically-twisted structures associated with this sunspot, and the corresponding brightening in the chromosphere as observed by the time-sequence of SOT/Ca II H line (3968 Å) images. The secondary, helically-twisted structure is found to be associated with the M8.9 flare event. The brightening starts six – seven minutes prior to the flare maximum with the appearance of a secondary, helically-twisted structure. The flare intensity maximizes as the secondary, helically-twisted structure moves away from the active region. This twisted flux tube, associated with the flare triggering, did not launch a CME. The location of the flare activity is found to coincide with the activation site of the helically-twisted structures.We conclude that the activation of successive helical twists (especially the second one) in the magnetic-flux tubes/ropes plays a crucial role in the energy build-up process and the triggering of the M-class solar flare without a coronal mass ejection (CME).

ON THE FLARE INDUCED HIGH-FREQUENCY GLOBAL WAVES IN THE SUN

Brajesh **Kumar**1, Savita Mathur2, R. A. Garc´ıa3, and P. Venkatakrishnan1
Astrophysical Journal Letters, 711:L12–L18, **2010** March

Recently, Karoff & Kjeldsen presented evidence of strong correlation between the energy in the high-frequency part ($5.3 < \nu < 8.3$ mHz) of the acoustic spectrum of the Sun and the solar X-ray flux. They have used disk-integrated intensity observations of the Sun obtained from the Variability of solar IRradiance and Gravity Oscillations instrument on board *Solar and Heliospheric Observatory* (*SOHO*) spacecraft. Similar signature of flares in velocity observations has not been confirmed till now. The study of low-degree high-frequency waves in the Sun is important for our understanding of the dynamics of the deeper solar layers. In this Letter, we present the analysis of the velocity observations of the Sun obtained from the Michelson and Doppler Imager (MDI) and the Global Oscillations at Low Frequencies (GOLF) instruments on board *SOHO* for some major flare events of the solar cycle 23. Application of wavelet techniques to the time series of disk-integrated velocity signals from the solar surface using the full-disk Dopplergrams obtained from the MDI clearly indicates that there is enhancement of high-frequency global waves in the Sun during the flares. This signature of flares is also visible in the Fourier Power Spectrum of these velocity oscillations. On the other hand, the analysis of disk-integrated velocity observations obtained from the GOLF shows only marginal evidence of effects of flares on high-frequency oscillations.

EVOLUTION OF SOLAR MAGNETIC FIELD AND ASSOCIATED MULTIWAVELENGTH PHENOMENA: FLARE EVENTS ON 2003 NOVEMBER 20

Pankaj **Kumar**1, P. K. Manoharan2 and Wahab Uddin1
ApJ 710 1195-1204, **2010**, **File**

We analyze Hα images, soft X-ray profiles, magnetograms, extreme ultra-violet images and, radio observations of two homologous flare events (M1.4/1N and M9.6/2B) on 2003 November 20 in the active region NOAA 10501 and study properties of reconnection between twisted filament systems, energy release, and associated launch of coronal mass ejections. During both events twisted filaments observed in Hα approached each other and initiated the flare processes. However, the second event showed the formation of cusp as the filaments interacted. The rotation of sunspots of opposite polarities, inferred from the magnetograms likely powered the twisted filaments and injection of helicity. Along the current sheet between these two opposite polarity sunspots, the shear was maximum, which could have caused the twist in the filament. At the time of interaction between filaments, the reconnection took place and flare emission in thermal and nonthermal energy ranges attained the maximum. The radio signatures revealed the opening of field lines resulting from the reconnection. The Hα images and radio data provide the inflow speed leading to reconnection and the scale size of the particle acceleration region. The first event produced a narrow and slow CME, whereas the later one was associated with a fast full halo CME. The halo CME signatures observed between the Sun and Earth using white-light and scintillation images and in situ measurements indicated the magnetic energy utilized in the expansion and propagation. The magnetic cloud signature at the Earth confirmed the flux rope ejected at the time of filament interaction and reconnection.

High-Energy Emission from a Solar Flare in Hard X-rays and Microwaves

M.R. **Kundu**, V.V. Grechnev, S.M. White, E.J. Schmahl, N.S. Meshalkina, L.K. Kashapova

E-print, Aug **2009**; Solar Phys, (**2009**) 260: 135–156; **File**

We investigate accelerated electron energy spectra for different sources in a large flare using simultaneous observations obtained with two instruments, the Nobeyama Radio Heliograph (NoRH) at 17 and 34 GHz, and the Reuven Ramaty High Energy Solar Spectroscopic Imager (RHESSI) at hard X-rays. This flare is one of the few in which emission up to energies exceeding 200 keV can be imaged in hard X-rays. Furthermore, we can investigate the spectra of individual sources up to this energy. We discuss and compare the HXR and microwave spectra and morphology. Although the event overall appears to correspond to the standard scenario with magnetic reconnection under an eruptive filament, several of its features do not seem to be consistent with popular flare models. In particular we find that (1) microwave emissions might be optically thick at high frequencies despite a low peak frequency in the total flux radio spectrum, presumably due to the inhomogeneity of the emitting source; (2) magnetic fields in high-frequency radio sources might be stronger than sometimes assumed; (3) sources spread over a very large volume can show matching evolution in their hard X-ray spectra that may provide a challenge to acceleration models. Our results emphasize the importance of studies of sunspot-associated flares and total flux measurements of radio bursts in the millimeter range. **17 June 2003**

Quasi-periodic pulsations in a solar flare with an unusual phase shift

Elena G. **Kupriyanova**, Larisa K. Kashapova, Tom Van Doorsselaere, Partha Chowdhury, Abhishek K. Srivastava, Yong-Jae Moon

MNRAS Volume 483, Issue 4 Pages 5499–5507 **2019**

https://arxiv.org/pdf/1812.09868.pdf

sci-hub.tw/10.1093/mnras/sty3480

Two kinds of processes could occur during the flare decay phase: processes of energy release or processes of energy relaxation. Quasi-periodic pulsations (QPPs) of the broadband emission are a good tool for the verification of mechanisms. We aim to study the processes during the decay phase of the X-class solar flare SOL**2014-03-29**T17:48. The observations in X-ray, microwave, and extreme ultraviolet (EUV) bands are exploited to study the fine temporal, parameters (emission measure, temperature) are studied using standard methods of correlation, Fourier, and wavelet analyses. It is found that the source of the QPPs is associated with the uniform post-flare loop. The X-ray source is located at the top of the arcade. QPPs with the similar characteristic time scales of P≈ 74--80 s are found in the X-ray (3--25 keV) and microwave (15.7 GHz) emissions. Besides, QPPs with the same period are found in the time profiles of both the temperature (Te) and emission measure (EM). The QPPs in temperature and the QPPs in emission measure demonstrate anti-phase behavior. The analysis reveals the quasi-periodic process of energy relaxation, without any additional source of energy during the decay phase. The periods of the QPPs are in a good agreement with second harmonic of standing slow magneto-acoustic wave in the arcade which could be triggered by a Moreton wave initiated by the flare in the direct vicinity of the arcade.

RHESSI Science Nuggets #379 **2020** http://sprg.ssl.berkeley.edu/~tohban/wiki/index.php/Quasi-periodic_pulsations_as_indicators_of_oscillatory_processes_in_solar_flares

Relationship of type III radio bursts with quasi-periodic pulsations in a solar flare

E. G. **Kupriyanova**, L. K. Kashapova, H. A. S. Reid, I. N. Myagkova

Solar Phys. **2016**

http://arxiv.org/pdf/1608.00129v1.pdf

We studied a solar flare with pronounced quasi-periodic pulsations detected in the microwave, X-ray, and radio bands. We used the methods of correlation, Fourier, and wavelet analyses to examine the temporal fine structures and relationships between the time profiles in each wave band. We found that the time profiles of the microwaves, hard X-rays and type III radio bursts vary quasi-periodically with the common period of 40-50 s. The average amplitude of the variations is high, above 30% of the background flux level and reaching 80% after the flare maximum. We did not find the periodicity in either the thermal X-ray flux component or source size dynamics. *Our findings indicate that the detected periodicity is likely to be associated with periodic dynamics in the injection of non-thermal electrons, that can be produced by periodic modulation of magnetic reconnection.* May 6, 2005

See CESRA highlight #846, Sept **2016** http://www.astro.gla.ac.uk/users/eduard/cesra/?p=846

Diagnostics of the acceleration modulation process based on quasi-periodic variations of are emission

Elena **Kupriyanova**_ , Hamish Reidy1, Larisa Kashapova2, and Irina Myagkova

CESRA **2016**, p.98

http://cesra2016.sciencesconf.org/conference/cesra2016/pages/CESRA2016_prog_abs_book_v3.pdf

We studied a solar are with pronounced quasi-periodic pulsations detected in the microwave, X-ray, and radio bands. We used the methods of correlation, Fourier, and wavelet analyses to examine the temporal _ne structures and relationships between the time pro_les in each wave band. We found that the time pro_les of the microwaves, hard X-rays and type III radio bursts vary quasi-periodically with the common period of 40{50 ~s. The average amplitude of the variations is high, above 30% of the background ux level and reaching 80% during the are maximum. We did not _nd the periodicity in either the thermal X-ray ux component or source size dynamics. Our _ndings indicate that the detected periodicity is likely to be associated with periodic dynamics in the injection of non-thermal electrons, that can be produced by periodic modulation of magnetic reconnection.

Specialist Discussion Meeting: 3D structure of the flare chromosphere

David **Kuridze**, Lyndsay Fletcher, Hugh Hudson

Astronomy & Geophysics (URL) **2023**

https://arxiv.org/ftp/arxiv/papers/2303/2303.16901.pdf

Spectral Characteristics and Formation Height of Off-Limb Flare Ribbons

D. **Kuridze**, M. Mathioudakis, P. Heinzel, J. Koza, H. Morgan, R. Oliver, A. F. Kowalski, J. C. Allred

ApJ **896** 120 **2020**

https://arxiv.org/pdf/2005.10924.pdf
https://iopscience.iop.org/article/10.3847/1538-4357/ab9603/pdf
Flare ribbons are bright manifestations of flare energy dissipation in the lower solar atmosphere. For the first time, we report on high-resolution imaging spectroscopy observations of flare ribbons situated off-limb in the Hβ and Ca II 8542 Å lines and make a detailed comparison with radiative hydrodynamic simulations. Observations of the X8.2-class solar flare SOL**2017-09-10**T16:06 UT obtained with the Swedish Solar Telescope reveal bright horizontal emission layers in Hβ line wing images located near the footpoints of the flare loops. The apparent separation between the ribbon observed in the Hβ wing and the nominal photospheric limb is about 300 - 500 km. The Ca II 8542 Å line wing images show much fainter ribbon emissions located right on the edge of the limb, without clear separation from the limb. RADYN models are used to investigate synthetic spectral line profiles for the flaring atmosphere, and good agreement is found with the observations. The simulations show that, towards the limb, where the line of sight is substantially oblique with respect to the vertical direction, the flaring atmosphere model reproduces the high contrast of the off-limb Hβ ribbons and their significant elevation above the photosphere. The ribbons in the Ca II 8542 Å line wing images are located deeper in the lower solar atmosphere with a lower contrast. A comparison of the height deposition of electron beam energy and the intensity contribution function shows that the Hβ line wing intensities can be an useful tracer of flare energy deposition in the lower solar atmosphere

Mapping the magnetic field of flare coronal loops

D. **Kuridze**, M. Mathioudakis, H. Morgan, R. Oliver, L. Kleint, T. V. Zaqarashvili, A. Reid, J. Koza, M. G. Löfdahl, T. Hillberg, V. Kukhianidze, A. Hanslmeier
ApJ **874, 126** **2019**
https://arxiv.org/pdf/1902.07514.pdf
Here we report on the unique observation of flaring coronal loops at the solar limb using high resolution imaging spectropolarimetry from the Swedish 1-meter Solar Telescope. The vantage position, orientation and nature of the chromospheric material that filled the flare loops allowed us to determine their magnetic field with unprecedented accuracy using the weak-field approximation method. Our analysis reveals coronal magnetic field strengths as high as 350 Gauss at heights up to 25 Mm above the solar limb. These measurements are substantially higher than a number of previous estimates and may have considerable implications for our current understanding of the extended solar atmosphere. **2017 September 10**
UKSP Nugget: #101 June **2019**
http://www.uksolphys.org/uksp-nugget/101-mapping-the-magnetic-field-of-solar-coronal-loops/

Spectropolarimetric Inversions of the Ca ii 8542 Å Line in an M-class Solar Flare

D. **Kuridze**1,2,3, V. M. J. Henriques2,4,5, M. Mathioudakis2, L. Rouppe van der Voort4,5, J. de la Cruz Rodríguez6, and M. Carlsson
2018 ApJ 860 10 DOI 10.3847/1538-4357/aac26d
We study the M1.9-class solar flare SOL**2015-09-27**T10:40 UT using high-resolution full Stokes imaging spectropolarimetry of the Ca ii 8542 Å line obtained with the CRISP imaging spectropolarimeter at the Swedish 1-m Solar Telescope. Spectropolarimetric inversions using the non-LTE code NICOLE are used to construct semiempirical models of the flaring atmosphere to investigate the structure and evolution of the flare temperature and magnetic field. A comparison of the temperature stratification in flaring and nonflaring areas reveals strong heating of the flare ribbon during the flare peak. The polarization signals of the ribbon in the chromosphere during the flare maximum become stronger when compared to its surroundings and to pre- and post-flare profiles. Furthermore, a comparison of the response functions to perturbations in the line-of-sight magnetic field and temperature in flaring and nonflaring atmospheres shows that during the flare, the Ca ii 8542 Å line is more sensitive to the lower atmosphere where the magnetic field is expected to be stronger. The chromospheric magnetic field was also determined with the weak-field approximation, which led to results similar to those obtained with the NICOLE inversions.

Spectroscopic inversions of the Ca ii 8542 Å line in a C-class solar flare

D. **Kuridze**, V. Henriques, M. Mathioudakis, J. Koza, T. V. Zaqarashvili, J. Rybák, A. Hanslmeier, F. P. Keenan
ApJ **2017**
https://arxiv.org/pdf/1708.00472.pdf
We study the C8.4 class solar flare SOL**2016-05-14**T11:34 UT using high-resolution spectral imaging in the Ca ii 8542 {\AA} line obtained with the CRISP imaging spectropolarimeter on the Swedish 1-m Solar Telescope. Spectroscopic inversions of the Ca ii 8542 {\AA} line using the non-LTE code NICOLE are used to investigate the evolution of the temperature and velocity structure in the flare chromosphere. A comparison of the temperature stratification in flaring and non-flaring areas reveals strong footpoint heating during the flare peak in the lower atmosphere. The temperature of the flaring footpoints between continuum optical depth at 500~nm, log $\tau500 \approx -2.5$ and -3.5 is $\sim 5-6.5$ kK, close to the flare peak, reducing gradually to ~ 5 kK. The temperature in the middle and upper chromosphere, between log $\tau500 \approx -3.5$ and -5.5, is estimated to be $\sim 6.5-20$ kK, decreasing to pre-flare temperatures, $\sim 5-10$ kK, after

approximately 15 minutes. However, the temperature stratification of the non-flaring areas is unchanged. The inverted velocity fields show that the flaring chromosphere is dominated by weak downflowing condensations at the Ca ii 8542 {\AA} formation height.

Observations and simulations of the Na I D1 line profiles in an M-class solar flare

D. **Kuridze**, M. Mathioudakis, D. J. Christian, A. F. Kowalski, D. B. Jess, S. D. T. Grant, T. Kawate, P. J. A. Simões, J. C. Allred, F. P. Keenan
ApJ **2016**
http://arxiv.org/pdf/1609.08120v1.pdf
We study the temporal evolution of the Na I D1 line profiles in the M3.9 flare **SOL2014-06-11**T21:03 UT, using high spectral resolution observations obtained with the IBIS instrument on the Dunn Solar Telescope combined with radiative hydrodynamic simulations. Our results show a significant increase in line core and wing intensities during the flare. The analysis of the line profiles from the flare ribbons reveal that the Na I D1 line has a central reversal with excess emission in the blue wing (blue asymmetry). We combine RADYN and RH simulations to synthesise Na I D1 line profiles of the flaring atmosphere and find good agreement with the observations. Heating with a beam of electrons modifies the radiation field in the flaring atmosphere and excites electrons from the ground state 3s 2S to the first excited state 3p 2P, which in turn modifies relative population of the two states. The change in temperature and the population density of the energy states make the sodium line profile revert from absorption into emission. Analysis of the simulated spectra also reveals that the Na I D1 flare profile asymmetries are produced by the velocity gradients generated %and opacity effects in the lower solar atmosphere.

Halpha line profile asymmetries and the chromospheric flare velocity field

D. **Kuridze**, M. Mathioudakis, P. J. A. Simões, L. Rouppe van der Voort, M. Carlsson, S. Jafarzadeh, J. C. Allred, A. F. Kowalski, M. Kennedy, L. Fletcher, D. Graham, F. P. Keenan
ApJ 813 125 **2015**
http://arxiv.org/pdf/1510.01877v1.pdf
The asymmetries observed in the line profiles of solar flares can provide important diagnostics of the properties and dynamics of the flaring atmosphere. In this paper the evolution of the Halpha and Ca II 8542 {\AA} lines are studied using high spatial, temporal and spectral resolution ground-based observations of an M1.1 flare obtained with the Swedish 1-m Solar Telescope. The temporal evolution of the Halpha line profiles from the flare kernel shows excess emission in the red wing (red asymmetry) before flare maximum, and excess in the blue wing (blue asymmetry) after maximum. However, the Ca II 8542 {\AA} line does not follow the same pattern, showing only a weak red asymmetry during the flare. RADYN simulations are used to synthesise spectral line profiles for the flaring atmosphere, and good agreement is found with the observations. We show that the red asymmetry observed in Halpha is not necessarily associated with plasma downflows, and the blue asymmetry may not be related to plasma upflows. Indeed, we conclude that the steep velocity gradients in the flaring chromosphere modifies the wavelength of the central reversal in the Halpha line profile. The shift in the wavelength of maximum opacity to shorter and longer wavelengths generates the red and blue asymmetries, respectively.

Evolution of Flare-accelerated Electrons in the Solar Corona and Chromosphere Revealed by Spatially Resolved Microwave and Hard X-Ray Analysis

Natsuha **Kuroda**, Gregory Fleishman, Dale Gary, Gelu Nita, Bin Chen, and Sijie Yu
EGU2020-3145 May **2020**
https://meetingorganizer.copernicus.org/EGU2020/displays/36057
Hard X-ray (HXR) and microwave (MW) observations are highly complementary for studying electron acceleration and transport processes in solar flares. In recent years, a new effort has been made in the MW domain using new high-resolution, multifrequency data from The Expanded Owens Valley Solar Array (EOVSA) and a breakthrough numerical modeling infrastructure that enables us to study properties of high-energy electrons in unprecedented cadence and quantitative detail. This study introduces the observation of an M1.2 flare that occurred on **2017 September 9** and analyzes the evolution of the nonthermal electrons in the corona based on EOVSA MW spectral imaging data. We find a significant spectral hardening of the MWemitting nonthermal electron population in the corona, using EOVSA lower-frequency (<7 GHz) observations over a selected 4-minute window of the flare's impulsive phase. We compare this spectral evolution with the evolution of the spectral index of nonthermal electrons emitting in the chromosphere, derived from HXR observations from the Reuven Ramaty High Energy Solar Spectroscopic Imager. We discuss the general picture of the evolution of the nonthermal electron population in this flare by incorporating observations at the two complementary wavelengths. We also make an estimate of the total energy of the nonthermal electrons contained in the observed coronal low-frequency MW source and discuss its temporal evolution.
Presentation #3145 https://presentations.copernicus.org/EGU2020/presentations-ST1.7.zip

Evolution of Flare-accelerated Electrons Quantified by Spatially Resolved Analysis

Natsuha **Kuroda**, Gregory D. Fleishman, Dale E. Gary, Gelu M. Nita, Bin Chen, Sijie Yu
Frontiers in Astronomy and Space Sciences, section Stellar and Solar Physics **2020**
https://arxiv.org/pdf/2004.13155.pdf
https://doi.org/10.3389/fspas.2020.00022

Nonthermal electrons accelerated in solar flares produce electromagnetic emission in two distinct, highly complementary domains - hard X-rays (HXRs) and microwaves (MWs). This paper reports MW imaging spectroscopy observations from the Expanded Owens Valley Solar Array of an M1.2 flare that occurred on **2017 September 9**, from which we deduce evolving coronal parameter maps. We analyze these data jointly with the complementary Reuven Ramaty High-Energy Solar Spectroscopic Imager HXR data to reveal the spatially-resolved evolution of the nonthermal electrons in the flaring volume. We find that the high-energy portion of the nonthermal electron distribution, responsible for the MW emission, displays a much more prominent evolution (in the form of strong spectral hardening) than the low-energy portion, responsible for the HXR emission. We show that the revealed trends are consistent with a single electron population evolving according to a simplified trap-plus-precipitation model with sustained injection/acceleration of nonthermal electrons, which produces a double-powerlaw with steadily increasing break energy.

Three-dimensional Forward-fit Modeling of the Hard X-Ray and the Microwave Emissions of the 2015 June 22 M6.5 Flare

Natsuha **Kuroda**, Dale E. Gary, Haimin Wang, Gregory Fleishman, Gelu M. Nita, Ju Jing
2018 *ApJ* **852** 32
https://arxiv.org/pdf/1712.07253.pdf

The well-established notion of a "common population" of the accelerated electrons simultaneously producing the hard X-ray (HXR) and the microwave (MW) emission during the flare impulsive phase has been challenged by some studies reporting the discrepancies between the HXR-inferred and the MW-inferred electron energy spectra. The traditional methods of their spectral inversion have some problems that can be mainly attributed to the unrealistic and the oversimplified treatment of the flare emission. To properly address this problem, we use a Non-linear Force Free Field (NLFFF) model extrapolated from an observed photospheric magnetogram as input to the three-dimensional, multi-wavelength modeling platform GX Simulator, and create a unified electron population model that can simultaneously reproduce the observed HXR and MW observations. We model the end of the impulsive phase of the **2015-06-22** M6.5 flare, and constrain the modeled electron spatial and energy parameters using observations made by the highest-resolving instruments currently available in two wavelengths, the Reuven Ramaty High Energy Solar Spectroscopic Imager (RHESSI) for HXR and the Expanded Owens Valley Solar Array (EOVSA) for MW. Our results suggest that the HXR-emitting electron population model fits the standard flare model with a broken power-law spectrum (E_break ~ 200 keV) that simultaneously produces the HXR footpoint emission and the MW high frequency emission. The model also includes an "HXR invisible" population of nonthermal electrons that are trapped in a large volume of magnetic field above the HXR-emitting loops, which is observable by its gyrosynchrotron (GS) radiation emitting mainly in MW low frequency range.

Observation of 2011-02-15 X2.2 flare in Hard X-ray and Microwave

Natsuha **Kuroda**, Haimin Wang, Dale E. Gary
ApJ **807** 124 **2015**
http://arxiv.org/pdf/1506.01424v1.pdf

Previous studies have shown that the energy release mechanism of some solar flares follow the Standard magnetic-reconnection model, but the detailed properties of high-energy electrons produced in the flare are still not well understood. We conducted a unique, multi-wavelength study that discloses the spatial, temporal and energy distributions of the accelerated electrons in the X2.2 solar flare on 2011, Feb. 15. We studied the source locations of seven distinct temporal peaks observed in hard X-ray (HXR) and microwave (MW) lightcurves using the Reuven Ramaty High Energy Solar Spectroscopic Imager (RHESSI) in 50 to 75 keV channels and Nobeyama Radioheliograph (NoRH) in 34 GHz, respectively. We found that the seven emission peaks did not come from seven spatially distinct sites in HXR and MW, but rather in HXR we observed a sudden change in location only between the second and the third peak, with the same pattern occurring, but evolving more slowly in MW. Comparison between the HXR lightcurve and the temporal variations in intensity in the two MW source kernels also confirmed that the seven peaks came predominantly from two sources, each with multiple temporal peaks. In addition, we studied the polarization properties of MW sources, and time delay between HXR and MW. We discuss our results in the context of the tether-cutting model. **2014 September 6**

Coupling between magnetic reconnection, energy release, and particle acceleration in the X17.2 2003 October 28 solar flare

Victoria G. **Kurt**1, Astrid M. Veronig2,3, Gregory D. Fleishman4,5, Jürgen Hinterreiter2,6, Johannes Tschernitz2 and Alexandra L. Lysenko7
A&A, 686, A195 (**2024**)
https://www.aanda.org/articles/aa/pdf/2024/06/aa49130-23.pdf
Context. The **2003 October 28** (X17.2) eruptive flare was a unique event. The coronal electric field and the π-decay γ-ray emission flux displayed the highest values ever inferred for solar flares.
Aims. Our aim is to reveal physical links between the magnetic reconnection process, energy release, and acceleration of electrons and ions to high energies in the chain of the magnetic energy transformations in the impulsive phase of the solar flare.
Methods. The global reconnection rate, φ(t), and the local reconnection rate (coronal electric field strength), Ec(r, t), were calculated from flare ribbon separation in Hα filtergrams and photospheric magnetic field maps. Then, HXRs measured by CORONAS-F/SPR-N and the derivative of the GOES SXR flux, İSXR(t) were used as proxies of the flare energy release evolution. The flare early rise phase, main raise phase, and main energy release phase were defined based on temporal profiles of the above proxies. The available results of INTEGRAL and CORONAS-F/SONG observations were combined with Konus-Wind data to quantify the time behavior of electron and proton acceleration. Prompt γ-ray lines and delayed 2.2 MeV line temporal profiles observed with Konus-Wind and INTEGRAL/SPI were used to detect and quantify the nuclei with energies of 10−70 MeV.
Results. The magnetic-reconnection rates, φ(t) and Ec(r, t), follow a common evolutionary pattern with the proxies of the flare energy released into high-energy electrons. The global and local reconnection rates reach their peaks at the end of the main rise phase of the flare. The spectral analysis of the high-energy γ-ray emission revealed a close association between the acceleration process efficiency and the reconnection rates. High-energy bremsstrahlung continuum and narrow γ-ray lines were observed in the main rise phase when Ec(r, t) of the positive (negative) polarity reached values of ∼120 V cm−1 (∼80 V cm−1). In the main energy release phase, the upper energy of the bremsstrahlung spectrum was significantly reduced and the pion-decay γ-ray emission appeared abruptly. We discuss the reasons why the change of the acceleration regime occurred along with the large-scale magnetic field restructuration of this flare.
Conclusions. The similarities between the proxies of the flare energy release with φ(t) and Ec(r, t) in the flare's main rise phase are in accordance with the reconnection models. We argue that the main energy release and proton acceleration up to subrelativistic energies began just when the reconnection rate was going through the maximum, that is, following a major change of the flare topology.

A physics-based method that can predict imminent large solar flares

Kusano, Iju, Bamba & Inoue
Science 31 Jul **2020**: Vol. 369, Issue 6503, pp. 587-591
DOI: 10.1126/science.aaz2511
https://science.sciencemag.org/content/369/6503/587/tab-pdf
https://science.sciencemag.org/content/369/6503/587
https://sci-hub.tw/10.1126/science.aaz2511
Solar flares are highly energetic events in the Sun's corona that affect Earth's space weather. The mechanism that drives the onset of solar flares is unknown, hampering efforts to forecast them, which mostly rely on empirical methods. We present the κ-scheme, a physics-based model to predict large solar flares through a critical condition of magnetohydrodynamic instability, triggered by magnetic reconnection. Analysis of the largest (X-class) flares from 2008 to 2019 (during solar cycle 24) shows that the κ-scheme predicts most imminent large solar flares, with a small number of exceptions for confined flares. We conclude that magnetic twist flux density, close to a magnetic polarity inversion line on the solar surface, determines when and where solar flares may occur and how large they can be.
6 Sep 2017
The sudden release of magnetic energy on the Sun drives powerful solar flares, which are difficult to predict. Kusano et al. derived physics-based thresholds for the onset of large solar flares and show how they can be predicted from routine solar observations (see the Perspective by Veronig). They tested their method using observations of the Sun from 2008 to 2019. In most cases, the method correctly identifies which regions will produce large flares within the next 20 hours, although there are some false positives and false negatives. The method also provides the exact location where each flare will begin and limits on how powerful it will be. Accurate predictions of solar flares could improve forecasts of space weather conditions around Earth.

A Challenge to Physics-based Prediction of Giant Solar Flares

K. **Kusano**
SCOSTEP-PRESTO ONLINE SEMINAR #1 May 26 (Tue), **2020**, 12:00-13:00 UT
Solar flares are catastrophic explosions in the solar corona and may potentially cause a severe space weather disaster. However, because the onset mechanism of solar flares is not yet well elucidated, most of the flare forecasts in operation rely on empirical methods. We recently developed a new physics-based model, called the κ-scheme, for predicting giant solar flares as one of the major outcomes of the Project for Solar-Terrestrial Environment Prediction (PSTEP), which is the Japanese nation-wide project for space weather and space climate study. The κ-scheme is able to predict imminent

giant solar flares through the critical condition of magnetohydrodynamic (MHD) instability triggered by magnetic reconnection. An analysis of the largest solar flares in solar cycle 24 indicates that the κ-scheme can provide precise information, including location and size, of possible giant solar flares with a small exception. Through this study, we also discovered that the magnetic twist flux density in the vicinity of the magnetic polarity inversion line (PIL) on the solar surface plays a crucial role in determining when, where, and how large solar flares may occur. Finally, we will discuss how important is the development of physics-based prediction to improve our predictive capability and the scientific understanding of solar-terrestrial system dynamics.

See Lin et al. (2020) sci-hub.tw/10.3847/1538-4357/ab822c

Park et al. (2020) sci-hub.tw/10.3847/1538-4357/ab65f0

MAGNETIC FIELD STRUCTURES TRIGGERING SOLAR FLARES AND CORONAL MASS EJECTIONS

K. **Kusano**1,4, Y. Bamba1, T. T. Yamamoto1, Y. Iida2,5, S. Toriumi2,5, and A. Asai

2012 ApJ 760 31

Solar flares and coronal mass ejections, the most catastrophic eruptions in our solar system, have been known to affect terrestrial environments and infrastructure. However, because their triggering mechanism is still not sufficiently understood, our capacity to predict the occurrence of solar eruptions and to forecast space weather is substantially hindered. Even though various models have been proposed to determine the onset of solar eruptions, the types of magnetic structures capable of triggering these eruptions are still unclear. In this study, we solved this problem by systematically surveying the nonlinear dynamics caused by a wide variety of magnetic structures in terms of three-dimensional magnetohydrodynamic simulations. As a result, we determined that two different types of small magnetic structures favor the onset of solar eruptions. These structures, which should appear near the magnetic polarity inversion line (PIL), include magnetic fluxes reversed to the potential component or the nonpotential component of major field on the PIL. In addition, we analyzed two large flares, the X-class flare on **2006 December 13** and the M-class flare on **2011 February 13**, using imaging data provided by the Hinode satellite, and we demonstrated that they conform to the simulation predictions. These results suggest that forecasting of solar eruptions is possible with sophisticated observation of a solar magnetic field, although the lead time must be limited by the timescale of changes in the small magnetic structures.

Large-scale contraction and subsequent disruption of coronal loops during various phases of the M6.2 flare associated with the confined flux rope eruption

Upendra **Kushwaha**, Bhuwan Joshi, Astrid M. Veronig, Yong-Jae Moon

ApJ **807** 101 **2015**

http://arxiv.org/pdf/1504.01888v1.pdf

We present a detailed multi-wavelength study of the M6.2 flare which was associated with a confined eruption of a prominence using TRACE, RHESSI, and NoRH observations. The pre-flare phase of this event is characterized by spectacular large-scale contraction of overlying extreme ultraviolet (EUV) coronal loops during which the loop system was subjected to an altitude decrease of ~20 Mm for an extended span of ~30 min. This contraction phase is accompanied by sequential EUV brightenings associated with hard X-ray (HXR) (up to 25 keV) and microwave (MW) sources from low-lying loops in the core of the flaring region which together with X-ray spectra indicate strong localized heating in the source region before the filament activation and associated M-class flare. With the onset of the impulsive phase of the M6.2 flare, we detect HXR and MW sources that exhibit intricate temporal and spatial evolution in relation with the fast rise of the prominence. Following the flare maximum, the filament eruption slowed down and subsequently confined within the large overlying active region loops; the event did not lead to a coronal mass ejection (CME). During the confinement process of the erupting prominence, we detect MW emission from the extended coronal region with multiple emission centroids which likely represent emission from hot blobs of plasma formed after the collapse of the expanding flux rope and entailing prominence material. RHESSI observations reveal high plasma temperature (~30 MK) and substantial non-thermal characteristics with electron spectral index (~5) during the impulsive phase of the flare. The time-evolution of thermal energy exhibits a good correspondence with the variations in cumulative non-thermal energy which suggest that the energy of accelerated particles efficiently converted to hot flare plasma implying an effective validation of the Neupert effect. **2004-07-14**

Impulsive Energy Release and Non-thermal Emission in a Confined M4.0 Flare Triggered by Rapidly Evolving Magnetic Structures

Upendra **Kushwaha**1, Bhuwan Joshi1, Kyung-Suk Cho2, Astrid Veronig3, Sanjiv Kumar Tiwari4, and S. K. Mathew

2014 ApJ 791 23

http://arxiv.org/pdf/1407.8115v2.pdf

We present observations of a confined M4.0 flare from NOAA 11302 on **2011 September 26**. Observations at high temporal, spatial, and spectral resolution from the Solar Dynamics Observatory, Reuven Ramaty High Energy Solar Spectroscopic Imager, and Nobeyama Radioheliograph observations enabled us to explore the possible triggering and energy release processes of this flare despite its very impulsive behavior and compact morphology. The flare light curves exhibit an abrupt rise of non-thermal emission with co-temporal hard X-ray (HXR) and microwave (MW) bursts that peaked instantly without any precursor emission. This stage was associated with HXR emission up to 200 keV that followed a power law with photon spectral index (γ) ~ 3. Another non-thermal peak, observed 32 s later, was more pronounced in the MW flux than the HXR profiles. Dual peaked structures in the MW and HXR light curves suggest a two-step magnetic reconnection process. Extreme ultraviolet (EUV) images exhibit a sequential evolution of the inner and outer core regions of magnetic loop systems while the overlying loop configuration remained unaltered. Combined observations in HXR, (E)UV, and Hα provide support for flare models involving the interaction of coronal loops. The magnetograms obtained by the Helioseismic and Magnetic Imager reveal emergence of magnetic flux that began ~five hr before the flare. However, the more crucial changes in the photospheric magnetic flux occurred about one minute prior to the flare onset with opposite polarity magnetic transients appearing at the early flare location within the inner core region. The spectral, temporal, and spatial properties of magnetic transients suggest that the sudden changes in the small-scale magnetic field have likely triggered the flare by destabilizing the highly sheared pre-flare magnetic configuration.

A statistical study of magnetic flux emergence in solar active regions prior to strongest flares

Alexander S. **Kutsenko**, Valentina I. Abramenko, Andrei A. Plotnikov
MNRAS **2021**
https://arxiv.org/pdf/2105.03886.pdf

Using the data on magnetic field maps and continuum intensity for Solar Cycles 23 and 24, we explored 100 active regions (ARs) that produced M5.0 or stronger flares. We focus on the presence/absence of the emergence of magnetic flux in these ARs 2-3 days before the strong flare onset. We found that 29 ARs in the sample emerged monotonously amidst quiet-Sun area. A major emergence of a new magnetic flux within pre-existing AR yielding the formation of a complex flare-productive configuration was observed in another 24 cases. For 30 ARs, an insignificant (in terms of the total magnetic flux of pre-existing AR) emergence of a new magnetic flux within the pre-existing magnetic configuration was observed; for some of them the emergence resulted in a formation of a configuration with a small δ-sunspot. 11 out of 100 ARs exhibited no signatures of magnetic flux emergence during the entire interval of observation. In 6 cases the emergence was in progress when the AR appeared on the Eastern limb, so that the classification and timing of emergence were not possible. We conclude that the recent flux emergence is not a necessary and/or sufficient condition for strong flaring of an AR. The flux emergence rate of analysed here flare-productive ARs was compared with that for flare-quiet ARs analysed in our previous studies. We revealed that the flare-productive ARs tend to display faster emergence than the flare-quiet ones.

On the possibility to probe the flare productivity of an active region on the early stage of emergence

Alexander S. **Kutsenko**, Valentina I. Abramenko, Olga K. Kutsenko
MNRAS Volume 501, Issue 4, March **2021**, Pages 6076–6082,
https://doi.org/10.1093/mnras/staa3548
https://arxiv.org/pdf/2011.12062.pdf

A long-standing problem is to predict the future flare productivity of an active region (AR) when it is on the stage of early emergence. The aim of this study is to probe two parameters of the photospheric magnetic field, both derived during the emergence phase of an AR, and to compare them with the flare productivity of the well-developed AR. The parameters are: (i) the index of the magnetic power spectrum (the slope of the spectrum) on the stage of emergence, and (ii) the flux emergence rate. Analysis of 243 emerging ARs showed that the magnetic power index increases from values typical for quiet-Sun regions to the values typical for mature ARs within a day while the emergence proceeds for several days; frequently, after the increase, the value of the power index undulates around some mean value with fluctuations being several time less than the growth of the power index during the emergence onset. For a subset of 34 flare-productive ARs we found no correlation between the power spectrum index at the stage of emergence and flare index derived from the entire interval of the AR's presence on the disc. At the same time, the flux emergence rate correlates well with the flare index (the Pearson's correlation coefficient is 0.74). We conclude that high flux emergence rate is a necessary condition for an AR to produce strong flares in the future, and so, the flux emergence rate can be used to probe the future flare productivity of the AR. **2014 Nov 24-28**
Table 1. The list of ARs and the derived parameters.

Magnetic Power Spectra of Emerging Active Regions

Olga K. **Kutsenko**, Alexander S. Kutsenko, Valentina I. Abramenko
Solar Phys. 294:102 **2019**
https://arxiv.org/pdf/1907.07952.pdf

sci-hub.se/10.1007/s11207-019-1498-3
Magnetic field data provided by the Helioseismic and Magnetic Imager on board the Solar Dynamics Observatory were utilized to explore the changes in the magnetic energy of four active regions (ARs) during their emergence. We found that at the very early stage of the magnetic flux emergence, an abrupt steepening of the magnetic power spectrum takes place leading to rapid increase of the absolute value of the negative spectra power index α in E(k) ~ kα. As the emergence proceeds, the energy increases at all scales simultaneously implying that elements of all sizes do appear in the photosphere. Meanwhile, the energy gain at scales larger than ≈10 Mm prevails as compared to that at smaller scales. Both direct (i.e., fragmentation of large structures into smaller ones) and inverse (i.e., merging of small magnetic features into larger elements) cascades are readily observed during the emergence. However, in the case of inverse cascade, the total energy gained at large scales exceeds the energy loss at smaller scales assuming simultaneous appearance of large-scale magnetic entities from beneath the photosphere. We conclude that most of the time the energy may grow at all scales. We also cannot support the point of view regarding the dominant role of the inverse cascade in the formation of an AR. Although the coalescence of small magnetic elements into larger pores and sunspots is observed, our analysis shows that the prevailed energy contribution to an AR comes from emergence of large-scale structures. **2010, May 29 – Jun 03, 2013, Apr 18 –21, 2013, Jun 26–30, 2015, Jan 24–28**

Extended statistical analysis of emerging solar active regions

A.S. **Kutsenko**, V.I. Abramenko, A.A. Pevtsov
MNRAS **2018**
https://arxiv.org/pdf/1811.12089.pdf
We use observations of line-of-sight magnetograms from Helioseismic and Magnetic Imager (HMI) on board of Solar Dynamics Observatory (SDO) to investigate polarity separation, magnetic flux, flux emergence rate, twist and tilt of solar emerging active regions. Functional dependence of polarity separation and maximum magnetic flux of an active region is in agreement with a simple model of flux emergence as the result of buoyancy forces. Our investigation did not reveal any strong dependence of emergence rate on twist properties of active regions.
flux-weighted centroids of opposite polarities **2015 January 16-19**

Electron acceleration and transport in the 2023-03-06 solar flare

Alexey **Kuznetsov**, Zhao Wu, Sergey Anfinogentov, Yang Su, Yao Chen
Frontiers in Astronomy and Space Sciences 11: 1407955. **2024**
doi: 10.3389/fspas.2024.1407955
https://arxiv.org/pdf/2405.18850
https://www.frontiersin.org/journals/astronomy-and-space-sciences/articles/10.3389/fspas.2024.1407955/full
We investigated in detail the M5.8 class solar flare that occurred on **2023-03-06**. This flare was one of the first strong flares observed by the Siberian Radioheliograph in the microwave range and the Advanced Space-based Solar Observatory in the X-ray range. The flare consisted of two separate flaring events (a “thermal” and a “cooler” ones), and was associated with (and probably triggered by) a filament eruption. During the first part of the flare, the microwave emission was produced in an arcade of relatively short and low flaring loops. During the second part of the flare, the microwave emission was produced by energetic electrons trapped near the top of a large-scale flaring loop; the evolution of the trapped electrons was mostly affected by the Coulomb collisions. Using the available observations and the GX Simulator tool, we created a 3D model of the flare, and estimated the parameters of the energetic electrons in it.

Stellar Superflares Observed Simultaneously with Kepler and XMM-Newton

Alexey A. **Kuznetsov**, Dmitrii Y. Kolotkov
ApJ **912** 81 **2021**
https://arxiv.org/pdf/2103.10866.pdf
https://iopscience.iop.org/article/10.3847/1538-4357/abf569/pdf
https://doi.org/10.3847/1538-4357/abf569
Solar and stellar flares are powerful events which produce intense radiation across the electromagnetic spectrum. Multiwavelength observations are highly important for understanding the nature of flares, because different flare-related processes reveal themselves in different spectral ranges. To study the correlation between thermal and nonthermal processes in stellar flares, we have searched the databases of Kepler (optical observations) and XMM-Newton (soft X-rays) for the flares observed simultaneously with both instruments; nine distinctive flares (with energies exceeding 1033 erg) on three stars (of K-M spectral classes) have been found. We have analyzed and compared the flare parameters in the optical and X-ray spectral ranges; we have also compared the obtained results with similar observations of solar flares. Most of the studied stellar flares released more energy in the optical range than in X-rays. In one flare, X-ray emission strongly dominated, which could be caused either by soft spectrum of energetic electrons or by a near-limb position of this flare. The X-ray flares were typically delayed with respect to and shorter than their optical counterparts, which is partially consistent with the Neupert effect. Using the scaling laws based on the magnetic

reconnection theory, we have estimated the characteristic magnetic field strengths in the stellar active regions and the sizes of these active regions as about 25−70 G and 250000−500000 km, respectively. The observed stellar superflares appear to be scaled-up versions of solar flares, with a similar underlying mechanism and nearly the same characteristic magnetic field values, but with much larger active region sizes.

Spatio-temporal dynamics of sources of hard X-ray pulsations in solar flares

S. A. **Kuznetsov**, I. V. Zimovets, A. S. Morgachev, A. B. Struminsky
Solar Phys. Volume 291, Issue 11, pp 3385–3426 **2016**
http://arxiv.org/pdf/1608.06594v1.pdf
We present systematic analysis of spatio-temporal evolution of sources of hard X-ray (HXR) pulsations in solar flares. We concentrate on disk flares whose impulsive phase are accompanied by a series of more than three peaks (pulsations) of HXR emission detected in the RHESSI 50-100 keV channel with 4-second cadence. **29 such flares** observed from February 2002 to June 2015 with time differences between successive peaks of 8-270 s are studied. The main observational result is that sources of HXR pulsations in all flares are not stationary, they demonstrate apparent displacements from pulsation to pulsation. The flares can be subdivided into two groups depending on character of dynamics of HXR sources. The group-1 consists of 16 flares (55%) with systematic dynamics of HXR sources from pulsation to pulsation with respect to a magnetic polarity inversion line (MPIL), which has simple extended trace on the photosphere. The group-2 consists of 13 flares (45%) with more chaotic displacements of HXR sources with respect to an MPIL having more complicated structure. Based on the observations we conclude that the mechanism of flare HXR pulsations is related to successive triggering of energy release in different magnetic loops. Group-1 flare regions consist of loops stacked into magnetic arcades extended along MPILs. Group-2 flare regions have more complicated magnetic structures and loops are arranged more chaotically. We also found that at least 14 (88%) group-1 flares and 11 (85%) group-2 flares are accompanied by coronal mass ejections, i.e. the majority of flares studied are eruptive events. This gives an indication that eruptive processes play important role in generation of HXR pulsations. We suggest that an erupting flux rope can act as a trigger of energy release. Its successive interaction with different loops can lead to apparent motion of HXR sources and to a series of HXR pulsations. **9 Nov 2002**,
Table 1. General information about the studied events.
See RHESSI Science Nuggets #285 Oct **2016**
http://sprg.ssl.berkeley.edu/~tohban/wiki/index.php/Spatio-Temporal_Dynamics_of_Flare_Hard_X-ray_Pulsations

Survey of Magnetic Helicity Injection in Regions Producing X-Class Flares

LaBonte, B. J., Georgoulis, M. K., & Rust, D. M.
E-print, Aug. **2007**; The Astrophysical Journal, 671:955Y963, 2007 December 10
we surveyed magnetic helicity injection into 48 X-flare producing active regions recorded by the MDI between 1996 July and 2005 July.
Most of the X-flare regions generated the helicity needed for a CME in a few days to a few hours.

An Explanation of Remarkable Emission-line Profiles in Post-flare Coronal Rain

Daniela A. **Lacatus**1, Philip G. Judge2, and Alina Donea
2017 ApJ 842 15
http://sci-hub.cc/10.3847/1538-4357/aa725d
https://arxiv.org/pdf/1707.07069.pdf
We study broad redshifted emission in chromospheric and transition region lines that appears to correspond to a form of post-flare coronal rain. Profiles of Mg ii, C ii, and Si iv lines were obtained using IRIS before, during, and after the X2.1 flare of **2015 March 11** (SOL2015-03-11T16:22). We analyze the profiles of the five transitions of Mg ii (the h and k transitions, and three lines belonging to the transitions). We use analytical methods to understand the unusual profiles, together with higher-resolution observational data of similar phenomena observed by Jing et al. The peculiar line ratios indicate anisotropic emission from the strands that have cross-strand line center optical depths (k line) of between 1 and 10. The lines are broadened by unresolved Alfvénic motions whose energy exceeds the radiation losses in the Mg ii lines by an order of magnitude. The decay of the line widths is accompanied by a decay in the brightness, suggesting a causal connection. If the plasma is 99% ionized, ion–neutral collisions can account for the dissipation; otherwise, a dynamical process seems necessary. Our work implies that the motions are initiated during the impulsive phase, to be dissipated as radiation over a period of an hour, predominantly by strong chromospheric lines. The coronal "rain" we observe is far more turbulent than most earlier reports have indicated, with implications for plasma heating mechanisms.

Alternative Waiting Time Statistics for the Lu and Hamilton Avalanche Model

Matías **Kychenthal**1,2 and Laura F. Morales1,2
2023 ApJ 946 84
https://iopscience.iop.org/article/10.3847/1538-4357/acb696/pdf

The solar corona hosts many explosive events. Among them, flares are some of the most energetic, rapidly releasing huge amounts of energy and, in the case of the largest ones, producing coronal mass ejections that have the potential to harm life on our planet. Therefore, there is great interest in attempting to foresee the occurrence of extreme solar flares. Avalanche models for solar flares have been used since the beginning of the 1990s to model the flaring corona in a simple and computationally inexpensive way. The pioneering and now most prevalent model in the literature was proposed by Lu and Hamilton. This model has been extremely useful to reproduce most of the main characteristic features observed in solar flares (e.g., the probability density function of a flare's energy) and, in recent years, has been used as the starting point to predict extreme flaring events. In this work, we revisit Lu and Hamilton's model and the very definition of waiting time for both extreme and all-sized events. We find that extreme avalanche statistics are well described by a log-normal distribution, in accordance with recent observations of solar flares.

Energy Definition and Minimization in Avalanche Models for Solar Flares

Henri **Lamarre**, Paul Charbonneau, Antoine Strugarek
Solar Phys. Volume 299, article number 13, **2024**
https://arxiv.org/pdf/2401.14503.pdf
https://doi.org/10.1007/s11207-024-02254-6
Self-organised critical avalanche models are a class of cellular automata that, despite their simplicity, can be applied to the modeling of solar (and stellar) flares and generate robust power-law distributions in event size measures. However, bridging the conceptual gap to both magnetohydrodynamics and real flare observations continues to prove challenging. In this paper, we focus on a specific, key aspect of this endeavour, namely the definition of magnetic energy and its consequences for the model's internal dynamics and energy release statistics. We show that the dual requirement of releasing energy and restoring local stability demands that the instability criterion and boundary conditions be set in a manner internally consistent with a given energy definition, otherwise unphysical behavior ensues, e.g., negative energy release. Working with three energy definitions previously used in the literature, we construct such internally consistent avalanche models and compare/contrast their energy release statistics. Using the same set of models, we also explore a recent proposal by Farhang et al. (2018, 2019), namely that avalanches/flares should maximize the amount of energy released by the lattice when instabilities are triggered. This tends to produce avalanches of shorter duration but higher peak energy release, but adding up to similar total energy release. For the three energy definition we tested, such avalanche models exhibit almost identical distributions of event size measures. Our results indicate that the key to reproduce solar-like power-law slopes in these size measures is lattice configurations in which most nodes remain relatively far from the instability threshold.

The FIP and Inverse-FIP Effects in Solar Flares

J. Martin **Laming**
2021 ApJ 909 17
https://iopscience.iop.org/article/10.3847/1538-4357/abd9c3/pdf
https://doi.org/10.3847/1538-4357/abd9c3
The inverse first ionization potential (FIP) effect, the depletion in the coronal abundance of elements like Fe, Mg, and Si that are ionized in the solar chromosphere relative to those that are neutral, has been identified in several solar flares. We give a more detailed discussion of the mechanism of fractionation by the ponderomotive force associated with magnetohydrodynamic waves, paying special attention to the conditions in which inverse-FIP fractionation arises in order to better understand its relation to the usual FIP effect, i.e., the enhancement of the coronal abundance of Fe, Mg, Si, etc. The FIP effect is generated by parallel propagating Alfvén waves, with either photospheric, or more likely coronal, origins. The inverse-FIP effect arises as upward-propagating fast-mode waves with an origin in the photosphere or below refract back downwards in the chromosphere where the Alfvén speed is increasing with altitude. We give a more physically motivated picture of the FIP fractionation, based on the wave refraction around inhomogeneities in the solar atmosphere, and inspired by previous discussions of analogous phenomena in the optical trapping of particles by laser beams. We apply these insights to modeling the fractionation and find good agreement with the observations of Katsuda et al. and Dennis et al.

Low Dimensional Convolutional Neural Network For Solar Flares GOES Time Series Classification

Vlad **Landa**, Yuval Reuveni
ApJS **258** 12 **2022**
https://arxiv.org/pdf/2101.12550.pdf
https://iopscience.iop.org/article/10.3847/1538-4365/ac37bc/pdf
https://doi.org/10.3847/1538-4365/ac37bc
Space weather phenomena such as solar flares, have massive destructive power when reaches certain amount of magnitude. Such high magnitude solar flare event can interfere space-earth radio communications and neutralize space-earth electronics equipment. In the current study, we explorer the deep learning approach to build a solar flare forecasting model and examine its limitations along with the ability of features extraction, based on the available time-

series data. For that purpose, we present a multi-layer 1D Convolutional Neural Network (CNN) to forecast solar flare events probability occurrence of M and X classes at 1,3,6,12,24,48,72,96 hours time frame. In order to train and evaluate the performance of the model, we utilised the available Geostationary Operational Environmental Satellite (GOES) X-ray time series data, ranged between July 1998 and January 2019, covering almost entirely the solar cycles 23 and 24. The forecasting model were trained and evaluated in two different scenarios (1) random selection and (2) chronological selection, which were compare afterward. Moreover we compare our results to those considered as state-of-the-art flare forecasting models, both with similar approaches and different ones.The majority of the results indicates that (1) chronological selection obtain a degradation factor of 3\% versus the random selection for the M class model and elevation factor of 2\% for the X class model. (2) When consider utilizing only X-ray time-series data, the suggested model achieve high score results compare to other studies. (3) The suggested model combined with solely X-ray time-series fails to distinguish between M class magnitude and X class magnitude solar flare events. All source code are available at this https URL

Hinode/EIS coronal magnetic field measurements at the onset of a C2 flare

Enrico **Landi**, Wenxian Li, Tomas Brage, Roger Hutton

ApJ **913** 1 **2021**

https://arxiv.org/pdf/2102.06072.pdf

https://iopscience.iop.org/article/10.3847/1538-4357/abf6d1/pdf

https://doi.org/10.3847/1538-4357/abf6d1

In the present work we study Hinode/EIS observations of an active region taken before, during and after a small C2.0 flare in order to monitor the evolution of the magnetic field evolution and its relation to the flare event. We find that while the flare left the active region itself unaltered, the event included a large Magnetic Field Enhancement (MFE), which consisted of a large increase of the magnetic field to strengths just short of 500~G in a rather small region where no magnetic field was measured before the flare. This MFE is observed during the impulsive phase of the flare at the footpoints of flare loops, its magnetic energy is sufficient to power the radiative losses of the entire flare, and has completely dissipated after the flare. We argue that the MFE might occur at the location of the reconnection event triggering the flare, and note that it formed within 22 minutes of the flare start (as given by the EIS raster return time). These results open the door to a new line of studies aimed at determining whether MFEs 1) can be flare precursor events, 2) can be used for Space Weather forecasts; and 3) what advance warning time they could allow; as well as to explore which physical processes lead to their formation and dissipation, whether such processes are the same in both long-duration and impulsive flares, and whether they can be predicted by theoretical models. **24-Aug-2007**
RHESSI #442 **2023** https://sprg.ssl.berkeley.edu/~tohban/wiki/index.php/A_possible_coronal_magnetic_flare_precursor

Predicting Solar Flares with Remote Sensing and Machine Learning

Erik **Larsen**

2021

https://arxiv.org/ftp/arxiv/papers/2110/2110.07658.pdf

High energy solar flares and coronal mass ejections have the potential to destroy Earth's ground and satellite infrastructures, causing trillions of dollars in damage and mass human suffering. Destruction of these critical systems would disable power grids and satellites, crippling communications and transportation. This would lead to food shortages and an inability to respond to emergencies. A solution to this impending problem is proposed herein using satellites in solar orbit that continuously monitor the Sun, use artificial intelligence and machine learning to calculate the probability of massive solar explosions from this sensed data, and then signal defense mechanisms that will mitigate the threat. With modern technology there may be only safeguards that can be implemented with enough warning, which is why the best algorithm must be identified and continuously trained with existing and new data to maximize true positive rates while minimizing false negatives. This paper conducts a survey of current machine learning models using open source solar flare prediction data. The rise of edge computing allows machine learning hardware to be placed on the same satellites as the sensor arrays, saving critical time by not having to transmit remote sensing data across the vast distances of space. A system of systems approach will allow enough warning for safety measures to be put into place mitigating the risk of disaster.

GOES class estimation for behind-the-limb solar flares using MESSENGER SAX

Erica **Lastufka**, Säm Krucker

ApJ **905** 161 **2020**

https://arxiv.org/pdf/2012.10221.pdf

https://doi.org/10.3847/1538-4357/abc5c2

Mercury mission MESSENGER's %(MErcury Surface, Space ENvironment, GEochemistry, and Ranging Solar Assembly for X-rays (SAX) observed almost 700 solar flares between May 28, 2007 and August 19, 2013, as **cataloged by \citet{dennisSOLARFLAREELEMENT2015}**. The SAX instrument, part of the X-ray Spectrometer (XRS), operated at 1 -- 10 keV, partially overlapping the energy range of the GOES X-ray spectrometers. SAX provides viewing angles different from the Earth-Sun line and can therefore be used as a GOES proxy for partially or fully

occulted flares as seen from Earth. For flares with GOES classes above C2 seen on-disk for both instruments, we found an empirical relationship between the soft X-ray (SXR) fluxes measured by both SAX and GOES. Due to the different energy response of the two SXR instruments, individual events can deviate on average by about a factor of two from the empirical relationship, implying that predictions of the GOES class of occulted flares from SAX data are therefore accurate to within the same factor.
The distinctive GOES energy response in combination with the multithermal nature of flares makes it difficult for any instrument, even other soft X-ray spectrometers, to provide a GOES proxy more accurate than a factor of two.
Table 2. Occulted flares observed by RHESSI and MESSENGER (2007-2013).

Multiwavelength Stereoscopic Observation of the 2013 May 1 Solar Flare and CME

Erica **Lastufka**1,2, Säm Krucker1,3, Ivan Zimovets4, Bulat Nizamov5, Stephen White6, Satoshi Masuda7, Dmitriy Golovin4, Maxim Litvak4, Igor Mitrofanov4, and Anton Sanin4
2019 ApJ 886 9
https://arxiv.org/pdf/2012.10179.pdf
https://sci-hub.st/10.3847/1538-4357/ab4a0a
A M-class behind-the-limb solar flare on **2013 May 1** (SOL2013-05-01T02:32), accompanied by a (~400 km s−1) coronal mass ejection (CME), was observed by several space-based observatories with different viewing angles. We investigated the RHESSI-observed occulted hard X-ray (HXR) emissions that originated at least 0.1 R_S above the flare site. Emissions below ~10 keV revealed a hot, extended (11 MK, >60") thermal source from the escaping CME core, with densities around 109 cm−3. In such a tenuous hot plasma, ionization times scales are several minutes, consistent with the nondetection of the hot CME core in SDO/AIA's 131 Å filter. The nonthermal RHESSI source originated from an even larger area (~100") at lower densities (108 cm−3) located above the hot core, but still behind the CME front. This indicates that the observed part of the nonthermal electrons are not responsible for heating the CME core. Possibly the hot core was heated by nonthermal electrons before it became visible from Earth, meaning that the unocculted part of the nonthermal emission likely originates from a more tenuous part of the CME core, where nonthermal electrons survive long enough to became visible from Earth. Simultaneous HXR spectra from the Mars Odyssey mission, which viewed the flare on disk, indicated that the number of nonthermal electrons >20 keV within the high coronal source is ~0.1%–0.5% compared with the number within the chromospheric flare ribbons. The detection of high coronal HXR sources in this moderate size event suggests that such sources are likely a common feature within solar eruptive events.

The Micro Solar Flare Apparutus (MiSolFA) Instrument Concept

Erica **Lastufka**, Diego Casadei, Gordon Hurford, Matej Kuhar, Gabriele Torre, Säm Krucker
Advances in Space Research **2019**
https://arxiv.org/pdf/1910.01825.pdf
The Micro Solar-Flare Apparatus (MiSolFA) is a compact X-ray imaging spectrometer designed for a small 6U micro-satellite. As a relatively inexpensive yet capable Earth-orbiting instrument, MiSolFA is designed to image the high-energy regions of solar flares from a different perspective than that of Solar Orbiter's STIX, operating from a highly elliptical heliocentric orbit. Two instruments working together in this way would provide a 3-dimensional view of X-ray emitting regions and can bypass the dynamic range limitation preventing simultaneous coronal and chromospheric imaging. Stereoscopic X-ray observations would also contain valuable information about the anisotropy of the flare-accelerated electron distribution. To perform these types of observations, MiSolFA must be capable of imaging sources with energies between 10 and 100 keV, with 10 arcsec angular resolution. MiSolFA's Imager will be the most compact X-ray imaging spectrometer in space. Scaling down the volume by a factor of ten from previous instrument designs requires special considerations. Here we present the design principles of the MiSolFA X-ray optics, discuss the necessary compromises, and evaluate the performance of the Engineering Model.

Coronal Mass Ejections with and without DH Type II Radio Bursts

M. Bendict **Lawrance** , A. Shanmugaraju, Bojan Vršnak
Solar Phys. **201**5
A statistical analysis of 135 out of 141 X-class flares observed during 1997 – 2012 with and without deca-hectometric (DH) type II radio bursts has been performed. It was found that 79 events (X-class flares and coronal mass ejections – Group I) were associated with DH type II radio bursts and 62 X-class flare events were not. Out of these 62 events without DH type IIs, 56 events (Group II) have location information, and they were selected for this study. Of these 56 events, only 32 were associated with CMEs. Most of the DH-associated X-class events (∼79 %) were halo CMEs, in contrast to 14 % in Group II. The average CME speed of the X-class flares associated with DH type IIs is 1555 km s−1, which is nearly twice that of the X-class flare-associated CMEs without DH event (744 km s−1). The X-class flares associated with DH radio bursts have a mean flare intensity (3.63×10−4 Wm−2) that is 38 % greater than that of X-class flares without DH radio bursts (2.23×10−4 Wm−2). In addition to the greater intensity, it is also found that the the duration and rise time of flares associated with DH radio emission (DH flares) is more than twice than that of the flares without DH radio emission. When the events were further divided into two categories with respect to their source locations in eastern and western regions, 65 % of the events in the radio-loud category (with DH radio bursts) are from

the western hemisphere and the remaining 35 % are from the eastern hemisphere. On the other hand, in the radio-quiet category (without DH radio bursts), nearly 60 % of the events are from the eastern hemisphere in contrast to those of the radio-loud category. It is found that 81 % of the events from eastern regions have flare durations > 30 min in the DH-flare category, in contrast to a nearly equal number from the western side for flare durations longer/shorter than 30 min. Similarly, the eastern events in the DH-flare category have a longer average rise-time of 34 min, while the western events have an average flare rise-time of 26 min. On the other hand, the CME speed and flare strength are found to be nearly equal among east and west side events, except that both these parameters are greater for events with DH type IIs

Extreme space weather events caused by super active regions during solar cycles 21-24

Gui-Ming **Le**, Gui-Ang Liu, Ming-Xian Zhao, Tian Mao, Ping-Guo Xu
Research in Astronomy and Astrophysics **2021**
https://arxiv.org/pdf/2103.00670.pdf **File**
Extreme space weather events including ≥X5.0 flares, ground level enhancement (GLE) events and super geomagnetic storms (Dst ≤ -250 nT) caused by super active regions (SARs) during solar cycles 21-24 were studied. The total number of ≥X5.0 solar flares was 62, 41 of them were X5.0-X9.9 flares and 21 of them were ≥X10.0 flares. We found that 83.9\% of the ≥X5.0 flares were produced by SARs. 78.05\% of the X5.0-X9.9 and 95.24\% of the ≥X10.0 solar flares were produced by SARs. 46 GLEs registered during solar cycles 21-24, and 25 GLEs were caused by SARs, indicating that 54.3\% of the GLEs were caused by SARs. 24 super geomagnetic storms were recorded during solar cycles 21-24, and 12 of them were caused by SARs, namely 50\% of the super geomagnetic storms are caused by SARs. It is found that only 29 SARs can produce ≥X5.0 flares, 15 SARs can produce GLEs and 10 SARs can produce super geomagnetic storms. Of the 51 SARs, only 33 SARs can produce at least one extreme space weather event, while none of the rest 18 SARs can produce an extreme space weather event. There were only 4 SARs, each of them can produce not only a ≥X5.0 flare, but also a GLE event and a super geomagnetic storm. Most of the extreme space weather events caused by the SARs appeared during solar cycles 22 and 23, especially for GLE events and super geomagnetic storms. The longitudinal distributions of source locations for the extreme space weather events caused by SARs were also studied.
28-30, October 2003
Table 1: The flares with intensities ≥X5.0 caused by SARs during solar cycles 21-24.
Table 2: The GLE events caused by SARs during solar cycles 21-24.
Table 3: The SGSs and the related ARs during solar cycles 21-24.

Statistical analysis of solar EUV and X-ray flux enhancements induced by solar flares and its implication to upper atmosphere

Le, Huijun; Liu, Libo; He, Han; Wan, Weixing
J. Geophys. Res., Vol. 116, No. A11, A11301, **2011; File**
http://dx.doi.org/10.1029/2011JA016704
The 0.1–0.8 nm X-ray flux data and 26–34 nm EUV flux data are used to statistically analyze the relationship between enhancement in X-ray flux and that in EUV flux during solar flares in 1996–2006. The EUV enhancement does not linearly increase with X-ray flux from C-class to X-class flares. Its uprising amplitude decreases with X-ray flux. The correlation coefficients between enhancements in EUV and X-ray flux for X, M and C-class flares are only 0.66, 0.58 and 0.54, respectively, which suggests that X-ray flux is not a good index for EUV flux during solar flares. Thus, for studying more accurately solar flare effect on the ionosphere/thermosphere system, one needs to use directly EUV flux measurements. One of important reasons for depressing relationship between X-ray and EUV is that the central meridian distance (CMD) of flare location can significantly affect EUV flux variation particularly for X-class flares: the larger value of CMD results in the smaller EUV enhancement. However, there are much smaller CMD effects on EUV enhancement for M and C-class flares. The solar disc images from SOHO/EIT are utilized to estimate the percentage contribution to total EUV enhancement from the flare region and from other region. The results show the larger percentage contribution from other region for the weaker flares, which would reduce the loss of EUV radiation due to limb location of flare and then weaken the CMD effect for weaker flares like M and C-class.

A Kinetic Transport Theory for Particle Acceleration and Transport in Regions of Multiple Contracting and Reconnecting Inertial-scale Flux Ropes

J. A. **le Roux**1,2, G. P. Zank1,2, G. M. Webb2, and O. Khabarova
2015 ApJ 801 112
Simulations of particle acceleration in turbulent plasma regions with multiple contracting and merging (reconnecting) magnetic islands emphasize the key role of temporary particle trapping in island structures for the efficient acceleration of particles to form hard power-law spectra. Statistical kinetic transport theories have been developed that capture the essential physics of particle acceleration in multi-island regions. The transport theory of Zank et al. is further developed by considering the acceleration effects of both the mean and the variance of the electric fields induced by the dynamics of multiple inertial-scale flux ropes. A focused transport equation is derived that includes new Fokker-Planck terms for

particle scattering and stochastic acceleration due to the variance in multiple flux-rope magnetic fields, plasma flows, and reconnection electric fields. A Parker transport equation is also derived in which a new expression for momentum diffusion appears, combining stochastic acceleration by particle scattering in the mean multi-flux-rope electric fields with acceleration by the variance in these electric fields. Test particle acceleration is modeled analytically considering drift acceleration by the variance in the induced electric fields of flux ropes in the slow supersonic, radially expanding solar wind. Hard power-law spectra occur for sufficiently strong inertial-scale flux ropes with an index modified by adiabatic cooling, solar wind advection, and diffusive escape from flux ropes. Flux ropes might be sufficiently strong behind interplanetary shocks where the index of suprathermal ion power-law spectra observed in the supersonic solar wind can be reproduced.

The Onset of Magnetic Reconnection in Dynamically Evolving Current Sheets

James **Leake**, Lars Daldorff, James Klimchuk

ApJ **973** 21 **2024**

https://arxiv.org/pdf/2406.04486

https://iopscience.iop.org/article/10.3847/1538-4357/ad5e71/pdf

We present the first results of three-dimensional (3D) numerical magnetohydrodynamic (MHD) simulations of the onset of magnetic reconnection via the tearing instability in dynamically thinning current sheets in the solar corona. In all our simulations, the onset of the non-linear tearing instability, which leads to the break-up of the thinning current sheet, does not occur until after the instability growth time becomes faster than the dynamic thinning time. Furthermore, as in previous 3D MHD simulations of static current sheets in the corona, for some parameters, the amount of magnetic shear is a fundamental switch-on parameter, which has consequences for coronal heating models. These results open up the possibility of using observable quantities of coronal current sheets to predict when they will break-up and release magnetic energy to power various energetic phenomena and/or heat the atmosphere.

Thermal Trigger for Solar Flares III: Effect of the Oblique Layer Fragmentation

Leonid **Ledentsov**

Solar Phys. **296**, Article number: 117 **2021**

https://arxiv.org/pdf/2107.03881.pdf

https://link.springer.com/content/pdf/10.1007/s11207-021-01862-w.pdf

https://doi.org/10.1007/s11207-021-01862-w

We consider the oblique fragmentation of the current layer as a result of the thermal instability described in Ledentsov (Sol. Phys. 296, 74, 2021a). It is shown that the fragmentation transverse to the current is a natural feature of the model. The fragmentation tilt does not exceed a few degrees for realistic preflare parameters of the coronal plasma. As a consequence, oblique fragmentation generally does not have a strong impact on the simulation results, however, extreme changes can reach an order of magnitude. Thus, oblique fragmentation can lead to a decrease in the estimate of the spatial period of the location of elementary energy release in solar flares to 0.1-1 Mm instead of 1-10 Mm obtained earlier.

Thermal Trigger for Solar Flares II: Effect of the Guide Magnetic Field

Leonid **Ledentsov**

Solar Phys. **296**, Article number: 93 **2021**

https://arxiv.org/pdf/2105.07516.pdf

https://link.springer.com/content/pdf/10.1007/s11207-021-01840-2.pdf

https://doi.org/10.1007/s11207-021-01840-2

We investigate the effect of the thermal imbalance on the structural stability of the magnetohydrodynamic model of the preflare current layer (Ledentsov, Sol. Phys. 296, 74, 2021). The piecewise homogeneous model of the current layer is supplemented by a magnetic field longitudinal with respect to the direction of the current. It is shown that the presence of a weak longitudinal field does not change the previously calculated spatial period of the thermal instability in the most expected range of the parameters of the preflare current layer and, moreover, contributes to the formation of the instability. On the other hand, a strong longitudinal magnetic field contributes to the spatial stabilization of the current layer.

Thermal Trigger for Solar Flares I: Fragmentation of the Preflare Current Layer

Leonid **Ledentsov**

Solar Phys. **296**, Article number: 74 **2021**

https://arxiv.org/pdf/2103.05664.pdf

https://link.springer.com/content/pdf/10.1007/s11207-021-01817-1.pdf

https://doi.org/10.1007/s11207-021-01817-1

We consider the effects of the heat balance on the structural stability of a preflare current layer. The problem of small perturbations is solved in the piecewise homogeneous MHD approximation taking into account the viscosity, the

electrical and thermal conductivity, and the radiative cooling. Solution of the problem allows the formation of an instability of a thermal nature. There is no external magnetic field inside the current layer in equilibrium state, but it can penetrate inside when the current layer is disturbed. Formation of a magnetic field perturbation inside the layer creates a dedicated frequency in a broadband disturbance subject to thermal instability. In the linear phase, the growth time of the instability is proportional to the characteristic time of radiative cooling of plasma and depends on the logarithmic derivatives of the radiative cooling function with respect to the plasma parameters. The instability results in transverse fragmentation of the current layer with a spatial period of 1-10 Mm along the layer in a wide range of coronal plasma parameters. The role of that instability in the triggering for the primary energy release in solar flares is discussed.

MHD discontinuities in solar flares: continuous transitions and plasma heating

L.S. **Ledentsov**, B.V. Somov

Advances in Space Research Volume 56, Issue 12, 15 December 2015, Pages 2779–2792 **2015**

http://www.sciencedirect.com/science/article/pii/S0273117715005700

The boundary conditions for the ideal MHD equations on a plane dis- continuity surface are investigated. It is shown that, for a given mass flux through a discontinuity, its type depends only on the relation between inclina- tion angles of a magnetic field. Moreover, the conservation laws on a surface of discontinuity allow changing a discontinuity type with gradual (continu- ous) changes in the conditions of plasma flow. Then there are the so-called transition solutions that satisfy simultaneously two types of discontinuities. We obtain all transition solutions on the basis of the complete system of boundary conditions for the MHD equations. We also found the expression describing a jump of internal energy of the plasma flowing through the dis- continuity. Firstly, this allows constructing a generalized scheme of possible continuous transitions between MHD discontinuities. Secondly, it enables the examination of the dependence of plasma heating by plasma density and configuration of the magnetic field near the discontinuity surface, i.e., by the type of the MHD discontinuity. It is shown that the best conditions for heating are carried out in the vicinity of a reconnecting current layer near the areas of reverse currents. The result can be helpful in explaining the temperature distributions inside the active regions in the solar corona during flares observed by modern space observatories in soft and hard X-rays.

Evolutionary of Discontinuous Plasma Flows in the Vicinity of Reconnecting Current Layers

Ledentsov, L. S.; Somov, B. V.

The Sun: New Challenges, Astrophysics and Space Science Proceedings, Volume 30. Springer-Verlag Berlin Heidelberg, **2012**, p. 117

The question about the interpretation of numerical experiments on magnetic reconnection in solar flares is considered. A correspondence between the standard classification of magnetohydrodynamic discontinuities and the parameters characterizing the mass flux through a discontinuity and the magnetic field configuration has been established within a classical formulation of the problem on discontinuous magnetohydrodynamic flows. A pictorial graphical representation of the relationship between the angles of the magnetic field vector relative to the normal to the discontinuity plane on both its sides has also been found. The relations between the parameters of a two-dimensional discontinuous flow have the simplest form in a frame of reference where the magnetic field lines (B) are parallel to the matter velocity (u) the de Hoffmann-Teller frame. The question about the transformation of the magnetic field configuration when passing to a "laboratory" frame of reference where (v ṡB)≠0, i.e., an electric field is present, is considered in this connection. The result is applied to the analytical solution of the problem on the magnetic field structure in the vicinity of a reconnecting current layer obtained previously by Bezrodnykh et al. The regions of nonevolutionary shocks are shown to appear near the endpoints of a current layer with reverse currents.

On discontinuous plasma flows in the vicinity of reconnecting current sheets in solar flares

Ledentsov, L. S.; Somov, B. V.

Astronomy Letters, Volume 37, Issue 2, pp.131-140, **2011**

The question about the interpretation of numerical experiments on magnetic reconnection in solar flares is considered. A correspondence between the standard classification of magnetohydrodynamic discontinuities and the parameters characterizing the mass flux through a discontinuity and the magnetic field configuration has been established within a classical formulation of the problem on discontinuous magnetohydrodynamic flows. A pictorial graphical representation of the relationship between the angles of the magnetic field vector relative to the normal to the discontinuity plane on both its sides has also been found. The relations between the parameters of a two-dimensional discontinuous flow have the simplest form in a frame of reference where the magnetic field lines (B) are parallel to the matter velocity (u)—the deHoffmann-Teller frame. The question about the transformation of the magnetic field configuration when passing to a “laboratory” frame of reference where $(v \cdot B) \neq 0$, i.e., an electric field is present, is considered in this connection. The result is applied to the analytical solution of the problem on the magnetic field structure in the vicinity of a reconnecting current sheet obtained previously by Bezrodnykh et al. The regions of nonevolutionary shocks are shown to appear near the endpoints of a current sheet with reverse currents.

Can Solar Limb Flare Prediction Be Properly Made by Extreme-ultraviolet Intensities?

Jaewon **Lee1**, Yong-Jae Moon1,2, Hyun-Jin Jeong2, Kangwoo Yi2, and Harim Lee2
2024 ApJL 971 L47
https://iopscience.iop.org/article/10.3847/2041-8213/ad6b9b/pdf

We address the question of whether the solar limb flare prediction can be properly made by EUV intensity, which has less projection effects than solar white light and magnetogram data. We develop empirical and multilayer perceptron (MLP) models to forecast the probability of a major solar limb flare within a day. We use Solar Dynamics Observatory (SDO)/Atmospheric Imaging Assembly (AIA) 94 and 131 Å that have high correlations and large slopes with X-ray flare fluxes from 2010 to 2022. We select 240 flares stronger than or equal to the M1.0 class and located near the limb region (60° or more in heliographic longitude). For input data, we use the limb intensity as the sum of SDO/AIA intensities in the limb region and the total intensity of the whole image. We compare the model performances using metrics such as the receiver operating characteristic—area under the curve. Our major results are as follows. First, we can forecast major solar limb flare occurrences with only SDO/AIA 94 and/or 131 Å intensities. Second, our models show better probability prediction than the climatological model. Third, both empirical (AUC = 0.85) and MLP (AUC = 0.84) models have similar performances, which are much better than a random forecast (AUC = 0.50). Finally, it is interesting to note that our model can forecast the flaring probability of all 52 events during the test period, while the models in the NASA/CCMC flare scoreboard can forecast only 22 events. From the above results, we can answer that the solar limb flare prediction using EUV intensity can be properly made.

Dimensionality of Solar Magnetic Reconnection **Review**

Jeongwoo **Lee**
Reviews of Modern Plasma Physics **2022**
https://link.springer.com/epdf/10.1007/s41614-022-00096-y
https://doi.org/10.1007/s41614-022-00096-y

Solar flares are the best examples of astrophysical magnetic reconnection in which the reconnection structure can be studied in detail. The structure is manifested through flare ribbons, intense optical and EUV emissions in footpoints of field lines attached to the coronal reconnection region. In the most common type of solar flares, two parallel ribbons appear and move away from each other, which could be related to the reconnection electric field under the theory of two-dimensional (2D) X-point reconnection, opening up a wide field of solar research. Another breakthrough came upon the discovery of circular ribbons, which implies a dome-shaped spine-fan structure capable of truly three dimensional (3D) null point reconnection. The variability of circular ribbons could also shed light on the reconnection electric field in the corona, but was relatively less attended. In this paper, we review selective topics in both types of flares with emphasis on the dimensionality of magnetic reconnection. Three types of reconnection: 2D X-point, 3D torsional, and 3D spine-fan reconnection are studied and associated with translational, rotational, and vibrational degrees of freedom. It is demonstrated that the dimensionality-based analysis of the observed dynamics of circular and parallel ribbons can facilitate a better understanding of the nature of solar magnetic reconnection. **1991-March-17, 2002 September 9, 2003-10-13, 2005-05-13, 2012-03-27, 2014-12-17, 2015-06-22**

Time Series Analysis of Photospheric Magnetic Parameters of Flare-quiet versus Flaring Active Regions: Scaling Properties of Fluctuations

Eo-Jin **Lee**, Sung-Hong Park, Yong-Jae Moon
Solar Phys. **295**, Article number: 123 **2020**
https://arxiv.org/pdf/2008.13085.pdf
https://link.springer.com/content/pdf/10.1007/s11207-020-01690-4.pdf

Time series of photospheric magnetic parameters of solar active regions (ARs) are used to answer whether scaling properties of fluctuations embedded in such time series help to distinguish between flare-quiet and flaring ARs. We examine a total of 118 flare-quiet and 118 flaring AR patches (called HARPs), which were observed from 2010 to 2016 by the Helioseismic and Magnetic Imager (HMI) on board the Solar Dynamics Observatory (SDO). Specifically, the scaling exponent of fluctuations is derived applying the Detrended Fluctuation Analysis (DFA) method to a dataset of 8-day time series of 18 photospheric magnetic parameters at 12-min cadence for all HARPs under investigation. We first find a statistically significant difference in the distribution of the scaling exponent between the flare-quiet and flaring HARPs, in particular for some space-averaged, signed parameters associated with magnetic field line twist, electric current density, and current helicity. The flaring HARPs tend to show higher values of the scaling exponent compared to those of the flare-quiet ones, even though there is considerable overlap between their distributions. In addition, for both the flare-quiet and flaring HARPs the DFA analysis indicates that (1) time series of most of various magnetic parameters under consideration are non-stationary, and (2) time series of the total unsigned magnetic flux and the mean photospheric magnetic free energy density in general present a non-stationary, persistent property, while the total unsigned flux near magnetic polarity inversion lines and parameters related to current density show a non-stationary, anti-persistent trend in their time series.

A Solar Magnetic-fan Flaring Arch Heated by Non-thermal Particles and Hot Plasma from an X-ray Jet Eruption

Kyoung-Sun **Lee**, Hirohisa Hara, Kyoko Watanabe, Anand D. Joshi, David H. Brooks, Shinsuke Imada, Avijeet Prasad, Phillip Dang, Toshifumi Shimizu, Sabrina L. Savage, Ronald Moore, Navdeep K. Panesar, Jeffrey W. Reep

ApJ **895** 42 **2020**

https://arxiv.org/pdf/2005.09875.pdf

https://doi.org/10.3847/1538-4357/ab8bce

We have investigated an M1.3 limb flare, which develops as a magnetic loop/arch that fans out from an X-ray jet. Using Hinode/EIS, we found that the temperature increases with height to a value of over 107 K at the loop-top during the flare. The measured Doppler velocity (redshifts of 100−500 km s−1) and the non-thermal velocity (≥100 km s−1) from Fe XXIV also increase with loop height. The electron density increases from 0.3×109 cm−3 early in the flare rise to 1.3×109 cm−3 after the flare peak. The 3-D structure of the loop derived with STEREO/EUVI indicates that the strong redshift in the loop-top region is due to upflowing plasma originating from the jet. Both hard X-ray and soft X-ray emission from RHESSI were only seen as footpoint brightenings during the impulsive phase of the flare, then, soft X-ray emission moves to the loop-top in the decay phase. Based on the temperature and density measurements and theoretical cooling models, the temperature evolution of the flare arch is consistent with impulsive heating during the jet eruption followed by conductive cooling via evaporation and minor prolonged heating in the top of the fan loop. Investigating the magnetic field topology and squashing factor map from SDO/HMI, we conclude *that the observed magnetic-fan flaring arch is mostly heated from low atmospheric reconnection accompanying the jet ejection, instead of from reconnection above the arch as expected in the standard flare model.* **2014 January 13**

Hinode/EIS Nuggets Aug **2020** http://solarb.mssl.ucl.ac.uk/SolarB/nuggets/nugget_2020aug.jsp

Heating and Eruption of a Solar Circular-ribbon Flare

Jeongwoo **Lee**1,2,3, Judith T. Karpen4, Chang Liu1,2,3, and Haimin Wang1,2,3

2020 ApJ 893 158

https://doi.org/10.3847/1538-4357/ab80c4

We studied a circular-ribbon flare, SOL**2014-12-17**T04:51, with emphasis on its thermal evolution as determined by the differential emission measure (DEM) inversion analysis of the extreme ultraviolet (EUV) images of the Atmospheric Imaging Assembly instrument on board the Solar Dynamics Observatory. Both temperature and emission measure start to rise much earlier than the flare, along with an eruption and formation of a hot halo over the fan structure. In the main flare phase, another set of ribbons forms inside the circular ribbon, and expands as expected for ribbons at the footpoints of a postflare arcade. An additional heating event further extends the decay phase, which is also characteristic of some eruptive flares. The basic magnetic configuration appears to be a fan–spine topology, rooted in a minority-polarity patch surrounded by majority-polarity flux. We suggest that reconnection at the null point begins well before the impulsive phase, when the null is distorted into a breakout current sheet, and that both flare and breakout reconnection are necessary in order to explain the subsequent local thermal evolution and the eruptive activities in this confined magnetic structure. Using local DEMs, we found a postflare temperature increase inside the fan surface, indicating that the so-called EUV late phase is due to continued heating in the flare loops.

Flare Productivity of Major Flaring Solar Active Regions: A Time-series Study of Photospheric Magnetic Properties

Eo-Jin **Lee**, Sung-Hong Park, Yong-Jae Moon

Solar Phys. 293:159 **2018**

https://arxiv.org/pdf/1810.12505.pdf

A solar active region (AR) that produces at least one M- or X-class major flare tends to produce multiple flares during its passage across the solar disk. It will be interesting if we can estimate how flare-productive a given major flaring AR is for a time interval of several days, by investigating time series of its photospheric magnetic field properties. For this, we studied 93 major flaring ARs observed from 2010 to 2016 by the Helioseismic and Magnetic Imager (HMI) on board the Solar Dynamics Observatory (SDO). More specifically, for each AR under study, the mean and fluctuation were calculated from an 8-day time series of each of 18 photospheric magnetic parameters extracted from the Space-weather HMI Active Region Patch (SHARP) vector magnetogram products at 12-min cadence. We then compared these with the AR's 8-day flare index, which is defined as the sum of soft X-ray peak fluxes of flares produced in the AR during the same interval of the 8-day SHARP parameter time series. As a result, it is found that the 8-day flare index is well correlated with the mean and/or fluctuation values of some magnetic parameters (with correlation coefficients of 0.6-0.7 in log-log space). Interestingly, the 8-day flare index shows a slightly better correlation with the fluctuation than the mean for the SHARP parameters associated with the surface integral of photospheric magnetic free energy density. We also discuss how the correlation varies if the 8-day flare index is compared with the mean or fluctuation calculated from an initial portion of the SHARP parameter time series.

Thermal and Nonthermal Emissions of a Composite Flare Derived from NoRH and SDO Observations

Jeongwoo **Lee**1,2, Stephen M. White3, Ju Jing4, Chang Liu4, Satoshi Masuda2, andJongchul Chae1
2017 ApJ 850 124

Differential emission measure (DEM) derived from the extreme ultraviolet (EUV) lines of theAtmospheric Imaging Assembly (AIA) on board the Solar Dynamic Observatory is used in the analysis of a solar flare observed by the Nobeyama Radioheliograph (NoRH). The target was a composite event consisting of an impulsive flare, SOL2015-06-21T01:42 (GOES class M2.0), and a gradual flare, SOL**2015-06-21**T02:36 (M2.6), for which separation of thermal plasma heating from nonthermal particle acceleration was of major interest. We have calculated the thermal free–free intensity maps with the AIA-derived DEM and compared them against the observed NoRH maps to attribute the difference to the nonthermal component. In this way, we were able to locate three distinct sources: the major source with thermal and nonthermal components mixed, a nonthermal source devoid of thermal particles, and a thermal source lacking microwave emission. Both the first and the second nonthermal sources produced impulsively rising 17 GHz intensities and moved away from the local magnetic polarization inversion lines in correlation with the flare radiation. In contrast, the thermal sources stay in fixed locations and show temporal variations of the temperature and emission measure uncorrelated with the flare radiation. We interpret these distinct properties as indicating that nonthermal sources are powered by magnetic reconnection and thermal sources passively receive energy from the nonthermal donor. The finding of these distinct properties between thermal and nonthermal sources demonstrates the microwave and EUV emission measure combined diagnostics.

IRIS, Hinode, SDO, and RHESSI observations of a white light flare produced directly by non-thermal electrons

Kyoung-Sun **Lee**, Shinsuke Imada, Kyoko Watanabe, Yumi Bamba, David H. Brooks
ApJ **836** 150 **2017**
https://arxiv.org/pdf/1701.06286v1.pdf

An X1.6 flare occurred in AR 12192 on **2014 October 22** at 14:02 UT and was observed by Hinode, IRIS, SDO, and RHESSI. We analyze a bright kernel which produces a white light (WL) flare with continuum enhancement and a hard X-ray (HXR) peak. Taking advantage of the spectroscopic observations of IRIS and Hinode/EIS, we measure the temporal variation of the plasma properties in the bright kernel in the chromosphere and corona. We found that explosive evaporation was observed when the WL emission occurred, even though the intensity enhancement in hotter lines is quite weak. The temporal correlation of the WL emission, HXR peak, and evaporation flows indicate that the WL emission was produced by accelerated electrons. To understand the white light emission process, we calculated the energy flux deposited by non- thermal electrons (observed by RHESSI) and compared it to the dissipated energy estimated from a chromospheric line (Mg II triplet) observed by IRIS. The deposited energy flux from the non-thermal electrons is about 3 ~ 7.7 X 10^(10) erg cm^(-2) s^(-1) for a given low energy cut-off of 30 ~ 40 keV, assuming the thick target model. The energy flux estimated from the temperature changes in the chromosphere measured using the Mg II subordinate line is about 4.6 - 6.7 X 10(9) erg cm^(-2) s^(-1): ~6-22% of the deposited energy. This comparison of estimated energy fluxes implies that the continuum enhancement was directly produced by the non-thermal electrons.
RHESSI Science Nuggets #334 October **2018**
http://sprg.ssl.berkeley.edu/~tohban/wiki/index.php/White-light_Emission_and_Non-thermal_Electrons

DEPENDENCE OF OCCURRENCE RATES OF SOLAR FLARES AND CORONAL MASS EJECTIONS ON THE SOLAR CYCLE PHASE AND THE IMPORTANCE OF LARGE-SCALE CONNECTIVITY

Kangjin **Lee**1, Y.-J. Moon1, and V. M. Nakariakov1,2
2016 ApJ 831 131 DOI 10.3847/0004-637X/831/2/131

We investigate the dependence of the occurrence rates of major solar flares (M- and X-class) and front-side halo coronal mass ejections (FHCMEs), observed from 1996 to 2013, on the solar cycle (SC) phase for six active McIntosh sunspot group classes: Fkc, Ekc, Dkc, Fki, Eki, and Dki. We classify SC phases as follows: (1) ascending phase of SC 23 (1996–1999), (2) maximum phase of SC 23 (2000–2002), (3) descending phase of SC 23 (2003–2008), and (4) ascending phase of SC 24 (2009–2013). We find that the occurrence rates of major flares and FHCMEs during the descending phase are noticeably higher than those during the other phases for most sunspot group classes. For the most active sunspot group class, Fkc, the occurrence rate of FHCMEs during the descending phase of SC 23 is three times as high as that during the ascending phase of SC 23. The potential of each McIntosh sunspot group class to produce major flares or FHCMEs is found to depend on the SC phase. The occurrence rates (R) of major flares and FHCMEs are strongly anti-correlated with the annual average latitude of the sunspot groups (L): for major flares and for FHCMEs. This finding indicates the possible role of large-scale coronal connectivity, e.g., trans-equatorial loops, in powerful energy releases. Interestingly, this relationship is very similar to that between the volumetric coronal heating rate and X-ray loop lengths, indicating common energy release mechanisms.

CORONAL THICK TARGET HARD X-RAY EMISSIONS AND RADIO EMISSIONS

Jeongwoo **Lee**1,2, Daye Lim2, G. S. Choe2, Kap-Sung Kim2, and Minhwan Jang

2013 ApJ 769 L11

A distinctive class of hard X-ray (HXR) sources located in the corona was recently found, which implies that the collisionally thick target model (CTTM) applies even to the corona. We investigated whether this idea can be independently verified by microwave radiations which have been known as the best companion to HXRs. This study is conducted on the GOES M2.3 class flare which occurred on **2002 September 9** and was observed by the Reuven Ramaty High-Energy Solar Spectroscopic Imager and the Owens Valley Solar Array. Interpreting the observed energy-dependent variation of HXR source size under the CTTM, the coronal density should be as high as 5 × 1011 cm–3 over a distance of up to 12". To explain the cutoff feature of the microwave spectrum at 3 GHz, however, we require a density no higher than 1 × 1011 cm–3. Additional constraints must be placed on the temperature and magnetic field of the coronal source in order to reproduce the microwave spectrum as a whole. First, a spectral feature called the Razin suppression requires a magnetic field in a range of 250-350 G along with high viewing angles around 75°. Second, to avoid excess fluxes at high frequencies due to the free-free emission that was not observed, we need a high temperature ≥2 × 107 K. These two microwave spectral features, Razin suppression and free-free emissions, become more significant at regions of high thermal plasma density and are essential for validating and determining additional parameters of the coronal HXR sources.

Solar Flare Occurrence Rate and Probability in Terms of the Sunspot Classification Supplemented with Sunspot Area and Its Changes

Kangjin **Lee**, Y.-J. Moon, Jin-Yi Lee, Kyoung-Sun Lee, Hyeonock Na

Solar Physics, December **2012**, Volume 281, Issue 2, pp 639-650

We investigate the solar flare occurrence rate and daily flare probability in terms of the sunspot classification supplemented with sunspot area and its changes. For this we use the NOAA active region data and GOES solar flare data for 15 years (from January 1996 to December 2010). We consider the most flare-productive 11 sunspot classes in the McIntosh sunspot group classification. Sunspot area and its changes can be a proxy of magnetic flux and its emergence/cancellation, respectively. We classify each sunspot group into two sub-groups by its area: “Large” and “Small”. In addition, for each group, we classify it into three sub-groups according to sunspot area changes: “Decrease”, “Steady”, and “Increase”. As a result, in the case of compact groups, their flare occurrence rates and daily flare probabilities noticeably increase with sunspot group area. We also find that the flare occurrence rates and daily flare probabilities for the “Increase” sub-groups are noticeably higher than those for the other sub-groups. In case of the (M+X)-class flares in the ‘Dkc’ group, the flare occurrence rate of the “Increase” sub-group is three times higher than that of the “Steady” sub-group. The mean flare occurrence rates and flare probabilities for all sunspot groups increase with the following order: “Decrease”, “Steady”, and “Increase”. Our results statistically demonstrate that magnetic flux and its emergence enhance the occurrence of major solar flares.

Collisionless turbulent transport and anisotropic electron heating in coronal flare loops

K. W. **Lee** and J. Büchner

A&A 535, A61 (**2011**)

Context. One of the hypotheses about the generation of the hard X-ray emissions (HXR) of the sun is that a strong electron-beam is first accelerated near the looptop, and then propagated down to the chromosphere. There the HXR emissions are generated by the bombardment of electrons via thick-target bremsstrahlung. Recently, the beam-plasma model has been questioned because streaming instabilities make the beam propagation doubtful. Another open question in solar flare models is the generation of anisotropic electron distributions deduced from microwave emissions. The question is whether one can find a mechanism, in addition to the generally considered mirror motion, that may cause the electron anisotropy in flare loops.

Aims. To understand the transport of coronal electron beams and the possible generation of electron anisotropic distribution in the course of the beam propagation, we simulated a beam-plasma return-current system. Our aim is to investigate the evolution of predicted streaming instabilities at the nonlinear stage and to determine the intensity of beam transport in coronal loops.

Methods. The linear instabilities and wave coupling in the beam-plasma return-current system are investigated by a multi-fluid dispersion analysis. We performed a two-dimensional electromagnetic particle-in-cell simulation to

understand the generation of turbulent transport and anisotropic electron heating at the nonlinear stage of the beam evolution.
Results. The beam-plasma return-current system is stablized at a late stage of evolution by a combined effect of 1) a relaxation of electron bulk drifts; and 2) a fast thermalization of the beam and return-current electrons in the drift direction. As a result, the downward electron beam continues to propagate in the coronal loop. Distinguishable parallel and perpendicular electron heating is observed, which is caused by turbulent deflection of electron beams. The electron distribution becomes anisotropic through different heating rates.
Conclusions. An electron beam injected from a solar flare looptop can continue to propagate stably despite a partial relaxation of its drift velocity. After drift relaxation and anisotropic electron heating, the slowed-down electron drifts and the ambient thermalized plasma create a stable beam-propagation environment because of the Landau damping effect. This electron beam can propagate stably at a modified drift speed down to the chromosphere, where it generates HXR radiation. We conclude that the beam plasma model is feasible for the HXR generation in a solar flare event. The observed anisotropic electron distribution is a direct consequence of turbulent deflections of the electron beams.

Parallel Motions of Coronal Hard X-ray Source and H® Ribbons

Jeongwoo **Lee** and Dale E. Gary
E-print, Aug 2008; Astrophysical Journal Letters, Vol. 685, No. 1: L87-L90, **2008**
http://solar.physics.montana.edu/cgi-bin/eprint/index.pl?entry=7776
http://www.journals.uchicago.edu/doi/abs/10.1086/592292
During solar flares H® ribbons form and often move away from the local magnetic polarity inversion line (PIL). While the motion perpendicular to the PIL has been taken as evidence for coronal magnetic reconnection in the so-called CSHKP standard model, the other velocity component parallel to the PIL is much less adopted as a property of the magnetic reconnection process. In this Letter we report an event in which the motion parallel to the PIL is found in both H® ribbons and a thermal hard X-ray source. Such commonality would indicate a link between the coronal magnetic reconnection and footpoint emissions as in the standard solar flare model. However, its direction implies a reconnection region that is increasing in length, a feature missing from the standard two-dimensional model. We present a modi¯ed framework in which the variation along the third dimension is allowed, in order to assess the e®ect of such a proper motion on estimation of the magnetic reconnection rate. Data used are hard X-ray maps from the *Reuven Ramaty High Energy Solar Spectroscopic Imager* (*RHESSI*), H® ¯lter grams of Big Bear Solar Observatory (BBSO), and the *SOHO* Michelson Doppler Imager (MDI) magnetogram obtained for the **2004 March 30** flare.

Magnetic Energy Release During the 2002 September 9 Solar Flare

Jeongwoo **Lee**, Dale E. Gary and G.S. Choe
Link: http://solar.njit.edu/preprints/lee1317.pdf

Radio Emissions from Solar Active Regions

Jeongwoo **Lee**
BBSO, Number: 1337, **2007**
This article reviews the efforts for understanding these radiative processes, and utilizing them as diagnostic tools in addressing a number of critical issues involved with active regions.

Deep Learning for Active Region Classification: A Systematic Study from Convolutional Neural Networks to Vision Transformers

Edoardo **Legnaro**, Sabrina Guastavino, Michele Piana, Anna Maria Massone
2024
https://arxiv.org/pdf/2410.17816
A solar active region can significantly disrupt the Sun Earth space environment, often leading to severe space weather events such as solar flares and coronal mass ejections. As a consequence, the automatic classification of active region groups is the crucial starting point for accurately and promptly predicting solar activity. This study presents our results concerned with the application of deep learning techniques to the classification of active region cutouts based on the Mount Wilson classification scheme. Specifically, we have explored the latest advancements in image classification architectures, from Convolutional Neural Networks to Vision Transformers, and reported on their performances for the active region classification task, showing that the crucial point for their effectiveness consists in a robust training process based on the latest advances in the field.

Do the solar flares originating from an individual active region follow a random process or a memory-dependent correlation?

W H **Lei**, C Li, F Chen, S J Zhong, Z G Xu, P F Chen

Monthly Notices of the Royal Astronomical Society, Volume 494, Issue 1, May **2020**, Pages 975–982, sci-hub.si/10.1093/mnras/staa688

We investigate the waiting time statistics of solar flares both in a flare-productive active region (AR 12673) of the solar cycle 24 and in a three-dimensional magnetohydrodynamic (MHD) simulated AR. The statistical models of a discrete random process and a continuous memorydependent process are applied to interpret the waiting time distributions (WTDs) of solar flares. Our results indicate that the occurrence of a solar flare in an individual AR maintains a certain amount of memory, and probably arises from MHD turbulence rather than from intermittent avalanches in a self-organized criticality system. It differs from the occurrence of 'super flares' when treating the star/Sun as a single non-linear system. **03-09 Sep 2017**

The chromospheric line-of-sight velocity variations in a solar microflare

U.M. **Leiko**, N.N. Kondrashova

Advances in Space Research, Volume 55, Issue 3, 1 February **2015**, Pages 886–890

http://www.sciencedirect.com/science/article/pii/S027311771400492X

The variations of the chromospheric line-of-sight velocity in the active region NOAA 11024 are studied before, during, and after a solar microflare on **2009 July 4**. At the day of the observations the main emergence phase was in this active region. The new emerging flux has interacted with the pre-existing magnetic field.

The spectropolarimetric observations were carried out with the French–Italian THEMIS telescope (Spain, Tenerife). We used Hα spectra of the high resolution obtained over 21 min. The spatial resolution was ~1 arcsec. The time interval between the spectra was 2.84 s. Doppler velocities were measured in the microflare location and its surroundings. We have revealed strong temporal variations of the line-of-sight velocity in the chromosphere. The velocities changed in the range −33–10 km/s. We revealed the velocity oscillations with the amplitude of 4–5 km/s. 12–14 min before the microflare both upward and downward motions with velocity values reaching about 20 km/s are found on the outer edge of the region studied. The amplitude of the oscillations increased. It may be the signature of the magnetic reconnection.

Properties of Flare-Imminent versus Flare-Quiet Active Regions from the Chromosphere through the Corona II: NonParametric Discriminant Analysis Results from the NWRA Classification Infrastructure (NCI)

KD **Leka**, Karin Dissauer, Graham Barnes, Eric L. Wagner

ApJ **942** 84 **2023**

https://arxiv.org/pdf/2212.11255.pdf

https://iopscience.iop.org/article/10.3847/1538-4357/ac9c04/pdf

A large sample of active-region-targeted time-series images from the Solar Dynamics Observatory / Atmospheric Imaging Assembly, the AIA Active Region Patch database ("AARPs", Paper I: Dissauer et al 2022) is used to investigate whether parameters describing the coronal, transition region, and chromospheric emission can differentiate a region that will imminently produce a solar flare from one that will not. Parametrizations based on moment analysis of direct and running-difference images provide for physically-interpretable results from nonparametric discriminant analysis. Across four event definitions including both 24hr and 6hr validity periods, 160 image-based parameters capture the general state of the atmosphere, rapid brightness changes, and longer-term intensity evolution. We find top Brier Skill Scores in the 0.07--0.33 range, True Skill Statistics in the 0.68--0.82 range (both depending on event definition), and Receiver Operating Characteristic Skill Scores above 0.8. Total emission can perform notably as can steeply increasing or decreasing brightness, although mean brightness measures do not, demonstrating the well-known active-region-size/flare-productivity relation. Once a region is flare productive, the active-region coronal plasma appears to stay hot. The 94AA filter data provides the most parameters with discriminating power, with indications that it benefits from sampling multiple physical regimes. In particular, classification success using higher-order moments of running difference images indicate a propensity for flare-imminent regions to display short-lived small-scale brightening events. Parameters describing the evolution of the corona can provide flare-imminent indicators, but at no preference over "static" parameters. Finally, all parameters and NPDA-derived probabilities are available to the community for additional research. **2011-07-26**

A Comparison of Flare Forecasting Methods. III. Systematic Behaviors of Operational Solar Flare Forecasting Systems **Review**?

K.D. **Leka**, Sung-Hong Park, Kanya Kusano, Jesse Andries, Graham Barnes, Suzy Bingham, D. Shaun Bloomfield, Aoife E. McCloskey, Veronique Delouille, David Falconer, Peter T. Gallagher, Manolis K. Georgoulis, Yuki Kubo, Kangjin Lee, Sangwoo Lee, Vasily Lobzin, JunChul Mun, Sophie A. Murray, Tarek

A.M. Hamad Nageem, Rami Qahwaji, Michael Sharpe, Rob Steenburgh, Graham Steward, Michael Terkildsen
ApJ **881** 101 **2019**
https://arxiv.org/pdf/1907.02909.pdf
sci-hub.se/10.3847/1538-4357/ab2e11
A workshop was recently held at Nagoya University (31 October - 02 November 2017), sponsored by the Center for International Collaborative Research, at the Institute for Space-Earth Environmental Research, Nagoya University, Japan, to quantitatively compare the performance of today's operational solar flare forecasting facilities. Building upon Paper I of this series (Barnes et al. 2016), in Paper II (Leka et al. 2019) we described the participating methods for this latest comparison effort, the evaluation methodology, and presented quantitative comparisons. In this paper we focus on the behavior and performance of the methods when evaluated in the context of broad implementation differences. Acknowledging the short testing interval available and the small number of methods available, we do find that forecast performance: 1) appears to improve by including persistence or prior flare activity, region evolution, and a human "forecaster in the loop"; 2) is hurt by restricting data to disk-center observations; 3) may benefit from long-term statistics, but mostly when then combined with modern data sources and statistical approaches. These trends are arguably weak and must be viewed with numerous caveats, as discussed both here and in Paper II. Following this present work, we present in Paper IV a novel analysis method to evaluate temporal patterns of forecasting errors of both types (i.e., misses and false alarms; Park et al. 2019). Hence, most importantly, with this series of papers we demonstrate the techniques for facilitating comparisons in the interest of establishing performance-positive methodologies.

A Comparison of Flare Forecasting Methods. II. Benchmarks, Metrics and Performance Results for Operational Solar Flare Forecasting Systems **Review?**

K.D. **Leka**, Sung-Hong Park, Kanya Kusano, Jesse Andries, Graham Barnes, Suzy Bingham, D. Shaun Bloomfield, Aoife E. McCloskey, Veronique Delouille, David Falconer, Peter T. Gallagher, Manolis K. Georgoulis, Yuki Kubo, Kangjin Lee, Sangwoo Lee, Vasily Lobzin, JunChul Mun, Sophie A. Murray, Tarek A.M. Hamad Nageem, Rami Qahwaji, Michael Sharpe, Rob Steenburgh, Graham Steward, Michael Terkildsen
Astrophysical Journal Supplement Series **243** 36 **2019**
https://arxiv.org/pdf/1907.02905.pdf
https://doi.org/10.3847/1538-4365/ab2e12
Solar flares are extremely energetic phenomena in our Solar System. Their impulsive, often drastic radiative increases, in particular at short wavelengths, bring immediate impacts that motivate solar physics and space weather research to understand solar flares to the point of being able to forecast them. As data and algorithms improve dramatically, questions must be asked concerning how well the forecasting performs; crucially, we must ask how to rigorously measure performance in order to critically gauge any improvements. Building upon earlier-developed methodology (Barnes et al, 2016, Paper I), international representatives of regional warning centers and research facilities assembled in 2017 at the Institute for Space-Earth Environmental Research, Nagoya University, Japan to - for the first time - directly compare the performance of operational solar flare forecasting methods. Multiple quantitative evaluation metrics are employed, with focus and discussion on evaluation methodologies given the restrictions of operational forecasting. Numerous methods performed consistently above the "no skill" level, although which method scored top marks is decisively a function of flare event definition and the metric used; there was no single winner. Following in this paper series we ask why the performances differ by examining implementation details (Leka et al. 2019, Paper III), and then we present a novel analysis method to evaluate temporal patterns of forecasting errors in (Park et al. 2019, Paper IV). With these works, this team presents a well-defined and robust methodology for evaluating solar flare forecasting methods in both research and operational frameworks, and today's performance benchmarks against which improvements and new methods may be compared.

Chapter 3 - Solar Flare Forecasting: Present Methods and Challenges **Review**

K.D.**Leka**, Graham Barnes
In: Extreme Events in Geospace
Origins, Predictability, and Consequences **Book**
Editor: Natalia **Buzulukova**, Elsevier, **2018**, 798 p. **File**
Chapter 3, Pages 65-98
See Site https://www.sciencedirect.com/science/article/pii/B9780128127001099921
Download PDF --> Download full book
http://sci-hub.do/10.1016/B978-0-12-812700-1.00003-0
Solar flares are one of the primary initiators of many space weather phenomena. Their fast initiation and orders-of-magnitude increase in high-energy electromagnetic radiation require true forecasting efforts. Today's probabilistic flare

forecasting capability is arguably not very good. When faced with specific questions regarding timing and magnitude of impending flares in the context of a flare-productive sunspot group, short-range targeted predictions are beyond the present science's capabilities. Such shortcomings may be of most serious consequence in the context of extreme solar flares—situations where a catastrophic flare event is highly likely, but when it will occur is both unknown and of great importance. This situation points to the need for better identification of a unique physical parameter space in which solar flares occur, for identifying the relevant physical trigger (or triggers), for the ability to estimate the likelihood that a trigger's presence will produce an event, and what size an event is expected. **March 7, 2012**

The NWRA Classification Infrastructure: Description and Extension to the Discriminant Analysis Flare Forecasting System (DAFFS)

K.D. **Leka**, Graham Barnes, Eric L. Wagner
Journal of Space Weather and Space Climate 8, A25 **2018**
https://arxiv.org/pdf/1802.06864.pdf
https://www.swsc-journal.org/articles/swsc/pdf/2018/01/swsc170078.pdf
A classification infrastructure built upon Discriminant Analysis has been developed at NorthWest Research Associates for examining the statistical differences between samples of two known populations. Originating to examine the physical differences between flare-quiet and flare-imminent solar active regions, we describe herein some details of the infrastructure including: parametrization of large datasets, schemes for handling "null" and "bad" data in multi-parameter analysis, application of non-parametric multi-dimensional Discriminant Analysis, an extension through Bayes' theorem to probabilistic classification, and methods invoked for evaluating classifier success. The classifier infrastructure is applicable to a wide range of scientific questions in solar physics. We demonstrate its application to the question of distinguishing flare-imminent from flare-quiet solar active regions, updating results from the original publications that were based on different data and much smaller sample sizes. Finally, as a demonstration of "Research to Operations" efforts in the space-weather forecasting context, we present the Discriminant Analysis Flare Forecasting System (DAFFS), a near-real-time operationally-running solar flare forecasting tool that was developed from the research-directed infrastructure. **6-8 Sept 2011 (4 spikes), 2014.03.18, 2016.04.17**

HELIOSEISMOLOGY OF PRE-EMERGING ACTIVE REGIONS. I. OVERVIEW, DATA, AND TARGET SELECTION CRITERIA

K. D. **Leka**1, G. Barnes1, A. C. Birch1,3, I. Gonzalez-Hernandez2, T. Dunn1, B. Javornik1, and D. C. Braun **2013** ApJ 762 130
This first paper in a series describes the design of a study testing whether pre-appearance signatures of solar magnetic active regions were detectable using various tools of local helioseismology. The ultimate goal is to understand flux-emergence mechanisms by setting observational constraints on pre-appearance subsurface changes, for comparison with results from simulation efforts. This first paper provides details of the data selection and preparation of the samples, each containing over 100 members, of two populations: regions on the Sun that produced a numbered NOAA active region, and a "control" sample of areas that did not. The seismology is performed on data from the GONG network; accompanying magnetic data from SOHO/MDI are used for co-temporal analysis of the surface magnetic field. Samples are drawn from 2001-2007, and each target is analyzed for 27.7 hr prior to an objectively determined time of emergence. The results of two analysis approaches are published separately: one based on averages of the seismology- and magnetic-derived signals over the samples, another based on Discriminant Analysis of these signals, for a statistical test of detectable differences between the two populations. We include here descriptions of a new potential-field calculation approach and the algorithm for matching sample distributions over multiple variables. We describe known sources of bias and the approaches used to mitigate them. We also describe unexpected bias sources uncovered during the course of the study and include a discussion of refinements that should be included in future work on this topic.

Sub-surface Plasma Flows and the Flare Productivity of Solar Active Regions

B **Lekshmi**, Kiran Jain, Rudolf W. Komm, Dibyendu Nandy
Front. Astron. Space Sci. 9:1020748 (**2022**)
https://arxiv.org/pdf/2210.09820.pdf
https://www.frontiersin.org/articles/10.3389/fspas.2022.1020748/pdf
The extreme space weather conditions resulting from high energetic events likes solar flares and Coronal Mass Ejections (CMEs) demand for reliable space weather forecasting. The magnetic flux tubes while rising through the convection zone gets twisted by the turbulent plasma flows, energizing the system and resulting in flares. We investigate the relationship between the subsurface plasma flows associated with flaring active regions and their surface magnetic flux and current helicity. The near-surface horizontal velocities derived from the ring-diagram analysis of active region patches using Global Oscillation Network Group (GONG) Doppler velocity measurements are used to compute the fluid dynamics descriptors like vertical divergence, vorticity and kinetic helicity used in this work. The flaring active regions are observed to have large value of vertical vorticity and kinetic helicity. Also, the horizontal flow divergence, vorticity, flux, kinetic and current helicities are observed to be significantly correlated and evolve in phase with each other. We observe that the integrated values of the above flow and magnetic parameters observed one day

prior to the flare are significantly correlated with the integrated flare intensity of the active region. Hence, we show that strong vorticity/kinetic helicities lead to larger active region twisting, presumably generating high-intensity flares.

The solar x-ray imager for GOES

James R. **Lemen**, Dexter W. Duncan, Christopher G. Edwards, Frank M. Friedlaender, Bruce K. Jurcevich, Mons D. Morrison, Larry A. Springer, Robert A. Stern, Jean-Pierre Wuelser, Marilyn E. Bruner, and Richard C. Catura

Proc. SPIE 5171, Telescopes and Instrumentation for Solar Astrophysics, (4 February **2004**);
https://sci-hub.tw/10.1117/12.507566

The next generation of the National Oceanic and Atmospheric Administration's (NOAA) Geo-Stationary Operational Environmental Satellite (GOES) spacecraft will include an X-ray telescope that will monitor the Sun for predicting solar energetic events and for providing information about the large-scale solar magnetic field. The Solar X-ray Imager that will be flown on the GOES N spacecraft in late 2004 makes use of a super-polished grazing incidence mirror, a highly efficient back-thinned CCD, and thin metalized filters to observe the million-degree corona with 10-arcsec resolution (5 arcsec pixel size). Full-sun images will be acquired with SXI on a one-minute cadence at wavelengths between approximately 10 and 60 Å. SXI data will be used to forecast 'space weather', i.e., the effects of charged particles that are produced at the Sun as they interact at the earth. Major contributors to space weather include: variations in the Sun's solar wind, solar flares, and solar mass ejections. Effects of space weather include: radiation damage and particle events in high-inclination orbit spacecraft, disruption of various kinds of communications equipment, degradation of navigational tools such as GPS, potential health hazards during space walks, and power blackouts. Data acquired by the SXI will additionally provide invaluable context information for upcoming solar missions such as STEREO and SDO. The Lockheed Martin Solar and Astrophysics Laboratory has prepared two flight model SXIs that are being readied for flight on the GOES N and GOES O or P spacecraft.

Large Eruptive and Confined Flares in Relation to the Solar Active Region Evolution

Fuyu **Li**1,2,3, Changhui Rao1,2,4, Huaning Wang2,5, Xinhua Zhao3, Nanbin Xiang6, Linhua Deng7, Haitang Li8, and Yu Liu8

2024 ApJL 976 L2
https://iopscience.iop.org/article/10.3847/2041-8213/ad8c37/pdf

Solar active regions (ARs) provide the required magnetic energy and the topology configuration for flares. Apart from conventional static magnetic parameters, the evolution of AR magnetic flux systems should have nonnegligible effects on magnetic energy store and the trigger mechanism of eruptions, which would promote the prediction for the flare using photospheric observations conveniently. Here we investigate 322 large (M- and X-class) flares from 2010 to 2019, almost the whole solar cycle 24. The flare occurrence rate is obviously higher in the developing phase, which should be due to the stronger shearing and complex configurations caused by affluent magnetic emergences. However, the probability of flare eruptions in decaying phases of ARs is obviously higher than that in the developing phase. The confined flares were in nearly equal counts to eruptive flares in developing phases, whereas the eruptive flares were half over confined flares in decaying phases. Yearly looking at flare eruption rates demonstrates the same conclusion. The relationship between sunspot group areas and confined/erupted flares also suggested that the strong field make constraints on the mass ejection, though it can contribute to flare productions. The flare indexes also show a similar trend. It is worth mentioning that all the X-class flares in the decaying phase were erupted, without the strong field constraint. The decaying of magnetic flux systems had facilitation effects on flare eruptions, which may be consequent on the splitting of magnetic flux systems.

The Evolution of Photospheric Current Density During an X9.3-Class Solar Flare

Li, HL (Li, Hai-Li) ; Liang, HF (Liang, Hong-Fei) ; Zhou, XP (Zhou, Xin-Ping) ; Liu, Y (Liu, Yu) ; Meng, N (Meng, Ni) ; Feng, YL (Feng, Yu-Long)

RESEARCH IN ASTRONOMY AND ASTROPHYSICS Volume 24 Issue 10 105013 **2024**
DOI 10.1088/1674-4527/ad709d

This paper deduced the temporal evolution of the magnetic field through a series of high-resolution vector magnetograms and calculated the fine distribution map of current density during an X9.3-class flare eruptions using Amp ère's law. The results show that a pair of conjugate current ribbons exist on both sides of the magnetic neutral line in this active region, and these conjugate current ribbons persist before, during, and after the flare. It was observed that the X9.3-class flare brightened in the form of a bright core and evolved into a double-ribbon flare over time. Importantly, the position of the double-ribbon flare matches the position of the current ribbons with high accuracy, and their morphologies are very similar. By investigating the complexity of current density and flare morphology, we discovered a potential connection between the eruption of major flares and the characteristics of current density.

Prediction of Large Solar Flares Based on SHARP and HED Magnetic Field Parameters

Xuebao **Li**, Xuefeng Li, Yanfang Zheng, Ting Li, Pengchao Yan, Hongwei Ye, Shunhuang Zhang, Xiaotian Wang, Yongshang Lv, Xusheng Huang
ApJ **276** 7 **2024**
https://arxiv.org/pdf/2410.18562
https://iopscience.iop.org/article/10.3847/1538-4365/ad8b2a/pdf
The existing flare prediction primarily relies on photospheric magnetic field parameters from the entire active region (AR), such as Space-Weather HMI Activity Region Patches (SHARP) parameters. However, these parameters may not capture the details the AR evolution preceding flares. The magnetic structure within the core area of an AR is essential for predicting large solar flares. This paper utilizes the area of high photospheric free energy density (HED region) as a proxy for the AR core region. We construct two datasets: SHARP and HED datasets. The ARs contained in both datasets are identical. Furthermore, the start and end times for the same AR in both datasets are identical. We develop six models for 24-hour solar flare forecasting, utilizing SHARP and HED datasets. We then compare their categorical and probabilistic forecasting performance. Additionally, we conduct an analysis of parameter importance. The main results are as follows: (1) Among the six solar flare prediction models, the models using HED parameters outperform those using SHARP parameters in both categorical and probabilistic prediction, indicating the important role of the HED region in the flare initiation process. (2) The Transformer flare prediction model stands out significantly in True Skill Statistic (TSS) and Brier Skill Score (BSS), surpassing the other models. (3) In parameter importance analysis, the total photospheric free magnetic energy density (Efree) within the HED parameters excels in both categorical and probabilistic forecasting. Similarly, among the SHARP parameters, the R_VALUE stands out as the most effective parameter for both categorical and probabilistic forecasting.

Enhanced Peak and Extended Cooling of the Extreme-ultraviolet Late Phase in a Confined Solar Flare

Shihan **Li**, Yu Dai, Mingde Ding, Jinhan Guo, Hao Wu
ApJ **977** 257 **2024**
https://arxiv.org/pdf/2410.18801
https://iopscience.iop.org/article/10.3847/1538-4357/ad8ba3/pdf
We present observations and analysis of an X1.8 non-eruptive solar flare on **2012 October 23**, which is characterized by an extremely large late-phase peak seen in the warm coronal extreme-ultraviolet (EUV) emissions (~ 3 MK), with the peak intensity over 1.4 times that of main flare peak. The flare is driven by a failed eruption of a magnetic flux rope (MFR), whose strong squeeze force acting on the overlying magnetic structures gives rise to an intense early heating of the late-phase loops. Based on differential emission measure (DEM) analysis, it is found that the late-phase loops experience a "longer-than-expected" cooling without the presence of any obvious additional heating, and meanwhile, their volume emission measure (EM) maintains a plateau level for a long time before turning into an evident decay. Without the need for an additional heating, we propose that the special thermodynamic evolution of the late-phase loops revealed in this flare might arise from loop cross-sectional expansions with height, which are evidenced by both direct measurements from EUV images and by magnetic field extrapolation. By blocking the losses of both heat flux and mass from the corona, such an upward cross-sectional expansion not only elongates the loop cooling time, but also more effectively sustains the loop density, therefore leading to a later-than-expected occurrence of the warm coronal late phase in combination with a sufficiently high late-phase peak. We further verify such a scenario by analytically solving the cooling process of a late-phase loop characterized by a variable cross section.

Very Long-periodic Pulsations Detected Simultaneously in a White-light Flare and Sunspot Penumbra

Dong **Li**1,2, Jincheng Wang2,3, and Yu Huang1
2024 ApJL 972 L2
https://iopscience.iop.org/article/10.3847/2041-8213/ad6cde/pdf
https://arxiv.org/pdf/2408.15706
We investigate the origin of very long-periodic pulsations in the white-light emission of an X6.4 flare on **2024 February 22** (SOL2024-02-22T22:08), which occurred at the edge of a sunspot group. The flare white-light fluxes reveal four successive and repetitive pulsations, which are simultaneously measured by the Helioseismic and Magnetic Imager and the White-light Solar Telescope. A quasi-period of 8.6−1.9+1.5 minutes, determined by the Morlet wavelet transform, is detected in the visible continuum channel. The modulation depth, which is defined as the ratio between the oscillatory amplitude and its long-term trend, is smaller than 0.1%, implying that the quasi-periodic pulsation (QPP) feature is a weak wave process. Imaging observations show that the X6.4 flare occurs near a sunspot group. Moreover, the white-light brightening is located in sunspot penumbra, and a similar quasi-period of about 8.5−1.8+1.6 minutes is identified in one penumbral location of the nearest sunspot. The map of Fourier power distribution suggests that a similar periodicity is universally existing in most parts of the penumbra that is close to the penumbral–photospheric boundary. Our observations support the scenario that the white-light QPP is probably modulated by the slow-mode magnetoacoustic gravity wave leaking from the sunspot penumbra.

Various Features of the X-class White-light Flares in Super Active Region NOAA 13664

Ying **Li**, Xiaofeng Liu, Zhichen Jing, Wei Chen, Qiao Li, Yang Su, De-Chao Song, M. D. Ding, Li Feng, Hui Li, Weiqun Gan

ApJL **972** L1 **2024**

https://arxiv.org/pdf/2408.05725 **File**

https://iopscience.iop.org/article/10.3847/2041-8213/ad6d6c/pdf

Super active region NOAA 13664 produced 12 X-class flares (including the largest one, an occulted X8.7 flare, in solar cycle 25 so far) during **2024 May 8-15** and 11 of them are identified as white-light flares. Here we present various features of these X-class white-light flares observed by the White-light Solar Telescope (WST) on board the Advanced Space-based Solar Observatory and the Helioseismic and Magnetic Imager (HMI) on board the Solar Dynamics Observatory. It is found that both the white-light emissions at WST 3600 Å (Balmer continuum) and HMI 6173 Å (Paschen continuum) show up in different regions of the sunspot group in these flares, including outside the sunspots and within the penumbra and umbra of the sunspots. They exhibit a point-, ribbon-, loop-, or ejecta-like shape, which can come from flare ribbons (or footpoints), flare loops, and plasma ejecta depending on the perspective view. The white-light duration and relative enhancement are measured and both parameters for 3600 Å emission have greater values than those for 6173 Å emission. It is also found that these white-light emissions are cospatial well with the hard X-ray (HXR) sources in the on-disk flares but have some offsets with the HXR emissions in the off-limb flares. In addition, it is interesting that the 3600 and 6173 Å emissions show different correlations with the peak HXR fluxes, with the former one more sensitive to the HXR emission. All these greatly help us understand the white-light flares of a large magnitude from a super active region on the Sun and also provide important insights into superflares on Sun-like stars. **2024 May: 8, 9, 10, 11, 12, 14, 15**

Table 1. Information of the 12 X-class Flares from Super AR NOAA 13664

Long-period energy releases during a C2.8 flare

Dong **Li**, Jianping Li, Jinhua Shen, Qiwu Song, Haisheng Ji, Zongjun Ning

A&A 690, A39 **2024**

https://arxiv.org/pdf/2408.01179

https://www.aanda.org/articles/aa/pdf/2024/10/aa50622-24.pdf

We investigated the intermittent energy-releasing processes by analyzing the long-period pulsations during a C2.8 flare on **2023 June 03**. The C2.8 flare shows three successive and repetitive pulsations in soft X-ray (SXR) and high-temperature extreme ultraviolet (EUV) emissions, which may imply three episodes of energy releases during the solar flare. The QPP period is estimated to be as long as about 7.5 minutes. EUV imaging observations suggest that these three pulsations come from the same flare area dominated by the hot loop system. Conversely, the flare radiation in wavelengths of radio/microwave, low-temperature EUV, ultraviolet (UV), and Ha only reveals the first pulsation, which may be associated with nonthermal electrons accelerated by magnetic reconnection. The other two pulsations in wavelengths of SXR and high-temperature EUV might be caused by the loop-loop interaction. Our observations indicate that the three episodes of energy releases during the C2.8 flare are triggered by different mechanisms, namely the accelerated electron via magnetic reconnection, and the loop-loop interaction in a complicated magnetic configuration.

Localizing Quasiperiodic Pulsations in Hard X-Ray, Microwave, and Lyα Emissions of an X6.4 Flare

Dong **Li**1,2, Zhenxiang Hong1,3, Zhenyong Hou4, and Yang Su1

2024 ApJ 970 77

https://iopscience.iop.org/article/10.3847/1538-4357/ad566c/pdf

https://arxiv.org/pdf/2408.05463

We report the simultaneous observations of quasiperiodic pulsations (QPPs) in wavelengths of hard X-ray (HXR), microwave, Lyα, and ultraviolet (UV) emissions during the impulsive phase of an X6.4 flare on **2024 February 22** (SOL2024-02-22T22:08). The X6.4 flare shows three repetitive and successive pulsations in HXR and microwave wavebands, and they have an extremely large modulation depth. The onset of flare QPPs is almost simultaneous with the start of magnetic cancellation between positive and negative fields. The wavelet power spectra suggest the presence of double periods, which are centered at ~200 and ~95 s, respectively. The long-period QPP can also be detected in Lyα and UV wavebands at the flare area, and it could be observed in the adjacent sunspot. Our observations indicate that the flare QPPs are most likely triggered by accelerated electrons that are associated with periodic magnetic reconnections. The long period at ~200 s is probably modulated by the slow magnetoacoustic wave originating from the neighboring sunspot, while the short period at ~95 s could be regarded as its second harmonic mode.

Spectral and Imaging Observations of a C2.3 White-Light Flare from the Advanced Space-Based Solar Observatory (ASO-S) and the Chinese Hα Solar Explorer (CHASE)

Qiao **Li**, Ying Li, Yang Su, Dechao Song, Hui Li, Li Feng, +++

Solar Phys. **299**, 73 **2024**
https://arxiv.org/pdf/2405.01308
https://doi.org/10.1007/s11207-024-02313-y
https://link.springer.com/content/pdf/10.1007/s11207-024-02313-y.pdf
Solar white-light flares are characterized by an enhancement in the optical continuum, which are usually large flares (say X- and M-class flares). Here we report a small C2.3 white-light flare (SOL**2022-12-20**T04:10) observed by the \emph{Advanced Space-based Solar Observatory} and the \emph{Chinese Hα Solar Explorer}. This flare exhibits an increase of ≈6.4\% in the photospheric Fe \textsc{i} line at 6569.2\,Å and {≈3.2\%} in the nearby continuum. The continuum at 3600\,Å also shows an enhancement of ≈4.7\%. The white-light brightening kernels are mainly located at the flare ribbons and co-spatial with nonthermal hard X-ray sources, which implies that the enhanced white-light emissions are related to nonthermal electron-beam heating. At the brightening kernels, the Fe \textsc{i} line displays an absorption profile that has a good Gaussian shape, with a redshift up to ≈1.7 km s−1, while the Hα line shows an emission profile though having a central reversal. The Hα line profile also shows a red or blue asymmetry caused by plasma flows with a velocity of several to tens of km s−1. It is interesting to find that the Hα asymmetry is opposite at the conjugate footpoints. It is also found that the CHASE continuum increase seems to be related to the change of photospheric magnetic field. Our study provides comprehensive characteristics of a small white-light flare that help understand the energy release process of white-light flares.

A Statistical Investigation of the Neupert Effect in Solar Flares Observed with ASO-S/HXI

Dong **Li**, Hanyang Dong, Wei Chen, Yang Su, Yu Huang, Zongjun Ning
Solar Phys. **299**, 57 **2024**
https://arxiv.org/pdf/2404.02653.pdf
https://doi.org/10.1007/s11207-024-02299-7
https://link.springer.com/article/10.1007/s11207-024-02299-7
Neupert effect refers to the strong correlation between the soft X-ray (SXR) light curve and the time-integrated hard X-rays (HXR) or microwave flux, which is frequently observed in solar flares. In this article, we therefore utilized the newly launched Hard X-ray Imager (HXI) on board the Advanced Space-based Solar Observatory to investigate the Neupert effect during solar flares. By checking the HXR light curves at 20-50 keV, a sample of 149 events that cover the flare impulsive phase were selected. Then, we performed a cross-correlation analysis between the HXR fluence (i.e., the time integral of the HXR flux) and the SXR 1-8 A flux measured by the Geostationary Operational Environmental Satellite. All the selected flares show high correlation coefficients (>0.90), which seem to be independent of the flare location and class. The HXR fluences tend to increase linearly with the SXR peak fluxes. Our observations indicate that all the selected flares obey the Neupert effect. **9 May 2023, 19 Jun 2023,**
Table 1.: Key parameters of the solar flares in this study 2022-2023

Survey of Magnetic Field Parameters Associated With Large Solar Flares

Ting **Li**, Yanfang Zheng, Xuefeng Li, Yijun Hou, Xuebao Li, Yining Zhang, Anqin Chen
ApJ **964** 159 **2024**
https://arxiv.org/pdf/2402.18890.pdf
https://iopscience.iop.org/article/10.3847/1538-4357/ad2e90/pdf
Until now, how the magnetic fields in M/X-class flaring active regions (ARs) differ from C-class flaring ARs remains unclear. Here, we calculate the key magnetic field parameters within the area of high photospheric free energy density (HED region) for 323 ARs (217 C- and 106 M/X-flaring ARs), including total photospheric free magnetic energy density Efree, total unsigned magnetic flux ΦHED, mean unsigned current helicity hc, length of the polarity inversion lines LPIL with a steep horizontal magnetic gradient, etc., and compare these with flare/coronal mass ejection (CME) properties. We first show the quantitative relations among the flare intensity, the eruptive character and ΦHED. We reveal that ΦHED is a measure for the GOES flux upper limit of the flares in a given region. For a given ΦHED, there exists the lower limit of FSXR for eruptive flares. This means that only the relatively strong flares with the large fraction of energy release compared to the total free energy are likely to generate a CME. We also find that the combinations of Efree-LPIL and Efree-hc present a good ability to distinguish between C-class and M/X-class flaring ARs. Using determined critical values of Efree and LPIL, one predicts correctly 93 out of 106 M/X-class flaring ARs and 159/217 C-class flaring ARs. The large LPIL or hc for M/X-class flaring ARs probably implies the presence of a compact current with twisted magnetic fields winding about it. **2014-11-07**

The White-light Emissions in Two X-class Flares Observed by ASO-S and CHASE

Ying **Li**, Zhichen Jing, De-Chao Song, Qiao Li, Jun Tian, Xiaofeng Liu, Ya Wang, M. D. Ding, Andrea Francesco Battaglia, Li Feng, Hui Li, Weiqun Gan
ApJL **963** L3 **2024**
https://arxiv.org/pdf/2402.07374.pdf
https://iopscience.iop.org/article/10.3847/2041-8213/ad27ca/pdf

The white-light continuum emissions in solar flares (i.e., white-light flares) are usually observed on the solar disk but, in a few cases, off the limb. Here we present on-disk as well as off-limb continuum emissions at 3600 Å (in the Balmer continuum) in an X2.1 flare (**SOL2023-03-03T17**:52) and an X1.5 flare (**SOL2023-08-07T20**:46), respectively, observed by the White-light Solar Telescope (WST) on the Advanced Space-based Solar Observatory (ASO-S). These continuum emissions are seen at the ribbons for the X2.1 flare and on loops during the X1.5 event, in which the latter also appears in the decay phase. These emissions also show up in the pseudo-continuum images at Fe I {\lambda}6173 from the Helioseismic and Magnetic Imager (HMI) on the Solar Dynamics Observatory (SDO). In addition, the ribbon sources in the X2.1 flare exhibit significant enhancements in the Fe I line at 6569.2 Å and the nearby continuum observed by the Chinese H{\alpha} Solar Explorer (CHASE). It is found that the on-disk continuum emissions in the X2.1 flare are related to a nonthermal electron-beam heating either directly or indirectly, while the off-limb emissions in the X1.5 flare are associated with thermal plasma cooling or due to Thomson scattering. These comprehensive continuum observations can provide good constraints on flare energy deposition models, which helps well understand the physical mechanism of white-light flares.

Observational signature of continuously operating drivers of decayless kink oscillation

Dong **Li**, Zhentong Li, Fanpeng Shi, Yang Su, Wei Chen, Fu Yu, Chuan Li, Ye Qiu, Yu Huang, Zongjun Ning

A&A 680, L15 **2023**

https://arxiv.org/pdf/2311.16434.pdf

https://www.aanda.org/articles/aa/pdf/2023/12/aa48075-23.pdf

Context. Decayless kink oscillations, which are nearly omnipresent in the solar corona, are believed to be driven by continuously operating energy supply.

Aims. In this Letter, we investigate an external continuous excitation of an apparent decayless oscillation during an X1.1 flare on **June 20, 2023** (SOL2023-06-20T16:42).

Methods. The decayless kink oscillation was identified in the coronal loop at extreme ultraviolet (EUV) wavelengths and the associated flare quasi-periodic pulsations (QPPs) were simultaneously observed in passbands of hard X-ray (HXR), microwave, and ultraviolet (UV) emissions.

Results. The kink oscillation is detected as a transverse oscillation of the coronal loop, which reveals five apparent cycles with an average period of about 130 ± 10 s. The oscillation amplitude does not show any significantly decay, suggesting a decayless oscillation. At the same time, the solar flare occurs in the vicinity of the oscillating loop and exhibits five main pulses in HXR, microwave, and UV emissions, which could be regarded as flare QPPs. They have similar periods of about 100–130 s, which may indicate successive and repetitive energy releases during the flare impulsive phase. The peak of each loop oscillation cycle appears to follow the pulse of the QPPs, suggesting that the transverse oscillation is closely associated with flare QPPs.

Conclusions. Our observations support the scenario where the repetitive energy released following flare QPPs could be invoked as external, continuously operating drivers of the apparent decayless kink oscillation.

Simultaneous detection of flare-associated kink oscillations and extreme-ultraviolet waves

Dong **Li**, Zhenyong Hou, Xianyong Bai, Chuan Li, Matthew Fang, Haisheng Zhao, Jincheng Wang, Zongjun Ning

Science China Technological Sciences **2023**

https://arxiv.org/pdf/2311.08767.pdf

Kink oscillations, which are frequently observed in coronal loops and prominences, are often accompanied by extreme-ultraviolet (EUV) waves. However, much more needs to be explored regarding the causal relationships between kink oscillations and EUV waves. In this article, we report the simultaneous detection of kink oscillations and EUV waves that are both associated with an X2.1 flare on 2023 March 03 (SOL**2023-03-03T17**:39). The kink oscillations, which are almost perpendicular to the axes of loop-like structures, are observed in three coronal loops and one prominence. One short loop shows in-phase oscillation within the same period of 5.2 minutes at three positions. This oscillation could be triggered by the pushing of an expanding loop and interpreted as the standing kink wave. Time lags are found between the kink oscillations of the short loop and two long loops, suggesting that the kink wave travels in different loops. The kink oscillations of one long loop and the prominence are possibly driven by the disturbance of the CME, and that of another long loop might be attributed to the interaction of the EUV wave. The onset time of the kink oscillation of the short loop is nearly same as the beginning of an EUV wave. This fact demonstrates that they are almost simultaneous. The EUV wave is most likely excited by the expanding loop structure and shows two components. The leading component is a fast coronal wave, and the trailing one could be due to the stretching magnetic field lines.

Deep Neural Networks of Solar Flare Forecasting for Complex Active Regions

Ming **Li**, Yanmei Cui, Yanmei Cui, and Bingxian Luo

Front. Astron. Space Sci. 10: 1177550. **2023**

doi: 10.3389/fspas.2023.1177550

https://www.frontiersin.org/articles/10.3389/fspas.2023.1177550/pdf
Solar flare forecasting is one of major components of operational space weather forecasting. Complex active regions (ARs) are the main source producing major flares, but only a few studies are carried out to establish flare forecasting models for these ARs. In this study, four deep learning models, called Complex Active Region Flare Forecasting Model (CARFFM)-1, −2, −3, and −4, are established. They take AR longitudinal magnetic fields, AR vector magnetic fields, AR longitudinal magnetic fields and the total unsigned magnetic flux in the neutral line region, AR vector magnetic fields and the total unsigned magnetic flux in the neutral region as input, respectively. These four models can predict the production of M-class or above flares in the complex ARs for the next 48 h. Through comparing the performance of the models, CARFFM-4 has the best forecasting ability, which has the most abundant input information. It is suggested that more valuable and rich input can improve the model performance. **2012 April 25, 2013 October 25**

Observational signatures of electron-driven chromospheric evaporation in a white-light flare

Dong **Li**, Chuan Li, Ye Qiu, Shihao Rao, Alexander Warmuth, Frederic Schuller, Haisheng Zhao, Fanpeng Shi, Jun Xu, Zongjun Ning

ApJ **954** 7 **2023**

https://arxiv.org/pdf/2306.15888.pdf
https://iopscience.iop.org/article/10.3847/1538-4357/ace256/pdf

We investigate observational signatures of explosive chromospheric evaporation during a white-light flare (WLF) that occurred on **2022 August 27**. Using the moment analysis, bisector techniques, and the Gaussian fitting method, red-shifted velocities of less than 20 km/s are detected in low-temperature spectral lines of Ha, C I and Si IV at the conjugated flare kernels, which could be regarded as downflows caused by chromospheric condensation. Blue-shifted velocities of about 30-40 km/s are found in the high-temperature line of Fe XXI, which can be interpreted as upflows driven by chromospheric evaporation. A nonthermal hard X-ray (HXR) source is co-spatial with one of the flare kernels, and the Doppler velocities are temporally correlated with the HXR fluxes. The nonthermal energy flux is estimated to be at least (1.3+-0.2)*10^10 erg/s/cm^2. The radiation enhancement at Fe I 6569.2 A and 6173 A suggests that the flare is a WLF. Moreover, the while-light emission at Fe I 6569.2 A is temporally and spatially correlated with the blue shift of Fe XXI line, suggesting that both the white-light enhancement and the chromospheric evaporation are triggered and driven by nonthermal electrons. All our observations support the scenario of an electron-driven explosive chromospheric evaporation in the WLF.

Traveling kink oscillations of coronal loops launched by a solar flare

Dong **Li**, Xianyong Bai, Hui Tian, Jiangtao Su, Zhenyong Hou, Yuanyong Deng, Kaifan Ji, Zongjun Ning

A&A 675, A169 **2023**

https://arxiv.org/pdf/2306.04973.pdf
https://www.aanda.org/articles/aa/pdf/2023/07/aa45812-22.pdf

We investigate the traveling kink oscillation triggered by a solar flare on **2022 September 29**. The observational data is mainly measured by the Solar Upper Transition Region Imager (SUTRI), the Atmospheric Imaging Assembly (AIA), and the Spectrometer/Telescope for Imaging X-rays (STIX). The transverse oscillations with apparent decaying in amplitudes, which are nearly perpendicular to the oscillating loop, are observed in passbands of SUTRI 465 A, AIA 171 A, and 193 A. The decaying oscillation is launched by a solar flare erupted closely to one footpoint of coronal loops, and then it propagates along several loops. Next, the traveling kink wave is evolved to a standing kink oscillation. To the best of our knowledge, this is the first report of the evolution of a traveling kink pulse to a standing kink wave along coronal loops. The standing kink oscillation along one coronal loop has a similar period of about 6.3 minutes at multiple wavelengths, and the decaying time is estimated to about 9.6-10.6 minutes. Finally, two dominant periods of 5.1 minutes and 2.0 minutes are detected in another oscillating loop, suggesting the coexistence of the fundamental and third harmonics.

Global energetics of solar powerful events on 6 September 2017

Dong **Li**, Alexander Warmuth, Jincheng Wang, Haisheng Zhao, Lei Lu, Qingmin Zhang, Nina Dresing, Rami Vainio, Christian Palmroos, Miikka Paassilta, Annamaria Fedeli, Marie Dominique

Research in Astron. Astrophys. **2023**

https://arxiv.org/pdf/2305.00381.pdf

Solar flares and coronal mass ejections (CMEs) are thought to be the most powerful events on the Sun. They can release energy as high as 10^32 erg in tens of minutes,and could produce solar energetic particles (SEPs) in the interplanetary space. We explore global energy budgets of solar major eruptions on **6 September 2017**, including the energy partition of a powerful solar flare, the energy budget of the accompanied CME and SEPs. In the wavelength range shortward of 222 nm, a major contribution of the flare radiated energy is in the soft X-ray (SXR) 0.1-7 nm domain. The flare energy radiated at wavelengths of Ly-alpha and middle ultraviolet is larger than that radiated in the extreme ultraviolet wavelength, but it is much less than that radiated in the SXR waveband. The total flare radiated energy could be comparable to the thermal and nonthermal energies. The energies carried by the major flare and its accompanied CME are roughly equal, and they are both powered by the magnetic free energy in the AR NOAA 12673. Moreover, the CME

is efficient in accelerating SEPs, and that the prompt component (whether it comes from the solar flare or the CME) contributes only a negligible fraction.

A Statistical Study of Short-period Decayless Oscillations of Coronal Loops in an Active Region

Dong **Li**1 and David M. Long2
2023 ApJ 944 8
https://iopscience.iop.org/article/10.3847/1538-4357/acacf4/pdf
https://arxiv.org/pdf/2212.08804.pdf
Coronal loop oscillations are common phenomena in the solar corona, which are often classified as decaying and decayless oscillations. Using the high-resolution observation measured by the Extreme Ultraviolet Imager (EUI) on board the Solar Orbiter, we statistically investigate small-scale transverse oscillations with short periods (<200 s) of coronal loops in an active region (AR), i.e., NOAA AR 12965. A total of 111 coronal loops are identified in EUI 174 Å images, and they all reveal transverse oscillations without any significant decaying, regarded as decayless oscillations. Oscillatory periods are measured from ∼11 to ∼185 s, with a median period of 40 s. Thus, they are also termed short-period oscillations. The corresponding loop lengths are measured from ∼10.5 to ∼30.2 Mm, and a strong dependence of oscillatory periods on loop lengths is established, indicating that the short-period oscillations are standing kink-mode waves in nature. Based on the coronal seismology, kink speeds are measured to be ∼330–1910 km s−1, and magnetic field strengths in coronal loops are estimated to be ∼4.1–25.2 G, while the energy flux carried by decayless kink oscillations lies in the range from roughly 7 to 9220 W m−2. Our estimations suggest that the wave energy carried by short-period decayless kink oscillations cannot support the coronal heating in the AR. **2022 March 17**

Particle Accelerations in a 2.5-dimensional Reconnecting Current Sheet in Turbulence

Yan **Li**1,2, Lei Ni1,2, Jing Ye1,2, Zhixing Mei1,2, and Jun Lin1,2,3
2022 ApJ 938 24
https://iopscience.iop.org/article/10.3847/1538-4357/ac8b6d/pdf
Electric field induced in magnetic reconnection is an efficient mechanism for generating energetic particles, but the detailed role it plays is still an open question in solar flares. In this work, accelerations of particles in an evolving reconnecting current sheet are investigated via the test-particle approach, and the electromagnetic field is taken in a self-consistent fashion from a 2.5D numerical experiment for the magnetic reconnection process in the corona. The plasma instabilities like the tearing mode in the current sheet produce magnetic islands in the sheet, and island merging occurs as well. For the motion of the magnetic island, it yields the occurrence of the opposite electric field at both endpoints of the island; hence, tracking the accelerated particles around magnetic islands suggests that the parallel acceleration does not apparently impact the energy gain of particles, but the perpendicular acceleration does. Furthermore, our results indicate that the impact of the guide field on the trajectory of accelerated particles in a more realistic electromagnetic configuration works only on those particles that are energetic enough. The energy spectra of both species show a single power-law shape. The higher-energy component of the power-law spectrum results from the particles that are trapped in the current sheet, while the escaped and partly trapped particles contribute to the lower-energy component of the spectrum. The evolution of the spectrum shows a soft-hard-soft pattern that has been observed in flares.

Flare Quasi-Periodic Pulsation Associated with Recurrent Jets

Dong **Li**, Fanpeng Shi, Haisheng Zhao, Shaolin Xiong, Liming Song, Wenxi Peng, Xinqiao Li, Wei Chen, and Zongjun Ning
Front. Astron. Space Sci. 9: 1032099. **2022**
doi: 10.3389/fspas.2022.1032099
https://arxiv.org/pdf/2209.10952.pdf
https://www.frontiersin.org/articles/10.3389/fspas.2022.1032099/pdf
Quasi-periodic pulsations (QPPs), which carry time features and plasma characteristics of flare emissions, are frequently observed in light curves of solar/stellar flares. In this study, we investigated non-stationary QPPs associated with recurrent jets during an M1.2 flare on **2022 July 14**. A quasi-period of ∼45±∼45±10 s, determined by the wavelet transform technique, is simultaneously identified at wavelengths of soft/hard X-ray and microwave emissions, which are recorded by the Gravitational Wave High-Energy Electromagnetic Counterpart All-sky Monitor, Fermi and the Nobeyama Radio Polarimeters, respectively. A group of recurrent jets with an intermittent cadence of about 45 ± 10 s are found in the Atmospheric Imaging Assembly (AIA) image series at 304 Å, but they are 180 s earlier than the flare QPP. All observational facts suggest that the flare QPPs could be excited by recurrent jets, and they should be associated with non-thermal electrons that are periodically accelerated by a repeated energy release process, such as repetitive magnetic reconnection. Moreover, the same quasi-period is discovered at double footpoints connected by a hot flare loop in AIA 94 Å, and the phase speed is measured to be ∼1,420 km s−1. Based on the differential emission measure, the average temperatures, number densities, and magnetic field strengths at the loop top and footpoint are estimated to be ∼7.7/6.7 MK, ∼7.5/3.6 × 1010 cm−3, and ∼143/99 G, respectively. Our measurements indicate that the 45-s QPP is probably modulated by the kink-mode wave of the flare loop.

The Lyman-α Emission in a C1.4 Solar Flare Observed by the Extreme Ultraviolet Imager aboard Solar Orbiter

Ying **Li**, Qiao Li, De-Chao Song, Andrea Francesco Battaglia, Hualin Xiao, Säm Krucker, Udo Schühle, Hui Li, Weiqun Gan, M. D. Ding

ApJ **936** 142 **2022**

https://arxiv.org/pdf/2208.06182.pdf

https://iopscience.iop.org/article/10.3847/1538-4357/ac897c/pdf

The hydrogen Lyman-α (H {\sc i} Lyα) emission during solar flares has rarely been studied in spatially resolved images and its physical origin has not been fully understood. In this paper, we present novel Lyα images for a C1.4 solar flare (SOL**2021-08-20**T22:00) from the Extreme Ultraviolet Imager aboard Solar Orbiter, together with multi-waveband and multi-perspective observations from the Solar Terrestrial Relations Observatory Ahead and the Solar Dynamics Observatory spacecraft. It is found that the Lyα emission has a good temporal correlation with the thermal emissions at 1--8 Å and 5--7 keV, indicating that the flaring Lyα is mainly produced by a thermal process in this small event. However, nonthermal electrons play a minor role in generating Lyα at flare ribbons during the rise phase of the flare, as revealed by the hard X-ray imaging and spectral fitting. Besides originating from flare ribbons, the Lyα emission can come from flare loops, likely caused by plasma heating and also cooling that happen in different flare phases. It is also found that the Lyα emission shows fairly similar features with the He {\sc ii} 304 Å emission in light curve and spatio-temporal variation along with small differences. These observational results improve our understanding of the Lyα emission in solar flares and also provide some insights for investigating the Lyα emission in stellar flares.

Knowledge-Informed Deep Neural Networks for Solar Flare Forecasting

Ming **Li**, Yanmei Cui,Bingxian Luo,Xianzhi Ao,Siqing Liu,Jingjing Wang,Shuxin Li,Chenxi Du,Xiaojing Sun,Xin Wang

Space Weather e2021SW002985 **2022**

https://doi.org/10.1029/2021SW002985

https://agupubs.onlinelibrary.wiley.com/doi/epdf/10.1029/2021SW002985

Recently, although various deep learning techniques have been applied to building space weather prediction models, a large amount of relevant prior knowledge of solar eruptions and magnetic properties is ignored during the model development. By integrating prior knowledge in flare production into the convolutional neural network (CNN) structures, we have developed a knowledge-informed deep neural network model aiming at forecasting solar flares. The line-of-sight magnetograms of Space-weather HMI Active Region Patches (SHARP) from May 2010 to December 2018 are selected. We have surveyed the relationships between solar flares and both the active region (AR) area and magnetic type. When integrating prior knowledge into the CNNs, three aspects are considered: 1) keeping the magnetic structure unchanged (data preprocessing) while filling SHARP magnetograms into squares; 2) grouping the data samples into two subsets according to different flare productivities (sample grouping); and 3) adding AR area as an extra input parameter to the CNN (extra input parameter implementation). Pure CNN model, Fusion model 1, and Fusion model 2 are built to forecast M-class or above flares in the next 48 hours, which involve data preprocessing, data preprocessing and sample grouping, and all the three aspects, respectively. Fusion model 2 which augments the most prior knowledge has the best performance. Our results imply that prior knowledge can play an important role in building deep learning flare forecasting models. In the future, adopting knowledge-informed deep neural networks will be an effective way to further improve the forecasting performance for other space weather events.

Quasi-periodic Accelerations of Energetic Particles during a Solar Flare

Dong **Li**, Wei Chen

ApJL **931** L28 **2022**

https://arxiv.org/abs/2205.07423

https://iopscience.iop.org/article/10.3847/2041-8213/ac6fd2/pdf

We report the observation of non-stationary Quasi-Periodic Pulsations (QPPs) in high-energy particles during the impulsive phase of an X4.8 flare on 2002 July 23 (SOL2002-07-23T00:35). The X4.8 flare was simultaneously measured by the Reuven Ramaty High Energy Solar Spectroscopic Imager, Nobeyama Radio Polarimeters, and Nobeyama Radioheliograph. The quasi-period of about 50 s, determined by the wavelet transform, is detected in the Gamma-ray line emission. Using the same method, a quasi-period of about 90 s is found in Gamma-ray continuum, hard X-ray (HXR) and radio emissions during almost the same time. Our observations suggest that the flare QPPs should be associated with energetic ions and nonthermal electrons that quasi-periodically accelerated by the repetitive magnetic reconnection. The different quasi-periods between Gamma-ray line and continuum/HXR/radio emissions indicate an apparent difference in acceleration or propagation between energetic ions and nonthermal electrons of this solar flare. **2002 July 23**

Detailed Thermal and Nonthermal Processes in an A-class Microflare

Zhentong **Li**1,2, Yang Su1,2, Astrid M. Veronig3, Shuting Kong4,5, Weiqun Gan1,2, and Wei Chen
2022 ApJ 930 147
https://iopscience.iop.org/article/10.3847/1538-4357/ac651c/pdf
How microflares behave and differ from large flares is an important question in flare studies. Although they have been extensively investigated, microflares are not fully understood in terms of their detailed energy release processes and the role of energetic electrons. A recent study on an A-class microflare suggests the existence of a nonthermal component down to 6.5 keV, indicating that accelerated electrons play an important role in microflares, as in large flares. Here, we revisit this event, and present a comprehensive, quantitative analysis of the energy release and plasma heating processes. Using careful differential emission measure (DEM) analysis, we calculate the thermal X-ray fluxes. By subtracting this multithermal component from the observed data, we confirm the existence of the remaining nonthermal component. In addition, we analyze the clear evaporation process and report the first imaging evidence for a low-energy cutoff of energetic electrons in EM maps of >10 MK plasma, which first appeared as two coronal sources significantly above the chromospheric footpoints. Detailed calculations of electron transport, based on the electron parameters and the evolution of loop dynamics, provide strong evidence of a beam-driven plasma heating process with a low-energy cutoff consistent with that derived independently from DEM analysis. This study reveals the important role of electron thermalization and low-energy cutoffs in the physical processes of microflares. **2017 August 21**

Modeling Electron Acceleration and Transport in the Early Impulsive Phase of the 2017 September 10 Solar Flare

Xiaocan **Li**, Fan Guo, Bin Chen, Chengcai Shen, Lindsay Glesener
ApJ **932** 92 **2022**
https://arxiv.org/pdf/2205.04946.pdf
https://iopscience.iop.org/article/10.3847/1538-4357/ac6efe/pdf
The X8.2-class limb flare on **September 10, 2017** is among the best studied solar flare events owing to its great similarity to the standard flare model and the broad coverage by multiple spacecraft and ground-based observations. These multiwavelength observations indicate that electron acceleration and transport are efficient in the reconnection and flare looptop regions. However, there lacks a comprehensive model for explaining and interpreting the multi-faceted observations. In this work, we model the electron acceleration and transport in the early impulsive phase of this flare. We solve the Parker transport equation that includes the primary acceleration mechanism during magnetic reconnection in the large-scale flare region modeled by MHD simulations. We find that electrons are accelerated up to several MeV and fill a large volume of the reconnection region, similar to the observations shown in microwaves. The electron spatial distribution and spectral shape in the looptop region agree well with those derived from the microwave and hard X-ray emissions before magnetic islands grow large and dominate the acceleration. Future emission modelings using the electron maps will enable direct comparison with microwave and hard X-ray observations. These results shed new light on the electron acceleration and transport in a broad region of solar flares within a data-constrained realistic flare geometry.

Three-dimensional Magnetic and Thermodynamic Structures of Solar Microflares

Z. F. **Li**, X. Cheng, F. Chen, J. Chen, M. D. Ding
ApJ **930** L7 **2022**
https://arxiv.org/pdf/2204.07762.pdf
https://iopscience.iop.org/article/10.3847/2041-8213/ac67aa/pdf
Microflares, one of small-scale solar activities, are believed to be caused by magnetic reconnection. Nevertheless, their three-dimensional (3D) magnetic structures, thermodynamic structures, and physical links to the reconnection have been unclear. In this Letter, based on high-resolution 3D radiative magnetohydrodynamic simulation of the quiet Sun spanning from the upper convection zone to the corona, we investigate 3D magnetic and thermodynamic structures of three homologous microflares. It is found that they originate from localized hot plasma embedded in the chromospheric environment at the height of 2--10 Mm above the photosphere and last for 3--10 minutes with released magnetic energy in the range of 1027−1028 erg. The heated plasma is almost co-spatial with the regions where the heating rate per particle is maximal. The 3D velocity field reveals a pair of converging flows with velocities of tens of km s−1 toward and outflows with velocities of about 100 km s−1 moving away from the hot plasma. These features support that magnetic reconnection plays a critical role in heating the localized chromospheric plasma to coronal temperature, giving rise to observed microflares. The magnetic topology analysis further discloses that the reconnection region is located near quasi-separators where both current density and squashing factors are maximal although the specific topology may vary from tether-cutting to fan-spine-like structure. **2020 May 20.**

Simultaneous Observations of Chromospheric Evaporation and Condensation during a C-class Flare

Dong **Li**, Zhenxiang Hong, Zongjun Ning
ApJ **926** 23 **2021**
https://arxiv.org/pdf/2112.06118.pdf

https://iopscience.iop.org/article/10.3847/1538-4357/ac426b/pdf
We explored simultaneous observations of chromospheric evaporation and condensation during the impulsive phase of a C6.7 flare on **9 May 2019**. The solar flare was simultaneously observed by multiple instruments, i.e., the New Vacuum Solar Telescope (NVST), the Interface Region Imaging Spectrograph, the Atmospheric Imaging Assembly (AIA), the Fermi, the Mingantu Spectral Radioheliograph, and the Nobeyama Radio Polarimeters. Using the single Gaussian fitting and the moment analysis technique, redshifted velocities at slow speeds of 15-19 km/s are found in the cool lines of C II and Si IV at one flare footpoint location. Red shifts are also seen in the H-alpha line-of-sight (LOS) velocity image measured by the NVST at double footpoints. Those red shifts with slow speeds can be regarded as the low-velocity downflows driven by the chromospheric condensation. Meanwhile, the converging motions from double footpoints to the loop top are found in the high-temperature EUV images, such as AIA 131 A, 94 A, and 335 A. Their apparent speeds are estimated to be roughly 126-210 km/s, which could be regarded as the high-velocity upflows caused by the chromospheric evaporation. The nonthermal energy flux is estimated to be about 5.7x10^10 erg/s/cm^2. The characteristic timescale is roughly equal to 1 minute. All these observational results suggest an explosive chromospheric evaporation during the flare impulsive phase. While a HXR/microwave pulse and a type III radio burst are found simultaneously, indicating that the explosive chromospheric evaporation is driven by the nonthermal electron.

Detection of Flare Multiperiodic Pulsations in Mid-ultraviolet Balmer Continuum, Lyα, Hard X-Ray, and Radio Emissions Simultaneously

Dong **Li**1,2, Mingyu Ge3, Marie Dominique4, Haisheng Zhao3, Gang Li3, Xiaobo Li3, Shuangnan Zhang3,5, Fangjun Lu3, Weiqun Gan1,6, and Zongjun Ning1,6
2021 ApJ 921 179
https://iopscience.iop.org/article/10.3847/1538-4357/ac1c05/pdf
https://doi.org/10.3847/1538-4357/ac1c05
Quasi-periodic pulsations (QPPs), which usually appear as temporal pulsations of the total flux, are frequently detected in the light curves of solar/stellar flares. In this study, we present the investigation of nonstationary QPPs with multiple periods during the impulsive phase of a powerful flare on **2017 September 6**, which were simultaneously measured by the Hard X-ray Modulation Telescope (Insight-HXMT), as well as the ground-based BLENSW. The multiple periods, detected by applying a wavelet transform and Lomb–Scargle periodogram to the detrended light curves, are found to be ∼20–55 s in the Lyα and mid-ultraviolet Balmer continuum emissions during the flare impulsive phase. Similar QPPs with multiple periods are also found in the hard X-ray emission and low-frequency radio emission. Our observations suggest that the flare QPPs could be related to nonthermal electrons accelerated by the repeated energy release process, i.e., triggering of repetitive magnetic reconnection, while the multiple periods might be modulated by the sausage oscillation of hot plasma loops. For the multiperiodic pulsations, other generation mechanisms could not be completely ruled out.

Magnetic Flux and Magnetic Non-potentiality of Active Regions in Eruptive and Confined Solar Flares

Ting **Li**, Anqin Chen, Yijun Hou, Astrid M. Veronig, Shuhong Yang, Jun Zhang
ApJ Letters **917** L29 **2021**
https://arxiv.org/pdf/2108.01299.pdf
https://iopscience.iop.org/article/10.3847/2041-8213/ac1a15/pdf
https://doi.org/10.3847/2041-8213/ac1a15
With the aim of understanding how the magnetic properties of active regions (ARs) control the eruptive character of solar flares, we analyze 719 flares of Geostationary Operational Environmental Satellite (GOES) class ≥C5.0 during 2010−2019. We carry out the first statistical study that investigates the flare-coronal mass ejections (CMEs) association rate as function of the flare intensity and the AR characteristics that produces the flare, in terms of its total unsigned magnetic flux (ΦAR). Our results show that the slope of the flare-CME association rate with flare intensity reveals a steep monotonic decrease with ΦAR. This means that flares of the same GOES class but originating from an AR of larger ΦAR, are much more likely confined. Based on an AR flux as high as 1.0×1024 Mx for solar-type stars, we estimate that the CME association rate in X100-class ``superflares" is no more than 50\%. For a sample of 132 flares ≥M2.0 class, we measure three non-potential parameters including the length of steep gradient polarity inversion line (LSGPIL), the total photospheric free magnetic energy (Efree) and the area with large shear angle (AΨ). We find that confined flares tend to have larger values of LSGPIL, Efree and AΨ compared to eruptive flares. Each non-potential parameter shows a moderate positive correlation with ΦAR. Our results imply that ΦAR is a decisive quantity describing the eruptive character of a flare, as it provides a global parameter relating to the strength of the background field confinement. **2011 February 15**
RHESSI Nuggets #414 **2021** https://sprg.ssl.berkeley.edu/~tohban/wiki/index.php/Confined_or_Eruptive%3F

Thermodynamic Evolution of Solar Flare Supra-arcade Downflows

Z. F. **Li**1,2, X. Cheng1,2,3, M. D. Ding1,2, Katharine K. Reeves4, DeOndre Kittrell4,5, Mark Weber4, and David E. McKenzie6

2021 ApJ 915 124
https://arxiv.org/pdf/2107.09215.pdf
https://iopscience.iop.org/article/10.3847/1538-4357/ac043e/pdf
https://doi.org/10.3847/1538-4357/ac043e
Solar flares are rapid energy release phenomena that appear as bright ribbons in the chromosphere and high temperature loops in the corona, respectively. Supra-arcade Downflows (SADs) are plasma voids that first come out above the flare loops and then move quickly toward the flare loop top during the decay phase of the flare. In our work, we study 20 SADs appearing in three flares. By differential emission measure (DEM) analysis, we calculate the DEM weighted average temperature and emission measure of the front region and the main body of SADs. It is found that the temperatures of the SAD front and body tend to increase during the course of SADs flowing downwards. The relationship between the pressure and temperature fits well with the adiabatic equation for both the SAD front and body, suggesting that the heating of SADs is mainly caused by adiabatic compression. Moreover, we also estimate the velocities of SADs via the Fourier Local Correlation Tracking method and find that increase of the temperature of the SAD front presents a correlation with the decrease of the SAD kinetic energy, while the SAD body does not, implying that the viscous process may also heat the SAD front in spite of a limited role. **2011.10.22, 2012.07.17, 2015.06.18**

The Acceleration of Charged Particles and Formation of Power-law Energy Spectra in Nonrelativistic Magnetic Reconnection

Xiaocan **Li**, Fan Guo, Yi-Hsin Liu
Physics of Plasmas **2021**
https://arxiv.org/pdf/2104.10732.pdf
Magnetic reconnection is a primary driver of particle acceleration processes in space and astrophysical plasmas. Understanding how particles are accelerated and the resulting particle energy spectra is among the central topics in reconnection studies. We review recent advances in addressing this problem in nonrelativistic reconnection that is relevant to space and solar plasmas and beyond. We focus on particle acceleration mechanisms, particle transport due to 3D reconnection physics, and their roles in forming power-law particle energy spectra. We conclude by pointing out the challenges in studying particle acceleration and transport in a large-scale reconnection layer and the relevant issues to be addressed in the future.

Three-dimensional magnetic reconnection in astrophysical plasmas **Review**

Ting **Li**, Eric Priest, Ruilong Guo
Proceedings of The Royal Society A **2021**
https://arxiv.org/pdf/2104.05174.pdf
Magnetic reconnection is a fundamental process in a laboratory, magnetospheric, solar and astrophysical plasma, whereby magnetic energy is converted into heat, bulk kinetic energy and fast particle energy. Its nature in two dimensions is much better understood than in three dimensions (3D), where its character is completely different and has many diverse aspects that are currently being explored. Here we focus on the magnetohydrodynamics of 3D reconnection in the plasma environment of the solar system, especially solar flares.
The theory of reconnection at null points, separators and quasi-separators is described, together with accounts of numerical simulations and observations of these three types of reconnection. The distinction between separator and quasi-separator reconnection is a theoretical one that is unimportant for the observations of energy release. A new paradigm for solar flares, in which 3D reconnection plays a central role, is proposed.

Methodology for In-flight Flat-field Calibration of the Lyman-alpha Solar Telescope (LST)

Jing-Wei **Li**, Hui Li, Ying Li, Li Feng, Yu Huang, Jie Zhao, Lei Lu, Bei-Li Ying, Jian-Chao Xue
Research in Astron. Astrophys. **2020**
https://arxiv.org/ftp/arxiv/papers/2012/2012.10110.pdf
Flat-field reflects the non-uniformity of the photometric response at the focal plane of an instrument, which uses digital image sensors, such as Charge Coupled Device (CCD) and Complementary Metal-Oxide-Semiconductor (CMOS). This non-uniformity must corrected before being used for scientific research. In this paper, we assess various candidate methods via simulation using available data so as to figure the in-flight flat-field calibration methodology for the Lyman-alpha Solar Telescope (LST). LST is one of the payloads for the Advanced Space-based Solar Observatory (ASO-S) mission and consists of three instruments: a White-light Solar Telescope (WST), a Solar Disk Imager (SDI) and a dual-waveband Solar Corona Imager (SCI). In our simulations, data from the Helioseismic and Magnetic Imager (HMI) and Atmospheric Imaging Assembly (AIA) onboard the Solar Dynamics Observatory (SDO) mission are used. Our results show that the normal KLL method is appropriate for in-flight flat-field calibration of WST and implementing a transmissive diffuser is applicable for SCI. For the in-flight flat-field calibration of SDI, we recommend the KLL method with off-pointing images with defocused resolution of around 18", and use the local correlation tracking (LCT) algorithm instead of limb-fitting to determine the relative dis-placements between different images.

Relation of Coronal Rain Originating from Coronal Condensations to Interchange Magnetic Reconnection

Leping **Li**1,2,3, Hardi Peter4, Lakshmi Pradeep Chitta4, and Hongqiang Song2
2020 ApJ 905 26
https://doi.org/10.3847/1538-4357/abc68c
Using extreme-ultraviolet images, we recently proposed a new and alternative formation mechanism for coronal rain along magnetically open field lines due to interchange magnetic reconnection. In this paper we report coronal rain at chromospheric and transition region temperatures originating from the coronal condensations facilitated by reconnection between open and closed coronal loops. For this, we employ the Interface Region Imaging Spectrograph (IRIS) and the Atmospheric Imaging Assembly (AIA) of the Solar Dynamics Observatory. Around **2013 October 19**, a coronal rain along curved paths was recorded by IRIS over the southeastern solar limb. Related to this, we found reconnection between a system of higher-lying open features and lower-lying closed loops that occurs repeatedly in AIA images. In this process, the higher-lying features form magnetic dips. In response, two sets of newly reconnected loops appear and retract away from the reconnection region. In the dips, seven events of cooling and condensation of coronal plasma repeatedly occur due to thermal instability over several days, from October 18 to 20. The condensations flow downward to the surface as coronal rain, with a mean interval between condensations of ~6.6 hr. In the cases where IRIS data were available we found the condensations to cool all the way down to chromospheric temperatures. Based on our observations we suggest that some of the coronal rain events observed at chromospheric temperatures could be explained by the new and alternative scenario for the formation of coronal rain, where the condensation is facilitated by interchange reconnection.

Large-scale particle acceleration during magnetic reconnection in solar flares

Xiaocan **Li**
Fleishman's Solar Physics Webinar 21-Aug-**2020**
https://youtu.be/Zga7ptZJWGI

An investigation of flare emissions at multiple wavelengths

Dong **Li**, Alexander Warmuth, Lei Lu, Zongjun Ning
Research in Astron. Astrophys (RAA) **2020**
https://arxiv.org/pdf/2009.04741.pdf
We report multi-wavelength observations of four solar flares on **2014 July 07**. We firstly select these flares according to the soft X-ray (SXR) and extreme ultraviolet (EUV) emissions recorded by the Extreme Ultraviolet Variability Experiment and Geostationary Orbiting Environmental Satellites. Then their locations and geometries are identified from the full-disk images measured by the Atmospheric Imaging Assembly (AIA), and the time delays among the light curves in different channels are identified. The electron number densities are estimated using the Differential Emission Measure method. We find that three of four flares show strong emissions in SXR channels and high temperature (>6 MK) EUV wavelengths during the impulsive phase, i.e., AIA 131 A and 94 A, and then they emit peak radiation subsequently in the middle temperature (~0.6-3 MK) EUV channels. Moreover, they last for a long time and have smaller electron densities, which are probably driven by the interaction of hot diffuse flare loops. Only one flare emits radiation at almost the same time in all the observed wavelengths, lasts for a relatively short time, and has a larger electron density. It is also accompanied by a type III radio burst. The bright emission at the EUV channel could be corresponding to the associated erupting filament.

Magnetic Flux of Active Regions Determining the Eruptive Character of Large Solar Flares

Ting **Li**, Yijun Hou, Shuhong Yang, Jun Zhang, Lijuan Liu, Astrid M. Veronig
ApJ **900** 128 **2020**
https://arxiv.org/pdf/2007.08127.pdf
https://doi.org/10.3847/1538-4357/aba6ef
We establish the largest eruptive/confined flare database to date and analyze 322 flares of \emph{GOES} class M1.0 and larger that occurred during 2010−2019, i.e., almost spanning the entire solar cycle 24. We find that the total unsigned magnetic flux (ΦAR) of active regions (ARs) is a key parameter in governing the eruptive character of large flares, with the proportion of eruptive flares exhibiting a strong anti-correlation with ΦAR. This means that an AR containing a large magnetic flux has a lower probability for the large flares it produces to be associated with a coronal mass ejection (CME). This finding is supported by the high positive correlation we obtained between the critical decay index height and ΦAR, implying that ARs with a larger ΦAR have a stronger magnetic confinement. Moreover, the confined flares originating from ARs larger than 1.0×1023 Mx have several characteristics in common: stable filament, slipping magnetic reconnection and strongly sheared post-flare loops. Our findings reveal new relations between the magnetic flux of ARs and the occurrence of CMEs in association with large flares. These relations obtained here provide quantitative criteria for forecasting CMEs and adverse space weather, and have also important implications for "superflares" on solar-type stars and stellar CMEs. **2011-10-02, 06 March 2012, 2012-07-10, 2014-10-22, 2014-10-24, 2014-12-19**

Preflare very long-periodic pulsations observed in Halpha emission before the onset of a solar flare

Dong **Li**, Song Feng, Wei Su, Yu Huang
A&A Lett 639, L5 **2020**
https://www.aanda.org/articles/aa/pdf/2020/07/aa38398-20.pdf

The very long-periodic pulsations during preflare phases (preflare-VLPs) were detected in the full-disk solar soft X-Ray (SXR) flux (see, Tan et al. 2016). They might be regarded as the precursors of solar flares, and could help us to well understand the trigger mechanism of solar flares. In this letter, we report a preflare-VLP event before the onset of an M1.1 circular-ribbon flare on **2015 October 16**. It was simultaneously observed in Halpha, SXR, and Extreme ultraviolet (EUV) wavelengths, which were recorded by the NVST, GOES, EVE, and AIA respectively. The preflare-VLP is identified as the repeat and quasi-periodic pulses in light curves during preflare phase, which might be modulated by LRC-circuit oscillation in the current-carrying plasma loop. The quasi-periodicity can be determined from the Fourier power spectrum with Markov chain Monte Carlo (MCMC)-based Bayesian (e.g., Liang et al. 2020), such as ~9.3 minutes. We firstly report a preflare-VLP event in the local Halpha line and EUV wavelength, which could be considered as the precursor of a solar flare. Therefore, it should be useful for the prediction of solar flares, especially for a powerful flare.

Large-scale particle acceleration during magnetic reconnection in solar flares

Xiaocan **Li** and Fan Guo
EGU2020-1959 May **2020**
https://meetingorganizer.copernicus.org/EGU2020/displays/36057

Magnetic reconnection is a primary driver of magnetic energy release and particle acceleration processes in space and astrophysical plasmas. Solar flares are a great example where observations have suggested that a large fraction of magnetic energy is converted into nonthermal particles and radiation. One of the major unsolved problems in reconnection studies is nonthermal particle acceleration. In the past decade or two, 2D kinetic simulations have been widely used and have identified several acceleration mechanisms in reconnection. Recent 3D simulations have shown that the reconnection layer naturally generates magnetic turbulence. Here we report our recent progresses in building a macroscopic model that includes these physics for explaining particle acceleration during solar flares. We show that, for sufficient large systems, high-energy particle acceleration processes can be well described as flow compression and shear. By means of 3D kinetic simulations, we found that the self-generated turbulence is essential for the formation of power-law electron energy spectrum in non-relativistic reconnection. Based on these results, we then proceed to solve an energetic particle transport equation in a compressible reconnection layer provided by high-Lundquist-number MHD simulations. Due to the compression effect, particles are accelerated to high energies and develop power-law energy distributions. The power-law index and maximum energy are both comparable to solar flare observations. This study clarifies the nature of particle acceleration in large-scale reconnection sites and initializes a framework for studying large-scale particle acceleration during solar flares.

Fleishman's webinar 21 Aug **2020**
https://youtu.be/Zga7ptZJWGI

Observations of a quasi-periodic pulsation in the coronal loop and microwave flux during a solar preflare phase

Dong **Li**, Ying Li, Lei Lu, Qingmin Zhang, Zongjun Ning, Sergey Anfinogentov
ApJL **2020**
https://arxiv.org/pdf/2003.09567.pdf

We report a quasi-periodic pulsation (QPP) event simultaneously detected from the spatial displacements of coronal loop at both EUV images and microwave emission during the preflare phase of a C1.1 flare on **2016 March 23**. Using the motion magnification technique, a low-amplitude transverse oscillation with the growing period is discovered in a diffuse coronal loop in Atmospheric Imaging Assembly (AIA) image sequences at wavelength of 171 A, and the initial oscillation period is estimated to be ~397 s with a slow growth rate of 0.045. At the same time, a QPP with growing periods from roughly 300 s to nearly 500 s is discovered in the microwave flux in the same active region. Based on the imaging observations measured at EUV wavelengths by the AIA and at microwave 17 GHz by Nobeyama Radioheliograph, the diffuse coronal loop and the microwave radiation source are found to be connected through a hot loop seen in AIA images at wavelength of 94 A. The growing period of the QPP should be related to the modulation of LRC-circuit oscillating process in a current-carrying plasma loop. The existence of electric currents may imply the non-potentialities in the source region during the preflare phase.

Quasi-periodic pulsation detected in Lyman-alpha emission during solar flares

Dong **Li**, Lei Lu, Zongjun Ning, Li Feng, Weiqun Gan, Hui Li
ApJ **893** 7 **2020**

https://arxiv.org/pdf/2003.01877.pdf
https://doi.org/10.3847/1538-4357/ab7cd1
We investigated the quasi-periodic pulsation (QPP) in Lyman-alpha, X-ray and extreme-ultraviolet (EUV) emissions during two solar flares, i.e., an X-class (**SOL2012-01-27T**) and a C-class (**SOL2016-02-08T**). The full-disk Lyman-alpha and X-Ray flux during these solar flares were recorded by the EUV Sensor and X-Ray Sensor on board the Geostationary Operational Environmental Satellite. The flare regions were located from the EUV images measured by the Atmospheric Imaging Assembly. The QPP could be identified as a series of regular and periodic peaks in the light curves, and its quasi-periodicity was determined from the global wavelet and Fourier power spectra. A quasi-periodicity at about 3 minutes is detected during the impulsive phase of the X-class flare, which could be explained as the acoustic wave in the chromosphere (e.g., Milligan et al. 2017). Interestingly, a quasi-periodicity at roughly 1 minute is discovered during the entire evolutionary phases of solar flares, including the precursor, impulsive, and gradual phases. This is the first report of 1-minute QPP in the Lyman-alpha emission during solar flares, in particular during the flare precursor. It may be interpreted as a self-oscillatory regime of the magnetic reconnection, such as magnetic dripping.

Predicting Solar Flares Using a Novel Deep Convolutional Neural Network

Xuebao **Li**, Yanfang Zheng, Xinshuo Wang, and Lulu Wang
Astrophysical Journal, 891:10 (11pp), **2020**
https://iopscience.iop.org/article/10.3847/1538-4357/ab6d04/pdf
Space weather forecasting is very important, and the prediction of space weather, especially for solar flares, has increasingly attracted research interests with the numerous recent breakthroughs in machine learning. In this study, we propose a novel convolutional neural network (CNN) model to make binary class prediction for both ≥C-class and ≥M-class flares within 24 hr. We collect magnetogram samples of solar active regions (ARs) provided by the Space-weather Helioseismic and Magnetic Imager Active Region Patches (SHARP) data from 2010 May to 2018 September. These samples are used to construct 10 separate data sets. Then, after training, validating, and testing our model, we compare the results of our model with previous studies in several metrics, with a focus on the true skill statistic (TSS). The major results are summarized as follows. (1) We propose a method of shuffle and split cross-validation (CV) based on AR segregation, which is the first attempt to verify the validity and stability of the model in flare prediction. (2) The proposed CNN model achieves a relatively high score of TSS = 0.749 ± 0.079 for ≥M-class prediction, and TSS = 0.679 ± 0.045 for ≥C-class prediction, which is greatly improved compared with previous studies. (3) The model trained on 10 CV data sets is considerably robust and stable in making flare prediction for both ≥C class and ≥M class. Our experimental results indicate that our proposed CNN model is a highly effective method for flare forecasting, with quite excellent prediction performance.

Quasi-periodic pulsations of gamma-ray emissions from a solar flare on 2017 September 06

D. **Li**, D. Y. Kolotkov, V. M. Nakariakov, L. Lu, Z. J. Ning
ApJ **888** 53 **2019**
https://arxiv.org/pdf/1912.01145.pdf
https://doi.org/10.3847/1538-4357/ab5e86
We investigate quasi-periodic pulsations (QPPs) of high-energy nonthermal emissions from an X9.3 flare (SOL2017-Sep-06T11:53), the most powerful flare since the beginning of solar cycle 24. The QPPs are identified as a series of regular and repeating peaks in the light curves in the gamma- and hard X-ray (HXR) channels recorded by the Konus-Wind, as well as the radio and microwave fluxes measured by the CALLISTO radio spectrograph during the impulsive phase. The periods are determined from the global wavelet and Fourier power spectra, as 24-30 s in the HXR and microwave channels which are associated with nonthermal electrons, and ~20 s in the gamma-ray band related to nonthermal ions. Both nonthermal electrons and ions may be accelerated by repetitive magnetic reconnection during the impulsive phase. However, we could not rule out other mechanisms such as the MHD oscillation in a sausage mode. The QPP detected in this study is useful for understanding the particle acceleration and dynamic process in solar flares and also bridging the gap between stellar and solar flares since the energy realm of the X9.3 solar flare is almost compared with a typical stellar flare.

Formation of Power-law Electron Energy Spectra in Three-dimensional Low-β Magnetic Reconnection

Xiaocan **Li**, Fan Guo, Hui Li, Adam Stanier, Patrick Kilian
ApJ **884** 118 **2019**
https://arxiv.org/pdf/1909.01911.pdf
https://doi.org/10.3847/1538-4357/ab4268
While observations have suggested that power-law electron energy spectra are a common outcome of strong energy release during magnetic reconnection, e.g., in solar flares, kinetic simulations have not been able to provide definite evidence of power-laws in energy spectra of non-relativistic reconnection. By means of 3D large-scale fully kinetic simulations, we study the formation of power-law electron energy spectra in non-relativistic low-β reconnection. We find that both the global spectrum integrated over the entire domain and local spectra within individual regions of the

reconnection layer have power-law tails with a spectral index p∼4 in the 3D simulation, which persist throughout the non-linear reconnection phase until saturation. In contrast, the spectrum in the 2D simulation rapidly evolves and quickly becomes soft. We show that 3D effects such as self-generated turbulence and chaotic magnetic field lines enable the transport of high-energy electrons across the reconnection layer and allow them to access several main acceleration regions. This leads to a sustained and nearly constant acceleration rate for electrons at different energies. We construct a model that explains the observed power-law spectral index in terms of the dynamical balance between particle acceleration and escape from main acceleration regions, which are defined based upon a threshold for the curvature drift acceleration term. This result could be important for explaining the formation of power-law energy spectrum in solar flares.

A Longitudinally Asymmetrical Kink Oscillation of Coronal Loop Caused by a Diagonally Placed Flare below the Loop System

Hongbo **Li**1, Hengqiang Feng1,2, Yu Liu3, Zhanjun Tian1, Jin Huang3,4, and Yuhu Miao
2019 ApJ 881 111
sci-hub.se/10.3847/1538-4357/ab2bf7
Although fast kink oscillations of coronal loops have been extensively studied for decades, details about their excitation, evolution, and damping remain elusive. Here, we present, for the first time, a longitudinally asymmetrical fast kink oscillation of a coronal loop that is excited by a GOES C-class flare located diagonally below the loop system. In this case, a damping-like phase and a growing-like phase are successively observed after the flare in different loop segments that are far from and close to the flare site, respectively. The investigation provides us with a new and valuable clue for the widely observed distinct deviations of fast kink oscillations from the sinusoidal pattern, especially for the local damping-like or growing-like phases associated with diagonally placed excitation sources, by illuminating a probable effect of the diagonally placed excitation source. **2015 June 18**

Two Types of Solar Confined Flares

Ting **Li**, Lijuan Liu, Yijun Hou, Jun Zhang
ApJS **881** 151 **2019**
https://arxiv.org/pdf/1907.04510.pdf **File**
https://doi.org/10.3847/1538-4357/ab3121
With the aim of understanding the physical mechanisms of confined flares, we selected 18 confined flares during 2011-2017, and classified the confined flares into two types based on their different dynamic properties and magnetic configurations. "Type I" of confined flares are characterized by slipping reconnection, strong shear, and stable filament. "Type II" flares have nearly no slipping reconnection, and have a configuration in potential state after the flare. Filament erupts but is confined by strong strapping field. "Type II" flares could be explained by 2D MHD models while "type I" flares need 3D MHD models. 7 flares of 18 (∼39 \%) belong to "type I" and 11 (∼61 \%) are "type II" confined flares. The post-flare loops (PFLs) of "type I" flares have a stronger non-potentiality, however, the PFLs in "type II" flares are weakly sheared. All the "type I" flares exhibit the ribbon elongations parallel to the polarity inversion line (PIL) at speeds of several tens of km s−1. For "type II" flares, only a small proportion shows the ribbon elongations along the PIL. We suggest that different magnetic topologies and reconnection scenarios dictate the distinct properties for the two types of flares. Slipping agnetic reconnections between multiple magnetic systems result in "type I" flares. For "type II" flares, magnetic reconnections occur in anti-parallel magnetic fields underlying the erupting filament. Our study shows that "type I" flares account for more than one third of the overall large confined flares, which should not be neglected in further studies. **2011 March 09, 2012 July 04, 2014 October 26,**
Table 1: Event list

Different Signatures of Chromospheric Evaporation in Two Solar Flares Observed with IRIS

Y. **Li**1,2, M. D. Ding3, J. Hong3, H. Li1, and W. Q. Gan1
2019 ApJ 879 30
https://iopscience.iop.org/article/10.3847/1538-4357/ab245a/pdf
We present different signatures of chromospheric evaporation in two solar flares observed by the Interface Region Imaging Spectrograph (IRIS). In the B1.6 flare on **2016 December 6** (SOL2016-12-06T10:40), the transition region Si iv line and the chromospheric C ii and Mg ii lines show blueshifts with low velocities up to 20 km s−1 at the flare loop footpoints in the rise phase, indicative of a gentle chromospheric evaporation. While in the C1.6 flare on **2015 December 19** (SOL2015-12-19T10:51), the Si iv, C ii, and Mg ii lines exhibit redshifts with velocities from several to tens of km s−1 at the footpoints, which might suggest an explosive chromospheric evaporation. Explosive evaporation has been observed in many flares that were captured by IRIS; however, gentle evaporation, especially manifested as blueshifts in the cool Si iv, C ii, and Mg ii lines, has scarcely been reported. Our results bring some new insights into chromospheric evaporation in the IRIS era.

Three-dimensional Magnetic Reconnection Triggering an X-class Confined Flare in Active Region 12192

Ting **Li**, Yijun Hou, Shuhong Yang, Jun Zhang
ApJ **2018**
https://arxiv.org/pdf/1811.03302.pdf
http://iopscience.iop.org/article/10.3847/1538-4357/aaefee/pdf
We present an extensive analysis of the X2.0-class confined flare on **2014 October 27** in the great active region AR 12192, observed by the \emph{Interface Region Imaging Spectrograph} and the \emph{Solar Dynamics Observatory}. The slipping motion of the substructures within the negative-polarity flare ribbon (R1) and continual reconnection-induced flows during the confined flare are first presented. The substructures within ribbon R1 were observed to slip in opposite directions at apparent speeds of 10-70 km s−1. The slipping motion exhibited the quasi-periodic pattern with a period of 80-110 s, which can be observed since the flare start and throughout the impulsive phase of the flare. Simultaneously quasi-periodic flows moved along a reverse-S shaped filament, with an average period of about 90 s. The period of reconnection-induced flows is similar to that of the slippage of ribbon substructures, implying the occurrence of quasi-periodic slipping magnetic reconnection. The spectral observations showed that the Si {\sc iv} line was blueshifted by 50-240 km s−1 at the location of the flows. During the process of the flare, the filament did not show the rise phase and was not associated with any failed eruption. The flare mainly consisted of two sets of magnetic systems, with both of their east ends anchoring in ribbon R1. We suggest that the slipping magnetic reconnection between two magnetic systems triggers the confined flare.

Solar jet-like features rooted on flare ribbons

Xiaohong **Li**, Jun Zhang, Shuhong Yang, Yijun Hou
Publications of the Astronomical Society of Japan 71, Issue 1, 1 January **2019**, 14
https://arxiv.org/pdf/1811.00281.pdf
Employing the high spatio-temporal Interface Region Imaging Spectrograph 1330 Å observations, we investigated the jet-like features that occurred during the X8.2 class flare in NOAA active region (AR) 12673 on **2017 September 10**. These jet-like features were rooted on the flare ribbons. We examined 15 features, and the mean values of the lifetimes, projected widths, lengths and velocities of these features were 87 s, 890 km, 2.7 Mm and 70 km s−1, respectively. We also observed many jet-like features which happened during the X1.0 class flare on **2014 October 25**. We studied the spectra at the base of a jet-like feature during its development. The Fe XXI 1354.08 Å line in the corona displays blueshift, while the Si IV 1402.77 Å line in the transition region exhibits redshift, which indicates the chromospheric evaporation. This is the first time that the jet-like features are reported to be rooted on the flare ribbons, and we suggest that these jet-like features were driven by the mechanism of chromospheric evaporation.

The Effect of Magnetic and Density Differences on the Fast Kink Oscillations of Neighboring Coronal Loops

Hongbo **Li**, Yu Liu
Solar Physics July **2018**, 293:105
http://sci-hub.tw/http://link.springer.com/10.1007/s11207-018-1327-0
It is reasonable that neighboring coronal loops may obtain similar momentum during a flare. The fast kink oscillations (FKOs) between them are thus mainly influenced by their physical differences. We discuss the dependencies of FKO on the physical properties of coronal loops in a low-β thin-tube approximation. From the analysis, we obtain the analytic relationship between the density [ρiρi] and magnetic field [B] of loops and the corresponding period [τ] and amplitude [A] of FKO, which may provide us with a powerful tool to diagnose the physical differences between neighboring loops.

Large-scale Compression Acceleration during Magnetic Reconnection in a Low-β Plasma

Xiaocan **Li**, Fan Guo, Hui Li, Shengtai Li
ApJ **866** 4 **2018**
https://arxiv.org/pdf/1807.03427.pdf
http://iopscience.iop.org/article/10.3847/1538-4357/aae07b/pdf
In solar flares and other astrophysical systems, a major challenge for solving particle acceleration problem associated with magnetic reconnection is the enormous scale separation between kinetic scales and observed reconnection scale. Because of this, it has been difficult to draw any definite conclusions by just using kinetic simulations. Particle acceleration model that solves energetic particle transport equation can capture the main acceleration physics found in kinetic simulations, and thus provide a practical way to make observable predictions and directly compare model results with observations. Here we study compression particle acceleration in magnetic reconnection by solving Parker (diffusion-advection) transport equation using velocity and magnetic fields from two-dimensional high-Lundquist-number magnetohydrodynamics (MHD) simulations of a low-β reconnection layer. We show that the compressible reconnection layer can give significant particle acceleration, leading to the formation of power-law particle energy distributions. We analyze the acceleration rate and find that the acceleration in the reconnection layer is a mixture of first order and second order Fermi processes. When including a guide field, we find the spectrum becomes steeper and

both the power-law cutoff energy and maximum particle energy decrease as plasma becomes less compressible. This model produces 2D particle distribution that one can use to generate radiation map and directly compare with solar flare observations. This provides a framework to explain particle acceleration at large-scale astrophysical reconnection sites, such as solar flares.

Non-damping oscillations at flaring loops

D. **Li**, D. Yuan, Y. N. Su, Q. M. Zhang, W. Su, Z. J. Ning
A&A 617, A86 **2018**
https://arxiv.org/pdf/1806.03573.pdf
Context. QPPs are usually detected as spatial displacements of coronal loops in imaging observations or as periodic shifts of line properties in spectroscopic observations. They are often applied for remote diagnostics of magnetic fields and plasma properties on the Sun.
Aims. We combine imaging and spectroscopic measurements of available space missions, and investigate the properties of non-damping oscillations at flaring loops.
Methods. We used the IRIS to measure the spectrum over a narrow slit. The double-component Gaussian fitting method was used to extract the line profile of Fe XXI 1354.08 A at "O I" window. The quasi-periodicity of loop oscillations were identified in the Fourier and wavelet spectra.
Results. A periodicity at about 40 s is detected in the line properties of Fe XXI, HXR emissions in GOES 1-8 A derivative, and Fermi 26-50 keV. The Doppler velocity and line width oscillate in phase, while a phase shift of about Pi/2 is detected between the Doppler velocity and peak intensity. The amplitudes of Doppler velocity and line width oscillation are about 2.2 km/s and 1.9 km/s, respectively, while peak intensity oscillate with amplitude at about 3.6% of the background emission. Meanwhile, a quasi-period of about 155 s is identified in the Doppler velocity and peak intensity of Fe XXI, and AIA 131 A intensity.
Conclusions. The oscillations at about 40 s are not damped significantly during the observation, it might be linked to the global kink modes of flaring loops. The periodicity at about 155 s is most likely a signature of recurring downflows after chromospheric evaporation along flaring loops. The magnetic field strengths of the flaring loops are estimated to be about 120-170 G using the MHD seismology diagnostics, which are consistent with the magnetic field modeling results using the flux rope insertion method. **6 Sept 2014**

Two Episodes of Magnetic Reconnections During a Confined Circular-ribbon Flare

Ting **Li**, Shuhong Yang, Qingmin Zhang, Yijun Hou, Jun Zhang
ApJ **859** 122 **2018**
https://arxiv.org/pdf/1804.05458.pdf
We analyze a unique event with an M1.8 confined circular-ribbon flare on **2016 February 13**, with successive formations of two circular ribbons at the same location. The flare had two distinct phases of UV and EUV emissions with an interval of about 270 s, of which the second peak was energetically more important. The first episode was accompanied by the eruption of a mini-filament and the fast elongation motion of a thin circular ribbon (CR1) along the counterclockwise direction at a speed of about 220 km/s. Two elongated spine-related ribbons were also observed, with the inner ribbon co-temporal with CR1 and the remote brightenings forming ~20 s later. In the second episode, another mini-filament erupted and formed a blowout jet. The second circular ribbon and two spine-related ribbons showed similar elongation motions with that during the first episode. The extrapolated 3D coronal magnetic fields reveal the existence of a fan-spine topology, together with a quasi-separatrix layer (QSL) halo surrounding the fan plane and another QSL structure outlining the inner spine. We suggest that continuous null-point reconnection between the filament and ambient open field occurs in each episode, leading to the sequential opening of the filament and significant shifts of the fan plane footprint. For the first time, we propose a compound eruption model of circular-ribbon flares consisting of two sets of successively formed ribbons and eruptions of multiple filaments in a fan-spine-type magnetic configuration.

The surge-like eruption of a miniature filament associated with circular flare ribbon

Haidong **Li**, Jiayan Yang, Yunchun Jiang, Yi Bi, Zhining Qu, Hechao Chen
Astrophysics and Space Science February **2018**, 363:26
http://sci-hub.tw/10.1007/s10509-017-3244-3
We present a study of a mini-filament erupting in association with a circular ribbon flare observed by NVST and SDO/AIA on **2014 March 17**. The filament was located at one footpoint region of a large loops. The potential field extrapolation shows that it was embedded under a magnetic null point configuration. First, we observed a brightening of the filament at the corresponding EUV images, close to one end of the filament. With time evolution, a circular flare ribbon was observed around the filament at the onset of the eruption, which is regarded as a signature of reconnection at the null point. After the filament activation, its eruption took the form of a surge, which ejected along one end of a large-scale closed coronal loops with a curtain-like shape. We conjecture that the null point reconnection may facilitate the eruption of the filament.

Observations of Electron-driven Evaporation during a Flare Precursor

Dong **Li**, Ying Li, Wei Su, Yu Huang, Zongjun Ning

ApJ **854** 26 **2018**

https://arxiv.org/pdf/1801.06755.pdf

http://sci-hub.tw/http://iopscience.iop.org/0004-637X/854/1/26/

We investigate the relationship between the blue shifts of a hot emission line and the nonthermal emissions in microwave and hard X-ray (HXR) wavelengths during the precursor of a solar flare on **2014 October 27**. The flare precursor is identified as a small but well-developed peak in soft X-ray and extreme-ultraviolet passbands before the GOES flare onset, which is accompanied by a pronounced burst in microwave 17 & 34 GHz and HXR 25-50 keV. The slit of Interface Region Imaging Spectrograph (IRIS) stays at one ribbon-like transient during the flare precursor, where shows visible nonthermal emissions in NoRH and RHESSI images. The IRIS spectroscopic observations show that the hot line of Fe XXI 1354.09 A (logT ~ 7.05) displays blue shifts, while the cool line of Si IV 1402.77 A (logT ~ 4.8) exhibits red shifts. The blue shifts and red shifts are well correlated to each other, indicative of an explosive chromospheric evaporation during the flare precursor particularly combining with a high nonthermal energy flux and a short characteristic timescale. In addition, the blue shifts of Fe XXI 1354.09 A are well correlated with the microwave and HXR emissions, implying that the explosive chromospheric evaporation during the flare precursor is driven by nonthermal electrons.

Spectroscopic Observations of a Current Sheet in a Solar Flare

Y. **Li**, J. C. Xue, M. D. Ding, X. Cheng, Y. Su, L. Feng, J. Hong, H. Li, W. Q. Gan

ApJ L **853** L15 **2018**

https://arxiv.org/pdf/1801.03631.pdf

https://iopscience.iop.org/article/10.3847/2041-8213/aaa6c0/pdf

Current sheet is believed to be the region of energy dissipation via magnetic reconnection in solar flares. However, its properties, for example, the dynamic process, have not been fully understood. Here we report a current sheet in a solar flare (SOL**2017-09-10**T16:06) that was clearly observed by the Atmospheric Imaging Assembly on board the Solar Dynamics Observatory as well as the EUV Imaging Spectrometer on Hinode. The high-resolution imaging and spectroscopic observations show that the current sheet is mainly visible in high temperature (>10 MK) passbands, particularly in the Fe XXIV 192.03 line with a formation temperature of ~18 MK. The hot Fe XXIV 192.03 line exhibits very large nonthermal velocities up to 200 km/s in the current sheet, suggesting that turbulent motions exist there. The largest turbulent velocity occurs at the edge of the current sheet, with some offset with the strongest line intensity. At the central part of the current sheet, the turbulent velocity is negatively correlated with the line intensity. From the line emission and turbulent features we obtain a thickness in the range of 7--11 Mm for the current sheet. These results suggest that the current sheet has internal fine and dynamic structures that may help the magnetic reconnection within it proceeds efficiently.

Doppler shift oscillations from a hot line observed by IRIS

Dong **Li**, Zongjun Ning, Yu Huang, N.-H. Chen, Qingmin Zhang, Yingna Su, Wei Su

ApJ **849** 113 **2017**

https://arxiv.org/pdf/1709.10059.pdf

We present a detailed investigation of the Doppler shift oscillations in a hot loop during an M1.7 flare on **2014 October 27** observed by the Interface Region Imaging Spectrograph. The periodic oscillations are observed in the Doppler shift of Fe XXI 1354.09 A (logT~7.05), and the dominant period is about 3.1 minutes. However, such 3.1-min oscillations are not found in the line-integrated intensity of Fe XXI 1354.09 A, AIA EUV fluxes, or microwave emissions. SDO/AIA and Hinode/XRT imaging observations indicate that the Doppler shift oscillations locate at the hot loop-top region (> 11MK). Moreover, the differential emission measure (DEM) results show that the temperature is increasing rapidly when the Doppler shift oscillates, but the number density does not exhibit the corresponding increases nor oscillations, implying that the flare loop is likely to oscillate in an incompressible mode. All these facts suggest that the Doppler shift oscillations at the shorter period are most likely the standing kink oscillations in a flare loop. Meanwhile, a longer period of about 10 minutes is identified in the time series of Doppler shift and line-integrated intensity, GOES SXR fluxes and AIA EUV light curves, indicating the periodic energy release in this flare, which may be caused by a slow mode wave.

Charged-particle acceleration in a reconnecting current sheet including multiple magnetic islands and a nonuniform background magnetic field

Y. **Li**1,2,3, N. Wu4 and J. Lin

A&A 605, A120 (**2017**)

https://www.aanda.org/articles/aa/pdf/2017/09/aa30026-16.pdf

Context. Charged particles are accelerated to high energies in solar flares. Although we know that magnetic reconnection is an efficient mechanism in generating energetic particles, the detailed role it plays in accelerating particles is still unknown.
Aims. We investigate particle acceleration by magnetic reconnection in the current sheet, including multiple islands and a guide field.
Methods. The long current sheet produced by the disruption in the corona magnetic field is usually not stable to various plasma instabilities, among which the tearing mode is the most important, and magnetic islands start to form in the current sheet when these instabilities develop. Two reverse processes are typically observed in the sheet: cascading of large islands to smaller ones, and merging of small islands into larger ones. Coalescent reconnection consequently takes place between two adjacent islands when merging occurs. The electric field induced by the coalescent reconnection is opposite to the electric field of the primary large-scale reconnection. We studied particle acceleration in such a current sheet and examined in detail the dynamic properties of electrons and protons in the current sheet through test particle approach.
Results. We found that some particles can be accelerated to high energies in a very short time, and some particles (near the coalescence reconnection site) are accelerated and decelerated back and forth by the primary and secondary electric fields. Particle motions show two distinct types along different trajectories: some particles are trapped around magnetic islands, and some escape from the current sheet mainly along open field lines. With the presence of a guide field, protons and electrons are found to eventually move in different directions. The energy spectra for both species follow a double power-law shape. The softer components of the power-law spectrum are due to the particles that are trapped and circulate around magnetic islands, while the particles that escape and are partly trapped contribute to the harder component of the spectrum. Finally, we also investigated the influences of the parameters for the reconnection process on the spectral feature.

Flare Ribbons Approach Observed by the Interface Region Imaging Spectrograph and the Solar Dynamics Observatory

Ting **Li**, Jun Zhang, Yijun Hou
ApJ **848** 32 **2017**
https://arxiv.org/pdf/1709.03216.pdf
We report flare ribbons approach (FRA) during a multiple-ribbon M-class flare on **2015 November 4** in NOAA AR 12443, obtained by the Interface Region Imaging Spectrograph and the Solar Dynamics Observatory. The flare consisted of a pair of main ribbons and two pairs of secondary ribbons. The two pairs of secondary ribbons were formed later than the appearance of main ribbons, with respective time delays of 15 and 19 minutes. The negative-polarity main ribbon spread outward faster than the first secondary ribbon with the same polarity in front of it, and thus the FRA was generated. Just before their encounter, the main ribbon was darkening drastically and its intensity decreased by about 70% in 2 minutes, implying the suppression of main-phase reconnection that produced two main ribbons. The FRA caused the deflection of the main ribbon to the direction of secondary ribbon with a deflection angle of about 60 degree. Post-approach arcade was formed about 2 minutes later and the downflows were detected along the new arcade with velocities of 35-40 km/s, indicative of the magnetic restructuring during the process of FRA. We suggest that there are three topological domains with footpoints outlined by the three pairs of ribbons. Close proximity of these domains leads to deflection of the ribbons in agreement with the magnetic field topology.

Spectroscopic Observations of Magnetic Reconnection and Chromospheric Evaporation in an X-shaped Solar Flare

Y. **Li**, M. Kelly, M. D. Ding, J. Qiu, X. S. Zhu, W. Q. Gan
ApJ **848** 118 **2017**
https://arxiv.org/pdf/1708.08586.pdf
http://iopscience.iop.org/article/10.3847/1538-4357/aa89e4/pdf
We present observations of distinct UV spectral properties at different locations during an atypical X-shaped flare (SOL**2014-11-09**T15:32) observed by the Interface Region Imaging Spectrograph (IRIS). In this flare, four chromospheric ribbons appear and converge at an X-point where a separator is anchored. Above the X-point, two sets of non-coplanar coronal loops approach laterally and reconnect at the separator. The IRIS slit was located close to the X-point, cutting across some of the flare ribbons and loops. Near the location of the separator, the Si IV 1402.77 A line exhibits significantly broadened line wings extending to 200 km/s but an unshifted line core. These spectral features suggest the presence of bidirectional flows possibly related to the separator reconnection. While at the flare ribbons, the hot Fe XXI 1354.08 A line shows blueshifts and the cool Si IV 1402.77 A, C II 1335.71 A, and Mg II 2803.52 A lines show evident redshifts up to a velocity of 80 km/s, which are consistent with the scenario of chromospheric evaporation/condensation.

Particle Acceleration during Magnetic Reconnection in a Low-beta Plasma

Xiaocan **Li**1,2,3, Fan Guo3, Hui Li3, and Gang Li1
2017 ApJ 843 21
http://iopscience.iop.org/article/10.3847/1538-4357/aa745e/pdf
Magnetic reconnection is a primary mechanism for particle energization in space and astrophysical plasmas. By carrying out two-dimensional (2D) fully kinetic simulations, we study particle acceleration during magnetic reconnection in plasmas with different plasma β (the ratio between the thermal pressure and the magnetic pressure). For the high-β cases, we do not observe significant particle acceleration. In the low-β regime ($\beta < 0.1$), we find that reconnection is efficient at energizing both electrons and ions. While the distribution of accelerated particles integrated over the whole simulation box appears highly non-thermal, it is actually the superposition of a series of distributions in different sectors of a 2D magnetic island. Each of those distributions has only a small non-thermal component compared with its thermal core. By tracking a large number of particles, we show that particles get energized in X-line regions, contracting magnetic islands, and magnetic island coalescence regions. We obtain the particle energization rate $\boldsymbol{j} \cdot \boldsymbol{E}$ by averaging over particle drift motions and find that it agrees well with the particle kinetic energy change. We quantify the contribution of curvature drift, gradient drift, polarization drift, magnetization, non-gyrotropic effect, and parallel electric field in different acceleration regions. We find that the major energization is due to particle curvature drift along the motional electric field. The other particle motions contribute less but may become important in different acceleration regions. The highly efficient particle energization in low-β plasmas may help us understand the strong particle energization in solar flares and accretion disk coronae.

Fundamental and Harmonic Oscillations in Neighboring Coronal Loops

Hongbo **Li**1,2,3, Yu Liu1,2, and Kuan Vai Tam
2017 ApJ 842 99
http://iopscience.iop.org.sci-hub.cc/0004-637X/842/2/99/
We present observations of multimode (fundamental and harmonic) oscillations in a loop system, which appear to be simultaneously excited by a GOES C-class flare. Analysis of the periodic oscillations reveals that (1) the primary loop with a period of P a ≈ 4 minutes and a secondary loop with two periods of P a ≈ 4 minutes and P b ≈ 2 minutes are detected simultaneously in closely spaced loop strands; (2) both oscillation components have their peak amplitudes near the loop apex, while in the second loop the low-frequency component P a dominates in a loop segment that is two times larger than the high-frequency component P b ; (3) the harmonic mode P b shows the largest deviation from a sinusoidal loop shape at the loop apex. We conclude that multiple harmonic modes with different displacement profiles can be excited simultaneously even in closely spaced strands, similar to the overtones of a violin string. **2015 June 18**

Quasi-periodic pulsations with multiple periods in hard X-ray emission

Dong **Li**, Qingmin Zhang
MNRAS **2017**
https://arxiv.org/pdf/1706.01680.pdf
We explore the quasi-periodic pulsations (QPPs) with multiple periods in hard X-ray (HXR) emission from Fermi/GBM during the impulsive phase of solar flare (SOL**2014-09-10)**. The completely new observational result is that the shorter periods appear at lower energies of the X-ray photons at the beginning and the longer periods appear at higher energies at the end, with some intersection of the periods at medium energies. We also find the shorter and then the longer periods during the same phase of this flare. Using the wavelet power spectrum and fast Fourier transform (FFT) spectrum, we analyze the normalized rapidly varying signal divided by its slowly varying signal, which is the smoothed original HXR flux. The periods of 27 s and 37 s are derived at lower energy channels between 17:25 UT and 17:29 UT, i.e., 12.0-27.3 keV and 27.3-50.9 keV. Then the periods of 27 s, 46 s and 60 s are observed at medium-energy channel from 17:26 UT to 17:33 UT, such as 50.9-102.3 keV. And the period of 80 s is detected at higher energy channel from 17:28 UT to 17:33 UT, such as 102.3-296.4 keV.

Explosive chromospheric evaporation driven by nonthermal electrons around one footpoint of a solar flare loop

Dong **Li**, Zongjun Ning, Yu Huang, Qingmin Zhang
ApJL 841 L9 **2017**
https://arxiv.org/pdf/1705.02448.pdf
http://sci-hub.cc/10.3847/2041-8213/aa71b0
We explore the temporal relationship between microwave/HXR emission and Doppler velocity during the impulsive phase of a solar flare on **2014 October 27** (SOL2014-10-27), which displays a pulse on the light curves in microwave (34 GHz) and hard X-ray (HXR, 25-50 keV) bands before the flare maximum. Imaging observation shows that this pulse mainly comes from one footpoint of a solar flare loop. The slit of Interface Region Imaging Spectrograph (IRIS)

stays at this footpoint during this solar flare. The Doppler velocities of Fe XXI 1354.09 A and Si IV 1402.77 A are extracted from the Gaussian fitting method. We find that the hot line of Fe XXI 1354.09 A (logT~7.05) in corona exhibits blue shift, while the cool line of Si IV 1402.77 A (logT~4.8) in transition region exhibits red shift, indicating explosive chromospheric evaporation. The evaporative upflows along the flare loop are also observed in the AIA 131 A image. To our knowledge, this is the first report of chromospheric evaporation evidence from both spectral and imaging observations in the same flare. Both microwave and HXR pulses are well correlated with the Doppler velocities, suggesting that the chromospheric evaporation is driven by nonthermal electrons around this footpoint of a solar flare loop.

Rotating Magnetic Structures Associated with a Quasi-circular Ribbon Flare

Haidong **Li**1,2, Yunchun Jiang1, Jiayan Yang1, Bo Yang1,2, Zhe Xu1,2, Junchao Hong1, and Yi Bi1
2017 ApJ 836 235 10.3847/1538-4357/aa5eac
http://sci-hub.cc/10.3847/1538-4357/aa5eac
We present the detection of a small eruption and the associated quasi-circular ribbon flare during the emergence of a bipole occurring on **2015 February 3**. Under a fan dome, a sigmoid was rooted in a single magnetic bipole, which was encircled by negative polarity. The nonlinear force-free field extrapolation shows the presence of twisted field lines, which can represent a sigmoid structure. The rotation of the magnetic bipole may cause the twisting of magnetic field lines. An initial brightening appeared at one of the footpoints of the sigmoid, where the positive polarity slides toward a nearby negative polarity field region. The sigmoid displayed an ascending motion and then interacted intensively with the spine-like field. This type of null point reconnection in corona led to a violent blowout jet, and a quasi-circular flare ribbon was also produced. The magnetic emergence and rotational motion are the main contributors to the energy buildup for the flare, while the cancellation and collision might act as a trigger.

Imaging Observations of Magnetic Reconnection in a Solar Eruptive Flare

Y. **Li**, X. Sun, M. D. Ding, J. Qiu, E. R. Priest
ApJ 835 190 **2017**
https://arxiv.org/pdf/1612.09417v1.pdf
https://iopscience.iop.org/article/10.3847/1538-4357/835/2/190/pdf
Solar flares are one of the most energetic events in the solar atmosphere. It is widely accepted that flares are powered by magnetic reconnection in the corona. An eruptive flare is usually accompanied by a coronal mass ejection, both of which are probably driven by the eruption of a magnetic flux rope (MFR). Here we report an eruptive flare on **2016 March 23** observed by the Atmospheric Imaging Assembly on board the Solar Dynamics Observatory. The extreme-ultraviolet imaging observations exhibit the clear rise and eruption of an MFR. In particular, the observations reveal solid evidence for magnetic reconnection from both the corona and chromosphere during the flare. Moreover, weak reconnection is observed before the start of the flare. We find that the preflare weak reconnection is of tether-cutting type and helps the MFR to rise slowly. Induced by a further rise of the MFR, strong reconnection occurs in the rise phases of the flare, which is temporally related to the MFR eruption. We also find that the magnetic reconnection is more of 3D-type in the early phase, as manifested in a strong-to-weak shear transition in flare loops, and becomes more 2D-like in the later phase, as shown by the apparent rising motion of an arcade of flare loops.

Quasi-periodic pulsations with periods that change depending on whether the pulsations have thermal or nonthermal components

Dong **Li**, Qingmin Zhang, Yu Huang, Zongjun Ning, Yingna Su
A&A **2016**
https://arxiv.org/pdf/1612.02677v1.pdf
Context. Quasi-periodic pulsations (QPPs) typically display periodic and regular peaks in the light curves during the flare emissions. Sometimes, QPPs show multiple periods at the same wavelength. However, changing periods in various channels are rare.
Aims. We report QPPs in a solar flare on **2014 October 27**. They showed a period change that depended on whether thermal or nonthermal components were included. The flare was simultaneously observed by many instruments.
Methods. Using the fast Fourier transform (FFT), we decomposed the light curves at multiple wavelengths into slowly varying and rapidly varying signals. Then we identified the QPPs as the regular and periodic peaks from the rapidly varying signals. The periods are derived with the wavelet method and confirmed based on the FFT spectra of the rapidly varying signals.
Results. We find a period of 50 s from the thermal emissions during the impulsive phase of the flare, that is, in the soft X-ray bands. At the same time, a period of about 100 s is detected from the nonthermal emissions, such as hard X-ray and microwave channels. The period ratio is exactly 2.0, which might be due to the modulations of the magnetic reconnection rate by the fundamental and harmonic modes of magnetohydrodynamic waves. Our results further show

that the 100 s period is present over a broad wavelength, such as hard X-rays, extreme-UV/UV, and microwave emissions, indicating the periodic magnetic reconnection in this flare.
Conclusions. To our knowledge, this is the first report about period changes from thermal to nonthermal components in a single flare that occur at almost the same time. This new observational finding could be a challenge to the theory of flare QPPs.

On the Power-Law Distributions of X-ray Fluxes from Solar Flares Observed with GOES

You-ping **Li**, Li Feng, Ping Zhang, Siming Liu, Weiqun Gan
Research in Astron. Astrophys (RAA) **2016**
http://arxiv.org/pdf/1609.03117v1.pdf
Power-law frequency distributions of the peak flux of solar flare X-ray emission have been studied extensively and attributed to a system of self-organized criticality (SOC). In this paper, we first show that, so long as the shape of the normalized light curve is not correlated with the peak flux, the flux histogram of solar flares also follows a power-law distribution with the same spectral index as the power-law frequency distribution of the peak flux, which may partially explain why power-law distributions are ubiquitous in the Universe. We then show that the spectral indexes of the histograms of soft X-ray fluxes observed by GOES satellites in two different energy channels are different: the higher energy channel has a harder distribution than the lower energy channel, which challenges the universal power-law distribution predicted by SOC models and implies a very soft distribution of thermal energy content of plasmas probed by the GOES. The temperature (T) distribution, on the other hand, approaches a power-law distribution with an index of 2 for high values of T. Application of SOC models to statistical properties of solar flares needs to be revisited.

Slipping Magnetic Reconnection of Flux Rope Structures as a Precursor to an Eruptive X-class Solar Flare

Ting **Li**, Kai Yang, Yijun Hou, Jun Zhang
ApJ 830 152 **2016**
http://arxiv.org/pdf/1608.02057v1.pdf
We present the quasi-periodic slipping motion of flux rope structures prior to the onset of an eruptive X-class flare on **2015 March 11**, obtained by the \emph{Interface Region Imaging Spectrograph} (\emph{IRIS}) and the \emph{Solar Dynamics Observatory} (\emph{SDO}). The slipping motion occurred at the north part of the flux rope and seemed to successively peel off the flux rope. The speed of the slippage was 30−40 km s−1, with an average period of 130±30 s. The Si {\sc iv} 1402.77 {\AA} line showed a redshift of 10−30 km s−1 and a line width of 50−120 km s−1 at the west legs of slipping structures, indicative of reconnection downflow. The slipping motion lasted about 40 min and the flux rope started to rise up slowly at the late stage of the slippage. Then an X2.1 flare was initiated and the flux rope was impulsively accelerated. One of the flare ribbons swept across a negative-polarity sunspot and the penumbral segments of the sunspot decayed rapidly after the flare. We studied the magnetic topology at the flaring region and the results showed the existence of a twisted flux rope, together with quasi-separatrix layers (QSLs) structures binding the flux rope. Our observations imply that quasi-periodic slipping magnetic reconnection occurs along the flux-rope-related QSLs in the preflare stage, which drives the later eruption of the flux rope and the associated flare.

Magnetic reconnection between a solar filament and nearby coronal loops

Leping **Li**, Jun Zhang, Hardi Peter, Eric Priest, Huadong Chen, Lijia Guo, Feng Chen, Duncan Mackay
Nature Physics **2016**
http://arxiv.org/pdf/1605.03320v1.pdf
Magnetic reconnection, the rearrangement of magnetic field topology, is a fundamental physical process in magnetized plasma systems all over the universe1,2. Its process is difficult to be directly observed. Coronal structures, such as coronal loops and filament spines, often sketch the magnetic field geometry and its changes in the solar corona3. Here we show a highly suggestive observation of magnetic reconnection between an erupting solar filament and its nearby coronal loops, resulting in changes in connection of the filament. X-type structures form when the erupting filament encounters the loops. The filament becomes straight, and bright current sheets form at the interfaces with the loops. Many plasmoids appear in these current sheets and propagate bi-directionally. The filament disconnects from the current sheets, which gradually disperse and disappear, reconnects to the loops, and becomes redirected to the loop footpoints. This evolution of the filament and the loops suggests successive magnetic reconnection predicted by theories1 but rarely detected with such clarity in observations. Our results on the formation, evolution, and disappearance of current sheets, confirm three-dimensional magnetic reconnection theory and have implications for the evolution of dissipation regions and the release of magnetic energy for reconnection in many magnetized plasma systems. **January 1, 2012**

Observations of an X-shaped Ribbon Flare in the Sun and Its Three-dimensional Magnetic Reconnection

Y. **Li**, J. Qiu, D. W. Longcope, M. D. Ding, K. Yang
ApJL **823** L13 **2016**
http://arxiv.org/pdf/1605.01833v1.pdf
We report evolution of an atypical X-shaped flare ribbon which provides novel observational evidence of three-dimensional (3D) magnetic reconnection at a separator. The flare occurred on **2014 November 9**. High-resolution slit-jaw 1330 A images from the Interface Region Imaging Spectrograph reveal four chromospheric flare ribbons that converge and form an X-shape. Flare brightening in the upper chromosphere spreads along the ribbons toward the center of the "X" (the X-point), and then spreads outward in a direction more perpendicular to the ribbons. These four ribbons are located in a quadrupolar magnetic field. Reconstruction of magnetic topology in the active region suggests the presence of a separator connecting to the X-point outlined by the ribbons. The inward motion of flare ribbons in the early stage therefore indicates 3D magnetic reconnection between two sets of non-coplanar loops that approach laterally, and reconnection proceeds downward along a section of vertical current sheet. Coronal loops are also observed by the Atmospheric Imaging Assembly on board the Solar Dynamics Observatory confirming the reconnection morphology illustrated by ribbon evolution.
See HMI Science Nuggets #53, May 2016 http://hmi.stanford.edu/hminuggets/?p=1552

Observations of solar flares with IRIS and SDO

D. **Li**, D.E. Innes, Z. J. Ning
A&A 587, A11 **2016**
http://arxiv.org/pdf/1512.05147v1.pdf
Context: Flare kernels brighten simultaneously in all SDO/AIA channels making it difficult to determine their temperature structure. IRIS is able to spectrally resolve Fe xxi emission from cold chromospheric brightenings, so can be used to infer the amount of Fe xxi emission in 131 channel. Aims: We use observations of two small solar flares seen by IRIS and SDO to compare the EMs deduced from the IRIS Fe xxi line and the AIA 131 channel to determine the fraction of Fe xxi emission in flare kernels in the 131 channel of AIA. Methods: Cotemporal and cospatial pseudo-raster AIA images are compared with the IRIS results.We use multi-Gaussian line fitting to separate the blending chromospheric emission so as to derive Fe xxi intensities and Doppler shifts in IRIS spectra. Results: We define loop and kernel regions based on the brightness of the 131 and 1600 {\AA} intensities. In the loop regions the Fe xxi EMs are typically 80% of the 131 ones, and range from 67% to 92%. Much of the scatter is due to small misalignments but the largest site with low Fe xxi contributions was probably affected by a recent injection of cool plasma into the loop. In flare kernels the contribution of Fe xxi increases from less than 10% at the low intensity 131 sites to 40-80% in the brighter kernels. Here the Fe xxi is superimposed on bright chromospheric emission and the Fe xxi line shows blue shifts, sometimes extending up to the edge of the spectral window, 200 km/s. Conclusions: The AIA 131 emission in flare loops is due to Fe xxi emission with a 10-20% contribution from continuum, Fe xxiii, and cooler background plasma emission. In bright flare kernels up to 52% of the 131 is from cooler plasma. The wide range seen in the kernels is caused by significant structure in the kernels which is seen as sharp gradients in Fe xxi EM at sites of molecular and transition region emission. **24-25 October 2013**

Observational Evidences of Electron-driven Evaporation in two Solar Flares

Dong **Li**, Zongjun Ning, Qingmin Zhang
ApJ 813 59 **2015**
http://arxiv.org/pdf/1509.07226v1.pdf
We have explored the relationship between hard X-ray (HXR) emissions and Doppler velocities caused by the chromospheric evaporation in two X1.6 class solar flares on **2014 September 10 and October 22**, respectively. Both events display double ribbons and Interface Region Imaging Spectrograph (IRIS) slit is fixed on one of their ribbons from the flare onset. The explosive evaporations are detected in these two flares. The coronal line of Fe XXI 1354.09 A shows blue shifts, but chromospheric line of C I 1354.29 A shows red shifts during the impulsive phase. The chromospheric evaporation tends to appear at the front of flare ribbon. Both Fe XXI and C I display their Doppler velocities with a `increase-peak-decrease' pattern which is well related to the `rising-maximum- decay' phase of HXR emissions. Such anti-correlation between HXR emissions and Fe XXI Doppler shifts, and correlation with C I Doppler shifts indicate the electron-driven evaporation in these two flares.

Heating and cooling of coronal loops observed by SDO

Li, L. P., Peter, H., Chen, F., and Zhang, J.
A&A, 583, A109 **2015**
E-print, Sept **2015**

http://ddl.escience.cn/f/sHZh
Context: One of the most prominent processes suggested to heat the corona to well above 106 K builds on nanoflares, short bursts of energy dissipation. Aims: We compare observations to model predictions to test the validity of the nanoflare process. Methods: Using extreme UV data from AIA/SDO and HMI/SDO line-of-sight magnetograms we study the spatial and temporal evolution of a set of loops in active region **AR 11850**. Results: We find a transient brightening of loops in emission from Fe xviii forming at about 7.2 MK while at the same time these loops dim in emission from lower temperatures. This points to a fast heating of the loop that goes along with evaporation of material that we observe as apparent upward motions in the image sequence. After this initial phases lasting for some 10 min, the loops brighten in a sequence of AIA channels showing cooler and cooler plasma, indicating the cooling of the loops over a time scale of about one hour. A comparison to the predictions from a 1D loop model shows that this observation supports the nanoflare process in (almost) all aspects. In addition, our observations show that the loops get broader while getting brighter, which cannot be understood in a 1D model. **September 24, 2013**

Chromospheric Evaporation in an X1.0 Flare on 2014 March 29 Observed with IRIS and EIS

Y. **Li**, M. D. Ding, J. Qiu, J. X. Cheng
ApJ **811** 7 **2015**
http://arxiv.org/pdf/1508.03927v1.pdf
Chromospheric evaporation refers to dynamic mass motions in flare loops as a result of rapid energy deposition in the chromosphere. These have been observed as blueshifts in X-ray and extreme-ultraviolet (EUV) spectral lines corresponding to upward motions at a few tens to a few hundreds of km/s. Past spectroscopic observations have also revealed a dominant stationary component, in addition to the blueshifted component, in emission lines formed at high temperatures (~10 MK). This is contradictory to evaporation models predicting predominant blueshifts in hot lines. The recently launched Interface Region Imaging Spectrograph (IRIS) provides high resolution imaging and spectroscopic observations that focus on the chromosphere and transition region in the UV passband. Using the new IRIS observations, combined with coordinated observations from the EUV Imaging Spectrometer, we study the chromospheric evaporation process from the upper chromosphere to corona during an X1.0 flare on 2014 March 29. We find evident evaporation signatures, characterized by Doppler shifts and line broadening, at two flare ribbons separating from each other, suggesting that chromospheric evaporation takes place in successively formed flaring loops throughout the flare. More importantly, we detect dominant blueshifts in the high temperature Fe XXI line (~10 MK), in agreement with theoretical predictions. We also find that, in this flare, gentle evaporation occurs at some locations in the rise phase of the flare, while explosive evaporation is detected at some other locations near the peak of the flare. There is a conversion from gentle to explosive evaporation as the flare evolves.

Sunspot Rotation and the M-class Flare in Solar Active Region NOAA 11158

Alexander **Li**, Yang Liu
Solar Phys. Volume 290, Issue 8, pp 2199-2209 **2015**
http://sun.stanford.edu/~yliu/papers/sunspotrotation_v5.pdf
In this paper, we measure the rotation of a sunspot in solar active region NOAA 11158 (Solar Target Identifier **SOL2011-02-15**) that was associated with anM-class flare. The flare occurred when the rotation rate of the sunspot reached its maximum. We further calculate the energy in the corona produced by the sunspot rotation. The energy accumulated in the corona before the flare reached 5.5? 1032 erg, sufficient for energy requirements for a moderately big solar eruption. This suggests that sunspot rotation, which is often observed in solar active regions, is an effective mechanism for building up magnetic energy in the corona.

Imaging and Spectral Observations of Quasi-Periodic Pulsations in a Solar Flare

D. **Li**, Z. J. Ning, Q. M. Zhang
ApJ **807** 72 **2015**
http://arxiv.org/pdf/1505.03252v1.pdf
We explore the Quasi-Periodic Pulsations (QPPs) in a solar flare observed by Fermi Gamma-ray Burst Monitor (GBM), Solar Dynamics Observatory (SDO), Solar Terrestrial Relations Observatory (STEREO), and Interface Region Imaging Spectrograph (IRIS) on **2014 September 10**. QPPs are identified as the regular and periodic peaks on the rapidly-varying components, which are the light curves after removing the slowly-varying components. The QPPs display only three peaks at the beginning on the hard X-ray (HXR) emissions, but ten peaks on the chromospheric and coronal line emissions, and more than seven peaks (each peak is corresponding to a type III burst on the dynamic spectra) at the radio emissions. An uniform quasi-period about 4 minutes are detected among them. AIA imaging observations exhibit that the 4-min QPPs originate from the flare ribbon, and tend to appear on the ribbon front. IRIS spectral observations show that each peak of the QPPs tends to a broad line width and a red Doppler velocity at C I, O IV, Si IV, and Fe XXI lines. Our findings indicate that the QPPs are produced by the non-thermal electrons which are accelerated by the induced quasi-periodic magnetic reconnections in this flare.

Diagnostics of Ellerman Bombs with High-resolution Spectral Data

Z. **Li**, C. Fang, Y. Guo, P. F. Chen, Z. Xu, W. Cao

Research in Astron. Astrophys. (RAA) **2015**

http://arxiv.org/pdf/1504.02538v1.pdf

Ellerman bombs (EBs) are tiny brightenings often observed near sunspots. The most impressive characteristic of the EB spectra is the two emission bumps in both wings of the Hα and \ion{Ca}{II} 8542 {\AA} lines. High-resolution spectral data of three small EBs were obtained on **2013 June 6** with the largest solar telescope, the 1.6 meter New Solar Telescope (NST), at the Big Bear Solar Observatory. The characteristics of these EBs are analyzed. The sizes of the EBs are in the range of 0.3\arcsec\--0.8\arcsec\ and their durations are only 3--5 minutes. Our semi-empirical atmospheric models indicate that the heating occurs around the temperature minimum region with a temperature increase of 2700--3000 K, which is surprisingly higher than previously thought. The radiative and kinetic energies are estimated to be as high as 5×1025--3.0×1026 ergs despite the small size of these EBs. Observations of the magnetic field show that the EBs appeared just in a parasitic region with mixed polarities and accompanied by mass motions. Nonlinear force-free field extrapolation reveals that the three EBs are connected with a series of magnetic field lines associated with bald patches, which strongly implies that these EBs should be produced by magnetic reconnection in the solar lower atmosphere. According to the lightcurves and the estimated magnetic reconnection rate, we propose that there is a three phase process in EBs: pre-heating, flaring and cooling phases.

Quasi-periodic Slipping Magnetic Reconnection During an X-class Solar Flare Observed by the Solar Dynamics Observatory and Interface Region Imaging Spectrograph

Ting **Li**, Jun Zhang

ApJL **804** L8 **2015**

http://arxiv.org/pdf/1504.01111v1.pdf

We firstly report the quasi-periodic slipping motion of flare loops during an eruptive X-class flare on **2014 September 10**. The slipping motion was investigated at a specific location along one of the two ribbons and can be observed throughout the impulsive phase of the flare. The apparent slipping velocity was 20-110 km/s and the associated period was 3−6 min. The footpoints of flare loops appeared as small-scale bright knots observed in 1400 {\AA}, corresponding to fine structures of the flare ribbon. These bright knots were observed to move along the southern part of the longer ribbon and also exhibited a quasi-periodic pattern. The Si IV 1402.77 {\AA} line was redshifted by 30-50 km/s at the locations of moving knots with a ~ 40-60 km/s line width, larger than other sites of the flare ribbon. We suggest that the quasi-periodic slipping reconnection is involved in this process and the redshift at the bright knots is probably indicative of reconnection downflow. The emission line of Si IV at the northern part of the longer ribbon also exhibited obvious redshifts of about 10-70 km/s in the impulsive phase of the flare, with the redshifts at the outer edges of the ribbon larger than those in the middle. The redshift velocities at post-flare loops reached about 80-100 km/s in the transition region.

Conversion from mutual helicity to self-helicity observed with IRIS

L. **Li**, H. Peter, F. Chen, J. Zhang

A&A, **2014**

http://www2.mps.mpg.de/data/outgoing/lileping/aa.pdf

Context. In the upper atmosphere of the Sun observations show convincing evidence for crossing and twisted structures, which are interpreted as mutual helicity and self-helicity.

Aims. We use observations with the new Interface Region Imaging Spectrograph (IRIS) to show the conversion of mutual helicity into self-helicity in coronal structures on the Sun.

Methods. Using far UV spectra and slit-jaw images from IRIS and coronal images and magnetograms from SDO, we investigated the evolution of two crossing loops in an active region, in particular, the properties of the Si IV line profile in cool loops.

Results. In the early stage two cool loops cross each other and accordingly have mutual helicity. The Doppler shifts in the loops indicate that they wind around each other. As a consequence, near the crossing point of the loops (interchange) reconnection sets in, which heats the plasma. This is consistent with the observed increase of the line width and of the appearance of the loops at higher temperatures. After this interaction, the two new loops run in parallel, and in one of them shows a clear spectral tilt of the Si IV line profile. This is indicative of a helical (twisting) motion, which is the same as to say that the loop has self-helicity.

Conclusions. The high spatial and spectral resolution of IRIS allowed us to see the conversion of mutual helicity to self-helicity in the (interchange) reconnection of two loops. This is observational evidence for earlier theoretical speculations. **2013-09-27**

Dynamics of double layers, ion acceleration and heat flux suppression during solar flares

T. C. **Li**, J. F. Drake, M. Swisdak

ApJ 793 7, **2014**

http://arxiv.org/pdf/1408.1511v1.pdf

Observations of flare-heated electrons in the corona typically suggest confinement of electrons. The confinement mechanism, however, remains unclear. The transport of coronal hot electrons into ambient plasma was recently investigated by particle-in-cell (PIC) simulations. Electron transport was significantly suppressed by the formation of a highly localized, nonlinear electrostatic electric potential in the form of a double layer (DL). In this work large-scale PIC simulations are performed to explore the dynamics of DLs in larger systems where, instead of a single DL, multiple DLs are generated. The primary DL accelerates return current electrons, resulting in high velocity electron beams that interact with ambient ions. This forms a Buneman unstable system that spawns more DLs. Trapping of heated return current electrons between multiple DLs strongly suppresses electron transport. DLs also accelerate ambient ions and produce strong ion flows over an extended region. This clarifies the mechanism by which hot electrons in the corona couple to and accelerate ions to form the solar wind. These new dynamics in larger systems reveal a more likely picture of DL development and their impact on the ambient plasma in the solar corona. They are applicable to the preparation for in-situ coronal space missions like the Solar Probe Plus.

On the Nature of the EUV Late Phase of Solar Flares

Y. **Li**, M. D. Ding, Y. Guo, Y. Dai

E-print, July 2014; ApJ, 793 85 **2014**

http://arxiv.org/pdf/1407.6041v1.pdf

The extreme-ultraviolet (EUV) late phase of solar flares is a second peak of warm coronal emissions (e.g., Fe XVI) for many minutes to a few hours after the GOES soft X-ray peak. It was first observed by the EUV Variability Experiment (EVE) on board the Solar Dynamics Observatory (SDO). The late phase emission originates from a second set of longer loops (late phase loops) that are higher than the main flaring loops. It is suggested as being caused by either additional heating or long-lasting cooling. In this paper, we study the role of long-lasting cooling and additional heating in producing the EUV late phase using the "enthalpy-based thermal evolution of loops" (EBTEL) model. We find that a long cooling process in late phase loops can well explain the presence of the EUV late phase emission, but we cannot exclude the possibility of additional heating in the decay phase. Moreover, we provide two preliminary methods based on the UV and EUV emissions from the Atmospheric Imaging Assembly (AIA) on board SDO to determine whether an additional heating plays some role or not in the late phase emission. Using nonlinear force-free field modeling, we study the magnetic configuration of the EUV late phase. It is found that the late phase can be generated either in hot spine field lines associated with a magnetic null point or in large-scale magnetic loops of multipolar magnetic fields. In this paper, we also discuss why the EUV late phase is usually observed in warm coronal emissions and why the majority of flares do not exhibit an EUV late phase**. 5-May-2010, 16-Oct-2010, 18-Feb-2011, 6-Sep-2011, 15-Nov-2011**

Heating and Dynamics of Two Flare Loop Systems Observed by AIA and EIS

Y. **Li**, J. Qiu, M. D. Ding

E-print, Dec **2013**; **2014** ApJ 781 120

We investigate heating and evolution of flare loops in a C4.7 two-ribbon flare on 2011 February 13. From SDO/AIA imaging observations, we can identify two sets of loops. Hinode/EIS spectroscopic observations reveal blueshifts at the feet of both sets of loops. The evolution and dynamics of the two sets are quite different. The first set of loops exhibits blueshifts for about 25 minutes followed by redshifts, while the second set shows stronger blueshifts, which are maintained for about one hour. The UV 1600 observation by AIA also shows that the feet of the second set of loops brighten twice. These suggest that continuous heating may be present in the second set of loops. We use spatially resolved UV light curves to infer heating rates in the few tens of individual loops comprising the two loop systems. With these heating rates, we then compute plasma evolution in these loops with the "enthalpy-based thermal evolution of loops" (EBTEL) model. The results show that, for the first set of loops, the synthetic EUV light curves from the model compare favorably with the observed light curves in six AIA channels and eight EIS spectral lines, and the computed mean enthalpy flow velocities also agree with the Doppler shift measurements by EIS. For the second set of loops modeled with twice-heating, there are some discrepancies between modeled and observed EUV light curves in low-temperature bands, and the model does not fully produce the prolonged blueshift signatures as observed. We discuss possible causes for the discrepancies.

Coronal Electron Confinement by Double Layers

T. C. **Li**, J. F. Drake, and M. Swisdak

2013 ApJ 778 144

In observations of flare-heated electrons in the solar corona, a longstanding problem is the unexplained prolonged lifetime of the electrons compared to their transit time across the source. This suggests confinement. Recent particle-in-cell (PIC) simulations, which explored the transport of pre-accelerated hot electrons through ambient cold plasma,

showed that the formation of a highly localized electrostatic potential drop, in the form of a double layer (DL), significantly inhibited the transport of hot electrons. The effectiveness of confinement by a DL is linked to the strength of the DL as defined by its potential drop. In this work, we investigate the scaling of the DL strength with the hot electron temperature by PIC simulations and find a linear scaling. We demonstrate that the strength is limited by the formation of parallel shocks. Based on this, we analytically determine the maximum DL strength, and also find a linear scaling with the hot electron temperature. The DL strength obtained from the analytic calculation is comparable to that from the simulations. At the maximum strength, the DL is capable of confining a significant fraction of hot electrons in the source.

ON THE SPECTRAL HARDENING AT 300 keV IN SOLAR FLARES
G. **Li**1, X. Kong1,2, G. Zank1, and Y. Chen
2013 ApJ 769 22
It has long been noted that the spectra of observed continuum emissions in many solar flares are consistent with double power laws with a hardening at energies 300 keV. It is now widely believed that at least in electron-dominated events, the hardening in the photon spectrum reflects an intrinsic hardening in the source electron spectrum. In this paper, we point out that a power-law spectrum of electrons with a hardening at high energies can be explained by the diffusive shock acceleration of electrons at a termination shock with a finite width. Our suggestion is based on an early analytical work by Drury et al., where the steady-state transport equation at a shock with a tanh profile was solved for a p-independent diffusion coefficient. Numerical simulations with a p-dependent diffusion coefficient show hardenings in the accelerated electron spectrum that are comparable with observations. One necessary condition for our proposed scenario to work is that high-energy electrons resonate with the inertial range of the MHD turbulence and low-energy electrons resonate with the dissipation range of the MHD turbulence at the acceleration site, and the spectrum of the dissipation range ~k –2.7. A ~k –2.7 dissipation range spectrum is consistent with recent solar wind observations.

ANALYSIS AND MODELING OF TWO FLARE LOOPS OBSERVED BY AIA AND EIS
Y. **Li**1,2,3, J. Qiu2, and M. D. Ding
2012 ApJ 758 52
We analyze and model an **M1.0 flare** observed by SDO/AIA and Hinode/EIS to investigate how flare loops are heated and evolve subsequently. The flare is composed of two distinctive loop systems observed in extreme ultraviolet (EUV) images. The UV 1600 Å emission at the feet of these loops exhibits a rapid rise, followed by enhanced emission in different EUV channels observed by the Atmospheric Imaging Assembly (AIA) and the EUV Imaging Spectrometer (EIS). Such behavior is indicative of impulsive energy deposit and the subsequent response in overlying coronal loops that evolve through different temperatures. Using the method we recently developed, we infer empirical heating functions from the rapid rise of the UV light curves for the two loop systems, respectively, treating them as two big loops with cross-sectional area of 5" by 5", and compute the plasma evolution in the loops using the EBTEL model. We compute the synthetic EUV light curves, which, with the limitation of the model, reasonably agree with observed light curves obtained in multiple AIA channels and EIS lines: they show the same evolution trend and their magnitudes are comparable by within a factor of two. Furthermore, we also compare the computed mean enthalpy flow velocity with the Doppler shift measurements by EIS during the decay phase of the two loops. Our results suggest that the two different loops with different heating functions as inferred from their footpoint UV emission, combined with their different lengths as measured from imaging observations, give rise to different coronal plasma evolution patterns captured both in the model and in observations.

SUPPRESSION OF ENERGETIC ELECTRON TRANSPORT IN FLARES BY DOUBLE LAYERS
T. C. **Li**, J. F. Drake, and M. Swisdak
2012 ApJ 757 20
During flares and coronal mass ejections, energetic electrons from coronal sources typically have very long lifetimes compared to the transit times across the systems, suggesting confinement in the source region. Particle-in-cell simulations are carried out to explore the mechanisms of energetic electron transport from the corona to the chromosphere and possible confinement. We set up an initial system of pre-accelerated hot electrons in contact with ambient cold electrons along the local magnetic field and let it evolve over time. Suppression of transport by a nonlinear, highly localized electrostatic electric field (in the form of a double layer) is observed after a short phase of free-streaming by hot electrons. The double layer (DL) emerges at the contact of the two electron populations. It is driven by an ion-electron streaming instability due to the drift of the back-streaming return current electrons interacting with the ions. The DL grows over time and supports a significant drop in temperature and hence reduces heat flux between the two regions that is sustained for the duration of the simulation. This study shows that transport suppression begins when the energetic electrons start to propagate away from a coronal acceleration site. It also implies confinement

of energetic electrons with kinetic energies less than the electrostatic energy of the DL for the DL lifetime, which is much longer than the electron transit time through the source region.

Acceleration of Electrons and Protons in Reconnecting Current Sheets Including Single or Multiple X-points

Y. **Li** and J. Lin

Solar Physics, Volume 279, Number 1 (**2012**), 91-113

Kinematic characteristics of electrons and protons in the magnetic reconnecting current sheet in the presence of a guide field are investigated. Particle trajectories are calculated for different values of the guide field by a test-particle calculation. The relationship between the final energy and the initial position has also been studied. We found that the addition of a guide field not only allows particles to get more energy and not only results in the separation of electrons and protons, but also causes the reconnecting electric field to selectively accelerate electrons and protons for different initial positions. The energy spectrum eventually obtained is the common power-law spectrum, and as the guide field increases, the index for the spectrum of electrons decreases rapidly. However, for a weak background magnetic field, proton spectra are not very sensitive to the guide field; but for a strong background field, the dependence of the spectrum index is similar to the electron spectrum. Meanwhile, kinematic characteristics of the accelerated particles in the current sheet including multiple X-points and O-points were also investigated. The result indicates that the existence of the multiple X- and O-points helps particles trapped in the accelerating region to gain more energy, and yields the double or multiple power-law feature.

STATISTICAL ANALYSES ON THERMAL ASPECTS OF SOLAR FLARES

Y. P. **Li**, W. Q. Gan and L. Feng

2012 ApJ 747 133

The frequency distribution of flare energies provides a crucial diagnostic to calculate the overall energy residing in flares and to estimate the role of flares in coronal heating. It often takes a power law as its functional form. We have analyzed various variables, including the thermal energies E th of 1843 flares at their peak time. They were recorded by both Geostationary Operational Environmental Satellites and Reuven Ramaty High-Energy Solar Spectroscopic Imager during the time period from 2002 to 2009 and are classified as flares greater than C 1.0. The relationship between different flare parameters is investigated. It is found that fitting the frequency distribution of E th to a power law results in an index of –2.38. We also investigate the corrected thermal energy E c_th, which represents the flare total thermal energy including the energy loss in the rising phase. Its corresponding power-law slope is –2.35. Compilation of the frequency distributions of the thermal energies from nanoflares, microflares, and flares in the present work and from other authors shows that power-law indices below –2.0 have covered the range from 1024 to 1032 erg. Whether this frequency distribution can provide sufficient energy to coronal heatings in active regions and the quiet Sun is discussed.

Study of the first productive active region in solar cycle 24

L. P. **Li**, J. Zhang, T. Li, S. H. Yang and Y. Z. Zhang

A&A 539, A7 (**2012**)

Context. The Sun is very quiet with less sunspots and activity since the beginning of solar cycle 24. However, the active region (**AR) 11045 emerged on February 5, 2010**, is associated with 43 (8 M- and 35 C-class) flares, 53 coronal mass ejections (CMEs), 29 filament eruptions, 19 extreme ultraviolet (EUV) waves and abundant jets, indicating that this AR is the first productive one of solar cycle 24.

Aims. We study the AR evolution and its associated activities, and also their relationships, to understand this productive AR.

Methods. We used SOHO/MDI magnetograms to study the magnetic fields, STEREO/SECCHI images to explore the activities, and GOES measurements to investigate the soft X-ray flux of the AR.

Results. During the AR evolution, six pairs of main magnetic fields emerged, and 93.1% flares and 82.75% filament eruption occurred in the emergence and stable phases of the magnetic flux. However, 43.4% CMEs occurred in the decaying phase, even though there were less flares. An example is given to show that an event is related to a flare, a filament eruption, a CME and an EUV wave from inner corona to outer corona in space, and the filament eruption and EUV wave occur near the peak time of the flare. Among the 29 filament eruptions, 79.3% are associated with CMEs, as well as 58.6%, associated with flares, and 34.5%, associated with EUV waves. During the 12-day active phase, 575 jets are detected with a daily occurrence rate of 49.3. This is the first time that so many jets have been identified in one AR, implying at least 575 lower magnetic reconnection processes during the AR evolution. We statistically studied these jets

along with the AR evolution, and noticed that the jets mostly occurred surrounding the emerging flux. We also investigated the spatio-temporal relationships between the jets and the flares, and find that the jets are usually rooted around the flare cores, and the soft X-ray flux is inverse correlated with the number of the jets, especially during the beginning 9 days since the AR emergence. In comparison with AR 11045, we studied the other newly emerging AR 11045, and obtained similar results. The relationships between the jets and the flares may well represent a scenario of two-step magnetic reconnection. Using schematic diagrams, we explain the remarkable magnetic field emergence, cancelation and shear motion of AR 11045, and its associated activities.

CORONAL JETS, MAGNETIC TOPOLOGIES, AND THE PRODUCTION OF INTERPLANETARY ELECTRON STREAMS

C. **Li**1,2, S. A. Matthews1, L. van Driel-Gesztelyi1,3,4, J. Sun1 and C. J. Owen

2011 ApJ 735 43

We investigate the acceleration source of the impulsive solar energetic particle (SEP) events on **2007 January 24**. Combining the in situ electron measurements and remote-sensing solar observations, as well as the calculated magnetic fields obtained from a potential-field source-surface model, we demonstrate that the jets associated with the hard X-ray flares and type-III radio bursts, rather than the slow and partial coronal mass ejections, are closely related to the production of interplanetary electron streams. The jets, originated from the well-connected active region (AR 10939) whose magnetic polarity structure favors the eruption, are observed to be forming in a coronal site, extending to a few solar radii, and having a good temporal correlation with the electron solar release. The open-field lines near the jet site are rooted in a negative polarity, along which energetic particles escape from the flaring AR to the near-Earth space, consistent with the in situ electron pitch angle distribution. The analysis enables us to propose a coronal magnetic topology relating the impulsive SEP events to their solar source.

On Integrated Hard X-Ray Broken-Up Spectra of Solar Flares

Y.P. **Li** · W.Q. Gan

Solar Phys (**2011**) 269: 59–66

The summation of two single power-law spectra with a rather big difference of the spectral indices and with comparable intensities looks like a broken-up spectrum. The spatially integrated hard X-rays contain contributions from different sources, like footpoint and looptop sources.Within the standard scenario of solar flares, the power-law index difference between the footpoints and looptop should be two. Taking the M7.6 flare on **24 October 2003** as an example, we showed that the hard X-ray spectrum itself for footpoints and looptop is a single power-law, but the spatially integrated spectrum presents a broken-up form. It is also shown that the time-integrated spectrum could present a broken-up form, although the spectrum in further refined intervals presents a single power-law. It is concluded that the integrated broken-up spectrum observed here is produced either by the summation of individual sources or by the temporal variation of a single source, not by the acceleration itself.

DIFFERENT PATTERNS OF CHROMOSPHERIC EVAPORATION IN A FLARING REGION OBSERVED WITH HINODE/EIS

Y. **Li** and M. D. Ding

2011 ApJ 727 98

We investigate the chromospheric evaporation in the flare of **2007 January 16** using line profiles observed by the Exterme-UV Imaging Spectrometer on board Hinode. Three points at flare ribbons of different magnetic polarities are analyzed in detail. We find that the three points show different patterns of upflows and downflows in the impulsive phase of the flare. The spectral lines at the first point are mostly blueshifted, with the hotter lines showing a dominant blueshifted component over the stationary one. At the second point, however, only weak upflows are detected; instead, notable downflows appear at high temperatures (up to 2.5-5.0 MK). The third point is similar to the second one only in that it shows evidence of multi-component downflows. While the evaporated plasma falling back down as warm rain is a possible cause of the redshifts at the second and third points, the different patterns of chromospheric evaporation at the three points imply the existence of different heating mechanisms in the flaring active region.

COMPARISON BETWEEN OBSERVATION AND SIMULATION OF MAGNETIC FIELD CHANGES ASSOCIATED WITH FLARES

Yixuan **Li**1, Ju Jing1, Yuhong Fan2, and Haimin Wang1

Astrophysical Journal Letters, 727:L19 (6pp), **2011** January

It has been a long-standing question in solar physics how magnetic field structure changes with eruptive events (e.g., flares and coronal mass ejections). In this Letter, we present the eruption-associated changes in the magnetic inclination angle, the horizontal component of magnetic field vectors, and the Lorentz force. The analysis is based on the observation of the X3.4 flare on **2006 December 13** and in comparison to the numerical simulation of Fan. Both observation and simulation show that (1) the magnetic inclination angle in the decayed peripheral penumbra increases, while that in the central area close to the flaring polarity inversion line (PIL) deceases after the flare; (2) the horizontal component of magnetic field increases at the lower altitude near the flaring PIL after the flare. The result suggests that the field lines at the flaring neutral line turn to more horizontal near the surface, that is in agreement with the prediction of Hudson et al.

STATISTICS OF FLARES SWEEPING ACROSS SUNSPOTS

Leping **Li** and Jun Zhang

Astrophysical Journal, 706:L17–L21, **2009** November; **File**

Flare ribbons are always dynamic and sometimes sweep across sunspots. After examining 588 (513 M-class and 75 X-class) flare events observed by the *TRACE* satellite and the *Hinode*/Solar Optical Telescope from 1998 May to 2009 May, we choose the event displaying one of the flare ribbons that completely sweeps across the umbra of a main sunspot of the corresponding active region, and finally obtain 20 (7 X-class and 13 M-class) events as our sample. In each event, we define the main sunspot completely swept across by the flare ribbon as the A-sunspot and its nearby opposite polarity sunspot as the B-sunspot. Observations show that the A-sunspot is a following polarity sunspot in 18 events and displays flux emergence in 13 cases. All of the B-sunspots are relatively simple, exhibiting either one main sunspot or one main sunspot and several small neighboring sunspots (pores). In two days prior to the flare occurrence, the A-sunspot rotates in all the cases, while the B-sunspot rotates in 19 events. The total rotating angle of the A-sunspot and B-sunspot rotates is 193◦ on average, and the rotating directions are the same in 12 events. In all cases; the A-sunspot and B-sunspot manifest shear motions with an average shearing angle of 28.◦5, and in 14 cases, the shearing direction is opposite to the rotating direction of the A-sunspot. We suggest that the emergence, the rotation, and the shear motions of the A-sunspot and B-sunspot result in the phenomenon that flare ribbons sweep across sunspots completely.

Solar source of energetic particles in interplanetary space during the 2006 December 13 event

C. **Li**, Y. Dai, J. -C. Vial, C. J. Owen, S. A. Matthews, Y. H. Tang, C. Fang, and A. N. Fazakerley

E-print, July **2009; File**, A&A

An X3.4 solar are and a fast halo coronal mass ejection (CME) occurred on 2006 December 13, accompanied by a high flux of energetic particles recorded both in near-Earth space and at ground level. **Our purpose is to provide evidence of flare acceleration in a major solar energetic particle (SEP) event**. We first present observations from ACE/EPAM, GOES, and the Apatity neutron monitor. It is found that the initial particle release time coincides with the flare emission and that the spectrum becomes softer and the anisotropy becomes weaker during particle injection, indicating that the acceleration source changes from a confined coronal site to a widespread interplanetary CME-driven shock. We then describe a comprehensive study of the associated flare active region. By use of imaging data from HINODE/SOT and SOHO/MDI magnetogram, we infer the flare magnetic reconnection rate in the form of the magnetic flux change rate. This correlates in time with the microwave emission, indicating a physical link between the flare magnetic reconnection and the acceleration of nonthermal particles. Combining radio spectrograph data from Huairou/NOAC, Culgoora/IPS, Learmonth/RSTN, and WAVES/WIND leads to a continuous and longlasting radio burst extending from a few GHz down to several kHz. Based on the photospheric vector magnetogram from Huairou/NOAC and the nonlinear force free field (NFFF) reconstruction method, we derive the 3D magnetic fi eld confi guration shortly after the eruption. Furthermore, we also compute coronal fi eld lines extending to a few solar radii using a potential- field source-surface (PFSS) model. *Both the so-called type III-l burst and the magnetic field configuration suggest that open-fi eld lines extend from the are active region into interplanetary space, allowing the accelerated and charged particles escape.*

Observations of The Magnetic Reconnection Signature of An M2 Flare on 2000 March 23

Leping **Li** and Jun Zhang

E-print, July **2009**, ApJ, 703:877–882, **2009, File**

Multi-wavelength observations of an M 2.0 flare event on **2000 March 23** in NOAA active region 8910 provide us a good chance to study the detailed structure and dynamics of the magnetic reconnection region. In the process of the flare, extreme ultraviolet (EUV) loops displayed two times of sideward motions upon a loop-top hard X-ray source with average velocities of 75 and 25.6 km/s, respectively. Meanwhile part of the loops disappeared and new post-flare loops formed. We consider these two motions to be the observational evidence of reconnection inflow, and find an X-shaped structure upon the post-flare loops during the period of the second motion. Two separations of the flare ribbons are associated with these two sideward motions, with average velocities of 3.3 and 1.3 km/s, separately. The sideward motions of the EUV loops and the separations of the flare ribbons are temporally consistent with two peaks of the X-ray flux. This indicates that there are two times of magnetic reconnection in the process of the flare. Using the observation of photospheric magnetic field, the velocities of the sideward motions and the separations, we deduce the corresponding coronal magnetic field strength to be about 13.2-15.2 G, and estimate the reconnection rates to be 0.05 and 0.02 for these two magnetic reconnection processes, respectively. Besides the sideward motions of EUV loops and the separations of flare ribbons, we also observe motions of bright points upward and downward along the EUV loops with velocities ranging from 45.4 to 556.7 km/s, which are thought to be the plasmoids accelerated in the current sheet and ejected upward and downward when magnetic reconnection occurs and energy releases. A cloud of bright material flowing outward from the loop-top hard X-ray source with an average velocity of 51 km/s in the process of the flare may be accelerated by the tension force of the newly reconnected magnetic field lines. All the observations can be explained by schematic diagrams of magnetic reconnection.

RADIO EMISSION FROM ACCELERATION SITES OF SOLAR FLARES
Yixuan **Li**1 and Gregory D. Fleishman1,2
Astrophysical Journal, 701:L52–L58, **2009** August
This Letter takes up the question of what radio emission is produced by electrons at the very acceleration site of a solar flare. Specifically, we calculate incoherent radio emission produced within two competing acceleration models—stochastic acceleration by cascading MHD turbulence and regular acceleration in collapsing magnetic traps. Our analysis clearly demonstrates that radio emission from acceleration sites (1) has sufficiently strong intensity to be observed by currently available radio instruments, and (2) has spectra and light curves that are distinctly different in these two competing models, which makes them observationally distinguishable. In particular, we suggest that some of the narrowband microwave and decimeter continuum bursts may be a signature of the stochastic acceleration in solar flares.

ON THE BRIGHTENING PROPAGATION OF POST-FLARE LOOPS OBSERVED BY TRACE
Leping **Li** et al **2009** ApJ 690 347-357
http://www.iop.org/EJ/abstract/0004-637X/690/1/347
Examining flare data observed by Transition Region and Coronal Explorer satellite from 1998 May to 2006 December, we choose 190 (151 M-class and 39 X-class) flare events which display post-flare loops (PFLs), observed by 171 Å and 195 Å wavelengths. One-hundred twenty-four of the 190 events exhibit flare ribbons (FRs), observed by 1600 Å images. We investigate the propagation of the brightening of these PFLs along the neutral lines and the separation of the FRs perpendicular to the neutral lines. Observations indicate that the footpoints of the initial brightening PFLs are always associated with the change of the photospheric magnetic fields. In most of the cases, the length of the FRs ranges from 20 Mm to 170 Mm. The propagating duration of the brightening is from 10 to 60 minutes, and from 10 to 70 minutes for the separating duration of the FRs. The velocities of the propagation and the separation range from 3 to 39 km s–1 and 3 to 15 km s–1, respectively. Both the propagating velocities and the separating velocities are associated with the flare strength and the length of the FRs. It appears that the propagation and the separation are dynamically coupled; the greater the propagating velocity, the faster the separation. Furthermore, a greater propagating velocity corresponds to a greater deceleration (or acceleration). These PFLs display three types of propagating patterns. In type I propagation, which includes about half of all the events, the brightening begins at the middle part of a set of PFLs, and propagates bidirectionally toward both of its ends. For type II, including 30% of all events, the brightening first appears at one end of a set of PFLs, then propagates to the other end. The remaining events belong to type III propagation, which display the initial brightening taking place at two (or more than two) positions on two (or more than two) sets of PFLs, then propagating bidirectionally along the neutral line. These three types of propagating patterns can be explained by a three-dimensional magnetic reconnection model. (See **Observational Analysis of Magnetic Reconnection Sequence,** Jiong **Qiu,** Astrophysical Journal, 692:1110–1124, **2009** February; **File)**

The Solar Magnetic Field and Coronal Dynamics of the Eruption on 2007 May 19
Y. **Li**, B. J. Lynch, G. Stenborg, J. G. Luhmann, K. E. J. Huttunen, B. T.

Welsch, P. C. Liewer, and A. Vourlidas
The Astrophysical Journal Letters, Vol. 681, No. 1: L37-L40, **2008**.
http://www.journals.uchicago.edu/doi/pdf/10.1086/590340
The solar eruption on 2007 May 19, from AR 10956 near solar disk center, consisted of a B9.5 flare (12:48 UT), a filament eruption, an EUV dimming, a coronal wave, and a multifront CME. The eruption was observed by the twin *STEREO* spacecraft at a separation angle of 8.5 . We report analysis of the source region photospheric _ magnetic field and its preeruption evolution using MDI magnetograms, the coronal magnetic field topology estimated via PFSS modeling, and the coronal dynamics of the eruption through *STEREO* EUVI wavelet-enhanced anaglyph movies. Despite its moderate magnitude and size, AR 10956 was a complex and highly nonpotential active region with a multipolar configuration, and hosted frequent flares, multiple filament eruptions, and CMEs.

In the 2 days prior to the May 19 eruption, the total unsigned magnetic flux of the region decreased by ~17%.

We interpret the photospheric magnetic field evolution, the coronal field topology, and the observed coronal dynamics in the context of current models of CME initiation and discuss the prospects for future MHD modeling inspired by these analyses.

Results from the Study of an M7.6 Flare and its Associated CME --

Hui **Li** and Youping Li, E-print, Dec 2006
Advances in Space Research, Volume 41, Issue 6, *Pages 962-968*, **2008**
An M7.6 flare was well observed on **October 24, 2003** in active region 10486 by a few instruments and satellites, including GOES, TRACE, SOHO, RHESSI and NoRH. Multi-wavelength study shows that this flare underwent two episodes. During the first episode, only a looptop source of <40 keV was observed in reconstructed RHESSI images, which showed shrinkage with a velocity of 12–14 km s^{-1} in a period of about 12 min. During the second process, in addition to the looptop source, two footpoint sources were observed in energy channel of as high as $\sim$200 keV. One of them showed fast propagation along one of the two TRACE 1600 Å flare ribbons and the 195 Å loop footpoints, which could be explained by successive magnetic reconnection. The associated CME showed a mass pickup process with decreasing center-of-mass velocity. The decrease of the CME kinetic energy and the increase of its potential energy lead to an almost constant total energy during the CME propagation. Our results reveal that the flare and its associated CME have comparable energy content, and the flare is of non-thermal property.

Interaction of magnetic field systems leading to an X1.7 flare due to large-scale flux tube emergence

H. **Li**, B. Schmieder, M.T. Song, and V. Bommier
E-print, Sept 2007; A&A 475, 1081-1091 (**2007**)
2005 September 13

Observational Studies of the X-Ray Quasi-Periodic Oscillations of a Solar Flare

Y.P. **Li** · W.Q. Gan
Solar Phys (**2008**) 247: 77–85
http://www.springerlink.com/content/f14t5w412g150114/fulltext.pdf
We study an M2.6 flare observed with RHESSI on **22 August 2005**. The light curves of the hard X-rays (counts and photon fluxes), the derived number fluxes, as well as the energy fluxes of energetic electrons all presented a damped quasi-periodic oscillation. The modulation depth of the hard X-rays increased with the energies. For the energy fluxes of energetic electrons, the modulation depth can be as high as 90%. During the oscillations, however, the plasma temperature had no apparent change. No correspondence was found between the motions of the flare loops and the quasi-periodic oscillations. We conclude that an oscillation with a high modulation depth for a period of about four minutes cannot be easily explained with the existing mechanisms.

Li, Y. P., Gan, W. Q. **The oscillatory shrinkage in TRACE 195 ºA loops during a flare impulsive phase**. ApJ 644, L97-L100, **2006**.

Magnetic-reconnection-driven Turbulence and Turbulent Reconnection Acceleration

Shi-Min **Liang**1, Jian-Fu Zhang1,2, Na-Na Gao1, and Hua-Ping Xiao1,2
2023 ApJ 952 93
https://iopscience.iop.org/article/10.3847/1538-4357/acdc18/pdf
This paper employs an MHD-PIC method to perform numerical simulations of magnetic-reconnection-driven turbulence and turbulent reconnection acceleration of particles. Focusing on the dynamics of the magnetic reconnection, the properties of self-driven turbulence, and the behavior of particle acceleration, we find the following: (1) When

reaching a statistically steady state of the self-driven turbulence, the magnetic energy is almost released by 50%, while the kinetic energy of the fluid increases by no more than 15%. (2) The properties of reconnection-driven turbulence are more complex than the traditional turbulence driven by an external force. (3) The strong magnetic field tends to enhance the turbulent reconnection efficiency to accelerate particles more efficiently, resulting in a hard spectral energy distribution. Our study provides a particular perspective on understanding turbulence properties and turbulent-reconnection-accelerated particles.

Chromospheric condensations and magnetic field in a C3.6-class flare studied via He I D3 spectro-polarimetry

Tine **Libbrecht**, Jaime de la Cruz Rodriguez, Sanja Danilovic, Jorrit Leenaarts, Hiva Pazira
A&A 621, A35 **2019**
https://arxiv.org/pdf/1806.06880.pdf
Context. Magnetic reconnection during flares takes place in the corona but a substantial part of flare energy is deposited in the chromosphere. However, high-resolution spectro-polarimetric chromospheric observations of flares are very rare. The most used observables are Ca II 8542 {\AA} and He I 10830 {\AA}. Aims. We aim to study the chromosphere during a C3.6 class flare via spectro-polarimetric observations of the He I D3 line. Methods. We present the first SST/CRISP spectro-polarimetric observations of He I D3. We analyze the data using the inversion code HAZEL, and estimate the LOS velocity and the magnetic field vector. Results. Strong He I D3 emission at the flare footpoints, as well as strong He I D3 absorption profiles tracing the flaring loops are observed during the flare. The He I D3 traveling emission kernels at the flare footpoints exhibit strong chromospheric condensations of up to ∼ 60 km/s at their leading edge. Our observations suggest that such condensations result in shocking the deep chromosphere, causing broad and modestly blueshifted He I D3 profiles indicating subsequent upflows. A strong and rather vertical magnetic field of up to ∼ 2500 G is measured in the flare footpoints, confirming that the He I D3 line is likely formed in the deep chromosphere at those locations. We provide chromospheric line-of-sight velocity and magnetic field maps obtained via He I D3 inversions. We propose a fan-spine configuration as the flare magnetic field topology. Conclusions. The He I D3 line is an excellent diagnostic to study the chromosphere during flares. The impact of strong condensations on the deep chromosphere has been observed. Detailed maps of the flare dynamics and the magnetic field are obtained. **2015-05-05**

Observations of Ellerman bomb emission features in He I D3 and He I 10830 Å

Tine **Libbrecht**, Jayant Joshi, Jaime de la Cruz Rodríguez, Jorrit Leenaarts, Andrés Asensio Ramos
A&A **2016**
https://arxiv.org/pdf/1610.01321v1.pdf
Context. Ellerman bombs (EBs) are short-lived emission features, characterized by extended wing emission in hydrogen Balmer lines. Until now, no distinct signature of EBs has been found in the He I 10830 {\AA} line, and conclusive observations of EBs in He I D 3 have never been reported. Aims. We aim to study the signature of EBs in neutral helium triplet lines.
Methods. The observations consist of 10 consecutive SST/TRIPPEL raster scans close to the limb, featuring the Hβ, He I D3 and He I 10830 {\AA} spectral regions. We also obtained raster scans with IRIS and make use of the SDO/AIA 1700 {\AA} channel. We use Hazel to invert the neutral helium triplet lines.
Results. Three EBs in our data show distinct emission signatures in neutral helium triplet lines, most prominently visible in the He I D3 line. The helium lines have two components: a broad and blue-shifted emission component associated with the EB, and a narrower absorption component formed in the overlying chromosphere. One of the EBs in our data shows evidence of strong velocity gradients in its emission component. The emission component of the other two EBs could be fitted using a constant slab. Our analysis hints towards thermal Doppler motions having a large contribution to the broadening for helium and IRIS lines. We conclude that the EBs must have high temperatures to exhibit emission signals in neutral helium triplet lines. An order of magnitude estimate places our observed EBs in the range of T∼2·104−105 K. **2015-08-01**

Ensemble Forecasting of Major Solar Flares with Short-, Mid-, and Long-term Active Region Properties

Daye **Lim**1, Yong-Jae Moon1, Eunsu Park1, Jongyeob Park2, Kangjin Lee1,3, Jin-Yi Lee4, and Soojeong Jang2
2019 ApJ 885 35
sci-hub.se/10.3847/1538-4357/ab45e7
We apply an ensemble technique for major flare prediction by considering short-, mid-, and long-term active region (AR) properties and their relative contributions. For this, we consider magnetic parameters from Solar Dynamics Observatory/Helioseismic and Magnetic Imager and flare lists from Geostationary Operational Environmental Satellites. In this study, we simultaneously consider flaring rates during short- (1 day), mid- (several days), and long-

term (several years) timeframes. In our model, the predicted rate is given by a weighted combination of the three rates such that the sum of their weights is 1. We calculate the Brier skill scores (BSSs) for investigating prediction performance and weights of these three terms to provide optimal results. The BSS (0.22) of the model with only long-term properties is higher than that with only short-term (0.07) or mid-term (0.08) properties. When short-/mid-term properties are additionally considered, the BSS is improved to 0.28/0.24. Our model has the best performance (BSS = 0.29) when all terms are considered, and their relative contributions to the short-, mid-, and long-term rates are 20%, 20%, and 60%, respectively. In addition, the model with three terms is more effective at predicting major flares in strong ARs. In view of the energy storage and release process, long-term magnetic properties may indicate the storage of magnetic free energy, while short- and mid-term flare history may reflect a recent trend of energy release process. Our results suggest that the performances of other existing flare models based on long-term properties should be improved by considering short- and/or mid-term flare history.

Forecast of Daily Major Flare Probability Using Relationships between Vector Magnetic Properties and Flaring Rates

Daye **Lim**, Yong-Jae Moon, Jongyeob Park, Eunsu Park, Kangjin Lee, Jin-Yi Lee, Soojeong Jang
Journal of the Korean Astronomical Society **2019**
https://arxiv.org/pdf/1907.11373.pdf
We develop forecast models of daily probability of major flares (M- and X-class) based on empirical relationships between photospheric magnetic parameters and daily flaring rates from May 2010 to April 2018. In this study, we consider ten magnetic parameters characterizing size, distribution, and non-potentiality of vector magnetic fields from Solar Dynamics Observatory (SDO)/Helioseismic and Magnetic Imager (HMI) and Geostationary Operational Environmental Satellites (GOES) X-ray flare data. The magnetic parameters are classified into three types: the total unsigned parameters, the total signed parameters, and the mean parameters. We divide the data into two sets chronologically: 70% for training and 30% for testing. The empirical relationships between the parameters and flaring rates are used to predict flare occurrence probabilities for a given magnetic parameter value. Major results of this study are as follows. First, major flare occurrence rates are well correlated with ten parameters having correlation coefficients above 0.85. Second, logarithmic values of flaring rates are well approximated by linear equations. Third, the total unsigned and signed parameters achieved better performance for predicting flares than the mean parameters in terms of verification measures of probabilistic and converted binary forecasts. We conclude that the total quantity of non-potentiality of magnetic fields is crucial for flare forecasting among the magnetic parameters considered in this study. When this model is applied for operational use, this model can be used using the data of 21:00 TAI with a slight underestimation of 2 - 6.3%. **2017 September 2 to 6**

Observation of a Large-scale Quasi-circular Secondary Ribbon associated with Successive Flares and a Halo CME

Eun-Kyung **Lim**, Vasyl Yurchyshyn, Pankaj Kumar, Kyuhyoun Cho, Chaowei Jiang, Sujin Kim, Heesu Yang, Jongchul Chae, Kyung-Suk Cho, Jeongwoo Lee
ApJ **850** 167 **2017**
https://arxiv.org/pdf/1711.00622.pdf
Solar flare ribbons provide an important clue to the magnetic reconnection process and associated magnetic field topology in the solar corona. We detected a large-scale secondary flare ribbon of a circular shape that developed in association with two successive M-class flares and one CME. The ribbon revealed interesting properties such as 1) a quasi-circular shape and enclosing the central active region; 2) the size as large as 500\arcsec\, by 650\arcsec\,, 3) successive brightenings in the clockwise direction at a speed of \kms{160} starting from the nearest position to the flaring sunspots, 4) radial contraction and expansion in the northern and the southern part, respectively at speeds of $\leq$ \kms{10}. Using multi-wavelength data from \textit{SDO}, \textit{RHESSI}, XRT, and Nobeyama, along with magnetic field extrapolations, we found that: 1) the secondary ribbon location is consistent with the field line footpoints of a fan-shaped magnetic structure that connects the flaring region and the ambient decaying field; 2) the second M2.6 flare occurred when the expanding coronal loops driven by the first M2.0 flare encountered the background decayed field. 3) Immediately after the second flare, the secondary ribbon developed along with dimming regions. Based on our findings, we suggest that interaction between the expanding sigmoid field and the overlying fan-shaped field triggered the secondary reconnection that resulted in the field opening and formation of the quasi-circular secondary ribbon. We thus conclude that interaction between the active region and the ambient large-scale fields should be taken into account to fully understand the entire eruption process. **2015 June 21**

Observations of a Series of Flares and Associated Jet-like Eruptions Driven by the Emergence of Twisted Magnetic Fields

Eun-Kyung **Lim**, Vasyl Yurchyshyn, Sung-Hong Park, Sujin Kim, Kyung-Suk Cho, Pankaj Kumar, Jongchul Chae, Heesu Yang, Kyuhyoun Cho, Donguk Song, Yeon-Han Kim
ApJ 817 39 **2016**

http://arxiv.org/pdf/1512.01330v1.pdf
We studied temporal changes of morphological and magnetic properties of a succession of four confined flares followed by an eruptive flare using the high-resolution New Solar Telescope (NST) operating at the Big Bear Solar Observatory (BBSO), Helioseismic and Magnetic Imager (HMI) magnetograms and Atmospheric Image Assembly (AIA) EUV images provided by Solar Dynamics Observatory (SDO). From the NST/Halpha and the SDO/AIA~304 A observations we found that each flare developed a jet structure that evolved in a manner similar to evolution of the blowout jet : 1) an inverted-Y shape jet appeared and drifted away from its initial position; 2) jets formed a curtain-like structure that consisted of many fine threads accompanied with subsequent brightenings near the footpoints of the fine threads; and finally 3) the jet showed a twisted structure visible near the flare maximum. Analysis of the HMI data showed that both the negative magnetic flux and the magnetic helicity have been gradually increasing in the positive polarity region indicating the continuous injection of magnetic twist before and during the series of flares. Based on these results, we suggest that the continuous emergence of twisted magnetic flux played an important role in producing a successive flares and developing a series of blowout jets. **2012-07-02**

Evolutionary Relationship between Sunspot Groups and Soft X-Ray Flares over Solar Cycles 21–25

Jiaqi **Lin** (**林家琪**)1,2, Feng Wang (**王锋**)1,2, Linhua Deng (邓林华)3,4, Hui Deng (邓辉)1,2, Ying Mei (**梅盈**)1,2, and Xiaojuan Zhang
2023 ApJ 958 1
https://iopscience.iop.org/article/10.3847/1538-4357/ad0469/pdf
Studying the interaction between solar flares and sunspot groups (SGs) is crucial for understanding and predicting solar activity. We examined the distribution, correlation, and flaring rates in the northern and southern hemispheres to reveal the relationship between different classes of soft X-ray (SXR) flares and different magnetic classifications of SGs. We discovered a significant north–south asymmetry in SXR flares and SG distribution over Solar Cycles (SC) 21–25. In the rising phase of SC24, the northern hemisphere's activity is significantly excessive. In the declining phase of SC24, the southern hemisphere's activity becomes significantly excessive. The total numbers of various SXR flares and SGs vary between the northern and southern hemispheres over the solar cycle. B-class flares are negatively correlated with all SGs at maximum but positively correlated at minimum. C-class flares correlate best with α and β SGs. M-class flares correlate best with βγδ and β SGs. X-class flares correlate highest with βγδ SGs. The flaring rate of each flare class is lowest for α SGs and highest for βγδ SGs. The flaring rates are higher in the southern hemisphere than in the northern hemisphere. Our results demonstrate that solar flares originate from different sources of solar active regions; the high-energy flares tend to be caused by more complex magnetic fields.

A New Parameter of the Photospheric Magnetic Field to Distinguish Eruptive-flare Producing Solar Active Regions

Pei Hsuan **Lin**1, Kanya Kusano1, Daikou Shiota2, Satoshi Inoue1, K. D. Leka1,3, and Yuta Mizuno1
2020 ApJ 894 20
sci-hub.tw/10.3847/1538-4357/ab822c
Solar flares and coronal mass ejections (CMEs) are eruptive phenomena caused by coronal magnetic fields. In particular, large eruptive events originate in active regions (AR) with strong surface magnetic fields. However, it is still unclear what determines the capability of an AR to specifically produce eruptive flares and CMEs, and this hinders our knowledge of the initiation mechanism for the eruptive component of these phenomena. In this study, we propose a new parameter r m to measure the possibility that a flare that occurs in an AR can be eruptive and produce a CME. The parameter r m is defined by the ratio of the magnetic flux of twist higher than a threshold T c to the surrounding—and specifically, the overlying—magnetic flux. The value of r m for each AR can be estimated using nonlinear force-free field extrapolation models of the coronal magnetic field. Based on the data obtained by the Solar Dynamics Observatory/Helioseismic and Magnetic Imager, we calculated the values of r m for 29 ARs at 51 times prior to flares larger than M5.0 class. We find that the footpoints of field lines with twist higher than 0.2 can represent the subsequent flare ribbons well, and field lines that overlie and "fence in" the highly twisted region will work to confine the eruption, generating confined flares. Discriminant function analysis is used to show that r m is moderately well able to distinguish ARs that have the capability of producing eruptive flares. **13-15 February 2011, 2014-01-07**
Table 1 Event List for Analysis (2011-2015)

Soft X-ray irradiance measured by the Solar Aspect Monitor on the Solar Dynamic Observatory Extreme ultraviolet Variability Experiment

C. Y. **Lin**, S. M. Bailey, A. Jones, D. Woodraska, A. Caspi, T. N. Woods, F. G. Eparvier, S. R. Wieman, L. V. Didkovsky

JGR **2016**
http://arxiv.org/pdf/1605.01444v1.pdf
The Solar Aspect Monitor (SAM) is a pinhole camera on the Extreme-ultraviolet Variability Experiment (EVE) aboard the Solar Dynamics Observatory (SDO). SAM projects the solar disk onto the CCD through a metallic filter designed to allow only solar photons shortward of 7 nm to pass. Contamination from energetic particles and out-of-band irradiance is, however, significant in the SAM observations. We present a technique for isolating the 0.01--7 nm integrated irradiance from the SAM signal to produce the first results of broadband irradiance for the time period from May 2010 to May 2014. The results of this analysis agree with a similar data product from EVE's EUV SpectroPhotometer (ESP) to within 25%. We compare our results with measurements from the Student Nitric Oxide Explorer (SNOE) Solar X-ray Photometer (SXP) and the Thermosphere Ionosphere Mesosphere Energetics and Dynamics (TIMED) Solar EUV Experiment (SEE) at similar levels of solar activity. We show that the full-disk SAM broadband results compare well to the other measurements of the 0.01--7 nm irradiance. We also explore SAM's capability toward resolving spatial contribution from regions of solar disk in irradiance and demonstrate this feature with a case study of several strong flares that erupted from active regions on **March 11, 2011**.

Energy Release and Particle Acceleration in Flares: Summary and Future Prospects

R.P. **Lin**
Space Sci Rev (**2011**) 159:421–445, **File** **A Review**
RHESSI measurements relevant to the fundamental processes of energy release and particle acceleration in flares are summarized. RHESSI's precise measurements of hard X-ray continuum spectra enable model-independent deconvolution to obtain the parent electron spectrum. Taking into account the effects of albedo, these show that the low energy cut-off to the electron power-law spectrum is typically ≲tens of keV, confirming that the accelerated electrons contain a large fraction of the energy released in flares. RHESSI has detected a high coronal hard X-ray source that is filled with accelerated electrons whose energy density is comparable to the magnetic-field energy density. This suggests an efficient conversion of energy, previously stored in the magnetic field, into the bulk acceleration of electrons. A new, collisionless (Hall) magnetic reconnection process has been identified through theory and simulations, and directly observed in space and in the laboratory; it should occur in the solar corona as well, with a reconnection rate fast enough for the energy release in flares. The reconnection process could result in the formation of multiple elongated magnetic islands, that then collapse to bulk-accelerate the electrons, rapidly enough to produce the observed hard X-ray emissions. RHESSI's pioneering γ-ray line imaging of energetic ions, revealing footpoints straddling a flare loop arcade, has provided strong evidence that ion acceleration is also related to magnetic reconnection. Flare particle acceleration is shown to have a close relationship to impulsive Solar Energetic Particle (SEP) events observed in the interplanetary medium, and also to both fast coronal mass ejections and gradual SEP events. New instrumentation to provide the high sensitivity and wide dynamic range hard X-ray and γ-ray measurements, plus energetic neutral atom (ENA) imaging of SEPs above ~2 $R_\odot$, will enable the next great leap forward in understanding particle acceleration and energy release is large solar eruptions—solar flares and associated fast coronal mass ejections (CMEs).

INVESTIGATION OF THICKNESS AND ELECTRICAL RESISTIVITY OF THE CURRENT SHEETS IN SOLAR ERUPTIONS

J. **Lin**[1,2], J. Li[3], Y.-K. Ko[2], and J. C. Raymond[2]
Astrophysical Journal, 693:1666–1677, **2009** March 10
http://www.iop.org/EJ/toc/-alert=43190/0004-637X/693/2
A discussion of the thickness of current sheets in solar eruptions, *d*, led Lin et al. in 2007 to estimate very large values for the effective resistivity, η_e. Here, we address some questions raised by that paper. We apply the limb synoptic map technique and find *d* between 5.0×10^4 and 4.6×10^5 km, increasing with both time and altitude. The possibility that large apparent *d* and η_e result from projection effects is examined and rejected.We derive theoretical scaling laws relating *d* to other observables that corroborate this conclusion and thus help confine both *d* and η_e to a reasonable range. The possible impact of our results on the existing models of particle acceleration in reconnecting current sheets is also briefly discussed.

Particle Acceleration by the Sun: Electrons, Hard X-rays/Gamma-rays **Review**

Lin R. P. et al.,
Space Sci. Rev. 124 (**2006**) 233.

Submerged Sources of Transient Acoustic Emission from Solar Flares

Charles **Lindsey**[1], J. C. Buitrago-Casas[2,3], Juan Carlos Martínez Oliveros[3], Douglas Braun[1], Angel D. Martínez[4], Valeria Quintero Ortega[4], Benjamín Calvo-Mozo[4], and Alina-Catalina Donea[5]

2020 ApJL 901 L9
https://doi.org/10.3847/2041-8213/abad2a
https://iopscience.iop.org/article/10.3847/2041-8213/abad2a/pdf
We report the discovery of ultra-impulsive acoustic emission from a solar flare, emission with a seismic signature that indicates submersion of its source approximately a Mm beneath the photosphere of the active region that hosted the flare. Just over two decades ago V. V. Zharkova and A. G. Kosovichev discovered the first acoustic transient released into the Sun's interior by a solar flare. These acoustic waves, refracted back upward to the solar surface after their release, make conspicuous Doppler ripples spreading outward from the flaring region that tell us a lot about their sources. The mechanism by which these transients are driven has stubbornly eluded our understanding. Some of the source regions, for example, are devoid of secondary Doppler, magnetic, or thermal disturbances in the outer atmosphere of the source regions that would signify the driving agent of an intense seismic transient in the outer atmosphere. In this study, we have applied helioseismic holography, a diagnostic based upon standard wave optics, to reconstruct a 3D image of the sources of acoustic waves emanating from the M9.3-class flare of **2011 July 30**. These images contain a source component that is submerged a full Mm beneath the active-region photosphere. The signature of acoustic sources this deep in the solar interior opens new considerations into the physics that must be involved in transient acoustic emission from flares—and possibly of flare physics at large. We develop analogies to seismicity remotely triggered by tremors from distant earthquakes, and consider prospects of new insight into the architecture of magnetic flux beneath flaring active regions.
RHESSI Science Nuggets #388 Sep **2020**
https://sprg.ssl.berkeley.edu/~tohban/wiki/index.php/Submerged_Flare_Acoustic_Sources
Flare acoustic radiation emanates from a source _inside_ the Sun.
HMI Science Nuggets #148 Dec 2020 http://hmi.stanford.edu/hminuggets/?p=3405

The Role of Magnetic Fields in Transient Seismic Emission Driven by Atmospheric Heating in Flares

C. **Lindsey**, A.-C. Donea, J. C. Martínez Oliveros, H. S. Hudson
Solar Physics, May **2014**, Volume 289, Issue 5, pp 1457-1469
http://arxiv.org/pdf/1303.3299v1.pdf
Transient seismic emission in flares remains largely mysterious. Its discoverers proposed that seismic transients are driven by impulsive heating of the flaring chromosphere. Simulations of such heating show strong shocks, but these are damped by heavy radiative losses as they proceed downward. Because compression of the gas the shock enters both heats it and increases its density, the radiative losses increase radically with the strength of the shock, leaving doubt that sufficient energy can penetrate into the solar interior to explain helioseismic signatures. We note that simulations to date have no account for strong, inclined magnetic fields characteristic of transient-seismic-source environments. A strong horizontal magnetic field, for example, greatly increases the compressional modulus of the chromospheric medium, greatly reducing compression of the gas, hence radiative losses. Inclined magnetic fields, then, must be fundamental to the role of impulsive heating in transient seismic emission.
This could explain the strong affinity of seismic sources to regions of strong, highly inclined penumbral magnetic fields, including the neutral lines separating opposing polarities in δ-configuration sunspots. The basic point, then, is that the role of inclined magnetic fields is fundamental to our understanding of the role of impulsive heating in transient seismic emission. Obliquely inclined magnetic fields will complicate simulations of impulsive heating considerably. However, horizontal magnetic fields, as a preliminary control simulation, can be incorporated into standard 1-D thick-target-heating simulations with a relatively simple adaptation of existing HD codes. 2005 January 15. **2011-02-15**

Peak Temperatures of Large Solar X-Ray Flares and Associated CME Speeds and Widths

A. G. **Ling** and S. W. Kahler
2020 ApJ 891 54
sci-hub.si/10.3847/1538-4357/ab6f6c
We recently repeated an earlier analysis by Garcia showing that large (≥M3.0) solar X-ray flares associated with solar energetic particle (SEP) events have significantly lower peak X-ray flux ratios R = (0.04–0.5 nm)/(0.1–0.8 nm), proxies for flare peak temperatures, than those without SEP events. As we expect SEP events to be produced by shocks ahead of fast coronal mass ejections (CMEs), a smaller R for an X-ray flare of a given peak flux Fp should also be more likely to be accompanied by a fast (Vcme > 1000 km s−1) CME. We confirm this expectation, examine the role played by the ratios R in correlations between Fp and CME speeds Vcme, and then compare CME widths W, Vcme, and R with each other. We consider an apparent conflict between a global scaling model of eruptive events showing Vcme scaling with higher R and our confirmation that the Garcia analysis implies that faster CMEs are associated with flares of lower R. The R values are examined for 16 large flares of the well-studied AR 12192, for which nearly all flares had no associated CMEs. Those flares share the same high values of R as other active region (AR) flares with no CMEs. We also find that small (<M3.0) flares of filament eruptions leading to SEP events share the lower R values of larger flares with fast CMEs.
Table 2 X-ray Flares and CME Speeds of FE SEP Events

Table 3 X-ray Flares > M3 and Associated CMEs and SEP Events (This table is available in its entirety in machine-readable form.)

Risks for Life on Habitable Planets from Superflares of Their Host Stars

Manasvi **Lingam**1,2 and Abraham Loeb
2017 ApJ 848 41
http://sci-hub.cc/10.3847/1538-4357/aa8e96
We explore some of the ramifications arising from superflares on the evolutionary history of Earth, other planets in the solar system, and exoplanets. We propose that the most powerful superflares can serve as plausible drivers of extinction events, and that their periodicity corresponds to certain patterns in the terrestrial fossil diversity record. On the other hand, weaker superflares may play a positive role in enabling the origin of life through the formation of key organic compounds. Superflares could also prove to be quite detrimental to the evolution of complex life on present-day Mars and exoplanets in the habitable zone of M- and K-dwarfs. We conclude that the risk posed by superflares has not been sufficiently appreciated, and that humanity might potentially witness a superflare event in the next $\sim 10^3$ years, leading to devastating economic and technological losses. In light of the many uncertainties and assumptions associated with our analysis, we recommend that these results should be viewed with due caution.

MULTISPECTRAL EMISSION OF THE SUN DURING THE FIRST WHOLE SUN MONTH: MAGNETOHYDRODYNAMIC SIMULATIONS

Roberto **Lionello** et al **2009** ApJ 690 902-912
http://www.iop.org/EJ/abstract/0004-637X/690/1/902
We demonstrate that a three-dimensional magnetohydrodynamic (MHD) simulation of the corona can model its global plasma density and temperature structure with sufficient accuracy to reproduce many of the multispectral properties of the corona observed in extreme ultraviolet (EUV) and X-ray emission. The key ingredient to this new type of global MHD model is the inclusion of energy transport processes (coronal heating, anisotropic thermal conduction, and radiative losses) in the energy equation. The calculation of these processes has previously been confined to one-dimensional loop models, idealized two-dimensional computations, and three-dimensional active region models. We refer to this as the thermodynamic MHD model, and we apply it to the time period of Carrington rotation 1913 (1996 August 22 to September 18). The form of the coronal heating term strongly affects the plasma density and temperature of the solutions. We perform our calculation for three different empirical heating models: (1) a heating function exponentially decreasing in radius; (2) the model of Schrijver et al.; and (3) a model reproducing the heating properties of the quiet Sun and active regions. We produce synthetic emission images from the density and temperature calculated with these three heating functions and quantitatively compare them with observations from EUV Imaging Telescope on the Solar and Heliospheric Observatory and the soft X-ray telescope on Yohkoh. Although none of the heating models provide a perfect match, heating models 2 and 3 provide a reasonable match to the observations.

The Solar Chromosphere Observed at 1 Hz and 0.''2 Resolution

Isabel **Lipartito**1, Philip G. Judge2, Kevin Reardon3,4, and Gianna Cauzzi
2014 ApJ 785 109
We recently reported extremely rapid changes in chromospheric fine structure observed using the IBIS instrument in the red wing of Hα. Here, we examine data obtained during the same observing run (2010 August 7), of a mature active region NOAA 11094. We analyze more IBIS data including wavelength scans and data from the Solar Dynamics Observatory, all from within a 30 minute interval. Using a slab radiative transfer model, we investigate the physical nature of fibrils in terms of tube-like versus sheet-like structures. Principal Component Analysis shows that the very rapid Hα variations in the line wings depend mostly on changes of line width and line shift, but for Ca II 854.2 the variations are dominated by changes in column densities. The tube model must be rejected for a small but significant class of fibrils undergoing very rapid changes. If our wing data arise from the same structures leading to "type II spicules," our analysis calls into question much recent work. Instead, the data do not reject the hypothesis that some fibrils are optical superpositions of plasma collected into sheets. We review how Parker's theory of tangential discontinuities naturally leads to plasma collecting into sheets, and show that the sheet picture is falsifiable. Chromospheric fine structures seem to be populated by both tubes and sheets. We assess the merits of spectral imaging versus slit spectroscopy for future studies.

HINODE OBSERVATIONS SUGGESTING THE PRESENCE OF A LOCAL SMALL-SCALE TURBULENT DYNAMO

B. W. **Lites**
2011 ApJ 737 52

Analysis of observations from the Hinode/Solar Optical Telescope spectropolarimeter (SP) yields results that are consistent with the operation of a small-scale turbulent dynamo in the upper solar convection zone. Examination of 45 Hinode data sets obtained in 2007 reveals only a very small correlation of the net polarity imbalance of the regions of the quiet Sun having very weak flux, relative to the polarity imbalance averaged over each data set. Further, there is no correlation of the average net unsigned flux of those regions of weakest flux with the average unsigned flux of each region studied. Positive correlations, especially of the net unsigned flux, should exist if the internetwork fields were to arise from dispersal of flux from active regions, so the absence of significant correlations supports the small-scale dynamo (SSD) scenario. Considering only regions of weakest flux, the net longitudinal flux increases slightly toward the limb, probably as the result of the dominance of horizontal fields higher in the photosphere. Inferred distributions of magnetic field strength as derived from inversions of Stokes profiles indicate that the magnetic energy of the quiet Sun observed at the resolution of the Hinode SP is dominated by the small fraction of field elements having kilo-Gauss strengths. Because these strong-field elements carry most of the imbalance of magnetic flux measured in each region, they likely arise primarily from dispersal of flux from active regions, rather than from an SSD.

A Maximum Entropy Argument for the Slopes of Power-law Particle Spectra in Solar Flares

Yuri E. **Litvinenko**

2019 ApJ 880 20

sci-hub.se/10.3847/1538-4357/ab2760

The maximum entropy formalism is used to infer the spectral index of power-law particle spectra in the heliosphere. The entropy-maximization argument by Brown et al. is revisited and generalized by relaxing the assumption of a particle spectrum extending to an infinite energy. The results for particle spectra with a finite upper cutoff energy are shown to be qualitatively different from those for spectra extending to infinity. The dependence of the predicted spectral index on the upper cutoff energy is determined. The relevance of the predicted values of the spectral index to the observed spectra of accelerated electrons in solar flares and ion tails in the solar wind is discussed.

Power-law spectra of energetic electrons in solar flares from the maximum entropy and dimensional considerations

Y.E.**Litvinenko**

Advances in Space Research Volume 63, Issue 4, 15 February **2019**, Pages 1466-1471

The maximum entropy formalism and dimensional analysis are used to derive a power-law spectrum of accelerated electrons in impulsive solar flares, where the particles can contain a significant fraction of the total flare energy. Entropy considerations are used to derive a power-law spectrum for a particle distribution characterised by its order of magnitude of energy. The derivation extends an earlier one-dimensional argument to the case of an isotropic three-dimensional particle distribution. Dimensional arguments employ the idea that the spectrum should reflect a balance between the processes of energy input into the corona and energy dissipation in solar flares. The governing parameters are suggested on theoretical grounds and shown to be consistent with solar flare observations. The flare electron flux, differential in the non-relativistic electron kinetic energy E, is predicted to scale as E-3. This scaling is in agreement with RHESSI measurements of the hard X-ray flux that is generated by deka-keV electrons, accelerated in intense solar flares

Time-dependent particle acceleration in a Fermi reservoir

Y. E. **Litvinenko**

A&A 544, A94 (**2012**)

Context. A steady model was presented by Burn, in which energy conservation is used to constrain the parameters of stochastic Fermi acceleration. A steady model, however, is unlikely to be adequate for particle acceleration in impulsive solar flares.

Aims. This paper describes a time-dependent model for particle acceleration in a Fermi reservoir

Methods. The calculation is based on the original formulation of stochastic acceleration by Fermi, with additional physically motivated assumptions about the turbulent and particle energy densities within the reservoir, that are similar to those of the steady analysis. The problem is reduced to an integro-differential equation that possesses an analytical solution.

Results. The model predicts the formation of a power-law differential energy spectrum N(E) ~ E-2, that is observable outside the reservoir. The predicted spectral index is independent of the parameters of the model. The results may help in understanding particle acceleration in solar flares and other astrophysical applications.

A New Approach of Data-driven Simulation and its Application to Solar Active Region 12673

Liu, ZP ; Jiang, CW ; Bian, XK ; Liu, QJ ; Zou, P ; Feng, XS

RAA Volume 24 Issue 12 Article Number 125005 **2024**

https://www.webofscience.com/wos/woscc/full-record/WOS:001372301700001DOI 10.1088/1674-4527/ad862b

The solar coronal magnetic field is a pivotal element in the study of eruptive phenomena, and understanding its dynamic evolution has long been a focal point in solar physics. Numerical models, driven directly by observation data, serve as indispensable tools in investigating the dynamics of the coronal magnetic field. This paper presents a new approach to electric field inversion, which involves modifying the electric field derived from the DAVE4VM velocity field using ideal Ohm's law. The time series of the modified electric field is used as a boundary condition to drive a magnetohydrodynamics model, which is applied to simulate the magnetic field evolution of active region 12673. The simulation results demonstrate that our method enhances the magnetic energy injection through the bottom boundary, as compared with energy injection calculated directly from the DAVE4VM code, and reproduces the evolution of the photospheric magnetic flux. The coronal magnetic field structure is also in morphological similarity to the coronal loops. This new approach will be applied to the high-accuracy simulation of eruption phenomena and provide more details on the dynamical evolution of the coronal magnetic field.

The Relationship between Kinetic and Magnetic Helicity in Solar Active Regions

Yang **Liu**1, Rudolf Komm2, Nicholas H. Brummell3, J. Todd Hoeksema1, Bhishek Manek4, and Gherardo Valori5

2024 ApJ 971 1

https://iopscience.iop.org/article/10.3847/1538-4357/ad58b7/pdf

Using Helioseismic and Magnetic Imager/Solar Dynamics Observatory data, we search for a relationship between kinetic helicity and magnetic helicity in solar active regions (ARs) using a sample of 62 ARs from 2010 May to 2015 May. The sample includes 32 mature ARs and 30 emerging ARs. We calculate kinetic helicity in the interior in the depth range from 0.6 to 11.6 Mm, magnetic helicity in the corona, helicity flux across the photosphere, and the magnetic twist and magnetic writhe of the ARs at the photosphere. From these data, relationships are found between magnetic helicity, helicity flux, and magnetic twist. However, magnetic writhe appears not to be related to the other magnetic quantities. No relationship is found between the kinetic helicity and any magnetic quantity. In particular, no relationship is found between the kinetic helicity and any of the following: magnetic helicity, magnetic helicity flux, magnetic twist, or magnetic writhe. These results suggest that (1) the magnetic helicity in the corona above ARs is mainly derived from the magnetic twist, and (2) the flow dynamics in the region from 0.6 to 11.6 Mm below the photosphere is not the primary source for the generation of magnetic helicity in ARs.

Solar flares and active regions in the Hale sector boundary in Solar Cycle 24

Claire L **Liu**, Junwei Zhao

MNRAS, Volume 527, Issue 2, January **2024**, Pages 1910–1914,

https://doi.org/10.1093/mnras/stad3298

https://academic.oup.com/mnras/article-pdf/527/2/1910/53252573/stad3298.pdf

Solar eruptions, such as flares and coronal mass ejections, have serious impacts on the Earth’s environment and human activity. Predicting the eruptions and therefore avoiding their damages is a main goal in the research community. Heliospheric current sheet (HCS), the boundary dividing the positive and negative magnetic fields that open up to the interplanetary space, is believed to be related with solar eruptions. The HCS consists of two types of boundaries: the Hale boundary and the non-Hale boundary, and the former is suggested in previous studies to be the region producing most of the solar flares. In this work, we explore relationships between Hale boundary, flares, and property of active regions (ARs). The HCS is determined from the magnetic field in the heliosphere calculated from the observed photospheric magnetic field using a potential field source surface model. We have analysed 8075 flares of C-class and above and 1652 ARs in the period from May 2010 to May 2019 in Solar Cycle 24. The following results are obtained: (1) 5957 flares (74±1 per cent) and 1212 ARs (73±2 per cent) are in the HCS; (2) among them, 70 per cent (±1 per cent) flares and 57 per cent (±3 per cent) ARs are in the Hale boundary; and (3) big ARs tend to emerge in the Hale boundary. We conclude that the HCS is related tightly to solar activity, and the Hale boundary is a region favoured to produce flares and to host large ARs.

Large Photospheric Doppler Shift in Solar Active Region 12673: I. Field-Aligned Flows

Jiayi **Liu**, Xudong Sun, Peter W. Schuck, Sarah A. Jaeggli, Brian T. Welsch, Carlos Quintero Noda

ApJ **955** 40 **2023**

https://arxiv.org/pdf/2307.09709.pdf

https://iopscience.iop.org/article/10.3847/1538-4357/ace907/pdf

Delta (δ) sunspots sometimes host fast photospheric flows along the central magnetic polarity inversion line (PIL). Here we study the strong Doppler shift signature in the central penumbral light bridge of solar active region NOAA 12673. Observations from the Helioseismic and Magnetic Imager (HMI) indicate highly sheared, strong magnetic fields. Large Doppler shifts up to 3.2 km s−1 appeared during the formation of the light bridge and persisted for about 16 hours. A

new velocity estimator, called DAVE4VMwDV, reveals fast converging and shearing motion along the PIL from HMI vector magnetograms, and recovers the observed Doppler signal much better than an old version of the algorithm. The inferred velocity vectors are largely (anti-)parallel to the inclined magnetic fields, suggesting that the observed Doppler shift contains significant contribution from the projected, field-aligned flows. High-resolution observations from the Hinode/Spectro-Polarimeter (SP) further exhibit a clear correlation between the Doppler velocity and the cosine of the magnetic inclination, which is in agreement with HMI results and consistent with a field-aligned flow of about 9.6 km s−1. The complex Stokes profiles suggest significant gradients of physical variables along the line of sight. We discuss the implications on the δ-spot magnetic structure and the flow-driving mechanism. **6 Sep 2017**

A Selective Up-sampling Method Applied Upon Unbalanced Data for Flare Prediction: Potential To Improve Model Performance

Siwei **Liu**, Jingjing Wang, Ming Li, Ming Li, Yanmei Cui, Yanmei Cui, Juan Guo, Yurong Shi, Bingxian Luo, and Siqing Liu

Front. Astron. Space Sci. 10:1082694. **2023**

doi: 10.3389/fspas.2023.1082694

https://www.frontiersin.org/articles/10.3389/fspas.2023.1082694/pdf

The Spaceweather HMI Active Region Patch (SHARP) parameters have been widely used to develop flare prediction models. The relatively small number of strong-flare events leads to an unbalanced dataset that prediction models can be sensitive to the unbalanced data and might lead to bias and limited performance. In this study, we adopted the logistic regression algorithm to develop a flare prediction model for the next 48 h based on the SHARP parameters. The model was trained with five different inputs. The first input was the original unbalanced dataset; the second and third inputs were obtained by using two widely used sampling methods from the original dataset, while the fourth input was the original dataset but accompanied by a weighted classifier. Based on the distribution properties of strong-flare occurrences related to SHARP parameters, we established a new selective up-sampling method and applied it to the mixed-up region (referred to as the confusing distribution areas consisting of both the strong-flare events and non-strong-flare events) to pick up the flare-related samples and add small random values to them and finally create a large number of flare-related samples that are very close to the ground truth. Thus, we obtained the fifth balanced dataset aiming to 1) promote the forecast capability in the mixed-up region and 2) increase the robustness of the model. We compared the model performance and found that the selective up-sampling method has potential to improve the model performance in strong-flare prediction with its F1 score reaching 0.5501 ± 0.1200, which is approximately 22% − 33% higher than other imbalance mitigation schemes.

Changes of Magnetic Energy and Helicity in Solar Active Regions from Major Flares

Yang **Liu**, Brian T. Welsch, Gherardo Valori, Manolis K. Georgoulis, Yang Guo, Etienne Pariat, Sung-Hong Park, Julia K. Thalmann

ApJ **942** 27 **2023**

https://arxiv.org/pdf/2211.09990.pdf

http://sun.stanford.edu/~yliu/papers/ChangeofHelicityEnergyinFlares.pdf

https://iopscience.iop.org/article/10.3847/1538-4357/aca3a6/pdf

Magnetic free energy powers solar flares and coronal mass ejections (CMEs), and the buildup of magnetic helicity might play a role in the development of unstable structures that subsequently erupt. To better understand the roles of energy and helicity in large flares and eruptions, we have characterized the evolution of magnetic energy and helicity associated with **21 X-class flares from 2010 to 2017**. Our sample includes both confined and eruptive events, with 6 and 15 in each category, respectively. Using HMI vector magnetic field observations from several hours before to several hours after each event, we employ (a) the Differential Affine Velocity Estimator for Vector Magnetograms (DAVE4VM) to determine the photospheric fluxes of energy and helicity, and (b) non-linear force-free field (NLFFF) extrapolations to estimate the coronal content of energy and helicity in source-region fields. Using Superposed Epoch analysis (SPE), we find, on average: (1) decreases in both magnetic energy and helicity, in both photospheric fluxes and coronal content, that persist for a few hours after eruptions, but no clear changes, notably in relative helicity, for confined events; (2) significant increases in the twist of photospheric fields in eruptive events, with twist uncertainties too large in confined events to constrain twist changes (and lower overall twist in confined events); and (3) on longer time scales (event time +12 hours), replenishment of free magnetic energy and helicity content to near pre-event levels for eruptive events. For eruptive events, magnetic helicity and free energy in coronal models clearly decrease after flares, with the amounts of decrease proportional to each region's pre-flare content. **2011 February 13–17, July 12, 2012**

Table 1. List of X-class flares in 13 ARs in our sample, all of which are within 50◦ from the central meridian and occurred after May 2010.

The Initiation and Back-reaction of the X5.4 Flare on 2012 March 7

Nian **Liu**1, Ju Jing1,2, Qiang Hu3, Satoshi Inoue1, and Haimin Wang1,2

2023 ApJ 946 64

https://iopscience.iop.org/article/10.3847/1538-4357/acbc15/pdf
In this paper, we study the evolution of the X5.4 flare (SOL**2012-03-07**T00:02) in NOAA Active Region 11429, focusing on its initiation mechanisms and back-reaction effects. To help our study, three-dimensional (3D) coronal magnetic field models are extrapolated from the photospheric magnetograms of the Helioseismic and Magnetic Imager on board the Solar Dynamics Observatory under the assumptions of nonlinear force-free field (NLFFF) and non-force-free field (non-FFF). We investigate the 3D magnetic structure and MHD kink instability, torus instability, and double-arc instability (DAI), and find that this flare is most likely triggered by the tether-cutting reconnection and the subsequent DAI. For the back-reactions of the flare, both NLFFF and non-FFF models clearly show an increase in horizontal magnetic field (Bh) and a decrease in inclination angle (ϕ) of the magnetic field near the polarity inversion line, from the photosphere up to a certain height (5 Mm and 8 Mm for non-FFF and NLFFF, respectively). In addition, the non-FFF model shows an enhancement of the downward Lorentz force acting on the photosphere, and the location of the enhancement spatially coincides with the location of the flare onset. The observed back-reaction is likely a consequence of magnetic reconnection.

Multi-instrument Comparative Study of Temperature, Number Density, and Emission Measure during the Precursor Phase of a Solar Flare

Nian **Liu**, Ju Jing, Yan Xu, Haimin Wang
Astrophysical Journal, 930:154 (10pp), **2022** May 10
https://arxiv.org/ftp/arxiv/papers/2302/2302.06825.pdf
We present a multi-instrument study of the two precursor brightenings prior to the M6.5 flare (SOL**2015-06-22**T18:23) in the NOAA Active Region 12371, with a focus on the temperature (T), electron number density (n), and emission measure (EM). The data used in this study were obtained from four instruments with a variety of wavelengths, i.e., the Solar Dynamics Observatory's Atmospheric Imaging Assembly (AIA), in six extreme ultraviolet (EUV) passbands; the Expanded Owens Valley Solar Array (EOVSA) in microwave (MW); the Reuven Ramaty High Energy Solar Spectroscopic Imager (RHESSI) in hard X-rays (HXR); and the Geostationary Operational Environmental Satellite (GOES) in soft X-rays (SXR). We compare the temporal variations of T, n, and EM derived from the different data sets. Here are the key results. (1) GOES SXR and AIA EUV have almost identical EM variations (1.5-3x10^48 per cm^3) and very similar T variations, from 8 to 15 million Kelvin (MK). (2) Listed from highest to lowest, EOVSA MW provides the highest temperature variations (15-60 MK), followed by RHESSI HXR (10-24 MK), then GOES SXR and AIA EUV (8-15 MK). (3) The EM variation from the RHESSI HXR measurements is always less than the values from AIA EUV and GOES SXR by at most 20 times. The number density variation from EOVSA MW is greater than the value from AIA EUV by at most 100 times. The results quantitatively describe the differences in the thermal parameters at the precursor phase, as measured by different instruments operating at different wavelength regimes and for different emission mechanisms.

Formation and Eruption of Hot Channels during an M6.5 Class Solar Flare

Yanjie **Liu**1,2, Yingna Su1,2, Rui Liu3, Jialin Chen1,2, Tie Liu4,5, and Haisheng Ji1,2
2022 ApJ 941 83
https://arxiv.org/pdf/2211.06060.pdf
https://iopscience.iop.org/article/10.3847/1538-4357/aca08c/pdf
We investigate the formation and eruption of hot channels associated with the M6.5 class flare (SOL 2015-06-22T18:23) that occurred in NOAA AR 12371 on **2015 June 22**. Two flare precursors are observed before the flare's main phase. Observations in 94 and 131 Å by SDO/AIA revealed the early morphology of the first hot channel as a group of hot loops, termed the seed hot channel. A few seed hot channels are formed above the polarity inversion line (PIL) and the formation is associated with the parallel motion of the footpoint brightenings along the PIL, which proceeds into the early stage of the flare main phase. During this process, seed hot channels build up and rise slowly, accelerating at the peak of the second precursor. They merge during the process of acceleration, forming a larger hot channel, which then forms an inverted-γ-shape kinking structure. Before the flare peak, the second kinking hot channel with negative crossing appears near the first kinking hot channel that erupted. The eruption of these two hot channels produces two peaks on the main flare's GOES light curve. The propagation of the footpoint brightenings along the PIL indicates that the first kinking hot channel may be formed due to zipper reconnection. The occurrence of merging between seed hot channels observed by AIA is supported by the extrapolated nonlinear force-free field models. The observed writhing motion of the first kinking hot channel may be driven by the Lorentz force.

Deep Learning Based Solar Flare Forecasting Model. II. Influence of Image Resolution

Sixuan **Liu**1,2,3, Long Xu1, Zhongrui Zhao1,2,3, R. Erdélyi4,5, Marianna B. Korsós5,6, and Xin Huang7,1
2022 ApJ 941 20
https://iopscience.iop.org/article/10.3847/1538-4357/ac99dc/pdf
Due to the accumulation of solar observational data and the development of data-driven algorithms, deep learning methods are widely applied to build a solar flare forecasting model. Most of the works focus on how to design or select proper deep networks for the forecasting task. Nevertheless, the influence of image resolution on the learning based

solar flare forecasting model has not been analyzed and discussed. In this Paper, we investigate the influence of the resolution of magnetograms on the accuracy of solar flare forecasting. We study the active regions by the Solar Dynamics Observatory/Helioseismic and Magnetic Imager (SDO/HMI) magnetograms from 2010 to 2019. Then, we downsample them to get a database containing active regions with several resolutions. Afterwards, three deep neural networks (i) AlexNet, (ii) ResNet-18, and (iii) SqueezeNet are implemented to evaluate the performance of solar flare forecasting compared to different resolutions of magnetogram. In experiments, we first did comparative experiments on our own simulated HMI database with different resolutions. Then we conducted experiments on two selected actual overlapping databases, Hinode–HMI and Michelson Doppler Imager–HMI, to reconfirm our conclusions. The experiment results show that all the selected deep learning networks are insensitive to the resolution to a certain extent. We visualized the regions of interest of the network from an interpretable perspective and found that the deep learning network pays more attention to the global features extracted from active regions that are not sensitive to local information in magnetograms. **2016 February 12**

On the nature of photospheric horizontal magnetic field increase in major solar flares

Lijuan **Liu**, Zhenjun Zhou, Yuming Wang, Xudong Sun, Guoqiang Wang
ApJL **934** L33 **2022**
https://arxiv.org/pdf/2207.12044.pdf
https://iopscience.iop.org/article/10.3847/2041-8213/ac83bf/pdf
Rapid increase of horizontal magnetic field (Bh) around the flaring polarity inversion line is the most prominent photospheric field change during flares. It is considered to be caused by the contraction of flare loops, the details behind which is still not fully understood. Here we investigate the Bh-increase in 35 major flares using HMI high-cadence vector magnetograms. We find that Bh-increase is always accompanied by the increase of field inclination. It usually initiates near the flare ribbons, showing step-like change in between the ribbons. In particular, its evolution in early flare phase shows close spatio-temporal correlation to flare ribbons. We further find that Bh-increase tends to have similar intensity in confined and eruptive flares, but larger spatial-extent in eruptive flares in a statistical sense. Its intensity and timescale have inverse and positive correlations to the initial ribbon separations, respectively. The results altogether are well consistent with a recent proposed scenario which suggests that the reconnection-driven contraction of flare loops enhances photospheric Bh according to the ideal induction equation, providing statistical evidence to the reconnection-driven origin for Bh-increase for the first time. **22 Jun 2015**
Table 1. Flare information and Bh-increase characteristics (2011-2017)

Apparent Footpoint Rotation and Writhe of Double Hot Channels in a Solar Flare

Yanjie **Liu**1,2, Yingna Su1,2, Rui Liu3, Jialin Chen1,2, Tie Liu4,5, and Haisheng Ji1,2
2022 ApJ 930 130
https://iopscience.iop.org/article/10.3847/1538-4357/ac63ac/pdf
We investigate the M6.5 class flare (SOL2015-06-22T18:23) occurring in NOAA Active Region 12371 on **2015 June 22**. This eruptive flare is associated with a halo coronal mass ejection with a speed of 1200 km s−1. The 94 Å observations by Atmospheric Image Assembly onboard Solar Dynamics Observatory show that one hot channel first rises up, then forms a kinking structure with negative crossing and erupts, which is followed by the eruption of another kinking hot channel with negative crossing at a similar location between the start and peak times of the flare. Consistent with the standard flare model, footpoint drifting of the two hot channels is observed during the eruption. More interestingly, the two footpoints of the first hot channel continue to drift and display an apparent clockwise rotation after leaving the area of the hook-shaped flare ribbons. This apparent rotation is along the high-Q region of the log Q map derived from the nonlinear force-free field extrapolation. Our analysis suggests that the apparent rotational motion is likely caused by magnetic reconnection between the first hot channel and the surrounding magnetic fields at the high-Q region during the unwrithing process. The unwrithing of the second hot channel is accompanied by a significant slipping motion of its right footpoint.

Investigation on the Spatiotemporal Structures of Supra-Arcade Spikes

Rui **Liu**, Yuming Wang
A&A **2021**
https://arxiv.org/pdf/2106.04752.pdf
The vertical current sheet (VCS) trailing coronal mass ejections (CMEs) is the key place where the flare energy release and the CME buildup take place through magnetic reconnection. It is often studied from the edge-on perspective for the morphological similarity with the two-dimensional ``standard'' picture, but its three dimensional structure can only be revealed when the flare arcade is observed side on. The structure and dynamics in the so-called supra-arcade region thus contain important clues to the physical processes in flares and CMEs. Here we focus on the supra-arcade spikes (SASs), interpreted as the VCS viewed side-on, to study their spatiotemporal structures. By identifying each individual spike during the decay phase of four selected flares, in which the associated CME is traversed by a near-Earth spacecraft, we found that the widths of spikes are log-normal distributed, while the Fourier power spectra of the overall supra-arcade EUV emission, including bright spikes and dark downflows as well as the diffuse background, are power-law distributed, in terms of either spatial frequency k or temporal frequency ν, which reflects the fragmentation of the VCS.

We demonstrate that coronal emission-line intensity observations dominated by Kolmogorov turbulence would exhibit a power spectrum of E(k)~k−13/3 or E(ν)~ν−7/2, which is consistent with our observations. By comparing the number of SASs and the turns of field lines as derived from the ICMEs, we found a consistent axial length of ~3.5 AU for three events with a CME speed of ~1000 km/s in the inner heliosphere, but a much longer axial length ~8 AU) for the fourth event with an exceptionally fast CME speed of ~1500 km/s, suggesting that this ICME is flattened and its `nose' has well passed the Earth when the spacecraft traversed its leg. **2011-Oct-22, 2013-Apr-11, 2013-Nov-07, 2014-Apr-02**

The Source Locations of Major Flares and CMEs in the Emerging Active Regions

Lijuan **Liu**, Yuming Wang, Zhenjun Zhou, Jun Cui
ApJ **909** 142 **2021**
https://arxiv.org/pdf/2101.07452.pdf
https://doi.org/10.3847/1538-4357/abde37
https://iopscience.iop.org/article/10.3847/1538-4357/abde37/pdf
Major flares and coronal mass ejections (CMEs) tend to originate from the compact polarity inversion lines (PILs) in the solar active regions (ARs). Recently, a scenario named as "collisional shearing" is proposed by \citet{Chintzoglou_2019} to explain the phenomenon, which suggests that the collision between different emerging bipoles is able to form the compact PIL, driving the shearing and flux cancellation that are responsible to the subsequent large activities. In this work, through tracking the evolution of 19 emerging ARs from their birth until they produce the first major flares or CMEs, we investigated the source PILs of the activities, i.e., the active PILs, to explore the generality of "collisional shearing". We find that none of the active PILs is the self PIL (sPIL) of a single bipole. We further find that 11 eruptions originate from the collisional PILs (cPILs) formed due to the collision between different bipoles, 6 from the conjoined systems of sPIL and cPIL, and 2 from the conjoined systems of sPIL and ePIL (external PIL between the AR and the nearby preexisting polarities). Collision accompanied by shearing and flux cancellation is found developing at all PILs prior to the eruptions, with 84% (16/19) cases having collisional length longer than 18~Mm. Moreover, we find that the magnitude of the flares is positively correlated with the collisional length of the active PILs, indicating that the intenser activities tend to originate from the PILs with severer collision. The results suggest that the "collisional shearing", i.e., bipole-bipole interaction during the flux emergence is a common process in driving the major activities in emerging ARs. **2010-06-11-12, 2011-02-17-18, 2012-02-18-19, 2012-03-21, 2013-06-18-19, 2013-10-13, 2013-10-13-16, 2013-11-05, 2013-11-08, 2014-06-10**
Table 2010-2014

Magnetic Reconnection Rate & X-line Spread in Collisionless Plasmas

Yi-Hsin **Liu**
Fleishman's webinar 16 Oct **2020**
https://youtu.be/lA7VufDjLG0

An Eruptive Circular-ribbon Flare with Extended Remote Brightenings

Chang **Liu**, Avijeet Prasad, Jeongwoo Lee, Haimin Wang
ApJ **899** 34 **2020**
https://arxiv.org/pdf/2007.14428.pdf
https://doi.org/10.3847/1538-4357/ab9cbe
We study an eruptive X1.1 circular-ribbon flare on **2013 November 10**, combining multiwavelength observations with a coronal field reconstruction using a non-force-free field method. In the first stage, a filament forms via magnetic reconnection between two mildly twisted sheared arcades, which are embedded under the fan dome associated with a null point. This reconnection seems to be driven by photospheric shearing and converging flows around the inner two arcade footpoints, consistent with the flare-related changes of transverse field. The southern portion of the filament rises upward due to torus instability and pushes against the null point. The induced null point reconnection then generates the circular ribbon and the initial remote brightening in the west, as accelerated electrons precipitate along the fan and propagate outward along quasi-separatix surfaces with high values of the squashing factor (Q) in the envelope fields, which have a curtain-like shape here. In the second stage, the southern end of the flux rope breaks away from the surface, sequentially disrupts the dome and overlying fields, and erupts in a whipping-like fashion to become a partial halo coronal mass ejection. This leads to an enhanced flare emission and fast-moving remote brightenings at the footpoints of the magnetic curtain, which span a remarkably broad region and are also associated with coronal dimmings. This is a rare example of eruptive circular-ribbon flares, in which the evolution of a flux rope from its formation to successful eruption out of the dome and the resulting unusually extended remote brightenings are completely observed.
RHESSI Science Nuggets #382 Sep **2020** https://sprg.ssl.berkeley.edu/~tohban/wiki/index.php/SOL2013-11-10_Eruptive_Circular-ribbon_Flare_with_Extended_Remote_Brightenings

The Eruption of Outer Spine-like Loops Leading to a Double-stage Circular-ribbon Flare

Chang **Liu**1,2,3, Jeongwoo Lee1,3, and Haimin Wang1,2,3

2019 ApJ 883 47
https://doi.org/10.3847/1538-4357/ab3923
Circular-ribbon flares occur in a confined magnetic structure, but can also be associated with coronal mass ejections (CMEs) when a filament embedded under the fan erupts. Here we study an M8.7 circular-ribbon flare (SOL**2014-12-17**T04:51), which is accompanied by a CME yet without a clear indication of filament eruption. Using a nonlinear force-free field model, we find that the outer spine-like loops form a magnetic flux rope (FR1) rooted at the edge of the fan, and that there is another flux rope (FR2) at the main magnetic polarity inversion line (PIL) under a fan-like flux rope FR3. We divide the event evolution into two stages by combining modeling results with EUV observations. The onset stage is featured with bidirectional jets that occurred between a filament and FR1, immediately followed by an upward motion of the latter. During this first stage, the inner/outer spine-related ribbons and the circular ribbon begin to brighten up. After about 10 minutes, another ejection stems from the main PIL region. In this second stage, all ribbons are significantly enhanced, and the twist of FR2 footpoints is decreased. We discuss these results in favor of a scenario where the initial reconnection between the filament and FR1 activates the latter to reconnect with FR3 with opposite twist. This produces larger scale erupting loops and consequently causes a weakening of FR3, which induces another eruption of FR2 from below. This event thus represents a new type of eruptive circular-ribbon flare caused by unstable outer spine-like loops.

Formation of a Magnetic Flux Rope in the Early Emergence Phase of NOAA Active Region 12673

Lijuan **Liu**, Xin Cheng, Yuming Wang, Zhenjun Zhou
ApJ 884 45 **2019**
https://arxiv.org/pdf/1908.06360.pdf
In this work, we investigate the formation of a magnetic flux rope (MFR) above the central polarity inversion line (PIL) of NOAA Active Region 12673 during its early emergence phase. Through analyzing the photospheric vector magnetic field, extreme ultraviolet (EUV) and ultraviolet (UV) images, extrapolated three-dimensional (3D) non-linear force-free fields (NLFFFs), as well as the photospheric motions, we find that with the successive emergence of different bipoles in the central region, the conjugate polarities separate, resulting in collision between the non-conjugated opposite polarities. Nearly-potential loops appear above the PIL at first, then get sheared and merge at the collision locations as evidenced by the appearance of a continuous EUV sigmoid on 2017 September 4, which also indicates the formation of an MFR. The 3D NLFFFs further reveal the gradual buildup of the MFR, accompanied by the appearance of two elongated bald patches (BPs) at the collision locations and a very low-lying hyperbolic flux tube configuration between the BPs. The final MFR has relatively steady axial flux and average twist number of around 2.1×1020~Mx and -1.5, respective. Shearing motions are found developing near the BPs when the collision occurs, with flux cancellation and UV brightenings being observed simultaneously, indicating the development of a process named as "collisional shearing" (firstly identified by Chintzoglou et al. 2019). The results clearly show that the MFR is formed by "collisional shearing", i.e., through shearing and flux cancellation driven by the collision between non-conjugated opposite polarities during their emergence.

Predicting Solar Flares Using a Long Short-Term Memory Network

Hao **Liu**, Chang Liu, Jason T. L. Wang, Haimin Wang
2019 *ApJ* **877** 121
https://arxiv.org/pdf/1905.07095.pdf
sci-hub.se/10.3847/1538-4357/ab1b3c
We present a long short-term memory (LSTM) network for predicting whether an active region (AR) would produce a gamma-class flare within the next 24 hours. We consider three gamma classes, namely >=M5.0 class, >=M class, and >=C class, and build three LSTM models separately, each corresponding to a gamma class. Each LSTM model is used to make predictions of its corresponding gamma-class flares. The essence of our approach is to model data samples in an AR as time series and use LSTMs to capture temporal information of the data samples. Each data sample has 40 features including 25 magnetic parameters obtained from the Space-weather HMI Active Region Patches (SHARP) and related data products as well as 15 flare history parameters. We survey the flare events that occurred from 2010 May to 2018 May, using the GOES X-ray flare catalogs provided by the National Centers for Environmental Information (NCEI), and select flares with identified ARs in the NCEI flare catalogs. These flare events are used to build the labels (positive vs. negative) of the data samples. Experimental results show that (i) using only 14-22 most important features including both flare history and magnetic parameters can achieve better performance than using all the 40 features together; (ii) our LSTM network outperforms related machine learning methods in predicting the labels of the data samples. To our knowledge, this is the first time that LSTMs have been used for solar flare prediction.

Energy Build-up and Triggering Leading to a M1.5 Flare on 1 August 2014

S. **Liu**, J. T. Su
Solar Physics December **2018**, 293:167
https://arxiv.org/pdf/1902.00333.pdf

The energy storage and trigger mechanisms of solar flares are important for understanding solar activity. We analyzed multi-wavelength observations of a M1.5 flare on **1 August 2014**, in active region NOAA 12127 (SOL2014-08-01T18:13). There are evident large-scale sunspot rotations in positive magnetic field of the main energy-release region before the eruption; the rotations contain both clockwise and counter-clockwise directions. Injection of magnetic helicity from the photosphere is prior to the flare. The sign of the helicity injection is reversed after the flare. It is found that both persistent larger-scale (≈one day≈one day) and impulse smaller-scale (≈one to two hours≈one to two hours) magnetic-flux emergences are associated with the flare. We conclude that larger-scale flux emergence, helicity injection, and sunspot rotation contribute to the energy build up, while the small-scale magnetic-flux emergence plays a crucial role in triggering the flare.

Evolution of Photospheric Vector Magnetic Field Associated with Moving Flare Ribbons As Seen By GST

Chang **Liu**, Wenda Cao, Jongchul Chae, Kwangsu Ahn, Debi Prasad Choudhary, Jeongwoo Lee, Rui Liu, Na Deng, Jiasheng Wang, Haimin Wang

ApJ **869** 21 **2018**

https://arxiv.org/pdf/1810.11733.pdf

sci-hub.tw/10.3847/1538-4357/aaecd0

The photospheric response to solar flares, also known as coronal back reaction, is often observed as sudden flare-induced changes in vector magnetic field and sunspot motions. However, it remains obscure whether evolving flare ribbons, the flare signature closest to the photosphere, are accompanied by changes in vector magnetic field therein. Here we explore the relationship between the dynamics of flare ribbons in the chromosphere and variations of magnetic fields in the underlying photosphere, using high-resolution off-band H-alpha images and near-infrared vector magnetograms of the M6.5 flare on **2015 June 22** observed with the 1.6 m Goode Solar Telescope. We find that changes of photospheric fields occur at the arrival of the flare ribbon front, thus propagating analogously to flare ribbons. In general, the horizontal field increases and the field lines become more inclined to the surface. When ribbons sweep through regions that undergo a rotational motion, the fields transiently turn more vertical with decreased horizontal field and inclination angle, and then restore and/or become more horizontal than before the ribbon arrival. The ribbon propagation decelerates near the sunspot rotation center, where the vertical field becomes permanently enhanced. Similar magnetic field changes are discernible in magnetograms from the Helioseismic and Magnetic Imager (HMI), and an inward collapse of coronal magnetic fields is inferred from the time sequence of non-linear force-free field models extrapolated from HMI magnetograms. We conclude that photospheric fields respond nearly instantaneously to magnetic reconnection in the corona.

Rapid buildup of a magnetic flux rope during a confined X2.2 class flare in NOAA AR 12673

Lijuan **Liu**, Xin Cheng, Yuming Wang, Zhenjun Zhou, Yang Guo, Jun cui

2018 *ApJL* **867** L5

https://iopscience.iop.org/article/10.3847/2041-8213/aae826/pdf

https://arxiv.org/pdf/1810.04424.pdf

sci-hub.tw/10.3847/2041-8213/aae826

Magnetic flux ropes (MFRs) are believed to be the core structure in solar eruptions, nevertheless, their formation remains intensely debated. Here we report a rapid buildup process of an MFR-system during a confined X2.2 class flare occurred on **2017 September 6** in NOAA AR 12673, three hours after which the structure erupted to a major coronal mass ejection (CME) accompanied by an X9.3 class flare. ***For the X2.2 flare, we do not find EUV dimmings, separation of its flare ribbons, or clear CME signatures, suggesting a confined flare.*** For the X9.3 flare, large-scale dimmings, separation of its flare ribbons, and a CME show it to be eruptive. By performing a time sequence of nonlinear force-free fields (NLFFFs) extrapolations we find that: until the eruptive flare, an MFR-system was located in the AR. During the confined flare, the axial flux and the lower bound of the magnetic helicity for the MFR-system were dramatically enhanced by about 86% and 260%, respectively, although the mean twist number was almost unchanged. During the eruptive flare, the three parameters were all significantly reduced. The results evidence the buildup and release of the MFR-system during the confined and the eruptive flare, respectively. The former may be achieved by flare reconnection. We also calculate the pre-flare distributions of the decay index above the main polarity inversion line (PIL) and find no significant difference. It indicates that the buildup of the magnetic flux and helicity of the MFR-system may play a role in facilitating its final eruption.

A Truly Global EUV Wave From the SOL2017-09-10 X8.2 Solar Flare-CME Eruption

Wei **Liu**, Meng Jin, Cooper Downs, Leon Ofman, Mark Cheung, Nariaki V. Nitta

ApJL **864** L24 **2018**

https://arxiv.org/pdf/1807.09847.pdf

http://iopscience.iop.org/article/10.3847/2041-8213/aad77b/pdf

We report SDO/AIA observations of an extraordinary global extreme ultraviolet (EUV) wave triggered by the X8.2 flare-CME eruption on **2017 September 10**. This was one of the best EUV waves ever observed with modern

instruments, yet likely the last one of such magnitudes of Solar Cycle 24 as the Sun heads toward the minimum. Its remarkable characteristics include: (1) The wave was observed, for the first time, to traverse the full-Sun corona over the entire visible solar disk and off-limb circumference, manifesting a truly global nature, owing to its exceptionally large amplitude, e.g., with EUV enhancements by up to 300% at 1.1 Rsun from the eruption. (2) This leads to strong transmissions (besides commonly observed reflections) in and out of both polar coronal holes, which are usually devoid of EUV waves. It has elevated wave speeds >2000 km/s within them, consistent with the expected higher fast-mode magnetosonic speeds. The coronal holes essentially serve as new "radiation centers" for the waves being refracted out of them, which then travel toward the equator and collide head-on, causing additional EUV enhancements. (3) The wave produces significant compressional heating to local plasma upon its impact, indicated by long-lasting EUV intensity changes and differential emission measure increases at higher temperatures (e.g., log T=6.2) accompanied by decreases at lower temperatures (log T=6.0). These characteristics signify the potential of such EUV waves for novel magnetic and thermal diagnostics of the solar corona {\it on global scales}.

Super Penumbral Chromospheric Flare

S. **Liu**, H.Q. Zhang, D. P. Choudhary, A. K. Srivastava, B. N. Dwivedi
Research in Astronomy and Astrophysics (RAA) **2018**
https://arxiv.org/pdf/1806.00232.pdf
We observed a C-class flare at the outer boundary of the super-penumbra of a sunspot. The flare was triggered by an emerging magnetic bipolar region that was obliquely oriented with respect to the super-penumbral fibrils. The flare started due to the low height magnetic reconnection of emerging magnetic flux with super-penumbral field resulting hot multi-temperature plasma flows in the inverse Evershed flow channel and its overlying atmosphere. The inverse Evershed flows in the chromosphere start from super penumbra towards sunspot that end at the outer boundary of the penumbra. The hot plasma flow towards the sunspot in the inverse Evershed channels show about 10 km s−1 higher velocity in Hα wavelengths compared to the plasma emissions at various temperatures as seen in different AIA filters. Even though these velocities are about seven times higher than the typical inverse-Evershed flow speeds, the flow is diminished at the outer boundary of the sunspot's penumbra. This suggests that the super-penumbral field lines that carry the inverse Evershed flows, are discontinued at the boundary where the penumbral field lines dive into the sun and these two sets of field lines are completely distinct. The discontinuity in the typical magnetic field and plasma properties at the adjoining of these two sets of field lines further leads the discontinuity in the characteristic magnetoacoustic and Alfv\'en speeds, therefore, stopping the plasma flows further on. The multi-temperature plasma in the inverse Evershed channels exhibits \textbf{possible} longitudinal oscillations initially during the onset of the flare, and later flows towards the sunspot. In the multi-temperature view, the different layers above the flare region have the mixture of supersonic as well as subsonic flows. **2012 October 25**

Electric-Current Neutralization, Magnetic Shear, and Eruptive Activity in Solar Active Regions

Yang **Liu**, Xudong Sun, Tibor Török, Viacheslav S. Titov, James E. Leake
ApJL **2017**
https://arxiv.org/pdf/1708.04411.pdf
http://sun.stanford.edu/~yliu/papers/curren_neutralization.pdf
The physical conditions that determine whether or not solar active regions (ARs) produce strong flares and coronal mass ejections (CMEs) are not yet well understood. Here we investigate the association between electric-current neutralization, magnetic shear along polarity inversion lines (PILs), and eruptive activity in four ARs; two emerging and two well-developed ones. We find that the CME-producing ARs are characterized by a strongly non-neutralized total current, while the total current in the ARs that did not produce CMEs is almost perfectly neutralized. The difference in the PIL-shear between these two groups is much less pronounced, which suggests that the degree of current-neutralization may serve as a better proxy for assessing the ability of ARs to produce CMEs. **2010−05−23, 2011-02-15, 9 March 2012, 2014−10−23**

Predicting Solar Flares Using SDO/HMI Vector Magnetic Data Product and Random Forest Algorithm

Chang **Liu**, Na Deng, Jason T. L. Wang, Haimin Wang
ApJ **843** 104 **2017**
https://arxiv.org/pdf/1706.02422.pdf
http://sci-hub.cc/10.3847/1538-4357/aa789b
Adverse space weather effects can often be traced to solar flares, prediction of which has drawn significant research interests. The Helioseismic and Magnetic Imager (HMI) produces full-disk vector magnetograms with continuous high cadence, while flare prediction efforts utilizing this unprecedented data source are still limited. Here we report results of flare prediction using physical parameters provided by the Space-weather HMI Active Region Patches (SHARP) and related data products. We survey X-ray flares occurred from 2010 May to 2016 December, and categorize their source regions into four classes (B, C, M, and X) according to the maximum GOES magnitude of flares they generated. We

then retrieve SHARP related parameters for each selected region at the beginning of its flare date to build a database. Finally, we train a machine-learning algorithm, called random forest (RF), to predict the occurrence of a certain class of flares in a given active region within 24 hours, evaluate the classifier performance using the 10-fold cross validation scheme, and characterize the results using standard performance metrics. Compared to previous works, our experiments indicate that using the HMI parameters and RF is a valid method for flare forecasting with fairly reasonable prediction performance. To our knowledge, this is the first time that RF is used to make multi-class predictions of solar flares. We also find that the total unsigned quantities of vertical current, current helicity, and flux near polarity inversion line are among the most important parameters for classifying flaring regions into different classes.
Table 5. 845 Samples of Flaring ARs

Short-term solar flare prediction using multi-model integration method

Jin-Fu **Liu**, Fei Li, Jie Wan and Da-Ren Yu
RAA **2017** Vol. 17 No. 4, 34
A multi-model integration method is proposed to develop a multi-source and heterogeneous model for short-term solar flare prediction. Different prediction models are constructed on the basis of extracted predictors from a pool of observation databases. The outputs of the base models are normalized first because these established models extract predictors from many data resources using different prediction methods. Then weighted integration of the base models is used to develop a multi-model integrated model (MIM). The weight set that single models assign is optimized by a genetic algorithm. Seven base models and data from Solar and Heliospheric Observatory/Michelson Doppler Imager longitudinal magnetograms are used to construct the MIM, and then its performance is evaluated by cross validation. Experimental results showed that the MIM outperforms any individual model in nearly every data group, and the richer the diversity of the base models, the better the performance of the MIM. Thus, integrating more diversified models, such as an expert system, a statistical model and a physical model, will greatly improve the performance of the MIM.

Relationship between Magnetic Field Properties and an X-class Flare in Active Region NOAA 9077

S. **Liu**, D. Liu
Advances in Space Research **2016**
https://arxiv.org/pdf/1902.00324.pdf
The magnetic field plays a key role in producing solar flares, so that the investigation on the relationship between the magnetic field properties and flares is significant. In this paper, based on the magnetic field extrapolated from the photospheric vector magnetograms of the active region NOAA 9077 obtained at Huairou Solar Observing Station, the magnetic field parameters including the height of field lines, force-free factor, free magnetic energy and inclination angle were studied with respect to an X-class flare in this region. We found that the magnetic field lines became lower and the ratio of number of closed field lines to those of open field lines increased after the flare. The force-free factor (α) attained a large value before the flare and then decreased after the flare for the closed field lines, while the open field lines showed the opposite tendency. Free energy reach to maximum before flare, then decrease after flare. The magnetic inclination angles showed opposite change trends after the flare for closed and open field lines. Therefore, we may conclude that non-potential energy released by flare mostly contained in the closed magnetic field lines. **14 July 2000**

Flare differentially rotates sunspot on Sun's surface

Chang **Liu**, Yan Xu, Wenda Cao, Na Deng, Jeongwoo Lee, Hugh S. Hudson, Dale E. Gary, Jiasheng Wang, Ju Jing, Haimin Wang
Nature Communications **2016**
https://arxiv.org/pdf/1610.02969v1.pdf
http://www.nature.com/articles/ncomms13104
Sunspots are concentrations of magnetic field visible on the solar surface (photosphere). It was considered implausible that solar flares, as resulted from magnetic reconnection in the tenuous corona, would cause a direct perturbation of the dense photosphere involving bulk motion. Here we report the sudden flare-induced rotation of a sunspot using the unprecedented spatiotemporal resolution of the 1.6 m New Solar Telescope, supplemented by magnetic data from the Solar Dynamics Observatory. It is clearly observed that the rotation is non-uniform over the sunspot: as the flare ribbon sweeps across, its different portions accelerate (up to 50 deg per hr) at different times corresponding to peaks of flare hard X-ray emission. The rotation may be driven by the surface Lorentz-force change due to the back reaction of coronal magnetic restructuring and is accompanied by a downward Poynting flux. These results have direct consequences for our understanding of energy and momentum transportation in the flare-related phenomena.
22 June 2015
See RHESSI Science Nuggets #284, Oct 2016
http://sprg.ssl.berkeley.edu/~tohban/wiki/index.php/Flare-induced_Impulsive_Sunspot_Rotation_caught_in_High_Resolution

Investigating Energetic X-Shaped Flares on the Outskirts of A Solar Active Region

Rui **Liu**, Jun Chen, Yuming Wang, Kai Liu

Scientific Reports **2016 File**

http://arxiv.org/pdf/1609.02713v1.pdf

Typical solar flares display two quasi-parallel, bright ribbons on the chromosphere. In between is the polarity inversion line (PIL) separating concentrated magnetic fluxes of opposite polarity in active regions (ARs). Intriguingly a series of flares exhibiting X-shaped ribbons occurred at the similar location on the outskirts of NOAA AR 11967, where magnetic fluxes were scattered, yet three of them were alarmingly energetic. The X shape, whose center coincided with hard X-ray emission, was similar in UV/EUV, which cannot be accommodated in the standard flare model. Mapping out magnetic connectivities in potential fields, we found that the X morphology was dictated by the intersection of two quasi-separatrix layers, i.e., a hyperbolic flux tube (HFT), within which a separator connecting a double null was embedded. This topology was not purely local but regulated by fluxes and flows over the whole AR. The nonlinear force-free field model suggested the formation of a current layer at the HFT, where the current dissipation can be mapped to the X-shaped ribbons via field-aligned heat conduction. These results highlight the critical role of HFTs in 3D magnetic reconnection and have important implications for astrophysical and laboratory plasmas. **2014 February 2**

Why is a flare-rich active region CME-poor?

Lijuan **Liu**, Yuming Wang, Jingxiu Wang, Chenglong Shen, Pinzhong Ye, Rui Liu, Jun Chen, Quanhao Zhang, S. Wang

2016 *ApJ* **826** 119

http://arxiv.org/pdf/1607.07531v1.pdf **File**

Solar active regions (ARs) are the major sources of two kinds of the most violent solar eruptions, namely flares and coronal mass ejections (CMEs). The largest AR in the past 24 years, NOAA AR 12192, crossed the visible disk from **2014 October 17 to 30**, unusually produced more than one hundred flares, including 32 M-class and 6 X-class ones, but only one small CME. Flares and CMEs are believed to be two phenomena in the same eruptive process. Why is such a flare-rich AR so CME-poor? We compared this AR with other four ARs; two were productive in both and two were inert. The investigation of the photospheric parameters based on the SDO/HMI vector magnetogram reveals that the flare-rich AR 12192, as the other two productive ARs, has larger magnetic flux, current and free magnetic energy than the two inert ARs, but contrast to the two productive ARs, it has no strong, concentrated current helicity along both sides of the flaring neutral line, indicating the absence of a mature magnetic structure consisting of highly sheared or twisted field lines. Furthermore, the decay index above the AR 12192 is relatively low, showing strong constraint. These results suggest that productive ARs are always large and have enough current and free energy to power flares, but whether or not a flare is accompanied by a CME is seemingly related to (1) if there is mature sheared or twisted core field serving as the seed of the CME, (2) if the constraint of the overlying arcades is weak enough. **2011-02-15, 2012-03-07, 2014-10-24**

Quasi-periodic Fast-mode Magnetosonic Wave Trains Within Coronal Waveguides Associated with Flares and CMEs

Wei **Liu**, Leon Ofman, Brittany Broder, Marian Karlicky, and Cooper Downs

Proceedings of the 14th International Solar Wind Conference, **201**5

http://sun.stanford.edu/~weiliu/research/publications/2016/2016AIP_WeiLiu_QFPs_SolWind14.pdf

Quasi-periodic, fast-mode, propagating wave trains (QFPs) are a new observational phenomenon recently discovered in the solar corona by the Solar Dynamics Observatory with extreme ultraviolet (EUV) imaging observations. They originate from flares and propagate at speeds up to ~2000 km s-1 within funnel-shaped waveguides in the wakes of coronal mass ejections (CMEs). QFPs can carry sufficient energy fluxes required for coronal heating during their occurrences. They can provide new diagnostics for the solar corona and their associated flares. We present recent observations of QFPs focusing on their spatio-temporal properties, temperature dependence, and statistical correlation with flares and CMEs. Of particular interest is the **2010-Aug-01** C3.2 flare with correlated QFPs and drifting zebra and fiber radio bursts, which might be different manifestations of the same fast-mode wave trains. We also discuss the potential roles of QFPs in accelerating and/or modulating the solar wind.

Structure, Stability, and Evolution of Magnetic Flux Ropes from the Perspective of Magnetic Twist

Rui **Liu**, Bernhard Kliem, Viacheslav S. Titov, Jun Chen, Yuming Wang, Haimin Wang, Chang Liu, Yan Xu, Thomas Wiegelmann

ApJ 818 148 **2016**

http://arxiv.org/pdf/1512.02338v1.pdf

We investigate the evolution of NOAA Active Region 11817 during **2013 August 10--12**, when it developed a complex field configuration and produced four confined, followed by two eruptive, flares. These C-and-above flares are all associated with a magnetic flux rope (MFR) located along the major polarity inversion line, where shearing and converging photospheric flows are present. Aided by the nonlinear force-free field modeling, we identify the MFR through mapping magnetic connectivities and computing the twist number Tw for each individual field line. The MFR is moderately twisted (|Tw|<2) and has a well-defined boundary of high squashing factor Q. We found that the field line with the extremum |Tw| is a reliable proxy of the rope axis, and that the MFR's peak |Tw| temporarily increases within half an hour before each flare while it decreases after the flare peak for both confined and eruptive flares. This pre-flare increase in |Tw| has little effect on the active region's free magnetic energy or any other parameters derived for the whole region, due to its moderate amount and the MFR's relatively small volume, while its decrease after flares is clearly associated with the stepwise decrease in free magnetic energy due to the flare. We suggest that Tw may serve as a useful parameter in forewarning the onset of eruption, and therefore, the consequent space weather effects. The helical kink instability is identified as the prime candidate onset mechanism for the considered flares.

Mg II Lines Observed during the X-class Flare on 29 March 2014 by the Interface Region Imaging Spectrograph

W. **Liu**, P. Heinzel, L. Kleint, J. Kasparova

Solar Phys. Volume 290, Issue 12, pp 3525-3543 **2015**

http://arxiv.org/pdf/1511.00480v1.pdf

Mg II lines represent one of the strongest emissions from the chromospheric plasma during solar flares. In this article, we studied the Mg II lines observed during the X1 flare on March 29 2014 (SOL2014-03-29T17:48) by IRIS. IRIS detected large intensity enhancements of the Mg II h and k lines, subordinate triplet lines, and several other metallic lines at the flare footpoints during this flare. We have used the advantage of the slit-scanning mode (rastering) of IRIS and performed, for the first time, a detailed analysis of spatial and temporal variations of the spectra. Moreover, we were also able to identify positions of strongest HXR emissions using RHESSI observations and to correlate them with the spatial and temporal evolution of Mg II spectra. The light curves of the Mg II lines increase and peak contemporarily with the HXR emissions but decay more gradually. There are large red asymmetries in the Mg II h and k lines after the flare peak. We see two spatially well separated groups of Mg II line profiles, non-reversed and reversed. In some cases, the Mg II footpoints with reversed profiles are correlated with HXR sources. We show the spatial and temporal behavior of several other line parameters (line metrics) and briefly discuss them. Finally, we have synthesized the Mg II k line using our non-LTE code with the MALI technique. Two kinds of models are considered, the flare model F2 of Machado et al. (1980) and the models of Ricchiazzi and Canfield (1983). Model F2 reproduces the peak intensity of the unreversed Mg II k profile at flare maximum but does not account for high wing intensities. On the other hand, the RC models show the sensitivity of Mg II line intensities to various electron-beam parameters. Our simulations also show that the microturbulence produces a broader line core, while the intense line wings are caused by an enhanced line source function.

A Circular-ribbon Solar Flare Following an Asymmetric Filament Eruption

Chang **Liu**, Na Deng, Rui Liu, Jeongwoo Lee, Etienne Pariat, Thomas Wiegelmann, Yang Liu, Lucia Kleint, Haimin Wang

ApJL 812 L19 **2015**

http://arxiv.org/pdf/1509.08414v1.pdf

The dynamic properties of flare ribbons and the often associated filament eruptions can provide crucial information on the flaring coronal magnetic field. This Letter analyzes the GOES-class X1.0 flare on **2014 March 29** (SOL2014-03-29T17:48), in which we found an asymmetric eruption of a sigmoidal filament and an ensuing circular flare ribbon. Initially both EUV images and a preflare nonlinear force-free field model show that the filament is embedded in magnetic fields with a fan-spine-like structure. In the first phase, which is defined by a weak but still increasing X-ray emission, the western portion of the sigmoidal filament arches upward and then remains quasi-static for about five minutes. The western fan-like and the outer spine-like fields display an ascending motion, and several associated ribbons begin to brighten. Also found is a bright EUV flow that streams down along the eastern fan-like field. In the second phase that includes the main peak of hard X-ray (HXR) emission, the filament erupts, leaving behind two major HXR sources formed around its central dip portion and a circular ribbon brightened sequentially. The expanding western fan-like field interacts intensively with the outer spine-like field, as clearly seen in running difference EUV images. We discuss these observations in favor of a scenario where the asymmetric eruption of the sigmoidal filament is initiated due to an MHD instability and further facilitated by reconnection at a quasi-null in corona; the latter is in turn enhanced by the filament eruption and subsequently produces the circular flare ribbon.

Extremely Large EUV Late Phase of Solar Flares

Kai **Liu**1,2, Yuming Wang1, Jie Zhang3, Xin Cheng4, Rui Liu1, and Chenglong Shen

2015 ApJ 802 35
http://arxiv.org/pdf/1504.05340v1.pdf
The second peak in the Fe xvi 33.5 nm line irradiance observed during solar flares by the Extreme-Ultraviolet Variability Experiment (EVE) is known as the EUV late phase. Our previous paper in 2013 by Liu et al. found that the main emissions in the late phase are originated from large-scale loop arcades that are closely connected to but different from the post-flare loops (PFLs), and we also proposed that a long cooling process without additional heating could explain the late phase. In this paper, we define the extremely large late phase because it not only has a bigger peak in the warm 33.5 irradiance profile, but also releases more EUV radiative energy than the main phase. Through detailed inspection of the EUV images from three points of view, it was discovered that aside from the later-phase loop arcades, the main contributor of the extremely large late phase is a hot structure that fails to erupt. This hot structure is identified as a flux rope, which is quickly energized by the flare reconnection and later on continuously produces the thermal energy during the gradual phase. Together with the late-phase loop arcades, the flux rope failing to erupt with the additional heating create the extremely large EUV late phase. **2010 November 5**.

Surface and Coronal Field Signatures of Implosions in Two Homologous Solar Flares
Chang **Liu**, Haimin Wang
HMI Science Nuggets, #30, **2014**
http://hmi.stanford.edu/hminuggets/?p=1008
By synthesizing the results of photospheric field change indicated by HMI observations and coronal field variation suggested by the NLFFF modeling, we study the flare-related 3D magnetic restructuring and find it consistent with the coronal implosion scenario in the low solar atmosphere. 2011/09/06-07

An Unorthodox X-Class Long-Duration Confined Flare
Rui **Liu**, Viacheslav S. Titov, Tingyu Gou, Yuming Wang, Kai Liu, Haimin Wang
E-print, May **2014, File**; ApJ, 790 8 **2014**
http://arxiv.org/pdf/1405.6774v1.pdf
https://iopscience.iop.org/article/10.1088/0004-637X/790/1/8/pdf
We report the observation of an X-class long-duration flare which is clearly confined. It appears as a compact-loop flare in the traditional EUV passbands (171 and 195 ?), but in the passbands sensitive to flare plasmas (94 and 131 ?), it exhibits a cusp-shaped structure above an arcade of loops like other long-duration events. Inspecting images in a running difference approach, we find that the seemingly diffuse, quasi-static cusp-shaped structure consists of multiple nested loops that repeatedly rise upward and disappear approaching the cusp edge. Over the gradual phase, we detect numerous episodes of loop rising, each lasting minutes. A differential emission measure analysis reveals that the temperature is highest at the top of the arcade and becomes cooler at higher altitudes within the cusp-shaped structure, contrary to typical long-duration flares. With a nonlinear force-free model, our analysis shows that the event mainly involves two adjacent sheared arcades separated by a T-type hyperbolic flux tube (HFT). One of the arcades harbors a magnetic flux rope, which is identified with a filament that survives the flare owing to the strong confining field. We conclude that a new emergence of magnetic flux in the other arcade triggers the flare, while the preexisting HFT and flux rope dictate the structure and dynamics of the flare loops and ribbons during the long-lasting decay phase, and that a quasi-separatrix layer high above the HFT could account for the cusp-shaped structure. **2011 November 3**.
Хорошее Введение.

A Statistical Study on Property of Spatial Magnetic Field for Solar Active Region
Liu Suo
Ap&ss **2014**
http://arxiv.org/pdf/1405.2149v1.pdf
Magnetic fields dominate most solar activities, there exist direct relations between solar flare and the distributions of magnetic field, and also its corresponding magnetic energy. In this paper, the statistical results about the relationships between the spatial magnetic field and solar flare are given basing on vector magnetic field observed by the Solar Magnetic Field Telescope (SMFT) at Huairou Solar Observing Station (HSOS). The spatial magnetic fields are obtained by extrapolated photosphere vector magnetic field observed by SMFT. There are 23 active regions with flare eruption are chosen as data samples, which were observed from 1997 to 2007. The results are as follows: 1. Magnetic field lines become lower after flare for 16(69%) active regions; 2. The free energy are decreased after flare for 17 (74%) active regions. It can conclude that for most active regions the changes of magnetic field after solar flare are coincident with the previous observations and studies.

Three-dimensional Magnetic Restructuring in Two Homologous Solar Flares in the Seismically
Active NOAA AR 11283

Chang **Liu**, Na Deng, Jeongwoo Lee, Thomas Wiegelmann, Chaowei Jiang, Brian R. Dennis, Yang Su, Alina Donea, Haimin Wang

ApJ, 795, 128 **2014**

http://arxiv.org/pdf/1409.6391v1.pdf

We carry out a comprehensive investigation comparing the three-dimensional magnetic field restructuring, flare energy release, and the helioseismic response, of two homologous flares, the **2011 September 6** X2.1 (FL1) and **September 7** X1.8 (FL2) flares in NOAA AR 11283. In our analysis, (1) a twisted flux rope (FR) collapses onto the surface at a speed of 1.5 km/s after a partial eruption in FL1. The FR then gradually grows to reach a higher altitude and collapses again at 3 km/s after a fuller eruption in FL2. Also, FL2 shows a larger decrease of the flux-weighted centroid separation of opposite magnetic polarities and a greater change of the horizontal field on the surface. These imply a more violent coronal implosion with corresponding more intense surface signatures in FL2. (2) The FR is inclined northward, and together with the ambient fields, it undergoes a southward turning after both events. This agrees with the asymmetric decay of the penumbra observed in the peripheral regions. (3) The amounts of free magnetic energy and nonthermal electron energy released during FL1 are comparable to those of FL2 within the uncertainties of the measurements. (4) No sunquake was detected in FL1; in contrast, FL2 produced two seismic emission sources S1 and S2 both lying in the penumbral regions. Interestingly, S1 and S2 are connected by magnetic loops, and the stronger source S2 has weaker vertical magnetic field. We discuss these results in relation to the implosion process in the low corona and the sunquake generation.

Plasmoid Ejections and Loop Contractions in an Eruptive M7.7 Solar Flare: Evidence of Particle Acceleration and Heating in Magnetic Reconnection Outflows

Wei **Liu**, Qingrong Chen, Vahe' Petrosian

E-print, March **2013**, ApJ

Where particle acceleration and plasma heating take place in relation to magnetic reconnection is a fundamental question for solar flares. We report analysis of an M7.7 flare on **2012 July 19** observed by SDO/AIA and RHESSI. Bi-directional outflows in forms of plasmoid ejections and contracting cusp-shaped loops originate between an erupting flux rope and underlying flare loops at speeds of typically 200-300 km/s up to 1050 km/s. These outflows are associated with spatially separated double coronal X-ray sources with centroid separation decreasing with energy. The highest temperature is located near the nonthermal X-ray loop-top source well below the original heights of contracting cusps near the inferred reconnection site. These observations suggest that the primary loci of particle acceleration and plasma heating are in the reconnection outflow regions, rather than the reconnection site itself. In addition, there is an initial ascent of the X-ray and EUV loop-top source prior to its recently recognized descent, which we ascribe to the interplay among multiple processes including the upward development of reconnection and the downward contractions of reconnected loops. The impulsive phase onset is delayed by 10~minutes from the start of the descent, but coincides with the rapid speed increases of the upward plasmoids, the individual loop shrinkages, and the overall loop-top descent, suggestive of an intimate relation of the energy release rate and reconnection outflow speed.

EVIDENCE FOR SOLAR TETHER-CUTTINGMAGNETIC RECONNECTION FROM CORONAL FIELD EXTRAPOLATIONS

CHANG **LIU**1, NA DENG1, JEONGWOO LEE1,2, THOMAS WIEGELMANN3, RONALD L. MOORE4, AND HAIMIN WANG1

E-print, Oct **2013**, http://arxiv.org/pdf/1310.5098v1.pdf; ApJL

Magnetic reconnection is one of the primarymechanisms for triggering solar eruptive events, but direct observation of its rapid process has been of challenge. In this Letter we present, using a nonlinear force-free field (NLFFF) extrapolation technique, a visualization of field line connectivity changes resulting fromtether-cutting reconnection over about 30 minutes during the **2011 February 13** M6.6 flare in NOAA AR 11158. Evidence for the tether-cutting reconnection was first collected through multiwavelength observations and then by the analysis of the field lines traced from positions of four conspicuous flare 1700 A footpoints observed at the event onset. Right before the flare, the four footpoints are located very close to the regions of local maxima of magnetic twist index. Especially, the field lines from the inner two footpoints form two strongly twisted flux bundles (up to ~1.2 turns), which

shear past each other and reach out close to the outer two footpoints, respectively. Immediately after the flare, the twist index of regions around the footpoints greatly diminish and the above field lines become low lying and less twisted (~0.6 turns), overarched by loops linking the later formed two flare ribbons. About 10% of the flux (~3×1019 Mx) from the inner footpoints has undergone a footpoint exchange. This portion of flux originates from the edge regions of the inner footpoints that are brightened first. These rapid changes of magnetic field connectivity inferred from the NLFFF extrapolation are consistent with the tether-cutting magnetic reconnection model.

He I D3 OBSERVATIONS OF THE 1984 MAY 22 M6.3 SOLAR FLARE
Chang **Liu**1, Yan Xu1, Na Deng1, Jeongwoo Lee1,2, Jifeng Zhang1,3, Debi Prasad Choudhary4, and Haimin Wang
2013 ApJ 774 60
The He I D3 line has a unique response to a flare impact on the low solar atmosphere and can be a powerful diagnostic tool for energy transport processes. Using images obtained from the recently digitized films of the Big Bear Solar Observatory, we report D3 observations of the M6.3 flare on 1984 May 22, which occurred in an active region with a circular magnetic polarity inversion line (PIL). The impulsive phase of the flare starts with a main elongated source that darkens in D3, inside of which bright emission kernels appear at the time of the initial small peak in hard X-rays (HXRs). These flare cores subsequently evolve into a sharp emission strand lying within the dark halo; this evolution occurs at the same time as the main peak in HXRs, reversing the overall source contrast from –5% to 5%. The radiated energy in D3 during the main peak is estimated to be about 1030 erg, which is comparable to that carried by nonthermal electrons above 20 keV. Afterward, the flare proceeds along the circular PIL in the counterclockwise direction to form a dark circular ribbon in D3, which apparently mirrors the bright ribbons in Hα and He I 10830 Å. All of these ribbons last for over one hour in the late gradual phase. We suggest that the present event resembles the so-called black-light flare that was proposed based on continuum images, and that D3 darkening and brightening features herein may be due to thermal conduction heating and the direct precipitation of high-energy electrons, respectively.

ON THE ORIGIN OF THE EXTREME-ULTRAVIOLET LATE PHASE OF SOLAR FLARES
Kai **Liu**1,2, Jie Zhang2, Yuming Wang1, and Xin Cheng
2013 ApJ 768 150
http://arxiv.org/pdf/1504.05333v1.pdf
Solar flares typically have an impulsive phase that is followed by a gradual phase as best seen in soft X-ray emissions. A recent discovery based on the EUV Variability Experiment observations on board the Solar Dynamics Observatory (SDO) reveals that some flares exhibit a second large peak separated from the first main phase peak by tens of minutes to hours, which is coined as the flare's EUV late phase. In this paper, we address the origin of the EUV late phase by analyzing in detail two late phase flares, an M2.9 flare on **2010 October 16** and an M1.4 flare on **2011 February 18**, using multi-passband imaging observations from the Atmospheric Imaging Assembly on board SDO. We find that (1) the late phase emission originates from a different magnetic loop system, which is much larger and higher than the main phase loop system. (2) The two loop systems have different thermal evolution. While the late phase loop arcade reaches its peak brightness progressively at a later time spanning for more than one hour from high to low temperatures, the main phase loop arcade reaches its peak brightness at almost the same time (within several minutes) in all temperatures. (3) Nevertheless, the two loop systems seem to be connected magnetically, forming an asymmetric magnetic quadruple configuration. (4) Further, the footpoint brightenings in UV wavelengths show a systematic delay of about one minute from the main flare region to the remote footpoint of the late phase arcade system. We argue that the EUV late phase is the result of a long-lasting cooling process in the larger magnetic arcade system.

IMPULSIVE THERMAL X-RAY EMISSION FROM A LOW-LYING CORONAL LOOP
Siming **Liu**, Youping Li1, and Lyndsay Fletcher
2013 ApJ 769 135
Understanding the relationship among different emission components plays an essential role in the study of particle acceleration and energy conversion in solar flares. In flares where gradual and impulsive emission components can be readily identified, the impulsive emission has been attributed to non-thermal particles. We carry out detailed analysis of Hα and X-ray observations of a GOES class B microflare loop on the solar disk. The impulsive hard X-ray emission, however, is found to be consistent with a hot, quasi-thermal origin, and there is little evidence of emission from chromospheric footpoints, which challenges conventional models of flares and reveals a class of microflares associated with dense loops. Hα observations indicate that the loop lies very low in the solar corona or even in the chromosphere and both emission and absorption materials evolve during the flare. The enhanced Hα emission may very well originate from the photosphere when the low-lying flare loop heats up the underlying chromosphere and reduces the corresponding Hα opacity. These observations may be compared with detailed modeling of flare loops with the internal kink instability, where the mode remains confined in space without apparent change in the global field shape, to uncover the underlying physical processes and to probe the structure of solar atmosphere.

Determining Heating Rates in Reconnection Formed Flare Loops of the M8.0 Flare on 2005 May 13

Wen-Juan **Liu**, Jiong Qiu, Dana W. Longcope, Amir Caspi

E-print, April **2013**; ApJ **2013** 770 111

We analyze and model an M8.0 flare on **2005 May 13** observed by the Transition Region and Coronal Explorer (TRACE) and Reuven Ramaty High Energy Solar Spectroscopic Imager (RHESSI) to determine the energy release rate from magnetic reconnection that forms and heats numerous flare loops. The flare exhibits two ribbons in UV 1600 {AA} emission. Analysis shows that the UV light curve at each flaring pixel rises impulsively within a few minutes, and decays slowly with a timescale longer than 10 minutes. Since the lower atmosphere (the transition region and chromosphere) responds to energy deposit nearly instantaneously, the rapid UV brightening is thought to reflect the energy release process in the newly formed flare loop rooted at the foot point. In this paper, we utilize the spatially resolved (down to 1″) UV light curves and the thick-target hard X-ray emission to construct heating functions of a few thousand flare loops anchored at the UV foot points, and compute plasma evolution in these loops using the Enthalpy-Based Thermal Evolution of Loops (EBTEL) model. The modeled coronal temperatures and densities of these flare loops are then used to calculate coronal radiation. The computed soft X-ray spectra and light curves compare favorably with those observed by RHESSI and by the Geostationary Operational Environmental Satellite (GOES) X-ray Sensor (XRS). The time-dependent transition region differential emission measure (DEM) for each loop during its decay phase is also computed with a simplified model and used to calculate the optically-thin C iv line emission, which dominates the UV 1600 {AA} bandpass during the flare. The computed C iv line emission decays at the same rate as observed. This study presents a method to constrain heating of reconnection-formed flare loops using all available observables independently, and provides insight into the physics of energy release and plasma heating during the flare. With this method, the lower limit of the total energy used to heat the flare loops in this event is estimated to be 1.22e31 ergs, of which only 1.9e30 ergs is carried by beam-driven upflows during the impulsive phase, suggesting that the coronal plasmas are predominantly heated in situ.

PLASMOID EJECTIONS AND LOOP CONTRACTIONS IN AN ERUPTIVE M7.7 SOLAR FLARE: EVIDENCE OF PARTICLE ACCELERATION AND HEATING IN MAGNETIC RECONNECTION OUTFLOWS

Wei **Liu**1,2, Qingrong Chen3, and Vahé Petrosian

2013 ApJ 767 168

Where particle acceleration and plasma heating take place in relation to magnetic reconnection is a fundamental question for solar flares. We report analysis of an M7.7 flare on **2012 July 19** observed by SDO/AIA and RHESSI. Bi-directional outflows in forms of plasmoid ejections and contracting cusp-shaped loops originate between an erupting flux rope and underlying flare loops at speeds of typically 200-300 km s–1 up to 1050 km s–1. These outflows are associated with spatially separated double coronal X-ray sources with centroid separation decreasing with energy. The highest temperature is located near the nonthermal X-ray loop-top source well below the original heights of contracting cusps near the inferred reconnection site. These observations suggest that the primary loci of particle acceleration and plasma heating are in the reconnection outflow regions, rather than the reconnection site itself. In addition, there is an initial ascent of the X-ray and EUV loop-top source prior to its recently recognized descent, which we ascribe to the interplay among multiple processes including the upward development of reconnection and the downward contractions of reconnected loops. The impulsive phase onset is delayed by 10 minutes from the start of the descent, but coincides with the rapid speed increases of the upward plasmoids, the individual loop shrinkages, and the overall loop-top descent, suggestive of an intimate relation of the energy release rate and reconnection outflow speed.

MAGNETIC ENERGY AND HELICITY IN TWO EMERGING ACTIVE REGIONS IN THE SUN

Y. **Liu**1 and P. W. Schuck

2012 ApJ 761 105

The magnetic energy and relative magnetic helicity in two emerging solar active regions, AR 11072 and AR 11158, are studied. They are computed by integrating over time the energy and relative helicity fluxes across the photosphere. The fluxes consist of two components: one from photospheric tangential flows that shear and braid field lines (shear term), the other from normal flows that advect magnetic flux into the corona (emergence term). For these active regions: (1) relative magnetic helicity in the active-region corona is mainly contributed by the shear term, (2) helicity fluxes from the emergence and the shear terms have the same sign, (3) magnetic energy in the corona (including both potential energy and free energy) is mainly contributed by the emergence term, and (4) energy fluxes from the emergence term and the shear term evolved consistently in phase during the entire flux emergence course. We also examine the apparent tangential velocity derived by tracking field-line footpoints using a simple tracking method. It is found that this velocity is more consistent with tangential plasma velocity than with the flux transport velocity, which agrees with the conclusion by Schuck.

CONTRACTING AND ERUPTING COMPONENTS OF SIGMOIDAL ACTIVE REGIONS

Rui **Liu**1,2, Chang Liu2, Tibor Török3, Yuming Wang1, and Haimin Wang

2012 ApJ 757 150

It has recently been noted that solar eruptions can be associated with the contraction of coronal loops that are not involved in magnetic reconnection processes. In this paper, we investigate five coronal eruptions originating from four sigmoidal active regions, using high-cadence, high-resolution narrowband EUV images obtained by the Solar Dynamic Observatory (SDO). The magnitudes of the flares associated with the eruptions range from GOES class B to class X. Owing to the high-sensitivity and broad temperature coverage of the Atmospheric Imaging Assembly (AIA) on board SDO, we are able to identify both the contracting and erupting components of the eruptions: the former is observed in cold AIA channels as the contracting coronal loops overlying the elbows of the sigmoid, and the latter is preferentially observed in warm/hot AIA channels as an expanding bubble originating from the center of the sigmoid. The initiation of eruption always precedes the contraction, and in the energetically mild events (B- and C-flares), it also precedes the increase in GOES soft X-ray fluxes. In the more energetic events, the eruption is simultaneous with the impulsive phase of the nonthermal hard X-ray emission. These observations confirm that loop contraction is an integrated process in eruptions with partially opened arcades. The consequence of contraction is a new equilibrium with reduced magnetic energy, as the contracting loops never regain their original positions. The contracting process is a direct consequence of flare energy release, as evidenced by the strong correlation of the maximal contracting speed, and strong anti-correlation of the time delay of contraction relative to expansion, with the peak soft X-ray flux. This is also implied by the relationship between contraction and expansion, i.e., their timing and speed.

RAPID CHANGES OF PHOTOSPHERIC MAGNETIC FIELD AFTER TETHER-CUTTING RECONNECTION AND MAGNETIC IMPLOSION

Chang **Liu**1, Na Deng1,2, Rui Liu1, Jeongwoo Lee3, Thomas Wiegelmann4, Ju Jing1, Yan Xu1, Shuo Wang1 and Haimin Wang

2012 ApJ 745 L4

The rapid, irreversible change of the photospheric magnetic field has been recognized as an important element of the solar flare process. This Letter reports such a rapid change of magnetic fields during the **2011 February 13** M6.6 flare in NOAA AR 11158 that we found from the vector magnetograms of the Helioseismic and Magnetic Imager (HMI) with 12 minute cadence. High-resolution magnetograms of Hinode that are available at ~–5.5, –1.5, 1.5, and 4 hr relative to the flare maximum are used to reconstruct a three-dimensional coronal magnetic field under the nonlinear force-free field (NLFFF) assumption. UV and hard X-ray images are also used to illuminate the magnetic field evolution and energy release. The rapid change is mainly detected by HMI in a compact region lying in the center of the magnetic sigmoid, where the mean horizontal field strength exhibited a significant increase of 28%. The region lies between the initial strong UV and hard X-ray sources in the chromosphere, which are cospatial with the central feet of the sigmoid according to the NLFFF model. The NLFFF model further shows that strong coronal currents are concentrated immediately above the region, and that, more intriguingly, the coronal current system underwent an apparent downward collapse after the sigmoid eruption. These results are discussed in favor of both the tether-cutting reconnection producing the flare and the ensuing implosion of the coronal field resulting from the energy release.

A Revisit of the Masuda Flare

Rui **Liu** · Yan Xu · Haimin Wang

Solar Phys (**2011**) 269: 67–82

https://link.springer.com/content/pdf/10.1007%2Fs11207-010-9688-z.pdf

We revisit the flare that occurred on **13 January 1992**, which is now universally termed the “Masuda flare”. The new analysis is motivated not just by its uniqueness despite the increasing number of coronal observations in hard X-rays, but also by the improvement of *Yohkoh* hard X-ray image processing, which was achieved after the intensive investigations on this celebrated event. Using an uncertainty analysis, we show that the hard X-ray coronal source is located closer to the soft X-ray loop by about 5000 km (or 7 arcsec) in the re-calibrated Hard X-ray Telescope (HXT) images than in the original ones. Specifically, the centroid of the M1-band (23 – 33 keV) coronal source is above the maximum brightness of the Soft X-ray Telescope (SXT) loop by 5000 ± 1000 km (9600 km in the original data) and above the apex of the SXT loop represented by the 30% brightness contour by 2000 ± 1000 km (~7000 km in the original data). The change is obviously significant, because most coronal sources are above the thermal loop by less than 6 arcsec. We suggest that this change may account for the discrepancy in the literature, *i.e.*, the spectrum of the coronal emission was reported to be extremely hard below ~20 keV in the pre-calibration investigations, whereas it was reported to be considerably softer in the literature after the recalibration done by Sato, Kosugi, and Makishima (*Pub. Astron. Soc. Japan* **51**, 127, 1999). Still, the coronal spectrum is flatter at lower energies than at higher energies, due to the lackof a similar, co-spatial source in the L-band (14 – 23 keV), for which a convincing explanation is absent.

CHROMOSPHERIC JET AND GROWING "LOOP" OBSERVED BY *HINODE*: NEW EVIDENCE OF FAN–SPINE MAGNETIC TOPOLOGY RESULTING FROM FLUX EMERGENCE

Wei **Liu**1,2, Thomas E. Berger1, Alan M. Title1, Theodore D. Tarbell1, and B. C. Low3

Astrophysical Journal, 728:103 (16pp), **2011** February

We present observations of a chromospheric jet and growing "loop" system that show new evidence of a fan–spine topology resulting from magnetic flux emergence. This event, occurring in an equatorial coronal hole on **2007 February 9**, was observed by the *Hinode* Solar Optical Telescope in the Ca ii H line in unprecedented detail. The predecessor of the jet is a bundle of fine material threads that extend above the chromosphere and appear to rotate about the bundle axis at ~50 km s-1 (period _200 s). These rotations or transverse oscillations propagate upward at velocities up to 786 km s-1. The bundle first slowly and then rapidly swings up, with the transition occurring at the onset of an A4.9 flare. A loop expands simultaneously in these two phases (velocity: 16–135 km s-1). Near the peak of the flare, the loop appears to rupture; simultaneous upward ejecta and mass downflows faster than free-fall appear in one of the loop legs. The material bundle then swings back in a whip-like manner and develops into a collimated jet, which is orientated along the inferred open-field lines with transverse oscillations continuing at slower rates. Some material falls back along smooth streamlines, showing no more oscillations. At low altitudes, the streamlines bifurcate at presumably a magnetic null point and bypass an inferred dome, depicting an inverted-Y geometry. These streamlines closely match in space the late Ca ii H loop and X-ray flare loop. These observations are consistent with the model that flux emergence in an open-field region leads to magnetic reconnection, forming a jet and fan–spine topology. We propose that the material bundle and collimated jet represent the outer spine in quasi-static and eruptive stages, respectively, and the growing loop is a two-dimensional projection of the three-dimensional fan surface.

FAST CONTRACTION OF CORONAL LOOPS AT THE FLARE PEAK

Rui **Liu** and Haimin Wang

Astrophysical Journal Letters, 714:L41–L46, **2010** May, **File**

BBSO #1417, **2010**

n **2005 September 8**, a coronal loop overlying the active region NOAA 10808 was observed in *TRACE* 171 Å to contract at ~100 km s-1 at the peak of an X5.4–2B flare at 21:05 UT. Prior to the fast contraction, the loop underwent a much slower contraction at ~6 km s-1 for about 8 minutes, initiating during the flare preheating phase. The sudden switch to fast contraction is presumably corresponding to the onset of the impulsive phase. The contraction resulted in the oscillation of a group of loops located below, with the period of about 10 minutes. Meanwhile, the contracting loop exhibited a similar oscillatory pattern superimposed on the dominant downward motion. We suggest that the fast contraction reflects a suddenly reduced magnetic pressure underneath due either to (1) the eruption of magnetic structures located at lower altitudes or to (2) the rapid conversion of magnetic free energy in the flare core region. Electrons accelerated in the shrinking trap formed by the contracting loop can theoretically contribute to a late-phase hard X-ray burst, which is associated with Type IV radio emission. To complement the X5.4 flare which was probably confined, a similar event observed in *SOHO*/EIT 195 Å on **2004 July 20** in an eruptive, M8.6 flare is briefly described, in which the contraction was followed by the expansion of the same loop leading up to a halo coronal mass ejection. These observations further substantiate the conjecture of coronal implosion and suggest coronal implosion as a new exciter mechanism for coronal loop oscillations.

Sigmoid-to-Flux-Rope Transition Leading to A Loop-Like Coronal Mass Ejection

Rui **Liu**1, Chang Liu1, Shuo Wang1, Na Deng, and Haimin Wang

E-print, Nov **2010**, ApJL, 725:L84–L90, **2010; File**

Sigmoids are one of the most important precursor structures for solar eruptions. In this Letter, we study a sigmoid eruption on **2010 August 1** with EUV data obtained by the Atmospheric Imaging Assembly (AIA) on board the Solar Dynamic Observatory (SDO). In AIA 94 \AA\ (Fe XVIII; 6 MK), topological reconfiguration due to tether-cutting reconnection is unambiguously observed for the first time, i.e., two opposite J-shaped loops reconnect to form a continuous S-shaped loop, whose central portion is dipped and aligned along the magnetic polarity inversion line (PIL), and a compact loop crossing the PIL. A causal relationship between photospheric flows and coronal tether-cutting reconnections is evidenced by the detection of persistent converging flows toward the PIL using line-of-sight magnetograms obtained by the Helioseismic and Magnetic Imager (HMI) on board SDO. The S-shaped loop remains in quasi-equilibrium in the lower corona for about 50 minutes, with the central dipped portion rising slowly at ~10 km s-1. The speed then increases to ~60 km s-1 about 10 minutes prior to the onset of a GOES-class C3.2 flare, as the S-shaped loop speeds up its transformation into an arch-shaped loop, which eventually leads to a loop-like coronal mass ejection (CME). The AIA observations combined with H? filtergrams as well as hard X-ray (HXR) imaging and spectroscopy

are consistent with most flare loops being formed by reconnection of the stretched legs of less-sheared J-shaped loops that envelopes the rising flux rope, in agreement with the standard tether-cutting scenario.

A Reconnecting Current Sheet Imaged in A Solar Flare

Rui **Liu**, Jeongwoo Lee, Tongjiang Wang, Guillermo Stenborg, Chang Liu, Haimin Wang
E-print, Sept 2010, **File** ; ApJL, 723, L28, **2010**

Magnetic reconnection changes the magnetic field topology and powers explosive events in astrophysical, space and laboratory plasmas. For flares and coronal mass ejections (CMEs) in the solar atmosphere, the standard model predicts the presence of a reconnecting current sheet, which has been the subject of considerable theoretical and numerical modeling over the last fifty years, yet direct, unambiguous observational verification has been absent. In this Letter we show a bright sheet structure of global length (>0.25 Rsun) and macroscopic width ((5 - 10)x10^3 km) distinctly above the cusp-shaped flaring loop, imaged during the flare rising phase in EUV. The sheet formed due to the stretch of a transequatorial loop system, and was accompanied by various reconnection signatures that have been dispersed in the literature. This unique event provides a comprehensive view of the reconnection geometry and dynamics in the solar corona. **2004 July 29, slow drifting radio continuum**

ELEMENTARY ENERGY RELEASE EVENTS IN FLARING LOOPS: EFFECTS OF CHROMOSPHERIC EVAPORATION ON X-RAYS

Siming Liu1, Feiran Han2 and Lyndsay Fletcher1
ApJ 709 58-66, **2010**

With the elementary energy release events introduced in a previous paper, we model the chromospheric evaporation in flaring loops. The thick-target hard X-ray (HXR) emission produced by electrons escaping from the acceleration region dominates the impulsive phase, and the thin-target emission from the acceleration region dominates the low-energy thermal component in the gradual phase, as observed in early impulsive flares. Quantitative details depend on properties of the thermal background, which leads to variations in the correlation between HXR flux and spectral index. For lower temperature and/or higher density of the background electrons, the HXRs both rise and decay more quickly with a plateau near the peak. The plateau is less prominent at higher energies. Given the complexity of transport of mass, momentum, and energy along loops in the impulsive phase, we propose a strategy to apply this single-zone energy release and electron acceleration model to observations of flares associated with single loops so that the energy release, electron acceleration, and evaporation processes may be studied quantitatively.

Coronal Implosion and Particle Acceleration in the Wake of a Filament Eruption

Rui **Liu**, & Haimin Wang
E-print, Aug **2009**; ApJL

We study the evolution of a group of TRACE 195 A coronal loops overlying a reverse S-shaped filament on **2001 June 15**. These loops were initially pushed upward with the filament ascending and kinking slowly, but as soon as the filament rose explosively, they began to contract at a speed of ~100 km/s, and sustained for at least 12 min, presumably due to the reduced magnetic pressure underneath with the filament escaping. Despite the contraction following the expansion, the loops of interest remained largely intact during the filament eruption, rather than formed via reconnection. These contracting loops naturally formed a shrinking trap, in which hot electrons of several keV, in an order of magnitude estimation, can be accelerated to nonthermal energies. A single hard X-ray burst, with no corresponding rise in GOES soft X-ray flux, was recorded by the Hard X-ray Telescope (HXT) on board Yohkoh, when the contracting loops expectedly approached the post-flare arcade originating from the filament eruption. HXT images reveal a coronal source distinctly above the top of the soft X-ray arcade by ~15". The injecting electron population for the coronal source (thin target) is hardening by ~1.5 powers relative to the footpoint emission (thick target), which is consistent with electron trapping in the weak diffusion limit. Although we can not rule out additional reconnection, observational evidences suggest that the shrinking coronal trap may play a significant role in the observed nonthermal hard X-ray emission during the flare decay phase.

Successive Solar Flares and Coronal Mass Ejections on 2005 September 13 from NOAA AR 10808

Chang **Liu**, Jeongwoo Lee, Marian Karlicky, Debi Prasad Choudhary, Na Deng, and Haimin Wang
E-print, Aug **2009; File**, ApJ, 703:757–768, **2009**

We present a multiwavelength study of the 2005 September 13 eruption from NOAA 10808 that produced total four flares and two fast coronal mass ejections (CMEs) within 1.5 hours. Our primary attention is paid to the fact that these eruptions occurred in close succession in time, and that all of them were located along an S-shaped magnetic polarity inversion line (PIL) of the active region. In our analysis, (1) the disturbance created by the first flare propagated southward along the PIL to cause a major filament eruption that led to the first CME and the associated second flare underneath. (2) The first CME partially removed the overlying magnetic fields over the northern Delta spot to allow the third flare and the second CME. (3) The ribbon separation during the fourth flare would indicate reclosing of the overlying field lines opened by the second CME. It is thus concluded that this series of flares and CMEs are interrelated to each other via magnetic reconnections between the expanding magnetic structure and the nearby magnetic fields. These results complement previous works made on this event with the suggested causal relationship among the successive eruptions.

COMBINED MODELING OF ACCELERATION, TRANSPORT, AND HYDRODYNAMIC RESPONSE IN SOLAR FLARES. I. THE NUMERICAL MODEL

Wei Liu1,2, Vahé Petrosian2 and John T. Mariska3

ApJ 702 1553-1566, **2009** doi: 10.1088/0004-637X/702/2/1553

Acceleration and transport of high-energy particles and fluid dynamics of atmospheric plasma are interrelated aspects of solar flares, but for convenience and simplicity they were artificially separated in the past. We present here self-consistently combined Fokker-Planck modeling of particles and hydrodynamic simulation of flare plasma. Energetic electrons are modeled with the Stanford unified code of acceleration, transport, and radiation, while plasma is modeled with the Naval Research Laboratory flux tube code. We calculated the collisional heating rate directly from the particle transport code, which is more accurate than those in previous studies based on approximate analytical solutions. We repeated the simulation of Mariska et al. with an injection of power law, downward-beamed electrons using the new heating rate. For this case, a ~10% difference was found from their old result. We also used a more realistic spectrum of injected electrons provided by the stochastic acceleration model, which has a smooth transition from a quasi-thermal background at low energies to a nonthermal tail at high energies. The inclusion of low-energy electrons results in relatively more heating in the corona (versus chromosphere) and thus a larger downward heat conduction flux. The interplay of electron heating, conduction, and radiative loss leads to stronger chromospheric evaporation than obtained in previous studies, which had a deficit in low-energy electrons due to an arbitrarily assumed low-energy cutoff. The energy and spatial distributions of energetic electrons and bremsstrahlung photons bear signatures of the changing density distribution caused by chromospheric evaporation. In particular, the density jump at the evaporation front gives rise to enhanced emission, which, in principle, can be imaged by X-ray telescopes. This model can be applied to investigate a variety of high-energy processes in solar, space, and astrophysical plasmas.

ELEMENTARY ENERGY RELEASE EVENTS IN SOLAR FLARES

Siming Liu and Lyndsay Fletcher

ApJ **701** L34-L38, **2009** doi: 10.1088/0004-637X/701/1/L34

Most theoretical investigations of particle acceleration during solar flares cannot be applied to observations for detailed study of the time evolution. We propose a phenomenological model for turbulence evolution and stochastic particle acceleration that links observations to the energy release and particle acceleration through two coefficients characterizing particle interactions with turbulent electromagnetic fields. In the linear regime the particle distribution does not affect the turbulence energy cascade. It is shown that electron acceleration critically depends on the intensity of small-scale turbulence and an impulsive nonthermal component only appears near the peak of the gradually evolving turbulence intensity. The model naturally reproduces the soft-hard-soft pattern of hard X-ray pulses, and we attribute the observed change in flux and spectral index correlation from the rise to decay phase of some pulses to changes in the background plasma. Detailed modeling of well observed individual events will probe the energy release processes.

HARD X-RAY EMISSION IN KINKING FILAMENTS

Rui **Liu**1, and David Alexander

Astrophysical Journal, 697:999–1009, **2009, File**

http://www.iop.org/EJ/toc/-alert=43190/0004-637X/697/2

We present an observational study on the impact of the dynamic evolution of kinking filaments on the production of hard X-ray (HXR) emission. The investigation of two kinking-filament events in this paper, occurring on 2003 June 12 and 2004 November 10, respectively, combined with our earlier study on the failed filament eruption of 2002 May 27, suggests that two distinct processes take place during the kink evolution, leading to HXR emission with different morphological connections to the overall magnetic configuration. The first phase of the evolution (Phase I) is characterized by compact HXR footpoint sources at the endpoints of the filament, and the second phase (Phase II) by a ribbon-like footpoint emission extending along the endpoints of the filament. The HXR emission in

both the **2002 May 27 and 2004 November 10** events shows a transition from Phase I to Phase II. In the 2002 May 27 event, coronal emission was observed to be associated with EUV brightening sheaths aligned along two filament legs in Phase I, while in Phase II, it was located near the projected crossing point of the kink. The coronal emission in the 2004 November 10 event does not exhibit a clear morphological transition as in the 2002 May 27 event, probably due to the filament's relatively small size. The 2003 June 12 event mostly features a Phase I emission, with a compact footpoint emission located at one end of the filament, and an elongated coronal source oriented along the same filament leg.We propose the following scenarios to explain the different flare morphology: magnetic reconnection in Phase I occurs as a result of the interactions of the two writhing filament legs; reconnection in Phase II occurs at an X-type magnetic topology beneath the filament arch when the filament ascends and expands.

RECONNECTION ELECTRIC FIELD AND HARDNESS OF X-RAY EMISSION OF SOLAR FLARES

CHANG **LIU** AND HAIMIN WANG

E-prinnt, March **2009**; ApJL **696** L27-L31 doi: 10.1088/0004-637X/696/1/L27 , 2009

http://arxiv.org/PS_cache/arxiv/pdf/0903/0903.3968v1.pdf

Magnetic reconnection is believed to be the prime mechanism to trigger solar flares and accelerate electrons up to energies of MeV. In the classical two-dimensional reconnection model, the separation motion of chromospheric ribbons manifests the successive reconnection that takes place higher up in the corona. Meanwhile, downward traveling energetic electrons bombard the dense chromosphere and create hard X-ray (HXR) emissions, which provide a valuable diagnostic of electron acceleration. Analyses of ribbon dynamics and HXR spectrum have been carried out separately. In this Letter, we report a study of the comparison of reconnection electric field measured from ribbon motion and hardness (spectral index) of X-ray emission derived from X-ray spectrum. Our survey of the maximum average reconnection electric field and the minimum overall spectral index for 13 two-ribbon flares show that they are strongly anti-correlated. The former is also strongly correlated with flare magnitude measured using the peak flux of soft X-ray emissions. These provide strong support for electron acceleration models based on the electric field generated at reconnecting current sheet during flares.

Hard X-ray Emission In Kinking Filaments

Rui **Liu** & David Alexander

BBSO, #1389, **2009, File** , http://solar.njit.edu/preprints/liu1389.pdf

We present an observational study on the impact of the dynamic evolution of kinking filaments on the production of hard X-ray (HXR) emission. The investigation of two kinking-filament events in this paper, occurring on **2003 June 12 and 2004 November 10**, respectively, combined with our earlier study on the failed filament eruption of **2002 May 27**, suggests that two distinct processes take place during the kink evolution, leading to HXR emission with different morphological connections to the overall magnetic configuration. The first phase of the evolution (Phase I) is characterized by compact HXR footpoint sources at the endpoints of the filament, and the second phase (Phase II) by a ribbon-like footpoint emission extending along the endpoints of the filament. The HXR emission in both the 2002 May 27 and 2004 November 10 events shows a transition from Phase I to Phase II. In the 2002 May 27 event, coronal emission was observed to be associated with EUV brightening sheaths aligned along two filament legs in Phase I, while in Phase II, it was located near the projected crossing point of the kink. The coronal emission in the 2004 November 10 event does not exhibit a clear morphological transition as in the 2002 May 27 event, probably due to the filament's relatively small size. The 2003 June 12 event mostly features a Phase I emission, with a compact footpoint emission located at one end of the filament, and an elongated coronal source oriented along the same filament leg. We propose the following scenarios to explain the different flare morphology: magnetic reconnection in Phase I occurs as a result of the interactions of the two writhing filament legs; reconnection in Phase II occurs at an X-type magnetic topology beneath the filament arch when the filament ascends and expands.

Implosion in a Coronal Eruption

Rui **Liu**, Haimin Wang, David Alexander

E-print, Feb **2009**; ApJ, **696** 121-135, doi: 10.1088/0004-637X/696/1/121 , **2009**

BBSO, #1388, **2009** http://solar.njit.edu/preprints/liu1388.pdf

We present the observations of the contraction of the EUV coronal loops overlying the flaring region during the pre-heating as well as the early impulsive phase of a GOES class C8.9 flare. During the relatively long, 6 min, pre-heating phase, hard X-ray count rates at lower energies (below 25 keV) as well as soft X-ray fluxes increase gradually and the flare emission is dominated by a thermal looptop source with the temperature of 20 - 30 MK. After the onset of impulsive hard X-ray bursts, the flare spectrum is composed of a thermal component of 17 - 20 MK, corresponding to the looptop emission, and a nonthermal component with the spectral index ~(3.5 - 4.5), corresponding to a pair of

conjugate footpoints. The contraction of the overlying coronal loops is associated with the converging motion of the conjugate footpoints and the downward motion of the looptop source. The expansion of the coronal loops following the contraction is associated with the enhancement in H-alpha emission in the flaring region, and the heating of an eruptive filament whose northern end is located close to the flaring region. The expansion eventually leads to the eruption of the whole magnetic structure and a fast coronal mass ejection. It is the first time that such a large scale contraction of the coronal loops overlying the flaring region has been documented, which is sustained for about 10 min at an average speed of ~5 km/s. Assuming that explosive chromospheric evaporation plays a significant role in compensating for the reduction of the magnetic pressure in the flaring region, we suggest that a prolonged pre-heating phase dominated by coronal thermal emission is a necessary condition for the observation of coronal implosion. The dense plasma accumulated in the corona during the pre-heating phase may effectively suppress explosive chromospheric evaporation, which explains the continuation of the observed implosion up to ~7 min into the impulsive phase. between 16:00 and 17:00 UT on **2005 July 30**

Episodic X-ray Emission Accompanying the Activation of an Eruptive Prominence: Evidence of Episodic Magnetic Reconnection

Wei W. **Liu**, Tong-Jiang Wang, Brian R. Dennis, Gordon D. Holman
E-print, Feb **2009**; ApJ
We present an X-ray imaging and spectroscopic study of a partially occulted (N16W93) **C7.7 flare on 2003 April 24** observed by RHESSI that accompanied a prominence eruption observed by TRACE. (1) The activation and rise of the prominence occurs during the preheating phase of the flare. The initial X-ray emission appears as a single coronal source at one leg of the prominence and it then splits into a double source. Such a source splitting happens three times, each coinciding with an increased X-ray flux and plasma temperature, suggestive of fast reconnection in a localized current sheet and an enhanced energy release rate. In the late stage of this phase, the prominence displays a helical structure. These observations are consistent with the tether-cutting or kink instability model for triggering solar eruptions. (2) *The eruption of the prominence takes place during the flare impulsive phase. Since then, there appear signatures predicted by the classical CSHKP model of two-ribbon flares occurring in a vertical current sheet trailing an eruption. These signatures include an EUV cusp and current-sheet-like feature (or ridge) above it. There is also X-ray emission along the EUV ridge both below and above the cusp, which in both regions appears closer to the cusp at higher energies in the thermal regime ($lesssim$20~keV). This trend is reversed in the nonthermal regime. (3) Spectral analysis indicates thermal X-rays from all sources throughout the flare, while during the impulsive phase there is additional nonthermal emission which primarily comes from the coronal source below the cusp.* This source also has a lower temperature ($T=20 pm 1$ vs.~$25 pm 1$ MK), a higher emission measure ($EM=[3.3 pm 0.4]$ vs.~$[1.2 pm 0.4] imes 10^{47} cm^{-3}$), and a much harder nonthermal spectrum (electron power-law index $delta=5.4 pm 0.4$ vs.~$8 pm 1$) than the upper sources.

ENERGY SPECTRUM OF THE ELECTRONS ACCELERATED BY A RECONNECTION ELECTRIC FIELD: EXPONENTIAL OR POWER LAW?

W. J. **Liu** et al **2009** ApJ 690 1633-1638
http://www.iop.org/EJ/abstract/0004-637X/690/2/1633
The direct current (DC) electric field near the reconnection region has been proposed as an effective mechanism to accelerate protons and electrons in solar flares. A power-law energy spectrum was generally claimed in the simulations of electron acceleration by the reconnection electric field. However in most of the literature, the electric and magnetic fields were chosen independently. In this paper, we perform test-particle simulations of electron acceleration in a reconnecting magnetic field, where both the electric and magnetic fields are adopted from numerical simulations of the MHD equations. It is found that the accelerated electrons present a truncated power-law energy spectrum with an exponential tail at high energies, which is analogous to the case of diffusive shock acceleration. The influences of reconnection parameters on the spectral feature are also investigated, such as the longitudinal and transverse components of the magnetic field and the size of the current sheet. It is suggested that the DC electric field alone might not be able to reproduce the observed single or double power-law distributions.

Solar Flares as Natural Particle Accelerators: A High-energy View from X-ray Observations and Theoretical Models

Wei **Liu**
2008; File of the book
http://solar.physics.montana.edu/cgi-bin/eprint/index.pl?entry=7644

Solar flares, which have significant space weather consequences, are natural particle accelerators and one of the most spectacular phenomena of solar activity. RHESSI is the most advanced solar X-ray and gamma-ray mission ever flown and has opened a new era in solar flare research following its launch in 2002. This **book** offers a glimpse of this active research area from a high-energy perspective and contains a comprehensive guideline for RHESSI data analysis. Its main theme is the investigation of particle acceleration and transport in solar flares. The strength of this book lies in its well-balanced account of the latest X-ray observations and theoretical models. The observational focus is on the morphology and spectra of imaged X-ray sources produced by nonthermal electrons or hot plasma. The modeling takes the novel approach of combining the Fokker-Planck treatment of the accelerated particles with the hydrodynamic treatment of the heated atmosphere. Applications of this modeling technique reach beyond the Sun to other exotic environments in the universe, such as extrasolar planetary auroras, stellar flares, and flares on accretion disks around neutron stars and black holes.
http://www.freebookspot.in/Comments.aspx?Element_ID=31543

Relationship between Powerful Flares and Dynamic Evolution of the Magnetic Field at the Solar Surface

Jihong **Liu** · Yin Zhang · Hongqi Zhang
Solar Phys (**2008)** 248: 67–84
http://www.springerlink.com/content/nh78261k82862778/fulltext.pdf
Powerful flares are closely related to the evolution of the complex magnetic field configuration at the solar surface. The strength of the magnetic field and speed of its evolution are two vital parameters in the study of the change of magnetic field in the solar atmosphere. We propose a dynamic and quantitative depiction of the changes in complexity of the active region: **E = u ↳ B**, where **u** is the velocity of the footpoint motion of the magnetic field lines and **B** is the magnetic field.

DOUBLE CORONAL HARD AND SOFT X-RAY SOURCE OBSERVED BY RHESSI: EVIDENCE FOR MAGNETIC RECONNECTION AND PARTICLE ACCELERATION IN SOLAR FLARES

Wei **Liu**, Vahe´ Petrosian, Brian R. Dennis, and Yan Wei Jiang
The Astrophysical Journal, 676:704Y716, **2008** March 20
http://www.journals.uchicago.edu/doi/pdf/10.1086/527538
We present data analysis and interpretation of an M1.4 class flare observed with the Reuven Ramaty High Energy Solar Spectroscopic Imager (RHESSI) on **2002 April 30**. This event, with its footpoints occulted by the solar limb, exhibits a rarely observed, but theoretically expected, double-source structure in the corona. The two coronal sources, observed over the 6Y30 keVrange, appear at different altitudes and show energy-dependent structures with the higher energy emission being closer together. Spectral analysis implies that the emission at higher energies in the inner region between the two sources is mainly nonthermal, while the emission at lower energies in the outer region is primarily thermal. The two sources are both visible for about 12 minutes and have similar light curves and power-law spectra above about 20 keV. These observations suggest that the magnetic reconnection site lies between the two sources. Bidirectional outflows of the released energy in the form of turbulence and/or particles from the reconnection site could be the source of the observed radiation. The spatially resolved thermal emission below about 15 keV, on the other hand, indicates that the lower source has a larger emission measure but a lower temperature than the upper source This is likely the result of the differences in the magnetic field and plasma density of the two sources.

THE SPATIAL DISTRIBUTION OF HARD X-RAY SPECTRAL INDEX AND LOCAL MAGNETIC RECONNECTION RATE

CHANG **LIU**,1 JEONGWOO LEE,2 JU JING,2 DALE E. GARY,2 AND HAIMIN WANG
E-print, Nov **2007**, ApJL
The rare phenomenon of ribbon-like hard X-ray (HXR) sources up to 100 keV found in the 2005 May 13 M8.0 flare observed with the Reuven Ramaty High Energy Solar Spectroscopic Imager provides detailed information on the spatial distribution of flare HXR emission.

Evolution of electron energy spectrum during solar flares

W. J. **Liu**, P. F. Chen, C. Fang, M. D. Ding
Advances in Space Research, Volume 39, Issue 9, p. 1394-1397, **2007**

Particle acceleration by direct-current electric field in the current sheet has been extensively studied, in which an electric and a magnetic field are generally prescribed, and a power law distribution of the electron energy is obtained. Based on MHD numerical simulations of flares, this paper aims at investigating the time evolution of the electron energy spectrum during solar flares. It turns out that the model reproduces the soft-hard-hard spectral feature which was observed in some flares.

RHESSI Observation of Chromospheric Evaporation

Wei **Liu**, Siming Liu, Yan Wei Jiang, and Vahe Petrosian
The Astrophysical Journal, 649:1124-1139, **2006**
Neupert effect

The Eruption from a Sigmoidal Solar Active Region on 2005 May 13

Chang **Liu**, Jeongwoo Lee, Vasyl Yurchyshyn, Na Deng, Kyung-Suk Cho, Marian Karlicky, and Haimin Wang
E-print, July **2007**
The most important finding is that the flare brightening starts in the core of the active region earlier than that of the rising motion of the flux rope. This timing clearly addresses one of the main issues in the magnetic eruption onset of sigmoid, namely, whether the eruption is initiated by an internal tether-cutting to allow the flux rope to rise upward or a flux rope rises due to a loss of equilibrium to later induce tether cutting below it. Our high time cadence SXI and Halpha data shows that the first scenario is relevant to this eruption. As other major findings, we have the RHESSI HXR images showing a change of the HXR source from a confined footpoint structure to an elongated ribbon-like structure after the flare maximum, which we relate to the sigmoid-to-arcade evolution. Radio dynamic spectrum shows a type II precursor that occurred at the time of expansion of the sigmoid and a drifting pulsating structure in the flare rising phase in HXR. Finally type II and III bursts are seen at the time of maximum HXR emission, simultaneous with the maximum reconnection rate derived from the flare ribbon motion in UV.

The Ribbon-like Hard X-Ray Emission in a Sigmoidal Solar Active Region

Chang **Liu**, Jeongwoo Lee, Dale E. Gary, and Haimin Wang
The Astrophysical Journal Letters, Volume 658, Number 2, Page L127, **2007**, **File**
http://www.journals.uchicago.edu/cgi-bin/resolve?ApJL21324]
13 May 2005

The X10 Flare on 29 October 2003: Was It Triggered by Magnetic Reconnection between Counter-Helical Fluxes?

Yu **Liu**, Hiroki Kurokawa[2], Chang Liu[3], David H. Brooks[2], Jingping Dun[2], Takako T. Ishii[2] and Hongqi Zhang
Solar Phys. 240 (2), Page: 253 – 262, **2007**
The X10 flare on 29 October 2003 resulted from *reconnection between magnetic flux tubes having opposite current helicity*.

The maximum magnetic flux in an active region

George **Livadiotis***a,b*,1 and Xenophon Moussas*b*,
Proceedings of the International Astronomical Union (2008), *N. Gopalswamy & D. F. Webb, eds.*, 4: 101-108, **2009**
http://journals.cambridge.org/action/displayIssue?jid=IAU&volumeId=4&seriesId=0&issueId=S257
The Photometric-Magnetic Dynamical model handles the evolution of an individual sunspot as an autonomous nonlinear, though integrable, dynamical system. The model considers the simultaneous interplay of two different interacted factors: The photometric and magnetic factors, respectively, characterizing the evolution of the sunspot visible area A on the photosphere, and the simultaneous evolution of the sunspot magnetic field strength B. All the possible sunspots are gathered in a specific region of the phase space (A, B). The separatrix of this phase space region determines the upper limit of the values of sunspot area and magnetic strength. Consequently, an upper limit of the magnetic flux in an active region is also determined, found to be ≈7.23 × 1023 Mx. This value is phenomenologically equal to the magnetic flux concentrated in the totality of the granules of the quite Sun. Hence, the magnetic flux concentrated in an active region cannot exceed the one concentrated in the whole photosphere.

Sunspots with the Strongest Magnetic Fields

W. **Livingston**, J. W. Harvey, O. V. Malanushenko and L. Webster
Solar Phys., 29(1-2), 41–68, 2006

Catalog of Hard X-ray Solar Flares Detected with Mars Odyssey/HEND from the Mars Orbit in 2001-2016

M.A. **Livshits**, I.V. Zimovets, D.V. Golovin, B.A. Nizamov, V.I. Vybornov, I.G. Mitrofanov, A.S. Kozyrev, M.L. Litvak, A.B. Sanin, V.I. Tretyakov
Astronomy Reports **2017**
https://arxiv.org/pdf/1706.01116.pdf
The study of nonstationary processes in the Sun is of great interest, and lately, multiwavelength observations and registration of magnetic fields are carried out by means of both ground-based telescopes and several specialized spacecraft (SC) on near-Earth orbits. However the acquisition of the new reliable information on their hard X-ray radiation remains demanded, in particular if the corresponding SC provide additional information, e.g. in regard to the flare observations from the directions other than the Sun-Earth direction. In this article we present a catalog of powerful solar flares registered by the High Energy Neutron Detector (HEND) device designed in the Space Research Institute (IKI) of Russian Academy of Sciences. HEND is mounted onboard the 2001 Mars Odyssey spacecraft. It worked successfully during the flight to Mars and currently operates in the near-Mars orbit. Besides neutrons, the HEND instrument is sensitive to the hard X-ray and gamma radiation. This radiation is registered by two scintillators: the outer one is sensitive to the photons above 40 keV and the inner one to the photons above 200 keV. The catalog was created with the new procedure of the data calibration. For most powerful 60 solar flares on the visible and on the far sides of the Sun (in respect to a terrestrial observer), we provide time profiles of flare radiation, summed over all the channels of X-ray and in some cases of gamma-ray bands as well as the spectra and characteristics of their power law approximation. We briefly discuss the results of the previous articles on the study of the Sun with HEND instrument and the potential of the further use of these data. **14 Jul 2005 , 12-Feb-2010**
TABLE II: Catalog of powerful solar flares (2001-2015).

Evidence of the Relationship between the Emerging Magnetic Fields, Electric Currents, and Solar Flares Observed on May 10, 2012

M.A. **Livshits**, I.Yu. Grigoryeva, I.I. Myshyakov, G.V. Rudenko
Astronomy Reports **2016**
http://arxiv.org/pdf/1604.07073v1.pdf
We have analyzed multi-wavelength observations and magnetic-field data for the solar flare of **May 10, 2012** (04:18 UT) and have detected a sign inversion of the signal in the line-of-sight magnetic measurements in the umbra of a small spot. This effect is associated, at least partly, with the emergence of a new magnetic field. Almost at the same time, a burst of hard X-rays was recorded, and a wave in the vacuum ultraviolet (EUV) range (a "sunquake") was generated due to the impact of the disturbance in the energy release range on the photosphere. At the beginning of the event, a sigmoid flare was recorded, but it did not spread, as it usually does, along the polarity inversion (neutral) line. SDO/HMI full-vector measurements were used to extrapolate the AR 11476 magnetic field to the corona, and the distribution of vertical currents jz in the photosphere was obtained. The distribution of currents in the active region shows that the relationship between them and the occurrence of flares is very intricate. We have corroborated that the expected "ideal" behavior of the current system before and after the flare (e.g., see (Sharykin and Kosovichev, 2015)) is observed only in the sigmoid region. The results obtained were compared with the observations of two other flares recorded in this AR on the same day, one of which was similar to the flare under discussion and the other was of different type. Our results confirm that the formation and eruption of large-scale magnetic flux ropes in sigmoid flares are associated with the shear motions in the photosphere and the emergence of twisted magnetic tubes, as well as with the subsequent development of the torus instability.

The magnetic virial theorem and the nature of flares on the Sun and other G stars

M.A. **Livshits**, G.V. Rudenko , M.M. Katsova , I.I. Myshyakov
Advances in Space Research, Volume 55, Issue 3, 1 February **2015**, Pages 920–926
http://www.sciencedirect.com/science/article/pii/S0273117714005389
Modern observations of magnetic fields confirm basic ideas obtained earlier by A.B. Severny about field changes that occur over the course of a flare. For interpretation of new data of the magnetic field vector, the methods of the non-linear force-free field (NLFFF) extrapolation were developed. As a test of these methods, we carried out the NLFFF extrapolation for the active region AR 11158 (February 2011) using the algorithm by Rudenko and Myshyakov (2009). This NLFFF approximation gives information on the magnetic field structure in the corona of active regions (AR). When considering the only total energy of non-stationary processes, it is possible to shift from the equations describing the structural features to considering the magnetic virial theorem. We obtain new analytic expression for the free energy

of the solar corona as a whole and discuss circumstances, which prevent using this analytic expression as a measure of the free energy of a size-limited AR, when magnetic fields of the photosphere of AR are not force-free. Observations and NLFFF extrapolation give the upper estimate of the energy of flares, which are able to occur in a given large active region. For the Sun, this value does not exceed 3×10^32 ergs. Because the average longitudinal magnetic fields of G stars (at an age of 1–2 Gyr) are ten-times stronger than the maximum magnetic field of the Sun as a star, the energy of solar-type stellar flares can only slightly exceed 10^34 ergs. These flares are associated with the energy deposit above the chromosphere and its subsequent release. Phenomena with the total energy up to 10^36 ergs which were registered also on the younger G stars have the nature which differs substantially from those non-stationary processes occurring on the Sun. **15 Feb 2011**

Culmination of the flare activity of Group 10786 in July 2005: X-Ray observations from near-mars and near-earth orbits

M. A. **Livshits**, D. V. Golovin, L. K. Kashapova, I. G. Mitrofanov, A. S. Kozyrev, M. L. Litvak, A. B. Sanin, V. I. Tret'yakov, W. Boynton and K. Shinohara, et al.
Astronomy Reports, Volume 55, Number 6, 551-560, **2011**
A detailed study of two major solar flares that occurred in Group 10786 at the time of its disappearance behind the western limb is presented. The flares **of July 14, 2005** were previously studied fairly poorly, as no RHESSI hard X-ray observations were available for themaxima of the twomost powerful of these flares. Observations carried out using the HEND equipment (on the Mars Odyssey spacecraft) developed at the Institute for Space Research in Moscow are used here to fill this gap. In the first flare, an intense, impulsive burst occurred at 07:23 UT, about 1.5 h after the onset of a weak, prolonged event. While processes in the neighborhood of the northern spot dominated in the flares of July 5–9, a powerful impulsive energy release on July 14 emerged when the flare process that originated in the North reached the southern spot. Our analysis of the flare activity of this medium-sized group reveals a gradual enhancement of the flare activity and a strong interaction between the acceleration above the magnetic-field neutral line and in the immediate vicinity of the spots. At the time of the culmination of the flare activity in the group on July 13 and 14, the pattern of nonstationary processes changes: fast coronal mass ejections form after a series of impulsive energy-release events. Spacecraft observations of the burst of July 14 after 11 UT at points separated in longitude (on RHESSI and Mars Odyssey) revealed clear anisotropy of the flare emission at energies exceeding 80 keV.

Localised acceleration of energetic particles by a weak shock in the solar corona

David M. **Long**, Hamish A. S. Reid, Gherardo Valori, Jennifer O'Kane
ApJ **2021**
https://arxiv.org/pdf/2108.05068.pdf
Globally-propagating shocks in the solar corona have long been studied to quantify their involvement in the acceleration of energetic particles. However, this work has tended to focus on large events associated with strong solar flares and fast coronal mass ejections (CMEs), where the waves are sufficiently fast to easily accelerate particles to high energies. Here we present observations of particle acceleration associated with a global wave event which occurred on **1 October 2011**. Using differential emission measure analysis, the global shock wave was found to be incredibly weak, with an Alfvén Mach number of ~1.008-1.013. Despite this, spatially-resolved type III radio emission was observed by the Nançay RadioHeliograph at distinct locations near the shock front, suggesting localised acceleration of energetic electrons. Further investigation using a magnetic field extrapolation identified a fan structure beneath a magnetic null located above the source active region, with the erupting CME contained within this topological feature. We propose that a reconfiguration of the coronal magnetic field driven by the erupting CME enabled the weak shock to accelerate particles along field lines initially contained within the fan and subsequently opened into the heliosphere, producing the observed type III emission. These results suggest that even weak global shocks in the solar corona can accelerate energetic particles via reconfiguration of the surrounding magnetic field.

Implications of High-density, High-temperature Ridges Observed in Some Two-ribbon Flares

Dana **Longcope**1 and Jiong Qiu1
2022 ApJ 941 160 **File**
https://iopscience.iop.org/article/10.3847/1538-4357/aca29a/pdf
Several two-ribbon solar flares observed on the disk, notably including the Bastille flare of 2000 July 14, show an extended ridge of plasma running along the loop tops of the post-reconnection arcade. In that and two more recent examples, the ridge is visible in emission by Fe xxiv at roughly 17 MK, with a high, steadily increasing emission measure suggesting an expanding column of very dense plasma. We find that ridges are consistent with overhead views of long, vertical plasma sheets, such as seen above certain limb flares. Those vertical features show enhanced temperature and density over their entire lengths, making explanations in terms of termination shocks and evaporation collision seem less plausible. We use observations of several ridge events to argue in favor of compression and heating

by slow magnetosonic shocks in the reconnection outflow. In this scenario, the ridge is built up as retracting flux piles hot, compressed plasma atop the post-flare arcade. Thanks to the overhead perspective offered by the ridge observations, we are able to measure the reconnection rate and show it to be consistent with the rate of increase in column emission measure across the ridge. This consistency supports the hypothesis that slow shocks and retraction compress the plasma seen in ridges, vertical plasma sheets, and possibly the high-temperature fans through which post-reconnection downflows are observed. Such a unified picture of these diverse features enhances our understanding of the role played by magnetic reconnection in solar flares. **14 Jul 2000, 18 Apr 2014, 28 Oct 2021**

Evidence for Downflows in the Narrow Plasma Sheet of 2017 September 10 and Their Significance for Flare Reconnection

Dana **Longcope**1, John Unverferth1, Courtney Klein1,2, Marika McCarthy1, and Eric Priest3
2018 ApJ 868 148
sci-hub.tw/10.3847/1538-4357/aaeac4
https://iopscience.iop.org/article/10.3847/1538-4357/aaeac4/pdf
Current sheets are believed to form in the wakes of erupting flux ropes and to enable the magnetic reconnection responsible for an associated flare. Multiwavelength observations of an eruption on **2017 September 10** show a long, linear feature widely taken as evidence of a current sheet viewed edge-on. The relation between the high-temperature, high-density plasma thus observed and any current sheet is not yet entirely clear. We estimate the magnetic field strength surrounding the sheet and conclude that approximately one-third of all flux in the active region was opened by the eruption. Subsequently decreasing field strength suggests that the open flux closed down over the next several hours through reconnection at a rate $\dot{\Phi} \simeq 5 \times 10^{17}$ Mx s−1. We find in AIA observations evidence of downward-moving, dark structures analogous to either supra-arcade downflows, more typically observed above flare arcades viewed face-on, or supra-arcade downflowing loops, previously reported in flares viewed in this perspective. These features suggest that the plasma sheet is composed of the magnetic flux retracting after being reconnected high above the arcade. We model flux tube retraction following reconnection to show that this process can generate high densities and temperatures as observed in the plasma sheet. The retracting flux tubes reach their highest temperatures at the end of their retraction, well below the site of reconnection, consistent with previous analysis of AIA and EIS data showing a peak in the plasma temperature near the base of this particular sheet.

A reconnection-driven model of the hard X-ray loop-top source from flare 2004-Feb-26

Dana **Longcope**, Jiong Qiu, Jasmine Brewer
2016 ApJ 833 211
https://arxiv.org/pdf/1610.07953v1.pdf
A compact X-class flare on 2004-Feb-26 showed a concentrated source of hard X-rays at the tops of the flare's loops. This was analyzed in previous work (Longcope et al. 2010), and interpreted as plasma heated and compressed by slow magnetosonic shocks generated during post-reconnection retraction of the flux. That work used analytic expressions from a thin flux tube (TFT) model, which neglected many potentially important factors such as thermal conduction and chromospheric evaporation. Here we use a numerical solution of the TFT equations to produce a more comprehensive and accurate model of the same flare, including those effects previously omitted. These simulations corroborate the prior hypothesis that slow mode shocks persist well after the retraction has ended, thus producing a compact, loop-top source instead of an elongated jet, as steady reconnection models predict. Thermal conduction leads to densities higher than analytic estimates had predicted, and evaporation enhances the density still higher, but at lower temperatures. X-ray light curves and spectra are synthesized by convolving the results from a single TFT simulation with the rate at which flux is reconnected, as measured through motion of flare ribbons, for example. These agree well with light curves observed by RHESSI and GOES and spectra from RHESSI. An image created from a superposition of TFT model runs resembles one produced from RHESSI observations. This suggests that the HXR loop-top source, at least the one observed in this flare, could be the result of slow magnetosonic shocks produced in fast reconnection models like Petschek's.

How gas-dynamic flare models powered by Petschek reconnection differ from those with ad hoc energy sources

Dana **Longcope**, Jim Klimchuk
2015 ApJ 813 131
http://arxiv.org/pdf/1510.05985v1.pdf
Aspects of solar flare dynamics, such as chromospheric evaporation and flare light-curves, have long been studied using one-dimensional models of plasma dynamics inside a static flare loop, subjected to some energy input. While extremely successful at explaining the observed characteristics of flares, all such models so far have specified energy input ad hoc, rather than deriving it self-consistently. There is broad consensus that flares are powered by magnetic energy released through reconnection. Recent work has generalized Petschek's basic reconnection scenario, topological change followed by field line retraction and shock heating, to permit its inclusion into a one-dimensional flare loop model. Here we

compare the gas dynamics driven by retraction and shocking to those from more conventional static loop models energized by ad hoc source terms. We find significant differences during the first minute, when retraction leads to larger kinetic energies and produces higher densities at the loop top, while ad hoc heating tends to rarify the loop top. The loop-top density concentration is related to the slow magnetosonic shock, characteristic of Petschek's model, but persists beyond the retraction phase occurring in the outflow jet. This offers an explanation for observed loop-top sources of X-ray and EUV emission, with advantages over that provided by ad hoc heating scenarios. The cooling phases of the two models are, however, notably similar to one another, suggesting observations at that stage will yield little information on the nature of energy input.

A simple model of chromospheric evaporation and condensation driven conductively in a solar flare

D. W. **Longcope**
ApJ, 795 10 **2014**
http://arxiv.org/pdf/1409.1886v1.pdf
Magnetic energy released in the corona by solar flares reaches the chromosphere where it drives characteristic upflows and downflows known as evaporation and condensation. These flows are studied here for the case where energy is transported to the chromosphere by thermal conduction. An analytic model is used to develop relations by which the density and velocity of each flow can be predicted from coronal parameters including the flare's energy flux F. These relations are explored and refined using a series of numerical investigations in which the transition region is represented by a simplified density jump. The maximum evaporation velocity, for example, is well approximated by $v_e \simeq 0.38(F/\rho_{co,0})1/3$, where $\rho_{co,0}$ is the mass density of the pre-flare corona. This and the other relations are found to fit simulations using more realistic models of the transition region both performed in this work, and taken from a variety of previously published investigations. These relations offer a novel and efficient means of simulating coronal reconnection without neglecting entirely the effects of evaporation.

Peristaltic Shocks: a model

Dana **Longcope** and Roger Scott
RHESSI Science Nugget , No. 207, Sept **2013**
http://sprg.ssl.berkeley.edu/~tohban/wiki/index.php/Peristaltic_Shocks:_a_model
Reconciling reconnection with high coronal preflare densities.
One possible resolution to this paradox would be a mechanism by which energy released by reconnection could be somehow transported across field lines onto the unreconnected flux. Such a mechanism would permit some evaporation in advance of the actual reconnection energy release on those field lines. This could also explain the high emission measure in the fan above a flaring arcade. In this scenario the fan would not correspond to the current sheet itself, but rather to a layer of pre-heated, and pre-loaded plasma surrounding the current sheet. It is through this layer that the remarkable supra-arcade downflows appear to descend, leaving behind them some form of trail or wake (Ref. [2]).

THE ROLE OF FAST MAGNETOSONIC WAVES IN THE RELEASE AND CONVERSION VIA RECONNECTION OF ENERGY STORED BY A CURRENT SHEET

D. W. **Longcope** and L. Tarr
2012 ApJ 756 192
Using a simple two-dimensional, zero-β model, we explore the manner by which reconnection at a current sheet releases and dissipates free magnetic energy. We find that only a small fraction (3%-11% depending on current-sheet size) of the energy is stored close enough to the current sheet to be dissipated abruptly by the reconnection process. The remaining energy, stored in the larger-scale field, is converted to kinetic energy in a fast magnetosonic disturbance propagating away from the reconnection site, carrying the initial current and generating reconnection-associated flows (inflow and outflow). Some of this reflects from the lower boundary (the photosphere) and refracts back to the X-point reconnection site. Most of this inward wave energy is reflected back again and continues to bounce between X-point and photosphere until it is gradually dissipated, over many transits. This phase of the energy dissipation process is thus global and lasts far longer than the initial purely local phase. In the process, a significant fraction of the energy (25%-60%) remains as undissipated fast magnetosonic waves propagating away from the reconnection site, primarily upward. This flare-generated wave is initiated by unbalanced Lorentz forces in the reconnection-disrupted current sheet, rather than by dissipation-generated pressure, as some previous models have assumed. Depending on the orientation of the initial current sheet, the wave front is either a rarefaction, with backward-directed flow, or a compression, with forward-directed flow.

A MODEL FOR THE ORIGIN OF HIGH DENSITY IN LOOPTOP X-RAY SOURCES

D. W. **Longcope** and S. E. Guidoni
2011 ApJ 740 73
Super-hot (SH) looptop sources, detected in some large solar flares, are compact sources of HXR emission with spectra matching thermal electron populations exceeding 30 MK. High observed emission measure (EM) and inference of electron thermalization within the small source region both provide evidence of high densities at the looptop, typically more than an order of magnitude above ambient. Where some investigators have suggested such density enhancement results from a rapid enhancement in the magnetic field strength, we propose an alternative model, based on Petschek reconnection, whereby looptop plasma is heated and compressed by slow magnetosonic shocks generated self-consistently through flux retraction following reconnection. Under steady conditions such shocks can enhance density by no more than a factor of four. These steady shock relations (Rankine-Hugoniot relations) turn out to be inapplicable to Petschek's model owing to transient effects of thermal conduction. The actual density enhancement can in fact exceed a factor of 10 over the entire reconnection outflow. An ensemble of flux tubes retracting following reconnection at an ensemble of distinct sites will have a collective EM proportional to the rate of flux tube production. This rate, distinct from the local reconnection rate within a single tube, can be measured separately through flare ribbon motion. Typical flux transfer rates and loop parameters yield EMs comparable to those observed in SH sources.

A Quantitative Model of Energy Release and Heating by Time-dependent, Localized Reconnection in a Flare with Thermal Loop-top X-ray Source

D.W. **Longcope** · A.C. Des Jardins · T. Carranza-Fulmer · J. Qiu
Solar Phys (**2010**) 267: 107–139
We present a quantitative model of the magnetic energy stored and then released through magnetic reconnection for a flare on **26 February 2004**. This flare, well observed by RHESSI and TRACE, shows evidence of non-thermal electrons for only a brief, early phase. Throughout the main period of energy release there is a super-hot (T _ 30 MK) plasma emitting thermal bremsstrahlung atop the flare loops. Our model describes the heating and compression of such a source by localized, transient magnetic reconnection. It is a threedimensional generalization of the Petschek model, whereby Alfvén-speed retraction following reconnection drives supersonic inflows parallel to the field lines, which form shocks: heating, compressing, and confining a loop-top plasma plug. The confining inflows provide longer life than a freely expanding or conductively cooling plasma of similar size and temperature. Superposition of successive transient episodes of localized reconnection across a current sheet produces an apparently persistent, localized source of high-temperature emission. The temperature of the source decreases smoothly on a time scale consistent with observations, far longer than the cooling time of a single plug. Built from a disordered collection of small plugs, the source need not have the coherent jet-like structure predicted by steady-state reconnection models. This new model predicts temperatures and emission measure consistent with the observations of 26 February 2004. Furthermore, the total energy released by the flare is found to be roughly consistent with that predicted by the model. Only a small fraction of the energy released appears in the super-hot source at any one time, but roughly a quarter of the flare energy is thermalized by the reconnection shocks over the course of the flare. All energy is presumed to ultimately appear in the lower-temperature (T _ 20 MK) post-flare loops. The number, size, and early appearance of these loops in TRACE's 171 Å band are consistent with the type of transient reconnection assumed in the model.

A Quantitative, Topological Model of Reconnection and Flux Rope Formation in a Two-Ribbon Flare

D.W. **Longcope** and C. Beveridge
E-print, Sept **2007**

Modeling and Measuring the Flux Reconnected and Ejected by the Two-Ribbon Flare/CME Event on 7 November 2004

Dana **Longcope** · Colin Beveridge · Jiong Qiu · B. Ravindra · Graham Barnes · Sergio Dasso
Solar Phys, (2007) 244: 45–73; DOI 10.1007/s11207-007-0330-7, **2007**

A solar flare driven by thermal conduction observed in mid-infrared

Fernando M. **López**, C. Guillermo Giménez de Castro, Cristina H. Mandrini, Paulo J. A. Simões, Germán D. Cristiani, Dale E. Gary, Carlos Francile, Pascal Démoulin

A&A 657, id.A51 **2022**
https://arxiv.org/pdf/2110.15751.pdf
https://www.aanda.org/articles/aa/pdf/2022/01/aa41967-21.pdf
https://doi.org/10.1051/0004-6361/202141967

The mid-infrared (mid-IR) range has been mostly unexplored for the investigation of solar flares. It is only recently that new mid-IR flare observations have begun opening a new window into the response and evolution of the solar chromosphere. These new observations have been mostly performed by the AR30T and BR30T telescopes that are operating in Argentina and Brazil, respectively. We present the analysis of SOL**2019-05-15**T19:24, a GOES class C2.0 solar flare observed at 30~THz (10 μm) by the ground-based telescope AR30T. Our aim is to characterize the evolution of the flaring atmosphere and the energy transport mechanism in the context of mid-IR emission. We performed a multi-wavelength analysis of the event by complementing the mid-IR data with diverse ground- and space-based data from the Solar Dynamics Observatory (SDO), the H--α Solar Telescope for Argentina (HASTA), and the Expanded Owens Valley Solar Array (EOVSA). Our study includes the analysis of the magnetic field evolution of the flaring region and of the development of the flare. The mid-IR images from AR30T show two bright and compact flare sources that are spatially associated with the flare kernels observed in ultraviolet (UV) by SDO. We confirm that the temporal association between mid-IR and UV fluxes previously reported for strong flares is also observed for this small flare. The EOVSA microwave data revealed flare spectra consistent with thermal free-free emission, which lead us to dismiss the existence of a significant number of non-thermal electrons. We thus consider thermal conduction as the primary mechanism responsible for energy transport. Our estimates for the thermal conduction energy and total radiated energy fall within the same order of magnitude, reinforcing our conclusions.

RHESSI Nuggets #425 Jan **2022**
https://sprg.ssl.berkeley.edu/~tohban/wiki/index.php/A_solar_flare_driven_by_thermal_conduction_observed_in_mid-infrared

Kink oscillations in a coronal loop arcade with finite plasma-β: effect of oblique propagation

I **Lopin**

Monthly Notices of the Royal Astronomical Society, Volume 514, Issue 3, August **2022**, Pages 4329–4342,
https://doi.org/10.1093/mnras/stac1502

Kink oscillations of a curved coronal slab with finite plasma-β, simulating a loop arcade, are examined. Perpendicular propagation, i.e. propagation along the arcade axis ($k_y > 0$) is taken into account. Two surface modes, labelled as faster and slower mode, are found to exist in the model. In the zero-β limit, the faster mode is a vertically polarized kink mode and the slower mode produces bending motions polarized along the arcade axis, provided $k_{-1}y k_{y-1}$ is of the order of or larger than the slab thickness a. Otherwise, if $k_{-1}y k_{y-1}$ is much less than a, the faster mode results in periodic displacement of a loop arcade along its axis and the slower mode has mixed properties. The phase speeds of both modes are very similar when $k_{-1}y \sim a k_{y-1} \sim a$, and they tend to the external and internal Alfvén speeds when $k_y \rightarrow 0$. As the internal plasma-β becomes finite and grows, the phase speed of the faster mode increases and that of the slower mode decreases. When $\beta_i > 0$, these modes are a superposition of vertical kink motions and those that are oriented along the arcade axis, both supplemented with the significant cross-averaged density perturbations. It seems promising to use the obtained results for interpreting quasi-periodic pulsations, in terms of kink oscillations of flaring high-β loops, provided the developed theory is applicable to the torroidal single loop model when choosing an appropriate k_y.

MHD Pulsations of Cylindrical Coronal Loops with Tangential Magnetic Discontinuity

I**. Lopin**1 and I. Nagorny2,3

2019 ApJ 882 134
https://doi.org/10.3847/1538-4357/ab32dc

We study the dispersive properties of the fast-sausage MHD mode in a cylindrical coronal loop with tangential magnetic discontinuity at its interface. To model this effect, we consider a straight axial magnetic field inside a coronal tube and a force-free twisted field in the external medium. The obtained dispersion relation was solved numerically and a number of limiting cases were explored analytically. The results indicate that the principal fast-sausage mode is trapped for all axial wavenumbers. Even a tiny magnetic discontinuity (or external twist) has a crucial effect on the global sausage mode. This mode is almost nondispersive in the long wavelength limit for small external twist, whereas it is strongly dispersive for large magnetic twist. In all cases the phase speed of the fundamental mode tends to the lower vicinity of the external Alfvén speed for small axial wavenumbers. The cutoffs of higher radial order modes were found reduced with respect to the reference model with a straight external field. The damping rate of the leaky modes grows as the external magnetic twist increases. Some applications of the developed theory to explain the observed quasi-periodic pulsations in flaring loops were given.

SAUSAGE WAVES IN TRANSVERSELY NONUNIFORM MONOLITHIC CORONAL TUBES

I. **Lopin**1 and I. Nagorny
2015 ApJ 810 87
We investigate fast sausage waves in a monolithic coronal magnetic tube, modeled as a local density inhomogeneity with a continuous radial profile. This work is a natural extension of our previous results, obtained for a slab loop model for the case of cylindrical geometry. Using Kneser's oscillating theorem, we provided the criteria for the existence of trapped and leaky wave regimes as a function of the profile features. For a number of density profiles there are only trapped modes for the entire range of longitudinal wave numbers. The phase speed of these modes tends toward the external Alfvén speed in the long wavelength limit. The generalized results were supported by the analytic solution of the wave equation for the specific density profiles. The approximate Wentzel–Kramers–Brillouin solutions allowed us to obtain the desired dispersion relations and to study their properties as a function of the profile parameters. The multicomponent quasi-periodic pulsations in flaring loops, observed on **2001 May 2 and 2002 July 3**, are interpreted in terms of the transversely fundamental trapped fast sausage mode with several longitudinal harmonics in a smooth coronal waveguide.

Fast Waves in Smooth Coronal Slab

I. **Lopin**1 and I. Nagorny
2015 ApJ 801 23
This work investigates the effect of transverse density structuring in coronal slab-like waveguides on the properties of fast waves. We generalized previous results obtained for the exponential and Epstein profiles to the case of an arbitrary transverse density distribution. The criteria are given to determine the possible (trapped or leaky) wave regime, depending on the type of density profile function. In particular, there are plasma slabs with transverse density structuring that support pure trapped fast waves for all wavelengths. Their phase speed is nearly equal to the external Alfvén speed for the typical parameters of coronal loops. Our findings are obtained on the basis of Kneser's oscillation theorem. To confirm the results, we analytically solved the wave equation evaluated at the cutoff point and the original wave equation for particular cases of transverse density distribution. We also used the WKB method and obtained approximate solutions of the wave equation at the cutoff point for an arbitrary transverse density profile. The analytic results were supplemented by numerical solutions of the obtained dispersion relations. The observed high-quality quasi-periodic pulsations of flaring loops are interpreted in terms of the trapped fundamental fast-sausage mode in a slab-like coronal waveguide.

Rapid variations of Si IV spectra in a flare observed by IRIS at a sub-second cadence

Juraj **Lorincik**, Vanessa Polito, Bart De Pontieu, Sijie Yu, Nabil Freij
Frontiers Astron. Space Sci. 9:1040945. **2022**
https://arxiv.org/pdf/2210.12205.pdf
https://doi.org/10.3389/fspas.2022.1040945
https://www.frontiersin.org/articles/10.3389/fspas.2022.1040945/pdf
We report on observations of highly-varying Si IV 1402.77 line profiles observed with the Interface Region Imaging Spectrograph (IRIS) during the M-class flare from **2022 January 18** at an unprecedented 0.8 s cadence. Moment analysis of this line observed in flare ribbon kernels showed that the intensity, Doppler velocity, and non-thermal broadening exhibited variations with periods below 10 s. These variations were found to be correlated with properties of the Gaussian fit to a well-resolved secondary component of the line redshifted by up to 70 km s−1, while the primary component was consistently observed near the rest wavelength of the line. A particularly high correlation was found between the non-thermal broadening of the line resulting from the moment analysis and the redshift of the secondary component. This means that the oscillatory enhancements in the line broadening were due to plasma flows (away from the observer) with varying properties. A simple de-projection of the Doppler velocities of the secondary component based on a three-dimensional reconstruction of flare loops rooted in the kernel suggests that the observed flows were caused by downflows and compatible with strong condensation flows recently predicted by numerical simulations. Furthermore, peaks of the intensity and the trends of Doppler velocity of the Gaussian fit to the secondary component (averaged in the ribbon) were found to correspond to one of the quasi-periodic pulsations (QPPs) detected during the event in the soft X-ray flux (as measured by the Geostationary Operational Environmental Satellite, GOES) and the microwave radio flux (as measured by the Expanded Owens Valley Solar Array, EOVSA). This result supports a scenario in which the QPPs were driven by repeated magnetic reconnection.
RHESSI Nuggets #440 **2023**
https://sprg.ssl.berkeley.edu/~tohban/wiki/index.php/Rapid_variations_of_Si_IV_spectra_in_a_flare_observed_by_IRIS_at_a_sub-second_cadence

Observation of super-Alfvénic slippage of reconnecting magnetic field lines on the Sun.

Lörinčík, J., Dudík, J., Sainz Dalda, A. et al.
Nat Astron (**2024**).
https://doi.org/10.1038/s41550-024-02396-4
https://www.nature.com/articles/s41550-024-02396-4.pdf

Slipping motions of magnetic field lines are a distinct signature of three-dimensional magnetic reconnection, a fundamental process driving solar and stellar flares. While being a key prediction of numerical experiments, the rapid super-Alfvénic field line slippage driven by the 'slip-running' reconnection has remained elusive in previous observations. New frontiers into exploring transient flare phenomena were introduced by recently designed high cadence observing programs of the Interface Region Imaging Spectrograph (IRIS). By exploiting high temporal resolution imagery (~2 s) of IRIS, here we reveal slipping motions of flare kernels at speeds reaching thousands of kilometres per second. The fast kernel motions are direct evidence of slip-running reconnection in quasi-separatrix layers, regions where magnetic field strongly changes its connectivity. Our results provide observational proof of theoretical predictions unaddressed for nearly two decades and extend the range of magnetic field configurations where reconnection-related phenomena can occur. **2022 Sep 25**
IRIS Nugget # Oct **2024** https://iris.lmsal.com/nugget

Blueshifted Si iv 1402.77 Å Line Profiles in a Moving Flare Kernel Observed by IRIS

Juraj **Lörinčík**1,2, Jaroslav Dudík3, and Vanessa Polito1,2
2022 ApJ 934 80
https://iopscience.iop.org/article/10.3847/1538-4357/ac78e2/pdf
We analyze the spectra of a slipping flare kernel observed during the **2015 June 22** M6.5-class flare by the Interface Region Imaging Spectrograph (IRIS). During the impulsive and peak phases of the flare, loops exhibiting an apparent slipping motion along the ribbons were observed in the 131 Å channel of SDO/AIA. The IRIS spectrograph slit observed a portion of the ribbons, including a moving kernel corresponding to a flare loop footpoint in Si iv, C ii, and Mg ii at a very-high 1 s cadence. The spectra observed in the kernel were mostly redshifted and exhibited pronounced red wings, as typically observed in large flares. However, in a small region in one of the ribbons, the Si iv 1402.77 Å line was partially blueshifted, with the corresponding Doppler velocity |vD| exceeding 50 km s−1. In the same region, the C ii 1334.53, 1335.66, and 1335.71 Å lines were weakly blueshifted (|vD| < 20 km s−1) and showed pronounced blue wings, which were also observed in the Mg ii k 2796.35 Å as well as the Mg ii triplet 2798.75 and 2798.82 Å lines. Using high-cadence AIA observations we found that the region where the blueshifts occurred corresponds to the accelerating kernel front as it moved through a weak field region. The IRIS observations with high resolution allowed us to capture the acceleration of the kernel under the slit for the first time. The unique observations of blueshifted chromospheric and TR lines provide new constraints for current models of flares.
IRIS Nugget 9 Aug 2022 https://iris.lmsal.com/nugget

Saddle-shaped solar flare arcades

Juraj **Lörinčík**, Jaroslav Dudík, Guillaume Aulanier
ApJ **909** L4 **2021**
https://arxiv.org/pdf/2102.10858.pdf
https://iopscience.iop.org/article/10.3847/2041-8213/abe7f7/pdf
https://doi.org/10.3847/2041-8213/abe7f7
Arcades of flare loops form as a consequence of magnetic reconnection powering solar flares and eruptions. We analyse the morphology and evolution of flare arcades that formed during five well-known eruptive flares. We show that the arcades have a common saddle-like shape. The saddles occur despite the fact that the flares were of different classes (C to X), occurred in different magnetic environments, and were observed in various projections. The saddles are related to the presence of longer, relatively-higher, and inclined flare loops, consistently observed at the ends of the arcades, which we term `cantles'. Our observations indicate that cantles typically join straight portions of flare ribbons with hooked extensions of the conjugate ribbons. The origin of the cantles is investigated in stereoscopic observations of the **2011 May 9** eruptive flare carried out by the Atmospheric Imaging Assembly (AIA) and Extreme Ultraviolet Imager (EUVI). The mutual separation of the instruments led to ideal observational conditions allowing for simultaneous analysis of the evolving cantle and the underlying ribbon hook. Based on our analysis we suggest that the formation of one of the cantles can be explained by magnetic reconnection between the erupting structure and its overlying arcades. We propose that the morphology of flare arcades can provide information about the reconnection geometries in which the individual flare loops originate. **2011-05-09, 2011-06-07, 2011-12-26, 2017-09-06, 2017-09-10**

Velocities of flare kernels and the mapping norm of field line connectivity

Juraj **Lörinčík**, Guillaume Aulanier, Jaroslav Dudík, Alena Zemanová, Elena Dzifčáková
ApJ **881** 68 **2019**
https://arxiv.org/pdf/1906.01880.pdf
sci-hub.se/10.3847/1538-4357/ab298f
We report on observations of flare ribbon kernels during the **2012 August 31** filament eruption. In the 1600\,\AA{} and 304\,\AA{} channels of the Atmospheric Imaging Assembly, flare kernels were observed to move along flare ribbons at velocities v‖ of up to 450 km\,s−1. Kernel velocities were found to be roughly anti-correlated with strength of the magnetic field. Apparent slipping motion of flare loops was observed in the 131\,\AA{} only for the slowest kernels

moving through strong-B region. In order to interpret the observed relation between BLOS and v‖, we examined distribution of the norm N, a quantity closely related to the slippage velocity. We then calculated the norm N of the quasi-separatrix layers (QSLs) in MHD model of a solar eruption adapted to the magnetic environment which qualitatively agrees to that of the observed event. We found that both the modelled N and velocities of kernels reach their highest values in the same weak-field regions, one located in the curved part of the ribbon hook and the other in the straight part of the conjugate ribbon located close to a parasitic polarity. Oppositely, lower values of the kernel velocities are seen at the tip of the ribbon hook, where the modelled N is low. Since the modelled distribution of N matches the observed dynamics of kernels, this supports that the kernel motions can be interpreted as a signature of QSL reconnection during the eruption.

Rotational effects on the negative magnetic pressure instability

Illa R. **Losada**, A. Brandenburg, N. Kleeorin, Dhrubaditya Mitra, I. Rogachevskii
E-print, March **2013**
Astron. Astrophys. 548, A49 (**2012**)
The surface layers of the Sun are strongly stratified. In the presence of turbulence with a weak mean magnetic field, a large-scale instability resulting in the formation of non-uniform magnetic structures, can be excited over the scale of many turbulent eddies or convection cells. This instability is caused by a negative contribution of turbulence to the effective (mean-field) magnetic pressure and has previously been discussed in connection with the formation of active regions and perhaps sunspots. We want to understand the effects of rotation on this instability in both two and three dimensions. We use mean-field magnetohydrodynamics in a parameter regime in which the properties of the negative effective magnetic pressure instability have previously been found to be in agreement with those of direct numerical simulations. We find that the instability is suppressed already for relatively slow rotation with Coriolis numbers (i.e. inverse Rossby numbers) around 0.2. The suppression is strongest at the equator. In the nonlinear regime, we find traveling wave solutions with propagation in the prograde direction at the equator with additional poleward migration away from the equator. The prograde rotation of the magnetic pattern near the equator is argued to be a possible explanation for the faster rotation speed of magnetic tracers found on the Sun. In the bulk of the domain, kinetic and current helicities are negative in the northern hemisphere and positive in the southern.

Investigation of a confined C-class flare in an arch filament system close to a regular sunspot

Rohan Eugene **Louis**
JGR **Volume124, Issue11** Pages 8255-8270 **2019**
https://arxiv.org/pdf/1910.05926.pdf
A moderate C1.1 class confined flare is investigated here, which occurred on **2013 September 24** at 22:56~UT, in an arch filament system close to a regular, unipolar sunspot. Spectro-polarimetric observations from the Tenerife Infrared Polarimeter at the 70 cm German Vacuum Tower Telescope were combined with data from the Helioseismic Magnetic Imager and the Atmospheric Imaging Assembly to identify the processes that triggered the flare. The legs of this arch filament were anchored in the leading sunspot and the network flux region of opposite polarity. The flare was driven by small-scale, flux cancellation at the weak neutral line underlying the arch filament which resulted in two small flaring events within an hour of the C1.1 flare. Flux cancellation was facilitated by the moat flow from the leading sunspot wherein small-scale magnetic fragments stream towards patches of pre-existing flux. The cancellation of flux led to the destabilization of the arch filament which was seen as an increase in the twist along the arch filament. The horizontal fields across the weak neutral line decay faster which cannot prevent the filament from rising that results in a two-ribbon flare at the neutral line. The arch filament unwinds as it rises, but is confined by the higher, overlying fields between the two polarities of the active region that decay much more slowly.

Triggering an eruptive flare by emerging flux in a solar active-region complex

Louis, Rohan E.; Kliem, Bernhard; Ravindra, B.; Chintzoglou, Georgios
Solar Phys. Volume 290, Issue 12, pp 3641-3662 **2015**
http://arxiv.org/pdf/1506.08035v1.pdf
A flare and fast coronal mass ejection originated between solar active regions NOAA 11514 and 11515 on **July 1, 2012** in response to flux emergence in front of the leading sunspot of the trailing region 11515. Analyzing the evolution of the photospheric magnetic flux and the coronal structure, we find that the flux emergence triggered the eruption by interaction with overlying flux in a non-standard way. The new flux neither had the opposite orientation nor a location near the polarity inversion line, which are favorable for strong reconnection with the arcade flux under which it emerged. Moreover, its flux content remained significantly smaller than that of the arcade (approximately 40 %). However, a loop system rooted in the trailing active region ran in part under the arcade between the active regions, passing over the site of flux emergence. The reconnection with the emerging flux, leading to a series of jet emissions into the loop system, caused a strong but confined rise of the loop system. This lifted the arcade between the two active regions, weakening its downward tension force and thus destabilizing the considerably sheared flux under the arcade. The complex event was also associated with supporting precursor activity in an enhanced network near the active regions, acting on the large-scale overlying flux, and with two simultaneous confined flares within the active regions.

Small scale chromospheric jets above a sunspot light bridge
Rohan E. **Louis**, Christian Beck, Kiyoshi Ichimoto
A&A, 567, A96, **2014**
http://arxiv.org/pdf/1406.0103v1.pdf
High-resolution broad-band filtergrams of active region NOAA 11271 in Ca ii H and G-band were obtained with the Solar Optical Telescope on board Hinode to identify the physical driver responsible for the dynamic and small-scale chromospheric jets above a sunspot light bridge. We identified the jets in the Ca images using a semi-automatic routine. The chromospheric jets consist of a bright, triangular-shaped blob that lies on the light bridge, while the apex of this blob extends into a spike-like structure which is bright against the dark umbral background. The majority of the jets have apparent lengths of less than 1000 km and about 30% of them have lengths between 1000-1600 km. They are oriented within +/-35 deg. to the normal of the light bridge axis. A majority of them are clustered near the central part within a 2 arcsec wide area. The jets are seen to move rapidly along the light bridge and a majority of them cannot be identified in successive images taken with a 2 min cadence. The jets are primarily located on one side of the light bridge and are directed into the umbral core. The Stokes profiles at/close to the location of the blobs on the LB exhibit both a significant net circular polarization and multiple components, including opposite-polarity lobes. The magnetic field diverges from the light bridge towards the umbral cores that it separates. In the photosphere there is a predominantly uni-directional flow with speeds of 100-150 m/s along the light bridge which is interrupted by a patch of weak motions that also moves along the light bridge. The dynamic short-lived jets above the LB seem to be guided by the magnetic field lines. Reconnection events are a likely trigger for such phenomenon since they occur at locations where the magnetic field changes orientation sharply. We find no clear relation between the jets and the photospheric flow pattern.
2011 August 19

Sunspot splitting triggering an eruptive flare
Rohan E. **Louis**, Klaus G. Puschmann, Bernhard Kliem, Horst Balthasar, Carsten Denker
E-print, Nov **2013**; A&A 562, A110 (**2014**)
We investigate how the splitting of the leading sunspot and associated flux emergence and cancellation in active region NOAA 11515 caused an eruptive M5.6 flare on **2012 July 2**. Our study employs multi-wavelength observations from HMI, AIA and ChroTel. Emerging flux formed a neutral line ahead of the leading sunspot and new satellite spots. The sunspot splitting caused a long-lasting flow toward this neutral line, where a filament formed. Further flux emergence, partly of mixed-polarity, as well as episodes of flux cancellation occurred repeatedly at the neutral line. Following a nearby C-class precursor flare with signs of interaction with the filament, the filament erupted nearly simultaneously with the onset of the M5.6 flare and evolved into a coronal mass ejection. The sunspot stretched without forming a light bridge, splitting unusually fast (within about a day, complete approximately 6 hours after the eruption) in two nearly equal parts. The front part separated strongly from the active region to approach the neighbouring active region where all its coronal magnetic connections were rooted. It also rotated rapidly (by 4.9 degree/hr) and caused significant shear flows at its edge. The eruption resulted from a complex sequence of processes in the (sub-)photosphere and corona. The persistent flows toward the neutral line likely caused the formation of a flux rope which held the filament. These flows and their associated flux cancellation, the emerging flux, and the precursor flare all contributed to the destabilization of the flux rope. We interpret the sunspot splitting as the separation of two flux bundles differently rooted in the convection zone and only temporarily joined in the spot. This explains the rotation as continued rise of the separating flux and implies that at least this part of the sunspot was still connected to its roots deep in the convection zone.

The relationship between chromospheric emissions and magnetic field strength
M. **Loukitcheva**1, 2, S. K**.** Solanki1, and S. M. White3
A&A 497, 273-285 (**2009**)
Aims. We analyze observational data from 4 instruments to study the correlations between chromospheric emission, spanning the heights from the temperature minimum region to the middle chromosphere, and photospheric magnetic field.
Methods. The data consist of radio images at 3.5 mm from the Berkeley-Illinois-Maryland Array (BIMA), UV images at 1600 Å from TRACE, Ca II K-line filtergrams from BBSO, and MDI/SOHO longitudinal photospheric magnetograms. For the first time interferometric millimeter data with the highest currently available resolution are included in such an analysis. We determine various parameters of the intensity maps and correlate the intensities with each other and with the magnetic field.
Results. The chromospheric diagnostics studied here show a pronounced similarity in their brightness structures and map out the underlying photospheric magnetic field relatively well. We find a power law to be a good representation of the relationship between photospheric magnetic field and emission from chromospheric diagnostics at all wavelengths. The dependence of chromospheric brightness on magnetic field is found to be different for network and internetwork regions.

The association of the Hale Sector Boundary with RHESSI solar flares and active longitudes

K. **Loumou**, I. G. Hannah, H. S. Hudson
A&A 618, A9 **2018**
https://arxiv.org/pdf/1808.05866.pdf
sci-hub.tw/10.1051/0004-6361/201731050
The heliospheric magnetic field (HMF) is structured into large sectors of positive and negative polarity. The parts of the boundary between these sectors where the change in polarity matches that of the leading-to-following sunspot polarity in that solar hemisphere, are called Hale Sector Boundaries (HSB). We investigate the flare occurrence rate near HSBs and the association between HSBs and active longitudes. Previous work determined the times HSBs were at solar central meridian, using the detection of the HMF sector boundary crossing at the Earth. In addition to this, we use a new approach which finds the HSB locations at all times by determining them from Potential Field Source Surface (PFSS) extrapolations of photospheric magnetograms. We use the RHESSI X-ray flare list for comparison to the HSB as it provides accurate flare locations over 14 years, from February 2002 to February 2016, covering both Cycles 23 and 24. For the active longitude positions we use previously published work based on sunspot observations. We find that the two methods of determining the HSB generally agree and that 41% (Cycle 23) and 47% (Cycle 24) of RHESSI flares occur within 30∘ of the PFSS determined-HSB. The behaviour of the HSBs varies over the two Cycles studied, and as expected they swap in hemisphere as the Cycles change. The HSBs and active longitudes do overlap but not consistently. They often move at different rates relative to each other (and the Carrington solar rotation rate) and these vary over each Cycle. The HSBs provide a useful additional activity indicator, particularly during periods when active longitudes are difficult to determine.

Magnetic reconnection: from the Sweet-Parker model to stochastic plasmoid chains

N. F. **Loureiro**, D. A. Uzdensky
Plasma Phys. Control. Fusion, EPS 2015 Special Issue **2015**
http://arxiv.org/pdf/1507.07756v1.pdf
Magnetic reconnection is the topological reconfiguration of the magnetic field in a plasma, accompanied by the violent release of energy and particle acceleration. Reconnection is as ubiquitous as plasmas themselves, with solar flares perhaps the most popular example. Over the last few years, the theoretical understanding of magnetic reconnection in large-scale fluid systems has undergone a major paradigm shift. The steady-state model of reconnection described by the famous Sweet-Parker (SP) theory, which dominated the field for ~50 years, has been replaced with an essentially time-dependent, bursty picture of the reconnection layer, dominated by the continuous formation and ejection of multiple secondary islands (plasmoids). Whereas in the SP model reconnection was predicted to be slow, a major implication of this new paradigm is that reconnection in fluid systems is fast (i.e., independent of the Lundquist number), provided that the system is large enough. This conceptual shift hinges on the realization that SP-like current layers are violently unstable to the plasmoid instability - implying, therefore, that such current sheets are super-critically unstable and thus can never form in the first place. This suggests that the formation of a current sheet and the subsequent reconnection process cannot be decoupled, as is commonly assumed. This paper provides an introductory-level overview of the recent developments in reconnection theory and simulations that led to this essentially new framework. We briefly discuss the role played by the plasmoid instability in selected applications, and describe some of the outstanding challenges that remain at the frontier of this subject. Amongst these are the analytical and numerical extension of the plasmoid instability to (i) 3D and (ii) non-MHD regimes. New results are reported in both cases.

Analyzing AIA Flare Observations Using Convolutional Neural Networks

Teri **Love***, Thomas Neukirch and Clare E. Parnell
Front. Astron. Space Sci., 26 June **2020** |
https://doi.org/10.3389/fspas.2020.00034
In order to efficiently analyse the vast amount of data generated by solar space missions and ground-based instruments, modern machine learning techniques such as decision trees, support vector machines (SVMs) and neural networks can be very useful. In this paper we present initial results from using a convolutional neural network (CNN) to analyse observations from the Atmospheric Imaging Assembly (AIA) in the 1,600Å wavelength. The data is pre-processed to locate flaring regions where flare ribbons are visible in the observations. The CNN is created and trained to automatically analyse the shape and position of the flare ribbons, by identifying whether each image belongs into one of four classes: two-ribbon flare, compact/circular ribbon flare, limb flare, or quiet Sun, with the final class acting as a control for any data included in the training or test sets where flaring regions are not present. The network created can classify flare ribbon observations into any of the four classes with a final accuracy of 94%. Initial results show that most of the images are correctly classified with the compact flare class being the only class where accuracy drops below 90% and some observations are wrongly classified as belonging to the limb class.

Observations of Extremely Strong Magnetic Fields in Active Region NOAA 12673 Using GST Magnetic Field Measurement

Vsevolod **Lozitsky**1, Vasyl Yurchyshyn2, Kwangsu Ahn2, and Haimin Wang3
2022 ApJ 928 41

https://iopscience.iop.org/article/10.3847/1538-4357/ac5518/pdf
We present a detailed study of very strong magnetic fields in the NOAA Active Region (AR) 12673, which was the most flare productive AR in solar cycle 24. It produced four X-class flares including the X9.3 flare on **2017 September 6** and the X8.2 limb event on September 10. Our analysis is based on direct measurements of full Zeeman splitting of the Fe i 1564.85 nm line using all Stokes I, Q, U, and V profiles. This approach allowed us to obtain reliable estimates of the magnitude of magnetic fields independent of the filling factor and atmosphere models. Thus, the strongest fields up to 5.5 kG were found in a light bridge (LB) of a spot, while in the dark umbra magnetic fields did not exceed 4 kG. In the case of the LB, the magnitude of the magnetic field is not related to the underlying continuum intensity, while in the case of umbral fields we observed a well-known anticorrelation between the continuum intensity and the field magnitude. In this study, the LB was cospatial with a polarity inversion line of δ-sunspot, and we speculate that the 5.5 kG strong horizontal fields may be associated with a compact twisted flux rope at or near the photosphere. A comparison of the depth of the Zeeman π and σ components showed that in the LB magnetic fields are, on average, more horizontal than those in the dark umbra.

Profiles of spectral lines, magnetic fields, and thermodynamical conditions in the X17.2/4B solar flare of 2003 October 28

V G **Lozitsky** E A Baranovsky N I Lozitska V P Tarashchuk
Monthly Notices of the Royal Astronomical Society, Volume 477, Issue 2, 21 June **2018**, Pages 2796–2803,
http://sci-hub.tw/10.1093/mnras/sty738
We analyse the peak phase of the exclusively powerful solar proton flare of **2003 October 28**,which had originated in the active region NOAA 0486. For studying the physical conditions in the flare, we used 12 spectral lines including lines from Fe I, Fe II, and the H α, H β, H γ, H δ lines observed with the Echelle spectrograph of the horizontal solar telescope of the Astronomical Observatory of the Taras Shevchenko National University of Kyiv. We found that this flare had a unique Balmer decrement, with the record ratio I (H β)/I(H α) = 1.68 of H β and H α intensities, which is unprecedented for all flares observed. In a place outside sunspots, the effective magnetic field measured by splitting 'center of gravity' I ± V profiles was found within the range of 0–200 G in the middle photosphere, till 1200 G in the upper photosphere and the temperature minimum zone and up to 500 G in the chromosphere. The essential broadening of the Fe I 5250.2 line versus the Fe I 5247.1 one was found indicating the presence of a strong (800–1100 G) 'turbulent' field in the middle photosphere. A semi-empirical model of the chromosphere constructed using the algorithms in PANDORA code has an interesting peculiarity, namely three discrete layers with an increased concentration and/or temperature, including a very dense and thin layer with the following parameters: the concentration of hydrogen nH = 1018 cm3, the thickness Δh = 3–5 km, and a height of h ≈ 1200 km above the photosphere.

Small-scale magnetic field diagnostics in solar flares using bisectors of I ± V profiles

V.G. **Lozitsky**
Advances in Space Research, Volume 55, Issue 3, 1 February **2015**, Pages 958–967
http://www.sciencedirect.com/science/article/pii/S0273117714005936
In the present study, spatially unresolved magnetic fields in solar flares are investigated by analyzing the fine structure of Zeeman splitting in two FeI lines. Namely, we consider bisector splitting of I ± V Stokes profiles in 5123.7 and 5233 Å lines. The analysis of bisector splitting functions (BSF) of the 5233 Å line averaged over 12 solar flares of different classes, from C5 to X1.4, reveals two distinct peaks, around Δλ = 80–110 mÅ and 170–200 mÅ. Such peculiarities indicate the unacceptability of weak field approximation for FeI 5233 line and need interpretation in the framework of inhomogeneous models with strong magnetic field components. Consequently, we argue that the named two peaks can reflect the existence of two discrete modes of subtelescopic magnetic fields with strengths about 6 and 12 kG in photospheric layers.

Automatic Solar Flare Detection Using the Solar Disk Imager Onboard the ASO-S Mission.

Lu, L., Tian, Z., Feng, L. et al.
Sol Phys 299, 72 (**2024**).
https://doi.org/10.1007/s11207-024-02310-1
https://link.springer.com/content/pdf/10.1007/s11207-024-02310-1.pdf
We present an automated solar flare detection software tool to automatically process solar observed images, detect and track solar flares, and finally compile an event catalog. It can identify and track flares that happen simultaneously or temporally close together. The method to identify a flare is based on the local intensity changes in macropixels. The basic characteristics, such as the time and location information of a flare, are determined with a triple-threshold scheme, with the first threshold (global threshold) to determine the occurrence (location) of the flare and the second and third thresholds (local thresholds) to determine the real start and end times of the flare. We have applied this tool to one month of continuous solar ultraviolet (UV) images obtained by the Solar Disk Imager (SDI) onboard the Advanced Space-based Solar Observatory (ASO-S), which show active phenomena such as flares, filaments or prominences, and solar jets. Our automated tool efficiently detected a total number of 226 solar events. After a visual inspection, we

found that only one event was misidentified (unrelated to an active event). We compared the detected events with the GOES X-ray flare list and found that our tool can detect 81% of GOES M-class and above flares (29 out of 36), from which we conclude that the intensity increase in SDI UV images can be considered as a good indicator of a solar flare.

Observational Signatures of Tearing Instability in the Current Sheet of a Solar Flare

Lei **Lu**, Li Feng, Alexander Warmuth, Astrid M. Veronig, Jing Huang, Siming Liu, Weiqun Gan, Zongjun Ning, Beili Ying, Guannan Gao

ApJ **924** L7 **2022**

https://arxiv.org/pdf/2112.07857.pdf

https://iopscience.iop.org/article/10.3847/2041-8213/ac42c6/pdf

https://doi.org/10.3847/2041-8213/ac42c6

Magnetic reconnection is a fundamental physical process converting magnetic energy into not only plasma energy but also particle energy in various astrophysical phenomena. In this letter, we show a unique dataset of a solar flare where various plasmoids were formed by a continually stretched current sheet. EUV images captured reconnection inflows, outflows, and particularly the recurring plasma blobs (plasmoids). X-ray images reveal nonthermal emission sources at the lower end of the current sheet, presumably as large plasmoids with a sufficiently amount of energetic electrons trapped in. In the radio domain, an upward slowly drifting pulsation structure, followed by a rare pair of oppositely drifting structures, was observed. These structures are supposed to map the evolution of the primary and the secondary plasmoids formed in the current sheet. Our results on plasmoids at different locations and scales shed important light on the dynamics, plasma heating, particle acceleration, and transport processes in the turbulent current sheet and provide observational evidence for the cascading magnetic reconnection process. **July 19, 2012**

Quasi-Periodic Pulsations Detected in Lyα and Nonthermal Emissions During Solar Flares

Lei **Lu**, Dong Li, Zongjun Ning, Li Feng, Weiqun Gan

Solar Phys. **296**, Article number: 130 **2021**

https://arxiv.org/pdf/2108.03820.pdf

https://link.springer.com/content/pdf/10.1007/s11207-021-01876-4.pdf

https://doi.org/10.1007/s11207-021-01876-4

We report quasi-periodic pulsations (QPPs) with double periods during three solar flares (viz. SOL**2011-Feb-15**T01:44, SOL**2011-Sep-25**T04:31, SOL**2012-May-17**T01:25). The flare QPPs were observed from light curves in Lyα, hard X-ray (HXR) and microwave emissions, with the Lyα emission recorded by the Geostationary Operational Environmental Satellite, the HXR emission recorded by the Reuven Ramaty High-Energy Solar Spectroscopic Imager and the Fermi Gamma-ray Burst Monitor, and the microwave emission recorded by the Nobeyama Radio Polarimeters and Radioheliograph. By using the Markov chain Monte Carlo (MCMC) method, QPPs with double periods of about two minutes and one minute were first found in the Lyα emission. Then using the same method, a QPP with nearly the same period of about two minutes was also found in HXR and microwave emissions. Considering the possible common origin (nonthermal electrons) between Lyα and HXR/microwave emission, we suggest that the two-minute QPP results from the periodic acceleration of nonthermal electrons during magnetic reconnections. The ratio between the double periods in the Lyα emission was found to be close to two, which is consistent with the theoretical expectation between the fundamental and harmonic modes. However, we cannot rule out other possible driving mechanisms for the one-minute QPPs in HXR/microwave emissions due to their relatively large deviations.

Catalog and Statistical Examinations of Lyα Solar Flares from GOES/EUVS-E Measurements

Lei **Lu**1,2, Li Feng1, Dong Li1,2, Beili Ying1, Hui Li1, Weiqun Gan1, Youping Li1,

2021 ApJS 253 29

https://iopscience.iop.org/article/10.3847/1538-4365/abd79b/pdf

https://doi.org/10.3847/1538-4365/abd79b

The Lyman-alpha (Lyα) line of neutral hydrogen at 121.6 nm is by far the brightest emission line in the vacuum ultraviolet spectral range of the Sun. The emission at this line could be a major energy input to the upper layers of the Earth's atmosphere, strongly impacting the geospace environment. The Geostationary Operational Environmental Satellite (GOES) series, starting with GOES-13, began to carry a multichannel Extreme UltraViolet Sensor (EUVS) with one channel (E-channel) targeting the Lyα line. In the present work, we produce a Lyα flare catalog from the GOES-15/EUVS-E data between 2010 April 8 and 2016 June 6 with an automatic flare detection algorithm. This algorithm is designed to search events at various scales and find their real start and end times. Based on the obtained flare list, statistics on the temporal behavior such as the duration, rise, and decay times, and the event asymmetries of Lyα flares is presented. On average (defined by the median of the distributions), the duration, rise and decay times of the flares were estimated to be 20.8 minutes, 5.6 minutes, and 14.2 minutes, respectively. We also discuss the frequency distributions of the peak flux and the fluence of Lyα flares, both of which reveal power-law behaviors with power-law indices of 2.71 ± 0.06 and 2.42 ± 0.06, respectively, implying that more flares are accumulated at small scales and these small-scale events play an important role in explaining the violent solar energy release.

Turbulence and Particle Acceleration in Collisionless Magnetic Reconnection: Effects of Temperature Inhomogeneity across Pre-reconnection Current Sheet

San **Lu**1 , V. Angelopoulos1 , A. V. Artemyev1,2 , P. L. Pritchett3 , J. Liu1 , A. Runov1 , A. Tenerani4 , C. Shi1 , and M. Velli1

The Astrophysical Journal, 878:109 (16pp), **2019**

https://iopscience.iop.org/article/10.3847/1538-4357/ab1f6b/pdf

Magnetic reconnection is an important process in various collisionless plasma environments because it reconfigures the magnetic field and releases magnetic energy to accelerate charged particles. Its dynamics depend critically on the properties of the pre-reconnection current sheet. One property in particular, cross-sheet temperature inhomogeneity, which is ubiquitous throughout the heliosphere, has been shown to increase reconnection outflow speed, energy conversion efficiency, and secondary island formation rate using twodimensional particle-in-cell simulations. Here we expand upon these findings, considering two cases with a long, thin current sheet, one with homogeneous temperature and one with inhomogeneous temperature across the current sheet. In the inhomogeneous temperature case, numerous secondary islands form continuously, which increases current sheet turbulence (well-developed cascade power spectra) at large wavenumbers. Current density, energy conversion, dissipation, and acceleration of high-energy particles are also enhanced relative to the homogenous temperature case. Our results suggest that inhomogeneous temperature profiles, which are realistic, need to be incorporated into studies of turbulence and particle acceleration in collisionless magnetic reconnection.

A Statistical Study of the Magnetic Imprints of X-Class Flares using SDO/HMI Vector Magnetograms

Zekun **Lu**, Weiguang Cao, Gaoxiang Jin, Yining Zhang, Mingde Ding, Yang Guo

ApJ **876** 133 **2018**

https://arxiv.org/pdf/1803.08310.pdf

sci-hub.se/10.3847/1538-4357/ab16d4

Magnetic imprints, the rapid and irreversible evolution of photospheric magnetic fields as a feedback from flares in the corona, have been confirmed by many previous studies. These studies showed that the horizontal field will permanently increase near the polarity inversion line (PIL) after eruptions, indicating that a more horizontal topology of photospheric magnetic field will be reconstructed. In this study, we analyze 17 near-disk X-class flares in 13 active regions (ARs) with heliographic angle no greater than 45 degrees since the launch of the Solar Dynamics Observatory (SDO). We find that confined flares without or with very weak CMEs tend to show very weak magnetic imprints on the photosphere. The imprint regions of the horizontal field could locate not only near the PIL but also near sunspot umbrae with strong vertical fields. Making use of the observed CME mass and speed, we find that the CMEs with larger momentums will bring into stronger magnetic imprints. Furthermore, a linear relationship, with a confidence coefficient 0.82, between the CME momentum and the change of Lorentz force is revealed. Based on that, we quantify the back reaction time to be 336 s, which could be further applied to independently estimate the CME mass. **2011.02.15, 2011.03.09, 2011.09.06, 2011.09.07, 2011.09.24, 2012.03.07, 2012.07.12, 2013.11.05, 2013.11.08, 2013.11.10, 2014.03.29, 2014.10.22, 2014.10.26 , 2014.11.07, 2014 December 20, 2015.03.11**

Table 1. List of 17 flare events from 13 ARs with heliographic angle no greater than 45°.

Probing the Effect of Cadence on the Estimates of Photospheric Energy and Helicity Injections in Eruptive Active Region NOAA AR 11158

E. **Lumme**, M. D. Kazachenko, G. H. Fisher, B. T. Welsch, J. Pomoell, E. K. J. Kilpua

Solar Physics June **2019**, 294:84

https://link.springer.com/content/pdf/10.1007%2Fs11207-019-1475-x.pdf

We study how the input-data cadence affects the photospheric energy and helicity injection estimates in eruptive NOAA Active Region 11158. We sample the novel 2.25-minute vector magnetogram and Dopplergram data from the Helioseismic and Magnetic Imager (HMI) instrument onboard the Solar Dynamics Observatory (SDO) spacecraft to create input datasets of variable cadences ranging from 2.25 minutes to 24 hours. We employ state-of-the-art data processing, velocity, and electric-field inversion methods for deriving estimates of the energy and helicity injections from these datasets. We find that the electric-field inversion methods that reproduce the observed magnetic-field evolution through the use of Faraday's law are more stable against variable cadence: the PDFI (PTD-Doppler-FLCT-Ideal, where PTD refers to Poloidal–Toroidal Decomposition, and FLCT to Fourier Local Correlation Tracking) electric-field inversion method produces consistent injection estimates for cadences from 2.25 minutes up to two hours, implying that the photospheric processes acting on time scales below two hours contribute little to the injections, or that they are below the sensitivity of the input data and the PDFI method. On other hand, the electric-field estimate derived from the output of DAVE4VM (Differential Affine Velocity Estimator for Vector Magnetograms), which does not fulfill Faraday's law exactly, produces significant variations in the energy and helicity injection estimates in the 2.25

minutes – two hours cadence range. We also present a third, novel DAVE4VM-based electric-field estimate, which corrects the poor inductivity of the raw DAVE4VM estimate. This method is less sensitive to the changes of cadence, but it still faces significant issues for the lowest of considered cadences (≥ two hours). We find several potential problems in both PDFI- and DAVE4VM-based injection estimates and conclude that the quality of both should be surveyed further in controlled environments. **11-17 Feb 2011**

Fundamental Transverse Vibrations of the Active Region Solar Corona

Manuel **Luna**, Ramon Oliver, Patrick Antolin, Inigo Arregui
A&A **2019**
https://arxiv.org/pdf/1907.05212.pdf
Some high-resolution observations have revealed that the active-region solar corona is filled with myriads of thin strands even in apparently uniform regions with no resolved loops. This fine structure can host collective oscillations involving a large portion of the corona due to the coupling of the motions of the neighbouring strands. We study these vibrations and the possible observational effects. Here we theoretically investigate the collective oscillations inherent to the fine structure of the corona. We have called them fundamental vibrations because they cannot exist in a uniform medium. We use the T-matrix technique to find the normal modes of random arrangements of parallel strands. We consider an increasing number of tubes to understand the vibrations of a huge number of tubes of a large portion of the corona. We additionally generate synthetic time-distance Doppler and line broadening diagrams of the vibrations of a coronal region to compare with observations. We have found that the fundamental vibrations are in the form of clusters of tubes where not all the tubes participate in the collective mode. The periods are distributed over a wide band of values. The width of the band increases with the number of strands but rapidly reaches an approximately constant value. The frequency band associated with the fine structure of the corona depends on the minimum separation between strands. We have found that the coupling between the strands is of large extent. The synthetic Dopplergrams and line-broadening maps show signatures of collective vibrations, not present in the case of purely random individual kink vibrations. We conclude that the fundamental vibrations of the corona can contribute to the energy budget of the corona and they may have an observational signature.

Flare Accelerated Electrons in Kappa-Distribution from X-Ray Spectra with Warm-Target Model

Yingjie **Luo** (1), Eduard P. Kontar (1), Debesh Bhattacharjee (1)
ApJ **974** 119 **2024**
https://arxiv.org/pdf/2408.00213
https://iopscience.iop.org/article/10.3847/1538-4357/ad6a59/pdf
X-ray observations provide essential and valuable insights into the acceleration and propagation of non-thermal electrons during solar flares. Improved X-ray spectral analysis requires a deeper understanding of the dynamics of energetic electrons. Previous studies have demonstrated that the dynamics of accelerated electrons of a few thermal speeds are more complex. To better describe the energetic electrons after injection, a model considering energy diffusion and thermalization effects in flare conditions (warm-target model) has recently been developed for Hard X-ray spectral analysis. This model has demonstrated how the low-energy cut-off, which can hardly be constrained in cold-target modeling, can be determined. However, the power-law form may not be the most suitable representation of injected electrons. The kappa distribution, which is proposed as a physical consequence of electron acceleration, has shown successful application in RHESSI spectral analysis. In this study, we employ the kappa-form injected electrons in the warm-target model to analyze two M-class flares, observed by RHESSI and STIX, respectively. The best-fit results show that the kappa-form energetic electron spectrum generates lower non-thermal energy when producing a similar photon spectrum in the fit range compared to the power-law form. We also demonstrated that the fit parameters associated with kappa-form electron spectrum can be well determined with small fit uncertainty. Further, the kappa distribution, which covers the entire electron energy range, enables the determination of key electron properties such as total electron number density and average energy in the flare site, providing valuable information on electron acceleration processes. **2011 February 24, 2022 March 28**
RHESSI Science Nuggets #470 **2024** https://sprg.ssl.berkeley.edu/~tohban/wiki/index.php/The_warm-target_model_and_kappa_distributions

Multiple Regions of Nonthermal Quasi-Periodic Pulsations during the Impulsive Phase of a Solar Flare

Yingjie **Luo**, Bin Chen, Sijie Yu, Marina Battaglia, Rohit Sharma
ApJ **940** 137 **2022**
https://arxiv.org/pdf/2210.06219.pdf
https://iopscience.iop.org/article/10.3847/1538-4357/ac997a/pdf

Flare-associated quasi-periodic pulsations (QPPs) in radio and X-ray wavelengths, particularly those related to nonthermal electrons, contain important information about the energy release and transport processes during flares. However, the paucity of spatially resolved observations of such QPPs with a fast time cadence has been an obstacle for us to further understand their physical nature. Here, we report observations of such a QPP event occurred during the impulsive phase of a C1.8-class eruptive solar flare using radio imaging spectroscopy data from the Karl G. Jansky Very Large Array (VLA) and complementary X-ray imaging and spectroscopy data. The radio QPPs, observed by the VLA in the 1--2 GHz with a sub-second cadence, are shown as three spatially distinct sources with different physical characteristics. Two radio sources are located near the conjugate footpoints of the erupting magnetic flux rope with opposite senses of polarization. One of the sources displays a QPP behavior with a ~5-s period. The third radio source, located at the top of the post-flare arcade, coincides with the location of an X-ray source and shares a similar period of ~25--45 s. We show that the two oppositely polarized radio sources are likely due to coherent electron cyclotron maser (ECM) emission. On the other hand, the looptop QPP source, observed in both radio and X-rays, is consistent with incoherent gyrosynchrotron and bremsstrahlung emission, respectively. We conclude that the concurrent, but spatially distinct QPP sources must involve multiple mechanisms which operate in different magnetic loop systems and at different periods. **February 18, 2016**.

Radio Spectral Imaging of an M8.4 Eruptive Solar Flare: Possible Evidence of a Termination Shock

Yingjie **Luo** (1), Bin Chen (1), Sijie Yu (1), Timothy S. Bastian (2), Samuel Krucker (3)
ApJ **911** 4 **2021**
https://arxiv.org/pdf/2102.06259.pdf
https://iopscience.iop.org/article/10.3847/1538-4357/abe5a4/pdf
https://doi.org/10.3847/1538-4357/abe5a4
Solar flare termination shocks have been suggested as one of the viable mechanisms for accelerating electrons and ions to high energies. Observational evidence of such shocks, however, remains rare. Using radio dynamic spectroscopic imaging of a long-duration C1.9 flare obtained by the Karl G. Jansky Very Large Array (VLA), Chen et al. (2015) suggested that a type of coherent radio bursts, referred to as "stochastic spike bursts", were radio signature of nonthermal electrons interacting with myriad density fluctuations at the front of a flare termination shock. Here we report another stochastic spike burst event recorded during the extended energy release phase of a long-duration M8.4-class eruptive flare on **2012 March 10**. VLA radio spectroscopic imaging of the spikes in 1.0--1.6 GHz shows that, similar to the case of Chen et al. (2015), the burst centroids form an extended, ~10"-long structure in the corona. By combining extreme ultraviolet imaging observations of the flare from two vantage points with hard X-ray and ultraviolet observations of the flare ribbon brightenings, we reconstruct the flare arcade in three dimensions. The results show that the spike source is located at ~60 Mm above the flare arcade where a diffuse supra-arcade fan and multitudes of plasma downflows are present. Although the flare arcade and ribbons seen during the impulsive phase do not allow us to clearly understand how the observed spike source location is connected to the flare geometry, cooling flare arcade observed two hours later suggest that the spikes are located in the above-the-loop-top region, where a termination shock presumably forms.

Estimating the Maximum Intensities of Soft X-ray Flares Using Extreme Value Theory

V. De la **Luz**, E. P. Balanzario, T. Tsiftsi
Solar Phys. **2018**
https://arxiv.org/pdf/1808.00105.pdf
Solar flares are one of the most energetic events in the solar system, their impact on Earth at ground level and its atmosphere remains under study. The repercussions of this phenomenon in our technological infrastructure includes radio blackouts and errors in geopositional and navigation systems that are considered natural hazards in ever more countries. Occurrence frequency and intensity of the most energetic solar flares are been taken into account in national programs for civil protection in order to reduce the risk and increase the resilience from Space Weather events. In this work we use the statistical theory of extreme values as well as other statistical methods in order to asses the magnitudes of the most extreme solar flare events expected to occur in a given period of time. We found that the data set under study presents a dual tail behaviour. Our results show that on average we can expect one solar flare greater than X23 each 25 years, that is to say, one such event each two solar cycles.

Reconnection Properties of Large-Scale Current Sheets During Coronal Mass Ejection Eruptions

B. J. **Lynch**, J. K. Edmondson, M. D. Kazachenko, S. E. Guidoni
2016 *ApJ* **826** 43
2014 http://arxiv.org/pdf/1410.1089v1.pdf

We present a detailed analysis of the properties of magnetic reconnection at large-scale current sheets in a high cadence version of the Lynch and Edmondson (2013) 2.5D MHD simulation of sympathetic magnetic breakout eruptions from a pseudostreamer source region. We examine the resistive tearing and breakup of the three main current sheets into chains of X- and O-type null points and follow the dynamics of magnetic island growth, their merging, transit, and ejection with the reconnection exhaust. For each current sheet, we quantify the evolution of the length-to-width aspect ratio (up to ~100:1), Lundquist number (~104), and reconnection rate (inflow-to-outflow ratios reaching ~0.15). We examine the statistical and spectral properties of the fluctuations in the current sheets resulting from the plasmoid instability, including the distribution of magnetic island width, mass, and flux content. We show that the temporal evolution of the spectral index of the reconnection-generated magnetic energy density fluctuations appear to reflect global properties of the current sheet evolution. Our results are in excellent agreement with recent, high resolution reconnection-in-a-box simulations even though our current sheets' formation, growth, and dynamics are intrinsically coupled to the global evolution of sequential sympathetic CME eruptions.

Cold Solar Flares. I. Microwave Domain

Alexandra L. **Lysenko**1, Stephen M. White2, Dmitry A. Zhdanov3, Nataliia S. Meshalkina3, Aleksander T. Altyntsev3, Galina G. Motorina1,4,5, and Gregory D. Fleishman6,7
2023 ApJ 954 122
https://iopscience.iop.org/article/10.3847/1538-4357/acea20/pdf
https://arxiv.org/pdf/2309.03993.pdf
We identify a set of ~100 "cold" solar flares and perform a statistical analysis of them in the microwave range. Cold flares are characterized by a weak thermal response relative to nonthermal emission. This work is a follow-up of a previous statistical study of cold flares, which focused on hard X-ray emission to quantify the flare nonthermal component. Here, we focus on the microwave emission. The thermal response is evaluated by the soft X-ray emission measured by the GOES X-ray sensors. We obtain spectral parameters of the flare gyrosynchrotron emission and reveal patterns of their temporal evolution. The main results of the previous statistical study are confirmed: as compared to a "mean" flare, the cold flares have shorter durations, higher spectral peak frequencies, and harder spectral indices above the spectral peak. Nonetheless, there are some cold flares with moderate and low peak frequencies. In the majority of cold flares, we find evidence of the Razin effect in the microwave spectra, indicative of rather dense flaring loops. We discuss the results in the context of the electron acceleration efficiency. **2010-06-12, 2012-07-10, 2012-07-06, 2012-07-14, 2012-08-15, 2013-04-24, 2014-01-08, 2014-06-29, 2014-11-21, 2015 May 8**

KW-Sun: The Konus-Wind Solar Flare Database in Hard X-Ray and Soft Gamma-Ray Ranges

A. L. **Lysenko**1, M. V. Ulanov1, A. A. Kuznetsov2, G. D. Fleishman3, D. D. Frederiks1, L. K. Kashapova2, Z. Ya. Sokolova1, D. S. Svinkin1, and A. E. Tsvetkova1
2022 ApJS 262 32
https://iopscience.iop.org/article/10.3847/1538-4365/ac8b87/pdf
We present a database of solar flares registered by the Konus-Wind instrument during more than 27 yr of operation, from 1994 November to now (2022 June). The constantly updated database (hereafter KW-Sun) contains over 1000 events detected in the instrument's triggered mode and is accessible online at http://www.ioffe.ru/LEA/kwsun/. For each flare, the database provides time-resolved energy spectra in energy range from ~20 keV to ~15 MeV in FITS format along with count-rate light curves in three wide-energy bands, G1 (~20–80 keV), G2 (~80–300 keV), and G3 (~300–1200 keV), with high time resolution (down to 16 ms) in ASCII and IDL SAV formats. This article focuses on the instrument capabilities in the context of solar observations, the structure of the KW-Sun data, and their intended usage. The presented homogeneous data set obtained in the broad energy range with high temporal resolution during more than two full solar cycles is beneficial for both statistical and case studies as well as a source of context data for solar flare research. **2017 September 6, 20 Jan 2022**

Gamma-ray emission from the impulsive phase of the 2017 September 06 X9.3 flare

Alexandra L. **Lysenko** (1), Sergey A. Anfinogentov (2), Dmitry D. Svinkin (1), Dmitry D. Frederiks (1), Gregory D. Fleishman
ApJ **877** 145 **2019**
https://arxiv.org/pdf/1904.10017.pdf
https://iopscience.iop.org/article/10.3847/1538-4357/ab1be0/pdf
We report hard X-ray and gamma-ray observations of the impulsive phase of the SOL2017-09-06T11:55 X9.3 solar flare. We focus on a high-energy part of the spectrum, >100 keV, and perform time resolved spectral analysis for a portion of the impulsive phase, recorded by the Konus-Wind experiment, that displayed prominent gamma-ray emission. Given a variety of possible emission components contributing to the gamma-ray emission, we employ a Bayesian inference to build the most probable fitting model. The analysis confidently revealed contributions from nuclear deexcitation lines, electron-positron annihilation line at 511 keV, and a neutron capture line at 2.223 MeV along

with two components of the bremsstrahlung continuum. The revealed time evolution of the spectral components is particularly interesting. The low-energy bremsstrahlung continuum shows a soft-hard-soft pattern typical for impulsive flares, while the high-energy one shows a persistent hardening at the course of the flare. The neutron capture line emission shows an unusually short time delay relative to the nuclear deexcitation line component, which implies that the production of neutrons was significantly reduced soon after the event onset. This in turn may imply a prominent softening of the accelerated proton spectrum at the course of the flare, similar to the observed softening of the low-energy component of the accelerated electrons responsible for the low-energy bremsstrahlung continuum. We discuss possible physical scenarios, which might result in the obtained relationships between these gamma-ray components.

A remarkable, but confused, coronal hard X-ray source

Alexandra **Lysenko**, Larisa Kashapova, Hugh Hudson
RHESSI Science Nuggets #325 June **2018**
http://sprg.ssl.berkeley.edu/~tohban/wiki/index.php/A_remarkable,_but_confused,_coronal_hard_X-ray_source
We report a probable occulted event in 1999 that had gone un-noticed previously, and could identify it spatially with SSRT as well as characterize its hard X-ray spectral evolution with Konus/WIND. It may be difficult to do much quantitative analysis on this particular event because of source confusion and the lack of RHESSI or even Yohkoh hard X-ray imaging, but this event adds one more case to the limited catalog of occulted solar hard X-ray coronal events.
1999-06-05, 2014-09-01

Statistics of "Cold" Early Impulsive Solar Flares in X-ray and Microwave domains

Alexandra L. **Lysenko**, Alexander T. Altyntsev, Natalia S. Meshalkina, Dmitriy Zhdanov, Gregory D. Fleishman
2018 ApJ 856 111
https://iopscience.iop.org/article/10.3847/1538-4357/aab271/pdf
https://arxiv.org/pdf/1802.09288.pdf
http://sci-hub.tw/http://iopscience.iop.org/0004-637X/856/2/111/
Solar flares often happen after a preflare / preheating phase, which is almost or entirely thermal. In contrast, there are the so-called early impulsive flares that do not show a (significant) preflare heating but instead often show the Neupert effect--a relationship where the impulsive phase is followed by a gradual, cumulative-like, thermal response. This has been interpreted as a dominance of nonthermal energy release at the impulsive phase, even though a similar phenomenology is expected if the thermal and nonthermal energies are released in comparable amounts at the impulsive phase. Nevertheless, some flares do show a good quantitative correspondence between the nonthermal electron energy input and plasma heating, in such cases the thermal response was weak, which results in calling them "cold" flares. We undertook a systematic search of such events among early impulsive flares registered by Konus-Wind instrument in the triggered mode from 11/1994 to 04/2017 and selected 27 cold flares based on relationships between HXR (Konus-Wind) and SXR (GOES) emission. For these events we put together all available microwave data from different instruments. We obtained temporal and spectral parameters of HXR and microwave emissions of the events and examined correlations between them. We found that, compared with a `mean' flare, the cold flares: (i) are weaker, shorter, and harder in the X-ray domain, (ii) are harder and shorter, but not weaker in the microwaves, (iii) have a significantly higher spectral peak frequencies in the microwaves. We discuss the possible physical reasons for these distinctions and implication of the finding. **1998-05-07, 1999-06-19, 1999-07-30, 1999-11-09, 1999-11-14, 1999-12-02, 2000-03-10, 2000-03-18, 2000-05-18, 2001-10-12, 2001-11-01, 2002-05-29, 2002-08-10, 2002-08-18, 2002-08-20, 2003-10-23, 2005-09-08, 2011-09-19, 2012-07-08, 2013-11-05, 2014-01-02, 2014-01-31, 2014-02-08, 2014-10-18, 2014-10-27, 2015-05-07**
TABLE 1 Konus-Wind cold solar flare list

KW-Sun: The Konus/WIND Hard X-ray Solar Flare Database

Alexandra **Lysenko** and the Konus/WIND Team
RHESSI Science Nuggets #287 Dec **2016**
http://sprg.ssl.berkeley.edu/~tohban/wiki/index.php/KW-Sun:_The_Konus/WIND_Hard_X-ray_Solar_Flare_Database
A Hale Cycle's worth of hard X-ray and soft gamma-ray flare observations.
We describe here KW-Sun, a large database of solar flare hard X-ray and soft γ-ray emission accumulated by the Konus/WIND experiment (Ref. [1]). Konus/WIND is a joint Russian-US experiment launched on November 1, 1994 for γ-ray burst and solar flare studies. The instrument has operated in interplanetary space since July of 2004, near the Lagrangian point L1, so it sees the Sun 24 hours a day, and thanks to being far from the Earth's magnetosphere it has an exceptionally stable background.
During more than 22 years of observations Konus/WIND has detected more than 1000 solar flares in trigger mode (Figure 1), which constitute the database. The KW-Sun database can be accessed via "http://www.ioffe.ru/LEA/kwsun/" (at the time of writing only the data for years 2012-2016 are available, the remaining data will be added shortly).
20 Dec 2002

Search and statistical analysis of ”cold” solar flares using X-ray and microwave data

Alexandra **Lysenko**∗†1 , Alexander Altyntsev2 , Valentin Pal’shin , Natalia Meshalkina2 , Dmitriy Zhdanov2 , and Gregory Fleishman

CESRA **2016** p.62

http://cesra2016.sciencesconf.org/conference/cesra2016/pages/CESRA2016_prog_abs_book_v3.pdf

There is a subclass of solar flares that show noticeable nonthermal emission followed by only a modest or delayed heating. Such events are referred to as ”cold” solar flares here for brevity. Some examples of such flares were described earlier as case studies. Those studies show that the reasons of such a behavior may be quite different from each other in various cold flares and may involve either dense or tenuous plasma in flaring loop(s), suppressed chromospheric evaporation, and interaction between system of flare loops. We undertook a systematic search for cold solar flare candidates using Hard X-ray (HXR) data from KonusWind and Soft X-ray (SXR) data from GOES. The formal criterion of an event to be flagged as a cold flare candidate was the absence of reported GOES event at the time of Konus-Wind trigger. This way, we found 41 events-candidates from 05/1998 to 02/2014. For these events we put together all available microwave data from different instruments including OVSA, NoRP, RSTN, and BBMS. We obtained temporal and spectral parameters of HXR, SXR, and microwave emissions of the candidates along with their energetics in HXR and examined different relationships between these characteristics. In the X-ray domain, a comparison has been made between our flare subset and a reference set composed of C and M GOES class flares detected by Konus-Wind in the trigger mode. We present the statistical results and examine which of our cold flare candidates demonstrate suppressed or delayed heating and discuss the likely causes of the apparent lack or delay of the thermal response.

Sun-as-a-star Study of an X-class Solar Flare with Spectroscopic Observations of CHASE

Y. L. **Ma**, Q. H. Lao, X. Cheng, B. T. Wang, Z. H. Zhao, S. H. Rao, C. Li, M. D. Ding

ApJ **966** 45 **2024**

https://arxiv.org/pdf/2403.09011.pdf

https://iopscience.iop.org/article/10.3847/1538-4357/ad3446/pdf

Sun-as-a-star spectroscopic characteristics of solar flares can be used as a benchmark for the detection and analyses of stellar flares. Here, we study the Sun-as-a-star properties of an X1.0 solar flare using high-resolution spectroscopic data obtained by the Chinese $\mathrm{H}\alpha$ Solar Explorer (CHASE). A noise reduction algorithm based on discrete Fourier transformation is first employed to enhance the signal-to-noise ratio of the space-integral $\mathrm{H}\alpha$ spectrum with a focus on its typical characteristics. For the flare of interest, we find that the average $\mathrm{H}\alpha$ profile displays a strong emission at the line center and an obvious line broadening. It also presents a clear red asymmetry, corresponding to a redshift velocity of around $50\mathrm{kms}\_1$ that slightly decreases with time, consistent with previous results. Furthermore, we study how the size of the space-integral region affects the characteristics of the flare Sun-as-a-star $\mathrm{H}\alpha$ profile. It is found that although the redshift velocity calculated from the $\mathrm{H}\alpha$ profile remains unchanged, the detectability of the characteristics weakens as the space-integral region becomes large. An upper limit for the size of the target region where the red asymmetry is detectable is estimated. It is also found that the intensity in $\mathrm{H}\alpha$ profiles, measured by the equivalent widths of the spectra, are significantly underestimated if the $\mathrm{H}\alpha$ spectra are further averaged in the time domain. **October 2, 2022**

Wave generation and energetic electron scattering in solar flares

Hanqing **Ma**, James F. Drake, Marc Swisdak

ApJ **954** 21 **2023**

https://arxiv.org/pdf/2307.04769.pdf

https://iopscience.iop.org/article/10.3847/1538-4357/ace59e/pdf

We conduct two-dimensional particle-in-cell simulations to investigate the scattering of electron heat flux by self-generated oblique electromagnetic waves. The heat flux is modeled as a bi-kappa distribution with a T_parallel > T_perp temperature anisotropy maintained by continuous injection at the boundaries. The anisotropic distribution excites oblique whistler waves and filamentary-like Weibel instabilities. Electron velocity distributions taken after the system has reached a steady state show that these in stabilities inhibit the heat flux and drive the total distributions towards isotropy. Electron trajectories in velocity space show a circular-like diffusion along constant energy surfaces in the wave frame. The key parameter controlling the scattering rate is the average speed, or drift speed vd, of the heat flux

compared with the electron Alfven speed vAe, with higher drift speeds producing stronger fluctua tions and a more significant reduction of the heat flux. Reducing the density of the electrons carrying the heat flux by 50% does not significantly affect the scattering rate. A scaling law for the electron scattering rate versus vd/vAe is deduced from the simulations. The implications of these results for understanding energetic electron transport during solar flare energy release are discussed.

A machine learning approach for computing solar flare locations in X-rays on-board Solar Orbiter/STIX

Paolo **Massa**, Simon Felix, László István Etesi, Ewan C. M. Dickson, Hualin Xiao, Francesco P. Ramunno, Merve Selcuk-Simsek, Brandon Panos, André Csillaghy, Säm Krucker
Conference paper accepted for an poster presentation to the ESA SPAICE CONFERENCE 17-19 September **2024**
https://arxiv.org/pdf/2408.16642
The Spectrometer/Telescope for Imaging X-rays (STIX) on-board the ESA Solar Orbiter mission retrieves the coordinates of solar flare locations by means of a specific sub-collimator, named the Coarse Flare Locator (CFL). When a solar flare occurs on the Sun, the emitted X-ray radiation casts the shadow of a peculiar "H-shaped" tungsten grid over the CFL X-ray detector. From measurements of the areas of the detector that are illuminated by the X-ray radiation, it is possible to retrieve the (x,y) coordinates of the flare location on the solar disk.
In this paper, we train a neural network on a dataset of real CFL observations to estimate the coordinates of solar flare locations. Further, we apply a post-training quantization technique specifically tailored to the adopted model architecture. This technique allows all computations to be in integer arithmetic at inference time, making the model compatible with the STIX computational requirements. We show that our model outperforms the currently adopted algorithm for estimating the flare locations from CFL data regarding prediction accuracy while requiring fewer parameters. We finally discuss possible future applications of the proposed model on-board STIX.

Lyman Continuum Observations of Solar Flares Using SDO/EVE

Marcos E. **Machado**, Ryan O. Milligan, Paulo J. A. Simoes
ApJ **869** 63 **2018**
https://arxiv.org/pdf/1810.10824.pdf
https://iopscience.iop.org/article/10.3847/1538-4357/aaec6e/pdf
The Extreme ultraviolet Variability Experiment was designed to observe the Sun-as-a-star in the extreme ultraviolet; a wavelength range that has remained spectrally unresolved for many years. It has provided a wealth of data on solar flares, perhaps most uniquely, on the Lyman spectrum of hydrogen at high cadence and moderate spectral resolution. In this paper we concentrate on the analysis of Lyman continuum (LyC) observations and its temporal evolution in a sample of six major solar flares. By fitting both the pre-flare and flare excess spectra with a blackbody function we show that the color temperature derived from the slope of LyC reveals temperatures in excess of 104 K in the six events studied; an increase of a few thousand Kelvin above quiet-Sun values (typically ~8000-9500 K). This was found to be as high as 17000 K for the **2017 September 6** X9.3 flare. Using these temperature values, and assuming a flaring area of 1018 cm2, estimates of the departure coefficient of hydrogen, b1, were calculated. It was found that b1 decreased from 102-103 in the quiet-Sun, to around unity during the flares. This implies that LyC is optically thick and formed in local thermodynamic equilibrium during flares. It also emanates from a relatively thin ($\lesssim$100 km) shell formed at deeper, denser layers than in the quiescent solar atmosphere. We show that in terms of temporal coverage and resolution, EVE gives a more comprehensive picture of the response of the chromosphere to the flare energy input with respect to those of the Skylab/Harvard College Observatory spatially resolved observations of the 1970's. **15−Feb−11, 30−Jul−11, 03−Nov−11, 06−Mar−12, 07−Jan−14, 2017 September 6**
RHESSI Science Nuggets #336 November **2018**
http://sprg.ssl.berkeley.edu/~tohban/wiki/index.php/Remembering_Marcos_Machado_via_his_research

Inverse Compton X-rays from relativistic flare electrons and positrons

A. L. **MacKinnon** and P. C. V. Mallik
A&A 510, A29 (**2010**)
Context. In solar flares, inverse Compton scattering (ICS) of photospheric photons might give rise to detectable hard X-ray photon fluxes from the corona where ambient densities are too low for significant bremsstrahlung or recombination. γ-ray lines and continuum in some large flares imply the presence of the necessary ~100 MeV electrons and positrons, the latter as by-products of GeV energy ions. Recent observations of coronal hard X-ray sources in particular prompt us to reconsider here the possible contribution of ICS.
Aims. We aim to evaluate the ICS X-ray fluxes to be expected from prescribed populations of relativistic electrons and positrons in the solar corona. The ultimate aim is to determine if ICS coronal X-ray sources might offer a new diagnostic window on relativistic electrons and ions in flares.

Methods. We use the complete formalism of ICS to calculate X-ray fluxes from possible populations of flare primary electrons and secondary positrons, paying attention to the incident photon angular distribution near the solar surface and thus improving on the assumption of isotropy made in previous solar discussions.
Results. Both primary electrons and secondary positrons produce very hard ICS X-ray spectra. The anisotropic primary radiation field results in pronounced centre-to-limb variation in predicted fluxes and spectra, with the most intense spectra, extending to the highest photon energies, expected from limb flares. Acceptable numbers of electrons or positrons could account for RHESSI coronal X/γ-ray sources.
Conclusions. Some coronal X-ray sources at least might be interpreted in terms of ICS by relativistic electrons or positrons, particularly when sources appear at such low ambient densities that bremsstrahlung appears implausible.

On the Possibility to Diagnose the Non-Maxwellian κ-Distributions from the Hinode/EIS EUV Spectra

Š. **Mackovjak**, E. Dzifčáková, J. Dudík
Solar Physics, January **2013**, Volume 282, Issue 1, pp 263-281
We investigate the possibility to diagnose the κ-distributions from the EUV spectra observed by the Hinode/EIS spectrometer. Observable lines of the most abundant elements except Fe are considered. Synthetic spectra for the κ-distributions with $\kappa=2-10$ and the Maxwellian distribution were calculated for a range of temperatures and electron densities. We find that only a small number of O, S, Ca, and Ni line ratios are sensitive to κ. A list of the best diagnostic options using transition region and coronal lines is provided. Usually, the line ratios sensitive to κ are also sensitive to electron density. Weak O iv lines are a notable exception. These lines offer greatest sensitivity to κ from all the lines observed by Hinode/EIS. Density diagnostics using lines of the non-Fe elements is discussed and the influence of κ on the diagnostics of electron density is presented. The density diagnostics using these non-Fe EIS lines are strongly affected by both known and unknown blends. Therefore, we performed the density diagnostics using the Fe xii – xiv lines. Subsequently, these proposed diagnostic methods for κ-distributions are tested using the spectral atlas obtained by Brown et al. (Astrophys. J. Suppl. 176, 511, 2008). These data do not provide conclusive evidence for the presence of κ-distributions due to possible plasma multithermality, a low observed signal-to-noise ratio, and unremovable or unknown blends.

Relationship between the topological skeleton, current concentrations, and 3D magnetic reconnection sites in the solar atmosphere

R. C. **Maclean**1, J. Büchner2, and E. R. Priest1
A&A 501, 321-333 (**2009**)
Aims. The aim of this work is to determine the relationship between the 3D structure of the coronal magnetic field, diagnosed by the topological skeleton, and current concentrations as potential sites of 3D reconnection.
Methods. We utilised the results of 3D numerical MHD simulations of an observed EUV bright point (BP) in the solar atmosphere. The simulations are based on MDI line-of-sight magnetogram data from 13 June 1998. We analysed the results of the simulations using the method of magnetic charge topology. Three different methods of reducing the magnetogram to a set of point magnetic sources are tested.
Results. Observations of the BP show a rotation of one of its main magnetic source regions. Numerical simulations of this rotational motion result in a localised build-up of parallel electric current, which is dissipated by anomalous resistivity, causing 3D magnetic reconnection and BP heating. The magnetic topological structure of the simulated BP was also calculated, and a portion of the topological separatrix surface bounding the magnetic flux of the rotating source region is found to correspond to the locations of current build-up and heating. All three magnetogram reduction methods produce similar results for the large-scale magnetic field structure.
Conclusions. Magnetic topology is a useful method for predicting the locations of coronal current concentrations, insofar as the results of our simulations show that strong integrated parallel electric fields are found only along topological separatrix surfaces. However, further investigation is necessary to determine exactly which parts of the reconstructed separatrices will host the electric currents. Topological magnetic field reconstructions also cast light on the location of coronal BP heating, which occurs as a result of the dissipation of the currents by 3D reconnection. The choice of the magnetogram reduction algorithm does not greatly affect the large-scale topological features of the resulting reconstructed magnetic field. Further work is required to compare these results with data for other observed BPs.

Lost and found sunquake in the 6 September 2011 flare caused by beam electrons

Connor **Macrae**, Sergei Zharkov, Valentina Zharkova, Malcolm Druett, Sarah Matthews, and Tomoko Kawate
A&A 619, A65 **2018**
http://computing.unn.ac.uk/staff/slmv5/kinetics/macrae1_quake_6sept_aa_paper_final.pdf
sci-hub.tw/10.1051/0004-6361/201832896

Active region NOAA 11283 produced two X-class flares on **6 and 7 September 2011** that have been well studied by many authors. The X2.1 class flare occurred on September 6, 2011 and was associated with the first of two homologous white light flares produced by this region, but no sunquake was found with it despite the one being detected in the second flare of **7 September 2011**. In this paper we present the first observation of a sunquake for the 6 September 2011 flare detected via statistical significance analysis of egression power and verified via directional holography and time-distance diagram. The surface wavefront exhibits directional preference in the north-west direction We interpret this sunquake and the associated flare emission with a combination of a radiative hydrodynamic model of a flaring atmosphere heated by electron beam and a hydrodynamic model of acoustic wave generation in the solar interior generated by a supersonic shock. The hydrodynamic model of the flaring atmosphere produces a hydrodynamic shock travelling with supersonic velocities towards the photosphere and beneath. For the first time we derive velocities (up to 140 km s-1) and onset time (about 50 seconds after flare onset) of the shock deposition at given depths of the interior. The shock parameters are confirmed by the radiative signatures in hard X-rays and white light emission observed from this flare. The shock propagation in the interior beneath the flare is found to generate acoustic waves elongated in the direction of shock propagation, that results in an anisotropic wavefront seen on the solar surface. Matching the detected seismic signatures on the solar surface with the acoustic wave front model derived for the simulated shock velocities, we infer that the shock has to be deposited under an angle of about 30◦ to the local solar vertical. Hence, the improved seismic detection technique combined with the double hydrodynamic model reported in this study opens new perspectives for observation and interpretation of seismic signatures in solar flares.

The magnetic topology of AR13664 leading to its first halo CME

David **MacTaggart**, Tom Williams, OPM Aslam
JGR **2024**
https://arxiv.org/pdf/2410.15964
In the first half of **May 2024**, the solar active region (AR)13664 was responsible for generating the strongest geomagnetic storm in over 20 years, through an enhanced production of X-class flares and coronal mass ejections (CMEs). A key factor in this production was the complex magnetic topology of AR13664. In this work, we investigate the region's magnetic topology related to the production of its first halo CME on **May 8th**. This is achieved by combining different observations of magnetic topology based on photospheric magnetic winding signatures and nonlinear force-free extrapolations, together with Atmospheric Imaging Assembly (AIA) observations at different wavelengths. We present evidence that the first halo CME, and its associated X1 flare, was created by an emerging bipole of twisted magnetic field, following the general picture of the standard flare model. The coincidence of the first large magnetic winding signature with the start time of the X1 flare, provides the onset time for the CME as well as the period of enhanced eruptive activity of the region - 04:36UT on May 8th. Finally, our topological analysis identifies the key topological sub-regions of AR13664 that can lead to subsequent eruptions, which will be useful for further studies of this region.

Direct evidence: twisted flux tube emergence creates solar active regions

David **MacTaggart**, Chris Prior, Breno Raphaldini, Paolo Romano, Salvatore Guglielmino
Nature Communications **volume 12**, Article number: 6621 **2021**
https://arxiv.org/ftp/arxiv/papers/2106/2106.11638.pdf
https://www.nature.com/articles/s41467-021-26981-7.pdf
The magnetic nature of the formation of solar active regions lies at the heart of understanding solar activity and, in particular, solar eruptions. A widespread model, used in many theoretical studies, simulations and the interpretation of observations, is that the basic structure of an active region is created by the emergence of a large tube of pre-twisted magnetic field. Despite plausible reasons and the availability of various proxies suggesting the accuracy of this model, there has not yet been a methodology that can clearly and directly identify the emergence of large pre-twisted magnetic flux tubes. Here, we present a clear signature of the emergence of pre-twisted magnetic flux tubes by investigating a robust topological quantity, called magnetic winding, in solar observations. This quantity detects the emerging magnetic topology despite the significant deformation experienced by the emerging magnetic field. Magnetic winding complements existing measures, such as magnetic helicity, by providing distinct information about field line topology, thus allowing for the direct identification of emerging twisted magnetic flux tubes. **October 11-13 2011**

The plasmoid instability in a confined solar flare

David **MacTaggart**, Lyndsay Fletcher
MNRAS **2019**
https://arxiv.org/pdf/1905.01201.pdf
Eruptive flares (EFs) are associated with erupting filaments and, in some models, filament eruption drives flare reconnection. Recently, however, observations of a confined flare (CF) have revealed all the hallmarks of an EF (impulsive phase, flare ribbons, etc.) without the filament eruption itself. Therefore, if the filament is not primarily responsible for impulsive flare reconnection, what is? In this Letter, we argue, based on mimimal requirements, that the plasmoid instability is a strong candidate for explaining the impulsive phase in the observed CF. We present

magnetohydrodynamic simulation results of the nonlinear development of the plasmoid instability, in a model active region magnetic field geometry, to strengthen our claim. We also discuss how the ideas described in this Letter can be generalised to other situations, including EFs.

Optimal Energy Growth in Current Sheets

David **MacTaggart**, Peter Stewart
Solar Phys. 292:148 **2017**
http://www.maths.gla.ac.uk/~dmactaggart/papers/dmac17c.pdf
In this paper, we investigate the possibility of transient growth in the linear perturbation of current sheets. The resistive magnetohydrodynamic (MHD) operator for a background field consisting of a current sheet is non-normal, meaning that associated eigenvalues and eigenmodes can be very sensitive to perturbation. In a linear stability analysis of a tearing current sheet, we show that modes that are damped as t\rightarrow\infty can produce transient energy growth, contributing faster growth rates and higher energy attainment (within a fixed finite time) than the unstable tearing mode found from normal-mode analysis. We determine the transient growth for tearing-stable and tearing-unstable regimes and discuss the consequences of our results for processes in the solar atmosphere, such as flares and coronal heating. Our results have significant potential impact on how fast current sheets can be disrupted. In particular, transient energy growth due to (asymptotically) damped modes may lead to accelerated current sheet thinning and, hence, a faster onset of the plasmoid instability, compared to the rate determined by the tearing mode alone.

The magnetic structure of surges in small-scale emerging flux regions⋆

D. **MacTaggart**1,2,3, S. L. Guglielmino4, A. L. Haynes5, R. Simitev1 and F. Zuccarello
A&A 576, A4 (**2015**)
Aims. We investigate the relationship between surges and magnetic reconnection during the emergence of small-scale active regions. In particular, to examine how the large-scale geometry of the magnetic field, shaped by different phases of reconnection, guides the flowing of surges.
Methods. We present three flux emergence models. The first model, and the simplest, consists of a region emerging into a horizontal ambient field that is initially parallel to the top of the emerging region. The second model is the same as the first but with an extra smaller emerging region which perturbs the main region. This is added to create a more complex magnetic topology and to test how this complicates the development of surges compared to the first model. The last model has a non-uniform ambient magnetic field to model the effects of emergence near a sunspot field and impose asymmetry on the system through the ambient magnetic field. At each stage, we trace the magnetic topology to identify the locations of reconnection. This allows for field lines to be plotted from different topological regions, highlighting how their geometry affects the development of surges.
Results. In the first model, we identify distinct phases of reconnection. Each phase is associated with a particular geometry for the magnetic field and this determines the paths of the surges. The second model follows a similar pattern to the first but with a more complex magnetic topology and extra eruptions. The third model highlights how an asymmetric ambient field can result in preferred locations for reconnection, subsequently guiding the direction of surges.
Conclusions. Each of the identified phases highlights the close connection between magnetic field geometry, reconnection and the flow of surges. These phases can now be detected observationally and may prove to be key signatures in determining whether or not an emerging region will produce a large-scale (CME-type) eruption.

Twisted flux tube emergence: rigid rise or nonlinear deformation?

D. **MacTaggart**
UKSP Nugget: 32, Feb **2013**
http://www.uksolphys.org/?p=5797
We have taken a flux emergence model, where the magnetic field expands into the atmosphere via the magnetic buoyancy instability, and shown that we can reproduce the observational signatures used as evidence for rigid emergence. This means that these signatures are not sufficient to determine which type of emergence is occurring. Although these studies do not categorically disprove rigid emergence, they cast a shadow of doubt over it. To achieve general acceptance, rigid emergence will have to undergo the same scrutiny as the ‘standard model’ of flux emergence. Although this model is highly nonlinear, each stage of the evolution has a sound physical basis with results that are testable by observations.

Flux emergence within mature solar active regions

D. **MacTaggart**
A&A 531, A108 **(2011)**
Aims. Recent insterest in flux emergence within mature active regions has led to several observational studies. Our aim is to model such a scenario and investigate the evolution of the system.

Methods. We solve the 3D MHD equations numerically with a Lagrangian-remap scheme. The mature active region is modelled, in the initial condition, with a potential field. The smaller emerging region is a twisted flux tube and is placed between the two polarities of the mature region. The polarities of the new flux are aligned the same way as those of the mature region. The new flux emerges closer to the main negative polarity than the main positive polarity. To investigate the effects of reconnection, the distribution of the parallel electric field is calculated throughout the simulation. The topology of the magnetic field is then studied in regions of interest indicated by the electric field distribution.
Results. The expansion of the new negative polarity is restricted due to the curvature of the overlying field and also because it is of the same sign. Reconnection is found to be strongest at low heights (below the corona) and along the outer side of the new positive polarity and its magnetic tongue. The effect of reconnection, in combination with the pressure between the two flux systems, is to resist the expansion of the new flux. The system then relaxes. Large-scale eruptions, such as CMEs, are not expected from the setup considered. At the new negative polarity, the high magnetic pressure can generate strong parallel electric fields which may lead to localized reconnection. The results of the model are in qualitative agreement with observations.

Research Note: Multiple eruptions from magnetic flux emergence:

D. **MacTaggart** and A.═W. Hood
A&A 508 (**2009**) 445-449
Aims. In this paper we study the effects of a toroidal magnetic flux tube emerging into a magnetized corona, with an emphasis on large-scale eruptions. The orientation of the fields is such that the two flux systems are almost antiparallel when they meet.
Methods. We follow the dynamic evolution of the system by solving the 3D MHD equations using a Lagrangian remap scheme.
Results. Multiple eruptions are found to occur. The physics of the trigger mechanisms is discussed and related to well-known eruption models.

Can magnetic breakout be achieved from multiple flux emergence?

MacTaggart, D., Hood, A.W.
E-print, May **2009**; A&A
We study the breakout model using multiple flux emergence to produce the magnetic configuration and the trigger. We do not impose any artificial motions on the boundaries. Once the original flux tube configuration is chosen the system is left to evolve itself. We perform non-linear simulations in 2.5D by solving the compressible and resistive MHD equations using a Lagrangian remap, shock capturing code (Lare2D). To produce a quadrupolar configuration from flux emergence we build on previous work where the interaction of two flux tubes forms the required quadrupole. Instead of imposing a shearing flow, a third flux tube is then allowed to emerge up through the central arcade. Breakout is not achieved in any of the experiments. This is due to the interaction of the third tube with the quadrupole and the effect of the plasma beta being O(1) at the photosphere and >= O(1) in the solar interior. When beta is of these orders, flows generated in the plasma can influence the magnetic field and so photospheric footpoints do not remain fixed.

Dynamics and plasma properties of an X-ray jet from SUMER, EIS, XRT, and EUVI A & B simultaneous observations*

M. S. **Madjarska**
A&A 526, A19 (**2011**)
Context. Small-scale transient phenomena in the quiet Sun are believed to play an important role in coronal heating and solar wind generation. One of them, called “X-ray jet”, is the subject of our study.
Aims. We intend to investigate the dynamics, evolution, and physical properties of this phenomenon.
Methods. We combine multi-instrument observations obtained simultaneously with the SUMER spectrometer onboard SoHO, with EIS and XRT onboard Hinode, and with EUVI/SECCHI onboard the Ahead and Behind STEREO spacecrafts. We derive plasma parameters such as temperatures and densities as well as dynamics by using spectral lines formed in the temperature range from 10 000 K to 12 MK. We also use an image difference technique to investigate the evolution of the complex structure of the studied phenomenon.
Results. With the available unique combination of data we were able to establish that the formation of a jet-like event is triggered by not one, but several energy depositions, which are most probably originating from magnetic reconnection. Each energy deposition is followed by the expulsion of pre-existing or newly reconnected loops and/or collimated flow along open magnetic field lines. We derived in great detail the dynamic process of X-ray jet formation and evolution. For the first time we also found spectroscopically a temperature of 12 MK (Fe xxiii 263.76 Å) and density of 4 × 1010 cm-3 in the quiet Sun, obtained from a pair of Fe xii lines with a maximum formation temperature of 1.3 × 106 K, in an energy deposition region. We point out a problem concerning an uncertainty in using the SUMER Mg x 624.9 Å line for coronal diagnostics. We clearly identified two types of up-flow: one collimated up-flow along open magnetic field

lines and a plasma cloud formed from the expelled BP loops. We also report a cooler down-flow along closed magnetic field lines. A comparison is made with a model developed by Moreno-Insertis et al. (2008).

‘Superflares’ on solar-type stars observed with Kepler

Hiroyuki **Maehara**.
RHESSI Science Nugget No. 253, June **2015**
http://sprg.ssl.berkeley.edu/~tohban/wiki/index.php/%22Superflares%22_on_solar-type_stars_observed_with_Kepler
Flare energies 10-1000 times those of the most powerful solar flares!
The long-term, high-precision and continuous observations of the large number of solar-type stars with Kepler enable us to detect not only exoplanets, its primary scientific objective, but also to observe flares. In particular we have found many "superflares" on other Sun-like stars. Our analysis of superflares on solar-type stars with the Kepler data reveals that the statistical properties of these stellar flares are similar to those of solar flares. These results suggest that both solar flares and superflares are caused by the same physical process (e.g. magnetic reconnection). Further detailed observations of superflare stars are needed to reveal whether superflare stars are really similar to the Sun and whether our Sun can produce superflares.

Structural properties of the solar flare-producing coronal current system developed in an emerging magnetic flux tube

Tetsuya **Magara**
Publications of the Astronomical Society of Japan, Volume 69, Issue 1, 1 February **2017**, 5
The activity of a magnetic structure formed in the solar corona depends on a coronal current system developed in the structure, which determines how an electric current flows in the corona. To investigate structural properties of the coronal current system responsible for producing a solar flare, we perform magnetohydrodynamic simulation of an emerging magnetic flux tube which forms a coronal magnetic structure. Investigation using fractal dimensional analysis and electric current streamlines reveals that the flare-producing coronal current system relies on a specific coronal current structure of two-dimensional spatiality, which has a sub-region where a nearly anti-parallel magnetic field configuration is spontaneously generated. We discuss the role of this locally generated anti-parallel magnetic field configuration in causing the reconnection of a three-dimensional magnetic field, which is a possible mechanism for producing a flare. We also discuss how the twist of a magnetic flux tube affects structural properties of a coronal current system, showing how much volume current flux is carried into the corona by an emerging flux tube. This gives a way to evaluate the activity of a coronal magnetic structure.

CHARACTERISTIC DEVELOPMENT OF MAGNETIC SHEAR IN A FLARE-PRODUCING SUNSPOT OBTAINED FROM VECTOR MAGNETIC FIELD MEASUREMENTS BY HINODE

T. **Magara**
2009 ApJ 702 386-391 doi: 10.1088/0004-637X/702/1/386
One of the promising models for the initiation of a solar flare requires observation-based information at the solar surface where the energy released during a flare is injected in the way limited by a real environment. *Hinode* provides a time series of vector-field maps of the photospheric magnetic field in NOAA10930 that shows strong flaring activity. We use these maps to investigate the structure and evolution of the magnetic field in a major sunspot of this active region. By dividing the sunspot into a number of small regions and assuming a linear force-free-field state in each divided region, we derive the spatial variation of magnetic shear and its temporal development in this sunspot. The magnetic shear first increases in magnitude and area with time, while it decreases before the onset of an X-class flare. A relation between the evolution of magnetic shear and the motions of an accompanying sunspot has also been found. We discuss the physical processes responsible for those observational features, suggesting that the characteristic development of magnetic shear in the major sunspot and the translational motion followed by rotational motion of the accompanying sunspot might be caused by the emergence of a twisted flux tube into the solar atmosphere.

FLARE-GENERATED TYPE II BURST WITHOUT ASSOCIATED CORONAL MASS EJECTION

J. **Magdalenić**1,2, C. Marqué1, A. N. Zhukov1,3, B. Vršnak2 and A. Veronig
2012 ApJ 746 152
We present a study of the solar coronal shock wave on **2005 November 14** associated with the GOES M3.9 flare that occurred close to the east limb (S06° E60°). The shock signature, a type II radio burst, had an unusually high starting frequency of about 800 MHz, indicating that the shock was formed at a rather low height. The position of the radio source, the direction of the shock wave propagation, and the coronal electron density were estimated using Nançay Radioheliograph observations and the dynamic spectrum of the Green Bank Solar Radio Burst Spectrometer. The soft X-ray, Hα, and Reuven Ramaty High Energy Solar Spectroscopic Imager observations show that the flare was compact, very impulsive, and of a rather high density and temperature, indicating a strong and impulsive increase of pressure in a small flare loop. The close association of the shock wave initiation with the impulsive energy release suggests that the impulsive increase of the pressure in the flare was the source of the shock wave. This is supported by the fact that,

contrary to the majority of events studied previously, no coronal mass ejection was detected in association with the shock wave, although the corresponding flare occurred close to the limb.

Numerical simulations of transverse oscillations in radiatively cooling coronal loops

N. **Magyar**, T. Van Doorsselaere, A. Marcu
Astronomy & Astrophysics (**2015**), Volume 582, id.A117, 8 pp
http://arxiv.org/pdf/1510.08760v1.pdf
We aim to study the influence of radiative cooling on the standing kink oscillations of a coronal loop. Using the FLASH code, we solved the 3D ideal magnetohydrodynamic equations. Our model consists of a straight, density enhanced and gravitationally stratified magnetic flux tube. We perturbed the system initially, leading to a transverse oscillation of the structure, and followed its evolution for a number of periods. A realistic radiative cooling is implemented. Results are compared to available analytical theory. We find that in the linear regime (i.e. low amplitude perturbation and slow cooling) the obtained period and damping time are in good agreement with theory. The cooling leads to an amplification of the oscillation amplitude. However, the difference between the cooling and non-cooling cases is small (around 6% after 6 oscillations). In high amplitude runs with realistic cooling, instabilities deform the loop, leading to increased damping. In this case, the difference between cooling and non-cooling is still negligible at around 12%. A set of simulations with higher density loops are also performed, to explore what happens when the cooling takes place in a very short time (tcool = 100 s). We strengthen the results of previous analytical studies that state that the amplification due to cooling is ineffective, and its influence on the oscillation characteristics is small, at least for the cases shown here. Furthermore, the presence of a relatively strong damping in the high amplitude runs even in the fast cooling case indicates that it is unlikely that cooling could alone account for the observed, **flare-related undamped oscillations** of coronal loops. These results may be significant in the field of coronal seismology, allowing its application to coronal loop oscillations with observed fading-out or cooling behaviour.

Photospheric Lorentz force changes in eruptive and confined solar flares

Samriddhi Sankar **Maity**, Ranadeep Sarkar, Piyali Chatterjee, Nandita Srivastava
ApJ **962** 86 **2024**
https://arxiv.org/pdf/2312.06787.pdf
https://iopscience.iop.org/article/10.3847/1538-4357/ad13f0/pdf
Solar flares are known to leave imprints on the magnetic field at the photosphere, often manifested as an abrupt and permanent change in the downward-directed Lorentz force in localized areas inside the active region. Our study aims to differentiate eruptive and confined solar flares based on the vertical Lorentz force variations. We select 26 eruptive and 11 confined major solar flares (stronger than the GOES M5 class) observed during 2011-2017. We analyze these flaring regions using SHARP vector-magnetograms obtained from the NASA's Helioseismic and Magnetic Imager (HMI). We also compare data corresponding to 2 synthetic flares from a δ--sunspot simulation reported in Chatterjee et al. [Phys. Rev. Lett. 116, 101101 (2016)]. We estimate the change in the horizontal magnetic field and the total Lorentz force integrated over an area around the polarity inversion line (PIL) that encompasses the location of the flare. Our results indicate a rapid increase of the horizontal magnetic field along the flaring PIL, accompanied by a significant change in the downward-directed Lorentz force in the same vicinity. Notably, we find that all the confined events under study exhibit a total change in Lorentz force of < 1.8×1022 dyne. This threshold plays an important factor in effectively distinguishing eruptive and confined flares. Further, our analysis suggests that the change in total Lorentz force also depends on the reconnection height in the solar corona during the associated flare onset. The results provide significant implications for understanding the flare-related upward impulse transmission for the associated coronal mass ejection.
2011 February 13, 2011 September 06, 2013 November 01, 2013-11-08, 2014-09-10, 2015 March 12
Table

Magnetic field topology by MDI data: Active region

N. G. **Makarenko**, I. S. Knyazeva and L. M. Karimova
Astronomy Letters, Volume 38, Number 8 (**2012**), 531-542
Pis'ma v Astronomicheskiı Zhurnal, **2012**, Vol. 38, No. 8, pp. 597–608.
Themain purpose of this paper is to describe the evolution of the magnetic field of active regions of the Sun in the context of Minkowski functionals: the Euler characteristic and perimeter calculated on the excursion set for a specified level. Themethods of geometry of random fields was applied to the MDI SOHO magnetogram, containing flaring active regions. The results demonstrated that morphological functional tracked the dynamic scenarios of the magnetic fields preceded by flares or accompanying them.

Using Coronal Loops to Reconstruct the Magnetic Field of an Active Region Before and After a Major Flare

A. **Malanushenko**, C. Schrijver, M. L. DeRosa, M. S. Wheatlan

E-print, Dec **2013**; **2014** ApJ 783 102
The shapes of solar coronal loops are sensitive to the presence of electrical currents that are the carriers of the nonpotential energy available for impulsive activity. We use this information in a new method for modeling the coronal magnetic field of AR 11158 as a nonlinear force-free field (NLFFF). The observations used are coronal images around time of major flare activity on **2011/02/15**, together with the surface line-of-sight magnetic field measurements. The data are from the Helioseismic and Magnetic Imager and Atmospheric Imaging Assembly (HMI and AIA, respectively) onboard the Solar Dynamics Observatory (SDO). The model fields are constrained to approximate the coronal loop configurations as closely as possible, while also subject to the force-free constraints. The method does not use transverse photospheric magnetic field components as input, and is thereby distinct from methods for modeling NLFFFs based on photospheric vector magnetograms. We validate the method using observations of AR 11158 at a time well before major flaring, and subsequently review the field evolution just prior to and following an X2.2 flare and associated eruption. The models indicate that the energy released during the instability is about 1x1032 erg, consistent with what is needed to power such a large eruptive flare. Immediately prior to the eruption the model field contains a compact sigmoid bundle of twisted flux that is not present in the post-eruption models, which is consistent with the observations. The core of that model structure is twisted by approx0.9 full turns about its axis.

MODELING STATISTICAL PROPERTIES OF SOLAR ACTIVE REGIONS THROUGH DIRECT NUMERICAL SIMULATIONS OF 3D-MHD TURBULENCE

Shiva Kumar **Malapaka**1,2 and Wolf-Christian Müller
2013 ApJ 774 84
Statistical properties of the Sun's photospheric turbulent magnetic field, especially those of the active regions (ARs), have been studied using the line-of-sight data from magnetograms taken by the Solar and Heliospheric Observatory and several other instruments. This includes structure functions and their exponents, flatness curves, and correlation functions. In these works, the dependence of structure function exponents (ζ_p) of the order of the structure functions (p) was modeled using a non-intermittent K41 model. It is now well known that the ARs are highly turbulent and are associated with strong intermittent events. In this paper, we compare some of the observations from Abramenko et al. with the log-Poisson model used for modeling intermittent MHD turbulent flows. Next, we analyze the structure function data obtained from the direct numerical simulations (DNS) of homogeneous, incompressible 3D-MHD turbulence in three cases: sustained by forcing, freely decaying, and a flow initially driven and later allowed to decay (case 3). The respective DNS replicate the properties seen in the plots of ζ_p against p of ARs. We also reproduce the trends and changes observed in intermittency in flatness and correlation functions of ARs. It is suggested from this analysis that an AR in the onset phase of a flare can be treated as a forced 3D-MHD turbulent system in its simplest form and that the flaring stage is representative of decaying 3D-MHD turbulence. It is also inferred that significant changes in intermittency from the initial onset phase of a flare to its final peak flaring phase are related to the time taken by the system to reach the initial onset phase.

DIRECT MEASUREMENTS OF MAGNETIC TWIST IN THE SOLAR CORONA

A. **Malanushenko**1, M. H. Yusuf2 and D. W. Longcope
2011 ApJ 736 97
In the present work, we study the evolution of magnetic helicity in the solar corona. We compare the rate of change of a quantity related to the magnetic helicity in the corona to the flux of magnetic helicity through the photosphere and find that the two rates are similar. This gives observational evidence that helicity flux across the photosphere is indeed what drives helicity changes in the solar corona during emergence. For the purposes of estimating coronal helicity, we neither assume a strictly linear force-free field nor attempt to construct a nonlinear force-free field. For each coronal loop evident in extreme ultraviolet, we find a best-matching line of a linear force-free field and allow the twist parameter α to be different for each line. This method was introduced and its applicability discussed in Malanushenko et al. The object of this study is emerging and rapidly rotating AR 9004 over about 80 hr. As a proxy for coronal helicity, we use the quantity α i Li /2 averaged over many reconstructed lines of magnetic field. We argue that it is approximately proportional to the "flux-normalized" helicity H/Φ2, where H is the helicity and Φ is the total enclosed magnetic flux of the active region. The time rate of change of such a quantity in the corona is found to be about 0.021 rad hr–1, which is comparable with the estimates for the same region obtained using other methods, which estimated the flux of normalized helicity to be about 0.016 rad hr

ADDITIVE SELF-HELICITY AS A KINK MODE THRESHOLD

A. Malanushenko[1], D. W. Longcope[1], Y. Fan[2] and S. E. Gibson[2]
ApJ 702 580-592, **2009** doi: 10.1088/0004-637X/702/1/580
In this paper, we propose that additive self-helicity, introduced by Longcope and Malanushenko, plays a role in the kink instability for complex equilibria, similar to twist helicity for thin flux tubes. We support this hypothesis by a

calculation of additive self-helicity of a twisted flux tube from the simulation of Fan and Gibson. As more twist gets introduced, the additive self-helicity increases, and the kink instability of the tube coincides with the drop of additive self-helicity, after the latter reaches the value of $H_A/\Phi^2 \approx 1.5$ (where Φ is the flux of the tube and H_A is the additive self-helicity). We compare the additive self-helicity to twist for a thin subportion of the tube to illustrate that H_A/Φ^2 is equal to the twist number, studied by Berger and Field, when the thin flux tube approximation is applicable. We suggest that the quantity H_A/Φ^2 could be treated as a generalization of a twist number, when the thin flux tube approximation is not applicable. A threshold on a generalized twist number might prove extremely useful studying complex equilibria, just as the twist number itself has proven useful studying idealized thin flux tubes. We explicitly describe a numerical method for calculating additive self-helicity, which includes an algorithm for identifying a domain occupied by a flux bundle and a method of calculating potential magnetic field confined to this domain. We also describe a numerical method to calculate twist of a thin flux tube, using a frame parallelly transported along the axis of the tube.

Coronal O VI emission observed with UVCS/SOHO during solar flares: Comparison with soft X-ray observations

S. **Mancuso**1, S. Giordano1 and J. C. Raymond2
A&A 591, A4 (**2016**)
http://www.aanda.org/articles/aa/pdf/2016/07/aa27036-15.pdf
In this work, we derive the O VI 1032 Å luminosity profiles of **58 flares**, during their impulsive phase, based on off-limb measurements by the Ultraviolet Coronagraph Spectrometer (UVCS) aboard the SOlar and Heliospheric Observatory (SOHO). The O VI luminosities from the transition region plasma (here defined as the region with temperatures $5.0 \leq \log T\,(K) \leq 6.0$) were inferred from the analysis of the resonantly scattered radiation of the O VI coronal ions. The temperature of maximum ionization for O VI is $\log T_{max}\,(K) = 5.47$. By comparison with simultaneous soft X-ray measurements, we investigate the likely source (chromospheric evaporation, footpoint emission, or heated prominence ejecta) for the transition region emission observed during the impulsive phase. In our study, we find evidence of the main characteristics predicted by the evaporation scenario. Specifically, most O VI flares precede the X-ray peaks typically by several minutes with a mean of 3.2 ± 0.1 min, and clear correlations are found between the soft X-ray and transition region luminosities following power laws with indices ~ 0.7 ± 0.3. Overall, the results are consistent with transition region emission originating from chromospheric evaporation; the thermal X-ray emission peaks after the emission from the evaporation flow as the loops fill with hot plasma. Finally, we were able to infer flow speeds in the range ~20−100 km s-1 for one-third of the events, 14 of which showed speeds between 60 and 80 km s-1. These values are compatible with those found through direct spectroscopic observations at transition region temperatures by the EUV Imaging Spectrometer (EIS) on board Hinode. **2003-03-20**
Table A.1. UVCS solar flare observations. (1997-2005)

Spectral Line Asymmetries of Hot Fe Lines in Multiloop Models

Revati S. **Mandage** and Stephen J. Bradshaw
2021 ApJ 908 128
https://iopscience.iop.org/article/10.3847/1538-4357/abd1d9/pdf
https://doi.org/10.3847/1538-4357/abd1d9
Extreme ultraviolet emission line profiles often show asymmetries, in the form of wing enhancements, during solar flares. Various explanations, ranging from magnetic disturbances to non-Maxwellian electron distributions to plasma turbulence have been proposed to explain these features. Plasma dynamics in a single loop can also satisfactorily explain line asymmetry. However, the presence of sub-resolution structures, confirmed by increasingly high-resolution observations, and observational difficulties in isolating a monolithic loop from nearby loops, necessitate detailed modeling efforts to investigate the effect of superposed dynamics on some line asymmetries. In the present work, we design multiloop models, representative of three possible loop configurations, to study how the resultant Fe xxiii spectral line profiles differ in each case and examine the differences between these multiloop models and the single loop model. We also briefly explore the role of a constant time delay in heating successive sub-loops on the spectral line shape. We find that for a multiloop model with sub-loops of the same length, heating time delay is an important factor that alters the line profile shape from the single loop case. Whereas, multiloop models with sub-loops of varied lengths predict significantly different line profiles, such as asymmetric lines for longer durations and with large blueshifts, without the necessity of introducing time delays.

Asymmetries and Broadenings of Spectral Lines in Strongly Charged Iron Produced during Solar Flares

Revati S. **Mandage** and Stephen J. Bradshaw
2020 ApJ 891 122
https://doi.org/10.3847/1538-4357/ab7340
Spatially resolved spectroscopic observations show wing enhancements and broadening in extreme ultraviolet emission lines, particularly in hot iron lines. Various explanations ranging from plasma turbulence and magnetic perturbations, to

nonthermal ion populations and multiple flows in unresolved structures have been proposed. In this work, we revisit the role of single loop plasma dynamics in spectral line shape by reproducing the wing enhancements of Fe xxiii and xxiv observed during a C-class solar flare using a single loop hydrodynamic model. We also run simulations with different loop lengths and the same beam parameters to investigate the role of loop length in line broadening and asymmetry. We find that the single loop model successfully reproduces line asymmetries and the loop length plays an important role in explaining some of the key observations such as the positive correlation between the Doppler shifts and line width, and broad but symmetric hot Fe lines.

On the non-Kolmogorov nature of flare-productive solar active regions

Revati S. **Mandage**, R.T.James McAteer
ApJ 833 237 **2016**
https://arxiv.org/pdf/1611.00830v1.pdf
A magnetic power spectral analysis is performed on 53 solar active regions, observed from August 2011 to July 2012. Magnetic field data obtained from the Helioseismic and Magnetic Imager, inverted as Active Region Patches, are used to study the evolution of the magnetic power index as each region rotates across the solar disk. Active regions are classified based on the number, and sizes, of solar flares they produce, in order to study the relationship between flare productivity and the magnetic power index. The choice of window size and inertial range plays a key role in determining the correct magnetic power index. The overall distribution of magnetic power indices has a range of 1.0−2.5. Flare-quiet regions peak at a value of 1.6, however flare-productive regions peak at a value of 2.2. Overall, the histogram of the distribution of power indices of flare-productive active regions is well separated from flare-quiet active regions. Only 12\% of flare-quiet regions exhibit an index greater than 2, whereas 90\% of flare-productive regions exhibit an index greater than 2. Flare-quiet regions exhibit a high temporal variance (i.e, the index fluctuates between high and low values), whereas flare-productive regions maintain an index greater than 2 for several days. This shows the importance of including the temporal evolution of active regions in flare prediction studies, and highlights the potential of a 2-3 day prediction window for space weather applications. **1-6 Aug 2011, 3-11 Nov 2011, 5-13 Nov 2011, 15-26 Jan 2012, 12-20 March 2012, 1-9 May 2012,**

Flare induced decay-less transverse oscillations in solar coronal loops

Sudip **Mandal**, Hui Tian, Hardi Peter
A&A 652, L3 **2021**
https://arxiv.org/pdf/2107.02247.pdf
https://www.aanda.org/articles/aa/pdf/2021/08/aa41542-21.pdf
https://doi.org/10.1051/0004-6361/202141542
Evidence of flare induced, large-amplitude, decay-less transverse oscillations is presented. A system of multi-thermal coronal loops as observed with the Atmospheric Imaging Assembly (AIA), exhibit decay-less transverse oscillations after a flare erupts nearby one of the loop footpoints. Measured oscillation periods lie between 4.2 min and 6.9 min wherein the displacement amplitudes range from 0.17 Mm to 1.16 Mm. A motion-magnification technique is employed to detect the pre-flare decay-less oscillations. These oscillations have similar periods (between 3.7 min and 5.0 min) like the previous ones but their amplitudes (0.04 Mm to 0.12 Mm) are found to be significantly smaller. No phase difference is found among oscillating threads of a loop when observed through a particular AIA channel or when their multi-channel signatures are compared. These features suggest that the occurrence of a flare in this case neither changed the nature of these oscillations (decaying vs decay-less) nor the oscillation periods. The only effect the flare has is to increase the oscillation amplitudes. **27-10-2014**

Topological Analysis of Emerging Bipole Clusters Producing Violent Solar Events

C.H. **Mandrini**, B. Schmieder, P. D?moulin, Y. Guo, G. Cristiani
E-print, Dec **2013**; Solar Phys., June **2014**, Volume 289, Issue 6, pp 2041-2071
During the rising phase of Solar Cycle 24 tremendous activity occurred on the Sun with fast and compact emergence of magnetic flux leading to bursts of flares (C to M and even X-class). We investigate the violent events occurring in the cluster of two active regions (ARs), NOAA numbers 11121 and 11123, observed in November **2010** with instruments onboard the Solar Dynamics Observatory and from Earth. Within one day the total magnetic flux increased by 70% with the emergence of new groups of bipoles in AR 11123. From all the events on **11 November**, we study, in particular, the ones starting at around 07:16 UT in GOES soft X-ray data and the brightenings preceding them. A magnetic-field topological analysis indicates the presence of null points, associated separatrices and quasi-separatrix layers (QSLs) where magnetic reconnection is prone to occur. The presence of null points is confirmed by a linear and a non-linear force-free magnetic-field model. Their locations and general characteristics are similar in both modelling approaches, which supports their robustness. However, in order to explain the full extension of the analysed event brightenings, which are not restricted to the photospheric traces of the null separatrices, we compute the locations of QSLs. Based on this more complete topological analysis, we propose a scenario to explain the origin of a low-energy event preceding a filament eruption, which is accompanied by a two-ribbon flare, and a consecutive confined flare in AR 11123. The results of our topology computation can also explain the locations of flare ribbons in two other events,

one preceding and one following the ones at 07:16 UT. Finally, this study provides further examples where flare-ribbon locations can be explained when compared to QSLs and only, partially, when using separatrices.

Magnetic energy release: flares and coronal mass ejections

Cristina H. **Mandrini**

Solar and Stellar Variability: Impact on Earth and Planets, Proceedings IAU Symposium No. 264, 2009, p. 257-266, A.G. Kosovichev, A.H. Andrei & J.-P. Rozelot, eds., **2010**, **File**

Free energy stored in the magnetic field is the source that powers solar and stellar activity at all temporal and spatial scales. The energy released during transient atmospheric events is contained in current-carrying magnetic fields that have emerged twisted and may be further stressed via motions in the lower atmospheric layers (i.e. loop-footpoint motions). Magnetic reconnection is thought to be the mechanism through which the stored magnetic energy is transformed into kinetic energy of accelerated particles and mass flows, and radiative energy along the whole electromagnetic spectrum. This mechanism works efficiently at scale lengths much below the spatial resolution of even the highest resolution solar instruments; however, it may imply a large-scale restructuring of the magnetic field inferred indirectly from the combined analysis of observations and models of the magnetic field topology. The aftermath of magnetic energy release includes events ranging from nanoflares, which are below our detection limit, to powerful flares, which may be accompanied by the ejection of large amounts of plasma and magnetic field (so called coronal mass ejections, CMEs), depending on the amount of total available free magnetic energy, the magnetic flux density distribution, the magnetic field configuration, etc. We describe key observational signatures of flares and CMEs on the Sun, their magnetic field topology, and discuss how the combined analysis of solar and interplanetary observations can be used to constrain the flare/CME ejection mechanism.

COMPANION EVENT AND PRECURSOR OF THE X17 FLARE ON 28 OCTOBER 2003

C.H. **MANDRINI**, P. DEMOULIN, B. SCHMIEDER et al.

Solar Physics (**2006**) 238: 293–312, **File**

this allows the filament to erupt in a way similar to that proposed by the breakout model, but with magnetic reconnection occurring at Quasi-Separatrix Layers (QSLs) rather than at a magnetic null point.

Generation of relativistic electrons at the termination shock in the solar flare region

G. **Mann**, A. M. Veronig, F. Schuller

A&A 686, A207 **2024**

https://arxiv.org/pdf/2404.12005.pdf

https://www.aanda.org/articles/aa/pdf/2024/06/aa49162-24.pdf

Context. Solar flares are accompanied by an enhanced emission of electromagnetic waves from the radio up to the γ-ray range. The associated hard X-ray and microwave radiation is generated by energetic electrons. These electrons play an important role, since they carry a substantial part of the energy released during a flare. The flare is generally understood as a manifestation of magnetic reconnection in the corona. The so-called standard CSHKP model is one of the most widely accepted models for eruptive flares. The solar flare event on **September 10, 2017** offers us a unique opportunity to study this model. The observations from the Expanded Owens Valley Solar Array (EOVSA) show that ≈ 1.6 × 104 electrons with energies > 300 keV are generated in the flare region. Aims. There are signatures in solar radio and extreme ultraviolet (EUV) observations as well as numerical simulations that a “termination shock” (TS) appears in the magnetic reconnection outflow region. Electrons accelerated at the TS can be considered to generate the loop-top hard X-ray sources. In contrast to previous studies, we investigate whether the heating of the plasma at the TS provides enough relativistic electrons needed for the hard X-ray and microwave emission observed during the solar X8.2 flare on September 10, 2017. Methods. We studied the heating of the plasma at the TS by evaluating the jump in the temperature across the shock by means of the Rankine-Hugoniot relationships under coronal circumstances measured during the event on **September 10, 2017**. The part of relativistic electrons was calculated in the heated downstream region. Results. In the magnetic reconnection outflow region, the plasma is strongly heated at the TS. Thus, there are enough energetic electrons in the tail of the electron distribution function (EDF) needed for the microwave and hard X-ray emission observed during the event on September 10, 2017. Conclusions. The generation of relativistic electrons at the TS is a possible mechanism of explaining the enhanced microwave and hard X-ray radiation emitted during flares.

Energetic electrons generated during solar flares

Gottfried **Mann**

Journal of Plasma Physics Volume 81, Issue 6 December **2015**, 475810601

https://www.cambridge.org/core/services/aop-cambridge-core/content/view/8A5D1B5591B173585BB12CF51EA2E67B/S0022377815001166a.pdf/energetic-electrons-generated-during-solar-flares.pdf

The Sun is a giant particle accelerator. During solar flares, magnetic field energy stored in the corona is suddenly released and transferred to local heating of the coronal plasma, mass motions (e.g. jets) and the generation of energetic particles, i.e. electrons, protons and heavy ions. Basically, a flare occurs as a local enhancement of the emission of electromagnetic radiation from the radio up to the ${\it\gamma}$-ray range on the Sun. That indicates the production of energetic electrons during flares. NASA's RHESSI mission has the aim to investigate electron acceleration processes by studying the Sun's X-ray and ${\it\gamma}$-ray emission with high spatial, temporal and spectral resolution, i.e. by means of imaging spectroscopy. A substantial part of the energy released during a flare is carried by these energetic electrons. Apart from them, solar energetic particles, i.e. protons and heavy ions, and coronal mass ejections play an important role in the energy budget of a flare. Here, we focus on electron acceleration. The way in which 10^{36} electrons are accelerated up to energies beyond 30 keV is one of the open questions in solar physics. A flare is considered as the manifestation of magnetic reconnection in the solar corona. Which mechanisms lead to the production of energetic electrons in the magnetic reconnection region is discussed in this paper. Two of them are described in more detail. **28 October 2003**
See CESRA highlight #1005 **2016** http://www.astro.gla.ac.uk/users/eduard/cesra/?p=1005

Electron acceleration at slow-mode shocks in the magnetic reconnection region in solar flares

Gottfried **Mann**∗1 , Henry Aurass , Hakan Oenel , and Alexander Warmuth
CESRA Abstract **2016**
http://cesra2016.sciencesconf.org/conference/cesra2016/pages/CESRA2016_prog_abs_book_v1.pdf
A solar flare appears as an sudden enhancement of the emission of electromagnetic radiation of the Sun covering a broad range of the spectrum from the radio up to the gamma-ray range. That indicates the generation of energetic electrons during flares, which are considered as the manifestation of magnetic reconnection in the solar corona. Spacecraft observations in the Earth's magnetosphere, as for instance by NASA's MMS mission, have shown that electrons can efficiently accelerated at the slow-mode shocks occurring in the magnetic reconnection region. This mechanism is applied to solar flares. Then, under coronal circumstances, enough electrons with energies > 30 ˜keV are generated in the magnetic reconnection region as required for the hard X-ray radiation during solar flares as observed by NASA's RHESSI mission

Budget of energetic electrons during solar flares in the framework of magnetic reconnection

G. **Mann** and A. Warmuth
A&A 528, A104 (**2011**)
Context. Among other things, solar flares are accompanied by the production of energetic electrons as seen in the nonthermal radio and X-ray radiation of the Sun. Observations of the *RHESSI* satellite show that 1032−1036 nonthermal electrons are produced per second during flares. They are related to an energy flux in the range 1018−1022 W. These electrons play an important role, since they carry a substantial part of the energy released during a flare.
Aims. In which way so many electrons are accelerated up to high energies during a fraction of a second is still an open question. By means of radio and hard X-ray data, we investigate under which conditions this acceleration happens in the corona.
Methods.The flare is considered in the framework of magnetic reconnection. The conditions in the acceleration region in the corona are deduced by using the conservation of the total electron number and energy.
Results.In the inflow region of the magnetic reconnection site, there are typical electron number densities of about 2.07Ч109 cm−3 and magnetic fields of about 46 G. These are regions with high Alfvén speeds of about 2200 km s−1. Then, sufficient energetic electrons (as required by the *RHESSI* observations) are only generated if the plasma inflow towards the reconnection site has Alfvén-Mach numbers in the range 0.1−1, which can lead to a super-Alfvénic outflow with speeds up to 3100 km s−1.

Generation of highly energetic electrons at reconnection outflow shocks during solar flares:

G. **Mann**, A. Warmuth and H. Aurass
A&A 494 (**2009**) 669-675
http://www.aanda.org/10.1051/0004-6361:200810099
Context. During solar flares a large amount of energy is suddenly released and partly transferred into energetic electrons. They are of special interest since a substantial part of the energy released during a flare is deposited into the energetic electrons. RHESSI observations, e.g. of the **2003 October 28** solar event, show that 10^{36} electrons with energies >20 keV are typically produced per second during large flares. They are related to a power of about 10^{22} W. It is still an open question in which way so many electrons are accelerated up to high energies during a fraction of a second.
Aims. Within the framework of the magnetic reconnection scenario, jets appear in the outflow region and can establish standing fast-mode shocks if they penetrate the surrounding plasma with super-Alfvénic speed. It is our aim to show that this shock can be the source of the energetic electrons produced during flares.

Methods. The electrons are regarded as energized by shock drift acceleration. The process is necessarily treated in a fully relativistic manner. The resulting distribution function of accelerated electrons is a loss-cone one and it allows to calculate the differential electron flux, which can be compared with RHESSI.
Results. The theoretically obtained fluxes of energetic electrons agree with the observed ones as demonstrated for the 2003 October 28 solar event.

Electron acceleration by the reconnection outflow shock during solar flares

G. **Mann**, H. Aurass and A. Warmuth
A&A 454, 969-974 (**2006**)
DOI: 10.1051/0004-6361:20064990

Coordinated observations between China and Europe to follow active region 12709

S. J. González **Manrique**, C. Kuckein, P. Gömöry, S. Yuan, Z. Xu, J. Rybák, H. Balthasar, P. Schwartz
Proceedings of IAUS 354 **2019**
https://arxiv.org/pdf/1912.08611.pdf
We present the first images of a coordinated campaign to follow active region NOAA 12709 on **2018 May 13** as part of a joint effort between three observatories (China-Europe). The active region was close to disk center and enclosed a small pore, a tight polarity inversion line and a filament in the chromosphere. The active region was observed with the 1.5-meter GREGOR solar telescope on Tenerife (Spain) with spectropolarimetry using GRIS in the He I 10830 Å spectral range and with HiFI using two broad-band filter channels. In addition, the Lomnicky Stit Observatory (LSO, Slovakia) recorded the same active region with the new Solar Chromospheric Detector (SCD) in spectroscopic mode at Hα 6562 Å. The third ground-based telescope was located at the Fuxian Solar Observatory (China), where the active region was observed with the 1-meter New Vacuum Solar Telescope (NVST), using the Multi-Channel High Resolution Imaging System at Hα 6562 Å. Overlapping images of the active region from all three telescopes will be shown as well as preliminary Doppler line-of-sight (LOS) velocities. The potential of such observations are discussed.

Temporal evolution of arch filaments as seen in He I 10 830 Å⋆

S. J. González **Manrique**1,2,3, C. Kuckein2, M. Collados4, C. Denker2, S. K. Solanki5,6, P. Gömöry1, M. Verma2, H. Balthasar2, A. Lagg5 and A. Diercke
A&A 617, A55 (**2018**)
http://sci-hub.tw/https://www.aanda.org/articles/aa/abs/2018/09/aa32684-18/aa32684-18.html
https://arxiv.org/pdf/1807.00728.pdf
Aims. We study the evolution of an arch filament system (AFS) and of its individual arch filaments to learn about the processes occurring in them.
Methods. We observed the AFS at the GREGOR solar telescope on Tenerife at high cadence with the very fast spectroscopic mode of the GREGOR Infrared Spectrograph (GRIS) in the He I 10 830 Å spectral range. The He I triplet profiles were fitted with analytic functions to infer line-of-sight (LOS) velocities to follow plasma motions within the AFS.
Results. We tracked the temporal evolution of an individual arch filament over its entire lifetime, as seen in the He I 10 830 Å triplet. The arch filament expanded in height and extended in length from 13″ to 21″. The lifetime of this arch filament is about 30 min. About 11 min after the arch filament is seen in He I, the loop top starts to rise with an average Doppler velocity of 6 km s−1. Only two minutes later, plasma drains down with supersonic velocities towards the footpoints reaching a peak velocity of up to 40 km s−1 in the chromosphere. The temporal evolution of He I 10 830 Å profiles near the leading pore showed almost ubiquitous dual red components of the He I triplet, indicating strong downflows, along with material nearly at rest within the same resolution element during the whole observing time.
Conclusions. We followed the arch filament as it carried plasma during its rise from the photosphere to the corona. The material then drained toward the photosphere, reaching supersonic velocities, along the legs of the arch filament. Our observational results support theoretical AFS models and aids in improving future models**. 2015 April 17**

Hinode EUV Imaging Spectrometer Observations of Solar Active Region Dynamics

John T. **Mariska**,1 Harry P. Warren,1 Ignacio Ugarte-Urra,2 David H. Brooks,2 David R. Williams,3 And Hirohisa Hara4
E-print, Oct 2007; PASJ
14 Dec 2006. http://arxiv.org/PS_cache/arxiv/pdf/0708/0708.4309v1.pdf
we find that significant intensity and Doppler-shift fluctuations as a function of time are present at a number of locations. These fluctuations appear to be similar to those observed in high-temperature emission lines with other spaceborne spectroscopic instruments.

Hard X-Ray Constraints on Small-Scale Coronal Heating Events

Andrew J. **Marsh**, David M. Smith, Lindsay Glesener, James A. Klimchuk, Stephen J. Bradshaw, Juliana Vievering, Iain G. Hannah, Steven Christe, Shin-nosuke Ishikawa, Sam Krucker

ApJ **2018**

https://arxiv.org/pdf/1808.02630.pdf

Much evidence suggests that the solar corona is heated impulsively, meaning that nanoflares may be ubiquitous in quiet and active regions (ARs). Hard X-ray (HXR) observations with unprecedented sensitivity >3~keV are now enabled by focusing instruments. We analyzed data from the \textit{Focusing Optics X-ray Solar Imager (FOXSI)} rocket and the \textit{Nuclear Spectroscopic Telescope Array (NuSTAR)} spacecraft to constrain properties of AR nanoflares simulated by the EBTEL field-line-averaged hydrodynamics code. We generated model X-ray spectra by computing differential emission measures for homogeneous nanoflare sequences with heating amplitudes H0, durations τ, delay times between events tN, and filling factors f. The single quiescent AR observed by \textit{FOXSI-2} on 2014 December 11 is well fit by nanoflare sequences with heating amplitudes 0.02 erg cm−3 s−1 < H0 < 13 erg cm−3 s−1 and a wide range of delay times and durations. We exclude delays between events shorter than ∼900 s at the 90\% confidence level for this region. Three of five regions observed by {\nustar} on **2014 November 1** are well fit by homogeneous nanoflare models, while two regions with higher fluxes are not. Generally, the {\nustar} count spectra are well fit by nanoflare sequences with smaller heating amplitudes, shorter delays, and shorter durations than the allowed \textit{FOXSI-2} models. These apparent discrepancies are likely due to differences in spectral coverage between the two instruments and intrinsic differences among the regions. Steady heating (tN = τ) was ruled out with >99\% confidence for all regions observed by either instrument.

First NuSTAR Limits on Quiet Sun Hard X-Ray Transient Events

Andrew J. **Marsh**1, David M. Smith1, Lindsay Glesener2 …….

2017 ApJ 849 131

https://arxiv.org/pdf/1711.05385.pdf

We present the first results of a search for transient hard X-ray (HXR) emission in the quiet solar corona with the Nuclear Spectroscopic Telescope Array (NuSTAR) satellite. While NuSTAR was designed as an astrophysics mission, it can observe the Sun above 2 keV with unprecedented sensitivity due to its pioneering use of focusing optics. NuSTAR first observed quiet-Sun regions on **2014 November 1**, although out-of-view active regions contributed a notable amount of background in the form of single-bounce (unfocused) X-rays. We conducted a search for quiet-Sun transient brightenings on timescales of 100 s and set upper limits on emission in two energy bands. We set 2.5–4 keV limits on brightenings with timescales of 100 s, expressed as the temperature T and emission measure EM of a thermal plasma. We also set 10–20 keV limits on brightenings with timescales of 30, 60, and 100 s, expressed as model-independent photon fluxes. The limits in both bands are well below previous HXR microflare detections, though not low enough to detect events of equivalent T and EM as quiet-Sun brightenings seen in soft X-ray observations. We expect future observations during solar minimum to increase the NuSTAR sensitivity by over two orders of magnitude due to higher instrument livetime and reduced solar background.

THREE-DIMENSIONAL CORONAL SLOW MODES: TOWARD THREE-DIMENSIONAL SEISMOLOGY

M. S. **Marsh**, R. W. Walsh and S. Plunkett

http://www.iop.org/EJ/toc/-alert=43190/0004-637X/697/2

2009 ApJ 697 1674-1680

On 2008 January 10, the twin Solar Terrestrial Relations Observatory A and B spacecraft conducted a high time cadence study of the solar corona with the Extreme-Ultraviolet Imager instruments with the aim of investigating coronal dynamics. Observations of the three-dimensional propagation of waves within active region coronal loops and a measurement of the true coronal slow mode speed are obtained. Intensity oscillations with a period of ≈12 minutes are observed to propagate outward from the base of a loop system, consistent with the slow magnetoacoustic mode. A novel analysis technique is applied to measure the wave phase velocity in the observations of the A and B spacecraft. These stereoscopic observations are used to infer the three-dimensional velocity vector of the wave propagation, with an inclination of 37° ± 6° to the local normal and a magnitude of 132 ± 9 and 132 ± 11 km s–1, giving the first measurement of the true coronal longitudinal slow mode speed, and an inferred temperature of 0.84 ± 0.12 MK and 0.84 ± 0.15 MK.

Ultra-impulsive Solar Flare Seismology

Angel D. **Martínez**1, Valeria Quintero Ortega1, J. C. Buitrago-Casas2,3, Juan Carlos Martínez Oliveros3, Benjamín Calvo-Mozo1, and Charles Lindsey4

2020 ApJL 895 L19

https://doi.org/10.3847/2041-8213/ab9173
We examine a strong, coherent, highly impulsive acoustic transient radiated into the solar interior by the flare SOL**20110730**T02:04-M9.3. The acoustic spectrum of this transient extends out to 10 mHz. The fine diffraction limit of this high-frequency component of the flare acoustic transient allows us to discriminate different source components in operation during the flare. Acoustic-source power density maps of the 10 mHz component show sources that are compact to within the now 760 km diffraction limit of local helioseismic diagnostics for this frequency. One of the acoustic sources found is bifurcated across a sharp penumbral magnetic boundary, the component in the stronger magnetic field temporally lagging its partner. The facility to discriminate this level of acoustic-source detail could open the door to a long sought after understanding of the mechanics of transient emission from solar flares, still a mystery two decades after its discovery. It also suggests that helioseismic observations of higher cadence and spatial resolution could reveal coherent acoustic emission at even higher frequencies, with proportionately further potential benefits to solar seismology and its growing domain of applications.

The Solar Corona: What Are The Remaining Fundamental Physical Questions?

(Invited Review)

Petrus C. **Martens**

Proceedings of the International Symposium on Solar-Terrestrial Physics, November 2012, Pune, India
Bull. Astron. Soc. India, **2013-2014**, in press.
http://solar.physics.montana.edu/martens/papers/martens-draft3.pdf; **File**
The two key unresolved physical questions in our knowledge of the solar corona are: (1) **How is the corona heated** to a temperature of several MK, and, directly related to that, why is the coronal emission structured in nearly constant cross-section loops? And, (2) **what is the mechanism that determines the onset of solar flares and eruptions**, and, again directly related, **can flares be predicted**? I will introduce these questions, discuss some proposed solutions that are not complete, and my view on getting to the full solutions.

Transient Artifacts in a Flare Observed by the Helioseismic and Magnetic Imager on the Solar Dynamics Observatory

J. C. **Martínez** Oliveros, C. Lindsey, H. S. Hudson, J. C. Buitrago Casas
Solar Physics, March **2014**, Volume 289, Issue 3, pp 809-819
The Helioseismic and Magnetic Imager (HMI) onboard the Solar Dynamics Observatory (SDO) provides a new tool for the systematic observation of white-light flares, including Doppler and magnetic information as well as continuum. In our initial analysis of the highly impulsive γ -ray flare SOL**2010-06-12**T00:57 (Martínez Oliveros et al., Solar Phys. 269, 269, 2011), we reported the signature of a strong blueshift in the two footpoint sources. Concerned that this might be an artifact due to aliasing peculiar to the HMI instrument, we undertook a comparative analysis of Global Oscillation Network Group (GONG++) observations of the same flare, using the PArametric Smearing Correction ALgorithm (PASCAL) algorithm to correct for artifacts caused by variations in atmospheric smearing. This analysis confirms the artifactual nature of the apparent blueshift in the HMI observations, finding weak redshifts at the footpoints instead. We describe the use of PASCAL with GONG++ observations as a complement to the SDO observations and discuss constraints imposed by the use of HMI far from its design conditions. With proper precautions, these data provide rich information on flares and transients.

Chromospheric and Coronal Observations of Solar Flares with the Helioseismic and Magnetic Imager

Juan-Carlos **Martinez**-Oliveros, S?m Krucker, Hugh S. Hudson, Pascal Saint-Hilaire, Hazel Bain, Charles Lindsey, Rick Bogart, Sebastien Couvidat, Phil Scherrer, Jesper Schou
E-print, Dec **2013**, ApJL
We report observations of white-light ejecta in the low corona, for two X-class flares on the **2013 May 13**, using data from the Helioseismic and Magnetic Imager (HMI) of the Solar Dynamics Observatory. At least two distinct kinds of sources appeared (chromospheric and coronal), in the early and later phases of flare development, in addition to the white-light footpoint sources commonly observed in the lower atmosphere. The gradual emissions have a clear identification with the classical loop-prominence system, but are brighter than expected and possibly seen here in the continuum rather than line emission. We find the HMI flux exceeds the radio/X-ray interpolation of the bremsstrahlung produced in the flare soft X-ray sources by at least one order of magnitude. This implies the participation of cooler sources that can produce free-bound continua and possibly line emission detectable by HMI. One of the early sources dynamically resembles "coronal rain", appearing at a maximum apparent height and moving toward the photosphere at an apparent constant projected speed of 134 ? 8 kms−1. Not much literature exists on the detection of optical continuum sources above the limb of the Sun by non-coronagraphic instruments, and these observations have potential implications for our basic understanding of flare development, since visible observations can in principle provide high spatial and temporal resolution.

THE HEIGHT OF A WHITE-LIGHT FLARE AND ITS HARD X-RAY SOURCES
Juan-Carlos **Martínez-Oliveros**1, Hugh S. Hudson1,2, Gordon J. Hurford1,3, Säm Krucker1,3, R. P. Lin1,4,5, Charles Lindsey6, Sebastien Couvidat7, Jesper Schou7, and W. T. Thompson
2012 ApJ 753 L26 http://arxiv.org/pdf/1206.0497v2.pdf
We describe observations of a white-light (WL) flare (SOL **2011-02-24** T07:35:00, M3.5) close to the limb of the Sun, from which we obtain estimates of the heights of the optical continuum sources and those of the associated hard X-ray (HXR) sources. For this purpose, we use HXR images from the Reuven Ramaty High Energy Spectroscopic Imager and optical images at 6173 Å from the Solar Dynamics Observatory. We find that the centroids of the impulsive-phase emissions in WL and HXRs (30-80 keV) match closely in central distance (angular displacement from Sun center), within uncertainties of order 02. This directly implies a common source height for these radiations, strengthening the connection between visible flare continuum formation and the accelerated electrons. We also estimate the absolute heights of these emissions as vertical distances from Sun center. Such a direct estimation has not been done previously, to our knowledge. Using a simultaneous 195 Å image from the Solar-Terrestrial RElations Observatory spacecraft to identify the heliographic coordinates of the flare footpoints, we determine mean heights above the photosphere (as normally defined; $\tau = 1$ at 5000 Å) of 305 ± 170 km and 195 ± 70 km, respectively, for the centroids of the HXR and WL footpoint sources of the flare. These heights are unexpectedly low in the atmosphere, and are consistent with the expected locations of $\tau = 1$ for the 6173 Å and the ~40 keV photons observed, respectively.

Seismic Emissions from a Highly Impulsive M6.7 Solar Flare
J.C. **Martinez-Oliveros**, H. Moradi, A-C. Donea
E-print, Jan 2008.
http://www.clique.monash.edu.au/SoPh_Martinez2.pdf
On **10 March 2001** the active region NOAA 9368 produced an unusually impulsive solar are in close proximity to the solar limb. Holographic analysis of the are shows a compact acoustic source strongly correlated with the impulsive hard X-ray, visible continuum, and radio emission.

To Rain or Not to Rain: Correlating GOES Flare Class and Coronal Rain Statistics
Emily I. **Mason**, Kara L. Kniezewski
ApJ **939** 21 **2022**
https://arxiv.org/pdf/2209.11283.pdf
https://iopscience.iop.org/article/10.3847/1538-4357/ac94d7/pdf
Post-flare arcades are well-known components of solar flare evolution, which have been observed for several decades. Coronal rain, cascades of catastrophically-cooled plasma, outline the loops and provide eye-catching evidence of the recent flare. These events are acknowledged to be common, but the scientific literature does not include any statistical overview documenting just how common the phenomenon actually is. This study reviews Solar Dynamics Observatory Atmospheric Imaging Assembly (SDO AIA) observations of 241 flares collected from the Space Weather Prediction Center (SWPC) database between 2011 and 2018. The flares cover the entire strength range of the C, M, and X GOES classes, and are distributed evenly across the SDO-observed majority of Solar Cycle 24. We find that post-flare arcade rain occurs for nearly all X and most M-class flares, but that it tapers off rapidly within C-class flares. There appears to be a cut-off point around C5, below which the occurrence of post-flare arcade rain drops significantly. There is also a general positive correlation between GOES class and the average duration of post-flare rain events. Post-flare arcade rain events in C-class flares appear to track with the sunspot number, providing a potential new tool for estimating, if not predicting, solar cycle strength. Furthermore, condensations appear to be suppressed in the shortest-length arcade loops of any class observed, suggesting that active region heating is height-constrained. These results open up further avenues for future research, including new methods to estimate energy deposition and to gain greater insight into steady active region heating. **2015-06-22**

Energetic Neutral Hydrogen from Large Solar Flares
Glenn **MASON**
RHESSI Science Nuggets №435 **2022**
https://sprg.ssl.berkeley.edu/~tohban/wiki/index.php/Energetic_Neutral_Hydrogen_from_Large_Solar_Flares
5 Dec 2006

Observations of Solar Coronal Rain in Null Point Topologies
E. I. **Mason**1, Spiro K. Antiochos2, and Nicholeen M. Viall
2019 ApJL 874 L33

sci-hub.se/10.3847/2041-8213/ab0c5d
https://arxiv.org/ftp/arxiv/papers/1904/1904.08982.pdf
Coronal rain is the well-known phenomenon in which hot plasma high in the Sun's corona undergoes rapid cooling (from ~106 to <104 K), condenses, and falls to the surface. Coronal rain appears frequently in active region coronal loops and is very common in post-flare loops. This Letter presents discovery observations, which show that coronal rain is ubiquitous in the commonly occurring coronal magnetic topology of a large (~100 Mm scale) embedded bipole very near a coronal hole boundary. Our observed structures formed when the photospheric decay of active-region-leading-sunspots resulted in a large parasitic polarity embedded in a background unipolar region. We observe coronal rain to appear within the legs of closed loops well under the fan surface, as well as preferentially near separatrices of the resulting coronal topology: the spine lines, null point, and fan surface. We analyze three events using SDO Atmospheric Imaging Assembly observations in the 304, 171, and 211 Å channels, as well as SDO Helioseismic and Magnetic Imager magnetograms. The frequency of rain formation and the ease with which it is observed strongly suggests that this phenomenon is generally present in null point topologies of this size scale. We argue that these rain events could be explained by the classic process of thermal nonequilibrium or via interchange reconnection at the null; it is also possible that both mechanisms are present. Further studies with higher spatial resolution data and MHD simulations will be required to determine the exact mechanism(s). **2015-04-11, 2015-04-16, 2015-04-28-29, 2015-05-04, 2016-02-15, 2016-02-20, 2016-02-27, 2016-03-12, 2016-03-15, 2016-04-16**

TESTING AUTOMATED SOLAR FLARE FORECASTING WITH 13 YEARS OF MICHELSON DOPPLER IMAGER MAGNETOGRAMS

J. P. **Mason** and J. T. Hoeksema
Astrophysical Journal, 723:634–640, **2010**
Flare occurrence is statistically associated with changes in several characteristics of the line-of-sight magnetic field in solar active regions (ARs).We calculated magnetic measures throughout the disk passage of 1075 ARs spanning solar cycle 23 to find a statistical relationship between the solar magnetic field and flares. This expansive study of over 71,000 magnetograms and 6000 flares uses superposed epoch (SPE) analysis to investigate changes in several magnetic measures surrounding flares and ARs completely lacking associated flares. The results were used to seek any flare associated signatures with the capability to recover weak systematic signals with SPE analysis. SPE analysis is a method of combining large sets of data series in a manner that yields concise information. This is achieved by aligning the temporal location of a specified flare in each time series, then calculating the statistical moments of the “overlapping” data. The best-calculated parameter, the gradient-weighted inversion-line length (GWILL), combines the primary polarity inversion line (PIL) length and the gradient across it. Therefore, GWILL is sensitive to complex field structures via the length of the PIL and shearing via the gradient. GWILL shows an average 35% increase during the 40 hr prior to X-class flares, a 16% increase before M-class flares, and 17% increase prior to B–C-class flares. ARs not associated with flares tend to decrease in GWILL during their disk passage. Gilbert and Heidke skill scores are also calculated and show that even GWILL is not a reliable parameter for predicting solar flares in real time.

STIX imaging I -- Concept

Paolo **Massa**, Gordon. J. Hurford, Anna Volpara, Matej Kuhar, et al.
Solar Phys. **298**, Article number: 114 **2023**
https://arxiv.org/pdf/2303.02485.pdf
https://doi.org/10.1007/s11207-023-02205-7
Aims. To provide a schematic mathematical description of the imaging concept of the Spectrometer/Telescope for Imaging X-rays (STIX) on board Solar Orbiter. The derived model is the fundamental starting point for both the interpretation of STIX data and the description of the data calibration process. Methods. We describe the STIX indirect imaging technique which is based on spatial modulation of the X-ray photon flux by means of tungsten grids. We show that each of 30 STIX imaging sub-collimators measures a complex Fourier component of the flaring X-ray source corresponding to a specific angular frequency. We also provide details about the count distribution model, which describes the relationship between the photon flux and the measured pixel counts. Results. We define the image reconstruction problem for STIX from both visibilities and photon counts. We provide an overview of the algorithms implemented for the solution of the imaging problem, and a comparison of the results obtained with these different methods in the case of the SOL**2022-03-31**T18 flaring event.

Efficient identification of pre-flare features in SDO/AIA images through use of spatial Fourier transforms

Paolo **Massa**, A Emslie, and A Emslie
Front. Astron. Space Sci. 9: 1040099. **2022**
https://doi.org/10.3389/fspas.2022.1040099
https://www.frontiersin.org/articles/10.3389/fspas.2022.1040099/pdf

In this “Methods” paper, we investigate how to compress SDO/AIA data by transforming the AIA source maps into the Fourier domain at a limited set of spatial frequency points. Specifically, we show that compression factors of one order of magnitude or more can be achieved without significant loss of information. The exploration of data compression techniques is motivated by our plan to train Neural Networks on AIA data to identify features that lead to a solar flare. Because the data is spatially resolved and polychromatic (as opposed to spatially-integrated, such as GOES, or monochromatic, such as magnetograms), the network can be trained to recognize features representing changes in plasma properties (e.g., temperature, density), in addition to temporal changes revealed by Sun-integrated data or physical restructuring revealed by monochromatic spatially-resolved data. However, given the immense size of a suitable training set of SDO/AIA data (more than 1011 pixels, requiring more than one TB of memory), some form of data compression scheme is highly desirable and, in this paper, we propose a Fourier based one. Numerical experiments show that, not only Fourier maps retain more information on the original AIA images compared to straightforward binning of spatial pixels, but also that certain types of changes in source structure (e.g., thinning or thickening of an elongated filamentary structure) may be equally, if not more, recognizable in the spatial frequency domain. We conclude by describing a program of work designed to exploit the use of spatial Fourier transform maps to identify features in four-dimensional data hypercubes containing spatial, spectral, and temporal information of the state of the solar plasma prior to possible flaring activity.

First Hard X-Ray Imaging Results by Solar Orbiter STIX

Paolo **Massa**, Andrea F. Battaglia, Anna Volpara, Hannah Collier, Gordon J. Hurford, +++
Solar Physics volume 297, Article number: 93 (**2022**)
https://link.springer.com/content/pdf/10.1007/s11207-022-02029-x.pdf
https://arxiv.org/pdf/2202.09334.pdf
The Spectrometer/Telescope for Imaging X-rays (STIX) is one of six remote sensing instruments on-board Solar Orbiter. The telescope applies an indirect imaging technique that uses the measurement of 30 visibilities, i.e., angular Fourier components of the solar flare X-ray source. Hence, the imaging problem for STIX consists of the Fourier inversion of the data measured by the instrument. In this work, we show that the visibility amplitude and phase calibration of 24 out of 30 STIX sub-collimators has reached a satisfactory level for scientific data exploitation and that a set of imaging methods is able to provide the first hard X-ray images of solar flares from Solar Orbiter. Four visibility-based image reconstruction methods and one count-based are applied to calibrated STIX observations of six events with GOES class between C4 and M4 that occurred in May 2021. The resulting reconstructions are compared to those provided by an optimization algorithm used for fitting the amplitudes of STIX visibilities. We show that the five imaging methods produce results morphologically consistent with the ones provided by the Atmospheric Imaging Assembly on board the Solar Dynamic Observatory (SDO/AIA) in UV wavelengths. The $\chi 2 \chi 2$ values and the parameters of the reconstructed sources are comparable between methods, thus confirming their robustness. **7,8,9 May 2021, 22 May 2021**

Imaging from STIX visibility amplitudes

Paolo **Massa**, Emma Perracchione, Sara Garbarino, Andrea F Battaglia, Federico Benvenuto, Michele Piana, Gordon Hurford, Sam Krucker
A&A **656**, A25 **2021**
https://arxiv.org/pdf/2108.04901.pdf
https://www.aanda.org/articles/aa/pdf/2021/12/aa40946-21.pdf
Aims: To provide the first demonstration of STIX Fourier-transform X-ray imaging using semi-calibrated (amplitude-only) visibility data acquired during the Solar Orbiter's cruise phase. Methods: We use a parametric imaging approach by which STIX visibility amplitudes are fitted by means of two non-linear optimization methods: a fast meta-heuristic technique inspired by social behavior, and a Bayesian Monte Carlo sampling method, which, although slower, provides better quantification of uncertainties. Results: When applied to a set of solar flare visibility amplitudes recorded by STIX on **November 18, 2020** the two parametric methods provide very coherent results. The analysis also demonstrates the ability of STIX to reconstruct high time resolution information and, from a spectral viewpoint, shows the reliability of a double-source scenario consistent with a thermal versus nonthermal interpretation. Conclusions: In this preliminary analysis of STIX imaging based only on visibility amplitudes, we formulate the imaging problem as a non-linear parametric issue we addressed by means of two high-performance optimization techniques that both showed the ability to sample the parametric space in an effective fashion, thus avoiding local minima.

A count-based imaging model for the Spectrometer/Telescope for Imaging X-rays (STIX) in Solar Orbiter

Paolo **Massa**, Michele Piana, Anna Maria Massone, Federico Benvenuto
A&A **2019**
https://arxiv.org/pdf/1902.08190.pdf
The Spectrometer/Telescope for Imaging X-rays (STIX) will look at solar flares across the hard X-ray window provided by the Solar Orbiter cluster. Similarly to the Reuven Ramaty High Energy Solar Spectroscopic Imager (RHESSI), STIX

is a visibility-based imaging instrument, which will ask for Fourier-based image reconstruction methods. However, in this paper we show that, as for RHESSI, also for STIX count-based imaging is possible. Specifically, here we introduce and illustrate a mathematical model that mimics the STIX data formation process as a projection from the incoming photon flux into a vector made of 120 count components. Then we test the reliability of Expectation Maximization for image reconstruction in the case of several simulated configurations typical of flare morphology.

Flux rope, hyperbolic flux tube, and late EUV phases in a non-eruptive circular-ribbon flare

S. **Masson**, E. Pariat, G. Valori, N. Deng, C. Liu, H. Wang, H. Reid
A&A **604**, A76 **2017**
https://arxiv.org/pdf/1704.01450.pdf

Context. The dynamics of ultraviolet (UV) emissions during solar flare provides constraints on the physical mechanisms involved in the trigger and the evolution of flares. In particular it provides some information on the location of the reconnection sites and the associated magnetic fluxes. In this respect, confined flares are far less understood than eruptive flares generating coronal mass ejections.
Aims. We present a detailed study of a confined circular flare dynamics associated with 3 UV late phases in order to understand more precisely which topological elements are present and how they constrain the dynamics of the flare.
Methods. We perform a non-linear force free field extrapolation of the confined flare observed with the HMI and AIA instruments onboard SDO. From the 3D magnetic field we compute the squashing factor and we analyse its distribution. Conjointly, we analyse the AIA EUV light curves and images in order to identify the post-flare loops, their temporal and thermal evolution. By combining both analysis we are able to propose a detailed scenario that explains the dynamics of the flare.
Results. Our topological analysis shows that in addition to a null-point topology with the fan separatrix, the spine lines and its surrounding Quasi-Separatix Layers halo (typical for a circular flare), a flux rope and its hyperbolic flux tube (HFT) are enclosed below the null. By comparing the magnetic field topology and the EUV post-flare loops we obtain an almost perfect match 1) between the footpoints of the separatrices and the EUV 1600 A ribbons and 2) between the HFT's field line footpoints and bright spots observed inside the circular ribbons. We showed, for the first time in a confined flare, that magnetic reconnection occured initially at the HFT, below the flux rope. Reconnection at the null point between the flux rope and the overlying field is only initiated in a second phase. In addition, we showed that the EUV late phase observed after the main flare episode are caused by the cooling loops of different length which have all reconnected at the null point during the impulsive phase.
Conclusions. Our analysis shows in one example that flux ropes are present in null-point topology not only for eruptive and jets events, but also for confined flares. This allows us to conjecture on the analogies between conditions that govern the generation of either jets, confined or eruptive flares. **Oct 22, 2011**

Interchange Slip-Running Reconnection and Sweeping SEP Beams

S. **Masson**, G. Aulanier, E. Pariat and K.-L. Klein
Solar Physics, Volume 276, Numbers 1-2, 199-217, **2012, File**

We present a new model to explain how particles (solar energetic particles; SEPs), accelerated at a reconnection site that is not magnetically connected to the Earth, could eventually propagate along the well-connected open flux tube. Our model is based on the results of a low-β resistive magnetohydrodynamics simulation of a three-dimensional line-tied and initially current-free bipole, which is embedded in a non-uniform open potential field. The topology of this configuration is that of an asymmetric coronal null point, with a closed fan surface and an open outer spine. When driven by slow photospheric shearing motions, field lines, initially fully anchored below the fan dome, reconnect at the null point, and jump to the open magnetic domain. This is the standard interchange mode as sketched and calculated in 2D. The key result in 3D is that reconnected open field lines located in the vicinity of the outer spine keep reconnecting continuously, across an open quasi-separatrix layer, as previously identified for non-open-null-point reconnection. The apparent slipping motion of these field lines leads to formation of an extended narrow magnetic flux tube at high altitude. Because of the slip-running reconnection, we conjecture that if energetic particles would be traveling through, or be accelerated inside, the diffusion region, they would be successively injected along continuously reconnecting field lines that are connected farther and farther from the spine. At the scale of the full Sun, owing to the super-radial expansion of field lines below 3 R ⊙, such energetic particles could easily be injected in field lines slipping over significant distances, and could eventually reach the distant flux tube that is well-connected to the Earth.

The nature of flare ribbons in coronal null-point topology

Masson, S., Pariat, E., Aulanier, G. and Schrijver, C. J.
E-print, June **2009**; ApJ, 700:559–578, **2009** July; **File**

Flare ribbons are commonly attributed to the low-altitude impact, along the footprints of separatrices or quasi-separatrix layers (QSLs), of particle beams accelerated through magnetic reconnection. If reconnection occurs at a three-dimensional coronal magnetic null point, the footprint of the dome-shaped fan surface would map a closed circular ribbon. This paper addresses the following issues: Does the entire circular ribbon brighten simultaneously, as expected

because all fan field lines pass through the null point? And since the spine separatrices are singular field lines, do spine-related ribbons look like compact kernels? What can we learn from these observations about current sheet formation and magnetic reconnection in a null-point topology? The present study addresses these questions by analyzing TRACE and SoHO/MDI observations of a confined flare presenting a circular ribbon. Using a potential field extrapolation, we linked the circular shape of the ribbon with the photospheric mapping of the fan field lines originating from a coronal null-point. Observations show that the flare ribbon outlining the fan-lines brightens sequentially along the counterclockwise direction and that the spine-related ribbons are elongated. Using the potential field extrapolation as initial condition, we conduct a low-beta resistive MHD simulation of this observed event. We drive the coronal evolution by line-tied diverging boundary motions, so as to emulate the observed photospheric flow pattern associated with some magnetic flux emergence. The numerical analyzis allows to explain several observed features of the confined flare. The vorticity induced in the fan by the prescribed motions causes the spines to tear apart along the fan. This leads to formation of a thin current sheet and induces null-point reconnection. We also find that the null point and its associated topological structure is embedded within QSLs, already present in the asymmetric potential field configuration. We find that the QSL footprints correspond to the observed elongated spine-ribbons. Finally, we observe that before and after reconnecting at the null point, all field lines undergo slipping and slip-running reconnection within the QSLs. Field lines, and therefore particle impacts, slip or slip-run according to their distance from the spine, in directions and over distances that are compatible with the observed dynamics of the ribbons.

Anna Maria **Massone**1, A. Gordon Emslie2, G. J. Hurford3, Marco Prato1,4, Eduard P. Kontar5, and Michele Piana1,6
Astrophysical Journal, 703:2004–2016, **2009**
RHESSI produces solar flare images with the finest angular and spectral resolutions ever achieved at hard X-ray energies. Because this instrument uses indirect, collimator-based imaging techniques, the “native” output of which is in the form of “visibilities” (two-dimensional spatial Fourier components of the image), the development and application of robust, accurate, visibility-based image reconstruction techniques is required. Recognizing that the density of spatial-frequency (*u*, *v*) coverage by *RHESSI* is much sparser than that normally encountered in radio astronomy, we therefore introduce amethod for image reconstruction from a relatively sparse distribution of sampled visibilities. The method involves spline interpolation at spatial frequencies less than the largest sampled frequency and the imposition of a positivity constraint on the image to reduce the ringing effects resulting from an unconstrained Fourier transform inversion procedure. Using simulated images consisting both of assumedmathematical forms and of the type of structure typically associated with solar flares, we validate the fidelity, accuracy, and robustness with which the new procedure recovers input images. The method faithfully recovers both single and multiple sources, both compact and extended, over a dynamic range of ~10 : 1. The performance of the method, which we term as uv_smooth, is compared with other *RHESSI* image reconstruction algorithms currently in use and its advantages summarized. We also illustrate the application of the method using *RHESSI* observations of four solar flares.

Extremely Microwave-Rich Solar Flare Observed with Nobeyama Radioheliograph

S. **Masuda**, M. Shimojo, T. Kawate, S. Ishikawa, and M. Ohno
Publ. Astron. Soc. Japan 65, 1 [6 pages] (**2013**) http://pasj.asj.or.jp/v65/sp1/65S001/65S001.pdf
A compact flare was observed with Nobeyama Radioheliograph (NoRH) slightly behind the west limb on **2011 March 10**. The microwave peak flux values at 17 and 34 GHz were about 210 and 133 sfu, respectively. From the correlation between the 17 GHz peak flux and the GOES 1–8 ˚A soft X-ray peak flux, M1.5-class is expected for this microwave flux. However, only the B1-level enhancement was detected in the GOES 1–8 ˚A soft X-ray light curve on the C1-level background during the flare period. In addition to microwaves, Suzaku detected hard X-ray emissions, even in the energy range above 100 keV. It is clear that high-energy electrons were effectively produced in this flare, while the thermal emission was very weak. Why did this flare have this unique feature? The following two cases are considered. One is the case that a magnetic trap for electrons works effectively, and that each electron continues to emit microwaves in its relatively long lifetime. The other is that the magnetic field around the looptop region is intense, and relatively a large number of lower-energy electrons emit microwaves. Considering the observational facts, such as the short duration and the small flare loop, the latter case is more plausible.

A loop-top hard X-ray source in a compact solar flare as evidence for magnetic reconnection

Masuda, S.; Kosugi, T.; Hara, H.; Tsuneta, S.; Ogawara, Y.
Nature, Volume 371, Issue 6497, pp. 495-497 (**1994**).
https://sci-hub.tw/10.1038/371495a0 **File**
SOLAR flares are thought to be the result of magnetic reconnection — the merging of antiparallel magnetic fields and the consequent release of magnetic energy. Flares are classified into two types1: compact and two-ribbon. The two-

ribbon flares, which appear as slowly-developing, long-lived large loops, are understood theoretically2-6 as arising from an eruption of a solar prominence that pulls magnetic field lines upward into the corona. As the field lines form an inverted Y-shaped structure and relax, the reconnection of the field lines takes place. This view has been supported by recent observations7-10. A different mechanism seemed to be required, however, to produce the short-lived, impulsive compact flares. Here we report observations made with the Yohkoh11 Hard X-ray Telescope12 and Soft X-ray Telescope13, which show a compact flare with a geometry similar to that of a two-ribbon flare. We identify the reconnection region as the site of particle acceleration, suggesting that the basic physics of the reconnection process (which remains uncertain) may be common to both types of flare. **13 Jan 1992, 17:25 UT, M2.0**

The periodic variations of a white-light flare observed with ULTRACAM

M. **Mathioudakis**, D.S. Bloomfield, D.B. Jess, V.S. Dhillon, T.R. Marsh
A&A **2006**
http://arxiv.org/pdf/astro-ph/0605196v1.pdf
High time resolution observations of a white--light flare on the active star EQ PegB show evidence of intensity variations with a period of approximately 10 s. The period drifts to longer values during the decay phase of the flare. If the oscillation is interpreted as an impulsively--excited, standing--acoustic wave in a flare loop, the period implies a loop length of 1.7 Mm and 3.4 Mm for the case of the fundamental mode and the second harmonic, respectively. However, the small loop lengths imply a very high modulation depth making the acoustic interpretation unlikely. A more realistic interpretation may be that of a fast--MHD wave, with the modulation of the emission being due to the magnetic field. Alternatively, the variations could be due to a series of reconnection events. The periodic signature may then arise as a result of the lateral separation of individual flare loops or current sheets with oscillatory dynamics (i.e. periodic reconnection). **November 4th 2003**

MULTI-WAVELENGTH SPECTROSCOPIC OBSERVATION OF EXTREME-ULTRAVIOLET JET IN AR 10960

Y. **Matsui**1, T. Yokoyama1, N. Kitagawa1, and S. Imada
2012 ApJ 759 15
We have studied the relationship between the velocity and temperature of a solar EUV jet. The highly accelerated jet occurred in the active region NOAA 10960 on **2007 June 5**. Multi-wavelength spectral observations with EIS/Hinode allow us to investigate Doppler velocities at a wide temperature range. We analyzed the three-dimensional angle of the jet from stereoscopic analysis with STEREO. Using this angle and Doppler velocity, we derived the true velocity of the jet. As a result, we found that the cool jet observed with He II 256 Å log10 Te [K] = 4.9 is accelerated to around 220 km s–1, which is over the upper limit of the chromospheric evaporation. The velocities observed with the other lines are below the upper limit of the chromospheric evaporation, while most of the velocities of the hot lines are higher than those of cool lines. We interpret that the chromospheric evaporation and magnetic acceleration occur simultaneously. A morphological interpretation of this event based on the reconnection model is given by utilizing the multi-instrumental observations.

Thermal responses in a coronal loop maintained by wave heating mechanisms

Takuma **Matsumoto**
MNRAS **2017**
https://arxiv.org/abs/1712.07377
A full 3-dimensional compressible magnetohydrodynamic (MHD) simulation is conducted to investigate the thermal responses of a coronal loop to the dynamic dissipation processes of MHD waves. When the foot points of the loop are randomly and continuously forced, the MHD waves become excited and propagate upward. Then, a high-temperature corona is produced naturally as the wave energy dissipates. The excited wave packets become non-linear just above the magnetic canopy, and the wave energy cascades into smaller spatial scales. Moreover, collisions between counter-propagating Alfv\'{e}n wave packets increase the heating rate, resulting in impulsive temperature increases. Our model demonstrates that the heating events in the wave-heated loops can be nanoflare-like in the sense that they are spatially localized and temporally intermittent.

The high-energy Sun - probing the origins of particle acceleration on our nearest star **Review**

S. A **Matthews**1 · H. A. S. Reid1 · D. Baker1 · D. S. Bloomfield2 · P. K. Browning3 · A. Calcines4 · G. Del Zanna5 · R. Erdelyi6,7,8 ·L. Fletcher9,10 · I. G. Hannah9 · N. Jeffrey2 · L. Klein11 · S. Krucker12 · E. Kontar9 · D. M. Long1 · A. MacKinnon9 · G. Mann13 ·M. Mathioudakis14 · R. Milligan14 · V. M. Nakariakov15 ·M. Pesce-Rollins16 · A. Y. Shih17 · D. Smith18 · A. Veronig19 · N. Vilmer11
Experimental Astronomy (**2021**)
https://doi.org/10.1007/s10686-021-09798-6
https://link.springer.com/content/pdf/10.1007/s10686-021-09798-6.pdf

As a frequent and energetic particle accelerator, our Sun provides us with an excellent astrophysical laboratory for understanding the fundamental process of particle acceleration. The exploitation of radiative diagnostics from electrons has shown that acceleration operates on sub-second time scales in a complex magnetic environment, where direct electric fields, wave turbulence, and shock waves all must contribute, although precise details are severely lacking. Ions were assumed to be accelerated in a similar manner to electrons, but γ-ray imaging confirmed that emission sources are spatially separated from X-ray sources, suggesting distinctly different acceleration mechanisms. Current X-ray and γ-ray spectroscopy provides only a basic understanding of accelerated particle spectra and the total energy budgets are therefore poorly constrained. Additionally, the recent detection of relativistic ion signatures lasting many hours, without an electron counterpart, is an enigma. We propose a single platform to directly measure the physical conditions present in the energy release sites and the environment in which the particles propagate and deposit their energy. To address this fundamental issue, we set out a suite of dedicated instruments that will probe both electrons and ions simultaneously to observe; high (seconds) temporal resolution photon spectra (4 keV – 150 MeV) with simultaneous imaging (1 keV – 30 MeV), polarization measurements (5–1000 keV) and high spatial and temporal resolution imaging spectroscopy in the UV/EUV/SXR (soft X-ray) regimes. These instruments will observe the broad range of radiative signatures produced in the solar atmosphere by accelerated particles.

Non-thermal distributions and energy transport in the solar flares

Sarah **Matthews**, Guilio del Zanna, Ariadna Calcines, Helen Mason, Mihalis Mathioudakis, Len Culhane, Louise Harra, Lidia van Driel-Gesztelyi, Lucie Green, David Long, Deb Baker, Gherardo Valori
Next Generation Solar Physics (NGSPM) white paper. Final report at: this http URL **2017**
https://arxiv.org/ftp/arxiv/papers/1712/1712.00773.pdf

Determining the energy transport mechanisms in flares remains a central goal in solar flares physics that is still not adequately answered by the 'standard flare model'. In particular, the relative roles of particles and/or waves as transport mechanisms, the contributions of low energy protons and ions to the overall flare budget, and the limits of low energy non-thermal electron distribution are questions that still cannot be adequately reconciled with current instrumentation. In this 'White Paper' submitted in response to the call for inputs to the Next Generation Solar Physics Mission review process initiated by JAXA, NASA and ESA in 2016, we outline the open questions in this area and possible instrumentation that could provide the required observations to help answer these and other flare-related questions.

SPECTROSCOPIC SIGNATURES RELATED TO A SUNQUAKE
S. A. **Matthews**1, L. K. Harra1, S. Zharkov2, and L. M. Green
2015 ApJ 812 35

The presence of flare-related acoustic emission (sunquakes (SQs)) in some flares, and only in specific locations within the flaring environment, represents a severe challenge to our current understanding of flare energy transport processes. In an attempt to contribute to understanding the origins of SQs we present a comparison of new spectral observations from Hinode's EUV imaging Spectrometer (EIS) and the Interface Region Imaging Spectrograph (IRIS) of the chromosphere, transition region, and corona above an SQ, and compare them to the spectra observed in a part of the flaring region with no acoustic signature. Evidence for the SQ is determined using both time–distance and acoustic holography methods, and we find that unlike many previous SQ detections, the signal is rather dispersed, but that the time–distance and 6 and 7 mHz sources converge at the same spatial location. We also see some evidence for different evolution at different frequencies, with an earlier peak at 7 mHz than at 6 mHz. Using EIS and IRIS spectroscopic measurements we find that in this location, at the time of the 7 mHz peak the spectral emission is significantly more intense, shows larger velocity shifts and substantially broader profiles than in the location with no SQ, and there is a good correlation between blueshifted, hot coronal, hard X-ray (HXR), and redshifted chromospheric emission, consistent with the idea of a strong downward motion driven by rapid heating by nonthermal electrons and the formation of chromospheric shocks. Exploiting the diagnostic potential of the Mg ii triplet lines, we also find evidence for a single large temperature increase deep in the atmosphere, which is consistent with this scenario. The time of the 6 mHz and time–distance peak signal coincides with a secondary peak in the energy release process, but in this case we find no evidence of HXR emission in the quake location, instead finding very broad spectral lines, strongly shifted to the red, indicating the possible presence of a significant flux of downward propagating Alfvén waves. **29-March- 2014**

Solar Particle Acceleration Radiation and Kinetics(SPARK)
A mission to understand the nature of particle acceleration **Review**

Sarah A. **Matthews**·David R. Williams·Karl-Ludwig Klein·Eduard P. Kontar·David M. Smith·Andreas Lagg·Sam Krucker·Gordon J. Hurford·Nicole Vilmer·Alexander L. MacKinnon· Valentina V. Zharkova·Lyndsay Fletcher·Iain G. Hannah·Philippa K. Browning·Davina E. Innes· Gerard Trottet·Clare Foullon·Valery M. Nakariakov·Lucie M. Green·Herve Lamoureux· Colin Forsyth ·David M. Walton·Mihalis Mathioudakis·Achim Gandorfer·Valentin Martinez-Pillet· Olivier Limousin·Erwin Verwichte·Silvia Dalla·Gottfried Mann·Henri Aurass·Thomas Neukirch
Exp Astron (**2012**) 33:237–269
sci-hub.se/10.1007/s10686-011-9260-3

https://www.academia.edu/24170833/Solar_Particle_Acceleration_Radiation_and_Kinetics_SPARK_?email_work_card=view-paper

In many cases particles are accelerated to relativistic energies and represent a substantial fraction of the total energyof the system, thus requiring extremely efficient acceleration processes. Theproduction of accelerated particles also appears coupled to magnetic field evo-lution in astrophysical plasmas through the turbulent magnetic fields producedby diffusive shock acceleration. Particle acceleration is thus a key componentin helping to understand the origin and evolution of magnetic structuresin, e.g. galaxies. The proximity of the Sun and the range of high-resolutiondiagnostics available within the solar atmosphere offers unique opportunities to study the processes involved in particle acceleration through the use of a combination of remote sensing observations of the radiative signatures of accelerated particles, and of their plasma and magnetic environment. TheSPARK concept targets the broad range of energy, spatial and temporal scalesover which particle acceleration occurs in the solar atmosphere, in order to de-termine how and where energetic particles are accelerated. SPARK combineshighly complementary imaging and spectroscopic observations of radiationfrom energetic electrons, protons and ions set in their plasma and magneticcontext. The payload comprises focusing-optics X-ray imaging covering therange from 1 to 60 keV; indirect HXR imaging and spectroscopy from 5 to 200keV, γ-ray spectroscopic imaging with high-resolution LaBr3 scintillators, andphotometry and source localisation at far-infrared wavelengths. The plasmaenvironmentof the regions of acceleration and interaction will be probed usingsoft X-ray imaging of the corona and vector magnetography of the photo-sphere and chromosphere. SPARK is designed for solar research. However, in addition it will be able to provide exciting new insights into the origin of particle acceleration in other regimes, including terrestrial gamma-ray flashes(TGF), the origin of γ-ray bursts, and the possible existence of axions. **January 6, 2004**

ANATOMY OF A SOLAR FLARE: MEASUREMENTS OF THE 2006 DECEMBER 14 X-CLASS FLARE WITH GONG, HINODE, AND RHESSI

S. A. **Matthews**1, S. Zharkov1 and V. V. Zharkova

2011 ApJ 739 71

Some of the most challenging observations to explain in the context of existing flare models are those related to the lower atmosphere and below the solar surface. Such observations, including changes in the photospheric magnetic field and seismic emission, indicate the poorly understood connections between energy release in the corona and its impact in the photosphere and the solar interior. Using data from Hinode, TRACE, RHESSI, and GONG we study the temporal and spatial evolution of the **2006 December 14** X-class flare in the chromosphere, photosphere, and the solar interior. We investigate the connections between the emission at various atmospheric depths, including acoustic signatures obtained by time-distance and holography methods from the GONG data. We report the horizontal displacements observed in the photosphere linked to the timing and locations of the acoustic signatures we believe to be associated with this flare, their vertical and horizontal displacement velocities, and their potential implications for current models of flare dynamics.

Generation and annihilation of three dimensional magnetic nulls in extrapolated solar coronal magnetic field: Data-based Implicit Large Eddy Simulation

Yogesh Kumar **Maurya** (1 and 2), Ramit Bhattacharyya (1), David I. Pontin (3)

2024

https://arxiv.org/pdf/2404.12034.pdf

Three-dimensional magnetic nulls are the points where magnetic field vanishes and are preferential sites for magnetic reconnection: a process which converts magnetic energy into heat and accelerates charged particles along with a rearrangement of magnetic field lines. In the solar corona, the reconnections manifest as coronal transients including solar flares, coronal mass ejections and coronal jets. The nulls are generally found to be collocated with complex active regions on the solar photosphere. Extrapolation of magnetic field from corresponding photospheric magnetogram indicate an abundance of these nulls in solar atmosphere. Nevertheless, their generation is still not well understood. Recently, Maurya et al. (2023) have demonstrated magnetic reconnection to be a cause for generation and annihilation of magnetic nulls through magnetohydrodynamics simulation, where the initial magnetic field is idealized to have a single radial null. This article further extends the study in a more realistic scenario where the initial magnetic field is constructed by extrapolating photospheric magnetogram data and hence, incorporates field line complexities inherent to a complex active region. For the purpose, the active region NOAA 11977 hosting a C6.6 class flare is selected. The simulation is initiated using non-force-free extrapolated magnetic field from the photospheric vector magnetogram at around 02:48:00 UT on **17 February 2014**, 16 minutes before the flare peak. The generation, annihilation and dynamics of nulls are explored by a complimentary usage of trilinear null detection technique and tracing of magnetic field line dynamics. It is found that the nulls can spontaneously generate/annihilate in pairs while preserving the topological degree and can have observational implications like footpoint brightenings. Magnetic reconnection is found to be the cause of such generation and annihilation.

Activity-related variations of high-degree p-mode amplitude, width, and energy in solar active regions

R. A. **Maurya**1,2, A. Ambastha2 and J. Chae

A&A 561, A123 (**2014**)

Context. Solar energetic transients such as flares and coronal mass ejections occur mostly within active regions (ARs) and release large amounts of energy, which is expected to excite acoustic waves by transferring the mechanical impulse of the thermal expansion of the flare on the photosphere. On the other hand, strong magnetic fields of AR sunspots absorb the power of the photospheric oscillation modes.

Aims. We study the properties of high-degree p-mode oscillations in flaring and dormant ARs and compare them with those in corresponding quiet regions (QRs) to find the association of the mode parameters with magnetic- and flare-related activities.

Methods. We computed the mode parameters using the ring-diagram technique. The magnetic-activity indices (MAIs) of ARs and QRs were determined from the line-of-sight magnetograms. The flare indices (FIs) of ARs were obtained from the GOES X-ray fluxes. Mode parameters were corrected for foreshortening, duty cycle, and MAI using multiple non-linear regression.

Results. Our analysis of several flaring and dormant ARs observed during the Carrington rotations 1980–2109 showed a strong association of the mode amplitude, width, and energy with magnetic and flare activities, although their changes are combined effects of foreshortening, duty cycle, magnetic-activity, flare-activity, and measurement uncertainties. We find that the largest reduction in mode amplitude and background power of an AR are caused by the angular distance of the AR from the solar disc centre. After correcting the mode parameters for foreshortening and duty cycle, we find that the mode amplitudes of flaring and dormant ARs are lower than in corresponding QRs reducing with increasing MAI, suggesting a stronger mode power suppression in ARs with larger magnetic fields. The mode widths in ARs are larger than in corresponding QRs and increase with MAI, indicating shorter lifetimes of modes in ARs than in QRs. The variations in mode amplitude and width with MAI are not same in different frequency bands. The largest amplification (reduction) in mode amplitude (mode width) of dormant ARs is found in the five-minute frequency band. The average mode energy of both the flaring and dormant ARs is smaller than in their corresponding QRs, reducing with increasing MAI. But the average mode energy reduction rate in flaring ARs is smaller than in dormant ARs. Moreover, the increase in mode width rate in dormant (flaring) ARs is followed by a decrease (increase) in the amplitude variation rate. Furthermore, including the mode corrections for MAI shows that mode amplitude and mode energy of flaring ARs escalate with FI, while the mode width shows an opposite trend, suggesting excitations of modes and growth in their lifetimes by flares. The increase (decrease) in mode amplitude (width) is larger in the five-minute and higher-frequency bands. The enhancement in width variation rate is followed by a rapid decline in the amplitude variation rate.

VELOCITY AND MAGNETIC TRANSIENTS DRIVEN BY THE X2.2 WHITE-LIGHT FLARE OF 2011 FEBRUARY 15 IN NOAA 11158

R. A. **Maurya**1,2, P. Vemareddy1 and A. Ambastha

2012 ApJ 747 134

http://arxiv.org/pdf/1106.4166v3.pdf

The first X-class flare of the current solar cycle 24 occurred in Active Region NOAA 11158 during its central meridian passage on **2011 February 15**. This two-ribbon white-light flare was observed by the Helioseismic and Magnetic Imager (HMI) on board the Solar Dynamics Observatory. During the peak phase of the flare, we detected magnetic and Doppler velocity (DV) transients appearing near the umbral boundary of the main sunspot. These transients persisted for a few minutes and showed spatial and temporal correspondence with the flare kernels. The observed magnetic polarity at the transients' locations underwent a sign reversal, together with a large enhancement in DVs. We explain this observational phenomenon using the HMI spectral data obtained before, during, and after the flare. These changes were reflected in the maps of the active region in all the Stokes parameters. Association of the transient features with various signatures of the flare and the cause and effects of their appearance are also presented on the basis of present theoretical models.

A Technique for Automated Determination of Flare Ribbon Separation and Energy Release

R. A. **Maurya** and A. Ambastha

Solar Phys. 262(2), 337-353, **2010**

We present a technique for automatic determination of flare ribbon separation and the energy released during the course of two-ribbon flares. We have used chromospheric Hα filtergrams and photospheric line-of-sight magnetograms to analyse flare ribbon separation and magnetic field structures, respectively. Flare ribbons were first enhanced and then extracted by the technique of “region growing”, *i.e.*, a morphological operator to help resolve the flare ribbons. Separation of flare ribbons was then estimated from the magnetic-polarity reversal line using an automatic technique implemented into an Interactive Data Language (IDL^{TM}) platform. Finally, the rate of flare-energy release was calculated using photospheric magnetic field data and the corresponding separation of the chromospheric Hα flare

ribbons. This method could be applied to measure the motion of any feature of interest (*e.g.*, intensity, magnetic, Doppler) from a given point of reference.

Transient Magnetic and Doppler Features Related to the White-Light Flares in NOAA 10486

R. A. **Maurya**, A. Ambastha
Solar Phys (**2009)** 258: 31–52
Rapidly moving transient features have been detected in magnetic and Doppler images of super-active region NOAA 10486 during the X17/4B flare of **28 October 2003** and the X10/2B flare of **29 October 2003**. Both these flares were extremely energetic white-light events. The transient features appeared during impulsive phases of the flares and moved with speeds ranging from 30 to 50 kms−1. These features were located near the previously reported compact acoustic (Donea and Lindsey, *Astrophys. J.* **630**, 1168, 2005) and seismic sources (Zharkova and Zharkov, *Astrophys. J.* **664**, 573, 2007). We examine the origin of these features and their relationship with various aspects of the flares, *viz.*, hard X-ray emission sources and flare kernels observed at different layers: *i*) photosphere (white-light continuum), *ii*) chromosphere (Hα 6563 Å), *iii*) temperature minimum region (UV 1600 Å), and *iv*) transition region (UV 284 Å).

Sympathetic solar flare: characteristics and homogeneities.

Mawad, R., Moussas, X.
Astrophys Space Sci 367, 107 (**2022**).
https://doi.org/10.1007/s10509-022-04145-3
https://link.springer.com/content/pdf/10.1007/s10509-022-04145-3.pdf
We studied 2204 sympathetic flares detected by the GOES during 1975–2017. Sympathetic flares have nearby, or homogeneous, GOES classes. The secondary solar flare is just a mirror image of the primary solar flare of the sympathetic flare. It has two types: 1) Twins: This type represents most of them (~78.6%). 2) Non-twins: It is an associated heterogeneous pair of solar flares. A negative relationship between the interval between the start times of primary and secondary flares was found with the duration of the primary flare with the solar cycle progress. Also, the stronger the solar cycle, the lower the maximum value of the timing ratio at the quiet Sun's epoch, while the timing ratio's value reaches a higher value during the weaker cycles. A positive relationship between the angular distance between pairs of sympathetic flares and SSN has been found. During the epoch of the active sun, the distance is as far as possible, while that distance becomes shorter during the epoch of the quiet sun. Sympathetic flares are equatorial in alignment. The higher inclination (slope of about −20° each cycle) is associated with the X-Class of the primary flare. It is more than this non-association. We found that the time series of inclinations is given a "Wings diagram" diagram.

Frozen-in Fractals All Around: Inferring the Large-Scale Effects of Small-Scale Magnetic Structure

R. T. James **McAteer**
Solar Phys. **2015**
The large-scale structure of the magnetic field in the solar corona provides the energy to power large-scale solar eruptive events. Our physical understanding of this structure, and hence our ability to predict these events, is limited by the type of data currently available. It is shown that the multifractal spectrum is a powerful tool to study this structure, by providing a physical connection between the details of photospheric magnetic gradients and current density at all size scales. This uses concepts associated with geometric measure theory and the theory of weakly differentiable functions to compare Ampère's law to the wavelet-transform modulus maximum method. The Hölder exponent provides a direct measure of the rate of change of current density across spatial size scales. As this measure is independent of many features of the data (pixel resolution, data size, data type, presence of quiet-Sun data), it provides a unique approach to studying magnetic-field complexity and hence a potentially powerful tool for a statistical prediction of solar-flare activity. Three specific predictions are provided to test this theory: the multifractal spectra will not be dependent on the data type or quality; quiet-Sun gradients will not persist with time; structures with high current densities at large size scales will be the source of energy storage for solar eruptive events.

25 Years of Self-organized Criticality: Numerical Detection Methods **Review**

R. T. James **McAteer**, Markus J. Aschwanden, Michaila Dimitropoulou, Manolis K. Georgoulis, Gunnar Pruessner, Laura Morales, Jack Ireland, Valentyna Abramenko
Space Science Reviews **2015**
The detection and characterization of self-organized criticality (SOC), in both real and simulated data, has undergone many significant revisions over the past 25 years. The explosive advances in the many numerical methods available for detecting, discriminating, and ultimately testing, SOC have played a critical role in developing our understanding of how systems experience and exhibit SOC. In this article, methods of detecting SOC are reviewed; from correlations to

complexity to critical quantities. A description of the basic autocorrelation method leads into a detailed analysis of application-oriented methods developed in the last 25 years. In the second half of this manuscript space-based, time-based and spatial-temporal methods are reviewed and the prevalence of power laws in nature is described, with an emphasis on event detection and characterization. The search for numerical methods to clearly and unambiguously detect SOC in data often leads us outside the comfort zone of our own disciplines—the answers to these questions are often obtained by studying the advances made in other fields of study. In addition, numerical detection methods often provide the optimum link between simulations and experiments in scientific research. We seek to explore this boundary where the rubber meets the road, to review this expanding field of research of numerical detection of SOC systems over the past 25 years, and to iterate forwards so as to provide some foresight and guidance into developing breakthroughs in this subject over the next quarter of a century.

The Bursty Nature of Solar Flare X-Ray Emission. II. The Neupert Effect

R. T. James **McAteer**1 and D. Shaun Bloomfield

2013 ApJ 776 66

We carry out a novel statistical test of the Neupert effect based on multifractal spectra. The multifractal spectrum is the number distribution of the strengths (i.e., the Hölder exponents) of bursts in a signal. This is tested on simulations and carried out on RHESSI X-ray data from a well observed GOES **X4.8** magnitude flare. The multifractal spectra is ideally suited to quantifying the relative smooth and bursty signals typically found in (thermal) soft X-ray and (non-thermal) hard X-ray data of solar flares. We show that light curves from all energies between 3 keV and 25 keV are statistically similar, suggesting that all these signals are dominated by the same (presumably thermal) emission. Emission lying between 25 keV and 100 keV probably contains some contribution from both thermal and non-thermal sources. The multifractal spectrum of a signal and that of its (cumulative) temporal integration are statistically similar (i.e., low residuals upon subtraction), but shifted by one in the peak Hölder exponent. We find the pairs of 3-6 keV and 100-300 keV emissions, the 6-12 keV and 100-300 keV emissions and the 12-25 keV and 100-300 keV emissions are all consistent with the Neupert effect. The best agreement with the Neupert effect is between the 12-25 keV and 100-300 keV pair, although possibly with some secondary source of thermal emission present.

Turbulence, complexity, and solar flares

R.T. James **McAteer**, 1, a, , , Peter T. Gallaghera and Paul A. Conlona

Adv. Space Res. 45(9), 1067-1074, **2010**

The issue of predicting solar flares is one of the most fundamental in physics, addressing issues of plasma physics, high-energy physics, and modelling of complex systems. It also poses societal consequences, with our ever-increasing need for accurate space weather forecasts. Solar flares arise naturally as a competition between an input (flux emergence and rearrangement) in the photosphere and an output (electrical current build up and resistive dissipation) in the corona. Although initially localised, this redistribution affects neighbouring regions and an avalanche occurs resulting in large scale eruptions of plasma, particles, and magnetic field. As flares are powered from the stressed field rooted in the photosphere, a study of the photospheric magnetic complexity can be used to both predict activity and understand the physics of the magnetic field. The magnetic energy spectrum and multifractal spectrum are highlighted as two possible approaches to this.

Measuring and modeling the rate of separator reconnection between an emerging and existing active region

Marika I. **McCarthy**, Dana W. Longcope, Anna Malanushenko, David E. McKenzie

ApJ **887** 140 **2019**

https://arxiv.org/pdf/1911.06340.pdf

https://doi.org/10.3847/1538-4357/ab55f0

Magnetic reconnection occurs when new flux emerges into the corona and becomes incorporated into the existing coronal field. A new active region (AR) emerging in the vicinity of an existing AR provides a convenient laboratory in which reconnection of this kind can be quantified. We use high time-cadence 171 Å data from SDO/AIA focused on new/old active region pair 11147/11149, to quantify reconnection. We identify new loops as brightenings within a strip of pixels between the regions. This strategy is premised on the assumption that the energy brightening a loop originates in magnetic reconnection. We catalog 301 loops observed in the 48-hour time period beginning with the emergence of AR 11149. The rate at which these loops appear between the two ARs is used to calculate the reconnection rate between them. We then fit these loops with magnetic field, solving for each loop's field strength, geometry, and twist (via its proxy, coronal α). We find the rate of newly-brightened flux overestimates the flux which could be undergoing reconnection. This excess can be explained by our finding that the interconnecting region is not at its lowest energy (constant-α) state; the extrapolations exhibit loop-to-loop variation in α. This flux overestimate may result from the slow emergence of AR 11149, allowing time for Taylor relaxation internal to the domain of the reconnected flux to bring the α distribution towards a single value which provides another mechanism for brightening loops after they are first created. **2011/01/21**

Reconnection and fast particle production in tokamak and solar plasmas

K.G.**McClements**

Advances in Space Research Volume 63, Issue 4, 15 February **2019**, Pages 1443-1452

Detailed in situ studies of magnetic reconnection and particle acceleration, which play a crucial role in the release and redistribution of energy in solar flares, can be performed in tokamak plasmas under conditions resembling those of the flaring solar corona. Recent measurements and modelling of fast particle production during reconnection events in the Mega-Amp Spherical Tokamak (MAST) are described. Specifically, observations in this device of electron acceleration during edge localised modes, and of both ion and electron acceleration during merging-compression plasma start-up, are presented, and possible implications of these studies for particle acceleration in flares are discussed. The results from MAST lend weight to the conjecture that large numbers of ions are accelerated to sub-MeV energies in flares.

Flare Forecasting Using the Evolution of McIntosh Sunspot Classifications

Aoife E. **McCloskey**, Peter T. Gallagher, D. Shaun Bloomfield

Journal of Space Weather and Space Climate 8, A34 **2018**

https://arxiv.org/pdf/1805.00919.pdf

https://www.swsc-journal.org/articles/swsc/pdf/2018/01/swsc170097.pdf

Most solar flares originate in sunspot groups, where magnetic field changes lead to energy build-up and release. However, few flare-forecasting methods use information of sunspot-group evolution, instead focusing on static point-in-time observations. Here, a new forecast method is presented based upon the 24-hr evolution in McIntosh classification of sunspot groups. Evolution-dependent $\geqslant$C1.0 and $\geqslant$M1.0 flaring rates are found from NOAA-numbered sunspot groups over December 1988 to June 1996 (Solar Cycle 22; SC22) before converting to probabilities assuming Poisson statistics. These flaring probabilities are used to generate operational forecasts for sunspot groups over July 1996 to December 2008 (SC23), with performance studied by verification metrics. Major findings are: i) considering Brier skill score (BSS) for $\geqslant$C1.0 flares, the evolution-dependent McIntosh-Poisson method (BSSevolution=0.09) performs better than the static McIntosh-Poisson method (BSSstatic=−0.09); ii) low BSS values arise partly from both methods over-forecasting SC23 flares from the SC22 rates, symptomatic of $\geqslant$C1.0 rates in SC23 being on average ≈80% of those in SC22 (with $\geqslant$M1.0 being ≈50%); iii) applying a bias-correction factor to reduce the SC22 rates used in forecasting SC23 flares yields modest improvement in skill relative to climatology for both methods (BSScorrstatic=0.09 and BSScorrevolution=0.20) and improved forecast reliability diagrams.

Flaring Rates and the Evolution of Sunspot Group McIntosh Classifications

Aoife E. **McCloskey** , Peter T. Gallagher, D. Shaun Bloomfield

Solar Phys. **2016**

http://arxiv.org/pdf/1607.00903v1.pdf

http://link.springer.com/article/10.1007/s11207-016-0933-y

Sunspot groups are the main source of solar flares, with the energy to power them being supplied by magnetic-field evolution (e.g. flux emergence or twisting/shearing). To date, few studies have investigated the statistical relation between sunspot-group evolution and flaring, with none considering evolution in the McIntosh classification scheme. Here we present a statistical analysis of sunspot groups from Solar Cycle 22, focusing on 24-hour changes in the three McIntosh classification components. Evolution-dependent ≥C1.0, ≥M1.0, and ≥X1.0 flaring rates are calculated, leading to the following results: i) flaring rates become increasingly higher for greater degrees of upward evolution through the McIntosh classes, with the opposite found for downward evolution; ii) the highest flaring rates are found for upward evolution from larger, more complex, classes (e.g. Zurich D- and E-classes evolving upward to F-class produce ≥C1.0 rates of 2.66±0.28 and 2.31±0.09 flares per 24 hours, respectively); iii) increasingly complex classes give higher rates for all flare magnitudes, even when sunspot groups do not evolve over 24 hours. These results support the hypothesis that injection of magnetic energy by flux emergence (i.e. increasing in Zurich or compactness classes) leads to a higher frequency and magnitude of flaring.

On Magnetic Activity Band Overlap, Interaction, and the Formation of Complex Solar Active Regions

Scott W. **McIntosh**, Robert J. Leamon

ApJL 796 L19 **2014**

http://arxiv.org/pdf/1410.6411v1.pdf

Recent work has revealed an phenomenological picture of the how the ~11-year sunspot cycle of Sun arises. The production and destruction of sunspots is a consequence of the latitudinal-temporal overlap and interaction of the toroidal magnetic flux systems that belong to the 22-year magnetic activity cycle and are rooted deep in the Sun's convective interior. We present a conceptually simple extension of this work, presenting a hypothesis on how complex active regions can form as a direct consequence of the intra- and extra-hemispheric interaction taking place in the solar interior. Furthermore, during specific portions of the sunspot cycle we anticipate that those complex active regions may

be particular susceptible to profoundly catastrophic breakdown---producing flares and coronal mass ejections of most severe magnitude.

Flare Nimbus

Susan **McKenna-Lawlor**: the flare "nimbus," its history and a new interpretation.
RHESSI Science Nugget, No. 178, June **2012**
The flare "nimbus," its history and a new interpretation.
http://sprg.ssl.berkeley.edu/~tohban/wiki/index.php/Flare_Nimbus

Discovery in 1960 of the Flare Nimbus Phenomenon and Changes with Time in Its Interpretation

Susan M. P. **McKenna-Lawlor**
Solar Physics, Volume 272, Number 2, 257-299, **2011**
During the International Geophysical Year (IGY, 1957/1958) Dunsink Observatory near Dublin in Ireland was a World Data Centre for Solar Activity. In this circumstance, Hα Lyot Heliograph records secured on a daily basis between 07:00 – 14:00 UT at the Cape of Good Hope (then an integral link in a network of similar instruments contributing during the IGY to global monitoring of solar chromospheric activity) were routinely sent to Dunsink for analysis and dissemination. The investigations carried out at Dunsink on these data resulted, inter alia, in the discovery of the Flare Nimbus phenomenon. The nimbus comprises a dark expanding halo seen in the plage regions around major flares at, or within a few minutes of, the time of flare maximum intensity in Hα light. It reaches its greatest extent about 30 minutes after flare maximum. Its maximum dimensions (estimated visually) lie in the range 2 – 4×105 km and its duration ranges from ~ 1 – 2 hours. Within the nimbus the striation pattern is either completely destroyed or loses its pre-flare configuration. An account of this phenomenon and its interpretation appeared primarily, although not exclusively, in the locally produced Dunsink Observatory Publications which are not now easily accessible to the world community of solar researchers. Also, at around the time when the nimbus was first identified and recorded in Lyot Heliograph data at several observatories, techniques in solar physics shifted towards high resolution narrow field observations. Under these conditions no further examples of the nimbus were recorded and the subject has remained dormant over several decades. The present paper again places the scientific results obtained with regard to the nimbus in the public domain, together with an account of the evolution within the scientific community of an explanation of this phenomenon. It is suggested here for the first time, in the light of present day data concerning coronal mass ejections (CMEs) and coronal **dimming**, that the nimbus provides a signature of CME-related reorganization of the magnetic field in the chromosphere (such that the transverse magnetic field component decreases and transforms into the line of sight component as the vector field stretches out). Coronal dimming provides a complementary signature of CME-related mass depletion in the corona.

DISTRIBUTION FUNCTIONS OF SIZES AND FLUXES DETERMINED FROM SUPRA-ARCADE DOWNFLOWS

D. E. **McKenzie**1 and S. L. Savage2
Astrophysical Journal Letters, 735:L6 (5pp), **2011, File**
The frequency distributions of sizes and fluxes of supra-arcade downflows (SADs) provide information about the process of their creation. For example, a fractal creation process may be expected to yield a power-law distribution of sizes and/or fluxes. We examine 120 cross-sectional areas and magnetic flux estimates found by Savage & McKenzie for SADs, and find that (1) the areas are consistent with a log-normal distribution and (2) the fluxes are consistent with both a log-normal and an exponential distribution. Neither set of measurements is compatible with a power-law distribution nor a normal distribution. As a demonstration of the applicability of these findings to improved understanding of reconnection, we consider a simple SAD growth scenario with minimal assumptions, capable of producing a log-normal distribution.

Flare Physics in the Hinode Era (Keynote)

David E. **McKenzie**
E-print, May **2009**, **File**; ASP Conference Series, Hinode-2 proceedings
Abstract. Hinode's manifest of instrumentation was conceived to investigate the magnetic connections through the photosphere, lower atmosphere, and corona. The complementarity of the instruments is indeed useful, as demonstrated in numerous flares and eruptions in just the first two years of operation. I will review some of the findings from Hinode's observations of flares to date. It is true, of course, that Hinode's capabilities have evolved since launch. These changes cause the planning of observations to be more complex, and the analysis to be less straightforward; but they do not diminish Hinode's ability to produce important observations of solar flares. On the contrary, Hinode is poised to

make truly surprising discoveries. I will explain why this is so, and why we should look forward to the challenge of the coming activity cycle.

QUANTITATIVE EXAMINATION OF SUPRA-ARCADE DOWNFLOWS IN ERUPTIVE SOLAR FLARES

D. E. **McKenzie** and Sabrina L. Savage
Astrophysical Journal, 697:1569–1577, **2009; File**
Downward motions above post-coronal mass ejection flare arcades are an unanticipated discovery of the *Yohkoh* mission, and have subsequently been detected with *TRACE*, *SOHO*/LASCO, *SOHO*/SUMER, and *Hinode*/XRT. These supra-arcade downflows are interpreted as outflows from magnetic reconnection, consistent with a three-dimensional generalization of the standard reconnection model of solar flares. We present results from our observational analyses of downflows, which include a semiautomated scheme for detection and measurement of speeds, sizes, and—for the first time—estimates of the magnetic flux associated with each shrinking flux tube. Though model dependent, these findings provide an empirical estimate of the magnetic flux participating in individual episodes of patchy magnetic reconnection, and the energy associated with the shrinkage of magnetic flux tubes.

Hinode XRT observations of a long-lasting coronal sigmoid

David E. **McKenzie** and Richard C. Canfield
E-print, May 2009; A&A Lett. (**2008**), v.481, L65-L68
http://solar.physics.montana.edu/mckenzie/Pubs/McKenzie-Canfield_XRTSigmoid_final.pdf
Aims: Coronal sigmoids are important sources of eruptions into interplanetary space, and a handful of models have been proposed to explain their characteristic S shape. However, the coronal X-ray images available to date have generally not had sufficient resolution to distinguish between these models. The goal of the present investigation is to determine whether the new observations from Hinode can help us to make such a distinction.
Methods: We present the first observations of a persistent coronal sigmoid obtained with the Hinode X-Ray Telescope (XRT). The excellent angular resolution of XRT (1 arcsec per pixel) and the sigmoid's location near disk center combined to provide an unprecedented view of the formation and eruption of this phenomenon. We compared the observed morphology with expectations inferred from two popular models of sigmoid formation, the bald-patch separatrix surface model and the kinking flux rope model.
Results: The images during the pre-eruptive phase show that the overall S shape of the sigmoid comprises two separate J-shaped bundles of many loops. The straight sections of the two J patterns lie anti-parallel to one another in the middle of the S, on opposite sides of the magnetic polarity inversion line. The images during the eruptive phase reveal that, before any soft X-ray flaring begins, a diffuse linear structure almost as long as the sigmoid lifts off from the middle of the S. It shows slight clockwise rotation. The X-ray flare begins with the appearance of a sheared arcade of short loops, in the area centered between the two J-shaped patterns of the sigmoid. Conclusions: Taken together, the observational findings provide strong support for the bald-patch separatrix surface model for this sigmoid.

The Link Between Non-Thermal Velocity and Free Magnetic Energy in Solar Flares

James **McKevitt**, Robert Jarolim, Sarah Matthews, Deborah Baker, Manuela Temmer, Astrid Veronig, Hamish Reid, Lucie Green
ApJL **961** L29 **2024**
https://arxiv.org/pdf/2401.07982.pdf
https://iopscience.iop.org/article/10.3847/2041-8213/ad1bee/pdf
The cause of excess spectral line broadening (non-thermal velocity) is not definitively known, but given its rise before and during flaring, the causal processes hold clues to understanding the triggers for the onset of reconnection and the release of free magnetic energy from the coronal magnetic field. A comparison of data during a 9-hour period from the extreme ultraviolet (EUV) Imaging Spectrometer (EIS) on the Hinode spacecraft - at a 3-minute cadence - and non-linear force-free field (NLFFF) extrapolations performed on Helioseismic and Magnetic Imager (HMI) magnetograms - at a 12-minute cadence - shows an inverse relationship between non-thermal velocity and free magnetic energy on short timescales during two X-class solar flares on **6 September 2017**. Analysis of these results supports suggestions that unresolved Doppler flows do not solely cause non-thermal broadening and instead other mechanisms like Alfvén wave propagation and isotropic turbulence have a greater influence.

Formation of the Lyman Continuum during Solar Flares

Shaun A. **McLaughlin**1, Ryan O. Milligan1,2, Graham S. Kerr2,3, Aaron J. Monson1, Paulo J. A. Simões4,5, and Mihalis Mathioudakis1
2023 ApJ 944 186
https://iopscience.iop.org/article/10.3847/1538-4357/acaf66/pdf

The Lyman continuum (LyC; <911.12 Å) forms at the top of the chromosphere in the quiet Sun, making LyC a powerful tool for probing the chromospheric plasma during solar flares. To understand the effects of nonthermal energy deposition in the chromosphere during flares, we analyzed LyC profiles from a grid of field-aligned radiative-hydrodynamic models generated using the RADYN code as part of the F-CHROMA project. The spectral response of LyC, the temporal evolution of the departure coefficient of hydrogen, b1, and the color temperature, Tc, in response to a range of nonthermal electron distribution functions, were investigated. The LyC intensity was seen to increase by 4–5.5 orders of magnitude during solar flares, responding most strongly to the nonthermal electron flux of the beam. Generally, b1 decreased from 102–103 to closer to unity during solar flares, indicating a stronger coupling to local conditions, while Tc increased from 8–9 to 10–16 kK. Tc was found to be approximately equal to the electron temperature of the plasma when b1 was at a minimum. Both optically thick and optically thin components of LyC were found to be in agreement with the interpretation of recent observations. The optically thick layer forms deeper in the chromosphere during a flare compared to quiescent periods, whereas the optically thin layers form at higher altitudes due to chromospheric evaporation, in low-temperature, high-density regions propagating upward. We put these results in the context of current and future missions.

Modelling Quasi-Periodic Pulsations in Solar and Stellar Flares **Review**

J. A. **McLaughlin**, V. M. Nakariakov, M. Dominique, P. Jelínek, S. Takasao
Space Science Reviews February **2018**, 214:45
https://link.springer.com/content/pdf/10.1007%2Fs11214-018-0478-5.pdf
https://arxiv.org/pdf/1802.04180.pdf
Solar flare emission is detected in all EM bands and variations in flux density of solar energetic particles. Often the EM radiation generated in solar and stellar flares shows a pronounced oscillatory pattern, with characteristic periods ranging from a fraction of a second to several minutes. These oscillations are referred to as quasi-periodic pulsations (QPPs), to emphasise that they often contain apparent amplitude and period modulation. We review the current understanding of quasi-periodic pulsations in solar and stellar flares. In particular, we focus on the possible physical mechanisms, with an emphasis on the underlying physics that generates the resultant range of periodicities. These physical mechanisms include MHD oscillations, self-oscillatory mechanisms, oscillatory reconnection/reconnection reversal, wave-driven reconnection, two loop coalescence, MHD flow over-stability, the equivalent LCR-contour mechanism, and thermal-dynamical cycles. We also provide a histogram of all QPP events published in the literature at this time. The occurrence of QPPs puts additional constraints on the interpretation and understanding of the fundamental processes operating in flares, e.g. magnetic energy liberation and particle acceleration. Therefore, a full understanding of QPPs is essential in order to work towards an integrated model of solar and stellar flares. **November 23, 1998, November 18, 2003,, 25 February 2014**

On the periodicity of oscillatory reconnection

J. A. **McLaughlin**1, J. O. Thurgood1 and D. MacTaggart
E-print, Dec **2012**; A&A 548, A98 (**2012**)
Context. Oscillatory reconnection is a time-dependent magnetic reconnection mechanism that naturally produces periodic outputs from aperiodic drivers.
Aims. This paper aims to quantify and measure the periodic nature of oscillatory reconnection for the first time.
Methods. We solve the compressible, resistive, nonlinear magnetohydrodynamics (MHD) equations using 2.5D numerical simulations.
Results. We identify two distinct periodic regimes: the impulsive and stationary phases. In the impulsive phase, we find the greater the amplitude of the initial velocity driver, the longer the resultant current sheet and the earlier its formation. In the stationary phase, we find that the oscillations are exponentially decaying and for driving amplitudes 6.3−126.2 km s-1, we measure stationary-phase periods in the range 56.3−78.9 s, i.e. these are high frequency (0.01−0.02 Hz) oscillations. In both phases, we find that the greater the amplitude of the initial velocity driver, the shorter the resultant period, but note that different physical processes and periods are associated with both phases.
Conclusions. We conclude that the oscillatory reconnection mechanism behaves akin to a damped harmonic oscillator.

The Multi-Instrument (EVE-RHESSI) DEM for Solar Flares, and Implications for Non-Thermal Emission

James M. **McTiernan**, Amir Caspi, Harry P. Warren
ApJ **881** 161 **2018**
https://arxiv.org/pdf/1805.12285.pdf
https://www.boulder.swri.edu/~amir/eprints/McTiernan_Caspi_Warren_2019_ApJ.pdf
Solar flare X-ray spectra are typically dominated by thermal bremsstrahlung emission in the soft X-ray (≲10 keV) energy range; for hard X-ray energies (≳30 keV), emission is typically non-thermal from beams of electrons. The low-energy extent of non-thermal emission has only been loosely quantified. It has been difficult to obtain a lower limit for a possible non-thermal cutoff energy due to the significantly dominant thermal emission.

Here we use solar flare data from the EUV Variability Experiment (EVE) on-board the Solar Dynamics Observatory (SDO) and X-ray data from the Reuven Ramaty High Energy Spectroscopic Imager (RHESSI) to calculate the Differential Emission Measure (DEM). This improvement over the isothermal approximation and any single-instrument DEM helps to resolve ambiguities in the range where thermal and non-thermal emission overlap, and to provide constraints on the low-energy cutoff.
In the model, thermal emission is from a DEM that is parametrized as multiple gaussians in Log(T). Non-thermal emission results from a photon spectrum obtained using a thick-target emission model. Spectra for both instruments are fit simultaneously in a self-consistent manner.
Our results have been obtained using a sample of 52 large (GOES X- and M-class) solar flares observed between February 2011 and February 2013. It turns out that it is often possible to determine low-energy cutoffs early (in the first two minutes) during large flares. Cutoff energies are typically low, less than 10 keV, with most values of the lower limits in the 5--7 keV range. **13 Feb 2011, 15 Feb 2011, 2011 February 16, 2011 July 30**
Tables
CESRA # 356 2019 http://sprg.ssl.berkeley.edu/~tohban/wiki/index.php/EVE-RHESSI_DEM_Models_and_the_Low-energy_Cutoff_for_Nonthermal_Electrons

The RHESSI Flare Catalog

Jim **McTiernan** and Hugh Hudson.
RHESSI Science Nuggets, No. 183, **2012**
http://sprg.ssl.berkeley.edu/~tohban/wiki/index.php/The_RHESSI_Flare_Catalog
The catalog is a powerful and convenient tool for overviews of the RHESSI flares.

RHESSI/GOES OBSERVATIONS OF THE NONFLARING SUN FROM 2002 TO 2006

J. M. **McTiernan**
The Astrophysical Journal, 697:94–99, **2009** May 20 doi:10.1088/0004-637X/697/1/94
In this work, we obtain the temperature (*T*) and emission measure (EM) for solar X-ray emission, using *RHESSI* and *GOES* data, at times for which there are no solar flares. Approximately 8700 time intervals during the *RHESSI* mission, from launch until 2006 August, are analyzed. We find that high-temperature emission, in the temperature range of 5–10 MK, is typically present during active times. When comparing temperature measurements, we find that *RHESSI* temperature measurements are consistently higher than *GOES* measurements, with smaller EM for *RHESSI*, but with values for the two instruments that are not necessarily well correlated.

Tuning up Fuzzy Inference Systems by using optimization algorithms for the classification of solar flares

Liz Angélica Ramos **Medina** (1), Alex Francisco Bustos Pinzón (1), Miguel A. Melgarejo (1), Santiago Vargas Domínguez (2) ((1) Universidad Distrital Francisco José de Caldas, Bogotá, Colombia (2) OAN - Universidad Nacional de Colombia, Bogotá, Colombia)
TECCIENCIA **2017**
https://arxiv.org/ftp/arxiv/papers/1706/1706.08163.pdf
In this work we describe the implementation and analysis of different optimization algorithms used for finding the best set of parameters for a Fuzzy Inference System intended to classify solar flares. The parameters will be identified among a universe of possible solutions for the algorithms, and the system will be tested in the particular case of dealing with the aim of classifying the solar flares.

Prevalence of non-stationarity in quasi-periodic pulsations (QPPs) associated with M- and X-class solar flares

Tishtrya **Mehta**, Anne-Marie Broomhall, Laura Hayes
MNRAS Volume 523, Issue 3, August 2023, Pages 3689–3698, **2023**
https://arxiv.org/pdf/2305.19737.pdf
https://scholar.google.com/scholar_url?url=https://academic.oup.com/mnras/advance-article-pdf
Quasi-periodic pulsations (QPPs) are frequently observed in solar and stellar flare emission, with recent studies suggesting that an increasing instantaneous period is a common characteristic of QPPs. Determining the prevalence of non-stationarity in QPPs contributes to a better understanding of which mechanisms are responsible in QPP generation. We obtain the rate of period evolution from QPPs in 98 M- and X-class flares from Solar Cycle 24 with average periods between 8-130s and investigate the prevalence of QPP non-stationarity. We also investigate whether the presence of a Coronal Mass Ejection (CME) impacts the period evolution of QPPs. We analyse soft X-ray lightcurves obtained from GOES' X-Ray Sensor (XRS) and assess the dominant periods in the impulsive and decay phases of the flares using the Fast Fourier Transform. We relate the rate of period evolution to flare duration, peak flare energy, and average QPP period. We find evidence of non-stationarity in 81% of the flares assessed, with most QPPs exhibiting a period evolution of less than 10s between the impulsive and decay phases, of which 66% exhibited an apparent period growth

and 14% showed an apparent period shrinkage. We find a positive correlation between the absolute magnitude of period evolution and the duration of the flare and no correlation between the period evolution of the QPPs and flare energy or CME presence. Furthermore, we conclude that non-stationarity is common in solar QPPs and must be accounted for in flare analysis. **21 Nov 2013**

Expansion and Compression of a Flash Loop System during the Flare on January 15, 2022 According to Ultraviolet and Microwave Data

V. F. **Melnikov, *** and N. S. Meshalkina
Geomagnetism and Aeronomy, **2023**, Vol. 63, No. 7, pp. 192–199.
In this paper, we study the dynamics of a single loop structure in a C1.3 flare on **January 15, 2022**.
A new type of behavior of flare loop was discovered. Unlike the previously known cases of visible contraction and expansion of flare loops in the phases of rise and decay of the flare radiation flux, respectively, the flare on **January 15, 2022** exhibited a directly opposite process: the loop increases in its height during the flare intensity rise phase and contracts during the decay phase. Characteristic changes in the height, duration, and rate of the expansion and contraction of the loop structure were established. An increase of the electric current in the loop during the rise phase and its decrease during the contraction phase are proposed as an explanation of this behavior.

Rethinking the solar flare paradigm

D. B. **Melrose**
Presented at First Asia_Pacific Conference on Plasma Physics, Chengdu, China, September 2017, to be published in Plasma Science and Technology, ID PST-2017-0486.R1 **2018**
https://arxiv.org/pdf/1803.10389.pdf
It is widely accepted that solar flares involve release of magnetic energy stored in the solar corona above an active region, but existing models do not include the explicitly time-dependent electrodynamics needed to describe such energy release. A flare paradigm is discussed that includes the electromotive force (EMF) as the driver of the flare, and the flare-associated current that links different regions where magnetic reconnection, electron acceleration, the acceleration of mass motions and current closure occur. The EMF becomes localized across regions where energy conversion occurs, and is involved in energy propagation between these regions.

Current-driven flare and CME models† **Review**

D. B. **Melrose**
JGR **2017**
http://sci-hub.cc/10.1002/2017JA024035
https://arxiv.org/pdf/1708.04367.pdf
Roles played by the currents in the impulsive phase of a solar flare and in a coronal mass ejection (CME) are reviewed. Solar flares are magnetic explosions: magnetic energy stored in unneutralized currents in coronal loops is released into energetic electrons in the impulsive phase and into mass motion in a CME. The energy release is due to a change in current configuration effectively reducing the net current path. A flare is driven by the electromotive force (EMF) due to the changing magnetic flux. The EMF drives a flare-associated current whose cross-field closure is achieved by redirection along field lines to the chromosphere and back. The essential roles that currents play are obscured in the "standard" model and are described incorrectly in circuit models. A semi-quantitative treatment of the energy and the EMF is provided by a multi-current model, in which the currents are constant and the change in the current paths is described by time-dependent inductances. There is no self-consistent model that includes the intrinsic time dependence, the EMF, the flare-associated current and the internal energy transport during a flare. The current, through magnetic helicity, plays an important role in a CME, with twist converted into writhe allowing the kink instability plus reconnection to lead to a new closed loop, and with the current-current force accelerating the CME through the torus instability.

Is Cyclotron Maser Emission in Solar Flares Driven by a Horseshoe Distribution?

D.B. **Melrose**, M.S. Wheatland
Solar Phys. **2016**
https://arxiv.org/pdf/1610.04299v1.pdf
Since the early 1980s, decimetric spike bursts have been attributed to electron cyclotron maser emission (ECME) by the electrons that produce hard X-ray bursts as they precipitate into the chromosphere in the impulsive phase of a solar flare. Spike bursts are regarded as analogous to the auroral kilometric radiation (AKR), which is associated with the precipitation of auroral electrons in a geomagnetic substorm. Originally, a loss-cone-driven version of ECME, developed for AKR, was applied to spike bursts, but it is now widely accepted that a different, horseshoe-driven, version of EMCE applies to AKR. We explore the implications of the assumption that horseshoe-driven ECME also applies to spike bursts. We develop a 1D model for the acceleration of the electrons by a parallel electric field, and show that under plausible assumptions it leads to a horseshoe distribution of electrons in a solar flare. A second

requirement for horseshoe-driven ECME is an extremely low plasma density, referred to as a density cavity. We argue that a coronal density cavity should develop in association with a hard X-ray burst, and that such a density cavity can overcome a long-standing problem with the escape of ECME through the second-harmonic absorption layer. Both the horseshoe distribution and the associated coronal density cavity are highly localized, and could not be resolved in the statistically large number of local precipitation regions needed to explain a hard X-ray burst. The model highlights the "number problem" in the supply of the electrons needed to explain a hard X-ray burst.

Bulk Energization of Electrons in Solar Flares by Alfvén Waves

D. B. **Melrose**, M. S. Wheatland

Solar Physics, March **2014**, Volume 289, Issue 3, pp 881-897

Bulk energization of electrons to 10 – 20 keV in solar flares is attributed to dissipation of Alfvén waves that transport energy and potential downward to an acceleration region near the chromosphere. The acceleration involves the parallel electric field that develops in the limit of inertial Alfvén waves (IAWs). A two-potential model for IAWs is used to relate the parallel potential to the cross-field potential transported by the waves. We identify a maximum parallel potential in terms of a maximum current density that corresponds to the threshold for the onset of anomalous resistivity. This maximum is of order 10 kV when the threshold is that for the Buneman instability. We argue that this restricts the cross-field potential in an Alfvén wave to about 10 kV. Effective dissipation requires a large number of up- and down-current paths associated with multiple Alfvén waves. The electron acceleration occurs in localized, transient, anomalously conducting regions (LTACRs) and is associated with the parallel electric field determined by Ohm's law with an anomalous resistivity. We introduce an idealized model in which the LTACRs are (upward-)current sheets, a few skin depths in thickness, separated by much larger regions of weaker return current. We show that this model can account semi-quantitatively for bulk energization.

Transfer of Energy, Potential, and Current by Alfv'en Waves in Solar Flares

D.B. **Melrose** and M.S. Wheatland

E-print, April **2013**; Solar Phys., **2013**, Volume 288, Issue 1, pp 223-240

Alfvén waves play three related roles in the impulsive phase of a solar flare: they transport energy from a generator region to an acceleration region; they map the cross-field potential (associated with the driven energy release) from the generator region onto the acceleration region; and within the acceleration region they damp by setting up a parallel electric field that accelerates electrons and transfers the wave energy to them. The Alfvén waves may also be regarded as setting up new closed current loops, with field-aligned currents that close across field lines at boundaries. A model is developed for large-amplitude Alfvén waves that shows how Alfvén waves play these roles in solar flares. A picket-fence structure for the current flow is incorporated into the model to account for the ``number problem" and the energy of the accelerated electrons.

MAGNETIC EXPLOSIONS: ROLE OF THE INDUCTIVE ELECTRIC FIELD

D. B. **Melrose**

2012 ApJ 749 59

Inclusion of the inductive electric field, E ind, due to the temporally changing B, in magnetic explosions is discussed, with emphasis on solar flares. Several roles played by E ind are identified: on a global scale, E ind produces the electromotive force that drives the explosion; the associated E ind × B drift is identified with the inflow of magnetic field lines into a reconnection region; the polarization current, associated with ∂E ind/∂t, implies a J × B force that accelerates this inflow; and the component of E ind parallel to B accelerates the energetic electrons that cause hard X-ray emission and type III radio bursts. Some simple models that describe these effects are presented. A resolution of the long-standing "number problem" in solar flares is suggested.

GENERIC MODEL FOR MAGNETIC EXPLOSIONS APPLIED TO SOLAR FLARES

D. B. **Melrose**

2012 ApJ 749 58

An accepted model for magnetospheric substorms is proposed as the basis for a generic model for magnetic explosions and is applied to solar flares. The model involves widely separated energy-release and particle-acceleration regions, with energy transported Alfvénically between them. On a global scale, these regions are coupled by a large-scale current that is set up during the explosion by redirection of pre-existing current associated with the stored magnetic energy. The explosion-related current is driven by an electromotive force (EMF) due to the changing magnetic flux enclosed by this current. The current path and the EMF are identified for an idealized quadrupolar model for a flare.

Modelling the influence of photospheric turbulence on solar flare statistics

M. **Mendoza**, A. Kaydul, L. de Arcangelis, J. S. Andrade Jr., H. J. Herrmann
2014
http://arxiv.org/pdf/1410.4542v1.pdf
Solar flares stem from the reconnection of twisted magnetic field lines in the solar photosphere. The energy and waiting time distributions of these events follow complex patterns that have been carefully considered in the past and that bear some resemblance with earthquakes and stockmarkets. Here we explore in detail the tangling motion of interacting flux tubes anchored in the plasma and the energy ejections resulting when they recombine. The mechanism for energy accumulation and release in the flow is reminiscent of self-organized criticality. From this model we suggest the origin for two important and widely studied properties of solar flare statistics, including the time-energy correlations. We first propose that the scale-free energy distribution of solar flares is largely due to the twist exerted by the vorticity of the turbulent photosphere. Second, the long-range temporal and time-energy correlations appear to arise from the tube-tube interactions. The agreement with satellite measurements is encouraging.

On Mid-Term Periodicities in Sunspot Groups and Flare Index

Blanca **Mendoza** and Víctor Manuel Velasco-Herrera
Solar Physics, Volume 271, Numbers 1-2, 169-182, **2011**
In this work we study the mid-term periodicities (MTPs), between 1 and 2 years, of the sunspot groups and the flare index (FI), by separating the data into hemispheres and spectral bands (SBs) according to the most significant periodicities presented by these phenomena. We found that the MTP of sunspot groups has a diminished power during the Modern Minimum and an increased power during the Modern Maximum, with the exception of cycle 20. For flares, the MTP has a diminished power during the low activity cycle 20, and an increased power during cycles 21 and 22. Therefore, for both sunspot groups and FI, cycle 20 shows a very diminished power followed by the active and higher-power cycles 21 and 22; cycle 23 shows a weaker power than cycles 21 and 22. It is uncertain whether MTP can be a precursor of a long-term minimum of solar activity or not, as has been previously suggested. Also, there is no one-to-one correlation between the cycle intensity and the importance of MTP. Concerning the quasi-biennial periodicities and the theory of two kinds of dynamos, we notice the tendency that higher-power cycles mean weaker coupling in the model. Concerning the hemispheric north-south asymmetry, for sunspot groups the southern hemisphere dominates in most of the SBs, while for FI the northern hemisphere dominates for all the SBs. Additionally, the time lag found between the two hemispheres indicates that the degrees of coupling in the photosphere for sunspot groups and in the corona for flares are between moderate and strong. Finally, the modulation shown by the MTP time series suggests that these periodicities are the product of chaotic quasi-periodic processes and not of stochastic processes.

A Machine Learning Enhanced Approach for Automated Sunquake Detection in Acoustic Emission Maps

Vanessa **Mercea**, Alin Razvan Paraschiv, Daniela Adriana Lacatus, Anca Marginean & Diana Besliu-Ionescu
Solar Physics volume 298, Article number: 4 (**2023**)
https://link.springer.com/content/pdf/10.1007/s11207-022-02081-7.pdf
Sunquakes are seismic emissions visible on the solar surface, associated with some solar flares. Although discovered in 1998, they have only recently become a more commonly detected phenomenon. Despite the availability of several manual detection guidelines, to our knowledge, the astrophysical data produced for sunquakes is new to the field of machine learning. Detecting sunquakes is a daunting task for human operators, and this work aims to ease and, if possible, to improve their detection. Thus, we introduce a dataset constructed from acoustic egression-power maps of solar active regions obtained for Solar Cycles 23 and 24 using the holography method. We then present a pedagogical approach to the application of machine-learning representation methods for sunquake detection using autoencoders, contrastive learning, object detection and recurrent techniques, which we enhance by introducing several custom, domain-specific data augmentation transformations. We address the main challenges of the automated sunquake-detection task, namely the very high noise patterns in and outside the active region shadow and the extreme class imbalance given by the limited number of frames that present sunquake signatures. With our trained models, we find temporal and spatial locations of peculiar acoustic emission and qualitatively associate them to eruptive and high energy emission. While noting that these models are still in a prototype stage, and there is much room for improvement in metrics and bias levels, we hypothesize that their agreement on example use cases has the potential to enable detection of weak solar acoustic manifestations.

Eruptions of Magnetic Ropes in Two Homologous Solar Events on 2002 June 1 and 2: a Key to Understanding of an Enigmatic Flare

N.S. **Meshalkina**, A.M. Uralov, V.V. Grechnev, A.T. Altyntsev, L.K. Kashapova

Pub. Astron. Soc. Japan 61, 791-, **2009. File**
http://arxiv.org/pdf/0908.0384v1.pdf
The goal of this paper is to understand the drivers, configurations, and scenarios of two similar eruptive events, which occurred in the same solar active region 9973 on **2002 June 1 and 2**. The June 2 event was previously studied by Sui, Holman, and Dennis (2006, 2008), who concluded that it was challenging for popular flare models. Using multi-spectral data, we analyze a combination of the two events. Each of the events exhibited an evolving cusp-like feature. We have revealed that these apparent ``cusps'' were most likely mimicked by twisted magnetic flux ropes, but unlikely to be related to the inverted Y-like magnetic configuration in the standard flare model. The ropes originated inside a funnel-like magnetic domain whose base was bounded by an EUV ring structure, and the top was associated with a coronal null point. The ropes appear to be the major drivers for the events, but their rise was not triggered by reconnection in the coronal null point. We propose a scenario and a three-dimensional scheme for these events in which the filament eruptions and flares were caused by interaction of the ropes.

Magnetically coupled atmosphere, fast sausage MHD waves, and forced magnetic field reconnection during the SOL2014-09-10T17:45 flare

Hana **Meszarosova**, Peter Gomory
A&A 643, A140 **2020**
https://arxiv.org/pdf/2010.01527.pdf
https://doi.org/10.1051/0004-6361/202038388
https://www.aanda.org/articles/aa/pdf/2020/11/aa38388-20.pdf
We study the physical properties and behavior of the solar atmosphere during the GOES X1.6 solar flare on **2014 September 10**. The steady plasma flows and the fast sausage MHD waves were analysed with the wavelet separation method. The magnetically coupled atmosphere and the forced magnetic field reconnection were studied with the help of the Vertical-Current Approximation Non-linear Force-Free Field code. We studied a mechanism of MHD wave transfer from the photosphere without dissipation or reflection before reaching the corona and a mechanism of the wave energy distribution over the solar corona. We report a common behavior of (extreme)ultraviolet steady plasma flows (speed of 15.3 -> 10.9 km/s) and fast sausage MHD waves (Alfven speed of 13.7 -> 10.3 km/s and characteristic periods of 1 587 -> 1 607 s), propagating in cylindrical plasma waveguides of the individual atmospheric layers (photosphere -> corona) observed by SDO/AIA/HMI and IRIS space instruments. A magnetically coupled solar atmosphere by a magnetic field flux tube above a sunspot umbra and a magnetic field reconnection forced by the waves were analysed. The solar seismology with trapped, leakage, and tunnelled modes of the waves, dissipating especially in the solar corona, is discussed with respect to its possible contribution to the outer atmosphere heating. We demonstrate that a dispersive nature of fast sausage MHD waves, which can easily generate the leaky and other modes propagating outside of their waveguide, and magnetic field flux tubes connecting the individual atmospheric layers can distribute the magnetic field energy across the active region. This mechanism can contribute to the coronal energy balance and to our knowledge on how the coronal heating is maintained.

Broadband microwave sub-second pulsations in an expanding coronal loop of the 2011 August 10 flare

Hana **Meszarosova**, Jan Rybak, Larisa Kashapova, Peter Gomory, Susanna Tokhchukova, Ivan Myshyakov
A&A **2016**
http://arxiv.org/pdf/1609.04217v1.pdf
We studied the characteristic physical properties and behavior of broadband microwave sub-second pulsations observed in an expanding coronal loop during the GOES C2.4 solar flare on **2011 August 10**. We found sub-second pulsations and other different burst groups in the complex radio spectrum. The broadband (bandwidth about 1 GHz) sub-second pulsations (temporal period range 0.07-1.49 s, no characteristic dominant period) lasted 70 s in the frequency range 4-7 GHz. These pulsations were not correlated at their individual frequencies, had no measurable frequency drift, and zero polarization. In these pulsations, we found the signatures of fast sausage magnetoacoustic waves with the characteristic periods of 0.7 and 2 s. The other radio bursts showed their characteristic frequency drifts in the range of -262-520 MHz/s. They helped us to derive average values of 20-80 G for the coronal magnetic field strength in the place of radio emission. It was revealed that the microwave event belongs to an expanding coronal loop with twisted sub-structures observed in the 131, 94, and 193 A SDO/AIA channels. Their slit-time diagrams were compared with the location of the radio source at 5.7 GHz to realize that the EUV intensity of the expanding loop increased just before the radio source triggering. We reveal two EUV bidirectional flows that are linked with the start time of the loop expansion. Their positions were close to the radio source and propagated with velocities within a range of 30-117 km/s. We demonstrate that periodic regime of the electron acceleration in a model of the quasi-periodic magnetic reconnection might be able to explain physical properties and behavior of the sub-second pulsations. The depolarization process of the microwave emission might be caused by a plasma turbulence in the radio source. Finally, the observed EUV flows might be linked with reconnection outflows.

Magnetoacoustic Waves Propagating along a Dense Slab and Harris Current Sheet and their Wavelet Spectra

Hana **Mészárosová**1, Marian Karlický1, Petr Jelínek1,2, and Ján Rybák
E-print, May 2014; **2014** ApJ 788 44.

Currently, there is a common endeavor to detect magnetoacoustic waves in solar flares. This paper contributes to this topic using an approach of numerical simulations. We studied a spatial and temporal evolution of impulsively generated fast and slow magnetoacoustic waves propagating along the dense slab and Harris current sheet using two-dimensional magnetohydrodynamic numerical models. Wave signals computed in numerical models were used for computations of the temporal and spatial wavelet spectra for their possible comparison with those obtained from observations. It is shown that these wavelet spectra allow us to estimate basic parameters of waveguides and perturbations. It was found that the wavelet spectra of waves in the dense slab and current sheet differ in additional wavelet components that appear in association with the main tadpole structure. These additional components are new details in the wavelet spectrum of the signal. While in the dense slab this additional component is always delayed after the tadpole head, in the current sheet this component always precedes the tadpole head. It could help distinguish a type of the waveguide in observed data. We present a technique based on wavelets that separates wave structures according to their spatial scales. This technique shows not only how to separate the magnetoacoustic waves and waveguide structure in observed data, where the waveguide structure is not known, but also how propagating magnetoacoustic waves would appear in observations with limited spatial resolutions. The possibilities detecting these waves in observed data are mentioned.

CORONAL TRAPPING OF ENERGETIC FLARE PARTICLES: Y OHKOH/HXT OBSERVATIONS

THOMAS R. **METCALF** AND DAVID ALEXANDER
ASTROPHYSICAL JOURNAL, 522:1108E1116, **1999** September **File**

We examine spectroscopic data from the Yohkoh Hard X-Ray Telescope in a search for spectral evidence of the coronal trapping of energetic particles during solar Nares. Two distinct particle populations with signi.cantly di.erent spectral properties are found to be present in three of the six Nares studied ; the .rst population is trapped in the corona, where it encounters a .. thick-thin II target, while the second population precipitates directly to the footpoints. In the remaining three events, a single population of energetic particles appear to be responsible for the observed hard X-ray emission, either via thermal bremsstrahlung (one case) or nonthermal thin-target emission (two cases). For the three events in which a trapped population is observed, the spectroscopic observations imply .rst that there is likely to be a single acceleration mechanism for both the trapped and the precipitating populations and second that the magnetic .eld geometry in these Nares is conducive to trapping in a con.ned region high in the corona, above the soft X-ray loops. Both conditions are consistent with magnetic reconnection models of Nares in which energetic particles are trapped between MHD slow-mode shocks attached to the reconnection region and a fast-mode shock formed by the reconnection outNow jet. **1991 Nov 19, 1992 Jan 13, 1992 Feb 17, 1992 Oct 04, 1993 Feb 17, 1993 Nov 30**

STEREO OBSERVATIONS OF ENERGETIC NEUTRAL HYDROGEN ATOMS DURING THE 2006 DECEMBER 5 SOLAR FLARE

R. A. **Mewaldt**, R. A. Leske, E. C. Stone, A. F. Barghouty, A. W. Labrador, C. M. S. Cohen, A. C. Cummings, A. J. Davis, T. T. von Rosenvinge, and M. E. Wiedenbeck
ApJL 693 L11-L15, **2009**
http://www.iop.org/EJ/abstract/1538-4357/693/1/L11

We report the discovery of energetic neutral hydrogen atoms (ENAs) emitted during the X9 solar event of **2006 December 5.** Beginning ~1 hr following the onset of this E79 flare, the Low Energy Telescopes (LETs) on both the STEREO A and B spacecraft observed a sudden burst of 1.6-15 MeV protons beginning hours before the onset of the main solar energetic particle event at Earth. More than 70% of these particles arrived from a longitude within ±10° of the Sun, consistent with the measurement resolution. The derived emission profile at the Sun had onset and peak times remarkably similar to the GOES soft X-ray profile and continued for more than an hour. The observed arrival directions and energy spectrum argue strongly that the particle events < 5 MeV were due to ENAs. To our knowledge, this is the first reported observation of ENA emission from a solar flare/coronal mass ejection. Possible origins for the production of ENAs in a large solar event are considered. We conclude that the observed ENAs were most likely produced in the high corona and that charge-transfer reactions between accelerated protons and partially stripped coronal ions are an important source of ENAs in solar events.

Diagnosing a Solar Flaring Core with Bidirectional Quasi-Periodic Fast Propagating Magnetoacoustic Waves

Yuhu **Miao**, Dong Li, Ding Yuan, Chaowei Jiang, Abouazza Elmhamdi, Mingyu Zhao, Sergey Anfinogentov
ApJL **908** L37 **2021**
https://arxiv.org/pdf/2101.12392.pdf
https://iopscience.iop.org/article/10.3847/2041-8213/abdfce/pdf
https://doi.org/10.3847/2041-8213/abdfce
Quasi-periodic fast propagating (QFP) waves are often excited by solar flares, and could be trapped in the coronal structure with low Alfvén speed, so they could be used as a diagnosing tool for both the flaring core and magnetic waveguide. As the periodicity of a QFP wave could originate from a periodic source or be dispersively waveguided, it is a key parameter for diagnosing the flaring core and waveguide. In this paper, we study two QFP waves excited by a GOES-class C1.3 solar flare occurring at active region NOAA 12734 on **8 March 2019**. Two QFP waves were guided by two oppositely oriented coronal funnel. The periods of two QFP waves were identical and were roughly equal to the period of the oscillatory signal in the X-ray and 17 GHz radio emission released by the flaring core. It is very likely that the two QFP waves could be periodically excited by the flaring core. Many features of this QFP wave event is consistent with the magnetic tuning fork model. We also investigated the seismological application with QFP waves, and found that the magnetic field inferred with magnetohydrodynamic seismology was consistent with that obtained in magnetic extrapolation model. Our study suggest that the QFP wave is a good tool for diagnosing both the flaring core and the magnetic waveguide.

Nonlinear Resonant Excitation of Fast Sausage Waves in Current-Carrying Coronal Loops

B. B. **Mikhalyaev**, D. B. Bembitov
Solar Physics, July **2014**
We consider a model of a coronal loop that is a cylindrical magnetic tube with two surface electric currents. Its principal sausage mode has no cut-off in the long-wavelength limit. For typical coronal conditions, the period of the mode is between one and a few minutes. The sausage mode of flaring loops could cause long-period pulsations observed in microwave and hard X-ray ranges. There are other examples of coronal oscillations: long-period pulsations of active-region quiet loops in the soft X-ray emission are observed. We assume that these can also be caused by sausage waves. The question arises of how the sausage waves are generated in quiet loops. We assume that they can be generated by torsional oscillations. This process can be described in the framework of the nonlinear three-wave interaction formalism. The periods of interacting torsional waves are similar to the periods of torsional oscillations observed in the solar atmosphere. The timescale of the sausage-wave excitation is not much longer than the periods of interacting waves, so that the sausage wave is excited before torsional waves are damped.

Observations of Chromospheric Flare Re-brightenings

C. H. **Miklenic**, A. M. Veronig, B. Vrsnak, and M. Barta
2010 ApJ 719 1750-1758; **File**
We investigate an active region that produced three C-class flares and one M-class flare within 2.5 hr. The morphology and location of the C-flares indicate that these events constitute a set of homologous flares. Radio observations indicate the occurrence of a downward-moving plasmoid during the impulsive phase of the M flare. We use TRACE 1700 Å filtergrams and SOHO Michelson Doppler Imager magnetograms to examine the character of the UV brightenings; i.e., we search for re-brightenings of former flare areas both across the series of events and within one and the same event. We find that essentially the same footpoints re-brighten in each C flare. Based on the progression of both the derived magnetic flux change rate and the observed Radio Solar Telescope Network microwave emission, we speculate about a further re-brightening during the decay phase of the M flare as a further member of the series of homologous flares. We conclude that the "postflare" field is driven to repeated eruption by continuous, shear-increasing, horizontal, photospheric flows, as one end of the involved magnetic arcade is anchored in the penumbra of a large sunspot. The observed motion pattern of the UV kernels indicates that the arcade evolves during the series of events from a both highly sheared and heavily entangled state to a still sheared but more organized state.
2004 July 23,

Temporal comparison of nonthermal flare emission and magnetic-flux change rates:

C.H.**Miklenic**, A.M.Veronig and B.Vrsnak

E-print, Oct 2009, **File**; A&A 499 (**2009**) 893-904

Context. To understand the mechanisms that trigger solar flares, we require models describing and quantifying observable responses to the original energy release process, since the coronal energy release site itself cannot be resolved with current technical equipment. Testing the usefulness of a particular model requires the comparison of its predictions with flare observations.

Aims. To test the standard flare model (CSHKP-model), we measured the magnetic-flux change rate in five flare events of different GOES classes using chromospheric/photospheric observations and compared its progression with observed nonthermal flare emission. We calculated the cumulated positive and negative magnetic flux participating in the reconnection process, as well as the total reconnection flux. Finally, we investigated the relations between the total reconnection flux, the GOES class of the events, and the linear velocity of the flare-associated CMEs.

Methods. Using high-cadence H α and TRACE 1600 Å image time-series data and MDI/SOHO magnetograms, we measured the required observables (newly brightened flare area and magnetic-field strength inside this area). RHESSI and INTEGRAL hard X-ray time profiles in nonthermal energy bands were used as observable proxies for the flare-energy release rate.

Results. We detected strong temporal correlations between the derived magnetic-flux change rate and the observed nonthermal emission of all events. The cumulated positive and negative fluxes, with flux ratios of between 0.64 and 1.35, were almost equivalent to each other. Total reconnection fluxes ranged between 1.8x1021 Mx for the weakest event (GOES class B9.5) and 15.5x1021 Mx for the most energetic one (GOES class X17.2). The amount of magnetic flux participating in the reconnection process was higher in more energetic events than in weaker ones. Flares with more reconnection flux were associated with faster CMEs.

Reconnection and energy release rates in a two-ribbon flare --

Miklenic, C. H., Veronig, A. M., Vrsnak, B., and Hanslmeier, A.

A&A 461 (**2007**) 697-706, **File**

*Aims.*The aim of this study was to derive the local reconnection rate (coronal electric field) and the global reconnection rate (magnetic flux change rate), as well as the energy release rate (Poynting flux), in a two-ribbon flare from chromospheric/photospheric observations. Furthermore, we tested whether equal shares of positive and negative magnetic flux are involved in the flare process.

*Methods.*A well-observed GOES M3.9 two-ribbon flare was analyzed. The required observables (ribbon expansion velocity, newly brightened area, and magnetic field strength at the ribbon front) were extracted from the TRACE 1600 Å and Kanzelhöhe H α image time series, and a SOHO MDI magnetogram. Furthermore, the ratio of the converted positive vs. negative magnetic flux was determined. Both RHESSI hard X-ray 20-60 keV full-disk time profiles and subregion time profiles derived from a time series of RHESSI images in the same energy range were used as independent, observable proxies for the energy release rate. The RHESSI images were also used to localize the sites where the bulk of the energy was deposited by fast electrons.

*Results.*We found good temporal correlations between the derived time profiles (local and global reconnection rate, Poynting flux) and observed HXR flux. The local reconnection-rate peak values ranged from $2.7\,\mathrm{V\,cm^{-1}}$ to $11.8\,\mathrm{V\,cm^{-1}}$, whereas the positive and the negative magnetic flux covered by the flare emission were equal within 5-10%.

*Conclusions.*The results indicate that the local reconnection rate, the global reconnection rate, and the energy release rate in a simple two-ribbon flare can be derived from chromospheric/photospheric observations. Furthermore, it was confirmed that equal shares of positive and negative magnetic flux participated in the reconnection process.

18 Nov 2003

Structure and Dynamics of Cool Flare Loops Observed by the Interface Region Imaging Spectrograph

K. **Mikuła**1, P. Heinzel2, W. Liu2, and A. Berlicki

2017 ApJ 845 30

http://sci-hub.cc/10.3847/1538-4357/aa7d4e

Flare loops were well observed with the Interface Region Imaging Spectrograph (IRIS) during the gradual phase of two solar flares on **2014 March 29 and 2015 June 22**. Cool flare loops are visible in various spectral lines formed at chromospheric and transition-region temperatures and exhibit large downflows which correspond to the standard scenario. The principal aim of this work is to analyze the structure and dynamics of cool flare loops observed in Mg ii lines. Synthetic profiles of the Mg ii h line are computed using the classical cloud model and assuming a uniform background intensity. In this paper, we study novel IRIS NUV observations of such loops in Mg ii h and k lines and also show the behavior of hotter lines detected in the FUV channel. We obtained the spatial evolution of the velocities: near the loop top, the flow velocities are small and they are increasing toward the loop legs. Moreover, from slit-jaw

image (SJI) movies, we observe some plasma upflows into the loops, which are also detectable in Mg iispectra. The brightness of the loops systematically decreases with increasing flow velocity, and we ascribe this to the effect of Doppler dimming, which works for Mg ii lines. Emission profiles of Mg ii were found to be extremely broad, and we explain this through the large unresolved non-thermal motions.

Intensity and velocity oscillations in a flaring active region

David C L **Millar**, Lyndsay Fletcher, Jayant Joshi
Monthly Notices of the Royal Astronomical Society, Volume 527, Issue 3, January **2024**, Pages 5916–5928,
https://doi.org/10.1093/mnras/stad3386
https://academic.oup.com/mnras/article-pdf/527/3/5916/54021982/stad3386.pdf
https://watermark.silverchair.com/stad3386.pdf
Chromospheric oscillations can give us insight into the physical environment in the solar atmosphere, both in quiet Sun and flaring conditions. Many authors have reported increases in the prevalence of 3-minute oscillations which are thought to be excited by events which impact the chromosphere such as flares. In this study, we utilized the Ca II 8542 Å line to study the oscillatory behaviour of the chromosphere in an active region which underwent two B-class flares. We analysed oscillations in both intensity and velocity, and found different behaviours in both. Intensity oscillations were most prevalent over the umbrae of sunspots and magnetic pores in the active region, and the extent of the area which contained significant oscillations was found to decrease when comparing times after the flares to before. By measuring the evolution of the magnetic field, we found that this could be because the areas surrounding the umbrae were becoming more ‘penumbral’ with an increase to the magnetic field inclination. Velocity oscillations were found across the active region both before and after the flares but were observed clearly in areas which were brightened by the second flare. By comparing to EUV imaging, it was seen that strong chromospheric velocity oscillations with 3–4-minute periods occurred at the same time and location as a flare loop cooling 30 min after the second flare peak. This could be evidence of disturbances in the loop exciting a response from the chromosphere at its acoustic cut-off frequency. **2013 June 13**

The effect of a solar flare on chromospheric oscillations

David C. L. **Millar**, Lyndsay Fletcher, Ryan O. Milligan
MNRAS **2020**
https://arxiv.org/pdf/2007.10301.pdf
Oscillations in the solar atmosphere have long been observed in quiet conditions, and increasingly also in data taken during solar flares. The chromosphere is known for its 3-minute signals, which are particularly strong over sunspot umbrae. These signals are thought to be driven by photospheric disturbances and their periods determined by the chromosphere's acoustic cut-off frequency. A small number of observations have shown the chromospheric 3-minute signals to be affected by energetic events such as solar flares, however the link between flare activity and these oscillatory signals remains unclear. In this work we present evidence of changes to the oscillatory structure of the chromosphere over a sunspot which occurs during the impulsive phase of an M1 flare. Using imaging data from the CRISP instrument across the Hα and Ca II 8542 Å spectral lines, we employed a method of fitting models to power spectra to produce maps of areas where there is evidence of oscillatory signals above a red noise background. Comparing results taken before and after the impulsive phase of the flare, we found that the oscillatory signals taken after the start of the flare differ in two ways: the locations of oscillatory signals had changed and the typical periods of the oscillations had tended to increase (in some cases increasing from <100s to ~200s). Both of these results can be explained by a restructuring of the magnetic field in the chromosphere during the flare activity, which is backed up by images of coronal loops showing clear changes to magnetic connectivity. These results represent one of the many ways that active regions can be affected by solar flare events. **2014-09-06**

Solar Irradiance Variability Due To Solar Flares Observed in Lyman-alpha Emission

Ryan O. **Milligan**
Solar Phys. **296**, Article number: 51 **2021**
https://arxiv.org/pdf/2102.00974.pdf
https://link.springer.com/content/pdf/10.1007/s11207-021-01796-3.pdf
https://doi.org/10.1007/s11207-021-01796-3
As the Lyman-alpha (Lya) line of neutral hydrogen is the brightest emission line in the solar spectrum, detecting increases in irradiance due to solar flares at this wavelength can be challenging due to the very high background. Previous studies that have focused on the largest flares have shown that even these extreme cases generate enhancements in Lya of only a few percent above the background. In this study, a superposed-epoch analysis was performed on ~8500 flares greater than B1 class to determine the contribution that flares make to changes in the solar EUV irradiance. Using the peak of the 1-8A X-ray emission as a fiducial time, the corresponding time series of 3123 B- and 4972 C-class flares observed in Lya emission by the EUV Sensor on GOES-15 were averaged to reduce background fluctuations and improve the flare signal. The summation of these weaker events showed that they

produced a 0.1-0.3% enhancement to the solar Lya irradiance. For comparison on average, the same technique was applied to 453 M- and 31 X-class flares, which resulted in a 1-4% increase in Lya emission. Flares were also averaged with respect to their heliographic angle to investigate any potential center-to-limb variation. For each GOES class, the relative enhancement in Lya at the flare peak was found to diminish for flares that occurred closer to the solar limb due to the opacity of the line, and/or foreshortening of the footpoints. One modest event included in the study, a C6.6 flare, exhibited an unusually high increase in Lya of 7% that may have been attributed to a failed filament eruption. Increases of this magnitude have hitherto only been associated with a small number of X-class flares. **9-11 Feb 2011, 13-15 Feb 2011, 18 Aug 2011, 4-5 May 2012, 17 Feb 2014**

Lyman-alpha Variability During Solar Flares Over Solar Cycle 24 Using GOES-15/EUVS-E

Ryan O. **Milligan**, Hugh S. Hudson, Phillip C. Chamberlin, Iain G. Hannah
Space Weather **Volume18, Issue7** e2019SW002331 **2020**
https://arxiv.org/pdf/1910.01364.pdf
https://agupubs.onlinelibrary.wiley.com/doi/epdf/10.1029/2019SW002331
The chromospheric Lyman-alpha line of neutral hydrogen (Lyα; 1216Å) is the strongest emission line in the solar spectrum. Fluctuations in Lyα are known to drive changes in planetary atmospheres, although few instruments have had the ability to capture rapid Lyα enhancements during solar flares. In this paper we describe flare-associated emissions via a statistical study of 477 M- and X-class flares as observed by the EUV Sensor on board the 15th Geostationary Operational Environmental Satellite, which has been monitoring the full-disk solar Lyα irradiance on 10s timescales over the course of Solar Cycle 24. The vast majority (95%) of these flares produced Lyα enhancements of 10% or less above background levels, with a maximum increase of ~30%. The irradiance in Lyα was found to exceed that of the 1-8 Å X-ray irradiance by as much as two orders of magnitude in some cases, although flares that occurred closer to the solar limb were found to exhibit less of a Lyα enhancement. This center-to-limb variation was verified through a joint observation of an X-class flare that appeared near the limb as viewed from Earth, but close to disk center as viewed by the MAVEN spacecraft in orbit around Mars. The frequency distribution of peak Lyα was found to have a power-law slope of 2.8±0.27, interestingly different from that of other observables. We also show that the data provide a clean timeseries for studies of ionospheric responses through a comparison with the Solar Flare Effect as observed by the Kakioka magnetometer. **15−Feb−11, 09−Aug−11, 07−Sep−11, 7−Mar−12, 13−May−13, 07−Jan−14, 10−Jun−14, 19 October 2014, 22−Oct−14, 5 May 2015**

Detection of 3-Minute Oscillations in Full-Disk Lyα Emission During A Solar Flare

Ryan O. **Milligan**, Bernhard Fleck, Jack Ireland, Lyndsay Fletcher, Brian R. Dennis
ApJL **848** L8 **2017**
https://arxiv.org/pdf/1709.09037.pdf
http://iopscience.iop.org/article/10.3847/2041-8213/aa8f3a/pdf
In this Letter we report the detection of chromospheric 3-minute oscillations in disk-integrated EUV irradiance observations during a solar flare. A wavelet analysis of detrended Lyman-alpha (from GOES/EUVS) and Lyman continuum (from SDO/EVE) emission from the **2011 February 15** X-class flare (SOL2011-02-15T01:56) revealed a ~3-minute period present during the flare's main phase. The formation temperature of this emission locates this radiation to the flare's chromospheric footpoints, and similar behaviour is found in the SDO/AIA 1600\AA\ and 1700\AA\ channels, which are dominated by chromospheric continuum. The implication is that the chromosphere responds dynamically at its acoustic cutoff frequency to an impulsive injection of energy. Since the 3-minute period was not found at hard X-ray energies (50-100 keV) in RHESSI data we can state that this 3-minute oscillation does not depend on the rate of energization of non-thermal electrons. However, a second period of 120 s found in both hard X-ray and chromospheric emission is consistent with episodic electron energization on 2-minute timescales. Our finding on the 3-minute oscillation suggests that chromospheric mechanical energy should be included in the flare energy budget, and the fluctuations in the Lyman-alpha line may influence the composition and dynamics of planetary atmospheres during periods of high activity.

Multi-Instrument Solar Flare Observations II: A SC24 Retrospective

Ryan **Milligan** and Jack Ireland.
RHESSI Science Nuggets #298 Apr **2017**
http://sprg.ssl.berkeley.edu/~tohban/wiki/index.php/Multi-Instrument_Solar_Flare_Observations_II:_A_SC24_retrospective
How the widget did in Cycle 24

Multi-Instrument Solar Flare Observations I: Solar Flare Finder

Ryan **Milligan**, Kim Tolbert
RHESSI Science Nuggets #297 Apr **2017**
http://sprg.ssl.berkeley.edu/~tohban/wiki/index.php/Multi-Instrument_Solar_Flare_Observations_I:_Solar_Flare_Finder
Retrospective searches for your favorite flare

On the Effectiveness of Multi-Instrument Solar Flare Observations During Solar Cycle 24

Ryan O. **Milligan**, Jack Ireland

Solar Phys. 293:18 **2018**

https://arxiv.org/pdf/1703.04412.pdf

https://link.springer.com/content/pdf/10.1007%2Fs11207-017-1233-x.pdf

Our current fleet of space-based solar observatories offer us a wealth of opportunities to study solar flares over a range of wavelengths, and the greatest advances in our understanding of flare physics often come from coordinated observations between different instruments. However, despite considerable effort to coordinate this armada of instruments over the years (e.g. through the Max Millennium Program of Solar Flare Research), there are few solar flares that have been observed by most or all available instruments simultaneously, due to the combination of each instrument's operational constraints. Here we describe a technique that retrospectively searches archival databases for flares jointly observed by RHESSI, SDO/EVE (MEGS-A and MEGS-B), Hinode/(EIS, SOT and XRT), and IRIS. Out of the 6,953 flares of GOES magnitude C1 or greater that we consider over the 6.5 years after the launch of SDO, 40 have been observed by six or more instruments simultaneously. The difficulty in scheduling co-ordinated observations for solar flare research is discussed with respect to instruments projected to begin operations during Solar Cycle 25, such as the Daniel K. Inouye Solar Telescope, Solar Orbiter and Solar Probe Plus. **4 February 2014**

Anomalous temporal behaviour of broadband Lyα observations during solar flares from SDO/EVE

Ryan O. **Milligan**1,2,3 and Phillip C. Chamberlin2

A&A 587, A123 (**2016**)

See 2015 http://arxiv.org/pdf/1506.02408v1.pdf

Although it is the most prominent emission line in the solar spectrum, there has been a notable lack of studies devoted to variations in Lyα emission during solar flares in recent years. However, the few examples that do exist have shown Lyα emission to be a substantial radiator of the total energy budget of solar flares (of the order of 10%). It is also a known driver of fluctuations in the Earth's ionosphere. The EUV Variability Experiment (EVE) on board the Solar Dynamics Observatory now provides broadband, photometric Lyα data at 10 s cadence with its Multiple EUV Grating Spectrograph-Photometer (MEGS-P) component, and has observed scores of solar flares in the 5 years since it was launched. However, the MEGS-P time profiles appear to display a rise time of tens of minutes around the time of the flare onset. This is in stark contrast to the rapid, impulsive increase observed in other intrinsically chromospheric features (Hα, Lyβ, LyC, C III, etc.). Furthermore, the emission detected by MEGS-P peaks around the time of the peak of thermal soft X-ray emission and not during the impulsive phase when energy deposition in the chromosphere (often assumed to be in the form of non-thermal electrons) is greatest. The time derivative of Lyα lightcurves also appears to resemble that of the time derivative of soft X-rays, reminiscent of the Neupert effect. Given that spectrally-resolved Lyα observations during flares from SORCE/SOLSTICE peak during the impulsive phase as expected, this suggests that the atypical behaviour of MEGS-P data is a manifestation of the broadband nature of the observations. This could imply that other lines and/or continuum emission that becomes enhanced during flares could be contributing to the passband. Users are hereby urged to exercise caution when interpreting broadband Lyα observations of solar flares. Comparisons have also been made with other broadband Lyα photometers such as PROBA2/LYRA and GOES/EUVS-E.

EUV Irradiance Observations from SDO/EVE as a Diagnostic of Solar Flares

Ryan O. **Milligan**

Conference proceedings for the symposium on "Solar and Stellar Flares and their Effects on the Planets" at the IAU General Assembly in Honolulu, HI, August **2015**

http://arxiv.org/pdf/1604.07793v1.pdf

For the past six years, the EUV Variability Experiment (EVE) onboard the Solar Dynamics Observatory has been monitoring changes in the Sun's extreme ultraviolet output over a range of timescales. Its primary function is to provide measurements of the solar spectral irradiance that is responsible for driving fluctuations in Earth's ionosphere and thermosphere. However, despite its modest spectral resolution and lack of spatial information, the EVE spectral range contains many lines and continua that have become invaluable for diagnosing the response of the lower solar atmosphere itself to an injection of energy, particularly during a flare's impulsive phase. In addition, high temperature emission lines can also be used to track changes in temperature and density of flaring plasma in the corona. The high precision of EVE observations are therefore crucial in helping us understand particle acceleration and energy transport mechanisms during solar flares, as well as the origins of the Sun's most geoeffective emission. **15−Feb−11, 07-Mar-11, 9 August 2011, 3 November 2011, 25-Oct-13**

Extreme Ultra-Violet Spectroscopy of the Lower Solar Atmosphere During Solar Flares (Invited Review)

Ryan O. **Milligan**
Solar Phys. **2015**
The extreme ultra-violet (EUV) portion of the solar spectrum contains a wealth of diagnostic tools for probing the lower solar atmosphere in response to an injection of energy, particularly during the impulsive phase of solar flares. These include temperature- and density-sensitive line ratios, Doppler-shifted emission lines, nonthermal broadening, abundance measurements, differential emission measure profiles, continuum temperatures and energetics, among others. In this article I review some of the recent advances that have been made using these techniques to infer physical properties of heated plasma at footpoint and ribbon locations during the initial stages of solar flares. I primarily focus on studies that have utilised spectroscopic EUV data from Hinode/EUV Imaging Spectrometer (EIS) and Solar Dynamics Observatory/EUV Variability Experiment (SDO/EVE), and I also provide some historical background and a summary of future spectroscopic instrumentation.

The Temporal Behaviour of Lyman-alpha Emission During Solar Flares From SDO/EVE

Ryan O. **Milligan**, Phillip C. Chamberlin
A&A **2015**
http://arxiv.org/pdf/1506.02408v1.pdf
Despite being the most prominent emission line in the solar spectrum, there has been a notable lack of studies devoted to variations in Lyman-alpha (Lyα) emission during solar flares in recent years. The few examples that do exist, however, have shown Lyα emission to be a substantial radiator of the total energy budget of solar flares (on the order of 10%). It is also a known driver of fluctuations in earth's ionosphere. The EUV Variability Experiment (EVE) onboard the Solar Dynamics Observatory now provides broadband, photometric Lyα data at 10 s cadence, and has observed scores of solar flares in the 5 years since it was launched. However, the time profiles appear to display a rise time of tens of minutes around the time of the flare onset. This is in stark contrast to the rapid, impulsive increase observed in other intrinsically chromospheric features (Hα, Lyβ, LyC, C III, etc.). Furthermore, the Lyα emission peaks around the time of the peak of thermal soft X-ray emission, rather than during the impulsive phase when energy deposition in the chromosphere - often assumed to be in the form of nonthermal electrons - is greatest. The time derivative of Lyα lightcurves also closely resembles that of the time derivative of soft X-rays, rather reminiscent of the Neupert Effect. To establish whether this atypical behaviour is a characteristic of flare heating in the lower solar atmosphere during explosive events, or a manifestation of the broadband nature of the EVE observations, comparisons have been made with spectrally-resolved Lyα measurements during flares from SORCE/SOLSTICE, and other broadband photometers such as PROBA2/LYRA and GOES/EUVS-E. **28 October 2003 , 15 February 2011**

Extreme Ultra-Violet Spectroscopy of the Flaring Solar Chromosphere **Review**

Ryan **Milligan**
Solar Physics, Volume 290, Issue 12, pp 3399-3423 **2015**
http://star.pst.qub.ac.uk/~rm/outgoing/milligan_solphys_2015.pdf
http://arxiv.org/pdf/1501.04829.pdf
The extreme ultraviolet portion of the solar spectrum contains a wealth of diagnostic tools for probing the lower solar atmosphere in response to an injection of energy, particularly during the impulsive phase of solar flares. These include temperature and density sensitive line ratios, Doppler shifted emission lines and nonthermal broadening, abundance measurements, Differential Emission Measure profiles, and continuum temperatures and energetics, among others. In this paper I shall review some of the advances made in recent years using these techniques, focusing primarily on studies that have utilized data from Hinode/EIS and SDO/EVE, while also providing some historical background and a summary of future spectroscopic instrumentation**. 14 December 2007. 15−Feb−2011, 9 March 2011.**
Table 1. Flares Whose Footpoints Were Observed by Hinode/EIS During the Impulsive Phase

The Redistribution of Nonthermal Electron Energy

Ryan **Milligan**
RHESSI Science Nugget, No. 230, **2014**
http://sprg.ssl.berkeley.edu/~tohban/wiki/index.php/RHESSI_Science_Nuggets
What we know about the dominant energy driving a solar flare.

The Radiated Energy Budget Of Chromospheric Plasma In A Major Solar Flare Deduced From Multi-Wavelength Observations

Ryan O. **Milligan**, Graham S. Kerr, Brian R. Dennis, Hugh S. Hudson, Lyndsay Fletcher, Joel C. Allred, Phillip C. Chamberlin, Jack Ireland, Mihalis Mathioudakis, & Francis P. Kennan

E-print, June **2014**; ApJ 793 70 **2014**
http://star.pst.qub.ac.uk/~rm/outgoing/milligan_apj_2014_preprint.pdf
http://arxiv.org/pdf/1406.7657v1.pdf
This paper presents measurements of the energy radiated by the lower solar atmosphere, at optical, UV, and EUV wavelengths, during an X-class solar flare (**SOL2011-02-15**T01:56) in response to an injection of energy assumed to be in the form of nonthermal electrons. Hard X-ray observations from RHESSI were used to track the evolution of the parameters of the nonthermal electron distribution to reveal the total power contained in flare accelerated electrons. By integrating over the duration of the impulsive phase, the total energy contained in the nonthermal electrons was found to be >2x1031 erg. The response of the lower solar atmosphere was measured in the free-bound EUV continua of H I (Lyman), He I, and He II, plus the emission lines of He II at 304A and H I (Lya) at 1216A by SDO/EVE, the UV continua at 1600A and 1700A by SDO/AIA, and the WL continuum at 4504A, 5550A, and 6684A, along with the Ca II H line at 3968A using Hinode/SOT. The summed energy detected by these instruments amounted to ~3x1030 erg; about 15% of the total nonthermal energy. The Lya line was found to dominate the measured radiative losses. Parameters of both the driving electron distribution and the resulting chromospheric response are presented in detail to encourage the numerical modelling of flare heating for this event, to determine the depth of the solar atmosphere at which these line and continuum processes originate, and the mechanism(s) responsible for their generation.

Continuum contributions to the SDO/AIA passbands during solar flares

Ryan **Milligan**
UKSP Nugget: 39, Sept **2013**
http://www.uksolphys.org/?p=7100
SDO/EVE sheds new light on flare free-free emission in the EUV.

Continuum Contributions to the SDO/AIA Passbands During Solar Flares

Ryan O. **Milligan** & Sarah A. McElroy
E-print, Aug **2013**; **2013** ApJ 777 12
Data from the Multiple EUV Grating Spectrograph (MEGS-A) component of the Extreme Ultraviolet Experiment (EVE) onboard the Solar Dynamics Observatory (SDO) were used to quantify the contribution of continuum emission to each of the EUV channels of the Atmospheric Imaging Assembly (AIA), also on SDO, during an X-class solar flare that occurred on **2011 February 15**. Both the pre-flare subtracted EVE spectra and fits to the associated free-free continuum were convolved with the AIA response functions of the seven EUV passbands at 10 s cadence throughout the course of the flare. It was found that 10-25% of the total emission in the 94A, 131A, 193A, and 335A passbands throughout the main phase of the flare was due to free-free emission. Reliable measurements could not be made for the 171A channel, while the continuum contribution to the 304A channel was negligible due to the presence of the strong He II emission line. Up to 50% of the emission in the 211A channel was found to be due to free-free emission around the peak of the flare, while an additional 20% was due to the recombination continuum of He II. The analysis was extended to a number of M- and X-class flares and it was found that the level of free-free emission contributing to the 171A and 211A passbands increased with increasing GOES class. These results suggest that the amount of continuum emission that contributes to AIA observations during flares is more significant than that stated in previous studies which used synthetic, rather than observed, spectra. These findings highlight the importance of spectroscopic observations carried out in conjunction with those from imaging instruments so that the data are interpreted correctly.

TIME-DEPENDENT DENSITY DIAGNOSTICS OF SOLAR FLARE PLASMAS USING SDO/EVE

Ryan O. **Milligan**, Michael B. Kennedy, Mihalis Mathioudakis, and Francis P. Keenan
2012 ApJ 755 L16
Temporally resolved electron density measurements of solar flare plasmas are presented using data from the EUV Variability Experiment (EVE) on board the Solar Dynamics Observatory. The EVE spectral range contains emission lines formed between 104 and 107 K, including transitions from highly ionized iron (10 MK). Using three density-sensitive Fe XXI ratios, peak electron densities of 1011.2-1012.1 cm–3 were found during four X-class flares. While previous measurements of densities at such high temperatures were made at only one point during a flaring event, EVE now allows the temporal evolution of these high-temperature densities to be determined at 10 s cadence. A comparison with GOES data revealed that the peak of the density time profiles for each line ratio correlated well with that of the emission measure time profile for each of the events studied.

Time Profiles of Solar Flare Densities

Ryan **Milligan** and Michael Kennedy.
RHESSI_Science_Nuggets, No. 176, May **2012**
The EUV spectra from EVE include nice density diagnostics.
See http://sprg.ssl.berkeley.edu/~tohban/wiki/index.php/Time_Profiles_of_Solar_Flare_Densities

9 August 2011

OBSERVATIONS OF ENHANCED EXTREME ULTRAVIOLET CONTINUA DURING AN X-CLASS SOLAR FLARE USING SDO/EVE
Ryan O. **Milligan**1, Phillip C. Chamberlin2, Hugh S. Hudson3, Thomas N. Woods4, Mihalis Mathioudakis1, Lyndsay Fletcher5, Adam F. Kowalski6 and Francis P. Keenan1
2012 ApJ 748 L14
Observations of extreme ultraviolet (EUV) emission from an X-class solar flare that occurred on **2011 February 15** at 01:44 UT are presented, obtained using the EUV Variability Experiment (EVE) on board the Solar Dynamics Observatory. The complete EVE spectral range covers the free-bound continua of H I (Lyman continuum), He I, and He II, with recombination edges at 91.2, 50.4, and 22.8 nm, respectively. By fitting the wavelength ranges blueward of each recombination edge with an exponential function, light curves of each of the integrated continua were generated over the course of the flare, as was emission from the free-free continuum (6.5-37 nm). The He II 30.4 nm and Lyα 121.6 nm lines, and soft X-ray (SXR; 0.1-0.8 nm) emission from GOES are also included for comparison. Each free-bound continuum was found to have a rapid rise phase at the flare onset similar to that seen in the 25-50 keV light curves from RHESSI, suggesting that they were formed by recombination with free electrons in the chromosphere. However, the free-free emission exhibited a slower rise phase seen also in the SXR emission from GOES, implying a predominantly coronal origin. By integrating over the entire flare the total energy emitted via each process was determined. We find that the flare energy in the EVE spectral range amounts to at most a few percent of the total flare energy, but EVE gives us a first comprehensive look at these diagnostically important continuum components.

Flare Observations of the EUV Continua
Ryan **Milligan**
RHESSI Science Nugget No. 167, Jan **2012**
http://sprg.ssl.berkeley.edu/~tohban/wiki/index.php/Flare_Observations_of_the_EUV_Continua
In this nugget we present new observations from the EUV Variability Experiment (EVE) instrument onboard SDO which show unambiguous, spectrally and temporally-resolved detections of the enhanced EUV continua during the first X-class flare of Solar Cycle 24. Here we focus on the free-free (bremsstrahlung) continuum, and on the free-bound (recombination) continua of hydrogen and helium. Although EVE was primarily designed to measure the variations in the solar EUV irradiance on a range of timescales, and with high precision, these data, in conjunction with X-ray observations from RHESSI, highlight EVE's ability to help answer long-standing, fundamental questions on solar flare energetics. **2011 February 15**

SPATIALLY RESOLVED NONTHERMAL LINE BROADENING DURING THE IMPULSIVE PHASE OF A SOLAR FLARE
Ryan O. **Milligan**
2011 ApJ 740 70
This paper presents a detailed study of excess line broadening in extreme ultraviolet (EUV) emission lines during the impulsive phase of a C-class solar flare. In this work, which utilizes data from the EUV Imaging Spectrometer on board Hinode, the broadened line profiles were observed to be cospatial with the two hard X-ray footpoints as observed by RHESSI. By plotting the derived nonthermal velocity for each pixel within the Fe XV and Fe XVI rasters against its corresponding Doppler velocity a strong correlation ($|r| > 0.59$) was found between the two parameters for one of the footpoints. This suggested that the excess broadening at these temperatures is due to a superposition of flows (turbulence), presumably as a result of chromospheric evaporation due to nonthermal electrons. Also presented are diagnostics of electron densities using five pairs of density-sensitive line ratios. Density maps derived using the Mg VII and Si X line pairs showed no appreciable increase in electron density at the footpoints, whereas the Fe XII, Fe XIII, and Fe XIV line pairs revealed densities approaching 1011.5 cm–3. Using this information, the nonthermal velocities derived from the widths of the two Fe XIV lines were plotted against their corresponding density values derived from their ratio. This showed that pixels with large nonthermal velocities were associated with pixels of moderately higher densities. This suggests that nonthermal broadening at these temperatures may have been due to enhanced densities at the footpoints, although estimates of the amount of opacity broadening and pressure broadening appeared to be negligible.

VELOCITY CHARACTERISTICS OF EVAPORATED PLASMA USING HINODE/EUV IMAGING SPECTROMETER
Ryan O. **Milligan** and Brian R. Dennis
ApJ 699 968-975, **2009**
This paper presents a detailed study of chromospheric evaporation using the EUV Imaging Spectrometer (EIS) onboard

Hinode in conjunction with hard X-ray (HXR) observations from *Reuven Ramaty High-Energy Solar Spectroscopic Imager* (*RHESSI*). The advanced capabilities of EIS were used to measure Doppler shifts in 15 emission lines covering the temperature range T = 0.05-16 MK during the impulsive phase of a C-class flare on **2007 December 14**. Blueshifts indicative of the evaporated material were observed in six emission lines from Fe XIV-XXIV (2-16 MK). Upflow velocity (v_{up}) was found to scale with temperature as v_{up} (km s^{-1}) $\approx$8-18T(MK). Although the hottest emission lines, Fe XXIII and Fe XXIV, exhibited upflows of >200 km s^{-1}, their line profiles were found to be dominated by a stationary component in contrast to the predictions of the standard flare model. Emission from O VI-Fe XIII lines (0.5-1.5 MK) was found to be redshifted by v_{down} (km s^{-1}) $\approx$60-17T (MK) and was interpreted as the downward-moving "plug" characteristic of explosive evaporation. These downflows occur at temperatures significantly higher than previously expected. Both upflows and downflows were spatially and temporally correlated with HXR emission observed by *RHESSI* that provided the properties of the electron beam deemed to be the driver of the evaporation. The energy flux of the electron beam was found to be $\gtrsim 5 \times 10^{10}$ erg cm^{-2} s^{-1}, consistent with the value required to drive explosive chromospheric evaporation from hydrodynamic simulations.

A Hot Microflare Observed With *RHESSI* and *Hinode*

Ryan O. **Milligan**

E-print, May **2008**; ApJL

RHESSI and *Hinode* observations of a GOES B-class flare are combined to investigate the origin of 15 MK plasma. The absence of any detectable hard X-ray emission coupled with weak blueshifted emission lines (indicating upward velocities averaging only 14 km s-1) suggests that this was a result of direct heating in the corona, as opposed to nonthermal electron precipitation causing chromospheric evaporation. These findings are in agreement with a recent hydrodynamical simulation of microflare plasmas which found that higher temperatures can be attained when less energy is used to accelerate electrons out of the thermal distribution. In addition, unusual redshifts in the 2 MK Fe XV line (indicating downward velocities of ~14 km s-1) were observed cospatial with one of the flare ribbons during the event. Downflows of such high temperature plasma are not predicted by any common flare model.

The Rotating Sunspot in AR 10930

Soonyoung **Min** · Jongchul Chae

Solar Phys (**2009**) 258: 203–217

We study the pattern and behavior of a rotating sunspot in Active Region 10930. The rotational angular speed has been extracted from the apparent motions of the sunspot determined by applying a new optical technique – called non-linear affine velocity estimator (NAVE) – to high-resolution G-band images taken by the *Solar Optical Telescope* (SOT) onboard the *Hinode* satellite. The structure and dynamics of coronal loops in this active region have been examined using the images obtained by the *X-Ray Telescope* (XRT) and the spectral data taken by the *Extreme-ultraviolet Imaging Spectrometer* (EIS), both also onboard *Hinode*. Our results are summarized as follows: *i*) The small sunspot of positive polarity rotated counterclockwise about its center by 540° during the period of five days. *ii*) Its angular velocity varied with the azimuth angle as well as the radial distance, being affected by the asymmetric shape of the umbra. *iii*) The angular velocity increased up to 8° h−1 until 13 December as the sunspot grew, and then decreased rapidly down to 3° h−1 on the next day as the sunspot decayed. *iv*) The coronal loops that connected the two sunspots became sigmoidal in shape. *v*) The coronal emissions from the regions around the rotating sunspot were blueshifted, which may indicate the expansion of the coronal loops. Our results suggest that the rotation of the sunspot may be closely related to the dynamic development of emerging twisted magnetic fields.

CORONAL ELECTRON DISTRIBUTION IN SOLAR FLARES: DRIFT-KINETIC MODEL

Takashi **Minoshima**1, Satoshi Masuda2, Yoshizumi Miyoshi2 and Kanya Kusano

2011 ApJ 732 111

Using a model of particle acceleration and transport in solar flares, we investigate the height distribution of coronal electrons by focusing on the energy-dependent pitch-angle scattering. When pitch-angle scattering is not included, the peak heights of loop-top electrons are constant, regardless of their energy, owing to the continuous acceleration and compression of the electrons via shrinkage of magnetic loops. On the other hand, under pitch-angle scattering, the electron heights are energy-dependent: intermediate-energy electrons are at a higher altitude, whereas lower and higher energy electrons are at lower altitudes. This implies that the intermediate-energy electrons are inhibited from following the shrinking field lines to lower altitudes because pitch-angle scattering causes efficient precipitation of these electrons into the footpoint and their subsequent loss from the loop. This result is qualitatively consistent with the position of the above-the-loop-top hard X-ray (HXR) source that is located above coronal HXR loops emitted by lower energy electrons and microwaves emitted by higher energy electrons. Quantitative agreement with observations might be

achieved by considering primary acceleration before the onset of loop shrinkage and additional pitch-angle scattering via wave-particle interactions.

MULTIWAVELENGTH OBSERVATION OF ELECTRON ACCELERATION IN THE 2006 DECEMBER 13 FLARE

T. **Minoshima**1,2, S. Imada3, T. Morimoto4, T. Kawate5, H. Koshiishi6, M. Kubo7, S. Inoue8, H. Isobe5, S. Masuda2,
S. Krucker9, and T. Yokoyama1
The Astrophysical Journal, 697:843–849, **2009** May 20 doi:10.1088/0004-637X/697/1/843
http://www.iop.org:80/EJ/toc/-alert=43190/0004-637X/697/1

We present a multiwavelength observation of a solar flare occurring on **2006 December 13** with *Hinode*, *RHESSI*, and the Nobeyama Radio Observatory to study the electron acceleration site and mechanism. The Solar Optical Telescope (SOT) on board *Hinode* observed elongated flare ribbons, and *RHESSI* observed double-footpoint hard X-ray (HXR) sources appearing in part of the ribbons. A photospheric vector magnetogram obtained from SOT reveals that the HXR sources are located at the region where horizontal magnetic fields change direction. The region is interpreted as the footpoint of magnetic separatrix. Microwave images taken with the Nobeyama Radioheliograph show a loop structure connecting the HXR sources. The brighter parts of the microwave intensity are located between the top and footpoints of the loop. We consider these observations as evidence of electron acceleration near the magnetic separatrix and injection parallel to the field line.

Comparative Analysis of Non-Thermal Emissions and Study of Electron Transport in a Solar Flare

T. **Minoshima**, T. Yokoyama, and N. Mitani
E-print, Oct 2007. Ap. J., 673:598Y 610, **2008**
http://www.journals.uchicago.edu/doi/pdf/10.1086/523884

We study nonthermal emission in a solar flare occurring on 2003 May 29 using RHESSI hard X-ray (HXR) and Nobeyama microwave observations. This flare shows several typical behaviors of HXR and microwave emission: time delay of microwave peaks relative to HXR peaks, loop-top microwave and footpoint HXR sources, and a harder electron energy distribution from the microwave spectrum than from the HXR spectrum. In addition, we found that the time profile of the spectral index of the higher energy (k100 keV) HXRs is similar to that of the microwaves, and is delayed relative to that of the lower energy (P100 keV) HXRs. We interpret these observations in terms of an electron transport model called trap-plus-precipitation. We numerically solved the spatially homogeneous Fokker-Planck equation to determine electron evolution in energy and pitch-angle space. By comparing observations with the behavior of HXR and microwave emission predicted by the model, we examine the pitch-angle distribution of the electrons injected into the flare site.We find that the observed spectral variations can be qualitatively explained if the injected electrons have a pitch-angle distribution concentrated perpendicular to the magnetic field lines rather than an isotropic distribution.

Solar Corona Thermal Background and Energy Spectrum of the Weak Solar Soft X-ray Bursts

I.K.**Mirzoeva**
2016
https://arxiv.org/pdf/1611.04525v1.pdf

We analyze the time profiles for weak solar soft X-ray bursts over the period 1995–1999 within the framework of the Interball–Tail Probe project. We have revealed a tendency for the peak of the energy spectrum of the time profiles for weak solar soft X-ray bursts to shift and their correlation with the thermal background.

Soft X-ray microflares

I. K. **Mirzoeva**
2015
http://arxiv.org/pdf/1509.05210v1.pdf

Soft X-ray solar bursts are studied within the framework of the Interball–Tail Probe project with the RF–15I–2 solar X-ray photometer–imager. The low-intensity microflares observed in September–December, 1995 are analyzed. Weak bursts with powers up to 10-8 W/m2 were detected. All the events were confirmed by GOES observations. Parameters of these microflares are determined. A physical mechanism for the low-intensity solar events is discussed.
The intensity distributions of the microflares are compiled. The energy distribution of solar flares is concluded to deviate from a power law. The lower limit of the solar-flare fluence

distribution is found. This conclusion is verified based on RHESSI data.
Correlations between the diurnal mean peaks of X-ray bursts of different classes and the daily means of the thermal background emission from the solar corona are revealed.
December 8-15, 1995, May 2 2002

Soft X-ray Spectral Diagnostics of Multi-thermal Plasma in Solar Flares with Chandrayaan-2 XSM

N. P. S. **Mithun**, Santosh V. Vadawale, Giulio Del Zanna, Yamini K. Rao, Bhuwan Joshi, Aveek Sarkar, Biswajit Mondal, P. Janardhan, Anil Bhardwaj, Helen E. Mason
ApJ **2022**
https://arxiv.org/pdf/2210.03364.pdf
Spectroscopic observations in X-ray wavelengths provide excellent diagnostics of the temperature distribution in solar flare plasma. The Solar X-ray Monitor (XSM) onboard the Chandrayaan-2 mission provides broad-band disk integrated soft X-ray solar spectral measurements in the energy range of 1-15 keV with high spectral resolution and time cadence. In this study, we analyse X-ray spectra of three representative GOES C-class flares obtained with the XSM to investigate the evolution of various plasma parameters during the course of the flares. Using the soft X-ray spectra consisting of the continuum and well-resolved line complexes of major elements like Mg, Si, and Fe, we investigate the validity of the isothermal and multi-thermal assumptions on the high temperature components of the flaring plasma. We show that the soft X-ray spectra during the impulsive phase of the high intensity flares are inconsistent with isothermal models and are best fitted with double peaked differential emission measure distributions where the temperature of the hotter component rises faster than that of the cooler component. The two distinct temperature components observed in DEM models during the impulsive phase of the flares suggest the presence of the directly heated plasma in the corona and evaporated plasma from the chromospheric footpoints. We also find that the abundances of low FIP elements Mg, Si, and Fe reduces from near coronal to near photospheric values during the rising phase of the flare and recovers back to coronal values during decay phase, which is also consistent with the chromospheric evaporation scenario. **2020-10-16, 2021-09-08, 2021-10-07**

Circular ribbon flare triggered from an incomplete fan-spine configuration⋆

Prabir K. **Mitra**1,2, Astrid M. Veronig1,3 and Bhuwan Joshi2
A&A 674, A154 (**2023**)
https://www.aanda.org/articles/aa/pdf/2023/06/aa46103-23.pdf
Context. Circular ribbon flares are characterised by circular, semi-circular, or elliptical ribbon brightenings. As the physics of such solar events involves a true 3D magnetic topology, they have been extensively studied in contemporary solar research.
Aims. In order to understand the triggering processes and the complex magnetic topology involved in circular ribbon flares, we carried out a thorough investigation of an M-class circular ribbon flare that originated within close proximity of a quasi-separatrix layer (QSL).
Methods. We combined multi-wavelength Atmospheric Imaging Assembly (AIA) and Reuven Ramaty High Energy Solar Spectroscopic Imager (RHESSI) observations with photospheric Helioseismic and Magnetic Imager (HMI) observations and coronal magnetic field modelling analysis using the non-linear force free field (NLFFF) model.
Results. The circular ribbon flare occurred from a complex magnetic configuration characterised by negative magnetic patches surrounded by positive-polarity regions on three sides. As the negative polarity patches were not surrounded by positive-polarity regions on all four sides, the corresponding coronal field was devoid of any null points. This led to the formation of an incomplete fan-spine-like configuration that deviated from classical fan-spine configurations in null-point topology. Further, an observationally identified QSL structure was situated within the active region, very close to the flaring region. The presence of the QSL was verified by the NLFFF modelling. The far end of the spine-like lines terminated very close to one footpoint location of the QSL lines. Our analysis suggests that activities at this location led to the activation of a flux rope situated within the fan-like lines and triggering of the circular ribbon flare via perturbation of the overall fan-spine-like structure. Further, we identified RHESSI X-ray sources from the footpoints of the QSL structure, which suggests that slipping reconnections can also lead to discernible signatures of particle acceleration. **12 March 2015**

Successive occurrences of quasi-circular ribbon flares in a fan-spine-like configuration involving hyperbolic flux tube

Prabir K. **Mitra** (USO/PRL), Bhuwan Joshi (USO/PRL)
MNRAS Volume 503, Issue 1, Pages 1017–1035, **2021**
https://arxiv.org/pdf/2101.08164.pdf
https://doi.org/10.1093/mnras/stab175
We present a comprehensive analysis of the formation and evolution of a fan-spine-like configuration that developed over a complex photospheric configuration where dispersed negative polarity regions were surrounded by positive polarity regions. This unique photospheric configuration, analogous to the geological "atoll" shape, hosted four

homologous flares within its boundary. Computation of the degree of squashing factor (Q) maps clearly revealed an elongated region of high Q-values between the inner and outer spine-like lines, implying the presence of an hyperbolic flux tube (HFT). The coronal region associated with the photospheric atoll configuration was distinctly identified in the form of a diffused dome-shaped bright structure directly observed in EUV images. A filament channel resided near the boundary of the atoll region. The activation and eruption of flux ropes from the filament channel led to the onset of four eruptive homologous quasi-circular ribbon flares within an interval of ≈11 hours. During the interval of the four flares, we observed continuous decay and cancellation of negative polarity flux within the atoll region. Accordingly, the apparent length of the HFT gradually reduced to a null-point-like configuration before the fourth flare. Prior to each flare, we observed localised brightening beneath the filaments which, together with flux cancellation, provided support for the tether-cutting model of solar eruption. The analysis of magnetic decay index revealed favourable conditions for the eruption, once the pre-activated flux ropes attained the critical heights for torus instability. **15-16 Feb 2014**

ERUPTIVE-IMPULSIVE HOMOLOGOUS M-CLASS FLARES ASSOCIATED WITH DOUBLE-DECKER FLUX ROPE CONFIGURATION IN MINI-SIGMOID OF NOAA 12673

Prabir K. **Mitra**,1, 2 Bhuwan Joshi,1 Astrid M. Veronig,3 Ramesh Chandra,4 K. Dissauer,3, 5 and Thomas Wiegelmann6

ApJ **900** 23 **2020**

https://arxiv.org/pdf/2007.11810.pdf

https://doi.org/10.3847/1538-4357/aba900

We present a multiwavelength analysis of two homologous, short lived, impulsive flares of GOES class M1.4 and M7.3, that occurred from a very localized mini-sigmoid region within the active region NOAA 12673 on **2017 September 7**. Both flares were associated with initial jet-like plasma ejection which for a brief amount of time moved toward east in a collimated manner before drastically changing direction toward southwest. Non-linear force-free field extrapolation reveals the presence of a compact double-decker flux rope configuration in the mini-sigmoid region prior to the flares. A set of open field lines originating near the active region which were most likely responsible for the anomalous dynamics of the erupted plasma, gave the earliest indication of an emerging coronal hole near the active region. The horizontal field distribution suggests a rapid decay of the field above the active region, implying high proneness of the flux rope system toward eruption. In view of the low coronal double-decker flux ropes and compact extreme ultra-violet (EUV) brightening beneath the filament along with associated photospheric magnetic field changes, our analysis supports the combination of initial tether-cutting reconnection and subsequent torus instability for driving the eruption.

Identification of Pre-flare Processes and Their Possible Role in Driving a Large-scale Flux Rope Eruption with Complex M-class Flare in the Active Region NOAA 12371

Prabir K. **Mitra**, Bhuwan Joshi, Avijeet Prasad

Solar Physics February **2020**, 295:29

https://link.springer.com/content/pdf/10.1007/s11207-020-1596-2.pdf

https://doi.org/10.1007/s11207-020-1596-2

https://arxiv.org/pdf/2002.05890.pdf

In this article, we study the origin of precursor flare activity and investigate its role towards triggering the eruption of a flux rope which resulted into a dual-peak M-class flare (SOL**2015-06-21**T02:36) in the active region NOAA 12371. The flare evolved in two distinct phases with peak flux levels of M2.1 and M2.6 at an interval of ≈54≈54 min. The active region exhibited striking moving magnetic features (MMFs) along with sunspot rotation. Nonlinear force-free field (NLFFF) modelling of the active region corona reveals a magnetic flux rope along the polarity inversion line in the trailing sunspot group which is observationally manifested by the co-spatial structures of an active region filament and a hot channel identified in the 304 and 94 Å images, respectively, from the Atmospheric Imaging Assembly (AIA). The active region underwent a prolonged phase of flux enhancement followed by a relatively shorter period of flux cancellation prior to the onset of the flare which led to the build up and activation of the flux rope. Extreme ultra-violet (EUV) images reveal localised and structured pre-flare emission, from the region of MMFs, adjacent to the location of the main flare. Our analysis reveals strong, localised regions of photospheric currents of opposite polarities at the precursor location, thereby making the region susceptible to small-scale magnetic reconnection. Precursor reconnection activity from this location most likely induced a slipping reconnection towards the northern leg of the hot channel which led to the destabilisation of the flux rope. The application of magnetic virial theorem suggests that there was an overall growth of magnetic free energy in the active region during the prolonged pre-flare phase which decayed rapidly after the hot channel eruption and its successful transformation into a halo coronal mass ejection (CME).

Pre-flare processes, flux rope activation, large-scale eruption and associated X-class flare from the active region NOAA 11875

Prabir K. **Mitra** (USO/PRL), Bhuwan Joshi (USO/PRL)

ApJ **884** 46 **2019**

https://arxiv.org/pdf/1908.04059.pdf

https://doi.org/10.3847/1538-4357/ab3a96
We present a multi-wavelength analysis of the eruption of a hot coronal channel associated with an X1.0 flare (**SOL2013-10-28T02**:03) from the active region NOAA 11875 by combining observations from AIA/SDO, HMI/SDO, RHESSI, and HiRAS. EUV images at high coronal temperatures indicated the presence of a hot channel at the core of the active region from the early pre-flare phase evidencing the pre-existence of a quasi-stable magnetic flux rope. The hot channel underwent an activation phase after a localized and prolonged pre-flare event occurring adjacent to one of its footpoints. Subsequently, the flux rope continued to rise slowly for ≈16 min during which soft X-ray flux gradually built-up characterizing a distinct precursor phase. The flux rope transitioned from the state of slow rise to the eruptive motion with the onset of the impulsive phase of the X1.0 flare. The eruptive expansion of the hot channel is accompanied by a series of type III radio bursts in association with impulsive rise of strong hard X-ray non-thermal emissions that included explicit hard X-ray sources of energies up to ≈50 keV from the coronal loops and ≈100 keV from their footpoint locations. Our study contains evidence that pre-flare activity occurring within the spatial extent of a stable flux rope can destabilize it toward eruption. Moreover, sudden transition of the flux rope from the state of slow rise to fast acceleration precisely bifurcated the precursor and the impulsive phases of the flare which points toward a feedback relationship between early CME dynamics and the strength of the large-scale magnetic reconnection.

Successive flux rope eruptions from δ-Sunspots region of NOAA 12673 and associated X-class eruptive flares on 2017 September 6

Prabir K. **Mitra** (USO/PRL, India), Bhuwan Joshi (USO/PRL, India), Avijeet Prasad (USO/PRL, India), Astrid M. Veronig (Univ. of Graz, Austria), R. Bhattacharyya (USO/PRL, India)
ApJ 869 69 **2018**
https://arxiv.org/pdf/1810.13146.pdf
In this paper, we present a multi-wavelength analysis of two X-class solar eruptive flares of classes X2.2 and X9.3 that occurred in the sigmoidal active region NOAA 12673 on **2017 September 6**, by combining observations of Atmospheric Imaging Assembly and Helioseismic Magnetic Imager instruments on board the Solar Dynamics Observatory. On the day of the reported activity, the photospheric structure of the active region displayed a very complex network of δ-sunspots that gave rise to the formation of a coronal sigmoid observed in the hot EUV channels. Both X-class flares initiated from the core of the sigmoid sequentially within an interval of ∼3 hours and progressed as a single "sigmoid--to--arcade" event. Differential emission measure analysis reveals strong heating of plasma at the core of the active region right from the pre-flare phase which further intensified and spatially expanded during each event. The identification of a pre-existing magnetic null by non-force-free-field modeling of the coronal magnetic fields at the location of early flare brightenings and remote faint ribbon-like structures during the pre-flare phase, which were magnetically connected with the core region, provide support for the breakout model of solar eruption. The magnetic extrapolations also reveal flux rope structures prior to both flares which are subsequently supported by the observations of the eruption of hot EUV channels. The second X-class flare diverged from the standard flare scenario in the evolution of two sets of flare ribbons, that are spatially well separated, providing firm evidence of magnetic reconnections at two coronal heights.

Solar microflares: a case study on temperatures and the Fe XVIII emission

Urmila **Mitra-Kraev**, Giulio Del Zanna
A&A 628, A134 **2019**
https://arxiv.org/pdf/1905.08579.pdf
https://doi.org/10.1051/0004-6361/201834856
In this paper, we discuss the temperature distribution and evolution of a microflare, simultaneously observed by Hinode XRT, EIS, and SDO AIA. We find using EIS lines that during peak emission the distribution is nearly isothermal and peaked around 4.5 MK. This temperature is in good agreement with that obtained from the XRT filter ratio, validating the use of XRT to study these small events, invisible by full-Sun X-ray monitors such as GOES. The increase in the estimated Fe XVIII emission in the AIA 94 {\AA} band can mostly be explained with the small temperature increase from the background temperatures. The presence of Fe XVIII emission does not guarantee that temperatures of 7 MK are reached, as is often assumed. We also revisit with new atomic data the temperatures measured by a SoHO SUMER observation of an active region which produced microflares, also finding low temperatures (3 - 4 MK) from an Fe XVIII / Ca XIV ratio. **2011-09-03**

Generation of fast magnetoacoustic waves in the corona by impulsive bursty reconnection

Sripan **Mondal**, A.K. Srivastava, David I. Pontin, Eric R. Priest, R. Kwon, Ding Yuan
ApJ **977** 235 **2024**
https://arxiv.org/pdf/2411.02180
https://iopscience.iop.org/article/10.3847/1538-4357/ad9022/pdf
Fast-mode magnetohydrodynamic (MHD) waves in the solar corona are often known to be produced by solar flares and eruptive prominences. We here simulate the effect of the interaction of an external perturbation on a magnetic null in

the solar corona which results in the formation of a current sheet (CS). Once the CS undergoes a sufficient extension in its length and squeezing of its width, it may go unstable to the formation of multiple impulsive plasmoids. Eventually, the plasmoids merge with one another to form larger plasmoids and/or are expelled from the sheet. The formation, motion and coalescence of plasmoids with each other and with magnetic Y-points at the outer periphery of the extended CS are found to generate wave-like perturbations. An analysis of the resultant quasi-periodic variations of pressure, density, velocity and magnetic field at certain locations in the model corona indicate that these waves are predominantly fast-mode magnetoacoustic waves. For typical coronal parameters, the resultant propagating waves carry an energy flux of 105 erg cm−2 s−1 to a large distance of at least 60 Mm away from the current sheet. In general, we suggest that both waves and reconnection play a role in heating the solar atmosphere and driving the solar wind and may interact with one another in a manner that we refer to as a "Symbiosis of WAves and Reconnection (SWAR)".

A Joint Microwave and Hard X-Ray Study Towards Understanding the Transport of Accelerated Electrons during an Eruptive Solar Flare

Surajit **Mondal**, Andrea F. Battaglia, Bin Chen, Sijie Yu
ApJ **966** 208 **2024**
https://arxiv.org/pdf/2404.14268.pdf
https://iopscience.iop.org/article/10.3847/1538-4357/ad3910/pdf
The standard flare model, despite its success, is limited in comprehensively explaining the various processes involving nonthermal particles. One such missing ingredient is a detailed understanding of the various processes involved during the transport of accelerated electrons from their site of acceleration to different parts of the flare region. Here we use simultaneous radio and X-ray observations from the Expanded Owens Valley Solar Array (EOVSA) and Spectrometer/Telescope for Imaging X-rays (STIX) onboard the Solar Orbiter (SolO), respectively, from two distinct viewing perspectives to study the electron transport processes. Through detailed spectral modeling of the coronal source using radio data and footpoint sources using X-ray spectra, we compare the nonthermal electron distribution at the coronal and footpoint sources. We find that the flux of nonthermal electrons precipitated at the footpoint is an order of magnitude greater than that trapped in the looptop, consistent with earlier works which primarily used X-ray for their studies. In addition, we find that the electron spectral indices obtained from X-ray footpoints is significantly softer than the spectral hardness of the nonthermal electron distribution in the corona. We interpret these differences based on transport effects and the difference in sensitivity of microwave and X-ray observations to different regimes of electron energies. Such an understanding is crucial for leveraging different diagnostic methods of nonthermal electrons simultaneously to achieve a more comprehensive understanding of the electron acceleration and transport processes of solar flares. **2021 May 7**

2.5D Magnetohydrodynamic Simulation of the Formation and Evolution of Plasmoids in Coronal Current Sheets

Sripan **Mondal**1, Abhishek K. Srivastava6,1, David I. Pontin2, Ding Yuan3,4, and Eric R. Priest5
2024 ApJ 963 139
https://iopscience.iop.org/article/10.3847/1538-4357/ad2079/pdf
In the present paper, using MPI-AMRVAC, we perform a 2.5D numerical magnetohydrodynamic simulation of the dynamics and associated thermodynamical evolution of an initially force-free Harris current sheet subjected to an external velocity perturbation under the condition of uniform resistivity. The amplitude of the magnetic field is taken to be 10 G, typical of the solar corona. We impose a Gaussian velocity pulse across this current sheet that mimics the interaction of fast magnetoacoustic waves with a current sheet in the corona. This leads to a variety of dynamics and plasma processes in the current sheet, which is initially quasi-static. The initial pulse interacts with the current sheet and splits into a pair of counterpropagating wavefronts, which form a rarefied region that leads to an inflow and a thinning of the current sheet. The thinning results in Petschek-type magnetic reconnection followed by a tearing instability and plasmoid formation. The reconnection outflows containing outward-moving plasmoids have accelerated motions with velocities ranging from 105 to 303 km s−1. The average temperature and density of the plasmoids are found to be 8 MK and twice the background density of the solar corona, respectively. These estimates of the velocity, temperature, and density of the plasmoids are similar to values reported from various solar coronal observations. Therefore, we infer that the external triggering of a quasi-static current sheet by a single-velocity pulse is capable of initiating magnetic reconnection and plasmoid formation in the absence of a localized enhancement of resistivity in the solar corona.

Determining the nanoflare heating frequency of an X-ray Bright Point observed by MaGIXS

Biswajit **Mondal**, P. S. Athiray, Amy R. Winebarger, Sabrina L. Savage, +++
ApJ **2024**
https://arxiv.org/pdf/2402.05036.pdf
Nanoflares are thought to be one of the prime candidates that can heat the solar corona to its multi-million kelvin temperature. Individual nanoflares are difficult to detect with the present generation instruments, however their presence can be inferred by comparing simulated nanoflare-heated plasma emissions with the observed emission. Using HYDRAD coronal loop simulations, we model the emission from an X-ray bright point (XBP) observed by the

Marshall Grazing Incidence X-ray Spectrometer (MaGIXS), along with nearest-available observations from the Atmospheric Imaging Assembly (AIA) onboard Solar Dynamics Observatory (SDO) and X-Ray Telescope (XRT) onboard Hinode observatory. The length and magnetic field strength of the coronal loops are derived from the linear-force-free extrapolation of the observed photospheric magnetogram by Helioseismic and Magnetic Imager (HMI) onboard SDO. Each loop is assumed to be heated by random nanoflares, whose magnitude and frequency are determined by the loop length and magnetic field strength. The simulation results are then compared and matched against the measured intensity from AIA, XRT, and MaGIXS. Our model results indicate the observed emissions from the XBP under study could be well matched by a distribution of nanoflares with average delay times 1500 s to 3000 s, which suggest that the heating is dominated by high-frequency events. Further, we demonstrate the high sensitivity of MaGIXS and XRT to diagnose the heating frequency using this method, while AIA passbands are found to be the least sensitive. **2021-07-30**

Reconnection-generated Plasma Flows in the Quasi-separatrix Layer in Localized Solar Corona

Sripan **Mondal**1, Abhishek K. Srivastava1, Sudheer K. Mishra2, K. Sangal1, Pradeep Kayshap3, Yang Guo4, David I Pontin5, Vadim M. Uritsky6, Leon Ofman6,7, Tongjiang Wang6
2023 ApJ 953 84
https://arxiv.org/pdf/2305.02277.pdf
https://iopscience.iop.org/article/10.3847/1538-4357/acd2da/pdf
Multiwavelength observations of the propagating disturbances (PDs), discovered by Atmospheric Imaging Assembly (AIA) on board Solar Dynamics Observatory (SDO), are analyzed to determine their driving mechanism and physical nature. Two magnetic strands in the localized corona are observed to approach and merge with each other, followed by the generation of brightening, which further propagates in a cusp-shaped magnetic channel. Differential emission measure analysis shows an occurrence of heating in this region of interest. We extrapolate potential magnetic field lines at coronal heights from the observed Helioseismic and Magnetic Imager vector magnetogram via Green's function method using MPI-AMRVAC. We analyze the field to locate magnetic nulls and quasi-separatrix layers (QSLs), which are preferential locations for magnetic reconnection. Dominant QSLs including a magnetic null are found to exist and match the geometry followed by PDs; therefore, this provides conclusive evidence of magnetic reconnection. In addition, spectroscopic analysis of Interface Region Imaging Spectrograph Si ivλ1393.77 line profiles show a rise of line width in the same time range depicting the presence of mass motion in the observed cusp-shaped region. PDs are observed to exhibit periodicities of around 4 minutes. The speeds of PDs measured by the surfing transform technique are close to each other in four different SDO/AIA bandpasses, i.e., 304, 171, 193, and 131 Å, excluding the interpretation of PDs in terms of slow magnetoacoustic waves. We describe comprehensively the observed PDs as quasiperiodic plasma flows generated as a result of periodic reconnection in the vicinity of a coronal magnetic null. **2021 April 17**

Evolution of Elemental Abundances During B-Class Solar Flares: Soft X-ray Spectral Measurements with Chandrayaan-2 XSM

Biswajit **Mondal**, Aveek Sarkar, Santosh V. Vadawale, N. P. S. Mithun, P. Janardhan, Giulio Del Zanna, Helen E. Mason, Urmila Mitra-Kraev, S. Narendranath
ApJ **920** 4 **2021**
https://arxiv.org/pdf/2107.07825.pdf
https://iopscience.iop.org/article/10.3847/1538-4357/ac14c1/pdf
https://doi.org/10.3847/1538-4357/ac14c1
The Solar X-ray Spectrometer (XSM) payload onboard Chandrayaan-2 provides disk-integrated solar spectra in the 1-15 keV energy range with an energy resolution of 180 eV (at 5.9 keV) and a cadence of 1~second. During the period from September 2019 to May 2020, covering the minimum of Solar Cycle 24, it observed nine B-class flares ranging from B1.3 to B4.5. Using time-resolved spectroscopic analysis during these flares, we examined the evolution of temperature, emission measure, and absolute elemental abundances of four elements -- Mg, Al, Si, and S. These are the first measurements of absolute abundances during such small flares and this study offers a unique insight into the evolution of absolute abundances as the flares evolve. Our results demonstrate that the abundances of these four elements decrease towards their photospheric values during the peak phase of the flares. During the decay phase, the abundances are observed to quickly return to their pre-flare coronal values. The depletion of elemental abundances during the flares is consistent with the standard flare model, suggesting the injection of fresh material into coronal loops as a result of chromospheric evaporation. To explain the quick recovery of the so-called coronal "First Ionization Potential (FIP) bias" we propose two scenarios based on the Ponderomotive force model. **2019 Sep 30-Oct 1; 2020 Mar 11, Apr 4-9, 30**

Deconstructing Photospheric Spectral Lines in Solar and Stellar Flares

Aaron J. **Monson**1, Mihalis Mathioudakis1, and Adam F. Kowalski2,3,4

2024 ApJ 963 40
https://iopscience.iop.org/article/10.3847/1538-4357/ad16da/pdf
During solar flares, spectral lines formed in the photosphere have been shown to exhibit changes to their profiles despite the challenges of energy transfer to these depths. Recent work has shown that deep-forming spectral lines are subject to significant contributions from regions above the photosphere throughout the flaring period, resulting in a composite emergent intensity profile from multiple layers of the atmosphere. We employ radiative–hydrodynamic and radiative transfer calculations to simulate the response of the solar/stellar atmosphere to electron beam heating and synthesize spectral lines of Fe i to investigate the line-of-sight velocity fields information available from Doppler shifts of the emergent intensity profile. By utilizing the contribution function to deconstruct the line profile shape into its constituent sources, we show that variations in the line profiles are primarily caused by changes in the chromosphere. Up-flows in this region were found to create blueshifts or false redshifts in the line core dependent on the relative contribution of the chromosphere compared to the photosphere. In extreme solar and stellar flare scenarios featuring explosive chromospheric condensations, redshifted transient components can dominate the temporal evolution of the profile shape, requiring a tertiary component consideration to fully characterize. We conclude that deep-forming lines require a multicomponent understanding and treatment, with different regions of the spectral line being useful for probing individual regions of the atmosphere's velocity flows.

Flare Induced Photospheric Velocity Diagnostics

Aaron J. **Monson**, Mihalis Mathioudakis, Aaron Reid, Ryan Milligan, David Kuridze
ApJ **915** 16 **2021**
https://arxiv.org/pdf/2105.02199.pdf
https://iopscience.iop.org/article/10.3847/1538-4357/abfda8/pdf
https://doi.org/10.3847/1538-4357/abfda8
We present radiative hydrodynamic simulations of solar flares generated by the RADYN and RH codes to study the perturbations induced in photospheric Fe I lines by electron beam heating. We investigate how variations in the beam parameters result in discernible differences in the induced photospheric velocities. Line synthesis revealed a significant chromospheric contribution to the line profiles resulting in an apparent red asymmetry by as much as 40 m/s close to the time of maximum beam heating which was not reflective of the upflow velocities that arose from the radiative hydrodynamic simulations at those times. The apparent redshift to the overall line profile was produced by significant chromospheric emission that was blueshifted by as much as 400 m/s and fills in the blue side of the near stationary photospheric absorption profile. The velocity information that can be retrieved from photospheric line profiles during flares must therefore be treated with care to mitigate the effects of higher parts of the atmosphere providing an erroneous velocity signal.

Triangulation Tracking of a Radially Propagating MHD Wave in the AIA 1600 Acoustic Power Maps in Active Region 12193

Teresa **Monsue**
Research Notes of the AAA **2018**
https://arxiv.org/pdf/1803.02447.pdf
For decades it has been established that the amount of energy released by solar flares excites the acoustic oscillations propagating on the surface of the Sun (Wolff 1972). It is believed that these flares can excite velocity oscillations in active regions, especially those regions where a higher class solar flare has taken place (Kumar 2006). However, questions arise as to how the behaviors of acoustic oscillations within such a chaotic environment can birth other waves of the MHD type. Can we observe such events? **October 24, 2014**

Temporal Evolution of Chromospheric Oscillations in Flaring Regions - A Pilot Study

Teresa **Monsue**, Frank Hill, Keivan G. Stassun
ApJ **2018**
https://arxiv.org/pdf/1803.02506.pdf
We have analyzed H-alpha intensity images obtained at a 1 minute cadence with the Global Oscillation Network Group (GONG) system to investigate the properties of oscillations in the 0-8 mHz frequency band at the location and time of strong M- and X-class flares. For each of three sub-regions within two flaring active regions, we extracted time series from multiple distinct positions, including the flare core and quieter surrounding areas. The time series were analyzed with a moving power map analysis to examine power as a function of frequency and time. We find that, in the flare core of all three sub-regions, the low-frequency power (~1-2 mHz) is substantially enhanced immediately prior to and after the flare, and that power at all frequencies up to 8 mHz is depleted at flare maximum. This depletion is both frequency and time dependent, which probably reflects the changing depths visible during the flare in the bandpass of the filter. These variations are not observed outside the flare cores. The depletion may indicate that acoustic energy is being converted into thermal energy at flare maximum, while the low-frequency enhancement may arise from an instability in the chromosphere and provide an early warning of the flare onset. Dark lanes of reduced wave power are also visible in

the power maps, which may arise from the interaction of the acoustic waves and the magnetic field. **2012 June 13, 2012 July 12**

Image patch analysis of sunspots and active regions II. Clustering via matrix factorization

Kevin R. **Moon**1*, Véronique Delouille2, Jimmy J. Li1, Ruben De Visscher2, Fraser Watson3 and Alfred O. Hero

J. Space Weather Space Clim., 6, A3 (**2016**) **Open Access**

http://www.swsc-journal.org/articles/swsc/pdf/2016/01/swsc150030.pdf

Context. Separating active regions that are quiet from potentially eruptive ones is a key issue in Space Weather applications. Traditional classification schemes such as Mount Wilson and McIntosh have been effective in relating an active region large scale magnetic configuration to its ability to produce eruptive events. However, their qualitative nature prevents systematic studies of an active region's evolution for example.

Aims. We introduce a new clustering of active regions that is based on the local geometry observed in Line of Sight magnetogram and continuum images.

Methods. We use a reduced-dimension representation of an active region that is obtained by factoring the corresponding data matrix comprised of local image patches. Two factorizations can be compared via the definition of appropriate metrics on the resulting factors. The distances obtained from these metrics are then used to cluster the active regions.

Results. We find that these metrics result in natural clusterings of active regions. The clusterings are related to large scale descriptors of an active region such as its size, its local magnetic field distribution, and its complexity as measured by the Mount Wilson classification scheme. We also find that including data focused on the neutral line of an active region can result in an increased correspondence between our clustering results and other active region descriptors such as the Mount Wilson classifications and the R-value.

Conclusions. Matrix factorization of image patches is a promising new way of characterizing active regions. We provide some recommendations for which metrics, matrix factorization techniques, and regions of interest to use to study active regions.

Image patch analysis of sunspots and active regions I. Intrinsic dimension and correlation analysis

Kevin R. **Moon**1*, Jimmy J. Li1, Véronique Delouille2, Ruben De Visscher2, Fraser Watson3 and Alfred O. Hero

J. Space Weather Space Clim., 6, A2 (**2016**) **Open Access**

http://www.swsc-journal.org/articles/swsc/pdf/2016/01/swsc150023.pdf

Context. The flare productivity of an active region is observed to be related to its spatial complexity. Mount Wilson or McIntosh sunspot classifications measure such complexity but in a categorical way, and may therefore not use all the information present in the observations. Moreover, such categorical schemes hinder a systematic study of an active region's evolution for example.

Aims. We propose fine-scale quantitative descriptors for an active region's complexity and relate them to the Mount Wilson classification. We analyze the local correlation structure within continuum and magnetogram data, as well as the cross-correlation between continuum and magnetogram data.

Methods. We compute the intrinsic dimension, partial correlation, and canonical correlation analysis (CCA) of image patches of continuum and magnetogram active region images taken from the SOHO-MDI instrument. We use masks of sunspots derived from continuum as well as larger masks of magnetic active regions derived from magnetogram to analyze separately the core part of an active region from its surrounding part.

Results. We find relationships between the complexity of an active region as measured by its Mount Wilson classification and the intrinsic dimension of its image patches. Partial correlation patterns exhibit approximately a third-order Markov structure. CCA reveals different patterns of correlation between continuum and magnetogram within the sunspots and in the region surrounding the sunspots.

Conclusions. Intrinsic dimension has the potential to distinguish simple from complex active regions. These results also pave the way for patch-based dictionary learning with a view toward automatic clustering of active regions.

STATISTICAL EVIDENCE FOR SYMPATHETIC FLARES

Y.-J. **Moon**,1,2 G. S. Choe,3 Y. D. Park,2 Haimin Wang,1 Peter T. Gallagher,1,4 Jongchul Chae,1,5 H. S. Yun,6 and Philip R. Goode1

ApJ 574:434–439, **2002**

https://iopscience.iop.org/article/10.1086/340945/pdf

https://iopscience.iop.org/article/10.1086/340945/pdf

Sympathetic flares are a pair of flares that occur almost simultaneously in different active regions, not by chance, but because of some physical connection. In this paper statistical evidence for the existence of sympathetic flares is presented. From GOES X-ray flare data, we have collected 48 pairs of near simultaneous flares whose positional

information and Yohkoh soft X-ray telescope images are available. To select the active regions that probably have sympathetic flares, we have estimated the ratio R of actual flaring overlap time to random-coincidence overlap time for 38 active region pairs. We have then compared the waiting-time distributions for the two different groups of active region pairs (R > 1 and R < 1) with corresponding nonstationary Poisson distributions. As a result, we find a remarkable overabundance of short waiting times for the group with R > 1. This is the first time such strong statistical evidence has been found for the existence of sympathetic flares. To examine the role of interconnecting coronal loops, we have also conducted the same analysis for two subgroups of the R > 1 group: one with interconnecting X-ray loops and the other without. We do not find any statistical evidence that the subgroup with interconnecting coronal loops is more likely to produce sympathetic flares than the subgroup without. For the subgroup with loops, we find that sympathetic flares favor active region pairs with transequatorial loops.

Stealth Non-standard-model Confined Flare Eruptions: Sudden Reconnection Events in Ostensibly Inert Magnetic Arches from Sunspots

Ronald L. **Moore**, Sanjiv K. Tiwari, Navdeep K. Panesar, V. Aparna, Alphonse C. Sterling
ApJ **975** 20 **2024**
https://arxiv.org/pdf/2408.09021 **File**
https://iopscience.iop.org/article/10.3847/1538-4357/ad71d2/pdf
We report seven examples of a long-ignored type of confined solar flare eruption that does not fit the standard model for confined flare eruptions. Because they are confined eruptions, do not fit the standard model, and unexpectedly erupt in ostensibly inert magnetic arches, we have named them stealth non-standard-model confined flare eruptions. Each of our flaring magnetic arches stems from a big sunspot. We tracked each eruption in full-cadence UV and EUV images from the Atmospheric Imaging Assembly (AIA) of Solar Dynamics Observatory (SDO) in combination with magnetograms from SDO's Helioseismic and Magnetic Imager (HMI). We present the onset and evolution of two eruptions in detail: one of six that each make two side-by-side main flare loops, and one that makes two crossed main flare loops. For these two cases, we present cartoons of the proposed pre-eruption field configuration and how sudden reconnection makes the flare ribbons and flare loops. Each of the seven eruptions is consistent with being made by sudden reconnection at an interface between two internal field strands of the magnetic arch, where they cross at a small (10 - 20 degrees) angle. These stealth non-standard-model confined flare eruptions therefore plausibly support the idea of E. N. Parker for coronal heating in solar coronal magnetic loops by nanoflare bursts of reconnection at interfaces of internal field strands that cross at angles of 10 - 20 degrees. **2012 Jan 8, 2013 Jan 14, 2013 Jun 27, 2014 Jan 23, 2014 Nov 19, 2014 Nov 20**

Joint MinXSS and RHESSI Flare X-ray Spectra between 1 and 15 keV

Chris **Moore**, Brian Dennis and the MinXSS Science
RHESSI Science Nuggets # 316 Feb **2018**
http://sprg.ssl.berkeley.edu/~tohban/wiki/index.php/Joint_MinXSS_and_RHESSI_Flare_X-ray_Spectra_between_1_and_15_keV
2016-07-23

Measurements and Modeling of Total Solar Irradiance in X-Class Solar Flares

Christopher Samuel **Moore**, Phillip Clyde Chamberlin, Rachel Hock
2015
http://arxiv.org/pdf/1509.06074v1.pdf
The Total Irradiance Monitor (TIM) from NASA's SOlar Radiation and Climate Experiment (SORCE) can detect changes in the Total Solar Irradiance (TSI) to a precision of 2 ppm, allowing observations of variations due to the largest X-Class solar ares for the first time. Presented here is a robust algorithm for determining the radiative output in the TIM TSI measurements, in both the impulsive and gradual phases, for the four solar ares presented in Woods et al. (2006), as well as an additional are measured on 2006 December 6. The radiative outputs for both phases of these five ares are then compared to the Vacuum Ultraviolet (VUV) irradiance output from the Flare Irradiance Spectral Model (FISM) in order to derive an empirical relationship between the FISM VUV model and the TIM TSI data output to estimate the TSI radiative output for eight other X-Class ares. This model provides the basis for the bolometric energy estimates for the solar ares analyzed in the Emslie et al. (2012) study.

Measurements and Modeling of Total Solar Irradiance in X-class Solar Flares

Christopher Samuel **Moore**1,2,3, Phillip Clyde Chamberlin4, and Rachel Hock
2014 ApJ 787 32
The Total Irradiance Monitor (TIM) from NASA's SOlar Radiation and Climate Experiment can detect changes in the total solar irradiance (TSI) to a precision of 2 ppm, allowing observations of variations due to the largest X-class solar

flares for the first time. Presented here is a robust algorithm for determining the radiative output in the TIM TSI measurements, in both the impulsive and gradual phases, for the **four solar flares presented in Woods et al**., as well as an additional flare measured on **2006 December 6**. The radiative outputs for both phases of these five flares are then compared to the vacuum ultraviolet (VUV) irradiance output from the Flare Irradiance Spectral Model (FISM) in order to derive an empirical relationship between the FISM VUV model and the TIM TSI data output to estimate the TSI radiative output for eight other X-class flares. This model provides the basis for the bolometric energy estimates for the solar flares analyzed in the Emslie et al. study.

THE LIMIT OF MAGNETIC-SHEAR ENERGY IN SOLAR ACTIVE REGIONS

Ronald L. **Moore**1, David A. Falconer1,2,3, and Alphonse C. Sterling
2012 ApJ 750 24

It has been found previously, by measuring from active-region magnetograms a proxy of the free energy in the active region's magnetic field, (1) that there is a sharp upper limit to the free energy the field can hold that increases with the amount of magnetic field in the active region, the active region's magnetic flux content, and (2) that most active regions are near this limit when their field explodes in a coronal mass ejection/flare eruption. That is, explosive active regions are concentrated in a main-sequence path bordering the free-energy-limit line in (flux content, free-energy proxy) phase space. Here, we present evidence that specifies the underlying magnetic condition that gives rise to the free-energy limit and the accompanying main sequence of explosive active regions. Using a suitable free-energy proxy measured from vector magnetograms of 44 active regions, we find evidence that (1) in active regions at and near their free-energy limit, the ratio of magnetic-shear free energy to the non-free magnetic energy the potential field would have is of the order of one in the core field, the field rooted along the neutral line, and (2) this ratio is progressively less in active regions progressively farther below their free-energy limit. Evidently, most active regions in which this core-field energy ratio is much less than one cannot be triggered to explode; as this ratio approaches one, most active regions become capable of exploding; and when this ratio is one, most active regions are compelled to explode.

Observed Aspects of Reconnection in Solar Eruptions **A Review**

Ronald L. **Moore** · Alphonse C. Sterling · G. Allen Gary · JonathanW. Cirtain · David A. Falconer
Space Sci Rev., 160:73–94, **2011, File**

The observed magnetic field configuration and signatures of reconnection in the large solar magnetic eruptions that make major flares and coronal mass ejections and in the much smaller magnetic eruptions that make X-ray jets are illustrated with cartoons and representative observed eruptions. The main reconnection signatures considered are the imaged bright emission from the heated plasma on reconnected field lines. In any of these eruptions, large or small, the magnetic field that drives the eruption and/or that drives the buildup to the eruption is initially a closed bipolar arcade. From the form and configuration of the magnetic field in and around the driving arcade and from the development of the reconnection signatures in coordination with the eruption, we infer that (1) at the onset of reconnection the reconnection current sheet is small compared to the driving arcade, and (2) the current sheet can grow to the size of the driving arcade only after reconnection starts and the unleashed erupting field dynamically forces the current sheet to grow much larger, building it up faster than the reconnection can tear it down. We conjecture that the fundamental reason the quasi-static pre-eruption field is prohibited from having a large current sheet is that the magnetic pressure is much greater than the plasma pressure in the chromosphere and low corona in eruptive solar magnetic fields.

Empirical Scaling Relations for the Photospheric Magnetic Elements of the Flaring and Non-Flaring Active Regions

M.A.**Moradhaseli**, M.Javaherian, N.Fathalian, H.Safari
Acta Astronomica, vol 71, no 2, p. 163-188, **2021**
https://arxiv.org/pdf/2109.12924.pdf

Here, we analyzed magnetic elements of the solar active regions (ARs) observed in the line-of-sight magnetograms (the 6173 Å~Fe \small{I} line) recorded with the Solar Dynamics Observatory (SDO)/Helioseismic and Magnetic Imager (HMI). The Yet Another Feature Tracking Algorithm (\textsf{YAFTA}) was employed to extract the statistical properties of these features (\textit{e.g.} filling factor, magnetic flux, and lifetime) within the areas of 180″×180″ inside the flaring AR (NOAA 12443) and the non-flaring AR (NOAA 12446) for **3 to 5 November 2015 and for 4 to 6 November 2015**, respectively. The mean filling factor of polarities was obtained to be about 0.49 for the flaring AR; this value was 0.08 for the non-flaring AR. Time series of the filling factors of the negative and positive polarities for the flaring AR showed anti-correlation (with the Pearson value of -0.80); while for the non-flaring AR, there was the strong positive correlation (with the Pearson value of 0.95). A power-law function was fitted to the frequency distributions of flux (F), size (S), and lifetime (T). Power exponents of the distributions of flux, size, and lifetime for the

flaring AR were obtained to be about -2.36, -3.11, and -1.70, respectively; these values of exponents for the non-flaring AR were found to be about -2.53, -3.42, and -1.61, respectively. ...

Relative field line helicity of a large eruptive solar active region

K. **Moraitis**, S. Patsourakos, A. Nindos
A&A 649, A107 **2021**
https://arxiv.org/pdf/2103.03643.pdf
https://www.aanda.org/articles/aa/pdf/2021/05/aa40384-21.pdf
https://doi.org/10.1051/0004-6361/202140384
Context. Magnetic helicity is a physical quantity of great importance in the study of astrophysical and natural plasmas. Although a density for helicity cannot be defined, a good proxy for it is field line helicity. The appropriate quantity for use in solar conditions is relative field line helicity (RFLH). Aims. This work aims to study in detail the behaviour of RFLH, for the first time, in a solar active region (AR). Methods. The target active region is the large, eruptive AR 11158. In order to compute RFLH and all other quantities of interest we use a non-linear force-free reconstruction of the AR coronal magnetic field of excelent quality. Results. We find that the photospheric morphology of RFLH is quite different than that of the magnetic field or of the electrical current, and this is not sensitive to the chosen gauge in the computation of RFLH. The value of helicity experiences a large decrease, 25% of its pre-flare value, during an X-class flare of the AR, a change that is also depicted in the photospheric morphology of RFLH. Moreover, the area of this change coincides with the area that encompasses the flux rope, the magnetic structure that later erupted. Conclusions. The use of RFLH can provide important information about the value and location of the magnetic helicity expelled from the solar atmosphere during eruptive events. **15 February 2011**

Magnetic helicity and eruptivity in active region 12673

K. **Moraitis**, X. Sun, E. Pariat, L. Linan
A&A 628, A50 **2019**
https://arxiv.org/abs/1907.06365
https://www.aanda.org/articles/aa/pdf/2019/08/aa35870-19.pdf
Context. In **September 2017** the largest X-class flare of Solar Cycle 24 occurred from the most active region (AR) of this cycle, AR 12673. The AR attracted much interest because of its unique morphological and evolution characteristics. Among the parameters examined in the AR was magnetic helicity, but either only approximately, and/or intermittently. Aims. This work is interested in studying the evolution of the relative magnetic helicity and of the two components of its decomposition, the non-potential, and the volume-threading one, in the time interval around the highest activity of AR 12673. Special emphasis is given on the study of the ratio of the non-potential to total helicity, that was recently proposed as an indicator of ARs eruptivity. Methods. For these, we first approximate the coronal magnetic field of the AR with two different optimization-based extrapolation procedures, and choose the one that produces the most reliable helicity value at each instant. Moreover, in one of these methods, we weight the optimization by the uncertainty estimates derived from the Helioseismic and Magnetic Imager (HMI) instrument, for the first time. We then follow an accurate method to compute all quantities of interest. Results. The first observational determination of the evolution of the non-potential to total helicity ratio seems to confirm the quality it has in indicating eruptivity. This ratio increases before the major flares of AR 12673, and afterwards it relaxes to smaller values. Additionally, the evolution patterns of the various helicity, and energy budgets of AR 12673 are discussed and compared with other works. **6 Sept 2017**

Predicting Extreme Solar Flare Events Using Lu and Hamilton Avalanche Model

L. F. **Morales** & N. A. Santos
Solar Physics volume 295, Article number: 155 (**2020**)
https://link.springer.com/content/pdf/10.1007/s11207-020-01713-0.pdf
Solar flares are the most powerful events in the solar atmosphere, releasing a huge amount of energy in a few minutes. Any progress in predicting when a flare of a big magnitude will occur is extremely important to evaluate the risk related to space weather. The Lu and Hamilton (Astrophys. J. Lett. 380, L89, 1991) self-organized criticality (SOC) model for solar flares is the one most conspicuous amongst the several avalanche models for flares that have been developed in the last 30 years. It has been very successful in reproducing some of the characteristic features of observed flares (e.g. probability density function of flare energy) and in the last years has been explored as a way of predicting extreme flaring events.
In this work, we study the predicting capabilities of Lu and Hamilton model by assessing the proximity to stability of the 2D lattice and studying the influence of the lattice structure in the generation of large avalanches. We find that the mean value of the lattice nodes bears enough information to predict large avalanches in more than half of the cases, making it a reliable precursor for forecasting purposes.

Hybrid simulations of chromospheric HXR flare sources

Z. **Moravec**, M. Varady, J. Kasparova, D. Kramolis

Astron. Nachr **2016**
http://arxiv.org/pdf/1601.07026v1.pdf
Recent measurements of vertical extents and positions of the chromospheric hard X-ray (HXR) flare sources based on Ramaty High-Energy Spectroscopic Imager (RHESSI) observations show a significant inconsistency with the theoretical predictions based on the standard collisional thick target model (CTTM). Using a hybrid flare code Flarix, we model simultaneously and self-consistently the propagation, scattering and energy losses of electron beams with power-law energy spectra and various initial pitch-angle distributions in a purely collisional approximation and concurrently the dynamic response of the heated chromosphere on timescales typical for RHESSI image reconstruction. The results of the simulations are used to model the time evolution of the vertical distribution of chromospheric HXR source within a singular (compact) loop. Adopting the typical RHESSI imaging times scales, energy dependent vertical sizes and positions as could be observed by RHESSI are presented.

Solar Flare 1/f Fluctuations from Amplitude Modulated Five Minute Oscillation

Masahiro **Morikawa**, Akika Nakamichi
2023
https://arxiv.org/pdf/2310.07288.pdf
We first study the solar flare time sequence based on the GOES16 data. We find that the power spectrum density of the low-energy (E\leq E_{mean}) flare shows 1/f fluctuations, but the high-energy (E>E_{mean}) flare shows a flat spectrum. Further, we found that the flare timing time-sequence shows 1/f fluctuations clearer. These facts indicate that the solar flare 1/f fluctuations are associated with low-energy phenomena. We investigate the origin of this 1/f fluctuations based on our recent proposal: 1/f fluctuations arise from amplitude modulation and demodulation. We speculate that this amplitude modulation is encoded by the resonance with the Solar Five-minute Oscillation (SFO) and demodulated by magnetic reconnection. We partially demonstrate this scenario by analyzing the SFO eigenmodes resolving the frequency degeneracy in the azimuthal order number m by solar rotation and resonance. Since 1/f fluctuation is robust, we speculate that the solar flare 1/f fluctuations may be inherited by the various phenomena around the Sun, such as the sunspot numbers and the cosmic rays. Finally, we compare the solar flares and the earthquakes, both showing 1/f fluctuations. Interestingly, the same analysis for solar flares is possible for earthquakes if we read SFO as Earth's Free Oscillation, and magnetic reconnection as fault rupture. Furthermore, we point out the possibility that the same analysis also applies to the activity of the black hole/disk system if we read SFO as the Quasi-Periodic Oscillation of a black hole.

Magnetic reconnection, plasmoids and numerical resolution

José María García **Morillo**, Alexandros Alexakis
J. Plasma Phys. **2024**
https://arxiv.org/pdf/2406.08951
Explaining fast magnetic reconnection in electrically conducting plasmas has been a theoretical challenge in plasma physics since its first description by Eugene N. Parker. In the recent years the observed reconnection rate has been shown by numerical simulations to be explained by the plasmoid instability that appears in highly conductive plasmas. In this work we show that the plasmoid instability is very sensitive to the numerical resolution used. It is shown that well resolved runs display no plasmoid instability even at Lundquist number as large as 5·105 achieved at resolutions of 327682 grid points. On the contrary in simulations that are under-resolved below a threshold, the plasmoid instability manifests itself with the formation of larger plasmoids the larger the under-resolving is. The present results thus question the description of the plasmoid instability as a mechanism for fast magnetic reconnection.

Observations of Chromospheric Anemone Jets with Hinode SOT and Hida Ca II Spectroheliogram

Morita, S., Shibata, K., Ueno, S., Ichimoto, K., Kitai, R., and Otsuji, K.
E-print, Feb **2010**
We present the first simultaneous observations of chromospheric "anemone" jets in solar active regions with Hinode SOT Ca II H broadband filetergram and Ca II K spetroheliogram on the Domeless Solar Telescope (DST) at Hida Observatory. During the coordinated observation, 9 chromospheric anemone jets were simultaneously observed with the two instruments. These observations revealed three important features, i.e.: (1) the jets are generated in the lower chromosphere, i.e. these cannot be seen in Ca II K3, (2) the length and lifetime of the jets are 0.4-5 Mm and 40-320 sec, (3) the apparent velocity of the jets with Hinode SOT are 3-24 km/s, while Ca II K3 component at the jets show blueshifts (in 5 events) in the range of 2- 6 km/s. The chromospheric anemone jets are associated with mixed polarity regions which are either small emerging flux regions or moving magnetic features. It is found that the Ca II K line often show red or blue asymmetry in K2/K1 component: the footpoint of the jets associated with emerging flux regions often show redshift (2-16 km/s), while the one with moving magnetic features show blueshift (around 5 km/s). Detailed analysis of magnetic evolution of the jet foaming regions revealed that the reconnection rate (or canceling rate) of the total magnetic flux at the footpoint of the jets are of order of 10^{16} Mx/s, and the resulting magnetic energy release rate (1.1-10) x 10^{24} erg/s, with the total energy release (1-13) x 10^{26} erg for the duration of the magnetic

cancellations, 130s. These are comparable to the estimated total energy, 10^{26} erg, in a single chromospheric anemone jet. In addition to Hida DST Ca II-K Spectroheliogram and Hinode SOT Ca II H broadband filetergram, we also used Hinode SOT magnetogram as well as Hida H alpha filtergram. An observation-based physical model of the jet is presented. The relation between chromospheric anemone jets and Ellerman bombs is discussed.

Solar Flares: Origin and Threat to our Civilization

Nils-Axel **Mörner**

a new monograph " **SOLAR FLARES: Investigations and selected Research**" , Chapter 1 P. 1-11 **2016**

See **File** Chernov_News on Zebra Patterns_ Flare Book.pdf

http://www.nova-authors.com/___Encrypted/WEB_Links_Storage/e-Books/978-1-53610-221-5_eBook.pdf

Determining the acceleration regions of in situ electrons using remote radio and X-ray observations

D. E. **Morosan**, N. Dresing, C. Palmroos, J. Gieseler, I. C. Jebaraj, A. Warmuth, A. Fedeli, S. Normo, J. Pomoell, E. K. J. Kilpua, P. Zucca, B. Dabrowski, A. Krankowski, G. Mann, C. Vocks, R. Vainio

A&A **2024**

https://arxiv.org/pdf/2412.06477

Solar energetic particles in the heliosphere are produced by flaring processes on the Sun or shocks driven by coronal mass ejections. These particles are regularly detected remotely as electromagnetic radiation (X-rays or radio emission), which they generate through various processes, or in situ by spacecraft monitoring the Sun and the heliosphere. We aim to combine remote-sensing and in situ observations of energetic electrons to determine the origin and acceleration mechanism of these particles. Here, we investigate the acceleration location, escape, and propagation directions of electron beams producing radio bursts observed with the Low Frequency Array (LOFAR), hard X-ray (HXR) emission and, in situ electrons observed at Solar Orbiter (SolO) on **3 October 2023**. These observations are combined with a three-dimensional (3D) representation of the electron acceleration locations and results from a magneto-hydrodynamic (MHD) model of the solar corona in order to investigate the origin and connectivity of electrons observed remotely at the Sun to in situ electrons. We observed a type II radio burst with good connectivity to SolO, where a significant electron event was detected. However, type III radio bursts and Hard X-rays were also observed co-temporally with the elctron event but likely connected to SolO by different far-sided field lines. The injection times of the SolO electrons are simultaneous with both the onset of the type II radio burst, the group of type III bursts and the presence of a second HXR peak, however, the most direct connection to SolO is that of the type II burst location. The in situ electron spectra point to shock acceleration of electrons with a short-term connection to the source region.

High-resolution observations of active region moss and its dynamics

R. J. **Morton**, J. A. McLaughlin

2014, ApJ **2014** 789 105

http://arxiv.org/pdf/1405.5694v1.pdf

The \textit{High resolution Coronal Imager (Hi-C)} has provided the sharpest view of the EUV corona to date. In this paper we exploit its impressive resolving power to provide the first analysis of the fine-scale structure of moss in an active region. The data reveal that the moss is made up of a collection of fine threads, that have widths with a mean and standard deviation of 440±190~km (Full Width Half Maximum). {The brightest moss emission is located at the visible head of the fine-scale structure and the fine structure appears to extend into the lower solar atmosphere.} The emission decreases along the features implying the lower sections are most likely dominated by cooler transition region plasma. These threads appear to be the cool, lower legs of the hot loops. In addition, the increased resolution allows for the first direct observation {of physical displacements of the moss fine-structure in a direction transverse to its central axis. Some of these transverse displacements demonstrate periodic behaviour, which we interpret as a signature of kink (Alfv\'enic) waves. Measurements of the properties of the transverse motions are made and the wave motions have} means and standard deviations of 55±37~km for the transverse displacement amplitude, 77±33~s for the period and 4.7±2.5~km/s for the velocity amplitude. The presence of waves in the transition region of hot loops could have important implications for the heating of active regions. **11-Jul-2012**

Chromospheric jets around the edges of sunspots⋆

R. J. **Morton**

A&A 543, A6 (**2012**)

Aims. Evidence is beginning to be put forward that demonstrates the role of the chromosphere in supplying energy and mass to the corona. We aim to assess the role of chromospheric jets in active region dynamics.

Methods. Using a combination of the Hinode/SOT Ca II H and TRACE 1550 Å and 1600 Å filters we examine chromospheric jets situated at the edge of a sunspot.
Results. Analysis reveals a near continuous series of jets, that raise chromospheric material into the low corona above a sunspot. The jets have average rise speeds of 30 km s-1 and a range of 10−100 km s-1. Enhanced emission observed at the jets leading edge suggests the formation of a shock front. Increased emission in TRACE bandpasses above the sunspot and the disappearance of the jets from the Ca II filter suggests that some of the chromospheric jet material is at least heated to ~0.1 MK. The evidence suggests that the jets could be a source of steady, low-level heating for active region features.

Simulating coronal condensation dynamics in 3D

S. P. **Moschou**, R. Keppens, C. Xia, X. Fang
2015
We present numerical simulations in 3D settings where coronal rain phenomena take place in a magnetic configuration of a quadrupolar arcade system. Our simulation is a magnetohydrodynamic simulation including anisotropic thermal conduction, optically thin radiative losses, and parametrised heating as main thermodynamical features to construct a realistic arcade configuration from chromospheric to coronal heights. The plasma evaporation from chromospheric and transition region heights eventually causes localised runaway condensation events and we witness the formation of plasma blobs due to thermal instability, that evolve dynamically in the heated arcade part and move gradually downwards due to interchange type dynamics. Unlike earlier 2.5D simulations, in this case there is no large scale prominence formation observed, but a continuous coronal rain develops which shows clear indications of Rayleigh-Taylor or interchange instability, that causes the denser plasma located above the transition region to fall down, as the system moves towards a more stable state. Linear stability analysis is used in the non-linear regime for gaining insight and giving a prediction of the system's evolution. After the plasma blobs descend through interchange, they follow the magnetic field topology more closely in the lower coronal regions, where they are guided by the magnetic dips.

Two-spacecraft reconstruction of a magnetic cloud and comparison to its solar source

C. **Mostl**1,2, C. Miklenic1, C.J. Farrugia3, M. Temmer2,4, A. Veronig1, A.B. Galvin3,
B. Vrsnak4, and H.K. Biernat1,2
E-print, Jan **2008**; Ann. Geophys.., 26, 3139–3152, **2008, File**
www.ann-geophys.net/26/3139/2008/
This paper compares properties of the source region with those inferred from satellite observations near Earth of the magnetic cloud which reached 1 AU on 20 November 2003. We use observations from space missions SOHO and TRACE together with ground-based data to study the magnetic structure of the active region NOAA 10501 containing a highly curved filament, and determine the reconnection rates and fluxes in an M4 flare on **18 November 2003** which is associated with a fast halo CME. This event has been linked before to the magnetic cloud on 20 November 2003. We model the near-Earth observations with the Grad-Shafranov reconstruction technique using a novel approach in which we optimize the results with two-spacecraft measurements of the solar wind plasma and magnetic field made by ACE and WIND. The two probes were separated by hundreds of Earth radii. They pass through the axis of the cloud which is inclined -50 degree to the ecliptic. The magnetic cloud orientation at 1 AU is consistent with an encounter with the heliospheric current sheet. We estimate that 50 % of its poloidal flux has been lost through reconnection in interplanetary space. By comparing the flare ribbon flux with the original cloud fluxes we infer a flux rope formation during the eruption, though uncertainties are still significant. The multi-spacecraft Grad-Shafranov method opens new vistas in probing of the spatial structure of magnetic clouds in STEREO-WIND/ACE coordinated studies.

Spatio-temporal energy partitioning in a non-thermally dominated two-loop solar flare

Galina G. **Motorina**, Gregory D. Fleishman, Eduard P. Kontar
ApJ Volume 890, Issue 1, id.75 **2020**
https://arxiv.org/pdf/2001.02009.pdf
https://iopscience.iop.org/article/10.3847/1538-4357/ab67d1/pdf
https://sci-hub.st/10.3847/1538-4357/ab67d1
Solar flares show remarkable variety of the energy partitioning between thermal and nonthermal components. Those with a prominent nonthermal component but only a modest thermal one are particularly well suited to study the direct effect of the nonthermal electrons on plasma heating. Here, we analyze such a well observed, impulsive single-spike nonthermal event, a **SOL2013-11-05T035054** solar flare, where the plasma heating can be entirely attributed to the energy losses of these impulsively accelerated electrons. Evolution of the energy budget of thermal and nonthermal components during the flare is analysed using X-ray, microwave, and EUV observations and three-dimensional modeling. The results suggest that (i) the flare geometry is consistent with a two-loop morphology and the magnetic energy is likely released due to interaction between these two loops; (ii) the released magnetic energy converted to the nonthermal energy of accelerated electrons only, which is subsequently converted to the thermal energy of the plasma;

(iii) the energy is partitioned in these two flaring loops in comparable amounts; (iv) one of these flaring loops remained relatively tenuous but rather hot, while the other remained relatively cool but denser than the first one. Therefore, this solar flare demonstrates an extreme efficiency of conversion of the free magnetic energy to the nonthermal energy of particle acceleration and the energy flow into two loops from the non-thermal to thermal one with a negligible direct heating.
RHESSI Science Nuggets #383 Sep **2020**
https://sprg.ssl.berkeley.edu/~tohban/wiki/index.php/Energy_Partitioning_in_a_Nonthermally_Dominated_Two-loop_Solar_Flare

Joint radio, EUV, and X-ray analysis of the 2013 November 5 cold flare

Galina **Motorina**∗1 , Eduard Kontar2 , and Gregory Fleishman3
CESRA **2016** p.63
http://cesra2016.sciencesconf.org/conference/cesra2016/pages/CESRA2016_prog_abs_book_v3.pdf
Solar flares, transient brightenings in the solar atmosphere seen throughout electromagnetic spectrum, demonstrate remarkable variety of the energy partitions between the thermal and nonthermal components. There are flares with a dominating or purely thermal component, i.e., with little or no non-thermal electrons visible. These flares strongly contrast with the flares in which the nonthermal component clearly dominates over the thermal one. Therefore, there is a puzzle as what leads to such extreme phenomena as purely 'thermal' and purely 'non-thermal' flares. It has recently been recognized that some flares with dominating nonthermal component are in fact 'cold flares' (Bastian et al. 2007; Fleishman et al. 2011; Masuda et al. 2013) in which no or so modest thermal plasma response is detected that these events are not even listed as GOES flares. Here we analyze a 05-Nov-2013 cold flare with a combination of radio (NoRH, NoRP, SSRT, BBMS), X-ray (RHESSI), and EUV (SDO) data to understand the relationship between the thermal and nonthermal components in this flare in detail. Before, there were no analysis of cold flares employing both RHESSI and SDO/AIA data, where RHESSI provides information of non-thermal energetic particles, and SDO/AIA characterizes the thermal response at lower temperatures, approximately 0.6 MK – 16 MK. The microwave spectral and imaging data taken from Nobeyama and BBMS/SSRT instruments put significant additional constraints on the magnetic field and number density at the source of the flare. With these data we build a consistent detailed picture of particle acceleration and plasma heating in this cold flare and attempt a 3D modeling of the flaring volume. Based on this analysis, we arrive at important conclusions about the energy release, particle acceleration, and plasma heating in solar flares.

Differential Emission Measure and Electron Distribution Function Reconstructed from RHESSI and SDO Observations

G.G. **Motorina**, E.P. Kontar
Geomagnetism and Aeronomy. Vol. 55. No. 7. **2015**
http://arxiv.org/pdf/1510.06755v1.pdf
To solve a number of problems in solar physics related to mechanisms of energy release in solar corona parameters of hot coronal plasma are required, such as energy distribution, emission measure, differential emission measure, and their evolution with time. Of special interest is the distribution of solar plasma by energies, which can evolve from a nearly Maxwellian distribution to a distribution with a more complex structure during a solar flare. The exact form of this distribution for low-energy particles, which receive the bulk of flare energy, is still poorly known; therefore, detailed investigations are required. We present a developed method of simultaneous fitting of data from two spacecrafts Solar Dynamics Observatory/Atmospheric Imaging Assembly (SDO/AIA) and Reuven Ramaty High Energy Solar Spectroscopic Imager (RHESSI), using a differential emission measure and a thin target model for the **August 14, 2010** flare event.

A detailed investigation of particle energisation mechanisms in models of collapsing magnetic traps

Kate **Mowbray**, Thomas Neukirch, James Threlfall
MNRAS Volume 536, Issue 1, January **2025**, Pages 609–623,
https://arxiv.org/pdf/2411.14881
https://doi.org/10.1093/mnras/stae2668
https://watermark.silverchair.com/stae2668.pdf
In this paper we provide a detailed investigation of the energisation processes in two-dimensional, two and a half-dimensional and three-dimensional collapsing magnetic trap models. Using kinematic magnetohydrodynamic models of collapsing magnetic traps, we examine the importance of Fermi acceleration in comparison with betatron acceleration in these models. We extend previous work by investigating particle orbits in two-dimensional models without and with a guide field component and from full three-dimensional models. We compare the outcomes for the different models and how they depend on the chosen initial conditions. While in the literature betatron acceleration has been emphasised as

the major mechanism for particle energisation in collapsing magnetic traps, we find that Fermi acceleration can play a significant role as well for particle orbits with suitable initial conditions.

Automatic detection of white-light flare kernels in SDO/HMI intensitygrams

L. **Mravcova** (1), M. Svanda
New Astronomy **2017**
https://arxiv.org/pdf/1706.00988.pdf
Solar flares with a broadband emission in the white-light range of the electromagnetic spectrum belong to most enigmatic phenomena on the Sun. The origin of the white-light emission is not entirely understood. We aim to systematically study the visible-light emission connected to solar flares in SDO/HMI observations. We developed a code for automatic detection of kernels of flares with HMI intensity brightenings and study properties of detected candidates. The code was tuned and tested and with a little effort, it could be applied to any suitable data set. By studying a few flare examples, we found indication that HMI intensity brightening might be an artefact of the simplified procedure used to compute HMI observables. **15 February 2011, 9 June 2011, 6th March 2012**

Plasma dynamics in the flaring loop observed by RHESSI

T. **Mrozek**, R. Falewicz, S. Kolomanski, M. Litwicka
A&A 659, A60 **2022**
https://arxiv.org/pdf/2112.11392.pdf
https://doi.org/10.1051/0004-6361/202039598
https://www.aanda.org/articles/aa/pdf/2022/03/aa39598-20.pdf
The thick-target model predicts that in flare foot points, we should observe lowering of HXR sources' altitude with increasing energy. The foot point of HXR sources result from the direct interaction of non-thermal electron beams with plasma in the lower part of the solar atmosphere, where the density increases rapidly. Therefore, we can estimate the plasma density distribution along the non-thermal electron beam directly from the observations of the altitude-energy relation obtained for the HXR foot point sources. The relation's shape is density-dependent and is also determined by the power-law distribution of non-thermal electrons. Additionally, during the impulsive phase these parameters may change dramatically. Thus, the interpretation of observed HXR foot point sources' altitudes is not straightforward and needs detailed numerical modelling of the electron precipitation process. The numerical model was calculated using the hydrodynamic 1D model with an application of the Fokker-Planck formalism for non-thermal beam precipitation. HXR data from RHESSI were used to trace chromospheric density changes during a non-thermal emission burst, in detail. We have found that the amount of mass that evaporated from the chromosphere is in good agreement with the ranges obtained from hydrodynamical modelling of a flaring loop, and from an analysis of observed emission measure in the loop top, and with specific scaling laws. Consistency between the obtained values shows that HXR images may provide an important constraint for models - a mass of plasma that evaporated due to a non-thermal electron beam depositing energy in the chromosphere. High-energy, non-thermal sources' (above 20 keV in this case) positions fit the column density changes obtained from the hydrodynamical model perfectly. Density changes seem to be less affected by the electrons' spectral index. **3 Aug 2002**

Solar Microflares Observed by SphinX and RHESSI

Tomasz **Mrozek**, Szymon Gburek, Marek Siarkowski, Barbara Sylwester…
Solar Phys (**2018**) 293:101
https://link.springer.com/content/pdf/10.1007%2Fs11207-018-1319-0.pdf
In 2009, the Russian Complex Orbital Observations Near-Earth of Activity of the Sun(CORONAS-Photon) spacecraft was launched, carrying the Polish Solar PHotometer In X-rays(SphinX). The SphinX was most sensitive in the spectral range 1.2 – 15 keV, thus an excellent opportunity appeared for comparison with the low-energy end of Ramaty High Energy Solar Spectroscopic Imager (RHESSI) spectra. Common spectral measurements with these instruments cover the range where most of the flare energy is accumulated. We have chosen four consecutive small solar events observed on **4 July 2009** at 13:43 UT, 13:48 UT, 13:52 UT, and 13:55 UT (RHESSI flare peak times) and used them to compare the data and results from the two instruments. Moreover, we included Geostationary Operational Environmental Satellite (GOES) records in our analysis. In practice, the range of comparison performed for SphinX and RHESSI is limited roughly to 3 – 6 keV. RHESSI fluxes measured with a use of one, four, and nine detectors in the 3 – 4 keV energy band agree with SphinX measurements. However, we observed that SphinX spectral irradiances are three times higher than those of RHESSI in the 4 – 6 keV energy band. This effect contributes to the difference in obtained emission measures, but the derived temperatures of plasma components are similar. RHESSI spectra were fitted using a model with two thermal components. We have found that the RHESSI hot component is in agreement with GOES, and the RHESSI hotter component fits the SphinX flaring component well. Moreover, we calculated the so-called thermodynamic measure and the total thermal energy content in the four microflares that we studied. The results obtained show that SphinX is a very sensitive complementary observatory for RHESSI and GOES.

EXPLOSIVE EVENTS AND THE EVOLUTION OF THE PHOTOSPHERIC MAGNETIC FIELD

K. **Muglach**1
Astrophysical Journal, 687:1398Y1405, **2008**
http://www.journals.uchicago.edu/doi/abs/10.1086/592065
Transition region explosive events have long been suggested as direct signatures of magnetic reconnection in the solar atmosphere. In seeking further observational evidence to support this interpretation, we study the relation between explosive events and the evolution of the solar magnetic field as seen in line-of-sight photospheric magnetograms. We find that about 38%of events show changes of the magnetic structure in the photosphere at the location of an explosive event over a time period of 1 hr. We also discuss potential ambiguities in the analysis of high-sensitivity magnetograms.

Long-Term Evolution of Magnetic Fields in Flaring Active Region NOAA 12673

Johan **Muhamad**, Muhamad Zamzam Nurzaman, Tiar Dani, Arun Relung Pamutri
Research in Astronomy and Astrophysics **2021**
https://arxiv.org/pdf/2110.07369.pdf
In this study, using full maps of the Sun observed by the Solar Dynamics Observatory and the Solar Terrestrial Relations Observatory, we identified that AR 12673 emerged in decayed AR 12665, which had survived for two solar rotations. Although both ARs emerged at the same location, they possessed different characteristics and different flare productivities. Therefore, it is important to study the long-term magnetic evolution of both ARs to identify the distinguishing characteristics of an AR that can produce large solar flares. We used the Spaceweather Helioseismic and Magnetic Imager Active Region Patch data to investigate the evolution of the photospheric magnetic field and other physical properties of the recurring ARs during five Carrington rotations. All these investigated parameters dynamically evolved through a series of solar rotations. We compared the long-term evolution of AR 12665 and AR 12673 to understand the differences in their flare-producing properties. We also studied the relation of the long-term evolution of these ARs with the presence of active longitude. We found that the magnetic flux and complexity of AR 12673 developed much faster than those of AR 12665. Our results confirmed that a strong emerging flux that emerged in the pre-existing AR near the active longitude created a very strong and complex AR that produced large flares.

A Study of Magnetic Field Characteristics of Flaring Active Region Based on Nonlinear Force-free Field Extrapolation

Johan **Muhamad**, Kanya Kusano, Satoshi Inoue, Yumi Bamba
ApJ **863** 162 **2018**
https://arxiv.org/pdf/1807.01436.pdf
Coronal magnetic fields are responsible for the onset of solar flares and solar eruptions. However, the type of magnetic field parameters that can be used to measure the critical condition for a solar eruption is still unclear. As an effort to understand the possible condition for a solar flare, we have examined the non-dimensional parameter κ introduced by Ishiguro & Kusano (2017), which contains information about magnetic twist distribution and magnetic flux in an active region (AR). We introduce a new parameter κ_*, as a proxy for κ, and we have analyzed the evolution of κ_* during the flaring period of an AR using the nonlinear force-free field (NLFFF) extrapolated from the photospheric vector magnetic field data. Using data from the Solar Dynamics Observatory (SDO)/Helioseismic and Magnetic Imager (HMI), we have calculated κ_* for the AR NOAA 11158 during its three-day flaring period. We found that κ_* increased to a certain level before two large flares and decreased significantly after their onset. The results suggest that κ_* may be used as an indicator of the necessary condition for the onset of a solar eruption in the AR. Based on this result, we propose a new method to assess the possibility of a large solar eruption from an AR by combining the parameter κ_* and information about the magnetic energy of the AR. **13-15 Feb 2011**

Magnetohydrodynamic Simulations for Studying Solar Flare Trigger Mechanism

J. **Muhamad**1,2, K. Kusano1, S. Inoue1,3, and D. Shiota
2017 ApJ 842 86
http://iopscience.iop.org.sci-hub.cc/0004-637X/842/2/86/
https://arxiv.org/pdf/1706.07153.pdf
In order to understand the flare trigger mechanism, we conduct three-dimensional magnetohydrodynamic simulations using a coronal magnetic field model derived from data observed by the Hinode satellite. Several types of magnetic bipoles are imposed into the photospheric boundary of the Nonlinear Force-free Field model of Active Region (AR) NOAA 10930 on **2006 December 13**, to investigate what kind of magnetic disturbance may trigger the flare. As a result, we confirm that certain small bipole fields, which emerge into the highly sheared global magnetic field of an AR, can effectively trigger a flare. These bipole fields can be classified into two groups based on their orientation relative to the polarity inversion line: the so-called opposite polarity, and reversed shear structures, as suggested by Kusano et al. We also investigate the structure of the footpoints of reconnected field lines. By comparing the distribution of reconstructed field lines and observed flare ribbons, the trigger structure of the flare can be inferred. Our simulation suggests that the data-constrained simulation, taking into account both the large-scale magnetic structure and small-

scale magnetic disturbance (such as emerging fluxes), is a good way to discover a flare-producing AR, which can be applied to space weather prediction.

Behaviour of molecular hydrogen emission in three solar flares

Sargam M. **Mulay**, Lyndsay Fletcher, Hugh Hudson, Nicolas Labrosse
MNRAS Volume 526, Issue 3, December 2023, Pages 4755–4767 **2023**
https://arxiv.org/ftp/arxiv/papers/2309/2309.07799.pdf
https://watermark.silverchair.com/stad2853.pdf

We have systematically investigated ultraviolet (UV) emission from molecular hydrogen (H2) using the Interface Region Imaging Spectrometer (IRIS), during three X-ray flares of C5.1, C9.7 and X1.0 classes on **Oct. 25, 2014**. Significant emission from five H2 spectral lines appeared in the flare ribbons, interpreted as photo-excitation (fluorescence) due to the absorption of UV radiation from two Si IV spectral lines. The H2 profiles were broad and consisted of two non-stationary components in red and in the blue wings of the line in addition to the stationary component. The red (blue) wing components showed small redshifts (blue shifts) of ~5-15 km s−1 (~5-10 km s−1). The nonthermal velocities were found to be ~5-15 km s−1. The interrelation between intensities of H2 lines and their branching ratios confirmed that H2 emission formed under optically thin plasma conditions. There is a strong spatial and temporal correlation between Si IV and H2 emission, but the H2 emission is more extended and diffuse, further suggesting H2 fluorescence, and - by analogy with flare "back-warming" providing a means to estimate the depth from which the H2 emission originates. We find that this is 1871±157 km and 1207±112 km below the source of the Si IV emission, in two different ribbon locations.

Thermodynamic evolution of a sigmoidal active region with associated flares

Sargam M. **Mulay**, Durgesh Tripathi, Helen Mason
MNRAS Volume 504, Issue 1, Pages 1201–1218 **2021**
https://arxiv.org/ftp/arxiv/papers/2103/2103.09561.pdf
https://watermark.silverchair.com/stab816.pdf
https://doi.org/10.1093/mnras/stab816

Active regions often show S-shaped structures in the corona called sigmoids. These are highly sheared and twisted loops formed along the polarity inversion line. They are considered to be one of the best pre-eruption signatures for CMEs. Here, we investigate the thermodynamic evolution of an on-disk sigmoid observed during **December 24-28, 2015**. For this purpose, we have employed Emission Measure (EM) and filter-ratio techniques on the observations recorded by the Atmospheric Imaging Assembly (AIA) onboard the Solar Dynamics Observatory (SDO) and X-ray Telescope (XRT) onboard Hinode. The EM analysis showed multi-thermal plasma along the sigmoid and provided a peak temperature of 10-12.5 MK for all observed flares. The sigmoidal structure showed emission from Fe XVIII (93.93 Å) and Fe XXI 128.75 Å) lines in the AIA 94 and 131 Å channels, respectively. Our results show that the hot plasma is often confined to very hot strands. The temperature obtained from the EM analysis was found to be in good agreement with that obtained using the XRT, AIA, and GOES filter-ratio methods. These results provide important constraints for the thermodynamic modeling of sigmoidal structures in the core of active regions. Moreover, this study also benchmarks different techniques available for temperature estimation in solar coronal structures. **24-28 Dec 2015**

Evidence of chromospheric molecular hydrogen emission in a solar flare observed by the IRIS satellite

Sargam M. **Mulay**, Lyndsay Fletcher
MNRAS Volume 504, Issue 2, June **2021**, Pages 2842–2852,
https://watermark.silverchair.com/stab367.pdf
https://doi.org/10.1093/mnras/stab367
https://arxiv.org/ftp/arxiv/papers/2102/2102.03329.pdf

We have carried out the first comprehensive investigation of enhanced line emission from molecular hydrogen, H2 at 1333.79 Å, observed at flare ribbons in SOL2014-04-18T13:03. The cool H2 emission is known to be fluorescently excited by Si IV 1402.77 Å UV radiation and provides a unique view of the temperature minimum region (TMR). Strong H2 emission was observed when the Si IV 1402.77 Å emission was bright during the flare impulsive phase and gradual decay phase, but it dimmed during the GOES peak. H2 line broadening showed non-thermal speeds in the range 7-18 km s−1, possibly corresponding to turbulent plasma flows. Small red (blue) shifts, up to 1.8 (4.9) km s−1 were measured. The intensity ratio of Si IV 1393.76 Å and Si IV 1402.77 Å confirmed that plasma was optically thin to Si IV (where the ratio = 2) during the impulsive phase of the flare in locations where strong H2 emission was observed. In contrast, the ratio differs from optically thin value of 2 in parts of ribbons, indicating a role for opacity effects. A strong

spatial and temporal correlation between H2 and Si IV emission was evident supporting the notion that fluorescent excitation is responsible. **April 18, 2014**

Flare-related Recurring Active Region Jets: Evidence for Very Hot Plasma

Sargam M. **Mulay** Sarah Matthews Takahiro Hasegawa Giulio Del Zanna Helen Mason Toshifumi Shimizu

Solar Physics December **2018**, 293:160

sci-hub.tw/10.1007/s11207-018-1376-4

We present a study of two active region jets (AR jets) that are associated with two C-class X-ray flares. The recurrent, homologous jets originated from the northern periphery of a sunspot. We confirm flare-like temperatures at the footpoints of these jets using spectroscopic observations of Fe xxiii (263.76 Å) and Fe xxiv (255.11 Å) emission lines. The emission measure loci method was used to obtain an isothermal temperature, and the results show a decrease (17.7 to 13.6 MK) in the temperature during the decay phase of the C 3.0 flare. The electron number densities at the footpoints were found to range from 1.7×10101.7×1010 to 2.0×1011 cm−32.0×1011 cm−3 using the Fe xiv line pair ratio. Nonthermal velocities were found to range from 34 – 100 km/s for Fe xxiv and 51 – 89 km/s for Fe xxiii. The plane-of-sky velocities were calculated to be 462±21462±21 and 228±23 km/s228±23 km/s for the two jets using the Atmospheric Imaging Assembly (AIA) 171 Å channel. The AIA light curves of the jet footpoint regions confirmed the temporal and spatial correlation between the two X-ray flares and the jet footpoint emission. The Gamma-ray Burst Monitor (GBM) also confirmed superhot plasma of 27 (25) MK with a nonthermal energy of 2.38×10262.38×1026 (2.87×10272.87×1027) ergs−1ergs−1 in the jet footpoint region during the rise (peak) phase of one of the flares. The temperatures of the jet footpoint regions obtained from EIS agree very well (within an uncertainty of 20%) with temperatures obtained from the Geostationary Environmental Operational Satellite (GOES) flux ratios. These results provide clear evidence for very hot plasma (>10 MK>10 MK) at the footpoints of the flare-related jets, and they confirm the heating and cooling of the plasma during the flares.

The Phenomena of Flares and CMEs in the Sun and Stars: Why Are the Energy Upper Limits in Both Phenomena Comparable?

D. J. **Mullan**1

2024 Res. Notes AAS 8 119

https://iopscience.iop.org/article/10.3847/2515-5172/ad4499

Solar/stellar flares which release large energies occur less frequently than those with small energies. Flare energies on a given star have not (yet) been observed to exceed Efm. Similarly, coronal mass ejections (CME's) with large kinetic energies (KE) on a given star also occur less frequently than those with small energies. The KE's of CME's on a given star have not (yet) been observed to exceed KEm. Interestingly, in any given star, Efm is found to be comparable in magnitude to KEm. This is puzzling since a one-to-one correlation between flares and CME's does not exist: some flares occur without any accompanying CME, and some CME's have no accompanying flare. Moreover, different types of MHD instabilities are believed to give rise to flares and CME's. The result Efm ≈ KEm could indicate support for Bemporad's conclusion: magnetic energy in the corona is in global equipartition with gravitational potential energy.

Frequencies of flare occurrence: Interaction Between convection and coronal loops

D. J. **Mullan**, R. R. Paudel

ApJ **854** 14 **2018**

https://arxiv.org/ftp/arxiv/papers/1801/1801.07708.pdf

Observations of solar and stellar flares have revealed the presence of power law dependences between the flare energy and the time interval between flares. Various models have been proposed to explain these dependences, and to explain the numerical value of the power law indices. Here, we propose a model in which convective flows in granules force the foot-points of coronal magnetic loops, which are frozen-in to photospheric gas, to undergo a random walk. In certain conditions, this can lead to a twist in the loop, which drives the loop unstable if the twist exceeds a critical value. The possibility that a solar flare is caused by such a twist-induced instability in a loop has been in the literature for decades. Here, we quantify the process in an approximate way with a view to replicating the power-law index. We find that, for relatively small flares, the random walk twisting model leads to a rather steep power law slope which agrees very well with the index derived from a sample of 56,000+ solar X-ray flares reported by the GOES satellites. For relatively large flares, we find that the slope of the power law is shallower. The empirical power law slopes reported for flare stars also have a range which overlaps with the slopes obtained here. We suggest that in the coolest stars, a significant change in slope should occur when the frozen-flux assumption breaks down due to low electrical conductivity.

Simultaneous Observation of Solar Neutrons from the ISS and High Mountain Observatories in association with a flare on July 8, 2014

Y. **Muraki**, D. Lopez, K. Koga, F. Kakimoto, T. Goka, L.X. Gonzalez, S.Masuda, Y. Matsubara, H. Matsumoto, P. Miranda, O. Okudaira, T. Obara, J. Salinas, T. Sako, S. Shibata, R.Ticona, Y. Tsunesada,J.F. Valdes-Galicia, K. Watanabe, T. Yamamoto
Proceeding of the 34th International Cosmic Ray Conference in Hague in August, 2015, **2015**
http://arxiv.org/ftp/arxiv/papers/1508/1508.04923.pdf
An M6.5-class flare was observed at N12E56 of the solar surface at 16:06 UT **on July 8, 2014**. In association with this flare, solar neutron detectors located on two high mountains, Mt. Sierra Negra and Chacaltaya and at the space station observed enhancements in the neutral channel. The authors analysed these data and a possible scenario of enhancements produced by high-energy protons and neutrons is proposed, using the data from continuous observation of a solar surface by the ultraviolet telescope onboard the Solar Dynamical Observatory (SDO).

UFCORIN: A Fully Automated Predictor of Solar Flares in GOES X-Ray Flux

Takayuki **Muranushi**, Takuya Shibayama, Yuko Hada Muranushi, Hiroaki Isobe, Shigeru Nemoto, Kenji Komazaki, Kazunari Shibata
Space Weather Volume 13, Issue 11 Pages 778–796 **2015**
http://arxiv.org/pdf/1507.08011v1.pdf
We have developed UFCORIN, a platform for studying and automating space weather prediction. Using our system we have tested 6,160 different combinations of SDO/HMI data as input data, and simulated the prediction of GOES X-ray flux for 2 years (2011-2012) with one-hour cadence. We have found that direct comparison of the true skill statistics (TSS) is ill-posed, and used the standard scores (z) of the TSS to compare the performance of the various prediction strategies. The best strategies we have found for predicting X, ≥M and ≥C class flares are better than the average of the 6,160 strategies by 2.3σ, 2.1σ, 3.8σ confidence levels, respectively. The best three's TSS values were 0.745±0.072, 0.481±0.017, and 0.557±0.043, respectively.

Three-dimensional numerical simulation of magnetohydrodynamic-gravity waves and vortices in the solar atmosphere

K. **Murawski**, I. Ballai, A.K. Srivastava, D. Lee
E-print, Sept **2013**, MNRAS
With the adaptation of the FLASH code we simulate magnetohydrodynamic-gravity waves and vortices as well as their response in the magnetized three-dimensional (3D) solar atmosphere at different heights to understand the localized energy transport processes. In the solar atmosphere strongly structured by gravitational and magnetic forces, we launch a localized velocity pulse (in horizontal and vertical components) within a bottom layer of 3D solar atmosphere modelled by initial VAL-IIIC conditions, which triggers waves and vortices. The rotation direction of vortices depends on the orientation of an initial perturbation. The vertical driver generates magnetoacoustic-gravity waves which result in oscillations of the transition region, and it leads to the eddies with their symmetry axis oriented vertically. The horizontal pulse excites all magnetohydrodynamic-gravity waves and horizontally oriented eddies. These waves propagate upwards, penetrate the transition region, and enter the solar corona. In the high-beta plasma regions the magnetic field lines move with the plasma and the temporal evolution show that they swirl with eddies. We estimate the energy fluxes carried out by the waves in the magnetized solar atmosphere and conclude that such wave dynamics and vortices may be significant in transporting the energy to sufficiently balance the energy losses in the localized corona. Moreover, the structure of the transition region highly affects such energy transports, and causes the channelling of the propagating waves into the inner corona.

HARD X-RAY IMAGING OF SOLAR FLARES USING INTERPOLATED VISIBILITIES

Entropy mode at a magnetic null point as a possible tool for indirect observation of nanoflares in the solar corona

K. **Murawski**1, T. V. Zaqarashvili2,4 and V. M. Nakariakov
A&A 533, A18 (**2011**)
Aims. We aim to explore the dynamics of the entropy mode perturbation excited by an energy release in the vicinity of a magnetic null point that is embedded in a gravitationally stratified solar corona.
Methods. We solve two-dimensional, time-dependent magnetohydrodynamic equations numerically to find spatial and temporal signatures of the entropy mode that is triggered impulsively by a spatially localized pulse of the gas pressure.
Results. We find that the properties of the entropy mode are determined by the sign of the initial pressure pulse. The initial increase in the gas pressure creates, together with the magnetoacoustic-gravity waves, a stationary void of the rarefied plasma at the launching place, associated with the entropy mode. In contrast, an initial decrease in the gas pressure, which corresponds to a rapid (or catastrophic) cooling, forms a blob of the dense plasma at the launching place.

Conclusions. The cool, dense blobs at magnetic null points may be observed in transition region and chromospheric spectral lines at coronal heights off the solar limb and may be associated with the places of nanoflare occurrence. Therefore, extensions of entropy mode studies may produce a diagnostic tool for indirect observations of nanoflares. The dense cool blobs may be affected by the gravity or carried by downflows, hence may initiate a coronal rain**.**

Neutron Production in Solar Flares

Ron **Murphy**, Gerry Share
RHESSI Science Nuggets #338 November **2018**
http://sprg.ssl.berkeley.edu/~tohban/wiki/index.php/Neutron_Production_in_Solar_Flares
Measurements of solar-flare neutrons, along with measurements of other flare emissions, are important diagnostic tools for understanding the flare process in general and ion acceleration in particular. There have been several RHESSI Nuggets written about detections of neutrons from solar flares (e.g. A, B, C). In this Nugget we discuss the physics of neutron production, and describe comparison of neutron calculations with measurements can be used to learn about ion acceleration in solar flares.
In the standard solar-flare model (Ref. [1]), electrons and ions are accelerated somehow via [magnetic reconnection], probably near the tops of closed coronal magnetic loops. These particles travel down the loop legs and interact with material at the loop footpoints. Nuclear interactions of the ions then produce excited and radioactive nuclei, neutrons, and pions.

Asymmetric Magnetic Reconnection in Weakly Ionized Chromospheric Plasmas

Nicholas A. **Murphy**1 and Vyacheslav S. Lukin
2015 ApJ 805 134
Realistic models of magnetic reconnection in the solar chromosphere must take into account that the plasma is partially ionized and that plasma conditions within any two magnetic flux bundles undergoing reconnection may not be the same. Asymmetric reconnection in the chromosphere may occur when newly emerged flux interacts with pre-existing, overlying flux. We present 2.5D simulations of asymmetric reconnection in weakly ionized, reacting plasmas where the magnetic field strengths, ion and neutral densities, and temperatures are different in each upstream region. The plasma and neutral components are evolved separately to allow non-equilibrium ionization. As in previous simulations of chromospheric reconnection, the current sheet thins to the scale of the neutral–ion mean free path and the ion and neutral outflows are strongly coupled. However, the ion and neutral inflows are asymmetrically decoupled. In cases with magnetic asymmetry, a net flow of neutrals through the current sheet from the weak-field (high-density) upstream region into the strong-field upstream region results from a neutral pressure gradient. Consequently, neutrals dragged along with the outflow are more likely to originate from the weak-field region. The Hall effect leads to the development of a characteristic quadrupole magnetic field modified by asymmetry, but the X-point geometry expected during Hall reconnection does not occur. All simulations show the development of plasmoids after an initial laminar phase.

ASYMMETRIC MAGNETIC RECONNECTION IN SOLAR FLARE AND CORONAL MASS EJECTION CURRENT SHEETS

N. A. **Murphy**1, M. P. Miralles1, C. L. Pope1,2, J. C. Raymond1, H. D. Winter1, K. K. Reeves1, D. B. Seaton3, A. A. van Ballegooijen1, and J. Lin
2012 ApJ 751 56
We present two-dimensional resistive magnetohydrodynamic simulations of line-tied asymmetric magnetic reconnection in the context of solar flare and coronal mass ejection current sheets. The reconnection process is made asymmetric along the inflow direction by allowing the initial upstream magnetic field strengths and densities to differ, and along the outflow direction by placing the initial perturbation near a conducting wall boundary that represents the photosphere. When the upstream magnetic fields are asymmetric, the post-flare loop structure is distorted into a characteristic skewed candle flame shape. The simulations can thus be used to provide constraints on the reconnection asymmetry in post-flare loops. More hard X-ray emission is expected to occur at the footpoint on the weak magnetic field side because energetic particles are more likely to escape the magnetic mirror there than at the strong magnetic field footpoint. The footpoint on the weak magnetic field side is predicted to move more quickly because of the requirement in two dimensions that equal amounts of flux must be reconnected from each upstream region. The X-line drifts away from the conducting wall in all simulations with asymmetric outflow and into the strong magnetic field region during most of the simulations with asymmetric inflow. There is net plasma flow across the X-line for both the inflow and outflow directions. The reconnection exhaust directed away from the obstructing wall is significantly faster

than the exhaust directed toward it. The asymmetric inflow condition allows net vorticity in the rising outflow plasmoid which would appear as rolling motions about the flux rope axis.

Flare forecasting at the Met Office Space Weather Operations Centre

Sophie A. **Murray**, Suzy Bingham, Michael Sharpe, David R. Jackson
SpaceWeather Quarterly Vol.14, Issue 2 p.18 **2017**
https://arxiv.org/pdf/1703.06754.pdf
http://onlinelibrary.wiley.com/doi/10.1002/swq.14/epdf
The Met Office Space Weather Operations Centre produces 24/7/365 space weather guidance, alerts, and forecasts to a wide range of government and commercial end users across the United Kingdom. Solar flare forecasts are one of its products, which are issued multiple times a day in two forms; forecasts for each active region on the solar disk over the next 24 hours, and full-disk forecasts for the next four days. Here the forecasting process is described in detail, as well as first verification of archived forecasts using methods commonly used in operational weather prediction. Real-time verification available for operational flare forecasting use is also described. The influence of human forecasters is highlighted, with human-edited forecasts outperforming original model results, and forecasting skill decreasing over longer forecast lead times.
UKSP Nuggets #79, 2017 www.uksolphys.org/?p=12998

Evidence for Partial Taylor Relaxation from Changes in Magnetic Geometry and Energy during a Solar Flare

Sophie A. **Murray**, D. Shaun Bloomfield, Peter T. Gallagher
E-print, Dec **2012**; A&A, A119 (**2013**)
http://arxiv.org/pdf/1212.5906v1.pdf
Solar flares are powered by energy stored in the coronal magnetic field, a portion of which is released when the field reconfigures into a lower energy state. Investigation of sunspot magnetic field topology during flare activity is useful to improve our understanding of flaring processes. Here we investigate the deviation of the non-linear field configuration from that of the linear and potential configurations, and study the free energy available leading up to and after a flare. The evolution of the magnetic field in NOAA region 10953 was examined using data from Hinode/SOT-SP, over a period of 12 hours leading up to and after a GOES B1.0 flare. Previous work on this region found pre- and post-flare changes in photospheric vector magnetic field parameters of flux elements outside the primary sunspot. 3D geometry was thus investigated using potential, linear force-free, and non-linear force-free field extrapolations in order to fully understand the evolution of the field lines. Traced field line geometrical and footpoint orientation differences show that the field does not completely relax to a fully potential or linear force-free state after the flare. Magnetic and free magnetic energies increase significantly ~ 6.5-2.5 hours before the flare by ~ 10^31 erg. After the flare, the non-linear force-free magnetic energy and free magnetic energies decrease but do not return to pre-flare 'quiet' values. The post-flare non-linear force-free field configuration is closer (but not equal) to that of the linear force-free field configuration than a potential one. However, the small degree of similarity suggests that partial Taylor relaxation has occurred over a time scale of ~ 3-4 hours. **2007 April 29**

The Evolution of Sunspot Magnetic Fields Associated with a Solar Flare

Sophie A. **Murray**, D. Shaun Bloomfield and Peter T. Gallagher
Solar Physics, Volume 277, Number 1, 45-57, **2012**
http://arxiv.org/pdf/1105.1978v1.pdf
Solar flares occur due to the sudden release of energy stored in active-region magnetic fields. To date, the precursors to flaring are still not fully understood, although there is evidence that flaring is related to changes in the topology or complexity of an active-region's magnetic field. Here, the evolution of the magnetic field in active region NOAA 10953 was examined using Hinode/SOT-SP data over a period of 12 hours leading up to and after **a GOES B1.0 flare**. A number of magnetic-field properties and low-order aspects of magnetic-field topology were extracted from two flux regions that exhibited increased Ca ii H emission during the flare. Pre-flare increases in vertical field strength, vertical current density, and inclination angle of $\approx 8°$ toward the vertical were observed in flux elements surrounding the primary sunspot. The vertical field strength and current density subsequently decreased in the post-flare state, with the inclination becoming more horizontal by $\approx 7°$. This behavior of the field vector may provide a physical basis for future flare-forecasting efforts. **29 April 2007**

Energetic electrons and coronal jets **Presentation**

Sophie **Musset**
Fleishman's Webinar 18 Dec **2020**

https://www.youtube.com/watch?v=4I57_w5IQu4&feature=youtu.be

Statistical study of hard X-ray emitting electrons associated with flare-related coronal jets

Sophie **Musset**, Mariana Jeunon, Lindsay Glesener

2019

https://arxiv.org/pdf/1903.10414.pdf

We present the statistical analysis of 33 flare-related coronal jets, and discuss the link between the jet and the flare properties in these events. We selected jets that were observed between 2010 and 2016 by the Atmospheric Imaging Assembly (AIA) on board the Solar Dynamic Observatory (SDO) and are temporally and spatially associated to flares observed by the Reuven Ramaty High Energy Solar Spectrometric Imager (RHESSI). For each jet, we calculated the jet duration and projected velocity in the plane of sky. The jet duration distribution has a median of 18.8 minutes. The projected velocities are between 31 km/s and 456 km/s with a median at 210 km/s. For each associated flare, we performed X-ray imaging and spectroscopy and identify non-thermal emission. Non-thermal emission was detected in only 1/4 of the event considered. We did not find a clear correlation between the flare thermal energy or SXR peak flux and the jet velocity. A moderate anti-correlation was found between the jet duration and the flare SXR peak flux. There is no preferential time delay between the flare and the jet. The X-ray emission is generally located at the base of the jet. The analysis presented in this paper suggests that the flare and jet are part of the same explosive event, that the jet is driven by the propagation of an Alfvenic perturbation, and that the energy partition between flare and jets varies substantially from one event to another. **Aug 2 2010**

APPENDIX: LIST OF EUV JETS (2010-2016)

Diffusive Transport of Energetic Electrons in the Solar Corona: X-ray and Radio Diagnostics

S. **Musset**, E. P. Kontar, N. Vilmer

A&A 610, A6 (**2018**)

https://arxiv.org/pdf/1710.00765.pdf

Imaging spectroscopy in X-rays with RHESSI provide the possibility to investigate the spatial evolution of the X-ray emitting electron distribution and therefore to study the transport effects on energetic electrons during solar flares. We study the energy dependence of the energetic electron scattering mean free path in the solar corona. We use the imaging spectroscopy technique with RHESSI to study the evolution of energetic electrons distribution in different part of the magnetic loop during the **2004 May 21** flare. These observations are compared with the radio observations of the gyrosynchrotron radiation of the same flare by Kuznetsov and Kontar (2015), and with the predictions of the diffusive transport model described by Kontar et al. (2014). The X-ray analysis shows a trapping of energetic electrons in the corona and a spectral hardening of the energetic electron distribution between the top of the loop and the footpoints. Coronal trapping of electrons is stronger for the radio-emitting electrons than for the X-ray-emitting electrons. These observations can be explained by the diffusive transport model derived by Kontar et al. (2014). We show that the combination of X-ray and radio diagnostics is a powerful tool to study electron transport in the solar corona in different energy domains. We show that the diffusive transport model can explain our observations; and in the range 25-500 keV, the electron scattering mean free path decreases with electron energy. We can estimate for the first time the scattering mean free path dependence on energy in the corona.

RHESSI Science Nuggets in October **2017** No. 309,

http://sprg.ssl.berkeley.edu/~tohban/wiki/index.php/Electron_Scattering_in_the_Flaring_Corona

High-energy Electrons and Electric Currents during a Flare

Sophie **Musset**, Nicole Vilmer, and Veronique Bommier.

RHESSI Science Nugget No. 255, June **2015**

http://sprg.ssl.berkeley.edu/~tohban/wiki/index.php/High-energy_Electrons_and_Electric_Currents_during_a_Flare

Photospheric vertical currents linked to sites of electron acceleration in the corona.

These observations show a spatial correlation between photospheric current ribbons and coronal X-ray sources. Moreover, for the first time, a conjoint evolution of hard X-ray emission and vertical current density at the photospheric level is observed during the course of a flare, and explained as the double consequence of the propagation of reconnection sites in the corona.

Hard X-ray emitting energetic electrons and photospheric electric currents

Sophie **Musset**, Nicole Vilmer, Véronique Bommier

A&A 580, A106 **2015**

http://arxiv.org/pdf/1506.02724v1.pdf

The energy released during solar flares is believed to be stored in non-potential magnetic fields associated with electric currents flowing in the corona. While no measurements of coronal electric currents are presently available, maps of photospheric electric currents can now be derived from SDO/HMI observations. Photospheric electric currents have been shown to be the tracers of the coronal electric currents. Particle acceleration can result from electric fields

associated with coronal electric currents. We revisit here some aspects of the relationship between particle acceleration in solar flares and electric currents in the active region.
We study the relation between the energetic electron interaction sites in the solar atmosphere, and the magnitudes and changes of vertical electric current densities measured at the photospheric level, during the X2.2 flare on **February 15 2011** in AR NOAA 11158.
X-ray images from RHESSI are overlaid on magnetic field and electric current density maps calculated from the spectropolarimetric measurements of SDO/HMI using the UNNOFIT inversion and Metcalf disambiguation codes. X-ray images are also compared with EUV images from SDO/AIA to complement the flare analysis.
Part of the elongated X-ray emissions from both thermal and non-thermal electrons overlay the elongated narrow current ribbons observed at the photospheric level. A new X-ray source at 50-100 keV (produced by non-thermal electrons) is observed in the course of the flare and is cospatial with a region in which new vertical photospheric currents appeared during the same period (increase of 15%). These observational results are discussed in the context of the scenarios in which magnetic reconnection (and subsequent plasma heating and particle acceleration) occurs at current-carrying layers in the corona.

Solar X-ray Emission Measured by the VernovMission During September – October of 2014

N. **Myagkova**, A. V. Bogomolov, L. K. Kashapova, V. V. Bogomolov, S. I. Svertilov, M. I. Panasyuk, E. A. Kuznetsova, G. V. Rozhkov
Solar Phys. Volume 291, Issue 11, pp 3439–3450 **2016**
Solar hard X-ray and γγ-ray emissions were measured by the Detector of the Roentgen and Gamma-ray Emissions (DRGE) instrument, which is part of the RELEC set of instruments operated onboard the Russian satellite Vernov, from July 8, 2014 until December 10, 2014 (on a solar-synchronous orbit with an apogee of 830 km, perigee of 640 km, and an inclination of 98.4∘98.4∘). RELEC measurements of 18 flares with X-ray energy >30 keV>30 keV, taken in September – October 2014, were connected with the same active region with the number AR 12172 during the first rotation and AR 12192 during the next one. These measurements were compared to the data obtained with RHESSI, Konus-Wind, Fermi Observatory, Radio Solar Telescope Net(RSTN), and the Nobeyama Radioheliograph (NoRH) operating at the same time. Quasi-periodicities with similar periods of 7±2 s7±2 s were found in about one third of all flares measured by RELEC (Vernov) from September 24 until October 30, 2014.

X-ray flares and coronal mass ejections (CMEs) during very quiet solar activity conditions of 2009

Kamsali **Nagaraja**, Praveen Kumar Basuvaraj, S. C. Chakravarty
Indian Journal of Pure and Applied Physics, **2018**
https://arxiv.org/pdf/2008.11157.pdf
Solar flares (SFs) are sudden brightening observed over the Sun surface which is associated with a large energy release. Flares with burst of Xray emission are normally followed by a mass ejection of electrons and ions from the solar atmosphere called Coronal Mass Ejections (CMEs). There is an evidence that solar magnetic field can change its configuration through reconnection and release energy, accelerating solar plasma causing SFs and CMEs. This study examines the SFs and CMEs data from SOHO and GOES satellites during the very low solar activity year of 2009 and moderately high solar activity of 2002. The results indicate that certain modifications in the existing mechanisms of generating SFs and CMEs would be necessary for developing more realistic forecast models affecting the space weather conditions.

Study of Time Evolution of Thermal and Non-Thermal Emission from an M-Class Solar Flare

Shunsaku **Nagasawa**, Tomoko Kawate, Noriyuki Narukage, Tadayuki Takahashi, Amir Caspi, Thomas N. Woods
ApJ **933** 173 **2022**
https://arxiv.org/pdf/2205.14369.pdf
https://iopscience.iop.org/article/10.3847/1538-4357/ac7532/pdf
We conduct a wide-band X-ray spectral analysis in the energy range of 1.5-100 keV to study the time evolution of the M7.6 class flare of **2016 July 23**, with the Miniature X-ray Solar Spectrometer (MinXSS) CubeSat and the Reuven Ramaty High Energy Solar Spectroscopic Imager (RHESSI) spacecraft. With the combination of MinXSS for soft X-rays and RHESSI for hard X-rays, a non-thermal component and three-temperature multi-thermal component -- "cool" (T≈ 3 MK), "hot" (T≈ 15 MK), and "super-hot" (T≈ 30 MK) -- were measured simultaneously. In addition, we successfully obtained the spectral evolution of the multi-thermal and non-thermal components with a 10 s cadence, which corresponds to the Alfvén time scale in the solar corona. We find that the emission measures of the cool and hot thermal components are drastically increasing more than hundreds of times and the super-hot thermal component is gradually appearing after the peak of the non-thermal emission. We also study the microwave spectra obtained by the Nobeyama Radio Polarimeters (NoRP), and we find that there is continuous gyro-synchrotron emission from mildly relativistic non-thermal electrons. In addition, we conducted a differential emission measure (DEM) analysis by using

Atmospheric Imaging Assembly (AIA) onboard the Solar Dynamics Observatory (SDO) and determine that the DEM of cool plasma increases within the flaring loop. We find that the cool and hot plasma components are associated with chromospheric evaporation. The super-hot plasma component could be explained by the thermalization of the non-thermal electrons trapped in the flaring loop.
RHESSI Science Nuggets #431 Jun **2022**
https://sprg.ssl.berkeley.edu/~tohban/wiki/index.php/Thermal/Nonthermal_with_MinXSS_and_RHESSI

Solar Flare Modified Complex Network

Amin **Najafi**, Amir Hossein Darooneh, Akbar Gheibi, and Nastaran Farhang
2020 ApJ 894 66
https://iopscience.iop.org/article/10.3847/1538-4357/ab8301/pdf
A constructive approach is developed to build the solar flare complex network by utilizing a visibility graph condition alongside the Abe–Suzuki method. Solar flare information such as position, start time, and peak flux is used for this purpose. The obtained characteristics of the topological features (such as the characteristic path length, power-law behavior of the probability distribution function of degrees, and the clustering coefficient) demonstrate the scale-free and small-world properties of the solar flare modified network. To explain the complexity of the constructed network, Omori's law as well as the universal scaling features are investigated. Furthermore, a nonextensive modification of the Gutenberg–Richter law is examined for the solar flare modified network using a q-stretched exponential model. Establishing a two-dimensional map for the configuration of 118 energetic main flares observed between 2006 and 2016, it is found that the main flares are located within the regions consisting of hubs (high-connectivity regions) of the network. A fractal dimension of the solar flare network of about 0.79 is also obtained.

Editorial to the Topical Collection: Oscillatory Processes in Solar and Stellar Coronae **Review**

Valery M. **Nakariakov**, Dipankar Banerjee, Bo Li, Tongjiang Wang, Ivan V. Zimovets & Maurizio Falanga
Space Science Reviews volume 218, Article number: 13 (**2022**)
https://link.springer.com/content/pdf/10.1007/s11214-022-00888-1.pdf

Quasi-periodic Pulsations in a Solar Microflare

V. M. **Nakariakov**1,2, S. Anfinogentov3, A. A. Storozhenko2, E. A. Kurochkin2, V. M. Bogod2,4, I. N. Sharykin3,5, and T. I. Kaltman2
2018 ApJ 859 154 DOI 10.3847/1538-4357/aabfb9
http://https//warwick.ac.uk/fac/sci/physics/research/cfsa/people/valery/research/eprints/Nakariakov_2018_ApJ_859_154.pdf
Irregular time evolution of the radio emission generated in a B2-class microflare (SOL**2017-01-25**T10:15), occurring on 2017 January 25 in active region 12,628, is studied. The microflare was apparently initiated by an appearance of an s-shaped loop, observed in the EUV band. The radio emission is associated with the nonthermal electrons detected with Ramaty High Energy Solar Spectroscopic Imager, and originates simultaneously from two opposite footpoints of a magnetic fan structure beginning at a sunspot. According to the active region geometry, the footpoints are situated in the meridional direction, and hence are observed by RATAN-600 simultaneously. The radio emission intensity signal, as well as the left-hand and right-hand circular polarization signals in the low-frequency band (3–4 GHz) show good correlation with each other, with the average characteristic time of the variation 1.4 ± 0.3 s. The polarization signal shows a time variation with the characteristic time of about 0.7 ± 0.2 s. The irregular quasi-periodic pulsations of the radio emission are likely to be caused by the superposition of the signals generated at the local electron plasma frequencies by the interaction of nonthermal electrons with the plasma at the footpoints. In this scenario, the precipitation rate of the nonthermal electrons at the opposite footpoints could be modulated by the superposition of fundamental and second harmonic modes of sausage oscillations, resulting in the observed different characteristic times of the intensity and polarization signals. However, other mechanisms, e.g., the oscillatory regime of loop coalescence or magnetic null point oscillation could not be rigorously excluded.

SLOW MAGNETOACOUSTIC WAVES IN TWO-RIBBON FLARES

V. M. **Nakariakov**1,2 and I. V. Zimovets3
Astrophysical Journal Letters, 730:L27 (4pp), **2011** April
We demonstrate that disturbances observed to propagate along the axis of the arcade in two-ribbon solar flares at the speed of a few tens of km s^{-1}, well below the Alfv´en and sound speeds, can be interpreted in terms of slow magnetoacoustic waves. The waves can propagate across the magnetic field, parallel to the magnetic neutral line, because of the wave-guiding effect due to the reflection from the footpoints. The perpendicular group speed of the perturbation is found to be a fraction of the sound speed, which is consistent with observations. The highest value of the group speed grows with the increase in the ratio of the sound and Alfv´en speeds. For a broad range of parameters, the highest value of the group speed corresponds to the propagation angle of 25°–28° to the magnetic

field. This effect can explain the temporal and spatial structure of quasi-periodic pulsations observed in two-ribbon flares.

Nuggets:
http://sprg.ssl.berkeley.edu/~tohban/wiki/index.php/Slow_Magnetoacoustic_Waves_in_Two-Ribbon_Flares

Oscillatory processes in solar flares

V M **Nakariakov**1, A R Inglis2, I V Zimovets3, C Foullon1, E Verwichte1, R Sych4 and I N Myagkova

E-print, Oct **2010, File**; Plasma Phys. Controlled Fusion (in press),

Electromagnetic (radio, visible-light, UV, EUV, X-ray and gamma-ray) emission generated by solar and stellar flares often contains pronounced quasi-periodic pulsations (QPP). Physical mechanisms responsible for the generation of long-period QPP (with the periods longer than one second) are likely to be associated with MHD processes. The observed modulation depths, periods and anharmonicity of QPP suggest that they can be linked with some kind of MHD auto-oscillations, e.g. an oscillatory regime of magnetic reconnection. Such regimes, of both spontaneous and induced nature, have been observed in resistive-MHD numerical simulations. The oscillations are essentially nonlinear and non-stationary. We demonstrate that a promising novel method for their analysis is the Empirical Mode Decomposition technique. **A review.**

QUASI-PERIODIC PULSATIONS IN THE GAMMA-RAY EMISSION OF A SOLAR FLARE

V. M. **Nakariakov**1, C. Foullon1, I. N. Myagkova2, and A. R. Inglis1

Astrophysical Journal Letters, 708:L47–L51, **2010** January

Quasi-periodic pulsations (QPPs) of gamma-ray emission with a period of about 40 s are found in a single loop X-class solar flare on **2005 January 1** at photon energies up to 2–6 MeV with the SOlar Neutrons and Gamma-rays (SONG) experiment aboard the CORONAS-Fmission. The oscillations are also found to be present in the microwave emission detected with the Nobeyama Radioheliograph, and in the hard X-ray and low energy gamma-ray channels of RHESSI. *Periodogram and correlation analysis shows that the 40 s QPPs of microwave, hard X-ray, and gamma ray emission are almost synchronous in all observation bands.* Analysis of the spatial structure of hard X-ray and low energy (80–225 keV) gamma-ray QPP with RHESSI reveals synchronous while asymmetric QPP at both footpoints of the flaring loop. The difference between the averaged hard X-ray fluxes coming from the two footpoint sources is found to oscillate with a period of about 13 s for five cycles in the highest emission stage of the flare. The proposed mechanism generating the 40 s QPP is a triggering of magnetic reconnection by a kink oscillation in a nearby loop. The 13 s periodicity could be produced by the second harmonics of the sausage mode of the flaring loop.

Quasi-Periodic Pulsations in Solar Flares **Review**

Nakariakov, V. M. and Melnikov, V. F.

Space Science Reviews **149**, pages119–151 **2009**

https://link.springer.com/content/pdf/10.1007/s11214-009-9536-3.pdf

Quasi-periodic pulsations (QPP) are a common feature of flaring energy releases in the solar atmosphere, observed in all bands, from radio to hard X-ray. In this review we concentrate on QPP with the periods longer than one second. Physical mechanisms responsible for the generation of long QPP split into two groups: ?load/unload? mechanisms and MHD oscillations. Load/unload mechanisms are repetitive regimes of flaring energy releases by magnetic reconnection or by other means. MHD oscillations can affect all elements of the flaring emission generation: triggering of reconnection and modulation of its rate, acceleration and dynamics of non-thermal electrons, and physical conditions in the emitting plasmas. In the case of MHD oscillations, the periodicity of QPP is determined either by the presence of some resonances, e.g. standing modes of plasma structures, or by wave dispersion. Periods and other parameters of QPP are linked with properties of flaring plasmas and their morphology. Observational investigation of the QPP generation mechanisms based upon the use of spatial information, broadband spectral coverage and multi-periodicity is discussed.

Coronal Elemental Abundances During A-Class Solar Flares Observed by Chandrayaan-2 XSM

Lakshitha **Nama**, Biswajit Mondal, S. Narendranath & K. T. Paul

Solar Physics volume 298, Article number: 55 (**2023**)

https://doi.org/10.1007/s11207-023-02142-5

The abundances of low first ionization potential (FIP) elements are three to four times higher in the closed loop active corona than in the photosphere, known as the FIP effect. Observations suggest that the abundances vary in different coronal structures. Here, we use the soft X-ray spectroscopic measurements from the Solar X-ray Monitor (XSM) onboard the Chandrayaan-2 orbiter to study the FIP effect in multiple A-class flares observed during the minimum of Solar Cycle 24. Using time-integrated spectral analysis, we derive the average temperature, emission measure, and the

abundances of four elements – Mg, Al, Si, and S. We find that the temperature and emission measure scales with the sub-class of flares while the measured abundances show an intermediate FIP bias for the lower A-flares (e.g. A1), while for the higher A-flares, the FIP bias is near unity. To investigate it further, we perform a time-resolved spectral analysis for a sample of the A-class flares and examine the evolution of temperature, emission measure, and abundances. We find that the abundances drop from the coronal values towards their photospheric values in the impulsive phase of the flares and, after the impulsive phase, they quickly return to the usual coronal values. The transition of the abundances from the coronal to photospheric values in the impulsive phase of the flares indicates the injection of fresh unfractionated material from the lower solar atmosphere to the corona due to chromospheric evaporation. However, explaining the quick recovery of the abundances from the photospheric to coronal values in the decay phase of the flare is challenging.

Sun-as-a-star Analysis of Hα Spectra of a Solar Flare Observed by SMART/SDDI: Time Evolution of Red Asymmetry and Line Broadening

Kosuke **Namekata**, Kiyoshi Ichimoto, Takako T. Ishii, Kazunari Shibata

ApJ **933** 209 **2022**

https://arxiv.org/pdf/2206.01395.pdf

https://iopscience.iop.org/article/10.3847/1538-4357/ac75cd/pdf

Stellar flares sometimes show red/blue asymmetries of Hα line, which can indicate chromospheric dynamics and prominence activations. However, the origin of asymmetries is not completely understood. For a deeper understanding of stellar data, we performed a Sun-as-a-star analysis of Hα line profiles of an M4.2-class solar flare showing dominant emissions from flare ribbons by using the data of the Solar Dynamics Doppler Imager onboard the Solar Magnetic Activity Research Telescope at Hida Observatory. The Sun-as-a-star Hα spectra of the flare show red asymmetry of up to ∼95 km s−1 and line broadening of up to ∼7.5 Å. The Sun-as-a-star Hα profiles are consistent with spectra from flare regions with weak intensity, but they take smaller redshift velocities and line widths by a factor of ∼2 than those with strong intensity. The redshift velocities, as well as line widths, peak out and decay more rapidly than the Hα equivalent widths, which is consistent with chromospheric condensation model and spatially-resolved flare spectra. This suggests that as a result of superposition, the nature of chromospheric condensation is observable even from stellar flare spectra. The time evolution of redshift velocities is found to be similar to that of luminosities of near-ultraviolet rays (1600 Å), while the time evolution of line broadening is similar to that of optical white lights. These Hα spectral behaviors in Sun-as-a-star view could be helpful to distinguish whether the origin of Hα red asymmetry of stellar flares is a flare ribbon or other phenomena. **2017 September 5**

Discovery of a Long-Duration Superflare on a Young Solar-Type Star EK Draconis with Nearly Similar Time Evolution for Hα and White-Light Emissions

Kosuke **Namekata**, Hiroyuki Maehara, Satoshi Honda, et al.

ApJL **2022**

https://arxiv.org/pdf/2201.09416.pdf

Young solar-type stars are known to show frequent "superflares", which may severely influence the habitable worlds on young planets via intense radiations and coronal mass ejections. Here we report an optical spectroscopic and photometric observation of a long-duration superflare on the young solar-type star EK Draconis (50-120 Myr age) with the Seimei telescope and Transiting Exoplanet Survey Satellite (TESS). The flare energy 2.6×1034 erg and white-light flare duration 2.2 hr are much larger than those of the largest solar flares, and this is the largest superflare on a solar-type star ever detected by optical spectroscopy. The Hα emission profile shows no significant line asymmetry, meaning no signature of a filament eruption, unlike the only previous detection of a superflare on this star (Namekata et al. 2021, Nat.Astron). Also, it did not show significant line broadening, indicating that the non-thermal heating at the flare footpoints are not essential or that the footpoints are behind the limb. The time evolution and duration of the Hα flare are surprisingly almost the same as those of the white-light flare, which is different from general M-dwarf (super-)flares and solar flares. This unexpected time evolution may suggest that different radiation mechanisms than general solar flares are predominant, as follows: (1) radiation from (off-limb) flare loops, and (2) re-radiation via radiative backwarming, in both of which the cooling timescales of flare loops could determine the timescales of Hα and white light.

Statistical Study of Solar White-light Flares and Comparison with Superflares on Solar-type Stars

Kosuke **Namekata**, Takahito Sakaue, Kyoko Watanabe, Ayumi Asai, Hiroyuki Maehara, Yuta Notsu, Shota Notsu, Satoshi Honda, Takako T. Ishii, Kai Ikuta,Daisaku Nogami, Kazunari Shibata

Proceedings of the IAUS340 **2018**

https://arxiv.org/pdf/1804.07122.pdf

Recently, many superflares on solar-type stars were discovered as white-light flares (WLFs). A correlation between the energies (E) and durations (t) of superflares is derived as t∝E0.39, and this can be theoretically explained by magnetic

reconnection (t∝E1/3). In this study, we carried out a statistical research on 50 solar WLFs with SDO/HMI to examine the t-E relation. As a result, the t-E relation on solar WLFs (t∝E0.38) is quite similar stellar superflares, but the durations of stellar superflares are much shorter than those extrapolated from solar WLFs. We present the following two interpretations; (1) in solar flares, the cooling timescale of WL emission may be longer than the reconnection one, and the decay time can be determined by the cooling timescale; (2) the distribution can be understood by applying a scaling law t∝E1/3B−5/3 derived from the magnetic reconnection theory.

Statistical Studies of Solar White-Light Flares and Comparisons with Superflares on Solar-type Stars

Kosuke **Namekata**, Takahito Sakaue, Kyoko Watanabe, Ayumi Asai, Hiroyuki Maehara, Yuta Notsu,Shota Notsu, Satoshi Honda, Takako Ishii, Kai Ikuta, Daisaku Nogami, Kazunari Shibata

ApJ **851** 91 **2017**

https://arxiv.org/pdf/1710.11325.pdf

Recently, many superflares on solar-type stars have been discovered as white-light flares (WLFs). The statistical study found a correlation between their energies (E) and durations (τ): τ∝E0.39 (Maehara et al. 2017 EP&S, 67, 59), similar to those of solar hard/soft X-ray flares: τ∝E0.2−0.33. This indicates a universal mechanism of energy release on solar and stellar flares, i.e., magnetic reconnection. We here carried out a statistical research on **50 solar WLFs** observed with \textit{SDO}/HMI and examined the correlation between the energies and durations. As a result, the E--τ relation on solar WLFs (τ∝E0.38) is quite similar to that on stellar superflares (τ∝E0.39). However, the durations of stellar superflares are one order of magnitude shorter than those expected from solar WLFs. We present the following two interpretations for the discrepancy. (1) In solar flares, the cooling timescale of WLFs may be longer than the reconnection one, and the decay time of solar WLFs can be elongated by the cooling effect. (2) The distribution can be understood by applying a scaling law (τ∝E1/3B−5/3) derived from the magnetic reconnection theory. In this case, the observed superflares are expected to have 2-4 times stronger magnetic field strength than solar flares. **15 Feb 2011, 18 Feb 2011, 31 Dec 2011,19 July 2012, 23 October 2012, 20 November 2012, 22 Oct 2014, 5 May 2015**

Table 1. Physical paremeters of flares. (2011-2015)

HMI Science Nuggets #77 Dec **2017** http://hmi.stanford.edu/hminuggets/?p=2066

Validation of a Scaling Law for the Coronal Magnetic Field Strengths and Loop Lengths of Solar and Stellar Flares

Kosuke **Namekata**, Takahito Sakaue, Kyoko Watanabe, Ayumi Asai, Kazunari Shibata

PASJ Volume 69, Issue 1, 1 February **2017**, 7

https://arxiv.org/pdf/1610.09811v1.pdf

Shibata & Yokoyama (1999, 2002) proposed a method of estimating the coronal magnetic field strengths (B) and magnetic loop lengths (L) of solar and stellar flares, on the basis of magnetohydrodynamic simulations of the magnetic reconnection model. Using the scaling law provided by Shibata & Yokoyama (1999, 2002), B and L are obtained as functions of the emission measure (EM=n2L3) and temperature (T) at the flare peak. Here, n is the coronal electron density of the flares. This scaling law enables the estimation of B and L for unresolved stellar flares from the observable physical quantities EM and T, which is helpful for studying stellar surface activities. To apply this scaling law to stellar flares, we discuss its validity for spatially resolved solar flares. EM and T were calculated from GOES soft X-ray flux data, and B and L are theoretically estimated using the scaling law. For the same flare events, B and L were also observationally estimated with images taken by Solar Dynamics Observatory (SDO)/ Helioseismic and Magnetic Imager (HMI) Magnetogram and Atmospheric Imaging Assembly (AIA) 94{\AA} pass band. As expected, a positive correlation was found between the theoretically and observationally estimated values. We interpret this result as indirect evidence that flares are caused by magnetic reconnection. Moreover, this analysis makes us confident in the validity of applying this scaling law to stellar flares as well as solar flares. **16 Feb 2011**

Twisted solar active region magnetic fields as drivers of space weather: Observational and theoretical investigations

Dibyendu **Nandy**, Duncan H. Mackay, Richard C. Canfield and P.C.H. Martens

Journal of Atmospheric and Solar-Terrestrial Physics

Volume 70, Issues 2-4, February **2008**, Pages 605-613

The properties and dynamics of magnetic fields on the Sun's photosphere and outer layers—notably those within solar active regions—govern the eruptive activity of the Sun. These photospheric magnetic fields also act as the evolving lower boundary of the Sun–Earth coupled system. Quantifying the physical attributes of these magnetic fields and exploring the mechanisms underlying their influence on the near-Earth space environment are of vital importance for forecasting and mitigating adverse space weather effects. In this context, we discuss here a novel technique for measuring twist in the magnetic field lines of solar active regions that does not invoke the force-free field assumption. Twist in solar active regions can play an important role in flaring activity and the initiation of CMEs via the kink instability mechanism; we outline a procedure for determining this solar active region eruptive potential. We also discuss how twist in active region magnetic fields can be used as inputs in simulations of the coronal and heliospheric

fields; specifically, we explore through simulations, the formation, evolution and ejection of magnetic flux ropes that originate in twisted magnetic structures. The results and ideas presented here are relevant for exploring the role of twisted solar active region magnetic fields and flux ropes as drivers of space weather in the Sun–Earth system.

Coronal Elemental Abundance: New Results from Soft X-Ray Spectroscopy of the Sun

Shyama **Narendranath**, P. Sreekumar, Netra S. Pillai, Singam Panini, K Sankarasubramanian & Juhani Huovelin

Solar Physics volume 295, Article number: 175 (**2020**)

https://link.springer.com/content/pdf/10.1007/s11207-020-01738-5.pdf

Elemental abundances in the solar corona are known to be different from those observed in the solar photosphere. The ratio of coronal to photospheric abundance shows a dependence on the first ionization potential (FIP) of the element. We estimate FIP bias from direct measurements of elemental abundances from soft X-ray spectra using data from multiple space missions covering a range of solar activity levels. This comprehensive analysis shows clear evidence for a decrease in FIP bias around the maximum intensity of the X-ray flare with coronal abundances briefly tending to photospheric values and a slow recovery as the flare decays. The departure from coronal abundances are larger for the low FIP elements Ca, Fe and Si than for S which have a mid FIP value. These changes in the degree of fractionation might provide inputs to model wave propagation through the chromosphere during flares. **1 May 2004, 26 June 2004, 2 January 2005, 5 July 2009, 6 January 2014**

Evidence of Electron Acceleration around the Reconnection X-point in a Solar Flare

Noriyuki **Narukage**, Masumi Shimojo, Taro Sakao

ApJ, 787 125 **2014**

http://arxiv.org/pdf/1404.3288v1.pdf

Particle acceleration is one of the most significant features that are ubiquitous among space and cosmic plasmas. It is most prominent during flares in the case of the Sun, with which huge amount of electromagnetic radiation and high-energy particles are expelled into the interplanetary space through acceleration of plasma particles in the corona. Though it has been well understood that energies of flares are supplied by the mechanism called magnetic reconnection based on the observations in X-rays and EUV with space telescopes, where and how in the flaring magnetic field plasmas are accelerated has remained unknown due to the low plasma density in the flaring corona. We here report the first observational identification of the energetic non-thermal electrons around the point of the ongoing magnetic reconnection (X-point); with the location of the X-point identified by soft X-ray imagery and the localized presence of non-thermal electrons identified from imaging-spectroscopic data at two microwave frequencies. Considering the existence of the reconnection outflows that carries both plasma particles and magnetic fields out from the X-point, our identified non-thermal microwave emissions around the X-point indicate that the electrons are accelerated around the reconnection X-point. Additionally, the plasma around the X-point was also thermally heated up to 10 MK. The estimated reconnection rate of this event is ~0.017.

Coronal-Temperature-Diagnostic Capability of the *Hinode*/*X-Ray Telescope* Based on Self-Consistent Calibration

N. **Narukage** · T. Sakao · R. Kano · H. Hara · M. Shimojo · T. Bando · F. Urayama · E. DeLuca · L. Golub · M. Weber · P. Grigis · J. Cirtain · S. Tsuneta

Solar Phys (**2011**) 269: 169–236

The *X-Ray Telescope* (XRT) onboard the *Hinode* satellite is an X-ray imager that observes the solar corona with unprecedentedly high angular resolution (consistent with its 1__ pixel size). XRT has nine X-ray analysis filters with different temperature responses. One of the most significant scientific features of this telescope is its capability of diagnosing coronal temperatures from less than 1 MK to more than 10 MK, which has never been accomplished before. To make full use of this capability, accurate calibration of the coronal temperature response of XRT is indispensable and is presented in this article. The effect of on-orbit contamination is also taken into account in the calibration. On the basis of our calibration results, we review the coronal-temperature-diagnostic capability of XRT.

Correlated Spatiotemporal Evolution of Extreme-Ultraviolet Ribbons and Hard X-rays in a Solar Flare

Stephen J. **Naus**, Jiong Qiu, C. Richard DeVore, Spiro K. Antiochos, Joel T. Dahlin, James F. Drake, Marc Swisdak, Vadim M. Uritsky

ApJ **926** 218 **2022**

https://arxiv.org/pdf/2109.15314.pdf

https://iopscience.iop.org/article/10.3847/1538-4357/ac4028/pdf

We analyze the structure and evolution of ribbons from the M7.3 SOL**2014-04-18**T13 flare using ultraviolet (UV) images from IRIS and SDO/AIA, magnetic data from SDO/HMI, hard X-ray (HXR) images from RHESSI, and light curves from Fermi/GBM, in order to infer properties of coronal magnetic reconnection. As the event progresses, two flare ribbons spread away from the magnetic polarity inversion line. The width of the newly brightened front along the extension of the ribbon is highly intermittent in both space and time, presumably reflecting non-uniformities in the structure and/or dynamics of the flare current sheet. Furthermore, the ribbon width grows most rapidly in regions exhibiting concentrated non-thermal HXR emission, with sharp increases slightly preceding the HXR bursts. The light curve of the ultraviolet emission matches the HXR light curve at photon energies above 25 keV. In other regions the ribbon-width evolution and light curves do not temporally correlate with the HXR emission. This indicates that the production of non-thermal electrons is highly non-uniform within the flare current sheet. Our results suggest a strong connection between the production of non-thermal electrons and the locally enhanced perpendicular extent of flare ribbon fronts, which in turn reflects inhomogeneous structure and/or reconnection dynamics of the current sheet. Despite this variability, the ribbon fronts remain nearly continuous, quasi-one-dimensional features. Thus, although the reconnecting coronal current sheets are highly structured, they remain quasi-two-dimensional and the magnetic energy release occurs systematically, rather than stochastically, through the volume of reconnecting magnetic flux.

On the Spontaneous Generation of Three-dimensional Magnetic Nulls

Sushree S. **Nayak**1, R. Bhattacharyya1, P. K. Smolarkiewicz2, Sanjay Kumar3, and A. Prasad4
2020 ApJ 892 44
sci-hub.si/10.3847/1538-4357/ab75bb

Three-dimensional magnetic nulls relate to magnetic topology, and are propitious for triggering solar coronal transients. Although abundant in nature, their generation is not established. This paper reports magnetohydrodynamic simulations indicating the nulls to be dissipative self-organized structures. Categorically, the results of two case studies are presented. First, a potential null located at the origin of a Cartesian coordinate system is subjected to a sinusoidal flow. The null is seen to bifurcate while conserving the net topological degree. Using the corresponding deformed magnetic field as an initial condition, the magnetofluid is subsequently evolved by dissipating its magnetic and kinetic energies through magnetic reconnection and viscous dissipation. In effect, a current-carrying null develops in the process. Second, another simulation is initiated with a modified Arnold–Beltrami–Childress (ABC) magnetic field which exerts a Lorentz force on the magnetofluid and has no nulls within the computational volume. Astoundingly, allowed the magnetofluid to relax, nulls having mixed topological degrees are generated. The modified ABC field being chaotic, the spontaneous appearance of nulls establishes emergence of ordered magnetic structures from chaos—a trait of self-organized structures—explaining their ubiquity in naturally existing plasmas.

A Data-constrained Magnetohydrodynamic Simulation of Successive Events of Blowout Jet and C-class Flare in NOAA AR 12615

Sushree S. **Nayak**1, R. Bhattacharyya1, A. Prasad2, Qiang Hu2, Sanjay Kumar3, and B. Joshi1
2019 ApJ 875 10
sci-hub.se/10.3847/1538-4357/ab0a0b

Magnetohydrodynamic simulation is carried out for the NOAA AR 12615 in the time span $t \in \{05:48, 06:18\}$ UT on **2016 December 5**; covering events of a blowout jet and a C1.2 flare. The events are selected based on the small interval between their occurrences, which provides us with an opportunity to explore two energetically different events of magnetic reconnection (MR) within the run time of a single magnetohydrodynamic (MHD) simulation. The simulation is initiated with magnetic field extrapolated from the vector magnetogram provided by the Helioseismic Magnetic Imager/Solar Dynamics Observatory, using a non-force-free approximation. The extrapolated Lorentz force is found to decay at a rate faster than the volume current density, making the higher corona to be effectively force-free while the Lorentz force affects only the lower corona and the photosphere—a desirable feature that agrees with the contemporary understanding. For the simulation, the plasma is idealized to be incompressible, thermally homogeneous and having perfect electrical conductivity. The results affirm MRs near a set of two three-dimensional (3D) magnetic nulls to be responsible for initiating the jet. Moreover, a flux rope located near the nulls contributes to the jet by changing its magnetic field lines from an anchored to an open topology. The scenario agrees with the standard mini-filament breakout model for blowout jets and provides its first demonstration from a 3D data-constrained MHD simulation where the computational output is reconciled with magnetogram(s) only once. The generation of flare ribbons is attributed to reconnections at a 3D null and a quasi-separatrix layer (QSL), highlighting the importance of topological complexity in flare initiation.

Magnetic field topology from non-force free extrapolation and magnetohydrodynamic simulation of its eventual dynamics

Sushree S. **Nayak**, R. Bhattacharyya, A. Prasad, Qiang Hu
Proc. IAU Symp. 340. **2018**
https://arxiv.org/pdf/1804.04814.pdf

Magnetic reconnections (MRs) for various magnetic field line (MFL) topologies are believed to be the initiators of various solar eruptive events like flares and coronal mass ejections (CMEs). Consequently, important is a thorough understanding and quantification of the MFL topology and their evolution which leads to MRs. Contemporary standard is to extrapolate the coronal MFLs using equilibrium models where the Lorentz force on the coronal plasma is zero everywhere, because either there is no current or the current is parallel to the magnetic field. In tandem, a non-force-free-field (NFFF) extrapolation scheme has evolved and allows for a Lorentz force which is non-zero only at the photosphere but asymptotically vanishes with height. The paper reports magnetohydrodynamic (MHD)- simulations initiated by NFFF extrapolation of the coronal MFLs for the active region NOAA 11158. Interestingly, quasi-separatrix layers (QSLs) which facilitate MRs are detected in the extrapolated MFLs. The AR 11158 is flare producing and, the paper makes an attempt to asses the role of QSLs in the flare onsets. **15th February, 2011**

Evolution of Characteristics of Vertical Electric Current and Magnetic Field in Active Regions of the Sun and Their Relation to Powerful Flares.

Nechaeva, A.B., Zimovets, I.V., Zubik, V.S. et al.
Geomagn. Aeron. 64, 150–171 (**2024**).
https://doi.org/10.1134/S0016793223601060
The study of evolution of magnetic field and electric currents in active regions of the Sun over a long-time interval is of interest for understanding the processes of energy accumulation and release in them, leading to various phenomena that affect space weather. In this study, based on the photospheric vector magnetograms of the helioseismic and magnetic imager instrument aboard the Solar Dynamics Observatory, the authors analyzed the evolution of a number of characteristics of the magnetic field and vertical electric current in three active regions, 11 158, 11 675, and 12 673, that produced M and X class flares, during the time from their origin in the eastern hemisphere, during passage through the solar disk, and until their disappearance near the western limb with a step of 2 h. The characteristics considered included: the power-law exponent of the probability density function of the absolute value of the vertical electric current density, the maximum absolute value of the vertical current density, the signed and unsigned total vertical currents and the unsigned total vertical and horizontal magnetic fluxes, the energy of the nonlinear force-free and potential magnetic fields, the free magnetic energy, and the number of islands with strong vertical current. Some regularities in the behavior of the characteristics considered are found, in particular, regarding the occurrence of solar flares. The correlation coefficients between pairs of these characteristics are calculated. Additionally, M. Aschwanden's approach is shown to be promising for predicting the maximum X-ray class of a flare by calculating the energy of the potential magnetic field in active regions. The results can be used to predict powerful solar flares.

IRIS burst properties in active regions

C. J. **Nelson**, L. Kleint
A&A 666, A66 **2022**
https://arxiv.org/pdf/2208.11013
https://www.aanda.org/articles/aa/pdf/2022/10/aa44375-22.pdf
Interface Region Imaging Spectrograph (IRIS) bursts are localised features thought to be driven by magnetic reconnection. Although these events are well-studied, it remains unknown whether their properties vary as their host active regions (ARs) evolve. Here, we aim to understand whether the measurable properties of IRIS bursts are consistent during the evolution of their host ARs. We study 42 dense 400-step rasters sampled by IRIS. These rasters each covered one of seven ARs, with each AR being sampled at least four times over a minimum of 48 hours. An automated detection algorithm is used to identify IRIS burst profiles. Data from the Solar Dynamics Observatory's Helioseismic and Magnetic Imager are also used to provide context about the co-spatial line-of-sight magnetic field. Of the rasters studied, 36 were found to contain IRIS burst profiles. Five ARs (11850, 11909, 11916, 12104, and 12139) contained IRIS burst profiles in each raster that sampled them whilst one AR (11871) was found to contain no such spectra at any time. A total of 4019 IRIS burst profiles belonging to 752 connected objects, which we define as parent IRIS bursts, were identified. IRIS burst profiles were only detected within compact regions in each raster, with these regions appearing to increase in size as the host ARs aged. No systematic changes in the frequency of IRIS burst profiles or the spectral characteristic of IRIS burst profiles through time were found for these ARs. Finally, 93 % of parent IRIS bursts with areas between 1 arcsec^2 and 4 arcsec^2 occurred co-spatial to bi-poles in the photosphere. Overall, IRIS bursts have remarkably consistent spectral and spatial properties throughout the evolution of ARs. These events predominantly form within the cores of larger and more complex ARs, with the regions containing these events appearing to increase in size as the host region itself evolves.

Small-Scale Structuring Of Ellerman Bombs at Solar Limb

C. J. **Nelson**, E. M. Scullion, J. G. Doyle, N. Freij, R. Erdélyi
ApJ, **2014**
http://arxiv.org/pdf/1410.5715v1.pdf
Ellerman bombs (EBs) have been widely studied in recent years due to their dynamic, explosive nature and apparent links to the underlying photospheric magnetic field implying that they may be formed by magnetic reconnection in the

photosphere. Despite a plethora of researches discussing the morphologies of EBs, there has been a limited investigation of how these events appear at the limb, specifically, whether they manifest as vertical extensions away from the disc. In this article, we make use of high-resolution, high-cadence observations of an AR at the solar limb, collected by the CRISP instrument, to identify EBs and infer their physical properties.
The upper atmosphere is also probed using the SDO/AIA. We analyse 22 EB events evident within these data, finding that 20 appear to follow a parabolic path away from the solar surface at an average speed of 9 km s^(-1), extending away from their source by 580 km, before retreating back at a similar speed. These results show strong evidence of vertical motions associated with EBs, possibly explaining the dynamical `flaring' (changing in area and intensity) observed in on-disc events. Two in-depth case studies are also presented which highlight the unique dynamical nature of EBs within the lower solar atmosphere. The viewing angle of these observations allows for a direct linkage between these EBs and other small-scale events in the H-alpha line wings, including a potential flux emergence scenario. The findings presented here suggest that EBs could have a wider-reaching influence on the solar atmosphere than previously thought, as we reveal a direct linkage between EBs and an emerging small-scale loop, and other near-by small-scale explosive events. However, as previous research found, these extensions do not appear to impact upon the H-alpha line core, and are not observed by the SDO/AIA EUV filters. **21st June 2012**.

Ellerman Bombs—Evidence for Magnetic Reconnection in the Lower Solar Atmosphere

C. J. **Nelson**1,2, S. Shelyag3, M. Mathioudakis4, J. G. Doyle1, M. S. Madjarska1, H. Uitenbroek5, and R. Erdélyi
2013 ApJ 779 125
The presence of photospheric magnetic reconnection has long been thought to give rise to short and impulsive events, such as Ellerman bombs (EBs) and Type II spicules. In this article, we combine high-resolution, high-cadence observations from the Interferometric BIdimensional Spectrometer and Rapid Oscillations in the Solar Atmosphere instruments at the Dunn Solar Telescope, National Solar Observatory, New Mexico, with co-aligned Solar Dynamics Observatory Atmospheric Imaging Assembly and Hinode Solar Optical Telescope (SOT) data to observe small-scale events situated within an active region. These data are then compared with state-of-the-art numerical simulations of the lower atmosphere made using the MURaM code. It is found that brightenings, in both the observations and the simulations, of the wings of the Hα line profile, interpreted as EBs, are often spatially correlated with increases in the intensity of the Fe I λ6302.5 line core. Bipolar regions inferred from Hinode/SOT magnetic field data show evidence of flux cancellation associated, co-spatially, with these EBs, suggesting that magnetic reconnection could be a driver of these high-energy events. Through the analysis of similar events in the simulated lower atmosphere, we are able to infer that line profiles analogous to the observations occur co-spatially with regions of strong opposite-polarity magnetic flux. These observed events and their simulated counterparts are interpreted as evidence of photospheric magnetic reconnection at scales observable using current observational instrumentation.

FORMATION OF PLASMOIDS IN MULTIPLE CURRENT SYSTEMS

M. J. **Nemati**, Z. X. Wang, and Lai Wei
2016 ApJ 821 128
We show that in systems with multiple current sheets, the reconnection rate can increase with increasing S. This is essentially different from the result in single current sheet systems where the reconnection rate usually decreases with increasing S or is independent of S. Such a resistive fast reconnection can be applied to account for the rapid events in multiple current systems of astrophysical, solar, and magnetic fusion plasmas.

Exploring the solar paradigm to explain stellar variability **Thesis-Review**

Nina-Elisabet **Nèmec**
2021
https://arxiv.org/pdf/2106.13183.pdf
The unprecedented precision of broadband stellar photometry achieved with the planet-hunting missions CoRoT and \textit{Kepler} initiated a new era in examining the magnetically-driven brightness variations of hundreds of thousands of stars. Such brightness variations are well studied and understood for the Sun. The plethora of data allows to accurately compare solar and stellar brightness variations. An intriguing question is whether the observed trends in the stellar photometric variability (e.g. the dependence of the variability on the stellar rotation period) can be explained by utilising the solar paradigm, in particular the physical concepts of brightness variations learnt from the Sun. The goal of this work is to find out, through comparison of observational and simulated data, if any physical concepts of solar brightness variability have to be altered to reproduce the distribution of Sun-like stars variabilities.

THEORY OF ENERGY STORAGE AND RELEASE IN THE SOLAR CORONA

Thomas **Neukirch**
Proceedings of the 11th European Solar Physics Meeting - The Dynamic Sun: Challenges for

*Theory and Observations, 11-16 September 2005 (ESA SP-596 or 600, December **2005**)*
Хороший обзор. **File,** **Review**

Unveiling Mass Transfer in Solar Flares: Insights from Elemental Abundance Evolutions Observed by Chang'E-2 Solar X-ray Monitor

Man-Hei **Ng**, Chi-Long Tang, Xiaoping Zhang, Kuan-Vai Tam, Peng-Fei Chen, Wudong Dong, Jing Li, Chi-Pui Tang
ApJ **972** 123 **2024**
https://arxiv.org/pdf/2407.02199
https://iopscience.iop.org/article/10.3847/1538-4357/ad5da3/pdf
Understanding how elemental abundances evolve during solar flares helps shed light on the mass and energy transfer between different solar atmospheric layers. However, prior studies have mostly concentrated on averaged abundances or specific flare phases, leaving a gap in exploring the comprehensive observations throughout the entire flare process. Consequently, investigations into this area are relatively scarce. Exploiting the Solar X-ray Monitor data obtained from the Chang'E-2 lunar orbiter, we present two comprehensive soft X-ray spectroscopic observations of flares in active regions, AR 11149 and 11158, demonstrating elemental abundance evolutions under different conditions. Our findings unveil the inverse first ionization potential (IFIP) effect during flares for Fe for the first time, and reaffirm its existence for Si. Additionally, we observed a rare depletion of elemental abundances, marking the second IFIP effect in flare decay phases. Our study offers a CSHKP model-based interpretation to elucidate the formation of both the FIP and IFIP effects in flare dynamics, with the inertia effect being incorporated into the ponderomotive force fractionation model.
January 28, 2011, February 21, 2011

The Merging of a Coronal Dimming and the Southern Polar Coronal Hole

Nawin **Ngampoopun**1, David M. Long1,2, Deborah Baker1, Lucie M. Green1, Stephanie L. Yardley1,3,4, Alexander W. James1,5, and Andy S. H. To
2023 ApJ 950 150
https://arxiv.org/pdf/2305.06106.pdf
https://iopscience.iop.org/article/10.3847/1538-4357/acd44e/pdf
We report on the merging between the southern polar coronal hole and an adjacent coronal dimming induced by a coronal mass ejection on **2022 March 18**, resulting in the merged region persisting for at least 72 hr. We use remote sensing data from multiple co-observing spacecraft to understand the physical processes during this merging event. The evolution of the merger is examined using Extreme-UltraViolet (EUV) images obtained from the Atmospheric Imaging Assembly on board the Solar Dynamic Observatory and Extreme Ultraviolet Imager, which is on board the Solar Orbiter spacecraft. The plasma dynamics are quantified using spectroscopic data obtained from the EUV Imaging Spectrometer on board Hinode. The photospheric magnetograms from the Helioseismic and Magnetic Imager are used to derive the magnetic field properties. To our knowledge, this work is the first spectroscopical analysis of the merging of two open-field structures. We find that the coronal hole and the coronal dimming become indistinguishable after the merging. The upflow speeds inside the coronal dimming become more similar to that of a coronal hole, with a mixture of plasma upflows and downflows observable after the merging. The brightening of the bright points and the appearance of coronal jets inside the merged region further imply ongoing reconnection processes. We propose that component reconnection between the coronal hole and coronal dimming fields plays an important role during this merging event because the footpoint switching resulting from the reconnection allows the coronal dimming to intrude onto the boundary of the southern polar coronal hole.

Onset of Secondary Instabilities and Plasma Heating during Magnetic Reconnection in Strongly Magnetized Regions of the Low Solar Atmosphere

Lei **Ni**1,2,3 and Vyacheslav S. Lukin
2018 ApJ 868 144
http://sci-hub.tw/10.3847/1538-4357/aaeb97
We numerically study magnetic reconnection on different spatial scales and at different heights in the weakly ionized plasma of the low solar atmosphere (around 300–800 km above the solar surface) within a reactive 2.5D multifluid plasma–neutral model. We consider a strongly magnetized plasma ($\beta \sim 6\%$) evolving from a force-free magnetic configuration and perturbed to initialize formation of a reconnection current sheet. On large scales, the resulting current sheets are observed to undergo a secondary "plasmoid" instability. A series of simulations at different scales demonstrates a cascading current sheet formation process that terminates for current sheets with width of 2 m and length of ~100 m, corresponding to the critical current sheet aspect ratio of ~50. We also observe that the plasmoid instability is the primary physical mechanism accelerating the magnetic reconnection in this plasma parameter regime. After plasmoid instabilities appear, the reconnection rate sharply increases to a value of ~0.035, observed to be independent of the Lundquist number. These characteristics are very similar to magnetic reconnection in fully ionized

plasmas. In this low-βguide-field reconnection regime, both the recombination and collisionless effects are observed to have a small contribution to the reconnection rate. The simulations show that it is difficult to heat the dense weakly ionized photospheric plasmas to above 2 × 104 K during the magnetic reconnection process. However, the plasmas in the low solar chromosphere can be heated above 3 × 104 K with reconnection magnetic fields of 500 G or stronger.

Magnetic reconnection in strongly magnetized regions of the low solar chromosphere

Lei **Ni**, Vyacheslav S. Lukin, Nicholas A. Murphy, Jun Lin
MR in TMR; v. December 5, **2017**
https://arxiv.org/pdf/1712.00582.pdf
Magnetic reconnection in strongly magnetized regions around the temperature minimum region of the low solar atmosphere is studied by employing MHD-based simulations of a partially ionized plasma within a reactive 2.5D multi-fluid model. It is shown that in the absence of magnetic nulls in a low β plasma the ionized and neutral fluid flows are well-coupled throughout the reconnection region. However, non-equilibrium ionization-recombination dynamics play a critical role in determining the structure of the reconnection region, lead to much lower temperature increases and a faster magnetic reconnection rate as compared to simulations that assume plasma to be in ionization-recombination equilibrium. The rate of ionization of the neutral component of the plasma is always faster than recombination within the current sheet region even when the initial plasma β is as high as β0=1.46. When the reconnecting magnetic field is in excess of a kilogauss and the plasma β is lower than 0.0145, the initially weakly ionized plasmas can become fully ionized within the reconnection region and the current sheet can be strongly heated to above 2.5×104~K, even as most of the collisionally dissipated magnetic energy is radiated away. The Hall effect increases the reconnection rate slightly, but in the absence of magnetic nulls it does not result in significant asymmetries or change the characteristics of the reconnection current sheet down to meter scales.

NUMERICAL EXPERIMENTS ON THE DETAILED ENERGY CONVERSION AND SPECTRUM STUDIES IN A CORONA CURRENT SHEET

Lei **Ni**1,2, Jun Lin1, Zhixing Mei 1, and Yan Li
2015 ApJ 812 92
http://arxiv.org/pdf/1512.08007v1.pdf
In this paper, we study the energy conversion and spectra in a corona current sheet (CS) by 2.5 dimensional MHD numerical simulations. Numerical results show that many Petschek-like fine structures with slow-mode shocks mediated by plasmoid instabilities develop during the magnetic reconnection process. The termination shocks can also be formed above the primary magnetic island and at the head of secondary islands. These shocks play important roles in generating thermal energy in a corona CS. For a numerical simulation with initial conditions close to the solar corona environment, the ratio of the generated thermal energy to the total dissipated magnetic energy is around 1/5 before secondary islands appear. After secondary islands appear, the generated thermal energy starts to increase sharply and this ratio can reach a value of about 3/5. In an environment with a relatively lower plasma density and plasma β, the plasma can be heated to a much higher temperature. After secondary islands appear, the one-dimensional energy spectra along the CS do not behave as a simple power law and the spectrum index increases with the wave number. The average spectrum index for the magnetic energy spectrum along the CS is about 1.8. The two-dimensional spectra intuitively show that part of the high energy is cascaded to large kx and ky space after secondary islands appear. The plasmoid distribution function calculated from numerical simulations behaves as a power law closer to in the intermediate ψ regime. By using the effective magnetic diffusivity is estimated to be about 1011 ~ 1012 m2 s−1.

IMPACT OF TEMPERATURE-DEPENDENT RESISTIVITY AND THERMAL CONDUCTION ON PLASMOID INSTABILITIES IN CURRENT SHEETS IN THE SOLAR CORONA

Lei **Ni**1,2, Ilia I. Roussev1,3, Jun Lin1, and Udo Ziegler
2012 ApJ 758 20
In this paper, we investigate, by means of two-dimensional magnetohydrodynamic simulations, the impact of temperature-dependent resistivity and thermal conduction on the development of plasmoid instabilities in reconnecting current sheets in the solar corona. We find that the plasma temperature in the current-sheet region increases with time and it becomes greater than that in the inflow region. As secondary magnetic islands appear, the highest temperature is not always found at the reconnection X-points, but also inside the secondary islands. One of the effects of anisotropic thermal conduction is to decrease the temperature of the reconnecting X-points and transfer the heat into the O-points, the plasmoids, where it gets trapped. In the cases with temperature-dependent magnetic diffusivity, η ~ T –3/2, the decrease in plasma temperature at the X-points leads to (1) an increase in the magnetic diffusivity until the characteristic time for magnetic diffusion becomes comparable to that of thermal conduction, (2) an increase in the reconnection rate, and (3) more efficient conversion of magnetic energy into thermal energy and kinetic energy of bulk motions. These results provide further explanation of the rapid release of magnetic energy into heat and kinetic energy seen during flares and coronal mass ejections. In this work, we demonstrate that the consideration of anisotropic thermal

conduction and Spitzer-type, temperature-dependent magnetic diffusivity, as in the real solar corona, are crucially important for explaining the occurrence of fast reconnection during solar eruptions.

Fragmentation of electric currents in the solar corona by plasma flows

D. H. **Nickeler**1, M. Karlický1, T. Wiegelmann2 and M. Kraus
E-print, Oct **2013**; A&A 556, A61 (**2013**)

Aims. We consider a magnetic configuration consisting of an arcade structure and a detached plasmoid, resulting from a magnetic reconnection process, as is typically found in connection with solar flares. We study spontaneous current fragmentation caused by shear and vortex plasma flows.
Methods. An exact analytical transformation method was applied to calculate self-consistent solutions of the nonlinear stationary magnetohydrodynamic equations. The assumption of incompressible field-aligned flows implies that both the Alfvén Mach number and the mass density are constant on field lines. We first calculated nonlinear magnetohydrostatic equilibria with the help of the Liouville method, emulating the scenario of a solar eruptive flare configuration with plasmoids (magnetic ropes or current-carrying loops in 3D) and flare arcade. Then a Mach number profile was constructed that describes the upflow along the open magnetic field lines and implements a vortex flow inside the plasmoid. This Mach number profile was used to map the magnetohydrostatic equilibrium to the stationary one.
Results. We find that current fragmentation takes place at different locations within our configuration. Steep gradients of the Alfvén Mach number are required, implying the strong influence of shear flows on current amplification and filamentation of the magnetohydrostatic current sheets. Crescent- or ring-like structures appear along the outer separatrix, butterfly structures between the upper and lower plasmoids, and strong current peaks close the lower boundary (photosphere). Furthermore, impressing an intrinsic small-scale structure on the upper plasmoid results in strong fragmentation of the plasmoid. Hence fragmentation of current sheets and plasmoids is an inherent property of magnetohydrodynamic theory.
Conclusions. Transformations from magnetohydrostatic into magnetohydrodynamic steady-states deliver fine-structures needed for plasma heating and acceleration of particles and bulk plasma flows in dissipative events that are typically connected to magnetic reconnection processes in flares and coronal mass ejections.

Self-consistent stationary MHD shear flows in the solar atmosphere as electric field generators

D.H. **Nickeler**, M. Karlicky, T. Wiegelmann, M. Kraus
A&A, **2014**
http://arxiv.org/pdf/1407.3227v1.pdf

Magnetic fields and flows in coronal structures, for example, in gradual phases in flares, can be described by 2D and 3D magnetohydrostatic (MHS) and steady magnetohydrodynamic (MHD) equilibria. Within a physically simplified, but exact mathematical model, we study the electric currents and corresponding electric fields generated by shear flows. Starting from exact and analytically calculated magnetic potential fields, we solveid the nonlinear MHD equations self-consistently. By applying a magnetic shear flow and assuming a nonideal MHD environment, we calculated an electric field via Faraday's law. The formal solution for the electromagnetic field allowed us to compute an expression of an effective resistivity similar to the collisionless Speiser resistivity. We find that the electric field can be highly spatially structured, or in other words, filamented. The electric field component parallel to the magnetic field is the dominant component and is high where the resistivity has a maximum. The electric field is a potential field, therefore, the highest energy gain of the particles can be directly derived from the corresponding voltage. In our example of a coronal post-flare scenario we obtain electron energies of tens of keV, which are on the same order of magnitude as found observationally. This energy serves as a source for heating and acceleration of particles.

Topological skeleton of the 2-D slightly non-ideal MHD system close to X-type magnetic null points – an analysis of the general solution for the generic case

D.H. **Nickeler**, M. Karlicky, and M. Barta
Ann. Geophys., 30, 1015-1023, **2012**

The appearance of eruptive space plasma processes, e.g. in eruptive flares as observed in the solar atmosphere, is usually assumed to be caused by magnetic reconnection, often connected with singular points of the magnetic field.
We are interested in the general relation between the eigenvalues of the Jacobians of the plasma velocity and the magnetic field and their relation to the shape of a spatially varying, localized non-idealness or resistivity, i.e. we are searching for the general solution. We perform a local analysis of almost all regular, generic, structurally stable non-ideal or resistive MHD solutions. Therefore we use Taylor expansions of the magnetic field, the velocity field and all other physical quantities, including the non-idealness, and with the method of comparison of coefficients, the non-linear resistive MHD system is solved analytically, locally in a close vicinity of the null point.
We get a parameterised general solution that provides us with the topological and geometrical skeleton of the resistive MHD fields. These local solutions provide us with the "roots" of field and streamlines around the null points of

basically all possible 2-D reconnection solutions. We prove mathematically that necessarily, the flow close to the magnetic X-point must also be of X-point type to guarantee positive dissipation of energy and annihilation of magnetic flux. We also prove that, if the non-idealness has only a one-dimensional, sheet-like structure, only one separatrix line can be crossed by the plasma flow, similar to known reconnective annihilation solutions.

Magnetic helicity of solar active regions

A. **Nindos**

Proceedings of the International Astronomical Union / Volume 4 / Symposium S257, pp 133 – 143, Published online: 16 Mapт **2009, File**

Magnetic helicity is a quantity that describes the linkage and twistedness/shear in the magnetic field. It has the unique feature that it is probably the only physical quantity which is approximately conserved even in resistive MHD. This makes magnetic helicity an ideal tool for the exploration of the physics of eruptive events. The concept of magnetic helicity can be used to monitor the whole history of a CME event from the emergence of twisted magnetic flux from the convective zone to the eruption and propagation of the CME into interplanetary space. In this article, I discuss the sources of the magnetic helicity injected into active regions and the role of magnetic helicity in the initiation of solar eruptions. **`Review`**

Detections of Multi-Periodic Oscillations during a Circular Ribbon Flare

Zongjun **Ning**, Ya Wang, Zhenxiang Xiang, Dong Li

Solar Phys. **297**, Article number: 2 **2022**

https://arxiv.org/pdf/2112.03446.pdf

We present the analysis of three kinds of oscillating behavior using multi-wavelength observations of the **10 November 2013** (SOL2013-11-10T05:14) circular-ribbon flare. This event is a typical circular-ribbon flare with an outer spine structure and homologous jets. We found three kinds of oscillations (or perturbation): i) flux oscillation (or QPP) with a dominant period of about 20 seconds at X-rays, EUV and microwave emissions, ii) periodic jets with an intermittent cadence of around 72 seconds, iii) outer loop perturbs a half cycle with the duration of about 168 seconds. Similar to the periodic jets that could be produced by a nonthermal process, like repeated magnetic reconnection, the flare QPP detected in thermal emissions could have the same origin as the oscillation seen in nonthermal emissions. The outer loop perturbation is possibly triggered by a blast wave driven by the circular-ribbon flare, or it might be modulated by the sausage wave or the slow magnetoacoustic wave. The results obtained provide data for further numerical study of the physical origin of flare oscillations.

Broken-up Spectra of the Loop-top Hard X-ray Source during a Solar Limb Flare

Hao **Ning**, Yao Chen, Jeongwoo Lee, Zhao Wu, Yang Su, Xiang-Liang Kong

Research in Astronomy and Astrophysics **19**, 173, **2019**

https://arxiv.org/pdf/1906.01284.pdf

Solar hard X-rays (HXRs) appear in the form of either footpoint sources or coronal sources, and each individual source provides its own critical information on acceleration of nonthermal electrons and plasma heating. Earlier studies found that the HXR emission in some events manifests a broken-up power-law spectrum with the break energy around a few hundred keV based on spatially-integrated spectral analysis, without distinguishing the contributions from individual sources. In this paper, we report the broken-up spectra of a coronal source studied using HXR data recorded by Ramaty High Energy Solar Spectroscopic Imager (RHESSI) during the **SOL2017-09-10T16**:06 (GOES class X8.2) flare. The flare occurred behind the western limb with its foot-point sources mostly occulted by the disk, and we could clearly identify such broken-up spectra pertaining solely to the coronal source during the flare peak time and after. Since a significant pileup effect on the RHESSI spectra is expected for this intense solar flare, we have selected the pileup correction factor, p=2. In this case, we found the resulting \textit{RHESSI} temperature (~30 MK) similar to the GOES soft X-ray temperature and break energies of 45--60 keV. Above the break energy the spectrum hardens with time from spectral index of 3.4 to 2.7, and the difference of spectral indices below and above the break energy increases from 1.5 to 5 with time. We, however, note that when p=2 is assumed, a single power-law fitting is also possible with the RHESSI temperature higher than the GOES temperature by ~10 MK. Possible scenarios for the broken-up spectra of the loop-top HXR source are briefly discussed.

RHESSI Nuggets #352 June **2019**

http://sprg.ssl.berkeley.edu/~tohban/wiki/index.php/Broken-up_hard_X-ray_spectra_found_for_a_loop-top_source_during_a_solar_limb_flare

Two-stage energy release process of a confined flare with double HXR peaks

Hao **Ning**, Yao Chen, Zhao Wu, Yang Su, Hui Tian, Gang Li, Guohui Du, Hongqiang Song

ApJ **854** 178 **2018**

https://arxiv.org/pdf/1801.06641.pdf

http://sci-hub.tw/http://iopscience.iop.org/0004-637X/854/2/178/

A complete understanding of the onset and subsequent evolution of confined flares has not been achieved. Earlier studies mainly analyzed disk events so as to reveal their magnetic topology and cause of confinement. In this study, taking advantage of a tandem of instruments working at different wavelengths of X-rays, EUVs, and microwaves, we present dynamic details of a confined flare observed on the northwestern limb of the solar disk on **July 24th, 2016**. The entire dynamic evolutionary process starting from its onset is consistent with a loop-loop interaction scenario. The X-ray profiles manifest an intriguing double-peak feature. From spectral fitting, it is found that the first peak is non-thermally dominated while the second peak is mostly multi-thermal with a hot (~10 MK) and a super-hot (~30 MK) component. This double-peak feature is unique in that the two peaks are clearly separated by 4 minutes, and the second peak reaches up to 25-50 keV; in addition, at energy bands above 3 keV the X-ray fluxes decline significantly between the two peaks. This, together with other available imaging and spectral data, manifest a two-stage energy release process. A comprehensive analysis is carried out to investigate the nature of this two-stage process. We conclude that the second stage with the hot and super-hot sources mainly involves direct heating through loop-loop reconnection at a relatively high altitude in the corona. The uniqueness of the event characteristics and complete data set make the study a nice addition to present literature on solar flares.

Emission Measure and Temperature Analysis of the Upper Coronal Source of a Solar Flare

Z. **Ning** , D. Li, Q. M. Zhang

Solar Physics Volume 291, Issue 6, pp 1783-1798 **2016**

An X-ray coronal source is usually seen above the reconnection site located above flare loops, while a second source appears in between this site and the loops. The first source is called the upper coronal source, the second the loop-top source. Both sources are thought to be related to the outflows from the magnetic reconnection site above the flare loops. Previous observations have shown that the upper coronal source has both a thermal and nonthermal component. In this article, we explore the spatial appearance of the upper coronal source in a solar flare observed by theReuven Ramaty High Energy Solar Spectroscopic Imager (RHESSI) and the Atmospheric Imaging Assembly onboard the Solar Dynamics Observatory (SDO/AIA) on **8 March 2011**. This event occurred at the limb with completely occulted loop footpoints. Both the loop-top and the upper coronal sources are well observed by RHESSI in X-rays. The loop-top source emission covers a wide energy range up to 50 keV, while the upper coronal source emits below 25 keV. The upper coronal source appears later (about two minutes) than the loop-top source, and the RHESSI X-ray spectral analysis shows that both sources have a temperature of 30 MK. This temperature is confirmed by the differential emission measure (DEM) analysis from SDO/AIA data. AIA observations show the counterparts in the ultraviolet (UV), and bidirectional outflows appear between AIA brightenings. The loop-top source seems to be located at the top of a hot and dense loop system, which expands with a speed of 10 kms−110 kms−1, while the upper coronal source moves faster upward with a speed of about 32 kms−132 kms−1 in the same time interval. The analysis of the spatial distribution of the emission measure and temperature indicates that the hot plasma itself or the heating region are possibly moving upward from the lower coronal region where the loop-top source appears. This is the reason that the upper coronal source appears later than the loop-top source.

Bi-directional flows in a C-class solar flare

Zongjun **Ning**

Astrophysics and Space Science January **2016**, 361:22

We have explored the bi-directional flows in a C-class solar flare observed by Solar Dynamic Observatory Atmospheric Imaging Assembly (SDO/AIA) on **2012 December 26**. This event occurs in a curved magnetic loop connecting a pair of negative and positive fields. The Reuven Ramaty High Energy Solar Spectroscopic Imager (RHESSI) observations show a X-ray source in 3–25 keV stayed at the loop top during the flare. High-cadence AIA observations exhibit many flows movement intermittently along the flare loop. In order to analyze these flows, firstly, the event is cut along the loop direction with a curved slit which is wide enough to include the bulk of ultraviolet (UV) and X-ray emissions. Secondly, after integration the flux along the slit width, we get the space-time slices at 9 AIA wavelengths and in RHESSI 3–25 keV. Thirdly, the derivative is done on the space-time slices. Many bi-directional flows are identified as the oblique streaks on the intensity-gradient space-time slices during the flare lifetime. They almost start from the same position near the loop top, where the X-ray emission is bright in 3–25 keV. Then they move toward the positive and the negative polarity footpoints simultaneously. Their average speed is directly measured about 230 kms−1, and they exhibit a typical quasi-period of about 3 minutes. The characteristics of these flows, such as bi-directional, simultaneous, symmetrical and quasi-periodic, are the observational constraints for acceleration theories.

Imaging Quasi-Periodic Fluctuations in a Simple Flare," by Zhongjun Ning: Time-series spectroscopy in a B8 flare.

Zongjun **Ning**, Hugh Hudson

RHESSI Nuggets, No. 221, **2014**
http://sprg.ssl.berkeley.edu/~tohban/wiki/index.php/Imaging_Quasi-Periodic_Oscillations_in_a_Simple_Flare
Time-series spectroscopy in a B8 flare.
Although these phenomena are quite numerous by now, there is no consensus yet on the meaning of the word "oscillation" in the solar context. In some cases it is not clear whether the repetitive outbursts are wave-like in nature, and so the word "pulsation" is also frequently used. Clearly the isolation of QPO emissions via imaging observations provides important clues to help identify the physics, and in this Nugget we describe RHESSI imaging observations of pulsations in the event SOL**2002-12-26**T05:52

Speed Distributions of Merging X-Ray Sources During Chromospheric Evaporation in Solar Flares

Zongjun **Ning**
Solar Physics, Volume 273, Number 1, 81-92, **2011**
We explore the speed distributions of X-ray source motions after the start of chromospheric evaporation in two Reuven Ramaty High Energy Solar Spectroscopic Imager (RHESSI) flares. First, we make CLEAN images at 15 energy bands with a 12 second integration window; then, we outline a flaring loop geometry to cover the looptop and footpoint sources as much as possible. Consistent with the previous steps, we find converging motion of the double footpoint sources along the flaring loop in these two events. This motion is dependent on the energy band and time and is typically seen at 3−25 keV, indicating a chromospheric evaporation origin. The speed distributions at various energy bands are measured for the **10 September 2002** flare, which exhibits a separation-to-mergence motion pattern well correlated with the rising-to-decay phases at 50−100 keV. **13 November 2003**

Hard X-ray Source Distributions on EUV Bright Kernels in a Solar Flare

Zongjun **Ning** ·Wenda Cao
Solar Phys (**2011**) 269: 283–293
We explore the hard X-ray source distributions of an C1.1 flare occurred on **14 December 2007**. Both Hinode/EIS and RHESSI observations are used. One of EIS rasters perfectly covers the double hard X-ray footpoints, where the EUV emission appears strong from the cool line of He ii (log T=4.7) to the hot line of Fe xvi (log T=6.4). We analyze RHESSI X-ray images at different energies and different times before the hard X-ray maximum. The results show a similar topology for the time-dependent source distribution (i.e. at 14:14:35 UT) as that for energy-dependent source distribution (i.e. at a given energy band of 6 – 9 keV) overlapped on EUV bright kernels, which seems to be consistent with the evaporation model.

Investigation of the Neupert Effect in the Various Intervals of Solar Flares

Zongjun **Ning** ·Wenda Cao
Solar Phys (**2010**) 264: 329–344; **File**
The *Reuven Ramaty High Energy Solar Spectroscopic Imager* (RHESSI) gives us a chance to investigate the theoretical Neupert effect using the correlation between the thermal-energy derivative and the nonthermal energy, or the thermal energy and the integral nonthermal energy. Based on this concept, we analyze four M-class RHESSI flares on **13 November 2003, 4 November 2004, 3 and 25 August 2005**. According to the evolution of the temperature [*T*], emission measure [EM], and thermal energy [*E*th], each event is divided into three phases during the nonthermal-energy input [d*E*nth d*t* in the units of erg s−1]. Phase 1is identified as the interval before the temperature maximum, while after the thermal-energy maximum is phase 3, between them is phase 2. We find that these four flares show the Neupert effect in phase 1, but not in phase 3. The Neupert effect still works well in the second phase, although the cooling becomes slightly important. We define the parameter μ in the relation of d*E*th d*t* **=** μd*E*nth*(t)*d*t* or *E*th*(t*0*)* **=** μ_ *t*00d*E*nth*(t)*d*t* d*t* when the cooling is ignored in phase 1. Considering the uncertainties in estimating the energy from the observations, it is not possible to precisely determine the fraction of the known energy in the nonthermal electrons transformed into the thermal energy of the hottest plasma observed by RHESSI. After a rough estimate of the flare volume and the assumption of the filling factor, we investigate the parameter μ in these four events. Its value ranges from 0.02 to 0.20, indicating that a small fraction (2%– 20%) of the nonthermal energy can be efficiently transformed into thermal energy, which is traced by the soft X-ray emission, and the bulk of the energy

is lost possibly due to cooling.

INVESTIGATION OF CHROMOSPHERIC EVAPORATION IN A NEUPERT-TYPE SOLAR FLARE

Zongjun **Ning**1 and Wenda Cao2
Astrophysical Journal, 717:1232–1242, **2010**
The Neupert effect implies a flare model in which the hard X-rays (HXRs) are produced by energetic electrons via electron-ion bremsstrahlung as they lose their energies in the chromosphere, while the soft X-rays (SXRs) are produced by thermal bremsstrahlung from "chromospheric evaporation" due to plasma being heated by those same electrons. Based on this concept, we investigate the evidence for chromospheric evaporation in a Neupert-type flare on **2004 October 30**. First, we demonstrate that this event is consistent with the Neupert effect. Using the *RHESSI* data, both thermal and nonthermal energies are derived after the onset of this flare. The high correlation between the derivative of the SXRs and HXRs and between the derivative of the thermal energy and nonthermal energy indicates that the 2004 October 30 flare is a Neupert-type event. Second, chromospheric evaporation is necessarily expected during the flare's rising phase.We analyze *RHESSI* images at different energies and different times around the flare maximum. The HXR emission tends to move the footpoints close to each other, finally merging them into a single source with the same position as the loop-top source. When the projection effect (due to this event being near the disk center) is taken into account, this fact can be regarded as the signature of chromospheric evaporation in the X-ray observations. *RHESSI* observations show three kinds of evidence that are consistent with the evaporation model. First, at a given instant, the higher energy X-rays originate from the deeper layers of the atmosphere or further away from the loop top. Second, in a given energy band, i.e., at 20–30 keV, the earlier X-rays originate from the deeper layers or further away from the loop top. Third, the X-ray footpoint sources at higher energies disappear at later times. Based on these characteristics, chromospheric evaporation took about 100 s for the 2004 October 30 flare. X-rays at all energy bands do not show evidence of evaporation probably because measurements are the most sensitive only between 12 and 30 keV. After measuring the source scale as a function of time, we roughly estimate the shrinkage velocities at different energies, for instance, 238 km s^{-1} for 12–15 keV, 285 km s^{-1} for 15–20 keV, and 846 km s^{-1} for 20–30 keV. If the evaporation processes primarily contribute to the source shrinkage, these values are considered as the evaporation velocities, indicating that the evaporation flow would be faster during the latter part of flare.

EVIDENCE OF CHROMOSPHERIC EVAPORATION IN THE 2004 DECEMBER 1 SOLAR FLARE

Zongjun **Ning**1, Wenda Cao2, Jing Huang3, Guangli Huang1, Yihua Yan3, and Hengqiang Feng4
Astrophysical Journal, 699:15–22, **2009**
http://www.iop.org:80/EJ/toc/-alert=43190/0004-637X/699/1
In this paper, we present the radio and hard X-ray evidence of chromospheric evaporation during an M1.0 flare which occurred on 2004 December 1. The radio emission was observed by the Solar Broadband Radio Dynamic Spectrometer in China, which yielded dynamic spectra of decimetric emission. The hard X-ray emission was observed by *RHESSI*. In the radio spectra, the burst is characterized by two groups of parallel-drifting structures, some of which change their drifting rates from positive to negative. Based on the standard flare model, we may explain these decimetric bursts in terms of chromospheric evaporation. On the other hand, *RHESSI* observations show that the hard X-ray emission in the energy range of 10–15 keV tends to rise from two footpoints to the looptop and eventually merges into a single looptop source, which is accepted as evidence of hard X-ray chromospheric evaporation. Such processes happened twice in this event. The drifting radio structures occurred between them, at the same time as the third hard X-ray peak was observed at 25–50 keV.

A complicated solar eruption event on 2003 October 26 Solar flare

Zongjun **Ning** · M.D. Ding · K.P. Qiu · H. Li · Y.N. Su · C. Fang
Astrophys Space Sci (**2008**) 315: 45–51
http://www.springerlink.com/content/h62353721477503x/
We present multi-wavelength observations of a complicated solar eruption event to associate with an X1.2 flare and a Coronal Mass Ejection (CME) on **2003 October 26**. The soft X-ray profile shows a possibility for occurrence of two flares with peaks around 06:20 and 07:00 UT. According to our observations, there are many evidences to show that they are corresponding to two energy releases. The first one produces type II, type III, moving type IV continua, a decimetric burst (DCIM) and strong emissions at Hα, 195 and 1600 Å; While the second energy release only produces a group of RS-III bursts, DCIM and Hα emissions. It appears that the first energy release is associated with a CME, while the second CME is quiet. Such observational difference between two energy releases is found indicating two magnetic reconnection processes occurrence with different plasma situation.

This indicates that the second energy release is restricted into lower corona and chromosphere, i.e. in the post-flare loops.

RHESSI Observations of the Neupert Effect in Three Solar Flares

Zongjun **Ning**
Solar Phys (**2008**) 248: 99–111
http://www.springerlink.com/content/826815l220869104/fulltext.pdf
Previous observations show that in many solar flares there is a causal correlation between the hard X-ray flux and the derivative of the soft X-ray flux. This so-called Neupert effect is indicative of a strong link between the primary energy release to accelerate particles and plasma heating. It suggests a flare model in which the hard X-rays are electron – ion bremsstrahlung produced by energetic electrons as they lose their energy in the lower corona and chromosphere and the soft X-rays are thermal bremsstrahlung from the "chromospheric evaporation" plasma heated by those same electrons.

we use the parameters derived from RHESSI observations to trace the primary energy release and the plasma response: The hard X-ray flux or spectral hardness is compared with the derivative of plasma thermal energy in three impulsive flares on **10 November 2002 and on 3 and 25 August 2005**. High correlations show that the Neupert effect does hold

Magnetic reconnection rate and spectral index for two double-ribbon flares

Zongjun **Ning**
Astrophys Space Sci (**2008**) 314: 137–143
http://www.springerlink.com/content/e7rx14436110j210/fulltext.pdf
We explore the correlations between the inferred reconnection rate and hard X-ray spectral hardness for two double-ribbon flares on **2003 November 1** and **2005 May 17** in this paper.

Microwave and Hard X-Ray Spectral Evolution for the 13 December 2006 Solar Flare

Zongjun **Ning**
Solar Phys (**2008**) 247: 53–62
http://www.springerlink.com/content/ew0324n62152062u/fulltext.pdf
This paper explores the time evolution of microwave and hard X-ray spectral indexes in the solar flare observed by Nobeyama Radio Polarimeters (NoRP) and the Ramaty High Energy Solar Spectroscopy Imager (RHESSI) on 13 December 2006. The microwave spectral index, γ_{MW}, is derived from the emissions at two frequencies, 17 and 35 GHz, and hard X-ray spectral index, γ_{HXR}, is derived from RHESSI spectra. Fifteen subpeaks are detected at the microwave and hard X-ray emissions. The microwave spectral indexes tend to be harder than hard X-ray spectral indexes during the flare, which is consistent with previous findings. All detected subpeaks follow the soft-hard-soft spectral behaviours in the hard X-ray rise-peak-decay phases. However, the corresponding microwave subpeaks display different spectral behaviour, such as soft-hard-soft, soft-hard-harder, soft-hard-soft **+** hard or irregular patterns. These contradictions reveal the complicated acceleration mechanism for low- and high-energy electrons during this event. It is also interesting

MICROWAVE AND HARD X-RAY SPECTRAL EVOLUTION IN TWO SOLAR FLARES

Zongjun **Ning**
The Astrophysical Journal, 659: L69–L72, **2007**
2004 May 21 and November 3.
Although the microwave and hard X-ray emission are produced by electrons at very different energies, a correlation between their spectral indices is found, indicating a common acceleration mechanism.

The Role of a Flux Rope Ejection in Three-dimensional Magnetohydrodynamic Simulation of a Solar Flare

Keisuke **Nishida**, Naoto Nishizuka and Kazunari Shibata
E-print, Aug 2013, ApJ
We investigated the dynamic evolution of a 3-dimensional (3D) flux rope eruption and magnetic reconnection process in a solar flare, by simply extending 2-dimensional (2D) resistive magnetohydrodynamic simulation model of solar flares with low beta plasma to 3D model. We succeeded in reproducing a current sheet and bi-directional reconnection outflows just below the flux rope during the eruption in our 3D simulations. We calculated four cases of a strongly twisted flux rope and a weakly twisted flux rope in 2D and 3D simulations. The time evolution of a weakly twisted flux rope in 3D simulation shows similar behaviors to 2D simulation, while a strongly twisted flux rope in 3D simulation shows clearly different time evolution from 2D simulation except for the initial phase evolution. The ejection speeds of both strongly and weakly twisted flux ropes in 3D simulations are larger than 2D simulations, and the reconnection

rates in 3D cases are also larger than 2D cases. This indicates a positive feedback between the ejection speed of a flux rope and the reconnection rate even in the 3D simulation, and we conclude that the plasmoid-induced reconnection model can be applied to 3D. We also found that small scale plasmoids are formed inside a current sheet and make it turbulent. These small scale plasmoid ejections has role in locally increasing reconnection rate intermittently as observed in solar flares, coupled with a global eruption of a flux rope.

NUMERICAL EXAMINATION OF PLASMOID-INDUCED RECONNECTION MODEL FOR SOLAR FLARES: THE RELATION BETWEEN PLASMOID VELOCITY AND RECONNECTION RATE

Keisuke **Nishida** et al **2009** ApJ 690 748-757
http://www.iop.org/EJ/abstract/0004-637X/690/1/748
The plasmoid-induced reconnection model explaining solar flares based on bursty reconnection produced by an ejecting plasmoid suggests a possible relation between the ejection velocity of a plasmoid and the rate of magnetic reconnection. In this study, we focus on the quantitative description of this relation. We performed magnetohydrodynamic simulations of solar flares by changing the values of resistivity and the plasmoid velocity. The plasmoid velocity has been changed by applying an additional force to the plasmoid to see how the plasmoid velocity affects the reconnection rate. An important result is that the reconnection rate has a positive correlation with the plasmoid velocity, which is consistent with the plasmoid-induced reconnection model for solar flares. We also discuss an observational result supporting this positive correlation.

Statistical and Observational Research on Solar Flare EUV Spectra and Geometrical Features

Shohei **Nishimoto**1, Kyoko Watanabe1, Shinsuke Imada2, Tomoko Kawate3, and Kyoung-Sun Lee4
2020 ApJ 904 31
https://doi.org/10.3847/1538-4357/abbacb
We performed statistical analysis on the flare emission data to examine parameters related to the flare extreme-ultraviolet (EUV) spectra. This study used the data from the Geostationary Operational Environmental Satellite X-ray Sensors to determine the fundamental flare parameters. The relationship between soft X-ray data and EUV emission data observed by the Extreme Ultraviolet Variability Experiment on board the Solar Dynamics Observatory (SDO) MEGS-A was investigated for 50 events. The results showed the hotter Fe line emissions have strong correlation with soft X-ray data in many cases. However, our statistical study revealed that EUV flare peak flux of Fe xv, Fe xvi and He ii lines have weak correlation with soft X-ray peak flux. In EUV line light curves, there was time difference in peak time, however the tendency to reach the peak in order from the hotter line to cooler line was not so clear. These results indicate that the temporal evolution of EUV emission can be roughly explained by soft X-ray data. However, the time changes of temperature and density distributions in the flare loop must be needed for accurate reproduction. Moreover, we compared the geometrical features of solar flares observed by the Atmospheric Imaging Assembly on board the SDO with the fundamental flare parameters for 32 events. The ribbon distance strongly correlated with both soft X-ray flare rise and decay times. This results indicate that the geometrical feature is essential parameter for predicting flare emission duration.

Operational solar flare prediction model using Deep Flare Net

Naoto **Nishizuka**, Yuki Kubo, Komei Sugiura, Mitsue Den, Mamoru Ishii
Earth, Planets and Space (EPS) **2021**
https://arxiv.org/pdf/2112.00977.pdf
We developed an operational solar flare prediction model using deep neural networks, named Deep Flare Net (DeFN). DeFN can issue probabilistic forecasts of solar flares in two categories, such as >=M-class and <M-class events or >=C-class and <C-class events, occurring in the next 24 h after observations and the maximum class of flares occurring in the next 24 h. DeFN is set to run every 6 h and has been operated since January 2019. The input database of solar observation images taken by the Solar Dynamic Observatory (SDO) is downloaded from the data archive operated by the Joint Science Operations Center (JSOC) of Stanford University. Active regions are automatically detected from magnetograms, and 79 features are extracted from each region nearly in real time using multiwavelength observation data. Flare labels are attached to the feature database, and then, the database is standardized and input into DeFN for prediction. DeFN was pretrained using the datasets obtained from 2010 to 2015. The model was evaluated with the skill score of the true skill statistics (TSS) and achieved predictions with TSS = 0.80 for >=M-class flares and TSS = 0.63 for >=C-class flares. For comparison, we evaluated the operationally forecast results from January 2019 to June 2020. We found that operational DeFN forecasts achieved TSS = 0.70 (0.84) for >=C-class flares with the probability threshold of 50 (40)%, although there were very few M-class flares during this period and we should continue monitoring the results for a longer time. Here, we adopted a chronological split to divide the database into two for training and testing. The chronological split appears suitable for evaluating operational models. Furthermore, we proposed the use of time-series cross-validation. The procedure achieved TSS = 0.70 for >=M-class flares and 0.59 for >=C-class flares using the datasets obtained from 2010 to 2017.

Reliable Probability Forecast of Solar Flares: Deep Flare Net-Reliable (DeFN-R)

Naoto **Nishizuka**, Yûki Kubo, Komei Sugiura, Mitsue Den, Mamoru Ishii

2020 *ApJ* **899** 150
https://arxiv.org/pdf/2007.02564.pdf
https://doi.org/10.3847/1538-4357/aba2f2

We developed a reliable probabilistic solar flare forecasting model using a deep neural network, named Deep Flare Net-Reliable (DeFN-R). The model can predict the maximum classes of flares that occur in the following 24 h after observing images, along with the event occurrence probability. We detected active regions from 3x10^5 solar images taken during 2010-2015 by Solar Dynamic Observatory and extracted 79 features for each region, which we annotated with flare occurrence labels of X-, M-, and C-classes. The extracted features are the same as used by Nishizuka et al. (2018); for example, line-of-sight/vector magnetograms in the photosphere, brightening in the corona, and the X-ray emissivity 1 and 2 h before an image. We adopted a chronological split of the database into two for training and testing in an operational setting: the dataset in 2010-2014 for training and the one in 2015 for testing. DeFN-R is composed of multilayer perceptrons formed by batch normalizations and skip connections. By tuning optimization methods, DeFN-R was trained to optimize the Brier skill score (BSS). As a result, we achieved BSS = 0.41 for >=C-class flare predictions and 0.30 for >=M-class flare predictions by improving the reliability diagram while keeping the relative operating characteristic curve almost the same. Note that DeFN is optimized for deterministic prediction, which is determined with a normalized threshold of 50%. On the other hand, DeFN-R is optimized for a probability forecast based on the observation event rate, whose probability threshold can be selected according to users' purposes.

Deep Flare Net (DeFN) model for solar flare prediction

Naoto **Nishizuka**, Komei Sugiura, Yuki Kubo, Mitsue Den, Mamoru Ishii

ApJ 858:113 (8pp) **2018**
https://arxiv.org/pdf/1805.03421.pdf
http://sci-hub.tw/10.3847/1538-4357/aab9a7

We developed a solar flare prediction model using a deep neural network (DNN), named Deep Flare Net (DeFN). The model can calculate the probability of flares occurring in the following 24 h in each active region, which is used to determine the most likely maximum classes of flares via a binary classification (e.g., >=M class versus <M class or >=C class versus <C class). From 3x10^5 observation images taken during 2010-2015 by Solar Dynamic Observatory, we automatically detected sunspots and calculated 79 features for each region, to which flare occurrence labels of X-, M-, and C-class were attached. We adopted the features used in Nishizuka et al. (2017) and added some features for operational prediction: coronal hot brightening at 131 A (T>=10^7 K) and the X-ray and 131 A intensity data 1 and 2 h before an image. For operational evaluation, we divided the database into two for training and testing: the dataset in 2010-2014 for training and the one in 2015 for testing. The DeFN model consists of deep multilayer neural networks, formed by adapting skip connections and batch normalizations. To statistically predict flares, the DeFN model was trained to optimize the skill score, i.e., the true skill statistic (TSS). As a result, we succeeded in predicting flares with TSS=0.80 for >=M-class flares and TSS=0.63 for >=C-class flares. Note that in usual DNN models, the prediction process is a black box. However, in the DeFN model, the features are manually selected, and it is possible to analyze which features are effective for prediction after evaluation. **6-8 March 2012, 9 March 2015**

Solar Flare Prediction Model with Three Machine-Learning Algorithms Using Ultraviolet Brightening and Vector Magnetogram

N. **Nishizuka**, K. Sugiura, Y. Kubo, M. Den, S. Watari, M. Ishii

2017 ApJ 835 156
https://arxiv.org/pdf/1611.01791v1.pdf

We developed a flare prediction model using machine learning, which is optimized to predict the maximum class of flares occurring in the following 24 h. Machine learning is used to devise algorithms that can learn from and make decisions on a huge amount of data. We used solar observation data during the period 2010-2015, such as vector magnetogram, ultraviolet (UV) emission, and soft X-ray emission taken by the Solar Dynamics Observatory and the Geostationary Operational Environmental Satellite. We detected active regions from the full-disk magnetogram, from which 60 features were extracted with their time differentials, including magnetic neutral lines, the current helicity, the UV brightening, and the flare history. After standardizing the feature database, we fully shuffled and randomly separated it into two for training and testing. To investigate which algorithm is best for flare prediction, we compared three machine learning algorithms: the support vector machine (SVM), k-nearest neighbors (k-NN), and extremely randomized trees (ERT). The prediction score, the true skill statistic (TSS), was higher than 0.9 with a fully shuffled dataset, which is higher than that for human forecasts. It was found that k-NN has the highest performance among the three algorithms. The ranking of the feature importance showed that the previous flare activity is most effective, followed by the length of magnetic neutral lines, the unsigned magnetic flux, the area of UV brightening, and the time differentials of features over 24 h, all of which are strongly correlated with the flux emergence dynamics in an active region. **2012 March 6**

Fermi Acceleration in Plasmoids interacting with Fast Shocks of Reconnection via Fractal Reconnection

N. **Nishizuka** and K. Shibata

E-print, Jan **2013**

We propose the particle acceleration model coupled with multiple plasmoid ejections in a solar flare. Unsteady reconnection produces plasmoids in a current sheet and ejects them out to the fast shocks, where particles in a plasmoid are reflected upstream the shock front by magnetic mirror effect. As the plasmoid passes through the shock front, the reflection distance becomes shorter and shorter driving Fermi acceleration, until it becomes proton Larmor radius. The fractal distribution of plasmoids may also have a role in naturally explaining the power-law spectrum in nonthermal emissions.

A LABORATORY EXPERIMENT OF MAGNETIC RECONNECTION: OUTFLOWS, HEATING, AND WAVES IN CHROMOSPHERIC JETS

N. **Nishizuka**1, Y. Hayashi2, H. Tanabe2, A. Kuwahata2, Y. Kaminou2, Y. Ono2, M. Inomoto2, and T. Shimizu

2012 ApJ 756 152

Hinode observations have revealed intermittent recurrent plasma ejections/jets in the chromosphere. These are interpreted as a result of non-perfectly anti-parallel magnetic reconnection, i.e., component reconnection, between a twisted magnetic flux tube and the pre-existing coronal/chromospheric magnetic field, though the fundamental physics of component reconnection is not revealed. In this paper, we experimentally reproduced the magnetic configuration and investigated the dynamics of plasma ejections, heating, and wave generation triggered by component reconnection in the chromosphere. We set plasma parameters as in the chromosphere (density 1014 cm–3, temperature 5-10 eV, i.e., (5-10) × 104 K, and reconnection magnetic field 200 G) using argon plasma. Our experiment shows bi-directional outflows with the speed of 5 km s–1 at maximum, ion heating in the downstream area over 30 eV, and magnetic fluctuations mainly at 5-10 μs period. We succeeded in qualitatively reproducing chromospheric jets, but quantitatively, we still have some differences between observations and experiments such as in jet velocity, total energy, and wave frequency. Some of them can be explained by the scale gap between solar and laboratory plasma, while the others are probably due to the difference in microscopy and macroscopy, collisionality, and the degree of ionization, which have not been achieved in our experiment.

SPECTROSCOPIC OBSERVATIONS OF CONTINUOUS OUTFLOWS AND PROPAGATING WAVES FROM NOAA 10942 WITH EXTREME ULTRAVIOLET IMAGING SPECTROMETER/HINODE

N. **Nishizuka**1 and H. Hara

2011 ApJ 737 L43

We focused on "sit-and-stare" observations of an outflow region at the edge of active region NOAA 10942 on **2007 February 20** obtained by the Extreme ultraviolet Imaging Spectrometer on board Hinode. We analyzed the data above the base of the outflow and found both continuous outflows and waves, which propagate from the base of the outflow. The spectra at the base of the outflow and at higher locations show different properties. The line profiles show blue-side asymmetry at the base of the outflow where nonthermal broadening becomes large because of fast upflows generated by heating events. On the other hand, at higher locations line profiles are symmetric and the intensity disturbances vary in phase with the velocity disturbances. The correlations between the intensity and velocity disturbances become noticeable at higher locations, so this indicates evidence of (at least locally) upward propagating slow-mode waves along the outflow. We also found a transient oscillation of different period in the wavelet spectrum. This indicates that a different wave is additionally observed during a limited period. High cadence spectroscopic observations revealed intermittent signatures of nonthermal velocities. Each of them seems to correspond to the base of the propagating disturbances. Furthermore, a jet was captured by the sit-and-stare observations across the slit. The similarity of line profiles of the outflow and the jet may indicate that the flows and waves originate in unresolved explosive events in the lower atmosphere of the corona.

STATISTICAL STUDY OF CHROMOSPHERIC ANEMONE JETS OBSERVED WITH HINODE/SOT

N. **Nishizuka**, T. Nakamura, T. Kawate, K. A. P. Singh and K. Shibata

2011 ApJ 731 43

The Solar Optical Telescope on board Hinode has revealed numerous tiny jets in all regions of the chromosphere outside of sunspots. A typical chromospheric anemone jet has a cusp-shaped structure and bright footpoint, similar to the shape of an X-ray anemone jet observed previously with the Soft X-ray Telescope on board Yohkoh. The similarity in the shapes of chromospheric and X-ray anemone jets suggests that chromospheric anemone jets are produced as a result of the magnetic reconnection between a small bipole (perhaps a tiny emerging flux) and a pre-existing uniform magnetic field in the lower chromosphere. We examine various chromospheric anemone jets in the solar active region near the solar limb and study the typical features (e.g., length, width, lifetime, and velocity) of the chromospheric anemone jets. Statistical studies show that chromospheric anemone jets have: (1) a typical length ~1.0-4.0 Mm, (2) a width ~100-400 km, (3) a lifetime ~100-500 s, and (4) a velocity ~5-20 km s–1. The velocity of the chromospheric anemone jets is comparable to the local Alfvén speed in the lower solar chromosphere (~10 km s–1). The histograms of chromospheric anemone jets near the limb and near the disk center show similar averages and shapes of distributions, suggesting that the characteristic behavior of chromospheric anemone jets is independent of whether they are observed on the disk or at the limb. The observed relationship between the velocity and length of chromospheric anemone jets shows that the jets do not follow ballistic motion but are more likely accelerated by some other mechanism. This is consistent with numerical simulations of chromospheric anemone jets.

MULTIPLE PLASMOID EJECTIONS AND ASSOCIATED HARD X-RAY BURSTS IN THE 2000 NOVEMBER 24 FLARE

N. **Nishizuka**1, H. Takasaki1,2, A. Asai3,4, and K. Shibata1
Astrophysical Journal, 711:1062–1072, **2010** March
The SoftX-ray Telescope (SXT) on board *Yohkoh* revealed that the ejection ofX-ray emitting plasmoid is sometimes observed in a solar flare. Itwas found that the ejected plasmoid is strongly accelerated during a peak in the hardX-ray (HXR) emission of the flare. In this paper, we present an examination of the *GOES* X 2.3 class flare that occurred at 14:51 UT on 2000 November 24. In the SXT images, we found “multiple” plasmoid ejections with velocities in the range of 250–1500 km s^{-1}, which showed blob-like or loop-like structures. Furthermore, we also found that each plasmoid ejection is associated with an impulsive burst of HXR emission. Although some correlation between plasmoid ejection and HXR emission has been discussed previously, our observation shows similar behavior for multiple plasmoid ejection such that each plasmoid ejection occurs during the strong energy release of the solar flare. As a result of temperature-emission measure analysis of such plasmoids, it was revealed that the apparent velocities and kinetic energies of the plasmoid ejections show a correlation with the peak intensities in the HXR emissions.

THE POWER-LAW DISTRIBUTION OF FLARE KERNELS AND FRACTAL CURRENT SHEETS IN A SOLAR FLARE

N. **Nishizuka**, A. Asai, H. Takasaki, H. Kurokawa, and K. Shibata
ApJL 694 L74-L78, **2009**
http://www.iop.org/EJ/abstract/1538-4357/694/1/L74
We report a detailed examination of the fine structure inside flare ribbons and the temporal evolution of this fine structure during the X2.5 solar flare that occurred on **2004 November 10**. We examine elementary bursts of the C IV (~1550 Å) emission lines seen as local transient brightenings inside the flare ribbons in the ultraviolet (1600 Å) images taken with Transition Region and Coronal Explorer, and we call them C IV kernels. This flare was also observed in Hα with the Sartorius 18 cm Refractor telescope at Kwasan observatory, Kyoto University, and in hard X-rays (HXR) with Reuven Ramaty High Energy Solar Spectroscopic Imager. Many C IV kernels, whose sizes were comparable to or less than 2", were found to brighten successively during the evolution of the flare ribbon. The majority of them were well correlated with the Hα kernels in both space and time, while some of them were associated with the HXR emission. These kernels were thought to be caused by the precipitation of nonthermal particles at the footpoints of the reconnecting flare loops. The time profiles of the C IV kernels showed intermittent bursts, whose peak intensity, duration, and time interval were well described by power-law distribution functions. This result is interpreted as evidence for "self-organized criticality" in avalanching behavior in a single flare event, or for fractal current sheets in the impulsive reconnection region.

GIANT CHROMOSPHERIC ANEMONE JET OBSERVED WITH *HINODE* AND COMPARISON WITH MAGNETOHYDRODYNAMIC SIMULATIONS: EVIDENCE OF PROPAGATING ALFVE´N WAVES AND MAGNETIC RECONNECTION

N. **Nishizuka**,1 M. Shimizu,2 T. Nakamura,1 K. Otsuji,1 T. J. Okamoto,3 Y. Katsukawa,3 and K. Shibata1
The Astrophysical Journal, 683: L83–L86, **2008**

http://www.journals.uchicago.edu/toc/apjl/2008/683/1
Hinode discovered a beautiful giant jet with both cool and hot components at the solar limb on **2007 February 9**. Simultaneous observations by the *Hinode* SOT, XRT, and *TRACE* 195 satellites revealed that hot (~5 # A 106 K) and cool (~104 K) jets were located side by side and that the hot jet preceded the associated cool jet (~1–2 minutes). A current-sheet-like structure was seen in optical (Ca ii H), EUV (195), and soft X-ray °A emissions, suggesting that magnetic reconnection is occurring in the transition region or upper chromosphere. Alfve´n waves were also observed with *Hinode* SOT. These propagated along the jet at velocities of ~200 km s with amplitudes (transverse velocity) of ~5–15 km s and a period of ~200 s. We performed two-dimensional _1 _1 MHD simulation of the jets on the basis of the emerging flux-reconnection model, by extending Yokoyama and Shibata's model. We extended the model with a more realistic initial condition (~106 K corona) and compared our model with multiwavelength observations. The improvement of the coronal temperature and density in the simulation model allowed for the first time the reproduction of the structure and evolution of both the cool and hot jets quantitatively, supporting the magnetic reconnection model. The generation and the propagation of Alfve´n waves are also reproduced self-consistently in the simulation model.

Observations of a high-quality quasi-periodic rapidly-propagating wave train using SDO/AIA

G. **Nistico**, D. J. Pascoe, V. M. Nakariakov
E-print, June **2014**; A&A 569, A12 (**2014**)
http://www2.warwick.ac.uk/fac/sci/physics/research/cfsa/people/nistico/publications/paper_wave_train.pdf
Context. We present a new event of quasi-periodic wave trains observed in EUV wavebands, rapidly-propagating away from an active region after a flare.
Aims. We measure parameters of a wave train observed on **7 December 2013** after an M2.1 flare, i.e. phase speeds, periods and wavelengths, in relationship to the local coronal environment and the energy sources.
Methods. We compare our observations with a numerical simulation of fast magnetoacoustic waves undergoing dispersive evolution and leakage in a coronal loop embedded in a potential magnetic field.
Results. The wave train is observed to propagate as several arc-shaped intensity disturbances, for almost half an hour, with a speed greater than 1000 km/s and a period of about 1 min. The wave train followed two different patterns of propagation, in accordance with the magnetic structure of the active region. The oscillatory signal is found to be of high quality, i.e. there is a large number (10 or more) of subsequent wave fronts observed. The observations are found to be consistent with the numerical simulation of a fast wave train generated by a localised impulsive energy release.
Conclusions. Transverse structuring in the corona can efficiently create and guide high quality quasi-periodic propagating fast wave trains.

Decaying and decayless transverse oscillations of a coronal loop⋆

G. **Nisticò**1, V. M. Nakariakov1,2 and E. Verwichte
A&A 552, A57 (**2013**)
Aims. We investigate kink oscillations of loops observed in an active region with the Atmospheric Imaging Assembly (AIA) instrument on board the Solar Dynamics Observatory (SDO) spacecraft before and after a flare.
Methods. The oscillations were depicted and analysed with time-distance maps, extracted from the cuts taken parallel or perpendicular to the loop axis. Moving loops were followed in time with steadily moving slits. The period of oscillations and its time variation were determined by best-fitting harmonic functions.
Results. We show that before and well after the occurrence of the flare, the loops experience low-amplitude decayless oscillations. The flare and the coronal mass ejection associated to it trigger large-amplitude oscillations that decay exponentially in time. The periods of the kink oscillations in both regimes (about 240 s) are similar. An empirical model of the phenomenon in terms of a damped linear oscillator excited by a continuous low-amplitude harmonic driver and by an impulsive high-amplitude driver is found to be consistent with the observations.

Data-Constrained Solar Modeling with GX Simulator

Gelu M. **Nita**, Gregory D. Fleishman, Alexey A. Kuznetsov, Sergey A. Anfinogentov, Alexey G. Stupishin, Eduard P. Kontar, Samuel J. Schonfeld, James A. Klimchuk, Dale E. Gary
ApJ **2023**
https://arxiv.org/pdf/2301.00795.pdf
To facilitate the study of solar active regions and flaring loops, we have created a modeling framework, the freely distributed GX Simulator IDL package, that combines 3D magnetic and plasma structures with thermal and non-thermal models of the chromosphere, transition region, and corona. The package has integrated tools to visualize the model data

cubes, compute multi-wavelength emission maps from them, and quantitatively compare the resulting maps with observations. Its object-based modular architecture, which runs on Windows, Mac, and Unix/Linux platforms, offers capabilities that include the ability to either import 3D density and temperature distribution models, or to assign numerically defined coronal or chromospheric temperatures and densities, or their distributions to each individual voxel. The application integrates FORTRAN and C++ libraries for fast calculation of radio emission (free-free, gyroresonance, and gyrosynchrotron emission) along with soft and hard X-ray and EUV codes developed in IDL. To facilitate the creation of models, we have developed a fully automatic model production pipeline that downloads the required SDO/HMI vector magnetic field data and (optionally) the contextual SDO/AIA images, performs potential or nonlinear force free field extrapolations, populates the magnetic field skeleton with parameterized heated plasma coronal models that assume either steady-state or impulsive plasma heating, and generates non-LTE density and temperature distribution models of the chromosphere that are constrained by photospheric measurements. The standardized models produced by this pipeline may be further customized through a set of interactive tools provided by the graphical user interface. Here we describe the GX Simulator framework and its applications.

New enhancements of the GX Simulator for studying solar flares and active regions

Gelu **Nita**

CESRA **2016** p.64

http://cesra2016.sciencesconf.org/conference/cesra2016/pages/CESRA2016_prog_abs_book_v3.pdf

Study of solar active regions and flaring loops requires analysis of imaging data obtained in multiple wavelength domains with differing spatial resolution, in a framework supplied by advanced 3D physical models. To facilitate such studies, we have developed our simulation package, GX Simulator, which we maintain, continuously enhance, and distribute through the SolarSoft repository, (ftp://sohoftp.nascom.nasa.gov/solarsoft/packages/GX Simulator/). The object-based architecture of the GX Simulator, which runs on Windows, Mac and Unix platforms, offers important capabilities including the abilities to import 3D density and temperature distribution models, or to assign to each individual voxel numerically defined Differential Emission Measure distributions; to apply parametric heating models involving average properties of the magnetic field lines crossing a given voxel volume; to create magnetic flux tubes and populate them with user-defined nonuniform thermal plasma and anisotropic, nonuniform, nonthermal electron distributions; to compute and investigate the spatial and spectral properties of radio, EUV, and X-ray emission calculated from the model, and to compare the model-derived images and spectra with observational data. The application integrates shared-object libraries containing fast free-free, gyrosynchrotron, and gyroresonance emission codes developed in FORTRAN and C++, and soft and hard X-ray and EUV codes developed in IDL. In this presentation we report on the most recent added capabilities, such as non-uniform grid rendering from an arbitrary viewing perspective and enhanced options of importing observational maps (both CEA and SHARP SDO maps are now supported), which will be part of the soon to be released new version of the tool.

3D Radio and X-Ray Modeling and Data Analysis Software: Revealing Flare Complexity

Gelu M. **Nita**, Gregory D. Fleishman, Alexey A. Kuznetsov, Eduard P. Kontar, Dale E. Gary

ApJ, 799:236 **2015**

http://arxiv.org/pdf/1409.0896v1.pdf

http://sci-hub.tw/10.1088/0004-637X/799/2/236

We have undertaken a major enhancement of our IDL-based simulation tools developed earlier for modeling microwave and X-ray emission. The object-based architecture provides an interactive graphical user interface that allows the user to import photospheric magnetic field maps and perform magnetic field extrapolations to almost instantly generate 3D magnetic field models, to investigate the magnetic topology of these models by interactively creating magnetic field lines and associated magnetic flux tubes, to populate the flux tubes with user-defined nonuniform thermal plasma and anisotropic, nonuniform, nonthermal electron distributions; to investigate the spatial and spectral properties of radio and X-ray emission calculated from the model, and to compare the model-derived images and spectra with observational data. The application integrates shared-object libraries containing fast gyrosynchrotron emission codes developed in FORTRAN and C++, soft and hard X-ray codes developed in IDL, a FORTRAN-based potential-field extrapolation routine and an IDL-based linear force free field extrapolation routine. The interactive interface allows users to add any user-defined radiation code that adheres to our interface standards, as well as user-defined magnetic field extrapolation routines. Here we use this tool to analyze a simple single-loop flare and use the model to constrain the 3D structure of the magnetic flaring loop and 3D spatial distribution of the fast electrons inside this loop. We iteratively compute multi-frequency microwave and multi-energy X-ray images from realistic magnetic fluxtubes obtained from an extrapolation of a magnetogram taken prior to the flare, and compare them with imaging data obtained by SDO, NoRH, and RHESSI instruments. We use this event to illustrate use of the tool for general interpretation of solar flares to address disparate problems in solar physics. **4-Aug-2011**

Effects of Magnetic Shear and Thermodynamic Asymmetry on Spontaneous Magnetohydrodynamic Reconnection

Shin-ya **Nitta** and Koji Kondoh

2022 ApJ 936 125
https://iopscience.iop.org/article/10.3847/1538-4357/ac729f/pdf
The spontaneous evolution of magnetic reconnection in generalized situations (with thermodynamic asymmetry regarding the current sheet and magnetic shear) is investigated using a two-dimensional magnetohydrodynamic simulation. We focus on the asymptotic state of temporal evolution, i.e., the self-similarly expanding phase. (1) A long fast-mode shock is generated in front of the shorter plasmoid as in the shear-less thermodynamically asymmetric case; however, the sheared magnetic component weakens the shock. This fast shock may work as a particle acceleration site. (2) The shorter plasmoid-side plasma infiltrates the longer plasmoid across the current sheet. Then, the plasmas from both sides of the current sheet coexist on the same magnetic field lines in the longer plasmoid. This may result in efficient plasma mixing. (3) The thermodynamic asymmetry and magnetic shear drastically decrease the reconnection rate in many orders of magnitude.

CRITICAL DIFFERENCES OF ASYMMETRIC MAGNETIC RECONNECTION FROM STANDARD MODELS

S. **Nitta**, T. Wada, T. Fuchida, and K. Kondoh
2016 ApJ 828 63
We have clarified the structure of asymmetric magnetic reconnection in detail as the result of the spontaneous evolutionary process. The asymmetry is imposed as ratio k of the magnetic field strength in both sides of the initial current sheet (CS) in the isothermal equilibrium. The MHD simulation is carried out by the HLLD code for the long-term temporal evolution with very high spatial resolution. The resultant structure is drastically different from the symmetric case (e.g., the Petschek model) even for slight asymmetry k = 2. (1) The velocity distribution in the reconnection jet clearly shows a two-layered structure, i.e., the high-speed sub-layer in which the flow is almost field aligned and the acceleration sub-layer. (2) Higher beta side (HBS) plasma is caught in a lower beta side plasmoid. This suggests a new plasma mixing process in the reconnection events. (3) A new large strong fast shock in front of the plasmoid forms in the HBS. This can be a new particle acceleration site in the reconnection system. These critical properties that have not been reported in previous works suggest that we contribute to a better and more detailed knowledge of the reconnection of the standard model for the symmetric magnetic reconnection system.

The Association of Solar Flares with Coronal Mass Ejections During the Extended Solar Minimum

Nitta, N. V., Aschwanden, A. M., Freeland, S. L., Lemen, J. R., Wuelser, J.-P., Zarro, D. M.
E-print, Aug **2013, File**; Solar Phys. April **2014**, Volume 289, Issue 4, pp 1257-1277
We study the association of solar flares with coronal mass ejections (CMEs) during the deep, extended solar minimum of 2007-2009, using extreme-ultraviolet (EUV) and white-light (coronagraph) images from the Solar Terrestrial Relations Observatory (STEREO). Although all of the fast (v > 900 km s-1) and wide (theta > 100 deg) CMEs are associated with a flare that is at least identified in GOES soft X-ray light curves, a majority of flares with relatively high X-ray intensity for the deep solar minimum (e.g. >=1 10-6 W m-2 or C1) are not associated with CMEs. Intense flares tend to occur in active regions with strong and complex photospheric magnetic field, but the active regions that produce CME-associated flares tend to be small, including those that have no sunspots and therefore no NOAA active-region numbers. Other factors on scales comparable to and larger than active regions seem to exist that contribute to the association of flares with CMEs. We find the possible low coronal signatures of CMEs, namely eruptions, dimmings, EUV waves, and Type III bursts, in 91%, 74%, 57%, and 74%, respectively, of the 35 flares that we associate with CMEs. None of these observables can fully replace direct observations of CMEs by coronagraphs.
14 May 2007. 3 June 2007, **2007-12-31, 2009-02-13,**
Table 2. Coronal waves observed by EUVI during March 2007 -December 2009

Soft X-ray Fluxes of Major Flares Far Behind the Limb as Estimated Using STEREO EUV Images

N. V. **Nitta**, M. J. Aschwanden, P. F. Boerner, S. L. Freeland, J. R. Lemen, J.-P. Wuelser
E-print, May **2013, File;** Solar Physics, November **2013**, Volume 288, Issue 1, pp 241-254
With increasing solar activity since 2010, many flares from the backside of the Sun have been observed by the Extreme Ultraviolet Imager (EUVI) on either of the twin STEREO spacecraft. Our objective is to estimate their X-ray peak fluxes from EUVI data by finding a relation of the EUVI with GOES X-ray fluxes. Because of the presence of the Fe xxiv line at 192 Å, the response of the EUVI 195 Å channel has a secondary broad peak around 15 MK, and its fluxes closely trace X-ray fluxes during the rise phase of flares. If the flare plasma is isothermal, the EUVI flux should be directly proportional to the GOES flux. In reality, the multithermal nature of the flare and other factors complicate the estimation of the X-ray fluxes from EUVI observations. We discuss the uncertainties, by comparing GOES fluxes with the high cadence EUV data from the Atmospheric Imaging Assembly (AIA) on board the Solar Dynamics Observatory

(SDO). We conclude that the EUVI 195 Å data can provide estimates of the X-ray peak fluxes of intense flares (e.g., above M4 in the GOES scale) to small uncertainties. Lastly we show examples of intense flares from regions far behind the limb, some of which show eruptive signatures in AIA images.

Clear Detection of Chromospheric Evaporation Upflows with High Spatial/Temporal Resolution by Hinode XRT

S. **Nitta**, S. Imada and T. T. Yamamoto
Solar Physics, Volume 276, Numbers 1-2, 183-197, **2012**
We find clear evidence for typical chromospheric evaporation associated with small transient brightenings, using the data from the X-ray Telescope (XRT) onboard Hinode. We found 13 events, each having a pair of evaporation upflows arising almost symmetrically from both foot points of a magnetic loop. These facts strongly support the standard flare model based on the magnetic reconnection. The apparent upflow velocities of three of the events are ≈500 kms−1, while those of the other events are ≈100 kms−1. This is the first clear direct detection of evaporating upflow motion in soft X-ray images from Hinode/XRT; such images were obtained with high cadence (≈60 s) and high spatial resolution (1 arcsec).

AN ALTERNATIVE VIEW OF THE "MASUDA" FLARE

Nariaki V. **Nitta**1, Samuel L. Freeland1, andWei Liu1,2
Astrophysical Journal Letters, 725:L28–L33, **2010, File**
The limb flare on 1992 January 13, the so-called Masuda flare, has stimulated scientists to refine theory of solar flares based on two-dimensional magnetic reconnection. This is primarily because of the hard X-ray (HXR) source seen above the clearly defined flare loop, and the outward motions in soft X-rays (SXRs) interpreted as "plasmoid" ejections. We have revisited *Yohkoh* HXR and SXR data for this and other limb flares and found that the Masuda flare is still unique in terms of the location and spectral properties of the coronal HXR source. However, the outward motions in SXR outside the flare loop may not be as simply characterized as plasmoid ejections as in other flares, nor are they particularly fast. The motions appear complex partly because we also see trans-equatorial loops in motion, one of whose legs anchors close to the main flare loop. It is possible that these large-scale loops represent post-flare loops, and that the flare may also be explained in terms of three-dimensional quadrupolar reconnection, similar to those flares where a pair of two loops exchange their footpoints through magnetic reconnection. It appears that expansion and brightening of large-scale loops offset from the main flare loop are not common, possibly providing a reason for the unusual coronal HXR source in the Masuda flare.

Coronal Jet Observed by Hinode As The Source Of A 3He-rich Solar Energetic Particle Event

Nariaki V. **Nitta**1, Glenn M. Mason2, Mark E. Wiedenbeck3,4, Christina M. S. Cohen4, S¨am Krucker5, Iain G. Hannah5, Masumi Shimojo6 and Kazunari Shibata7
E-print, Feb 2008; ApJL, 675:L125–L128, **2008** March 10
http://www.journals.uchicago.edu/doi/pdf/10.1086/533438
We study the solar source of the 3He-rich solar energetic particle (SEP) event observed on 2006 November 18.

New estimation of non-thermal electrons energetics in the giant solar flare on 28 October 2003 based on Mars Odyssey observations

B.A. **Nizamov**, I.V. Zimovets, D.V. Golovin, A.B. Sanin, M.L. Litvak, V.I. Tretyakov, I.G. Mitrofanov, A.S. Kozyrev
Journal of Atmospheric and Solar-Terrestrial Physics **2018**
https://arxiv.org/pdf/1804.00313.pdf
A new estimation of the total number and energy of non-thermal electrons produced in the giant (>X17) solar flare on 2003 October 28 is presented based on the analysis of observations of hard X-ray (HXR) emission by the High Energy Neutron Detector (HEND) onboard the Mars Odyssey spacecraft orbiting Mars. This is done to complement the estimation of non-thermal electron energy based on the RHESSI data, which missed the peak of the flare impulsive phase. We used different models to make this estimation, including the widespread thick and warm target models. We found that, depending on the model used and the low-energy cutoff (Ec) of non-thermal electrons, the estimate of their total energy in the entire flare can vary from 1.6×1032 to 5.7×1033 ergs. The lowest estimate, 1.6×1032 ergs, obtained

within the thick target model and fixed Ec=46 keV, is consistent (within the factor of 2) with the estimate based on RHESSI data (E>5.6×1031 ergs). In this case, non-thermal electrons accelerated in the peak of the flare impulsive phase missed by RHESSI contained approximately 40% of the total energy of non-thermal electrons of the entire flare. The highest value, 5.7×1033 ergs, obtained with the thick target model and fixed Ec=10 keV, which is comparable to the estimate for another giant flare on 2003 November 4, looks abnormally high, since it exceeds the total non-potential magnetic energy of the parent active region (2.9×1033 ergs). Our estimates also show that the total number and energetics of the HXR-producing electrons in the flare region is a few times larger than that of the population of energetic electrons impulsively injected into the interplanetary space from the Sun.

DECONSTRUCTING ACTIVE REGION AR10961 USING *STEREO*, *HINODE*, *TRACE*, AND *SOHO*

Jane B. **Noglik**1, Robert W. Walsh1, Rhona C. Maclean2, and M. S. Marsh1
Astrophysical Journal, 703:1923–1938, **2009** October
Active region 10961 was observed over a five-day period (**2007 July 2–6**) by instrumentation on-board *STEREO*, *Hinode*, *TRACE*, and *SOHO*. As it progressed from Sun's center to the solar limb, a comprehensive analysis of the extreme ultraviolet, X-ray, and magnetic field data reveals clearly observable changes in the global nature of the region. Temperature analyses undertaken using *STEREO* Extreme Ultraviolet Imager double filter ratios and X-ray imaging telescope single and combined filter ratios demonstrate an overall cooling of the region from between 1.6–3.0 MK to 1.0–2.0 MK over the five days. Similarly, *Hinode* Extreme Ultraviolet Imaging Spectrograph density measurements show a corresponding increase in density of 27%. Moss, cool (1 MK) outer loop areas, and hotter core loop regions were examined and compared with potential magnetic field extrapolations from *SOHO* Michelson Doppler Imager magnetogram data. In particular, it was found that the potential field model was able to predict the structure of the hotter X-ray loops and that the larger cool loops seen in 171 Å images appeared to follow the separatrix surfaces. The reasons behind the high-density moss regions only observed on one side of the active region are examined further.

An Analysis of the Sunspot Groups and Flares of Solar Cycle 23

Donald C. **Norquist**
Solar Phys (**2011**) 269: 111–127
Designing a statistical solar flare forecasting technique can benefit greatly from knowledge of the flare frequency of occurrence with respect to sunspot groups. This study analyzed sunspot groups and H⟨ and X-ray flares reported for the period 1997 – 2007. Annual catalogs were constructed, listing the days that numbered sunspot groups were observed (designated sunspot group-days, SSG-Ds) and for each day a record for each associated H⟨ flare of importance category one or greater and normal or bright brightness and for each X-ray flare of intensity C 5 or higher. The catalogs were then analyzed to produce frequency distributions of SSG-Ds by year, sunspot group class, likelihood of producing at least one flare overall and by sunspot group class, and frequency of occurrence of numbers of flares per day and flare intensity category. Only 3% of SSG-Ds produced a substantial H⟨ flare and 7% had a significant X-ray flare. We found that mature, complex sunspot groups were more likely than simple sunspot groups to produce a flare, but the latter were more prevalent than the former. More than half of the SSG-Ds with flares had a maximum intensity flare greater than the lowest category (C-class of intensity five and higher). The fact that certain sunspot group classes had flaring probabilities significantly higher than the combined probabilities of the intensity categories when all SSG-Ds were considered suggest that it might be best to first predict the flaring probability. For sunspot groups found likely to flare, a separate diagnosis of maximum flare intensity category appears feasible.

Do Kepler Superflare Stars Really Include Slowly Rotating Sun-like Stars?—Results Using APO 3.5 m Telescope Spectroscopic Observations and Gaia-DR2 Data

Notsu, Yuta; Maehara, Hiroyuki; Honda, Satoshi; Hawley, Suzanne L.; ....
2019 ApJ...876...58N
https://arxiv.org/pdf/1904.00142.pdf
We report the latest view of Kepler solar-type (G-type main-sequence) superflare stars, including recent updates with Apache Point Observatory (APO) 3.5 m telescope spectroscopic observations and Gaia-DR2 data. First, we newly conducted APO 3.5 m spectroscopic observations of 18 superflare stars found from Kepler 1-minute time-cadence data. More than half (43 stars) are confirmed to be "single" stars, among 64 superflare stars in total that have been spectroscopically investigated so far in this APO 3.5 m and our previous Subaru/HDS observations. The measurements of v sin i (projected rotational velocity) and chromospheric lines (Ca II H and K and Ca II λ8542) support that the

brightness variation of superflare stars is caused by the rotation of a star with large starspots. We then investigated the statistical properties of Kepler solar-type superflare stars by incorporating Gaia-DR2 stellar radius estimates. As a result, the maximum superflare energy continuously decreases as the rotation period P rot increases. Superflares with energies ≲5 × 1034 erg occur on old, slowly rotating Sun-like stars (P rot ∼ 25 days) approximately once every 2000─3000 yr, while young, rapidly rotating stars with P rot ∼ a few days have superflares up to 1036 erg. The maximum starspot area does not depend on the rotation period when the star is young, but as the rotation slows down, it starts to steeply decrease at P rot ≳ 12 days for Sun-like stars. These two decreasing trends are consistent since the magnetic energy stored around starspots explains the flare energy, but other factors like spot magnetic structure should also be considered.
CEASRA #354 2019
http://sprg.ssl.berkeley.edu/~tohban/wiki/index.php/Do_Kepler_Superflare_Stars_Really_Include_Slowly_Rotating_Sun-like_Stars%3F

High Dispersion Spectroscopy of solar-type superflare stars

Yuta **Notsu**
RHESSI Science Nugget No. 254, June **2015**
http://sprg.ssl.berkeley.edu/~tohban/wiki/index.php/High_Dispersion_Spectroscopy_of_solar-type_superflare_stars
The results of these observations and analysis confirm that stars similar to the Sun can have superflares if they have large starspots. In the future, in addition to the continuing spectroscopic observations with Subaru Telescope, we will conduct observations with the Kyoto University Okayama 3.8 m telescope, which is now under construction.

Three-Dimensional Reconstruction and Thermal Modeling of Observed Loops

Federico A. **Nuevo**, Cecilia Mac Cormack, Marcelo C. López Fuentes, Alberto M. Vásquez & Cristina H. Mandrini
Solar Physics volume 295, Article number: 171 (**2020**)
https://link.springer.com/content/pdf/10.1007/s11207-020-01739-4.pdf
https://arxiv.org/pdf/2011.09575.pdf
Due to their characteristic temperature and density, loop structures in active regions (ARs) can be seen bright in extreme ultraviolet (EUV) and soft X-ray images. The semiempirical determination of the three-dimensional (3D) distribution of basic physical parameters (electronic density and temperature, and magnetic field) is a key constraint for coronal heating models. In this work we develop a technique for the study of EUV bright loops based on differential emission measure (DEM) analysis and we first apply it to AR structures observed by the {Atmospheric Imaging Assembly} (AIA) on board the {Solar Dynamics Observatory} (SDO). The 3D structure and intensity of the magnetic field of the observed EUV loops are modelled using force-free field extrapolations based on magnetograms taken by the {Helioseismic and Magnetic Imager} (HMI) on board SDO. In this work we report the results obtained for several bright loops identified in different ARs. Our analysis indicates that the mean and width of the temperature distributions are nearly invariant along the loop lengths. For a particular loop we study its temporal evolution and find that these characteristics remain approximately constant for most of its life time. The appearance and disappearance of this loop occurs at time-scales much shorter than its life time of ≈2.5 hours. The results of this analysis are compared with numerical simulations using the zero-dimensional (0D) hydrodynamic model, Enthalpy-Based Thermal Evolution of Loops (EBTEL). We study two alternative heating scenarios: first, we apply a constant heating rate assuming loops in quasi-static equilibrium, and second, we heat the loops using impulsive events or nanoflares. We find that all the observed loops are overdense with respect to a quasi-static equilibrium solution and that the nanoflare heating better reproduces the observed densities and temperatures. **11-29-2010**

Response of Hinode XRT to quiet Sun, active region and flare plasma

B. **O'Dwyer**, G. Del Zanna and H. E. Mason
E-print, May 2014; A&A 561, A20 (**2014**)
http://www.damtp.cam.ac.uk/user/astro/gd232/research/papers/odwyer_etal_2014.pdf
Aims. We examine the response of the Hinode X-Ray Telescope (XRT), using simultaneous observations with the Hinode Extreme-ultraviolet Imaging Spectrometer (EIS), for a flare, an active region and a quiet Sun region. We also examine the relative intensity calibration of EIS and XRT.
Methods. EIS differential emission measure distribution (DEM) curves were used to create synthetic spectra with the CHIANTI atomic database. The contribution of spectral lines and continuum emission to each of the XRT channels was determined from the synthetic spectra, which were then convolved with the effective area of each XRT channel. The predicted total count rates for each channel were compared with the observed count rates. The effects of varying elemental abundances and the temperature range for the inversion were investigated. DEMs obtained from the XRT bands were also computed and compared to those obtained with EIS.
Results. For the active region observations, the observed XRT count rates for most of the channels are in reasonable agreement with those predicted using EIS observations, but are dependent on the elemental abundances chosen. Significant discrepancies between predicted and observed count rates were found and are discussed for the adjacent

quiet Sun region and also for the flare. Synthetic spectra and continuum emission contributing to the XRT channels are presented and discussed for the active region, quiet Sun and flare observations.

SDO/AIA response to coronal hole, quiet Sun, active region, and flare plasma

B. **O'Dwyer**1, G. Del Zanna1, H. E. Mason1,M. A. Weber2, and D. Tripathi1
A&A 521, A21, **2010, File**

Aims. We examine the contribution of spectral lines and continuum emission to the EUV channels of the Atmospheric Imaging Assembly (AIA) on the Solar Dynamics Observatory (SDO) in different regions of the solar atmosphere.
Methods.Synthetic spectra were obtained using the CHIANTI atomic database and sample differential emission measures for coronal hole, quiet Sun, active region and flare plasma. These synthetic spectra were convolved with the effective area of each channel, in order to determine the dominant contribution in different regions of the solar atmosphere.
Results. We highlight the contribution of particular spectral lines which under certain conditions can affect the interpretation of SDO/AIA data.

Three-dimensional magnetic reconnection in a collapsing coronal loop system

Aidan M. **O'Flannagain**, Shane A. Maloney, Peter T. Gallagher, Philippa Browning, Jose Refojo
A&A **2018**
https://arxiv.org/pdf/1806.09365.pdf

Magnetic reconnection is believed to be the primary mechanism by which non-potential energy stored in coronal magnetic fields is rapidly released during solar eruptive events. Unfortunately, owing to the small spatial scales on which reconnection is thought to occur, it is not directly observable in the solar corona. However, larger scale processes, such as associated inflow and outflow, and signatures of accelerated particles have been put forward as evidence of reconnection. We explore the origin of a persistent Type I radio source that accompanies a coronal X--shaped structure during its passage across the disk. Of particular interest is the time range around a partial collapse of the structure that is associated with inflow, outflow, and signatures of particle acceleration. Imaging radio observations from the NRH were used to localise the radio source. SDO AIA EUV observations from the same time period were analysed, looking for evidence of inflows and outflows. Further \texttt{mpole} magnetic reconstructions using SDO HMI observations allowed the magnetic connectivity associated with the radio source to be determined. The Type I radio source was well aligned with a magnetic separator identified in the extrapolations. During the partial collapse, gradual (1 km/s) and fast (5 km/s) inflow phases and fast (30 km/s) and rapid (80-100 km/s) outflow phases were observed, resulting in an estimated reconnection rate of ~ 0.06. The radio source brightening and dimming was found to be co-temporal with increased soft x-ray emission in both RHESSI and GOES. We interpret the brightening and dimming of the radio emission as evidence for accelerated electrons in the reconnection region responding to a gradual fall and rapid rise in electric drift velocity, in response to the inflowing and outflowing field lines. These results present a comprehensive example of 3D null-point reconnection**. 2 – 12 July 2013**

Solar Hard X-ray Source Sizes in a Beam-Heated and Ionised Chromosphere

A. **O'Flannagain**, J. C. Brown, P. T. Gallagher
2015 *ApJ* **799** 127
http://arxiv.org/pdf/1411.5168v1.pdf

Solar flare hard X-rays (HXRs) are produced as bremsstrahlung when an accelerated population of electrons interacts with the dense chromospheric plasma. HXR observations presented by using the Ramaty High-Energy Solar Spectroscopic Imager (RHESSI) have shown that HXR source sizes are 3-6 times more extended in height than those predicted by the standard collisional thick target model (CTTM). Several possible explanations have been put forward including the multi-threaded nature of flare loops, pitch-angle scattering, and magnetic mirroring. However, the nonuniform ionisation (NUI) structure along the path of the electron beam has not been fully explored as a solution to this problem. Ionised plasma is known to be less effective at producing nonthermal bremsstrahlung HXRs when compared to neutral plasma. If the peak HXR emission was produced in a locally ionised region within the chromosphere, the intensity of emission will be preferentially reduced around this peak, resulting in a more extended source. Due to this effect, along with the associated density enhancement in the upper chromosphere, injection of a beam of electrons into a partially ionised plasma should result in a HXR source which is substantially more vertically extended relative to that for a neutral target. Here we present the results of a modification to the CTTM which takes into account both a localised form of chromospheric NUI and an increased target density. We find 50 keV HXR source widths, with and without the inclusion of a locally ionised region, of ~3 Mm and ~0.7 Mm, respectively. This helps to provide a theoretical solution to the currently open question of overly-extended HXR sources.

Solar flare X-ray source motion as a response to electron spectral hardening

A. M. **O'Flannagain**1, P. T. Gallagher1, J. C. Brown2, R. O. Milligan3, and G. D. Holman4

A&A 555, A21 (**2013**)
Context. Solar flare hard X-rays (HXRs) are thought to be produced by nonthermal coronal electrons stopping in the chromosphere or remaining trapped in the corona. The collisional thick target model (CTTM) predicts that more energetic electrons penetrate to greater column depths along the flare loop. This requires that sources produced by harder power-law injection spectra should appear further down the legs or footpoints of a flareloop. Therefore, the frequently observed hardening of the injected power-law electron spectrum during flare onset should be concurrent with a descending hard X-ray source.
Aims. We test this implication of the CTTM by comparing its predicted HXR source locations with those derived from observations of a solar flare which exhibits a nonthermally-dominated spectrum before the peak in HXRs, known as an early impulsive event.
Methods. The HXR images and spectra of an early impulsive C-class flare were obtained using the Ramaty High-Energy Solar Spectroscopic Imager (RHESSI). Images were reconstructed to produce HXR source height evolutions for three energy bands. Spatially integrated spectral analysis was performed to isolate nonthermal emission and to determine the power-law index of the electron injection spectrum. The observed height-time evolutions were then fitted with CTTM-based simulated heights for each energy, using the electron spectral indices derived from the RHESSI spectra.
Results. The flare emission was found to be dominantly nonthermal above ~7 keV, with emission of thermal and nonthermal X-rays likely to be simultaneously observable below that energy. The density structure required for a good match between model and observed source heights agreed with previous studies of flare loop densities.
Conclusions. The CTTM has been used to produce a descent of model HXR source heights that compares well with observations of this event. Based on this interpretation, downward motion of nonthermal sources should occur in any flare where there is spectral hardening in the electron distribution during a flare. However, this is often masked by thermal emission associated with flare plasma preheating. To date, flare models that predict transfer of energy from the corona to the chromosphere by means other than a flux of nonthermal electrons do not predict this observed source descent. Therefore, flares such as this will be key in explaining this elusive energy transfer process.
28 November 2002

Hard X-rays in Descent

Aidan **O'Flannagain** and John Brown
RHESSI Science Nugget, No. 201, May **2013**
http://sprg.ssl.berkeley.edu/~tohban/wiki/index.php/Hard_X-rays_in_Descent
A novel test of the thick-target model for hard X-ray emission.

Excitation and Damping of Slow Magnetosonic Waves in Flaring Hot Coronal Loops: Effects of Compressive Viscosity

Leon **Ofman**, Tongjiang Wang
ApJ **926** 64 **2022**
https://arxiv.org/pdf/2111.10696.pdf
https://iopscience.iop.org/article/10.3847/1538-4357/ac4090/pdf
Slow magnetosonic waves associated with flares were observed in coronal loops by SOHO/SUMER, SDO/AIA in various EUV bandpasses, and other instruments. The excitation and damping of slow magnetosonic waves provides information on the magnetic, temperature, and density structure of the loops. Recently, it was found using 1.5D models that the thermal conduction is suppressed and compressive viscosity is enhanced in hot (T>6 MK) flaring coronal loops. We model the excitation and dissipation of slow magnetosonic waves in hot coronal loops with realistic magnetic geometry, enhanced density, and temperature (compared to background corona) guided by EUV observations using 3D MHD visco-resistive model. The effects of compressive viscosity tensor component along the magnetic field are included with classical and enhanced viscosity coefficient values for the first time in 3D MHD coronal loop model. The waves are excited by a velocity pulse at the footpoint of the loop at coronal lower boundary. The modeling results demonstrate the excitation of the slow magnetosonic waves and nonlinear coupling to other wave modes, such as the kink and fast magnetosonic. We find significant leakage of the waves from the hot coronal loops with small effect of viscous dissipation in cooler (6MK) loops, and more significant effects of viscous dissipation in hotter (10.5MK) coronal loops. Our results demonstrate that nonlinear 3D MHD models are required to fully account for various wave couplings, damping, standing wave formation, and viscous dissipation in hot flaring coronal loops. Our viscous 3D MHD code provides a new tool for improved coronal seismology. **28 December 2013, 24 January 2015**

Quasi-periodic Counter-propagating Fast Magnetosonic Wave Trains from Neighboring Flares: SDO/AIA Observations and 3D MHD Modeling

Leon **Ofman**1,2,5 and Wei Liu3,4,6
2018 ApJ 860 54
https://arxiv.org/pdf/1805.00365.pdf

Since their discovery by the Solar Dynamics Observatory/Atmospheric Imaging Assembly (AIA) in the extreme ultraviolet, rapid (phase speeds of ~1000 km s−1), quasi-periodic, fast-mode propagating (QFP) wave trains have been observed accompanying many solar flares. They typically propagate in funnel-like structures associated with the expanding magnetic field topology of the active regions (ARs). The waves provide information on the associated flare pulsations and the magnetic structure through coronal seismology (CS). The reported waves usually originate from a single localized source associated with the flare. Here we report the first detection of counter-propagating QFPs associated with two neighboring flares on **2013 May 22**, apparently connected by large-scale, trans-equatorial coronal loops. We present the first results of a 3D MHD model of counter-propagating QFPs in an idealized bipolar AR. We investigate the excitation, propagation, nonlinearity, and interaction of the counter-propagating waves for a range of key model parameters, such as the properties of the sources and the background magnetic structure. In addition to QFPs, we also find evidence of trapped fast- (kink) and slow-mode waves associated with the event. We apply CS to determine the magnetic field strength in an oscillating loop during the event. Our model results are in qualitative agreement with the AIA-observed counter-propagating waves and used to identify the various MHD wave modes associated with the observed event, providing insights into their linear and nonlinear interactions. Our observations provide the first direct evidence of counter-propagating fast magnetosonic waves that can potentially lead to turbulent cascade and carry significant energy flux for coronal heating in low-corona magnetic structures.

Three dimensional MHD Modeling of Vertical Kink Oscillations in an Active Region Plasma Curtain

Leon **Ofman**, Marzia Parisi, Abhishek K. Srivastava
A&A 582, A75 **2015**
http://arxiv.org/pdf/1505.05427v1.pdf
Observations on **2011 August 9** of an X6.9-class flare in active region (AR) 11263 by the Atmospheric Imaging Assembly (AIA) on-board the Solar Dynamics Observatory (SDO), were followed by a rare detection of vertical kink oscillations in a large-scale coronal active region plasma curtain in EUV coronal lines. The damped oscillations with periods in the range 8.8-14.9 min were detected and analyzed recently. Our aim is to study the generation and propagation of the MHD oscillations in the plasma curtain taking into account realistic 3D magnetic and density structure of the curtain. We also aim at testing and improving coronal seismology for more accurate determination of the magnetic field than with standard method. We use the observed morphological and dynamical conditions, as well as plasma properties of the coronal curtain based on Differential Emission Measure (DEM) analysis to initialize a 3D MHD model of its vertical and transverse oscillations by implementing the impulsively excited velocity pulse mimicking the flare generated nonlinear fast magnetosonic propagating disturbance interacting with the curtain obliquely. The model is simplified by utilizing initial dipole magnetic field, isothermal energy equation, and gravitationally stratified density guided by observational parameters. Using the 3D MHD model, we are able to reproduce the details of the vertical oscillations and study the process of their excitation by nonlinear fast magnetosonic pulse, propagation, and damping, finding agreement with the observations. We estimate the accuracy of simplified slab-based coronal seismology by comparing the determined magnetic field strength to actual values from the 3D MHD modeling results and demonstrate the importance of taking into account more realistic magnetic geometry and density for improving coronal seismology.

MODELING SUPER-FAST MAGNETOSONIC WAVES OBSERVED BY SDO IN ACTIVE REGION FUNNELS

L. **Ofman**1,2,5, W. Liu3,4, A. Title3 and M. Aschwanden
2011 ApJ 740 L33
Recently, quasi-periodic, rapidly propagating waves have been observed in extreme ultraviolet by the Solar Dynamics Observatory/Atmospheric Imaging Assembly (AIA) instrument in about 10 flare/coronal mass ejection (CME) events thus far. A typical example is the **2010 August 1** C3.2 flare/CME event that exhibited arc-shaped wave trains propagating in an active region (AR) magnetic funnel with ~5% intensity variations at speeds in the range of 1000-2000 km s–1. The fast temporal cadence and high sensitivity of AIA enabled the detection of these waves. We identify them as fast magnetosonic waves driven quasi-periodically at the base of the flaring region and develop a three-dimensional MHD model of the event. For the initial state we utilize the dipole magnetic field to model the AR and include gravitationally stratified density at coronal temperature. At the coronal base of the AR, we excite the fast magnetosonic wave by periodic velocity pulsations in the photospheric plane confined to a funnel of magnetic field lines. The excited fast magnetosonic waves have similar amplitude, wavelength, and propagation speeds as the observed wave trains. Based on the simulation results, we discuss the possible excitation mechanism of the waves, their dynamical properties, and the use of the observations for coronal MHD seismology.

General aspects of hard X-ray flares observed by HINOTORI Gradual burst and impulsive burst

Ohki, K.; Takakura, T.; Tsuneta, S.; Nitta, N.
Solar Physics vol. 86, July **1983**, p. 301-311; Discussion, p. 312

http://articles.adsabs.harvard.edu/full/1983SoPh...86..301O
http://articles.adsabs.harvard.edu/cgi-bin/nph-iarticle_query?1983SoPh...86..301O&data_type=PDF_HIGH&whole_paper=YES&type=PRINTER&filetype=.pdf
Observational results are presented for five gradual and four impulsive type events from the hard X-ray imaging and spectrometer instruments on the Hinotori satellite. Four sets of differences are clearly observed between the gradual and impulsive type bursts. Hard X-ray images are found to show the existence of a large coronal source for each gradual burst and a wide variety of source structures for impulsive bursts. The source heights of the impulsive bursts are found to be low. All gradual bursts are found to exhibit power-law spectra, whereas impulsive bursts exhibit exponential thermal spectra at least before the maximum phase. Energy-dependent peak delays are found only in gradual bursts. It is concluded that two different acceleration and emission mechanisms are involved with these two kinds of hard X-ray bursts.

Maximum Energy of Particles in Plasmas

Mitsuo **Oka**, Kazuo Makishima, Toshio Terasawa
ApJ **2024**
https://arxiv.org/pdf/2412.00564
Particles are accelerated to very high, non-thermal energies in space, solar, and astrophysical plasma environments. In cosmic ray physics, the "Hillas limit" is often used as a rough estimate (or the necessary condition) of the maximum energy of particles. This limit is based on the concepts of one-shot direct acceleration by a system-wide motional electric field, as well as stochastic and diffusive acceleration in strongly turbulent environments. However, it remains unclear how well this limit explains the actual observed maximum energies of particles. Here we show, based on a systematic review, that the observed maximum energy of particles -- those in space, solar, astrophysical, and laboratory environments -- often reach the energy predicted by the Hillas limit. We also found several exceptions, such as electrons in solar flares and jet-terminal lobes of radio galaxies, as well as protons in planetary radiation belts, where deviations from this limit occur. We discuss possible causes of such deviations, and we argue in particular that there is a good chance of detecting ultra-high-energy (~100 GeV) solar flare electrons that have not yet been detected. We anticipate that this study will facilitate further interdisciplinary discussions on the maximum energy of particles and the underlying mechanisms of particle acceleration in diverse plasma environments.

Particle acceleration in solar flares with imaging-spectroscopy in soft X-rays

Mitsuo **Oka**, Amir Caspi, Bin Chen, Mark Cheung, James Drake, Dale Gary, Lindsay Glesener, Fan Guo, Hantao Ji, Xiaocan Li, Takuma Nakamura, Noriyuki Narukage, Katharine Reeves, Pascal Saint-Hilaire, Taro Sakao, Chengcai Shen, Amy Winebarger, Tom Woods
White paper submitted to the Decadal Survey for Solar and Space Physics (Heliophysics) 2024-2033; **2023**
https://arxiv.org/ftp/arxiv/papers/2306/2306.04909.pdf
Particles are accelerated to very high, non-thermal energies during explosive energy-release phenomena in space, solar, and astrophysical plasma environments. In the case of solar flares, it has been established that magnetic reconnection plays an important role for releasing the magnetic energy, but it remains unclear if or how magnetic reconnection can further explain particle acceleration during flares. Here we argue that the key issue is the lack of understanding of the precise context of particle acceleration but it can be overcome, in the near future, by performing imaging-spectroscopy in soft X-rays (SXRs). Such observations should be complemented by observations in other wavelengths such as extreme-ultraviolets (EUVs), microwaves, hard X-rays (HXRs), and gamma-rays. Also, numerical simulations will be crucial for further narrowing down the particle acceleration mechanism in the context revealed by the observations. Of all these efforts, imaging-spectroscopy in SXRs, if successfully applied to large limb flares, will be a milestone in our challenge of understanding electron acceleration in solar flares and beyond, i.e. the Plasma Universe.

Electron Power-Law Spectra in Solar and Space Plasmas **Review**

M. **Oka**, J. Birn, M. Battaglia, C. C. Chaston, S. M. Hatch, G. Livadiotis, S. Imada, Y. Miyoshi, M. Kuhar, F. Effenberger, E. Eriksson, Y. V. Khotyaintsev, A. Retinò
Space Science Reviews 2018, 214:82 **2018**
https://arxiv.org/pdf/1805.09278.pdf
https://link.springer.com/content/pdf/10.1007%2Fs11214-018-0515-4.pdf
Particles are accelerated to very high, non-thermal energies in solar and space plasma environments. While energy spectra of accelerated electrons often exhibit a power law, it remains unclear how electrons are accelerated to high energies and what processes determine the power-law index \delta. Here, we review previous observations of the power-law index \delta in a variety of different plasma environments with a particular focus on sub-relativistic electrons. It appears that in regions more closely related to magnetic reconnection (such as the `above-the-looptop' solar hard X-ray source and the plasma sheet in Earth's magnetotail), the spectra are typically soft (\delta \gtrsim 4). This is in contrast to the typically hard spectra (\delta \lesssim 4) that are observed in coincidence with shocks. The difference implies that shocks are more efficient in producing a larger non-thermal fraction of electron energies when compared to

magnetic reconnection. A caveat is that during active times in Earth's magnetotail, \delta values seem spatially uniform in the plasma sheet, while power-law distributions still exist even in quiet times. The role of magnetotail reconnection in the electron power-law formation could therefore be confounded with these background conditions. Because different regions have been studied with different instrumentations and methodologies, we point out a need for more systematic and coordinated studies of power-law distributions for a better understanding of possible scaling laws in particle acceleration as well as their universality.

4.1 Solar Energetic Particles (SEPs)

KAPPA DISTRIBUTION MODEL FOR HARD X-RAY CORONAL SOURCES OF SOLAR FLARES

M. **Oka**1, S. Ishikawa1,2, P. Saint-Hilaire1, S. Krucker1,3, and R. P. Lin
2013 ApJ 764 6

Solar flares produce hard X-ray emission, the photon spectrum of which is often represented by a combination of thermal and power-law distributions. However, the estimates of the number and total energy of non-thermal electrons are sensitive to the determination of the power-law cutoff energy. Here, we revisit an "above-the-loop" coronal source observed by RHESSI on **2007 December 31** and show that a kappa distribution model can also be used to fit its spectrum. Because the kappa distribution has a Maxwellian-like core in addition to a high-energy power-law tail, the emission measure and temperature of the instantaneous electrons can be derived without assuming the cutoff energy. Moreover, the non-thermal fractions of electron number/energy densities can be uniquely estimated because they are functions of only the power-law index. With the kappa distribution model, we estimated that the total electron density of the coronal source region was ~2.4 × 1010 cm–3. We also estimated without assuming the source volume that a moderate fraction (~20%) of electrons in the source region was non-thermal and carried ~52% of the total electron energy. The temperature was 28 MK, and the power-law index δ of the electron density distribution was –4.3. These results are compared to the conventional power-law models with and without a thermal core component.

Electron Energy Partition in the Above-the-looptop Solar Hard X-Ray Sources

Mitsuo **Oka**1, Säm Krucker1,2, Hugh S. Hudson1,3, and Pascal Saint-Hilaire
ApJ 799 129 **2015**

Solar flares produce non-thermal electrons with energies up to tens of MeVs. To understand the origin of energetic electrons, coronal hard X-ray (HXR) sources, in particular above-the-looptop sources, have been studied extensively. However, it still remains unclear how energies are partitioned between thermal and non-thermal electrons within the above-the-looptop source. Here we show that the kappa distribution, when compared to conventional spectral models, can better characterize the above-the-looptop HXRs ($\gtrsim$15 keV) observed in four different cases. The widely used conventional model (i.e., the combined thermal plus power-law distribution) can also fit the data, but it returns unreasonable parameter values due to a non-physical sharp lower-energy cutoff Ec. In two cases, extreme-ultraviolet data were available from SDO/AIA and the kappa distribution was still consistent with the analysis of differential emission measure. Based on the kappa distribution model, we found that the **2012 July 19** flare showed the largest non-thermal fraction of electron energies about 50%, suggesting equipartition of energies. Considering the results of particle-in-cell simulations, as well as density estimates of the four cases studied, we propose a scenario in which electron acceleration is achieved primarily by collisionless magnetic reconnection, but the electron energy partition in the above-the-looptop source depends on the source density. In low-density above-the-looptop regions (few times 109 cm–3), the enhanced non-thermal tail can remain and a prominent HXR source is created, whereas in higher-densities (>1010 cm–3), the non-thermal tail is suppressed or thermalized by Coulomb collisions.

Above-the-Looptop Sources

Mitsuo **Oka** and Sa"m Krucker.
RHESSI Science Nugget No. 244, Jan **2015**
http://sprg.ssl.berkeley.edu/~tohban/wiki/index.php/Above-the-Looptop_Sources

While previous studies suggested that all electrons are accelerated to form a power-law (See the Nugget "Acceleration-region Densities"), we have proposed that the kappa distribution model (i.e., a Maxwellian-like core combined with a power-law tail) can equally fit the X-ray data from the above-the-looptop source (see our previous nugget "Kappa Distribution"). In this Nugget (See also Ref.[2]), we report an expanded study of the above-the-looptop sources, finding two cases with significantly enhanced non-thermal tail (hard X-ray) distributions, and two cases of less-enhanced non-thermal tail (Figure 2). With the kappa distribution model, we found that the flare **SOL2012-0719** showed the largest non-thermal fractions of electron number density (20%) and electron energy density (50%) whereas the **SOL2013-05-13** event showed the smallest non-thermal fractions of electron number density (6%) and electron energy density (16%). These results can be discussed in the context of magnetic reconnection, as described below.
Electron distribution functions in coronal sources explained.

Kappa Distribution

Mitsuo **Oka**
RHESSI Science Nugget No. 192, **2013**
http://sprg.ssl.berkeley.edu/~tohban/wiki/index.php/Kappa_Distribution
A simpler function fits both thermal and non-thermal hard X-ray components simultaneously.
With this in mind, we have revisited an 'above-the-loop' coronal X-ray source observed by RHESSI on 2007 December 31 and showed that the so-called kappa distribution can also be used to represent the energy spectrum. Because the kappa distribution has a Maxwellian-like core connected smoothly to the high-energy power-law tail, the emission measure and temperature of the instantaneous electrons can be derived without assuming a cutoff energy. Furthermore, the non-thermal fractions of electron number/energy densities can be uniquely estimated because they are functions of the power-law index only. **2007 December 31**

Statistical Properties of Superflares on Solar-type Stars: Results Using All of the Kepler Primary Mission Data

Soshi **Okamoto**, Yuta Notsu, Hiroyuki Maehara, Kosuke Namekata, Satoshi Honda, Kai Ikuta, Daisaku Nogami, Kazunari Shibata
2021 *ApJ* **906** 72
https://arxiv.org/pdf/2011.02117.pdf
https://iopscience.iop.org/article/10.3847/1538-4357/abc8f5/pdf
https://doi.org/10.3847/1538-4357/abc8f5
We report the latest statistical analyses of superflares on solar-type (G-type main-sequence; effective temperature is 5100 -- 6000 K) stars using all of the Kepler primary mission data, and Gaia-DR2 (Data Release 2) catalog. We updated the flare detection method from our previous studies by using high-pass filter to remove rotational variations caused by starspots. We also examined the sample biases on the frequency of superflares, taking into account gyrochronology and flare detection completeness. The sample size of solar-type stars and Sun-like stars (effective temperature is 5600 - 6000 K and rotation period is over 20 days in solar-type stars) are ∼4 and ∼12 times, respectively, compared with Notsu et al. (2019, ApJ, 876, 58). As a result, we found 2341 superflares on 265 solar-type stars, and 26 superflares on 15 Sun-like stars: the former increased from 527 to 2341 and the latter from 3 to 26 events compared with our previous study. This enabled us to have a more well-established view on the statistical properties of superflares. The observed upper limit of the flare energy decreases as the rotation period increases in solar-type stars. The frequency of superflares decreases as the stellar rotation period increases. The maximum energy we found on Sun-like stars is 4×1034 erg. Our analysis of Sun-like stars suggest that the Sun can cause superflares with energies of ∼7×1033 erg (∼X700-class flares) and ∼1×1034 erg (∼X1000-class flares) once every ∼3,000 years and ∼6,000 years, respectively.

Development of a method for determining the search window for solar flare neutrinos

K. **Okamoto**, Y. Nakano, S. Masuda, Y. Itow, M. Miyake, T. Terasawa, S. Ito, M. Nakahata
Solar Phys. **295**, Article number: 133 **2019**
https://arxiv.org/pdf/1909.10715.pdf
https://link.springer.com/content/pdf/10.1007/s11207-020-01706-z.pdf
Neutrinos generated during solar flares remain elusive. However, after 50 years of discussion and search, the potential knowledge unleashed by their discovery keeps the search crucial. Neutrinos associated with solar flares provide information on otherwise poorly known particle acceleration mechanisms during solar flare. For neutrino detectors, the separation between atmospheric neutrinos and solar flare neutrinos is technically encumbered by an energy band overlap. To improve differentiation from background neutrinos, we developed a method to determine the temporal search window for neutrino production during solar flares. Our method is based on data recorded by solar satellites, such as Geostationary Operational Environmental Satellite (GOES), Reuven Ramaty High Energy Solar Spectroscopic Imager (RHESSI), and GEOTAIL. In this study, we selected **23 solar flares above the X5.0 class** that occurred between 1996 and 2018. We analyzed the light curves of soft X-rays, hard X-rays, γ-rays, line γ-rays from neutron capture as well as the derivative of soft X-rays. The average search windows are determined as follows: 4,178 s for soft X-ray, 700 s for derivative of soft X-ray, 944 s for hard X-ray (100-800 keV), 1,586 s for line γ-ray from neutron captures, and 776 s for hard X-ray (above 50 keV). This method allows neutrino detectors to improve their sensitivity to solar flare neutrinos. **July 23, 2002, October 28, 2003, October 29, 2003, November 2, 2003, November 4, 2003, January 20, 2005**
Table 3. List of solar flares selected for this study.

Observations of Thomson scattering from a loop-prominence system

Juan Carlos Martínez **Oliveros**, Juan Camilo Guevara Gómez, Pascal Saint-Hilaire, Hugh Hudson, Säm Krucker
ApJ **936** 56 **2022**
https://arxiv.org/pdf/2208.06007.pdf
https://iopscience.iop.org/article/10.3847/1538-4357/ac83b7/pdf

We describe observations of the white-light structures in the low corona following the X8.2 flare SOL**2017-09-10**, as observed in full Stokes parameters by the Helioseismic and Magnetic Imager (HMI) of the Solar Dynamics Observatory. These data show both bright loops and a diffuse emission region above them. We interpret the loops as the white-light counterpart of a classical loop-prominence system, intermediate between the hot X-ray loops and coronal rain. The diffuse emission external to the loops is linearly polarized and has a natural interpretation in terms of Thomson scattering from the hot plasma seen prior to its cooling and recombination. The polarimetric data from HMI enable us to distinguish this contribution of scattering from the HMI pseudo-continuum measurement, and to make a direct estimation of the coronal mass in the polarized source. For a snapshot at 16:19~UT, we estimate a mass 8×1014~g. We further conclude that the volumetric filling factor of this source is near unity.

THE HEIGHT OF A WHITE-LIGHT FLARE AND ITS HARD X-RAY SOURCES

Juan-Carlos Martínez **Oliveros**1, Hugh S. Hudson1,2, Gordon J. Hurford1,3, Säm Krucker1,3, R. P. Lin1,4,5, Charles Lindsey6, Sebastien Couvidat7, Jesper Schou7, and W. T. Thompson
2012 ApJ 753 L26

We describe observations of a white-light (WL) flare (**SOL2011-02-24T07:35:00, M3.5**) close to the limb of the Sun, from which we obtain estimates of the heights of the optical continuum sources and those of the associated hard X-ray (HXR) sources. For this purpose, we use HXR images from the Reuven Ramaty High Energy Spectroscopic Imager and optical images at 6173 Å from the Solar Dynamics Observatory. We find that the centroids of the impulsive-phase emissions in WL and HXRs (30-80 keV) match closely in central distance (angular displacement from Sun center), within uncertainties of order 02. This directly implies a common source height for these radiations, strengthening the connection between visible flare continuum formation and the accelerated electrons. We also estimate the absolute heights of these emissions as vertical distances from Sun center. Such a direct estimation has not been done previously, to our knowledge. Using a simultaneous 195 Å image from the Solar-Terrestrial RElations Observatory spacecraft to identify the heliographic coordinates of the flare footpoints, we determine mean heights above the photosphere (as normally defined; $\tau = 1$ at 5000 Å) of 305 ± 170 km and 195 ± 70 km, respectively, for the centroids of the HXR and WL footpoint sources of the flare. These heights are unexpectedly low in the atmosphere, and are consistent with the expected locations of $\tau = 1$ for the 6173 Å and the ~40 keV photons observed, respectively.

Imaging Spectroscopy of a White-Light Solar Flare

J.C. Martínez **Oliveros** · S. Couvidat · J. Schou · S. Krucker · C. Lindsey · H.S. Hudson · P. Scherrer
Solar Phys (**2011**) 269: 269–281

We report observations of a white-light solar flare (**SOL2010-06-12T00:57, M2.0**) observed by the Helioseismic Magnetic Imager (HMI) on the Solar Dynamics Observatory (SDO) and the Reuven Ramaty High Energy Solar Spectroscopic Imager (RHESSI). The HMI data give us the first space-based high-resolution imaging spectroscopy of a white-light flare, including continuum, Doppler, and magnetic signatures for the photospheric Fe i line at 6173.34 Å and its neighboring continuum. In the impulsive phase of the flare, a bright white-light kernel appears in each of the two magnetic footpoints. When the flare occurred, the spectral coverage of the HMI filtergrams (six equidistant samples spanning ±172 mÅ around nominal line center) encompassed the line core and the blue continuum sufficiently far from the core to eliminate significant Doppler crosstalk in the latter, which is otherwise a possibility for the extreme conditions in a white-light flare. RHESSI obtained complete hard X-ray and γ-ray spectra (this was the first γ-ray flare of Cycle 24). The Fe i line appears to be shifted to the blue during the flare but does not go into emission; the contrast is nearly constant across the line profile. We did not detect a seismic wave from this event. The HMI data suggest stepwise changes of the line-of-sight magnetic field in the white-light footpoints.

Black and White Flares

J.C.M. **Oliveros** & C. Lindsey
RHESSI Science Nugget, 24 Jan **2011**
http://sprg.ssl.berkeley.edu/~tohban/wiki/index.php/Black_and_White_Flares

With the newly-launched Solar Dynamics Observatory (SDO) we now have new tools to study the important phenomenon of the white-light flare. Much to our surprise, though, the first gamma-ray flare of the SDO era turned out to be a negative flare! This event was **SOL2010-06-12T00:57, naming it unambiguously by the new IAU convention**. Such a phenomenon is known for other stars but had never been credibly reported for the Sun. Theories have been waiting in the wings for such an observation, so we were very pleased to find it well-observed by many spacecraft and ground-based observatories, the only downside being that RHESSI could only observe photometrically, not as an imager, because observations of the Crab Nebula required pointing away from Sun center.

The Periodic and Temporal Behaviors of Solar X-Ray Flares in Solar Cycles 23 and 24

Jacob **Oloketuyi**1,2,3, Yu Liu1,2,4, and Mingyu Zhao
2019 ApJ 874 20

https://doi.org/10.3847/1538-4357/ab064c
The recent solar cycles 23 and 24 are thought to be unusually quiet with more prolonged periods. Both sunspot groups and solar soft X-ray (SXR) flares show a decline in numbers comparable to cycles 21 and 22. In order to understand the periodic variations and distributions of solar flares with the sunspot group numbers in these cycles, this study investigates the periodicities and distributions of the solar SXR flares, 36354 in total (B (13351) 36.7%, C (20699) 56.9%, M (2141) 5.9%, and X (163) 0.45%) between 1996 July and 2016 December. The continuous wavelet transforms and cross-correlation methods were used to carry out the study. First, we found that the B- class flare number is asynchronous and negatively correlated with the sunspot group numbers. The flare class exhibits deviation when sunspot group numbers rise or fall around 100. The other class flares are in phase, synchronous with the sunspot group numbers. The C-class flares show the highest level of correlation of 0.868 with sunspot group numbers. A different number of short and intermediate periodicities was also noticed among the flare classes. Notable 256-day periodicity is found for B flares, 7, 64, and 300 days for C, 32, 64, and 256 days for M flares, and 40, 32, and 25 days for X flares. The difference in periodic variations of the flare classes could be attributed to the magnetic flux system of sunspot groups producing them.

Fermi-LAT observations of the 2017 September 10th solar flare

Nicola **Omodei**, Melissa Pesce-Rollins, Francesco Longo, Alice Allafort, Säm Krucker
ApJL **2018**
https://arxiv.org/pdf/1803.07654.pdf
The Fermi-Large Area Telescope (LAT) detection of the X8.2 GOES class solar flare of **2017 September 10** provides for the first time observations of a long duration high-energy gamma-ray flare associated with a Ground Level Enhancement (GLE). The >100 MeV emission from this flare lasted for more than 12 hours covering both the impulsive and extended phase. We present the localization of the gamma-ray emission and find that it is consistent with the active region (AR) from which the flare occurred over a period lasting more than 6 hours contrary to what was found for the 2012 March 7 flares. The temporal variation of the proton index inferred from the gamma-ray data seems to suggest two phases in acceleration of the proton population. Based on timing arguments we interpret the second phase to be tied to the acceleration mechanism powering the GLE, believed to be particle acceleration at a coronal shock driven by the CME.

Generation of Large Scale Electric Fields in Coronal Flare Circuits

Onel. H.; Mann, G.
E-print, July **2012**, Cent. Eur. Astropys. Bull. 33 (**2009**), 1, 141-154
A large number of energetic electrons are generated during solar flares. They carry a substantial part of the flare released energy but how these electrons are created is not fully understood yet. This paper suggests that plasma motion in an active region in the photosphere is the source of large electric currents. These currents can be described by macroscopic circuits. Under special circumstances currents can establish in the corona along magnetic field lines. The energy released by these currents when moderate assumptions for the local conditions are made, is found be comparable to the flare energy.

Electron Energy Spectra and e-e Bremsstrahlung from Anisotropic Electron Distributions in Extreme Solar Flares

I. D. **Oparin**, Yu. E. Charikov, E. P. Ovchinnikova, A. N. Shabalin
2020
https://arxiv.org/pdf/2012.07908.pdf
We study the electron energy spectra of two powerful solar flares SOL**2003-10-28**T 11:06:16 (GOES class X17.2) and SOL**2002-07-23**T00:18:16 (X4.8) on the basis of HXR and gamma-ray spectra obtained from RHESSI data. Electron-electron (e-e) bremsstrahlung makes a significant contribution to the X-ray flux at energies above 500 keV. In X-ray flux calculations different electron pitch-angle distributions were considered: quasi-transverse and quasi-longitudinal. It was shown that breaks in hard X-ray spectra occur on energies $\epsilon \approx 100$ keV with photon spectral-index difference $\Delta\gamma \geq 1$ in the case of quasi-longitudinal anisotropy and hard power-law electron energy spectra. We deduce the parameters of non-thermal electrons energy spectra from RHESSI data for the extreme solar flares of 2003 October 28 and 2002 July 23. After including e-e bremsstrahlung, the non-thermal electrons energy spectra obtained in the thick-target model can be fitted using power-law with spectral index $\delta \approx 5$. For the 2002 July 23 flare, there is a pronounced asymmetry towards the southern footpoint, starting from energies above 100 keV. The separation of HXR sources at energies above 100 keV may be related to a feature of relativistic electron transport in flaring loops.

Perspectives of current-layer diagnostics in solar flares

A. V. **Oreshina** and I. V. Oreshina
A&A 558, A16 (**2013**)
http://arxiv.org/pdf/1404.4434v1.pdf

Context. A reconnecting current layer is a “heart” of a solar flare, because it is a place of magnetic-field energy release. However, there are no direct observations of these layers.
Aims. The aim of our work is to understand why we actually do not directly observe current layers and what we need to do it in the future.
Methods. The method is based on a simple mathematical model of a super-hot ($T \gtrsim 10^8$ K) turbulent-current layer (SHTCL) and a model of plasma heating by the layer.
Results. The models allow us to study a correspondence between the main characteristics of the layer, such as temperature and dimensions, and the observational features, such as differential and integral emission measure of heated plasma, intensity of spectral lines Fe xxvi (1.78 and 1.51 Å) and Ni xxvii (1.59 Å). This method provides a theoretical basis for determining parameters of the current layer from observations.
Conclusions. Observations of SHTCLs are difficult, because the spectral line intensities are faint, but it is theoretically possible in the future. Observations in X-ray range 1.5–1.8 Å with high spectral resolution (better than 0.01 Å) and high temporal resolution (seconds) are needed. It is also very important to interpret the observations using a multi-temperature approach instead of the usual single or double temperature method.

Magnetic-topology evolution in NOAA AR 10501 on 2003 November 18

A.V. **Oreshina**, I.V. Oreshina, and B.V. Somov
A&A, 538, A138, **2012, File**
Context.NOAA AR 10501 produced three flares on 2003 November 18. Two of them were associated with coronal mass ejections (CMEs).
Aims.We model the magnetic-field structure of the active region, study the magnetic-topology evolution, and propose a scenario of the observed events.
Methods.The coronal magnetic field is reconstructed using a topological model (also called magnetic-charge model). We present an automatic method of choosing the magnetic charges for the case where the charges are located beneath the photosphere. The new method improves quantitative analysis of magnetograms and makes processing faster.
Results.We demonstrate that coronal conditions became more favourable for magnetic reconnection before the flaring events. It is also shown that the magnetic-field configuration at the time of both CMEs was critical, close to what is called “topological trigger”. We assume that the topological trigger played a key role in the initiation of these CMEs.

A FAST METHOD FOR CONSTRUCTING MAGNETIC FIELD MODELS OF SOLAR ACTIVE REGIONS

I.V. **Oreshina**1 and B.V. Somov1
EAS Publications Series, Vol. ?, **2012, File**
A new method is proposed for automatic choosing the so-called magnetic “charges" that are necessary to model the coronal magnetic field in solar ARs. The method makes the quantitative analysis of large-scale magnetic field fast, easy, and reliable that allows us to study the evolution of ARs on short time scales.

On the heat conduction in a high-temperature plasma in solar flares

A.V. **Oreshina** and B. V. Somov
Astronomy Letters, Volume 37, Number 10, 726-736, **2011**
Pis’ma v Astronomicheskiĭ Zhurnal, **2011**, Vol. 37, No. 10, pp. 789–800.
We have developed three types of mathematical models to describe the mechanisms of plasma heating in the corona by intense heat fluxes from a super-hot ($T_e \gtrsim 10^8$ K) reconnecting current layer in connection with the problem of energy transport in solar flares. We show that the heat fluxes calculated within the framework of self-similar solutions using Fourier’s classical law exceed considerably the real energy fluxes known from present-day multi-wavelength observations of flares. This is because the conditions for the applicability of ordinary heat conduction due to Coulomb collisions of thermal plasma electrons are violated. Introducing anomalous heat conduction due to the interaction of thermal runaway electrons with ion-acoustic turbulence does not give a simple solution of the problem, because it produces unstable temperature profiles. The models incorporating the effect of collisional heat flux relaxation describe better the heat transport in flares than Fourier’s law and anomalous heat conduction.

Flare Kernels May be Smaller than You Think: Modelling the Radiative Response of Chromospheric Plasma Adjacent to a Solar Flare

Christopher M. J. **Osborne**, Lyndsay Fletcher
MNRAS **2022**
https://arxiv.org/pdf/2209.03238
Numerical models of solar flares typically focus on the behaviour of directly-heated flare models, adopting magnetic field- aligned, plane-parallel methodologies. With high spatial- and spectral-resolution ground-based optical observations of flares, it is essential also to understand the response of the plasma surrounding these strongly heated

volumes. We investigate the effects of the extreme radiation field produced by a heated column of flare plasma on an adjacent slab of chromospheric plasma, using a two-dimensional radiative transfer model and considering the time-dependent solution to the atomic level populations and electron density throughout this model. The outgoing spectra of Hα and Ca II 854.2 nm synthesised from our slab show significant spatial-, time-, and wavelength-dependent variations (both enhancements and reductions) in the line cores, extending on order 1 Mm into the non-flaring slab due to the incident transverse radiation field from the flaring boundary. This may lead to significant overestimates of the sizes of directly-heated flare kernels, if line-core observations are used. However, the radiation field alone is insufficient to drive any significant changes in continuum intensity, due to the typical photospheric depths at which they forms, so continuum sources will not have an apparent increase in size. We show that the line formation regions near the flaring boundary can be driven upwards in altitude by over 1 Mm despite the primary thermodynamic parameters (other than electron density) being held horizontally uniform. This work shows that in simple models these effects are significant and should be considered further in future flare modelling and interpretation.

On the importance of Ca II photoionization by the hydrogen lyman transitions in solar flare models

C M J **Osborne**, P Heinzel, J Kašparová, L Fletcher
Monthly Notices of the Royal Astronomical Society, Volume 507, Issue 2, October **2021**, Pages 1972–1978,
https://scholar.google.com/scholar_url?url=https://academic.oup.com/mnras/article-pdf
https://doi.org/10.1093/mnras/stab2156
The forward fitting of solar flare observations with radiation–hydrodynamic simulations is a common technique for learning about energy deposition and atmospheric evolution during these explosive events. A frequent spectral line choice for this process is Ca II 854.2 nm due to its formation in the chromosphere and substantial variability. It is important to ensure that this line is accurately modelled to obtain the correct interpretation of observations. Here, we investigate the importance of photoionization of Ca II to Ca III by the hydrogen Lyman transitions, whilst the Lyman continuum is typically considered in this context in simulations, the associated bound–bound transitions are not. This investigation uses two RADYN flare simulations and reprocesses the radiative transfer using the Lightweaver framework which accounts for the overlapping of all active transitions. The Ca II 854.2 nm line profiles are found to vary significantly due to photoionization by the Lyman lines, showing notably different shapes and even reversed asymmetries. Finally, we investigate to what extent these effects modify the energy balance of the simulation and the implications on future radiation–hydrodynamic simulations. There is found to be a 10–15 per cent change in detailed optically thick radiative losses from considering these photoionization effects on the calcium lines in the two simulations presented, demonstrating the importance of considering these effects in a self-consistent way.

RADYNVERSION: Learning to Invert a Solar Flare Atmosphere with Invertible Neural Networks

Christopher M. J. **Osborne**, John A. Armstrong, Lyndsay Fletcher
ApJ **873** 128 **2019**
https://arxiv.org/pdf/1901.08626.pdf
https://doi.org/10.3847/1538-4357/ab07b4
During a solar flare, it is believed that reconnection takes place in the corona followed by fast energy transport to the chromosphere. The resulting intense heating strongly disturbs the chromospheric structure, and induces complex radiation hydrodynamic effects. Interpreting the physics of the flaring solar atmosphere is one of the most challenging tasks in solar physics. Here we present a novel deep learning approach, an invertible neural network, to understanding the chromospheric physics of a flaring solar atmosphere via the inversion of observed solar line profiles in H{\alpha} and Ca II {\lambda}8542. Our network is trained using flare simulations from the 1D radiation hydrodynamics code RADYN as the expected atmosphere and line profile. This model is then applied to single pixels from an observation of an M1.1 solar flare taken with SST/CRISP instrument just after the flare onset. The inverted atmospheres obtained from observations provide physical information on the electron number density, temperature and bulk velocity flow of the plasma throughout the solar atmosphere ranging from 0-10 Mm in height. The density and temperature profiles appear consistent with the expected atmospheric response, and the bulk plasma velocity provides the gradients needed to produce the broad spectral lines whilst also predicting the expected chromospheric evaporation from flare heating. We conclude that we have taught our novel algorithm the physics of a solar flare according to RADYN and that this can be confidently used for the analysis of flare data taken in these two wavelengths. This algorithm can also be adapted for a menagerie of inverse problems providing extremely fast (~10 {\mu}s) inversion samples. **2014/09/06**

Particle energisation in a collapsing magnetic trap model: the relativistic regime

Solmaz Eradat **Oskoui**, Thomas Neukirch
A&A, 567, A131, **2014**,
http://arxiv.org/pdf/1406.6196v1.pdf
In solar flares, a large number of charged particles is accelerated to high energies. By which physical processes this is achieved is one of the main open problems in solar physics. It has been suggested that during a flare, regions of the

rapidly relaxing magnetic field can form a collapsing magnetic trap (CMT) and that this trap may contribute to particle energisation.} In this Research Note we focus on a particular analytical CMT model based on kinematic magnetohydrodynamics. Previous investigations of particle acceleration for this CMT model focused on the non-relativistic energy regime. It is the specific aim of this Research Note to extend the previous work to relativistic particle energies. Particle orbits were calculated numerically using the relativistic guiding centre equations. We also calculated particle orbits using the non-relativistic guiding centre equations for comparison. For mildly relativistic energies the relativistic and non-relativistic particle orbits mainly agree well, but clear deviations are seen for higher energies. In particular, the final particle energies obtained from the relativistic calculations are systematically lower than the energies reached from the corresponding non-relativistic calculations, and the mirror points of the relativistic orbits are systematically higher than for the corresponding non-relativistic orbits. While the overall behaviour of particle orbits in CMTs does not differ qualitatively when using the relativistic guiding centre equations, there are a few systematic quantitative differences between relativistic and non-relativistic particle dynamics.

Loss cone evolution and particle escape in collapsing magnetic trap models in solar flares

Solmaz Eradat **Oskoui**, Thomas Neukirch and Keith James Grady
A&A 563, A73 (**2014**)
Context. Collapsing magnetic traps (CMTs) have been suggested as one possible mechanism responsible for the acceleration of high-energy particles during solar flares. An important question regarding the CMT acceleration mechanism is which particle orbits escape and which are trapped during the time evolution of a CMT. While some models predict the escape of the majority of particle orbits, other more sophisticated CMT models show that, in particular, the highest-energy particles remain trapped at all times. The exact prediction is not straightforward because both the loss cone angle and the particle orbit pitch angle evolve in time in a CMT.
Aims. Our aim is to gain a better understanding of the conditions leading to either particle orbit escape or trapping in CMTs.
Methods. We present a detailed investigation of the time evolution of particle orbit pitch angles in the CMT model of Giuliani and collaborators and compare this with the time evolution of the loss cone angle. The non-relativistic guiding centre approximation is used to calculate the particle orbits. We also use simplified models to corroborate the findings of the particle orbit calculations.
Results. We find that there is a critical initial pitch angle for each field line of a CMT that divides trapped and escaping particle orbits. This critical initial pitch angle is greater than the initial loss cone angle, but smaller than the asymptotic (final) loss cone angle for that field line. As the final loss cone angle in CMTs is larger than the initial loss cone angle, particle orbits with pitch angles that cross into the loss cone during their time evolution will escape whereas all other particle orbits are trapped. We find that in realistic CMT models, Fermi acceleration will only dominate in the initial phase of the CMT evolution and, in this case, can reduce the pitch angle, but that betatron acceleration will dominate for later stages of the CMT evolution leading to a systematic increase of the pitch angle. Whether a particle escapes or remains trapped depends critically on the relative importance of the two acceleration mechanisms, which cannot be decoupled in more sophisticated CMT models.

Connecting Flares and Transient Mass-loss Events in Magnetically Active Stars

Rachel A. **Osten**1,3 and Scott J. Wolk
2015 ApJ 809 79
http://arxiv.org/pdf/1506.04994v1.pdf
We explore the ramification of associating the energetics of extreme magnetic reconnection events with transient mass-loss in a stellar analogy with solar eruptive events. We establish energy partitions relative to the total bolometric radiated flare energy for different observed components of stellar flares and show that there is rough agreement for these values with solar flares. We apply an equipartition between the bolometric radiated flare energy and kinetic energy in an accompanying mass ejection, seen in solar eruptive events and expected from reconnection. This allows an integrated flare rate in a particular waveband to be used to estimate the amount of associated transient mass-loss. This approach is supported by a good correspondence between observational flare signatures on high flaring rate stars and the Sun, which suggests a common physical origin. If the frequent and extreme flares that young solar-like stars and low-mass stars experience are accompanied by transient mass-loss in the form of coronal mass ejections, then the cumulative effect of this mass-loss could be large. We find that for young solar-like stars and active M dwarfs, the total mass lost due to transient magnetic eruptions could have significant impacts on disk evolution, and thus planet formation, and also exoplanet habitability.

Sun-as-a-star Analysis of the X1.6 Flare on 2023 August 5: Dynamics of Post-flare Loops in Spatially Integrated Observational Data

Takato **Otsu**, Ayumi Asai, Kai Ikuta, Kazunari Shibata
ApJL **974** L13 **2024**
https://arxiv.org/pdf/2409.07630
https://iopscience.iop.org/article/10.3847/2041-8213/ad7a70/pdf

Post-flare loops are loop-like plasmas observed during the decay phase of solar flares, and they are expected to exist for stellar flares. However, it is unclear how post-flare loops are observed in stellar flares' cases. To clarify behaviors of post-flare loops in spatially integrated data, we performed the Sun-as-a-star analysis of the X1.6 flare that occurred on **2023 August 5**, using GOES X-ray flux (∼107 K), extreme ultraviolet (EUV) images taken by Atmospheric Imaging Assembly onboard the Solar Dynamic Observatory (≥104.9 K) and Hα data taken by Solar Dynamics Doppler Imager on board the Solar Magnetic Activity Research Telescope at Hida Observatory, Kyoto University (∼104 K). As a result, this flare showed signatures corresponding to the important dynamics of the post-flare loops even in the spatially integrated data: (1) The Hα light curve showed two distinct peaks corresponding to the flare ribbons and the post-flare loops. The plasma cooling in the post-flare loops generated different peak times in soft X-rays, EUV, and Hα light curves. (2) Downflows were confirmed as simultaneous redshifted/blueshifted absorptions in the Hα spectra. (3) The apparent rise of post-flare loops was recognized as a slowing of the decay for the Hα light curve. These results are keys to investigating stellar post-flare loops with spatially integrated data. We also discuss the dependence of our results on flare locations and their possible applications to stellar observations.

Multiwavelength Sun-as-a-star Analysis of the M8.7 Flare on 2022 October 2 Using Hα and EUV Spectra Taken by SMART/SDDI and SDO/EVE

Takato **Otsu**, Ayumi Asai

ApJ **964** 75 **2024**

https://arxiv.org/pdf/2402.00589.pdf

https://iopscience.iop.org/article/10.3847/1538-4357/ad24ec/pdf

This paper presents a multiwavelength Sun-as-a-star analysis of the M8.7 flare on **2022 October 2**, which were associated with a filament eruption and the following coronal mass ejection. The Sun-as-a-star analysis was performed using Hα data taken by Solar Dynamics Doppler Imager on board the Solar Magnetic Activity Research Telescope at Hida Observatory, Kyoto University and full-disk integrated extreme ultraviolet (EUV) spectra taken by the Extreme ultraviolet Variability Experiment (EVE) on board the Solar Dynamics Observatory. The Sun-as-a-star Hα spectra showed blueshifted absorption corresponding to the filament eruption. Furthermore, the EVE O {\sc v} 629.7 Å spectra showed blueshifted brightening, which can also be attributed to the filament eruption. Even when the blueshifted absorption became almost invisible in the Sun-as-a-star Hα spectra, the O {\sc v} blueshifted brightening up to −400 km s−1 was still clearly visible. This result indicates that even when the shifted components--which are expected to originate from stellar eruptions--become almost invisible in the spatially integrated stellar Hα spectra, the erupting materials may still be present and observable in EUV spectra. Additionally, the Sun-as-a-star Hα and O {\sc v} spectra exhibited redshifted absorption and brightening, respectively, during the decay phase of the flare. These components probably originate from the post-flare loops, providing clues for the multi-temperature nature of the post-flare loops in the spatially integrated observation. Our Sun-as-a-star results suggest that the combination of Hα and EUV lines allows the investigation of the multi-temperature structure and temporal development of stellar active phenomena even in spatially integrated spectra.

RHESSI Science Nuggets #467 **2024** https://sprg.ssl.berkeley.edu/~tohban/wiki/index.php/Sun-as-a-star_Analysis_of_the_M8.7_Flare_on_2022_October_2_Using_H-alpha_and_EUV_Spectra_Taken_by_SMART/SDDI_and_SDO/EVE

Sun-as-a-star Analyses of Various Solar Active Events Using Hα Spectral Images Taken by SMART/SDDI

Takato **Otsu**, Ayumi Asai, Kiyoshi Ichimoto, Takako T. Ishii, Kosuke Namekata

ApJ **939** 98 **2022**

https://arxiv.org/pdf/2210.02819.pdf

https://iopscience.iop.org/article/10.3847/1538-4357/ac9730/pdf

Sun-as-a-star analyses, in which observational data is spatially integrated, are useful for interpreting stellar data. For future applications to stellar observations, we performed Sun-as-a-star analyses of Hα spectra for various active events on the Sun, not only for flares and filament eruptions/surges on the solar disk, but also for eruptions of off limb prominences using Hα spectral images taken by the Solar Magnetic Activity Research Telescope / Solar Dynamics Doppler Imager (SMART/SDDI) at Hida Observatory, Kyoto University. All the analyzed events show emission relative to the pre-event state and the changes in their Hα equivalent widths are all on the orders of 10−4 Å. Sun-as-a-star Hα spectra exhibit different features depending on the causes of the emission: (i) Flares show emission at the Hα line center, together with red asymmetry and line broadening, as reported in a previous study. (ii) Filament eruptions with and without flares show emission near the Hα line center, accompanied by blue-/red-shifted absorption. Notably, disappearance of dark filaments leads to the apparent enhancement of the Hα line center emission. (iii) Eruptions of off limb prominences show blue-/red-shifted emission. These spectral features enable us to identify the active phenomena on Sun-like stars. We have also found that even the filament eruptions showing red-shifted absorptions in Sun-as-a-star Hα spectra lead to coronal mass ejections (CMEs). This result suggests that even if the falling components of stellar filament eruptions are detected as red-shifted absorptions in Hα spectra, such stellar filament eruptions may also

develop into CMEs. **2016 November 5, 2017 February 19, 2017 April 2, 2017 April 23, 2017 June 19, 2017 September 8, 2021 April 19 – 20, 2021 May 5**
Table 1. List of events analyzed in this paper 2016-2021

Temporal and Periodic Variations of the Solar Flare Index During the Last Four Solar Cycles and Their Association with Selected Geomagnetic-Activity Parameters

Atila **Ozguc**, Ali Kilcik & Vasyl Yurchyshyn
Solar Physics volume 297, Article number: 112 (**2022**)
https://doi.org/10.1007/s11207-022-02049-7
We studied the temporal and periodic variations of the monthly solar flare index (FI) and selected geomagnetic-activity parameters (Ap, Dst, Scalar B, and aa) measured during Solar Cycles 21 – 24 (from January 1, 1975 to December 31, 2020) and report the following findings: 1) all data sets except the FI peak values gradually decreased after 1992, while the FI peak values began their gradual decrease in 1982; 2) all data sets show double or multiple peaks during the maximum phase of solar cycles; 3) the FI shows meaningful correlations with the investigated geomagnetic-activity parameters; 4) the 11-year sunspot-cycle periodicity and periodicities lower than 3.9 months were observed in all data sets without exception; 5) the FI time series exhibits a unique period of 4.8 – 5.2 months that is not present in all the other indices, while geomagnetic aa, Ap, and Dst indices show a unique 6 – 6.1 months periodicity that does not appear in the scalar B and FI; 6) crosswavelet transform (XWT) spectra between FI and other parameters generally show phase mixing in the short (2 – 8 months) period range, while all parameters used in this study were found to be inphase and highly correlated with the 11-year solar-activity period. All these results show that the FI variations are one of the main drivers of the geomagnetic activity.

Automatic Detection of Magnetic delta in Sunspot Groups

Sreejith **Padinhatteeri**, Paul A. Higgins, D. Shaun Bloomfield, Peter T. Gallagher
Solar Phys. **2015**
http://arxiv.org/pdf/1510.06413v1.pdf
Large and magnetically complex sunspot groups are known to be associated with flares. To date, the Mount Wilson scheme has been used to classify sunspot groups based on their morphological and magnetic properties. The most flare prolific class, the delta sunspot-group, is characterised by opposite polarity umbrae within a common penumbra, separated by less than 2 degrees. In this article, we present a new system, called the Solar Monitor Active Region Tracker - Delta Finder (SMART-DF), that can be used to automatically detect and classify magnetic deltas in near-realtime. Using continuum images and magnetograms from the Helioseismic and Magnetic Imager (HMI) onboard NASA's Solar Dynamics Observatory (SDO), we first estimate distances between opposite polarity umbrae. Opposite polarity pairs having distances of less that 2 degrees are then identified, and if these pairs are found to share a common penumbra, they are identified as a magnetic delta configuration. The algorithm was compared to manual delta detections reported by the Space Weather Prediction Center (SWPC), operated by the National Oceanic and Atmospheric Administration (NOAA). SMART-DF detected 21 out of 23 active regions (ARs) that were marked as delta spots by NOAA during 2011 - 2012 (within +/- 60 degrees longitude). SMART-DF in addition detected five ARs which were not announced as delta spots by NOAA. The near-relatime operation of SMART-DF resulted in many deltas being identified in advance of NOAA's daily notification. SMART-DF will be integrated with SolarMonitor (www.solarmonitor.org) and the near-realtime information will be available to the public.
2011-09-27, 2012-03-09, 2013-10-11, 2014-10-20

A Prospective New Diagnostic Technique for Distinguishing Eruptive and Non-Eruptive Active Regions

P. **Pagano**, D.H. Mackay, S.L. Yardley
ApJ **883** 112 **2019**
https://arxiv.org/pdf/1908.09223.pdf
https://doi.org/10.3847/1538-4357/ab3e42
Active regions are the source of the majority of magnetic flux rope ejections that become Coronal Mass Ejections (CMEs). To identify in advance which active regions will produce an ejection is key for both space weather prediction tools and future science missions such as Solar Orbiter. The aim of this study is to develop a new technique to identify which active regions are more likely to generate magnetic flux rope ejections. The new technique will aim to: (i) produce timely space weather warnings and (ii) open the way to a qualified selection of observational targets for space-borne instruments. We use a data-driven Non-linear Force-Free Field (NLFFF) model to describe the 3D evolution of the magnetic field of a set of active regions. We determine a metric to distinguish eruptive from non-eruptive active regions based on the Lorentz force. Furthermore, using a subset of the observed magnetograms, we run a series of simulations to test whether the time evolution of the metric can be predicted. The identified metric successfully differentiates active regions observed to produce eruptions from the non-eruptive ones in our data sample. A meaningful prediction of the metric can be made between 6 to 16 hours in advance. This initial study presents an interesting first step in the prediction of CME onset using only LOS magnetogram observations combined with NLFFF modelling.

Future studies will address how to generalise the model such that it can be used in a more operational sense and for a variety of simulation approaches. **2012.08.29-09.02**
Table 1. Properties of the active regions analysed in this study (2012-2015)

A SURVEY OF SOFT X-RAY LIMB FLARE IMAGES: THE RELATION BETWEEN THEIR STRUCTURE IN THE CORONA AND OTHER PHYSICAL PARAMETERS

R. **Pallavicini**,* S. Serio,| and G. S. VaianaI
ApJ 216:108-122, **1977**
https://ui.adsabs.harvard.edu/link_gateway/1977ApJ...216..108P/ADS_PDF
A survey of soft X-ray limb flare images obtained by the S-054 experiment on board Skylab is presented. From a morphological point of view, limb flares have been subdivided into three groups : (A) flares characterized by compact loop structures; (B) flares with a pointlike appearance ; (C) flares with large and diffuse systems of loops. The significance of this subdivision is investigated with the aid of plasma parameters determined by combining the S-054 spatially resolved observations with full-disk data obtained by the Solrad 9 satellite. From a comparison of the spatial structure with physical parameters such as height, volume, energy density, and characteristic times, and from the correlation with white-light coronal transients and Ha active prominences, the existence of two physically distinct classes of flares is established: class I, which consists of both morphological groups A and B, and class II, which comprises only events of group C.
Events of class I are compact flares with smaller volume (~ 1026-1027 cm3) and lower height (^104 km); faster rise and decay times, and shorter duration (~tens of minutes). They have higher energy density (~ 102 -103 ergs cm-3), do not appear to be associated with white-light coronal transients, and are located very low at the base of active regions; their entire structure is bright, with a tendency to be brighter in the lower sections. Events of class II are long-enduring events (~hours) with longer rise and decay times and greater height (~5 x 104 km). They have larger volume (~ 1028 - 1029 cm3) and lower energy density (10-102 ergs cm-3) and are associated with prominence eruption or activation and with white-light coronal transients. The large and diffuse systems of loops characteristic of these events are generally brighter at the top,
A model is proposed which qualitatively accounts for the observed differences between the two classes of flares. In particular, it is suggested that compact flares of class I are loops filled from below by evaporated chromospheric material, while flares of class II are probably produced by direct heating of cool condensed material present at coronal heights in the form of a prominence.
TABLE 2 Characteristics of Selected S-054 Limb Events (1973-74)

Exploring the Origin of Solar Energetic Electrons I: Constraining the Properties of the Acceleration Region Plasma Environment

Ross **Pallister**, Natasha L. S. Jeffrey
ApJ **958** 18 **2023**
https://arxiv.org/pdf/2310.04229.pdf
https://iopscience.iop.org/article/10.3847/1538-4357/ad0035/pdf
Solar flare electron acceleration is an efficient process, but its properties (mechanism, location) are not well constrained. Via hard X-ray (HXR) emission, we routinely observe energetic electrons at the Sun, and sometimes we detect energetic electrons in interplanetary space. We examine if the plasma properties of an acceleration region (size, temperature, density) can be constrained from in-situ observations, helping to locate the acceleration region in the corona, and infer the relationship between electrons observed in-situ and at the Sun. We model the transport of energetic electrons, accounting for collisional and non-collisional effects, from the corona into the heliosphere (to 1.0 AU). In the corona, electrons are transported through a hot, over-dense region. We test if the properties of this region can be extracted from electron spectra (fluence and peak flux) at different heliospheric locations. We find that cold, dense coronal regions significantly reduce the energy at which we see the peak flux and fluence for distributions measured out to 1.0 AU, the degree of which correlates with the temperature and density of plasma in the region. Where instrument energy resolution is insufficient to differentiate the corresponding peak values, the spectral ratio of [7-10) to [4-7) keV can be more readily identified and demonstrates the same relationship. If flare electrons detected in-situ are produced in, and/or transported through hot, over-dense regions close to HXR-emitting electrons, then this plasma signature should be present in their lower-energy spectra (1-20 keV), observable at varying heliospheric distances with missions such as Solar Orbiter.

Spatially Separated Electron and Proton Beams in a Simulated Solar Coronal Jet

Ross **Pallister**1, Peter F. Wyper2, David I. Pontin1,3, C. Richard DeVore4, and Federica Chiti1
2021 ApJ 923 163

https://iopscience.iop.org/article/10.3847/1538-4357/ac2e6d/pdf
https://doi.org/10.3847/1538-4357/ac2e6d
Magnetic reconnection is widely accepted to be a major contributor to nonthermal particle acceleration in the solar atmosphere. In this paper we investigate particle acceleration during the impulsive phase of a coronal jet, which involves bursty reconnection at a magnetic null point. A test-particle approach is employed, using electromagnetic fields from a magnetohydrodynamic simulation of such a jet. Protons and electrons are found to be accelerated nonthermally both downwards toward the domain's lower boundary and the solar photosphere, and outwards along the axis of the coronal jet and into the heliosphere. A key finding is that a circular ribbon of particle deposition on the photosphere is predicted, with the protons and electrons concentrated in different parts of the ribbon. Furthermore, the outgoing protons and electrons form two spatially separated beams parallel to the axis of the jet, signatures that may be observable in in-situ observations of the heliosphere.

Proton acceleration at tearing coronal null-point current sheets

R. **Pallister**1, D. I. Pontin1 and P. F. Wyper2
A&A 622, A207 (**2019**)
https://www.aanda.org/articles/aa/pdf/2019/02/aa34284-18.pdf
Context. Non-thermal particle acceleration in the solar corona is thought to constitute a substantial part of the energy budget of explosive events such as solar flares. One well-established mechanism of non-thermal acceleration is directly via fields in current sheets.
Aims. In this paper we study proton acceleration during “spine-fan reconnection” at a 3D magnetic null point. This type of reconnection has recently been implicated in some flares known as circular-ribbon flares. It has also recently been discovered that the reconnecting current sheet may undergo a non-linear tearing-type instability. This tearing leads to the formation of flux ropes and quasi-turbulent dynamics.
Methods. A predictor-corrector test particle code is used to model the trajectories of protons at different stages of sheet tearing: when the sheet is intact, just after the formation of the first major flux rope, and once the non-linear phase of the instability has become more fully developed. The fields for these proton trajectories were taken from snapshots of a 3D magnetohydrodynamics simulation treated as three static field geometries represented by interpolated grids. Acceleration in the intact current sheet is compared to earlier simulations of infinite static current sheets and then used as a control case with which to compare the later snapshots.
Results. Protons are found to be predominantly accelerated along the fan surface, especially in the absence of current sheet tearing. Most of the highest energy protons are accelerated in the main body of the current sheet, along the direction of strongest parallel electric field. A high energy tail is present in the kinetic energy distribution. After tearing commences, this direct acceleration no longer dominates and acceleration in the outflow regions makes a proportionally greater contribution. Sheet tearing appears overall to hinder the acceleration of protons in the fan plane, at least in the absence of time-dependent acceleration mechanisms. Some correlation is found between high energy protons and locations of flux ropes formed by the instability, but the nature of the link remains at present unclear.

Konus-Wind and Helicon-Coronas-F Observations of Solar Flares

V. D. **Pal'shin**, Yu. E. Charikov, R. L. Aptekar, S. V. Golenetskii, A. A. Kokomov, D. S. Svinkin, Z. Ya. Sokolova, M. V. Ulanov, D. D. Frederiks, A. E. Tsvetkova
Ge&Ae, 54, 943 (**2014**)
http://arxiv.org/pdf/1412.2015v1.pdf
https://link.springer.com/content/pdf/10.1134/S0016793214070093.pdf
Results of solar flare observations obtained in the Konus-Wind experiment from November, 1994 to December, 2013 and in the Helicon Coronas-F experiment during its operation from 2001 to 2005, are presented. For the periods indicated Konus-Wind detected in the trigger mode 834 solar flares, and Helicon-Coronas-F detected more than 300 solar flares.
A description of the instruments and data processing techniques are given. As an example, the analysis of the spectral evolution of the flares SOL**2012-11-08**T02:19 (M 1.7) and SOL**2002-03-10**T01:34 (C5.1) is made with the Konus-Wind data and the flare SOL**2003-10-26**T06:11 (X1.2) is analyzed in the 2.223 MeV deuterium line with the Helicon-Coronas-F data.

Embedding Ordinality to Binary Loss Function for Improving Solar Flare Forecasting

Chetraj **Pandey**, Anli Ji, Jinsu Hong, Rafal A. Angryk, Berkay Aydin
DSAA 2024 conference **2024**
https://arxiv.org/pdf/2408.11768
In this paper, we propose a novel loss function aimed at optimizing the binary flare prediction problem by embedding the intrinsic ordinal flare characteristics into the binary cross-entropy (BCE) loss function. This modification is intended to provide the model with better guidance based on the ordinal characteristics of the data and improve the overall performance of the models. For our experiments, we employ a ResNet34-based model with transfer learning to

predict ≥M-class flares by utilizing the shape-based features of magnetograms of active region (AR) patches spanning from −90◦ to +90◦ of solar longitude as our input data. We use a composite skill score (CSS) as our evaluation metric, which is calculated as the geometric mean of the True Skill Score (TSS) and the Heidke Skill Score (HSS) to rank and compare our models' performance. The primary contributions of this work are as follows: (i) We introduce a novel approach to encode ordinality into a binary loss function showing an application to solar flare prediction, (ii) We enhance solar flare forecasting by enabling flare predictions for each AR across the entire solar disk, without any longitudinal restrictions, and evaluate and compare performance. (iii) Our candidate model, optimized with the proposed loss function, shows an improvement of ∼7%, ∼4%, and ∼3% for AR patches within ±30◦, ±60◦, and ±90◦ of solar longitude, respectively in terms of CSS, when compared with standard BCE. Additionally, we demonstrate the ability to issue flare forecasts for ARs in near-limb regions (regions between ±60◦ to ±90◦) with a CSS=0.34 (TSS=0.50 and HSS=0.23), expanding the scope of AR-based models for solar flare prediction. This advances the reliability of solar flare forecasts, leading to more effective prediction capabilities.
substantial text overlap with arXiv:2406.11054

Advancing Solar Flare Prediction using Deep Learning with Active Region Patches

Chetraj **Pandey**, Temitope Adeyeha, Jinsu Hong, Rafal A. Angryk, Berkay Aydin
European Conference on Machine Learning and Principles and Practice of Knowledge Discovery in Databases, (ECML PKDD), **2024**
https://arxiv.org/pdf/2406.11054
In this paper, we introduce a novel methodology for leveraging shape-based characteristics of magnetograms of active region (AR) patches and provide a novel capability for predicting solar flares covering the entirety of the solar disk (AR patches spanning from -90◦ to +90◦ of solar longitude). We create three deep learning models: (i) ResNet34, (ii) MobileNet, and (iii) MobileViT to predict ≥M-class flares and assess the efficacy of these models across various ranges of solar longitude. Given the inherent imbalance in our data, we employ augmentation techniques alongside undersampling during the model training phase, while maintaining imbalanced partitions in the testing data for realistic evaluation. We use a composite skill score (CSS) as our evaluation metric, computed as the geometric mean of the True Skill Score (TSS) and the Heidke Skill Score (HSS) to rank and compare models. The primary contributions of this work are as follows: (i) We introduce a novel capability in solar flare prediction that allows predicting flares for each ARs throughout the solar disk and evaluate and compare the performance, (ii) Our candidate model (MobileNet) achieves a CSS=0.51 (TSS=0.60 and HSS=0.44), CSS=0.51 (TSS=0.59 and HSS=0.44), and CSS=0.48 (TSS=0.56 and HSS=0.40) for AR patches within ±30◦, ±60◦, ±90◦ of solar longitude respectively. Additionally, we demonstrate the ability to issue flare forecasts for ARs in near-limb regions (regions between ±60◦ to ±90 ◦) with a CSS=0.39 (TSS=0.48 and HSS=0.32), expanding the scope of AR-based models for solar flare prediction. This advancement opens new avenues for more reliable prediction of solar flares, thereby contributing to improved forecasting capabilities.

Unveiling the Potential of Deep Learning Models for Solar Flare Prediction in Near-Limb Regions

Chetraj **Pandey**, Rafal A. Angryk, Berkay Aydin
the 22nd International Conference on Machine Learning and Applications (ICMLA), **2023**
https://arxiv.org/pdf/2309.14483.pdf
This study aims to evaluate the performance of deep learning models in predicting ≥M-class solar flares with a prediction window of 24 hours, using hourly sampled full-disk line-of-sight (LoS) magnetogram images, particularly focusing on the often overlooked flare events corresponding to the near-limb regions (beyond ±70◦ of the solar disk). We trained three well-known deep learning architectures--AlexNet, VGG16, and ResNet34 using transfer learning and compared and evaluated the overall performance of our models using true skill statistics (TSS) and Heidke skill score (HSS) and computed recall scores to understand the prediction sensitivity in central and near-limb regions for both X- and M-class flares. The following points summarize the key findings of our study: (1) The highest overall performance was observed with the AlexNet-based model, which achieved an average TSS∼0.53 and HSS∼0.37; (2) Further, a spatial analysis of recall scores disclosed that for the near-limb events, the VGG16- and ResNet34-based models exhibited superior prediction sensitivity. The best results, however, were seen with the ResNet34-based model for the near-limb flares, where the average recall was approximately 0.59 (the recall for X- and M-class was 0.81 and 0.56 respectively) and (3) Our research findings demonstrate that our models are capable of discerning complex spatial patterns from full-disk magnetograms and exhibit skill in predicting solar flares, even in the vicinity of near-limb regions. This ability holds substantial importance for operational flare forecasting systems. **2013- 01-09**

Towards Interpretable Solar Flare Prediction with Attention-based Deep Neural Networks

Chetraj **Pandey**, Anli Ji, Rafal A. Angryk, Berkay Aydin
The 6th International Conference on Artificial Intelligence and Knowledge Engineering (AIKE), **2023**
https://arxiv.org/pdf/2309.04558.pdf

Solar flare prediction is a central problem in space weather forecasting and recent developments in machine learning and deep learning accelerated the adoption of complex models for data-driven solar flare forecasting. In this work, we developed an attention-based deep learning model as an improvement over the standard convolutional neural network (CNN) pipeline to perform full-disk binary flare predictions for the occurrence of ≥M1.0-class flares within the next 24 hours. For this task, we collected compressed images created from full-disk line-of-sight (LoS) magnetograms. We used data-augmented oversampling to address the class imbalance issue and used true skill statistic (TSS) and Heidke skill score (HSS) as the evaluation metrics. Furthermore, we interpreted our model by overlaying attention maps on input magnetograms and visualized the important regions focused on by the model that led to the eventual decision. The significant findings of this study are: (i) We successfully implemented an attention-based full-disk flare predictor ready for operational forecasting where the candidate model achieves an average TSS=0.54±0.03 and HSS=0.37±0.07. (ii) we demonstrated that our full-disk model can learn conspicuous features corresponding to active regions from full-disk magnetogram images, and (iii) our experimental evaluation suggests that our model can predict near-limb flares with adept skill and the predictions are based on relevant active regions (ARs) or AR characteristics from full-disk magnetograms. **13 May 2013**

Exploring Deep Learning for Full-disk Solar Flare Prediction with Empirical Insights from Guided Grad-CAM Explanations

Chetraj **Pandey**, Anli Ji, Trisha Nandakumar, Rafal A. Angryk, Berkay Aydin
the 10th IEEE International Conference On Data Science And Advanced Analytics (DSAA 2023) **2023**
https://arxiv.org/pdf/2308.15712.pdf
This study progresses solar flare prediction research by presenting a full-disk deep-learning model to forecast ≥M-class solar flares and evaluating its efficacy on both central (within ±70∘) and near-limb (beyond ±70∘) events, showcasing qualitative assessment of post hoc explanations for the model's predictions, and providing empirical findings from human-centered quantitative assessments of these explanations. Our model is trained using hourly full-disk line-of-sight magnetogram images to predict ≥M-class solar flares within the subsequent 24-hour prediction window. Additionally, we apply the Guided Gradient-weighted Class Activation Mapping (Guided Grad-CAM) attribution method to interpret our model's predictions and evaluate the explanations. Our analysis unveils that full-disk solar flare predictions correspond with active region characteristics. The following points represent the most important findings of our study: (1) Our deep learning models achieved an average true skill statistic (TSS) of ∼0.51 and a Heidke skill score (HSS) of ∼0.38, exhibiting skill to predict solar flares where for central locations the average recall is ∼0.75 (recall values for X- and M-class are 0.95 and 0.73 respectively) and for the near-limb flares the average recall is ∼0.52 (recall values for X- and M-class are 0.74 and 0.50 respectively); (2) qualitative examination of the model's explanations reveals that it discerns and leverages features linked to active regions in both central and near-limb locations within full-disk magnetograms to produce respective predictions. In essence, our models grasp the shape and texture-based properties of flaring active regions, even in proximity to limb areas -- a novel and essential capability with considerable significance for operational forecasting systems.

Explainable Deep Learning-based Solar Flare Prediction with post hoc Attention for Operational Forecasting

Chetraj **Pandey**, Rafal A. Angryk, Manolis K. Georgoulis, Berkay Aydin
the 26th International Conference on Discovery Science (DS2023) **2023**
https://arxiv.org/pdf/2308.02682.pdf
This paper presents a post hoc analysis of a deep learning-based full-disk solar flare prediction model. We used hourly full-disk line-of-sight magnetogram images and selected binary prediction mode to predict the occurrence of ≥M1.0-class flares within 24 hours. We leveraged custom data augmentation and sample weighting to counter the inherent class-imbalance problem and used true skill statistic and Heidke skill score as evaluation metrics. Recent advancements in gradient-based attention methods allow us to interpret models by sending gradient signals to assign the burden of the decision on the input features. We interpret our model using three post hoc attention methods: (i) Guided Gradient-weighted Class Activation Mapping, (ii) Deep Shapley Additive Explanations, and (iii) Integrated Gradients. Our analysis shows that full-disk predictions of solar flares align with characteristics related to the active regions. The key findings of this study are: (1) We demonstrate that our full disk model can tangibly locate and predict near-limb solar flares, which is a critical feature for operational flare forecasting, (2) Our candidate model achieves an average TSS=0.51±0.05 and HSS=0.38±0.08, and (3) Our evaluation suggests that these models can learn conspicuous features corresponding to active regions from full-disk magnetograms. : **2014-01-05, 2011-09-22**

Explaining Full-disk Deep Learning Model for Solar Flare Prediction using Attribution Methods

Chetraj **Pandey**, Rafal A. Angryk, Berkay Aydin

Preprint accepted at European Conference on Machine Learning and Principles and Practice of Knowledge Discovery in Databases (ECML-PKDD) **2023**
https://arxiv.org/pdf/2307.15878.pdf
This paper contributes to the growing body of research on deep learning methods for solar flare prediction, primarily focusing on highly overlooked near-limb flares and utilizing the attribution methods to provide a post hoc qualitative explanation of the model's predictions. We present a solar flare prediction model, which is trained using hourly full-disk line-of-sight magnetogram images and employs a binary prediction mode to forecast ≥M-class flares that may occur within the following 24-hour period. To address the class imbalance, we employ a fusion of data augmentation and class weighting techniques; and evaluate the overall performance of our model using the true skill statistic (TSS) and Heidke skill score (HSS). Moreover, we applied three attribution methods, namely Guided Gradient-weighted Class Activation Mapping, Integrated Gradients, and Deep Shapley Additive Explanations, to interpret and cross-validate our model's predictions with the explanations. Our analysis revealed that full-disk prediction of solar flares aligns with characteristics related to active regions (ARs). In particular, the key findings of this study are: (1) our deep learning models achieved an average TSS=0.51 and HSS=0.35, and the results further demonstrate a competent capability to predict near-limb solar flares and (2) the qualitative analysis of the model explanation indicates that our model identifies and uses features associated with ARs in central and near-limb locations from full-disk magnetograms to make corresponding predictions. In other words, our models learn the shape and texture-based characteristics of flaring ARs even at near-limb areas, which is a novel and critical capability with significant implications for operational forecasting.

Towards coupling full-disk and active region-based flare prediction for operational space weather forecasting.

Pandey C, Ji A, Angryk RA, Georgoulis MK and Aydin B
(**2022**) Front. Astron. Space Sci. 9: 897301.
https://www.frontiersin.org/articles/10.3389/fspas.2022.897301/pdf
https://arxiv.org/pdf/2209.07406
Solar flare prediction is a central problem in space weather forecasting and has captivated the attention of a wide spectrum of researchers due to recent advances in both remote sensing as well as machine learning and deep learning approaches. The experimental findings based on both machine and deep learning models reveal significant performance improvements for task specific datasets. Along with building models, the practice of deploying such models to production environments under operational settings is a more complex and often time-consuming process which is often not addressed directly in research settings. We present a set of new heuristic approaches to train and deploy an operational solar flare prediction system for ≥M1.0-class flares with two prediction modes: full-disk and active region-based. In full-disk mode, predictions are performed on full-disk line-of-sight magnetograms using deep learning models whereas in active region-based models, predictions are issued for each active region individually using multivariate time series data instances. The outputs from individual active region forecasts and full-disk predictors are combined to a final full-disk prediction result with a meta-model. We utilized an equal weighted average ensemble of two base learners' flare probabilities as our baseline meta learner and improved the capabilities of our two base learners by training a logistic regression model. The major findings of this study are: 1) We successfully coupled two heterogeneous flare prediction models trained with different datasets and model architecture to predict a full-disk flare probability for next 24 h, 2) Our proposed ensembling model, i.e., logistic regression, improves on the predictive performance of two base learners and the baseline meta learner measured in terms of two widely used metrics True Skill Statistic (TSS) and Heidke Skill Score (HSS), and 3) Our result analysis suggests that the logistic regression-based ensemble (Meta-FP) improves on the full-disk model (base learner) by ∼9% in terms TSS and ∼10% in terms of HSS. Similarly, it improves on the AR-based model (base learner) by ∼17% and ∼20% in terms of TSS and HSS respectively. Finally, when compared to the baseline meta model, it improves on TSS by ∼10% and HSS by ∼15%.

Destabilization of a Solar Prominence/Filament Field System by a Series of Eight Homologous Eruptive Flares

Navdeep K. **Panesar**, Alphonse C. Sterling, Davina E. Innes, Ronald L. Moore
ApJ **811** 5 **2015**
http://arxiv.org/pdf/1508.01952v1.pdf
Homologous flares are flares that occur repetitively in the same active region, with similar structure and morphology. A series of at least eight homologous flares occurred in active region NOAA 11237 over **16 - 17 June 2011**. A nearby prominence/filament was rooted in the active region, and situated near the bottom of a coronal cavity. The active region was on the southeast solar limb as seen from SDO/AIA, and on the disk as viewed from STEREO/EUVI-B. The dual perspective allows us to study in detail behavior of the prominence/filament material entrained in the magnetic field of the repeatedly-erupting system. Each of the eruptions was mainly confined, but expelled hot material into the prominence/filament cavity system (PFCS). The field carrying and containing the ejected hot material interacted with the PFCS and caused it to inflate, resulting in a step-wise rise of the PFCS approximately in step with the homologous eruptions. The eighth eruption triggered the PFCS to move outward slowly, accompanied by a weak coronal dimming. As this slow PFCS eruption was underway, a final ejective flare occurred in the core of the active region, resulting in

strong dimming in the EUVI-B images and expulsion of a coronal mass ejection (CME). A plausible scenario is that the repeated homologous flares could have gradually destabilized the PFCS, and its subsequent eruption removed field above the acitive region and in turn led to the ejective flare, strong dimming, and CME.

Multilayer Mirror Based High-Resolution Solar Soft X-Ray Spectrometer

S. S. **Panini**1*, S. Narendranath2*, P. Sreekumar3 and K. Sankarasubramanian2
Front. Astron. Space Sci., **2021** |
https://www.frontiersin.org/articles/10.3389/fspas.2021.647828/full
https://www.frontiersin.org/articles/10.3389/fspas.2021.647828/pdf https://doi.org/10.3389/fspas.2021.647828
Soft X-ray spectroscopy of the Sun is an important tool to understand the coronal dynamics and composition. The solar coronal X-ray spectrum below 1 keV is the least explored with high-resolution spectroscopy. Recent observations with Hinode XRT using coarse spectroscopy along with high-resolution imaging have shown that abundances in the coronae have variability associated with structures on the Sun. Disk averaged abundances with better spectral resolution spectrometers show time variability associated with flares. Both spatial and temporal variabilities seem to be related to changes in the magnetic field topology. Understanding such short term variabilities is necessary to model the underlying dynamics and mixing of material between different layers of the Sun. A Sensitive high-resolution spectrometer that covers the range in plasma temperatures and emission line complexes would uniquely reveal the entire evolution of flares. We are investigating a design of a multi-layer mirror-based X-ray spectrograph in the spectral range from 0.5 to 7 keV. The instrument operates in four asynchronous spectral channels operating one at a time. The multi-layer mirror placed at the focus of a Wolter type I telescope reflects a narrow band X-rays to the CCD which is placed at Nasmyth defocus. Converging X-rays from the front end optics helps to increase the spectral range of each channel while preserving the spectral resolution. This design is estimated to achieve a spectral resolution of 20 eV in the spectral range of 0.5–7 keV. With such high spectral resolution, we can resolve individual spectral features e.g., 6.7 keV Fe complex which can be used to diagnose high-temperature transient plasma during flares. The instrument design estimated performance and the science capabilities of this instrument will be discussed in detail in the paper.

Identifying preflare spectral features using explainable artificial intelligence

Brandon **Panos**, Lucia Kleint, Jonas Zbinden
A&A 671, A73 **2023**
https://arxiv.org/pdf/2301.01560.pdf
https://doi.org/10.1051/0004-6361/202244835
https://www.aanda.org/articles/aa/pdf/2023/03/aa44835-22.pdf
The prediction of solar flares is of practical and scientific interest; however, many machine learning methods used for this prediction task do not provide the physical explanations behind a model's performance. We made use of two recently developed explainable artificial intelligence techniques called gradient-weighted class activation mapping (Grad-CAM) and expected gradients (EG) to reveal the decision-making process behind a high-performance neural network that has been trained to distinguish between MgII spectra derived from flaring and nonflaring active regions, a fact that can be applied to the task of short timescale flare forecasting. The two techniques generate visual explanations (heatmaps) that can be projected back onto the spectra, allowing for the identification of features that are strongly associated with precursory flare activity. We automated the search for explainable interpretations on the level of individual wavelengths, and provide multiple examples of flare prediction using IRIS spectral data, finding that prediction scores in general increase before flare onset. Large IRIS rasters that cover a significant portion of the active region and coincide with small preflare brightenings both in IRIS and SDO/AIA images tend to lead to better forecasts. The models reveal that MgII triplet emission, flows, as well as broad and highly asymmetric spectra are all important for the task of flare prediction. Additionally, we find that intensity is only weakly correlated to a spectrum's prediction score, meaning that low intensity spectra can still be of great importance for the flare prediction task, and that 78% of the time, the position of the model's maximum attention along the slit during the preflare phase is predictive of the location of the flare's maximum UV emission. **2014-02-12, 2014-06-11, 2015-03-11, 2015-06-22**

Exploring mutual information between IRIS spectral lines. II. Calculating the most probable response in all spectral windows

Brandon **Panos**, Lucia Kleint
2021 *ApJ* **915** 77
https://arxiv.org/pdf/2106.03463.pdf
https://iopscience.iop.org/article/10.3847/1538-4357/ac00c0/pdf
https://doi.org/10.3847/1538-4357/ac00c0
A three-dimensional picture of the solar atmosphere's thermodynamics can be obtained by jointly analyzing multiple spectral lines that span many formation heights. In paper I, we found strong correlations between spectral shapes from a variety of different ions during solar flares in comparison to the quiet Sun. We extend these techniques to address the following questions: which regions of the solar atmosphere are most connected during a solar flare, and what are the most likely responses across several spectral windows based on the observation of a single Mg II spectrum? Our models

are derived from several million IRIS spectra collected from 21 M- and X-class flares. We applied this framework to archetypal Mg II flare spectra, and analyzed the results from a multi-line perspective. We find that (1) the line correlations from the photosphere to the transition region are highest in flare ribbons. (2) Blue-shifted reversals appear simultaneously in Mg II, C II, and Si IV during the impulsive phase, with Si IV displaying possible optical depth effects. Fe II shows signs of strong emission, indicating deep early heating. (3) The Mg II line appears to typically evolve a blue-shifted reversal that later returns to line center and becomes single peaked within 1-3 minutes. The widths of these single peaked profiles slowly erode with time. During the later flare stages, strong red wing enhancements indicating coronal rain are evident in Mg II, C II, and Si IV. Our framework is easily adaptable to any multi-line data set, and enables comprehensive statistical analyses of the atmospheric behavior in different spectral windows. **29 Mar 2014, 10 Sep 2014, 27 Oct 2014, 15 Jun 2015, 22 Jun 2015**
TABLE 1 Flare observations (2014-2015)

Exploring mutual information between IRIS spectral lines. I. Correlations between spectral lines during solar flares and within the quiet Sun

Brandon **Panos**, Lucia Kleint, Sviatoslav Voloshynovskiy
2021 *ApJ* **912** 121
https://arxiv.org/pdf/2104.12161.pdf
https://iopscience.iop.org/article/10.3847/1538-4357/abf11b/pdf
https://doi.org/10.3847/1538-4357/abf11b
Spectral lines allow us to probe the thermodynamics of the solar atmosphere, but the shape of a single spectral line may be similar for different thermodynamic solutions. Multiline analyses are therefore crucial, but computationally cumbersome. We investigate correlations between several chromospheric and transition region lines to restrain the thermodynamic solutions of the solar atmosphere during flares. We used machine-learning methods to capture the statistical dependencies between 6 spectral lines sourced from 21 large solar flares observed by NASA's Interface Region Imaging Spectrograph (IRIS). The techniques are based on an information-theoretic quantity called mutual information (MI), which captures both linear and nonlinear correlations between spectral lines. The MI is estimated using both a categorical and numeric method, and performed separately for a collection of quiet Sun and flaring observations. Both approaches return consistent results, indicating weak correlations between spectral lines under quiet Sun conditions, and substantially enhanced correlations under flaring conditions, with some line-pairs such as Mg II and C II having a normalized MI score as high as 0.5. We find that certain spectral lines couple more readily than others, indicating a coherence in the solar atmosphere over many scale heights during flares, and that all line-pairs are correlated to the GOES derivative, indicating a positive relationship between correlation strength and energy input. Our methods provide a highly stable and flexible framework for quantifying dependencies between the physical quantities of the solar atmosphere, allowing us to obtain a three-dimensional picture of its state.
TABLE 2 Flare observations 2014-2015

Real-time flare prediction based on distinctions between flaring and non-flaring active region spectra

Brandon **Panos**, Lucia Kleint
2020 *ApJ* **891** 17
https://arxiv.org/pdf/1911.12621.pdf
https://doi.org/10.3847/1538-4357/ab700b
With machine learning entering into the awareness of the heliophysics community, solar flare prediction has become a topic of increased interest. Although machine learning models have advanced with each successive publication, the input data has remained largely fixed on magnetic features. Despite this increased model complexity, results seem to indicate that photospheric magnetic field data alone may not be a wholly sufficient source of data for flare prediction. For the first time we have extended the study of flare prediction to spectral data. In this work, we use Deep Neural Networks to monitor the changes of several features derived from the strong resonant Mg II h&k lines observed by IRIS. The features in descending order of predictive capability are: The triplet emission at 2798.77 Å, line core intensity, total continuum emission between the h&k line cores, the k/h ratio, line-width, followed by several other line features such as asymmetry and line center. Regions that are about to flare generate spectra which are distinguishable from non-flaring active region spectra. Our algorithm can correctly identify pre-flare spectra approximately 35 minutes before the start of the flare, with an 80% accuracy, precision and recall. This accuracy monotonically increases to 90% as we move closer in time to the start of the flare. Our study indicates that spectral data alone can lead to good predictive models and should be considered as an additional source of information alongside photospheric magnetograms.

Identifying Typical Mg ii Flare Spectra Using Machine Learning

Brandon **Panos**1,2, Lucia Kleint1,3, Cedric Huwyler1, Säm Krucker1,4, Martin Melchior1,
2018 ApJ 861 62
http://sci-hub.tw/10.3847/1538-4357/aac779

The Interface Region Imaging Spectrograph (IRIS) performs solar observations over a large range of atmospheric heights, including the chromosphere where the majority of flare energy is dissipated. The strong Mg ii h&k spectral lines are capable of providing excellent atmospheric diagnostics, but have not been fully utilized for flaring atmospheres. We aim to investigate whether the physics of the chromosphere is identical for all flare observations by analyzing if there are certain spectra that occur in all flares. To achieve this, we automatically analyze hundreds of thousands of Mg ii h&k-line profiles from a set of 33 flares and use a machine learning technique, which we call supervised hierarchical k-means, to cluster all profile shapes. We identify a single peaked Mg ii profile, in contrast to the double-peaked quiet Sun profiles, appearing in every flare. Additionally, we find extremely broad profiles with characteristic blueshifted central reversals appearing at the front of fast-moving flare ribbons. These profiles occur during the impulsive phase of the flare, and we present results of their temporal and spatial correlation with non-thermal hard X-ray signatures, suggesting that flare-accelerated electrons play an important role in the formation of these profiles. The ratio of the integrated Mg ii h&k lines can also serve as an opacity diagnostic, and we find higher opacities during each flare maximum. Our study shows that machine learning is a powerful tool for large scale statistical solar analyses.

First Imaging Observation of Standing Slow Wave in Coronal Fan loops

V. **Pant**, A. Tiwari, D. Yuan, D. Banerjee

ApJL **2017**

https://arxiv.org/pdf/1708.06946.pdf

We observe intensity oscillations along coronal fan loops associated with the active region AR 11428. The intensity oscillations were triggered by blast waves which were generated due to X-class flares in the distant active region AR 11429. To characterise the nature of oscillations, we created time-distance maps along the fan loops and noted that the intensity oscillations at two ends of the loops were out of phase. As we move along the fan loop, the amplitude of the oscillations first decreased and then increased. The out-of-phase nature together with the amplitude variation along the loop implies that these oscillations are very likely to be standing waves. The period of the oscillations are estimated to be ∼27 min, damping time to be ∼45 min and phase velocity projected in the plane of sky ∼ 65-83 km s−1. The projected phase speeds were in the range of acoustic speed of coronal plasma at about 0.6 MK which further indicates that these are slow waves. To best of our knowledge, this is the first report on the existence of the standing slow waves in non-flaring fan loops. **2012 March 7**

Spectroscopy of Very Hot Plasma in Non-flaring Parts of a Solar Limb Active Region: Spatial and Temporal Properties

Susanna **Parenti**1, Giulio del Zanna2, Antonino Petralia3, Fabio Reale3,4, Luca Teriaca5, Paola Testa6, and Helen E. Mason

2017 ApJ 846 25

In this work we investigate the thermal structure of an off-limb active region (AR) in various non-flaring areas, as it provides key information on the way these structures are heated. In particular, we concentrate on the very hot component (>3 MK) as it is a crucial element to distinguish between different heating mechanisms. We present an analysis using Fe and Ca emission lines from both the Solar Ultraviolet Measurement of Emitted Radiation (SUMER) on board the Solar and Heliospheric Observatory (SOHO) and the EUV Imaging Spectrometer (EIS) on board Hinode. A data set covering all ionization stages from Fe x to Fe xix has been used for the thermal analysis (both differential emission measure and emission measure, EM). Ca xiv is used for the SUMER-EIS radiometric cross calibration. We show that the very hot plasma is present and persistent almost everywhere in the core of the limb AR. The off-limb AR is clearly structured in Fe xviii. Almost everywhere, the EM analysis reveals plasma at 10 MK (visible in Fe xix emission), which is down to 0.1% of EM of the main 3 MK plasma. We estimate the power-law index of the hot tail of the EM to be between −8.5 and −4.4. However, the question about the possible existence of a small minor peak at around 10 MK remains open. The absence in some part of the AR of the Fe xix and Fe xxiii lines (which fall into our spectral range) enables us to determine an upper limit on the EM at these temperatures. Our results include a new Ca xiv943.59 Å atomic model.

Hinode/EIS Nugget May 2018 http://solarb.mssl.ucl.ac.uk/SolarB/nuggets/nugget_2018may.jsp

Post-flare evolution of AR 10923 with Hinode/XRT

S. **Parenti**, F. Reale and K. K. Reeves

A&A 517, A41 (**2010**)

Context. Flares are dynamic events which involve rapid changes in coronal magnetic topology end energy release. Even if they may be localized phenomena, the magnetic disturbance at their origin may propagate and be effective in a larger part of the active region.

Aims. We investigate the temporal evolution of a flaring active region with respect to the loops morphology, the temperature, and emission measure distributions.

Methods. We consider Hinode/XRT data of a the **2006 November 12th C1.1 flare**. We inspect the evolution of the morphology of the flaring region also with the aid of TRACE data. XRT filter ratios are used to derive temperature and emission measure maps and evolution.
Results. The analyzed flare includes several brightenings. We identify a coherent sequence of tangled and relaxed loop structures before, during, and after the brightenings. Although the thermal information is incomplete because of pixel saturation at the flare peak, thermal maps show fine, evolving spatial structuring. Temperature and emission measure variations show up in great detail, and we are able to detect a secondary heating of larger loops close to the proper flaring region. Finally we estimate the amount of energy released in these flaring loops during the flare decay.

THREE-DIMENSIONAL MODELING OF QUASI-HOMOLOGOUS SOLAR JETS

E. **Pariat**1, S. K. Antiochos2, and C. R. DeVore3
Astrophysical Journal, 714:1762–1778, **2010** May
Recent solar observations (e.g., obtained with *Hinode* and *STEREO*) have revealed that coronal jets are a more frequent phenomenon than previously believed. This higher frequency results, in part, from the fact that jets exhibit a homologous behavior: successive jets recur at the same location with similar morphological features. We present the results of three-dimensional (3D) numerical simulations of our model for coronal jets. This study demonstrates the ability of the model to generate recurrent 3D untwisting quasi-homologous jets when a stress is constantly applied at the photospheric boundary. The homology results from the property of the 3D nullpoint system to relax to a state topologically similar to its initial configuration. In addition, we find two distinct regimes of reconnection in the simulations: an impulsive 3D mode involving a helical rotating current sheet that generates the jet and a quasi-steady mode that occurs in a 2D-like current sheet located along the fan between the sheared spines. We argue that these different regimes can explain the observed link between jets and plumes.

CURRENT BUILDUP IN EMERGING SERPENTINE FLUX TUBES

E. **Pariat**1,3, S. Masson2, and G. Aulanier2
Astrophysical Journal, 701:1911–1921, **2009** August
The increase of magnetic flux in the solar atmosphere during active-region formation involves the transport of the magnetic field from the solar convection zone through the lowest layers of the solar atmosphere, through which the plasma β changes from > 1 to < 1 with altitude. The crossing of this magnetic transition zone requires the magnetic field to adopt a serpentine shape also known as the sea-serpent topology. In the frame of the resistive flux-emergence model, the rising of the magnetic flux is believed to be dynamically driven by a succession of magnetic reconnections which are commonly observed in emerging flux regions as Ellerman bombs. Using a data-driven, three-dimensional (3D) magnetohydrodynamic numerical simulation of flux emergence occurring in active region 10191 on 2002 November 16–17, we study the development of 3D electric current sheets. We show that these currents buildup along the 3D serpentine magnetic-field structure as a result of photospheric diverging horizontal line-tied motions that emulate the observed photospheric evolution. We observe that reconnection can not only develop following a pinching evolution of the serpentine field line, as usually assumed in two-dimensional geometry, but can also result from 3D shearing deformation of the magnetic structure. In addition, we report for the first time on the observation in the UV domain with the *Transition Region and Coronal Explorer* (*TRACE*) of extremely transient loop-like features, appearing within the emerging flux domain, which link several Ellermam bombs with one another. We argue that these loop transients can be explained as a consequence of the currents that build up along the serpentine magnetic field.

A Model for Solar Polar Jets

E. **Pariat**, S. K. Antiochos & C. R. DeVore
E-print, Oct **2008**
http://solar.physics.montana.edu/cgi-bin/eprint/index.pl?entry=8566
We propose a model for the jetting activity that is commonly observed in the Sun's corona, especially in the open-field regions of polar coronal holes. Magnetic reconnection is the process driving the jets and a relevant magnetic configuration is the well known null-point and fan-separatrix topology. The primary challenge in explaining the observations is that reconnection must occur in a short-duration energetic burst, rather than quasi-continuously as is implied by the observations of long-lived structures in coronal holes, such as polar plumes. The key idea underlying our model for jets is that reconnection is forbidden for an axisymmetric null-point topology. Consequently, by imposing a twisting motion that maintains the axisymmetry, magnetic stress can be built up to high levels until an ideal instability breaks the symmetry and leads to an explosive release of energy via reconnection. Using three-dimensional magnetohydrodynamic simulations, we demonstrate that this mechanism does produce massive, high-speed jets driven by nonlinear Alfv'en waves. We discuss the implications of our results for observations of the solar corona.

Magnetic Helicity Flux across Solar Active Region Photospheres: II. Association of Hemispheric Sign Preference with Flaring Activity during Solar Cycle 24

Sung-Hong **Park**, K. D. Leka, Kanya Kusano

ApJ **2021**

https://arxiv.org/pdf/2102.13331.pdf

In our earlier study of this series (Park et al. 2020, Paper I), we examined the hemispheric sign preference (HSP) of magnetic helicity flux dH/dt across photospheric surfaces of 4802 samples of 1105 unique active regions (ARs) observed during solar cycle 24. Here, we investigate any association of the HSP, expressed as a degree of compliance, with flaring activity, analyzing the same set of dH/dt estimates as used in Paper I. The AR samples under investigation are assigned to heliographic regions (HRs) defined in the Carrington longitude-latitude plane with a grid spacing of 45◦ in longitude and 15◦ in latitude. For AR samples in each of the defined HRs, we calculate the degree of HSP compliance and the average soft X-ray flare index. The strongest flaring activity is found to be in one distinctive HR with an extremely low HSP compliance of 41% as compared to the mean and standard deviation of 62% and 7%, respectively, over all HRs. This sole HR shows an anti-HSP (i.e., less than 50%) and includes the highly flare-productive AR NOAA 12673, however this AR is not uniquely responsible for the HR's low HSP. We also find that all HRs with the highest flaring activity are located in the southern hemisphere, and they tend to have lower degrees of HSP compliance. These findings point to the presence of localized regions of the convection zone with enhanced turbulence, imparting a greater magnetic complexity and a higher flaring rate to some rising magnetic flux tubes.

A Comparison of Flare Forecasting Methods. IV. Evaluating Consecutive-Day Forecasting Patterns

Sung-Hong **Park**, K. D. Leka, Kanya Kusano, Jesse Andries, Graham Barnes, Suzy Bingham, D. Shaun Bloomfield, Aoife E. McCloskey, Veronique Delouille, David Falconer, Peter T. Gallagher, Manolis K. Georgoulis, Yuki Kubo, Kangjin Lee, Sangwoo Lee, Vasily Lobzin, JunChul Mun, Sophie A. Murray, Tarek A. M. Hamad Nageem, Rami Qahwaji, Michael Sharpe, Rob A. Steenburgh, Graham Steward, Michael Terkildsen

ApJ **890** 124 **2020**

https://arxiv.org/pdf/2001.02808.pdf

https://doi.org/10.3847/1538-4357/ab65f0

sci-hub.tw/10.3847/1538-4357/ab65f0

A crucial challenge to successful flare prediction is forecasting periods that transition between "flare-quiet" and "flare-active". Building on earlier studies in this series (Barnes et al. 2016; Leka et al. 2019a,b) in which we describe methodology, details, and results of flare forecasting comparison efforts, we focus here on patterns of forecast outcomes (success and failure) over multi-day periods. A novel analysis is developed to evaluate forecasting success in the context of catching the first event of flare-active periods, and conversely, of correctly predicting declining flare activity. We demonstrate these evaluation methods graphically and quantitatively as they provide both quick comparative evaluations and options for detailed analysis. For the testing interval 2016-2017, we determine the relative frequency distribution of two-day dichotomous forecast outcomes for three different event histories (i.e., event/event, no-event/event and event/no-event), and use it to highlight performance differences between forecasting methods. A trend is identified across all forecasting methods that a high/low forecast probability on day-1 remains high/low on day-2 even though flaring activity is transitioning. For M-class and larger flares, we find that explicitly including persistence or prior flare history in computing forecasts helps to improve overall forecast performance. It is also found that using magnetic/modern data leads to improvement in catching the first-event/first-no-event transitions. Finally, 15% of major (i.e., M-class or above) flare days over the testing interval were effectively missed due to a lack of observations from instruments away from the Earth-Sun line. **2016-01-01, 2016-08-07, 2017-07-03, 2017-10-20**

Application of the Deep Convolutional Neural Network to the Forecast of Solar Flare Occurrence Using Full-disk Solar Magnetograms

Eunsu **Park**, Yong-Jae Moon, Seulki Shin, Kangwoo Yi, Daye Lim, Harim Lee, and Gyungin Shin

2018 ApJ 869 91

sci-hub.tw/10.3847/1538-4357/aaed40

In this study, we present the application of the Convolutional Neural Network (CNN) to the forecast of solar flare occurrence. For this, we consider three CNN models (two pretrained models, AlexNet and GoogLeNet, and one newly proposed model). Our inputs are SOHO/Michelson Doppler Imager (from 1996 May to 2010 December) and SDO/Helioseismic and Magnetic Imager (from 2011 January to 2017 June) full-disk magnetograms at 00:00 UT. Model outputs are the "Yes or No" of daily flare occurrence (C, M, and X classes) and they are compared with GOESobservations. We train the models using the input data and observations from 1996 to 2008, covering the entire solar cycle 23, and test them using the data sets from 2009 to 2017, covering solar cycle 24. Then we compare the results of the CNN models with those of three previous flare forecast models in view of statistical scores. The major

results from this study are as follows. First, we successfully apply CNN to the full-disk solar magnetograms without any preprocessing or feature extraction. Second, the results of our CNN models are slightly better in Heidke skill score and true skill statistics, and considerably better in false alarm ratio (FAR) and critical success index than the previous solar flare forecasting models. Third, our proposed model has better values of all statistical scores except for FAR, than the other two pretrained models. Our results indicate a sufficient possibility that deep learning methods can improve the capability of the solar flare forecast as well as similar types of forecast problems.

Photospheric Shear Flows in Solar Active Regions and Their Relation to Flare Occurrence

Sung-Hong **Park**, Jordan A. Guerra, Peter T. Gallagher, Manolis K. Georgoulis, D. Shaun Bloomfield
Solar Phys. 293:114 **2018**
https://arxiv.org/pdf/1807.07714.pdf
http://sci-hub.tw/https://link.springer.com/article/10.1007/s11207-018-1336-z
Solar active regions (ARs) that produce major flares typically exhibit strong plasma shear flows around photospheric magnetic polarity inversion lines (MPILs). It is therefore important to quantitatively measure such photospheric shear flows in ARs for a better understanding of their relation to flare occurrence. Photospheric flow fields were determined by applying the Differential Affine Velocity Estimator for Vector Magnetograms (DAVE4VM) method to a large data set of 2,548 co-aligned pairs of AR vector magnetograms with 12-min separation over the period 2012-2016. From each AR flow-field map, three shear-flow parameters were derived corresponding to the mean (<S>), maximum (S_max) and integral (S_sum) shear-flow speeds along strong-gradient, strong-field MPIL segments. We calculated flaring rates within 24 hr as a function of each shear-flow parameter, and also investigated the relation between the parameters and the waiting time ({\tau}) until the next major flare (class M1.0 or above) after the parameter observation. In general, it is found that the larger S_sum an AR has, the more likely it is for the AR to produce flares within 24 hr. It is also found that among ARs which produce major flares, if one has a larger value of S_sum then {\tau} generally gets shorter. These results suggest that large ARs with widespread and/or strong shear flows along MPILs tend to not only be more flare productive, but also produce major flares within 24 hr or less. **26 September 2015**

Study of Magnetic Helicity Injection in the Active Regions NOAA 9236 Producing Multiple Flare-associated CME Events

Sung-Hong **Park**, Kanya Kusano, Kyung-Suk Cho, Jongchul Chae, Su-Chan Bong, Pankaj Kumar, So-Young Park, Yeon-Han Kim, Young-Deuk Park
E-print, Aug **2013**; ApJ
To better understand a preferred magnetic field configuration and its evolution during Coronal Mass Ejection events, we investigated the spatial and temporal evolution of photospheric magnetic fields in the active region NOAA 9236 that produced eight flare-associated CMEs during the time period of **2000 November 23-26**. The time variations of the total magnetic helicity injection rate and the total unsigned magnetic flux are determined and examined not only in the entire active region but also in some local regions such as the main sunspots and the CME-associated flaring regions using SOHO/MDI magnetogram data. As a result, we found that: (1) in the sunspots, a large amount of postive (right-handed) magnetic helicity was injected during most of the examined time period, (2) in the flare region, there was a continuous injection of negative (left-handed) magnetic helicity during the entire period, accompanied by a large increase of the unsigned magnetic flux, and (3) the flaring regions were mainly composed of emerging bipoles of magnetic fragments in which magnetic field lines have substantially favorable conditions for making reconnection with large-scale, overlying, and oppositely directed magnetic field lines connecting the main sunspots. These observational findings can also be well explained by some MHD numerical simulations for CME initiation (e.g., reconnection-favored emerging flux models). We therefore conclude that reconnection-favored magnetic fields in the flaring emerging flux regions play a crucial role in producing the multiple flare-associated CMEs in NOAA 9236.

PARTICLE-IN-CELL SIMULATIONS OF PARTICLE ENERGIZATION VIA SHOCK DRIFT ACCELERATION FROM LOW MACH NUMBER QUASI-PERPENDICULAR SHOCKS IN SOLAR FLARES

Jaehong **Park**1,2, Chuang Ren1,2,3, Jared C. Workman1,4, and Eric G. Blackman
2013 ApJ 765 147
Low Mach number, high beta fast mode shocks can occur in the magnetic reconnection outflows of solar flares. These shocks, which occur above flare loop tops, may provide the electron energization responsible for some of the observed hard X-rays and contemporaneous radio emission. Here we present new two-dimensional particle-in-cell simulations of low Mach number/high beta quasi-perpendicular shocks. The simulations show that electrons above a certain energy threshold experience shock-drift-acceleration. The transition energy between the thermal and non-thermal spectrum and the spectral index from the simulations are consistent with some of the X-ray spectra from RHESSI in the energy regime of E 40 ~ 100 keV. Plasma instabilities associated with the shock structure such as the modified-two-stream and the electron whistler instabilities are identified using numerical solutions of the kinetic dispersion relations. We also

show that the results from PIC simulations with reduced ion/electron mass ratio can be scaled to those with the realistic mass ratio.

Radio Emission from Masuda Sources

S.-H. **Park** and G.D. Fleishman

BBSO preprint #1440, **2010,** Solar Phys (2010) 266: 323–335

We note that different models, providing comparably good interpretation of the hard X-ray properties of so-called Masuda sources, can make distinctly different predictions for the radio emission produced at the Masuda source by the same population of accelerated electrons. Accordingly, we calculate the radio emission within a few competing models, *i.e.*, those involving magnetic, turbulent, and collisional trapping of the fast electrons in the coronal source. We show that even available incomplete radio observations of the classical Masuda event and a Masuda-like event on **31 December 2007**, recently reported by Krucker *et al*. (*Astrophys. J*. 714, 1108, 2010) are highly valuable in restricting the physical model of the source. Furthermore, our study proposes that combination of more complete high resolution X-ray and radio observations can allow unambiguous distinction between the competing Masuda source models.

STUDY OF MAGNETIC HELICITY IN SOLAR ACTIVE REGIONS AND ITS RELATIONSHIP WITH SOLAR ERUPTIONS

Sung-Hong **Park**

Thesis, **2010, File**

http://solar.njit.edu/SolarPhDStudents.htm

It is generally believed that eruptive phenomena in the solar atmosphere such as solar flares and coronal mass ejections (CMEs) occur in solar active regions with complex magnetic structures. The magnetic complexity is quantified in terms of twists, kinks, and interlinkages of magnetic field lines. Magnetic helicity has been recognized as a useful measure for these properties of a given magnetic field system. Magnetic helicity studies have been naturally directed to the energy buildup and instability leading to solar eruptions. However, in spite of many years of study, detailed aspects of initiation mechanisms of eruptive events are still not well understood. The objective of this dissertation is to understand a long-term (a few days) variation of magnetic helicity in active regions and its relationship with flares and CMEs.

Time Evolution of Coronal Magnetic Helicity in the Flaring Active Region NOAA 10930

Sung-Hong **Park**, Jongchul Chae, Ju Jing, Changyi Tan, Haimin Wang

ApJ, **2010**, 720, 1102-1107

To study the three-dimensional (3D) magnetic field topology and its long-term evolution associated with the X3.4 flare of **2006 December 13**, we investigate the coronal relative magnetic helicity in the flaring active region (AR) NOAA 10930 during the time period of December 8-14. The coronal helicity is calculated based on the 3D nonlinear force-free magnetic fields reconstructed by the weighted optimization method of Wiegelmann, and is compared with the amount of helicity injected through the photospheric surface of the AR. The helicity injection is determined from the magnetic helicity flux density proposed by Pariat et al. using Solar and Heliospheric Observatory/Michelson Doppler Imager magnetograms. The major findings of this study are the following. (1) The time profile of the coronal helicity shows a good correlation with that of the helicity accumulation by injection through the surface. (2) The coronal helicity of the AR is estimated to be -4.3$times$10^{43} Mx^{2} just before the X3.4 flare. (3) This flare is preceded not only by a large increase of negative helicity, -3.2$times$10^{43} Mx^{2}, in the corona over ~1.5 days but also by noticeable injections of positive helicity though the photospheric surface around the flaring magnetic polarity inversion line during the time period of the channel structure development. We conjecture that the occurrence of the X3.4 flare is involved with the positive helicity injection into an existing system of negative helicity.

Productivity of Solar Flares and Magnetic Helicity Injection in Active Regions

Sung-Hong **Park**, Jongchul Chae and Haimin Wang

BBSO Preprint #1425, Astrophysical Journal, 718:43–51, **2010** July

The main objective of this study is to better understand how magnetic helicity injection in an active region (AR) is related to the occurrence and intensity of solar flares. We therefore investigate magnetic helicity injection rate and unsigned magnetic flux, as a reference. In total, 378 ARs are analyzed using *SOHO*/MDI magnetograms. The 24 hr averaged helicity injection rate and unsigned magnetic flux are compared with the flare index and the flare-productive probability in next 24 hr following a measurement. In addition, we study the variation of helicity over a span of several days around the times of the 19 flares above M5.0 which occurred in selected strong flare-productive ARs. The major findings of this study are as follows: (1) for a sub-sample of 91 large ARs with unsigned magnetic fluxes in the range from 3 to 5 x 10^{22} Mx, there is a difference in magnetic helicity injection rate between flaring ARs and non-flaring ARs

by a factor of 2; (2) the GOES C-flare-productive probability as a function of helicity injection displays a sharp boundary between flare-productive ARs and flare-quiet ones; (3) the history of helicity injection before all the 19 major flares displayed a common characteristic: a significant helicity accumulation of (3—45) x 10^{42} Mx^2 during a phase of monotonically increasing helicity over 0.5—2 days. Our results support the notion that helicity injection is important in flares, but it is not effective to use it alone for the purpose of flare forecast. It is necessary to find a way to better characterize the time history of helicity injection as well as its spatial distribution inside ARs.

The Variation of Relative Magnetic Helicity Around Major Flares

Sung-Hong **Park**, Jeongwoo Lee, G.S. Choe, Jongchul Chae, Hyewon Jeong, Guo Yang, Ju Jing and Haimin Wang

E-print, Aug 2008; BBSO Preprint #1364, **2008;** Astrophysical Journal, Vol. 686, No. 2

http://solar.njit.edu/preprints/park1364.pdf

http://www.journals.uchicago.edu/doi/abs/10.1086/591117

We have investigated the variation of magnetic helicity over a span of several days around the times of eleven X-class flares which occurred in seven active regions (NOAA 9672, 10030, 10314, 10486, 10564, 10696, and 10720) using the magnetograms taken by the Michelson Doppler Imager (MDI) on board the Solar and Heliospheric Observatory (SOHO). As a major result we found that each of these major flares was preceded by a significant helicity accumulation, $(1.8–16)\times10^{42}$ Mx^2 over a long period (0.5–a few days). Another finding is that the helicity accumulates at a nearly constant rate, $(4.5–48)\times10^{40}$ Mx^2 hr^{-1}, and then becomes nearly constant before the flares. This led us to distinguish the helicity variation into two phases: a phase of monotonically increasing helicity and the following phase of relatively constant helicity. As expected, the amount of helicity accumulated shows a modest correlation with time-integrated soft X-ray flux during flares. However, the average helicity change rate in the first phase shows even stronger correlation with the time-integrated soft X-ray flux. We discuss the physical implications of this result and the possibility that this characteristic helicity variation pattern can be used as an early warning sign for solar eruptions.

Modeling a Propagating Sawtooth Flare Ribbon Structure as a Tearing Mode in the Presence of Velocity Shear

Jacob **Parker**, Dana Longcope

2017 *ApJ* **847** 30

https://arxiv.org/pdf/1709.04534.pdf

On **April 18, 2014** (SOL2014-04-18T13:03) an M-class flare was observed by IRIS. The associated flare ribbon contained a quasi-periodic sawtooth pattern that was observed to propagate along the ribbon, perpendicular to the IRIS spectral slit, with a phase velocity of ∼15 km s−1. This motion resulted in periodicities in both intensity and Doppler velocity along the slit. These periodicities were reported to be approximately ±0.5arcseconds in position and ±20 km s−1 in velocity and were measured to be ∼180◦ out of phase with one another. This quasi-periodic behavior has been attributed by others to bursty or patchy reconnection and slipping occurring during three-dimensional magnetic reconnection. While able to account for periodicities in both intensity and Doppler velocity these suggestions do not explicitly account for the phase velocity of the entire sawtooth structure, or for the relative phasing of the oscillations. Here we propose that the observations can be explained by a tearing mode instability occurring at a current sheet across which there is also a velocity shear. Using a linear model of this instability we reproduce the relative phase of the oscillations, as well as the phase velocity of the sawtooth structure. We suggest a geometry and local plasma parameters for the April 18 flare which would support our hypothesis. Under this proposal the combined spectral and spatial IRIS observations of this flare may provide the most compelling evidence to date of a tearing mode occurring in the solar magnetic field.

THE DETECTION OF NUMEROUS MAGNETIC SEPARATORS IN A THREE-DIMENSIONAL MAGNETOHYDRODYNAMIC MODEL OF SOLAR EMERGING FLUX

C. E. **Parnell**, R. C. Maclean, and A. L. Haynes

Astrophysical Journal Letters, 725:L214–L218, **2010**

Magnetic separators in three-dimensional (3D) magnetic fields are believed to be often associated with locations of magnetic reconnection. In this preliminary study, we investigate this relationship using data from a numerical resistive 3D MHD experiment of a solar flux emergence event. For the first time separators are detected in complex magnetic fields resulting from a 3D resistiveMHDmodel of flux emergence. Two snapshots of the model, taken from different stages of its evolution, are analyzed. Numerous separators are found in both snapshots, and their properties, including their geometry, length, relationship to the magnetic null points, and integrated parallel electric field are studied. The separators reside at the junctions between the emerging flux, the overlying field, and two other flux domains that are newly formed by reconnection. The long separators, which connect clusters of nulls that lie either side of the emerging flux, pass through spatially localized regions of high parallel electric field and correspond to local maxima in integrated parallel electric field. These factors indicate that strong magnetic reconnection takes place

along many of the separators, and that separators play a key role during the interaction of emerging and overlying flux.

Bayesian Analysis of Quasi-periodic Pulsations in Stellar Flares

D. J. **Pascoe**, A. Smyrli, T. Van Doorsselaere, and A.-M. Broomhall
ApJ **2020**
https://www.dropbox.com/s/xin4fn2vgqk7ung/bayesian_analysis_qpps.pdf
Quasi-periodic pulsations (QPPs) are routinely observed in a range of wavelengths during flares but in most cases the mechanism responsible is unknown. We present a method to detect and characterise QPPs in time series such as light curves for solar or stellar flares based on forward modelling and Bayesian analysis. We include models for QPPs as oscillations with finite lifetimes and non-monotonic amplitude modulation, such as wave trains formed by dispersive evolution in structured plasmas. By quantitatively comparing different models using Bayes factors we characterise the QPPs according to five properties; sinusoidal or non-sinusoidal, finite or indefinite duration, symmetric or asymmetric perturbations, monotonic or non-monotonic amplitude modulation, and constant or varying period of oscillation. We demonstrate our method and show examples of these five characteristics by analysing QPPs in white light stellar flares observed by the Kepler space telescope. Different combinations of properties may be able to identify particular physical mechanisms and so improve our understanding of QPPs and allow their use as seismological diagnostics. We propose three observational classes of QPPs can be distinguished; decaying harmonic oscillations, finite wave trains, and non-sinusoidal pulsations.

Seismology of contracting and expanding coronal loops using damping of kink oscillations by mode coupling

D.J. **Pascoe**, A.J.B. Russell, S.A. Anfinogentov, P.J.A. Simões, C.R. Goddard, V.M. Nakariakov, L. Fletcher
A&A 607, A8 **2017**
http://www2.warwick.ac.uk/fac/sci/physics/staff/research/davidpascoe/seis_contract.pdf
https://www.aanda.org/articles/aa/pdf/2017/11/aa30915-17.pdf
Aims. We extend recently developed seismological methods to analyse oscillating loops which feature a large initial shift in the equilibrium position and investigate additional observational signatures related to the loop environment and oscillation driver.
Methods. We model the motion of coronal loops as a kink oscillation damped by mode coupling, accounting for any change in loop length and the possible presence of parallel harmonics in addition to the fundamental mode. We apply our model to a loop which rapidly contracts due to a post-flare implosion (SOL**2012-03-09**) and a loop with a large lateral displacement (SOL**2012-10-20**).
Results. The seismological method is used to calculate plasma parameters of the oscillating loops including the transverse density profile, magnetic field strength, and phase mixing timescale. For SOL2012-03-09 the period of oscillation has a linear correlation with the contracting motion and suggests the kink speed remains constant during the oscillation. The implosion excitation mechanism is found to be associated with an absence of additional parallel harmonics.
Conclusions. The improved Bayesian analysis of the coronal loop motion allows for accurate seismology of plasma parameters, and the evolution of the period of oscillation compared with the background trend can be used to distinguish between loop motions in the plane of the loop and those perpendicular to it. The seismologically inferred kink speed and density contrast imply sub-Alfvénic ($MA = 0.16 \pm 0.03$) propagation of the magnetic reconfiguration associated with the implosion, as opposed to triggering by a wave propagating at the Alfvén speed.

Predicting Solar Flares Using Time Series Analysis

Lucas A. **Pauker**1, Monica G. Bobra2, and Eric Jonas3
2019 Res. Notes AAS 3 157
https://iopscience.iop.org/article/10.3847/2515-5172/ab4db0
Rapidly emerging magnetic flux on the solar surface often indicates a greater likelihood of a solar flare (e.g., Leka & Barnes 2003). In this study, we attempt to answer the following question: Is there a characteristic pattern in the time evolution of magnetic flux or other physical parameters that distinguish flaring active regions from quiet ones?

Antipodal Flares

B. **Pecos** and B. Paul
RHESSI Science Nugget, No. 197, Apr **2013**
Flares occur at opposite ends of a solar diameter, with striking consequences.
http://sprg.ssl.berkeley.edu/~tohban/wiki/index.php/Antipodal_Flares

A Survey of the Hard X-Ray Characteristics of Seismically Active and Quiet White-Light Flares

Pedram, E., & Matthews, S. A.
2012, Solar Physics, 277, 317-335
Various mechanisms have been proposed to explain how seismic waves can be generated during a solar flare, several of which include a major role for accelerated electrons. To address this question further, we have selected two samples of white-light flares (WLFs): one that has associated sunquakes, and one that does not. We focus particularly on the spatial characteristics of the hard X-ray (HXR) and WL emission, and the HXR spectral characteristics associated with the flares in both samples, including spectral hardness, HXR source size, and total injected electron power. Coupling the determined rate of energy deposition with the area over which the energy is being deposited suggests that in general the acoustically active flares are associated with a larger and more impulsive deposition of electron energy. However, this does not always correspond to a higher WL contrast.

Spectral and Imaging Observations of a White-light Flare in the Mid-Infrared

M **Penn**, S Krucker, H Hudson, M Jhabvala, D Jennings, A Lunsford, P Kaufmann
2016 ApJL **819** L30
http://arxiv.org/pdf/1512.04449v1.pdf
We report high-resolution observations at mid-infrared wavelengths of a minor solar flare, SOL**2014-09-24**T17T17:50 (C7.0), using Quantum Well Infrared Photodetector (QWIP) cameras at an auxiliary of the McMath-Pierce telescope. The flare emissions, the first simultaneous observations in two mid-infrared bands at 5 μm and 8 μm with white-light and hard X-ray coverage, revealed impulsive time variability with increases on time scales of ∼4∼s followed by exponential decay at ∼10 s in two bright regions separated by about 13". The brightest source is compact, unresolved spatially at the diffraction limit (1.3" at 5 μm). We identify the IR sources as flare ribbons also seen in white-light emission at 6173∼\AA∼observed by SDO/HMI, with twin hard X-ray sources observed by RHESSI, and with EUV sources (e.g., 94∼\AA) observed by SDO/AIA. The two infrared points have closely the same flux density (fν, W/m2Hz) and extrapolate to a level about an order of magnitude below that observed in the visible band by HMI, but with a flux more than two orders of magnitude above the free-free continuum from the hot (∼15 MK) coronal flare loop observed in the X-ray range. The observations suggest that the IR emission is optically thin, this constraint and others suggest major contributions from a density less than about 3×1013∼cm−3. We tentatively interpret this emission mechanism as predominantly free-free emission in a highly ionized but cool and rather dense chromospheric region.

Temporal Defocusing as a Depth Diagnostic of Submerged Sources of Transient Acoustic Emission from Solar Flares

Savannah **Perez-Piel**, Juan Camilo Buitrago-Casas, Juan Carlos Martínez Oliveros & Charles Lindsey
Solar Physics volume 298, Article number: 77 (**2023**)
https://link.springer.com/content/pdf/10.1007/s11207-023-02163-0.pdf
Helioseismic holography applied to HMI observations of a sunquake associated with the SOL**20140207**T10:29M1.9 flare hosted by NOAA AR11968 shows the signature of a compact submerged acoustic source. In the 9 – 11-mHz bandpass, this source appears to be at a depth of 2 Mm. This is nearly double the depth of the highly impulsive acoustic transient, referred to as an ultra-impulsive transient source recently found in the SOL**20110730**T02:09M9.3 flare, emerging from NOAA AR11261 in 2011. The latter source was compound, having multiple surface components overlaying a single submerged component. Many of the sources observed have evidence of being constituted of multiple components, some of which are staggered in depth. The helioseismic source of the flare of 2014-02-07 is distinguished by the apparent absence of a strong shallow compact overlying source component matching the character of those apparent in the flare of **2011-07-30**. This suggests that the volume several Mm beneath active-region photospheres could possibly harbor many more ultra-impulsive transient acoustic sources than the rarities that have so far appeared in familiar surface-focal-plane diagnostics. Based on weak surface signatures that appear in place of the strong ones, we find a temporal delay between weak surface and strong submerged sources similar to that found between surface-and-submerged sources in the flare of 2011-07-30. While it remains highly speculative based on the limited statistics we have at this point, this temporal delay supports a model in which the submerged source is perturbed by some presently invisible triggering disturbance that propagates downward from the flaring outer atmosphere at ∼ 5 km s−1. This is slower than the sound speed anywhere in the 0 – 2-Mm depth range. However, this potentially could be an Alfvèn speed if submerged magnetic flux densities along which the trigger propagates are as high as possible. The standard local-helioseismic diagnostics we have used in the past have been heavily reinforced in this study by a powerful new control resource found in the recognition of temporal defocusing of compact transient sources. In particular, its tight relationship to the standard spatial defocusing upon which helioseismic holography has capitalized from its early advent.

The Structure and Dynamics of a Bright Point as seen with Hinode, SoHO and TRACE

D. **P'erez-Su'arez**, R.C. Maclean, J.G. Doyle and M.S. Madjarska
E-print, Oct 2008, A&A, 492 (**2008**) 575-583
http://www.aanda.org/10.1051/0004-6361:200809507
Our aim is to determine the plasma properties of a coronal bright point and compare its magnetic topology extrapolated from magnetogram data with its appearance in X-ray images. We analyse spectroscopic data obtained with EIS/Hinode, Ca II H and G-band images from SOT/Hinode, UV images from TRACE, X-ray images from XRT/Hinode and high-resolution/high-cadence magnetogram data from MDI/SoHO. The BP comprises several coronal loops as seen in the X-ray images, while the chromospheric structure consists of tens of small bright points as seen in Ca II H. An excellent correlation exists between the Ca II BPs and increases in the magnetic field, implying that the Ca II H passband is a good indicator for the concentration of magnetic flux. Doppler velocities between 6 and 15 km/s are derived from the Fe XII and Fe XIII lines for the BP region, while for Fe XIV and Si VII they are in the range from -15 to +15 km/s. The coronal electron density is 3.7$ imes$10^{9} cm^{-3}. An excellent correlation is found between the positive magnetic flux and the X-ray light-curves. The remarkable agreement between the extrapolated magnetic field configuration and some of the loops composing the BP as seen in the X-ray images suggests that a large fraction of the magnetic field in the bright point is close to potential. The close correlation between the positive magnetic flux and the X-ray emission suggests that energy released by magnetic reconnection is stimulated by flux emergence or cancellation.

Fermi Large Area Telescope observations of high-energy gamma-ray emission from behind-the-limb solar flares

Melissa **Pesce-Rollins**, Nicola Omodei, Vahe' Petrosian, Wei Liu, Fatima Rubio da Costa, Alice Allafort, for the Fermi-LAT Collaboration
The 34th International Cosmic Ray Conference Proceedings **2015**
http://arxiv.org/pdf/1507.04303v1.pdf
Fermi-LAT >30 MeV observations have increased the number of detected solar flares by almost a factor of 10 with respect to previous space observations. These sample both the impulsive and long duration phases of GOES M and X class flares. Of particular interest is the recent detections of three solar flares whose position behind the limb was confirmed by the STEREO-B spacecraft. While gamma-ray emission up to tens of MeV resulting from proton interactions has been detected before from occulted solar flares, the significance of these particular events lies in the fact that these are the first detections of >100 MeV gamma-ray emission from footpoint-occulted flares. We will present the Fermi-LAT, RHESSI and STEREO observations of these flares and discuss the various emission scenarios for these sources and implications for the particle acceleration mechanisms.
2013 Oct 11, 2014 Jan 06, 2014 Sep 01

First detection of >100 MeV gamma rays associated with a behind-the-limb solar flare

Melissa **Pesce-Rollins**, Nicola Omodei, Vahe' Petrosian, Wei Liu, Fatima Rubio da Costa, Alice Allafort, Qingrong Chen
ApJL **2015**
http://arxiv.org/pdf/1505.03480v1.pdf **File**
We report the first detection of >100 MeV gamma rays associated with a behind-the-limb solar flare, which presents a unique opportunity to probe the underlying physics of high-energy flare emission and particle acceleration. On **2013 October 11** a GOES M1.5 class solar flare occurred ~ 9.9 degrees behind the solar limb as observed by STEREO-B. RHESSI observed hard X-ray emission above the limb, most likely from the flare loop-top, as the footpoints were occulted. Surprisingly, the Fermi Large Area Telescope (LAT) detected >100 MeV gamma-rays for ~30 minutes with energies up to GeV. The LAT emission centroid is consistent with the RHESSI hard X-ray source, but its uncertainty does not constrain the source to be located there. The gamma-ray spectra can be adequately described by bremsstrahlung radiation from relativistic electrons having a relatively hard power-law spectrum with a high-energy exponential cutoff, or by the decay of pions produced by accelerated protons and ions with an isotropic pitch-angle distribution and a power-law spectrum with a number index of ~3.8. We show that high optical depths rule out the gamma rays originating from the flare site and a high-corona trap model requires very unusual conditions, so a scenario in which some of the particles accelerated by the CME shock travel to the visible side of the Sun to produce the observed gamma rays may be at work.

SDO AIA and EVE observations and modelling of solar flare loops

P. **Petkaki**1, G. Del Zanna1, H. E. Mason1 and S. J. Bradshaw
A&A 547, A25 (**2012**)
We present imaging and spectroscopic observations of an isolated C1-class solar flare, obtained with the Atmospheric Imaging Assembly (AIA) and Extreme ultraviolet Variability Experiment (EVE) on the Solar Dynamics Observatory (SDO). We obtain excellent agreement between the peak flare temperatures estimated using the EVE spectra with those obtained from GOES and, most importantly, from the ratio of the 94 Å and 131 Å AIA channels, which are found to be dominated by Fe xviii and Fe xxi. These results confirm that these two AIA bands can be reliably used to provide

temperature diagnostics for the peak and gradual phases of solar flares. The flare kernels, probable sources of chromospheric evaporation, are seen as strong localised emission in the AIA bands at the footpoints of flare loops. The flare loops are close to isothermal during the gradual phase. We have run several hydrodynamic simulations (using the HYDRAD code) to study the cooling of the flare loops. We find good overall agreement between observed and predicted electron temperatures and densities when a gradual increase and decrease of the heating is assumed.

Acceleration of charged particles by fluctuating and steady electric fields in a X-type magnetic field

Panagiota **Petkaki** and Alexander L. MacKinnon
Advances in Space Research, Volume 48, Issue 5, 1 September **2011**, Pages 884-898
Release of stored magnetic energy via particle acceleration is a characteristic feature of astrophysical plasmas. Magnetic reconnection is one of the mechanisms for releasing energy from magnetized plasmas. Collisionless magnetic reconnection could provide both the energy release mechanism and the particle accelerator in space plasmas. Here we studied particle acceleration when fluctuating (in-time) electric fields are superposed on an static X-type magnetic field in collisionless hot solar plasma. This system is chosen to mimic the reconnective dissipation of a linear MHD disturbance. Our results are compared to particle acceleration from constant electric field superposed on an X-type magnetic field. The constant electric field configuration represents the effects of steady state magnetic reconnection. Time evolution of ion and electron distributions are obtained by numerically integrating particle trajectories. The frequencies of the electric field represent a turbulent range of waves. Depending on the frequency and amplitude of the electric field, electrons and ions are accelerated to different degrees and have energy distributions of bimodal form consisting of a lower energy part and a high energy tail. For frequencies (ω in dimensioless units) in the range $0.5 \omega 1.0$ a substantial fraction (20%–30%) of the proton distribution is accelerated to gamma-ray producing energies. For frequencies in the range $1 \omega 100.0$ the bulk of the electron distribution is accelerated to hard X-ray producing energies. The acceleration mechanism is important for solar flares and solar noise storms but it could be applicable to all collisionless astrophysical plasmas.

Thermal structure of a hot non-flaring corona from Hinode/EIS

A. **Petralia**1, F. Reale1,2, P. Testa3 and G. Del Zanna
A&A 564, A3 (**2014**)
http://www.aanda.org/articles/aa/pdf/2014/04/aa22998-13.pdf
Aims. In previous studies, a very hot plasma component has been diagnosed in solar active regions through the images in three different narrow-band channels of Atmospheric Imaging Assembly (AIA) on board the Solar Dynamics Observatory (SDO). This diagnostic from extreme ultraviolet (EUV) imaging data has also been supported by the matching morphology of emission in the hot Ca XVII line, as observed with Extreme-Ultraviolet Imaging Spectrometer (EIS) on board Hinode. This evidence is debated because of the unknown distribution of the emission measure along the line of sight. Here we investigate in detail the thermal distribution of one such region using EUV spectroscopic data.
Methods. In an active region observed with SDO/AIA, Hinode/EIS, and X-ray telescope (XRT), we select a sub-region with a very hot plasma component and another cooler sub-region for comparison. The average spectrum is extracted for both, and 14 intense lines are selected for analysis that probe the $5.5 < \log T < 7$ temperature range uniformly. From these lines, the emission measure distributions are reconstructed with the Markov-chain Monte Carlo method. Results are cross-checked in comparison with the two sub-regions, with a different inversion method, with the morphology of the images, and with the addition of fluxes measured with narrow, and broadband imagers.
Results. We find that, whereas the cool region has a flat and featureless distribution that drops at temperature $\log T \geq 6.3$, the distribution of the hot region shows a well-defined peak at $\log T = 6.6$ and gradually decreasing trends on both sides, thus supporting the very hot nature of the hot component diagnosed with imagers. The other cross-checks are consistent with this result.
Conclusions. This study provides a completion of the analysis of active region components, and the resulting scenario supports the presence of a minor very hot plasma component in the core, with temperatures $\log T > 6.6$.
2011September 13

Abrupt Changes in the Photospheric Magnetic Field, Lorentz Force, and Magnetic Shear during 15 X-class Flares

Gordon J. D. **Petrie**
2019 ApJSup 240 11
sci-hub.tw/10.3847/1538-4365/aaef2f
During major solar flares, the photospheric magnetic field of the flaring active region is often observed to change abruptly, permanently, and significantly. Here we analyze vector magnetograms covering 15 X-class flares observed in 11 active regions by the Solar Dynamic ObservatoryHelioseismic and Magnetic Imager. Resolving magnetic changes using a reference potential field, more complex magnetic field, Lorentz force, and magnetic shear changes could be analyzed than previously. In each case, physical and coherent patterns of change were found. Generally the dominant change was in the horizontal field component that strengthened in the central structure, accompanied there by a

downward Lorentz force change and strengthening of horizontal magnetic shear consistent with magnetic implosion, with weaker changes of opposite sign in neighboring and peripheral regions including sunspots. In most cases this central structure was a strong, sheared photospheric magnetic neutral line, but in one case it was an isolated unipolar sunspot. Magnetic relaxation in the vertical direction was typical throughout the flaring regions. Unique in this study was the behavior at bald-patch structures during the X-class flares of **2017 September 6** in NOAA Active Region 12673. During the X9.3 flare, the horizontal and vertical field components weakened and the shear relaxed in horizontal and vertical directions, indicating a large free magnetic energy source for the flare. The magnetic changes at the bald patches exhibited evidence of organized vertical magnetic flux reduction during three X-class flares, not found at other structures, suggesting the greater possibilities of magnetic reconfiguration and energy release at bald patches.
Erratum: **2019** *ApJS* **242** 30 https://iopscience.iop.org/article/10.3847/1538-4365/ab245c/pdf

Photospheric and Coronal Observations of Abrupt Magnetic Restructuring in Two Flaring Active Regions

G. J. D. **Petrie**
Solar Phys. Volume 291, Issue 3, pp 791-821 **2016**
For **two major X-class flares** observed by the Solar Dynamics Observatory (SDO) and the Solar TErrestrial RElations Observatory Ahead (STEREO-A) spacecraft when they were close to quadrature, we compare major, abrupt changes in the photospheric magnetic vector field to changes in the observed coronal magnetic structure during the two flares. The Lorentz force changes in strong photospheric fields within active regions are estimated from time series of SDO Helioseismic and Magnetic Imager (HMI) vector magnetograms. These show that the major changes occurred in each case near the main neutral line of the region and in two neighboring twisted opposite-polarity sunspots. In each case the horizontal parallel field strengthened significantly near the neutral line while the azimuthal field in the sunspots decreased, suggesting that a flux rope joining the two sunspots collapsed across the neutral line with reduced magnetic pressure because of a reduced field twist component. At the same time, the coronal extreme ultraviolet (EUV) loop structure was observed by the Atmospheric Imaging Assembly (AIA) onboard SDO and the Extreme Ultraviolet Imager (EUVI) on STEREO-A to decrease significantly in height during each eruption, discontinuous changes signifying ejection of magnetized plasma, and outward-propagating continuous but abrupt changes consistent with loop contraction. An asymmetry in the observed EUV loop changes during one of the flares matches an asymmetry in the photospheric magnetic changes associated with that flare. The observations are discussed in terms of the well-known tether-cutting and breakout flare initiation models.

When the tail wags the dog: solar surface magnetic effects of flares observed by HMI

Gordon **Petrie**
HMI Science Nuggets, #8, March **2014**
http://hmi.stanford.edu/hminuggets/?p=539
Analysis of HMI vector magnetic field data before and after a flare illustrate how the energy released can result in a collapse of loop structures, and how the effects can be observed on the solar surface.

Estimating flare-related photospheric Lorentz force vector changes within active regions

Gordon **Petrie**
Solar Phys., 2014, Volume 289, Issue 10, pp 3663-3680, **2014**
http://arxiv.org/pdf/1403.6156v1.pdf
It is shown that expressions for the global Lorentz force associated with a flaring active region derived by Fisher et al. (2012) can be used to estimate the Lorentz forces for strong fields in large structures over photospheric subdomains within active regions. Gary's (2001) model for the stratified solar atmosphere is used to demonstrate that in large-scale structures with typical horizontal magnetic length scale >>300 km and with strong magnetic fields ($\geq$1 kG at the τ=1 opacity layer at 5000 \AA), the Lorentz force acting on the photosphere may be approximated by a surface integral based on photospheric boundary data alone. These conditions cover many of the sunspot fields and major neutral lines that have been studied using Fisher et al.'s expressions over the past few years. The method gives a reasonable estimate of Lorentz force changes associated with a flare based on photospheric magnetogram observations provided that the Lorentz force changes associated with the flare have a lasting effect on the observed fields, and are not immediately erased by post-flare equilibration processes.

A Spatio-temporal Description of the Abrupt Changes in the Photospheric Magnetic and Lorentz-Force Vectors During the 15 February 2011 X2.2 Flare

G. J. D. **Petrie**
Solar Physics, October **2013**, Volume 287, Issue 1-2, pp 415-440
The active region NOAA 11158 produced the first X-class flare of Solar Cycle 24, an X2.2 flare at 01:44 UT on **15 February 2011**. The Helioseismic and Magnetic Imager (HMI) instrument on the Solar Dynamics Observatory (SDO)

satellite produces 12-minute, 0.5″ pixel−1 vector magnetograms. Here we analyze a series of these data covering a 12-hour interval centered at the time of this flare. We describe the spatial distributions of the photospheric magnetic changes associated with the flare, including the abrupt changes in the field vector, vertical electric current and Lorentz-force vector acting on the solar interior. We also describe these parameters' temporal evolution. The abrupt magnetic changes were concentrated near the neutral line and in two neighboring sunspots. Near the neutral line, the field vectors became stronger and more horizontal during the flare and the shear increased. This was due to an increase in strength of the horizontal field components near the neutral line, most significant in the horizontal component parallel to the neutral line but the perpendicular component also increased in strength. The vertical component did not show a significant, permanent overall change at the neutral line. The increase in field strength at the neutral line was accompanied by a compensating decrease in field strength in the surrounding volume. In the two sunspots near the neutral line the integrated azimuthal field abruptly decreased during the flare but this change was permanent in only one of the spots. There was a large, abrupt, downward vertical Lorentz-force change acting on the solar interior during the flare, consistent with results of past analyses and recent theoretical work. The horizontal Lorentz force acted in opposite directions along each side of neutral line, with the two sunspots at each end subject to abrupt torsional forces relaxing their magnetic twist. These shearing forces were consistent with a contraction of field and decrease of shear near the neutral line, whereas the field itself became more sheared as a result of the field collapsing towards the neutral line from the surrounding volume. The Lorentz forces acting on the atmospheric volume above the photosphere were equal and opposite.

THE ABRUPT CHANGES IN THE PHOTOSPHERIC MAGNETIC AND LORENTZ FORCE VECTORS DURING SIX MAJOR NEUTRAL-LINE FLARES

G. J. D. **Petrie**

2012 ApJ 759 50

We analyze the spatial and temporal variations of the abrupt photospheric magnetic changes associated with six major flares using 12 minute, 05 pixel–1 vector magnetograms from NASA's Helioseismic and Magnetic Imager instrument on the Solar Dynamics Observatory satellite. The six major flares occurred near the main magnetic neutral lines of four active regions, NOAA 11158, 11166, 11283, and 11429. During all six flares the neutral-line field vectors became stronger and more horizontal, in each case almost entirely due to strengthening of the horizontal field components parallel to the neutral line. In all six cases the neutral-line pre-flare fields were more vertical than the reference potential fields, and collapsed abruptly and permanently closer to potential-field tilt angles during every flare, implying that the relaxation of magnetic stress associated with non-potential tilt angles plays a major role during major flares. The shear angle with respect to the reference potential field did not show such a pattern, demonstrating that flare processes do not generally relieve magnetic stresses associated with photospheric magnetic shear. The horizontal fields became significantly and permanently more aligned with the neutral line during the four largest flares, suggesting that the collapsing field is on average more aligned with the neutral line than the pre-flare neutral-line field. The vertical Lorentz force had a large, abrupt, permanent downward change during each of the flares, consistent with loop collapse. The horizontal Lorentz force changes acted mostly parallel to the neutral line in opposite directions on each side, a signature of the fields contracting during the flare, pulling the two sides of the neutral line toward each other. The greater effect of the flares on field tilt than on shear may be explained by photospheric line-tying.

ABRUPT LONGITUDINAL MAGNETIC FIELD CHANGES IN FLARING ACTIVE REGIONS

G. J. D. **Petrie**1 and J. J. Sudol2

Astrophysical Journal, 724:1218–1237, **2010**

We characterize the changes in the longitudinal photospheric magnetic field during 38 X-class and 39 M-class flares within 65◦ of disk center using 1 minute GONG magnetograms. In all 77 cases, we identify at least one site in the flaring active region where clear, permanent, stepwise field changes occurred. The median duration of the field changes was about 15 minutes and was approximately equal for X-class and for M-class flares. The absolute values of the field changes ranged from the detection limit of ~10 G to as high as ~450 G in two exceptional cases. The median value was 69 G. Field changes were significantly stronger for X-class than for M-class flares and for limb flares than for disk-center flares. Longitudinal field changes less than 100 G tended to decrease longitudinal field strengths, both close to disk center and close to the limb, while field changes greater than 100 G showed no such pattern. Likewise, longitudinal flux strengths tended to decrease during flares. Flux changes, particularly net flux changes near disk center, correlated better than local field changes with *GOES* peak X-ray flux. The strongest longitudinal field and flux changes occurred in flares observed close to the limb.We estimate the change of Lorentz force associated with each flare and find that this is large enough in some cases to power seismic waves. We find that longitudinal field decreases would likely outnumber increases at all parts of the solar disk within 65◦ of disk center, as in our observations, if photospheric field tilts increase during flares as predicted by Hudson et al.

Implications of loop-top origin for microwave, hard X-ray, and low-energy gamma-ray emissions from behind the limb flares

Vahé **Petrosian**
ApJ **2018**
https://arxiv.org/pdf/1808.07161.pdf
http://iopscience.iop.org/article/10.3847/1538-4357/aadd07/pdf
The Fermi gamma-ray Space Telescope (Fermi) has detected hard X-ray (HXR) and gamma-ray photons from three flares, which according to \stereo occurred in active regions behind the limb of the Sun as delineated by near Earth instruments. For two of these flares \r has provided HXR images with sources located just above the limb, presumably from the loop top (LT) region of a relatively large loop. Fermi-Gamma-ray Burst Monitor has detected HXRs and gamma-rays, and RSTN has detected microwaves emissions with similar light curves. This paper presents a quantitative analysis of these multi-wavelength observations assuming that HXRs and microwaves are produced by electrons accelerated at the LT source, with emphasize on the importance of the proper treatment of escape of the particles from the acceleration-source region and the trans-relativistic nature of the analysis. The observed spectra are used to determine the magnetic field and relativistic electron spectra. It is found that a simple power-law in momentum (with cut off above a few 100 MeV) agrees with all observations, but in energy space a broken power law spectrum (steepening at rest mass energy) may be required. It is also shown that the production of the >100 MeV photons detected by The Fermi-Large Area Telescope at the LT source would require more energy compared to photospheric emission. These energies are smaller than that required for electrons, so that the possibility that all the emissions originate in the LT cannot be ruled out on energetic grounds. However, the differences in the light curves and emission centroids of HXRs and >100 MeV gamma-rays favour a different source for the latter. **2013 − 10 – 11, 2014 − 09 − 01**

PARTICLE ACCELERATION IN SOLAR FLARES AND ASSOCIATED CME SHOCKS

Vahé **Petrosian**
2016 ApJ 830 28 DOI 10.3847/0004-637X/830/1/28
https://arxiv.org/pdf/1605.04022v1.pdf
Observations relating the characteristics of electrons seen near Earth (solar energetic particles [SEPs]) and those producing flare radiation show that in certain (prompt) events the origin of both populations appears to be the flare site, which shows strong correlation between the number and spectral index of SEP and hard X-ray radiating electrons, but in others (delayed), which are associated with fast coronal mass ejections (CMEs), this relation is complex and SEPs tend to be harder. Prompt event spectral relation disagrees with that expected in thick or thin target models. We show that using a more accurate treatment of the transport of the accelerated electrons to the footpoints and to Earth can account for this discrepancy. Our results are consistent with those found by Chen & Petrosian for two flares using nonparametric inversion methods, according to which we have weak diffusion conditions, and trapping mediated by magnetic field convergence. The weaker correlations and harder spectra of delayed events can come about by reacceleration of electrons in the CME shock environment. We describe under what conditions such a hardening can be achieved. Using this (acceleration at the flare and reacceleration in the CME) scenario, we show that we can describe the similar dichotomy that exists between the so-called impulsive, highly enriched (3He and heavy ions), and softer SEP events and stronger, more gradual SEP events with near-normal ionic abundances and harder spectra. These methods can be used to distinguish the acceleration mechanisms and to constrain their characteristics.

Stochastic Acceleration by Turbulence

Vahé **Petrosian**
Space Science Reviews volume 173, pages535–556(**2012**)
https://link.springer.com/content/pdf/10.1007/s11214-012-9900-6.pdf
The subject of this paper is stochastic acceleration by plasma turbulence, a process akin to the original model proposed by Fermi. We review the relative merits of different acceleration models, in particular the so called first order Fermi acceleration by shocks and second order Fermi by stochastic processes, and point out that plasma waves or turbulence play an important role in all mechanisms of acceleration. Thus, stochastic acceleration by turbulence is active in most situations. We also show that it is the most efficient mechanism of acceleration of relatively cool non relativistic thermal background magnetized plasma particles. In addition, it can preferentially accelerate electrons relative to protons as is needed in many astrophysical radiating sources, where usually there are no indications of presence of shocks. We also point out that a hybrid acceleration mechanism consisting of initial acceleration by turbulence of background particles followed by a second stage acceleration by a shock has many attractive features. It is demonstrated that the above scenarios can account for many signatures of the accelerated electrons, protons and other ions, in particular 3He and 4He, seen directly as Solar Energetic Particles and through the radiation they produce in solar flares.
Stochastic Acceleration in Solar Flares

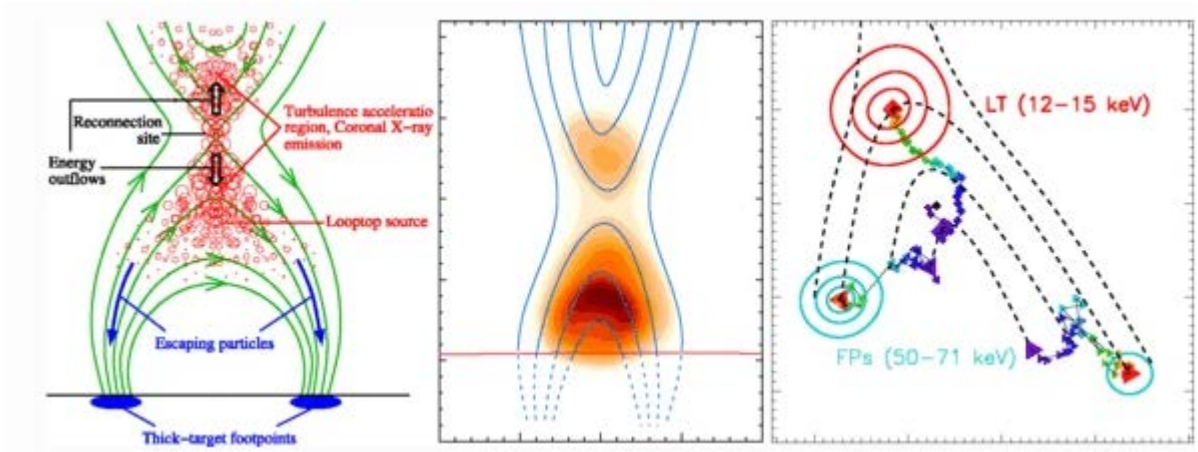

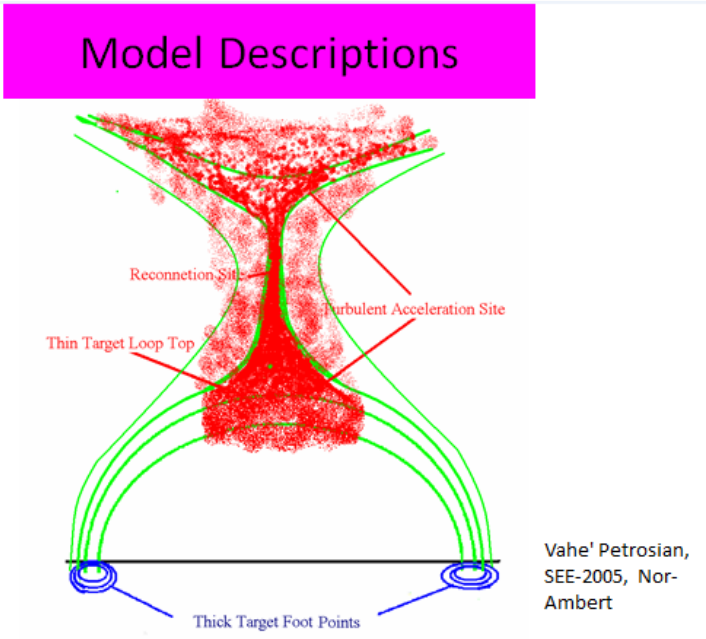

Derivation of Stochastic Acceleration Model Characteristics for Solar Flares from RHESSI Hard X-ray Observations

Vahé **Petrosian** and Qingrong Chen

ApJ **712** L131-L134, **2010**

The model of stochastic acceleration of particles by turbulence has been successful in explaining many observed features of solar flares. Here, we demonstrate a new method to obtain the accelerated electron spectrum and important acceleration model parameters from the high-resolution hard X-ray (HXR) observations provided by *RHESSI*. In our model, electrons accelerated at or very near the loop top (LT) produce thin target bremsstrahlung emission there and then escape downward producing thick target emission at the loop footpoints (FPs). Based on the electron flux spectral images obtained by the regularized spectral inversion of the *RHESSI* count visibilities, we derive several important parameters for the acceleration model. We apply this procedure to the **2003 November 3** solar flare, which shows an LT source up to 100-150 keV in HXR with a relatively flat spectrum in addition to two FP sources. The results imply the presence of strong scattering and a high density of turbulence energy with a steep spectrum in the acceleration region.

Particle Acceleration in Solar Flares and Enrichment of 3He and Heavy Ions

Vah´e **Petrosian**

E-print, July_Aug **2008, File**

Хороший обзор по ускорению.

We discuss possible mechanisms of acceleration of particles in solar flares and show that turbulence plays an important role in all the mechanism. It is also argued that stochastic particle acceleration by turbulent plasma waves is the most likely mechanism for production of the high energy electrons and ions responsible for observed radiative signatures of solar flares and for solar energetic particle or SEPs, and that the predictions of this model agrees well with many past and recent high spectral and temporal

observations of solar flares. It is shown that, in addition, the model explains many features of SEPs that accompany flares. In particular we show that it can successfully explain the observed extreme enhancement, relative to photospheric values, of 3He ions and the relative spectra of 3He and 4He. It has also the potential of explaining the relative abundances of most ions including the increasing enhancements of heavy ions with ion mass or mass-to-charge ratio.

What Helicity Can Tell us About Solar Magnetic Fields

Alexei A. **Pevtsov**

E-print, Feb **2008**; J. Astrophys. Astr.

Concept of magnetic/current helicity was introduced to solar physics about 15 years ago. Earlier studies led to discovery of such fundamental properties as hemispheric helicity rule, and role of helicity in magnetic reconnection and solar eruptions. Later, the concept was successfully applied in studies of different solar processes from solar dynamo to flare and CME phenomena. Although no silver bullet, helicity has proven to be a very useful .tool. in answering many still puzzling questions about origin and evolution of solar magnetic fields. I present an overview of some helicity studies and briefly analyze their findings.

Case study on the identification and classification of small-scale flow patterns in flaring active region

E. **Philishvili**1,2, B. M. Shergelashvili3,2,4, S. Buitendag5, J. Raes1, S. Poedts1,6 and M. L. Khodachenko3,7,8

A&A 645, A52 (**2021**)

https://arxiv.org/pdf/2011.07634.pdf

https://doi.org/10.1051/0004-6361/202038895

Context. We propose a novel methodology to identity flows in the solar atmosphere and classify their velocities as either supersonic, subsonic, or sonic.

Aims. The proposed methodology consists of three parts. First, an algorithm is applied to the Solar Dynamics Observatory (SDO) image data to locate and track flows, resulting in the trajectory of each flow over time. Thereafter, the differential emission measure inversion method is applied to six Atmospheric Imaging Assembly (AIA) channels along the trajectory of each flow in order to estimate its background temperature and sound speed. Finally, we classify each flow as supersonic, subsonic, or sonic by performing simultaneous hypothesis tests on whether the velocity bounds of the flow are larger, smaller, or equal to the background sound speed.

Methods. The proposed methodology was applied to the SDO image data from the 171 Å spectral line for the date **6 March 2012** from 12:22:00 to 12:35:00 and again for the date **9 March 2012** from 03:00:00 to 03:24:00. Eighteen plasma flows were detected, 11 of which were classified as supersonic, 3 as subsonic, and 3 as sonic at a 70% level of significance. Out of all these cases, 2 flows cannot be strictly ascribed to one of the respective categories as they change from the subsonic state to supersonic and vice versa. We labeled them as a subclass of transonic flows.

Results. The proposed methodology provides an automatic and scalable solution to identify small-scale flows and to classify their velocities as either supersonic, subsonic, or sonic. It can be used to characterize the physical properties of the solar atmosphere.

Conclusions. We identified and classified small-scale flow patterns in flaring loops. The results show that the flows can be classified into four classes: sub-, super-, trans-sonic, and sonic. The flows occur in the complex structure of the active region magnetic loops. The detected flows from AIA images can be analyzed in combination with the other high-resolution observational data, such as Hi-C 2.1 data, and be used for the development of theories describing the physical conditions responsible for the formation of flow patterns.

Quasi-oscillatory dynamics observed in ascending phase of the flare on March 6, 2012. E. **Philishvili**1,2 , B.M. Shergelashvili3,2,5 , T.V. Zaqarashvili4,2 , V. Kukhianidze2 , G. Ramishvili2 , M. Khodachenko3,6 , S. Poedts1 , P. De Causmaecker

A&A 600, A67 **2017**

https://arxiv.org/pdf/1612.09562v1.pdf

Context. The dynamics of the flaring loops in active region (AR) 11429 are studied. The observed dynamics consist of several evolution stages of the flaring loop system during both the ascending and descending phases of the registered M-class flare. The dynamical properties can also be classified by different types of magnetic reconnection, related plasma ejection and aperiodic flows, quasi-periodic oscillatory motions, and rapid temperature and density changes, among others. The focus of the present paper is on a specific time interval during the ascending (pre-flare) phase.

Aims. The goal is to understand the quasi-periodic behavior in both space and time of the magnetic loop structures during the considered time interval.

Methods.We have studied the characteristic location, motion, and periodicity properties of the flaring loops by examining space-time diagrams and intensity variation analysis along the coronal magnetic loops using AIA intensity and HMI magnetogram images (from the Solar Dynamics Observatory(SDO)).
Results. We detected bright plasma blobs along the coronal loop during the ascending phase of the solar flare, the intensity variations of which clearly show quasi-periodic behavior. We also determined the periods of these oscillations.
Conclusions. Two different interpretations are presented for the observed dynamics. Firstly, the oscillations are interpreted as the manifestation of non-fundamental harmonics of longitudinal standing acoustic oscillations driven by the thermodynamically nonequilibrium background (with time variable density and temperature). The second possible interpretation we provide is that the observed bright blobs could be a signature of a strongly twisted coronal loop that is kink unstable. **6 March 2012**

Highly ionized Calcium and Argon X-ray spectra from a large solar flare

K.J.H.**Phillips**, J.Sylwester, B.Sylwester, M.Kowalinski, M.Siarkowski, W. Trzebinski, S.Plocieniak, Z.Kordylewski
ApJ **2018**
https://arxiv.org/pdf/1806.08584.pdf
X-ray lines of helium-like calcium (\ion{Ca}{19}) between 3.17~\AA\ and 3.21~\AA\ and associated \ion{Ca}{18} dielectronic satellites have previously been observed in solar flare spectra, and their excitation mechanisms are well established. Dielectronic satellites of lower ionization stages (\ion{Ca}{17}~--~\ion{Ca}{15}) are not as well characterized. Several spectra during a large solar flare in 2001 by the DIOGENESS X-ray spectrometer on the {\em CORONAS-F}\/ spacecraft show the \ion{Ca}{17} and \ion{Ca}{16} satellites as well as lines of ionized argon (\ion{Ar}{17}, \ion{Ar}{16}) including dielectronic satellites. The DIOGENESS spectra are compared with spectra from a synthesis code developed here based on an isothermal assumption with various atomic sources including dielectronic satellite data from the Cowan Hartree--Fock code. Best-fit comparisons are made by varying the temperature as the code's input (Ar/Ca abundance ratio fixed at 0.33); close agreement is achieved although with adjustments to some ion fractions. The derived temperature is close to that derived from the two {\em GOES}\/ X-ray channels, TGOES. Some lines are identified for the first time. Similar spectra from the {\em P78-1}\/ spacecraft and the Alcator C-Mod tokamak have also been analyzed and similar agreement obtained. The importance of blends of calcium and argon lines is emphasized, affecting line ratios used for temperature diagnostics. This analysis will be applied to the {\em Solar Maximum Mission}\/ Bent Crystal Spectrometer archive and to X-ray spectra expected from the ChemiX instrument on the Sun-orbiting {\em Interhelioprobe}\/ spacecraft, while the relevance to X-ray spectra from non-solar sources is indicated. **25 Aug 2001**

THE SOLAR FLARE IRON ABUNDANCE

K. J. H. **Phillips**1 and B. R. Dennis
2012 ApJ 748 52
The abundance of iron is measured from emission line complexes at 6.65 keV (Fe line) and 8 keV (Fe/Ni line) in RHESSI X-ray spectra during solar flares. Spectra during long-duration flares with steady declines were selected, with an isothermal assumption and improved data analysis methods over previous work. Two spectral fitting models give comparable results, viz., an iron abundance that is lower than previous coronal values but higher than photospheric values. In the preferred method, the estimated Fe abundance is A(Fe) = 7.91 ± 0.10 (on a logarithmic scale, with A(H) = 12) or 2.6 ± 0.6 times the photospheric Fe abundance. Our estimate is based on a detailed analysis of 1898 spectra taken during 20 flares. No variation from flare to flare is indicated. This argues for a fractionation mechanism similar to quiet-Sun plasma. The new value of A(Fe) has important implications for radiation loss curves, which are estimated.

AI-FLARES: Artificial Intelligence for the Analysis of Solar Flares Data **Review**

Michele **Piana**, Federico Benvenuto, Anna Maria Massone, Cristina Campi, Sabrina Guastavino, Francesco Marchetti, Paolo Massa, Emma Perracchione, Anna Volpara
2024
https://arxiv.org/pdf/2401.01104.pdf
AI-FLARES (Artificial Intelligence for the Analysis of Solar Flares Data) is a research project funded by the Agenzia Spaziale Italiana and by the Istituto Nazionale di Astrofisica within the framework of the ``Attività di Studio per la Comunità Scientifica Nazionale Sole, Sistema Solare ed Esopianeti" program. The topic addressed by this project was the development and use of computational methods for the analysis of remote sensing space data associated to solar flare emission. This paper overviews the main results obtained by the project, with specific focus on solar flare forecasting, reconstruction of morphologies of the flaring sources, and interpretation of acceleration mechanisms triggered by solar flares. **September 25 2011**,

Flare forecasting and feature ranking using SDO/HMI data

Michele **Piana**, Cristina Campi, Federico Benvenuto, Sabrina Guastavano, Anna Maria Massone
Nuovo Cimento **2018**
https://arxiv.org/pdf/1812.07258.pdf
We describe here the application of a machine learning method for flare forecasting using vectors of properties extracted from images provided by the Helioseismic and Magnetic Imager in the Solar Dynamics Observatory (SDO/HMI). We also discuss how the method can be used to quantitatively assess the impact of such properties on the prediction process.

FLARECAST: an I4.0 technology for space weather using satellite data

Michele **Piana**, Anna Maria Massone, Federico Benvenuto, Cristina Campi
IEEE Italy Session - 4th International Forum on Research and Technologies for Society and Industry **2018**
https://arxiv.org/ftp/arxiv/papers/1806/1806.08560.pdf
'Flare Likelihood and Region Eruption Forecasting (FLARECAST)' is a Horizon 2020 project, which realized a technological platform for machine learning algorithms, with the objective of providing the space weather community with a prediction service for solar flares. This paper describes the FLARECAST service and shows how the methods implemented in the platform allow both flare prediction and a quantitative assessment of how the information contained in the space data utilized in the analysis may impact the forecasting process.

Comprehensive Analysis of the Geoeffective Solar Event of 21 June 2015: Effects on the Magnetosphere, Plasmasphere, and Ionosphere Systems

Mirko **Piersanti**, Tommaso Alberti, Alessandro Bemporad …
Solar Physics November **2017**, 292:169
https://link.springer.com/content/pdf/10.1007%2Fs11207-017-1186-0.pdf
A full-halo coronal mass ejection (CME) left the Sun on 21 June 2015 from active region (AR) NOAA 12371. It encountered Earth on 22 June 2015 and generated a strong geomagnetic storm whose minimum Dst value was −204 nT. The CME was associated with an M2-class flare observed at 01:42 UT, located near disk center (N12 E16). Using satellite data from solar, heliospheric, and magnetospheric missions and ground-based instruments, we performed a comprehensive Sun-to-Earth analysis. In particular, we analyzed the active region evolution using ground-based and satellite instruments (Big Bear Solar Observatory (BBSO), Interface Region Imaging Spectrograph (IRIS), Hinode, Atmospheric Imaging Assembly (AIA) onboard the Solar Dynamics Observatory (SDO), Reuven Ramaty High Energy Solar Spectroscopic Imager(RHESSI), covering Hαα, EUV, UV, and X-ray data); the AR magnetograms, using data from SDO/Helioseismic and Magnetic Imager (HMI); the high-energy particle data, using the Payload for Antimatter Matter Exploration and Light-nuclei Astrophysics (PAMELA) instrument; and the Rome neutron monitor measurements to assess the effects of the interplanetary perturbation on cosmic-ray intensity. We also evaluated the 1 – 8 Å soft X-ray data and the ∼1∼1 MHz type III radio burst time-integrated intensity (or fluence) of the flare in order to predict the associated solar energetic particle (SEP) event using the model developed by Laurenza et al. (Space Weather7(4), 2009). In addition, using ground-based observations from lower to higher latitudes (International Real-time Magnetic Observatory Network (INTERMAGNET) and European Quasi-Meridional Magnetometer Array (EMMA)), we reconstructed the ionospheric current system associated with the geomagnetic sudden impulse (SI). Furthermore, Super Dual Auroral Radar Network (SuperDARN) measurements were used to image the global ionospheric polar convection during the SI and during the principal phases of the geomagnetic storm. In addition, to investigate the influence of the disturbed electric field on the low-latitude ionosphere induced by geomagnetic storms, we focused on the morphology of the crests of the equatorial ionospheric anomaly by the simultaneous use of the Global Navigation Satellite System (GNSS) receivers, ionosondes, and Langmuir probes onboard the Swarm constellation satellites. Moreover, we investigated the dynamics of the plasmasphere during the different phases of the geomagnetic storm by examining the time evolution of the radial profiles of the equatorial plasma mass density derived from field line resonances detected at the EMMA network (1.5<L<6.51.5<L<6.5). Finally, we present the general features of the geomagnetic response to the CME by applying innovative data analysis tools that allow us to investigate the time variation of ground-based observations of the Earth's magnetic field during the associated geomagnetic storm.

KINK WAVES IN AN ACTIVE REGION DYNAMIC FIBRIL

A. **Pietarila**1, R. Aznar Cuadrado2, J. Hirzberger2 and S. K. Solanki
2011 ApJ 739 92
We present high spatial and temporal resolution Ca II 8542 Å observations of a kink wave in an on-disk chromospheric active region fibril. The properties of the wave are similar to those observed in off-limb spicules. From the observed phase and period of the wave we determine a lower limit for the field strength in the chromospheric active region fibril

located at the edge of a sunspot to be a few hundred gauss. We find indications that the event was triggered by a small-scale reconnection event higher up in the atmosphere.

Analysis of Solar-like X-Class Flare on Wolf 359 Observed Simultaneously with TESS and XMM-Newton

Małgorzata **Pietras** (1), Robert Falewicz (1 and 2), Marek Siarkowski (3), Anna Kepa (3), Kamil Bicz (1 and 2), Paweł Preś

ApJ **2023**

https://arxiv.org/pdf/2307.08425.pdf

We present an analysis of a flare on the Wolf 359 star based on simultaneous observations of TESS and XMM-Newton. A stellar flare with energy comparable to an X-class solar flare is analyzed on this star for the first time. The main goal of the study was to determine whether the same physical processes drive and occur in stellar flares as in the solar flares. We tried to estimate the flare class by various direct and indirect methods. Light curves and spectra in different energy ranges were used to determine the parameters and profiles of the flare. From the XMM-Newton EPIC-pn X-ray data, we estimated the temperature and emission measure during the flare. The thermodynamical timescale and the loop semi-length were also determined with two different methods. The RGS spectra enabled us to calculate the differential emission measure (DEM) distributions. The obtained DEM distributions have three components at temperature values of 3 MK, 7 MK, and 16-17 MK. The analysis of the line ratio in helium-like triplets allowed us to determine the plasma electron density. Our results for the flare loop on Wolf 359 were compared to typical parameters for solar flares observed with GOES and RHESSI. This supports our conclusion that the processes taking place in stellar flares are like those in solar flares. The determined geometrical parameters of the phenomenon do not differ from the values of analogs occurring on the Sun.

Statistical Analysis of Stellar Flares from the First Three Years of TESS Observations

M. **Pietras**1, R. Falewicz1,2, M. Siarkowski3, K. Bicz1, and P. Preś1

2022 ApJ 935 143

https://iopscience.iop.org/article/10.3847/1538-4357/ac8352/pdf

In this paper, we study stellar light curves from the Transiting Exoplanet Survey Satellite (TESS) for the presence of stellar flares. The main aim is to detect stellar flares using 2 minute cadence data and to perform a statistical analysis. To find and analyze stellar flares, we prepared the automatic software WARPFINDER. We implemented three methods described in this paper: trend, difference, and profile fitting. Automated searches for flares was accompanied by visual inspection. Using our software we analyzed the 2 minute cadence light curves of 330,000 stars located in the first 39 sectors of TESS observations. As a result, we detected over 25,000 stars showing flare activity with the total number of more than 140,000 flares. This means that about 7.7% of all the analyzed objects are flaring stars. The estimated flare energies range between 1031 and 1036 erg. We prepared a preliminary preview of the statistical distribution of parameters such as the flare duration, amplitude, and energy, and compared it with previous results. The relationship between stellar activity and spectral type, temperature, and mass was also statistically analyzed. Based on the scaling laws, we estimated the average values of the magnetic field strength and length of the flare loops. In our work, we used both single (about 60%), and double (about 40%) flare profiles to fit the observational data. The components of the double profile are supposed to be related to the direct heating of the photosphere by nonthermal electrons and back-warming processes.

Spectral variations within solar flare ribbons

A.G.M. **Pietrow**, M.K. Druett, V. Singh

A&A 685, A137 **2024**

https://arxiv.org/pdf/2402.10611.pdf

https://www.aanda.org/articles/aa/pdf/2024/05/aa48839-23.pdf

Context. Solar flare ribbons are intense brightenings of principally chromospheric material that are responsible for a large fraction of the chromospheric emission in solar and stellar flares. We present an on-disc observation of flare ribbon substructures in an X9.3-class flare observed by the Swedish 1-m Solar Telescope. Aims. We identify categories of ribbon substructures seen in the Ca ii 8542 Å, Hα, and Ca ii K lines, focusing on their spatial locations and their (spectro-)polarimetric properties.

Methods. Color Collapsed Plotting (COCOPLOT) software is used to assist in identifying areas of interest.

Results. We present five categories of spectral profiles within the general body of the flare ribbon: (1) Extremely broadened spectral line profiles, where the standard Fabry-Perot interferometer wavelength windows (≈ 70 km s−1) are insufficiently wide to allow for a complete analysis of the dynamics and atmospheric conditions. The mechanisms causing this degree of this broadening are not yet clearly understood. (2) Long-lived, dense kernels that manifest as more saturated chromospheric line profiles with lower signal in both Stokes parameters. They are interpreted as

footpoints of bunched magnetic field loops, whose chromospheric lines form at greater heights than the nearby areas. (3) Doppler-shifted leading edges of the flare ribbon in regions that transiently display lower Stokes signals due to the emission dominating at greater heights in the atmosphere. (4) Condensed coronal rain overlapping the flare ribbons in the line of sight, producing exceptionally high Doppler shifts near the footpoints. (5) Compact blue-shifted areas close to areas with coronal rain down-flows, which are interpreted as material that is thrown up as a result of the down-flowing material impacting the chromosphere. Additionally, a ribbon formation height of about 700 km with respect to penumbral features is estimated using correlating structures on the ribbon and the underlying photosphere. Conclusions. When selecting areas of flare ribbon for more general analysis, especially small regions consisting of a few pixels or low-resolution averages, it is important to be aware of the variety of substructures present within a flare ribbon, and of the spatial context that can produce these differences. General behaviors across the ribbon should not be inferred from regions that show localized differences. **6 Sep 2017**

A comparative study of two X2.2 and X9.3 solar flares observed with HARPS-N: Reconciling Sun-as-a-star spectroscopy and high-spatial resolution solar observations in the context of the solar-stellar connection

A. G. M. **Pietrow**, M. Cretignier, M. K. Druett, J. D. Alvarado-Gómez, +++
A&A 682, A46 **2024**
https://arxiv.org/pdf/2309.03373.pdf
https://www.aanda.org/articles/aa/pdf/2024/02/aa47895-23.pdf
Stellar flares cannot be spatially resolved, which complicates ascertaining the physical processes behind particular spectral signatures. Due to their proximity to Earth, solar flares can serve as a stepping stone for understanding their stellar counterparts, especially when using a Sun-as-a-star instrument and in combination with spatially resolved observations. We aim to understand the disk-integrated spectral behaviors of a confined X2.2 solar flare and its eruptive X9.3 successor as measured by HARPS-N. The behavior of multiple photospheric and chromospheric spectral lines are investigated by means of activity indices and contrast profiles. A number of different photospheric lines were also investigated by means of equivalent widths, and radial velocity measures, which are then related to physical processes directly observed in high-resolution observations made with the Swedish 1-meter Solar Telescope and SDO Our findings suggest a relationship between the evolving shapes of contrast profile time and the flare locations, which assists in constraining flare locations in disk-integrated observations. In addition, an upward bias was found in flare statistics based on activity indices derived from the Ca II H & K lines. In this case, much smaller flares cause a similar increase in the activity index as that produced by larger flares. Hα-based activity indices do not show this bias and are therefore less susceptible to activity jitter. Sodium line profiles show a strongly asymmetric response during flare activity, which is best captured with a newly defined asymmetrical sodium activity index. A strong flare response was detected in Mn I line profiles, which is unexpected and calls for further exploration. Intensity increases in Hα, Hβ, and certain spectral windows of AIA before the flare onset suggest their potential use as short-term flare predictors. **6 September 2017**

Physical properties of a fan-shaped jet backlit by an X9.3 flare

A.G.M. **Pietrow**, M. Druett, J. de la Cruz Rodriguez, F. Calvo, D. Kiselman
A&A **2021**
https://arxiv.org/pdf/2110.10541.pdf
Fan-shaped jets can be observed above light bridges and are driven by reconnection of the vertical umbral field with the more horizontal field above the light bridges. Because these jets are not fully opaque in chromospheric lines, one cannot study their spectra without the highly complex considerations of radiative transfer in spectral lines from the atmosphere behind the fan. We get around this by taking advantage of a unique set of observations of the Hα line along with the Ca II 8542 and Ca II K lines obtained with the Swedish 1-m Solar Telescope where a fan-shaped jet was backlit by an X9.3 flare. The Hα flare ribbon emission profiles from behind the fan are highly broadened and flattened, allowing us to investigate the fan as if it were backlit by continuous emission. Using this model we derived the opacity and velocity of the material in the jet and what we believe to be the first observationally derived estimate of the mass and density of material in a fan-shaped jet. Using inversions of Ca II 8542 emission via STiC, we were also able to estimate the temperature in the jet. Finally, we use the masses and POS and LOS velocities as functions of time to investigate the downward supply of energy and momentum to the photosphere in the collapse of this jet, and evaluate it as a potential driver for a sunquake beneath. We found that the physical properties of the fan material are reasonably chromospheric in nature, with a temperature of 7050 ± 250 K and a mean density of 2 ± 0.3 × 10−11 g cm−3. The total mass observed in \halpha~ was found to be 3.9 ± 0.7 × 1013g and the kinetic energy delivered to the base of the fan in its collapse was nearly two orders of magnitude below typical sunquake energies. We therefore rule out this jet as the sunquake driver, but cannot completely rule out larger fan jets as potential drivers. **6 Sep 2017**

Ubiquitous quiet-Sun jets

V. Martínez **Pillet**1, J. C. del Toro Iniesta2 and C. Quintero Noda
A&A 530, A111 (**2011**)

Aims. We attempt to identify the same quiet-Sun jets in the Hinode spectropolarimeter (SP) data set.
Methods. We generate combinations of linear polarization magnetograms with blue- and redshifted far-wing circular polarization magnetograms to allow an easy identification of the quiet-Sun jets.
Results. The jets are identified in the Hinode data where both red- and blueshifted cases are often found in pairs. They appear next to regions of transverse fields that exhibit quiet-Sun neutral lines. They also have a clear tendency to occur in the outer boundary of the granules. These regions always display highly displaced and anomalous Stokes V profiles.
Conclusions. The quiet Sun is pervaded with jets formed when new field regions emerge at granular scales loaded with horizontal field lines that interact with their surroundings. This interaction is suggestive of some form of reconnection of the involved field lines that generates the observed high speed flows**.**

Thermal and non-thermal emission from reconnecting twisted coronal loops

R. **Pinto**, M. Gordovskyy, P.K. Browning, N. Vilmer
A&A 585, A159 **2016**
http://arxiv.org/pdf/1506.01251v2.pdf
Context. Twisted magnetic fields should be ubiquitous in the solar corona, particularly in flare-producing active regions where the magnetic fields are strongly non-potential. The magnetic energy contained in such twisted fields can be released during solar flares and other explosive phenomena. It has recently been shown that reconnection in helical magnetic coronal loops results in plasma heating and particle acceleration distributed within a large volume, including the lower coronal and chromospheric sections of the loops. Hence, the magnetic reconnection and particle acceleration scenario involving magnetic helicity can be a viable alternative to the standard flare model, where particles are accelerated only in a small volume located in the upper corona.
Aims. The key goal of this study is to investigate the links and observational signatures of plasma heating and particle acceleration in kink-unstable twisted coronal loops.
Methods. We used a combination of magnetohydrodynamic (MHD) simulations and test-particle methods. These simulations describe the development of kink instability and magnetic reconnection in twisted coronal loops using resistive compressible MHD and incorporate atmospheric stratification and large-scale loop curvature. The resulting distributions of hot plasma let us estimate thermal X-ray emission intensities. With the electric and magnetic fields we obtained, we calculated electron trajectories using the guiding-centre approximation. These trajectories combined with the MHD plasma density distributions let us deduce synthetic hard X-ray bremsstrahlung intensities.
Results. Our simulations emphasise that the geometry of the emission patterns produced by hot plasma in flaring twisted coronal loops can differ from the actual geometry of the underlying magnetic fields. In particular, the twist angles revealed by the emission threads (soft X-ray thermal emission; SXR) are consistently lower than the field-line twist present at the onset of the kink instability. Hard X-ray (HXR) emission that is due to the interaction of energetic electrons with the stratified background is concentrated at the loop foot-points in these simulations, even though the electrons are accelerated everywhere within the coronal volume of the loop. The maximum of the HXR emission consistently precedes that of SXR emission, with the HXR light curve being approximately proportional to the temporal derivative of the SXR light curve.

Soft X-ray emission in kink-unstable coronal loops

R. F. **Pinto**, N. Vilmer, A. S. Brun
A&A, 576, A37 2015
http://arxiv.org/pdf/1401.0916v2.pdf
Context. Solar flares are associated with intense soft X-ray emission generated by the hot flaring plasma in coronal magnetic loops. Kink unstable twisted flux-ropes provide a source of magnetic energy which can be released impulsively and account for the heating of the plasma in flares. Aims. We investigate the temporal, spectral and spatial evolution of the properties of the thermal continuum X-ray emission produced in such kink-unstable magnetic flux-ropes and we discuss the results of the simulations with respect to solar flare observations. Methods. We compute the temporal evolution of the thermal X-ray emission in kink-unstable coronal loops based on a series of MHD numerical simulations. The numerical setup used consists of a highly twisted loop embedded in a region of uniform and untwisted background coronal magnetic field. We let the kink instability develop, compute the evolution of the plasma properties in the loop (density, temperature) without accounting for mass exchange with the chromosphere. We then deduce the X-ray emission properties of the plasma during the whole flaring episode. Results. During the initial (linear) phase of the instability plasma heating is mostly adiabatic (due to compression). Ohmic diffusion takes over as the instability saturates, leading to strong and impulsive heating (up to more than 20 MK), to a quick enhancement of X-ray emission and to the hardening of the thermal X-ray spectrum. The temperature distribution of the plasma becomes broad, with the emission measure depending strongly on temperature. Significant emission measures arise for plasma at temperatures higher than 9 MK. The magnetic flux-rope then relaxes progressively towards a lower energy state as it reconnects with the background flux. The loop plasma suffers smaller sporadic heating events but cools down globally by thermal conduction. The total thermal X-ray emission slowly fades away during this phase, and the high temperature component of emission measure distribution converges to the power-law distribution EM $\propto$ T^(−4.2). The amount of twist deduced

directly from the X-ray emission patterns is considerably lower than the maximum magnetic twist in the simulated flux-ropes.
See RHESSI Science Nugget No. 249, March **2015**
http://sprg.ssl.berkeley.edu/~tohban/wiki/index.php/Soft_X-ray_emission_in_kink-unstable_coronal_loops

Synergy of Stochastic and Systematic Energization of Plasmas during Turbulent Reconnection

Theophilos **Pisokas**, Loukas Vlahos, and Heinz Isliker
2018 ApJ 852 64
http://sci-hub.tw/10.3847/1538-4357/aaa1e0

The important characteristic of turbulent reconnection is that it combines large-scale magnetic disturbances $(\delta B/B \sim 1)$ with randomly distributed unstable current sheets (UCSs). Many well-known nonlinear MHD structures (strong turbulence, current sheet(s), shock(s)) lead asymptotically to the state of turbulent reconnection. We analyze in this article, for the first time, the energization of electrons and ions in a large-scale environment that combines large-amplitude disturbances propagating with sub-Alfvénic speed with UCSs. The magnetic disturbances interact stochastically (second-order Fermi) with the charged particles and play a crucial role in the heating of the particles, while the UCSs interact systematically (first-order Fermi) and play a crucial role in the formation of the high-energy tail. The synergy of stochastic and systematic acceleration provided by the mixture of magnetic disturbances and UCSs influences the energetics of the thermal and nonthermal particles, the power-law index, and the length of time the particles remain inside the energy release volume. We show that this synergy can explain the observed very fast and impulsive particle acceleration and the slightly delayed formation of a superhot particle population.
CESRA Highlight #1773 Feb **2018** http://www.astro.gla.ac.uk/users/eduard/cesra/?p=1773

Stochastic Fermi Energization of Coronal Plasma during explosive magnetic energy release

Theophilos **Pisokas**, Loukas Vlahos, Heinz Isliker, Vassilios Tsiolis, Anastasios Anastasiadis
ApJ **2016**
https://arxiv.org/pdf/1612.04246v1.pdf

The aim of this study is to analyze the interaction of charged particles (ions and electrons) with randomly formed particle scatterers (e.g.\ large scale local "magnetic fluctuations" or "coherent magnetic irregularities"), using the set up proposed initially by \cite{Fermi49}. These scatterers are formed by the explosive magnetic energy release and propagate with the Alfv\'en speed along the irregular magnetic fields. They are large scale local fluctuations (δB/B≈1), randomly distributed inside the unstable magnetic topology and will here be called {\bf Alfv\'enic Scatterers (AS)}. We constructed a 3D grid on which a small fraction of randomly chosen grid points are acting as AS. In particular, we study how a large number of test particles evolve inside a collection of AS, analyzing the evolution of their energy distribution and their escape time distribution. We use a well established method to estimate the transport coefficients directly from the trajectories of the particles. Using the estimated transport coefficients and solving the Fokker-Planck (FP) equation numerically, we can recover the energy distribution of the particles. We have shown that the Stochastic Fermi Energization (SFE) of mildly relativistic and relativistic plasma can heat and accelerate the tail of the ambient particle distribution as predicted by \citet{Parker58} and \citet{Ramaty79}. The temperature of the hot plasma and the tail of the energetic particles depend on the mean free path (λsc) of the particles between the scatterers inside the energization volume.
See Introduction

FAST DIFFERENTIAL EMISSION MEASURE INVERSION OF SOLAR CORONAL DATA

Joseph **Plowman**, Charles Kankelborg, and Petrus Martens
2013 ApJ 771 2

We present a fast method for reconstructing differential emission measures (DEMs) using solar coronal data. The method consists of a fast, simple regularized inversion in conjunction with an iteration scheme for removal of residual negative emission measure. On average, it computes over 1000 DEMs s–1 for a sample active region observed by the Atmospheric Imaging Assembly (AIA) on the Solar Dynamics Observatory, and achieves reduced chi-squared of order unity with no negative emission in all but a few test cases. The high performance of this method is especially relevant in the context of AIA, which images of order one million solar pixels per second. This paper describes the method, analyzes its fidelity, compares its performance and results with other DEM methods, and applies it to an active region and loop observed by AIA and by the Extreme-ultraviolet Imaging Spectrometer on Hinode.

A new catalogue of solar flare events from soft x-ray GOES signal in the period 1986-2020

Nicola **Plutino**, Francesco Berrilli, Dario Del Moro, Luca Giovannelli
Advances in Space Research Volume 71, Issue 4, 15 February **2023**, Pages 2048-2058
https://arxiv.org/pdf/2211.10189.pdf
https://doi.org/10.1016/j.asr.2022.11.020

Solar flares, along with other sun-originated events such as Coronal Mass Ejections, fast solar wind streams, and solar energetic particles are among the most relevant events in Space Weather. Moreover, solar flares are the most energetic processes that occur in our solar system. The in-depth study of their occurrence statistics, both over extended periods or during individual solar cycles, allows us to improve and constrain the basic physical models of their origin. Increasing the number of detected events, especially those of lower intensity, and the number of physical parameters that describe the detected flares is, therefore, a mandatory goal. In this paper, we present a computationally efficient algorithm for the detection of solar flares in the soft-X solar flux provided by the GOES (NASA/NOAA) satellite constellation. Our code produces a new flare catalogue increasing the number of events with respect to the official GOES list. In addition to increasing the number of identified events, the catalogue contains information such as: an estimate of the total energy released, start and end time of the event, possible overlap with other events, background level of the GOES X-ray emission close to the revealed event. After a detailed description of the detection algorithm, we carry out a preliminary analysis of the flares reported in our catalogue and compare our results with the official list of GOES for the period from 1998 to 2020. **2 Nov 1987, 1 Jan 2001, 3 Mar 2001**

X8.2 Solar flare on the rear side of the solar disk: An evidence for the current sheet as a mechanism for cosmic ray acceleration

I.M. **Podgorny** 1 , A.I. Podgorny 2
Sun and Geosphere, **2019**; 14/1: 13 -19
http://newserver.stil.bas.bg/SUNGEO//00SGArhiv/SG_v14_No1_2019-pp-13-19.pdf
The X8.2 flare occurred on 2017 September 11 during the minimum period of solar activity. The flare is appeared over the active region AR12673. This active region produces two large and many small flares. The solar cosmic rays have been observed in association with the X8.2 flare. The active region at that time is situated on the back side of the Sun disk behind the Western limb. The front of the accelerated protons flux arrives to the Earth with the delay not exceeding the proton flight time from the Sun. Such proton propagation can occur only along the lines of the interplanetary magnetic field. The solar proton acceleration takes place by electric filed along a singular line of the current sheet above an active region. There is no reason to believe that the mechanisms of cosmic ray acceleration on the Sun and other stars are of different nature. The results of observations of accelerated electrons on the SOHO/EPHIN instrument show that electrons are accelerated and propagated during flares together with protons. At the same time, a simple analysis of the GOES results leads to the conclusion that the flux of relativistic electrons does not show any connection with the recorded solar cosmic rays. Currently, this contradiction cannot be explained. Photos in spectral lines of ions obtained on the SDO spacecraft are used to study the pre-flare state and flare development. The source of flare radiation in the spectral lines of the highly ionized irons FeXXIV and FeXXIII is observed in the corona outside the solar limb. The emission of these spectral lines sharply increases during appearing of flare X-ray radiation. The energy release of a flare occurs in the corona above an active region. The temperature in the flare is greater than 20 MK. The size of the hot plasma cloud is ~1010 cm.

Current sheets in corona and X-ray sources for flares above the active region 10365

A.I. **Podgorny**, I.M. Podgorny, N.S. Meshalkina
Journal of Atmospheric and Solar-Terrestrial Physics Volume 180, November **2018** Pages 16-25
sci-hub.tw/10.1016/j.jastp.2018.02.009
The coincidence of current sheets positions obtained from results of numerical MHD simulation for flares **May 27, 2003** at 02:53 UT and **May 29, 2003** at 00:51 UT with positions of observed X-ray sources confirm the mechanism of solar flareaccording to which the magnetic energy of the current sheet is released in corona above an active region. To study the magnetic field configuration obtained from 3D MHD simulation, the system of graphic presentation is developed. Magnetic fieldlines in 3D space have a complex configuration near a current sheet above the active region which can be investigated using the developed system of visualization. The physical meaning of the processes in the current sheet is best demonstrated by the lines in the plane of the current sheet configuration which are tangential to the projections of the magnetic field vectors on this plane. Position of such lines defines the magnetic forces, which create the current sheet and then destroy it, when the system turns into an unstable state. Analysis of magnetic lines in large area above the active region allows make a preliminary conclusion about existence of the magnetic lines that connect the hard X-ray sources and the current sheet.

Diagnostic of a Solar Flare via Analyses of Emission in Spectral Lines of Highly Ionized Iron

I. M. **Podgorny** 1 , A. I. Podgorny
Astronomy Reports October **2018**, Volume 62, Issue 10, pp 696–704
Astronomicheskii Zhurnal, 2018, Vol. 95, No. 10, pp. 735–744
https://link.springer.com/content/pdf/10.1134%2FS1063772918100074.pdf
An analysis of the dynamics of the electron temperature of the solar atmosphere in regions where solar flares appear is presented. The temperatures are estimated from the emission in spectral lines of ions with various degrees of ionization. The emission of ionized helium and highly ionized iron was used. Images of preflare states and of flares from the archive of the American SDO spacecraft are analyzed. A solar flare is usually preceded by the registration of a bright

glowing structure above the action region, with a temperature exceeding that of the corona. This preflare structure (~1010 cm) is identified with the development of a system of currents, which, according to numerical simulations, is responsible for the accumulation of energy above the active region before the flare. After several tens of hours of a slow increase in the brightness of the preflare glow in the 94 Å iron (FeXVIII) line, the emission in the 193 Å line of FeXXIV increases sharply, indicating a flare-like growth of the temperature up to at least 20 MK. This growth of the emission coincides with the onset of the solar flare. The observed dynamics of the emission in spectral lines of highly ionized ions is consistent with an electrodynamic model of a solar flare based on the accumulation of magnetic energy in a current sheet above the active region and the explosive release of the stored energy. Studies of mechanisms for solar flares are of special importance in connection with the discovery of solar cosmic rays. Information from the worldwide network of neutron monitors and from the GOES spacecraft has made it possible to firmly state that the source of solar rays is solar flares, not shocks generated by such flares. It cannot be ruled out that a similar mechanism, not shocks, is also responsible for the acceleration of cosmic rays in the Galaxy.

Diagnostics of Solar Flares by Analyzing the Spectral Lines Emission of Highly Ionized Irons

I. M. **Podgorny** 1 , A. I. Podgorny

Proceedings of Ninth Workshop “Solar Influences on the Magnetosphere, Ionosphere and Atmosphere” Sunny Beach, Bulgaria, May 30 - June 3, **2017**, p. 01-07

http://ws-sozopol.stil.bas.bg/2017Sunny/Proceedings2017_V3.pdf

The photos of the pre-flare development observed in the spectral lines of highly ionized iron (SDO AIA apparatus) indicate the energy accumulation for a flare in the corona in the pre-flare local (about 1010 cm) high temperature structure. The pre-flare structures in the corona are observed in UV spectral lines of ions FeXXIV, FeXXIII, FeXVIII several hours before big solar flares. During a flare the emission of the UV spectral lines in the corona are increased explosively. These phenomena can be used for prediction of solar cosmic rays. Information obtained from the worldwide neutron monitor network and measurements on GOES spacecraft demonstrates unambiguously that solar cosmic rays are generated in solar flares. These phenomena are well described by the solar flare electrodynamical model, created on the basis of the observational data and the numerical magnetohydrodynamic simulation using the initial and boundary conditions, taken from the active regions observation before the flare. It is impossible to exclude that the similar mechanism of particle acceleration is responsible for galactic cosmic rays generation. Now all published mechanisms of cosmic ray generation are based on unproven assumptions. These assumptions are not confirmed by longterm observations. With the modern concept of cosmic rays, a fundamentally important question arises: can the mechanism of proton acceleration in solar flares explain the acceleration of particles of galactic cosmic rays. **10.09.2014**

Magnetic field configuration in corona and X-ray sources for the flare from May 27, 2003 at 02:53

A.I. **Podgorny**, I. M. Podgorny, N. S. Meshalkina.

Sun and Geosphere, **2017**; 12/2: 85 -92

http://newserver.stil.bas.bg/SUNGEO//00SGArhiv/SG_v12_No2_2017-pp-85-92.pdf

Numerical MHD simulation above the real active region of the solar corona shows the current sheet creation before a flare. The system of graphic output is developed here, which permits to study the magnetic field configuration obtained from the presented MHD simulation. The physical meaning of the flare energy accumulation and rapid release processes is best demonstrated by the lines in the plane of the current sheet configuration which are tangential to the projections of the magnetic field vectors on this plane. The magnetic j×B/c forces are perpendicular to these lines. Position of such lines defines the magnetic forces, which create the current sheet and then destroy it, when the system transforms in unstable state. The magnetic lines can be analyzed in complicated magnetic configuration near a current sheet and in corona above the active region using the developed graphical system.

Magnetic field distribution in the flare productive active region NOAA 10720

I.M. **Podgorny**, A.I. Podgorny

Journal of Atmospheric and Solar-Terrestrial Physics, Volume 92, January **2013**, Pages 59–64

Association of the active region NOAA 10720 magnetic flux and flare appearance is investigated. Distributions of the normal magnetic component in the active region are calculated in the potential approximation using SOHO MDI line-of-sight magnetic measurements. During traveling along the solar disk the magnetic flux of the active region increases up to 4×1022 Mx. The X class solar flares appear, when the magnetic flux reaches . It is shown that the magnetic flux and the magnetic field distribution in the active region in the long duration X3.8 flare **January 17, 2005** do not reveal considerable change. During the flare X3.8 magnetic energy flow from the photosphere is not observed. The obtained results show that flare energy released in the corona has been accumulated during the preflare time. This conclusion supports the flare model based on the conception of flare energy accumulation in the magnetic field of a coronal current sheet.

MHD simulation of magnetic field configuration above the active region NOAA 10365

A.I. **Podgorny**, I.M. Podgorny
Advances in Space Research, Volume 50, Issue 10, **2012**, Pages 1445–1449
The current sheet (CS) creation before a flare in the vicinity of a singular line above the active region NOAA 10365 is shown in numerical experiments. Such a way the possibility of energy accumulation for a solar flare is demonstrated. These data and results of observation confirm the electrodynamical solar flare model that explains solar flares and CME appearance during CS disruption. The model explains also all phenomena observed in flares. For correct reproduction of the real boundary conditions the magnetic flux between spots should be taken into account. The full system of 3D MHD equations are solved using the PERESVET code. For setting the boundary conditions the method of photospheric magnetic maps is used. Such a method permits to take into account all evolution of photospherical magnetic field during several days before the flare.

Magnetic flux in an active solar region and its correlation with flares

A. I. **Podgorny** & I. M. Podgorny
Astronomy Reports, Volume 55 Number 7, 629-636, **2011**
The correlation between the magnetic flux in an active solar region and associated powerful solar flares is studied. The behavior of the active regions AR **10486** and AR **10365** is considered. These regions produced a series of class X flares as they crossed the solar disk. The flares appeared when the magnetic flux exceeded 1022 Mx. The magnetic flux remained constant during all the flares except for one. During this flare, the flux decreased by about 10%; this impulsive decrease of the flux was also recorded in the absence of flares. No energy flux from the photosphere to the corona at the time of the flare was observed. The behavior of the photospheric field in AR 10486 and AR 10365 is consistent with a slow accumulation of energy in the corona and the explosive release of energy stored in the magnetic field of a current sheet above an active region during the flare.
Original Russian Text - Astronomicheskii Zhurnal, 2011, Vol. 88, No. 7, pp. 684–691, 2011

A Model of a Solar Flare: Comparisons with Observations of High-Energy Processes

A. I. **Podgorny** and I. M. Podgorny
*Astronomy Reports, **2006**, Vol. 50, No. 10, pp. 842–850 (Astronomicheskiĭ Zhurnal, 2006, Vol. 83, No. 10, pp. 940–949).*

Real-time Flare Detection in Ground-based H α Imaging at Kanzelh?he Observatory

Poetzi, Werner, Veronig, A.M., Riegler, G., Amerstorfer, U., Pock, Th., Temmer, M., Polanec, W., Baumgartner, D.J.
Solar Phys., **201**4
http://arxiv.org/pdf/1411.3896v2.pdf
Kanzelh\"ohe Observatory (KSO) regularly performs high-cadence full-disk imaging of the solar chromosphere in the Hα and CaIIK spectrallines as well as the solar photosphere in white-light. In the frame of ESA's Space Situational Awareness (SSA) programme, a new system for real-time Hα data provision and automatic flare detection was developed at KSO. The data and events detected are published in near real-time at ESA's SSA Space Weather portal (this http URL). In this paper, we describe the Hα instrument, the image recognition algorithms developed, the implementation into the KSO Hα observing system and present the evaluation results of the real-time data provision and flare detection for a period of five months. The Hα data provision worked in 99.96% of the images, with a mean time lag between image recording and online provision of 4s. Within the given criteria for the automatic image recognition system (at least three Hα images are needed for a positive detection), all flares with an area ≥50 micro-hemispheres and located within 60◦ of the Sun's center that occurred during the KSO observing times were detected, in total a number of 87 events. The automatically determined flare importance and brightness classes were correct in ∼85%. The mean flare positions in heliographic longitude and latitude were correct within ∼1◦. The median of the absolute differences for the flare start times and peak times from the automatic detections in comparison to the official NOAA (and KSO) visual flare reports were 3 min (1 min).

Modeling Global Magnetic-Flux Emergence in Bipolar Solar-Active Regions.

Poisson, M., López Fuentes, M., Mandrini, C.H. et al.
Sol Phys 299, 56 (**2024**).
https://doi.org/10.1007/s11207-024-02303-0
Active regions (ARs) appear in the solar atmosphere as a consequence of the emergence of magnetic-flux ropes (FR). In this study, we use Bayesian methods to analyze line-of-sight magnetograms of emerging ARs. We employ a FR model consisting of a half-torus field structure based on eight parameters. The goal is to derive constrained physical parameters of the originating FR that are consistent with the observations. Specifically, we aim to obtain a precise

estimation of the AR tilt angle and magnetic twist at different stages of the emergence process. To achieve this, we propose four temporal methods that correlate the field-parameter evolutions with a single coherent FR. These methods differ from each other in the size of the explored parameter space. We test the methods on four bipolar ARs observed with the Michelson Doppler Imager on board the Solar and Heliospheric Observatory. We find that tilt angles are typically consistent between the temporal methods, improving previous estimations at all stages of the emergence. The twist sign derived from the temporal methods is consistent with previous estimations. The standard errors of all the methods used are similar, indicating that they model the observations equally well. These results indicate that the proposed methods can be used to obtain global magnetic parameters of ARs during their early evolution. The derived parameters contribute to a better understanding of the formation of FRs, and the role of ARs in the magnetic recycling process along the solar cycle.

Multi-wavelength observations and modelling of a microflare: constraining non-thermal particle acceleration

Vanessa **Polito** [1,2], Marianne Peterson [3], Lindsay Glesener [3], Paola Testa [4], Sijie Yu [5], Katharine K. Reeves [4], Xudong Sun [6], Jessie Duncan [7]
Front. Astron. Space Sci. 10: 1214901. **2023**
https://www.frontiersin.org/articles/10.3389/fspas.2023.1214901/pdf
In this work we analyze a small B-class flare that occurred on **29 April 2021** and was observed simultaneously by the Interface Region Imaging Spectrograph (IRIS) and the Nuclear Spectroscopic Telescope Array (NuSTAR) X-ray instrument. The IRIS observations of the ribbon of the flare show peculiar spectral characteristics that are typical signatures of energy deposition by non-thermal electrons in the lower atmosphere. The presence of the non-thermal particles is also confirmed directly by fitting the NuSTAR spectral observations. We show that, by combining IRIS and NuSTAR multi-wavelength observations from the corona to the lower atmosphere with hydrodynamic simulations using the RADYN code, we can provide strict constraints on electron-beam heated flare models. This work presents the first NuSTAR, IRIS and RADYN joint analysis of a non-thermal microflare, and presents a self-consistent picture of the flare-accelerated electrons in the corona and the chromospheric response to those electrons. **April 29th 2021**
IRIS Nugget 14 Aug **2023** https://iris.lmsal.com/nugget

Solar Flare Ribbon Fronts I: Constraining flare energy deposition with IRIS spectroscopy

Vanessa **Polito**, Graham S. Kerr, Yan Xu, Viacheslav M. Sadykov, Juraj Lorincik
https://arxiv.org/pdf/2211.05333.pdf
ApJ **944** 104 **2023**
https://arxiv.org/pdf/2211.05333.pdf
https://iopscience.iop.org/article/10.3847/1538-4357/acaf7c/pdf
Lower atmospheric lines show peculiar profiles at the leading edge of ribbons during solar flares. In particular, increased absorption of the BBSO/GST \hei~10830~Å line \citep[e.g.][]{Xu2016}, as well as broad and centrally reversed profiles in the spectra of the \mgii~and \cii~lines observed by the \iris~satellite \citep[e.g.][]{Panos2018,Panos2021a} have been reported. In this work, we aim to understand the physical origin of the \iris\ ribbon front line profiles, which seem to be common of many, if not all, flares. To achieve this, we quantify the spectral properties of the \iris~\mgii~ribbon front profiles during four large flares and perform a detailed comparison with a grid of radiative hydrodynamic models using the \radynfp~code. We also studied their transition region counterparts, finding that these ribbon front locations are regions where transition region emission and chromospheric evaporation are considerably weaker compared to other parts of the ribbons. Based on our comparison between the \iris~observations and modelling, our interpretation is that there are different heating regimes at play in the leading and trailing regions of the ribbons. More specifically, we suggest that bombardment of the chromosphere by more gradual and modest non-thermal electron energy fluxes can qualitatively explain the \iris~observations at the ribbon front, while stronger and more impulsive energy fluxes are required to drive chromospheric evaporation and more intense TR emission. Our results provide a possible physical origin for the peculiar behaviour of the \iris~chromospheric lines in the ribbon leading edge and new constraints for the flare models. **2014-08-01, 2014-09-10, 2014-10-27, 2015-06-22**

Can the Superposition of Evaporative Flows Explain Broad Fe xxi Profiles during Solar Flares?

Vanessa **Polito**1, Paola Testa1, and Bart De Pontieu2,3
2019 ApJL 879 L17
sci-hub.se/10.3847/2041-8213/ab290b
The observation of the high-temperature ($\gtrsim$10 MK) Fe xxi 1354.1 Å line with the Interface Region Imaging Spectrograph has provided significant insights into the chromospheric evaporation process in flares. In particular, the line is often observed to be completely blueshifted, in contrast to previous observations at lower spatial and spectral resolution, and in agreement with predictions from theoretical models. Interestingly, the line is also observed to be mostly symmetric and significantly broader than expected from thermal motions (assuming the peak formation temperature of the ion is in equilibrium). One popular interpretation for the nonthermal broadening is the superposition

of flows from different loop strands. In this work, we test this scenario by forward-modeling the Fe xxi line profile assuming different possible observational scenarios using hydrodynamic simulations of multi-thread flare loops with the 1D RADYN code. Our results indicate that the superposition of flows alone cannot easily reproduce both the symmetry and the significant broadening of the line and that some other physical process, such as turbulence, or a much larger ion temperature than previously expected, likely needs to be invoked in order to explain the observed profiles. **2014 September 10**
RHESSI Nuggets #377 April **2020** http://sprg.ssl.berkeley.edu/~tohban/wiki/index.php/Broad_symmetrical_Doppler-shifted_Fe_XXI_line_profiles

Possible Signatures of a Termination Shock in the 2014 March 29 X-class Flare Observed by IRIS

Vanessa **Polito**1, Giselle Galan2, Katharine K. Reeves1, and Sophie Musset3
2018 ApJ 865 161
sci-hub.tw/10.3847/1538-4357/aadada
The standard model of flares predicts the existence of a fast-mode magnetohydrodynamic shock above the looptops, also known as termination shock (TS), as the result of the downward-directed outflow reconnection jets colliding with the closed magnetic loops. A crucial spectral signature of a TS is the presence of large Doppler shifts in the spectra of high-temperature lines (≥10 MK), which has been rarely observed so far. Using high-resolution observations of the Fe xxi line with the Interface Region Imaging Spectrograph (IRIS), we detect large redshifts (≈200 km s−1) at the top of the bright looptop arcade of the X1-class flare on 2014 March 29. In some cases, the redshifts are accompanied by faint simultaneous Fe xxi blueshifts of about −250 km s−1. The values of red and blueshifts are in agreement with recent modeling of Fe xxi spectra downflow of the reconnection site and previous spectroscopic observations with higher temperature lines. The locations where we observe the Fe xxi shifts are co-spatial with 30–70 keV hard X-ray sources detected by the Reuven Ramaty High Energy Solar Spectroscopic Imager (RHESSI), indicating that nonthermal electrons are located above the flare loops. We speculate that our results are consistent with the presence of a TS in flare reconnection models.

Broad Non-Gaussian Fe XXIV Line Profiles in the Impulsive Phase of the 2017 September 10 X8.3 class Flare Observed by Hinode/EIS

Vanessa **Polito**, Jaroslav Dudík, Jana Kašparová, Elena Dzifčáková, Katharine K. Reeves, Paola Testa, Bin Chen
2018 ApJ 864 63
https://arxiv.org/pdf/1807.09361.pdf
http://sci-hub.tw/http://iopscience.iop.org/article/10.3847/1538-4357/aad62d/meta
We analyze the spectra of high temperature \fexxiv~lines observed by \emph{Hinode}/EIS during the impulsive phase of the X8.3--class flare on **September 10, 2017**. The line profiles are broad, show pronounced wings, and clearly depart from a single Gaussian shape. The lines can be well fitted with κ distributions, with values of κvarying between~≈1.7 to 3. The regions where we observe the non-Gaussian profiles coincide with the location of high-energy (≈100--300 keV) HXR sources observed by \emph{RHESSI}, suggesting the presence of particle acceleration or turbulence, also confirmed by the observations of a non-thermal microwave sources with the \emph{Expanded Owens Valley Solar Array} (EOVSA) at and above the HXR looptop source. We also investigate the effect of taking into account κ distributions in the temperature diagnostics based on the ratio of the \fexxiii~263.76~\AA~and \fexxiv~255.1~\AA~EIS lines. We found that these lines can be formed at much higher temperatures than expected (up to log(T\,[K])\,≈\,7.8), if departures from Maxwellian distributions are taken into account. Although larger line widths are expected because of these higher formation temperatures, the observed line widths still imply non-thermal broadening in excess of ~200\,\kps. The non-thermal broadening related to HXR emission is better interpreted by turbulence rather than chromospheric evaporation.

Investigating the Response of Loop Plasma to Nanoflare Heating Using RADYN Simulations

V. **Polito**1, P. Testa1, J. Allred2, B. De Pontieu3,4,5, M. Carlsson4,5, T. M. D. Pereira4,5,Milan Gošić3,6, and Fabio Reale7
2018 ApJ 856 178
http://sci-hub.tw/http://iopscience.iop.org/0004-637X/856/2/178/
https://arxiv.org/pdf/1804.05970.pdf
We present the results of 1D hydrodynamic simulations of coronal loops that are subject to nanoflares, caused by either in situ thermal heating or nonthermal electron (NTE) beams. The synthesized intensity and Doppler shifts can be directly compared with Interface Region Imaging Spectrograph (IRIS) and Atmospheric Imaging Assembly (AIA) observations of rapid variability in the transition region (TR) of coronal loops, associated with transient coronal heating. We find that NTEs with high enough low-energy cutoff (E_C) deposit energy in the lower TR and chromosphere, causing blueshifts (up to ~20 km s−1) in the IRIS Si iv lines, which thermal conduction cannot reproduce. The E_C threshold value for the blueshifts depends on the total energy of the events (≈5 keV for 1024 erg, up to 15 keV for

1025 erg). The observed footpoint emission intensity and flows, combined with the simulations, can provide constraints on both the energy of the heating event and E_C. The response of the loop plasma to nanoflares depends crucially on the electron density: significant Si iv intensity enhancements and flows are observed only for initially low-density loops (<109 cm−3). This provides a possible explanation of the relative scarcity of observations of significant moss variability. While the TR response to single heating episodes can be clearly observed, the predicted coronal emission (AIA 94 Å) for single strands is below current detectability and can only be observed when several strands are heated closely in time. Finally, we show that the analysis of the IRIS Mg ii chromospheric lines can help further constrain the properties of the heating mechanisms.

Analysis and modelling of recurrent solar flares observed with Hinode/EIS on March 9, 2012

V. **Polito**, G. Del Zanna, G. Valori, E. Pariat, H. E. Mason, J. Dudik, M. Janvier
A&A 601, A39 **(2017)**
https://arxiv.org/pdf/1612.03504v1.pdf

Three homologous C-class flares and one last M-class flare were observed by both the Solar Dynamics Observatory (SDO) and the Hinode EUV Imaging Spectrometer (EIS) in the AR 11429 on **March 9, 2012**. All the recurrent flares occurred within a short interval of time (less than 4 hours), showed very similar plasma morphology and were all confined, until the last one when a large-scale eruption occurred. The C-class flares are characterized by the appearance, at approximatively the same locations, of two bright and compact footpoint sources of ≈∼3--10∼MK evaporating plasma, and a semi-circular ribbon. During all the flares, the continuous brightening of a spine-like hot plasma (≈∼10∼MK) structure is also observed. Spectroscopic observations with Hinode/EIS are used to measure and compare the blueshift velocities in the \fexxiii\ emission line and the electron number density at the flare footpoints for each flare. Similar velocities, of the order of 150--200∼km∼s−1, are observed during the C2.0 and C4.7 confined flares, in agreement with the values reported by other authors in the study of the last M1.8 class flare. On the other hand, lower electron number densities and temperatures tend to be observed in flares with lower peak soft X-ray flux.In order to investigate the homologous nature of the flares, we performed a Non-Linear Force-Free Field (NLFFF) extrapolation of the 3D magnetic field configuration in the corona. The NLFFF extrapolation and the Quasi-Separatrix Layers (QSLs) provide the magnetic field context which explains the location of the kernels, spine-like and semi-circular brightenings observed in the (non-eruptive) flares. Given the absence of a coronal null point, we argue that the homologous flares were all generated by the continuous recurrence of bald patch reconnection.

SIMULTANEOUS IRIS AND HINODE/EIS OBSERVATIONS AND MODELING OF THE 2014 OCTOBER 27 X2.0 CLASS FLARE

V. **Polito**1, J. W. Reep1,2, K. K. Reeves3, P. J. A. Simões4, J. Dudík5, G. Del Zanna1, H. E. Mason1, and L. Golub
2016 ApJ 816 89

We present a study of the X2-class flare which occurred on **2014 October 27** and was observed with the Interface Region Imaging Spectrograph (IRIS) and the EUV Imaging Spectrometer (EIS) on board the Hinode satellite. Thanks to the high cadence and spatial resolution of the IRIS and EIS instruments, we are able to compare simultaneous observations of the Fe xxi 1354.08 Å and Fe xxiii 263.77 Å high-temperature emission (10 MK) in the flare ribbon during the chromospheric evaporation phase. We find that IRIS observes completely blueshifted Fe xxi line profiles, up to 200 km s−1 during the rise phase of the flare, indicating that the site of the plasma upflows is resolved by IRIS. In contrast, the Fe xxiii line is often asymmetric, which we interpret as being due to the lower spatial resolution of EIS. Temperature estimates from SDO/AIA and Hinode/XRT show that hot emission (log(T[K]) > 7.2) is first concentrated at the footpoints before filling the loops. Density-sensitive lines from IRIS and EIS give estimates of electron number density of 1012 cm−3 in the transition region lines and 1010 cm−3 in the coronal lines during the impulsive phase. In order to compare the observational results against theoretical predictions, we have run a simulation of a flare loop undergoing heating using the HYDRAD 1D hydro code. We find that the simulated plasma parameters are close to the observed values that are obtained with IRIS, Hinode, and AIA. These results support an electron beam heating model rather than a purely thermal conduction model as the driving mechanism for this flare.
See UKSP Nugget #61, Sept **2015**
http://www.uksolphys.org/uksp-nugget/61-simultaneous-iris-and-hinodeeis-observation-and-modelling-of-an-x-class-flare/ **27 October 2014**

JOINT HIGH TEMPERATURE OBSERVATION OF A SMALL C6.5 SOLAR FLARE WITH IRIS/EIS/AIA

Polito V., Reeves, K.K., Del Zanna, G., Golub, L., Mason, H.E.
2015 *ApJ* **803** 84
http://www.damtp.cam.ac.uk/user/astro/papers/polito+2015.pdf

We present the observation of a C6.5 class flare on **2014 February 3**, obtained with the Interface Region Imaging Spectrograph (IRIS) and the EUV Imaging Spectrometer (EIS) on board HINODE. We follow the details of the impulsive phase with IRIS and the gradual decay phase with both IRIS and EIS. The IRIS Slit-Jaw Imager and Atmospheric Imaging Assembly (AIA) are used to precisely co-align the two sets of spectroscopic observations. Of particular interest is the Fe XXI 1354.08 ? spectral line, which is the highest temperature emission (~ 10 MK) observed in the IRIS wavelength range. We show the evolution of the Fe XXI profiles during the impulsive phase of the flare at the same ribbon location with a 75 s temporal cadence. Totally blue-shifted (~ 82 km s-1) profiles are found at the very early phase of the flare and gradually decrease in about 6 minutes. This result is consistent with 1-D model predictions during chromospheric evaporation in flares. The blue shifted components also exhibit large non-thermal broadening, which decrease simultaneously with the blue-shifted velocity. After the evaporation first occurs, the Fe XXI intensity progressively moves from the footpoints to the top of the hot flare loops seen in the AIA 131 ? images, where the emission is observed to be at rest and thermal. Emission measure estimates from IRIS/EIS/AIA observations during the gradual phase show isothermal loop top structures cooling from about 13.5 MK to 12 MK with electron densities of the order ~ 5 − 6 ? 10^10 cm −3 .

Time-dependent Data-driven Modeling of Active Region Evolution Using Energy-optimized Photospheric Electric Fields

Jens **Pomoell**, Erkka Lumme, Emilia Kilpua
Solar Physics April **2019**, 294:41
https://link.springer.com/content/pdf/10.1007%2Fs11207-019-1430-x.pdf
In this work, we present results of a time-dependent data-driven numerical simulation developed to study the dynamics of coronal active region magnetic fields. The evolving boundary condition driving the model, the photospheric electric field, is inverted using a time sequence of vector magnetograms as input. We invert three distinct electric field datasets for a single active region. All three electric fields reproduce the observed evolution of the normal component of the magnetic field. Two of the datasets are constructed so as to match the energy input into the corona to that provided by a reference estimate. Using the three inversions as input to a time-dependent magnetofrictional model, we study the response of the coronal magnetic field to the driving electric fields. The simulations reveal the magnetic field evolution to be sensitive to the input electric field despite the normal component of the magnetic field evolving identically and the total energy injection being largely similar. Thus, we demonstrate that the total energy injection is not sufficient to characterize the evolution of the coronal magnetic field: coronal evolution can be very different despite similar energy injections. We find the relative helicity to be an important additional metric that allows one to distinguish the simulations. In particular, the simulation with the highest relative helicity content produces a coronal flux rope that subsequently erupts, largely in agreement with extreme-ultraviolet imaging observations of the corresponding event. Our results suggest that time-dependent data-driven simulations that employ carefully constructed driving boundary conditions offer a valuable tool for modeling and characterizing the evolution of coronal magnetic fields. **2012.06.11-15**

Stochastic Acceleration of Electrons by Fast Magnetosonic Waves in Solar Flares: the Effects of Anisotropy in Velocity andWavenumber Space

Peera **Pongkitiwanichaku**l, Benjamin D. G. Chandran
2014 ApJ 796 45
http://arxiv.org/pdf/1406.0802v1.pdf
We develop a model for stochastic acceleration of electrons in solar flares. As in several previous models, the electrons are accelerated by turbulent fast magnetosonic waves ("fast waves") via transit-time-damping (TTD) interactions. (In TTD interactions, fast waves act like moving magnetic mirrors that push the electrons parallel or anti-parallel to the magnetic field). We also include the effects of Coulomb collisions and the waves' parallel electric fields. Unlike previous models, our model is two-dimensional in both momentum space and wavenumber space and takes into account the anisotropy of the wave power spectrum Fk and electron distribution function fe. We use weak turbulence theory and quasilinear theory to obtain a set of equations that describes the coupled evolution of Fk and fe. We solve these equations numerically and find that the electron distribution function develops a power-law-like non-thermal tail within a restricted range of energies E∈(Ent, Emax). We obtain approximate analytic expressions for Ent and Emax, which describe how these minimum and maximum energies depend upon parameters such as the electron number density and the rate at which fast-wave energy is injected into the acceleration region at large scales. We contrast our results with previous studies that assume that Fk and fe are isotropic, and we compare one of our numerical calculations with the time-dependent hard-x-ray spectrum observed during the June 27, 1980 flare. In our numerical calculations, the electron energy spectra are softer (steeper) than in models with isotropic Fk and fe and closer to the values inferred from observations of solar flares.

THE EFFECTS OF WAVE ESCAPE ON FAST MAGNETOSONIC WAVE TURBULENCE IN SOLAR FLARES

Peera **Pongkitiwanichakul**1, Benjamin D. G. Chandran1, Judith T. Karpen2, and C. Richard DeVor

2012 ApJ 757 72
One of the leading models for electron acceleration in solar flares is stochastic acceleration by weakly turbulent fast magnetosonic waves ("fast waves"). In this model, large-scale flows triggered by magnetic reconnection excite large-wavelength fast waves, and fast-wave energy then cascades from large wavelengths to small wavelengths. Electron acceleration by large-wavelength fast waves is weak, and so the model relies on the small-wavelength waves produced by the turbulent cascade. In order for the model to work, the energy cascade time for large-wavelength fast waves must be shorter than the time required for the waves to propagate out of the solar-flare acceleration region. To investigate the effects of wave escape, we solve the wave kinetic equation for fast waves in weak turbulence theory, supplemented with a homogeneous wave-loss term. We find that the amplitude of large-wavelength fast waves must exceed a minimum threshold in order for a significant fraction of the wave energy to cascade to small wavelengths before the waves leave the acceleration region. We evaluate this threshold as a function of the dominant wavelength of the fast waves that are initially excited by reconnection outflows.

Magnetic reconnection: MHD theory and modelling. **Review**

Pontin, D.I., Priest, E.R.
Living Rev Sol Phys 19, 1 (**2022**).
https://link.springer.com/content/pdf/10.1007/s41116-022-00032-9.pdf
In this review we focus on the fundamental theory of magnetohydrodynamic reconnection, together with applications to understanding a wide range of dynamic processes in the solar corona, such as flares, jets, coronal mass ejections, the solar wind and coronal heating. We summarise only briefly the related topics of collisionless reconnection, non-thermal particle acceleration, and reconnection in systems other than the corona. We introduce several preliminary topics that are necessary before the subtleties of reconnection can be fully described: these include null points (Sects. 2.1–2.2), other topological and geometrical features such as separatrices, separators and quasi-separatrix layers (Sects. 2.3, 2.6), the conservation of magnetic flux and field lines (Sect. 3), and magnetic helicity (Sect. 4.6). Formation of current sheets in two- and three-dimensional fields is reviewed in Sect. 5. These set the scene for a discussion of the definition and properties of reconnection in three dimensions that covers the conditions for reconnection, the failure of the concept of a flux velocity, the nature of diffusion, and the differences between two-dimensional and three-dimensional reconnection (Sect. 4). Classical 2D models are briefly presented, including magnetic annihilation (Sect. 6), slow and fast regimes of steady reconnection (Sect. 7), and non-steady reconnection such as the tearing mode (Sect. 8). Then three routes to fast reconnection in a collisional or collisionless medium are described (Sect. 9). The remainder of the review is dedicated to our current understanding of how magnetic reconnection operates in three dimensions and in complex magnetic fields such as that of the Sun’s corona. In Sects. 10–12, 14.1 the different regimes of reconnection that are possible in three dimensions are summarised, including at a null point, separator, quasi-separator or a braid. The role of 3D reconnection in solar flares (Sect. 13) is reviewed, as well as in coronal heating (Sect. 14), and the release of the solar wind (Sect. 15.2). Extensions including the role of reconnection in the magnetosphere (Sect. 15.3), the link between reconnection and turbulence (Sect. 16), and the role of reconnection in particle acceleration (Sect. 17) are briefly mentioned.

Why are flare ribbons associated with the spines of magnetic null points generically elongated?

D. I. **Pontin**, K. Galsgaard, P. Demoulin
Solar Phys. Volume 291, Issue 6, pp 1681-1710 **2016**
http://arxiv.org/pdf/1605.05704v1.pdf
Coronal magnetic null points exist in abundance as demonstrated by extrapolations of the coronal field, and have been inferred to be important for a broad range of energetic events. These null points and their associated separatrix and spine field lines represent discontinuities of the field line mapping, making them preferential locations for reconnection. This field line mapping also exhibits strong gradients adjacent to the separatrix (fan) and spine field lines, that can be analysed using the `squashing factor', Q. In this paper we make a detailed analysis of the distribution of Q in the presence of magnetic nulls. While Q is formally infinite on both the spine and fan of the null, the decay of Q away from these structures is shown in general to depend strongly on the null-point structure. For the generic case of a non-radially-symmetric null, Q decays most slowly away from the spine/fan in the direction in which |B| increases most slowly. In particular, this demonstrates that the extended, elliptical high-Q halo around the spine footpoints observed by Masson et al. (Astrophys. J., 700, 559, 2009) is a generic feature. This extension of the Q halos around the spine/fan footpoints is important for diagnosing the regions of the photosphere that are magnetically connected to any current layer that forms at the null. In light of this, we discuss how our results can be used to interpret the geometry of observed flare ribbons in `circular ribbon flares', in which typically a coronal null is implicated. We conclude that both the physics in the vicinity of the null and how this is related to the extension of Q away from the spine/fan can be used in tandem to understand observational signatures of reconnection at coronal null points.

The effect of reconnection on the structure of the Sun's open-closed-flux boundary

D. I. **Pontin**, P. F. Wyper
ApJ **2015**
http://arxiv.org/pdf/1502.01311v1.pdf
Global magnetic field extrapolations are now revealing the huge complexity of the Sun's corona, and in particular the structure of the boundary between open and closed magnetic flux. Moreover, recent developments indicate that magnetic reconnection in the corona likely occurs in highly fragmented current layers, and that this typically leads to a dramatic increase in the topological complexity beyond that of the equilibrium field. In this paper we investigate the consequences of reconnection at the open-closed flux boundary ("interchange reconnection") in a fragmented current layer. We demonstrate that it leads to a situation in which magnetic flux (and therefore plasma) from open and closed field regions is efficiently mixed together. This corresponds to an increase in the length and complexity of the open-closed boundary. Thus, whenever reconnection occurs at a null point or separator of the open-closed boundary, the associated separatrix arc of the so-called "S-web" in the high corona becomes not a single line but a band of finite thickness within which the open-closed flux boundary is highly structured. This has significant implications for the acceleration of the slow solar wind, for which the interaction of open and closed field is thought to be important, and may also explain the coronal origins of certain solar energetic particles. The topological structures examined contain magnetic null points, separatrices and separators, and include a model for a pseudo-streamer. The potential for understanding both the large scale morphology and fine structure observed in flare ribbons associated with coronal nulls is also discussed.

The structure of current layers and degree of field line braiding in coronal loops

D. I. **Pontin**, G. Hornig
ApJ **2014**
http://arxiv.org/pdf/1411.2845v1.pdf
One proposed resolution to the long-standing problem of solar coronal heating involves the buildup of magnetic energy in the corona due to turbulent motions at the photosphere that braid the coronal field, and the subsequent release of this energy via magnetic reconnection. In this paper the ideal relaxation of braided magnetic fields modelling solar coronal loops is followed. A sequence of loops with increasing braid complexity is considered, with the aim of understanding how this complexity influences the development of small scales in the magnetic field, and thus the energy available for heating. It is demonstrated that the ideally accessible force-free equilibrium for these braided fields contains current layers of finite thickness. It is further shown that for any such braided field, if a force-free equilibrium exists then it should contain current layers whose thickness is determined by length scales in the field line mapping. The thickness and intensity of the current layers follow scaling laws, and this allows us to extrapolate beyond the numerically accessible parameter regime and to place an upper bound on the braid complexity possible at coronal plasma parameters. At this threshold level the braided loop contains 1026—1028 ergs of available free magnetic energy, more than sufficient for a large nanoflare.

ON THE NATURE OF RECONNECTION AT A SOLAR CORONAL NULL POINT ABOVE A SEPARATRIX DOME

D. I. **Pontin**1, E. R. Priest2, and K. Galsgaard
2013 ApJ 774 154
Three-dimensional magnetic null points are ubiquitous in the solar corona and in any generic mixed-polarity magnetic field. We consider magnetic reconnection at an isolated coronal null point whose fan field lines form a dome structure. Using analytical and computational models, we demonstrate several features of spine-fan reconnection at such a null, including the fact that substantial magnetic flux transfer from one region of field line connectivity to another can occur. The flux transfer occurs across the current sheet that forms around the null point during spine-fan reconnection, and there is no separator present. Also, flipping of magnetic field lines takes place in a manner similar to that observed in the quasi-separatrix layer or slip-running reconnection.

Theory of magnetic reconnection in solar and astrophysical plasmas **Review**

D. I. **Pontin**
Philosophical Transactions of the Royal Society A: Mathematical, Physical and Engineering Sciences, vol. 370, issue 1970, pp. 3169-3192, **2012**
http://sci-hub.tw/10.1098/rsta.2011.0501
Magnetic reconnection is a fundamental process in a plasma that facilitates the release of energy stored in the magnetic field by permitting a change in the magnetic topology. In this article we present a review of the current state of understanding of magnetic reconnection. We discuss theoretical results regarding the formation of current sheets in complex 3D magnetic fields, and describe the fundamental differences between reconnection in two and three dimensions. We go on to outline recent developments in modelling of reconnection with kinetic theory, as well as in the MHD framework where a number of new 3D reconnection regimes have been identified. We discuss evidence from

observations and simulations of solar system plasmas that support this theory, and summarise some prominent locations in which this new reconnection theory is relevant in astrophysical plasmas.

Forced magnetic reconnection and plasmoid coalescence
I. Magnetohydrodynamic simulations

M. A. **Potter**, P. K. Browning and M. Gordovskyy
A&A 623, A15 (**2019**)
https://doi.org/10.1051/0004-6361/201833565
sci-hub.tw/10.1051/0004-6361/201833565

Context. Forced magnetic reconnection, a reconnection event triggered by external perturbation, should be ubiquitous in the solar corona. Energy released during such cases can be much greater than that which was introduced by the perturbation. The exact dynamics of magnetic reconnection events are determined by the structure and complexity of the reconnection region: the thickness of reconnecting layers, the field curvature; the presence, shapes and sizes of magnetic islands. It is unclear how the properties of the external perturbation and the initial current sheet affect the reconnection region properties, and thereby the reconnection dynamics and energy release profile.
Aims. We investigate the effect of the form of the external perturbation and initial current sheet on the evolution of the reconnection region and the energy release process. Chiefly we explore the non-linear interactions between multiple, simultaneous perturbations, which represent more realistic scenarios. Future work will use these results in test particle simulations to investigate particle acceleration over multiple reconnection events.
Methods. Simulations are performed using Lare2d, a 2.5D Lagrangian-remap solver for the visco-resistive MHD equations. The model of forced reconnection is extended to include superpositions of sinusoidal driving disturbances, including localised Gaussian perturbations. A transient perturbation is applied to the boundaries of a region containing a force-free current sheet. The simulation domain is sufficiently wide to allow multiple magnetic islands to form and coalesce.
Results. Island coalescence contributes significantly to energy release and involves rapid reconnection. Long wavelength modes in perturbations dominate the evolution, without the presence of which reconnection is either slow, as in the case of short wavelength modes, or the initial current sheet remains stable, as in the case of noise perturbations. Multiple perturbations combine in a highly non-linear manner: reconnection is typically faster than when either disturbance is applied individually, with multiple low-energy events contributing to the same total energy release.

THE OPTICAL DEPTH OF WHITE-LIGHT FLARE CONTINUUM

Hugh **Potts**, Hugh Hudson1, Lyndsay Fletcher, and Declan Diver
Astrophysical Journal, 722:1514–1521, **2010**

The white-light continuum emission of a solar flare remains a puzzle as regards its height of formation and its emission mechanism(s). This continuum and its extension into the near-UV contain the bulk of the energy radiated by a flare, and so its explanation is a high priority. We describe a method to determine the optical depth of the emitting layer and apply it to the well-studied flare of **2002 July 15**, making use ofMDI pseudo-continuum intensity images. We find the optical depth of the visible continuum in all flare images, including an impulsive ribbon to be small, consistent with the observation of Balmer and Paschen edges in other events.

An Event-Based Verification Scheme for the Real-Time Flare Detection System at Kanzelhöhe Observatory

W. **Pötzi**, . M. Veronig, M. Temmer
Solar Physics June **2018**, 293:94
https://link.springer.com/content/pdf/10.1007%2Fs11207-018-1312-7.pdf

In the framework of the Space Situational Awareness program of the European Space Agency (ESA/SSA), an automatic flare detection system was developed at Kanzelhöhe Observatory (KSO). The system has been in operation since mid-2013. The event detection algorithm was upgraded in September 2017. All data back to 2014 was reprocessed using the new algorithm. In order to evaluate both algorithms, we apply verification measures that are commonly used for forecast validation. In order to overcome the problem of rare events, which biases the verification measures, we introduce a new event-based method. We divide the timeline of the Hαα observations into positive events (flaring period) and negative events (quiet period), independent of the length of each event. In total, 329 positive and negative events were detected between 2014 and 2016. The hit rate for the new algorithm reached 96% (just five events were missed) and a false-alarm ratio of 17%. This is a significant improvement of the algorithm, as the original system had a hit rate of 85% and a false-alarm ratio of 33%. The true skill score and the Heidke skill score both reach values of 0.8 for the new algorithm; originally, they were at 0.5. The mean flare positions are accurate within ±1±1 heliographic degree for both algorithms, and the peak times improve from a mean difference of 1.7±2.9 minutes1.7±2.9 minutes to 1.3±2.3 minutes1.3±2.3 minutes. The flare start times that had been systematically late by about 3 minutes as determined by the original algorithm, now match the visual inspection within −0.47±4.10 minutes−0.47±4.10 minutes. **22 August 2015**

Real-time flare detection in ground-based Hα imaging at Kanzelhöhe Observatory

Werner **Pötzi**, Astrid M. Veronig, Gernot Riegler, Ute Amerstorfer, Thomas Pock, Manuela Temmer, Wolfgang Polanec, Dietmar J. Baumgartner

Solar Physics, Volume 290, Issue 3, pp 951-977 **2014**

http://arxiv.org/pdf/1411.3896v2.pdf

Kanzelh\"ohe Observatory (KSO) regularly performs high-cadence full-disk imaging of the solar chromosphere in the Hα and CaIIK spectrallines as well as the solar photosphere in white-light. In the frame of ESA's Space Situational Awareness (SSA) programme, a new system for real-time Hα data provision and automatic flare detection was developed at KSO. The data and events detected are published in near real-time at ESA's SSA Space Weather portal (this http URL). In this paper, we describe the Hα instrument, the image recognition algorithms developed, the implementation into the KSO Hα observing system and present the evaluation results of the real-time data provision and flare detection for a period of five months. The Hα data provision worked in 99.96% of the images, with a mean time lag between image recording and online provision of 4s. Within the given criteria for the automatic image recognition system (at least three Hα images are needed for a positive detection), all flares with an area ≥50 micro-hemispheres and located within 60◦ of the Sun's center that occurred during the KSO observing times were detected, in total a number of 87 events. The automatically determined flare importance and brightness classes were correct in ∼85%. The mean flare positions in heliographic longitude and latitude were correct within ∼1◦. The median of the absolute differences for the flare start times and peak times from the automatic detections in comparison to the official NOAA (and KSO) visual flare reports were 3 min (1 min).

Compressive oscillations in hot coronal loops: Are sloshing oscillations and standing slow waves independent?

S. Krishna **Prasad**, T. Van Doorsselaere

ApJ **914** 81 **2021**

https://arxiv.org/pdf/2104.12038.pdf

https://iopscience.iop.org/article/10.3847/1538-4357/abfb01/pdf

https://doi.org/10.3847/1538-4357/abfb01

Employing high-resolution EUV imaging observations from SDO/AIA, we analyse a compressive plasma oscillation in a hot coronal loop triggered by a C-class flare near one of its foot points as first studied by Kumar et al. We investigate the oscillation properties in both the 131{\,}Å and 94{\,}Å channels and find that what appears as a pure sloshing oscillation in the 131{\,}Å channel actually transforms into a standing wave in the 94{\,}Å channel at a later time. This is the first clear evidence of such transformation confirming the results of a recent numerical study which suggests that these two oscillations are not independent phenomena. We introduce a new analytical expression to properly fit the sloshing phase of an oscillation and extract the oscillation properties. For the AIA 131{\,}Å channel, the obtained oscillation period and damping time are 608±4{\,}s and 431±20{\,}s, respectively during the sloshing phase. The corresponding values for the AIA 94{\,}Å channel are 617±3{\,}s and 828±50{\,}s. During the standing phase that is observed only in the AIA 94{\,}Å channel, the oscillation period and damping time have increased to 791±5{\,}s and 1598±138{\,}s, respectively. The plasma temperature obtained from the DEM analysis indicates substantial cooling of the plasma during the oscillation. Considering this, we show that the observed oscillation properties and the associated changes are compatible with damping due to thermal conduction. We further demonstrate that the absence of a standing phase in the 131{\,}Å channel is a consequence of cooling plasma besides the faster decay of oscillation in this channel. **2012-05-07**

Magnetohydrodynamic Simulation of Magnetic Null-point Reconnections and Coronal dimmings during the X2.1 flare in NOAA AR 11283

Avijeet **Prasad**, Karin Dissauer, Qiang Hu, R. Bhattacharyya, Astrid M. Veronig, Sanjay Kumar, Bhuwan Joshi

ApJ **903** 129 **2020**

https://arxiv.org/pdf/2009.11109.pdf

https://doi.org/10.3847/1538-4357/abb8d2

The magnetohydrodynamics of active region NOAA 11283 is simulated using an initial non-force-free magnetic field extrapolated from its photospheric vector magnetogram. We focus on the magnetic reconnections at a magnetic null point that participated in the X2.1 flare on **2011 September 6** around 22:21 UT (SOL2011-09-06T22:21X2.1) followed by the appearance of circular flare ribbons and coronal dimmings. The initial magnetic field from extrapolation displays a three-dimensional (3D) null topology overlying a sheared arcade. Prior to the flare, magnetic loops rise due to the initial Lorentz force, and reconnect at the 3D null, leading to expansion and loss of confined plasma that produce the observed pre-flare coronal dimmings. Further, the simulated dynamics documents the transfer of twist from the arcade

to the overlying loops through reconnections, developing a flux rope. The non-parallel field lines comprising the rope and lower-lying arcades form an X-type geometry. Importantly, the simultaneous reconnections at the 3D null and the X-type geometry can explain the observed circular and parallel flare ribbons. Reconnections at the 3D null transform closed inner spine field lines into open field lines of the outer spine. The footpoints of these open field lines correspond to a ring-shaped coronal dimming region, tracing the dome. Further, the flux rope bifurcates because of these reconnections which also results in the generation of open magnetic field lines. The plasma loss along the open field lines can potentially explain the observed coronal dimming.

Magnetohydrodynamic simulation of magnetic null-point reconnections in NOAA AR12192 initiated with an extrapolated non-force-free-field

A. **Prasad**, R. Bhattacharyya, Qiang Hu, Sanjay Kumar, Sushree S. Nayak
ApJ **860** 96 **2018**
https://arxiv.org/pdf/1805.00635.pdf
Magnetohydrodynamics of the solar corona is simulated numerically. The simulation is initialized with an extrapolated non-force-free magnetic field using the vector magnetogram of the active region (AR) NOAA 12192 obtained on the solar photosphere. Particularly, we focus on the magnetic reconnections occurring close to a magnetic null-point that resulted in appearance of circular chromospheric flare ribbons on **October 24, 2014** around 21:21 UT, after peak of an X3.1 flare. The extrapolated field lines show the presence of the three-dimensional (3D) null near one of the polarity inversion lines---where the flare was observed. In the subsequent numerical simulation, we find magnetic reconnections occurring near the null point, where the magnetic field lines from the fan-plane of the 3D null form a X-type configuration with underlying arcade field lines. The footpoints of the dome-shaped field lines, inherent to the 3D null, show high gradients of the squashing factor. We find slipping reconnections at these quasi-separatrix layers, which are co-located with the post-flare circular brightening observed at the chromospheric heights. This demonstrates the viability of the initial non-force-free field along with the dynamics it initiates. Moreover, the initial field and its simulated evolution is found to be devoid of any flux rope, which is in congruence with the confined nature of the flare.

Study of magnetic field topology of active region 12192 using an extrapolated non-force-free magnetic field

A. **Prasad**, R. Bhattacharyya, Q. Hu, S. S. Nayak, Sanjay Kumar
Proc. IAU Symp. 340 **2018**
https://arxiv.org/pdf/1804.04354.pdf
The solar active region (AR) 12192 was one of the most flare productive region of solar cycle 24, which produced many X-class flares; the most energetic being an X3.1 flare on **October 24, 2014** at 21:10 UT. Customarily, such events are believed to be triggered by magnetic reconnection in coronal magnetic fields. Here we use the vector magnetograms from solar photosphere, obtained from Heliospheric Magnetic Imager (HMI) to investigate the magnetic field topology prior to the X3.1 event, and ascertain the conditions that might have caused the flare. To infer the coronal magnetic field, a novel non-force-free field (NFFF) extrapolation technique of the photospheric field is used, which suitably mimics the Lorentz forces present in the photospheric plasma. We also highlight the presence of magnetic null points and quasi-separatrix layers (QSLs) in the magnetic field topology, which are preferred sites for magnetic reconnections and discuss the probable reconnection scenarios.

THE LOCATION OF CENTROIDS IN PHOTON AND ELECTRON MAPS OF SOLAR FLARES

Marco **Prato**1,2, A. Gordon Emslie3, Eduard P. Kontar4, Anna Maria Massone2, and Michele Piana2,5
Astrophysical Journal, 706:917–922, **2009** November
We explore the use of centroid coordinates as a means to identify the “locations” of electron–proton bremsstrahlung hard X-ray sources in solar flares. Differences between the coordinates of the electron and photon centroids are derived and explained. For electron propagation in a collision-dominated target, with either a uniform or an exponential density profile, the position of the electron centroid can be calculated analytically. We compare these analytic forms to data from a flare event on **2002 February 20.** We first spectrally invert the native photon visibility data to obtain “electron visibilities,” which are in turn used to construct electron flux images at various electron energies *E*. Centroids of these maps are then obtained by straightforward numerical integration over the electron maps. This comparison allows us to infer the density structure in the two compact sources visible, and we discuss the (somewhat unexpected) results thus obtained.

Time-dependent data-driven coronal simulations of AR 12673 from emergence to eruption

D. J. **Price**, J. Pomoell, E. Lumme and E. K. J. Kilpua
A&A 628, A114 (**2019**)
DOI: 10.1051/0004-6361/201935535
Aims. We present a detailed study of the magnetic evolution of AR 12673 using a magnetofrictional modelling approach.

Methods. The fully data-driven and time-dependent model was driven with maps of the photospheric electric field, inverted from vector magnetogram observations obtained from the Helioseismic and Magnetic Imager (HMI) on board the Solar Dynamics Observatory (SDO). Our analysis was aided by studying the evolution of metrics such as the free magnetic energy and the current-carrying helicity budget of the domain, maps of the squashing factor and twist, and plots of the current density. These allowed us to better understand the dynamic nature of the magnetic topology.
Results. Our simulation captured the time-dependent nature of the active region and the erupting flux rope associated with the X-class flares on **6 September 2017**, including the largest of solar cycle 24. Additionally, our results suggest a possible threshold for eruptions in the ratio of current-carrying helicity to relative helicity.
Conclusion. The flux rope was found to be a combination of two structures that partially combine during the eruption process. Our time-dependent data-driven magnetofrictional model is shown to be capable of generating magnetic fields consistent with extreme ultraviolet (EUV) observations.

Magnetic reconnection on the Sun: ESPD Senior Prize Lecture **Review**

E. **Priest**
Advances in Space Research Volume 71, Issue 4, 15 February **2023**, Pages 1856-1865
https://reader.elsevier.com/reader/sd/pii/S0273117722002149
Magnetic reconnection is a fundamental process for changing the magnetic topology and converting magnetic energy into other forms on the Sun, such as heat, flow energy and fast particle energy. In two dimensions it is fairly well understood, although some aspects still need to be developed. In three dimensions, it behaves very differently and a substantial body of theory and numerical experiment has now been built up, including reconnection at null points, separators and quasi-separators.
Some aspects of solar flares can be understood with 2D reconnection models, but other aspects such as the shapes of flare ribbons, the acceleration of particles and the creation of twist in erupting flux ropes need a 3D understanding. A paradigm shift in our understanding of coronal heating by reconnection has been stimulated by dramatic new observations of photospheric flux cancellation from SUNRISE and from SST together with the realisation that it may well be driving nanoflare heating events and possibly campfires.

The Creation of Twist by Reconnection of Flux Tubes

E. R. **Priest** & D. W. Longcope
Solar Physics volume 295, Article number: 48 (**2020**)
https://link.springer.com/content/pdf/10.1007/s11207-020-01608-0.pdf
sci-hub.si/10.1007/s11207-020-01608-0
A fundamental process in a plasma is the magnetic reconnection of one pair of flux tubes (such as solar coronal loops) to produce a new pair. During this process magnetic helicity is conserved, but mutual helicity can be transformed to self-helicity, so that the new tubes acquire twist. However, until recently, when Wright (Astrophys. J. 878, 102, 2019) supplied a solution, the partition of self-helicity between the two tubes was an outstanding puzzle. Here we examine Wright's result in detail and apply it to a variety of cases. The simplest case, which Wright himself used to illustrate the result, is that of thin ribbons or flux sheets. We first explicitly apply his method to the usually expected standard case (when the tubes approach one another without twisting before reconnection) and confirm his result is valid for flux sheaths and tubes as well as sheets.
For the reconnection of sheets, it is shown that the orientation of the sheets needs to be chosen carefully. For flux sheaths and tubes, Wright's results are demonstrated to hold for the standard case. There is both a local and a global aspect to the effect of reconnection. The local effect of reconnection is to produce an equipartition of the added self-helicity (and therefore of twist), but the extra global effect of the location and orientation of the feet of the sheet, shell or tube in general adds different amounts of magnetic helicity to the two structures.
It is important, as Wright realized, to account for any twist or writhe already existing in the fluxes prior to reconnection. Here we show explicitly that, if a section of a flux sheet is twisted by a multiple of π with its ends held fixed and is then reconnected with another sheet, then the effect of the reconnection is to add that multiple of π to one sheet and subtract it from the other, while conserving the total helicity. If, on the other hand, the central part of a flux sheath is twisted before reconnection by any angle, then the effect of reconnection is to add that amount of twist to one sheath and subtract it from the other, while conserving the total helicity. Thus, for the local part of the process in both sheets and sheaths, there is no longer helicity equipartition

Evolution of Magnetic Helicity During Eruptive Flares and Coronal Mass Ejections

Eric **Priest**, Dana Longcope, Miho Janvier
Solar Phys. Volume 291, Issue 7, pp 2017–2036 **2016**
http://arxiv.org/pdf/1607.03874v1.pdf
During eruptive solar flares and coronal mass ejections, a non-pot{\-}ential magnetic arcade with much excess magnetic energy goes unstable and reconnects. It produces a twisted erupting flux rope and leaves behind a sheared arcade of hot coronal loops. We suggest that: the twist of the erupting flux rope can be determined from conservation of magnetic flux and magnetic helicity and equipartition of magnetic helicity. It depends on the geometry of the initial pre-eruptive structure.

Two cases are considered, in the first of which a flux rope is not present initially but is created during the eruption by the reconnection. In the second case, a flux rope is present under the arcade in the pre-eruptive state, and the effect of the eruption and reconnection is to add an amount of magnetic helicity that depends on the fluxes of the rope and arcade and the geometry.

Hydrogen Emission in Type II White-light Solar Flares

Ondřej **Procházka**, Aaron Reid, Mihalis Mathioudakis
2019
https://arxiv.org/pdf/1907.10888.pdf
Type II WLFs have weak Balmer line emission and no Balmer jump. We carried out a set of radiative hydrodynamic simulations to understand how the hydrogen radiative losses vary with the electron beam parameters and more specifically with the low energy cutoff. Our results have revealed that for low energy beams, the excess flare Lyman emission diminishes with increasing low energy cutoff as the energy deposited into the top chromosphere is low compared to the energy deposited into the deeper layers. Some Balmer excess emission is always present and is driven primarily by direct heating from the beam with a minor contribution from Lyman continuum backwarming. The absence of Lyman excess emission in electron beam models with high low energy cutoff is a prominent spectral signature of type II WLFs.

Reproducing Type II White-Light Solar Flare Observations with Electron and Proton Beam Simulations

Ondřej **Procházka**, Aaron Reid, Ryan O. Milligan, Paulo J. A. Simões, Joel C. Allred, Mihalis Mathioudakis
2018 *ApJ* **862** 76
https://arxiv.org/pdf/1806.00249.pdf
We investigate the cause of the suppressed Balmer series and the origin of the white-light continuum emission in the X1.0 class solar flare on **2014 June 11**. We use radiative hydrodynamic simulations to model the response of the flaring atmosphere to both electron and proton beams which are energetically constrained using RHESSI and Fermi observations. A comparison of synthetic spectra with the observations allow us to narrow the range of beam fluxes and low energy cut-off that may be applicable to this event. We conclude that the electron and proton beams that can reproduce the observed spectral features are those that have relatively low fluxes and high values for the low energy cut-off. While electron beams shift the upper chromosphere and transition region to greater geometrical heights, proton beams with a similar flux leave these areas of the atmosphere relatively undisturbed. It is easier for proton beams to penetrate to the deeper layers and not deposit their energy in the upper chromosphere where the Balmer lines are formed. The relatively weak particle beams that are applicable to this flare do not cause a significant shift of the τ=1 surface and the observed excess WL emission is optically thin.

Suppression of Hydrogen Emission in an X-class White-light Solar Flare

Ondřej **Procházka**1, Ryan O. Milligan1,2,3, Joel C. Allred2, Adam F. Kowalski4,5, Pavel Kotrč6, and Mihalis Mathioudakis
2017 ApJ 837 46
http://sci-hub.cc/10.3847/1538-4357/aa5da8
We present unique NUV observations of a well-observed X-class flare from NOAA 12087 obtained at the Ondřejov Observatory. The flare shows a strong white-light continuum but no detectable emission in the higher Balmer and Lyman lines. Reuven Ramaty High-Energy Solar Spectroscopic Imager and Fermi observations indicate an extremely hard X-ray spectrum and γ-ray emission. We use the RADYN radiative hydrodynamic code to perform two types of simulations: one where an energy of 3 × 1011 erg cm−2 s−1 is deposited by an electron beam with a spectral index of ≈3, and a second where the same energy is applied directly to the photosphere. The combination of observations and simulations allows us to conclude that the white-light emission and the suppression or complete lack of hydrogen emission lines is best explained by a model where the dominant energy deposition layer is located in the lower layers of the solar atmosphere, rather than the chromosphere. **2014 June 11**
See RHESSI nuggets #296, March 2017
http://sprg.ssl.berkeley.edu/~tohban/wiki/index.php/Suppression_of_Hydrogen_Emission_in_an_X-class_White-light_Solar_Flare

Reflection of fast magnetosonic waves near magnetic reconnection region

Elena **Provornikova**, J. Martin Laming, Vyacheslav S. Lukin
ApJ **2018**
https://arxiv.org/pdf/1803.11212.pdf
Magnetic reconnection in the solar corona is thought to be unstable to the formation of multiple interacting plasmoids, and previous studies have shown that plasmoid dynamics can trigger MHD waves of different modes propagating outward from the reconnection site. However, variations in plasma parameters and magnetic field strength in the

vicinity of a coronal reconnection site may lead to wave reflection and mode conversion. In this paper we investigate the reflection and refraction of fast magnetoacoustic waves near a reconnection site. Under a justified assumption of an analytically specified Alfv\'{e}n speed profile, we derive and solve analytically the full wave equation governing propagation of fast mode waves in a non-uniform background plasma without recourse to the small-wavelength approximation. We show that the waves undergo reflection near the reconnection current sheet due to the Alfv\'en speed gradient and that the reflection efficiently depends on the plasma-β parameter as well as on the wave frequency. In particular, we find that waves are reflected more efficiently near reconnection sites in a low-β plasma which is typical for the solar coronal conditions. Also, the reflection is larger for lower frequency waves while high frequency waves propagate outward from the reconnection region almost without the reflection. We discuss the implications of efficient wave reflection near magnetic reconnection sites in strongly magnetized coronal plasma for particle acceleration, and also the effect this might have on First Ionization Potential (FIP) fractionation by the ponderomotive force of these waves in the chromosphere.

Plasma compression in magnetic reconnection regions in the solar corona

Elena **Provornikova**, John Martin Laming, Vyacheslav S. Lukin
2016 ApJ 825 55
http://arxiv.org/pdf/1604.07325v1.pdf
It has been proposed that particles bouncing between magnetized flows converging in a reconnection region can be accelerated by the first order Fermi mechanism. Analytical considerations of this mechanism have shown that the spectral index of accelerated particles is related to the total plasma compression within the reconnection region similarly to the case of diffusive shock acceleration mechanism. As a first step to investigate the efficiency of Fermi acceleration in reconnection regions in producing hard energy spectra of particles in the solar corona, we explore the degree of plasma compression that can be achieved at reconnection sites. In particular, we aim to determine the conditions for the strong compressions to form. Using a two-dimensional resistive MHD numerical model we consider a set of magnetic field configurations where magnetic reconnection can occur including a Harris current sheet, a force-free current sheet, and two merging flux ropes. Plasma parameters are taken to be characteristic of the solar corona. Numerical simulations show that strong plasma compressions (≥ 4) in the reconnection regions can form when the plasma heating due to reconnection is efficiently removed by fast thermal conduction or radiative cooling process. The radiative cooling process which is negligible in the typical 1 MK corona can play an important role in the low corona/transition region. It is found that plasma compression is expected to be strongest in low-beta plasma $\beta \sim 0.01-0.07$ at reconnection magnetic nulls.

Scaling laws of quasi-periodic pulsations in solar flares

C. E. **Pugh**, A.-M. Broomhall, V. M. Nakariakov
A&A 624, A65 **2019**
https://arxiv.org/pdf/1902.09627.pdf
sci-hub.se/10.1051/0004-6361/201834455
Quasi-periodic pulsations (QPPs) are a common feature of solar flares, but previously there has been a lack of observational evidence to support any of the theoretical models that might explain the origin of QPPs. We aimed to determine if there are any relationships between the QPP period and other properties of the flaring region, using the sample of flares with QPPs from Pugh et al. (2017b). If any relationships exist then these can be compared with scaling laws for the theoretical QPP mechanisms. To obtain the flaring region properties we made use of the AIA 1600 and HMI data. The AIA 1600 images allow the flare ribbons to be seen while the HMI magnetograms allow the positive and negative magnetic polarity ribbons to be distinguished and the magnetic properties determined. The ribbon properties calculated in this study were the ribbon separation distance, area, total unsigned magnetic flux, and average magnetic field strength. Only the flares that occurred within \pm 60° of the solar disk centre were included, which meant a sample of 20 flares with 22 QPP signals. Positive correlations were found between the QPP period and the ribbon properties. The strongest correlations were with the separation distance and magnetic flux. Because these ribbon properties also correlate with the flare duration, and the relationship between the QPP period and flare duration may be influenced by observational bias, we also made use of simulated data to check if artificial correlations could be introduced. These simulations show that although QPPs cannot be detected for certain combinations of QPP period and flare duration, this does not introduce an apparent correlation. There is evidence of relationships between the QPP period and flare ribbon properties, and in the future the derived scaling laws between these properties can be compared to equivalent scaling laws for theoretical QPP mechanisms. **2014-10-25**
Table 1: List of flares with QPPs used in this study (2014)

Properties of quasi-periodic pulsations in solar flares from a single active region

C. E. **Pugh**, V. M. Nakariakov, A.-M. Broomhall, A. V. Bogomolov, I. N. Myagkova
A&A 608, A101 **2017**
https://arxiv.org/pdf/1709.09472.pdf

We investigate the properties of a set of solar flares originating from a single active region (AR) that exhibit QPPs, and look for signs of the QPP periods relating to AR properties. The AR studied, best known as NOAA 12192, was unusually long-lived and produced 181 flares. Data from the GOES, EVE, Fermi, Vernov and NoRH observatories were used to determine if QPPs were present in the flares. For the soft X-ray GOES and EVE data, the time derivative of the signal was used. Power spectra of the time series data (without any form of detrending) were inspected, and flares with a peak above the 95% confidence level in the spectrum were labelled as having candidate QPPs. The confidence levels were determined taking account of uncertainties and the possible presence of red noise. AR properties were determined using HMI line of sight magnetograms. A total of 37 flares (20% of the sample) show good evidence of having QPPs, and some of the pulsations can be seen in data from multiple instruments and in different wavebands. The QPP periods show a weak correlation with the flare amplitude and duration, but this may be due to an observational bias. A stronger correlation was found between the QPP period and duration of the QPP signal, which can be partially but not entirely explained by observational constraints. No correlations were found with the AR area, bipole separation, or average magnetic field strength. The fact that a substantial fraction of the flare sample showed evidence of QPPs using a strict detection method with minimal processing of the data demonstrates that these QPPs are a real phenomenon, which cannot be explained by the presence of red noise or the superposition of multiple unrelated flares. The lack of correlation between the QPP periods and AR properties implies that the small-scale structure of the AR is important, and/or that different QPP mechanisms act in different cases. **2014 September 22-30, 2014 October 19-27, 2014 November 16-23**

Significance testing for quasi-periodic pulsations in solar and stellar flares

C. E. **Pugh**, A.-M. Broomhall, V. M. Nakariakov
A&A 602, A47 **2017**
https://arxiv.org/pdf/1703.07294.pdf
The robust detection of quasi-periodic pulsations (QPPs) in solar and stellar flares has been the topic of recent debate. In light of this, we have adapted a method described by Vaughan (2005) to aid with the search for QPPs in flare time series data. The method identifies statistically significant periodic signals in power spectra, and properly accounts for red noise as well as the uncertainties associated with the data. We show how the method can be further developed to be used with rebinned power spectra, allowing us to detect QPPs whose signal is spread over more than one frequency bin. An advantage of these methods is that there is no need to detrend the data prior to creating the power spectrum. Examples are given where the methods have been applied to synthetic data, as well as real flare time series data with candidate QPPs from the Nobeyama Radioheliograph. These show that, despite the transient nature of QPPs, peaks corresponding to the QPPs can be seen at a significant level in the power spectrum without any form of detrending or other processing of the original time series data, providing the background trends are not too steep. **22-Oct-14, 24-Oct-14, 29-Oct-14,**

Evidence for similar processes occurring in stellar superflares and solar flares

Chloe E. **Pugh**, Valery M. Nakariakov & Anne-Marie Broomhall
UKSP Nuggets of **2016** №66
http://www.uksolphys.org/uksp-nugget/66-evidence-for-similar-processes-occurring-in-stellar-superflares-and-solar-flares/

Statistical Properties of Quasi-Periodic Pulsations in White-Light Flares Observed With Kepler

C. E. **Pugh**, D. J. Armstrong, V. M. Nakariakov, A.-M. Broomhall
Monthly Notices of the Royal Astronomical Society **2016**
http://arxiv.org/pdf/1604.03018v1.pdf
We embark on a study of quasi-periodic pulsations (QPPs) in the decay phase of white-light stellar flares observed by Kepler. Out of the 1439 flares on 216 different stars detected in the short-cadence data using an automated search, 56 flares are found to have pronounced QPP-like signatures in the light curve, of which 11 have stable decaying oscillations. No correlation is found between the QPP period and the stellar temperature, radius, rotation period and surface gravity, suggesting that the QPPs are independent of global stellar parameters. Hence they are likely to be the result of processes occurring in the local environment. There is also no significant correlation between the QPP period and flare energy, however there is evidence that the period scales with the QPP decay time for the Gaussian damping scenario, but not to a significant degree for the exponentially damped case. This same scaling has been observed for MHD oscillations on the Sun, suggesting that they could be the cause of the QPPs in those flares. Scaling laws of the flare energy are also investigated, supporting previous reports of a strong correlation between the flare energy and stellar temperature/radius. A negative correlation between the flare energy and stellar surface gravity is also found.

Multi-point study of the energy release and transport in the 28 March 2022, M4-flare using STIX, EUI, and AIA during the first Solar Orbiter nominal mission perihelion

Stefan **Purkhart**, Astrid M. Veronig, Ewan C. M. Dickson, Andrea Francesco Battaglia, Säm Krucker, Robert Jarolim, Bernhard Kliem, Karin Dissauer, Tatiana Podladchikova
A&A 679, A99 **2023**
https://arxiv.org/pdf/2310.02038.pdf
https://www.aanda.org/articles/aa/pdf/2023/11/aa46354-23.pdf
We present a case study of an M4-class flare on **28 March 2022**, near Solar Orbiter's first science perihelion (0.33 AU). Solar Orbiter was 83.5° west of the Sun-Earth line, making the event appear near the eastern limb, while Earth-orbiting spacecraft observed it near the disk center. The timing and location of the STIX X-ray sources were related to the plasma evolution observed in the EUV by the Extreme Ultraviolet Imager (EUI) on Solar Orbiter and the Atmospheric Imaging Assembly (AIA) on the Solar Dynamics Observatory, and to the chromospheric response observed in 1600 Å by AIA. We performed differential emission measure (DEM) analysis to further characterize the flaring plasma at different subvolumes. The pre-flare magnetic field configuration was analyzed using a nonlinear force-free (NLFF) extrapolation. In addition to the two classical hard X-ray (HXR) footpoints at the ends of the flaring loops, later in the event we observe a nonthermal HXR source at one of the anchor points of the erupting filament. The evolution of the AIA 1600~Å footpoints indicates that this change in footpoint location represents a discontinuity in an otherwise continuous westward motion of the footpoints throughout the flare. The NLFF extrapolation suggests that strongly sheared field lines close to, or possibly even part of, the erupting filament reconnected with a weakly sheared arcade during the first HXR peak. The remainder of these field lines reconnected later in the event, producing the HXR peak at the southern filament footpoint. Our results show that the reconnection between field lines with very different shear in the early phase of the flare plays a crucial role in understanding the motion of the HXR footpoint during later parts of the flare. This generalizes simpler models, such as whipping reconnection, which only consider reconnection propagating along uniformly sheared arcades.
SO Nuggets #24 **2023** **https://www.cosmos.esa.int/web/solar-orbiter/-/science-nugget-understanding-stix-hard-x-ray-source-motions-using-field-extrapolations**

Nanoflare distributions over solar cycle 24 based on SDO/AIA differential emission measure observations

Stefan **Purkhart**, Astrid M. Veronig
A&A 661, A149 **2022**
https://arxiv.org/pdf/2203.11625.pdf
https://www.aanda.org/articles/aa/pdf/2022/05/aa43234-22.pdf
Nanoflares in quiet-Sun regions during solar cycle 24 are studied with the best available plasma diagnostics to derive their energy distribution and contribution to coronal heating during different levels of solar activity. Extreme ultraviolet (EUV) filters of the Atmospheric Imaging Assembly (AIA) onboard the Solar Dynamics Observatory (SDO) are used. We analyze 30 AIA/SDO image series between 2011 and 2018, each covering a 400×400 arcsec quiet-Sun field-of-view over two hours with a 12-second cadence. Differential emission measure (DEM) analysis is used to derive the emission measure (EM) and temperature evolution for each pixel. We detect nanoflares as EM-enhancements using a threshold-based algorithm and derive their thermal energy from the DEM observations. Nanoflare energy distributions follow power-laws that show slight variations in steepness (α= 2.02 to 2.47) but no correlation to the solar activity level. The combined nanoflare distribution of all data sets covers five orders of magnitude in event energies (1024 to 1029 erg) with a power-law index α=2.28±0.03. The derived mean energy flux of (3.7±1.6)×104 erg cm−2 s−1 is one order of magnitude smaller than the coronal heating requirement. We find no correlation between the derived energy flux and solar activity. Analysis of the spatial distribution reveals clusters of high energy flux (up to 3×105 erg cm−2 s−1) surrounded by extended regions with lower activity. Comparisons with magnetograms from the Helioseismic and Magnetic Imager (HMI) demonstrate that high-activity clusters are located preferentially in the magnetic network and above regions of enhanced magnetic flux density.

Tracing Field Lines That Are Reconnecting or Expanding or Both

Jiong **Qiu**
Frontiers in Astronomy and Space Sciences, vol. 11, id. 1401846,
2024
https://doi.org/10.3389/fspas.2024.1401846
https://arxiv.org/pdf/2409.04573
Explosive energy release in the solar atmosphere is driven magnetically, but mechanisms triggering the onset of the eruption remain in debate. In the case of flares and CMEs, ideal or non-ideal instabilities usually occur in the corona, but direct observations and diagnostics there are difficult to obtain. To overcome this difficulty, we analyze observational signatures in the upper chromosphere or transition region, in particular, brightenings and dimmings at the feet of coronal magnetic structures. In this paper, we examine the time evolution of spatially resolved light curves in two eruptive flares, and identify a variety of tempo-spatial sequences of brightenings and dimmings, such as dimming

followed by brightening, and dimming preceded by brightening. These brightening-dimming sequences are indicative of the configuration of energy release in the form of plasma heating or bulk motion. We demonstrate the potential of using these analyses to diagnose properties of magnetic reconnection and plasma expansion in the corona during the early stage of the eruption. **2011 June 21, 2012-07-12**

Three types of solar coronal rain during magnetic reconnection between open and closed magnetic

Fangfang **Qiao**, Leping Li, Hui Tian, Zhenyong Hou, Hongqiang Song, Kaifan Ji, Zheng Sun
ApJ **2024**
https://arxiv.org/pdf/2408.05736
Coronal rain (CR) is a crucial part of the mass cycle between the corona and chromosphere. It includes the flare-driven CR and two types of quiescent CR separately along the non-flaring active region closed loops and along the open structures, labeled as types I, II, and III CR, respectively. Among them, types I and III CR are generally associated with magnetic reconnection. In this study, employing data taken by the Solar Dynamics Observatory (SDO) and the Solar Upper Transition Region Imager (SUTRI) on **2022 October 11**, we report three types of CR during an interchange reconnection between open and closed magnetic filed structures above the southeastern solar limb. The open and closed structures converge, with the formation of current sheet at the interface, and reconnect. The newly-formed closed and open structures then recede from the reconnection region. During the reconnection, coronal condensation occurs along the reconnecting closed loops, and falls toward the solar surface along both loop legs as the type II CR. Subsequently, condensation happens in the newly-formed closed loops, and moves down toward the solar surface along both loop legs as the type I CR. Magnetic dips of the reconnecting open structures form during the reconnection. In the dips, condensation occurs, and propagates along the open structures toward the solar surface as the type III CR. Our results suggest that the reconnection rate may be crucial for the formation of types I and III CR during the reconnection.

The Role of Magnetic Shear in Reconnection-Driven Flare Energy Release

J. **Qiu**, M. Alaoui, S. K. Antiochos, J. T. Dahlin, M. Swisdak, J. F. Drake, A. Robison, C. R. DeVore, V. M. Uritsky
ApJ **955** 34 **2023**
https://arxiv.org/pdf/2306.14419.pdf
https://iopscience.iop.org/article/10.3847/1538-4357/acebeb/pdf
Using observations from the Solar Dynamics Observatory's Atmosphere Imaging Assembly and the Ramaty High Energy Solar Spectroscopic Imager, we present novel measurements of the shear of post-reconnection flare loops (PRFLs) in SOL**20141218**T21:40 and study its evolution with respect to magnetic reconnection and flare emission. Two quasi-parallel ribbons form adjacent to the magnetic polarity inversion line (PIL), spreading in time first parallel to the PIL and then mostly in a perpendicular direction. We measure magnetic reconnection rate from the ribbon evolution, and also the shear angle of a large number of PRFLs observed in extreme ultraviolet passbands ($\lesssim$1 MK). For the first time, the shear angle measurements are conducted using several complementary techniques allowing for a cross-validation of the results. In this flare, the total reconnection rate is much enhanced before a sharp increase of the hard X-ray emission, and the median shear decreases from 60∘-70∘ to 20∘, on a time scale of ten minutes. We find a correlation between the shear-modulated total reconnection rate and the non-thermal electron flux. These results confirm the strong-to-weak shear evolution suggested in previous observational studies and reproduced in numerical models, and also confirm that, in this flare, reconnection is not an efficient producer of energetic non-thermal electrons during the first ten minutes when the strongly sheared PRFLs are formed. We conclude that an intermediate shear angle, $\leq$40∘, is needed for efficient particle acceleration via reconnection, and we propose a theoretical interpretation.

Properties and Energetics of Magnetic Reconnection: I. Evolution of Flare Ribbons

Jiong **Qiu**, Jianxia Cheng
Solar Phys. **297**, Article number: 80 **2022**
https://arxiv.org/pdf/2205.03004.pdf
https://doi.org/10.1007/s11207-022-02003-7
In this article, we measure the mean magnetic shear from the morphological evolution of flare ribbons, and examine the evolution of flare thermal and non-thermal X-ray emissions during the progress of flare reconnection. We analyze three eruptive flares and three confined flares ranging from GOES class C8.0 to M7.0. They exhibit well-defined two ribbons along the magnetic polarity inversion line (PIL), and have been observed by the Atmospheric Imaging Assembly and the Ramaty High Energy Solar Spectroscopic Imager from the onset of the flare throughout the impulsive phase. The analysis confirms the strong-to-weak shear evolution in the core region of the flare, and the flare hard X-ray emission rises as the shear decreases. In eruptive flares in this sample, significant non-thermal hard X-ray emission lags the ultraviolet emission from flare ribbons, and rises rapidly when the shear is modest. In all flares, we observe that the plasma temperature rises in the early phase when the flare ribbons rapidly spread along the PIL and the shear is high. We compare these results with prior studies, and discuss their implications, as well as complications, related to physical

mechanisms governing energy partition during flare reconnection. **2013-08-12, 2014-05-10, 2014-08-25, 2014-12-17, 2014-12-18, 2015-01-29**

The Neupert Effect of Flare UltraViolet and Soft X-ray Emissions

Jiong **Qiu**
ApJ **909** 99 **2021**
https://arxiv.org/pdf/2101.11069.pdf
https://iopscience.iop.org/article/10.3847/1538-4357/abe0b3/pdf
https://doi.org/10.3847/1538-4357/abe0b3
We model the Neupert effect that relates flare heating energy with the observed SXR emission. The traditional form of the Neupert effect refers to the correlation between the time-integrated HXR or microwave light curve and the SXR light curve. In this paper, instead, we use as the proxy for heating energy the ultraviolet (UV) emission at the foot-points of flare loops, and modify the model of the Neupert effect by taking into account the discrete nature of flare heating as well as cooling. In the modified empirical model, spatially resolved UV lightcurves from the transition region or upper chromosphere are each convolved with a kernel function characterizing the decay of the flare loop emission. Contributions by all loops are summed to compare with the observed total SXR emission. The model has successfully reproduced the observed SXR emission from its rise to decay. To estimate heating energies in flare loops, we also employ the UV Foot-point Calorimeter (UFC) method that infers heating rates in flare loops from these UV light curves and models evolution of flare loops with a zero-dimensional hydrodynamic code. The experiments show that a multitude of impulsive heating events do not well reproduce the observed flare SXR light curve, but a two-phase heating model leads to better agreement with observations. Comparison of the two models of the Neupert effect further allows us to calibrate the UFC method, and improve the estimate of heating rates in flare loops continuously formed by magnetic reconnection throughout the flare evolution. **2005-05-13, 2011-04-22, 2011-12-26, 2013-08-12, 2013-08-30, 2014-02-05, 04-18, 05-10, 06-15, 09-28, 11-09, 12-01, 04, 17, 19**
Table 1. Properties of Flares and Model Parameters (2005-2014)
RHESSI Science Nugget, No. **403**, Mar **2021**
https://sprg.ssl.berkeley.edu/~tohban/wiki/index.php/The_Neupert_Effect_Revisited

The Magnetic Topology and Eruption Mechanism of a Multiple-ribbon Flare

Ye **Qiu**, Yang Guo, M. D. Ding, Ze Zhong
ApJ **901** 13 **2020**
https://arxiv.org/pdf/2008.08866.pdf
https://doi.org/10.3847/1538-4357/abae5b
Multiple-ribbon flares are usually complex in their magnetic topologies and eruption mechanisms. In this paper, we investigate an X2.1 flare (SOL**2015-03-11**T16:22) that occurred in active region 12297 near the center of the solar disk by both potential and nonlinear force-free field models extrapolated with the data observed by the Helioseismic and Magnetic Imager (HMI) on board Solar Dynamics Observatory (SDO). We calculate the three-dimensional squashing degree distribution. The results reveal that there are two flux ropes in this active region, covered by a large scale hyperbolic flux tube (HFT), which is the intersection of quasi-separatrix layers with a null point embedded in it. When the background magnetic field diminishes due to the separation of the northwest dipole and the flux cancellation, the central flux rope rises up forming the two brightest central ribbons. It then squeezes the upper lying HFT structure to generate further brightenings. This very energetic flare with a complex shape is accompanied by a coronal mass ejection (CME). We adopt the simplified line-tied force-balance equation of the current ring model and assign the observed value of the decay index to the equation to simulate the acceleration profile of the CME in the early stage. It is found that the path with an inclination of 45◦ from radial best fits the profile of the actual acceleration.

Observational Properties of Solar Flare Ribbons

Jiong **Qiu**
Fleishman's webinar 17 July **2020**
https://youtu.be/QTtF1GHxrC8

Elongation of Flare Ribbons

Jiong **Qiu**1, Dana W. Longcope1, Paul A. Cassak2, and Eric R. Priest
2017 ApJ 838 17 DOI 10.3847/1538-4357/aa6341
http://sci-hub.cc/10.3847/1538-4357/aa6341
https://arxiv.org/pdf/1707.02478.pdf
We present an analysis of the apparent elongation motion of flare ribbons along the polarity inversion line (PIL), as well as the shear of flare loops in several two-ribbon flares. Flare ribbons and loops spread along the PIL at a speed ranging from a few to a hundred km s−1. The shear measured from conjugate footpoints is consistent with the measurement from flare loops, and both show the decrease of shear toward a potential field as a flare evolves and ribbons and loops

spread along the PIL. Flares exhibiting fast bidirectional elongation appear to have a strong shear, which may indicate a large magnetic guide field relative to the reconnection field in the coronal current sheet. We discuss how the analysis of ribbon motion could help infer properties in the corona where reconnection takes place. **2005 May 13, 2000 Jul 14, 2004 Nov 07, 2005 Jan 15 , 2011 Sep 13, 2011 Dec 26,**
Table 1 Properties of Flare Ribbon Elongation

LONG DURATION FLARE EMISSION: IMPULSIVE HEATING OR GRADUAL HEATING?

Jiong **Qiu** and Dana W. Longcope
ApJ 820 14 **2016**
http://arxiv.org/pdf/1604.05342v1.pdf
Flare emissions in X-ray and EUV wavelengths have previously been modeled as the plasma response to impulsive heating from magnetic reconnection. Some flares exhibit gradually evolving X-ray and EUV light curves, which are believed to result from superposition of an extended sequence of impulsive heating events occurring in different adjacent loops or even unresolved threads within each loop. In this paper, we apply this approach to a long duration two-ribbon flare SOL**2011-09-13**T22 observed by the Atmosphere Imaging Assembly (AIA). We find that to reconcile with observed signatures of flare emission in multiple EUV wavelengths, each thread should be heated in two phases, an intense impulsive heating followed by a gradual, low-rate heating tail that is attenuated over 20–30 minutes. Each AIA resolved single loop may be composed of several such threads. The two-phase heating scenario is supported by modeling with both a zero-dimensional and a 1D hydrodynamic code. We discuss viable physical mechanisms for the two-phase heating in a post-reconnection thread.

ULTRAVIOLET AND EXTREME-ULTRAVIOLET EMISSIONS AT THE FLARE FOOTPOINTS OBSERVED BY ATMOSPHERE IMAGING ASSEMBLY

Jiong **Qiu**, Zoe Sturrock, Dana W. Longcope, James A. Klimchuk, and Wen-Juan Liu
E-prunt, Aug **2013; 2013** ApJ 774 14
http://arxiv.org/pdf/1305.6899v1.pdf
http://solar.physics.montana.edu/qiuj/publication/apj_qiu_2013.pdf
A solar flare is composed of impulsive energy release events by magnetic reconnection, which forms and heats flare loops. Recent studies have revealed a two-phase evolution pattern of UV 1600 ? emission at the feet of these loops: a rapid pulse lasting for a few seconds to a few minutes, followed by a gradual decay on timescales of a few tens of minutes. Multiple band EUV observations by the Atmosphere Imaging Assembly further reveal very similar signatures. These two phases represent different but related signatures of an impulsive energy release in the corona. The rapid pulse is an immediate response of the lower atmosphere to an intense thermal conduction flux resulting from the sudden heating of the corona to high temperatures (we rule out energetic particles due to a lack of significant hard X-ray emission). The gradual phase is associated with the cooling of hot plasma that has been evaporated into the corona. The observed footpoint emission is again powered by thermal conduction (and enthalpy), but now during a period when approximate steady-state conditions are established in the loop. UV and EUV light curves of individual pixels may therefore be separated into contributions from two distinct physical mechanisms to shed light on the nature of energy transport in a flare. We demonstrate this technique using coordinated, spatially resolved observations of UV and EUV emissions from the footpoints of a C3.2 thermal flare. **2010 August 1**.

Hard X-ray Spikes Observed by RHESSI

Jiong **Qiu**
RHESSI Science Nugget, No. 191, **2013**
New software allows RHESSI to study rapid time variations, in spite of the image modulation.
RHESSI capabilities have allowed us to continue the decades-long effort to study rapidly evolving hard X-ray bursts. These observations may hold the key to uncover fundamental scales of energy release in solar flares. The most prominent hard X-ray spikes from a sample of RHESSI flares exhibit similar temporal properties as those discovered in SMM flares in the 70s and BATSE flares in the 90s. **17 March 2002**

Solar flare hard X-ray spikes observed by RHESSI: a case study

J. **Qiu**, J. X. Cheng, G. J. Hurford, Y. Xu, and H. Wang
E-print, Oct **2012**, A&A, 547, A72 (2012)
Context. Fast-varying hard X-ray spikes of subsecond time scales were discovered by space telescopes in the 70s and 80s, and are also observed by the Ramaty High Energy S olar S pectroscopic Imager (RHESSI). These events indicate that the flare energy release is fragmented.

Aims. In this paper, we analyze hard X-ray spikes observed by RHESSI to understand their temporal, spectral, and spatial properties.
Methods. A recently developed demodulation code was applied to hard X-ray light curves in several energy bands observed by RHESSI. Hard X-ray spikes were selected from the demodulated flare light curves. We measured the spike duration, the energydependent time delay, and count spectral index of these spikes. We also located the hard X-ray source emitting these spikes from RHESSI mapping that was coordinated with imaging observations in visible and UV wavelengths.
Results. We identify quickly varying structures of 1 s during the rise of hard X-rays in five flares. These hard X-ray spikes can be observed at photon energies over 100 keV. They exhibit sharp rise and decay with a duration (FWHM) of less than 1 s. Energydependent time lags are present in some spikes. It is seen that the spikes exhibit harder spectra than underlying components, typically by 0.5 in the spectral index when they are fitted to power-law distributions. RHESSI clean maps at 25?100 keV with an integration of 2 s centered on the peak of the spikes suggest that hard X-ray spikes are primarily emitted by double foot-point sources in magnetic fields of opposite polarities.With the RHESSI mapping resolution of 4", the hard X-ray spike maps do not exhibit detectable difference in the spatial structure from sources emitting underlying components. Coordinated high-resolution imaging UV and infrared observations confirm that hard X-ray spikes are produced in magnetic structures embedded in the same magnetic environment of the underlying components. The coordinated high-cadence TRACE UV observations of one event possibly reveal new structures on spatial scales < 1-2"at the time of the spike superposed on the underlying component. They are probably sources of hard X-ray spikes. **2002-Mar-17, 2002-Aug-30, 2003-Oct-29, 2005-Jan-17, 2005-Jan-19**

HEATING OF FLARE LOOPS WITH OBSERVATIONALLY CONSTRAINED HEATING FUNCTIONS

Jiong **Qiu**, Wen-Juan Liu, and Dana W. Longcope
2012 ApJ 752 124
We analyze high-cadence high-resolution observations of a C3.2 flare obtained by AIA/SDO on **2010 August 1**. The flare is a long-duration event with soft X-ray and EUV radiation lasting for over 4 hr. Analysis suggests that magnetic reconnection and formation of new loops continue for more than 2 hr. Furthermore, the UV 1600 Å observations show that each of the individual pixels at the feet of flare loops is brightened instantaneously with a timescale of a few minutes, and decays over a much longer timescale of more than 30 minutes. We use these spatially resolved UV light curves during the rise phase to construct empirical heating functions for individual flare loops, and model heating of coronal plasmas in these loops. The total coronal radiation of these flare loops are compared with soft X-ray and EUV radiation fluxes measured by GOES and AIA. This study presents a method to observationally infer heating functions in numerous flare loops that are formed and heated sequentially by reconnection throughout the flare, and provides a very useful constraint to coronal heating models.

RECONNECTION AND ENERGETICS IN TWO-RIBBON FLARES: A REVISIT OF THE BASTILLE-DAY FLARE

Jiong **Qiu**1, WenJuan Liu1, Nicholas Hill2, and Maria Kazachenko1
Astrophysical Journal, 725:319–330, **2010, File**
https://iopscience.iop.org/article/10.1088/0004-637X/725/1/319/pdf
We conduct a semi-quantitative analysis of two-ribbon flares to investigate the observational relationship between magnetic reconnection and energetics by revisiting the Bastille-day flare, particularly the UV and hard X-ray (HXR) observations. The analysis establishes that prominent UV emission is primarily produced by precipitating electrons that also produce HXRs. In addition, reconnection and subsequent energy release along adjacent field lines along the polarity inversion line (PIL) combined with elongated decay of UV emission may account for the observed extended UV ribbons whereas HXR sources with rapid decay appear mostly as compact kernels. Observations also show that HXR sources and UV brightenings exhibit an organized parallel motion along the magnetic PIL during the rise of the flare, and then the perpendicular expansion of UV ribbons dominate during the peak. With a 2.5 dimensional approximation with the assumed translational dimension along the PIL, we derive geometric properties of UV ribbons and infer the pattern of reconnection as with a varying magnetic guide field during reconnection. It is shown that HXR and UV emissions evolve in a similar way to reconnection rates determined by the perpendicular “motion.” The analysis suggests that a relatively strong guide field may be present during the rise of the flare, whereas particle acceleration and non-thermal energy release are probably more efficient with an enhanced reconnection rate with a relatively weak guide field.We discuss the role of the guide field in reconnection and particle energization, as well as novel observational experiments that may be conducted to shed new light on these issues.

Kernels and Ribbons (Revisiting the Bastille Day Flare)

Jiong **QIU**
2010 June 14

http://sprg.ssl.berkeley.edu/~tohban/wiki/index.php/Kernels_and_Ribbons

Evaluating Mean Magnetic Field in Flare Loops

Jiong **Qiu** · Dale E. Gary · Gregory D. Fleishman
Solar Phys (**2009**) 255: 107–118, DOI 10.1007/s11207-009-9316-y
https://sci-hub.do/10.1007/s11207-009-9316-y **File**

We analyze multiple-wavelength observations of a two-ribbon flare exhibiting apparent expansion motion of the flare ribbons in the lower atmosphere and rising motion of X-ray emission at the top of newly-formed flare loops. We evaluate magnetic reconnection rate in terms of $V_r B_r$ by measuring the ribbon-expansion velocity (V_r) and the chromospheric magnetic field (B_r) swept by the ribbons. We also measure the velocity (V_t) of the apparent rising motion of the loop-top X-ray source, and estimate the mean magnetic field (B_t) at the top of newly-formed flare loops using the relation $\_V_tB_t\_ \approx \_V_rB_r\_$, namely, conservation of reconnection flux along flare loops. For this flare, B_t is found to be 120 and 60 G, respectively, during two emission peaks five minutes apart in the impulsive phase. An estimate of the magnetic field in flare loops is also achieved by analyzing the microwave and hard X-ray spectral observations, yielding $B =$ 250 and 120 G at the two emission peaks, respectively. The measured B from the microwave spectrum is an appropriately-weighted value of magnetic field from the loop top to the loop leg. Therefore, the two methods to evaluate coronal magnetic field in flaring loops produce fully-consistent results in this event.
19 October 2001.

Observational Analysis of Magnetic Reconnection Sequence

Jiong **Qiu**
E-print, Oct 2008; Astrophysical Journal, 692:1110–1124, **2009** February; **File**
http://solar.physics.montana.edu/cgi-bin/eprint/index.pl?entry=8622

We conduct comprehensive analysis of an X2.0 flare to derive quantities indicative of magnetic reconnection in solar corona by following temporally and spatially resolved flare ribbon evolution in the lower atmosphere. The analysis reveals a macroscopically distinctive two-stage reconnection (Moore et al. 2001) marked by a clear division in morphological evolution, reconnection rate, and energy release rate. ***During the first stage, the flare brightening starts at and primarily spreads along the polarity inverion line (PIL) with the maximum apparent speed comparable to the local Alfven speed. The second stage is dominated by ribbon expansion perpendicular to the PIL*** at a fraction of the local Alfven speed. We further develop a data analysis approach, namely "reconnection sequence analysis", to determine the connectivity and reconnection flux during the flare between a dozen magnetic sources defined from partitioning the photospheric magnetogram. It is found that magnetic reconnection proceeds sequentially between magnetic cells, and the observationally measured reconnection flux in major cells compares favorably with computations by a topological model of magnetic reconnection. The 3D evolution of magnetic reconnection is discussed with respect to its implication on helicity transfer and energy release through reconnection. **7 Nov 2004**
(See ON THE BRIGHTENING PROPAGATION OF POST-FLARE LOOPS OBSERVED BY TRACE, Leping Li et al 2009 ApJ 690 347-357)

Flare Induced Sunquake Signatures in the Ultraviolet as Observed by the Atmospheric Imaging Assembly

Sean **Quinn**, Mihalis Mathioudakis, Christopher J. Nelson, Ryan O. Milligan, Aaron Reid, David B. Jess
ApJ **920** 25 **2021**
https://arxiv.org/pdf/2105.05704.pdf
https://iopscience.iop.org/article/10.3847/1538-4357/ac0139/pdf
https://doi.org/10.3847/1538-4357/ac0139

Sunquakes (SQs) have been routinely observed in the solar photosphere, but it is only recently that signatures of these events have been detected in the chromosphere. We investigate whether signatures of SQs are common in Ultraviolet (UV) continua, which sample the solar plasma several hundred km above where SQs are typically detected. We analyse observations from the Solar Dynamics Observatory's Atmospheric Imaging Assembly (SDO/AIA) 1600 Å and 1700 Å passbands, for SQ signatures induced by the flares of Solar Cycle 24. We base our analysis on the 62 SQs detected in the recent statistical study presented by Sharykin & Zosovichev (2020). We find that 9 out of 62 SQ candidates produced a response that is clearly detected in running difference images from the AIA 1600 Å and 1700 Å channels. A binary frequency filter with a width of 2 mHz, centred on 6 mHz, was applied to the data. The first signature of each SQ was detected at distances between 5.2 Mm to 25.7 Mm from the associated flare ribbon. Time-distance and regression analysis allowed us to calculate the apparent transverse velocities of the SQs in the UV datasets and found maximum velocities as high as 41 km s-1, 87 Mm away from the SQ source. Our analysis shows that flare induced SQ signatures can be detected in the SDO/AIA 1600 Å and 1700 Å passbands, hinting at their presence in the lower chromosphere.

There was no apparent correlation between GOES flare classification, and the appearance of the SQ at these heights.
15.02.2011, 2012 February 04, 2012 July 04, 23.10.2012, 05.11.2013, 2014 February 02, 04.02.2014, 22.08.2015, 06.09.2017
Table 1. The 25 flares that produced some response associated with a SQ
HMI Science Nuggets #171 http://hmi.stanford.edu/hminuggets/?p=3783

Kelvin-Helmholtz instability and collapse of a twisted magnetic null point with anisotropic viscosity

James **Quinn**, David MacTaggart, Radostin Simitev
A&A 650, A143 (**2021**)
https://www.aanda.org/articles/aa/pdf/2021/06/aa40460-21.pdf
https://doi.org/10.1051/0004-6361/202140460
https://arxiv.org/pdf/2102.00761.pdf
Context: Magnetic null points are associated with high-energy coronal phenomena such as solar flares and are often sites of reconnection and particle acceleration. Dynamic twisting of a magnetic null point can generate a Kelvin-Helmholtz instability (KHI) within its fan plane and, under continued twisting, can instigate spine-fan reconnection and an associated collapse of the null point.
Aim: This article aims to compare the effects of isotropic and anisotropic viscosity in simulations of the KHI and collapse in a dynamically twisted magnetic null point.
Methods: Simulations were performed using the 3D magnetohydrodynamics code Lare3d with a custom anisotropic viscosity module. A pair of high resolution simulations was performed, one using isotropic viscosity and another using anisotropic viscosity, keeping all other factors identical, and the results analysed in detail. A further parameter study was performed over a range of values for viscosity and resistivity.
Results: Both viscosity models permit the growth of the Kelvin-Helmholtz instability and the eventual collapse of the null point. Over all studied parameters, anisotropic viscosity allows a faster growing instability, while isotropic viscosity damps the instability to the extent of stabilisation in some cases. Although the viscous heating associated with anisotropic viscosity is generally smaller, the ohmic heating dominates and is enhanced by the current sheets generated by the instability, leading to a greater overall heating rate when using anisotropic viscosity. The collapse of the null point occurs significantly sooner when anisotropic viscosity is employed.

The Chromospheric Response to the Sunquake generated by the X9.3 Flare of NOAA 12673

Sean **Quinn**, Aaron Reid, Mihalis Mathioudakis, Christopher Nelson, S. Krishna Prasad, Sergei Zharkov
2019 ApJ **881** 82
https://arxiv.org/pdf/1906.08545.pdf
https://doi.org/10.3847/1538-4357/ab2c9e
Active region NOAA 12673 was extremely volatile in 2017 September, producing many solar flares, including the largest of solar cycle 24, an X9.3 flare of **06 September 2017**. It has been reported that this flare produced a number of sunquakes along the flare ribbon (Sharykin & Kosovichev 2018; Zhao & Chen 2018). We have used co-temporal and co-spatial Helioseismic and Magnetic Imager (HMI) line-of-sight (LOS) and Swedish 1-m Solar Telescope observations to show evidence of the chromospheric response to these sunquakes. Analysis of the Ca II 8542 \AA\space line profiles of the wavefronts revealed that the crests produced a strong blue asymmetry, whereas the troughs produced at most a very slight red asymmetry. We used the combined HMI, SST datasets to create time-distance diagrams and derive the apparent transverse velocity and acceleration of the response. These velocities ranged from 4.5 km s−1 to 29.5 km s−1 with a constant acceleration of 8.6 x 10−3 km s−2. We employed NICOLE inversions, in addition to the Center-of-Gravity (COG) method to derive LOS velocities ranging 2.4 km s−1 to 3.2 km s−1. Both techniques show that the crests are created by upflows. We believe that this is the first chromospheric signature of a flare induced sunquake.
HMI Science Nuggets #129 **2019** http://hmi.stanford.edu/hminuggets/?p=3053

Prediction of Solar Flares Using Unique Signatures of Magnetic Field Images

Abbas **Raboonik**, Hossein Safari, Nasibe Alipour, Michael S. Wheatland
ApJ **2016**
https://arxiv.org/abs/1610.03222
Prediction of solar flares is an important task in solar physics. The occurrence of solar flares is highly dependent on the structure and the topology of solar magnetic fields. A new method for predicting large (M and X class) flares is presented, which uses machine learning methods applied to the Zernike moments of magnetograms observed by the Helioseismic and Magnetic Imager (HMI) onboard the Solar Dynamics Observatory (SDO) for a period of six years from 2 June 2010 to 1 August 2016. Magnetic field images consisting of the radial component of the magnetic field are converted to finite sets of Zernike moments and fed to the Support Vector Machine (SVM) classifier. Zernike moments have the capability to elicit unique features from any 2-D image, which may allow more accurate classification. The

results indicate whether an arbitrary active region has the potential to produce at least one large flare. We show that the majority of large flares can be predicted within 48 hours before their occurrence, with only 10 false negatives out of 385 flaring active region magnetograms, and 21 false positives out of 179 non-flaring active region magnetograms. Our method may provide a useful tool for prediction of solar flares which can be employed alongside other forecasting methods. **2011-12-27 , 2012-05-09, 2012-06-14**

First Comparison of FLARIX Simulations with MSDP Observation of the C1.6 Solar Flare in the Hα Line of Hydrogen

Krzysztof **Radziszewski**4, Petr Heinzel, Jana Kašparová, Michalina Litwicka, Arkadiusz Berlicki, Paweł Rudawy, and Robert Falewicz

2024 ApJ 977 132

https://iopscience.iop.org/article/10.3847/1538-4357/ad8ba9/pdf

The primary objective of this study is to develop a time-dependent model of the flaring atmosphere based on observational data. Here, we present, for the first time, a comparison between numerical simulations of the flaring emission, specifically focusing on the hydrogen Hα line, utilizing the FLARIX code and spectral observations of a compact C1.6 GOES-class flare observed on **2012 September 10**, by the MSDP imaging spectrograph installed at the Białków Observatory. The Multichannel Subtractive Double Pass imaging spectrograph spectral data, collected with a temporal resolution as fine as 50 ms, enabled a comprehensive analysis of Hα line profiles and light curves measured within an area of the flare's emission. An initial atmospheric model close to VAL-C, with a modified temperature in the upper chromosphere, was employed in simulations. To enhance temporal resolution, modulations of the nonthermal electron (NTE) beam's parameters were introduced based on variations in observed hard X-ray (HXR) flux (using RHESSI data). The synthesized Hα line profiles were compared with the observed spectra. During the impulsive phase of the flare, the evolution of the observed and synthetic Hα line intensity agrees, but discrepancies were found in intensities at specific wavelengths of the Hα line profile. Fluctuations in the energy flux of NTEs exhibited a strong correlation with the Hα emission during the HXR pulse. After considering various effects (such as the filling factor FF = 0.20) that could influence observed emissions, relatively good agreement between theoretical and observed lines was achieved.

The depth and the vertical extent of the energy deposition layer in a medium-class solar flare

Krzysztof **Radziszewski**, Robert Falewicz, Pawel Rudawy

ApJ **903** 28 **2020**

https://arxiv.org/pdf/2009.06064.pdf

https://doi.org/10.3847/1538-4357/abb706

We analyze here variations of the position and the vertical extent of the energy deposition layer (EDL) in the C1.6 \textit{GOES}-class solar flare observed at 10:20 UT on **2012 September 10**. The variations of the EDL are contrasted with the variations of the spectra and emission intensities recorded in the Hα line with the very high time resolution using the MSDP spectrograph at Białk{ó}w Observatory.

The flare radiated hard X-rays (HXR) detectable up to a energy of 70 keV. A numerical model of the flare used in the analysis assumes that the non-thermal electrons (NTEs) carried the external energy to the flare. The NTEs energy flux was derived from a non-thermal component seen in \textit{RHESSI} spectra. The main geometrical parameters of the flare were derived using restored \textit{RHESSI} imaging data.

We found that the variations of the X-ray fluxes recorded in various energy bands and the variations of the Hα intensities were well correlated in time during the pre-impulsive and impulsive phases of the flare and they agreed with the variations of the calculated position and vertical extent of the EDL. The variations of the emission noticed in various parts of the Hα line profile were caused by individual episodes of energy deposition by the beams of NTEs of various energy spectra on various depths in the chromospheric plasma. These results supplement our previous findings for the solar flare on **21 June 2013**, having nearly the same \textit{GOES}-class of C1.1 but HXR emission below 34 keV only \citep{2017ApJ...847...84F} (hereafter Paper I).

Variations of Flaring Kernel Sizes in Various Parts of the Hα Line Profile

K. **Radziszewski**, P. Rudawy

Solar Physics, June **2013**, Volume 284, Issue 2, pp 397-404,

We analyze the temporal variations of the sizes and emission intensities of 31 flaring kernels in various parts of the Hα line profile. We have found that the areas of all kernels decrease systematically when observed in consecutive wavelengths toward the wings of the Hα line, but their areas and emission intensity vary in time. Our results are in agreement with the commonly accepted model of the wine-glass-shaped lower parts of the magnetic flaring loops channelling high-energy variable particle beams toward the chromospheric plasma.

High time-resolution spectral-imaging data used in our work were collected using the Large Coronagraph and Horizontal Telescope equipped with the Multi-channel Subtractive Double Pass Spectrograph and the Solar Eclipse Coronal Imaging System (MSDP-SECIS) at the Białków Observatory of the University of Wrocław, Poland.
Table: July 2003 - Aug 2005

High time resolution observations of solar Hα flares. II. Search for signatures of electron beam heating

K. **Radziszewski**1, P. Rudawy1 and K. J. H. Phillips2
A&A 535, A123 (**2011**)
Aims. The Hα emission of solar flare kernels and associated hard X-ray (HXR) emission often show similar time variations but their light curves are shifted in time by energy transfer mechanisms. We searched for fast radiative response of the chromosphere in the Hα line as a signature of electron beam heating.
Methods. We investigate the time differences with sub-second resolution between the Hα line emission observed with a Multi-channel Subtractive Double Pass (MSDP) spectrograph on the Large Coronagraph and Horizontal Telescope at Białków Observatory, Poland, and HXR emission recorded by the RHESSI spacecraft during several flares, greatly extending our earlier analysis (Paper I) to flares between 2003 and 2005.
Results. For 16 Hα flaring kernels, observed in 12 solar flares, we made 72 measurements of time delays between local maxima of the RHESSI X-ray and Hα emissions. For most kernels, there is an excellent correlation between time variations in the Hα line emission (at line centre and in the line wings) and HXR (20–50 keV) flux, with the Hα emission following features in the HXR light curves generally by a short time lapse $\Delta t = 1–2$ s, sometimes significantly longer (10–18 s). We also found a strong spatial correlation.
Conclusions. Owing to our larger number of time measurements than in previous studies, the distribution of Δt values shows a much clearer pattern, with many examples of short (1–2 s) delays of the Hα emission, but with some flares showing longer (10–18 s) delays. The former are consistent with energy transfer along the flaring loop legs by non-thermal electron beams, the latter to the passage of conduction fronts.

X-ray and H-alpha Flare Impulses,

K. **Radziszewski** and P. Rudawy
RHESSI Science Nugget, No. 163, **2011**
http://sprg.ssl.berkeley.edu/~tohban/wiki/index.php/X-ray_and_H-alpha_Flare_Impulses
Strikingly precise correlations of H-alpha kernels and hard X-ray bursts.
2003 July 16, 2005 July 12

Sizes of flaring kernels in various parts of the H-alpha line profile

K. **Radziszewski** and P. Rudawy
E-print, May **2008**, Manuscript prepared for Ann. Geophys.
http://www.astro.uni.wroc.pl/ludzie/rudawy/rad2.pdf
In this paper we present new results of spectraphotometrical investigations of the flaring kernels sizes and their intensities measured simultaneously in various parts of the H-alpha line profile. Our investigations were based on the very high temporal resolution spectral-imaging observations of the solar flares collected with Large Coronagraph (LC), Multi-channel Subtractive Double Pass Spectrograph and Solar Eclipse Coronal Imaging System (MSDP-SECIS) at Bialkow Observatory (University of Wroclaw, Poland). We have found that the areas of the investigated individual flaring kernels vary in time and in wavelengths as well as the intensities and areas of the H-alpha flaring kernels decreased systematically when observed in consecutive wavelengths toward the wings of the H-alpha line. Our result could be explained as an effect of the cone-shaped lower parts of the magnetic loops channeling high energy particle beams exciting chromospheric plasma.

High Time Resolution Observations of Solar H-alpha Flares –

I -- K. **Radziszewski**, P. Rudawy, K. J. H. Phillips
A&A E -print, Oct **2006**
good time correlations between X-ray flux variations and variations of the H-alpha emission of the selected bright flaring kernels

IMAGING SPECTROSCOPY USING AIA DIFFRACTION PATTERNS IN CONJUNCTION WITH RHESSI AND EVE OBSERVATIONS

Claire L. **Raftery**1, Säm Krucker2 and Robert P. Lin
2011 ApJ 743 L27
Extreme-ultraviolet (EUV) spectroscopy is a very powerful tool that can be used for probing the dynamic response of the solar corona and chromosphere during solar flares. Here we present a unique application of observations from the Atmospheric Imaging Assembly (AIA) on board the Solar Dynamics Observatory using the artifacts of diffraction and dispersion. Using these techniques we can achieve imaging spectroscopy at the resolution of AIA (06 plate scale) and at the revolutionary cadence of the instrument (nominally 12 s) for the brightest (saturated) pixels during solar flares. Analyzing the dispersion and diffraction effects that are observed as a result of the support grids used for the instrument's front filters, we can achieve up to 0.5 Å spectral resolution across the EUV, optically thin passbands. Here we describe the technique used and present the first result of its application—the emission measure distribution for a single pixel at the top of a flaring loop. We analyze the AIA dispersion spectrum in conjunction with Extreme Ultraviolet Variability Experiment observations and spectroscopic and imaging results from the Reuven Ramaty High Energy Solar Spectroscopic Imager.

Multi-wavelength observations and modelling of a canonical solar flare

C. L. **Raftery**[1, 2], P. T. Gallagher[1], R. O. Milligan[2], and J. A. Klimchuk[2]
A&A 494, 1127-1136 (**2009**), DOI: 10.1051/0004-6361:200810437; **File**
Aims. We investigate the temporal evolution of temperature, emission measure, energy loss, and velocity in a C-class solar flare from both observational and theoretical perspectives.
Methods. The properties of the flare were derived by following the systematic cooling of the plasma through the response functions of a number of instruments – the Reuven Ramaty High Energy Solar Spectroscopic Imager (RHESSI; >5 MK), GOES-12 (5–30 MK), the Transition Region and Coronal Explorer (TRACE 171 Å; 1 MK), and the Coronal Diagnostic Spectrometer (CDS; ~0.03–8 MK). These measurements were studied in combination with simulations from the 0-D enthalpy based thermal evolution of loops (EBTEL) model.
Results. At the flare onset, upflows of ~90 km s^{-1} and low-level emission were observed in Fe XIX, consistent with pre-flare heating and gentle chromospheric evaporation. During the impulsive phase, upflows of ~80 km s^{-1} in Fe XIX and simultaneous downflows of ~20 km s^{-1} in He I and O V were observed, indicating explosive chromospheric evaporation. The plasma was subsequently found to reach a peak temperature of >13 MK in approximately 10 min. Using EBTEL, conduction was found to be the dominant loss mechanism during the initial ~300 s of the decay phase. It was also found to be responsible for driving gentle chromospheric evaporation during this period. As the temperature fell below ~8 MK, and for the next ~4000 s, radiative losses were determined to dominate over conductive losses. The radiative loss phase was accompanied by significant downflows of <40 km s^{-1} in O V.
Conclusions. This is the first extensive study of the evolution of a canonical solar flare using both spectroscopic and broad-band instruments in conjunction with a 0-D hydrodynamic model. While our results are in broad agreement with the standard flare model, the simulations suggest that both conductive and non-thermal beam heating play important roles in heating the flare plasma during the impulsive phase of at least this event.
ILWS WORKSHOP 2006, GOA, FEBRUARY 19-20, 2006

Effects of sunspot umbral rotation in the onset of flares

K. Sundara **Raman**

Solar synthetic imaging: Introducing denoising diffusion probabilistic models on SDO/AIA data

Francesco P. **Ramunno**, S. Hackstein, V. Kinakh, M. Drozdova, G. Quetant, A. Csillaghy, S. Voloshynovskiy
A&A 686, A285 **2024**
https://arxiv.org/pdf/2404.02552.pdf
https://doi.org/10.1051/0004-6361/202347860
https://www.aanda.org/articles/aa/pdf/2024/06/aa47860-23.pdf
Given the rarity of significant solar flares compared to smaller ones, training effective machine learning models for solar activity forecasting is challenging due to insufficient data. This study proposes using generative deep learning models, specifically a Denoising Diffusion Probabilistic Model (DDPM), to create synthetic images of solar phenomena, including flares of varying intensities. By employing a dataset from the AIA instrument aboard the SDO spacecraft, focusing on the 171 Å band that captures various solar activities, and classifying images with GOES X-ray measurements based on flare intensity, we aim to address the data scarcity issue. The DDPM's performance is evaluated using cluster metrics, Frechet Inception Distance (FID), and F1-score, showcasing promising results in generating realistic solar imagery. We conduct two experiments: one to train a supervised classifier for event identification and

another for basic flare prediction, demonstrating the value of synthetic data in managing imbalanced datasets. This research underscores the potential of DDPMs in solar data analysis and forecasting, suggesting further exploration into their capabilities for solar flare prediction and application in other deep learning and physical tasks.

Relationship between Successive Flares in the Same Active Region and Space-Weather HMI Active Region Patch (SHARP) Parameters

Hao **Ran**, Ying D. Liu, Yang Guo, Rui Wang
ApJ **937** 43 **2022**
https://arxiv.org/pdf/2207.07254.pdf
https://iopscience.iop.org/article/10.3847/1538-4357/ac80fa/pdf
A solar active region (AR) may produce multiple notable flares during its passage across the solar disk. We investigate successive flares from flare-eruptive active regions, and explore their relationship with solar magnetic parameters. We examine six ARs in this study, each with at least one major flare above X1.0. The Space-Weather HMI Active Region Patch (SHARP) is employed in this study to parameterize the ARs. We aim to identify the most flare-related SHARP parameters and lay foundation for future practical flare forecasts. We first evaluate the correlation coefficients between the SHARP parameters and the successive flare production. Then we adopt a Natural Gradient Boost (NGBoost) method to analyze the relationship between the SHARP parameters and the successive flare bursts. Based on the correlation analysis and the importance distribution returned from NGBoost, we select 8 most flare-related SHARP parameters. Finally, we discuss the physical meanings of the 8 selected parameters and their relationship with flare production. **13-18 Feb 2011, 8-11 Mar 2011, 5-10 Sep 2011, 4-12 Mar 2012, 26-31 Mar 2014, 1-7 Sep 2017**

Multi-wavelength observations of a B-class flare using XSM, AIA, and XRT

Yamini K. **Rao**, B. Mondal, Giulio Del Zanna, N. P. S. Mithun, S. V. Vadawale, K. K. Reeves, Helen E. Mason, Anil Bhardwaj
ApJ **958** 190 **2023**
https://arxiv.org/pdf/2308.14912
https://iopscience.iop.org/article/10.3847/1538-4357/acf46a/pdf
We present multi-wavelength observations by Chandrayaan-2/XSM, SDO/AIA and Hinode/XRT of a B-class flare observed on **25th February, 2021**, originating from an active region (AR 12804) near the North-West limb. The microflare lasts for approx 30 mins and is composed of hot loops reaching temperatures of 10 MK. We report excellent agreement (within 20 percent) for the average effective temperatures obtained at the flare peak from all the three instruments, which have different temperature sensitivities. The XRT filter combination of Be-thin and Be-med provides an excellent opportunity to measure the high-temperatures in such microflare events. The elemental abundances during the evolution of the microflare are also studied and observed to drop towards photospheric values at the flare peak time, compared to coronal values during the rise and decay phase. This is consistent with previous XSM studies.

RT-2 DETECTION OF QUASI-PERIODIC PULSATIONS IN THE 2009 JULY 5 SOLAR HARD X-RAY FLARE

A. R. **Rao**1, J. P. Malkar1, M. K. Hingar1, V. K. Agrawal1,2, S. K. Chakrabarti3,4, A. Nandi2,4, D. Debnath4, T. B. Kotoch4, T. R. Chidambaram5, P. Vinod5, S. Sreekumar5, Y. D. Kotov6, A. S. Buslov6, V. N. Yurov6, V. G. Tyshkevich6, A. I. Arkhangelskij6, R. A. Zyatkov6, S. Shaheda Begum7, and P. K. Manoharan7
Astrophysical Journal, 714:1142–1148, **2010** May
We present the results of an analysis of hard X-ray observations of the C2.7 solar flare detected by the RT-2 experiment on board the *Coronas–Photon* satellite.We detect hard X-ray pulsations at periods of ~12 s and ~15 s. We find a marginal evidence for a decrease in period with time.We have augmented these results using the publicly available data from the *RHESSI* satellite. We present a spectral analysis and measure the spectral parameters.

Role of Transients in the Sustainability of Solar Coronal Plumes

N.-E. **Raouafi**1 and G. Stenborg
2014 ApJ 787 118.
We report on the role of small-scale, transient magnetic activity in the formation and evolution of solar coronal plumes. Three plumes within equatorial coronal holes are analyzed over the span of several days based on the Solar Dynamic Observatory (SDO)/Atmospheric Imaging Assembly 171 Å and 193 Å images and SDO/Helioseismic and Magnetic Imager line-of-sight magnetograms. The focus is on the role of transient structures at the footpoints in sustaining coronal plumes for relatively long periods of time (i.e., several days). The appearance of plumes is a gradual and lengthy process. In some cases, the initial stages of plume formation are marked by the appearance of pillar-like structures whose footpoints are the sources of transient brightenings. In addition to nominal jets occurring prior to and during the development of plumes, the data show that a large number of small jets (i.e., "jetlets") and plume transient

bright points (PTBPs) occur on timescales of tens of seconds to a few minutes. These features are the result of quasi-random cancellations of fragmented and diffuse minority magnetic polarity with the dominant unipolar magnetic field concentration over an extended period of time. They unambiguously reflect a highly dynamical evolution at the footpoints and are seemingly the main energy source for plumes. This suggests a tendency for plumes to be dependent on the occurrence of transients (i.e., jetlets, and PTBPs) resulting from low-rate magnetic reconnection. The decay phase of plumes is characterized by gradual fainting and multiple rejuvenations as a result of the dispersal of the unipolar magnetic concentration and its precipitation into multiple magnetic centers.

OBSERVATIONAL EVIDENCE FOR CORONAL TWISTED FLUX ROPE
N.-E. **Raouafi**
ApJ 691 L128-L132 **2009**
http://www.iop.org/EJ/abstract/1538-4357/691/2/L128
Multi-instrument data sets of NOAA AR10938 on 2007 January 16 (e.g., Hinode, STEREO, GOES, MLSO, and ISOON Hα) are utilized to study the fine structure and evolution of a magnetic loop system exhibiting multiple crossing threads, whose arrangement and individual shapes are very suggestive of individual field lines in a flux rope. The footpoints of the magnetic threads are closely rooted into pores and plage areas. A C-class flare recorded by GOES at approximately 2:35 UT near one of the footpoints of the multi-thread system (along with a wisp of loop material shown by EUV data) led to the brightening of the magnetic structure revealing its fine structure with several threads that indicate a high degree of linking (suggesting a left-handed helical pattern as shown by the filament structure formed later on). EUV observations by Hinode/EIS of hot spectral lines at 2:46 UT show a complex structure of coronal loops. The same features were observed about 20 minutes later in X-ray images from Hinode/XRT and about 30 minutes further in EUV images of STEREO/SECCHI/EUVI with much better resolution. Hα and 304 Å images revealed the presence of several filament fibrils in the same area. They evolved a few hours later into a denser structure seemingly showing a helical pattern, which persisted or several days forming a segment of a larger-scale filament. The present observations provide an important indication for a flux robe as a precursor of a solar filament.

Global and local dynamics of X-flare-producing active regions during solar cycle 25 peak phase

B. **Raphaldini**1⋆, M. Dikpati1, A. S. W. Teruya2, K. Jain3, A. A. Norton4 and S. W. McIntosh1,5
A&A, 691, A3 (**2024**)
https://www.aanda.org/articles/aa/pdf/2024/11/aa51428-24.pdf
Context. The configuration of the longitudinally elongated region that active regions (ARs) cluster around, known as a toroid belt, has been shown to be an indicator of intense activity. In particular, complex ARs at locations in the north and/or south toroids tend to appear “tipped-away” with respect to each other. On the other hand, magnetic helicity has been used as an indicator of flare activity in ARs.
Aims. As solar cycle (SC) 25 approaches its peak, a number of significant (X-class) flares have been produced. Here, we investigate the circumstances surrounding two of the most flare-prolific ARs of solar cycle 25, namely, ARs 13590 and 13514. Two aspects of the evolution of these ARs are investigated in this work: the global-scale magnetic toroid configuration and small-scale magnetic field morphology and topology – before, during, and after the onset of major flares.
Methods. We studied the global morphology of the solar magnetic fields near intense flares in terms of the spatial distribution of ARs on magnetic fields synoptic maps. On AR scales, we analyzed the magnetic helicity accumulation, as well as its current-carrying and potential components.
Results. Our results are consistent with major flare-prolific ARs from solar cycles 23 and 24. In particular, we observe a consistent dominance of current-carrying magnetic helicity at the time of major flares. The evolution of global magnetic toroids, indicating the occurrence of flare-prolific ARs in the tipped-away portion of the toroid, together with the local dynamics of complex ARs, could offer a few weeks of lead time to prepare for upcoming space weather hazards. **7-28 Dec 2023, 14-28 Feb 2024**

Deciphering Pre-solar-storm Features Of September-2017 Storm From Global And Local Dynamics

Breno **Raphaldini**, Mausumi Dikpati, Aimee A. Norton, Andre S. W. Teruya, Scott W. McIntosh, Christopher B. Prior, David MacTaggart
ApJ **958** 175 **2023**
https://arxiv.org/pdf/2309.16775.pdf
https://iopscience.iop.org/article/10.3847/1538-4357/acfef0/pdf
We investigate whether global toroid patterns and the local magnetic field topology of solar active region AR12673 together can hindcast occurrence of the biggest X-flare of solar cycle (SC)-24. Magnetic toroid patterns (narrow latitude-belts warped in longitude, in which active regions are tightly bound) derived from surface distributions of active regions, prior/during AR12673 emergence, reveal that the portions of the South-toroid containing AR12673 was not tipped-away from its north-toroid counterpart at that longitude, unlike the 2003 Halloween storms scenario. During

the minimum-phase there were too few emergences to determine multi-mode longitudinal toroid patterns. A new emergence within AR12673 produced a complex/non-potential structure, which led to rapid build-up of helicity/winding that triggered the biggest X-flare of SC-24, suggesting that this minimum-phase storm can be anticipated several hours before its occurrence. However, global patterns and local dynamics for a peak-phase storm, such as that from AR11263, behaved like 2003 Halloween storms, producing the third biggest X-flare of SC-24. AR11263 was present at the longitude where the North/South toroids tipped-away from each other. While global toroid patterns indicate that pre-storm features can be forecast with a lead-time of a few months, its application on observational data can be complicated by complex interactions with turbulent flows. Complex/non-potential field structure development hours before the storm are necessary for short term prediction. We infer that minimum-phase storms cannot be forecast accurately more than a few hours ahead, while flare-prone active regions in peak-phase may be anticipated much earlier, possibly months ahead from global toroid patterns.

Magnetic Winding as an Indicator of Flare Activity in Solar Active Regions

Breno **Raphaldini**1, Christopher B. Prior1, and David MacTaggart2
2022 ApJ 927 156
https://iopscience.iop.org/article/10.3847/1538-4357/ac4df9/pdf
Magnetic helicity is a measure of the entanglement of magnetic field lines used to characterize the complexity of solar active region (AR) magnetic fields. Previous attempts to use helicity-based indicators to predict solar eruptive/flaring events have shown promise but not been universally successful. Here we investigate the use of a quantity associated with the magnetic helicity, the magnetic winding, as a means to predict flaring activity. This quantity represents the fundamental entanglement of magnetic field lines and is independent of the magnetic field strength. We use vector magnetogram data derived from the Helioseismic Magnetic Imager (HMI) to calculate the evolution and distribution of the magnetic winding flux associated with five different ARs, three of them with little flaring activity/nonflaring (AR 11318, AR 12119, AR 12285) and two highly active with X-class flares (AR 11158, AR 12673). We decompose these quantities into "current-carrying" and "potential" parts. It is shown that the ARs that show flaring/eruptive activity have significant contributions to the winding input from the current-carrying part of the field. A significant and rapid input of current-carrying winding is found to be a precursor of flaring/eruptive activity, and, in conjunction with the helicity, sharp inputs of both quantities are found to precede individual flaring events by several hours. This suggests that the emergence/submergence of topologically complex current-carrying field is an important element for the ignition of AR flaring. **AR 11158 , 11318, 12119, 12285, 12673**

CURRENT SHEETS FORMATION IN TANGLED CORONAL MAGNETIC FIELDS

A. F. **Rappazzo**1,2 and E. N. Parker
2013 ApJ 773 L2
We investigate the dynamical evolution of magnetic fields in closed regions of solar and stellar coronae. To understand under which conditions current sheets form, we examine dissipative and ideal reduced magnetohydrodynamic models in Cartesian geometry, where two magnetic field components are present: the strong guide field B 0, extended along the axial direction, and the dynamical orthogonal field b. Magnetic field lines thread the system along the axial direction that spans the length L and are line-tied at the top and bottom plates. The magnetic field b initially has only large scales, with its gradient (current) length scale of the order of ℓ b . We identify the magnetic intensity threshold b/B 0 ~ ℓ b /L. For values of b below this threshold, field-line tension inhibits the formation of current sheets, while above the threshold they form quickly on fast ideal timescales. In the ideal case, above the magnetic threshold, we show that current sheets thickness decreases in time until it becomes smaller than the grid resolution, with the analyticity strip width δ decreasing at least exponentially, after which the simulations become underresolved.

FIELD LINES TWISTING IN A NOISY CORONA: IMPLICATIONS FOR ENERGY STORAGE AND RELEASE, AND INITIATION OF SOLAR ERUPTIONS

A.F. **Rappazzo**1, M. Velli2, and G. Einaudi
2013 ApJ 771 76
We present simulations modeling closed regions of the solar corona threaded by a strong magnetic field where localized photospheric vortical motions twist the coronal field lines. The linear and nonlinear dynamics are investigated in the reduced magnetohydrodynamic regime in Cartesian geometry. Initially the magnetic field lines get twisted and the system becomes unstable to the internal kink mode, confirming and extending previous results. As typical in this kind of investigations, where initial conditions implement smooth fields and flux-tubes, we have neglected fluctuations and the fields are laminar until the instability sets in. However, previous investigations indicate that fluctuations, excited by photospheric motions and coronal dynamics, are naturally present at all scales in the coronal fields. Thus, in order to understand the effect of a photospheric vortex on a more realistic corona, we continue the simulations after kink instability sets in, when turbulent fluctuations have already developed in the corona. In the nonlinear stage the system never returns to the simple initial state with ordered twisted field lines, and kink instability does not occur again. Nevertheless, field lines get twisted, although in a disordered way, and energy accumulates at large scales through an inverse cascade. This energy can subsequently be released in micro-flares or larger flares, when interaction with

neighboring structures occurs or via other mechanisms. The impact on coronal dynamics and coronal mass ejections initiation is discussed.

PIXEL ANALYSIS OF PHOTOSPHERIC SPECTRAL DATA. I. PLASMA DYNAMICS
Anthony P. **Rasca**1,3,4, James Chen1,4, and Alexei A. Pevtsov
2016 ApJ 832 53
Recent observations of the photosphere using high spatial and temporal resolution show small dynamic features at or below the current resolving limits. A new pixel dynamics method has been developed to analyze spectral profiles and quantify changes in line displacement, width, asymmetry, and peakedness of photospheric absorption lines. The algorithm evaluates variations of line profile properties in each pixel and determines the statistics of such fluctuations averaged over all pixels in a given region. The method has been used to derive statistical characteristics of pixel fluctuations in observed quiet-Sun regions, an active region with no eruption, and an active region with an ongoing eruption. Using Stokes I images from the Vector Spectromagnetograph (VSM) of the Synoptic Optical Long-term Investigations of the Sun (SOLIS) telescope on **2012 March 13**, variations in line width and peakedness of Fe i 6301.5 Å are shown to have a distinct spatial and temporal relationship with an M7.9 X-ray flare in NOAA 11429. This relationship is observed as stationary and contiguous patches of pixels adjacent to a sunspot exhibiting intense flattening in the line profile and line-center displacement as the X-ray flare approaches peak intensity, which is not present in area scans of the non-eruptive active region. The analysis of pixel dynamics allows one to extract quantitative information on differences in plasma dynamics on sub-pixel scales in these photospheric regions. The analysis can be extended to include the Stokes parameters and study signatures of vector components of magnetic fields and coupled plasma properties.

Electron re-acceleration and HXR emission
Heather **Ratcliffe** and Marian Karlicky.
RHESSI Science Nugget No. 194, Feb **2013**
http://sprg.ssl.berkeley.edu/~tohban/wiki/index.php/Electron_re-acceleration_and_HXR_emission
Can wave-particle interaction solve the electron number problem?
During solar flares, vast amounts of energy are released from the Sun's magnetic field, part of which leads to particle acceleration. Fast electrons thus produced can propagate along a coronal magnetic loop, and produce Hard X-ray (HXR) emission at its footpoints by collisional bremsstrahlung in the dense chromosphere. This HXR emission is one of the primary diagnostics of energetic electrons, and is usually interpreted using the "thick target" model. This assumes, among other things, that the distribution function of the emitting electrons is modified only by collisions. However, when such fast electron beams propagate in a plasma, Langmuir (plasma) waves are generated. These waves are strongly affected by density inhomogeneities, or by wave-wave interactions, and this evolution can have significant effects on the electron distribution. Several simulation methods are applicable in this situation. In this Nugget we show some quasilinear and PIC (particle-in-cell) simulations of the electron evolution and briefly discuss the effects on HXR emission.

DENSITY FLUCTUATIONS AND THE ACCELERATION OF ELECTRONS BY BEAM-GENERATED LANGMUIR WAVES IN THE SOLAR CORONA
H. **Ratcliffe**, N. H. Bian, and E. P. Kontar
2012 ApJ 761 176
Non-thermal electron populations are observed throughout the heliosphere. The relaxation of an electron beam is known to produce Langmuir waves which, in turn, may substantially modify the electron distribution function. As the Langmuir waves are refracted by background density gradients and as the solar and heliospheric plasma density is naturally perturbed with various levels of inhomogeneity, the interaction of Langmuir waves with non-thermal electrons in inhomogeneous plasmas is an important topic. We investigate the role played by ambient density fluctuations on the beam-plasma relaxation, focusing on the effect of acceleration of beam electrons. The scattering of Langmuir waves off turbulent density fluctuations is modeled as a wavenumber diffusion process which is implemented in numerical simulations of the one-dimensional quasilinear kinetic equations describing the beam relaxation. The results show that a substantial number of beam electrons are accelerated when the diffusive timescale in wavenumber space τ_D is of the order of the quasilinear timescale τ_{ql}, while when $\tau_D \gg \tau_{ql}$, the beam relaxation is suppressed. Plasma inhomogeneities are therefore an important means of energy redistribution for waves and hence electrons, and so must be taken into account when interpreting, for example, hard X-ray or Type III emission from flare-accelerated electrons.

EVOLUTION OF SPINNING AND BRAIDING HELICITY FLUXES IN SOLAR ACTIVE REGION NOAA 10930

B. **Ravindra**1, Keiji Yoshimura2 and Sergio Dasso
2011 ApJ 743 33
The line-of-sight magnetograms from Solar Optical Telescope Narrowband Filter Imager observations of NOAA Active Region 10930 have been used to study the evolution of spinning and braiding helicities over a period of five days starting from 2006 December 9. The north (N) polarity sunspot was the follower and the south (S) polarity sunspot was the leader. The N-polarity sunspot in the active region was rotating in the counterclockwise direction. The rate of rotation was small during the first two days of observations and it increased up to 8° hr–1 on the third day of the observations. On the fourth and fifth days it remained at 4° hr–1 with small undulations in its magnitude. The sunspot rotated about 260° in the last three days. The S-polarity sunspot did not complete more than 20° in five days. However, it changed its direction of rotation five times over a period of five days and injected both the positive and negative type of spin helicity fluxes into the corona. Through the five days, both the positive and negative sunspot regions injected equal amounts of spin helicity. The total injected helicity is predominantly negative in sign. However, the sign of the spin and braiding helicity fluxes computed over all the regions were reversed from negative to positive five times during the five-day period of observations. The reversal in spinning helicity flux was found before the onset of the X3.4-class flare, too. Though, the rotating sunspot has been observed in this active region, the braiding helicity has contributed more to the total accumulated helicity than the spinning helicity. The accumulated helicity is in excess of –7 × 1043 Mx2 over a period of five days. Before the X3.4-class flare that occurred on **2006 December 13**, the rotation speed and spin helicity flux increased in the S-polarity sunspot. Before the flare, the total injected helicity was larger than –6 × 1043 Mx2. The observed reversal in the sign of spinning and braiding helicity fluxes could be the signature of the emergence of a twisted flux tube, which acquires the writhe of an opposite sign. The magnetic cloud associated with the ejected mass has carried about –7 × 1041 Mx2 of helicity. A time integration of helicity flux of about 1.2 hr integrated backward in time of the observation of the coronal mass ejection is sufficient for this event.

EVOLUTION OF CURRENTS OF OPPOSITE SIGNS IN THE FLARE-PRODUCTIVE SOLAR ACTIVE REGION NOAA 10930

B. **Ravindra**1, P. Venkatakrishnan2, Sanjiv Kumar Tiwari2,3 and R. Bhattacharyya
2011 ApJ 740 19
Analysis of a time series of high spatial resolution vector magnetograms of the active region NOAA 10930 available from the Solar Optical Telescope SpectroPolarimeter on board Hinode revealed that there is a mixture of upward and downward currents in the two footpoints of an emerging flux rope. The flux emergence rate is almost the same in both the polarities. We observe that along with an increase in magnetic flux, the net current in each polarity increases initially for about three days after which it decreases. This net current is characterized by having exactly opposite signs in each polarity while its magnitude remains almost the same most of the time. The decrease of the net current in both the polarities is due to the increase of current having a sign opposite to that of the net current. The dominant current, with the same sign as the net current, is seen to increase first and then decreases during the major X-class flares. Evolution of non-dominant current appears to be a necessary condition for flare initiation. The above observations can be plausibly explained in terms of the superposition of two different force-free states resulting in a non-zero Lorentz force in the corona. This Lorentz force then pushes the coronal plasma and might facilitate the magnetic reconnection required for flares. Also, the evolution of the net current is found to follow the evolution of magnetic shear at the polarity inversion line.

Spatial Offsets in Flare-CME Current Sheets

John C. **Raymond**1, Silvio Giordano2, and Angela Ciaravella3
2017 ApJ 843 121
http://sci-hub.cc/10.3847/1538-4357/aa7848
https://arxiv.org/pdf/1706.03090.pdf
Magnetic reconnection plays an integral part in nearly all models of solar flares and coronal mass ejections (CMEs). The reconnection heats and accelerates the plasma, produces energetic electrons and ions, and changes the magnetic topology to form magnetic flux ropes and to allow CMEs to escape. Structures that appear between flare loops and CME cores in optical, UV, EUV, and X-ray observations have been identified as current sheets and have been interpreted in terms of the nature of the reconnection process and the energetics of the events. Many of these studies have used UV spectral observations of high temperature emission features in the [Fe xviii] and Si xii lines. In this paper, we discuss several surprising cases in which the [Fe xviii] and Si xii emission peaks are spatially offset from each other. We discuss interpretations based on asymmetric reconnection, on a thin reconnection region within a broader streamer-like structure, and on projection effects. Some events seem to be easily interpreted as the projection of a sheet that is extended along the line of sight that is viewed an angle, but a physical interpretation in terms of asymmetric reconnection is also plausible. Other events favor an interpretation as a thin current sheet embedded in a streamer-like structure. **1997 May 5, 2002 January 10, 2003 January 3, 2003 June 13, 2003 November 4**
Table 1 UVCS Current Sheet Observations Selected for this Study (1997-2003)

Observational Aspects of Particle Acceleration in Large Solar Flares **Review**

John C. **Raymond** · Säm Krucker · Robert P. Lin · Vahé Petrosian

Space Sci. Rev., 173:197–221, **2012, File**

Solar flares efficiently accelerate electrons to several tens of MeV and ions to 10 GeV. The acceleration is usually thought to be associated with magnetic reconnection occurring high in the corona, though a shock produced by the CoronalMass Ejection (CME) associated with a flare can also accelerate particles. Diagnostic information comes from emission at the acceleration site, direct observations of Solar Energetic Particles (SEPs), and emission at radio wavelengths by escaping particles, but mostly from emission from the chromosphere produced when the energetic particles bombard the footpoints magnetically connected to the acceleration region. This paper provides a review of observations that bear upon the acceleration mechanism.

Plasma sloshing in pulse-heated solar and stellar coronal loops

F. **Reale**

2016

http://arxiv.org/pdf/1607.01329v1.pdf

There is evidence that coronal heating is highly intermittent, and flares are the high energy extreme. The properties of the heat pulses are difficult to constrain. Here hydrodynamic loop modeling shows that several large amplitude oscillations (~ 20% in density) are triggered in flare light curves if the duration of the heat pulse is shorter that the sound crossing time of the flaring loop. The reason is that the plasma has not enough time to reach pressure equilibrium during the heating and traveling pressure fronts develop. The period is a few minutes for typical solar coronal loops, dictated by the sound crossing time in the decay phase. The long period and large amplitude make these oscillations different from typical MHD waves. This diagnostic can be applied both to observations of solar and stellar flares and to future observations of non-flaring loops at high resolution.

POST-FLARE ULTRAVIOLET LIGHT CURVES EXPLAINED WITH THERMAL INSTABILITY OF LOOP PLASMA

F. **Reale**1,2, E. Landi3 and S. Orlando

2012 ApJ 746 18

In the present work, we study the C8 flare that occurred on **2000 September 26** at 19:49 UT and observed by the Solar and Heliospheric Observatory/Solar Ultraviolet Measurement of Emitted Radiation spectrometer from the beginning of the impulsive phase to well beyond the disappearance in the X-rays. The emission first decayed progressively through equilibrium states until the plasma reached 2-3 MK. Then, a series of cooler lines, i.e., Ca X, Ca VII, Ne VI, O IV, and Si III (formed in the temperature range log T = 4.3-6.3 under equilibrium conditions), are emitted at the same time and all evolve in a similar way. Here, we show that the simultaneous emission of lines with such a different formation temperature is due to thermal instability occurring in the flaring plasma as soon as it has cooled below ~2 MK. We can qualitatively reproduce the relative start time of the light curves of each line in the correct order with a simple (and standard) model of a single flaring loop. The agreement with the observed light curves is greatly improved, and a slower evolution of the line emission is predicted, if we assume that the model loop consists of an ensemble of subloops or strands heated at slightly different times. Our analysis can be useful for flare observations with the Solar Dynamics Observatory/Extreme ultraviolet Variability Experiment.

VIDENCE OF WIDESPREAD HOT PLASMA IN A NONFLARING CORONAL ACTIVE REGION FROM *HINODE/X-RAY TELESCOPE*

Fabio **Reale**1,5, Paola Testa2, James A. Klimchuk3, and Susanna Parenti

Astrophysical Journal, 698:756–765, **2009**

http://www.iop.org/EJ/toc/-alert=43190/0004-637X/698/1

Nanoflares, short and intense heat pulses within spatially unresolved magnetic strands, are now considered a leading candidate to solve the coronal heating problem. However, the frequent occurrence of nanoflares requires that flare-hot plasma be present in the corona at all times. Its detection has proved elusive until now, in part because the intensities are predicted to be very faint. Here, we report on the analysis of an active region observed with five filters by *Hinode/X-Ray Telescope (XRT)* in **2006 November**. We have used the filter ratio method to derive maps of temperature and emission measure (EM) both in soft and hard ratios. These maps are approximate in that the plasma is assumed to be isothermal along each line of sight. Nonetheless, the hardest available ratio reveals the clear presence of plasma around 10 MK. To obtain more detailed information about the plasma properties, we have performed Monte Carlo simulations assuming a variety of nonisothermal EM distributions along the lines of sight. We find that the observed filter ratios imply bi-modal distributions consisting of a strong cool ($\log T \sim 6.3 - 6.5$) component and a weaker (few percent) and hotter ($6.6 < \log T < 7.2$) component. The data are consistent with bi-modal distributions along all lines of sight, i.e., throughout the active region. We also find that the isothermal temperature inferred from a filter ratio depends sensitively on the precise temperature of the cool component. A slight shift of this component can cause the hot component to be obscured

in a hard ratio measurement. Consequently, temperature maps made in hard and soft ratios tend to be anticorrelated. We conclude that this observation supports the presence of widespread nanoflaring activity in the active region.

Modeling Time-Variable Elemental Abundances in Coronal Loop Simulations

Jeffrey W. **Reep**, John Unverferth, Will T. Barnes, Sherry Chhabra
ApJL **2024**
https://arxiv.org/pdf/2406.04473

Numerous recent X-ray observations of coronal loops in both active regions (ARs) and solar flares have shown clearly that elemental abundances vary with time. Over the course of a flare, they have been found to move from coronal values towards photospheric values near the flare peak, before slowly returning to coronal values during the gradual phase. Coronal loop models typically assume that the elemental abundances are fixed, however. In this work, we introduce a time-variable abundance factor into the 0D ebtel++ code that models the changes due to chromospheric evaporation in order to understand how this affects coronal loop cooling. We find that for strong heating events ($\gtrsim 1$ erg s^{-1} cm^{-3}), the abundances quickly tend towards photospheric values. For smaller heating rates, the abundances fall somewhere between coronal and photospheric values, causing the loop to cool more quickly than the time-fixed photospheric cases (typical flare simulations) and more slowly than time-fixed coronal cases (typical AR simulations). This suggests heating rates in quiescent AR loops no larger than $\approx$0.1 erg s^{-1} cm^{-3} to be consistent with recent measurements of abundance factors $f \gtrsim 2$.

Understanding the Duration of Solar and Stellar Flares at Various Wavelengths

Jeffrey W. **Reep**, Vladimir S. Airapetian
ApJ **958** 9 **2023**
https://arxiv.org/pdf/2306.03765.pdf **File**
https://iopscience.iop.org/article/10.3847/1538-4357/acf45a/pdf

Recent irradiance measurements from numerous heliophysics and astrophysics missions including SDO, GOES, Kepler, TESS, Chandra, XMM-Newton, and NICER have provided critical input in understanding the physics of the most powerful transient events on the Sun and magnetically active stars, solar and stellar flares. The light curves of flare events from the Sun and stars show remarkably similar shapes, typically with a sharp rise and protracted decay phase. The duration of solar and stellar flares has been found to be correlated with the intensity of the event in some wavelengths, such as white light, but not in other wavelengths, such as soft X-rays, but it is not evident why this is the case. In this study, we use a radiative hydrodynamics code to examine factors affecting the duration of flare emission at various wavelengths. The duration of a light curve depends on the temperature of the plasma, the height in the atmosphere at which the emission forms, and the relative importance of cooling due to radiation, thermal conduction, and enthalpy flux. We find that there is a clear distinction between emission that forms low in the atmosphere and responds directly to heating, and emission that forms in the corona, indirectly responding to heating-induced chromospheric evaporation, a facet of the Neupert effect. We discuss the implications of our results to a wide range of flare energies.

Estimating the X-Ray Irradiance of the 2003 October 28 Solar Flare

Jeffrey W. **Reep**1
2022 Res. Notes AAS 6 240
https://iopscience.iop.org/article/10.3847/2515-5172/aca293

The **2003 October 28 X24** solar flare was saturated in GOES XRS/A for about 10 minutes, near the peak of the event. By using RHESSI X-ray spectral fits during that same time period, the XRS/A time series of the flare and derived quantities like temperature and emission measure can be estimated.

Solar Flare Irradiance: Observations and Physical Modeling

Jeffrey W. **Reep**, David E. Siskind, Harry P. Warren
ApJ **927** 103 **2021**
https://arxiv.org/pdf/2110.06310.pdf
https://iopscience.iop.org/article/10.3847/1538-4357/ac4784/pdf

We examine SDO/EVE data to better understand solar flare irradiance, and how that irradiance may vary for large events. We measure scaling laws relating GOES flare classes to irradiance in 21 lines measured with SDO/EVE, formed across a wide range of temperatures, and find that this scaling depends on the line formation temperature. We extrapolate these irradiance values to large events, exceeding X10. In order to create full spectra, however, we need a physical model of the irradiance. We present the first results of a new physical model of solar flare irradiance, NRLFLARE, that sums together a series of flare loops to calculate the spectral irradiance ranging from the X-rays through the far ultraviolet (~ 0 to 1250 Angstroms), constrained by GOES/XRS observations. We test this model against SDO/EVE data. The model spectra and time evolution compares well in high temperature emission, but cooler

lines show large discrepancies. We speculate that the discrepancies are likely due to both a non-uniform cross section of the flaring loops as well as opacity effects. We then show that allowing the cross-sectional area to vary with height significantly improves agreement with observations, and is therefore a crucial parameter needed to accurately model the intensity of spectral lines, particularly in the transition region from $4.7 < \log T < 6.0$. **15 December 2010, 3 November 2011, 7 March 2012, 14 March 2012**

Forecasting the Remaining Duration of an Ongoing Solar Flare

Jeffrey W. **Reep**, Will T. Barnes
Space Weather e2021SW002754 **2021**
https://arxiv.org/pdf/2103.03957.pdf
https://agupubs.onlinelibrary.wiley.com/doi/epdf/10.1029/2021SW002754
https://doi.org/10.1029/2021SW002754
The solar X-ray irradiance is significantly heightened during the course of a solar flare, which can cause radio blackouts due to ionization of the atoms in the ionosphere. As the duration of a solar flare is not related to the size of that flare, it is not directly clear how long those blackouts can persist. Using a random forest regression model trained on data taken from X-ray light curves, we have developed a direct forecasting method that predicts how long the event will remain above background levels. We test this on a large collection of flares observed with GOES-15, and show that it generally outperforms simple linear regression. This forecast is computationally light enough to be performed in real time, allowing for the prediction to be made during the course of a flare. **2012-09-01, 2012-10-20, 2013-11-05-06, 2014-09-10, 2015-11-23, 2016-03-12**

Simulating Solar Flare Irradiance with Multithreaded Models of Flare Arcades

Jeffrey W. **Reep**, Harry P. Warren, Christopher S. Moore, Crisel Suarez, Laura A. Hayes
ApJ **895** 30 **2020**
https://arxiv.org/pdf/2003.10505.pdf
https://doi.org/10.3847/1538-4357/ab89a0
Understanding how energy is released in flares is one of the central problems of solar and stellar astrophysics. Observations of high temperature flare plasma hold many potential clues as to the nature of this energy release. It is clear, however, that flares are not composed of a few impulsively heated loops, but are the result of heating on many small-scale threads that are energized over time, making it difficult to compare observations and numerical simulations in detail. Several previous studies have shown that it is possible to reproduce some aspects of the observed emission by considering the flare as a sequence of independently heated loops, but these studies generally focus on small-scale features while ignoring the global features of the flare. In this paper, we develop a multithreaded model that encompasses the time-varying geometry and heating rate for a series of successively-heated loops comprising an arcade. To validate, we compare with spectral observations of five flares made with the MinXSS CubeSat as well as light curves measured with GOES/XRS and SDO/AIA. We show that this model can successfully reproduce the light curves and quasi-periodic pulsations in GOES/XRS, the soft X-ray spectra seen with MinXSS, and the light curves in various AIA passbands. The AIA light curves are most consistent with long duration heating, but elemental abundances cannot be constrained with the model. Finally, we show how this model can be used to extrapolate to spectra of extreme events that can predict irradiance across a wide wavelength range including unobserved wavelengths. **21 Jul 2016, 23 Jul 2016, 29 Nov 2016, 01 Apr 2017**

Electron Beams Cannot Directly Produce Coronal Rain

Jeffrey W. **Reep**, Patrick Antolin, Stephen J. Bradshaw
ApJ **890** 100 **2020**
https://arxiv.org/pdf/2002.07669.pdf
https://doi.org/10.3847/1538-4357/ab6bdc
Coronal rain is ubiquitous in flare loops, forming shortly after the onset of the solar flare. Rain is thought to be caused by a thermal instability, a localized runaway cooling of material in the corona. The models that demonstrate this require extremely long duration heating on the order of the radiative cooling time, localized near the footpoints of the loops. In flares, electron beams are thought to be the primary energy transport mechanism, driving strong footpoint heating during the impulsive phase that causes evaporation, filling and heating flare loops. Electron beams, however, do not act for a long period of time, and even supposing that they did, their heating would not remain localized at the footpoints. With a series of numerical experiments, we show directly that these two issues mean that electron beams are incapable of causing the formation of rain in flare loops. This result suggests that either there is another mechanism acting in flare loops responsible for rain, or that the modeling of the cooling of flare loops is somehow deficient. To adequately describe flares, the standard model must address this issue to account for the presence of coronal rain.

What determines the X-ray intensity and duration of a solar flare?

Jeffrey W. **Reep**, Kalman J. Knizhnik

ApJ **874** 157 **2019**
https://arxiv.org/pdf/1903.10564.pdf
sci-hub.se/10.3847/1538-4357/ab0ae7
https://ui.adsabs.harvard.edu/link_gateway/2019ApJ...874..157R/PUB_PDF
Solar flares are observed and classified according to their intensity measured with the GOES X-ray Sensors. We show that the duration of a flare, as measured by the full width at half maximum (FWHM) in GOES is not related to the size of the flare as measured by GOES intensity. The durations of X-class flares range from a few minutes to a few hours, and the same is true of M- and C-class flares. In this work, we therefore examine the statistical relationships between the basic properties of flares -- temperature, emission measure, energy, etc. -- in comparison to both their size and duration. We find that the size of the flare is directly related to all of these basic properties, as previously found by many authors. The duration is not so clear. When examining the whole data set, the duration appears to be independent of all of these properties. In larger flares, however, there are direct correlations between the GOES FWHM and magnetic reconnection flux and ribbon area. We discuss the possible explanations, finding that this discrepancy may be due to large uncertainties in small flares, though we cannot rule out the possibility that the driving physical processes are different in smaller flares than larger ones. We discuss the implications of this result and how it relates to the magnetic reconnection process that releases energy in flares. **2 Nov. 2013**

On the Synthesis of GOES Light Curves from Numerical Models

Jeffrey W. **Reep** and Harry P. Warren
2018 Res. Notes AAS 2 48
http://iopscience.iop.org/article/10.3847/2515-5172/aaca2b
Numerical simulations of solar flares are often used to produce synthetic GOES light curves that can be compared against data (e.g., Warren 2006; Reep & Toriumi 2017; Zhu et al. 2018). There are a few different methods that have been used in the past to synthesize these light curves, but the literature does not generally discuss advantages and disadvantages of each method. In this note, we briefly discuss three different methods that can be used.

Efficient Calculation of Non-Local Thermodynamic Equilibrium Effects in Multithreaded Hydrodynamic Simulations of Solar Flares

Jeffrey W. **Reep**, Stephen J. Bradshaw, Nicholas A. Crump, Harry P. Warren
ApJ **871** 18 **2018**
https://arxiv.org/pdf/1806.09574.pdf
sci-hub.tw/10.3847/1538-4357/aaf580
Understanding the dynamics of the solar chromosphere is crucial to understanding the transport of energy across the atmosphere, especially in impulsive heating events. The chromosphere is optically thick and described by non-local thermodynamic equilibrium (NLTE), often making observations difficult to interpret. There is also considerable evidence that the atmosphere is filamented and that current instruments do not sufficiently resolve small scale features. In flares, for example, it is likely that multithreaded models are required to describe and understand the heating process. The combination of NLTE effects and multithreaded modeling requires computationally demanding calculations, which has motivated the development of a model that can efficiently treat both. We describe the implementation of a solver in a hydrodynamic code for the hydrogen level populations that approximates the NLTE solutions. We derive an accurate electron density across the chromosphere and corona that includes the effects of non-equilibrium ionization for helium and metals. We show the effects of this solver on simulations, which we then use to synthesize light curves and Doppler shifts of spectral lines, with a post-processing radiative transfer code. We demonstrate the utility of this model on multithreaded simulations, where we simulate IRIS observations of a small flare. We show that observed velocities in Mg II, C II, and O I can be explained with a multithreaded model of loops subject to electron beam heating, so long as NLTE effects are treated. The synthesized intensities, however, do not match observed ones very well, which we suggest is primarily due to assumptions about the initial atmosphere. We briefly show how altering the initial atmosphere can drastically alter line profiles and derived quantities, and suggest that it should be tuned to preflare observations for better agreement.

The Duration of Energy Deposition on Unresolved Flaring Loops in the Solar Corona

Jeffrey W. **Reep**, Vanessa Polito, Harry P. Warren, Nicholas A. Crump
2018 *ApJ* **856** 149
https://arxiv.org/pdf/1802.08884.pdf
http://sci-hub.tw/http://iopscience.iop.org/0004-637X/856/2/149/
Solar flares form and release energy across a large number of magnetic loops. The global parameters of flares, such as the total energy released, duration, physical size, etc., are routinely measured, and the hydrodynamics of a coronal loop subjected to intense heating have been extensively studied. It is not clear, however, how many loops comprise a flare, nor how the total energy is partitioned between them. In this work, we employ a hydrodynamic model to better understand the energy partition by synthesizing Si IV and Fe XXI line emission and comparing to observations of these

lines with IRIS. We find that the observed temporal evolution of the Doppler shifts holds important information on the heating duration. To demonstrate this we first examine a single loop model, and find that the properties of chromospheric evaporation seen in Fe XXI can be reproduced by loops heated for long durations, while persistent red-shifts seen in Si IV cannot be reproduced by any single loop model. We then examine a multi-threaded model, assuming both a fixed heating duration on all loops, and a distribution of heating durations. For a fixed heating duration, we find that durations of 100 -- 200 s do a fair job of reproducing both the red- and blue-shifts, while a distribution of durations, with a median of about 50 -- 100 s, does a better job. Finally, we compare our simulations directly to observations of an M-class flare seen by IRIS, and find good agreement between the modeled and observed values given these constraints. **March 12, 2015**

The direct relation between the duration of magnetic reconnection and the evolution of GOES light curves in solar flares

Jeffrey W **Reep**, Shin Toriumi
ApJ **851** 4 **2017**
https://arxiv.org/pdf/1711.00422.pdf
GOES soft X-ray light curves are used to measure the timing and duration of solar flare emission. The timing and duration of the magnetic reconnection and subsequent energy release which drives solar flares are unknown, though the light curves are presumably related. It is therefore critical to understand the physics which connects the two: how does the time scale of reconnection produce an observed GOES light curve? In this work, we model the formation and expansion of an arcade of loops with a hydrodynamic model, which we then use to synthesize GOES light curves. We calculate the FWHM and the e-folding decay time of the light curves and compare them to the separation of the centroids of the two ribbons which the arcade spans, which is representative of the size scale of the loops. We reproduce a linear relation between the two, as found observationally in previous work. We show that this demonstrates a direct connection between the duration of energy release and the evolution of these light curves. We also show that the cooling processes of individual loops comprising the flare arcade directly affect the measured time scales. From the clear consistency between the observed and modeled linearity, we conclude that the primary factors that control the flare time scales are the duration of reconnection and the loop lengths. **6 Mar 2012, 5 Nov 2013, 22 June 2015**

Science Objective: Understanding Energy Transport by Alfvénic Waves in Solar Flares

Jeffrey W. **Reep**, Harry P. Warren, James E. Leake, Lucas A. Tarr, Alexander J.B. Russell, Graham S. Kerr, Hugh S. Hudson
Next Generation Solar Physics Mission White paper, **2017**
https://arxiv.org/pdf/1702.01667.pdf
Solar flares are driven by the release of magnetic energy from reconnection events in the solar corona, whereafter energy is transported to the chromosphere, heating the plasma and causing the characteristic radiative losses. In the collisional thick-target model, electrons accelerated to energies exceeding 10 keV traverse the corona and impact the chromosphere, where they deposit their energy through collisions with the much denser plasma in the lower atmosphere. While there are undoubtedly high energy non-thermal electrons accelerated in flares, it is unclear whether these electron beams are the sole mechanism of energy transport, or whether they only dominate in certain phases of the flare's evolution. Alfv\'enic waves are generated during the post-reconnection relaxation of magnetic field lines, so it is important to examine their role in energy transport.

Transition Region and Chromospheric Signatures of Impulsive Heating Events. II. Modeling

Jeffrey W. **Reep**, Harry P. Warren, Nicholas A. Crump, Paulo J.A. Simoes
ApJ **827** 145 **2016**
http://arxiv.org/pdf/1607.06684v1.pdf
Results from the Solar Maximum Mission showed a close connection between the hard X-ray and transition region emission in solar flares. Analogously, the modern combination of RHESSI and IRIS data can inform the details of heating processes in ways never before possible. We study a small event that was observed with RHESSI, IRIS, SDO, and Hinode, allowing us to strongly constrain the heating and hydrodynamical properties of the flare, with detailed observations presented in a previous paper. Long duration red-shifts of transition region lines observed in this event, as well as many other events, are fundamentally incompatible with chromospheric condensation on a single loop. We combine RHESSI and IRIS data to measure the energy partition among the many magnetic strands that comprise the flare. Using that observationally determined energy partition, we show that a proper multi-threaded model can reproduce these red-shifts in magnitude, duration, and line intensity, while simultaneously being well constrained by the observed density, temperature, and emission measure. We comment on the implications for both RHESSI and IRIS observations of flares in general, namely that: (1) a single loop model is inconsistent with long duration red-shifts, among other observables; (2) the average time between energization of strands is less than 10 seconds, which implies that for a hard X-ray burst lasting ten minutes, there were at least 60 strands within a single IRIS pixel located on the flare ribbon; (3) the majority of these strands were explosively heated with energy distribution well described by a

power law of slope ≈−1.6; (4) the multi-stranded model reproduces the observed line profiles, peak temperatures, differential emission measure distributions, and densities. **19−Nov−14**

Non-thermal recombinationin solar flares and microflares

Jeffrey **Reep** and John Brown
RHESSI Science Nuggets No. 275, June 6: **2016**
http://sprg.ssl.berkeley.edu/~tohban/wiki/index.php/Non-thermal_recombination_in_solar_flares_and_microflares

Amended results for hard X-ray emission by non-thermal thick target recombination in solar flares

Jeffrey W. **Reep**, John C. Brown
ApJ **824** 90 **2016**
http://arxiv.org/pdf/1604.04607v1.pdf
Brown & Mallik 2008 and the Brown et al. 2010 corrigendum of it presented expressions for non-thermal recombination (NTR) in the collisionally thin- and thick-target regimes, claiming that the process could account for a substantial part of hard X-ray continuum in solar flares usually attributed entirely to thermal and non-thermal bremsstrahlung (NTB). However, we have found the thick-target expression to become unphysical for low cut-offs in the injected electron energy spectrum. We trace this to an error in the derivation, derive a corrected version which is real-valued and continuous for all photon energies and cut-offs, and show that, for thick targets, Brown et al. over-estimated NTR emission at small photon energies. The regime of small cut-offs and large spectral indices involve large (reducing) correction factors but in some other thick-target parameter regimes NTR/NTB can still be of order unity. We comment on the importance of these results to flare and to microflare modeling and spectral fitting. An empirical fit to our results shows that the peak NTR contribution comprises over half the hard X-ray signal if delta > 6 (E_0c/4 keV)^(0.4).

Alfvénic Wave Heating of the Upper Chromosphere in Flares

Jeffrey W. **Reep**, Alexander J.B. Russell
ApJL 818 L20 **2016**
http://arxiv.org/pdf/1601.01969v1.pdf
We have developed a numerical model of flare heating due to the dissipation of Alfv\'enic waves propagating from the corona to the chromosphere. With this model, we present an investigation of the key parameters of these waves on the energy transport, heating, and subsequent dynamics. For sufficiently high frequencies and perpendicular wave numbers, the waves dissipate significantly in the upper chromosphere, strongly heating it to flare temperatures. This heating can then drive strong chromospheric evaporation, bringing hot and dense plasma to the corona. We therefore find three important conclusions: (1) Alfv\'enic waves, propagating from the corona to the chromosphere, are capable of heating the upper chromosphere and the corona, (2) the atmospheric response to heating due to the dissipation of Alfv\'enic waves can be strikingly similar to heating by an electron beam, and (3) this heating can produce explosive evaporation.

X-ray Source Heights in a Solar Flare: Thick-target versus Thermal Conduction Front Heating

Jeffrey W. **Reep**, Stephen J. Bradshaw, Gordon D. Holman
ApJ 818 44 **2016**
http://arxiv.org/pdf/1512.08978v1.pdf
Observations of solar flares with RHESSI have shown X-ray sources traveling along flaring loops, from the corona down to the chromosphere and back up. The **28 November 2002** C1.1 flare, first observed with RHESSI by Sui et al. 2006 and quantitatively analyzed by O'Flannagain et al. 2013, very clearly shows this behavior. By employing numerical experiments, we use these observations of X-ray source height motions as a constraint to distinguish between heating due to a non-thermal electron beam and in situ energy deposition in the corona. We find that both heating scenarios can reproduce the observed light curves, but our results favor non-thermal heating. In situ heating is inconsistent with the observed X-ray source morphology and always gives a height dispersion with photon energy opposite to what is observed.

Optimal Electron Energies for Driving Chromospheric Evaporation in Solar Flares

Reep, J.W., Bradshaw, S.J., & Alexander, D.
ApJ **808** 177 **2015**

http://arxiv.org/pdf/1506.08115v1.pdf
In the standard model of solar flares, energy deposition by a beam of electrons drives strong chromospheric evaporation leading to a significantly denser corona and much brighter emission across the spectrum. Chromospheric evaporation was examined in great detail by Fisher, Canfield, & McClymont (1985a,b,c), who described a distinction between two different regimes, termed explosive and gentle evaporation. In this work, we examine the importance of electron energy and stopping depths on the two regimes and on the atmospheric response. We find that with explosive evaporation, the atmospheric response does not depend strongly on electron energy. In the case of gentle evaporation, lower energy electrons are significantly more efficient at heating the atmosphere and driving up-flows sooner than higher energy electrons. We also find that the threshold between explosive and gentle evaporation is not fixed at a given beam energy flux, but also depends strongly on the electron energy and duration of heating. Further, at low electron energies, a much weaker beam flux is required to drive explosive evaporation.

Flare Heating by Mildly Non-thermal Particles

Reep, J.W.
RHESSI Science Nugget No. 245, Jun **2015**
http://sprg.ssl.berkeley.edu/~tohban/wiki/index.php/Flare_Heating_by_Mildly_Non-thermal_Particles
Sorting out nonthermal distributions via HYDRAD simulations.
The atmospheric response to heating by mildly non-thermal particles is extremely similar to direct in situ heating of the plasma. Strong chromospheric evaporation can be driven both through a particle beam and by a thermal conduction front. Further, the X-ray emissions as might be seen by RHESSI can be nearly indistinguishable. The explanation for this behavior is simple: the stopping depths of low-energy electrons are significantly less than for high energy electrons, so that low-energy electrons will deposit their energy in the corona, even at low densities [Ref. 4]. The heating by an electron beam would then be nearly the same as direct plasma heating. The main conclusion of this Nugget is simply that caution must be taken to conclude that a heating event (whether it be a flare, nanoflare, or something else) does not have electron acceleration.

On the sensitivity of the GOES flare classification to properties of the electron beam in the thick target model

Reep, J.W., Bradshaw, S.J., McAteer R.T.J.
E-print, Oct **2013**, http://arxiv.org/pdf/1310.3242v1.pdf; **2013** ApJ 778 76
The collisional thick target model, wherein a large number of electrons are accelerated down a flaring loop, can be used to explain many observed properties of solar flares. In this study, we focus on the sensitivity of GOES flare classification to the properties of the thick target model. Using a hydrodynamic model with RHESSI-derived electron beam parameters, we explore the effects of the beam energy flux (or total non-thermal energy), the cut-off energy, and the spectral index of the electron distribution on the soft X-rays (SXRs) observed by GOES. We conclude that (1) the GOES class is proportional to the non-thermal energy for in the low energy passband (1-8 AA) and in the high energy passband (0.5-4 AA); (2) the GOES class is only weakly dependent on the spectral index in both passbands; (3) increases in the cut-off will increase the flux in the 0.5-4 AA passband, but decrease the flux in the 1-8 AA passband, while decreases in the cut-off will cause a decrease in the 0.5-4 AA passband and a slight increase in the 1-8 AA passband. **2002-04-15, 2002-07-23**

Diagnosing the time-dependence of active region core heating from the emission measure: II. Nanoflare trains

Jeffrey W. **Reep**, Stephen J. Bradshaw, James A. Klimchuk
E-print, March **2013**
The time-dependence of heating in solar active regions can be studied by analyzing the slope of the emission measure distribution cool-ward of the peak. In a previous study we showed that low-frequency heating can account for 0\% to 77\% of active region core emission measures. We now turn our attention to heating by a finite succession of impulsive events for which the timescale between events on a single magnetic strand is shorter than the cooling timescale. We refer to this scenario as a ``nanoflare train" and explore a parameter space of heating and coronal loop properties with a hydrodynamic model. Our conclusions are: (1) nanoflare trains are consistent with 86\% to 100\% of observed active region cores when uncertainties in the atomic data are properly accounted for; (2) steeper slopes are found for larger values of the ratio of the train duration Delta_H to the post-train cooling and draining timescale Delta_C, where Delta_H depends on the number of heating events, the event duration and the time interval between successive events (au_C); (3) au_C may be diagnosed from the width of the hot component of the emission measure provided that the temperature bins are much smaller than 0.1~dex; (4) the slope of the emission measure alone is not sufficient to provide information about any timescale associated with heating - the length and density of the heated structure must be measured for Delta_H to be uniquely extracted from the ratio Delta_H/Delta_C.

Pre-emergence Signatures Of Horizontal Divergent Flows In Solar Active Regions

T. **Rees-Crockford**, C. J. Nelson, M. Mathioudakis

ApJ **2022**

https://arxiv.org/pdf/2210.06276.pdf

Solar active regions (ARs) play a fundamental role in driving many of the geo-effective eruptions which propagate into the Solar System. However, we are still unable to consistently predict where and when ARs will occur across the solar disk by identifying pre-emergence signatures in observables such as the Doppler velocity (without using Helioseismic methods). Here we aim to determine the earliest time at which pre-emergence signatures, specifically the Horizontal Divergent Flow (HDF), can be confidently detected using data from the Solar Dynamics Observatory's Helioseismic and Magnetic Imager (SDO/HMI). Initially, we follow previous studies using the thresholding method, which searches for significant increases in the number of pixels that display a specific line-of-sight velocity. We expand this method to more velocity windows and conduct a basic parameter study investigating the effect of cadence on the inferred results. Our findings agree with previous studies with 37.5% of ARs displaying a HDF, with average lead times between the HDF and flux emergence of 58 minutes. We present a new potential signature of flux emergence which manifests as cadence-independent transient disruptions to the amplitudes of multiple velocity windows and recover potential pre-emergence signatures for 10 of the 16 ARs studied, with lead times of 60-156 minutes. Several effects can influence both the estimated times of both HDF and flux emergence suggesting that one may need to combine Doppler and magnetic field data to get a reliable indicator of continued flux emergence.

A window into magnetic reconnection: IRIS observations of the consequences of reconnection during solar flares **Review**

Katharine **Reeves**

Front. Astron. Space Sci. 9: 1041951. **2022 File**

https://doi.org/10.3389/fspas.2022.1041951

https://www.frontiersin.org/articles/10.3389/fspas.2022.1041951/pdf

Magnetic reconnection is a dynamic process that occurs in solar flares in a tenuous and hot environment. High-cadence, high-spatial resolution spectroscopic observations with the Interface Region Imaging Spectrometer (IRIS) have provided a unique window into the reconnection process that occurs during solar flares. IRIS has observed many consequences of the reconnection process, including detailed observations of outflows that are thought to be indicative of reconnection, possible observations of the termination shocks that are predicted by-products of reconnection, and observations of flare ribbons which are imprints of the reconnection process in the chromosphere. This paper will review these observations and put them in the context of flare models that predict reconnection signatures. **2014 March 29 , 2014 April 18 , 2014 April 19, 2014 August 29, 2014 November 9, 2016 December 6**

Hot Plasma Flows and Oscillations in the Loop-top Region During the September 10 2017 X8.2 Solar Flare

Katharine K. **Reeves**, Vanessa Polito, Bin Chen, Giselle Galan, Sijie Yu, Wei Liu, Gang Li

ApJ **905** 165 **2020**

https://arxiv.org/pdf/2010.12049.pdf

https://doi.org/10.3847/1538-4357/abc4e0

In this study, we investigate motions in the hot plasma above the flare loops during the 2017 September 10 X8.2 flare event. We examine the region to the south of the main flare arcade, where there is data from the Interface Region Imaging Spectrograph (IRIS), and the Extreme ultraviolet Imaging Spectrometer (EIS) on Hinode. We find that there are initial blue shifts of 20--60 km/s observed in this region in the Fe XXI line in IRIS and the Fe XXIV line in EIS, and that the locations of these blue shifts move southward along the arcade over the course of about 10 min. The cadence of IRIS allows us to follow the evolution of these flows, and we find that at each location where there is an initial blue shift in the Fe XXIV line, there are damped oscillations in the Doppler velocity with periods of ~400 s. We conclude that these periods are independent of loop length, ruling out magnetoacoustic standing modes as a possible mechanism. Microwave observations from the Expanded Owens Valley Solar Array (EOVSA) indicate that there are non-thermal emissions in the region where the Doppler shifts are observed, indicating that accelerated particles are present. We suggest that the flows and oscillations are due to motions of the magnetic field that are caused by reconnection outflows disturbing the loop-top region.

ATMOSPHERIC IMAGING ASSEMBLY OBSERVATIONS OF HOT FLARE PLASMA

Katharine K. **Reeves** and Leon Golub

2011 ApJ 727 L52, **File**

We present observations of hot plasma from solar eruptions recorded by the Atmospheric Imaging Assembly (AIA) on the Solar Dynamics Observatory. AIA is the first narrowband instrument capable of taking images of hot plasma in the 5-15 MK range. We find that there are hot structures above flare loops, and that they are typically more diffuse and nebulous than the well-defined flare loops. Because of the narrowband response, high sensitivity, and high spatial

resolution of AIA, these supra-arcade structures are visible in exquisite detail, particularly in the 131 Å and 94 Å channels. In one event, a C4.9 flare observed on **2010 November 3**, hot plasma is seen to outline an erupting plasmoid and possibly a current sheet. We compare hot plasma observed with AIA to structures observed with the X-Ray Telescope on the Hinode mission and find that the plasma imaged in AIA contains more fine detail. These new AIA observations show that supra-arcade flare structures and coronal mass ejections are highly structured not only in space and time, but also in temperature. This thermal structuring is expected, based on modeling efforts, but has now been imaged directly for the first time over a large range of temperatures.

Field Line Shrinkage in Flares Observed by the X-Ray Telescope on Hinode

Katharine K. **Reeves**, Daniel B. Seaton, Terry G. Forbes
E-print, Nov 2007, ApJ, 675:868Y874, **2008**
http://www.journals.uchicago.edu/doi/pdf/10.1086/526336
The X-Ray Telescope on **Hinode** has observed individual loops of plasma moving downward in a manner that is consistent with field line shrinkage in the aftermath of reconnection at higher altitudes.
We measure the shrinkage in both of these events, and find that it is 17-27%, which is consistent with theoretical predictions.
The STEREO mission provides an unprecedented opportunity to reconstruct the 3D configuration of solar features. In this work, we combine SECCHI/EUVI data from both spacecraft by means of a local correlation tracking method. The technique allows an automatic (without user intervention) matching of pixels in both images. This information is then used to triangulate the 3D coordinates of each pixel. We use the method in order to reconstruct and analyze the 3D structure of active regions. In particular, we focus on the extraction of coronal loop heights, observed nearly simultaneously in the 171, 195 and 284 Å passbands. We compare the properties of loops in the different wavelengths and extract valuable information regarding their geometry. In particular, we demonstrate that some loops that look co-spatial in the 171 Å and 195 Å images have in fact different heights and thus occupy different volumes. Our results have important implications for multi-wavelength studies of coronal loops, especially for calculations using filter-ratio techniques.

Sparkling Extreme-ultraviolet Bright Dots Observed with Hi-C

S. **Régnier**1, C. E. Alexander1, R. W. Walsh1, A. R. Winebarger2, J. Cirtain2, L. Golub3, K. E. Korreck3, N. Mitchell4, S. Platt4, M. Weber3, B. De Pontieu5, A. Title5, K. Kobayashi6, S. Kuzin7, and C. E. DeForest
2014 ApJ 784 134
Observing the Sun at high time and spatial scales is a step toward understanding the finest and fundamental scales of heating events in the solar corona. The high-resolution coronal (Hi-C) instrument has provided the highest spatial and temporal resolution images of the solar corona in the EUV wavelength range to date. Hi-C observed an active region on **2012 July 11** that exhibits several interesting features in the EUV line at 193 Å. One of them is the existence of short, small brightenings "sparkling" at the edge of the active region; we call these EUV bright dots (EBDs). Individual EBDs have a characteristic duration of 25 s with a characteristic length of 680 km. These brightenings are not fully resolved by the SDO/AIA instrument at the same wavelength; however, they can be identified with respect to the Hi-C location of the EBDs. In addition, EBDs are seen in other chromospheric/coronal channels of SDO/AIA, which suggests a temperature between 0.5 and 1.5 MK. Based on their frequency in the Hi-C time series, we define four different categories of EBDs: single peak, double peak, long duration, and bursty. Based on a potential field extrapolation from an SDO/HMI magnetogram, the EBDs appear at the footpoints of large-scale, trans-equatorial coronal loops. The Hi-C observations provide the first evidence of small-scale EUV heating events at the base of these coronal loops, which have a free magnetic energy of the order of 1026 erg.

Relationship between photospheric currents and coronal magnetic helicity for force-free bipolar fields

S. **R´egnier**
E-print, March, **2009**; A&A
http://solar.physics.montana.edu/cgi-bin/eprint/index.pl?entry=9715
The origin and evolution of the magnetic helicity in the solar corona are not well understood. For instance, the magnetic helicity of an active region is often about 10^42 Mx^2 (10^26 Wb^2), but the observed processes whereby it is thought to be injected into the corona do not yet provide an accurate estimate of the resulting magnetic helicity budget or time evolution. The variation in magnetic helicity is important for understanding the physics of flares, coronal mass ejections, and their associated magnetic clouds. To shed light on this topic, we investigate here the changes in magnetic helicity due to electric currents in the corona for a single twisted flux tube that may model characteristic coronal structures such as active region filaments, sigmoids, or coronal loops. For a bipolar photospheric magnetic field and several distributions of current, we extrapolated the coronal field as a nonlinear force-free field. We then computed the

relative magnetic helicity, as well as the self and mutual helicities. Starting from a magnetic configuration with a moderate amount of current, the amount of magnetic helicity can increase by 2 orders of magnitude when the maximum current strength is increased by a factor of 2. The high sensitivity of magnetic helicity to the current density can partially explain discrepancies between measured values on the photosphere, in the corona, and in magnetic clouds. Our conclusion is that the magnetic helicity strongly depends on both the strength of the current density and also on its distribution. Only improved measurements of current density at the photospheric level will advance our knowledge of the magnetic helicity content in the solar atmosphere.

Self-consistent nanoflare heating in model active regions: MHD avalanches

J **Reid**, J Threlfall, A W Hood

MNRAS, Volume 518, Issue 1, January **2023**, Pages 1584–1600,

https://doi.org/10.1093/mnras/stac3188

Straightened cylindrical models of coronal loops have been standard for decades, and shown to support nanoflare-like heating, but the influence of geometric curvature in models upon the heating produced has not been discussed in depth. Heating, its spatiotemporal distributions, and the associated mechanisms responsible are discussed, and compared with those from straightened models of a coronal loop. Previously, magnetohydrodynamic avalanches have been generalized to curved loops, and shown to be viable. From that study, the associated heating is analysed and discussed in depth. Heating is seen to arise from processes originally instigated, yet not dominated, by magnetic reconnection, producing bursty, aperiodic nanoflares, dispersed evenly throughout the corona, but with a modest bias away from footpoints. One novelty arising is the simultaneous yet independent occurrence of nanoflare-like events at disjoint sites along individual strands, anticipating some features recently seen in ‘campfires’ by Solar Orbiter. With a view to future refinements in the model and to the inclusion of additional physical effects, the implications of this analysis are discussed.

Chromospheric Bubbles in Solar Flares

A. **Reid**1, B. Zhigulin1, M. Carlsson2,3, and M. Mathioudakis1

2020 ApJL 894 L21

https://arxiv.org/pdf/2005.10586.pdf

https://doi.org/10.3847/2041-8213/ab8d1e

We analyze a grid of radiative hydrodynamic simulations of solar flares to study the energy balance and response of the atmosphere to nonthermal electron beam heating. The appearance of chromospheric bubbles is one of the most notable features that we find in the simulations. These pockets of chromospheric plasma get trapped between the transition region and the lower atmosphere as it is superheated by the particle beam. The chromospheric bubbles are seen in the synthetic spectra, appearing as an additional component to Balmer line profiles with high Doppler velocities as high as 200 km s−1. Their signatures are also visible in the wings of Ca ii 8542 Å line profiles. These bubbles of chromospheric plasma are driven upward by a wave front that is induced by the shock of energy deposition, and require a specific heating rate and atmospheric location to manifest.

Chromospheric Inversions of a Micro-flaring Region

A. **Reid**, V. Henriques, M. Mathioudakis, J. G. Doyle, T. Ray

ApJ **2017**

https://arxiv.org/pdf/1707.00029.pdf

We use spectropolarimetric observations of the Ca II 8542~\AA\ line, taken from the Swedish 1-m Solar Telescope (SST), in an attempt to recover dynamic activity in a micro-flaring region near a sunspot via inversions. These inversions show localized mean temperature enhancements of ~1000~K in the chromosphere and upper photosphere, along with co-spatial bi-directional Doppler shifting of 5 - 10 km s−1. This heating also extends along a nearby chromospheric fibril, co-spatial to 10 - 15 km s−1 down-flows. Strong magnetic flux cancellation is also apparent in one of the footpoints, concentrated in the chromosphere. This event more closely resembles that of an Ellerman Bomb (EB), though placed slightly higher in the atmosphere than is typically observed. **2014 July 28**

Magnetic Flux Cancellation in Ellerman Bombs

A. **Reid**, M. Mathioudakis, J. G. Doyle, E. Scullion, V. Henriques, C. Nelson, T. Ray

ApJ **2016**

http://arxiv.org/pdf/1603.07100v1.pdf

Ellerman Bombs (EBs) are often found co-spatial with bipolar photospheric magnetic fields. We use Hα imaging spectroscopy along with Fe I 6302.5 \AA\ spectro-polarimetry from the Swedish 1-m Solar Telescope (SST), combined with data from the Solar Dynamic Observatory (SDO) to study EBs and the evolution of the local magnetic fields at EB locations. The EBs are found via an EB detection and tracking algorithm. We find, using NICOLE inversions of the spectro-polarimetric data, that on average (3.43 ± 0.49) x 1024 ergs of stored magnetic energy disappears from the bipolar region during the EBs burning. The inversions also show flux cancellation rates of 1014 - 1015 Mx s−1, and temperature enhancements of 200 K at the detection footpoints. We investigate near-simultaneous flaring of EBs due to

co-temporal flux emergence from a sunspot, which shows a decrease in transverse velocity when interacting with an existing, stationary area of opposite polarity magnetic flux and the EBs are formed. We also show that these EBs can get fueled further by additional, faster moving, negative magnetic flux regions. **2014 June 5**

The Low-High-Low Starting Frequency Trend in Groups of Type III Bursts," by Hamish Reid. The type III radio bursts echo the pattern of flare energy release.

Hamish **Reid**
RHESSI Science Nuggets, #242, December **2014**
The type III radio bursts echo the pattern of flare energy release. **10-Mar-2003, 18-Mar-2003**

The Low-High-Low Trend of Type III Radio Burst Starting Frequencies and Solar Flare Hard X-rays

Hamish A. S. **Reid**, Nicole Vilmer, Eduard P. Kontar
A&A, **2014**
http://arxiv.org/pdf/1403.1839v1.pdf
Using simultaneous X-ray and radio observations from solar flares, we investigate the link between the type III radio burst starting frequency and hard X-ray spectral index. For a proportion of events the relation derived between the starting height (frequency) of type III radio bursts and the electron beam velocity spectral index (deduced from X-rays) is used to infer the spatial properties (height and size) of the electron beam acceleration region. Both quantities can be related to the distance travelled before an electron beam becomes unstable to Langmuir waves. To obtain a list of suitable events we considered the RHESSI catalogue of X-ray flares and the Phoenix 2 catalogue of type III radio bursts. From the 200 events that showed both type III and X-ray signatures, we selected 30 events which had simultaneous emission in both wavelengths, good signal to noise in the X-ray domain and > 20 seconds duration. We find that > 50 % of the selected events show a good correlation between the starting frequencies of the groups of type III bursts and the hard X-ray spectral indices. A low-high-low trend for the starting frequency of type III bursts is frequently observed. Assuming a background electron density model and the thick target approximation for X-ray observations, this leads to a correlation between starting heights of the type III emission and the beam electron spectral index. Using this correlation we infer the altitude and vertical extents of the flare acceleration regions. We find heights from 183 Mm down to 25 Mm while the sizes range from 13 Mm to 2 Mm. These values agree with previous work that places an extended flare acceleration region high in the corona. We analyse the assumptions required and explore possible extensions to our assumed model. We discuss these results with respect to the acceleration heights and sizes derived from X-ray observations alone. **Table**
14-Feb- 2002,20-Feb-2002, 19-Jul-2002, 10-Mar-2003, 18-Mar-2003, 26 Apr-2003, 9-Jun-2003, 9-Jul-2003, 22-Oct-2003, 28-May-2004, 25 Jul-2004

X-ray and UV investigation into the magnetic connectivity of a solar flare

H. A. S. **Reid**, N. Vilmer, G. Aulanier, E. Pariat
E-print, Oct **2012;** A&A 547, A52 **(2012)**
We investigate the X-ray and UV emission detected by RHESSI and TRACE in the context of a solar flare on the **16th November 2002** with the goal of better understanding the evolution of the flare. We analysed the characteristics of the X-ray emission in the 12-25 and 25-50 keV energy range while we looked at the UV emission at 1600 angstrom. The flare appears to have two distinct phases of emission separated by a 25-second time delay, with the first phase being energetically more important. We found good temporal and spatial agreement between the 25-50 keV X-rays and the most intense areas of the 1600 angstrom UV emission. We also observed an extended 100-arcsecond < 25 keV source that appears coronal in nature and connects two separated UV ribbons later in the flare. Using the observational properties in X-ray and UV wavelengths, we propose two explanations for the flare evolution in relation to the spine/fan magnetic field topology and the accelerated electrons. We find that a combination of quasi separatrix layer reconnection and null-point reconnection is required to account for the observed properties of the X-ray and UV emission.

Characteristics of the flare acceleration region derived from simultaneous hard X-ray and radio observations

H. A. S. **Reid**1,2, N. Vilmer2 and E. P. Kontar1
A&A, Volume 529, A66, 8 p. May **2011**
We investigate the type III radio bursts and X-ray signatures of accelerated electrons in a well-observed solar flare in order to find the spatial properties of the acceleration region. Combining simultaneous RHESSI hard X-ray flare data and radio data from Phoenix-2 and the Nançay radioheliograph, the outward transport of flare accelerated electrons is analysed. The observations show that the starting frequencies of type III bursts are anti-correlated with the HXR spectral index of solar flare accelerated electrons. We demonstrate both analytically and numerically that the type III

burst starting location is dependent upon the accelerated electron spectral index and the spatial acceleration region size, but weakly dependent on the density of energetic electrons for relatively intense electron beams. Using this relationship and the observed anti-correlation, we estimate the height and vertical extent of the acceleration region, giving values of around 50 Mm and 10 Mm, respectively. The inferred acceleration height and size suggest that electrons are accelerated well above the soft X-ray loop-top, which could be consistent with the electron acceleration between 40 Mm and 60 Mm above the flaring loop.

EVIDENCE THAT TEMPORAL CHANGES IN SOLAR SUBSURFACE HELICITY PRECEDE ACTIVE REGION FLARING

A. A. **Reinard**1, J. Henthorn2, R. Komm3, and F. Hill3

Astrophysical Journal Letters, 710:L121–L125, **2010** February

We report on the analysis of subsurface vorticity/helicity measurements for flare producing and quiet active regions. We have developed a parameter to investigate whether large, decreasing kinetic helicity density commonly occurs prior to active region flaring. This new parameter is effective at separating flaring and non-flaring active regions and even separates among C-, M-, and X-class flare producing regions. In addition, this parameter provides advance notice of flare occurrence, as it increases 2–3 days before the flare occurs. These results are striking on an average basis, though on an individual basis there is still considerable overlap between flare associated and non-flare associated values. We propose the following qualitative scenario for flare production: subsurface rotational kinetic energy twists the magnetic field lines into an unstable configuration, resulting in explosive reconnection and a flare.

Comprehensive radiative MHD simulations of eruptive flares above collisional polarity inversion lines

Matthias **Rempel**, Georgios Chintzoglou, Mark C. M. Cheung, Yuhong Fan, Lucia Kleint

ApJ **955** 105 **2023**

https://arxiv.org/pdf/2303.05299.pdf

https://iopscience.iop.org/article/10.3847/1538-4357/aced4d/pdf

We present a new simulation setup using the MURaM radiative MHD code that allows to study the formation of collisional polarity inversion lines (cPILs) in the photosphere and the coronal response including flares. In the setup we start with a bipolar sunspot configuration and set the spots on collision course by imposing the appropriate velocity field at the footpoints in the subphotospheric boundary. We vary parameters such as the initial spot separation, collision speed and collision distance. While all setups lead to the formation of a sigmoid structure, only the cases with a close passing of the spots cause flares and mass eruptions. The energy release is in the 1−2×1031 ergs range, putting the simulated flares into the upper C to lower M-class range. While the case with the more distant passing of the spots does not lead to a flare, the corona is nonetheless substantially heated, suggesting non-eruptive energy release mechanisms. We focus our discussion on two setups that differ in spot coherence and resulting cPIL length. We find different timings in the transition from a sheared magnetic arcade (SMA) to magnetic flux rope (MFR); the setup with a short cPIL produces a MFR during the eruption, while the MFR is pre-existing in the setup with a longer cPIL. While both result in flares of comparable strength, only the setup with pre-existing MFR produces a CME.

Towards data-driven modeling and real-time prediction of solar flares and coronal mass ejections

M. **Rempel**, Y. Fan, M. Dikpati, A. Malanushenko (HAO/NCAR), M. D. Kazachenko (CU/NSO), M. C. M. Cheung, G. Chintzoglou (LMSAL), X. Sun (U. of Hawaii), G. H. Fisher (U. of Berkeley), T. Y. Chen (Columbia)

Heliophysics 2050 White Paper **2023**

https://arxiv.org/ftp/arxiv/papers/2212/2212.14384.pdf

Modeling of transient events in the solar atmosphere requires the confluence of 3 critical elements: (1) model sophistication, (2) data availability, and (3) data assimilation. This white paper describes required advances that will enable statistical flare and CME forecasting (e.g. eruption probability and timing, estimation of strength, and CME details, such as speed and magnetic field orientation) similar to weather prediction on Earth.

Observations of Current Sheet Heating in X-Ray during a Solar Flare

A. A **Reva**1, S. A. Bogachev1, I. P. Loboda1, A. S. Ulyanov1, and A. S. Kirichenko1

2022 ApJ 931 93

https://iopscience.iop.org/article/10.3847/1538-4357/ac6b3d/pdf

https://arxiv.org/pdf/2306.02355.pdf

In the solar corona, magnetic reconnection occurs due to the finite resistivity of the plasma. At the same time, this resistivity leads to ohmic heating. Therefore, the reconnecting current sheet should heat the surrounding plasma. This paper presents experimental evidence of such plasma heating being caused by magnetic reconnection. We observed the effect during a C1.4 solar flare on **2003 February 16** at the active region NOAA 10278, near the solar limb. Thanks to

such a location, we successfully identified all the principal elements of the flare: the flare arcade, the flux rope, and, most importantly, the presumed position of the current sheet. By analyzing the monochromatic X-ray images of the Sun obtained by the CORONAS-F/SPIRIT instrument in the Mg xii 8.42 Å spectral line, we detected a high-temperature ($T \geq 4$ MK) emission at the predicted location of the current sheet. The high-temperature emission appeared during the CME's impulsive acceleration phase. We believe that this additionally confirms that the plasma heating around the current sheet and the magnetic reconnection inside the current sheet are strongly connected.

CME-Flare Association and the Role of Reconnection in CME Acceleration.

Reva, A., Loboda, I., Bogachev, S. & Alexey Kirichenko
Sol Phys 299, 55 (**2024**).
https://doi.org/10.1007/s11207-024-02302-1
The association of coronal mass ejections (CMEs) with flares is related to the question of whether reconnection is necessary for the CME eruption. Indeed, if reconnection happens during a CME eruption, the plasma is heated, which can be observed as a flare. In this work, we study the CME-flare association using data obtained with the Mg XII spectroheliograph on board the *Complex Orbital Observations Near-Earth of Activity on the Sun* (CORONAS-F) satellite. This instrument is sensitive only to the emission of plasma with a temperature greater than 4 MK, which makes it a convenient tool for detection of flaring activity. During our analysis, we first searched for CMEs detected during the Mg XII observations by the *Large Angle and Spectroscopic Coronagraph* (LASCO). Then, we visually checked the Mg XII images for flaring activity. We found that during the Mg XII observations (2001 – 2003), 198 CMEs were detected by LASCO. One hundred sixty of them (81%) are associated with flares seen in the Mg XII images. The strength of flares associated with ***narrow CMEs*** – *jet-like ejecta* – is uniformly distributed in the A – C GOES class range. The speed of narrow CMEs does not depend on the flare strength. For normal CMEs (motion of both magnetic field and plasma), the flare strength varies from A to X class with a peak of the distribution at the C level. The median speed and the kinetic energy of normal CMEs weakly depend on flare strength for weak flares (below C) and strongly for strong ones (M and X). Our results suggest that at solar maximum reconnection occurs during most CMEs. For strong flares (M and X), the reconnection is a dominant acceleration mechanism. For weak flares (C and below), other mechanisms start to play a bigger role.

CORONAS/SPIRIT Mg XII and Nanoflares

Anton **Reva**
RHESSI Science Nuggets #335 October **2018**
http://sprg.ssl.berkeley.edu/~tohban/wiki/index.php/CORONAS/SPIRIT_Mg_XII_and_Nanoflares
The CORONAS-F/SPIRIT data constrain the high-temperature DEM levels in the solar corona, and do not find any evidence for the "smoking gun" signature expected for nanoflare heating. Because the instrument is uniquely monochromatic, and because of the extent of the data, these constraints are the most direct ones yet published.

Estimate of the Upper Limit on Hot Plasma Differential Emission Measure (DEM) in Non-Flaring Active Regions and Nanoflare Frequency Based on the Mg xiiSpectroheliograph Data from CORONAS-F/SPIRIT

Anton **Reva**, Artem Ulyanov, Alexey Kirichenko, Sergey Bogachev, Sergey Kuzin
Solar Physics October **2018**, 293:140
https://link.springer.com/content/pdf/10.1007%2Fs11207-018-1363-9.pdf
Nanoflare-heating theory predicts steady hot-plasma emission in non-flaring active regions. It is hard to find this emission with conventional non-monochromatic imagers (such as the Atmospheric Imaging Assembly or the X-Ray Telescope), because their images contain a cool-temperature background. In this work, we search for hot plasma in non-flaring active regions using the Mg xii spectroheliograph onboard the Complex Orbital Observations Near-Earth of Activity on the Sun (CORONAS)-F/SPectroheliographIc X-ray Imaging Telescope (SPIRIT). This instrument acquired monochromatic images of the solar corona in the Mg xii 8.42 Å line, which emits only at temperatures higher than 4 MK. The Mg xii images only contain the signal from hot plasma, without any low-temperature background. We studied the hot plasma in active regions using SPIRIT data from 18 – 28 February 2002. During this period, the Mg xiispectroheliograph worked with a 105-second cadence almost without data gaps. Hot plasma was observed only in the flaring active regions. We did not observe any hot plasma in non-flaring active regions. The hot-plasma column emission measure in the non-flaring active region is not expected to exceed 3×10243×1024 cm−5. The hot differential emission measure is lower than 0.01% of the DEM of the main temperature component. The absence of Mg xii emission in the non-flaring active regions can be explained by weak and frequent nanoflares (with a delay of less than 500 seconds) or by very short and intense nanoflares that lead to non-equilibrium ionization.

BREAKOUT RECONNECTION OBSERVED BY THE TESIS EUV TELESCOPE

A. A. **Reva**, A. S. Ulyanov, S. V. Shestov, and S. V. Kuzin

2016 ApJ 816 90
http://arxiv.org/pdf/1601.04511v1.pdf
We present experimental evidence of the coronal mass ejection (CME) breakout reconnection, observed by the TESIS EUV telescope. The telescope could observe solar corona up to 2 R⊙ from the Sun center in the Fe 171 Å line. Starting from **2009 April 8**, TESIS observed an active region (AR) that had a quadrupolar structure with an X-point 0.5 R⊙ above photosphere. A magnetic field reconstructed from the Michelson Doppler Imager data also has a multipolar structure with an X-point above the AR. At 21:45 UT on April 9, the loops near the X-point started to move away from each other with a velocity of ≈7 km s−1. At 01:15 UT on April 10, a bright stripe appeared between the loops, and the flux in the GOES 0.5–4 Å channel increased. We interpret the loops' sideways motion and the bright stripe as evidence of the breakout reconnection. At 01:45 UT, the loops below the X-point started to slowly move up. At 15:10 UT, the CME started to accelerate impulsively, while at the same time a flare arcade formed below the CME. After 15:50 UT, the CME moved with constant velocity. The CME evolution precisely followed the breakout model scenario.

Wave-like Formation of Hot Loop Arcades

A. **Reva** , S. Shestov, I. Zimovets, S. Bogachev, S. Kuzin
Solar Physics Volume 290, Issue 10, pp 2909-2921 **2015**
http://arxiv.org/pdf/1510.02319v1.pdf
We present observations of hot arcades made with the Mg xii spectroheliograph onboard the CORONAS-F mission, which provides monochromatic images of hot plasma in the Mg xii 8.42 Å resonance line. The arcades were observed to form above the polarity inversion line between active regions NOAA 09847 and 09848 at four successive episodes: at 09:18, 14:13, and 22:28 UT on **28 February 2002**, and at 00:40 UT on **1 March 2002**. The evolution of the arcades can be described as: a) a small flare (precursor) appeared near the edge of the still invisible arcade, b) the arcade brightened in a wave-like manner – closer loops brightened earlier, and c) the arcade intensity gradually decreased in ≈1 h. The estimated wave speed was ≈700 kms−1, and the distance between the hot loops was ≈50 Mm. The arcades formed without visible changes in their magnetic structure. The arcades were probably heated up by the instabilities of the current sheet above the arcade, which were caused by a magnetohydrodynamic wave excited by the precursor.

Investigation of Hot X-Ray Points (HXPs) Using Spectroheliograph Mg xii Experiment Data from CORONAS-F/SPIRIT

A. **Reva**, S. Shestov, S. Bogachev and S. Kuzin
Solar Physics, Volume 276, Numbers 1-2, 97-112, **2012**
http://arxiv.org/pdf/1509.07367v1.pdf

Observations in the Mg xii 8.42 Å line onboard the CORONAS-F satellite have revealed compact high temperature objects – hot X-ray points (HXPs) – and their major physical parameters were investigated. Time dependencies of temperature, emission measure, intensity, and electron density were measured for 169 HXPs. HXPs can be divided into two groups by their temperature variations: those with gradually decreasing temperature and those with rapidly decreasing temperature. HXP plasma temperatures lie in the range of 5−40 MK, the emission measure is 1045−1048 cm−3, and the electron density is above 1010 cm−3, which exceeds the electron density in the quiet Sun (108−109 cm−3). HXP lifetimes vary between 5−100 minutes, significantly longer than the conductive cooling time. This means that throughout a HXP's lifetime, the energy release process continues, which helps to maintain its high temperature. A HXP's thermal energy is not greater than 1028 erg, and the total energy which is released in HXPs does not exceed 1030 erg. HXPs differ in their physical properties from other flare-like microevents, such as microflares, X-ray bright points, and nanoflares.

DYNAMICS OF THE FLARING LOOP SYSTEM OF 2005 AUGUST 22 OBSERVED IN MICROWAVES AND HARD X-RAYS

V. E. **Reznikova**1,2, V. F. Melnikov1,3, H. Ji4, and K. Shibasaki1
Astrophysical Journal, 724:171–181, **2010**
We studied the spatial dynamics of the flaring loop in the **2005 August 22** event using microwave (NoRH) and hard X-ray (*RHESSI*) observations together with complementary data from *SOHO*/MDI, SMART at Hida, *SOHO*/EIT, and *TRACE*.We have found that (1) the pre-flare morphology of the active region exhibits a strongly sheared arcade seen in Hα and the J-shape filament seen in EUV; (2) energy release and high-energy electron acceleration occur in a sequence along the extensive arcade; (3) the shear angle and the parallel (to the magnetic neutral line) component of the footpoint (FP) distance steadily decrease during the flare process; (4) the radio loop shrinks in length and height during the first emission peak, and later it grows; after the fourth peak the simultaneous descending of the brightest loop and formation of a new microwave loop at a higher altitude occur; (5) the hard X-ray coronal source

is located higher than the microwave loop apex and shows faster upward motion; (6) the first peak on microwave time profiles is present in both the loop top and FP regions. However, the emission peaks that follow are present only in the FP regions.We conclude that after the first emission peak the acceleration site is located over the flaring arcade and particles are accelerated along magnetic field lines.We make use of the collapsing magnetic trap model to understand some observational effects.

MHD Wave Refraction and the Acoustic Halo Effect around Solar Active Regions: A 3D Study

Carlos **Rijs**, Hamed Moradi, Damien Przybylski, and Paul S. Cally
2015 ApJ 801 27
An enhancement in high-frequency acoustic power is commonly observed in the solar photosphere and chromosphere surrounding magnetic active regions. We perform three-dimensional linear forward wave modeling with a simple wavelet pulse acoustic source to ascertain whether the formation of the acoustic halo is caused by MHD mode conversion through regions of moderate and inclined magnetic fields. This conversion type is most efficient when high frequency waves from below intersect magnetic field lines at a large angle. We find a strong relationship between halo formation and the equipartition surface at which the Alfvén speed a matches the sound speed c, lending support to the theory that photospheric and chromospheric halo enhancement is due to the creation and subsequent reflection of magnetically dominated fast waves from essentially acoustic waves as they cross a = c. In simulations where we have capped a such that waves are not permitted to refract after reaching the a= c height, halos are non-existent, which suggests that the power enhancement is wholly dependent on returning fast waves. We also reproduce some of the observed halo properties, such as a dual 6 and 8 mHz enhancement structure and a spatial spreading of the halo with height.

Stochastic Electron Acceleration by Temperature Anisotropy Instabilities under Solar Flare Plasma Conditions

Mario **Riquelme**5,1, Alvaro Osorio1, Daniel Verscharen2,3, and Lorenzo Sironi4
2022 ApJ 924 52
https://arxiv.org/pdf/2103.05805.pdf
https://iopscience.iop.org/article/10.3847/1538-4357/ac3e67/pdf
Using 2D particle-in-cell plasma simulations, we study electron acceleration by temperature anisotropy instabilities, assuming conditions typical of above-the-loop-top sources in solar flares. We focus on the long-term effect of $T_{e,\perp} > T_{e,\parallel}$ instabilities by driving the anisotropy growth during the entire simulation time through imposing a shearing or a compressing plasma velocity ($T_{e,\perp}$ and $T_{e,\parallel}$ are the temperatures perpendicular and parallel to the magnetic field). This magnetic growth makes $T_{e,\perp}/T_{e,\parallel}$ grow due to electron magnetic moment conservation, and amplifies the ratio ω_{ce}/ω_{pe} from ~ 0.53 to ~ 2 (ω_{ce} and ω_{pe} are the electron cyclotron and plasma frequencies, respectively). In the regime $\omega_{ce}/\omega_{pe} \lesssim 1.2$–$1.7$, the instability is dominated by oblique, quasi-electrostatic modes, and the acceleration is inefficient. When ω_{ce}/ω_{pe} has grown to $\omega_{ce}/\omega_{pe} \gtrsim 1.2$–$1.7$, electrons are efficiently accelerated by the inelastic scattering provided by unstable parallel, electromagnetic z modes. After ω_{ce}/ω_{pe} reaches ~ 2, the electron energy spectra show nonthermal tails that differ between the shearing and compressing cases. In the shearing case, the tail resembles a power law of index $\alpha_s \sim 2.9$ plus a high-energy bump reaching ~ 300 keV. In the compressing runs, $\alpha_s \sim 3.7$ with a spectral break above ~ 500 keV. This difference can be explained by the different temperature evolutions in these two types of simulations, suggesting that a critical role is played by the type of anisotropy driving, ω_{ce}/ω_{pe}, and the electron temperature in the efficiency of the acceleration.

Clustering Behavior in Solar Flare Dynamics

Elmer C. **Rivera**1, Jay R. Johnson1, Jonathan Homan1, and Simon Wing2
2022 ApJL 937 L8
https://iopscience.iop.org/article/10.3847/2041-8213/ac8de9/pdf
The solar magnetic activity cycle provides energy input that is released in intense bursts of radiation known as solar flares. As such, the dynamics of the activity cycle is embedded in the sequence of times between the flare events. Recent analysis shows that solar flares exhibit memory on different timescales. These previous studies showed that the time ordering of flare events is not random, but rather there is dependence between successive flares. In the present work, the clustering of flares is demonstrated through a straightforward nonparametric method where the cumulative distribution function of successive flares is compared with the cumulative distribution function of surrogate sequences of flares obtained by random permutation of flares. The random permutation is performed within rate-variable Bayesian blocks during which the flare rate is assumed to be constant. Differences between the cumulative distribution functions are substantial on a timescale around 3 hr, suggesting that flare recurrence on that timescale is more likely than would be expected if the waiting time were drawn from a nonstationary Poisson process.

Scattering of energetic electrons by heat-flux-driven whistlers in flares

G. T. **Roberg-Clark**, O. V. Agapitov, J. F. Drake, M. M. Swisdak

2019 *ApJ* **887** 190

https://arxiv.org/pdf/1908.06481.pdf

https://doi.org/10.3847/1538-4357/ab5114

The scattering of electrons by heat-flux-driven whistler waves is explored with particle-in-cell (PIC) simulations relevant to the transport of energetic electrons in flares and the solar wind. The simulations are initiated with a large heat flux that is produced using a kappa distribution of electrons with positive velocity and a cold return current beam. This system represents energetic electrons escaping from a reconnection-driven energy release site. This heat flux system drives large amplitude oblique whistler waves propagating both along and against the heat flux, as well as electron acoustic waves. While the waves are dominantly driven by the low energy electrons, including the cold return current beam, the energetic electrons resonate with and are scattered by the whistlers on time scales of the order of a hundred electron cyclotron times. Electron perpendicular energy is increased while the field-aligned electron heat flux is suppressed. The resulting scattering mean-free-paths of energetic electrons are small compared with the typical scale size of energy release sites in flares, which might lead to the effective confinement of energetic electrons that is required for the production of very energetic particles.

Tracing the signatures of a quiet Sun nanoflare

Rebecca A. **Robinson**1,2 and Mats Carlsson1,2

A&A 677, A36 (**2023**)

https://www.aanda.org/articles/aa/pdf/2023/09/aa47089-23.pdf

Context. Nanoflare-scale reconnection events are difficult to detect, and even when they are detected, it is tricky to reconstruct the details and trigger mechanisms that power them. However, numerical models of nanoflare-scale reconnection can provide context to observations of small-scale reconnection events via the comparison of synthetic observables to observed signatures of the nanoflare.

Aims. We aim to demonstrate how a simulated nanoflare event would look if it were observed by the Solar Dynamics Observatory Atmospheric Imaging Assembly (SDO/AIA) and the upcoming Multi-slit Solar Explorer (MUSE). The goal is to determine the details (if any) of nanoflare-scale reconnection events that could reasonably be captured by current and future instruments.

Methods. We calculated synthetic observables from a quiet Sun simulation of a nanoflare-scale reconnection event, including integrated intensities of Fe IX at 171.073 Å and Fe XII at 195.119 Å. Then, we degraded the synthetic observables to SDO/AIA and MUSE resolutions in order to determine whether the instruments are capable of capturing the details of the reconnection event.

Results. We determine that even small-scale reconnection events in the quiet Sun can be detected by both SDO/AIA and MUSE. In the 171 channel of each instrument, it is possible to discern details of the two bidirectional jets that emanate from the reconnection site. These two bidirectional jets correspond to two different magnetic features undergoing large-angle reconnection with an overlying horizontal field in the corona. In the 193 channel of SDO/AIA, it is only possible to see one set of bidirectional jets, which corresponds to the most energetic reconnecting feature. However, the calculated count rate for AIA 193 is not sufficient for a reliable observation.

Conclusions. Quiet Sun activity is detectable with SDO/AIA and will be detectable with the future MUSE mission. It is possible to detect bidirectional jets with both instruments, which can give context clues as to the mechanisms causing the nanoflare event. The resolution and spectral information of MUSE will give a much more detailed observation of the event, making it much easier to reconstruct a possible trigger mechanism. However, we must be careful in our interpretations of observations when we have limited information, as vastly different physical processes can produce similar observational signatures.

Analyzing the Sequence of Phases Leading to the Formation of the Active Region 13664, with Potential Carrington-like Characteristics

Paolo **Romano**, Abouazza Elmhamdi, Alessandro Marassi, Lidia Contarino

2024 *ApJL* **973** L31

https://arxiv.org/pdf/2409.04408

https://iopscience.iop.org/article/10.3847/2041-8213/ad77cb/pdf

Several recurrent X-class flares from Active Region (AR) 13664 have triggered a severe G5-class geomagnetic storm between May 10 and 11, 2024. The morphology and compactness of this AR closely resemble the active region responsible for the famous Carrington Event of 1859. Although the induced geomagnetic currents produced a value of the Dst index, probably, an order of magnitude weaker than that of the Carrington Event, the characteristics of AR 13664 warrant special attention. Understanding the mechanisms of magnetic field emergence and transformation in the solar atmosphere that lead to the formation of such an extensive, compact and complex AR is crucial. Our analysis of the emerging flux and horizontal motions of the magnetic structures observed in the photosphere reveals the fundamental role of a sequence of emerging bipoles at the same latitude and longitude, followed by converging and shear motions. This temporal order of processes frequently invoked in magnetohydrodynamic models - emergence,

converging motions, and shear motions - is critical for the storage of magnetic energy preceding strong solar eruptions that, under the right timing, location and direction conditions, can trigger severe space weather events at Earth.

On the evolution of a sub-C class flare: a showcase for the capabilities of the revamped Catania Solar Telescope

Paolo **Romano**, Salvo L. Guglielmino, Pierfrancesco Costa, Mariachiara Falco, Salvatore Buttaccio, Alessandro Costa, Eugenio Martinetti, Giovanni Occhipinti, Daniele Spadaro, Rita Ventura, Giuseppe E. Capuano, Francesca Zuccarello

Solar Phys. **297**, Article number: 7 **2022**

https://arxiv.org/pdf/2111.08972.pdf

https://link.springer.com/content/pdf/10.1007/s11207-021-01932-z.pdf

https://doi.org/10.1007/s11207-021-01932-z

Solar flares are occasionally responsible for severe Space Weather events, which can affect space-borne and ground-based infrastructures, endangering anthropic technological activities and even human health and safety. Thus, an essential activity in the framework of Space Weather monitoring is devoted to the observation of the activity level of the Sun.

In this context, the acquisition system of the Catania Solar Telescope has been recently upgraded in order to improve its contribution to the European Space Agency (ESA) - Space Weather Service Network through the ESA Portal, which represents the main asset for Space Weather in Europe.

Here, we describe the hardware and software upgrades of the Catania Solar Telescope and the main data products provided by this facility, which include full-disc images of the photosphere and chromosphere, together with a detailed characterization of the sunspot groups. As a showcase of the observational capabilities of the revamped Catania Solar Telescope, we report the analysis of a B5.4 class flare occurred on **2020 December 7**, simultaneously observed by the IRIS and SDO satellites.

Two strong white-light solar flares in AR NOAA 12673 as potential clues for stellar superflares

Paolo **Romano**, Abouazza Elmhamdi, Ayman Kordi

Solar Physics 294:4 **2019**

https://arxiv.org/pdf/1812.04581.pdf

Recently, two strong homologous white light flares of X-GOES class occurred on the Sun on **Sept. 06, 2017**, providing a rare exceptional opportunity to study the mechanisms responsible for the formation of the magnetic field configurations suitable for the manifestation of such yet enigmatic eruptive events and their effects in the lower layers of the solar atmosphere.

Using photospheric vector magnetograms, taken before the beginning of the two X-class events, as boundary conditions to reconstruct the non−linear coronal magnetic field configuration, we identified two related 3D null points located at low heights above the photosphere (i.e. in very low corona). These null points are most likely responsible for the triggering of the two strong X-GOES class flares. We deduced that their formation at such low altitudes may plausibly be ascribed to the peculiar photospheric horizontal motions of the main magnetic structures of the hosting Active Region NOAA 12673.

These events can be adopted as a hint for a possible interpretation of the activity of young G-type stars, recently reported by the Kepler mission. We argued that a possible explanation of the acceleration of huge numbers of particles producing white light emission, during the Sept. 6 events as well as during white light flares in young Sun-like stars, might be attributed to the special accompanying conditions of the occurrence of magnetic reconnection at low altitudes of their atmospheres.

Homologous White Light Solar Flares Driven by Photospheric Shear Motions

P. **Romano**1, A. Elmhamdi2, M. Falco1, P. Costa1, A. S. Kordi2, H. A. Al-Trabulsy2, and R. M. Al-Shammari

2018 ApJL 852 L10 **File**

http://iopscience.iop.org.sci-hub.tw/2041-8205/852/1/L10/

https://arxiv.org/pdf/1812.04252.pdf

We describe the peculiarity of two recurrent white light flares that occurred on **2017 September 06**, in the super active region NOAA 12673, with a time interval, between their peaks, of about 3 hr. These events of the X2.2 and X9.3 GOES classes are very important, not only for their high level of emission and for the visible effects on the lower layers of the solar atmosphere, which are discernible as clear white light ribbons, but also for the strong horizontal photospheric motions, which seemed to drive them. In fact, we observed the displacement of a negative umbra located in the main delta spot of the active region for several hours before the flare occurrence. We measured velocities of up to 0.6 km s−1. The strong and persistent shear motion of the photospheric structures, together with the high intensity of the magnetic flux involved in these events, can be considered responsible for the new energy that is continuously supplied

to the magnetic system. From the timing of the emissions at different wavelengths, we were able to provide some constraints for the modeling of such events.
RHESSI Nuggets #341 Dec **2018**
http://sprg.ssl.berkeley.edu/~tohban/wiki/index.php/Homologous_White_Light_Solar_Flares

Observation of a 3D magnetic null point

P. **Romano**, M. Falco, S. L. Guglielmino, M. Murabito
ApJ **837** 173 **2017**
https://arxiv.org/pdf/1703.00665.pdf
We describe high resolution observations of a GOES B-class flare characterized by a circular ribbon at chromospheric level, corresponding to the network at photospheric level. We interpret the flare as a consequence of a magnetic reconnection event occurred at a three-dimensional (3D) coronal null point located above the supergranular cell. The potential field extrapolation of the photospheric magnetic field indicates that the circular chromospheric ribbon is cospatial with the fan footpoints, while the ribbons of the inner and outer spines look like compact kernels. We found new interesting observational aspects that need to be explained by models: 1) a loop corresponding to the outer spine became brighter a few minutes before the onset of the flare; 2) the circular ribbon was formed by several adjacent compact kernels characterized by a size of 1"-2"; 3) the kernels with stronger intensity emission were located at the outer footpoint of the darker filaments departing radially from the center of the supergranular cell; 4) these kernels start to brighten sequentially in clockwise direction; 5) the site of the 3D null point and the shape of the outer spine were detected by RHESSI in the low energy channel between 6.0 and 12.0 keV. Taking into account all these features and the length scales of the magnetic systems involved by the event we argued that the low intensity of the flare may be ascribed to the low amount of magnetic flux and to its symmetric configuration. **2015 May 20**

Recurrent flares in active region NOAA 11283

P. **Romano**, F. Zuccarello, S. L. Guglielmino, F. Berrilli, R. Bruno, V. Carbone, G. Consolini, M. de Lauretis, D. Del Moro, A. Elmhamdi et al. (14 more)
A&A 582, A55 (**2015**)
Context. Flares and coronal mass ejections (CMEs) are solar phenomena that are not yet fully understood. Several investigations have been performed to single out their related physical parameters that can be used as indices of the magnetic complexity leading to their occurrence.
Aims. In order to shed light on the occurrence of recurrent flares and subsequent associated CMEs, we studied the active region NOAA **11283** where recurrent M and X GOES-class flares and CMEs occurred.
Methods. We use vector magnetograms taken by HMI/SDO to calculate the horizontal velocity fields of the photospheric magnetic structures, the shear and the dip angles of the magnetic field, the magnetic helicity flux distribution, and the Poynting fluxes across the photosphere due to the emergence and the shearing of the magnetic field.
Results. Although we do not observe consistent emerging magnetic flux through the photosphere during the observation time interval, we detected a monotonic increase of the magnetic helicity accumulated in the corona. We found that both the shear and the dip angles have high values along the main polarity inversion line (PIL) before and after all the events. We also note that before the main flare of X2.1 GOES class, the shearing motions seem to inject a more significant energy than the energy injected by the emergence of the magnetic field.
Conclusions. We conclude that the very long duration (about 4 days) of the horizontal displacement of the main photospheric magnetic structures along the PIL has a primary role in the energy release during the recurrent flares. This peculiar horizontal velocity field also contributes to the monotonic injection of magnetic helicity into the corona. This process, coupled with the high shear and dip angles along the main PIL, appears to be responsible for the consecutive events of loss of equilibrium leading to the recurrent flares and CMEs.

Flare occurrence and the spatial distribution of the magnetic helicity flux

P. **Romano**1 and F. Zuccarello
A&A 535, A1 (**2011**)
Context. The accumulation of magnetic helicity via emergence of new magnetic flux and/or shearing photospheric motions is considered an important tool for understanding the processes that lead to eruptive phenomena.
Aims. We highlight a specific aspect of the magnetic helicity accumulation, providing new observational evidence of the role played by the interaction of magnetic field systems that are characterized by opposite signs of the magnetic helicity flux in triggering solar eruptions.
Methods. The amount of magnetic helicity injected into the corona through the photosphere in a sample of active regions (ARs) during their passage across the solar disk was measured by inferring the apparent motion of photospheric footpoints of magnetic field lines from a time series of MDI full-disk line-of-sight magnetograms. The temporal variation of the maps of magnetic helicity flux was analysed by measuring the fragmentation of the patches that are

characterized by the flux of magnetic helicity. The temporal correlation between the number of these patches and the flare and coronal mass ejection (CME) occurrence has also been studied.
Results. The fragmentation of the patches singled out in the maps of the magnetic helicity flux provides a useful indication of the evolution of the AR complexity. The more fragmented the maps of the magnetic helicity flux are, the higher is the flare and CME frequency. Moreover, most of the events occur for low values (~3 ÷ 17) of the difference of the number of patches with opposite signs of magnetic helicity flux.
Conclusions. These results indicate that not only the accumulation of magnetic helicity in the corona, but also its positive and negative fragmentation and distribution should be taken into account to provide a more confident indication of AR complexity and flare/CME productivity. In particular, the interaction of magnetic systems characterized by opposite sign of magnetic helicity flux may be responsible for many observed eruptions.

An M1.5 Flare Triggered by a Multireconnection Process

P. **Romano** · F. Zuccarello · L. Contarino
Solar Phys (**2007**) 240: 49–61
The analysis of full-disk SOHO/MDI magnetograms and of WL and
171 E TRACE images shows in fact that both flux emergence and horizontal displacements
of photospheric flux concentrations have a key role in triggering the event.

Photospheric magnetic evolution of super active regions:

P. **Romano** and F. Zuccarello
A&A 474 (**2007**) 633-637
We studied the magnetic flux evolution in 26 super active regions observed on the solar disc from Jan. 1, 2000 to Dec. 31, 2006, in order to determine a physical relationship between flares and some properties of the photospheric magnetic fields.
The deviations from magnetic polarity balance and the length of the inversion lines characterized by a horizontal magnetic gradient greater than 0.3 G km^{-1} seem to have a major role in producing a magnetic field topology able to trigger flares.

A Catalog of Solar Flare Events Observed by the SOHO/EIT

Sumanth A. **Rotti**, Petrus C.H. Martens, Berkay Aydin
ApJ S **249** 20 **2020**
https://arxiv.org/pdf/2007.05586.pdf
https://doi.org/10.3847/1538-4365/ab9a42
https://iopscience.iop.org/article/10.3847/1538-4365/ab9a42/pdf
We have compiled a catalog of solar flares as observed by the Extreme ultraviolet Imaging Telescope (EIT) aboard the Solar and Heliospheric Observatory (SOHO) spacecraft and the GOES spacecraft over a span from 1997 to 2010. During mid-1998, the cadence of EIT images was revised from two images per day to 12 minutes. However, the low temporal resolution causes significant data gaps in capturing much of the flaring phenomenon. Therefore, we monitor possible errors in flare detection by flare parameters such as temporal overlap, observational wavelength, and considering full field of view (FOV) images. We consider the GOES flare catalog as the primary source. We describe the technique used to enhance the GOES detected flares using the Extreme Ultraviolet (EUV) image captured by the EIT instrument. In order to detect brightenings, we subtract the images with a maximum cadence of 25 minutes. We have downloaded and analyzed the EIT data via the Virtual Solar Observatory (VSO). This flare dataset from the SOHO/EIT period proves indispensable to the process of the solar flare predictions as the instrument has covered most of Solar Cycle 23.

Evolution of the Ratio of Mg II Intensities During Solar Flares

Soumya **Roy**, Durgesh Tripathi
ApJ **964** 106 **2024**
https://arxiv.org/pdf/2402.11189.pdf
https://iopscience.iop.org/article/10.3847/1538-4357/ad2a46/pdf
The Mg II k \& h line intensity ratios can be used to probe the characteristics of the plasma in the solar atmosphere. In this study, using the observations recorded by the Interface Region Imaging Spectrometer (IRIS), we study the variation of the Mg II k \& h intensity ratio for three flares belonging to X-class, M-class, and C-class, throughout their evolution. We also study the k-to-h intensity ratio as a function of magnetic flux density obtained from the line-of-sight magnetograms recorded by the Helioseismic and Magnetic Imager (HMI) on board the Solar Dynamics Observatory (SDO). Our results reveal that while the intensity ratios are independent of magnetic flux density, they show significant changes during the evolution of the C-class and M-class flares. The intensity ratios start to increase at the start of the flare and peak during the impulsive phase before the flare peak and decrease rapidly thereafter. The values of the ratios

fall even below the pre-flare level during the peak and decline phases of the flare. These results are important in light of the heating and cooling of localized plasma and provide further constraints on the understanding of flare physics. **Oct 22, 2014, Feb 3, 2015, Nov 4, 2015**
IRIS Nugget 12 Apr **2024** https://iris.lmsal.com/nugget

The Lorentz force at work: multi-phase magnetohydrodynamics throughout a flare lifespan

Wenzhi **Ruan**, Rony Keppens, Limei Yan, Patrick Antolin
ApJ 967:82 **2024**
https://arxiv.org/pdf/2403.19204.pdf
https://iopscience.iop.org/article/10.3847/1538-4357/ad3915/pdf **File**
The hour-long, gradual phase of solar flares is well-observed across the electromagnetic spectrum, demonstrating many multi-phase aspects, where cold condensations form within the heated post-flare system, but a complete three-dimensional (3D) model is lacking. Using a state-of-the-art 3D magnetohydrodynamic simulation, we identify the key role played by the Lorentz force through the entire flare lifespan, and show that slow variations in the post-flare magnetic field achieve the bulk of the energy release. Synthetic images in multiple passbands closely match flare observations, and we quantify the role of conductive, radiative and Lorentz force work contributions from flare onset to decay. This highlights how the non-force-free nature of the magnetic topology is crucial to trigger Rayleigh-Taylor dynamics, observed as waving coronal rays in extreme ultraviolet observations. Our C-class solar flare reproduces multi-phase aspects such as post-flare coronal rain. In agreement with observations, we find strands of cooler plasma forming spontaneously by catastrophic cooling, leading to cool plasma draining down the post-flare loops. As there is force balance between magnetic pressure and tension and the plasma pressure in gradual-phase flare loops, this has potential for coronal seismology to decipher the magnetic field strength variation from observations. **June 22, 2015, May 22, 2013, September 10, 2017**

MHD turbulence formation in solar flares: 3D simulation and synthetic observations

Wenzhi **Ruan**, Limei Yan, Rony Keppens
2023 *ApJ* **947** 67
https://arxiv.org/pdf/2210.09856.pdf
https://iopscience.iop.org/article/10.3847/1538-4357/ac9b4e/pdf
Turbulent plasma motion is common in the universe, and invoked in solar flares to drive effective acceleration leading to high energy electrons. Unresolved mass motions are frequently detected in flares from extreme ultraviolet (EUV) observations, which are often regarded as turbulence. However, how this plasma turbulence forms during the flare is still largely a mystery. Here we successfully reproduce observed turbulence in our 3D magnetohydrodynamic simulation where the magnetic reconnection process is included. The turbulence forms as a result of an intricate non-linear interaction between the reconnection outflows and the magnetic arcades below the reconnection site, in which the shear-flow driven Kelvin-Helmholtz Instability (KHI) plays a key role for generating turbulent vortices. The turbulence is produced above high density flare loops, and then propagates to chromospheric footpoints along the magnetic field as Alfvenic perturbations. High turbulent velocities above 200 km s^-1 can be found around the termination shock, while the low atmosphere reaches turbulent velocities of 10 km s^-1 at a layer where the number density is about 10^11 cm^-3. The turbulent region with maximum non-thermal velocity coincides with the region where the observed high-energy electrons are concentrated, demonstrating the potential role of turbulence in acceleration. Synthetic views in EUV and fitted Hinode-EIS spectra show excellent agreement with observational results. An energy analysis demonstrates that more than 10% of the reconnection downflow kinetic energy can be converted to turbulent energy via KHI.

When hot meets cold: post-flare coronal rain

Wenzhi **Ruan**, Yuhao Zhou, Rony Keppens
ApJL **920** L15 **2021**
https://arxiv.org/pdf/2109.11873.pdf
https://iopscience.iop.org/article/10.3847/2041-8213/ac27b0/pdf
https://doi.org/10.3847/2041-8213/ac27b0
Most solar flares demonstrate a prolonged, hourlong post-flare (or gradual) phase, characterized by arcade-like, post-flare loops (PFLs) visible in many extreme ultraviolet (EUV) passbands. These coronal loops are filled with hot -- ~30MK -- and dense plasma, evaporated from the chromosphere during the impulsive phase of the flare, and they very gradually recover to normal coronal density and temperature conditions. During this gradual cooling down to ~1MK regimes, much cooler -- ~0.01MK -- and denser coronal rain is frequently observed inside PFLs. Understanding PFL dynamics in this long-duration, gradual phase is crucial to the entire corona-chromosphere mass and energy cycle. Here we report a simulation in which a solar flare evolves from pre-flare, over impulsive phase all the way into its gradual phase, which successfully reproduces post-flare coronal rain. This rain results from catastrophic cooling caused by thermal instability, and we analyse the entire mass and energy budget evolution driving this sudden

condensation phenomenon. We find that the runaway cooling and rain formation also induces the appearance of dark post-flare loop systems, as observed in EUV channels. We confirm and augment earlier observational findings, suggesting that thermal conduction and radiative losses alternately dominate the cooling of PFLs.

A fully self-consistent model for solar flares

Wenzhi **Ruan**, Chun Xia, Rony Keppens
ApJ **896** 97 **2020**
https://arxiv.org/pdf/2005.08578.pdf
https://sci-hub.st/https://iopscience.iop.org/article/10.3847/1538-4357/ab93db
https://iopscience.iop.org/article/10.3847/1538-4357/ab93db/pdf
The 'standard solar' flare model collects all physical ingredients identified by multi-wavelength observations of our Sun: magnetic reconnection, fast particle acceleration and the resulting emission at various wavelengths, especially in soft to hard X-ray channels. Its cartoon representation is found throughout textbooks on solar and plasma astrophysics, and guides interpretations of unresolved energetic flaring events on other stars, accretion disks and jets. To date, a fully self-consistent model that reproduces the standard scenario in all its facets is lacking, since this requires the combination of a large scale, multi-dimensional magnetohydrodynamic (MHD) plasma description with a realistic fast electron treatment. Here, we demonstrate such a novel combination, where MHD combines with an analytic fast electron model, adjusted to handle time-evolving, reconnecting magnetic fields and particle trapping. This allows to study (1) the role of fast electron deposition in the triggering of chromospheric evaporation flows; (2) the physical mechanisms that generate various hard X-ray sources at chromospheric footpoints or looptops; and (3) the relationship between soft X-ray and hard X-ray fluxes throughout the entire flare loop evolution. For the first time, this self-consistent solar flare model demonstrates the observationally suggested relationship between flux swept out by the hard X-ray footpoint regions, and the actual reconnection rate at the X-point, which is a major unknown in flaring scenarios. We also demonstrate that a looptop hard X-ray source can result from fast electron trapping.
RHESSI Nuggets # 393 **2020** https://sprg.ssl.berkeley.edu/~tohban/wiki/index.php/Self-Consistent_Flare_Model

Extreme-ultraviolet and X-Ray Emission of Turbulent Solar Flare Loops

Wenzhi **Ruan** (1), Chun Xia (1,2), Rony Keppens
2019 ApJL 877 L11
https://iopscience.iop.org/article/10.3847/2041-8213/ab1f78/pdf
Turbulence has been observed in flare loops and is believed to be crucial for the acceleration of particles and in the emission of X-ray photons in flares, but how the turbulence is produced is still an open question. A scenario proposed by Fang et al. suggests that fast evaporation flows from flare loop footpoints can produce turbulence in the looptop via the Kelvin–Helmholtz instability (KHI). We revisit and improve on this scenario and study how the KHI turbulence influences extreme-ultraviolet (EUV) and X-ray emission. A 2.5D numerical simulation is performed in which we incorporate the penetration of high-energy electrons as a spatio-temporal dependent trigger for chromospheric evaporation flows. EUV, soft X-ray (SXR), and hard X-ray (HXR) emission are synthesized based on the evolving plasma parameters and given energetic electron spectra. KHI turbulence leads to clear brightness fluctuations in the EUV, SXR, and HXR emission, with the SXR light curve demonstrating a clear quasi-periodic pulsation (QPP) with period of 26 s. This QPP derives from a locally trapped, fast standing wave that resonates in between KHI vortices. The spectral profile of the Fe xxi 1354 line is also synthesized and found to be broadened due to the turbulent motion of plasma. HXR tends to mimic the variation of SXR flux and the footpoint HXR spectrum is flatter than the looptop HXR spectrum.

Solar flares and Kelvin-Helmholtz instabilities: A parameter survey

Wenzhi **Ruan** (1), Chun Xia (1,2), Rony Keppens
A&A **2018**
https://arxiv.org/pdf/1809.02410.pdf
Hard X-ray (HXR) sources are frequently observed near the top of solar flare loops, and the emission is widely ascribed to bremsstrahlung. We here revisit an alternative scenario which stresses the importance of *inverse Compton processes* and the Kelvin- Helmholtz instability (KHI) proposed by Fang et al. (2016). This scenario adds a novel ingredient to the standard flare model, where evaporation flows from flare-impacted chromospheric foot-points interact with each other near the loop top and produce turbulence via KHI. The turbulence can act as a trapping region and as an efficient accelerator to provide energetic electrons, which scatter soft X-ray (SXR) photons to HXR photons via the inverse Compton mechanism. This paper focuses on the trigger of the KHI and the resulting turbulence in this new scenario. We perform a parameter survey to investigate the necessary ingredients to obtain KHI through interaction of chromospheric evaporation flows. When turbulence is produced in the loop apex, an index of -5/3 can be found in the spectra of velocity and magnetic field fluctuations. The KHI development and the generation of turbulence are controlled by the amount of energy deposited in the chromospheric foot-points and the time scale of its energy deposition, but typical values for M class flares show the KHI development routinely. Asymmetry of energy deposition

determines the location where the turbulence is produced, and the synthesized SXR light curve shows a clear periodic signal related to the sloshing motion of the vortex pattern created by the KHI.

Gradual Magnetic Evolution of Sunspot Structure and Filament-Corona Dynamics Associated with the X1.8 Flare in AR 11283

Guiping **Ruan**, Yao Chen, Haimin Wang
ApJ 812 120 **2015**
http://arxiv.org/pdf/1509.04407.pdf
In this paper, we present a study on persistent and gradual penumbral decay and correlated decline of the photospheric transverse field component during 10-20 hours before a major flare (X1.8) eruption on **2011 September 7**. This long-term pre-eruption behavior is corroborated with the well-imaged pre-flare filament rising, the consistent expansion of coronal arcades overlying the filament, as well as the NLFFF modelling results in the literature. We suggest that both the long-term pre-flare penumbral decay and the transverse field decline are the photospheric manifestation of the gradual rise of the coronal filament-flux rope system. We also suggest that a C3 flare and subsequent reconnection process preceding the X1.8 flare play an important role in triggering the later major eruption.

Plasma heating in the initial phase of solar flares

P. **Rudawy**1, M. Siarkowski2 and R. Falewicz1
Solar and Stellar Variability: Impact on Earth and Planets, Proceedings IAU Symposium No. 264, **2009**, p. 282-284, A.G. Kosovichev, A.H. Andrei & J.-P. Rozelot, eds.
Y:\obridko\otchet09
In this paper we analyze soft and hard X-ray emission of the **2002 September 20** M1.8 GOES class solar flare observed by RHESSI and GOES satellites, where soft X-ray emission precedes the onset of the main bulk hard X-ray emission by »5 min. This suggests that an additional heating mechanism may be at work at the early beginning of the flare. However RHESSI spectra indicate presence of the non-thermal electrons also before impulsive phase. So, we assumed that a dominant energy transport mechanism during rise phase of solar flares is electron beam-driven evaporation. We used non-thermal electron beams derived from RHESSI spectra as the heating source in a hydrodynamic model of the analyzed flare. We showed that energy delivered by non-thermal electron beams is sufficient to heat the flare loop to temperatures in which it emits soft X-ray closely following the GOES 1-8 °A light-curve.

Validity of NLFFF Optimization Reconstruction

G. V. **Rudenko**, I. S. Dmitrienko
Solar Phys. **2020**
https://arxiv.org/pdf/2001.05660.pdf
We evaluate validity of NLFFF extrapolation performed with Optimization class (OPTI) codes. While explaining inevitable for OPTI partial non-solenoidality caused by the gas pressure notable role in pressure balance at photospheric heights and by mathematical aspects related to optimization and BVP (boundary value problem), we justify elimination of the non-solenoidal component (postprocessing) from the OPTI result obtained. In essence, postprocessing converts the entire non-solenoidal part into a solenoidal force part, which possibly reflects factual deviation of magnetic field from its force-free pproximation on the photosphere and in the solar corona. Two forms of postprocessing have been analyzed in this paper.Postprocessing I eliminates the non-solenoidal component without changing transverse field at the measurement level, and Postprocessing II leaves the field normal component unchanged. Extrapolation, postprocessing, and then comparison of metric and energy characteristics are performed over AR 11158 active region for a small fragment of its evolution containing the February X-class flare.Our version of OPTI code showed that free energy decreased by ∼1032 erg within 1 hour, which corresponds to theoretical estimations of the flare-caused magnetic energy loss. This result differs significantly from the one in Sun et al. (2012).Therefore, we also comment on some features of our OPTI code implementation, which may cause significant differences between our results and those obtained using the Wiegelmann (2004) version of OPTI code in study by Sun et al. (2012). **2011/02/-14-15**

Flux-Rope Mediated Turbulent Magnetic Reconnection

Alexander J. B. **Russell**
ApJ **2024**
https://arxiv.org/pdf/2406.16149
We present a new model of magnetic reconnection in the presence of turbulence, applicable when the magnetic helicity is non-zero. The new model differs from the Lazarian-Vishniac turbulent reconnection theory by emphasizing the role of locally coherent magnetic structures, whose existence is shown to be permitted by the properties of magnetic field line separation in turbulent plasma. Local coherence allows storage of magnetic helicity inside the reconnection layer and we argue that helicity conservation produces locally coherent twisted flux ropes. We then introduce the "Alfvén

horizon" to explain why the global reconnection rate can be governed by locally coherent magnetic field structure instead of by field line wandering, formally extending to 3D the principle that reconnection can be made fast by fragmentation of the global current layer. Coherence is shown to dominate over field line dispersion if the anisotropy of the turbulence at the perpendicular scale matching the thickness of a marginally stable current layer exceeds the aspect ratio of the current layer. Finally, we conjecture that turbulence generated within the reconnection layer may produce a balance of anisotropies that maintains the system in the flux-rope mediated regime. The new model successfully accounts for the major features of 3D numerical simulations of self-generated turbulent reconnection, including reconnection rates of 0.01 in resistive MHD and 0.1 with collisionless physics.

Alfvén Waves in Solar Flares **Review**

Alexander J. B. **Russell**

"Alfvén Waves Across Heliophysics: Progress, Challenges, and Opportunities" (American Geophysical Union). **2023**

https://arxiv.org/pdf/2311.02144.pdf

Solar flares are dramatic events in which magnetic reconnection in the corona leads to heating of plasma to tens of MK and acceleration of particles to high energies. They also centrally involve transport between the corona (where the magnetic reconnection occurs) and the lower solar atmosphere (where most energy is radiated from). There is substantial evidence for the presence of Alfvénic waves/turbulence in solar flares, for example, in the ubiquitous nonthermal broadening of flare spectral lines. The physical role that Alfvénic waves have in the flare has attracted considerable attention, especially since 2007-2010. This article reviews what spectroscopic observations reveal about the properties and importance of Alfvénic waves, turbulence and transport in solar flares; mechanisms for wave excitation by magnetic reconnection at high Lundquist numbers and braking of the sunward reconnection jet; and models of wave energy transport to the lower atmosphere and the resulting heating and dynamics. The article finishes with discussion of the outlook for new progress.

A unified view of coronal loop contraction and oscillation in flares

Alexander J. B. **Russell**, Paulos J. A. Simoes, Lyndsay Fletcher

A&A 581, A8 **2015**

http://arxiv.org/pdf/1506.07716v1.pdf

http://www.aanda.org/articles/aa/pdf/2015/09/aa25746-15.pdf

Context: Transverse loop oscillations and loop contractions are commonly associated with solar flares, but the two types of motion have traditionally been regarded as separate phenomena.

Aims: We present an observation of coronal loops contracting and oscillating following onset of a flare. We aim to explain why both behaviours are seen together and why only some of the loops oscillate.

Methods: A time sequence of SDO/AIA 171 \r{A} images is analysed to identify positions of coronal loops following the onset of M6.4 flare SOL**2012-03-09**T03:53. We focus on five loops in particular, all of which contract during the flare, with three of them oscillating as well. A simple model is then developed for contraction and oscillation of a coronal loop.

Results: We propose that coronal loop contractions and oscillations can occur in a single response to removal of magnetic energy from the corona. Our model reproduces the various types of loop motion observed and explains why the highest loops oscillate during their contraction while no oscillation is detected for the shortest contracting loops. The proposed framework suggests that loop motions can be used as a diagnostic for the removal of coronal magnetic energy by flares, while rapid decrease of coronal magnetic energy is a newly-identified excitation mechanism for transverse loop oscillations.

See http://www.uksolphys.org/uksp-nugget/62-coronal-loop-contraction-and-oscillation-in-flares/

Solar flares and focused energy transport by MHD waves

A. J. B. **Russell**1⋆ and D. J. Stackhouse2

A&A 558, A76 (**2013**)

Context. Transport of flare energy from the corona to the chromosphere has traditionally been assigned to electron beams; however, interest has recently been renewed in magnetohydrodynamic (MHD) waves as a complementary or alternative mechanism.

Aims. We determine whether, and under what conditions, MHD waves deliver spatially localised energy to the chromosphere, as required if MHD waves are to contribute to emission from flare ribbons and kernels. This paper also highlights several properties of MHD waves that are relevant to solar flares and demonstrates their application to the flare problem.

Methods. Transport is investigated using a magnetic arcade model and 2.5D MHD simulations. Different wave polarisations are considered and the effect of fine structuring transverse to the magnetic field is also examined. Ray tracing provides additional insight into the evolution of waveguided fast waves.

Results. Alfvén waves are very effective at delivering energy fluxes to small areas of chromosphere, localisation being enhanced by magnetic field convergence and phase mixing. Fast waves, in the absence of fine coronal structure, are more suited to powering emission from diffuse rather than compact sources; however, fast waves can be strongly localised by coronal waveguides, in which case focused energy is best transported to the chromosphere when waveguides are directly excited by the energy release.
Conclusions. MHD waves pass an important test for inclusion in future flare models.

On The Solar Origins of Open Magnetic Fields in the Heliosphere

Rust, D.M., Haggerty, D.K., Georgoulis, M.K., Sheeley, N.R., Wang, Y.-M., DeRosa, M.L., Schriver, C.J.
E-print, Oct 2008; ApJ, v. 687, 635–645, **2008**
http://www.journals.uchicago.edu/doi/abs/10.1086/592017
A combination of heliospheric and solar data was used to identify open magnetic fields stretching from the lower corona to Earth orbit. 35 near-relativistic electron beams detected at the ACE spacecraft ??labeled?? the heliospheric segments of the open fields. An X-ray flare occurred<20 minutes before injection of the electrons in 25 events. These flares labeled the solar segment of the open fields. The flares occurred in western-hemisphere active regions (ARs) with *coronal holes whose polarity agreed with the polarity of the beam-carrying interplanetary fields in 23 of the 25 events.* We conclude that electron beams reach 1 AU from open AR fields adjacent to flare sites. The Wang & Sheeley implementation of the potential-field source-surface model successfully identified the open fields in 36% of cases. Success meant that the open fields reached the source surface within 3 heliographic deg of the interplanetary magnetic field connected to ACE at 1 AU. Inclusion of five near misses improves the success rate to 56%. The success rate for the Schrijver & DeRosa PFSS implementation was 50%. Our results suggest that, even if the input magnetic data are updated frequently, the PFSS models succeed in only 50% of cases to identify the coronal segment of open fields. Development of other techniques is in its infancy.

Triangulation of Hard X-Ray Sources in an X-Class Solar Flare with ASO-S/HXI and Solar Orbiter/STIX.

Ryan, D.F., Massa, P., Battaglia, A.F. et al.
Sol Phys 299, 114 (**2024**).
https://doi.org/10.1007/s11207-024-02341-8
https://link.springer.com/content/pdf/10.1007/s11207-024-02341-8.pdf
HXI on ASO-S and STIX onboard Solar Orbiter are the first simultaneously operating solar hard X-ray imaging spectrometers. ASO-S's low Earth orbit and Solar Orbiter's periodic displacement from the Sun–Earth line enables multi-viewpoint solar hard X-ray spectroscopic imaging analysis for the first time. Here, we demonstrate the potential of this new capability by reporting the first results of 3D triangulation of hard X-ray sources in the SOL**2023-12-31**T21:55 X5 flare. HXI and STIX observed the flare near the east limb with an observer separation angle of 18°. We triangulated the brightest regions within each source, which enabled us to characterise the large-scale hard X-ray geometry of the flare. The footpoints were found to be in the chromosphere within uncertainty, as expected, while the thermal looptop source was centred at an altitude of 15.1 ± 1 Mm. Given the footpoint separation, this implies a more elongated magnetic-loop structure than predicted by a semi-circular model. These results show the strong diagnostic power of joint HXI and STIX observations for understanding the 3D geometry of solar flares. We conclude by discussing the next steps required to fully exploit their potential.

3D evolution of a solar flare thermal X-ray loop-top source⋆

D. F. **Ryan**1, S. Laube1, B. Nicula2, S. Krucker1,3, S. A. Maloney4, A. F. Battaglia1,5, A. Warmuth6, A. Csillaghy1 and D. Müller7
A&A 681, A61 (**2024**)
https://www.aanda.org/articles/aa/pdf/2024/01/aa47212-23.pdf
Context. The recent launch of Solar Orbiter has placed a solar X-ray imager (Spectrometer/Telescope for Imaging X-rays; STIX) beyond Earth orbit for the first time. This introduces the possibility of deriving the 3D locations and volumes of solar X-ray sources by combining STIX observations with those of Earth-orbiting instruments such as the Hinode X-ray Telescope (XRT). These measurements promise to improve our understanding of the evolution and energetics of solar flares. However, substantial design differences between STIX and XRT present important challenges that must first be overcome.
Aims. We aim to: 1) explore the validity of combining STIX and XRT for 3D analysis given their different designs, 2) understand uncertainties associated with 3D reconstruction and their impact on the derived volume and thermodynamic properties, 3) determine the validity of the scaling law that is traditionally used to estimate source volumes from single-viewpoint observations, 4) chart the temporal evolution of the location, volume, and thermodynamic properties of a thermal X-ray loop-top source of a flare based on a 3D reconstruction for the first time.
Methods. The **SOL2021-05-07T18**:43 M3.9-class flare is analysed using co-temporal observations from STIX and XRT, which, at the time, were separated by an angle of 95.4° relative to the flare site. The 3D reconstruction is

performed via elliptical tie-pointing and the visualisation by JHelioviewer, which is enabled by new features developed for this project. Uncertainties associated with the 3D reconstruction are derived from an examination of projection effects given the observer separation angle and the source orientation and elongation.
Results. Firstly, we show that it is valid to combine STIX 6–10 keV and XRT Be-thick observations for 3D analysis for the flare examined in this study. However, the validity of doing so in other cases may depend on the nature of the observed source. Therefore, careful consideration should be given on a case-by-case basis. Secondly, the optimal observer separation angle for 3D reconstruction is 90° ± 5°, but the uncertainties are still relatively small in the range 90° ± 20°. Other angles are viable, but are associated with higher uncertainties, which can be quantified. Thirdly, the traditional area-to-volume scaling law may overestimate the 3D-derived volume of the thermal X-ray loop-top source studied here by over a factor of 2. This is beyond the uncertainty of the 3D reconstruction. The X-ray source was not very asymmetric, and so the overestimation may be greater for more elongated sources. In addition, the degree of overestimation can vary with time and viewing angle, demonstrating that the true source geometry can evolve differently in different dimensions. 3D reconstruction is therefore necessary to derive more reliable volumes. Simply applying a modified scaling law to single-viewpoint observations is not sufficient. Finally, the vertical motion of the X-ray source is consistent with previous observations of limb flares. This indicates that 3D reconstruction by elliptical tie-pointing provides reliable 3D locations. The uncertainties of thermodynamic properties derived from volume, temperature, and/or emission measure are dominated by those of the volume. In contrast to single-viewpoint studies, observationally constrained volume uncertainties can be assigned via 3D reconstruction, which lends quantifiable credibility to scientific conclusions drawn from the derived thermodynamic properties. **2021-05-07**

Effects of flare definitions on the statistics of derived flare distributions

Daniel F. **Ryan**, Marie Dominique, Dan Seaton, Koen Stegen, Arthur White
2016 A&A 592, A133
http://arxiv.org/pdf/1606.04472v1.pdf

The statistical examination of solar flares is crucial to revealing their global characteristics and behaviour. Such examinations can tackle large-scale science questions or give context to detailed single-event studies. However, they are often performed using standard but basic flare detection algorithms relying on arbitrary thresholds. This arbitrariness may lead to important scientific conclusions being drawn from results caused by subjective choices in algorithms rather than the true nature of the Sun. In this paper, we explore the effect of the arbitrary thresholds used in the GOES (Geostationary Operational Environmental Satellite) event list and LYRA (Large Yield RAdiometer) Flare Finder algorithms. We find that there is a small but significant relationship between the power law exponent of the GOES flare peak flux frequency distribution and the flare start thresholds of the algorithms. We also find that the power law exponents of these distributions are not stable, but appear to steepen with increasing peak flux. This implies that the observed flare size distribution may not be a power law at all. We show that depending on the true value of the exponent of the flare size distribution, this deviation from a power law may be due to flares missed by the flare detection algorithms. However, it is not possible determine the true exponent from GOES/XRS observations. Additionally we find that the PROBA2/LYRA flare size distributions are artificially steep and clearly non-power law. We show that this is consistent with an insufficient degradation correction. This means that PROBA2/LYRA should not be used for flare statistics or energetics unless degradation is adequately accounted for. However, it can be used to study variations over shorter timescales and for space weather monitoring.

The Compatibility of Flare Temperatures Observed with AIA, GOES, and RHESSI

Daniel F. **Ryan**, Aidan M. O'Flannagain, Markus J. Aschwanden…
Solar Physics, July **2014**, Volume 289, Issue 7, pp 2547-2563

We test the compatibility and biases of multi-thermal flare DEM (differential emission measure) peak temperatures determined with AIA with those determined by GOES and RHESSI using the isothermal assumption. In a set of 149 M- and X-class flares observed during the first two years of the SDO mission, AIA finds DEM peak temperatures at the time of the peak GOES 1 – 8 Å flux to have an average of T p=12.0±2.9 MK and Gaussian DEM widths of log10(σ T)=0.50±0.13. From GOES observations of the same 149 events, a mean temperature of T p=15.6±2.4 MK is inferred, which is systematically higher by a factor of T GOES/T AIA=1.4±0.4. We demonstrate that this discrepancy results from the isothermal assumption in the inversion of the GOES filter ratio. From isothermal fits to photon spectra at energies of $\epsilon \approx 6-12$ keV of 61 of these events, RHESSI finds the temperature to be higher still by a factor of T RHESSI/T AIA=1.9±1.0. We find that this is partly a consequence of the isothermal assumption. However, RHESSI is not sensitive to the low-temperature range of the DEM peak, and thus RHESSI samples only the high-temperature tail of the DEM function. This can also contribute to the discrepancy between AIA and RHESSI temperatures. The higher flare temperatures found by GOES and RHESSI imply correspondingly lower emission measures. We conclude that self-consistent flare DEM temperatures and emission measures require simultaneous fitting of EUV (AIA) and soft X-ray (GOES and RHESSI) fluxes.

Decay-phase Cooling and Inferred Heating of M- and X-class Solar Flares

Daniel F. **Ryan**1,2,3, Phillip C. Chamberlin2, Ryan O. Milligan2,3,4, and Peter T. Gallagher
2013 ApJ 778 68.
http://arxiv.org/pdf/1401.4079v1.pdf

In this paper, the cooling of 72 M- and X-class flares is examined using GOES/XRS and SDO/EVE. The observed cooling rates are quantified and the observed total cooling times are compared with the predictions of an analytical zero-dimensional hydrodynamic model. We find that the model does not fit the observations well, but does provide a well-defined lower limit on a flare's total cooling time. The discrepancy between observations and the model is then assumed to be primarily due to heating during the decay phase. The decay-phase heating necessary to account for the discrepancy is quantified and found be ~50% of the total thermally radiated energy, as calculated with GOES. This decay-phase heating is found to scale with the observed peak thermal energy. It is predicted that approximating the total thermal energy from the peak is minimally affected by the decay-phase heating in small flares. However, in the most energetic flares the decay-phase heating inferred from the model can be several times greater than the peak thermal energy.

The Thermal Properties of Solar Flares over Three Solar Cycles Using GOES X-Ray Observations

Ryan, Daniel F.; Milligan, Ryan O.; Gallagher, Peter T.; Dennis, Brian R.; Tolbert, A. Kim; Schwartz, Richard A.; Young, C. Alex
E-print, March **2013**

Solar flare X-ray emission results from rapidly increasing temperatures and emission measures in flaring active region loops. To date, observations from the X-Ray Sensor (XRS) on board the Geostationary Operational Environmental Satellite (GOES) have been used to derive these properties, but have been limited by a number of factors, including the lack of a consistent background subtraction method capable of being automatically applied to large numbers of flares. In this paper, we describe an automated Temperature and Emission measure-Based Background Subtraction method (TEBBS), that builds on the methods of Bornmann. Our algorithm ensures that the derived temperature is always greater than the instrumental limit and the pre-flare background temperature, and that the temperature and emission measure are increasing during the flare rise phase. Additionally, TEBBS utilizes the improved estimates of GOES temperatures and emission measures from White et al. TEBBS was successfully applied to over 50,000 solar flares occurring over nearly three solar cycles (1980-2007), and used to create an extensive catalog of the solar flare thermal properties. We confirm that the peak emission measure and total radiative losses scale with background subtracted GOES X-ray flux as power laws, while the peak temperature scales logarithmically. As expected, the peak emission measure shows an increasing trend with peak temperature, although the total radiative losses do not. While these results are comparable to previous studies, we find that flares of a given GOES class have lower peak temperatures and higher peak emission measures than previously reported. The TEBBS database of flare thermal plasma properties is publicly available at **http://www.SolarMonitor.org/TEBBS/.**

The Thermal Properties of Solar Flares over Three Solar Cycles Using GOES X-Ray Observations

Daniel F. **Ryan**, Ryan O. Milligan, Peter T. Gallagher, Brian R. Dennis, A. Kim Tolbert, Richard A. Schwartz, C. Alex Young
ApJS Volume 202, Issue 2, article id. 11, **2012**
https://iopscience.iop.org/article/10.1088/0067-0049/202/2/11/pdf

Solar flare X-ray emission results from rapidly increasing temperatures and emission measures in flaring active region loops. To date, observations from the X-Ray Sensor (XRS) onboard the Geostationary Operational Environmental Satellite (GOES) have been used to derive these properties, but have been limited by a number of factors, including the lack of a consistent background subtraction method capable of being automatically applied to large numbers of flares. In this paper, we describe an automated temperature and emission measure-based background subtraction method (TEBBS), which builds on the methods of Bornmann (1990). Our algorithm ensures that the derived temperature is always greater than the instrumental limit and the pre-flare background temperature, and that the temperature and emission measure are increasing during the flare rise phase. Additionally, TEBBS utilizes the improved estimates of GOES temperatures and emission measures from White et al. (2005). TEBBS was successfully applied to over 50,000 solar flares occurring over nearly three solar cycles (1980-2007), and used to create an extensive catalog of the solar flare thermal properties. We confirm that the peak emission measure and total radiative losses scale with background subtracted GOES X-ray flux as power-laws, while the peak temperature scales logarithmically. As expected, the peak emission measure shows an increasing trend with peak temperature, although the total radiative losses do not. While these results are comparable to previous studies, we find that flares of a given GOES class have lower peak temperatures and higher peak emission measures than previously reported. The resulting TEBBS database of thermal

flare plasma properties is publicly available on Solar Monitor (www.solarmonitor.org/TEBBS/) and will be available on Heliophysics Integrated Observatory (www.helio-vo.eu).

FLARES PRODUCING WELL-ORGANIZED POST-FLARE ARCADES (SLINKIES) HAVE EARLY PRECURSORS

M. P. **Ryutova**1, Z. Frank2, H. Hagenaar2 and T. Berger
2011 ApJ 733 125
Exploding loop systems producing X-ray flares often, but not always, bifurcate into a long-living, well-organized system of multi-threaded loop arcades resembling solenoidal slinkies. The physical conditions that cause or prevent this process are not known. To address this problem, we examined most of the major (X-class) flares that occurred during the last decade and found that the flares that bifurcate into long-living slinky arcades have different signatures than those that do not "produce" such structures. The most striking difference is that, in all cases of slinky formation, GOES high energy proton flux becomes significantly enhanced 10-24 hr before the flare occurs. No such effect was found prior to the "non-slinky" flares. This fact may be associated with the difference between energy production by a given active region and the amount of energy required to bring the entire system into the form of well-organized, self-similar loop arcades. As an example illustrating the process of post-flare slinky formation, we present observations taken with the Hinode satellite, in several wavelengths, showing a time sequence of pre-flare and flare activity, followed by the formation of dynamically stable, well-organized structures. One of the important features revealed is that post-flare coronal slinky formation is preceded by scale invariant structure formation in the underlying chromosphere/transition region. We suggest that the observed regularities can be understood within the framework of self-organized critical dynamics characterized by scale invariant structure formation with critical parameters largely determined by energy saturation level. The observed regularities per se may serve as a long-term precursor of strong flares and may help to study predictability of system behavior.

Propagation of the Alfvén Wave and Induced Perturbations in the Vicinity of a 3D Proper Magnetic Null Point

S. **Sabri**1, H. Ebadi1, and S. Poedts2,3
2022 ApJ 924 126
https://iopscience.iop.org/article/10.3847/1538-4357/ac3b5f/pdf
The aim of the present work is to study the propagation of the Alfvén wave around a 3D proper magnetic null point and its accompanying perturbations. In this line, the shock-capturing Godunov-type PLUTO code is used to solve the magnetohydrodynamic (MHD) equations. It is found that the Alfvén wave propagates toward the null point at the fan plane and the wave−wave interaction could be the main reason for the Alfvén wave energy dissipation, ehile, at two other planes including the spine axis, the Alfvén wave spreads toward the spine axis and accumulates along it. Furthermore, the fast magnetoacoustic wave moves toward the null point at the fan plane and also at two other planes including the spine axis. The fast magnetoacoustic wave also refracts around the null point without any significant accumulation along the spine axis. Finally, the slow mode moves toward the null point at the fan plane. It is illustrated that, at the x,z plane, in addition to the refraction of the slow wave around the null point, there is an accumulation of the slow mode along the spine axis, while, at the other plane including the spine axis, the slow magnetoacoustic wave refracts around the null point. Moreover, it is found that the 3D structure results in the high amplitude of MHD wave energy in comparison with the 2.5D structure. Finally, it is found that the Alfvén wave gives its energy to the induced fast and slow magnetoacoustic waves and they have more time to heat the plasma.

Can Proton Beam Heating Flare Models Explain Sunquakes?

Viacheslav **Sadykov**, John Stefan, Alexander Kosovichev, Joel Allred, Graham S Kerr, Andrey Stejko, Adam Kowalski
ApJ **2023**
https://arxiv.org/pdf/2306.13162.pdf
SDO/HMI observations reveal a class of solar flares with substantial energy and momentum impacts in the photosphere, concurrent with white-light emission and helioseismic responses, known as sunquakes. Previous radiative hydrodynamic modeling has demonstrated the challenges of explaining sunquakes in the framework of the standard flare model of `electron beam' heating. One of the possibilities to explain the sunquakes and other signatures of the photospheric impact is to consider additional heating mechanisms involved in solar flares, for example, via flare-accelerated protons. In this work, we analyze a set of single-loop RADYN+FP simulations where the atmosphere is heated by non-thermal power-law-distributed proton beams which can penetrate deeper than the electron beams into the low atmospheric layers. Using the output of the RADYN models, we calculate synthetic Fe I 6173 A line Stokes profiles and from those the line-of-sight (LOS) observables of the SDO/HMI instrument, as well as the 3D helioseismic response and compare them with the corresponding observational characteristics. These initial results show that the models with proton beam heating can produce the enhancement of the HMI continuum observable and explain qualitatively generation of sunquakes. The continuum observable enhancement is evident in all models but is more

prominent in ones with Ec≥500 keV. In contrast, the models with Ec≤100 keV provide a stronger sunquake-like helioseismic impact according to the 3D acoustic modeling, suggesting that low-energy (deka- and hecto-keV) protons have an important role in the generation of sunquakes.

Response of SDO/HMI observables to heating of the solar atmosphere by precipitating high-energy electrons

Viacheslav M **Sadykov**, Alexander G Kosovichev, Irina N Kitiashvili, Graham S Kerr
2019
https://arxiv.org/pdf/1906.10788.pdf

We perform modeling of the line-of-sight (LOS) observables of the Helioseismic and Magnetic Imager (HMI) onboard the Solar Dynamics Observatory (SDO) for models of the solar atmosphere heated by precipitating high-energy electrons during solar flares. The radiative hydrodynamic (RADYN) flare models are obtained from the F-CHROMA database. The Stokes profiles for the Fe 6173 A line observed by SDO/HMI are calculated using the radiative transfer code RH1.5D assuming statistical equilibrium for atomic level populations and imposing a 100 G or 1000 G uniform vertical magnetic field. The SDO/HMI data processing pipeline algorithm is applied to derive the observables (continuum intensity, line depth, Doppler velocity, LOS magnetic field). Our results reveal that the deviations of the observables from the actual spectroscopic line parameters can reach 0.7 km/s for Doppler velocities and almost 100 G for the LOS magnetic field for the flare models with an average deposited energy flux of ≥5.0×1010 erg cm−2 s−1. Such deviations are significantly smaller for weaker flares with lower deposited energy fluxes. The LOS magnetic field observable does not reverse its sign for any considered flare model. The results show that sharp magnetic transients in SDO/HMI observations during solar flares may partly be due to rapid changes of the line profile. These changes are likely caused by heating of the atmosphere by accelerated electrons and should be interpreted with caution.

Statistical study of properties of the Soft X-ray emission during solar flares

Viacheslav M **Sadykov**, Alexander G Kosovichev, Irina N Kitiashvili, Alexander Frolov
ApJ **874** 19 **2018**
https://arxiv.org/pdf/1810.05610.pdf

We present a statistical analysis of properties of the Soft X-Ray (SXR) emission, plasma temperature (T), and emission measure (EM), derived from GOES observations of flares in 2002-2017. The temperature and emission measures are obtained using the TEBBS algorithm (Ryan et al. 2012), which delivers reliable results together with uncertainties even for weak B-class flare events. More than 96% of flares demonstrate a sequential appearance of T, SXR, and EM peaks, in agreement with the expected behavior of the chromospheric evaporation process. The relative number of such flares increases with increasing the SXR peak flux. The SXR peak is closer in time to the T peak for B-class flares than for >=C-class flares, while it is very close to the EM peak for MX-class flares. We define flares as "T-controlled events" if the SXR-T time delay is at least two times shorter than the EM-SXR delay, and as "EM-controlled events" if the EM-SXR delay is at least two times shorter than the SXR-T delay. For any considered flare class range, the T-controlled events compared to EM-controlled events have: a) higher EM but lower T; b) longer durations and shorter relative growth times; c) longer FWHM and characteristic decay times. Interpretation of these statistical results based on a dynamic loop model suggests that for flares of the same class range, the T-controlled events are developed in longer loops than the EM-controlled events.

Statistical Study of Chromospheric Evaporation in Impulsive Phase of Solar Flares

Viacheslav M **Sadykov**, Alexander G Kosovichev, Ivan N Sharykin, Graham S Kerr
ApJ **871** 2 **2019**
https://arxiv.org/pdf/1805.10729.pdf
sci-hub.tw/10.3847/1538-4357/aaf6b0

We present a statistical study of chromospheric evaporation in solar flares using simultaneous observations by the RHESSI X-ray telescope and the IRIS UV spectrograph. The results are compared with radiation hydrodynamic flare models from the F-CHROMA RADYN database. For each event, we study spatially-resolved Doppler shifts of spectral lines formed in the transition region (C II 1334.5 A) and hot coronal plasma (Fe XXI 1354.1 A) to investigate the dynamics of the solar atmosphere during the flare impulsive phase. We estimate the energy fluxes deposited by high-energy electrons using X-ray imaging spectroscopy and assuming the standard thick-target model. Using the RADYN flare models, the RH 1.5D radiative transfer code and the Chianti atomic line database, we calculate C II and Fe XXI line profiles and compare with the observations. While the models predict a correlation between the Doppler shifts and deposited energy flux for both lines, this was only observed in the C II data, and not in the Fe XXI data. In addition, the C II and Fe XXI Doppler shifts are not correlated with each other in the observations and strongly correlated in models. Several quantitative discrepancies are found between the observations and models: the Fe XXI Doppler shifts are substantially stronger in the models than in the data, the C II mean blueshifts are absent in the observations but predicted by the models. The transition energy between "gentle" and "explosive" evaporation regimes derived from the observations ([Math Processing Error]~erg~cm[Math Processing Error]~s[Math Processing Error]) and the models ([Math Processing Error]~erg~cm[Math Processing Error]~s[Math Processing Error]) are comparable with each other.

The results illustrate, for the first time, observational relationships among the processes of chromospheric evaporation, response of the colder layers, and the flare energy flux deposited by high-energy electrons. **2014-02-13, 2014-03-29, 2014-06-12, 2014-06-13, 2015-03-11, 2015-08-27**

Interactive Multi-Instrument Database of Solar Flares

Viacheslav M **Sadykov**, Rishabh Gupta, Alexander G Kosovichev, Vincent Oria, Gelu M Nita
Astrophysical Journal Supplement Series, Volume 231, Issue 1, article id. 6 **2017**
https://arxiv.org/pdf/1702.02991.pdf
https://iopscience.iop.org/article/10.3847/1538-4365/aa79a9/pdf
Solar flares represent a complicated physical phenomenon observed in a broad range of the electromagnetic spectrum, from radiowaves to gamma-rays. For a complete understanding of the flares it is necessary to perform a combined multi-wavelength analysis using observations from many satellites and ground-based observatories. For efficient data search, integration of different flare lists and representation of observational data, we have developed the Interactive Multi-Instrument Database of Solar Flares (this https URL). The web database if fully functional and allows the user to search for uniquely-identified flare events based on their physical descriptors and availability of observations of a particular set of instruments. Currently the data from three primary flare lists (GOES, RHESSI and HEK) and a variety of other event catalogs (Hinode, Fermi GBM, Konus-Wind, OVSA flare catalogs, CACTus CME catalog, Filament eruption catalog) and observing logs (IRIS and Nobeyama coverage), are integrated, and an additional set of physical descriptors (temperature and emission measure) is provided along with observing summary, data links and multi-wavelength light curves for each flare event since January, 2002. We think that the created instrument will allow researchers significantly speed up the search of events of interest for statistical and case studies.

Relationships Between Characteristics of the Line-of-Sight Magnetic Field and Solar Flare Forecasts

Viacheslav M **Sadykov**, Alexander G Kosovichev
2017 *ApJ* **849** 148
https://arxiv.org/pdf/1704.03423.pdf
We analyze the relationship between the flare X-ray peak flux, and characteristics of the polarity inversion line (PIL) and active regions (ARs), derived from line-of-sight (LOS) magnetograms. The PIL detection algorithm based on a magnetogram segmentation procedure is applied for each AR with 1 hr cadence. The PIL and AR characteristics are associated with the AR flare history and divided into flaring and nonflaring cases. Effectiveness of the derived characteristics for flare forecasting is determined by the number of nonflaring cases separated from flaring cases by a certain threshold, and by their Fisher ranking score. The Support Vector Machine (SVM) classifier trained only on the PIL characteristics is used for the flare prediction. We have obtained the following results: (1) the PIL characteristics are more effective than global characteristics of ARs, (2) the highest True Skill Statistics (TSS) values of 0.76 ± 0.03 for ≥M1.0 flares and 0.84 ± 0.07 for ≥X1.0 flares are obtained using the "Sigmoid" SVM kernel, (3) the TSS scores obtained using only the LOS magnetograms are slightly lower than the scores obtained using vector magnetograms, but significantly better than current expert-based predictions, (4) for prediction of ≥M1.0 class flares 74.4% of all cases, and 91.2% for ≥X1.0 class, can be pre-classified as negative with no significant effect on the results, (5) the inclusion of global AR characteristics does not improve the forecast. The study confirms the unique role of the PIL region characteristics in the flare initiation process, and demonstrates possibilities of flare forecasting using only the LOS magnetograms.. **2011-02-16**

Relationship between chromospheric evaporation and magnetic field topology in M-class solar flare

V.M. **Sadykov**, A.G. Kosovichev, I.N. Sharykin, I.V. Zimovets, S. Vargas Dominguez
2016 *ApJ* **828** 4
http://arxiv.org/pdf/1604.05346v1.pdf
Chromospheric evaporation is observed as Doppler blueshift during solar flares. It plays one of key roles in dynamics and energetics of solar flares, however, its mechanism is still unknown. In this paper we present a detailed analysis of spatially-resolved multi-wavelength observations of chromospheric evaporation during an M 1.0 class solar flare (SOL**2014-06-12**T21:12) using data from the NASA's IRIS (Interface Region Imaging Spectrograph) and HMI/SDO (Helioseismic and Magnetic Imager onboard Solar Dynamics Observatory) telescopes, and VIS/NST (Visible Imaging Spectrometer at New Solar Telescope) high-resolution observations, covering the temperature range from 10^4 K to 10^7 K. The results show that the averaged over the region Fe XXI blueshift of the hot evaporating plasma is delayed relative to the C II redshift of the relatively cold chromospheric plasma by about 1 min. The spatial distribution of the delays is not uniform across the region and can be as long as 2 min in several zones. Using vector magnetograms from HMI we reconstruct the magnetic field topology and the quasi-separatrix layer (QSL) and find that the blueshift delay regions as well as the H-alpha flare ribbons are connected to the region of magnetic polarity inversion line (PIL) and an expanding flux rope via a system of low-lying loop arcades with height < ~4.5 Mm. This allows us to propose an

interpretation of the chromospheric evaporation based on the geometry of local magnetic fields, and the primary energy source associated with the PIL.

Properties of Chromospheric Evaporation and Plasma Dynamics of a Solar Flare from Iris

Viacheslav M. **Sadykov**1,2,3,4, Santiago Vargas Dominguez1,5, Alexander G. Kosovichev1,2, Ivan N. Sharykin3, Alexei B. Struminsky3,4, and Ivan Zimovets

2015 ApJ 805 167

The dynamics of hot chromospheric plasma of solar flares is a key to understanding the mechanisms of flare energy release and particle acceleration. A moderate M1.0 class flare of **2014 June 12**, (SOL2014-06-12T21:12) was simultaneously observed by NASA's Interface Region Imaging Spectrograph (IRIS) and other spacecraft, and also by the New Solar Telescope at the BBSO. This paper presents the first part of our investigation focused on analysis of the IRIS data. Our analysis of the IRIS data in different spectral lines reveals a strong redshifted jet-like flow with a speed of ~100 km s−1 of the chromospheric material before the flare. Strong nonthermal emission of the C ii k 1334.5 Å line, formed in the chromosphere–corona transition region, is observed at the beginning of the impulsive phase in several small (with a size of ~1") points. It is also found that the C ii k line is redshifted across the flaring region before, during, and after the impulsive phase. A peak of integrated emission of the hot (1.1 ▪ 107 K) plasma in the Fe xxi 1354.1 Å line is detected approximately five minutes after the integrated emission peak of the lower temperature C ii k. A strong blueshift of the Fe xxi line across the flaring region corresponds to evaporation flows of the hot chromospheric plasma with a speed of 50 km s−1. Additional analysis of the RHESSI data supports the idea that the upper chromospheric dynamics observed byIRIS has features of "gentle" evaporation driven by heating of the solar chromosphere by accelerated electrons and by a heat flux from the flare energy release site.

Analysis of IRIS and NST observations of the 12.06.2014 flare event

Viacheslav M. **Sadykov**, Santiago Vargas Dominguez, Alexander G. Kosovichev, Ivan N. Sharykin

2014

http://arxiv.org/pdf/1412.0172v1.pdf

We present results of analysis of a M1.0 class flare event of **12 June, 2014** (SOL2014-06-12T21:12), observed with the NASA's Interface Region Imaging Spectrograph (IRIS) mission and New Solar Telescope (NST) at Big Bear Solar Observatory (BBSO). The IRIS observed this event in the coarse raster mode and obtained high-resolution UV spectra and Slit-Jaw (SJ) images for almost the whole flaring region. Our analysis of the IRIS data in different spectral lines reveals strong redshifted fluxes of the chromospheric material before the flare. It is also found that most of the chromospheric and transition region lines are redshifted across the flaring region during the flare. Expansion of a photospheric flux-rope structure is observed in the high-resolution images from the NST with the Broadband Filter Imager (BFI) using the TiO filter. Emission of the hot (20 MK) coronal Fe XXI line is detected ~400 seconds after the emission peaks of the lower temperature lines in the O I IRIS spectral window. We found that the Fe XXI line is blueshifted across the flaring region. This corresponds to evaporation flow with a speed of 50 km/s of the chromospheric plasma heated to the high temperature, as predicted by hydrodynamic flare models.

From Chromospheric Evaporation to Coronal Rain: An Investigation of the Mass and Energy Cycle of a Flare

Seray **Sahin**, Patrick Antolin

ApJ **970** 106 **2024**

https://arxiv.org/pdf/2406.02280

https://iopscience.iop.org/article/10.3847/1538-4357/ad4ed9/pdf

Chromospheric evaporation (CE) and coronal rain (CR) represent two crucial phenomena encompassing the circulation of mass and energy during solar flares. While CE marks the start of the hot inflow into the flaring loop, CR marks the end, indicating the outflow in the form of cool and dense condensations. With \textit{IRIS} and \textit{AIA/SDO}, we examine and compare the evolution, dynamics, morphology, and energetics of the CR and CE during a C2.1 flare. The CE is directly observed in imaging and spectra in the \ion{Fe}{XXI} line with \textit{IRIS} and in the \ion{Fe}{XVIII} line of AIA, with upward average total speeds of 138±[35] km~s−1 and a temperature of [9.03±3.28]×106~K. An explosive to gentle CE transition is observed, with an apparent reduction in turbulence. From quiescent to gradual flare phase, the amount and density of CR increases by a factor of ≈4.4 and 6, respectively. The rain's velocity increases by a 1.4, in agreement with gas pressure drag. In contrast, the clump widths variation is negligible. The location and morphology of CE match closely those of the rain showers, with similar CE sub-structure to the rain strands, reflecting fundamental scales of mass and energy transport. We obtain a CR outflow mass three times larger than the CE inflow mass, suggesting the presence of unresolved CE, perhaps at higher temperatures. The CR energy corresponds to half that of the CE. These results suggest an essential role of coronal rain in the mass-energy cycle of a flare. **2014 September 17**

Prevalence of Thermal Nonequilibrium over an Active Region

Seray **Şahin**1 and Patrick Antolin1

2022 ApJL 931 L27

https://iopscience.iop.org/article/10.3847/2041-8213/ac6fe9/pdf

https://arxiv.org/pdf/2205.10794.pdf

Recent observations have shown that besides the characteristic multimillion degree component, the corona also contains a large amount of cool material called coronal rain, whose clumps are 10–100 times cooler and denser than the surroundings and are often organized in larger events, termed showers. Thermal instability (TI) within a coronal loop in a state of thermal nonequilibrium (TNE) is the leading mechanism behind the formation of coronal rain but no investigation on showers exists to date. In this study, we conduct a morphological and thermodynamic multiwavelength study of coronal rain showers observed in an active region (AR) off-limb with IRIS and the Solar Dynamics Observatory, spanning chromospheric to transition region and coronal temperatures. Rain showers were found to be widespread across the AR over the 5.45 hr observing time, with an average length, width, and duration of 27.37 ± 11.95 Mm, 2.14 ± 0.74 Mm, and 35.22 ± 20.35 minutes, respectively. We find a good correspondence between showers and the cooling coronal structures consistent with the TNE–TI scenario, thereby properly identifying coronal loops in the "coronal veil", including the strong expansion at low heights and an almost zero expansion in the corona. This agrees with previous work suggesting that the observed zero expansion in the EUV is due to specific cross-field temperature distribution. We estimate the total number of showers to be 155 ± 40, leading to a TNE volume of 4.56 ± [3.71] × 1028 cm3, i.e., on the same order of the AR volume. This suggests a prevalence of TNE over the AR indicating strongly stratified and high-frequency heating on average. **2017 June 2**

Evolution of magnetic fields and energy release processes during homologous eruptive flares

Suraj **Sahu** (USO/PRL), Bhuwan Joshi (USO/PRL), Avijeet Prasad (University of Oslo), Kyung-Suk Cho (SSD/KASI)

ApJ **943** 70 **2023**

https://arxiv.org/pdf/2212.04150.pdf

https://iopscience.iop.org/article/10.3847/1538-4357/acac2d/pdf

We explore the processes of repetitive build-up and explosive release of magnetic energy together with the formation of magnetic flux ropes that eventually resulted into three homologous eruptive flares of successively increasing intensities (i.e., M2.0, M2.6, and X1.0). The flares originated from NOAA active region 12017 during **2014 March 28-29**. EUV observations and magnetogram measurements together with coronal magnetic field modeling suggest that the flares were triggered by the eruption of flux ropes embedded by a densely packed system of loops within a small part of the active region. In X-rays, the first and second events show similar evolution with single, compact sources, while the third event exhibits multiple emission centroids with a set of strong non-thermal conjugate sources at 50-100 keV during the HXR peak. The photospheric magnetic field over an interval of approximately 44 hr encompassing the three flares undergoes important phases of emergence and cancellation processes together with significant changes near the polarity inversion lines within the flaring region. Our observations point toward the tether-cutting mechanism as the plausible triggering process of the eruptions. Between the second and third event, we observe a prominent phase of flux emergence which temporally correlates with the build-up phase of free magnetic energy in the active region corona. In conclusion, our analysis reveals an efficient coupling between the rapidly evolving photospheric and coronal magnetic fields in the active region that led to a continued phase of the build-up of free energy, resulting into the homologous flares of successively increasing intensities. **Spikes**

HXR emission from an activated flux rope and subsequent evolution of an eruptive long duration solar flare

Suraj **Sahu**, Bhuwan Joshi, Prabir K. Mitra, Astrid M. Veronig, V. Yurchyshyn

ApJ **897** 157 **2020**

https://arxiv.org/pdf/2005.06221.pdf

https://doi.org/10.3847/1538-4357/ab962b

In this paper, we present a comprehensive study of the evolutionary phases of a major M6.6 long duration event (LDE) with special emphasize on its pre-flare phase. The event occurred in NOAA 12371 on **2015 June 22**. A remarkable aspect of the event was an active pre-flare phase lasting for about an hour during which a hot EUV coronal channel was in build-up stage and displayed co-spatial hard X-ray (HXR) emission up to energies of 25 keV. As such, this is the first evidence of HXR coronal channel. The coronal magnetic field configuration based on NLFFF modeling clearly exhibited a magnetic flux rope (MFR) oriented along the polarity inversion line (PIL) and co-spatial with the coronal channel. We observed significant changes in the AR's photospheric magnetic field during an extended period of ≈42 hours in the form of rotation of sunspots, moving magnetic features, and flux cancellation along the PIL. Prior to the flare onset, the MFR underwent a slow rise phase (≈14 km s−1) for ≈12 min which we attribute to the faster build-up and activation of the MFR by tether-cutting reconnection occurring at multiple locations along the MFR itself. The sudden transition in the kinematic evolution of the MFR from the phase of slow to fast rise (≈109 km s−1 with

acceleration ≈110 m s−2) precisely divides the pre-flare and impulsive phase of the flare, which points toward the feedback process between the early dynamics of the eruption and the strength of the flare magnetic reconnection.

Grid-based imaging of X-rays and gamma-rays with high angular resolution

Pascal **Saint-Hilaire** ∗ , Albert Y. Shih, Gordon J. Hurford, Brian Dennis
In the 'Handbook of X-ray and Gamma-Ray Astrophysics' **2022**
http://sprg.ssl.berkeley.edu/~shilaire/papers/Grid_imaging_in_X_rays_and_gamma_ray.pdf
This chapter contains an overview of the basic principles of X-ray and gamma-ray imaging for astronomy that achieve high angular resolution with nonfocusing optics. Specific topics include systems with single-grid masks, with pairs of grids known as bi-grid collimators, and with more than two grids known as multigrid collimators. A discussion of each type is given along with advantages and limitations of the various design options and descriptions of actual implementations. **1980 April 30, January 20, 2005, 7-9 May 2021**

X-RAY EMISSION FROM THE BASE OF A CURRENT SHEET IN THE WAKE OF A CORONAL MASS EJECTION

P. **Saint-Hilaire**, S. Krucker, and R.P. Lin
E-print, May **2009, File**; ApJ, 699:245–253, **2009, File**
Following a coronal mass ejection (CME) which started on **2002 November 26**, RHESSI observed for 12 hr an X-ray source above the solar limb, at altitudes between 0.1 and 0.3 R_S above the photosphere. The Geostationary Operational Environmental Satellite baseline was remarkably high throughout this event. The X-ray source?s temperature peaked around 10?11 MK, and its emission measure increased throughout this time interval. Higher up, at 0.7 R_S, hot (initially >8 MK) plasma has been observed by Ultraviolet Coronograph Spectrometer on Solar and Heliospheric Observatory for 2.3 days. This hot plasma was interpreted as the signature of a current sheet (CS) trailing the CME. The thermal energy content of the X-ray source is more than an order of magnitude larger than in the CS. Hence, it could be the source of the hot plasma in the CS, although CS heating by magnetic reconnection within it cannot be discounted. To better characterize the X-ray spectrum, we have used novel techniques (back-projection-based and visibility-based) for long integration (several hours) imaging spectroscopy. There is no observed non-thermal hard X-ray bremsstrahlung emission, leading to the conclusion that there is either very little particle acceleration occurring in the vicinity of this post-flare X-ray source, or that either the photon spectral index would have had to be uncharacteristically (in flare parlance) high (γ >= 8) and/or the low-energy cutoff very low (Ec <= 6 keV).

THE X-RAY DETECTABILITY OF ELECTRON BEAMS ESCAPING FROM THE SUN

Pascal **Saint-Hilaire**, S¨am Krucker, Steven Christe, and Robert P. Lin
Astrophysical Journal, 696:941–952, **2009** May
http://www.iop.org/EJ/toc/-alert=43190/0004-637X/696/1
We study the detectability and characterization of electron beams as they leave their acceleration site in the low corona toward interplanetary space through their nonthermal X-ray bremsstrahlung emission. We demonstrate that the largest interplanetary electron beams (_10^{35} electrons above 10 keV) can be detected in X-rays with current and future instrumentation, such as *RHESSI* or the X-Ray Telescope (XRT) onboard *Hinode*.We make a list of optimal observing conditions and beam characteristics. Amongst others, good imaging (as opposed to mere localization or detection in spatially integrated data) is required for proper characterization, putting the requirement on the number of escaping electrons (above 10 keV) to _3 Ч 10^{36} for *RHESSI*, _3 Ч 10^{35} for *Hinode*/XRT, and _10^{33} electrons for the *FOXSI* sounding rocket scheduled to fly in 2011. Moreover, we have found that simple modeling hints at the possibility that coronal soft X-ray jets could be the result of local heating by propagating electron beams.

A Trigger Mechanism of Magnetic Reconnection and Particle Acceleration during Thinning of the Current Sheet

S. **Saito** and J. I. Sakai
Page 793 [http://www.journals.uchicago.edu/cgi-bin/resolve?ApJ64916]
The generated magnetic islands successively coalesce and the magnetic energy is converted into plasma kinetic energy. Through the coalescence, high-energy electrons are quasi-periodically produced. (Type III groups ?)

Continuous Plasma Outflows from the Edge of a Solar Active Region as a Possible Source of Solar Wind.

Sakao, T., Kano, R., Narukage, N., Kotoku, J., Bando, T., DeLuca, E.E.,

Lundquist, L.L., Tsuneta, S., Harra, L.K., Katsukawa, Y., Kubo, M., Hara, H., Matsuzaki, K., Shimojo, M., Bookbinder, J.A., Golub, L., Korreck, K.E., Su, Y., Shibasaki, K., Shimizu, T., Nakatani, I., **2007**. Science 318, 1585–1588.

Probability Distribution Functions of Solar and Stellar Flares

Takashi **Sakurai**
Physics, vol. 5, issue 1, pp. 11-23 **2022**
https://arxiv.org/ftp/arxiv/papers/2212/2212.02678.pdf
https://www.mdpi.com/2624-8174/5/1/2
We studied the soft X-ray data of solar flares and found that the distribution functions of flare fluence are successfully modeled by tapered power law or gamma function distributions whose power exponent is slightly smaller than 2, indicating that the total energy of the flare populations is mostly contributed from a small number of large flares. The largest possible solar flares in 1000 years are predicted to be around X70 in terms of the GOES flare class. We also studied superflares (more energetic than solar flares) from solar-type stars, and found that their power exponent in the fitting of the gamma function distribution is around 1.05, much flatter than solar flares. The distribution function of stellar flare energy extrapolated downward does not connect to the distribution function of solar flare energy.

Hard X-Ray Spectral Evolution and Production of Solar Energetic Particle Events during the January 2005 X-Class Flares

R. **Saldanha**, Sam Krucker, and R. P. Lin
The Astrophysical Journal, Vol. 673, No. 2: 1169-1173, **2008**; **File**
http://www.journals.uchicago.edu/doi/pdf/10.1086/524929
High-resolution hard X-ray observations provided by the Reuven Ramaty High Energy Solar Spectroscopic Imager (RHESSI) are used to study the spectral evolution of _50Y200 keV nonthermal electron bremsstrahlung emissions of five X-class flares observed during the January 2005 solar storm events. Four of these flares show progressive spectral hardening during at least some hard X-ray peaks, while only one event shows the otherwise more commonly observed soft-hard-soft behavior. Imaging observations reveal that_50Y100 keV nonthermal electron bremsstrahlung emissions originate from footpoints of flare loops at all times, including during times of progressive spectral hardening, indicating that the spectral hardening component is produced by precipitating electrons, and not by electrons trapped in the corona. The four flares with progressive spectral hardening are all related to solar energetic particle (SEP) events, while the only X-class flare with soft-hard-soft behavior is not. This finding is consistent with earlier studies, suggesting that electron acceleration and transport in flares is somehow linked to the production of SEPs escaping into interplanetary space.

Plasma Heating Induced by Tadpole-Like Downflows in the Flaring Solar Corona

Tanmoy **Samanta**, Hui Tian, Bin Chen, Katharine K. Reeves, Mark C. M. Cheung, Angelos Vourlidas, Dipankar Banerjee
The Innovation 2(1), 100083 (**2021**)
https://arxiv.org/ftp/arxiv/papers/2103/2103.14257.pdf
https://doi.org/10.1016/j.xinn.2021.100083
As one of the most spectacular energy release events in the solar system, solar flares are generally powered by magnetic reconnection in the solar corona. As a result of the re-arrangement of magnetic field topology after the reconnection process, a series of new loop-like magnetic structures are often formed and are known as flare loops. A hot diffuse region, consisting of around 5-10 MK plasma, is also observed above the loops and is called a supra-arcade fan. Often, dark, tadpole-like structures are seen to descend through the bright supra-arcade fans. It remains unclear what role these so-called supra-arcade downflows (SADs) play in heating the flaring coronal plasma. Here we show a unique flare observation, where many SADs collide with the flare loops and strongly heat the loops to a temperature of 10-20 MK. Several of these interactions generate clear signatures of quasi-periodic enhancement in the full-Sun-integrated soft X-ray emission, providing an alternative interpretation for quasi-periodic pulsations that are commonly observed during solar and stellar flares**. 2013 April 11**

Probabilistic solar flare forecasting using historical magnetogram data

Kiera van der **Sande**, Andrés Muñoz-Jaramillo, Subhamoy Chatterjee
ApJ **2023**
https://arxiv.org/pdf/2308.15410.pdf
Solar flare forecasting research using machine learning (ML) has focused on high resolution magnetogram data from the SDO/HMI era covering Solar Cycle 24 and the start of Solar Cycle 25, with some efforts looking back to SOHO/MDI for data from Solar Cycle 23. In this paper, we consider over 4 solar cycles of daily historical magnetogram data from multiple instruments. This is the first attempt to take advantage of this historical data for ML-

based flare forecasting. We apply a convolutional neural network (CNN) to extract features from full-disk magnetograms together with a logistic regression model to incorporate scalar features based on magnetograms and flaring history. We use an ensemble approach to generate calibrated probabilistic forecasts of M-class or larger flares in the next 24 hours. Overall, we find that including historical data improves forecasting skill and reliability. We show that single frame magnetograms do not contain significantly more relevant information than can be summarized in a small number of scalar features, and that flaring history has greater predictive power than our CNN-extracted features. This indicates the importance of including temporal information in flare forecasting models.

Machine learning correlation of SDO/AIA EUV images to GOES/XRS X-ray flare magnitudes

Kiera van der **Sande**, Natasha Flyer, Thomas Berger, and Riana Gagnon
Front. Astron. Space Sci. 9:1031211. **2022**
https://www.frontiersin.org/articles/10.3389/fspas.2022.1031211/pdf
https://doi.org/10.3389/fspas.2022.1031211
Supervised Machine Learning (ML) models for solar flare prediction rely on accurate labels for a given input data set, commonly obtained from the GOES/XRS X-ray flare catalog. With increasing interest in utilizing ultraviolet (UV) and extreme ultraviolet (EUV) image data as input to these models, we seek to understand if flaring activity can be defined and quantified using EUV data alone. This would allow us to move away from the GOES single pixel measurement definition of flares and use the same data we use for flare prediction for label creation. In this work, we present a Solar Dynamics Observatory (SDO) Atmospheric Imaging Assembly (AIA)-based flare catalog covering flare of GOES X-ray magnitudes C, M and X from 2010 to 2017. We use active region (AR) cutouts of full disk AIA images to match the corresponding SDO/Helioseismic and Magnetic Imager (HMI) SHARPS (Space weather HMI Active Region Patches) that have been extensively used in ML flare prediction studies, thus allowing for labeling of AR number as well as flare magnitude and timing. Flare start, peak, and end times are defined using a peak-finding algorithm on AIA time series data obtained by summing the intensity across the AIA cutouts. An extremely randomized trees (ERT) regression model is used to map SDO/AIA flare magnitudes to GOES X-ray magnitude, achieving a low-variance regression. We find an accurate overlap on 85% of M/X flares between our resulting AIA catalog and the GOES flare catalog. However, we also discover a number of large flares unrecorded or mislabeled in the GOES catalog**. 2010/10/16, 2012/07/12,, 2014/01/01, 2015/01/04.**

Comparison of STEREO/EUVI Loops with Potential Magnetic Field Models

A. W. **Sandman**, M. J. Aschwanden[2], M. L. DeRosa[2], J. P. Wülser[2] and D. Alexander
E-print, June 2009**;** Solar Phys. (**2009**) 259: 1–11
The *Solar Terrestrial Relations Observatory* (STEREO) provides the first opportunity to triangulate the three-dimensional coordinates of active region loops simultaneously from two different vantage points in space. Three-dimensional coordinates of the coronal magnetic field have been calculated with theoretical magnetic field models for decades, but it is only with the recent availability of STEREO data that a rigorous, quantitative comparison between observed loop geometries and theoretical magnetic field models can be performed. Such a comparison provides a valuable opportunity to assess the validity of theoretical magnetic field models. Here we measure the misalignment angles between model magnetic fields and observed coronal loops in three active regions, as observed with the Extreme Ultraviolet Imager (EUVI) on STEREO on 30 April, 9 May, and 19 May 2007. We perform stereoscopic triangulation of some 100 – 200 EUVI loops in each active region and compute extrapolated magnetic field lines using magnetogram information from the Michelson Doppler Imager (MDI) on the *Solar and Heliospheric Observatory* (SOHO). We examine two different magnetic extrapolation methods: (1) a potential field and (2) a radially stretched potential field that conserves the magnetic divergence. *We find considerable disagreement between each theoretical model and the observed loop geometries, with an average misalignment angle on the order of 20° – 40°. We conclude that there is a need for either more suitable (coronal rather than photospheric) magnetic field measurements or more realistic field extrapolation models.*

Trigger Mechanism of Solar Subflares in a Braided Coronal Magnetic Structure

Sanjiv K. Tiwari, Caroline E. Alexander, Amy R. Winebarger, Ronald L. Moore
ApJL, **2014**
http://arxiv.org/pdf/1410.4260v1.pdf
Fine-scale braiding of coronal magnetic loops by continuous footpoint motions may power coronal heating via nanoflares, which are spontaneous fine-scale bursts of internal reconnection. An initial nanoflare may trigger an avalanche of reconnection of the braids, making a microflare or larger subflare. In contrast to this internal triggering of subflares, we observe external triggering of subflares in a braided coronal magnetic field observed by the {\it High-resolution Coronal Imager (Hi-C)}. We track the development of these subflares using 12 s cadence images acquired by {\it SDO}/AIA in 1600, 193, 94 \AA, and registered magnetograms of {\it SDO}/HMI, over four hours centered on the {\it Hi-C} observing time. These data show numerous recurring small-scale brightenings in transition-region emission happening on polarity inversion lines where flux cancellation is occurring. We present in detail an example of an apparent burst of reconnection of two loops in the transition region under the braided coronal field, appropriate for

releasing a short reconnected loop downward and a longer reconnected loop upward. The short loop presumably submerges into the photosphere, participating in observed flux cancellation. A subflare in the overlying braided magnetic field is apparently triggered by the disturbance of the braided field by the reconnection-released upward loop. At least 10 subflares observed in this braided structure appear to be triggered this way. How common this external trigger mechanism for coronal subflares is in other active regions, and how important it is for coronal heating in general, remain to be seen. **11 July 2012,**

Reorganization of Photospheric Magnetic Fields in Active Regions During Energetic Flares

J. C. **Santos** , C. M. Wrasse

Solar Phys. Volume 291, Issue 4, pp 1107-1114 **2016**

The reorganization of the photospheric magnetic field may be important for flaring activity. In this work we use the time evolution of the magnetic power spectra to identify for which length scales the reorganization of the active region magnetic field is most closely related to energetic flares. Our results show that the reorganization occurs mainly for length scales larger than 12.6 Mm and may start much before the time of the flare, but the time evolution of magnetic power spectra does not show regular patterns. An analysis of the dissipation spectra suggests that the dissipation takes place at all spatial scales, including small wavenumbers in which more energy is available.

3D MHD simulations of electric current development in a rotating sunspot: active region NOAA 8210

J. C. **Santos**1,2, J. Büchner1 and A. Otto

A&A 535, A111 (**2011**)

Context. Active region (AR) 8210 was the host of many flares and coronal mass ejections (CMEs). Studies of its temporal evolution indicated that the clockwise rotation of a negative magnetic polarity, together with the motion of a positive polarity located close to it are a major source of magnetic energy to the corona above.

Aims. Search for the mechanisms of energy storage and release above AR8210. For this sake we locate the current system generated by the photospheric plasma motion suggested as source of coronal energy supply above AR8210 and compare it with the location of identified flaring regions.

Methods. We simulated the reaction of the corona using a three-dimensional (3D) MagnetoHydroDynamic (MHD) model. The initial coronal magnetic field is extrapolated out of the observed line-of-sight (LOS) component of the photospheric magnetic field. The corresponding photospheric plasma motion is imposed close to the bottom boundary of the simulation box. Current dependent resistivity and compressibility of the plasma are considered in the model.

Results. The horizontal plasma motion causes a current system that spatially coincides with the flaring region associated to AR8210. Particularly, the rotation of the plasma over the main negative polarity gives rise to strong currents localized over the main negative polarity, i.e. close to the position of a flare site. Above this region a strong magnetic field divergence is indicated by large differential flux tube volumes. Intense currents also form along the eastern border of a positive polarity region, over a polarity inversion line (PIL), in a site where a flare appears later. The southward motion of a positive flux concentration generates a current system extending mainly along the eastern border of it, over a polarity inversion line. Magnetic energy is deposited mainly over the main negative polarity, where the major flare activity is observed at later times.

Conclusions. The two patterns of photospheric plasma motion suggested as being responsible for the flaring activity of AR8210 generate current systems spatially coincident with the flaring area associated to this active region. These currents generate magnetic fields that contribute to the increase in magnetic energy inside the simulation volume. The transport of magnetic flux by the photospheric plasma motion also contributes to the redistribution of magnetic energy. The increase in magnetic energy occurs mainly over the main negative polarity and close to where a strong current system is formed. We conclude that in the case of AR8210 the rotation of the negative polarity region is the main contributor to its flare activity. The southward motion of a positive magnetic flux concentration plays an important role in the formation of current systems at its eastern border.

On the relation between DC current locations and an EUV bright point: A case study

J. C. **Santos**[1, 2], J. Büchner[1], M. S. Madjarska[1], and M. V. Alves

A&A 490, 345-352 (**2008**), DOI: 10.1051/0004-6361:200809975

Context. Motion of the photospheric plasma forces the footpoints of magnetic flux tubes to move. This can give rise to electric currents in the solar atmosphere. The dissipation of these electric currents and the consequent heating of the solar plasma may be responsible for the formation of Extreme-UltraViolet (EUV) and X-ray bright points. Earlier bright point models usually consider either the emergence or the canceling of photospheric magnetic features as being responsible for reconnection causing the bright point.

Aims. We investigate the consequences of different patterns of horizontal photospheric plasma motion for the generation of electric currents in the solar atmosphere and locate them with respect to an observed EUV bright point. The goal is to find out whether these currents might be responsible for the heating of bright points.

Results. A comparison with data obtained by TRACE in the 1550 Å channel and by the EIT in the 195 Å channel shows that the region where the strongest current concentrations are formed coincides with the region where the EUV bright point appears.

Efficiency of solar microflares in accelerating electrons when rooted in a sunspot⋆

Jonas **Saqri**1, Astrid M. Veronig1,2, Andrea Francesco Battaglia3,4, Ewan C. M. Dickson1, Dale E. Gary5 and Säm Krucker3,6

A&A 683, A41 (**2024**)

https://arxiv.org/pdf/2312.06856.pdf

https://www.aanda.org/articles/aa/pdf/2024/03/aa48295-23.pdf

https://doi.org/10.1051/0004-6361/202348295

Context. The spectral shape of the X-ray emission in solar flares varies with the event size, with small flares generally exhibiting softer spectra than large events, indicative of a relatively lower number of accelerated electrons at higher energies.

Aims. We investigate two microflares of GOES classes A9 and C1 (after background subtraction) observed by STIX onboard Solar Orbiter with exceptionally strong nonthermal emission. We complement the hard X-ray imaging and spectral analysis by STIX with co-temporal observations in the (E)UV and visual range by AIA and HMI to investigate what makes these microflares so efficient in high-energy particle acceleration.

Methods. We made a preselection of events in the STIX flare catalog based on the ratio of the thermal to nonthermal quicklook X-ray emission. The STIX spectrogram science data were used to perform spectral fitting to identify the non-thermal and thermal components. The STIX X-ray images were reconstructed to analyze the spatial distribution of the precipitating electrons and the hard X-ray emission they produce. The EUV images from SDO/AIA and SDO/HMI LOS magnetograms were analyzed to better understand the magnetic environment and the chromospheric and coronal response. For the A9 event, EOVSA microwave observations were available, allowing for image reconstruction in the radio domain.

Results. We performed case studies of two microflares observed by STIX on **October 11, 2021 and November 10, 2022**, which showed unusually hard microflare X-ray spectra with power-law indices of the electron flux distributions of $\delta = (2.98 \pm 0.25)$ and $\delta = (4.08 \pm 0.23)$, during their non-thermal peaks and photon energies up to 76 keV and 50 keV, respectively. For both events under study, we found that one footpoint is located within a sunspot covering areas with mean magnetic flux densities in excess of 1500 G, suggesting that the hard electron spectra are caused by the strong magnetic fields the flare loops are rooted in. Additionally, we revisited a previously published unusually hard RHESSI microflare and found that in this event, there was also one flare kernel located within a sunspot, which corroborates the result from the two hard STIX microflares under study in this work.

Conclusions. The characteristics of the strong photospheric magnetic fields inside the sunspot umbrae and penumbrae where flare loops are rooted play an important role in the generation of exceptionally hard X-ray spectra in these microflares. **November 17, 2006**

Multi-point study of the energy release and impulsive CME dynamics in an eruptive C7 flare

J. **Saqri**, A. M. Veronig, E. C. M. Dickson, T. Podladchikova, A. Warmuth, H. Xiao, D. E. Gary, A. F. Battaglia, S. Krucker

A&A **2023**

https://arxiv.org/pdf/2302.11232.pdf

Context. The energy release in eruptive flares and the kinematics of the associated coronal mass ejections (CMEs) are interlinked and require favorable observing positions as both on–disk and off–limb signatures are necessary to characterize these events. Aims. We combine observations from different vantage points to perform a detailed study of a long duration eruptive C7 class flare that occurred on **17 April 2021** and was partially occulted from Earth view. The dynamics and thermal properties of the flare-related plasma flows, the flaring arcade, and the energy releases and particle acceleration are studied together with the kinematic evolution of the associated CME in order to place this long duration event in context of previous eruptive flare studies. Methods. We use data from the Spectrometer-Telescope for Imaging X-rays (STIX) onboard the Solar Orbiter to analyze the spectral characteristics, timing, and spatial distribution of the flare X-ray emission. Data from the Extreme Ultraviolet Imager (EUVI) onboard the Solar TErrestrial RElations Observatory-Ahead (STEREO-A) spacecraft are used for context images as well as to track the ejected plasma close to the Sun. With Atmospheric Imaging Assembly extreme ultraviolet (EUV) images from the Solar Dynamics Observatory, the flare is observed off–limb and differential emission measure maps are reconstructed. The coronagraphs onboard STEREO-A are used to track the CME out to around 8 R.

Results. The flare showed hard X-ray (HXR) bursts over the duration of an hour in two phases lasting from 16:04 UT to 17:05 UT. During the first phase, a strong increase in emission from hot plasma and impulsive acceleration of the CME was observed. The CME acceleration profile shows a three-part evolution of slow rise, acceleration, and propagation in line with the first STIX HXR burst phase, which is triggered by a rising hot (14 MK) plasmoid. During the CME acceleration phase, we find signatures of ongoing magnetic reconnection behind the erupting structure, in agreement with the standard eruptive flare scenario. The subsequent HXR bursts that occur about 30 minutes after the primary

CME acceleration show a spectral hardening (from $\delta \approx 7$ to $\delta \approx 4$) but do not correspond to further CME acceleration and chromospheric evaporation. Therefore, the CME-flare feedback relationship may only be of significance within the first 25 minutes of the event under study, as thereafter the flare and the CME eruption evolve independently of each other.

Multi-instrument STIX microflare study

J. **Saqri**, A.M. Veronig, A. Warmuth, E.C.M. Dickson, A.F. Battaglia, T. Podladchikova, H. Xiao, M. Battaglia, G.J. Hurford, S. Krucker
A&A 659, A52 **2022**
https://arxiv.org/pdf/2201.00712.pdf
https://doi.org/10.1051/0004-6361/202142373
https://www.aanda.org/articles/aa/pdf/2022/03/aa42373-21.pdf

Context. During its commissioning phase in 2020, the Spectrometer/Telescope for Imaging X-rays (STIX) on board the Solar Orbiter spacecraft observed 69 microflares. The two largest events from this set (of GOES class B2 and B6), both of which were observed on-disk from the spacecraft as well as from Earth, are analysed in terms of the spatial, temporal and spectral characteristics. Aims. We complement observations from the STIX instrument with EUV imagery from SDO/AIA and GOES soft X-ray data to add imaging and plasma diagnostics over different temperature ranges for a detailed microflare case study in terms of energy release and transport.
Methods. We use data from GOES for SXR plasma diagnostics and SDO/AIA for high cadence EUV imaging and the reconstruction of differential emission measure (DEM) maps of the thermal flare plasma. The reconstructed DEM profiles are used to study the temporal evolution of thermal flare plasma in the kernels and loops independently. We derive the time evolution of the flare plasma parameters (EM, T) and thermal energy from STIX, GOES and AIA observations, and study STIX spectra to determine the nonthermal emission from accelerated electrons.
Results. Spectral fitting of the STIX data shows clear nonthermal emission for both microflares under study. For both events the plasma temperature and EM derived from STIX, GOES as well as the reconstructed DEM maps differ in absolute values and timing with AIA (sensitive to lower plasma temperatures) lagging behind. The deduced plasma parameters from either method roughly agree with values in the literature for microflares as do the nonthermal fit parameters from STIX. This finding is corroborated by the Neupert effect exhibited between the time derivative of the GOES SXR emission and the STIX HXR profiles. For the B6 event where such an analysis was possible, the nonthermal energy deduced from STIX roughly coincides with the lower estimates of the thermal energy requirement deduced from the SXR and EUV emissions.
Conclusions. The observed Neupert effects and impulsive/ gradual phases indicate that both events under study are consistent with the standard chromospheric evaporation flare scenario. For the B6 event on **June 7th, 2020**, this interpretation is further supported by the temporal evolution seen in the DEM profiles of the flare ribbons and loops. For this event we further find that accelerated electrons can roughly account for the required thermal energy. The **June 6th, 2020** event demonstrates that STIX can detect nonthermal emission for GOES class B2 events albeit smaller than the background rate level. We demonstrate for the first time how detailed multi-instrument studies of solar flares can be performed with STIX.

Lorentz Force Evolution Reveals the Energy Buildup Processes during Recurrent Eruptive Solar Flares

Ranadeep **Sarkar**, Nandita Srivastava, Astrid M. Veronig
ApJL **885** L17 **2019**
https://arxiv.org/pdf/1910.13264.pdf
sci-hub.se/10.3847/2041-8213/ab4da2

The energy release and build-up processes in the solar corona have significant implications in particular for the case of large recurrent flares, which pose challenging questions about the conditions that lead to the episodic energy release processes. It is not yet clear whether these events occur due to the continuous supply of free magnetic energy to the solar corona or because not all of the available free magnetic energy is released during a single major flaring event. In order to address this question, we report on the evolution of photospheric magnetic field and the associated net Lorentz force changes in ARs 11261 and 11283, each of which gave rise to recurrent eruptive M- and X-class flares. Our study reveals that after the abrupt downward changes during each flare, the net Lorentz force increases by (2-5)x10^22 dyne in between the successive flares. This distinct rebuild-up of net Lorentz forces is the first observational evidence found in the evolution of any non-potential parameter of solar active regions (ARs), which suggests that new energy was supplied to the ARs in order to produce the recurrent large flares. The rebuild-up of magnetic free energy of the ARs is further confirmed by the observations of continuous shearing motion of moving magnetic features of opposite polarities near the polarity inversion line. The evolutionary pattern of the net Lorentz force changes reported in this study has significant implications, in particular, for the forecasting of recurrent large eruptive flares from the same AR and hence the chances of interaction between the associated CMEs. **2011/08/03-04, 2011/09/06-07**
RHESSI Science Nuggets # 364 Dec **2019**

http://sprg.ssl.berkeley.edu/~tohban/wiki/index.php/Lorentz_Force_Evolution_Reveals_the_Energy_Build-up_Processes_during_Recurrent_Eruptive_Solar_Flares

A Comparative Study of the Eruptive and Non-Eruptive Flares Produced by the Largest Active Region of Solar Cycle 24

Ranadeep **Sarkar**, Nandita Srivastava
Solar Phys. 293:16 **2018**
https://arxiv.org/pdf/1801.00473.pdf
https://link.springer.com/content/pdf/10.1007%2Fs11207-017-1235-8.pdf
We investigate the morphological and magnetic characteristics of solar active region (AR) NOAA 12192. AR 12192 was the largest region of Solar Cycle 24; it underwent noticeable growth and produced 6 X-class flares, 22 M-class flares, and 53 C-class flares in the course of its disc passage. However, the most peculiar fact of this AR is that it was associated with only one CME in spite of producing several X-class flares. In this work, we carry out a comparative study between the eruptive and non-eruptive flares produced by AR 12192. We find that the magnitude of abrupt and permanent changes in the horizontal magnetic field and Lorentz force are significantly smaller in the case of the confined flares compared to the eruptive one. We present the areal evolution of AR 12192 during its disc passage. We find the flare-related morphological changes to be weaker during the confined flares, whereas the eruptive flare exhibits a rapid and permanent disappearance of penumbral area away from the magnetic neutral line after the flare. Furthermore, from the extrapolated nonlinear force-free magnetic field, we examine the overlying coronal magnetic environment over the eruptive and non-eruptive zones of the AR. We find that the critical decay index for the onset of torus instability was achieved at a lower height over the eruptive flaring region, than for the non-eruptive core area. These results suggest that the decay rate of the gradient of overlying magnetic field strength may play a decisive role to determine the CME productivity of the AR. In addition, the magnitude of changes in the flare-related magnetic characteristics are found to be well correlated with the nature of solar eruptions. **2014.10.22-25**

Simulating coronal loop implosion and compressible wave modes in a flare hit active region

Aveek **Sarkar**, Bhargav Vaidya, Soumitra Hazra, Jishnu Bhattacharyya
ApJ **851** 120 **2017**
https://arxiv.org/pdf/1711.05273.pdf
There is considerable observational evidence of implosion of magnetic loop systems inside solar coronal active regions following high energy events like solar flares. In this work, we propose that such collapse can be modeled in three dimensions quite accurately within the framework of ideal magnetohydrodynamics. We furthermore argue that the dynamics of loop implosion is only sensitive to the transmitted disturbance of one or more of the system variables, e.g. velocity generated at the event site. This indicates that to understand loop implosion, it is sensible to leave the event site out of the simulated active region. Towards our goal, a velocity pulse is introduced to model the transmitted disturbance generated at the event site. Magnetic field lines inside our simulated active region are traced in real time, and it is demonstrated that the subsequent dynamics of the simulated loops closely resemble observed imploding loops. Our work highlights the role of plasma β in regards to the rigidity of the loop systems and how that might affect the imploding loops' dynamics. Compressible magnetohydrodynamic modes such as kink and sausage are also shown to be generated during such processes, in accordance with observations.

Statistical techniques for the detection and analysis of solar explosive events⋆

L. M. **Sarro**1 and A. Berihuete
A&A 528, A62 (**2011**)
Context. Solar explosive events are commonly explained as small-scale magnetic reconnection events, although an unambiguous confirmation of this scenario remains elusive owing to the lack of spatial resolution and the statistical analysis of sufficiently large samples of this type of events.
Aims. We propose a sound statistical treatment of data cubes consisting of a temporal sequence of long-slit spectra of the solar atmosphere. The analysis comprises all stages from the explosive event detection to its characterization and the subsequent sample study.
Methods. We designed two complementary approaches based on the combination of standard statistical techniques (the robust principal component analysis in one approach and wavelet decomposition and independent component analysis in the second) to obtain least biased samples. These techniques are implemented in the spirit of letting the data speak for themselves. The analysis is carried out for two spectral lines: the C iv line at 1548.2 Å and the Ne viii line at 770.4 Å.
Results. We find significant differences between the characteristics of the line profiles emitted in the proximities of two active regions, and in the quiet Sun, most visible in the relative importance of a separate population of red shifted profiles. We also find a higher frequency of explosive events near the active regions, and in the C iv line. The distribution of the explosive events characteristics is interpreted in the light of recent numerical simulations. Finally, we point out several regions of the parameter space where the reconnection model has to be refined in order to explain the observations.

YOHKOH/WBS Recalibration and a Comprehensive Catalogue of Solar Flares Observed by YOHKOH SXT, HXT and WBS Instruments

J. **Sato**, Y. Matsumoto, K. Yoshimura, S. Kubo, J. Kotoku, S. Masuda, M. Sawa, K. Suga, M. Yoshimori, T. Kosugi & T. Watanabe

Solar Physics, Volume 236, Issue 2, pp.351-368, **2006**

https://link.springer.com/content/pdf/10.1007/s11207-006-1831-5.pdf

The flare catalogue of the Yohkoh mission is compiled and linked to this article as an electronic supplement. For showing flare characteristics over wide energy range concisely, we provide the images of Hard X-ray Telescope (HXT) and the Soft X-ray Telescope (SXT), and the spectra of Hard X-ray Spectrometer (HXS) and Gamma-Ray Spectrometer (GRS) with the Wide Band Spectrometer (WBS) time profiles. The energy versus pulse height (PH) data channels in HXS and GRS are re-calibrated by using the data of the whole mission period. Secular gain changes are recognized in HXS, and the characteristics of power-law flare spectra simultaneously observed by HXT and HXS confirms the trend. The GRS gains are different for the flare observations during the previous maximum and for the current maximum. The total of 33 γ -ray events are observed, and for 12 of them γ-ray flare spectra are obtained. **27 Oct 1991, 16 Jul 1992, 6 Nov 1997**

LOW-ALTITUDE RECONNECTION INFLOW-OUTFLOW OBSERVATIONS DURING A 2010 NOVEMBER 3 SOLAR ERUPTION

Sabrina L. **Savage**1, Gordon Holman1, Katharine K. Reeves2, Daniel B. Seaton3, David E. McKenzie4, and Yang Su

2012 ApJ 754 13

For a solar flare occurring on **2010 November 3**, we present observations using several SDO/AIA extreme-ultraviolet (EUV) passbands of an erupting flux rope followed by inflows sweeping into a current sheet region. The inflows are soon followed by outflows appearing to originate from near the termination point of the inflowing motion—an observation in line with standard magnetic reconnection models. We measure average inflow plane-of-sky speeds to range from ~150 to 690 km s–1 with the initial, high-temperature inflows being the fastest. Using the inflow speeds and a range of Alfvén speeds, we estimate the Alfvénic Mach number which appears to decrease with time. We also provide inflow and outflow times with respect to RHESSI count rates and find that the fast, high-temperature inflows occur simultaneously with a peak in the RHESSI thermal light curve. Five candidate inflow-outflow pairs are identified with no more than a minute delay between detections. The inflow speeds of these pairs are measured to be ~102 km s–1 with outflow speeds ranging from ~102 to 103 km s–1—indicating acceleration during the reconnection process. The fastest of these outflows are in the form of apparently traveling density enhancements along the legs of the loops rather than the loop apexes themselves. These flows could possibly either be accelerated plasma, shocks, or waves prompted by reconnection. The measurements presented here show an order of magnitude difference between the retraction speeds of the loops and the speed of the density enhancements within the loops—presumably exiting the reconnection site.

RE-INTERPRETATION OF SUPRA-ARCADE DOWNFLOWS IN SOLAR FLARES

Sabrina L. **Savage**1, David E. McKenzie2 and Katharine K. Reeves

2012 ApJ 747 L40

Following the eruption of a filament from a flaring active region, sunward-flowing voids are often seen above developing post-eruption arcades. First discovered using the soft X-ray telescope aboard Yohkoh, these supra-arcade downflows (SADs) are now an expected observation of extreme ultra-violet and soft X-ray coronal imagers and spectrographs (e.g, TRACE, SOHO/SUMER, Hinode/XRT, SDO/AIA). Observations made prior to the operation of AIA suggested that these plasma voids (which are seen in contrast to bright, high-temperature plasma associated with current sheets) are the cross-sections of evacuated flux tubes retracting from reconnection sites high in the corona. The high temperature imaging afforded by AIA's 131, 94, and 193 Å channels coupled with the fast temporal cadence allows for unprecedented scrutiny of the voids. For a flare occurring on **2011 October 22**, we provide evidence suggesting that SADs, instead of being the cross-sections of relatively large, evacuated flux tubes, are actually wakes (i.e., trailing regions of low density) created by the retraction of much thinner tubes. This re-interpretation is a significant shift in the fundamental understanding of SADs, as the features once thought to be identifiable as the shrinking loops themselves now appear to be "side effects" of the passage of the loops through the supra-arcade plasma. In light of the fact that previous measurements have attributed to the shrinking loops characteristics that may instead belong to their wakes, we discuss the implications of this new interpretation on previous parameter estimations and on reconnection theory.

QUANTITATIVE EXAMINATION OF A LARGE SAMPLE OF SUPRA-ARCADE DOWNFLOWS IN ERUPTIVE SOLAR FLARES

Sabrina L. **Savage**1,2 and David E. McKenzie2

The Astrophysical Journal, 730:98 (16pp), **2011** April
Sunward-flowing voids above post-coronal mass ejection flare arcades were first discovered using the soft X-ray telescope aboard *Yohkoh* and have since been observed with *TRACE* (extreme ultraviolet (EUV)), *SOHO*/LASCO (white light), *SOHO*/SUMER (EUV spectra), and *Hinode*/XRT (soft X-rays). Supra-arcade downflow (SAD) observations suggest that they are the cross-sections of thin flux tubes retracting from a reconnection site high in the corona. Supra-arcade downflowing loops (SADLs) have also been observed under similar circumstances and are theorized to be SADs viewed from a perpendicular angle. Although previous studies have focused on dark flows because they are easier to detect and complementary spectral data analysis reveals their magnetic nature, the signal intensity of the flows actually ranges from dark to bright. This implies that newly reconnected coronal loops can contain a range of hot plasma density. Previous studies have presented detailed SAD observations for a small number of flares. In this paper, we present a **substantial SADs and SADLs flare catalog**. We have applied semiautomatic detection software to several of these events to detect and track individual downflows thereby providing statistically significant samples of parameters such as velocity, acceleration, area, magnetic flux, shrinkage energy, and reconnection rate. We discuss these measurements (particularly the unexpected result of the speeds being an order of magnitude slower than the assumed Alfv´en speed), how they were obtained, and potential impact on reconnection models.

RECONNECTION OUTFLOWS AND CURRENT SHEET OBSERVED WITH *HINODE*/XRT IN THE 2008 APRIL 9 "CARTWHEEL CME" FLARE
Sabrina L. **Savage**1, David E. McKenzie1, Katharine K. Reeves2, Terry G. Forbes3, and Dana W. Longcope1
Astrophysical Journal, 722:329–342, **2010, File**
Supra-arcade downflows (SADs) have been observed with *Yohkoh*/SXT (soft X-rays (SXR)), *TRACE* (extreme ultraviolet (EUV)), *SOHO*/LASCO (white light), *SOHO*/SUMER (EUV spectra), and *Hinode*/XRT (SXR). Characteristics such as low emissivity and trajectories, which slow as they reach the top of the arcade, are consistent with post-reconnection magnetic flux tubes retracting from a reconnection site high in the corona until they reach a lower-energy magnetic configuration. Viewed from a perpendicular angle, SADs should appear as shrinking loops rather than downflowing voids. We present X-ray Telescope (XRT) observations of supra-arcade downflowing loops (SADLs) following a coronal mass ejection (CME) on 2008 April 9 and show that their speeds and decelerations are consistent with those determined for SADs. We also present evidence for a possible current sheet observed during this flare that extends between the flare arcade and the CME. Additionally, we show a correlation between reconnection outflows observed with XRT and outgoing flows observed with LASCO.

The two solar flares diagnostics based on the soft X-ray emission recording
Mikhail I.**Savchenko**, Pavel V.VataginVadim P.LazutkovDmitriy V.Skorodumov, Igor V.KudryavtsevYuriy E.Charikov
St. Petersburg Polytechnical University Journal: Physics and Mathematics
Volume 3, Issue 3, October **2017**, Pages 292-297
https://www.sciencedirect.com/science/article/pii/S240572231730097X
The time history of the temperature and the emission measure of the solar flare plasma have been studied relying upon the experimental data on the soft X-rays recorded by the IRIS spectrometer on **June 29, 2002** (F1) and **March 27, 2003** (F2). F1 was a thermal flare and was not accompanied by hard X-rays. This data analysis revealed that at least two sequential energy-release processes occurred during the F1 event. The F2 event took place behind the limb, so only the top part of the flare loop being the soft X-ray source was recorded by the satellite-based spectrometer. From this data analysis it appeared that fast plasma heating occurred in the initial stage of F2 and then the flare region expanded and the emission measure of flare plasma increased.

The Relation between Solar Eruption Topologies and Observed Flare Features II: Dynamical Evolution
A. **Savcheva**, E. Pariat, S. McKillop, P. McCauley, E. Hanson, Y. Su, & E. DeLuca
2016 ApJ 817 43
http://www.pergamentum.com/eprint/savcheva_etal_ribbonsA_II.pdf
A long established goal of solar physics is to build understanding of solar eruptions and develop flare and CME forecasting models. In this paper, we continue our investigation of non-linear forces free field (NLFFF) models by comparing topological properties of the solutions to the evolution of the flare ribbons. In particular, we show that data constrained NLFFF models of three erupting sigmoid regions (**SOL2010-04-08, SOL2010-08-07, and SOL2012-05-**

12) built to reproduce the active region magnetic field in the pre-flare state can be rendered unstable and the subsequent sequence of unstable solutions produce quasi-separatrix layers (QSLs) that match the flare ribbon evolution as observed by SDO/AIA. We begin with a best-fit equilibrium model for the pre-flare active region; we than add axial flux to the flux rope in the model to move it across the stability boundary; at this point the magnetofrictional code no longer converges to an equilibrium solution, the flux rope rises as the solutions are iterated. We interpret the sequence of magnetofrictional steps as an evolution of the active region as the flare/CME begins. The magnetic field solutions at different steps are compared with the flare ribbons. The results are fully consistent with the 3D extension of the standard flare/CME model. Our ability to capture essential topological features of flaring active regions with a non-dynamic magneto-frictional code strongly suggests that the pre-flare, large scale topological structures are preserved as the flux rope becomes unstable and lifts off.

The Relation between Solar Eruption Topologies and Observed Flare Features I: Flare Ribbons

A. **Savcheva**, E. Pariat, S. McKillop, P. McCauley, E. Hanson, Y. Su, E. Werner, E. E. DeLuca
2015 *ApJ* **810** 96
http://arxiv.org/pdf/1506.03452v1.pdf
In this paper we present a topological magnetic field investigation of seven two-ribbon flares in sigmoidal active regions observed with Hinode, STEREO, and SDO. We first derive the 3D coronal magnetic field structure of all regions using marginally unstable 3D coronal magnetic field models created with the flux rope insertion method. The unstable models have been shown to be a good model of the flaring magnetic field configurations. Regions are selected based on their pre-flare configurations along with the appearance and observational coverage of flare ribbons, and the model is constrained using pre-flare features observed in extreme ultraviolet and X-ray passbands. We perform a topology analysis of the models by computing the squashing factor, Q, in order to determine the locations of prominent quasi-separatrix layers (QSLs). QSLs from these maps are compared to flare ribbons at their full extents. We show that in all cases the straight segments of the two J-shaped ribbons are matched very well by the flux-rope-related QSLs, and the matches to the hooked segments are less consistent but still good for most cases. In addition, we show that these QSLs overlay ridges in the electric current density maps. This study is the largest sample of regions with QSLs derived from 3D coronal magnetic field models, and it shows that the magnetofrictional modeling technique that we employ gives a very good representation of flaring regions, with the power to predict flare ribbon locations in the event of a flare following the time of the model.
SOL2007-02-12T07:30:00L075C297 SOL2007-12-07T04:20:00L085C296 SOL2010-04-08T02:35:00L110C176 SOL2010-08-07T17:55:00L100C002 SOL2012-05-08T09:21:00L108C232 SOL2013-03-15T05:46:00L116C077 SOL2013-04-11T06:55:00L110C071

FIELD TOPOLOGY ANALYSIS OF A LONG-LASTING CORONAL SIGMOID

A. S. **Savcheva**1,2, A. A. van Ballegooijen2 and E. E. DeLuca
2012 ApJ 744 78
We present the first field topology analysis based on nonlinear force-free field (NLFFF) models of a long-lasting coronal sigmoid observed in **2007 February 7-12** with the X-Ray Telescope on Hinode. The NLFFF models are built with the flux rope insertion method and give the three-dimensional coronal magnetic field as constrained by observed coronal loop structures and photospheric magnetograms. Based on these models, we have computed horizontal maps of the current and the squashing factor Q for 25 different heights in the corona for all six days of the evolution of the region. We use the squashing factor to quantify the degree of change of the field line linkage and to identify prominent quasi-separatrix layers (QSLs). We discuss the major properties of these QSL maps and devise a way to pick out important QSLs since our calculation cannot reach high values of Q. The complexity in the QSL maps reflects the high degree of fragmentation of the photospheric field. We find main QSLs and current concentrations that outline the flux rope cavity and that become characteristically S-shaped during the evolution of the sigmoid. We note that, although intermittent bald patches exist along the length of the sigmoid during its whole evolution, the flux rope remains stable for several days. However, shortly after the topology of the field exhibits hyperbolic flux tubes (HFT) on February 7 and February 12 the sigmoid loses equilibrium and produces two B-class flares and associated coronal mass ejections (CMEs). The location of the most elevated part of the HFT in our model coincides with the inferred locations of the two flares. Therefore, we suggest that the presence of an HFT in a coronal magnetic configuration may be an indication that the system is ready to erupt. We offer a scenario in which magnetic reconnection at the HFT drives the system toward the marginally stable state. Once this state is reached, loss of equilibrium occurs via the torus instability, producing a CME.

Non-Linear Force-Free Modeling of a Long-Lasting Coronal Sigmoid

Antonia **Savcheva** and Adrian van Ballegooijen
E-print, Sept **2009**; ApJ, 703(2), 1766-1777, **2009**

A study of the magnetic configuration and evolution of a long-lasting quiescent coronal sigmoid is presented. The sigmoid was observed by {it Hinode}/XRT and TRACE between **2007 Feb 6 and Feb 12** when it finally erupted. We construct non-linear force-free field models for several observations during this period, using the flux rope insertion method. The high spatial and temporal resolution of XRT allows us to finely select best-fit models that match the observations. The modeling shows that a highly sheared field, consisting of a weakly twisted flux rope inbedded in a potential field, very well describes the structure of the X-ray sigmoid. The flux rope reaches a stable equilibrium, but its axial flux is close to the stability limit of about $5 imes 10^{20}$ Mx. The relative magnetic helicity increases with time from Feb 8 until just prior to the eruption on Feb 12. We study the spatial distribution of the torsion parameter $alpha$ in the vicinity of the flux rope, and find that it has a hollow-core distribution, i.e., electric currents are concentrated in a current layer at the boundary between the flux rope and its surroundings. The current layer is located near the Bald Patch Separatrix Surface (BPSS) of the magnetic configuration, and the X-ray emission appears to come from this current layer/BPSS, consistent with the Titov & D'{e}moulin model. We find that the twist angle Phi of the magnetic field increases with time to about $2 pi$ just prior to the eruption, but never reaches the value necessary for the kink instability.

Identification of multiple hard X-ray sources in solar flares: A Bayesian analysis of the February 20 2002 event

Federica **Scacchiano**, Alberto Sorrentino, A Gordon Emslie, Anna Maria Massone, Michele Piana
ApJ **2018**
https://arxiv.org/pdf/1801.09141.pdf
Hard X-ray emission in solar flares is typically characterized by a number of discrete sources, each with its own spectral, temporal, and spatial variability. Establishing the relationship amongst these sources is critical to determine the role of each in the energy release and transport processes that occur within the flare. In this paper we present a novel method to identify and characterize each source of hard X-ray emission. In particular, the method permits a quantitative determination of the most likely number of subsources present, and of the relative probabilities that the hard X-ray emission in a given subregion of the flare is represented by a complicated multiple source structure or by a simpler single source. We apply the method to a well-studied flare on **2002~February~20** in order to assess competing claims as to the number of chromospheric footpoint sources present, and hence to the complexity of the underlying magnetic geometry/toplogy. Contrary to previous claims of the need for multiple sources to account for the chromospheric hard X-ray emission at different locations and times, we find that a simple two-footpoint-plus-coronal-source model is the most probable explanation for the data. We also find that one of the footpoint sources moves quite rapidly throughout the event, a factor that presumably complicated previous analyses. The inferred velocity of the footpoint corresponds to a very high induced electric field, compatible with those in thin reconnecting current sheets.

The effects of resistivity on oscillatory reconnection and consequences for solar flare Quasi Periodic Pulsations

Luiz A. C. A. **Schiavo**, James Stewart, Philippa K. Browning
2024
https://arxiv.org/pdf/2410.14563
Quasi-periodic pulsations (QPPs) are often observed in flare emissions. While these may reveal much about the time-dependent reconnection involved in flare energy release, the underlying mechanisms are still poorly understood. In this paper, we use 2D magnetohydrodynamic simulations to investigate the magnetic reconnection in two merging flux ropes, focusing on the effects of the resistivity on the time variation of the reconnection. We consider both uniform resistivity and current-dependent anomalous resistivity profiles. Our findings reveal that resistivity plays a critical role in controlling the reconnection dynamics, including reconnection rate oscillations and the rate of decay of the reconnection rate. Resistivity also influences the oscillations in emitted gyrosynchrotron radiation. However, in contrast to this strong influence of resistivity on reconnection rates, we observed a different behaviour for the emitted waves, whose frequencies are almost independent of resistivity variations.

Self-similar solutions of oscillatory reconnection: parameter study of magnetic field strength and background temperature

Luiz A. C. A. **Schiavo**, Gert J. J. Botha, James A. McLaughlin
ApJ **975** 10 **2024**
https://arxiv.org/pdf/2409.12130
https://iopscience.iop.org/article/10.3847/1538-4357/ad7600/pdf
Oscillatory reconnection is a specific type of time-dependent reconnection which involves periodic changes in the magnetic topology of a null point. The mechanism has been reported for a variety of magnetic field strengths and configurations, background temperatures and densities. All these studies report an oscillation in the current density at the null point, but also report a variety of periods, amplitudes and overall behaviors. We conduct a parametric study for equilibrium magnetic field strength and initial background temperature, solving 2D resistive MHD equations around a

magnetic X-point. We introduce a parameter space for the ratio of internal-to-magnetic energy and find self-similar solutions for simulations where this ratio is below 0.1 (which represents a magnetically-dominated environment or, equivalently, a low-beta plasma). Self-similarity can be seen in oscillations in the current density at the null (including amplitude and period), Ohmic heating and the temperature generated via reconnection jets. The parameter space of energy ratios also allows us to contextualize previous studies of the oscillatory reconnection mechanism and bring those different studies together into a single unified understanding.

The Cold Shoulder: Emission Measure Distributions of Active Region Cores

J.T. **Schmelz** and S. Pathak
EIS nugget, July **2013**
We have used EIS, XRT, and xrt_dem_iterative2 to determine the EMD(T) of eight inter-moss areas located in the cores of five different active regions. We then calculated b, where EMD(T) $\propto$ Tb, between Log T = 6.0 and the temperature of the peak of the EMD. For regions (1) and (2) in AR 11113 the exponents were rather large, indicating that steady heating was most likely dominating. The steady-heating model of Winebarger (2011) resembles the EMD for these regions.
For regions (3) and (5-8), b was lower, indication nanoflare heating. Our results are consistent with those of O'Dwyer et al. (2013), who suggested that active region age could be a strong indicator of the dominant heating. Older regions are more likely to be dominated by steady heating, while younger regions show more evidence of nanoflares.

HINODE X-RAY TELESCOPE DETECTION OF HOT EMISSION FROM QUIESCENT ACTIVE REGIONS: A NANOFLARE SIGNATURE?

J. T. **Schmelz** et al
ApJ 693 L131-L135 **2009**
http://www.iop.org/EJ/abstract/1538-4357/693/2/L131
The X-Ray Telescope (XRT) on the Japanese/USA/UK Hinode (Solar-B) spacecraft has detected emission from a quiescent active region core that is consistent with nanoflare heating. The fluxes from 10 broadband X-ray filters and filter combinations were used to construct differential emission measure (DEM) curves. In addition to the expected active region peak at log T = 6.3-6.5, we find a high-temperature component with significant emission measure at log T > 7.0. This emission measure is weak compared to the main peak—the DEM is down by almost three orders of magnitude—which accounts of the fact that it has not been observed with earlier instruments. It is also consistent with spectra of quiescent active regions: no Fe XIX lines are observed in a CHIANTI synthetic spectrum generated using the XRT DEM distribution. The DEM result is successfully reproduced with a simple two-component nanoflare model.

Empirical atmosphere model in a mini flare during magnetic reconnection

Brigitte **Schmieder**, Reetika Joshi, Ramesh Chandra, Guillaume Aulanier, Akiko Tei, Petr Heinzel, James Tomin, Nicole Vilmer, Veronique Bommier
HVAR proceedings **2021**
Cent. Eur. Astrophys. Bull. vol (**2021**) 1, 5
https://arxiv.org/pdf/2112.06790.pdf
A spatio-temporal analysis of IRIS spectra of MgII, CII, and SiIV ions allows us to study the dynamics and the stratification of the flare atmosphere along the line of sight during the magnetic reconnection phase at the jet base. Strong asymmetric MgII and CII line profiles with extended blue wings observed at the reconnection site are interpreted by the presence of two chromospheric temperature clouds: one explosive cloud with blueshifts at 290 km/s and one cloud with smaller Doppler shift (around 36 km/s). Simultaneously at the same location a mini flare was observed with strong emission in multi temperatures (AIA), in several spectral IRIS lines (e.g. Oiv and Siiv, Mgii), absorption of identified chromospheric lines in Siiv line profile, enhancement of the Balmer continuum and X-ray emission by FERMI/GBM. With the standard thick-target flare model we calculate the energy of non thermal electrons observed by FERMI and compare it to the energy radiated by the Balmer continuum emission. We show that the low energy input by non thermal electrons above 20 keV was still sufficient to produce the excess of Balmer continuum. **March 22, 2019**

Solar Active Region Electric Currents Before and During Eruptive Flares **Review**

Brigitte **Schmieder**, Guillaume Aulanier
AGU book , A&A **2019**
https://arxiv.org/pdf/1903.04050.pdf
The chapter "Solar Active Region Electric Currents Before and During Eruptive Flares" is a discussion on electric currents in the pre-eruption state and in the course of eruptions of solar magnetic structures, using information from solar observations, nonlinear force-free field extrapolations relying on these observations, and three-dimensional magnetohydrodynamic (MHD) models. The discussion addresses the issue of neutralized vs. non-neutralized currents in

active regions and concludes that MHD models are able to explain non-neutralized currents in active regions by the existence of strong magnetic shear along the polarity inversion lines, thus confirming previous observations that already contained this result. The models have also captured the essence of the behavior of electric currents in active regions during solar eruptions, predicting current-density increases and decreases inside flare ribbons and in the interior of expanding flux ropes respectively. The observed photospheric current density maps, inferred from vector magnetic field observations, exhibit similar whirling ribbon patterns to the MHD model results, that are interpreted as the signatures of flux ropes and of quasi-separatrix layers (QSLs) between the magnetic systems in active regions. Enhancement of the total current in these QSLs during the eruptions and decreasing current densities at the footpoint of erupting flux ropes, has been confirmed in the observations. **February 15, 2011 , September 10, 2014**

Extreme solar storms based on solar magnetic field

Brigitte **Schmieder**

Varsiti Conference in Varna June 2016 **2017**

https://arxiv.org/pdf/1708.01790.pdf **File**

Many questions have to be answered before understanding the relationship between the emerging magnetic flux through the solar surface and the extreme geoeffective events. Which threshold determines the onset of the eruption? What is the upper limit in energy for a flare? Is the size of sunspot the only criteria to get extreme solar events?
Based on observations of previous solar cycles, and theory, the main ingredients for getting X ray class flares and large Interplanetary Corona Mass Ejections e.g. the built up of the electric current in the corona, are presented such as the existence of magnetic free energy, magnetic helicity, twist and stress in active regions. The upper limit of solar flare energy in space research era and the possible chances to get super-flares and extreme solar events can be predicted using MHD simulation of coronal mass ejections. **September 1, 1859, July 25 1946, April 4-5, 1947, August 1972, October 28 2003, October 28, October 29 and November 4, November 17 2003, October 2014.**

Flare-CME models: an observational perspective **Review**

Schmieder B., Aulanier G., Vrsnak B.

Solar Phys. *Solar and Stellar Flares: Observations, Simulations, and Synergies Volume 290, Issue 12, pp 3457-3486* **2015 File**

http://www.lesia.obspm.fr/perso/guillaume-aulanier/73_2015.FlareCmeObs.pdf

Eruptions, flares, and coronal mass ejection (CMEs) are due to physical phenomena mainly driven by an initially force-free current-carrying magnetic field.We review some key observations relevant to the current theoretical trigger mechanisms of the eruption and to the energy release via reconnection. Sigmoids observed in X-rays and UV, as well as the pattern (double J-shaped) of electric currents in the photosphere show clear evidence of the existence of currents parallel to the magnetic field and can be the signature of a flux rope that is detectable in CMEs. The magnetic helicity of filaments and active regions is an interesting indirectly measurable parameter because it can quantify the twist of the flux rope. On the other hand, the magnetic helicity of the solar structures allows us to associate solar eruptions and magnetic clouds in the heliosphere. The magnetic topology analysis based on the 3D magnetic field extrapolated from vector magnetograms is a good tool for identifying the reconnection locations (null points and/or the 3D large volumes ? hyperbolic flux tube, HFT). Flares are associated more with quasi-separatrix layers (QSLs) and HFTs than with a single null point, which is a relatively rare case. We review various mechanisms that have been proposed to trigger CMEs and their observable signatures: by "breaking" the field lines overlying the flux rope or by reconnection below the flux rope to reduce the magnetic tension, or by letting the flux rope to expand until it reaches a minimum threshold height (loss of equilibrium or torus instability). Additional mechanisms are commonly operating in the solar atmosphere. Examples of observations are presented throughout the article and are discussed in this framework.
15 May 2001, 12 September 2005, 14 September 2005, November 2010 forming AR 11123, 15 February 2011, 6 September 2011

Actors of the main activity in large complex centres during the 23 solar cycle maximum

B. **Schmieder** a,*, P. Dermoulin a, E. Pariat a, T. ToËroËk a,1, G. Molodij a, C.H. Mandrini b, S. Dasso b, R. Chandra c, W. Uddin d, P. Kumar d, P.K. Manoharan e, P. Venkatakrishnan f, N. Srivastava

Advances in Space Research 47 (**2011**) 2081–2091, **File**

During the maximum of Solar Cycle 23, large active regions had a long life, spanning several solar rotations, and produced large numbers of X-class flares and CMEs, some of them associated to magnetic clouds (MCs). This is the case for the Halloween active regions in 2003. The most geoeffective MC of the cycle (Dst = _457) had its source during the disk passage of one of these active regions (NOAA 10501) on 18 November 2003. Such an activity was presumably due to continuous emerging magnetic flux that was observed during this passage. Moreover, the region exhibited a complex topology with multiple domains of different magnetic helicities. The complexity was observed to reach such unprecedented levels that a detailed multi-wavelength analysis is necessary to precisely identify the solar sources of CMEs and MCs. Magnetic clouds are identified using in situ measurements and interplanetary scintillation (IPS) data. Results from these two different sets of data are also compared.

The nonpotentiality of coronae of solar active regions, the dynamics of the surface magnetic field, and the potential for large flares

C.J. **Schrijver**

ApJ 820 103 **2016**

http://arxiv.org/pdf/1602.07244v1.pdf

Flares and eruptions from solar active regions are associated with atmospheric electrical currents accompanying distortions of the coronal field away from a lowest-energy potential state. In order to better understand the origin of these currents and their role in M- and X-class flares, I review all active-region observations made with SDO/HMI and SDO/AIA from 2010/05 through 2014/10 within approximately 40 degrees from disk center. I select the roughly 4% of all regions that display a distinctly nonpotential coronal configuration in loops with a length comparable to the scale of the active region, and all that emit GOES X-class flares. The data for 41 regions confirm, with a single exception, that strong-field, high-gradient polarity inversion lines (SHILs) created during emergence of magnetic flux into, and related displacement within, pre-existing active regions are associated with X-class flares. Obvious nonpotentiality in the active region-scale loops occurs in 6 of 10 selected regions with X-class flares, all with relatively long SHILs along their primary polarity inversion line, or with a long internal filament there. Nonpotentiality can exist in active regions well past the flux-emergence phase, often with reduced or absent flaring. I conclude that the dynamics of the flux involved in the compact SHILs is of preeminent importance for the large-flare potential of active regions within the next day, but that their associated currents may not reveal themselves in active region-scale nonpotentiality. In contrast, active region-scale nonpotentiality, which can persist for many days, may inform us about the eruption potential other than those from SHILs which is almost never associated with X-class flaring. **01.07.2010, 15.02.11, 09.03.2011, 23.02.2011, 20.06.2011, 07.07.2011, 28.03.2012, 04.12.2011, 06.03.2012, 12.07.2012, 03.12.2012, 10.06.2013, 08.11.2013, 10.11.2013, 07.01.2014, 29.03.2014, 10.09.2014, 24.10.2014,**

The set of 41 selected regions with 78 distinct dates is listed in Table 1.

A Statistical Study of Distant Consequences of Large Solar Energetic Events

Carolus J. **Schrijver**, Paul A. Higgins

Solar Phys. Volume 290, Issue 10, pp 2943-2950 **2015**

http://arxiv.org/pdf/1509.05680v1.pdf **File**

Large solar flares and eruptions may influence remote regions through perturbations in the outer-atmospheric magnetic field, leading to causally related events outside of the primary or triggering eruptions that are referred to as "sympathetic events." We quantify the occurrence of sympathetic events using the full-disk observations by the Atmospheric Imaging Assembly onboard the Solar Dynamics Observatory associated with all flares of GOES class M5 or larger from 01 May 2010 through 31 December 2014. Using a superposed-epoch analysis, we find an increase in the rate of flares, filament eruptions, and substantial sprays and surges more than 20 degrees away from the primary flares within the first four hours at a significance of 1.8 standard deviations. We also find that the rate of distant events drops by two standard deviations, or a factor of 1.2, when comparing intervals between 4 hours and 24 hours before and after the start times of the primary large flares. We discuss the evidence for the concluding hypothesis that the gradual evolution leading to the large flare and the impulsive release of the energy in that flare both contribute to the destabilization of magnetic configurations in distant active regions and quiet-Sun areas. These effects appear to leave distant regions, in an ensemble sense, in a more stable state, so that fewer energetic events happen for at least a day following large energetic events**. 2011-09-07**

Table 1. 18 flares with no distant events within 24 hours; 13 flares with one distant event within 24 hours; 16 flares with two or more distant events within 24 hours:

THE 2011 FEBRUARY 15 X2 FLARE, RIBBONS, CORONAL FRONT, AND MASS EJECTION: INTERPRETING THE THREE-DIMENSIONAL VIEWS FROM THE SOLAR DYNAMICS OBSERVATORY AND STEREO GUIDED BY MAGNETOHYDRODYNAMIC FLUX-ROPE MODELING

Carolus J. **Schrijver**1, Guillaume Aulanier2, Alan M. Title1, Etienne Pariat2 and Cecile Delannée

E-print, June **2011**, **File**; **2011** ApJ 738 167, **File?**

The **2011 February 15** X2.2 flare and associated Earth-directed halo coronal mass ejection were observed in unprecedented detail with high resolution in spatial, temporal, and thermal dimensions by the Atmospheric Imaging Assembly (AIA) on the Solar Dynamics Observatory, as well as by instruments on the two STEREO spacecraft, then at near-quadrature relative to the Sun-Earth line. These observations enable us to see expanding loops from a flux-rope-like structure over the shearing polarity-inversion line between the central δ-spot groups of AR 11158, developing a propagating coronal front ("EIT wave"), and eventually forming the coronal mass ejection moving into the inner heliosphere. The observations support the interpretation that all of these features, including the "EIT wave," are signatures of an expanding volume traced by loops (much larger than the flux rope only), surrounded by a moving front rather than predominantly wave-like perturbations; this interpretation is supported by previously published MHD

models for active-region and global scales. The lateral expansion of the eruption is limited to the local helmet-streamer structure and halts at the edges of a large-scale domain of connectivity (in the process exciting loop oscillations at the edge of the southern polar coronal hole). The AIA observations reveal that plasma warming occurs within the expansion front as it propagates over quiet Sun areas. This warming causes dimming in the 171 Å (Fe IX and Fe X) channel and brightening in the 193 and 211 Å (Fe XII-XIV) channels along the entire front, while there is weak 131 Å (Fe VIII and Fe XXI) emission in some directions. An analysis of the AIA response functions shows that sections of the front running over the quiet Sun are consistent with adiabatic warming; other sections may require additional heating which MHD modeling suggests could be caused by Joule dissipation. Although for the events studied here the effects of volumetric expansion are much more obvious than true wave phenomena, we discuss how different magnetic environments within and around the erupting region can lead to the signatures of either or both of these aspects.

Long-range magnetic couplings between solar flares and coronal mass ejections observed by SDO and STEREO

C.J. **Schrijver** and A.M. Title

E-print, 18 Jan **2011**, **File**; JGR, 116, A04108, doi:10.1029/2010JA016224, **2011**

The combination of SDO and STEREO observations enable us to view much of the solar surface and atmosphere simultaneously and continuously. These near-global observations often show near-synchronous long-distance interactions between magnetic domains that exhibit flares, eruptions, and frequent minor forms of activity. Here, we analyze a series of flares, filament eruptions, coronal mass ejections, and related events which occurred on **2010/08/01-02**. These events extend over a full hemisphere of the Sun, only two-thirds of which is visible from the Earth's perspective. The combination of coronal observations and global field modeling reveals the many connections between these events by magnetic field lines, particularly those at topological divides. We find that all events of substantial coronal activity, including those where flares and eruptions initiate, are connected by a system of separatrices, separators, and quasi-separatrix layers, with little activity within the deep interiors of domains of connectivity. We conclude that for this sequence of events the evolution of field on the hemisphere invisible from Earth's perspective is essential to the evolution, and possibly even to the initiation, of the flares and eruptions over an area that spans at least 180 degrees in longitude. Our findings emphasize that the search for the factors that play a role in the initiation and evolution of eruptive and explosive phenomena, sought after for improved space-weather forecasting, requires knowledge of much, if not all, of the solar surface field.

Driving Major Solar Flares and Eruptions: A Review

Carolus J. **Schrijver**

Advances in Space Research

Volume 43, Issue 5, 2 March **2009**, Pages 739-755; **File**

This review focuses on the processes that energize and trigger M- and X-class solar flares and associated flux-rope destabilizations. Numerical modeling of specific solar regions is hampered by uncertain coronal-field reconstructions and by poorly understood magnetic reconnection; these limitations result in uncertain estimates of field topology, energy, and helicity. The primary advances in understanding field destabilizations therefore come from the combination of generic numerical experiments with interpretation of sets of observations. These suggest a critical role for the emergence of twisted flux ropes into pre-existing strong field for many, if not all, of the active regions that produce M- or X-class flares. The flux and internal twist of the emerging ropes appear to play as important a role in determining whether an eruption will develop predominantly as flare, confined eruption, or CME, as do the properties of the embedding field. Based on reviewed literature, I outline a scenario for major flares and eruptions that combines flux-rope emergence, mass draining, near-surface reconnection, and the interaction with the surrounding field. Whether deterministic forecasting is in principle possible remains to be seen: to date no reliable such forecasts can be made. Large-sample studies based on long-duration, comprehensive observations of active regions from their emergence through their flaring phase are needed to help us better understand these complex phenomena.

Non-linear force-free field modeling of a solar active region around the time of a major flare and coronal mass ejection

C.J. **Schrijver**1, M.L. DeRosa1, T. Metcalf2, G. Barnes2, B. Lites3, T. Tarbell1, J. McTiernan4, G. Valori5, T. Wiegelmann6, M.S. Wheatland7, T. Amari8, G. Aulanier9, P. D´emoulin9, M. Fuhrmann10, K. Kusano11, S. R´egnier12, J.K. Thalmann6

E-print, Nov 2007, ApJ Vol. 675, No. 2: 1637-1644, **2008**.

http://www.journals.uchicago.edu/doi/pdf/10.1086/527413
13 Dec 2006
Solar flares and coronal mass ejections are associated with rapid changes in field connectivity and powered by the partial dissipation of electrical currents in the solar atmosphere. A critical unanswered question is whether the currents involved are induced by the motion of pre-existing atmospheric magnetic flux subject to surface plasma flows, or whether these currents are associated with the emergence of flux from within the solar convective zone. We address this problem by applying state-of-the-art nonlinear force-free field (NLFFF) modeling to the highest resolution and quality vector-magnetographic data observed by the recently launched **Hinode** satellite on NOAA Active Region 10930 around the time of a powerful X3.4 flare. We compute 14 NLFFF models with 4 different codes and a variety of boundary conditions. We find that the model fields differ markedly in geometry, energy content, and force-freeness. We discuss the relative merits of these models in a general critique of present abilities to model.

A characteristic magnetic field pattern associated with all major solar flares and its use in flare forecasting –

Carolus J. **Schrijver**
2007, ApJL, 655, L117, doi: 10.1086/511857
https://iopscience.iop.org/article/10.1086/511857/pdf
Solar flares result from some electromagnetic instability that occurs within regions of relatively strong magnetic field in the Sun's atmosphere. The processes that enable and trigger these flares remain topics of intense study and debate. I analyze observations of 289 X- and M-class flares and over 2500 active region magnetograms to discover (1) that large flares, without exception, are associated with pronounced high-gradient polarity-separation lines, while (2) the free energy that emerges with these fibrils is converted into flare energy in a broad spectrum of flare magnitudes that may well be selected at random from a power-law distribution up to a maximum value. This maximum is proportional to the total unsigned flux R within ~15 Mm of strong-field, high-gradient polarity-separation lines, which are a characteristic appearance of magnetic fibrils carrying electrical currents as they emerge through the photosphere. Measurement of R is readily automated, and R can therefore be used effectively for flare forecasting. The probability for major flares to occur within 24 hr of the measurement of R approaches unity for active regions with the highest values of R around 2×10^{21} Mx. For regions with $R \lesssim 10^{19}$ Mx, no M- or X-class flares occur within a day.

Soft X-Ray Observations of Quiescent Solar Active Regions using Novel Dual-zone Aperture X-ray Solar Spectrometer (DAXSS)

Bennet D. **Schwab**, Robert H. A. Sewell, Thomas N. Woods, Amir Caspi, James Paul Mason, Christopher Moore
ApJ **2020**
https://arxiv.org/pdf/2008.11313.pdf
The Dual-zone Aperture X-ray Solar Spectrometer (DAXSS) was flown on **2018 June18** on the NASA 36.336 sounding rocket flight and obtained the highest resolution to date for solar soft X-ray (SXR) spectra over a broad energy range. This observation was during a time with quiescent (non-flaring) small active regions on the solar disk and when the 10.7 cm radio flux (F10.7) was 75 solar flux units (1 sfu = 10-22 W/m^2/Hz). The DAXSS instrument consists of a LASP-developed dual-zone aperture and a commercial X-ray spectrometer from Amptek that measures solar full-disk irradiance from 0.5-20 keV with a resolving power of 20 near 1 keV. This paper discusses the novel design of the spectrometer and the instrument characterization techniques. Additionally,the solar measurements obtained from the 2018 sounding rocket flight are analyzed using CHIANTI spectral models to fit the temperatures, emission measures, and relative elemental abundances of the solar corona plasma. The abundance of iron was found to be 35 percent higher than expected in the quiescent sun's corona suggesting either that our spectral models require additional sophistication or that the underlying atomic database may require updates. Future long-term systematic observations of this spectral range are needed. DAXSS will fly on the INSPIRESat-1 CubeSat in late-2020, and its SXR spectral data could provide further insight into the sources of coronal heating through modeling the changes of relative elemental abundances during developments of active regions and solar flaring events.

A flare in the deep solar atmosphere

Richard **Schwartz**, Hugh Hudson
RHESSI Science Nugget No. 282, **2016**
http://sprg.ssl.berkeley.edu/~tohban/wiki/index.php/A_flare_in_the_deep_solar_atmosphere

In this Nugget we report a singular set of observations of a very short-lived GOES event, well-observed by RHESSI and Fermi at high temperatures, which we argue to have taken place in the deepest solar atmosphere. In fact the duration of the GOES event is only about 15 seconds (FWHM) in the soft channel (1-8 A), very unusual indeed. As noted, the X-ray data strongly suggest a compact, low-altitude source. These have a standard interpretation in terms of flux transfer between compact and large-scale fields.
2016-09-19

DESAT: an SSW tool for SDO/AIA image de-saturation

Richard A **Schwartz**, Gabriele Torre, Anna Maria Massone, Michele Piana
Inverse Problems, **2015**
http://arxiv.org/pdf/1503.02302v1.pdf
Saturation affects a significant rate of images recorded by the Atmospheric Imaging Assembly on the Solar Dynamics Observatory. This paper describes a computational method and a technological pipeline for the de-saturation of such images, based on several mathematical ingredients like Expectation Maximization, image correlation and interpolation. An analysis of the computational properties and demands of the pipeline, together with an assessment of its reliability are performed against a set of data recorded from the **Feburary 25 2014** flaring event.

A Systematic Approach to the Reconstruction of Saturated SDO/AIA Images

Richard A **Schwartz**, Gabriele Torre, Michele Piana
ApJL, 793 L23 **2014**
http://arxiv.org/pdf/1407.7343v1.pdf
EUV images of solar flares provided by the Atmospheric Imaging Assembly onboard the Solar Dynamics Observatory (SDO/AIA) are often affected by saturation effects in their core, physically most interesting region. We introduce an image reconstruction procedure that allows recovering information in the primary saturation domain using the secondary images produced by the diffraction fringes as input data. Such a procedure is based on standard image-processing tools like correlation, convolution, and back-projection. Its effectiveness is tested in the case of SDO/AIA observations of the **July 8 2013** flaring event.

The Halloween Flares and Large-Scale Correlations

Richard **Schwartz** and Hugh Hudson
RHESSI Halloween Nugget, Oct **2013**
http://sprg.ssl.berkeley.edu/~tohban/wiki/index.php/The_Halloween_Flares_and_Large-Scale_Correlations
The celebrated phenomena of the "Halloween Flares" of 2003 have just reappeared, though more weakly, in **October 2013**. In the waning phase of the previous sunspot maximum, a remarkable group of apparently independent sunspot groups appeared within a few days of one another. Something like this has just happened, or is just happening, in the declining phase of our current sunspot maximum ([Cycle 24]). For reasons unknown in detail, and probably unknowable any time soon, the organization of solar activity visible at the surface has large-scale correlations in space and time, meaning that flares bunch up in a highly non-random manner:

Identification of Multiple Hard X-Ray Sources in Solar Flares: A Bayesian Analysis of the 2002 February 20 Event

Federica **Sciacchitano**1, Alberto Sorrentino1,2, A Gordon Emslie3, Anna Maria Massone2, and Michele Piana1,2
2018 ApJ 862 68
http://sci-hub.tw/http://iopscience.iop.org/article/10.3847/1538-4357/aacc27/meta
The hard X-ray emission in a solar flare is typically characterized by a number of discrete sources, each with its own spectral, temporal, and spatial variability. Establishing the relationship among these sources is critical to determining the role of each in the energy release and transport processes that occur within the flare. In this paper we present a novel method to identify and characterize each source of hard X-ray emission. The method permits a quantitative determination of the most likely number of subsources present, and of the relative probabilities that the hard X-ray emission in a given subregion of the flare is represented by a complicated multiple source structure or by a simpler single source. We apply the method to a well-studied flare on **2002 February 20** in order to assess competing claims as to the number of chromospheric footpoint sources present, and hence to the complexity of the underlying magnetic geometry/topology. Contrary to previous claims of the need for multiple sources to account for the chromospheric hard X-ray emission at different locations and times, we find that a simple two-footpoint-plus-coronal-source model is the most probable explanation for the data. We also find that one of the footpoint sources moves quite rapidly throughout the event, a factor that presumably complicated previous analyses. The inferred velocity of the footpoint corresponds to a very high induced electric field, compatible with the fields in thin reconnecting current sheets.

Using Flare Rates to Search for Stellar Activity Cycles

Matthew T. **Scoggins**1, James. R. A. Davenport2,3, and Kevin R. Covey1
2019 Res. Notes AAS 3 137
https://iopscience.iop.org/article/10.3847/2515-5172/ab45a0
Measuring the prevalence and duration of activity cycles gives insight into the origin of stellar magnetic dynamos. Traditional techniques for detecting activity cycles include: monitoring integrated flux measurements (Kopp et al. 2016), chromospheric emission lines (Duncan et al. 1991), and starspot tracking (Messina & Guinan 2002; Montet et al. 2017). However, these techniques face challenges such as photometric precision, or limited spectroscopic sample sizes. Flares, however, are easily detectable for stars even out to kpc distances, and can be surveyed for many stars simultaneously using wide-field photometric surveys. Encouragingly, *the Sun's flare rate varies by a factor of 10 between solar maximum and minimum* (e.g., Veronig et al. 2002; Aschwanden & Freeland 2012).

INFERRING THE MAGNETOHYDRODYNAMIC STRUCTURE OF SOLAR FLARE SUPRA-ARCADE PLASMAS FROM A DATA-ASSIMILATED FIELD TRANSPORT MODEL

Roger B. **Scott**, David E. McKenzie, and Dana W. Longcope
2016 ApJ 819 56
Supra-arcade fans are highly dynamic structures that form in the region above post-reconnection flare arcades. In these features the plasma density and temperature evolve on the scale of a few seconds, despite the much slower dynamics of the underlying arcade. Further, the motion of supra-arcade plasma plumes appears to be inconsistent with the low-beta conditions that are often assumed to exist in the solar corona. In order to understand the nature of these highly debated structures, it is, therefore, important to investigate the interplay of the magnetic field with the plasma. Here we present a technique for inferring the underlying magnetohydrodynamic processes that might lead to the types of motions seen in supra-arcade structures. Taking as a case study the **2011 October 22** event, we begin with extreme-ultraviolet observations and develop a time-dependent velocity field that is consistent with both continuity and local correlation tracking. We then assimilate this velocity field into a simplified magnetohydrodynamic simulation, which deals simultaneously with regions of high and low signal-to-noise ratio, thereby allowing the magnetic field to evolve self-consistently with the fluid. Ultimately, we extract the missing contributions from the momentum equation in order to estimate the relative strength of the various forcing terms. In this way we are able to make estimates of the plasma beta, as well as predict the spectral character and total power of Alfvén waves radiated from the supra-arcade region.

Observing the formation of flare-driven coronal rain

E. **Scullion**, L. Rouppe Van Der Voort, P. Antolin, S. Wedemeyer, G. Vissers, E. P. Kontar, P. Gallagher
ApJ **833** 184 **2016**
https://arxiv.org/pdf/1610.09255v1.pdf
Flare-driven coronal rain can manifest from rapidly cooled plasma condensations near coronal loop-tops in thermally unstable post-flare arcades. We detect 5 phases that characterise the post-flare decay: heating, evaporation, conductive cooling dominance for ~120 s, radiative / enthalpy cooling dominance for ~4700 s and finally catastrophic cooling occurring within 35-124 s leading to rain strands with s periodicity of 55-70 s. We find an excellent agreement between the observations and model predictions of the dominant cooling timescales and the onset of catastrophic cooling. At the rain formation site we detect co-moving, multi-thermal rain clumps that undergo catastrophic cooling from ~1 MK to ~22000 K. During catastrophic cooling the plasma cools at a maximum rate of 22700 K s-1 in multiple loop-top sources. We calculated the density of the EUV plasma from the DEM of the multi-thermal source employing regularised inversion. Assuming a pressure balance, we estimate the density of the chromospheric component of rain to be 9.21x10^11 +-1.76x10^11 cm-3 which is comparable with quiescent coronal rain densities. With up to 8 parallel strands in the EUV loop cross section, we calculate the mass loss rate from the post-flare arcade to be as much as 1.98x10^12 +/-4.95x10^11 g s-1. Finally, we reveal a close proximity between the model predictions of 10^5.8 K and the observed properties between 10^5.9 K and 10^6.2 K, that defines the temperature onset of catastrophic cooling. The close correspondence between the observations and numerical models suggests that indeed acoustic waves (with a sound travel time of 68 s) could play an important role in redistributing energy and sustaining the enthalpy-based radiative cooling. **01-07-2012**

Unresolved Fine-scale Structure in Solar Coronal Loop-tops

E. **Scullion**1,2, L. Rouppe van der Voort1, S. Wedemeyer1, and P. Antolin
2014 ApJ 797 36
http://arxiv.org/pdf/1409.1920v1.pdf
New and advanced space-based observing facilities continue to lower the resolution limit and detect solar coronal loops in greater detail. We continue to discover even finer substructures within coronal loop cross-sections, in order to understand the nature of the solar corona. Here, we push this lower limit further to search for the finest coronal loop

substructures, through taking advantage of the resolving power of the Swedish 1 m Solar Telescope/CRisp Imaging Spectro-Polarimeter (CRISP), together with co-observations from the Solar Dynamics Observatory/Atmospheric Image Assembly (AIA). High-resolution imaging of the chromospheric H? 656.28 nm spectral line core and wings can, under certain circumstances, allow one to deduce the topology of the local magnetic environment of the solar atmosphere where its observed. Here, we study post-flare coronal loops, which become filled with evaporated chromosphere that rapidly condenses into chromospheric clumps of plasma (detectable in H?) known as a coronal rain, to investigate their fine-scale structure. We identify, through analysis of three data sets, large-scale catastrophic cooling in coronal loop-tops and the existence of multi-thermal, multi-stranded substructures. Many cool strands even extend fully intact from loop-top to footpoint. We discover that coronal loop fine-scale strands can appear bunched with as many as eight parallel strands within an AIA coronal loop cross-section. The strand number density versus cross-sectional width distribution, as detected by CRISP within AIA-defined coronal loops, most likely peaks at well below 100 km, and currently, 69% of the substructure strands are statistically unresolved in AIA coronal loops. **1-2 July 2012, 24th Sept. 2011,**

Observations of an Eruptive Solar Flare in the Extended EUV Solar Corona

Daniel B. **Seaton**, Jonathan M. Darnel
2018 ApJL **852** L9
https://arxiv.org/pdf/1712.06003.pdf
http://iopscience.iop.org.sci-hub.tw/2041-8205/852/1/L9/
https://iopscience.iop.org/article/10.3847/2041-8213/aaa28e/pdf
We present observations of a powerful solar eruption, accompanied by an X8.2 solar flare, from NOAA Active Region 12673 on **2017 September 10** by the ***Solar Ultraviolet Imager (SUVI) on the GOES-16 spacecraft***. SUVI is noteworthy for its relatively large field of view, which allows it to image solar phenomena to heights approaching 2 solar radii. These observations include the detection of an apparent current sheet associated with magnetic reconnection in the wake of the eruption, and evidence of an extreme-ultraviolet wave at some of the largest heights ever reported. We discuss the acceleration of the nascent coronal mass ejection to approximately 2000 km s-1 at about 1.5 solar radii. We compare these observations with models of eruptions and eruption-related phenomena. We also describe the SUVI data and discuss how the scientific community can access SUVI observations of the event.

Observations of the Formation, Development, and Structure of a Current Sheet in an Eruptive Solar Flare

Daniel B. **Seaton**1,2, Allison E. Bartz3, and Jonathan M. Darnel
2017 ApJ 835 139
https://arxiv.org/pdf/1610.06905v1.pdf
We present Atmospheric Imaging Assembly observations of a structure we interpret as a current sheet associated with an X4.9 flare and coronal mass ejection that occurred on **2014 February 25** in NOAA Active Region 11990. We characterize the properties of the current sheet, finding that the sheet remains on the order of a few thousand kilometers thick for much of the duration of the event and that its temperature generally ranged between 8 and 10 MK. We also note the presence of other phenomena believed to be associated with magnetic reconnection in current sheets, including supra-arcade downflows and shrinking loops. We estimate that the rate of reconnection during the event was M A ≈ 0.004–0.007, a value consistent with model predictions. We conclude with a discussion of the implications of this event for reconnection-based eruption models.

Theoretical and Observational Evidence for Coriolis Effects in Coronal Magnetic Fields Via Direct Current Driven Flaring Events

Darryl Z. **Seligman**, Leslie A. Rogers, Adina D. Feinstein, Mark R. Krumholz, James R. Beattie, Christoph Federrath, Fred C. Adams, Marco Fatuzzo, Maximilian N. Günther
ApJ **929** 54 **2022**
https://arxiv.org/pdf/2201.03697.pdf
https://iopscience.iop.org/article/10.3847/1538-4357/ac5b69/pdf
All stars produce explosive surface events such as flares and coronal mass ejections. These events are driven by the release of energy stored in coronal magnetic fields, generated by the stellar dynamo. However, it remains unclear if the energy deposition in the magnetic fields is driven by direct or alternating currents. Recently, we presented observational measurements of the flare intensity distributions for a sample of ∼105 stars across the main sequence observed by TESS, all of which exhibited power-law distributions similar to those observed in the Sun, albeit with varying slopes. Here we investigate the mechanisms required to produce such a distribution of flaring events via direct current energy deposition, in which coronal magnetic fields braid, reconnect, and produce flares. We adopt a topological model for this process which produces a power-law distribution of energetic flaring events. We expand this model to include the Coriolis effect, which we demonstrate produces a shallower distribution of flare energies in stars that rotate more rapidly (corresponding to a weaker decline in occurrence rates toward increasing flare energies). We present tentative evidence for the predicted rotation-power-law index correlation in the observations. We advocate for future

observations of stellar flares that would improve our measurements of the power-law exponents, and yield key insights into the underlying dynamo mechanisms that underpin the self-similar flare intensity distributions.

Call and Response: A Time-Resolved Study of Chromospheric Evaporation in a Large Solar Flare

Sean G. **Sellers**, Ryan O. Milligan, R. T. James McAteer
ApJ **936** 85 **2022**
https://arxiv.org/pdf/2208.14347.pdf
https://iopscience.iop.org/article/10.3847/1538-4357/ac87a9/pdf
We studied an X1.6 solar flare produced by NOAA AR 12602 on **2014 October 22**. The entirety of this event was covered by RHESSI, IRIS, and Hinode/EIS, allowing analysis of the chromospheric response to a nonthermal electron driver. We derived the energy contained in nonthermal electrons via RHESSI spectral fitting, and linked the time-dependent parameters of this call to the response in Doppler velocity, density, and nonthermal width across a broad temperature range. The total energy injected was 4.8×1030 erg, and lasted 352 seconds. This energy drove explosive chromospheric evaporation, with a delineation in both Doppler and nonthermal velocities at the flow reversal temperature, between 1.35--1.82 MK. The time of peak electron injection (14:06 UT) corresponded to the time of highest velocities. At this time, we found 200 km s−1 blueshifts in the core of Fe XXIV, which is typically assumed to be at rest. Shortly before this time, the nonthermal electron population had the shallowest spectral index (≈ 6), corresponding to the peak nonthermal velocity in Si IV and Fe XXI. Nonthermal velocities in Fe XIV, formed near the flow reversal temperature were low, and not correlated with density or Doppler velocity. Nonthermal velocities in ions with similar temperatures were observed to increase and correlate with Doppler velocities, implying unresolved flows surrounding the flow reversal point. This study provides a comprehensive, time-resolved set of chromospheric diagnostics for a large X-class flare, along with a time-resolved energy injection profile, ideal for further modeling studies.

On the Distinct Periodicities of Sunspot Counts in Flaring and Non-flaring Active Regions

Stefano **Sello**
2017
https://arxiv.org/pdf/1707.01900.pdf
In a recent work, Kilcik et al. (2017), have detected the temporal and periodic behavior of sunspot counts (SSC) in flaring (i.e. C, M, or X class flares), and non-flaring active regions for the last two solar cycles, covering the period: 1996 - 2016. The main results obtained are: 1) The temporal behavior of monthly means of daily total SSC in flaring and non-flaring active regions are different and these differences are also varying from cycle to cycle; 2) The periodicities detected in SSC of flaring and non-flaring active regions are quite different and these variations are also different from one cycle to another; the highest detected period in the flaring active regions is 113 days, while there are much higher periodicities (327, 312, and 256 days) in non-flaring regions. The detection of typical different periodicities in flaring and non-flaring regions can suggests both important differences and physical interpretation in the magneto-hydrodynamic behavior of the Sun. For this reason in the present paper we show a further periodicity analysis of the sunspot counts in flaring and in non-flaring active regions using the same data source of that used by the above cited authors and applying a powerful wavelet analysis tool which is particularly useful to detect multiscale features of complex unsteady and unevenly sampled time series. In order to futher support the differences and similarities found in the time behavior of SSC in flaring and non-flaring regions, we also computed the behavior of the wavelet entropy, a proper time function which allow us to measure the degree of complexity in the dynamics of the related time series.

From eruption to post-flare rain: A 2.5D MHD model⋆

Samrat **Sen**1,2,3, Avijeet Prasad4,5, Valeriia Liakh3 and Rony Keppens3
A&A, 688, A64 (**2024**)
https://arxiv.org/pdf/2405.10688
https://www.aanda.org/articles/aa/pdf/2024/08/aa49767-24.pdf
Context. Erupting magnetic flux ropes play an important role in producing solar flares, whereas fine-scale condensed coronal rain is often found in post-flare loops. However, the formation of the MFRs in the pre-flare stage and how this leads to coronal rain in a post-eruption magnetic loop is not fully understood.
Aims. We explore the formation and eruption of MFRs, followed by the appearance of coronal rain in the post-flare loops to understand the magnetic and thermodynamic properties of eruptive events and their multi-thermal aspects in the solar atmosphere.
Methods. We performed a resistive-magnetohydrodynamic simulation with the open-source code MPI-AMRVAC to explore the evolution of sheared magnetic arcades that can lead to flux rope eruptions. The system was in mechanical imbalance at the initial state and evolved self-consistently in a nonadiabatic atmosphere under the influence of radiative losses, thermal conduction, and background heating. We used an additional level of adaptive mesh refinement to achieve the smallest cell size of ≈32.7 km in each direction to reveal the fine structures in the system.

Results. The system achieves a semi-equilibrium state after a short transient evolution from its initial mechanically imbalanced condition. A series of erupting MFRs is formed due to spontaneous magnetic reconnection across current sheets that are created underneath the erupting flux ropes. A gradual development of thermal imbalance is noted at a loop top in the post-eruption phase, which leads to catastrophic cooling and to the formation of condensations. We obtain plasma blobs that fall down along the magnetic loop in the form of coronal rain. The dynamical and thermodynamic properties of these cool condensations agree well with observations of post-flare coronal rain. Conclusions. Our simulation supports the development and eruption of multiple MFRs and the formation of coronal rain in post-flare loops. This is one of the key aspects required to reveal the mystery of coronal heating in the solar atmosphere.

Thermally enhanced tearing in solar current sheets: explosive reconnection with plasmoid-trapped condensations

Samrat **Sen**, Rony Keppens
A&A 666, A28 **2022**
https://arxiv.org/pdf/2208.04355.pdf
https://www.aanda.org/articles/aa/pdf/2022/10/aa44152-22.pdf
https://doi.org/10.1051/0004-6361/202244152
In flare-relevant current sheets, tearing instability may trigger explosive reconnection and plasmoid formation. We explore how the thermal and tearing modes reinforce each other in the fragmentation of a current sheet in the solar corona through an explosive reconnection process, characterized by the formation of plasmoids which interact and trap condensing plasma. We use a resistive magnetohydrodynamic (MHD) simulation of a 2D current layer, incorporating the non-adiabatic effects of optically thin radiative energy loss and background heating using \texttt{MPI-AMRVAC}. Our parametric survey explores different resistivities and plasma-β to quantify the instability growth rate in the linear and nonlinear regimes. We notice that for dimensionless resistivity values within 10−4−5×10−3, we get explosive behavior where thermal instability and tearing behavior reinforce each other. This is clearly below the usual critical Lundquist number range of pure resistive explosive plasmoid formation. The non-linear growth rates follow weak power-law dependency with resistivity. The fragmentation of the current sheet and the formation of the plasmoids in the nonlinear phase of the evolution due to the thermal and tearing instabilities are obtained. The formation of plasmoids is noticed for the Lundquist number (SL) range 4.6×103−2.34×105. We quantify the temporal variation of the plasmoid numbers and the density filling factor of the plasmoids for different physical conditions. We also find that the maximum plasmoid numbers scale as S0.223L. Within the nonlinearly coalescing plasmoid chains, localized cool condensations gather, realizing density and temperature contrasts similar to coronal rain or prominences.

Energy distribution of solar flare events

S. **Sen**, A. Mangalam, R. Ramesh (Indian Institute of Astrophysics)
Proceedings of IAU Symposium 340 **2018**
https://arxiv.org/pdf/1805.08431.pdf
Observational evidence of the braiding of magnetic field lines has been reported. The magnetic reconnection within the loop (nanoflares) and with other loops (microflares) disentangle the field. The coronal field then reorganizes itself to attain a force-free field configuration. We have evaluated the power law index of the energy distribution f(E)=f0E−α by using a model of relaxation incorporating different profile functions of winding number distribution f(w) based on braided topologies. We study the radio signatures that occur in the solar corona using the radio data obtained from the Gauribidanur Radio Observatory (IIA) and extract the power law index by using the Statistic-sensitive nonlinear iterative peak clipping (SNIP) algorithm. We see that the power law index obtained from the model is in good agreement with the calculated value from the radio data observation.

Proton Acceleration in Low-β Magnetic Reconnection with Energetic Particle Feedback

Jeongbhin **Seo**, Fan Guo, Xiaocan Li, and Hui Li
2024 ApJ 977 146
https://iopscience.iop.org/article/10.3847/1538-4357/ad8e64/pdf
Magnetic reconnection regions in space and astrophysics are known as active particle acceleration sites. There is ample evidence showing that energetic particles can take a substantial amount of converted energy during magnetic reconnection. However, there has been a lack of studies understanding the backreaction of energetic particles at magnetohydrodynamical scales in magnetic reconnection. To address this, we have developed a new computational method to explore the feedback by nonthermal energetic particles. This approach considers the backreaction from these energetic particles by incorporating their pressure into magnetohydrodynamics (MHD) equations. The pressure of the energetic particles is evaluated from their distribution evolved through Parker's transport equation, solved using stochastic differential equations (SDEs), so we coin the name MHD-SDE. Applying this method to low-β magnetic reconnection simulations, we find that reconnection is capable of accelerating a large fraction of energetic particles that contain a substantial amount of energy. When the feedback from these particles is included, their pressure suppresses the compression structures generated by magnetic reconnection, thereby mediating particle energization. Consequently,

the feedback from energetic particles results in a steeper power-law energy spectrum. These findings suggest that feedback from nonthermal energetic particles plays a crucial role in magnetic reconnection and particle acceleration.

Temporal and Spatial Characteristics of Hard X-Ray Sources in Flare Model with a Vertical Current Sheet

Alexander N. **Shabalin**, Evgeniia P. Ovchinnikova, Yuri E. Charikov
ApJ **954** 58 **2023**
https://arxiv.org/pdf/2308.05718.pdf
https://iopscience.iop.org/article/10.3847/1538-4357/acea5e/pdf
We analyzed changes in the height of the coronal hard X-ray (HXR) source for flares SOL**2013-05-13**T01:50 and SOL**2013-05-13**T15:51. Analysis of the Reuven Ramaty High Energy Solar Spectroscopic Imager data revealed the downward motion of the HXR source and the separation of the sources by energy and height. In the early stages of the flares, a negative correlation was found between the HXR source area in the corona and HXR flux. For the SOL**2013-05-13**T15:51 event, an increasing trend in the time delay spectra at the footpoints was obtained. For both events, the spectra of the time delays in the coronal HXR source showed a decreasing trend across the energies in certain flare phases. To interpret the observed phenomena, we considered a flare model of collapsing traps and calculated the distribution functions of accelerated electrons along the magnetic loop using a nonstationary relativistic kinetic equation. This approach considers betatron and Fermi first-order acceleration mechanisms. The increasing trend of the time delay spectra at the footpoints was explained by the high mirror ratio in the magnetic loop and betatron acceleration mechanism. The observed features in the spatial and temporal behavior of the HXR sources, such as the negative correlation between the HXR source area and HXR flux, can be interpreted by the collapsing trap model.
RHESSI Nuggets #453 **2023**
https://sprg.ssl.berkeley.edu/~tohban/wiki/index.php/Temporal_and_Spatial_Characteristics_of_Hard_X-Ray_Sources_in_Flare_Model_with_Vertical_Current_Sheet

A statistical study of CME-associated flare during the solar cycle 24

AMK **Shaltout**; Eid A Amin; M.M. Beheary; R. H. Hamid
Advances in Space Research Volume 63, Issue 7, 1 April **2019**, Pages 2300-2311
https://www.sciencedirect.com/science/article/pii/S0273117718309359?dgcid=raven_sd_via_email
We investigate on the relationship between flares and coronal mass ejections (CMEs) in which a flare started before and after the CME events which differ in their physical properties, indicating potentially different initiation mechanisms. The physical properties of two types flare-correlated CME remain an interesting and important question in space weather. We study the relationship between flares and CMEs using a different approach requiring both temporal and spatial constraints during the period from December 1, 2008 to April 30, 2017 in which the CMEs data were acquired by SOHO/LASCO (Solar and Heliospheric Observatory/Large Angle Spectrometric Coronagraph) over the solar cycle 24. The soft X-ray flare flux data, such as flare class, location, onset time and integrated flux, are collected from Geostationary Environmental satellite (GOES) \textbf{and XRT Flare catalogs}. We selected 301 CMEs-flares pairs applying simultaneously temporal and spatial constraints in all events for the distinguish between two associated CME-flare types. We study the correlated properties of coincident flares and CMEs during this period, specifically separating the sample into two types: flares that precede a CME and flares that follow a CME. We found an opposite correlation relationship between the acceleration and velocity of CMEs in the After- and Before-CMEs events. We found a log-log relation between the width and mass of CMEs in the two associated types. The CMEs and flares properties show that there were significant differences in all physical parameters such as (mass, angular width, kinetic energy, speed and acceleration) between two flare-associated CME types.

Spatial and Spectral Evolution of Microwave and X-Ray Sources During the Solar Limb Flare on February 5, 2023.

Shamsutdinova, J.N., Kashapova, L.K., Li, Z. et al.
Sol Phys 299, 80 (**2024**).
https://doi.org/10.1007/s11207-024-02331-w
We present an empirical scenario of the energy release process during a solar limb flare on **February 5, 2023**. This event was observed by the Siberian Radioheliograph (SRH) within the 3 – 12 GHz range and the Advanced Space-based Solar Observatory / Hard X-ray Imager (ASO-S/HXI) within 10 – 300 keV range. The combination of these data allowed us to use information not only about the spectral features but also about the spatial evolution of the flare. The main source of the energy released was a small compact loop which was revealed in both the X-ray and microwave ranges. During the early phases of the flare evolution, a spectral analysis of microwave emission showed that thermal gyrosynchrotron emission turned to gyrosynchrotron emission of nonthermal electrons. This indicated the transition from the heating process to the acceleration processes. Spectral indices derived from hard X-ray and microwave data closely agree with each other and show the classical soft–hard–soft scenario of acceleration. The hardening of the average microwave spectrum at the end of the impulsive phase was caused by the contribution of jet emission to microwaves rather than by peculiarities of the acceleration processes.

HARD–SOFT–HARD FLARE SPECTRA AND THEIR ENERGY DEPENDENCE IN SPECTRAL EVOLUTION OF A SOLAR HARD X-RAY FLARE
Chengwen **Shao**1,2 and Guangli Huang
Astrophysical Journal, 694:L162–L165, **2009**
http://www.iop.org/EJ/toc/-alert=43191/1538-4357/694/2
In this Letter, we studied the time evolution of the energy-dependent spectral indices for the **2004 November 3** solar hard X-ray flare observed by *RHESSI*. The common soft–hard–soft (SHS) pattern spectra were found at the lower energies, while a new feature, hard–soft–hard (HSH), was found at higher energies for each subpeak. As the energy increases, the SHS pattern is gradually converted into the HSH pattern. Some possible explanations for the spectral evolution and its energy dependence are discussed, such as the return current.

COMPARATIVE STUDY OF SOLAR HXR FLARE SPECTRA IN LOOPTOP AND FOOTPOINT SOURCES
Chengwen **Shao** et al **2009** ApJ 691 299-305
http://www.iop.org/EJ/abstract/0004-637X/691/1/299
In this paper, 28 peaks and subpeaks are selected in 13 RHESSI hard X-ray (HXR) flares with a single-loop structure. One looptop (LT) source is observed at lower energies, and two footpoint (FP) sources are observed at higher energies in these flares. The HXR flare spectra in the LT and FP sources are studied statistically. It is found that the LT spectral index (γLT) is well correlated with the FP spectral index (γFP) for larger values of γLT, while γLT is anticorrelated with γFP for smaller values of γLT. This new statistical result may be explained by the different relationships between the photon fluxes and spectral indices in the LT and FP sources, as well as by the nonthermal thin-target model with a larger low-cutoff energy.

Characteristics of Sustained >100 γ-ray Emission Associated with Solar Flares
G. H. **Share**, R. J. Murphy, A. K. Tolbert, B. R. Dennis, S. M. White, R. A. Schwartz, and A. J. Tylka
ApJ Supplement **2017**
http://www.astro.umd.edu/~share/publications/share_2017.pdf **File**
We characterize and provide a catalog of thirty >100 MeV sustained γ-ray emission (SGRE) events observed by Fermi LAT. These events are temporally and spectrally distinct from the associated solar flares. Their spectra are consistent with decay of pions produced by >300 MeV protons and are not consistent with electron bremsstrahlung. SGRE start times range from CME onset to two hours later. Their durations range from about four minutes to twenty hours and appear to be correlated with durations of >100 MeV SEP proton events. The >300 MeV protons producing SGRE have spectra that can be fit with power laws with a mean index of ∼4 and RMS spread of 1.8. γ-ray line measurements indicate that SGRE proton spectra are steeper above 300 MeV than they are below 300 MeV. The number of SGRE protons >500 MeV is on average about ten times more than the number in the associated flare and about fifty to one hundred times less than the number in the accompanying SEP. SGRE can extend tens of degrees from the flare site. Sustained bremsstrahlung from MeV electrons was observed in one SGRE event. Flare >100 keV X-ray emission appears to be associated with SGRE and with intense SEPs. From this observation, we provide arguments that lead us to propose that sub-MeV to MeV protons escaping from the flare contribute to the seed population that is accelerated by shocks onto open field lines to produce SEPs and onto field lines returning to the Sun to produce SGRE. **3 June 1983?, 2011-02-24, 2011 March 7, 2011-05-29, 2011-06-02, 2011-06-07, 2011-08-04, 2011-08-09, 2011-09-06, 2011-09-07, 2011-09-24, 22-Jan-12, 2012-01-23, 2012-01-27, 2012-03-04, 2012-03-05, 06-Mar-12, 2012 March 7, 2012-03-09, 2012-03-10, 2012-03-13, 2012-05-17, 2012-06-03, 2012-07-06, 2012-10-23, 2012-11-27, 2013-04-11, 2013-05-13, 2013-05-14, 2013-05-15, 2013-10-11, 2013-10-25, 2013-10-28, 2014 February 25, 2014-09-01, 2015-06-21**
Table 1. LAT Sustained >100 MeV Emission (SGRE) Events from June 2008 to December 2016
Table 4. Onset Times of CMEs, Type II Radio, and SGREs
Table A1. Solar Eruptive Events from June 2008 to May 2012
Table C2. Spectral Characteristics of Sustained-Emission Events
Table E3. Radio Bursts from LAT Sustained >100 MeV Events

Relationship Between Flares and GLEs
Gerald **Share**1,2, Ronald Murphy2
Presentation at "Ground Level Enhancement (GLE)"
Comparative Data Analysis Workshop (CDAW), LMSAL, Jan 6-9, **2009**

Source-region characteristics of anemone active regions in the ascending phase of solar cycle 24

R. **Sharma** and C. Cid
A&A 642, A233 (2020)
https://www.aanda.org/articles/aa/pdf/2020/10/aa38927-20.pdf
https://doi.org/10.1051/0004-6361/202038927
https://sci-hub.st/https://www.aanda.org/articles/aa/abs/2020/10/aa38927-20/aa38927-20.html
Context. Active regions in close proximity to coronal holes, also known as anemone regions, are the best candidates for studying the interaction between closed and open magnetic field topologies at the Sun. Statistical investigation of their source-region characteristics can provide vital clues regarding their possible association with energetic events, relevant from space weather perspectives.
Aims. The main goal of our study is to understand the distinct properties of flaring and non-flaring anemone active regions and their host coronal holes, by examining spatial and magnetic field distributions during the rise phase of the solar cycle, in the years 2011–2014.
Methods. Anemone regions were identified from the minimum-distance threshold, estimated using the data available in the online catalogs for on-disk active regions and coronal holes. Along with the source-region area and magnetic field characteristics, associated filament and flare cases were also located. Regions with and without flare events were further selected for a detailed statistical examination to understand the major properties of the energetic events, both eruptive and confined, at the anemone-type active regions.
Results. Identified anemone regions showed weak asymmetry in their spatial distribution over the solar disk, with yearly average independent from mean sunspot number trend, during the rise phase of solar cycle 24. With the progression in solar cycle, the area and minimum-distance parameters indicated a decreasing trend in their magnitudes, while the magnetic field characteristics indicated an increase in their estimated magnitudes. More than half of the regions in our database had an association with a filament structure, and nearly a third were linked with a magnetic reconnection (flare) event. Anemone regions with and without flares had clear distinctions in their source-region characteristics evident from the distribution of their properties and density analysis. The key differences included larger area and magnetic field magnitudes for flaring anemone regions, along with smaller distances between the centers of the active region and its host coronal hole. **06 September 2011**

Radio and X-ray Observations of Short-lived Episodes of Electron Acceleration in a Solar Microflare

Rohit **Sharma**, Marina Battaglia, Yingjie Luo, Bin Chen, Sijie Yu
ApJ **904** 94 **2020**
https://arxiv.org/pdf/2009.14497.pdf
https://doi.org/10.3847/1538-4357/abbd96
Solar flares are sudden energy release events in the solar corona, resulting from magnetic reconnection, that accelerates particles and heats the ambient plasma. During a flare, there are often multiple, temporally and spatially separated individual energy release episodes that can be difficult to resolve depending on the observing instrument. We present multi-wavelength imaging and spectroscopy observations of multiple electron acceleration episodes during a GOES B1.7-class two-ribbon flare on **2012 February 25**, observed simultaneously with the Karl G. Jansky Very Large Array (VLA) at 1--2 GHz, the Reuven Ramatay High Energy Solar Spectroscopic Imager (RHESSI) in X-rays, and the Solar Dynamics Observatory in extreme ultraviolet (EUV). During the initial phase of the flare, five radio bursts were observed. A nonthermal X-ray source was seen co-temporal, but not co-spatial, with the first three radio bursts. Their radio spectra are interpreted as optically thick gyrosynchrotron emission. By fitting the radio spectra with a gyrosynchrotron model, we derive the magnetic field strength and nonthermal electron spectral parameters in each acceleration episode. Notably, the nonthermal parameters derived from X-rays differ considerably from the nonthermal parameters inferred from the radio. The observations are indicative of multiple, co-temporal acceleration episodes during the impulsive phase of a solar microflare. The X-ray and radio burst sources likely originate from separate electron distributions in different magnetic loops.
CESRA #2832 March **2021** http://www.astro.gla.ac.uk/users/eduard/cesra/?p=2832

On the Bright Loop Top Emission in Post Eruption Arcades

Rohit **Sharma**, Durgesh Tripathi, Hiroaki Isobe, Avyarthana Ghosh
ApJ **2016**
http://arxiv.org/pdf/1603.04959v1.pdf
The observations of post eruption arcades (PEAs) in X-rays and EUV reveal strong localised brightenings at the loop top regions. The origin of these brightenings and their dynamics is not well understood to date. Here, we study the dynamics of PEAs using one-dimensional hydrodynamic modelling with the focus on the the understanding of the formation of localised brightening.Our findings suggest that these brightenings are the result of collisions between the counter-streaming chromospheric evaporation from both the foot points. We further perform forward modelling of the emission observed in simulated results in various spectral lines observed by the Extreme-Ultraviolet Imaging Telescope

aboard Hinode. The forward modelled intensities in various spectral lines are in close agreement with a flare observed in **December 17, 2006** by EIS.

Sunquakes of Solar Cycle 24

I.N. **Sharykin**, A.G. Kosovichev
ApJ **2019**
https://arxiv.org/pdf/1911.04197.pdf
The paper presents results of a search for helioseismic events (sunquakes) produced by M-X class solar flares during Solar Cycle 24. The search is performed by analyzing photospheric Dopplergrams from Helioseismic Magnetic Imager (HMI). Among the total number of 500 M-X class flares, 82 helioseismic events were detected. This result is quite unexpected, since it was previously thought that sunquakes were very rare and observed mainly in strong flares. However, our analysis has shown that there many strong sunquakes were produced by solar flares of low M class, while in some powerful X-class flares helioseismic waves were not observed or were weak. Our analysis also revealed several active regions characterized by the most efficient generation of helioseismic waves during flares. We found that the sunquake power correlates with the maximum value of soft X-ray flux time derivative better than with the X-ray class, indicating that the sunquake mechanism is associated with high-energy particles. We also show that the seismically active flares are more impulsive than the flares without photospheric and helioseismic perturbations. We present a new catalog of helioseismic solar flares, which opens opportunities for performing statistical studies to better understand physics of sunquakes as well as flare energy release and transport. **October 23, 2012, November 5, 2013**
Table 2011-2017

Flare Energy Release at the Magnetic Field Polarity Inversion Line During M1.2 Solar Flare of 2015 March 15.
II. Investigation of Photospheric Electric Current and Magnetic Field Variations Using HMI 135-second Vector Magnetograms

I.N. **Sharykin**, I.V. Zimovets, I.I.Myshyakov
2020 *ApJ* **893** 159
https://arxiv.org/pdf/1905.03352.pdf
https://doi.org/10.3847/1538-4357/ab84ef
This work is a continuation of Paper I (Sharykin et al. 2018) devoted to analysis of nonthermal electron dynamics and plasma heating in the confined M1.2 class solar flare SOL2015-03-15T22:43 revealing energy release in the highly sheared interacting magnetic loops in the low corona, above the polarity inversion line (PIL). The scope of the present work is to make the first extensive quantitative analysis of the photospheric magnetic field and photospheric vertical electric current (PVEC) dynamics in the PIL region using new vector magnetograms obtained with the Helioseismic and Magnetic Imager (HMI) onboard the Solar Dynamics Observatory (SDO) with high temporal resolution of 135 s. Data analysis revealed sharp changes of the magnetic structure and PVEC associated with the flare onset near the PIL. It was found that the strongest plasma heating and electron acceleration were associated with the largest increase of the magnetic reconnection rate, total PVEC and effective PVEC density in the flare ribbons. Observations and non-linear force-free field (NLFFF) extrapolations have shown that the magnetic field structure around the PIL is consistent with the tether-cutting magnetic reconnection (TCMR) geometry. We gave qualitative interpretation of the observed dynamics of the flare ribbons, magnetic field and PVEC, and electron acceleration, within the TCMR scenario.

Flare Energy Release in the Magnetic Field Polarity Inversion Line During M1.2 Solar Flare of March 15, 2015.
I. Onset of Plasma Heating and Electrons Acceleration

I.N. **Sharykin**, I.V. Zimovets, I.I. Myshyakov, N.S. Meshalkina
2018 *ApJ* **864** 156
https://arxiv.org/pdf/1805.05792.pdf
http://sci-hub.tw/http://iopscience.iop.org/article/10.3847/1538-4357/aada15/meta
We present the study of SOL**2015-03-15** M1.2 flare, revealing acceleration of electrons and plasma heating in the sheared twisted magnetic structure in the polarity inversion line (PIL). The scope is to make the analysis of nonthermal electrons dynamics and plasma heating in the highly stressed magnetic loops interacting in the PIL by using X-ray, microwave, ultraviolet, and optical observations. It is found that the most probable scenario for the energy release in the PIL is the tether-cutting magnetic reconnection between the low-lying (3 Mm above the photosphere) magnetic loops within a twisted magnetic flux rope. Energetic electrons with the hardest spectrum were appeared at the onset of plasma heating up to the super-hot temperature of 40 MK. These electrons are localized in a thin magnetic channel with width of around 0.5 Mm with high average magnetic field of about 1200 G. The plasma beta in the super-hot region is less than 0.01. The estimated density of accelerated electrons is about 10^9 cm^-3 that is much less than the super-hot plasma density. The energy density flux of non-thermal electrons is estimated up to 3x10^12 ergs cm^-2s^-1 that is much higher than in the currently available radiative hydrodynamic models. These results revealed that one need to

develop new self-consisting flare models reproducing 3D magnetic reconnection in the PIL with strong magnetic field, spatial filamentation of energy release, formation of high energy density populations of nonthermal electrons and appearance of the super-hot plasma.

Onset of Photospheric Impacts and Helioseismic Waves in X9.3 Solar Flare of September 6, 2017

Ivan N. **Sharykin**, Alexander G. Kosovichev
ApJ **864(1)** 86 **2018**
https://arxiv.org/pdf/1804.06565.pdf
https://iopscience.iop.org/article/10.3847/1538-4357/aad558/pdf
The X9.3 flare of **September 6, 2017**, was the most powerful flare of Solar Cycle 24. It generated strong white-light emission and multiple helioseismic waves (sunquakes). By using data from Helioseismic and Magnetic Imager (HMI) onboard the Solar Dynamics Observatory (SDO) as well as hard X-ray data from KONUS instrument onboard WIND spacecraft, and Anti-Coincidence System (ACS) onboard the INTERGRAL space observatory, we investigate spatio-temporal dynamics of photospheric emission sources, identify sources of helioseismic waves and compare the flare photospheric dynamics with the hard X-ray (HXR) temporal profiles. The results show that the photospheric flare impacts started to develop in compact regions in close vicinity of the magnetic polarity inversion line (PIL) in the pre-impulsive phase before detection of the HXR emission. The initial photospheric disturbances were localized in the region of strong horizontal magnetic field of the PIL, and, thus, are likely associated with a compact sheared magnetic structure elongated along the PIL. The acoustic egression power maps revealed two primary sources of generation of sunquakes, which were associated with places of the strongest photospheric impacts in the pre-impulsive phase and the early impulsive phase. This can explain the two types of helioseismic waves observed in this flare. Analysis of the high-cadence HMI filtergrams suggests that the flare energy release developed in the form of sequential involvement of compact low-lying magnetic loops that were sheared along the PIL.
HMI Science Nuggets in September **2018** #110 hmi.stanford.edu/hminuggets/?p=2649

Investigation of Relationship Between High-Energy X-ray Sources and Photospheric Impact of X1.8 Solar Flare of October 23, 2012

Ivan N **Sharykin**, Alexander G Kosovichev, Viacheslav M Sadykov, Ivan V Zimovets, Ivan I Myshyakov
2017 *ApJ* **843** 67
https://arxiv.org/pdf/1703.03767.pdf
http://sci-hub.cc/10.3847/1538-4357/aa77f1
The X-class solar flare of **October 23, 2012,** generated continuum photospheric emission and a strong helioseismic wave ("**sunquake**") that points to an intensive energy release in the dense part of the solar atmosphere. We study properties of the energy release with high temporal and spatial resolutions, using photospheric data from Helioseismic Magnetic Imager (HMI) onboard Solar Dynamics Observatory (SDO), and hard X-ray observations made by Ramaty High-Energy Solar Spectroscopic Imager (RHESSI). For this analysis we use level-1 HMI data (filtergrams), obtained by scanning the Fe I line (6731 \AA) with time cadence of$\sim$3.6 s and spatial resolution of $\sim$0.5″ per pixel. It is found that the photospheric disturbances spatially coincide with the region of the hard X-ray emission but are delayed by $\lesssim$4seconds. This delay is consistent with predictions of the RADYN models. However, the models fail to explain the magnitude of the observed variations of the HMI lines. The data indicate that the photospheric impact might be caused by the electron energy flux substantially higher than that in the current flare radiative hydrodynamic models.

Solar flares with similar soft but different hard X-ray emissions: case and statistical studies

Ivan N. **Sharykin**, Alexei B. Struminsky, Ivan V. Zimovets, Wei-Qun Gan
Research in Astronomy and Astrophysics (RAA) Vol 16, No 1 (**2016**) paper 5
From the Reuven Ramaty High Energy Solar Spectroscopic Imager (RHESSI) catalog we select events which have approximately the same GOES class (high C - low M or 500–1200 counts s−1within the RHESSI 6–12 keV energy band), but with different maximal energies of detected hard X-rays. The selected events are subdivided into two groups: (1) flares with X-ray emissions observed by RHESSI up to only 50 keV and (2) flares with hard X-ray emission observed also above 50 keV. The main task is to understand observational peculiarities of these two flare groups. We use RHESSI X-ray data to obtain spectral and spatial information in order to find differences between selected groups. Spectra and images are analyzed in detail for six events (case study). For a larger number of samples (85 and 28 flares in the low-energy and high-energy groups respectively) we only make some generalizations. In spectral analysis we use the thick-target model for hard X-ray emission and one temperature assumption for thermal soft X-ray emission. RHESSI X-ray images are used for determination of flare region sizes. Although thermal and spatial properties of these two groups of flares are not easily distinguishable, power law indices of hard X-rays show significant differences. Events from the high-energy group generally have a harder spectrum. Therefore, the efficiency

of chromospheric evaporation is not sensitive to the hardness of nonthermal electron spectra but rather depends on the total energy flux of nonthermal electrons.

Flare Energy Release in the Lower Solar Atmosphere Near the Magnetic Field Polarity Inversion Line

I.N. **Sharykin**, V.M. Sadykov, A.G. Kosovichev, S. Vargas-Dominguez, I.V. Zimovets
Astrophysical Journal, Volume 840, Issue 2, article id. 84, 13 pp. (**2017**)
https://arxiv.org/abs/1801.04921

We study flare processes in the solar atmosphere using observational data for a M1-class flare of **June 12, 2014**, obtained by New Solar Telescope (NST/BBSO) and Helioseismic Magnetic Imager (HMI/SDO). The main goal is to understand triggers and manifestations of the flare energy release in the photosphere and chromosphere using high-resolution optical observations and magnetic field measurements. We analyze optical images, HMI Dopplergrams and vector magnetograms, and use Non-Linear Force-Free Field (NLFFF) extrapolations for reconstruction of the magnetic topology and electric currents. The NLFFF modelling reveals interaction of two magnetic flux ropes with oppositely directed magnetic field in the PIL. These flux ropes are observed as a compact sheared arcade along the PIL in the high-resolution broad-band continuum images from NST. In the vicinity of PIL, the NST H alpha observations reveal formation of a thin three-ribbon structure corresponding to a small-scale photospheric magnetic arcade. The observational results evidence in favor of location of the primary energy release site in the chromospheric plasma with strong electric currents concentrated near the polarity inversion line. In this case, magnetic reconnection is triggered by the interacting magnetic flux ropes forming a current sheet elongated along the PIL.
substantial text overlap with arXiv:1604.05380

Observational Investigation of Energy Release in the Lower Solar Atmosphere of a Solar Flare

I. N. **Sharykin**, V. M. Sadykov, A. G. Kosovichev, S. Vargas-Dominguez, I. V. Zimovets
2017 ApJ 840 84
http://arxiv.org/pdf/1604.05380v1.pdf

We study flare processes in the lower solar atmosphere using observational data for a M1-class flare of **June 12, 2014**, obtained by New Solar Telescope (NST/BBSO) and Helioseismic Magnetic Imager (HMI/SDO). The main goal is to understand triggers and manifestations of the flare energy release in the lower layers of the solar atmosphere (the photosphere and chromosphere) using high-resolution optical observations and magnetic field measurements. We analyze optical images, HMI Dopplergrams and vector magnetograms, and use Non-Linear Force-Free Field (NLFFF) extrapolations for reconstruction of the magnetic topology. The NLFFF modelling reveals interaction of oppositely directed magnetic flux-tubes in the PIL. These two interacting magnetic flux tubes are observed as a compact sheared arcade along the PIL in the high-resolution broad-band continuum images from NST. In the vicinity of the PIL, the NST H alpha observations reveal formation of a thin three-ribbon structure corresponding to the small-scale photospheric magnetic arcade. Presented observational results evidence in favor of location of the primary energy release site in the dense chromosphere where plasma is partially ionized in the region of strong electric currents concentrated near the polarity inversion line. Magnetic reconnection may be triggered by two interacting magnetic flux tubes with forming current sheet elongated along the PIL.

Energy Release and Initiation of a Sunquake in a C-class Flare

I. N. **Sharykin**1,2, A. G. Kosovichev1,3,4, and I. V. Zimovets
2015 ApJ 807 102
http://arxiv.org/pdf/1405.5912v1.pdf
http://sci-hub.cc/10.3847/1538-4357/aa6dfd

We present an analysis of the C7.0 solar flare from **2013 February 17**, revealing a strong helioseismic response (sunquake) caused by a compact impact observed with the Helioseismic and Magnetic Imager on board the Solar Dynamics Observatory (SDO) in the low atmosphere. This is the weakest known C-class flare generating a sunquake event. To investigate the possible mechanisms of this event and understand the role of accelerated charged particles and photospheric electric currents, we use data from three space observatories: RHESSI, SDO, and Geostationary Operational Environmental Satellite. We find that the photospheric flare impact does not spatially correspond to the strongest hard X-ray emission source, but both of these events are parts of the same energy release. Our analysis reveals a close association of the flare energy release with a rapid increase in the electric currents and suggests that the sunquake initiation is unlikely to be caused by the impact of high-energy electrons, but may be associated with rapid current dissipation or a localized impulsive Lorentz force in the lower layers of the solar atmosphere.

Dynamics of Electric Currents, Magnetic Field Topology and Helioseismic Response of a Solar Flare

I. N. **Sharykin**, A. G. Kosovichev

2015 *ApJ* **808** 72

http://arxiv.org/pdf/1502.05190v1.pdf

The solar flare on **July 30, 2011** was of a modest X-ray class (M9.3), but it made a strong photospheric impact and produced a "sunquake," observed with the Helioseismic and Magnetic Imager (HMI) on NASA's Solar Dynamics Observatory (SDO). In addition to the helioseismic waves (also observed with the SDO/AIA instrument), the flare caused a large expanding area of white-light emission and was accompanied by substantial restructuring of magnetic fields, leading to the rapid formation of a sunspot structure in the flare region. The flare produced no significant hard X-ray emission and no coronal mass ejection. This indicates that the flare energy release was mostly confined to the lower atmosphere. The absence of significant coronal mass ejection rules out magnetic rope eruption as a mechanism of helioseismic waves. We discuss the connectivity of the flare energy release with the electric currents dynamics and show the potential importance of high-speed plasma flows in the lower solar atmosphere during the flare energy release.

Plasma Heating to Super-Hot Temperatures (>30 MK) in the August 9, 2011 Solar Flare

I.N. **Sharykin**, A.B. Struminsky, I.V. Zimovets

Astronomy Letters Volume 41, Issue 1-2, pp 53-66 **2015**

Pis'ma v Astronomicheskiĭ Zhurnal, **2015**, Vol. 41, Nos. 1–2, pp. 57–71.

http://arxiv.org/pdf/1502.03220v1.pdf

We investigate the August 9, 2011 solar flare of X-ray class X6.9, the "hottest" flare from 2000 to 2012, with a peak plasma temperature according to GOES data of 32.5 MK. Our goal is to determine the cause of such an anomalously high plasma temperature and to investigate the energy balance in the flare region with allowance made for the presence of a super-hot plasma (>30 MK). We analyze the RHESSI, GOES, AIA/SDO, and EVE/SDO data and discuss the spatial structure of the flare region and the results of our spectral analysis of its X-ray emission. Our analysis of the RHESSI X-ray spectra is performed in the one-temperature and two-temperature approximations by taking into account the emission of hot (20 MK) and super-hot (45 MK) plasmas. The hard X-ray spectrum in both models is fitted by power laws. The observed peculiarities of the flare are shown to be better explained in terms of the two-temperature model, in which the super-hot plasma is located at the flare loop tops (or in the magnetic cusp region). The formation of the super-hot plasma can be associated with its heating through primary energy release and with the suppression of thermal conduction. The anomalously high temperature (32.5 MK according to GOES) is most likely to be an artefact of the method for calculating the temperature based on two-channel GOES measurements in the one-temperature approximation applied to the emission of a multi-temperature flare plasma with a minor contribution from the low-temperature part of the differential emission measure.

August 9, 2011 (X6.9) and July 23, 2002

Onset of Electron Acceleration in a Flare Loop

I.N. **Sharykin**, S. Liu, L. Fletcher

2014 ApJ 793 25.

http://arxiv.org/pdf/1408.1413v1.pdf

We carried out detailed analysis of X-ray and radio observations of a simple flare loop that occurred on **12th August 2002**, with the impulsive hard X-ray (HXR) light curves dominated by a single pulse. The emission spectra of the early impulsive phase are consistent with an isothermal model in the coronal loop with a temperature reaching several keVs. A power-law high-energy spectral tail is evident near the HXR peak time, in accordance with the appearance of footpoints at high energies, and is well correlated with the radio emission. The energy content of the thermal component keeps increasing gradually after the disappearance of this nonthermal component. These results suggest that electron acceleration only covers a central period of a longer and more gradual energy dissipation process and that the electron transport within the loop plays a crucial role in the formation of the inferred power-law electron distribution. The spectral index of power-law photons shows a very gradual evolution indicating a quasi-steady state of the electron accelerator, which is confirmed by radio observations. These results are consistent with the theory of stochastic electron acceleration from a thermal background. Advanced modeling with coupled electron acceleration and spatial transport processes is needed to explain these observations more quantitatively, which may reveal the dependence of the electron acceleration on the spatial structure of the acceleration region.

Energy Release and Initiation of Sunquake in C-class Flare

I.N. **Sharykin**, A.G. Kosovichev, I.V. Zimovets

2014

http://arxiv.org/pdf/1405.5912v1.pdf

We present analysis of a C-class solar flare of **Febrary 17, 2013**, revealing a strong helioseismic response caused by a very compact impact in the photosphere. This is the first detection of sunquake in C-class flares. To investigate possible mechanisms of generation of this sunquake, and to understand the role of accelerated charged particles and photospheric electric currents, we use data from three space observatories: Ramaty High Energy Solar Spectroscopic Imager (RHESSI), Solar Dynamics Observatory (SDO) and Geostationary Operational Environmental Satellite (GOES). We find that the sunquake impulse does not spatially correspond to the HXR emission source, but both of these events are parts of the same energy release. Our analysis reveals a close association of the flare energy release with a rapid increase of the electric currents, and suggests that the sunquake initiation can be explained by a rapid current dissipation or by a localized impulsive Lorentz force.

Fine structure of flare ribbons and evolution of electric currents

I.N. **Sharykin**, A.G. Kosovichev
2014 ApJ 788 L18
http://arxiv.org/pdf/1404.5104v1.pdf
Emission of solar flares across the electromagnetic spectrum is often observed in the form of two expanding ribbons. The standard flare model explains the flare ribbons as footpoints of magnetic arcades, emitting due to interaction of energetic particles with the chromospheric plasma. However, the physics of this interaction and properties of the accelerated particles are still unknown. We present results of multiwavelength observations of C2.1 flare of **August 15, 2013**, observed with New Solar Telescope (NST) of Big Bear Solar Observatory, Solar Dynamics Observatory (SDO), GOES and FERMI spacecraft. The observations reveal previously unresolved sub-arcsecond structure of the flare ribbons in regions of strong magnetic field consisting from numerous small-scale bright knots. We observe red-blue asymmetry of H α flare ribbons with a width as small as 100 km. We discuss the relationship between the ribbons and vertical electric currents estimated from vector magnetograms, and show that Joule heating can be responsible for energization of H α knots in the ribbons.

Simulation Models for Exploring Magnetic Reconnection **Review**

Michael **Shay**, Subash Adhikari, Naoki Beesho, Joachim Birn, +++
Chapter 5.2 of ISSI Book on Magnetic Reconnection, Space Science Reviews **2024**
https://arxiv.org/pdf/2406.05901
Simulations have played a critical role in the advancement of our knowledge of magnetic reconnection. However, due to the inherently multiscale nature of reconnection, it is impossible to simulate all physics at all scales. For this reason, a wide range of simulation methods have been crafted to study particular aspects and consequences of magnetic reconnection. This chapter reviews many of these methods, laying out critical assumptions, numerical techniques, and giving examples of scientific results. Plasma models described include magnetohydrodynamics (MHD), Hall MHD, Hybrid, kinetic particle-in-cell (PIC), kinetic Vlasov, Fluid models with embedded PIC, Fluid models with direct feedback from energetic populations, and the Rice Convection Model (RCM).

Atmospheric Response to of an Active Region to new Small Flux Emergence

D.L. **Shelton**, L.K. Harra, L.M. Green
Solar Phys. Volume 290, Issue 3, pp 753-770 **2015**
http://arxiv.org/pdf/1412.5623v1.pdf
We investigate the atmospheric response to a small emerging flux region (EFR) that occurred in the positive polarity of Active Region 11236 on **23-24 June 2011**. Data from the \textit{Solar Dynamics Observatory's Atmopheric Imaging Assembly} (AIA), the \textit{Helioseismic and Magnetic Imager} (HMI) and Hinode's \textit{EUV imaging spectrometer} (EIS) are used to determine the atmospheric response to new flux emerging into a pre-existing active region.
Brightenings are seen forming in the upper photosphere, chromosphere, and corona over the EFR's location whilst flux cancellation is observed in the photosphere. The impact of the flux emergence is far reaching, with new large-scale coronal loops forming up to 43 Mm from the EFR and coronal upflow enhancements of approximately 10 km s−1 on the north side of the EFR. Jets are seen forming in the chromosphere and the corona over the emerging serpentine field. This is the first time that coronal jets have been seen over the serpentine field.

Flows and magnetic field structures in reconnection regions of simulations of the solar atmosphere: do flux pile-up models work?

S. **Shelyag**, Y. E. Litvinenko, V. Fedun, G. Verth, J.J. González-Avilés, F.S. Guzmán
A&A **2018**
https://arxiv.org/pdf/1809.00587.pdf
We study the process of magnetic field annihilation and reconnection in simulations of magnetised solar photosphere and chromosphere with magnetic fields of opposite polarities and constant numerical resistivity. Exact analytical

solutions for reconnective annihilations are used to interpret the features of magnetic reconnection in simulations of flux cancellation in the solar atmosphere. We use MURaM high-resolution photospheric radiative magneto-convection simulations to demonstrate the presence of magnetic field reconnection consistent with the magnetic flux pile-up models. Also, a simulated data-driven chromospheric magneto-hydrodynamic simulation is used to demonstrate magnetic field and flow structures, which are similar to the ones theoretically predicted. Both simulations demonstrate flow and magnetic field structures roughly consistent with accelerated reconnection with magnetic flux pile-up. The presence of standard Sweet-Parker type reconnection is also demonstrated in stronger photospheric magnetic fields.

Energy-releasing Process for the 2013 May 13 X1.7 Limb Flare: A Continued Study

Jinhua **Shen**1,2, Jianping Li3, Yu Huang3, Dong Li3, Yingna Su3, and Haisheng Ji3
2023 ApJ 950 71
https://iopscience.iop.org/article/10.3847/1538-4357/accc8c/pdf
In this paper, we reanalyze the X1.7 class limb flare that occurred on **2013 May 13** (SOL2013-05-13T01:56 UT), concentrating on the energy-releasing process using microwave observations mainly made by Nobeyama and X-ray observations made by RHESSI. The analysis was carried out in the context of EUV observations made by the Atmospheric Imaging Assembly on board Solar Dynamics Observatory. First, we complement the initiation process by showing that the initiation occurred together with material falling from a large-scale overlying prominence, a signature of drainage instability. The usual downward and upward motions of the microwave and X-ray sources are observed from their evolution. However, the microwave source's height shows a recurrent decrease and increase during its overall upward motion; it shows a kind of recurrent contraction and expansion. The time period of the recurrent contraction and expansion corresponds to the period of post-contraction oscillation of EUV loops, and the oscillatory motions are closely correlated with four microwave/hard X-ray peaks that unusually increased nonthermal emission levels by several times. X-ray spectra get hardened during the oscillation. In addition, the rapid contraction of magnetic loops located on the outside of the erupting flux rope occurs 5 minutes after the onset of the flare, showing that the contraction of the peripheral magnetic loops is more likely due to the vortex and sink flows generated by an upward erupting magnetic flux rope rather than a coronal implosion. The results can provide more insight into the physics of dynamic coronal magnetic field and particle acceleration during solar flares.

Non-thermal Broadening of IRIS Fe XXI Lines Caused by Turbulent Plasma Flows in the Magnetic Reconnection Region During Solar Eruptions

Chengcai **Shen**, Vanessa Polito, Katharine K. Reeves, Bin Chen, Sijie Yu, Xiaoyan Xie
2022
https://arxiv.org/pdf/2211.07428.pdf
Magnetic reconnection is the key mechanism for energy release in solar eruptions, where the high-temperature emission is the primary diagnostic for investigating the plasma properties during the reconnection process. Non-thermal broadening of high-temperature lines has been observed in both the reconnection current sheet (CS) and flare loop-top regions by UV spectrometers, but its origin remains unclear. In this work, we use a recently developed three-dimensional magnetohydrodynamic (MHD) simulation to model magnetic reconnection in the standard solar flare geometry and reveal highly dynamic plasma flows in the reconnection regions. We calculate the synthetic profiles of the Fe XXI 1354 Å~line observed by the Interface Region Imaging Spectrograph (IRIS) spacecraft by using parameters of the MHD model, including plasma density, temperature, and velocity. Our model shows that the turbulent bulk plasma flows in the CS and flare loop-top regions are responsible for the non-thermal broadening of the Fe XXI emission line. The modeled non-thermal velocity ranges from tens of km s−1 to more than two hundred km s−1, which is consistent with the IRIS observations. Simulated 2D spectral line maps around the reconnection region also reveal highly dynamic downwflow structures where the high non-thermal velocity is large, which is consistent with the observations as well. **2015-03-07-08**

Coronal Quasi-periodic Fast-mode Propagating Wave Trains **Review**

Yuandeng **Shen**, Xinping Zhou, Yadan Duan, Zehao Tang, Chengrui Zhou, Song Tan
Solar Phys. **2022**
https://arxiv.org/pdf/2112.14959.pdf **File**
QFP wave trains in the corona have been studied intensively in the past decade, thanks to the full-disk, high spatiotemporal resolution, and wide-temperature coverage observations taken by the SDO/AIA. In AIA observations, QFP wave trains are seen to consist of multiple coherent and concentric wavefronts emanating successively near the epicenter of the accompanying flares; they propagate outwardly either along or across coronal loops at fast-mode magnetosonic speeds from several hundred to more than 2000 km/s, and their periods are in the range of tens of seconds to several minutes. Based on the distinct different properties of QFP wave trains, they might be divided into two distinct categories including narrow and broad ones. For most QFP wave trains, some of their periods are similar to those of quasi-periodic pulsations (QPPs) in the accompanying flares, indicating that they are probably different manifestations of the same physical process. Currently, candidate generation mechanisms for QFP wave trains include two main categories: pulsed energy excitation mechanism in association with magnetic reconnection and dispersion evolution

mechanism related to the dispersive evolution of impulsively generated broadband perturbations. In addition, the generation of some QFP wave trains might be driven by the leakage of three and five minute oscillations from the lower atmosphere. As one of the new discoveries of SDO, QFP wave trains provide a new tool for coronal seismology to probe the corona parameters, and they are also useful for diagnosing the generation of QPPs, flare processes including energy release and particle accelerations. This review aims to summarize the main observational and theoretical results of the spatially-resolved QFP wave trains in extreme ultraviolet observations, and states briefly a number of questions that deserve further investigations. **2010 September 08, 2011 February 14, 2011 May 30, 2012 April 24, 2013 May 22, 2014 November 03, 2015 April 16**

Table 1. Physical parameters of the published QFP wave trains

The Origin of Underdense Plasma Downflows Associated with Magnetic Reconnection in Solar Flares

Chengcai **Shen**, Bin Chen, Katharine K. Reeves, Sijie Yu, Vanessa Polito, Xiaoyan Xie

Nature Astronomy **volume 6**, pages1–2 (**2022**)

https://arxiv.org/pdf/2111.11407.pdf

https://doi.org/10.1038/s41550-021-01570-2

Magnetic reconnection is a universal process that powers explosive energy release events such as solar flares, geomagnetic substorms, and some astrophysical jets. A characteristic feature of magnetic reconnection is the production of fast reconnection outflow jets near the plasma Alfvén speeds. In eruptive solar flares, dark, finger-shaped plasma downflows moving toward the flare arcade have been commonly regarded as the principal observational evidence for such reconnection-driven outflows. However, they often show a speed much slower than that expected in reconnection theories, challenging the reconnection-driven energy release scenario in standard flare models. Here, we present a three-dimensional magnetohydrodynamics model of solar flares. By comparing the model-predictions with the observed plasma downflow features, we conclude that these dark downflows are self-organized structures formed in a turbulent interface region below the flare termination shock where the outflows meet the flare arcade, a phenomenon analogous to the formation of similar structures in supernova remnants. This interface region hosts a myriad of turbulent flows, electron currents, and shocks, crucial for flare energy release and particle acceleration. **2015 June 28**

Round-Trip Slipping Magnetic Reconnection Observed in a Fan-Spine Jet

Yuandeng **Shen**, Zhining Qu, Chengrui Zhou, Yadan Duan, Zehao Tang, Ding Yuan

ApJL **885** L11 **2019**

https://arxiv.org/pdf/1910.05472.pdf

https://iopscience.iop.org/article/10.3847/2041-8213/ab4cf3/pdf

A solar jet on **2014 July 31**, which was accompanied by a GOES C1.3 flare and a mini-filament eruption at the jet base, was studied by using observations taken by the New Vacuum Solar Telescope and the Solar Dynamic Observatory. Magnetic field extrapolation revealed that the jet was confined in a fan-spine magnetic system that hosts a null point at the height of about 9 Mm from the solar surface. An inner flare ribbon surrounded by an outer circular ribbon and a remote ribbon were observed to be associated with the eruption, in which the inner and remote ribbons respectively located at the footprints of the inner and outer spines, while the circular one manifested the footprint of the fan structure. It is interesting that the circular ribbon's west part showed an interesting round-trip slipping motion, while the inner ribbon and the circular ribbon's east part displayed a northward slipping motion. Our analysis results indicate that the slipping motions of the inner and the circular flare ribbons reflected the slipping magnetic reconnection process in the fan quasi-separatrix layer, while the remote ribbon was associated with the magnetic reconnection at the null point. In addition, the filament eruption was probably triggered by the magnetic cancellation around its south end, which further drove the slipping reconnection in the fan quasi-separatrix layer and the reconnection at the null point.

The Dynamical Behavior of Reconnection-driven Termination Shocks in Solar Flares: Magnetohydrodynamic Simulations

Chengcai **Shen**, Xiangliang Kong, Fan Guo, John C. Raymond, Bin Chen

ApJ **869** 116 **2018**

https://arxiv.org/pdf/1812.01189.pdf

sci-hub.tw/10.3847/1538-4357/aaeed3

In eruptive solar flares, termination shocks (TSs), formed when high-speed reconnection outflows collide with closed dense flaring loops, are believed to be one of the possible candidates for plasma heating and particle acceleration. In this work, we perform resistive magnetohydrodynamic simulations in a classic Kopp-Pneuman flare configuration to study the formation and evolution of TSs, and analyze in detail the dynamic features of TSs and variations of the shock strength in space and time. This research focuses on the fast reconnection phase when plasmoids form and produce small-scale structures inside the flare current sheet. It is found that the TS emerges once the downward outflow colliding with closed magnetic loops becomes super-magnetosonic, and immediately becomes highly dynamical. The morphology of a TS can be flat, oblique, or curved depending on the detailed interactions between the outflows/plasmoids and the highly dynamic plasma in the looptop region. The TS becomes weaker when a plasmoid is

crossing through, or may even be destroyed by well developed plasmoids and then re-constructed above the plasmoids. We also perform detailed statistical analysis on important physical quantities along and across the shock front. The density and temperature ratios range from 1 to 3 across the TS front, and the pressure ratio typically has larger values up to 10. We show that weak guide fields do not strongly affect the Mach number and compression ratios, and the TS length becomes slightly larger in the case with thermal conduction.

INITIATION PROCESSES FOR THE 2013 MAY 13 X1.7 LIMB FLARE

Jinhua **Shen**1,2, Ya Wang3,4, Tuanhui Zhou3,5, and Haisheng Ji3,5
2017 ApJ 835 43
http://iopscience.iop.org.sci-hub.cc/0004-637X/835/1/43/
For the X1.7 class flare on **2013 May 13** (SOL2013-05-13T01:53), its initiation process was well observed by the Atmospheric Imaging Assembly (AIA) on board the Solar Dynamic Observatory and the Extreme UltraViolet Imager (EUVI) on board STEREO-B . The initiation process incorporates the following phenomena: an X-ray precursor that started ~9 minutes before flare onset, two hot magnetic loops (as seen with AIA hot channels) forming a sigmoidal core magnetic structure (as seen with the EUVI), a rapidly formed magnetic flux rope (MFR) that expands outward, and a flare loop that contracts inward. The two hot magnetic loops were activated after the occurrence of the X-ray precursor. After activation, magnetic reconnection occurred between the two hot magnetic loops (inside the sigmoid structure), which produced the expanding MFR and the contracting flare loop (CFL). The MFR and CFL can only be seen with AIA hot and cool channels, respectively. For this flare, the real initiation time can be regarded as being from the starting time of the precursor, and its impulsive phase started when the MFR began its fast expansion. In addition, the CFL and the growing postflare magnetic loops are different loop systems, and the CFL was the product of magnetic reconnection between sheared magnetic fields that also produced the MFR.

Well-observed Dynamics of Flaring and Peripheral Coronal Magnetic Loops during an M-class Limb Flare

Jinhua **Shen**1, Tuanhui Zhou2,3, Haisheng Ji2,3, Thomas Wiegelmann4, Bernd Inhester4, and Li Feng
2014 ApJ 791 83
In this paper, we present a variety of well-observed dynamic behaviors for the flaring and peripheral magnetic loops of the M6.6 class extreme limb flare that occurred on **2011 February 24** (SOL2011-02-24T07:20) from EUV observations by the Atmospheric Imaging Assembly on the Solar Dynamics Observatory and X-ray observations by RHESSI. The flaring loop motion confirms the earlier contraction-expansion picture. We find that the U-shaped trajectory delineated by the X-ray corona source of the flare roughly follows the direction of a filament eruption associated with the flare. Different temperature structures of the coronal source during the contraction and expansion phases strongly suggest different kinds of magnetic reconnection processes. For some peripheral loops, we discover that their dynamics are closely correlated with the filament eruption. During the slow rising to abrupt, fast rising of the filament, overlying peripheral magnetic loops display different responses. Two magnetic loops on the elbow of the active region had a slow descending motion followed by an abrupt successive fast contraction, while magnetic loops on the top of the filament were pushed outward, slowly being inflated for a while and then erupting as a moving front. We show that the filament activation and eruption play a dominant role in determining the dynamics of the overlying peripheral coronal magnetic loops.

OBSERVATIONAL STUDY OF THE QUASI-PERIODIC FAST-PROPAGATING MAGNETOSONIC WAVES AND THE ASSOCIATED FLARE ON 2011 MAY 30

Yuandeng **Shen**1,2 and Yu Liu
2012 ApJ 753 53
https://iopscience.iop.org/article/10.1088/0004-637X/753/1/53/pdf
On **2011 May 30**, quasi-periodic fast-propagating (QFP) magnetosonic waves accompanied by a C2.8 flare were directly imaged by the Atmospheric Imaging Assembly instrument on board the Solar Dynamics Observatory. The QFP waves successively emanated from the flare kernel, they propagated along a cluster of open coronal loops with a phase speed of ~834 km s–1 during the flare's rising phase, and the multiple arc-shaped wave trains can be fitted with a series of concentric circles. We generate the k - ω diagram of the Fourier power and find a straight ridge that represents the dispersion relation of the waves. Along the ridge, we find a lot of prominent nodes which represent the available frequencies of the QFP waves. On the other hand, the frequencies of the flare are also obtained by analyzing the flare light curves using the wavelet technique. The results indicate that almost all the main frequencies of the flare are consistent with those of the QFP waves. This suggests that the flare and the QFP waves were possibly excited by a common physical origin. On the other hand, a few low frequencies (e.g., 2.5 mHz (400 s) and 0.7 mHz (1428 s)) revealed by the k - ω diagram cannot be found in the accompanying flare. We propose that these low frequencies were

possibly due to the leakage of the pressure-driven p-mode oscillations from the photosphere into the low corona, which should be a noticeable mechanism for driving the QFP waves observed in the corona.

NUMERICAL EXPERIMENTS ON FINE STRUCTURE WITHIN RECONNECTING CURRENT SHEETS IN SOLAR FLARES

Chengcai **Shen**1,2, Jun Lin1,3 and Nicholas A. Murphy
2011 ApJ 737 14

We perform resistive magnetohydrodynamic simulations to study the internal structure of current sheets that form during solar eruptions. The simulations start with a vertical current sheet in mechanical and thermal equilibrium that separates two regions of the magnetic field with opposite polarity which are line-tied at the lower boundary representing the photosphere. Reconnection commences gradually due to an initially imposed perturbation, but becomes faster when plasmoids form and produce small-scale structures inside the current sheet. These structures include magnetic islands or plasma blobs flowing in both directions along the sheet, and X-points between pairs of adjacent islands. Among these X-points, a principal one exists at which the reconnection rate reaches maximum. A fluid stagnation point (S-point) in the sheet appeared where the reconnection outflow bifurcates. The S-point and the principal X-point (PX-point) are not co-located in space though they are very close to one another. Their relative positions alternate as reconnection progresses and determine the direction of motion of individual magnetic islands. Newly formed islands move upward if the S-point is located above the PX-point, and downward if the S-point is below the PX-point. Merging of magnetic islands was observed occasionally between islands moving in the same direction. Reconnected plasma flow was observed to move faster than blobs nearby.

KINEMATICS AND FINE STRUCTURE OF AN UNWINDING POLAR JET OBSERVED BY THE SOLAR DYNAMIC OBSERVATORY/ATMOSPHERIC IMAGING ASSEMBLY

Yuandeng **Shen**1,2,3, Yu Liu1,3, Jiangtao Su3,4 and Ahmed Ibrahim
2011 ApJ 735 L43

We present an observational study of the kinematics and fine structure of an unwinding polar jet, with high temporal and spatial observations taken by the Atmospheric Imaging Assembly on board the Solar Dynamic Observatory and the Solar Magnetic Activity Research Telescope. During the rising period, the shape of the jet resembled a cylinder with helical structures on the surface, while the mass of the jet was mainly distributed on the cylinder's shell. In the radial direction, the jet expanded successively at its western side and underwent three distinct phases: the gradually expanding phase, the fast expanding phase, and the steady phase. Each phase lasted for about 12 minutes. The angular speed of the unwinding motion of the jet and the twist transferred into the outer corona during the eruption are estimated to be 11.1 × 10–3 rad s–1 (period = 564 s) and 1.17-2.55 turns (or 2.34-5.1π), respectively. On the other hand, by calculating the azimuthal component of the magnetic field in the jet and comparing the free energy stored in the non-potential magnetic field with the jet's total energy, we find that the non-potential magnetic field in the jet is enough to supply the energy for the ejection. These new observational results strongly support the scenario that the jets are driven by the magnetic twist, which is stored in the twisted closed field of a small bipole, and released through magnetic reconnection between the bipole and its ambient open field.

EARLY ABNORMAL TEMPERATURE STRUCTURE OF X-RAY LOOP-TOP SOURCE OF SOLAR FLARES

Jinhua **Shen**,1,2 Tuanhui Zhou,2 Haisheng Ji,2,3 Na Wang,1 Wenda Cao,3 and Haimin Wang3
Astrophysical Journal, 686: L37–L40, **2008** October
http://www.journals.uchicago.edu/doi/pdf/10.1086/592835

This Letter is to investigate the physics of a newly discovered phenomenon—contracting flare loops in the early phase of solar flares. In classical flare models, which were constructed based on the phenomenon of the expansion of flare loops, an energy releasing site is put above flare loops. These models can predict that there is a vertical temperature gradient in the top of flare loops due to heat conduction and cooling effects. Therefore, the centroid of an X-ray loop-top source at higher energy bands will be higher in altitude, which we can define as the normal temperature distribution. With observations made by *RHESSI*, we analyzed 10 M- or X-class flares (9 limb flares). For all these flares, the movement of loop-top sources shows an obvious U-shaped trajectory, which we take as the signature of contraction-to-expansion of flare loops. We find that, for all these flares, a normal temperature distribution does exist, but only along the path of expansion. The temperature distribution along the path of contraction is abnormal, showing no spatial order at all. The result suggests that magnetic reconnection processes in the contraction and expansion phases of these solar flares are different.

Categorization model of moving small-scale intensity enhancements in solar active regions

B.M. **Shergelashvili**, E. Philishvili, S. Buitendag, S. Poedts, M. Khodachenko
A&A **2022**
https://arxiv.org/pdf/2203.06285.pdf
The small-scale moving intensity enhancements remotely observed in the extreme ultraviolet images of the solar active regions, which we refer to as active region moving campfires (ARMCs), are related to local plasma temperature and/or density enhancements. Their dynamics is driven by the physical processes in the entire coronal plasma. Our previous study of ARMCs indicates that they have characteristic velocities at around the background sound speed. The main goal of our work is to carry out a simultaneous analysis of EUV images from two observational missions, SDO/AIA and Hi-C 2.1. The aims of the performed cross-validating analysis of both SDO/AIA and Hi-C 2.1 data were to reveal how the observed moving features are distributed over the studied active region, **AR12712**, test the existence of different groups of ARMCs with distinct physical characteristics. We use the statistical model of intensity centroid convergence and tracking that was developed in our previous paper. Furthermore, a Gaussian mixture model fit of the observed complex of moving ARMCs is elaborated to reveal the existence of distinct ARMC groups and to study the physical characteristics of these different groups. In data from the 171Å, 193Å and 211Å channels of SDO/AIA, we identified several groups of ARMCs with respect to both blob intensity and velocity profiles. The existence of such groups is confirmed by the cross-validation of the 172Å data sets from Hi-C 2.1. The ARMCs studied in this paper have characteristic velocities in the range of the typical sound speeds in coronal loops. Hence, these moving objects differ from the well-known rapid Alfvénic velocity jets from magnetic reconnection sites. This is also proven by the fact that ARMCs propagate along the active region magnetic structure (strands). The nature of the discovered statistical grouping of the ARMC events is not known. **29 May 2018**

Extreme Ultraviolet Spectra of Solar Flares from the Extreme Ultraviolet Spectroheliograph SPIRIT Onboard the CORONAS-F Satellite

S. **Shestov**, A. Reva1, and S. Kuzin
2014 ApJ 780 15
http://arxiv.org/pdf/1510.03652v1.pdf
We present detailed extreme ultraviolet (EUV) spectra of four large solar flares: M5.6, X1.3, X3.4, and X17 classes in the spectral ranges 176-207 Å and 280-330 Å. These spectra were obtained by the slitless spectroheliograph SPIRIT onboard the CORONAS-F satellite. To our knowledge, these are the first detailed EUV spectra of large flares obtained with a spectral resolution of ~0.1 Å. We performed a comprehensive analysis of the obtained spectra and provide identification of the observed spectral lines. The identification was performed based on the calculation of synthetic spectra (the CHIANTI database was used), with simultaneous calculations of the differential emission measure (DEM) and density of the emitting plasma. More than 50 intense lines are present in the spectra that correspond to a temperature range of T = 0.5-16 MK; most of the lines belong to Fe, Ni, Ca, Mg, and Si ions. In all the considered flares, intense hot lines from Ca XVII, Ca XVIII, Fe XX, Fe XXII, and Fe XXIV are observed. The calculated DEMs have a peak at T ~ 10 MK. The densities were determined using Fe XI-Fe XIII lines and averaged 6.5 × 109 cm–3. We also discuss the identification, accuracy, and major discrepancies of the spectral line intensity prediction.
2001 September 16, 2001 December 28, 2004 July 16, and 2005 September 7.

Asymmetric Hard X-ray Radiation of Two Ribbons in a Thermal-Dominated C-Class Flare

Guanglu **Shi**, Li Feng, Jun Chen, Beili Ying, Shuting Li, Qiao Li, Hui Li, Ying Li, Kaifan Ji, Yu Huang, Weiqun Gan, the LST team
Solar Phys. **299**, 104 **2024**
https://arxiv.org/pdf/2407.13099
https://doi.org/10.1007/s11207-024-02349-0
The asymmetry in hard X-ray (HXR) emission at the footpoints (FPs) of flare loops is a ubiquitous feature closely associated with nonthermal electron transport. We analyze the asymmetric HXR radiation at two flare ribbons which is thermal-dominated during a long-duration C4.4 flare that occurred on **March 20, 2023**, combining multi-view and multi-waveband observations from the ASO-S, SolO, and SDO spacecraft. We find that the H I Lyα emission captures similar features to the He II λ304 in both light curve and spatio-temporal evolution of a pair of conjugate flare ribbons. The spectra and imaging analysis of the HXR emission, detected by STIX in 4-18 keV, reveal that the two-ribbon flare radiation is thermal dominated by over 95%, and the radiation source mainly concentrates on the northern ribbon, leading to an asymmetric distribution. To understand the underlying reasons for the HXR radiation asymmetry, we extrapolate the magnetic field within the active region using the NLFFF model. For 78% of the magnetic field lines starting from the northern flare ribbon, their lengths from the loop-tops (LTs) to the northern FPs are shorter than those to the southern FPs. For 62% of the field lines, their magnetic field strengths at the southern FPs exceed those at the northern FPs. In addition, considering the larger density, ≈1.0×1010 cm−3, of the low-lying flare loops (< 32 Mm), we find the shorter path from the LT to the northern FP enables more electrons to reach the northern FP more easily after collisions with the surrounding plasma. Therefore, in this thermal-dominated C-class flare, the asymmetric location of the flare LT relative to its two FPs plays a dominant role in the HXR radiation asymmetry, while such asymmetry is

also slightly influenced by the magnetic mirror effect resulting in larger HXR radiation at the FPs with weaker magnetic strength.

Multiwavelength Observations of Quasiperiodic Pulsations in the Impulsive Phase of an Eruptive Flare with the Hard X-Ray Imager On Board ASO-S and Other Instruments.

Shi, F., Li, D., Ning, Z. et al.
Sol Phys 299, 30 (**2024**).
https://doi.org/10.1007/s11207-024-02272-4
We investigated the quasiperiodic pulsations (QPPs) of the X1.2 solar flare (SOL**2023-01-06**T00:57) based on multi-instrument observations, especially the Hard X-ray Imager (HXI) on board the Advanced Space-based Solar Observatory (ASO-S). The quasiperiod of ≈27 s was identified in hard X-rays (HXR) and microwaves using the Markov Chain Monte Carlo method, while no corresponding oscillation was found in soft X-rays. The HXI imaging demonstrates that HXR pulsations arise from the double-footpoint HXR sources. Moreover, the fluctuation of ≈27 s period was also present in the nonthermal electron power-law index derived from the X-ray spectra, which is the signature of periodic electron acceleration/precipitation during the impulsive phase. The electron spectral indices not only exhibited the well-known “soft–hard–soft” evolution, but also showed the negative correlation with the HXR pulsations. These results suggest that QPPs directly originate from quasiperiodic injections of accelerated electrons into flare-loop footpoints. We also discuss the possible generation mechanisms for QPPs.

Are Quasi-periodic Pulsations Independent of Loop Oscillations in Solar Flare?

Fanpeng **Shi** (**史帆鹏**)1,2, Dong Li (**李**东)1,2, Zongjun Ning (**宁宗**军)1,2, Yangfan Guo (**郭**杨帆)3, Song Feng (冯松)4, and Jun Xu (**徐俊**)1,2
2023 ApJ 958 39
https://iopscience.iop.org/article/10.3847/1538-4357/acf7c2/pdf
We investigated oscillations in an M8.7 solar flare (SOL**2014-10-22**), including quasi-periodic pulsations (QPPs) in light curves and Doppler shift oscillations in the flare loops. Using Bayesian-based Markov Chain Monte Carlo, Fast Fourier Transform, and wavelet analysis method, QPPs were identified at microwave and hard X-ray wave bands during the impulsive phase, and the dominant period is 40–50 s. They should be associated with a repetitive energy release process, which accelerates nonthermal electrons periodically. On the other hand, we cannot rule out the possibility of the modulation of external waves because of the lower temporal resolution of spectroscopic observation. However, almost immediately after QPPs, a minority of flare loops display their Doppler velocity oscillations with a significant period of ∼4 minutes, which are observed by the Interface Region Imaging Spectrograph at the coronal line Fe xxi 1354.08 Å (T ∼ 107 K), while its intensity and width show no similar oscillation. Our observations suggest that flare loop oscillations are most likely the fast kink mode waves with a phase speed of ∼840 km s−1. The magnetic field strength in flare loops was estimated to be 54–69 G via the coronal seismology. The QPPs and loop oscillation could be independent of each other in this event.

Excitation of Multi-periodic Kink Motions in Solar Flare Loops: Possible Application to Quasi-periodic Pulsations

Mijie **Shi**, Bo Li, Shao-Xia Chen, Mingzhe Guo, Shengju Yuan
ApJL **943** L19 **2023**
https://arxiv.org/pdf/2301.05382.pdf
https://iopscience.iop.org/article/10.3847/2041-8213/acb3c6/pdf
Magnetohydrodynamic (MHD) waves are often invoked to interpret quasi-periodic pulsations (QPPs) in solar flares. We study the response of a straight flare loop to a kink-like velocity perturbation using three-dimensional MHD simulations and forward model the microwave emissions using the fast gyrosynchrotron code. Kink motions with two periodicities are simultaneously generated,with the long-period component P_L = 57s being attributed to the radial fundamental kink mode and the short-period component P_S=5.8s to the first leaky kink mode. Forward modeling results show that the two-periodic oscillations are detectable in the microwave intensities for some lines of sight. Increasing the beam size to (1")^2 does not wipe out the microwave oscillations. We propose that the first leaky kink mode is a promising candidate mechanism to account for short-period QPPs. Radio telescopes with high spatial resolutions can help distinguish between this new mechanism with such customary interpretations as sausage modes.

Synthetic Emissions of the Fe XXI 1354 Å Line from Flare Loops Experiencing Fundamental Fast Sausage Oscillations

Mijie **Shi**, Bo Li, Zhenghua Huang, Shaoxia Chen
ApJ **2019**
https://arxiv.org/pdf/1902.06087.pdf

Inspired by recent IRIS observations, we forward model the response of the Fe XXI 1354 \AA\ line to fundamental, standing, linear fast sausage modes (FSMs) in flare loops. Starting with the fluid parameters for an FSM in a straight tube with equilibrium parameters largely compatible with the IRIS measurements, we synthesize the line profiles by incorporating the non-Equilibrium Ionization (NEI) effect in the computation of the contribution function. We find that both the intensity and Doppler shift oscillate at the wave period (P). The phase difference between the two differs from the expected value (90◦) only slightly because NEI plays only a marginal role in determining the ionic fraction of Fe XXI in the examined dense loop. The Doppler width modulations, however, posses an asymmetry in the first and second halves of a wave period, leading to a secondary periodicity at P/2 in addition to the primary one at P. This behavior results from the competition between the broadening due to bulk flow and that due to temperature variations, with the latter being stronger but not overwhelmingly so. These expected signatures, with the exception of the Doppler width, are largely consistent with the IRIS measurements, thereby corroborating the reported detection of a fundamental FSM. The forward modeled signatures are useful for identifying fundamental FSMs in flare loops from measurements of the Fe \MyRoman{21} 1354 \AA\ line with instruments similar to IRIS, even though a much higher cadence is required for the expected behavior in the Doppler widths to be detected.

The Kelvin Force and Loop-Top Concentration

Kiyoto **Shibasaki**
RHESSI Nuggets #307 September **2017**
http://sprg.ssl.berkeley.edu/~tohban/wiki/index.php/The_Kelvin_Force_and_Loop-Top_Concentration
New physics can explain the perplexing overpressure at the flare looptop regions.

Numerical Study on Excitation of Turbulence and Oscillation in Above-the-loop-top Region of a Solar Flare

Kengo **Shibata**, Shinsuke Takasao, Katharine K. Reeves
ApJ **943** 106 **2023**
https://arxiv.org/pdf/2212.05802.pdf
https://iopscience.iop.org/article/10.3847/1538-4357/acaa9c/pdf
Extreme ultraviolet imaging spectroscopic observations often show an increase in line width around the loop-top or above-loop-top (ALT) region of solar flares, suggestive of turbulence. In addition, recent spectroscopic observations found the oscillation in the Doppler velocity around the ALT region. We performed three-dimensional magnetohydrodynamic (MHD) simulations to investigate the dynamics in the ALT region, with a particular focus on the generation of turbulence and the excitation of the oscillatory motion. We found a rapid growth of MHD instabilities around the upper parts of the ALT region (arms of the magnetic tuning fork). The instabilities grow more rapidly than the magnetic Rayleigh-Taylor-type instabilities at the density interface beneath the reconnecting current sheet. Eventually, the ALT region is filled with turbulent flows. The arms of the magnetic tuning fork have bad-curvature and transonic flows. Therefore, we consider that the rapidly growing instabilities are combinations of pressure-driven and centrifugally driven Rayleigh-Taylor-type instabilities. Despite the presence of turbulent flows, the ALT region shows a coherent oscillation driven by the backflow of the reconnection jet. We examine the numerical results by re-analyzing the solar flare presented in Reeves et al. 2020. We find that the highest non-thermal velocity is always at the uppermost visible edge of the ALT region, where oscillations are present. This result is consistent with our models. We also argue that the turbulent magnetic field has a significant impact on the confinement of non-thermal electrons in the ALT region. **2017 10 September**

Fractal Reconnection in Solar and Stellar Environments

Kazunari **Shibata**, Shinsuke Takasao
2016 "Magnetic Reconnection: Concepts and Applications", Springer-Verlag, W. D. Gonzalez and E. N. Parker, eds.
http://arxiv.org/pdf/1606.09401v1.pdf
Recent space based observations of the Sun revealed that magnetic reconnection is ubiquitous in the solar atmosphere, ranging from small scale reconnection (observed as nanoflares) to large scale one (observed as long duration flares or giant arcades). Often the magnetic reconnection events are associated with mass ejections or jets, which seem to be closely related to multiple plasmoid ejections from fractal current sheet. The bursty radio and hard X-ray emissions from flares also suggest the fractal reconnection and associated particle acceleration. We shall discuss recent observations and theories related to the plasmoid-induced-reconnection and the fractal reconnection in solar flares, and their implication to reconnection physics and particle acceleration. Recent findings of many superflares on solar type stars that has extended the applicability of the fractal reconnection model of solar flares to much a wider parameter space suitable for stellar flares are also discussed.

Solar Flares: Magnetohydrodynamic Processes"

Review

Kazunari **Shibata** and Tetsuya Magara

Living **Reviews** in Solar Physics, 8, (**2011**), 6

http://www.livingreviews.org/lrsp-2011-6

This paper outlines the current understanding of solar flares, mainly focused on magnetohydrodynamic (MHD) processes responsible for producing a flare. Observations show that flares are one of the most explosive phenomena in the atmosphere of the Sun, releasing a huge amount of energy up to about 1032 erg on the timescale of hours. Flares involve the heating of plasma, mass ejection, and particle acceleration that generates high-energy particles. The key physical processes for producing a flare are: the emergence of magnetic field from the solar interior to the solar atmosphere (flux emergence), local enhancement of electric current in the corona (formation of a current sheet), and rapid dissipation of electric current (magnetic reconnection) that causes shock heating, mass ejection, and particle acceleration. The evolution toward the onset of a flare is rather quasi-static when free energy is accumulated in the form of coronal electric current (field-aligned current, more precisely), while the dissipation of coronal current proceeds rapidly, producing various dynamic events that affect lower atmospheres such as the chromosphere and photosphere. Flares manifest such rapid dissipation of coronal current, and their theoretical modeling has been developed in accordance with observations, in which numerical simulations proved to be a strong tool reproducing the time-dependent, nonlinear evolution of a flare. We review the models proposed to explain the physical mechanism of flares, giving an comprehensive explanation of the key processes mentioned above. We start with basic properties of flares, then go into the details of energy build-up, release and transport in flares where magnetic reconnection works as the central engine to produce a flare.

RHESSI OBSERVATIONS OF THE PROPORTIONAL ACCELERATION OF RELATIVISTIC >0.3 MeV ELECTRONS AND >30 MeV PROTONS IN SOLAR FLARES

A. Y. **Shih**1, R. P. Lin1, and D.M. Smith2

Astrophysical Journal, 698:L152–L157, **2009, File**

http://www.iop.org:80/EJ/toc/-alert=43191/1538-4357/698/2

We analyze all *RHESSI* measurements from 2002 to 2005 (29 flare events) of the 2.223 MeV neutroncapture γ -ray line and >0.3 MeV electron bremsstrahlung continuum emissions, produced by >30 MeV accelerated protons (depending on assumptions) and >0.3 MeV accelerated electrons, respectively. We find a close proportionality between the two emissions over >3 orders of magnitude in fluence, from the largest flares down to the limits of detectability. This implies that the processes in flares that accelerate electrons above 0.3 MeV and protons above 30 MeV are closely related, and that the relative acceleration of these two populations is roughly independent of flare size. We find an overall weak correlation between the 2.223 MeV fluence and the peak *GOES* 1–8 Å soft X-ray (SXR) flux, but with a close proportionality for flares with 2.223 MeV fluence above a threshold of 50 ph cm^{-2} (equivalent to ~2 Ч 10^{31} protons >30 MeV). Below this threshold the flares usually have large (M-class or higher) but generally uncorrelated excess SXR emission. Thus, above this threshold it appears that flares reach a maximum efficiency for >30 MeV proton and relativistic (>0.3 MeV) electron acceleration, with proportionate amounts of energy going to flare SXR thermal emission and to >50 keV electrons. Finally, we find that the electron-to-proton ratios—J_e(0.5 MeV)/J_p (10 MeV)—in these flares, obtained from the γ -ray observations, are about 2 orders of magnitude larger than the ratios in gradual solar energetic particle (SEP) events, but are comparable with ratios in impulsive SEP events.

Simultaneous ALMA-Hinode-IRIS observations on footpoint signatures of a soft X-ray loop-like microflare

Toshifumi **Shimizu**, Masumi Shimojo, Masashi Abe

ApJ **922** 113 **2021**

https://arxiv.org/pdf/2109.11215.pdf

https://iopscience.iop.org/article/10.3847/1538-4357/ac27a4/pdf

https://doi.org/10.3847/1538-4357/ac27a4

Microflares have been considered to be among the major energy input sources to form active solar corona. To investigate the response of the low atmosphere to events, we conducted an ALMA observation at 3 mm coordinated with IRIS and Hinode observations, on **March 19, 2017**. During the observations, a soft X-ray loop-type microflare (active-region transient brightening) was captured using Hinode X-ray telescope in high temporal cadence. A brightening loop footpoint is located within narrow field of views ALMA, IRIS slit-jaw imager, and Hinode spectro-polarimeter. Counterparts of the microflare at the footpoint were detected in Si IV and ALMA images, while the counterparts were less apparent in C II and Mg II k images. Their impulsive time profiles exhibit the Neupert effect pertaining to soft X-ray intensity evolution. The magnitude of thermal energy measured using ALMA was approximately 100 times smaller than that measured in the corona. These results suggest that impulsive counterparts can

be detected in the transition region and upper chromosphere where the plasma is thermally heated via impinging non-thermal particles. Our energy evaluation indicates a deficit of accelerated particles that impinge the footpoints for a small class of soft X-ray microflares. The footpoint counterparts consist of several brightening kernels, all of which are located in weak (void) magnetic areas formed in patchy distribution of strong magnetic flux at the photospheric level. The kernels provide a conceptual image in which the transient energy release occurs at multiple locations on the sheaths of magnetic flux bundles in the corona.
RHESSI Nuggets #420 **2021**
https://sprg.ssl.berkeley.edu/~tohban/wiki/index.php/First_look_at_ALMA/HInode/IRIS_microflares

3D magnetic field configuration of small-scale reconnection events in the solar plasma atmosphere **Review**

T. **Shimizu**
Physics of Plasmas **2015**
http://arxiv.org/ftp/arxiv/papers/1508/1508.05481.pdf
The outer solar atmosphere, i.e., the corona and the chromosphere, is replete with small energy-release events, which are accompanied by transient brightening and jet-like ejections. These events are considered to be magnetic reconnection events in the solar plasma, and their dynamics have been studied using recent advanced observations from the Hinode spacecraft and other observatories in space and on the ground. These events occur at different locations in the solar atmosphere, and vary in their morphology and amount of the released energy. The magnetic field configurations of these reconnection events are inferred based on observations of magnetic fields at the photospheric level. Observations suggest that these magnetic configurations can be classified into two groups. In the first group, two anti-parallel magnetic fields reconnect to each other, yielding a 2D emerging flux configuration. In the second group, helical or twisted magnetic flux tubes are parallel or at a relative angle to each other. Reconnection can occur only between anti-parallel components of the magnetic flux tubes and may be referred to as component reconnection. The latter configuration type may be more important for the larger class of small-scale reconnection events. The two types of magnetic configurations can be compared to counter-helicity and co-helicity configurations, respectively, in laboratory plasma collision experiments.

High speed photospheric material flow observed at the polarity inversion line of a delta-type sunspot producing an X5.4 flare on 7 March 2012

Shimizu, T., Lites, B.W., and Bamba, Y.
E-print, June **2014**; PASJ, Hinode special issue 66 (SP1), S14 (1–10) **2014**
http://arxiv.org/pdf/1406.1617v1.pdf
http://pasj.oxfordjournals.org/content/66/SP1/S14.full.pdf+html
Solar flares abruptly release the free energy stored as a non-potential magnetic field in the corona and may be accompanied by eruptions of the coronal plasma. Formation of a non-potential magnetic field and the mechanisms for triggering the onset of flares are still poorly understood. In particular, photospheric dynamics observed near those polarity inversion lines that are sites of major flare production have not been well observed with high spatial resolution spectro-polarimetry. This paper reports on a remarkable high-speed material flow observed along the polarity inversion line located between flare ribbons at the main energy release side of an X5.4 flare on **7 March 2012**. Observations were carried out by the spectro-polarimeter of the Solar Optical Telescope onboard Hinode. The high-speed material flow was observed in the horizontally-oriented magnetic field formed nearly parallel to the polarity inversion line. This flow persisted from at least 6 hours before the onset of the flare, and continued for at least several hours after the onset of the flare. Observations suggest that the observed material flow represents neither the emergence nor convergence of the magnetic flux. Rather, it may be considered to be material flow working both to increase the magnetic shear along the polarity inversion line and to develop magnetic structures favorable for the onset of the eruptive flare.

MAGNETOHYDRODYNAMICS STUDY OF THREE-DIMENSIONAL FAST MAGNETIC RECONNECTION FOR INTERMITTENT SNAKE-LIKE DOWNFLOWS IN SOLAR FLARES

T. **Shimizu**, K. Kondo1,4, M. Ugai2,5 and K. Shibata
ApJ 707 420-427, **2009**
Three-dimensional instability of the spontaneous fast magnetic reconnection is studied with magnetohydrodynamics (MHD) simulation, where the two-dimensional model of the spontaneous fast magnetic reconnection is destabilized in three dimensions. In two-dimensional models, every plasma condition is assumed to be uniform in the sheet current direction. In that case, it is well known that the two-dimensional fast magnetic reconnection can be caused by current-driven anomalous resistivity, when an initial resistive disturbance is locally put in a one-dimensional current sheet. In this paper, it is studied whether the two-dimensional fast magnetic reconnection can be destabilized or not when the

initial resistive disturbance is three dimensional, i.e., that which has weak fluctuations in the sheet current direction. According to our study, the two-dimensional fast magnetic reconnection is developed to the three-dimensional intermittent fast magnetic reconnection which is strongly localized in the sheet current direction. The resulting fast magnetic reconnection repeats to randomly eject three-dimensional magnetic loops which are very similar to the intermittent downflows observed in solar flares. In fact, in some observations of solar flares, the current sheet seems to be approximately one dimensional, but the fast magnetic reconnection is strongly localized in the sheet current direction, i.e., fully three dimensional. In addition, the observed plasma downflows as snake-like curves. It is shown that those observed features are consistent with our numerical MHD study.

HINODE **OBSERVATION OF THE MAGNETIC FIELDS IN A SUNSPOT LIGHT BRIDGE ACCOMPANIED BY LONG-LASTING CHROMOSPHERIC PLASMA EJECTIONS**

Toshifumi **Shimizu**1, Yukio Katsukawa2, Masahito Kubo3, Bruce W. Lites3, Kiyoshi Ichimoto4, Yoshinori Suematsu2, Saku Tsuneta2, Shin'ichi Nagata4, Richard A. Shine5, and Theodore D. Tarbell5
Astrophysical Journal, 696:L66–L69, 2009 May
http://www.iop.org/EJ/toc/-alert=43192/1538-4357/696/1

We present high-resolutionmagnetic fieldmeasurements of a sunspot light bridge (LB) that produced chromospheric plasma ejections intermittently and recurrently for more than 1 day. The observations were carried out with the *Hinode* Solar Optical Telescope on **2007 April 29 and 30**. The spectro-polarimeter reveals obliquely oriented magnetic fields with vertical electric current density higher than 100 mA m^{-2} along the LB. The observations suggest that current-carrying highly twisted magnetic flux tubes are trapped below a cusp-shaped magnetic structure along the LB. The presence of trapped current-carrying flux tubes is essential for causing longlasting chromospheric plasma ejections at the interface with pre-existing vertically oriented umbral fields. A bidirectional jet was clearly detected, suggesting magnetic reconnections occurring at very low altitudes, slightly above the height where the vector magnetic fields are measured. Moreover, we found another strong vertical electric current on the interface between the current-carrying flux tube and pre-existing umbral field, which might be a direct detection of the currents flowing in the current sheet formed at the magnetic reconnection sites.

THE CORRELATION AMONG THE RISE VELOCITY OF A SOFT X-RAY LOOP, THE EJECTION VELOCITY OF A PLASMOID, AND THE HEIGHT ABOVE THE LOOP TOP OF THE HARD X-RAY SOURCE IN MASUDA-TYPE FLARES, AND ITS INTERPRETATION BASED ON THE RECONNECTION MODEL OF FLARES

M. **Shimizu**,1 K. Nishida,2 H. Takasaki,3 D. Shiota,4 T. Magara,4 and K. Shibata2
Astrophysical Journal, 683: L203–L206, **2008**
http://www.journals.uchicago.edu/toc/apjl/2008/683/2

One of the most important results on solar flares obtained by *Yohkoh* is finding impulsive compact-loop flares associated with a hard X-ray (HXR) loop-top source well above a soft X-ray (SXR) loop, which are called Masuda-type flares. This finding supports the reconnection model of flares in which magnetic reconnection occurs above the closed loop observed in the soft X-ray during a flare. Although this model qualitatively explains the observed feature of Masuda-type flares, quantitative investigations into physical processes in these flares are still insufficient, which is the main subject of this Letter. We used 15 Masuda-type flares (seven are newly found and eight are previously reported) to examine the correlation among the rise velocity of an SXR loop, the ejection velocity of a plasmoid, and the height of the HXR source above the SXR loop (i.e., the difference in the apparent heights of the HXR and SXR sources). The main conclusion is that there is a positive correlation among these three quantities, and we explain the physical origin of this correlation using a reconnection model of flares.

FREQUENT OCCURRENCE OF HIGH-SPEED LOCAL MASS DOWNFLOWS ON THE SOLAR SURFACE

T. **Shimizu**,1 B. W. Lites,2 Y. Katsukawa,3 K. Ichimoto,3 Y. Suematsu,3 S. Tsuneta,3 S. Nagata,4 M. Kubo,2 R. A. Shine,5 and T. D. Tarbell5
The Astrophysical Journal, 680:1467-1476, **2008** June 20
http://www.journals.uchicago.edu/doi/pdf/10.1086/588775

We report on new spectropolarimetric measurements with simultaneous filter imaging observation, revealing the frequent appearance of polarization signals indicating high-speed, probably supersonic, downflows that are associated with at least three different configurations of magnetic fields in the solar photosphere.

Development of Daily Maximum Flare-Flux Forecast Models for Strong Solar Flares

Seulki **Shin**, Jin-Yi Lee, Yong-Jae Moon , Hyoungseok Chu, Jongyeob Park

Solar Phys. Volume 291, Issue 3, pp 897-909 **2016**

We have developed a set of daily maximum flare-flux forecast models for strong flares (M- and X-class) using multiple linear regression (MLR) and artificial neural network (ANN) methods. Our input parameters are solar-activity data from January 1996 to December 2013 such as sunspot area, X-ray maximum, and weighted total flare flux of the previous day, as well as mean flare rates of McIntosh sunspot group (Zpc) and Mount Wilson magnetic classifications. For a training dataset, we used 61 events each of C-, M-, and X-class from January 1996 to December 2004. For a testing dataset, we used all events from January 2005 to November 2013. A comparison between our maximum flare-flux models and NOAA model based on true skill statistics (TSS) shows that the MLR model for X-class and the average of all flares (M+XM+X-class) are much better than the NOAA model. According to the hitting fraction (HF), which is defined as a fraction of events satisfying the condition that the absolute differences of predicted and observed flare flux on a logarithm scale are smaller than or equal to 0.5, our models successfully forecast the maximum flare flux of about two-thirds of the events for strong flares. Since all input parameters for our models are easily available, the models can be operated steadily and automatically on a daily basis for space-weather services.

PLASMA HEATING IN THE VERY EARLY PHASE OF SOLAR FLARES

M. **Siarkowski**1, R. Falewicz2, and P. Rudawy2

The Astrophysical Journal, 705:L143–L147, **2009**

In this Letter, we analyze soft X-ray (SXR) and hard X-ray (HXR) emission of the **2002 September 20** M1.8 *GOES* class solar flare observed by the *RHESSI* and *GOES* satellites. In this flare event, SXR emission precedes the onset of the main bulk HXR emission by ~5 minutes. This suggests that an additional heating mechanism may be at work at the early beginning of the flare. However, *RHESSI* spectra indicate a presence of the non-thermal electrons also before the impulsive phase. So, we assumed that a dominant energy transport mechanism during the rise phase of solar flares is electron-beam-driven evaporation. We used non-thermal electron beams derived from *RHESSI* spectra as the heating source in a hydrodynamic model of the analyzed flare. We showed that energy delivered by non-thermal electron beams is sufficient to heat the flare loop to temperatures in which it emits SXR closely following the *GOES* 1–8 Å light curve. We also analyze the number of non-thermal electrons, the low-energy cutoff, electron spectral indices, and the changes of these parameters with time.

Statistical analysis of the onset temperature of solar flares in 2010-2011

Douglas Félix da **Silva**, Li Hui, Paulo J. A. Simões, Adriana Valio, Joaquim C. E. R., Hugh S. Hudson, Paulo J. A. Simoes, Lyndsay Fletcher, Laura A. Hayes, Iain G. Hannah

MNRAS Volume 525, Issue 3, November **2023**, Pages 4143–4148
https://arxiv.org/pdf/2308.11017.pdf
https://doi.org/10.1093/mnras/stad2244

Understanding the physical processes that trigger solar flares is paramount to help with forecasting space weather and mitigating the effects on our technological infrastructure. A previously unknown phenomenon was recently identified in solar flares: the plasma temperature, derived from soft X-ray (SXR) data, at the onset of four flares, was revealed to be in the range 10-15 MK, without evidence of gradual heating. To investigate how common the hot-onset phenomenon may be, we extend this investigation to solar flares of B1.2- X6.9 classes recorded by the X-ray Sensor (XRS) on-board the GOES-14 and GOES-15 satellites between 2010 and 2011. For this statistical study, we employed the same methodology as in recent work, where the pre-flare SXR flux of each flare is obtained manually, and the temperature and emission measure values are obtained by the flux ratio of the two GOES/XRS channels using the standard software. From 3224 events listed in the GOES flare catalog for 2010-2011, we have selected and analyzed 745 events for which the flare heliographic location was provided in the list, to investigate center-to-limb effects of the hot-onset phenomenon. Our results show that 559 out of 745 flares (75%) exhibit an onset temperature above 8.6 MK (the first quartile), with respective log10 of the emission measure values between 46.0 - 47.25 cm-3, indicating that small amounts of plasma are quickly heated to high temperatures. These results suggest that the hot-onset phenomenon is very common in solar flares. **20 Jan 2010, 14 Feb 2011, 3 Sep 2011**

Broken Power-law Energy Spectra of the Accelerated Electrons Detected in Radio and Hard X-Rays during the SOL2013-05-13 Event

Douglas Félix da **Silva**1,2 and Adriana Valio2

2021 ApJL 915 L1
https://doi.org/10.3847/2041-8213/ac0726

https://iopscience.iop.org/article/10.3847/2041-8213/ac0726/pdf
Solar flares, resulting from magnetic activity of the Sun, are among the most energetic events in the solar system and in extreme cases directly affect our highly technological society. In this work, we analyze a solar flare detected at millimeter and centimeter wavelengths, as well as X-rays above 1 MeV. Observations of solar flares at these energy bands provide diagnostics of the energetic accelerated electrons and the magnetic fields where the emission is produced. During the SOL**2013-05-13** solar flare, radio data were obtained by the telescope system POlarisation Emission of Millimeter Activity at the Sun, which observes the Sun at 45 and 90 GHz with polarization measurements, and at microwaves (1–15 GHz) by the Radio Solar Telescope Network. For the same event, X-ray emission was detected by the RHESSI and Fermi satellites. Spectra at both wavelengths were constructed and fit separately to yield the accelerated electron energy distribution that produced the emission. The optically thin radio spectral index was calculated by fitting the Ramaty model of gyrosynchrotron emission to the observed radio spectrum, whereas the hard X-ray spectral index was obtained from the spectral fit assuming a thermal emission model plus a nonthermal broken power-law distribution. Finally, both spectral indexes were compared and confirmed that the index obtained from the radio spectrum agrees with the index of the X-ray spectrum for energies above the break energy of ~600 keV. Thus, the hard X-rays more energetic than 600 keV and high radio frequencies of solar flares are emitted by the same population of high-energy accelerated electrons. This result indicates that the accelerated electrons have an energy distribution best represented by a broken power law, with a breakup above energies around 1 MeV.

Submillimeter radiation as the thermal component of the Neupert Effect

Jorge Fernando Valle **Silva**, C. Guillermo Giménez de Castro, Paulo José de Aguiar Simões, Jean-Pierre Raulin
Solar Phys. **2019**
https://arxiv.org/pdf/1909.01435.pdf
The Neupert effect is the empirical observation that the time evolution of non-thermal emission (e.g. hard X-rays) is frequently proportional to the time derivative of the thermal emission flux (soft X-rays), or, vice versa, that time integrated non-thermal flux is proportional to thermal flux. We analyzed the GOES M2.2 event SOL**2011-02-14**T17:25, and found that the 212 GHz emission plays quite well the role of the thermal component of the Neupert effect. We show that the maximum of the hard X-ray flux for energies above 50 keV is coincident in time with the time-derivative of the 212 GHz flux, within the uncertainties. The microwave flux density at 15.4 GHz, produced by optically thin gyrosynchrotron mechanism, and hard-X rays above 25 keV mark the typical impulsive phase, and have similar time evolution. On the other hand, the 12 GHz emission is delayed by about 25 seconds with respect of the microwave and hard X-ray peak. We argue that this delay cannot be explained by magnetic trapping of non-thermal electrons. With all the observational evidence, we suggest that the 212 GHz emission is produced by thermal bremsstrahlung, initially in the chromosphere, and shifting to optically thin emission from thehot coronal loops at the end of the gradual phase.

The behavior of the spotless active regions during the solar minimum 23-24

Alexandre J. Oliveira e **Silva**, Caius L. Selhorst
Living Around Active Stars Proceedings IAU Symposium No. 328, 2016 **2017**
https://arxiv.org/pdf/1703.00926.pdf
In this work, we analysed the physical parameters of the spotless actives regions observed during solar minimum 23 - 24 (2007 - 2010). The study was based on radio maps at 17~GHz obtained by Imager (MDI) on board the Solar and Heliospheric Observatory (SOHO). The results shows that the spotless active regions presents the same radio characteristics of a ordinary one, they can live in the solar surface for long periods (>10 days), and also can present small flares.

Millimeter Observation of Solar Flares with Polarization

Silva, D. F.; Valio, A. B. M.
Ground-based Solar Observations in the Space Instrumentation Era
ASP Conference Series, Vol. 504, p. 55, **2016**
http://aspbooks.org/publications/504/055.pdf
We present the investigation of two solar flares on **February 17 and May 13, 2013**, studied in radio from 5 to 405 GHz (RSTN, POEMAS, SST), and in X-rays up to 300 keV (FERMI and RHESSI). The objective of this work is to study the evolution and energy distribution of the population of accelerated electrons and the magnetic field configuration. For this we constructed and fit the radio spectrum by a gyro synchrotron model. The optically thin spectral indices from radio observations were compared to that of the hard X-rays, showing that the radio spectral index is harder than the latter by 2. These flares also presented 10-15 % circular polarized emission at 45 and 90 GHz that suggests that the sources are located at different legs of an asymmetric loop.

Precise timing of solar flare footpoint sources from mid-infrared observations

Paulo J. A. **Simões**, Lyndsay Fletcher, Hugh S. Hudson, Graham S. Kerr, Matt Penn, Karla F. Lopez
MNRAS **2024**

https://arxiv.org/pdf/2406.11361
Solar flares are powerful particle accelerators, and in the accepted standard flare model most of the flare energy is transported from a coronal energy-release region by accelerated electrons which stop collisionally in the chromosphere, heating and ionising the plasma, producing a broadband enhancement to the solar radiative output. We present a time-delay analysis of the infrared emission from two chromospheric sources in the flare SOL**2014-09-24**T17:50 taken at the McMath-Pierce telescope. By cross-correlating the intensity signals, measured with 1s cadence, from the two spatially resolved infrared sources we find a delay of 0.75 ± 0.07 s at 8.2 μm, where the uncertainties are quantified by a Monte Carlo analysis. The sources correlate well in brightness but have a time lag larger than can be reasonably explained by the energy transport dominated by non-thermal electrons precipitating from a single acceleration site in the corona. If interpreted as a time-of-flight difference between electrons traveling to each footpoint, we estimate time delays between 0.14 s and 0.42 s, for a reconnection site at the interior quasi-separatrix layer or at the null-point of the spine-fan topology inferred for this event. We employed modelling of electron transport via time-dependent Fokker-Planck and radiative hydrodynamic simulations to evaluate other possible sources of time-delay in the generation of the IR emission, such as differing ionisation timescales under different chromospheric conditions. Our results demonstrate that they are also unable to account for this discrepancy. This flare appears to require energy transport by some means other than electron beams originating in the corona.
RHESSI Science Nuggets #457 **2023**
https://sprg.ssl.berkeley.edu/~tohban/wiki/index.php/Precise_timing_of_flare_footpoint_sources_from_mid-infrared_observations

Precise timing of flare footpoint sources from mid-infrared observations

Paulo **SIMÕES** et al.
RHESSI Science Nuggets #457 **2023**
https://sprg.ssl.berkeley.edu/~tohban/wiki/index.php/Precise_timing_of_flare_footpoint_sources_from_mid-infrared_observations
2014-09-24

The spectral content of SDO/AIA 1600 and 1700 Å filters from flare and plage observations

Paulo J. A. **Simões**, Hamish A. S. Reid, Ryan O. Milligan, Lyndsay Fletcher
ApJ 870 114 **2019**
https://arxiv.org/pdf/1808.01488.pdf
sci-hub.tw/10.3847/1538-4357/aaf28d
The strong enhancement of the ultraviolet emission during solar flares is usually taken as an indication of plasma heating in the low solar atmosphere caused by the deposition of the energy released during these events. Images taken with broadband ultraviolet filters by the Transition Region and Coronal Explorer (TRACE) and Atmospheric Imaging Assembly (AIA 1600 and 1700 \AA) have revealed the morphology and evolution of flare ribbons in great detail. However, the spectral content of these images is still largely unknown. Without the knowledge of the spectral contribution to these UV filters, the use of these rich imaging datasets is severely limited. Aiming to solve this issue, we estimate the spectral contributions of the AIA UV flare and plage images using high-resolution spectra in the range 1300 to 1900 \AA\ from the Skylab NRL SO82B spectrograph. We find that the flare excess emission in AIA 1600 \AA\ is composed of the C IV 1550 \AA\ doublet (26\%), Si I continua (20\%), with smaller contributions from many other chromospheric lines such as C I 1561 and 1656 \AA\ multiplets, He II 1640 \AA, Si ii 1526 and 1533 \AA. For the AIA 1700 \AA\ band, C I 1656 \AA\ multiplet is the main contributor (38\%), followed by He II 1640 (17\%), and accompanied by a multitude of other chromospheric lines, with minimal contribution from the continuum. Our results can be generalized to state that the AIA UV flare excess emission is of chromospheric origin, while plage emission is dominated by photospheric continuum emission in both channels. **1973-09-07**

Formation of the thermal infrared continuum in solar flares

Paulo J. A. **Simões**1, Graham S. Kerr1⋆, Lyndsay Fletcher1, Hugh S. Hudson1,2, C. Guillermo Giménez de Castro3 and Matt Penn
A&A 605, A125 (**2017**)
https://www.aanda.org/articles/aa/pdf/2017/09/aa30856-17.pdf
Aims. Observations of the Sun with the Atacama Large Millimeter Array have now started, and the thermal infrared will regularly be accessible from the NSF's Daniel K. Inouye Solar Telescope. Motivated by the prospect of these new data, and by recent flare observations in the mid infrared, we set out here to model and understand the source of the infrared continuum in flares, and to explore its diagnostic capability for the physical conditions in the flare atmosphere. Methods. We use the one-dimensional (1D) radiation hydrodynamics code RADYN to calculate mid-infrared continuum emission from model atmospheres undergoing sudden deposition of energy by non-thermal electrons. Results. We identify and characterise the main continuum thermal emission processes relevant to flare intensity enhancement in the mid- to far-infrared (2–200 μm) spectral range as free-free emission on neutrals and ions. We find that the infrared intensity evolution tracks the energy input to within a second, albeit with a lingering intensity

enhancement, and provides a very direct indication of the evolution of the atmospheric ionisation. The prediction of highly impulsive emission means that, on these timescales, the atmospheric hydrodynamics need not be considered in analysing the mid-IR signatures. **24−Sep−14**

Tracking flare chromospheric ionisation in the infrared

Paulo **Simões**, Lyndsay Fletcher, Hugh Hudson …
UKSP Nuggets # 78, **2017.**
http://www.uksolphys.org/uksp-nugget/78-tracking-flare-chromospheric-ionisation-in-the-infrared/
Infrared observations of solar flare chromospheric sources look like they will provide useful flare diagnostics, being both a prompt response to the energy input, and directly related to the evolution of ionisation in the chromosphere. We have also been able to show [3] that as the flare rises to its peak IR intensity, the brightness temperature maps very closely the evolution of electron density where the contribution function peaks, offering the possibility that the IR brightness temperature can be used to track something like the chromospheric 'total electron content'. Flare observations in the infrared continuum are rare at present, but this will change with the Daniel K. Inouye Solar Telescope which will be able to observe parts of the IR continuum between 1 and 5 μm, initially, though with capability to go out to 10μm in the future.

Formation of the thermal infrared continuum in solar flares

Paulo J. A. **Simões** (1), Graham S. Kerr (1 and 5), Lyndsay Fletcher (1), Hugh S. Hudson (1 and 2), C. Guillermo Giménez de Castro (3), Matt Penn
A&A **2017**
https://arxiv.org/pdf/1706.09867.pdf
Observations of the Sun with the Atacama Large Millimeter Array have now started, and the thermal infrared will regularly be accessible from the NSF's Daniel K. Inouye Solar Telescope. Motivated by the prospect of these new data, and by recent flare observations in the mid infrared, we set out here to model and understand the source of the infrared continuum in flares, and to explore its diagnostic capability for the physical conditions in the flare atmosphere. We use the 1D radiation hydrodynamics code RADYN to calculate mid-infrared continuum emission from model atmospheres undergoing sudden deposition of energy by non-thermal electrons. We identify and characterise the main continuum thermal emission processes relevant to flare intensity enhancement in the mid- to far-infrared (2-200 μm) spectral range as free-free emission on neutrals and ions. We find that the infrared intensity evolution tracks the energy input to within a second, albeit with a lingering intensity enhancement, and provides a very direct indication of the evolution of the atmospheric ionization. The prediction of highly impulsive emission means that, on these timescales, the atmospheric hydrodynamics need not be considered in analysing the mid-IR signatures.

Observations and modelling of Helium lines in solar flares

Paulo J. A. **Simões**, Lyndsay Fletcher, Nicolas Labrosse, Graham S. Kerr
Proceedings of the Coimbra Solar Physics Meeting 2015: Ground-based Solar Observations in the Space Instrumentation Era; Astronomical Society of the Pacific Conference Series **201**5
http://arxiv.org/pdf/1512.03477v1.pdf
We explore the response of the He II 304 {\AA} and He I 584 {\AA} line intensities to electron beam heating in solar flares using radiative hydrodynamic simulations. Comparing different electron beams parameters, we found that the intensities of both He lines are very sensitive to the energy flux deposited in the chromosphere, or more specifically to the heating rate, with He II 304 {\AA} being more sensitive to the heating than He I 584 {\AA}. Therefore, the He line ratio increases for larger heating rates in the chromosphere. A similar trend is found in observations, using SDO/EVE He irradiance ratios and estimates of the electron beam energy rate obtained from hard X-ray data. From the simulations, we also found that spectral index of the electrons can affect the He ratio but a similar effect was not found in the observations. **2011-02-15, 2011-07-30, 2011-08-04, 2014-01-01**

Impulsive Heating of Solar Flare Ribbons Above 10 MK

Paulo J. A. **Simões**, David R. Graham, Lyndsay Fletcher
Solar Phys. Volume 290, Issue 12, pp 3573-3591 **2015**
http://arxiv.org/pdf/1505.03384v1.pdf
The chromospheric response to the input of flare energy is marked by extended extreme ultraviolet (EUV) ribbons and hard X-ray (HXR) footpoints. These are usually explained as the result of heating and bremsstrahlung emission from accelerated electrons colliding in the dense chromospheric plasma. We present evidence of impulsive heating of flare ribbons above 10 MK in a two-ribbon flare. We analyse the impulsive phase of **SOL2013-11-09**T06:38, a C2.6 class

event using data from Atmospheric Imaging Assembly (AIA) on board of Solar Dynamics Observatory (SDO) and the Reuven Ramaty High Energy Solar Spectroscopic Imager (RHESSI) to derive the temperature, emission measure and differential emission measure of the flaring regions and investigate the evolution of the plasma in the flaring ribbons. The ribbons were visible at all SDO/AIA EUV/UV wavelengths, in particular, at 94 and 131 \AA\ filters, sensitive to temperatures of 8 MK and 12 MK. Time evolution of the emission measure of the plasma above 10 MK at the ribbons has a peak near the HXR peak time. The presence of hot plasma in the lower atmosphere is further confirmed by RHESSI imaging spectroscopy analysis, which shows resolved sources at 11-13 MK associated with at least one ribbon. We found that collisional beam heating can only marginally explain the necessary power to heat the 10 MK plasma at the ribbons.

Direct observation of the energy release site in a solar flare by SDO/AIA, Hinode/EIS and RHESSI

Paulo J. A. **Simões**, David R. Graham, Lyndsay Fletcher
A&A 577, A68 **2015**
http://arxiv.org/pdf/1503.01491v1.pdf
We present direct evidence for the detection of the main energy release site in a non-eruptive solar flare, **SOL2013-11-09**T06:38UT. This GOES C2.7 event was characterised by two flaring ribbons and a compact, bright coronal source located between them, which is the focus of our study. We use imaging from SDO/AIA, and imaging spectroscopy from RHESSI to characterise the thermal and non-thermal emission from the coronal source, and EUV spectroscopy from the Hinode/EIS, which scanned the coronal source during the impulsive peak, to analyse Doppler shifts in Fe XII and Fe XXIV emission lines, and determine the source density. The coronal source exhibited an impulsive emission lightcurve in all AIA filters during the impulsive phase. RHESSI hard X-ray images indicate both thermal and non-thermal emission at the coronal source, and its plasma temperature derived from RHESSI imaging spectroscopy shows an impulsive rise, reaching a maximum at 12-13 MK about 10 seconds prior to the hard X-ray peak. High redshifts associated with this bright source indicate downflows of 40-250 km/s at a broad range of temperatures, interpreted as loop shrinkage and/or outflows along the magnetic field. Outflows from the coronal source towards each ribbon are also observed by AIA images at 171, 193, 211, 304 and 1600 A. The electron density of the source obtained from a Fe XIV line pair is 1011.50which is collisionally thick to electrons with energy up to 45-65 keV, responsible for the source's non-thermal X-ray emission. We conclude that the bright coronal source is the location of the main release of magnetic energy in this flare, with a geometry consistent with component reconnection between crossing, current-carrying loops. We argue that the energy that can be released via reconnection, based on observational estimates, can plausibly account for the non-thermal energetics of the flare.

Soft X-ray Pulsations in Solar Flares

Paulo J. A. **Simões**, Hugh S. Hudson, Lyndsay Fletcher
Solar Phys. Volume 290, Issue 12, pp 3625-3639 **2015**
http://arxiv.org/pdf/1412.3045v1.pdf
https://sci-hub.ru/10.1007/s11207-015-0691-2
The soft X-ray emissions of solar flares come mainly from the bright coronal loops at the highest temperatures normally achieved in the flare process. Their ubiquity has led to their use as a standard measure of flare occurrence and energy, although the bulk of the total flare energy goes elsewhere. Recently Dolla et al. (2012) noted quasi-periodic pulsations (QPP) in the soft X-ray signature of the X-class flare SOL**2011-02-15**, as observed by the standard photometric data from the GOES (Geostationary Operational Environmental Satellite) spacecraft. We analyze the suitability of the GOES data for this kind of analysis and find them to be generally valuable after Sept. 2010 (GOES-15). We then extend Dolla et al. results to a list of X-class flares from Cycle 24, and show that most of them display QPP in the impulsive phase. During the impulsive phase the footpoints of the newly-forming flare loops may also contribute to the observed soft X-ray variations. The QPP show up cleanly in both channels of the GOES data, making use of time-series of irradiance differences (the digital time derivative on the 2-s sampling). We show that there is minimal phase difference between the differenced GOES energy channels, nor between them and the hard X-ray variations on short time scales. We deploy different techniques to characterize the GOES QPP, finding no systematic patterns in spite of their general prevalence and usually no strong signature of a strict periodicity. The QPP may also appear on somewhat longer time scales during the later gradual phase, possibly with a greater tendency towards coherence, but the sampling noise in GOES difference data for large irradiance values makes these more uncertain. We note that the QPP of the impulsive phase can result from broadband variations, for example in red-noise power law distribution, in the flare development from its basic plasma instability. **2011-09-07, 14−May−13, 15−May−13, 28−Oct−13, 10−Nov−13, 25−Feb−14, 25−Apr−14**
Table 1. X-class flares of Cycle 24, along with the results of the wavelet analysis.

SDO observations of a flare’s coronal “implosion”

Paulo **Simões**, L. Fletcher, H. Hudson & A. Russell
UKSP Nugget: 42, Dec **2013**.
http://www.uksolphys.org/?p=7616
The corona collapses at the start of a flare.
The diffusion timescale for magnetic field in the corona is long but the impulsive phase of a flare is short, so most of the energy must come from a reduction in volume (i.e. from the shortening of the current-carrying field) somewhere in the configuration [2], referred to as the 'implosion'.

Implosion of Coronal Loops during the Impulsive Phase of a Solar Flare

P. J. A. **Simões**1, L. Fletcher1, H. S. Hudson1,2, and A. J. B. Russell
2013 ApJ 777 152
We study the relationship between implosive motions in a solar flare, and the energy redistribution in the form of oscillatory structures and particle acceleration. The flare **SOL2012-03-09**T03:53 (M6.4) shows clear evidence for an irreversible (stepwise) coronal implosion. Extreme-ultraviolet (EUV) images show at least four groups of coronal loops at different heights overlying the flaring core undergoing fast contraction during the impulsive phase of the flare. These contractions start around a minute after the flare onset, and the rate of contraction is closely associated with the intensity of the hard X-ray and microwave emissions. They also seem to have a close relationship with the dimming associated with the formation of the coronal mass ejection and a global EUV wave. Several studies now have detected contracting motions in the corona during solar flares that can be interpreted as the implosion necessary to release energy. Our results confirm this, and tighten the association with the flare impulsive phase. We add to the phenomenology by noting the presence of oscillatory variations revealed by Geostationary Operational Environmental Satellite soft X-rays (SXR) and spatially integrated EUV emission at 94 and 335 Å. We identify pulsations of 60 s in SXR and EUV data, which we interpret as persistent, semi-regular compressions of the flaring core region which modulate the plasma temperature and emission measure. The loop oscillations, observed over a large region, also allow us to provide rough estimates of the energy temporarily stored in the eigenmodes of the active-region structure as it approaches its new equilibrium.

The Flare that Time Forgot

Paulo **Simoes** and Hugh Hudson
RHESSI Science Nuggets, October **2013**, No. 209
http://sprg.ssl.berkeley.edu/~tohban/wiki/index.php/The_Flare_that_Time_Forgot
The Masuda flare. But, there was only really the one event, and many have commented how unusual it was. Was this type of event worth the fuss?

Implosion and Oscillation

Paulo **Simões** and Hugh Hudson.
RHESSI Science Nugget No. 204, **2013**
http://sprg.ssl.berkeley.edu/~tohban/wiki/index.php/Implosion_and_Oscillation
The flare implosion originates in the lower solar atmosphere and creates oscillations visible even in GOES soft X-rays.
SOL2012-03-09 (M6.4)

Too few? Too many?

Simoes, P. J. A. and Kontar, E. P.
RHESSI Science Nugget, No. 200, **2013**
We analysed four well-observed events in which the common loop structure could be identified in HXR: two footpoint sources at higher photon energies and a looptop source at lower energies.
Our conclusion is that the accelerated electrons must be subject to magnetic trapping and/or pitch-angle scattering, keeping a fraction of the population trapped inside the coronal loops.
2002 July 23, 2003 Nov 02, 2011 Feb 24, 2011 Sept 24

Implications for electron acceleration and transport from non-thermal electron rates at looptop and footpoint sources in solar flares

Simoes, P. J. A. and Kontar, E. P.
E-print, Feb **2013**; A&A, 551, A135 (**2013**)
The interrelation of hard X-ray (HXR) emitting sources and the underlying physics of electron acceleration and transport presents one of the major questions in high-energy solar flare physics. Spatially resolved observations of solar

flares often demonstrate the presence of well-separated sources of bremsstrahlung emission, so-called coronal and footpoint sources. Using spatially resolved X-ray observations by the Reuven Ramaty High Energy Solar Spectroscopic Imager (RHESSI) and recently improved imaging techniques, we investigate in detail the spatially resolved electron distributions in a few well-observed solar flares. The selected flares can be interpreted as having a standard geometry with chromospheric HXR footpoint sources related to thick-target X-ray emission and the coronal sources characterised by a combination of thermal and thin-target bremsstrahlung. Using imaging spectroscopy techniques, we deduce the characteristic electron rates and spectral indices required to explain the coronal and footpoint X-ray sources. We found that, during the impulsive phase, the electron rate at the looptop is several times (a factor of 1.7-8) higher than at the footpoints. The results suggest that a sufficient number of electrons accelerated in the looptop explain the precipitation into the footpoints and imply that electrons accumulate in the looptop. We discuss these results in terms of magnetic trapping, pitch-angle scattering, and injection properties. Our conclusion is that the accelerated electrons must be subject to magnetic trapping and/or pitch-angle scattering, keeping a fraction of the population trapped inside the coronal loops. These findings put strong constraints on the particle transport in the coronal source and provide quantitative limits on deka-keV electron trapping/scattering in the coronal source.
2002 July 23, 2003 Nov 02, 2011 Feb 24, 2011 Sept 24

Study of reconnection rates and light curves in solar flares from low and mid chromosphere

G **Sindhuja** Nandita Srivastava A M Veronig W Pötzi
Monthly Notices of the Royal Astronomical Society, Volume 482, Issue 3, 21 January **2019**, Pages 3744–3756
sci-hub.tw/10.1093/mnras/sty2887
We study the flare evolution process using both H α and Ca–K data sets to understand the variations between the two. The reconnection rates and fluxes from low and mid chromosphere using the high cadence Ca–K and H α time lapse images and low-noise 720-s Helioseismic Magnetic Imager line-of-sight magnetograms, respectively, are studied. From the past studies it is understood that the surface magnetic flux swept by the flare ribbons relates to a global reconnection rate. Therefore in order to measure the abovesaid parameters, the observables like the newly brightened area and magnetic field of the area are calculated. We report the results of the analysis carried out for nine flare events observed during 2010–2015 from Kanzelhöhe Solar Observatory for Solar and Environmental Research. The parameters like reconnection flux and reconnection rate estimated using Ca–K and H α images are compared. We infer that the reconnection flux parameter estimated from Ca–K and H α follow a similar trend and shows a linear relation in the log–log plot. Further our study also reveals that Ca–K light curve during the course of the flare is dominated by impulsive and gradual components and follows the trend of the non-thermally dominated Reuven Ramaty High Energy Solar Spectroscopic Imager (RHESSI) (25–50 keV) light curves. Whereas, H α light curve is dominated by a gradual component and follows the trend and shape of the thermally dominated RHESSI HXR (6-12 keV) light curves. **2014 Feb 13-14,2014 May 10, 22 Oct 14, 2015 Apr 9**
Table 1. List of flares under study together with the source AR and associated CMEs.

The Missing Cool Corona in the Flat Magnetic Field around Solar Active Regions

Talwinder **Singh**, Alphonse C. Sterling, Ronald L. Moore
ApJ **909** 57 **2021**
https://arxiv.org/pdf/2012.15406.pdf
https://iopscience.iop.org/article/10.3847/1538-4357/abd7f2/pdf
https://doi.org/10.3847/1538-4357/abd7f2
SDO/AIA images the full solar disk in several EUV bands that are each sensitive to coronal plasma emissions of one or more specific temperatures. We observe that when isolated active regions (ARs) are on the disk, full-disk images in some of the coronal EUV channels show the outskirts of the AR as a dark moat surrounding the AR. Here we present seven specific examples, selected from time periods when there was only a single AR present on the disk. Visually, we observe the moat to be most prominent in the AIA 171 Angstrom band, which has the most sensitivity to emission from plasma at log10 T = 5.8. By examining the 1D line-of-sight emission measure temperature distribution found from six AIA EUV channels, we find the intensity of the moat to be most depressed over the temperature range log10 T ~ 5.7 - 6.2 for most of the cases. We argue that the dark moat exists because the pressure from the strong magnetic field that splays out from the AR presses down on underlying magnetic loops, flattening those loops -- along with the lowest of the AR's own loops over the moat -- to a low altitude. Those loops, which would normally emit the bulk of the 171 Angstrom emission, are restricted to heights above the surface that are too low to have 171 Angstrom-emitting plasmas sustained in them, according to Antiochos & Noci (1986), while hotter EUV-emitting plasmas are sustained in the overlying higher-altitude long AR-rooted coronal loops. This potentially explains the low-coronal-temperature dark moats surrounding the ARs. **2014 Dec 17, 2018 Feb 11, 2018 Apr 25, 2018 May 30, 2018 Jun 17, 2018 Jul 14, 2019 Feb 20, 2019 Apr 15**

Dynamic Evolution of Current Sheets, Ideal Tearing, Plasmoid Formation and Generalized Fractal Reconnection Scaling Relations

K. A. P. **Singh**1,2, Fulvia Pucci3,4, Anna Tenerani5, Kazunari Shibata2, Andrew Hillier6, and Marco Velli7
2019 ApJ 881 52
sci-hub.se/10.3847/1538-4357/ab2b99
Magnetic reconnection may be the fundamental process allowing energy stored in magnetic fields to be released abruptly, with solar flares and coronal mass ejection being archetypal natural plasma examples. Magnetic reconnection is much too slow of a process to be efficient on the large scales, but accelerates once small enough scales are formed in the system. For this reason, the fractal reconnection scenario was introduced to explain explosive events in the solar atmosphere; it was based on the recursive triggering and collapse via tearing instability of a current sheet originally thinned during the rise of a filament in the solar corona. Here we compare the different fractal reconnection scenarios that have been proposed, and derive generalized scaling relations for the recursive triggering of fast, "ideal" —i.e., Lundquist number independent—tearing in collapsing current sheet configurations with arbitrary current profile shapes. An important result is that the Sweet–Parker scaling with Lundquist number, if interpreted as the aspect ratio of the singular layer in an ideally unstable sheet, is universal and does not depend on the details of the current profile in the sheet. Such a scaling, however, must not be interpreted in terms of stationary reconnection, rather it defines a step in the accelerating sequence of events of the ideal tearing mediated fractal cascade. We calculate scalings for the expected number of plasmoids for such generic profiles and realistic Lundquist numbers, showing that in ideal tearing scenarios a smaller number of plasmoids, by orders of magnitude, is generated compared to the original fractal model.

GPS as a solar observational instrument: Real-time estimation of EUV photons flux rate during strong, medium, and weak solar flares

Talwinder **Singh**, Manuel Hernandez-Pajares, Enric Monte, Alberto Garcia-Rigo, Germán Olivares-Pulido
JGR December **2015** Vol: 120, Pages: 10,840–10,850
http://onlinelibrary.wiley.com/doi/10.1002/2015JA021824/pdf
In this manuscript, the authors show how the Global Navigation Satellite Systems, GNSS (exemplified in the Global Positioning System, GPS), can be efficiently used for a very different purpose from that for which it was designed as an accurate Solar observational tool, already operational from the open global GPS measurements available in real-time, and with some advantages regarding dedicated instruments onboard spacecraft. The very high correlation of the solar extreme ultraviolet (EUV) photon flux rate in the 26–34 mm spectral band, obtained from the solar EUV monitor instrument onboard the SOHO spacecraft during Solar flares, is shown with the GNSS solar flare activity indicator (GSFLAI). The GSFLAI is defined as the gradient of the ionospheric vertical total electron content rate versus the cosine of the Solar zenith angle in the day hemisphere (which filters out nonsolar over ionization), and it is measured from data collected by a global network of dual frequency GPS receivers (giving in this way continuous coverage). GSFLAI for 60 X class flares, 320 M class flares, and 300 C class flares, occurred since 2001, were directly compared with the EUV solar flux rate data to show existing correlations. It was found that the GSFLAI and EUV flux rate present the same linear relationship for all classes of flares, not only the strong and medium intensity ones, X and M class, as in previous works, but also for the weakest C class solar flares, which is a remarkable result.

Nonlinear Instability and Intermittent Nature of Magnetic Reconnection in Solar Chromosphere

K.A.P. **Singh**, Andrew Hillier, H. Isobe, K. Shibata
PASJ 10 **2015**
http://arxiv.org/pdf/1602.01999v1.pdf
The recent observations of Singh et al. (2012) have shown multiple plasma ejections and the intermittent nature of magnetic reconnection in the solar chromosphere, highlighting the need for fast reconnection to occur in highly collisional plasma. However, the physical process through which fast magnetic reconnection occurs in partially ionized plasma, like the solar chromosphere, is still poorly understood. It has been shown that for sufficiently high magnetic Reynolds numbers, Sweet-Parker current sheets can become unstable leading to tearing mode instability and plasmoid formation, but when dealing with a partially ionized plasma the strength of coupling between the ions and neutrals plays a fundamental role in determining the dynamics of the system. We propose that as the reconnecting current sheet thins and the tearing instability develops, plasmoid formation passes through strongly, intermediately, and weakly coupled (or decoupled) regimes, with the time scale for the tearing mode instability depending on the frictional coupling between ions and neutrals. We present calculations for the relevant time scales for fractal tearing in all three regimes. We show that as a result of the tearing mode instability and the subsequent non-linear instability due to the plasmoid-dominated reconnection, the Sweet-Parker current sheet tends to have a fractal-like structure, and when the chromospheric magnetic field is sufficiently strong the tearing instability can reach down to kinetic scales, which are hypothesized to be necessary for fast reconnection.

Chromospheric Anemone Jets and Magnetic Reconnection in Partially Ionized Solar Atmosphere

K.A.P **Singh**, K. Shibata, N. Nishizuka, and H. Isobe
Physics of Plasmas, Volume 18, 111210 (**2011**)
The solar optical telescope onboard Hinode with temporal resolution of less than 5 s and spatial resolution of 150 km has observed the lower solar atmosphere with an unprecedented detail. This has led to many important findings, one of them is the discovery of chromospheric anemone jets in the solar chromosphere. The chromospheric anemone jets are ubiquitous in solar chromosphere and statistical studies show that the typical length, life time and energy of the chromospheric anemone jets are much smaller than the coronal events (e.g., jets/flares/CMEs). Among various observational parameters, the apparent length and maximum velocity shows good correlation. The velocity of chromospheric anemone jets is comparable to the local Alfvén speed in the lower solar chromosphere. Since the discovery of chromospheric anemone jets by Hinode, several evidences of magnetic reconnection in chromospheric anemone jets have been found and these observations are summarized in this paper. These observations clearly suggest that reconnection occurs quite rapidly as well as intermittently in the solar chromosphere. In the solar corona, anomalous resistivity arises due to various collisionless processes. Previous MHD simulations show that reconnection becomes fast as well as strongly time-dependent due to anomalous resistivity. Such processes would not arise in the solar chromosphere which is fully collisional and partially-ionized. So, it is unclear how the rapid and strongly time-dependent reconnection would occur in the solar chromosphere. It is quite likely that the Hall and ambipolar diffusion are present in the solar chromosphere and they could play an important role in driving such rapid, strongly time-dependent reconnection in the solar chromosphere.

A Comparative Analysis of Machine Learning Models for Solar Flare Forecasting: Identifying High Performing Active Region Flare Indicators

Suvadip **Sinha**, Om Gupta, Vishal Singh, B. Lekshmi, Dibyendu Nandy, Dhrubaditya Mitra, Saikat Chatterjee, Sourangshu Bhattacharya, Saptarshi Chatterjee, Nandita Srivastava, Axel Brandenburg
ApJ **935** 45 **2022**
https://arxiv.org/pdf/2204.05910.pdf
https://iopscience.iop.org/article/10.3847/1538-4357/ac7955/pdf
Solar flares create adverse space weather impacting space and Earth-based technologies. However, the difficulty of forecasting flares, and by extension severe space weather, is accentuated by the lack of any unique flare trigger or a single physical pathway. Studies indicate that multiple physical properties contribute to active region flare potential, compounding the challenge. Recent developments in Machine Learning (ML) have enabled analysis of higher dimensional data leading to increasingly better flare forecasting techniques. However, consensus on high-performing flare predictors remains elusive. In the most comprehensive study till date, we conduct a comparative analysis of four popular ML techniques (K-Nearest Neighbor, Logistic Regression, Random Forest Classifier, and Support Vector Machine) by training these on magnetic parameters obtained from the Helioseismic Magnetic Imager (HMI) onboard the Solar Dynamics Observatory (SDO) during the entirety of solar cycle 24. We demonstrate that Logistic Regression and Support Vector Machine algorithms perform extremely well in forecasting active region flaring potential. The logistic regression algorithm returns the highest true skill score of 0.967±0.018, possibly the highest classification performance achieved with any parametric study alone. From a comparative assessment, we establish that the magnetic properties like total current helicity, total vertical current density, total unsigned flux, R_value, and total absolute twist are the top-performing flare indicators. We also introduce and analyze two new performance metrics, namely, Severe and Clear Space Weather indicators. Our analysis constrains the most successful ML algorithms and identifies physical parameters that contribute most to active region flare productivity.

Particle heating and acceleration by reconnecting and nonreconnecting current sheets

Nikos **Sioulas**1,2, Heinz Isliker1 and Loukas Vlahos1
A&A 657, A8 (**2022**)
https://www.aanda.org/articles/aa/pdf/2022/01/aa41361-21.pdf
https://doi.org/10.1051/0004-6361/202141361
In this article, we study the physics of charged particle energization inside a strongly turbulent plasma, where current sheets naturally appear in evolving large-scale magnetic topologies, but they are split into two populations of fractally distributed reconnecting and nonreconnecting current sheets (CS). In particular, we implemented a Monte Carlo simulation to analyze the effects of the fractality and we study how the synergy of energization at reconnecting CSs and at nonreconnecting CSs affects the heating, the power-law high energy tail, the escape time, and the acceleration time of electrons and ions. The reconnecting current sheets systematically accelerate particles and play a key role in the formation of the power-law tail in energy distributions. On the other hand, the stochastic energization of particles through their interaction with nonreconnecting CSs can account for the heating of the solar corona and the impulsive heating during solar flares. The combination of the two acceleration mechanisms (stochastic and systematic), commonly present in many explosive events of various sizes, influences the steady-state energy distribution, as well as the transport properties of the particles in position- and energy-space. Our results also suggest that the heating and acceleration characteristics of ions and electrons are similar, the only difference being the time scales required to reach a steady state.

Stationary and impulsive injection of electron beams in converging magnetic field:

T. V. **Siversky** and V. V. Zharkova
A&A 504 (**2009**) 1057-1070
http://www.aanda.org/10.1051/0004-6361/200912341
Aims. We study time-dependent precipitation of an electron beam injected into a flaring atmosphere with a converging magnetic field by considering collisional and Ohmic losses with anisotropic scattering and pitch angle diffusion. Two injection regimes are investigated: short impulse and stationary injection. The effects of converging magnetic fields with different spatial profiles are compared and the energy deposition produced by the precipitating electrons at different depths and regimes is calculated.
Methods. The time dependent Fokker-Planck equation for electron distribution in depth, energy and pitch angle was solved numerically by using the summary approximation method.
Results. Steady state injection was found to be established for beam electrons 0.07–0.2 s after the injection onset depending on the initial beam parameters. Energy deposition by a stationary beam is strongly dependent on a self-induced electric field but more weakly dependent on a magnetic field convergence. Energy depositions by short electron impulses are found to be insensitive to the self-induced electric field but are strongly affected by magnetic convergence. Short beam impulses are shown to produce sharp asymmetric hard X-ray bursts on a timescale of the order of tens of milliseconds, often observed in solar flares.

Pulsations of microwave emission from a solar flare in a twisted loop caused by intrinsic MHD oscillations

C. **Smith**, M. Gordovskyy, P.K. Browning
MNRAS **2022**
https://arxiv.org/pdf/2201.08419.pdf
We present results revealing microwave pulsations produced in a model of a flaring twisted solar coronal loop, without any external oscillatory driver. Two types of oscillations are identified: slowly-decaying oscillations with a period of about 70-75s and amplitude of about 5-10% seen in loops both with and without energetic electrons, and oscillations with period of about 40s and amplitude of a few tens of percent observed only in loops with energetic electrons for about 100s after onset of fast energy release. We interpret the longer-period oscillations as the result of a standing kink mode modulating the average magnetic field strength in the loop, whilst the short-period intermittent oscillations associated with energetic electrons are likely to be produced by fast variations of the electric field which produces energetic electrons in this scenario. The slowly-decaying oscillations can explain the quasi-periodic pulsations often observed in the flaring corona.

Information Theoretical Approach to Understanding Flare Waiting Times

Jesse M. **Snelling**, Jay R. Johnson, Jake Willard, Yosia Nurhan, Jonathan Homan, and Simon Wing
2020 ApJ 899 148
https://doi.org/10.3847/1538-4357/aba7b9
There is not currently a consensus on the process responsible for producing the waiting time distribution of solar flares. This study presents an information theoretical approach to determining whether solar flare data are significantly distinguishable from a nonstationary Poisson process. A study of solar flares stronger than C1 class detected by the Geostationary Operational Environmental Satellite from 1975 to 2017 was performed. A sequence of waiting times (time elapsed between adjacent X-ray flare peaks) was constructed from the data. Surrogate waiting time sequences were produced using a time-varying Poisson firing rate from the Bayesian block procedure. Utilizing Shannon entropy, the mutual information of time-lagged waiting time distributions was computed for both the original data and the surrogates using a method of discretization by binning. When the entire period is considered, we see that when compared to carefully constructed surrogates, there is a significant elevation of mutual information on a timescale of approximately 30 hr, demonstrating that flares are confidently related to subsequent flares, contradicting the null hypothesis that flares are produced by a nonstationary Poisson process. When only 4 yr subsets of the data are considered, we see that at relatively small timescales (on the order of 10–30 hr), solar flare waiting times have a significant impact on subsequent flares. When corrected for the number of points in each considered time window, there is no correlation between the magnitude of significance and position in the solar cycle.

Onset of 2D magnetic reconnection in the solar photosphere, chromosphere and corona

B. **Snow**, G. J.J. Botha, J. A. McLaughlin, A. Hillier
2017 A&A
https://arxiv.org/pdf/1711.00683.pdf
We investigate the onset of 2D time-dependent magnetic reconnection that is triggered using an external velocity driver located away from, and perpendicular to, an equilibrium Harris current sheet. Previous studies have typically utilised an internal trigger to initiate reconnection, e.g. initial conditions centred on the current sheet. Numerical simulations

solving the compressible, resistive magnetohydrodynamics equations were performed to investigate the reconnection onset within different atmospheric layers of the Sun, namely the corona, chromosphere and photosphere. A reconnecting state is reached for all atmospheric heights considered, with the dominant physics being highly dependent on atmospheric conditions. The coronal case achieves a sharp rise in electric field for a range of velocity drivers. For the chromosphere, we find a larger velocity amplitude is required to trigger reconnection. For the photospheric environment, the electric field is highly dependent on the inflow speed; a sharp increase in electric field is obtained only as the velocity entering the reconnection region approaches the Alfven speed. Additionally, the role of ambipolar diffusion is investigated for the chromospheric case and we find that the ambipolar diffusion alters the structure of the current density in the inflow region. The rate at which flux enters the reconnection region is controlled by the inflow velocity. This determines all aspects of the reconnection start-up process, i.e. the early onset of reconnection is dominated by the advection term in Ohms law in all atmospheric layers. A lower plasma-β enhances reconnection and creates a large change in the electric field. A high plasma-β hinders the reconnection, yielding a sharp rise in the electric field only when the velocity flowing into the reconnection region approaches the local Alfven speed.

Effects of flares on solar high-degree helioseismic acoustic mode amplitudes

M. Cristina Rabello **Soares**, Frederic Baudin, Vanessa G. Teixeira
MNRAS Volume 505, Issue 1, Pages 293–303, **2021**
https://arxiv.org/pdf/2102.13181.pdf
https://doi.org/10.1093/mnras/stab1277
Several attempts have been made to observe whether solar flares excite acoustic modes since Wolff (1972) suggested this possibility. Moreover, the rapid progress of asteroseismology and the study of stellar flares makes the study of these phenomena in the Sun important to inform our study of the influence of the more energetic stellar flares on asteroseismic acoustic modes.
We look for the impact of flares on the amplitude of solar acoustic modes and other effects that are also affecting the mode amplitude. Solar acoustic mode amplitudes are known to be sensitive to magnetic fields. As flares usually occur in the presence of strong magnetic fields and most likely are the by-product of magnetic reconnection, we show how the magnetic field in and around the flaring region affects the mode amplitude. The mode amplitudes were obtained using ring-diagram analysis, which was first applied to a single event, the largest flare in the space age (the `Halloween Flare', SOL**2003-10-28**T11:00), using MDI data. Then, using HMI data, the analysis was applied to the regions corresponding to the flares observed during the high activity phase of cycle 24 and that fall into two groups. These two groups consist of small (10-60 erg cm−2 s−1) and large (>1200 erg cm−2 s−1) peak-flux flares, based on the Heliophysics Event Knowledgebase (HEK).
After applying several corrections in order to take into account several sources of bias, we did not find any amplification in the inferred mode amplitude due to flaring activity, within a 10% uncertainty.
RHESSI Nuggets #408 April **2021**
https://sprg.ssl.berkeley.edu/~tohban/wiki/index.php/Effects_of_Flares_on_Solar_p-modes

Slipping reconnection in a solar flare observed in high resolution with the GREGOR solar telescope

M. **Sobotka**, J. Dudík, C. Denker, H. Balthasar, J. Jurčák, W. Liu, T. Berkefeld, M. Collados Vera, A. Feller, A. Hofmann, F. Kneer, C. Kuckein, A. Lagg, R. E. Louis, O. von der Lühe, H. Nicklas, R. Schlichenmaier, D. Schmidt, W. Schmidt, M. Sigwarth, S. K. Solanki, D. Soltau, J. Staude, K. G. Strassmeier, R. Volkmer, T. Waldmann
A&A **2016**
http://arxiv.org/pdf/1605.00464v1.pdf
A small flare ribbon above a sunspot umbra in active region 12205 was observed on **November 7, 2014**, at 12:00 UT in the blue imaging channel of the 1.5 m GREGOR telescope, using a 1 A Ca II H interference filter. Context observations from the Atmospheric Imaging Assembly (AIA) onboard the Solar Dynamics Observatory (SDO), the Solar Optical Telescope (SOT) onboard Hinode, and the Interface Region Imaging Spectrograph (IRIS) show that this ribbon is part of a larger one that extends through the neighboring positive polarities and also participates in several other flares within the active region. We reconstructed a time series of 140 seconds of Ca II H images by means of the multiframe blind deconvolution method, which resulted in spatial and temporal resolutions of 0.1 arcsec and 1 s. Light curves and horizontal velocities of small-scale bright knots in the observed flare ribbon were measured. Some knots are stationary, but three move along the ribbon with speeds of 7-11 km/s. Two of them move in the opposite direction and exhibit highly correlated intensity changes, which provides evidence of a slipping reconnection at small spatial scales.

DIRECT IMAGING OF FINE STRUCTURE IN THE CHROMOSPHERE OF A SUNSPOT UMBRA

H. Socas-Navarro1, S. W. McIntosh2, R. Centeno2, A. G. de Wijn2 and B. W. Lites2
ApJ 696 1683-1688 doi: 10.1088/0004-637X/696/2/1683, **2009**
High-resolution imaging observations from the Hinode spacecraft in the Ca II H line are employed to study the dynamics of the chromosphere above a sunspot. We find that umbral flashes and other brightenings produced by the oscillation are extremely rich in fine structure, even beyond the resolving limit of our observations (0.″22). The umbra is tremendously dynamic to the point that our time cadence of 20 s does not suffice to resolve the fast lateral (probably apparent) motion of the emission source. Some bright elements in our data set move with horizontal propagation speeds of 30 km s–1. We have detected filamentary structures inside the umbra (some of which have a horizontal extension of ~1500 km) which, to our best knowledge, had not been reported before. The power spectra of the intensity fluctuations reveal a few distinct areas with different properties within the umbra that seem to correspond with the umbral cores that form it. Inside each one of these areas the dominant frequencies of the oscillation are coherent, but they vary considerably from one core to another.

String confinement of super-strong magnetic fields

A A **Solov'ev**
Monthly Notices of the Royal Astronomical Society, Volume 515, Issue 4, **2022**, Pages 4981–4989,
https://doi.org/10.1093/mnras/stac1818
A new class of force-free solutions for a horizontal magnetic filament with a circular cross-section is found, in which the magnetic field strength on the axis significantly (up to 2–3 orders of magnitude and more) exceeds the strength of the longitudinal external field that keeps the rope from lateral expansion. A weak transverse field leads to a small deviation from the force-free field structure and results in a density deficit and an increase in temperature on the rope axis. The possibility of a flare release of magnetic energy is shown when critical values of the longitudinal electric current density in the filament are reached at which ‘anomalous resistance’ occurs, caused by the development of the current ion-sound plasma instability. It turns out to be much larger than the usual Coulomb resistance. The following values are determined: the scale of the current dissipation region, the electric field strength in it, which significantly exceeds the Dreicer value, and the possible energy of accelerated charged particles (up to hundreds of MeV). The critical density of the longitudinal current at which the plasma turbulence is excited does not depend on the presence of a super-strong field on the flux-rope axis, so that the current density depends only on the electron concentration, temperature, and anomalous conductivity. However, super-strong magnetic fields can manifest themselves in the fact that, in their presence, the excitation of plasma instabilities can occur at sufficiently high electron concentrations. This effect may explain the large number of accelerated particles sometimes observed in solar flares.

FLARE ENERGY RELEASE IN MAGNETIC FLUX ROPE COMPRESSED BY THE CONVERGENT SUNSPOTS

Solov’ev1,2 A.A., Kirichek1 E.A.
Астрономия-**2018** Том 2 Солнечно-земная физика – современное состояние и перспективы С.230
http://www.izmiran.ru/library/eaas2018/eaas-2018-2.pdf
In paper [1] a new mechanism of solar flares caused by the convergence of two magnetic centers (sunspots) was suggested. According to [1], the strong X-class flare does not occur at the moment of closest approach of spots, but arises at the stage of their divergence. The authors obtained a number of empirical regularities typical for this mechanism. We propose the theoretical MHD model of the accumulation of free magnetic energy in the flux rope compressed between two approaching sunspots. This energy is released later as a power flare at the stage of their divergence.

Does the region of flare-energy release work as a vacuum-cleaner?,

Solov'ev, A., Murawski, K.,
Astrophysics and Space Science 350, 11, **2014**,
We aim to explore the unusual flare event which took place in the solar atmosphere on **September 22, 2011** and propose its theoretical interpretation. We analyze the process of energy release in the twisted magnetic flux-rope associated with the event, assuming the excitation of anomalous resistivity of turbulent plasma in the rope, and solve numerically nonlinear two-dimensional (2D) magnetohydrodynamic (MHD) equations. The analytical approach to the problem of flare-energy release show that the conditions of excitation of anomalous resistivity can be satisfied in the twisted magnetic flux-rope whose parameters fits well the SDO observational findings. One of the most remarkable properties of the flare phenomenon under the present consideration was the permanent sucking of the coronal/chromospheric gas from the very remote points to the flare filament, i.e. into the low-lying hot region of the flare energy release. This unusual phenomenon has been simulated by numerical methods in terms of ideal MHD. The numerical results reveal that siphon back-flow exhibits characteristic spatial signatures which mimic the observational

findings. The flare-energy release region, as a part of strongly twisted magnetic flux-rope, is able to work as a vacuum-cleaner.

Plasma Astrophysics, Part I: Fundamental and Practice,
Second Edition, Springer SBM, New York, **2012**
B.V. **Somov**,
Свободный доступ к электронной версии
http://dx.doi.org/10.1007/978-1-4614-4283-7

Plasma Astrophysics, Part II: Reconnection and Flares,
Second Edition, Springer SBM, New York, **2012**
B.V. **Somov**,
Свободный доступ к электронной версии
http://dx.doi.org/10.1007/978-1-4614-4295-0

On the magnetic reconnection of electric currents in solar flares

B. V. **Somov**
Astronomy Letters, Volume 38, Number 2, 128-138, **2012**
Astronomicheskiĭ Zhurnal, **2012**, Vol. 38, No. 2, pp. 149–160.
The role of the electric currents distributed over the volume of an active region on the Sun is considered from the standpoint of solar flare physics. We suggest including the electric currents in a topological model of the magnetic field in an active region. Typical values of the mutual inductance and the interaction energy of the coronal electric currents flowing along magnetic loops have been estimated for the M7/1N flare on **April 27, 2006**. We show that if these currents actually make a significant contribution to the flare energetics, then they must manifest themselves in the photosphericmagnetic fields. Depending on their orientation, the distributed currents can both help and hinder reconnection in the current layer at the separator during the flare. Asymmetric reconnection of the currents is accompanied by their interruption and an inductive change in energy. The reconnection of currents in flares differs significantly from the ordinary coalescence instability of magnetic islands in current layers. Highly accurate measurements of the magnetic fields in active regions are needed for a quantitative analysis of the role of distributed currents in solar flares.

Overview of open issues in the physics of large solar flares

B. V. **SOMOV,** S. I. BEZRODNYKH, L. S. LEDENTSOV
Astronomical and Astrophysical Transactions (*AApTr*), 2010/**2011**, Vol. 27, Issue 1, pp. 69–81, **File**
A broad variety of observational methods allows us to see the effect of magnetic reconnection in high-temperature strongly-magnetized plasma of the solar corona. Some specific features of the large-scale reconnection in large solar flares are summarized in this **review** but they are not investigated in detail yet. For example, an analysis of the topological peculiarities of magnetic field in active regions clearly shows that the so-called topological trigger phenomenon is necessary to allow for in order to construct realistic models for large solar flares and Coronal Mass Ejections (CMEs). However this is not a simple task. We discuss also some new analytical models of magnetic reconnection in a current layer with attached MHD discontinuities. In the context of the numerical simulations on reconnection, a question on their interpretation is considered. Some new results obtained recently are briefly reviewed together with new questions of the solar flare physics to be studied.

Magnetic reconnection and topological trigger in physics of large solar flares

Somov B.V.
Asian Journal of Physics, Vol. 17, Nos. 2-3, 421-454, **2008; File**
Solar flares are accessible to a broad variety of observational methods to see and investigate the {\em magnetic reconnection} phenomenon in high-temperature strongly-magnetized plasma of the solar corona. An analysis of the topological peculiarities of magnetic field in active regions shows that the {\em topological trigger} effect is necessary to allow for in order to construct models for large eruptive flares. The topological trigger is not a resistive instability which leads to a change of the topology of the field configuration from pre- to post reconnection state. On the contrary, the topological trigger is a quick change of the global topology, which dictates the fast reconnection of collisional or collisionless nature. The current state of the art and development potential of the theory of collisionless reconnection in

the strong magnetic fields related to large flares are briefly reviewed. Particle acceleration is considered in collapsing magnetic traps created by reconnection. In order to explain the formation of coronal X-ray sources, the Fermi acceleration and betatron mechanism are simultaneously taken into account analytically in a collisionless approximation. Finally, the emphasis is on urgent unsolved problems of solar flare physics.

B.V. **Somov**, Moscow State University, Moskva, Russia

Plasma Astrophysics, Part I

Fundamentals and Practice

Series: Astrophysics and Space Science Library, Vol. 391, **2012**

Plasma Astrophysics, Part II

Reconnection and Flares

Series: Astrophysics and Space Science Library, Vol. 392, **2012**

This two-part book is devoted to classic fundamentals and current practices and perspectives of modern plasma astrophysics. This first part uniquely covers all the basic principles and practical tools required for understanding and work in plasma astrophysics. More than 25% of the text is updated from the first edition, including new figures, equations and entire sections on topics such as magnetic reconnection and the Grad-Shafranov equation.

The book is aimed at professional researchers in astrophysics, but it will also be useful to graduate students in space sciences, geophysics, applied physics and mathematics, especially those seeking a unified view of plasma physics and fluid mechanics.

Plasma Astrophysics, Part I

Fundamentals and Practice

Series: Astrophysics and Space Science Library , Vol. 340

Volume package Plasma Astrophysics, Part I and II

Somov, Boris V.

2006, XV, 437 p., 78 illus., 4 in colour, Hardcover

Plasma Astrophysics, Part II

Reconnection and Flares

Series: Astrophysics and Space Science Library , Vol. 341

Volume package??Plasma??Astrophysics??Part??I??and??II??

Somov, Boris V.

2007, XII, 428 p., 78 illus., 4 in colour, Hardcover

The triggering process of an X-class solar flare on a small quadrupolar active region

Qiao **Song**, Jing-Song Wang, Xiaoxin Zhang, Hechao Chen, Shuhong Yang, Zhenyong Hou, Yijun Hou, Qian Ye, Peng Zhang, Xiuqing Hu, Jinping Dun, Weiguo Zong, Xianyong Bai, Bo Chen, Lingping He, Kefei Song

ApJ **959** 53 **2023**

https://arxiv.org/pdf/2309.09414.pdf

https://iopscience.iop.org/article/10.3847/1538-4357/acf836/pdf

The occurrence of X-class solar flares and their potential impact on the space weather often receive great attention than other flares. But predicting when and where an X-class flare will occur is still a challenge. With the multi-wavelength observation from the Solar Dynamics Observatory and FengYun- 3E satellite, we investigate the triggering of a GOES X1.0 flare occurring in the NOAA active region (AR) 12887. Our results show that this unique X-class flare is bred in a relatively small but complex quadrupolar AR. Before the X-class flare, two filaments (F1 and F2) exist below a null-point topology of the quadrupolar AR. Magnetic field extrapolation and observation reveal that F1 and F2 correspond to two magnetic flux ropes with the same chirality and their adjacent feet rooted at nonconjugated opposite polarities, respectively. Interestingly, these two polarities collide rapidly, accompanied by photospheric magnetic flux emergence, cancellation and shear motion in the AR center. Above this site, F1 and F2 subsequently intersect and merge to a longer filament (F3) via a tether-cutting-like reconnection process. As a result, the F3 rises and erupts, involving the large-scale arcades overlying filament and the quadrupolar magnetic field above the AR, and eventually leads to the eruption of the X-class flare with a quasi-X-shaped flare ribbon and a coronal mass ejection. It suggests that the rapid collision of nonconjugated opposite polarities provides a key condition for the triggering of this X-class flare, and also provides a featured case for flare trigger mechanism and space weather forecasting. **28 Oct 2021**

Spectral Observations and Modeling of a Solar White-light Flare Observed by CHASE

De-Chao **Song**, Jun Tian, Y. Li, M. D. Ding, Yang Su, Sijie Yu, Jie Hong, Ye Qiu, Shihao Rao, Xiaofeng Liu, Qiao Li, Xingyao Chen, Chuan Li, Cheng Fang
ApJ **952** L6 **2023**
https://arxiv.org/pdf/2307.12641.pdf
https://iopscience.iop.org/article/10.3847/2041-8213/ace18c/pdf
The heating mechanisms of solar white-light flares remain unclear. We present an X1.0 white-light flare on **2022 October 2** (SOL2022-10-02T20:25) observed by the Chinese \ha\ Solar Explorer (CHASE) that provides two-dimensional spectra in the visible light for the full solar disk with a seeing-free condition. The flare shows a prominent enhancement of ∼40\% in the photospheric \fe\ line at 6569.2 Å, and the nearby continuum also exhibits a maximum enhancement of ∼40\%. For the continuum near the \fe\ line at 6173 Å from the Helioseismic and Magnetic Imager (HMI) on board the Solar Dynamics Observatory (SDO), it is enhanced up to ∼20\%. At the white-light kernels, the \fe\ line at 6569.2 Å has a symmetric Gaussian profile that is still in absorption and the Hα line at 6562.8 Å displays a very broad emission profile with a central reversal plus a red or blue asymmetry. The white-light kernels are co-spatial with the microwave footpoint sources observed by the Expanded Owens Valley Solar Array (EOVSA) and the time profile of the white-light emission matches that of the hard X-ray emission above 30 keV from the Gamma-ray Burst Monitor (GBM) on Fermi. These facts indicate that the white-light emission is qualitatively related to a nonthermal electron beam. We also perform a radiative hydrodynamic simulation with the electron beam parameters constrained by the hard X-ray observations from Fermi/GBM. The result reveals that the white-light enhancement cannot be well explained by a pure electron-beam heating together with its induced radiative backwarming but may need additional heating sources such as \alfven\ waves.

A White-light Flare Powered by Magnetic Reconnection in the Lower Solar Atmosphere

Yongliang **Song**, Hui Tian, Xiaoshuai Zhu, Yajie Chen, Mei Zhang, Jingwen Zhang
ApJL **893** L13 **2020**
https://arxiv.org/pdf/2003.11747.pdf
https://doi.org/10.3847/2041-8213/ab83fa
White-light flares (WLFs), first observed in 1859, refer to a type of solar flares showing an obvious enhancement of the visible continuum emission. This type of enhancement often occurs in most energetic flares, and is usually interpreted as a consequence of efficient heating in the lower solar atmosphere through non-thermal electrons propagating downward from the energy release site in the corona. However, this coronal-reconnection model has difficulty in explaining the recently discovered small WLFs. Here we report a C2.3 white-light flare, which are associated with several observational phenomena: fast decrease in opposite-polarity photospheric magnetic fluxes, disappearance of two adjacent pores, significant heating of the lower chromosphere, negligible increase of hard X-ray flux, and an associated U-shaped magnetic field configuration. All these suggest that this white-light flare is powered by magnetic reconnection in the lower part of the solar atmosphere rather than by reconnection higher up in the corona. **2016 November 30**

Investigation of white-light emission in circular-ribbon flares

Yongliang **Song**, Hui Tian
ApJ **867** 159 **2018**
https://arxiv.org/pdf/1810.02958.pdf
sci-hub.tw/10.3847/1538-4357/aae5d1
Using observations by the Solar Dynamics Observatory from June 2010 to December 2017, we have performed the first statistical investigation of circular-ribbon flares (CFs) and examined the white-light emission in these CFs. We find 90 CFs occurring in 36 active regions (ARs), including 8 X-class, 34 M-class, 48 C- and B-class flares. The occurrence rate of white-light flares (WLFs) is 100\% (8/8) for X-class CFs, ∼62\% (21/34) for M-class CFs, and ∼8\% (4/48) for C- and B-class CFs. Sometimes we observe several CFs in a single AR, and nearly all of them are WLFs. Compared to normal CFs, CFs with white-light enhancement tend to have a shorter duration, smaller size, stronger electric current and more complicated magnetic field. We find that for X-class WLFs, the white-light enhancement is positively correlated with the flare class, implying that the white-light enhancement is largely determined by the amount of released energy. However, there is no such correlation for M- and C-class WLFs, suggesting that other factors such as the time scale, spatial scale and magnetic field complexity may play important roles in the generation of white-light emission if the released energy is not high enough. **2011 September 6, 2011.09.07, 2012.05.10, 2013 November 5, 2015.10.16, 2016.11.30**
Table 1. List of circular-ribbon flares (2011-2017)
HMI Science Nuggets #115 Dec 2018 http://hmi.stanford.edu/hminuggets/?p=2725

Observations of white-light flares in NOAA active region 11515: high occurrence rate and relationship with magnetic transients

Y. L. **Song**, H. Tian, M. Zhang, M. D. Ding
A&A 613, A69 **2018**

https://arxiv.org/pdf/1801.04371.pdf
https://www.aanda.org/articles/aa/pdf/2018/05/aa31817-17.pdf
There are two goals in this study. One is to investigate how frequently white-light flares (WLFs) occur in a flare-productive active region (NOAA active region 11515). The other is to investigate the relationship between WLFs and magnetic transients (MTs). We use the full-disk continuum filtergrams and line-of-sight magnetograms taken by SDO/HMI to identify WLFs and MTs, respectively. Images taken by SDO/AIA are also used to show the morphology of the flares in the upper atmosphere. We found at least 20 WLFs out of a total of 70 flares above C class (28.6%) in NOAA active region 11515 during its passage across the solar disk. Each of these WLFs occurred in a small region, with a short duration of about 5 minutes. The enhancement of white-light continuum intensity is usually small, with an average enhancement of 8.1%. The 20 WLFs observed were found along an unusual configuration of the magnetic field characterized by a narrow ribbon of negative field. Furthermore, the WLFs were found to be accompanied by MTs, with radical changes in magnetic field strength (or even a sign reversal) observed during the flare. In contrast, there is no obvious signature of MTs in those 50 flares without white-light enhancements. Our results suggest that WLFs occur much more frequently than what was previously thought, with most WLFs being fairly weak enhancements. This may explain why WLFs are not frequently reported. Our observations also suggest that MTs and WLFs are closely related and appear co-spatial and co-temporal, when considering HMI data. A larger enhancement of WL emission is often accompanied by a larger change of the line-of-sight component of the unsigned magnetic field. Considering the close relationship between MTs and WLFs, many previously reported flares with MTs may be WLFs. **2012.07.03-06**
Table 1. Information of the white-light flares detected in NOAA AR 11515

Observations of a white-light flare associated with a filament eruption

Y. L. **Song**, Y. Guo, H. Tian, X. S. Zhu, M. Zhang, Y. J. Zhu
ApJ **854** 64 **2018**
https://arxiv.org/pdf/1801.04408.pdf
http://sci-hub.tw/http://iopscience.iop.org/0004-637X/854/1/64/
We present observations of an M5.7 white-light flare (WLF) associated with a small filament eruption in NOAA active region 11476 on **2012 May 10**. During this flare, a circular flare ribbon appeared in the east and a remote brightening occurred in the northwest of the active region. Multi-wavelength data are employed to analyze the WLF, including white light (WL), ultraviolet, extreme ultraviolet, hard X-ray (HXR) and microwave. A close spatial and temporal relationship between the WL, HXR and microwave emissions is found in this WLF. However, the peak time of the WL emission lagged that of the HXR and microwave emissions by about 1-2 minutes. Such a result tends to support the back-warming mechanism for the WL emission. Interestingly, the enhanced WL emission occurred at the two footpoints of the filament. Through forced and potential field extrapolations, we find that the three-dimensional magnetic field in the flare region has a fan-spine feature and that a flux rope lies under the dome-like field structure. We describe the entire process of flare evolution into several steps, each producing the sequent brightening below the filament, the circular flare ribbons and the WL enhancement respectively. We suggest that reconnection between the magnetic field of the filament and the overlying magnetic field or reconnection within the flux rope leads to the WL enhancement.

On the relationship between sunspot structure and magnetic field changes associated with solar flares

Yongliang **Song**, Mei Zhang
2016 *ApJ* **826** 173
http://arxiv.org/pdf/1605.01163v1.pdf
Many previous studies have shown that magnetic fields as well as sunspot structures present rapid and irreversible changes associated with solar flares. In this paper we first use five X-class flares observed by SDO/HMI to show that not only the magnetic fields and sunspot structures do show rapid, irreversible changes but also these changes are closely related, both spatially and temporally. The magnitudes of the correlation coefficients between the temporal variations of horizontal magnetic field and sunspot intensity are all larger than 0.90, with a maximum value of 0.99 and an average value of 0.96. Then using four active regions in quiescent times, three observed and one simulated, we show that in sunspot penumbra regions there also exists a close correlation between sunspot intensity and horizontal magnetic field strength, in addition to the well-known one between sunspot intensity and normal magnetic field strength. Connecting these two observational phenomena, we show that the sunspot structure change and the magnetic field change are the two facets of the same phenomena of solar flares, one change might be induced by the change of the other due to a linear correlation between sunspot intensity and magnetic field strength out of a local force balance.
2011. 02. 15, 2011. 09. 06, 2012. 03. 07, 2014. 11. 07, 2014. 12. 20

Dark Post-Flare Loops Observed by Solar Dynamics Observatory

Qiao **Song**, Jing-Song Wang, Xueshang Feng, Xiaoxin Zhang
ApJ **821** 83 **2016**
http://arxiv.org/pdf/1604.01510v1.pdf

Solar post-flare loops (PFLs) are arcade-like loop systems that appear during the gradual phases of eruptive flares. The extreme ultraviolet (EUV) observations from the Atmospheric Imaging Assembly (AIA) on board the Solar Dynamics Observatory (SDO) allow us to investigate the fine structures in PFLs. In this work, we focus on studying the dark post-flare loops (DPFLs) during X-class flares, which are more evident in SDO/AIA data than in previous EUV data. We identify and analyze the DPFLs observed by SDO and find that: (1) the DPFLs of an X5.4 flare have an average lifetime of 10.0 ± 5.5 minutes, an average width of 1022 ± 339 km, and an average maximum length of 33 ± 10 Mm, (2) blob-like falling features with a size close to the resolution of SDO/AIA are identified in the DPFLs and they have an average velocity of 76 ±19 km s−1, and (3) the average widths of the DPFLs slightly increase with the characteristic temperatures in AIA 304, 171, 193, and 211 {\AA} channels. Our investigation shows that DPFLs are found in all of the 20 cases within this study, which suggests that they are a common phenomenon in X-class flares and are probably produced by the same mechanism that creates coronal rain. **2011-09-22, 2011-09-24, 2012=01=27, 2012 March 7. 2012-07-12, 2014 February 25**
Table 1: List of 20 X-class flares in Solar Cycle 24 (Zhang et al. 2014) and DPFL time of the flares

Flares and magnetic non-potentiality of NOAA AR 11158

Qiao **Song**, Jun Zhang, Shu-Hong Yang, Yang Liu
E-print, Jan **2013**
Magnetic non-potentiality is important for understanding flares and other solar activities in active regions (ARs). Five non-potential parameters, i.e. Electric current, current helicity, source field, photospheric free energy, and angular shear, are calculated to quantify the non-potentiality of NOAA AR 11158. Benefitting from the high spatial resolution, high cadence and continuous temporal coverage of vector magnetograms from the Helioseismic and Magnetic Imager onboard the Solar Dynamics Observatory, both the long-term evolution of the AR and the rapid change during flares are studied. We confirm that, compared with the magnetic flux, the magnetic non-potentiality has a closer connection with the flare, and the emerging flux regions are important for understanding the magnetic non-potentiality and flares. The main results are as follows. (1) The vortex in the source field directly displays the deflection of the horizontal magnetic field. The deflection corresponds to the fast rotating sunspot with a time delay, which suggests that the sunspot rotation leads to an increase in the non-potentiality. (2) Two areas that have evident changes in the azimuth of the vector magnetic field are found near the magnetic polarity inversion line. The change rates of the azimuth are about 1.3? h−1 and 3.6? h−1, respectively. (3) Rapid and prominent increases are found in the variation of helicity during four flares in the regions where their initial brightening occurs. The recovery of the increases takes 3?4 h for the two biggest flares (X2.2 and M6.6), but only takes about 2 h for the two other smaller flares (M2.2 and M1.6). **2011 February 12 to 16**

CO-ANALYSIS OF SOLAR MICROWAVE AND HARD X-RAY SPECTRAL EVOLUTIONS. I. IN TWO FREQUENCY OR ENERGY RANGES

Qiwu **Song**1, Guangli Huang1 and Hiroshi Nakajima
2011 ApJ 734 113
Solar microwave and hard X-ray spectral evolutions are co-analyzed in the **2000 June 10 and 2002 April 10** flares, and are simultaneously observed by the Owens-Valley Solar Array in the microwave band and by Yohkoh/Hard X-ray Telescope or RHESSI in the hard X-ray band, with multiple subpeaks in their light curves. The microwave and hard X-ray spectra are fitted by a power law in two frequency ranges of the optical thin part and two photon energy ranges, respectively. Similar to an earlier event in Shao & Huang, the well-known soft-hard-soft pattern of the lower energy range changed to the hard-soft-hard (HSH) pattern of the higher energy range during the spectral evolution of each subpeak in both hard X-ray flares. This energy dependence is actually supported by a positive correlation between the overall light curves and spectral evolution in the lower energy range, while it becomes an anti-correlation in the higher energy range. Regarding microwave data, the HSH pattern appears in the spectral evolution of each subpeak in the lower frequency range, which is somewhat similar to Huang & Nakajima. However, it returns back to the well-known pattern of soft-hard-harder for the overall spectral evolution in the higher frequency range of both events. This frequency dependence is confirmed by an anti-correlation between the overall light curves and spectral evolution in the lower frequency range, but it becomes a positive correlation in the higher frequency range. The possible mechanisms are discussed, respectively, for reasons why hard X-ray and microwave spectral evolutions have different patterns in different energy and frequency intervals.

Statistical Assessment of Photospheric Magnetic Features in Imminent Solar Flares Predictions

Hui **Song**, Vasyl Yurchyshyn, Ju Jing, Changyi Tan, V.I. Abramenko and Haimin Wang
BBSO, Number: 1338, 2007; Solar Phys (**2009**) 254: 101–125
Abstract: In this study we used the ordinal logistic regression method to establish a prediction model, which estimates the probability for each solar active region to produce X-, M- or C-class flares during the next 1-day time period. Three predictive

parameters are: (1) total unsigned magnetic flux T_{flux}, which is a measure of an active region's size, (2) the length of strong-gradient neutral line L_{gnl}, which describes the global non-potentiality of an active region, and (3) total magnetic dissipation E_{diss}, which is another proxy measure of an active region's non-potentiality. They are all derived from SOHO MDI magnetograms. The ordinal response variable is the different level of solar flares magnitude. By analyzing 230 active regions, L_{gnl} is proved to be the most powerful predictor, if only one predictor is chosen. Compared with the current predictions methods used by Solar Monitor at Solar Data Analysis Center (SDAC) and NOAA Space Environment Center (SEC), the ordinal logistic model using L_{gnl} and T_{flux} as predictors demonstrated its automaticity, simpleness and fairly high prediction accuracy. To our knowledge, this is the first time the ordinal logistic regression model was used in solar physics to predict solar flares.

Exhaustive study of three-time periods of solar activity due to single active regions: sunspot, flare, CME, and, geo-effective characteristics

Shirsh Lata **Soni**, Manohar Lal Yadav, Radhe Syam Gupta, Pyare lal Verma
Astrophysics and space science journal **2020**
https://arxiv.org/ftp/arxiv/papers/2012/2012.04853.pdf
In this paper, we present the multi-wavelength study of a high level of solar activity during which a single active region produced multiple flares/CMEs. According to the sunspot observations, the current solar cycle 24 manifest to be less intense in comparison with the previous recent sunspot cycles. In the course of the current sunspot cycle 24, several small and large sunspot groups have produced various moderate and intense flare/CME events. There are a few active regions with a large number of flaring activities passed across the visible disk of the Sun during 2012-2015. In this study, we consider the three periods **22-29 Oct 2013, 01-08 Nov 2013, and 25 Oct- 08-Nov 2014**, during which 228 flares have been observed. Considering only active regions near the central part of the disk, 59 CMEs (halo or partial) have been reported among which only 39 events are associated with flares. We conclude that an active region with a larger area, more complex morphology and stronger magnetic field has a comparatively higher possibility of producing extremely fast CMEs (speed > 1500 km/sec). So that among the 5 X class flares of the reported periods, 3 of them (60%) are associated with a CME. The lift-off time for CME-flare associated events has a +15 to+30 minute time interval range after the occurrence time of associated flares suggesting that the flares produce the CMEs. Additionally, we compiled the geomagnetic storms occurring within1-5 days after the CME onset. 10% of the 59 CMEs are related to a magnetic storm but all are moderate storms.

Multi-wavelength Study of Energetic Processes during Solar Flares occurrence

Shirsh Lata **Soni**, Radhe Shyam Gupta, Adya Prasad Mishra
Research in astronomy and Astrophysics **2020**
https://arxiv.org/ftp/arxiv/papers/2005/2005.11829.pdf
This paper is an attempt to understand the physical processes occurring in different layers of solar atmosphere during a solar flare. For a complete understanding of the flare we must analyze multi-wavelength datasets, as emission at different wavelength originates from different layers of the solar atmosphere. Also, flares are transient and localized events observed to occur at all longitudes. With these considerations, we have carried out multi-wavelength analysis of two representative flare events. One event occurred close to the centre of the solar disk and other occurred close to the limb. In the former case, we examine the emission from the lower layers of the solar atmosphere. Therefore the chromospheres, transition region and also the photospheric magneto-gram can be analyzed. On the other hand, in near-limb event, coronal features can be clearly studied. In this paper, the first event studied is the M 1.1 class flare from the active region NOAA 10649 located at S10E14 and the second event is the M 1.4 class flare from the active region NOAA 10713 located at S12W90. In both cases, we have observed the excellent multi-wavelength data sets. The observations from multi-instrumental data clearly shows that flares occur in the vicinity of sunspots. These are regions of strong magnetic field with mixed polarity. **17 July 2004, 29 December2004**

On the differences in the periodic behaviour of magnetic helicity flux in flaring active regions with and without X-class events

Sz. **Soós**, M. B. Korsós, H. Morgan, R. Erdélyi
ApJ **925** 129 **2022**
https://arxiv.org/pdf/2112.05933.pdf
https://iopscience.iop.org/article/10.3847/1538-4357/ac4094/pdf
Observational pre-cursors of large solar flares provide a basis for future operational systems for forecasting. Here, we study the evolution of the normalized emergence (EM), shearing (SH) and total (T) magnetic helicity flux components for 14 flaring with at least one X-class flare) and 14 non-flaring (< M5-class flares) active regions (ARs) using the Spaceweather Helioseismic Magnetic Imager Active Region Patches vector magnetic field data. Each of the selected ARs contain a δ-type spot. The three helicity components of these ARs were analyzed using wavelet analysis. Localised

peaks of the wavelet power spectrum (WPS) were identified and statistically investigated. We find that: i) the probability density function of the identified WPS peaks for all the EM, SH and T profiles can be fitted with a set of Gaussian functions centered at distinct periods between ~ 3 to 20 hours. ii) There is a noticeable difference in the distribution of periods found in the EM profiles between the flaring and non-flaring ARs, while no significant difference is found in the SH and T profiles. iii) In flaring ARs, the distributions of the shorter EM/SH/T periods (< 10 hrs) split up into two groups after flares, while the longer periods (> 10 hrs) do not change. iv) When the EM periodicity does not contain harmonics, the ARs do not host a large energetic flare. Finally, v) significant power at long periods (~ 20 hour) in the T and EM components may serve as pre-cursor for large energetic flares.
Table 1. Summary table of the studied 28 active regions (AR 11158-12740)

Analysis of Lower Hybrid Drift Waves in Kappa Distributions over Solar Atmosphere

Antony **Soosaleon**, Blesson Jose
2021
https://arxiv.org/pdf/2102.01323.pdf
Kappa distributions and with loss cone features have been frequently observed with flares emissions with the signatures of Lower hybrid waves. We have analysed the plasma with Kappa distributions and with loss cone features for the drift wave instabilities in perpendicular propagation for Large flare and Normal flare and Coronal condition . While analysing the growth/damping rate, we understand that the growth of propagation of EM waves increases with kappa distribution index for all the three cases. In comparing the propagation large flare shows lesser growth in compared with the normal and the coronal plasmas. When added the loss cone features to Kappa distributions, we find that the damping of EM wave propagation takes place. The damping rate EM waves is increases with perpendicular temperature and loss cone index l, in all the three cases but damping is very high for large flare and then normal in comparision with coronal condition. This shows that the lower hybrid damping may be the source of coronal heating.

Sign singularity and flares in solar active region NOAA 11158

Luca **Sorriso-Valvo**, Gaetano De Vita, Maria D. Kazachenko, Sam Krucker, Leonardo Primavera,Sergio Servidio, Antonio Vecchio, Brian T. Welsch, George H. Fisher, Fabio Lepreti, Vincenzo Carbone
2015 *ApJ* **801** 36
http://arxiv.org/pdf/1501.04279v1.pdf
Solar Active Region NOAA 11158 has hosted a number of strong flares, including one X2.2 event. The complexity of current density and current helicity are studied through cancellation analysis of their sign-singular measure, which features power-law scaling. Spectral analysis is also performed, revealing the presence of two separate scaling ranges with different spectral index. The time evolution of parameters is discussed. Sudden changes of the cancellation exponents at the time of large flares, and the presence of correlation with EUV and X-ray flux, suggest that eruption of large flares can be linked to the small scale properties of the current structures. **10-17 Feb 2011**, **2011/02/15**

A CRITICAL EXAMINATION OF THE FUNDAMENTAL ASSUMPTIONS OF SOLAR FLARE AND CORONAL MASS EJECTION MODELS

D. S. **Spicer**1, R. Bingham2,3, and R. Harrison
2013 ApJ 768 8
The fundamental assumptions of conventional solar flare and coronal mass ejection (CME) theory are re-examined. In particular, the common theoretical assumption that magnetic energy that drives flares and CMEs can be stored in situ in the corona with sufficient energy density is found wanting. In addition, the observational constraint that flares and CMEs produce non-thermal electrons with fluxes of order 1034-1036 electrons s–1, with energies of order 10-20 keV, must also be explained. This constraint when imposed on the "standard model" for flares and CMEs is found to miss the mark by many orders of magnitude. We suggest, in conclusion, there are really only two possible ways to explain the requirements of observations and theory: flares and CMEs are caused by mass-loaded prominences or driven directly by emerging magnetized flux.

Velocity Response of the Observed Explosive Events in the Lower Solar Atmosphere. I. Formation of the Flowing Cool-loop System

A. K. **Srivastava**1, Yamini K. Rao1, P. Konkol2, K. Murawski2, M. Mathioudakis3, Sanjiv K. Tiwari4,5, E. Scullion6, J. G. Doyle7, and B. N. Dwivedi1
2020 ApJ 894 155
https://doi.org/10.3847/1538-4357/ab86bb
We observe plasma flows in cool loops using the Slit-Jaw Imager on board the Interface Region Imaging Spectrometer (IRIS). Huang et al. observed unusually broadened Si iv 1403 Å line profiles at the footpoints of such loops that were attributed to signatures of explosive events (EEs). We have chosen one such unidirectional flowing cool-loop system observed by IRIS where one of the footpoints is associated with significantly broadened Si iv line profiles. The line-profile broadening indirectly indicates the occurrence of numerous EEs below the transition region (TR), while it

directly infers a large velocity enhancement/perturbation, further causing the plasma flows in the observed loop system. The observed features are implemented in a model atmosphere in which a low-lying bipolar magnetic field system is perturbed in the chromosphere by a velocity pulse with a maximum amplitude of 200 km s−1. The data-driven 2D numerical simulation shows that the plasma motions evolve in a similar manner as observed by IRIS in the form of flowing plasma filling the skeleton of a cool-loop system. We compare the spatio-temporal evolution of the cool-loop system in the framework of our model with the observations, and conclude that their formation is mostly associated with the velocity response of the transient energy release above their footpoints in the chromosphere/TR. Our observations and modeling results suggest that the velocity responses most likely associated to the EEs could be one of the main candidates for the dynamics and energetics of the flowing cool-loop systems in the lower solar atmosphere.

MHD Seismology as a Tool to Diagnose the Coronae of X-ray Active Sun-like Flaring Stars

A.K. **Srivastava**, S. Lalitha

E-print, Sept **2013**, The Proceedings of ISSTP-2012

It is now well accepted that the detection of impulsively generated multiple MHD modes are potentially used in diagnosing the local plasma conditions of the solar corona. Analogously, such analyses can also be significantly used in diagnosing the coronae of X-ray active Sun-like stars. In the present paper, we briefly review the detection of MHD modes in coronae of some X-ray active Sun-like stars, e.g. Proxima Centauri, XI-Boo etc using XMM-Newton observations, and discuss the implications in deriving physical information about their localized magnetic atmosphere. We conclude that the refinement in the MHD seismology of solar corona is also providing the best analogy to develop the stellar seismology of magnetically active and flaring Sun-like stars to deduce the local physical conditions of their coronae.

X6.9-class Flare Induced Vertical Kink Oscillations in a Large-Scale Plasma Curtain as Observed by SDO/AIA

A.K. **Srivastava**, M. Goossens

E-print, Sept **2013**; **2013** ApJ 777 17

We present rare observational evidence of vertical kink oscillations in a laminar and diffused large-scale plasma curtain as observed by the Atmospheric Imaging Assembly (AIA) on board the Solar Dynamics Observatory (SDO). The X6.9 class flare in the Active Region 11263 on **09 August 2011**, induces a global large-scale disturbance that propagates in a narrow lane above the plasma curtain and creates a low density region that appears as a dimming in the observational image data. This large-scale propagating disturbance acts as a non-periodic driver that interacts asymmetrically and obliquely with the top of the plasma curtain, and triggers the observed oscillations. In the deeper layers of the curtain, we find evidence of vertical kink oscillations with two periods (795 s and 530 s). On the magnetic surface of the curtain where the density is inhomogeneous due to the coronal dimming, non-decaying vertical oscillations are also observed (period approx 763-896 s). We infer that the global large-scale disturbance triggers vertical kink oscillations in the deeper layers as well as on the surface of the large-scale plasma curtain. The properties of the excited waves strongly depend on the local plasma and magnetic field conditions.

Discovery of the Sausage-Pinch Instability in Solar Corona

Abhi K. **Srivastava**1, R. Erdélyi2, V. Fedun2, P. Kayshap1, N.C. Joshi1, D. Tripathi

UKSP nugget 34, **2013.** http://www.uksolphys.org/?p=6158

A wide range of MHD instabilities have been observed in recent years in association with various solar dynamical processes. An instability known as the sausage instability (m = 0) mode, which is theoretically investigated in astrophysical plasma [7,9,10], has – to the best of our knowledge - not yet been observed in the solar atmosphere (although it is worth mentioning that sausage oscillations of the stable flux-tubes are well-observed [11,12,13]). In this nugget, we outline in brief the discovery of the sausage-pinch instability in the solar corona, in an activated partial filament eruption observed by SDO/AIA.

These types of magnetic instabilities can act as canonical plasma processes to trigger large-scale solar eruptions**.**

12 September 2011

OBSERVATIONAL EVIDENCE OF SAUSAGE-PINCH INSTABILITY IN SOLAR CORONA BY SDO/AIA

A. K. **Srivastava**1, R. Erdélyi2, Durgesh Tripathi3, V. Fedun2,4, N. C. Joshi1, and P. Kayshap

2013 ApJ 765 L42

We present the first observational evidence of the evolution of sausage-pinch instability in active region 11295 during a prominence eruption using data recorded on **2011 September 12** by the Atmospheric Imaging Assembly (AIA) onboard the Solar Dynamics Observatory (SDO). We have identified a magnetic flux tube visible in AIA 304 Å that shows curvatures on its surface with variable cross-sections as well as enhanced brightness. These curvatures evolved and thereafter smoothed out within a timescale of a minute. The curved locations on the flux tube exhibit a radial outward enhancement of the surface of about 1-2 Mm (a factor of two larger than the original thickness of the flux tube) from

the equilibrium position. AIA 193 Å snapshots also show the formation of bright knots and narrow regions in-between at the four locations as that of 304 Å along the flux tube where plasma emission is larger compared to the background. The formation of bright knots over an entire flux tube as well as the narrow regions in <60 s may be the morphological signature of the sausage instability. We also find the flows of confined plasma (propagation of brightness) in these bright knots along the field lines, which indicates the dynamicity of the flux tube that probably causes the dominance of the longitudinal field component over short temporal scales. The observed longitudinal motion of the plasma frozen in the magnetic field lines further vanishes the formed curvatures and plasma confinements as well as growth of instability to stabilize the flux tube.

Multiwavelength Observations of Supersonic Plasma Blob Triggered by Reconnection-Generated Velocity Pulse in AR10808

A.K. **Srivastava**, R. Erdélyi, K. Murawski, Pankaj Kumar
Solar Phys., 281(2), 729-747, **2012**
Using multi-wavelength observations of Solar and Heliospheric Observatory (SoHO)/Michelson Doppler Imager (MDI), Transition Region and Coronal Explorer (TRACE, 171 Å), and Hα from Culgoora Solar Observatory at Narrabri, Australia, we present a unique observational signature of a propagating supersonic plasma blob before an M6.2-class solar flare in active region 10808 on **9 September 2005**. The blob was observed between 05:27 UT and 05:32 UT with almost a constant shape for the first 2 – 3 min, and thereafter it quickly vanished in the corona. The observed lower-bound speed of the blob is estimated as ≈ 215 km s−1 in its dynamical phase. The evidence of the blob with almost similar shape and velocity concurrent in Hα and TRACE 171 Å images supports its formation by a multi-temperature plasma. The energy release by a recurrent three-dimensional reconnection process via the separator dome below the magnetic null point, between the emerging flux and pre-existing field lines in the lower solar atmosphere, is found to be the driver of a radial velocity pulse outwards that accelerates this plasma blob in the solar atmosphere. In support of identification of the possible driver of the observed eruption, we solve the two-dimensional ideal magnetohydrodynamic equations numerically to simulate the observed supersonic plasma blob. The numerical modelling closely match the observed velocity, evolution of multi-temperature plasma, and quick vanishing of the blob found in the observations. Under typical coronal conditions, such blobs may also carry an energy flux of 7.0×106 erg cm−2 s−1 to balance the coronal losses above active regions.

OBSERVATIONS OF POST-FLARE PLASMA DYNAMICS DURING AN M1.0 FLARE IN AR11093 BY THE SOLAR DYNAMICS OBSERVATORY/ATMOSPHERIC IMAGING ASSEMBLY*

Abhishek K. **Srivastava**1,2 and K. Murawski
2012 ApJ 744 173
We observe the motion of cool and hot plasma in a multi-stranded post-flare loop (PFL) system that evolved in the decay phase of a two-ribbon M1.0 class flare in AR 11093 on **2010 August 7** using the Solar Dynamics Observatory/Atmospheric Imaging Assembly 304 Å and 171 Å filters. The moving intensity feature and its reflected counterpart are observed in the loop system at multiple temperatures. The observed hot counterpart of the plasma probably envelopes the cool confined plasma and moves comparatively faster (~34 km s–1) than the latter (29 km s–1) in the form of a spreading intensity feature. The propagating plasma and intensity reflect from the region of another footpoint of the loop. The subsonic speed of the moving plasma and associated intensity feature may be most likely evolved in the PFL system through impulsive flare heating processes. Complementing our observations of moving multi-temperature intensity features in the PFL system and its reflection, we also attempt to solve two-dimensional ideal magnetohydrodynamic equations numerically using the VAL-IIIC atmosphere as an initial condition to simulate the observed plasma dynamics. We consider a localized thermal pulse impulsively generated near one footpoint of the loop system during the flare processes, which is launched along the magnetic field lines at the solar chromosphere. The pulse steepens into a slow shock at higher altitudes while moving along this loop system, which triggers plasma perturbations that closely exhibit the observed plasma dynamics.

Transient induced MHD oscillations : A tool to probe the solar active regions

Srivastava, Abhishek K.; Nakariakov, V. M.; Dwivedi, B. N.; Kumar, Pankaj
E-print, Oct **2011**. Proc. of the 1st Asian-Pacific Solar Phys. Meeting
Solar transients and eruptive phenomena which are ubiquitous in the solar atmosphere, can shed new light to the understanding of the outstanding problems like coronal heating and the solar wind acceleration. Observations in the entire electromagnetic spectrum of such dynamical processes of large and small-scale transient/eruptive events, with highly dynamic magnetic field configuration, and energetic particles, provide crucial information about the plasma processes at mega-Kelvin temperature embedded in a complex magnetic field, and also energy build-up/energy-release processes, taking place in such events. One of the most important phenomenological aspects of solar eruptive phenomena is the induced magnetohydrodynamic (MHD) waves generated during these energetic processes, which carry a potential signature to probing the solar active regions. In this paper, we briefly review the recent trends of the

transient (e.g., flares) induced quasi-periodic oscillations in the solar atmosphere and discuss their implications in diagnosing the solar active regions, providing the clue to understanding local plasma dynamics and heating.

Observation of Kink Instability as Driver of Recurrent Flares in AR 10960

Srivastava, A. K.; Kumar, Pankaj; Zaqarashvili, T. V.; Filippov, B. P.; Khodachenko, M. L.; Uddin, Wahab
E-print Jan **2011**; Publication in Advances in Geosciences

We study the active region NOAA 10960, which produces two flare events (B5.0, M8.9) on **04 June 2007**. We find the observational signature of right handed helical twists in the loop system associated with this active region. The first B5.0 flare starts with the activation of helical twist showing ~3 turns. However, after ~20 minutes another helical twist (with ~2 turns) appears, which triggers M8.9 flare. Both helical structures were closely associated with a small positive polarity sunspot in the AR. We interpret these observations as evidence of kink instability, which triggers the recurrent solar flares.

OBSERVATION OF KINK INSTABILITY DURING SMALL B5.0 SOLAR FLARE ON 2007 JUNE 4

A. K. **Srivastava**1, T. V. Zaqarashvili2,3, Pankaj Kumar1, and M. L. Khodachenko2
Astrophysical Journal, 715:292–299, **2010** May

Using multi-wavelength observations of *SOHO*/MDI, SOT–*Hinode*/blue-continuum (4504 Å), *G* band (4305 Å), Ca ii H (3968 Å), and TRACE 171 Å, we present the observational signature of a highly twisted magnetic loop in AR 10960 during the period 04:43 UT–04:52 UT on 2007 June 4. SOT–*Hinode*/blue-continuum (4504 Å) observations show that penumbral filaments of positive polarity sunspot have counterclockwise twist, which may be caused by the clockwise rotation of the spot umbrae. The coronal loop, whose one footpoint is anchored in this sunspot, shows strong right-handed twist in chromospheric SOT–*Hinode*/Ca ii H (3968 Å) and coronal TRACE 171Å images. The length and the radius of the loop are $L \sim 80$ Mm and $a \sim 4.0$ Mm, respectively. The distance between neighboring turns of magnetic field lines (i.e., pitch) is estimated as ≈10 Mm. The total twist angle, $\sqrt{} \sim 12\pi$ (estimated for the homogeneous distribution of the twist along the loop), is much larger than the Kruskal–Shafranov instability criterion. We detected clear double structure of the loop top during 04:47 UT–04:51 UT on TRACE 171Å images, which is consistent with simulated kink instability in curved coronal loops.We suggest that the kink instability of this twisted magnetic loop triggered a B5.0 class solar flare, which occurred between 04:40 UT and 04:51 UT in this active region.

Spatially inhomogeneous acceleration of electrons in solar flares

Duncan J. **Stackhouse**, Eduard P. Kontar
A&A 612, A64 **2018**
https://arxiv.org/pdf/1801.04743.pdf
sci-hub.se/10.1051/0004-6361/201730708

The imaging spectroscopy capabilities of the Reuven Ramaty high energy solar spectroscopic imager (RHESSI) enable the examination of the accelerated electron distribution throughout a solar flare region. In particular, it has been revealed that the energisation of these particles takes place over a region of finite size, sometimes resolved by RHESSI observations. In this paper, we present, for the first time, a spatially distributed acceleration model and investigate the role of inhomogeneous acceleration on the observed X-ray emission properties. We have modelled transport explicitly examining scatter-free and diffusive transport within the acceleration region and compare with the analytic leaky-box solution. The results show the importance of including this spatial variation when modelling electron acceleration in solar flares. The presence of an inhomogeneous, extended acceleration region produces a spectral index that is, in most cases, different from the simple leaky-box prediction. In particular, it results in a generally softer spectral index than predicted by the leaky-box solution, for both scatter-free and diffusive transport, and thus should be taken into account when modelling stochastic acceleration in solar flares. **2011 Feb 24**

Analysis and Modeling of High-frequency Emission and Deep Seismic Sources of Sunquakes

John T. **Stefan**1 and Alexander G. Kosovichev1,2
2022 ApJL 937 L26
https://arxiv.org/pdf/2209.11286.pdf
https://iopscience.iop.org/article/10.3847/2041-8213/ac8f92/pdf

Recent work published by Lindsey et al. find evidence for a deep and compact seismic source for the sunquake associated with the **2011 July 30** M9.3 flare, as well as seismic emission extending up to 10 mHz. We examine the sunquake independently, and a possible wave front is found in the 8 mHz band, though no wave front is easily discernible in the 10 mHz band. Additionally, we perform numerical simulations of seismic excitation modeled with the reported parameters and changes in the power spectra with increasing depth of the excitation source are examined. It is

found that the peak frequency decreases for increasing depths, but a shallow minimum is indicated between z = 0 and z = −840 km. Analysis of the suspected wave front of the M9.3 sunquake finds that the power spectrum of the reported seismic emission is close to that of background oscillations, though with a peak frequency noticeably lower than the background peak. Additionally, it is found that the amplitude of the source estimated by Lindsey et al. is too low to produce the observed wave front.

Estimation of Key Sunquake Parameters through Hydrodynamic Modeling and Cross-Correlation Analysis

John T. **Stefan**, Alexander G. Kosovichev
ApJ **2019**
https://arxiv.org/pdf/1911.06839.pdf
Sunquakes are one of the more distinct secondary phenomena related to solar flares, where energy deposition in the lower layers of the Sun's atmosphere excites acoustic waves easily visible in HMI dopplergrams. We explore two possible sources of sunquakes in the context of the electron beam hypothesis, as an instantaneous transfer of momentum and as a gradual applied force. We model the sunquake excitation and compare with five observed sunquake events using a cross-correlation analysis. We find that at least half the events studied are consistent with the electron beam hypothesis and estimate the energy required to excite the sunquakes to be within the range determined by previous studies. **2012 Oct 23, 2013 Nov 5, 2014 Mar 29, 2015 Sep 30, 2017 Sep 6**

A novel technique to measure intensity fluctuations in EUV images and to detect coronal sound waves nearby active regions*

G. **Stenborg**1, E. Marsch2, A. Vourlidas3, R. Howard3 and K. Baldwin4
A&A 526, A58 (**2011**)
Context. In the past years, evidence for the existence of outward-moving (Doppler blue-shifted) plasma and slow-mode magneto-acoustic propagating waves in various magnetic field structures (loops in particular) in the solar corona has been found in ultraviolet images and spectra. Yet their origin and possible connection to and importance for the mass and energy supply to the corona and solar wind is still unclear. There has been increasing interest in this problem thanks to the high-resolution observations available from the extreme ultraviolet (EUV) imagers on the Solar TErrestrial RElationships Observatory (STEREO) and the EUV spectrometer on the Hinode mission.
Aims. Flows and waves exist in the corona, and their signatures appear in EUV imaging observations but are extremely difficult to analyse quantitatively because of their weak intensity. Hence, such information is currently available mostly from spectroscopic observations that are restricted in their spatial and temporal coverage. To understand the nature and origin of these fluctuations, imaging observations are essential. Here, we present measurements of the speed of intensity fluctuations observed along apparently open field lines with the Extreme UltraViolet Imagers (EUVI) onboard the STEREO mission. One aim of our paper is to demonstrate that we can make reliable kinematic measurements from these EUV images, thereby complementing and extending the spectroscopic measurements and opening up the full corona for such an analysis. Another aim is to examine the assumptions that lead to flow versus wave interpretation for these fluctuations.
Methods. We have developed a novel image-processing method by fusing well established techniques for the kinematic analysis of coronal mass ejections (CME) with standard wavelet analysis. The power of our method lies with its ability to recover weak intensity fluctuations along individual magnetic structures at any orientation , anywhere within the full solar disk , and using standard synoptic observing sequences (cadence <3 min) without the need for special observation plans.
Results. Using information from both EUVI imagers, we obtained wave phase speeds with values on the order of 60–90 km s-1, compatible with those obtained by other previous measurements. Moreover, we studied the periodicity of the observed fluctuations and established a predominance of a 16-min period, and other periods that seem to be multiples of an underlying 8-min period.
Conclusions. The validation of our analysis technique opens up new possibilities for the study of coronal flows and waves, by extending it to the full disk and to a larger number of coronal structures than has been possible previously. It opens up a new scientific capability for the EUV observations from the recently launched Solar Dynamics Observatory. Here we clearly establish the ubiquitous existence of sound waves which continuously propagate along apparently open magnetic field lines.

Scattering Polarization in Solar Flares

Jiri **Stepan** and Petr Heinzel
RHESSI Science Nuggets, October **2013**, No. 210
http://sprg.ssl.berkeley.edu/~tohban/wiki/index.php/Scattering_Polarization_in_Solar_Flares
We call the direct excitation of polarization "impact polarization." Like any process creating spectral line polarization, impact polarization results from an anisotropy of the medium in which the lines are formed. In particular, the impact-polarization models assume that the distribution of velocities of particles is not isotropic. If the atoms of the plasmas

collide with these anisotropically moving particles, the subsequent photons emitted from the atoms are linearly polarized. (see **2013** ApJ 778 L6)

The nature of separator current layers in MHS equilibria I. Current parallel to the separator

J. E. H. **Stevenson**, C. E. Parnell, E. R. Priest and A. L. Haynes
A&A 573, A44 (**2015**)
Context. Separators, which are in many ways the three-dimensional equivalent to two-dimensional nulls, are important sites for magnetic reconnection. Magnetic reconnection occurs in strong current layers which have very short length scales.
Aims. The aim of this work is to explore the nature of current layers around separators. A separator is a special field line which lies along the intersection of two separatrix surfaces and forms the boundary between four topologically distinct flux domains. In particular, here the current layer about a separator that joins two 3D nulls and lies along the intersection of their separatrix surfaces is investigated.
Methods. A magnetic configuration containing a single separator embedded in a uniform plasma with a uniform electric current parallel to the separator is considered. This initial magnetic setup, which is not in equilibrium, relaxes in a non-resistive manner to form an equilibrium. The relaxation is achieved using the 3D MHD code, Lare3d, with resistivity set to zero. A series of experiments with varying initial current are run to investigate the characteristics of the resulting current layers present in the final (quasi-)equilibrium states.
Results. In each experiment, the separator collapses and a current layer forms along it. The dimensions and strength of the current layer increase with initial current. It is found that separator current layers formed from current parallel to the separator are twisted. Also the collapse of the separator is a process that evolves like an infinite-time singularity where the length, width and peak current in the layer grow slowly whilst the depth of the current layer decreases.

Automatic recognition of complex magnetic regions on the Sun in GONG magnetogram images and prediction of flares: Techniques for the flare warning program Flarecast

Steward, Graham A.; Lobzin, Vasili V.; Wilkinson, Phil J.; Cairns, Iver H.; Robinson, Peter A.
Space Weather, Vol. 9, No. 11, S11004, **2011**
http://dx.doi.org/10.1029/2011SW000703
In the present paper, Global Oscillation Network Group (GONG) solar magnetograms are used to automatically identify active regions by thresholding the line-of-sight component of the solar magnetic field. The flare potential of the regions is predicted by locating strong-gradient polarity inversion lines (SPILs) and estimating their parameters. The parameters of interest are the length of the SPIL, a proxy for its curvature; the maximum west-east and south-north gradients of the magnetic field in its vicinity; and a sum of the magnetic field gradients, the summation being performed along the SPIL. Analysis for thresholding of one, two, and three parameters and the corresponding probabilities for correct prediction of flares are presented and compared. The probability for correct prediction of X-ray flares of class C or greater in a 24 h window exceeds 88%, while the probability of false alarms is less than 10% if the decision rule involves thresholding of three specific parameters. These parameters are the steepest south-north gradient of the magnetic field, the maximum curvature of the SPILs, and the length of the longest SPIL, all being calculated for the entire region rather than for a particular SPIL. The steepest south-north gradient of the magnetic field is also used to estimate the probabilities for a flare to belong to classes C, M, or X. These techniques are now implemented in the flare warning program **Flarecast**. The first automatically predicted M- and X-class flares are presented, and Flarecast is found to predict well the observed X-ray flares.

Oscillatory reconnection and waves driven by merging magnetic flux ropes in solar flares

J. **Stewart**, P.K. Browning, M. Gordovskyy
MNRAS **2022**
https://arxiv.org/pdf/2205.03106.pdf
Oscillatory reconnection is a process that has been suggested to underlie several solar and stellar phenomena, and is likely to play an important role in transient events such as flares. Quasi-periodic pulsations (QPPs) in flare emissions may be a manifestation of oscillatory reconnection, but the underlying mechanisms remain uncertain. In this paper, we present 2D magnetohydrodynamic (MHD) simulations of two current-carrying magnetic flux ropes with an out-of-plane magnetic field undergoing oscillatory reconnection in which the two flux ropes merge into a single flux rope. We find that oscillatory reconnection can occur intrinsically without an external oscillatory driver during flux rope coalescence, which may occur both during large-scale coronal loop interactions and the merging of plasmoids in fragmented current

sheets. Furthermore, we demonstrate that radially propagating non-linear waves are produced in the aftermath of flux rope coalescence, due to the post-reconnection oscillations of the merged flux rope. The behaviour of these waves is found to be almost independent of the initial out-of-plane magnetic field. It is estimated that the waves emitted through merging coronal loops and merging plasmoids in loop-top current sheets would have a typical phase speed of 90 km/s and 900 km/s respectively. It is possible that the properties of the waves emitted during flux rope coalescence could be used as a diagnostic tool to determine physical parameters within a coalescing region.

Solar flare hard X-rays from the anchor points of an eruptive filament

Muriel Zoë **Stiefel**, Andrea Francesco Battaglia, Krzysztof Barczynski, Hannah Collier, Anna Volpara, Paolo Massa, Conrad Schwanitz, Sofia Tynelius, Louise Harra, Säm Krucker

A&A **2022**

https://arxiv.org/pdf/2212.11327.pdf

Context. We present an analysis of a GOES M1.8 flare with excellent observational coverage in UV, EUV, and X-ray, including observations from the instruments IRIS, SDO with AIA, Hinode/EIS, Hinode/XRT, and Solar Orbiter with the Spectrometer/Telescope for Imaging X-rays (STIX). Hard X-ray emission is often observed at the footpoints of flare loops and is occasionally observed in the corona. In this flare, four nonthermal hard X-ray sources are seen.
Aim. Our aim is to understand why we can observe four individual nonthermal sources in this flare and how we can characterize the physical properties of these four sources.
Methods. We used the multiwavelength approach to analyze the flare and characterize the four sources. To do this, we combined imaging at different wavelengths and spectroscopic fitting in the EUV and X-ray range.
Results. The flare is eruptive with an associated coronal mass ejection, and it shows the classical flare picture of a heated flare loop seen in EUV and X-rays, and two nonthermal hard X-ray footpoints at the loop ends. In addition to the main flare sources, we observed two outer sources in the UV, EUV, and nonthermal X-ray range located away from the main flare loop to the east and west. The two outer sources are clearly correlated in time, and they are only seen during the first two minutes of the impulsive phase, which lasts a total of about four minutes.
Conclusions. Based on the analysis, we determine that the outer sources are the anchor points of an erupting filament. The hard X-ray emission is interpreted as flare-accelerated electrons that are injected upward into the filament and then precipitate along the filament toward the chromosphere, producing Bremsstrahlung. While sources like this have been speculated to exist, this is the first report of their detection. **23 September 2021**

RHESSI Science Nuggets #450 **2023** https://sprg.ssl.berkeley.edu/~tohban/wiki/index.php/Solar_flare_hard_X-rays_from_the_anchor_points_of_an_eruptive_filament

RHESSI Microflares: I. X-Ray Properties and Multiwavelength Characteristics

S. **Stoiser** · A.M. Veronig · H. Aurass · A. Hanslmeier

Solar Phys (**2007**) 246: 339–364

http://www.springerlink.com/content/91154m0718683066/fulltext.pdf

Spectral and Imaging Diagnostics of Spatially-Extended Turbulent Electron Acceleration and Transport in Solar Flares

Morgan **Stores**, Natasha L. S. Jeffrey, James A. McLaughlin

ApJ **2023**

https://arxiv.org/pdf/2301.13682.pdf

Solar flares are efficient particle accelerators with a large fraction of released magnetic energy (10-50%) converted into energetic particles such as hard X-ray producing electrons. This energy transfer process is not well constrained, with competing theories regarding the acceleration mechanism(s), including MHD turbulence. We perform a detailed parameter study examining how various properties of the acceleration region, including its spatial extent and the spatial distribution of turbulence, affect the observed electron properties, such as those routinely determined from X-ray imaging and spectroscopy. Here, a time-independent Fokker-Planck equation is used to describe the acceleration and transport of flare electrons through a coronal plasma of finite temperature. Motivated by recent non-thermal line broadening observations that suggested extended regions of turbulence in coronal loops, an extended turbulent acceleration region is incorporated into the model. We produce outputs for the density weighted electron flux, a quantity directly related to observed X-rays, modelled in energy and space from the corona to chromosphere. We find that by combining several spectral and imaging diagnostics (such as spectral index differences or ratios, energy or spatial-dependent flux ratios, and electron depths into the chromosphere) the acceleration properties, including the timescale and velocity dependence, can be constrained alongside the spatial properties. Our diagnostics provide a foundation for constraining the properties of acceleration in an individual flare from X-ray imaging spectroscopy alone, and can be applied to past, current and future observations including those from RHESSI and Solar Orbiter.

RHESSI nugget #448 2023 https://sprg.ssl.berkeley.edu/~tohban/wiki/index.php/Diagnostics_of_Spatially-Extended_Turbulent_Acceleration_and_Transport

The Spatial and Temporal Variations of Turbulence in a Solar Flare

Morgan **Stores**, Natasha L. S. Jeffrey, Eduard P. Kontar
ApJ **923** 40 **2021**
https://arxiv.org/pdf/2110.01542.pdf
https://iopscience.iop.org/article/10.3847/1538-4357/ac2c65/pdf
https://doi.org/10.3847/1538-4357/ac2c65
Magnetohydrodynamic (MHD) plasma turbulence is believed to play a vital role in the production of energetic electrons during solar flares and the non-thermal broadening of spectral lines is a key sign of this turbulence. Here, we determine how flare turbulence evolves in time and space using spectral profiles of Fe xxiv, Fe xxiii and Fe xvi, observed by Hinode/EIS. Maps of non-thermal velocity are created for times covering the X-ray rise, peak, and decay. For the first time, the creation of kinetic energy density maps reveal where energy is available for energization, suggesting that similar levels of energy may be available to heat and/or accelerate electrons in large regions of the flare. We find that turbulence is distributed throughout the entire flare; often greatest in the coronal loop tops, and decaying at different rates at different locations. For hotter ions (Fe xxiv and Fe xxiii), the non-thermal velocity decreases as the flare evolves and during/after the X-ray peak shows a clear spatial variation decreasing linearly from the loop apex towards the ribbon. For the cooler ion (Fe xvi), the non-thermal velocity remains relativity constant throughout the flare, but steeply increases in one region corresponding to the southern ribbon, peaking just prior to the peak in hard X-rays before declining. The results suggest turbulence has a more complex temporal and spatial structure than previously assumed, while newly introduced turbulent kinetic energy maps show the availability of the energy and identify important spatial inhomogeneities in the macroscopic plasma motions leading to turbulence. **2013-05-15**

Predictive Capabilities of Avalanche Models for Solar Flares

A. **Strugarek**, P. Charbonneau
Solar Physics, Volume 289, Issue 11, pp 4137-4150 **2014**
We assess the predictive capabilities of various classes of avalanche models for solar flares. We demonstrate that avalanche models cannot generally be used to predict specific events because of their high sensitivity to the embedded stochastic process. We show that deterministically driven models can nevertheless alleviate this caveat and be efficiently used for predictions of large events. Our results suggest a new approach for predictions of large (typically X-class) solar flares based on simple and computationally inexpensive avalanche models.

Deterministically Driven Avalanche Models of Solar Flares

Antoine **Strugarek**, Paul Charbonneau, Richard Joseph, Dorian Pirot
E-print, March **2014**; Solar Phys. August **2014**, Volume 289, Issue 8, pp 2993-3015
We develop and discuss the properties of a new class of lattice-based avalanche models of solar flares. These models are readily amenable to a relatively unambiguous physical interpretation in terms of slow twisting of a coronal loop. They share similarities with other avalanche models, such as the classical stick–slip self-organized critical model of earthquakes, in that they are driven globally by a fully deterministic energy-loading process. The model design leads to a systematic deficit of small-scale avalanches. In some portions of model space, mid-size and large avalanching behavior is scale-free, being characterized by event size distributions that have the form of power-laws with index values, which, in some parameter regimes, compare favorably to those inferred from solar EUV and X-ray flare data. For models using conservative or near-conservative redistribution rules, a population of large, quasiperiodic avalanches can also appear. Although without direct counterparts in the observational global statistics of flare energy release, this latter behavior may be relevant to recurrent flaring in individual coronal loops. This class of models could provide a basis for the prediction of large solar flares.

Burst-on-Tail (BOT)

Alexei **Struminsky** and Ivan Zimovets
RHESSI Science Nugget, No. 195, March **2013**
http://sprg.ssl.berkeley.edu/~tohban/wiki/index.php/Burst-on-Tail_(BOT)
A highly non-thermal development in the late phase of the flare process.
In this Nugget we present an outstanding example of strong electron acceleration in a solar flare without a visible response in soft X-ray emission and propose its possible interpretations. **SOL2003-10-26**

Oscillatory reconnection and waves driven by merging magnetic flux ropes in solar flares

J **Stewart**, P K Browning, M Gordovskyy
Monthly Notices of the Royal Astronomical Society, Volume 513, Issue 4, July **2022**, Pages 5224–5237,
https://doi.org/10.1093/mnras/stac1286
Oscillatory reconnection is a process that has been suggested to underlie several solar and stellar phenomena, and is likely to play an important role in transient events such as flares. Quasi-periodic pulsations in flare emissions may be a manifestation of oscillatory reconnection, but the underlying mechanisms remain uncertain. In this paper, we present

2D magnetohydrodynamic simulations of two current-carrying magnetic flux ropes with an out-of-plane magnetic field undergoing oscillatory reconnection in which the two flux ropes merge into a single flux rope. We find that oscillatory reconnection can occur intrinsically without an external oscillatory driver during flux rope coalescence, which may occur both during large-scale coronal loop interactions and the merging of plasmoids in fragmented current sheets. Furthermore, we demonstrate that radially propagating non-linear waves are produced in the aftermath of flux rope coalescence, due to the post-reconnection oscillations of the merged flux rope. The behaviour of these waves is found to be almost independent of the initial out-of-plane magnetic field. It is estimated that the waves emitted through merging coronal loops and merging plasmoids in loop-top current sheets would have a typical phase speed of 90 and 900 km s−1, respectively. It is possible that the properties of the waves emitted during flux rope coalescence could be used as a diagnostic tool to determine physical parameters within a coalescing region.

Automatic recognition of complex magnetic regions on the Sun in SDO magnetogram images and prediction of flares: Techniques and results for the revised flare prediction program Flarecast

Graham **Steward**, Vasili Lobzin, Iver H. Cairns, Bo Li, David Neudegg
Space Weather Volume 15, Issue 9 September **2017** Pages 1151–1164 DOI 10.1002/2017SW001595
In the present paper, solar magnetograms provided by the Helioseismic and Magnetic Imager onboard Solar Dynamics Observatory spacecraft are used to identify active regions automatically by thresholding the line-of-sight component of the solar magnetic field. The flare potential of the regions is predicted by locating potential active regions with strong-gradient polarity inversion lines (SPILs) and estimating 18 physically relevant parameters of these regions. In particular, parameters of interest include the sum of north-south gradients, sum of east-west gradients, length of SPIL, and total integrated magnetic flux. For deterministic prediction of flares, analyses for thresholding of single parameters and different combinations, which include up to four parameters, are presented and compared. If the false alarm rate does not exceed 10% (20%), the probabilities for correct prediction of X-ray flares of class M and greater, M5 and greater, and X in the 24 h window are 71% (86%), 84% (96%), and 94% (100%), respectively. These probabilities are for the best four-parameter technique found. A technique for probabilistic forecasting was also developed. These deterministic and probabilistic techniques will be implemented in a revised version of the flare warning program, Flarecast, which will be operational in the Australian Space Forecast Centre.

Solar flare hard X-rays from the anchor points of an eruptive filament

Muriel Zoë **Stiefel**1, Andrea Francesco Battaglia1,2, Krzysztof Barczynski1,3, Hannah Collier1,2, Anna Volpara4, Paolo Massa5, Conrad Schwanitz1,3, Sofia Tynelius1, Louise Harra3,1 and Säm Krucker2,6
A&A 670, A89 (**2023**)
ww.aanda.org/articles/aa/pdf/2023/02/aa45044-22.pdf
Context. We present an analysis of a GOES M1.8 flare with excellent observational coverage in UV, extreme-UV (EUV), and X-ray, including observations from the Interface Region Imaging Spectrograph (IRIS), from the Solar Dynamics Observatory (SDO) with the Atmospheric Imaging Assembly (AIA), from the Hinode/EUV Imaging Spectrometer (EIS), from the Hinode/X-ray Telescope (XRT), and from Solar Orbiter with the Spectrometer/Telescope for Imaging X-rays (STIX). Hard X-ray emission is often observed at the footpoints of flare loops and is occasionally observed in the corona. In this flare, four nonthermal hard X-ray sources are seen.
Aims. Our aim is to understand why we can observe four individual nonthermal sources in this flare and how we can characterize the physical properties of these four sources.
Methods. We used the multiwavelength approach to analyze the flare and characterize the four sources. To do this, we combined imaging at different wavelengths and spectroscopic fitting in the EUV and X-ray range.
Results. The flare is eruptive with an associated coronal mass ejection, and it shows the classical flare picture of a heated flare loop seen in EUV and X-rays, and two nonthermal hard X-ray footpoints at the loop ends. In addition to the main flare sources, we observed two outer sources in the UV, EUV, and nonthermal X-ray range located away from the main flare loop to the east and west. The two outer sources are clearly correlated in time, and they are only seen during the first two minutes of the impulsive phase, which lasts a total of about four minutes.
Conclusions. Based on the analysis, we determine that the outer sources are the anchor points of an erupting filament. The hard X-ray emission is interpreted as flare-accelerated electrons that are injected upward into the filament and then precipitate along the filament toward the chromosphere, producing Bremsstrahlung. While sources like this have been speculated to exist, this is the first report of their detection. **23 September 2021**
Solar Orbiter nugget #13 **2023** https://www.cosmos.esa.int/web/solar-orbiter/-/science-nugget-solar-flare-hard-x-rays-from-the-anchor-points-of-an-eruptive-filament

The Tests and Calibrations of the Hard X-ray Imager Aboard ASO-S.

Su, Y., Zhang, Z., Chen, W. et al.
Sol Phys 299, 153 (**2024**).
https://doi.org/10.1007/s11207-024-02392-x
https://link.springer.com/content/pdf/10.1007/s11207-024-02392-x.pdf

The Hard X-ray Imager (HXI) aboard the Advanced Space-based Solar Observatory (ASO-S) is an instrument designed to observe hard X-ray (HXR) spectra and images of solar flares. Having 91 subcollimators to modulate incident X-rays, HXI can obtain 91 modulation data and 45 visibilities to reconstruct images with a spatial resolution as high as ∼3.1 arcsec. HXI was launched on 9 October 2022 and powered up on 17 October 2022. After the on-orbit testing phase lasting for three months, HXI was ready for regular observations on 18 January 2023. With fine-tuning of the detectors and electronics, we were able to expand the energy range from ∼30 – 200 keV to ∼10 keV – 300 keV, which significantly raised the scientific values of the data and the number of detected flare events. This paper presents the changes and improvements of HXI instrument since 2019, the important ground tests, on-orbit tests, and calibration works. We also present the light curves, spectra, and reconstructed images of one flare observed by HXI on **6 January 2023.**

Determination of Differential Emission Measure from Solar Extreme Ultraviolet Images

Yang **Su**1,2, Astrid M. Veronig3, Iain G. Hannah4, Mark C. M. Cheung5, Brian R. Dennis6, Gordon D. Holman6, Weiqun Gan1,2, and Youping Li1
2018 ApJL 856 L17
http://iopscience.iop.org/article/10.3847/2041-8213/aab436/pdf
The Atmospheric Imaging Assembly (AIA) on board the Solar Dynamic Observatory (SDO) has been providing high-cadence, high-resolution, full-disk UV-visible/extreme ultraviolet (EUV) images since 2010, with the best time coverage among all the solar missions. A number of codes have been developed to extract plasma differential emission measures (DEMs) from AIA images. Although widely used, they cannot effectively constrain the DEM at flaring temperatures with AIA data alone. This often results in much higher X-ray fluxes than observed. One way to solve the problem is by adding more constraint from other data sets (such as soft X-ray images and fluxes). However, the spatial information of plasma DEMs are lost in many cases. In this Letter, we present a different approach to constrain the DEMs. We tested the sparse inversion code and show that the default settings reproduce X-ray fluxes that could be too high. Based on the tests with both simulated and observed AIA data, we provided recommended settings of basis functions and tolerances. The new DEM solutions derived from AIA images alone are much more consistent with (thermal) X-ray observations, and provide valuable information by mapping the thermal plasma from ~0.3 to ~30 MK. Such improvement is a key step in understanding the nature of individual X-ray sources, and particularly important for studies of flare initiation. **2013 November 10-13**

High-resolution Observations of Flares in an Arch Filament System

Yingna **Su**1,2, Rui Liu3,4, Shangwei Li1,5, Wenda Cao6,7, Kwangsu Ahn6, and Haisheng Ji
2018 ApJ 855 77
http://sci-hub.tw/http://iopscience.iop.org/0004-637X/855/2/77/
https://arxiv.org/pdf/1803.06085.pdf
We study five sequential solar flares (SOL**2015-08-07**) occurring in Active Region 12396 observed with the Goode Solar Telescope (GST) at the Big Bear Solar Observatory, complemented by Interface Region Imaging Spectrograph and SDO observations. The main flaring region is an arch filament system (AFS) consisting of multiple bundles of dark filament threads enclosed by semicircular flare ribbons. We study the magnetic configuration and evolution of the active region by constructing coronal magnetic field models based on SDO/HMI magnetograms using two independent methods, i.e., the nonlinear force-free field (NLFFF) extrapolation and the flux rope insertion method. The models consist of multiple flux ropes with mixed signs of helicity, i.e., positive (negative) in the northern (southern) region, which is consistent with the GST observations of multiple filament bundles. The footprints of quasi-separatrix layers (QSLs) derived from the extrapolated NLFFF compare favorably with the observed flare ribbons. An interesting double-ribbon fine structure located at the east border of the AFS is consistent with the fine structure of the QSL's footprint. Moreover, magnetic field lines traced along the semicircular footprint of a dome-like QSL surrounding the AFS are connected to the regions of significant helicity and Poynting flux injection. The maps of magnetic twist show that positive twist became dominant as time progressed, which is consistent with the injection of positive helicity before the flares. We hence conclude that these circular shaped flares are caused by 3D magnetic reconnection at the QSLs associated with the AFS possessing mixed signs of helicity.

Statistical Study of Free Magnetic Energy and Flare Productivity of Solar Active Regions

J. T. **Su**1,2,3, J. Jing1, S. Wang1,2, T. Wiegelmann4, and H. M. Wang
ApJ 788 150, **2014**
http://arxiv.org/pdf/1405.2131v1.pdf
Photospheric vector magnetograms from the Helioseismic and Magnetic Imager on board the Solar Dynamic Observatory are utilized as the boundary conditions to extrapolate both nonlinear force-free and potential magnetic fields in solar corona. Based on the extrapolations, we are able to determine the free magnetic energy (FME) stored in active regions (ARs). Over 3000 vector magnetograms in 61 ARs were analyzed. We compare FME with the ARs' flare

index (FI) and find that there is a weak correlation (<60%) between FME and FI. FME shows slightly improved flare predictability relative to the total unsigned magnetic flux of ARs in the following two aspects: (1) the flare productivity predicted by FME is higher than that predicted by magnetic flux and (2) the correlation between FI and FME is higher than that between FI and magnetic flux. However, this improvement is not significant enough to make a substantial difference in time-accumulated FI, rather than individual flare, predictions.

Table 2. Information of 61 chosen ARs

Imaging coronal magnetic-field reconnection in a solar flare

Su, Y., Veronig, A. M., Holman, G. D., Dennis, B. R., Wang, T. J., Temmer, M., Gan, W. Q.
E-print, July **2013, File**; Nature Physics Volume: 9 Issue: 8 Pages: 489-493, **2013**

Magnetic-field reconnection is believed to play a fundamental role in magnetized plasma systems throughout the Universe1, including planetary magnetospheres, magnetars and accretion disks around black holes. This letter present extreme ultraviolet and X-ray observations of a solar flare showing magnetic reconnection with a level of clarity not previously achieved. The multi-wavelength extreme ultraviolet observations from SDO/AIA show inflowing cool loops and newly formed, outflowing hot loops, as predicted. RHESSI X-ray spectra and images simultaneously show the appearance of plasma heated to >10 MK at the expected locations. These two data sets provide solid visual evidence of magnetic reconnection producing a solar flare, validating the basic physical mechanism of popular flare models. However, new features are also observed that need to be included in reconnection and flare studies, such as three-dimensional non-uniform, non-steady and asymmetric evolution. **2011 August 17**

OBSERVATIONS OF A TWO-STAGE SOLAR ERUPTIVE EVENT (SEE): EVIDENCE FOR SECONDARY HEATING

Yang **Su**1,2,3, Brian R. Dennis1, Gordon D. Holman1, Tongjiang Wang1,2, Phillip C. Chamberlin1, Sabrina Savage1 and Astrid Veronig
2012 ApJ 746 L5

We present RHESSI, SDO/AIA, SOHO/LASCO, STEREO, and GOES observations of a partially occulted solar eruptive event that occurred at the southwest limb on **2011 March 8**. The GOES X-ray light curve shows two peaks separated by almost 2 hr that we interpret as two stages of a single event associated with the delayed eruption of a coronal mass ejection (CME). A hot flux rope formed during the first stage and continued expanding and rising throughout the event. The speed of the flux rope decreased from ~120 to 14 km s–1 during the decay phase of the first stage and increased again during the second stage to become the CME with a speed of ~516 km s–1. RHESSI and GOES data analyses show that the plasma temperature reached over 20 MK in the first stage, then decreased to ~10 MK and increased to 15 MK in the second stage. This event provides clear evidence for a secondary heating phase. The enhanced EUV and X-ray emission came from the high corona (~60 arcsec above the limb) in the second stage, ~40 arcsec higher than the site of the initial flare emission. STEREO-A on-disk observations indicate that the post-flare loops during this stage were of larger scale sizes and spatially distinct from those in the first stage.

IMAGING OBSERVATIONS OF QUASI-PERIODIC PULSATIONS IN SOLAR FLARE LOOPS WITH SDO/AIA

J. T. **Su**1, Y. D. Shen2, Y. Liu2, Y. Liu3, and X. J. Mao
2012 ApJ 755 113

Quasi-periodic pulsations (QPPs) of flaring emission with periods from a few seconds to tens of minutes have been widely detected from radio bands to γ-ray emissions. However, in the past the spatial information of pulsations could not be utilized well due to the instrument limits. We report here imaging observations of the QPPs in three loop sections during a C1.7 flare with periods of P = 24 s-3 minutes by means of the extreme-ultraviolet 171 Å channel of the Atmospheric Imaging Assembly (AIA) instrument on board the Solar Dynamics Observatory. We confirm that the QPPs with the shortest period of 24 s were not of an artifact produced by the Nyquist frequency of the AIA 12 s cadence. The QPPs in the three loop sections were interconnected and closely associated with the flare. The detected perturbations propagated along the loops at speeds of 65-200 km s–1, close to those of acoustic waves in them. The loops were made up of many bright blobs arranged in alternating bright and dark changes in intensity (spatial periodical distribution) with the wavelengths 2.4-5 Mm (as if they were magnetohydrodynamic waves). Furthermore, in the time-distance diagrams, the detected perturbation wavelengths of the QPPs are estimated to be ~10 Mm, which evidently do not fit the above ones of the spatial periodic distributions and produce a difference of a factor of 2-4 with them. It is suggested that the short QPPs with periods P < 60 s were possibly sausage-mode oscillations and the long QPPs with periods P > 60 s were the higher (e.g., >2nd) harmonics of slow magnetoacoustic waves.

EXTREME-ULTRAVIOLET MULTI-WAVELENGTH OBSERVATIONS OF QUASI-PERIODIC PULSATIONS IN A SOLAR POST-FLARE CUSP-SHAPE LOOP WITH SDO/AIA

J. T. **Su**1, Y. D. Shen2, and Y. Liu

2012 ApJ 754 43

We present extreme-ultraviolet multi-wavelength observations with the SDO/AIA instruments of quasi-periodic pulsations (QPPs) propagating along a cusp-shaped loop formed after an M2.2 flare on the Sun. Our motivation is to detect whether there were slow-mode magnetoacoustic waves propagating along its protruding flux tube. To this end, with fast Fourier transform we extract the short (<3 minutes) and long (>3 minutes) period components of the QPPs from time-space diagrams of the tube slices. We find that velocity differences did exist among the short/long-period components of different wavelengths, but only one event in the long-period ones showed they were greater than the measurement errors (e.g., 65 km s–1), which were 330 km s–1 detected in 171 Å, 590 km s–1 in 211 Å, and 180 km s–1 in 304 Å. The intensity modulation in all wavelengths is found to be very large, e.g., ~60% of the emission trend for an event in the 171 Å passband, which would be an order of magnitude higher than the perturbation of the plasma density in the slow-mode magnetoacoustic waves. Moreover, only the QPPs with upward velocities of 50-300 km s–1 are found in the tube, and the downward ones of several tens of kilometers are never unambiguously detected. Therefore, most of the QPP events under study were likely the episodic outflows along the tube, and the one with a supersonic speed of 590 km s–1 may be a kink wave.

Two-Stage SEE shows reconnection

Yang **Su** and Brian Dennis:

RHESSI science nugget No. 158, 8 Sept **2011**

http://sprg.ssl.berkeley.edu/~tohban/wiki/index.php/Two-stage_SEE_Shows_Reconnection

A beautiful eruptive event (a SEE) appears to show reconnection in an example of the new EVE "super-late" phase of a flare. We report here on an event on **8 March 2011** with similar strong evidence for a second stage of energy release high in the corona.

OBSERVATIONS AND MAGNETIC FIELD MODELING OF THE FLARE/CORONAL MASS EJECTION EVENT ON 2010 APRIL 8

Yingna **Su**1, Vincent Surges1,2, Adriaan van Ballegooijen1, Edward DeLuca1 and Leon Golub

2011 ApJ 734 53, **File**

We present a study of the flare/coronal mass ejection event that occurred in Active Region 11060 on **2010 April 8**. This event also involves a filament eruption, EIT wave, and coronal dimming. Prior to the flare onset and filament eruption, both SDO/AIA and STEREO/EUVI observe a nearly horizontal filament ejection along the internal polarity inversion line, where flux cancellations frequently occur as observed by SDO/HMI. Using the flux-rope insertion method developed by van Ballegooijen, we construct a grid of magnetic field models using two magneto-frictional relaxation methods. We find that the poloidal flux is significantly reduced during the relaxation process, though one relaxation method preserves the poloidal flux better than the other. The best-fit pre-flare NLFFF model is constrained by matching the coronal loops observed by SDO/AIA and Hinode/XRT. We find that the axial flux in this model is very close to the threshold of instability. For the model that becomes unstable due to an increase of the axial flux, the reconnected field lines below the X-point closely match the observed highly sheared flare loops at the event onset. The footpoints of the erupting flux rope are located around the coronal dimming regions. Both observational and modeling results support the premise that this event may be initiated by catastrophic loss of equilibrium caused by an increase of the axial flux in the flux rope, which is driven by flux cancellations.

OBSERVATIONAL EVIDENCE OF CHANGING PHOTOSPHERIC VECTOR MAGNETIC FIELDS ASSOCIATED WITH SOLAR FLARES

J. T. **Su**1,2, J. Jing1, H. M. Wang1, X. J. Mao2,3, X. F. Wang2, H. Q. Zhang2, Y. Y. Deng2, J. Guo2 and G. P. Wang

2011 ApJ 733 94

Recent observations have provided evidence that the solar photospheric magnetic fields could have rapid and permanent changes in both longitudinal and transverse components associated with major flares. As a result, the Lorentz force (LF) acting on the solar photosphere and solar interior could be perturbed, and the change of LF is always nearly in the downward direction. However, these rapid and permanent changes have not been systematically investigated, yet, using vector magnetograms. In this paper, we analyze photospheric vector magnetograms covering five flares to study the evolution of photospheric magnetic fields. In particular, we investigate two-dimensional spatial distributions of the

changing LF. Around the major flaring polarity inversion line, the net change of the LF is directed downward in an area of ~1019 cm2 for X-class flares. For all events, the white-light observations show that sunspots darken in this location after flares, and magnetic fields become more inclined, which is consistent with the ideas put forward by Hudson et al. and Fisher et al., and observations.

EVIDENCE FOR THE FULL HARD X-RAY SPECTRAL SIGNATURE OF NONUNIFORM IONIZATION IN A SOLAR FLARE

Yang **Su**1,2,3, Gordon D. Holman2 and Brian R. Dennis
2011 ApJ 731 106
The hard X-ray (HXR) emission from solar flares is observed primarily from the footpoints of flare magnetic loops, where nonthermal electrons are understood to emit thick-target bremsstrahlung as they stream from the fully ionized hot corona to the denser, cooler, and partially ionized chromosphere. The change in the plasma ionization along the path of the electrons should result in a characteristic upward break and corresponding flattening of the X-ray spectrum with increasing energy at lower energies, and a downward break at higher energies. Due to the presence of thermal emission, the upward break usually cannot be observed. We report the first evidence for both breaks in spectra measured with the Reuven Ramaty High Energy Solar Spectroscopic Imager (RHESSI) during the GOES X1.2 class flare that happened on 2002 October 31. The RHESSI X-ray spectral analysis shows both the breakup at ~49 keV and the breakdown at ~134 keV at the HXR peak time. The time evolution of both breaks also agrees with the nonuniform ionization (NUI) model. Other possible explanations for the breaks are considered, but the NUI model provides the simplest explanation for the spectral shape and its time evolution. We find that the average column density of the fully ionized plasma changed from 2 ×1019 cm–2 in the rise phase to 7 ×1021 cm–2 after the peak. This indicates that plasma in the target was heated and became ionized during the flare, in agreement with heating by the nonthermal electrons and chromospheric evaporation expected in the collisional thick-target model.

OBSERVATIONAL EVIDENCE OF UNWINDING AND CHIRALITY CHANGING IN PENUMBRAL FILAMENTS BY HINODE

Jiangtao **Su**1,2, Yu Liu3, Hongqi Zhang1,2, Xinjie Mao4, Yin Zhang1,2 and Han He1,2
ApJ 710 170-179, **2010**
In this paper, we present a very important and quite controversial observational property of penumbral filaments that may exhibit twisting motions and change their chirality. Using high-resolution observations from the Solar Optical Telescope on board *Hinode*, we study the unwinding and twisting motions in the penumbral filaments of active region NOAA 10930. Penumbral filaments, including those to the northwest of the magnetic polarity inversion line (PIL) and those inside the PIL region, are found to make unwinding motions associated with the decrease of their right-handed twists. After unwinding, the filaments inside the PIL region are found to twist continuously to develop left-handed twists in them. Moreover, we find the filament elongating, expanding, splitting, and the screw pitch decreasing in the unwinding process and, getting shorter, shrinking, merging, and the screw pitch increasing in the twisting process. These observational results indicate that penumbral filaments are more inclined to be twisted magnetic flux tubes in nature.

On classification of RHESSI flares

Yang **Su**, W.Q. Gan and Y.P. Li
Advances in Space Research, Volume 41, Issue 6, **2008**, Pages 988-991
https://sci-hub.tw/10.1016/j.asr.2007.07.010
Based on the light curves and images of RHESSI flares, we tried to make a preliminary classification of solar flares. Three basic types of flares seem to be existed: accordantly gradual flares, accordantly impulsive flares, and early impulsive flares. The proportion for each type is given. The possible physical meaning related to different types is discussed. **27 Feb 2002, 14 July 2002, 3 Aug 2002**

Flare Energy Build-Up in a Decaying Active Region Near a Coronal Hole

Yingna **Su**1,2, Adriaan van Ballegooijen1, Brigitte Schmieder3, Arkadiusz Berlicki4,5,3, Yang Guo3, Leon Golub1,Guangli Huang2
E-print, Aug **2009**; ApJ, 704:341–353, **2009** October, **File**
A B1.7 two-ribbon flare occurred in a highly non-potential decaying active region near a coronal hole at 10:00 UT on **May 17, 2008**. This flare is ?large? in the sense that it involves the entire region, and it is associated with both a filament eruption and a CME. We present multi-wavelength observations from EUV (TRACE, STEREO/EUVI), X-rays (Hinode/XRT), and Hα (THEMIS, BBSO) prior to, during and after the flare. Prior to the flare, the region contained two filaments. The long J-shaped sheared loops corresponding to the southern filament were evolved from two short loop systems, which happened around 22:00 UT after a filament eruption on May 16. Formation of highly sheared loops in the south eastern part of the region was observed by STEREO 8 hours before the flare. We also perform non-linear force free field (NLFFF) modeling for the region at two times prior to the flare, using the flux rope insertion method.

The models include the non-force-free effect of magnetic buoyancy in the photosphere. The best-fit NLFFF models show good fit to observations both in the corona (X-ray and EUV loops) and chromosphere (Hα filament). We find that the horizontal fields in the photosphere are relatively insensitive to the present of flux ropes in the corona. The axial flux of the flux rope in the NLFFF model on May 17 is twice that on May 16, and the model on May 17 is only marginally stable. We also find that the quasi-circular flare ribbons are associated with the separatrix between open and closed fields. This observation and NLFFF modeling suggest that this flare may be triggered by the reconnection at the null point on the separatrix surface.

LOCAL TWIST AND CURRENT HELICITY DISTRIBUTIONS OF ACTIVE REGION NOAA 10930

J. T. **Su**1,2, T. Sakurai1, Y. Suematsu1, M. Hagino1, and Yu Liu3
Astrophysical Journal, 697:L103–L107, **2009** June 1 doi:10.1088/0004-637X/697/2/L103
Hinode high-quality vector magnetograms and *G*-band data are utilized to study the distributions of local twist α_z and current helicity h_c on the active region of NOAA 10930. The new findings are as follows. (1) The patches of positive and negative helicities were intermixed showing a mesh pattern in the umbra and a thread pattern in the penumbra. (2) For its main stable sunspot (MSS), there was a positive-helicity patch accounting for ~43% of the umbra area surrounding the inner umbra, which had a predominantly negative helicity. For its minor rotating sunspot (MRS), there was a negative-helicity patch appearing in the umbra. (3) The fine distributions of α_z and h_c on a penumbral filament indicated that it may be possible for the two opposite helicities to coexist in a filament and their magnitudes were nearly equivalent.

Evolution of the Sheared Magnetic Fields of two X-class Flares Observed by Hinode/XRT

Yingna **Su**, Leon Golub, Adriaan Van Ballegooijen, Edward Deluca, Kathy Reeves, Taro Sakao, Ryohei Kano, Noriyuki Narukage, and Kiyoto Shibasaki
E-print, August 2007
We present multi-wavelength observations of the evolution of the sheared magnetic fields in NOAA Active Region 10930, where two X-class flares occurred on **2006 December 13 and December 14**, respectively. Observations made with the X-ray Telescope (XRT) and the Solar Optical Telescope (SOT) aboard Hinode suggest that the gradual formation of the sheared magnetic fields in this active region is caused by the rotation and west-to-east motion of an emerging sunspot. In the pre-flare phase of the two flares, XRT shows several highly sheared X-ray loops in the core field region, corresponding to a filament seen in the TRACE EUV observations. XRT observations also show that part of the sheared core field erupted, and another part of the sheared core field stayed behind during the flares, which may explain why a large part of the filament is still seen by TRACE after the flare. About 2-3 hours after the peak of each flare, the core field becomes visible in XRT again, and shows a highly sheared inner and less sheared outer structure. We also find that the post-flare core field is clearly less sheared than the pre-flare core field, which is consistent with the idea that the energy released during the flares is stored in the highly sheared fields prior to the flare.

Analysis of magnetic shear in an X17 solar flare on October 28, 2003 –

Y.N. **Su**, L. Golub, A.A. Van Ballegooijen, M. Gros
Solar Physics (2006) 236: 325–349
a clear decrease in the shear of the flare footpoints during the flare.

A STATISTICAL STUDY OF SHEAR MOTION OF THE FOOTPOINTS IN TWO-RIBBON FLARES

Yingna **Su**, Leon Golub,2 and Adriaan A. Van Ballegooijen2
The Astrophysical Journal, 655:606-614, 2007, file
A statistical investigation of shear motion of the ultraviolet (UV) or extreme-ultraviolet (EUV) footpoints in 50 two-ribbon flares, using the high spatial resolution data obtained in 1998-2005 by TRACE.
Table, M- and X-class flares.

Estimations of Elemental Abundances During Solar Flares Observed in Soft X-rays by the MinXSS-1 CubeSat Mission

Crisel **Suarez**, Christopher S. Moore
ApJ 957 14 **2023**
https://arxiv.org/pdf/2308.16235.pdf
https://iopscience.iop.org/article/10.3847/1538-4357/acf0c2/pdf
Solar flares are complex phenomena emitting all types of electromagnetic radiation, and accelerating particles on timescales of minutes, converting magnetic energy to thermal, radiative, and kinetic energy through magnetic

reconnections. As a result, local plasma can be heated to temperatures in excess of 20 MK. During the soft X-ray (SXR) solar flare peak, the elemental abundance of low first-ionization potential (FIP) elements are typically observed to be depleted from coronal values. We explored the abundance variations using disk-integrated solar spectra from the Miniature X-ray Solar Spectrometer CubeSat-1 (MinXSS-1). MinXSS-1 is sensitive to the 1-12 keV energy range with an effective 0.25 keV full-width at half-maximum (FWHM) resolution at 5.9 keV. During the year-long mission of MinXSS-1, between May 2016 - May 2017, 21 flares with intermittent data downlinks were observed ranging from C to M class. We examine the time evolution of temperature, volume emission measure, and elemental abundances of Fe, Ca, Si, S, and Ar with CHIANTI spectral models near the peak SXR emission times observed in the MinXSS-1 data. We determined the average absolute abundance of A(Fe) = 7.81, A(Ca) = 6.84, A(S) = 7.28, A(Si) = 7.90, and A(Ar) = 6.56. These abundances are depleted from coronal values during the SXR peak compared to non-flaring times. The elemental abundance values that are depleted from their coronal values are consistent with the process of chromospheric evaporation, in which the lower atmospheric plasma fills the coronal loops. **2016-07-21-23**
Table 2016-2017

Emission measure distribution for diffuse regions in active regions

Srividya **Subramanian**
EIS Nugget, Dec **2014**
http://solarb.mssl.ucl.ac.uk/SolarB/nuggets/nugget_2014dec.jsp

Emission Measure Distribution for Diffuse Regions in Solar Active Regions

Srividya **Subramanian**, Durgesh Tripathi, James A. Klimchuk, Helen E. Mason
ApJ, ApJ 795 76 **2014**
http://arxiv.org/pdf/1409.1447v1.pdf
Our knowledge of the diffuse emission that encompasses active regions is very limited. In the present paper we investigate two off-limb active regions, namely AR10939 and AR10961, to probe the underlying heating mechanisms. For this purpose we have used spectral observations from Hinode/EIS and employed the emission measure (EM) technique to obtain the thermal structure of these diffuse regions. Our results show that the characteristic EM distributions of the diffuse emission regions peak at log T = 6.25 and the cool-ward slopes are in the range 1.4 - 3.3. This suggests that both low as well as high frequency nanoflare heating events are at work. Our results provide additional constraints on the properties of these diffuse emission regions and their contribution to the background/foreground when active region cores are observed on-disk. **2007 Jan 26, (2007 Aug 01-08, AR 10961)**

What is the true nature of blinkers?

S. **Subramanian**1, M. S. Madjarska1, J. G. Doyle1 and D. Bewsher
A&A 538, A50 (**2012**)
Aims. The aim of this work is to identify the true nature of the transient EUV brightenings, called blinkers.
Methods. Co-spatial and co-temporal multi-instrument data, including imaging (EUVI/STEREO, XRT and SOT/Hinode), spectroscopic (CDS/SoHO and EIS/Hinode) and magnetogram (SOT/Hinode) data, of an isolated equatorial coronal hole were used. An automatic program for identifying transient brightenings in CDS O v 629 Å, EUVI 171 Å and XRT was applied.
Results. We identified 28 blinker groups in the CDS O v 629 Å raster images. All CDS O v 629 Å blinkers showed counterparts in EUVI 171 Å and 304 Å images. We classified these blinkers into two categories, one associated with coronal counterparts and other with no coronal counterparts as seen in XRT images and EIS Fe xii 195.12 Å raster images. Around two-thirds of the blinkers show coronal counterparts and correspond to various events like EUV/X-ray jets, brightenings in coronal bright points or foot-point brightenings of larger loops. These brightenings occur repetitively and have a lifetime of around 40 min at transition region temperatures. The remaining blinker groups with no coronal counterpart in XRT and EIS Fe xii 195.12 Å appear as point-like brightenings and have chromospheric/transition region origin. They take place only once and have a lifetime of around 20 min. In general, lifetimes of blinkers are different at different wavelengths, i.e. different temperatures, decreasing from the chromosphere to the corona.
Conclusions. This work shows that the term blinker covers a range of phenomena. Blinkers are the EUV response of various transient events originating at coronal, transition region and chromospheric heights. Hence, events associated with blinkers contribute to the formation and maintenance of the temperature gradient in the transition region and the corona.
See May **2012** Hinode EIS Nugget:
http://msslxr.mssl.ucl.ac.uk:8080/SolarB/nuggets/nugget_2012may.jsp

A question raised from the observation of dynamic cusp formation: When and where does particle acceleration occur?

Linhui **Sui**, Gordon D. Holman, & Brian R. Dennis

E-print, Oct 2007, Adv. Space Res. Volume 41, Issue 6, **2008**, Pages 976-983
We present observations of a C9.4 flare on **2002 June 2** in EUV (TRACE) and X-rays (RHESSI). The multiwavelength data reveal: (1) the involvement of a quadrupole magnetic configuration; (2) loop expansion and ribbon motion in the pre-impulsive phase; (3) gradual formation of a new compact loop with a long cusp at the top during the impulsive phase of the flare; (4) appearance of a large, twisted loop above the cusp expanding outward immediately after the hard X-ray peak; and (5) X-ray emission observed only from the new compact loop and the cusp. In particular, the gradual formation of an EUV cusp feature is very clear. The observations also reveal the timing of the cusp formation and particle acceleration: most of the impulsive hard X-rays (>25 keV) were emitted before the cusp was seen. This suggests that fast reconnection occurred during the restructuring of the magnetic configuration, resulting in more efficient particle acceleration, while the reconnection slowed after the cusp was completely formed and the magnetic geometry was stabilized. This observation is consistent with the observations obtained with Yohkoh/Soft X-ray Telescope (SXT) that soft X-ray cusp structures only appear after the major impulsive energy release in solar flares. These observations have important implications for the modeling of magnetic reconnection and particle acceleration.

Nonthermal X-Ray Spectral Flattening toward Low Energies in Early Impulsive Flares

Sui, Linhui; Holman, Gordon D.; Dennis, Brian R.
Astrophysical Journal, Volume 670, Issue 1, pp. 862-871. **2007**
https://iopscience.iop.org/article/10.1086/522198/pdf
The determination of the low-energy cutoff to nonthermal electron distributions is critical to the calculation of the nonthermal energy in solar flares. The most direct evidence for low-energy cutoffs is flattening of the power-law, nonthermal X-ray spectra at low energies. However, because of the plasma preheating often seen in flares, the thermal emissions at low energies may hide such spectral flattening of the nonthermal component. We select a category of flares, which we call ``early impulsive flares," in which the >25 keV hard X-ray (HXR) flux increase is delayed by less than 30 s after the flux increase at lower energies. Thus, the plasma preheating in these flares is minimal, so the nonthermal spectrum can be determined to lower energies than in flares with significant preheating. Out of a sample of 33 early impulsive flares observed by the Ramaty High Energy Solar Spectroscopy Imager (RHESSI), nine showed spectral flattening toward low energies. In these events, the break energy of the double power-law fit to the HXR spectra lies in the range 10-50 keV, significantly lower than the value we have seen for other flares that do not show such early impulsive emissions. In particular, it correlates with the HXR flux. After correcting the spatially integrated spectra for albedo from isotropically emitted X-rays and using RHESSI imaging spectroscopy to exclude the extended albedo halo, we find that albedo associated with isotropic or nearly isotropic electrons can only account for the spectral flattening in three flares near Sun center. The spectral flattening in the remaining six flares is found to be consistent with the existence of a low-energy cutoff in the electron spectrum, falling in the range 15-50 keV, which also correlates with the HXR flux. **. 26 Feb 2002, 22 Apr 2002, 2002 June 2, 29 June 2002, 14 Nov 2002**
2. EARLY IMPULSIVE FLARES

Motion of 3-6 keV Nonthermal Sources along the Legs of a Flare Loop

Sui, Linhui; Holman, Gordon D.; Dennis, Brian R.
Astrophysical Journal, Volume 645, Issue 2, pp. L157-L160. **2006**
https://iopscience.iop.org/article/10.1086/506325/pdf
Observations of nonthermal X-ray sources are critical to the study of electron acceleration and transport in solar flares. Strong thermal emission radiated from the preheated plasma before the flare impulsive phase often makes it difficult to detect low-energy X-ray sources that are produced by relatively low-energy nonthermal electrons. Knowledge of the distribution of these low-energy nonthermal electrons is particularly important in determining the total nonthermal electron energy in solar flares. We report on an ``early impulsive flare" in which impulsive hard X-ray emission was seen early in the flare before the soft X-ray emission had risen significantly, indicating limited plasma preheating. Early in the flare, RHESSI <25 keV images show coronal sources that moved first downward and then upward along the legs of a flare loop. In particular, the 3-6 keV source appeared as a single coronal source at the start of the flare, and then it evolved into two coronal sources moving down along the two legs of the loop. After nearly reaching the two footpoints at the hard X-ray peak, the two sources moved back up to the looptop again. RHESSI images and light curves all indicate that nonthermal emission dominated at energies as low as 3-6 keV. We suggest that the evolution of both the spectral index and the low-energy cutoff of the injected electron distribution could result in the accelerated electrons reaching a lower altitude along the legs of the dense flare loop and hence result in the observed downward and upward motions of the nonthermal sources. **2002 November 28**

Evidence for the formation of a large-scale current sheet in a solar flare.

Sui, L., Holman, G. D.
ApJ 596, L251-L254, **2003**.

Extraordinary Magnetic Flux Emergence Rate Preceding the May 2024 Extreme Geomagnetic Disturbances

Xudong **Sun**1, Aimee Norton2, Shin Toriumi3, Peter Schuck4, Jie Zhang
HMI Science Nuggets #4216 June **2024**
http://hmi.stanford.edu/hminuggets/?p=4216
NOAA active regions 13664/8, the solar source region responsible for the **May 2024** extreme geomagnetic disturbances that caused the largest geomagnetic storm since 2003, broke the record of magnetic flux emergence rate in the SDO era. **6-12 May 2024**

Magnetic helicity evolution during active region emergence and subsequent flare productivity

Zheng **Sun**, Ting Li, Quan Wang, Shangbin Yang, Mei Zhang, Yajie Chen
A&A 686, A148 **2024**
https://arxiv.org/pdf/2403.18354.pdf
https://www.aanda.org/articles/aa/pdf/2024/06/aa48734-23.pdf
Aims. Solar active regions (ARs), which are formed by flux emergence, serve as the primary sources of solar eruptions. However, the specific physical mechanism that governs the emergence process and its relationship with flare productivity remains to be thoroughly understood. Methods. We examined 136 emerging ARs, focusing on the evolution of their magnetic helicity and magnetic energy during the emergence phase. Based on the relation between helicity accumulation and magnetic flux evolution, we categorized the samples and investigated their flare productivity. Results. The emerging ARs we studied can be categorized into three types, Type-I, Type-II, and Type-III, and they account for 52.2%, 25%, and 22.8% of the total number in our sample, respectively. Type-I ARs exhibit a synchronous increase in both the magnetic flux and magnetic helicity, while the magnetic helicity in Type-II ARs displays a lag in increasing behind the magnetic flux. Type-III ARs show obvious helicity injections of opposite signs. Significantly, 90% of the flare-productive ARs (flare index > 6) were identified as Type-I ARs, suggesting that this type of AR has a higher potential to become flare productive. In contrast, Type-II and Type-III ARs exhibited a low and moderate likelihood of becoming active, respectively. Our statistical analysis also revealed that Type-I ARs accumulate more magnetic helicity and energy, far beyond what is found in Type-II and Type-III ARs. Moreover, we observed that flare-productive ARs consistently accumulate a significant amount of helicity and energy during their emergence phase. Conclusions. These findings provide valuable insight into the flux emergence phenomena, offering promising possibilities for early-stage predictions of solar eruptions. **2012-11-25-27, 2013-06-11-14, 2016-03-12-14**

Deep Learning–based Solar Flare Forecasting Model. III. Extracting Precursors from EUV Images

Dezhi **Sun**1,2, Xin Huang3,1, Zhongrui Zhao1,2, and Long Xu1
2023 ApJS 266 8
https://iopscience.iop.org/article/10.3847/1538-4365/acc248/pdf
A solar flare is one of the most intense solar activities, and flare forecasting is necessary to avoid its destructive impact on the near-Earth space environment and technological infrastructure. Previous studies have demonstrated the importance of the photospheric magnetic field in the occurrence of flares. Therefore, most of the input data in traditional solar flare forecasting models are magnetograms of active regions. The magnetic field of the photosphere is routinely measured and observed, but the magnetic field of the corona is not. Hence, the goal of our work is to test whether precursors can be extracted from coronal multiwavelength images of active regions and to build a flare-forecasting model. Therefore, we investigated the effect of using extreme ultraviolet (EUV) images (at 94, 131, 171, 193, 211, and 335 Å) of the active region on solar flare forecasting. We generated a data set consisting of EUV images of the active regions observed by the Solar Dynamics Observatory/Atmospheric Imaging Assembly from 2010 to 2016. Based on this data set, a deep-learning method was used to extract precursors from EUV multiwavelength images. The test results of the forecasting model were discussed and analyzed, and the following conclusions were drawn. (1) Each wavelength achieved good results using the EUV multiwavelength images for flare forecasting. The 94 Å wavelength demonstrated the best result among the single-wavelength results. (2) Among the combined multiwavelength results, the best fusion results were obtained for all six wavelengths. **2012 March 7, 2015 Sep 27**

Solar Flare Forecast Using 3D Convolutional Neural Networks

Pengchao **Sun**3,1, Wei Dai3,1, Weiqi Ding1, Song Feng4,1, Yanmei Cui2, Bo Liang1, Zeyin Dong1, and Yunfei Yang1
2022 ApJ 941 1
https://iopscience.iop.org/article/10.3847/1538-4357/ac9e53/pdf
Solar flares are immense energy explosions in the solar atmosphere and severely influence space weather. So, forecasting solar flare eruptions is extremely important. Spatial distribution and evolution of active region (AR) magnetic fields are closely related to flare eruptions. In this paper, we simultaneously utilized the two characteristics to build two flare-forecast models using three-dimensional convolutional neural networks (3D CNNs). The two models forecast whether an AR would erupt a ≥C- or ≥M-class flare within the next 24 hr, respectively. The magnetogram

sequences provided by the Space-weather Helioseismic and Magnetic Imager Active Region Patches are selected to train our models. We used several performance metrics, such as true skill statistics (TSS), to evaluate our models. The TSS scores of the ≥C and ≥M models reach 0.756 and 0.826, respectively, indicating that our models have superior forecast performance. We used the the gradient-weighted class activation mapping (Grad-CAM) method to visually explain our flare-forecast models. The Grad-CAM illustrates that the 3D CNNs may extract the spatial distribution and evolution of AR magnetic fields simultaneously for flare forecasts. So, the 3D CNN method is valid for flare forecasts, and it utilizes the characteristics related to flare eruptions.

Predicting Solar Flares Using CNN and LSTM on Two Solar Cycles of Active Region Data

Zeyu **Sun**, Monica G. Bobra, Xiantong Wang, Yu Wang, Hu Sun, Tamas Gombosi, Yang Chen, Alfred Hero

ApJ **931** 163 **2022**

https://arxiv.org/pdf/2204.03710.pdf

https://iopscience.iop.org/article/10.3847/1538-4357/ac64a6/pdf

We consider the flare prediction problem that distinguishes flare-imminent active regions that produce an M- or X-class flare in the future 24 hours, from quiet active regions that do not produce any flare within ±24 hours. Using line-of-sight magnetograms and parameters of active regions in two data products covering Solar Cycle 23 and 24, we train and evaluate two deep learning algorithms -- CNN and LSTM -- and their stacking ensembles. The decisions of CNN are explained using visual attribution methods. We have the following three main findings. (1) LSTM trained on data from two solar cycles achieves significantly higher True Skill Scores (TSS) than that trained on data from a single solar cycle with a confidence level of at least 0.95. (2) On data from Solar Cycle 23, a stacking ensemble that combines predictions from LSTM and CNN using the TSS criterion achieves significantly higher TSS than the "select-best" strategy with a confidence level of at least 0.95. (3) A visual attribution method called Integrated Gradients is able to attribute the CNN's predictions of flares to the emerging magnetic flux in the active region. It also reveals a limitation of CNN as a flare prediction method using line-of-sight magnetograms: it treats the polarity artifact of line-of-sight magnetograms as positive evidence of flares.

Improved and Interpretable Solar Flare Predictions with Spatial & Topological Features of the Polarity-Inversion-Line Masked Magnetograms

Hu **Sun**,Ward Manchester IV,Yang Chen

Space Weather **Volume19, Issue12** e2021SW002837 **2021**

https://agupubs.onlinelibrary.wiley.com/doi/epdf/10.1029/2021SW002837

https://doi.org/10.1029/2021SW002837

Many current research efforts undertake the solar flare classification task using the Space-weather HMI Active Region Patch (SHARP) parameters as the predictors. The SHARP parameters are scalar quantities based on spatial average or integration of physical quantities derived from the vector magnetic field, which loses information of the two-dimensional spatial distribution of the field and related quantities. In this paper, we construct two new sets of spatial features to expand the feature set used for the flare classification task. The first set uses the idea of topological data analysis to summarize the geometric information of the distributions of various SHARP quantities across active regions. The second set utilizes tools coming from spatial statistics to analyze the vertical magnetic field component Br and summarize its spatial variations and clustering patterns. All features are constructed within regions near the polarity inversion lines (PILs) and classification performances using the new features are compared against those using SHARP parameters (also along the PIL). We found that using the new features can improve the skill scores of the flare classification model and new features tend to have higher feature importance, especially the spatial statistics features. This potentially suggests that even using a single magnetic field component, Br, instead of all SHARP parameters, one can still derive strongly predictive features for flare classification. **2011.02.13**

Non-Neutralized Electric Current of Active Regions Explained as a Projection Effect

Xudong **Sun**, Mark C. M. Cheung

Solar Phys. **296**, Article number: 7 **2021**

https://arxiv.org/pdf/2011.11873.pdf

https://link.springer.com/content/pdf/10.1007/s11207-020-01742-9.pdf

Active regions (ARs) often possess an observed net electric current in a single magnetic polarity. We show that such "non-neutralized" currents can arise from a geometric projection effect when a twisted flux tube obliquely intersects the photosphere. To this end, we emulate surface maps of an emerging AR by sampling horizontal slices of a semi-torus flux tube at various heights. Although the tube has no net toroidal current, its poloidal current, when projected along the vertical direction, amounts to a significant non-neutralized component on the surface. If the tube emerges only partially as in realistic settings, the non-neutralized current will 1) develop as double ribbons near the sheared polarity inversion line, (2) positively correlate with the twist, and 3) reach its maximum before the magnetic flux. The projection effect may be important to the photospheric current distribution, in particular during the early stages of flux emergence.

Interpreting LSTM Prediction on Solar Flare Eruption with Time-series Clustering

Hu **Sun** (1), Ward Manchester (2), Zhenbang Jiao (1), Xiantong Wang (2), Yang Chen

ApJ **2020**

https://arxiv.org/pdf/1912.12360.pdf

We conduct a post hoc analysis of solar flare predictions made by a Long Short Term Memory (LSTM) model employing data in the form of Space-weather HMI Active Region Patches (SHARP) parameters. These data are distinguished in that the parameters are calculated from data in proximity to the magnetic polarity inversion line where the flares originate. We train the the LSTM model for binary classification to provide a prediction score for the probability of M/X class flares to occur in next hour. We then develop a dimension-reduction technique to reduce the dimensions of SHARP parameter (LSTM inputs) and demonstrate the different patterns of SHARP parameters corresponding to the transition from low to high prediction score. Our work shows that a subset of SHARP parameters contain the key signals that strong solar flare eruptions are imminent. The dynamics of these parameters have a highly uniform trajectory for many events whose LSTM prediction scores for M/X class flares transition from very low to very high. The results suggest that there exist a few threshold values of a subset of SHARP parameters when surpassed could indicate a high probability of strong flare eruption. Our method has distilled the knowledge of solar flare eruption learnt by deep learning model and provides a more interpretable approximation where more physics related insights could be derived.

Appendix A Summary of Sudden Transition Cases (2011-2017)

Expansion of Solar Coronal Hot Electrons in an Inhomogeneous Magnetic Field: 1-D PIC Simulation

Jicheng **Sun**, Xinliang Gao, Yangguang Ke, Quanming Lu, Xueyi Wang, Shui Wang

ApJ **887** 96 **2019**

https://arxiv.org/ftp/arxiv/papers/1911/1911.07207.pdf

https://doi.org/10.3847/1538-4357/ab5060

The expansion of hot electrons in flaring magnetic loops is crucial to understanding the dynamics of solar flares. In this paper we investigate, for the first time, the transport of hot electrons in a magnetic mirror field based on a 1-D particle-in-cell (PIC) simulation. The hot electrons with small pitch angle transport into the cold plasma, which leads to the generation of Langmuir waves in the cold plasma and ion acoustic waves in the hot plasma. The large pitch angle electrons can be confined by the magnetic mirror, resulting in the different evolution time scale between electron parallel and perpendicular temperature. This will cause the formation of electron temperature anisotropy, which can generate the whistler waves near the interface between hot electrons and cold electrons. The whistler waves can scatter the large pitch angle electrons to smaller value through the cyclotron resonance, leading to electrons escaping from the hot region. These results indicate that the whistler waves may play an important role in the transport of electrons in flaring magnetic loops. The findings from this study provide some new insights to understand the electron dynamics of solar flares.

Super-Flaring Active Region 12673 Has One of the Fastest Magnetic Flux Emergence Ever Observed

Xudong **Sun**, Aimee A. Norton

Research Notes of the AAS **1** 24 **2017**

https://arxiv.org/pdf/1711.08383.pdf

http://iopscience.iop.org/article/10.3847/2515-5172/aa9be9

The flux emergence rate of AR 12673 is greater than any values reported in the literature of which we are aware.

6 Sept 2017

Investigating the Magnetic Imprints of Major Solar Eruptions with SDO/HMI High-Cadence Vector Magnetograms

Xudong **Sun**, J. Todd Hoeksema, Yang Liu, Maria Kazachenko, Ruizhu Chen

ApJ **2017**

https://arxiv.org/pdf/1702.07338.pdf

The solar active region photospheric magnetic field evolves rapidly during major eruptive events, suggesting appreciable feedback from the corona. The new high-cadence (90 s or 135 s) vector magnetogram dataset from the Helioseismic and Magnetic Imager (HMI) is suited for investigating these "magnetic imprints". Observations of an archetypical event, SOL**2011-02-15T01**:56, show the following trends. Firstly, the horizontal magnetic field component (Bh) exhibits permanent, step-like changes with a time scale of several minutes, whereas the radial component (Br) varies less. Secondly, Bh near the main polarity inversion line increases significantly during the earlier phase of the associated flare, whereas Bh in the periphery decreases at later times with smaller magnitudes. Thirdly, transient artifacts coincide with enhanced flare emission, where the Stokes profiles are no longer adequately modeled under

standard settings, and the inferred magnetic field becomes unreliable. Our results corroborate previous findings, remove certain ambiguities that arise from line-of-sight only or lower-cadence vector observations, and provide insights on the momentum processes during solar eruption. The dataset may also be useful to the study of sunquakes and data-driven modeling of the solar corona.

Why Is the Great Solar Active Region 12192 CME-Poor?

Xudong **Sun**, Monica G. Bobra, J. Todd Hoeksema, Yang Liu, Yan Li, Chenglong Shen, Sebastien Couvidat, Aimee A. Norton, George H. Fisher

ApJL **2015**

http://arxiv.org/pdf/1502.06950v1.pdf

Solar active region (AR) **12192 of October 2014** hosts the largest sunspot group in 24 years. It is the most prolific flaring site of Cycle 24, but surprisingly produced no coronal mass ejection (CME) from the core region during its disk passage. Here, we study the magnetic conditions that prevented eruption and the consequences that ensued. We find AR 12192 to be "big but mild"; its core region exhibits weaker non-potentiality, stronger overlying field, and smaller flare-related field changes compared to two other major flare-CME-productive ARs (11429 and 11158). These differences are present in the intensive-type indices (e.g., means) but generally not the extensive ones (e.g., totals). AR 12192's large amount of magnetic free energy does not translate into CME productivity. The unexpected behavior suggests that AR eruptiveness is limited by some relative measure of magnetic non-potentiality over the restriction of background field, and that confined flares may leave weaker photospheric and coronal imprints compared to their eruptive counterparts. **18-28 Oct 2014, 2012-03-07, 2011-02-15**

Хорошее Введение про confined and eruptive flares.

See also HMI Science Nuggets, No. 37, April 2015

http://hmi.stanford.edu/hminuggets/?p=1153

Erratum: ApJL, 850:L43 (1pp), **2017** December 1

Dynamic Evolution of an X-shaped Structure above a Trans-equatorial Quadrupole Solar Active Region Group

J. Q. **Sun**, X. Cheng, Y. Guo, M. D. Ding, Y. Li

ApJL, **2014**

http://arxiv.org/pdf/1405.1563v1.pdf

In the solar corona, magnetic reconnection usually takes place at the singular configuration of magnetic field, in particular near a magnetic null owing to its high susceptibility to perturbations. In this Letter, we report a rare X-shaped structure, encompassing a magnetic null, above a trans-equatorial quadrupole active region group that is well observed by the Atmospheric Imaging Assembly (AIA). The observations show that this X-shaped structure is visible in all AIA EUV passbands and stably exists for days. However, possibly induced by flare activities at the northern part of the quadrupole active region group, the X-shaped structure starts to destabilize and meanwhile a jet erupted near its center at 15:05 UT on **2013 October 7**. Through the non-linear force-free field modeling, we identify a magnetic null, which is above the quadrupole polarities and well corresponds to the X-shaped structure. After the jet eruption, the temperature and emission measure of the plasma near the X-shaped structure rise from 2.3 MK and 1.2x10^27 cm-5 at 15:01 UT to 5.4 MK and 3.7x10^27 cm-5 at 15:36 UT, respectively, revealed by the differential emission measure analysis, indicating that magnetic reconnection most likely takes place there to heat the plasma. Moreover, the height of the null has an increase of 10 Mm, which is most likely due to the partial opening of the field lines near the fan surface that makes the null underneath rise to seek for a new equilibrium.

Differential Emission Measure Analysis of A Limb Solar Flare on 2012 July 19

J. Q. **Sun**, X. Cheng, M. D. Ding

2014 ApJ 786 73

http://arxiv.org/pdf/1403.6202v2.pdf

We perform Differential Emission Measure (DEM) analysis of an M7.7 flare that occurred on 2012 July 19 and was well observed by the Atmospheric Imaging Assembly (AIA) aboard the Solar Dynamic Observatory. Using the observational data with unprecedented high temporal and spatial resolution from six AIA coronal passbands, we calculate the DEM of the flare and derive the time series of maps of DEM-weighted temperature and emission measure (EM). It is found that, during the flare, the highest EM region is located in the flare loop top with a value varying between 8.4 10^28 cm^-5 and 2.5 10^30 cm^-5. The temperature there rises from 8 MK at about 04:40 UT (the initial rise phase) to a maximum value of 13 MK at about 05:20 UT (the hard X-ray peak). Moreover, we find a hot region that is above the flare loop top with a temperature even up to 16 MK. We also analyze the DEM properties of the reconnection site. The temperature and density there are not as high as that in the loop top and the flux rope, indicating that the main heating may not take place inside the reconnection site. In the end, we examine the dynamic behavior of the flare loops. Along the flare loop, both the temperature and the EM are the highest in the loop top and gradually

decrease towards the footpoints. In the northern footpoint, an upward force appears with a biggest value in the impulsive phase, which we conjecture originates from chromospheric evaporation.

Hot Spine Loops and the Nature of a Late-Phase Solar Flare

Xudong **Sun**, J. Todd Hoeksema, Yang Liu, Guillaume Aulanier, Yingna Su, Iain G. Hannah, Rachel A. Hock

E-print, Oct **2013**; **2013** ApJ 77, 139.

http://arxiv.org/pdf/1310.1438v1.pdf

The fan-spine magnetic topology is believed to be responsible for many curious features in solar explosive events. A spine field line links distinct flux domains, but direct observation of such feature has been rare. Here we report a unique event observed by the Solar Dynamic Observatory where a set of hot coronal loops (over 10 MK) connected to a quasi-circular chromospheric ribbon at one end and a remote brightening at the other. Magnetic field extrapolation suggests these loops are partly tracer of the evolving spine field line. Continuous slipping- and null-point-type reconnections were likely at work, energizing the loop plasma and transferring magnetic flux within and across the fan quasi-separatrix layer. We argue that the initial reconnection is of the "breakout" type, which then transitioned to a more violent flare reconnection with an eruption from the fan dome. Significant magnetic field changes are expected and indeed ensued. This event also features an extreme-ultraviolet (EUV) late phase, i.e. a delayed secondary emission peak in warm EUV lines (about 2-7 MK). We show that this peak comes from the cooling of large post-reconnection loops beside and above the compact fan, a direct product of eruption in such topological settings. The long cooling time of the large arcades contributes to the long delay; additional heating may also be required. Our result demonstrates the critical nature of cross-scale magnetic coupling - topological change in a sub-system may lead to explosions on a much larger scale. **2011 November 15**

A NON-RADIAL ERUPTION IN A QUADRUPOLAR MAGNETIC CONFIGURATION WITH A CORONAL NULL

Xudong **Sun**, J. Todd Hoeksema1, Yang Liu, Qingrong Chen, and Keiji Hayashi

2012 ApJ 757 149

We report one of the several homologous non-radial eruptions from NOAA active region (AR) 11158 that are strongly modulated by the local magnetic field as observed with the Solar Dynamic Observatory. A small bipole emerged in the sunspot complex and subsequently created a quadrupolar flux system. Nonlinear force-free field extrapolation from vector magnetograms reveals its energetic nature: the fast-shearing bipole accumulated ~2 × 1031 erg free energy (10% of AR total) over just one day despite its relatively small magnetic flux (5% of AR total). During the eruption, the ejected plasma followed a highly inclined trajectory, over 60° with respect to the radial direction, forming a jet-like, inverted-Y-shaped structure in its wake. Field extrapolation suggests complicated magnetic connectivity with a coronal null point, which is favorable of reconnection between different flux components in the quadrupolar system. Indeed, multiple pairs of flare ribbons brightened simultaneously, and coronal reconnection signatures appeared near the inferred null. Part of the magnetic setting resembles that of a blowout-type jet; the observed inverted-Y structure likely outlines the open field lines along the separatrix surface. Owing to the asymmetrical photospheric flux distribution, the confining magnetic pressure decreases much faster horizontally than upward. This special field geometry likely guided the non-radial eruption during its initial stage.

EVOLUTION OF MAGNETIC FIELD AND ENERGY IN A MAJOR ERUPTIVE ACTIVE REGION BASED ON SDO/HMI OBSERVATION

Xudong **Sun**1,2, J. Todd Hoeksema1, Yang Liu1, Thomas Wiegelmann3, Keiji Hayashi1, Qingrong Chen2 and Julia Thalmann

2012 ApJ 748 77

We report the evolution of the magnetic field and its energy in NOAA active region 11158 over five days based on a vector magnetogram series from the Helioseismic and Magnetic Imager (HMI) on board the Solar Dynamic Observatory (SDO). Fast flux emergence and strong shearing motion led to a quadrupolar sunspot complex that produced several major eruptions, including the first X-class flare of Solar Cycle 24. Extrapolated nonlinear force-free coronal fields show substantial electric current and free energy increase during early flux emergence near a low-lying sigmoidal filament with a sheared kilogauss field in the filament channel. The computed magnetic free energy reaches a maximum of ~2.6 × 1032 erg, about 50% of which is stored below 6 Mm. It decreases by ~0.3 × 1032 erg within 1 hr of the X-class flare, which is likely an underestimation of the actual energy loss. During the flare, the photospheric field changed rapidly: the horizontal field was enhanced by 28% in the core region, becoming more inclined and more parallel to the polarity inversion line. Such change is consistent with the conjectured coronal field "implosion" and is supported by the coronal loop retraction observed by the Atmospheric Imaging Assembly (AIA). The extrapolated field

becomes more "compact" after the flare, with shorter loops in the core region, probably because of reconnection. The coronal field becomes slightly more sheared in the lowest layer, relaxes faster with height, and is overall less energetic.

The EIS flare catalogue 1 year anniversary

Jian **Sun**, Lucie Green and Deb Baker
Hinode/EIS Nugget, Feb **2012**
http://msslxr.mssl.ucl.ac.uk:8080/SolarB/nuggets/nugget_2012feb.jsp
The catalogue is accessed via the Hinode/EIS website **http://msslxr.mssl.ucl.ac.uk:8080/SolarB/eisflarecat.jsp** hosted at UCL-MSSL. Flare events can be seen by year in the lists or the database can be searched. Once a flare event is identified, a link takes you to a summary page showing the location of the EIS observations overlaid on a full Sun context image and also a timeline showing the EIS observations against the context of the GOES X-ray data (see Figure 1). Both context images show whether the observations are slit or slot and the details of the slit/slot width. From this same page you can view thumbnails of the EIS data, download the data files and find more information on the EIS study that was used.

CME productivity associated with Solar Flare peak X-ray emission flux

G.S.**Suryanarayana** K.M.Balakrishna
Advances in Space Research Volume 61, Issue 9, 1 May **2018**, Pages 2482-2489
http://sci-hub.tw/http://linkinghub.elsevier.com/retrieve/pii/S0273117718301236
It is often noticed that the occurrence rate of Coronal Mass Ejections (CMEs) increases with increase in flare duration where peak flux too increase. However, there is no complete association between the duration and peak flux. Distinct characteristics have been reported for active regions (ARs) where flares and CMEs occur in contrast to ARs where flares alone occur. It is observed that peak flux of flares is higher when associated with CMEs compared to peak flux of flares with which CMEs are not associated. In other words, it is likely that flare duration and peak flux are independently affected by distinct active region dynamics. Hence, we examine the relative ability of flare duration and peak flux in enhancing the CME productivity. We report that CME productivity is distinctly higher in association with the enhancement of flare peak flux in comparison to corresponding enhancement of flare duration.

Abnormal rotation rates of sunspots and durations of associated flares

G. S. **Suryanarayana**, K. M. Hiremath, S. P. Bagare and M. Hegde
A&A 580, A25 (**2015**), **File**
http://www.aanda.org/articles/aa/pdf/2015/08/aa23389-14.pdf
Context. Short-duration and long-duration flares are important in terms of their association with coronal heating and coronal mass ejections, respectively. Sunspot motions in the photosphere have been known to be associated with flare occurrences.
Aims. We study the association between the abnormal rotation rates (longitudinal displacement in a given latitude in contrast with the rotation of spots around their umbral centre) of sunspots and flare duration.
Methods. We compute the rotation rates of sunspots for different days during their evolution. We consider rotation rates that are in excess of one standard deviation as abnormal rotation rates. Also, the duration of time between the initial and final stages of the flares are computed.
Results. Using Kodaikanal Observatory white light picture and GOES soft X-ray flare data, we find that a good we find that duration of flare is independent of sunspot area.
Conclusions. The present study suggests that sub-surface dynamics plays a dominant role in determining the duration and rate of dissipation of energy during flares. **2000.01.13-16, 2000.02.05-09, 2000.02.14, 2000.02.29-03.03, 2000.03.10-22, 2000.04.02-09**
Хорошее Введение

Plasma Heating in a Post Eruption Current Sheet: A Case Study Based on Ultraviolet, Soft, and Hard X-Ray Data

R. **Susino**1,3, A. Bemporad1, and Säm Krucker
2013 ApJ 777 93
Off-limb observations of the solar corona after coronal mass ejections (CMEs) often show strong, compact, and persistent UV sources behind the eruption. They are primarily observed by the SOHO/UVCS instrument in the "hot" [Fe XVIII] λ974 line and are usually interpreted as a signature of plasma heating due to magnetic reconnection in the post-CME current sheet (CS). Nevertheless, the physical process itself and the altitude of the main energy release are currently not fully understood. In this work, we study the evolution of plasma heating after the CME of **2004 July 28** by comparing UV spectra acquired by UVCS with soft and hard X-ray (SXR, HXR) images of the post-flare loops taken by GOES/SXI and RHESSI. The X-ray data show a long-lasting extended source that is rising upward, toward the high-temperature source detected by UVCS. UVCS data show the presence of significant non-thermal broadening in the CS (a signature of turbulent motions) and a strong density gradient across the CS region. The thermal energy released in the

HXR source is on the order of ~1032 erg, a factor ~2-5 larger than the energy required to explain the high-temperature plasma sampled by UVCS. Nevertheless, the very different time evolutions of SXR and HXR sources compared with the UV emission suggest that reconnection occurring above the post-eruption arcades is not directly responsible for the high-temperature plasma sampled higher up by UVCS. We conclude that an additional plasma heating mechanism (such as turbulent reconnection) in the CS is likely required.

The Evolution of the Net Twist Current and the Net Shear Current in Active Region NOAA 10930

Yogita **Suthar**, P. Venkatakrishnan, B. Ravindra, S. N. A. Jaaffrey
Solar Phys., July **2014**, Volume 289, Issue 7, pp 2459-2471
The electric current exists because of the non-potential magnetic field in solar active regions. We present the evolution of net current in the solar active region NOAA 10930 as the sum of shear current and twist current by using 27 high-resolution vector magnetograms obtained with Hinode/SOT-SP during 9 – 15 December 2006. This active region was highly eruptive and produced a large number of flares ranging from B to X class. We derived local distribution of shear and twist current densities in this active region and studied the evolution of net shear current (NSC) and net twist current (NTC) in the N-polarity and S-polarity regions separately. We found the following: i) The twist current density was dominant in the umbrae. ii) The footpoint of the emerging flux rope showed a dominant twist current. iii) The shear current density and twist current density appeared in alternate bands around the umbrae. iv) On the scale of the active region, NTC was always larger than NSC. v) Both NTC and NSC decreased after the onset of an X3.4 class flare that occurred on **13 December 2006**.

FLARING SOLAR HALE SECTOR BOUNDARIES

L. **Svalgaard**1, I. G. Hannah2 and H. S. Hudson
2011 ApJ 733 49
http://arxiv.org/pdf/1010.2710v2.pdf
The sector structure that organizes the magnetic field of the solar wind into large-scale domains has a clear pattern in the photospheric magnetic field as well. The rotation rate, 27-28.5 days, implies an effectively rigid rotation originating deeper in the solar interior than the sunspots. The photospheric magnetic field is known to be concentrated near that portion (the Hale boundary) in each solar hemisphere, where the change in magnetic sector polarity matches that between the leading and following sunspot polarities in active regions in the respective hemispheres. We report here that flares and microflares also concentrate at the Hale boundaries, implying that flux emergence and the creation of free magnetic energy in the corona also have a direct cause in the deep interior.

Evolution and motions of magnetic fragments during the active region formation and decay: A statistical study

Michal **Švanda** (1 and 2), M. Sobotka (1), L. Mravcová (2 and 1), T. Výbošťoková (3)
A&A **2021**
https://arxiv.org/pdf/2102.02807.pdf
Context: The evolution of solar active regions is still not fully understood. The growth and decay of active regions have mostly been studied in case-by-case studies.
Aims: Instead of studying the evolution of active regions case by case, we performed a large-scale statistical study to find indications for the statistically most frequent scenario.
Methods: We studied a large sample of active regions recorded by the Helioseismic and Magnetic Imager instrument. The sample was split into two groups: forming (367 members) and decaying (679 members) active regions. We tracked individual dark features (i.e. those that are assumed to be intensity counterparts of magnetised fragments from small objects to proper sunspots) and followed their evolution. We investigated the statistically most often locations of fragment merging and splitting as well as their properties.
Results: Our results confirm that statistically, sunspots form by merging events of smaller fragments. The coalescence process is driven by turbulent diffusion in a process similar to random-walk, where supergranular flows seem to play an important role. The number of appearing fragments does not seem to significantly correlate with the number of sunspots formed. The formation seems to be consistent with the magnetic field accumulation. Statistically, the merging occurs most often between a large and a much smaller object. The decay of the active region seems to take place preferably by a process similar to the erosion. **AR11076**

Understanding the HMI pseudocontinuum in white-light solar flares

M. **Svanda** (1 and 2), Jan Jurcak (1), Jana Kasparova (1), Lucia Kleint
ApJ **860** 144 **2018**
https://arxiv.org/pdf/1805.03369.pdf
We analyse observations of the X9.3 solar flare (SOL**2017-09-06**T11:53) observed by SDO/HMI and Hinode/SOT. Our aim is to learn about the nature of the HMI pseudocontinuum Ic used as a proxy for the white-light continuum. From

model atmospheres retrieved by an inversion code applied to the Stokes profiles observed by the Hinode satellite we synthesise profiles of the FeI 617.3 nm line and compare them to HMI observations. Based on a pixel-by-pixel comparison we show that the value of Ic represents the continuum level well in quiet-Sun regions only. In magnetised regions it suffers from a simplistic algorithm that is applied to a complex line shape. During this flare both instruments also registered emission profiles in the flare ribbons. Such emission profiles are poorly represented by the six spectral points of HMI, the used algorithm does not account for emission profiles in general, and thus the derived pseudocontinuum intensity does not approximate the continuum value properly.
RHESSI – Science Nuggets #324 May 2018
http://sprg.ssl.berkeley.edu/~tohban/wiki/index.php/Understanding_HMI_pseudocontinuum_in_white-light_flares

Large-scale horizontal flows in the solar photosphere
V. Possible evidence for the disconnection of bipolar sunspot groups from their magnetic roots

M. **Švanda**1, 2, 3, M. Klvaňa2, and M. Sobotka2
A&A 506, 875-884 **(2009**)
In a recent paper (Švanda et al. 2008, A&A, 477, 285) we pointed out that, based on the tracking of Doppler features in the full-disc MDI Dopplergrams, the active regions display two dynamically different regimes. We speculated that this could be a manifestation of the sudden change in the active regions dynamics, caused by the dynamic disconnection of sunspots from their magnetic roots as proposed by Schüssler & Rempel (2005, A&A, 441, 337). Here we investigate the dynamic behaviour of the active regions recorded in the high-cadence MDI data over the last solar cycle in order to confirm the predictions in the Schüssler's & Rempel's paper. We find that, after drastic reduction of the sample, which is done to avoid disturbing effects, a large fraction of active regions displays a sudden decrease in the rotation speed, which is compatible with the mechanism of the dynamic disconnection of sunspots from their parental magnetic structures.

The Misnomer of “Post-Flare Loops”

Zdenˇek **Švestka**
Solar Phys (**2007**) 246: 393–397, **File**
https://link.springer.com/content/pdf/10.1007%2Fs11207-007-9088-1.pdf
Attention is drawn to the fact that the term “post-flare loops” is incorrect and should be avoided, because the loops are parts of the flare itself. Two other names for these loop systems are suggested.

Ссылаться на этот обзор
VARIETIES OF CORONALMASS EJECTIONS AND THEIR RELATION TO FLARES
ZDENˇEK **ŠVESTKA** **Review**
Space Science Reviews **95:** 135–146, **2001**
https://sci-hub.ru/10.1023/A:1005225208925
Most coronal mass ejections (CMEs) start as coronal storms which are caused by an opening of channels of closed field lines along the zero line of the longitudinal magnetic field. This can happen along any zero line on the Sun where the configuration is destabilized. If the opening includes a zero line inside an active region, one observes a chromospheric flare. If this does not happen, no flare is associated with the CME in the chromosphere, but the process, as well as the response in the corona (a Long Decay Event in X-rays) remains the same. The only difference between flare-associated and non-flare-associated CMEs is the strength of the magnetic field in the region of the field line opening. This can explain essentially all differences which have been observed between these two kinds of CMEs. However, there are obviously also other sources of CMEs, different from coronal storms: sprays (giving rise to narrow, pointed ejections), erupting interconnecting loops (often destabilized by flares), and growing coronal holes. This paper tries to summarize and interpret observations which support this general picture, and demonstrates that both CMEs and flares must be properly discussed in any study of solar-terrestrial relations.

Eruptive Solar Flares, ed. Z. **Svestka**
Svestka, Z., &Cliver, E.W. , et al. **1992**, in Eruptive Solar Flares, ed. Z. Svestka (Berlin: Springer), 1

HISTORY AND BASIC CHARACTERISTICS OF ERUPTIVE FLARES
Svestka, Z., &Cliver, E.W. , **1992, File**
https://sci-hub.ru/10.1007/3-540-55246-4_70
We review the evolution of our knowledge and understanding of the eruptive

(dynamic, two-ribbon) flare phenomenon.
In the conclusion, we summarize the basic characteristics of eruptive flares.

Solar flares - The gradual phase **Review**

Zdenˇek **Švestka**
Solar Phys (**1989**) V. 121, No 1-2 p. 399-417; Discussion, p. 500 **File**
https://link.springer.com/content/pdf/10.1007/BF00161709.pdf
There are two kinds of the gradual phase of flares: (1) flares in which all the energy is released within the impulsive phase, and the gradual phase is simply the cooling of the heated flare plasma (confined flares) and (2) flares in which the energy release continues during the gradual phase (dynamic flares). The simplest case of the former, the single-loop flare, and the associated phenomena of coronal 'tongues', flaring arches, and bright surges are briefly addressed. Dynamic flares are discussed in more detail, including the Kopp and Pneuman (1976) model of these flares, subsequent modifications of the model, loop shrinking, giant postflare X-ray arches, radio type IV events and noise storms, complex structures of dynamic flares, and small dynamic flares. Flare hybrids are briefly addressed.

On the varieties of solar flares.

Švestka, Z.:
In: Neidig, D.F. (ed.) The Lower Atmosphere of Solar Flares, Proceedings of the Solar Maximum Mission Symposium, Sunspot, NM, Aug. 20 – 24, 1985 (A87-26201 10-92), Sunspot, NM, National Solar Observatory, **1986**, 332. ADS.
http://articles.adsabs.harvard.edu/pdf/1986lasf.conf..332S
An attempt is made to classify flares starting with two axiomatic assumptions: (1) that a flare is a short-lived release of energy in consequence of a rearrangement of the magnetic structure, and (2) the mode of energy release is a reconnection of magnetic field lines. Somewhat surprisingly, in spite of the enormous diversity of the flare phenomena, two classes are derived: dynamic flares and confined flares, where the confined flares may be subdivided in two subclasses. All the other varieties may be due to differences in the boundary conditions of the flare process. The paper discusses the various factors which cause the varieties in flares, and the association of the two basic types of flares with different kinds of radiation and with othere active phenomena on the Sun.

The reported durations of GOES Soft X-Ray flares in different solar cycles

Bill **Swalwell**, Silvia Dalla, Stephen Kahler, Stephen White, Alan Ling, Rodney Viereck, and Astrid Veronig
Space Weather **Volume16, Issue6** Pages 660-666 **2018**
https://arxiv.org/pdf/1805.10246.pdf
http://sci-hub.tw/https://onlinelibrary.wiley.com/doi/abs/10.1029/2018SW001886
The Geostationary Orbital Environmental Satellites (GOES) Soft X-ray (SXR) sensors have provided data relating to, \textit{inter alia}, the time, intensity and duration of solar flares since the 1970s. The GOES SXR Flare List has become the standard reference catalogue for solar flares and is widely used in solar physics research and space weather. We report here that in the current version of the list there are significant **differences between the mean duration of flares which occurred before May 1997 and the mean duration of flares thereafter.** Our analysis shows that the reported flare timings for the pre-May 1997 data were not based on the same criteria as is currently the case. This finding has serious implications for all those who used flare duration (or fluence, which depends on the chosen start and end times) as part of their analysis of pre-May 1997 solar events, or statistical analyses of large samples of flares, \textit{e.g.} as part of the assessment of a Solar Energetic Particle forecasting algorithm.

Fine wave structure of umbral flashes

R. **Sych**, M. Wang
A&A **2017**
https://arxiv.org/pdf/1710.08100.pdf
Context. Umbral flashes (UFs) are most common phenomenon of wave processes in sunspots. Studying the relationship between wave time dynamics and UF origin requires further investigating their fine spatial and height structure. Aims. We investigated the association between a short-time increase in the variations of 3-minute EUV emission at footpoints of coronal magnetic loops and the UF emergence in sunspot umbrae. Methods. We applied the Pixelized Wavelet Filtering (PWF) technique to analyze a cube of the images obtained by SDO/AIA at 1600{\AA}, 304{\AA}, and 171{\AA} to study the spatio-temporal dynamic of oscillations in individual magnetic loops. The time-distance plots were used to obtain the wave front propagation velocity. We used the magnetic field extrapolation for SDO/HMI magnetograms to obtain localization of the magnetic loop footpoins. Results. For the first time, we obtained 2D images of fine wave processes in magnetic structures of different scales related to umbral flashes. UFs sources were mainly localized at the magnetic loop footpoints anchored in an umbra.We revealed two types UFs, point and extended. The

first type is related to the footpoints of open field lines, the second is associated with the closed. The time dynamics of UFs shows an increase the oscillations before the peak value within one low-frequency wave train. It is shown that the maxima of oscillation trains coincide with the peak intensity of umbral flashes. Conclusions. The sunspot wave dynamics showed a relation between the localization of oscillations power peak at the coronal magnetic loop footpoints and the UF origin. The spatial structure of the UF sources, their power and lifetime are determined by the cut-off frequency of the waves for the detected waveguides. We concluded that UFs are a process of short-time increase of the wave activity at the footpoints of magnetic loops. **December 8, 2010**

MHD waves in sunspots **Review**

Robert **Sych**
Chapter in AGU Monograph **2015**
http://arxiv.org/pdf/1509.06466v1.pdf
The review addresses the spatial frequency morphology of sources of sunspot oscillations and waves, including their localization, size, oscillation periods, height localization with the mechanism of cut-off frequency that forms the observed emission variability. Dynamic of sunspot wave processes, provides the information about the structure of wave fronts and their time variations, investigates the oscillation frequency transformation depending on the wave energy is shown. The initializing solar flares caused by trigger agents like magnetoacoustic waves, accelerated particle beams, and shocks are discussed. Special attention is paid to the relation between the flare reconnection periodic initialization and the dynamics of sunspot slow magnetoacoustic waves. A short review of theoretical models of sunspot oscillations is provided.

Sunspot waves and flare energy release

R. **Sych**, M. Karlický, A. Altyntsev, J. Dudík, L. Kashapova
A&A, 577, A43 **2014**
http://arxiv.org/pdf/1409.2947v1.pdf
We address a possibility of the flare process initiation and further maintenance of its energy release due to a transformation of sunspot longitudinal waves into transverse magnetic loop oscillations with initiation of reconnection. This leads to heating maintaining after the energy release peak and formation of a flat stage on the X-ray profile. We applied the time-distance plots and pixel wavelet filtration (PWF) methods to obtain spatio-temporal distribution of wave power variations in SDO/AIA data. To find magnetic waveguides, we used magnetic field extrapolation of SDO/HMI magnetograms. The propagation velocity of wave fronts was measured from their spatial locations at specific times. In correlation curves of the 17 GHz (NoRH) radio emission we found a monotonous energy amplification of 3-min waves in the sunspot umbra before the **2012 June 7** flare. This dynamics agrees with an increase in the wave-train length in coronal loops (SDO/AIA, 171 {\AA}) reaching the maximum 30 minutes prior to the flare onset. A peculiarity of this flare time profile in soft X-rays (RHESSI, 3-25 keV) is maintaining the constant level of the flare emission for 10 minutes after the short impulse phase, which indicates at the energy release continuation. Throughout this time, we found 30-sec period transverse oscillations of the flare loop in the radio-frequency range (NoRH, 17 GHz). This periodicity is apparently related to the transformation of propagating longitudinal 3-min waves from the sunspot into the loop transverse oscillations. The magnetic field extrapolation showed the existence of the magnetic waveguide (loop) connecting the sunspot with the energy release region. A flare loop heating can be caused by the interaction (reconnections) of this transversally oscillating waveguide with the underlying twisted loops.

Relationship between wave processes in sunspots and quasi-periodic pulsations in active region flares

R. **Sych**, V.M. Nakariakov, M. Karlicky, and S. Anfinogentov
E-print, Aug **2009**, A&A, 505 (**2009**) 791-799
http://www.aanda.org/10.1051/0004-6361/200912132
A phenomenological relationship between oscillations in a sunspot and quasi-periodic pulsations in flaring energy releases at an active region above the sunspot, is established. The analysis of the microwave emission recorded by the Nobeyama Radioheliograph at 17 GHz shows a gradual increase in the power of the 3-min oscillation train in the sunspot associated with AR 10756 before flares in this active region. The flaring light curves are found to be bursty with a period of 3 min. Our analysis of the spatial distribution of the 3-min oscillation power implies that the oscillations follow from sunspots along coronal loops towards the flaring site. It is proposed that quasi-periodic pulsations in the flaring energy releases can be triggered by 3-min slow magnetoacoustic waves leaking from sunspots.
28, 30 Apr, 1 May 2005

New Solar Flare Calcium Abundances with no Surprises: Results from the SMM Bent Crystal Spectrometer

J. **Sylwester**, B. Sylwester, K.J.H. Phillips, A. Kepa

ApJ **930** 77 **2022**
https://arxiv.org/pdf/2203.02257.pdf
https://iopscience.iop.org/article/10.3847/1538-4357/ac5b0d/pdf
The calcium abundance in flare plasmas is estimated using X-ray spectra from the Solar Maximum Mission Bent Crystal Spectrometer (BCS) during the decays of 194 flares (GOES classifications from B6.4 to X13) occurring between 1980 and 1989. Previous work by Sylwester et al. found that the abundance varied from flare to flare. That analysis is improved on here using updated instrument parameters and by including all calcium lines viewed by the BCS instead of only the resonance line, so greatly enhancing the photon count statistics. The abundance variations are confirmed with the average abundance, A(Ca) (expressed logarithmically with A(H)=12), equal to 6.77±0.20 for 194 flares (141 of which are new in this study). This range corresponds to factors of between 1.7 and 7.2 larger than the photospheric abundance and so our results are in line with a ``FIP" (first ionization potential) effect whereby low-FIP elements like Ca (FIP = 6.11~eV) have enhanced coronal abundances. The Ca flare abundance is uncorrelated with solar activity indices, but weak correlations are suggested with GOES flare class and duration (larger A(Ca) for smaller and shorter flares). The ponderomotive force theory of Laming explaining the FIP effect gives a range of parameters within which our estimates of A(Ca) agree with the theory. However, this then gives rise to disagreements with previous estimates of the flare silicon and sulfur abundances, although those of argon and iron are in good agreement. Small adjustments of the theory may thus be necessary.
Table 1. SMM BCS flares in this analysis 1980

A Unique Resource for Solar Flare Diagnostic Studies: the SMM Bent Crystal Spectrometer

J. **Sylwester**, B. Sylwester, K. J. H. Phillips. A. Kepa, C. G. Rapley
ApJ **894** 137 **2020**
https://arxiv.org/pdf/2004.03241.pdf
https://doi.org/10.3847/1538-4357/ab86ba
The {\em Bent Crystal Spectrometer}\/ (BCS) on the NASA {\em Solar Maximum Mission}\/ spacecraft observed the X-ray spectra of numerous solar flares during the periods 1980 February to November and 1984~--~1989. The instrument, the first of its kind to use curved crystal technology, observed the resonance lines of He-like Ca (\caxix) and Fe (\fexxv) and neighboring satellite lines, allowing the study of the rapid evolution of flare plasma temperature, turbulence, mass motions etc. To date there has not been a solar X-ray spectrometer with comparable spectral and time resolution, while subsequent solar cycles have delivered far fewer and less intense flares. The BCS data archive thus offers an unparalleled resource for flare studies. A recent re-assessment of the BCS calibration and its operations is extended here by using data during a spacecraft scan in the course of a flare on 1980 November~6 that highlights small deformations in the crystal curvature of the important channel~1 (viewing lines of \caxix\ and satellites). The results explain long-standing anomalies in spectral line ratios which have been widely discussed in the past. We also provide an in-flight estimation of the BCS collimator field of view which improves the absolute intensity calibration of the BCS. The BCS channel~1 background is shown to be entirely due to solar continuum radiation, confirming earlier analyses implying a time-variable flare abundance of Ca. We suggest that BCS high-resolution \caxix\ and \fexxv\ line spectra be used as templates for the analysis of X-ray spectra of non-solar sources.

RESIK SOLAR X-RAY FLARE ELEMENT ABUNDANCES ON A NON-ISOTHERMAL ASSUMPTION

B. **Sylwester**, K. J. H. Phillips, J. Sylwester, A.. Kepa
ApJ **805** 49 **2015**
http://arxiv.org/pdf/1503.00979.pdf
Solar X-ray spectra from the RESIK crystal spectrometer on the CORONAS-F spacecraft (spectral range 3.3-6.1A are analyzed for thirty-three flares using a method to derive abundances of Si, S, Ar, and K, emission lines of which feature prominently in the spectra. For each spectrum, the method first optimizes element abundances then derives the differential emission measure as a function of temperature based on a procedure given by Sylwester et al. and Withbroe. This contrasts with our previous analyses of RESIK spectra in which an isothermal assumption was used. The revised abundances (on a logarithmic scale with A(H) = 12) averaged for all the flares in the analysis are A(Si) = 7.53 +/- 0.08 (previously 7.89 +/- 0.13), A(S) = 6.91 +/- 0.07 (7.16 +/- 0.17), A(Ar) = 6.47 +/- 0.08 (6.45 +/- 0.07), and A(K) = 5.73 +/- 0.19 (5.86 +/- 0.20), with little evidence for time variations of abundances within the evolution of each flare. Our previous estimates of the Ar and K flare abundances are thus confirmed by this analysis but those for Si and S are reduced. This suggests the flare abundances of Si and Ar are very close to the photospheric abundance or solar proxies, while S is significantly less than photospheric and the K abundance is much higher than photospheric. These estimates differ to some extent from those in which a single enhancement factor applies to elements with first ionization potential less than 10~eV. **Table 2. RESIK Flares in this Analysis**
2003 January 7, 2003 February 6

X-ray Flare Spectra from the DIOGENESS Spectrometer and its concept applied to ChemiX on the Interhelioprobe spacecraft

J. **Sylwester**, Z. Kordylewski, S. Plocieniak, M. Siarkowski, M. Kowalinski, S. Nowak, W. Trzebinski, M. Steslicki, B. Sylwester, E. Stanczyk, R. Zawerbny, Z. Szaforz, K. J. H. Phillips, F. Farnik, A. Stepanov
Solar Phys., **2015**
http://arxiv.org/pdf/1411.0850v1.pdf
The DIOGENESS X-ray crystal spectrometer on the CORONAS-F spacecraft operated for a single month (25~August to 17~September) in 2001 but in its short lifetime obtained one hundred and forty high-resolution spectra from some eight solar flares with GOES importance ranging from C9 to X5. The instrument included four scanning flat crystals with wavelength ranges covering the regions of Si XIII (6.65 Angstroms), S XV (5.04 Angstroms), and Ca XIX (3.18 Angstroms) X-ray lines and associated dielectronic satellites. Two crystals covering the Ca XIX lines were oriented in a ``Dopplerometer'' manner, i.e. such that spatial and spectral displacements both of which commonly occur in flares can be separated. We describe the DIOGENESS spectrometer and the spectra obtained during flares which include lines not hitherto seen from spacecraft instruments. An instrument with very similar concept is presently being built for the two Russian Interhelioprobe spacecraft due for launch in 2020 and 2022 that will make a near-encounter (perihelion approx. 0.3 a.u.) to the Sun in its orbit. We outline the results that are likely to be obtained. Aug. 25, Aug. 30, Sept. 2, Sept. 3, Sept. 16 **2001**

Solar Flare Composition and Thermodynamics from RESIK X-ray Spectra

B. **Sylwester**, J. Sylwester, K. J. H. Phillips, A. Kepa, T. Mrosek
2014, ApJ 787 122
http://arxiv.org/pdf/1404.5775v2.pdf
Previous estimates of the solar flare abundances of Si, S, Cl, Ar, and K from the RESIK X-ray crystal spectrometer on board the CORONAS-F spacecraft were made on the assumption of isothermal X-ray emission. We investigate the effect on these estimates by relaxing this assumption and instead determining the differential emission measure (DEM) or thermal structure of the emitting plasma by re-analyzing RESIK data for a GOES class M1.0 flare on 2002 November~14 (SOL**2002-11-14**T22:26) for which there was good data coverage. The analysis method uses a maximum-likelihood (Withbroe--Sylwester) routine for evaluating the DEM. In a first step, called here AbuOpt, an optimized set of abundances of Si, S, Ar, and K is found that is consistent with the observed spectra. With these abundances, the differential emission measure evolution during the flare is found. The abundance optimization leads to revised abundances of silicon and sulfur in the flare plasma: A(S)=6.94±0.06 and A(Si)=7.56±0.08 (on a logarithmic scale with A(H)=12). Previously determined abundances of Ar, K, and Cl from an isothermal assumption are still the preferred values. During the flare's maximum phase, the X-ray-emitting plasma has a basically two-temperature structure, with the cooler plasma with approximately constant temperature (3--6~MK) and a hotter plasma with temperature 16−21~MK. Using imaging data from the RHESSI hard X-ray spacecraft, the emission volume of the hot plasma is deduced from which lower limits of the electron density Ne and the thermal content of the plasma are given.

X-ray Flare Spectra from the DIOGENESS Spectrometer and Its Concept Applied to ChemiX on the Interhelioprobe Spacecraft

Janusz **Sylwester**, Zbigniew Kordylewski, Stefan Płocieniak …
Solar Phys. Volume 290, Issue 12, pp 3683-3697 **2015 Open Access**
The DIOGENESS X-ray crystal spectrometer on the CORONAS-F spacecraft operated only for a single month (25 August to 17 September) in 2001, but in its short lifetime obtained one hundred and forty high-resolution spectra of eight solar flares with GOES importance ranging from C9 to X5. The instrument included four scanning flat crystals with wavelength ranges covering the regions of Si xiii (6.65 Å), S xv (5.04 Å), and Ca xix (3.18 Å) X-ray lines and associated dielectronic satellites. Two crystals covering the Ca xix lines were oriented in a “dopplerometer” manner, i.e. such that spatial and spectral displacements, both of which commonly occur in flares, can be separated. We describe the DIOGENESS spectrometer and the spectra obtained during flares that include lines not hitherto seen from spacecraft instruments. An instrument with a very similar concept is currently being built for the two Russian Interhelioprobe spacecraft that are scheduled for launch in 2020 and 2022 and will make a near-encounter (perihelion ~ 0.3 AU) with the Sun in its orbit. We outline the results that are likely to be obtained.

THE SOLAR FLARE CHLORINE ABUNDANCE FROM RESIK X-RAY SPECTRA

B. **Sylwester**1, K. J. H. Phillips2, J. Sylwester1 and V. D. Kuznetsov
2011 ApJ 738 49
The abundance of chlorine is determined from X-ray spectra obtained with the RESIK instrument on CORONAS-F during solar flares between 2002 and 2003. Using weak lines of He-like Cl, Cl XVI, between 4.44 and 4.50 Å, and with temperatures and emission measures from GOES on an isothermal assumption, we obtained A(Cl) = 5.75 ± 0.26 on a scale A(H) = 12. The uncertainty reflects an approximately a factor of two scatter in measured line fluxes. Nevertheless, our value represents what is probably the best solar determination yet obtained. It is higher by factors of 1.8 and 2.7 than Cl abundance estimates from an infrared sunspot spectrum and nearby H II regions. The constancy of the RESIK

abundance values over a large range of flares (GOES class from below C1 to X1) argues for any fractionation that may be present in the low solar atmosphere to be independent of the degree of solar activity.

Chromospheric and coronal heating and jet acceleration due to reconnection driven by flux cancellation. II. Cancellation of two magnetic polarities of unequal flux

Syntelis P., Priest E. R

A&A **2021**

https://arxiv.org/pdf/2103.16184.pdf

Context. Recent observations have shown that magnetic flux cancellation occurs at the photosphere more frequently than previously thought.
Aims. In order to understand the energy release by reconnection driven by flux cancellation, we previously studied a simple model of two cancelling polarities of equal flux. Here, we further develop our analysis to achieve a more general setup where the two cancelling polarities have unequal magnetic fluxes and where many new features are revealed.
Methods. We carried out an analytical study of the cancellation of two magnetic fragments of unequal and opposite flux that approach one another and are located in an overlying horizontal magnetic field.
Results. The energy release as microflares and nanoflares occurs in two main phases. During phase 1a, a separator is formed and reconnection is driven at it as it rises to a maximum height and then moves back down to the photosphere, heating the plasma and accelerating plasma jets in the process. During phase 1b, once the separator moves back to the photosphere, it bifurcates into two null points. Reconnection is no longer driven at the separator and an isolated magnetic domain connecting the two polarities is formed. During phase 2, the polarities cancel out at the photosphere as magnetic flux submerges below the photosphere and as reconnection occurs at and above the photosphere and plasma jets and a mini-filament eruption can be produced.

Eruptions and Flaring Activity in Emerging Quadrupolar Regions

P. **Syntelis**, E. J. Lee, C. W. Fairbairn, V. Archontis, A. W. Hood

A&A **2019**

https://arxiv.org/pdf/1909.01446.pdf

Context. Some of the most dynamic active regions are associated with complex photospheric magnetic configurations such as quadrupolar regions, and especially ones with a δ-spot configuration and a strong Polarity Inversion Line (PIL). Aims. We study the formation and eruption of magnetic flux ropes in quadrupolar regions. Methods. 3D MHD simulations of the partial emergence of a highly twisted flux tube from the solar interior into a non-magnetized stratified atmosphere. Results. We emerge two Ω-shaped loops forming a quadrupolar region. The emerging flux forms two initially separated bipoles, that later come in contact creating a δ-spot central region. Above the two bipoles, two magnetic lobes expand and interact through a series of current sheets at the interface between them. Two recurrent confined eruptions are produced. In both cases, reconnection between sheared low-lying field lines forms a flux rope. Reconnection between the two lobes high in the atmosphere forms retracting field lines that push against the flux rope, creating a current sheet between them. It also forms a third magnetic lobe between the two emerged ones, that later acts as a strapping field. The flux rope eruptions are triggered when the reconnection between the flux ropes and the field above them becomes efficient enough to remove the tension of the overlying field. These reconnection events occur internally in the system. The first erupting flux rope almost fully reconnects with the overlying field. The second eruption is confined by the overlying field. During the confined eruption, the flux rope is enhanced in size, flux and twist, similar to confined-flare-to-flux-rope observations. Proxies of the emission reveal the two erupting filaments channels. A flare arcade is formed only in the second eruption due to the longer-lasting and more efficient reconnection below the flux rope.

Quasi-periodic pulsations in hard X-rays of partially occulted solar flares

Ż. **Szaforz**, M. Tomczak

Advances in Space Research Volume 64, Issue 5, 1 September **2019**, Pages 1100-1111

https://sci-hub.se/10.1016/j.asr.2019.06.006

We investigated solar flares partially occulted by the solar disk observed by the Yohkoh satellite. We found that about 30–40% of them show quasi-periodic pulsations (QPPs) in hard X-rays (HXR). A lack of usually brighter footpoint sources allowed us to reconstruct coronal HXR sources with a higher quality. We analyzed 28 partially occulted flares showing the QPPs and for the first time present results for such events as a group. In our opinion, the majority of the observed HXR loop-top sources can be explained as successive compression and rarefaction of magnetic traps described in a model of oscillating magnetic traps (OMT). In this model a particular value of a ratio between the diameter of traps and the period of pulsations is postulated. In our modification of this model, different values of the ratio are possible, with the exception of a lower range, where low values of magnetic field strength and high values of electron density number can excess the plasma-β parameter above unity (ballooning instability). **2 December 1991**
Table 1 List of partially occulted flares with the QPPs found in the Yohkoh HXT Flare Catalogue (1991-2001)
Fig. 3. The SXT images of *28 partially occulted flares*

Testing the Model of Oscillating Magnetic Traps

Ż. **Szaforz**, M. Tomczak

Solar Phys., **2015**, Volume 290, Issue 1, pp 115-127

The aim of this paper is to test the model of oscillating magnetic traps (the OMT model), proposed by Jakimiec and Tomczak (Solar Phys. 261, 233, 2010). This model describes the process of excitation of quasi-periodic pulsations (QPPs) observed during solar flares. In the OMT model energetic electrons are accelerated within a triangular, cusp-like structure situated between the reconnection point and the top of a flare loop as seen in soft X-rays. We analyzed QPPs in hard X-ray light curves for 23 flares as observed by Yohkoh. Three independent methods were used. We also used hard X-ray images to localize magnetic traps and soft X-ray images to diagnose thermal plasmas inside the traps. We found that the majority of the observed pulsation periods correlates with the diameters of oscillating magnetic traps, as was predicted by the OMT model. We also found that the electron number density of plasma inside the magnetic traps in the time of pulsation disappearance is strongly connected with the pulsation period. We conclude that the observations are consistent with the predictions of the OMT model for the analyzed set of flares.

Coronal Magnetic Field Structure and Evolution for Flaring AR 11117 and Its Surroundings

Tilaye **Tadesse**, T. Wiegelmann, B. Inhester, A. Pevtsov

Solar Physics, November **2012**, Volume 281, Issue 1, pp 53-65

In this study, photospheric vector magnetograms obtained with the Synoptic Optical Long-term Investigations of the Sun (SOLIS) survey are used as boundary conditions to model three-dimensional nonlinear force-free (NLFF) coronal magnetic fields as a sequence of NLFF equilibria in spherical geometry. We study the coronal magnetic field structure inside an active region and its temporal evolution. We compare the magnetic field configuration obtained from NLFF extrapolation before and after the flaring event in active region (AR) 11117 and its surroundings observed on **27 October 2010**, and we also compare the magnetic field topologies and the magnetic energy densities and study the connectivities between AR 11117 and its surroundings. During the investigated time period, we estimate the change in free magnetic energy from before to after the flare to be 1.74×1032 erg, which represents about 13.5 % of the NLFF magnetic energy before the flare. In this study, we find that electric currents from AR 11117 to its surroundings were disrupted after the flare.

Magnetic Connectivity Between Active Regions 10987, 10988, and 10989 by Means of Nonlinear Force-Free Field Extrapolation

Tilaye **Tadesse**, T. Wiegelmann, B. Inhester and A. Pevtsov

Solar Physics, Volume 277, Number 1, 119-130, **2012**

Extrapolation codes for modelling the magnetic field in the corona in Cartesian geometry do not take the curvature of the Sun's surface into account and can only be applied to relatively small areas, e.g., a single active region. We apply a method for nonlinear force-free coronal magnetic field modelling of photospheric vector magnetograms in spherical geometry which allows us to study the connectivity between multi-active regions. We use Vector Spectromagnetograph (VSM) data from the Synoptic Optical Long-term Investigations of the Sun (SOLIS) survey to model the coronal magnetic field, where we study three neighbouring magnetically connected active regions (ARs 10987, 10988, 10989) observed on 28, 29, and 30 March 2008, respectively. We compare the magnetic field topologies and the magnetic energy densities and study the connectivities between the active regions. We have studied the time evolution of the magnetic field over the period of three days and found no major changes in topologies, as there was no major eruption event. From this study we have concluded that active regions are much more connected magnetically than the electric current.

Time-resolved emission from bright hot pixels of an active region observed in the EUV band with SDO/AIA and multi-stranded loop modeling

E. **Tajfirouze**, F. Reale, A. Petralia, P. Testa

ApJ 816, Issue 1, article id. 12 **2016**

http://arxiv.org/pdf/1510.07524v1.pdf

Evidence for small amounts of very hot plasma has been found in active regions and might be the indication of an impulsive heating, released at spatial scales smaller than the cross section of a single loop. We investigate the heating and substructure of coronal loops in the core of one such active region by analyzing the light curves in the smallest resolution elements of solar observations in two EUV channels (94 A and 335 A) from the Atmospheric Imaging Assembly on-board the Solar Dynamics Observatory. We model the evolution of a bundle of strands heated by a storm of nanoflares by means of a hydrodynamic 0D loop model (EBTEL). The light curves obtained from the random combination of those of single strands are compared to the observed light curves either in a single pixel or in a row of pixels, simultaneously in the two channels and using two independent methods: an artificial intelligent system (Probabilistic Neural Network, PNN) and a simple cross-correlation technique. We explore the space of the parameters

to constrain the distribution of the heat pulses, their duration and their spatial size, and, as a feedback on the data, their signatures on the light curves. From both methods the best agreement is obtained for a relatively large population of events (1000) with a short duration (less than 1 min) and a relatively shallow distribution (power law with index 1.5) in a limited energy range (1.5 decades). The feedback on the data indicates that bumps in the light curves, especially in the 94 A channel, are signatures of a heating excess that occurred a few minutes before. **28 October 2010**,

EUV Flickering of Solar Coronal Loops: A New Diagnostic of Coronal Heating

Tajfirouze, E.; Reale, F.; Peres, G.; Testa, P.
ApJL 817, Issue 2, article id. L11, 6 pp. (**2016**)
http://arxiv.org/pdf/1601.03935v1.pdf
A previous work of ours found the best agreement between EUV light curves observed in an active region core (with evidence of super-hot plasma) and those predicted from a model with a random combination of many pulse-heated strands with a power-law energy distribution. We extend that work by including spatially resolved strand modeling and by studying the evolution of emission along the loops in the EUV 94 " and 335 " channels of the Atmospheric Imaging Assembly on board the Solar Dynamics Observatory. Using the best parameters of the previous work as the input of the present one, we find that the amplitude of the random fluctuations driven by the random heat pulses increases from the bottom to the top of the loop in the 94 " channel and from the top to the bottom in the 335 " channel. This prediction is confirmed by the observation of a set of aligned neighboring pixels along a bright arc of an active region core. Maps of pixel fluctuations may therefore provide easy diagnostics of nanoflaring regions.

Quasi-periodic oscillations in flares and coronal mass ejections associated with magnetic reconnection

Takuya **Takahashi**, Jiong Qiu, Kazunari Shibata
ApJ **848** 102 **2017**
https://arxiv.org/pdf/1709.05234.pdf
We propose a mechanism for quasi-periodic oscillations of both coronal mass ejections (CMEs) and flare loops as related to magnetic reconnection in eruptive solar flares. We perform two-dimensional numerical MHD simulations of magnetic flux rope eruption, with three different values of the global Lundquist number. In the low Lundquist number run, no oscillatory behavior is found. In the moderate Lunquist number run, on the other hand, quasi-periodic oscillations are excited both at the bottom of the flux rope and at the flare loop-top. In the high Lundquist number run, quasi-periodic oscillations are also excited; in the meanwhile, the dynamics become turbulent due to the formation of multiple plasmoids in the reconnection current sheet. In high and moderate Lundquist number runs, thin reconnection jet collide with the flux rope bottom or flare loop-top and dig them deeply. Steep oblique shocks are formed as termination shocks where reconnection jet is bent (rather than decelerated) in horizontal direction, resulting in supersonic back-flows. The structure becomes unstable, and quasi-periodic oscillation of supersonic back-flows appear at locally confined high-beta region at both the flux rope bottom and flare loop-top. We compare the observational characteristics of quasi-periodic oscillations in erupting flux ropes, post-CME current sheets, flare ribbons and light curves, with corresponding dynamical structures found in our simulation. **2014 April 18**

Analysis of the Solar Flare Index for Solar Cycles 18 – 24: Extremely Deep Gnevyshev Gap in the Chromosphere

Jouni **Takalo**
Solar Phys. **2023**
https://arxiv.org/pdf/2306.04239.pdf
We study the solar flare index (SFI) for the solar cycles 18\,--\,24. We find that SFI has deeper Gnevyshev gap (GG) in its first principal component than other atmospheric parameters. The GG is extremely clear especially in the even cycles.
The GG of the SFI appears about a half year later as a drop in the interplanetary magnetic field near the Earth and in the geomagnetic Ap-index. The instantaneous response of the magnetic field to solar flares, however, shows about two to three days after the eruption as a high, sharp peak in the cross-correlation of the SFI and Ap-index and as a lower peak in SFI vs. IMF B cross-correlation. We confirm these rapid responses using superposed-epoch analysis.
The most active flare cycles during 1944-2020 are the Cycles 19 and 21. The Cycle 18 has very strong SFI days as much as Cycle 22, but it has least nonzero SFI days in the whole interval. Interestingly Cycle 20 can be compared to the Cycles 23 and 24 in its low flare activity, although it locates between the most active SFI cycles.

OBSERVATIONAL EVIDENCE OF PARTICLE ACCELERATION ASSOCIATED WITH PLASMOID MOTIONS

Shinsuke **Takasao**1, Ayumi Asai2,3, Hiroaki Isobe3,4, and Kazunari Shibata
2016 ApJ 828 103
https://arxiv.org/pdf/1611.00108v1.pdf

We report a strong association between the particle acceleration and plasma motions found in the **2010 August 18** solar flare. The plasma motions are tracked in the extreme ultraviolet (EUV) images taken by the Atmospheric Imaging Assembly (AIA) on board the Solar Dynamics Observatory and the Extreme UltraViolet Imager (EUVI) on the Solar Terrestrial Relations Observatory spacecraft Ahead, and the signature of particle acceleration was investigated by using Nobeyama Radioheliograph data. In our previous paper, we reported that in EUV images many plasma blobs appeared in the current sheet above the flare arcade. They were ejected bidirectionally along the current sheet, and the blobs that were ejected sunward collided with the flare arcade. Some of them collided or merged with each other before they were ejected from the current sheet. We discovered impulsive radio bursts associated with such plasma motions (ejection, coalescence, and collision with the post flare loops). The radio bursts are considered to be the gyrosynchrotron radiation by nonthermal high energy electrons. In addition, the stereoscopic observation by AIA and EUVI suggests that plasma blobs had a three-dimensionally elongated structure. We consider that the plasma blobs were three-dimensional plasmoids (i.e., flux ropes) moving in a current sheet. We believe that our observation provides clear evidence of particle acceleration associated with the plasmoid motions. We discuss possible acceleration mechanisms on the basis of our results.

ABOVE-THE-LOOP-TOP OSCILLATION AND QUASI-PERIODIC CORONAL WAVE GENERATION IN SOLAR FLARES

Shinsuke **Takasao**1,3 and Kazunari Shibata

2016 ApJ 823 150

http://arxiv.org/pdf/1606.09354v1.pdf

Observations revealed that various kinds of oscillations are excited in solar flare regions. Quasi-periodic pulsations (QPPs) in flare emissions are commonly observed in a wide range of wavelengths. Recent observations have found that fast-mode magnetohydrodynamic (MHD) waves are quasi-periodically emitted from some flaring sites (quasi-periodic propagating fast-mode magnetoacoustic waves; QPFs). Both QPPs and QPFs imply a cyclic disturbance originating from the flaring sites. However, the physical mechanisms remain puzzling. By performing a set of two-dimensional MHD simulations of a solar flare, we discovered the local oscillation above the loops filled with evaporated plasma (above-the-loop-top region) and the generation of QPFs from such oscillating regions. Unlike all previous models for QPFs, our model includes essential physics for solar flares such as magnetic reconnection, heat conduction, and chromospheric evaporation. We revealed that QPFs can be spontaneously excited by the above-the-loop-top oscillation. We found that this oscillation is controlled by the backflow of the reconnection outflow. The new model revealed that flare loops and the above-the-loop-top region are full of shocks and waves, which is different from the previous expectations based on a standard flare model and previous simulations. In this paper, we show the QPF generation process based on our new picture of flare loops and will briefly discuss a possible relationship between QPFs and QPPs. Our findings will change the current view of solar flares to a new view in which they are a very dynamic phenomenon full of shocks and waves.

Magnetohydrodynamic shocks in and above post-flare loops: two-dimensional simulation and a simplified model

Shinsuke **Takasao**, Takuma Matsumoto, Naoki Nakamura, Kazunari Shibata

ApJ **805** 135 **2015**

http://arxiv.org/pdf/1504.05700v1.pdf

Solar flares are an explosive phenomenon, where super-sonic flows and shocks are expected in and above the post-flare loops. To understand the dynamics of post-flare loops, a two-dimensional magnetohydrodynamic (2D MHD) simulation of a solar flare has been carried out. We found new shock structures in and above the post-flare loops, which were not resolved in the previous work by Yokoyama and Shibata 2001. To study the dynamics of flows along the reconnected magnetic field, kinematics and energetics of the plasma are investigated along selected field lines. It is found that shocks are crucial to determine the thermal and flow structures in the post-flare loops. On the basis of the 2D MHD simulation, we have developed a new post-flare loop model which we call the pseudo-2D MHD model. The model is based on the 1D MHD equations, where all the variables depend on one space dimension and all the three components of the magnetic and velocity fields are considered. Our pseudo-2D model includes many features of the multi-dimensional MHD processes related to magnetic reconnection (particularly MHD shocks), which the previous 1D hydrodynamic models are not able to include. We compare the shock formation and energetics of a specific field line in the 2D calculation with those in our pseudo-2D MHD model, and we found that they give similar results. This model will allow us to study the evolution of the post-flare loops in a wide parameter space without expensive computational cost and without neglecting important physics associated with magnetic reconnection.

SIMULTANEOUS OBSERVATION OF RECONNECTION INFLOW AND OUTFLOW ASSOCIATED WITH THE 2010 AUGUST 18 SOLAR FLARE

Shinsuke **Takasao**1,2, Ayumi Asai3, Hiroaki Isobe3 and Kazunari Shibata

2012 ApJ 745 L6
We report the simultaneous extreme-ultraviolet observation of magnetic reconnection inflow and outflow in a flare on **2010 August 18** observed by the Atmospheric Imaging Assembly on board the Solar Dynamics Observatory. We found that during the rise phase of the flare, some plasma blobs appeared in the sheet structure above the hot loops. The plasma blobs were ejected bidirectionally along the sheet structure (outflow), at the same time as the threads visible in extreme-ultraviolet images moved toward the sheet structure (inflow). The upward and downward ejection velocities are 220-460 km s–1 and 250-280 km s–1, respectively. The inflow speed changed from 90 km s–1 to 12 km s–1 in 5 minutes. By using these velocities, we estimated the nondimensional reconnection rate, which we found to vary during this period from 0.20 to 0.055. We also found that the plasma blobs in the sheet structure collided or merged with each other before they were ejected from the sheet structure. We hypothesize that the sheet structure is the current sheet and that these plasma blobs are plasmoids or magnetic islands, which could be important for understanding the dynamics of the reconnection region.

Evolution and Flare Activity of Delta-Sunspots in Cycle 23

Kan **Takizawa**, Reizaburo Kitai
Solar Phys. Volume 290, Issue 7, pp 2093-2116 **2015**
http://arxiv.org/pdf/1507.06453v1.pdf
The emergence and magnetic evolution of solar active regions (ARs) of beta-gamma-delta type, which are known to be highly flare-productive, were studied with the SOHO/MDI data in Cycle 23. We selected 31 ARs that can be observed from their birth phase, as unbiased samples for our study. From the analysis of the magnetic topology (twist and writhe), we obtained the following results. i) Emerging beta-gamma-delta ARs can be classified into three topological types as "quasi-beta", "writhed" and "top-to-top". ii) Among them, the "writhed" and "top-to-top" types tend to show high flare activity. iii) As the signs of twist and writhe agree with each other in most cases of the "writhed" type (12 cases out of 13), we propose a magnetic model in which the emerging flux regions in a beta-gamma-delta AR are not separated but united as a single structure below the solar surface. iv) Almost all the "writhed"-type ARs have downward knotted structures in the mid portion of the magnetic flux tube. This, we believe, is the essential property of beta-gamma-delta ARs. v) The flare activity of beta-gamma-delta ARs is highly correlated not only with the sunspot area but also with the magnetic complexity. vi) We suggest that there is a possible scaling-law between the flare index and the maximum umbral area. **26-31 July 2002, 11-16 January 2005, 29 Nov-5 Dec 2005**
Table 1. Summary of parameters for 31 ARs studied.

The Effect of Resistivity on the Periodicity of Oscillatory Reconnection

Jordan **Talbot**1, James A. McLaughlin1, Gert J. J. Botha1, and Mark Hancock1
2024 ApJ 965 133
https://iopscience.iop.org/article/10.3847/1538-4357/ad2a5d/pdf
The oscillatory reconnection mechanism is investigated for a parameter study of eight orders of magnitude of resistivity, with a particular interest in the evolution of the oscillating current density at the null point and its associated periodicity. The resistive, nonlinear MHD simulations are solved in 2.5D for different levels of resistivity. Three methods (wavelet analysis, Fourier transform, and ANOVA) are used to investigate the effect of resistivity versus resultant period. It is found that there is an independence between the level of background resistivity and the period of the oscillatory reconnection mechanism. Conversely, it is found that resistivity has a significant effect on the maximum amplitude of the current density and the nature of its decay rate, as well as the magnitude of ohmic heating at the null.

The relationships among solar flare impulsiveness, energy release, and ribbon development

Cole A **Tamburri**, Maria D Kazachenko, Adam F Kowalski
ApJ **966** 94 **2024**
https://arxiv.org/pdf/2403.02457.pdf
https://iopscience.iop.org/article/10.3847/1538-4357/ad3047/pdf
We develop the impulsiveness index, a new classification system for solar flares using the SDO/EVE 304 Å Sun-as-a-star light curves. Impulsiveness classifies events based on the duration and intensity of the initial high-energy deposition of energy into the chromosphere. In stellar flare U-band light curves, Kowalski et al. (2013) found that impulsiveness is related to quantities such as a proxy for the Balmer jump ratio. However, the lack of direct spatial resolution in stellar flares limits our ability to explain this phenomenon. We calculate impulsiveness for 1368 solar flares between 04/2010 and 05/2014. We divide events into categories of low, mid, and high impulsiveness. We find, in a sample of 480 flares, that events with high maximum reconnection rate tend to also have high impulsiveness. For six case studies, we compare impulsiveness to magnetic shear, ribbon evolution, and energy release. We find that the end of the 304 Å light curve rise phase in these case studies corresponds to the cessation of PIL-parallel ribbon motion, while PIL-perpendicular motion persists afterward in most cases. The measured guide field ratio for low and mid-impulsiveness case study flares decreases about an order of magnitude during the impulsive flare phase. Finally, we find that, in four of the six case studies, flares with higher, more persistent shear tend to have low impulsiveness. Our study suggests that

impulsiveness may be related to other properties of the impulsive phase, though more work is needed to verify this relationship and apply our findings to stellar flare physics. **2012 Nov 20, 2013 May 16, 2013 Oct 13, 2013 Oct 15, 2014 Apr 4, 2014 Apr 15**

Statistical Investigation of the Kinematic and Thermal Properties of Supra-arcade Downflows Observed During a Solar Flare

Guangyu **Tan**, Yijun Hou, Hui Tian
MNRAS Volume 522, Issue 3, July **2023**, Pages 4468–4480,
https://doi.org/10.1093/mnras/stad1228
https://arxiv.org/pdf/2208.14737.pdf

Supra-arcade downflows (SADs) are dark structures descending towards post-reconnection flare loops observed in extreme ultraviolet or X-ray observations and are closely related to magnetic reconnection during solar flares. Due to the lack of statistical study on SADs in a single flare, evolutions of kinematic and thermal properties of SADs during the flare process still remain obscure. In this work, we identified 81 SADs in a flare that occurred on **2013 May 22** using observations of the Atmospheric Imaging Assembly (AIA) on the Solar Dynamics Observatory (SDO). The kinematic properties of each SAD, including the appearance time, height, projective velocity, and acceleration were recorded. We found that the appearance heights of SADs become larger during the flare, which is likely due to the lift of the bottom of the plasma sheet. In the flare decay phase, the region where SADs mainly appear moves from the north part to the south side possibly related to a secondary eruption in the south side. The trajectories of most SADs can be fitted by one or two deceleration processes, while some special ones have positive accelerations during the descent. For the thermal properties, we selected 54 SADs, whose front and body could be clearly distinguished from the surrounding during the entire descent, to perform Differential Emission Measure analysis. It is revealed that the temperatures of the SAD front and body tend to increase during their downward courses, and the relationship between the density and temperature indicates that the heating is mainly caused by adiabatic compression.

The early evolution of solar flaring plasma loops

Baolin **Tan**
Universe **2021** *7*(10), 378;
https://www.mdpi.com/2218-1997/7/10/378/pdf
https://doi.org/10.3390/universe7100378
https://arxiv.org/ftp/arxiv/papers/2110/2110.07846.pdf

Plasma loops are the elementary structures of solar flaring active regions which dominate the whole processes of flaring eruptions. The standard flare models are well explained the evolution and eruption after magnetic reconnection around the hot cusp-structure above the top of plasma loops, however, the early evolution of the plasma loops before the onset of magnetic reconnection has been poorly understood. Considering that magnetic-gradients are ubiquitous in solar plasma loops, this work applies the magnetic-gradient pumping (MGP) mechanism to study the early evolution of flaring plasma loops. The results indicate that the early evolution depend on the magnetic field distribution and the geometry of the plasma loops which dominates the balance between the accumulation and dissipation of energy around loop-tops. Driven by MGP process, both of the density and temperature as well as the plasma beta value around the looptop will increase in the early phase of the plasma loops evolution. In fact, the solar plasma loops will have two distinct evolutionary results: the low, initial dense plasma loops with relatively strong magnetic fields tend to be stable for their maximum beta value always smaller than the critical value, while the higher, initial dilute solar plasma loops with relatively weak magnetic fields tend to be unstable for their beta values exceeding the critical value at a time of about one hour after the formation of the solar magnetized plasma loop. The latter may produce ballooning instability and finally trigger the following magnetic reconnection and eruptions. These physical scenarios may provide us a new viewpoint to understand the nature and origin of solar flares.

Energy and spectral analysis of confined solar flares from radio and X-ray observations

Chengming **Tan**, Karl-Ludwig Klein, Yihua Yan, Satoshi Masuda, Baolin Tan, Jing Huang, Guowu Yuan
Research in Astronomy and Astrophysics **2021**
https://arxiv.org/pdf/2108.02601.pdf

The energy and spectral shape of radio bursts may help us understand the generation mechanism of solar eruptions, including solar flares, CMEs, eruptive filaments, and various scales of jets. The different kinds of flares may have different characteristics of energy and spectral distribution. In this work, we selected 10 mostly confined flare events during **October 2014** to investigate their overall spectral behavior and the energy emitted in microwaves by using radio observations from microwaves to interplanetary radio waves, and X-ray observations of GOES, RHESSI, and Fermi/GBM. We found that: All the confined flare events were associated with a microwave continuum burst extending to frequencies of 9.4 - 15.4 GHz, and the peak frequencies of all confined flare events are higher than 4.995 GHz and lower than or equal to 17 GHz. The median value is around 9 GHz. The microwave burst energy (or fluence) as well as the peak frequency are found to provide useful criteria to estimate the power of solar flares. The observations imply that the magnetic field in confined flares tends to be stronger than that in 412 flares studied by Nita et al. 2004. All 10 events

studied did not produce detectable hard X-rays with energies above 300 keV indicating the lack of efficient acceleration of electrons to high energies in the confined flares. **18, 22, 24, 27, 28, 29 Oct 2014**

Very Long-period Pulsations before the Onset of Solar Flares

Baolin **Tan**, Zhiqiang Yu, Jing Huang, Chengming Tan, Yin Zhang
ApJ 833 206 **2016**
https://arxiv.org/pdf/1610.09291v1.pdf
Solar flares are the most powerful explosions occurring in the solar system, which may lead to disastrous space weather events and impact various aspects of our Earth. So far, it is still a big challenge in modern astrophysics to understand the origin of solar flares and predict their onset. Based on the analysis of soft X-ray emission observed by the Geostationary Operational Environmental Satellite (GOES), this work reported a new discovery of very long-periodic pulsations occurred in the preflare phase before the onset of solar flares (preflare-VLPs). These pulsations are typically with period of 8 - 30 min and last for about 1 - 2 hours. They are possibly generated from LRC oscillations of plasma loops where electric current dominates the physical process during magnetic energy accumulation in the source region. The preflare-VLP provides an essential information for understanding the triggering mechanism and origin of solar flares, and may help us to response to solar explosions and the corresponding disastrous space weather events as a convenient precursory indicator. **13 July 2012, 25 Oct 2013, 19 Oct 2014, 26 October 2014, 5 May 2015**

Diagnose Physical Conditions Near the Flare Energy-release Sites from Observations of Solar Microwave Type III Bursts

Baolin **Tan**, Marian Karlicky, Hana Meszarosova, Guangli Huang
Research in Astron. & Astrophys. (RAA), **201**5
http://arxiv.org/pdf/1511.08863v1.pdf
In the physics of solar flares, it is crucial to diagnose the physical conditions near the flare energy-release sites. However, so far it is unclear how do diagnose these physical conditions. Solar microwave type III burst is believed to be a sensitive signature of the primary energy release and electron accelerations in solar flares. This work takes into account the effect of magnetic field on the plasma density and developed s set of formulas which can be used to estimate the plasma density, temperature, magnetic field near the magnetic reconnection site and particle acceleration region, and the velocity and energy of electron beams. We applied these formulas to three groups of microwave type III pairs in a X-class flare, and obtained some reasonable and interesting results. This method can be applied to other microwave type III bursts to diagnose the physical conditions of source regions, and provide some basic information to understand the intrinsic nature and fundamental processes occurring near the flare energy-release sites. **13 Dec 2006**

SMALL-SCALE MICROWAVE BURSTS IN LONG-DURATION SOLAR FLARES

Baolin **Tan**
2013 ApJ 773 165
Solar small-scale microwave bursts (SMBs), including microwave dot, spike, and narrow-band type III bursts, are characterized by very short timescales, narrow frequency bandwidth, and very high brightness temperatures. Based on observations of the Chinese Solar Broadband Radio Spectrometer at Huairou with superhigh cadence and frequency resolution, this work presents an intensive investigation of SMBs in several flares that occurred in active region NOAA 10720 during **2005 January 14-21**. Especially for long-duration flares, the SMBs occurred not only in the early rising and impulsive phase, but also in the flare decay phase and even after the end of the flare. These SMBs are strong bursts with inferred brightness temperatures of at least 8.18 × 1011-1.92 × 1013 K, very short lifetimes of 5-18 ms, relative frequency bandwidths of 0.7%-3.5%, and superhigh frequency drifting rates. Together with their obviously different polarizations from background emission (the quiet Sun, and the underlying flaring broadband continuum), such SMBs should be individual, independent strong coherent bursts related to some non-thermal energy release and the production of energetic particles in a small-scale source region. These facts show the existence of small-scale strong non-thermal energy releasing activities after the flare maxima, which is meaningful for predicting space weather. Physical analysis indicates that a plasma mechanism may be the most favorable candidate for the formation of SMBs. From the plasma mechanism, the velocities and kinetic energy of fast electrons can be deduced and the region of electron acceleration can also be tracked.

Evolution of Evershed and Shear Flows Associated with the X3.4 Flare of 2006 December 13

Changyi **Tan**, P.F. Chen, Valentyna Abramenko and Haimin Wang
BBSO Preprint #1363, 2008; *ApJ* **690** 1820-1828, **2009**
http://www.iop.org/EJ/abstract/0004-637X/690/2/1820
http://solar.njit.edu/preprints/tan1363.pdf
Rapid and irreversible penumbral decays related to X-class flares have been found in a number of studies. Since the Evershed flows are closely associated with morphology of sunspot penumbra, we use the state-of-art Hinode data to track Evershed flow in flaring active regions as well as shear flows close to the flaring neutral line. This paper concentrates on the study of AR 10930 around the time of an X3.4 flare on December 13, 2006. We utilize the seeing-free solar optical telescope G-band and *Stokes-V* data as tracers to obtain the horizontal component of the Evershed and shear flows by local correlation tracking. We find that: (1) An obvious

penumbral decay appears in this active region intimately associated with the X3.4 flare. (2) The mean magnitude of the horizontal speeds of the Evershed flows within the penumbra decay areas varies from 0.4 to 1 km s^{-1} temporally and spatially. (3) The Evershed flows decrease before the flare eruption in two of the four penumbral decay areas. (4) The mean shear flows along the magnetic neutral of this δ-sunspot started to decrease before the flare and continue to decrease for another hour after the flare. The magnitude of this flow apparently dropped from 0.2 to 0.06 km s^{-1}. (5) Quasi-periodic oscillating behavior of the plasma flows is observed in both Evershed flows and shear flows. We propose that the decays of the penumbra and the Evershed flow are related to the magnetic rearrangement involved in the CME/flare events.

Solar Flare Prediction Based on the Fusion of Multiple Deep-learning Models

Rongxin **Tang**1,2,3, Wenti Liao1,2, Zhou Chen1,2,4,5, Xunwen Zeng2, Jing-song Wang5, Bingxian Luo6,7, Yanhong Chen6, Yanmei Cui6, Meng Zhou2, Xiaohua Deng2Show full author list

2021 ApJS 257 50

https://doi.org/10.3847/1538-4365/ac249e

https://iopscience.iop.org/article/10.3847/1538-4365/ac249e/pdf

Solar flare formation mechanisms and their corresponding predictions have commonly been difficult topics in solar physics for decades. The traditional forecasting method manually constructs a statistical relationship between the measured values of solar active regions and solar flares that cannot fully utilize the information related to solar flares contained in observational data. In this article, we first used neural-network methods driven by the measured magnetogram and magnetic characteristic parameters of the sunspot group to learn the prediction model and predict solar flares. The prediction fusion model is based on a deep neural network, convolutional neural network, and bidirectional long short-term memory neural network and can predict whether a sunspot group will have a flare event above class M or class C in the next 24 or 48 hr. The real skill statistics (TSS) and F1 scores were used to evaluate the performances of our fusion model. The test results clearly show that this fusion model can make full use of the information related to solar flares and combine the advantages of each independent model to capture the evolution characteristics of solar flares, which is a much better performance than traditional statistical prediction models or any single machine-learning method. We also proposed two frameworks, namely F1_FFM and TSS_FFM, which optimize the F1 score and TSS score, respectively. The cross validation results show that they have their respective advantages in the F1 score and TSS score.

Parametric Evolution of Power-law Energy Spectra of Flare Accelerated Electrons in the Solar Atmosphere

J. F. **Tang**1,2,3, D. J. Wu2, L. Chen2, L. Xu4, and B. L. Tan3

2020 ApJ 904 1

https://doi.org/10.3847/1538-4357/abc2ca

It is well known that solar hard X-ray bursts (HXRs) and solar radio bursts (SRBs) from solar flares both are produced directly by fast electron beams (FEBs) traveling through the solar atmosphere. The observed characteristics of HXRs and SRBs sensitively depend on the energy distribution of FEBs, which are believed commonly to have a power-law energy spectrum. When FEBs propagating in the solar atmosphere, however, their energy spectra can considerably vary due to the interaction with the atmospheric plasmas and this may significantly influence the observational characteristics of the producing HXRs and SRBs. In the present paper, based on flare atmospheric models, we investigate the parametric evolution of power-law spectra of FEBs due to their energy losses when propagating along flaring loops. The results show that an initially single power-law spectrum with a lower-energy cutoff can evolve into a more complex double power-law spectrum or a broken power-law spectrum with multi-breaking knees because of the dependence of the energy loss on the initial energies. The possible effects of the energy-spectral evolution of FEBs on observational characteristics of their HXR flares and SRBs are discussed. The present results are helpful to understand the physics of dynamical spectra of HXRs and SRBs from solar flares.

Observational Signatures of Impulsively Heated Coronal Loops: Power-Law Distribution of Energies

Y. **Taroyan**, R. Erdélyi & S. J. Bradshaw

Solar Physics, Volume 269, Number 2, 295-307, **2011**

It has been established that small scale heating events, known as nanoflares, are important for solar coronal heating if the power-law distribution of their energies has a slope α steeper than −2 (α<−2). Forward modeling of impulsively heated coronal loops with a set of prescribed power-law indices α is performed. The power-law distribution is incorporated into the governing equations of motion through an impulsive heating term. The results are converted into synthetic Hinode/EIS observations in the 40″ imaging mode, using a selection of spectral lines formed at various temperatures. It is shown that the intensities of the emission lines and their standard deviations are sensitive to changes in α. A method based on a combination of observations and forward modeling is proposed for determining whether the heating in a particular case is due to small or large scale events. The method is extended and applied to a loop structure that consists of multiple strands.

On Excited Frequencies for Alfvén Waves in a Coronal Arcade

Lucas A. **Tarr**

2017 ApJ 847 1

The normal modes of oscillation for a magnetic arcade are used to analytically solve an initial value problem and estimate the power spectra of wave frequencies generated by a reconnection event in the solar corona. Over a realistic range of parameters, I find that such a disturbance generates a peak power at ~10 s $^{\mathrm{mHz}}$ frequency and substantial power up to $^{\sim 4\ \mathrm{Hz}}$. The cadence and sensitivity of current instrumentation does not allow observations of oscillations at these frequencies, but in the near future, new instrumentation will be able to probe this regime and observationally determine its energetic importance.

Quiescent Reconnection Rate Between Emerging Active Regions and Preexisting Field, with Associated Heating: NOAA AR 11112

Lucas A. **Tarr**, Dana W. Longcope, David E. McKenzie, Keiji Yoshimura

Solar Physics, September **2014**, Volume 289, Issue 9, pp 3331-3349

When magnetic flux emerges from beneath the photosphere, it displaces the preexisting field in the corona, and a current sheet generally forms at the boundary between the old and new magnetic domains. Reconnection in the current sheet relaxes this highly stressed configuration to a lower energy state. This scenario is most familiar and most often studied in flares, where the flux transfer is rapid. We present here a study of steady, quiescent flux transfer occurring at a rate three orders of magnitude lower than that in a large flare. In particular, we quantify the reconnection rate and the related energy release that occurred as the new polarity emerged to form NOAA Active Region 11112 (**SOL16 October 2010**T00:00:00L205C117) within a region of preexisting flux. A bright, low-lying kernel of coronal loops above the emerging polarity, observed with the Atmospheric Imaging Assembly onboard the Solar Dynamics Observatory and the X-ray Telescope onboard Hinode, originally showed magnetic connectivity only between regions of newly emerged flux when overlaid on magnetograms from the Helioseismic and Magnetic Imager. Over the course of several days, this bright kernel advanced into the preexisting flux. The advancement of an easily visible boundary into the old flux regions allows measuring the rate of reconnection between old and new magnetic domains. We compare the reconnection rate with the inferred heating of the coronal plasma. To our knowledge, this is the first measurement of steady, quiescent heating related to reconnection. We determined that the newly emerged flux reconnects at a fairly steady rate of 0.38×10^{16} Mx s^{-1} over two days, while the radiated power varies between $(2-8)\times10^{25}$ erg s^{-1} over the same time. We found that as much as 40 % of the total emerged flux at any given time may have reconnected. The total amounts of transferred flux ($\sim 1\times10^{21}$ Mx) and radiated energy ($\sim 7.2\times10^{30}$ ergs) are comparable to that of a large M- or small X-class flare, but are stretched out over 45 hours.

CALCULATING SEPARATE MAGNETIC FREE ENERGY ESTIMATES FOR ACTIVE REGIONS PRODUCING MULTIPLE FLARES: NOAA AR11158

Lucas **Tarr**, Dana Longcope, and Margaret Millhouse

2013 ApJ 770 4

It is well known that photospheric flux emergence is an important process for stressing coronal fields and storing magnetic free energy, which may then be released during a flare. The Helioseismic and Magnetic Imager (HMI) on board the Solar Dynamics Observatory (SDO) captured the entire emergence of NOAA AR 11158. This region emerged as two distinct bipoles, possibly connected underneath the photosphere, yet characterized by different photospheric field evolutions and fluxes. The combined active region complex produced 15 GOES C-class, two M-class, and the X2.2 Valentine's Day Flare during **the four days after initial emergence on 2011 February 12.** The M and X class flares are of particular interest because they are nonhomologous, involving different subregions of the active region. We use a Magnetic Charge Topology together with the Minimum Current Corona model of the coronal field to model field evolution of the complex. Combining this with observations of flare ribbons in the 1600 Å channel of the Atmospheric Imaging Assembly on board SDO, we propose a minimization algorithm for estimating the amount of reconnected flux and resulting drop in magnetic free energy during a flare. For the **M6.6, M2.2, and X2.2 flares**, we find a flux exchange of 4.2×10^{20} Mx, 2.0×10^{20} Mx, and 21.0×10^{20} Mx, respectively, resulting in free energy drops of 3.89×10^{30} erg, 2.62×10^{30} erg, and 1.68×10^{32} erg.

CALCULATING ENERGY STORAGE DUE TO TOPOLOGICAL CHANGES IN EMERGING ACTIVE REGION NOAA AR 11112

Lucas **Tarr** and Dana Longcope

2012 ApJ 749 64

The minimum current corona model provides a way to estimate stored coronal energy using the number of field lines connecting regions of positive and negative photospheric flux. This information is quantified by the net flux connecting pairs of opposing regions in a connectivity matrix. Changes in the coronal magnetic field, due to processes such as magnetic reconnection, manifest themselves as changes in the connectivity matrix. However, the connectivity matrix

will also change when flux sources emerge or submerge through the photosphere, as often happens in active regions. We have developed an algorithm to estimate the changes in flux due to emergence and submergence of magnetic flux sources. These estimated changes must be accounted for in order to quantify storage and release of magnetic energy in the corona. To perform this calculation over extended periods of time, we must additionally have a consistently labeled connectivity matrix over the entire observational time span. We have therefore developed an automated tracking algorithm to generate a consistent connectivity matrix as the photospheric source regions evolve over time. We have applied this method to NOAA Active Region 11112, which underwent a GOES M2.9 class flare around 19:00 on **2010 October 16**th, and calculated a lower bound on the free magnetic energy buildup of ~8.25 × 1030 erg over 3 days.

Limb Event Brightenings (LEBs) with fast ejection using IRIS mission Observations

E. **Tavabi**, S. Koutchmy, L. Golub
Solar Phys. **2015**
http://arxiv.org/ftp/arxiv/papers/1507/1507.06794.pdf
The Interface Region Imaging Spectrograph (IRIS) of the recently commissioned NASA Small Explorer mission provides significantly more complete and higher resolution spectral coverage of the dynamical conditions inside the chromosphere and Transition Region (TR) than has heretofore been available. Near the solar limb high temporal, spatial (0"3) and spectral resolution observations from ultraviolet IRIS spectra reveal high-energy limb event brightenings (LEBs) at low chromospheric height, near 1 Mm height above the limb. They can be characterized as explosive events producing jets. We selected 2 events showing spectra of a confined eruption just off or near the quiet Sun limb, the jet part showing obvious moving material with short duration large Doppler shifts in three directions identified as macro-spicules on slit-jaw (SJ) images in SiIV and HeII 304. The events are analyzed from a sequence of very close rasters taken near the central meridian and the South Pole limb. The processed SJ images and the simultaneously observed fast spectral sequences with large Doppler shifts, with a pair of red shifted elements together with a faster blue shifted element from almost the same position, are analyzed. Shifts correspond to velocities up to 100 km/s in projection on the plane of the limb. The occurrence of erupting spicules and macrospicules from these regions is noticed from images taken before and after the spectra. The cool low-FIP element simultaneous line emissions of the MgII h & k resonance lines do not clearly show a similar signature due to optical thickness effects but SiIV broad band SJ images do. The bidirectional plasma jets ejected from a small reconnection site are interpreted as the result of coronal loop-loop interactions leading to reconnection in nearby sites. **Oct. 10, 2013**

Blue wing enhancement of the chromospheric Mg II h and k lines in a solar flare

Akiko **Tei**, Takahito Sakaue, Tekanori J. Okamoto, Tomoko Kawate, Petr Heinzel, Satoru Ueno, Ayumi Asai, Kiyoshi Ichimoto, Kazunari Shibata
PASJ 70, Issue 6, **2018**
https://arxiv.org/pdf/1803.05237.pdf
We performed coordinated observations of AR 12205, which produced a C-class flare on **2014 November 11**, with the Interface Region Imaging Spectrograph (IRIS) and the Domeless Solar Telescope (DST) at Hida Observatory. Using spectral data in the Si IV 1403 \AA, C II 1335 \AA, and Mg II h and k lines from IRIS and the Ca II K, Ca II 8542 \AA, and Hα lines from DST, we investigated a moving flare kernel during the flare. In the Mg II h line, the leading edge of the flare kernel showed the intensity enhancement in the blue wing, and the smaller intensity of the blue-side peak (h2v) than that of the red-side one (h2r). The blueshift lasted for 9-48 s with a typical speed of 10.1 ± 2.6 km s−1 and it was followed by the high intensity and the large redshift with a speed of up to 51 km s−1 detected in the Mg II h line. The large redshift was a common property for all six lines but the blueshift prior to it was found only in the Mg II lines. A cloud modeling of the Mg II h line suggests that the blue wing enhancement with such peak difference can be caused by a chromospheric-temperature (cool) upflow. We discuss a scenario in which an upflow of cool plasma is lifted up by expanding hot plasma owing to the deep penetration of non-thermal electrons into the chromosphere. Furthermore, we found that the blueshift persisted without any subsequent redshift in the leading edge of the flare kernel during its decaying phase. The cause of such long-lasting blueshift is also discussed. 2014-11-11
RHESSI Science Nugget, No. 321, April 2018 http://sprg.ssl.berkeley.edu/~tohban/wiki/index.php/Blue-wing_enhancement_of_the_Mg_II_h_and_k_lines_in_a_flare

Investigating the Soft X-ray Spectra of Solar Flare Onsets

Anant **Telikicherla**, Thomas N. Woods, Bennet D. Schwab
ApJ **966** 198 **2024**
https://arxiv.org/pdf/2403.05992.pdf
https://iopscience.iop.org/article/10.3847/1538-4357/ad37f6/pdf
In this study we present the analysis of six solar flare events that occurred in 2022, using new data from the third-generation Miniature X-Ray Solar Spectrometer (MinXSS), also known as the Dual-zone Aperture X-ray Solar Spectrometer (DAXSS). The primary focus of this study is on the flare's "onset phase", which is characterized by elevated soft X-ray emissions even before the flare's impulsive phase. We analyze the temporal evolution of plasma temperature, emission measure, and elemental abundance factors during the flare onset phase, by fitting the DAXSS

spectra with the Astrophysical Plasma Emission Code (APEC) model. The model fitting results indicate that the flaring-plasma is already at a high temperature (10-15 MK) during the onset period. The temperature rises during the onset phase, followed by a decrease and subsequent increase during the impulsive phase. Elemental abundance factors show a trend of falling below pre-flare values during the onset phase, with some recovery before the impulsive phase. During the impulsive phase, the abundance factors decrease from elevated coronal values to about photospheric values. We also analyze images from the 193 Angstrom channel of the Atmospheric Imaging Assembly (AIA), highlighting the formation or brightening of coronal loop structures during the onset phase. Two distinct onset loop configurations are observed which are referred to as 1-loop and 2-loop onsets. Both DAXSS and AIA observations indicate that the flare onset phase exhibits similar hot coronal plasma properties as the impulsive phase, suggesting that the onset phase may act as a preconditioning effect for some flares. **2022-03-06, 2022-03-15, 2022-03-29, 2022-04-19, 2022-08-15, 2022-08-18**

Space weather: the solar perspective -- an update to Schwenn (2006) Review

Manuela **Temmer**
Living Reviews in Solar Physics **2021**
https://arxiv.org/pdf/2104.04261.pdf
https://link.springer.com/content/pdf/10.1007/s41116-021-00030-3.pdf
The Sun, as an active star, is the driver of energetic phenomena that structure interplanetary space and affect planetary atmospheres. The effects of Space Weather on Earth and the solar system is of increasing importance as human spaceflight is preparing for lunar and Mars missions. This review is focusing on the solar perspective of the Space Weather relevant phenomena, coronal mass ejections (CMEs), flares, solar energetic particles (SEPs), and solar wind stream interaction regions (SIR). With the advent of the STEREO mission (launched in 2006), literally, new perspectives were provided that enabled for the first time to study coronal structures and the evolution of activity phenomena in three dimensions. New imaging capabilities, covering the entire Sun-Earth distance range, allowed to seamlessly connect CMEs and their interplanetary counterparts measured in-situ (so called ICMEs). This vastly increased our knowledge and understanding of the dynamics of interplanetary space due to solar activity and fostered the development of Space Weather forecasting models. Moreover, we are facing challenging times gathering new data from two extraordinary missions, NASA's Parker Solar Probe (launched in 2018) and ESA's Solar Orbiter (launched in 2020), that will in the near future provide more detailed insight into the solar wind evolution and image CMEs from view points never approached before. The current review builds upon the Living Reviews paper by Schwenn from 2006, updating on the Space Weather relevant CME-flare-SEP phenomena from the solar perspective, as observed from multiple viewpoints and their concomitant solar surface signatures**. 5-8 Dec 1981, 13-16 Aug 1982, 12 July 2007, December 12, 2008, December 22, 2009, 10 Jun 2010, June 12-13, 2010, 28 Oct 2003, November 18, 2003, 6-8 Aug 2007, March 7, 2011, August 9, 2011, March 7–11, 2012: May 17, 2012, June 30, 2012, 2-4 Dec 2012, June 14, 2012, February 25, 2014, August 24, 2014, January 1, 2016, September 6, 2017, 6-12 Sep 2017,**

On Flare-CME Characteristics from Sun to Earth Combining Remote-Sensing Image Data with In SituMeasurements Supported by Modeling

Manuela **Temmer**, Julia K. Thalmann, Karin Dissauer, Astrid M. Veronig, Johannes Tschernitz, Jürgen Hinterreiter, Luciano Rodriguez
Solar Physics July **2017**, 292:93
https://link.springer.com/content/pdf/10.1007%2Fs11207-017-1112-5.pdf
https://arxiv.org/pdf/1703.00694.pdf
We analyze the well-observed flare and coronal mass ejection (CME) from **1 October 2011** (SOL2011-10-01T09:18) covering the complete chain of effects – from Sun to Earth – to better understand the dynamic evolution of the CME and its embedded magnetic field. We study in detail the solar surface and atmosphere associated with the flare and CME using the Solar Dynamics Observatory (SDO) and ground-based instruments. We also track the CME signature off-limb with combined extreme ultraviolet (EUV) and white-light data from the Solar Terrestrial Relations Observatory (STEREO). By applying the graduated cylindrical shell (GCS) reconstruction method and total mass to stereoscopic STEREO-SOHO (Solar and Heliospheric Observatory) coronagraph data, we track the temporal and spatial evolution of the CME in the interplanetary space and derive its geometry and 3D mass. We combine the GCS and Lundquist model results to derive the axial flux and helicity of the magnetic cloud (MC) from in situmeasurements from Wind. This is compared to nonlinear force-free (NLFF) model results, as well as to the reconnected magnetic flux derived from the flare ribbons (flare reconnection flux) and the magnetic flux encompassed by the associated dimming (dimming flux). We find that magnetic reconnection processes were already ongoing before the start of the impulsive flare phase, adding magnetic flux to the flux rope before its final eruption. The dimming flux increases by more than 25% after the end of the flare, indicating that magnetic flux is still added to the flux rope after eruption. Hence, the derived flare reconnection flux is most probably a lower limit for estimating the magnetic flux within the flux rope. We find that the magnetic helicity and axial magnetic flux are lower in the interplanetary space by ~ 50% and 75%, respectively, possibly indicating an erosion process. A CME mass increase of 10% is observed over a range of ~4--

20 R⊙~4--20 R⊙. The temporal evolution of the CME-associated core-dimming regions supports the scenario that fast outflows might supply additional mass to the rear part of the CME.

Relation between CME Acceleration Profile and Flare Energy Release derived from Combined STEREO and RHESSI Observations

Temmer, M.1; Veronig, A.M.1; Vrsnak, B.2
Fraiburg ESP Meeting **2008**, **Presentation**
In the standard flare/CME picture magnetic reconnection occurs in a current sheet formed behind the CME, which may provide a feedback relationship between both phenomena. To study the relationship of the large-scale CME acceleration and the energy release in the associated flare we analyze three well observed events. The observations cover the early (low corona) evolution of the CMEs with the EUVI instruments aboard the twin STEREO spacecraft and the RHESSI hard Xray emission of the associated flare. Since the flare hard X-rays are due to fast electrons, they provide the most direct indicator of the evolution of the flare energy release in the flare. The results are compared to case studies for halo-CMEs where a close synchronization between the CME acceleration and the flare energy release was found (**Temmer et al., ApJ, 2008, 673, L95**).

ACCELERATION IN FAST HALO CMEs AND SYNCHRONIZED FLARE HXR BURSTS

M. **Temmer**, A. M. Veronig, B. Vrsˇnak, J. Rybaˊk, P. Go꞉mo꞉ry, S. Stoiser, and D. Maricˇic
The Astrophysical Journal, 673: L95–L98, **2008, File**
We study two well-observed, fast halo CMEs **(2005.01.17; 2006.07.06)**, covering the full CME kinematics including the initiation and impulsive acceleration phase, and their associated flares. We find a close synchronization between the CME acceleration profile and the flare energy release as indicated by the *RHESSI* hard X-ray flux onsets, as well as peaks occur simultaneously within 5 minutes. These findings indicate a close physical connection between both phenomena and are interpreted in terms of a feedback relationship between the CME dynamics and the reconnection process in the current sheet beneath the CME.

WIDESPREAD NANOFLARE VARIABILITY DETECTED WITH HINODE/X-RAY TELESCOPE IN A SOLAR ACTIVE REGION

Sergio **Terzo**1,4, Fabio Reale1,4, Marco Miceli1,4, James A. Klimchuk2, Ryouhei Kano3 and Saku Tsuneta
2011 ApJ 736 111
It is generally agreed that small impulsive energy bursts called nanoflares are responsible for at least some of the Sun's hot corona, but whether they are the explanation for most of the multimillion-degree plasma has been a matter of ongoing debate. We present here evidence that nanoflares are widespread in an active region observed by the X-Ray Telescope on board the Hinode mission. The distributions of intensity fluctuations have small but important asymmetries, whether taken from individual pixels, multipixel subregions, or the entire active region. Negative fluctuations (corresponding to reduced intensity) are greater in number but weaker in amplitude, so that the median fluctuation is negative compared to a mean of zero. Using Monte Carlo simulations, we show that only part of this asymmetry can be explained by Poisson photon statistics. The remainder is explainable through a tendency for exponentially decreasing intensity, such as would be expected from a cooling plasma produced from a nanoflare. We suggest that nanoflares are a universal heating process within active regions.

On the Coronal Temperature in Solar Microflares

Paola **Testa**1 and Fabio Reale2,3
2020 ApJ 902 31
https://doi.org/10.3847/1538-4357/abb36e
We present a study of solar imaging and spectral observations of a microflare, focusing on the temperature diagnostics provided by the Atmospheric Imaging Assembly (AIA) on board the Solar Dynamics Observatory, and the Extreme-Ultraviolet Imaging Spectrometer (EIS) on board Hinode. Our data analysis, in particular from the emission in the 131 and 94 Å channels, indicates that the heated plasma reaches temperatures of $\gtrsim$10 MK, at odds with a previous analysis of the same event, and we discuss the reason for the discrepancy. A particularly interesting aspect is the likely presence of the Fe xxiii 263.76 Å line, though weak, in EIS spectra in the early phases of the event, supporting the presence of high temperature plasma. Hydrodynamic 1D modeling of a single loop heated with a 3 minute pulse to 12–15 MK reproduces well most observed features along one of the brightening loops, including intensities in the AIA hot channels and their temporal variability, as well as the intensity, Doppler shift, and line width of the EIS Fe xxiii line, and its timing relative to the AIA emission. Overall, we obtain a coherent scenario of a typical microflaring loop system and provide constraints on the intensity of the energy release as well as its spatial and temporal distribution, both along and across the loop.

IRIS Observations of Short-term Variability in Moss Associated with Transient Hot Coronal Loops

Testa, Paola ; Polito, Vanessa ; De Pontieu, Bart
The Astrophysical Journal, Volume 889, Issue 2, id.124, 23 pp. (**2020**)
https://iopscience.iop.org/article/10.3847/1538-4357/ab63cf/pdf
We observed rapid variability (≲60 s) at the footpoints of transient, hot (∼8-10 MK) coronal loops in active region cores, with the Interface Region Imaging Spectrograph (IRIS). The high spatial (∼0"33) and temporal (≲5-10 s) resolution of IRIS is often crucial for the detection of this variability. We show how, in combination with 1D RADYN loop modeling, these IRIS spectral observations of the transition region (TR) and chromosphere provide powerful diagnostics of the properties of coronal heating and energy transport (thermal conduction or nonthermal electrons, NTEs). Our simulations of nanoflare-heated loops indicate that emission in the Mg II triplet can be used as a sensitive diagnostic for nonthermal particles. In our events, we observe a large variety of IRIS spectral properties (intensity, Doppler shifts, broadening, chromospheric/TR line ratios, Mg II triplet emission) even for different footpoints of the same coronal events. In several events, we find spectroscopic evidence for NTEs (e.g., TR blueshifts and Mg II triplet emission), suggesting that particle acceleration can occur even for very small magnetic reconnection events, which are generally below the detection threshold of hard X-ray instruments that provide direct detection of emission of nonthermal particles.
IRIS Nugget Jan **2022** https://iris.lmsal.com/nugget?cmd=view-pod&pubDate=2022-01-10

HIGH SPATIAL RESOLUTION Fe xii OBSERVATIONS OF SOLAR ACTIVE REGIONS
Paola **Testa**1, Bart De Pontieu2,3, and Viggo Hansteen
2016 ApJ 827 99
We use UV spectral observations of active regions with the Interface Region Imaging Spectrograph(IRIS) to investigate the properties of the coronal Fe xii 1349.4 Å emission at unprecedented high spatial resolution (~0.33"). We find that by using appropriate observational strategies (i.e., long exposures, lossless compression), Fe xii emission can be studied with IRIS at high spatial and spectral resolution, at least for high-density plasma (e.g., post-flare loops and active region moss). We find that upper transition region (TR; moss) Fe xii emission shows very small average Doppler redshifts (v_D ~ 3 km s−1) as well as modest non-thermal velocities (with an average of ~24 km s−1 and the peak of the distribution at ~15 km s−1). The observed distribution of Doppler shifts appears to be compatible with advanced three-dimensional radiative MHD simulations in which impulsive heating is concentrated at the TR footpoints of a hot corona. While the non-thermal broadening of Fe xii 1349.4 Å peaks at similar values as lower resolution simultaneous Hinode Extreme Ultraviolet Imaging Spectrometer (EIS) measurements of Fe xii195 Å, IRIS observations show a previously undetected tail of increased non-thermal broadening that might be suggestive of the presence of subarcsecond heating events. We find that IRIS andEIS non-thermal line broadening measurements are affected by instrumental effects that can only be removed through careful analysis. Our results also reveal an unexplained discrepancy between observed 195.1/1349.4 Å Fe xii intensity ratios and those predicted by the CHIANTI atomic database.

Evidence of Non-Thermal Particles in Coronal Loops Heated Impulsively by Nanoflares
Paola **Testa** (1), Bart De Pontieu (2,3), Joel Allred (4), Mats Carlsson (3), Fabio Reale (5), Adrian Daw (4), Viggo Hansteen (3), Juan Martinez-Sykora (6), Wei Liu (2,7), Ed DeLuca (1), Leon Golub (1), Sean McKillop (1), Kathy Reeves (1), Steve Saar (1), Hui Tian (1), Jim Lemen (2), Alan Title (2), Paul Boerner (2), Neal Hurlburt (2), Ted Tarbell (2), J.P. Wuelser (2), Lucia Kleint (2,6), Charles Kankelborg (8), Sarah Jaeggli (8)
Science, **2014**
Movies are available at: http://www.lmsal.com/~ptesta/iris_science_mov/
http://arxiv.org/pdf/1410.6130v1.pdf
The physical processes causing energy exchange between the Sun's hot corona and its cool lower atmosphere remain poorly understood. The chromosphere and transition region (TR) form an interface region between the surface and the corona that is highly sensitive to the coronal heating mechanism. High resolution observations with the Interface Region Imaging Spectrograph (IRIS) reveal rapid variability (about 20 to 60 seconds) of intensity and velocity on small spatial scales at the footpoints of hot dynamic coronal loops. The observations are consistent with numerical simulations of heating by beams of non-thermal electrons, which are generated in small impulsive heating events called "coronal nanoflares". The accelerated electrons deposit a sizable fraction of their energy in the chromosphere and TR. Our analysis provides tight constraints on the properties of such electron beams and new diagnostics for their presence in the nonflaring corona. 2013-11-09

OBSERVING CORONAL NANOFLARES IN ACTIVE REGION MOSS
Paola **Testa**1, Bart De Pontieu2, Juan Martínez-Sykora2,3, Ed DeLuca1, Viggo Hansteen4, Jonathan Cirtain5, Amy Winebarger5, Leon Golub1, Ken Kobayashi5, Kelly Korreck1, Sergey Kuzin6, Robert Walsh7, Craig DeForest8, Alan Title2, and Mark Webe
2013 ApJ 770 L1

The High-resolution Coronal Imager (Hi-C) has provided Fe XII 193Å images of the upper transition region moss at an unprecedented spatial (~0."3-0."4) and temporal (5.5 s) resolution. The Hi-C observations show in some moss regions variability on timescales down to ~15 s, significantly shorter than the minute-scale variability typically found in previous observations of moss, therefore challenging the conclusion of moss being heated in a mostly steady manner. These rapid variability moss regions are located at the footpoints of bright hot coronal loops observed by the Solar Dynamics Observatory/Atmospheric Imaging Assembly in the 94 Å channel, and by the Hinode/X-Ray Telescope. The configuration of these loops is highly dynamic, and suggestive of slipping reconnection. We interpret these events as signatures of heating events associated with reconnection occurring in the overlying hot coronal loops, i.e., coronal nanoflares. We estimate the order of magnitude of the energy in these events to be of at least a few 1023 erg, also supporting the nanoflare scenario. These Hi-C observations suggest that future observations at comparable high spatial and temporal resolution, with more extensive temperature coverage, are required to determine the exact characteristics of the heating mechanism(s).

HINODE/EIS SPECTROSCOPIC VALIDATION OF VERY HOT PLASMA IMAGED WITH THE SOLAR DYNAMICS OBSERVATORY IN NON-FLARING ACTIVE REGION CORES

Paola **Testa**1 and Fabio Reale

2012 ApJ 750 L10

We use coronal imaging observations with the Solar Dynamics Observatory/Atmospheric Imaging Assembly (AIA), and Hinode/Extreme-ultraviolet Imaging Spectrometer (EIS) spectral data to explore the potential of narrowband EUV imaging data for diagnosing the presence of hot (T 5 MK) coronal plasma in active regions. We analyze observations of two active regions (AR 11281, AR 11289) with simultaneous AIA imaging and EIS spectral data, including the Ca XVII line (at 192.8 Å), which is one of the few lines in the EIS spectral bands sensitive to hot coronal plasma even outside flares. After careful co-alignment of the imaging and spectral data, we compare the morphology in a three-color image combining the 171, 335, and 94 Å AIA spectral bands, with the image obtained for Ca XVII emission from the analysis of EIS spectra. We find that in the selected active regions the Ca XVII emission is strong only in very limited areas, showing striking similarities with the features bright in the 94 Å (and 335 Å) AIA channels and weak in the 171 Å band. We conclude that AIA imaging observations of the solar corona can be used to track hot plasma (6-8 MK), and so to study its spatial variability and temporal evolution at high spatial and temporal resolution.

TEMPERATURE DISTRIBUTION OF A NON-FLARING ACTIVE REGION FROM SIMULTANEOUS *HINODE* XRT AND EIS OBSERVATIONS

Paola **Testa**1, Fabio Reale2,3, Enrico Landi4, Edward E. DeLuca1, and Vinay Kashyap1

Astrophysical Journal, 728:30 (12pp), **2011**

We analyze coordinated *Hinode* X-ray Telescope (XRT) and Extreme Ultraviolet Imaging Spectrometer (EIS) observations of a non-flaring active region to investigate the thermal properties of coronal plasma taking advantage of the complementary diagnostics provided by the two instruments. In particular, we want to explore the presence of hot plasma in non-flaring regions. Independent temperature analyses from the XRT multi-filter data set, and the EIS spectra, including the instrument entire wavelength range, provide a cross-check of the different temperature diagnostics techniques applicable to broadband and spectral data, respectively, and insights into cross-calibration of the two instruments. The emission measure distributions, (EM(*T*)), we derive from the two data sets have similar width and peak temperature, but show a systematic shift of the absolute values, the EIS (EM(*T*)) being smaller than the XRT (EM(*T*)) by approximately a factor two. We explore possible causes of this discrepancy, and we discuss the influence of the assumptions for the plasma element abundances. Specifically, we find that the disagreement between the results from the two instruments is significantly mitigated by assuming chemical composition closer to the solar photospheric composition rather than the often adopted “coronal” composition.We find that the data do not provide conclusive evidence on the high temperature (log *T* (K) _ 6.5) tail of the plasma temperature distribution, however, suggesting its presence to a level in agreement with recent findings for other non-flaring regions.

On the reliability of relative helicities deduced from nonlinear force-free coronal models

Julia K. **Thalmann**, X. Sun, K. Moraitis, M. Gupta

A&A 643, A153 **2020**

https://arxiv.org/pdf/2009.05287.pdf

https://doi.org/10.1051/0004-6361/202038921

We study the relative helicity of active region (AR) NOAA~12673 during a ten-hour time interval centered around a preceding X2.2 flare (SOL**2017-09-06**T08:57) and also including an eruptive X9.3 flare that occurred three hours later (SOL**2017-09-06**T11:53). In particular, we aim for a reliable estimate of the normalized self-helicity of the current-carrying magnetic field, the so-called helicity ratio |HJ|/|HV|, a promising candidate to quantity the eruptive potential of solar ARs. Using SDO/HMI vector magnetic field data as an input, we employ nonlinear force-free (NLFF) coronal magnetic field models using an optimization approach. The corresponding relative helicity, and related quantities, are

computed using a finite-volume method. From multiple time series of NLFF models based on different choices of free model parameters, we are able to assess the spread of |HJ|/|HV|, and to estimate its uncertainty. In comparison to earlier works, we favor the non-solenoidal contribution to the free magnetic energy, |Emix|/EJ,s, as selection criterion regarding the required solenoidal quality of the NLFF models for subsequent relative helicity analysis. As a recipe for a reliable estimate of the relative magnetic helicity (and related quantities), we recommend to employ multiple NLFF model time series based on different combinations of free model parameters, to retain only those which satisfy $|Emix|/EJ,s \leq 0.2$ at a certain time instant, to subsequently compute mean estimates, and to use the spread of the individually contributing values as an indication for the uncertainty.

On the Factors Determining the Eruptive Character of Solar Flares

Julia K. **Thalmann**

Magnetic helicity budget of solar active regions prolific of eruptive and confined flares

J. K. **Thalmann**, K. Moraitis, L. Linan, E. Pariat, G. Valori, K. Dalmasse
ApJ **887** 64 **2019**
https://arxiv.org/pdf/1910.06563.pdf
https://doi.org/10.3847/1538-4357/ab4e15
We compare the coronal magnetic energy and helicity of two solar active regions (ARs), prolific in major eruptive (AR~11158) and confined (AR~12192) flaring, and analyze the potential of deduced proxies to forecast upcoming flares. Based on nonlinear force-free (NLFF) coronal magnetic field models with a high degree of solenoidality, and applying three different computational methods to investigate the coronal magnetic helicity, we are able to draw conclusions with a high level of confidence. Based on real observations of two solar ARs we checked trends regarding the potential eruptivity of the active-region corona, as suggested earlier in works that were based on numerical simulations, or solar observations. Our results support that the ratio of current-carrying to total helicity, |HJ|/|HV|, shows a strong ability to indicate the eruptive potential of a solar AR. However, |HJ|/|HV| seems not to be indicative for the magnitude or type of an upcoming flare (confined or eruptive). Interpreted in context with earlier observational studies, our findings furthermore support that the total relative helicity normalized to the magnetic flux at the NLFF model's lower boundary, HV/ϕ2, represents no indicator for the eruptivity. **2011 February 14, 2014 October 24**
HMI Science Nuggets #145 Oct 2020 http://hmi.stanford.edu/hminuggets/?p=3370

Temporal and spatial relationship of flare signatures and the force-free coronal magnetic field

Julia K. **Thalmann**, Astrid M. Veronig, Yang Su
ApJ **826** 143 **2016**
http://arxiv.org/pdf/1605.03703v1.pdf
We investigate the plasma and magnetic environment of active region NOAA 11261 on **2 August 2011** around a GOES M1.4 flare/CME (SOL2011-08-02T06:19). We compare coronal emission at (extreme) ultraviolet and X-ray wavelengths, using SDO AIA and RHESSI images, in order to identify the relative timing and locations of reconnection-related sources. We trace flare ribbon signatures at ultraviolet wavelengths, in order to pin down the intersection of previously reconnected flaring loops at the lower solar atmosphere. These locations are used to calculate field lines from 3D nonlinear force-free magnetic field models, established on the basis of SDO HMI photospheric vector magnetic field maps. With this procedure, we analyze the quasi-static time evolution of the coronal model magnetic field previously involved in magnetic reconnection. This allows us, for the first time, to estimate the elevation speed of the current sheet's lower tip during an on-disk observed flare, as a few kilometers per second. Comparison to post-flare loops observed later above the limb in STEREO EUVI images supports this velocity estimate. Furthermore, we provide evidence for an implosion of parts of the flaring coronal model magnetic field, and identify the corresponding coronal sub-volumes associated to the loss of magnetic energy. Finally, we spatially relate the build up of magnetic energy in the 3D models to highly sheared fields, established due to dynamic relative motions of polarity patches within the active region.
Хорошее Введение

Exceptions to the rule: the X-flares of AR 2192 Lacking Coronal Mass Ejections

Thalmann, J. K.; Su, Y.; Temmer, M.; Veronig, A. M.
Ground-based Solar Observations in the Space Instrumentation Era
ASP Conference Series, Vol. 504, p. 203, **2016**
http://aspbooks.org/publications/504/203.pdf
NOAA Active region (AR) 2192, that was present on the Sun in October 2014, was the largest region which occurred since November 1990 (see Figure 1). The huge size accompanied by a very high activity level, was quite unexpected as it appeared during the unusually weak solar cycle 24. Nevertheless, the AR turned out to be one of the most prolific flaring ARs of cycle 24. It produced in total 6 X, 29 M, 79 C flares during its disk passage from October 18-29, 2014

(see Figure 2). Surprisingly, all flares greater than GOES class M5 and X were confined, i.e. had no coronal mass ejections (CME) associated. All the flare events had some obvious similarity in morphology, as they were located in the core of the AR and revealed only minor separation motion away from the neutral line but a large initial separation of the conjugate flare ribbons. In the paper by Thalmann et al. (2015) we describe the series of flares and give details about the confined X1.6 flare event from October 22, 2014 as well as the single eruptive M4.0 flare event from October 24, 2014. The study of the X1.6 flare revealed a large initial separation of flare ribbons together with recurrent flare brightenings, which were related to two episodes of enhanced hard X-ray emission as derived from RHESSI observations. This suggests that magnetic field structures connected to specific regions were repeatedly involved in the process of reconnection and energy release. Opposite to the central location of the sequence of confined events within the AR, a single eruptive (M4.0) event occurred on the outskirt of the AR in the vicinity of open magnetic fields. Our investigations revealed a predominantly north-south oriented magnetic system of arcade fields overlying the AR that could have preserved the magnetic arcade to erupt, and consequently kept the energy release trapped in a localized volume of magnetic field high up in the corona (as supported by the absence of a lateral motion of the flare ribbons and the recurrent brightenings within them). We conclude that the background magnetic field configuration is an essential parameter for deriving the “eruptiveness” of flare events. Sun et al. (2015) supports this conclusion and derived for this AR a quite slow decay of the strength of the overlying magnetic field (decay index; see Török & Kliem 2005). Interestingly, our magnetic field modellings revealed no flux rope inherent to the AR, indicating that further investigations are needed. In a recent paper by Veronig $ Polanec (2015), who investigated in more detail the X-flares using also ground-based observations in Hα from Kanzelhöhe Observatory (Pötzi et al. 2015), it was shown that such confined events could be explained by the emerging-flux model, where newly emerging small flux tubes reconnect with pre-existing large coronal loops. **October 22, 2014, October 24, 2014**

The Exceptional Aspects of the Confined X-class Flares of Solar Active Region 2192

Julia K. **Thalmann**, Yang Su, Manuela Temmer, Astrid M. Veronig
Proceedings IAU Symposium No. S320, "Solar and Stellar Flares and Their Effects on Planets" **2016**
http://arxiv.org/pdf/1605.03712v1.pdf

During late October 2014, active region NOAA 2192 caused an unusual high level of solar activity, within an otherwise weak solar cycle. While crossing the solar disk, during a period of 11 days, it was the source of 114 flares of GOES class C1.0 and larger, including 29 M- and 6 X-flares. Surprisingly, none of the major flares (GOES class M5.0 and larger) was accompanied by a coronal mass ejection, contrary to statistical tendencies found in the past. From modeling the coronal magnetic field of NOAA 2192 and its surrounding, we suspect that the cause of the confined character of the flares is the strong surrounding and overlying large-scale magnetic field. Furthermore, we find evidence for multiple magnetic reconnection processes within a single flare, during which electrons were accelerated to unusual high energies. **October 22,23,24 2014**

The Confined X-class Flares of Solar Active Region 2192

J.K. **Thalmann**, Y. Su, M. Temmer, A. M. Veronig
ApJL **801** L23 **2015**
http://arxiv.org/pdf/1502.05157v1.pdf
The unusually large NOAA active region 2192, observed in **October 2014**, was outstanding in its productivity of major two-ribbon flares without coronal mass ejections. On a large scale, a predominantly north-south oriented magnetic system of arcade fields served as a strong, also lateral, confinement for a series of large two-ribbon flares originating from the core of the active region. The large initial separation of the flare ribbons, together with an almost absent growth in ribbon separation, suggests a confined reconnection site high up in the corona. Based on a detailed analysis of the confined X1.6 flare on October 22, we show how exceptional the flaring of this active region was. We provide evidence for repeated energy release, indicating that the same magnetic field structures were repeatedly involved in magnetic reconnection. We find that a large number of electrons was accelerated to non-thermal energies, revealing a steep power law spectrum, but that only a small fraction was accelerated to high energies. The total non-thermal energy in electrons derived (on the order of 10^25 J) is considerably higher than that in eruptive flares of class X1, and corresponds to about 10\% of the excess magnetic energy present in the active-region corona. **Oct 19 05:03 UT (X1.1), Oct 22 14:28 UT (X1.6), Oct 24 22:41 UT (X3.1), Oct 25 17:08 UT (X1.0), Oct 26 10:56 UT (X2.0), and Oct 27 14:47 UT (X2.0).**
Erratum: 2017 ***ApJL*** 844 L27 http://iopscience.iop.org/article/10.3847/2041-8213/aa7f6f/pdf

Forecasting Solar Flares by Data Assimilation in Sandpile Models

Christian **Thibeault**, Antoine Strugarek, Paul Charbonneau, Benoit Tremblay
Solar Phys. **297**, Article number: 125 **2022**
https://arxiv.org/pdf/2206.13583.pdf
https://doi.org/10.1007/s11207-022-02055-9

The prediction of solar flares is still a significant challenge in space weather research, with no techniques currently capable of producing reliable forecasts performing significantly above climatology. In this paper, we present a flare forecasting technique using data assimilation coupled with computationally inexpensive cellular automata called sandpile models. Our data assimilation algorithm uses the simulated annealing method to find an optimal initial condition that reproduces well an energy-release time series. We present and empirically analyze the predictive capabilities of three sandpile models, namely the Lu and Hamilton model (LH) and two deterministically-driven models (D). Despite their stochastic elements, we show that deterministically-driven models display temporal correlations between simulated events, a needed condition for data assimilation. We present our new data assimilation algorithm and demonstrate its success in assimilating synthetic observations produced by the avalanche models themselves. We then apply our method to GOES X-Ray time series for 11 active regions having generated multiple X-class flares in the course of their lifetime. We demonstrate that for such large flares, our data assimilation scheme substantially increases the success of ``All-Clear'' forecasts, as compared to model climatology.

A time dependent relation between EUV solar flare light-curves from lines with differing formation temperatures

Edward M.B. **Thiemann**, Francis G. Eparvier and Thomas N. Woods
J. Space Weather Space Clim. **2017**, 7, A36
https://www.swsc-journal.org/articles/swsc/pdf/2017/01/swsc170050.pdf
https://arxiv.org/pdf/1703.02995.pdf
Extreme ultraviolet (EUV) solar flare emissions evolve in time as the emitting plasma heats and then cools. Although accurately modeling this evolution has been historically difficult, especially for empirical relationships, it is important for understanding processes at the Sun, as well as for their influence on planetary atmospheres. With a goal to improve empirical flare models, a new simple empirical expression is derived to predict how cool emissions evolve based on the evolution of a hotter emission. This technique is initially developed by studying 12 flares in detail observed by the EUV variability experiment (EVE) onboard the Solar Dynamics Observatory (SDO). Then, over 1100 flares observed by EVE are analyzed to validate these relationships. The Cargill and Enthalpy Based Thermal Evolution of Loops (EBTEL) flare cooling models are used to show that this empirical relationship implies the energy radiated by a population of hotter formed ions is approximately proportional to the energy exciting a population of cooler formed ions emitting when the peak formation temperatures of the two lines are up to 72% of each other and above 2 MK. These results have practical implications for improving flare irradiance empirical modeling and for identifying key emission lines for future monitoring of flares for space weather operations; and also provide insight into the cooling processes of flare plasma. **26 March 2002, 14 Aug 2010, 8 March 2011, 15 May 2011, 22 Sept 2011, 2 Oct 2011, 5 March 2012, 7 May 2012, 9 May 2012, 11 May 2012, 17 May 2012, 5 July 2012, 11 Apr 2013**

Center-to-Limb Variability of Hot Coronal EUV Emissions During Solar Flares

Edward **Thiemann**, Phillip Chamberlin, Francis Eparvier, Luke Epp
Solar Phys. 293:19 **2018**
https://arxiv.org/ftp/arxiv/papers/1710/1710.02498.pdf
https://link.springer.com/content/pdf/10.1007%2Fs11207-018-1244-2.pdf
It is generally accepted that densities of quiet sun and active region plasma are sufficiently low to justify the optically thin approximation, and it is commonly used in the analysis of line emissions from plasma in the solar corona. However, densities of solar flare loops are substantially higher, compromising the optically thin approximation. This study begins with a radiative transfer model that uses typical solar flare densities and geometries to show that hot coronal emission lines are not generally optically thin. Further, the model demonstrates that the observed integrated line intensity should exhibit center-to-limb variability (CTLV), with flares observed near the limb being dimmer than those occurring near disk-center. The model predictions are validated with an analysis of nearly 300 flares observed by EVE on SDO that uses 6 lines, with peak formation temperatures between 8.9 and 15.8 MK, to show limb flares are systematically dimmer than disk-center flares. The data are then used to show that the electron column density along the line-of-sight typically increases by 4.44 x 1019 cm-2 for limb flares over the disk-center flare value. It is shown that CTLV of hot coronal emissions reduces the amount of ionizing radiation propagating into the solar system, and changes the relative intensities of lines and bands commonly used for spectral analysis.

RHESSI and General Relativity

Bill **Thompson** and Hugh Hudson
RHESSI Science Nuggets No. 260, Sept **2015**
http://sprg.ssl.berkeley.edu/~tohban/wiki/index.php/RHESSI_and_General_Relativity

Flare particle acceleration in the interaction of twisted coronal flux ropes

J. **Threlfall**, A. W. Hood, P. K. Browning
2018 A&A 611, A40
https://arxiv.org/pdf/1801.02907.pdf
The aim of this work is to investigate and characterise non-thermal particle behaviour in a three-dimensional (3D) magnetohydrodynamical (MHD) model of unstable multi-threaded flaring coronal loops. We have used a numerical scheme which solves the relativistic guiding centre approximation to study the motion of electrons and protons. The scheme uses snapshots from high resolution numerical MHD simulations of coronal loops containing two threads, where a single thread becomes unstable and (in one case) destabilises and merges with an additional thread. The particle responses to the reconnection and fragmentation in MHD simulations of two loop threads are examined in detail. We illustrate the role played by uniform background resistivity and distinguish this from the role of anomalous resistivity using orbits in an MHD simulation where only one thread becomes unstable without destabilising further loop threads. We examine the (scalable) orbit energy gains and final positions recovered at different stages of a second MHD simulation wherein a secondary loop thread is destabilised by (and merges with) the first thread. We compare these results with other theoretical particle acceleration models in the context of observed energetic particle populations during solar flares.

Particle Acceleration Due to Coronal Non-null Magnetic Reconnection

James **Threlfall**, Thomas Neukirch, Clare Elizabeth Parnell
Solar Physics March **2017**, 292:45
Various topological features, for example magnetic null points and separators, have been inferred as likely sites of magnetic reconnection and particle acceleration in the solar atmosphere. In fact, magnetic reconnection is not constrained to solely take place at or near such topological features and may also take place in the absence of such features. Studies of particle acceleration using non-topological reconnection experiments embedded in the solar atmosphere are uncommon. We aim to investigate and characterise particle behaviour in a model of magnetic reconnection which causes an arcade of solar coronal magnetic field to twist and form an erupting flux rope, crucially in the absence of any common topological features where reconnection is often thought to occur. We use a numerical scheme that evolves the gyro-averaged orbit equations of single electrons and protons in time and space, and simulate the gyromotion of particles in a fully analytical global field model. We observe and discuss how the magnetic and electric fields of the model and the initial conditions of each orbit may lead to acceleration of protons and electrons up to 2 MeV in energy (depending on model parameters). We describe the morphology of time-dependent acceleration and impact sites for each particle species and compare our findings to those recovered by topologically based studies of three-dimensional (3D) reconnection and particle acceleration. We also broadly compare aspects of our findings to general observational features typically seen during two-ribbon flare events.

Particle dynamics in a non-flaring solar active region model

J. **Threlfall**, Ph.-A. Bourdin, T. Neukirch, C. E. Parnell
A&A 587, A4 **2016**
http://arxiv.org/pdf/1510.04211v1.pdf
The aim of this work is to investigate and characterise particle behaviour in a (observationally-driven) 3D MHD model of the solar atmosphere above a slowly evolving, non-flaring active region. We use a relativistic guiding-centre particle code to investigate particle acceleration in a single snapshot of the 3D MHD simulation. Despite the lack of flare-like behaviour in the active region, direct acceleration of electrons and protons to non-thermal energies ($\lesssim$420MeV) was found, yielding spectra with high-energy tails which conform to a power law. Examples of particle dynamics, including particle trapping caused by local electric rather than magnetic field effects, are observed and discussed, together with implications for future experiments which simulate non-flaring active region heating and reconnection. **14th Nov 2007**
See UKSP Nuggets #72, Sept **2016**
http://www.uksolphys.org/uksp-nugget/72-particle-dynamics-in-a-non-flaring-solar-active-region-model/

Particle acceleration at reconnecting separator current layers

J. **Threlfall**, J. E. H. Stevenson, C. E. Parnell, T. Neukirch
A&A 585, A95 (**2016**)
http://arxiv.org/pdf/1510.04215v1.pdf
The aim of this work is to investigate and characterise particle behaviour in a 3D MHD model of a reconnecting magnetic separator. We use a relativistic guiding-centre test-particle code to investigate electron and proton acceleration in snapshots from 3D MHD separator reconnection experiments, and compare the results with findings from an analytical separator reconnection model studied in a previous investigation. The behaviour (and acceleration) of large distributions of particles are examined in detail for both analytical and numerical separator reconnection models. Differences in acceleration sites are recovered and discussed, together with the dependence of final particle energy ranges upon the dimensions of the models and the stage of the (time-dependent) MHD reconnection event. We discuss the implications of these results for observed magnetic separators in the solar corona.

Particle acceleration at a reconnecting magnetic separator

J. **Threlfall**, T. Neukirch, C. E. Parnell, S. Eradat Oskoui
A&A 574, A7 (**2015**)
http://arxiv.org/pdf/1410.6465v1.pdf

While the exact acceleration mechanism of energetic particles during solar flares is (as yet) unknown, magnetic reconnection plays a key role both in the release of stored magnetic energy of the solar corona and the magnetic restructuring during a flare. Recent work has shown that special field lines, called separators, are common sites of reconnection in 3D numerical experiments. To date, 3D separator reconnection sites have received little attention as particle accelerators. We investigate the effectiveness of separator reconnection as a particle acceleration mechanism for electrons and protons. We study the particle acceleration using a relativistic guiding-centre particle code in a time-dependent kinematic model of magnetic reconnection at a separator. The effect upon particle behaviour of initial position, pitch angle and initial kinetic energy are examined in detail, both for specific (single) particle examples and for large distributions of initial conditions. The separator reconnection model contains several free parameters and we study the effect of changing these parameters upon particle acceleration, in particular in view of the final particle energy ranges which agree with observed energy spectra.

First comparison of wave observations from CoMP and AIA/SDO

J. **Threlfall**1, I. De Moortel1, S. W. McIntosh2 and C. Bethge
A&A 556, A124 (**2013**)

Context. Waves have long been thought to contribute to the heating of the solar corona and the generation of the solar wind. Recent observations have demonstrated evidence of quasi-periodic longitudinal disturbances and ubiquitous transverse wave propagation in many different coronal environments.
Aims. This paper investigates signatures of different types of oscillatory behaviour, both above the solar limb and on-disk, by comparing findings from the Coronal Multi-channel Polarimeter (CoMP) and the Atmospheric Imaging Assembly (AIA) on-board the Solar Dynamics Observatory (SDO) for the same active region.
Methods. We study both transverse and longitudinal motion by comparing and contrasting time-distance images of parallel and perpendicular cuts along/across active region fan loops. Comparisons between parallel space-time diagram features in CoMP Doppler velocity and transverse oscillations in AIA images are made, together with space-time analysis of propagating quasi-periodic intensity features seen near the base of loops in AIA.
Results. Signatures of transverse motions are observed along the same magnetic structure using CoMP Doppler velocity (vphase = 600 → 750 km s-1, P = 3 → 6 min) and in AIA/SDO above the limb (P = 3 → 8 min). Quasi-periodic intensity features (vphase = 100 → 200 km s-1, P = 6 → 11 min) also travel along the base of the same structure. On the disk, signatures of both transverse and longitudinal intensity features were observed by AIA, and both show similar properties to signatures found along structures anchored in the same active region three days earlier above the limb. Correlated features are recovered by space-time analysis of neighbouring tracks over perpendicular distances of ≲2.6 Mm.

Nonlinear wave propagation and reconnection at magnetic X-points in the Hall MHD regime

J. **Threlfall**1, C. E. Parnell1, I. De Moortel1, K. G. McClements2 and T. D. Arber
A&A 544, A24 (**2012**)

Context. The highly dynamical, complex nature of the solar atmosphere naturally implies the presence of waves in a topologically varied magnetic environment. Here, the interaction of waves with topological features such as null points is inevitable and potentially important for energetics. The low resistivity of the solar coronal plasma implies that non-magnetohydrodynamic (MHD) effects should be considered in studies of magnetic energy release in this environment.
Aims. This paper investigates the role of the Hall term in the propagation and dissipation of waves, their interaction with 2D magnetic X-points and the nature of the resulting reconnection.
Methods. A Lagrangian remap shock-capturing code (Lare2d) was used to study the evolution of an initial fast magnetoacoustic wave annulus for a range of values of the ion skin depth (δi) in resistive Hall MHD. A magnetic null-point finding algorithm was also used to locate and track the evolution of the multiple null-points that are formed in the system.
Results. Depending on the ratio of ion skin depth to system size, our model demonstrates that Hall effects can play a key role in the wave-null interaction. In particular, the initial fast-wave pulse now consists of whistler and ion-cyclotron components; the dispersive nature of the whistler wave leads to (i) earlier interaction with the null; (ii) the creation of multiple additional, transient nulls and, hence, an increased number of energy release sites. In the Hall regime, the relevant timescales (such as the onset of reconnection and the period of the oscillatory relaxation) of the system are reduced significantly, and the reconnection rate is enhanced.

Implosive Collapse about Magnetic Null Points: A Quantitative Comparison between 2D and 3D Nulls

Jonathan O. **Thurgood**1,2, David I. Pontin1, and James A. McLaughlin2

2018 ApJ 855 50
http://iopscience.iop.org/article/10.3847/1538-4357/aab0a0/pdf
Null collapse is an implosive process whereby MHD waves focus their energy in the vicinity of a null point, forming a current sheet and initiating magnetic reconnection. We consider, for the first time, the case of collapsing 3D magnetic null points in nonlinear, resistive MHD using numerical simulation, exploring key physical aspects of the system as well as performing a detailed parameter study. We find that within a particular plane containing the 3D null, the plasma and current density enhancements resulting from the collapse are quantitatively and qualitatively as per the 2D case in both the linear and nonlinear collapse regimes. However, the scaling with resistivity of the 3D reconnection rate—which is a global quantity—is found to be less favorable when the magnetic null point is more rotationally symmetric, due to the action of increased magnetic back-pressure. Furthermore, we find that, with increasing ambient plasma pressure, the collapse can be throttled, as is the case for 2D nulls. We discuss this pressure-limiting in the context of fast reconnection in the solar atmosphere and suggest mechanisms by which it may be overcome. We also discuss the implications of the results in the context of null collapse as a trigger mechanism of Oscillatory Reconnection, a time-dependent reconnection mechanism, and also within the wider subject of wave–null point interactions. We conclude that, in general, increasingly rotationally asymmetric nulls will be more favorable in terms of magnetic energy release via null collapse than their more symmetric counterparts.
UKSP Nuggets #92 July **2018** www.uksolphys.org/?p=14413

Three-dimensional oscillatory magnetic reconnection

J.O. **Thurgood**, D.I. Pontin, J.A. McLaughlin
ApJ **2017**
https://arxiv.org/pdf/1706.09662.pdf
Here we detail the dynamic evolution of localised reconnection regions about three-dimensional (3D) magnetic null points by using numerical simulation. We demonstrate for the first time that reconnection triggered by the localised collapse of a 3D null point due to an external MHD wave involves a self-generated oscillation, whereby the current sheet and outflow jets undergo a reconnection reversal process during which back-pressure formation at the jet heads acts to prise open the collapsed field before overshooting the equilibrium into an opposite-polarity configuration. The discovery that reconnection at fully 3D nulls can proceed naturally in a time-dependent and periodic fashion is suggestive that oscillatory reconnection mechanisms may play a role in explaining periodicity in astrophysical phenomena associated with magnetic reconnection, such as the observed quasi-periodicity of solar and stellar flare emission. Furthermore, we find a consequence of oscillatory reconnection is the generation of a plethora of freely-propagating MHD waves which escape the vicinity of the reconnection region

Evaluation of different recipes for chromospheric radiative losses in solar flares

J.**Tian**, J.Hong, Y.Li, M.D.Ding
A&A 668, A96 **2022**
https://arxiv.org/pdf/2210.04461
https://www.aanda.org/articles/aa/pdf/2022/12/aa44615-22.pdf
Context. Radiative losses are an indispensable part in the numerical simulation of flares. Detailed calculations could be computationally expensive, especially in the chromosphere. There have been some approximate recipes for chromospheric radiative losses in flares, yet their feasibility in flare simulations needs further evaluation.
Aims. We aim to evaluate the performance of different recipes for chromospheric radiative losses in flare simulations.
Methods. We compare the atmospheric structure and line profiles in beam-heated flares calculated with detailed radiative losses and the approximate recipes.
Results. Both GF90 and HCD22 recipes provide acceptable total radiative losses compared with detailed one, but there are discrepancies in the different atmospheric layers during the different evolutionary phases, which leads to misestimations of temperature and line intensity. The recipe of GF90 overestimates the coolings in the upper chromosphere greatly when temperature exceeds 10^5 K, which also affects the flare evolution and line asymmetries. Radiative heating in the middle chromosphere only functions in the initial stage and could be safely neglected. However, radiative heating from Lyman continuum could dominate near the transition region.

Multi-episode Chromospheric Evaporation Observed in a Solar Flare

H. **Tian**1 and N.-H. Chen
2018 ApJ 856 34 10.3847/1538-4357/aab15a
With observations of the Interface Region Imaging Spectrograph (IRIS), we study chromospheric heating and evaporation during an M1.6 flare SOL**2015-03-12**T11:50. At the flare ribbons, the Mgii 2791.59 Å line shows quasi-periodic short-duration red-wing enhancement, which is likely related to repetitive chromospheric condensation as a result of episodic heating. On the contrary, the Si iv 1402.77 Å line reveals a persistent red-wing asymmetry in both the impulsive and decay phases, suggesting that this line responds to both cooling downflows and chromospheric

condensation. The first two episodes of red-wing enhancement occurred around 11:42 UT and 11:45 UT, when two moving brightenings indicative of heating fronts crossed the IRIS slit. The greatly enhanced red wings of the Si iv and Mg ii lines at these occasions are accompanied by an obvious increase in the line intensities and the HXR flux, suggesting two episodes of energy injection into the lower atmosphere in the form of nonthermal electrons. The Mg ii k/h ratio has a small value of ~1.2 at the ribbons and decreases to ~1.1 at these two occasions. Correspondingly, the Fe xxi 1354 Å line reveals two episodes of chromospheric evaporation, which is characterized as a smooth decrease of the blueshift from ~300 km s−1 to nearly zero within ~3 minutes. The Fexxi 1354 Å line is entirely blueshifted in the first episode, while it appears to contain a nearly stationary component and a blueshifted component in the second episode. Additional episodes of blueshifted Fe xxi emission are found around the northern ribbon in the decay phase, though no obvious response is detected in the Si iv and Mg ii emission. We have also examined the Fe xxiemission at the flare loop top and identified a secondary component with a ~200 km s−1 redshift, which possibly results from the downward moving reconnection outflow. Our analysis also yields a rest wavelength of 1354.0878 ± 0.0072 Å for this Fe xxi line.

Magnetic reconnection at the earliest stage of solar flux emergence

Hui **Tian**, Xiaoshuai Zhu, Hardi Peter, Jie Zhao, Tanmoy Samanta, Yajie Chen

ApJ 854 174 **2018**

https://arxiv.org/pdf/1801.06785.pdf

http://sci-hub.tw/http://iopscience.iop.org/0004-637X/854/2/174/

On **2016 September 20**, the Interface Region Imaging Spectrograph observed an active region during its earliest emerging phase for almost 7 hours. The Helioseismic and Magnetic Imager on board the Solar Dynamics Observatory observed continuous emergence of small-scale magnetic bipoles with a rate of ~1016Mx~s−1. The emergence of magnetic fluxes and interactions between different polarities lead to frequent occurrence of ultraviolet (UV) bursts, which exhibit as intense transient brightenings in the 1400 \AA{} images. In the meantime, discrete small patches with the same magnetic polarity tend to move together and merge, leading to enhancement of the magnetic fields and thus formation of pores (small sunspots) at some locations. The spectra of these UV bursts are characterized by the superposition of several chromospheric absorption lines on the greatly broadened profiles of some emission lines formed at typical transition region temperatures, suggesting heating of the local materials to a few tens of thousands of kelvin in the lower atmosphere by magnetic reconnection. Some bursts reveal blue and red shifts of ~100~km~s−1 at neighboring pixels, indicating the spatially resolved bidirectional reconnection outflows. Many such bursts appear to be associated with the cancellation of magnetic fluxes with a rate of the order of ~1015 Mx~s−1. We also investigate the three-dimensional magnetic field topology through a magneto-hydrostatic model and find that a small fraction of the bursts are associated with bald patches (magnetic dips). Finally, we find that almost all bursts are located in regions of large squashing factor at the height of ~1 Mm, reinforcing our conclusion that these bursts are produced through reconnection in the lower atmosphere.

HMI Science Nuggets #87 Feb **2018** http://hmi.stanford.edu/hminuggets/?p=2275

Multi-episode chromospheric evaporation observed in a solar flare

H. **Tian**, N.-H. Chen

ApJ **2018**

https://arxiv.org/pdf/1801.04370.pdf

With observations of IRIS, we study chromospheric heating and evaporation during an M1.6 flare SOL**2015-03-12**T11:50. At the flare ribbons, the Mg II 2791.59 line shows quasi-periodic short-duration red-wing enhancement, which is likely related to repetitive chromospheric condensation as a result of episodic heating. On the contrary, the Si IV 1402.77 line reveals a persistent red-wing asymmetry in both the impulsive and decay phases, suggesting that this line responds to both cooling downflows and chromospheric condensation. The first two episodes of red-wing enhancement occurred around 11:42 UT and 11:45 UT, when two moving brightenings indicative of heating fronts crossed the IRIS slit. The greatly enhanced red wings of the Si IV and Mg II lines at these occasions are accompanied by an obvious increase in the line intensities and the HXR flux, suggesting two episodes of energy injection into the lower atmosphere in the form of nonthermal electrons. The Mg II k/h ratio has a small value of ~1.2 at the ribbons and decreases to ~1.1 at these two occasions. Correspondingly, the Fe XXI 1354 line reveals two episodes of chromospheric evaporation, which is characterized as a smooth decrease of the blue shift from ~300 km/s to nearly zero within ~3 minutes. The Fe XXI 1354 line is entirely blueshifted in the first episode, while appears to contain a nearly stationary component and a blueshifted component in the second episode. More episodes of blueshifted Fe XXI emission is found around the northern ribbon in the decay phase, though no obvious response is detected in the Si IV and Mg II emission. We have also examined the Fe XXI emission at the flare loop top and identified a secondary component with a ~200 km/s red shift, which possibly results from the downward moving reconnection outflow. Our analysis also suggests a reference wavelength of 1354.0878 Angstrom for this Fe XXI line.

Global sausage oscillation of solar flare loops detected by the Interface Region Imaging Spectrograph

Hui **Tian**, Peter R. Young, Katharine K. Reeves, Tongjiang Wang, Patrick Antolin, Bin Chen, Jiansen He
ApJL 823 L16 **2016**

An observation from the Interface Region Imaging Spectrograph reveals coherent oscillations in the loops of an M1.6 flare on **2015 March 12**. Both the intensity and Doppler shift of Fe~{\sc{xxi}}~1354.08\AA{}~show clear oscillations with a period of ~25 seconds. Remarkably similar oscillations were also detected in the soft X-ray flux recorded by the Geostationary Operational Environmental Satellites (GOES). With an estimated phase speed of ~2420~km~s−1 and a derived electron density of at least 5.4×1010 cm−3, the observed short-period oscillation is most likely the global fast sausage mode of a hot flare loop. We find a phase shift of ~π/2 (1/4 period) between the Doppler shift oscillation and the intensity/GOES oscillations, which is consistent with a recent forward modeling study of the sausage mode. The observed oscillation requires a density contrast between the flare loop and coronal background of a factor ⩾42. The estimated phase speed of the global mode provides an lower limit of the Alfv\'en speed outside the flare loop. We also find an increase of the oscillation period, which might be caused by the separation of the loop footpoints with time.

Temporal evolution of chromospheric evaporation: case studies of the M1.1 flare on 2014 September 6 and X1.6 flare on 2014 September 10

Hui **Tian**, Peter R. Young, Katharine K. Reeves, Bin Chen, Wei Liu, Sean McKillop
ApJ 811 139 **2015**
http://arxiv.org/pdf/1505.02736v1.pdf

Observations from IRIS allow us to study the chromospheric heating and evaporation processes during solar flares with unprecedented high resolution and high cadence. We track the complete evolution of ~11 MK evaporation flows in the M1.1 flare on **2014 September 6 and the X1.6 flare on 2014 September 10**. These hot flows, as indicated by the entirely blueshifted Fe xxi 1354.08 emission line, evolve smoothly with a velocity decreasing from ~200 km/s to almost stationary within a few minutes. The velocity decrease appears to be exponential in time, especially for the X1.6 flare. There is a good correlation between the flow velocity and the energy deposition rate as represented by the RHESSI hard X-Ray flux, or the time derivative of the soft X-Ray flux observed by GOES and the HINODE/XRT, which is in general agreement with models of nonthermal electron heating. The maximum blue shift of Fe xxi appears approximately at the same time as or slightly after the impulsive enhancement of the UV continuum and the Mg ii 2798.8 line emission, demonstrating that the hot evaporation flow is closely related to heating of the lower chromosphere. In the M1.1 flare, the maximum Fe XXI blue shift, the peaks of RHESSI hard X-Ray flux and the time derivative of GOES flux occur at roughly the same time. In the X1.6 flare, the maximum blue shift is found slightly before the peak time of the soft X-Ray derivative, a result that is qualitatively consistent with a recent radiative hydrodynamic simulation (RADYN) of chromospheric evaporation. Finally, while the hot Fe xxi 1354.08 line is entirely blueshifted with no obvious rest component, cool chromospheric and transition region lines like Si iv 1402.77 are often not entirely redshifted but just reveal an obvious enhancement in the red wing of the line profiles at the flare ribbons, suggesting a faster speed of chromospheric condensation than previously thought.

Imaging and spectroscopic observations of magnetic reconnection and chromospheric evaporation in a solar flare

Hui **Tian**, Gang Li, Katharine K. Reeves, John C. Raymond, Fan Guo, Wei Liu, Bin Chen, Nicholas A. Murphy
ApJL **797** 88 **2014**
http://arxiv.org/pdf/1411.2301v1.pdf

Magnetic reconnection is believed to be the dominant energy release mechanism in solar flares. The standard flare model predicts both downward and upward outflow plasmas with speeds close to the coronal Alfv\'{e}n speed. Yet, spectroscopic observations of such outflows, especially the downflows, are extremely rare. With observations of the newly launched Interface Region Imaging Spectrograph (IRIS), we report the detection of greatly redshifted (~125 km s-1 along line of ight) Fe {\sc{xxi}} 1354.08\AA{} emission line with a ~100 km s−1 nonthermal width at the reconnection site of a flare. The redshifted Fe {\sc{xxi}} feature coincides spatially with the loop-top X-Ray source observed by the Reuven Ramaty High Energy Solar Spectroscopic Imager (RHESSI). We interpret this large redshift as the signature of downward-moving reconnection outflow/hot retracting loops. Imaging observations from both IRIS and the Atmospheric Imaging Assembly (AIA) onboard the Solar Dynamics Observatory (SDO) also reveal the eruption and reconnection processes. Fast downward-propagating blobs along these loops are also found from cool emission lines (e.g., Si {\sc{iv}}, O {\sc{iv}}, C {\sc{ii}}, Mg {\sc{ii}}) and images of AIA and IRIS. Furthermore, the entire Fe {\sc{xxi}} line is blueshifted by ~260 km s−1 at the loop footpoints, where the cool lines mentioned above all exhibit obvious redshift, a result that is consistent with the scenario of chromospheric evaporation induced by downward-propagating nonthermal electrons from the reconnection site. **2014 April 19.**

THE SPECTROSCOPIC SIGNATURE OF QUASI-PERIODIC UPFLOWS IN ACTIVE REGION TIMESERIES

Hui **Tian**1, Scott W. McIntosh1 and Bart De Pontieu

2011 ApJ 727 L37

Quasi-periodic propagating disturbances are frequently observed in coronal intensity image sequences. These disturbances have historically been interpreted as being the signature of slow-mode magnetoacoustic waves propagating into the corona. The detailed analysis of Hinode EUV Imaging Spectrometer (EIS) timeseries observations of an active region (known to contain propagating disturbances) shows strongly correlated, quasi-periodic, oscillations in intensity, Doppler shift, and line width. No frequency doubling is visible in the latter. The enhancements in the moments of the line profile are generally accompanied by a faint, quasi-periodically occurring, excess emission at ~100 km s–1 in the blue wing of coronal emission lines. The correspondence of quasi-periodic excess wing emission and the moments of the line profile indicates that repetitive high-velocity upflows are responsible for the oscillatory behavior observed. Furthermore, we show that the same quasi-periodic upflows can be directly identified in a simultaneous image sequence obtained by the Hinode X-Ray Telescope. These results are consistent with the recent assertion of De Pontieu & McIntosh that the wave interpretation of the data is not unique. Indeed, given that several instances are seen to propagate along the direction of the EIS slit that clearly shows in-phase, quasi-periodic variations of intensity, velocity, width (without frequency doubling), and blue wing enhanced emission, this data set would appear to provide a compelling example that upflows are more likely to be the main cause of the quasi-periodicities observed here, as such correspondences are hard to reconcile in the wave paradigm.

ON ASYMMETRY OF MAGNETIC HELICITY IN EMERGING ACTIVE REGIONS: HIGH-RESOLUTION OBSERVATIONS

Lirong **Tian**1, Pascal D´emoulin2, David Alexander1, and Chunming Zhu1

Astrophysical Journal, 727:28 (13pp), **2011** January

We employ the DAVE (differential affine velocity estimator) tracking technique on a time series of Michelson Doppler Imager (MDI)/1 minute high spatial resolution line-of-sight magnetograms to measure the photospheric flow velocity for three newly emerging bipolar active regions (ARs). We separately calculate the magnetic helicity injection rate of the leading and following polarities to confirm or refute the magnetic helicity asymmetry, found by Tian & Alexander using MDI/96 minute low spatial resolution magnetograms. Our results demonstrate that the magnetic helicity asymmetry is robust, being present in the three ARs studied, two of which have an observed balance of the magnetic flux. The magnetic helicity injection rate measured is found to depend little on the window size selected, but does depend on the time interval used between the two successive magnetograms being tracked. It is found that the measurement of the magnetic helicity injection rate performs well for a window size between 12 ↳ 10 and 18 ↳ 15 pixels and at a time interval ⊗*t* = 10 minutes. Moreover, the short-lived magnetic structures, 10–60 minutes, are found to contribute 30%–50% of themagnetic helicity injection rate. Comparing with the results calculated by MDI/96 minute data, we find that the MDI/96 minute data, in general, can outline the main trend of the magnetic properties, but they significantly underestimate the magnetic flux in strong field regions and are not appropriate for quantitative tracking studies, so provide a poor estimate of the amount of magnetic helicity injected into the corona.

On Asymmetry of Magnetic Helicity in Emerging Active Regions: High Resolution Observations

Lirong **Tian**, Pascal Demoulin, David Alexander, Chunming Zhu

E-print Oct **2010**, ApJ

We employ the DAVE (differential affine velocity estimator, Schuck 2005; 2006) tracking technique on a time series of MDI/1m high spatial resolution line-of-sight manetograms to measure the photospheric flow velocity for three newly emerging bipolar active regions. We separately calculate the magnetic helicity injection rate of the leading and following polarities to confirm or refute the magnetic helicity asymmetry, found by Tian & Alexander (2009) using MDI/96m low spatial resolution magnetograms. Our results demonstrate that the magnetic helicity asymmetry is robust being present in the three active regions studied, two of which have an observed balance of the magnetic flux. The magnetic helicity injection rate measured is found to depend little on the window size selected, but does depend on the time interval used between the two successive magnetograms tracked. It is found that the measurement of the magnetic helicity injection rate performs well for a window size between 12X10 and 18X15 pixels, and at a time interval Δt=10 minutes. Moreover, the short-lived magnetic structures, 10-60 minutes, are found to contribute 30-50% of the magnetic helicity injection rate. Comparing with the results calculated by MDI/96m data, we find that the MDI/96m data, in general, can outline the main trend of the magnetic properties, but they significantly underestimate the magnetic flux in strong field region and are not appropriate for quantitative tracking studies, so provide a poor estimate of the amount of magnetic helicity injected into the corona.

ASYMMETRY OF HELICITY INJECTION FLUX IN EMERGING ACTIVE REGIONS
Lirong **Tian** and David Alexander
Astrophysical Journal, 695:1012–1023, **2009** April
http://www.iop.org/EJ/toc/-alert=43190/0004-637X/695/2
Observational and modeling results indicate that typically the leading magnetic field of bipolar active regions (ARs) is often spatially more compact,while more dispersed and fragmented in following polarity. In this paper,we address the origin of this morphological asymmetry, which is not well understood. Although it may be assumed that, in an emerging ∧-shaped flux tube, those portions of the flux tube in which the magnetic field has a higher twist may maintain its coherence more readily, this has not been tested observationally. To assess this possibility, it is important to characterize the nature of the fragmentation and asymmetry in solar ARs and this provides the motivation for this paper. We separately calculate the distribution of the helicity flux injected in the leading and following polarities of 15 emerging bipolar ARs, using the Michelson Doppler Image 96 minute line-of-sight magnetograms and a local correlation tracking technique. We find from this statistical study that the leading (compact) polarity injects several times more helicity flux than the following (fragmented) one (typically 3–10 times). This result suggests that the leading polarity of the ∧-shaped flux tube possesses a much larger amount of twist than the following field prior to emergence. We argue that the helicity asymmetry between the leading and following magnetic field for the ARs studied here results in the observed magnetic field asymmetry of the two polarities due to an imbalance in the magnetic tension of the emerging flux tube. We suggest that the observed imbalance in the helicity distribution results from a difference in the speed of emergence between the leading and following legs of an inclined ∧-shaped flux tube. In addition, there is also the effect of magnetic flux imbalance between the two polarities with the fragmented following polarity displaying spatial fluctuation in both the magnitude and sign of helicity measured.

Origins of coronal energy and helicity in NOAA 10030

Lirong **Tian**1, David Alexander1, and Richard Nightingale2
E-print, April 2008; ApJ, 684:747-756, **2008**
http://www.journals.uchicago.edu/doi/pdf/10.1086/590234
Exploring the origins of coronal helicity and energy, as well as determining the mechanisms that lead to coronal energy release, are fundamental topics in solar physics. Using MDI/96 minute line-of-sight and HSOS vector magnetograms in conjunction with TRACE white light and UV (1600 AA) images and BBSO/H_alpha and SOHO/EIT (195 AA), we find in active region NOAA 10030 that a large positive polarity sunspot, located in the center of the region, exhibited significant counter-clockwise rotation, which continued for six days during the period, **July 12-18, 2002**. This rotating sunspot was related to the formation of inverse-S-shaped filaments, left-handed twist of the vector magnetic fields, and the production of strong negative vertical current, but exhibited little emergence of magnetic flux. In all, five M-class and two X-class flares were produced around this rotating sunspot over the six day period. The observed characteristics of the strongly rotating sunspot suggest that sunspots can undergo strong intrinsic rotation, the source of which may originate below the photosphere and can play a significant role in helicity production and injection and energy buildup in the corona. A sunspot with negative magnetic polarity showed fast and significant emergence in the eastern portion of the active region, and moved north-eastward over several days, but exhibited little rotation. The moving sunspot also exhibited the formation of inverse-S-shaped filaments, left-handed twist of vector magnetic fields and coronal structure, and the production of stronger positive current. The observed characteristics of the emerging sunspot suggest that significant emergence of twisted magnetic fields may not always result in the rotation of the associated sunspots, but do play also a very important role in the coronal helicity accumulation and free-energy build-up.

What is the Most Important Origin of the Coronal Helicity?

Lirong **Tian**
Subsurface and Atmospheric Influences on Solar Activity
ASP Conference Series, Vol. 383, c **2008**
R. Howe, R. W. Komm, K. S. Balasubramaniam, and G. J. D. Petrie, eds.
http://spacibm.rice.edu/~alicetlr/publications/2008b.pdf
23 active regions (ARs) with well-defined SXR sigmoids are selected to study what is the most important origin of the coronal helicity--the emergence of magnetic fields or the photospheric horizontal motions. The redial magnetic flux of each polarity, the helicity injection rate, and total helicity flux (Delta H_{lct}) are calculated using local correlation tracking technique and MDI 96m line-of-sight magnetograms, and the helicity budget of the differential rotation (Delta H_{rot}) is also extimated. It is found that six ARs inject helicity flux greater than 10^{43} Mx^2,(Delta H =Delta H_{lct}-Delta H_{rot}), in a sample of seven ARs with emerging magnetic flux greater than 10^{22} Mx. On the other hand, in sixteen ARs with emerging magnetic flux less than 10^{22} Mx, only 4 ARs injected the helicity flux greater than 10^{43} Mx^2, which denotes the main comtribution of the horizontal motions. The statitical results suggest that the horizontal motions are not important to the coronal helicity injection when there is little magnetic field emergence.

ON THE ORIGIN OF MAGNETIC HELICITY IN THE SOLAR CORONA
Lirong **Tian** and David Alexander
The Astrophysical Journal, 673:532-543, **2008**
http://www.journals.uchicago.edu/doi/pdf/10.1086/524129
Twenty-three active regions associated with pronounced sigmoidal structure in Yohkoh soft X-ray observations are selected to investigate the origin of magnetic helicity in the solar corona.
These statistical results signify that the strong emergence of magnetic field is the most important origin of the coronal helicity, while horizontal motions and differential rotation are insufficient to explain the measured helicity injection flux. Furthermore, the study of the helicity injection in nineteen newly emerging active regions confirms the result on the important role played by strong magnetic flux emergence in controlling the injection of magnetic helicity into the solar corona.

1997 MAY 12 CORONAL MASS EJECTION EVENT.
I. A SIMPLIFIED MODEL OF THE PREERUPTIVE MAGNETIC STRUCTURE
V. S. **Titov**, Z. Mikic, J. A. Linker, and R. Lionello
http://www.journals.uchicago.edu/doi/pdf/10.1086/527280
The Astrophysical Journal, 675:1614Y1628, 2008 March 10
A simple model of the coronal magnetic field prior to the coronal mass ejection (CME) eruption on 1997May 12 is developed. First, the magnetic field is constructed by superimposing a large-scale background field and a localized bipolar field to model the active region (AR) in the current-free approximation. Second, this potential configuration is quasi-statically sheared by photospheric vortex motions applied to two flux concentrations of the AR. Third, the resulting force-free field is then evolved by canceling the photospheric magnetic flux with the help of an appropriate tangential electric field applied to the central part of the AR. To understand the structure of the modeled configuration, we use the field linemapping technique by generalizing it to spherical geometry.We demonstrate that the initial potential configuration contains a hyperbolic flux tube (HFT) which is a union of two intersecting quasi-separatrix layers. This HFT provides a partition of the closed magnetic flux between the AR and the global solar magnetic field. Such a partition is approximate since the entire flux distribution is perfectly continuous. The vortex motions applied to the AR interlock the field lines in the coronal volume to form additionally two newHFTs pinched into thin current layers.Reconnection in these current layers helps to redistribute the magnetic flux and current within the AR in the flux-cancellation phase. In this phase, a magnetic flux rope is formed together with a bald patch separatrix surface wrapping around the rope. Other important implications of the identified structural features of the modeled configuration are also discussed.

Trigger Mechanism of Solar Subflares in a Braided Coronal Magnetic Structure
Sanjiv K. **Tiwari**, Caroline E. Alexander, Amy R. Winebarger, Ronald L. Moore
ApJL, 795 L24 **2014**
http://arxiv.org/pdf/1410.4260v1.pdf
Fine-scale braiding of coronal magnetic loops by continuous footpoint motions may power coronal heating via nanoflares, which are spontaneous fine-scale bursts of internal reconnection. An initial nanoflare may trigger an avalanche of reconnection of the braids, making a microflare or larger subflare. In contrast to this internal triggering of subflares, we observe external triggering of subflares in a braided coronal magnetic field observed by the {\it High-resolution Coronal Imager (Hi-C)}. We track the development of these subflares using 12 s cadence images acquired by {\it SDO}/AIA in 1600, 193, 94 \AA, and registered magnetograms of {\it SDO}/HMI, over four hours centered on the {\it Hi-C} observing time. These data show numerous recurring small-scale brightenings in transition-region emission happening on polarity inversion lines where flux cancellation is occurring. We present in detail an example of an apparent burst of reconnection of two loops in the transition region under the braided coronal field, appropriate for releasing a short reconnected loop downward and a longer reconnected loop upward. The short loop presumably submerges into the photosphere, participating in observed flux cancellation. A subflare in the overlying braided magnetic field is apparently triggered by the disturbance of the braided field by the reconnection-released upward loop. At least 10 subflares observed in this braided structure appear to be triggered this way. How common this external trigger mechanism for coronal subflares is in other active regions, and how important it is for coronal heating in general, remain to be seen. **11July 2012**

MAGNETIC NON-POTENTIALITY OF SOLAR ACTIVE REGIONS AND PEAK X-RAY FLUX OF THE ASSOCIATED FLARES
Sanjiv Kumar **Tiwari**, P. Venkatakrishnan, and Sanjay Gosain
Astrophysical Journal, 721:622–629, **2010** September, **File**
Predicting the severity of solar eruptive phenomena such as flares and coronal mass ejections remains a great

challenge despite concerted efforts to do so over the past several decades. However, the advent of high-quality vector magnetograms obtained from *Hinode* (SOT/SP) has increased the possibility of meeting this challenge. In particular, the spatially averaged signed shear angle (SASSA) seems to be a unique parameter for quantifying the non-potentiality of active regions.We demonstrate the usefulness of the SASSA for predicting flare severity. For this purpose, we present case studies of the evolution of magnetic non-potentiality using 115 vector magnetograms of four active regions, namely, ARs NOAA 10930, 10960, 10961, and 10963 during 2006 December 8–15, 2007 June 3–10, 2007 June 28–July 5, and 2007 July 10–17, respectively. The NOAA ARs 10930 and 10960 were very active and produced X and M class flares, respectively, along with many smaller X-ray flares. On the other hand, the NOAA ARs 10961 and 10963 were relatively less active and produced only very small (mostly A- and B-class) flares. For this study, we have used a large number of high-resolution vector magnetograms obtained from *Hinode* (SOT/SP). Our analysis shows that **the peak X-ray flux of the most intense solar flare emanating from the active regions depends on the magnitude of the SASSA at the time of the flare**. This finding of the existence of a lower limit of the SASSA for a given class of X-ray flares will be very useful for space weather forecasting. We have also studied another non-potentiality parameter called the mean weighted shear angle (MWSA) of the vector magnetograms along with the SASSA. We find that the MWSA does not show such distinction as the SASSA for upper limits of the *GOES* X-ray flux of solar flares; however, both the quantities show similar trends during the evolution of all active regions studied.

Spatially Resolved Plasma Composition Evolution in a Solar Flare -- The Effect of Reconnection Outflow

Andy S.H. **To**, David H. Brooks, Shinsuke Imada, Ryan J. French, Lidia van Driel-Gesztelyi, Deborah Baker, David M. Long, William Ashfield IV, Laura A. Hayes

A&A 691, A95 **2024**

https://arxiv.org/pdf/2409.18188?

https://www.aanda.org/articles/aa/pdf/2024/11/aa49246-24.pdf

Context. Solar flares exhibit complex variations in elemental abundances compared to photospheric values. These abundance variations, characterized by the first ionization potential (FIP) bias, remain challenging to interpret.
Aims. We aim to (1) examine the spatial and temporal evolution of coronal abundances in the X8.2 flare on **2017 September 10**, and (2) provide a new scenario to interpret the often observed high FIP bias loop top, and provide further insight into differences between spatially resolved and Sun-as-a-star flare composition measurements.
Methods. We analyzed 12 Hinode/Extreme-ultraviolet Imaging Spectrometer (EIS) raster scans spanning 3.5 hours, employing both Ca XIV 193.87 Å/Ar XIV 194.40 Å and Fe XVI 262.98 Å/S XIII 256.69 Å composition diagnostics to derive FIP bias values. We used the Markov Chain Monte Carlo (MCMC) differential emission measure (DEM) method to obtain the distribution of plasma temperatures, which forms the basis for the FIP bias calculations.
Results. Both the Ca/Ar and Fe/S composition diagnostics consistently show that flare loop tops maintain high FIP bias values of > 2–6, with peak phase values exceeding 4, over the extended duration, while footpoints exhibit photospheric FIP bias of ∼1. The consistency between these two diagnostics forms the basis for our interpretation of the abundance variations.
Conclusions. We propose that this variation arises from a combination of two distinct processes: high FIP bias plasma downflows from the plasma sheet confined to loop tops, and chromospheric evaporation filling the loop footpoints with low FIP bias plasma. Mixing between these two sources produces the observed gradient. Our observations show that the localized high FIP bias signature at loop tops is likely diluted by the bright footpoint emission in spatially averaged measurements. The spatially resolved spectroscopic observations enabled by EIS prove critical for revealing this complex abundance variation in loops. Furthermore, our observations show clear evidence that the origin of hot flare plasma in flaring loops consists of a combination of both directly heated plasma in the corona and from ablated chromospheric material; and our results provide valuable insights into the formation and composition of loop top brightenings, also known as EUV knots, which are a common feature at the tops of flare loops.

RHESSI Nuggets #476 **2024**

https://heliowiki.smce.nasa.gov/wiki/index.php/Spatially_resolved_plasma_composition_evolution_in_a_solar_flare

Reconnection outflow feeds abundance variations.

The Evolution of Plasma Composition During a Solar Flare

Andy S.H. **To**, David M. Long, Deborah Baker, David H. Brooks, Lidia van Driel-Gesztelyi, J. Martin Laming, Gherardo Valori

ApJ **911** 86 **2021**

https://arxiv.org/pdf/2102.09985.pdf

https://iopscience.iop.org/article/10.3847/1538-4357/abe85a/pdf

https://doi.org/10.3847/1538-4357/abe85a

We analyse the coronal elemental abundances during a small flare using Hinode/EIS observations. Compared to the pre-flare elemental abundances, we observed a strong increase in coronal abundance of Ca XIV 193.84 Å, an emission line

with low first ionisation potential (FIP < 10 eV), as quantified by the ratio Ca/Ar during the flare. This is in contrast to the unchanged abundance ratio observed using Si X 258.38 Å/S X 264.23 Å. We propose two different mechanisms to explain the different composition results. Firstly, the small flare-induced heating could have ionised S, but not the noble gas Ar, so that the flare-driven Alfvén waves brought up Si, S and Ca in tandem via the ponderomotive force which acts on ions. Secondly, the location of the flare in strong magnetic fields between two sunspots may suggest fractionation occurred in the low chromosphere, where the background gas is neutral H. In this region, high-FIP S could behave more like a low-FIP than a high-FIP element. The physical interpretations proposed generate new insights into the evolution of plasma abundances in the solar atmosphere during flaring, and suggests that current models must be updated to reflect dynamic rather than just static scenarios. **2-5 Feb 2014**

Flare Hybrids **Review**

M. **Tomczak**, P. Dubieniecki
Solar Physics Volume 290, Issue 12, pp 3611-3623 **2015**
http://arxiv.org/pdf/1504.03165v1.pdf
http://link.springer.com/journal/11207/290/12/page/1
https://link.springer.com/content/pdf/10.1007/s11207-015-0688-x.pdf
Svestka (Solar Phys. 1989, 121, 399) on the basis of the Solar Maximum Mission observations introduced a new class of flares, the so-called flare hybrids. When they start, they look as typical compact flares (phase 1), but later on they look like flares with arcades of magnetic loops (phase 2). We summarize the features of flare hybrids in soft and hard X-rays as well as in extreme-ultraviolet; these allow us to distinguish them from other flares. Additional energy release or long plasma cooling timescales have been suggested as possible cause of phase 2. Estimations of frequency of flare hybrids have been given. Magnetic configurations supporting their origin have been presented. In our opinion, flare hybrids are quite frequent and a difference between lengths of two interacting systems of magnetic loops is a crucial parameter for recognizing their features. **1992-11-05, 1992-09-09, 5 NOV 1992**

Multiperiodicity in quasi-periodic pulsations of flare hard X-rays: a case study

M. **Tomczak**, Z. Szaforz
Central European Astrophysical Bulletin, Cent. Eur. Astrophys. Bull. 38, 111. **2014**
http://arxiv.org/pdf/1412.2173v1.pdf
We present a case study of the solar flare (SOL**2001-10-02**T17:31) that showed quasi-periodic pulsations (QPPs) in hard X-rays with two simultaneously excited periods, P_1 = 26-31 s and P_2 = 110 s. Complete evolution of the flare recorded by the Yohkoh telescopes, together with the patrol SOHO/EIT images, allowed us to identify magnetic structures responsible for particular periods and to propose an overall scenario which is consistent with the available observations. Namely, we suggest that emerging magnetic flux initiated the reconnection with legs of a large arcade of coronal loops that had been present in an active region for several days. The reconnection excited MHD oscillations in both magnetic structures simultaneously: period P_1 was generated in the emerging loop and in a loop being a result of the reconnection; period P_2 occurred in the arcade. Both resonators produced photons of different spectra. We anticipate that multiperiodicity in hard X-rays can be a common feature of flare hybrids, i.e. the events, in which magnetic structures of different sizes interact.

The YOHKOH survey of partially occulted flares in hard X-rays

M. **Tomczak**
A&A 502, 665-678 (**2009**)
Context. Modern solar X-ray imagers do not completely resolve the problem of deriving detailed diagnostics of faint hard X-ray sources in the presence of stronger ones. This is the case for the impulsive phase of solar flares in which footpoint sources are usually stronger than loop-top ones.
Aims. Flares that are partially occulted by the solar limb provide the most hopeful source of knowledge about hard X-ray loop-top sources. This work attempts to fill the gap between the published survey of partially occulted flares observed by RHESSI (Krucker & Lin 2008, ApJ, 673, 1181) and the extensive *Yohkoh* database.
Methods. Among the 1286 flares in the *Yohkoh* Hard X-ray Telescope Flare Catalogue (Sato et al. 2006, Sol. Phys., 236, 351), for which the hard X-ray images were presented, we identified 98 events that occurred behind the solar limb. We investigated their hard X-ray spectra and spatial structure.
Results. In most cases, we found that the hard X-ray spectrum of partially occulted flares consists of two components, non-thermal and thermal, which are cospatial to within 4 arcsec. For rest events, the components are separated, the non-thermal component clearly appearing to be situated higher. The photon energy spectra of the partially occulted flares are systematically steeper than spectra of the non-occulted flares. We can explain this difference as a consequence of intrinsically dissimilar conditions in coronal parts of flares, in comparison with the footpoints that usually dominate the hard X-ray emission of disk flares. At least two reasons for the difference should be taken into consideration: (1)

stronger contamination of hard X-rays by emission from thermal plasma; and (2) different mechanisms in which non-thermal electrons radiate their energy. For events unbiased by the thermal component, the difference, $\Delta\gamma = \bar{\gamma}_{LT} - \bar{\gamma}_{FP}$, equals 1.5. We found a lack of correlation between the altitude of flares and the hard X-ray power-law index γ.
Conclusions. A schematic picture, in which a thin-target mechanism is responsible for the hard X-ray emission of loop-top sources and a thick-target mechanism for emission by footpoint sources, is modified by the presence of some coronal thick-target sources. Some of these sources exhibit evidence of magnetic trapping. For the characteristics of flares is conclusive the local magnetic configuration in which they occur.

Solar Sources of Flares and CMEs **Review**

Shin **Toriumi**
Proceedings of the IAU Symposium No. 388 **2024**
https://arxiv.org/pdf/2409.16353
Strong solar flares and coronal mass ejections (CMEs) are prone to originate within and near active regions (ARs) with a high magnetic complexity. Therefore, to better understand the generation mechanism of flares and the resultant CME eruption and to gain insight into their stellar counterparts, it is crucial to reveal how solar flare-productive ARs are generated and developed. In this review, first, we summarize some general aspects of solar flares and key observational characteristics of such ARs. Then, we discuss a series of flux emergence simulations that were performed to elucidate the subsurface origins of their complexity and introduce state-of-the-art models that consider the effect of turbulent thermal convection. Future flare observations using SOLAR-C, a next-generation high-throughput extreme ultraviolet spectroscopy mission, are also discussed.

Solar Flares and Magnetic Helicity **Review**

Shin **Toriumi**, Sung-Hong Park
A chapter in the AGU book "Helicities in Geophysics, Astrophysics and Beyond" **2022**
https://arxiv.org/pdf/2204.06010.pdf
Solar flares and coronal mass ejections are the largest energy release phenomena in the current solar system. They cause drastic enhancements of electromagnetic waves of various wavelengths and sometimes eject coronal material into the interplanetary space, disturbing the magnetic surroundings of orbiting planets including the Earth. It is generally accepted that solar flares are a phenomenon in which magnetic energy stored in the solar atmosphere above an active region is suddenly released through magnetic reconnection. Therefore, to elucidate the nature of solar flares, it is critical to estimate the complexity of the magnetic field and track its evolution. Magnetic helicity, a measure of the twist of coronal magnetic structures, is thus used to quantify and characterize the complexity of flare-productive active regions. This chapter provides an overview of solar flares and discusses how the different concepts of magnetic helicity are used to understand and predict solar flares. **1997 November 3, 2000 February 27, 2001 October 25, 2007-04-30, 2011 February 14-15, 2014 October 24**

Flux emergence and generation of flare-productive active regions

Shin **Toriumi**
Advances in Space Research **2021**
https://arxiv.org/pdf/2105.09961.pdf
Solar flares and coronal mass ejections are among the most prominent manifestations of the magnetic activity of the Sun. The strongest events of them tend to occur in active regions (ARs) that are large, complex, and dynamically evolving. However, it is not clear what the key observational features of such ARs are, and how these features are produced. This article answers these fundamental questions based on morphological and magnetic characteristics of flare-productive ARs and their evolutionary processes, i.e., large-scale flux emergence and subsequent AR formation, which have been revealed in observational and theoretical studies. We also present the latest modeling of flare-productive ARs achieved using the most realistic flux emergence simulations in a very deep computational domain. Finally, this review discusses the future perspective pertaining to relationships of flaring solar ARs with the global-scale dynamo and stellar superflares. **13 Feb 2011, 7 Mar 2012, 7 Jan 2014, 29 Mar 2014**

Flare-productive active regions **Review**

Shin **Toriumi**, Haimin Wang
Living Reviews in Solar Physics **16**: 3 **2019**
https://arxiv.org/pdf/1904.12027.pdf
sci-hub.do/10.1007/s41116-019-0019-7
Strong solar flares and coronal mass ejections, here defined not only as the bursts of electromagnetic radiation but as the entire process in which magnetic energy is released through magnetic reconnection and plasma instability, emanate from active regions (ARs) in which high magnetic non-potentiality resides in a wide variety of forms. This review focuses on the formation and evolution of flare-productive ARs from both observational and theoretical points of view.

Starting from a general introduction of the genesis of ARs and solar flares, we give an overview of the key observational features during the long-term evolution in the pre-flare state, the rapid changes in the magnetic field associated with the flare occurrence, and the physical mechanisms behind these phenomena. Our picture of flare-productive ARs is summarized as follows: subject to the turbulent convection, the rising magnetic flux in the interior deforms into a complex structure and gains high non-potentiality; as the flux appears on the surface, an AR with large free magnetic energy and helicity is built, which is represented by delta-sunspots, sheared polarity inversion lines, magnetic flux ropes, etc; the flare occurs when sufficient magnetic energy has accumulated, and the drastic coronal evolution affects magnetic fields even in the photosphere. We show that the improvement of observational instruments and modeling capabilities has significantly advanced our understanding in the last decades. Finally, we discuss the outstanding issues and future perspective and further broaden our scope to the possible applications of our knowledge to space-weather forecasting, extreme events in history, and corresponding stellar activities. **1859 September 1, 1946 July 25, 3 August 1972, 2000 Jun 6, 2001 Apr 9, 2001 Aug 25, 2003 Oct 28, 2003 Oct 29, 2003 Nov 2, 2006 Dec 13, February 12, 2007, 5-7 Dec 2007, 12-16 Feb 2011, 2012 March 7, 2012 July 02, 2014 Oct 24, 2015 June 22, 2015 August 19, 3-7 Sep 2017**

Numerical Simulations of Flare-productive Active Regions: delta-sunspots, Sheared Polarity Inversion Lines, Energy Storage, and Predictions

Shin **Toriumi**, Shinsuke Takasao

ApJ **850** 39 **2017**

https://arxiv.org/pdf/1710.08926.pdf

https://iopscience.iop.org/article/10.3847/1538-4357/aa95c2/pdf

Solar active regions (ARs) that produce strong flares and coronal mass ejections (CMEs) are known to have a relatively high non-potentiality and are characterized by delta-sunspots and sheared magnetic structures. In this study, we conduct a series of flux emergence simulations from the convection zone to the corona and model four types of active regions that have been observationally suggested to cause strong flares, namely the Spot-Spot, Spot-Satellite, Quadrupole, and Inter-AR cases. As a result, we confirm that delta-spot formation is due to the complex geometry and interaction of emerging magnetic fields, with finding that the strong-field, high-gradient, highly-sheared polarity inversion line (PIL) is created by the combined effect of the advection, stretching, and compression of magnetic fields. We show that free magnetic energy builds up in the form of a current sheet above the PIL. It is also revealed that photospheric magnetic parameters that predict flare eruptions reflect the stored free energy with high accuracy, while CME-predicting parameters indicate the magnetic relationship between flaring zones and entire ARs.

Magnetic Properties of Solar Active Regions that Govern Large Solar Flares and Eruptions

Shin **Toriumi**, Carolus J. Schrijver, Louise K. Harra, Hugh Hudson, Kaori Nagashima

ApJ **2017 834** 56

https://arxiv.org/pdf/1611.05047v1.pdf

https://iopscience.iop.org/article/10.3847/1538-4357/834/1/56/pdf

Solar flares and coronal mass ejections (CMEs), especially the larger ones, emanate from active regions (ARs). With the aim to understand the magnetic properties that govern such flares and eruptions, we systematically survey all flare events with GOES levels of >=M5.0 within 45 deg from disk center between May 2010 and April 2016. These criteria lead to a total of 51 flares from 29 ARs, for which we analyze the observational data obtained by the Solar Dynamics Observatory. More than 80% of the 29 ARs are found to exhibit delta-sunspots and at least three ARs violate Hale's polarity rule. The flare durations are approximately proportional to the distance between the two flare ribbons, to the total magnetic flux inside the ribbons, and to the ribbon area. From our study, one of the parameters that clearly determine whether a given flare event is CME-eruptive or not is the ribbon area normalized by the sunspot area, which may indicate that the structural relationship between the flaring region and the entire AR controls CME productivity. AR characterization show that even X-class events do not require delta-sunspots or strong-field, high-gradient polarity inversion lines. An investigation of historical observational data suggests the possibility that the largest solar ARs, with magnetic flux of 2x10^23 Mx, might be able to produce "superflares" with energies of order of 10^34 erg. The proportionality between the flare durations and magnetic energies is consistent with stellar flare observations, suggesting a common physical background for solar and stellar flares.

Table 1. Properties of Flare Events Table A1. Measured Parameters of Flare Events

1946-07-25, 2011-02-13, 2011-02-15, 2011-03-09, 2011-07-30, 2011-08-03, 2011-08-04, 2012-01-23, 2012-03-07, 2012-03-09, 2012-03-10, 2012-05-10, 2012-07-02, 2012-07-04, 2012-07-05, 2012-07-12, 2013-04-11, 2013-10-24, 2013-11-01, 2013-11-03, 2013-11-05, 2013-11-08, 2013-11-10, 2013-12-31, 2014-01-07, 2014-02-04, 2014-03-29, 2014-04-18, 2014-09-10, 2014-09-28, 2014-10-22, 2014-10-24, 2014-10-25, 2014-10-26, 2014-10-27, 2014-11-07, 2014-12-04, 2014-12-17, 2014-12-18, 2014-12-20, 2015-03-10, 2015-03-11, 2015-06-22, 2015-06-25, 2015-08-24, 2015-09-28,

HMI Science Nuggets #65. **SDO Reveals the Properties of Flare-productive Sunspot Regions**

http://hmi.stanford.edu/hminuggets/?p=1786

LIGHT BRIDGE IN A DEVELOPING ACTIVE REGION. II. NUMERICAL SIMULATION OF FLUX EMERGENCE AND LIGHT BRIDGE FORMATION

Shin **Toriumi**1, Mark C. M. Cheung2, and Yukio Katsukawa

2015 ApJ 811 138

Light bridges, the bright structure dividing umbrae in sunspot regions, show various activity events. In Paper I, we reported on an analysis of multi-wavelength observations of a light bridge in a developing active region (AR) and concluded that the activity events are caused by magnetic reconnection driven by magnetconvective evolution. The aim of this second paper is to investigate the detailed magnetic and velocity structures and the formation mechanism of light bridges. For this purpose, we analyze numerical simulation data from a radiative magnetohydrodynamics model of an emerging AR. We find that a weakly magnetized plasma upflow in the near-surface layers of the convection zone is entrained between the emerging magnetic bundles that appear as pores at the solar surface. This convective upflow continuously transports horizontal fields to the surface layer and creates a light bridge structure. Due to the magnetic shear between the horizontal fields of the bridge and the vertical fields of the ambient pores, an elongated cusp-shaped current layer is formed above the bridge, which may be favorable for magnetic reconnection. The striking correspondence between the observational results of Paper I and the numerical results of this paper provides a consistent physical picture of light bridges. The dynamic activity phenomena occur as a natural result of the bridge formation and its convective nature, which has much in common with those of umbral dots and penumbral filaments.

LIGHT BRIDGE IN A DEVELOPING ACTIVE REGION. I. OBSERVATION OF LIGHT BRIDGE AND ITS DYNAMIC ACTIVITY PHENOMENA

Shin **Toriumi**1, Yukio Katsukawa1, and Mark C. M. Cheung

2015 ApJ 811 137

http://arxiv.org/pdf/1509.00183v1.pdf

Light bridges, the bright structures that divide the umbra of sunspots and pores into smaller pieces, are known to produce a wide variety of activity events in solar active regions (ARs). It is also known that the light bridges appear in the assembling process of nascent sunspots. The ultimate goal of this series of papers is to reveal the nature of light bridges in developing ARs and the occurrence of activity events associated with the light bridge structures from both observational and numerical approaches. In this first paper, exploiting the observational data obtained by Hinode, the Interface Region Imaging Spectrograph, and the Solar Dynamics Observatory, we investigate the detailed structure of the light bridge in **NOAA AR 11974** and its dynamic activity phenomena. As a result, we find that the light bridge has a weak, horizontal magnetic field, which is transported from the interior by a large-scale convective upflow and is surrounded by strong, vertical fields of adjacent pores. In the chromosphere above the bridge, a transient brightening occurs repeatedly and intermittently, followed by a recurrent dark surge ejection into higher altitudes. Our analysis indicates that the brightening is the plasma heating due to magnetic reconnection at lower altitudes, while the dark surge is the cool, dense plasma ejected from the reconnection region. From the observational results, we conclude that the dynamic activity observed in a light bridge structure such as chromospheric brightenings and dark surge ejections are driven by magnetoconvective evolution within the light bridge and its interaction with the surrounding magnetic fields.

Observations and modeling of the solar flux emergence **Review**

Shin **TORIUMI**

Publ. Astron. Soc. Japan (**2014**) 66 (SP1), S6 (1–10)

http://pasj.oxfordjournals.org/content/66/SP1/S6.full.pdf+html

In a wide variety of magnetic activity phenomena occurring in the Sun, flux emergence is one of the most prominent events. It is important to study flux emergence since this is the process that transports the magnetic flux from the deep interior to the upper atmosphere, creates active regions, and sometimes causes catastrophic flaring eruptions. Recent observations have revealed that flux emergence ranges from the formation of large-scale active regions including sunspots to small-scale events observable only with advanced instruments, covering a very broad spectrum of scale involved. In addition, helioseismology may allow us to investigate the process even before the flux itself appears at the visible surface of the Sun. At the same time, recent development in the numerical modeling of flux emergence opens the door to a further understanding of physical processes, such as resistive and convective emergence. In this paper, we

review the observational and numerical progress in the field of flux emergence study, while focusing particularly on three important aspects: emergence in the interior, the first appearance in the surface layer, and their relation with flaring activity. Based on these studies, we also discuss what should be investigated in the future.

Statistical Analysis of the Horizontal Divergent Flow in Emerging Solar Active Regions

Shin **Toriumi**, Keiji Hayashi, Takaaki Yokoyama
ApJ, **2014**
http://arxiv.org/pdf/1408.2383v1.pdf

Solar active regions (ARs) are thought to be formed by magnetic fields from the convection zone. Our flux emergence simulations revealed that a strong horizontal divergent flow (HDF) of unmagnetized plasma appears at the photosphere before the flux begins to emerge. In our earlier study, we analyzed HMI data for a single AR and confirmed presence of this precursor plasma flow in the actual Sun. In this paper, as an extension of our earlier study, we conducted a statistical analysis of the HDFs to further investigate their characteristics and better determine the properties. From SDO/HMI data, we picked up 23 flux emergence events over a period of 14 months, the total flux of which ranges from 10^{20} to 10^{22} Mx. Out of 23 selected events, 6 clear HDFs were detected by the method we developed in our earlier study, and 7 HDFs detected by visual inspection were added to this statistic analysis. We found that the duration of the HDF is on average 61 minutes and the maximum HDF speed is on average 3.1 km s^{-1}. We also estimated the rising speed of the subsurface magnetic flux to be 0.6-1.4 km s^{-1}. These values are highly consistent with our previous one-event analysis as well as our simulation results. The observation results lead us to the conclusion that the HDF is rather a common feature in the earliest phase of AR emergence. Moreover, our HDF analysis has capability of determining the subsurface properties of emerging fields that cannot be directly measured.
Fig. 7.— ARs analyzed in this study. (Left) SDO/HMI magnetogram.

Formation of a Flare-Productive Active Region: Observation and Numerical Simulation of NOAA AR 11158

S. **Toriumi**, Y. Iida, K. Kusano, Y. Bamba, S. Imada
Solar Phys., Volume 289, Issue 9, pp 3351-3369, **2014**
http://arxiv.org/pdf/1403.4029v1.pdf

We present a comparison of the Solar Dynamics Observatory (SDO) analysis of NOAA Active Region (AR) 11158 and numerical simulations of flux-tube emergence, aiming to investigate the formation process of this flare-productive AR. First, we use SDO/Helioseismic and Magnetic Imager (HMI) magnetograms to investigate the photospheric evolution and Atmospheric Imaging Assembly (AIA) data to analyze the relevant coronal structures. Key features of this quadrupolar region are a long sheared polarity inversion line (PIL) in the central δ-sunspots and a coronal arcade above the PIL. We find that these features are responsible for the production of intense flares, including an X2.2-class event. Based on the observations, we then propose two possible models for the creation of AR 11158 and conduct flux-emergence simulations of the two cases to reproduce this AR. Case 1 is the emergence of a single flux tube, which is split into two in the convection zone and emerges at two locations, while Case 2 is the emergence of two isolated but neighboring tubes. We find that, in Case 1, a sheared PIL and a coronal arcade are created in the middle of the region, which agrees with the AR 11158 observation. However, Case 2 never builds a clear PIL, which deviates from the observation. Therefore, we conclude that the flare-productive AR 11158 is, between the two cases, more likely to be created from a single split emerging flux than from two independent flux bundles.

THE MAGNETIC SYSTEMS TRIGGERING THE M6.6 CLASS SOLAR FLARE IN NOAA ACTIVE REGION 11158

Shin **Toriumi**1,4, Yusuke Iida1,5, Yumi Bamba2, Kanya Kusano2,6, Shinsuke Imada2, and Satoshi Inoue
2013 ApJ 773 128

We report a detailed event analysis of the M6.6 class flare in the active region (AR) NOAA 11158 on **2011 February 13**. AR 11158, which consisted of two major emerging bipoles, showed prominent activity including one X- and several M-class flares. In order to investigate the magnetic structures related to the M6.6 event, particularly the formation process of a flare-triggering magnetic region, we analyzed multiple spacecraft observations and numerical results of a flare simulation. We observed that, in the center of this quadrupolar AR, a highly sheared polarity inversion line (PIL) was formed through proper motions of the major magnetic elements, which built a sheared coronal arcade lying over the PIL. The observations lend support to the interpretation that the target flare was triggered by a localized magnetic region that had an intrusive structure, namely, a positive polarity penetrating into a negative counterpart. The geometrical relationship between the sheared coronal arcade and the triggering region is consistent with the theoretical flare model based on the previous numerical study. We found that the formation of the trigger region was due to the continuous accumulation of small-scale magnetic patches. A few hours before the flare occurred, the series of emerged/advected patches reconnected with a pre-existing field. Finally, the abrupt flare eruption of the M6.6 event

started around 17:30 UT. Our analysis suggests that in the process of triggering flare activity, all magnetic systems on multiple scales are included, not only the entire AR evolution but also the fine magnetic elements.

DETECTION OF THE HORIZONTAL DIVERGENT FLOW PRIOR TO THE SOLAR FLUX EMERGENCE

S. **Toriumi**1, K. Hayashi2, and T. Yokoyama
2012 ApJ 751 154
It is widely accepted that solar active regions including sunspots are formed by the emerging magnetic flux from the deep convection zone. In previous numerical simulations, we found that the horizontal divergent flow (HDF) occurs before the flux emergence at the photospheric height. This paper reports the HDF detection prior to the flux emergence of NOAA AR 11081, which is located away from the disk center. We use SDO/HMI data to study the temporal changes of the Doppler and magnetic patterns from those of the reference quiet Sun. As a result, the HDF appearance is found to come before the flux emergence by about 100 minutes. Also, the horizontal speed of the HDF during this time gap is estimated to be 0.6-1.5 km s–1, up to 2.3 km s–1. The HDF is caused by the plasma escaping horizontally from the rising magnetic flux. And the interval between the HDF and the flux emergence may reflect the latency during which the magnetic flux beneath the solar surface is waiting for the instability onset to the further emergence. Moreover, SMART Hα images show that the chromospheric plages appear about 14 minutes later, located cospatial with the photospheric pores. This indicates that the plages are caused by plasma flowing down along the magnetic fields that connect the pores at their footpoints. One important result of observing the HDF may be the possibility of predicting the sunspot appearances that occur in several hours.

NUMERICAL EXPERIMENTS ON THE TWO-STEP EMERGENCE OF TWISTED MAGNETIC FLUX TUBES IN THE SUN

S. **Toriumi** and T. Yokoyama
2011 ApJ 735 126
We present the new results of the two-dimensional numerical experiments on the cross-sectional evolution of a twisted magnetic flux tube rising from the deeper solar convection zone (–20,000 km) to the corona through the surface. The initial depth is 10 times deeper than most of the previous calculations focusing on the flux emergence from the uppermost convection zone. We find that the evolution is illustrated by the following two-step process. The initial tube rises due to its buoyancy, subject to aerodynamic drag due to the external flow. Because of the azimuthal component of the magnetic field, the tube maintains its coherency and does not deform to become a vortex roll pair. When the flux tube approaches the photosphere and expands sufficiently, the plasma on the rising tube accumulates to suppress the tube's emergence. Therefore, the flux decelerates and extends horizontally beneath the surface. This new finding owes to our large-scale simulation, which simultaneously calculates the dynamics within the interior as well as above the surface. As the magnetic pressure gradient increases around the surface, magnetic buoyancy instability is triggered locally and, as a result, the flux rises further into the solar corona. We also find that the deceleration occurs at a higher altitude than assumed in our previous experiment using magnetic flux sheets. By conducting parametric studies, we investigate the conditions for the two-step emergence of the rising flux tube: field strength 1.5 × 104 G and the twist 5.0 × 10–4 km–1 at –20,000 km depth.

Dependence of the Magnetic Energy of Solar Active Regions on the Twist Intensity of the Initial Flux Tubes

Shin **Toriumi**, Takehiro Miyagoshi, Takaaki Yokoyama, Hiroaki Isobe, and Kazunari Shibata
E-print Jan **2011**, PASJ
We present a series of numerical experiments that model the evolution of magnetic flux tubes with a different amount of initial twist. As a result of calculations, tightly twisted tubes reveal a rapid two-step emergence to the atmosphere with a slight slowdown at the surface, while weakly twisted tubes show a slow two-step emergence waiting longer the secondary instability to be triggered. This picture of the two-step emergence is highly consistent with recent observations. These tubes show multiple magnetic domes above the surface, indicating that the secondary emergence is caused by interchange mode of magnetic buoyancy instability. As for the weakest twist case, the tube exhibits an elongated photospheric structure and never rises into the corona. The formation of the photospheric structure is due to inward magnetic tension force of the azimuthal field component of the rising flux tube (i.e., tube's twist). When the twist is weak, azimuthal field cannot hold the tube's coherency, and the tube extends laterally at the subadiabatic surface. In addition, we newly find that the total magnetic energy measured above the surface depends on the initial twist. Strong twist tubes follow the initial relation between the twist and the magnetic energy, while weak twist tubes deviates from this relation, because these tubes store their magnetic energy in the photospheric structures.

Distribution of Electric Currents in Solar Active Regions

Tibor **Torok**, James E. Leake, Viacheslav S. Titov, Vasilis Archontis, Zoran Mikić, Mark G. Linton, K?vin Dalmasse, Guillaume Aulanier, Bernhard Kliem
E-print, Jan **2014**; **2014** ApJ 782 L10
http://arxiv.org/pdf/1401.2931v1.pdf
There has been a long-lasting debate on the question of whether or not electric currents in solar active regions are neutralized. That is, whether or not the main (or direct) coronal currents connecting the active region polarities are surrounded by shielding (or return) currents of equal total value and opposite direction. Both theory and observations are not yet fully conclusive regarding this question, and numerical simulations have, surprisingly, barely been used to address it. Here we quantify the evolution of electric currents during the formation of a bipolar active region by considering a three-dimensional magnetohydrodynamic simulation of the emergence of a sub-photospheric, current-neutralized magnetic flux rope into the solar atmosphere. We find that a strong deviation from current neutralization develops simultaneously with the onset of significant flux emergence into the corona, accompanied by the development of substantial magnetic shear along the active region's polarity inversion line. After the region has formed and flux emergence has ceased, the strong magnetic fields in the region's center are connected solely by direct currents, and the total direct current is several times larger than the total return current. These results suggest that active regions, the main sources of coronal mass ejections and flares, are born with substantial net currents, in agreement with recent observations. Furthermore, they support eruption models that employ pre-eruption magnetic fields containing such currents.

FAN–SPINE TOPOLOGY FORMATION THROUGH TWO-STEP RECONNECTION DRIVEN BY TWISTED FLUX EMERGENCE
T. **T¨or¨ok**1, G. Aulanier1, B. Schmieder1, K. K. Reeves2, and L. Golub2
Astrophysical Journal, 704:485–495, **2009** October
We address the formation of three-dimensional nullpoint topologies in the solar corona by combining *Hinode/* X-ray Telescope (XRT) observations of a small dynamic limb event, which occurred beside a non-erupting prominence cavity, with a three-dimensional (3D) zero-β magnetohydrodynamics (MHD) simulation. To this end, we model the boundary-driven "kinematic" emergence of a compact, intense, and uniformly twisted flux tube into a potential field arcade that overlies a weakly twisted coronal flux rope. The expansion of the emerging flux in the corona gives rise to the formation of a nullpoint at the interface of the emerging and the pre-existing fields. We unveil a two-step reconnection process at the nullpoint that eventually yields the formation of a broad 3D fan–spine configuration above the emerging bipole. The first reconnection involves emerging fields and a set of large-scale arcade field lines. It results in the launch of a torsional MHD wave that propagates along the arcades, and in the formation of a sheared loop system on one side of the emerging flux. The second reconnection occurs between these newly formed loops and remote arcade fields, and yields the formation of a second loop system on the opposite side of the emerging flux. The two loop systems collectively display an anenome pattern that is located below the fan surface. The flux that surrounds the inner spine field line of the nullpoint retains a fraction of the emerged twist, while the remaining twist is evacuated along the reconnected arcades. The nature and timing of the features which occur in the simulation do qualititatively reproduce those observed by XRT in the particular event studied in this paper. Moreover, the two-step reconnection process suggests a new consistent and generic model for the formation of anemone regions in the solar corona.
2007 April 24,

Inverse diffraction for the Atmospheric Imaging Assembly in the Solar Dynamics Observatory

Gabriele **Torre**, Richard A Schwartz, Federico Benvenuto, Anna Maria Massone, Michele Piana
Inverse Problems, **2015**
http://arxiv.org/pdf/1501.07805v1.pdf
The Atmospheric Imaging Assembly in the Solar Dynamics Observatory provides full Sun images every 1 seconds in each of 7 Extreme Ultraviolet passbands. However, for a significant amount of these images, saturation affects their most intense core, preventing scientists from a full exploitation of their physical meaning. In this paper we describe a mathematical and automatic procedure for the recovery of information in the primary saturation region based on a correlation/inversion analysis of the diffraction pattern associated to the telescope observations. Further, we suggest an interpolation-based method for determining the image background that allows the recovery of information also in the region of secondary saturation (blooming).
September 6 2011,

EMPIRICAL DETERMINATION OF THE ENERGY LOSS RATE OF ACCELERATED ELECTRONS IN A WELL-OBSERVED SOLAR FLARE
Gabriele **Torre**1, Nicola Pinamonti1, A. Gordon Emslie2, Jingnan Guo1, Anna Maria Massone3, and Michele Piana

2012 ApJ 751 129
We present electron images of an extended solar flare source, deduced from RHESSI hard X-ray imaging spectroscopy data. We apply the electron continuity equation to these maps in order to determine empirically the form of the energy loss rate for the bremsstrahlung-emitting electrons. We show that this form is consistent with an energy transport model involving Coulomb collisions in a target with a temperature of about 2 × 107 K, with a continuous injection of fresh deka-keV electrons at a rate of approximately 10–2 electrons s–1 per ambient electron**.**

A data driven kinetic approach to coronal heating

A. **Toutountzi**1, L. Vlahos1, H. Isliker1, K. Moraitis2, M. Georgoulis2, and G. Chintzoglou
A&A **2016**
http://arxiv.org/pdf/1603.07129v1.pdf
Aims. Coronal heating through the explosive release of magnetic energy remains an open problem in solar physics. Several one-dimensional hydrodynamical models have been developed over the last decade, using simple approaches for the way energy is
deposited and transported in the coronal plasma, namely by inserting “nanoflares” in the form of “hot spots” at random sites and times. Our aim in this work is to investigate the problem from a different perspective.
Methods. With the help of a nonlinear force-free extrapolation method we reconstruct the coronal magnetic field of a well-studied solar active region (NOAA AR 11158) using an observed photospheric vector magnetogram of the region as the required boundary condition. We then determine the locations, energy contents, and volumes of unstable areas (i.e., areas prone to releasing energy) within the active-region corona. These areas include strong gradients in the magnetic field and are naturally connected to three-dimensional current sheets. The statistical distributions of these volumes, their fractal structure and corresponding fractal dimension as well as their electric currentdensity distribution are then inferred. Further adopting a simple model for the resistivity, we estimate the key characteristics of the fractally distributed electric fields. We then follow the behavior of thousands of particles (electrons and ions), obeying an initial Maxwellian distribution with temperature 10 eV, monitoring their trajectories and energization obtained by encountering the electric fields enveloped by unstable volumes. For computational convenience, the spatial resolution of the magnetic field reconstruction (hundreds of km) is much coarser than the particles’ mean free path, which is 0.1 − 1 km in the low corona.
Results. The presence of collisions traps the bulk of the plasma around the unstable current sheets (UCS) and only a tail of the distribution of the electrons and ions gain substantial energy. Assuming that the distance between the UCS can be as small as the collisional mean free path, we find that the low active-region corona is heated to 100-200 eV, corresponding to temperatures in excess of 2 MK, within tens of seconds for electrons and thousands of seconds for ions. Our main result is that fractally distributed nanoflares inside the active region, following the statistical properties of the extrapolated magnetic fields, can heat electrons and ions with minor enhancements of the local resistivity due to the fragmentation of electric fields inside the driven complex magnetic topology.
Conclusions. The active region solar corona can be naturally heated by fractally distributed swarms of nanoflares that we simulate here as energy dissipation episodes in UCS. This could be extended for the quiet Sun corona, provided that currently undetected nanoflares are sufficient in number and occurrence frequency. February 11-16, 2011

Plasma Motions and Turbulent Magnetic Diffusivity of Active Region AR 12158 Using a Minimum Energy Functional and Non-Force-Free Reconstructions of Vector Magnetograms

Benoit **Tremblay**, Alain Vincent
Solar Phys. January **2017**, 292:2
We present a generalization of the resistive minimum-energy fit (MEF-R: Tremblay and Vincent, *Solar Phys.* **290**, 437, 2015) for non-force-free (NFF) magnetic fields. InMEF-R, an extremum principle is used to infer two-dimensional maps of plasma motions [$\boldsymbol{v}(x, y)$] and magnetic eddy diffusivity [$\eta_{\mathrm{eddy}}(x, y)$] at the photosphere. These reconstructions could be used as boundary conditions in data-driven simulations or in data assimilation. The algorithm is validated using the analytical model of a resistive expanding spheromak by Rakowski, Laming, and Lyutikov (*Astrophys. J.* **730**, 30, 2011). We study the flaring Active Region AR 12158 using a series of magnetograms and Dopplergrams provided by the *Helioseismic and Magnetic Imager* (HMI) onboard the *Solar Dynamics Observatory* (SDO). The results are discussed for a non-force-free magnetic-field reconstruction [$\boldsymbol{B}_{\mathrm{NFF}}$] (Hu and Dasgupta in *Solar Phys.* **247**, 87, 2008). We found that the vertical plasma velocities [$v_z(x, y)$] inferred using MEF-R are very similar to the observed Doppler velocities [$v_r(x, y)$]. Finally, we study the potential spatial correlation between microturbulent velocities and significant values of $\eta_{\mathrm{eddy}}(x, y)$. **10 September 2014**

Reconstruct Photospheric Velocity and Magnetic Diffusivity in Active Regions from Observed Magnetograms and Dopplergrams

Benoit **Tremblay**, Alain Vincent
Solar Phys. February **2015**, Volume 290, Issue 2, pp 437-466
We introduce MEF-R, a generalization of the minimum energy fit (MEF; Longcope, Astrophys. J.612, 1181, 2004) to a non-ideal (resistive) gas. The new technique requires both vector magnetograms and Doppler velocities as input fields.

However, in the case of active regions observed only with the Michelson–Doppler Imager (MDI) onboard the Solar and Heliospheric Observatory (SOHO) such as AR 9077, we have only access to line-of-sight magnetograms. We reconstruct two-dimensional maps of the magnetic diffusivity η(x,y) together with velocity components v x (x,y), v y (x,y), and v z (x,y) under the linear force-free magnetic field approximation. Computed maps for v z (x,y) very well match the Doppler velocities v r (x,y). We find the average value $\langle\eta\rangle \approx 108$ m2 s−1 with a standard deviation of ≈ 1010 m2 s−1. Such high values of η(x,y) are to be expected at some places since our magnetic diffusivity is actually eddy-diffusivity. Inside AR 9077, the maps of η(x,y) do not resemble closely the maps from classical models of the magnetic diffusivity, but they are closer to η as a function of temperature than to ηas a function of electric current density.

Transient Formation of Loops in the Core of an Active Region

Durgesh **Tripathi**1
2021 ApJ 909 105
https://doi.org/10.3847/1538-4357/abdd2e
We study the formation of transient loops in the core of the AR 11890. For this purpose, we have used the observations recorded by the Atmospheric Imaging Assembly (AIA) and the Interface Region Imaging Spectrograph (IRIS). For photospheric field configuration, we have used the line-of-sight (LOS) magnetograms obtained from the Helioseismic and Magnetic Imager. The transient is simultaneously observed in all the UV and EUV channels of AIA and the three slit-jaw images from IRIS. The coexistence of the transient in all AIA and IRIS SJI channels suggests the transient's multithermal nature. The transient consists of short loops located at the base of the transient, as well as long loops. A differential emission measure analysis shows that the transient has a clumpy structure. The highest emission observed at the base is within the temperature bin of $\log T = 6.65$–6.95. We observe the longer loops at a similar temperature, albeit very feeble. Using LOS magnetograms, we conclude that the magnetic reconnection may have caused the transient. Our observations further suggest that the physics of the formation of such transients may be similar to those of typical coronal jets, albeit in different topological configurations. Such multiwavelength observations shed light on the formation of hot plasma in the solar corona and provide further essential constraints on modeling the thermodynamics of such transients.

EMISSION MEASURE DISTRIBUTION AND HEATING OF TWO ACTIVE REGION CORES

Durgesh **Tripathi**1,2, James A. Klimchuk3 and Helen E. Mason
2011 ApJ 740 111
Using data from the Extreme-ultraviolet Imaging Spectrometer aboard Hinode, we have studied the coronal plasma in the core of two active regions. Concentrating on the area between opposite polarity moss, we found emission measure distributions having an approximate power-law form EMT 2.4 from log T = 5.5 up to a peak at log T = 6.55. We show that the observations compare very favorably with a simple model of nanoflare-heated loop strands. They also appear to be consistent with more sophisticated nanoflare models. However, in the absence of additional constraints, steady heating is also a viable explanation.

EVIDENCE OF IMPULSIVE HEATING IN ACTIVE REGION CORE LOOPS

Durgesh **Tripathi**1, Helen E. Mason1, and James A. Klimchuk2
Astrophysical Journal, 723:713–718, **2010**
Using a full spectral scan of an active region from the Extreme-Ultraviolet Imaging Spectrometer (EIS) we have obtained emission measure EM(T) distributions in two different moss regions within the same active region.We have compared these with theoretical transition region EMs derived for three limiting cases, namely, static equilibrium, strong condensation, and strong evaporation from Klimchuk et al. The EM distributions in both the moss regions are strikingly similar and show a monotonically increasing trend from log T [K] = 5.15–6.3. Using photospheric abundances, we obtain a consistent EM distribution for all ions. Comparing the observed and theoretical EM distributions, we find that the observed EM distribution is best explained by the strong condensation case (EM_{con}), suggesting that a downward enthalpy flux plays an important and possibly dominant role in powering the transition region moss emission. The downflows could be due to unresolved coronal plasma that is cooling and draining after having been impulsively heated. This supports the idea that the hot loops (with temperatures of 3–5 MK) seen in the core of active regions are heated by nanoflares.

Temperature Tomography of a Coronal Sigmoid Supporting the Gradual Formation of a Flux Rope

Durgesh **Tripathi**1, Bernhard Kliem, Helen E. Mason1, Peter R. Young3, 5, and Lucie M. Green

E-print, April **2009,** Astrophysical Journal, 698:L27–L32, **2009, File**
Multi-wavelength observations of a sigmoidal (S-shaped) solar coronal source by the EUV Imaging Spectrometer and the X-ray Telescope aboard the **Hinode spacecraft and by the EUV Imager aboard STEREO** are reported. The data reveal the coexistence of a pair of J-shaped hot arcs at temperatures T>2 MK with an S-shaped structure at somewhat lower temperatures T~1.3 MK. The middle section of the S-shaped structure runs along the polarity inversion line of the photospheric field, bridging the gap between the arcs. Flux cancellation occurs at the same location in the photosphere. The sigmoid forms in the gradual decay phase of the active region, which does not experience an eruption. These findings correspond to the expected signatures of a flux rope forming, or being augmented, gradually by a topology transformation inside a magnetic arcade. In such a transformation, the plasma on newly formed helical field lines in the outer flux shell of the rope (S-shaped in projection) is expected to enter a cooling phase once the reconnection of their parent field line pairs (double-J shaped in projection) is complete. Thus, the data support the conjecture that flux ropes can exist in the corona prior to eruptive activity.

A bright coronal downflow seen in multi-wavelength observations: evidence of a bifurcating flux-rope?

D. **Tripathi**, S.K. Solanki, H.E. Mason, D.F. Webb
E-print, July **2007**
To study the origin and characteristics of a bright coronal downflow seen after a coronal mass ejection associated with erupting prominences on 5~March 2000.
The origin of the downflow was likely to have been magnetic reconnection taking place inside the erupting flux rope that led to its bifurcation.

EIT and TRACE responses to flare plasma –

D. **Tripathi**, G. Del Zanna, H. E. Mason, C. Chifor
A&A Letters, E-print, Oct **2006**

Origin of the 30 THz emission detected during the 2012 March 13 solar flare at 17:20 UT

G. **Trottet**, J.-P. Raulin, A. MacKinnon, G. Giménez de Castro, P.J.A. Simões, D. Cabezas, V. de La Luz, M. Luoni, P. Kaufmann
Soar Phys. **2015**
http://arxiv.org/pdf/1509.06336v1.pdf
Solar observations in the infrared domain can bring important clues on the response of the low solar atmosphere to primary energy released during flares. At present the infrared continuum has been detected at 30 THz (10 μm) in only a few flares. In this work we present a detailed multi-frequency analysis of SOL2012-03-13, including observations at radio millimeter and sub-millimeter wavelengths, in hard X-rays (HXR), gamma-rays (GR), H-alpha, and white-light. HXR/GR spectral analysis shows that the event is a GR line flare and allows estimating the numbers of and energy contents in electrons, protons and alpha particles produced during the flare. The energy spectrum of the electrons producing the HXR/GR continuum is consistent with a broken power-law with an energy break at ~800 keV. It is shown that the high-energy part (above ~800 keV) of this distribution is responsible for the high-frequency radio emission (> 20 GHz) detected during the flare. By comparing the 30 THz emission expected from semi-empirical and time-independent models of the quiet and flare atmospheres, we find that most (~80%) of the observed 30 THz radiation can be attributed to thermal free-free emission of an optically-thin source. Using the F2 flare atmospheric model this thin source is found to be at temperatures T~8000 K and is located well above the minimum temperature region. We argue that the chromospheric heating, which results in 80% of the 30 THz excess radiation, can be due to energy deposition by non-thermal flare accelerated electrons, protons and alpha particles. The remaining 20% of the 30 THz excess emission is found to be radiated from an optically-thick atmospheric layer at T~5000 K, below the temperature minimum region, where direct heating by non-thermal particles is insufficient to account for the observed infrared radiation.

Dreicer electric field definition and runaway electrons in solar flares

Yu.T. **Tsap**, A.V. Stepanov, Yu.G. Kopylova
Research in Astron. Astrophys. **2024**
https://arxiv.org/pdf/2401.04591.pdf
We analyse electron acceleration by a large-scale electric field E in a collisional hydrogen plasma under the solar flare coronal conditions based on approaches proposed by Dreicer and Spitzer for the dynamic friction force of electrons. The Dreicer electric field EDr is determined as a critical electric field at which the entire electron population runs away. Two regimes of strong (E≲EDr) and weak (E≪EDr) electric field are discussed. It is shown that the commonly used formal definition of the Dreicer field leads to an overestimation of its value by about five times. The critical velocity at which the electrons of the ``tail" of the Maxwell distribution become runaway under the action of the sub-Dreiser electric fields turns out to be underestimated by 3–√ times in some works because the Coulomb collisions between

runaway and thermal electrons are not taken into account. The electron acceleration by sub-Dreicer electric fields generated in the solar corona faces difficulties.

Electron acceleration and hard X-ray emission from SOL2013-11-09

Yuri **Tsap** and Galina Motorina.
RHESSI Science Nugget No. 273, May **2016**
http://sprg.ssl.berkeley.edu/~tohban/wiki/index.php/Electron_acceleration_and_hard_X-ray_emission_from_SOL2013-1
Testing the thick-target model in an interesting flare!

On the origin of 140 GHz emission from the 4 July 2012 solar flare

Yuriy T. **Tsap**, Victoria V. Smirnova, Alexander S. Morgachev, Galina G. Motorina, Eduard P. Kontar, Valery G. Nagnibeda, Polina V. Strekalova
Advances in Space Research, V. 57, I. 7, p. 1449-1455 **2016**; DOI: 10.1016/j.asr.2015.12.037
http://arxiv.org/pdf/1604.01530v1.pdf
The sub-THz event observed on the **4 July 2012** with the Bauman Moscow State Technical University Radio Telescope RT-7.5 at 93 and 140~GHz as well as Kislovodsk and Metsahovi radio telescopes, Radio Solar Telescope Network (RSTN), GOES, RHESSI, and SDO orbital stations is analyzed. The spectral flux between 93 and 140 GHz has been observed increasing with frequency. On the basis of the SDO/AIA data the differential emission measure has been calculated. It is shown that the thermal coronal plasma with the temperature above 0.5~MK cannot be responsible for the observed sub-THz flare emission. The non-thermal gyrosynchrotron mechanism can be responsible for the microwave emission near 10~GHz but the observed millimeter spectral characteristics are likely to be produced by the thermal bremsstrahlung emission from plasma with a temperature of about 0.1~MK.

Chromospheric evaporation and pitch angle diffusion of trapped electrons in solar flare coronal loops

Yuriy T. **Tsap**, Yulia G. Kopylov, , Alexander V. Stepanov
Advances in Space Research, Volume 55, Issue 3, 1 February **2015**, Pages 791–794
http://www.sciencedirect.com/science/article/pii/S0273117714002841
The peculiarities of time delays between the peaks of hard X-ray and microwave emissions within the framework of the trap-plus-precipitation model are studied. Using the continuity equation it has been shown that time delays strongly depend on the chromospheric evaporation in the case of the Coulomb pitch angle diffusion of trapped electrons into the loss–cone. Based on the obtained results the origin of time delays as well as the role of Coulomb collisions in flare coronal loops are discussed.

TRAPPED ENERGETIC ELECTRONS OF CORONAL LOOPS IN THE DECAY PHASE OF SOLAR FLARES

Yuriy **Tsap**, Jing Huang, Yihua Yan
ИКИ, **2014**, Сессия: Солнце
http://plasma2014.cosmos.ru/presentations

Reconnection fluxes in eruptive and confined flares and implications for superflares on the Sun

Johannes **Tschernitz**, Astrid M. Veronig, Julia K. Thalmann, Jürgen Hinterreiter, Werner Pötzi
2018 *ApJ* **853** 41
https://arxiv.org/pdf/1712.04701.pdf
https://iopscience.iop.org/article/10.3847/1538-4357/aaa199/pdf
We use Hα filtergrams from Kanzelh¨ohe Observatory together with SDO HMI and SOHO MDI magnetograms to derive magnetic reconnection fluxes and rates. The flare reconnection flux is strongly correlated with the peak of the GOES 1-8 ˚A soft X-ray flux (c=0.92, in log-log space), both for confined and eruptive flares. Confined flares of a certain GOES class exhibit smaller ribbon areas but larger magnetic flux densities in the flare ribbons (by a factor of 2). In the largest events, up to ≈50% of the magnetic flux of the active region (AR) causing the flare is involved in the flare magnetic reconnection. These findings allow us to extrapolate toward the largest solar flares possible. A complex solar AR hosting a magnetic flux of 2·1023 Mx, which is in line with the largest AR fluxes directly measured, is capable of producing an X80 flare, which corresponds to a bolometric energy of about 7 · 1032 ergs. Using a magnetic flux estimate of 6 · 1023 Mx for the largest solar AR observed, we find that flares of GOES class ≈X500 could be produced (Ebol ≈ 3 · 1033 ergs). These estimates suggest that the present day's Sun is capable of producing flares and related

space weather events that may be more than an order of magnitude stronger than have been observed to date. **2011 November 9, 2014 May 10**
Table 2. List of events. (2000-2015)
Table 3. Flare reconnection fluxes ϕ, reconnection rates ˙ϕ and peak of GOES 1-8 ˚A SXR flux derivate F˙ SXR.

Extreme Value Analysis of Solar Flare Events

T. **Tsiftsi** V. De la Luz
Space Weather 16?, 12, 1984-1996 **2018**
http://sci-hub.tw/10.1029/2018SW001958
Space weather events such as solar flares can be harmful for life and infrastructure on Earth or in near-Earth orbit. In this paper we employ extreme value theory to model extreme solar flare events; extreme value theory offers the appropriate tools for the study and estimation of probabilities for extrapolation to ranges outside of those that have already been observed. In this work the data points used are inherently independent and realistic confidence intervals are offered with respect to the estimates of future solar flare events. The data used in this study are peak X-ray fluxes provided by National Oceanic and Atmospheric Administration that form a series of distinct flare events. The expected return levels for Carrington- or Halloween storm-like events were calculated with the outcome that the existing data predict similar events happening in 110 and 38 years, respectively, which are consistent with the results and inferences provided by Elvidge and Angling (2018, https://doi.org/10.1002/2017SW001727). We also make a preliminary analysis of the implications of solar seasonality and found its effect on extreme flare events to be statistically insignificant.

Particle acceleration by sub-proton cyclotron frequency spectrum of dispersive Alfven waves in inhomogeneous solar coronal plasmas

D. **Tsiklauri**
MNRAS **2024**
https://arxiv.org/pdf/2312.14616.pdf
The problem of explaining observed soft X-ray fluxes during solar flares, which invokes acceleration of large fraction of electrons, if the acceleration takes places at the solar coronal loop-top, can potentially be solved by postulating that flare at loop-top creates dispersive Alfven waves (DAWs) which propagate towards the foot-points. As DAWs move in progressively denser parts of the loop (due to gravitational stratification) the large fraction of electrons is no longer needed. Here we extend our previous results by considering f−1 frequency spectrum of DAWs and add He++ ions using fully kinetic particle-in-cell (PIC) simulations. We consider cases when transverse density gradient is in the range 4−40c/ωpe and DAW driving frequency is 0.3−0.6ωcp. We find that (i) The frequency spectrum case does not affect electron acceleration fraction in the like-to-like cases, but few times larger percentage of He++ heating is seen due to ion cyclotron resonance; (ii) In cases when counter propagating DAWs collide multiple-times, much larger electron and ion acceleration fractions are found, but the process is intermittent in time. This is because intensive heating (temperature increase) makes the-above-thermal-fraction smaller; Also more isotropic velocity distributions are seen; (iii) Development of kink oscillations occurs when DAWs collide; (iv) Scaling of the magnetic fluctuations power spectrum steepening in the higher-density regions is seen, due to wave refraction. Our PIC runs produce much steeper slopes than the orginal spectrum, indicating that the electron-scale physics has a notable effect of DAW spectrum evolution.

Three dimensional particle-in-cell simulation of particle acceleration by circularly polarised inertial Alfven waves in a transversely inhomogeneous plasma

D. **Tsiklauri**
E-print, Aug **2012**; Physics of Plasmas, in-press, September 2012 issue
The process of particle acceleration by left-hand, circularly polarised inertial Alfvén waves (IAW) in a transversely inhomogeneous plasma is studied using 3D particle-in-cell simulation. A cylindrical tube with, transverse to the background magnetic field, inhomogeneity scale of the order of ion inertial length is considered on which IAWs with frequency 0.3 omegaci are launched that are allowed to develop three wavelength. As a result time-varying parallel electric fields are generated in the density gradient regions which accelerate electrons in the parallel to magnetic field direction. Driven perpendicular electric field of IAWs also heats ions in the transverse direction. Such numerical setup is relevant for solar flaring loops and earth auroral zone. This first, 3D, fully-kinetic simulation demonstrates electron acceleration efficiency in the density inhomogeneity regions, along the magnetic field, of the order of 45% and ion heating, in the transverse to the magnetic field direction, of 75%. The latter is a factor of two times higher than the previous 2.5D analogous study and is in accordance with solar flare particle acceleration observations. We find that the generated parallel electric field is localised in the density inhomogeneity region and rotates in the same direction and with the same angular frequency as the initially launched IAW. Our numerical simulations seem also to suggest that the "knee" often found in the solar flare electron spectra can alternatively be interpreted as the Landau damping (Cerenkov resonance effect) of IAWs due to the wave-particle interactions.

Two-dimensional time evolution of beam-plasma instability in the presence of binary collisions

S. F. **Tigik**1, L. F. Ziebell1, P. H. Yoon2,3 and E. P. Kontar
A&A 586, A19 (**2016**) **Open Access**
http://www.aanda.org/articles/aa/pdf/2016/02/aa27271-15.pdf
Energetic electrons produced during solar flares are known to be responsible for generating solar type III radio bursts. The radio emission is a byproduct of Langmuir wave generation via beam-plasma interaction and nonlinear wave-wave and wave-particle interaction processes. In addition to type III radio bursts, electrons traveling downwards toward the chromosphere lead to the hard X-ray emission via electron-ion collisions. Recently, the role of Langmuir waves on the X-ray-producing electrons has been identified as important, because Langmuir waves may alter the electron distribution, thereby affecting the X-ray profile. Both Coulomb collisions and wave-particle interactions lead electrons to scattering and energy exchange that necessitates considering the two-dimensional (2D) problem in velocity space. The present paper investigates the influence of binary collisions on the beam-plasma instability development in 2D in order to elucidate the nonlinear dynamics of Langmuir waves and binary collisions. The significance of the present findings in the context of solar physics is discussed.

Millimeter and X-Ray Emission from the 5 July 2012 Solar Flare

Y. T. **Tsap**, V. V. Smirnova, G. G. Motorina, A. S. Morgachev, S. A. Kuznetsov, V. G. Nagnibeda, V. S. Ryzhov
Solar Physics March **2018**, 293:50
http://sci-hub.tw/http://link.springer.com/10.1007/s11207-018-1269-6
The **5 July 2012** solar flare SOL2012-07-05T11:44 (11:39 – 11:49 UT) with an increasing millimeter spectrum between 93 and 140 GHz is considered. We use space and ground-based observations in X-ray, extreme ultraviolet, microwave, and millimeter wave ranges obtained with the Reuven Ramaty High-Energy Solar Spectroscopic Imager, Solar Dynamics Observatory(SDO), Geostationary Operational Environmental Satellite, Radio Solar Telescope Network, and Bauman Moscow State Technical University millimeter radio telescope RT-7.5. The main parameters of thermal and accelerated electrons were determined through X-ray spectral fitting assuming the homogeneous thermal source and thick-target model. From the data of the Atmospheric Imaging Assembly/SDO and differential-emission-measure calculations it is shown that the thermal coronal plasma gives a negligible contribution to the millimeter flare emission. Model calculations suggest that the observed increase of millimeter spectral flux with frequency is determined by gyrosynchrotron emission of high-energy (≳300≳300 keV) electrons in the chromosphere. The consequences of the results are discussed in the light of the flare-energy-release mechanisms.

On the origin of 140 GHz emission from the 4 July 2012 solar flare

Yuriy T. **Tsap**, Victoria V. Smirnova, Alexander S. Morgachev, Galina G. Motorina, Eduard P. Kontar,Valery G. Nagnibeda, Polina V. Strekalova
2016
http://arxiv.org/pdf/1604.01530v1.pdf
The sub-THz event observed on the **4 July 2012** with the Bauman Moscow State Technical University Radio Telescope RT-7.5 at 93 and 140~GHz as well as Kislovodsk and Mets\"ahovi radio telescopes, Radio Solar Telescope Network (RSTN), GOES, RHESSI, and SDO orbital stations is analyzed. The spectral flux between 93 and 140 GHz has been observed increasing with frequency. On the basis of the SDO/AIA data the differential emission measure has been calculated. It is shown that the thermal coronal plasma with the temperature above 0.5~MK cannot be responsible for the observed sub-THz flare emission. The non-thermal gyrosynchrotron mechanism can be responsible for the microwave emission near 10~GHz but the observed millimeter spectral characteristics are likely to be produced by the thermal bremsstrahlung emission from plasma with a temperature of about 0.1~MK.

Extreme Value Analysis of Solar Flare Events

Thomai **Tsiftsi**, Victor De la Luz
Space Weather **2018**
https://arxiv.org/pdf/1802.06100.pdf
Space weather events such as solar flares can be harmful for life and infrastructure on earth or in near-earth orbit. In this paper we employ extreme value theory (EVT) to model extreme solar flare events; EVT offers the appropriate tools for the study and estimation of probabilities for extrapolation to ranges outside of those that have already been observed. In the past such phenomena have been modelled as following a power law which may gives poor estimates of such events due to overestimation. The data used in the study were X-ray fluxes from NOAA/GOES and the expected return levels for Carrington or Halloween like events were calculated with the outcome that the existing data predict similar events happening in 110 and 38 years respectively.

Electron plasma wake field acceleration in solar coronal and chromospheric plasmas

David **Tsiklauri** (Queen Mary University of London)
Phys. Plasmas **2017**
https://arxiv.org/pdf/1706.05265.pdf
Three dimensional, particle-in-cell, fully electromagnetic simulations of electron plasma wake field acceleration applicable to solar atmosphere are presented. It is established that injecting driving and trailing electron bunches into solar coronal and chromospheric plasmas, results in electric fields (−(20−5)×106 V/m), leading to acceleration of the trailing bunch up to 52 MeV, starting from initial 36 MeV. The results provide one of potentially important mechanisms for the extreme energetic solar flare electrons, invoking plasma wake field acceleration.

Online Catalog of Activity Events of Solar Cycle 24 Related to Active Regions.

Tsvetkov, T., Nakeva, Y. & Petrov, N.
Sol Phys 299, 125 (**2024**).
https://doi.org/10.1007/s11207-024-02351-6
We present a statistical study on the relationship of solar dynamic events (solar flares and coronal mass ejections) with active regions during Solar Cycle 24 (December 2008–December 2019). Combining data from NOAA Space Weather Prediction Center and observations of Large Angle and Spectrometric Coronagraph (LASCO) onboard the Solar and Heliospheric Observatory (SOHO) spacecraft, we found that more than a half of the coronal mass ejections were generated inside active regions. Geostationary Operational Environmental Satellite (GOES) soft X-ray flare listing data completed our study showing that almost 83% of Solar Cycle 24 flares are connected with active regions. Finally, we summarize the details for the related phenomena into an online catalog based on a list of all 1533 active regions that produced at least one flare and/or coronal mass ejection during Solar Cycle 24 and explore their properties like flare class, coronal mass ejection speed, and angular width paying special attention to the most powerful and threatful to Earth solar events.

Superflares, chromospheric activities and photometric variabilities of solar-type stars from the second-year observation of TESS and spectra of LAMOST

Zuo-Lin **Tu**, Ming Yang, H.-F. Wang, F. Y. Wang
ApJS **253** 35 **2021**
https://arxiv.org/pdf/2101.02901.pdf
https://iopscience.iop.org/article/10.3847/1538-4365/abda3c/pdf
https://doi.org/10.3847/1538-4365/abda3c
In this work, 1272 superflares on 311 stars are collected from 22,539 solar-type stars from the second-year observation of Transiting Exoplanet Survey Satellite ({\em TESS}), which almost covered northern hemisphere of the sky. Three superflare stars contain hot Jupiter candidates or ultra short-period planet candidates. We obtain $\gamma=-1.76\pm0.11$ of the correlation between flare frequency and flare energy ($dN/dE \propto E^{-\gamma}$) for all superflares, and get $\beta=0.42\pm0.01$ of the correlation between superflare duration and energy ($T_{duration} \propto E^{\beta}$), which supports that similar mechanism is shared by stellar superflares and solar flares. Stellar photometric variability (Rvar) is estimated for all solar-type stars, and the relation of $E \propto Rvar^{3/2}$ is included. Indicator of chromospheric activity (S-index) is obtained by using data from the Large Sky Area Multi-Object Fiber Spectroscopic Telescope (LAMOST) for 7454 solar-type stars. Distributions of these two properties indicate that the Sun is generally less active than superflare stars. We find that saturation-like feature of $Rvar \sim 0.1$ may be the reason for superflare energy saturating around 1036 erg. TIC93277807 was captured by {\em TESS} first-year mission and generated the most energetic superflare. This superflare is valuable and unique to be treated as an extreme event, which may be generated by different mechanisms rather than that of other superflares.

THE MAGNETIC ENERGY-HELICITY DIAGRAM OF SOLAR ACTIVE REGIONS

Kostas **Tziotziou**1, Manolis K. Georgoulis1,3, and Nour-Eddine Raouafi
2012 ApJ 759 L4
Using a recently proposed nonlinear force-free method designed for single-vector magnetograms of solar active regions, we calculate the instantaneous free magnetic energy and relative magnetic helicity budgets in 162 vector magnetograms corresponding to 42 different active regions. We find a statistically robust, monotonic correlation between the free magnetic energy and the relative magnetic helicity in the studied regions. This correlation implies that magnetic helicity, in addition to free magnetic energy, may be an essential ingredient for major solar eruptions. Eruptive active regions appear well segregated from non-eruptive ones in both free energy and relative helicity with major (at least M-class) flares occurring in active regions with free energy and relative helicity exceeding 4 × 1031 erg and 2 × 1042 Mx2, respectively. The helicity threshold agrees well with estimates of the helicity contents of typical coronal mass ejections.

OBSERVATIONS OF MULTIPLE SURGES ASSOCIATED WITH MAGNETIC ACTIVITIES IN AR 10484 ON 2003 OCTOBER 25

Wahab **Uddin**1, B. Schmieder2, R. Chandra3, Abhishek K. Srivastava1, Pankaj Kumar4, and S. Bisht

2012 ApJ 752 70

We present a multi-wavelength study of recurrent surges observed in Hα, UV (Solar and Heliospheric Observatory (SOHO)/EIT), and Radio (Learmonth, Australia) from the super-active region NOAA 10484 on 2003 October 25. Several bright structures visible in Hα and UV corresponding to subflares are also observed at the base of each surge. Type III bursts are triggered and RHESSI X-ray sources are evident with surge activity. The major surge consists of bunches of ejective paths forming a fan-shaped region with an angular size of (65°) during its maximum phase. The ejection speed reaches up to ~200 km s–1. The SOHO/Michelson Doppler Imager magnetograms reveal that a large dipole emerges from the east side of the active region on 2003 October 18-20, a few days before the surges. **On 2003 October 25,** the major sunspots were surrounded by "moat regions" with moving magnetic features (MMFs). Parasitic fragmented positive polarities were pushed by the ambient dispersion motion of the MMFs and annihilated with negative polarities at the borders of the moat region of the following spot to produce flares and surges. A topology analysis of the global Sun using Potential Field Source Surface shows that the fan structures visible in the EIT 171 Å images follow magnetic field lines connecting the present active region to a preceding active region in the southeast. Radio observations of Type III bursts indicate that they are coincident with the surges, suggesting that magnetic reconnection is the driver mechanism. The magnetic energy released by the reconnection is transformed into plasma heating and provides the kinetic energy for the ejections. A lack of a radio signature in the high corona suggests that the surges are confined to follow the closed field lines in the fans. We conclude that these cool surges may have some local heating effects in the closed loops, but probably play a minor role in global coronal heating and the surge material does not escape to the solar wind.

Extremely Energetic 4B/X17.2 Flare and Associated Phenomena

Wahab **Uddin**∗, Ramesh Chandra & Syed Salman Ali

J. Astrophys. Astr. (**2006**) **27,** 267–276

http://www.ias.ac.in/jaa/junsep2006/JAA22.pdf

We observed 4B/X17.2 flare in H*α* from super-active region NOAA 10486 at ARIES, Nainital. This is one of the largest flares of current solar cycle 23, which occurred near the Sun's center and produced extremely energetic emission almost at allwavelengths from γ -ray to radiowaves. The flare is associated with a bright/fast full-halo earth directed CME, strong type II, type III and type IV radio bursts, an intense proton event and GLE. This flare is well observed bySOHO,RHESSI andTRACE. Our H*α* observations show the stretching/de-twisting and eruption of helically twisted S shaped (sigmoid) filament in the south–west direction of the active region with bright shock front followed by rapid increase in intensity and area of the gigantic flare. The flare shows almost similar evolution in H*α*, EUV and UV. We measure the speed of H*α* ribbon separation and the mean value is ∼ 70 km s−1. This is used together with photospheric magnetic field to infer a magnetic reconnection rate at three HXR sources at the flare maximum. In this paper, we also discuss the energetics of active region filament, flare and associated CME.

Orientation of X-Ray Bright Points in the Quiet Sun

K. **Ueda**, R. Kano, S. Tsuneta & H. Shibahashi

Solar Phys., 261, No. 1, Page: 77 – 85, **2010**

Thanks to the high-resolution images from the X-ray telescope (XRT) aboard the *Hinode* satellite, X-ray bright points (XBPs) in the quiet region of the Sun are resolved and can be seen to have complex loop-like structures. We measure the orientation of such loop structures for 488 XBPs picked up in 26 snapshot X-ray images near the disk center. The distribution of the orientation is slightly but clearly biased to the east−west direction: the random distribution is rejected with a significance level of 1% by the χ^2-test. The distribution is similar to the orientation distribution for the bipolar magnetic fields. The XBP orientation is, however, much more random than that of the bipolar magnetic fields with similar size. 24% of the XBPs are due to emerging bipoles, while the remaining 76% are due to chance encounters of opposite polarities.

DETERMINING HEATING TIME SCALES IN SOLAR ACTIVE REGION CORES FROM AIA/*SDO* FE XVIII IMAGES

IGNACIO **UGARTE-URRA**1 AND HARRY P. WARREN2

E-print, Jan **2014**; **2014** ApJ 783 12

We present a study of the frequency of transient brightenings in the core of solar active regions as observed in the Fe XVIII line component of AIA/*SDO* 94 °A filter images. The Fe XVIII emission is isolated using an

empirical correction to remove the contribution of “warm” emission to this channel. Comparing with simultaneous observations from EIS/*Hinode*, we find that the variability observed in Fe XVIII is strongly correlated with the emission from lines formed at similar temperatures. We examine the evolution of loops in the cores of active regions at various stages of evolution. Using a newly developed event detection algorithm we characterize the distribution of event frequency, duration, and magnitude in these active regions. These distributions are similar for regions of similar age and show a consistent pattern as the regions age. This suggests that these characteristics are important constraints for models of solar active regions. We find that the typical frequency of the intensity fluctuations is about 1400 s for any given line-of-sight, i.e. about 2–3 events per hour. Using the EBTEL 0D hydrodynamic model, however, we show that this only sets a lower limit on the heating frequency along that line-of-sight. **2011/08/04, 2011/11/08, 2011/12/05, 2012/04/22, 2012/05/18**

TEMPORAL VARIABILITY OF ACTIVE REGION OUTFLOWS

Ignacio **Ugarte-Urra**1 and Harry P. Warren2
2011 ApJ 730 37
Recent observations from the Extreme-ultraviolet Imaging Spectrometer (EIS) on board Hinode have shown that low-density areas on the periphery of active regions are characterized by strong blueshifts in the emission of spectral lines formed at 1 MK. These Doppler shifts have been associated with outward propagating disturbances observed with extreme-ultraviolet and soft X-ray imagers. Since these instruments can have broad temperature responses, we investigate these intensity fluctuations using the monochromatic imaging capabilities of the EIS wide slit (slot) and confirm their 1 MK nature. We also look into their spectral temporal variability using narrow slit observations and present the first Doppler movies of the outflow regions. We find that the Fe XII 195.119 Å blueshifted spectral profiles at their footpoints exhibit transient blue wing enhancements on timescales as short as the 5 minute cadence. We have also looked at the fan peripheral loops observed at 0.6 MK in Si VII 275.368 Å in those regions and find no sign of the recurrent outward propagating disturbances with velocities of 40-130 km s–1 seen in Fe XII. We do observe downward trends (15-20 km s–1) consistent with the characteristic redshifts measured at their footpoints. We, therefore, find no evidence that the structures at these two temperatures and the intensity fluctuations they exhibit are related to one another.

Active Region Transition Region Loop Populations and Their Relationship to the Corona

Ignacio **Ugarte-Urra**, Harry P. Warren, and David H. Brooks
ApJ 695, 642-651, **2009**
http://www.iop.org/EJ/toc/-alert=43190/0004-637X/695/1
The relationships among coronal loop structures at different temperatures are not settled. Previous studies have suggested that coronal loops in the core of an active region (AR) are not seen cooling through lower temperatures and therefore are steadily heated. If loops were cooling, the transition regionwould be an ideal temperature regime to look for a signature of their evolution. The Extreme-ultraviolet Imaging Spectrometer on ***Hinode*** provides monochromatic images of the solar transition region and corona at an unprecedented cadence and spatial resolution, making it an ideal instrument to shed light on this issue. Analysis of observations of AR 10978 taken in 2007 December 8–19 indicates that there are two dominant loop populations in the AR: (1) core multitemperature loops that undergo a continuous process of heating and cooling in the full observed temperature range 0.4–2.5MK and even higher as shown by the X-Ray Telescope and (2) peripheral loops which evolve mostly in the temperature range 0.4–1.3MK. Loops at transition region temperatures can reach heights of 150 Mm in the corona above the limb and develop downflows with velocities in the range of 39–105 km s^{-1}.

Solar extreme ultraviolet variability as a proxy for nanoflare heating diagnostics

Artem **Ulyanov**, Anton Reva, Alexey Kirichenko, Ivan Loboda and Sergey Bogachev
A&A 683, A88 (**2024**)
https://www.aanda.org/articles/aa/pdf/2024/03/aa48425-23.pdf
Aims. We aim to improve the existing techniques to probe the nanoflare hypothesis for the coronal heating problem. For this purpose, we propose using the solar extreme ultraviolet (EUV) emission variability registered with modern space-based imagers.
Methods. We followed a novel model-based approach. As a starting point, we used the EBTEL 0d hydrodynamic model. We integrated the arising system of stochastic differential equations to calculate the covariance matrix for plasma parameters. We then employed a Taylor expansion technique to relate model parameters with observable EUV intensity variation statistics.
Results. We found that in the high-frequency approximation, the variability of the EUV emission is defined by the dimensionless factor ϖ, which is inversely proportional to the frequency. We calculated the factor ϖ throughout the solar disk and found that it does not exceed 0.01, except for the finite number of compact regions. The distribution of ϖ follows the power law with an index of ≈ -2.6. To validate our approach, we used it to probe the temperature of

the coronal plasma. We show that the line-of-sight temperature distribution is close to homogeneous with a mode of ≈1.25 MK, which is in perfect agreement with the results of the spectroscopic diagnostics.

Direct Evidence for Magnetic Reconnection in a Solar EUV Nanoflare

Artem S. **Ulyanov**, Sergey A. Bogachev, Ivan P. Loboda, Anton A. Reva, Alexey S. Kirichenko
Solar Physics September **2019**, 294:128
https://link.springer.com/content/pdf/10.1007%2Fs11207-019-1472-0.pdf
sci-hub.se/10.1007/s11207-019-1472-0
We provide observational evidence that the mechanism of solar EUV nanoflares may be close to the standard flare model. The object of our study was a nanoflare on **25 February 2011**, for which we determined a plasma temperature of 3.1 MK, a total thermal energy of 6.2×1025 erg, and an electric-current distribution that reaches its maximum at a height of ≈1.5 Mm. Despite the lack of spatial resolution, we reconstructed the 3D magnetic configuration for this event in the potential and non-linear force-free-field interpolations. As a result, we identified four null-points, two of which were coincident with the region of maximal energy release. The nanoflare was initiated by a new small-scale magnetic flux, which appeared on the photosphere about 15 – 20 minutes before the nanoflare. The total free energy stored in the region before the nanoflare was ≈8.9×1025 erg. Only about two-thirds of this amount was transferred into the plasma heating and EUV radiation. We posit that the remaining energy could be transferred during particle acceleration and plasma motions, which are still inaccessible for direct observations in nanoflares.

Examining Flux Tube Interactions as a Cause of Sub-alfvénic Outflow

John **Unverferth**1 and Dana Longcope2
2021 ApJ 923 248
https://iopscience.iop.org/article/10.3847/1538-4357/ac312e/pdf
https://iopscience.iop.org/article/10.3847/1538-4357/ac312e/pdf
https://doi.org/10.3847/1538-4357/ac312e
In accepted models, magnetic tension drives reconnected magnetic flux away from the reconnection site at the local Alfvén speed. Numerous observational signatures of these outflows have been identified in solar flares, notable among them being supra-arcade downflows (SADs), almost none move at the Alfvén speed as predicted by models. Well-studied examples of SADs or SAD loops found in the flare of **2017 September 10** (SOL2017-09-10T15:35:00) move at a quarter or less of the expected Alfvén speed. Among those reasons posited to explain such discrepancies is the possibility that reconnected flux experiences a drag force during its outflow. Drag has not been included in previous reconnection models. Here, we develop the first such model in order to test the possibility that drag can explain sub-alfveńic reconnection outflows. Our model uses thin flux tube dynamics, previously shown to match features of flare observations other than outflow speed, including for the 2017 September 10 flare. We supplement the dynamics with a drag force representing the tube's interaction with surrounding plasma through the formation of a wake. The wake's width appears as a parameter in the force. We perform simulations, varying the drag parameter and synthesizing EUV observations, to test whether a drag force can produce a reasonable fit to observed features of the September 10 flare. We find that that slower retraction increases the brightness of emission and lowers the temperature of the synthetic plasma sheet. With proper choice of parameters the drag enables the simulation to agree reasonably with the observations.

Modeling Observable Differences in Flare Loop Evolution due to Reconnection Location and Current Sheet Structure

John **Unverferth** and Dana Longcope
2020 ApJ 894 148
https://doi.org/10.3847/1538-4357/ab88cf
Flare reconnection is expected to occur at some point within a large-scale coronal current sheet. The structure of the magnetic field outside this sheet is almost certain to affect the flare, especially its energy release. Different models for reconnection have invoked different structures for the current sheet's magnetic field and different locations for the reconnection electric field within it. Models invoking Petschek-type reconnection often use a uniform field. Others invoke a field bounded by two Y-points with a field strength maximum between them and propose this maximum as the site of the reconnection electric field. Still other models, such as the collapsing trap model, require that the field strength peak at or near the edge of the current sheet and propose that reconnection occurs above this peak. At present there is no agreement as to where reconnection might occur within a global current sheet. We study the post-reconnection dynamics under all these scenarios, seeking potentially observable differences between them. We find that reconnection occurring above the point of strongest field leads to the highest density and the highest emission measure of the hottest material. This scenario offers a possible explanation of superhot coronal sources seen in some flares.

Effects of the Canopy and Flux Tube Anchoring on Evaporation Flow of a Solar Flare

John **Unverferth** and Dana Longcope
2018 ApJ 859 170

Spectroscopic observations of flare ribbons typically show chromospheric evaporation flows, which are subsonic for their high temperatures. This contrasts with many numerical simulations where evaporation is typically supersonic. These simulations typically assume flow along a flux tube with a uniform cross-sectional area. A simple model of the magnetic canopy, however, includes many regions of low magnetic field strength, where flux tubes achieve local maxima in their cross-sectional area. These are analgous to a chamber in a flow tube. We find that one-third of all field lines in a model have some form of chamber through which evaporation flow must pass. Using a one-dimensional isothermal hydrodynamic code, we simulated supersonic flow through an assortment of chambers and found that a subset of solutions exhibit a stationary standing shock within the chamber. These shocked solutions have slower and denser upflows than a flow through a uniform tube would. We use our solution to construct synthetic spectral lines and find that the shocked solutions show higher emission and lower Doppler shifts. When these synthetic lines are combined into an ensemble representing a single canopy cell, the composite line appears slower, even subsonic, than expected due to the outsized contribution from shocked solutions.

Nanoflare Heating of the Solar Corona Observed in X-rays

Vishal **Upendran**, Durgesh Tripathi, N.P.S. Mithun, Santosh Vadawale, Anil Bhardwaj
ApJ Letters **2022**
https://arxiv.org/pdf/2211.02324.pdf
The existence of the million-degree corona above the cooler photosphere is an unsolved problem in astrophysics. Detailed study of quiescent corona that exists regardless of the phase of the solar cycle may provide fruitful hints towards resolving this conundrum. However, the properties of heating mechanisms can be obtained only statistically in these regions due to their unresolved nature. Here, we develop a two-step inversion scheme based on the machine learning scheme of Upendran & Tripathi (2021a) for the empirical impulsive heating model of Pauluhn & Solanki (2007), and apply it to disk integrated flux measurements of the quiet corona as measured by the X-ray solar monitor (XSM) onboard Chandrayaan - 2. We use data in three energy passbands, viz., 1 - 1.3 keV, 1.3 - 2.3 keV, and 1 - 2.3 keV, and estimate the typical impulsive event frequencies, timescales, amplitudes, and the distribution of amplitudes. We find that the impulsive events occur at a frequency of ≈25 events per minute with a typical lifetime of ≈10 minutes. They are characterized by a power law distribution with a slope $\alpha \leq 2.0$. The typical amplitudes of these events lie in an energy range of 1021 - 1024 ergs, with a typical radiative loss of about ≈103 erg cm−2 s−1 in the energy range of 1 - 2.3 keV. These results provide further constraints on the properties of sub-pixel impulsive events in maintaining the quiet solar corona.

The First AGILE Solar Flare Catalog

Alessandro **Ursi**, Nicolò Parmiggiani, Mauro Messerotti, Alberto Pellizzoni, Carlotta Pittori, Francesco Longo, Francesco Verrecchia, Andrea Argan, Andrea Bulgarelli, Marco Tavani, Patrizio Tempesta, Fabio D'Amico
ApJS **267** 9 **2023**
https://arxiv.org/pdf/2305.14957.pdf
https://iopscience.iop.org/article/10.3847/1538-4365/acd4b6/pdf
We report the Astrorivelatore Gamma ad Immagini LEggero (AGILE) observations of solar flares, detected by the on board anticoincidence system in the 80-200 keV energy range, from 2007 May 1st to 2022 August 31st. In more than 15 yr, AGILE detected 5003 X-ray, minute-lasting transients, compatible with a solar origin. A cross-correlation of these transients with the Geostationary Operational Environmental Satellites (GOES) official solar flare database allowed to associate an intensity class (i.e., B, C, M, or X) to 3572 of them, for which we investigated the main temporal and intensity parameters. The AGILE data clearly revealed the solar activity covering the last stages of the 23rd cycle, the whole 24th cycle, and the beginning of the current 25th cycle. In order to compare our results with other space missions operating in the high-energy range, we also analyzed the public lists of solar flares reported by RHESSI and Fermi Gamma-ray Burst Monitor. This catalog reports 1424 events not contained in the GOES official dataset, which, after statistical comparisons, are compatible with low-intensity, short-duration solar flares.
Besides providing a further dataset of solar flares detected in the hard X-ray range, this study allowed to point out two main features: a longer persistence of the decay phase in the high-energy regime, with respect to the soft X-rays, and a tendency of the flare maximum to be reached earlier in the soft X-rays with respect to the hard X-rays. ***Both these aspects support a two-phase acceleration mechanism of electrons in the solar atmosphere.*** **2013 April 24**

Extreme Solar Events: Setting up a Paradigm **Review**

Usoskin, I., Miyake, F., Baroni, M. et al.
Space Sci Rev 219, 73 (**2023**).
https://doi.org/10.1007/s11214-023-01018-1
https://link.springer.com/content/pdf/10.1007/s11214-023-01018-1.pdf **File**
The Sun is magnetically active and often produces eruptive events on different energetic and temporal scales. Until recently, the upper limit of such events was unknown and believed to be roughly represented by direct instrumental observations. However, two types of extreme events were discovered recently: extreme solar energetic particle events on the multi-millennial time scale and super-flares on sun-like stars. Both discoveries imply that the Sun might rarely

produce events, called extreme solar events (ESE), whose energy could be orders of magnitude greater than anything we have observed during recent decades. During the years following these discoveries, great progress has been achieved in collecting observational evidence, uncovering new events, making statistical analyses, and developing theoretical modelling. The ESE paradigm lives and is being developed. On the other hand, many outstanding questions still remain open and new ones emerge. Here we present an overview of the current state of the art and the forming paradigm of ESE from different points of view: solar physics, stellar–solar projections, cosmogenic-isotope data, modelling, historical data, as well as terrestrial, technological and societal effects of ESEs. Special focus is paid to open questions and further developments. This review is based on the joint work of the International Space Science Institute (ISSI) team #510 (2020–2022). 7176 BCE and 5259 BCE, **5410 BCE, 1279 CE, 1052 CE, 1859, 4-6 Dec 2006, 13 Dec 2006**

The size distribution of magnetic bright points derived from Hinode/SOT observations

D. **Utz**1, A. Hanslmeier1, C. Möstl1, 2, R. Muller3, A. Veronig1, and H. Muthsam4
A&A 498, 289-293 (2009), DOI: 10.1051/0004-6361/200810867
Context. Magnetic bright points (MBPs) are small-scale magnetic features in the solar photosphere. They may be a possible source of coronal heating by rapid footpoint motions that cause magnetohydrodynamical waves. The number and size distribution are of vital importance in estimating the small scale-magnetic-field energy.
Aims. The size distribution of MBPs is derived for G-band images acquired by the Hinode/SOT instrument.
Methods. For identification purposes, a new automated segmentation and identification algorithm was developed.
Results. For a sampling of 0.108 arcsec/pixel, we derived a mean diameter of $^{(218 \pm 48)}$ km for the MBPs. For the full resolved data set with a sampling of 0.054 arcsec/pixel, the size distribution shifted to a mean diameter of $^{(166 \pm 31)}$ km. The determined diameters are consistent with earlier published values. The shift is most probably due to the different spatial sampling.
Conclusions. We conclude that the smallest magnetic elements in the solar photosphere cannot yet be resolved by G-band observations. The influence of discretisation effects (sampling) has also not yet been investigated sufficiently.

Magnetic Reconnection Onset via Disruption of a Forming Current Sheet by the Tearing Instability

Dmitri A. **Uzdensky**, Nuno F. Loureiro
2014
http://arxiv.org/pdf/1411.4295v1.pdf
The recent realization that Sweet-Parker current sheets are violently unstable to the secondary tearing (plasmoid) instability implies that such current sheets cannot occur in real systems. This suggests that, in order to understand the onset of magnetic reconnection, one needs to consider the growth of the tearing instability in a current layer as it is being formed. Such an analysis is performed here in the context of nonlinear resistive MHD for a generic time-dependent equilibrium representing a gradually forming current sheet. It is shown that two regimes, single-island and multi-island, are possible, depending on the rate of current sheet formation. A simple model is used to compute the criterion for transition between these two regimes, as well as the reconnection onset time and the current sheet parameters at that moment. For typical solar corona parameters this model yields results consistent with observations.

Observations of the Quiet Sun During the Deepest Solar Minimum of the Past Century with Chandrayaan-2 XSM -- Sub-A Class Microflares Outside Active Regions

Santosh V. **Vadawale**, N. P. S. Mithun, Biswajit Mondal, Aveek Sarkar, P. Janardhan, Bhuwan Joshi, Anil Bhardwaj, M. Shanmugam, Arpit R. Patel, Hitesh Kumar L. Adalja, Shiv Kumar Goyal, Tinkal Ladiya, Neeraj Kumar Tiwari, Nishant Singh, Sushil Kumar
ApJL **912** L13 **2021**
https://arxiv.org/pdf/2103.16644.pdf
https://iopscience.iop.org/article/10.3847/2041-8213/abf0b0/pdf
https://doi.org/10.3847/2041-8213/abf0b0
Solar flares, with energies ranging over several orders of magnitude, result from impulsive release of energy due to magnetic reconnection in the corona. Barring a handful, almost all microflares observed in X-rays are associated with the solar active regions. Here we present, for the first time, a comprehensive analysis of a large sample of quiet Sun microflares observed in soft X-rays by the Solar X-ray Monitor (XSM) on board the Chandrayaan-2 mission during the 2019-20 solar minimum. A total of 98 microflares having peak flux below GOES A-level were observed by the XSM during observations spanning 76 days. By using the derived plasma temperature and emission measure of these events obtained by fitting the XSM spectra along with volume estimates from concurrent imaging observations in EUV with the Solar Dynamics Observatory/Atmospheric Imaging Assembly (SDO/AIA), we estimated their thermal energies to be ranging from 3e26 to 6e27 erg. We present the frequency distribution of the quiet Sun microflares with energy and discuss the implications of these observations of small-scale magnetic reconnection events outside active regions on coronal heating. **12-29 Sep 2019, 24 Feb-24 Mar 2020**

Table 1. Micoflares observed by XSM in the quiet Sun period

Particle Acceleration Mechanisms **Tutorial** **Review**

Rami **Vainio** and Alexandr Afanasiev

In: O.E. Malandraki, N.B. Crosby (eds.), Solar Particle Radiation Storms Forecasting and Analysis Chapter 3, **2018**

https://link.springer.com/content/pdf/10.1007%2F978-3-319-60051-2.pdf

File Malandraki_Crosby_SEPs_Forecasting and Analysis_Book.pdf

This chapter provides a short tutorial review on particle acceleration in dynamic electromagnetic fields under scenarios relevant to the problem of particle acceleration in the solar corona and solar wind during solar eruptions. It concentrates on fundamental aspects of the acceleration process and refrains from presenting detailed modeling of the specific conditions in solar eruptive plasmas. All particle acceleration mechanisms (in the solar corona) are related to electric fields that can persist in the highly conductive plasma: either electrostatic (or potential) or inductive related to temporally variable magnetic fields through Faraday's law. Mechanisms involving both kinds of fields are included in the tutorial.

Solar flare catalog from 3 years of Chandrayaan-2 XSM observations

Aravind Bharathi **Valluvan**, Ashwin Goyal, Devansh Jain, Abhinna Sundar Samantaray, Abhilash Sarwade, Kasiviswanathan Sankarasubramanian

Solar Phys. Volume 299, article number 8 **2024**

https://arxiv.org/pdf/2312.09191.pdf

https://doi.org/10.1007/s11207-023-02244-0

We present a catalog of 6266 solar flares detected by the X-Ray Solar Monitor onboard the Chandrayaan-2 lunar orbiter between 1.55 and 12.4 keV (1 and 8 Å) **from 2019 September 12 to 2022 November 4**, including 1469 type A flares. The catalog represents the first large sample, including both type A, hot thermal flares, and type B, impulsive flares, with a sub-A class sensitive instrument. We also detect 213 sub-A and 1330 A class flares. Individual flares are fit with an exponentially-modified Gaussian function and multi-flare groups are decomposed into individual flares. We validate our findings with flare catalogs made using visual inspection as well as automatic pipelines on Geostationary Operational Environmental Satellite and Solar Dynamics Observatory data. We find a clear bimodality in the ratio of the width to decay time between type A and B flares. We infer a power-law index of $\alpha_F=1.92\pm0.09$ for the background-subtracted peak flux distribution of XSM flares, which is consistent with the value ~2 reported in the literature. We also infer $\alpha_F=1.90\pm0.09$ for type B, and $\alpha_F=1.94\pm0.08$ for type A flares, which has previously not been reported in the literature. These comparable values hint at a similarity in their generative processes.

Time Evolution of Force-Free Parameter and Free Magnetic Energy in Active Region NOAA 10365

G. **Valori**, P. Romano, A. Malanushenko, I. Ermolli, F. Giorgi, K. Steed, L. van Driel-Gesztelyi, F. Zuccarello, J.-M. Malherbe

Solar Phys., February **2015**, Volume 290, Issue 2, pp 491-506

We describe the variation of the accumulated coronal helicity derived from the magnetic helicity flux through the photosphere in active region (AR) NOAA 10365, where several large flares and coronal mass ejections (CMEs) occurred. We used SOHO/MDI full-disk line-of-sight magnetograms to measure the helicity flux, and the integral of GOES X-ray flux as a proxy of the coronal energy variations due to flares or CMEs. Using the linear force-free field model, we transformed the accumulated helicity flux into a time sequence of the force-free parameter α accounting for flares or CMEs via the proxy derived from GOES observations. This method can be used to derive the value of α at different times during the AR evolution, and is a partial alternative to the commonly used match of field lines with EUV loops. By combining the accumulated helicity obtained from the observations with the linear force-free theory, we describe the main phases of the emergence process of the AR, and relate them temporally with the occurrence of flares or CMEs. Additionally, a comparison with the loop-matching method of fixing alpha at each time independently shows that the proposed method may be helpful in avoiding unrealistic or undetermined values of alpha that may originate from an insufficient quality of the image used to identify coronal loops at a given time. For the relative intensity of the considered events, the linear force-free field theory implies that there is a direct correlation between the released energy on the one hand and the product of the coronal helicity with the variation of α due to the event on the other. Therefore, the higher the value of the accumulated coronal helicity, the smaller the force-free parameter variation required to produce the same decrease in the free energy during the CMEs.

Reconnection brightenings in the quiet solar photosphere

Luc H. M. Rouppe **van der Voort**, Robert J. Rutten, Gregal J. M. Vissers

A&A **2016**

http://arxiv.org/pdf/1606.03675v1.pdf

We describe a new quiet-Sun phenomenon which we call "Quiet-Sun Ellerman-like Brightenings" (QSEB). QSEBs are similar to Ellerman bombs (EB) in some respects but differ significantly in others. EBs are transient brightenings of the wings of the Balmer H-alpha line that mark strong-field photospheric reconnection in complex active regions. QSEBs are similar but smaller and less intense Balmer-wing brightenings that occur in quiet areas away from active regions. In the H-alpha wing we measure typical lengths of less than 0.5 arcsec, widths of 0.21 arcsec, and lifetimes of less than a minute. We discovered them using high-quality H-alpha imaging spectrometry from the Swedish 1-m Solar Telescope (SST) and show that in lesser-quality data they cannot be distinguished from more ubiquitous facular brightenings, nor in the ultraviolet diagnostics currently available from space platforms. We add evidence from concurrent SST spectropolarimetry that QSEBs also mark photospheric reconnection events, but in quiet regions on the solar surface.

Quasi-periodic pulsations in solar and stellar flares: an overview of recent results **Review**

Tom **Van Doorsselaere**, Elena G. Kupriyanova, Ding Yuan
Solar Phys. Volume 291, Issue 11, pp 3143–3164 **2016**
http://arxiv.org/pdf/1609.02689v1.pdf
https://perswww.kuleuven.be/~u0041608/docs/2016qppreview.pdf
Quasi-periodic pulsations (or QPPs) are periodic intensity variations in the flare emission, across all wavelength bands. In this paper, we review the observational and modelling achievements since the previous review on this topic by Nakariakov & Melnikov (2009). In recent years, it has become clear that QPPs are an inherent feature of solar flares, because almost all flares exhibit QPPs. Moreover, it is now firmly established that QPPs often show multiple periods. We also review possible mechanisms for generating QPPs. Up to now, it has not been possible to conclusively identify the triggering mechanism or cause of QPPs. The lack of this identification currently hampers possible seismological inferences of flare plasma parameters. QPPs in stellar flares have been detected for a long time, and the high quality data of the Kepler mission allows to study the QPP more systematically. However, it has not been conclusively shown whether the time scales of stellar QPPs are different or the same as those in solar flares.

LYRA OBSERVATIONS OF TWO OSCILLATION MODES IN A SINGLE FLARE

T. **Van Doorsselaere**1,5, A. De Groof2, J. Zender3, D. Berghmans4 and M. Goossens
2011 ApJ 740 90
We analyze light curves from the LYRA irradiance experiment on board PROBA2 during the flare of **2010 February 8**. We see both long- and short-period oscillations during the flare. The long-period oscillation is interpreted in terms of standing slow sausage modes; the short-period oscillation is thought to be a standing fast sausage mode. The simultaneous presence of two oscillation modes in the same flaring structure allows for new coronal seismological applications. The periods are used to find seismological estimates of the plasma-β and the density contrast of the flaring loop. Also the wave mode number is estimated from the observed periods.

Evolution of Active Regions **Review**

van Driel-Gesztelyi, Lidia and Green, Lucie M.
Living Reviews in Solar Physics PUB.NO. lrsp-2015-1, Sept **2015**
http://solarphysics.livingreviews.org/Articles/lrsp-2015-1/
The evolution of active regions (AR) from their emergence through their long decay process is of fundamental importance in solar physics. Since large-scale flux is generated by the deep-seated dynamo, the observed characteristics of flux emergence and that of the subsequent decay provide vital clues as well as boundary conditions for dynamo models. Throughout their evolution, ARs are centres of magnetic activity, with the level and type of activity phenomena being dependent on the evolutionary stage of the AR. As new flux emerges into a pre-existing magnetic environment, its evolution leads to re-configuration of small-and large-scale magnetic connectivities. The decay process of ARs spreads the once-concentrated magnetic flux over an ever-increasing area. Though most of the flux disappears through small-scale cancellation processes, it is the remnant of large-scale AR fields that is able to reverse the polarity of the poles and build up new polar fields. In this Living Review the emphasis is put on what we have learned from observations, which is put in the context of modelling and simulation efforts when interpreting them. For another, modelling-focused Living Review on the sub-surface evolution and emergence of magnetic flux see Fan (2009). In this first version we focus on the evolution of dominantly bipolar ARs.

Shock-drift accelerated electrons and n-distribution

M. **Vandas** and M. Karlický
A&A 591, A127 (**2016**)
Aims. By analyzing soft X-ray spectra observed during the impulsive phase of several solar flares, the n-distribution function of superthermal electrons has been detected. In the paper we try to answer the question of whether electrons with this type of distribution function can be produced in a shock, e.g. in a flare termination shock.
Methods. We use analytical and numerical methods to compute distribution functions of electrons accelerated by a shock.

Results. We analytically derive the distribution functions of reflected electrons at quasi-perpendicular shocks. We also consider the influence of the electrostatic cross-shock potential, shock curvature, and the role of the upstream seed population on these distributions. The computed distributions are compared with the n-distributions. We found that a high-energy part of the distribution of electrons reflected at a quasi-perpendicular shock can be very well fitted by the n-distribution in all the cases we studied. This provides a chance to detect the flare termination shock.

Active region upflows: 1. Multi-instrument observations

K. **Vanninathan**, M.S. Madjarska, K. Galsgaard, Z. Huang, J.G. Doyle
A&A **2015**
http://arxiv.org/pdf/1509.05624v1.pdf
Upflows at the edges of active regions (ARs) are studied by spatially and temporally combining multi-instrument observations obtained with EIS/Hinode, AIA and HMI/SDO and IBIS/NSO, to derive their plasma parameters. This information is used for benchmarking data-driven modelling of the upflows (Galsgaard et al., 2015). The studied AR upflow displays blueshifted emission of 5-20 km/s in Fe XII and Fe XIII and its average electron density is 1.8x10^9 cm^3 at 1 MK. The time variation of the density shows no significant change (in a 3sigma error). The plasma density along a single loop drops by 50% over a distance of 20000 km. We find a second velocity component in the blue wing of the Fe XII and Fe XIII lines at 105 km/s. This component is persistent during the whole observing period of 3.5 hours with variations of only 15 km/s. We also study the evolution of the photospheric magnetic field and find that magnetic flux diffusion is responsible for the formation of the upflow region. High cadence Halpha observations of the chromosphere at the footpoints of the upflow region show no significant jet-like (spicule/rapid blue excursion) activity to account for several hours/days of plasma upflow. Using an image enhancement technique, we show that the coronal structures seen in the AIA 193A channel is comparable to the EIS Fe XII images, while images in the AIA 171A channel reveals additional loops that are a result of contribution from cooler emission to this channel. Our results suggest that at chromospheric heights there are no signatures that support the possible contribution of spicules to AR upflows. We suggest that magnetic flux diffusion is responsible for the formation of the coronal upflows. The existence of two velocity components possibly indicate the presence of two different flows which are produced by two different physical mechanisms, e.g. magnetic reconnection and pressure-driven.

Evidence for a White-light Flare on 10 September 1886

J.M. **Vaquero**, M. Vázquez, J. Sánchez Almeida
Solar Phys. 292:33 **2017**
https://arxiv.org/pdf/1701.05910v1.pdf
We present evidence for the occurrence of a white-light flare on **10 September 1886**. It represents the third of such rare events reported in the history of astronomy. The flare was mentioned by Valderrama (1886, L'Astronomie 5, 388). In this article we have used the original logbook of the observer, J. Valderrama y Aguilar, an amateur astronomer that lived in Madrid and Santa Cruz de Tenerife at that time.

Modifications of thick-target model: re-acceleration of electron beams by static and stochastic electric fields

M. **Varady**1,2, M. Karlický2, Z. Moravec1 and J. Kašparová
A&A 563, A51 (**2014**)
Context. The collisional thick-target model (CTTM) of the impulsive phase of solar flares, together with the famous Carmichael, Sturrock, Hirayama, and Kopp-Pneuman (CSHKP) model, presented for many years a “standard” model, which straightforwardly explained many observational aspects of flares. On the other hand, many critical issues appear when the concept is scrutinised theoretically or with the new generation of hard X-ray (HXR) observations. The famous “electron number problem” or problems related to transport of enormous particle fluxes though the corona represent only two of them. To resolve the discrepancies, several modifications of the CTTM appeared.
Aims. We study two of them based on the global and local re-acceleration of non-thermal electrons by static and stochastic electric fields during their transport from the coronal acceleration site to the thick-target region in the chromosphere. We concentrate on a comparison of the non-thermal electron distribution functions, chromospheric energy deposits, and HXR spectra obtained for both considered modifications with the CTTM itself.
Methods. The results were obtained using a relativistic test-particle approach. We simulated the transport of non-thermal electrons with a power-law spectrum including the influence of scattering, energy losses, magnetic mirroring, and also the effects of the electric fields corresponding to both modifications of the CTTM.
Results. We show that both modifications of the CTTM change the outcome of the chromospheric bombardment in several aspects. The modifications lead to an increase in chromospheric energy deposit, change of its spatial distribution, and a substantial increase in the corresponding HXR spectrum intensity.
Conclusions. The re-acceleration in both models reduces the demands on the efficiency of the primary coronal accelerator, on the electron fluxes transported from the corona downwards, and on the total number of accelerated coronal electrons during flares.

Confinedness of an X3.1 class solar flare occurred in NOAA 12192: Analysis from multi-instruments observations

N. **Vasantharaju**, F. Zuccarello, F. Ferrente, S. L. Guglielmino
ApJ **950** 183 **2023**
https://arxiv.org/pdf/2304.12156.pdf
https://iopscience.iop.org/article/10.3847/1538-4357/accfff/pdf
The non-association of coronal mass ejections with high energetic flares is sparse. For this reason, the magnetic conditions required for the confinedness of major flares is a topic of active research. Using multi-instrument observations, we investigated the evolution and effects of confinedness in an X3.1 flare, which occurred in active region (AR) 12192. The decrease of net fluxes in the brightening regions, near the footpoints of the multi-sigmoidal AR in photosphere and chromosphere, indicative of flux cancellation favouring tether-cutting reconnection (TCR), is observed using the magnetic field observations of HMI/SDO and SOT/Hinode, respectively. The analysis of spectropolarimetric data obtained by the Interferometric Bidimensional Spectrometer over the brightening regions suggests untwisting of field lines, which further supports TCR. Filaments near polarity inversion line region, resulted from TCR of low lying sheared loops, undergo merging and form an elongated filament. The temperature and density differences between footpoints of the merged filament, revealed by DEM analysis, caused streaming and counter-streaming of plasma flow along the filament and unloads at its footpoints with an average velocity of ≈ 40 km s−1. This results in decrease of mass of the filament (density decreased by >50%), leading to its rise and expansion outwards. However, due to strong strapping flux, the filament separates itself instead of erupting. Further, the evolution of non-potential parameters describes the characteristics of confinedness of the flare. Our study suggests that the sigmoid-filament system exhibits upward catastrophe due to mass unloading, but gets suppressed by strong confinement of external poloidal field. **24 October 2014**

Magnetic Imprints of Eruptive and Noneruptive Solar Flares as Observed by Solar Dynamics Observatory

N. **Vasantharaju**1,2, P. Vemareddy1, B. Ravindra1, and V. H. Doddamani3
2022 ApJ 927 86
https://iopscience.iop.org/article/10.3847/1538-4357/ac4d8c/pdf
The abrupt and permanent changes of the photospheric magnetic field in the localized regions of active regions during solar flares, called magnetic imprints (MIs), have been observed for nearly the past three decades. The well-known coronal implosion model is assumed to explain such flare-associated changes but the complete physical understanding is still missing and debatable. In this study, we made a systematic analysis of flare-related changes of the photospheric magnetic field during 21 flares (14 eruptive and seven noneruptive) using the 135 s cadence vector magnetogram data obtained from the Helioseismic and Magnetic Imager. The MI regions for eruptive flares are found to be strongly localized, whereas the majority of noneruptive events (>70%) have scattered imprint regions. To quantify the strength of the MIs, we derived the integrated change of horizontal field and the total change of Lorentz force over an area. These quantities correlate well with the flare strength, irrespective of whether flares are eruptive or not, or have a short or long duration. Further, the free energy (FE), determined from virial theorem estimates, exhibits a statistically significant downward trend that starts around the flare time and is observed in the majority of flares. The change of FE during flares does not depend on eruptivity but has a strong positive correlation (≈0.8) with the Lorentz force change, indicating that part of the FE released would penetrate the photosphere. While these results strongly favor the idea of significant feedback from the corona on the photospheric magnetic field, the characteristics of MIs are quite indistinguishable from flares being eruptive or not. **15 Feb 2011, 9 Mar 2011, 30 Jul 2011, 6 Mar 2012, 11 Apr 2013, 28 oct 2013, 8 Nov 2013, 2 Feb 2014, 24 Oct 2014, 23 May 2015, 22 Jun 2015,**
Table 1 List of 21 Flare Events from 17 ARs and their Associated Magnetic Properties

Statistical study of magnetic non-potential measures in confined and eruptive flares

N. **Vasantharaju**, P. Vemareddy, B. Ravindra, V. H. Doddamani
ApJ **860** 58 **2018**
https://arxiv.org/pdf/1805.02348.pdf
Using the HMI/SDO vector magnetic field observations, we studied the relation of degree of magnetic non-potentiality with the observed flare/CME in active regions. From a sample of 77 flare/CME cases, we found a general relation that degree of non-potentiality is positively correlated with the flare strength and the associated CME speeds. Since the magnetic flux in the flare-ribbon area is more related to the reconnection, we trace the strong gradient polarity inversion line (SGPIL), Schrijver's R value manually along the flare-ribbon extent. Manually detected SGPIL length and R values show higher correlation with the flare strength and CME speed than the automatically traced values without flare-ribbon information. It highlights the difficulty of predicting the flare strength and CME speed a priori from the pre-flare magnetograms used in flare prediction models. Although the total, potential magnetic energy proxies show weak positive correlation, the decrease in free energy exhibits higher correlation (0.56) with the flare strength and CME speed. Moreover, the eruptive flares have threshold of SGPIL length (31Mm), R value (1.6×1019Mx), free-energy decrease (2×1031erg) compared to confined ones. In 90\% eruptive flares, the decay-index curve is steeper

reaching ncrit=1.5 within 42Mm, whereas it is beyond 42Mm in >70% confined flares. While indicating the improved statistics in the predictive capability of the AR eruptive behavior with the flare-ribbon information, our study provides threshold magnetic properties for a flare to be eruptive. **15 Feb 2011, March 7, 2012**

Nature of helicity injection in non-erupting solar active regions

P. **Vemareddy**
MNRAS **2022**
https://arxiv.org/pdf/2208.03228
Using time-sequence vector magnetic field and coronal observations from \textit{Solar Dynamics Observatory}, we report the observations of the magnetic field evolution and coronal activity in four emerging active regions (ARs). The ARs emerge with leading polarity being the same as for the majority of ARs in a hemisphere of solar cycle 24. After emergence, the magnetic polarities separate each other without building a sheared polarity inversion line. In all four ARs, the magnetic fields are driven by foot point motions such that the sign of the helicity injection (dH/dt) in the first half of the evolution is changed to the opposite sign in the later part of the observation time. This successive injection of opposite helicity is also consistent with the sign of mean force-free twist parameter (αav). Further, the EUV light curves of the ARs in 94Å~and GOES X-ray flux reveal flaring activity below C-class magnitude. Importantly, the white-light coronagraph images in conjunction with the AR images in AIA 94 Å~delineate the absence of associated CMEs with the studied ARs. These observations imply that the ARs with successive injection of opposite sign magnetic helicity are not favorable to twisted flux rope formation with excess coronal helicity, and therefore are unable to launch CMEs, according to recent reports. This study provides the characteristics of helicity flux evolution in the ARs referring to the conservative property of magnetic helicity and more such studies would help to quantify the eruptive capability of a given AR. **17–22 Apr, 2012, 24–29 Jul, 2015, 25–30 Mar, 2017, 29 Mar–03 Apr, 2017**

Magnetic Structure in Successively Erupting Active Regions: Comparison of Flare-Ribbons with Quasi-Separatrix Layers

P. **Vemareddy**
Front. Phys 9:749479 **2021**
https://arxiv.org/pdf/2109.14583.pdf
https://www.frontiersin.org/articles/10.3389/fphy.2021.749479/pdf
https://doi.org/10.3389/fphy.2021.749479
This paper studies the magnetic topology of successively erupting active regions (ARs) 11429 and 12371. Employing vector magnetic field observations from Helioseismic and Magnetic Imager, the pre-eruptive magnetic structure is reconstructed by a model of non-linear force-free field (NLFFF). For all the five CMEs from these ARs, the pre-eruptive magnetic structure identifies an inverse-S sigmoid consistent with the coronal plasma tracers in EUV observations. In all the eruption cases, the quasi-separatrix layers (QSLs) of Large Q values are continuously enclosing core field bipolar regions in which inverse-S shaped flare ribbons are observed. These QSLs essentially represent the large connectivity gradients between the domains of twisted core flux within the inner bipolar region and the surrounding potential like arcade. It is consistent with the observed field structure largely with the sheared arcade. The QSL maps in the chromosphere are compared with the flare-ribbons observed at the peak time of the flares. The flare ribbons are largely inverse-S shape morphology with their continuity of visibility is missing in the observations. For the CMEs in the AR 12371, the QSLs outline the flare ribbons as a combination of two inverse J-shape sections with their straight parts being separated. These QSLs are typical with the weakly twisted flux rope. Similarly, for the CMEs in the AR 11429, the QSLs are co-spatial with the flare ribbons both in the middle of the PIL and in the hook sections. In the frame work of standard model of eruptions, the observed flare ribbons are the characteristic of the pre-eruptive magnetic structure being sigmoid which is reproduced by {\bf the} NLFFF model with a weakly twisted flux rope at the core. **7-11 Mar 2012, 17-25 Jun 2015**

Relation of Non-neutralized electric currents and the activity in active regions

P. **Vemareddy**
RHESSI Science Nuggets #386 Oct **2020**
https://sprg.ssl.berkeley.edu/~tohban/wiki/index.php/Relation_of_Non-neutralized_electric_currents_and_the_activity_in_active_regions **March 7, 2012**

Degree of electric current neutralization and the activity in solar active regions

P. **Vemareddy**
MNRAS Volume 486, Issue 4, July **2019**, Pages 4936–4946,
https://arxiv.org/pdf/1904.02648.pdf
https://watermark.silverchair.com/stz1020.pdf

Using time-sequence vector magnetic field observation from Helioseismic and Magnetic Imager, we examined the connection of non-neutralized currents and the observed activity in 20 solar active regions (ARs). The net current in a given magnetic polarity is algebraic sum of direct current (DC) and return current (RC) and the ratio |DC/RC| is a measure of degree of net current neutralization (NCN). In the emerging ARs, the non-neutrality of these currents builds with the onset of flux emergence, following the relaxation to neutrality during the separation motion of bipolar regions. Accordingly, some emerging ARs are source regions of CMEs occurring at the time of higher level non-neutrality. ARs in the post-emergence phase can be CME productive provided they have interacting bipolar regions with converging and shearing motions. In these cases, the net current evolves with higher level (>1.3) of non-neutrality. Differently, the |DC/RC| in flaring and quiet ARs vary near unity. In all the AR samples, the |DC/RC| is higher for chiral current density than that for vertical current density. Owing to the fact that the non-neutralized currents arise in the vicinity of sheared polarity-inversion-lines (SPILs), the profiles of the total length of SPIL segments and the degree of NCN follow each other with a positive correlation. We find that the SPIL is localized as small segments in flaring-ARs, whereas it is long continuous in CME-producing ARs. These observations demonstrate the dividing line between the CMEs and flares with the difference being in global or local nature of magnetic shear in the AR that reflected in non-neutralized currents. **Table** 1. Details of the active regions in this study (2012-2016)

Very fast helicity injection leading to critically stable state and large eruptive activity in solar active region NOAA 12673

P. **Vemareddy**

ApJ **872** 182 **2019**

https://arxiv.org/abs/1901.09358

https://doi.org/10.3847/1538-4357/ab0200

Using the photospheric magnetic and coronal observations of Solar Dynamics Observatory, we studied the build-up and eruption of coronal non-potential magnetic structure in emerging active region (AR) 12673. The velocity field derived from tracked vector-magnetograms indicates persistent shear and converging motions of flux regions about the polarity inversion line (PIL). A major helicity injection occurs during rapid flux emergence consistent with the very fast flux emergence phase. While this helicity flux builds-up the sigmoid by September 4, the helicity injection by the continued shear and converging motions in the later evolution contributes to sigmoid sustenance and its core field twist as a manifestation of the flux rope which erupts after exceeding critical value of twist. Moreover, the total length of sheared PIL segments correlates with the non-neutralized current and maintains a higher value in both the polarity regions as a signature of eruptive capability of the AR according to the flux rope models. The modelled magnetic field qualitatively reproduces the sigmoidal structure capturing major features like twisted core flux as flux rope, and hook-shaped parts connecting at the middle of the PIL. Study of quasi-separatrix-layers reveals that the sheared arcade, enclosing the flux rope, is stressed to a critically stable state and its coronal height becomes doubled from September 4-6. While demonstrating the fast injection of helicity per unit flux as the crucial factor for severe space-weather events, this study explains the formation of the flux rope and recurrent eruptive nature of the AR by the critically stable state of sheared arcade early on September 6. **4-6 Sept 2017**

Study of Three-Dimensional Magnetic Structure and the Successive Eruptive Nature of Active Region 12371

P. **Vemareddy**, P. Demóulin

ApJ **2018**

https://arxiv.org/pdf/1803.04728.pdf

We study the magnetic structure of successively erupting sigmoid in active region 12371 by modeling the quasi-static coronal field evolution with non-linear force-free field (NLFFF) equilibria. HMI/SDO vector magnetograms are used as input to the NLFFF model. In all eruption events, the modeled structure resembles the observed pre-eruptive coronal sigmoid and the NLFFF core-field is a combination of double inverse J-shaped and inverse-S field-lines with dips touching the photosphere. Such field-lines are formed by flux-cancellation reconnection of opposite-J field-lines at bald-patch locations. It implies the formation of a weakly twisted flux-rope from large scale sheared arcade field lines. Later on, this flux-rope undergo coronal tether-cutting reconnection until a CME is triggered. The modeled structure captured these major features of sigmoid-to-arcade-to-sigmoid transformation, that is being recurrent under continuous photospheric flux motions. Calculations of the field-line twist reveal a fractional increase followed by a decrease of the number of pixels having a range of twist. This traces the buildup process of a twisted core-field by slow photospheric motions and the relaxation after eruption, respectively. Our study infers that the large eruptivity of this AR is due to a steep decrease of the background coronal field meeting the torus instability criteria at low height (\approx 40 Mm) in contrast to non-eruptive ARs. **18-25 June, 2015**

RHESSI Science Nuggets №318 March **2018**

http://sprg.ssl.berkeley.edu/~tohban/wiki/index.php/Homologous_CME/flares_from_AR_12371

Successive Injection of Opposite Magnetic Helicity in Solar Active Region NOAA 11928

P. **Vemareddy**, P. Démoulin

A&A **2016**
https://arxiv.org/pdf/1611.00699v1.pdf
Understanding the nature and evolution of the photospheric helicity flux transfer is a key to reveal the role of magnetic helicity in coronal dynamics of solar active regions. Using SDO/HMI photospheric vector magnetograms and the derived flow velocity field, we computed boundary driven helicity flux with a 12 minute cadence during the emergence of AR 11928. Accounting the foot point connectivity defined by non-linear force-free magnetic extrapolations, we derived and analyzed the corrected distribution of helicity flux maps. The photospheric helicity flux injection is found to changes sign during the steady emergence of the AR. This reversal is confirmed with the evolution of the photospheric electric currents and with the coronal connectivity as observed in EUV wavelengths with SDO/AIA. During about the three first days of emergence, the AR coronal helicity is positive while later on the field configuration is close to a potential field. As theoretically expected, the magnetic helicity cancelation is associated to enhanced coronal activity. The study suggests a boundary driven transformation of the chirality in the global AR magnetic structure. This may be the result of the emergence of a flux rope with positive twist around its apex while it has negative twist in its legs. The origin of such mixed helicity flux rope in the convective zone is challenging for models.
2013.12.17-20

Flux Emergence in the Solar Active Region NOAA 11158: The Evolution of Net Current

P. **Vemareddy**, P. Venkatakrishnan, S. Karthikreddy
Research in Astronomy and Astrophysics, Vol 15, No 9 1547-1558 (**2015**)
http://arxiv.org/pdf/1502.05458v1.pdf
We present a detailed investigation on the evolution of observed net vertical current using a time series of vector magnetograms of the active region (AR) NOAA 11158 obtained from Helioseismic Magnetic Imager. We also discuss the relation of net current to the observed eruptive events. The AR evolved from βγ to βγδ configuration over a period of 6 days. The AR had two sub-regions of activity with opposite chirality: one dominated by sunspot rotation producing a strong CME, the other showing large shear motions producing a strong flare. The net current in each polarity over the CME producing sub-region increased to a maximum and then decreased when the sunspots got separated. The time profile of net current in this sub-region followed the time profile of the rotation rate of the S-polarity sunspot of the same sub-region. The net current in the flaring sub-region showed a sudden increase at the time of the strong flare and remained unchanged till the end of the observation, while the sunspots maintained their close proximity. The systematic evolution of the observed net current is seen to follow the time evolution of total length of strongly sheared polarity inversion lines in both the sub-regions. The observed photospheric net current could be explained as an inevitable product of the emergence of a twisted flux rope, from a higher pressure confinement below the photosphere into the lower pressure environment of the photosphere. **February 13-16, 2011**

Quasi-Static 3D-Magnetic Field Evolution in Solar Active Region NOAA 11166 Associated with X1.5 Flare

P. **Vemareddy**, and T. Wiegelmann
E-print, July **2014**; ApJ, **2014** 792 40
http://arxiv.org/pdf/1406.7823v1.pdf
We study the quasi-static evolution of coronal magnetic fields constructed from the Non Linear Force Free Field (NLFFF) approximation aiming to understand the relation between the magnetic field topology and ribbon emission during an X1.5 flare in active region (AR) NOAA 11166. The flare with a quasi-elliptical, and two remote ribbons occurred on **March 9, 2011** at 23:13UT over a positive flux region surrounded by negative flux at the center of the bipolar AR. Our analysis of the coronal magnetic structure with potential and NLFFF solutions unveiled the existence of a single magnetic null point associated with a fan-spine topology and is co-spatial with the hard X-ray source. The footpoints of the fan separatrix surface agree with the inner edge of the quasi-elliptical ribbon and the outer spine is linked to one of the remote ribbons. During the evolution, the slow footpoint motions stressed the fieldlines along the polarity inversion line and caused electric current layers in the corona around the fan separatrix surface. These current layers trigger magnetic reconnection as a consequence of dissipating currents, which are visible as cusped shape structures at lower heights. The reconnection process reorganised the magnetic field topology whose signatures are observed at the separatrices/QSL structure both in the photosphere and corona during the pre-to-post flare evolution. In agreement with previous numerical studies, our results suggest that the line-tied footpoint motions perturb the fan-spine system and cause null point reconnection, which eventually causes the flare emission at the footpoints of the fieldlines.

ON THE INJECTION OF HELICITY BY THE SHEARING MOTION OF FLUXES IN RELATION TO FLARES AND CORONAL MASS EJECTIONS

P. **Vemareddy**1, A. Ambastha1, R. A. Maurya2, and J. Chae
2012 ApJ 761 86
http://arxiv.org/pdf/1202.5195v2.pdf

An investigation of helicity injection by photospheric shear motions is carried out for two active regions (ARs), NOAA 11158 and 11166, using line-of-sight magnetic field observations obtained from the Helioseismic and Magnetic Imager on board the Solar Dynamics Observatory. We derived the horizontal velocities in the ARs from the differential affine velocity estimator (DAVE) technique. Persistent strong shear motions at maximum velocities in the range of 0.6-0.9 km s–1 along the magnetic polarity inversion line and outward flows from the peripheral regions of the sunspots were observed in the two ARs. The helicities injected in NOAA 11158 and 11166 during their six-day evolution period were estimated as 14.16 × 1042 Mx2 and 9.5 × 1042 Mx2, respectively. The estimated injection rates decreased up to 13% by increasing the time interval between the magnetograms from 12 minutes to 36 minutes, and increased up to 9% by decreasing the DAVE window size from 21 × 18 to 9 × 6 pixel2, resulting in 10% variation in the accumulated helicity. In both ARs, the flare-prone regions (R2) had inhomogeneous helicity flux distribution with mixed helicities of both signs and coronal mass ejection (CME) prone regions had almost homogeneous distribution of helicity flux dominated by a single sign. The temporal profiles of helicity injection showed impulsive variations during some flares/CMEs due to negative helicity injection into the dominant region of positive helicity flux. A quantitative analysis reveals a marginally significant association of helicity flux with CMEs but not flares in AR 11158, while for the AR 11166, we find a marginally significant association of helicity flux with flares but not CMEs, providing evidence of the role of helicity injection at localized sites of the events. These short-term variations of helicity flux are further discussed in view of possible flare-related effects. This study suggests that flux motions and spatial distribution of helicity injection are important to understanding the complex nature of the magnetic flux system of the AR, and how it can lead to conditions favorable for eruptive events.

ON THE ROLE OF ROTATING SUNSPOTS IN THE ACTIVITY OF SOLAR ACTIVE REGION NOAA 11158

P. **Vemareddy**1, A. Ambastha1, and R. A. Maurya
2012 ApJ 761 60
http://arxiv.org/pdf/1210.3912v1.pdf

We study the role of rotating sunspots in relation to the evolution of various physical parameters characterizing the non-potentiality of the active region (AR) NOAA 11158 and its eruptive events using the magnetic field data from the Helioseismic and Magnetic Imager (HMI) and multi-wavelength observations from the Atmospheric Imaging Assembly (AIA) on board the Solar Dynamics Observatory. From the evolutionary study of HMI intensity and AIA channels, it is observed that the AR consists of two major rotating sunspots, one connected to a flare-prone region and another with coronal mass ejection (CME). The constructed space-time intensity maps reveal that the sunspots exhibited peak rotation rates coinciding with the occurrence of major eruptive events. Further, temporal profiles of twist parameters, namely, average shear angle, αav, αbest, derived from HMI vector magnetograms, and the rate of helicity injection, obtained from the horizontal flux motions of HMI line-of-sight magnetograms, correspond well with the rotational profile of the sunspot in the CME-prone region, giving predominant evidence of rotational motion causing magnetic non-potentiality. Moreover, the mean value of free energy from the virial theorem calculated at the photospheric level shows a clear step-down decrease at the onset time of the flares revealing unambiguous evidence of energy release intermittently that is stored by flux emergence and/or motions in pre-flare phases. Additionally, distribution of helicity injection is homogeneous in the CME-prone region while in the flare-prone region it is not and often changes sign. This study provides a clear picture that both proper and rotational motions of the observed fluxes played significant roles in enhancing the magnetic non-potentiality of the AR by injecting helicity, twisting the magnetic fields and thereby increasing the free energy, leading to favorable conditions for the observed transient activity.

Filament Eruption in NOAA 11093 Leading to a Two-Ribbon M1.0 Class Flare and CME

P. **Vemareddy**, R. A. Maurya and A. Ambastha
Solar Physics, Volume 277, Number 2, 337-354, **2012**
http://arxiv.org/pdf/1103.3168v2.pdf

We present a multi-wavelength analysis of an eruption event that occurred in active region NOAA 11093 on **7 August 2010**, using data obtained from SDO, STEREO, RHESSI, and the GONG Hα network telescope. From these observations, we inferred that an upward slow rising motion of an inverse S-shaped filament lying along the polarity inversion line resulted in a CME subsequent to a two-ribbon flare. Interaction of overlying field lines across the filament with the side-lobe field lines, associated EUV brightening, and flux emergence/cancelation around the filament were the observational signatures of the processes leading to its destabilization and the onset of eruption. Moreover, the time profile of the rising motion of the filament/flux rope corresponded well with flare characteristics, viz., the reconnection rate and hard X-ray emission profiles. The flux rope was accelerated to the maximum velocity as a CME at the peak phase of the flare, followed by deceleration to an average velocity of 590 km s−1. We suggest that the observed emergence/cancelation of magnetic fluxes near the filament caused it to rise, resulting in the tethers to cut and

reconnection to take place beneath the filament; in agreement with the tether-cutting model. The corresponding increase/decrease in positive/negative photospheric fluxes found in the post-peak phase of the eruption provides unambiguous evidence of reconnection as a consequence of tether cutting.

Solar Flare Distributions: Lognormal Instead of Power Law?

Cis **Verbeeck**1, Emil Kraaikamp1, Daniel F. Ryan2, and Olena Podladchikova1
Astrophysical Journal, 884:50 (16pp), **2019**
https://iopscience.iop.org/article/10.3847/1538-4357/ab3425/pdf
In many statistical solar flare studies, power laws are claimed and exponents derived by fitting a line to a log–log histogram. It is well known that this approach is statistically unstable, and very large statistics are needed to produce reliable exponent estimates. This may explain part of the observed divergence in power-law exponents in various studies. Moreover, the question is seldom addressed to what extent the data really do support power-law behavior. In this paper, we perform a comprehensive study of 6924 flares detected in SDO/AIA 9.4 nm images by the Solar Demon flare detection software between 2010 May 13 and 2018 March 16 and 9601 flares detected during the same period in GOES/XRS data by the LYRAFF flare detection software. We apply robust statistics to the SDO/AIA 9.4 nm peak intensity and the GOES/XRS raw peak flux, background-subtracted peak flux, and background-subtracted fluence and find clear indications that most background-corrected data are not well described by a power law and that all are better described by a lognormal distribution, while the raw GOES/XRS peak flux is best described by a power law. This may explain the success of power-law fits in flare studies using uncorrected data. The behavior of flare distributions has important implications for large-scale science questions such as coronal heating and the nature of solar flares. The apparent lognormal character of flare distributions in our data sets suggests that the assumed power-law nature of flares and its consequences need to be reexamined with great care.2014-03-29

A Multi-wavelength Analysis of Active Regions and Sunspots by Comparison of Automatic Detection Algorithms

C. **Verbeeck**, P. A. Higgins, T. Colak, F. T. Watson, V. Delouille, B. Mampaey, R. Qahwaji
Solar Physics, March **2013**, Volume 283, Issue 1, pp 67-95
Since the Solar Dynamics Observatory (SDO) began recording ≈ 1 TB of data per day, there has been an increased need to automatically extract features and events for further analysis. Here we compare the overall detection performance, correlations between extracted properties, and usability for feature tracking of four solar feature-detection algorithms: the Solar Monitor Active Region Tracker (SMART) detects active regions in line-of-sight magnetograms; the Automated Solar Activity Prediction code (ASAP) detects sunspots and pores in white-light continuum images; the Sunspot Tracking And Recognition Algorithm (STARA) detects sunspots in white-light continuum images; the Spatial Possibilistic Clustering Algorithm (SPoCA) automatically segments solar EUV images into active regions (AR), coronal holes (CH), and quiet Sun (QS). One month of data from the Solar and Heliospheric Observatory (SOHO)/Michelson Doppler Imager (MDI) and SOHO/Extreme Ultraviolet Imaging Telescope (EIT) instruments during **12 May – 23 June 2003** is analysed. The overall detection performance of each algorithm is benchmarked against National Oceanic and Atmospheric Administration (NOAA) and Solar Influences Data Analysis Center (SIDC) catalogues using various feature properties such as total sunspot area, which shows good agreement, and the number of features detected, which shows poor agreement. Principal Component Analysis indicates a clear distinction between photospheric properties, which are highly correlated to the first component and account for 52.86% of variability in the data set, and coronal properties, which are moderately correlated to both the first and second principal components. Finally, case studies of NOAA 10377 and 10365 are conducted to determine algorithm stability for tracking the evolution of individual features. We find that magnetic flux and total sunspot area are the best indicators of active-region emergence. Additionally, for NOAA 10365, it is shown that the onset of flaring occurs during both periods of magnetic-flux emergence and complexity development.

On the origin of two X-class flares in active region NOAA 12673 - Shear flows and head-on collision of new and pre-existing flux

M. **Verma**
A&A 612, A101 **2018**
https://arxiv.org/pdf/1801.08368.pdf
Flare-prolific active region NOAA 12673 produced consecutive X2.2 and X9.3 flares on **06/09/2017**. To scrutinize the morphological, magnetic, and horizontal flow properties associated with these flares, a 7-hour time-series was used consisting of continuum images, line-of-sight/vector magnetograms, and 1600 {\AA} UV images. These data were acquired with the SDO HMI and AIA. The white-light flare emission differed for both flares, while the X2.2 flare displayed localized, confined flare kernels, the X9.3 flare exhibited a two-ribbon structure. In contrast, the excess UV emission exhibited a similar structure for both flares, but with larger areal extent for the X9.3 flare. These two flares represented a scenario, where the first confined flare acted as precursor, setting up the stage for the more extended flare. Difference maps for continuum and magnetograms revealed locations of significant changes, i.e., penumbral decay and umbral strengthening. The curved magnetic polarity inversion line in the {\delta}-spot was the fulcrum of most changes.

Horizontal proper motions were computed using the DAVE4VM. Persistent flow features included (1) strong shear flows along the polarity inversion line, where the negative, parasitic polarity tried to bypass the majority, positive-polarity part of the {\delta}-spot in the north, (2) a group of positive-polarity spots, which moved around the {\delta}-spot in the south, moving away from the {\delta}-spot with significant horizontal flow speeds, and (3) intense moat flows partially surrounding the penumbra of several sunspots, which became weaker in regions with penumbral decay. The enhanced flare activity has its origin in the head-on collision of newly emerging flux with an already existing regular, {\alpha}-spot.

Flows in and around active region NOAA12118 observed with the GREGOR solar telescope and SDO/HMI

M. **Verma**, C. Denker, H. Balthasar, C. Kuckein, S.J. González Manrique, M. Sobotka,
ASP Conf. Series - Coimbra solar physics meeting: Grounds-based solar observations in the space instrumentation era , I. Dorotovic, C. Fischer, and M. Temmer (eds.) **2016**
http://arxiv.org/pdf/1603.01109v1.pdf
Accurate measurements of magnetic and velocity fields in and around solar active regions are key to unlocking the mysteries of the formation and the decay of sunspots. High spatial resolution image and spectral sequences with a high cadence obtained with the GREGOR solar telescope give us an opportunity to scrutinize 3-D flow fields with local correlation tracking and imaging spectroscopy. We present GREGOR early science data acquired in 2014 July - August with the GREGOR Fabry-P\'erot Interferometer and the Blue Imaging Channel. Time-series of blue continuum (? 450.6 nm) images of the small active region NOAA 12118 were restored with the speckle masking technique to derive horizontal proper motions and to track the evolution of morphological changes. In addition, high-resolution observations are discussed in the context of synoptic data from the Solar Dynamics Observatory. **2014 July 18**.

Horizontal flow fields observed in Hinode G-band images
III. The decay of a satellite sunspot and the role of magnetic flux removal in flaring

M. **Verma** and C. Denker
A&A 545, A92 (**2012**)
Context. Emergence of magnetic flux plays an important role in the initiation of flares. However, the role of submerging magnetic flux in prompting flares is more ambiguous, not the least because of the scarcity of observations.
Aims. The flare-prolific active region NOAA 10930 offered both a developing δ-spot and a decaying satellite sunspot of opposite polarity. The objective of this study is to characterize the photometric decay of the satellite sunspot as well as the evolution of photospheric and chromospheric horizontal proper motions in its surroundings.
Methods. We apply the local correlation tracking technique to a 16-h time-series of Hinode G-band and Ca ii H images and study the horizontal proper motions in the vicinity of the satellite sunspot on 2006 December 7. Decorrelation times were computed to measure the lifetime of solar features in intensity and flow maps.
Results. We observed shear flows in the dominant umbral cores of the satellite sunspot. These flows vanished once the penumbra had disappeared. This slow penumbral decay had an average rate of 152 Mm2 day-1 over an 11-h period. Typical lifetimes of intensity features derived from an autocorrelation analysis are 3–5 min for granulation, 25–35 min for G-band bright points, and up to 200−235 min for penumbrae, umbrae, and pores. Long-lived intensity features (i.e., the dominant umbral cores) are not related to long-lived flow features in the northern part of the sunspot, where flux removal, slowly decaying penumbrae, and persistent horizontal flows of up to 1 km s-1 contribute to the erosion of the sunspot. Finally, the restructuring of magnetic field topology was responsible for a homologous M2.0 flare, which shared many characteristics with an X6.5 flare on the previous day.
Conclusions. Notwithstanding the prominent role of δ-spots in flaring, we conclude based on the decomposition of the satellite sunspot, the evolution of the surrounding flow fields, and the timing of the M2.0 flare that the vanishing magnetic flux in the decaying satellite sunspot played an instrumental role in triggering the homologous M2.0 flare and the eruption of a small Hα filament. The strong magnetic field gradients of the neighboring δ-spot merely provided the vehicle for the strongest flare emission about 10 min after the onset of the flare.

Can we predict solar flares?

Astrid M. **Veronig**
Science 31 Jul **2020**: Vol. 369, Issue 6503, pp. 504-505
DOI: 10.1126/science.abb6150
https://sci-hub.tw/10.1126/science.abb6150
https://science.sciencemag.org/content/369/6503/504
Flares from the Sun are the strongest explosions in our Solar System. They can cause severe space weather disturbances, posing a hazard to astronauts and technological systems in space and on the ground. Solar flares have an immediate impact in the form of enhanced radiation and energetic particles in as little as 8 min after the start of the event. Reliable prediction methods for flares are needed to provide longer warning times. However, pinning down the flare onset conditions is necessary for reliable predictions and is still a struggle (1). On page 587 of this issue, Kusano et al. (2) introduce a method to predict and successfully test for large imminent flares.

Magnetic Reconnection Rates and Energy Release in a Confined X-class Flare

A.M. **Veronig**, W. Polanec

Solar Phys. Volume 290, Issue 10, pp 2923-2942 **2015**

http://arxiv.org/pdf/1509.07089v1.pdf

We study the energy-release process in the confined X1.6 flare that occurred on **22 October 2014** in AR 12171. Magnetic-reconnection rates and reconnection fluxes are derived from three different data sets: space-based data from the Atmospheric Imaging Assembly (AIA) 1600 {\AA} filter onboard the Solar Dynamics Observatory (SDO) and ground-based Hα and Ca II K filtergrams from Kanzelh\"ohe Observatory. The magnetic-reconnection rates determined from the three data sets all closely resemble the temporal profile of the hard X-rays measured by the Ramaty High Energy Solar Spectroscopic Imager (RHESSI), which are a proxy for the flare energy released into high-energy electrons. The total magnetic-reconnection flux derived lies between 4.1×1021 Mx (AIA 1600 {\AA}) and 7.9×1021 Mx (Hα), which corresponds to about 2 to 4% of the total unsigned flux of the strong source AR. Comparison of the magnetic-reconnection flux dependence on the GOES class for 27 eruptive events collected from previous studies (covering B to >X10 class flares) reveals a correlation coefficient of ≈0.8 in double-logarithmic space. The confined X1.6 class flare under study lies well within the distribution of the eruptive flares. The event shows a large initial separation of the flare ribbons and no separation motion during the flare. In addition, we note enhanced emission at flare-ribbon structures and hot loops connecting these structures before the event starts. These observations are consistent with the emerging-flux model, where newly emerging small flux tubes reconnect with pre-existing large coronal loops.

MULTIWAVELENGTH IMAGING AND SPECTROSCOPY OF CHROMOSPHERIC EVAPORATION IN AN M-CLASS SOLAR FLARE

A. M. **Veronig** 1, J. Rybák 2, P. Gömöry 2,3, S. Berkebile-Stoiser 1, M. Temmer 1,4, W. Otruba 3, B. Vršnak 5, W. Pötzi 3 and D. Baumgartner

2010 ApJ 719 655

We study spectroscopic observations of chromospheric evaporation mass flows in comparison with the energy input by electron beams derived from hard X-ray (HXR) data for the white-light M2.5 flare of **2006 July 6**. The event was captured in high-cadence spectroscopic observing mode by SOHO/CDS combined with high-cadence imaging at various wavelengths in the visible, extreme ultraviolet, and X-ray domain during the joint observing campaign JOP171. During the flare peak, we observe downflows in the He I and O V lines formed in the chromosphere and transition region, respectively, and simultaneous upflows in the hot coronal Si XII line. The energy deposition rate by electron beams derived from RHESSI HXR observations is suggestive of explosive chromospheric evaporation, consistent with the observed plasma motions. However, for a later distinct X-ray burst, where the site of the strongest energy deposition is exactly located on the Coronal Diagnostics Spectrometer (CDS) slit, the situation is intriguing. The O V transition region line spectra show the evolution of double components, indicative of the superposition of a stationary plasma volume and upflowing plasma elements with high velocities (up to 280 km s–1) in single CDS pixels on the flare ribbon. However, the energy input by electrons during this period is too small to drive explosive chromospheric evaporation. These unexpected findings indicate that the flaring transition region is much more dynamic, complex, and fine structured than is captured in single-loop hydrodynamic simulations.

Temporal aspects and frequency distributions of solar soft X-ray flares

A. **Veronig**1, M. Temmer1, A. Hanslmeier1, W. Otruba2, and M. Messerotti3

A&A 382, 1070–1080 (**2002**)

DOI: 10.1051/0004-6361:20011694

https://sci-hub.ru/10.1051/0004-6361:20011694

A statistical analysis of almost 50 000 soft X-ray (SXR) flares observed by GOES during the period 1976–2000 is presented. On the basis of this extensive data set, statistics on temporal properties of soft X-ray flares, such as duration, rise and decay times with regard to the SXR flare classes is presented. Correlations among distinct flare parameters, i.e. SXR peak flux, fluence and characteristic times, and frequency distributions of flare occurrence as function of the peak flux, the fluence and the duration are derived. We discuss the results of the analysis with respect to statistical flare models, the idea of coronal heating by nanoflares, and elaborate on implications of the obtained results on the Neupert effect in solar flares.

A Survey of Nanoflare Properties in Active Regions Observed with the Solar Dynamics Observatory

Nicholeen M. **Viall** and James A. Klimchuk

2017 ApJ 842 108

http://iopscience.iop.org.sci-hub.cc/0004-637X/842/2/108/

In this paper, we examine 15 different active regions (ARs) observed with the Solar Dynamics Observatory and analyze their nanoflare properties. We have recently developed a technique that systematically identifies and measures plasma temperature dynamics by computing time lags between light curves. The time lag method tests whether the plasma is maintained at a steady temperature, or if it is dynamic, undergoing heating and cooling cycles. An important aspect of our technique is that it analyzes both observationally distinct coronal loops as well as the much more prevalent diffuse emission between them. We find that the widespread cooling reported previously for NOAA AR 11082 is a generic property of all ARs. The results are consistent with impulsive nanoflare heating followed by slower cooling. Only occasionally, however, is there full cooling from above 7 MK to well below 1 MK. More often, the plasma cools to approximately 1–2 MK before being reheated by another nanoflare. These same 15 ARs were first studied by Warren et al. We find that the degree of cooling is not well correlated with the reported slopes of the emission measure distribution. We also conclude that the Fe xviii emitting plasma that they measured is mostly in a state of cooling. These results support the idea that nanoflares have a distribution of energies and frequencies, with the average delay between successive events on an individual flux tube being comparable to the plasma cooling timescale.

The Transition Region Response to a Coronal Nanoflare: Forward Modeling and Observations in SDO/AIA

Nicholeen M. **Viall** and James A. Klimchuk

2015 ApJ 799 58

The corona and transition region (TR) are fundamentally coupled through the processes of thermal conduction and mass exchange. It is not possible to understand one without the other. Yet the temperature-dependent emissions from the two locations behave quite differently in the aftermath of an impulsive heating event such as a coronal nanoflare. Whereas the corona cools sequentially, emitting first at higher temperatures and then at lower temperatures, the TR is multithermal and the emission at all temperatures responds in unison. We have previously applied the automated time lag technique of Viall & Klimchuk to disk observations of an active region (AR) made by the Atmospheric Imaging Assembly (AIA) on the Solar Dynamics Observatory. Lines of sight passing through coronal plasma show clear evidence for post-nanoflare cooling, while lines of sight intersecting the TR footpoints of coronal strands show zero time lag. In this paper, we use the EBTEL hydrodynamics code to demonstrate that this is precisely the expected behavior when the corona is heated by nanoflares. We also apply the time lag technique for the first time to off-limb observations of an AR. Since TR emission is not present above the limb, the occurrence of zero time lags is greatly diminished, supporting the conclusion that zero time lags measured on the disk are due to TR plasma. Lastly, we show that the "coronal" channels in AIA can be dominated by bright TR emission. When defined in a physically meaningful way, the TR reaches a temperature of roughly 60% the peak temperature in a flux tube. The TR resulting from impulsive heating can extend to 3 MK and higher, well within the range of the "coronal" AIA channels.

Table 1 ARs are Ordered in Increasing Total Unsigned Magnetic Flux, Following WWB2012 (2010-2011)

PATTERNS OF NANOFLARE STORM HEATING EXHIBITED BY AN ACTIVE REGION OBSERVED WITH SOLAR DYNAMICS OBSERVATORY/ATMOSPHERIC IMAGING ASSEMBLY

Nicholeen M. **Viall** and James A. Klimchuk

2011 ApJ 738 24, **2011**

It is largely agreed that many coronal loops—those observed at a temperature of about 1 MK—are bundles of unresolved strands that are heated by storms of impulsive nanoflares. The nature of coronal heating in hotter loops and in the very important but largely ignored diffuse component of active regions is much less clear. Are these regions also heated impulsively, or is the heating quasi-steady? The spectacular new data from the Atmospheric Imaging Assembly (AIA) telescopes on the Solar Dynamics Observatory offer an excellent opportunity to address this question. We analyze the light curves of coronal loops and the diffuse corona in six different AIA channels and compare them with the predicted light curves from theoretical models. Light curves in the different AIA channels reach their peak intensities with predictable orderings as a function the nanoflare storm properties. We show that while some sets of light curves exhibit clear evidence of cooling after nanoflare storms, other cases are less straightforward to interpret. Complications arise because of line-of-sight integration through many different structures, the broadband nature of the AIA channels, and because physical properties can change substantially depending on the magnitude of the energy release. Nevertheless, the light curves exhibit predictable and understandable patterns consistent with impulsive nanoflare heating.

SMESE: A SMall Explorer for Solar Eruptions

J.-C. **Vial**, F. Auchère[a], J. Chang[b], C. Fang[c], W.Q. Gan[b], K.-L. Klein[d], J.-Y. Prado[e], G. Trottet[d], C. Wang[f] and Y.H. Yan[g]

Advances in Space Research
Volume 40, Issue 12, **2007**, Pages 1787-1801
The SMall Explorer for Solar Eruptions (SMESE) mission is a microsatellite proposed by France and China. The payload of SMESE consists of three packages: LYOT (a Lyman α imager and a Lyman α coronagraph), DESIR (an Infra-Red Telescope working at 35–80 and 100–250 μm), and HEBS (a High-Energy Burst Spectrometer working in X- and γ-rays). a launch around 2012–2013

Stellar flares, superflares and coronal mass ejections -- entering the Big data era **Review**

Krisztián **Vida**, Zsolt Kővári, Martin Leitzinger, Petra Odert, Katalin Oláh, Bálint Seli, Levente Kriskovics, Robert Greimel, Anna Görgei
Universe **2024**
https://arxiv.org/pdf/2407.16446
Flares, sometimes accompanied by coronal mass ejections (CMEs), are the result of sudden changes in the magnetic field of stars with high energy release through magnetic reconnection, which can be observed across a wide range of the electromagnetic spectrum from radio waves to the optical range to X-rays. In our observational review, we attempt to collect some fundamental new results, which can largely be linked to the Big data era that has arrived due to the expansion of space photometric observations of the last two decades. We list the different types of stars showing flare activity, their observation strategies, and discuss how their main stellar properties relate to the characteristics of the flares (or even CMEs) they emit. Our goal is to focus, without claiming to be complete, on those results that may in one way or another challenge the "standard" flare model based on the solar paradigm. **2024 May 10**

FOXSI-2 Solar Microflares II: Hard X-ray Imaging Spectroscopy and Flare Energetics

Juliana T. **Vievering**, Lindsay Glesener, P. S. Athiray, Juan Camilo Buitrago-Casas, Sophie Musset, Daniel Ryan, Shin-nosuke Ishikawa, Jessie Duncan, Steven Christe, Säm Krucker
2021 *ApJ* **913** 15
https://arxiv.org/pdf/2011.04753.pdf
https://iopscience.iop.org/article/10.3847/1538-4357/abf145/pdf
https://doi.org/10.3847/1538-4357/abf145
We study the nature of energy release and transfer for two sub-A class solar microflares observed during the second flight of the Focusing Optics X-ray Solar Imager (FOXSI-2) sounding rocket experiment on **2014 December 11**. FOXSI is the first solar-dedicated instrument to utilize focusing optics to image the Sun in the hard X-ray (HXR) regime, sensitive to the energy range 4-20 keV. Through spectral analysis of the two microflares using an optically thin isothermal plasma model, we find evidence for plasma heated to temperatures of ~10 MK and emissions measures down to ~1044 cm−3. Though nonthermal emission was not detected for the FOXSI-2 microflares, a study of the parameter space for possible hidden nonthermal components shows that there could be enough energy in nonthermal electrons to account for the thermal energy in microflare 1, indicating that this flare is plausibly consistent with the standard thick-target model. With a solar-optimized design and improvements in HXR focusing optics, FOXSI-2 offers approximately five times greater sensitivity at 10 keV than the Nuclear Spectroscopic Telescope Array (NuSTAR) for typical microflare observations and allows for the first direct imaging spectroscopy of solar HXRs with an angular resolution at scales relevant for microflares. Harnessing these improved capabilities to study the evolution of small-scale events, we find evidence for spatial and temporal complexity during a sub-A class flare. These studies in combination with contemporanous observations by the Atmospheric Imaging Assembly onboard the Solar Dynamics Observatory (SDO/AIA) indicate that the evolution of these small microflares is more similar to that of large flares than to the single burst of energy expected for a nanoflare.
RHESSI Nuggets #396 Dec **2020** https://sprg.ssl.berkeley.edu/~tohban/wiki/index.php/Investigation_of_Small-Scale_Energy_Releases_in_Hard_X-rays_with_%E2%80%8BFOXSI

ENERGETIC PARTICLES IN THE SOLAR ATMOSPHERE **Review**

N. **Vilmer**1 and S. Musset2
SF2A-2019: Proceedings of the Annual meeting of the French Society of Astronomy and Astrophysics. Eds.: P. Di Matteo, O. Creevey, A. Crida, G. Kordopatis, J. Malzac, J.-B. Marquette, M. N'Diaye, O. Venot, **2019**, pp 283-289
http://sf2a.eu/proceedings/2019/2019/vilmer.pdf
http://sf2a.eu/proceedings/2019/2019sf2a.conf..0283V.pdf
The Sun is an efficient particle accelerator. These particles play a major role in the active Sun because they contain a large amount of the magnetic energy released during flares. Energetic electrons and ions interact with the solar atmosphere and produce high-energy X-rays and γ-rays. Energetic particles can also escape to the corona and interplanetary medium and may eventually reach the Earth's orbit. It is currently admitted that solar flares are powered by magnetic energy previously stored in the coronal magnetic field and that magnetic energy release is likely to occur on coronal current sheets along regions of strong gradient of magnetic connectivity. Particle transport from the

acceleration region to the emission sites must also be considered to infer properties of the accelerated particles (and thus of the acceleration processes) from the observations of their radiation. In this paper, we will present the results of some recent studies using RHESSI observations: relationship found in some flares between ribbons of electric currents observed at the photospheric level and the flare energetic electrons traced by their X-ray emissions. We will also present some results on electron transport in solar flares and comment on the role of scattering in this process. We will finally describe some recent results from FERMI/LAT observations on the production of GeV protons in connection with solar flares and/or coronal mass ejections. **23 July 2002, 21 May 2004, 15 Feb 2011, 2014 February 25**
3 FERMI/LAT observations of long duration γ-ray events

Energetic electrons in the solar atmosphere as diagnosed from their radio and Hard X-ray signatures.

Nicole **Vilmer**∗1 and Hamish Reid
CESRA **2016** p.66
http://cesra2016.sciencesconf.org/conference/cesra2016/pages/CESRA2016_prog_abs_book_v3.pdf
Efficient particle acceleration is observed in association with solar flares. X-ray and radio emissions provide valuable information on the properties of electron acceleration, interaction and propagation in the solar atmosphere. In particular, radio emission from electron beams produced in association with solar flares provides crucial information on the relationship and connections between energetic electrons in the corona and electrons measured in situ. In this talk, we will address the question of the relation between escaping electrons that generate type III emissions in the corona and in the interplanetary medium and electrons confined to the lower atmosphere of the Sun that produce HXRs. We will present here the results of a study based on ten years of data (2002-2011) starting with a selection of 'coronal' type III bursts above 100 MHz. We use X-ray flare information from RHESSI (flares above 6 keV) to produce a list of more than 300 coronal type III bursts associated with X-ray emissions (see Reid and Vilmer, 2016). For these associated events, we will characterize the relative timings, the X-ray and radio intensities and the associated GOES class. We will also examine the percentage of the 'coronal' type III bursts associated with an interplanetary signature (i.e. an interplanetary type III burst detected below 12 MHz by the Wind/Waves experiment) and whether the association between coronal types III and interplanetary types III depends on the characteristics of the propagating electron beams. We will further describe how these studies can be continued in the future using the combination of ground-based measurements with Solar Orbiter and Solar Probe + observations.

Properties of Energetic Ions in the Solar Atmosphere from γ-Ray and Neutron Observations

N. **Vilmer**, A. L. MacKinnon and G. J. Hurford
Space Sci. Rev., 159:167–224, **2011, File** **A Review**
Gamma-rays and neutrons are the only sources of information on energetic ions present during solar flares and on properties of these ions when they interact in the solar atmosphere. The production of γ-rays and neutrons results from convolution of the nuclear cross-sections with the ion distribution functions in the atmosphere. The observed γ-ray and neutron fluxes thus provide useful diagnostics for the properties of energetic ions, yielding strong constraints on acceleration mechanisms as well as properties of the interaction sites. The problem of ion transport between the accelerating and interaction sites must also be addressed to infer as much information as possible on the properties of the primary ion accelerator. In the last couple of decades, both theoretical and observational developments have led to substantial progress in understanding the origin of solar γ-rays and neutrons. This chapter reviews recent developments in the study of solar γ-rays and of solar neutrons at the time of the RHESSI era. The unprecedented quality of the RHESSI data reveals γ-ray line shapes for the first time and provides γ-ray images. Our previous understanding of the properties of energetic ions based on measurements from the former solar cycles is also summarized. The new results—obtained owing both to the gain in spectral resolution (both with RHESSI and with the non solar-dedicated INTEGRAL/SPI instrument) and to the pioneering imaging technique in the γ-ray domain—are presented in the context of this previous knowledge. Still open questions are emphasized in the last section of the chapter and future perspectives on this field are briefly discussed.

Numerical Simulation of a Solar Active Region. I: Bastille Day Flare

Alain **Vincent**, Paul Charbonneau and Caroline Dubé
Solar Physics, Volume 278, Number 2 (**2012**), 367-391
We present three-dimensional unsteady modeling and numerical simulations of a coronal active region, carried out within the compressible single-fluid MHD approximation. We focus on AR 9077 on **14 July 2000**, and the triggering of the X5.7 GOES X-ray class "Bastille Day" flare. We simulate only the lower corona, although we include a virtual photosphere and chromosphere below. The boundary conditions at the base of this layer are set using temperature maps from line intensities and line-of-sight magnetograms (SOHO/MDI). From the latter, we generate vector magnetograms using the force-free approximation; these vector magnetograms are then used to produce the boundary condition on the

velocity field using a minimum energy principle (Longcope, Astrophys. J. 612, 1181, 2004). The reconnection process is modeled through a dynamical hyper-resistivity which is activated when the current exceeds a critical value (Klimas et al., J. Geophys. Res. 109, 2218, 2004). Comparing the time series of X-ray fluxes recorded by GOES with modeled time series of various mean physical variables such as current density, Poynting energy flux, or radiative loss inside the active region, we can demonstrate that the model properly captures the evolution of an active region over a day and, in particular, is able to explain the initiation of the flare at the observed time.

Non-LTE inversions of a confined X2.2 flare: I. Vector magnetic field in the photosphere and chromosphere

G. J. M. **Vissers**, S. Danilovic, J. de la Cruz Rodriguez, J. Leenaarts, R. Morosin, C. J. Diaz Baso, A. Reid, J. Pomoell, D. J. Price, S. Inoue

A&A 645, A1 **2021**

https://arxiv.org/pdf/2009.01537.pdf

https://doi.org/10.1051/0004-6361/202038900

Context. Obtaining an accurate measurement of magnetic field vector in the solar atmosphere is essential for studying changes in field topology during flares and reliably modelling space weather.

Aims. We tackle this problem by applying various inversion methods to a confined X2.2 flare that occurred in NOAA AR 12673 on **6 September 2017** and comparing the photospheric and chromospheric magnetic field vector with the results of two numerical models of this event.

Methods. We obtained the photospheric magnetic field from Milne-Eddington and (non-)local thermal equilibrium (non-LTE) inversions of Hinode SOT/SP Fe I 6301.5 Å and 6302.5 Å. The chromospheric field was obtained from a spatially regularised weak-field approximation (WFA) and non-LTE inversions of Ca II 8542 Å observed with CRISP at the Swedish 1 m Solar Telescope. We investigated the field strengths and photosphere-to-chromosphere shear in the field vector.

Results. The LTE- and non-LTE-inferred photospheric magnetic field components are strongly correlated across several optical depths in the atmosphere, with a tendency towards a stronger field and higher temperatures in the non-LTE inversions. For the chromospheric field, the non-LTE inversions correlate well with the spatially regularised WFA, especially in terms of the line-of-sight field strength and field vector orientation. The photosphere exhibits coherent strong-field patches of over 4.5 kG, co-located with similar concentrations exceeding 3 kG in the chromosphere. The obtained field strengths are up to two to three times higher than in the numerical models, while the photosphere-to-chromosphere shear close to the polarity inversion line is more concentrated and structured.

Conclusions. In the photosphere, the assumption of LTE for Fe I line formation does not yield significantly different magnetic field results in comparison to the non-LTE case, while Milne-Eddington inversions fail to reproduce the magnetic field vector orientation where Fe I is in emission. In the chromosphere, the non-LTE-inferred field is excellently approximated by the spatially regularised WFA. Our inversions confirm the locations of flux rope footpoints that have been predicted by numerical models. However, pre-processing and lower spatial resolution lead to weaker and smoother field in the models than what our data indicate. This highlights the need for higher spatial resolution in the models to better constrain pre-eruptive flux ropes.

Ellerman bombs at high resolution III. Simultaneous observations with IRIS and SST

Gregal J. M. **Vissers**, Luc H. M. Rouppe van der Voort, Robert J. Rutten, Mats Carlsson, Bart De Pontieu

ApJ 812 11 **2015**

http://arxiv.org/pdf/1507.00435v1.pdf

Ellerman bombs are transient brightenings of the extended wings of the solar Balmer lines in emerging active regions. We describe their properties in the ultraviolet lines sampled by the Interface Region Imaging Spectrograph (IRIS), using simultaneous imaging spectroscopy in Hα with the Swedish 1-m Solar Telescope (SST) and ultraviolet images from the Solar Dynamics Observatory for Ellerman bomb detection and identification. We select multiple co-observed Ellerman bombs for detailed analysis. The IRIS spectra strengthen the view that Ellerman bombs mark reconnection between bipolar kilogauss fluxtubes with the reconnection and the resulting bi-directional jet located within the solar photosphere and shielded by overlying chromospheric fibrils in the cores of strong lines. The spectra suggest that the reconnecting photospheric gas underneath is heated sufficiently to momentarily reach stages of ionization normally assigned to the transition region and the corona. We also analyze similar outburst phenomena that we classify as small flaring arch filaments and ascribe to higher-located reconnection. They have different morphology and produce hot arches in million-Kelvin diagnostics. **2013 Sep 6, 2014 Jun 14, 2014 Jun 15**

Variation of the electron flux spectrum along a solar flare loop as inferred from STIX hard X-ray observations

Anna **Volpara**, Paolo Massa, Sam Krucker, A Gordon Emslie, Michele Piana, Anna Maria Massone

A&A 684, A185 (**2024**)

https://arxiv.org/pdf/2311.07148.pdf
Regularized imaging spectroscopy was introduced for the construction of electron flux images at different energies from count visibilities recorded by the Reuven Ramaty High Energy Solar Spectroscopic Imager (RHESSI). In this work we seek to extend this approach to data from the Spectrometer/Telescope for Imaging X-rays (STIX) on-board the Solar Orbiter mission. Our aims are to demonstrate the feasibility of regularized imaging spectroscopy as a method for analysis of STIX data, and also to show how such analysis can lead to insights into the physical processes affecting the nonthermal electrons responsible for the hard X-ray emission observed by STIX. STIX records imaging data in an intrinsically different manner from RHESSI. Rather than sweeping the angular frequency plane in a set of concentric circles (one circle per detector), STIX uses 30 collimators, each corresponding to a specific angular frequency. In this paper we derive an appropriate modification of the previous computational approach for the analysis of the visibilities observed by STIX. This approach also allows for the observed count data to be placed into non-uniformly-spaced energy bins. We show that the regularized imaging spectroscopy approach is not only feasible for analysis of the visibilities observed by STIX, but also more reliable. Application of the regularized imaging spectroscopy technique to several well-observed flares reveals details of the variation of the electron flux spectrum throughout the flare sources. We conclude that the visibility-based regularized imaging spectroscopy approach is well-suited to analysis of STIX data. We also use STIX electron flux spectral images to track, for the first time, the behavior of the accelerated electrons during their path from the acceleration site in the solar corona toward the chromosphere . **2021-05-08, 2022-09-29**

Role of electron inertia and reconnection dynamics in a stressed X-point collapse with a guide-field

J. Graf **von der Pahlen** and D. Tsiklauri
A&A 595, A84 (**2016**)
Aims. In previous simulations of collisionless 2D magnetic reconnection it was consistently found that the term in the generalised Ohm’s law that breaks the frozen-in condition is the divergence of the electron pressure tensor’s non-gyrotropic components. The motivation for this study is to investigate the effect of the variation of the guide-field on the reconnection mechanism in simulations of X-point collapse, and the related changes in reconnection dynamics.
Methods. A fully relativistic particle-in-cell (PIC) code was used to model X-point collapse with a guide-field in two and three spatial dimensions.
Results. We show that in a 2D X-point collapse with a guide-field close to the strength of the in-plane field, the increased induced shear flows along the diffusion region lead to a new reconnection regime in which electron inertial terms play a dominant role at the X-point. This transition is marked by the emergence of a magnetic island – and hence a second reconnection site – as well as electron flow vortices moving along the current sheet. The reconnection electric field at the X-point is shown to exceed all lower guide-field cases for a brief period, indicating a strong burst in reconnection. By extending the simulation to three spatial dimensions it is shown that the locations of vortices along the current sheet (visualised by their Q-value) vary in the out-of-plane direction, producing tilted vortex tubes. The vortex tubes on opposite sides of the diffusion region are tilted in opposite directions, similarly to bifurcated current sheets in oblique tearing-mode reconnection. The tilt angles of vortex tubes were compared to a theoretical estimation and were found to be a good match. Particle velocity distribution functions for different guide-field runs, for 2.5D and 3D simulations, are analysed and compared.

Magnetic Reconnection in an X-point Collapse

Jan Graf **von der Pahlen** and D. Tsiklauri
UKSP Nugget: 41. Dec **2013**
http://www.uksolphys.org/uksp-nugget/41-magnetic-reconnection-in-an-x-point-collapse/
The research presented in this nugget [3] is an extension of the works of [1,2], where collisionless magnetic reconnection in a stressed X-point collapse was investigated using a 2.5D PIC code (i.e. a PIC code over a domain with two spatial dimensions and three particle velocity components). The same set-up was used in this simulation, also including ‘closed’ boundary conditions, where particles are reflected at the boundary and magnetic flux is conserved, fixing magnetic field lines. The alternative boundary conditions introduced here are ‘open’ i.e. allowing particles and magnetic flux to escape at the boundary. Further, a uniform out-of-plane magnetic field (guide-field), ranging from 0.1 to 1 the characteristic in-plane field strength (BP), was introduced.

Contrastive Representation Learning for Predicting Solar Flares from Extremely Imbalanced Multivariate Time Series Data

Onur **Vural**, Shah Muhammad Hamdi, Soukaina Filali Boubrahimi
ICMLA 2024 on September 7 **2024**
https://arxiv.org/pdf/2410.00312
Major solar flares are abrupt surges in the Sun's magnetic flux, presenting significant risks to technological infrastructure. In view of this, effectively predicting major flares from solar active region magnetic field data through machine learning methods becomes highly important in space weather research. Magnetic field data can be represented

in multivariate time series modality where the data displays an extreme class imbalance due to the rarity of major flare events. In time series classification-based flare prediction, the use of contrastive representation learning methods has been relatively limited. In this paper, we introduce CONTREX, a novel contrastive representation learning approach for multivariate time series data, addressing challenges of temporal dependencies and extreme class imbalance. Our method involves extracting dynamic features from the multivariate time series instances, deriving two extremes from positive and negative class feature vectors that provide maximum separation capability, and training a sequence representation embedding module with the original multivariate time series data guided by our novel contrastive reconstruction loss to generate embeddings aligned with the extreme points. These embeddings capture essential time series characteristics and enhance discriminative power. Our approach shows promising solar flare prediction results on the Space Weather Analytics for Solar Flares (SWAN-SF) multivariate time series benchmark dataset against baseline methods.

Mars Odyssey/HEND and RHESSI

Vadim **Vybornov** and Michael A. Livshits
RHESSI Science Nugget No. 202, June **2013**
We discuss observations of flares visible from the Earth, as a check on the HEND calibrations, and then show observations from the solar hemisphere (the "backside") invisible from Earth. **27 Oct 2002**

Solar Flare Prediction and Feature Selection using Light Gradient Boosting Machine Algorithm

Vysakh P. A., Prateek Mayank
Solar Phys. 298, Article number: 137 **2023**
https://arxiv.org/pdf/2310.19332.pdf
Solar flares are among the most severe space weather phenomena, and they have the capacity to generate radiation storms and radio disruptions on Earth. The accurate prediction of solar flare events remains a significant challenge, requiring continuous monitoring and identification of specific features that can aid in forecasting this phenomenon, particularly for different classes of solar flares. In this study, we aim to forecast C and M class solar flares utilising a machine-learning algorithm, namely the Light Gradient Boosting Machine. We have utilised a dataset spanning 9 years, obtained from the Space-weather Helioseismic and Magnetic Imager Active Region Patches (SHARP), with a temporal resolution of 1 hour. A total of 37 flare features were considered in our analysis, comprising of 25 active region parameters and 12 flare history features. To address the issue of class imbalance in solar flare data, we employed the Synthetic Minority Oversampling Technique (SMOTE). We used two labeling approaches in our study: a fixed 24-hour window label and a varying window that considers the changing nature of solar activity. Then, the developed machine learning algorithm was trained and tested using forecast verification metrics, with an emphasis on evaluating the true skill statistic (TSS). Furthermore, we implemented a feature selection algorithm to determine **the most significant features from the pool of 37 features that could distinguish between flaring and non-flaring active regions**. We found that utilising a limited set of useful features resulted in improved prediction performance. For the 24-hour prediction window, we achieved a TSS of 0.63 (0.69) and accuracy of 0.90 (0.97) for ≥C (≥M) class solar flares.

Solar Flare Detection Method using Rn-222 Radioactive Source

Jonathan **Walg**, Yaniv Zigel, Anatoly Rodnianski, Itzhak Orion
2020
https://arxiv.org/ftp/arxiv/papers/2002/2002.02787.pdf
arXiv:1902.10131
Solar neutrino detection is known to be a very challenging task, due to the minuscule absorption cross-section and mass of the neutrino. One research showed that relative large solar-flares affected the decay-rates of Mn-54 in December 2006. Since most the radiation emitted during a solar flare are blocked before reaching the earth surface, it should be assumed that such decay-rate changes could be due to neutrino flux increase from the sun, in which only neutrinos can penetrate the radionuclide. This study employs the Rn-222 radioactive source for the task of solar flare detection, based on the prediction that it will provide a stable gamma ray counting rate. In order to ascertain counting stability, three counting systems were constructed to track the count-rate changes. The signal processing approach was applied in the raw data analysis. The Rn-222 count-rate measurements showed several radiation counting dips, indicating that the radioactive nuclide can be affected by order of magnitude neutrino flux change from the sun. We conclude that using the cooled Radon source obtained the clearest responses, and therefore this is the preferable system for detecting neutrino emissions from a controlled source.

Pre-Flare Flows in the Corona

A.J. **Wallace** · L.K. Harra · L. van Driel-Gesztelyi · L.M. Green · S.A. Matthews
Solar Phys (**2010**) 267: 361–375
Solar flares take place in regions of strong magnetic fields and are generally accepted to be the result of a resistive instability leading to magnetic reconnection. When new

flux emerges into a pre-existing active region it can act as a flare and coronal mass ejection trigger. In this study we observed active region 10955 after the emergence of small-scale additional flux at the magnetic inversion line. We found that flaring began when additional positive flux levels exceeded 1.38 Ч 10^{20} Mx (maxwell), approximately 7 h after the initial flux emergence. We focussed on the pre-flare activity of one B-class flare that occurred on the following day. The earliest indication of activity was a rise in the non-thermal velocity one hour before the flare. 40 min before flaring began, brightenings and pre-flare flows were observed along two loop systems in the corona, involving the new flux and the preexisting active region loops. We discuss the possibility that reconnection between the new flux and pre-existing loops before the flare drives the flows by either generating slow mode magnetoacoustic waves or a pressure gradient between the newly reconnected loops. The subsequent B-class flare originated from fast reconnection of the same loop systems as the pre-flare flows.

Unveiling key factors in solar eruptions leading to the solar superstorm in 2024 May

Rui **Wang**1,2,3⋆, Ying D. Liu1,2,3, Xiaowei Zhao4,5 and Huidong Hu1,2

A&A 692, A112 (**2024**)

https://arxiv.org/pdf/2410.00891 **File**

https://doi.org/10.1051/0004-6361/202452008

https://www.aanda.org/articles/aa/pdf/2024/12/aa52008-24.pdf

NOAA active region (AR) 13664/8 produced the most intense geomagnetic effects since the Halloween event of 2003. The resulting extreme solar storm is thought to be the consequence of multiple interacting coronal mass ejections (CMEs). Notably, this AR exhibits exceptionally rapid magnetic flux emergence. The eruptions on which we focus all occurred along collisional polarity inversion lines (PILs) through collisional shearing during a three-day period of extraordinarily high flux emergence (∼1021 Mx h−1). Our key findings reveal how photospheric magnetic configurations in eruption sources influence solar superstorm formation and geomagnetic responses, and link exceptionally strong flux emergence to sequential homologous eruptions: (1) We identified the source regions of seven halo CMEs that were distributed primarily along two distinct PILs. This distribution suggests two groups of homologous CMEs. (2) The variations in the magnetic flux emergence rates in the source regions are correlated with the CME intensities. This might explain the two contrasting cases of complex ejecta that are observed at Earth. (3) Our calculations of the magnetic field gradients around the CME source regions show strong correlations with eruptions. This provides crucial insights into solar eruption mechanisms and enhances our prediction capabilities for future events.
May 2024: 4-12, 8, 9, 10,11

Exploring Standing and Reflected Slow-mode Waves in Flaring Coronal Loops: A Parametric Study Using 2.5D MHD Modeling

Tongjiang **Wang**, Leon Ofman, Stephen J. Bradshaw

Solar Phys. **299**, 37 **2024**

https://arxiv.org/pdf/2403.02464.pdf

https://doi.org/10.1007/s11207-024-02285-z

Recent observations of reflected propagating and standing slow-mode waves in hot flaring coronal loops have spurred our investigation into their underlying excitation and damping mechanisms. To understand these processes, we conduct 2.5D magnetohydrodynamic (MHD) simulations using an arcade active region model that includes a hot and dense loop. Our simulations allow for in-depth parametric investigations complementing and expanding our previous 3D MHD modeling results. We excite these waves in two distinct models as motivated by observations from the SDO/AIA. Model 1 incorporates classical compressive viscosity coefficient, while Model 2 adopts a 10-times enhanced viscosity coefficient. We find that: (1) Our 2.5D MHD simulations reinforce previous conclusions derived from 1D and 3D MHD models that significantly enhanced viscosity is crucial for the rapid excitation of standing slow waves with damping times consistent with observations by Wang et al. (2015). (2) We uncover that nonlinearity in Model 1 delays the conversion of a reflected propagating wave into a standing wave. In contrast, Model 2 exhibits a much weak influence of nonlinearity. (3) Our results reveal that the transverse temperature structure holds more influence on wave behavior than the density structure. In Model 1, increased loop temperature contrast significantly enhances wave trapping within the structure, mitigating the impact of temperature-dependent viscous damping. Conversely, in Model 2, the impact of temperature structure on wave behavior weakens in comparison to the effect of viscosity. (4) Model 1 displays evident nonlinear coupling to the fast and kink magnetoacoustic waves and pronounced wave leakage into the corona. However, analyzing three observed wave events by SDO/AIA aligns with Model 2 predictions, providing further support for the substantial viscosity increase.

A Strong-flare Prediction Model Developed Using a Machine-learning Algorithm Based on the Video Data Sets of the Solar Magnetic Field of Active Regions

Jingjing **Wang**1,2, Bingxian Luo1,2,3, Siqing Liu1,2,3, and Yue Zhang4

2023 ApJS 269 54
https://iopscience.iop.org/article/10.3847/1538-4365/ad036d/pdf
It is well accepted that the physical properties obtained from the solar magnetic field observations of active regions (ARs) are related to solar eruptions. These properties consist of temporal features that might reflect the evolution process of ARs, and spatial features that might reflect the graphic properties of ARs. In this study, we generated video data sets with timescales of 1 day and image data sets of the SHARP radial magnetic field of the ARs from 2010 May to 2020 December. For the ARs that evolved from "quiet" to "active" and erupted the first strong flares in 4 days, we extract and investigate both the temporal and spatial features of ARs from videos, aiming to capture the evolution properties of their magnetic field structures during their transition process from "quiet" (non–strong flaring) to "active" (strong flaring). We then conduct a comparative analysis of the model performance by video input and single-image input, as well as of the effect of the model performance variation with the prediction window up to 3 days. We find that for those ARs that erupted the first strong flares in 4 days, the temporal features that reflect their evolution from "quiet" to "active" before the first strong flares can be recognized and extracted from the video data sets by our network. These features turn out to be important predictors that can effectively improve strong-flare prediction, especially by reducing the false alarms in a nearly 2 day prediction window.
Introduction

Enhanced three-minute oscillation above a sunspot during a solar flare
Ya **Wang**, Lyndsay Fletcher, Sargam Mulay, Haisheng Ji, Wenda Cao
ApJ **961** 231 **2023**
https://arxiv.org/pdf/2311.17223.pdf
https://iopscience.iop.org/article/10.3847/1538-4357/ad10a9/pdf
Three-minute oscillations are a common phenomenon in the solar chromosphere above a sunspot. Oscillations can be affected by the energy release process related to solar flares. In this paper, we report on an enhanced oscillation in flare event SOL**2012-07-05**T21:42 with a period of around three minutes, that occurred at the location of a flare ribbon at a sunspot umbra-penumbra boundary, and was observed both in chromo-spheric and coronal passbands. An analysis of this oscillation was carried out using simultaneous ground-based observations from the Goode Solar Telescope (GST) at the Big Bear Solar Observatory (BBSO) and space-based observations from the Solar Dynamics Observatory (SDO). A frequency shift was observed before and after the flare, with the running penumbral wave that was present with a period of about 200 s before the flare co-existing with a strengthened oscillation with a period of 180 s at the same locations after the flare. We also found a phase difference between different passbands, with the oscillation occurring from high-temperature to low-temperature passbands. Theoretically, the change in frequency is strongly dependent on the variation of the inclination of the magnetic field and the chromospheric temperature. Following an analysis of the properties of the region, we find the frequency change is caused by the slight decrease of the magnetic inclination angle to the local vertical. In addition, we suggest that the enhanced three-minute oscillation is related to the additional heating, maybe due to the downflow, during the EUV late phase of the flare.

Spectral Features of the Solar Transition Region and Chromospheric Lines at Flare Ribbons Observed with IRIS
L. F. **Wang**1,2, Y. Li3,4, Q. Li3,4, X. Cheng1,2, and M. D. Ding1,2
2023 ApJS 268 62
https://arxiv.org/pdf/2308.11275.pdf
https://iopscience.iop.org/article/10.3847/1538-4365/acf127/pdf
We report on the spectral features of the Si ivλ1402.77, C iiλ1334.53, and Mg iih or k lines, formed in the layers from the transition region to the chromosphere, in three two-ribbon flares (with X, M, and C class) observed with IRIS. All three lines show significant redshifts within the main flare ribbons, which mainly originate from the chromospheric condensation during the flares. The average redshift velocities of the Si iv line within the main ribbons are 56.6, 25.6, and 10.5 km s−1 for the X-, M-, and C-class flares, respectively, which show a decreasing tendency with the flare class. The C ii and Mg ii lines show a similar tendency but with smaller velocities compared to the Si iv line. Additionally, the Mg iih or k line shows a blue-wing enhancement in the three flares, in particular at the flare ribbon fronts, which is supposed to be caused by an upflow in the upper chromosphere due to the heating of the atmosphere. Moreover, the Mg iih or k line exhibits a central reversal at the flare ribbons but turns to pure emission shortly after 1–4 minutes. Correspondingly, the C ii line also shows a central reversal but in a smaller region. However, for the Si iv line, the central reversal is only found in the X-class flare. As usual, the central reversal of these lines can be caused by the opacity effect. This implies that, in addition to the optically thick lines (C ii and Mg ii lines), the Si iv line can become optically thick in a strong flare, which is likely related to the nonthermal electron beam heating. **2015 Dec 19, 2022 Jan 18, 2022 Mar 30**

Three-dimensional Turbulent Reconnection within Solar Flare Current Sheet
Yulei **Wang**, Xin Cheng, Mingde Ding, Zhaoyuan Liu, Jian Liu, Xiaojue Zhu

ApJL **954** L36 **2023**
https://arxiv.org/pdf/2308.10494.pdf
https://iopscience.iop.org/article/10.3847/2041-8213/acf19d/pdf
Solar flares can release coronal magnetic energy explosively and may impact the safety of near-earth space environments. Their structures and properties on macroscale have been interpreted successfully by the generally-accepted two-dimension standard model invoking magnetic reconnection theory as the key energy conversion mechanism. Nevertheless, some momentous dynamical features as discovered by recent high-resolution observations remain elusive. Here, we report a self-consistent high-resolution three-dimension magnetohydrodynamical simulation of turbulent magnetic reconnection within a flare current sheet. It is found that fragmented current patches of different scales are spontaneously generated with a well-developed turbulence spectrum at the current sheet, as well as at the flare loop-top region. The close coupling of tearing-mode and Kelvin-Helmholtz instabilities plays a critical role in developing turbulent reconnection and in forming dynamical structures with synthetic observables in good agreement with realistic observations. The sophisticated modeling makes a paradigm shift from the traditional to three-dimension turbulent reconnection model unifying flare dynamical structures of different scales.

Towards a live homogeneous database of solar active regions based on SOHO/MDI and SDO/HMI synoptic magnetograms. I. Automatic detection and calibration

Ruihui **Wang**, Jie Jiang, Yukun Luo
Astrophysical Journal Supplement Series **268** 55 **2023**
https://arxiv.org/pdf/2308.06914.pdf **File**
https://iopscience.iop.org/article/10.3847/1538-4365/acef1b/pdf **File**
Recent studies indicate that a small number of rogue solar active regions (ARs) may have a significant impact on the end-of-cycle polar field and the long-term behavior of solar activity. The impact of individual ARs can be qualified based on their magnetic field distribution. This motivates us to build a live homogeneous AR database in a series of papers. As the first of the series, we develop a method to automatically detect ARs from 1996 onwards based on SOHO/MDI and SDO/HMI synoptic magnetograms. The method shows its advantages in excluding decayed ARs and unipolar regions and being compatible with any available synoptic magnetograms. The identified AR flux and area are calibrated based on the co-temporal SDO/HMI and SOHO/MDI data. The homogeneity and reliability of the database are further verified by comparing it with other relevant databases. We find that ARs with weaker flux have a weaker cycle dependence. Stronger ARs show the weaker cycle 24 compared with cycle 23. Several basic parameters, namely, location, area, and flux of negative and positive polarities of identified ARs are provided in the paper. This paves the way for AR's new parameters quantifying the impact on the long-term behavior of solar activity to be presented in the subsequent paper of the series. The constantly updated database covering more than two full solar cycles will be beneficial for the understanding and prediction of the solar cycle. The database and the detection codes are accessible online.
The detection algorithm and full database of detected ARs are freely accessible at https://github.com/Wang-Ruihui/Alive-homogeneous-database-of-solar-active-regions

Change ratios of magnetic helicity and magnetic free energy during major solar flares

Quan **Wang**, Mei Zhang, Shangbin Yang, Xiao Yang, Xiaoshuai Zhu
RAA **2023**
https://arxiv.org/pdf/2308.05366.pdf **File**
Magnetic helicity is an important concept in solar physics, with a number of theoretical statements pointing out the important role of magnetic helicity in solar flares and coronal mass ejections (CMEs). Here we construct a sample of 47 solar flares, which contains **18 no-CME-associated confined flares and 29 CME-associated eruptive flares**. We calculate the change ratios of magnetic helicity and magnetic free energy before and after these 47 flares. Our calculations show that the change ratios of magnetic helicity and magnetic free energy show distinct different distributions in confined flares and eruptive flares. The median value of the change ratios of magnetic helicity in confined flares is −0.8%, while this number is −14.5% for eruptive flares. For the magnetic free energy, the median value of the change ratios is −4.3% for confined flares, whereas this number is −14.6% for eruptive flares. This statistical result, using observational data, is well consistent with the theoretical understandings that magnetic helicity is approximately conserved in the magnetic reconnection, as shown by confined flares, and the CMEs take away magnetic helicity from the corona, as shown by eruptive flares.
Table 1. Information and results of the **18 confined flare** events 2012-2017
Table 2. Information and results of the **29 eruptive flare** events 2011-2017

Sequential Remote Brightenings and Co-spatial Fast Downflows during Two Successive Flares

B. T. **Wang**, X. Cheng, C. Li, J. Chen, M. D. Ding
ApJ **953** 172 **2023**

https://arxiv.org/pdf/2306.15991.pdf
https://iopscience.iop.org/article/10.3847/1538-4357/ace319/pdf
Remote brightenings often appear at outskirts of source active regions of solar eruptive events, nevertheless, their origin remains to be ascertained. In this study, we report imaging and spectroscopic observations of sequential remote brightenings with a combination of Hα Imaging Spectrograph (HIS) onboard the Chinese Hα Solar Explorer (CHASE), which is the first space-based solar telescope of China, and the Solar Dynamics Observatory. It is found that, during two successive M-class flares occurring on **2022 August 17**, multiple ribbon-like brightenings appeared in sequence away from the flaring active region. Meanwhile, abundant cool filament materials moved downward to the sequential remote brightenings as visible at the Hα red wing with a line-of-sight speed up to 70 km s−1. The extrapolated three-dimensional magnetic field configuration shows that the sequential remote brightenings correspond to the footpoints of closed ambient field lines whose conjugate footpoints are rooted in the main flare site. We suggest that the sequential remote brightenings are most likely caused by the heating of interchange reconnection between the erupting flux rope and closed ambient field, during which the rope-hosting filament materials are transferred to the periphery of flaring active region along the closed ambient field rather than to the interplanetary space like in the scenario of the slow solar wind formation.

Efficient Electron Acceleration Driven by Flux Rope Evolution during Turbulent Reconnection

Z. **Wang**1,2, A. Vaivads2, H. S. Fu1,3, J. B. Cao1,3, and Y. Y. Liu1,3
2023 ApJ 946 39
https://iopscience.iop.org/article/10.3847/1538-4357/acbd3e/pdf
Magnetic flux ropes or magnetic islands are important structures responsible for electron acceleration and energy conversion during turbulent reconnection. However, the evolution of flux ropes and the corresponding electron acceleration process still remain open questions. In this paper, we present a comparative study of flux ropes observed by the Magnetospheric Multiscale mission in the outflow region during an example of turbulent reconnection in Earth's magnetotail. Interestingly, we find the farther the flux rope is away from the X-line, the bigger the size of the flux rope and the slower it moves. We estimate the power density converted at the observed flux ropes via the three fundamental electron acceleration mechanisms: Fermi, betatron, and parallel electric field. The dominant acceleration mechanism at all three flux ropes is the betatron mechanism. The flux rope that is closest to the X-line, having the smallest size and the fastest moving velocity, is the most efficient in accelerating electrons. Significant energy also returns from particles to fields around the flux ropes, which may facilitate the turbulence in the reconnection outflow region. **2020 August 3**

Precursor Identification for Strong Flares Based On Anomaly Detection Algorithm

Jingjing **Wang**, Bingxian Luo, and Siqing Liu
Front. Astron. Space Sci. 9:1037863. **2022**
doi: 10.3389/fspas.2022.1037863
https://www.frontiersin.org/articles/10.3389/fspas.2022.1037863/pdf
In this study, we assume that the magnetic configuration of active regions (ARs) in quiet periods has certain similarities and can be considered “normal” features. While there are some other magnetic features of active regions that are related to strong flares, they can be considered the precursor of strong flares and “anomaly” features. Our study aims to identify those “anomalies” and apply them in strong-flare forecasting. An unsupervised auto-encoder network has been used to understand and memorize these “normal” features, and then, based on the mean squared errors between the pictures of the ARs and the corresponding reconstructed pictures derived by the network, an anomaly detection algorithm has been adopted to identify the precursor for strong flares and develop a strong-flare classification model. The strong-flare classification model reaches an F1 score of 0.8139, an accuracy of 0.8954, a recall of 0.8785, and a precision of 0.7581. Moreover, for those correctly predicted strong-flare events (94 M-class flares and above), the model reaches an average first warning time of 45.24 h. The results indicate that the anomaly detection algorithm can be used in precursor identification for strong flares and help in both improving strong-flare prediction accuracy and enlarging the time in advance. Also, the obtained average maximum warning period for strong-flare prediction (nearly 2 days) will be useful for future applications for space-weather solar flare prediction. **15 Feb 2011. 22 Oct 2014**
HMI Nuggets #187 **2022** http://hmi.stanford.edu/hminuggets/?p=4015

Current-sheet Oscillations Caused by Kelvin-Helmholtz Instability at the Loop Top of Solar Flares

Yulei **Wang**, Xin Cheng, Zining Ren, Mingde Ding
ApJL **931** L32 **2022**
https://arxiv.org/pdf/2205.10361.pdf
https://iopscience.iop.org/article/10.3847/2041-8213/ac715a/pdf
Current sheets (CSs), long stretching structures of magnetic reconnection above solar flare loops, are usually observed to oscillate, their origins, however, are still puzzled at present. Based on a high-resolution 2.5-dimensional MHD simulation of magnetic reconnection, we explore the formation mechanism of the CS oscillations. We find that large-

amplitude transverse waves are excited by the Kelvin-Helmholtz instability (KHI) at the highly turbulent cusp-shaped region. The perturbations propagate upward along the CS with a phase speed close to local Alfvén speed thus resulting in the CS oscillations we observe. Though the perturbations damp after propagating for a long distance, the CS oscillations are still detectable. In terms of detected CS oscillations, with a combination of differential emission measure technique, we propose a new method for measuring the magnetic field strength of the CSs and its distribution in height. **2011-10-22**

Annihilation of Magnetic Islands at the Top of Solar Flare Loops

Yulei **Wang**, Xin Cheng, Mingde Ding, Quanming Lu
ApJ 923:227 **2021**
https://arxiv.org/pdf/2110.08526.pdf
https://iopscience.iop.org/article/10.3847/1538-4357/ac3142/pdf
The dynamics of magnetic reconnection in the solar current sheet (CS) is studied by high-resolution 2.5-dimensional MHD simulation. With the commence of magnetic reconnection, a number of magnetic islands are formed intermittently and move quickly upward and downward along the CS. When colliding with the semi-closed flux of flare loops, the downflow islands cause a second reconnection with a rate even comparable with that in the main CS. Though the time-integrated magnetic energy release is still dominated by the reconnection in main CS, the second reconnection can release substantial magnetic energy, annihilating the main islands and generating secondary islands with various scales at the flare loop top. The distribution function of the flux of the second islands is found to follow a power-law varying from $f(\psi)\sim\psi-1$ (small scale) to $\psi-2$ (large scale), which seems to be independent with background plasma β and if including thermal conduction. However, the spatial scale and the strength of the termination shocks driven by main reconnection outflows or islands decrease if β increases or thermal conduction is included. We suggest that the annihilation of magnetic islands at the flare loop top, which is not included in the standard flare model, plays a non-negligible role in releasing magnetic energy to heat flare plasma and accelerate particles.

Slow-Mode Magnetoacoustic Waves in Coronal Loops **Review**

Tongjiang **Wang**, Leon Ofman, Ding Yuan, Fabio Reale, Dmitrii Y. Kolotkov, Abhishek K. Srivastava
Space Science Reviews **2021**
https://arxiv.org/pdf/2102.11376.pdf
Rapidly decaying long-period oscillations often occur in hot coronal loops of active regions associated with small (or micro-) flares. This kind of wave activity was first discovered with the SOHO/SUMER spectrometer from Doppler velocity measurements of hot emission lines, thus also often called "SUMER" oscillations. They were mainly interpreted as global (or fundamental mode) standing slow magnetoacoustic waves. In addition, increasing evidence has suggested that the decaying harmonic type of pulsations detected in light curves of solar and stellar flares are likely caused by standing slow-mode waves. The study of slow magnetoacoustic waves in coronal loops has become a topic of particular interest in connection with coronal seismology. We review recent results from SDO/AIA and Hinode/XRT observations that have detected both standing and reflected intensity oscillations in hot flaring loops showing the physical properties (e.g., oscillation periods, decay times, and triggers) in accord with the SUMER oscillations. We also review recent advances in theory and numerical modeling of slow-mode waves focusing on the wave excitation and damping mechanisms. MHD simulations in 1D, 2D and 3D have been dedicated to understanding the physical conditions for the generation of a reflected propagating or a standing wave by impulsive heating. Various damping mechanisms and their analysis methods are summarized. Calculations based on linear theory suggest that the non-ideal MHD effects such as thermal conduction, compressive viscosity, and optically thin radiation may dominate in damping of slow-mode waves in coronal loops of different physical conditions. Finally, an overview is given of several important seismological applications such as determination of transport coefficients and heating function.

Naked emergence of an anti-Hale active region
I. Overall evolution and magnetic properties⋆

Jincheng **Wang**1,2,3, Xiaoli Yan1,3, Defang Kong1,3, Zhike Xue1,3, Liheng Yang1,3, Qiaoling Li1,4, Yan Zhang1,4 and Hao Li5,6
A&A 652, A55 (**2021**)
https://arxiv.org/abs/2106.02786
https://www.aanda.org/articles/aa/pdf/2021/08/aa40685-21.pdf
https://doi.org/10.1051/0004-6361/202140685
Aims. In order to understand the emergence of the active region, we investigate the emerging process and magnetic properties of a naked anti-Hale active region during the period between **August 24 to 25, 2018**.
Methods. Using the data from Helioseismic and Magnetic Imager on board the Soar Dynamic Observatory and the New Vacuum Solar Telescope, we calculated different evolving parameters (such as pole separation, tilt angle) and magnetic parameters (such as vertical electric current, force-free parameter, relative magnetic helicity) during the emergence of the active region. With these calculated parameters and some reasonable assumptions, we use two different methods to estimate the twist of the active region.

Results. The magnetic flux and pole separation continue increasing while the tilt angle exhibits a decreasing pattern during the emergence of the active region. The increase of the pole separation is mainly contributed as a result of the enhancement in the longitude direction. A power-law relationship between pole separation and total flux is found during the emergence of the active region. On the other hand, it is found that both the positive and negative electric currents increased equivalently and the average flux-weighted force-free parameter $\tilde{\alpha}$ remains almost consistently positive, on the order of ∼10−8 m−1. The relative magnetic helicity is mainly contributed by the shear term, while the relative magnetic helicity injection flux of the shear term changes its sign at the latter stage of the emergence. The twist number of the whole active region remains on the order of 10−1 turns during the emergence of the active region. Conclusions. We find that the magnetic flux tube with low twist also could emerge into the solar atmosphere.

Erupting Magnetic Flux Rope Affects Running Penumbral Waves

Wensi **Wang**, Rui Liu
A&A **2021**
https://arxiv.org/pdf/2101.04915.pdf
Context. It is well known that solar flares have broad impacts on the low atmosphere, but it is largely unknown how they affect sunspot waves and oscillations. It is also under debate as to whether the flare-induced photospheric changes are due to the momentum conservation with coronal mass ejections or due to magnetic reconnection. Aims. To shed light on the so-called "back reaction" of solar eruptions, we investigated how running penumbral waves (RPWs) at one foot of an erupting magnetic flux rope (MFR) responds to the rope buildup and subsequent erosion. Results. During the rope-buildup stage, the western foot of the rope, which is completely enclosed by a hooked ribbon, expands rapidly and consequently overlaps a sunspot penumbra. This converts the original penumbral field into the rope field, which is associated with a transient increase in electric currents flowing through the ribbon-swept penumbral region. During the rope-erosion stage, the rope foot shrinks as the eastern section of the hooked ribbon slowly sweeps the same penumbral region, where the rope field is converted into flare loops. This conversion induces mixed effects on the photospheric field inclination but heats up the low atmosphere at the footpoints of these flare loops to transition-region temperatures, therefore resulting in the post-eruption RPWs with an enhanced contrast in the 1600A passband and an extended bandwidth to low frequencies at 3-5 mHz, compared with the pre-eruption RPWs that peak at 6 mHz. Conclusions. This observation clearly demonstrates that it is the magnetic reconnection in the corona that impacts the low atmosphere and leads to the changing behaviors of RPWs, which, in turn, offer a new window to diagnose flare reconnections. **2015 November 4**
See Paper I Wang, W., Liu, R., Wang, Y., et al. 2017, Nature communications, 8, 1330

High-resolution He I 10830 Å Narrowband Imaging for an M-class Flare. III. EUV Late Phase

Ya **Wang**1,2, Haisheng Ji1,3, Alexander Warmuth4, Ying Li1, and Wenda Cao5
2020 ApJ 905 126
https://doi.org/10.3847/1538-4357/abc47a
In this paper, we report the EUV late phase for the M1.8 class flare on **2012 July 5** in the active region (AR) 11515. The late phase is shown by the prominent appearance of EUV emission at 131 Å of two additional flare loop systems (flare arcades 2 and 3, as named in this paper) other than the main flare loop (flare arcade 1), as observed by the Atmospheric Imaging Assembly (AIA) on board the Solar Dynamic Observatory (SDO). Three sets of flare arcades connect four flare ribbons, which forms an asymmetric quadrupole magnetic field configuration. While the emission from flare arcade 2, linking the pair of secondary flare ribbons, and arcade 3, linking one of the main flare ribbons and one of the secondary flare ribbons, conjointly contributes to the EUV late phase, their heating mechanisms are quite different. While the brightening of flare arcade 2 is the result of disturbance created by the eruption of EUV hot channels to the overlying coronal magnetic field, the heating of flare arcade 3 was closely associated with two rapid contractions of the overlying filament threads during the partial eruption of the filament. The contractions are discernible in He i 10830 Å images and have signatures in the EUV wavelengths of AIA. The two rapid contractions are the result of a sudden drop in magnetic pressure after the eruption of two hot channels. Clear evidence suggests that magnetic reconnection may occur between the contracting filament threads and the low-lying magnetic field.

High Resolution Observations of Solar Flares

Haimin **Wang**
Fleishman's Solar Physics Webinar 18-Sep-**2020**
https://youtu.be/GZWctGWzvTY
2 Jul 2012, 6 Jul 2012, 11 Aug 2013, 15 Aug 2013, 17 Aug 2013, 1 Aug 2014, 22 Jun 2015, 10 Jun 2018

Three-Dimensional Magnetic and Velocity Structures of Active Region 12673

Haimin **Wang**, Bin Chen, Ju Jing, Sijie Yu, Chang Liu, Vasyl Yurchyshyn, Kwangsu Ahn, Takenori Okamoto, Shin Toriumi, Wenda Cao, Dale Gary

EGU2020 presentation #2234 **File**

Solar Flare Predictive Features Derived from Polarity Inversion Line Masks in Active Regions Using an Unsupervised Machine Learning Algorithm

Jingjing **Wang**, Yuhang Zhang, Shea A. Hess Webber, Siqing Liu, Xuejie Meng, and Tieyan Wang
2020 ApJ 892 140
https://doi.org/10.3847/1538-4357/ab7b6c
sci-hub.tw/10.3847/1538-4357/ab7b6c
The properties of the polarity inversion line (PIL) in solar active regions (ARs) are strongly correlated to flare occurrences. The PIL mask, enclosing the PIL areas, has shown significant potential for improving machine-learning-based flare prediction models. In this study, an unsupervised machine-learning algorithm, Kernel Principle Component Analysis (KPCA), is adopted to directly derive features from the PIL mask and difference PIL mask, and use those features to classify ARs into two categories—non-strong flaring ARs and strong-flaring (M-class and above flares) ARs—for time-in-advance from one hour to 72 hr at a 1 hr cadence. The two best features are selected from the KPCA results to develop random-forest classifiers for predicting flares, and the models are then evaluated and compared to similar models based on the R value and difference R value. The results show that the features derived from the PIL masks by KPCA are effective in predicting flare occurrence, with overall better Fisher ranking scores and similar predictive statistics as the R value characteristics. **2017 September 6**
HMI Science Nuggets, #**140**, **2020** http://hmi.stanford.edu/hminuggets/?p=3263

Predicting solar flares with machine learning: investigating solar cycle dependence

Xiantong **Wang**, Yang Chen, Gabor Toth, Ward B. Manchester, Tamas I. Gombosi, Alfred O. Hero, Zhenbang Jiao, Hu Sun, Meng Jin, Yang Liu
2020 *ApJ* **895** 3
https://arxiv.org/pdf/1912.00502.pdf
https://doi.org/10.3847/1538-4357/ab89ac
A deep learning network, Long-Short Term Memory (LSTM) network, is used in this work to predict whether the maximum flare class an active region (AR) will produce in the next 24 hours is class Γ. We considered Γ are ≥M, ≥C and any flare class. The essence of using LSTM, which is a recurrent neural network, is its capability to capture temporal information of the data samples. The input features are time sequences of 20 magnetic parameters from SHARPs - Space-weather HMI Active Region Patches. We analyzed active regions from June 2010 to Dec 2018, using the Geostationary Operational Environmental Satellite (GOES) X-ray flare catalogs and label the data samples with identified ARs in the GOES X-ray flare catalogs. Our results (i) shows consistent skill scores with recently published results using LSTMs and better than the previous work using single time input (eg. DeFN) (ii) The skill scores from the model show essential differences when different years of data was chosen for training and testing.

Further Evidence for Looplike Fine Structure inside "Unipolar" Active Region Plages

Y.-M. **Wang**, I. Ugarte-Urra, and J. W. Reep
2019 ApJ 885 34
sci-hub.se/10.3847/1538-4357/ab45f6
Earlier studies using extreme-ultraviolet images and line-of-sight magnetograms from the Solar Dynamics Observatory (SDO) have suggested that active region (AR) plages and strong network concentrations often have small, looplike features embedded within them, even though no minority-polarity flux is visible in the corresponding magnetograms. Because of the unexpected nature of these findings, we have searched the SDO database for examples of inverted-Y structures rooted inside "unipolar" plages, with such jetlike structures being interpreted as evidence for magnetic reconnection between small bipoles and the dominant-polarity field. Several illustrative cases are presented from the period of 2013–2015, all of which are associated with transient outflows from AR "moss." The triangular or dome-shaped bases have horizontal dimensions of ~2–4 Mm, corresponding to ~1–3 granular diameters. We also note that the spongy-textured Fe ix 17.1 nm moss is not confined to plages, but may extend into regions where the photospheric field is relatively weak or even has mixed polarity. We again find a tendency for bright coronal loops seen in the 17.1, 19.3, and 21.1 nm passbands to show looplike fine structure and compact brightenings at their footpoints. These observations provide further confirmation that present-day magnetograms are significantly underrepresenting the amount of minority-polarity flux inside AR plages and again suggest that footpoint reconnection and small-scale flux cancellation may play a major role in coronal heating, both inside and outside ARs. **2013 April 30, 2013 May 4-5, 2014 September 14, 2014 December 1, 2014 December 13, 2014 December 15, 2015 April 18, 2015 May 5, 2015 October 23, 2015 November 5, 2015 December 19.**

Parameters Derived from the SDO/HMI Vector Magnetic Field Data: Potential to Improve Machine-learning-based Solar Flare Prediction Models

Jingjing **Wang**1, Siqing Liu1,2, Xianzhi Ao1, Yuhang Zhang3, Tieyan Wang4, and Yang Liu5

2019 ApJ 884 175
sci-hub.se/10.3847/1538-4357/ab441b
It is well established that solar flares and coronal mass ejections (CMEs) are powered by the free magnetic energy stored in volumetric electric currents in the corona, predominantly in active regions (ARs). Much effort has been made to search for eruption-related signatures from magnetic field observed mostly in the photosphere; and the signatures are further employed for predicting flares and CMEs. The parameters in the Space-weather HMI Active Region Patches (SHARP) data from the Solar Dynamics Observatory/HMI observation of vector magnetic field are designed and generated for this purpose. In this paper, we report research done on modification of these SHARP parameters with an attempt to improve flare prediction. The newly modified parameters are weighed heavily by magnetic polarity inversion lines (PIL) with high magnetic gradient, as suggested by Schrijver, by multiplying the parameters with a PIL mask. We demonstrate that the number of the parameters that can well discriminate erupted and nonerupted ARs increases significantly by a factor of two, in comparison with the original parameters. This improvement suggests that the high-gradient PILs are tightly related with solar eruption that agrees with previous studies. This also provides new data that possess potential to improve the machine-learning-based solar flare prediction models. **2011 February 15**

Determination of transport coefficients by coronal seismology of flare-induced slow-mode waves: Numerical parametric study of 1D loop model

Tongjiang **Wang**, Leon Ofman
ApJ **886** 2 **2019**
https://arxiv.org/pdf/1909.10910.pdf
sci-hub.se/10.3847/1538-4357/ab478f
Recent studies of a flaring loop oscillation event on **2013 December 28** observed by the Atmospheric Imaging Assembly (AIA) of the Solar Dynamics Observatory (SDO) have revealed the suppression of thermal conduction and significant enhancement of compressive viscosity in hot (∼10 MK) plasma. In this study we aim at developing a new coronal seismology method for determining the transport coefficients based on a parametric study of wave properties using a 1D nonlinear MHD loop model in combination with the linear theory. The simulations suggest a two-step scheme: we first determine the effective thermal conduction coefficient from the observed phase shift between temperature and density perturbations as this physical parameter is insensitive to the unknown viscosity; then from the loop model with the obtained thermal conduction coefficient, we determine the effective viscosity coefficient from the observed decay time using the parametric modeling. With this new seismology technique we are able to quantify the suppression of thermal conductivity by a factor of about 3 and the enhancement of viscosity coefficient by a factor of 10 in the studied flaring loop. Using the loop model with these refined transport coefficients, we study the excitation of slow magnetoacoustic waves by launching a flow pulse from one footpoint. The simulation can self-consistently produce the fundamental standing wave on a timescale in agreement with the observation.

Roles of photospheric motions and flux emergence in the major solar eruption on 2017 September 6

Rui **Wang**, Ying D. Liu, J. Todd Hoeksema, I.V. Zimovets, Yang Liu
ApJ **2018**
https://arxiv.org/pdf/1810.13092.pdf
We study the magnetic field evolution in the active region (AR) 12673 that produced the largest solar flare in the past decade on **2017 September 6**. Fast flux emergence is one of the most prominent features of this AR. We calculate the magnetic helicity from photospheric tangential flows that shear and braid field lines (shear-helicity), and from normal flows that advect twisted magnetic flux into the corona (emergence-helicity), respectively. Our results show that the emergence-helicity accumulated in the corona is −1.6×1043 Mx2 before the major eruption, while the shear-helicity accumulated in the corona is −6×1043 Mx2, which contributes about 79\% of the total helicity. The shear-helicity flux is dominant throughout the overall investigated emergence phase. Our results imply that the emerged fields initially contain relatively low helicity. Much more helicity is built up by shearing and converging flows acting on preexisted and emerging flux. Shearing motions are getting stronger with the flux emergence, and especially on both sides of the polarity inversion line of the core field region. The evolution of the vertical currents shows that most of the intense currents do not appear initially with the emergence of the flux, which implies that most of the emerging flux is probably not strongly current-carrying. The helical magnetic fields (flux rope) in the core field region are probably formed by long-term photospheric motions. The shearing and converging motions are continuously generated driven by the flux emergence. AR 12673 is a representative as photospheric motions contribute most of the nonpotentiality in the AR with vigorous flux emergence.

High-resolution He i 10830 Å Narrowband Imaging for an M-class Flare. II. Multiple Hot Channels: Their Origin and Destination

Ya **Wang**1,2, Yingna Su1,3, Jinhua Shen4, Xu Yang5, Wenda Cao5, and Haisheng Ji1,3
2018 ApJ 859 148 DOI 10.3847/1538-4357/aac0f7

In this paper, we report our second-part result for the M1.8 class flare on **2012 July 5**, with an emphasis on the initiation process for the flare-associated filament eruption. The data set consists of high-resolution narrowband images in He i 10830 Å and broadband images in TiO 7057 Å taken at Big Bear Solar Observatory with the 1.6 m aperture Goode Solar Telescope. EUV images in different passbands observed by the Atmospheric Imaging Assembly on board the Solar Dynamics Observatory are used to distinguish hot plasma from cool plasma structures during the flare process. High-resolution 10830 Å images clearly show that, below the horizontal fibrils, which correspond to the filament's spine in full-disk Hα images, a sheared arch filament system (AFS) lies across the penumbra and surrounding satellite sunspots, between which continuous shearing motion is observed. Before the eruption, three microflares occurred successively and were followed by the appearance of three EUV hot channels. Two hot channels erupted, producing two flaring sites and two major peaks in GOES soft X-ray light curves; however, one hot channel's eruption failed. The 10830 Å imaging enables us to trace the first two hot channels to their very early stage, which is signified by the rising of the AFS after the first two precursors. Continuous flux emergence and localized flare-associated cancellation are observed under the AFS. In addition, EUV ejections were observed during the formation of the EUV hot channels. These observations support the fact that the hot channels are the result of magnetic reconnections during precursors.

Effect of transport coefficients on excitation of flare-induced standing slow-mode waves in coronal loops

Tongjiang **Wang**, Leon Ofman, Xudong Sun, Sami K Solanki, Joseph M Davila

ApJ **2018**

https://arxiv.org/pdf/1805.03282.pdf

Standing slow-mode waves have been recently observed in flaring loops by the Atmospheric Imaging Assembly (AIA) of the Solar Dynamics Observatory (SDO). By means of the coronal seismology technique transport coefficients in hot (~10 MK) plasma were determined by Wang et al.(2015, Paper I), revealing that thermal conductivity is nearly suppressed and compressive viscosity is enhanced by more than an order of magnitude. In this study we use 1D nonlinear MHD simulations to validate the predicted results from the linear theory and investigate the standing slow-mode wave excitation mechanism. We first explore the wave trigger based on the magnetic field extrapolation and flare emission features. Using a flow pulse driven at one footpoint we simulate the wave excitation in two types of loop models: model 1 with the classical transport coefficients and model 2 with the seismology-determined transport coefficients. We find that model 2 can form the standing wave pattern (within about one period) from initial propagating disturbances much faster than model 1, in better agreement with the observations. Simulations of the harmonic waves and the Fourier decomposition analysis show that the scaling law between damping time (τ) and wave period (P) follows $\tau \propto P2$ in model 2, while $\tau \propto P$ in model 1. This indicates that the largely enhanced viscosity efficiently increases the dissipation of higher harmonic components, favoring the quick formation of the fundamental standing mode. Our study suggests that observational constraints on the transport coefficients are important in understanding both, the wave excitation and damping mechanisms. **2013 December 28**

Unambiguous Evidence of Coronal Implosions During Solar Eruptions and Flares

Juntao **Wang**, P. J. A. Simoes, L. Fletcher

ApJ **859** 25 **2018**

https://arxiv.org/pdf/1804.02354.pdf

http://sci-hub.tw/http://iopscience.iop.org/0004-637X/859/1/25/

In the implosion conjecture, coronal loops contract as the result of magnetic energy release in solar eruptions and flares. However, after almost two decades, observations of this phenomenon are still rare, and most of previous reports are plagued by projection effects so that loop contraction could be either true implosion or just a change in loop inclination. In this paper, to demonstrate the reality of loop contractions in the global coronal dynamics, we present four events with the continuously contracting loops in an almost edge-on geometry from the perspective of SDO/AIA, which are free from the ambiguity caused by the projection effects, also supplemented by contemporary observations from STEREO for examination. In the wider context of observations, simulations and theories, we argue that the implosion conjecture is valid in interpreting these events. Furthermore, distinct properties of the events allow us to identify two physical categories of implosion. One type demonstrates a rapid contraction at the beginning of the flare impulsive phase, as magnetic free energy is removed rapidly by a filament eruption. The other type, which has no visible eruption, shows a continuous loop shrinkage during the entire flare impulsive phase which we suggest manifests the ongoing conversion of magnetic free energy in a coronal volume. Corresponding scenarios are described, which can provide reasonable explanations for the observations. We also point out that implosions may be suppressed in cases when a heavily-mass-loaded filament is involved, possibly serving as an alternative account for their observational rarity. **2011-09-14, 2014-02-17, 2016-04-08, 2016-11-22**

Evolution of Photospheric Flow and Magnetic Fields Associated with The 2015 June 22 M6.5 Flare

Jiasheng **Wang**, Chang Liu, Na deng, Haimin Wang

2018 ApJ 853 143
https://arxiv.org/pdf/1801.03486.pdf
http://sci-hub.tw/http://iopscience.iop.org/0004-637X/853/2/143/
The evolution of photospheric flow and magnetic fields before and after flares can provide important information regarding the flare triggering and back reaction processes. However, such studies on the flow field are rare due to the paucity of high-resolution observations covering the entire flaring period. Here we study the structural evolution of penumbra and shear flows associated with the **2015 June 22** M6.5 flare in NOAA AR 12371, using high-resolution imaging observation in the TiO band taken by the 1.6~m Goode Solar Telescope at Big Bear Solar Observatory, with the aid of the differential affine velocity estimator method for flow tracking. The accompanied photospheric vector magnetic field changes are also analyzed using data from the Helioseismic and Magnetic Imager. As a result, we found, for a penumbral segment in the negative field adjacent to the magnetic polarity inversion line (PIL), an enhancement of penumbral flows (up to an unusually high value of \sm2~\kms) and extension of penumbral fibrils after the first peak of the flare hard X-ray (HXR) emission. We also found an area at the PIL, which is co-spatial with a precursor brightening kernel, exhibits a gradual increase of shear flow velocity (up to \sm0.9~\kms) after the flare. The enhancing penumbral and shear flow regions are also accompanied by an increase of horizontal field and decrease of magnetic inclination angle(measured from the solar surface). These results are discussed in the context of the theory of back reaction of coronal restructuring on the photosphere as a result of flare energy release.

Observations of Reconnection Flows in a Flare on the Solar Disk

Juntao **Wang**, P. J. A. Simoes, N. L. S. Jeffrey, L. Fletcher, P. J. Wright, I. G. Hannah
ApJL **847** L1 **2017**
https://arxiv.org/pdf/1708.08706.pdf
http://iopscience.iop.org/article/10.3847/2041-8213/aa8904/pdf
Magnetic reconnection is a well-accepted part of the theory of solar eruptive events, though the evidence is still circumstantial. Intrinsic to the reconnection picture of a solar eruptive event, particularly in the standard model for two-ribbon flares ("CSHKP" model), are an advective flow of magnetized plasma into the reconnection region, expansion of field above the reconnection region as a flux rope erupts, retraction of heated post-reconnection loops, and downflows of cooling plasma along those loops. We report on a unique set of SDO/AIA imaging and Hinode/EIS spectroscopic observations of the disk flare SOL**2016-03-23**T03:54 in which all four flows are present simultaneously. This includes spectroscopic evidence for a plasma upflow in association with large-scale expanding closed inflow field. The reconnection inflows are symmetric, and consistent with fast reconnection, and the post-reconnection loops show a clear cooling and deceleration as they retract. Observations of coronal reconnection flows are still rare, and most events are observed at the solar limb, obscured by complex foregrounds, making their relationship to the flare ribbons, cusp field and arcades formed in the lower atmosphere difficult to interpret. The disk location and favorable perspective of this event have removed these ambiguities giving a clear picture of the reconnection dynamics.

On Critical Height of Torus Instability in Two-Ribbon Solar Flares

Dong **Wang**, Rui Liu, Yuming Wang, Kai Liu, Jun Chen, Jiajia Liu, Zhenjun Zhou, Min Zhang
ApJL **2017**
https://arxiv.org/pdf/1706.03169.pdf
We studied the background field for 60 two-ribbon flares of M-and-above classes during 2011--2015. These flares are categorized into two groups, i.e., \emph{eruptive} and \emph{confined} flares, based on whether a flare is associated with a coronal mass ejection or not. The background field of source active regions is approximated by a potential field extrapolated from the Bz component of vector magnetograms provided by the Helioseismic and Magnetic Imager. We calculated the decay index n of the background field above the flaring polarity inversion line, and defined a critical height hcrit corresponding to the theoretical threshold (ncrit=1.5) of the torus instability. We found that hcrit is approximately half of the distance between the centroids of opposite polarities in active regions, and that the distribution of hcrit is bimodal: it is significantly higher for confined flares than for eruptive ones. The decay index increases monotonously with increasing height for 86\% (84\%) of the eruptive (confined) flares but displays a saddle-like profile for the rest 14\% (16\%), which are found exclusively in active regions of multipolar field configuration. Moreover, n at the saddle bottom is significantly smaller in confined flares than that in eruptive ones. These results highlight the critical role of background field in regulating the eruptive behavior of two-ribbon flares. **2012-03-14, 2014-02-04, 2014-10-22**
Table 1. Flare list ('E' for **eruptive** flares, 'C' for **confined** flares.)
HMI Science Nuggets #71 Sept 2017 http://hmi.stanford.edu/hminuggets/?p=1956

High-resolution observations of flare precursors in the low solar atmosphere

Haimin **Wang**, Chang Liu, Kwangsu Ahn, Yan Xu, Ju Jing, Na Deng, Nengyi Huang, Rui Liu, Kanya Kusano, Gregory D. Fleishman, Dale E. Gary, Wenda Cao

Nature Astronomy 1, 0085 **2017**
https://arxiv.org/pdf/1703.09866.pdf
http://www.nature.com/articles/s41550-017-0085
Solar flares are generally believed to be powered by free magnetic energy stored in the corona, but the build up of coronal energy alone may be insufficient for the imminent flare occurrence. The flare onset mechanism is a critical but less understood problem, insights into which could be gained from small-scale energy releases known as precursors, which are observed as small pre-flare brightenings in various wavelengths, and also from certain small-scale magnetic configurations such as the opposite polarity fluxes, where magnetic orientation of small bipoles is opposite to that of the ambient main polarities. However, high-resolution observations of flare precursors together with the associated photospheric magnetic field dynamics are lacking. Here we study precursors of a flare using unprecedented spatiotemporal resolution of the 1.6 m New Solar Telescope, complemented by novel microwave data. Two episodes of precursor brightenings are initiated at a small-scale magnetic channel (a form of opposite polarity fluxes) with multiple polarity inversions and enhanced magnetic fluxes and currents, lying near the footpoints of sheared magnetic loops. The low-atmospheric origin of these precursor emissions is corroborated by microwave spectra. We propose that the emerging magnetic channel field interacts with the sheared arcades to cause precursor brightenings at the main flare core region. These high-resolution results provide evidence of low-atmospheric small-scale energy release and possible relationship to the onset of the main flare. **22 June 2015**

High resolution He I 10830 Å narrow-band imaging of an M-class flare. I - analysis of sunspot dynamics during flaring

Ya **Wang**, Yingna Su, Zhenxiang Hong, Zhicheng Zeng, Kaifan Ji, Philip R. Goode, Wenda Cao, Haisheng Ji
ApJ 833 250 **2016**
https://arxiv.org/pdf/1610.09227v1.pdf
In this paper, we report our first-step results of high resolution He\,\textsc{i} 10830 \AA\ narrow-band imaging (bandpass: 0.5 {\AA}) of an M1.8 class two-ribbon flare on **July 5, 2012**. The flare was observed with the 1.6 meter aperture New Solar Telescope at Big Bear Solar Observatory. For this unique data set, sunspot dynamics during flaring were analyzed for the first time. By directly imaging the upper chromosphere, running penumbral waves are clearly seen as an outward extension of umbral flashes, both take the form of absorption in the 10830 \AA\ narrow-band images. From a space-time image made of a slit cutting across a flare ribbon and the sunspot, we find that the dark lanes for umbral flashes and penumbral waves are obviously broadened after the flare. The most prominent feature is the sudden appearance of an oscillating absorption strip inside the ribbon when it sweeps into the sunspot's penumbral and umbral regions. During each oscillation, outwardly propagating umbral flashes and subsequent penumbral waves rush out into the inwardly sweeping ribbon, followed by a returning of the absorption strip with similar speed. We tentatively explain the phenomena as the result of a sudden increase in the density of ortho-Helium atoms in the area of the sunspot being excited by the flare's EUV illumination. This explanation is based on the observation that 10830 \AA\ absorption around the sunspot area gets enhanced during the flare. Nevertheless, questions are still open and we need further well-devised observations to investigate the behavior of sunspot dynamics during flares.

Arcade Implosion Caused by a Filament Eruption in a Flare

Juntao **Wang**, P. J. A. Simoes, L. Fletcher, J. K. Thalmann, H. S. Hudson, I. G. Hannah
ApJ 833 221 **2016**
https://arxiv.org/pdf/1610.05931v1.pdf **File**
Coronal implosions - the convergence motion of plasmas and entrained magnetic field in the corona due to a reduction in magnetic pressure - can help to locate and track sites of magnetic energy release or redistribution during solar flares and eruptions. We report here on the analysis of a well-observed implosion in the form of an arcade contraction associated with a filament eruption, during the C3.5 flare SOL**2013-06-19**T07:29. A sequence of events including magnetic flux-rope instability and distortion, followed by filament eruption and arcade implosion, lead us to conclude that the implosion arises from the transfer of magnetic energy from beneath the arcade as part of the global magnetic instability, rather than due to local magnetic energy dissipation in the flare. The observed net contraction of the imploding loops, which is found also in nonlinear force-free field extrapolations, reflects a permanent reduction of magnetic energy underneath the arcade. This event shows that, in addition to resulting in expansion or eruption of overlying field, flux-rope instability can also simultaneously implode unopened field due to magnetic energy transfer. It demonstrates the "partial opening of the field" scenario, which is one of the ways in 3D to produce a magnetic eruption without violating the Aly-Sturrock hypothesis. In the framework of this observation we also propose a unification of three main concepts for active region magnetic evolution, namely the metastable eruption model, the implosion conjecture, and the standard "CSHKP" flare model.

Waves in Solar Coronal Loops **Review**

Wang, Tongjiang
Wiley Book **2016**
http://onlinelibrary.wiley.com/doi/10.1002/9781119055006.ch23/summary
The corona is visible in the optical band only during a total solar eclipse or with a coronagraph. Coronal loops are believed to be plasma-filled closed magnetic flux anchored in the photosphere. Based on the temperature regime, they are generally classified into cool, warm, and hot loops. The magnetized coronal structures support propagation of various types of magnetohydrodynamics (MHD) waves. This chapter reviews the recent progress made in studies based on observations of four types of wave phenomena mainly occurring in coronal loops of active regions, including: flare-excited slow-mode waves; impulsively excited kink-mode waves; propagating slow magnetoacoustic waves; and ubiquitous propagating kink (Alfvénic) waves. This review not only comprehensively discusses these waves and coronal seismology but also topics that are newly emerging or hotly debated in order to provide the reader with useful guidance on further studies.

THE MECHANISMS OF ELECTRON ACCELERATION DURING MULTIPLE X LINE MAGNETIC RECONNECTION WITH A GUIDE FIELD
Huanyu **Wang**1,2, Quanming Lu1,2, Can Huang1,2, and Shui Wang
2016 ApJ 821 84
The interactions between magnetic islands are considered to play an important role in electron acceleration during magnetic reconnection. In this paper, two-dimensional particle-in-cell simulations are performed to study electron acceleration during multiple X line reconnection with a guide field. Because the electrons remain almost magnetized, we can analyze the contributions of the parallel electric field, Fermi, and betatron mechanisms to electron acceleration during the evolution of magnetic reconnection through comparison with a guide-center theory. The results show that with the magnetic reconnection proceeding, two magnetic islands are formed in the simulation domain. Next, the electrons are accelerated by both the parallel electric field in the vicinity of the X lines and the Fermi mechanism due to the contraction of the two magnetic islands. Then, the two magnetic islands begin to merge into one, and, in such a process, the electrons can be accelerated by both the parallel electric field and betatron mechanisms. During the betatron acceleration, the electrons are locally accelerated in the regions where the magnetic field is piled up by the high-speed flow from the X line. At last, when the coalescence of the two islands into one big island finishes, the electrons can be further accelerated by the Fermi mechanism because of the contraction of the big island. With the increase of the guide field, the contributions of the Fermi and betatron mechanisms to electron acceleration become less and less important. When the guide field is sufficiently large, the contributions of the Fermi and betatron mechanisms are almost negligible.

Evidence of thermal conduction suppression in hot coronal loops: Supplementary results
Tongjiang **Wang**, Leon Ofman, Xudong Sun, Elena Provornikova, Joseph M. Davila
Proceedings of IAUS 320, **2015**
http://arxiv.org/pdf/1510.02750v1.pdf
Slow magnetoacoustic waves were first detected in hot (>6 MK) flare loops by the SOHO/SUMER spectrometer as Doppler shift oscillations in Fe XIX and Fe XXI lines. Recently, such longitudinal waves have been found by SDO/AIA in the 94 and 131 \AA\ channels. Wang et al. (2015) reported the first AIA event revealing signatures in agreement with a fundamental standing slow-mode wave, and found quantitative evidence for thermal conduction suppression from the temperature and density perturbations in the hot loop plasma of $\gtrsim 9$ MK. The present study extends the work of Wang et al. (2015) by using an alternative approach. We determine the polytropic index directly based on the polytropic assumption instead of invoking the linear approximation. The same results are obtained as in the linear approximation, indicating that the nonlinearity effect is negligible. We find that the flare loop cools slower (by a factor of 2-4) than expected from the classical Spitzer conductive cooling, approximately consistent with the result of conduction suppression obtained from the wave analysis. The modified Spitzer cooling timescales based on the nonlocal conduction approximation are consistent with the observed, suggesting that nonlocal conduction may account for the observed conduction suppression in this event. In addition, the conduction suppression mechanism predicts that larger flares may tend to be hotter than expected by the EM-T relation derived by Shibata & Yokoyama (2002).
28.12.2013

Evidence of thermal conduction suppression in a solar flaring loop by coronal seismology of slow-mode waves
Tongjiang **Wang**, Leon Ofman, Xudong Sun, Elena Provornikova, Joseph M. Davila
ApJL **811** L13 **2015**
http://arxiv.org/pdf/1509.00920v1.pdf
Analysis of a longitudinal wave event observed by the Atmospheric Imaging Assembly (AIA) onboard the Solar Dynamics Observatory (SDO) is presented. A time sequence of 131 A images reveals that a C-class flare occurred at one footpoint of a large loop and triggered an intensity disturbance (enhancement) propagating along it. The spatial

features and temporal evolution suggest that a fundamental standing slow-mode wave could be set up quickly after meeting of two initial disturbances from the opposite footpoints. The oscillations have a period of ~12 min and a decay time of ~9 min. The measured phase speed of 500±50 km/s matches the sound speed in the heated loop of ~10 MK, confirming that the observed waves are of slow mode. We derive the time-dependent temperature and electron density wave signals from six AIA extreme-ultraviolet (EUV) channels, and find that they are nearly in phase.The measured polytropic index from the temperature and density perturbations is 1.64±0.08 close to the adiabatic index of 5/3 for an ideal monatomic gas. The interpretation based on a 1D linear MHD model suggests that the thermal conductivity is suppressed by at least a factor of 3 in the hot flare loop at 9 MK and above. The viscosity coefficient is determined by coronal seismology from the observed wave when only considering the compressive viscosity dissipation. We find that to interpret the rapid wave damping, the classical compressive viscosity coefficient needs to be enhanced by a factor of 15 as the upper limit. **2013 December 28**

Thermodynamic Spectrum of Solar Flares Based on SDO/EVE Observations: Techniques and First Results

Yuming **Wang**, Zhenjun Zhou, Jie Zhang, Kai Liu, Rui Liu, Chenglong Shen, Phillip C. Chamberlin **2015**

http://arxiv.org/pdf/1507.08895v1.pdf

SDO/EVE provide rich information of the thermodynamic processes of solar activities, particularly of solar flares. Here, we develop a method to construct thermodynamic spectrum (TDS) charts based on the EVE spectral lines. Reading from the charts, we are able to easily recognize if there is a late phase following a main phase of a flare, and able to learn the begin, peak and end times of the flare as well as the drift of the temperature, i.e., the cooling rate, of the heated plasma during the flare. Through four M-class flares of different types, we illustrate which thermodynamic information can be revealed from the TDS charts. Further, we investigate the TDS charts of all the flares greater than M5.0, and some interesting results are achieved. First, there are two distinct drift patterns, called Type I and Type II. For Type I flares, the enhanced emission drifts from high to low temperture, whereas for Type II flares, the drift is somewhat reversed, suggesting a more violent and durable heating during Type II flares than Type I flares. Second, for late-phase flares, the peak intensity ratio of the late phase to the main phase read from the TDS chart is roughly correlated with the flare class identified by GOES SXR, and the flares with a stronger late phase are all confined. We believe that the re-deposition of the energy carried by a flux rope, that unsuccessfully erupts out, into thermal emissions is responsible for the strong late phase found in a confined flare. These results provide us new clues to advance our understanding of the thermodynamic processes of solar flares and associated solar eruptions, e.g., coronal mass ejections.

3.1. A **confined flare** on 2011 September 8
3.2. A confined flare with a late phase on 2010 November 5
3.3. An **eruptive flare** on 2011 March 8
3.4. An eruptive flare with a late phase on 2010 October 16
4.2. The **late-phase flares**
Table 3: SXR information of selected flares
Table 4: Late-phase flares

2010 October 16, 2012 October 22, 2010 November 5, 15 Feb 2011, 2011 March 8, 9 Aug 2011, 7 Sept 2011, 2011 September 8, 22 Sept 2011, 27 Jan 2012, 14 May 2013, 7 Jan 2014

Structure and Evolution of Magnetic Fields Associated with Solar Eruptions (Invited Review)

Haimin **Wang**, Chang Liu

Research in Astronomy and Astrophysics, 15, 145 **2015**

http://arxiv.org/pdf/1412.8676v1.pdf **File**

This paper reviews the studies of solar photospheric magnetic field evolution in active regions and its relationship to solar flares. It is divided into two topics, the magnetic structure and evolution leading to solar eruptions and the rapid changes of photospheric magnetic field associated with eruptions. For the first topic, we describe the magnetic complexity, new flux emergence, flux cancellation, shear motions, sunspot rotation, and magnetic helicity injection, which may all contribute to the storage and buildup of energy and triggering of solar eruptions. For the second topic, we concentrate on the observations of rapid and irreversible changes of photospheric magnetic field associated with flares, and the implication on the restructuring of three-dimensional magnetic field. In particular, we emphasize the recent advances in observations of photospheric magnetic field, as state-of-the-art observing facilities (such as Hinode and Solar Dynamic Observatory) become available. The linkage between observations and theories and future prospectives in this research area are also discussed. **1989 March 10, 6 June 2000, 9 Apr 2001,2001 September 24, 24-26 Oct 2001, 28 and 29 Oct 2003, 2003 November 2., 2003 November 29, 5-8 N0v 2004, 2006 December 6, 2006 December 13, 12-16 Feb 2011, 2011 February 13., 2011 February 15, 2011 July 2, 2012 March 7**

Sudden Photospheric Motion and Sunspot Rotation Associated with the X2.2 Flare on 2011 February 15

Shuo **Wang**, Chang Liu, Na Deng, Haimin Wang
E-print, Jan **2014**; **2014** ApJ 782 L31
http://arxiv.org/pdf/1401.7957v1.pdf

The Helioseismic and Magnetic Imager provides 45 s cadence intensity images and 720 s cadence vector magnetograms. These unprecedented high-cadence and high-resolution data give us a unique opportunity to study the change of photospheric flows and sunspot rotations associated with flares. By using the differential affine velocity estimator method and the Fourier local correlation tracking method separately, we calculate velocity and vorticity of photospheric flows in the flaring NOAA AR 11158, and investigate their temporal evolution around the X2.2 flare on 2011 February 15. It is found that the shear flow around the flaring magnetic polarity inversion line exhibits a sudden decrease, and both of the two main sunspots undergo a sudden change in rotational motion during the impulsive phase of the flare. These results are discussed in the context of the Lorentz-force change that was proposed by Hudson et al. (2008) and Fisher et al. (2012). This mechanism can explain the connections between the rapid and irreversible photospheric vector magnetic field change and the observed short-term motions associated with the flare. In particular, the torque provided by the horizontal Lorentz force change agrees with what is required for the measured angular acceleration.

Three-ribbon Solar Flares: What Do They Imply for the 3D Magnetic Field Structure?

Haimin **Wang**, Chang Liu
HMI Science Nuggets, #21, **2014**
http://hmi.stanford.edu/hminuggets/?p=851

Solar flares are often seen with two chromospheric ribbons, which lie in opposite magnetic polarities and run parallel to the magnetic polarity inversion line (PIL), evidencing the standard flare geometry. With high-resolution observations, flares with a closed circular-like ribbon have also been revealed (Ref. 1 and references therein). The associated surface magnetic field configuration usually consists of a parasitic region encompassed by the opposite-polarity field, forming a circular PIL. Besides the circular ribbon, an inner and an outer (remote) ribbons are usually found. Some flares also exhibit surge-like eruptions from the area of the circular ribbon. In interpreting these events, the fan-spine magnetic topology is involved, where the dome-shaped fan portrays the closed separatrix surface, and the inner and outer spine field lines in different connectivity domains pass through a coronal null point.

Study of Two Successive Three-Ribbon Solar Flares on 2012 July 6

Haimin **Wang**, Chang Liu, Na Deng, Zhicheng Zeng, Yan Xu, Ju Jing and Wenda Cao
E-print, Dec **2013**; **2014** ApJ 781 L23
http://arxiv.org/pdf/1312.6649v1.pdf

This Letter reports two rarely observed three-ribbon flares (M1.9 and C9.2) on **2012 July 6** in NOAA AR 11515, which we found with Halpha observations of 0.1" resolution from the New Solar Telescope and CaII H images from Hinode. The flaring site is characterized with an intriguing "fish-bone-like" morphology evidenced by both Halpha images and a nonlinear force-free field (NLFFF) extrapolation, where two semi-parallel rows of low-lying, sheared loops connect an elongated, parasitic negative field with the sandwiching positive fields. The NLFFF model also shows that the two rows of loops are asymmetric in height and have opposite twists, and are enveloped by large-scale field lines including open fields. The two flares occurred in succession in half an hour and are located at the two ends of the flaring region. The three ribbons of each flare run parallel to the PIL, with the outer two lying in the positive field and the central one in the negative field. Both flares show surge-like flows in Halpha apparently toward the remote region, while the C9.2 flare is also accompanied by EUV jets possibly along the open field lines. Interestingly, the 12-25 keV hard X-ray sources of the C9.2 flare first line up with the central ribbon then shift to concentrate on the top of the higher branch of loops. These results are discussed in favor of reconnection along the coronal null-line producing the three flare ribbons and the associated ejections.

On the Strength of the Hemispheric Rule and the Origin of Active-region Helicity

Y.-M. **Wang**
2013 ApJ 775 L46

Vector magnetograph and morphological observations have shown that the solar magnetic field tends to have negative (positive) helicity in the northern (southern) hemisphere, although only ~60%-70% of active regions appear to obey this "hemispheric rule." In contrast, at least ~80% of quiescent filaments and filament channels that form during the decay of active regions follow the rule. We attribute this discrepancy to the difficulty in determining the helicity sign of newly emerged active regions, which are dominated by their current-free component; as the transverse field is canceled at the polarity inversion lines, however, the axial component becomes dominant there, allowing a more reliable determination of the original active-region chirality. We thus deduce that the hemispheric rule is far stronger than generally assumed, and cannot be explained by stochastic processes. Earlier studies have shown that the twist associated with the axial tilt of active regions is too small to account for the observed helicity; here, both tilt and twist are induced by the Coriolis force acting on the diverging flow in the emerging flux tube. However, in addition to this east-west expansion about the apex of the loop, each of its legs must expand continually in cross section during its rise through the convection zone, thereby acquiring a further twist through the Coriolis force. Since this transverse pressure effect is not limited by drag or tension forces, the final twist depends mainly on the rise time, and may be large enough to explain the observed active-region helicity.

THREE-DIMENSIONAL MAGNETOHYDRODYNAMIC MODELING OF PROPAGATING DISTURBANCES IN FAN-LIKE CORONAL LOOPS
Tongjiang **Wang**1,2, Leon Ofman1,2,3, and Joseph M. Davila
2013 ApJ 775 L23
Quasi-periodic propagating intensity disturbances (PDs) have been observed in large coronal loops in EUV images over a decade, and are widely accepted to be slow magnetosonic waves. However, spectroscopic observations from Hinode/EIS revealed their association with persistent coronal upflows, making this interpretation debatable. Motivated by the scenario that the coronal upflows could be the cumulative result of numerous individual flow pulses generated by sporadic heating events (nanoflares) at the loop base, we construct a velocity driver with repetitive tiny pulses, whose energy frequency distribution follows the flare power-law scaling. We then perform three-dimensional MHD modeling of an idealized bipolar active region by applying this broadband velocity driver at the footpoints of large coronal loops which appear open in the computational domain. Our model successfully reproduces the PDs with similar features as the observed, and shows that any upflow pulses inevitably excite slow magnetosonic wave disturbances propagating along the loop. We find that the generated PDs are dominated by the wave signature as their propagation speeds are consistent with the wave speed in the presence of flows, and the injected flows rapidly decelerate with height. Our simulation results suggest that the observed PDs and associated persistent upflows may be produced by small-scale impulsive heating events (nanoflares) at the loop base in the corona, and that the flows and waves may both contribute to the PDs at lower heights.

STUDY OF RAPID FORMATION OF A δ SUNSPOT ASSOCIATED WITH THE 2012 JULY 2 C7.4 FLARE USING HIGH-RESOLUTION OBSERVATIONS OF THE NEW SOLAR TELESCOPE
Haimin **Wang**1, Chang Liu1, Shuo Wang1, Na Deng1, Yan Xu1, Ju Jing1, and Wenda Cao
2013 ApJ 774 L24
Rapid, irreversible changes of magnetic topology and sunspot structure associated with flares have been systematically observed in recent years. The most striking features include the increase of the horizontal field at the polarity inversion line (PIL) and the co-spatial penumbral darkening. A likely explanation of the above phenomenon is the back reaction to the coronal restructuring after eruptions: a coronal mass ejection carries the upward momentum while the downward momentum compresses the field lines near the PIL. Previous studies could only use low-resolution (above 1") magnetograms and white-light images. Therefore, the changes are mostly observed for X-class flares. Taking advantage of the 0."1 spatial resolution and 15 s temporal cadence of the New Solar Telescope at the Big Bear Solar Observatory, we report in detail the rapid formation of sunspot penumbra at the PIL associated with the C7.4 flare on **2012 July 2**. It is unambiguously shown that the solar granulation pattern evolves to an alternating dark and bright fibril structure, the typical pattern of penumbra. Interestingly, the appearance of such a penumbra creates a new δ sunspot. The penumbral formation is also accompanied by the enhancement of the horizontal field observed using vector magnetograms from the Helioseismic and Magnetic Imager. We explain our observations as being due to the eruption of a flux rope following magnetic cancellation at the PIL. Subsequently, the re-closed arcade fields are pushed down toward the surface to form the new penumbra. NLFFF extrapolation clearly shows both the flux rope close to the surface and the overlying fields.

Study of Rapid Formation of a Delta Sunspot Associated with the 2012 July 2 C7.4 Flare Using High-resolution Observations of New Solar Telescope
Haimin **Wang**, Chang Liu, Shuo Wang, Na Deng, Yan Xu, Ju Jing and Wenda Cao
E-print, Aug **2013**, ApJL

Rapid, irreversible changes of magnetic topology and sunspot structure associated with flares have been systematically observed in recent years. The most striking features include the increase of horizontal field at the polarity inversion line (PIL) and the co-spatial penumbral darkening. A likely explanation of the above phenomenon is the back reaction to the coronal restructuring after eruptions: a coronal mass ejection carries the upward momentum while the downward momentum compresses the field lines near the PIL. Previous studies could only use low resolution (above 1") magnetograms and white-light images. Therefore, the changes are mostly observed for X-class flares. Taking advantage of the 0.1" spatial resolution and 15s temporal cadence of the New Solar Telescope at Big Bear Solar Observatory, we report in detail the rapid formation of sunspot penumbra at the PIL associated with the C7.4 flare on **2012 July 2**. It is unambiguously shown that the solar granulation pattern evolves to alternating dark and bright fibril structure, the typical pattern of penumbra. Interestingly, the appearance of such a penumbra creates a new delta sunspot. The penumbral formation is also accompanied by the enhancement of horizontal field observed using vector magnetograms from the Helioseismic and Magnetic Imager. We explain our observations as due to the eruption of a flux rope following magnetic cancellation at the PIL. Subsequently the re-closed arcade fields are pushed down towards the surface to form the new penumbra. NLFFF extrapolation clearly shows both the flux rope close to the surface and the overlying fields.

CIRCULAR RIBBON FLARES AND HOMOLOGOUS JETS

Haimin **Wang** and Chang Liu

2012 ApJ 760 101

Solar flare emissions in the chromosphere often appear as elongated ribbons on both sides of the magnetic polarity inversion line (PIL), which has been regarded as evidence of a typical configuration of magnetic reconnection. However, flares having a circular ribbon have rarely been reported, although it is expected in the fan-spine magnetic topology involving reconnection at a three-dimensional (3D) coronal null point. We present five circular ribbon flares with associated surges, using high-resolution and high-cadence Hα blue wing observations obtained from the recently digitized films of Big Bear Solar Observatory. In all the events, a central parasitic magnetic field is encompassed by the opposite polarity, forming a circular PIL traced by filament material. Consequently, a flare kernel at the center is surrounded by a circular flare ribbon. The four homologous jet-related flares on **1991 March 17 and 18** are of particular interest, as (1) the circular ribbons brighten sequentially, with cospatial surges, rather than simultaneously, (2) the central flare kernels show an intriguing "round-trip" motion and become elongated, and (3) remote brightenings occur at a region with the same magnetic polarity as the central parasitic field and are co-temporal with a separate phase of flare emissions. In another flare on **1991 February 25**, the circular flare emission and surge activity occur successively, and the event could be associated with magnetic flux cancellation across the circular PIL. We discuss the implications of these observations combining circular flare ribbons, homologous jets, and remote brightenings for understanding the dynamics of 3D magnetic restructuring.

THE RELATIONSHIP BETWEEN THE SUDDEN CHANGE OF THE LORENTZ FORCE AND THE MAGNITUDE OF ASSOCIATED FLARES

Shuo **Wang**, Chang Liu, and Haimin Wang

2012 ApJ 757 L5

The rapid and irreversible change of photospheric magnetic fields associated with flares has been confirmed by many recent studies. These studies showed that the photospheric magnetic fields respond to coronal field restructuring and turn to a more horizontal state near the magnetic polarity inversion line (PIL) after eruptions. Recent theoretical work has shown that the change in the Lorentz force associated with a magnetic eruption will lead to such a field configuration at the photosphere. The Helioseismic Magnetic Imager has been providing unprecedented full-disk vector magnetograms covering the rising phase of the solar cycle 24. In this study, we analyze 18 flares in four active regions, with GOES X-ray class ranging from C4.7 to X5.4. We find that there are permanent and rapid changes of magnetic field around the flaring PIL, the most notable of which is the increase of the transverse magnetic field. The changes of fields integrated over the area and the derived change of Lorentz force both show a strong correlation with flare magnitude. It is the first time that such magnetic field changes have been observed even for C-class flares. Furthermore, for seven events with associated coronal mass ejections (CMEs), we use an estimate of the impulse provided by the Lorentz force, plus the observed CME velocity, to estimate the CME mass. We find that if the timescale of the back reaction is short, i.e., in the order of 10 s, the derived values of CME mass (~1015 g) generally agree with those reported in literature.

RAPID TRANSITION OF UNCOMBED PENUMBRAE TO FACULAE DURING LARGE FLARES

Haimin **Wang**1, Na Deng1,2 and Chang Liu

2012 ApJ 748 76

In the past two decades, the complex nature of sunspots has been disclosed with high-resolution observations. One of the most important findings is the "uncombed" penumbral structure, where a more horizontal magnetic component

carrying most of Evershed flows is embedded in a more vertical magnetic background. The penumbral bright grains are locations of hot upflows and dark fibrils are locations of horizontal flows that are guided by a nearly horizontal magnetic field. On the other hand, it was found that flares may change the topology of sunspots in δ configuration: the structure at the flaring polarity inversion line becomes darkened while sections of peripheral penumbrae may disappear quickly and permanently associated with flares. The high spatial and temporal resolution observations obtained with the Hinode/Solar Optical Telescope provide an excellent opportunity to study the evolution of penumbral fine structures associated with major flares. Taking advantage of two near-limb events, we found that in sections of peripheral penumbrae swept by flare ribbons the dark fibrils completely disappear, while the bright grains evolve into faculae that are signatures of vertical magnetic flux tubes. The corresponding magnetic fluxes measured in the decaying penumbrae show stepwise changes temporally correlated with the flares. These observations suggest that the horizontal magnetic field component of the penumbra could be straightened upward (i.e., turning from horizontal to vertical) due to magnetic field restructuring associated with flares, which results in the transition of penumbrae to faculae.

RESPONSE OF THE PHOTOSPHERIC MAGNETIC FIELD TO THE X2.2 FLARE ON 2011 FEBRUARY 15

Shuo **Wang**1, Chang Liu1, Rui Liu1, Na Deng1, Yang Liu2 and Haimin Wang
2012 ApJ 745 L17

It is well known that the long-term evolution of the photospheric magnetic field plays an important role in building up free energy to power solar eruptions. Observations, despite being controversial, have also revealed a rapid and permanent variation of the photospheric magnetic field in response to the coronal magnetic field restructuring during the eruption. The Helioseismic and Magnetic Imager instrument (HMI) on board the newly launched Solar Dynamics Observatory produces seeing-free full-disk vector magnetograms at consistently high resolution and high cadence, which finally makes possible an unambiguous and comprehensive study of this important back-reaction process. In this study, we present a near disk-center, GOES-class X2.2 flare, which occurred in NOAA AR 11158 on **2011 February 15**. Using the magnetic field measurements made by HMI, we obtained the first solid evidence of a rapid (in about 30 minutes) and irreversible enhancement in the horizontal magnetic field at the flaring magnetic polarity inversion line (PIL) by a magnitude of ~30%. It is also shown that the photospheric field becomes more sheared and more inclined. This field evolution is unequivocally associated with the flare occurrence in this sigmoidal active region, with the enhancement area located in between the two chromospheric flare ribbons and the initial conjugate hard X-ray footpoints. These results strongly corroborate our previous conjecture that the photospheric magnetic field near the PIL must become more horizontal after eruptions, which could be related to the newly formed low-lying fields resulting from the tether-cutting reconnection.

Slow-Mode Oscillations of Hot Loops Excited at Flaring Footpoints

Tongjiang **Wang**, Wei Liu, Leon Ofman, Joseph M. Davila
(Submitted on 16 Jun **2017**)
5th Hinode Meeting: Exploring the Active Sun, ASP Conference Series, Vol. 456, eds. by L. Golub, I. De Moortel, and T. Shimizu, 127, **2012**
https://arxiv.org/pdf/1706.05427.pdf

The analysis of a hot loop oscillation event using SOHO/SUMER, GOES/SXI, and RHESSI observations is presented. Damped Doppler shift oscillations were detected in the Fe XIX line by SUMER, and interpreted as a fundamental standing slow mode. The evolution of soft X-ray emission from GOES/SXI and hard X-ray sources from RHESSI suggests that the oscillations of a large loop are triggered by a small flare, which may be produced by interaction (local reconnection) of this large loop with a small loop at its footpoint. This study provides clear evidence supporting our early conjecture that the slow-mode standing waves in hot coronal loops are excited by impulsive heating (small or microflares) at the loop's footpoint. **2003 April 24**

Evidence of Two-Stage Magnetic Reconnection in the 2005 January 15 X2.6 Flare

Pu **Wang**1, Yixuan Li2, Mingde Ding1, Haisheng Ji3;4, Haimin Wang
BBSO Preprint #1474, **2011**; New Astronomy

We analyze in detail the X2.6 flare that occurred on **2005 January 15** in the NOAA AR 10720 using multiwavelength observations. There are several interesting properties of the flare that reveal possible two-stage magnetic reconnection similar to that in the physical picture of tether-cutting, where the magnetic fields of two separate loop systems reconnect at the flare core region, and subsequently a large flux rope forms, erupts, and breaks open the overlying arcade fields. The observed manifestations include: (1) remote Hα brightenings appear minutes before the main phase of the flare; (2) separation of the flare ribbons has a slow and a fast phase, and the flare hard X-ray emission appears in the later fast phase; (3) rapid transverse field enhancement near the magnetic polarity inversion line (PIL) is found to be associated with the flare. We conclude that the flare occurrence fits the tether-cutting reconnection picture in a special way, in which there are three flare ribbons outlining the sigmoid configuration. We also discuss this event in the context of what

was predicted by Hudson, Fisher, & Welsch (2008), where the Lorentz force near the flaring PIL drops after the flare and consequently the magnetic field lines there turn to be more horizontal as we observed.

OBSERVATIONAL EVIDENCE OF BACK REACTION ON THE SOLAR SURFACE ASSOCIATED WITH CORONAL MAGNETIC RESTRUCTURING IN SOLAR ERUPTIONS
Haimin **Wang** and Chang Liu
Astrophysical Journal Letters, 716:L195–L199, **2010** June
Most models of solar eruptions assume that coronal field lines are anchored in the dense photosphere and thus the photospheric magnetic fields would not have rapid, irreversible changes associated with eruptions resulted from the coronal magnetic reconnection. Motivated by the recent work of Hudson et al. on quantitatively evaluating the back reaction due to energy release from the coronal fields, in this Letter we synthesize our previous studies and present analysis of new events about flare-related changes of photospheric magnetic fields. For the 11 X-class flares where vector magnetograms are available, we always find an increase of transverse field at the polarity inversion line (PIL) although only four events had measurements with 1 minute temporal resolution. We also discuss 18 events with 1 minute cadence line-of-sight magnetogram observation, which all show prominent changes of magnetic flux contained in the flaring δ spot region. Except in one case, the observed limbward flux increases while diskward flux decreases rapidly and irreversibly after flares. This observational evidence provides support, either directly or indirectly, for the theory and prediction of Hudson et al. that the photospheric magnetic fields must respond to coronal field restructuring and turn to a more horizontal state near the PIL after eruptions.

FOOTPOINT MOTIONS AS EVIDENCE FOR PATCHY RECONNECTIONS IN AN M9.1 SOLAR FLARE
Lin **Wang**
Astrophysical Journal, 694:247–256, **2009** March
http://www.iop.org/EJ/article/-alert=43190/0004-637X/694/1/247/apj_694_1_247.pdf
We present an investigation on the UV footpoint motions of an M9.1 two-ribbon solar flare that occurred on **2004 July 22**, employing the *TRACE* 1700 Å images and a magnetogram observed by *SOHO*/MDI. In the beginning, we found that the UV footpoints spread a two-dimensional distribution in, especially, the negative magnetic region, rather than a quasi-one-dimensional distribution as expected. Based on an assumption, we extract the information of the footpoints and link them into trajectories. From the results, we find some unexpected motion patterns and features, such as bidirectional elongations of footpoints, large angles between the footpoint trajectories, a "merging" pattern of the motion, and an apparent prevalence of motions along the iso-Gauss contours over those along the gradient of the magnetic field. We suggest that the quasi-three-dimensional CSHKP model with a uniform arcade may be inapplicable to the flare, in spite of the two-ribbon appearance. Instead, the **"patchy reconnection"** concept presented by Klimchuk in 1997 may be appropriate.Only a fraction of the magnetic field participates in the energetic reconnection. The elongations may offer crucial restrictions on the excitation of the reconnections. The large angles and the "merging" process may imply a chaotic geometry of the reconnection subsystems, rather than a symmetrical one. The prevalence may offer an important clue in solar flare studies.

MAGNETIC CHANGES IN THE COURSE OF THE X7.1 SOLAR FLARE ON 2005 JANUARY 20
Jingxiu **Wang** et al **2009** ApJ 690 862-874, **File**
http://www.iop.org/EJ/abstract/0004-637X/690/1/862
Rapid magnetic changes in the course of the X7.1 solar flare on **2005 January 20** at the photosphere in the host active region (AR), NOAA AR 10720, are diagnosed. The database for this study consists of Huairou vector magnetograms, Transition Region and Coronal Explorer (TRACE) white light and UV/EUV images, RHESSI hard X-ray, and Solar and Heliospheric Observatory EUV observations. For such an event that is close to but not on the solar west limb (N12 W58), the projection effects in the observed vector magnetograms are untangled by combining an intuitive geometric analysis and a transformation of the magnetograms into the heliographic coordination system. The magnetic changes in the horizontal magnetic fields are emphasized. We find definitive evidence of weakening in the horizontal magnetic fields in a few isolated patches in the outskirts of this δ-sunspot group and strengthening in the horizontal fields (HFs) in an extended area centralized at the magnetic neutral line between major sunspots of opposite polarities. The rapid magnetic changes take place at the level of 100-300 G, several factors of ten of the noise level. The identified HF changes are consistent with the darkening of inner penumbrae and weakening of outer penumbrae in this δ-sunspot group. The enhanced HFs spatially coincide with the TRACE 1550 Å rope-like structures lying low above the magnetic neutral line. Unexpectedly, during the flare, the lower lying rope-like structures remain in place, though they exhibit episodic disturbance and brightening, while the outer EUV loops are impulsively expanding. The rapid magnetic changes manifest an impulsive input of free magnetic energy in the photosphere, resulting from an impulsive growth of

a new emerging flux region (EFR) along the magnetic neutral line. The facts of the increasing core fields in magnetic nonpotentiality, the continued disturbance of the inner rope-like structures, and the breakout of the outer loops during the major flare cannot be interpreted by any single flare model. However, the nature of magnetohydrodynamical catastrophe is clearly implied for the flare triggering.

Study of White-Light Flares Observed by Hinode

Haimin **Wang**
BBSO Preprint, #1373, **2008**
http://solar.njit.edu/preprints/wang1373.pdf
White-light flares are considered as the most energetic flaring events that are observable in optical broad-band continuum of solar spectrum. They have not been commonly observed. Observations of white-light flares with sub-arcsecond resolution have been very rare. The continuous high resolution observations of Hinode provide an unique opportunity to systematically study the white-light flares with a spatial resolution around 0.2 arcsec.We surveyed all the flares above GOES magnitude C5.0 since the launch of Hinode in 2006 October, 13 of them were covered by Hinode G-band observations.We analyzed the peak contrast and equivalent area (calculated via integrated excess emission contrast) of these flares as a function of GOES X-ray flux, and found that the cut-off visibility is likely around M1 flares under the observing limit of Hinode. Many other observational and physical factors should affect the visibility of white-light flares; as the observing conditions are improved, smaller flares are likely to have detectable white-light emissions. We are cautious that this limit visibility is an overestimate, as G-band observations contains emissions from upper atmosphere. Among 13 events analyzed, only the M8.7 flare of **2007 June 4** had near-simultaneous observations in both G-band and blue continuum. The blue continuum had a peak contrast of 94% vs. 175% in G-band for this event. The equivalent area in blue continuum is an order of magnitude lower than that in G-band. Very recently, Jess et al. studied a C2.0 flare with a peak contrast of 300% in blue continuum. Comparing to the events presented in this Letter, that event is probably a unusual white-light flare: a very small kernel with a large contrast that can be detected in high resolution observations.

STUDY OF MAGNETIC CHANNEL STRUCTURE IN ACTIVE REGION 10930

Haimin **Wang**,1, 2 Ju Jing,1, 2 Changyi Tan,1, 2 Thomas Wiegelmann,3 and Masahito Kubo4
Astrophysical Journal, 687:658Y667, **2008**
http://www.journals.uchicago.edu/doi/abs/10.1086/592082
The concept of ‘‘magnetic channel’’ was first introduced by Zirin & Wang. They were defined as a series of oppositely directed vertical-field inversions separated by extremely narrow elongated transverse fields. In this paper, we utilized unprecedented filtergraph and spectropolarimetry observations from Hinode, and studied the evolution and physical properties of channel structure of AR 10930 in detail.We found the following: (1) Channels are associated with new flux emergence in the middle of existing penumbra connecting the _ sunspot. (2) The width of each channel is in the order of 100 or less. (3) The line-of-sight magnetic gradient is highest in the channel, 2.4Y4.9 G km_1. (4) The fields are highly sheared and inclined with a median shear angle around 64_ and inclination angle around 25_. (5) Using nonlinear force-free field (NLFF) extrapolation, we derive a near surface current system carrying electric current in the order of 5 ; 1011 A. (6) The X3.4 flare on 2006 December 13 occurred during the period that the channels rapidly formed, but a few hours before the maximum phase of channel structure development. Based on the observational evidence, we propose that the channels are formed during the emergence of a sequence of magnetic bipoles that are squeezed in the compact penumbra of the _ sunspot and they are highly nonpotential. Formation of channels might be a precursor of major flares.

A STATISTICAL STUDY OF SOLAR ACTIVE REGIONS THAT PRODUCE EXTREMELY FAST CORONAL MASS EJECTIONS

Yuming **Wang**1, 2 and Jie Zhang
The Astrophysical Journal, 680:1516-1522, **2008**
http://www.journals.uchicago.edu/doi/pdf/10.1086/587619
We present statistical results on the properties of the solar source regions that produced the 57 fastest (_1500 km s_1) front-side coronal mass ejections (CMEs) from 1996 June to 2007 January. The properties of these fast-CMEY producing regions, 35 in total, are compared with those of all 1143 active regions (ARs) in the period studied. An automated method, based on SOHO MDI magnetic synoptic charts, is used to select and characterize the ARs. For

each, a set of parameters is derived that includes the areas (positive, negative, and total, denoted A_P, A_N, and A_T, respectively), the magnetic fluxes (positive, negative, and total, F_P, F_N, and F_T), the average magnetic field strength (B_{avg}), a quasi elongation (e) characterizing the overall shape of the AR, the number and length of polarity inversion lines (PILs, or neutral lines, N_{PIL} and L_{PIL}, respectively), and the average and maximum magnetic gradient on the PILs (GOP_{avg} and GOP_{max}). Our statistical analysis shows a general trend between the scales of an AR and the likelihood of its producing a fast CME; that is, the larger the geometric size (A_T), the larger the magnetic flux (F_T), the stronger the magnetic field (B_{avg}), and the more complex the magnetic configuration (N_{PIL} and L_{PIL}), the greater the possibility of producing a fast CME. When all the ARs are sorted into three evenly sized groups with low, intermediate, and high values of these parameters, we find that for all the parameters, more than 60% of extremely fast CMEs are from the high-value group. The two PIL parameters are the best indicators of fast-CME production, with more than 80% coming from the high-value group.

SUCCESSIVE FLARING DURING THE 2005 SEPTEMBER 13 ERUPTION

Haimin **Wang**, Chang Liu, Ju Jing, and Vasyl Yurchyshyn

The Astrophysical Journal, 671:973Y977, **2007** December 10; File

We report a detailed analysis of successive flaring during the X1.5 event in theNOAAAR 0808 on 2005 September 13.We identify a filament lying at the southeast boundary of the active region as the physical linkage between the two flares in close succession. It is noticeable that the filament erupted_13 minutes after the initial flare onset at_19:22UT near the central magnetic polarity inversion line (PIL). During this time period, the filament only showed a slow rising; meanwhile, a spatially associated large magnetic loop with one leg connecting to the initial flaring site began to brighten in the TRACE 195 8 channel. After _19:35 UT, the filament abruptly erupted together with the bright TRACE loop. Besides the moving ribbons at the first flaring site, the filament eruption caused a secondary flare identified with another set of moving ribbons. This event thus provides a clear evidence for the successive flaring where the initial flare destabilizes the nearby flux loop system, leading to the filament eruption with the second flare. We also identify the initial flare core by finding rapid, irreversible enhancements of the photospheric transverse magnetic fields at a section of the PIL.

A COMPARATIVE STUDY BETWEEN ERUPTIVE X-CLASS FLARES ASSOCIATED WITH CORONAL MASS EJECTIONS AND CONFINED X-CLASS FLARES

Yuming **Wang**1,2 and Jie Zhang

Astrophysical Journal, 665:1428Y1438, **2007** August; **File**

We examine the two kinds of major energetic phenomena that occur in the solar atmosphere: eruptive and confined events. The former describes flares with associated coronal mass ejections (CMEs), while the latter denotes flares without associated CMEs.We find that about 90% of X-class flares are eruptive, but the remaining 10% are confined. To probe why the largest energy releases could be either eruptive or confined, we investigate four X-class events from each of the two types. Both sets of events are selected to have very similar intensities (X1.0 to X3.6) and duration (rise time under 13 minutes and decay time over 9 minutes) in soft X-ray observations, to reduce any bias due to flare size on CME occurrence. We find that the occurrence of eruption (or confinement) is sensitive to the displacement of the location of the energy release, defined as the distance between the flare site and the flux-weighted magnetic center of the source active region. The displacement is 6Y17Mmfor confined events but as large as 22Y37Mmfor eruptive events. This means that confined events occur closer to the magnetic center, while the eruptive events tend to occur close to the edge of active regions.We use the potential field source-surface model to infer the coronal magnetic field above the source active regions and calculate the flux ratio of low (<1.1 R_) to high (_1.1 R_) corona.We find that the confined events have a lower ratio (<5.7) than the eruptive events (>7.1). These results imply that a stronger overlying arcade field may prevent energy releases in the low corona from being eruptive, resulting in flares, but without CMEs. **Table.**

Solar Trans-equatorial Activity

Jingxiu **Wang** · Yuzong Zhang · Guiping Zhou · Louise K. Harra · David R.Williams · Yunchun Jiang

Solar Phys (**2007**) 244: 75–94

We have found that solar flares in NOAA active region (AR) 10696 were often associated with large-scale trans-equatorial activities. These trans-equatorial activities appeared to be very common and manifest themselves through *i*) the formation and eruption of trans-equatorial loops (TELs), *ii*) the formation and eruption of trans-equatorial filaments (TEFs), and *iii*) the trans-equatorial brightening (TEB) in the chromosphere. It is determined that the TEF was formed following episodic plasma ejecta from flares occurring in the AR. The TEF eruption was associated with a trans-equatorial flare. All flares in the AR that were accompanied by trans-equatorial activities were associated with halo coronal mass ejections (CMEs). It was noticed that one or several major flares in the AR were followed by an increase of brightness and nonpotentiality of a TEL. These coupled events had a lifetime of more than 12 hours. In addition their associated halo CMEs always had a positive acceleration, indicating prolonged magnetic reconnections in the outer corona at high altitudes.

Flarelike brightenings of active region loops observed with SUMER

T. J. **Wang**, D. E. Innes, S. K. Solanki, W. Curdt

Proc. of 11th European Solar Physics Meeting, **2005**
http://arxiv.org/pdf/1510.00337v1.pdf
Coronal loops on the east limb of the Sun were observed by SUMER on SOHO for several days. Small flare-like brightenings are detected very frequently in the hot flare line Fe~{\small XIX}. We find that the relatively intense events are in good coincidence with the transient brightenings seen by Yohkoh/SXT. A statistical analysis shows that these brightenings have durations of 5-84 min and extensions along the slit of 2-67 Mm. The integrated energy observed in Fe~{\small XIX} for each event is in the range of 3×1018−5×1023 ergs, and the estimated thermal energy ranges from 1026−1029 ergs. Application of the statistical method proposed by Parnell \& Jupp (2000) yields a value of 1.5 to 1.8 for the index of a power law relation between the frequency of the events and the radiated energy in Fe~{\small XIX}, and a value of 1.7 to 1.8 for the index of the frequency distribution of the thermal energy in the energy range >1027 ergs. We examine the possibility that these small brightenings give a big contribution to heating of the active region corona. **16−20 September 2000, 25−30 September 2000**

Initial features of an X-class flare observed with SUMER and TRACE

T. J. **Wang**, S. K. Solanki, D. E. Innes, W. Curdt
SOLMAG 2002. Proc. the Magnetic Coupling of the Solar Atmosphere Euroconference and IAU Colloquium 188, Ed. H. Sawaya-Lacoste. ESA SP-505. Noordwijk, Netherlands: ESA Publications Division, ISBN 92-9092-815-8, **2002**, p. 607 - 610 **2018**
https://arxiv.org/pdf/1805.10418.pdf
A class X1.5 flare started on the solar limb at 00:43 UT on **21 April 2002**, which was associated with a CME observed at 01:27 UT by LASCO C2. The coordinated analyses of this flare include TRACE 195 {\AA} images and SUMER spectra in lines of Fe XXI, Fe XII, and C II. We find that: 1) The flare began with a jet seen by TRACE, which was detected by SUMER in the C II line as a strong brightening with blue shifts up to 170 km s[Math Processing Error]. At that time only weak emission was detected in Fe XII and Fe XXI. 2) Subsequently, a weak looplike brightening started south of the jet, moving outwards with an average speed of about 150 km s[Math Processing Error]. The SUMER spectra responded this moving loop as separatingly brightenings, visible only in the Fe XXI line. The southwards moving component contains red- and blue-shifted emission features and has an apparent speed of [Math Processing Error]120 km s[Math Processing Error]. The absence of signatures in Fe XII and C II lines indicates that the moving weak loop seen by TRACE corresponds to the emission from very hot plasma, in a blend line in the 195 {\AA} bandpass due to Fe XXIV formed at T > 10 MK. 3) The trigger mechanism of the flare and associated CME can be interpreted in the same way as that proposed by Wang et al. (2002) for an event with similar initial features.

A Comparative Study between Eruptive X-Class Flares Associated with Coronal Mass Ejections and Confined X-Class Flares

Yuming **Wang**1,2 and Jie Zhang1
2007 ApJ 665 1428
https://iopscience.iop.org/article/10.1086/519765/pdf
We examine the two kinds of major energetic phenomena that occur in the solar atmosphere: eruptive and confined events. The former describes flares with associated coronal mass ejections (CMEs), while the latter denotes flares without associated CMEs. We find that about 90% of X-class flares are eruptive, but the remaining 10% are confined. To probe why the largest energy releases could be either eruptive or confined, we investigate four X-class events from each of the two types. Both sets of events are selected to have very similar intensities (X1.0 to X3.6) and duration (rise time under 13 minutes and decay time over 9 minutes) in soft X-ray observations, to reduce any bias due to flare size on CME occurrence. We find that the occurrence of eruption (or confinement) is sensitive to the displacement of the location of the energy release, defined as the distance between the flare site and the flux-weighted magnetic center of the source active region. The displacement is 6-17 Mm for confined events but as large as 22-37 Mm for eruptive events. This means that confined events occur closer to the magnetic center, while the eruptive events tend to occur close to the edge of active regions. We use the potential field source-surface model to infer the coronal magnetic field above the source active regions and calculate the flux ratio of low (<1.1 R⊙) to high (≥1.1 R⊙) corona. We find that the confined events have a lower ratio (<5.7) than the eruptive events (>7.1). These results imply that a stronger overlying arcade field may prevent energy releases in the low corona from being eruptive, resulting in flares, but without CMEs. **1998 May 2, 2000 Mar 2, 2000 Jun 6, 2000 Sep 30, 2000 Nov 24, 2001 Apr 2, 2001 Jun 23, 2003 Jun 9, 2004 Feb 26, 2004 Jul 15, 2004 Jul 16, 2004 Jul 17, 2004 Oct 30**
TABLE 1 Confined X-Class Flares from 1996 to 2004 and Selected Eruptive Flares

COMPARISON OF THE 1998 APRIL 29 M6.8 AND 1998 NOVEMBER 5 M8.4 FLARES

HAIMIN **WANG**, PHILIP R. GOODE, CARSTEN DENKER, GUO YANG, VASYL YURCHISHIN. NARIAKI NITTA, JOSEPH B. GURMAN, CHRIS ST. CYR, AND ALEXANDER G. KOSOVICHEV
ASTROPHYSICAL JOURNAL, 536:971И981, **2000, File**
We combined, and analyzed in detail, the Ha and magnetograph data from Big Bear Solar Observatory

(BBSO), full-disk magnetograms from the Michelson Doppler Imager (MDI) on board Solar and Heliospheric Observatory (SOHO), coronagraph data from the Large Angle Spectrometric Coronagraph (LASCO) of SOHO, Fe XII 195 data from the Extreme ultraviolet Imaging Telescope (EIT) of SOHO, A_ and Yohkoh soft X-ray telescope (SXT) data of the M6.8 Care of 1998 April 29 in National Oceanic and Atmospheric Administration (NOAA) region 8375 and the M8.4 Care of 1998 November 5 in NOAA region 8384. These two Cares have remarkable similarities :
1. Partial halo coronal mass ejections (CMEs) were observed for both events. For the 1998 April 29 event, even though the Care occurred in the southeast of the disk center, the ejected material moved predominantly across the equator, and the central part of the CME occurred in the northeast limb. The direction in which the cusp points in the postCare SXT images determines the dominant direction of the CMEs.
2. Coronal dimming was clearly observed in EIT Fe XII 195 for both but was not observed in A_ Yohkoh SXT for either event. Dimming started 2 hr before the onset of the Cares, indicating large-scale coronal restructuring before both Cares.
3. No global or local photospheric magnetic Peld change was detected from either event ; in particular, no magnetic Peld change was found in the dimming areas.
4. Both events lasted several hours and, thus, could be classiPed as long duration events (LDEs). However, they are di†erent in the following important aspects. For the 1998 April 29 event, the Care and the CME are associated with an erupting Plament in which the two initial ribbons were well connected and then gradually separated. SXT preCare images show the classical S-shape sheared conPguration (sigmoid structure). For the 1998 November 5 event, two initial ribbons were well separated, and the SXT preCare image shows the interaction of at least two loops. In addition, no Plament eruption was observed. We conclude that even though these two events resulted in similar coronal consequences, they are due to two distinct physical processes : eruption of sheared loops and interaction of two loops.

Thermal-nonthermal energy partition in solar flares derived from X-ray, EUV, and bolometric observations

Alexander **Warmuth**, Gottfried Mann
A&A 644, A172 **2020**
https://arxiv.org/pdf/2011.04442.pdf
https://doi.org/10.1051/0004-6361/202039529
https://www.aanda.org/articles/aa/pdf/2020/12/aa39529-20.pdf
In solar flares, energy is released impulsively and is partly converted into thermal energy of hot plasmas and kinetic energy of accelerated nonthermal particles. Despite numerous efforts, no consensus on quantifying this energy balance has yet been reached. We aim to understand the reasons for the contradicting results on energy partition obtained by various recent studies. We considered five recent studies that address the thermal-nonthermal energy partition in solar flares. Their results are reviewed, and their methods are compared and discussed in detail. The main uncertainties in deriving the energy partition are identified as (a) the derivation of the differential emission measure (DEM) distribution and (b) the role of the conductive energy loss for the thermal component, as well as (c) the determination of the low-energy cutoff for the injected electrons. The bolometric radiated energy, as a proxy for the total energy released in the flare, is a useful independent constraint on both thermal and nonthermal energetics. In most of the cases, the derived energetics are consistent with this constraint. There are indications that the thermal-nonthermal energy partition changes with flare strength: in weak flares, there appears to be a deficit of energetic electrons, while the injected nonthermal energy is sufficient to account for the thermal component in strong flares. This behavior is identified as the main cause of the dissimilar results in the studies we considered. The changing partition has two important consequences: (a) an additional direct (i.e. non-beam) heating mechanism has to be present, and (b) considering that the bolometric emission originates mainly from deeper atmospheric layers, conduction or waves are required as additional energy transport mechanisms.

The STIX Aspect System (SAS): The Optical Aspect System of the Spectrometer/Telescope for Imaging X-Rays (STIX) on Solar Orbiter

A. **Warmuth**, H. Önel, […], K. Ber
Solar Physics volume 295, Article number: 90 (**2020**)
https://link.springer.com/content/pdf/10.1007/s11207-020-01660-w.pdf
The Spectrometer/Telescope for Imaging X-rays (STIX) is a remote sensing instrument on Solar Orbiter that observes the hard X-ray bremsstrahlung emission of solar flares. This paper describes the STIX Aspect System (SAS), a subunit that measures the pointing of STIX relative to the Sun with a precision of ±4″±4″, which is required to accurately localize the reconstructed X-ray images on the Sun. The operating principle of the SAS is based on an optical lens that images the Sun onto a plate that is perforated by small apertures arranged in a cross-shaped configuration of four radial arms. The light passing through the apertures of each arm is detected by a photodiode. Variations of spacecraft pointing and of distance from the Sun cause the solar image to move over different apertures, leading to a modulation of the

measured lightcurves. These signals are used by ground analysis to calculate the locations of the solar limb, and hence the pointing of the telescope.

Constraints on energy release in solar flares from RHESSI and GOES X-ray observations II. Energetics and energy partition

A. **Warmuth** and G. Mann

A&A 588, A116 **(2016)** **10.1051/0004-6361/201527475**

Aims. We derive constraints on energy release, transport and conversion processes in solar flares based on a detailed characterization of the physical parameters of both the thermal plasma and the accelerated nonthermal electrons based on X-ray observations. In particular, we address the questions of whether the energy required to heat the thermal plasma can be supplied by nonthermal particles, and how the energetics derived from X-rays compare to the total bolometric radiated energy.
Methods. Time series of spectral fits and images for 24 flares ranging from GOES class C3.4 to X17.2 were obtained using RHESSI hard X-ray observations. This has been supplemented by GOES soft X-ray fluxes. In our companion Paper I, we have used this data set to obtain the basic physical parameters for the thermal plasma (using the isothermal approximation) and the injected energetic electrons (assuming the thick-target model). Here, we used this data set to derive the flare energetics, including thermal energy, radiative and conductive energy loss, gravitational and flow energy of the plasma, and kinetic energy of the injected electrons. We studied how the thermal energies compare to the energy in nonthermal electrons, and how the various energetics and energy partition depend on flare importance.
Results. All flare energetics show a good to excellent correlation with the peak GOES flux. The gravitational energy of the evaporated plasma and the kinetic energy of plasma flows can be neglected in the discussion of flare energetics. The radiative energy losses are comparable to the maximum thermal energy, while the conductive losses are considerably higher than the maximum thermal energy, especially in weaker flares. The total heating requirement of the hot plasma amounts to ≈50% of the total bolometric energy loss, with the conductive losses as a major contribution. The nonthermal energy input by energetic electrons is not sufficient to account for the total heating requirements of the hot plasma or for the bolometric losses, in particular in weak flares.
Conclusions. Our results support the standard model of solar flares, with the following modifications. (1) Heating the hot thermal plasma and supplying the bolometric radiated energy requires an additional non-beam heating mechanism. (2) Strong conductive losses are a necessary additional energy transport process that transfers the energy released in the corona to the lower (and denser) atmospheric layers, where the bulk of the released energy is efficiently radiated away at longer wavelengths (EUV, UV, and white light) by cooler material.

Constraints on energy release in solar flares from RHESSI and GOES X-ray observations I. Physical parameters and scalings

A. **Warmuth** and G. Mann

A&A 588, A115 **(2016)**

http://www.aanda.org/articles/aa/pdf/2016/04/aa27474-15.pdf

Aims. We constrain energy release and particle acceleration processes in solar flares by means of comprehensively characterizing the physical parameters of both the thermal plasma and the accelerated nonthermal particles using X-ray data. Our aim is to bridge the gap between detailed case studies and large statistical studies.
Methods. We obtained time series of spectral fits and images for 24 flares ranging from GOES class C3.4 to X17.2 using RHESSI hard X-ray observations. These data were used to derive basic physical parameters for the thermal plasma (using the isothermal approximation) and the injected nonthermal electrons (assuming the thick-target model). For the thermal component, this was supplemented by GOES soft X-ray data. We derived the ranges and distributions of the various parameters, the scaling with flare importance, and the relation between thermal parameters derived from RHESSI and GOES. Finally, we investigated the relation between thermal and nonthermal parameters.
Results. Temperature and emission measure of the thermal plasma are strongly correlated with the peak GOES X-ray flux. Higher emission measures result both from a larger source volume and a higher density, with the latter effect being more important. RHESSI consistently gives higher temperatures and lower emission measures than GOES does, which is a signature of a multithermal plasma. The discrepancy between RHESSI and GOES is particularly pronounced in the early flare phase, when the thermal X-ray sources tend to be large and located higher in the corona. The energy input rate by nonthermal electrons is correlated with temperature and with the increase rate of emission measure and thermal energy.
Conclusions. The derived relations between RHESSI- and GOES-derived thermal parameters and the relation between thermal parameters and energy input by nonthermal electrons are consistent with a two-component model of the thermal flare plasma. Both RHESSI and GOES observe a cooler plasma component (≈10−25 MK) that is generated by chromospheric evaporation caused by a nonthermal electron beam. In addition, a hotter component (≥25 MK) is only detected by RHESSI; this component is more consistent with direct in situ heating of coronal plasma. With the exception of the early impulsive phase, RHESSI observes a combination of the evaporated and the directly heated component.

Table 1. Overview of the 24 analyzed flares.

Thermal and nonthermal hard X-ray source sizes in solar flares obtained from RHESSI observations
II. Scaling relations and temporal evolution

A. **Warmuth** and G. Mann

A&A 552, A87 **(2013)**
http://www.aanda.org/articles/aa/pdf/2016/04/aa27475-15.pdf

Context. A thorough understanding of solar flares requires determining the physical parameters of both the hot thermal plasma and the accelerated nonthermal electrons. This can be provided by hard X-ray (HXR) observations. In addition to HXR spectroscopy, imaging is needed to measure the geometric HXR source sizes. These parameters may vary as a function of flare size, importance, and time.
Aims. We determine the scaling relations of the geometric source parameters of both thermal and nonthermal HXR sources with respect to length scale and flare importance, and we characterize their temporal evolution. This is required for further studies involving parameters such as thermal energies, plasma densities, and current densities.
Methods. In a previous paper, we obtained time series of the geometric HXR source sizes (thermal and nonthermal) for 24 flares from GOES class C3.4 to X17.2 using the RHESSI instrument. Here, we investigate how themal volumes, nonthermal footpoint areas, and footpoint separations depend on the flare length scale and GOES importance. In addition,we study the time evolution of these geometric parameters. Table: 2002-2003.
Results. The increase in the thermal source volume with length scale is slightly below a Euclidian scaling, but not too far from it. The thermal source volume is correlated with GOES class, which contrasts with what was found for RHESSI microflares. The nonthermal footpoint areas, on the other hand, are not well-correlated with either length scale or GOES class. With regard to temporal evolution, the RHESSI thermal source volumes tend to show a more complex behavior than the simple growth-decline pattern typical of flares observed in EUV. In most events, the thermal volume shows a rapid initial rise to a peak in the early impulsive phase. This peak is correlated with the initial downward motion of the coronal source, and is consistent with the notion of initially contracting magnetic field lines.
Conclusions. The behavior of the geometric parameters of thermal and nonthermal HXR sources is generally consistent with the standard model of eruptive solar flares: a quasi-Euclidian scaling of volume with length scale, an initially decreasing thermal volume due to field line shrinking, followed by an increase in both volume and footpoint separation with time as the arcade of reconnected flare loops grows. However, the thermal volume is not the dominant factor in determining thermal energy, as well as thermal SXR and HXR flux. Electron density and/or temperature seem to be more important parameters in this respect. **2002 Apr. 10**

Thermal and nonthermal hard X-ray source sizes in solar flares obtained from RHESSI observations
I. Observations and evaluation of methods

A. **Warmuth** and G. Mann

A&A 552, A86 (**2013**)

Context. In solar flares, a large amount of thermal and nonthermal energy is released impulsively in the form of heated plasma and accelerated particles. These processes can be studied via hard X-ray (HXR) diagnostics. In addition to spectroscopic observations, a thorough understanding of the thermal and nonthermal particle populations requires the knowledge of the HXR source sizes.
Aims. We derive the geometric source parameters of both thermal coronal sources and the nonthermal HXR footpoints in solar flares. We compare and evaluate four different methods for obtaining source sizes, and then derive the most reliable source sizes, as well as the systematic uncertainties.
Methods. We obtained time series of HXR images for 24 flares from GOES class C3.4 to X17.2 using the RHESSI instrument. The four imaging techniques employed are CLEAN, Pixon, visibility forward fit, and MEM_NJIT. From this data set, we derived the geometric parameters of the thermal HXR sources and the nonthermal footpoints. Using the different imaging techniques allowed us to quantify systematic measurement uncertainties.
Results. We find that the different methods give consistent results on HXR source sizes. The correlations are very good for the thermal sources, and somewhat lower for the footpoints. The MEM_NJIT algorithm gives systematically smaller sizes than the other methods, possibly a result of over-resolution. Thermal source volumes are in the range of 2 × 1025−1.2 × 1028 cm3 (with a median relative uncertainty of 30%), and nonthermal footpoint areas in the range of 2 × 1016−6 × 1017 cm2 (median relative uncertainty: 40%). The thermal volumes of our sample are in the same range as those derived for microflares, which would imply that source size is not an important parameter for flare energetics.
Conclusions. Using different imaging algorithms for determining HXR source sizes offers the advantage that uncertainties can be better quantified thus making the derived parameters more reliable. Combined with geometric parameters that were derived as time series in a larger number of flares, this will allow the study of the scaling relations and the temporal evolution of thermal and nonthermal HXR sources.

RAPID CHANGES OF ELECTRON ACCELERATION CHARACTERISTICS AT THE END OF THE IMPULSIVE PHASE OF AN X-CLASS SOLAR FLARE

Alexander **Warmuth**1, Gordon D. Holman2, Brian R. Dennis2, Gottfried Mann1, Henry Aurass1, and Ryan O. Milligan2

Astrophysical Journal, 699:917–922, **2009, File**

http://www.iop.org/EJ/toc/-alert=43190/0004-637X/699/1

obtained with *RHESSI*. This flare exhibits HXR pulses during the impulsive phase, with a particularly pronounced peak at the end of the impulsive phase. This peak is associated with HXR emission up to high energies (>300 keV) but does not show any Neupert effect (i.e., no simultaneous rise in soft X-rays). Fitting the spatially integrated photon spectra with a Maxwellian plus a nonthermal thick-target component reveals that the data are consistent with a high low-energy cutoff (≈ 100 keV) of the energetic electrons during the late peak. The high lowenergy cutoff straightforwardly explains the lack of a Neupert effect—while highly energetic electrons are produced efficiently, there is a lack of low-energy electrons that usually contain the bulk of the total energy. Hence, the energy input into the chromosphere remains too small to trigger chromospheric evaporation. This observation shows that the characteristics of electron acceleration can change dramatically and rapidly at the end of the impulsive phase of solar flares. This could be evidence for physically distinct acceleration processes acting in the same event, or alternatively for a sudden shift in the characteristic parameters of the accelerator. Using radio observations and comparing HXR images with magnetograms, we conclude that changes in the strength and the topology of the magnetic field in which the accelerator is working are responsible for the profound changes in the injected electron spectrum.

Modelling shock drift acceleration of electrons at the reconnection outflow termination shock in solar flares - Observational constraints and parametric study:

A. **Warmuth**, G. Mann and H. Aurass

A&A 494 (**2009**) 677-691

http://www.aanda.org/10.1051/0004-6361:200810101

Context. The acceleration of electrons to nonthermal energies in solar flares is one of the main unsolved questions in solar physics. One possibility for producing these energetic electrons is acceleration at the reconnection outflow termination shock (TS).

Aims. By comparing theoretical results with observations of nonthermal electrons, we determine whether shock drift acceleration (SDA) at the TS is a viable electron acceleration mechanism.

Methods. We used radio observations to constrain the characteristics of the TS, and hard X-ray observations provided by *RHESSI*, *INTEGRAL*, and *HXRS* to obtain the characteristics of the injected electrons. Invoking relativistic shock-drift acceleration at the TS, we calculated electron flux spectra, which are then compared with the corresponding observational results from *RHESSI*. A parametric study of the model allows us to answer the question under which conditions the TS is a viable electron accelerator.

Results. SDA at the TS is able to reproduce the required fluxes and kinetic power of nonthermal electrons in solar flares as long as there is significant heating of the outflow jet and a sufficiently large shock area. A prediction of the model is that the flux and power of injected electrons is higher than the values that are usually given by fitting observed spectra, since the low-energy cutoff is generally below 10 keV. The synthetic spectra are consistent with the observed spectral indices up to ≈100 keV. Beyond that, they soften too quickly. Possibly this is because we have not yet considered various additional effects, such as multiple reflections at the shock or some form of preacceleration. The observed relation between electron flux and spectral index is reproduced by the model, as well as the temporal evolution of the energetic electrons. We conclude that SDA at the TS is a viable electron acceleration mechanism that deserves further study.

Constraining Electron Acceleration at a Standing Shock with HXR and Radio Observations

Warmuth, A.; Mann, G.; Aurass, H.

Central European Astrophysical Bulletin (CEAB), **2007**CEAB...31..135W

The acceleration of electrons to non-thermal energies in solar flares is one of the main unsolved questions in solar physics. One possibility for the production of these energetic electrons is acceleration at the reconnection outflow termination shock (TS). We use radio observations to constrain the characteristics of the TS, and hard X-ray and γ-ray observations provided by RHESSI and INTEGRAL to obtain the characteristics of the injected differential electron flux. Invoking relativistic shock-drift acceleration at the TS, we calculate differential electron fluxes, which are then compared with the observations. This approach allows us to answer the question if, and under which conditions, the TS is a viable electron accelerator.

Data-driven model of the solar corona above an active region

J. **Warnecke** and H. Peter

A&A 623, L12 (**2019**)
https://www.aanda.org/articles/aa/pdf/2019/04/aa35385-19.pdf
Aims. We aim to reproduce the structure of the corona above a solar active region as seen in the extreme ultraviolet (EUV) using a three-dimensional magnetohydrodynamic (3D MHD) model.
Methods. The 3D MHD data-driven model solves the induction equation and the mass, momentum, and energy balance. To drive the system, we feed the observed evolution of the magnetic field in the photosphere of the active region AR 12139 into the bottom boundary. This creates a hot corona above the cool photosphere in a self-consistent way. We synthesize the coronal EUV emission from the densities and temperatures in the model and compare this to the actual coronal observations.
Results. We are able to reproduce the overall appearance and key features of the corona in this active region on a qualitative level. The model shows long loops, fan loops, compact loops, and diffuse emission forming at the same locations and at similar times as in the observation. Furthermore, the low-intensity contrast of the model loops in EUV matches the observations.
Conclusions. In our model the energy input into the corona is similar as in the scenarios of fieldline-braiding or flux-tube tectonics, that is, energy is transported to the corona through the driving of the vertical magnetic field by horizontal photospheric motions. The success of our model shows the central role that this process plays for the structure, dynamics, and heating of the corona. **16 August 2014**

Spectroscopic Observations of Current Sheet Formation and Evolution

Harry P. **Warren**, David H. Brooks, Ignacio Ugarte-Urra, Jeffrey W. Reep, Nicholas A. Crump, George A. Doschek
2018 *ApJ* **854** 122
https://arxiv.org/pdf/1711.10826.pdf
https://iopscience.iop.org/article/10.3847/1538-4357/aaa9b8/pdf
We report on the structure and evolution of a current sheet that formed in the wake of an eruptive X8.3 flare observed at the west limb of the Sun on **September 10, 2017**. Using observations from the EUV Imaging Spectrometer (EIS) on Hinode and the Atmospheric Imaging Assembly (AIA) on the Solar Dynamics Observatory (SDO), we find that plasma in the current sheet reaches temperatures of about 20 MK and that the range of temperatures is relatively narrow. The highest temperatures occur at the base of the current sheet, in the region near the top of the post-flare loop arcade. The broadest high temperature line profiles, in contrast, occur at the largest observed heights. Further, line broadening is strong very early in the flare and diminishes over time. The current sheet can be observed in the AIA 211 and 171 channels, which have a considerable contribution from thermal bremsstrahlung at flare temperatures. Comparisons of the emission measure in these channels with other EIS wavelengths and AIA channels dominated by Fe line emission indicate a coronal composition and suggest that the current sheet is formed by the heating of plasma already in the corona. Taken together, these observations suggest that some flare heating occurs in the current sheet while additional energy is released as newly reconnected field lines relax and become more dipolar.
Hinode/ EIS Nugget March 2018 http://solarb.mssl.ucl.ac.uk/SolarB/nuggets/nugget_2018mar.jsp

Transition Region and Chromospheric Signatures of Impulsive Heating Events. I. Observations

Harry P. **Warren**, Jeffrey W. Reep, Nicholas A. Crump, Paulo J. A. Simoes
ApJ 829 35 **2016**
http://arxiv.org/pdf/1606.09045v1.pdf
We exploit the high spatial resolution and high cadence of the Interface Region Imaging Spectrograph (IRIS) to investigate the response of the transition region and chromosphere to energy deposition during a small flare. Simultaneous observations from RHESSI provide constraints on the energetic electrons precipitating into the flare footpoints while observations of XRT, AIA, and EIS allow us to measure the temperatures and emission measures from the resulting flare loops. We find clear evidence for heating over an extended period on the spatial scale of a single IRIS pixel. During the impulsive phase of this event the intensities in each pixel for the Si IV 1402.770, C II 1334.535, Mg II 2796.354 and O I 1355.598 emission lines are characterized by numerous, small-scale bursts typically lasting 60s or less. Red shifts are observed in Si IV, C II, and Mg II during the impulsive phase. Mg II shows red-shifts during the bursts and stationary emission at other times. The Si IV and C II profiles, in contrast, are observed to be red-shifted at all times during the impulsive phase. These persistent red-shifts are a challenge for one-dimensional hydrodynamic models, which predict only short-duration downflows in response to impulsive heating. We conjecture that energy is being released on many small-scale filaments with a power-law distribution of heating rates. 2014-11-19

Abundances in Solar Flares

Harry **Warren**
RHESSI Science Nuggets, No. 224, **2014**
http://sprg.ssl.berkeley.edu/~tohban/wiki/index.php/Abundances_in_Solar_Flares

wrinkles in the FIP effect for flares.

OBSERVATIONS OF THERMAL FLARE PLASMA WITH THE EUV VARIABILITY EXPERIMENT
Harry P. **Warren**1, John T. Mariska2, and George A. Doschek
2013 ApJ 770 116
One of the defining characteristics of a solar flare is the impulsive formation of very high temperature plasma. The properties of the thermal emission are not well understood, however, and the analysis of solar flare observations is often predicated on the assumption that the flare plasma is isothermal. The EUV Variability Experiment (EVE) on the Solar Dynamics Observatory provides spectrally resolved observations of emission lines that span a wide range of temperatures (e.g., Fe XV-Fe XXIV) and allow for thermal flare plasma to be studied in detail. In this paper we describe a method for computing the differential emission measure distribution in a flare using EVE observations and apply it to several representative events. We find that in all phases of the flare the differential emission measure distribution is broad. Comparisons of EVE spectra with calculations based on parameters derived from the Geostationary Operational Environmental Satellites soft X-ray fluxes indicate that the isothermal approximation is generally a poor representation of the thermal structure of a flare.

A SYSTEMATIC SURVEY OF HIGH-TEMPERATURE EMISSION IN SOLAR ACTIVE REGIONS
Harry P. **Warren**1, Amy R. Winebarger2, and David H. Brooks
2012 ApJ 759 141
The recent analysis of observations taken with the EUV Imaging Spectrometer and X-Ray Telescope instruments on Hinode suggests that well-constrained measurements of the temperature distribution in solar active regions can finally be made. Such measurements are critical for constraining theories of coronal heating. Past analysis, however, has suffered from limited sample sizes and large uncertainties at temperatures between 5 and 10 MK. Here we present a systematic study of the differential emission measure distribution in 15 active region cores. We focus on measurements in the "inter-moss" region, that is, the region between the loop footpoints, where the observations are easier to interpret. To reduce the uncertainties at the highest temperatures we present a new method for isolating the Fe XVIII emission in the AIA/SDO 94 Å channel. The resulting differential emission measure distributions confirm our previous analysis showing that the temperature distribution in an active region core is often strongly peaked near 4 MK. We characterize the properties of the emission distribution as a function of the total unsigned magnetic flux. We find that the amount of high-temperature emission in the active region core is correlated with the total unsigned magnetic flux, while the emission at lower temperatures, in contrast, is inversely related. These results provide compelling evidence that high-temperature active region emission is often close to equilibrium, although weaker active regions may be dominated by evolving million degree loops in the core.

OBSERVATIONS OF RECONNECTING FLARE LOOPS WITH THE ATMOSPHERIC IMAGING ASSEMBLY
Harry P. **Warren**, Casey M. O'Brien1 and Neil R. Sheeley, Jr.
2011 ApJ 742 92
Perhaps the most compelling evidence for the role of magnetic reconnection in solar flares comes from the supra-arcade downflows that have been observed above many post-flare loop arcades. These downflows are thought to be related to highly non-potential field lines that have reconnected and are propagating away from the current sheet. We present new observations of supra-arcade downflows taken with the Atmospheric Imaging Assembly (AIA) on the Solar Dynamics Observatory (SDO). The morphology and dynamics of the downflows observed with AIA provide new evidence for the role of magnetic reconnection in solar flares. With these new observations we are able to measure downflows originating at larger heights than in previous studies. We find, however, that the initial velocities measured here (~144 km s–1) are well below the Alfvén speed expected in the lower corona, and consistent with previous results. We also find no evidence that the downflows brighten with time, as would be expected from chromospheric evaporation. These observations suggest that simple two-dimensional models cannot explain the detailed observations of solar flares.

THE TEMPERATURE DEPENDENCE OF SOLAR ACTIVE REGION OUTFLOWS
Harry P. **Warren**, Ignacio Ugarte-Urra1, Peter R. Young1, and Guillermo Stenborg2
Astrophysical Journal, 727:58 (5pp), **2011** January
Spectroscopic observations with the EUV Imaging Spectrometer (EIS) on *Hinode* have revealed large areas of high-speed outflows at the periphery of many solar active regions. These outflows are of interest because they may connect to the heliosphere and contribute to the solar wind. In this paper, we use slit rasters from EIS in combination

with narrowband slot imaging to study the temperature dependence and morphology of an outflow region and show that it is more complicated than previously thought. Outflows are observed primarily in emission lines from Fe xi to Fe xv. Observations at lower temperatures (Si vii), in contrast, show bright fan-like structures that are dominated by inflows. These data also indicate that the morphology of the outflows and the fans is different, outflows are observed in regions where there is no emission in Si vii. This suggests that the fans, which are often associated with outflows in studies involving imaging data, are not directly related to the active region outflows.

EVIDENCE FOR STEADY HEATING: OBSERVATIONS OF AN ACTIVE REGION CORE WITH HINODE AND TRACE

Harry P. Warren1, Amy R. Winebarger2 and David H. Brooks1,3
2010 ApJ 711 228-238
The timescale for energy release is an important parameter for constraining the coronal heating mechanism. Observations of "warm" coronal loops (~1 MK) have indicated that the heating is impulsive and that coronal plasma is far from equilibrium. In contrast, observations at higher temperatures (~3 MK) have generally been consistent with steady heating models. Previous observations, however, have not been able to exclude the possibility that the high temperature loops are actually composed of many small-scale threads that are in various stages of heating and cooling and only appear to be in equilibrium. With new observations from the EUV Imaging Spectrometer and X-ray Telescope (XRT) on *Hinode* we have the ability to investigate the properties of high temperature coronal plasma in extraordinary detail. We examine the emission in the core of an active region and find three independent lines of evidence for steady heating. We find that the emission observed in XRT is generally steady for hours, with a fluctuation level of approximately 15% in an individual pixel. Short-lived impulsive heating events are observed, but they appear to be unrelated to the steady emission that dominates the active region. Furthermore, we find no evidence for warm emission that is spatially correlated with the hot emission, as would be expected if the high temperature loops are the result of impulsive heating. Finally, we also find that intensities in the "moss," the footpoints of high temperature loops, are consistent with steady heating models provided that we account for the local expansion of the loop from the base of the transition region to the corona. In combination, these results provide strong evidence that the heating in the core of an active region is effectively steady, that is, the time between heating events is short relative to the relevant radiative and conductive cooling times.

Observation and Modeling of Coronal "Moss" With the EUV Imaging Spectrometer on *Hinode*

Harry P. **Warren**, Amy R. Winebarger, John T. Mariska, George A. Doschek, and Hirohisa Hara
The Astrophysical Journal, Vol. 677, No. 2: 1395-1400, **2008**.

Emission Line Intensity Ratios of Fe xxvi/ xxv/ xxiv in Solar Flares Observed by Hinotori

Tetsuya **Watanabe**1
2024 ApJ 965 41
https://iopscience.iop.org/article/10.3847/1538-4357/ad298c/pdf
High-resolution spectra observed by the Solar X-ray spectrometer on board the Hinotori mission are revisited. Flat crystals slightly offset to the satellite spin axis produce automatic spectral scans for emission lines emerging from highly charged iron ions in solar flares every half-spin time period. All the downlinked data of the mission are converted to FITS format and major flare spectral data are revived as IDL save files in ISAS/DARTS. Based on these data sets, single-temperature fits are performed for the emission line complex of highly charged iron ions in the wavelength range of 1.75–1.95 Å and compared with theoretical predictions. Synthetic spectra with single electron temperatures estimated from j/w line-intensity ratios fit fairly well for Fe xxiv and Fe xxiii lines in the wavelength range of 1.85–1.88 Å, while intensity ratios of Fe xxv lines (x, y, z) and the inner-shell excitation line of Fe xxiv (q) to the Fe xxv resonance line (w) have systematic excesses. Empirical relations for the observed line ratios are derived. Ion fractions of Fe+25/Fe+24 estimated by intensity ratios of Lyα/w in the temperature range of log Te=7.25–7.45 are consistent with values in ionization equilibrium, and the remaining excesses of the Fe xxv line ratios may suggest problems with the atomic parameters or atomic modeling. **1981 October 7**

White-light Emission and Chromospheric Response by an X1.8-class Flare on 2012 October 23

Kyoko **Watanabe**1 and Shinsuke Imada2
2020 ApJ 891 88
sci-hub.si/10.3847/1538-4357/ab711b
On **2012 October 23**, a strong white-light emission, associated with an X1.8-class flare, was observed by the Solar Optical Telescope on board the Hinode satellite. White-light kernels were clearly observed along the Ca ii H

ribbons. RHESSI also observed hard X-ray emissions that were almost located on the white-light kernels. The total energy of the white-light emission was and the total energy of the accelerated electrons was almost of the same order when we used 40 keV as the lower energy cutoff. The white-light emission appears to have originated from nonthermal electrons in these energies. Moreover, the EUV imaging spectrometer on board the Hinode satellite performed a raster scan over this flaring active region and the flare occurred during the scan. Over the white-light kernels, we observed redshifts of a few tens of km s−1 in Fe xii. It appears that these EUV responses originated from some accelerated electrons due to the solar flare and they are considered to be the source of the white-light emission. In fact, the electron density of the white-light kernels was less than , which is sufficiently low for nonthermal electrons to penetrate into the photosphere.

Characteristics that Produce White-Light Enhancements in Solar Flares Observed by Hinode/SOT

Kyoko **Watanabe**, Jun Kitagawa, Satoshi Masuda
ApJ **850** 204 **2017**
https://arxiv.org/pdf/1710.09531.pdf

To understand the conditions that produce white-light (WL) enhancements in solar flares, a statistical analysis of visible continuum data as observed by Hinode/Solar Optical Telescope (SOT) was performed. In this study, approximately 100 flare events from M- and X-class flares were selected. The time period during which the data were recorded spans from January 2011 to February 2016. Of these events, approximately half are classified as white-light flares (WLFs), whereas the remaining events do not show any enhancements of the visible continuum (non-WLF; NWL). In order to determine the existence of WL emission, running difference images of not only the Hinode/SOT WL (G-band, blue, green, and red filter) data but also the Solar Dynamics Observatory/Helioseismic and Magnetic Imager continuum data are used. A comparison between these two groups of WL data in terms of duration, temperature, emission measure of GOES soft X-rays, distance between EUV flare ribbons, strength of hard X-rays, and photospheric magnetic field strength was undertaken. In this statistical study, WLF events are characterized by a shorter time-scale and shorter ribbon distance compared with NWL events. From the scatter plots of the duration of soft X-rays and the energy of non-thermal electrons, a clear distinction between WLF and NWL events can be made. It is found that the precipitation of large amounts of accelerated electrons within a short time period plays a key role in generating WL enhancements. Finally, it was demonstrated that the coronal magnetic field strength in the flare region is one of the most important factors that allow the individual identification of WLF events from NWL events. **2015 March 11, 2012 July 12**
Table 1. WLF event list and physical parameters from GOES & SDO data. (2011-2015)

Emission Height and Temperature Distribution of White-Light Emission Observed by Hinode/SOT from the 2012 January 27 X-class Solar Flare

Kyoko **Watanabe**, Toshifumi Shimizu, Satoshi Masuda, Kiyoshi Ichimoto, and Masanori Ohno
E-print, Oct **2013**; ApJ, 776, 123 (**2013**)

White-light emissions were observed from an X1.7 class solar flare on **2012 January 27**, using three continuum bands (red, green, and blue) of the Solar Optical Telescope on board the Hinode satellite. This event occurred near the solar limb, and so differences in the locations of the various emissions are consistent with differences in heights above the photosphere of the various emission sources. Under this interpretation, our observations are consistent with the white-light emissions occurring at the lowest levels of where the Ca II H emission occurs. Moreover, the centers of the source regions of the red, green, and blue wavelengths of the white-light emissions are significantly displaced from each other, suggesting that those respective emissions are emanating from progressively lower heights in the solar atmosphere. The temperature distribution was also calculated from the white-light data, and we found the lower-layer emission to have a higher temperature. This indicates that high-energy particles penetrated down to near the photosphere, and deposited heat into the ambient lower layers of the atmosphere.

Production of High-Temperature Plasmas During the Early Phases of a C9.7 Flare. II. Bi-directional Flows Suggestive of Reconnection in a Pre-flare Brightening Region

T. **Watanabe**, H. Hara, A. C. Sterling, L. K. Harra
Solar Physics, November **2012**, Volume 281, Issue 1, pp 87-99

The **6 June 2007** 16:55 UT flare was well observed with high time-cadence sparse raster scans by the EUV Imaging Spectrometer (EIS) on board the Hinode spacecraft. The observation covers an active region area of 240 arcsec × 240 arcsec with the 1 arcsec slit in about 160 seconds.
We describe here spectral properties of a “pre-flare brightening” to this flare, which started about nine minutes prior to flare-ribbon onset. This flare brightening looks like two small loops apparently having a cusp-shape structure about 40 – 50 arcsec west of the main flaring loops, which show dynamic behavior in velocity during the early phases of the flare: The He ii line at 256.32 Å shows the existence of a bi-directional flow along the Sun–Earth line of sight of about −70 and +100 km s−1. On the other hand, the Fe xvi line at 262.98 Å formed at higher coronal temperatures shows only a slight increase in intensity at the location of these loops, and the Fe xxiii line at 263.76 Å barely appears. Electron

density at the site derived from the intensity ratios of the Fe xiv line pair at 264.78 Å and 274.20 Å is lower than the average of 109.3 cm−3 in other parts of the active-region outskirts. Combining a time series of STEREO-A/B SECCHI-EUVI 171 Å images, we conclude that the pre-flare-brightening region may be heated via magnetic reconnection taking place as a result of loop–loop interaction**.**

Hinode Flare Catalogue

K. **Watanabe**, S. Masuda and T. Segawa
Solar Phys. Volume 279, Number 1, 317-322 **2012; File**
We describe a catalogue of solar flares observed by the three instruments (SOT, XRT, EIS) onboard the Hinode satellite. From the launch of the Hinode satellite in September 2006 until late 2011, about 5000 solar flares (larger than A-class in the GOES classification) occurred during the five-year period of Hinode observations, and more than half of them were captured by the Hinode telescopes. Observation information for RHESSI and Nobeyama Radioheliograph are also included in the catalogue. This catalogue is distributed to users through the Internet. It will be useful and helpful for scientists in surveying flares to be analyzed, facilitate access to Hinode data, and help advance data analysis activities among the world solar community**.** **http://st4a.stelab.nagoya-u.ac.jp/hinode_flare/**

ELLERMAN BOMBS AT HIGH RESOLUTION. I. MORPHOLOGICAL EVIDENCE FOR PHOTOSPHERIC RECONNECTION

Hiroko **Watanabe**1, Gregal Vissers2, Reizaburo Kitai1, Luc Rouppe van der Voort2 and Robert J. Rutten
2011 ApJ 736 71
High-resolution imaging-spectroscopy movies of solar active region NOAA 10998 obtained with the Crisp Imaging Spectropolarimeter at the Swedish 1-m Solar Telescope show very bright, rapidly flickering, flame-like features that appear intermittently in the wings of the Balmer Hα line in a region with moat flows and likely some flux emergence. They show up at regular Hα blue-wing bright points that outline the magnetic network, but flare upward with much larger brightness and distinct "jet" morphology seen from aside in the limbward view of these movies. We classify these features as Ellerman bombs and present a morphological study of their appearance at the unprecedented spatial, temporal, and spectral resolution of these observations. The bombs appear along the magnetic network with footpoint extents up to 900 km. They show apparent travel away from the spot along the pre-existing network at speeds of about 1 km s–1. The bombs flare repetitively with much rapid variation at timescales of seconds only, in the form of upward jet-shaped brightness features. These reach heights of 600-1200 km and tend to show blueshifts; some show bi-directional Doppler signature and some seem accompanied with an Hα surge. They are not seen in the core of Hα due to shielding by overlying chromospheric fibrils. The network where they originate has normal properties. The morphology of these jets strongly supports deep-seated photospheric reconnection of emergent or moat-driven magnetic flux with pre-existing strong vertical network fields as the mechanism underlying the Ellerman bomb phenomenon.

PRODUCTION OF HIGH-TEMPERATURE PLASMAS DURING THE EARLY PHASES OF A C9.7 FLARE

Tetsuya **Watanabe** 1,2, Hirohisa Hara 1,2, Alphonse C. Sterling 3,4 and Louise K. Harra 5
2010 ApJ 719 213
Explosive chromospheric evaporation is predicted from some current solar flare models. In this paper, we analyze a flare with high time cadence raster scans with the EUV Imaging Spectrometer (EIS) on board the Hinode spacecraft. This observation covers an area of 240" × 240", with the 1" slit in about 160 s. The early phases of a C9.7 flare that occurred on **2007 June 6** were well observed. The purpose of our analysis is to study for the first time the spatially resolved spectra of high-temperature plasma, especially from Fe XXIII and Fe XXIV, allowing us to explore the explosive chromospheric evaporation scenario further. Sections of raster images obtained between 17:20:09 and 17:20:29 (UT) show a few bright patches of emission from Fe XXIII/Fe XXIV lines at the footpoints of the flaring loops; these footpoints were not clearly seen in the images taken earlier, between 17:17:30 and 17:17:49 (UT). Fe XXIII spectra at these footpoints show dominating blueshifted components of –(300 to 400) km s–1, while Fe XV/XIV lines are nearly stationary; Fe XII lines and/or lower temperature lines show slightly redshifted features, and Fe VIII and Si VII to He II lines show ~+50 km s–1 redshifted components. The density of the 1.5-2 MK plasma at these footpoints is estimated to be 3 × 1010 cm–3 by the Fe XIII/XIV line pairs around the maximum of the flare. High-temperature loops connecting the footpoints appear in the Fe XXIII/XXIV images taken over 17:22:49-17:23:08 (UT) which is near the flare peak. Line profiles of these high-temperature lines at this flare peak time show only slowly moving components. The concurrent cooler Fe XVII line at 254.8 Å is relatively weak, indicating the predominance of high-temperature plasma (>107 K) in these loops. The characteristics observed during the early phases of this flare are consistent with the scenario of explosive chromospheric evaporation.

G-BAND AND HARD X-RAY EMISSIONS OF THE 2006 DECEMBER 14 FLARE OBSERVED BY *HINODE*/SOT AND *RHESSI*

Kyoko **Watanabe**1, S¨am Krucker2, Hugh Hudson2, Toshifumi Shimizu1, Satoshi Masuda3, and Kiyoshi Ichimoto4

Astrophysical Journal, 715:651–655, **2010** May; **File**

We report on *G*-band emission observed by the Solar Optical Telescope on board the *Hinode* satellite in association with the X1.5-class flare on **2006 December 14**. The *G*-band enhancements originate from the footpoints of flaring coronal magnetic loops, coinciding with nonthermal hard X-ray bremsstrahlung sources observed by the *Reuven Ramaty High Energy Solar Spectroscopic Imager*. At the available 2 minute cadence, the *G*-band and hard X-ray intensities are furthermore well correlated in time. Assuming that the *G*-band enhancements are continuum emission from a blackbody, we derived the total radiative losses of the white-light flare (white-light power). If the *G*-band enhancements additionally have a contribution from lines, the derived values are overestimates. We compare the white-light power with the power in hard X-ray producing electrons using the thick-target assumption. Independent of the cutoff energy of the accelerated electron spectrum, the white-light power and the power of accelerated electrons are roughly proportional. Using the observed upper limit of ~30 keV for the cutoff energy, the hard X-ray producing electrons provide at least a factor of 2 more power than needed to produce the white-light emission. For electrons above 40 keV, the powers roughly match for all four of the time intervals available during the impulsive phase. Hence, the flare-accelerated electrons contain enough energy to produce the white-light flare emissions. The observed correlation in time, space, and power strongly suggests that electron acceleration and white-light production in solar flares are closely related. However, the results also call attention to the inconsistency in apparent source heights of the hard X-ray (chromosphere) and white-light (upper photosphere) sources.

25 Years of Self-organized Criticality: Concepts and Controversies **Review**

Nicholas W. **Watkins**, Gunnar Pruessner, Sandra C. Chapman, Norma B. Crosby, Henrik J. Jensen

Space Science Reviews **2015**

Introduced by the late Per Bak and his colleagues, self-organized criticality (SOC) has been one of the most stimulating concepts to come out of statistical mechanics and condensed matter theory in the last few decades, and has played a significant role in the development of complexity science. SOC, and more generally fractals and power laws, have attracted much comment, ranging from the very positive to the polemical. The other papers (Aschwanden et al. in Space Sci. Rev., 2014, this issue; McAteer et al. in Space Sci. Rev., 2015, this issue; Sharma et al. in Space Sci. Rev. 2015, in preparation) in this special issue showcase the considerable body of observations in solar, magnetospheric and fusion plasma inspired by the SOC idea, and expose the fertile role the new paradigm has played in approaches to modeling and understanding multiscale plasma instabilities. This very broad impact, and the necessary process of adapting a scientific hypothesis to the conditions of a given physical system, has meant that SOC as studied in these fields has sometimes differed significantly from the definition originally given by its creators. In Bak's own field of theoretical physics there are significant observational and theoretical open questions, even 25 years on (Pruessner 2012). One aim of the present review is to address the dichotomy between the great reception SOC has received in some areas, and its shortcomings, as they became manifest in the controversies it triggered. Our article tries to clear up what we think are misunderstandings of SOC in fields more remote from its origins in statistical mechanics, condensed matter and dynamical systems by revisiting Bak, Tang and Wiesenfeld's original papers.

Erratum to: 25 Years of Self-organized Criticality: Concepts and Controversies

Observation of a Flare and Filament Eruption in Lyman-αα on 8 September 2011 by the PRoject for OnBoard Autonomy/Large Yield Radiometer (PROBA2/LYRA)

L. **Wauters**, M. Dominique, R. Milligan, I. E. Dammasch, M. Kretzschmar & J. Machol

Solar Physics volume 297, Article number: 36 (**2022**)

https://link.springer.com/content/pdf/10.1007/s11207-022-01963-0.pdf

The Large Yield Radiometer (LYRA) instrument onboard the PRoject for OnBoard Autonomy (PROBA2) observes the solar irradiance in four channels in the UV–EUV. One of these channels is centered around the hydrogen line at 121.6 nm. The solar Lyman-αα emission line is an optically thick line mostly formed in the chromosphere. Although it is one of the strongest lines of the solar spectrum, only a limited number of instruments provided observations of solar flares in Lyman-αα, and those observations differ significantly in shape, durations, and amplitude. We focus on an event that happened on **8 September 2011** (SOL2011-09-08T15:46). This event, an M6.7 flare, was associated with a filament eruption that happened during the decaying phase of the flare. Most of the irradiance fluctuations observed in the Lyman-αα time series are synchronized with nonthermal emission fluctuations, as is predicted by flare models. However, there is a late-phase peak in Lyman-αα observations that rather correlates with the timing of the filament eruption. We demonstrate that the eruption of the filament is at the origin of this peak.

Correction: ***Solar Physics*** volume 297**,** Article number: **39 (2022)**

Understanding Problem Forecasts of ISEST Campaign Flare-CME Events

David **Webb**, Nariaki Nitta

Solar Physics October **2017**, 292:142

The goal of the International Study of Earth-affecting Solar Transients (ISEST) project as part of the Variability of the Sun and Its Terrestrial Impact (VarSITI) program is to understand the origin, evolution, and propagation of solar transients through the space between the Sun and Earth, and to improve our prediction capability for space weather. A goal of ISEST Working Group 4 (Campaign Events) is to study a set of well-observed Sun-to-Earth events to develop an understanding of why some events are successfully forecast (textbook cases), whereas others become problem or failed forecasts. In this article we study six cases during the rise of Solar Cycle 24 that highlight forecasting problems. Likely source coronal mass ejections (CMEs) were identified in all six cases, but the related solar surface activity ranged from uncertain or weak to X-class flares. The geoeffects ranged from none to severe as in the two Sun–Earth events in 2015 that caused severe storms. These events were chosen to illustrate some key problems in understanding the chain from cause to geoeffect. **6 Jan. 2012, 7 – 9 Mar. 2012, 12 – 14 July 2012, 23 – 24 July 2012, 4 – 8 Oct. 2012, 15 – 17 Mar. 2013, 1 June 2013, 7 – 9 Jan. 2014, 10 – 13 Sep. 2014, 15 – 17 Mar. 2015, 21 – 24 June 2015**

Episodic energy release during the main- and post-impulsive phase of a solar flare

Yuqian **Wei**, Bin Chen, Sijie Yu, Haimin Wang, Yixian Zhang, Lindsay Glesener

ApJ **964** 174 **2024**

https://arxiv.org/pdf/2403.00985.pdf

https://iopscience.iop.org/article/10.3847/1538-4357/ad2e8f/pdf

When and where the magnetic field energy is released and converted in eruptive solar flares remains an outstanding topic in solar physics. To shed light on this question, here we report multi-wavelength observations of a C9.4-class eruptive limb flare that occurred on **2017 August 20**. The flare, accompanied by a magnetic flux rope eruption and a white light coronal mass ejection, features three post-impulsive X-ray and microwave bursts immediately following its main impulsive phase. For each burst, both microwave and X-ray imaging suggest that the non-thermal electrons are located in the above-the-loop-top region. Interestingly, contrary to many other flares, the peak flux of the three post-impulsive microwave and X-ray bursts shows an increase for later bursts. Spectral analysis reveals that the sources have a hardening spectral index, suggesting a more efficient electron acceleration into the later post-impulsive bursts. We observe a positive correlation between the acceleration of the magnetic flux rope and the non-thermal energy release during the post-impulsive bursts in the same event. Intriguingly, different from some other eruptive events, this correlation does not hold for the main impulse phase of this event, which we interpret as energy release due to the tether-cutting reconnection before the primary flux rope acceleration occurs. In addition, using footpoint brightenings at conjugate flare ribbons, a weakening reconnection guide field is inferred, which may also contribute to the hardening of the non-thermal electrons during the post-impulsive phase. **2017 August 20**

The Photospheric Imprints of Coronal Electric Currents

Brian T. **Welsch**

ApJ **2022**

https://arxiv.org/pdf/2211.01911.pdf

Flares and coronal mass ejections are powered by magnetic energy stored in coronal electric currents. Here, we explore the nature of coronal currents in observed and model active region (ARs) by studying manifestations of these currents in photospheric vector magnetograms. We employ Gauss's separation method, recently introduced to the solar physics literature, to partition the photospheric field into three distinct components, each arising from a separate source: (i) currents passing through the photosphere, (ii) currents flowing below it, and (iii) currents flowing above it. We refer to component (iii) as the photospheric imprint of coronal currents. In both AR 10930 and AR 11158, photospheric imprints exhibit large-scale, spatially coherent structures along these regions' central, sheared polarity inversion lines (PILs) that are consistent with coronal currents flowing horizontally above these PILs, similar to recent findings in AR 12673 by Schuck et al. (2022). We find similar photospheric imprints in a simple model of a non-potential AR with known currents. We find that flare-associated changes in photospheric imprints in AR 11158 accord with earlier reports that near-PIL fields become more horizontal, consistent with the "implosion" scenario. We hypothesize that this evolution effectively shortens, in an overall sense, current-carrying coronal fields, leading to decreased inductive energy (DIE) in the coronal field. We further hypothesize that, in the hours prior to flares, parts of the coronal field slowly expand, in a process we deem coronal inflation (CI) -- essentially, the inverse of the implosion process. Both of these hypotheses are testable with non-potential coronal field extrapolations. **2006/12/12, 2011/02/15**

SWAP Observations of Post-flare Giant Arches in the Long-Duration 14 October 2014 Solar Eruption

Matthew J. **West** and Daniel B. Seaton

ApJL **2015**
http://arxiv.org/pdf/1502.00801v1.pdf
On **14 October 2014** the Sun Watcher with Active Pixels and Image Processing (SWAP) EUV solar telescope on-board the Project for On-Board Autonomy 2 (PROBA2) spacecraft observed an eruption that led to the formation of perhaps the largest post-eruptive loop system seen in the solar corona in solar cycle 24. The initial eruption occurred at about 18:30 UT on 14 October, behind the East Solar limb, and was observed as a a coronal mass ejection and an M2.2 solar flare. In the 48 hours following the eruption, the associated post-eruptive loops grew to a height of approximately 400000 km (>0.5 solar-radii) at rates between 2-6 km/s. We conclude from our observations of this event that ordinary post-eruptive loops and so-called post-flare giant arches are fundamentally the same and are formed by the same magnetic reconnection mechanism.

Photospheric response to a flare

Michael S. **Wheatland**, Donald B. Melrose, Alpha Mastrano
ApJ **864** 159 **2018**
https://arxiv.org/pdf/1808.03097.pdf
http://sci-hub.tw/http://iopscience.iop.org/article/10.3847/1538-4357/aad8ae/meta
Flares produce sudden and permanent changes in the horizontal photospheric magnetic field. In particular flares generally produce increased magnetic shear in the photospheric field along the neutral line. Recent observations show also that flares can produce sudden photospheric motion. We present a model for the observed changes as the response of the photosphere to a large-amplitude shear Alfv\'{e}n wave propagating down from the corona on either side of the neutral line. The Alfv\'{e}nic front is assumed to impact the photosphere close to the neutral line first, and then successively further away with time, such that the line of impact coincides with the flare ribbon. The wave introduces magnetic shear and velocity shear. The magnetic shear introduced at the photosphere has the same sign on either side of the neutral line, while the velocity shear has the opposite sign. We discuss the possibility that this process is responsible for particle acceleration in flares. **22 June 2015**
RHESSI Science Nuggets #332 October **2018**
http://sprg.ssl.berkeley.edu/~tohban/wiki/index.php/Photospheric_response_to_a_flare

Estimating Electric Current Densities in Solar Active Regions

M. S. **Wheatland**
Solar Phys. **2015**
Electric currents in solar active regions are thought to provide the energy released via magnetic reconnection in solar flares. Vertical electric current densities J z at the photosphere may be estimated from vector magnetogram data, subject to substantial uncertainties. The values provide boundary conditions for nonlinear force-free modelling of active region magnetic fields. A method is presented for estimating values of J z taking into account uncertainties in vector magnetogram field values, and minimisingJ2zacross the active region. The method is demonstrated using the boundary values of the field for a force-free twisted bipole, with the addition of noise at randomly chosen locations.

ANTI-PHASE SIGNATURE OF FLARE GENERATED TRANSVERSE LOOP OSCILLATIONS

R. S. **White**, E. Verwichte, and C. Foullon
2013 ApJ 774 104
Transverse loop oscillations observed by the Atmospheric Imaging Assembly instrument on the Solar Dynamics Observatory spacecraft are studied after an impulsive solar flare eruption on **2012 May 8**. We have found that a transversely oscillating coronal loop seen in the 171 Å bandpass oscillates in anti-phase with respect to adjacent larger loops seen in the 193 Å and 211 Å bandpasses. These unusual oscillations are analyzed to investigate the excitation mechanism responsible for their initial inwardly directed anti-phase behavior. The transverse oscillations are analyzed by constructing space-time diagrams from cuts made parallel to the projected loop displacements. The displacement time oscillation profiles are background subtracted and fitted with a damped cosine curve that includes a linear change in the period with time. The local magnetic topology of the active region is modeled using potential field source surface extrapolation. It reveals that the loops are anchored in different topological regions with foot point locations identified on either side of the EUV flare peak emission source. In this context, the oscillation characteristics indicate that the excitation mechanism is closely linked to the local magnetic field topology and the reconnection generated wave dynamics in the active region rather than following an external flare blast wave. We discuss how observations such as these may serve to identify reconnection processes in similar quadrupolar active regions.

First observation of a transverse vertical oscillation during the formation of a hot post-flare loop

R. S. **White**, E. Verwichte and C. Foullon

A&A 545, A129 (**2012**)
Aims. We report and analyse the first observation of a transverse oscillation in a hot coronal loop with the Atmospheric Imaging Assembly (AIA) on the Solar Dynamics Observatory (SDO), following a linked coronal-flare mass-ejection event on the **3 November 2010**. The oscillating coronal loop is observed off the east solar limb and exclusively in the 131 Å and 94 Å bandpasses, indicating a loop plasma of temperature in the range of 9–11 MK. Furthermore, the loop is not observed to cool into the other AIA channels, but just disappears from all bandpasses at the end of the oscillation.
Methods. A time series analysis of the loop oscillation is conducted by taking several cuts at different positions along the loop, estimating the transverse displacements over time for two strands in the loop and fitting those with a damped cosine curve. Intensity time variations, both along the loop and for a series of cut cross-sections, are investigated. Using a three-dimensional loop geometry obtained from a comparison of STEREO-B/EUVI and AIA images, we model different modes of transverse oscillations in the uniformly filled loop.
Results. Our time series analysis reveals a period of 302 ± 14 s (291 ± 9 s) and a damping time of 306 ± 43 s (487 ± 125 s) for the first (second) loop strand. A spatial phase shift along the loop of approximately 180° suggests that we observe a higher order harmonic. Intensity oscillations are consistent with an interpretation in terms of a vertically polarised mode. Our forward modelling suggests that the loop oscillates as either a second or third order harmonic of this mode.
Conclusions. This is the first observation of a transverse loop oscillation observed exclusively in the hot coronal lines. The loop oscillation is vertically polarised and is dominated by a higher order harmonic mode. We conclude that the excitation mechanism of this 5 min period oscillation is directly connected with the reconnection processes that form the post flare loop, which differs from the blast wave excitation mechanism often proposed as the cause of cooler transverse loop oscillations.

Solar Flare Sounding Rocket Campaign
A White Paper on the Scientific Motivation and Feasibility of Introducing Routine Solar Flare Campaigns for Sounding Rockets

A. **Winebarger**, L. Glesener, K. Reeves
Solar News 1 Aug **2019**
https://rscience.gsfc.nasa.gov/keydocs/SolarFlareCampaign.pdf

A Statistical Study to Determine the Origin of Long-Duration Gamma-ray Flares

Lisa M. **Winter**, Valerie Bernstein, Nicola Omodei, Melissa Pesce-Rollins
ApJ **864** 39 **2018**
https://arxiv.org/pdf/1807.06001.pdf **File**
http://sci-hub.tw/10.3847/1538-4357/aad3c0
Two scenarios have been proposed to account for sustained ≥30\,MeV gamma-ray emission in solar flares: (1) prolonged particle acceleration/trapping involving large-scale magnetic loops at the flare site, and (2) precipitation of high-energy (> 300 MeV) protons accelerated at coronal/interplanetary shock waves. To determine which of these scenarios is more likely, we examine the associated soft X-ray flares, coronal mass ejections (CMEs), and solar energetic proton events (SEPs) for: (a) the long-duration gamma-ray flares (LDGRFs) observed by the Large Area Telescope (LAT) on \Fermi, and (b) delayed and/or spatially-extended high-energy gamma-ray flares observed by the Gamma-ray Spectrometer on the Solar Maximum Mission, the Gamma-1 telescope on the Gamma satellite, and the Energetic Gamma-Ray Experiment Telescope on the Compton Gamma-Ray Observatory. For the \Fermi data set of 11 LDGRFs with >100 MeV emission lasting for ≥∼2 hours, we search for associations and reverse associations between LDGRFs, X-ray flares, CMEs, and SEPs, i.e., beginning with the gamma-ray flares and also, in turn, with X-class soft X-ray flares, fast (≥ 1500 km s−1) and wide CMEs, and intense (peak flux ≥2.67×10−3 protons cm−2 s−1 sr−1, with peak to background ratio > 1.38) > 300 MeV SEPs at 1 A.U. While LDGRFs tend to be associated with bright X-class flares, we find that only 1/3 of the X-class flares during the time of \Fermi monitoring coincide with an LDGRF. However, nearly all fast, wide CMEs are associated with an LDGRF. These preliminary association analyses favor the proton precipitation scenario, although there is a prominent counter-example of a potentially magnetically well-connected solar eruption with > 100 MeV emission for ∼10 h for which the near-Earth > 300 MeV proton intensity did not rise above background. **2011.03.07, 2012.01.27, 2012.03.07,**
TABLE 1 *Properties of Fermi LAT Gamma-Ray Flares 2011-2015*
TABLE 2 *Properties of X-class flares without Fermi LAT Gamma-Ray Flares*
TABLE 3 *Properties of Pre-Fermi LAT Gamma-Ray Flares 1982-1991*

Using the Maximum X-ray Flux Ratio and X-ray Background to Predict Solar Flare Class

Lisa M. **Winter**, K. Balasubramaniam
JGR or Space Weather **2015**
http://arxiv.org/pdf/1504.00294v1.pdf

We present the discovery of a relationship between the maximum ratio of the flare flux (namely, 0.5-4 Ang to the 1-8 Ang flux) and non-flare background (namely, the 1-8 Ang background flux), which clearly separates flares into classes by peak flux level. We established this relationship based on an analysis of the Geostationary Operational Environmental Satellites (GOES) X-ray observations of ~ 50,000 X, M, C, and B flares derived from the NOAA/SWPC flares catalog. Employing a combination of machine learning techniques (K-nearest neighbors and nearest-centroid algorithms) we show a separation of the observed parameters for the different peak flaring energies. This analysis is validated by successfully predicting the flare classes for 100% of the X-class flares, 76% of the M-class flares, 80% of the C-class flares and 81% of the B-class flares for solar cycle 24, based on the training of the parametric extracts for solar flares in cycles 22-23. **Aug 09 2011**

Frequency Distribution of Acoustic Oscillation in the Solar Atmosphere During Flare Event

A. **Wiśniewska**1,2, E. Chmielewska3, K. Radziszewski3, M. Roth2, and J. Staiger2
2019 ApJ 886 32
https://doi.org/10.3847/1538-4357/ab487c
We present a study of multi-wavelength observations, of a C 2.3 solar flare in Active Region NOAA 12353, observed on **2015 May 23**, which reveal new properties of acoustic waves in the flaring region. The space-, and ground-based data measured by the HELioseismological Large Regions Interferometric Device, operating at the Vacuum Tower Telescope, the Atmospheric Imaging Assembly (AIA), and Helioseismic and Magnetic Imager on board the Solar Dynamic Observatory, were used in this paper. First, using power spectra of solar oscillations, we identified the dominant frequencies and their location at seven different atmospheric levels before and after the flare event. Second, based on AIA observations taken in six Extreme Ultraviolet filters, we derived Differential Emission Measure (DEM) profiles and DEM maps of the flare. Finally, we confirm the sigma shape of the magnetic field in the active area, directly related to the flare. Our results are as follows: the high-frequency waves ($\nu > 5$ mHz) in the photosphere, in both cases, before and after the flare, are generated at the footpoints of the chromospheric loop, while in the chromosphere (Hα line), before the event the power enhancement exhibits the maximum of flare emission, and after the eruption the enhancement by all frequencies is observed only in the post-flare loop area. Moreover, the power of oscillation in the pores surrounding the area before the flare has a random character, while after the flare oscillation power is concentrated in the pore, and weakened outside of. We conclude that accurate detection of high-frequency acoustic waves in active regions can lead to faster and easier prediction of high-energy events.

WHAT IS THE RELATIONSHIP BETWEEN PHOTOSPHERIC FLOW FIELDS AND SOLAR FLARES?

Brian T. **Welsch**1, Yan Li1, Peter W. Schuck2, and George H. Fisher1
Astrophysical Journal, 705:821–843, **2009** November
We estimated photospheric velocities by separately applying the Fourier Local Correlation Tracking and Differential Affine Velocity Estimator methods to 2708 co-registered pairs of *SOHO*/MDI magnetograms, with nominal 96 minute cadence and ~2_ pixels, from 46 active regions (ARs) from 1996 to 1998 over the time interval τ_{45} when each AR was within 45◦ of disk center. For each magnetogram pair, we computed the reprojected, average estimated radial magnetic field, $\tilde{} B_R$; and each tracking method produced an independently estimated flow field, **u**. We then quantitatively characterized these magnetic and flow fields by computing several extensive and intensive properties of each; extensive properties scale with AR size, while intensive properties do not depend directly on AR size. Intensive flow properties included moments of speeds, horizontal divergences, and radial curls; extensive flow properties included sums of these properties over each AR, and a crude proxy for the ideal Poynting flux, $S_R = \_|\mathbf{u}| \tilde{} B_R$. Several quantities derived from $\tilde{} B_R$ were also computed, including: √, the total unsigned flux; R, a measure of the unsigned flux near strong-field polarity inversion lines; and $\_ \tilde{} B_R$. Next, using correlation and discriminant analysis, we investigated the associations between these properties and flares from the *GOES* flare catalog, when averaged over both τ_{45} and shorter time windows of 6 and 24 hr. Our AR sample included both flaring and flare-quiet ARs; the latter did not flare above *GOES* C1.0 level during τ_{45}. Among magnetic properties, we found R to be most strongly associated with flare flux. Among extensive flow properties, the proxy Poynting flux, S_R, was most strongly associated with flare flux, at a level comparable to that of R. All intensive flow properties studied were more poorly associated with flare flux than these extensive properties. Past flare activity was also associated with future flare occurrence. The largest coefficients of determination from correlations with flare flux that we performed are~ 0.25, implying no single variable that we considered can explain the majority of variability in average flare flux.

Estimating electric current densities in solar active regions

M.S. **Wheatland**
Solar Phys. Volume 290, Issue 4, pp 1147-1157 **2015**
http://arxiv.org/pdf/1503.02741v1.pdf
Electric currents in solar active regions are thought to provide the energy released via magnetic reconnection in solar flares. Vertical electric current densities Jz at the photosphere may be estimated from vector magnetogram data, subject to substantial uncertainties. The values provide boundary conditions for nonlinear force- free modelling of active region magnetic fields. A method is presented for estimating values of Jz taking into account uncertainties in vector magnetogram field values, and minimizing J2z across the active region. The method is demonstrated using the boundary values of the field for a force-free twisted bipole, with the addition of noise at randomly chosen locations.

The Energetics of a Flaring Solar Active Region and Observed Flare Statistics

M. S. **Wheatland**
The Astrophysical Journal, Vol. 679, No. 2: 1621-1628, **2008**.
http://www.journals.uchicago.edu/doi/abs/10.1086/587871
A stochastic model for the energy of a flaring solar active region is presented, generalizing and extending the approach of Wheatland and Glukhov. The probability distribution for the free energy of an active region is described by the solution to a master equation involving deterministic energy input and random jump transitions downward in energy (solar flares). It is shown how two observable distributions, the flare frequency-energy distribution and the flare waiting-time distribution, may be derived from the steady state solution to the master equation, for given choices for the energy input and for the rates of flare transitions. An efficient method of numerical solution of the steady state master equation is presented. Solutions appropriate for flaring, involving a constant rate of energy input and powerlaw distributed jump transition rates, are numerically investigated. The flarelike solutions exhibit power-law flare frequency-energy distributions below a high-energy rollover, set by the largest energy the active region is likely to have. The solutions also exhibit approximately exponential (i.e., Poisson) waiting-time distributions, despite the rate of flaring depending on the free energy of the system.

Including Flare Sympathy in a Model for Solar Flare Statistics

M. S. **Wheatland** and I. J. D. Craig, Solar Physics, Volume 238 Number 1, p. 73-86, **2006**

The Relationship Between Solar Radio and Hard X-ray Emission **A Review**

S. M. **White**1,5, A. O. Benz2, S. Christe3, F. F´arn´ık4, M. R. Kundu5, G. Mann6, Z. Ning7, J.-P. Raulin8, A. V. R. Silva-V´alio8, P. Saint-Hilaire9, N. Vilmer10, and A.Warmuth6
Space Sci. Rev., 159:225–261, **2011, File**
This **review** discusses the complementary relationship between radio and hard X-ray observations of the Sun using primarily results from the era of the *Reuven Ramaty High Energy Solar Spectroscopic Imager* satellite. A primary focus of joint radio and hard X-ray studies of solar flares uses observations of nonthermal gyrosynchrotron emission at radio wavelengths and bremsstrahlung hard X-rays to study the properties of electrons accelerated in the main flare site, since it is well established that these two emissions show very similar temporal behavior. A quantitative prescription is given for comparing the electron energy distributions derived separately from the two wavelength ranges: this is an important application with the potential for measuring the magnetic field strength in the flaring region, and reveals significant differences between the electrons in different energy ranges. Examples of the use of simultaneous data from the two wavelength ranges to derive physical conditions are then discussed, including the case of microflares, and the comparison of images at radio and hard X-ray wavelengths is presented. There have been puzzling results obtained from observations of solar flares at millimeter and submillimeter wavelengths, and the comparison of these results with corresponding hard X-ray data is presented. Finally, the review discusses the association of hard X-ray releases with radio emission at decimeter and meter wavelengths, which is dominated by plasma emission (at lower frequencies) and electron cyclotron maser emission (at higher frequencies), both coherent emission mechanisms that require small numbers of energetic electrons. These comparisons show broad general associations but detailed correspondence remains more elusive.

Timing Issues for 2005 Jan 20

Stephen **White**
Presentation at “Ground Level Enhancement (GLE)”
Comparative Data Analysis Workshop (CDAW), LMSAL, Jan 6-9, **2009**
Address the relative contributions of “flare” and “CME” accelerated particles to SEPs

The Dependence of Solar Flare Magnitude on sunspot Area During Activity Cycle 24

Lucy **Will**1, Ellis A. Avallone2, and Xudong Sun

2022 Res. Notes AAS 6 37
We measure the sunspot areas of activity cycle 24 using ten years of continuum images from the Helioseismic and Magnetic Imager, and compare them with the peak flare soft X-ray flux from the Geostationary Operational Environmental Satellite. We find that the sunspot area in our sample is positively correlated with the magnitude of the largest flare they produce. Complex spot groups with βγδ magnetic classification tend to be larger and more likely to produce intense flares. Our findings are qualitatively consistent with previous studies.

Investigating the Efficacy of Topologically Derived Time-Series for Flare Forecasting. I. Dataset Preparation

Thomas **Williams**, Christopher B. Prior, David MacTaggart
ApJ **2024**
https://arxiv.org/pdf/2412.04335
The accurate forecasting of solar flares is considered a key goal within the solar physics and space weather communities. There is significant potential for flare prediction to be improved by incorporating topological fluxes of magnetogram datasets, without the need to invoke three-dimensional magnetic field extrapolations. Topological quantities such as magnetic helicity and magnetic winding have shown significant potential towards this aim, and provide spatio-temporal information about the complexity of active region magnetic fields. This study develops time-series that are derived from the spatial fluxes of helicity and winding that show significant potential for solar flare prediction. It is demonstrated that time-series signals, which correlate with flare onset times, also exhibit clear spatial correlations with eruptive activity; establishing a potential causal relationship. A significant database of helicity and winding fluxes and associated time series across 144 active regions is generated using SHARP data processed with the ARTop code that forms the basis of the time-series and spatial investigations conducted here. We find that a number of time-series in this dataset often exhibit extremal signals that occur 1-8 hours before a flare. This, publicly available, living dataset will allow users to incorporate these data into their own flare prediction algorithms.

Evidence from EIS for axial filament rotation before a large flare

Williams, D. R., Harra, L. K., Brooks, D. H., Imada, S., Hansteen, V. H.
E-print, Feb. 2009; PASJ (Vol. 61, No. 3, June **2009**
http://www.mssl.ucl.ac.uk/~drw/papers/antisymvel/v4_erupfil.pdf
In this article, we present observations made with the Extreme-ultraviolet Imaging Spectrometer (EIS) on-board the Hinode solar satellite, of an active region filament in the He II emission line at 256.32 ?. The host active region (AR 10930) produces an X-class flare during these observations. We measure Doppler shifts with apparent velocities of up to 20 km/s, which are antisymmetric about the filament length and occur several minutes before the flare?s impulsive phase. This is indicative of a rotation of the filament, which is in turn consistent with expansion of a twisted flux rope due to the MHD helical kink instability. This is the first time that such an observation has been possible in this transition-region line, and we note that the signature observed occurs before the first indications of pre-flare activity in the GOES solar soft X-ray flux, suggesting that the filament begins to destabilise in tandem with a reorganistation of the local magnetic field. We suggest that this expansion is triggered by the decrease of magnetic tension around, and/or total pressure above, the filament. **13 Dec 2006**

Magnetic reconnection in flux-tubes undergoing spinning footpoint motions

A. L. **Wilmot-Smith** and I. De Moortel
A&A 473 (**2007**) 615-623 (Section 'The Sun')
http://www.aanda.org/10.1051/0004-6361:20077455

Identifying Observables That Can Differentiate Between Impulsive and Footpoint Heating: Time Lags and Intensity Ratios

Amy R. **Winebarger**1, Roberto Lionello2, Cooper Downs2, Zoran Mikić2, and Jon Linker2
2018 ApJ 865 111 DOi 10.3847/1538-4357/aad9fb
Observations of solar coronal loops have identified several common loop characteristics, including that loops appear to cool and have higher than expected densities. Two potential heating scenarios have been suggested to explain these observations. One scenario is that the loops are formed by many strands, each heated independently by a series of small-scale impulsive heating events, or nanoflares. Another hypothesis is that the heating is quasi-steady and highly stratified, i.e., "footpoint heating"; such heating can drive thermal nonequilibrium in some structures depending on the scale height and magnitude of the energy deposition, and the geometry of the structure. Studies of both types of heating have found that they can qualitatively reproduce the observed loop properties. The goal of this paper is to identify observables that can be used to differentiate between these two heating scenarios. To do this, we use a single loop geometry. For footpoint heating, we vary the heating magnitude and stratification, for impulsive heating, we vary the heating magnitude. We use one-dimensional hydrodynamic codes to calculate the resulting temperature and density evolution. We convolve the temperature and density with the response functions of four EUV channels of the

Atmospheric Imaging Assembly and one filter channel of Hinode's X-ray Telescope. We consider two principal diagnostics: the time lag between the appearance of the loop in two different channels, and the ratio of the peak intensities of the loop in the two channels. Based on this limited data set, we find (1) that footpoint heating can predict longer time lags than impulsive heating in some channel pairs, (2) that footpoint heating can predict zero or negative time lags in some channel pairs, (3) that the intensity ratio expected from impulsive heating is confined to a narrow range, while footpoint heating predicts a wider range of intensity ratios, and (4) that the range of temperatures expected in impulsive heating is broader than the range of temperatures expected in footpoint heating. This preliminary study identifies observables that may be useful in discriminating between heating models in future work.

DETECTING NANOFLARE HEATING EVENTS IN SUBARCSECOND INTER-MOSS LOOPS USING Hi-C

Amy R. **Winebarger**1, Robert W. Walsh2, Ronald Moore1, Bart De Pontieu3, Viggo Hansteen4, Jonathan Cirtain1, Leon Golub5, Ken Kobayashi6, Kelly Korreck5, Craig DeForest7, Mark Weber5, Alan Title3, and Sergey Kuzin

2013 ApJ 771 21

The High-resolution Coronal Imager (Hi-C) flew aboard a NASA sounding rocket on **2012 July 11** and captured roughly 345 s of high-spatial and temporal resolution images of the solar corona in a narrowband 193 Å channel. In this paper, we analyze a set of rapidly evolving loops that appear in an inter-moss region. We select six loops that both appear in and fade out of the Hi-C images during the short flight. From the Hi-C data, we determine the size and lifetimes of the loops and characterize whether these loops appear simultaneously along their length or first appear at one footpoint before appearing at the other. Using co-aligned, co-temporal data from multiple channels of the Atmospheric Imaging Assembly on the Solar Dynamics Observatory, we determine the temperature and density of the loops. We find the loops consist of cool (~105 K), dense (~1010 cm–3) plasma. Their required thermal energy and their observed evolution suggest they result from impulsive heating similar in magnitude to nanoflares. Comparisons with advanced numerical simulations indicate that such dense, cold and short-lived loops are a natural consequence of impulsive magnetic energy release by reconnection of braided magnetic field at low heights in the solar atmosphere.

USING A DIFFERENTIAL EMISSION MEASURE AND DENSITY MEASUREMENTS IN AN ACTIVE REGION CORE TO TEST A STEADY HEATING MODEL

Amy R. **Winebarger**1, Joan T. Schmelz2, Harry P. Warren3, Steve H. Saar4 and Vinay L. Kashyap

2011 ApJ 740 2

The frequency of heating events in the corona is an important constraint on the coronal heating mechanisms. Observations indicate that the intensities and velocities measured in active region cores are effectively steady, suggesting that heating events occur rapidly enough to keep high-temperature active region loops close to equilibrium. In this paper, we couple observations of active region (AR) 10955 made with the X-Ray Telescope and the EUV Imaging Spectrometer on board Hinode to test a simple steady heating model. First we calculate the differential emission measure (DEM) of the apex region of the loops in the active region core. We find the DEM to be broad and peaked around 3 MK. We then determine the densities in the corresponding footpoint regions. Using potential field extrapolations to approximate the loop lengths and the density-sensitive line ratios to infer the magnitude of the heating, we build a steady heating model for the active region core and find that we can match the general properties of the observed DEM for the temperature range of $6.3 < \log T < 6.7$. This model, for the first time, accounts for the base pressure, loop length, and distribution of apex temperatures of the core loops. We find that the density-sensitive spectral line intensities and the bulk of the hot emission in the active region core are consistent with steady heating. We also find, however, that the steady heating model cannot address the emission observed at lower temperatures. This emission may be due to foreground or background structures, or may indicate that the heating in the core is more complicated. Different heating scenarios must be tested to determine if they have the same level of agreement.

Using the maximum X-ray flux ratio and X-ray background to predict solar flare class

L. M. **Winter**, K. Balasubramaniam

Space Weather Volume 13, Issue 5 May **2015** Pages 286–297

http://arxiv.org/pdf/1504.00294v1.pdf

We present the discovery of a relationship between the maximum ratio of the flare flux (namely, 0.5–4 Å to the 1–8 Å flux) and nonflare background (namely, the 1–8 Å background flux), which clearly separates flares into classes by peak flux level. We established this relationship based on an analysis of the Geostationary Operational Environmental Satellites X-ray observations of ~ 50,000 X, M, C, and flares derived from the NOAA/Space Weather Prediction Center flares catalog. Employing a combination of machine learning techniques (K-nearest neighbors and nearest centroid algorithms) we show a separation of the observed parameters for the different peak flaring energies. This analysis is validated by successfully predicting the flare classes for 100% of the X-class flares, 76% of the M-class flares, 80% of the C-class flares, and 81% of the B-class flares for solar cycle 24, based on the training of the parametric extracts for solar flares in cycles 22–23.

SIMULATING THE EFFECTS OF INITIAL PITCH-ANGLE DISTRIBUTIONS ON SOLAR FLARES

Henry D. **Winter**1, Petrus Martens2 and Katharine K. Reeves

2011 ApJ 735 103

In this work, we model both the thermal and non-thermal components of solar flares. The model we use, HYLOOP, combines a hydrodynamic equation solver with a non-thermal particle tracking code to simulate the thermal and non-thermal dynamics and emission of solar flares. In order to test the effects of pitch-angle distribution on flare dynamics and emission, a series of flares is simulated with non-thermal electron beams injected at the loop apex. The pitch-angle distribution of each beam is described by a single parameter and allowed to vary from flare to flare. We use the results of these simulations to generate synthetic hard and soft X-ray emissions (HXR and SXR). The light curves of the flares in Hinode's X-ray Telescope passbands show a distinct signal that is highly dependent on pitch-angle distribution. The simulated HXR emission in the 3-6 keV bandpass shows the formation and evolution of emission sources that correspond well to the observations of pre-impulsive flares. This ability to test theoretical models of thermal and non-thermal flare dynamics directly with observations allows for the investigation of a wide range of physical processes governing the evolution of solar flares. We find that the initial pitch-angle distribution of non-thermal particle populations has a profound effect on loop top HXR and SXR emission and that apparent motion of HXR is a natural consequence of non-thermal particle evolution in a magnetic trap.

Long-period oscillations in the lower solar atmosphere prior to flare events

A. **Wiśniewska**1, M. B. Korsós2,3,5, I. Kontogiannis1, Sz. Soós3,5 and R. Erdélyi4,3,5

A&A, 686, A224 (**2024**)

https://www.aanda.org/articles/aa/pdf/2024/06/aa48606-23.pdf

Context. Multiple studies have identified a range of oscillation periods in active regions, from 3−5 min to long-period oscillations that last from tens of minutes to several hours. Recently, it was also suggested that these periods are connected with eruptive activity in the active regions. Thus, it is essential to understand the relation between oscillations in solar active regions and their solar eruption activity.

Aims. We investigate the long-period oscillations of NOAA 12353 prior to a series of C-class flares and correlate the findings with the 3- to 5-min oscillations that were previously studied in the same active region. The objective of this work is to elucidate the presence of various oscillations with long periods in the lower solar atmosphere both before and after the flare events.

Methods. To detect long-period oscillations, we assessed the emergence, shearing, and total magnetic helicity flux components from the photosphere to the top of the chromosphere. To analyze the magnetic helicity flux in the lower solar atmosphere, we used linear force-free field extrapolation to construct a model of the magnetic field structure of the active region. Subsequently, the location of long-period oscillations in the active region was probed by examining the spectral energy density of the measured intensity signal in the 1700 Å, 1600 Å, and 304 Å channels of the Atmospheric Imaging Assembly (AIA) of the Solar Dynamics Observatory (SDO). Significant oscillation periods were determined by means of a wavelet analysis.

Results. Based on the evolution of the three magnetic helicity flux components, 3- to 8-h periods were found both before and after the flare events, spanning from the photosphere to the chromosphere. These 3- to 8-h periods were also evident throughout the active region in the photosphere in the 1700 Å channel. Observations of AIA 1600 Å and 304 Å channels, which cover the chromosphere to the transition region, revealed oscillations of 3−8 h near the region in which the flare occurred. The spatial distribution of the measured long-period oscillations mirror the previously reported distribution of 3- to 5-min oscillations in NOAA 12353 that were seen both before and after the flares.

Conclusions. This case study suggest that the varying oscillation properties in a solar active region could be indicative of future flaring activity. **2015 May 21-23**

Frequency Distribution of Acoustic Oscillation in the Solar Atmosphere During Flare Event

A. **Wisniewska**, E. Chmielewska, K. Radziszewski, M. Roth, J. Staiger

2019 ApJ 886 32

https://doi.org/10.3847/1538-4357/ab487c

https://arxiv.org/ftp/arxiv/papers/2203/2203.02420.pdf

We present a study of multi-wavelength observations, of a C 2.3 solar flare in Active Region NOAA 12353, observed on **2015 May 23**, which reveal new properties of acoustic waves in the flaring region. The space-, and ground-based data measured by the HELioseismological Large Regions Interferometric Device, operating at the Vacuum Tower Telescope, the Atmospheric Imaging Assembly, and Helioseismic and Magnetic Imager on board the Solar Dynamic Observatory, were used in this paper. First, using power spectra of solar oscillations, we identified the dominant frequencies and their location at seven different atmospheric levels before and after the flare event. Second, based on AIA observations taken in six Extreme Ultraviolet filters, we derived Differential Emission Measure (DEM) profiles and DEM maps of the flare. Finally, we confirm the {\sigma}-classification of the magnetic field in the active area, directly related to the flare. Our results are as follows: the high-frequency waves ({\nu}>5 mHz) in the photosphere, in

both cases, before and after the flare, are generated at the foot-points of the chromospheric loop, while in the chromosphere (H{\alpha} line), before the event the power enhancement exhibits for maximum of flare emission, and after the eruption the enhancement by all frequencies is observed only in the post flare loop area. Moreover, the power of oscillation in the pores surrounding area before the flare has a random character, while after the flare oscillation's power is concentrated in the pore, and weakened outside of. We conclude that the accurate detection of high-frequency acoustic waves in the active regions can lead to faster and easier prediction of high-energy events.

3D Numerical Simulation of Kink-driven Rayleigh–Taylor Instability Leading to Fast Magnetic Reconnection

Pakorn **Wongwaitayakornkul**1, Hui Li2, and Paul M. Bellan1
2020 ApJL 895 L7
https://doi.org/10.3847/2041-8213/ab8e35
Fast magnetic reconnection involving non-MHD microscale physics is believed to underlie both solar eruptions and laboratory plasma current disruptions. While there is extensive research on both the MHD macroscale physics and the non-MHD microscale physics, the process by which large-scale MHD couples to the microscale physics is not well understood. An MHD instability cascade from a kink to a secondary Rayleigh–Taylor instability in the Caltech astrophysical jet laboratory experiment provides new insights into this coupling and motivates a 3D numerical simulation of this transition from large to small scale. A critical finding from the simulation is that the axial magnetic field inside the current-carrying dense plasma must exceed the field outside. In addition, the simulation verifies a theoretical prediction and experimental observation that, depending on the strength of the effective gravity produced by the primary kink instability, the secondary instability can be Rayleigh–Taylor or mini-kink. Finally, it is shown that the kink-driven Rayleigh–Taylor instability generates a localized electric field sufficiently strong to accelerate electrons to very high energy.

Unsupervised Machine Learning for the Identification of Preflare Spectroscopic Signatures

Magnus M. **Woods**1,2, Alberto Sainz Dalda1,2,3, and Bart De Pontieu2,4,5
2021 ApJ 922 137
https://iopscience.iop.org/article/10.3847/1538-4357/ac2667/pdf
https://doi.org/10.3847/1538-4357/ac2667
The study of the preflare environment is of great importance to understanding what drives solar flares. k-means clustering, an unsupervised machine-learning technique, has the ability to cluster large data set in a way that would be impractical or impossible for a human to do. In this paper we present a study using k-means clustering to identify possible preflare signatures in spectroscopic observations of the Mg ii h and k spectral lines made by NASA's Interface Region Imaging Spectrometer. Our analysis finds that spectral profiles showing single-peak Mg ii h and k and single-peaked emission in the Mg ii UV triplet lines are associated with preflare activity up to 40 minutes prior to flaring. Subsequent inversions of these spectral profiles reveal increased temperature and electron density in the chromosphere, which suggest that significant heating events in the chromosphere may be associated with precursor signals to flares.

Serial Flaring in an Active Region: Exploring Why Only One Flare Is Eruptive

Magnus M. **Woods**1,2,3,4, Satoshi Inoue2, Louise K. Harra1, Sarah A. Matthews1, and Kanya Kusano2
2020 ApJ **890** 84
https://iopscience.iop.org/article/10.3847/1538-4357/ab6bc8/pdf
Over a four hour period between **2014 June 12–13** a series of three flares were observed within AR 12087. This sequence of flares started with a non-eruptive M-class flare, followed by a non-eruptive C-class flare, and finally ended with a second C-class flare that had an associated filament eruption. In this paper we combine spectroscopic analysis of Interface Region Imaging Spectrometer observations of the Si iv line during the three flares along with a series of nonlinear force-free field (NLFFF) extrapolations in order to investigate the conditions that lead the final flare to be eruptive. From this analysis it is found to be unlikely that the eruption was triggered by either kink instability or by tether-cutting reconnection, allowing the flux rope to rise into a region where it would be susceptible to the torus instability. The NLFFF modeling does, however, suggest that the overlying magnetic field has a fan-spine topology, raising the possibility that breakout reconnection occurring during the first two flares weakened the overlying field, allowing the flux rope to erupt in the subsequent third flare.
HMI Science Nuggets #135 March **2020** http://hmi.stanford.edu/hminuggets/?p=3155

Observations and Modelling of the Pre-Flare Period of the 29 March 2014 X1 Flare

M. M. **Woods**, L. K. Harra, S. A.Matthews, D. H. Mackay, S. Dacie, D. M. Long
Solar Phys. 292:38 **2017**
https://arxiv.org/pdf/1701.06457v1.pdf
On the **29 March 2014** NOAA active region (AR) 12017 produced an X1 flare which was simultaneously observed by an unprecedented number of observatories. We have investigated the pre-flare period of this flare from 14:00 UT until 19:00 UT using joint observations made by the Interface Region Imaging Spectrometer (IRIS) and the Hinode Extreme

Ultraviolet Imaging Spectrometer (EIS). Spectral lines providing coverage of the solar atmosphere from chromosphere to the corona were analysed to investigate pre-flare activity within the AR. The results of the investigation have revealed evidence of strongly blue-shifted plasma flows, with velocities up to 200 km/s, being observed 40 minutes prior to flaring. These flows are located along the filament present in the active region and are both spatially discrete and transient. In order to constrain the possible explanations for this activity, we undertake non-potential magnetic field modelling of the active region. This modelling indicates the existence of a weakly twisted flux rope along the polarity inversion line in the region where a filament and the strong pre-flare flows are observed. We then discuss how these observations relate to the current models of flare triggering. We conclude that the most likely drivers of the observed activity are internal reconnection in the flux rope, early onset of the flare reconnection, or tether cutting reconnection along the filament.

See UKSP Nugget #77 **2017** http://www.uksolphys.org/uksp-nugget/77-just-before-an-x-class-flare/

IRIS Nugget **2021-08-10** https://iris.lmsal.com/nugget?cmd=view-pod&pubDate=2021-08-10 **2015-03-11**

New Solar Irradiance Measurements from the Miniature X-Ray Solar Spectrometer CubeSat

Thomas N. **Woods**, Amir Caspi, Phillip C. Chamberlin, Andrew Jones, Richard Kohnert, James Paul Mason, Christopher S. Moore, Scott Palo, Colden Rouleau, Stanley C. Solomon, Janet Machol, Rodney Viereck

ApJL **2016**

https://arxiv.org/pdf/1610.01936v1.pdf

The goal of the Miniature X-ray Solar Spectrometer (MinXSS) CubeSat is to explore the energy distribution of soft X-ray (SXR) emissions from the quiescent Sun, active regions, and during solar flares, and to model the impact on Earth's ionosphere and thermosphere. The energy emitted in the SXR range (0.1 to 10 keV) can vary by more than a factor of 100, yet we have limited spectral measurements in the SXRs to accurately quantify the spectral dependence of this variability. The MinXSS primary science instrument is an Amptek, Inc. X123 X-ray spectrometer that has an energy range of 0.5-30 keV with a nominal 0.15 keV energy resolution. Two flight models have been built. The first, MinXSS-1, has been making science observations since 2016 June 9, and has observed numerous flares, including 40 C-class and 7 M-class flares. These SXR spectral measurements have advantages over broadband SXR observations, such as providing the capability to derive multiple-temperature components and elemental abundances of coronal plasma, improved irradiance accuracy, and higher resolution spectral irradiance as input to planetary ionosphere simulations. MinXSS spectra obtained during the **M5.0 flare on 2016 July 23** highlight these advantages, and indicate how the elemental abundance changes from primarily coronal to more photospheric during the flare. MinXSS-1 observations are compared to the Geostationary Operational Environmental Satellite (GOES) X-Ray Sensor (XRS) measurements of SXR irradiance and estimated corona temperature. Additionally, a suggested improvement to the calibration of the GOES XRS data is presented.

New Solar Extreme-ultraviolet Irradiance Observations during Flares

Woods, Thomas N.; Hock, Rachel; Eparvier, Frank; Jones, Andrew R.; Chamberlin, Phillip C.; Klimchuk, James A.; Didkovsky, Leonid; Judge, Darrell; Mariska, John; Warren, Harry; Schrijver, Carolus J.; Webb, David F.; Bailey, Scott; Tobiska, W. Kent

Astrophysical Journal, Volume 739, Issue 2, article id. 59, 13 pp. (**2011**)

New solar extreme-ultraviolet (EUV) irradiance observations from the NASA Solar Dynamics Observatory (SDO) EUV Variability Experiment provide full coverage in the EUV range from 0.1 to 106 nm and continuously at a cadence of 10 s for spectra at 0.1 nm resolution and even faster, 0.25 s, for six EUV bands. These observations can be decomposed into four distinct characteristics during flares. First, the emissions that dominate during the flare's impulsive phase are the transition region emissions, such as the He II 30.4 nm. Second, the hot coronal emissions above 5 MK dominate during the gradual phase and are highly correlated with the GOES X-ray. A third flare characteristic in the EUV is coronal dimming, seen best in the cool corona, such as the Fe IX 17.1 nm. As the post-flare loops reconnect and cool, many of the EUV coronal emissions peak a few minutes after the GOES X-ray peak. *One interesting variation of the post-eruptive loop reconnection is that warm coronal emissions (e.g., Fe XVI 33.5 nm) sometimes exhibit a second large peak separated from the primary flare event by many minutes to hours, with EUV emission originating not from the original flare site and its immediate vicinity, but rather from a volume of higher loops. We refer to this second peak as the EUV late phase.* The characterization of many flares during the SDO mission is provided, including quantification of the spectral irradiance from the EUV late phase that cannot be inferred from GOES X-ray diagnostics.

Extreme Ultraviolet Late-Phase Flares: Before and During the Solar Dynamics Observatory Mission

Thomas N. **Woods**

Solar Phys., Volume 289, Issue 9, pp 3391-3401, **2014; File**
http://arxiv.org/pdf/1401.5811v1.pdf
The solar extreme-ultraviolet (EUV) observations from the Solar Dynamics Observatory (SDO) have revealed interesting characteristics of warm coronal emissions, such as Fe xvi 335 Å emission, which peak soon after the hot coronal X-ray emissions peak during a flare and then sometimes peak for a second time hours after the X-ray flare peak. This flare type, with two warm coronal emission peaks but only one X-ray peak, has been named the EUV late phase (Woods et al., Astrophys. J. 739, 59, 2011). These flares have the distinct properties of i) having a complex magnetic-field structure with two initial sets of coronal loops, with one upper set overlaying a lower set, ii) having an eruptive flare initiated in the lower set and disturbing both loop sets, iii) having the hot coronal emissions emitted only from the lower set in conjunction with the X-ray peak, and iv) having the first peak of the warm coronal emissions associated with the lower set and its second peak emitted from the upper set many minutes to hours after the first peak and without a second X-ray enhancement. The disturbance of the coronal loops by the eruption is at about the same time, but the relaxation and cooling down of the heated coronal loops during the post-flare reconnections have different time scales with the longer, upper loops being significantly delayed from the lower loops. The difference in these cooling time scales is related to the difference between the two peak times of the warm coronal emission and is also apparent in the decay profile of the X-ray emissions having two distinct decays, with the first decay slope being steeper (faster) and the delayed decay slope being smaller (slower) during the time of the warm-coronal-emission second peak. The frequency and relationship of the EUV late-phase decay times between the Fe xvi 335 Å two flare peaks and X-ray decay slopes are examined using three years of SDO/EUV Variability Experiment (EVE) data, and the X-ray dual-decay character is then exploited to estimate the frequency of EUV late-phase flares during the past four solar cycles. This study indicates that the frequency of EUV late-phase flares peaks before and after each solar-cycle minimum.
8 July 1996 , 4 May 2010, 24 December 2012

NEW SOLAR EXTREME-ULTRAVIOLET IRRADIANCE OBSERVATIONS DURING FLARES

Thomas N. **Woods**1,9, Rachel Hock1, Frank Eparvier1, Andrew R. Jones1, Phillip C. Chamberlin2, James A. Klimchuk2, Leonid Didkovsky3, Darrell Judge3, John Mariska4, Harry Warren4, Carolus J. Schrijver5, David F. Webb6, Scott Bailey7 and W. Kent Tobiska
2011 ApJ 739 59**, File**
New solar extreme-ultraviolet (EUV) irradiance observations from the NASA Solar Dynamics Observatory (SDO) EUV Variability Experiment provide full coverage in the EUV range from 0.1 to 106 nm and continuously at a cadence of 10 s for spectra at 0.1 nm resolution and even faster, 0.25 s, for six EUV bands. These observations can be decomposed into four distinct characteristics during flares. First, the emissions that dominate during the flare's impulsive phase are the transition region emissions, such as the He II 30.4 nm. Second, the hot coronal emissions above 5 MK dominate during the gradual phase and are highly correlated with the GOES X-ray. A third flare characteristic in the EUV is coronal dimming, seen best in the cool corona, such as the Fe IX 17.1 nm. As the post-flare loops reconnect and cool, many of the EUV coronal emissions peak a few minutes after the GOES X-ray peak. One interesting variation of the post-eruptive loop reconnection is that warm coronal emissions (e.g., Fe XVI 33.5 nm) sometimes exhibit a second large peak separated from the primary flare event by many minutes to hours, with EUV emission originating not from the original flare site and its immediate vicinity, but rather from a volume of higher loops. We refer to this second peak as the EUV late phase. The characterization of many flares during the SDO mission is provided, including quantification of the spectral irradiance from the EUV late phase that cannot be inferred from GOES X-ray diagnostics.

Microflare Heating of a Solar Active Region Observed with NuSTAR, Hinode/XRT, and SDO/AIA

Paul J. **Wright**, Iain G. Hannah, Brian W. Grefenstette, Lindsay Glesener, Säm Krucker, Hugh S. Hudson, David M. Smith, Andrew J. Marsh, Stephen M. White, Matej Kuhar
ApJ **2017**
https://arxiv.org/pdf/1706.06108.pdf
http://iopscience.iop.org/article/10.3847/1538-4357/aa7a59/pdf
NuSTAR is a highly sensitive focusing hard X-ray (HXR) telescope and has observed several small microflares in its initial solar pointings. In this paper, we present the first joint observation of a microflare with NuSTAR and Hinode/XRT on **2015 April 29** at ~11:29 UT. This microflare shows heating of material to several million Kelvin, observed in Soft X-rays (SXRs) with Hinode/XRT, and was faintly visible in Extreme Ultraviolet (EUV) with SDO/AIA. For three of the four NuSTAR observations of this region (pre-, decay, and post phases) the spectrum is well fitted by a single thermal model of 3.2-3.5 MK, but the spectrum during the impulsive phase shows additional emission up to 10 MK, emission equivalent to A0.1 GOES class. We recover the differential emission measure (DEM) using SDO/AIA, Hinode/XRT, and NuSTAR, giving unprecedented coverage in temperature. We find the pre-flare DEM peaks at ~3 MK and falls off sharply by 5 MK; but during the microflare's impulsive phase the emission above 3 MK is brighter and extends to 10 MK, giving a heating rate of about 2.5×1025 erg s−1. As the NuSTAR spectrum is purely thermal we determined upper-limits on the possible non-thermal bremsstrahlung emission. We find that for the accelerated electrons to be the source of the heating requires a power-law spectrum of $\delta \geq 7$ with a low energy cut-off

Ec≲7 keV. In summary, this first NuSTAR microflare strongly resembles much more powerful flares.
UK Solar Physics (UKSP) – Nuggets #84 **2017** www.uksolphys.org/?p=13616

Persistent Upflows and Downflows at Active Region boundaries Observed by SUTRI and AIA

Yuchuan **Wu**, Zhenyong Hou, Wenxian Li, Xianyong Bai, Yongliang Song, Xiao Yang, Ziyao Hu, Yuanyong Deng, Kaifan Ji

ApJ **965** 109 **2024**

https://arxiv.org/pdf/2403.07422.pdf

https://iopscience.iop.org/article/10.3847/1538-4357/ad3358/pdf

Upflows and downflows at active region (AR) boundaries have been frequently observed with spectroscopic observations at extreme ultraviolet (EUV) passbands. In this paper, we report the coexistence of upflows and downflows at the AR boundaries with imaging observations from the Solar Upper Transition Region Imager (SUTRI) and the Atmospheric Imaging Assembly (AIA). With their observations from **2022 September 21 to 2022 September 30**, we find 17 persistent opposite flows occurring along the AR coronal loops. The upflows are prominent in the AIA 193 Åimages with a velocity of 50-200 km/s, while the downflows are best seen in the SUTRI 465 Åand AIA 131 Åimages with a slower velocity of tens of kilometers per second (characteristic temperatures (log T(K)) for 193 Å, 465 Åand 131 Åare 6.2, 5.7, 5.6, respectively). We also analyze the center-to-limb variation of the velocities for both upflows and downflows. The simultaneous observations of downflows and upflows can be explained by the chromosphere-corona mass-cycling process, in which the localized chromospheric plasma is impulsively heated to coronal temperature forming a upflow and then these upflows experience radiative cooling producing a downflow with the previously heated plasma returning to the lower atmosphere. In particular, the persistent downflows seen by SUTRI provide strong evidence of the cooling process in the mass cycle. For upflows associated with open loops, part of the plasma is able to escape outward and into the heliosphere as solar wind.

Highly Energetic Electrons Accelerated in Strong Solar Flares as a Preferred Driver of Sunquakes

H. **Wu**, Y. Dai, M. D. Ding

ApJL **943** L6 **2023**

https://arxiv.org/pdf/2301.02865.pdf

https://iopscience.iop.org/article/10.3847/2041-8213/acb0d1/pdf

Sunquakes are enhanced seismic waves excited in some energetic solar flares. Up to now, their origin has still been controversial. In this Letter, we select and study 20 strong flares in Solar Cycle 24, whose impulse phase is fully captured by the \emph{Reuven Ramaty High Energy Solar Spectroscopic Imager} (\emph{RHESSI}). For 11 out of 12 sunquake-active flares in our sample, the hard X-ray (HXR) emission shows a good temporal and spatial correlation with the white-light (WL) enhancement and the sunquake. Spectral analysis also reveals a harder photon spectrum that extends to several hundred keV, implying a considerable population of flare-accelerated nonthermal electrons at high energies. Quantitatively, the total energy of electrons above 300 keV in sunquake-active flares is systematically different from that in sunquake-quiet flares, while the difference is marginal for electrons above 50 keV. All these facts support highly energetic electrons as a preferred driver of the sunquakes. Such an electron-driven scenario can be reasonably accommodated in the framework of a recently proposed selection rule for sunquake generation. For the remaining one event, the sunquake epicenter is cospatial with a magnetic imprint, i.e., a permanent change of magnetic field on the photosphere. Quantitative calculation shows that the flare-induced downward Lorentz force can do enough work to power the sunquake, acting as a viable sunquake driver for this specific event. **9 Aug 2011, 24 Sep 2011, 2012 October 23, 27 Oct 2014,**

Table 1. List of the Flares under study and the Sunquake Information 2011-2017

On the origin of hard X-ray emissions from the behind-the-limb flare on 2014 September 1

Yihong **Wu**, Alexis P. Rouillard, Athanasios Kouloumvakos, Rami Vainio, Alexandr N. Afanasiev, Illya Plotnikov, Ronald J. Murphy, Gottfried J. Mann, Alexander Warmuth

ApJ **909** 163 **2021**

https://arxiv.org/pdf/2101.05401.pdf

https://doi.org/10.3847/1538-4357/abdc20

The origin of hard X-rays and gamma-rays emitted from the solar atmosphere during occulted solar flares is still debated. The hard X-ray emissions could come from flaring loop tops rising above the limb or Coronal Mass Ejections (CME) shock waves, two by-products of energetic solar storms. For the shock scenario to work, accelerated particles must be released on magnetic field lines rooted on the visible disk and precipitate. We present a new Monte Carlo code that computes particle acceleration at shocks propagating along large coronal magnetic loops. A first implementation of the model is carried out for the **2014 September 1** event and the modeled electron spectra are compared with those inferred from Fermi Gamma-ray Burst Monitor (GBM) measurements. When particle diffusion processes are invoked our model can reproduce the hard electron spectra measured by GBM nearly ten minutes after the estimated on-disk hard X-rays appear to have ceased from the flare site.

Microwave imaging of a hot flux rope structure during the pre-impulsive stage of an eruptive M7.7 solar flare

Z. **Wu**, Y. Chen, G. Huang, H. Nakajima, H. Song, V. Melnikov, W. Liu, G. Li, K. Chandrashekhar, F. Jiao
ApJL 820 L29 **2016**
http://arxiv.org/pdf/1603.02777v1.pdf

Corona structures and processes during the pre-impulsive stage of solar eruption are crucial to understanding the physics leading to the subsequent explosive energy release. Here we present the first microwave imaging study of a hot flux rope structure during the pre-impulsive stage of an eruptive M7.7 solar flare, with the Nobeyama Radioheliograph (NoRH) at 17 GHz. The flux rope is also observed by the SDO/AIA in its hot passbands of 94 and 131 \AA\. In the microwave data, it is revealed as an overall arcade-like structure consisting of several intensity enhancements bridged by generally weak emissions, with brightness temperatures (TB) varying from ~10,000~K to ~20,000 K. Locations of microwave intensity enhancements along the structure remain relatively fixed at certain specific parts of the flux rope, indicating that the distribution of emitting electrons is affected by the large scale magnetic configuration of the twisted flux rope. Wavelet analysis shows a pronounced 2-min period of the microwave TB variation during the pre-impulsive stage of interest. The period agrees well with that reported for AIA sunward-contracting loops and upward ejective plasmoids (suggested to be reconnection outflows). This suggests that both periodicities are controlled by the same reconnection process that takes place intermittently at a 2-min time scale. We infer that at least a part of the emission is excited by non-thermal energetic electrons via the gyro-synchrotron mechanism. The study demonstrates the potential of microwave imaging in exploring the flux rope magnetic geometry and relevant reconnection process during the onset of solar eruption. **19 July 2012**

Research Note

Electron acceleration in the turbulent reconnecting current sheets in solar flares

G. P. **Wu**1 and G. L. Huang2
A&A 502, 341-344 (**2009**)
DOI: 10.1051/0004-6361/200811494

Context. We investigate the nonlinear evolution of the electron distribution in the presence of the strong inductive electric field in the reconnecting current sheets (RCS) of solar flares.
Aims. We aim to study the characteristics of nonthermal electron-beam plasma instability and its influence on electron acceleration in RCS.
Methods. Including the external inductive field, the one-dimensional Vlasov simulation is performed with a realistic mass ratio for the first time.
Results. Our principal findings are as follows: 1) the Buneman instability can be quickly excited on the timescale of 10^{-7} s for the typical parameters of solar flares. After saturation, the beam-plasma instabilities are excited due to the non-Maxwellian electron distribution; 2) the final velocity of the electrons trapped by these waves is of the same order as the phase speed of the waves, while the untrapped electrons continue to be accelerated; 3) the inferred anomalous resistance of the current sheet and the energy conversion rate are basically of the same order as those previously estimated, e.g., “the analysis of Martens”.
Conclusions. The Buneman instability is excited on the timescale of 10^{-7} s and the wave-particle resonant interaction limits the low-energy electrons to be further accelerated in RCS.

Is Flare Ribbon Fine Structure Related to Tearing in the Flare Current Sheet?

P. F. **Wyper**1 and D. I. Pontin2,3
2021 ApJ 920 102
https://iopscience.iop.org/article/10.3847/1538-4357/ac1943/pdf
https://doi.org/10.3847/1538-4357/ac1943
https://arxiv.org/pdf/2108.10966.pdf

Observations of solar flare ribbons show significant fine structure in the form of breaking wavelike perturbations and spirals. The origin of this structure is not well understood, but one possibility is that it is related to the tearing instability in the flare current sheet. Here we study this connection by constructing an analytical 3D magnetic field representative of an erupting flux rope with a flare current sheet below it. We introduce small-scale flux ropes representative of those formed during a tearing instability in the current layer, and use the squashing factor on the solar surface to identify the shape of the presumed flare ribbons and fine structure. Our analysis suggests there is a direct link between flare ribbon fine structure and flare current sheet tearing, with the majority of the ribbon fine structure related to oblique tearing modes. Depending upon the size, location, and twist of the small-scale flux ropes, breaking wavelike and spiral features within the hooks and straight sections of the flare ribbon can be formed that are qualitatively similar to observations. We also show that the handedness of the spirals/waves must be the same as the handedness of the hooks of the main ribbon. We conclude that tearing in the flare current layer is a likely explanation for spirals and wavelike features in flare ribbons. **2014 September 10**

THREE-DIMENSIONAL SIMULATIONS OF TEARING AND INTERMITTENCY IN CORONAL JETS

P. F. **Wyper**1, C. R. DeVore2, J. T. Karpen2, and B. J. Lynch

2016 ApJ 827 4

Observations of coronal jets increasingly suggest that local fragmentation and intermittency play an important role in the dynamics of these events. In this work, we investigate this fragmentation in high-resolution simulations of jets in the closed-field corona. We study two realizations of the embedded-bipole model, whereby impulsive helical outflows are driven by reconnection between twisted and untwisted field across the domed fan plane of a magnetic null. We find that the reconnection region fragments following the onset of a tearing-like instability, producing multiple magnetic null points and flux-rope structures within the current layer. The flux ropes formed within the weak-field region in the center of the current layer are associated with "blobs" of density enhancement that become filamentary threads as the flux ropes are ejected from the layer, whereupon new flux ropes form behind them. This repeated formation and ejection of flux ropes provides a natural explanation for the intermittent outflows, bright blobs of emission, and filamentary structure observed in some jets. Additional observational signatures of this process are discussed. Essentially all jet models invoke reconnection between regions of locally closed and locally open field as the jet-generation mechanism. Therefore, we suggest that this repeated tearing process should occur at the separatrix surface between the two flux systems in all jets. A schematic picture of tearing-mediated jet reconnection in three dimensions is outlined.

Spine-fan reconnection
The influence of temporal and spatial variation in the driver

P. F. **Wyper**1, R. Jain1 and D. I. Pontin

A&A 545, A78 (**2012**)

Context. From observations, the atmosphere of the Sun has been shown to be highly dynamic with perturbations of the magnetic field often lacking temporal or spatial symmetry. Despite this, studies of the spine-fan reconnection mode at 3D nulls have so far focused on the very idealised case with symmetric driving of a fixed spatial extent.

Aims. We investigate the spine-fan reconnection process for less idealised cases, focusing on asymmetric driving and drivers with different length scales. We look at the initial current sheet formation and whether the scalings developed in the idealised models are robust in more realistic situations.

Methods. The investigation was carried out by numerically solving the resistive compressible 3D magnetohydrodynamic equations in a Cartesian box containing a linear null point. The spine-fan collapse was driven at the null through tangential boundary driving of the spine foot points.

Results. We find significant differences in the initial current sheet formation with asymmetric driving. Notable is the displacement of the null point position as a function of driving velocity and resistivity (η). However, the scaling relations developed in the idealised case are found to be robust (albeit at reduced amplitudes) despite this extra complexity. Lastly, the spatial variation is also shown to play an important role in the initial current sheet formation through controlling the displacement of the spine foot points.

Conclusions. We conclude that during the early stages of spine-fan reconnection both the temporal and spatial nature of the driving play important roles, with the idealised symmetrically driven case giving a “best case” for the rate of current development and connectivity change. As the most interesting eruptive events occur in relatively short time frames this work clearly shows the need for high temporal and spatial knowledge of the flows for accurate interpretation of the reconnection scenario. Lastly, since the scalings developed in the idealised case remain robust with more complex driving we can be more confident of their use in interpreting reconnection in complex magnetic field structures.

A New Solar Hard X-ray Image Reconstruction Algorithm for ASO-S/HXI Based on Deep Learning.

Xia, Y., Su, Y., Liu, H. et al.

Sol Phys 299, 158 (**2024**).

https://doi.org/10.1007/s11207-024-02399-4

Most solar hard X-ray (HXR) imagers in the past and current solar missions obtain X-ray images via Fourier transform imaging technology, which requires proper imaging algorithms to reconstruct images from spatially-modulated or temporally-modulated signals. A variety of algorithms have been developed during the last 50 years for the characteristics of respective instruments. In this work, we present a new imaging algorithm developed based on deep learning for the Hard X-ray Imager (HXI) onboard the Advanced Space-based Solar Observatory (ASO-S) and the preliminary test results of the algorithm with both simulated data and observations. We first created a training dataset by obtaining modulation data from simulated HXR images of single, double and loop-shaped sources, respectively, and the patterns of HXI sub-collimators. Then, we introduced machine-learning algorithm to develop a pattern-based deep learning network model: HXI_DLA, which can directly produce an image from modulation counts. After training the model with simple sources, we tested DLA for simple sources, extended sources, and double sources for imaging dynamic range. Finally, we compared CLEAN and DLA images reconstructed from HXI observations of three flares. Overall, these imaging tests revealed that the current HXI_DLA method produces comparable image result to those

from the widely used imaging method CLEAN. In some cases, DLA images are even slightly better. Besides, HXI_DLA is super fast for imaging and parameter-free. Although this is only the first step towards a fully developed and practical DLA method, the tests have shown the potential of deep learning in the field of solar hard X-ray imaging.

Plasma heating and nanoflare caused by slow-mode wave in a coronal loop

Fanxiaoyu **Xia**, Tongjiang Wang, Yang Su, Jie Zhao, Qingmin Zhang, Astrid M. Veronig, Weiqun Gan
ApJL **936** L13 **2022**
https://arxiv.org/pdf/2208.10029.pdf
https://iopscience.iop.org/article/10.3847/2041-8213/ac8afe/pdf
We present a detailed analysis of a reflecting intensity perturbation in a large coronal loop that appeared as sloshing oscillation and lasted for at least one and a half periods. The perturbation is initiated by a microflare at one footpoint of the loop, propagates along the loop and is eventually reflected at the remote footpoint where significant brightenings are observed in all the AIA extreme-ultraviolet (EUV) channels. This unique observation provides us with the opportunity to better understand not only the thermal properties and damping mechanisms of the sloshing oscillation, but also the energy transfer at the remote footpoint. Based on differential emission measures (DEM) analysis and the technique of coronal seismology, we find that 1) the calculated local sound speed is consistent with the observed propagation speed of the perturbation during the oscillation, which is suggestive of a slow magnetoacoustic wave; 2) thermal conduction is the major damping mechanism of the wave but additional damping mechanism such as anomalous enhancement of compressive viscosity or wave leakage is also required to account for the rapid decay of the observed waves; 3) the wave produced a nanoflare at the remote footpoint, with a peak thermal energy of ∼1024−1025 erg. This work provides a consistent picture of the magnetoacoustic wave propagation and reflection in a coronal loop, and reports the first solid evidence of a wave-induced nanoflare. The results reveal new clues for further simulation studies and may help solving the coronal heating problem. **2014 June 10**

Detection of Energy Cutoffs in Flare-accelerated Electrons

Fanxiaoyu **Xia**1,2, Yang Su1,2, Wen Wang3, Linghua Wang3, Alexander Warmuth4, Weiqun Gan1,2, and Youping Li1,2
2021 ApJ 908 111
https://iopscience.iop.org/article/10.3847/1538-4357/abce5c/pdf
Energy cutoffs in electron distribution define the lower and upper limits on the energy range of energetic electrons accelerated in solar flares. They are crucial parameters for understanding particle acceleration processes and energy budgets. Their signatures have been reported in studies of flattened flare X-ray spectra, i.e., the impulsive emission of nonthermal bremsstrahlung from energetic electrons impacting ambient, thermal plasma. However, these observations have not provided unambiguous constraints on the cutoffs. Moreover, other processes may result in similar spectral features. Even the existence and necessity of cutoffs as physical parameters of energetic electrons have been under debate. Here we report a search for their signatures in flare-accelerated electrons with two approaches, i.e., in both X-ray spectra and solar energetic particle (SEP) events. These represent two different electron populations, but may contain information of the same acceleration process. By studying a special group of late impulsive flares, and a group of selected SEP events, we found evidence of cutoffs revealed in both X-ray spectra and SEP electron distributions. In particular, we found for the first time consistent low- and high-energy cutoffs in both hard X-ray-producing and escaping electrons in two events. We also showed the importance of high-energy cutoff in studies of spectral shapes. These results provide evidence of cutoffs in flare-accelerated energetic electrons and new clues for constraining electron distribution parameters and particle acceleration models. **23 Oct 2003, 14 Aug 2004, 7 Nov 2004, 6 Dec 2006, 18 Nov 2012, 16 Apr 2015**
Table 1 Late Impulsive X-Ray Bursts and Two Selected SEP-related Flare Events (2002-2015)

PARTICLE ACCELERATION AND TRANSPORT DURING 3D CME ERUPTIONS

Qian **Xia**,1 Joel T. Dahlin,2 , ∗ Valentina Zharkova,1 and Spiro K. Antiochos3
ApJ **2020**
https://solargsm.com/wp-content/uploads/2020/04/xia_etal_ArmTP_apj2020.pdf
We calculate particle acceleration during corona mass ejection (CME) eruptions using combined magnetohydrodynamic (MHD) and test-particle models. The 2.5D/3D CMEs are generated via the breakout mechanism. In this scenario a reconnection at the “breakout” current sheet (CS) above the flux rope initiates the CME eruption by destabilizing a quasi-static force balance. Reconnection at the flare CS below the erupting flux rope drives the fast acceleration of the CME, which forms flare loops below and produces the energetic particles observed in flares. For test-particle simulations, two times are selected during the impulsive and decay phases of the eruption. Particles are revealed to be accelerated more efficiently in the flare CS rather than in the breakout CS even in the presence of large magnetic islands. Particles are first accelerated in the CSs (with or without magnetic islands) by the reconnection electric field mainly through particle curvature drift. We find, as expected, that accelerated particles precipitate into the chromosphere, or become trapped in the loop top by magnetic mirrors, or escape to interplanetary space along open field lines. Some trapped particles are reaccelerated, either via reinjection to the flare CS or through a local Betatron-

type acceleration associated with compression of the magnetic field. The energetic particles produce relatively hard energy spectra during the impulsive phase. During the gradual phase, the relaxation of magnetic field shear reduces the guiding field in the flare CS, which leads to a decrease in particle energization efficiency. Important implications of our results for observations of particle acceleration in the solar coronal jets are also discussed.

Particle acceleration in coalescent and squashed magnetic islands II. Particle-In-cell approach

Q.**Xia** and V. Zharkova

A&A 635, A116 **2020**

http://mpee.northumbria.ac.uk/staff/slmv5/kinetics/AA_islands_PIC_2col_accept2020.pdf

https://doi.org/10.1051/0004-6361/201936420

Aims. Particles are known to have efficient acceleration in reconnecting current sheets with multiple magnetic islands, formed during a reconnection process. Using test particle approach, the recent investigation of particle dynamics in 3D magnetic islands, or current sheets with multiple X- and O-null points revealed that the particle energy gains are higher in squashed magnetic islands than in coalescent ones. However, this approach did not consider the ambient plasma feedback to the presence of accelerated particles, which a□ects their distributions within the acceleration region.
Methods. In the current paper, we use the particle-in-cell (PIC) approach to investigate further particle acceleration in 3D Harris-type reconnecting current sheets with coalescent (merging) and squashed (contracting) magnetic islands with different magnetic field topologies, ambient densities ranging 10^8 - 10^{12} m^3, proton-to-electron mass ratios, and island aspect ratios.
Results. In current sheets with single or multiple X-nullpoints, accelerated particles of opposite charges are separated and ejected into the opposite semiplanes from the current sheet midplane, generating a strong polarisation electric field across a current sheet. Particles of the same charge form two populations: transit and bounced particles, with very different energy and asymmetric pitch-angle distributions, which can be distinguished from observations. In some cases the difference in energy gains by transit and bounced particles leads to turbulence generated by Buneman instability. In magnetic island topology, the different reconnection electric fields in squashed and coalescent islands impose different particle drift motions. This makes particle acceleration more efficient in squashed magnetic islands than in coalescent ones. The spectral indices of electron energy spectra are 4.2 for coalescent and 4.0 for squashed islands, which are lower than reported from the test-particle approach. The particles accelerated in magnetic islands are found trapped in the midplane of squashed islands, and shifted as clouds towards the X-nullpoints in coalescent ones.
Conclusions. In reconnecting current sheets with multiple X- and O-nullpoints particles are found accelerated on a much shorter spatial scale and gain higher energies than near a single X-nullpoint. The distinct density and pitch- angle distributions of particles with high and low energy detected with the PIC approach can help to distinguish the observational features of accelerated particles.

Particle acceleration in coalescent and squashed magnetic islands I. Test particle approach

Q.**Xia** and V. Zharkova

A&A **2018**

http://computing.unn.ac.uk/staff/slmv5/kinetics/xia_zharkova_islands_TP_aa18.pdf

Aims. Magnetic reconnection in large Harris-type reconnecting current sheets (RCSs) with a single X-nullpoint often leads to occurrence of magnetic islands with multiple O- and X-nullpoints. Over time these magnetic islands become squashed, or coalescent with two islands merging, as it has been observed indirectly during coronal mass ejection and by in-situ observations in the heliosphere and magnetotail. These points emphasize the importance of understanding the basic energising processes of ambient particles dragged into current sheets with magnetic islands of different configuration.
Methods. Trajectories of protons and electrons accelerated by a reconnection electric field are investigated using a test particle approach in RCSs with different 3D magnetic field topologies defined analytically for multiple X- and O-nullpoints. Trajectories, densities and energy distributions are explored for 106 thermal particles dragged into the current sheets from different sides and distances.
Results. This study confrms that protons and electrons accelerated in magnetic islands in a presence of strong guiding field are ejected from a current sheet into the opposite semiplanes with respect to its midplane. Particles are found to escape O-nullpoints only through the neighbouring X-nullpoints along (not across) the midplane following the separation law for electrons and protons in a given magnetic topology. Particles gain energy either inside O-nullpoints or in a vicinity of X-nullpoints that often leads to electron clouds formed about the X-nullpoint between the O-nullpoints. Electrons are shown to be able to gain sub-relativistic energies in a single magnetic island. Energy spectra of accelerated particles are close to power laws with spectral indices varying from 1.1 to 2.4. The more squashed the islands the larger the difference between the energy gains by transit and bounced particles. Their energy spectra are often with double maxima leading to fast growing turbulence.
Conclusions. Particles are shown to gain most energy in multiple X-nullpoints between O-nullpoints (or magnetic islands). This leads to a formation of electron clouds between magnetic islands. Particle energy gains are much larger in squashed islands than in coalescent ones. In summary, particle acceleration by a reconnection electric field in magnetic islands is much more effective than in an RCS with a single X-nullpoint.

The data center for the Spectrometer and Telescope for Imaging X-rays (STIX) on board Solar Orbiter https://datacenter.stix.i4ds.net/stix

Hualin **Xiao**1, Shane Maloney2, Säm Krucker1, Ewan Dickson3, Paolo Massa4, Erica Lastufka1, Andrea Francesco Battaglia1,5, László Etesi1, Nicky Hochmuth6, Frédéric Schuller7, Daniel F. Ryan1, Olivier Limousin8, Hannah Collier1,5, Alexander Warmuth7 and Michele Piana9,10
A&A 673, A142 (**2023**)
https://www.aanda.org/articles/aa/pdf/2023/05/aa46031-23.pdf
Context. The Spectrometer and Telescope for Imaging X-rays (STIX) on board Solar Orbiter observes solar X-ray emission in the range of 4–150 keV and produces spectra and images of solar flares over a wide range of flare magnitudes. During nominal operation, STIX continuously generates data. A constant data flow requires fully automated data-processing pipelines to process and analyze the data, and a data platform to manage, visualize, and distribute the data products to the scientific community.
Aims. The STIX Data Center has been built to fulfill these needs. In this paper, we outline its main components to help the community better understand the tools and data it provides.
Methods. The STIX Data Center is operated at the University of Applied Sciences and Arts Northwestern Switzerland (FHNW) and consists of automated processing pipelines and a data platform. The pipelines process STIX telemetry data, perform common analysis tasks, and generate data products at different processing levels. They have been designed to operate fully automatically with minimal human intervention. The data platform provides web-based user interfaces and application programmable interfaces for searching and downloading STIX data products.
Results. The STIX Data Center has been operating successfully for more than two years. The platform facilitates instrument operations and provides vital support to STIX data users. 7 Oct 2022, 26 Jan 2023
https://datacenter.stix.i4ds.net/stix

Probing turbulence in solar flares from SDO/AIA emission lines

Xiaoyan **Xie**1 Gang Li2* Katharine K. Reeves11
Front. Astron. Space Sci. Volume 11 : 1383746 **2024** |
https://doi.org/10.3389/fspas.2024.1383746
https://www.frontiersin.org/journals/astronomy-and-space-sciences/articles/10.3389/fspas.2024.1383746/full
Multiple pieces of evidence have revealed the important role of turbulence in physical processes in solar eruptions, from particle acceleration to the suppression of conductive cooling. Radio observations of density variation have established a Kolmogorov-like spectrum for solar wind density disturbance. Close to the Sun, measurements from extreme ultraviolet (EUV) bands have been used to examine turbulence in the solar atmosphere. The Atmospheric Imaging Assembly onboard the Solar Dynamics Observatory (SDO/AIA) has been frequently used for diagnosing plasma properties due to its complex coverage of temperature response. We compute structure functions (SFs) using SDO/AIA emission measurements for two example of plasma sheets. With the relationship
of $v \sim b \sim \delta n$ and $\delta I \sim \delta(n0+\delta n)2 \sim \delta n \delta I \sim \delta(n0+\delta n)2 \sim \delta n$ (v, b, δn, and δI are turbulent velocity, magnetic field, number density, and intensity, respectively, and n0 is the background density), SFs of δI can be regarded as a proxy for those of the turbulent v and b fields in the plasma sheet. We show that by properly accounting for the radial dependence of the emission line intensity, an SF method is capable of probing the presence of turbulence from SDO/AIA emission lines. Compared to in situ observations, performing SFs on EUV emissions is advantageous in studying turbulence behavior in the wave-vector space, and it opens a new window for investigating turbulence from massive SDO/AIA observations.

Statistical Study of the Kinetic Features of Supra-arcade Downflows Detected from Multiple Solar Flares

Xiaoyan **Xie**1,2,3, Katharine K. Reeves2, Chengcai Shen2, and Joshua D. Ingram4,2
2022 ApJ 933 15
https://iopscience.iop.org/article/10.3847/1538-4357/ac695d/pdf
We have developed a tracking algorithm to determine the speeds of supra-arcade downflows (SADs) and set up a system to automatically track SADs and measure some interesting parameters. By conducting an analysis of six flares observed by the Atmospheric Imaging Assembly on the Solar Dynamics Observatory, we detect more smaller and slower SADs than prior work, due to the higher spatial resolution of our observational data. The inclusion of these events with smaller and slower SADs directly results in lower median velocities and widths than in prior work, but the fitted distributions and evolutions of the parameters still show good consistency with prior work. The observed distributions of the widths, speeds, and lifetimes of SADs are consistent with log-normal distributions, indicating that random and unstable processes are responsible for generating SADs during solar eruptions. Also, we find that the fastest SADs occur at approximately the middle of the height ranges. The number of SADs in each image versus time shows that there are "rest phases" of SADs, when few SADs are seen. These findings support the idea that SADs originate from a fluid instability. We compare our results with a numerical simulation that generates SADs using a mixture of the Rayleigh–Taylor instability and the Richtmyer–Meshkov instability, and find that the simulation generates quantities

that are consistent with our observational results. **2011 Oct 22, 2012 Jan 16, 2012 Jan 27, 2012 Jul 17, 2013 May 22, 2015 Jun 18,**
Table 1 Basic Information about the Flares Examined in This Study,

Numerical experiments on dynamic evolution of a CME-flare current sheet

Xiaoyan **Xie**, Zhixing Mei, Chengcai Shen, Qiangwei Cai, Jing Ye, Katharine K Reeves, Ilia I Roussev, Jun Lin
MNRAS Volume 509, Issue 1, January **2022**, Pages 406–420,
https://doi.org/10.1093/mnras/stab2954
In this paper, we performed magnetohydrodynamics numerical experiments to look into the dynamic behaviour of the current sheet (CS) between the coronal mass ejection (CME) and the associated solar flare, especially the CS oscillation and plasmoid motions in coronal conditions. During the evolution, the disrupting magnetic configuration becomes asymmetric first in the buffer region at the bottom of the CME bubble. The Rayleigh−Taylor instability in the buffer region and the deflected motion of the plasma driven by the termination shock at the bottom of the CME bubble cause the buffer region to oscillate around the y-axis. The local oscillation propagates downwards through the CS, prompting an overall CS oscillation. As the buffer region grows, the oscillation period becomes longer, increasing from about 30 s to about 16 min. Meanwhile, there is another separated oscillation with a period between 0.25 and 1.5 min in the cusp region of the flare generated by velocity shearing. The tearing mode instability yields formations of plasmoids inside the CS. The motions of all the plasmoids observed in the experiment accelerate, which implies that the large-scale CME/flare CS itself in the true eruptive event is filled with the diffusion region according the the standard theory of magnetic reconnection.

Study of Ribbon Separation and Magnetic Reconnection Rates in a Two-Ribbon Flare

W. **Xie**, H. Zhang, H. Wang
Solar Physics, Volume 254 Number 2, Page: 271 – 283, **2009**
In this paper, we present a study of the correlation between the speed of flare ribbon separation and the magnetic flux density during the **10 April 2001** solar flare. The study includes the section of the neutral line containing the flare core and its peripheral area. This event shows clear two-ribbon structure and inhomogeneous magnetic fields along the ribbons, so the spatial correlation and distribution of the flare and magnetic parameters can be studied. A weak negative correlation is found between the ribbon separation speed (V_r) and the longitudinal magnetic flux density (B_z). This correlation is the weakest around the peak of the flare. Spatially, the correlation is also weakest at the positions of the hard X-ray (HXR) sources. In addition, we estimate the magnetic reconnection rate (electric field strength in the reconnection region E_{rec}) by combining the speed of flare ribbons and the longitudinal magnetic flux density. During flare evolution, the time profiles of the magnetic reconnection rate are similar to that of the ribbon separation speed, and the speeds of ribbon separation are relatively slow in the strong magnetic fields (*i.e.*, V_r is negatively correlated with B_z). However, along the flare ribbons, E_{rec} fluctuates in a small range except near the HXR source. A localized enhancement of the reconnection rate corresponds to the position of the HXR source.

Extreme Red-wing Enhancements of UV Lines During the 2022 March 30 X1.3 Solar Flare

Yan **Xu**, Graham S. Kerr, Vanessa Polito, Nengyi Huang, Ju Jing, Haimin Wang
ApJ **958** 67 **2023**
https://arxiv.org/pdf/2309.05745.pdf
https://iopscience.iop.org/article/10.3847/1538-4357/acf8c6/pdf
Here we present the study of a compact emission source during an X1.3 flare on **2022-March-30**. Within a ∼41∼s period (17:34:48 UT to 17:35:29 UT), IRIS observations show spectral lines of Mg II, C II and Si IV with extremely broadened, asymmetric red-wings. This source of interest (SOI) is compact, ∼ 1\arcsec.6, and is located in the wake of a passing ribbon. Two methods were applied to measure the Doppler velocities associated with these red wings: spectral moments and multi-Gaussian fits. The spectral moments method considers the averaged shift of the lines, which are 85 km s−1, 125 km s−1 and 115 km s−1 for the Mg II, C II and Si IV lines respectively. The red-most Gaussian fit suggests a Doppler velocity up to ∼160 km s−1 in all of the three lines. Downward mass motions with such high speeds are very atypical, with most chromospheric downflows in flares on the order 10-100 km s−1. Furthermore, EUV emission is strong within flaring loops connecting two flare ribbons located mainly to the east of the central flare region. The EUV loops that connect the SOI and its counterpart source in the opposite field are much less brightened, indicating that the density and/or temperature is comparatively low. These observations suggest a very fast downflowing plasma in transition region and upper chromosphere, that decelerates rapidly since there is no equivalently strong shift of the O I chromospheric lines. This unusual observation presents a challenge that models of the solar atmosphere's response to flares must be able to explain.
IRIS Nugget # Sep **2023** https://iris.lmsal.com/nugget

Multi-Passband Observations of A Solar Flare over the He I 10830 Å line

Yan **Xu**, Xu Yang, Graham S. Kerr, Vanessa Polito, Viacheslav M. Sadykov, Ju Jing, Wenda Cao, Haimin Wang
ApJ Letters **924** L18 **2022**
https://arxiv.org/pdf/2112.09949.pdf
https://iopscience.iop.org/article/10.3847/2041-8213/ac447c/pdf
https://doi.org/10.3847/2041-8213/ac447c
This study presents a C3.0 flare observed by the BBSO/GST and IRIS, on **2018-May-28** around 17:10 UT. The Near Infrared Imaging Spectropolarimeter (NIRIS) of GST was set to spectral imaging mode to scan five spectral positions at ± 0.8 Å, ± 0.4 Åand line center of He I 10830. At the flare ribbon's leading edge the line is observed to undergo enhanced absorption, while the rest of the ribbon is observed to be in emission. When in emission, the contrast compared to the pre-flare ranges from about 30 % to nearly 100 % at different spectral positions. Two types of spectra, "convex" shape with higher intensity at line core and "concave" shape with higher emission in the line wings, are found at the trailing and peak flaring areas, respectively. On the ribbon front, negative contrasts, or enhanced absorption, of about ∼10%−20% appear in all five wavelengths. This observation strongly suggests that the negative flares observed in He I 10830 with mono-filtergram previously were not caused by pure Doppler shifts of this spectral line. Instead, the enhanced absorption appears to be a consequence of flare energy injection, namely non-thermal collisional ionization of helium caused by the precipitation of high energy electrons, as found in our recent numerical modeling results. In addition, though not strictly simultaneous, observations of Mg II from the IRIS spacecraft, show an obvious central reversal pattern at the locations where enhanced absorption of He I 10830 is seen, which is in consistent with previous observations.

Transient rotation of photospheric vector magnetic fields associated with a solar flare

Yan **Xu**, Wenda Cao, Kwangsu Ahn, Ju Jing, Chang Liu, Jongchul Chae, Nengyi Huang, Na Deng, Dale E. Gary, Haimin Wang
Nature Communications **2018**
https://www.nature.com/articles/s41467-017-02509-w.pdf
https://arxiv.org/pdf/1801.03171.pdf
As one of the most violent eruptions on the Sun, flares are believed to be powered by magnetic reconnection. The fundamental physics involving the release, transfer and deposition of energy have been studied extensively. Taking advantage of the unprecedented resolution provided by the 1.6-m Goode Solar Telescope, here we show a sudden rotation of vector magnetic fields, about 12∘-20∘ counterclockwise, associated with a flare. Unlike the permanent changes reported previously, the azimuth-angle change is transient and co-spatial/temporal with Hα emission. The measured azimuth angle becomes closer to that in potential fields suggesting untwist of flare loops. The magnetograms were obtained in the near infrared at 1.56~μm, which is minimally affected by flare emission and no intensity profile change was detected. We believe that these transient changes are real and discuss the possible explanations in which the high energy electron beams or Alfve´n waves play a crucial role. **June 22, 2015**

Homologous Circular-ribbon Flares Driven by Twisted Flux Emergence

Z. **Xu**1, K. Yang2, Y. Guo2, J. Zhao3, Z. J. Zhao1, and L. Kashapova
2017 ApJ 851 30
http://sci-hub.tw/10.3847/1538-4357/aa9995
In this paper, we report two homologous circular-ribbon flares associated with two filament eruptions. They were well observed by the New Vacuum Solar Telescope and the Solar Dynamics Observatory on **2014 March 5**. Prior to the flare, two small-scale filaments enclosed by a circular pre-flare brightening lie along the circular polarity inversion line around the parasitic polarity, which has shown a continuous rotation since its first appearance. Two filaments eventually erupt in sequence associated with two homologous circular-ribbon flares and display an apparent writhing signature. Supplemented by the nonlinear force-free field extrapolation and the magnetic field squashing factor investigation, the following are revealed. (1) This event involves the emergence of magnetic flux ropes into a pre-existing polarity area, which yields the formation of a 3D null-point topology in the corona. (2) Continuous input of the free energy in the form of a flux rope from beneath the photosphere may drive a breakout-type reconnection occurring high in the corona, supported by the pre-flare brightening. (3) This initiation reconnection could release the constraint on the flux rope and trigger the MHD instability to first make filament F1 lose equilibrium. The subsequent more violent magnetic reconnection with the overlying flux is driven during the filament rising. In return, the eruption of filament F2 is further facilitated by the reduction of the magnetic tension force above. These two processes form a positive feedback to each other to cause the energetic mass eruption and flare.
HMI Science Nuggets #78 **2018** http://hmi.stanford.edu/hminuggets/?p=2107

Sudden Penumbral Reappearance and Umbral Motion Induced by an M7.9 Solar Flare

Zhe **Xu**1,2,3, Yunchun Jiang1,3, Jiayan Yang1,3, Junchao Hong1,3, and Haidong Li
2017 ApJL 840 L21

http://iopscience.iop.org.sci-hub.cc/2041-8205/840/2/L21/
The sudden flare-related changes of sunspot structures have been recognized as the photospheric responses to the solar eruptions in the corona. In this study, we report two distinctive sunspots variations associated with the flare SOL**2015-06-25**T08:16 (M7.9). Along the flaring polarity inversion line (PIL), the originally decayed penumbra showed a sudden reappearance, with the horizontal fields increasing in the direction of the penumbral fibrils aligned. On the other hand, the small umbra, where the reappearing penumbra rooted, had a sudden northeastward motion, toward the north part of a large sunspot located in the other side of PIL. Based on the calculation of Lorentz force changes, the area of penumbral reappearance mainly suffered a downward pressure, while the umbra region was dominated by the northeastward lateral pressure. These observations can be well understood as a result of coronal fields contraction, which can be deduced from the nonlinear force-free field extrapolation model. It also confirms the implosion idea that the restructuring of coronal fields could impact the solar surface and interior.

RAPID PENUMBRA AND LORENTZ FORCE CHANGES IN AN X1.0 SOLAR FLARE
Zhe **Xu**1,2, Yunchun Jiang1, Jiayang Yang1, Bo Yang1,2, and Yi Bi
2016 ApJ 820 L21
We present observations of the violent changes in photospheric magnetic structures associated with an X1.1 flare, which occurred in a compact ?-configuration region in the following part of AR 11890 on **2013 November 8**. In both central and peripheral penumbra regions of the small ? sunspot, these changes took place abruptly and permanently in the reverse direction during the flare: the inner/outer penumbra darkened/disappeared, where the magnetic fields became more horizontal/vertical. Particularly, the Lorentz force (LF) changes in the central/peripheral region had a downward/upward and inward direction, meaning that the local pressure from the upper atmosphere was enhanced/released. It indicates that the LF changes might be responsible for the penumbra changes. These observations can be well explained as the photospheric response to the coronal field reconstruction within the framework of the magnetic implosion theory and the back reaction model of flares.

Ultra-narrow Negative Flare Front Observed in Helium-10830~Å using the 1.6 m New Solar Telescope

Yan **Xu**, Wenda Cao, Mingde Ding, Lucia Kleint, Jiangtao Su, Chang Liu, Haisheng Ji, Jongchul Chae, Ju Jing, Kyuhyoun Cho, Kyungsuk Cho, Dale Gary, Haimin Wang
ApJ 819 89 **2016**
http://arxiv.org/pdf/1601.04729v1.pdf
https://iopscience.iop.org/article/10.3847/0004-637X/819/2/89/pdf
Solar flares are sudden flashes of brightness on the Sun and are often associated with coronal mass ejections and solar energetic particles which have adverse effects in the near Earth environment. By definition, flares are usually referred to bright features resulting from excess emission. Using the newly commissioned 1.6~m New Solar Telescope at Big Bear Solar Observatory, here we show a striking "negative" flare with a narrow, but unambiguous "dark" moving front observed in He I 10830 \AA, which is as narrow as 340 km and is associated with distinct spectral characteristics in H-alpha and Mg II lines. Theoretically, such negative contrast in He I 10830 \AA\ can be produced under special circumstances, by nonthermal-electron collisions, or photoionization followed by recombination. Our discovery, made possible due to unprecedented spatial resolution, confirms the presence of the required plasma conditions and provides unique information in understanding the energy release and radiative transfer in astronomical objects **2013 Aug. 17, 2014 Aug. 01**

Comparison of Emission Properties of two Homologous Flares in AR 11283

Yan **Xu**, Ju Jing, Shuo Wang, Haimin Wang
ApJ, **2014**
http://arxiv.org/pdf/1404.6577v1.pdf
Large, complex, active regions may produce multiple flares within a certain period of one or two days. These flares could occur in the same location with similar morphologies, commonly referred to as homologous flares. In **2011 September,** active region NOAA 11283 produced a pair of homologous flares on the **6th and 7th**, respectively. Both of them were white-light (WL) flares, as captured by the Helioseismic and Magnetic Imager (HMI) onboard the Solar Dynamics Observatory in visible continuum at 617.3 nm which is believed to originate from the deep solar atmosphere.We investigate the WL emission of these X-class flares with HMIs seeing-free imaging spectroscopy. The durations of impulsive peaks in the continuum are about 4 minutes. We compare the WL with hard X-ray (HXR) observations for the September 6 flare and find a good correlation between the continuum and HXR both spatially and temporally. In absence of RHESSI data during the second flare on September 7, the derivative of the GOES soft X-ray is used and also found to be well correlated temporally with the continuum. We measure the contrast enhancements, characteristic sizes, and HXR fluxes of the twin flares, which are similar for both flares, indicating analogous triggering and heating processes. However, the September 7 flare was associated with conspicuous sunquake signals whereas no

seismic wave was detected during the flare on September 6. Therefore, this comparison suggests that the particle bombardment may not play a dominant role in producing the sunquake events studied in this paper.

Anomalous resistivity in beam-return currents and hard-X ray spectra of solar flares

L. **Xu**1,2, L. Chen1 and D. J. Wu
A&A 550, A63 (**2013**)

Context. Observations of hard-X ray (HXR) spectra from solar flares show that there is noncollisional energy loss when energetic beam electrons are transported along the flare loop from their acceleration site above the looptop in the corona to the loop footpoints in the chromosphere.
Aims. This paper investigates anomalous (i.e., noncollisional) resistivity due to the effective collision by the wave-particle interaction in the beam-return current system of a flare and its effect on the HXR spectral evolution between the looptop and footpoint sources.
Methods. To attribute the noncollisional energy loss to an induced electric field by the beam current, the induced electric field is estimated by the spectral evolution between the looptop and footpoint sources, which is deduced from the standard thin-thick target model. To include collisional and anomalous resistivity caused by the ion-acoustic wave turbulence excited by the return current, the necessary excited level and the excited condition are discussed for the steady-state case in which the return current density driven by the induced electric field in terms of Ohm's law is required to be equal to the beam current density.
Results. The results show that including the anomalous resistivity can reasonably remove the discrepancy between observations and predictions. Meanwhile, the necessary excited level for the ion-acoustic turbulence is tens times of the thermal noise of electrostatic fluctuations in the background plasma, which is an ordinary and low excited level that is easily satisfied.
Conclusions. This indicates that the microscopic kinetics of plasma particles possibly play an important and critical role in understanding the dynamics of beam-return current systems in the solar atmosphere and in the physics of solar flares.

CHARACTERISTIC SIZE OF FLARE KERNELS IN THE VISIBLE AND NEAR-INFRARED CONTINUA

Yan **Xu**1, Wenda Cao2, Ju Jing1, and Haimin Wang
2012 ApJ 750 L7

In this Letter, we present a new approach to estimate the formation height of visible and near-infrared emission of an X10 flare. The sizes of flare emission cores in three wavelengths are accurately measured during the peak of the flare. The source size is the largest in the G band at 4308 Å and shrinks toward longer wavelengths, namely the green continuum at 5200 Å and NIR at 15600 Å, where the emission is believed to originate from the deeper atmosphere. This size-wavelength variation is likely explained by the direct heating model as electrons need to move along converging field lines from the corona to the photosphere. Therefore, one can observe the smallest source, which in our case is 065 ± 002 in the bottom layer (represented by NIR), and observe relatively larger kernels in upper layers of 103 ± 014 and 196 ± 027, using the green continuum and G band, respectively. We then compare the source sizes with a simple magnetic geometry to derive the formation height of the white-light sources and magnetic pressure in different layers inside the flare loop.

DUAL-STAGE RECONNECTION DURING SOLAR FLARES OBSERVED IN HARD X-RAY

Yan **Xu**1, Ju Jing1, Wenda Cao2, and Haimin Wang1
Astrophysical Journal Letters, 709:L142–L145, **2010** February, **File**

In this Letter, we present hard X-ray (HXR) observation by the *Reuven Ramaty High Energy Solar Spectroscopic Imager* of the **2003 October 29** X10 flare. Two pairs of HXR conjugate footpoints have been identified during the early impulsive phase. This geometric configuration is very much in the manner predicted by the "tether-cutting" scenario first proposed by Moore & Roumeliotis. The HXR light curves show that the outer pair of footpoints disappeared much faster than the other pair. This temporal behavior further confirms that this event is a good example of the "tether-cutting" model. In addition, we reconstructed a three-dimensional magnetic field based on the nonlinear force-free extrapolation and found that each pair of HXR footpoints were indeed linked by corresponding magnetic field lines.

High Resolution Observations of White-Light Emissions from the Opacity Minimum during an X-class Flare

Yan **Xu**, Wenda Cao, Ju Jing, and Haimin Wang
E-print, March **2010**, BBSO preprint #1432, **2010**, Astron. Nachr.

Using high cadence, high resolution near infrared (NIR) observations of the X10 white-light flare (WLF) on **2003 October 29**, we investigated the evolution of the core-halo structure of white-light emission during the two-second

period flare peak. We found that size and intensity of the halo remained almost constant in the range of 10~Mm^2. However, the core area was very compact and expanded rapidly from about 1~Mm^2 to 4~Mm^2.At the same time, the total emission of the core increased nearly twenty times. This distinct behavior indicates that different heating mechanisms might be responsible for core and halo emissions. In addition to the temporal analysis, we compared the intensity enhancements of the flare core and halo. The result shows that the halo contrast increased by about 8% compared to the flare-quiet region, which could be explained by a combination of direct-heating and backwarming models.

RHESSI HARD X-RAY IMAGING SPECTROSCOPY OF EXTENDED SOURCES AND THE PHYSICAL PROPERTIES OF ELECTRON ACCELERATION REGIONS IN SOLAR FLARES
Yan **Xu**, A. Gordon Emslie,1 and G. J. Hurford2
The Astrophysical Journal, 673:576–585, **2008**
http://www.journals.uchicago.edu/doi/pdf/10.1086/524184
In this study we present the results of a newapproach to studying the acceleration and propagation of bremsstrahlung producing electrons in solar flares. The method involves an analysis of the size of extended solar flare structures as a function of photon energy. Hard X-ray images from 10 M-class limb events, observed by the Reuven Ramaty High Energy Solar Spectroscopic Imager (RHESSI) to have the general form of a single extended source, were analyzed by forward fitting to the source visibilities in each energy band. On average the source sizes *l* increased slowlywith photon energy E as $l \sim E^{1/2}$. This behavior is consistent neither with the predictions of a single-loop thermal model nor with a model in which nonthermal electrons are injected into a constant-density structure from a compact acceleration region. While a nonuniform density distribution along the flare loop can in principle reconcile the data with a nonthermal collisional model with point-source injection, the resulting density profiles are highly questionable. On the other hand, the data are consistent with a nonthermal collisional model that incorporates an extended acceleration region, perhaps in combination with a localized thermal source. We present best-fit results on the density and length of this acceleration region. To our knowledge, this is the first quantitative empirical analysis of the physical characteristics of electron acceleration regions in solar flares.

Decay of Solar Pores Driven by Small-scale Magnetic Reconnection Episodes

Zhike **Xue**1,2,3, Xiaoli Yan1,3, Liheng Yang1,2,3, Jie Chen2, Jincheng Wang1,3, Qiaoling Li4, and Li Zhao1,3
2021 ApJL 919 L29
https://iopscience.iop.org/article/10.3847/2041-8213/ac2733/pdf
https://doi.org/10.3847/2041-8213/ac2733
We present the relationships between the disappearances of two small pores, magnetic cancellations, and magnetic reconnection episodes in the NOAA AR 12778 on 2020 October 26 with high-resolution observations of the New Vacuum Solar Telescope and the Solar Dynamics Observatory. Two emerging positive polarities (P1 and P2) approach a negative polarity (N1) with velocities of 0.26 and 0.42 km s−1, respectively. Then, two small-scale magnetic reconnection episodes occur between a series of magnetic loops that are rooted in these polarities. The reconnection inflow velocities are around 4.0 km s−1 which is faster than the movements of P1 and P2. Compared with the first magnetic reconnection episode, more magnetic free energy is released in the second reconnection episode due to the greater magnetic strength of P2. Subsequently, magnetic cancellation occurs first between P1 and N1, and then between P2 and N1. At the same time, the pores S1 (N1) and S2 (P2) decay and disappear. The area decay rate of the small pore S2 is estimated to be 7.3 Mm2 hr−1, which is larger than previously reported cases. And the flux decay rate of S2 is 5.1 × 1019 Mx hr−1, similar to the results obtained in the larger sunspots. We conclude that the magnetic reconnection episodes may be caused by both the movement of the magnetic polarities and the plasma dynamics themselves. The decay and disappearance of the small pores and the polarities are driven by magnetic reconnection episodes and then flux submergence. We suggest that a magnetic reconnection episode is a more efficient mechanism for the disappearance of solar pores.

Observations of Magnetic Reconnection with Large Separatrix Angles and Separatrix Jets above the Solar Surface

Z. K. **Xue**1,2,3, X. L. Yan1,3, L. H. Yang1,2,3, J. Chen2, J. C. Wang1,3, Z. Liu1,3,4, K. H. Lee5, and L. C. Lee5,6
2021 ApJ 915 17
https://iopscience.iop.org/article/10.3847/1538-4357/abfb71/pdf
https://doi.org/10.3847/1538-4357/abfb71
We analyze six cases of magnetic reconnection with large separatrix angles and separatrix jets observed on the solar disk. The separatrix angle is defined as the angle between the two separatrices on the two sides of the outflow region. The plasma jets are observed immediately downstream of the separatrices. The morphological characteristics and magnetic field configurations of all magnetic reconnections are displayed. At the same time, we calculate several

physical parameters of each case, which include the inflow velocity (from 2.3 to 24 km s−1), the outflow velocity (from 1.9 to 43 km s−1), the separatrix jet velocity (from 13 to 82 km s−1), the width (from 0.42 × 103 to 1.2 × 103 km) and length (from 1.4 × 103 to 4.3 × 103 km) of the current sheet, and the separatrix angle θsep (from 72° to 128°). We find that the outflow velocity, the separatrix jet velocity, and the width and length of the current sheet are positively related to the inflow velocity, but the separatrix angle does not depend on the inflow velocity and it is related to the initial magnetic field configuration before magnetic reconnection. Meanwhile, the velocities of the outflow and the separatrix jet decrease with increasing $|\theta_{sep} - 90^{\circ}|$, indicating that when the separatrix angle is close to 90°, the jet and the outflow reach their maximum velocities. These observations are compared with the results of the theoretical model and the numerical simulation.

Thermodynamical Evolution of Supra-Arcade Downflows

Jianchao **Xue**, Yang Su, Hui Li, Xiaozhou Zhao

ApJ **898** 88 **2020**

https://arxiv.org/pdf/2007.11205.pdf

https://doi.org/10.3847/1538-4357/ab9a3d

Supra-arcade downflows (SADs) are dark, teardrop-shaped features descending upon flare arcades. They are thought to be the results of magnetic reconnection, but the detailed formation mechanism of SADs and their relationship to flare energy release are still unclear. In this work, we explore the thermodynamical properties of SADs in the **2011 October 22** limb flare using the observations of the Solar Dynamics Observatory/Atmospheric Imaging Assembly and an improved Differential Emission Measure (DEM) technique. Different heating events around SADs are identified and the propagation speeds of plasma heating are calculated. The first heating event starts with the increase of the emission measure at temperatures higher than 5 MK, about 2.8 minutes before the arrival of the first studied SAD. Its propagation speed is about 140 km/s, a little faster than the speed of the SAD. However, the other two events have fast propagation speeds more than 700 km/s. We suspect that the first heating event can be explained by adiabatic compression, but the others may have different causes. Besides, we observed that SADs can push away their surrounding spikes. The formation of SADs is further explained on the basis of patchy and bursty magnetic reconnection that reconnection outflows may push away surrounding plasma and leave dark lanes behind them. The reliability of the DEM results, heating and cooling mechanisms, and other SAD explanations are discussed.

Spectral and Imaging Observations of a Current Sheet Region in a Small-scale Magnetic Reconnection Event

Zhike **Xue**1,2, Xiaoli Yan1,2, Liheng Yang1,2, Jincheng Wang1,2, Song Feng3,Qiaoling Li1,2,4, Kaifan Ji1,2, and Li Zhao1,

2018 ApJL 858 L4

http://sci-hub.tw/http://iopscience.iop.org/2041-8205/858/1/L4/

We report a possible current sheet region associated with a small-scale magnetic reconnection event by using the spectral and imaging observations of the Interface Region Imaging Spectrograph(IRIS) and the magnetograms obtained by the Solar Dynamics Observatory on **2016 August 08**. The length and width of the current sheet region are estimated to be from 1.4 ± 0.1 Mm to 3.0 ± 0.3 Mm and from 0.34 ± 0.01 Mm to 0.64 ± 0.09 Mm, respectively. The evolutions of the length of the current sheet region are positively correlated with that of the width. These measurements are among the smallest reported. When the IRIS slit scans the current sheet region, the spectroscopic observations show that the Si iv line is broadened in the current sheet region and the plasma has a blueshifted feature at the middle and a redshifted feature at the ends of the current sheet region. The maximum measured blueshifted and redshifted Doppler velocities are −20.8 ± 0.9 and 34.1 ± 0.4 km s−1, respectively. Additionally, the electron number densities of the plasma in the current sheet region are computed to be around 1011 cm−3 based on the spectrums of the two O ivlines. The emergence, movement, and cancellation of a small sunspot with negative polarity are observed during the formation and shift of the current sheet region. We suggest that the occurrence and evolution of the magnetic reconnection are driven by the movement of the small sunspot in the photosphere.

Photospheric Pore Rotation Associated with a C-class Flare from Spectropolarimetric Observations with DKIST

Rahul **Yadav**, Maria D. Kazachenko, Andrey N. Afanasyev, Gianna Cauzzi, Kevin Reardon

ApJL **973** L10 **2024**

https://arxiv.org/pdf/2408.16956

https://iopscience.iop.org/article/10.3847/2041-8213/ad758d/pdf

We present high-resolution observations of a C4.1-class solar flare (SOL**2023-05-03T20**:53) in AR 13293 from the ViSP and VBI instruments at the DKIST. The fast cadence, good resolution, and high polarimetric sensitivity of ViSP data provide a unique opportunity to explore the photospheric magnetic fields before and during the flare. We infer the magnetic field vector in the photosphere from the Fe I 6302 line using Milne-Eddington inversions. Combined analysis of the inverted data and VBI images reveals the presence of two oppositely-polarity pores exhibiting rotational motion

both prior to and throughout the flare event. Data-driven simulations further reveal a complex magnetic field topology above the rotating pores, including a null-point-like configuration. We observed a 30% relative change in the horizontal component (δFh) of Lorentz force at the flare peak time and roughly no change in the radial component. We find that the changes in δFh are the most likely driver of the observed pore rotation. These findings collectively suggest that the back-reaction of magnetic field line reconfiguration in the corona may influence the magnetic morphology and rotation of pores in the photosphere on a significantly smaller scale.

A statistical study of magnetic field changes in the photosphere during solar flares using high-cadence vector magnetograms and their association with flare ribbons

Rahul **Yadav**, Maria D. Kazachenko
ApJ **944** 215 **2022**
https://arxiv.org/pdf/2210.14264.pdf
https://iopscience.iop.org/article/10.3847/1538-4357/acaa9d/pdf
Abrupt and permanent photospheric magnetic field changes have been observed in many flares. It is believed that such changes are related to the reconfiguration of magnetic field lines, however, the real origin is still unclear. In this study we analyze 37 flares to understand the magnetic field vector changes in the photosphere using high-cadence (135 s) vector magnetograms obtained from the HMI/SDO. We also co-align these magnetogram sequences with flare ribbon images (1600 Å), obtained from the AIA/SDO, to understand how the field change is associated with the ribbon morphology. We find that the permanent change in the horizontal component lies near the polarity inversion line, whereas the vertical component pixels are less pronounced and distributed in small patches. We also find that the pixels exhibiting ultraviolet emission are not always associated with permanent field change. In 84% of 37 events the UV emission starts early by several minutes compared to the field change start time for the pixels showing both UV emission and permanent horizontal field change. The field change properties show no relation with the size of active regions, but are strongly related to the flare ribbon properties like ribbon magnetic flux and ribbon area. The permanent field change duration is strongly correlated with the GOES flaring duration, with an average value of 29% of total GOES flare time. Our analysis suggests that the change in photospheric magnetic field is caused by combination of two scenarios: contraction of flare loops driven by magnetic reconnection and coronal implosion. **15 Feb 2011**
Table 1. List of 37 flares. 2010-2015

On the radiative losses in the chromosphere during a C-class flare

Rahul **Yadav**, J. de la Cruz Rodríguez, Graham S. Kerr, C. J. Díaz Baso, Jorrit Leenaarts
A&A 665, A50 **2022**
https://arxiv.org/pdf/2207.02840
https://www.aanda.org/articles/aa/pdf/2022/09/aa43440-22.pdf
Solar flares release an enormous amount of energy in the corona. A substantial fraction of this energy is transported to the lower atmosphere, which results in chromospheric heating. The mechanisms that transport energy to the lower solar atmosphere during a flare are still not fully understood. We aim to estimate the temporal evolution of the radiative losses in the chromosphere at the footpoints of a C-class flare, in order to set observational constraints on the electron beam parameters of a RADYN flare simulation. We estimated the radiative losses from hydrogen, and singly ionized Ca and Mg using semi-empirical model atmospheres. To estimate the integrated radiative losses in the chromosphere the net cooling rates were integrated between the temperature minimum and the height where the temperature reaches 10 kK. The stratification of the net cooling rate suggests that the Ca IR triplet lines are responsible for most of the radiative losses in the flaring atmosphere. During the flare peak time, the contribution from Ca II H & K and Mg II h & k lines are strong and comparable to the Ca IR triplet (∼32 kW m−2). Since our flare is a relatively weak event the chromosphere is not heated above 11 kK, which in turn yields a subdued Ly{\alpha} contribution (∼7 kW m−2). The temporal evolution of total integrated radiative losses exhibits sharply-rising losses (0.4 kW m−2 s−1) and a relatively slow decay (0.23 kW~m−2 s−1). The maximum value of total radiative losses is reached around the flare peak time, and can go up to 175 kW m−2 for a single pixel located at footpoint. After a small parameter study, we find the best model-data consistency in terms of the amplitude of radiative losses and the overall atmospheric structure with a RADYN flare simulation in the injected energy flux of 5×1010 erg s−1 cm−2. **2019-05-06**

Stratification of physical parameters in a C-class solar flare using multi-line observations

Rahul **Yadav**, C. J. D. Baso, J. de la Cruz Rodr'iguez, F. Calvo, R. Morosin
A&A 649, A106 **2021**
https://arxiv.org/pdf/2011.02953.pdf
https://doi.org/10.1051/0004-6361/202039857
We present high-resolution and multi-line observations of a C2-class solar flare, occurred in NOAA AR 12740 on **May 6, 2019**. The rise, peak and decay phases of the flare were recorded continuously and quasi-simultaneously in the Ca II K line with the CHROMIS instrument, the Ca II 8542 and Fe I 6173 Å lines with the CRISP instrument at the SST. The observations in the chromospheric Ca II lines exhibit intense brightening near the flare footpoints. At these locations, a non-LTE inversion code was employed to infer the temperature, magnetic field, line-of-sight (LOS) velocity and

microturbulent velocity stratification in the flaring atmosphere. During the flare peak time, the LOS velocity shows both upflows and downflows around the flare footpoints in the upper chromosphere and lower chromosphere, respectively. Moreover, the temporal analysis of the LOS magnetic field at the flarepoints exhibits a maximum change of ~600 G. After the flare, the LOS magnetic field decreases to the non-flaring value, exhibiting no permanent or step-wise change. The analysis of response functions to the temperature, LOS magnetic field and velocity shows that the Ca II lines exhibit enhanced sensitivity to the deeper layers (i.e., log_t ~ -3) of the flaring atmosphere, whereas for the non-flaring atmosphere they are mainly sensitive around log_t ~ -4. We suggest that a fraction of the apparent increase in the LOS magnetic field at the flare footpoints may be due to the increase in the sensitivity of the Ca II 8542 Å line in the deeper layers, where the field strength is relatively stronger. The rest can be due to magnetic field reconfiguration during the flare. Our observations illustrate that even a less intense C-class flare can heat the deeper layers of the solar chromosphere, mainly at the flare footpoints, without affecting the photosphere.

TIME VARIATION AND STATISTICAL STUDIES OF MAGNETIC HELICITY INJECTION IN SOLAR MAGNETIC REGIONS

Tetsuya T. **Yamamoto**1 and T. Sakurai
Astrophysical Journal, 698:928–937, **2009**
http://www.iop.org/EJ/toc/-alert=43190/0004-637X/698/1
In this study, we analyzed the helicity injection in solar active regions statistically with the method proposed by Kusano et al. We investigated the variation in helicity injection as an active region evolves and the statistical distribution
of helicity injection against the magnetic flux (√) and the latitude. The temporal evolution of active regions is divided into three phases (“emergence,” “active,” and “decay” phases). We studied one emergence-phase region, 13 active-phase regions, and five decay-phase regions. The total number of helicity injection rates we obtained is 1476. We found the following results. The dispersions (standard deviations) in the helicity injection rates are proportional to $\sqrt{}^{-0.47}$ in the active-phase regions and to $\sqrt{}^{-0.34}$ in the decay-phase regions. The dispersion for the emergence-phase region, 0.046 day^{-1}, is larger than those for the active-phase regions, 0.004–0.03 day^{-1}, and those for the decay-phase regions, 0.004–0.01 day^{-1}. The average helicity injection rates of the active-phase regions show the latitude dependence, which is consistent with the “hemispheric rule” of helical structures in the solar atmosphere, while those of the decay-phase regions are inconsistent with the hemispheric rule. The average helicity injection rates for the active-phase regions, 0.003–0.03 day^{-1}, are larger than that for the emergence-phase region, 0.0045 day^{-1}, and those for the decay-phase regions, $<$0.002 day^{-1}. These dependences of the helicity injection rates give us clues on the generation mechanism of helicity and the evolution of the magnetic field in the solar convection zone.

A Data-constrained Magnetohydrodynamic Simulation of the X1.0 Solar Flare of 2021 October 28

Daiki **Yamasaki**, Satoshi Inoue, Yumi Bamba, Jeongwoo Lee, Haimin Wang
ApJ **940** 119 **2022**
https://arxiv.org/pdf/2210.14563 **File**
https://iopscience.iop.org/article/10.3847/1538-4357/ac9df4/pdf
The solar active region NOAA 12887 produced a strong X1.0 flare on **2021 October 28**, which exhibits X-shaped flare ribbons and a circle-shaped erupting filament. To understand the eruption process with these characteristics, we conducted a data-constrained magnetohydrodynamics simulation using a nonlinear force-free field of the active region about an hour before the flare as the initial condition. Our simulation reproduces the filament eruption observed in the Ha images of GONG and the 304 angstrom images of SDO/AIA and suggests that two mechanisms can possibly contribute to the magnetic eruption. One is the torus instability of the pre-existing magnetic flux rope (MFR), and the other is upward pushing by magnetic loops newly formed below the MFR via continuous magnetic reconnection between two sheared magnetic arcades. The presence of this reconnection is evidenced by the SDO/AIA observations of the 1600 angstrom brightening in the footpoints of the sheared arcades at the flare onset. To clarify which process is more essential for the eruption, we performed an experimental simulation in which the reconnection between the sheared field lines is suppressed. In this case too, the MFR could erupt, but at a much reduced rising speed. We interpret this result as indicating that the eruption is not only driven by the torus instability, but additionally accelerated by newly formed and rising magnetic loops under continuous reconnection.

Evolution of the Non-potential Magnetic Field in the Solar Active Region 12673 Based on a Nonlinear Force-free Modeling

Daiki **Yamasaki**, Satoshi Inoue, Shin'ichi Nagata, Kiyoshi Ichimoto
ApJ **908** 132 **2021**
https://arxiv.org/pdf/2012.01008.pdf
https://iopscience.iop.org/article/10.3847/1538-4357/abcfbb/pdf

https://doi.org/10.3847/1538-4357/abcfbb
Active region (AR) 12673 produced many M-class and several X-class flares, one of which being an X9.3 flare, which is recorded as the largest solar flare in solar cycle 24. We studied the evolution of the three-dimensional flare-productive magnetic field within AR 12673, using a time series of nonlinear force-free field extrapolations of every 12 hours from September 4th 00:00 UT to 6th 00:00 UT. Our analysis found that three magnetic flux ropes (MFRs) are formed by September 4th, one of which produced the X9.3 flare on September 6th. One MFR has positive magnetic twist which is a different sign from other two MFRs. Since the temporal evolution of the magnetic flux of the MFR accumulating the positive twist is consistent with the profile of the GOES X-ray flux well observed from September 4th to 6th, we suggest that the formation of the MFR having the positive twist is closely related to the occurrence of the M-class flares including an M5.5 flare. We further found a magnetic null in the magnetic field surrounding the MFRs, in particular, above the MFR having positive twist before the M5.5 flare which is the largest M-flare observed during this period. By comparing with the AIA 1600 angstrom images, we found that the footpoints of the overlying field lines are anchored to the area where the brightening was initially observed. Therefore, we suggest that reconnection induced by the torus instability of the positively twisted MFR at the null possibly drived the M5.5 flare. **4 Sep 2017**

Extreme Solar Flare Prediction Using Residual Networks with HMI Magnetograms and Intensitygrams

Juyoung **Yun**, Jungmin Shin
SPAICE Conference **2024**
https://arxiv.org/pdf/2405.14750
Solar flares, especially C, M, and X class, pose significant risks to satellite operations, communication systems, and power grids. We present a novel approach for predicting extreme solar flares using HMI intensitygrams and magnetograms. By detecting sunspots from intensitygrams and extracting magnetic field patches from magnetograms, we train a Residual Network (ResNet) to classify extreme class flares. Our model demonstrates high accuracy, offering a robust tool for predicting extreme solar flares and improving space weather forecasting. Additionally, we show that HMI magnetograms provide more useful data for deep learning compared to other SDO AIA images by better capturing features critical for predicting flare magnitudes. This study underscores the importance of identifying magnetic fields in solar flare prediction, marking a significant advancement in solar activity prediction with practical implications for mitigating space weather impacts. **2022-01-16**

Characteristic time of stellar flares on Sun-like stars

Y **Yan**, H He, C Li, A Esamdin, B L Tan, L Y Zhang, H Wang
MNRAS: Letters, Volume 505, Issue 1, **2021**, Pages L79–L83,
https://doi.org/10.1093/mnrasl/slab055
https://academic.oup.com/mnrasl/article-abstract/505/1/L79/6297375
Using the short-cadence data (1-min interval) of the Kepler space telescope, we conducted a statistical analysis for the characteristic time of stellar flares on Sun-like stars (SLS). Akin to solar flares, stellar flares show rise and decay light-curve profiles, which reflect the two distinct phases (rise phase and decay phase) of the flare process. We derived characteristic times of the two phases for stellar flares of SLS, resulting in a median rise time of about 5.9 min and a median decay time of 22.6 min. It is found that both the rise time and the decay time of the stellar flares follow a lognormal distribution. The peak positions of the lognormal distributions for flare rise time and decay time are 3.5 min and 14.8 min, respectively. These time values for stellar flares are similar to the time-scale of solar flares, which supports the idea that stellar flares and solar flares have the same physical mechanism. The statistical results obtained in this work for SLS can be a benchmark of flare characteristic times when comparing with other types of stars.

Research progress based on observations of the New Vacuum Solar Telescope **Review**

Xiaoli **Yan**, Zhong Liu, Jun Zhang, Zhi Xu
SCIENCE CHINA Technological Sciences **2019**
https://arxiv.org/pdf/1910.09127.pdf
The purpose of this paper is to introduce the main scientific results made by the one-meter New Vacuum Solar Telescope (NVST), which was put into commission on 2010. NVST is one of the large aperture solar telescopes in the world, located on the shore of Fuxian lake of Yunnan province in China, aiming at serving solar physicists by providing them with high resolution photospheric and chromospheric observational data. Based on the data from NVST and complementary observations from space (e.g., Hinode, SDO and IRIS, etc), dozens of scientific papers have been published with a wide range of topics concentrating mainly on dynamics and activities of fine-scale magnetic structures and their roles in the eruptions of active-region filaments and flares. The achievements include dynamic characteristics of photospheric bright points, umbral dots, penumbral waves, and sunspot/light bridge oscillation, observational evidence of small-scale magnetic reconnection, and fine-scale dynamic structure of prominences. All these new results will shed light on the better understanding of solar eruptive activities. Data release, observation proposals, and future research subjects are introduced and discussed.

Bright points. Umbral dot, penumbral wave. Sunspot light bridge. Formation, fine-scale structures, and eruption mechanism of solar filaments. Fine structure of solar prominences. Filament formation. Magnetic structures of active-region filaments. Filament eruption. Small-scale magnetic reconnection in the solar eruptions. Release of twist in a filament by magnetic reconnection. Interchange magnetic reconnection between a filament and nearby open fields. Magnetic reconnection between a twisted arch filament system and coronal loops. Magnetic reconnection between two active-region filaments. Oscillatory magnetic reconnection. Small-scale eruptive activities. Mini-filaments and jets. Formation and trigger mechanism of solar flares

Simultaneous observation of a flux rope eruption and magnetic reconnection during an X-class solar flare

X.L. **Yan**, L.H. Yang, Z.K. Xue, Z.X. Mei, D.F. Kong, J.C. Wang, Q.L. Li
ApJL **853** L18 **2018**
https://arxiv.org/pdf/1801.02738.pdf
https://iopscience.iop.org/article/10.3847/2041-8213/aaa6c2/pdf
In this letter, we present a spectacular eruptive flare (X8.2) associated with a coronal mass ejection (CME) on **2017 September 10** at the west limb of the Sun. A flux rope eruption is followed by the inflow, the formation of a current sheet and a cusp structure, which were simultaneously observed during the occurrence of this flare. The hierarchical layers of the cusp-shaped structure are well observed in 131 \AA\ observation. The scenario that can be created from these observations is very consistent with the predictions of some eruptive models. Except for the characteristics mentioned above in the process of the flare predicted by classical eruption models, the current sheet separating into several small current sheets is also observed at the final stage of the flux rope eruption. The quantitative calculation of the velocities and accelerations of the inflow, hot cusp structure, and post-flare loops is presented. The width of the current sheet is estimated to be about 3 [Math Processing Error] [Math Processing Error] km. These observations are very useful to understand the process of solar eruptions.

Successive X-class flares and coronal mass ejections driven by shearing motion and sunspot rotation in active region NOAA 12673

X.L. **Yan**, J.C. Wang, G.M. Pan, D.F. Kong, Z.K. Xue, L.H. Yang, Q.L. Li
2018 *ApJ* **856** 79
https://arxiv.org/pdf/1801.02290.pdf
http://sci-hub.tw/http://iopscience.iop.org/0004-637X/856/1/79/
We present a clear case study on the occurrence of two successive X-class flares including a decade-class flare (X9.3) and two coronal mass ejections (CMEs) triggered by shearing motion and sunspot rotation in active region NOAA 12673 on 2017 September 6. A shearing motion between the main sunspots with opposite polarities started on September 5 and even lasted after the second X-class flare on September 6. Moreover, the main sunspot with negative polarity rotated around its umbral center and another main sunspot with positive polarity also exhibited a slow rotation. The sunspot with negative polarity at the northwest of active region also began to rotate counter-clockwise before the onset of the first X-class flare. The successive formation and eruption of two S-shaped structures were closely related to the counter-clockwise rotation of three sunspots. It is also found that the rotation of sunspots is faster during four hours prior to the onset of the flares than the period before. The existence of a flux rope is found prior to the onset of two flares by using non-linear force free field extrapolation based on the vector magnetograms observed by SDO/HMI. These results suggest that shearing motion and sunspot rotation play an important role in the buildup of the free energy and the formation of flux ropes in the corona which produces solar flares and CMEs.
CESRA #97 **2018** http://hmi.stanford.edu/hminuggets/?p=2452

The Eruption of a Small-scale Emerging Flux Rope as the Driver of an M-class Flare and of a Coronal Mass Ejection

X. L. **Yan**1,2,3, C. W. Jiang4, Z. K. Xue1,3, J. C. Wang1,5, E. R. Priest6, L. H. Yang1,3, D. F. Kong1,2,3, W. D. Cao7, and H. S. Ji8
2017 ApJ 845 18
https://arxiv.org/pdf/1707.00073.pdf
http://sci-hub.cc/10.3847/1538-4357/aa7e29
Solar flares and coronal mass ejections are the most powerful explosions in the Sun. They are major sources of potentially destructive space weather conditions. However, the possible causes of their initiation remain controversial. Using high-resolution data observed by the New Solar Telescope of Big Bear Solar Observaotry, supplemented by Solar Dynamics Observatoryobservations, we present unusual observations of a small-scale emerging flux rope near a large sunspot, whose eruption produced an M-class flare and a coronal mass ejection. The presence of the small-scale flux rope was indicated by static nonlinear force-free field extrapolation as well as data-driven magnetohydrodynamics modeling of the dynamic evolution of the coronal three-dimensional magnetic field. During the emergence of the flux

rope, rotation of satellite sunspots at the footpoints of the flux rope was observed. Meanwhile, the Lorentz force, magnetic energy, vertical current, and transverse fields were increasing during this phase. The free energy from the magnetic flux emergence and twisting magnetic fields is sufficient to power the M-class flare. These observations present, for the first time, the complete process, from the emergence of the small-scale flux rope, to the production of solar eruptions. **24 Aug 2015**

SUNSPOT ROTATION, SIGMOIDAL FILAMENT, FLARE, AND CORONAL MASS EJECTION: THE EVENT ON 2000 FEBRUARY 10

X. L. **Yan**1,2, Z. Q. Qu1, D. F. Kong1,2, and C. L. Xu

2012 ApJ 754 16

We find that a sunspot with positive polarity had an obvious counterclockwise rotation and resulted in the formation and eruption of an inverse S-shaped filament in NOAA Active Region 08858 from **2000 February 9 to 10**. The sunspot had two umbrae which rotated around each other by 195° within about 24 hr. The average rotation rate was nearly 8° hr–1. The fastest rotation in the photosphere took place during 14:00 UT to 22:01 UT on February 9, with a rotation rate of nearly 16° hr–1. The fastest rotation in the chromosphere and the corona took place during 15:28 UT to 19:00 UT on February 9, with a rotation rate of nearly 20° hr–1. Interestingly, the rapid increase of the positive magnetic flux occurred only during the fastest rotation of the rotating sunspot, the bright loop-shaped structure, and the filament. During the sunspot rotation, the inverse S-shaped filament gradually formed in the EUV filament channel. The filament experienced two eruptions. In the first eruption, the filament rose quickly and then the filament loops carrying the cool and the hot material were seen to spiral counterclockwise into the sunspot. About 10 minutes later, the filament became active and finally erupted. The filament eruption was accompanied with a C-class flare and a halo coronal mass ejection. These results provide evidence that sunspot rotation plays an important role in the formation and eruption of the sigmoidal active-region filament.

PARTICLE ACCELERATION BY FAST MODES IN SOLAR FLARES

Huirong **Yan**,1 A. Lazarian,2 and Vahe´ Petrosian3

Astrophysical Journal, 684:1461-1468, **2008**

http://www.journals.uchicago.edu/toc/apj/2008/684/2

We address the problem of particle acceleration in solar flares by fast modes which may be excited during the reconnection and undergo cascade and are subjected to damping.We extend the calculations beyond the quasi-linear approximation and compare the acceleration and scattering by transit time damping and gyroresonance interactions. We find that the acceleration is dominated by the so-called transit time damping mechanism. We estimate the total energy transferred into particles and show that our approach provides sufficiently accurate results.We compare this rate with the energy-loss rate. Scattering by fast modes appears to be sufficient to prevent the protons from escaping the system during the acceleration. Confinement of electrons, on the other hand, requires the existence of plasma waves. Electrons can be accelerated to GeV energies through the process described here for solar flare conditions.

Rapid rotation of a sunspot associated with flares:

X. L. **Yan** and Z. Q. Qu

A&A 468 (**2007**) 1083-1088 (Section 'The Sun')

http://www.aanda.org/10.1051/0004-6361:20077064

Active region NOAA 10424 observed on August 5, 2003 is studied in detail by using TRACE, SOHO/MDI, BBSO H α monograph, and GOES data.

It is shown that there is a close relationship between the sunspot rotation and the emerging kinked magnetic Ω-loops, where the flares occur.

A Possible Mechanism for "Late Phase" in Stellar White-Light Flares

Kai E. **Yang**, Xudong Sun, Graham S. Kerr, Hugh S. Hudson

ApJ **959** 54 **2023**

https://arxiv.org/pdf/2310.19316.pdf

https://iopscience.iop.org/article/10.3847/1538-4357/ad077d/pdf

M-dwarf flares observed by the \textit{Transiting Exoplanet Survey Satellite} (\textit{TESS}) sometimes exhibit a "peak-bump" light-curve morphology, characterized by a secondary, gradual peak well after the main, impulsive peak. A similar "late phase" is frequently detected in solar flares observed in the extreme-ultraviolet from longer hot coronal loops distinct from the impulsive flare structures. White-light emission has also been observed in off-limb solar flare loops. Here, we perform a suite of one-dimensional hydrodynamic loop simulations for M-dwarf flares inspired by these solar examples. Our results suggest that coronal plasma condensation following impulsive flare heating can yield high electron number density in the loop, allowing it to contribute significantly to the optical light curves via free-bound

and free-free emission mechanisms. Our simulation results qualitatively agree with \textit{TESS} observations: the longer evolutionary time scale of coronal loops produces a distinct, secondary emission peak; its intensity increases with the injected flare energy. **We argue that coronal plasma condensation is a possible mechanism for the \textit{TESS} late-phase flares.**

Image Super-resolution Methods for FY-3E X-EUVI 195 Å Solar Images

Qinglin **Yang**1,2, Zhou Chen2,3,4, Rongxin Tang2,3, Xiaohua Deng2,3, and Jinsong Wang4
2023 ApJS 265 36
https://iopscience.iop.org/article/10.3847/1538-4365/acb3b9/pdf
olar eruptions and the solar wind are sources of space weather disturbances, and extreme-ultraviolet (EUV) observations are widely used to research solar activity and space weather forecasts. Fengyun-3E is equipped with the Solar X-ray and Extreme Ultraviolet Imager, which can observe EUV imaging data. Limited by the lower resolution, however, we research super-resolution techniques to improve the data quality. Traditional image interpolation methods have limited expressive ability, while deep-learning methods can learn to reconstruct high-quality images through training on paired data sets. There is a wide variety of super-resolution models. We try these three representative models: Real-ESRGAN combined with generative adversarial networks, residual channel-attention networks (RCAN) based on channel attention, and SwinIR, based on self-attention. Instruments on different satellites differ in observation time, angle, and resolution, so we selected Solar Dynamics Observatory/Atmospheric Imaging Assembly (SDO/AIA) 193 Å images with similar wavelengths as a reference and used a feature-based method for image registration to eliminate slight deformations to build training data sets. Finally, we compare the above methods in their evaluation metrics and visual quality. RCAN has the highest peak signal-to-noise ratio and structural similarity evaluation. Real-ESRGAN model is the best in the Learned Perceptual Image Patch Similarity index, and its results visually show that it has more highly detailed textures. The corrected super-resolution results can complement the SDO/AIA data to provide solar EUV images with a higher temporal resolution for space weather forecasting and solar physics research. **2021-10-28, 2022-06-08**

Weak Bidirectional Outflows and Flare Current Sheet in a Solar Coronal Jet Driven by the Eruption of a Minifilament

Jiayan **Yang**1, Junchao Hong1, Bo Yang1, Yi Bi1, and Zhe Xu1
2023 ApJ 942 86
https://iopscience.iop.org/article/10.3847/1538-4357/aca66f/pdf
Different from the classical emerging-flux model for solar jets, recent studies proposed that the great majority of solar coronal jets are triggered by minifilament eruptions and two magnetic reconnection processes should take place during the course, named as external reconnection (breakout reconnection) and internal reconnection (flare reconnection). With the excellent data of the Solar Dynamics Observatory, we present the observational signatures of these two magnetic reconnection processes during a solar coronal jet that occurred in a huge coronal hole of northern hemisphere. The jet was triggered by the eruption of a minifilament that located at a coronal bright point in the coronal hole. Weak bidirectional outflows were observed when the erupting minifilament approached the ambient open field, ejecting along the triggered jet spire and the jet base simultaneously. In addition, a flare current sheet occurred after the eruption of the minifilament, connecting the jet spire and the jet bright point (or flare). We suggest the occurrence of the weak bidirectional outflows and the flare current sheet correspond to the external and the internal reconnections, respectively. Prior to the eruption of the minifilament and the jet, photospheric magnetic flux cancellation maintained for more than 7 hr in the source region, and the positive flux decreased for about 28.6% during this period. So, consistent with the recent observations, the trigger mechanism of the minifilament eruption and the following jet in this event may be flux cancellation rather than flux emergence. **2011 May 29**

Formation of a Solar Filament by Magnetic Reconnection and Associated Chromospheric Evaporation and Subsequent Coronal Condensation

Bo **Yang**, Jiayan Yang, Yi Bi, Junchao Hong, Zhe Xu
ApJ Letters **2021**
https://arxiv.org/pdf/2110.10951.pdf
We present the first observation of a solar filament formed by magnetic reconnection and associated chromospheric evaporation and subsequent coronal condensation. Driven by shearing motion during flux emergence, a sequential tether-cutting reconnection processes occurred and resulted in an M1.3 confined flare accompany with the formation of a sigmoid structure. It is found that the flare had a conjugate compact footpoint brightenings, which correspond to the footpoints of the sigmoid. Furthermore, observational evidence of explosive evaporation is well diagnosed at the conjugate footpoint brightenings in the impulsive phase of the flare. After the flare, continuous cool condensations formed at about the middle section of the sigmoid and then moved in opposite directions along the sigmoid, eventually leading to the formation of the filament. These observations suggest that magnetic reconnection not only can form the magnetic field structure of the filament, but also heat their chromospheric footpoints during their formation and drive chromospheric evaporation. As a result, the heated chromospheric plasma may be evaporated into the magnetic field

structure of the filament, where the accumulated hot plasma might suffer from thermal instability or thermal non-equilibrium, causing catastrophic cooling and coronal condensation to form the cool dense material of the filament. This observation lends strong support to the evaporative-condensation model and highlights the crucial role of magnetic reconnection in forming both the magnetic field structure and the cool dense material of filaments. **2014 February 2**

Radiative Hydrodynamic Simulations of the Spectral Characteristics of Solar White-light Flares

Yu-Tong **Yang**, Jie Hong, Ying Li, Ming-De Ding, Hui Li
Research in Astronomy and Astrophysics (RAA) Volume 21, Issue 1, id.001, **2021**
https://arxiv.org/pdf/2007.08850.pdf
As one of the most violent activities in the solar atmosphere, white-light flares (WLFs) are generally known for their enhanced white-light (or continuum) emission, which primarily originates in the solar lower atmosphere. However, we know little about how white-light emission is produced. In this study, we aim to investigate the response of the continua at 3600Åand 4250Å and also the Hα and Lyα lines during WLFs modeled with radiative hydrodynamics simulations. We take non-thermal electron beams as the energy source for the WLFs in two different initial atmospheres and vary their parameters. Our results show that the model with non-thermal electron beam heating can clearly show enhancements in the continua at 3600Å and 4250Å\ as well as in the Hα and Lyα lines. A larger electron beam flux, a smaller spectral index, or a penumbral initial atmosphere leads to a stronger emission increase at 3600Å, 4250Å and in the Hα line. For the Lyα line, however, it is more preferably enhanced in a quiet-Sun initial atmosphere with a larger spectral index of the electron beam. It is also notable that the continua at 3600Å and 4250Å and the Hα line exhibit a dimming at the beginning of the heating and reach their peak emissions later than the peak time of the heating function, while the Lyα line does not show such behaviors. These results can be served as a reference for analyzing future WLF observations.

Imaging and spectral study on the null point of a fan-spine structure during a solar flare

Shuhong **Yang**, Qingmin Zhang, Zhi Xu, Jun Zhang, Ze Zhong, Yang Guo
ApJ 898:101 **2020**
https://arxiv.org/pdf/2005.09613.pdf
https://iopscience.iop.org/article/10.3847/1538-4357/ab9ac7/pdf
Using the multi-instrument observations, we make the first simultaneous imaging and spectral study on the null point of a fan-spine magnetic topology during a solar flare. When magnetic reconnection occurs at the null point, the fan-spine configuration brightens in the (extreme-)ultraviolet channels. In the Hα images, the fan-spine structure is partly filled and outlined by the bi-directional material flows ejected from the reconnection site. The extrapolated coronal magnetic field confirms the existence of the fan-spine topology. Before and after the flare peak, the total velocity of the outflows is estimated to be about 60 km s−1. During the flare, the Si IV line profile at the reconnection region is enhanced both in the blue-wing and red-wing. At the flare peak time, the total velocity of the outflows is found to be 144 km s−1. Superposed on the Si IV profile, there are several deep absorption lines with the blueshift of several tens of km s−1. The reason is inferred to be that the bright reconnection region observed in Si IV channel is located under the cooler material appearing as dark features in the Hα line. The blueshifted absorption lines indicate the movement of the cooler material toward the observer. The depth of the absorption lines also depends on the amount of cooler material. These results imply that this kind of spectral profiles can be used as a tool to diagnose the properties of cooler material above reconnection site. **22 March 2019**.

Two-step evolution of a rising flux rope resulting in a confined solar flare

Shuhong **Yang**, Jun Zhang, Qiao Song, Yi Bi, Ting Li
ApJ **878** 38 **2019**
https://arxiv.org/pdf/1905.00808.pdf
https://iopscience.iop.org/article/10.3847/1538-4357/ab1f67/pdf
Combining the Solar Dynamics Observatory and the New Vacuum Solar Telescope observations, we study a confined flare triggered by a rising flux rope within the trailing sunspots of active region 12733. The flux rope lying above the sheared polarity inversion line can be constructed through magnetic extrapolation but could not be detected in multi-wavelength images at the pre-flare stage. The conspicuous shearing motions between the opposite-polarity fields in the photosphere are considered to be responsible for the flux rope formation. The maximum twist of the flux rope is as high as -1.76, and then the flux rope rises due to the kink instability. Only when the flare starts can the flux rope be observed in high-temperature wavelengths. The differential emission measure results confirm that this flux rope is a high-temperature structure. Associated with the rising flux rope, there appear many post-flare loops and a pair of flare ribbons. When the rising flux rope meets and reconnects with the large-scale overlying field lines, a set of large-scale twisted loops are formed, and two flare ribbons propagating in opposite directions appear on the outskirts of the former ribbons, indicating that the twist of the flux rope is transferred to a much larger system. These results imply that the external reconnection between the rising flux rope and the large-scale overlying loops plays an important role in the confined flare formation. **26 January 2019**

Observational Evidence of Magnetic Reconnection Associated with Magnetic Flux Cancellation

Bo **Yang**1,2,3, Jiayan Yang1,2, Yi Bi1,2, Junchao Hong1,2, Haidong Li1,2, Zhe Xu1,2,4, and Hechao Chen
2018 ApJ 861 135 DOI 10.3847/1538-4357/aac37f

Using high spatial and temporal data from the Solar Dynamics Observatory (SDO) and the Interface Region Imaging Spectrograph (IRIS), several observational signatures of magnetic reconnection in the course of magnetic flux cancellation are presented, including two loop–loop interaction processes, multiple plasma blob ejections, and a sheet-like structure that appeared above the flux cancellation sites with a Y-shaped and an inverted Y-shaped end. The IRIS 1400 Å observations show that the plasma blobs were ejected from the tip of the Y-shaped ends of the sheet-like structure. Obvious photospheric magnetic flux cancellation occurred after the first loop–loop interaction and continued until the end of the observation. Complemented by the nonlinear force-free field extrapolation, we found that two sets of magnetic field lines, which revealed an X-shaped configuration, aligned well with the interacted coronal loops. Moreover, a magnetic null point was found to be situated at about 0.9 Mm height, which was right above the flux cancellation sites and located between the two sets of magnetic field lines. These results suggest that the flux cancellation might be a result of the submergence of magnetic field lines following a magnetic reconnection that occurs in the lower atmosphere of the Sun, and the ejected plasma blobs should be plasmoids created in the sheet-like structure due to the tearing-mode instability. This observation reveals a detailed magnetic field structure and a dynamic process above the flux cancellation sites and will help us to understand magnetic reconnection in the lower atmosphere of the Sun.

Mini-filament Eruptions Triggering Confined Solar Flares Observed by ONSET and SDO

Shuhong **Yang**, Jun Zhang
ApJL **2018**
https://arxiv.org/pdf/1806.01763.pdf

Using the observations from the Optical and Near-infrared Solar Eruption Tracer and the Solar Dynamics Observatory, we study an M5.7 flare in AR 11476 on **2012 May 10** and a micro-flare in the quiet Sun on **2017 March 23**. Before the onset of each flare, there is a reverse S-shaped filament above the polarity inversion line. Then the filaments become unstable and begin to rise. The rising filaments gain the upper hand over the tension force of the dome-like overlying loops and thus successfully erupt outward. The footpoints of the reconnecting overlying loops successively brighten and are observed as two flare ribbons, while the newly formed low-lying loops appear as the post-flare loops. These eruptions are similar to the classical model of successful filament eruptions associated with coronal mass ejections. However, the erupting filaments in this study move along large-scale lines and eventually reach the remote solar surface, i.e., no filament material is ejected into the interplanetary space. Thus both the flares are confined ones. These results reveal that some successful filament eruptions can trigger confined flares. Our observations also imply that this kind of filament eruptions may be ubiquitous on the Sun, from active regions with large flares to the quiet Sun with micro-flares.

Automated Solar Flare Detection and Feature Extraction in High-Resolution and Full-Disk H αα Images

Meng **Yang**, Yu Tian, Yangyi Liu, Changhui Rao
Solar Physics May **2018**, 293:81
https://link.springer.com/content/pdf/10.1007%2Fs11207-018-1300-y.pdf

In this article, an automated solar flare detection method applied to both full-disk and local high-resolution Hαα images is proposed. An adaptive gray threshold and an area threshold are used to segment the flare region. Features of each detected flare event are extracted, e.g. the start, peak, and end time, the importance class, and the brightness class. Experimental results have verified that the proposed method can obtain more stable and accurate segmentation results than previous works on full-disk images from Big Bear Solar Observatory (BBSO) and Kanzelhöhe Observatory for Solar and Environmental Research (KSO), and satisfying segmentation results on high-resolution images from the Goode Solar Telescope (GST). Moreover, the extracted flare features correlate well with the data given by KSO. The method may be able to implement a more complicated statistical analysis of Hαα solar flares.
22 June 2015, 2 April 2017, 20 August 2017

Observationally quantified reconnection providing a viable mechanism for active region coronal heating

Kai E. **Yang**, Dana W. Longcope, M. D. Ding, Yang Guo
2018
https://arxiv.org/pdf/1802.06206.pdf

The heating of the Sun's corona has been explained by several different mechanisms including wave dissipation and magnetic reconnection. While both have been shown capable of supplying the requisite power, neither has been used in a quantitative model of observations fed by measured inputs. Here we show that impulsive reconnection is capable of producing an active region corona agreeing both qualitatively and quantitatively with extreme-ultraviolet observations. We calculate the heating power proportional to the velocity difference between magnetic footpoints and the photospheric plasma, called the non-ideal velocity. The length scale of flux elements reconnected in the corona is found to be around 160 km. The differential emission measure of the model corona agrees with that derived using multi-wavelength images. Synthesized extreme-ultraviolet images resemble observations both in their loop-dominated appearance and their intensity histograms. This work provides compelling evidence that impulsive reconnection events are a viable mechanism for heating the corona.

Block-induced complex structures building the flare-productive solar active region 12673

Shuhong **Yang**, Jun Zhang, Xiaoshuai Zhu, Qiao Song
ApJL **849** L21 **2017**
https://arxiv.org/pdf/1710.06545.pdf
http://sci-hub.tw/10.3847/2041-8213/aa9476
Solar active region (AR) 12673 produced 4 X-class, 27 M-class, and numerous lower class flares during its passage across the visible solar disk in **September 2017**. Our study is to answer the questions why this AR was so flare-productive and how the X9.3 flare, the largest one of the last decade, took place. We find that there was a sunspot in the initial several days, and then two bipolar regions emerged nearby it successively. Due to the standing of the pre-existing sunspot, the movement of the bipoles was blocked, while the pre-existing sunspot maintained its quasi-circular shaped umbra only with the disappearance of a part of penumbra. Thus, the bipolar patches were significantly distorted, and the opposite polarities formed two semi-circular shaped structures. After that, two sequences of new bipolar regions emerged within the narrow semi-circular zone, and the bipolar patches separated along the curved channel. The new bipoles sheared and interacted with the previous ones, forming a complex topological system, during which numerous flares occurred. At the highly sheared region, a great deal of free energy was accumulated. On **September 6,** one negative patch near the polarity inversion line began to rapidly rotate and shear with the surrounding positive fields, and consequently the X9.3 flare erupted. Our results reveal that the block-induced complex structures built the flare-productive AR and the X9.3 flare was triggered by an erupting filament due to the kink instability. To better illustrate this process, a block-induced eruption model is proposed for the first time.

A STATISTICAL STUDY OF FLARE PRODUCTIVITY ASSOCIATED WITH SUNSPOT PROPERTIES IN DIFFERENT MAGNETIC TYPES OF ACTIVE REGIONS

Ya-Hui **Yang**1, Min-Shiu Hsieh2, Hsiu-Shan Yu3, and P. F. Chen4
2017 ApJ 834 150 **File**
http://sci-hub.cc/doi/10.3847/1538-4357/834/2/150
It is often believed that intense flares preferentially originate from the large-size active regions (ARs) with strong magnetic fields and complex magnetic configurations. This work investigates the dependence of flare activity on the AR properties and clarifies the influence of AR magnetic parameters on the flare productivity, based on two data sets of daily sunspot and flare information as well as the GOES soft X-ray measurements and HMI vector magnetograms. By considering the evolution of magnetic complexity, we find that flare behaviors are quite different in the short- and long-lived complex ARs and the ARs with more complex magnetic configurations are likely to host more impulsive and intense flares. Furthermore, we investigate several magnetic quantities and perform the two-sample Kolmogorov–Smirnov test to examine the similarity/difference between two populations in different types of ARs. Our results demonstrate that the total source field strength on the photosphere has a good correlation with the flare activity in complex ARs. It is noted that intense flares tend to occur at the regions of strong source field in combination with an intermediate field-weighted shear angle. This result implies that the magnetic free energy provided by a complex AR could be high enough to trigger a flare eruption even with a moderate magnetic shear on the photosphere. We thus suggest that the magnetic free energy represented by the source field rather than the photospheric magnetic complexity is a better quantity to characterize the flare productivity of an AR, especially for the occurrence of intense flares.
1-5 Sept 2011, 6-10 Nov 2013, 6-10 July 2014

OBSERVATIONS OF THE GROWTH OF AN ACTIVE REGION FILAMENT

Bo **Yang**1,2, Yunchun Jiang1, Jiayan Yang1, Yi Bi1,2, and Haidong Li
2016 ApJ 830 16
We present observations of the growth of an active region filament caused by magnetic interactions among the filament and its adjacent superpenumbral filament (SF) and dark thread-like structures (T). Multistep reconnections are identified during the whole growing process. Magnetic flux convergence and cancellation occurring at the positive footpoint region of the filament is the first step reconnection, which resulted in the filament bifurcating into two sets of intertwined threads. One set anchored in situ, while the other set moved toward and interacted with the SF and part of T.

This indicates the second step reconnection, which gave rise to the disappearance of the SF and the formation of a long thread-like structure that connects the far ends of the filament and T. The long thread-like structure further interacted with the T and then separated into two parts, representing the third step reconnection. Finally, another similar long thread-like structure, which intertwined with the fixed filament threads, appeared. H α observations show that this twisted structure is a longer sinistral filament. Based on the observed photospheric vector magnetograms, we performed a non-linear force-free field extrapolation to reconstruct the magnetic fields above the photosphere and found that the coronal magnetic field lines associated with the filament consists of two twisted flux ropes winding around each other. These results suggest that magnetic interactions among filaments and their adjacent SFs and T could lead to the growth of the filaments, and the filament is probably supported in a flux rope.

Quantifying the Topology and Evolution of a Magnetic Flux Rope Associated with Multi-flare Activities

Kai **Yang**, Yang Guo, M. D. Ding
ApJ **824** 148 **2016**
http://arxiv.org/pdf/1604.07502v1.pdf
Magnetic flux rope (MFR) plays an important role in solar activities. A quantitative assessment of the topology of an MFR and its evolution is crucial for a better understanding of the relationship between the MFR and the associated activities. In this paper, we investigate the magnetic field of active region 12017 from **2014 March 28 to 29**, where 12 flares were triggered by the intermittent eruptions of a filament (either successful or confined). Using the vector magnetic field data from the Helioseismic and Magnetic Imager on board the \textit{Solar Dynamics Observatory}, we calculate the magnetic energy and helicity injection in the active region, and extrapolate the 3D magnetic field with a nonlinear force-free field model. From the extrapolations, we find an MFR that is cospatial with the filament. We further determine the configuration of this MFR by a closed quasi-separatrix layer (QSL) around it. Then, we calculate the twist number and the magnetic helicity for the field lines composing the MFR. The results show that the closed QSL structure surrounding the MFR gets smaller as a consequence of the flare occurrence. We also find that the flares in our sample are mainly triggered by kink instability. Moreover, the twist number varies more sensitively than other parameters to the occurrence of flares.

On the 2012 October 23 circular ribbon flare: emission features and magnetic topology

Kai **Yang**, Yang Guo, M. D. Ding
2015 *ApJ* **806** 171
http://arxiv.org/pdf/1505.02914v1.pdf
Circular ribbon flares are usually related to spine-fan type magnetic topology containing null-points. In this paper, we investigate an X-class circular ribbon flare on 2012 October 23, using the multi-wavelength data from the \textit{Solar Dynamics Observatory}, \textit{Hinode}, and the \textit{Ramaty High Energy Solar Spectroscopic Imager}. In \ion{Ca}{2} H emission, the flare showed three ribbons with two highly elongated ones inside and outside a quasi-circular one, respectively. A hot channel was displayed in the extreme ultraviolet (EUV) emissions that infers the existence of a magnetic flux rope. Two hard X-ray (HXR) sources in the 12--25 keV energy band were located at the footpoints of this hot channel. Using a nonlinear force-free magnetic field extrapolation, we identify three topological structures: (1) a 3D null-point, (2) a flux rope below the fan of the null-point, and (3) a large-scale quasi-separatrix layers (QSL) induced by the quadrupolar-like magnetic field of the active region. We find that the null-point is embedded within the large-scale QSL. In our case, all three identified topological structures must be considered to explain all the emission features associated with the observed flare. Besides, the HXR sources are regarded as the consequence of the reconnection within or near the border of the flux rope.

Magnetic reconnection between small-scale loops observed with the New Vacuum Solar Telescope

Shuhong **Yang**, Jun Zhang, and Yongyuan Xiang
ApJL, **798** L11 **2015**.
Animations: http://ourstar.bao.ac.cn/~shuhongyang/files/apjl_reconnection/
Using the high tempo-spatial resolution H α images observed with the New Vacuum Solar Telescope, we report the solid observational evidence of magnetic reconnection between two sets of small-scale anti-parallel loops with an X-shaped topology. The reconnection process contains two steps: a slow step with the duration of more than several tens of minutes, and a rapid step lasting for only about three minutes. During the slow reconnection, two sets of anti-parallel loops reconnect gradually, and new loops are formed and stacked together. During the rapid reconnection, the anti-parallel loops approach each other quickly, and then the rapid reconnection takes place, resulting in the disappearance of former loops. In the meantime, new loops are formed and separate. The region between the approaching loops is brightened, and the thickness and length of this region are determined to be about 420 km and 1.4 Mm, respectively. During the rapid reconnection process, obvious brightenings at the reconnection site and apparent material ejections

outward along reconnected loops are observed. These observed signatures are consistent with predictions by reconnection models. We suggest that the successive slow reconnection changes the conditions around the reconnection site and triggers instabilities, thus leading to the rapid approach of the anti-parallel loops and resulting in the rapid reconnection. **2014 February 3,**

Fine Structures and Overlying Loops of Confined Solar Flares

Shuhong **Yang**, Jun Zhang, and Yongyuan Xiang
ApL, 793 L28 **2014**
http://arxiv.org/pdf/1412.1314v1.pdf
http://arxiv.org/pdf/1409.0471v1.pdf
Using the H$ α observations from the New Vacuum Solar Telescope at Fuxian Solar Observatory, we focus on the fine structures of three confined flares and the issue why all the three flares are confined instead of eruptive. All the three confined flares take place successively at the same location and have similar morphologies, so can be termed homologous confined flares. In the simultaneous images obtained by the Solar Dynamics Observatory, many large-scale coronal loops above the confined flares are clearly observed in multi-wavelengths. At the pre-flare stage, two dipoles emerge near the negative sunspot, and the dipolar patches are connected by small loops appearing as arch-shaped H$ α fibrils. There exists a reconnection between the small loops, and thus the H$ α fibrils change their configuration. The reconnection also occurs between a set of emerging H$ α fibrils and a set of pre-existing large loops, which are rooted in the negative sunspot, a nearby positive patch, and some remote positive faculae, forming a typical three-legged structure. During the flare processes, the overlying loops, some of which are tracked by activated dark materials, do not break out. These direct observations may illustrate the physical mechanism of confined flares, i.e., magnetic reconnection between the emerging loops and the pre-existing loops triggers flares and the overlying loops prevent the flares from being eruptive. 2013 October 12

Magnetic-Reconnection Generated Shock Waves as a Driver of Surges

Heesu **Yang**, Jongchul Chae , Eun-Kyung Lim, Kyoung-Sun Lee , Hyungmin Park , Dong-uk Song , Kyuhyoun Cho
E-print, April **2014**; ApJL
http://astro.snu.ac.kr/~yang/ms_hsyang.pdf
We found that a surge consists of multiple shock features. In our high spatio-temporal spectroscopic observation of the surge using Fast Imaging Solar Spectrograph of the 1.6 meter New Solar Telescope at Big Bear Solar Observatory, each shock is identified with the sudden appearance of an absorption feature at the blue wings of the Ca II 8542 ? line and Hα line that gradually shifts to the red wings. The shock features are overlapped with one another with an time interval of 110 s, which is much shorter than the duration of each shock feature 300 - 400 s. This finding suggests that the multiple shocks may not have been originated from a train of sinusoidal waves generated by oscillations and flows in the photosphere. As we found the signature of the magnetic flux cancellations at the base of the surge, we conclude that the multiple shock waves in charge of the surge were generated by the magnetic reconnection in the low atmosphere associated with the flux cancellation.

Characteristics of the Photospheric Magnetic Field Associated with Solar Flare Initiation

Ya-Hui **Yang**1, P. F. Chen2, Min-Shiu Hsieh3, S. T. Wu4, Han He5, and Tsung-Che Tsa
2014 ApJ 786 72
The physical environment governing the solar flare initiation is not fully understood, although there are significant efforts to address the relationship between magnetic non-potential parameters and early flare signatures. In this study, we attempt to characterize the flare initiation based on the processed Helioseismic and Magnetic Imager vector magnetograms, Atmospheric Imaging Assembly 1600 Å, and RHESSI hard X-ray observations. Three flare events, the M6.6 flare on **2011 February 13**, the X2.2 flare on **2011 February 15**, and the X2.1 flare on **2011 September 6**, in two active regions AR 11158 and AR 11283 are investigated. We analyze the source field strength in the photosphere, which is defined as the magnitude of the observed magnetic field deviation from the potential field. It is found that one of the strong source field regions above the magnetic polarity inversion line well connects the initial bright kernels of two conjugate ribbons. The results imply that the distribution of the photospheric source field strength can be used to locate the initiation site of flaring loops regardless of the configuration of pre-flare magnetic fields or the evolution of active regions. Moreover, the field configuration in the strong source field regions tends to become more inclined after flares, which is consistent with the coronal implosion scenario. We also employ a fast method to derive the total current density from the photospheric vector magnetogram in the framework of force-free field. This method can provide fast

estimation of photospheric current density within a reasonable accuracy without appealing for the more accurate calculation from a model extrapolation.

Properties of Solar Ephemeral Regions at the Emergence Stage

Shuhong **Yang**, Jun Zhang
E-print, Dec **2013**; ApJ
For the first time, we statistically study the properties of ephemeral regions (ERs) and quantitatively determine their parameters at the emergence stage based on a sample of 2988 ERs observed by the Solar Dynamics Observatory. During the emergence process, there are three kinds of kinematic performances, i.e., separation of dipolar patches, shift of ER's magnetic centroid, and rotation of ER's axis. The average emergence duration, flux emergence rate, separation velocity, shift velocity, and angular speed are 49.3 min, 2.6 ? 10^15 Mx s^−1, 1.1 km s^−1, 0.9 km s^−1, and 0degr.6 min^−1, respectively. At the end of emergence, the mean magnetic flux, separation distance, shift distance, and rotation angle are 9.3 ? 10^18 Mx, 4.7 Mm, 1.1 Mm, and 12degr.9, respectively. We also find that the higher the ER magnetic flux is, (1) the longer the emergence lasts, (2) the higher the flux emergence rate is, (3) the further the two polarities separate, (4) the lower the separation velocity is, (5) the larger the shift distance is, (6) the slower the ER shifts, and (7) the lower the rotation speed is. However, the rotation angle seems not to depend on the magnetic flux. Not only at the start time, but also at the end time, the ERs are randomly oriented in both the northern and the southern hemispheres. Besides, neither the anticlockwise rotated ERs, nor the clockwise rotated ones dominate the northern or the southern hemisphere.

Hard X-ray Footpoint Asymmetry

Ya-Hui **YANG**
RHESSI Science Nugget, No. 212, Nov **2013**
http://sprg.ssl.berkeley.edu/~tohban/wiki/index.php/Hard_X-ray_Footpoint_Asymmetry
Our statistical results show that 75% of the strong HXR footpoints coincide with the weaker magnetic field strengths, which is qualitatively consistent with the prediction of an asymmetric magnetic mirror scenario. Even so, it must be emphasized that the properties of HXR footpoint asymmetry are also affected by other transport effects and coronal acceleration process besides the asymmetric magnetic mirror. It is difficult to attribute the footpoint asymmetry purely to a single effect for solar flares. It would be worthwhile to investigate further the causes of footpoint asymmetry reversal during different flaring periods or between different energy ranges.

Magnetic Nonpotentiality in Photospheric Active Regions as a Predictor of Solar Flares

Xiao **Yang**, GangHua Lin, HongQi Zhang, XinJie Mao
E-print, Aug **2013**, **2013** ApJ 774 L27
Based on several magnetic nonpotentiality parameters obtained from the vector photospheric active region magnetograms obtained with the Solar Magnetic Field Telescope at the Huairou Solar Observing Station over two solar cycles, a machine learning model has been constructed to predict the occurrence of flares in the corresponding active region within a certain time window. The Support Vector Classifier, a widely used general classifier, is applied to build and test the prediction models. Several classical verification measures are adopted to assess the quality of the predictions. We investigate different flare levels within various time windows, and thus it is possible to estimate the rough classes and erupting times of flares for particular active regions. Several combinations of predictors have been tested in the experiments. The True Skill Statistics are higher than 0.36 in 97% of cases and the Heidke Skill Scores range from 0.23 to 0.48. The predictors derived from longitudinal magnetic fields do perform well, however they are less sensitive in predicting large flares. Employing the nonpotentiality predictors from vector fields improves the performance of predicting large flares of magnitude geqM5.0 and geqX1.0.

ASYMMETRY OF HARD X-RAY EMISSIONS AT CONJUGATE FOOTPOINTS IN SOLAR FLARES

Ya-Hui **Yang**1, C. Z. Cheng2,3, Säm Krucker4,5, Min-Shiu Hsieh6, and Nai-Hwa Chen
2012 ApJ 756 42
The chromospheric double hard X-ray (HXR) sources generally appear at the conjugate footpoints of flaring loops with asymmetric flux distributions. The behavior of such HXR footpoint asymmetry should be affected by several effects simultaneously and cannot be attributed to a single effect easily. In this study, we attempt to address the properties of photospheric magnetic fields in the areas coinciding with asymmetric HXR footpoints based on RHESSI observations during 2002-2009. A total of 172 time intervals in 22 flares closed to the solar disk center with available pre-flare MDI magnetograms are investigated. The strong HXR footpoint is found to preferentially (75%) locate at the region with weak magnetic field strength, which is qualitatively consistent with the asymmetric magnetic mirror scenario. The HXR

footpoint fluxes become more asymmetric when the footpoints move to the areas with more asymmetric field strength. A feature of asymmetry reversal between different energy ranges is observed in some flares, although no significant energy dependence of footpoint asymmetry is found in our statistical results. We also investigated the possible causes of time-dependent HXR footpoint asymmetry by examining the **2004 November 4** M5.4 flare and the **2004 November 6** M3.6 flare. By comparing the estimated asymmetry quantities with the HXR light curves, the asymmetry reversal in the late period of the M5.4 flare is mainly attributed to the difference of coronal energy release or acceleration processes in different periods, while it is associated with the location changes of HXR footpoints moving to different magnetic field regions in the M3.6 flare.

A Statistical Study on Photospheric Magnetic Nonpotentiality of Active Regions and Its Relationship with Flares During Solar Cycles 22 - 23

Xiao **Yang**, HongQi Zhang, Yu Gao, Juan Guo and GangHua Lin

E-print, July **2012**, Solar Phys**.** Volume 280, Number 1 (2012), 165-181

A statistical study is carried out on the photospheric magnetic nonpotentiality in solar active regions and its relationship with associated flares. We select 2173 photospheric vector magnetograms from 1106 active regions observed by the Solar Magnetic Field Telescope at Huairou Solar Observing Station, National Astronomical Observatories of China, in the period of 1988 ? 2008, which covers most of the 22nd and 23rd solar cycles. We have computed the mean planar magnetic shear angle (overline{Deltaphi}), mean shear angle of the vector magnetic field (overline{Deltapsi}), mean absolute vertical current density (overline{|Jz|}), mean absolute current helicity density (overline{|hc|}), absolute twist parameter (α av|), mean free magnetic energy density (overline{ hofree}), effective distance of the longitudinal magnetic field (dE), and modified effective distance (dEm) of each photospheric vector magnetogram. Parameters overline{|hc|}, overline{ hofree}, and dEm show higher correlations with the evolution of the solar cycle. The Pearson linear correlation coefficients between these three parameters and the yearly mean sunspot number are all larger than 0.59. Parameters overline{Deltaphi}, overline{Deltapsi}, overline{|Jz|}, α av|, and dE show only weak correlations with the solar cycle, though the nonpotentiality and the complexity of active regions are greater in the activity maximum periods than in the minimum periods. All of the eight parameters show positive correlations with the flare productivity of active regions, and the combination of different nonpotentiality parameters may be effective in predicting the flaring probability of active regions.

ESTIMATION OF THE RECONNECTION ELECTRIC FIELD IN THE 2003 OCTOBER 29 X10 FLARE

Ya-Hui **Yang**1, C. Z. Cheng1,2,3, Säm Krucker4,5 and Min-Shiu

2011 ApJ 732 15

The electric field in the reconnecting current sheet of the 2003 October 29 X10 flare is estimated to be a few kV m–1 in this study, based on the rate of change in the photospheric magnetic flux in the newly brightened areas of Transition Region and Coronal Explorer (TRACE) UV ribbons. For comparison, the motion speed of Reuven Ramaty High Energy Solar Spectroscopic Imager (RHESSI) hard X-ray (HXR) footpoints and the photospheric magnetic field strength are also used for the electric field calculation. This X10 flare event is selected due to its distinct two-phase HXR kernel motion, two arcade systems with different magnetic shear, and the high cadence and complete coverage of the TRACE 1600 Å Michelson Doppler Imager (MDI) magnetogram and RHESSI HXR observations. We pay particular attention to the electric field characteristics in different flare phases, as well as the temporal correlation with the HXR emission and its power-law spectral index and the photospheric magnetic field strength. We found that in the early impulsive phase, the reconnection electric field peaks just before the HXR emission peaks and the energy spectrum hardens. The result is consistent with the scenario that more particles are accelerated to higher energies by larger reconnection electric fields and then precipitate into the lower chromosphere to produce stronger HXR emissions. Such a particle acceleration mechanism plays its most significant role in the impulsive phase of this flare. In addition, our results provide evidence that the highly sheared magnetic field lines are mapped to the magnetic reconnection diffusion region to produce a large reconnection electric field.

Magnetic helicity accumulation and tilt angle evolution of newly emerging active regions

S. **Yang**1, 2, H. Zhang1, and J. Büchner2

A&A 502, 333-340 (**2009**)

DOI: 10.1051/0004-6361/200810032

Context. It has been known for years that there is a general dominance of negative (positive) helicity of active regions (ARs) in the northern (southern) solar hemisphere. For a better understanding of the role of helicity in the evolution of

active regions, it is necessary to know more about the accumulation of helicity during the emergence of active regions. In particular, different conclusions were drawn in the past about the relationship between the accumulated helicity and the writhe of active regions.
Aims. We investigate the accumulation of helicity in newly emerging simple bipolar solar active regions. We also investigate the relation between the accumulated helicity and writhe.
Methods. We obtain helicity accumulation by applying Fast Fourier Transforms (FFT) and local correlation tracking (LCT) to MDI data. We deduce the writhe of the active regions according to the evolution of the tilt angle between the connecting line of the weighting centers of opposite polarities in the ARs.

Results. It is found that the accumulated helicity is proportional to the exponent of magnetic flux $(|H| \propto \Phi^{1.85})$ in the 58 selected newly emerged simple ARs. 74% of ARs have a negative (positive) helicity when the above defined tilt angle rotates clockwise (counter-clockwise). This means that the accumulated helicity and writhe have the same sign for most of the investigated ARs according to the tilt angle evolution of ARs. We also found that 56% (57.6%) of these ARs in the northern (southern) photosphere provide negative (positive) helicity to the corona in the course of the emergence of magnetic flux.

MAGNETIC HELICITY EXCHANGE BETWEEN NEIGHBORING ACTIVE REGIONS

S. **Yang**, J. B¨ uchner2, and H. Zhang1
Astrophysical Journal, 695:L25–L30, **2009** April
http://www.iop.org/EJ/toc/-alert=43192/1538-4357/695/1
Addressing the long-lasting problem of the magnetic helicity distribution in the solar corona, a proof for magnetic helicity exchange between two neighboring emerging active regions (ARs) was found: when AR 9188 emerged, it first started to accumulate positive helicity, while the later neighboring emerging AR 9192 accumulated negative helicity. At a later time, after the bright connecting loops became visible between the two ARs, AR 9188 also suddenly started to gain negative helicity. At the same time AR 9192 started to loose negative helicity. It was found that the magnetic helicity fluxes of the two ARs changed simultaneously by almost the same amount. At one instant it was even possible to determine that the connecting loop between the two ARs carried negative helicity. We excluded the possibility that magnetic flux emergence was causing the observed variation of the magnetic helicity. Hence, magnetic helicity was indeed transferred from the late emerging AR 9192 to AR 9188 via an unbalanced magnetic torque along the loop. Such kinds of helicity transfer might be a common mechanism of redistribution of magnetic helicity in the solar atmosphere, which has just not been widely observed yet.
8-9 Oct 2000.

A STATISTICAL STUDY OF HARD X-RAY FOOTPOINT MOTIONS IN LARGE SOLAR FLARES

Ya-Hui **Yang**1, C. Z. Cheng1,2, S¨am Krucker3, R. P. Lin3,4, andW. H. Ip
Astrophysical Journal, 693:132–139, **2009** March 1
A statistical analysis of the temporal evolution of hard X-ray (HXR) footpoint motions in 27 M- and X-class solar flares observed by the Reuven Ramaty High Energy Solar Spectroscopic Imager is presented. Extreme UV images from TRACE and SOHO/EIT, Hα images, and magnetograms from SOHO/MDI are used to put the HXR footpoint motions in context of flare ribbons and the magnetic neutral line. Footpoint motions are often found to be complex making a statistical analysis difficult. In an attempt to simplify the analysis, each event was searched for motions predominantly parallel and predominantly perpendicular to the neutral line or flare ribbons. Four kinds of complex motions are described and their relationships to the possible magnetic reconnection processes are discussed. In the soft X-ray (SXR) rise phase, motions along the neutral line or flare ribbons are most common (20 out of 27) and only two events show perpendicular motions (for the remaining five events a simple classification was not possible). However, at later times around the SXR peak, perpendicular motion is more frequently observed (~ 40%) than motions along the neutral line or ribbons ~ 27%). The preference of HXR kernels appearing at the footpoints of highly-sheared magnetic loops at the start of the SXR rise phase is consistent with the magnetic reconnection theory that the reconnection occurring at sheared magnetic arcade field lines produces most HXR energy release in the impulsive phase of large flares.

Widespread Occurrence of High-Velocity Upflows in Solar Active Regions

S. L. **Yardley**, D. H. Brooks, D. Baker
A&A 650, L10 **2021**
https://arxiv.org/pdf/2106.01396.pdf
https://www.aanda.org/articles/aa/pdf/2021/06/aa41131-21.pdf
https://doi.org/10.1051/0004-6361/202141131

We performed a systematic study of 12 active regions (ARs) with a broad range of areas, magnetic flux and associated solar activity in order to determine whether there are upflows present at the AR boundaries and if these upflows exist, whether there is a high speed asymmetric blue wing component present in the upflows. To identify the presence and locations of the AR upflows we derive relative Doppler velocity maps by fitting a Gaussian function to {\it Hinode}/EIS Fe XII 192.394\,Å line profiles. To determine whether there is a high speed asymmetric component present in the AR upflows we fit a double Gaussian function to the Fe XII 192.394\,Å mean spectrum that is computed in a region of interest situated in the AR upflows. Upflows are observed at both the east and west boundaries of all ARs in our sample with average upflow velocities ranging between -5 to -26~km s−1. A blue wing asymmetry is present in every line profile. The intensity ratio between the minor high speed asymmetric Gaussian component compared to the main component is relatively small for the majority of regions however, in a minority of cases (8/30) the ratios are large and range between 20 to 56~\%. These results suggest that upflows and the high speed asymmetric blue wing component are a common feature of all ARs. **31 Jan 2011, 15 Apr 2011**
Table 1. The NOAA ARs and EIS data used in this study (2010-2011)

A Comparative Study of Confined and Eruptive Solar Flares using Microwave Observations

Yashiro, S.; Akiyama, S.; Masuda, S.; Shimojo, M.; Asai, A.; Imada, S.; Gopalswamy, N.
American Geophysical Union, Fall Meeting **2015**, **abstract** #SH43B-2447
It is well known that about 10% X-class solar flares are not associated with coronal mass ejections (CMEs). These flares are referred to as confined flares, which are not associated with mass or energetic particles leaving the Sun. However, electrons are accelerated to MeV energies as indicated by the presence of microwave emission with a turnover frequency of ~15 GHz (Gopalswamy et al. 2009, IAU Symposium 257, p. 283). In this paper, we extend the study of confined flares to lower soft X-ray flare sizes (M and above) that occurred in the time window of the Nobeyama Radioheliograph (NoRH). We also make use of the microwave spectral information from the Nobeyama Radio Polarimeters (NoRP). During 1996 - 2014, NoRH and NoRP observed 663 flares with size M1.0 or larger. Using the CME observations made by SOHO/LASCO and STEREO/SECCHI, we found 215 flares with definite CME association (eruptive flares) and 202 flares that definitely lacked CMEs (confined flares). The remaining 146 flares whose CME association is unclear are excluded from the analysis. We examined the peak brightness temperature and the spatial size obtained by NoRH. Although there is a large overlap between the two populations in these properties, we found that microwave sources with the largest spatial extent and highest brightness temperature are associated with eruptive flares. Spectral analysis using NoRP data showed a tendency that more confined flares had higher turnover frequency (≥17 GHz). We also compare the NoRH images with the photospheric magnetograms to understand the difference in the magnetic structure of the two types of flare sources.

Three-dimensional simulation of thermodynamics on confined turbulence in a large-scale CME-flare current sheet

Jing **Ye**, John C. Raymond, Zhixing Mei, Qiangwei Cai, Yuhao Chen, Yan Li, Jun Lin
ApJ **2023**
https://arxiv.org/pdf/2308.09496.pdf
Turbulence plays a key role for forming the complex geometry of the large-scale current sheet (CS) and fast energy release in a solar eruption. In this paper, we present full 3D high-resolution simulations for the process of a moderate Coronal Mass Ejection (CME) and the thermodynamical evolution of the highly confined CS. Copious elongated blobs are generated due to tearing and plasmoid instabilities giving rise to a higher reconnection rate and undergo the splitting, merging and kinking processes in a more complex way in 3D. A detailed thermodynamical analysis shows that the CS is mainly heated by adiabatic and numerical viscous terms, and thermal conduction is the dominant factor that balances the energy inside the CS. Accordingly, the temperature of the CS reaches to a maximum of about 20 MK and the range of temperatures is relatively narrow. From the face-on view in the synthetic Atmospheric Imaging Assembly 131 A˚, the downflowing structures with similar morphology to supra-arcade downflows are mainly located between the post-flare loops and loop-top, while moving blobs can extend spikes higher above the loop-top. The downward-moving plasmoids can keep the twisted magnetic field configuration until the annihilation at the flare loop-top, indicating that plasmoid reconnection dominates in the lower CS. Meanwhile, the upward-moving ones turn into turbulent structures before arriving at the bottom of the CME, implying that turbulent reconnection dominates in the upper CS. The spatial distributions of the turbulent energy and anisotropy are addressed, which show a significant variation in the spectra with height.

Detailed analysis of dynamic evolution of three Active Regions before flare and CME occurrence at the photospheric level

Yudong **Ye**, M. B. Korsos, R. Erdelyi
Advances in Space Research Volume 61, Issue 2, 15 January **2018**, Pages 673-682
https://arxiv.org/pdf/1801.00430.pdf
We present a combined analysis of the applications of the weighted horizontal magnetic gradient (denoted as WG_M in Korsos et al., ApJ, 802, L21, 2015) method and the magnetic helicity tool (Berger & Field, JFM, 147, 133, 1984)

employed for three active regions (ARs), namely NOAA AR11261, AR11283 and AR11429. All three active regions produced series flares and CMEs. We followed the evolution of the components of the WG_M and the magnetic helicity before the flare and CME occurrences. We found an unique and mutually shared behavior, called the U-shaped pattern, of the weighted distance component of WG_M and of the shearing component of the helicity flux before the flare and CME eruptions. This common pattern is associated with the decreasing-receding phase yet reported only known to be a necessary feature prior to solar flare eruption(s), but found now at the same time in the evolution of the shearing helicity parameter. This result leads to the conclusion that (i) the shearing motion of photospheric magnetic field may be a key driver for the solar eruption in addition to the flux emerging process, and that (ii) the found decreasing-approaching pattern in the evolution of shearing helicity may be another precursor indicator for improving the forecasting of solar eruptions. **30/07/-04/08/ 2011, 06-09/09/2011, 05-10/03/2012**

Irreversible Rapid Changes of Magnetic Field Associated with the 2012 October 23 Circular Near-limb X1.8 Flare

Dandan **Ye**, Chang Liu, Haimin Wang
Research in Astronomy and Astrophysics **(**RAA) **2016**
http://arxiv.org/pdf/1602.02080v1.pdf
It has been found that photospheric magnetic fields can change in accordance with the three-dimensional magnetic field restructuring following solar eruptions. Previous studies mainly use vector magnetic field data taken for events near the disk center. In this paper, we analyze the magnetic field evolution associated with the 2012 October 23 X1.8 flare in NOAA AR 11598 that is close to the solar limb, using both the 45 s cadence line-of-sight and 12 minute cadence vector magnetograms from the Helioseismic and Magnetic Imager on board Solar Dynamic Observatory. This flare is classified as a circular-ribbon flare with spine-fan type magnetic topology containing a null point. In the line-of-sight magnetograms, there are two apparent polarity inversion lines (PIL). The PIL closer to the limb is affected more by the projection effect. Between these two PILs there lie positive polarity magnetic fields, which are surrounded by negative polarity fields outside the PILs. We find that after the flare, both the apparent limb-ward and disk-ward negative fluxes decrease, while the positive flux in-between increases. We also find that the horizontal magnetic fields have a significant increase along the disk-ward PIL, while in surrounding area, they decrease. Synthesizing the observed field changes, we conclude that the magnetic fields collapse toward the surface above the disk-ward PIL as depicted in the coronal implosion scenario, while the peripheral field turns to a more vertical configuration after the flare. We also suggest that this event is an asymmetric circular-ribbon flare: a flux rope is likely present above the disk-ward PIL. Its eruption causes the instability of the entire fan-spine structure and the implosion near that PIL.

Automated Driving for Global Nonpotential Simulations of the Solar Corona

Anthony R. **Yeates**1 and Prantika Bhowmik1
2022 ApJ 935 13
https://iopscience.iop.org/article/10.3847/1538-4357/ac7de4/pdf
We describe a new automated technique for active region emergence in coronal magnetic field models, based on the inversion of the electric field locally from a single line-of-sight magnetogram for each region. The technique preserves the arbitrary shapes of magnetic field distribution associated with individual active regions and incorporates emerging magnetic helicity (twist) in a parametrized manner through a noninductive electric field component. We test the technique with global magnetofrictional simulations of the coronal magnetic field during Solar Cycle 24 Maximum from 2011 June 1 to 2011 December 31. The active regions are determined in a fully automated and objective way using Spaceweather HMI Active Region Patch (SHARP) data. Our primary aim is to constrain two free parameters in the emergence algorithm: the duration of emergence and the twist parameter for each individual active region. While the duration has a limited effect on the resulting coronal magnetic field, changing the sign and amplitude of the twist parameters profoundly influences the amount of nonpotentiality generated in the global coronal magnetic field. We explore the possibility of constraining both the magnitude and sign of the twist parameter using estimates of the current helicity derived from vector magnetograms and supplied in the SHARP metadata for each region. Using the observed sign of twist for each region reduces the overall nonpotentiality in the corona, highlighting the importance of scatter in the emerging active region helicities. **17 Nov 2012**

Modulational Instability of Fast Sausage Mode as One of the Possible Mechanisms for Quasiperiodic Pulsations during Solar Flares

Naga Varun **Yelagandula**1
2021 ApJ 923 131
https://iopscience.iop.org/article/10.3847/1538-4357/ac2e07/pdf
https://doi.org/10.3847/1538-4357/ac2e07
Quasiperiodic pulsations (QPPs) are frequently observed in the entire range of the electromagnetic spectrum during solar flares, and there can be many possible mechanisms leading to this phenomenon. In the present work, we demonstrate the possibility of the generation of QPPs by a nonlinear fast sausage mode in a coronal loop. The coronal loop itself is represented by an infinitely long homogenous magnetic flux tube, which in many cases is a good

approximation, and the nonlinearity of the fast sausage mode is modeled by the nonlinear Schrödinger equation (NSE) with a cubic nonlinearity. We have shown that the frequency-renormalized plane wave solution, which happens to be an exact solution of the NSE, transforms into a series of quasiperiodic oscillations (QPOs) due to the so-called modulational instability or the Benjamin–Feir instability. Our numerical solutions show that such QPOs evolve at almost every point above a certain height along the magnetic flux tube, which represents the coronal loop. As the fast sausage mode perturbs the plasma density strongly, the density perturbations caused by the QPOs of the nonlinear fast sausage mode correspondingly modulate the radiation throughout the electromagnetic spectrum, resulting in the emergence of the corresponding QPPs. This mechanism should therefore be able to describe some of the observed QPPs.

Feature Selection on a Flare Forecasting Testbed: A Comparative Study of 24 Methods

Atharv **Yeoleka**, Sagar Patel, Shreejaa Talla, Krishna Rukmini Puthucode, Azim Ahmadzadeh, Viacheslav M. Sadykov, Rafal A. Angryk

IEEE ICDM 2021, SFE-TSDM Workshop **2021**

https://arxiv.org/pdf/2109.14770.pdf

The Space-Weather ANalytics for Solar Flares (SWAN-SF) is a multivariate time series benchmark dataset recently created to serve the heliophysics community as a testbed for solar flare forecasting models. SWAN-SF contains 54 unique features, with 24 quantitative features computed from the photospheric magnetic field maps of active regions, describing their precedent flare activity. In this study, for the first time, we systematically attacked the problem of quantifying the relevance of these features to the ambitious task of flare forecasting. We implemented an end-to-end pipeline for preprocessing, feature selection, and evaluation phases. We incorporated 24 Feature Subset Selection (FSS) algorithms, including multivariate and univariate, supervised and unsupervised, wrappers and filters. We methodologically compared the results of different FSS algorithms, both on the multivariate time series and vectorized formats, and tested their correlation and reliability, to the extent possible, by using the selected features for flare forecasting on unseen data, in univariate and multivariate fashions. We concluded our investigation with a report of the best FSS methods in terms of their top-k features, and the analysis of the findings. We wish the reproducibility of our study and the availability of the data allow the future attempts be comparable with our findings and themselves.

Application of Deep Reinforcement Learning to Major Solar Flare Forecasting

Kangwoo **Yi**1, Yong-Jae Moon1,2, and Hyun-Jin Jeong2

2023 ApJS 265 34

https://iopscience.iop.org/article/10.3847/1538-4365/acb76d/pdf

In this study, we present the application of deep reinforcement learning to the forecasting of major solar flares. For this, we consider full-disk magnetograms at 00:00 UT from the Solar and Heliospheric Observatory/Michelson Doppler Imager (1996–2010) and the Solar Dynamics Observatory/Helioseismic and Magnetic Imager (2011–2019), as well as Geostationary Operational Environmental Satellite X-ray flare data. We apply Deep Q-Network (DQN) and Double DQN, which are popular deep reinforcement learning methods, to predict "Yes or No" for daily M- and X-class flare occurrence. The reward functions, consisting of four rewards for true positive, false positive, false negative, and true negative, are used for our models. The major results of this study are as follows. First, our deep-learning models successfully predict major solar flares with good skill scores, such as HSS, F1, TSS, and ApSS. Second, the performance of our models depends on the reward function, learning method, and target agent update time. Third, the performance of our deep-learning models is noticeably better than that of a convolutional neural network (CNN) model with the same structure: 0.38 (CNN) to 0.44 (ours) for HSS, 0.47 to 0.52 for F1, 0.53 to 0.59 for TSS, and 0.09 to 0.12 for ApSS.

Visual Explanation of a Deep Learning Solar Flare Forecast Model and Its Relationship to Physical Parameters

Kangwoo **Yi**1, Yong-Jae Moon1,2, Daye Lim2, Eunsu Park2, and Harim Lee2

2021 ApJ 910 8

https://iopscience.iop.org/article/10.3847/1538-4357/abdebe/pdf

https://doi.org/10.3847/1538-4357/abdebe

In this study, we present a visual explanation of a deep learning solar flare forecast model and its relationship to physical parameters of solar active regions (ARs). For this, we use full-disk magnetograms at 00:00 UT from the Solar and Heliospheric Observatory/Michelson Doppler Imager and the Solar Dynamics Observatory/Helioseismic and Magnetic Imager, physical parameters from the Space-weather HMI Active Region Patch (SHARP), and Geostationary Operational Environmental Satellite X-ray flare data. Our deep learning flare forecast model based on the Convolutional Neural Network (CNN) predicts "Yes" or "No" for the daily occurrence of C-, M-, and X-class flares. We interpret the model using two CNN attribution methods (guided backpropagation and Gradient-weighted Class Activation Mapping [Grad-CAM]) that provide quantitative information on explaining the model. We find that our deep learning flare forecasting model is intimately related to AR physical properties that have also been distinguished in previous studies as holding significant predictive ability. Major results of this study are as follows. First, we

successfully apply our deep learning models to the forecast of daily solar flare occurrence with TSS = 0.65, without any preprocessing to extract features from data. Second, using the attribution methods, we find that the polarity inversion line is an important feature for the deep learning flare forecasting model. Third, the ARs with high Grad-CAM values produce more flares than those with low Grad-CAM values. Fourth, nine SHARP parameters such as total unsigned vertical current, total unsigned current helicity, total unsigned flux, and total photospheric magnetic free energy density are well correlated with Grad-CAM values.

Forecast of Major Solar X-Ray Flare Flux Profiles Using Novel Deep Learning Models

Kangwoo **Yi**, Yong-Jae Moon, Gyungin Shin, and Daye Lim
2020 ApJL 890 L5
https://doi.org/10.3847/2041-8213/ab701b
In this Letter, we present the application of a couple of novel deep learning models to the forecast of major solar X-ray flare flux profiles. These models are based on a sequence-to-sequence framework using long short-term memory cell and an attention mechanism. For this, we use Geostationary Operational Environmental Satellite 10 X-ray flux data from 1998 August to 2006 April. Seven hundred sixty events are used for training and 85 for testing. The models forecast 30 minutes of X-ray flux profiles during the rise phase of the solar flare with a minute time cadence. We evaluate the models using the 10-fold cross-validation and rms error (RMSE) based on flux profiles and RMSE based on its peak flux. For comparison we consider two simple deep learning models and four conventional regression models. Major results of this study are as follows. First, we successfully apply our deep learning models to the forecast of solar flare X-ray flux profiles, without any preprocessing to extract features from data. Second, our proposed models outperform the other models. Third, our models achieve better performance for forecasting X-ray flux profiles with low-peak fluxes than those with high-peak fluxes. Fourth, our models successfully predict flare duration with high correlations for both all cases and cases at peak times. Our study indicates that our deep learning models can be useful for forecasting time-series data in astronomy and space weather, even for impulsive events such as major flares.

Formation Mechanism of Soft X-Ray Transient Trans-Equatorial Loop System

Masaki **Yokoyama** · Satoshi Masuda
Solar Phys (**2009**) 254: 285–296
The Soft X-ray Telescope (SXT) onboard *Yohkoh* often observed large-scale coronal loops connecting two active regions situated in opposite hemispheres. These are the trans-equatorial loop systems (TLSs). The formation mechanism of TLSs is not yet known. We analyzed a TLS observed simultaneously with *Yohkoh*/SXT and a coronagraph (SOHO/LASCO-C1). SOHO/LASCO-C1 observed loop expansion and eruption at the west solar limb. *Yohkoh*/SXT observed a rising motion (chromospheric evaporation) of hot and dense plasmas from the active regions located at the footpoints of the loop. Important results of our analyses are that (1) the loop eruption and the rising motion of the plasmas were simultaneous, (2) the TLS had a cusp-like appearance, and (3) the highest temperature region of the TLS was located above the bright loop seen in soft X rays. These observational results (loop expansion, eruption, and chromospheric evaporation) suggest that this bright (high-density) TLS was created by the same mechanism by which a solar flare occurs, namely, magnetic reconnection. In this paper, we propose a formation mechanism of the TLS that forms between two independent active regions. **28-30 May 1998**

The first OPEA model for solar X-ray flares

E **Yoldaş**, H A Dal
MNRAS, Volume 517, Issue 2, December **2022**, Pages 1937–1945,
https://doi.org/10.1093/mnras/stac2814
In this study, the flares detected in the solar hard X-ray (λ0.5–4.0 Å) data accumulated by the Geostationary Operational Environmental Satellite (GOES) from 2001 March–May were analysed. For the first time in the literature, the One Phase Exponential Association (OPEA) model was derived for the Sun and, for the first time, over X-ray data. 1014 flares were detected in the analysis. Contrary to expectations, it was seen that the flares can be modelled with three different OPEA models, not one model. The Plateau value was found to be 5.053 ± 0.110 s with the half-time of 2316.12 s for the flares during 2001 March, while it was 5.676 ± 0.138 s with the half-time of 3967.59 s for 2001 April and 5.338 ± 0.080 s with the half-time of 2755.66 s for 2001 May. The results indicate that the models exhibit a fluctuation in their form time by time. This means that there is a phenomenon that changes the energy of flares obtained in three consecutive months. We also demonstrate that the linear parts of the flare cumulative frequency distributions obtained in these data interestingly show a separation.

The Temperature and Density of a Solar Flare Kernel Measured from Extreme Ultraviolet Lines of O IV

Peter R. **Young**
ApJ **966** 102 **2024**
https://arxiv.org/pdf/2401.12390.pdf
https://iopscience.iop.org/article/10.3847/1538-4357/ad37fc/pdf

Previously-unexplored diagnostics of O IV in the extreme ultraviolet region 260-280 A are used to derive a temperature and density for a solar flare kernel observed on **2012 March 9** with the Extreme ultraviolet Imaging Spectrometer on the Hinode satellite. Seven lines from the 2s 2p^2 - 2s 2p 3s transition array between 271.99 and 272.31 A are both temperature and density sensitive relative to the line at 279.93 A. The temperature, T, is constrained with the 268.02/279.93 ratio, giving a value of log (T/K)=5.10 +/- 0.03. The ratio 272.13/279.93 then yields an electron number density, N_e, of log (N_e/cm^-3) = 12.55 with a lower limit of 11.91, and an upper limit of 14.40. The O IV emitting volume is estimated to be 0.4 arcsec (300 km) across. Additional O IV lines at 196, 207 and 260 A are consistent with the derived temperature and density but have larger uncertainties from the radiometric calibration and blending. Density diagnostics of O V and Mg VII from the same spectrum are consistent with a constant pressure of 10^17.0 K cm^-3 through the transition region. The temperature derived from O IV supports recent results that O IV is formed around 0.15 dex lower at high densities compared to standard "zero-density" ionization balance calculations.

A Spectroscopic Measurement of High Velocity Spray Plasma from an M-class Flare and Coronal Mass Ejection

Peter R. **Young**
Adv. Sp. Research Volume 71, Issue 4, 15 February **2023**, Pages 1900-1906
https://arxiv.org/pdf/2204.09542.pdf
https://doi.org/10.1016/j.asr.2022.06.002
Coronal mass ejection spray plasma associated with the M1.5-class flare of **16 February 2011** is found to exhibit a Doppler blue-shift of 850 km/s - the largest value yet reported from ultraviolet (UV) or extreme ultraviolet (EUV) spectroscopy of the solar disk and inner corona. The observation is unusual in that the emission line (Fe XII 193.51 A) is not observed directly, but the Doppler shift is so large that the blue-shifted component appears in a wavelength window at 192.82 A, intended to observe lines of O V, Fe XI and Ca XVII. The Fe XII 195.12 A emission line is used as a proxy for the rest component of 193.51 A. The observation highlights the risks of using narrow wavelength windows for spectrometer observations when observing highly-dynamic solar phenomena. The consequences of large Doppler shifts for ultraviolet solar spectrometers, including the upcoming Multi-slit Solar Explorer (MUSE) mission, are discussed.

Solar Ultraviolet Bursts **Review**

Peter R. **Young**, Hui Tian, Hardi Peter, Robert J. Rutten, Chris J. Nelson, Zhenghua Huang, ...
Space Science Reviews December **2018**, 214:120
https://link.springer.com/content/pdf/10.1007%2Fs11214-018-0551-0.pdf
https://arxiv.org/pdf/1805.05850.pdf
The term "ultraviolet (UV) burst" is introduced to describe small, intense, transient brightenings in ultraviolet images of solar active regions. We inventorize their properties and provide a definition based on image sequences in transition-region lines. Coronal signatures are rare, and most bursts are associated with small-scale, canceling opposite-polarity fields in the photosphere that occur in emerging flux regions, moving magnetic features in sunspot moats, and sunspot light bridges. We also compare UV bursts with similar transition-region phenomena found previously in solar ultraviolet spectrometry and with similar phenomena at optical wavelengths, in particular Ellerman bombs. Akin to the latter, UV bursts are probably small-scale magnetic reconnection events occurring in the low atmosphere, at photospheric and/or chromospheric heights. Their intense emission in lines with optically thin formation gives unique diagnostic opportunities for studying the physics of magnetic reconnection in the low solar atmosphere.
Oct 22-23, 2013, 2013 December 6, 2014 March 4, 2014 June 15., 26 Oct 2016

A Si IV/O IV electron density diagnostic for the analysis of IRIS solar spectra

P.R. **Young**, F.P. Keenan, R.O. Milligan, H. Peter
ApJ **2018**
https://arxiv.org/pdf/1803.01721.pdf
Solar spectra of ultraviolet bursts and flare ribbons from the Interface Region Imaging Spectrograph (IRIS) have suggested high electron densities of >1012 cm−3 at transition region temperatures of 0.1 MK, based on large intensity ratios of Si IV λ1402.77 to O IV λ1401.16. In this work a rare observation of the weak O IV λ1343.51 line is reported from an X-class flare that peaked at 21:41 UT on **2014 October 24**. This line is used to develop a theoretical prediction of the Si IV λ1402.77 to O IV λ1401.16 ratio as a function of density that is recommended to be used in the high density regime. The method makes use of new pressure-dependent ionization fractions that take account of the suppression of dielectronic recombination at high densities. It is applied to two sequences of flare kernel observations from the October 24 flare. The first shows densities that vary between 3×1012 to 3×1013 cm−3 over a seven minute period, while the second location shows stable density values of around 2×1012 cm−3 over a three minute period.

The 2014 March 29 X-flare: sub-arcsecond resolution observations of Fe XXI 1354.1

Peter **Young**, Hui Tian, Sarah Jaeggli
ApJ, **799** 218 **2014**
http://arxiv.org/pdf/1409.8603v1.pdf
The Interface Region Imaging Spectrometer (IRIS) is the first solar instrument to observe ~10 MK plasma at subarcsecond spatial resolution through imaging spectroscopy of the Fe XXI 1354.1 forbidden line. IRIS observations of the X1 class flare that occurred on 2014 March 29 at 17:48 UT reveal Fe XXI emission from both the flare ribbons and the post-flare loop arcade. Fe XXI appears at the ribbon locations around 75 seconds after the ribbons appear in the chromospheric continuum, and 1354.1 shows blue-shifts of 100-200 km/s, suggesting hot plasma upflow into the corona. The Fe XXI ribbon emission is compact with a spatial extent of <2", and can extend beyond the chromospheric ribbon locations. Examples are found of both decreasing and increasing blue-shift in the direction away from the ribbon locations, and blue-shifts were present for at least 6 minutes after the flare peak. The post-flare loop arcade, seen in Atmospheric Imaging Assembly (AIA) 131 A filtergram images that are dominated by Fe XXI, exhibited bright loop-tops with an asymmetric intensity distribution. The sizes of the loop-tops are resolved by IRIS at > 1", and line widths in the loop-tops are not broader than in the loop-legs suggesting the loop-tops are not sites of enhanced turbulence. Line-of-sight speeds in the loop arcade are typically <10 km/s, and mean non-thermal motions fall from 43 km/s at the flare peak to 26 km/s six minutes later. If the average velocity in the loop arcade is assumed to be at rest, then it implies a new reference wavelength for the Fe XXI line of 1354.106 +/- 0.023 A.

PROPERTIES OF A SOLAR FLARE KERNEL OBSERVED BY HINODE AND SDO

P. R. **Young**1, G. A. Doschek2, H. P. Warren2, and H. Hara
2013 ApJ 766 127
Flare kernels are compact features located in the solar chromosphere that are the sites of rapid heating and plasma upflow during the rise phase of flares. An example is presented from a M1.1 class flare in active region AR 11158 observed on **2011 February 16** 07:44 UT for which the location of the upflow region seen by EUV Imaging Spectrometer (EIS) can be precisely aligned to high spatial resolution images obtained by the Atmospheric Imaging Assembly (AIA) and Helioseismic and Magnetic Imager (HMI) on board the Solar Dynamics Observatory (SDO). A string of bright flare kernels is found to be aligned with a ridge of strong magnetic field, and one kernel site is highlighted for which an upflow speed of 400 km s–1 is measured in lines formed at 10-30 MK. The line-of-sight magnetic field strength at this location is 1000 G. Emission over a continuous range of temperatures down to the chromosphere is found, and the kernels have a similar morphology at all temperatures and are spatially coincident with sizes at the resolution limit of the AIA instrument (400 km). For temperatures of 0.3-3.0 MK the EIS emission lines show multiple velocity components, with the dominant component becoming more blueshifted with temperature from a redshift of 35 km s–1 at 0.3 MK to a blueshift of 60 km s–1 at 3.0 MK. Emission lines from 1.5-3.0 MK show a weak redshifted component at around 60-70 km s–1 implying multi-directional flows at the kernel site. Significant non-thermal broadening corresponding to velocities of 120 km s–1 is found at 10-30 MK, and the electron density in the kernel, measured at 2 MK, is 3.4 × 1010 cm–3. Finally, the Fe XXIV λ192.03/λ255.11 ratio suggests that the EIS calibration has changed since launch, with the long wavelength channel less sensitive than the short wavelength channel by around a factor two.

High-precision density measurements in the solar corona - I.=Analysis methods and results for Fe XII and Fe XIII:

P. R.**Young**, T.Watanabe, H.Hara and J. T.Mariska
A&A 495 (**2009**) 587-606
Aims. The EUV Imaging Spectrometer (EIS) instrument on board the Hinode satellite has access to some of the best coronal density diagnostics, and the high sensitivity of the instrument now allows electron number density, N_e, measurements to an unprecedented precision of up to $\pm$5% in active regions. This paper gives a thorough overview of data analysis issues for the best diagnostics of Fe XII and Fe XIII and assesses the accuracy of the measurements. Methods. Two density diagnostics each from Fe XII (λ186.88/λ195.12 and λ196.64/λ195.12) and Fe XIII (λ196.54/λ202.04 and λ203.82/λ202.04) are analysed in two active region datasets from 2007 May 3 and 6 that yield densities in the range $8.5 \leq \log(N_e/\mathrm{cm}^{-3}) \leq 11.0$. The densities are derived using v5.2 of the CHIANTI atomic database. Blending, line fitting, and instrumental issues are discussed, and line fit parameters presented. Results. The Fe XII and Fe XIII diagnostics show broadly the same trend in density across the active region, consistent with their similar temperatures of formation. However, the high precision of the EIS measurements demonstrates significant discrepancies of up to 0.5 dex in derived $\log N_e$ values, with Fe XII always giving higher densities than Fe XIII. The discrepancies may partly be due to real physical differences between the emitting regions of the two

plasmas, but the dominant factor lies in the atomic models of the two ions. Two specific problems are identified for Fe XII λ196.64 and Fe XIII λ203.82: the former is found to be underestimated in strength by the CHIANTI atomic model, while the high-density limit of the λ203.82/λ202.04 ratio appears to be inaccurate in the CHIANTI atomic model. The small grating tilt of the EIS instrument is found to be very significant when deriving densities from emission lines separated by more than a few angstroms. Revised wavelengths of 196.518 ± 0.003 Å and 196.647 ± 0.003 Å are suggested for the Fe XIII λ196.54 and Fe XII λ196.64 lines, respectively.

On the intensity ratio variation of the Si IV 1394/1403 Å lines during solar flares

Hao-Cheng **Yu**, J. Hong, M. D. Ding

A&A **2023**

https://arxiv.org/pdf/2306.08296.pdf

Context. The Si IV lines at 1394 Å and 1403 Å form in the solar atmosphere at a temperature of ∼104.8 K. They are usually considered optically thin, but their opacity can be enhanced during solar flares. Traditionally, the intensity ratio of these lines are used as an indicator of the optical thickness. However, observations have shown a wavelength-dependent intensity ratio profile r(Δλ) of the the 1394 Å to 1403 Å lines.
Aims. We aim to study the variation of the intensity ratio profile in solar flares and the physical reasons behind it.
Method. The Si IV lines and their intensity ratio profiles are calculated from the one-dimensional radiative hydrodynamics flare model with non-thermal electron heating.
Result. During flares, r(Δλ) is smaller than 2 at the line core but larger than 2 at the line wings. We attribute the deviation of the ratio from 2 to two effects: the resonance scattering effect and the opacity effect. Resonance scattering increases the population ratio of the upper levels of the two lines, and as a result, increases r(Δλ), in all wavelengths. The opacity effect decreases r(Δλ), especially at the line core where the opacity is larger. These two effects compete with each other and cause the U-shape of r(Δλ).

Imaging and Spectroscopic Observations of the Dynamic Processes in Limb Solar Flares

Ke **Yu**, Y. Li, Jie Hong, De-Chao Song, M. D. Ding

ApJ **935** 8 **2022**

https://arxiv.org/pdf/2207.05925.pdf

https://iopscience.iop.org/article/10.3847/1538-4357/ac7e46/pdf

We investigate various dynamic processes including magnetic reconnection, chromospheric evaporation, and coronal rain draining in two limb solar flares through imaging and spectroscopic observations from the Interface Region Imaging Spectrograph (IRIS) and the Atmospheric Imaging Assembly (AIA) on board the Solar Dynamics Observatory. In the early phase of the flares, a bright and dense loop-top structure with a cusp-like shape can be seen in multi-wavelength images, which is co-spatial with the hard X-ray 25--50 keV emission. In particular, intermittent magnetic reconnection downflows are detected in the time-space maps of AIA 304 Å. The reconnection downflows are manifested as redshifts on one half of the loops and blueshifts on the other half in the IRIS Si {\sc iv} 1393.76 Å line due to a projection effect. The Si {\sc iv} profiles exhibit complex features (say, multi-peak) with a relatively larger width at the loop-top region. During the impulsive phase, chromospheric evaporation is observed in both AIA images and the IRIS Fe {\sc xxi} 1354.08 Å line. Upward motions can be seen from AIA 131 Å images. The Fe {\sc xxi} line is significantly enhanced and shows a good Gaussian shape. In the gradual phase, warm rains are observed as downward moving plasmas in AIA 304 Å images. Both the Si {\sc iv} and Fe {\sc xxi} lines show a relatively symmetric shape with a larger width around the loop top. These results provide observational evidence for various dynamic processes involved in and are crucial to understand the energy release process of solar flares. **2014 October 29 and 30**

Statistical Studies on Modified Neupert Effect★

YU Wen-hui a b c, LI You-ping a b, GAN Wei-qun a b

Chinese Astronomy and Astrophysics Volume 45, Issue 1, **2021**, Pages 82-98

https://doi.org/10.1016/j.chinastron.2021.02.006

https://www.sciencedirect.com/science/article/abs/pii/S0275106221000060

https://sci-hub.ru/10.1016/j.chinastron.2021.02.006

The qualitative description of the Neupert effect is that there is a causal relationship between the pulse component (hard X-ray, microwave burst) and the gradual component (soft X-ray emission) in a flare. The initial energy of the flare is released in the form of accelerating particles. The energetic particles produce HXR (hard X-ray) via nonthermal electron-ion bremsstrahlung as they lose their energies in the chromosphere. The SXR (soft X-ray) emission of the flare is the response of energetic particles injected into the chromosphere. According to the quantitative description of the classic Neupert effect, SXR should reach maximum instantly at the end of HXR emission (sign of nonthermal electron injection). However, previous observations have found that for quite a number of flares the SXR peak time (t2) is significantly later than the end time of HXR (t1) ($\tau=t2-t1,\tau>0$), deviating from the classic Neupert effect. In order to study the events deviating from the classic Neupert effect or not, we checked the RHESSI (Reuven Ramaty High

Energy Solar Spectroscopic Imager) and GOES (Geostationary Operational Environmental Satellites) events list from 2002 to 2015, and found out flare samples that have simple lightcurves at 25–50 keV together with other criteria. A total of 276 flare samples were finally selected. We have analysed the τ distribution of these flares, as well as the relationship between the loop length (represented by the distance between two footpoint sources d) and τ. We found that: (1) 227 sample flares present τ>0, which means that about 82% of total samples deviate from the classical Neupert effect; (2) there is a roughly linear correlation between τ and d, that is, the longer the loop is, the later the maximum time of SXR with respect to the end of HXR; (3) there seems to have a critical distance, within which the classic Neupert effect works. These results confirm the necessity of modifying Neupert effect, and expound its physical significance. **2002-02-26, 2002−11−14, 2005−05−16, 2013−07−04, 2013-10-22**

Magnetic Reconnection during the Post-impulsive Phase of a Long-duration Solar Flare: Bidirectional Outflows as a Cause of Microwave and X-Ray Bursts

Sijie **Yu** (余思捷)1, Bin Chen (陈彬)1, Katharine K. Reeves2, Dale E. Gary1, Sophie Musset3,4, Gregory D. Fleishman1, Gelu M. Nita1, and Lindsay Glesener4

2020 ApJ 900 17

https://arxiv.org/pdf/2007.10443.pdf **File**

https://doi.org/10.3847/1538-4357/aba8a6

Magnetic reconnection plays a crucial role in powering solar flares, production of energetic particles, and plasma heating. However, where the magnetic reconnections occur, how and where the released magnetic energy is transported, and how it is converted to other forms remain unclear. Here we report recurring bidirectional plasma outflows located within a large-scale plasma sheet observed in extreme-ultraviolet emission and scattered white light during the post-impulsive gradual phase of the X8.2 solar flare on **2017 September 10**. Each of the bidirectional outflows originates in the plasma sheet from a discrete site, identified as a magnetic reconnection site. These reconnection sites reside at very low altitudes (<180 Mm, or 0.26 R ⊙) above the top of the flare arcade, a distance only <3% of the total length of a plasma sheet that extends to at least 10 R ⊙. Each arrival of sunward outflows at the loop-top region appears to coincide with an impulsive microwave and X-ray burst dominated by a hot source (10–20 MK) at the loop top and a nonthermal microwave burst located in the loop-leg region. We propose that the reconnection outflows transport the magnetic energy released at localized magnetic reconnection sites outward in the form of kinetic energy flux and/or electromagnetic Poynting flux. The sunward-directed energy flux induces particle acceleration and plasma heating in the post-flare arcades, observed as the hot and nonthermal flare emissions.

IRIS Si IV Line Profiles at Flare Ribbons as Indications of Chromospheric Condensation

Ke **Yu**, Y. Li, M. D. Ding, D. Li, Yi-An Zhou, Jie Hong

ApJ **896** 154 **2020**

https://arxiv.org/pdf/2005.02029.pdf

https://iopscience.iop.org/article/10.3847/1538-4357/ab9014/pdf

We present temporal variations of the Si IV line profiles at the flare ribbons in three solar flares observed by the Interface Region Imaging Spectrograph (IRIS). In the M1.1 flare on **2014 September 6** and the X1.6 flare on **2014 September 10**, the Si IV line profiles evolve from wholly redshifted to red-wing enhanced with the flare development. However, in the B1.8 flare on **2016 December 2**, the Si IV line profiles are wholly redshifted throughout the flare evolution. We fit the wholly redshifted line profiles with a single Gaussian function but the red-asymmetric ones with a double Gaussian function to deduce the corresponding Doppler velocities. In addition, we find that hard X-ray emission above 25 keV shows up in the two large flares, implying a nonthermal electron beam heating. In the microflare, there only appears weak hard X-ray emission up to 12 keV, indicative of a thermal heating mostly. We interpret the redshifts or red asymmetries of the Si IV line at the ribbons in the three flares as spectral manifestations of chromospheric condensation. We propose that whether the line appears to be wholly redshifted or red-asymmetric depends on the heating mechanisms and also on the propagation of the condensation.

Magnetic Reconnection During the Post-Impulsive Phase of a Long-Duration Solar Flare: Bi-Directional Outflows as a Cause of Microwave and X-ray Bursts

Sijie **Yu** (1), Bin Chen (1), Katharine K. Reeves (2), Dale E. Gary (1), Sophie Musset (3 and 4), Gregory D. Fleishman (1), Gelu M. Nita (1), Lindsay Glesener (4)

ApJ Volume 900, Issue 1, id.17 **2020**

https://arxiv.org/pdf/2007.10443.pdf **File**

Magnetic reconnection plays a crucial role in powering solar flares, production of energetic particles, and plasma heating. However, where the magnetic reconnections occur, how and where the released magnetic energy is transported, and how it is converted to other forms remain unclear. Here we report recurring bi-directional plasma outflows located within a large-scale plasma sheet observed in extreme ultraviolet emission and scattered white light during the post-impulsive gradual phase of the X8.2 solar flare on **2017 September 10**. Each of the bi-directional outflows originates in the plasma sheet from a discrete site, identified as a magnetic reconnection site. These reconnection sites reside at very

low altitudes (<180 Mm, or 0.26 R⊙) above the top of the flare arcade, a distance only <3% of the total length of a plasma sheet that extends to at least 10 R⊙. Each arrival of sunward outflows at the looptop region appears to coincide with an impulsive microwave and X-ray burst dominated by a hot source (10-20 MK) at the looptop, which is immediately followed by a nonthermal microwave burst located in the loopleg region. We propose that the reconnection outflows transport the magnetic energy released at localized magnetic reconnection sites outward in the form of kinetic energy flux and/or electromagnetic Poynting flux. The sunward-directed energy flux induces particle acceleration and plasma heating in the post-flare arcades, observed as the hot and nonthermal flare emissions.
CESRA Nuggets #2711 Oct **2020** http://www.astro.gla.ac.uk/users/eduard/cesra/?p=2711

Possible Detection of Subsecond-Period Propagating Magnetohydrodynamics Waves in Post-Reconnection Magnetic Loops during a Two-Ribbon Solar Flare

Sijie **Yu** (1), Bin Chen
ApJ **872** 71 **2019**
https://arxiv.org/pdf/1901.05379.pdf
https://iopscience.iop.org/article/10.3847/1538-4357/aaff6d/pdf
https://web.njit.edu/~binchen/download/publications/Yu_Chen_2019/Yu_Chen_2019.pdf
Solar flares involve the sudden release of magnetic energy in the solar corona. Accelerated nonthermal electrons have been often invoked as the primary means for transporting the bulk of the released energy to the lower solar atmosphere. However, significant challenges remain for this scenario, especially in accounting for the large number of accelerated electrons inferred from observations. Propagating magnetohydrodynamics (MHD) waves, particularly those with subsecond/second-scale periods, have been proposed as an alternative means for transporting the released flare energy likely alongside the electron beams, while observational evidence remains elusive. Here we report a possible detection of such waves in the late impulsive phase of a two-ribbon flare. This is based on ultra-high cadence dynamic imaging spectroscopic observations of a peculiar type of decimetric radio bursts obtained by the Karl G. Jansky Very Large Array. Radio imaging at each time and frequency pixel allows us to trace the spatiotemporal motion of the source, which agrees with the implications of the frequency drift pattern in the dynamic spectrum. The radio source, propagating at 1000--2000 km s−1 in projection, shows close spatial and temporal association with transient brightenings on the flare ribbon. In addition, multitudes of subsecond-period oscillations are present in the radio emission. We interpret the observed radio bursts as \edit1{short-period} MHD wave packets propagating along newly reconnected magnetic flux tubes linking to the flare ribbon. The estimated energy flux carried by the waves is comparable to that needed for accounting for the plasma heating during the late impulsive phase of this flare. **2014 November 01**
RHESSI Science Nuggets #343 2019 http://sprg.ssl.berkeley.edu/~tohban/wiki/index.php/Short-Period_Waves
CESRA Nuggets #2166 March **2019** http://www.astro.gla.ac.uk/users/eduard/cesra/?p=2166

Short-term Solar Flare Level Prediction Using a Bayesian Network Approach

*Daren **Yu**, Xin Huang, Huaning Wang, Yanmei Cui, Qinghua Hu, and Rui Zhou*
ApJ **710** 869-877, **2010**
A Bayesian network approach for short-term solar flare level prediction has been proposed based on three sequences of photospheric magnetic field parameters extracted from *Solar and Heliospheric Observatory*/Michelson Doppler Imager longitudinal magnetograms. The magnetic measures, the maximum horizontal gradient, the length of neutral line, and the number of singular points do not have determinate relationships with solar flares, so the solar flare level prediction is considered as an uncertainty reasoning process modeled by the Bayesian network. The qualitative network structure which describes conditional independent relationships among magnetic field parameters and the quantitative conditional probability tables which determine the probabilistic values for each variable are learned from the data set. Seven sequential features—the maximum, the mean, the root mean square, the standard deviation, the shape factor, the crest factor, and the pulse factor—are extracted to reduce the dimensions of the raw sequences. Two Bayesian network models are built using raw sequential data (BN_R) and feature extracted data (BN_F), respectively. The explanations of these models are consistent with physical analyses of experts. The performances of the BN_R and the BN_F appear comparable with other methods. More importantly, the comprehensibility of the Bayesian network models is better than other methods.

SHORT-TERM SOLAR FLARE PREDICTION USING MULTIRESOLUTION PREDICTORS

Daren Yu1, Xin Huang1, Qinghua Hu1, Rui Zhou1, Huaning Wang2 and Yanmei Cui3
ApJ 709 321-326, **2010**
Multiresolution predictors of solar flares are constructed by a wavelet transform and sequential feature extraction method. Three predictors—the maximum horizontal gradient, the length of neutral line, and the number of singular points—are extracted from *Solar and Heliospheric Observatory*/Michelson Doppler Imager longitudinal magnetograms. A maximal overlap discrete wavelet transform is used to decompose the sequence of predictors into four frequency bands. In each band, four sequential features—the maximum, the mean, the standard deviation, and the root mean square—are extracted. The multiresolution predictors in the low-frequency band reflect trends in the evolution of newly

emerging fluxes. The multiresolution predictors in the high-frequency band reflect the changing rates in emerging flux regions. The variation of emerging fluxes is decoupled by wavelet transform in different frequency bands. The information amount of these multiresolution predictors is evaluated by the information gain ratio. It is found that the multiresolution predictors in the lowest and highest frequency bands contain the most information. Based on these predictors, a C4.5 decision tree algorithm is used to build the short-term solar flare prediction model. It is found that the performance of the short-term solar flare prediction model based on the multiresolution predictors is greatly improved.

Short-Term Solar Flare Prediction Using a Sequential Supervised Learning Method

Daren **Yu**[1], Xin Huang[1], Huaning Wang[2] and Yanmei Cui

Solar Phys. Volume 255, Number 1, p. 91-105, **2009**

Solar flares are powered by the energy stored in magnetic fields, so evolutionary information of the magnetic field is important for short-term prediction of solar flares. However, the existing solar flare prediction models only use the current information of the active region. A sequential supervised learning method is introduced to add the evolutionary information of the active region into a prediction model. The maximum horizontal gradient, the length of the neutral line, and the number of singular points extracted from SOHO/MDI longitudinal magnetograms are used in the model to describe the nonpotentiality and complexity of the photospheric magnetic field. The evolutionary characteristics of the predictors are analyzed by using autocorrelation functions and mutual information functions. The analysis results indicate that a flare is influenced by the 3-day photospheric magnetic field information before flare eruption. A sliding-window method is used to add evolutionary information of the predictors into machine learning algorithms, then C4.5 decision tree and learning vector quantization are employed to predict the flare level within 48 hours. Experimental results indicate that the performance of the short-term solar flare prediction model within the sequential supervised learning framework is significantly improved.

A Compact Source for Quasi-Periodic Pulsation in an M-class Solar Flare

Ding **Yuan**, Song Feng, Dong Li, Zhongjun Ning, Baolin Tan

ApJL **886** L25 **2019**

https://arxiv.org/pdf/1911.05217.pdf

sci-hub.se/10.3847/2041-8213/ab5648

Quasi-periodic pulsations (QPP) are usually found in the light curves of solar and stellar flares, they carry the features of time characteristics and plasma emission of the flaring core, and could be used to diagnose the coronas of the Sun and remote stars. In this study, we combined the Atmospheric Imaging Assembly (AIA) onboard the Solar Dynamics Observatory and the Nobeyama Radioheliograph (NoRH) to observe an M7.7 class flare occurred at active region 11520 on **19 July 2012**. A QPP was detected both in the AIA $131\unit{Å}$ bandpass and the NoRH $17\unit{GHz}$ channel, it had a period of about four minutes. In the spatial distribution of Fourier power, we found that this QPP originated from a compact source and that it overlapped with the X-ray source above the loop top. The plasma emission intensities in the AIA $131\unit{Å}$ bandpass were highly correlated within this region. The source region is further segmented into stripes that oscillated with distinctive phases. Evidence in this event suggests that this QPP was likely to be generated by intermittent energy injection into the reconnection region.

Multi-layered Kelvin-Helmholtz Instability in the Solar Corona

Ding **Yuan**, Yuandeng Shen, Yu Liu, Xueshang Feng, Rony Keppens

ApJ **2019**

https://arxiv.org/pdf/1910.05710.pdf

The Kelvin-Helmholtz (KH) instability is commonly found in many astrophysical, laboratory, and space plasmas. It could mix plasma components of different properties and convert dynamic fluid energy from large scale structure to smaller ones. In this study, we combined the ground-based New Vacuum Solar Telescope (NVST) and the Solar Dynamic Observatories (SDO) / Atmospheric Imaging Assembly (AIA) to observe the plasma dynamics associated with active region 12673 on **09 September 2017**. In this multi-temperature view, we identified three adjacent layers of plasma flowing at different speeds, and detected KH instabilities at their interfaces. We could unambiguously track a typical KH vortex and measure its motion. We found that the speed of this vortex suddenly tripled at a certain stage. This acceleration was synchronized with the enhancements in emission measure and average intensity of the 193 Å data. We interpret this as evidence that KH instability triggers plasma heating. The intriguing feature in this event is that the KH instability observed in the NVST channel was nearly complementary to that in the AIA 193 Å. Such a multi-thermal energy exchange process is easily overlooked in previous studies, as the cold plasma component is usually not visible in the extreme ultraviolet channels that are only sensitive to high temperature plasma emissions. Our finding indicates that embedded cold layers could interact with hot plasma as invisible matters. We speculate that this process could occur at a variety of length scales and could contribute to plasma heating.

Forward Modelling of Standing Kink Modes in Coronal Loops II. Applications

Ding **Yuan**, Tom Van Doorsselaere
2016
http://arxiv.org/pdf/1602.07598v1.pdf
Magnetohydrodynamic waves are believed to play a significant role in coronal heating, and could be used for remote diagnostics of solar plasma. Both the heating and diagnostic applications rely on a correct inversion (or backward modelling) of the observables into the thermal and magnetic structures of the plasma. However, owing to the limited availability of observables, this is an ill-posed issue. Forward Modelling is to establish a plausible mapping of plasma structuring into observables. In this study, we set up forward models of standing kink modes in coronal loops and simulate optically thin emissions in the extreme ultraviolet bandpasses, and then adjust plasma parameters and viewing angles to match three events of transverse loop oscillations observed by the Solar Dynamics Observatory/Atmospheric Imaging Assembly. We demonstrate that forward models could be effectively used to identify the oscillation overtone and polarization, to reproduce the general profile of oscillation amplitude and phase, and to predict multiple harmonic periodicities in the associated emission intensity and loop width variation.
16 Oct 2010, 03 Nov 2010, 6 Sept 2011

Forward Modelling of Standing Slow Modes in Flaring Coronal Loops

D. **Yuan**, T. Van Doorsselaere, D. Banerjee, P. Antolin
ApJ **807** 98 **2015**
http://arxiv.org/pdf/1504.07475v1.pdf
Standing slow mode waves in hot flaring loops are exclusively observed in spectrometers and are used to diagnose the magnetic field strength and temperature of the loop structure. Due to the lack of spatial information, the longitudinal mode cannot be effectively identified. In this study, we simulate standing slow mode waves in flaring loops and compare the synthesized line emission properties with SUMER spectrographic and SDO/AIA imaging observations. We find that the emission intensity and line width oscillations are a quarter period out of phase with Doppler shift velocity both in time and spatial domain, which can be used to identify a standing slow mode wave from spectroscopic observations. However, the longitudinal overtones could be only measured with the assistance of imagers. We find emission intensity asymmetry in the positive and negative modulations, this is because the contribution function pertaining to the atomic emission process responds differently to positive and negative temperature variations. One may detect \textbf{half} periodicity close to the loop apex, where emission intensity modulation is relatively small. The line-of-sight projection affects the observation of Doppler shift significantly. A more accurate estimate of the amplitude of velocity perturbation is obtained by de-projecting the Doppler shift by a factor of $1-2\theta/\pi$rather than the traditionally used $\cos\theta$. \textbf{If a loop is heated to the hotter wing, the intensity modulation could be overwhelmed by background emission, while the Doppler shift velocity could still be detected to a certain extent.

Distinct propagating fast wave trains associated with flaring energy releases

D. **Yuan**1, Y. Shen2, Y. Liu2, V. M. Nakariakov1,3, B. Tan4 and J. Huan
A&A 554, A144 (**2013**)
Context. Large-scale fast waves with perturbation of the EUV emission intensity are well resolved in both temporal and spatial scale by SDO/AIA. These waves are prone to propagate along the magnetic field line.
Aims. We aim to probe the link between propagating fast wave trains and flaring energy releases. By measuring the wave parameters, we reveal their nature and investigate the potential to diagnose the energy source and waveguide.
Methods. The spatial and temporal evolution of the wave amplitude and propagating speed are studied. The correlation of individual wave trains with flare-generated radio bursts is tested.
Results. The propagating wave pattern comprises distinct wave trains with varying periods and wavelengths. This characteristic signature is consistent with the patterns formed by waveguide dispersion, when different spectral components propagate at different phase and group speeds. The wave train releases are found to be highly correlated in start time with the radio bursts emitted by the non-thermal electrons that were accelerated in bursty energy releases. The wave amplitude is seen to reach the maximum midway during its course. This can be caused by a combined effect of the waveguide spread in the transverse direction and density stratification. The transverse amplitude distribution perpendicular to the wave vector is found to follow approximately a Gaussian profile. The spatial structure is consistent with the kink mode that is polarised along the line-of-sight. The propagating speed is subject to deceleration from ~735−845 km s-1 to ~600 km s-1. This could be caused by the decrease in the local Alfvén speed and/or the projection effect.

Magnetic field re-configuration associated with a slow rise eruptive X1.2 flare in NOAA active region 11944

Vasyl **Yurchyshyn**, Xu Yang, Gelu Nita, Gregory Fleishman, Valentina Abramenko, Satoshi Inoue, Eun-

Kyung Lim, and Wenda Cao
Front. Astron. Space Sci. 9:816523 **2022**
https://www.frontiersin.org/articles/10.3389/fspas.2022.816523/full
https://doi.org/10.3389/fspas.2022.816523
http://www.bbso.njit.edu/~vayur/ar11944_final.pdf **File**
Using multi-wavelength observations, we analysed magnetic field variations associated with a gradual X1.2 flare that erupted on **January 7, 2014** in active region (AR) NOAA 11944 located near the disk center. A fast coronal mass ejection (CME) was observed following the flare, which was noticeably deflected in the south-west direction. A chromospheric filament was observed at the eruption site prior to and after the flare. We used SDO/HMI data to perform non-linear force-free field (NLFFF) extrapolation of coronal magnetic fields above the AR and to study the evolution of AR magnetic fields prior to the eruption. The extrapolated (model) data allowed us to detect signatures of several magnetic flux ropes (MFRs) present at the eruption site several hours before the event. The eruption site was located under slanted sunspot fields with a varying decay index of 1.0-1.5. That might have caused the erupting fields to slide along this slanted magnetic boundary rather than vertically erupt, thus explaining the slow rise of the flare as well as the observed direction of the resulting CME. We employed sign-singularity tools to quantify the evolutionary changes in the model twist and observed current helicity data, and found rapid and coordinated variations of current systems in both data sets prior to the event as well as their rapid exhaustion after the event onset.

High-resolution Observations of a White-light Flare with NST

V. **Yurchyshyn**1,2, P. Kumar2, V. Abramenko3,4, Y. Xu5, P. R. Goode1, K.-S. Cho2,6, and E.-K. Lim
2017 ApJ 838 32
Using high-resolution data from the New Solar Telescope, we studied fine spatial and temporal details of an M1.3 white-light (WL) flare, which was one of three homologous solar flares (C6.8, M1.3, and M2.3) observed in close proximity to the west solar limb on **2014 October 29** in NOAA active region 12192. We report that the TiO WL flare consists of compact and intense cores surrounded by less intense spatial halos. The strong and compact WL cores were measured to be Mm across, with an area of about 1014 cm2. Several TiO features were not cospatial with Hα flare ribbons and were displaced toward the disk center by about 500 km, which suggests that the TiO and Hα radiation probably did not originate in the same chromospheric volume. The observed TiO intensity enhancements are not normally distributed and are structured by the magnetic field of the penumbra.
See High Resolution Temporal and Spatial Structure of a White Light Flare, by Vasyl **Yurchyshyn**.
RHESSI Science Nuggets #299: April **2017**
http://sprg.ssl.berkeley.edu/~tohban/wiki/index.php/High_Resolution_Temporal_and_Spatial_Structure_of_a_White_Light_Flare
The biggest solar telescope finds still smaller scales for white-light flare kernels.

Multiwavelength Observations of a Slow Raise, Multi-Step X1.6 Flare and the Associated Eruption

Yurchyshyn, V., Kumar, P., Cho, K.S., Lim, E.K., & Abramenko, V.
ApJ 812 172 **2015**
http://www.bbso.njit.edu/~vayur/x1.6flare.pdf
Using multi-wavelength observations we studied a slow rise, multi-step X1.6 flare that began on **November 7, 2014** as a localized eruption of core fields inside a \delta-sunspot and later engulfed the entire active region. This flare event was associated with formation of two systems of post eruption arcades and several J-shaped flare ribbons showing extremely fine details, irreversible changes in the photospheric magnetic fields, and it was accompanied by a fast and wide coronal mass ejection. Data from the Solar Dynamics Observatory, IRIS spacecraft along with the ground based data from the New Solar Telescope (NST) present evidence that i) the flare and the eruption were directly triggered by a flux emergence that occurred inside a \delta--sunspot at the boundary between two umbrae; ii) this event represented an example of the formation of an unstable flux rope observed only in hot AIA channels (131 and 94 Å) and LASCO C2 coronagraph images; iii) the global post eruption arcade spanned the entire AR and was due to global scale reconnection occurring at heights of about one solar radii, indicating on the global spatial and temporal scale of the eruption.

High Resolution Observations of Chromospheric Jets in Sunspot Umbra

Yurchyshyn, V., Abramenko, V., Kosovichev, A., and Goode, P.
E-print, April **2014,** ApJ, 787 58, **2014**
http://www.bbso.njit.edu/~vayur/spikes/VYurchyshyn_Spikes.pdf
Recent observations of sunspot's umbra suggested that it may be finely structured at a sub-arcsecond scale representing a mix of hot and cool plasma elements. In this study we report the first detailed observations of the umbral spikes, which are cool jet-like structures seen in the chromosphere of an umbra. The spikes are cone-shaped features with a typical height of 0.5-1.0 Mm and a width of about 0.1 Mm. Their life time ranges from 2 to 3 min and they tend to re-

appear at the same location. The spikes are not associated with photospheric umbral dots and they rather tend to occur above darkest parts of the umbra, where magnetic fields are strongest. The spikes exhibit up and down oscillatory motions and their spectral evolution suggests that they might be driven by upward propagating shocks generated by photospheric oscillations. It is worth noting that triggering of the running penumbral waves seems to occur during the interval when the spikes reach their maximum height. **14 June 2013**

ON THE ORIGIN OF INTERGRANULAR JETS

V. B. **Yurchyshyn**1, P. R. Goode1, V. I. Abramenko1 and O. Steiner
BBSO Preprint 1484, **2011, 2011** ApJ 736 L35

We observe that intergranular jets, originating in the intergranular space surrounding individual granules, tend to be associated with granular fragmentation, in particular, with the formation and evolution of a bright granular lane (BGL) within individual granules. The BGLs have recently been identified as vortex tubes by Steiner et al. We further discover the development of a well-defined bright grain located between the BGL and the dark intergranular lane to which it is connected. Signatures of a BGL may reach the lower chromosphere and can be detected in off-band Hα images. Simulations also indicate that vortex tubes are frequently associated with small-scale magnetic fields. We speculate that the intergranular jets detected in the New Solar Telescope (NST) data may result from the interaction between the turbulent small-scale fields associated with the vortex tube and the larger-scale fields existing in the intergranular lanes. The intergranular jets are much smaller and weaker than all previously known jet-like events. At the same time, they appear much more numerous than the larger events, leading us to the speculation that the total energy release and mass transport by these tiny events may not be negligible in the energy and mass-flux balance near the temperature minimum atop the photosphere. The study is based on the photospheric TiO broadband (1.0 nm) filter data acquired with the 1.6 m NST operating at the Big Bear Solar Observatory. The data set also includes NST off-band Hα images collected through a Zeiss Lyot filter with a passband of 0.025 nm.

Variations of Current Helicity in Active Region 10930 as Inferred from Hinode Spectropolarimeter Data and Cancellation Exponent

V. **Yurchyshyn**, V. Abramenko and H. Watanabe
BBSO #1464, **2010; File;** Proceedings of Hinode 3 meeting, ASP Conference Series

Current helicity derived from vector magnetograms possesses a well-pronounced scaling behavior, which can be studied by introducing a signed measure and calculating the power-law exponent (cancellation exponent). The time variations of this exponent seem to be related to flare activity of an active region. Here we focus on changes of current helicity in active region NOAA 10930 as derived from a set of Hinode spectropolarimeter data. Our findings are that the cancellation exponent first strongly increased on Dec 11 then rapidly decreased after a small sunspot-satellite developed. Afterward, the cancellation exponent began its gradual increase without significant new magnetic flux emergence. These two different modes of behavior may indicate different processes that ultimately led to an eruption: the first process is rapid injection of current helicity, while the second process is gradual redistribution of injected helicity over all spatial scales in the active region.

Magnetic Field, Hα, and RHESSI Observations of the 2002 July 23 Gamma-Ray Flare

Yurchyshyn, Vasyl; Wang, Haimin; Abramenko, Valentyna; Spirock, Thomas J.; Krucker, Säm
Astrophysical Journal, 605:546–553, **2004; File**

In this paper we examine two aspects of the **2002 July 23** gamma-ray flare by using multiwavelength observations. First, the data suggest that the interaction of the erupted field with an overlying large-scale coronal field can explain the offset between the gamma-ray and the hard X-ray sources observed in this event. Second, we pay attention to rapid and permanent changes in the photospheric magnetic field associated with the flare. MDI and BBSO magnetograms show that the following magnetic flux had rapidly decreased by 1 ; 10^{20} Mx immediately after the flare, while the leading polarity was gradually increasing for several hours after the flare. Our study also suggests that the changes were most probably associated with the emergence of new flux and the reorientation of the magnetic field lines. We interpret the magnetograph and spectral data for this event in terms of the tether-cutting model.

Ejection of cool plasma into the hot corona⋆

P. **Zacharias**1⋆⋆, H. Peter2 and S. Bingert
A&A 532, A112 (**2011**)

Context. The corona is highly dynamic and shows transient events on various scales in space and time. Most of these features are related to changes in the magnetic field structure or impulsive heating caused by the conversion of magnetic to thermal energy.
Aims. We investigate the processes that lead to the formation, ejection and fall of a confined plasma ejection that was observed in a numerical experiment of the solar corona. By quantifying physical parameters such as mass, velocity, and orientation of the plasma ejection relative to the magnetic field, we provide a description of the nature of this particular plasma ejection.
Methods. The time-dependent three-dimensional magnetohydrodynamic (3D MHD) equations are solved in a box extending from the chromosphere, which serves as a reservoir for mass and energy, to the lower corona. The plasma is heated by currents that are induced through field line braiding as a consequence of photospheric motions included in the model. Spectra of optically thin emission lines in the extreme ultraviolet range are synthesized, and magnetic field lines are traced over time. We determine the trajectory of the plasma ejection and identify anomalies in the profiles of the plasma parameters.
Results. Following strong heating just above the chromosphere, the pressure rapidly increases, leading to a hydrodynamic explosion above the upper chromosphere in the low transition region. The explosion drives the plasma, which needs to follow the magnetic field lines. The ejection is then moving more or less ballistically along the loop-like field lines and eventually drops down onto the surface of the Sun. The speed of the ejection is in the range of the sound speed, well below the Alfvén velocity.
Conclusions. The plasma ejection observed in a numerical experiment of the solar corona is basically a hydrodynamic phenomenon, whereas the rise of the heating rate is of magnetic nature. The granular motions in the photosphere lead (by chance) to a strong braiding of the magnetic field lines at the location of the explosion that in turn is causing strong currents which are dissipated. Future studies need to determine if this process is a ubiquitous phenomenon on the Sun on small scales. Data from the Atmospheric Imaging Assembly on the Solar Dynamics Observatory (AIA/SDO) might provide the relevant information.

Unraveling the Trigger Mechanism of Explosive Reconnection in Partially Ionized Solar Plasma

Abdullah **Zafar**, Lei Ni, Jun Lin, Ahmad Ali
ApJ **2024**
https://arxiv.org/pdf/2407.01915
Plasmoid instability is usually accounted for the onset of fast reconnection events observed in astrophysical plasmas. However, the measured reconnection rate from observations can be one order of magnitude higher than that derived from MHD simulations. In this study, we present the results of magnetic reconnection in the partially ionized low solar atmosphere based on 2.5D magnetohydrodynamics (MHD) simulations. The whole reconnection process covers two different fast reconnection phases. In the first phase, the slow Sweet-Parker reconnection transits to the plasmoid-mediated reconnection, and the reconnection rate reaches about 0.02. In the second phase, a faster explosive reconnection appears, with the reconnection rate reaching above 0.06. At the same time, a sharp decrease in plasma temperature and density at the principle X-point is observed which is associated with the strong radiative cooling, the ejection of hot plasma from the local reconnection region or the motion of principle X-point from hot and denser region to cool and less dense one along the narrow current sheet. This causes gas pressure depletion and the increasing of magnetic diffusion at the main X-point, resulting in the local Petschek-like reconnection and a violent and rapid increase in the reconnection rate. This study for the first time reveals a common phenomenon that the plasmoid dominated reconnection transits to an explosive faster reconnection with the rate approaching the order of 0.1 in partially ionized plasma in the MHD scale.

Rayleigh–Taylor Instability and Excitation of Super-Dreicer Electric Fields in the Solar Chromosphere

V. V. **Zaitsev**, P. V. Kronshtadtov, A. V. Stepanov
Solar Phys. Volume 291, Issue 11, pp 3451–3459 **2016**
Within the framework of the long-standing so-called “number problem” in the physics of solar flares, we consider the excitation of a super-Dreicer electric field at the leading edge of the electric current pulse that occurs at the chromospheric legs of a coronal magnetic loop as a result of the magnetic Rayleigh–Taylor instability. It is shown that for a sufficiently strong electric current, \(I_{0} \ge 10^{10}~\mbox{A}\), the current pulse propagates in the non-linear mode and generates a strong longitudinal electric field \(E_{z}\), which strongly depends on the current (\(E_{z} \propto I_{0}^{3}\)) and can exceed the Dreicer field (\(E_{z} > E_{\mathrm{D}}\)). In this case, the bulk of electrons in the site of the current pulse is in a runaway mode, and the energy release rate in the chromosphere increases

significantly. Super-Dreicer electric fields also provide injection of protons into the regime of acceleration by Langmuir turbulence generated by fast electrons at the leading edge of the electric current pulse. The electric field at the pulse edge can exceed the Dreicer field starting from the chromosphere level with the number density \(n \approx 10^{13}~\mbox{cm}^{-3}\). At a lower current \(I_{0} < 10^{10}~\mbox{A}\), a super-Dreicer mode at the higher levels of the chromosphere with \(n < 10^{12}~\mbox{cm}^{-3}\) occurs.

Particle Acceleration and Plasma Heating in the Chromosphere

V. V. **Zaitsev**, A. V. Stepanov

Solar Phys. Volume 290, Issue 12, pp 3559-3572 **2015**

We propose a new mechanism of electron acceleration and plasma heating in the solar chromosphere, based on the magnetic Rayleigh–Taylor instability. The instability develops at the chromospheric footpoints of a flare loop and deforms the local magnetic field. As a result, the electric current in the loop varies, and a resulting inductive electric field appears. A pulse of the induced electric field, together with the pulse of the electric current, propagates along the loop with the Alfvén velocity and begins to accelerate electrons up to an energy of about 1 MeV. Accelerated particles are thermalized in the dense layers of the chromosphere with the plasma density n≈1014--1015 cm−3, heating them to a temperature of about several million degrees. Joule dissipation of the electric current pulse heats the chromosphere at heights that correspond to densities n≤1011--1013 c. Observations with the New Solar Telescope at Big Bear Solar Observatory indicate that chromospheric footpoints of coronal loops might be heated to coronal temperatures and that hot plasma might be injected upwards, which brightens ultra-fine loops from the photosphere to the base of the corona. Thereby, recent observations of the Sun and the model we propose stimulate a déjà vu – they are reminiscent of the concept of the chromospheric flare.

A SOHO/UVCS study of coronal outflows at the edge of an active region complex

L. **Zangrilli**1 and G. Poletto

A&A 545, A8 (**2012**)

Context. In the past, active regions (ARs) have been suggested as a possible source of the slow solar wind. Their role as solar wind contributors has recently been supported by HINODE observations at low coronal levels.

Aims. Our purpose is to determine whether outflows at the edges of ARs can be detected in higher layers of the corona, supporting the low-corona evidence for the occurrence of wind streams from ARs.

Methods. Data acquired by SOHO/UVCS on January 2, 1998, at altitudes ranging from 1.5 to 2.3 solar radii at mid latitudes, were used to infer the physical properties of an AR complex at the time of its limb passage. To this end, the Doppler dimming technique was applied to UVCS observations of the H i Lyα and O vi doublet lines at 1031.9 and 1037.6 Å.

Results. Outflow speeds (and electron densities) were inferred: outflows, at speeds increasing with height, turn out to be confined within a narrow channel at the edge of closed loop systems within the AR. Our results are compared with those obtained by other authors with different techniques.

Conclusions. Our results support the assumption that ARs are sources of slow wind. To our knowledge these are the first direct measurements of AR flows in the intermediate corona. Tentative profiles of the speed vs. heliocentric altitudes at heliocentric distances between ≈ 1.5 and ≈ 2.3 solar radii show that AR flows are faster than streams from equatorial coronal holes.

Investigating and comparing the IRIS spectral lines Mg II, Si IV, and C II for flare precursor diagnostics

Jonas **Zbinden**1,2,⋆, Lucia Kleint1,2 and Brandon Panos1,2

A&A, 689, A72 (**2024**)

https://www.aanda.org/articles/aa/pdf/2024/09/aa47824-23.pdf

Context. Reliably predicting solar flares can mitigate the risks of technological damage and enhance scientific output by providing reliable pointings for observational campaigns. Flare precursors in the spectral line Mg II have been identified.

Aims. We extend previous studies by examining the presence of flare precursors in additional spectral lines, such as Si IV and C II, over longer time windows, and for more observations.

Methods. We trained neural networks and XGBoost decision trees to distinguish spectra observed from active regions that lead to a flare and those that did not. To enhance the information within each observation, we tested different masking methods to preprocess the data.

Results. We find average classification true skill statistics (TSS) scores of 0.53 for Mg II, 0.44 for Si IV, and 0.42 for C II. We speculate that Mg II h&k performs best because it samples the highest formation height range, and is sensitive to heating and density changes in the mid- to upper chromosphere. The flaring area relative to the field of view has a large effect on the model classification score and needs to be accounted for. Combining spectral lines has proven difficult, due to the difference in areas of high probability for an imminent flare between different lines.

Conclusions. Our models extract information from all three lines, independent of observational bias or GOES X-ray flux precursors, implying that the physics encoded in a combination of high resolution spectral data could be useful for flare forecasting.

Flare Expansion to a Magnetic Rope Accompanied by Rare Radio Bursts

Alena **Zemanová**, Marian Karlický, Jana Kašparová, and Jaroslav Dudík
2020 ApJ 905 111
https://doi.org/10.3847/1538-4357/abc424
We present multispectral analysis (radio, Hα, ultraviolet (UV)/extreme ultraviolet (EUV), and hard X-ray) of a confined flare from **2015 March 12**. This flare started within the active region NOAA 12 297 and then it expanded into a large preexisting magnetic rope embedded with a cold filament. The expansion started with several brightenings located along the rope. This process was accompanied by a group of slowly positively drifting bursts in the 0.8–2 GHz range. The frequency drift of these bursts was 45–100 MHz s−1. One of the bursts had an S-like form. During the brightening of the rope we observed a unique bright EUV structure transverse to the rope axis. The structure was observed in a broad range of temperatures and it moved along the rope with the velocity of about 240 km s−1. When the structure dissipated, we saw a plasma further following twisted threads in the rope. The observed slowly positively drifting bursts were interpreted considering particle beams and we show that one with the S-like form could be explained by the beam propagating through the helical structure of the magnetic rope. The bright structure transverse to the rope axis was interpreted considering line-of-sight effects and the dissipation-spreading process, which we found to be more likely.

Causal Attention Deep-learning Model for Solar Flare Forecasting

Xinze **Zhang**1,2, Long Xu3, Zihan Li1, and Xin Huang3
2024 ApJS 274 38
https://iopscience.iop.org/article/10.3847/1538-4365/ad7386/pdf
Solar flares originate from the sudden release of energy stored in the magnetic field of the active region on the Sun, but the trigger for flares is still uncertain. Currently, deep-learning-based solar flare prediction models have achieved good results and are widely recognized. However, these models focus more on data correlation rather than causality. An ideal flare prediction model should probe into the causes/triggers of solar flares, and diagnose the precursors of flares rather than just correlation analysis. To extract more informative precursors of flares from magnetograms, while suppressing the interference of confounding factors, a causal attention module is introduced to disentangle causal and confounder features from the input features. To address the problem of imbalanced positive and negative samples in the data set, an adaptive data set split mechanism is proposed. It divides the data set into several balanced subsets of positive and negative samples, and dynamically adjusts the subsets according to the model's prediction results during the training process. The experimental results demonstrate that our proposed model achieves 4.08%, 8.38%, and 2.19% higher accuracy, true skill score, and area under the receiver operating characteristic curve than the baseline model. Additionally, the class-specific heatmaps by using the gradient-weighted class activation mapping method reveal that our proposed model generally focuses on the polarity inverse line of active regions, well in line with theoretical study.

Transverse oscillation of prominence and filament induced by an EUV wave from the farside of the Sun

Yanjie **Zhang**, Qingmin Zhang, De-chao Song, Haisheng Ji
ApJ **2024**
https://arxiv.org/pdf/2401.15858.pdf
In this paper, we report our multi-angle observations of the transverse oscillation of a prominence and a filament induced by an EUV wave originating from the farside of the Sun on **2014 September 1**. The prominence oscillation was simultaneously observed by both Atmospheric Imaging Assembly (AIA) onboard the Solar Dynamics Observatory (SDO) spacecraft and Extreme-UltraViolet Imager (EUVI) onboard the Behind Solar Terrestrial Relations Observatory (STEREO) spacecraft. The speed of the shock travelling in the interplanetary space exceeds that of the EUV wave, and the coronal dimming area experiences minimal growth. This indicates that the shock wave is driven by the CME, while the EUV wave freely propagates after the lateral motion of the CME flanks has stopped. The observed oscillation direction of the prominence, determined through three-dimensional reconstruction, further supports this point. Moreover, The detailed investigation of the oscillations in the prominence and filament induced by the EUV wave reveals initial amplitudes of 16.08 and 2.15 Mm, periods of 1769 and 1863 s, damping time scales of 2640 and 1259 s, and damping ratios of 1.49 and 0.68, respectively. The radial component of magnetic field, as derived from the prominence and filament oscillation measurements, was estimated to be 5.4 G and 4.1 G, respectively. In turn, utilizing the onset times of both the prominence and filament oscillation, the average speeds of the EUV wave are determined to be 498 km s−1 and 451 km s−1, respectively.

Quasiperiodic Oscillations of Flare Loops and Slipping Motion of Ribbon Substructures during a C-class Flare

Yining **Zhang**1,2, Ting Li1,2,3, and Jing Ye4,5,6
2024 ApJ 972 122
https://arxiv.org/pdf/2407.03639
https://iopscience.iop.org/article/10.3847/1538-4357/ad5e69/pdf
Quasiperiodic oscillations in solar-flaring emission have been observed over the past few decades. To date, the underpinning processes resulting in the quasiperiodic oscillations remain unknown. In this paper, we report a unique event that exhibits both the long-duration quasiperiodic intensity oscillations of flare loops and the quasiperiodic slipping motion of ribbon substructures during a C9.1-class flare (SOL**2015-03-15**-T01:15), using the observations from the Solar Dynamics Observatory and Interface Region Imaging Spectrograph. The high-temperature flare loops rooted in the straight part of ribbons display a "bright–dim" intensity oscillation, with a period of about 4.5 minutes. The oscillation starts just after the flare onset and lasts over 3 hr. Meanwhile, the substructures within the ribbon tip display the quasiperiodic slipping motion along the ribbon at 1400 Å images, which has a similar periodicity to the stationary intensity oscillation of the flare loops in the straight part of the flare ribbons. We suggest that the quasiperiodic pattern is probably related to the loop-top dynamics caused by the reconnection outflow impinging on the flare loops.

Circular-ribbon flares and the related activities **Review**

Qingmin **Zhang**
Reviews of Modern Plasma Physics **2024**
https://arxiv.org/pdf/2401.16101.pdf
Solar flares are an impulsive increase of emissions as a result of impetuous release of magnetic free energy. In this paper, I will present the recent progress on circular-ribbon flares (CRFs) and their related activities, including coronal jets, filaments, coronal mass ejections (CMEs), radio bursts, coronal dimmings, and coronal loop oscillations. Owing to the prevalence of three-dimensional (3D) magnetic null points and the corresponding fan-spine topology in the solar atmosphere, CRFs are regularly observed in ultraviolet (UV), extreme-ultraviolet (EUV), and Hα passbands. Spine reconnection and fan reconnection around the null points are predominantly responsible for the energy release and subsequent particle acceleration. Slipping reconnection at quasi-separatrix layers (QSLs) may explain the sequential brightening or rapid degradation of the circular ribbons. Periodic or quasi-periodic acceleration and precipitation of nonthermal particles in the chromo- sphere produce observed quasi-periodic pulsations (QPPs) of CRFs in multiple altitudes as well as wavelengths. Like two-ribbon flares, the injected high-energy particles result in explosive evaporation in circular and inner ribbons, which is characterized by simultaneous blueshifts in the coronal emission lines and redshifts in the chromospheric emission lines. Homologous CRFs residing in the same active region present similar morphology, evolution, and energy partition. The peculiar topology of CRFs with closed outer spines facilitates remote brightenings and EUV late phases, which are uncommon in tworibbon flares. Besides, CRFs are often accompanied by coronal jets, type III radio bursts, CMEs, shock waves, coronal dimmings, and kink oscillations in coronal loops and filaments. Magnetohydrodynamics numerical simulations are very helpful to understand the key problems that are still unclear up to now. Multiwavelength and multipoint observations with state-of-the-art instruments are enormously desired to make a breakthrough. The findings in CRFs are important for a comprehensive understanding of solar flares and have implication for stellar flares. **2002-11-16, 2010-10-16, 2011-02-08, 6 Sep 2011, 7 Sep 2011, 23 Sep 2011, 2011-10-22, 2011-11-15, 2012 May 10 , 2012-07-14, 13 Jan 2013, 2013-03-02, 2013 November 5-6-7, 10 Nov 2013, 5 Mar 2014, 2014-04-16, 2014-08-24, 2014-12-17, 18 Dec 2014, 2015 March 10, 2015-04-20-21, 16 Oct 2015, 2016-01-09**

A Flare Observed in Coronal, Transition Region and Helium I 10830 ? Emissions

Zhicheng **Zeng**, Jiong Qiu, Wenda Cao, Philip G. Judge
2014 ApJ 793 87
http://arxiv.org/pdf/1408.0236v1.pdf
On **June 17, 2012**, we observed the evolution of a C-class flare associated with the eruption of a filament near a large sunspot in the active region NOAA 11504. We obtained high spatial resolution filtergrams using the 1.6 m New Solar Telescope at the Big Bear Solar Observatory in broad-band TiO at 706 nm (bandpass:10 ?) and He I 10830 ? narrow-band (bandpass: 0.5 ?, centered 0.25 ? to the blue). We analyze the spatio-temporal behavior of the He I 10830 ? data, which were obtained over a 90" X 90" field of view with a cadence of 10 sec. We also analyze simultaneous data from the Atmospheric Imaging Assembly and Extreme Ultraviolet Variability Experiment instruments on board the Solar Dynamics Observatory spacecraft, and data from Reuven Ramaty High Energy Solar Spectroscopic Imager and GOES spacecrafts. Non-thermal effects are ignored in this analysis. Several quantitative aspects of the data, as well as models derived using the "0D" Enthalpy-Based Thermal Evolution of Loops model (EBTEL: Klimchuk et al. 2008) code, indicate that the triplet states of the 10830 ? multiplet are populated by photoionization of chromospheric plasma followed by radiative recombination. Surprisingly, the He II 304 ? line is reasonably well matched by standard emission measure calculations, along with the C IV emission which dominates the AIA 1600 ? channel during flares. This work lends support to some of our previous work combining X-ray, EUV and UV data of flares to build models of energy transport from corona to chromosphere.

Quasi-periodic oscillations of flare loops and slipping motion of ribbon substructures during a C-class flare

Yining **Zhang**, Ting Li, Jing Ye

ApJ **2024**

https://arxiv.org/pdf/2407.03639

Quasi-periodic oscillations in solar flaring emission have been observed over the past few decades. To date, the underpinning processes resulting in the quasi-periodic oscillations remain unknown. In this paper, we report a unique event that exhibits both the long-duration quasi-periodic intensity oscillations of flare loops and the quasi-periodic slipping motion of ribbon substructures during a C9.1-class flare (SOL2015-03-15-T01:15), using the observations from Solar Dynamics Observatory and Interface Region Imaging Spectrograph. The high-temperature flare loops rooted in the straight part of ribbons display a "bright-dim" intensity oscillation, with a period of about 4.5 minutes. The oscillation starts just after the flare onset and lasts over 3 hours. Meanwhile, the substructures within the ribbon tip display the quasi-periodic slipping motion along the ribbon at 1400 Åimages which has a similar periodicity to the stationary intensity oscillation of the flare loops in the straight part of the flare ribbons. We suggest that the quasi-periodic pattern is probably related to the loop-top dynamics caused by the reconnection outflow impinging on the flare loops. **2015 March 15**

Plasma Dynamics and Nonthermal Particle Acceleration in 3D Nonrelativistic Magnetic Reconnection

Qile **Zhang**, Fan Guo, William Daughton, Xiaocan Li, Hui Li

ApJ **2024**

https://arxiv.org/pdf/2404.08807.pdf

Understanding plasma dynamics and nonthermal particle acceleration in 3D magnetic reconnection has been a long-standing challenge. In this paper, we explore these problems by performing large-scale fully kinetic simulations of multi-xline plasmoid reconnection with various parameters in both the weak and strong guide field regimes. In each regime, we have identified its unique 3D dynamics that leads to field-line chaos and efficient acceleration, and we have achieved nonthermal acceleration of both electrons and protons into power-law spectra. The spectral indices agree well with a simple Fermi acceleration theory that includes guide field dependence. In the low-guide-field regime, the flux-rope kink instability governs the 3D dynamics for efficient acceleration. The weak dependence of the spectra on the ion-to-electron mass ratio and β ($\ll 1$) implies that the particles are sufficiently magnetized for Fermi acceleration in our simulations. While both electrons and protons are injected at reconnection exhausts, protons are primarily injected by perpendicular electric fields through Fermi reflections and electrons are injected by a combination of perpendicular and parallel electric fields. The magnetic power spectra agree with in-situ magnetotail observations, and the spectral index may reflect a reconnection-driven size distribution of plasmoids instead of Goldreich-Sridhar vortex cascade. As the guide field becomes stronger, the oblique flux ropes of large sizes capture the main 3D dynamics for efficient acceleration. Intriguingly, the oblique flux ropes can also run into flux-rope kink instability to drive extra 3D dynamics. This work has broad implications for 3D reconnection dynamics and particle acceleration in heliophysics and astrophysics.

Energetics of a solar flare and a coronal mass ejection generated by a hot channel eruption

Qingmin **Zhang**, Weilin Teng, Dong Li, Jun Dai, Yanjie Zhang

ApJ **958** 85 **2023**

https://arxiv.org/pdf/2310.14010.pdf

https://iopscience.iop.org/article/10.3847/1538-4357/ad05bc/pdf

Hot channels (HCs) are prevalent in the solar corona and play a critical role in driving flares and CMEs. In this paper, we estimate the energy contents of an X1.4 eruptive flare with a fast CME generated by a HC eruption on **2011 September 22**. Originating from NOAA AR11302, the HC is the most dramatic feature in 131 and 94 Å images observed by SDO/AIA. The flare is simultaneously observed by SDO/AIA, RHESSI, and STEREO-B/EUVI. The CME is simultaneously detected by the white-light coronagraphs of SOHO/LASCO and STEREO-B/COR1. Using multiwavelength and multiview observations of the eruption, various energy components of the HC, flare, and CME are calculated. The thermal and kinetic energies of the HC are (1.77±0.61)×1030 erg and (2.90±0.79)×1030 erg, respectively. The peak thermal energy of the flare and total radiative loss of SXR-emitting plasma are (1.63±0.04)×1031 erg and (1.03−1.31)×1031 erg, respectively. The ratio between the thermal energies of HC and flare is 0.11±0.03, suggesting that thermal energy of the HC is not negligible. The kinetic and potential energies of the CME are (3.43±0.94)×1031 erg and (2.66±0.49)×1030 erg, yielding a total energy of (3.69±0.98)×1031 erg for the CME. Continuous heating of the HC is required to balance the rapid cooling by heat conduction, which probably originate from intermittent magnetic reconnection at the flare current sheet. Our investigation may provide insight into the buildup, release, and conversion of energies in large-scale solar eruptions.

Observations of magnetic reconnection and particle acceleration locations in solar coronal jets

Yixian **Zhang**, Sophie Musset, Lindsay Glesener, Navdeep Panesar, Gregory Fleishman

ApJ **943** 180 **2023**

https://arxiv.org/pdf/2207.05668.pdf

https://iopscience.iop.org/article/10.3847/1538-4357/aca654/pdf

We present a multi-wavelength analysis of two flare-related jets on **November 13, 2014**, using data from SDO/AIA, RHESSI, Hinode/XRT, and IRIS. Unlike most coronal jets where hard X-ray (HXR) emissions are usually observed near the jet base, in these events HXR emissions are found at several locations, including in the corona. We carry out the first differential emission measure (DEM) analysis that combines both AIA (and XRT when available) bandpass filter data and RHESSI HXR measurements for coronal jets, and obtain self-consistent results across a wide temperature range and into non-thermal energies. In both events, hot plasma first appeared at the jet base, but as the base plasma gradually cooled, hot plasma also appeared near the jet top. Moreover, non-thermal electrons, while only mildly energetic, are found in multiple HXR locations and contain a large amount of total energy. Particularly, the energetic electrons that produced the HXR sources at the jet top were accelerated near the top location, rather than traveling from a reconnection site at the jet base. This means that there was more than one particle acceleration site in each event. Jet velocities are consistent with previous studies, including upward and downward velocities around ~200 km/s and ~100 km/s respectively, and fast outflows of 400-700 km/s. We also examine the energy partition in the later event, and find that the non-thermal energy in accelerated electrons is most significant compared to other energy forms considered. We discuss the interpretations and provide constraints on mechanisms for coronal jet formation.

RHESSI Science Nuggets #445 Mar **2023**

https://sprg.ssl.berkeley.edu/~tohban/wiki/index.php/Particle_Acceleration_in_Two_Coronal_Jets

Multi-species Ion Acceleration in 3D Magnetic Reconnection

Qile **Zhang**, Fan Guo, William Daughton, Hui Li, Ari Le, Tai Phan, Mihir Desai

2022

https://arxiv.org/pdf/2210.04113.pdf

Magnetic reconnection drives explosive particle acceleration in a wide range of space and astrophysical applications. The energized particles often include multiple species (electrons, protons, heavy ions), but the underlying acceleration mechanism is poorly understood. In-situ observations of these minority heavy ions offer a more stringent test of acceleration mechanisms, but the multi-scale nature of reconnection hinders studies on heavy-ion acceleration. Here we employ hybrid simulations (fluid electron, kinetic ions) to capture 3D reconnection over an unprecedented range of scales. For the first time, our simulations demonstrate nonthermal acceleration of all available ion species into power-law spectra. The reconnection layers consist of fragmented kinking flux ropes as part of the reconnection-driven turbulence, which produces field-line chaos critical for accelerating all species. The upstream ion velocities influence the first Fermi reflection for injection. Then lower charge/mass species initiate Fermi acceleration at later times as they interact with growing flux ropes. The resulting spectra have similar power-law indices ($p \sim 4.5$), but different maximum energy/nucleon $\propto$(charge/mass)α, with $\alpha \sim 0.6$ for low plasma β, and with p and α increasing as β approaches unity. These findings are consistent with observations at heliospheric current sheets and the magnetotail, and provide strong evidence suggesting Fermi acceleration as the dominant ion-acceleration mechanism.

Solar Flare Index Prediction Using SDO/HMI Vector Magnetic Data Products with Statistical and Machine Learning Methods

Hewei **Zhang**, Qin Li, Yanxing Yang, Ju Jing, Jason T.L. Wang, Haimin Wang, Zuofeng Shang

ApJS **263** 28 **2022**

https://arxiv.org/pdf/2209.13779.pdf

https://iopscience.iop.org/article/10.3847/1538-4365/ac9b17/pdf

Solar flares, especially the M- and X-class flares, are often associated with coronal mass ejections (CMEs). They are the most important sources of space weather effects, that can severely impact the near-Earth environment. Thus it is essential to forecast flares (especially the M-and X-class ones) to mitigate their destructive and hazardous consequences. Here, we introduce several statistical and Machine Learning approaches to the prediction of the AR's Flare Index (FI) that quantifies the flare productivity of an AR by taking into account the numbers of different class flares within a certain time interval. Specifically, our sample includes 563 ARs appeared on solar disk from May 2010 to Dec 2017. The 25 magnetic parameters, provided by the Space-weather HMI Active Region Patches (SHARP) from Helioseismic and Magnetic Imager (HMI) on board the Solar Dynamics Observatory (SDO), characterize coronal magnetic energy stored in ARs by proxy and are used as the predictors. We investigate the relationship between these SHARP parameters and the FI of ARs with a machine-learning algorithm (spline regression) and the resampling method (Synthetic Minority Over-Sampling Technique for Regression with Gaussian Noise, short by SMOGN). Based on the established relationship, we are able to predict the value of FIs for a given AR within the next 1-day period. Compared with other 4 popular machine learning algorithms, our methods improve the accuracy of FI prediction, especially for large FI. In addition, we sort the importance of SHARP parameters by Borda Count method calculated from the ranks that are rendered by 9 different machine learning methods.

First detection of transverse vertical oscillation during the expansion of coronal loops

Qingmin **Zhang**, Chuan Li, Dong Li, Ye Qiu, Yanjie Zhang, Yiwei Ni

ApJL **2022**

https://arxiv.org/pdf/2209.00194.pdf

In this Letter, we perform a detailed analysis of the M5.5-class eruptive flare occurring in active region 12929 on **2022 January 20**. The eruption of a hot channel generates a fast coronal mass ejection (CME) and a dome-shaped extreme-ultraviolet (EUV) wave at speeds of 740−860 km s−1. The CME is associated with a type II radio burst, implying that the EUV wave is a fast-mode shock wave. During the impulsive phase, the flare shows quasi-periodic pulsations (QPPs) in EUV, hard X-ray, and radio wavelengths. The periods of QPPs range from 18 s to 113 s, indicating that flare energy is released and nonthermal electrons are accelerated intermittently with multiple time scales. The interaction between the EUV wave and low-lying adjacent coronal loops (ACLs) results in contraction, expansion, and transverse vertical oscillation of ACLs. The speed of contraction in 171, 193, and 211 Å is higher than that in 304 Å. The periods of oscillation are 253 s and 275 s in 304 Å and 171 Å, respectively. A new scenario is proposed to explain the interaction. The equation that interprets the contraction and oscillation of the overlying coronal loops above a flare core can also interpret the expansion and oscillation of ACLs, suggesting that the two phenomena are the same in essence.

Sunspot shearing and sudden retraction motion associated with the 2013 August 17 M3.3 Flare

Yanjie **Zhang**, Zhe Xu, Qingmin Zhang, Jun Dai, Haisheng Ji

ApJ **933** L20 **2022**

https://arxiv.org/pdf/2206.09156.pdf

https://iopscience.iop.org/article/10.3847/2041-8213/ac79b7/pdf

In this Letter, we give a detailed analysis to the M3.3 class flare that occurred on **August 17, 2013** (SOL2013-08-17T18:16). It presents a clear picture of mutual magnetic interaction initially from the photosphere to the corona via the abrupt rapid shearing motion of a small sunspot before the flare, and then suddenly from the corona back to the photosphere via the sudden retraction motion of the same sunspot during the flare impulsive phase. About 10 hours before the flare, a small sunspot in the active region NOAA 11818 started to move northeast along a magnetic polarity inversion line (PIL), creating a shearing motion that changed the quasi-static state of the active region. A filament right above the PIL was activated following the movement of the sunspot and then got partially erupted. The eruption eventually led to the M3.3 flare. The sunspot was then suddenly pulled back to the opposite direction upon the flare onset. During the backward motion, the Lorentz force underwent a simultaneous impulsive change both in magnitude and direction. Its directional change is found to be conformable with the retraction motion. The observation provides direct evidence for the role of the shearing motion of the sunspot in powering and triggering the flare. It especially confirms that the abrupt motion of a sunspot during a solar flare is the result of a back reaction caused by the reconfiguration of the coronal magnetic field.

Two-dimensional modeling of the tearing-mode-governed magnetic reconnection in the large-scale current sheet above the two-ribbon flare

Yining **Zhang**, Jing Ye, Zhixing Mei, Yan Li, Jun Lin

Research in Astronomy and Astrophysics **2022**

https://arxiv.org/pdf/2206.04484.pdf

We attempt to model magnetic reconnection during the two-ribbon flare in the gravitationally stratified solar atmosphere with the Lundquist number of S=106 using 2D simulations. We found that the tearing mode instability leads to the inhomogeneous turbulence inside the reconnecting current sheet (CS) and invokes the fast phase of reconnection. Fast reconnection brings an extra dissipation of magnetic field which enhances the reconnection rate in an apparent way. The energy spectrum in the CS shows the power-law pattern and the dynamics of plasmoids governs the associated spectral index. We noticed that the energy dissipation occurs at a scale lko of 100-200~km, and the associated CS thickness ranges from 1500 to 2500~km, which follows the Taylor scale lT=lkoS1/6. The termination shock(TS) appears in the turbulent region above flare loops, which is an important contributor to heating flare loops. Substantial magnetic energy is converted into both kinetic and thermal energies via TS, and the cumulative heating rate is greater than the rate of the kinetic energy transfer. In addition, the turbulence is somehow amplified by TS, of which the amplitude is related to the local geometry of the TS.

Implications for additional plasma heating driving the extreme-ultraviolet late phase of a solar flare with microwave imaging spectroscopy

Jiale **Zhang**, Bin Chen, Sijie Yu, Hui Tian, Yuqian Wei, Hechao Chen, Guangyu Tan, Yingjie Luo, Xingyao Chen

ApJ **2022**

https://arxiv.org/pdf/2205.03518.pdf **File**

Extreme-ultraviolet late phase (ELP) refers to the second extreme-ultraviolet (EUV) radiation enhancement observed in certain solar flares, which usually occurs tens of minutes to several hours after the peak of soft X-ray emission. The coronal loop system that hosts the ELP emission is often different from the main flaring arcade, and the enhanced EUV emission therein may imply an additional heating process. However, the origin of the ELP remains rather unclear. Here we present the analysis of a C1.4 flare that features such an ELP, which is also observed in microwave wavelengths by the Expanded Owens Valley Solar Array (EOVSA). Similar to the case of the ELP, we find a gradual microwave enhancement that occurs about three minutes after the main impulsive phase microwave peaks. Radio sources coincide with both footpoints of the ELP loops and spectral fits on the time-varying microwave spectra demonstrate a clear deviation of the electron distribution from the Maxwellian case, which could result from injected nonthermal electrons or nonuniform heating to the footpoint plasma. We further point out that the delayed microwave enhancement suggests the presence of an additional heating process, which could be responsible for the evaporation of heated plasma that fills the ELP loops, producing the prolonged ELP emission. **July 14th, 2017**

Statistical analysis of circular-ribbon flares

Yanjie **Zhang**, Qingmin Zhang, Dechao Song, Shuting Li, Jun Dai, Zhe Xu, Haisheng Ji
Astrophysical Journal Supplement Series **260** 19 **2022**
https://arxiv.org/pdf/2203.12819.pdf
https://iopscience.iop.org/article/10.3847/1538-4365/ac5f4c/pdf
Circular-ribbon flares (CFs) are a special type of solar flares owing to their particular magnetic topology. In this paper, we conducted a comprehensive statistical analysis of 134 CFs from 2011 September to 2017 June, including four B-class, 82 C-class, 40 M-class, and eight X-class flares, respectively. The flares were observed by the Atmospheric Imaging Assembly (AIA) on board the Solar Dynamics Observatory (SDO) spacecraft. The physical properties of CFs are derived, including the location, area (ACF), equivalent radius (rCF) assuming a semi-spherical fan dome, lifetime (τCF), and peak SXR flux in 1−8 Å. It is found that all CFs are located in active regions, with the latitudes between -30∘ and 30∘. The distributions of areas and lifetimes could be fitted with a log-normal function. There is a positive correlation between the lifetime and area. The peak SXR flux in 1−8 Å is well in accord with a power-law distribution with an index of −1.42. For the 134 CFs, 57\% of them are accompanied by remote brightenings or ribbons. A positive correlation exists between the total length (LRB) and average distance (DRB) of remote brightenings. About 47\% and 51\% of the 134 CFs are related to type III radio bursts and jets, respectively. The association rates are independent of flare energies. About 38\% of CFs are related to mini-filament eruptions, and the association rates increase with flare classes. Only 28\% of CFs are related to CMEs, meaning that a majority of them are confined rather than eruptive events. There is a positive correlation between the CME speed and peak SXR flux in 1−8 Å, and faster CMEs tend to be wider. **7 Sep 2011, 8 May 2012, 13 Jan 2013, 10 Nov 2013, 28 Dec 2013, 18 Apr 2014, 17 Dec 2014, 16 Oct 2015**
Table 1. List of 134 Circular-ribbon Flares 2011-2017

X-ray fine structure of a limb solar flare revealed by Insight-HXMT, RHESSI and Fermi

Ping **Zhang**, Wei Wang, Yang Su, Shuangnan Zhang, Liming Song, Fangjun Lu, Shu Zhang
Research in A&A Volume 22, Issue 5, id.055006, 9 pp **2022**
https://arxiv.org/pdf/2202.12600.pdf
We conduct a detailed analysis of an M1.3 limb flare occurring on **2017 July 3**, which have the X-ray observations recorded by multiple hard X-ray telescopes, including Hard X-ray Modulation Telescope (Insight-HXMT), Ramaty High Energy Solar Spectroscopic Imager (RHESSI), and The Fermi Gamma-ray Space Telescope (FERMI). Joint analysis has also used the EUV imaging data from the Atmospheric Imaging Assembly (AIA) aboard the Solar Dynamic Observatory. The hard X-ray spectral and imaging evolution suggest a lower corona source, and the non-thermal broken power law distribution has a rather low break energy ~ 15 keV. The EUV imaging shows a rather stable plasma configuration before the hard X-ray peak phase, and accompanied by a filament eruption during the hard X-ray flare peak phase. Hard X-ray image reconstruction from RHESSI data only shows one foot point source. We also determined the DEM for the peak phase by SDO/AIA data. The integrated EM beyond 10 MK at foot point onset after the peak phase, while the > 10 MK source around reconnection site began to fade. The evolution of EM and hard X-ray source supports lower corona plasma heating after non-thermal energy dissipation. The combination of hard X-ray spectra and images during the limb flare provides the understanding on the interchange of non-thermal and thermal energies, and relation between lower corona heating and the upper corona instability.
RHESSI Science Nuggets №428 Mar **2022** https://sprg.ssl.berkeley.edu/~tohban/wiki/index.php/Solar_Hard_X-rays_with_Insight

Non-thermal electron energization during the impulsive phase of an X9.3 flare revealed by Insight-HXMT

P. **Zhang**, W. Wang, Y. Su, L.M. Song, C.K. Li, D.K. Zhou, S.N. Zhang, H. Tian, S.M. Liu, H.S. Zhao, S. Zhang
ApJ **918** 42 **2021**
https://arxiv.org/pdf/2106.09506.pdf

https://iopscience.iop.org/article/10.3847/1538-4357/ac0cfb/pdf
https://doi.org/10.3847/1538-4357/ac0cfb
The X9.3 flare SOL**20170906**T11:55 was observed by the CsI detector aboard the first Chinese X-ray observatory Hard X-ray Modulation telescope (Insight-HXMT). By using wavelets method, we report about 22 s quasiperiodic pulsations(QPPs) during the impulsive phase. And the spectra from 100 keV to 800 keV showed the evolution with the gamma-ray flux, of a power-law photon index from ∼1.8 before the peak, ∼2.0 around the flare peak, to ∼1.8 again. The gyrosynchrotron microwave spectral analysis reveals a $36.6 \pm 0.6 \arcsec$ radius gyrosynchrotron source with mean transverse magnetic field around 608.2 Gauss, and the penetrated ≥ 10 keV non-thermal electron density is about 106.7cm−3 at peak time. The magnetic field strength followed the evolution of high-frequency radio flux. Further gyrosynchrotron source modeling analysis implies that there exists a quite steady gyrosynchrotron source, the non-thermal electron density and transverse magnetic field evolution are similar to higher-frequency light curves. The temporally spectral analysis reveals that those non-thermal electrons are accelerated by repeated magnetic reconnection, likely from a lower corona source.

Efficient Nonthermal Ion and Electron Acceleration Enabled by the Flux-Rope Kink Instability in 3D Nonrelativistic Magnetic Reconnection

Qile **Zhang**, Fan Guo, William Daughton, Xiaocan Li, Hui Li
2021
https://arxiv.org/pdf/2105.04521.pdf
The relaxation of field-line tension during magnetic reconnection gives rise to a universal Fermi acceleration process involving the curvature drift of particles. However, the efficiency of this mechanism is limited by the trapping of energetic particles within flux ropes. Using 3D fully kinetic simulations, we demonstrate that the flux-rope kink instability leads to field-line chaos in weak-guide-field regimes where the Fermi mechanism is most efficient, thus allowing particles to transport out of flux ropes and undergo further acceleration. As a consequence, both ions and electrons develop clear power-law energy spectra which contain a significant fraction of the released energy. The low-energy bounds are determined by the injection physics, while the high-energy cutoffs are limited only by the system size. These results have strong relevance to observations of nonthermal particle acceleration in both the magnetotail and solar corona.

Energy partition in a confined flare with an extreme-ultraviolet late phase

Q. M. **Zhang**, J. X. Cheng, Y. Dai, K. V. Tam, A. A. Xu
A&A 650, A88 **2021**
https://arxiv.org/pdf/2104.03677.pdf
https://www.aanda.org/articles/aa/pdf/2021/06/aa38082-20.pdf
https://doi.org/10.1051/0004-6361/202038082
In this paper, we reanalyze the M1.2 confined flare with a large extreme-ultraviolet (EUV) late phase on **2011 September 9**, focusing on its energy partition. The radiation (∼5.4×1030 erg) in 1−70 Å is nearly eleven times larger than the radiation in 70−370 Å, and is nearly 180 times larger than the radiation in 1−8 Å. The peak thermal energy of the post-flare loops is estimated to be (1.7−1.8)×1030 erg based on a simplified schematic cartoon. Based on previous results of Enthalpy-Based Thermal Evolution of Loops (EBTEL) simulation, the energy inputs in the main flaring loops and late-phase loops are (1.5−3.8)×1029 erg and 7.7×1029 erg, respectively. The nonthermal energy ((1.7−2.2)×1030 erg) of the flare-accelerated electrons is comparable to the peak thermal energy and is sufficient to provide the energy input of the main flaring loops and late-phase loops. The magnetic free energy (9.1×1031 erg) before flare is large enough to provide the heating requirement and radiation, indicating that the magnetic free energy is adequate to power the flare.

Spectroscopic observations of a flare-related coronal jet

Q. M. **Zhang**, Z. H. Huang, Y. J. Hou, D. Li, Z. J. Ning, Z. Wu
A&A **2021**
https://arxiv.org/pdf/2101.06629.pdf
Coronal jets are ubiquitous in active regions (ARs) and coronal holes. In this paper, we study a coronal jet related to a C3.4 circular-ribbon flare in active region 12434 on **2015 October 16**. Two minifilaments were located under a 3D fan-spine structure before flare. The flare was generated by the eruption of one filament. The kinetic evolution of the jet was divided into two phases: a slow rise phase at a speed of ∼131 km s−1 and a fast rise phase at a speed of ∼363 km s−1 in the plane-of-sky. The slow rise phase may correspond to the impulsive reconnection at the breakout current sheet. The fast rise phase may correspond to magnetic reconnection at the flare current sheet. The transition between the two phases occurred at ∼09:00:40 UT. The blueshifted Doppler velocities of the jet in the Si {\sc iv} 1402.80 Å line range from -34 to -120 km s−1. The accelerated high-energy electrons are composed of three groups. Those propagating upward along open field generate type \textrm{III} radio bursts, while those propagating downward produce HXR emissions and drive chromospheric condensation observed in the Si {\sc iv} line. The electrons trapped in the rising filament generate a microwave burst lasting for ≤40 s. Bidirectional outflows at the base of jet are manifested by

significant line broadenings of the Si {\sc iv} line. The blueshifted Doppler velocities of outflows range from -13 to -101 km s−1. The redshifted Doppler velocities of outflows range from ∼17 to ∼170 km s−1. Our multiwavelength observations of the flare-related jet are in favor of the breakout jet model and are important for understanding the acceleration and transport of nonthermal electrons.

Simultaneous transverse oscillations of a coronal loop and a filament excited by a circular-ribbon flare

Q. M. **Zhang**
A&A 642, A159 **2020**
https://arxiv.org/pdf/2008.01451.pdf
https://doi.org/10.1051/0004-6361/202038557To investigate the excitation of kink oscillations in coronal loops and filaments, a C3.4 circular-ribbon flare (CRF) associated with a blowout jet in active region 12434 on **2015 October 16** is analyzed. The flare excited small-amplitude kink oscillation of a remote coronal loop. The oscillation lasted for ≥4 cycles without significant damping. The amplitude and period are 0.3±0.1 Mm and 207±12 s. Interestingly, the flare also excited transverse oscillation of a remote filament. The oscillation lasted for ∼3.5 cycles with decaying amplitudes. The initial amplitude is 1.7−2.2 Mm. The period and damping time are 437−475 s and 1142−1600 s. The starting times of simultaneous oscillations of coronal loop and filament were concurrent with the hard X-ray peak time. Though small in size and short in lifetime, the flare set off a chain reaction. It generated a bright secondary flare ribbon (SFR) in the chromosphere, remote brightening (RB) that was cospatial with the filament, and intermittent, jet-like flow propagating in the northeast direction. The loop oscillation is most probably excited by the flare-induced blast wave at a speed of ≥1300 km s−1. The excitation of the filament oscillation is more complicated. The blast wave triggers secondary magnetic reconnection far from the main flare, which not only heats the local plasma to higher temperatures (SFR and RB), but produces jet-like flow (i.e., reconnection outflow) as well. The filament is disturbed by the secondary magnetic reconnection and experiences transverse oscillation. The findings give new insight into the excitation of transverse oscillations of coronal loops and filaments.

Transverse coronal loop oscillations excited by homologous circular-ribbon flares

Q. M. **Zhang**, J. Dai, Z. Xu, D. Li, L. Lu, K. V. Tam, A. A. Xu
A&A 638, A32 **2020**
https://arxiv.org/pdf/2005.02067.pdf
https://www.aanda.org/articles/aa/pdf/2020/06/aa38233-20.pdf
We report our multiwavelength observations of two homologous circular-ribbon flares (CRFs) in active region 11991 on **2014 March 5**, focusing on the transverse oscillations of an extreme-ultraviolet (EUV) loop excited by the flares. The transverse oscillations are of fast standing kink-mode. The first-stage oscillation triggered by the C2.8 flare is decayless with lower amplitudes (310−510 km). The periods (115−118 s) in different wavelengths are nearly the same, indicating coherent oscillations. The magnetic field of the loop is estimated to be 65−78 G. The second-stage oscillation triggered by the M1.0 flare is decaying with larger amplitudes (1250−1280 km). The periods decreases from 117 s in 211 Å to 70 s in 171 Å, implying a decrease of loop length or an implosion after a gradual expansion. The damping time, being 147−315 s, increases with the period, so that the values of τ/P are close to each other in different wavelengths. The thickness of the inhomogeneous layer is estimated to be ∼0\farcs45 under the assumption of resonant absorption. This is the first observation of the excitation of two kink-mode loop oscillations by two sympathetic flares. The results are important for understanding of the excitation of kink oscillations of coronal loops and hence the energy balance in the solar corona. Our findings also validate the prevalence of significantly amplified amplitudes of oscillations by successive drivers.

Fast degradation of the circular flare ribbon on 2014 August 24

Q. M. **Zhang**, S. H. Yang, T. Li, Y. J. Hou, Y. Li
A&A L 636, L11 **2020**
https://arxiv.org/pdf/2004.06837.pdf
https://doi.org/10.1051/0004-6361/202038072
The separation and elongation motions of solar flare ribbons have extensively been investigated. The degradation and disappearance of ribbons have rarely been explored. In this paper, we report our multiwavelength observations of a C5.5 circular-ribbon flare associated with two jets (jet1 and jet2) on **2014 August 24**, focusing on the fast degradation of the outer circular ribbon (CR). The flare, consisting of a short inner ribbon (IR) and outer CR, was triggered by the eruption of a minifilament. The brightness of IR and outer CR reached their maxima simultaneously at ∼04:58 UT in all AIA wavelengths. Subsequently, the short eastern part of CR faded out quickly in 1600 Å but gradually in EUV wavelengths. The long western part of CR degraded in the counterclockwise direction and experienced a deceleration. The degradation was distinctly divided into two phases: phase I with faster apparent speeds (58−69 km s−1) and phase II with slower apparent speeds (29−35 km s−1). The second phase stopped at ∼05:10 UT when the western CR totally disappeared. Besides the outward propagation of jet1, the jet spire experienced untwisting motion in the counterclockwise direction during 04:55−05:00 UT. We conclude that the event can be explained by the breakout jet

model. The coherent brightenings of the IR and CR at ~04:58 UT may result from the impulsive interchange reconnection near the null point, whereas sub-Alfvénic slipping motion of the western CR in the counterclockwise direction indicates the occurrence of slipping magnetic reconnection. Another possible explanation of the quick disappearance of the hot loops connecting to the western CR is that they are simply reconnected sequentially without the need for significant slippage after the null point reconnection.

Longitudinal filament oscillations enhanced by two C-class flares

Q. M. **Zhang**, J. H. Guo, K. V. Tam, A. A. Xu

A&A 635, A132 **2020**

https://arxiv.org/pdf/2001.01250.pdf

https://doi.org/10.1051/0004-6361/201937291

Context. Large-amplitude, longitudinal filament oscillations triggered by solar flares have been well established in the literature. However, filament oscillations enhanced by flares have never been reported.

Aims. In this paper we report the multiwavelength observations of a very long filament in active region (AR) 11112 on **2010 October 18**. The filament was composed of two parts, the eastern part (EP) and the western part (WP). We focus on longitudinal oscillations of the EP, which were enhanced by two homologous C-class flares in the same AR.

Methods. The filament was observed in Hα wavelength by the Global Oscillation Network Group and in extreme ultraviolet wavelengths by the Atmospheric Imaging Assembly on board the Solar Dynamics Observatory (SDO). Line-of-sight magnetograms were provided by the Helioseismic and Magnetic Imager on board SDO. The global three-dimensional magnetic fields were obtained using the potential field source surface modeling. Soft X-ray light curves of the two flares were recorded by the GOES spacecraft. White light images of the corona were observed by the LASCO/C2 coronagraph on board SOHO. To reproduce part of the observations, we perform one-dimensional, hydrodynamic numerical simulations using the MPI-AMRVAC code.

Results. The C1.3 flare was confined without a coronal mass ejection (CME). Both EP and WP of the filament were slightly disturbed and survived the flare. After 5 h, eruption of the WP generated a C2.6 flare and a narrow jet-like CME. Three oscillating threads (thda, thdb, thdc) are obviously identified in the EP, and their oscillations are naturally divided into three phases by the two flares. The initial amplitude ranges from 1.6 to 30 Mm with a mean value of ~14 Mm. The period ranges from 34 to 73 min with a mean value of ~53 min. The curvature radii of the magnetic dips are estimated to be 29 to 133 Mm with a mean value of ~74 Mm. The damping times ranges from ~62 to ~96 min with a mean value of ~82 min. The value of τ/P is between 1.2 and 1.8. For thda in the EP, the amplitudes were enhanced by the two flares from 6.1 Mm to 6.8 Mm after the C1.3 flare, and further to 21.4 Mm after the C2.6 flare. The period variation as a result of perturbation from the flares was within 20%. The attenuation became faster after the C2.6 flare.

Conclusions. To the best of our knowledge, this is the first report of large-amplitude, longitudinal filament oscillations enhanced by flares. Numerical simulations reproduce the oscillations of thda very well. The simulated amplitudes and periods are close to the observed values, while the damping time in the last phase is longer, implying additional mechanisms should be taken into account apart from radiative loss.

Remote coronal dimmings related to a circular-ribbon flare

Q. M. **Zhang**, R. S. Zheng

A&A **2020**

https://arxiv.org/pdf/1912.09618.pdf

In this paper, multiwavelength observations of remote coronal dimmings related to an M1.1 circular-ribbon flare (CRF) in active region (AR) 12434 are reported. The confined flare without a CME was observed by AIA and HMI on board SDO on **2015 October 16**. Global three-dimensional (3D) magnetic fields before flare were obtained using the potential field source surface modeling. A few minutes before the flare hard X-ray peak time (06:13:48 UT), small-scale, weak dimming appeared ~240$\arcsec$ away from the flare site, which can be observed by AIA only in 131 and 171 Å. Afterwards, long and narrow dimmings became evident in all AIA EUV passbands except 304 Å, while localized core dimming was not clearly observed near the flare site. The large-area dimmings extended southeastward and the areas increased gradually. The total area of dimmings reaches (1.2±0.4)×104 Mm2 in 193 Å. The maximal relative intensity decreases in 171 and 193 Å reach 90\% and 80\%, respectively. Subsequently, the dimmings began to replenish and the area decreased slowly, lasting for ≥3 hr. The remote dimmings and AR 12434 were connected by large-scale coronal loops. The remote dimmings were associated with the southwest footpoints of coronal loops with weak negative polarities. Possible origins of remote dimmings are discussed.

A magnetic confinement nuclear fusion mechanism for solar flares

Ying-Zhi **Zhang**

Research in Astronomy and Astrophysics **2019**

https://arxiv.org/pdf/1912.00193.pdf

We propose a magnetic confinement nuclear fusion mechanism for the evolution of a solar flare in solar atmosphere. The mechanism agree with two observed characteristics of explosive flares and coronal mass ejections (CMEs) that

have proved to be very difficult to explain with previous mechanisms: the huge enrichments of 3He and the high energy gamma ray radiation. The twisted magnetic flux rope is a typical structure during the solar flares, which is closely related to the solar active region that magnetic fields have almost complete control over the plasma. Consequently, the plasma inside the flux rope is heated to more than 1.0×107 K by adiabatic compression process, and then the thermonuclear fusion can take place in the flux rope accompanied with high energy gamma rays. We utilize the time-dependent ideal 2.5-dimensional magnetohydrodynamic (MHD) simulation to demonstrate the physical mechanism for producing flares, which reveals three stages of flare development with process of magnetic energy conversion and intense release during the solar flares and CMEs in solar atmosphere. Furthermore, we discuss the relationship between magnetic reconnection and solar eruptions.

Energy partition in two M-class circular-ribbon flares

Q. M. **Zhang**, J. X. Cheng, L. Feng, Y. Su, L. Lu, Y. Huang, D. Li, T. H. Zhou, J. L. Chen
ApJ **883** 124 **2019**
https://arxiv.org/pdf/1908.02685.pdf
https://iopscience.iop.org/article/10.3847/1538-4357/ab3a52/pdf
In this paper, we investigate the energy partition of two homologous M1.1 circular-ribbon flares (CRFs) in active region (AR) 12434. They were observed by \textit{SDO}, \textit{GOES}, and \textit{RHESSI} on **2015 October 15 and 16**, respectively. The peak thermal energy, nonthermal energy of flare-accelerated electrons, total radiative loss of hot plasma, and radiant energies in 1−8 {\AA} and 1−70 {\AA} of the flares are calculated. The two flares have similar energetics. The peak thermal energies are (1.94±0.13)×1030 erg. The nonthermal energies in flare-accelerated electrons are (3.9±0.7)×1030 erg. The radiative outputs of the flare loops in 1−70 {\AA}, which are ∼200 times greater than the outputs in 1−8 {\AA}, account for ∼62.5\% of the peak thermal energies. The radiative losses of SXR-emitting plasma are one order of magnitude lower than the peak thermal energies. Therefore, the total heating requirements of flare loops including radiative loss are (2.1±0.1)×1030 erg, which could sufficiently be supplied by nonthermal electrons.

Imaging observations of chromospheric evaporation in a circular-ribbon flare

Q. M. **Zhang**, D. Li, Y. Huang
ApJ 870 109 **2019**
https://arxiv.org/pdf/1811.11363.pdf
http://iopscience.iop.org/article/10.3847/1538-4357/aaf4b7/pdf
In this paper, we report our multiwavelength imaging observations of chromospheric evaporation in a C5.5 circular-ribbon flare (CRF) on **2014 August 24**. The flare was observed by the Atmospheric Imaging Assembly (AIA) on board the \textit{Solar Dynamics Observatory} (\textit{SDO}), X-ray Telescope (XRT) on board the \textit{Hinode} spacecraft, and ground-based Nobeyama Radioheliograph (NoRH). The CRF consisted of a discrete circular ribbon with a diameter of ∼1$\arcmin$ and a short inner ribbon observed in ultraviolet (UV), extreme-ultraviolet (EUV), soft X-ray (SXR), and especially in 17 GHz. The peak time (∼04:58 UT) of the flare in 17 GHz coincided with that in UV 1600 Å and SXR derivative as a hard X-ray proxy, implying the peak time of impulsive energy deposition in the lower atmosphere. Shortly after the peak time, converging motion and filling process in the flare loop were revealed in AIA 131 Å and two XRT filters (Be_thin and Be_med), which are clear evidence for chromospheric evaporation upflows. The chromospheric evaporation lasted for ∼6 minutes until ∼05:04 UT. The temperature, density, and apparent velocities of the upflows are ∼107 K, ∼1.8×1010 cm−3, and 50−630 km s−1 with a mean value of ∼170 km s−1. By comparison with previous models, we are able to estimate that energies above 5×1010 erg cm−2 s−1 are likely needed to explain the observational results. Since heating by thermal conduction does not seem to provide enough energy, alternative mechanisms such as nonthermal electrons or Alfvénic waves might need to be invoked.

Impulsive radio and hard X-ray emission from an M-class flare

Ping **Zhang**1,2,4, Yang Guo3, Lu Wang1,2 and Siming Liu
A&A 615, A48 (**2018**)
https://www.aanda.org/articles/aa/pdf/2018/07/aa31274-17.pdf
Context. Impulsive radio and hard X-ray emission from large solar flares are usually attributed to a hard distribution of high-energy electrons accelerated in the energy dissipation process of magnetic reconnection.
Aims. We report the detection of impulsive radio and hard X-ray emissions produced by a population of energetic electrons with a very soft distribution in an M-class flare: SOL**2015-08-27**T05:45 .
Methods. The absence of impulsive emission at 34 GHz and hard X-ray emission above 50 keV and the presence of distinct impulsive emission at 17 GHz and lower frequencies and in the 25–50 keV X-ray band imply a very soft distribution of energetic electrons producing the impulsive radio emission via the gyro-synchrotron process, and impulsive X-rays via bremsstrahlung.
Results. The spectrum of the impulsive hard X-ray emission can be fitted equally well with a power-law model with an index of ∼6.5 or a super-hot thermal model with a temperature as high as 100 MK. Imaging observations in the extreme-UV and X-ray bands and extrapolation of the magnetic field structure using a nonlinear force-free model show that energetic electrons trapped in coronal loops are responsible for these impulsive emissions.

Conclusions. Since the index of the power-law model is nearly constant during the impulsive phase, the power-law distribution or the super-hot component should be produced by a bulk energization process such as the Fermi and betatron acceleration of collapsing magnetic loops.

Propagating wave in active region-loops, located over the solar disk observed by the Interface Region Imaging Spectrograph

B. **Zhang**, Y. J. Hou, J. Zhang
A&A **2018**
https://arxiv.org/pdf/1801.02880.pdf
We aim to ascertain the physical parameters of a propagating wave over the solar disk detected by the Interface Region Imaging Spectrograph (IRIS). Using imaging data from the IRIS and the Solar Dynamic Observatory (SDO), we tracked bright spots to determine the parameters of a propagating transverse wave in active region (AR) loops triggered by activation of a filament. Deriving the Doppler velocity of Si IV line from spectral observations of IRIS, we have determined the rotating directions of active region loops which are relevant to the wave. On **2015 December 19**, a filament was located on the polarity inversion line of the NOAA AR 12470. The filament was activated and then caused a C 1.1 two-ribbon flare. Between the flare ribbons, two rotation motions of a set of bright loops were observed to appear in turn with opposite directions. Following the end of the second rotation, a propagating wave and an associated transverse oscillation were detected in these bright loops. In 1400 A channel, there was bright material flowing along the loops in a wave-like manner, with a period of ~128 s and a mean amplitude of ~880 km. For the transverse oscillation, we tracked a given loop and determine the transverse positions of the tracking loop in a limited longitudinal range. In both of 1400 A and 171 A channels, approximately four periods are distinguished during the transverse oscillation. The mean period of the oscillation is estimated as ~143 s and the displacement amplitude as between ~1370 km and ~690 km. We interpret these oscillations as a propagating kink wave and obtain its speed of ~1400 km s-1. Our observations reveal that a flare associated with filament activation could trigger a kink propagating wave in active region loops over the solar disk.

Simultaneous transverse and longitudinal oscillations in a quiescent prominence triggered by a coronal jet

Qingmin **Zhang**, Dong Li, Zongjun Ning
ApJ **2017**
https://arxiv.org/pdf/1711.00670.pdf
In this paper, we report our multiwavelength observations of the simultaneous transverse and longitudinal oscillations in a quiescent prominence on **2015 June 29**. A C2.4 flare took place in active region 12373, which was associated with a pair of short ribbons and a remote ribbon. During the impulsive phase of the flare, a coronal jet spurted out of the primary flare site and propagated in the northwest direction at an apparent speed of ~224 km s−1. Part of the jet stopped near the remote ribbon. The remaining part continued moving forward before stopping to the east of prominence. Once the jet encountered the prominence, it pushed the prominence to oscillate periodically. The transverse oscillation of the eastern part (EP) of prominence can be divided into two phases. In phase I, the initial amplitude, velocity, period, and damping timescale are ~4.5 Mm, ~20 km s−1, ~25 minutes, and ~7.5 hr, respectively. In phase II, the initial amplitude increases to ~11.3 Mm while the initial velocity halves to ~10 km s−1. The period increases by a factor of ~3.5. The western part (WP) of prominence also experienced transverse oscillation. The initial amplitude is only ~2 Mm and the velocity is less than 10 km s−1. The period (~27 minutes) is slightly longer than that of EP in phase I. To the east of prominence, a handful of horizontal threads experienced longitudinal oscillation. The initial amplitude, velocity, period, and damping timescale are ~52 Mm, ~50 km s−1, ~99 minutes, and 2.5 hr, respectively. To our knowledge, this is the first report of simultaneous transverse and longitudinal prominence oscillations triggered by a coronal jet.

Are complex magnetic field structures responsible for the confined X-class flares in super active region 12192?

Jun **Zhang**, Ting Li, Huadong Chen
ApJ **845** 54 **2017**
https://arxiv.org/pdf/1707.03171.pdf
http://sci-hub.cc/10.3847/1538-4357/aa7e7d
From **2014 October 19 to 27**, six X-class flares occurred in super active region (AR) 12192. They were all confined flares and were not followed by coronal mass ejections (CMEs). To examine the structures of the four flares close to the solar disk center from October 22 to 26, we employ firstly composite triple-time images in each flare process to display {the stratified structure} of these flare loops. The loop structures of each flare in both lower (171 {\AA}) and higher (131 {\AA}) temperature channels are complex, e.g., the flare loops rooting at flare ribbons are sheared or twisted (enwound) together, and the complex structures have not been destroyed during the flares. For the first flare, although the flare loop system appears as a spindle shape, we can estimate their structure from observations, with lengths ranging

from 130 to 300 Mm, heights from 65 to 150 Mm, widths at the middle part of the spindle from 40 to 100 Mm, and shear angles from 16∘ to 90∘. Moreover, the flare ribbons display irregular movements, such as the left ribbon fragments of the flare on 22 swept a small region repeatedly, and the both ribbons of the flare on 26 moved along the same direction, instead of separating from each other. These irregular movements also imply that the corresponding flare loops are complex, e.g. several sets of flare loops are twisted together. Although previous studies suggest that the background magnetic fields prevent confined flares from erupting, we firstly suggest based on these observations that the complex flare loop structures may be responsible for these confined flares. **2014 September 10, October 22, 24, 25, 26 2014**

Photospheric Magnetic Free Energy Density of Solar Active Regions

Hongqi **Zhang**
Solar Phys. **2016**
We present the photospheric energy density of magnetic fields in two solar active regions (one of them recurrent) inferred from observational vector magnetograms, and compare it with other available differently defined energy parameters of magnetic fields in the photosphere. We analyze the magnetic fields in Active Regions NOAA 6580-6619-6659 and 11158. The quantity \(\frac{1}{4\pi}{\mathbf{B}}_{n}\cdot{\mathbf{B}}_{p}\) is an important energy parameter that reflects the contribution of magnetic shear to the difference between the potential (\(\mathbf{B}_{p}\)) and the non-potential magnetic field (\(\mathbf{B}_{n}\)), and also the contribution to the free magnetic energy near the magnetic neutral lines in the active regions. It is found that the photospheric mean magnetic energy density shows clear changes before the powerful solar flares in Active Region NOAA 11158, which is consistent with the change in magnetic fields in the flaring lower atmosphere. **April 14, 1991, May 11, 1991, June 9, 1991, 13-16 Feb 2011**

Pre-flare coronal dimmings

Q. M. **Zhang**, Y. N. Su, H. S. Ji
A&A 598, A3 (**2017**)
https://arxiv.org/pdf/1611.08371v1.pdf
In this paper, we focus on the pre-flare coronal dimmings. We report our multiwavelength observations of the GOES X1.6 solar flare and the accompanying halo CME produced by the eruption of a sigmoidal magnetic flux rope (MFR) in NOAA active region (AR) 12158 on **2014 September 10**. The eruption was observed by the Atmospheric Imaging Assembly (AIA) aboard the Solar Dynamic Observatory (SDO). The photospheric line-of-sight magnetograms were observed by the Helioseismic and Magnetic Imager (HMI) aboard SDO. The soft X-ray (SXR) fluxes were recorded by the GOES spacecraft. The halo CME was observed by the white light coronagraphs of the Large Angle Spectroscopic Coronagraph (LASCO) aboard SOHO.} {About 96 minutes before the onset of flare/CME, narrow pre-flare coronal dimmings appeared at the two ends of the twisted MFR. They extended very slowly with their intensities decreasing with time, while their apparent widths (8−9 Mm) nearly kept constant. During the impulsive and decay phases of flare, typical fanlike twin dimmings appeared and expanded with much larger extent and lower intensities than the pre-flare dimmings. The percentage of 171 {\AA} intensity decrease reaches 40\%. The pre-flare dimmings are most striking in 171, 193, and 211 {\AA} with formation temperatures of 0.6−2.5 MK. The northern part of the pre-flare dimmings could also be recognized in 131 and 335 {\AA}.} To our knowledge, this is the first detailed study of pre-flare coronal dimmings, which can be explained by the density depletion as a result of the gradual expansion of the coronal loop system surrounding the MFR during the slow rise of the MFR.

Chromospheric Condensation and Quasi-periodic Pulsations in a Circular-ribbon Flare

Q. M. **Zhang**, D. Li, Z. J. Ning
ApJ 832 65 **2016**
http://arxiv.org/pdf/1609.03165v1.pdf
In this paper, we report our multiwavelength observations of the C3.1 circular-ribbon flare SOL**2015-10-16**T10:20 in AR 12434. The flare consisted of a circular flare ribbon (CFR), an inner flare ribbon (IFR) inside, and a pair of short parallel flare ribbons (PFRs). During the impulsive phase of the flare, "two-step" raster observations of \textit{IRIS} with a cadence of 6 s and an exposure time of 2 s show plasma downflow at the CFR in the Si {\sc iv} λ 1402.77 line, suggesting chromospheric condensation. The downflow speeds first increased rapidly from a few km s−1 to the peak values of 45−52 kms−1, before decreasing gradually to the initial levels. The decay timescales of condensation were 3−4 minutes, indicating ongoing magnetic reconnection. Interestingly, the downflow speeds are positively correlated with logarithm of the Si {\sc iv} line intensity and time derivative of the \textit{GOES} soft X-ray (SXR) flux in 1−8 {\AA}. The radio dynamic spectra are characterized by a type \Rmnum{3} radio burst associated with the flare, which implies that the chromospheric condensation was most probably driven by nonthermal electrons. Using an analytical expression and the peak Doppler velocity, we derived the lower limit of energy flux of the precipitating electrons, i.e., 0.65×1010 erg cm−2 s−1. The Si {\sc iv} line intensity and SXR derivative show quasi-periodic pulsations with periods of 32−42 s.

Photospheric Magnetic Free Energy Density of Solar Active Regions

Hongqi **Zhang**
Solar Phys. Volume 291, Issue 12, pp 3501–3517 **2016**
http://arxiv.org/pdf/1608.07805v1.pdf
We present the photospheric energy density of magnetic fields in two solar active regions inferred from observational vector magnetograms, and compare it with the possible different defined energy parameters of magnetic fields in the photosphere. We analyze the magnetic fields in active region NOAA 6580-6619-6659 and 11158. It is noticed that the quantity 1/4pi Bn.Bp is an important energy parameter that reflects the contribution of magnetic shear on the difference between the potential magnetic field (Bp) and non-potential one (Bn), and also the contribution to the free magnetic energy near the magnetic neutral lines in the active regions. It is found that the photospheric mean magnetic energy density changes obviously before the powerful solar flares in the active region NOAA 11158, it is consistent with the change of magnetic fields in the lower atmosphere with flares. **1991 June, 2011 February 15**

Explosive Chromospheric Evaporation in a Circular-ribbon Flare

Q. M. **Zhang**, D. Li, Z. J. Ning, Y. N. Su, H. S. Ji, Y. Guo
ApJ **827** 27 **2016**
http://arxiv.org/pdf/1605.02823v1.pdf
In this paper, we report our multiwavelength observations of the C4.2 circular-ribbon flare in active region (AR) 12434 on **2015 October 16**. The short-lived flare was associated with positive magnetic polarities and a negative polarity inside, as revealed by the photospheric line-of-sight magnetograms. Such magnetic pattern is strongly indicative of a magnetic null point and spine-fan configuration in the corona. The flare was triggered by the eruption of a mini-filament residing in the AR, which produced the inner flare ribbon (IFR) and the southern part of a closed circular flare ribbon (CFR). When the eruptive filament reached the null point, it triggered null point magnetic reconnection with the ambient open field and generated the bright CFR and a blowout jet. Raster observations of the \textit{Interface Region Imaging Spectrograph} (\textit{IRIS}) show plasma upflow at speed of 35−120 km s−1 in the Fe {\sc xxi} 1354.09 {\AA} line (logT≈7.05) and downflow at speed of 10−60 km s−1 in the Si {\sc iv} 1393.77 {\AA} line (logT≈4.8) at certain locations of the CFR and IFR during the impulsive phase of flare, indicating explosive chromospheric evaporation. Coincidence of the single HXR source at 12−25 keV with the IFR and calculation based on the thick-target model suggest that the explosive evaporation was most probably driven by nonthermal electrons.

Secondary Flare Ribbons Observed by the Solar Dynamics Observatory

Jun **Zhang**, Ting Li, and Shuhong Yang
2014 ApJ 782 L27
Using the observations from the Atmospheric Imaging Assembly (AIA) and the Helioseismic and Magnetic Imager on board the Solar Dynamics Observatory, we statistically investigate the flare ribbons (FRs) of **19 X-class flares of the 24th solar cycle from 2010 June to 2013 August**. Of these 19 flares, the source regions of 16 can be observed by AIA and the FRs of each flare are well detected, and 11 of the 16 display multiple ribbons. Based on the ribbon brightness and the relationship between the ribbons and post-flare loops, we divide the multiple ribbons into two types: normal FRs, which are connected by post-flare loops and have been extensively investigated, and secondary flare ribbons (SFRs), which are weaker than the FRs, not connected by post-flare loops, and always have a short lifetime. Of the 11 SFRs, 10 appear simultaneously with the FRs, and none of them have post-flare loops. The last one, on the other hand, appears 80 minutes later than the FR, lasts almost two hours, and also has no post-flare loops detected. We suggest that the magnetic reconnection associated with this SFR is triggered by the blast wave that results from the main flare. These observations imply that in some flare processes, more than two sets of magnetic loops or more than twice the number of magnetic reconnections are involved.

Electron Acceleration in a Dynamically Evolved Current Sheet Under Solar Coronal Conditions

Shaohua **Zhang**, A. M. Du, Xueshang Feng, Xin Cao, Quanming Lu, Liping Yang, Gengxiong Chen, Ying Zhang
Solar Physics. May **2014**, Volume 289, Issue 5, pp 1607-1623
Electron acceleration in a drastically evolved current sheet under solar coronal conditions is investigated via the combined 2.5-dimensional (2.5D) resistive magnetohydrodynamics (MHD) and test-particle approaches. Having a high magnetic Reynolds number (105), the long, thin current sheet is torn into a chain of magnetic islands, which grow in size and coalesce with each other. The acceleration of electrons is explored in three typical evolution phases: when several large magnetic islands are formed (phase 1), two of these islands are approaching each other (phase 2), and almost merging into a “monster” magnetic island (phase 3). The results show that for all three phases electrons with an initial Maxwell distribution evolve into a heavy-tailed distribution and more than 20 % of the electrons can be accelerated higher than 200 keV within 0.1 second and some of them can even be energized up to MeV ranges. The lower-energy electrons are located away from the magnetic separatrices and the higher-energy electrons are inside the magnetic islands. The most energetic electrons have a tendency to be around the outer regions of the magnetic islands

or to appear in the small secondary magnetic islands. It is the trapping effect of the magnetic islands and the distributions of E p that determine the acceleration and spatial distributions of the energetic electrons.

A swirling flare-related EUV jet

Q. M. **Zhang** and H. S. Ji

E-print, Dec **2013**, A&A 561, A134 (**2014**)

We report our observations of a swirling flare-related EUV jet on **2011 October 15** at the edge of NOAA active region 11314.} {We utilised the multiwavelength observations in the extreme-ultraviolet (EUV) passbands from the Atmospheric Imaging Assembly (AIA) aboard the Solar Dynamics Observatory (SDO). We extracted a wide slit along the jet axis and 12 thin slits across its axis to investigate the longitudinal motion and transverse rotation. We also used data from the Extreme-Ultraviolet Imager (EUVI) aboard the Solar TErrestrial RElations Observatory (STEREO) spacecraft to investigate the three-dimensional (3D) structure of the jet. Gound-based Hα images from the El Teide as a member of the Global Oscillation Network Group (GONG) provide a good opportunity to explore the relationship between the cool surge and hot jet. Line-of-sight magnetograms from the Helioseismic and Magnetic Imager (HMI) aboard SDO enable us to study the magnetic evolution of the flare/jet event. We carried out potential-field extrapolation to figure out the magnetic configuration associated with the jet.} {The onset of jet eruption coincided with the start time of C1.6 flare impulsive phase. The initial velocity and acceleration of the longitudinal motion were 254pm10 km s-1 and -97pm5 m s-2, respectively. The jet presented helical structure and transverse swirling motion at the beginning of its eruption. The counter-clockwise rotation slowed down from an average velocity of ~122 km s-1 to ~80 km s-1. The interwinding thick threads of the jet untwisted into multiple thin threads during the rotation that lasted for 1 cycle with a period of ~7 min and an amplitude that increases from ~3.2 Mm at the bottom to ~11 Mm at the upper part. Afterwards, the curtain-like leading edge of the jet continued rising without rotation, leaving a dimming region behind before falling back to the solar surface. The appearance/disappearance of dimming corresponded to the longitudinal ascending/descending motions of jet. Cospatial Hα surge and EUV dimming imply that the dimming resulted from the absorption of hot EUV emission by cool surge. The flare/jet event was caused by continuous magnetic cancellation before the start of flare. The jet was associated with the open magnetic fields at the edge of AR 11314.

Magnetic Reconnection: From "Open" Extreme-ultraviolet Loops to Closed Post-flare Ones Observed by SDO

Jun **Zhang**1, Shuhong Yang1, Ting Li1, Yuzong Zhang1, Leping Li1, and Chaowei Jiang

E-print, Nov **2013; 2013** ApJ 776 57

We employ Solar Dynamics Observatory observations and select three well-observed events including two flares and one extreme-ultraviolet (EUV) brightening. During the three events, the EUV loops clearly changed. One event was related to a major solar flare that took place on **2012 July 12** in active region NOAA AR 11520. "Open" EUV loops rooted in a facula of the AR deflected to the post-flare loops and then merged with them while the flare ribbon approached the facula. Meanwhile, "open" EUV loops rooted in a pore disappeared from top to bottom as the flare ribbon swept over the pore. The loop evolution was similar in the low-temperature channels (e.g., 171 Å) and the high-temperature channels (e.g., 94 Å). The coronal magnetic fields extrapolated from the photospheric vector magnetograms also show that the fields apparently "open" prior to the flare become closed after it. The other two events were associated with a B1.1 flare on **2010 May 24** and an EUV brightening on **2013 January 03**, respectively. During both of these two events, some "open" loops either disappeared or darkened before the formation of new closed loops. We suggest that the observations reproduce the picture predicted by the standard magnetic reconnection model: "open" magnetic fields become closed due to reconnection, manifesting as a transformation from "open" EUV loops to closed post-flare ones.

EMERGING DIMMINGS OF ACTIVE REGIONS OBSERVED BY THE SOLAR DYNAMICS OBSERVATORY

Jun **Zhang**1, Shuhong Yang1, Yang Liu2, and Xudong Sun

2012 ApJ 760 L29

Using the observations from the Atmospheric Imaging Assembly and the Helioseismic and Magnetic Imager on board the Solar Dynamics Observatory, we statistically investigate the emerging dimmings (EDs) of 24 isolated active regions (IARs) from 2010 June to 2011 May. All the IARs show EDs in lower-temperature lines (e.g., 171 Å) at their early emerging stages. Meanwhile, in higher temperature lines (e.g., 211 Å), the ED regions brighten continuously. There are two types of EDs: fan-shaped and halo-shaped. There are 19 fan-shaped EDs and 5 halo-shaped ones. The EDs appear to be delayed by several to more than ten hours relative to the first emergence of the IARs. The shortest delay is 3.6 hr and the longest is 19.0 hr. The EDs last from 3.3 hr to 14.2 hr, with a mean duration of 8.3 hr. Before the appearance of the EDs, the emergence rate of the magnetic flux of the IARs is between 1.2 × 1019 Mx hr–1 to 1.4 × 1020 Mx hr–1. The larger the emergence rate is, the shorter the delay time is. While the dimmings appear, the magnetic flux of the IARs ranges from 8.8 × 1019 Mx to 1.3 × 1021 Mx. These observations imply that the reconfiguration of the coronal magnetic fields due to reconnection between the newly emerging flux and the surrounding existing fields results in a

new thermal distribution which leads to a dimming for the cooler channel (171 Å) and brightening in the warmer channels.

Statistical Studies on the Excess Peak Flux in Soft X-rays and EUV Bands from Solar Flares

D. H. **Zhang**, L. Cai, A. Ercha, Y. Q. Hao and Z. Xiao
Solar Physics, Volume 280, Number 1 (**2012**), 183-196
Based on the solar X-ray data in the band of 0.1 – 0.8 nm observed by Geostationary Operational Environmental Satellites (GOES), the XUV and EUV data in the bands of 26 – 34 nm and 0.1 – 50 nm observed by the Solar EUV Monitor (SEM) onboard the Solar and Heliospheric Observatory (SOHO), a statistical analysis on the excess peak flux (the pre-flare flux is subtracted) in two SEM bands during M- and X-class flares from 1998 to 2007 is given. The average ratio of the excess peak flux to the pre-flare flux for the M-class flares is 5.5 %±3.7 % and that for the X-class flares is 16 %±11 %. The excess peak fluxes in two SEM bands are positively correlated with the X-ray flare class; with the increase in the X-ray flare class, the excess peak flux in two SEM bands increases. However, a large dispersion in the excess peak flux in the SEM bands and their ratio is found for the same X-ray flare class. The relationship between the excess peak fluxes of the two SEM bands also shows large dispersion. It is considered that the diversity we found in the flare spectral irradiance is caused by many variable factors related to the structure and evolution of solar flares.

MAGNETIC HELICITY TRANSPORTED BY FLUX EMERGENCE AND SHUFFLING MOTIONS IN SOLAR ACTIVE REGION NOAA 10930

Y**. Zhang**1,2, R. Kitai2, and K. Takizawa
2012 ApJ 751 85
We present a new methodology which can determine magnetic helicity transport by the passage of helical magnetic field lines from the sub-photosphere and the shuffling motions of footpoints of preexisting coronal field lines separately. It is well known that only the velocity component, which is perpendicular to the magnetic field ($\upsilon \perp B$), has contributed to the helicity accumulation. Here, we demonstrate that $\upsilon \perp B$ can be deduced from a horizontal motion and vector magnetograms under a simple relation of $\upsilon t = \mu t + (\upsilon n / Bn) B t$, as suggested by Démoulin & Berger. Then after dividing $\upsilon \perp B$ into two components, as one is tangential and the other is normal to the solar surface, we can determine both terms of helicity transport. Active region (AR) NOAA 10930 is analyzed as an example during its solar disk center passage by using data obtained by the Spectropolarimeter and the Narrowband Filter Imager of Solar Optical Telescope on board Hinode. We find that in our calculation the helicity injection by flux emergence and shuffling motions have the same sign. During the period we studied, the main contribution of helicity accumulation comes from the flux emergence effect, while the dynamic transient evolution comes from the shuffling motions effect. Our observational results further indicate that for this AR the apparent rotational motion in the following sunspot is the real shuffling motions on the solar surface.

Statistical Properties of Solar Active Regions Obtained from an Automatic Detection System and the Computational Biases

Jie **Zhang**, Yuming Wang and Yang Liu
2010 ApJ 723 1006-1018, **File**
We have developed a computational software system to automate the process of identifying solar active regions (ARs) and quantifying their physical properties based on high-resolution synoptic magnetograms constructed from Michelson Doppler Imager (MDI; on board the SOHO spacecraft) images from 1996 to 2008. The system, based on morphological analysis and intensity thresholding, has four functional modules: (1) intensity segmentation to obtain kernel pixels, (2) a morphological opening operation to erase small kernels, which effectively remove ephemeral regions and magnetic fragments in decayed ARs, (3) region growing to extend kernels to full AR size, and (4) the morphological closing operation to merge/group regions with a small spatial gap. We calculate the basic physical parameters of the 1730 ARs identified by the auto system. The mean and maximum magnetic flux of individual ARs are 1.67 × 1022 Mx and 1.97 × 1023 Mx, while that per Carrington rotation are 1.83 × 1023 Mx and 6.96 × 1023 Mx, respectively. The frequency distributions of ARs with respect to both area size and magnetic flux follow a log-normal function. However, when we decrease the detection thresholds and thus increase the number of detected ARs, the frequency distribution largely follows a power-law function. We also find that the equatorward drifting motion of the AR bands with solar cycle can be described by a linear function superposed with intermittent reverse driftings. The average drifting speed over one solar cycle is or 0.708 ± 0.015 m s-1.

FINE MAGNETIC FEATURES AND CHIRALITY IN SOLAR ACTIVE REGION NOAA 10930

Hongqi **Zhang**
Astrophysical Journal, 716:1493–1502, **2010** June
In this paper, we present fine magnetic features near the magnetic inversion line in the solar active region NOAA

10930. The high-resolution vector magnetograms obtained by *Hinode* allow detailed analyses around magnetic fibrils in the active region. The analyses are based on the fact that the electric current density can be divided into two components: the shear component caused by the magnetic inhomogeneity and the twist component caused by the magnetic field twist. The relationships between magnetic field, electric current density, and its two components are examined. It is found that the individual magnetic fibrils are dominated by the current density component caused by the magnetic inhomogeneity, while the large-scale magnetic region is generally dominated by the electric current component associated with the magnetic twist. The microstructure of the magnetic field in the solar atmosphere is far from the force-free field. The current mainly flows around the magnetic flux fibrils in the active regions.

A Statistical Study on the Relationship between the Transport Rate of Magnetic Helicity and Solar Flares

Yin **Zhang**, Baolin Tan, Yihua Yan
E-print, Sept **2009;** Astrophysical Journal, 704:1622–1627, **2009** October
We present in this paper a statistical study of which is aimed at understanding the fact that some flares (type I flare) are associated with sharp variations of the transport rate of the magnetic helicity (dH/dt) and others not (type II flare). The sample consists of 49 M-class and X-class flares which produced by 9 isolated active regions. Used high temporal magnetograms obtained by the Michelson Doppler Imager (MDI) instrument on the Solar and Heliospheric Observatory (SOHO), we calculate the temporal variation of dH/dt during the flaring time, and compare its profile with the soft X-ray flux. We find that type I flares have longer duration and higher peak flux in soft X-ray than type II flares. Furthermore, the ratio of total unsigned magnetic flux of the host active region to that of the visible solar disk is also higher for type I flares, while the total flux itself is independent of the flare type. Our results show that whether the flare is associated with sharp variations of dH/dt depends on the properties of the flare and of its host active region. The relationship between dH/dt and microwave bursts is also discussed.

Relationship between Rotating Sunspots and Flares

Yin **Zhang** · Jihong Liu · Hongqi Zhang
Solar Phys (**2008**) 247: 39–52
http://www.springerlink.com/content/w54x26500vx51732/fulltext.pdf
Active Region (AR) NOAA 10486 was a super AR in the declining phase of solar cycle 23. Dominated by the rapidly rotating positive polarity of an extensive δ sunspot, it produced several powerful flare-CMEs. We study the evolution and properties of the rotational motion of the major poles of positive polarities and estimate the accumulated helicity injected by them.We also present two homologous flares that occurred in the immediate periphery of the rotating sunspots.
This suggests that the rotational motions of sunspots not only relate to the transport of magnetic energy and complexity from the low atmosphere to the corona but may also play a key role in the onset of the homologous flares.

Interaction between a Fast Rotating Sunspot and Ephemeral Regions as the Origin of the Major Solar Event on 2006 December 13

Jun **Zhang**, Leping Li, and Qiao Song
The Astrophysical Journal Letters, Volume 662, Number 1, Page L35-L38, **2007**
The major solar event on 2006 December 13 is characterized by the approximately simultaneous occurrence of a heap of hot ejecta, a great two-ribbon flare, and an extended Earth-directed coronal mass ejection. We examine the magnetic field and sunspot evolution in NOAA AR 10930, the source region of the event, while it transited the solar disk center from December 10 to 13. We find that the obvious changes in the active region associated with the event are the development of magnetic shear, the appearance of ephemeral regions, and fast rotation of a smaller sunspot. Around the area of the magnetic neutral line of the active region, interaction between the fast rotating sunspot and the ephemeral regions triggers continual brightening and finally the major flare. This indicates that only after the sunspot rotates up to 200° does the major event take place. The sunspot rotates at least 240° about its center, the largest sunspot rotation angle that has been reported.

Comprehensive Analysis of a Filament-embedding Solar Active Region at Different Stages of Evolution

Jie **Zhao**1, Fu Yu1, Sarah E. Gibson2, Yuhong Fan2, Yang Su1,3, Ying Li1,3, Jun Dai1, Hui Li1,3, Chuan Li4,5,6, Pengfei Chen4,5Show full author list
2024 ApJL 965 L16
https://iopscience.iop.org/article/10.3847/2041-8213/ad3555/pdf
Active regions are the brightest structures seen in the solar corona, so their physical properties hold important clues to the physical mechanisms underlying coronal heating. In this work, we present a comprehensive study for a filament-embedding active region as determined from observations from multiple facilities including the Chinese Hα Solar Explorer. We find three types of dynamic features that correspond to different thermal and magnetic properties, i.e., the

overlying loops—1 MK cool loops, the moss region—2–3 MK hot loops' footprints, and the sigmoidal filament. The overlying cool loops, which have a potential field, always show Doppler blueshifts at the east footprint and Doppler redshifts at the west, indicating a pattern of "siphon flow." The moss-brightening regions, which sustain the hot loops that have a moderate sheared field, always show downward Doppler redshifts at the chromosphere, which could be a signature of plasma condensing into the inner region adjacent to the filament. The sigmoidal filament, which has strongly sheared field lines along the polarity inversion line, however, shows a different Doppler velocity pattern in its middle part, i.e., an upward Doppler blueshift at the double-J-shaped stage indicating tether-cutting reconnection during the filament channel formation and then a downward redshift showing the plasma condensation for the sigmoidal filament formation. The present work shows overall properties of the filament-embedding active region, constraining the heating mechanisms of different parts of the active region and providing hints regarding the mass loading of the embedded filament. **2022 February 14–17**

SDO/HMI Captured Another Limb Flare in Continuum Intensity → 2022 May 3

Junwei **Zhao**, Wei Liu, Jean-Claude Vial
HMI Science Nuggets #179 May **2022** http://hmi.stanford.edu/hminuggets/?p=3900

A Survey and Statistical Study of Off-Limb Events Observed in SDO/HMI Continuum Intensity.

Zhao, J.S., Liu, Y.
Sol Phys 298, 148 (**2023**).
https://doi.org/10.1007/s11207-023-02240-4
Several strong eruptive events that occurred near the solar limb were reported generating off-limb features detectable in the SDO/HMI's continuum intensity. These observations offer new insights into the emission mechanisms of off-limb flaring loops, magnetic strength in the loops, and electron density distributions, among others. However, only a limited number of such events were reported, and it is unclear whether off-limb white-light features are popular or only associated with specific eruptions. In this study, we surveyed all the flaring events that occurred between May 2010 and August 2023 with a magnitude stronger than M2.0 and a heliographic longitude larger than 65◦. We found that among the 189 flares that met our selection criteria, 78 (41.3%) had off-limb features associated with them. Further statistical analysis showed, unsurprisingly, that the stronger the flare, the more likely it has an off-limb white-light feature, and the closer the flare is to the limb, the more likely an off-limb feature is detectable. We then categorized these off-limb white-light events into four types, closed-loop eruptions, open-loop eruptions, fast ejection, and flare arcades, and identified the events with visible flare ribbons. Coupling two examples of the white-light observations with simultaneous UV/EUV observations, we demonstrate the usefulness of the former in studying the flare dynamics and emission mechanisms. Our catalogue provides a rather complete list of the off-limb white-light events, which will benefit the community interested in studying such events.

White-light Continuum Observation of the Off-limb Loops of the SOL2017-09-10 X8.2 Flare: Temporal and Spatial Variations

Junwei **Zhao**, Wei Liu, Jean-Claude Vial
ApJ Letters **921** L26 **2021**
https://arxiv.org/pdf/2110.14130.pdf
https://iopscience.iop.org/article/10.3847/2041-8213/ac3339/pdf
https://doi.org/10.3847/2041-8213/ac3339
Observations of the Sun's off-limb white-light (WL) flares offer rare opportunities to study the energy release and transport mechanisms in flare loops. One of the best such events was SOL2017-09-10, an X8.2 flare that occurred near the Sun's west limb on **2017 September 10** and produced a WL loop system lasting more than 60 minutes and reaching an altitude higher than 30 Mm. The event was well observed by a suite of ground- and space-based instruments, including the Solar Dynamics Observatory/Helioseismic and Magnetic Imager (SDO/HMI) that captured its off-limb loops in WL continuum near Fe I 6173 A, and the Atmospheric Imager Assembly (SDO/AIA) that observed its ultraviolet (UV) and extreme-ultraviolet (EUV) counterparts. We found quasi-periodic pulsations in the WL and UV emissions at the flare loop-top with a period around 8.0 min. Each pulsation appears to have an EUV counterpart that occurs earlier in time and higher in altitude. Despite many similarities in the WL and UV images and light curves, the WL flux at the loop-top continues to grow for about 16 minutes while the UV fluxes gradually decay. We discuss the implication of these unprecedented observations on the understanding of the enigmatic off-limb WL flare emission mechanisms.
HMI Science Nuggets #167 Oct **2021** http://hmi.stanford.edu/hminuggets/?p=3713

Waves of Magnetic-field Variations Observed in a Flare-excited Sunquake Event

Junwei **Zhao**1 and Ruizhu Chen1,2
2018 ApJL 860 L29 DOI 10.3847/2041-8213/aacbd6

We report on the detection of waves of magnetic-field variations that were associated with flare-excited sunquake waves. An X-9.3 flare that occurred on **2017 September 6** excited strong sunquakes, and the sunquake waves were observed sweeping across the flare's host active region. This rare event gives us an unprecedented opportunity to study responses of magnetic field to passing sunquake waves. A wave of magnetic-field variations was observed in each of the two sunspots that the sunquake waves swept through, and the time–distance relations for the waves observed in magnetic field and Doppler velocity are similar. The phase relations measured between, as well as the oscillatory power distributions calculated from, the Doppler velocity variations and magnetic-field variations associated with the sunquake waves are compared with those obtained from the background waves in the same areas of the sunspot umbra and penumbra separately. The phase relations seem to favor the theory that the waves of magnetic variations are owing to opacity changes associated with the passing sunquake waves. The comparisons of phases and power distributions indicate that the background magnetic variations observed in sunspots are a combination of various wave modes, and fast magnetoacoustic waves only account for a fraction of those magnetic variations.
HMI Science Nuggets #105 **2018** http://hmi.stanford.edu/hminuggets/?p=2579

Hooked flare ribbons and flux-rope related QSL footprints

Jie **Zhao**, Stuart A. Gilchrist, Guillaume Aulanier, Brigitte Schmieder, Etienne Pariat, Hui Li
ApJ **823** 62 **2014**
http://arxiv.org/pdf/1603.07563v1.pdf
We studied the magnetic topology of active region 12158 on **2014 September 10** and compared it with the observations before and early in the flare which begins at 17:21 UT (SOL2014-09-10T17:45:00). Our results show that the sigmoidal structure and flare ribbons of this active region observed by SDO/AIA can be well reproduced from a Grad-Rubin non linear force free field extrapolation method. Various inverse-S and -J shaped magnetic field lines, that surround a coronal flux rope, coincide with the sigmoid as observed in different extreme ultraviolet wavelengths, including its multi-threaded curved ends. Also, the observed distribution of surface currents in the magnetic polarity where it was not prescribed is well reproduced. This validates our numerical implementation and set-up of the Grad-Rubin method. The modeled double inverse-J shaped Quasi-Separatrix Layer (QSL) footprints match the observed flare ribbons during the rising phase of the flare, including their hooked parts. The spiral-like shape of the latter may be related to a complex pre-eruptive flux rope with more than one turn of twist, as obtained in the model. These ribbon-associated flux-rope QSL-footprints are consistent with the new standard flare model in 3D, with the presence of a hyperbolic flux tube located below an inverse tear drop shaped coronal QSL. This is a new step forward forecasting the locations of reconnection and ribbons in solar flares, and the geometrical properties of eruptive flux ropes.
See **ERRATUM** **2016** ***ApJ*** 825 **80**

Temporal Evolution of the Magnetic Topology of the NOAA Active Region 11158

Jie **Zhao**, Hui Li, Etienne Pariat, Brigitte Schmieder, Yang Guo, Thomas Wiegelmann
2014, ApJ
http://arxiv.org/pdf/1404.5004v1.pdf
We studied the temporal evolution of the magnetic topology of the active region (AR) 11158 based on the reconstructed three-dimensional magnetic elds in the corona. The non-linear force-free eld (NLFFF) extrapolation method was applied to the 12 minutes cadence data obtained with the Helioseismic and Magnetic Imager (HMI) onboard the Solar Dynamics Observatory (SDO) during ve days. By calculating the squashing degree factor Q in the volume, the derived quasi-separatrix layers (QSLs) show that this AR has an overall topology, resulting from a magnetic quadrupole, including an hyperbolic ux tube (HFT) con guration which is relatively stable at the time scale of the are (1 □ 2 hours). A strong QSL, which corresponds to some highly sheared arcades that might be related to the formation of a ux rope, is prominent just before the **M6.6 and X2.2** ares, respectively. These facts indicate the close relationship between the strong QSL and the high are productivity of AR 11158. In addition, with a close inspection of the topology, we found a small-scale HFT which has an inverse teardrop structure above the aforementioned QSL before the X2.2 are. It indicates the existence of magnetic ux rope at this place. Even though a global con guration (HFT) is recognized in this AR, it turns out that the large-scale HFT only plays a secondary role during the eruption. In nal, we dismiss a trigger based on the breakout model and highlight the central role of the ux rope in the related eruption.

Statistical Study of Emerging Flux Regions and the Upper Atmosphere Response

Zhao, Jie; Li, Hui
E-print, July **2012**, RAA
We statistically study the property of emerging flux regions (EFRs) and the upper solar atmosphere response to the flux emergence by using data from the Helioseismic and Magnetic Imager (HMI) and the Atmospheric Imaging Assembly (AIA) on board the Solar Dynamics Observatory (SDO). Parameters including the total emerged flux, the flux growth rate, the maximum area, the duration of the emergence and the separation speed of the opposite polarities are adopted to delineate the property of the EFRs. The response of the upper atmosphere is addressed by the response of the

atmosphere at different wavelengths (and thus at different temperatures). According to our results, the total emerged fluxes are in the range of (0.44 -- 11.2)x1019 Mx while the maximum area ranges from 17 to 182 arcsec^2. The durations of the emergence are between 1 and 12 hours, which are positively correlated to both the total emerged flux and the maximum area. The maximum distances between the opposite polarities are 7 -- 25 arcsec and are also correlated to the duration positively. The separation speeds are from 0.05 to 1.08 km s-1, negatively correlated to the duration. The derived flux growth rates are (0.1 -- 1.3)x1019 Mx hr-1, which are positively correlated to the total emerging flux. The upper atmosphere responds to the flux emergence in the 1600AA chromospheric line first, and then tens and hundreds of seconds later, in coronal lines, such as the 171AA (T=105.8 K) and 211AA (T=106.3 K) lines almost simultaneously, suggesting the successively heating of atmosphere from the chromosphere to the corona.

Determination of the Topology Skeleton of Magnetic Fields in a Solar Active Region *

Hui **Zhao**, Jing-Xiu Wang1, Jun Zhang1, Chi-Jie Xiao1 and Hai-Min Wang2
Chin. J. Astron. Astrophys. Vol. 8 (**2008**), No. 2, 133–145
http://www.chjaa.org

Magnetic topology has been a key to the understanding of magnetic energy release mechanism. Based on observed vector magnetograms, we have determined the threedimensional (3D) topology skeleton of the magnetic fields in the active region **NOAA 10720 (15 January 2005)**. The skeleton consists of six 3D magnetic nulls and a network of corresponding spines, fans, and null-null lines. For the first time, we have identified a spiral magnetic null in Sun's corona. The magnetic lines of force twisted around the spine of the null, forming a 'magnetic wreath' with excess of free magnetic energy and resembling observed brightening structures at extraultraviolet (EUV) wavebands. We found clear evidence of topology eruptions which are referred to as catastrophic changes of topology skeleton associated with a coronal mass ejection (CME) and an explosive X-ray flare. These results shed new lights on the structural complexity and its role in explosive magnetic activity. The concept of flux rope has been widely used in modelling explosive magnetic activity, although their observational identity is rather obscure or, at least, lacking of necessary details up to date.We suggest that the magnetic wreath associated with the 3D spiral null is likely an important class of the physical entity of flux ropes.

Plasma turbulence generated in 3D current sheet with magnetic islands

Zharkova V. and Xia, Q
Frontiers in Space Physics Volume 8 | Article 665998 **2021**
https://solargsm.com/wp-content/uploads/2021/10/frontiers_cs_turb.pdf
https://www.frontiersin.org/articles/10.3389/fspas.2021.665998/pdf
https://doi.org/10.3389/fspas.2021.665998

In this paper we aim to investigate the kinetic turbulence in a reconnecting current sheet (RCS) with X- and O-nullpoints and to explore its link to the features of accelerated particles. We carry out simulations of magnetic reconnection in a thin current sheet with 3D magnetic field topology affected by tearing instability until the formation of two large magnetic islands using particle-in-cell (PIC) approach. The model utilises a strong guiding field that leads to separation of the particles of opposite charges, generation of a strong polarisation electric field across the RCS and suppression of kink instability in the 'out-of-plane' direction. The accelerated particles of the same charge entering an RCS from the opposite edges are shown accelerated to different energies forming the `bump-in-tail' velocity distributions that, in turn, can generates plasma turbulence in different locations. The turbulence-generated waves produced by either electron or proton beams can be identified from the energy spectra of electromagnetic field fluctuations in the phase and frequency domains. From the phase space analysis we gather that the kinetic turbulence may be generated by accelerated particle beams, which are later found to evolve into a phase-space hole indicating the beam breakage. This happens at some distance from the particle entrance into an RCS, e.g. about 7di (ion inertial depth) for the electron beam and 12di for the proton beam. In a wavenumber space the spectral index of the power spectrum of the turbulent magnetic field near the ion inertial length is found to be -2.7 that is consistent with other estimations. The collective turbulence power spectra are consistent with the high-frequency fluctuations of perpendicular electric field, or upper hybrid waves, to occur in a vicinity of X-nullpoints, where the Langmuir (LW) can be generated by accelerated electrons with high growth rates, while further from X-nullponts or on the edges of magnetic islands, where electrons become ejected and start moving across the magnetic field lines, Bernstein waves can be generated. The frequency spectra of high and low-frequency waves are explored in the kinetic turbulence in parallel and perpendicular directions to the local magnetic field showing noticeable lower hybrid turbulence occurring between the electron's gyro- and plasma frequencies seen also in the wavelet spectra. Fluctuation of the perpendicular electric field component of turbulence can be consistent with the oblique whistler waves generated on the ambient density fluctuations by intense electron beams. This study brings attention to a key role of particle acceleration in generation kinetic turbulence inside current sheets.

Sunquake with a second bounce, other sunquakes, and emission associated with the X9.3 flare of 6 September 2017. I. Observations

Sergei **Zharkov**1, Sarah Matthews2, Valentina Zharkova3, Malcolm Druett4, Satoshi Inoue5, Ingolf E. Dammasch6 and Connor Macrae1

A&A 639, A78 (**2020**)
https://www.aanda.org/articles/aa/pdf/2020/07/aa36755-19.pdf
https://www.aanda.org/articles/aa/pdf/forth/aa36755-19.pdf

Aims. The 6 September 2017 X9.3 solar flare produced very unique observations of magnetic field transients and a few seismic responses, or sunquakes, detected by the Helioseismic and Magnetic Imager (HMI) instrument aboard Solar Dynamic Observatory (SDO) spacecraft, including the strongest sunquake ever reported. This flare was one of a few flares occurring within a few days or hours in the same active region. Despite numerous reports of the fast variations of magnetic field, and seismic and white light emission, no attempts were made to interpret the flare features using multi-wavelength observations. In this study, we attempt to produce the summary of available observations of the most powerful flare of the 6 September 2017 obtained using instruments with different spatial resolutions (this paper) and to provide possible interpretation of the flaring events, which occurred in the locations of some seismic sources (a companion Paper II).
Methods. We employed non-linear force-free field extrapolations followed by magnetohydrodynamic simulations in order to identify the presence of several magnetic flux ropes prior to the initiation of this X9.3 flare. Sunquakes were observed using the directional holography and time–distance diagram detection techniques. The high-resolution method to detect the Hα line kernels in the CRISP instrument at the diffraction level limit was also applied.
Results. We explore the available γ-ray (GR), hard X-ray (HXR), Lyman-α, and extreme ultra-violet (EUV) emission for this flare comprising two flaring events observed by space- and ground-based instruments with different spatial resolutions. For each flaring event we detect a few seismic sources, or sunquakes, using Dopplergrams from the HMI/SDO instrument coinciding with the kernels of Hα line emission with strong redshifts and white light sources. The properties of sunquakes were explored simultaneously with the observations of HXR (with KONUS/WIND and the Reuven Ramaty High Energy Solar Spectroscopic Imager payload), EUV (with the Atmospheric Imaging Assembly (AIA/SDO and the EUV Imaging Spectrometer aboard Hinode payload), Hα line emission (with the CRisp Imaging Spectro-Polarimeter (CRISP) in the Swedish Solar Telescope), and white light emission (with HMI/SDO). The locations of sunquake and Hα kernels are associated with the footpoints of magnetic flux ropes formed immediately before the X9.3 flare onset.
Conclusions. For the first time we present the detection of the largest sunquake ever recorded with the first and second bounces of acoustic waves generated in the solar interior, the ripples of which appear at a short distance of 5–8 Mm from the initial flare location. Four other sunquakes were also detected, one of which is likely to have occurred 10 min later in the same location as the largest sunquake. Possible parameters of flaring atmospheres in the locations with sunquakes are discussed using available temporal and spatial coverage of hard X-ray, GR, EUV, hydrogen Hα-line, and white light emission in preparation for their use in an interpretation to be given in Paper II.

Properties of the 15 February 2011 Flare Seismic Sources

S. **Zharkov**, L. M. Green, S. A. Matthews, V. V. Zharkova

Solar Physics, June **2013**, Volume 284, Issue 2, pp 315-327

The first near-side X-class flare of Solar Cycle 24 occurred in February 2011 (SOL2011-02-05T01:55) and produced a very strong seismic response in the photosphere. One sunquake was reported by Kosovichev (Astrophys. J. Lett. 734, L15, 2011), followed by the discovery of a second sunquake by Zharkov, Green, Matthews et al. (Astrophys. J. Lett. 741, L35, 2011). The flare had a two-ribbon structure and was associated with a flux-rope eruption and a halo coronal mass ejection (CME) as reported in the CACTus catalogue. Following the discovery of the second sunquake and the spatial association of both sources with the locations of the feet of the erupting flux rope (Zharkov, Green, Matthews et al., Astrophys. J. Lett. 741, L35, 2011), we present here a more detailed analysis of the observed photospheric changes in and around the seismic sources. These sunquakes are quite unusual, taking place early in the impulsive stage of the flare, with the seismic sources showing little hard X-ray (HXR) emission, and strongest X-ray emission sources located in the flare ribbons. We present a directional time–distance diagram computed for the second source, which clearly shows a ridge corresponding to the travelling acoustic-wave packet and find that the sunquake at the second source happened about 45 seconds to one minute earlier than the first source. Using acoustic holography we report different frequency responses of the two sources. We find strong downflows at both seismic locations and a supersonic horizontal motion at the second site of acoustic-wave excitation.

COMPARISON OF SEISMIC SIGNATURES OF FLARES OBTAINED BY SOHO/MICHELSON DOPPLER IMAGER AND GONG INSTRUMENTS

S. **Zharkov**1, V. V. Zharkova2 and S. A. Matthews

2011 ApJ 739 70

The first observations of seismic responses to solar flares were carried out using time-distance (TD) and holography techniques applied to SOHO/Michelson Doppler Imager (MDI) Dopplergrams obtained from space and unaffected by terrestrial atmospheric disturbances. However, the ground-based network GONG is potentially a very valuable source of sunquake observations, especially in cases where space observations are unavailable. In this paper, we present an updated technique for pre-processing of GONG observations for the application of subjacent vantage holography. Using this method and TD diagrams, we investigate several sunquakes observed in association with M- and X-class solar flares and compare the outcomes with those reported earlier using MDI data. In both GONG and MDI data sets, for the first time, we also detect the TD ridge associated with the **2001 September 9** flare. Our results show reassuringly positive identification of sunquakes from GONG data that can provide further information about the physics of seismic processes associated with solar flares.

Statistical properties of H -alpha flares in relation to sunspots and active regions in the cycle 23

Zharkov S.I. and Zharkova V.V.
E-print, Nov **2009**, JASTP
The statistical properties of H flare occurrences compared with those of sunspot and active region areas in the cycle 23. The flare numbers in the cycle 23 of all significances and locations are obtained from the Solar Geophysical Data (SGD) and the other data was taken from the automated Solar Feature Catalogs (SFC, http://solar.inf.brad.ac.uk). The average monthly flare occurrences during the whole cycle correlate closely with the total and cumulative areas of active regions and sunspots. The cumulative distribution of solar flare occurrences at different latitudes in the northern and southern hemispheres versus the time reveal a strong asymmetry with a domination of one or other hemispheres similar to the cumulative distributions of sunspots and active regions. Although the sunspot area asymmetry lags the flare occurrence asymmetry by about time of a few months at the ascending phase of the cycle and up to 12 months in the descending one. The latitudinal distribution of flare occurrences in the whole period reveal a well defined maximum at 18◦ in the northern and two maxima at 14◦ and 20◦ in the southern hemisphere. The longitudinal distributions of flare occurrence residuals of the running values and those averaged with a one year filter reveal a set of persistent longitudes in the opposite hemispheres lasting for about 1.0-1.5 years and changing quickly a few times over the cycle phases.

Pitch-angle distribution of accelerated electrons in 3D current sheets with magnetic islands

V. **Zharkova** and Q. Xia
A&A **2021**
https://solargsm.com/wp-content/uploads/2021/02/zharkova_xia_PADs_aa21.pdf
This research aims to explore variations of electron pitch-angle distribution (PAD) during spacecraft cross reconnecting current sheets (RCSs) with magnetic islands. The results can benchmark the sampled characteristic features with realistic PADs derived from in-situ observations. Particle motion is simulated in 2.5D Harris-type RCSs using particle-in-cell (PIC) method considering the plasma feedback to electromagnetic fields. We evaluate particle energy gains and PADs in different locations and under the different directions of passing the current sheet by a virtual spacecraft. The RCS parameters are comparable to heliosphere and solar wind conditions. The energy gains and the PADs of particles would change depending on the specific topology of magnetic fields. Besides, the observed PADs also depend on the crossing paths of the spacecraft. When the guiding field is weak, the bi-directional electron beams (strahls) are mainly present inside the islands and located closely above/below the X-nullpoints in the inflow regions. The magnetic field relaxation near X-nullpoint converts the PADs towards 90 degrees. As the guiding field becomes larger, the regions with bi-directional strahls are compressed towards small areas in the exhausts of RCSs. Mono-directional strahls are quasi-parallel to the magnetic field lines near the X-nullpoint due to the dominant Fermi-type magnetic curvature drift acceleration. Meanwhile, the high-energy electrons confined inside magnetic islands create PADs about 90 degrees. Our results link the electron PADs to local magnetic structures and directions of spacecraft crossings. This can help explain a variety of the PAD features reported in the recent observations in the solar wind and the Earth's magnetosphere.

Sunquake with a second bounce, other sunquakes, and emission associated with the X9.3 flare of 6 September 2017. II. Proposed interpretation

Valentina **Zharkova**1 , Sergei Zharkov2 , Malcolm Druett3 , Sarah Matthews4 , and Satoshi Inoue5
A&A 639, A79 **2020**
https://www.aanda.org/articles/aa/pdf/2020/07/aa37885-20.pdf
https://solargsm.com/wp-content/uploads/2020/05/Zharkova_et-al_6sept17_aa20.pdf
In this paper we present the interpretation of the observations of the flare from **6 September 2017** reported in Paper 1. These include gamma-ray (GR), hard X-ray (HXR), soft X-rays (SXR), Lyα line, extreme ultraviolet (EUV), Hα, and white light (WL) emission, which were recorded during the two flaring events 1 (FE1) and 2 (FE2) that occurred at 11:55:37 UT (FE1) and 12:06:40 UT (FE2). Paper 1 also reported the first detection of the sunquake with first and second bounces of seismic waves combined with four other sunquakes in different locations supported with the

observations of HXR, GR, EUV, Hα, and WL emission with strongly varying spatial resolution and temporal coverage. In the current Paper 2, we propose some likely scenarios for heating of flaring atmospheres in the footpoints with sunquakes which were supported with EUV and Hα emission. We used a range of parameters derived from the HXR, EUV, and Hα line observations to generate hydrodynamic models, which can account for the blueshifts derived from the EUV emission and the redshifts observed with the EUV Imaging Spectrometer (EIS) in the He II line and by the CRisp Imaging Spectro-Polarimeter (CRISP) in the Swedish Solar Telescope (SST) in Hα line emission. The parameters of hydrodynamic shocks produced by different beams in flaring atmospheres were used as the initial conditions for another type of hydrodynamic models that were developed for acoustic wave propagation in the solar interior. These models simulate the sets of acoustic waves produced in the interior by the hydrodynamic shocks from atmospheres above deposited in different footpoints of magnetic loops. The Hα line profiles with large redshifts in three kernels (two in FE1 and one in FE2) were interpreted with the full non-local thermodynamic equilibrium (NLTE) radiative simulations in all optically thick transitions (Lyman lines and continuum Hα, Hβ, and Pα) applied for flaring atmospheres with fast downward motions while considering thermal and non-thermal excitation and ionisation of hydrogen atoms by energetic power-law electron beams. The observed Hα line profiles in three kernels were fit with the simulate blue wing emission of the Hα line profiles shifted significantly (by 4-6 Å) towards the line red wings, because of strong downward motions with velocities about 300 km s-1 by the shocks generated in flaring atmospheres by powerful beams. The flaring atmosphere associated with the largest sunquake (seismic source 2 in FE1) is found consistent with being induced by a strong hydrodynamic shock produced by a mixed beam deposited at an angle of -30◦ from the local vertical. We explain the occurrence of a second bounce in the largest sunquake by a stronger momentum delivered by the shock generated in the flaring atmosphere by a mixed beam and deeper depths of the interior where this shock was deposited. Indeed, the shock with mixed beam parameters is found deposited deeply into the interior beneath the flaring atmosphere under the angle to the local vertical that would allow the acoustic waves generated in the direction closer to the surface to conserve enough energy for the second bounces from the interior layers and from the photosphere. The wave characteristics of seismic sources 1 and 3 (in FE1) were consistent with those produced by the shocks generated by similar mixed beams deposited at the angles -(0 - 10)◦ (seismic source 1) and +30◦ (seismic source 3) to the local vertical. The differences of seismic signatures produced in the flares of **6 September 2011** and 2017 are also discussed.

Beam electrons as sources of Hα ribbons in a C-class flare

Valentina **Zharkova**, Malcolm Druett and Eamon Scullion (Northumbria)
UK Solar Physics (UKSP) – Nuggets #83. **2017** www.uksolphys.org/?p=13393
New flare simulations explain a decades-old redshift mystery.
Observations of solar flare onsets show a rapid increase of hard and soft X-rays, ultra-violet emission with large Doppler blue-shifts associated with plasma upflows, and Hα emission with red-shifts up to 1–4 Å [1, 2, 3]. Modern radiative hydrodynamic models account well for blue-shifted emission, but struggle to reproduce closely the red-shifted Hα lines observed at the flare onset. Here we present a joint hydrodynamic and radiative model showing that during the first seconds of beam injection the effects caused by beam electrons can reproduce Hα line profiles with large red-shifts closely matching those observed in a C1.5 flare by the Swedish Solar Telescope. The model also accounts for the timing and magnitude of upward plasma motion to the corona observed 29 s after the event onset in 171 Å by the Atmospheric Imaging Assembly/Solar Dynamics Observatory. **30th June 2013**

Analytical solutions of continuity equation for joint collisional and Ohmic energy losses and their effects on hard X-ray emission. II. Mixed energy losses

Zharkova V.V. and Dobranskis R.R.
MNRAS **2016**
http://mnras.oxfordjournals.org/content/early/2016/03/07/mnras.stw500.full.pdf?keytype=ref&ijkey=zcVKoDhBj8zNW7o
In this paper we consider simultaneous analytical solutions of continuity equations for electron beam precipitation a) in collisional losses and b) in Ohmic losses, or mixed energy losses (MEL), by applying the iterative method to calculate the resulting differential densities at given precipitation depth. The differential densities of precipitating electrons derived from the analytical solutions for mixed energy losses reveal increased flattening at energies below 10-30 keV compared to a pure collisional case. This flattening becomes stronger with an increasing precipitation depth turning into a positive slope at greater precipitation depths in the chromosphere resulting in a differential density distribution with maximum that shifts towards higher energies with increase of a column depth. While the differential densities combining precipitating and returning electrons are higher at lower energies than those for a pure collisional case. The resulting hard X-ray (HXR) emission produced by the beams with different initial energy fluxes and spectral indices is calculated using the MEL approach for different ratios between the differential densities of precipitating and returning electrons. The number of returning electrons can be even further enhanced by a magnetic mirroring, not considered in the present model, while dominating at lower atmospheric depths where the magnetic convergence and magnitude are the highest. The proposed MEL approach provides an opportunity to account simultaneously for both collisional and ohmic losses in flaring events, which can be used for a quick spectral fitting of HXR spectra and evaluation of a fraction of returning electrons versus precipitating ones. The semi-analytical MEL approach is used for spectral fitting to

RHESSI observations of nine C, M and X class flares revealing a close fit to the observations and good resemblance to numerical FP solutions. **01 Oct 2012, 23 Oct 2012, 25 Oct 2013, 19 Dec 2013, 08 Jan 2014, 13 Jan 2014, 17 Jan 2014,**

On the Generation of Hydrodynamic Shocks by Mixed Beams and Occurrence of Sunquakes in Flares

Valentina **Zharkova** , Sergei Zharkov

Solar Physics November **2015**, Volume 290, Issue 11, pp 3163-3188

Observations of solar flares with sunquakes by space- and ground-based instruments reveal essentially different dynamics of seismic events in different flares. Some sunquakes are found to be closely associated with the locations of hard X-ray (HXR) and white-light (WL) emission, while others are located outside either of them. In this article we investigate possible sources causing a seismic response in a form of hydrodynamic shocks produced by the injection of mixed (electron plus proton) beams, discuss the velocities of these shocks, and the depths where they deposit the bulk of their energy and momentum. The simulation of hydrodynamic shocks in flaring atmospheres induced by electron-rich and proton-rich beams reveals that the linear depth of the shock termination is shifted beneath the level of the quiet solar photosphere on a distance from 200 to 5000 km. The parameters of these atmospheric hydrodynamic shocks are used as initial condition for another hydrodynamic model developed for acoustic-wave propagation in the solar interior (Zharkov, Mon. Not. Roy. Astron. Soc. 431, 3414, 2013). The model reveals that the depth of energy and momentum deposition by the atmospheric shocks strongly affects the propagation velocity of the acoustic-wave packet in the interior. The locations of the first bounces from the photosphere of acoustic waves generated in the vicinity of a flare are seen as ripples on the solar surface, or sunquakes. Mixed proton-dominated beams are found to produce a strong supersonic shock at depths 200 – 300 km under the level of the quiet-Sun photosphere and in this way produce well-observable acoustic waves, while electron-dominated beams create a slightly supersonic shock propagating down to 5000 km under the photosphere. This shock can only generate acoustic waves at the top layers beneath the photosphere since the shock velocity very quickly drops below the local sound speed. The distance Δ of the first bounce of the generated acoustic waves is discussed in relation to the minimal phase velocities of wave packets defined by the acoustic cutoff frequency and the parameters of atmospheric shock termination beneath the photosphere.

Particle acceleration in 3D single current sheets formed in the solar corona and heliosphere: PIC approach

Zharkova V.V. and Siversky T

Journal of Physics, Conference Series (JPCS), **2015**, 642, 012032

http://computing.unn.ac.uk/staff/slmv5/kinetics/zharkova_aiac15_v3.pdf

Acceleration of protons and electrons in a reconnecting current sheet (RCS) is investigated with the test particle and particle-in-cell (PIC) approaches in a 3D magnetic topology. PIC simulations confirm a spatial separation of electrons and protons with respect to the midplane depending on the guiding field. Simulation reveals that the separation occurs in magnetic topologies with strong guiding fields and lasts as long as the particles are kept dragged into a current sheet. This separation produces a polarisation electric field induced by the plasma feedback to a presence of accelerated particles, which shape can change from symmetric towards the midplane (for weak guiding field) to fully asymmetric (for strong guiding field). Particles are found accelerated at a midplane of any current sheets present in the heliosphere to the energies up to hundred keV for electrons and hundred MeV for protons. The maximum energy gained by particles during their motion inside the current sheet is defined by its magnetic field topology (the ratio of magnetic field components), the side and location from the X-nullpoint, where the particles enter a current sheet. In strong magnetic fields of the solar corona with weaker guiding fields, electrons are found circulating about the midplane to large distances where proton are getting accelerated, creating about the current sheet midplane clouds of high energy electrons, which can be the source of hard X-ray emission in the coronal sources of flares. These electrons are ejected into the same footpoint as protons after the latter reach the energy sufficient to break from a current sheet. In a weaker magnetic field of the heliosphere the bounced electrons with lower energies cannot reach the midplane turning instead at some distance D before the current sheet midplane by 180 degrees from their initial motion. Also the beams of accelerated transit and bounced particles are found to generate turbulent electric fields in a form of Langmuir waves (electrons) or ion-acoustic waves (protons).

Recent Advances in Understanding Particle Acceleration Processes in Solar Flares **Review**

V.V. **Zharkova** · K. Arzner · A.O. Benz · P. Browning · C. Dauphin · A.G. Emslie · L. Fletcher · E.P. Kontar · G. Mann · M. Onofri · V. Petrosian · R. Turkmani · N. Vilmer · L. Vlahos

Space Sci Rev (**2011**) 159:357–420, **File**

We **review** basic theoretical concepts in particle acceleration, with particular emphasis on processes likely to occur in regions of magnetic reconnection. Several new developments are discussed, including detailed studies of reconnection in three-dimensional magnetic field configurations (e.g., current sheets, collapsing traps, separatrix regions) and stochastic acceleration in a turbulent environment. Fluid, test-particle, and particle-in-cell approaches are used and results compared. While these studies show considerable promise in accounting for the various observational manifestations of solar flares, they are limited by a number of factors, mostly relating to available computational power. Not the least of these issues is the need to explicitly incorporate the electrodynamic feedback of the accelerated particles themselves on the environment in which they are accelerated. A brief prognosis for future advancement is offered.

Diagnostics of electron beam properties from the simultaneous hard X-ray and microwave emission in the 2001 March 10 flare

V. V. **Zharkova**, N. S. Meshalkina, L. K. Kashapova, A. A. Kuznetsov and A. T. Altyntsev
E-print May, **2011,** A&A 532, A17 (**2011**)

Context. Microwave (MW) and hard X-ray (HXR) data are thought to be powerful means of investigating the mechanisms of particle acceleration and precipitation in solar flares, reflecting different aspects of electron interaction with ambient particles in the presence of a magnetic field. Simultaneous simulation of HXR and MW emission with the same populations of electrons is still a big challenge for interpreting observations of real events. Recent progress in simulations of particle kinetics with the time-dependent Fokker-Planck (FP) approach offers an opportunity to produce this interpretation.
Aims. In this paper we apply the FP kinetic model of precipitation of electron beam with energy range from 12 keV to 1.2 MeV to the interpretation of X-ray and MW emissions observed in the flare of **2001 March 10**.
Methods. The theoretical HXR and MW emissions were calculated by using the distribution functions of electron beams found by solving time-dependent approach in a converging magnetic field for anisotropic scattering of beam electrons on the ambient particles in Coloumb collisions and Ohmic losses.
Results. The simultaneously observed HXR photon spectra and frequency distribution of MW emission and polarization were fit by those simulated from FP models that include the effects of electric field induced by beam electrons and precipitation onto a converging magnetic loop. Magnetic field strengths in the footpoints on the photosphere were updated with newly calibrated SOHO/MDI data. The observed HXR energy spectrum above 10 keV is shown to be a double power law that was precisely fit by the photon HXR spectrum simulated for the model including the self-induced electric field but without magnetic convergence. The MW emission simulated for different models of electron precipitation revealed a better fit (above 90% confidence level) to the observed distribution at higher frequencies for the models combining collisions and electric field effects with a moderate magnetic field convergence of two. The MW simulations were able to reproduce closely the main features of the MW emission observed at higher frequencies: the spectral index, the frequency of peak intensity and the frequency of the MW polarization reversal, while at lower frequencies the simulated MW intensities are lower than the observed ones.

THE EFFECTS OF ELECTRON-BEAM-INDUCED ELECTRIC FIELD ON THE GENERATION OF LANGMUIR TURBULENCE IN FLARING ATMOSPHERES

Valentina V. **Zharkova** and Taras V. Siversky
2011 ApJ 733 33

The precipitation of an electron beam injected into the solar atmosphere is studied for the generation of Langmuir wave turbulence in the presence of collisional and Ohmic losses. The system of quasi-linear time-dependent kinetic equations describing the evolution of beams and Langmuir waves is solved by using the summary approximation method. It is found that at upper atmospheric levels the self-induced electric field suppresses the generation of Langmuir turbulence to very small regions below injection. With further precipitation into deeper atmosphere the initial single power-law distributions of beam electrons are transformed into energy distributions with maxima at lower energies formed by collisional and Ohmic energy depletion. The electrons with lower energies (<20 keV) generate on large spatial scales intense low-hybrid and high-hybrid Langmuir waves with well-defined patterns in the corona while higher energy electrons generate moderate low-hybrid waves in the chromosphere. The maximum wave density appears at the maximum of the ambient density. The self-induced electric field reduces the level and makes the regions with low-hybrid Langmuir turbulence narrower in the corona and upper chromosphere. The higher the beam energy flux or its self-induced electric field, the narrower the regions with Langmuir turbulence. High-hybrid Langmuir waves in the form of multiple patterns in space (in the corona) and energy (below 20 keV) are found to be generated only by a very intense electron beam. The number of patterns in both dimensions is also shown to be significantly reduced by the self-induced electric field.

The effect of energetic particle beams on the chromospheric emission of the 25th July 2004 flare

Zharkova V.V., Kashapova L.K., Chornogor S.N. and Andrienko O,V.
E-print Oct **2010**, MNRAS

In this paper a role of particle beams for generation of a close spatial and temporal correlation between hard H-ray (HXR) energy and Hα line emission bursts in the solar flare of **25 July 2004** is discussed. The light curves in HXR emission and Hα line revealed the pre-flare and main flare events correlated with the variations of a line-of-sight (LOS) magnetic flux. HXR emission shows the three main bursts during the main flare phase which are accompanied by Hα intensity increases. The latter appear in 10 locations (kernels) at different times in succession; the kernel locations are associated with strong magnetic sources situated on the opposite sides from the magnetic neutral line (MNL). The appearance of Hα kernels in the pre-flare event and those at the start of the main event are correlated very closely (within a few seconds) with the HXR emission observed by RHESSI (HXR+Hα kernels), while the appearance of some other ones, not associated with HXR emission, was delayed by ten of seconds. Electron beam parameters were derived from the RHESSI spectra in where the observed HXR photon flux was corrected for the self-induced electric field effect. Possible implications of this electric field on production of the transient magnetic fields observed during the flare are discussed. The Hα emission observed during the first burst was simulated in hydrodynamic atmospheres for 5 level plus continuum hydrogen atom with the full non-LTE approach combining radiative, thermal and non-thermal excitation and ionization by an electron beam with the derived parameters. The simulated temporal profiles of Hα emission produced by non-thermal hydrogen excitation revealed a very good fit to the observed ones in the HXR+Hα kernels and 10-20 s delays in the other kernels. This allows to speculate that Hα emission in these kernels is caused mainly by electrons in the HXR+Hα kernels and mainly by protons in the other ones.

Diagnostics of energetic electrons with anisotropic distributions in solar flares I. Hard X-rays bremsstrahlung emission

Zharkova V.V., Kuznetsov A.A. and Siversky T.V.
E-print, Nov 2009, A&A, 512, A8 (**2010**)
http://www.aanda.org/10.1051/0004-6361/200811486

Aims. The paper aims are to simulate steady-state distributions of electrons beams precipitating in collisional and Ohmic losses with pitch angle anisotropy into a flaring atmosphere with converging magnetic field and to apply these to the interpretation of HXR photon spectra, directivity and polarization observed for different photon energies and positions of flares.
Methods. Summary approximation method is applied to time-dependent Fokker-Planck equation splitting a temporal derivative equally between the derivatives in depth, energy and pitch angles and finding the solutions in forward and backward directions for each variable.
Results. For softer beams there is a noticeable flattening of the photon spectra at lower energies caused by the self-induced electric field which increases for larger viewing angles. For the models with electric field the HXR emission with lower energies (30 keV) becomes directed mainly upwards at upper atmospheric levels owing to the increased number of particles moving upwards, while at the deeper layers it becomes again directed downwards. The polarization maximum shifts to higher energies with every precipitation depth approaching 25 keV for the models with pure collisions and 100 keV for the models with return currents. At deeper layers the polarization decreases because of the izotropization of electrons by collisions. The maximum polarization is observed at the viewing angle of 90◦ becoming shifted to lower angles for softer beams. The integrated polarization and directivity shows dependence on a magnetic field convergence for harder beams while for softer beam the directivity is strongly affected by the self-induced electric field changing from downward to upward one at upper atmospheric depths.
Conclusions. The proposed precipitation model for an electron beam with wider pitch angle dispersion of 0.2 taking into account collisional and Ohmic losses allowed us to fit the double power law HXR photon spectra with a spectrum flattening at lower energies observed in the flares of **20 and 23 July 2002**. The observed directivity of HXR photons of 20 keV derived for a large number of flares located from the disk center to limb is also well reproduced by the theoretical directivity calculated for an electron beam with a very narrow pitch angle dispersion of 0.02. The simulated polarization of such the narrowly-directed electron beam fits up to 90% of all the available polarimetric observations carried out at various locations on the solar disk.

Energy Dissipation in Magnetohydrodynamic Turbulence: Coherent Structures or "Nanoflares"?

Vladimir **Zhdankin**, Stanislav Boldyrev, Jean Carlos Perez, Steven M. Tobias

ApJ, 795 127 **2014**

http://arxiv.org/pdf/1409.3285v1.pdf

We investigate the intermittency of energy dissipation in magnetohydrodynamic (MHD) turbulence by identifying dissipative structures and measuring their characteristic scales. We find that the probability distribution of energy dissipation rates exhibits a power law tail with index very close to the critical value of -2.0, which indicates that structures of all intensities contribute equally to energy dissipation. We find that energy dissipation is uniformly spread among coherent structures with lengths and widths in the inertial range. At the same time, these structures have thicknesses deep within the dissipative regime. As the Reynolds number is increased, structures become thinner and more numerous, while the energy dissipation continues to occur mainly in large-scale coherent structures. This implies that in the limit of high Reynolds number, energy dissipation occurs in thin, tightly packed current sheets which nevertheless span a continuum of scales up to the system size, exhibiting features of both coherent structures and nanoflares previously conjectured as a coronal heating mechanism.

Kelvin--Helmholtz Instability in Solar Atmosphere Jets

I. **Zhelyazkov**

2014 J. Astrophys. Astr.

http://arxiv.org/pdf/1411.6472v1.pdf

In this article I have discussed the recent approaches in studying the Kelvin--Helmholtz (KH) instability of magnetohydrodynamic (MHD) waves propagating in solar atmosphere jets. The main focus is on the modeling the KH instability developing in coronal mass ejections in view of its (instability) contribution to triggering a wave turbulence subsequently leading to an effective coronal heating. KH instability of MHD waves in coronal active regions recently observed and imaged in unprecedented detail in EUV thanks to the high cadence, high-resolution observations by \emph{SDO}/AIA instrument, and spectroscopic observations by \emph{Hinode}/EIS instrument is a challenge for modeling this event. It is shown that considering the solar mass flows of coronal mass ejections as moving cylindrical twisted magnetic flux tubes the imaged instability can be explained in terms of unstable m=−3 MHD mode. Obtained critical jet speeds for the instability onset as well as the linear wave growth rates are in good agreement with observational data.

Kelvin--Helmholtz instability of magnetohydrodynamic waves propagating on solar surges

I. **Zhelyazkov**, R. Chandra, A. K. Srivastava, T. Mishonov

2014

http://arxiv.org/pdf/1411.6481v1.pdf

In the present paper, we study the evolutionary conditions for Kelvin--Helmholtz (KH) instability in a high-temperature solar surge observed in NOAA AR11271 using the Solar Dynamics Observatory data on 2011 August 25. We study the propagation of normal MHD modes in a flux tube considering the two cases, notably of untwisted magnetic flux tube and the twisted one. The numerical solution to the dispersion relation shows that the kink (m=1) wave traveling in an untwisted flux tube becomes unstable if the jet speed exceeds 1060 km\,s−1 -- a speed which is inaccessible for solar surges. A weak twist (the ratio of azimuthal to longitudinal magnetic field component) of the internal magnetic field in the range of 0.025--0.2 does not change substantially the critical flow velocity. Thus, one implies that, in general, the kink mode is stable against the KH instability. It turns out, however, that the m=−2 and m=−3 MHD modes can become unstable when the twist parameter has values between 0.2 and 0.4. Therefore, the corresponding critical jet speed for instability onset lies in the range of 93.5--99.3 km\,s1. The instability wave growth rate, depending on the value of the wavelength, is of the order of several dozen inverse milliseconds. It remains to be seen whether these predictions will be observationally validated in future in the coronal jet-like structures in abundant measure.

Multiclass solar flare forecasting models with different deep learning algorithms

Yanfang **Zheng** and others

Monthly Notices of the Royal Astronomical Society, Volume 521, Issue 4, June **2023**, Pages 5384–5399,

https://doi.org/10.1093/mnras/stad839

https://watermark.silverchair.com/stad839.pdf

We develop a Hybrid Bidirectional Long and Short-Term Memory based on attention mechanism (HBiLSTM-Attention) model and a BiLSTM-Attention model for multiclass flare forecasting within 24 h. We construct a new data base containing 10 separate data sets with magnetogram images and magnetic field parameters. Based on the same data base, for the first time we compare the multiclass forecasting performance of our proposed HBiLSTM-Attention model, BiLSTM-Attention model, and three other deep-learning models based on Convolutional Neural Network (CNN-based) from two aspects of categorical performance with the true skill statistic (TSS) and probabilistic performance with the Brier skill score (BSS). The major results are as follows. (1) The TSS values of our proposed model are 0.692 ± 0.042,

0.475 ± 0.038, 0.642 ± 0.043, 0.754 ± 0.062, 0.692 ± 0.042, and 0.708 ± 0.052 for No-flare, C, M, X, ≥C, and ≥M class, respectively, which are better than those of the BiLSTM-Attention model, and much better than those of the three other CNN-based models. (2) Our proposed model achieves the scores of BSS = 0.498 ± 0.061, 0.202 ± 0.037, 0.209 ± 0.050, −0.271 ± 0.180, 0.498 ± 0.061, 0.268 ± 0.056 for No-flare, C, M, X, ≥C, and ≥M class, respectively, outperforming the other four models in every class except for X class. (3) To our knowledge, HBiLSTM-Attention is the first multiclass flare forecasting model based on magnetic field parameters and deep learning, and achieves promising prediction performance. Moreover, this is the first attempt to investigate the reliability of probabilistic prediction for multiclass flares.

Solar Flare Prediction with the Hybrid Deep Convolutional Neural Network

Yanfang **Zheng1**, Xuebao Li1, and Xinshuo Wang
2019 ApJ 885 73
https://iopscience.iop.org/article/10.3847/1538-4357/ab46bd/pdf
We propose a hybrid Convolutional Neural Network (CNN) model (Model 2) and modify a popular CNN model (Model 1) to predict multiclass solar flare occurrence within 24 hr. We collect samples of solar active regions provided by the Space-weather Helioseismic and Magnetic Imager Active Region Patches data from 2010 May to 2018 September. These samples are categorized into four classes (No-flare, C, M, and X), containing 10 separate data sets. Then after training, validating, and testing our models, we compare the results with previous studies in forecast verification metrics with an emphasis on the true skill statistic (TSS). The main results are summarized as follows. (1) This is the first time that the CNN models are used to make multiclass predictions of solar flare. (2) Model 2 has better values of all statistical scores than Model 1 in every class. (3) Model 2 achieves relatively high average scores of TSS = 0.768 for No-flare class, 0.538 for C class, 0.534 for M class, and 0.552 for X class, which are the best results from the existing literatures. (4) Model 2 also can be used to make binary class flare predictions for ≥M-class major flares, and the performance yields a TSS with 0.749 ± 0.079. (5) Model 2 obtains fairly good scores in other metrics for both multiclass flare predictions and ≥M-class major flare predictions. We surmise that some crucial features extracted automatically by our models may have not been excavated before and could provide important clues for studying the mechanism of flare.

Sunspots rotation and magnetic transients associated with flares in NOAA AR 11429

Jianchuan **Zheng**, Zhiliang Yang, Jianpeng Guo, Kaiming Guo, Hui Huang, Xuan Song, Weixing Wan
Research in Astronomy and Astrophysics (RAA) **2017**
https://arxiv.org/pdf/1704.08018.pdf
We analyze sunspots rotation and magnetic transients in NOAA AR 11429 during two X-class (X5.4 and X1.3) flares using the data from the Helioseismic and Magnetic Imager on board the \emph{Solar Dynamics Observatory}. A large leading sunspot with positive magnetic polarity rotated counterclockwise. As expected, the rotation was significantly affected by the two flares. The magnetic transients induced by the flares were clearly evident in the sunspots with negative polarity. They were moving across the sunspots with speed of order 3−7 km s−1. Furthermore, the trend of magnetic flux evolution of these sunspots exhibited changes associated with the flares. These results may shed light on the understanding of the evolution of sunspots. **5-7 March 2012**

Slipping magnetic reconnections with multiple flare ribbons during an X-class solar flare

Ruisheng **Zheng**, Yao Chen, Bing Wang
ApJ 823 136 **2016**
http://arxiv.org/pdf/1604.04982v1.pdf
https://iopscience.iop.org/article/10.3847/0004-637X/823/2/136/pdf
With the observations of the Solar Dynamics Observatory, we present the slipping magnetic reconnections with multiple flare ribbons (FRs) during an X1.2 eruptive flare on **2014 January 7**. A center negative polarity was surrounded by several positive ones, and there appeared three FRs. The three FRs showed apparent slipping motions, and hook structures formed at their ends. Due to the moving footpoints of the erupting structures, one tight semi-circular hook disappeared after the slippage along its inner and outer edge, and coronal dimmings formed within the hook. The east hook also faded as a result of the magnetic reconnection between the arcades of a remote filament and a hot loop that was impulsively heated by the under flare loops. Our results are accordant with the slipping magnetic reconnection regime in 3D standard model for eruptive flares. We suggest that complex structures of the flare is likely a consequence of the more complex flux distribution in the photosphere, and the eruption involves at least two magnetic reconnections.

Semicircular-like Secondary Flare Ribbons Associated with a Failed Eruption

R. **Zheng**1, M. B. Korsós1,2, and R. Erdélyi

2015 ApJ 809 45
Flare ribbons (FRs) are one of the most apparent signatures of solar flares and have been treated as an indicator of magnetic reconnection. Drawing upon the observations from the Solar Dynamics Observatory, we present semicircular-like secondary FRs (SFRs) of a C2.3 flare on **2013 June 19**. Before the flare eruption, two bipoles in this core region subsequently emerged. Due to the interaction between the two bipoles, a tether-cutting eruption took place in the core region. The SFRs, surrounding the core region nearly simultaneously with the flare onset, were much weaker than the two normal FRs. Two ends of the SFRs experienced a separation and extension movement, but the middle part of the SFRs hardly expanded outward. We find SFRs are closely associated with the footpoint brightenings of some small loops around the core region. The eruption was confined by transequatorial loops (TLs), which resulted in the plasma material falling in the north end of the TLs and remote brightenings showing up in the south end of the TLs. The disappearance of the faint (filament) material during the emergence of the SFRs could indicate another eruption. We conclude that two or more magnetic reconnections are involved in this event and propose that SFRs consisting of a small part of true FRs resulted from the second magnetic reconnection and bright footpoints of loop clusters likely heated by the main flare.

Solar Flares and the Axion Quark Nugget Dark Matter Model

Ariel **Zhitnitsky**
JCAP **2018**
https://arxiv.org/pdf/1801.01509.pdf
We advocate the idea that the nanoflares conjectured by Parker long ago to resolve the corona heating problem, may also trigger the larger solar flares. The arguments are based on the model where emission of extreme ultra violet (EUV) radiation and soft x-rays from the Sun are powered externally by incident dark matter particles within the Axion Quark Nugget (AQN) Dark Matter Model. The corresponding annihilation events of the AQNs with the solar material are identified with nanoflares. This model gives a very reasonable intensity of EUV radiation without adjustments of any parameters in the model. When the same nuggets enter the regions with high magnetic field they serve as the triggers igniting the magnetic reconnections which eventually may lead to much larger flares. Technically, the magnetic reconnection is ignited due to the shock wave which inevitably develops when the dark matter nuggets enter the solar atmosphere with velocity $v\sim 10^{-3}c$ which is much higher than the speed of sound cs, such that the Mach number $M=v/cs\gg 1$. These shock waves generate very strong and very short impulses expressed in terms of pressure $\Delta p/p\sim M2$ and temperature $\Delta T/T\sim M2$ in vicinity of (would be) magnetic reconnection area. We find that this mechanism is consistent with x -ray observations as well as with observed jet like morphology of the initial stage of the flares. The mechanism is also consistent with the observed scaling of the flare distribution $dN\sim W^{-\alpha}dW$ as a function of the flare's energy W. We also speculate that the same nuggets may trigger the sunquakes which are known to be correlated with large flares.

Extreme-ultraviolet Late Phase in Homologous Solar Flares from a Complex Active Region

Y. **Zhong**, Y. Dai, M. D. Ding
ApJ **916** 37 **2021**
https://doi.org/10.3847/1538-4357/ac0430
https://arxiv.org/pdf/2105.10069.pdf
https://iopscience.iop.org/article/10.3847/1538-4357/ac0430/pdf
Recent observations in extreme-ultraviolet (EUV) wavelengths reveal a new late phase in some solar flares, which is seen as a second peak in warm coronal emissions (~3 MK) several tens of minutes to a few hours after the soft X-ray (SXR) peak. The origin of the EUV late phase (ELP) is explained by either a long-lasting cooling process in the long ELP loops, or a delayed energy ejection into the ELP loops well after the main flare heating. Using the observations with the \emph{Solar Dynamics Observatory} (\emph{SDO}), we investigate the production of the ELP in six homologous flares (F1--F6) originating from a complex active region (AR) NOAA 11283, with an emphasis on the emission characteristics of the flares. It is found that the main production mechanism of the ELP changes from additional heating in flare F1 to long-lasting cooling in flares F3--F6, with both mechanisms playing a role in flare F2. The transition is evidenced by an abrupt decrease of the time lag of the ELP peak, and the long-lasting cooling process in the majority of the flares is validated by a positive correlation between the flare ribbon fluence and the ELP peak intensity. We attribute the change in ELP production mechanism to an enhancement of the envelope magnetic field above the AR, which facilitates a more prompt and energetic heating of the ELP loops. In addition, the last and the only confined flare F6 exhibits an extremely large ELP. The different emission pattern revealed in this flare may reflect a different energy partitioning inside the ELP loops, which is due to a different magnetic reconnection process. **2011: August 31 to September 11, September 6, 7, 8, 9.**

Transition from circular-ribbon to parallel-ribbon flares associated with a bifurcated magnetic flux rope

Z. **Zhong**, Y. Guo, M. D. Ding, C. Fang, Q. Hao
ApJ **871** 105 **2019**

https://arxiv.org/pdf/1812.10223.pdf
Magnetic flux ropes play a key role in triggering solar flares in the solar atmosphere. In this paper, we investigate the evolution of active region NOAA 12268 within 36 hours from **2015 January 29 to 30**, during which a flux rope was formed and three M-class and three C-class flares were triggered without coronal mass ejections. During the evolution of the active region, the flare emission seen in the Hα and ultraviolet wavebands changed from a circular shape (plus an adjacent conjugated ribbon and a remote ribbon) to three relatively straight and parallel ribbons. Based on a series of reconstructed nonlinear force-free fields, we find sheared or twisted magnetic field lines and a large-scale quasi-separatrix layer (QSL) associated with 3D null points in a quadrupolar magnetic field. These features always existed and constantly evolved during the two days. The twist of the flux rope was gradually accumulated that eventually led to its instability. Around the flux rope, there were some topological structures, including a bald patch, a hyperbolic flux tube and a torus QSL. We discuss how the particular magnetic structure and its evolution produce the flare emission. In particular, the bifurcation of the flux rope can explain the transition of the flares from circular to parallel ribbons. We propose a two-stage evolution of the magnetic structure and its associated flares. In the first stage, sheared arcades under the dome-like large-scale QSL were gradually transformed into a flux rope through magnetic reconnection, which produced the circular ribbon flare. In the second stage, the flux rope bifurcated to form the three relatively straight and parallel flare ribbons.

On the origin of a broad QFP wave train: unwinding jet as the driver

Xinping **Zhou**, Zehao Tang, Zhining Qu, Ke Yu, Chengrui Zhou, Yuqi Xiang, Ahmed Ahmed Ibrahim, Yuandeng Shen
ApJ **2024**
https://arxiv.org/pdf/2409.17741
Large-scale extreme-ultraviolet (EUV) waves commonly exhibit as single wavefront and are believed to be caused by coronal mass ejections (CMEs). Utilizing high spatiotemporal resolution imaging observations from the Solar Dynamics Observatory, we present two sequentially generated wave trains originating from the same active region: a narrow quasiperiodic fast-propagating (QFP) wave train that propagates along the coronal loop system above the jet and a broad QFP wave train that travels along the solar surface beneath the jet. The measurements indicate that the narrow QFP wave train and the accompanying flare's quasiperiodic pulsations (QPPs) have nearly identical onsets and periods. This result suggests that the accompanying flare process excites the observed narrow QFP wave train. However, the broad QFP wave train starts approximately 2 minutes before the QPPs of the flare, but consistent with the interaction between the unwinding jet and the solar surface. Moreover, we find that the \zx{period of the broad QFP wave train, approximately 130\,s, closely matches that of the unwinding jet}. This period is significantly longer than the 30\,s period of the accompanying flare's QPPs. Based on these findings, we propose that the intermittent energy release of the accompanying flare excited the narrow QFP wave train confined propagating in the coronal loop system. The unwinding jet, rather than the intermittent energy release in the accompanying flare, triggered the broad QFP wave train propagating along the solar surface. **2011 January 27**

Resolved magnetohydrodynamic wave lensing in the solar corona

Xinping **Zhou**, Yuandeng Shen, Ding Yuan, Rony Keppens, Xiaozhou Zhao, Libo Fu, Zehao Tang, Jiaoyang Wang, Chengrui Zhou
Nature Communications 15, 3281 (**2024**)
https://arxiv.org/pdf/2404.12044.pdf
Electromagnetic wave lensing, a common physical phenomenon recognized in visible light for centuries, finds extensive applications in manipulating light in optical systems such as telescopes and cameras. Magnetohydrodynamic wave is a common perturbation phenomenon in the corona. By using high spatio-temporal resolution observations from the Solar Dynamics Observatory, here, we report the observation of a magnetohydrodynamic wave lensing in the highly ionized and magnetized coronal plasma, where quasi-periodic wavefronts emanated from a flare converged at a specific point after traversing a coronal hole. The entire process resembles an electromagnetic wave lensing from the source to the focus. Meanwhile, the magnetohydrodynamic wave lensing is well reproduced through a magnetohydrodynamic numerical simulation with full spatio-temporal resolution. We further investigate potential applications for coronal seismology, as the lensing process encodes information on the Alfvén speed, in conjunction with favorable geometric and density variations. **2011 February 24**

Consecutive Narrow and Broad Quasi-periodic Fast-propagating Wave Trains Associated with a Flare

Xinping **Zhou**, Yuandeng Shen, Chengrui Zhou, Zehao Tang, Ahmed Ahmed Ibrahim
ScChG **2024**
https://arxiv.org/pdf/2401.06661.pdf
The excitation mechanism of coronal quasi-period fast-propagating (QFP) wave trains remains unresolved. Using Atmospheric Imaging Assembly onboard the Solar Dynamics Observatory observations, we study a narrow and a broad QFP wave train excited one after another during the successive eruptions of filaments hosted within a fan-spine

magnetic system on **2013 October 20**. The consecutive occurrence of these two types of QFP wave trains in the same event provides an excellent opportunity to explore their excitation mechanisms and compare their physical parameters. Our observational results reveal that narrow and broad QFP wave trains exhibit distinct speeds, periods, energy fluxes, and relative intensity amplitudes, although originating from the same active region and being associated with the same {\em GOES} C2.9 flare. Using wavelet analysis, we find that the narrow QFP wave train shares a similar period with the flare itself, suggesting its possible excitation through the pulsed energy release in the magnetic reconnection process that generated the accompanying flare. On the other hand, the broad QFP wave train appears to be associated with the energy pulses released by the successive expansion and unwinding of filament threads. Additionally, it is plausible that the broad QFP wave train was also excited by the sequential stretching of closed magnetic field lines driven by the erupting filament. These findings shed light on the different excitation mechanisms and origins of the QFP wave trains.

Recurrent narrow quasi-periodic fast-propagating wave trains excited by the intermittent energy release in the accompanying solar flare

Xinping **Zhou**, Yuandeng Shen, Hongfei Liang, Zhining Qu, Yadan Duan, Zehao Tang, Chengrui Zhou, Song Tan

ApJ **941** 59 **2022**

https://arxiv.org/pdf/2211.14488.pdf

https://iopscience.iop.org/article/10.3847/1538-4357/aca1b6/pdf

About the driven mechanisms of the quasi-periodic fast-propagating (QFP) wave trains, there exist two dominant competing physical explanations: associated with the flaring energy release or attributed to the waveguide dispersion. Employing Solar Dynamics Observatory (SDO) Atmospheric Imaging Assembly (AIA) 171 A images, we investigated a series of QFP wave trains composed of multiple wavefronts propagating along a loop system during the accompanying flare on **2011 November 11**. The wave trains showed a high correlation in start time with the energy release of the accompanying flare. Measurements show that the wave trains phase speed is almost consistent with its group speed with a value of about 1000 km s-1, indicating that the wave trains should not be dispersed waves. The period of the wave trains was the same as that of the oscillatory signal in X ray emissions released by the flare. Thus we propose that the QFP wave trains were most likely triggered by the flare rather than by dispersion. We investigated the seismological application with the QFP waves and then obtained that the magnetic field strength of the waveguide was about 10 Gauss. Meanwhile, we also estimated that the energy flux of the wave trains was about 1.2X105 erg cm-2 s-1.

Observations of a Flare-ignited broad Quasi-periodic Fast-propagating wave train

Xinping **Zhou**, Yuandeng Shen, Ying D. Liu, Huidong Hu, Jiangtao Su, Zehao Tang, Chengrui Zhou, Yadan Duan, Song Tan

ApJL **930** L5 **2022**

https://arxiv.org/pdf/2204.05603.pdf

https://iopscience.iop.org/article/10.3847/2041-8213/ac651e/pdf

Large-scale Extreme-ultraviolet (EUV) waves are frequently observed as an accompanying phenomenon of flares and coronal mass ejections (CMEs). Previous studies mainly focus on EUV waves with single wavefronts that are generally thought to be driven by the lateral expansion of CMEs. Using high spatio-temporal resolution multi-angle imaging observations taken by the Solar Dynamic Observatory and the Solar Terrestrial Relations Observatory, we present the observation of a broad quasi-periodic fast propagating (QFP) wave train composed of multiple wavefronts along the solar surface during the rising phase of a GOES M3.5 flare on **2011 February 24**. The wave train transmitted through a lunate coronal hole (CH) with a speed of 840 +/-67 km/s, and the wavefronts showed an intriguing refraction effect when they passed through the boundaries of the CH. Due to the lunate shape of the CH, the transmitted wavefronts from the north and south arms of the CH started to approach each other and finally collided, leading to the significant intensity enhancement at the collision site. This enhancement might hint the occurrence of interference between the two transmitted wave trains. The estimated magnetosonic Mach number of the wave train is about 1.13, which indicates that the observed wave train was a weak shock. Period analysis reveals that the period of wave train was ~90 seconds, in good agreement with that of the accompanying flare. Based on our analysis results, we conclude that the broad QFP wave train was a large-amplitude fast-mode magnetosonic wave or a weak shock driven by some non-linear energy release processes in the accompanying flare.

Diagnosing the Optically Thick/Thin Features Using the Intensity Ratio of Si IV Resonance Lines in Solar Flares

Yi-an **Zhou**, Jie Hong, Y. LI, M.D. Ding

ApJ **2022**

https://arxiv.org/pdf/2201.05305.pdf

In the optically thin regime, the intensity ratio of the two Si IV resonance lines (1394 and 1403 Å) are theoretically the same as the ratio of their oscillator strengths, which is exactly 2. Here, we study the ratio of the integrated intensity of the Si IV lines ($R=\int I1394(\lambda)d\lambda/\int I1403(\lambda)d\lambda$) and the ratio of intensity at each wavelength point

(r(Δλ)=I1394(Δλ)/I1403(Δλ)) in two solar flares observed by the Interface Region Imaging Spectrograph. We find that at flare ribbons, the ratio R ranges from 1.8 to 2.3 and would generally decrease when the ribbons sweep across the slit position. Besides, the distribution of r(Δλ) shows a descending trend from the blue wing to the red wing. In loop cases, the Si IV line presents a wide profile with a central reversal. The ratio R deviates little from 2, but the ratio r(Δλ) can vary from 1.3 near the line center to greater than 2 in the line wings. Hence we conclude that in flare conditions, the ratio r(Δλ) varies across the line, due to the variation of the opacity at the line center and line wings. We notice that, although the ratio r(Δλ) could present a value which deviates from 2 as a result of the opacity effect near the line center, the ratio R is still close to 2. Therefore, caution should be taken when using the ratio of the integrated intensity of the Si IV lines to diagnose the opacity effect. **2014 April 18, 2017 September 9**

Resolving Two Distinct Thermal X-ray Components in a compound Solar Flare

Zhenjun **Zhou**, Rui Liu, Jianqing Sun, Jie Zhang, Mingde Ding, Yuming Wang, Xiaoyu Yu, Lijuan Liu, Jun Cui

ApJ **925** 132 **2022**

https://arxiv.org/pdf/2112.04652.pdf

https://iopscience.iop.org/article/10.3847/1538-4357/ac3bbe/pdf **File**

X-ray emission provides the most direct diagnostics of the energy-release process in solar flares. Occasionally, a superhot X-ray source is found to be above hot flare loops of ~10 MK temperature. While the origin of the superhot plasma is still elusive, it has conjured up an intriguing image of in-situ plasma heating near the reconnection site high above the flare loops, in contrast to the conventional picture of chromospheric evaporation. Here we investigate an extremely long-duration solar flare, in which EUV images show two distinct flare loop systems that appear successively along a Gamma-shaped polarity inversion line (PIL). When both flare loop systems are present, the HXR spectrum is found to be well fitted by combining a hot component (Te ~12 MK) and a superhot component (Te ~30 MK). Associated with a fast CME, the superhot X-ray source is located at top of the flare arcade that appears earlier, straddling and extending along the long "arm" of the Gamma-shaped PIL. Associated with a slow CME, the hot X-ray source is located at the top of the flare arcade that appears later and sits astride the short "arm" of the Gamma-shaped PIL. Aided by observations from a different viewing angle, we are able to verify that the superhot X-ray source is above the hot one in projection, but the two sources belong to different flare loop systems. Thus, this case study provides a stereoscopic observation explaining the co-existence of superhot and hot X-ray emitting plasmas in solar flares. **2012 July 17**

RHESSI Science Nuggets #423 **2021**

https://sprg.ssl.berkeley.edu/~tohban/wiki/index.php/Resolving_two_distinct_thermal_X-ray_components

Spectroscopic Observations of High-speed Downflows in a C1.7 Solar Flare

Yi-An **Zhou**, Y. Li, M. D. Ding, Jie Hong, Ke Yu

ApJ **904** 95 **2020**

https://arxiv.org/pdf/2009.06158.pdf

https://doi.org/10.3847/1538-4357/abb77c

In this paper, we analyze the high-resolution UV spectra for a C1.7 solar flare (SOL**2017-09-09**T06:51) observed by the \textit{Interface Region Imaging Spectrograph} (\textit{IRIS}). {We focus on the spectroscopic observations at the locations where the cool lines of \ion{Si}{4} 1402.8 Å (~104.8 K) and \ion{C}{2} 1334.5/1335.7 Å (~104.4 K) reveal significant redshifts with Doppler velocities up to ~150 km s−1.} These redshifts appear in the rise phase of the flare, then increase rapidly, reach the maximum in a few minutes, and proceed into the decay phase. Combining the images from \textit{IRIS} and Atmospheric Imaging Assembly (AIA) on board the {\em Solar Dynamics Observatory} ({\em SDO}), we propose that the redshifts in the cool lines are caused by the downflows in the transition region and upper chromospheric layers, which likely result from a magnetic reconnection leading to the flare. In addition, the cool \ion{Si}{4} and \ion{C}{2} lines show gentle redshifts (a few tens of km s−1) at some other locations, which manifest some distinct features from the above locations. This is supposed to originate from a different physical process.

Extreme-ultraviolet Late Phase Caused by Magnetic Reconnection over Quadrupolar Magnetic Configuration in a Solar Flare

Zhenjun **Zhou**, Xin Cheng, Lijuan Liu, Yu Dai, Yuming Wang, Jun Cui

2019 *ApJ* **878** 46

https://arxiv.org/pdf/1905.00549.pdf

sci-hub.se/10.3847/1538-4357/ab1d5c

A second emission enhancement in warm coronal extreme-ultraviolet (EUV) lines (about 2-7 MK) during some solar flares is known as the EUV late phase. Imaging observations confirm that the late phase emission originates from a set of longer or higher loops than the main flare loops. Nevertheless, some questions remain controversial: What is the relationship between these two loop systems? What is the heating source of late phase emission, a heating accompany the main phase heating or occuring quite later? In this paper, we present clear evidence for heating source in a late-

phase solar flare: magnetic reconnection of overlying field in a quadrupolar magnetic configuration. The event is triggered by an erupted core structure that eventually leads to a coronal mass ejection (CME). Cusp feature and its shrinkage motion high in the late-phase emission region are the manifestation of the later phase reconnection following the main flare reconnection. Using the enthalpy-based thermal evolution of loops (EBTEL) model, we reasonably reproduce the late-phase emissions in some EUV lines. We suggest that a continuous additional heating is responsible for the appearance of the elongated EUV late phase. **2014 April 25**

Toward Understanding the 3D Structure and Evolution of Magnetic Flux Ropes in an Extremely Long Duration Eruptive Flare

Zhenjun **Zhou** , Jie Zhang4, Yuming Wang1,3, Rui Liu1,5, and Georgios Chintzoglou
2017 ApJ 851 133 **File**
http://iopscience.iop.org.sci-hub.tw/0004-637X/851/2/133/
In this work, we analyze the initial eruptive process of an extremely long duration C7.7-class flare that occurred on **2011 June 21**. The flare had a 2 hr long rise time in soft X-ray emission, which is much longer than the rise time of most solar flares, including both impulsive and gradual ones. Combining the facts that the flare occurred near the disk center as seen by the Solar Dynamic Observatory (SDO) but near the limb as seen by two Solar Terrestrial Relations Observatory(STEREO) spacecraft, we are able to track the evolution of the eruption in 3D in a rare slow-motion manner. The time sequence of the observed large-scale EUV hot channel structure in the Atmospheric Imaging Assembly (AIA) high-temperature passbands of 94 and 131 Å clearly shows the process of how the sigmoid structure prior to the eruption was transformed into a near-potential post-eruption loop arcade. We believe that the observed sigmoid represents the structure of a twisted magnetic flux rope (MFR), which has reached a height of about 60 Mm at the onset of the eruption. We argue that the onset of the flare precursor phase is likely triggered by the loss of the magnetohydrodynamic equilibrium of a preexisting MFR, which leads to the slow rise of the flux rope. The rising motion of the flux rope leads to the formation of a vertical current sheet underneath, triggering the fast magnetic reconnection that in turn leads to the main phase of the flare and fast acceleration of the flux rope.

ELECTRON ACCELERATION BY CASCADING RECONNECTION IN THE SOLAR CORONA. II. RESISTIVE ELECTRIC FIELD EFFECTS

X. **Zhou**1,2, J. Büchner2, M. Bárta2,3, W. Gan1, and S. Liu
2016 ApJ 827 94
We investigate electron acceleration by electric fields induced by cascading reconnections in current sheets trailing coronal mass ejections via a test particle approach in the framework of the guiding-center approximation. Although the resistive electric field is much weaker than the inductive electric field, the electron acceleration is still dominated by the former. Anomalous resistivity η is switched on only in regions where the current carrier's drift velocity is large enough. As a consequence, electron acceleration is very sensitive to the spatial distribution of the resistive electric fields, and electrons accelerated in different segments of the current sheet have different characteristics. Due to the geometry of the 2.5-dimensional electromagnetic fields and strong resistive electric field accelerations, accelerated high-energy electrons can be trapped in the corona, precipitating into the chromosphere or escaping into interplanetary space. The trapped and precipitating electrons can reach a few MeV within 1 s and have a very hard energy distribution. Spatial structure of the acceleration sites may also introduce breaks in the electron energy distribution. Most of the interplanetary electrons reach hundreds of keV with a softer distribution. To compare with observations of solar flares and electrons in solar energetic particle events, we derive hard X-ray spectra produced by the trapped and precipitating electrons, fluxes of the precipitating and interplanetary electrons, and electron spatial distributions.

Electron acceleration by cascading reconnection in the solar corona I Magnetic gradient and curvature effects

X. **Zhou**, J. Büchner, M. Barta, W. Gan, S. Liu
A&A **2015**
http://arxiv.org/pdf/1504.06486v1.pdf
Aims: We investigate the electron acceleration in convective electric fields of cascading magnetic reconnection in a flaring solar corona and show the resulting hard X-ray (HXR) radiation spectra caused by Bremsstrahlung for the coronal source. Methods: We perform test particle calculation of electron motions in the framework of a guiding center approximation. The electromagnetic fields and their derivatives along electron trajectories are obtained by linearly interpolating the results of high-resolution adaptive mesh refinement (AMR) MHD simulations of cascading magnetic reconnection. Hard X-ray (HXR) spectra are calculated using an optically thin Bremsstrahlung model. Results: Magnetic gradients and curvatures in cascading reconnection current sheet accelerate electrons: trapped in magnetic islands, precipitating to the chromosphere and ejected into the interplanetary space. The final location of an electron is determined by its initial position, pitch angle and velocity. These initial conditions also influence electron acceleration efficiency. Most of electrons have enhanced perpendicular energy. Trapped electrons are considered to cause the observed bright spots along coronal mass ejection CME-trailing current sheets as well as the flare loop-top HXR emissions.

Converging motion of conjugate flaring kernels during two large solar flares

Tuanhui **Zhou**, Haisheng Ji and Guangli Huang

Advances in Space Research , Volume 41, Issue 8, **2008**, Pages 1195-1201

In this paper, we analyze the footpoint motion of two large solar flares using observations made by the Transition Region and Coronal Explorer (TRACE) and Reuven Ramaty High Energy Solar Spectroscopic Imager (*RHESSI*). The two flares are the **M5.7 flare of March 14, 2002 and the X10 flare of October 29, 2003.** They are both classical two-ribbon flares as observed in TRACE 1600 or 171 Å images and have long-duration conjugate hard X-ray (HXR) footpoint emission. We use the 'center-of-mass' method to locate the centroids of the UV/EUV flare ribbons. The results are: (1) The conjugate UV/EUV ribbons and HXR footpoints of the two flares show a converging (inward) motion during the impulsive phase. For the two flares, the converging motion lasts about 3 and 10 min, respectively. The usual separation (outward) motion for the flare ribbons and footpoints take place only after the converging motion. (2) During the inward and the outward motion, the conjugate ribbons and footpoints of the two events exhibit a strong unshear motion. In obtaining above results, TRACE UV/EUV and *RHESSI* HXR data show an overall agreement. The two events demonstrate that the magnetic reconnection for the flares occurs in highly sheared magnetic field. Furthermore, the results support the magnetic model constructed by Ji et al. [Ji, H., Huang, G., Wang, H. Astrophys. J. 660, 893–900, 2007], who proposed that the contracting motion of flaring loops is the signature of the relaxation of sheared magnetic fields.

Quasi-Simultaneous Flux Emergence in the Events of October – November 2003

Guiping **Zhou** · Jingxiu Wang · Yuming Wang · Yuzong Zhang

Solar Phys (**2007**) 244: 13–24; **File**

From late October to the beginning of November 2003, a series of intense solar eruptive events took place on the Sun. More than six active regions (ARs), including three large ARs (NOAA numbers AR 10484, AR 10486, and AR 10488), were involved in the activity. Among the six ARs, four of them bear obviously quasi-simultaneous emergence of magnetic flux. Based on the global Hα and SOHO/EIT EUV observations, we found that a very long filament channel went through the six ARs. This implies that there is a magnetic connection among these ARs. The idea of large-scale magnetic connectivity among the Ars is supported by the consistency of the same chirality in the three major ARs and in their associated magnetic clouds. Although the detailed mechanisms for the quasi-simultaneous flux emergence and the large-scale flux system formation need to be extensively investigated, the observations provide new clues in studying the global solar activity.

Modeling Mg II h, k and Triplet Lines at Solar Flare Ribbons

Yingjie **Zhu**, Adam F. Kowalski, Hui Tian, Han Uitenbroek, Mats Carlsson, Joel C. Allred

2019 *ApJ* **879** 19

https://arxiv.org/pdf/1904.12285.pdf

sci-hub.se/10.3847/1538-4357/ab2238

Observations from the \textit{Interface Region Imaging Spectrograph} (\textsl{IRIS}) often reveal significantly broadened and non-reversed profiles of the Mg II h, k and triplet lines at flare ribbons. To understand the formation of these optically thick Mg II lines, we perform plane parallel radiative hydrodynamics modeling with the RADYN code, and then recalculate the Mg II line profiles from RADYN atmosphere snapshots using the radiative transfer code RH. We find that the current RH code significantly underestimates the Mg II h \& k Stark widths. By implementing semi-classical perturbation approximation results of quadratic Stark broadening from the STARK-B database in the RH code, the Stark broadenings are found to be one order of magnitude larger than those calculated from the current RH code. However, the improved Stark widths are still too small, and another factor of 30 has to be multiplied to reproduce the significantly broadened lines and adjacent continuum seen in observations. Non-thermal electrons, magnetic fields, three-dimensional effects or electron density effect may account for this factor. Without modifying the RADYN atmosphere, we have also reproduced non-reversed Mg II h \& k profiles, which appear when the electron beam energy flux is decreasing. These profiles are formed at an electron density of ∼8×1014 cm−3 and a temperature of ∼1.4×104 K, where the source function slightly deviates from the Planck function. Our investigation also demonstrates that at flare ribbons the triplet lines are formed in the upper chromosphere, close to the formation heights of the h \& k lines. **2014 March 29**

Two-Phase Heating in Flaring Loops

Chunming **Zhu**, Jiong Qiu, Dana W. Longcope

ApJ **856** 27 **2018**

https://arxiv.org/pdf/1802.00871.pdf

We analyze and model a C5.7 two-ribbon solar flare observed by SDO, Hinode and GOES on **2011 December 26**. The flare is made of many loops formed and heated successively over one and half hours, and their footpoints are brightened in the UV 1600 A before enhanced soft X-ray and EUV missions are observed in flare loops. Assuming that anchored at each brightened UV pixel is a half flaring loop, we identify more than 6,700 half flaring loops, and infer the heating rate of each loop from the UV light curve at the foot-point. In each half loop, the heating rate consists of two phases, an intense impulsive heating followed by a low-rate heating persistent for more than 20 minutes. Using these heating rates, we simulate the evolution of their coronal temperatures and densities with the model of "enthalpy-based thermal evolution of loops" (EBTEL). In the model, suppression of thermal conduction is also considered. This model successfully reproduces total soft X-ray and EUV light curves observed in fifteen pass-bands by four instruments GOES, AIA, XRT, and EVE. In this flare, a total energy of 4.9x10^30 ergs is required to heat the corona, around 40% of this energy is in the slow heating phase. About two fifth of the total energy used to heat the corona is radiated by the coronal plasmas, and the other three fifth transported to the lower atmosphere by thermal conduction.

Evolution of a Current Sheet in a Solar Flare

Chunming **Zhu**, Rui Liu, David Alexander, R.T. James McAteer
2016 *ApJ* **821** L29
http://arxiv.org/pdf/1603.07062v1.pdf
We report multi-wavelength and multi-viewpoint observations of a solar eruptive event which involves loop-loop interactions. During a C2.0 flare, motions associated with inflowing and outflowing plasma provide evidence for ongoing magnetic reconnection. The flare loop top and a rising "concave-up" feature are connected by a current-sheet-like structure (CSLS). The physical properties (thickness, length, temperature, and density) of the CSLS are evaluated. In regions adjacent to the CSLS, the EUV emission (characteristic temperature at 1.6 MK) begins to increase more than ten minutes prior to the onset of the flare, and steeply decreases during the decay phase. The reduction of the emission resembles that expected from coronal dimming. The dynamics of this event imply a magnetic reconnection rate in the range 0.01 -- 0.05. **2013 December 10**

Complex Flare Dynamics Initiated by a Filament-Filament Interaction

Chunming **Zhu**, Rui Liu, David Alexander, Xudong Sun, James McAteer
2015 ApJ 813 60
http://arxiv.org/pdf/1507.05889v1.pdf
We report on an eruption involving a relatively rare filament-filament interaction on **2013 June 21**, observed by SDO and STEREO-B. The two filaments were separated in height within AR 11777. The onset of the eruption of the lower filament was accompanied simultaneously by the apparent descent of the upper filament resulting in a convergence and direct interaction of the two filaments. The interaction was accompanied by the heating of plasmas surrounding the upper filament and the subsequent coalescence of the filaments into a magnetically complex structure, whose eruption was associated with an M2.9 class solar flare. Magnetic loop shrinkage and descending dark voids were observed at different locations as part of the large flare energy release giving us a unique insight into these dynamic flare phenomena.

Successive Coronal Mass Ejections Associated with Weak Solar Energetic Particle Events

Bin **Zhuang**, Noé Lugaz, Tingyu Gou, Liuguan Ding
ApJ **921** 6 **2021**
https://arxiv.org/pdf/2109.02225.pdf
https://iopscience.iop.org/article/10.3847/1538-4357/ac17e9/pdf
https://doi.org/10.3847/1538-4357/ac17e9
The scenario of twin coronal mass ejections (CMEs), i.e., a fast and wide primary CME (priCME) preceded by previous CMEs (preCMEs), has been found to be favorable to a more efficient particle acceleration in large solar energetic particle (SEP) events. Here, we study 19 events during 2007--2014 associated with twin-CME eruptions but without large SEP observations at L1 point. We combine remote-sensing and in situ observations from multiple spacecraft to investigate the role of magnetic connectivity in SEP detection and the CME information in 3-dimensional (3D) space. We study one-on-one correlations of the priCME 3D speed, flare intensity, suprathermal backgrounds, and height of CME-CME interaction with the SEP intensity. Among these, the priCME speed is found to correlate with the SEP peak intensity at the highest level. We use the projection correlation method to analyze the correlations between combinations of these multiple independent factors and the SEP peak intensity. We find that the only combination of two or more parameters that has higher correlation with the SEP peak intensity than the CME speed is the CME speed combined with the propagation direction. This further supports the dominant role of the priCME in controlling the SEP enhancements, and emphasizes the consideration of the latitudinal effect. Overall, the magnetic connectivity in longitude as well as latitude and the relatively lower priCME speed may explain the existence of the twin-CME SEP-poor events. The role of the barrier effect of preCME(s) is discussed for an event on **2013 October 28.**
Table 1:: Twin-CME (L1-point) SEP-poor events during 2007– 2014
Table 2:: Twin-CME (L1-point) large SEP events in solar cycle 24

Topological Quantification of the "Anemone" (Branching) Solar Flares

Evgeny V. **Zhuzhoma**, Vladislav S. Medvedev, Yurii V. Dumin, Boris V. Somov
Physica D **2021**
https://arxiv.org/pdf/2111.06730.pdf
Here, using the methods of dynamical systems and Morse-Smale theory, we derive a few universal topological relations between the numbers of the null points and sources of various kinds with arbitrary arrangement in the above-mentioned structures. Such relations can be a valuable tool both for a quantification of the already-observed anemone flares and for a prediction of the new ones in complex magnetic configurations.

Cylindrical and Spherical Pistons as Drivers of MHD Shocks

Tomislav **Žic** · Bojan Vršnak · Manuela Temmer · Carla Jacobs
Solar Phys (**2008**) 253: 237–247
We consider an expanding three-dimensional (3-D) piston as a driver of an MHD shock wave. It is assumed that the source-region surface accelerates over a certain time interval to achieve a particular maximum velocity. Such an expansion creates a large-amplitude wave in the ambient plasma. Owing to the nonlinear evolution of the wave front, its profile steepens and after a certain time and distance a discontinuity forms, marking the onset of the shock formation. We investigate how the formation time and distance depend on the acceleration phase duration, the maximum expansion velocity (defining also acceleration), the Alfvén velocity (defining also Mach number), and the initial size of the piston. The model differs from the 1-D case, since in the 3-D evolution, a decrease of the wave amplitude with distance must be taken into account. We present basic results, focusing on the timing of the shock formation in the low- and high-plasma-beta environment. We find that the shockformation time and the shock-formation distance are (1) approximately proportional to the acceleration phase duration; (2) shorter for a higher expansion velocity; (3) larger in a higher Alfvén speed environment; (4) only weakly dependent on the initial source size; (5) shorter for a stronger acceleration; and (6) shorter for a larger Alfvén Mach number of the source surface expansion. To create a shock causing a high-frequency type II burst and the Moreton wave, the source region expansion should, according to our results, achieve a velocity on the order of 1000 km s^{-1} within a few minutes, in a low Alfvén velocity environment.

When it rippled in one place and exploded in another

Ivan **Zimovets**
RHESSI Science Nuggets #465 Dec **2023**
https://sprg.ssl.berkeley.edu/~tohban/wiki/index.php/When_it_rippled_in_one_place_and_exploded_in_another
5 Nov 2013

Quasi-Periodic Energy Release in a Three-Ribbon Solar Flare

Ivan **Zimovets**, Ivan Sharykin & Ivan Myshyakov
Solar Physics volume 296, Article number: 188 (**2021**)
https://link.springer.com/content/pdf/10.1007/s11207-021-01936-9.pdf
https://doi.org/10.1007/s11207-021-01936-9
Quasi-periodic pulsations (QPPs) are found in solar flares of various magnetic morphologies, e.g. in two-ribbon or circular-ribbon flares, and the mechanisms of their generation are not yet clear. Here we present the first detailed analysis of QPPs (with a period P=54±13 seconds) found in the Ramaty High Energy Solar Spectroscopic Imager (RHESSI) observations of a relatively rare three-ribbon M1.1 class flare that occurred on **5 July 2012** (SOL**2012-07-05T06:49**). QPPs are manifested in the temporal profiles of temperature [TT] and emission measure [EMEM] of "super-hot" ($T_s \approx 30 - 50$ MK) plasma but are almost invisible in the profiles of "hot" ($T_h \approx 15 - 20$ MK) plasma parameters when approximating X-ray spectra of the flare with the bremsstrahlung spectrum of a two-temperature thermal (Maxwellian) plasma. In addition, QPPs with a similar period are found in the temporal profiles of the flux and spectral index of nonthermal electrons if the observed X-ray spectra are approximated by a combination of the bremsstrahlung spectra of a single-temperature plasma and nonthermal electrons with a power-law energy distribution. QPPs are not well expressed in the X-ray flux according to RHESSI and GOES data, or in radio data. The QPPs are accompanied by apparent systematic movement of a single X-ray source at a low speed of 34±21 km s^{-1} along the central flare ribbon over a narrow (<5 Mm) "tongue" of negative magnetic polarity, elongated (≈20 Mm) between two areas of positive polarity. The results of magnetic extrapolation in the nonlinear force-free field (NLFFF) approximation show that the X-ray source could move along curved and twisted field lines between two sheared flare arcades. It is worth noting that in the homologous three-ribbon M6.1 flare (SOL**2012-07-05T11:39**), which occurred in the same region about five hours later, the X-ray sources moved much less systematically and did not produce similar QPPs. We interpret the observed QPPs as a result of successive episodes of energy release in different spatial locations. In each pulsation, $\approx(1 - 4)\times 10^{29}$ erg is released in the form of thermal energy of hot and super-hot plasmas (or accelerated electrons), which is comparable with the energy of a microflare. The total kinetic energy released during all QPPs is $\approx(0.7 - 3.5)\times 10^{30}$ erg, which is about an order of magnitude less than the free magnetic energy $\approx 1.56\times 10^{31}$ erg released in the flare region. We discuss possible propagating triggers of the quasi-periodic energy release (slow magnetoacoustic waves, asymmetric rise of curved/twisted field lines, flapping

oscillations, and thermal instability in a reconnecting current sheet) and argue that the current state of available mechanisms and observations does not allow us to reach an unambiguous conclusion.

Quasi-Periodic Pulsations in Solar and Stellar Flares: A Review of Underpinning Physical Mechanisms and Their Predicted Observational Signatures

I. V. **Zimovets**, J. A. McLaughlin, A. K. Srivastava, D. Y. Kolotkov, A. A. Kuznetsov, E. G. Kupriyanova, I.-H. Cho, A. R. Inglis, F. Reale, D. J. Pascoe, H. Tian, D. Yuan, D. Li & Q. M. Zhang
Space Science Reviews volume 217, Article number: 66 (**2021**)
https://link.springer.com/content/pdf/10.1007/s11214-021-00840-9.pdf
https://doi.org/10.1007/s11214-021-00840-9

The phenomenon of quasi-periodic pulsations (QPPs) in solar and stellar flares has been known for over 50 years and significant progress has been made in this research area. It has become clear that QPPs are not rare—they are found in many flares and, therefore, robust flare models should reproduce their properties in a natural way. At least fifteen mechanisms/models have been developed to explain QPPs in solar flares, which mainly assume the presence of magnetohydrodynamic (MHD) oscillations in coronal structures (magnetic loops and current sheets) or quasi-periodic regimes of magnetic reconnection. We review the most important and interesting results on flare QPPs, with an emphasis on the results of recent years, and we present the predicted and prominent observational signatures of each of the fifteen mechanisms. However, it is not yet possible to draw an unambiguous conclusion as to the correct underlying QPP mechanism because of the qualitative, rather than quantitative, nature of most of the models and also due to insufficient observational information on the physical properties of the flare region, in particular the spatial structure of the QPP source. We also review QPPs in stellar flares, where progress is largely based on solar-stellar analogies, suggesting similarities in the physical processes in flare regions on the Sun and magnetoactive stars. The presence of QPPs with similar properties in solar and stellar flares is, in itself, a strong additional argument in favor of the likelihood of solar-stellar analogies. Hence, advancing our understanding of QPPs in solar flares provides an important additional channel of information about stellar flares. However, further work in both theory/simulations and in observations is needed. **1972 May 16, 1998 May 8, 29 May 2003, February 15, 2011, 2012-07-19, 26 Oct 2014, 09 November 2014, 2014 December 17, 2015 March 12, 5 May 2015, 2015 November 04, September 10, 2017**

Relationships between Photospheric Vertical Electric Currents and Hard X-Ray Sources in Solar Flares: Statistical Study

I.V. **Zimovets**, I.N. Sharykin, W.Q. Gan
ApJ **891** 138 **2020**
https://arxiv.org/pdf/2002.06646.pdf
https://doi.org/10.3847/1538-4357/ab75be

There are still debates whether particle acceleration in solar flares may occur due to interruption of electric currents flowing along magnetic loops. To contribute to this problem, we performed the first statistical study of relationships between flare hard X-ray (HXR; 50−100 keV) sources observed by the \textit{Ramaty High-Energy Solar Spectroscopic Imager} (RHESSI) and photospheric vertical electric currents (PVECs, jr) calculated using vector magnetograms obtained with the Helioseismic and Magnetic Imager (HMI) on-board the \textit{Solar Dynamics Observatory} (SDO). A sample of 48 flares, from C3.0 to X3.1 class, observed in central part of the solar disk by both instruments in 2010--2015 was analyzed. We found that ≈70\% of all HXR sources overlapped with islands or ribbons of enhanced (|jr|≳104 statampere~cm−2) PVECs. However, less than ≈40\% of the HXR sources overlapped with PVEC maxima, with an accuracy of ±3″. More than in half of the flares there were HXR sources outside regions of enhanced PVECs. We found no correlation between intensity of the HXR sources and PVEC density or total PVEC under them. No systematic dissipation of PVECs under the HXR sources was found during the flares. Collectively, the results do not support the current-interruption flare models. However, the results indicate the importance of the presence of longitudinal currents in flare regions. Understanding of their specific role in the processes of energy release, plasma heating, and acceleration of particles requires further investigation. **2010-10-16, 2011-09-26, 2011-12-25, 2012-06-03, 2012-07-06,**
Table 1. Information on the solar flares studied (2010-2015)

Density distribution of photospheric vertical electric currents in flare active regions of the Sun

I.V. **Zimovets** (1), A.B. Nechaeva (1 and 2), I.N. Sharykin (1), W.Q. Gan (3)
2019
https://arxiv.org/pdf/1908.09016.pdf

Solar active regions contain electric currents. Information on the distribution of currents is important for understanding the processes of energy release on the surface of the Sun and in the overlying layers. The paper presents an analysis of the probability density function (PDF) of the absolute value of the photospheric vertical electric current density (|jz|) in 48 active regions before and after flares in 2010--2017. Calculation of |jz| is performed by applying the differential form of Ampere's circuital law to photospheric vector magnetograms obtained from observations of the Helioseismic and Magnetic Imager (HMI) instrument onboard the Solar Dynamics Observatory (SDO). It has been established that for the

studied active regions PDF(|jz|) is described by the Gauss function in the low-|jz| region (|jz|<10110±1321 statampere/cm2) and the decaying power-law function in the region of higher |jz| values. Also, for some active regions PDF(|jz|) can be described by the special kappa-function. The distributions of the parameters of the approximating functions are obtained using the least squares method. The average absolute value of the power-law function index is 3.69±0.51, and 3.99±0.51 of the kappa-function. No systematic changes in parameters during the flares are detected. An explicit connection between the parameters and the flare X-ray class, as well as with the Hale magnetic class of the active regions, is not found. Arguments are presented in favor of the suggestion that the Gaussian distribution in the low-value region of PDF(|jz|) represents noise in the data, while the power-law "tail" reflects the nature of electric currents in the solar active regions. **03.08.2011, 29.09.2014**

Magnetic Structure of Solar Flare Regions Producing Hard X-Ray Pulsations

I.V. **Zimovets**, R. Wang, Y.D. Liu, C.C. Wang, S.A. Kuznetsov, I.N. Sharykin, A.B. Struminsky, V.M. Nakariakov

JASTP Volume 174, September **2018**, Pages 17-27

https://reader.elsevier.com/reader/sd/57C406616EBCC7F3D96944EB109BA6D4F5D66AE6550663538F70F573EDBECEA44C3F56C5ECD99D9123B1BAFD853872E3

We present analysis of the magnetic field in seven solar flare regions accompanied by the pulsations of hard X-ray (HXR) emission. These flares were studied by Kuznetsov et al. (2016) (Paper I), and chosen here because of the availability of the vector magnetograms for their parent active regions (ARs) obtained with the SDO/HMI data. In Paper I, based on the observations only, it was suggested that a magnetic flux rope (MFR) might play an important role in the process of generation of the HXR pulsations. The goal of the present paper is to test this hypothesis by using the extrapolation of magnetic field with the non-linear force-free field (NLFFF) method. Having done this, we found that before each flare indeed there was an MFR elongated along and above a magnetic polarity inversion line (MPIL) on the photosphere. In two flare regions the sources of the HXR pulsations were located at the footpoints of different magnetic field lines wrapping around the central axis, and constituting an MFR by themselves. In five other flares the parent field lines of the HXR pulsations were not a part of an MFR, but surrounded it in the form of an arcade of magnetic loops. These results show that, at least in the analyzed cases, the “single flare loop” models do not satisfy the observations and magnetic field modeling, while are consistent with the concept that the HXR pulsations are a consequence of successive episodes of energy release and electron acceleration in different magnetic flux tubes (loops) of a complex AR. An MFR could generate HXR pulsations by triggering episodes of magnetic reconnection in different loops in the course of its non-uniform evolution along an MPIL. However, since three events studied here were confined flares, actual eruptions may not be required to trigger sequential particle acceleration episodes in the magnetic systems containing an MFR.

15-Feb-2011, 07-Jun-2011, 06-Sep-2011, 18-Apr-2014, 22- Oct-2014, 24-Oct-2014, and 09-Nov-2014

Magnetic Structure and Electric Currents in Solar Flare Regions Producing Hard X-Ray Pulsations

I.V. **Zimovets**, R. Wang, Y.D. Liu, C.C. Wang, S.A. Kuznetsov, I.N. Sharykin, A.B. Struminsky, V.M. Nakariakov

Solar Phys. **2017**

https://arxiv.org/pdf/1708.01869.pdf

https://reader.elsevier.com/reader/sd/D943F3EDFFA19652E63E628B39C4696C309935683003CD5FBC75683B316096AEE20F06928C0501F3965BF0549093FDB1

We present analysis of magnetic field and vertical electric currents (VECs) in seven solar flare regions accompanied by pulsations of hard X-ray (HXR) emission. These flares were studied by Kuznetsov et al. (2016) and chosen here because of the availability of the vector magnetograms for their parent active regions (ARs) obtained with the SDO/HMI data. By extrapolation of magnetic field with the non-linear force-free field (NLFFF) method we found that before each flare there was a magnetic flux rope (MFR) elongated along and above a magnetic polarity inversion line (MPIL) on the photosphere. In two flare regions the sources of the HXR pulsations were located at footpoints of different magnetic field lines wrapping around the central axis, and constituting an MFR by themselves. In five other flares the parent field lines of the HXR pulsations were not a part of an MFR, but surrounded it in the form of an arcade of magnetic loops. Also, we found that in three out of seven events the sources of the HXR pulsations were located in vicinity of enhanced ($\gtrsim$104~statampere~cm^{-2}) regions of VECs on the photosphere, having the form of extended ribbons elongated ($\gtrsim$10~Mm) mainly along an MPIL. In four remaining events VECs are concentrated in multiple tiny ($\lesssim$5~Mm) islands scattered around the MPIL. In general, the HXR sources are found to locate close but out of the sites of the highest VECs on the photosphere. There are no significant correlations between intensity of the HXR sources and characteristics of VECs and magnetic field components (as well as of their evolution in time) on the photosphere beneath the HXR sources. All these observational results are in favor of the concept that the HXR pulsations are a consequence of successive episodes of energy release in different magnetic flux tubes of a complex AR triggered by

non-uniform eruption of an MFR. **15-Feb-2011, 07-Jun-2011, 06-Sep-2011, 18-Apr-2014, 22- Oct-2014, 24-Oct-2014, and 09-Nov-2014**

Spatio-Temporal Dynamics of Flare Hard X-ray Pulsations

I. V. **Zimovets**, S. A. Kuznetsov & A. B. Struminsky
RHESSI Science Nuggets #285 Oct **2016**
http://sprg.ssl.berkeley.edu/~tohban/wiki/index.php/Spatio-Temporal_Dynamics_of_Flare_Hard_X-ray_Pulsations
The goal of the present work is to perform systematic analysis of spatio-temporal evolution of sources of the HXR pulsations in a large set of flares observed with RHESSI between 2002 and 2015. We emphasize that our study is not accented on the finding and analysis of the quasi-periodicities. Our approach is more general. We are interested in all flares which are accompanied by multiple HRX pulsations/peaks seen in the RHESSI data, no matter whether they are quasi-periodic (in the above sense) or not.
Two main results of our systematic analysis of large set of solar flares with HXR pulsations are:
1) The sources of HXR pulsations in all studied flares were not persistent: the spatial locations of the HXR sources changed in time from one pulsation peak to another;
2) The majority of flares (83%) were associated with CMEs and, thus, were eruptive events, i.e. were accompanied by eruptive processes - sudden ejections of filaments and/or magnetic structures such as magnetic flux ropes and arcades of magnetic loops.
In our view, the crucial role in generation of pulsations, as well as in excitation of coronal loops oscillations (see, e.g., Ref. [3]), is played by unstable eruptive magnetic structures. **2002-11-09, 2002-08-20**

Excitation of kink oscillations of coronal loops: statistical study

Zimovets, I.V., Nakariakov, V.M.
A&A, 577, A4 **2015**
E-print, Dec **2014**
Context. Solar flares are often accompanied by kink (transverse) oscillations of coronal loops. Despite intensive study of these oscillations in recent years mechanisms for their excitation remain unrevealed.
Aims. To clarify the excitation mechanisms for kink oscillations of coronal loops.
Methods. We analyse 58 kink oscillation events observed by the Atmospheric Imaging Assembly (AIA) onboard the Solar Dynamics Observatory (SDO) during its first four years (2010-2014) with the use of the JHelioviewer. Association of these oscillation events with flares, lower coronal eruptions and plasma ejections, coronal mass ejections (CMEs) and coronal type II radio bursts is studied.
Results. It is found that 44 out of these 58 oscillation events (76%) were associated with CMEs observed in the white light emission. Moreover, 57 events (98%) were accompanied by lower coronal eruptions/ejections (LCEs) observed in the EUV band in the parental active regions. An LCE was not clearly seen only in one event but it was definitely associated with a CME. The main observational finding is that the kink oscillations were excited by the deviation of loops from their equilibria by a nearby LCEs in 55 events (95%). In 3 remaining events it was difficult to reliably determine the cause of the oscillations because of limitations of the observational data. We also found that 53 events (91%) were associated with flares. In five remaining events the parental active regions were behind the limb and we could not directly see flare sites. It indicates that there is a close relationship between these two kinds of the solar activity. However, the estimated speeds of a hypothetical driver of kink oscillations by flares were found to be low than 500 km/s in 80% of cases. Such low speeds are not in favour of the association of the oscillation excitation with a shock wave, as it has usually been assumed. The fact that only 23 (40%) of the oscillation events were found to be associated with coronal type II radio bursts is also against the shock wave mechanism for the excitation of kink oscillations.
Conclusions. The performed statistical analysis shows that the most probable mechanism for the excitation of kink oscillations of coronal loops is the deviation of loops from their equilibrium by nearby eruptions or plasma ejections rather than a blast shock wave ignited by a flare.
7 Jan 2013

Fine structure of the sources of quasi-periodic pulsations in “single-loop” solar flares

I. V. **Zimovets**, S. A. Kuznetsov & A. B. Struminsky
Astronomy Letters, April **2013**, Volume 39, Issue 4, pp 267-278
Pis’ma v Astronomicheskiĭ Zhurnal, **2013**, Vol. 39, No. 4, pp. 297–309.
Analysis of the observational data obtained with a high angular resolution in the ranges of vacuum ultraviolet (1″, TRACE) and hard X-ray (4″, RHESSI) emissions in some solar flares previously considered “single-loop” ones shows that they are not such flares. The thick single loops with a diameter of 13″–21″ observed in these flares in the microwave range with an angular resolution of 5″–10″ (NoRH) are actually arcades of thinner loops with a diameter of less than 3″. In this case, the observed quasi-periodic pulsations of microwave emission are not a consequence of the oscillations of an isolated thick loop, as is usually assumed, but a result of the successive involvement of many relatively thinner loops in the process of flare energy release. The established facts impose significant constraints on the generation models of pulsations in flares. **March 14, 2002, JULY 22, 2004**

Non-thermal “Burst-on-Tail” of Long-Duration Solar Event on 26 October 2003

I. **Zimovets**, A. Struminsky

Solar Physics, December **2012**, Volume 281, Issue 2, pp 749-763

Observations of a rare long-duration solar event of GOES class X1.2 from **26 October 2003** are presented. This event showed a pronounced burst of hard X-ray and microwave emission, which was extremely delayed (> 60 min) with respect to the main impulsive phase and did not have any significant response visible in soft X-ray emission. We refer to this phenomenon as a “burst-on-tail”. Based on TRACE observations of the growing flare arcade and some simplified estimation, we explain why a reaction of active region plasma to accelerated electrons may change drastically over time. We suggest that, during the “burst-on-tail”, non-thermal electrons were injected into magnetic loops of larger spatial scale than during the impulsive phase bursts, thus resulting in much smaller values of plasma temperature and emission measure in their coronal volume, and hence little soft X-ray flux. The nature of the long gap between the main impulsive phase and the “burst-on-tail” is, however, still an open question.

Observations of Double-Periodic X-Ray Emission in Interacting Systems of Solar Flare Loops

I.V. **Zimovets** · A.B. Struminsky

Solar Phys (**2010**) 263: 163–174

We investigate the M1.8 solar flare of **20 October 2002**. The flare was accompanied by quasi-periodic pulsations (QPP) of both thermal and nonthermal hard X-ray emissions (HXR) observed by RHESSI in the 3 – 50 keV energy range. Analysis of the HXR time profiles in different energy channels made with the Lomb periodogram has indicated two statistically significant time periods of about 16 and 36 s. The 36 s QPP were observed only in the nonthermal HXR emission in the impulsive phase of the flare. The 16 s QPP were found in thermal and nonthermal HXR emission both in the impulsive and in the decay phases of the flare. Imaging analysis of the flare region, the determined time periods of the QPP, and the estimated physical parameters of the flare loops allowed us to interpret the observed QPP in terms of MHD oscillations excited in two spatially separated, but interacting systems of flaring loops.

Imaging Observations of Quasi-Periodic Pulsatory Nonthermal Emission in Two-Ribbon Solar Flares

I.V. **Zimovets** · A.B. Struminsky

Solar Phys (**2009**) 258: 69–88

Using RHESSI and some auxiliary observations we examine possible connections between the spatial and temporal structure of nonthermal hard X-ray (HXR) emission sources from the two-ribbon flares of **29 May 2003** and **19 January 2005**. In each of these events quasi-periodic pulsations (QPP) with time period of 1 – 3 minutes are evident in both hard X rays and microwaves. The sources of nonthermal HXR emission are situated mainly at the footpoints of the flare arcade loops observed by TRACE and the SOHO/EIT instrument in the EUV range. At least one of the sources moves systematically during and after the QPP phase in each flare. The sources move predominantly parallel to the magnetic inversion line during the 29 May flare and along flare ribbons during the QPP phase of both flares. By contrast, the sources start to show movement perpendicular to the flare ribbons with velocity comparable to that along the ribbons’ movement after the QPP phase. The sources of each pulse are localized in distinct parts of the ribbon during the QPP phase. The measured velocity of the sources and the estimated energy release rate do not correlate well with the flux of the HXR emission calculated from these sources. The sources of microwaves and thermal HXRs are situated near the apex of the flare loop arcade and are not stationary either. Almost all of the QPP as well as some pulses of nonthermal HXR emission during the post-QPP phase reveal soft – hard – soft spectral behavior, indicating separate acts of electron acceleration and injection. In our opinion at least two different flare scenarios based on the Nakariakov *et al.* (2006, *Astron. Astrophys.* **452**, 343) model and on the idea of current-carrying loop coalescence are suitable for interpreting the observations. However, it is currently not possible to choose between them owing to observational limitations.

Continuous Null-Point Magnetic Reconnection Builds Up a Torus Unstable Magnetic Flux Rope Triggering the X9.3 Flare in Solar Active Region~12673

Peng **Zou**, Chaowei Jiang, Fengsi Wei, Xueshang Feng, Pingbing Zuo, Yi Wang

ApJ **890** 10 **2020**

https://arxiv.org/pdf/2001.04633.pdf

https://doi.org/10.3847/1538-4357/ab6aa8

Two X-class solar flares occurred on **2017 September 6** from active region NOAA 12673: the first one is a confined X2.2 flare, and it is followed only ~3 hours later by the second one, which is the strongest flare in solar cycle 24, reaching X9.3 class and accompanied with a coronal mass ejection. Why these two X-class flares occurred in the same position with similar magnetic configurations, but one is eruptive while the other is not? Here we track the coronal magnetic field evolution via nonlinear force-free field extrapolations from a time sequence of vector magnetograms with high cadence. A detailed analysis of the magnetic field shows that a magnetic flux rope (MFR) forms and grows gradually before the first flare, and shortly afterwards, the MFR's growth is significantly enhanced with a much faster rise in height, from far below the threshold of torus instability to above it, while the magnetic twist only increases mildly. Combining EUV observations and the magnetic field extrapolation, we found that overlying the MFR is a null-point magnetic topology, where recurrent brightening is seen after the first flare. We thus suggest a scenario to interpret the occurrence of the two flares. The first flare occurred since the MFR reached a high enough height to activate the null point, and its continuous expansion forces the null-point reconnection recurrently. Such reconnection weakens the overlying field, allowing the MFR to rise faster, which eventually crosses the threshold of torus instability and triggers the second, eruptive flare.

A Two-Step Magnetic Reconnection in a Confined X-class Flare in Solar Active Region 12673

Peng **Zou**, Chaowei Jiang, Xueshang Feng, Pingbing Zuo, Yi Wang, Fengsi Wei

2019 ApJ 870 97

sci-hub.tw/10.3847/1538-4357/aaf3b7

https://arxiv.org/pdf/1811.09005.pdf

Solar flares are often associated with coronal eruptions, but there are confined ones without eruption, even for some X-class flares. How such large flares occurred and why they are confined are still not well understood. Here we studied a confined X2.2 flare in NOAA 12673 on **2017 September 6**. It exhibits two episodes of flare brightening with rather complex, atypical ribbons. Based on topology analysis of extrapolated coronal magnetic field, we revealed that there is a two-step magnetic reconnection process during the flare. Prior to the flare, there is a magnetic flux rope (MFR) with one leg rooted in a rotating sunspot. Neighboring to the leg is a magnetic null-point structure. The sunspot drives the MFR to expand, pushing magnetic flux to the null point, and reconnection is first triggered there. The disturbance from the null-point reconnection triggers the second reconnection, i.e., a tether-cutting reconnection below the rope. However, these two reconnections failed to produce an eruption, because the rope is firmly held by its strapping flux. Furthermore, we compared this flare with an eruptive X9.3 flare in the same region with 2 hours later, which has a similar MFR configuration. The key difference between them is that, for the confined flare, the MFR is fully below the threshold of torus instability, while for the eruptive one, the MFR reaches entirely above the threshold. This study provides a good evidence supporting that reconnection alone may not be able to trigger eruption, rather, MHD instability plays a more important role.

Continuum enhancements, line profiles and magnetic field evolution during consecutive flares

Francesca **Zuccarello**, Salvo L. Guglielmino, Vincenzo Capparelli, Mihalis Mathioudakis, Peter H. Keys, Serena Criscuoli, Mariachiara Falco, Mariarita Murabito

ApJ **889** 65 **2020**

https://arxiv.org/pdf/1912.00859.pdf

https://iopscience.iop.org/article/10.3847/1538-4357/ab621f/pdf

During solar flares, magnetic energy can be converted into electromagnetic radiation from radio waves to γ rays. Enhancements in the continuum at visible wavelengths give rise to white-light flares, as well as continuum enhancements in the FUV and NUV passbands. In addition, the strong energy release in these events can lead to the rearrangement of the magnetic field at the photospheric level, causing morphological changes in large and stable magnetic structures like sunspots. In this context, we describe observations acquired by satellite instruments (IRIS, SDO/HMI, Hinode/SOT) and ground-based telescopes (ROSA/DST) during two consecutive C7.0 and X1.6 flares occurred in active region NOAA 12205 on **2014 November 7**. The flare was accompanied by an eruption. The results of the analysis show the presence of continuum enhancements during the evolution of the events, observed both in ROSA images and in \textit{IRIS} spectra. In the latter, a prominent blue-shifted component is observed at the onset of the eruption. We investigate the role played by the evolution of the δ sunspots of the active region in the flare triggering, and finally we discuss the changes in the penumbrae surrounding these sunspots as a further consequence of these flares.

Continuum emission enhancements and penumbral changes observed during flares by IRIS, ROSA, and Hinode

F. **Zuccarello**, S.L. Guglielmino, V. Capparelli, M. Mathioudakis, P. Keys, L. Fletcher, S. Criscuoli, M. Falco, M. Murabito

Nuovo Cimento C as proceeding of the Third Meeting of the Italian Solar and Heliospheric Community **2019**

https://arxiv.org/pdf/1901.01732.pdf
In this paper we describe observations acquired by satellite instruments (Hinode/SOT and IRIS) and ground-based telescopes (ROSA@DST) during two consecutive C7.0 and X1.6 flares occurred in active region NOAA 12205 on **2014 November 7**. The analysis of these data show the presence of continuum enhancements during the evolution of the events, observed both in ROSA images and in IRIS spectra. Moreover, we analyze the role played by the evolution of the δ sunspots of the active region in the flare triggering, indicating the disappearance of a large portion of penumbra around these sunspots.

Vortex and Sink Flows in Eruptive Flares as a Model for Coronal Implosions

F. P. **Zuccarello**1,2,5, G. Aulanier2, J. Dudík3, P. Démoulin2, B. Schmieder2, and S. A. Gilchrist4
2017 ApJ 837 115
http://iopscience.iop.org.sci-hub.cc/0004-637X/837/2/115/
Eruptive flares are sudden releases of magnetic energy that involve many phenomena, several of which can be explained by the standard 2D flare model and its realizations in 3D. We analyze a 3D magnetohydrodynamics simulation, in the framework of this model, that naturally explains the contraction of coronal loops in the proximity of the flare sites, as well as the inflow toward the region above the cusp-shaped loops. We find that two vorticity arcs located along the flanks of the erupting magnetic flux rope are generated as soon as the eruption begins. The magnetic arcades above the flux rope legs are then subjected to expansion, rotation, or contraction depending on which part of the vortex flow advects them. In addition to the vortices, an inward-directed magnetic pressure gradient exists in the current sheet below the magnetic flux rope. It results in the formation of a sink that is maintained by reconnection. We conclude that coronal loop apparent implosions observed during eruptive flares are the result of hydromagnetic effects related to the generation of vortex and sink flows when a flux rope moves in a magnetized environment.

The transition from eruptive to confined flares in the same active region

F. P. **Zuccarello**, R. Chandra, B. Schmieder, G. Aulanier, R. Joshi
A&A 601, A26 **2017**
https://arxiv.org/pdf/1702.02477.pdf **File**
Solar flares are sudden and violent releases of magnetic energy in the solar atmosphere that can be divided in eruptive flares, when plasma is ejected from the solar atmosphere, resulting in a coronal mass ejection (CME), and confined flares when no CME is associated with the flare. We present a case-study showing the evolution of key topological structures, such as spines and fans which may determine the eruptive versus non-eruptive behavior of the series of eruptive flares, followed by confined flares, which are all originating from the same site. To study the connectivity of the different flux domains and their evolution, we compute a potential magnetic field model of the active region. Quasi-separatrix layers are retrieved from the magnetic field extrapolation. The change of behavior of the flares from one day to the next -eruptive to confined- can be attributed to the change of orientation of the magnetic field below the fan with respect to the orientation of the overlaying spine, rather than an overall change in the stability of the large scale field. Flares tend to be more-and-more confined when the field that supports the filament and the overlying field gradually become less-and-less anti-parallel, as a direct result of changes in the photospheric flux distribution, being themselves driven by continuous shearing motions of the different magnetic flux concentrations. **2014 April 15**
See **Introduction**

Vortex and sink flows in eruptive flares as a model for coronal implosions

Francesco P. **Zuccarello**, Guillaume Aulanier, Jaroslav Dudík, Pascal Démoulin, Brigitte Schmieder, Stuart A. Gilchrist
ApJ **2017**
https://arxiv.org/pdf/1702.00199v1.pdf
Eruptive flares are sudden releases of magnetic energy that involve many phenomena, several of which can be explained by the standard 2D flare model and its realizations in three-dimensions. We analyze a three-dimensional magnetohydrodynamics simulation in the framework of this model that naturally explains the contraction of coronal loops in the proximity of the flare sites, as well as the inflow towards the region above the cusp-shaped loops.
We find that two vorticity arcs located along the flanks of the erupting magnetic flux rope are generated as soon as the eruption begins. The magnetic arcades above the flux-rope legs are then subjected to expansion, rotation or contraction depending on which part of the vortex-flow advects them. In addition to the vortices, an inward-directed magnetic pressure gradient exists in the current sheet below the magnetic flux rope. It results in the formation of a sink that is maintained by reconnection.
We conclude that coronal loop apparent implosions observed during eruptive flares are the result of hydro-magnetic effects related to the generation of vortex- and sink-flows when a flux rope moves in a magnetized environment.

The X17.2 flare occurred in NOAA 10486: an example of filament destabilization caused by a domino effect:

F. **Zuccarello**, P. Romano, F. Farnik, M. Karlicky, L. Contarino, V. Battiato, S.═L. Guglielmino, M. Comparato and I. Ugarte-Urra
A&A 493 (2009) 629-637

Context. It is now possible to distinguish between two main models describing the mechanisms responsible for eruptive flares : the standard model, which assumes that most of the energy is released, by magnetic reconnection, in the region hosting the core of a sheared magnetic field, and the breakout model, which assumes reconnection occurs at first in a magnetic arcade overlaying the eruptive features.
Aims. We analyze the phenomena observed in NOAA 10486 before and during an X17.2 flare that occurred on 2003 October 28, to study the relationship between the pre-flare and flare phases and determine which model is the most suitable for interpreting this event.
Methods. We performed an analysis of multiwavelength data set available for the event using radio data (0.8–4.5 GHz), images in the visible range (WL and H^{α}), EUV images (1600 and 195 Å), and X-ray data, as well as MDI longitudinal magnetograms. We determined the temporal sequence of events occurring before and during the X17.2 flare and the magnetic field configuration in the linear force-free field approximation.
Results. The active region was characterized by a multiple arcade configuration and the X17.2 flare was preceded, by ~2 h, by the partial eruption of one filament. This eruption caused reconnection at null points located in the low atmosphere and a decrease in magnetic tension in the coronal field lines overlaying other filaments present in the active region. As a consequence, these filaments were destabilized and the X17.2 flare occurred.
Conclusions. The phenomena observed in NOAA 10486 before and during the X17.2 flare cannot be explained by a simple scenario such as the standard or breakout model, but instead in terms of a so-called domino effect, involving a sequence of destabilizing processes that triggered the flare.

Дифференциальная мера эмиссии солнечных нановспышек, определенная с помощью алгоритма SITES.

Белов С.А., Леденцов Л.С., Завершинский Д.И., Богачёв С.А.
СОЛНЕЧНО-ЗЕМНАЯ ФИЗИКА Том 10 № 2 , **2024** С. 4–14.
https://naukaru.ru/ru/storage/viewWindow/159165

В работе представлены результаты исследования возможностей алгоритма SITES (Solar Iterative Temperature Emission Solver) [Morgan, Pickering, 2019] для восстановления дифференциальной меры эмиссии (ДМЭ) источника по его излучению в нескольких участках электромагнитного спектра в контексте наблюдения солнечных нановспышек прибором AIA/SDO. Метод SITES был реализован на языке программирования Python и впервые был применен для построения ДМЭ нановспышек. С этой целью мы проверили эффективность работы алгоритма на модельных одно- и двухпиковых ДМЭ при температурах, характерных для солнечных нановспышек. Результаты тестирования говорят о том, что алгоритм SITES может быть ограниченно применим для исследования ДМЭ нановспышек в однопиковом приближении. Алгоритм обладает сочетанием хорошей точности и высокой скорости счета в исследуемой области температур от 1 до 3 МК. Особенности ДМЭ нановспышек, восстановленных методом SITES, были изучены на основе найденной нами ранее выборки из 58855 событий, наблюдавшихся в 2019 г. с помощью AIA/SDO. Полученные результаты подтверждают, что характерная температура плазмы в нановспышках составляет 1–2 МК. Восстановленные ДМЭ нановспышек, как правило, имеют один максимум внутри этого диапазона, однако полученное нами для всех вспышек распределение по температуре формирует два кластера с максимумами при 1.2 и 1.7 МК. Мы интерпретируем это как возможное свидетельство существования двух типов солнечных нановспышек, но данный результат требует дополнительного подтверждения.

ТЕМП ФОРМИРОВАНИЯ СОЛНЕЧНЫХ НАНОВСПЫШЕК В РАЗЛИЧНЫХ СПЕКТРАЛЬНЫХ ДИАПАЗОНАХ

Белов С.А., Завершинский Д.И., Богачев С.А., Леденцов Л.С.
АЖ Том: 100Номер: 12 Год: 2023 Страницы: 1322-1331
DOI: 10.31857/S0004629923120010

Частота и темп формирования солнечных нановспышек (НВ) измерены в 6 корональных спектральных диапазонах (094, 131, 171, 193, 211, 335 Å) и одном, относящимся к переходному слою (304 Å). Были использованы данные SDO/AIA, полученные в минимуме солнечной активности в мае 2019 г. Мы проанализировали одну и ту же область Солнца размером 360\textquotedblleft×720\textquotedblleft во всех каналах на протяжении интервала времени 1 ч. Для поиска НВ во всех спектральных диапазонах мы применили одинаковый алгоритм, основанный на анализе амплитуды быстрых уярчений на изображениях. Частота и темп НВ, как можно ожидать, существенно различаются в различных диапазонах. Для порога 5σ наибольшая частота НВ, 207 $с^{-1}$, измерена в канале 171 Å. Далее следуют спектральные диапазоны 193 Å (85% от канала 171 Å), 211 Å (74%) и 131 Å (63%). Мы не смогли достоверно измерить частоту в каналах 094 и 335 Å, но установили, что

она составляет менее 15% от частоты в канале 171 Å. В канале 304 Å мы обнаружили большое число уярчений, которые не имеют соответствия в короне. Тем не менее около 40% корональных НВ имеют соответствие в линии 304 Å, с порогом выше 5σ.

ЭЛЕКТРОСТАТИЧЕСКАЯ ТУРБУЛЕНТНОСТЬ В ПЕРЕПАДАХ ЭЛЕКТРОННОЙ ТЕМПЕРАТУРЫ СОЛНЕЧНОЙ АТМОСФЕРЫ

БЕСПАЛОВ П.А.1, САВИНА О.Н

ПАЖ Том: 41Номер: 10 Год: **2015** Страницы: 651

Обсуждается связь процессов образования и свойств переходного слоя солнечной атмосферы, характеризующегося резким градиентом электронной температуры, с электростатической турбулентностью, обеспечивающей высокую эффективную частоту соударений электронов и низкую теплопроводность среды. Получена простая зависимость величины шумового электрического поля в переходном слое от эффективной частоты соударений. Для трубки относительно слабого магнитного поля, проходящей из хромосферы в корону, на основе известных экспериментальных моделей солнечной атмосферы оценен высотный ход теплопроводности и величина шумовых электрических полей.

РАСПРЕДЕЛЕНИЕ НАНОВСПЫШЕК В МИНИМУМЕ СОЛНЕЧНОЙ АКТИВНОСТИ

БОГАЧЁВ С. А.[*1]

ГиА Том: 63Номер: 4 Год: 2023 Страницы: 488-495

Мы используем данные телескопа Atmospheric Imaging Assembly (AIA) на космическом аппарате Solar Dynamics Observatory (SDO) в канале 171 Å, чтобы исследовать пространственное распределение вспышек малой энергии (нановспышек). Мы исследовали два периода: 20.05.2019 с 12:00 UT до 13:00 UT и 10.05.2020 с 12:00 UT до 13:00 UT. Всего нами было найдено 87 974 нановспышки со средним темпом формирования 6.0×10^{-21} см$^{-2}$ с$^{-1}$. Для солнечных широт от 0° до 50° темп формирования нановспышек является примерно равномерным со среднеквадратичным отклонением около 25%. Нами обнаружена асимметрия в темпе формирования нановспышек в южном и северном полушариях Солнца: темп формирования нановспышек в южном полушарии был на 34–42% больше, чем в северном. В этот период такая же асимметрия наблюдалась и для обычных вспышек. Мы также обнаружили слабую зависимость темпа формирования нановспышек от солнечного цикла: число нановспышек растет при более высокой активности Солнца.

ИЗМЕРЕНИЕ ЭНЕРГЕТИЧЕСКОГО РАСПРЕДЕЛЕНИЯ НАНОВСПЫШЕКМАЛОЙ МОЩНОСТИ

Богачёв С.А., Ерхова Н.Ф.

СЗФ Том: 9Номер: 1 Год: **2023** Страницы: 3-9

https://elibrary.ru/download/elibrary_50417067_38172738.pdf

В работе предложен метод измерения энергетического распределения вспышек малой энергии (нановспышек) в области ниже 10^{23} эрг. В качестве примера измерен спектр нановспышек в области 10^{21}-10^{26} эрг для двух участков спокойной короны Солнца, наблюдавшихся телескопом SDO/AIA в канале 171 Å в мае 2019 г. Показано, что спектр нановспышек является степенным в области энергий 10^{22}-10^{26} эрг. Наклон спектра в этой области является постоянным, т. е. не зависит от энергии. Ниже 10^{22} эрг начинается завал спектра. Для энергий менее 10^{21} эрг метод не дает статистически значимых результатов из-за высоких погрешностей. Результаты исследования указывают, что солнечные нановспышки могут быть обнаружены вплоть до энергий 10^{21}-10^{22} эрг. Ранее сообщалось об измерениях спектра только в области 10^{23} эрг и выше. Полный поток энергии нановспышек в области выше 10^{22} эрг для исследованных участков короны составил P »$2 \cdot 10^4$ эрг·см$^{-2}$·с$^{-1}$, что примерно в 15 раз меньше, чем требуется для полной компенсации тепловых потерь короны. **20 мая 2019**

Effect of Coulomb collisions on the particle acceleration in collapsing magnetic traps .

С. А. **Богачев,** Б. В. Сомов,

Письма в АЖ, 35, 63 (**2009**). **File.**

Abstract The problem of particle acceleration in collapsing magnetic traps in the solar corona has been solved by taking into account the particle scattering and braking in the high-temperature plasma of solar flares. The Coulomb collisions are shown to be weak in traps with lifetimes t l < 10 s and strong for t l > 100 s. In the approximation of strong collisions, collapsing magnetic traps are capable of confining up to 20% of the injected particles in the corona for a long time. In the collisionless approximation, this value exceeds 90%. The question about the observational manifestations of collisions is examined. For collision times comparable to t l , the electron spectrumat energies above 10 keV is shown to be a double-power-law one. Such spectra were found by the RHESSI satellite in flares.

ПОСТРОЕНИЕ СВЕТОВЫХ КРИВЫХ СОЛНЕЧНЫХ ВСПЫШЕК В ЛИНИИ Hα

БОРОВИК А.В.1, КОНЯЕВ П.А.2, ЖДАНОВ А.А.1

Г и А Том: 56Номер: 5 Год: **2016** Страницы: 547-557
Представлены результаты исследования ряда факторов, влияющих на построение световых кривых солнечных вспышек в линии Hα. Установлено, что вид световой кривой зависит от способа измерения интенсивности, размера окна измерений, колебаний яркости участков спокойной хромосферы (реперных областей). Реальную картину развития вспышечного процесса показывают световые кривые, построенные по максимальной интенсивности вспышки. Предложен метод отбора “реперных областей”.

РАСПРЕДЕЛЕНИЕ СОЛНЕЧНЫХ ВСПЫШЕК МАЛОЙ МОЩНОСТИ ПО ВРЕМЕНИ ПОДЪЕМА ЯРКОСТИ К МАКСИМУМУ

БОРОВИК А.В.1, ЖДАНОВ А.А.1

СОЛНЕЧНО-ЗЕМНАЯ ФИЗИКА Том: 4Номер: 3 Год: **2018** Страницы: 5-16
По сообщениям международного вспышечного патруля за 1972-2010 гг. сформирована электронная база данных, включающая параметры более 123 тысяч солнечных вспышек в линии Hα. Для классов площади и баллов вспышек определены средние продолжительности флэш-фаз. Показано, что с ростом класса площади время подъема яркости вспышек к максимуму увеличивается. Для классов яркости эта тенденция проявляется в более слабой форме. Самые короткие флэш-фазы имеют вспышки взрывного типа и вспышки с единственным центром повышенной яркости внутри вспышечной области, самые продолжительные - двухленточные вспышки и вспышки, демонстрирующие несколько максимумов интенсивности. Выделено 572 случая со временами подъема более 60 мин. Большинство (80 %) таких сверхпродолжительных вспышек имеют более короткую главную фазу. Установлено, что вспышки малой мощности с точки зрения особенностей развития не отличаются от крупных. Они так же, как и мощные вспышки, сопровождаются активизацией и исчезновением волокон, могут иметь взрывную фазу и многократные всплески интенсивности. Среди малых встречаются такие, которые покрывают тени солнечных пятен, а также двухленточные и белые вспышки.

Динамика жесткого рентгеновского, гамма- и микроволнового излучения солнечных вспышек, продуцированных активной областью 0069 в августе 2002 г.

А. В. **Богомолов**, Л. К. Кашапова, И. Н. Мягкова, Ю. Т. Цап
Астрономический журнал , 91(3), **2014**, С. 211-222
Проведен поиск закономерностей в изменении характеристик вспышечного солнечного излучения по мере развития активной области NOAA 0069 в период с **14 по 24 августа 2002** г. Прибором СОНГ (Солнечные Нейтроны и Гамма-кванты), установленным на борту российской солнечной обсерватории КОРОНАС-Ф, было зарегистрировано жесткое рентгеновское и гамма-излучение во время 9 из 30 вспышек класса выше C5, произошедших в данной активной области в указанный период времени. Было получено, что по мере развития данной активной области наблюдалась тенденция к нарастанию потока рентгеновского и гамма-излучения в максимумах вспышек, а также к уменьшению показателя спектра жесткого рентгеновского излучения, причем вспышки с более жестким спектром излучения происходили в тени пятна, т.е. в области наиболее сильных магнитных полей.

Динамика мелкомасштабных магнитных полей перед малыми и крупными солнечными вспышками.

Боровик А.В., Жданов А.А.
СОЛНЕЧНО-ЗЕМНАЯ ФИЗИКА Том 9 № 4 , 2023 С. 44–53
https://naukaru.ru/ru/storage/viewWindow/138049
По данным наблюдений SDO (Solar Dynamics Observatory) исследовалась динамика продольного магнитного поля активной области (АО) NOAA 12673. За время прохождения АО по диску Солнца пятна и фоновые поля в ней показывали сложные траектории движения, при этом наблюдалось образование многочисленных короткоживущих локальных мелкомасштабных линий раздела полярностей (ЛЛРП), которые формировались при появлении в АО новых магнитных потоков и их сближении с полями противоположной полярности. Протяженность таких ЛЛРП составляла менее 15000 км (~20 угл. сек), время существования — несколько часов. Исследование вспышечной активности NOAA 12673 показало, что вспышки малой мощности (оптический класс S, площадь <2 кв. град) обычно происходят вблизи ЛЛРП. Перед малыми вспышками, а также перед крупной вспышкой **06.09.2017** (оптический балл 3B, рентгеновский класс X9.3) на ограниченных участках локальных и главной ЛРП АО наблюдались сдвиговые напряжения магнитного поля и рост gradH: в области вспышек малой мощности — до значений 1.3–1.5 Гс/км, в области крупной вспышки — 3–3.5 Гс/км. Полученные результаты свидетельствуют о том, что перед малыми и крупными вспышками продольное магнитное поле ведет себя аналогичным образом.

СОЛНЕЧНЫЕ ВСПЫШКИ МАЛОЙ МОЩНОСТИ В ЛИНИИ H_α : РЕЗУЛЬТАТЫ ИССЛЕДОВАНИЙ

Боровик А.В.

Изв. КрАО Том: 119 Номер: 1 Год: 2023 Страницы: 27-41

В работе обобщаются результаты многолетних исследований вспышек малой мощности в линии Hα (оптический класс S), полученные с использованием данных международного вспышечного патруля, наблюдательных материалов в линии 6563 Å Байкальской астрофизической обсерватории ИСЗФ СО РАН и телескопов GONG, наблюдений обсерваторий SDO, SOHO и Kitt Peak. В результате проведенных исследований получены уточненные, статистически достоверные и наиболее полные на сегодняшний день данные о пространственно-временных параметрах солнечных вспышек, оценена их полная энергия в оптическом диапазоне длин волн. Установлено, что вспышки малой мощности (малые вспышки) образуют на Солнце плотные скопления - центры вспышечной активности (ЦВА), связанные с областями всплывающих магнитных потоков. Обнаружено, что такие вспышки возникают вблизи локальных мелкомасштабных короткоживущих линий раздела полярности (ЛЛРП) продольного магнитного поля. Одной из выявленных закономерностей возникновения малых вспышек является возрастание градиента магнитного поля на отдельных участках ЛЛРП в области вспышки. Продолжительность роста составляет от 40 минут до 1.5 часов. Максимального градиента (1.3-1.5 Гс/км) магнитное поле достигает на момент возникновения вспышки. Результаты исследования показывают, что вспышки малой мощности обладают схожими с крупными вспышками сценариями развития: сопровождаются активизациями и эрупцией волокон, имеют взрывную фазу, сопровождаются излучением разной мощности в рентгеновском и радиодиапазонах, потоками протонов. Среди них встречаются вспышки, покрывающие тени солнечных пятен, двухленточные и белые вспышки. Полученные результаты могут быть использованы для диагностики нестационарных процессов на Солнце, прогноза солнечной активности и геоэффективных солнечных событий.

Малые солнечные вспышки и локальные линии раздела полярности продольного магнитного поля активной области.

Боровик А. В., Жданов А. А.

СОЛНЕЧНО-ЗЕМНАЯ ФИЗИКА Том 8. **2022**. № 1 С. 19-23.
https://naukaru.ru/ru/storage/viewWindow/87252

По фотосферным данным и данным о продольном магнитном поле со спутника SDO, а также по наблюдениям в линии Hα на наземных станциях GONG исследована вспышечная активность группы солнечных пятен NOAA 12673, которая в сентябре 2017 г. произвела крупнейшую за последнее десятилетие вспышку класса X9.3. Активная область отличалась бурным развитием и сложными топологией и динамикой магнитного поля. Установлено, что в активной области на протяжении практически всего времени развития вследствие движений разнополярных магнитных потоков и их сближений происходило формирование многочисленных локальных линий раздела полярностей (ЛЛРП) магнитного поля. Обнаружено, что малые солнечные вспышки тесным образом связаны с ЛЛРП и возникают на тех участках ЛЛРП, где градиент продольного магнитного поля со временем достигает максимальных значений. **3-4 Сент 2017**

СОЛНЕЧНЫЕ ВСПЫШКИ МАЛОЙ МОЩНОСТИ В ОПТИЧЕСКОМ И РЕНТГЕНОВСКОМ ДИАПАЗОНАХ ДЛИН ВОЛН В 21-24-М СОЛНЕЧНЫХ ЦИКЛАХ

БОРОВИК А.В.1, ЖДАНОВ А.А.1

СОЛНЕЧНО-ЗЕМНАЯ ФИЗИКА Том: 6Номер: 3 Год: **2020** Страницы: 18-25

По данным в оптическом и рентгеновском диапазонах длин волн проанализирована вспышечная активность Солнца за 21-24-й циклы. Показано, что на протяжении последних четырех циклов активность Солнца постепенно снижалась. По отношению к 21-му циклу (самому активному за последние 50 лет) в 24-м цикле произошло в 4.4 раза меньше оптических крупных вспышек классов площади 2-4, в 8.2 раза меньше вспышек класса 1 и в 4.1 раза меньше малых вспышек (MB) оптического класса S. Число вспышек рентгеновского класса X уменьшилось в 3.7 раз, класса M - в 3.2 раза. Это подтверждает влияние вековых трендов активности Солнца на пиковые значения вспышечной активности в одиннадцатилетних циклах. Показано, что оптические вспышки малой мощности могут сопровождаться потоками протонов и всплесками рентгеновского излучения разной мощности, в том числе класса X. В мягком рентгене диапазоны излучения для оптических MB и вспышек высоких классов в значительной степени перекрываются. Подтверждено, что рентгеновское излучение солнечных вспышек возникает в среднем на 2 мин раньше оптического. Для оптических MB и вспышек класса 1 максимум излучения в рентгеновском диапазоне наступает позже максимума излучения в оптическом диапазоне примерно на 1 мин, для вспышек классов 2-4 - на 2 мин.

Процессы энерговыделения в солнечных вспышках малой мощности.

Боровик А.В., Жданов А.А.

СОЛНЕЧНО-ЗЕМНАЯ ФИЗИКА Том 5 Номер 4 С. 3–11. **2019**
https://naukaru.ru/ru/storage/viewWindow/43508

По данным международного вспышечного патруля за 1972–2010 гг. [http://www.ngdc. noaa.gov/stp/space-weather/solar-data/solar-features/so-lar-flares/] выполнены статистические исследования малых солнечных вспышек (класс площади S). Установлена высокая корреляционная зависимость между продолжительностью вспышек и временем подъема яркости к максимуму. Получены новые данные по относительным временам подъема яркости (отношение времени подъема к общей продолжительности вспышки). Установлено, что

распределения Тотн малых солнечных вспышек содержат ряд максимумов с наиболее значимыми 0.2, 0.25, 0.33 и 0.5. При переходе от вспышек низких оптических классов к более крупным вспышкам максимумы постепенно исчезают. Получены распределения солнечных вспышек по энергии в оптическом диапазоне длин волн, свидетельствующие о том, что интервалы энергий вспышек разного класса площади в значительной степени перекрываются. До 9.5 % малых вспышек попадает в интервал энергий крупных солнечных вспышек (класс площади 2–4). Еще более значительное перекрытие — со вспышками класса площади 1.

Статистические исследования солнечных вспышек малой мощности.

Боровик А.В., Жданов А.А.
СОЛНЕЧНО-ЗЕМНАЯ ФИЗИКА Том 4 Номер 2 **2018**
https://naukaru.ru/ru/nauka/article/19917/view
Работа является продолжением серии работ, посвященных исследованию временных параметров солнечных вспышек в линии Hα. По данным международного вспышечного патруля за период 1972–2010 гг. определены средние продолжительности вспышек различных баллов и классов пло-щади. Установлено, что 94.6 % вспышек имеют продолжительность не более 60 мин. Для 90 % вспышек с мин время жизни составляет 2.1–3.3 ч. В редких случаях вспышки могут существовать порядка 12 ч. Время жизни мощных солнечных вспышек не превышает 8.3 ч. Установлено, что продолжительности солнечных вспышек зависят от особенностей их развития. Самые короткие времена жизни имеют вспышки с одним центром повышенной яркости внутри вспышечной области, самые продолжительные — двухленточные вспышки и вспышки, демонстрирующие несколько всплесков интенсивности. Подтверждено, что с увеличением класса площади и яркости вспышек их продолжительность увеличивается.

СТАТИСТИЧЕСКИЕ ИССЛЕДОВАНИЯ СОЛНЕЧНЫХ ВСПЫШЕК МАЛОЙ МОЩНОСТИ. РАСПРЕДЕЛЕНИЯ ВСПЫШЕК ПО ПЛОЩАДИ, ЯРКОСТИ И БАЛЛАМ

Боровик А.В., Жданов А.А.
СОЛНЕЧНО-ЗЕМНАЯ ФИЗИКА Том: 3Номер: 1 Год: **2017** С. 34-45
Создана электронная база данных для 123801 солнечных вспышек, произошедших на Солнце с 1972 по 2010 гг. Основу составили каталоги Solar Geophysical Data (SGD) и квартального бюллетеня (Quarterly Bulletin on Solar Activity). С помощью разработанного пакета программ проведена предварительная статистическая обработка данных. Первые результаты позволили выявить ряд новых особенностей в распределении параметров солнечных вспышек, отличных от полученных ранее. Установлено, что более 90 % всех происходящих на Солнце вспышек имеют малую мощность. Самый многочисленный класс составляют вспышки балла SF (64 %). Вспышечная активность показывает хорошо выраженную цикличность и высокую корреляцию с числами Вольфа. Самые высокие коэффициенты корреляции имеют вспышки классов площади S и 1. Существует также высокая корреляция между отдельными классами вспышек: S и 1, 1 и (2-4). Полученные ранее [Mitra et al., 1972] результаты, свидетельствующие о превалировании на Солнце вспышек балла SN (47 %) и существовании значимых пиков в распределении для вспышек баллов SN и 1N, не подтвердились. Распределение числа солнечных вспышек с ростом оптического балла имеет плавный спад без существенных отклонений. С ростом оптического балла происходит постепенное перераспределение вспышек в сторону увеличения класса яркости. Большее число вспышек баллов SN и 1N, присутствующее на распределениях [Mitra et al., 1972], по всей вероятности, связано с недостаточной статистикой.

ВОЗНИКНОВЕНИЕ ЖЕСТКОГО РЕНТГЕНОВСКОГО ИЗЛУЧЕНИЯ ПРИ СЛАБЫХ НЕСТАЦИОНАРНЫХ ПРОЦЕССАХ В АКТИВНЫХ ОБЛАСТЯХ

Выборнов В.И. 1 , Григорьева И.Ю. 2 , Лившиц М.А. 1 , Иванов Е.Ф. 3
«Солнечная и солнечно-земная физика – **2014**», Санкт-Петербург, Пулково, 20 – 24 октября
Стр. 91-94
http://www.gao.spb.ru/russian/publ-s/conf_2014/conf_2014.pdf
We investigate solar A7-C6 flares, accompanied by the X-rays with energies E > 30keV, registered on the Suzaku satellite. Most events with hard X-rays arise in groups with a spot area of S > 500 mvh, a significant part of them develops during the decay phase of the powerful events and near the solar limb. As an example of events occurred on the disk, we examined flares on **17.11.05 and 19.05.07**. Due to the joint analysis of X-ray (Suzaku), microwaves (RATAN-600, SSRT) and magnetic field data (SOHO/MDI, SOT/Hinode) we are localized the sources of emission with a power-law spectrum with E > 30keV. These sources are situated apparently near to a small region of particle acceleration in these weak flares. We found new source in the polarized microwaves which is associated with acceleration and located over the neutral line in the region of high magnetic field strengths. Particles are accelerated more effectively when in this small region the new magnetic field emerges.

НАБЛЮДЕНИЯ МОЩНОЙ ВСПЫШКИ 27 ОКТЯБРЯ 2002 Г., ПРОИЗОШЕДШЕЙ НА ОБРАТНОЙ СТОРОНЕ СОЛНЦА

Выборнов В.И., Лившиц М.А., Кашапова Л.К., Митрофанов И.Г., Головин Д.В., Козырев А.С., Литвак М.Л., Санин А.Б., Третьяков В.И., Бойнтон В., Шинохара К., Хамара Д.
АЖ, 89(10), 888, **2012**
Анализируются результаты наблюдений мощной солнечной вспышки 27 октября 2002 г. в жесткой рентгеновской области и микроволновом диапазоне. Вспышка наблюдалась с околомарсианской орбиты аппаратурой HEND, разработанной в ИКИ РАН и установленной на космическом аппарате Mars-Odyssey. Хотя для земного наблюдателя эта мощная вспышка наблюдалась далеко за восточным лимбом Солнца, связанный с ней протяженный источник зарегистрирован RHESSI в области энергий до примерно 60 кэВ. Эруптивное событие наблюдалось в микроволновом диапазоне на обсерватории Nobeyama. По характеристикам рентгеновского излучения находится спектр электронов, ответственных за рассматриваемые излучения в рамках толстой мишени для наблюдений с околомарсианской и тонкой мишени – с околоземной орбиты. Выводы сопоставляются с результатами микроволновых наблюдений. Обсуждаются условия распространения электронов в солнечной короне.

Метод обнаружения нового магнитного потока на основе его скейлинговых свойств – **Головко** А.А., Салахутдинова И.И.
Солнечно-земная физика, **2014**

Вспышечная активность на Солнце и особенности выхода новых магнитных потоков в 2011-2013 гг.
А.А.**Головко**
ИКИ-**2014**, Сессия: Солнце
http://plasma2014.cosmos.ru/presentations
Периоды усиления вспышечной активности в течение 2011-2013 гг. соответствуют интервалам аномального поведения фотосферного магнитного поля, когда новый магнитный поток одной полярности увеличивается, в то время как поток противоположной полярности уменьшается.
Обнаруженный факт можно объяснить выходом новых порций крупномасштабного магнитного поля и их взаимодействием со старым магнитным полем.

А.А.**Головко,** И.И.Салахутдинова, АЖ, Т. 89, С. 458, **2012**

РАДИОИЗЛУЧЕНИЕ СОЛНЕЧНОЙ ВСПЫШКИ 12.02.2010 г. И РЕЖИМЫ УСКОРЕНИЯ ЭЛЕКТРОНОВ
Р. В. **Горгуца**1, В. А. Ковалев1, И. Г. Костюченко2, А. К. Маркеев1, Д. Е. Соболев1, В. В. Фомичев
ГЕОМАГНЕТИЗМ И АЭРОНОМИЯ, **2015**, том 55, № 3, с. 1–5
При анализе данных наблюдений радиовсплесков, полученных в ИЗМИРАН с помощью спектро_ графов метрового диапазона и радиометров на фиксированных частотах, использован дифферен_ циальный метод, с помощью которого обнаружено двухступенчатое (быстрое + медленное по срав_ нению с экспоненциальным законом) поведение потоков радиоизлучения на фазах возрастания и спада. Показано, что наблюдаемый быстрый режим возрастания потока на частоте 3013 МГц, со_ провождаемый уменьшением временно&го масштаба, может быть связан с быстрым режимом уско_ рения электронов, ответственных за магнитотормозное излучение вспышки в микроволновом диа_ пазоне.

МНОГОВОЛНОВЫЕ НАБЛЮДЕНИЯ ВСПЫШКИ 10 МАЯ 2012: УСКОРЕНИЕ ЧАСТИЦ И ВСПЛЫТИЕ МАГНИТНОГО ПОЛЯ
Григорьева И.Ю.1, Кузнецов А.А.2, Мешалкина Н.С.2, Мышьяков И.И.2
Пулково «Солнечная и солнечно-земная физика – **2015**», с.99
We present a study of the dynamics of a GOES M5.7 class flare, which occurred on 10 May 2012 in NOAA 11476, in a small group of spots near the neutral line of the local magnetic field. The properties of the hard X-ray (HXR) and microwave (MW) radiation associated with this flare are analyzed. The HXR spectra are constructed according to the Space Telescope Konus-WIND and RHESSI. Detailed analysis of one-dimensional SSRT observations (5.7 GHz) and NoRP polarimeters is made. Two-dimensional radio images (SSRT and NoRH) are reconstructed. The LOS-magnetogram (SDO / HMI) detected the emergence of a new magnetic flux in a small region adjacent to the north-west of one of the EUV flare activity centers (according to SDO / AIA). Comprehensive analysis shows that the increase in the MW radiation and in the HXR occurred almost simultaneously. Two polarized MW bursts with different

properties are registered. The second burst was accompanied by appearance of a HXRsource (with energies up to 100 keV) in the loop top. We estimate the changes in the magnetic flux associated with the emergence of a new field with opposite polarity. These results directly suggest a link between the development of non-stationary processes (such as the current amplification and highly efficient particle acceleration) with the magnetic flux emergence. Such dramatic effects usually do not occur near the neutral line, but only in the events associated with large sunspots (like in powerful flares on 14 July 2000 and 20 May 2005).

НАБЛЮДЕНИЯ ЖЕСТКОГО РЕНТГЕНОВСКОГО ИЗЛУЧЕНИЯ СЛАБЫХ ВСПЫШЕК
И.Ю. **Григорьева**, М.А. Лившиц
ИКИ-**2014**, Сессия: Солнце
http://plasma2014.cosmos.ru/presentations
В некоторых слабых вспышках наблюдаются фотоны со степенным дифференциальным спектром в области 50-200 кэВ.
В активных областях, где развиваются эти вспышки B-C баллов, в дополнении к микроволновому источнику над пятном формируется источник поляризованного излучения с обратным знаком поляризации.
Для проанализированных случаев показано, что нагрев плазмы и ускорение электронов связаны с процессом всплытия нового магнитного поля в близи линии раздела полярности.
В предположении нелинейных бессиловых полей в короне всплытие магнитного поля приводит к накоплению свободной энергии на низких высотах хромосфы. И изменения в системе токов активной области приводит к слабым вспышечным процессам. В этой модели, полученные выше результаты, свидетельствуют об ускорении частиц в мелкомасштабных элементах.

ЭВОЛЮЦИЯ АКТИВНЫХ ОБЛАСТЕЙ НА СОЛНЦЕ: ВЫЯВЛЕНИЕ НОВОГО МАГНИТНОГО ПОЛЯ МЕТОДОМ МУЛЬТИФРАКТАЛЬНОГО СЕГМЕНТИРОВАНИЯ

ГОЛОВКО А.А.1, САЛАХУТДИНОВА И.И
АЖ Том: 92Номер: 8 Год: **2015** Страницы: 650

Идентификация новых магнитных потоков методом мультифрактального сегментирования применена для изучения закономерностей эволюции активных областей и комплексов активности. Использованы магнитограммы SOLIS, MDI SOHO и SOT Hinode. По наблюдениям активной области **26-28 октября 2003** г. № 10488 по каталогу данных NOAA обнаружена значительная вариабельность участков нового магнитного потока с характерным временем 1-2 ч. Уширение мультифрактального спектра в участках магнитограмм, соответствующих новому магнитному потоку, обусловливает его визуализацию на сегментированных мультифрактальных изображениях, соответствующих минимальным фрактальным размерностям. По данным за 2010-2014 гг. исследованы некоторые закономерности выхода новых магнитных потоков в 24-м солнечном

цикле. На всех этапах развития цикла преобладает положительная корреляция временн х вариаций площади новых магнитных потоков N- и S-полярности. Постепенное убывание коэффициента корреляции от 2010 к 2014 гг. можно объяснить прогрессирующим усложнением связей между активными областями, приводящим к кластеризации их в комплексы активности.х вариаций площади новых магнитных потоков N- и S-полярности. Постепенное убывание коэффициента корреляции от 2010 к 2014 гг. можно объяснить прогрессирующим усложнением связей между активными областями, приводящим к кластеризации их в комплексы активности.

Григорьева И.Ю., Струминский А.Б., Шаховская А.Н. **О наблюдательных свидетельствах перестройки магнитной конфигурации активных областей в тепловом/нетепловом излучении, связанном с солнечными вспышками X7.1 20.01.05, M5.1 17.05.12**
Сборник трудов XXVI Всероссийской ежегодной конференции по физике Солнца «Солнце и солнечно-земная физика – 2022» ГАО РАН.
http://www.gaoran.ru/russian/solphys/2022/book/conf2022.pdf

Активные области минимума прошедшего солнечного цикла: связь нагрева плазмы с электрическими токами
И. Ю. **Григорьева**, М. А. Лившиц, Г. В. Руденко, И. И. Мышьяков
Астрономический журнал, 90(8) - **2013**, С. 665-675
Проанализирована совокупность данных о небольших активных областях (АО) на Солнце за три года (2007–2009 гг.). Показано, что в очень спокойных условиях (при низком уровне рентгеновского фона) форма корональных петель некоторых АО достаточно хорошо соответствует ходу силовых линий, вычисленному в

потенциальном приближении. Это относится к нескольким АО (например, к группе 10999 в июне 2008 г.), где вспышки мощнее B3 вообще не наблюдались. Микроволновое излучение этой АО, зарегистрированное на РАТАН-600, было очень слабым и поляризация фактически отсутствовала. В большинстве групп наблюдались субвспышки. На примере группы 10933 (январь 2007 г.) продемонстрировано, что для таких АО характерно возрастание мягкого рентгеновского излучения от нескольких до десяти раз, одновременно с некоторым увеличением потока микроволнового излучения. При этом к северо-западу от основного пятна АО 10933 развивается источник с противоположным направлением поляризации. Серия магнитограмм SOHO/MDI (а также Hinode) показывает, что перед развитием этого поляризованного источника происходит всплытие нового магнитного поля, продолжающееся несколько часов 8 января 2007 г. С использованием наблюдений полного вектора магнитного поля (данные Hinode) и метода нелинейной экстраполяции бессиловых магнитных полей получена оценка плотности тока на поверхностях, располагающихся на различных высотах. Проинтегрированный по высоте ток существенно усилен в двух узлах над нейтральной линией поля вблизи места основного всплытия поля. Таким образом, подтверждается то, что всплытие нового магнитного поля является основным фактором эволюции АО на всех стадиях их существования. Развитие этих представлений может помочь в выяснении взаимосвязи между усилением токов, нагревом плазмы и ускорением частиц, как в слабых АО, так и в мощных комплексах активности.

УСКОРЕНИЕ ЭЛЕКТРОНОВ В МАГНИТНЫХ ЛОВУШКАХ СОЛНЕЧНОЙ ВСПЫШКИ: МОДЕЛЬНЫЕ СВОЙСТВА И ИХ НАБЛЮДАТЕЛЬНЫЕ ПОДТВЕРЖДЕНИЯ

ГРИЦЫК П.А.1, СОМОВ Б.В.1

ПАЖ Том: 43Номер: 9 Год: **2017** Страницы: 676

С помощью аналитического решения кинетического уравнения мы исследовали модельные свойства коронального и хромосферного источников жесткого рентгеновского излучения в лимбовой вспышке **19 июля 2012** г. В приближении толстой мишени с обратным током мы рассчитали спектр излучения в основаниях вспышечной петли и показали, что он согласуется с наблюдаемым. Спектр коронального источника, расположенного над вспышечной петлей, рассчитан в приближении тонкой мишени. При этом показатель наклона спектра жесткого рентгеновского излучения воспроизводится очень точно, но интенсивность коронального излучения в несколько раз ниже наблюдаемой. Ранее нами было показано, что это противоречие полностью устраняется, если учесть дополнительное (относительно первичного ускорения в пересоединяющем токовом слое) ускорение электронов в корональной магнитной ловушке, которая сжимается в поперечном направлении и уменьшается по длине во время импульсной фазы вспышки. В настоящей статье мы детально исследуем данный эффект в контексте более реалистичного сценария вспышки, когда за время всплеска в жестком рентгеновском диапазоне существовал целый ансамбль ловушек, каждая из которых находилась на разных этапах своей эволюции: формирование, коллапс, уничтожение. Полученные в работе результаты указывают не только на существование ускорения Ферми первого порядка и бетатронного нагрева электронов в солнечных вспышках, но и на высокую их эффективность. На примере высокоточных наблюдений конкретной вспышки предсказанные ранее теоретические особенности модели находят убедительные подтверждения.

АНАЛИТИЧЕСКАЯ МОДЕЛЬ РАСПРОСТРАНЕНИЯ ТЕПЛОВЫХ УБЕГАЮЩИХ ЭЛЕКТРОНОВ В СОЛНЕЧНЫХ ВСПЫШКАХ

ГРИЦЫК П.А.1, СОМОВ Б.В.1

ПАЖ Том: 45Номер: 4 Год: **2019** Страницы: 279-289

Природа жесткого рентгеновского излучения солнечных вспышек хорошо известна. Наблюдаемое излучение как в короне, так и в хромосфере состоит из двух компонент: нетепловой и тепловой. Нетепловая компонента обусловлена тормозным излучением ускоренных электронов, тепловая - тормозным излучением нагретых электронов плазмы. Вследствие того, что спектры нетеплового и теплового жесткого рентгеновского излучения частично перекрываются, их корректная интерпретация напрямую зависит от точности кинетических моделей, описывающих распространение в атмосфере Солнца убегающих электронов тепловой и нетепловой природы. Эволюция функции распределения последних, т.е. электронов, ускоренных в области магнитного пересоединения, точно описывается в приближении современных моделей толстой мишени с обратным током. В настоящей работе рассмотрена модель теплового убегания электронов и найдено аналитическое решение соответствующего кинетического уравнения, в котором учтены кулоновские столкновения. Сделаны оценки степени поляризации излучения, которая не превышает $\sim 5\%$. Полученная функция распределения может быть также использована для расчета спектра теплового рентгеновского излучения и, как следствие, интерпретации наблюдений тепловой компоненты в рентгеновском спектре вспышки.

РЕНТГЕНОВСКОЕ И МИКРОВОЛНОВОЕ ИЗЛУЧЕНИЕ СОЛНЕЧНОЙ ВСПЫШКИ 19 ИЮЛЯ 2012 ГОДА: ВЫСОКОТОЧНЫЕ НАБЛЮДЕНИЯ И КИНЕТИЧЕСКИЕ МОДЕЛИ

ГРИЦЫК П.А.1, СОМОВ Б.В.1

ПАЖ Том: 42Номер: 8 Год: **2016** Страницы: 586

Солнечная вспышка класса M7.7 **19 июля 2012** г. в 05:58 UT наблюдалась с высоким пространственным, временным и спектральным разрешением в жестком рентгеновском и оптическом диапазонах. Вспышка имела место на краю солнечного диска, что позволило увидеть относительное расположение коронального и хромосферного источников рентгеновского излучения, определить их спектры. Для объяснения наблюдений коронального и незакрытого солнечным лимбом хромосферного источников мы применяем аккуратную аналитическую модель кинетического поведения ускоренных электронов во вспышке. Хромосферный источник жесткого рентгеновского излучения интерпретируется в приближении толстой мишени с обратным током, а корональный - в приближении тонкой мишени. Полученные оценки показателей наклона спектров жесткого рентгеновского излучения обоих источников согласуются с результатами наблюдений. Однако рассчитанная интенсивность излучения коронального источника в несколько раз ниже наблюдаемой. Учет эффекта ускорения быстрых электронов в коллапсирующей магнитной ловушке позволил нам устранить это противоречие. В результате моделирования получена оценка плотности потока энергии, переносимой электронами с энергиями выше 15 кэВ, которая составляет $\sim 5 \times 10^{10}$ erg cm^{-2} s^{-1}, что в ~5 раз превышает значения, характерные для модели толстой мишени без обратного тока. С целью независимой проверки модели рассчитан спектр микроволнового излучения в диапазоне 1-50 ГГц, который соответствует имеющимся данным радионаблюдений.

Связь множественности источников жесткого рентгеновского излучения солнечных вспышек со множественностью -особенностей магнитного поля

О. Г. **Ден**1, И. В. Зимовец

АЖ, **2014**, #7, С. 569-577

Исследована импульсная фаза мощной солнечной вспышки **13 сентября 2005** г. (UT), наблюдавшейся космическим аппаратом RHESSI в диапазоне жесткого рентгеновского излучения (кэВ). Проведено пространственное сопоставление наблюдавшихся в этом диапазоне множественных источников излучения и рассчитанных для вспышечной области -особенностей магнитного поля. Показано, что совокупности источников жесткого рентгеновского излучения можно сопоставить совокупность -особенностей - мест возможного первичного энерговыделения вспышки. Силовые линии магнитного поля, пущенные из окрестности найденных магнитных особенностей, оканчиваются в хромосфере в окрестности наблюдавшихся источников жесткого рентгеновского излучения. Вопрос о том, каким образом множественные магнитные особенности вовлекаются в процесс энерговыделения практически одновременно, требует дальнейшего изучения.

О НАИБОЛЕЕ ТИПИЧНОЙ СТРУКТУРЕ ТРЕХМЕРНОГО МАГНИТНОГО ПЕРЕСОЕДИНЕНИЯ

ДУМИН Ю.В.1,2, СОМОВ Б.В.

ПАЖ Том: 42Номер: 11 Год: **2016** Страницы: 850

В связи с проблемой магнитного пересоединения в турбулентной астрофизической плазме с сильным магнитным полем, в частности, в солнечных вспышках, мы рассчитали вероятность возникновения различных топологических структур трехмерного пересоединения в нулевой точке случайного магнитного поля. Установлено, что доминирующую роль играет специфическая неосесимметричная структура с шестью асимптотическими направлениями - “шестихвостка”, называемая также “неправильным радиальным нулем”. Все остальные структуры, в частности, осесимметричные (“правильные радиальные нули”) реализуются с гораздо меньшей вероятностью. Принципиальной особенностью “шестихвостки” является то, что на больших расстояниях она приближенно редуцируется к классической двумерной структуре X-типа.

ФИЗИЧЕСКИЕ СВОЙСТВА СПОКОЙНОГО ПЕРЕХОДНОГО СЛОЯ МЕЖДУ КОРОНОЙ И ХРОМОСФЕРОЙ СОЛНЦА

ДУНИН-БАРКОВСКАЯ О.В.1, СОМОВ Б.В.1

ПАЖ Том: 42 Номер: 12 Год: **2016** Страницы: 908

Представлены результаты исследований физических свойств переходного слоя между короной и хромосферой Солнца в спокойных областях. Здесь структура атмосферы Солнца определяется взаимодействием магнитных полей над фотосферой. Они концентрируются в тонкие трубки, внутри которых велика напряженность поля. Исследовано, как в зависимости от скорости плазмы на хромосферной границе переходного слоя меняются распределения температуры, концентрации и скорости плазмы вдоль магнитной трубки, один конец которой находится в хромосфере, а другой - в короне. Рассмотрены два предельных случая: горизонтально и вертикально расположенная магнитная трубка. Для различных концентраций плазмы определены диапазоны скоростей на хромосферной границе переходного слоя, для которых в переходном слое не должны

возбуждаться ударные волны. Показано, что наиболее благоприятными для возбуждения ударных волн в переходном слое являются направленные вниз течения плазмы в его основании. Для всех рассчитанных вариантов переходного слоя показано, что перенос тепловой энергии вдоль магнитных трубок может быть хорошо описан в приближении классической электронной столкновительной теплопроводности вплоть до очень больших скоростей в основании переходного слоя. Рассчитанное жесткое ультрафиолетовое (EUV) излучение хорошо согласуется с современными космическими наблюдениями Солнца.

МЕТОД ПОИСКА НАНОВСПЫШЕК И ИХ ПРОСТРАНСТВЕННОЕ РАСПРЕДЕЛЕНИЕ В КОРОНЕ СОЛНЦА

Завершинский Д.И., Богачёв С.А., Белов С.А., Леденцов Л.С.
ПАЖ Том: 48Номер: 9 Год: **2022** Страницы: 665-675
Солнечные нановспышки – мелкомасштабные события, которые могут играть значительную роль в нагреве короны. Из-за слабой величины сигнала поиск и исследование нановспышек представляют собой непростую задачу, которая по-разному решается разными авторами. Мы представляем собственный метод регистрации нановспышек, который, по нашему мнению, позволяет эффективно измерять темп формирования нановспышек, а также их пространственное распределение на изображениях Солнца в вакуумном УФ диапазоне спектра. Мы исследовали серию из 300 изображений Солнца, полученных телескопом SDO/AIA в канале 171 Å в период низкой активности Солнца (с 12:00 UT по 13:00 UT **20 мая 2019** г.) и определили темп формирования нановспышек: P≈4.23×10−21 см−2 с−1, который оказался в согласии с результатами других авторов, а также исследовали зависимость P от гелиографической широты и яркости короны Солнца. Согласно нашим результатам, темп формирования нановспышек не зависит от гелиошироты, что отличается от поведения обычных вспышек, формирующихся в узких поясах активности. Также обнаружена связь между величиной P [пикс−1 ч−1] и светимостью короны I [отсчеты]: lgP=−2.27+0.00327I. Мы оцениваем наши результаты как благоприятные для теории нагрева короны нановспышками.

ГЕНЕРАЦИЯ СУПЕРДРАЙСЕРОВСКИХ ЭЛЕКТРИЧЕСКИХ ПОЛЕЙ В СОЛНЕЧНОЙ ХРОМОСФЕРЕ

Зайцев В.В.1, Кронштадтов П.В.1, Степанов А.В.
Пулково *«Солнечная и солнечно-земная физика – **2015** с.149*
Excitation of the electric field on the front of the current pulse that occurs at the footpoints of a coronal magnetic loop as a result of the magnetic Rayleigh-Taylor instability is considered. For the time of ≈ / ≈ 5 ÷ 25 A A ᴛ l V s (where l is the scale of a plasma tongue invading the magnetic loop due to the Rayleigh-Taylor instability) a disturbance associated with the tension of the magnetic field B (r, t) ϕ , "running away" from the region of instability with the Alfven speed. As a result, a pulse of electric current I (z V t) z A − with a scale of Δξ ≈ l begins to propagate along the magnetic loop. Therewith the inductive electric field z E on the pulse front appears, directed along of the loop axis, i.e., capable of accelerating particles. For sufficiently high current value, B ρ > p ϕ 2 / 8 , a non-linear regime of propagation of the electric current pulse is realized and quite high longitudinal electric field is generated E I V c a B l z z A z≈ 2 3 / 4 2 2 which depending on the current magnitude can exceed the Dreicer field.

Корональные магнитные арки

Зайцев В.В., Степанов А.В.
УФН, т.178(11), 1165-1204, **2008, Файл**
Physics Uspekhi, Volume 51, Issue 11, pp. 1123-1160 (**2008**).
The goal of this review is to outline some new ideas in the physics of coronal magnetic loops, the fundamental structural elements of the atmospheres of the Sun and flaring stars, which are involved in phenomena such as stellar coronal heating, flare energy release, charged particle acceleration, and the modulation of optical, radio, and X-ray emissions. The Alfvén–Carlqvist view of a coronal loop as an equivalent electric circuit allows a good physical understanding of loop processes. Describing coronal loops as MHD-resonators explains various ways in which flaring emissions from the Sun and stars are modulated, whereas modeling them by magnetic mirror traps allows one to describe the dynamics and emission of high-energy particles. Based on these approaches, loop plasma and fast particle parameters are obtained and models for flare energy release and stellar corona heating are developed.

ПРЕДВСПЫШЕЧНЫЕ РЕНТГЕНОВСКИЕ ПУЛЬСАЦИИ С ИСТОЧНИКАМИ ВНЕ АКТИВНОЙ ОБЛАСТИ ОСНОВНОЙ ВСПЫШКИ

Зимовец И.В., Шарыкин И.Н., Кальтман Т.И., Ступишин А.Г., Низамов Б.А.

Г и А Том: 63Номер: 5 Год: **2023** Страницы: 547-560
Ранее мы показали, что по характеру расположения источников предвспышечных рентгеновских пульсаций относительно основной солнечной вспышки события разделяются по крайней мере на два типа: в событиях типа I источники пульсаций и основной вспышки находятся в одной активной области (АО), а в событиях типа II – в разных. В данной работе представлен анализ события типа II, в котором по данным космической обсерватории Ramaty High-Energy Solar Spectroscopic Imager (RHESSI) рентгеновские источники предвспышечных квазипериодических пульсаций (с периодом P = 1.5 ± 0.1 мин), начавшихся в ~18:02 UT, располагались в АО 11 884 в Западном полушарии, а источники основной вспышки M1.0 SOL**2013-11-05**T18:08 в АО 11 890 в Восточном полушарии. Пульсации также наблюдались с помощью Gamma-Ray Burst Monitor (GBM) на борту космической обсерватории Fermi и X-Ray Sensor (XRS) на борту Geostationary Operational Environmental Satellite (GOES), что исключает возможность их искусственного происхождения.. По данным Atmospheric Imaging Assembly (AIA) на борту Solar Dynamics Observatory (SDO) в экстремальном ультрафиолетовом диапазоне установлено, что источники пульсаций располагались в основании корональных струй (джетов), истекавших со скоростями ~100–1500 км/с. Расстояние между АО 11 884 и АО 11 890 составляло ~1.4 RS. Плазме струй потребовалось бы ~17–250 мин, чтобы достичь АО 11 890, что намного больше времени межу началом пульсаций (струй) и вспышкой (~6 мин), к тому же в картинной плоскости струи истекали в противоположном (западном) от активной области вспышки направлении. В короне не наблюдались петли, соединяющие АО 11 884 и АО 11 890. Более того, не обнаружено соединения этих областей силовыми линиями магнитного поля, экстраполированного с фотосферы в корону в потенциальном приближении. Эти аргументы свидетельствуют о том, что струи (и связанные с ними пульсации) не могли быть триггером вспышки. Таким образом, представлен яркий пример события, в котором не было физической связи между предвспышечными рентгеновскими пульсациями (и струями) и последовавшей за ними вспышкой. Это событие демонстрирует важное значение пространственно-разрешенных наблюдений при исследовании пульсаций на Солнце и звездах..
RHESSI Science Nuggets #465 Dec **2023**
https://sprg.ssl.berkeley.edu/~tohban/wiki/index.php/When_it_rippled_in_one_place_and_exploded_in_another

Зимовец И.В., Шарыкин И.Н., Кальтман Т.И., Ступишин А.Г., Низамов Б.А.
Предвспышечные пульсации с источниками вне активной области основной вспышки Сборник трудов XXVI Всероссийской ежегодной конференции по физике Солнца «Солнце и солнечно-земная физика – 2022» ГАО РАН.
http://www.gaoran.ru/russian/solphys/2022/book/conf2022.pdf

ИСТОЧНИКИ ДЛИННОПЕРИОДНЫХ РЕНТГЕНОВСКИХ ПУЛЬСАЦИЙ ПЕРЕД НАЧАЛОМ СОЛНЕЧНЫХ ВСПЫШЕК

Зимовец И.В., Нечаева А.Б., Шарыкин И.Н., Низамов Б.А.
Г и А Том: 62Номер: 4 Год: 2022 Страницы: 436-455
В работе [Tan et al., 2016] утверждается, что перед значительной долей (26–46%) “изолированных” солнечных вспышек наблюдаются длиннопериодные (с периодом P = 1.9–47.3 мин и длительностью 1–2 ч) квазипериодические пульсации (КПП) в диапазоне мягкого рентгеновского излучения. Результаты получены по данным инструмента GOES/XRS без пространственного разрешения. В данной работе мы выполнили анализ источников таких КПП перед 35 “изолированными” вспышками класса X на основе “quick-look” изображений RHESSI в диапазоне 6–12 кэВ и установили, что события можно разделить на два типа. В событиях типа I источники всех КПП и основной вспышки располагаются в одной активной области (АО) на Солнце, тогда как в событиях типа II источники по крайней мере части КПП располагаются в другой АО, нежели АО вспышки. Более детальный анализ двух событий типа I и трех событий типа II с помощью изображений RHESSI в рентгеновском и SDO/AIA в ультрафиолетовом диапазонах показывает, что источники рентгеновских пульсаций в одной АО располагаются в разных местах (в пределах ~20 Мм друг от друга и от основной вспышки), причем их появление соответствует появлению новых петлеобразных ультрафиолетовых источников. Мы приводим наблюдательные аргументы в пользу того, что предполагаемые в работе [Tan et al., 2016] механизмы, основанные на осцилляциях корональных петель как LRC электрических контуров или МГД-осцилляциях петель, маловероятны. Более перспективными для объяснения рассматриваемых КПП представляется механизм осциллирующего пересоединения. В событиях типа I оно происходит в одной АО, тогда как в событиях типа II оно может происходить параллельно в нескольких разнесенных АО, и для объяснения этого обстоятельства требуется предположить когерентность подфотосферного всплытия магнитных потоков в разных участках Солнца. Это предположение требует дальнейшей проверки.

О СВЯЗИ ВСПЫШЕЧНЫХ ИСТОЧНИКОВ ЖЕСТКОГО РЕНТГЕНОВСКОГО ИЗЛУЧЕНИЯ

И ЭЛЕКТРИЧЕСКИХ ТОКОВ НА ФОТОСФЕРЕ
Зимовец И.В., Шарыкин И.Н.
Пулково «Солнечная и солнечно-земная физика – **2015** с.153
There are some evidences that initial energy release and acceleration of electrons, at least in some solar flares, can occur inside magnetic tubes with strong electric currents, in the transition region and chromosphere, rather than in the corona. We report preliminary results of observational study of spatial relationship between hard X-ray (HXR; ≥50keV) sources detected by RHESSI in 12 flares and vertical currents in parental active regions (AOs) calculated using the HMI/SDO photospheric vector magnetograms. We found that in all flares at least one HXR source was in a region of strong currents within 10%–90% of the maximum current of an entire AO. Integral currents (of the same sign) across the HXR sources were in the range of 1.1–9.5.1011 A. We also found that there were multiple regions of strong currents in each AO where HXR sources were not detected. These results give evidence that there is link between flare HXR sources and strong vertical currents on the photosphere. However, this link is not clear. It seems that strong vertical currents is necessary but not sufficient condition for generation of flare HXR sources. This work should be expanded to try to find sufficient condition. **03.08.2011**

Статистика вспышек в комплексах активности на Солнце
Исаева Е.С.
Диссертация **2023**

РЕНТГЕНОВСКИЕ ВСПЫШКИ И КОМПЛЕКСЫ АКТИВНОСТИ НА СОЛНЦЕ В 24 ЦИКЛЕ

ИСАЕВА Е. С.[1,2], ТОМОЗОВ В. М.[2], ЯЗЕВ С. А.
АСТРОНОМИЧЕСКИЙ ЖУРНАЛ Том: 97 Номер: 1 Год: **2020** Страницы: 64-72
Проанализирована статистическая связь комплексов активности (КА) на Солнце и солнечных вспышек с рентгеновскими классами GOES выше M1.0 (744 события) в течение 24 цикла солнечной активности (до января 2019 г.). Все группы пятен разбиты на три класса: в ядрах КА, в ветвях КА, за пределами КА. Показано, что 78% вспышек указанных классов происходят преимущественно в группах пятен, расположенных в ядрах и в ветвях КА. Удельное число вспышек в ядрах КА в 2.5 раза превышает соответствующий параметр в ветвях КА и за пределами КА. С КА связаны 87% LDE-вспышек указанных классов, 82% всех сильных протонных вспышек, генерирующих потоки энергичных протонов на орбите Земли, а также 74% всех гамма-вспышек в 24 цикле.

ПРОТОННЫЕ ВСПЫШКИ В КОМПЛЕКСАХ АКТИВНОСТИ НА СОЛНЦЕ: ВОЗМОЖНЫЕ ПРИЧИНЫ И СЛЕДСТВИЯ

ИСАЕВА Е.С.[1,2], **ТОМОЗОВ В.М.**[1,2], **ЯЗЕВ С.А.**[1,2]

СОЛНЕЧНО-ЗЕМНАЯ ФИЗИКА Том: 95Номер: 3 Год: 2018 Страницы: 256-264
Вспышки на Солнце, которые сопровождались потоками частиц на орбите Земли, превышающими 10 частиц на квадратный сантиметр в секунду с энергией более 10 МэВ в 24 цикле, происходили преимущественно в комплексах активности (в 82%)и в 80% случаев не далее, чем в 20 гелиографических градусах от ближайших корональных дыр. При этом рентгеновский класс вспышек плохо коррелирует с потоком протонов на орбите Земли. В статье обосновывается гипотеза о том, что выход частиц в гелиосферу обусловлен существованием долгоживущих магнитных каналов, позволяющих обеспечить перенос ускоренных вспышкой частиц в пограничную область открытой магнитной структуры корональных дыр. Обсуждается возможный вклад процессов обменного пересоединения как в формирование таких каналов, так и роль обменного пересоединения в генерации самих вспышек.

РЕНТГЕНОВСКИЕ ВСПЫШКИ И КОМПЛЕКСЫ АКТИВНОСТИ НА СОЛНЦЕ

ИСАЕВА Е.С.[1], **ЯЗЕВ С.А.**[2,3]

СОЛНЕЧНО-ЗЕМНАЯ ФИЗИКА Номер: 22 (135) Год: 2013 Страницы: 3-11
Проанализирована связь комплексов активности (КА) на Солнце и солнечных вспышек рентгеновских классов выше M0 на фазе роста 24-го цикла солнечной активности (до апреля 2012 г.). Все группы пятен разбиты на три класса: в ядрах КА, в ветвях КА, за пределами КА. Показано, что вспышки происходят преимущественно в группах пятен, расположенных в ядрах и в ветвях КА. Для вспышек рентгеновского класса X не отмечено особой роли ядер КА (в группах пятен вне КА наблюдается такое же число X-вспышек), но суммарная мощность вспышек класса X в ядрах КА оказывается выше, чем в активных областях вне КА. LDE-вспышки (long decay events, или вспышки с длительным затуханием всплеска (более 4 ч) в мягком рентгеновском излучении) происходят преимущественно в КА, при этом наиболее мощные события наблюдаются в основном в ветвях, а не в ядрах КА. Показано, что в течение фазы роста 24-го цикла вспышечная деятельность проявлялась в виде всплесков продолжительностью около двух солнечных оборотов. Эти всплески хорошо коррелируют с импульсами пятнообразовательной деятельности Солнца, связанными с активностью КА. В исследуемый период девять из одиннадцати мощных протонных вспышек произошли в КА.

ЭРУПТИВНЫЕ ПРОЦЕССЫ В НАЧАЛЕ РАЗВИТИЯ МОЩНЫХ ВСПЫШЕЧНО-АКТИВНЫХ ОБЛАСТЕЙ НА СОЛНЦЕ

Л. К. **Кашапова**1, М. А. Лившиц

АСТРОНОМИЧЕСКИЙЖУРНАЛ, **2008**, том 85,№12, с. 1129–1142 **File**

Изучается эволюция больших центров активности на Солнце и выясняются условия, приводящие к мощным нестационарным процессам. В дополнение к рассматриваемым в таких случаях обычным факторам (изменение площади пятен, структуры магнитных полей и характера движений), изучается вопрос о том, насколько наблюдения собственно нестационарных процессов (вспышек и связанных с ними корональных выбросов массы) могут быть полезны для предсказания развития таких процессов в ходе последующей эволюции центра активности. Данная проблема обсуждается на примере мощной группы10486 октября 2003 г., наблюдения которой удалось провести еще до выхода этой группына восточный лимб, используя наблюдения на космическом аппарате, располагающемся на околомарсианской орбите. Для событий 2003 г. появилась возможность строить изображения вспышек в различных спектральных диапазонах, и можно было подробно изучать высокоэнергичные процессы в изолированной в начале своего развития группе 486 и затем в событиях связанных между собой групп 486 и 484. Анализ своеобразного первого периода развития группы486 показал, что в дальнейшем можно ожидать усиления активности не только вследствие всплытия новых магнитных потоков (и групп-сателлитов), но и взаимодействия и синхронизации двух, а затем и трех больших групп конца октября 2003 г. Иначе говоря, появление экстремально мощных нестационарных процессов связано в данном случае с относительно более высоким вкладом крупномасштабных магнитных полей. Сделанные выводы сопоставляются с результатами изучения характера движений и магнитных полей в обсуждаемом центре активности за время всего прохождения по диску с **21 октября по 5 ноября 2003** г. 21,23, 24 октября 2003

Широтные распределения солнечных микровспышек и высокотемпературной плазмы в минимуме солнечной активности.

Кириченко А.С., Лобода И.П., Рева А.А., Ульянов А.С., Богачев С.А.

СЗФ, Т 9, №2, С. 5–11 **2023**

https://naukaru.ru/ru/storage/viewWindow/121954

В работе проанализировано распределение по широте высокотемпературной плазмы (T> 4 МК) и рентгеновских микровспышек на солнечном диске в период низкой активности Солнца в 2009 г. Распределение микровспышек классов A0.1–A1.0 содержит пояса, характерные для обычных вспышек класса B и выше. Всего нами зарегистрировано 526 микровспышек, большинство из которых, около 96 %, наблюдалось на высоких широтах. Около 4 % микровспышек было обнаружено около экватора. Мы полагаем, что они сформированы остаточным магнитным полем предыдущего , 23-го цикла активности. Обычные вспышки класса B и выше в этот период около экватора почти не наблюдались. Число микровспышек в южном полушарии в этот период было незначительно выше, чем в северном. Это отличается от распределения обычных вспышек, для которых ранее сообщалось о доминировании северного полушария по числу вспышек.

ДЛИТЕЛЬНЫЙ НАГРЕВ ПЛАЗМЫ В СОЛНЕЧНЫХ МИКРОВСПЫШКАХ РЕНТГЕНОВСКОГО КЛАССА A1.0 И НИЖЕ

КИРИЧЕНКО А. С.1, БОГАЧЕВ С. А.

Письма в АЖ, т.39, №11, стр. 884, **2013**

Представлены результаты исследования трех солнечных микровспышек рентгеновского класса порядка A1.0 и ниже, наблюдавшихся в минимуме солнечной активности в 2009 году: вспышка **19.04.2009** (класс A0.38), вспышка **24.06.2009** (класс A0.47), вспышка **18.07.2009** (класс A2.2). Отличительной особенностью данных событий от других микровспышек низких рентгеновских классов являлось поддержание высокой температуры плазмы (МК) на фазе спада излучения спустя значительное время после максимума вспышки. Времена жизни высокотемпературного источника излучения в короне во всех трех случаях существенно превышают времена его теплопроводного и лучистого охлаждения, а тепловая энергия, выделяемая на фазе спада вспышки, на порядок превышает тепловую энергию, высвобождаемую во время ее импульсной фазы. Высказано предположение, что длительное поддержание высокой температуры плазмы в микровспышках низких рентгеновских классов может осуществляться за счет процесса магнитного пересоединения, связанного с выбросами массы из области вспышки. Время жизни горячей плазмы в короне в этом случае может заметно превышать время охлаждения плазмы. Исследование показало, что во всех трех исследованных микровспышках действительно происходила эрупция вещества.

СКИН-СЛОЙ ЭРУПТИВНОГО МАГНИТНОГО ЖГУТА В КРУПНЫХ СОЛНЕЧНЫХ ВСПЫШКАХ

КИЧИГИН Г.Н.1, МИРОШНИЧЕНКО Л.И.2,3, СИДОРОВ В.И.4, ЯЗЕВ С.А.1

ГЕОМАГНЕТИЗМ И АЭРОНОМИЯ Том: 56Номер: 4 Год: **2016** Страницы: 423-430

Эволюция магнитного поля вспышечно-активных областей Солнца из геометрии и топологии HMI/SDO-магнитограмм

И. С. **Князева**, Н. Г. Макаренко

Астрономический журнал, **2014**, Том 91, Номер 3, С. 200-210

Представлены апробация и дальнейшее развитие топологических подходов для анализа магнитного поля Солнца. С целью описания и диагностики предвспышечной динамики магнитного поля активных областей Солнца по HMI-магнитограммам обсерватории SDO использован аппарат, основанный на методах геометрии случайных полей, математической морфологии и топологии и масштабируемого пространства (scale-space). Полученные результаты показали, что предложенный формализм позволяет диагностировать предвспышечную динамику для практически представляющих интерес интервалов времени.

О ФОРМИРОВАНИИ НИТЕПОДОБНЫХ СТРУКТУР НА РАННЕЙ ФАЗЕ СОЛНЕЧНЫХ ВСПЫШЕК

В. А. **Ковалев**, *, Е. Д. Куретовab, Е. С. Куркинab

ФИЗИКА ПЛАЗМЫ, **2020**, том 46, № 4, с. 351–357

Предложена модель, описывающая начальную фазу вспышечного нагрева в короне Солнца. Уравнение энергии для вспышечной плазмы в магнитной трубке приведено к двумерному уравнению теплопроводности с нелинейным объемным источником, обеспечивающим нагрев плазмы в режиме с обострением, и нелинейным анизотропным коэффициентом теплопроводности. Показано, что взрывной нагрев плазмы может сопровождаться формированием высокотемпературных структур, вытянутых вдоль магнитной трубки.

Микроволновый индикатор потенциальной геоэффективности и жгутовая магнитная структура солнечной активной области.

Кудрявцева А.В., Мышьяков И.И., Уралов А.М., Гречнев В.В.

СЗФ Том 7. **2021**. № 1. С. 3–12.

https://naukaru.ru/ru/storage/viewWindow/66383

Выполнен анализ присутствия микроволнового источника над нейтральной линией (ИНЛ) в суперактивной области NOAA 12673, породившей ряд геоэффективных событий в сентябре 2017 г. Для оценки положения ИНЛ использовались данные Сибирского радиогелиографа в диапазоне 4–8 ГГц и Радиогелиографа Нобеяма на частоте 17 ГГц. Расчет коронального магнитного поля в нелинейном бессиловом приближении выявил протяженную структуру, состоящую из взаимосвязанных магнитных жгутов, расположенных практически по всей длине главной линии раздела полярностей фотосферного магнитного поля. ИНЛ проецируется в зону максимальных значений горизонтального магнитного поля — основной энергосо-держащей части этой структуры. В ходе каждой вспышки балла X активная область теряла магнитную спиральность и становилась источником КВМ. **6-7 Sep 2017**

ПОЛЯРИЗАЦИЯ ЖЕСТКОГО РЕНТГЕНОВСКОГО ИЗЛУЧЕНИЯ ПРИ ДЛИТЕЛЬНОЙ И ИМПУЛЬСНОЙ ИНЖЕКЦИИ РЕЛЯТИВИСТСКИХ ЭЛЕКТРОНОВ ВО ВСПЫШЕЧНУЮ ПЕТЛЮ

Кудрявцев И.В.1,2, Мельников В.Ф.2, Чариков Ю.Е.1,3

Пулково «Солнечная и солнечно-земная физика – **2015** с.239

In this paper a comparison of polarization properties of impulsive and gradual HXR bursts on the basis of theoretical analysis of their emissions is conducted. Numerical simulation is carried out for the impulsive and gradual injections, lasting a few seconds, and a few tens of seconds, respectively. In the latter case one can speak on a quasi-stationary mode of changes of the angular distribution of nonthermal electrons. Various cases of the angular dependence of the injected electrons are considered. To obtain the parameters of HXR, the relativistic kinetic equation for fast electrons and the relativistic bremsstrahlung cross-section are used. The differences in the dynamics of the degree of polarization are discussed. For example, in the case of the impulsive injection, the degree of polarization rapidly decreases after reaching the peak rate of the injected electrons due to the effect of fast isotropization of electrons in the process of their scattering on the background plasma particles. In the case of the gradual injection, a high value (25–50%) of polarization degree remains during tens of seconds

after the intensity peak and can be experimentally registered even now.

ИССЛЕДОВАНИЕ ПРОСТРАНСТВЕННОЙ ДИНАМИКИ ИСТОЧНИКОВ КВАЗИПЕРИОДИЧЕСКИХ ПУЛЬСАЦИЙ ЖЕСТКОГО РЕНТГЕНОВСКОГО ИЗЛУЧЕНИЯ СОЛНЕЧНЫХ ВСПЫШЕК

Кузнецов С.А.1,2, Моргачев А.С.1,2, Зимовец И.В.3, Струминский А.Б.
Пулково «Солнечная и солнечно-земная физика – **2015** с. 249
We present a brief description of the method, which we are currently developing for study physical properties of quasi-periodic pulsations in solar flare with hard X-ray emission. The preliminary analysis of the M4.6-class flare of **9 November 2002** is given as an example. It is shown that the double footpoint-like hard X-ray (25–50 keV) sources move along the magnetic neutral line in course of the flare. This can be interpreted as successive involvement of new flaring loops of the magnetic arcade into the energy release process. Our observational results are in agreement with some previous works on this topic. Description of the systematic study of this phenomenon for a large number of events will be presented later.

ЭВОЛЮЦИЯ СОЛНЕЧНОЙ ВСПЫШКИ SOL 2013-05-17: АНАЛИЗ ОПТИЧЕСКИХ СПЕКТРОВ (СЕРИЯ БАЛЬМЕРА) И КВАЗИПЕРИОДИЧЕСКИЕ ПУЛЬСАЦИИ

Купряков Ю.А., Бычков К.В., Белова О.М., Горшков А.Б., Barta M.
Изв. КрАО Том: 119Номер: 4 Год: 2023 Страницы: 5-11
Цель работы - изучение поведения кривых интенсивности излучения в линиях Hϵ, Hβ и Hα в процессе развития вспышки и сравнение результатов с расчетными значениями. Наблюдения проводились на горизонтальной солнечной установке HSFA-2 (Ondˇrejov Observatory). Для обработки была отобрана вспышка 2013-05-17 класса M 3.2 в активной области NOAA 11748, для которой были определены абсолютные значения потоков в спектральных линиях. Показано, что наблюдениям удовлетворяет модель нагрева хромосферного газа потоком магнитогидродинамических волн из конвективной зоны и его ионизация и возбуждение потоком надтепловых частиц из короны. Выполнены расчеты в линиях водорода с учетом основных процессов, определяющих излучение газа, непрозрачного в спектральных линиях. Плоский декремент бальмеровской серии свидетельствует о неоднородности излучающей области по вертикали. Поиск квазипериодических пульсаций показал, что в данной вспышке они обнаруживаются только в линии Hα с уровнем значимости 95 %. В других спектральных диапазонах они отсутствуют.

Квазипериодические пульсации в солнечных и звездных вспышках. Обзор Review

Куприянова Е.Г., Колотков Д.Ю., Накаряков В.М., Кауфман А.С.
СОЛНЕЧНО-ЗЕМНАЯ ФИЗИКА Том 6. **2020**. № 1 С. 3–29.
https://naukaru.ru/ru/storage/viewWindow/50116
https://naukaru.ru/en/storage/viewWindow/50357
В статье представлен обзор современного состояния исследований колебательных процессов в солнечных и звездных вспышках, основанных на наблюдательных данных наземных и космических инструментов с высоким временны́м, пространственным и спектральным разрешением в разных диапазонах электромагнитного спектра. Рассматриваются механизмы генерации вспышечного излучения и его квазипериодической модуляции. Обсуждаются сходство и различие солнечных и звездных вспышек, а также связанные с этим проблемы супервспышек на Солнце и космической погоды. Показано, что квазипериодические пульсации (КПП) вспышечного излучения являются эффективным инструментом диагностики как самих вспышечных процессов, так и параметров тепловой плазмы и ускоренных частиц. Рассматриваются виды КПП, их статистические свойства и методы анализа с учетом нестационарности параметров КПП. Сделан обзор предполагаемых механизмов КПП и открытых вопросов. **2005-05-06, 2013-05-14, 29 Mar 2014**

Долгопериодические пульсации теплового микроволнового излучения солнечной вспышки 2 июня 2007 г. по данным с высоким пространственным разрешением

Е. Г. **Куприянова**, В. Ф. Мельников, В. М. Пузыня, К. Шибасаки, Х. С. Джи
АЖ, т. 91, №8, С. 662-667, **2014**
На основе данных радиогелиографа Нобеяма (NoRH) на 17 ГГц с высоким угловым и временным разрешением в тепловой компоненте микроволнового излучения вспышечной петли 02.06.2007 на Солнце обнаружены и исследованы квазипериодические пульсации с постоянными во времени периодами в диапазоне от 55 до 250 с. Выделены колебания с периодом около 110–120 с, отличающиеся от других своей синфазностью вдоль оси петли. Наблюдаемые периодичности вероятнее всего вызваны модуляцией радиоизлучения медленными магнитозвуковыми волнами, захваченными в филаментированной вспышечной петле.

МЕТОД ОЦЕНКИ ПРОСТРАНСТВЕННОГО ПЕРИОДА ЭНЕРГОВЫДЕЛЕНИЯ В СОЛНЕЧНЫХ ВСПЫШКАХ

Леденцов Л.С.
ПАЖ Том: 49Номер: 11 Год: **2023** Страницы: 819-828

С целью анализа современных спутниковых наблюдений аркад вспышечных корональных петель предложен метод оценки пространственного периода энерговыделения в солнечных вспышках. Метод основывается на применении анализа Фурье к разностным изображениям вспышечных аркад в далеком ультрафиолетовом диапазоне. Работа метода продемонстрирована на примере наблюдения Бастильской вспышки с космического аппарата TRACE в канале 171 Å. Среднее значение пространственного периода энерговыделения в Бастильской вспышке, определенное предложенным методом, составляет 5–8 Мм, что хорошо согласуется со сценарием развития тепловой неустойчивости предвспышечного токового слоя в солнечных вспышках.

ТЕПЛОВАЯ НЕУСТОЙЧИВОСТЬ ПЕРЕСОЕДИНЯЮЩЕГО ТОКОВОГО СЛОЯ В СОЛНЕЧНЫХ ВСПЫШКАХ

ЛЕДЕНЦОВ Л.С.1, СОМОВ Б.В.

ПАЖ Том: 42 Номер: 12 Год: **2016** Страницы: 925

С целью интерпретации современных спутниковых наблюдений последовательного увеличения яркости корональных петель в солнечных вспышках мы решили задачу об устойчивости малых продольных возмущений однородного пересоединяющего токового слоя. В рамках магнитогидродинамического приближения показано, что условием неустойчивости служит эффективное подавление теплопроводности плазмы возмущением магнитного поля внутри слоя. Неустойчивость в линейной фазе нарастет за характерное время лучистого охлаждения плазмы. В результате неустойчивости в токовом слое может образовываться периодическая структура холодных и горячих волокон, расположенных поперек направления электрического тока. Предлагаемый механизм тепловой неустойчивости пересоединяющего токового слоя может быть полезен для объяснения последовательного увеличения яркости, “поджига”, вспышечных петель в солнечных вспышках.

КАТАЛОГ ЖЕСТКИХ РЕНТГЕНОВСКИХ ВСПЫШЕК НА СОЛНЦЕ, ЗАРЕГИСТРИРОВАННЫХ С ОКОЛОМАРСИАНСКОЙ ОРБИТЫ MARS ODYSSEY/HEND В 2001-2016 ГГ

ЛИВШИЦ М.А.1, ЗИМОВЕЦ И.В.2, ГОЛОВИН Д.В.2, НИЗАМОВ Б.А.3,4, ВЫБОРНОВ В.И.2, МИТРОФАНОВ И.Г.2, КОЗЫРЕВ А.С.2, ЛИТВАК М.Л.2, САНИН А.Б.2, ТРЕТЬЯ

АЖ Том: 94Номер: 9 Год: **2017** Страницы: 778-792

Изучение нестационарных процессов на Солнце представляет большой интерес, и в последние годы многоволновые наблюдения излучения и регистрация магнитных полей проводятся как наземными телескопами, так и несколькими специализированными космическими аппаратами на околоземных орбитах. Однако получение новой надежной информации о жестком рентгеновском излучении остается востребованным, особенно, если соответствующие космические аппараты обеспечивают дополнительную информацию, например, при наблюдениях вспышек с иных направлений, отличающихся от направления Солнце-Земля. В статье представлен каталог мощных солнечных вспышек, зарегистрированных прибором High Energy Neutron Detector(HEND), разработанным в Институте космических исследований РАН. Прибор HEND установлен на космическом аппарате "2001 Mars Odyssey", успешно работал при полете к Марсу и в настоящее время функционирует на околомарсианской орбите. Помимо нейтронов, аппаратура HEND чувствительна к жесткому рентгеновскому (до 300 кэВ) и гамма-излучению (выше 300 кэВ). Это излучение регистрируется двумя сцинтилляторами: внешний сцинтиллятор регистрирует фотоны с энергиями выше 40 кэВ, внутренний - свыше 200 кэВ. При создании каталога проведена новая процедура калибровки данных. Кратко обсуждаются методы калибровки внешнего детектора. Для 60 наиболее мощных солнечных вспышек на видимой с Земли и обратной сторонах Солнца приведены временные профили излучения, суммированные по всем каналам рентгеновского, а в некоторых случаях и гамма-диапазонов, спектры и характеристики их степенной аппроксимации. Кратко обсуждаются результаты прежних работ по изучению Солнца с аппаратурой HEND и возможности дальнейшего использования этих данных.

НАБЛЮДАТЕЛЬНЫЕ СВИДЕТЕЛЬСТВА СВЯЗИ ВСПЛЫТИЯ МАГНИТНЫХ ПОЛЕЙ, ТОКОВ И СОЛНЕЧНЫХ ВСПЫШЕК 10 МАЯ 2012 Г.

М. А. **Лившиц**,1, * И. Ю. Григорьева,2, ** И. И. Мышьяков,3, *** Г. В. Руденко

АЖ Том: 93 Номер: 10 Страницы: 907 **2016**

Мы проанализировали многоволновые наблюдения и данные о магнитном поле солнечной вспышки **10 мая 2012** г. (04:18 UT). Было зарегистрировано обращение знака сигнала в измерениях магнитного поля вдоль луча зрения в тени небольшого пятна. Этот эффект, по крайней мере, частично, связан со всплытием нового магнитного поля. Практически одновременно с этим, произошел всплеск жесткого рентгеновского излучения, и возникла волна в диапазонах вакуумного ультрафиолета (ВУФ) – «солнцетрясение», связанная с воздействием

возмущения в области энерговыделения на фотосферу. В начале события зарегистрировано появление вспышки типа "сигмоид», но она не распространилась, как обычно, вдоль нейтральной линии. По данным о полном векторе (SDO/HMI) была проведена экстраполяция магнитных полей активной области (АО) 11476 в корону и получено распределение вертикальных токов jz на фотосфере. Известно, что при изучении распределения токов во всей АО, связь между ними и возникновением вспышек очень сложная. В данном случае мы подтвердили, что ожидаемая "идеальная» связь и изменение системы токов до и после вспышки, описанная, например, в работе Шарыкина и Косовичева, реализуются только в области сигмоида. Проведено сравнение результатов с наблюдениями двух вспышек этой АО в этот день, одна из которых имела другой тип, а другая – аналогична исследуемой. Эти результаты – аргумент в пользу того, что формирование и выброс крупномасштабных замагниченных жгутов в сигмоидных вспышках связаны с влиянием сдвиговых движений в фотосфере и выносом спиральности в магнитной трубке и дальнейшим развитием неустойчивости тороидального плазменного шнура.

Связь нетепловых и газодинамических процессов в мощных солнечных вспышках

Лившиц М.А.1, Кашапова Л.К.

Геом. и аэрон. №7 **2012**

Связь между газодинамическими процессами и ускорением частиц иллюстрируется на трех примерах. Во вспышке **6 июля 2006** г наблюдения позволяют убедиться в реализации процесса взрывного испарения хромосферы в импульсной фазе. Кроме того, связанный с этой вспышкой СМЕ отражает процесс первичного выделения энергии. В мощной лимбовой вспышке **14 июля 2005** г СМЕ, наблюдающийся во внешних слоях короны, вероятно, является следствием неоднократного энерговыделения и выбросов плазмы. Об этом, по-видимому, свидетельствует дополнительное излучение в дециметровом диапазоне, характерное обычно для постэруптивных процессов. Один пример слабой вспышки на фазе затухания мощного явления **15 апреля 2001** г также сопровождается дециметровым всплеском.

МОЩНЫЕ НЕСТАЦИОНАРНЫЕ ПРОЦЕССЫ НА СОЛНЦЕ: ПРОСТРАНСТВЕННО-ВРЕМЕННАЯ СТРУКТУРА И ЭФФЕКТИВНОЕ УСКОРЕНИЕ ЧАСТИЦ

ЛИВШИЦ М.А.

Солнечно=земн. Физика Номер: 12-1 Год: **2008** Страницы: 3-4

Обобщаются сведения о высокоэнергичных процессах на Солнце. Уточняется классификация вспышек и обосновывается точка зрения о том, что корональный выброс массы и собственно вспышка являются проявлениями одного и того же общего процесса, по крайней мере в случае самых мощных событий. Затем проанализированы данные об ускорении электронов (RHESSI, «Марс-Одиссей») и протонов. Показано, что существование двух пиков жесткого рентгеновского излучения, разнесенных на 10-20 мин, и эволюция спектров этого излучения свидетельствуют о двух эпизодах ускорения. Проанализированы спектры 172 протонных возрастаний, отождествляемых с отношением потоков протонов с энергиями более 10 и 100 МэВ около Земли. Оказалось, эти спектры остаются практически теми же самыми у большинства мощных вспышек при благоприят-ных условиях выхода из короны и распространения частиц в межпланетном пространстве. Это является аргументом в пользу инвариантности основных черт эффективного ускорения частиц в мощных событиях. Этот процесс происходит на взрывной фазе вспышки, и его источник располагается низко, непосредственно над хромосферой, в области, примыкающей к пятнам. Имеются основания полагать, что при этом происходит быстрое одновременное ускорение электронов и протонов с захватом некоторой доли частиц в магнитные ловушки. Существует, однако, небольшое количество событий, в которых уже на постэ-руптивной фазе развития вспышки из короны выходит дополнительное количество протонов с энергией до 10-30 МэВ. Ана-лиз этих случаев с более мягким спектром частиц скорее свидетельствует о дополнительном ускорении частиц на корональ-ных высотах (около 30 000 км), чем об облегчении выхода частиц из ловушек. В статье оценен вклад потока протонов с энер-гией более 10 МэВ, возникающего на постэруптивной фазе вспышки, в общий поток частиц в максимуме протонного возрас-тания и кратко обсуждаются возможные механизмы ускорения частиц на значительных высотах в короне.

Рентгеновское и гамма-излучение солнечных вспышек **Review**

А. Л. **Лысенко**1, Д. Д. Фредерикс1, Г. Д. Флейшман1,2, Р. Л. Аптекарь1, А. Т. Алтынцев3, С. В. Голенецкий1, Д. С. Свинкин1, М. В. Уланов1, А. Е. Цветкова1, А. В. Ридная1

УФН **2020** **File**

Приводится краткий обзор современного состояния и актуальных проблем физики солнечных вспышек, которые можно прояснить методами рентгеновской и гамма-астрономии. Подробно рассмотрены несколько вопросов, среди которых – условия и механизмы ускорения электронов во вспышке, распределение вспышечной энергии между тепловой и нетепловой компонентами, гамма-излучение вспышек и его динамика,

пространственная структура источников в рентгеновском и гамма-диапазонах. В данном контексте обсуждаются последние результаты российско-американского эксперимента Konus-Wind, отметившего в 2019 г. 25-летие непрерывной работы в космосе.

ПРОЯВЛЕНИЯ НАГРЕВА В НАЧАЛЕ ВСПЫШКИ 29 ИЮНЯ 2012 Г

МЕШАЛКИНА Н.С.[1], **АЛТЫНЦЕВ А.Т.**[1]

СОЛНЕЧНО-ЗЕМНАЯ ФИЗИКА Том: 10 Номер: 3 Год: 2024 Страницы: 13-20

Анализ данных GOES для вспышки SOL2012-06-29T04:09 класса C4.6 показывает тепловой характер энерговыделения в течение нескольких минут перед импульсной стадией. Нагрев плазмы до температур выше 10 МК приводит к появлению струй плазмы вдоль открытых силовых линий и в больших петлях. В работе исследуется взаимосвязь нагретой плазмы со вспышечной структурой и ее динамикой по данным наблюдений в рентгеновском, крайнем ультрафиолетовом и радиоволновом диапазонах. Особое внимание привлекает обнаружение на динамических спектрах тонких временных структур узкополосного радиоизлучения до и после импульсной стадии вспышки. На начальной стадии наблюдаются широкополосные импульсы в дециметровом диапазоне, которые можно связать с формированием тепловых фронтов в струях. Серия сверхъярких всплесков в сантиметровом диапазоне, характеризующихся частотным дрейфом, наблюдается после окончания импульсного энерговыделения в ядре вспышки. По данным Сибирского солнечного радиотелескопа (5.7 ГГц) было установлено, что источники этих субсекундных всплесков находятся в удаленном основании крупномасштабной вспышечной петли.

Мешалкина Н.С., Мельников В.Ф. Расширение и сжатие системы вспышечных петель во время вспышки 15.01.2022 по данным в ультрафиолетовом и микроволновом диапазонах **Сборник трудов XXVI Всероссийской ежегодной конференции по физике Солнца «Солнце и солнечно-земная физика – 2022» ГАО РАН.**
http://www.gaoran.ru/russian/solphys/2022/book/conf2022.pdf

Динамика нагрева плазмы и энергетических распределений ускоренных электронов во время солнечных вспышек по данным рентгеновского и ультрафиолетового излучения
Моторина Г.Г.
Диссертация. ГАО. **2017**
http://www.gaoran.ru/russian/diss/Motorina_diss.pdf
https://arxiv.org/ftp/arxiv/papers/1710/1710.10652.pdf
The aim of the thesis is the study of properties of solar flares via reconstruction of energy distributions of accelerated/heated electrons, diagnostics of flare plasma based on EUV and X-ray observations, as well as the estimation of the thermal balance within the "standard" flare model. The X-ray data were obtained from the Ramaty High Energy Solar Spectroscopic Imager (RHESSI) and the Russian solar observatory KORONAS-F (IRIS experiment). The EUV data were obtained from the Solar Dynamics Observatory / Atmospheric Imaging Assembly (SDO/AIA). In the first chapter a new technique is presented, which allowed to determine at first the photon spectra based on the KORONAS-F/IRIS observations and then to reconstruct the energy spectra of the emitting electrons using the random search method and the Tikhonov regularization method. In the second chapter the developed technique of simultaneously fitting the model differential emission measure functions (DEM) to RHESSI and SDO/AIA data is introduced, which allowed to infer the electron distribution from X-ray and EUV observations. The proposed method allows to reconstruct of both the spectra of accelerated/heated electrons and the basic parameters of the flare plasma, such as temperature, emission measure, total electron number density, and flare energy. In addition, the analytical function suitable for both DEM analysis and mean electron flux spectra in flares has been developed and applied, as well as kappa-distribution in the form of differential emission measure. The thermal balance and hard X-ray emission of coronal loops from different flare regions within the "standard" flare model is considered in the third chapter. This thesis is based on the next papers: Motorina et al., TePh, 2012, Motorina & Kontar, Ge&Ae, 2015, Battaglia et al., ApJ, 2015, Motorina et al., TePh, 2016, Tsap et al., Ge&Ae, 2016. **15 апреля 2002, 23 июля 2002, 26 июля 2002, 19 января 2005, 23.08.2005, 14 Aug 2010, 09.11.2013, 8 мая 2015**

ИССЛЕДОВАНИЕ ПРОЦЕССОВ ОХЛАЖДЕНИЯ НА ФАЗЕ СПАДА СОЛНЕЧНЫХ И ЗВЕЗДНЫХ ВСПЫШЕК

МОТЫК И.Д.[*1], **КАШАПОВА Л.К.**[*1]

АЖ Том: 99Номер: 11 Год: **2022** Страницы: 1008-1015

Работа посвящена исследованию процессов охлаждения и потери энергии на фазе спада вспышек. Именно во время этой фазы одновременно с процессами охлаждения и потери энергии могут возникать различные волновые процессы, приводящие к дополнительному энерговыделению, что делает ее интересным объектом исследования. Считается, что охлаждение вспышечной плазмы на фазе спада происходит за счет двух процессов – теплопроводности и потерь за счет излучения. В начале доминирует процесс теплопроводности, а затем наступает полное доминирование процесса потерь за счет излучения. Мы провели анализ средних временн{\cyrery}'х профилей солнечных вспышек в полосах SDO/AIA 304, 1600 и 1700 Å и среднего временно́го профиля вспышки в белом свете карлика спектрального класса M4. Для описания временн{\cyrery}'х профилей была предложена аналитическая модель, основанная на известных формулах поведения температуры. Результаты анализа с помощью разработанной модели показали, что доминирование процесса охлаждения за счет потерь на излучение для полосы SDO/AIA 304 Å наступает раньше, чем это определено в стандартной модели. Для других спектральных полос процесс потерь за счет излучения практически все время доминирует на фазе спада. Сравнение результатов, полученных для вспышек на красном карлике M4 и в солнечных вспышках, показало, что процессы охлаждения в солнечных и звездных вспышках схожи и зависят от структуры атмосферы. Предложенная аналитическая модель может использоваться для разделения классической формы затухания и накладывающихся на нее процессов энерговыделения.

ЭВОЛЮЦИЯ ХАРАКТЕРИСТИК ВЕРТИКАЛЬНОГО ЭЛЕКТРИЧЕСКОГО ТОКА И МАГНИТНОГО ПОЛЯ В АКТИВНЫХ ОБЛАСТЯХ СОЛНЦА И ИХ СВЯЗЬ С МОЩНЫМИ ВСПЫШКАМИ

Нечаева А.Б., Зимовец И.В., Зубик В.С., Шарыкин И.Н.

ГиА Том: 64Номер: 2 Год: 2024 Страницы: 175-198

Изучение эволюции магнитного поля и электрических токов в активных областях Солнца на длительном интервале времени представляет интерес для понимания процессов накопления и выделения энергии в них, приводящих к разнообразным явлениям, оказывающим влияние на космическую погоду. В этой работе на основе фотосферных векторных магнитограмм инструмента Helioseismic and Magnetic Imager на борту Solar Dynamics Observatory был проведен анализ эволюции ряда характеристик магнитного поля и вертикального электрического тока в трех активных областях 11158, 11675 и 12673, произведших вспышки классов M и X, на протяжении времени от их зарождения в восточном полушарии, во время прохождения по солнечному диску и до исчезновения вблизи западного лимба с шагом 2 часа. Рассматриваемые характеристики включали в себя: показатель степенной функции плотности вероятности абсолютного значения плотности вертикального электрического тока, максимум абсолютного значения плотности вертикального тока, знаковый и беззнаковый вертикальный ток, беззнаковые вертикальный и горизонтальный магнитные потоки, энергия нелинейного бессилового и потенциального магнитного поля, свободная магнитная энергия, а также количество островов с сильными вертикальными токами. Найдены некоторые закономерности в поведении рассматриваемых характеристик при эволюции активных областей, в частности относительно возникновения вспышек. Рассчитаны коэффициенты корреляции между парами всех рассматриваемых характеристик. Дополнительно, показана перспективность подхода М. Ашвандена для прогнозирования максимального рентгеновского класса вспышки на основе вычисления энергии потенциального магнитного поля в активных областях. Полученные результаты могут использоваться при прогнозировании мощных солнечных вспышек.

Evolution of the Photospheric Magnetic Field and Coronal Null Points before Solar Flares

А. В. **Орешина**, Б. В. Сомов,

Письма в АЖ, **35**, 234-240 (**2009**). (See ADS)

Based on a topological model for the magnetic field of a solar active region (AR), we suggest a criterion for the existence of magnetic null points on the separators in the corona. With the problem of predicting solar flares in mind, we have revealed a model parameter whose decrease means that the AR evolves toward a major eruptive flare. We analyze the magnetic field evolution for AR 9077 within two days before the Bastille Day flare on **July 14, 2000.** The coronal conditions are shown to have become more favorable for magnetic reconnection, which led to a 3B/X5.7 eruptive flare.

Analytical Description of Charged Particle Motion in a Reconnecting Current Sheet

А. В. **Орешина**, Б. В. Сомов,

Письма в АЖ, **35**, 221-233 (**2009**). (See ADS)

Abstract—We have obtained an analytical solution to the equation of motion in the guiding center approximation for nonrelativistic charged particles in a reconnecting current sheet with a three-component magnetic field. Given the electric field attributable to magnetic reconnection, the solution describes stable and unstable three-dimensional particle orbits. We have found the domain of input parameters at which the motion is stable. A physical interpretation of the processes affecting the stability of the motion is given. Charge separation is shown to take place in the sheet during the motion: oppositely charged particles are localized mostly in different regions of the current sheet. A formula is derived for the particle energy in stable and unstable orbits. The results obtained by numerical and analytical methods are compared.

ФИЗИЧЕСКИЙ МЕХАНИЗМ СОЛНЕЧНОЙ ВСПЫШКИ, ОСНОВАННЫЙ НА НАКОПЛЕНИИ ЭНЕРГИИ В МАГНИТНОМ ПОЛЕ ТОКОВОГО СЛОЯ В СОЛНЕЧНОЙ КОРОНЕ

Подгорный И.М., Подгорный А.И.

КОСМИЧЕСКИЕ ИССЛЕДОВАНИЯ Том: 57Номер: 6 Год: **2019** Страницы: 403-422

DOI: 10.1134/S0023420619060062

Во время солнечной вспышки за несколько десятков минут освобождается магнитная энергия ~1032 эрг. Неизменность магнитного поля на солнечной поверхности во время вспышек доказывает появление вспышки в короне. Анализ динамики электронной температуры солнечной атмосферы дает независимое доказательство коронального происхождения вспышки. Появление вспышки в короне объясняется освобождением энергии, накопленной в магнитном поле токового слоя. Для исследования вспышечной ситуации проводилось численное МГД моделирование над реальной активной областью. Результаты моделирования показали появление токового слоя, положение которого совпадает с положением наблюдаемого источника теплового рентгеновского излучения. Разработана методика проведения расчетов в реальном масштабе времени. Основываясь на механизме освобождения энергии в токовом слое предложена электродинамическая модель солнечной вспышки, объясняющая ее основные наблюдаемые проявления. Источники жесткого рентгеновского излучения появляются вследствие торможения в нижних плотных слоях солнечной атмосферы пучков электронов, ускоренных в продольных токах. Ускорение солнечных космических лучей происходит в токовом слое электрическим полем $E = -V \times B/c$, а не в ударных волнах.

ГЕНЕРАЦИЯ ТОКОВОГО СЛОЯ В КОРОНЕ, АККУМУЛИРУЮЩЕГО ЭНЕРГИЮ ДЛЯ ВСПЫШКИ

Подгорный1 А.И., Подгорный2 И.М.

Астрономия-**2018** Том 2 Солнечно-земная физика – современное состояние и перспективы с. 190
http://www.izmiran.ru/library/eaas2018/eaas-2018-2.pdf
The flare mechanism based on the energy accumulation in the magnetic field of a current sheet explains the slow energy accumulation in corona and then its explosive release. The position of the current sheet obtained by numerical MHD simulation above a real active region coincides with the position of source of flare thermal X-ray emission. Flare energy accumulation is demonstrated by positions of 2D magnetic field lines in the plane perpendicular to the magnetic vector in the point of the current density maximum.

УСКОРЕНИЕ СОЛНЕЧНЫХ КОСМИЧЕСКИХ ЛУЧЕЙ ВО ВСПЫШЕЧНОМ ТОКОВОМ СЛОЕ И ИХ РАСПРОСТРАНЕНИЕ В МЕЖПЛАНЕТНОМ ПРОСТРАНСТВЕ

ПОДГОРНЫЙ А.И.1, ПОДГОРНЫЙ И.М.
АЖ Том: 92Номер: 9 Год: **2015** Страницы: 767
Анализ данных космических аппаратов GOES показал, что быстрая компонента протонов высокой энергии приходит к Земле от вспышки, происшедшей на западной части солнечного диска, с пролетным временем, а запаздывающая компонента начинает регистрироваться через несколько часов. Ускорение всех протонов происходит во вспышке единым механизмом. Частицы быстрой компоненты распространяются вдоль магнитных линий спирали Архимеда, которые связывают вспышку с Землей. Быстрая компонента не регистрируется на Земле от вспышек, происшедших на восточной части солнечного диска. Частицы от таких вспышек не попадают на линию магнитного поля, связывающую вспышку с Землей. Эти частицы достигают Земли, перемещаясь поперек межпланетного магнитного поля. Захваченные магнитным полем частицы переносятся солнечным ветром благодаря вмороженности межпланетного магнитного поля в плазму и диффундируют поперек поля. Длительность запаздывающей компоненты достигает нескольких суток.

ДИНАМИКА МАГНИТНОГО ПОЛЯ АКТИВНЫХ ОБЛАСТЕЙ В ПРЕДВСПЫШЕЧНОМ СОСТОЯНИИ И ВО ВРЕМЯ СОЛНЕЧНЫХ ВСПЫШЕК

ПОДГОРНЫЙ А.И.1, ПОДГОРНЫЙ И.М.2, МЕШАЛКИНА Н.С.
АЖ Том: 92 Номер: 8 Год: **2015** Страницы: 669
Проведен анализ вспышечной активности активных областей Солнца NOAA **10656, 11429, 10930**. Показано сохранение во время вспышки не только магнитного потока с точностью до 2%, но и распределения магнитного поля в активной области. Анализ подтвердил ранее опубликованные авторами выводы о возникновении больших (класса X) солнечных вспышек при магнитных потоках активных областей больших 10^{22} Мкс. Для возникновения большой вспышки недостаточно только большого магнитного потока активной области. Показано, что распределение поля активной области перед вспышкой должно иметь сложную структуру типа $\beta\gamma\delta$. Такие активные области могут создавать в короне особые линии магнитного поля, в окрестности которых формируются токовые слои. Над простыми, дипольного типа ативными областями магнитные линии имеют арочную форму, особые линии отсутствуют, и токовые слои образоваться не могут. Дипольного типа активные области не производят вспышек. Дисбаланс магнитного потока активной области и скорость нарастания магнитного потока не являются признаками появления вспышки.

НАКОПЛЕНИЕ МАГНИТНОЙ ЭНЕРГИИ В КОРОНАЛЬНОМ ТОКОВОМ СЛОЕ В ПРЕДВСПЫШЕЧНОМ СОСТОЯНИИ АКТИВНОЙ ОБЛАСТИ СОЛНЦА

И.М. **Подгорный**, А.И. Подгорный
ИКИ-**2014**, Сессия: Солнце
http://plasma2014.cosmos.ru/presentations
1. Необходимое условие возникновения большой вспышки (класса X) – возрастание магнитного потока АО Ф > 10^22 Макс.
2. Вспышки происходят над АО со сложной конфигурация магнитного поля. Простые биполярные АО вспышек не производят.
3. Распределение B в АО сохраняется во время большинства в том числе и больших вспышек.
4. Полученные результаты показывают, что энергия вспышки выделяется высоко в короне, и токи, ответственные за аккумулированную для вспышки энергию локализованы в короне. Такой токовой системой может быть **токовый слой**.

ВСПЫШЕЧНОЕ ИЗЛУЧЕНИЕ СОБЫТИЯ 04.05.2022 И ЕГО МИЛЛИМЕТРОВАЯ КОМПОНЕНТА

Смирнова В.В., Цап Ю.Т., Рыжов В.С., Моторина Г.Г., Моргачев А.С., Барта М.
ГиА Том: 63Номер: 5 Год: **2023** Страницы: 561-569

На основе наблюдений на радиотелескопе РТ-7.5 МГТУ им. Н.Э. Баумана на волне 3.2 мм (93 ГГц), а также других (Сибирского радиогелиографа, Solar Dynamics Observatory (SDO), радиообсерватории Metsähovi) наземных и космических инструментах исследовано происхождение миллиметрового излучения солнечной вспышки SOL**2022-05-04T08**:45 рентгеновского класса M5.7. Анализ временны́х профилей излучения в рентгеновском и сантиметровом диапазонах показал, что миллиметровый источник излучения едва ли связан с горячей (5 × 105–107 K) корональной плазмой. Об этом также свидетельствует оценка суб-ТГц потока излучающей горячей плазмы по данным AIA/SDO, который оказался значительно меньше наблюдаемых значений. Получены указания о развитии тепловой неустойчивости во вспышечных ультрафиолетовых петлях. Обосновывается связь миллиметровой компоненты вспышки с тепловым источником в хромосфере Солнца.

МАГНИТНЫЕ ЖГУТЫ С ТОКОВОЙ ОБОЛОЧКОЙ КАК ВСПЫШЕЧНЫЕ СОЛНЕЧНЫЕ СТРУКТУРЫ

СОЛОВЬЕВ А.А.[1], **КИРИЧЕК Е.А.**[1]

ПАЖ Том: 50 Номер: 9 Год: 2024 Страницы: 616-624

Модели бессиловых магнитных жгутов различаются по их внутренней токовой структуре: в одном случае сильные электрические токи сосредоточены на оси жгута, а в другом - в тонкой периферической оболочке. В настоящей работе проводится сравнительный анализ трех новых моделей второго типа. Все бессиловые магнитные жгуты имеют одно общее физическое свойство, приводящее к вспышечному энерговыделению: при выходе вершины петельного жгута в хромосферу и корону Солнца, внешнее давление, удерживающее жгут от бокового расширения, неуклонно падает; при некотором критическом его уменьшении продольное магнитное поле жгута стремится к нулю на поверхности смены знака токов. При этом азимутальный ток jϕ(r) и бессиловой параметр α(r), приближаясь к разрыву на этой поверхности, начинают неограниченно расти вблизи нее. Это приводит к возбуждению плазменной ионно-звуковой неустойчивости, резкому понижению проводимости плазмы, быстрой диссипации магнитной энергии в жгуте и генерации супер-дрейсеровских электрических полей. Совокупность таких процессов в сочетании с эффектом Паркера - выравниванием с альвеновской скоростью вращательного момента (torque) вдоль оси жгута - хорошо описывает основные проявления солнечной вспышки.

МАГНИТОГИДРОСТАТИКА ВЕРТИКАЛЬНОЙ СИЛОВОЙ ТРУБКИ В СОЛНЕЧНОЙ АТМОСФЕРЕ: КОРОНАЛЬНЫЕ ПЕТЛИ, МОДЕЛЬ КОЛЬЦЕВОГО ВСПЫШЕЧНОГО ВОЛОКНА

СОЛОВЬЕВ А.А.1, КИРИЧЕК Е.А

ПАЖ 41(5) 234 **2015**

Магнитогидростатическая теория скрученной магнитной силовой трубки (жгута), погруженной в реалистическую солнечную атмосферу, впервые представлена в замкнутой аналитической форме. Выведены общие формулы, позволяющие рассчитывать равновесные распределения плотности, давления и температуры плазмы внутри аксиальносимметричной вертикальной силовой трубки по ее магнитной структуре, которая предполагается известной (заданной). Построена аналитическая модель свободной от магнитного поля внешней гидростатической среды - солнечной атмосферы, в которой использован температурный профиль полуэмпирической табличной модели Авретта [illegible] формул рассчитано распределение параметров плазмы в скрученной магнитной силовой трубке при небольших отклонениях ее внутренней магнитной структуры от бессиловой. Поперечное сечение трубки не меняется с высотой, поэтому полученную модель можно применять для описания вертикальных частей корональных петель. Найдено, что при превышении скрученности поля над бессиловым состоянием плотность плазмы в магнитной трубке растет, а при уменьшении скрученности поля по сравнению с бессиловым уровнем - падает. Это свойство скрученной магнитной трубки имеет принципиальное значение для обоснования механизма вспышечного энерговыделения в магнитных жгутах. Рассмотрена модель вспышки в кольцевой хромосферной конфигурации.

НОВЫЕ НАПРАВЛЕНИЯ В ФИЗИКЕ СОЛНЕЧНЫХ ВСПЫШЕК

10 minute review

Б.В. **Сомов**

ИКИ-**2014**, Сессия: Солнце
http://plasma2014.cosmos.ru/presentations

О магнитном пересоединении электрических токов в солнечных вспышках,

Сомов Б.В.,

Письма в Астрон. журн., 38, 149, 2012

Новые результаты и новые вопросы в физике больших солнечных вспышек

Б.В. **Сомов**

Презентация, ИКИ, февр. **2009; File**

РАСШИРЕНИЕ ИСТОЧНИКА МЯГКОГО РЕНТГЕНОВСКОГО ИЗЛУЧЕНИЯ И ‘‘МАГНИТНАЯ ДЕТОНАЦИЯ’’ В СОЛНЕЧНЫХ ВСПЫШКАХ

Струминский А.Б., Садовский А.М., Григорьева И.Ю.

ПАЖ Том: 49Номер: 11 Год: 2023 Страницы: 806-818
DOI: 10.31857/S0320010823110086

Регистрация радиоизлучения солнечных вспышек на частотах ниже ~2 ГГц позволяет делать верхние оценки характерного размера источника мягкого рентгеновского (SXR) излучения $L(t)$ в предположении, что плотность $n(t)$ определяется плазменной частотой ν_p. Если SXR источник с большей плотностью находится внутри радиоисточника, то размер SXR источника будет$L(t)<(EM(t)/2n(t)^2)^{1/3}$, где $EM(t)$ — мера эмиссии. Для трех вспышек (C7.2 **22.12.2009**), (M2.9 **06.07.2012**) и (X1.1 **06.07.2012**) рассчитываются скорости расширения SXR источника $V(t)\sim dL(t)/dt$, которые сравниваются с оценками скорости звука и альвеновской скорости. Под “магнитной детонацией” мы понимаем процесс распространения магнитного пересоединения со сверхзвуковой скоростью в эруптивных вспышках. “Магнитная детонация” и последующий корональный выброс массы (КВМ) реализовывались во вспышках (C7.2 22.12.2009) и (X1.1 06.07.2012), в которых сверхзвуковые и сверхальвеновские скорости достигались, если плотность SXR источника была ниже 2.1×10^9 и 7.4×10^8 см$^{-3}$ (ν_p<410 и <245 МГц) соответственно. “Магнитной детонации” и КВМ не было во вспышке (M2.9 06.07.2012), частоты радиоизлучения которой были только выше 1415 МГц ($n>2.5\times10^{10}$ см$^{-3}$). Для “магнитной детонации” во вспышке (X1.1 06.07.2012) сделаны оценки величин магнитного поля, напряженности электрического поля пересоединения, потока плазмы и массы КВМ.

СВЯЗЬ МЕЖДУ ДЛИТЕЛЬНОСТЬЮ И ВЕЛИЧИНОЙ УСКОРЕНИЯ КОРОНАЛЬНЫХ ВЫБРОСОВ МАССЫ

Струминский А. Б., Григорьева И. Ю., Логачев Ю. И., Садовский А. М.

ГЕОМАГНЕТИЗМ И АЭРОНОМИЯ Том: 61Номер: 6 Год: 2021 Страницы: 683-693
DOI: 10.31857/S001679402105014X

Исследуется вопрос о том, какая последовательность процессов на Солнце приводит к положительной обратной связи между движением и нагревом плазмы, ускорением электронов, а в итоге, к формированию корональных выбросов массы, ударных волн и ускорению протонов. Для этого проведен анализ солнечных событий, связанных с тремя импульсными вспышками: M2.9 **6 июля 2012** г., X2.2 и X9.3 **6 сентября 2017** г. и одной длительной вспышкой M3.7 **7 марта 2011** г. Электроны ускорялись до релятивистских энергий во всех четырех вспышках, но две последние сопровождались корональными выбросами массы, ударными волнами и ускорением протонов с энергией >300 МэВ. Найдено два отличия вспышек без корональных выбросов массы. Первое отличие – были ограничены высотой, которая характерна для радиоизлучения 1415 МГц (верхняя хромосфера). Второе отличие – максимум меры эмиссии в них запаздывал относительно максимума температуры на время менее 2 мин. Если считать, что вспышка и корональные выбросы массы черпают энергию из одного резервуара, то время запаздывания можно рассматривать как характерное время ускорения корональных выбросов массы – существование дополнительного оттока энергии. Из теоретических оценок максимальной величины ускорения корональных выбросов массы, значений их минимальной и максимальной скорости следует возможный разброс времени ускорения корональных выбросов массы. Сравнения оценок и наблюдений показывает, что необходимая длительность ускорения для реализации межпланетного коронального выброса массы была достигнута в событиях M3.7 7 марта 2011 г. и X9.3 6 сентября 2017 г.

ПРОГНОЗИРОВАНИЕ СОЛНЕЧНЫХ ВСПЫШЕК И ФОНОВЫХ ПОТОКОВ РЕНТГЕНОВСКОГО ИЗЛУЧЕНИЯ ПО ДАННЫМ СИНОПТИЧЕСКИХ НАЗЕМНЫХ НАБЛЮДЕНИЙ С ПОМОЩЬЮ МЕТОДОВ МАШИННОГО ОБУЧЕНИЯ

ТЛАТОВ А.Г.*1, ИЛЛАРИОНОВ Е.А.2, БЕРЕЗИН И.А.1, ШРАМКО А.Д.

Косм. Исслед. Том: 58Номер: 6 Год: **2020** Страницы: 479-484

В работе представлены модели машинного обучения для прогнозирования мощных солнечных вспышек и фоновых потоков рентгеновского излучения в диапазоне 1–8 Å. Для прогнозирования солнечных вспышек на следующий день использовалась информация о текущем уровне солнечной активности, получаемая с наземных синоптических наблюдений, таких как характеристики солнечных пятен, потоки радиоизлучения на длинах волн 10.7 и 5 см, а также уровень фонового потока и количества солнечных вспышек текущего дня, полученных со спутника GOES. Для прогнозирования фоновых потоков рентгеновского излучения использовались только данные наземных телескопов. Показана высокая эффективность прогноза на следующий день. Нейронные сеть обучалась на данных, доступных с 2002 г.

ГАММА-ВСПЫШКИ И КОМПЛЕКСЫ АКТИВНОСТИ НА СОЛНЦЕ

ТОМОЗОВ В.М.1, ЯЗЕВ С.А.*1, ИСАЕВА Е.С.

АЖ Том: 97Номер: 8 Год: **2020** Страницы: 695-704

Проведен анализ мощных вспышечных событий из каталога Share и др. с длительной фазой гамма- излучения с целью объяснения особенностей импульсной и длительных фаз таких вспышек и выявления их связи с комплексами активности и корональными дырами. Показано, что 74% таких событий оказались тесно связанными с комплексами активности. Качественно продемонстрирована связь процессов ускорения частиц в ходе развития вспышки с изменениями магнитной топологии во вспышечной области и с эволюцией

коронального выброса массы. Обсуждаются возможная связь корональных дыр с комплексами активности и роль “обменного” пересоединения в этих процессах.

РАСПРЕДЕЛЕНИЕ ЭНЕРГИИ НАНОВСПЫШЕК В МИНИМУМЕ И НА ФАЗЕ РОСТА 24 СОЛНЕЧНОГО ЦИКЛА

А. С. **Ульянов**, С. А. Богачёв, А. А. Рева, А. С. Кириченко, И. П. Лобода

ПАЖ Том: 45Номер: 4 Год: **2019** Страницы: 290-300

Представлено распределение по энергиям слабых эмиссионных событий (нановспышек) в короне Солнца, измеренное для двух стадий 24-го солнечного цикла, - в минимуме и в начале роста солнечной активности. Исследование проведено по данным двух инструментов, ТЕСИС/КОРОНАС-ФОТОН (для минимума цикла; 2009 г.) и AIA/SDO (фаза роста, 2010–2011 гг.), для которых мы применили единый алгоритм детектирования событий. Собранная нами база составляет более 10^5вспышек. Для всех событий мы измерили поток излучения в ВУФ-диапазоне спектра и определили тепловую энергию, которая находилась в диапазоне от 10^{23} до 10^{26} эрг и была распределенной по степенному закону: $N(E)dE \sim N^{-\alpha}dE$ ...

Филатов Л.В., Мельников В.Ф. Ускорение нетепловых электронов при согласованном взаимодействии с турбулентностью вистлеров во вспышечной петле ……

Сборник трудов XXVI Всероссийской ежегодной конференции по физике Солнца «Солнце и солнечно-земная физика – 2022» ГАО РАН.

http://www.gaoran.ru/russian/solphys/2022/book/conf2022.pdf

СТРУКТУРА И ФИЗИЧЕСКИЕ УСЛОВИЯ В НА-ПЕТЛЯХ ВСПЫШКИ БАЛЛА М7.7

ФИРСТОВА Н.М.1, ПОЛЯКОВ В.И.

ПАЖ Том: 43Номер: 11 Год: **2017** Страницы: 845-856

Вспышка балла М7.7 **19 июля 2012** г. представляет собой наиболее яркий пример вспышки "Масуда" с четко определенным вторым рентгеновским источником выше вершины петли. Поведение системы петель, сопровождающих эту вспышку, подробно исследовано Лиу и др. по данным Reuven Ramaty High Energy Solar Spectroscopic Imager (RHESSI) и Solar Dynamics Observatory/Atmospheric Imaging Assembly (SDO/AIA). Мы провели на Большом солнечном вакуумном телескопе (БСВТ) спектральные и фильтровые наблюдения На-петель в этой вспышке. Основные физические параметры в петлях этой особенной вспышки в целом совпадают с известными данными в На-петлях. Однако электронная концентрация 1011 см-3 и интегральная интенсивность 12% непрерывного излучения центра солнечного диска являются довольно высокими, если учесть, что наблюдения получены почти через 3 ч после начала вспышки. Проведена оценка скорости подъема аркады петель (^3.5 км/с) и разности высот между На-петлями и петлями в 94 А, которая составляет ^2 х 104 км.

СВЯЗЬ МЕЖДУ ПОЯВЛЕНИЕМ ИСТОЧНИКОВ ГАММА-ИЗЛУЧЕНИЯ И УДАРНОЙ ЛИНЕЙНОЙ ПОЛЯРИЗАЦИЕЙ ЛИНИИ Н ВО ВСПЫШКЕ 23 ИЮЛЯ 2002 ГОДА

ФИРСТОВА Н.М.

ПАЖ Том: 41Номер: 10 Год: **2015** Страницы: 642

При спектро-поляриметрических наблюдениях на Большом солнечном вакуумном телескопе вспышки балла 2В/4.8Х **23 июля 2002** г. нами в южной ленте была обнаружена ударная линейная поляризация. Максимальная поляризация превысила 10 . В целом поляризация наблюдалась только в течение 6 мин из почти 2 ч наблюдений этой вспышки. Профили линии Н имели в это время глубокое самообращение в центре. В настоящей работе проведено сопоставление наблюденной на БСВТ с данными Reuven Ramaty High Energy Solar Spectroscopic Imager (RHESSI), где впервые были получены местоположения -излучения. При точном сопоставлении выяснилось, что эффекты в линии Н наблюдались на участке <10, который был расположен между двумя рентгеновскими источниками в южной ленте. В этом же месте, по данным RHESSI, наблюдался источник -излучения, обусловленный потоком высокоэнергичных (1 МэВ) электронов. События в короне и в верхней хромосфере совпадают с наблюденными эффектами в линии Н также и по времени. В работе делается предположение, что два рентгеновских источника представляют собой общее основание южной ветви петли, раздвоенное из-за высыпания высокоэнергичных электронов. Предполагается, что внедрение этих электронов в плотные слои хромосферы могло привести к ударной поляризации и провалу интенсивности в линии Н в южной ленте вспышки в отличие от северной ленты, где наблюдался типичный источник жесткого рентгена с энергией 20 120 кэВ, самообращение в цен

ПОПЕРЕЧНЫЕ ГРАДИЕНТЫ ПРОДОЛЬНОГО МАГНИТНОГО ПОЛЯ В АКТИВНЫХ ОБЛАСТЯХ С РАЗНЫМ УРОВНЕМ ВСПЫШЕЧНОЙ ПРОДУКТИВНОСТИ: РАЗЛИЧНЫЕ ПОДХОДЫ К ВЫЧИСЛЕНИЮ, ДИНАМИКА И ВЕРОЯТНЫЕ КРИТИЧЕСКИЕ ЗНАЧЕНИЯ

ФУРСЯК ЮРИЙ

Изв. КрАО Том: 118Номер: 3 Год: 2022 Страницы: 39-57
https://www.elibrary.ru/download/elibrary_49967263_79839761.pdf

Основной задачей исследования является анализ величины и динамики поперечной составляющей градиента продольного магнитного поля в активных областях (АО) с различным уровнем вспышечной продуктивности. В работе использованы данные о пространственном распределении на уровне фотосферы Солнца Bz-компоненты вектора магнитного поля, предоставляемые инструментом Helioseismic and Magnetic Imager (HMI) на борту Solar Dynamics Observatory (SDO). Для анализа отобраны 13 АО: 6 областей с низкой активностью и 7 с высокой, из них две области с дополнительным всплытием магнитного потока. Мониторинг каждой из областей осуществлялся на протяжении 3–5 суток в пределах 30–35 гелиографических градусов относительно центрального меридиана. Рассмотрены два подхода к вычислению градиента продольного магнитного поля – современный, требующий магнитографических данных высокого пространственного разрешения, и классический. Для каждого подхода определены параметры, характеризующие градиент продольного магнитного поля в АО. Для современного подхода это средняя по АО величина поперечной составляющей градиента продольного магнитного поля $< \nabla \perp Bz >$, для классического подхода – максимальное значение поперечной составляющей градиента продольного магнитного поля совокупности пар пятен в АО ($max(\nabla \perp Bz)$). Динамика выбранных параметров сопоставлена с уровнем вспышечной продуктивности АО. Показано, что: 1. Существуют пороговые значения параметров, характеризующих градиент продольного магнитного поля АО. Для величины $< \nabla \perp Bz >$ критическое значение равно 0.08 Гс км$^{-1}$, а для параметра $max(\nabla \perp Bz)$ – 0.115 Гс км$^{-1}$. 2. Первые мощные вспышки рентгеновских классов M и выше наблюдаются в АО через 23–25 часов после превышения вышеуказанными параметрами соответствующих критических значений.

МОРФОЛОГИЯ, ДИНАМИКА И ОСОБЕННОСТИ МАГНИТНОЙ КОНФИГУРАЦИИ АКТИВНЫХ ОБЛАСТЕЙ ПЕРЕД ВСПЫШКАМИ РЕНТГЕНОВСКОГО КЛАССА X

Фурсяк Ю.А.

Пулково «Солнечная и солнечно-земная физика – **2015**», с.371

We analyzed morphological and evolutionary characteristics of several active regions in the solar cycle 24, that launched at least two or more X-class flares. Transverse gradients of the longitudinal magnetic field, proper motions of sunspots, as well as features of the magnetic configuration of sunspot groups before the powerful flare were investigated. We used data from SDO/HMI (magnetic fields of active regions), X-ray flux data from the spacecraft GOES-15, and information about the magnetic fields of sunspots obtained from the Tower Solar Telescope TST-2 of the Crimean Astrophysical Observatory and the Mt. Wilson 150-foot Solar Telescope. We found that during at least 1–2 days before the launch of the first Xclass flare, the magnetic gradient has to exceed the Severny's critical threshold of 0.1 G/km. **04-08.09.2011, 04-08.03.2012, 09-17.10.2013, 21-27.10.2014**

ТЕМПЕРАТУРА СТОЛКНОВИТЕЛЬНОЙ ПЛАЗМЫ И БЕТАТРОННОЕ УСКОРЕНИЕ КВАЗИТЕПЛОВЫХ ЭЛЕКТРОНОВ В СОЛНЕЧНЫХ ВСПЫШКАХ

ЦАП Ю. Т.[*1], **МЕЛЬНИКОВ В. Ф.**[*2]

ПАЖ Том: 49Номер: 4 Год: **2023** Страницы: 289-298

На основе модели коллапсирующей магнитной ловушки рассмотрено влияние температуры максвелловской вспышечной плазмы на эффективность бетатронного ускорения квазитепловых быстрых электронов в области каспа корональных петель. Показано, что увеличение температуры приводит к резкому росту (на 6–8 порядков) числа квазитепловых электронов, способных преодолеть "барьер кулоновских потерь". Это предполагает необходимость преднагрева фоновой плазмы в области каспа до $\gtrsim$10 МК, за которое может отвечать бетатронный механизм. Обсуждается связь между импульсной фазой вспышечного энерговыделения и рентгеновскими предвестниками солнечных вспышек.

УСКОРЕНИЕ ЭЛЕКТРОНОВ И СУБСЕКУНДНЫЕ ВРЕМЕННЫЕ ЗАДЕРЖКИ ЖЕСТКОГО РЕНТГЕНОВСКОГО ИЗЛУЧЕНИЯ СОЛНЕЧНЫХ ВСПЫШЕК ПО ДАННЫМ РОССИЙСКОГО СПУТНИКА ЛОМОНОСОВ

Цап Ю.Т., Петров В.Л., Яшин И.В., Богомолов В.В., Богомолов А.В., Свертилов С.И., Панасюк М.И., Гольдварг Т.Б., Моторина Г.Г., Копылова Ю.Г., Мягкова И.Н.

ПАЖ Том: 56Номер: 6 Год: **2018** Страницы: 404-409

На основе спутниковых наблюдений, полученных с помощью блоков детектирования рентгеновского и гамма-излучения (БДРГ/Ломоносов), используя методы цифровой фильтрации, проведен анализ временных задержек

между секундными пульсациями временных профилей жесткого рентгеновского излучения различных диапазонов солнечной вспышки **21.VII.2016** г. Показано, что скорости счета квантов в энергетических каналах 10–20, 20–35 и 35–60 кэВ, зарегистрированные на БДРГ/Ломоносов, являются коррелированными с точностью до 0.1 с. Это сравнительно хорошо согласуется с результатами наблюдений на гамма-мониторе Gamma-ray Burst Monitor, установленном на спутнике Fermi, и предполагает эффективное ускорение заряженных частиц на протяжении всей длины вспышечной магнитной арки.

ВРЕМЕННЫЕ ЗАДЕРЖКИ НЕТЕПЛОВОГО ИЗЛУЧЕНИЯ СОЛНЕЧНЫХ ВСПЫШЕК ПО НАБЛЮДЕНИЯМ НА КОРОНАС-Ф

ЦАП Ю.Т.1,2, СТЕПАНОВ А.В.2, КАШАПОВА Л.К.3, МЯГКОВА И.Н.4, БОГОМОЛОВ А.В.4,КОПЫЛОВА Ю.Г.2, ГОЛЬДВАРГ Т.Б.

Косм. Исслед. Том: 54Номер: 4 Год: **2016** Страницы: 302-307

In 2001–2003, the X-ray and microwave observations of ten solar flares of M- and X-classes were carried out by the CORONAS-F orbital station, the RSTN Sun service, and Nobeyama radio polarimeters. Based on these observations, a correlation analysis of time profiles of nonthermal radiation was performed. On average, hard X-ray radiation outstrips the microwave radiation in 9 events, i.e., time delays are positive. The appearance of negative delays is associated with effective scattering of accelerated electrons in pitch angles, where the length of the free path of a particle is less than the half-length of a flare loop. The additional indications are obtained in favor of the need to account for the effect of magnetic mirrors on the dynamics of energetic particles in the coronal arches.

УСКОРЕНИЕ ЭЛЕКТРОНОВ И НАГРЕВ ВСПЫШЕЧНОЙ ПЛАЗМЫ КОРОНАЛЬНЫХ ПЕТЕЛЬ

Цап Ю.Т.1,2, Моторина Г.Г.2, Копылова Ю.Г.

Пулково «Солнечная и солнечно-земная физика – **2015**», с.379

The peculiarities of the SXR and HXR time profiles as well as the temperature and the emission measure of the **23 August 2005** (M3.0) and **9 November 2013** (C2.7) solar flares based on observations with RHESSI satellite are analysed. The dynamics of main parameters of the thermal coronal plasma was studied. The spectral index, integral flux, and low energy cutoff were found using the HXR spectrum fitting. It has been shown that the HXR peaks can be delayed with respect to the temperature ones. In terms of the energy balance and the relationship of HXR emission from the loop top and footpoints evidences in favor of an important role of the Joule dissipation and the electron acceleration in the chromosphere have been obtained.

МОДУЛИРОВАННЫЕ ВСПЫШКОЙ 3- И 5-МИНУТНЫЕ КОЛЕБАНИЯ КАК СРЕДСТВО ЗОНДИРОВАНИЯ СОЛНЕЧНОЙ АТМОСФЕРЫ

А. А. **Челпанов**, Н. И. Кобанов

АЖ т. 97, №4, 341-347, **2020**

Мы применяем новый подход для измерения временных задержек магнитогидродинамических волн, распространяющихся в солнечной атмосфере. Малая вспышка в факельной области послужила модулятором уже существующих в хромосфере 3- и 5-минутных колебаний. Амплитуда этих колебаний увеличилась в несколько раз, что сделало возможным легко фиксировать образовавшийся волновой цуг при его распространении вверх через слои солнечной атмосферы. Такой кратковременный и хорошо выраженный волновой цуг служит удобным инструментом для определения скорости распространяющихся магнитогидродинамических волн, поскольку он позволяет избежать неопределенностей в измерении фазового сдвига, которые возникают в обычных условиях. Преимущество использования амплитудной модуляции от малой вспышки состоит в том, что это дает возможность исследовать атмосферу Солнца в условиях, приближенных к условиям в невозмущенной атмосфере.

Вариации магнитного поля в акивнной области NOAA 10486 и их связь с рентгеновскими вспышками и корональными выбросами масс

О. В. Чумак[1], Х.-К. Цанг[2], Ж. Гуо[2]

Астрономический журнал, **2008, С. 946-960**

На основе магнитограмм SOHO/MDI проанализированы временны̀е изменения параметров магнитного поля активной области (АО) NOAA 10486, входившей в большой комплекс активности 23-го солнечного цикла, в течение ее прохождения по диску Солнца с **26 по 31 октября 2003 г.** Результаты сопоставлены с рентгеновскими вспышками в этой АО и параметрами корональных выбросов массы, ассоциированных с данной АО. Рассмотрены временны̀е вариации распределений по величине поля полного магнитного потока (Fa), имбаланса потоков северной и южной полярностей (Im), сложности(Co) как меры взаимоперекрытия противоположных полярностей, угла наклона магнитной оси (An). Временны̀е вариации свободной энергии, накопленной в токовых слоях АО, отслеживались с помощью специально введенного параметра (Sh). Получены следующие результаты. Во-первых, параметры Fa, Im, Co, An, Sh количественно идентифицируют текущее

состояние АО и позволяют отслеживать и анализировать динамическую эволюцию ее магнитного поля. Во-вторых, вариации распределений по величине магнитного поля и средние значения параметров Fa, Im, Co, An и Sh связаны со вспышками и корональными выбросами массы и демонстрируют значительную амплитуду. В-третьих, параметр Sh, характеризующий непотенциальность магнитного поля в областях, примыкающих к главной нейтральной линии, демонстрирует рост своих значений перед эруптивными событиями и представляет особый интерес в плане мониторинга состояния АО в реальном времени. В-четвертых, магнитное поле АО обнаруживает своеобразную “квазиупругость” — структура поля после активных событий восстанавливается в среднем за 1–3 ч.

Шабалин А.Н., Овчинникова Е.П., Чариков Ю.Е. Корональные источники жесткого рентгеновского излучения в моделях солнечных вспышек с вертикальным токовым слоем: наблюдения и моделирование …

Сборник трудов XXVI Всероссийской ежегодной конференции по физике Солнца «Солнце и солнечно-земная физика – 2022» ГАО РАН.

http://www.gaoran.ru/russian/solphys/2022/book/conf2022.pdf

ВЛИЯНИЕ ФЛУКТУАЦИЙ МАГНИТНОГО ПОЛЯ ВСПЫШЕЧНОЙ ПЕТЛИ НА ЭНЕРГЕТИЧЕСКИЙ СПЕКТР И ПРОСТРАНСТВЕННОЕ РАСПРЕДЕЛЕНИЕ ЖЕСТКОГО РЕНТГЕНОВСКОГО ИЗЛУЧЕНИЯ

Шабалин А.Н.1, Чариков Ю.Е

Пулково «Солнечная и солнечно-земная физика – **2015**», с.383

It is shown that turbulent pitch-angle scattering leads to increasing of Hard X-Ray intensity predominantly in loop’s footpoints for isotropic initial electron source and contrary strengthening at looptop for anisotropic beams for δB/B = 10-3.

РАСЧЕТ СТЕПЕНИ ЛИНЕЙНОЙ ПОЛЯРИЗАЦИИ ИЗЛУЧЕНИЯ ЛИНИИ Hα, ВОЗБУЖДАЕМОЙ ПРОТОНАМИ, ВО ВСПЫШКАХ СОЛНЦА

ШАПОЧКИН М. Б.*

АЖ Том: 98Номер: 4 Год: **2021** Страницы: 305-313

Приводится оригинальный аналитический расчет степени линейной поляризации линий Hα во время солнечных вспышек, вызванной анизотропными протонами, когда в хромосфере Солнца температура тепловых протонов больше температуры тепловых электронов. Анализируются зависимости степени линейной поляризации от параметров функции распределения тепловых и нетепловых протонов во время вспышек Солнца. Обсуждается диагностика вспышечной плазмы.

НАБЛЮДЕНИЕ ГЕЛИОСЕЙСМИЧЕСКИ АКТИВНОЙ СОЛНЕЧНОЙ ВСПЫШКИ С МАЛЫМ ПОТОКОМ ЖЕСТКОГО РЕНТГЕНОВСКОГО ИЗЛУЧЕНИЯ ДО 50 КЭВ

ШАРЫКИН И.Н.[1], **ЗИМОВЕЦ И.В.**[1], **КОСОВИЧЕВ А.Г.**[2], **МЫШЬЯКОВ И.И.**[3]

ПАЖ Том: 50Номер: 3 Год: **2024** Страницы: 233-250

Рассматривается солнечная вспышка класса M1.1, произошедшая **5 июля 2012** г. в 06:49 UT. Событие уникально тем фактом, что в нем было обнаружено гелиосейсмическое возмущение, несмотря на малый поток жесткого рентгеновского излучения в диапазоне 25-50 кэВ и очень мягкий спектр по данным RHESSI. Как правило, большинство известных солнцетрясений детектировалось в солнечных вспышках с большими потоками жесткого рентгеновского излучения на высоких энергиях (как минимум до 100-300 кэВ). Рассматриваемое событие противоречит популярной гипотезе о генерации солнцетрясений пучками ускоренных электронов высоких энергий. Анализ доступных рентгеновских спектров по данным RHESSI показывает, что их можно объяснить двумя способами. Рентгеновский спектр в диапазоне 25-50 кэВ объясняется степенным распределением ускоренных электронов с индексом 7-9, либо наличием сверхгорячей плазмы с температурой T ~ 30-60 МК. В том и другом случае мы имеем дело с электронами относительно низких энергий, которые либо являлись причиной генерации солнцетрясения, либо их следует рассматривать как вторичное (сопутствующее) явление по отношению к истинной причине фотосферного возмущения. Впервые для гелиосейсмически активной солнечной вспышки приводятся результаты совместного анализа рентгеновских и микроволновых спектров. Анализ показывает, что спектры в обоих диапазонах, могут хорошо объясняться излучением сверхгорячей замагниченной плазмы, а не ускоренными электронами с мягким спектром. Но также возможно объяснение спектров при рассмотрении ускоренных электронов, частично захваченных в магнитную ловушку. Получены оценки параметров тепловой плазмы, ускоренных электронов, потоков энергий различных видов. Проведен анализ динамики ультрафиолетовых и рентгеновских источников излучения. Также приводится анализ структуры магнитного поля по векторным магнитограммам и нелинейной бессиловой экстраполяции коронального магнитного поля. Обсуждаются механизмы генерации гелиосейсмического возмущения во время данной солнечной вспышки. Вероятно, эруптивный процесс мог быть как первичной, так и вторичной причиной

солнцетрясения. Появление сверхгорячей плазмы в короне могло привести к формированию распространяющихся тепловых фронтов в нижние слои солнечной атмосферы, где возбуждаются гелиосейсмические волны. Анализ не позволяет исключать и возможность генерации солнцетрясения ускоренными электронами с мягким спектром.

НАГРЕВ ПЛАЗМЫ ДО СВЕРХВЫСОКИХ ТЕМПЕРАТУР (МК) В СОЛНЕЧНОЙ ВСПЫШКЕ 9 АВГУСТА 2011 ГОДА

ШАРЫКИН И.Н.1, СТРУМИНСКИЙ А.Б.1,2, ЗИМОВЕЦ И.В.

ПАЖ Том: 41Номер: 1 Год: **2015** Страницы: 57

Astronomy Letters Volume 41, Issue 1-2, pp 53-66 **2015**

http://arxiv.org/pdf/1502.03220v1.pdf

Исследуется солнечная вспышка 9 августа 2011 г. рентгеновского класса X6.9, которая является самой “горячей” вспышкой с 2000 по 2012 гг., с максимальной температурой плазмы по данным GOES МК. Целью работы является определение причины такой аномально высокой температуры плазмы, а также исследование энергетического баланса во вспышечной области с учетом наличия сверхгорячей плазмы (МК). Мы анализируем данные RHESSI, GOES, AIA/SDO и EVE/SDO, обсуждаем пространственную структуру вспышечной области и результаты спектрального анализа ее рентгеновского излучения. Анализ рентгеновских спектров по данным RHESSI проводится в рамках одно- и двухтемпературного приближения с учетом излучения горячей (МК) и сверхгорячей (МК) плазмы. Спектр жесткого рентгеновского излучения в обеих моделях аппроксимируется степенными функциями. Показано, что наблюдаемые особенности вспышки лучше объясняются с помощью двухтемпературной модели, в которой сверхгорячая плазма располагается в вершинах вспышечных петель (или области магнитного каспа). Формирование сверхгорячей плазмы может быть связано с ее нагревом за счет первоначального энерговыделения и подавлением теплопроводности. Аномально высокая температура (33 МК по GOES) скорее всего является артефактом метода расчета температуры по двухканальным измерениям GOES в рамках однотемпературного приближения, примененного к излучению многотемпературной вспышечной плазмы с малым вкладом низкотемпературной части дифференциальной меры эмиссии.

РОЛЬ ВЫБРОСОВ ПЛАЗМЫ В РАЗВИТИИ МОЩНЫХ СОЛНЕЧНЫХ ВСПЫШЕК РАЗЛИЧНОЙ ДЛИТЕЛЬНОСТИ

А. Н. **Шаховская**1, М. А. Ли вши ц2, И. М. Черток2

АСТРОНОМИЧЕСКИЙЖУРНАЛ, **2006***, том 83,№12, с. 1128–1141*

Современные наблюдения показывают, что достаточно мощный выброс плазмы сопровождается формированием системы корональных петель и появлением двух лент, светящихся близ их оснований. Однако в одних случаях двухленточная вспышка длится, например, в мягком рентгеновском диапазоне много часов, в других — затухает в течение десятков минут. На примере четырех мощных вспышек **15–18 июля 2002** г. исследуется вопрос о причинах, влияющих на длительность вспышек. На основе разнообразных наземных и спутниковых наблюдений показано, что кратковременные быстрые события включали в себя коллимированные (узкие) выбросы плазмы в северном направлении и последующее формирование компактных петель в головной части активной области. В одном из событий, вслед за мощным выбросом в широком телесном угле в восточном направлении, в хвостовой части области сформировалась протяженная арочная система, определившая длительный характер вспышки. Есть основания полагать, что в тех событиях, где присутствуют коллимированные (узкие) выбросы и соответствующие узкие детали корональных выбросов массы (КВМ), система корональных петель образуется, но постэруптивное энерговыделение не возникает или выражено очень слабо, энергия из этой области не поступает вниз, и плазма в корональных петлях свободно высвечивается. В отличие от этих быстрых вспышек, широкий выброс и крупномасштабный яркий КВМсопровождаютсяформированием и длительным существованием протяженной арочной системы. Таким образом, мощные нестационарные процессы на Солнце включают в себя крупномасштабный КВМ и собственно вспышку, в которых реализация процесса пересоединения вместе с эволюцией вынесенной наружу плазмы определяют характер конкретного явления.

АКТИВНЫЕ ОБЛАСТИ НА СОЛНЦЕ С ПОВЫШЕННОЙ ВСПЫШЕЧНОЙ АКТИВНОСТЬЮ В 24 ЦИКЛЕ

ЯЗЕВ С. А.*1,2, ИСАЕВА Е. С.1,2, ИШМУХАМЕТОВА Ю. В.1

АЖ Том: 98 Номер: 6 Год: **2021** Страницы: 506-517

Проанализированы активные области (АО) на Солнце, отличающиеся высокими значениями вспышечного индекса и в то же время развивавшиеся вне комплексов активности (КА). Таких объектов в 24 цикле выделено 13. Показано, что эти АО относятся к разряду сравнительно долгоживущих крупных групп пятен, отличающихся повышенной скоростью роста площади. Эти АО входят в состав комплексов АО, соединяются с

другими АО системами высоких корональных систем, включая трансэкваториальные. Часть таких АО ассоциируется авторами с короткоживущими (менее 3 кэррингтоновских оборотов) комплексами активности, часть является компонентами комплексов активных областей. Все 13 рассмотренные АО находились рядом с корональными дырами.